GEOTECHNICAL AND GEOPHYSICAL SITE CHARACTERISATION 5

ISC'5

Barry M. Lehane,
Hugo E. Acosta-Martínez &
Richard Kelly
Editors

VOLUME 1

Proceedings of the

5TH INTERNATIONAL CONFERENCE ON GEOTECHNICAL AND GEOPHYSICAL SITE CHARACTERISATION

IN PURSUIT OF BEST PRACTICE

ISC'5, Gold Coast, Queensland, Australia, September 5–9, 2016

SIMSG ISSMGE

AUSTRALIAN GEOMECHANICS SOCIETY

GEOTECHNICAL AND GEOPHYSICAL SITE CHARACTERISATION 5

PROCEEDINGS OF THE FIFTH INTERNATIONAL CONFERENCE ON GEOTECHNICAL AND GEOPHYSICAL SITE CHARACTERISATION (ISSMGE TC-102 – ISC'5), GOLD COAST, QUEENSLAND, AUSTRALIA, 5-9 SEPTEMBER 2016

Geotechnical and Geophysical Site Characterisation 5

Editors

Barry M. Lehane
School of Civil, Environmental & Mining Engineering, The University of Western Australia, Australia

Hugo E. Acosta-Martínez
AECOM, Perth, Australia

Richard Kelly
SMEC and The University of Newcastle, New South Wales, Australia

VOLUME 1

AUSTRALIAN GEOMECHANICS SOCIETY

Published by: Australian Geomechanics Society
PO Box 955, St Ives, NSW 2075, Australia
e-mail: secretary@australiangeomechanics.org
www.australiangeomechanics.org

For Volume 1, ISBN 978-0-9946261-1-0
For Volume 2, ISBN 978-0-9946261-2-7

 ISBN 978-0-9946261-1-0

Table of contents

Introduction XIX

VOLUME 1

Seventh James K. Mitchell Lecture and keynote papers

The Seventh James K. Mitchell Lecture: Characterization of silt/sand soils 3
A-B. Huang

Evaluating effective stress parameters and undrained shear strengths of soft-firm clays from CPTu and DMT 19
P.W. Mayne

Characterizing mine tailings for geotechnical design 41
K. Been

New tools and directions in offshore site investigation 57
M.F. Randolph

Geotechnical site investigation in energetic nearshore zones: opportunities & challenges 69
N. Stark

Evaluating liquefaction and lateral spreading in interbedded sand, silt and clay deposits using the cone penetrometer 81
R.W. Boulanger, D.M. Moug, S.K. Munter, A.B. Price & J.T. DeJong

The GP sampler: a new innovation in core sampling 99
K. Mori & K. Sakai

Simulation of the cone penetration test: discrete and continuum approaches 125
A. Gens, M. Arroyo, J. Butlanska, L. Monforte, J.M. Carbonell, M. Ciantia, & C. O'Sullivan

Geophysical properties of soils 135
J.C. Santamarina & J. Park

Session Reports

Geophysics, 1 147
S. Foti

Geophysics, 2 155
K. Suto

Case histories, 1 159
S. Buttling

Case histories, 2 167
M. Arroyo

General site characterisation 173
J. Wierzbicki

Pavements and fills 181
B. Look

Sampling and laboratory 191
J.A. Pineda

Rocks and residual soil characterisation 199
E.A.G. Marques

Interpretation and design of in situ tests 205
J.T. DeJong

Design using in-situ tests 211
A. Klar

Liquefaction assessment 217
A.V. da Fonseca, C. Ramos & M. Cubrinovski

Application of statistical techniques 233
M.B. Jaksa

Non-standard materials and tailings 239
F. Schnaid

Developments in technology and standards 245
F.A.B. Danziger & T. Lunne

Penetration testing 251
J. Puechen

Pressuremeter and dilatometer 259
S. Burlon, W. Frikha & P. Monaco

Theme 1. Developments in Technology & Standards

Integration of invasive and non-invasive techniques in ground characterisation 273
S.D. Ekanayake, C.J. Leo, D.S. Liyanapathirana & P. Harutoonian

In-situ determination of soil deformation modulus and the wave velocity parameters using the Panda 3® 279
E. Escobar, M.A. Benz Navarrete, R. Gourvès, P. Breul & B. Chevalier

Comparison of Unified and European soil classification systems 285
M.S. Kovacevic, D. Juric-Kacunic & L. Libric

Televiewer imaging of boreholes; benefits and considerations for interpretation in the absence of physical rock core 291
G.T.C. McKenna & S.L. Roberts-Kelly

Additional parameters measured in a single CPT, click-on modules for the digital cone 297
M. Woollard, O. Storteboom, T. Länsivaara & J. Selänpää

Correction for CPT fs errors due to variation in sleeve diameter 303
M. Holtrigter & A. Thorp

Reduced pressuremeter test time procedure and new analysis method 309
K. Iskander

Earth pressure evaluation and safety assessment employing a novel measurement device – The Inclinodeformeter 315
G.M. Ausweger & F. Tschuchnigg

Theme 2. Penetration Testing

Correlation of p-wave velocity and SPT-N on volcanic soils in Costa Rica 323
S.J. Ibanez, S. Ortiz-Palacio, V. López-Ausin & J.A. Porres-Benito

Strength assessment of frozen soils by instrumented Dynamic Cone Penetrometer 329
S.Y. Kim, W-T. Hong, J-S. Lee & Y. Kim

The SPT N-value errors examined with digital technology 333
B. Look

SPT test: An approach to predicting undrained shear strength based on energy concepts 339
J.A. Lukiantchuki

Rotation speed analysis in SPT-T test by type of soil 345
R.R. Nuñez, T.T.C. Piovan & A.S.P. Peixoto

Critical appraisal of T-bar penetration tests 351
J. Peuchen & J. Terwindt

Free-falling full-flow penetrometer for marine material characterization – analytical solution 357
S. Pinkert

CPTu in consolidating soils 363
P.P. Rahardjo, B.W. Anggoro & A. Wirawan

Effect of rotation rate on shear vane results in a silty tailings 369
D. Reid

Analysis of instrumented sharp cone tests performed in a sensitive clay of Quebec 375
V. Silvestri & C. Tabib

Theme 3. Interpretation of In-Situ Testing

Relative densities and void ratios derived from CPT data using in situ field calibration 383
T. Biryaltseva, T. Mörz, S. Brandt, S. Kreiter, U. Gerdes & B. Ossig

Relative density prediction based on in-situ and laboratory measurements of shear wave velocity 389
T. Biryaltseva, T. Lunne, S. Kreiter & T. Mörz

Strain moduli of alluvial soils from CPT, DMT, Vs, and lab tests 395
G. Bosco & P. Monaco

Virtual T-bar penetrometer tests using Discrete Element Method 401
L.S. Carvalho, J.R.M.S. Oliveira, C.A.B. Vasconcellos, M.E.S. Marques, M.G. Teixeira & J.A. Lukiantchuki

Correlations between SPT and CPT data for a sedimentary tropical silty sand deposit in Brazil 407
Y.D. Costa, E.S. Cunha & C.L. Costa & A.C. Pereira

Finite element modeling of cone penetration test in weakly cemented sand 413
R. Debasis, S.D. Kumar, D. Arghya & G. Saswati

Cylindrical cavity expansion analysis applied to the interpretation of variable rate cone penetration in tailings 419
G. Dienstmann, F. Schnaid & S. Maghous

Reliability of soil porosity estimation from seismic wave velocities 425
S. Foti & F. Passeri

Discrete Element Method modeling studies of the interactions between soils and in-Situ testing devices 431
J.D. Frost, A. Martinez, J. Su & T. Xu

Identification of the influence of overconsolidation effect on subsoil's stiffness by a CPTU method 437
Z. Młynarek, J. Wierzbicki & T. Lunne

Application and tentative validation of soil behavior classification chart based on drilling parameter measurements 443
P. Reiffsteck, J. Benoît, M. Hamel & J.-M. Vaillant

Calibrating CPT relative density and strength correlations for a laboratory fine sand 449
J.A. Schneider, J.R. Giampa, A.S. Bradshaw & J.T. Newgard

On the determination of the undrained shear strength from vane shear testing in soft clays 455
L.J. Wilson, G.P. Kouretzis, J.A. Pineda & R.B. Kelly

Use of shear wave velocity to estimate stress history and undrained shear strength of clays 461
S.S. Agaiby & P.W. Mayne

Permeability profile of a planosol based on in situ falling head permeability tests 467
C.A.B. Bastos & D.F. Fagundes

Influence of penetration rate on CPTU measurements in saturated silty soils 473
M.F. García Martínez, L. Tonni, G. Gottardi & I. Rocchi

Dissipation tests in saline environment 479
E. Imre, D. Bishop, L. Bates, S. Fityus, Z. Bakacsi, K. Rajkai & M. Juhász

Some comments on the CPTu and DMT dissipation tests 485
E. Imre, D. Bishop, L. Bates, S. Fityus, Z. Hortobagyi & M. Juhász

Estimation of soil hydraulic conductivity assisted by numerical tools – two case studies 491
R. Karim, M.M. Rahman & D. Hughes

Effect of soil stiffness on cone penetration response in soft-stiff-soft clays 497
H. Ma, Y. Hu, M. Zhou & M.S. Hossain

A method for predicting the undrained shear strength from piezocone dissipation tests: case studies 503
E. Odebrecht, F. Mantaras & F. Schnaid

Monotonic and dilatory excess pore water dissipations in silt following CPTU at variable penetration rate 509
P. Paniagua, R. Carroll, J.-S. L'Heureux & S. Nordal

Estimating K_0 in sandy soils using the CPT 515
P.K. Robertson

Effects of suction on CPT results and soil classification 521
A.R. Russell & D. Reid

Theme 4. Laboratory Testing and Sampling

Engineering characterization of a leached marine clay using Sherbrooke block samples 529
H.A. Amundsen, A. Emdal & V. Thakur

Undrained shear strength and anisotropic yield surface of diatomaceous mudstone 535
N. Arsalan, M. Akaishi & M. Sugiyama

Laboratory measurement of sensitivity of carbonate soils 541
N. Boukpeti & B.M. Lehane

Maximum shear modulus of a Brazilian lateritic soil from in situ and laboratory tests 547
L. Décourt, J.M. de Camargo Barros, O.C.B. Gandolfo, A.R.Q. Filho & F.D. Penna

Engineering properties and cone factor of Onsøy clay, Louiseville clay and Mexico City clay 553
H. Hirabayashi, H. Saegusa, M. Tanaka, T. Fukasawa & R. Tomita

Influence of phosphate dispersing agents on particle size distribution of soil fines 559
A. Kaur & G.C. Fanourakis

The influence of in-situ effective stress on sample quality for intermediate soils 565
C.P. Krage, B.M. Albin, J.T. DeJong & D.J. DeGroot

Offshore prediction of sampler penetration and recovery using CPTs 571
N. Ramsey

Experience with gel-push sampling in New Zealand 577
M.E. Stringer, M. Cubrinovski & I. Haycock

Definition of failure in cyclic direct simple shear tests on normally consolidated kaolin clay and presentation of shear strain contour diagrams 583
D. Zografou, N. Boukpeti, S.M. Gourvenec & C.D. O'Loughlin

Theme 5. Liquefaction Assessments

Standard Penetration Test-based assessment of seismic soil liquefaction potential of Urmia, Iran 591
H. Bahadori & A. Hasheminezhad

Liquefaction assessment based on combined use of CPT and shear wave velocity measurement 597
Z. Bán, A. Mahler, T.J. Katona & E. Győri

The determination of factor of safety against liquefaction and post-liquefaction settlement 603
P.R. Klibbe

Soil classification and liquefaction evaluation using Screw Driving Sounding 609
S.Y. Mirjafari, R.P. Orense & N. Suemasa

Combined use of SDMT-CPTU results for site characterization and liquefaction analysis of canal levees 615
P. Monaco, L. Tonni, G. Gottardi, M. Marchi, L. Martelli, S. Amoroso & L. Simeoni

Estimating the cyclic softening of clays of five different sites at Matsyapuri, Willingdon Island, Kochin, Kerala, India 621
R.R. Phule, P. Kurangale, R. Alone, V. Gabhale, N. Pawar & K. Birajdar

Field measurements of the variability in shear strain and pore pressure generation in Christchurch soils 627
J.N. Roberts, K.H. Stokoe, S. Hwang, B.R. Cox, Y. Wang, F.M. Men & S. van Ballegooy

Liquefaction assessment CPTu tests in a site in South of Portugal 633
C. Rodrigues, S. Amoroso, N. Cruz & A. Viana da Fonseca

Evaluation of DMT-based liquefaction triggering curves based on field case histories 639
K.M. Rollins, T.K. Remund & S. Amoroso

Liquefaction resistance of gravelly soil from Becker penetrometer (BPT) and Chinese dynamic cone penetrometer (DPT) 645
K.M. Rollins, T.L. Youd & M. Talbot

New developed soundings to assess liquefaction potential of soils 651
S. Sawada

Comparison of liquefaction evaluation based on SPT and geophysical tests (case study: Mahabad dam, Iran) 657
M.M. Shahrabi, F. Jafarzadeh, A.A. Garakani, N. Eskandari, M. Banikheir & H. F. Jahromi

Fines content correction factors for SPT N values – liquefaction resistance correlation 663
M.M. Shahien

A surface seismic approach to liquefaction 669
S. Castellaro & R. Panzeri

Theme 6. Pavements and Fills

Evaluation of rockfill embankments by field tests in Siraf Refinery Complex site, Iran 677
E. Asghari-Kaljahi, N. Nasrollahi & Z. Kheyrouri

Control of soil compaction in pavement layers: a new approach using the dynamic cone penetrometer (DCP) 683
A. Belincanta, J.A. Lukiantchuki & J.H.C. Reis

A new indirect tensile testing setup to determine stiffness properties of lightly stabilised granular materials 689
D.K. Paul, R. Gnanendran & M.J.I. Alam

New and innovative approach to ensuring quality of quarry source materials in Queensland road infrastructure construction 695
A. Dissanayake & P. Evans

Correlation between the results of the PLT and CBR tests to determine the elasticity modulus 701
A. Hajiannia, M.T. Dorobati, S. Kasaeian & S.B. Baghbadorani

Characterization of railroad track substructures using dynamic and static cone penetrometer 707
W-T. Hong, S. Kang, J-S. Lee, Y-H. Byun & C-Y. Choi

Suggested QC criteria for deep compaction using the CPT 711
P.K. Robertson

Proposed performance criteria for earthwork construction quality control 717
A. Sawangsuriya, S. Wachiraporn, S. Sirisak & W. Lawanwisut

Collapse settlement and strength characteristics of unsaturated soils with different degrees of compaction 723
A.M. Shahnoory & M. Sugiyama

Geotechnical characterization of a heterogeneous unsuitable stockpile 729
K. Rengifo, F. Herrera & L. de la Cruz

Verification of an impact rolling compaction trial using various in situ testing methods 735
B.T. Scott, M.B. Jaksa & E. Syamsuddin

Theme 7. Pressuremeter and Dilatometer

Pressuremeter tests in the hard soils and soft rocks of Arak Aluminum Plant site, Iran 743
E. Asghari-Kaljahi, Z. Khalili & S. Yasrobi

Stress-strain response of fine silica sand using a miniature pressuremeter
A.A. Bagbag, J.P. Doherty & B.M. Lehane 749

Use of flat dilatometer in Ontario
L.F. Cao, S.M. Peaker & S. Ahmad 755

Self-boring pressuremeter tests at the National Field Testing Facility, Ballina NSW
F.M. Gaone, J.P. Doherty & S.M. Gourvenec 761

Practice of the PENCEL pressuremeter in foundations design
F. Messaoud & P.J. Cosentino 767

In situ characteristics of Manhattan glacial deposits from pressuremeter tests
C.E. Ho 773

Membrane correction for pressuremeter test
J. Monnet, D. Mahmutovic & L. Boutonnier 779

New DMT method for evaluating soil unit weight in soft to firm clays
Z. Ouyang & P.W. Mayne 785

Evolution of deformation parameters during cyclic expansion tests at several experimental test sites
P. Reiffsteck, S. Fanelli & G. Desanneaux 791

Ground property characterization from in-situ tests: opportunities offered by measuring thrust during Flat Plate Dilatometer testing
J.H. Schmertmann & D.K. Crapps 797

Interpretation of the instrumented DMT (iDMT)- a more accurate estimation of p_0
H. Shen, W. Haegeman & H. Peiffer 803

Determination of E_m from Ménard pressuremeter tests for gneiss residual soils
T.Q. Silva, E.S. Cândido, E.A.G. Marques & E. Minette 809

Author index 813

VOLUME 2

Theme 8. Geophysics

Multi-dimensional Electrical Resistivity Tomography (ERT) for the mapping of the zones with (or without) cavities in Hofuf KSA
S.N. Abduljauwad, H.R. Ahmed, M.A. Shafiq & M. Abdul-Waheed 819

Preliminary results of P-wave and S-wave measurements by seismic dilatometer test (SPDMT) in Mirandola (Italy)
S. Amoroso, C. Comina, S. Foti & D. Marchetti 825

Geophysical characterisation of marine and quick clay sites: field and laboratory tests 831
S. Bazin, H. Anschütz, G. Sauvin, T.E. Helle, S. Gribben, S. Donohue & M. Long

Near-surface geophysical scanning for exemplar landslide projects in Poland 837
Z. Bednarczyk

Imagery of nonlinear soil behaviour using in-situ and laboratory tests 843
K. Çami, J. Garcia, L.-F. Bonilla-Hidalgo, J.-L. Tacita & S. Perlo

An investigation into the effects of material properties on shear wave velocity in rocks/soils 849
N. Campbell, C. Fenton & S. Tallett-Williams

Integrated use of terrestrial laser scanning and thermal imagery for characterization of hydrothermally altered granites 855
J.S. Coggan, D.M. Pascoe, M.L. Eyre & J.H. Howe

Soil discrimination using an electrical logging method 861
M. Fujii, K. Watanabe, T. Fukaya & K. Takechi

Inversion of effective phase velocity seismic surface wave data by partial least squares regression 867
G. Heymann, D.N. Wilke & S. Kok

Use of GPR on two sites with voids to enable safer work and targeted probing 873
C.G.C. Hughes, K.J. Read & M. Watson

Assessment of underground karst caves using geophysical tests: a case study for Lajamgir dam site, Iran 879
F. Jafarzadeh, M.M. Shahrabi, M. Banikheir, N. Eskandari, A.A. Garakani & H. F. Jahromi

A comparison of in-situ and laboratory resistivity measurements in soft clay 883
R.B. Kelly, J.A. Pineda & L. Suwal

Geophysical characterisation for dredging of the Marine Industry Park, Darwin 887
J. Lean & S. Williams

Generalization and standardization of multi-station surface wave method for site investigation 893
C.P. Lin & C.H. Lin

Characterisation of small strain rock modulus from ultrasonic pulse velocity testing 899
B. Look, S. Schneider & C. Gallage

Use of geophysical logs to map aquifers electrofacies 905
R. Macari, A.S.P. Peixoto & G.G. Nery

Multichannel Analysis of Surface Waves (MASW) for offshore geotechnical investigations 911
T. McGrath, M. Long, P. O'Connor, A. Trafford & D. Ward

In-situ detection of sensitive clays from a geophysical perspective 917
A.A. Pfaffhuber, S. Bazin, K. Kåsin, H. Anschütz, R. Sandven, A. Montafia, A.S. Gylland & M. Long

Regional geotechnical railway corridor mapping using airborne electromagnetics 923
A.A. Pfaffhuber, H. Anschütz, T. Ørbech, S. Bazin, A.O.K. Lysdahl, M. Vöge, G. Sauvin, I.-K. Waarum, H.C. Smebye, K. Kåsin, G. Grøneng, A.-L. Berggren, J.B. Pedersen & N. Foged

Fractures location on karstified limestone surfaces by electrical resistivity tomography characterization 929
J.A. Porres-Benito, S.J. Ibanez, S. Ortiz-Palacio & V. López-Ausín

Site characterization of seismic stations based on downhole tests to 30 m depth in South Korea 935
C.G. Sun, J.M. Jeong, K.S. Kim & I.S. Jang

Design and application of a low-cost, 3D printed crosshole seismic system - Preliminary assessment 941
M.B. Sylvain, M.A. Pando, M.J. Whelan, V.O. Ogunro & Y. Park

S-wave borehole tomography for geotechnical site characterization 947
J.K. von Ketelhodt, T. Fechner & M.P.E. de Kleine

Analysis of active MASW test data for a convergent shear wave velocity profile 951
S.S. Kashyap, A.M. Krishna & A. Dey

Development of an unmanned aircraft mounted software defined ground penetrating radar 957
J.F. Fitter, A.B. McCallum & J. X. Leon

Simplified seismic soil classification: the velocity-frequency-impedance (VfZ) matrix 963
S. Castellaro

The complementarity of HV and dispersion curves 967
S. Castellaro

Theme 9. General Site Characterisation

Characterisation of Halden silt 975
Ø. Blaker, R. Carroll, J.-S. L'Heureux & M. Klug

In situ behavior of clay soils over different drought-rewetting conditions 981
A. Denis, R. Fabre & J.F. Lataste

Geotechnical site investigations for dredging works - Port of Townsville 987
M. Jaditager & N. Sivakugan

Using multi-channel analysis of surface waves and cone penetrometer tests to delineate an in-filled palaeochannel during routine investigations - A Christchurch earthquake case study 991
R. Kamuhangire, T. Plunket & C. Rüegg

CPTU crossing existing boreholes in the soil 997
K. Kåsin

Effect of inter-particle strength on K_0 correlation for granular materials 1003
J. Lee, G. Kim, I. Kim, D. Kim, & B. Byun

Soil behaviour type of the Sarapuí II test site 1009
P.F. Nejaim, G.M.F. Jannuzzi & F.A.B. Danziger

Geophysical and in situ testing applied to site characterisation for non-engineered structures in developing regions 1015
S. Ortiz-Palacio, S. Ibáñez García, V. López-Ausín & J.A. Porres-Benito

Geotechnical characterization of Ballina clay 1021
J.A. Pineda, R.B. Kelly, L. Suwal, L. Bates & S.W. Sloan

Geotechnical parameters of soft soil in Macaé – Rio de Janeiro 1029
L.M.M. Povoa, P.N.C. Nascimento, P.C.A. Maia & V.S. Singui

Geophysical and geotechnical characterisation of the Saltwater Creek bridge site, Morten Bay rail project, Queensland, Australia 1033
A. Purwodihardjo, T. Rahiman, M. Parsons & J. Kruger

CPT, DMT and MASW allowing economic design of a large residential project over soft soils 1039
N.B. Schofield & R.W. Burke

A 2016 case for public geotechnical databases 1045
T. Thompson

Site characterization and seismic response analysis in the area of Collemaggio, L'Aquila (Italy) 1051
G. Totani, P. Monaco, F. Totani, G. Lanzo, A. Pagliaroli, S. Amoroso & D. Marchetti

Geotechnical and geophysical site characterization of a nuclear power plant site in United Arab Emirates 1057
S. Parashar, R. Rice, P. Asprouda, H. Al Hammadi & J.D. Lee

Theme 10. Characterisation in Rock and Residual Soil

Continuous-interval seismic piezocone testing in Piedmont residuum 1065
S.S. Agaiby, E. Cargill, T. Ku & P.W. Mayne

Assessment of results of CPT tests in porous lateritic unsaturated soil from Campinas, Brazil 1071
P.J.R. Albuquerque & T.G. Rodriguez

Piezocone tests in residual soils: a Portuguese experience in granitic soils 1077
N. Cruz, J. Cruz, F. Martins, C. Rodrigues & M. Cruz

A method to assess rock strength and excavatability of diamondiferous kimberlite ore through in situ rock testing 1083
S. Elbaz, D. Crawford & M. Tuck

Evaluation of the vulnerability of rock weathering based on monitoring using photogrammetry 1087
D.H. Kim, I. Gratchev, E. Oh & A.S. Balasubramaniam

In-situ rock stress determined by hydraulic fracturing test in Singapore 1093
K. Kimura, T. Yasuda, S. L. Chiam & K. H. Goay

Use of the Light Falling Weight Deflectometer (LFWD) as a site investigation tool for residual soils and weak rock 1099
D. Lacey, B. Look & D. Marks

Morphology and geotechnical characterization of a phyllite weathering profile developed under tropical climate 1105
M.F. Leão & E.A.G. Marques

Evaluation of the engineering properties of the weathered layer in Korea 1111
S.H. Lee, B.H. Jo & C. Chung

Impact of rock mass strength parameters on low wall stability assessment outcomes in open-cut coal mines 1117
J. Li, N. Tucker & J.K. Todd

Investigation the results of Plate Load Test using rigid plates in weak rock masses: a case study 1123
M.G. Nik, B. Abrah & E.G. Samani

Characterization of unsaturated tropical soil site by in situ tests 1129
B.P. Rocha, R.A. dos Santos, R.C. Bezerra, R.A. Rodrigues & H.L. Giacheti

G-γ decay curves in granitic residual soils by seismic dilatometer 1137
C. Rodrigues, S. Amoroso, N. Cruz & J. Cruz

A consideration on the shear strength characteristics of unsaturated volcanic soils 1143
A.S. Samim & M. Sugiyama

Characterisation of a lateritic soil using laboratory and in-situ tests 1149
W. Shi, B.M. Lehane, A. Gower & S. Terzaghi

Theme 11. Characterisation of Non-standard soils

Estimation of undrained shear strength for peat using CPT 1157
H. Hayashi & T. Hayashi

A review of the unconfined compressive strength of microbial induced calcite precipitation treated soils 1161
R.N. Hora, M.M. Rahman, S. Beecham & R. Karim

Challenges with sampling coarse-grained permafrost: an experience in Svalbard 1167
T.M.H. Le, M. Wold & M.G. Bærverfjord

Collapse settlement and strength characteristics of unsaturated soils with different degrees of compaction 1173
A.M. Shahnoory & M. Sugiyama

Prediction of swelling potential of Sudanese clayey sand (SC) soils 1179
H. Shammat & M.A. Osman

Theme 12. Design Using In-situ tests

Evaluation of tip resistance to auger drilling 1187
G.G. Boldyrev & G.A. Novichkov

Characterisation of a Norwegian quick clay using a piezoball penetrometer 1193
N. Boylan, A. Bihs, M. Long, M.F. Randolph & S. Nordal

Observing friction fatigue on calcareous material 1199
D. Denes

Data driven design - a vision for an automated approach 1205
J.P. Doherty & B.M. Lehane

The Smithfield Bypass project – Justifiable need for a second stage piezocone testing 1211
L.E. Ezeajugh

Soil strength in the Murray River determined from a free falling penetrometer 1217
A. Fawaz, A. Teoh, D.W. Airey & T. Hubble

Correlations of regional (Poland) geotechnical parameters on the basis of CPTU and DMT tests 1223
T. Godlewski

Evaluating the OCR and permeability of cutoff wall using CPTU results 1229
X.P. Li, G.J. Cai, J. Lin, S.Y. Liu & A.J. Puppala

Evaluation of relative density and liquefaction potential with CPT in reclaimed calcareous sand 1235
P. Mengé, K. Vinck, M. Van den Broeck, P.O. Van Impe & W.F. Van Impe

Use of CPTU for the assessment of the stiffness model of subsoil 1241
Z. Młynarek, J. Wierzbicki & W. Wołyński

Empirical estimation of soil unit weight and undrained shear strength from shear wave velocity measurements 1247
S.W. Moon & T. Ku

Small strain stiffness assessments from in situ tests – revisited 1253
J.J.M. Powell, L. Dhimitri, D. Ward & A.P. Butcher

Case studies on variability in soils and driven pile performance 1259
W.A. Prakoso

Evaluation of CPT- based ultimate lateral pile resistance in sand 1265
H.Y. Qin & W.D. Guo

Interpretation of CPT data for pile loading behavior - inverse estimation of void ratio over depth 1271
K.-F. Seitz, E. Heins, A. Carstensen & J. Grabe

Interpretation of shear strength data for construction on mine tailings deposits 1275
D.J. Williams

Estimation of shear wave velocity based on SPT profile data 1281
F. Yi & F.P. Yi

Application of dynamic cone penetrometer for measuring active thaw layer depth 1287
H-K. Yoon, Y.S. Kim, S.S. Hong, Y-H. Byun & J-S. Lee

Theme 13. Case Histories

Two-dimensional non-linear dynamic response of a heap leach pad located in Peru 1291
F.C. Perez & J.D. Ale

Ultimate resistance and settlement of foundations using Ménard pressuremeter test results: case of bored piles 1297
R. Bahar, N. Alimrina & L. Djerbal

Applicability of CPT to determine geotechnical properties of sand deposits to an Uruguayan gas plant 1303
A.W.R. Barreto & B.L.C.G. Árabe

Study on seismic response analysis in "Vincenzo Bellini" Garden area by Seismic Dilatometer Marchetti tests 1309
A. Cavallaro, S. Grasso & A. Ferraro

Predicted and measured behavior of a tall building in a lateritic clay 1315
L. Décourt, C. Grotta Jr., A.S.D. Penna & G.C. Campos

Remedial measures to facilitate the construction of stable bridge approach fills: a case study 1321
V. Diyaljee

Subsidence characterisation for a proposed concrete shaft using a 250m deep inclinometer borehole - Huntly East Coalmine, New Zealand 1327
Z. Du, M. Balks, V. Moon, P. Page, R. Winter & L. Cunningham

Subsurface compacted rubble raft technology for ground improvement 1331
Z. Du & M.A. Shahin

A4 motorway operation in the area of linear discontinuous surface deformations 1337
M. Grygierek & J. Kawalec

Effects of additional excavation on critical slip surface of stabilized walls with soil nailing 1343
A. Hajiannia, M.T. Dorobati, S.B. Baghbadorani & S. Kasaeian

Field investigation of the performance of soft soil reinforcement with inclined pile 1349
A.T. Harianto, L. Samang, B. Suheriyatna & Y. Sandyutama

Static load testing of concrete free reticulated micropiles system 1353
A. Mehdizadeh, M.M. Disfani, R. Evans, E. Gad, A. Escobar & W. Jennings

A comparative analysis of the stability of a slope in an overconsolidated clay pit based on CPT and DMT measurements 1359
H. Peiffer

How many drillings are necessary? A case study 1365
M. Premstaller

Elastic and non-elastic response of pile-raft system embedded in soft clay 1369
M.V. Shah, A.R. Gandhi & D.V. Jakhodiya

Geotechnical monitoring of in situ heater test 1375
K. Sosna & J. Záruba

Site investigation, monitoring and stability analysis of a built-up slope involved by gas pipeline explosion 1381
G. Totani, F. Totani, P. Monaco & L. Simeoni

A preliminary design of ground improvement by grouted stone columns for a shopping centre 1387
A.M. Ünver & İ.S. Ünver

Comparison of pile design following two standards: EC7 and AS2159 1393
S. Buttling

Different response of apparently identical structures: a far-field lesson from the Mirandola (Italy) 2012 earthquake 1405
S. Castellaro

In-situ performance assessment of ballasted railway track stabilised using geosynthetics and shock mats 1411
S. Nimbalkar & B. Indraratna

Measuring and comparing soil parameters for a large bridge on East coast of United States 1417
R. Failmezger, G. Sedran & D. Marchetti

Behavior of a model shallow foundation on reinforced sandy sloped fill under cyclic loading 1423
M.J.I. Alam, C.T. Gnanendran & S.R. Lo

Theme 14. Application of Statistical Techniques

Frequency spectrum “Bell-curve” fitting as a component of SCPT interval velocity accuracy assessment 1431
E. Baziw & G. Verbeek

Enhanced data interpretation: combining in-situ test data by Bayesian updating 1437
J. Huang, R.B. Kelly & S.W. Sloan

Calibration of Vs prediction model based on SPT-N using conditional probability theory 1443
T. Kishida & C-C. Tsai

Identification of geologic depositional variations using CPT-based conditional probability mapping 1447
C.P. Krage, J.T. DeJong & R.W. Boulanger

Probabilistic assessment of laterally loaded pile performance in sand 1453
B.M. Lehane, F. Glisic & J.P. Doherty

Stochastic waveform inversion for probabilistic geotechnical site characterization
S.S. Parida, K. Sett & P. Singla 1459

Automatic methodology to predict grain size class from dynamic penetration test using neural networks 1465
C. Sastre, M. Benz, R. Gourvès, P. Breul & C. Bacconnet

Quantifying and reducing uncertainty in down-hole shear wave velocities using signal stacking 1471
M.A. Styler & I. Weemees

3D mapping of organic layers by means of CPTU and statistical data analysis 1481
J. Wierzbicki, A. Smaga, K. Stefaniak & W. Wołyński

Assessment of ground improvement on silt based on spatial variability analysis of CPTU data 1487
H.F. Zou, G.J. Cai, S.Y. Liu, J. Lin, T.V. Bheemasetti & A.J. Puppala

Theme 15. Environmental Testing

Observed influence of ambient temperature variations on the analysis of ground thermal response tests 1495
S. Colls

Monitoring the plume of potassium chloride from wells used as ground improvement in highly sensitive clays 1501
T.E. Helle, P. Aagaard, A. Emdal & S. Nordal

The effects of preload surcharge on arsenic and aluminium mobilization in pyritic sediment 1507
O. Karikari-Yeboaha, W. Skinner & J. Addai-Mensah

Electrical conductivity breakthrough curve of soil column with residual diesel fuel 1513
M. Oh & Y.S. Kim

Experimental study on water content and density effects on dielectric permittivity of selected Victorian soils 1517
A. Orangi, D.S. Langley, N.M. Withers & G.A. Narsilio

In-situ soil water content estimation using new capacitive based sensors 1523
A. Orangi, N.M. Withers, D.S. Langley & G.A. Narsilio

Site characterization for a new refinery in a disposal area for bituminous residue 1529
B. Pasqualini, E. Nicotera, A. Liberati, R. Marcellini, P. Ascari & R. Galbiati

Influence of periodic hydrocarbon contaminated bentonite on strength and settlement characteristics of stone column 1535
M.V. Shah & H.C. Chokhawala

A preliminary study on evaluating the performance of aged landfill covers using DC and CC resistivity methods 1541
Y.X. Wu, Y.H. Wang & X. Zhang

Assessment of the infiltration capacity of a retention pond by the TDR measurements 1547
I.A. Ichola & C. Anzoras

Author index 1553

 ISBN 978-0-9946261-1-0

Introduction

Site characterisation is an essential component of the geotechnical design required for projects involving deep and shallow foundations, basements, slopes, tunnels, roads, embankments, mine tailings, seismic hazard assessments, site remediation and ground improvement. The Fifth International Conference on Geotechnical and Geophysical Site Characterisation (ISC'5) was held from September 5th to 9th 2016, on the Gold Coast about 100 km south of Brisbane in Queensland, Australia. This fifth conference follows the successful series of international conferences held in Atlanta (ISC'1, 1998), Porto (ISC'2, 2004), Taipei (ISC'3, 2008) and Porto de Galinhas, Brazil (ISC'4, 2012). The series is promoted by the International Society of Soil Mechanics and Geotechnical Engineering (ISSMGE) and managed by the ISSMGE Technical Committee, TC102 (Ground Property Characterization from In-Situ Tests).

These two volume proceedings contain 237 papers, which were presented by geotechnical researchers and practitioners from 50 countries. Eight keynote papers and 16 session report papers are presented by outstanding experts in the field. The Seventh James K. Mitchell Lecture presented by Prof. An-Bin Huang is also included. The papers have been sorted into 15 general themes, namely: 1. Developments in technology and standards; 2. Penetration testing; 3. Interpretation of in-situ testing; 4. Laboratory testing and sampling; 5. Liquefaction assessments; 6. Pavements and fills; 7. Pressuremeter and dilatometer; 8. Geophysics; 9. General site characterisation; 10. Characterisation in rock and residual soil; 11. Characterisation of non-standard soils; 12. Design using in-situ tests; 13. Case histories; 14. Application of statistical techniques and 15. Environmental testing. The Seventh James K. Mitchell lecture, keynote papers and session report papers are provided at the beginning of Volume 1.

The editors would like to thank all of the members of TC102 for their ongoing support as well as all experts involved in reviewing the selected papers. We are particularly grateful to all keynote lecturers, session reporters and authors for their contribution to the state-of-the-art, as presented in these proceedings. We are most grateful for the financial support provided by the Australian Geomechanics Society.

Barry M. Lehane
University of Western Australia, Australia

Hugo E. Acosta-Martínez
AECOM, Australia

Richard Kelly
SMEC and the University of Newcastle, Australia

Keynote lectures

Geotechnical and Geophysical Site Characterisation 5 – Lehane, Acosta-Martínez & Kelly (Eds)
ISBN 978-0-9946261-1-0

The Seventh James K. Mitchell Lecture: Characterization of silt/sand soils

A.B. Huang
National Chiao Tung University, Hsinchu, TAIWAN

ABSTRACT: The term silt/sand or M/S is proposed as an inclusive abbreviation of soils that can span from sand with very little silt, silty sand to pure silt. It is generally believed that sands with fines (particles passing #200 sieve) tend to be more compressible. Because of their low permeability, cone penetration tests (CPT) in sands with fines can be partially drained. High compressibility makes the soil more contractive and thus showing lower resistance in undrained shearing. Significant ground subsidence can also be associated with the high compressibility of M/S/ soils. For CPT in granular soils with similar density and stress states, the high compressibility and partial drainage can both contribute to lower cone tip resistance. Natural granular soils are likely to contain fines than being clean (fines content < 5%). Studies on M/S soils are far less than those on clean sands. Because of the unique geological setting, the author had the opportunity to work with a local M/S deposit in Central Western Taiwan in the past 25 years. Procedures for laboratory soil element tests as well as CPT calibration tests using reconstituted specimens have been developed and a series of tests performed. Practical undisturbed sampling techniques in M/S soils were experimented and applied. Methods to correlate cyclic strength, fines contents and cone tip resistance in M/S deposit were proposed. The concepts of equivalent granular void ratio and state parameter were experimented in compiling the test data. The paper describes the new characterization techniques developed and lessons learned in the interpretation of test data for the studied M/S soils.

1 INTRODUCTION

1.1 *Origin of the studied soil deposit*

Parts of the Western and Southern Taiwan are covered by a thick deposit of alluvial material. The alluvial material originated from the central mountain range that lies on the east side of Taiwan in a north-south direction as shown in Figure 1. The central mountain range was created by the collision between the Philippine Sea plate and Eurasian plate. The plate movements were also responsible for frequent and strong earthquakes in this region. Typhoon is another form of natural hazards that brought in heavy rainfalls. Earthquakes weakened the rock formations in the central mountain range which were mostly sedimentary and metamorphic in nature. Rainfalls created landslides and debris flows, the eroded soil eventually deposited and formed the land on the west side of Taiwan. The process of transportation by rapidly flowing streams ground the fractured rock into sand and silt particles before deposition on the west plain, to a thickness of several hundred meters. The island of Taiwan has one of the highest density of population in the world. The continued industrial, agricultural and infrastructure developments created constant struggles for more land and water resources.

Because of the above reasons, the author had the opportunities to conduct research and consulting activities that relate to the characterization of the soil deposits in this region. The activities included:

1. Calibration of cone penetration tests (CPT) for a land reclamation project in Mai Liao (see Figure 1) in the mid-1990's. The original goal was to develop guidelines for the interpretation of CPT in M/S soil for quality assurance of field densification.
2. Dynamic soil property characterization after the Chi Chi earthquake in 1999. Cyclic triaxial tests were performed on reconstituted and natural M/S soils.
3. The design and construction of various infrastructure projects that demanded undisturbed M/S soil samples be taken with reasonable costs.
4. Evaluation of the mechanisms of ground subsidence along the west coast of Taiwan.
5. Development of geotechnical design parameters for the Fu Hai offshore wind farm.

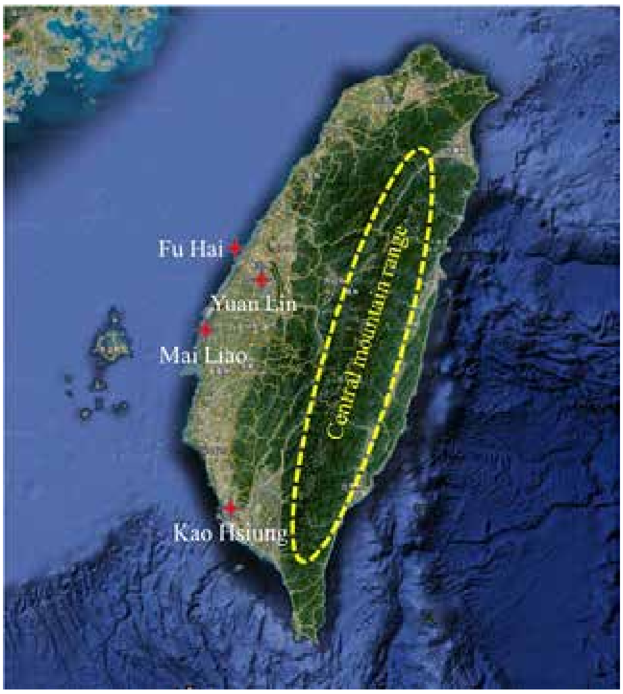

Figure 1. The central mountain range and west plain of Taiwan (from Google)

The above activities provided the opportunities for various aspects of laboratory and field tests to be undertaken that eventually lead to a more comprehensive study on the M/S soils in this region.

1.2 *Physical properties of the silt/sand soils studied*

Mai Liao Sand (MLS) represents a typical alluvial soil deposit in Central Western Taiwan (see Figure 1). The term Mai Liao Sand is used loosely as most of the tests to be reported in the paper involve mixture of sand and silt. A few metric tons of MLS was acquired from a land reclamation site. Figure 2 shows the typical grain size distribution curves of MLS samples taken from the land reclamation site. The natural soil deposit in the field could have a much wider variation of fines contents. The sand retrieved from the reclamation site was washed and sieved through a #200 sieve to separate the fines (particles passing the #200 sieve) from the sand particles. The specific gravity of clean MLS sand particles had an average value of 2.69 and the fines had an average specific gravity of 2.71. X-ray diffraction analysis of MLS showed significant amounts of muscovite and chlorite, in addition to quartz, as indicated in Table 1. The sand particles retained on #200 sieve were angular and platy as indicated in the scanning electron microscope photograph shown in Figure 3. The grain characteristics are apparently affected by the parental rocks which included shale, slate and schist, in addition to sandstone. The fines passing #200 sieve had a liquid limit of 32 and a plasticity index less than 8. Figure 4 shows the variation of minimum (e_{min}) and maximum (e_{max}) void ratios of MLS as the fines contents changed from 0 to 80%. Details on the determination of e_{min} and e_{max} are described in Huang et al. (2004).

Table 1 Mineral contents of MLS (Huang et al., 2004)

Mineral	Coarse, %	Fines, %
Quartz	75.4	20.0
Clinochlore	10.9	29.4
Muscovite	8.6	48.1
Feldspar	5.1	2.5

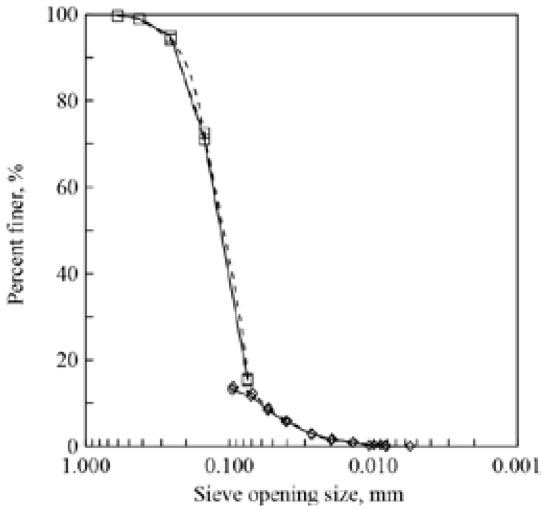

Figure 2. Grain size distribution of MLS (Huang and Chuang, 2011)

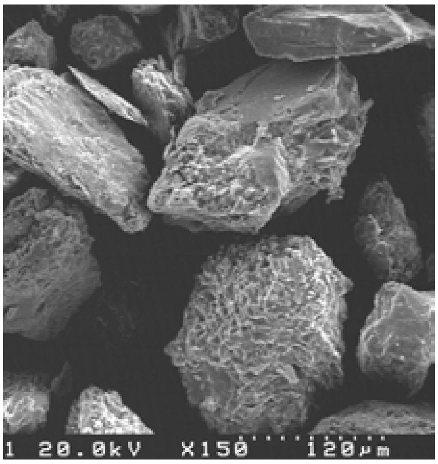

Figure 3. Scanning electron microscope photograph of MLS particles retained on #200 sieve (Huang and Chuang, 2011)

Affected by its mineral contents, MLS was significantly more compressible then typical clean quartz sand reported in literature (Huang et al., 1999 and 2004). Studies on the effects of fines on engineering properties of granular soils have included a wide spectrum of gradations that span from clean sand, silty sand, clayey sand, sandy silt to pure silt. The unified soil classification of these soils can vary from SP, SW-SM, SM, SM-SC to ML, depending on the amounts and characteristics of the fines. The term silt/sand (M/S) is proposed to serve as an abbreviated term to describe inclusively, granular soils with a possibility of some cohesion and wide range of gradations.

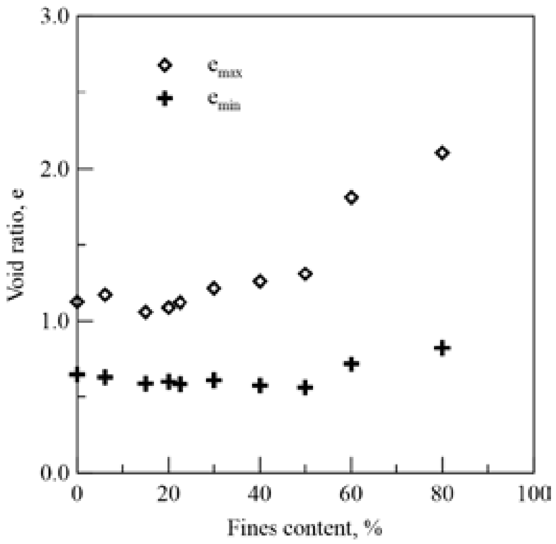

Figure 4. Minimum and maximum void ratios versus fines contents (Huang and Chuang, 2011)

2 LABORATORY TESTS ON RECONSTITUTED M/S SPECIMENS

2.1 *M/S soil as a binary packing*

There is still a lack of consensus as to what role the fines content plays in relation to cyclic strength. Some studies showed that the fines content has a stabilizing effect, while others indicate no effect, and still others claim a destabilizing effect. The available studies have mostly been concentrated on laboratory tests using reconstituted specimens. The reconstituted M/S specimens were often made of mixtures of clean quartz (e.g., Ottawa) sand with crushed silica, kaolin or other types of natural silt. These mixtures of sand and fines, or gap graded artificial soils have been compared to those of coarse and fine spherical grains (Lade et al., 1998), or a binary packing. For M/S soils under the same void ratio, and fines content below a threshold value, cyclic strength decreases with fines content. This trend is reversed when fines content exceeds the threshold. As the diameter ratio, D_{ratio} of the coarse grains over that of the fine grains exceeded approximately 7, one can expect a bilinear correlation between the minimum void ratio (e_{min}) and fines content. The e_{min} reaches its lowest value as the fines content approaches 30%, as conceptually described in Figure 5.

Figure 5 implies that as fines content approaches 30%, the binary packing becomes unstable unless the grain mixture is in a denser state (hence lower void ratio). Thus the threshold fines content should correspond to that when the packing is at its least stable state, provided the M/S soil gradation is close to binary. Some of the studies on artificial silty sand specimens, mostly of silica in nature, have demonstrated that the threshold fines content, generally ranged from 25 to 45% (Koester, 1994; Polito, 1999; and Xenaki & Athanasopoulos, 2003). The concept of binary packing provided a scientific basis to describe the potential trend of M/S soil behaviors and their relationship with fines contents.

The distinct element method (DEM) simulations reported by Ng et al. (2016) showed that the trough of the e-fines content relationship became less obvious as the D_{ratio} decreased to 5. For MLS, with its D_{ratio} slightly larger than 3, the existence of a threshold fines content was even less obvious as shown in Figure 5.

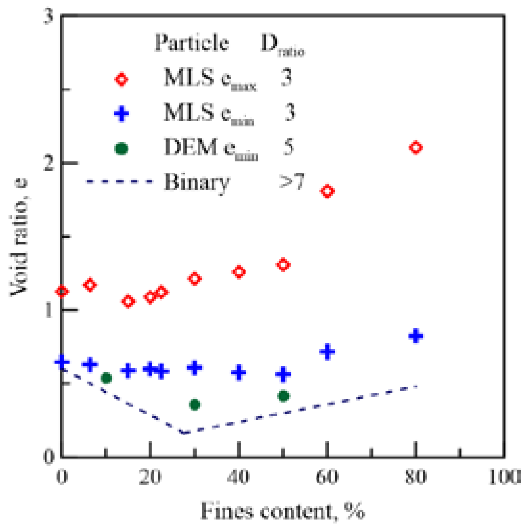

Figure 5. Effects of fines on void ratios (after Ng et al., 2016)

Based on the binary packing model, a series of void ratio indices that relate the active grain contacts (i.e., the soil skeleton) to fines contents have been proposed and evolved in the past (Thevanayagam et al., 2002). The intergranular contact index void ratio, e* (Thevanayagam, 2000) or simply the equivalent granular void ratio defined as:

$$e^* = \frac{e+(1-b)FC}{1-(1-b)FC} \quad (1)$$

where
e = void ratio
b = parameter reflects fraction of fines participating in the force structure of the solid skeleton
FC = fines content in decimal

The value of b ranges from 0 to 1. A higher b corresponds to an increase of contribution of fines in the force structure of the soil skeleton. The value of b is believed to be mostly related to grain size ratio (χ) between the lower 10% fractile of the coarse (D_{10}) and medium size (d_{50}) of fine particles (i.e., $\chi = D_{10}/d_{50}$), and fines content of the M/S soil. The value of b can be determined empirically or semi-empirically (Rahman et al., 2008).

Rahman et al. (2008) reported that for certain M/S soils, a series of void ratio (e) based critical state lines that correspond to various fines contents can be collapsed into one by replacing e with e*. This unified e* based critical state line should be close to or the same as that of zero fines content where e* = e.

2.2 *Element tests on reconstituted MLS specimens*

A series of isotropically consolidated undrained monotonic and cyclic triaxial tests on reconstituted MLS specimens have been conducted by the author. The monotonic triaxial tests were performed on specimens prepared by moist tamping (MT) method. The MT method can be used to create specimens with a wide range of initial densities. This series of isotropically consolidated, undrained monotonic axial compression tests (CIU) provided data to establish the critical state loci and hence the critical state lines.

Figure 6 depicts selected isotropic consolidation curves from this series of CIU tests. The initial void ratio (e_o) marked in Figure 6 represents the void ratio when the specimen was prepared, prior to saturation and consolidation. The void ratios (e) included in Figure 6 are back calculated, based on the post-consolidation void ratios determined from the water content of the specimen, after the test was completed. Details of obtaining post-consolidation void ratio for triaxial specimens are given in Huang et al. (2004).

The e_{min} and e_{max} are marked on the figure. In general, the compressibility increased with fines content and p', and decreased as the specimen became denser. The void ratio after applying the initial consolidation stress 10 kPa could be significantly less than e_o. When the fines contents reached 50%, the application of initial confining stress and the saturation process caused enough compression that the consolidation curves were almost indistinguishable among specimens with different e_o values. It is thus imperative that the post-consolidation void ratio be used in presenting M/S data that involve density states.

For the monotonic shearing tests performed, the critical state friction angle ($\emptyset'_{crit}$) ranged from 30.2° to 30.9° regardless of the fines content, indicating that the coarse and fine MLS particles had similar grain to grain frictional behavior.

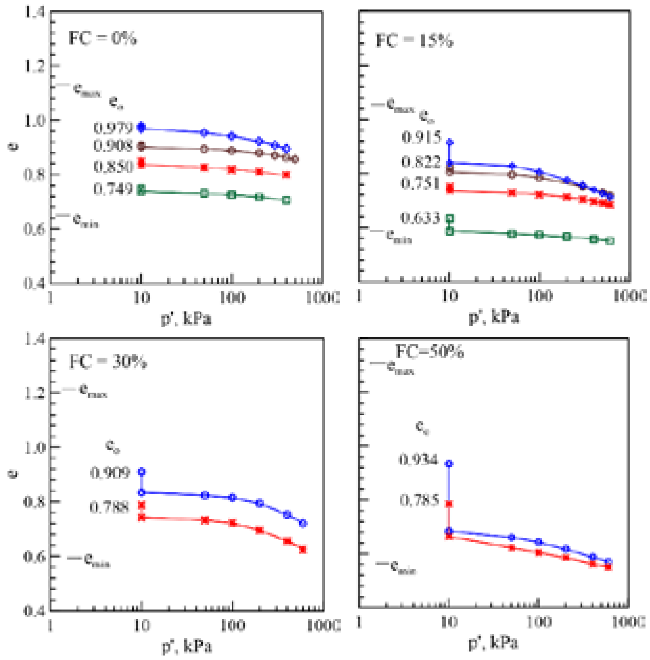

Figure 6. Isotropic consolidation curves of MLS with various fines contents (after Huang et al., 2004).

Figure 7 shows the void ratio, e based critical state loci that correspond to fines contents of 0, 15 and 30%. The critical state loci for each of the three types of fines contents were more or less parallel to each other but moved downward as the fines content increased. Similar phenomenon has also been reported by Kikumoto et al. (2009). No meaningful critical state line could be obtained from the monotonic triaxial tests for FC≥50%, therefore it is not reported in Figure 7.

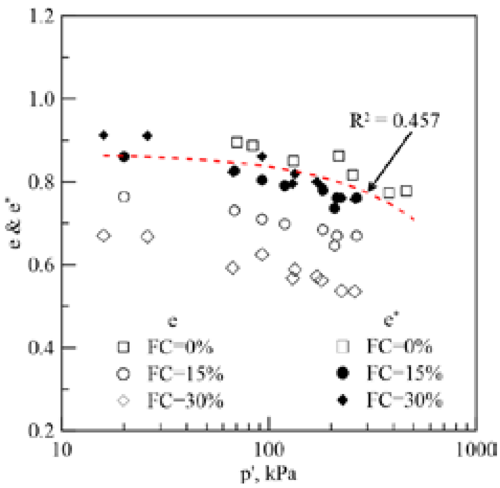

Figure 7. The e based and e* based critical state loci under different fines contents (Huang & Chuang, 2011)

Soil element tests also included cyclic triaxial tests where the specimen was consolidated under an isotropic effective confining stress p' and then subjected to a cyclic deviator stress, σ_d in axial direction. Three to five cyclic triaxial tests were performed with various amplitude of $\sigma_d/2p'$. The cyclic resistance ratio (CRR) is used to represent the cyclic strength. CRR is defined as the $\sigma_d/2p'$ that produced an axial strain of 5% in double amplitude in 20 cycles of uniform load application. For cyclic triaxial tests, the specimens were made by water sedimentation (WS) and dry deposition (DD), in addition to MT method. The additional specimen preparation methods were chosen to evaluate the effects of soil fabric. Readers are referred to Huang et al. (2004) and Huang & Chuang (2011) for details of the specimen preparation and triaxial test procedures for this series of laboratory tests. It should be noted that as fines contents exceed 15%, the above described axial strain of 5% in double amplitude does not necessarily correspond to soil flow failure (i.e., the effective confining stress becomes zero as the applied p' is completely offset by the cyclic stress induced pore pressure). In other words, the soil specimen was softened under the cyclic loading conditions but the applied p' was not completely offset by the developed pore pressure.

The e-CRR and e*-CRR correlations for specimens prepared by WS method are presented in Figures 8. Due to high compressibility of the fines, post consolidation void ratio higher than 0.75 would be excessively loose and very difficult to make for specimens with FC larger than 15%. On the other hand, specimens with FC less than 15% are significantly less compressible, a void ratio less than 0.75 would be rather dense. Because of these reasons, only a narrow window of common void ratios can be found in Figure 8 where comparison of the cyclic strength with different fines contents can be made. The results included in Figure 8 show that, for void ratios around 0.75, CRR decreases with FC. Similar trend was also noticed for MLS specimens prepared by other methods (i.e., MT and DD methods) and when FC extended beyond 50%.

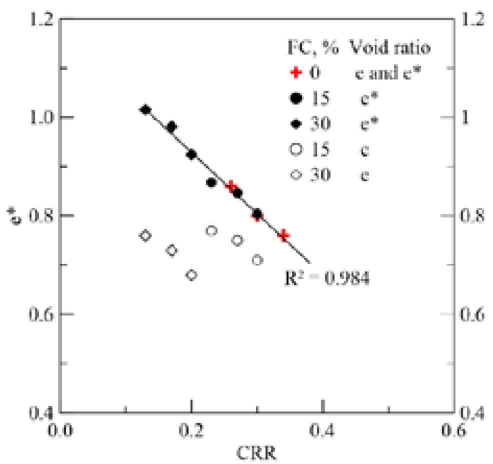

Figure 8. Correlating CRR with e and e* (Huang & Chuang, 2011)

For specimens with the same FC, lower void ratio corresponds to a denser state and hence higher CRR. However, there are apparently separate e-CRR correlations for different fines contents as indicated in Figure 8. An important value of the equivalent void ratio would be to achieve a single and unified e*-CRR correlation. For MLS, the ratio of D_{10} (= 0.08mm) over d_{50} (= 0.044mm) (χ) was 1.82. Huang & Chuang (2011) used a trial and error procedure to optimize the b parameter of Equation (1). For a b parameter of approximately 0.6, a unified and consistent e*-CRR correlation can be obtained for the three types of fines contents as shown in Figure 8. Note that for FC = 0%, e=e*. It is interesting to note that the e* based critical state loci also tend to collapse into a single correlation close to that of zero fines content where e* = e as shown in Figure 7. For the set of data in Figure 7, the e* was calculated using the same b parameter determined earlier.

Figure 9 shows a plot of CRR versus state parameter (Ψ) for MLS with FC = 0, 15 and 30% reported by Huang & Chuang (2011). The state parameter is defined as the difference between the current void ratio (e) and that on the critical state line for a given effective mean normal stress (p'). It reflects the dilatancy of a given soil that considers the effects of density and confining stress. The results depicted in Figure 9 have similar trend but with a much more scattered $\Psi -$ CRR correlation when compared to those reported by Jefferies and Been (2006) for clean quartz sands where CRR increases as Ψ becomes increasingly negative.

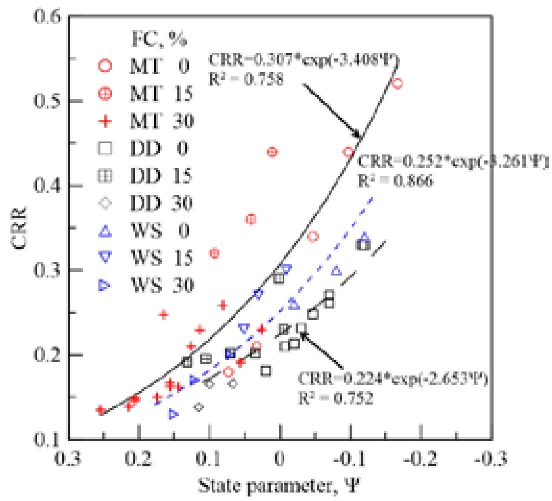

Figure 9. Correlation between cyclic strength and state parameter Ψ for MLS test data (Huang & Chuang, 2011)

The state parameters of MLS extend into the positive side (Ψ>0) much more so than those reported by Jefferies and Been (2006). This is a reflection of the compressive nature of MLS grains and more contractive behavior during shear. For specimens with the same state parameter, the cyclic resistance ratio (CRR) of MT specimens are the highest and those of DD specimens are the lowest. This is consistent with the earlier findings reported by Huang et al. (2004) which indicated that for specimens with the same void ratio, CRR from MT specimens are the highest and those from DD specimens are the lowest. For data of the same specimen preparation group, those with high fines contents are clustered further towards the positive side of the state parameter axis and lower CRR values. This is again a reflection of the higher compressibility associated with M/S mixtures with higher fines contents.

To use the state parameter derived from void ratio, e would require a separate critical state line for the M/S mixtures with different fines contents. For the tests on MLS reported herein, only three types of fines contents are involved. For natural M/S soils, there can be numerous possibilities of fines contents. Thus, it is conceivable that an impractically large number of laboratory tests are required to provide the series of critical state lines that correspond to all given fines contents unless a fines content based interpolation scheme can be effectively used to determine these critical state lines. This drawback may be reduced or minimized by invoking the equivalent granular void ratio e* in the determination of critical state line. Figure 7 shows the void ratio, e based critical state loci that correspond to each of the three types of fines contents along with those computed based on e*. The state parameter determined based on e* of the soil specimen and the unified e*-p' critical state line is referred to as the equivalent granular state parameter (Ψ*). A plot of Ψ* versus CRR for specimens prepared by the three methods are shown in Figure 10. Similar trend between CRR and Ψ* as those observed in Figure 9 can be found in Figure 10. The CRR-Ψ* data show much improved R^2 values in fitting with the corresponding exponential curves. Apparently, the determination of Ψ* based on e* and a single, unified e*-p' critical state line is much less noisy than deriving Ψ using e and separate e-p' critical state lines for each type of fines content.

Many important lessons can be learned from the series of soil element tests on reconstituted MLS specimens, these include:

- For M/S soils, the density state should be referenced in terms of void ratio, rather than relative density as the relative density can often exceed 100%.
- The post consolidation void ratio, or the void ratio just prior to the shearing test should be used to represent the density state of the specimen.
- The method of reconstituting the specimen does affect the shear strength measurements. For a given state parameter, the moist tamping (MT) method seemed to yield the highest CRR while dry deposition (DD) method provides the lowest CRR. It is conceivable however, that this sequence may vary for soils with different origin.
- The use of e* and Ψ* can help in streamlining the critical state lines and correlations among e*, Ψ* and cyclic strength.

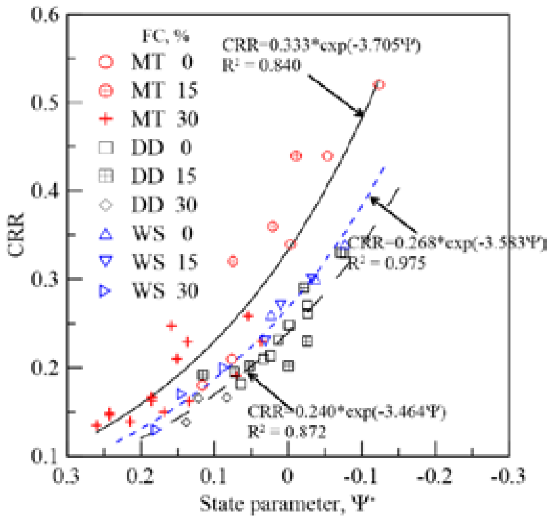

Figure 10. Correlation between cyclic strength and equivalent granular state parameter Ψ* for MLS test data (Huang & Chuang, 2011)

2.3 *CPT calibration tests in MLS*

An advantage of calibration chamber tests is that uniform, repeatable soil specimens can be created under known density and stress states. Figure 11 shows a schematic view of the calibration chamber used to calibrate CPT in MLS. It was designed for 525 mm diameter and 760 - 815 mm high specimens. The relatively small chamber size was utilized for ease of specimen saturation, back-pressuring and handling. The chamber was designed to provide constant stress lateral boundary conditions only. The piston at the bottom of the specimen controlled vertical stress. The main interest in performing CPT calibration tests in M/S soils such as MLS is to evaluate the effects of soil compressibility and partial drainage on test results.

A series of CPT was performed in MLS using the calibration chamber system shown in Figure 11. The chamber specimens were prepared by dry deposition (DD) method. A comparison of cone tip resistance with pore pressure effect correction (q_T) from CPT performed in dry and saturated specimens with fines contents of 15, 30 and 50% are presented in Figure 12. Other than saturation, the test pairs had the same density and stress conditions. When FC = 15%, the q_T in dry and saturated specimens agreed within 6%, after reaching a penetration depth of 300 mm. We can conclude that CPT performed in MLS with fines contents less than 15% may be considered a drained test. When FC ≥ 30%, q_T in a dry specimen could be more than twice the value as in a saturated specimen. It is apparent that as fines content exceeded 30%, the CPT could no longer be considered a drained test.

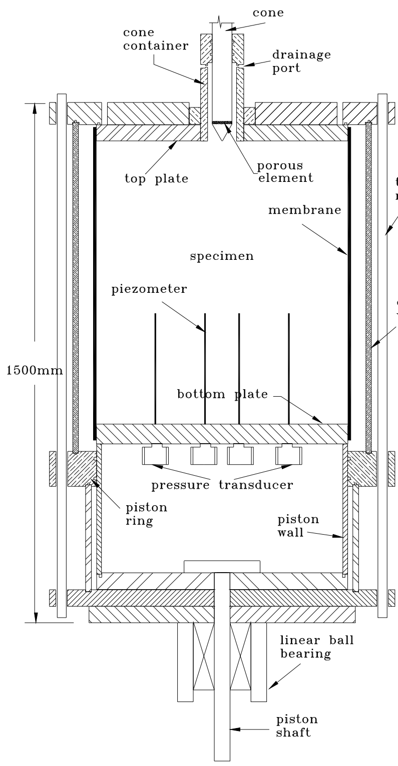

Figure 11. Schematic view of the calibration chamber

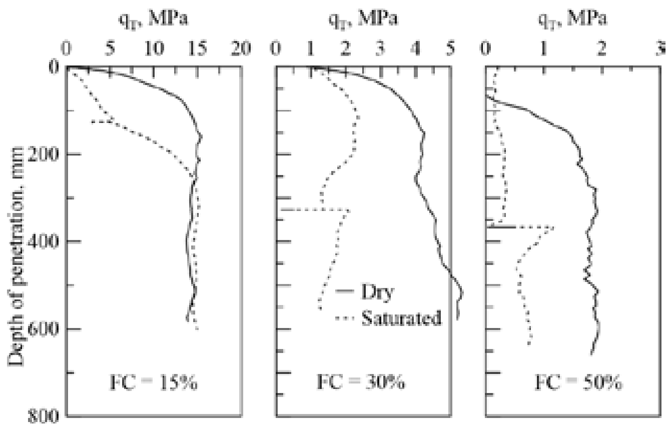

Figure 12. CPT in dry and saturated MLS with different fines contents

Where the CPT in saturated specimens was interrupted for excess pore pressure dissipation, the time required to dissipate 50% of the excess pore pressure measured at u2 position, or t_{50} changed from a few seconds to a few minutes as the fines contents increased from 15 to 50%. As depicted in Figure 12, immediately upon resumption of cone penetration, there was a sudden increase of q_T in saturated specimens with FC = 30 and 50%. For CPT under partially drained conditions, the penetration induced pore pressure was significant enough to lower the q_T values. The pore pressure dissipation after interruption of the cone penetration densified the surrounding soil. Within a short period when the cone penetration resumed, the induced pore pressure was not fully developed and that caused an increase of q_T above those prior to the interruption. McNeilan & Bugno (1984) reported similar experience of CPT in offshore California silts. The increases in q_T and sleeve friction, f_s were referred to as setups by McNeilan & Bugno (1984). The setup generally diminished with further penetration.

The effects of compressibility on drained CPT in MLS can best be demonstrated when compared with the general trend of cone tip resistance, q_T – relative density, D_r correlations in normally consolidated clean quartz sands with different compressibility as shown in Figure 13. The MLS data points clustered around the correlations for high compressibility clean quartz sand. For CPT in overconsolidated MLS with FC=15%, some of the data had relative densities exceeding 100%. As explained earlier, the high relative density was due to high compressibility of MLS with FC=15% and therefore significant void ratio reduction after application of the confining stress.

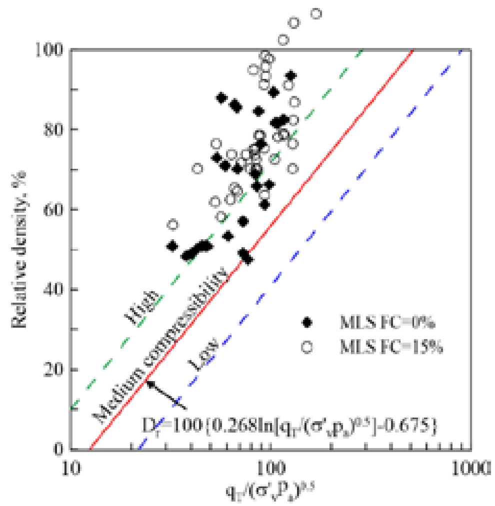

Figure 13. Comparison of normalized q_T with those in normally consolidated clean quartz sands (after Mayne, 2006)

Figure 14 shows a comparison of cone tip resistance in MLS with FC ranged from 0 to 50% and those in clean quartz sands (i.e., Ticino and Da Nang sands) as well as a calcareous (Quiou) sand. The MLS specimens were saturated when FC = 30 and 50%. Therefore, Figure 14 enables the combined effects of soil compressibility and partial drainage be evaluated by comparing with the test results of those in clean quartz sand and crushable sand. The comparison shows that under similar void ratio, the cone tip resistance in MLS with FC = 30 and 50% can be significantly lower than those in Ticino and Da Nang sands. Although with generally lower void ratio, the cone tip resistances in MLS with FC = 0 and 15% (drained CPT) are comparable with those in crushable Quiou sand.

In general q_T in MLS is significantly more stress dependent than density dependent. Because of this reason, the normalized cone tip resistance has a rather poor correlation with the state parameter.

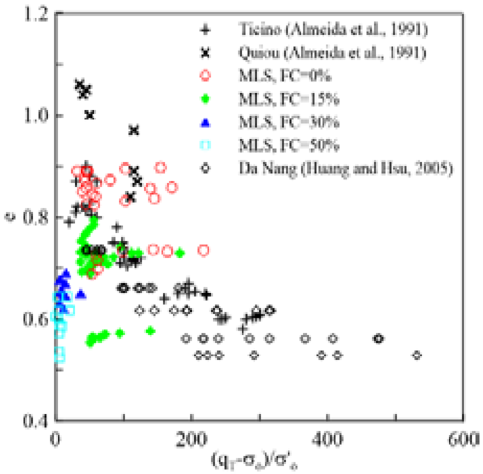

Figure 14. Comparison of normalized q_T with other sands

2.4 *Specimen preparation by mist pluviation*

Kuerbis & Vaid (1988) stated that an ideal specimen reconstitution technique for cohesionless soils must be able to (1) produce all density ranges of the in situ deposits, (2) have a uniform packing throughout, (3) be saturated for undrained tests, (4) prevent particle segregation, and (5) simulate the deposition process. Studies (e.g., Høeg et al., 2000) have suggested that the water sedimentation (WS) method is the most promising in reproducing the soil fabric of a natural silty sand deposit but particle segregation must be avoided. In the water sedimentation method, dry soil particles are pluviated into deaired water. The WS simulates the process of alluvial deposition, or that of hydraulic fills. To minimize particle segregation, the WS soil specimens are usually prepared in thin layers and the process can be time consuming. To adopt any of the three specimen reconstitution techniques (i.e., MT, DD and WS) described above for preparation of calibration chamber specimens would be time consuming and prone to create non-uniformity.

Huang et al. (2015) developed a mist pluviation method that can be used to reconstitute silty sand specimens for soil element as well as calibration chamber (or physical modeling) tests. The mist pluviation (MP) method retains parts of the WS processes, but with an addition of a mist zone that mixes soil particles with water droplets while falling through air. The mist pluviation method is named after the process of soil placement and the medium in which the soil falls through. A schematic diagram of this approach is shown in Figure 15.

To initiate specimen preparation, dry soil in the storage compartment is continuously released by gravity. The soil particles are dropped into a cloud of water droplets (with rated diameter of 130 μm, about the same as the mean diameter of MLS sand grains) or mist zone generated by a series of water spray nozzles. Soil particles with different sizes and water droplets mixed into aggregates with similar diameters in the mist zone, before falling to the thin water film on the surface of the deposited soils. Adjustment can be made to change the size of water droplets and dry soil drop rates. Segregation is minimized because the similar diameters of the soil/water aggregates. To create a uniform deposition, a steady rate of dry soil discharge is required. The soil specimen is extremely loose immediately after pluviation. Consolidation is required to reach a higher density.

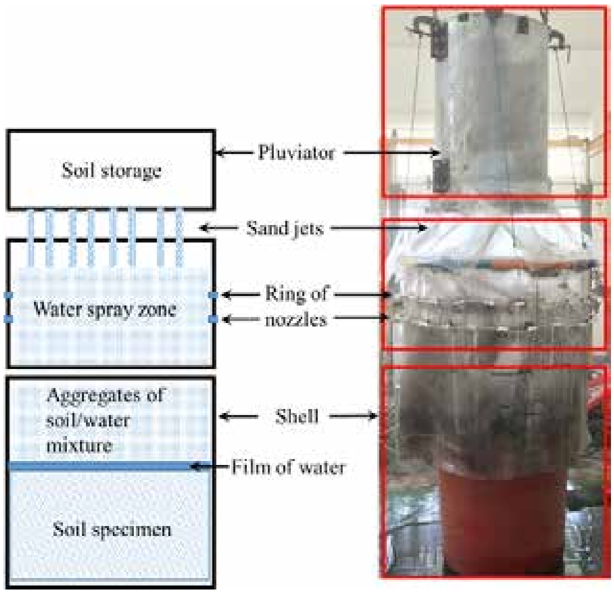

Figure 15. Laboratory setup for mist pluviation

Figure 16 shows the isotropically consolidated undrained compression (CIU) test results of MLS specimens with two different FC's prepared by MP and MT methods under an effective consolidation stress σ_c' of 100 kPa. The results reveal that the MP specimens clearly showed a more dilatant and strain-hardening behavior in comparison with those of MT specimens. The homogeneity of MP specimens with regard to void ratio (or *w*) and FC was evaluated with measurements of the layering slices and annular portions for each layer. The results show that both vertical and lateral variations of FC or *w* were small and randomly distributed, indicating that the MP method can produce homogeneous specimens, regardless of the FC and particle gradations (Huang et al., 2015).

3 FIELD SAMPLING AND LAB TESTS

Taking undisturbed or high quality samples in low cohesion soils has always been a difficult task. The available reports on the undisturbed sampling in clean sand below ground water table have mostly been limited to the ground freezing method. By freezing the ground water, the sand particles and their matrix were fixed in the frozen ground. The sand samples were taken by coring and remained frozen until laboratory shearing test. Experience has indicated that the cyclic strength of undisturbed specimens taken by ground freezing method can be significantly higher than that of reconstituted specimens with similar densities

(Ishihara, 1993). The process of ground freezing however, is time consuming and prohibitively expensive. Høeg et al. (2000) had limited success in their attempt to obtain natural silt samples at 3m below ground surface using a 50 mm inside diameter Swedish Geotechnical Institute piston sampler under ambient temperature, in the capillary zone right above the ground water table. The vibration during transportation and specimen extrusion from the sampling tube can cause disturbance to the silty soil samples as indicated by Høeg et al. (2000). Konrad et al. (1995) reported their success in obtaining undisturbed sand samples using Laval sampler, from below the ground water table without freezing. A 200mm diameter and 500mm high sample can be obtained with the Laval sampler. In order to prevent soil structure damage during transportation for low cohesion sand, Konrad et al. (1995) developed a method to freeze the Laval sample above ground.

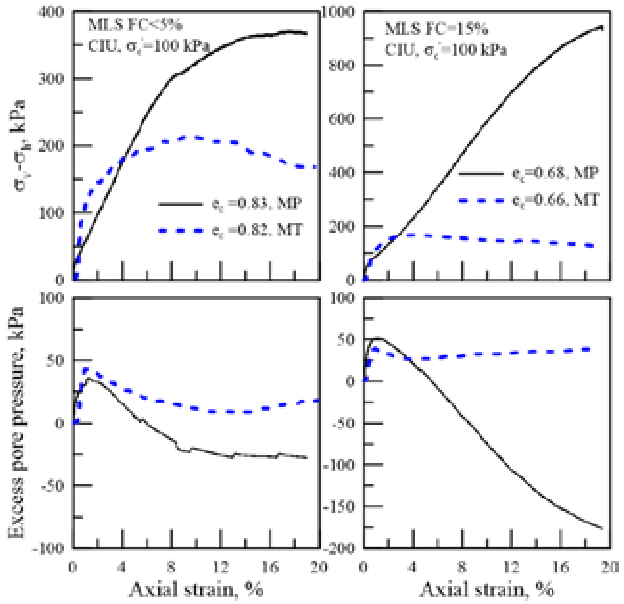

Figure 16. Comparison of monotonic undrained response between MP and MT methods (Huang et al., 2015)

Huang & Huang (2007) reported the use of Laval sampler to take undisturbed samples in M/S soil at a test site in Yuan Lin (see Figure 1) in Central Taiwan. The Laval sampler as schematically described in Figure 17 was developed at Laval University (La Rochelle et al., 1981), originally for taking high quality samples in sensitive clay. The boreholes were extended by a 330 mm diameter fishtail device using a mixture of bentonite and barite as the drill mud. To take a sample, the drill rig pushes the sampling tube into the bottom of the borehole while rotating the overcoring tube. The steel teeth and cutters were located at 20mm behind the bottom of the sampling tube. During penetration, the head valve was kept open to allow drill mud circulation and thus removal of soil cuttings.

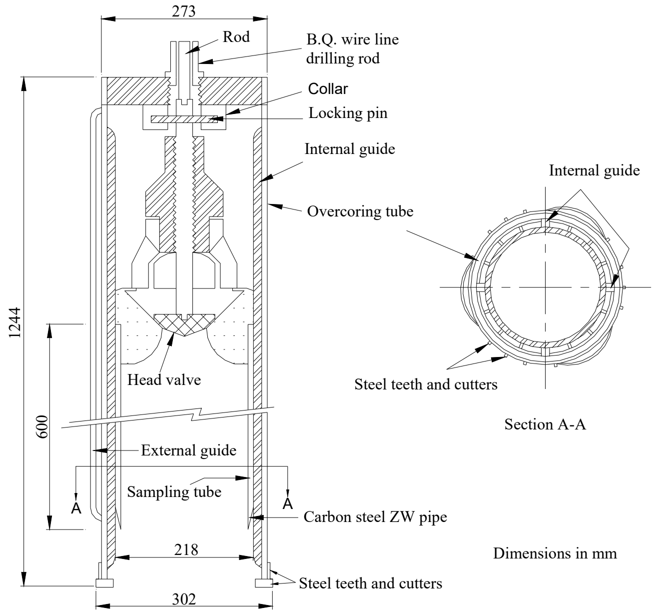

Figure 17. Schematic view of the Laval sampler (after La Rochelle et al., 1981)

Samples taken from soil layers expected to have medium or high fines contents (FC close or exceeds 50%) were extruded on site, cut into 120 to 180mm long segments and placed on a pre-waxed wooden board. The sealed samples were kept in a moisturized container during transportation and laboratory storage. Samples taken from soil layers expected to have low fines contents (FC < 50%) remained in the sampling tube and kept vertical until it was completely frozen above ground. A procedure referred to as the unidirectional freezing reported by Konrad et al. (1995) was followed to solidify the sample without causing volume change. The soil along with the sampling tube was placed in a Styrofoam lined wooden box and gradually frozen from top of the sample by dry ice at -80ºC. A backpressure equal to the water head within the sample was applied by means of a nylon tubing connected to the bottom of the sample to ensure that no water can drain under gravity. The bottom drainage and backpressure assured pore water drainage only due to water volume expansion during freezing. The amount of expelled water and temperature at the bottom of the soil sample were monitored as the freezing progressed. The freezing process took 15 to 24 hours, upon which the temperature at the bottom reached below 0ºC. Figure 18 depicts a record of time versus expelled water volume and temperature measured at the bottom of soil sample with FC = 18%. The frozen samples were stored in a freezer during shipping and laboratory storage until the time of shearing test.

Four, 70 mm diameter specimens could be cored from a 170mm long section of Laval sample therefore assuring all four specimens came from the same depth in ground; a rather desirable feature for cyclic triaxial tests. The specimen was kept frozen during this preparation stage. Thawing took place after the specimen was seated in the triaxial cell following a slow thawing procedure reported by Hofmann (1997) under a confining stress of 20 kPa and a cell water temperature of 5ºC. The amount of water absorbed by the specimen and the change of specimen height were monitored during the thawing process.

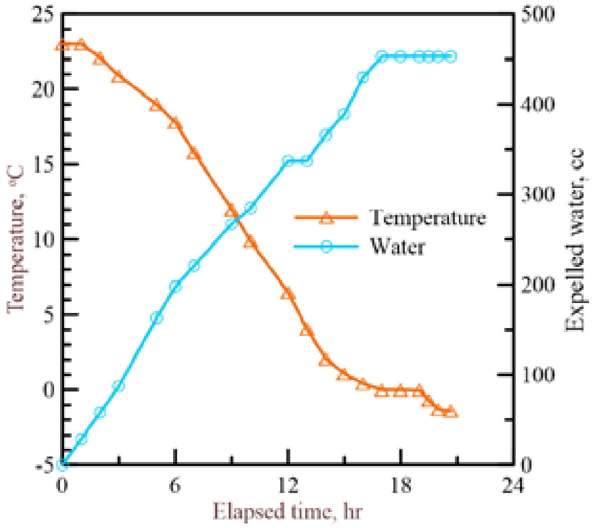

Figure 18. Water volume expelled and temperature variation with time (Huang et al., 2009)

Figure 19 shows a comparison of shear wave velocity, V_s taken from the cyclic triaxial test specimens and those from different field measurements, normalized with respect to σ'_v or V_{s1}. V_{s1} is computed as described by Andrus & Stokoe (2000) where

$$V_{s1} = V_s(\sigma_{atm}/\sigma'_v)^{0.25} \qquad (2)$$

where σ_{atm} is the reference atmospheric pressure of 100 kPa. The field shear wave velocity measurements included P-S logging and seismic piezo-cone penetration tests (SCPTU). The depths of the V_{s1} from Laval samples (LS) are in reference to those where the samples were taken. For laboratory measurements using bender elements, V_s=V_{s1} as the specimens were under an effective confining stress (σ'_c) of 100 kPa, which is also isotropic (σ'_c=σ'_v). Although there were some scattering among the field measurements, the laboratory V_{s1}values are comparable to those of field measurements. The discrepancies of V_{s1} values from different sources may well be due to differences in shearing modes and applied lateral stress for the case of bender element tests.

The gel-push sampler developed in Japan (Tani & Kaneko, 2006; Lee et al., 2006) as schematically shown in Figure 20 is a modified version from a 75mm Osterberg piston sampler (also known as a Japanese sampler). Sand sample was taken by pushing the gel-push sampler as typically done for piston sampling in clays. Because of the high frictional resistance in granular soils, it is usually difficult to retrieve sand sample by pushing. The gel-push sampler injects a water soluble polymeric lubricant (the gel) from the sampler shoe to facilitate push sampling. A shutter located at the tip of the sampler remained open during pushing. A slight reverse motion by injecting water into the gel chamber triggers the closure of the shutter before the sample is retrieved. The closed shutter prevents the sample from falling during withdrawal. Upon withdrawal of the sampling tube above ground, the ends of the tube were sealed with Styrofoam plugs. No freezing was conducted for the samples. The sampling tubes were stored in a well cushioned container for transportation. An accelerometer was attached to the sampling tube where the acceleration readings were continuously recorded during shipping.

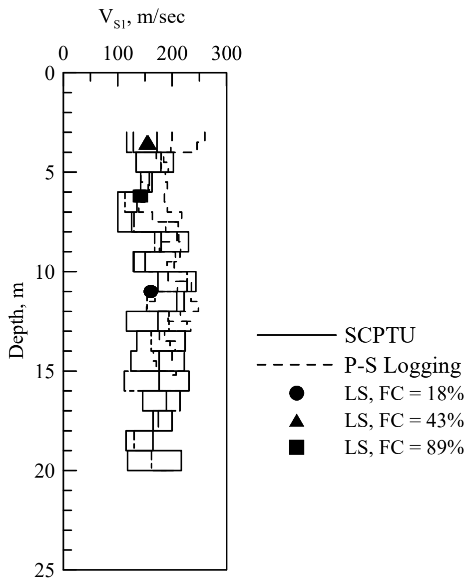

Figure 19. Comparison of laboratory and field V_{s1} measurements in YLS.

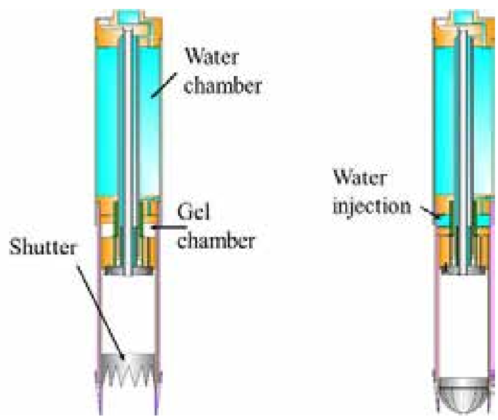

Figure 20. Schematic views of the gel-push sampler (after Lee et al., 2006).

The soil sample extruded out of the gel-push sampler was trimmed to a diameter of 70mm to fit the triaxial testing device and remove a shell of soil that was impregnated by the gel during field sampling. The trimmed soil specimen was inserted directly into a rubber membrane lined sample holder. A layer of sponge was placed between the rubber membrane and the metal split mold. The sponge was compressed initially by the application of vacuum to give room for insertion of the soil specimen. Upon release of vacuum, the sponge expansion provides a confining stress on the granular soil specimen until the specimen is seated in the triaxial cell and vacuum resumed through the drainage lines. By maintaining the confining stress the sample holder minimizes the chance of disturbance during triaxial test set up.

Figure 21 shows the comparison between the V_s measurements taken in the gel push specimens in a triaxial cell using bender elements and those from the field seismic cone penetration tests (SCPTU). The specimens were then used for cyclic triaxial tests (CTX) or K_o consolidation undrained, axial compression (CK_oU-AC) triaxial tests. All triaxial specimens were consolidated to σ'_v comparable to the in situ overburden stress prior to shearing. For the most part, the laboratory V_s falls within or close to the range of those from SCPTU at comparable depths.

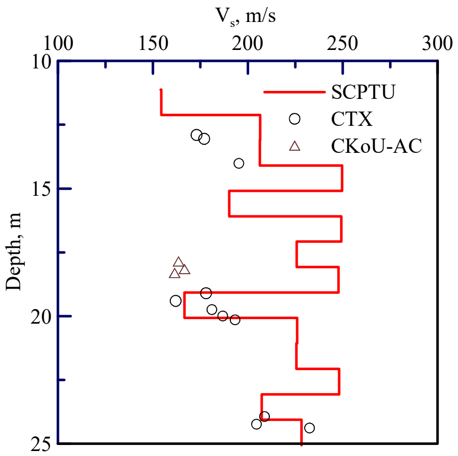

Figure 21. Comparison of Vs between the bender element and SCPTU measurements (Huang et al., 2008).

4 CORRELATING CRR WITH q_T AND V_s

Due to the cost and difficulties involved in undisturbed sampling in cohesionless soils, the cyclic resistance ratio (CRR) required for liquefaction potential assessment has been inferred from empirical correlations between CRR and field test results under the framework of simplified procedure (Youd et al., 2001). The simplified procedure using CPT has been based on q_T normalized to an effective vertical stress, σ'_v as follows:

$$q_{T1N} = (q_T/\sigma_{atm})(\sigma_{atm}/\sigma'_v)^n \tag{3}$$

where
σ_{atm} = atmospheric pressure of 100 kPa
n = exponent that varies with soil type

The exponent n = 1.0 in the case of clayey soils (soil behavior type index, $I_c > 2.60$), n = 0.5 for clean sands (I_c = 1.64), and intermediate values of n apply for mixtures of sand and silt. Some iteration may be required for the selection of n and computation of I_c. In any case, $n \leq 1$. Readers are referred to Robertson (2009) for details on the determination of I_c and n.

The CRR-q_{T1N} correlations have generally been established empirically according to field observations. Although different in magnitude and/or format, most available CRR-q_{T1N} correlations for sands that contain fines suggest that a given CRR should correspond to a lower q_{T1N} as fines content increases (e.g., Stark & Olson, 1995; Robertson & Wride, 1998). Thus, an adjustment of q_{T1N} is required when CPT is used for liquefaction potential assessment in silty sand under the simplified procedure. Despite of the significant impact of fines content adjustment on the outcome of liquefaction potential assessment, little explanation has been offered to justify such adjustment (Ishihara, 1993; Youd et al., 2001).

By comparing the CRR and q_{T1N} from CPT calibration tests in reconstituted specimens with comparable fines contents, density and stress states, it was possible to verify the CRR-q_{T1N} correlation by direct comparisons for MLS as shown in Figure 22. The CRR values were determined based on cyclic strength obtained from a series of cyclic triaxial tests. The inference of CRR under anisotropic stress conditions from isotropically consolidated cyclic triaxial tests (CRR_{CTX}) followed the procedure by Ishihara (1996) as,

$$\mathrm{CRR} = CRR_{CTX}\frac{1+2K}{3} \tag{4}$$

Where K = ratio of effective horizontal stress, σ'_h over effective vertical stress, σ'_v

All laboratory cyclic triaxial and CPT calibration tests involving MLS used well mixed homogeneous specimens. The results as shown in Figure 22 indicate that the fines content adjustment becomes significant only when the fines start affecting the drainage conditions in CPT and thus result in a group of data points with distinctly lower q_{T1N}. The laboratory study in MLS seems to suggest that a more effective q_{T1N} adjustment scheme should be based on CPT drainage conditions rather than fines content. Cyclic shearing is always undrained regardless of fines contents. CPT can be drained or partially drained depending on the soil conditions. It is understandable that some adjustment is applied before entering the CRR-q_{T1N} correlation when CPT changes from drained to partially drained. However, the adjustment should be related to drainage conditions in CPT and not directly to fines contents.

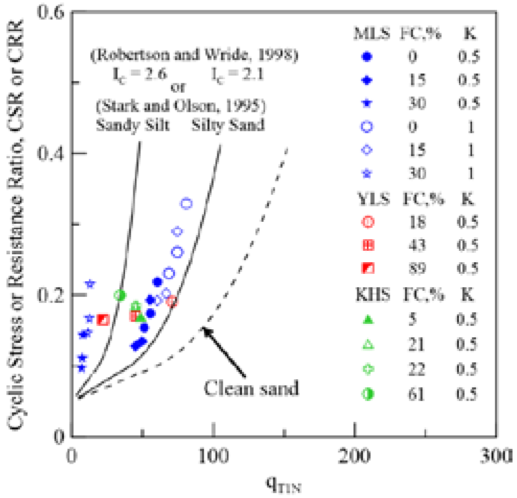

Figure 22. Laboratory and field calibrations of CRR-q_{T1N} correlations.

Considering the importance of drainage during cone penetration in an M/S deposit, attempts were made in the field tests to ascertain the drainage conditions associated with CPTU. A series of CPTU using a standard cone (cone cross sectional area=10cm^2) penetrating at 20mm/sec (the standard CPTU), a large cone (cone cross sectional area=15cm^2) penetrating at 20mm/sec (the large CPTU), and a standard cone penetrating at 1mm/sec (the slow CPTU) were conducted at the Yuan Lin test site. The pore pressure element was located immediately behind the cone face, at the u_2 position. Profiles of fines contents according to SPT specimens, CTPU results that include friction ratio, R_f (=f_s/q_T x100%) from tests at Yuan Lin site are shown in Figure 23. The results indicated no significant differences in q_T among three types of CPTU, considering drastic differences in cone size and/or penetration rate. Because of the time consuming nature, slow CPTU was conducted only in depth levels where Laval samples were taken. The u_2 values from large CPTU were mostly identical to those from the standard CPTU. The u_2 in slow CPTU matched well with the hydrostatic pressure u_o, indicating that 1mm/sec was slow enough to allow the penetration induced pore pressure to fully dissipate and reach equilibrium in most part with the surrounding hydrostatic pressure. The R_f values from slow CPTU were consistently higher than those of standard and large CPTU. No consistent correlation between the increase in R_f and soil fines contents could be identified. During CPTU, the soil element ahead of the cone tip experiences an increase in mean normal stress as the cone tip approaches. This increased stress is released as the soil element passes the base of the cone face and thus a reduction in lateral stress against the friction sleeve immediately behind the cone tip. In a slow CPTU, more time is allowed for the soil element to creep towards the friction sleeve and develop higher lateral stress against the friction sleeve and thus higher f_s. This creeping is believed to be the main cause of the increase in f_s or R_f when cone penetration rate was reduced from 20 to 1 mm/sec as the change in penetration rate did not have significant effects on q_T.

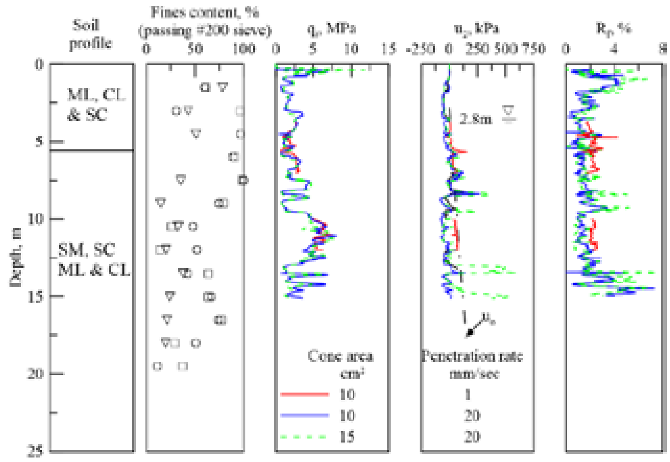

Figure 23. CPTU profiles from Yuan Lin site (after Huang, 2009).

Profiles of fines contents according to gel-push samples and results from standard and slow CPTU performed at a Kao Hsiung test site (see Figure 1) are shown in Figure 24. The slow CPTU was conducted from 9.8 to 25m, the same depth range where gel-push samples were taken at Kao Hsiung site. The results in terms of q_T, u_2 and R_f and their relationship with penetration rates are very similar to those from Yuan Lin site. No significant differences in q_T and u_2 were noticed from CPTU with a 20 times difference in penetration rate.

At Yuan Lin site, the standard CPTU was coupled with pore pressure dissipation tests from 3.5 to 12.5m, at 1m intervals. The same was included in the standard CPTU at Kao Hsiung site from 9.8 to 20.8m. In a pore pressure dissipation test, the cone penetration was suspended while u_2 was continuously recorded until it reached equilibrium with u_o. Figures 25 and 26 compare parts of the q_T, f_s profiles obtained from the field CPTU at two test sites and those from CPTU in reconstituted MLS specimens in a calibration chamber. The field data are the enlarged segments of the corresponding profiles included in Figures 23 and 24. This enlargement allows the change in q_T and f_s and its relationship with pore pressure dissipation tests to be visualized. The MLS specimens with fines contents at 30 and 50% were prepared by MT method where the sand and fines were fully mixed. The MLS specimen was saturated under a back pressure of 300 kPa during CPTU calibration test. A pore pressure dissipation test was conducted in MLS at 0.3-0.4m depth in the calibration chamber. For CPTU in MLS, there were distinct setups as referred to by McNeilan and Bugno (1984) or significant increase in q_T and f_s immediately following the pore pressure dissipation test or the start of the subsequent push. For the field CPTU where the fines contents could exceed 50%, the pore pressure dissipation tests were basically evidenced by a sharp decrease (due to suspension of the cone penetration) and regain of q_T and f_s values as penetration resumed, without significant setups.

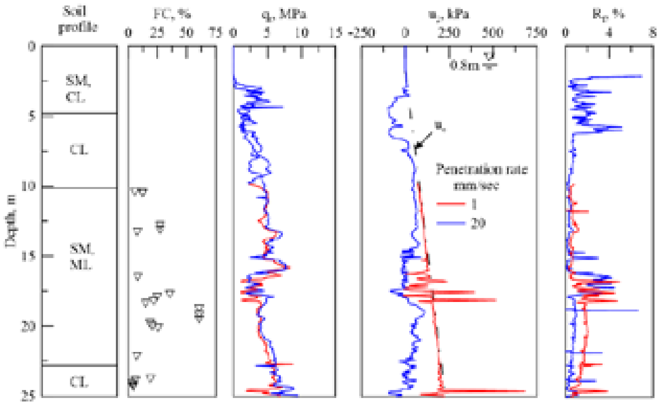

Figure 24. CPTU profiles from Kao Hsiung site (after Huang, 2009).

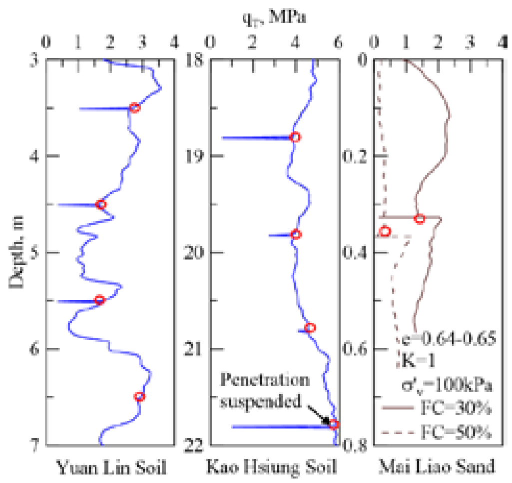

Figure 25. Setup in q_T following pore pressure dissipation (Huang et al., 2009)

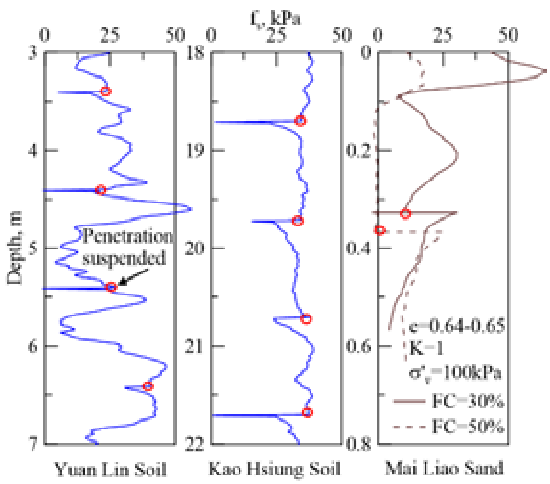

Figure 26. Setup in f_s following pore pressure dissipation (Huang et al., 2009)

Figure 27 compares the t_{50} values among the field and laboratory CPTU and their relationships with fines contents. The t_{50} was defined as the time required for u_2 to change from its initial value immediately upon penetration suspension to gain 50% of its full range of variation until a plateau in u_2 was reached. For laboratory CPTU in MLS, t_{50} increased significantly as fines content changed from 0 to 50%. No clear trend between t_{50} and fines contents could be identified from field tests, even where the fines contents reached as high as 89%.

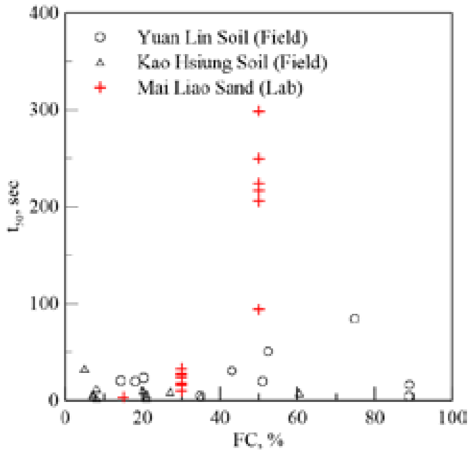

Figure 27. t_{50} versus fines contents (Huang et al., 2009)

The laboratory CPTU in MLS presented above indicated that at fines contents above 30%, CPTU behaved as a partially drained test. The effects of partial drainage were demonstrated by the presence of significant setups following a pore pressure dissipation test and clear trend between fines contents and t_{50} as shown in Figure 27. The field CPTU at both test sites were close to drained conditions even when the overall fines contents reached as high as 100%. The drastic differences in the effects of fines contents on t_{50} between CPTU in laboratory prepared, well mixed silty sand and natural silt/sand in the field are likely due to the heterogeneity existed in natural soil. It is believed that the presence of closely spaced free draining sand layers made the field CPTU behave as a drained test in a silty soil mass, thus resulted in low t_{50} even when the overall fines contents were high.

Cyclic triaxial tests using specimens from Laval samples from Yuan Lin site (YLS) were conducted to determine their CRR. Similarly, CRR values were measured using the gel push samples from Kao Hsiung site (KHS). The CRR from the natural soil specimens were then compared with field CPTU data to establish their CRR-q_{T1N} correlations. A K value of 0.5 was used to infer the field CRR values. At much wider range of fines contents, the lateral spread of CRR-q_{T1N} data points based on tests in YLS and KHS shown in Figure 22 was less than those suggested by the available CRR-q_{T1N} correlations.

Using bender elements, the V_s can be measured on the same soil specimen of cyclic shearing test. The CRR-V_{s1} correlation can thus be conveniently calibrated completely based on laboratory tests (Huang et al., 2004 and Baxter et al., 2008). Figure 28 shows CRR-V_{s1} data points from reconstituted MLS specimens and Laval samples of YLS. A K value of 0.5 was used to infer the field CRR values from cyclic triaxial tests as previously described. Again, there was no evidence of separate CRR-V_{s1} correlations due to differences in fines contents as suggested by Andrus & Stokoe (2000). It should be noted that drainage should have no effects on small strain shear wave velocity measurement.

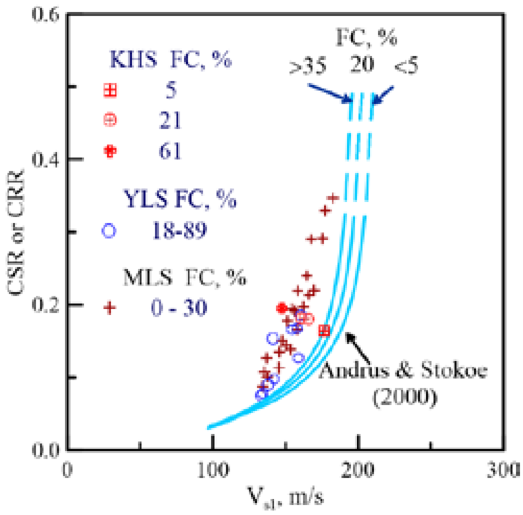

Figure 28. The CRR-V_{s1} correlations.

5 SUBSIDENCE DUE TO REPEATED COMPRESSION

Ground subsidence from excessive groundwater pumping has been a serious problem in many parts of the world. In the alluvial fan of Central Western Taiwan, the ground subsidence has reached as much as 2 m in the past few decades. The ground subsidence threatens the operation of the high speed rail, induces prolonged flooding, and causes sea water intrusion in the region. As described earlier, the compressible M/S soils are the predominant deposit in this region. Based on field monitoring, Hung et al. (2012) reported that the major compression was observed in the soil or aquifer layer at depths from 52 to 153 m, where the accumulated compression of 63.4 cm occurred from 1990 to 2010. This compression corresponds to an average vertical strain of approximately 0.6%. Figure 29 shows the soil compression from multi-point borehole extensometer readings and ground water level fluctuations according to an open end piezometer installed at a depth of 150m. The ground water level albeit fluctuated on a short term basis, had actually risen by approximately 10 m in that period of 20 years shown in Figure 29. The fluctuation was believed to be caused by tidal variations and ground water pumping for irrigation and industrial purposes which were temporal and repeated mostly on a daily basis. The ground water pumping was not excessive enough to permanently lower the ground water table.

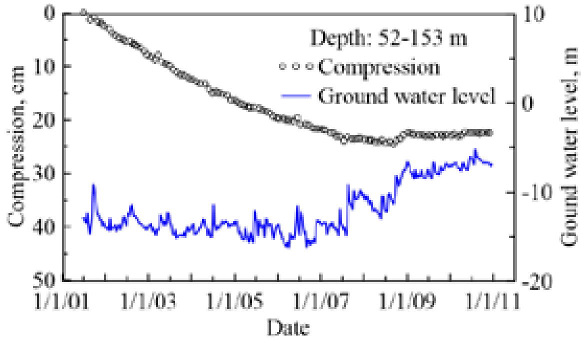

Figure 29. History of soil compression and ground water level variations (Chang et al., 2016)

The M/S soil layer or aquifer within the depth range shown in Figure 29 consisted mostly of fine to coarse sand with occasional layers of gravel with practically no clays. The change in effective stress associated with the ground water level fluctuation was not sufficient to cause the measured soil compression considering the typical compressibility of granular soils in this region, if the compression was solely induced by static soil consolidation. Thus, the conventional thinking of ground subsidence associated with soft soil consolidation induced by static stress increase due to the lowering of ground water table is not able to explain the phenomenon of excessive ground subsidence in this region.

Chang et al. (2016) postulated that the ground subsidence could be a result of repeated loading/unloading induced by the continuous and long term fluctuation of pore water pressure. The phenomenon would be similar to deformation of a pavement subgrade due to repeated traffic loading. A shakedown theory (e.g., Koiter, 1960) has been used to describe this elasto-plastic soil behavior under repeated loading. For ground subsidence, however, the loading was believed to be caused by pore pressure (i.e., effective stress) fluctuation instead of surface loading.

A K_o triaxial consolidation system was setup to study the ground subsidence due to pore pressure fluctuations. Figure 30 shows the stress strain relationship from a test on an M/S specimen made of quartz sand mixed with 20 % mica (by weight). A sinusoidal pore pressure variation from an initial back pressure of 150 kPa was applied while maintain a constant total vertical stress of 350 kPa to the soil specimen under K_o conditions. The amplitude of pore pressure and thus vertical effective stress fluctuation ranged from 10 to a maximum of 95 kPa. Figure 30 shows that as predicted by the shakedown theory, the accumulated axial strains from repeated loading/unloading are much more significant than those from a single loop of stress increase. The rate of strain accumulation reduced significantly as the number of repeated load cycle increased, again as predicted by the shakedown theory. As depicted in Figure 31, with 20% of mica content (MC), the strain accumulation in the M/S specimen is much more significant than that in clean quartz sand (MC = 0%). Also, for the tested soil specimen, a 0.6% axial strain can be easily reached with an amplitude of approximately 20 kPa pore pressure fluctuation as shown in Figure 31.

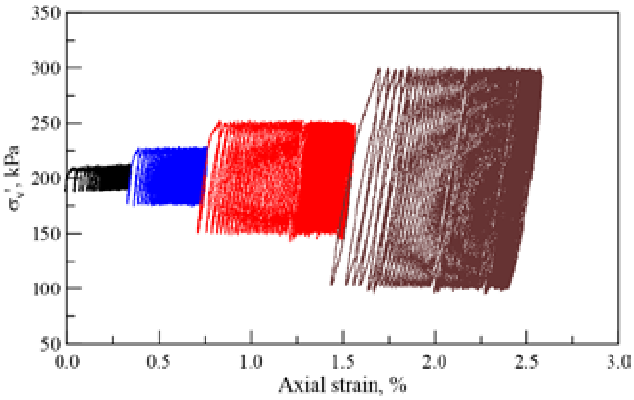

Figure 30. Repeated loading induced axial strain accumulation (Chang et al., 2016)

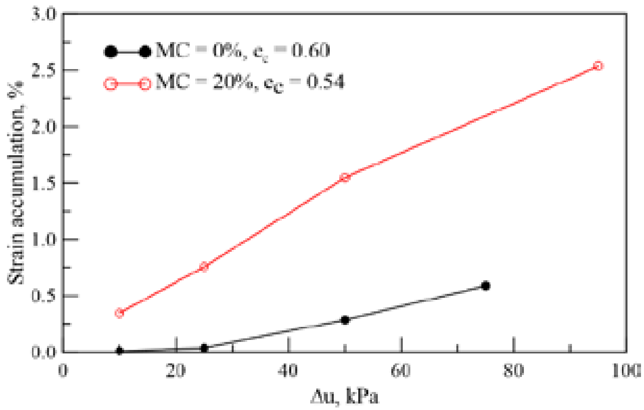

Figure 31. Effects of fines content on strain accumulation (Chang et al., 2016)

6 CONCLUDING REMARKS

Based on the series of studies described above, the following conclusions can be drawn:

- For M/S soils, good quality soil samples can be taken with reasonable costs. As such, undisturbed soil samples should be taken on a more regular basis when necessary.
- In reporting the test data of laboratory soil element or physical model tests, the post consolidation void ratio e_c should be used to represent the density state of the specimen. The use of relative density for M/S soils can be missleading and should be avoided.
- The fines and grain characteristics of the coarse particles can make the M/S soil much more compressible than typical clean quartz sands. For CPT in well mixed homogeneous M/S soils, the effects of partial drainage can make the cone tip resistance significantly less than those in clean quartz sand under similar density and stress states.
- For field CPTU, partial drainage should not be assumed simply because of the overall soil fines contents or soil behavior type index. Due to soil heterogeneity and closely spaced free draining soil layers, the CPTU can be drained in soils with high overall fines contents. The drainage conditions should be verified with simple procedures such as the pore pressure dissipation tests. In assessing the liquefaction potential using the simplified procedure, the fines content adjustment should not be used unless it is verified that the cone penetration is indeed partially drained. Or we should consider drainage adjustment, not fines content adjustment.
- The use of equivalent granular void ratio, e* and equivalent granular state parameter, Ψ* can be very helpful in streamlining the effects of fines on various engineering properties of M/S soils. A single critical state line that is based on e* can be applied for a wide range of fines contents. The number of tests required to establish e* based critical state line is much less than that needed to determine a series of critical state lines for the individual fines contents involved.
- The correlation between CRR and Ψ or Ψ* appears promising. To integrate CRR-Ψ correlation into the simplified procedure for liquefaction potential assessment would require a reliable correlation between Ψ (or Ψ*) and an in situ test method which is still lacking.
- Mist pluviation demonstrated its potential as a means to reconstitute specimens for soil element as well as physical model tests. Homogeneous M/S specimens with more dilatant behavior than those of MT specimens can be made in a continuous process and with efficiency.
- The effects of high compressibility can also be responsible for ground subsidence. Initial test results have indicated that repeated pore pressure fluctuation can induce significant strain accumulation.

7 REFERENCES

Almeida, M.S.S., Jamiolkowski, M. & Peterson, R.W. 1991 Preliminary results of CPT tests in calcareous Quoiu sand. Proceedings, *First International Symposium on Calibration Chamber Testing*, Potsdam, New York, pp.41-54.

Andrus, R.D. & Stokoe, K.H., II. 2000. Liquefaction resistance of soils from shear-wave velocity. Journal of Geotechnical and Geoenvironmental Engineering, ASCE, Vol.126, No.11, pp.1015-1025.

Baxter, C. D. P., Bradshaw, A. S., Green, R. A. & Wang, J. H. 2008. Correlation between cyclic resistance and shear-wave velocity for Providence silts. Journal of Geotechnical and Geoenvironmental Engineering, Vol. 134, No. 1, pp. 37 - 46.

Chang, W.J., Chou, S.H. & Huang, A.B. 2016. Simulation of the effects of repeated groundwater pumping using Cyclic K_o consolidation. Submitted to Acta Geotechnica for consideration of publication.

Høeg, K. Dyvik, R. & Sandbaekken, G. 2000. Strength of undisturbed versus reconstituted silt and silty sand Specimens.

Journal of Geotechnical and Geoenvironmental Engineering, ASCE 126(7):606-617.
Hofmann, B.A. 1997. In situ ground freezing to obtain undisturbed samples of loose sand for liquefaction assessment. Ph.D. thesis, Department of Civil and Environmental Engineering, University of Alberta, Edmonton, Alberta, Canada.
Huang, A.B., Hsu, H.H., & Chang, J.W. 1999. The behavior of a compressible silty fine sand. *Canadian Geotechnical Journal*36(1): 88-101.
Huang, Y.T, Huang, A.B., Kuo, Y.C. & Tsai, M.D. 2004. A laboratory study on the undrained strength of a silty sand from Central Western Taiwan. Soil Dynamics and Earthquake Engineering, Vol.24, No.9-10, pp.733-743.
Huang, A.B. & Hsu, H.H. 2005. Cone penetration tests under simulated field conditions. Geotechnique, Vol.LV, No.5, pp.345-354.
Huang, A.B. & Huang, Y.T. 2007. Undisturbed sampling and laboratory shearing tests on a sand with various fines contents. Soils and Foundations, Vol.47, No.4, pp.771-781.
Huang, A.B., Tai, Y.Y., Lee, W.F., & Ishihara, K. 2008. Sampling and field characterization of the silty sand in central and southern Taiwan. Proceedings, The 3rd International Conference on Site Characterization, Taipei, pp.1457-1463.
Huang, A.B., Tai, Y.Y., Lee, W.F. & Huang, Y.T. 2009. Field evaluation of the cyclic strength versus cone tip resistance correlation in silty sands. Soils and Foundations, Vol.49, No.4, pp.557-568.
Huang, A.B. & Chuang, S.Y. 2011. Correlating cyclic strength with fines contents through state parameters. Soils and Foundations, Vol. 51 No. 6, pp.991-1001.
Huang, A.B., Chang, W.J., Hsu, H.H. & Huang, Y.J. 2015. A mist pluviation method for reconstituting silty sand specimens. Engineering Geology, Vol.188, pp.1-9.
Hung, W. C., Hwang, C., Liou, J. C., Lin, Y. S. & Yang, H. L. 2012. Modeling aquifer-system compaction and predicting land subsidence in central Taiwan. Engineering Geology Journal, Vol. 147-148, pp. 78-90.
Ishihara, K. 1993. Liquefaction and flow failure during earthquakes. Geotechnique 43, No.3, pp.351-415.
Ishihara, K. 1996. Soil behavior in earthquake geotechnics. Clarendon Press, Oxford, UK, 350p.
Jefferies, M.G. & Been., K. 2006. Soil liquefaction – A critical state approach. Taylor and Francis, London, 479p.
Kikumoto, M. Muir Wood, D. & Russell, A. 2009. Particle crushing and deformation behavior. Soils and Foundations, Vol.50, No.4, pp.547-563.
Koester, J.P. 1994. The influence of fines type and content on cyclic strength. Prakash S & Dakoulas P, editors. *Groundfailures under seismic conditions. ASCE Geotechnical Special Publication*44.:17–33.
Koiter, W. T. 1960. General theorems for elastic–plastic solids. In Progress in solid mechanics (ed I. N. Sneddon & R. Hill), pp. 165–221. Amsterdam: North Holland.
Konrad, J.M., St-Laurent, S. Gilbert, F., & Leroueil, S. 1995. Sand sampling below the water table using the 200 mm diameter Laval sampler. *Canadian Geotechnical Journal* 32:1079-1086.
Kuerbis, R. & Vaid, V.P. 1988. Sand sample preparation - the slurry deposition method. Soils and Foundations, 28(4):107-118.
Lade, P.V., Liggio, C.D., & Yamamuro, J.A. 1998. Effects of non-plastic fines on minimum and maximum void ratios of sand. *ASTM Geotechnical Testing Journal*21(4):336-347.
La Rochelle, P., Sarrailh, J., Tavenas, F., Roy, M. & Laroueil, S. 1981. Causes of sampling disturbance and design of a new sampler for sensitive soils. *Canadian Geotechnical Journal*18(1):52-66.
Lee, J.T., Wang, C.C., Ho, Y.T. & Huang, A.B. 2013. Characterization of reservoir sediment with differential pressure sensored flat dilatometer and piezo-penetrometer. Acta Geotechnica, Issue 4, pp 373-380.
Lee, W. F., Liao, H. J., & Ishihara, K. 2006. A study on engineering properties of Kaohsiung silty sand. (in Chinese), Internal Research Report, Taiwan Construction Research Institute, Taipei, Taiwan:204p.
Mayne, P.W. 2006. The 2006 James K. Mitchell lecture: Undisturbed sand strength from seismic cone tests. Geomechanics and Geoengineering, Vol. 1 (4), Taylor & Francis, London: 239-247.
McNeilan, T.W., & Bugno, W.T. 1984. Cone penetration test results in offshore California silts. *Symposium on Strength Testing of Marine Sediments: Laboratory and In-Situ Measurements*, San Diego, ASTM STP 883:55-71.
Ng, T.T., Zhou, W., & Chang X.L. 2016. Effect of particle shape and fine content on the behavior of binary mixture. Journal of Engineering Mechanics, 10.1061/(ASCE) EM.1943-7889.0001070 , C4016008.
Polito, C.P. 1999. The effects of nonplastic and plastic fines on the liquefaction of sandy soils, Ph.D. Thesis, Virginia Polytechnic Institute and State University, Blacksburg, Virginia.
Rahman, M. M., Lo, S. R. & Gnanendran, C. T. 2008. On equivalent granular void ratio and steady state behavior of loose sand with fines. Canadian Geotechnical Journal, Vol. 45, pp.1439 - 1456.
Robertson, P. K. 2009. Interpretation of cone penetration tests – a unified approach. Canadian Geotechnical Journal, Vol. 46, pp. 1337 - 1355.
Robertson, P. K. & Wride, C. E. 1998. Evaluating cyclic liquefaction potential using the cone penetration test. Canadian Geotechnical Journal, Vol. 35, pp. 442 - 459.
Stark, T. D. & Olson, S. M. 1995. Liquefaction resistance using CPT and field case histories. Journal of Geotechnical Engineering Division, Vol. 121, No. 12, p. 856 - 869.
Tani, K. & Kaneko, S. 2006. Method of recovering undisturbed samples using water-soluble thick polymer. (in Japanese) Tsuchi-to-Kiso, *Journal of Japanese Geotechnical Society* 54(4):145-148.
Thevanayagam, S. 2000. Liquefaction potential and undrained fragility of silty soils. Proceedings, 12th World Conference on Earthquake Engineering, Aukland, New Zealand, edited by R. Park, New Zealand Society of Earthquake Engineering, Upper Hutt, New Zealand, Paper 2383.
Thevanayagam, S., Thenthan, T., Mohan, S. & Liang, J. 2002. Undrained fragility of clean sands, silty sands, and sandy silt. *Journal of Geotechnical and Geoenvironmental Engineering, ASCE*128(10):849-859.
Xenaki, V.C. & Athanasopoulos, G.A. 2003. Liquefaction resistance of sand–silt mixtures: an experimental investigation of the effect of fines. Soil Dynamics and Earthquake Engineering23:183-194.
Yamamuro, J.A. & Wood, F.M., 2004. Effect of depositional method on the undrained behavior and microstructure of sand with silt. *Soil Dynamics and Earthquake Engineering* 24(9-10):751-760.
Youd, T.L., Idriss, I.M., Andrus, R.D., Arango, I., Castro, G., Christian, J.T., Dobry, R., Liam Finn, W.D., Harder Jr., L.F., Hynes, M.E., Ishihara, K., Koester, J.P., Liao, S.S.C., Marcuson III, W.F., Martin, G.R., Mitchell, J.K., Moriwaki, Y., Power, M.S., Robertson, P.K., Seed, R.B., & Stokoe II, K.H. 2001. Liquefaction resistance of soils: summary report from the 1996 NCEER and 1998 NCEER/NSF workshops on evaluation of liquefaction resistance of soils. *Journal of Geotechnical and Geoenvironmental Engineering, ASCE*127(10):817-833.

Geotechnical and Geophysical Site Characterisation 5 – Lehane, Acosta-Martínez & Kelly (Eds)

Evaluating effective stress parameters and undrained shear strengths of soft-firm clays from CPTu and DMT

P.W. Mayne
Georgia Institute of Technology, Atlanta, Georgia, USA

ABSTRACT: Results from piezocone penetration (CPTu) and flat dilatometer tests (DMT) can be used to evaluate the stratigraphy, soil types, and a suite of engineering parameters that are needed for geotechnical analysis and design, especially for finite element methods (FEM). Of particular interest herein is the utilization of in-situ test data for assessing the effective stress strength envelope (c' and ϕ') in soft to firm clays, as well as undrained shear strengths (s_u), since many FEM codes have built-in constitutive soil models that are based on critical-state soil mechanics and require effective stress parameters as input. An existing undrained limit plasticity solution for evaluating ϕ' in clays from CPTu is reviewed and then extended to the DMT via a link established thru spherical cavity expansion theory. Laboratory and field results on soft Bothkennar clay at the British national test site and additional CPTu data in clays are used to illustrate the methodologies.

1 INTRODUCTION

1.1 *Site investigation*

Soft to firm clays are commonly found offshore and onshore in marginal areas of construction, particularly coastal regions, lakeshores, and near waterways and rivers. As a result, construction issues arise concerning suitable bearing capacity of shallow and deep foundations, stability of embankments, earth-retention walls, and excavations, as well as concerns related to time rate of consolidation and long-term settlements. While laboratory testing programs are necessary, in-situ measurements from piezocone and dilatometer soundings allow the fast collection of data on these soft soils with immediate applications for the evaluation of geoengineering parameters for analysis and design.

1.2 *Geoparameters from CPT*

A fairly good number of soil engineering parameters have been defined and identified in order to represent the complexities of soil behavioral characteristics. A set of common-used and necessary geoparameters obtained from cone penetration testing (CPT) for analyses is listed in Table 1, yet this is far from a complete and comprehensive listing of all that have been implemented in practice (Lunne et al. 1997; Mayne 2007).

Readings from the CPT can include: cone resistance (q_t), sleeve friction (f_s), and penetration porewater pressure (u_2), as well as time to reach 50% consolidation during dissipation (t_{50}) and downhole shear wave velocity (V_s), thus designated SCPTù. The SCPTù is a particularly efficient and expedient means for site-specific subsurface investigations, as multiple measurements are collected from a single sounding as depicted in Figure 1. At a standard rate of push of 20 mm/s, the q_t, f_s, and u_2 readings are taken every 10 to 50 mm, while the t_{50} and/or V_s can be obtained every one meter.

Table 1. Common geoparameters for representing the behavior of soft-firm clays from CPT data

Symbol	Parameter	Readings
SBT	Soil behavior type	Uses CPT index I_c
I_c	CPT material index	I_c = *fctn* (Q_{tn} and F)
γ_t	Unit weight	from f_s reading
σ_{vo}	Overburden stress	$\sigma_{vo} = \int \gamma_t\, dz$
u_0	Hydrostatic pressure	Δu dissipations
σ_{vo}'	Effective stress	$\sigma_{vo}' = \sigma_{vo} - u_0$
σ_p'	Preconsolidation stress	σ_p' = *fctn* (q_{net}, I_c)
YSR	Yield stress ratio	YSR = σ_p'/σ_{vo}'
c'	Effective cohesion intercept	NTH method
ϕ'	Effective friction angle	NTH method
s_u	Undrained shear strength	N_{kt} factor
D'	Constrained modulus	$D' \approx 5{\cdot}q_{net}$
G_0	Small-strain modulus	V_s data
G	Shear modulus	G_0 and τ/τ_{max}
c_{vh}	Coefficient of consolidation	Δu dissipation
K_0	Lateral stress coefficient	ϕ' and YSR
k	Hydraulic conductivity	Δu dissipations

Notes: NTH = Norwegian Institute of Technology; τ/τ_{max} = mobilized strength; τ = shear stress; τ_{max} = shear strength.

The penetrometer readings provide the net cone resistance ($q_{net} = q_t - \sigma_{vo}$) and excess porewater pressure ($\Delta u = u_2 - u_0$), as well as the effective cone tip resistance ($q_E = q_t - u_2$). Dimensionless CPT parameters have been developed to give: (a) normalized cone tip resistance: $Q = q_{net}/\sigma_{vo}'$, (b) normalized sleeve friction: $F = 100 \cdot f_s/q_{net}$, and (c) normalized porewater pressure parameter: $B_q = \Delta u/q_{net}$. Later, an updated version of Q is detailed and designated Q_{tn} that is needed in determining the CPT material index (I_c) which finds application in soil behavioral classification (Robertson 2009), as well as the assessment of the yield stress or preconsolidation stress (σ_p') and other geoparameters (Mayne 2015).

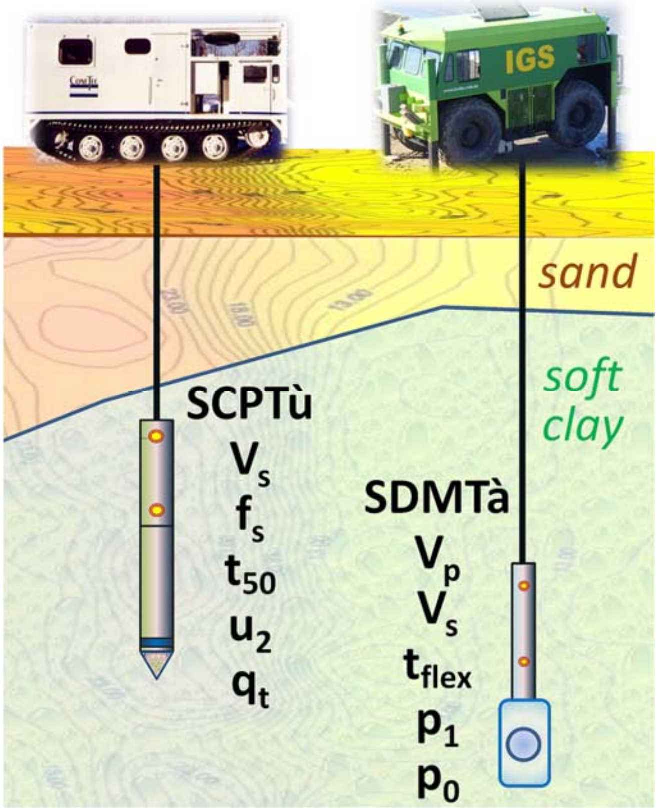

Figure 1. Multiple readings captured by a single sounding using seismic piezocone (SCPTù) and seismic dilatometer (SDMTà).

1.3 *Geoparameters from DMT*

A similar suite of geoparameters is found from the results of flat plate dilatometer tests (DMT), as initially identified by Marchetti (1980). In the DMT, two pressure readings are taken at each 0.2-m depth interval: (a) A-reading corrected to p_0 (contact pressure); and (b) B-reading corrected to p_1 (expansion pressure). These provide three DMT indices: (1) soil material index: $I_D = (p_1-p_0)/(p_0-u_0)$; (2) dilatometer modulus: $E_D = 34.7 \cdot (p_1-p_0)$; and (3) horizontal stress index: $K_D = (p_0-u_0)/\sigma_{vo}'$.

Additional readings can be taken during the DMT, including: (a) dissipation A-readings to get time for degree of consolidation (e.g., t_{flex}), (b) P-wave arrival to obtain V_p = compression wave velocity; (c) S-wave arrival to obtain V_s = shear wave velocity (Marchetti et al. 2008); (d) C-readings which are the membrane position of A-reading but taken during deflation, and (e) blade thrust readings. For the set of p_0, p_1, t_{flex}, V_p, and V_s measurements, the test can be designated SDMTà (Figure 1).

Details concerning the interpretation of soil engineering parameters from the DMT are provided in Marchetti et al. (2001) and Marchetti (2015). Two geoparameters which have not been evaluated in soft to firm clays using the DMT include: (1) effective stress friction angle (ϕ') and (2) effective cohesion intercept (c'). A methodology for their assessment from DMT readings in clay is proposed herein.

2 SOIL CLASSIFICATION BY CPT

2.1 *Soil behavioral type*

During CPT, soil types are usually identified indirectly since samples are not normally taken. The soil types can be assessed using one or more different approaches that rely on the direct measurements or post-processed readings, as indicated in Table 2. An alternative means to classify soil types in-situ is via the vision cone (VisCPT) whereby a video-cam records the images of soil particles passing a sapphire window (Ghalib et al. 2000).

Table 2. Methods for Soil Type Identification by CPT

Method	Procedure	Reference
"Rules of Thumb"	1. Clean sands: $q_t > 50\ \sigma_{atm}$ $u_2 \approx u_0$ 2. Clays: $q_t > 50\ \sigma_{atm}$ 2.1 Intact: $u_2 \approx u_0$ 2.2 Fissured: $u_2 < 0$	Mayne, et al. (2002)
Soil behavioral charts	Non-normalized: 1. q_t vs f_s 2. ($q_t - u_2$) vs. f_s	Fellenius & Eslami (2000)
Soil behavioral charts	Normalized charts: 1. Q vs F 2. Q vs B_q	Lunne et al. (1997)
Soil behavior type (SBT)	CPT material index. I_c where $I_c = fctn(Q_{tn}, F)$	Robertson (2009)
Probability based relationships	Statistical estimates of sand, silt, and clay contents	Tümay, et al. (2011)

One of the most popular methods in use today utilizes soil behavioral type (SBT) charts based on Q, F, and B_q, termed *SBTn* since the three piezocone readings are normalized. This system classifies soils into 9 distinct zones that are presented in either log Q vs. log F charts or log Q vs B_q charts, or both (Lunne et al. 1997). The general layout for the Q-F chart is shown in Figure 2.

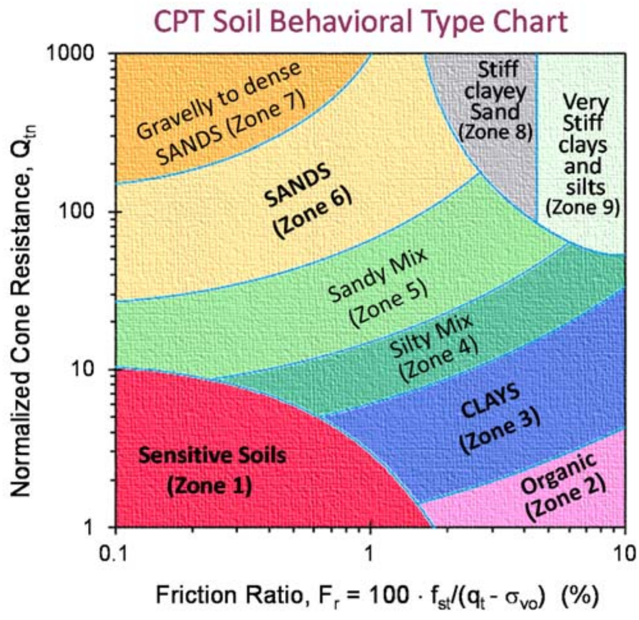

Figure 2. Chart for 9-zonal soil behavioral types from CPTu Q versus F (after Robertson 2009)

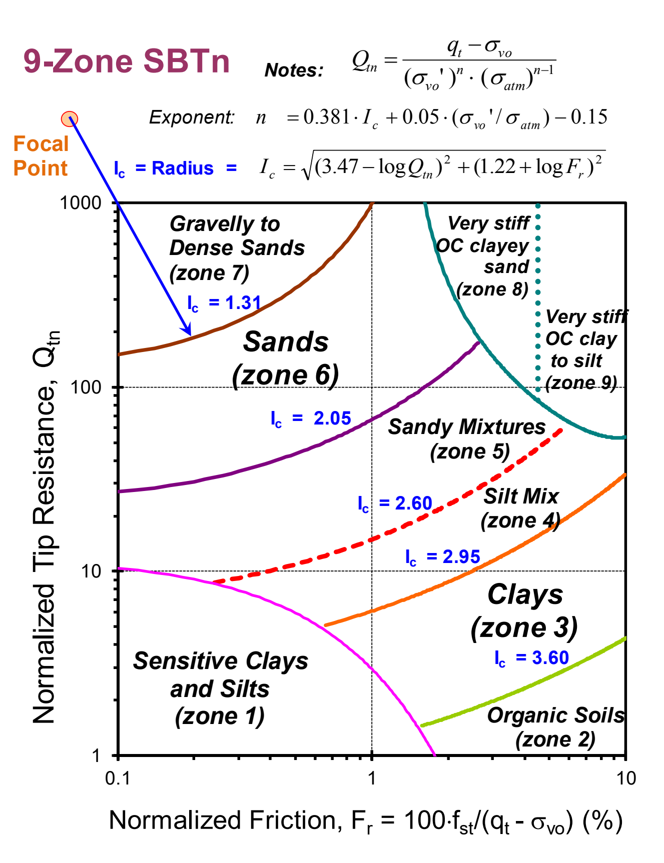

Figure 3. Definition of CPT material index I_c for Q versus F chart (after Robertson 2009)

2.2 *CPT material index, I_c*

The CPT material index I_c represents a family of the radii of a sets of circles which separate soil behavioral zones 2 through 7 in the log Q vs. log F chart, as shown by Figure 3. The index is given by:

$$I_c = \sqrt{(3.47 - \log Q)^2 + (1.22 + \log F)^2} \quad (1)$$

using the initial values of Q and F described previously. Then, a revised value of normalized cone resistance is defined:

$$Q_{tn} = \frac{(q_t - \sigma_{vo})/\sigma_{atm}}{(\sigma_{vo}'/\sigma_{atm})^n} \quad (2)$$

where the exponent "n" is determined from (Robertson 2009):

$$n = 0.381 \cdot I_c + 0.05 \cdot (\sigma_{vo}'/\sigma_{atm}) - 0.05 \leq 1.0 \quad (3)$$

and the index I_c is recalculated. Iteration converges quickly and generally only 3 cycles are needed to secure the operational I_c at each depth.

Algorithms are available to cull the CPTu data for zone 1 (soft sensitive clays) and zones 8 and 9 (stiff overconsolidated clays and sands). Once these three zones are identified, the material index I_c is used to separate zones 2 through 7, so all easily implemented on a spreadsheet or programmable software code.

Sensitive clays of Zone 1 are identified when:

$$Q_{tn} < 12 \cdot \exp(-1.4 \cdot F) \quad (4)$$

Overconsolidated soils of Zone 8 ($1.5 < F < 4.5\%$) and Zone 9 ($F \geq 4.5\%$) are found when:

$$Q_{tn} \geq [0.006(F-0.9) - 0.0004(F-0.9)^2 - 0.002]^{-1} \quad (5)$$

Then, the remaining soil types are identified by the CPT material index: Zone 2 (organic soils: $I_c \geq 3.60$); Zone 3 (clays: $2.95 \leq I_c < 3.60$); Zone 4 (silt mixtures: $2.60 \leq I_c < 2.95$); Zone 5 (sand mixtures: $2.05 \leq I_c < 2.60$); Zone 6 (sands: $1.31 \leq I_c < 2.05$); and Zone 7 (gravelly to dense sands: $I_c \leq 1.31$). The red dashed line at $I_c = 2.60$ represents an approximate boundary separating *drained* ($I_c < 2.60$) from undrained behavior ($I_c > 2.60$).

A similar CPTu material index has been developed for the 9 SBTn zones to represent the log Q vs. B_q diagrams, designated $I_{Q\text{-}Bq}$ by Torrez-Cruz (2015).

An alternate means to normalize the porewater pressures readings is through the parameter $\Delta u/\sigma_{vo}'$ that is used by Schneider et al. (2008) where the graph of log Q vs $\Delta u/\sigma_{vo}'$ provides various soil behavioral type zones. Schneider et al. (2012) derive corresponding equations that delineate the SBTs for both the Q-F and Q-$\Delta u/\sigma_{vo}'$ plots. They also provide data from a variety of field sites to populate the graphs and show the regions of drained, partially drained, and undrained behavior.

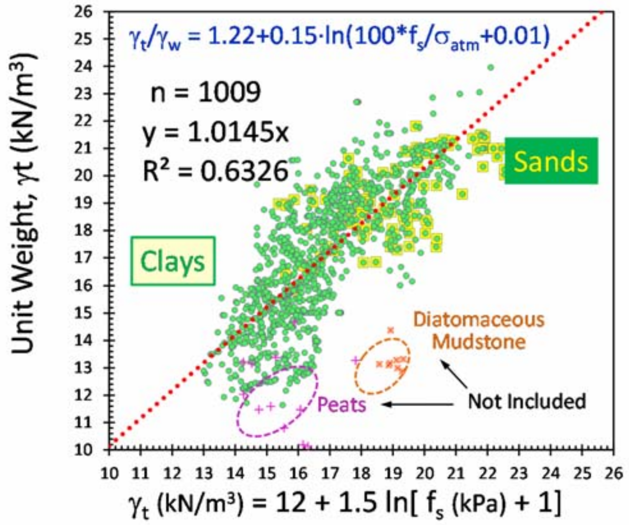

Figure 4. Soil unit weight from CPT sleeve friction reading

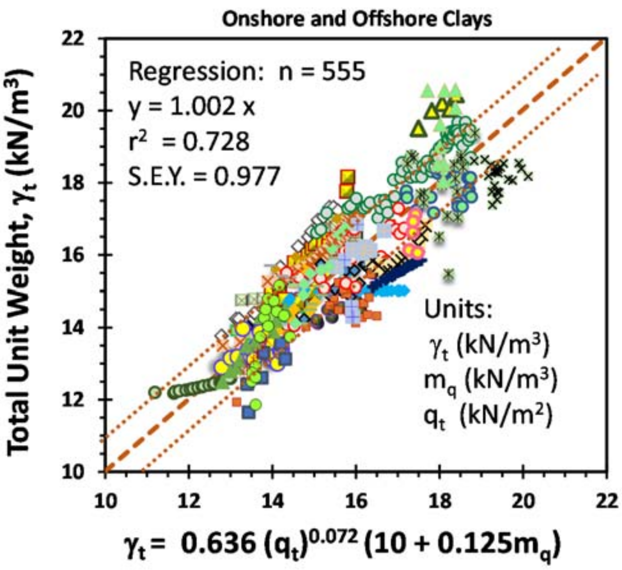

Figure 5. Soil unit weight of soft-firm clays from cone resistance (q_t) and resistance-depth ratio (m_q).

2.3 *Soil unit weight*

The use of normalized piezocone parameters requires the evaluation of total and effective overburden stresses ($\sigma_{vo}' = \sigma_{vo} - u_0$), where $\sigma_{vo} = \int \gamma_t\, dz$ and u_0 = hydrostatic porewater pressure. Therefore, an indirect assessment of unit weight (γ_t) is needed.

A general assessment of soil unit weight from CPT for a variety of soil types has been found related to the sleeve friction, as shown by Figure 4 (Mayne 2014):

$$\gamma_t/\gamma_w = 1.22 + 0.15 \cdot \ln\,(100\, f_s/\sigma_{atm}+0.01) \qquad (6)$$

For soft-firm clays, the cone resistance exhibits a linear trend with depth that can be represented by the parameter $m_q = \Delta q_t/\Delta z$, termed the resistance-depth ratio. Two sets of regressions on q_t data both with and without an intercept (b = 0) giving similar slope values m_q are indicative of normally-consolidated (NC) to lightly-overconsolidated (LOC) clays (Mayne & Peuchen 2012). In contrast, different m_q slope values from the two regressions are characteristic of overconsolidated soils and thus the method is not applicable. It has been observed that the range of m_q in soft-firm clays generally occurs when the ratio m_q < 80 kN/m³ (Mayne 2014).

For soft to firm clays, the resistance-depth ratio m_q gives an estimate of the average soil total unit weight over the depth of the deposit:

$$\gamma_t/\gamma_w \;=\; 1 \;+\; 0.125\; m_q/\gamma_w \qquad (7)$$

It is interesting to note that the resistance-depth ratio has the same units as unit weight, thus can be employed as a normalizing parameter in the same manner that atmospheric pressure (σ_{atm}) is used for stress.

To capture variations in the unit weight with depth, a more elaborate trend is shown in Figure 5 in terms of q_t and m_q (Mayne & Peuchen 2012). This can be expressed in dimensionless form:

$$\gamma_t/\gamma_w \;= 0.886 \cdot (q_t/\sigma_{atm})^{0.072}\,[1+ 0.125 \cdot m_q/\gamma_w] \qquad (8)$$

2.4 *Unit weights at Bothkennar*

The estimating of soil unit weights from CPTu in soft clay are illustrated with a case study. For the Bothkennar site in Scotland, two sets of piezocone data were utilized from field testing by Nash et al. (1992a) and Powell & Lunne (2005), as presented in Figure 6. The agreement between the early sounding and later series is quite evident.

The evaluation of the m_q parameter is shown in Figure 7a, giving a value of the resistance-depth ratio: m_q = 54 kN/m³. This can be input into equation (7) to give an estimated γ_t = 16.7 kN/m³ which agrees well as an overall value when compared with lab unit weights obtained from Delft and piston type samples taken at the site that are shown in Figure 7b (Hight et al. 2003).

A slightly improved profile of estimated unit weight with depth is obtained using both the cone resistance q_t together with the m_q parameter, as seen by Figure 7b, per equation (8). Here, the profile of unit weight decreases slightly in the crust and then increases slightly with depth in the soft clay.

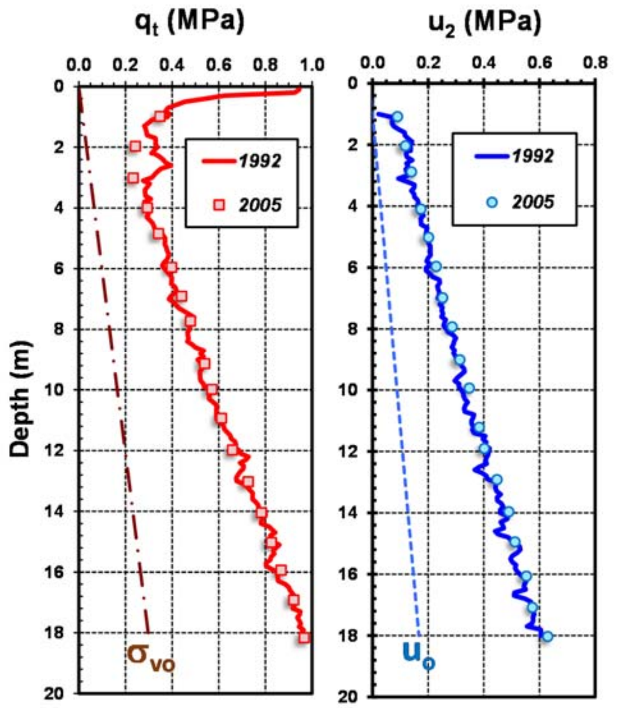

Figure 6. Results from two sets of piezocone sounding series at Bothkennar clay test site, UK (data from Nash et al. 1992 and Powell & Lunne 2005).

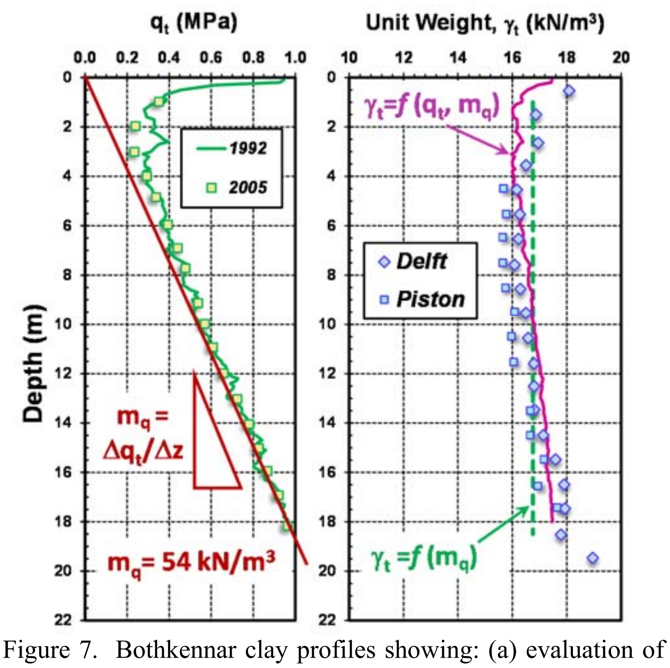

Figure 7. Bothkennar clay profiles showing: (a) evaluation of m_q ratio; (b) measured and estimated soil unit weights.

3 EFFECTIVE STRESS FRICTION ANGLE OF CLAY FROM PIEZOCONE

The prevailing shear strength of soils depends upon the frictional characteristics of soils, stress path, initial anisotropic state of stress, degree of drainage, direction of loading, and many other factors. Commonly, two extreme cases are sought for saturated geomaterials: (1) drained strength ($\Delta u = 0$) with corresponding effective stress friction angle (ϕ') and effective cohesion intercept (c'); and (2) undrained shear strength ($s_u = c_u$) corresponding to constant volume ($\Delta V/V_0 = 0$).

3.1 *Effective stress friction angle*

Since the piezocone takes measures of both total stress changes (q_t) and porewater pressures (u_2) during penetration into soil, the principle of effective stress can be realized (Sandven 1990). In the case of soft to firm clays, it can be taken that $c' = 0$ and the effective friction angle (ϕ') can be evaluated using the NTH (Norwegian Institute of Technology) solution detailed by Senneset et al. (1989) and Sandven & Watn (1995).

For the general case, undrained penetration is represented by:

$$q_{net} = (N_q - 1)\cdot(\sigma_{vo}' + a') - N_u \cdot \Delta u_2 \tag{9}$$

where the attraction $a' = c'\cdot\cot\phi'$ and N_q = bearing capacity factor for end bearing or tip resistance is given by:

$$N_q = \tan^2(45° + \phi'/2)\cdot\exp[(\pi - 2\beta)\cdot\tan\phi'] \tag{10}$$

and β = angle of plastification which dictates the size of the failure zone. The term N_u is the bearing factor for porewater pressure (Senneset & Janbu 1985):

$$N_u = 6\cdot\tan\phi'\cdot(1 + \tan\phi') \tag{11}$$

Additional details are given by Sandven (1990) regarding the terms of attraction (a') and angle of plastification (β). The cone resistance number (N_m) is defined as:

$$N_m = \frac{q_t - \sigma_{vo}}{\sigma_{vo}' + c'\cdot\cot\phi'} = \frac{N_q - 1}{1 + N_u \cdot B_q} \tag{12}$$

A discussion of evaluating the effective cohesion intercept c' is provided in a later section of this paper.

For the case when $c' = 0$, the parameter N_m is identical to the normalized cone resistance (Q) and the relationship becomes:

$$Q = \frac{N_q - 1}{1 + N_u \cdot B_q} = \frac{q_t - \sigma_{vo}}{\sigma_{vo}'} \tag{13}$$

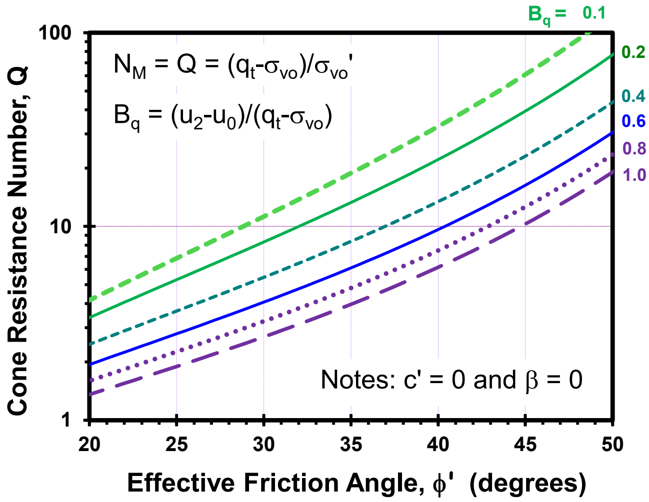

Figure 8. NTH graphical solution for ϕ' in terms of Q and B_q for simple case when c' = and β = 0.

Therefore, for the simplified case when β = 0 and c' = 0, the undrained limit plasticity solution relates Q to effective stress friction angle ϕ' and parameter B_q:

$$Q = \frac{\tan^2(45° + \phi'/2)\cdot\exp(\pi\cdot\tan\phi') - 1}{1 + 6\cdot\tan\phi'\cdot(1+\tan\phi')\cdot B_q} \qquad (14)$$

as presented graphically in Figure 8.

An approximate inversion of the NTH solution has been developed for individual values of Q and B_q for the case when c' = 0 and β = 0 (Mayne 2007):

$$\phi' = 29.5°\cdot B_q^{0.121}\cdot[0.256 + 0.336\cdot B_q + \log Q] \qquad (15)$$

This is applicable for the specific ranges of porewater pressure parameter ($0.1 < B_q < 1$) and effective stress friction angles (20° < ϕ' < 45°).

3.2 *NTH application to Bothkennar CPTu data*

The NTH method is applied to the piezocone data from Bothkennar, Scotland (reported earlier in Figure 6). Figure 9 presents a plot of Δu_2 vs. q_{net} and gives regression best fit line slopes B_q = 0.62 and 0.65, respectively, for the 1992 and 2005 data sets.

Similarly, plots of q_{net} vs. σ_{vo}' are shown in Figure 10 and regression lines indicate N_m = Q = 5.22 and 5.17, respectively. The regressions were completed using best fit line options with forced intercepts of zero, as the assumption here is that c' = 0. Using the paired values of Q and B_q input into Figure 8 give NTH-evaluated ϕ' = 32.9° and 33.3°, respectively.

Extensive laboratory programs and in-situ field tests of Bothkennar clay have been accomplished over the past three decades (Hight et al. 2003). These include many series of laboratory triaxials tests on both undisturbed and remolded samples taken by a variety of high quality samplers and different laboratories.

Results from a particular set produced by Allman & Atkinson (1992) are shown in Figure 11. These include several modes of shearing: triaxial compression (CK_0UC, CK_0DC) and extension (CK_0UE, CK_0DE) tests from both undrained and drained stress paths, all confirming that the characteristic ϕ' = 34° for Bothkennar clay.

Using the approximate expression for ϕ' = *fctn* (Q, B_q), Figure 12 presents the derived profiles of ϕ' with depth at Bothkennar using the two sets of CPTu data. These show good agreement with the summary ϕ' = 34° from the laboratory triaxial data, with slightly conservative evaluations by the CPTu approach.

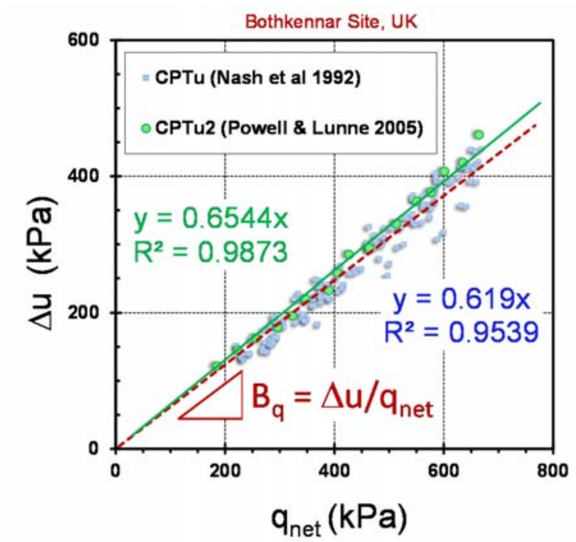

Figure 9. Plot of excess porewater pressure vs. net cone resistance from Bothkennar CPTu data.

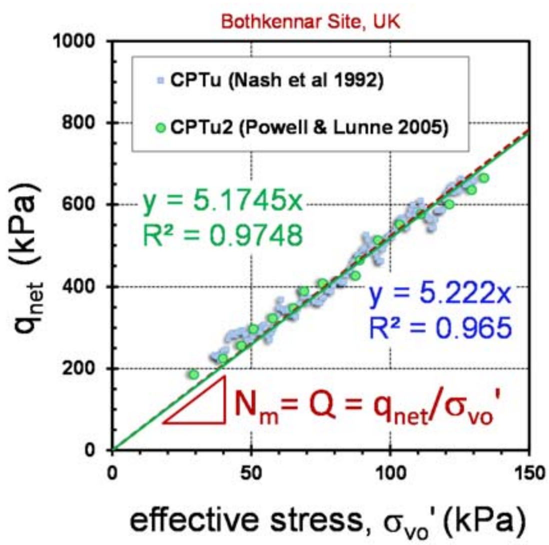

Figure 10. Plot of net cone resistance vs. effective overburden stress from Bothkennar CPTu data.

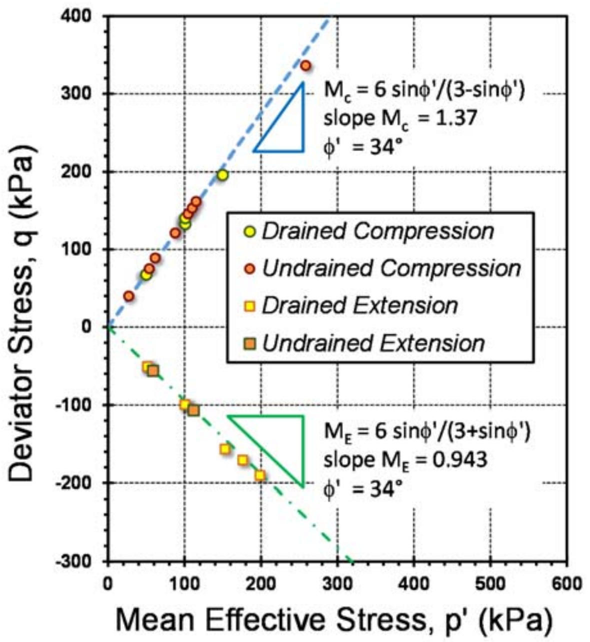

Figure 11. Results from triaxial tests on Bothkennar soft clay reported by Allman & Atkinson (1992).

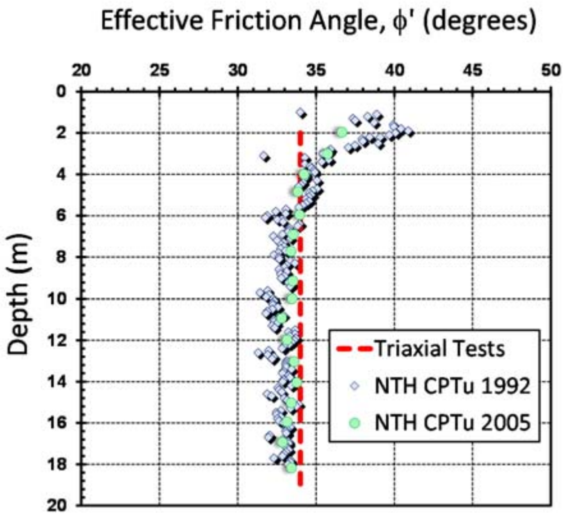

Figure 12. Profile of ϕ' at Bothkennar clay using CPTu Q and B_q and approximate NTH solution.

4 UNDRAINED STRENGTH PARAMETERS FROM PIEZOCONE

Undrained shear strength (s_u) is a total stress parameter measured at constant volume. The mode of shearing affects the magnitude of undrained shear strength in soft to firm clays. For instance, the Bothkennar clay has a family of s_u profiles that have been obtained from a variety of different lab and field tests. Figure 13 shows a relative sampling that indicate the hierarchy of s_u from highest to lowest: field vane tests (FVT), triaxial compression (TC), simple shear (SS), and triaxial extension (TE).

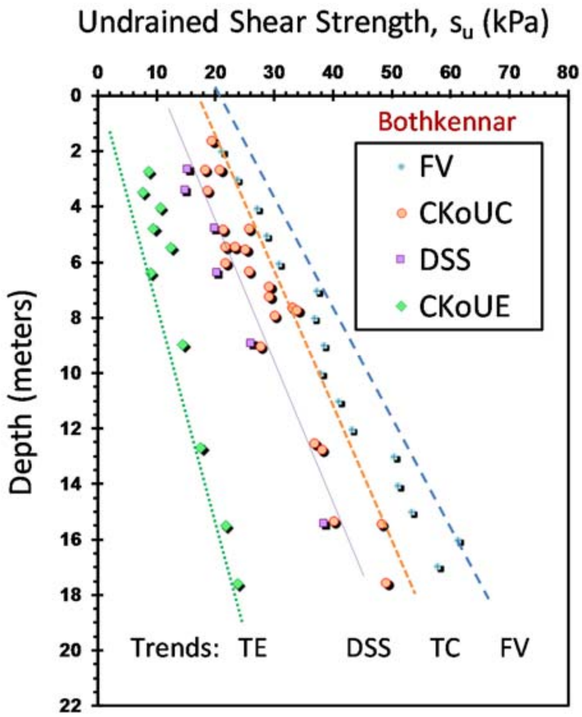

Figure 13. Family of s_u profiles for Bothkennar soft clay (data from Hight et al. 2003).

4.1 *Undrained shear strength from piezocone*

For CPT results, the undrained shear strength (s_u) is most often interpreted in terms of the net cone tip resistance. If the triaxial compression mode is taken as the relevant type of undrained shear strength (s_{uc}), then:

$$s_{uc} = \frac{q_{net}}{N_{kt}} \tag{16}$$

where N_{kt} = bearing factor for net tip resistance.

For CPTu in soft to firm clays, Lunne et al. (2005) recommend a value N_{kt} = 12 for s_{uc}. A study of piezocone data on 3 onshore and 11 offshore clays by Low et al. (2010) found the range: $8.6 \leq N_{kt} \leq 15.3$, with a mean value of N_{kt} = 11.9 for triaxial compression mode. Similarly, a larger study of 51 soft to firm intact clays found a mean value of N_{kt} = 11.8 for s_{uc} corresponding to the CAUC triaxial mode (Mayne et al. 2015).

For other shearing modes, other operational values of N_{kt} must be used. For instance, Low et al. (2010) found a mean N_{kt} = 13.6 for the lab average strength (s_{uAVE}) from triaxial compression, simple shear, and triaxial extension (range: $10.6 \leq N_{kt} \leq 17.4$), which is close to a simple shear mode (s_{uSS}). For calibration with the field vane (s_{uv}), they determined N_{kt} averages 13.3 with a range: $10.8 \leq N_{kt} \leq 19.9$.

Similarly, the undrained shear strength can be expressed in terms of the excess porewater pressures during penetration ($\Delta u = u_2 - u_0$):

$$s_{uc} = \frac{\Delta u}{N_{\Delta u}} \tag{17}$$

where $N_{\Delta u}$ = bearing factor for excess porewater pressures. For the triaxial compression mode, Lunne (2010) recommends a value of $N_{\Delta u} = 6$ for preliminary work or initial estimates until calibrated with laboratory tests on undisturbed samples. From their study, Low et al. (2010) indicate a mean value of $N_{\Delta u} = 5.88$, while the study by Mayne, Peuchen, & Baltoukas (2015) found a representative $N_{\Delta u} = 6.5$.

4.2 *Spherical cavity expansion*

For undrained shear, the spherical cavity expansion (SCE) solutions formulated by Vesic (1972, 1977) are interesting because they relate s_u to both q_{net} and excess porewater pressures (Δu):

$$N_{kt} = 4/3 \cdot [\ln(I_R) + 1] + \pi/2 + 1 \tag{18}$$

$$N_{\Delta u} = 4/3 \cdot \ln(I_R) \tag{19}$$

where $I_R = G/s_u$ = rigidity index and G = shear modulus. The rigidity index can also be considered as the reciprocal of a reference shear strain (γ_{ref}), thus $I_R = 1/\gamma_{ref}$. Adopting a characteristic shear strain at peak strength or failure of 1%, or $\gamma_{ref} = 0.01$, corresponds to an assumed default value of $I_R = 100$.

In truth, the shoulder position of excess porewater pressure measurements by piezocone (Δu_2) is comprised of two components: octahedral and shear-induced. For young to aged normally-consolidated clays with OCRs < 2, the shear induced portion is rather small compared to the octahedral portion (Baligh 1980; Burns & Mayne 2002). Therefore, as a first approximation to Δu in clays, SCE provides the octahedral component alone.

Since the undrained strength is given by:

$$s_{uc} = \frac{q_{net}}{N_{kt}} = \frac{\Delta u}{N_{\Delta u}} \tag{20}$$

It is noted that the parameter B_q interrelates the two bearing factors (Lunne 2010):

$$N_{\Delta u} = B_q \cdot N_{kt} \tag{21}$$

Therefore, spherical cavity expansion allows for a direct interrelationship between Δu_2 and q_{net} expressed simply as a function of rigidity index, as shown in Figure 14. In support of this notion, piezocone data from 34 soft-firm clay sites (Mayne & Peuchen 2012) are shown to validate the SCE relationships and the operational values of rigidity index are seen to fall within the range: $10 < I_R < 1000$. The data are separated into two groups comprised of 19 offshore clays and 15 onshore clay deposits.

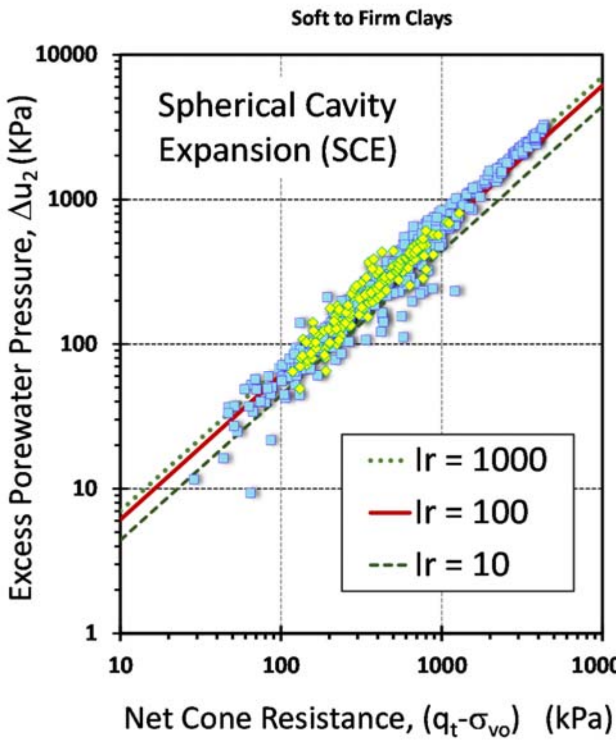

Figure 14. SCE relationship between Δu_2 and q_{net} with piezocone data from 15 onshore clays (yellow dots) and 19 offshore clays (blue dots).

Combining equations (18), (19), and (21), we find that rigidity index is simply a function of the porewater pressure parameter B_q:

$$I_R = \exp\left(\frac{2.93 \cdot B_q}{1 - B_q}\right) \tag{22}$$

For the data ranges shown in Figure 14, the operational range of $B_q = \Delta u/q_{net}$ varies from 0.45 to 0.75 with a central value of B_q of around 0.60. Statistical regression analyses on the onshore and offshore data gave mean B_q values of 0.62 and 0.69, respectively.

4.3 *SCE evaluated s_u from CPTu*

Substituting the SCE backfigured I_R back into the expressions for bearing factor terms, we obtain the following:

$$N_{kt} = \frac{3.90}{1 - B_q} \tag{23}$$

$$N_{\Delta u} = \frac{3.90}{(1/B_q) - 1} \tag{24}$$

The SCE relationships between the bearing factors N_{kt} and $N_{\Delta u}$ with B_q are shown in Figure 15. Superimposed over these lines are the backfigured values from the study reported by Mayne, et al. (2015), with considerable scatter evident in the data.

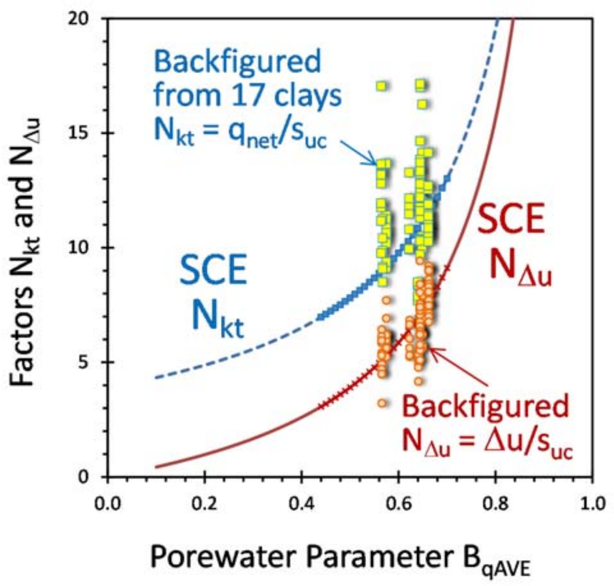

Figure 15. SCE relationships between cone bearing factors N_{kt} and $N_{\Delta u}$ with porewater parameter B_q. Data from piezocone tests and CAUC triaxial compression mode, s_{uc}.

In this endeavor, constant values of the bearing factors for any given clay are found using the average B_{qAVE} from the Δu vs. q_{net} plot. The SCE expressions can then be stated:

$$s_{uc} = \frac{q_{net}}{3.90} \cdot (1 - B_{qAVE}) \quad (25)$$

$$s_{uc} = \frac{\Delta u}{3.90} \cdot [(1/B_{qAVE}) - 1] \quad (26)$$

The application of the mean $B_{qAVE} = 0.65$ from the 2005 CPTu series of data for Bothkennar clay is used to provide assessments of s_{uc} profiles at the site based from both q_{net} and Δu, as shown in Figure 16. These are seen to be comparable, perhaps slightly high, when compared to the laboratory series of CAUC triaxial data from the site.

An alternative to the above approach is to utilize the specific B_q value at each elevation to drive the SCE solutions for the N_{kt} and $N_{\Delta u}$ factors, thus both variables with depth. In this case, both the q_{net} and Δu readings give the same exact profile of s_{uc}. In fact, the direct solution for s_u is given simply as:

$$s_{uc} = \frac{q_t - u_2 - \sigma_{vo}'}{3.90} \quad (27)$$

Using this approach, the derived profiles of s_{uc} for both the 1992 and 2005 soundings are shown in Figure 17. The 1992 sounding was digitized in more detail at approximate 0.1-m intervals, while the 2005 sounding was digitized at coarser 1-m intervals as a check to verify the quality of the earlier CPTu data. Thus, while this approach also gives relatively reasonable agreement with both the lab triaxial compression results and field vane data, the resulting profiles shows more variability and skittishness at any given elevation, specifically the finer data from 1992 vintage.

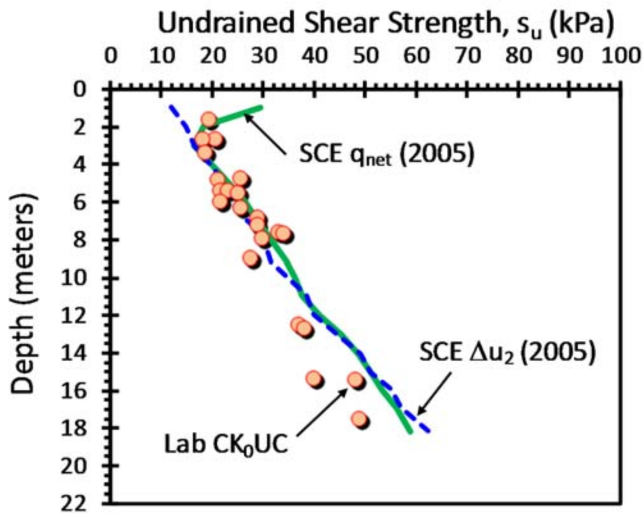

Figure 16. Profiles of s_{uc} at Bothkennar using SCE solutions for q_{net} and Δu with the average value of B_q.

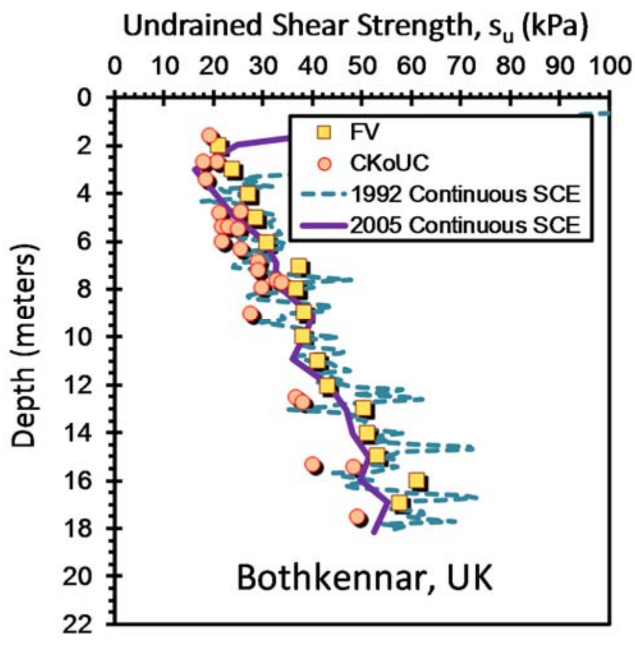

Figure 17. Profiles of undrained shear strength at Bothkennar using continuous B_q data.

4.4. *Strength from effective cone resistance*

Another option for assessing s_u in clays is via the effective cone resistance (Lunne et al. 1997):

$$s_u = \frac{q_t - u_2}{N_{ke}} \qquad (28)$$

where N_{ke} is a bearing factor averaging about 8.0 in soft-firm clays (Mayne et al. 2015). Yet in consideration of SCE theory alone per equation (27), this relationship cannot be expressed in this form.

In the case of a hybrid SCE model with critical state soil mechanics (CSSM), however, it can be expressed in terms of effective cone resistance where the bearing term for CIUC triaxial is found as (Chen & Mayne 1993):

$$N_{ke} = 2/M_c + 3.90 \qquad (29)$$

where M_c = q-p' frictional parameter for triaxial compression as shown in Figure 11.

5 EFFECTIVE STRESS STRENGTH PARAMETERS OF CLAY FROM DMT

5.1 *Equivalent porewater pressures from DMT*

The contact pressures (p_0) from DMT readings in clays appear to be dominated by the porewater pressures induced during blade insertion (Mayne 2006). For soft to firm intact clays, the assertion can be made that:

$$\Delta u = p_0 - u_0 \qquad (30)$$

which allows for the net contact pressure to be expressed in terms of SCE:

$$p_0 - u_0 = 4/3 \cdot s_u \cdot \ln(I_R) \qquad (31)$$

5.2 *Cavity expansion link for DMT*

Spherical cavity expansion also expresses the magnitude of change in horizontal stress for probes pushed into clay:

$$\Delta\sigma_h = 4/3 \cdot s_u \cdot (\ln I_R + 1) \qquad (32)$$

As a first approximation, the net expansion pressure from the flat dilatometer can be considered as a measure of this horizontal stress change:

$$\Delta\sigma_h = p_1 - u_0 \qquad (33)$$

From (16) and (18), the net cone resistance is expressed directly from SCE as:

$$q_{net} = 4/3 \cdot s_u \cdot (\ln I_R + 1) + \pi/2 + 1 \qquad (34)$$

and by combining equations (31) through (34), an equivalent net cone resistance can be found in terms of the dilatometer pressures:

$$q_{net} = 2.93 \cdot p_1 - 1.93 \cdot p_0 - u_0 \qquad (35)$$

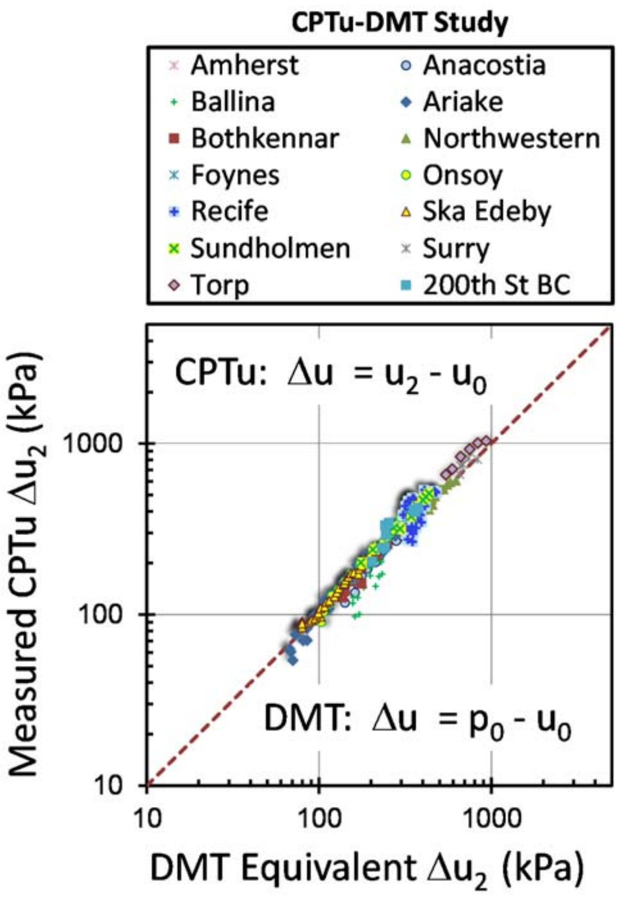

Figure 18. Measured CPTu Δu_2 versus DMT-equivalent excess porewater pressure: $\Delta u = p_0 - u_0$.

5.3 *CPTu-DMT database in clays*

An in-situ database of 12 clays that were subjected to both piezocone and flat dilatometer tests was compiled to validate the CPTu-DMT interrelationships. Figure 18 shows the measured excess porewater pressures (Δu_2) from piezocone tests vs. the equivalent Δu calculated from flat plate dilatometer tests according to equation (31). These are seen to be quite comparable and the results are consistent with the earlier observations by Mayne & Bachus (1989) for a variety of clays.

Similarly, Figure 19 shows the net cone resistance ($q_{net} = q_t - \sigma_{vo}$) from CPTu soundings at the same elevations in the same clays are plotted vs. the equivalent q_{net} obtained from DMT readings per equation (35). Again, the results are comparable.

5.4 *Equivalent NTH method for DMT*

These findings allow for the application of the NTH undrained limit plasticity solution to flat dilatometer tests in clays in assessing the effective stress friction angle (ϕ'). In particular, the tentative use would be restricted to soft-firm NC-LOC clays where c' = 0 is a common assumption. As noted previously for the CPTu, two options are available for obtaining ϕ' using the NTH solution: (1) individual plots of q_{netDMT} vs. σ_{vo}' to obtain N_m and Δu_{DMT} vs. q_{netDMT} to obtain B_{qDMT}; and (2) approximate ϕ' expression using equivalent Q_{DMT} and B_{qDMT} which are given by:

$$Q_{DMT} = \frac{2.93 \cdot p_1 - 1.93 \cdot p_0 - u_0}{\sigma_{vo}'} \tag{36}$$

$$B_q = \frac{p_0 - u_0}{2.93 \cdot p_1 - 1.93 \cdot p_0 - u_0} \tag{37}$$

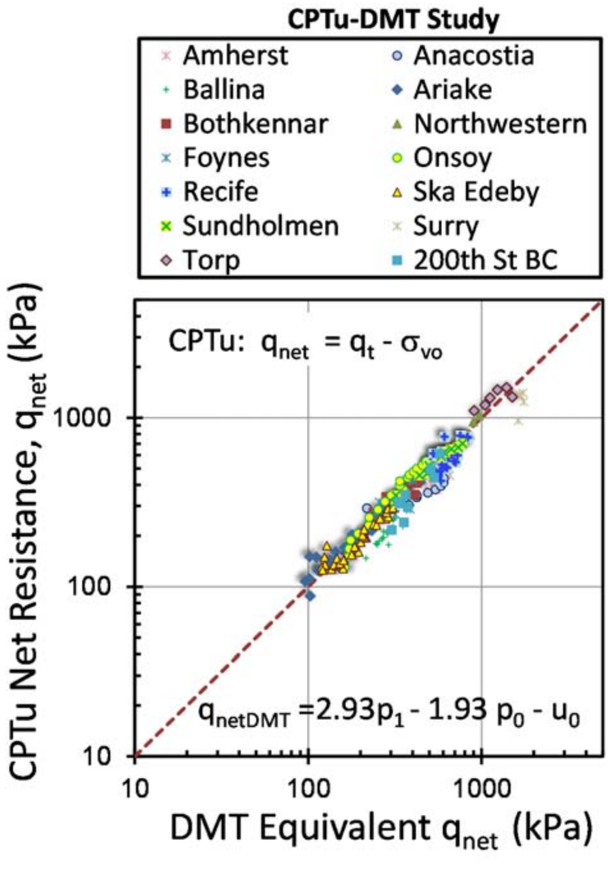

Figure 19. Measured CPTu q_{net} versus DMT-equivalent net cone resistance: q_{net}.

5.5 *Application to Bothkennar DMT data*

The results of a representative DMT sounding at the Bothkennar soft clay site are reported by Hight et al. (2003) and shown in Figure 20 with the associated DMT material index (I_D) profile. The p_0 and p_1 readings are seen to increase approximately linearly with depth with the contact pressures ranging from 137 to 500 kPa and the expansion pressures varying from 175 to 600 kPa in the depth range from 2 m to 16 m. Groundwater is approximately 1 m deep.

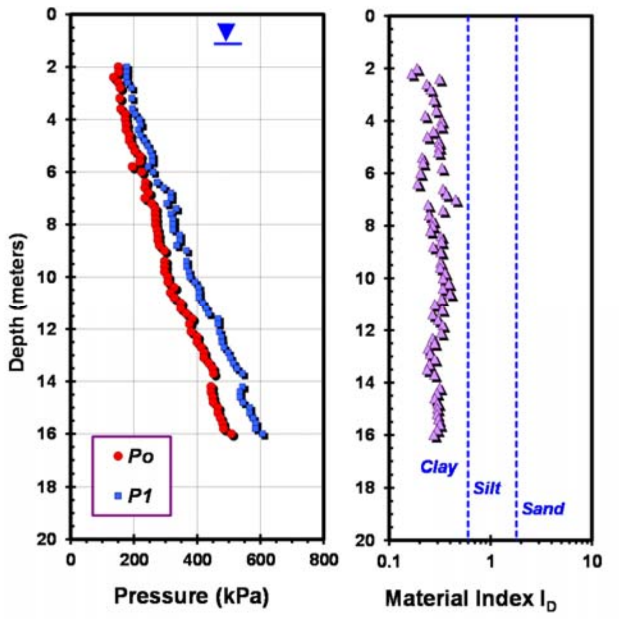

Figure 20. Representative DMT sounding at Bothkennar clay site (data from Hight et al. 2003).

The post-processing of equivalent Δu vs q_{net} is presented in Figure 21, giving an equivalent B_{qDMT} = 0.54. Similarly, the plotting of equivalent q_{netDMT} vs. effective overburden stress in Figure 22 gives a slope where $N_m = Q = 5.64$. Using either Figure 8 or equation (14) with these values gives an operational friction angle ϕ' = 32.6°. Referring once more to Figure 11 that hosts the effective stress strength envelope for undrained and drained triaxial compression and extension test results on Bothkennar clay (Allman & Atkinson 1992), the characteristic ϕ' = 34° from the laboratory series is seen to be in general agreement with the in-situ evaluations.

Alternatively, the approximate NTH solution using derived profiles of Q_{DMT} and B_{qDMT} per equations (34) and (35) are presented in Figure 23a. These can be processed at all elevations using equation (15) to produce a profile of ϕ' with depth, indicating a range 32° < ϕ' < 35° in the depth range of 4 to 16 m.

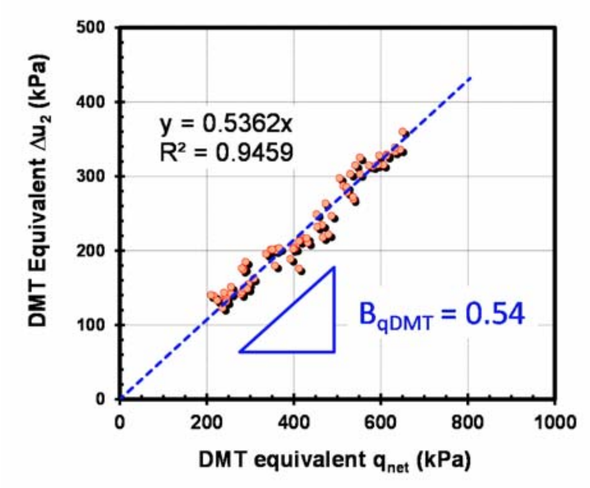

Figure 21. Post-processing DMT data to obtain equivalent B_q parameter at Bothkennar.

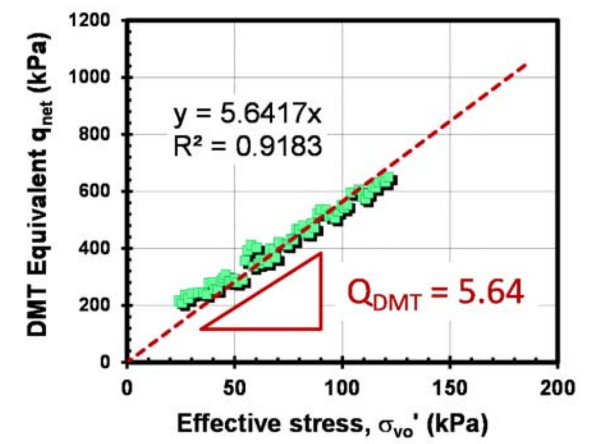

Figure 22. Post-processing to obtain DMT-equivalent Q in Bothkennar soft clay.

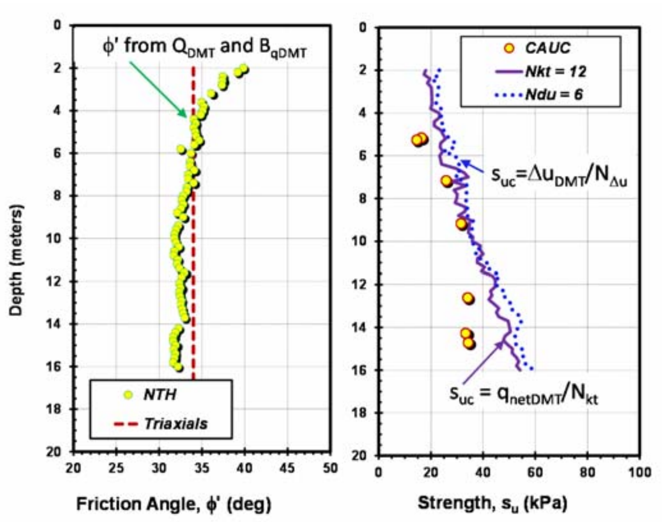

(a) (b)

Figure 23. Profiles at Bothkennar: (a) ϕ' from approximate NTH solution using Q_{DMT} and B_{qDMT}; (b) shear strength in triaxial compression (s_{uc}) using q_{netDMT} and Δu_{DMT}

Of additional note, the equivalent profiles of q_{netDMT} and Δu_{DMT} can be used with the classical N_{kt} = 12 and $N_{\Delta u}$ = 6 approach given by equations (16) and (17) to evaluate the undrained shear strengths, as presented in Figure 23b. These are seen to be somewhat comparable with lab TC tests on undisturbed samples for depths < 12 m but do appear to overpredict s_{uc} at greater depths.

6 EFFECTIVE STRESS COHESION INTERCEPT

6.1 *NTH Solution for c'*

The NTH solution can also provide an evaluation of both Mohr-Coulomb parameters: c' and ϕ'. In the general case, the cone resistance number given by equation (12) is expressed:

$$N_m = \frac{\tan^2(45° + \tfrac{1}{2}\phi')\cdot \exp[(\pi - 2\beta)\cdot \tan\phi'] - 1}{1 + 6\cdot \tan\phi' \cdot (1 + \tan\phi')\cdot B_q} \quad (38)$$

When plotting q_{net} vs. σ_{vo}' to obtain the slope N_m, a negative intercept on the σ_{vo}' axis is the value of attraction a' = c'·cotϕ'. An approximate inversion of (38) to give ϕ' directly from N_m, β, and B_q can be formulated as:

$$\phi' \approx 30°\cdot 10^{0.0035\beta}\cdot B_q^{0.121}\cdot[0.256+0.336\cdot B_q+\log N_m] \quad (39)$$

which is valid for the following parametric ranges: 20° ≤ ϕ' ≤ 40°, -30° ≤ β ≤ +20°, and 0.1 ≤ B_q ≤ 1.0. The evaluation of c' from CPTu data in clays is best illustrated by an example, as provided subsequently.

6.2 *Effective cohesion intercept of Bothkennar clay*

The critical state line (CSL) for Bothkennar clay was shown in Figure 11 as adequately represented by ϕ' = 34° and c' = 0. These values correspond to triaxial tests performed on reconstituted specimens of the clay, as well as to triaxial compression tests on undisturbed clay when evaluated at q_{max}. For a failure envelope taken at larger strains, or for overconsolidated states, it is possible to assign an apparent cohesion intercept value.

Post-processing the two sets of CPTu results from Bothkennar (1992 series and 2005 series) are shown in Figure 24, in this case allowing a general linear expression with both slope (m) and intercept (b). This is in contrast to the same data presented earlier in Figure 10 where the linear trend was forced through the origin. The slope of q_{net} versus σ_{vo}' plotting averages N_m = 4.68. The ratio of the slope (m) to the ordinate axis intercept (b) gives the attraction (a') which is the negative intercept on the abscissa axis: a' = m/b. For Bothkennar, the average a' = 10.3 kPa. The corresponding B_q parameter remains unchanged, as per Figure 9, and averages B_q = 0.64. Adopting β = 0°, the inverted NTH solution gives the following Mohr-

Coulomb effective stress strength parameters: ϕ' = 31.7° and c' = 6.4 kPa.

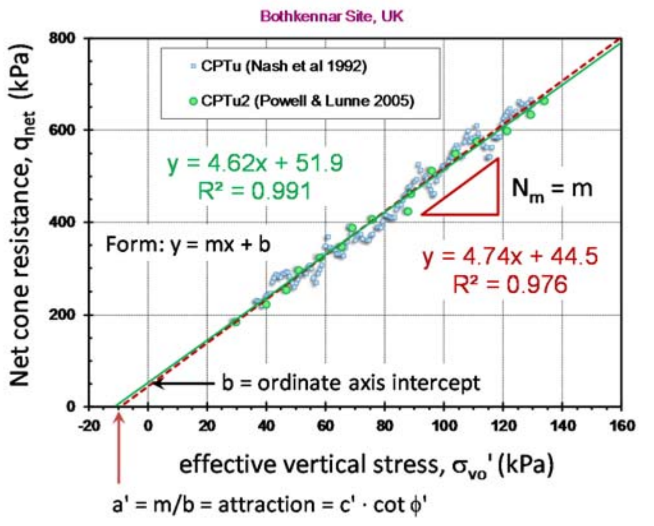

Figure 24. Evaluation of N_m and attraction a' in Bothkennar clay (alternate CPTu post-processing to that in Figure 10).

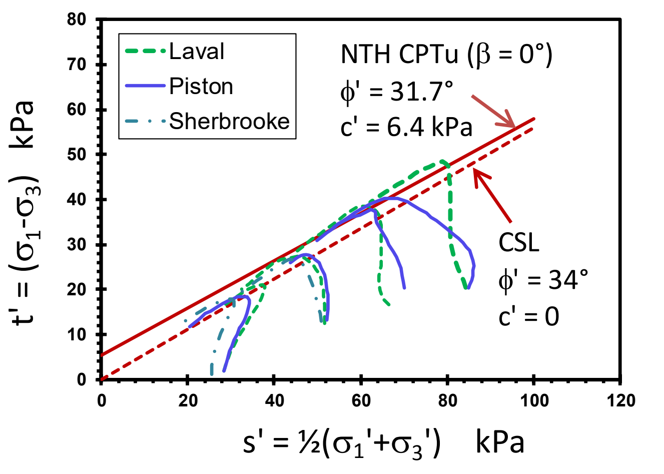

Figure 25. Triaxial stress paths for undisturbed Bothkennar clay (data from Hight et al. 1992) and superimposed c'-ϕ' derived parameters from NTH CPTu analyses.

These c'-ϕ' parameters are compared to CAUC triaxial tests on undisturbed specimens of Bothkennar clay in Figure 25. The CAUC tests include three separate series from high-quality sampling at the national test site using Laval, piston, and Sherbrooke type samplers (Hight et al. 1992). The CSL frictional characteristics represented by c' = 0 and ϕ' = 34° are shown for reference (Allman & Atkinson 1992). On the t-s' plot, these correspond to a slope angle α = 29.2° and intercept a* = c'·cosϕ' = 0. Superimposed over the individual stress paths are the NTH CPTu-derived parameters (ϕ' = 31.7° and c' = 6.4 kPa). Here, the corresponding t-s' parameters are given as: angle α = 27.7° and intercept a* = c'·cosϕ' = 5.4 kPa. Overall, the agreement between the Mohr-Coulomb envelope and laboratory triaxial data is reasonable.

6.3 *Alternative relationships for c'*

Notably, c' = 0 is a common assumption for soft to firm clays with OCRs < 2. Nevertheless, some stability analyses involving natural slopes, excavations, and soil nail walls require an assessment of c' for limit equilibrium and/or finite element studies. Also, overconsolidated soils may show an apparent cohesion intercept and friction angle.

Guidance on the selection and magnitude of c' can be found in a few other sources. Mayne & Stewart (1988) review data from CIUC and CAUC triaxial data on 16 different NC to OC clays and conclude that the effective cohesion intercept relates to the effective preconsolidation stress, expressed as the ratio c'/σ_p':

$$0.03 < c'/\sigma_p' < 0.06 \tag{40}$$

Mesri & Abdel-Ghaffar (1993) review 60 slope failures in clays and backfigure strength parameters from stability analyses finding that:

$$0.003 < c'/\sigma_p' < 0.11 \tag{41}$$

Sorensen & Okkel (2013) report that a common guideline in Scandinavia is that:

$$c' \approx 0.1\, s_u \tag{42}$$

A simplified approach to undrained strength assessment for embankment stability analyses on soft clays is well documented (Jamiolkowski et al. 1985) and more recently confirmed for offshore applications (DeGroot et al. 2011):

$$\text{DSS:}\quad s_u = 0.23\, \sigma_p' \tag{43a}$$

$$\text{TC:}\quad s_u = 0.29\, \sigma_p' \tag{43b}$$

Thus combining (42) with (43b) indicates:

$$c' \approx 0.03\, \sigma_p' \tag{44}$$

which is consistent with the aforementioned triaxial trends given by equation (40) and backfigured slope stability strength parameters given by (41).

In fact, for uncemented clays and silts, especially those that are NC-LOC, the effective cohesion intercept (c') is a pseudo-parameter as it appears to be an extrapolated value from the yield surface when force-fitting a linear expression for strength (i.e., Mohr-Coulomb envelope: $\tau_{max} = c' + \sigma'\cdot\tan\phi'$). A generalized yield surface is shown in Figure 26 in terms of Cambridge q-p' space with the CSL. That portion of the curved yield surface that extends above the CSL in the OC region can be extended back to an intercept on the ordinate axis, giving an apparent effective intercept: $q_c' = 2c'\cdot\cot\phi'\cdot M_c$.

For the Bothkennar clay, Hight et al. (2003) present the results of the interpreted yield surface from stress path testing, as shown on Figure 27. Here, the axes are normalized to the corresponding preconsolidation stress (σ_p') to account for the various sampling depths and the fact that σ_p' generally increases with depth.

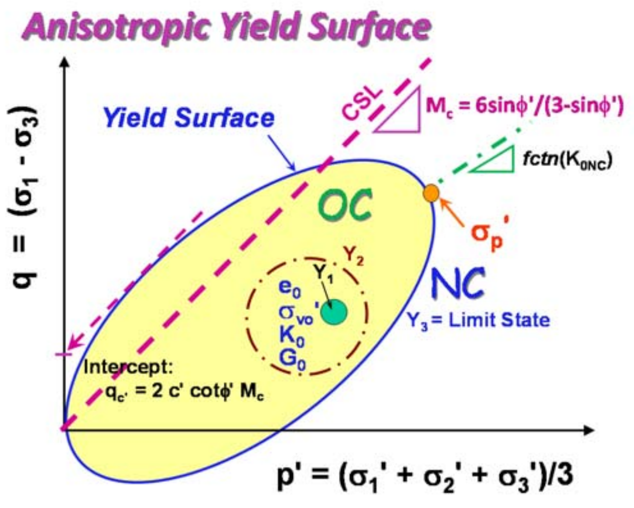

Figure 26. Generalized yield surface in q-p' space with projection giving an apparent effective cohesion intercept.

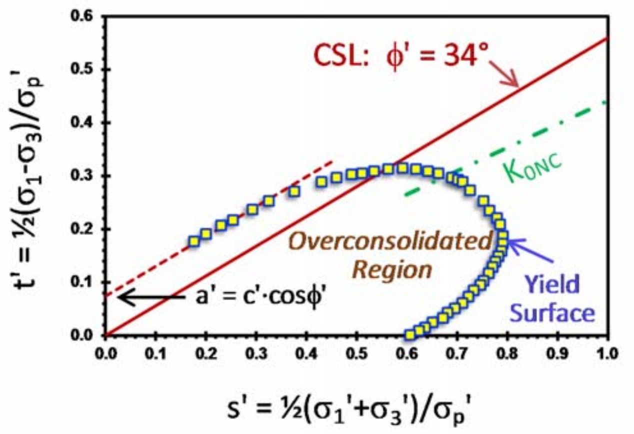

Figure 27. Yield surface for Bothkennar clay in t-s' space.

Thus, one outstanding question relates to the applicable value of σ_p' for normalization of the derived c' from the NTH solution on CPTu and/or DMT soundings, since the analysis of data is performed over the entire depth of the sounding. One possibility is to use the value of σ_p' at an effective stress equal to one atmosphere: $\sigma_{vo}' = \sigma_{atm}$, while another might consider use of the overconsolidation difference: OCD = (σ_p' - σ_{vo}')/σ_{atm}. However, the OCD really pertains to soils that are mechanically prestressed, such as removal of overburden by erosion, glaciation, or excavation (Locat et al. 2003). For some NC-LOC clays, there has been erosion but perhaps most of the observed preconsolidation has been due to other mechanisms such as secondary compression and ageing, groundwater fluctuations, diagenesis, and/or other factors.

7 STRESS HISTORY

In-situ tests are often used to give an initial first look at the stress history of clay deposits, as well as to supplement the more definitive results of one-dimensional consolidation tests on high-quality specimens. The CPT and DMT are particularly advantageous in this regard because they collect data at frequent depth intervals of 20 and 200 mm, respectively, whereas other tests (e.g., VST, PMT) provide readings on the order of 1 to 1.5 m intervals.

The CPT and DMT data in clays can be interpreted using empirical methods (e.g., Larsson & Åhnberg 2005), analytical approaches (e.g., Konrad & Law 1987; Mayne 2001, 2007), and/or numerical solutions (Yu & Mitchell 1998; Finno 1993). Herein, the simple SCE solutions will be applied to soft to firm NC-LOC clays.

7.1 *SCE solution for OCR from CPTu*

Critical state soil mechanics (CSSM) provides a link between undrained shear strength and stress history in terms of overconsolidation ratio: OCR = σ_p'/σ_{vo}', where σ_p' = preconsolidation stress or effective yield stress. For the case of triaxial shearing of isotropically consolidated specimens (CIUC):

$$s_{uc} = \left(\frac{M_c}{2}\right)\left(\frac{OCR}{2}\right)^{\Lambda} \sigma_{vo}' \qquad (45)$$

where $\Lambda = 1 - C_s/C_c$ = plastic volumetric strain ratio, C_s = swelling index, and C_c = virgin compression index. For most clays and silts, the value of Λ is about 0.8 to 0.9 (Jamiolkowski et al. 1985; Larson & Åhnberg 2005). Combining (16), (18) and (45) yields an expression for OCR in terms of normalized cone resistance: $Q = q_{net}/\sigma'_{v0}$ (Mayne 1991):

$$OCR = 2 \cdot \left[\frac{Q}{M_c \cdot \{\tfrac{2}{3} \cdot (1 + \ln I_R) + \tfrac{\pi}{2} + \tfrac{1}{2}\}}\right]^{1/\Lambda} \qquad (46)$$

Similarly, an expression can be found in terms of normalized excess porewater pressure:

$$OCR = 2 \cdot \left[\frac{\Delta u / \sigma_{vo}'}{\tfrac{2}{3} \cdot M_c \cdot \ln I_R}\right]^{1/\Lambda} \qquad (47)$$

As a first approximation, the power law formats can be removed by assuming that $\Lambda = 1$. Then, the expression in (46) can be reduced to provide a direct evaluation of the preconsolidation stress in terms of net cone resistance:

$$\sigma_p' \approx \frac{q_{net}}{M_c \cdot (1 + \frac{1}{3}\ln I_R)} \tag{48}$$

Similarly, equation (47) is reduced to relate the yield stress in terms of excess porewater pressure:

$$\sigma_p' \approx \frac{\Delta u}{\frac{1}{3} M_c \cdot \ln I_R} \tag{49}$$

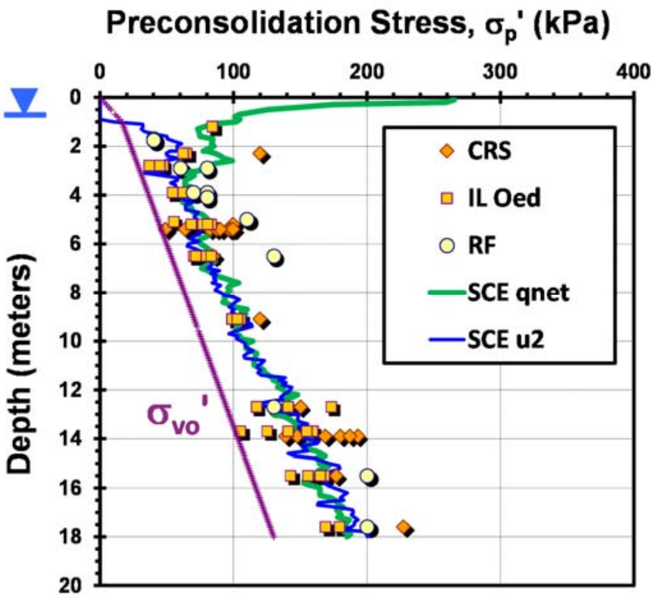

Figure 28. SCE-CPTu estimated and laboratory measured profiles of σ_p' at Bothkennar soft clay site.

7.2 *Application of SCE-CPTu-OCR to Bothkennar*

The SCE solutions for stress history evaluation can be applied to the Bothkennar CPTu data. All parameters are found from the post-processing of the sounding results. The value of $M_c = 1.37$ is found from the CSL $\phi' = 34°$ using the NTH effective penetration theory, as detailed earlier in Section 3.2. An operational value of rigidity index (I_R) is determined from the average B_q using equation (22). The overall $B_q = 0.619$ provides $I_R = 116$ for the CPTu reported by Nash et al. (1992a).

Consequently, for the Bothkennar clay, the SCE expressions become simply: $\sigma_p' = 0.28\ q_{net}$ and $\sigma_p' = 0.46\ \Delta u_2$. In Figure 28, these two CPT profiles are compared with three series of consolidation tests available from an extensive laboratory testing program conducted for the site (Nash et al. 1992b). One-dimensional consolidation tests included: (a) incremental-load type by Bristol University; (b) constant-rate-of-strain (CRS) types by Bristol Polytechnic; and (c) restricted flow (RF) tests at Oxford University. It can be seen that the piezocone profiles derived from q_{net} and Δu readings give very good agreement with the laboratory reference values.

7.3 *SCE solution for OCR from DMT*

Using the SCE link established in Section 5, a companion set of analytical solutions can be established for the flat dilatometer test in clays. For the net resistance relationships given by (46) and (48), the equivalent simplified expression for the DMT becomes:

$$\sigma_p' \approx \frac{2.93 p_1 - 1.93 p_0 - u_0}{M_c \cdot (1 + \frac{1}{3}\ln I_R)} \tag{50}$$

For the second case where $p_0 \approx u_2$, then equations (47) and (49) provide the relationship:

$$\sigma_p' \approx \frac{p_0 - u_0}{\frac{1}{3} M_c \cdot \ln I_R} \tag{51}$$

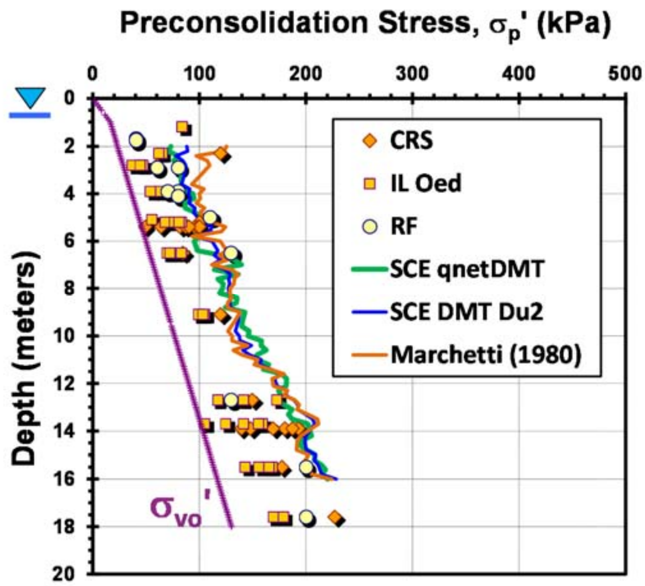

Figure 29. SCE-DMT estimated and laboratory measured profiles of σ_p' at Bothkennar soft clay site.

7.4 *Application of SCE-DMT-OCR to Bothkennar*

The SCE solutions for stress history from DMT readings can be applied to the Bothkennar data set. Again, the $M_c = 1.37$ is found from the CSL $\phi' = 34°$ characteristic value. The post-processing of the Δu_{DMT} vs. q_{netDMT} in Figure 21 gives an equivalent $B_{qDMT} = 0.54$. From equation (22), the backfigured $I_R = 31$ which seems a bit lower than the CPTu-estimated value of 116. Luckily, the results are not highly sensitive the value of I_R.

A comparison of the two DMT profiles for σ_p' are presented with the three series of laboratory consolidometer tests in Figure 29. It is evident that the DMT estimates are on the high side of the results, perhaps because of the underestimation of the operational I_R value. Also shown for comparison is the conventional interpretation of OCR from the K_D parameter given by Marchetti (1980). This too matches toward the high side when compared with the lab benchmark values.

8 CALIBRATION OF NTH METHOD FOR CPTU

8.1 *Effective friction angles of clays*

A good number of natural clays have effective stress friction angles that are around 30°, as measured by triaxial compression tests. A review of effective frictional envelopes and yield surfaces of 50 worldwide deposits by Diaz-Rodriguez, et al. (1992) showed the full range: 17.5° < ϕ' < 43° for natural clays. A recent statistical review of measured ϕ' from 453 different clays (Mayne 2012, 2013) found that the mean and standard deviations averages ϕ' = 28.61° ± 5.05° when determined using triaxial compression tests (CAUC and CIUC).

For several natural Norwegian clays, Sandven (1990) calibrated the NTH CPTu solution with effective friction angles measured by triaxial compression tests on undisturbed samples, with values of ϕ' in the general ranges as noted above.

8.2. *Clay chamber tests*

A study of data from mini-piezocone penetrometers in calibration chamber tests found that the NTH gave good predictions for prepared deposits of clays, mostly having used kaolin and/or kaolinite-sand mixtures in the testing programs (Ouyang et al. 2016). Chamber test results from mini-CPTu series performed at one research group (Swedish Geotechnical Institute) and 8 universities were compiled for review (Cornell, Cambridge, LSU, Purdue, Oxford, Sheffield, Sangmyung, University of Western Australia). An interesting aspect of kaolinitic clays is that the clay mineral has a rather low friction angle (20° < ϕ' < 23°), whereas when mixed with sands and/or fine silica, a higher frictional characteristic is observed: 30° < ϕ' < 33°, similar to natural clays, as discussed by Rossato et al. (1992).

A comparison of triaxial-measured versus CPTu-calculated ϕ' using the NTH solution is presented in Figure 30. Kaolinite and kaolin-mixtures predominate here and are shown by circles. Results from Bothkennar clay (Section 3.2), are also shown, albeit its mineralogy is primarily illite with additional constituents of quartz, feldspar, mica, chlorite, and kaolinite. Overall, very good agreement is noted for this dataset. Note also that an improved estimate (close to 1:1 line) is made if the assumed β = - 5°.

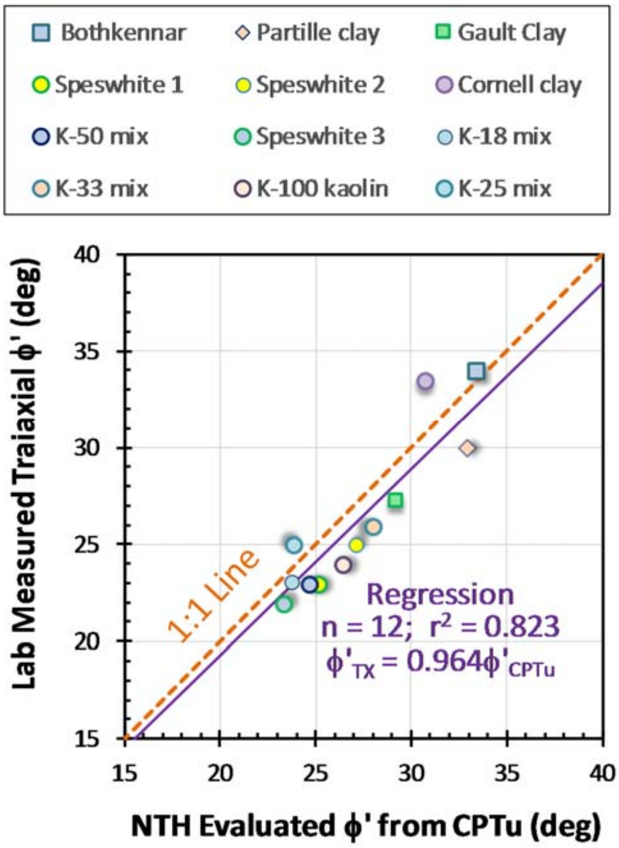

Figure 30. Calibration of NTH CPTu solution using data from clay calibration chamber tests (data from Ouyang et al. 2016).

9 DRAINAGE CONSIDERATIONS

9.1 *Drained versus undrained*

The concepts of drained vs. undrained behavior have been clarified through the framework of critical state soil mechanics and indicate that an infinite number of stress paths may lie in between these two extreme condidtions (Schofield & Wroth, 1968; Wood 1990; Mayne et al. 2009; Holtz et al. 2011). These notions have recently been examined experimentally by the introduction of in-situ twitch testing, whereby the rate of the test is varied to assess drainage characteristics and/or strain rate effects (Randolph 2004). Twitch testing has been accomplished using CPT and CPTu, T-bar, ball penetrometers, and vanes.

9.2 *Centrifuge CPT twitch tests in kaolin*

A series of CPTu twitch tests in centrifuge deposits of normally-consolidated kaolin clay are reported by Schneider et al. (2007). A mini-piezocone of diameter d = 10 mm was used in tests at accelerations of 160 g. The CPT velocity (v) was varied from 3 mm/s to 0.0004 mm/s and the recorded responses in measured q_t and u_2 were used to prepare Figures 31 and 32. A normalized velocity is defined as:

$$V = v \cdot d / c_v \tag{52}$$

where v = probe velocity, d = probe diameter, and c_v = coefficient of consolidation. For the NC kaolin, the reported values: $0.060 < c_v < 0.076$ mm²/s.

DeJong et al. (2013) have reported that essentially undrained behavior occurs when $V > 30$, while drained behavior with low porewater pressure response ($B_q < 0.1$) is observed when $V < 0.3$. These thresholds generally appear valid for the kaolin CPTu tests shown, albeit perhaps a slightly higher V limit for the undrained domain. The intermediate values of V correspond to partially drained or partly undrained conditions.

The changes in cone tip resistance with penetration rate can be represented in terms of normalized cone resistance (Q) and an algorithm suggested by DeJong et al. (2013):

$$\frac{Q}{Q_{ref}} \approx 1 + \left(\frac{(Q_{drained}/Q_{ref}) - 1}{1 + (V/V_{50})^c} \right) \tag{53}$$

where $Q = q_{net}/\sigma'_{vo}$, $Q_{drained}$ is the normalized cone resistance for fully drained penetration (i.e., when $B_q = 0$), Q_{ref} = reference value of normalized cone resistance, often taken at undrained conditions, $Q_{undrained}$ which normally occurs at maximum B_q. The value of normalized velocity when excess porewater pressures are half their maximum values is designated as a reference value, V_{50}. Finally, the exponent c is a fitting parameter.

Following a similar representation for Δu_2, a modified version of the algorithm for normalized porewater pressures given by DeJong et al. (2013) can be expressed by:

$$\frac{B_q}{B_{q-ref}} \approx 1 - \frac{1}{1 + (V/V_{50})^c} \tag{54}$$

The fitting parameters for the centrifuge CPTs in kaolin shown as red dashed lines in Figures 31 and 32 are: $Q_{drained} = 7$; $Q_{ref} = Q_{undrained} = 3.2$, $V_{50} = 6$, $c = 1$, and $B_{q-ref} = 0.55$.

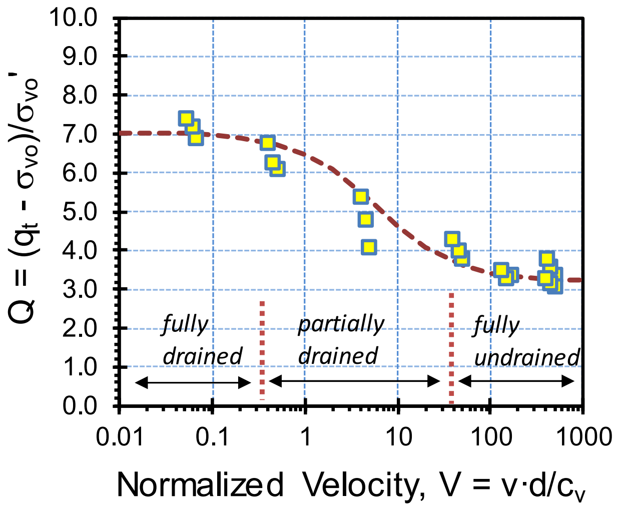

Figure 31. Centrifuge CPT cone resistance versus normalized velocity in kaolin (data from Schneider et al. 2007)

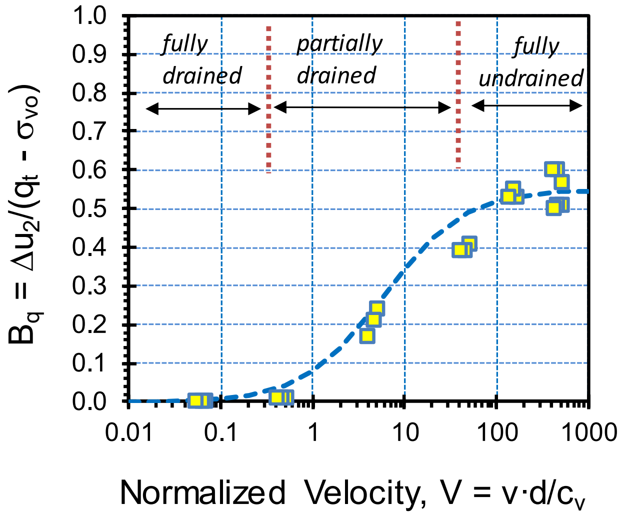

Figure 32. Centrifuge CPT porewater pressure response versus normalized velocity in kaolin (data from Schneider et al. 2007)

9.3 *Soil behavioral charts in Q-B_q space*

As indicated earlier in Sections 2.1 and 2.2, results from piezocone tests can be plotted in Q-B_q space to ascertain soil behavioral type (SBT). As noted by Schneider (2009) and DeJong et al. (2013), these empirical charts are based on CPT data taken at the standard rate of 20 mm/s. Changes in CPT results due to rate effects will not be recognized by these SBT charts. Thus, the only valid points from the centrifuge tests for soil identification are the paired Q and B_q values from the undrained range, as shown in Figure 33. As the rate is decreased, the data appear to shift up and to the left into the silt mixture zone.

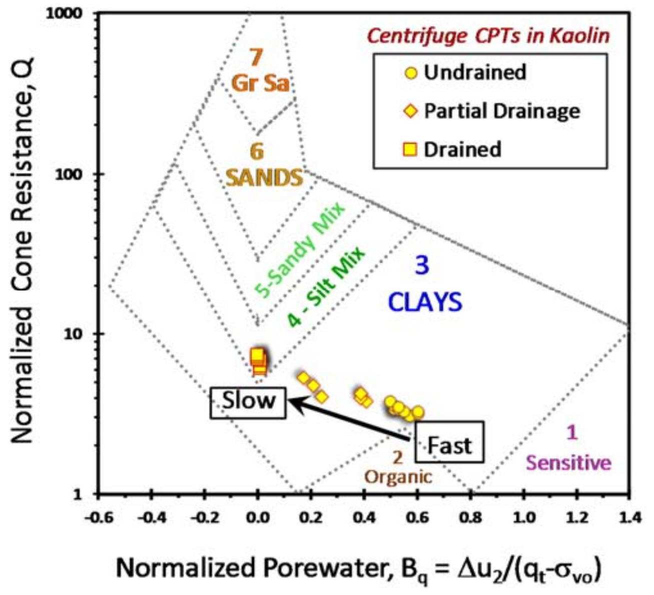

Figure 33. Centrifuge CPT data from twitch testing in kaolin plotted in SBT Q-B_q space.

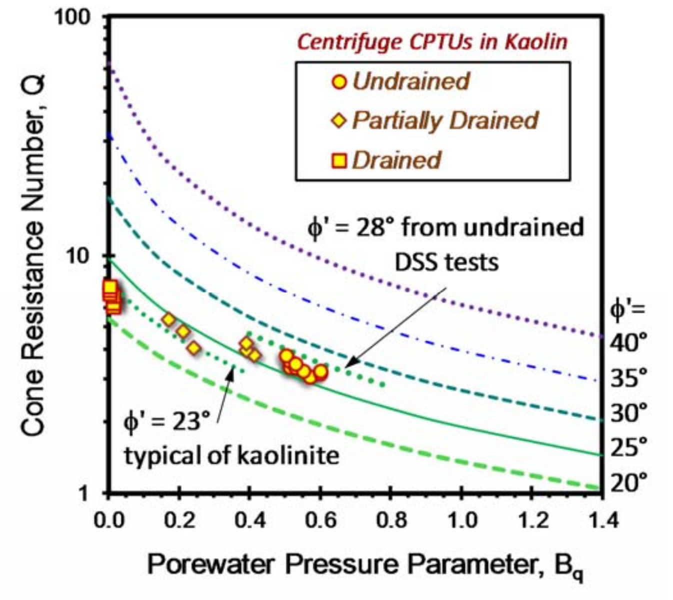

Figure 34. NTH solution for effective friction angle presented in Q-B_q space. Data from CPT twitch testing in centrifuge kaolin deposits also shown.

9.4 *NTH solution presented in Q-B_q space*

For the case where c' = 0, the NTH solution is simply expressed in terms of normalized cone resistance and porewater pressure parameter. Thus, an alternate means of presenting the NTH solution of Figure 8 is in the format of the soil behavioral chart of Q versus B_q, as suggested by Ouyang et al. (2016) and illustrated in Figure 34.

The twitch test data from the CPT centrifuge experiments in kaolin are also shown and interestingly they more or less follow the same trends as the individual lines for specific ϕ' values. Since effective stress friction angle is a soil property, this should logically be expected with the same ϕ' realized in both the undrained and drained regions, as well as for intermediate partially drained cases.

The specific kaolin used in the centrifuge CPTu twitch testing program has an apparent effective stress friction angle ϕ' = 28°, as determined from the τ-σ_v' plots from undrained simple shear tests reported by Schneider (2009). For the undrained Q and B_q values, this gives rather good agreement, as evident in Figure 34. Then, as the CPTu penetration rates are decreased, the resulting increase in Q and corresponding decrease in B_q show an apparent reduction in friction angle towards a value ϕ' = 23°. This value is more in line with the well-known values for kaolinite and mineral version of kaolin, as discussed by Rossato et al. (1992) and Section 8.2.

The reasons behind this trend are not clearly understood at this time, but perhaps relate to a change in the angle of plastification (β) as the relative size of the failure region around the cone tip morphs from undrained to partially drained to drained conditions. Certainly additional research is needed to clarify this issue.

10 DISCUSSION

Several alternate theoretical solutions to represent cone penetration in clays have been documented (Konrad & Law 1987; Yu & Mitchell 1998; Low 2009). The choice of the Vesić (1977) cavity expansion solution was selected herein because a cone bearing factor $N_{kt} \approx 12 \pm 1$ associates with characteristic values of the porewater pressure parameter in soft clays: $B_q \approx 0.6 \pm 0.1$. Other solutions may prove more compatible in matching with available data in future studies (e.g., Lu et al. 2004; Low 2009; Schneider et al. 2012). Certainly, more complex algorithms are necessary to represent the porewater pressure response of sensitive clays ($B_q > 0.8$) and overconsolidated clays ($B_q < 0.4$), as well as fissured fine-grained geomaterials ($B_q < 0$). For instance, one approach is a hybrid SCE-CSSM approach (Burns & Mayne 2002).

With regard to undrained effective stress penetration, the NTH solution appears to be a unique analytical approach for CPTu in clays for assessing ϕ'. An empirical approach has been proposed by Keaveny & Mitchell (1986), however received less attention.

Finally, it is perhaps necessary to utilize numerical finite element or finite difference schemes (e.g., Abu-Farsakh et al. 2003) in a means to advance CPTu interpretations forward in an effective stress framework in order to detail a universal approach for evaluating ϕ' in overconsolidated clays, as well as the full range of soil materials encountered in geotechnics. These numerical solutions should be well calibrated with extensive series of penetration tests at various rates and include dissipatory porewater pressure versus time measurements for a comprehensive set of data, e.g. CPTu and piezoball data reported by Mahmoodzadeh and Randolph (2014).

11 CONCLUSIONS

Results from in-situ piezocone (CPTu) and flat dilatometer tests (DMT) in clays have traditionally been utilized for assessing total strength parameters, namely the undrained shear strength (s_u), often employed in limit equilibrium analyses and closed-form plasticity solutions for bearing capacity. Yet, modern geotechnical capabilities include finite element and finite difference modeling that require effective stress parameters (c' and ϕ'), thus giving the ability to predict field induced porewater pressure responses during construction.

As a consequence, it is of interest to review an existing NTH undrained effective stress limit plasticity solution for CPTu penetration in clays. This offers a means for evaluating ϕ' in soft clays (c' = 0), or alternatively a paired set of c' and ϕ' strength parameters. The NTH solution is extended to the DMT domain via links established from spherical cavity expansion (SCE) theory. Furthermore, interpretative procedures for clay stress history from CPTu readings can also be applied to DMT soundings. Laboratory and in-situ test results from the Bothkennar soft clay test site in the UK and data from other testing programs on clays are employed to illustrate the methodologies.

12 ACKNOWLEDGMENTS

The author appreciates the continued support of ConeTec Investigations of Richmond, BC and Design House Consultancy of New York, NY. Additional funding was provided by Fugro Engineers in Leidschendam, the US Dept. of Energy at Savannah River Site, and the Georgia Dept. of Transportation at Forest Park, Georgia USA.

13 REFERENCES

Abu-Farsakh, M., Tumay, M. & Voyiadjis, G. 2003. Numerical parametric study of piezocone penetration test in clays. *International J. of Geomechanics* Vol. 3 (2): 170-181.

Allman, M.A. & Atkinson, J.H. 1992. Mechanical properties of reconstituted Bothkennar soil. *Géotechnique* 42 (2): 289–301.

Baligh, M.M. 1986. Undrained deep penetration: pore pressures. *Geotechnique* 36 (4): 487-501.

Burns, S.E. & Mayne, P.W. 2002. Analytical cavity expansion-critical state model for piezocone dissipation in fine-grained soils. *Soils & Foundations* 42 (2): 131-137.

Chen, B.S.Y. and Mayne, P.W. 1993. Piezocone evaluation of undrained shear strength in clays. *Proc. 11th Southeast Asian Geotechnical Conference*, National Univ. of Singapore & Nanyang Technological Univ., Singapore: 91-98.

DeGroot, D.J., Lunne, T. & Tjelta, T.I. (2011). Recommended best practice for geotechnical site characterization of cohesive offshore sediments. *Frontiers in Offshore Geotechnics II* (Perth), Taylor & Francis, London: 33-57.

DeJong, J.D., Jaeger, R.A., Boulanger, R.W., Randolph, M.F. & Wahl, D.A.J. 2013. Variable penetration rate cone testing for characterization of intermediate soils. *Geotechnical & Geophysical Site Characterization 4*, Vol. 1 (Proc. ISC-4, Pernambuco), Taylor & Francis Group, London: 25-42.

Diaz-Rodriguez, J.A., Leroueil, S. & Aleman, J.D. 1992. Yielding of Mexico City clay and other natural clays. *J. Geotech. Engineering* 118 (7): 981-995.

Fellenius, B. H., & Eslami, A., 2000. Soil profile interpreted from CPTu data. *Proc. Geotechnical Engineering Conf.*, Asian Institute of Technology, Bangkok, Thailand, 18 p.

Finno, R.J. 1993. Analytical interpretation of dilatometer penetration in cohesive soils. *Geotechnique* 43(2): 241-254.

Ghalib, A., Hryciw, R., & Susila, E. 2000. Soil stratigraphy delineation by VisCPT. *Innovations & Applications in Geotechnical Site Characterization* (GSP No. 97), ASCE, Reston/VA: 65-79.

Hight, D.W., Böese, R., Butcher, A.P., Clayton, C.R.I. & Smith, P.R. 1992. Disturbance of the Bothkennar clay prior to laboratory testing. *Geotechnique* 42 (2): 199-217.

Hight, D.W., Paul, M.A., Barras, B.F., Nash, D.F.T., Smith, P.R., Jardine, R.J. & Edwards, D.H. 2003. The characterisation of the Bothkennar clay. *Characterization & Engineering Properties of Natural Soils*, Vol. 1, Swets & Zeitlinger, Lisse: 543-597.

Holtz, R.D., Kovacs, W.D. & Sheahan, T.C. 2011. *An Introduction to Geotechnical Engineering, 2nd Edition*, Pearson Educational, Upper Saddle River, NJ: 853 p,

Jamiolkowski, M., Ladd, C.C., Germaine, J.T. & Lancellotta, R. 1985. New developments in field and lab testing of soils. *Proc. 11th ICSMFE*, San Francisco: 57-153.

Keaveny, J.M. & Mitchell, J.K. 1986. Strength of fine-grained soils using the piezocone. *Use of In-Situ Tests in Geot. Engrg,* GSP 6, ASCE, Reston, Virginia: 668-685.

Konrad, J-M. & Law, K.T. 1987. Undrained shear strength from piezocone tests. *Canadian Geot. J.* 24 (3): 392-405.

Larsson, R. & Åhnberg, H. 2005. On the evaluation of undrained shear strength and preconsolidation pressure from common field tests in clay. *Canadian Geotechnical J.* 42 (4): 1221-1231.

Locat, J., Tanaka, H., Tan, T.S., Dasari, G.R. and Lee, H. 2003. Natural soils: geotechnical behavior and geological knowledge. *Characterization & Engrg. Properties of Natural Soils*, Vol. 1, Swets & Zeitlinger, Lisse: 3-28.

Low, H.E. 2009. Performance of penetrometers in deepwater soft soil characterisation. *PhD Thesis*. Centre for Offshore Foundation Systems, School of Civil & Resource Engrg., Univ. Western Australia: 300 p.

Low, H.E., Lunne, T., Andersen, K.H., Sjursen, M.A., Li, X. and Randolph, M.F. 2010. Estimation of intact and remoulded undrained shear strengths from penetration tests in soft clays. *Geotechnique* 60 (11): 843-859.

Lu, Q., Randolph, M.F., Hu, Y. & Bugarski, I.C. 2004. A numerical study of cone penetration in clay. *Geotechnique* 54 (4): 257-267.

Lunne, T., Robertson, P.K., and Powell, J.J.M. 1997. *The Cone Penetration Test in Geotechnical Practice*, EF Spon/Blackie Academic, Routledge Publishing, New York: 312 p.

Lunne, T., Randolph, M.F., Chung, S.F., Andersen, K.H. and Sjursen, M. 2005. Comparison of cone and t-bar factors in two onshore and one offshore clay sediments. *Frontiers in Offshore Geotechnics* (Proc. ISFOG-1, Perth), Taylor & Francis Group, London: 981-989.

Lunne, T. (2010). The CPT in offshore soil investigations - a historic perspective. *Proc. 2nd Intl. Symp. on Cone Penetration Testing*, Vol. 1, Huntington Beach, CA; Omnipress: 71-113. *www.cpt10.com.*

Mahmoodzadeh, H. & Randolph, M.F. 2014. Penetrometer testing: effect of partial consolidation on subsequent dissipation response. *J. Geotechnical & Geoenviron. Engrg*. Vol. 140 (6), 04014022.

Marchetti, S. 1980. In-situ tests by flat dilatometer. *Journal of Geotechnical Engrg.* 106 (GT3): 299–321.

Marchetti, S., Monaco, P., Totani, G. & Calabrese, M. 2001. The flat dilatometer test (DMT) in soil investigations. A report by the ISSMGE Committee TC16. Reprinted in *Proc. 3rd Intl. Conf. on the Flat Dilatometer*, Rome: 523-565.

Marchetti, D., Marchetti, S., Monaco, P. & Totani, G. 2008. Experience with seismic dilatometer in various soil types. *Geotechnical & Geophysical Site Characterization*, Vol. 2 (ISC-3, Taiwan), Taylor & Francis, London: 1339-1345.

Marchetti, S. 2015. Update. *Proceedings 3rd Intl. Conf. on Flat Dilatometer.* Rome: 299–321. www.dmt15.com

Mayne, P.W. & Stewart, H.E. 1988. Pore pressure response of K_0-consolidated clays. *Journal of Geotechnical Engineering*, Vol. 114 (11): 1340-1346.

Mayne, P.W. & Bachus, R.C. 1989. Penetration porewater pressures in clay by CPTU, DMT, and SBP. *Proc., 12th Intl. Conf. on Soil Mech. & Foundation Engineering*, Vol. 1, Rio de Janeiro: 291-294.

Mayne, P.W. 1991. Determination of OCR in clays by piezocone tests using cavity expansion and critical state concepts. *Soils and Foundations*, Vol. 31 (2), June: 65-76.

Mayne, P.W. 2001. Stress-strain-strength-flow parameters from enhanced in-situ tests. *Proc. International Conf. on In-Situ Measurement of Soil Properties & Case Histories* (In-Situ 2001), Bali, Indonesia: 27-47.

Mayne, P.W., Christopher, B., Berg, R., and DeJong, J. 2002. *Subsurface Investigations - Geot. Site Characterization*. Publication No. FHWA-NHI-01-031, National Highway Institute, Federal Highway Admin., Washington, D.C., 301 p

Mayne, P.W. 2006. Interrelationships of DMT and CPTU readings in soft clays, *Flat Dilatometer Testing* (Proc. 2nd Intl. Conf. DMT), Washington, DC: 231-236.

Mayne, P.W. 2007. In-situ test calibrations for evaluating soil parameters, *Characterization & Engineering Properties of Natural Soils*, Vol. 3 (Proc. Singapore 2006), Taylor & Francis Group, London: 1602-1652.

Mayne, P.W. 2007. *Synthesis 368 on Cone Penetration Test*. (NCHRP), Transportation Research Board, National Academy Press, Washington DC: 120 p. www.trb.org

Mayne, P.W., Coop, M.R., Springman, S., Huang, A-B., & Zornberg, J. 2009. SOA-1: Geomaterial behavior and testing. Proc. *17th Intl. Conf. Soil Mechanics & Geot. Engrg*., Vol. 4 (ICSMGE, Alexandria), Millpress/IOS Press, Rotterdam: 2777-2872.

Mayne, P.W. 2012. Invited keynote: Quandary in geomaterial characterization: new vs. old. *Shaking the Foundations of GeoEngineering Education* (Proc. Univ. Ireland, Galway), Taylor & Francis Group, London: 15-26.

Mayne, P.W. 2013. Updating our geotechnical curricula via a balanced approach of in-situ, laboratory, and geophysical testing of soil. *Proc. 61st Annual Geotechnical Conference*, Minnesota Geot. Society, Univ. Minnesota, St. Paul: 65-86.

Mayne, P.W. 2014. Keynote: Interpretation of geotechnical parameters from seismic piezocone tests. *Proceedings, 3rd Intl. Symposium on Cone Penetration Testing*, (CPT'14, Las Vegas): 47-73. www.cpt14.com

Mayne, P.W. and Peuchen, J. 2012. Unit weight trends with cone resistance in soft to firm clays. *Geotechnical and Geophysical Site Characterization 4,* Vol. 1 (Proc. ISC-4, Pernambuco), CRC Press, London: 903-910.

Mayne, P.W., Peuchen, J. & Baltoukas, D. 2015. Piezocone evaluation of undrained strength in soft to firm offshore clays. *Frontiers in Offshore Geotechnnics III*, Vol. 2 (Proc. ISFOG-3, Oslo), Taylor & Francis, London: 1091-1096.

Mayne, P.W. 2015. Keynote lecture: In-situ geocharacterization of soils in the year 2016 and beyond. *Advances in Soil Mechanics, Vol. 5: Geotechnical Synergy* (Proc. PCSMGE, Buenos Aires), IOS Press, Amsterdam: 139-161.

Mesri, G. & Abdel-Ghaffar, M.E.M. 1993. Cohesion intercept in effective stress-stability analysis. *J. Geotechnical Engineering* 119 (8): 1229-1249.

Nash, D.F.T., Powell, J.J.M. & Lloyd, I.M. 1992a. Initial investigations of the soft clay testbed site at Bothkennar clay site. *Géotechnique* 42(2): 163–181.

Nash, D.F.T., Sills, G.C. & Davison, L.R. 1992b. One-dimensional consolidation testing of soft clay from Bothkennar. *Geotechnique* 42 (2): 241-256.

Ouyang, Z., Mayne, P.W. & Sharp,.J. 2016. Review of clay chamber tests using miniature cone and piezocone penetrometers, *Proc. GeoVancouver 2016*, (69th Canadian Geotechnical Conference): www.cgs.ca

Powell, J.J.M. & Lunne, T. 2005. A comparison of different sized piezocones in UK clays. *Proc. ICSMGE*, Vol. 1 (Osaka), Millpress/IOS, Rotterdam: 729-734.

Randolph, M.F. 2004. Characterization of soft sediments for offshore applications. *Geotechnical & Geophysical Site Characterization*, Vol. 1 (Proc. ISC-2, Porto), Millpress, Rotterdam: 209-232.

Robertson, P.K. 2009. Cone penetration testing: a unified approach. *Canadian Geotechnical J.* 46 (11): 1337-1355.

Rossato, G., Ninis, N., and Jardine, R.1992. Properties of some kaolin-based model clay soils. *Geotechnical Testing Journal,* Vol. 15, No. 2, ASTM: 166-179.

Sandven, R. 1990. Strength and deformation properties of fine grained soils obtained from piezocone tests. *PhD Dissertation*, Institutt for Geoteknikk, Norwegian Inst. of Technology (NTH), Trondheim: 600 p.

Sandven, R. & Watn, A. 1995. Soil classification and parameter evaluation from piezocone tests. *Proc. 2nd Intl. Symp. on Cone Penetration Testing* (CPT'95, Linköping), Vol. 3, Swedish Geotechnical Society: 35-55.

Schneider, J.A. 2009. Separating influences of yield stress ratio and partial drainage on piezocone response. *Australia Geomechanics Journal* 44 (3): 1-18.

Schneider, J.A., Lehane, B.M. & Schnaid, F. 2007. Velocity effects on piezocone measurements in normally and overconsolidated clays. *Intl. J. of Physical Modelling in Geotechnics*, Vol. 7, Issue 2: 23-34.

Schneider, J.A., Randolph, M.F., Mayne, P.W., & Ramsey, N.R. 2008. Analysis of factors influencing soil classification using normalized piezocone tip resistance and pore pressure parameters. *Journal of Geotechnical & Geoenvironmental Engrg*. 134 (11): 1569-1586.

Schneider, J.A., Hotstream, J.N., Mayne, P.W. & Randolph, M.F. 2012. Comparing CPTu Q-F and Q-$\Delta u_2/\sigma_{vo}'$ soil classification charts. *Geotechnique Letters*, Vol. 2 (4): 209-215.

Schofield, A.N. & Wroth, C.P. 1968. *Critical State Soil Mechanics*, McGraw-Hill, London: 310 p. Download PDF version from: www.geotechnique.info

Senneset, K. & Janbu, N. 1985. Shear strength parameters obtained from static cone penetration tests. *Strength Testing of Marine Sediments*. Special Tech Publ. 883, ASTM, West Conshohocken, PA: 41-54.

Senneset, K., Sandven, R. & Janbu, N. 1989. Evaluation of soil parameters from piezocone tests. *In-Situ Testing of Soil Properties for Transportation, Transportation Res. Record 1235*. National Research Council, Washington DC: 24-37.

Sorensen, K.K. & Okkels, N. 2013. Correlation between drained shear strength and plasticity index of undisturbed overconsolidated clays. *Proc. 18th Intl. Conf. Soil Mech. & Geot. Engrg.*, Paris: 423-428.

Torrez-Cruz, L.A. 2015. CPT-based soil type classification in a platinum tailings storage facility. *From Fundamentals to Applications in Geotechnics*, Part 1 (Proc. 15th PCSMGE, Buenos Aires), IOS Press, Rotterdam: 406-413.

Tümay, M.T., HatipKarasulu, Y., Młynarek, Z., & Wierzbicki, J. 2011. Effectiveness of CPT-based classification methods for identification of subsoil stratigraphy. *Proc. 15th European Conf. on Soil Mechanics & Geot. Engineering,* Athens, Greece, Vol. 1, IOS/Millpress, Rotterdam: 91-98.

Vesić, A.S. 1972. Expansion of cavities in infinite soil mass. *Journal of the Soil Mechanics & Foundations Division* (ASCE), Vol. 98 (SM3): 265-290.

Vesić, A.S. 1977. *Design of Pile Foundations, NCHRP Synthesis No. 42*, Transportation Research Board, National Academy Press, Washington, DC: 68 pages.

Wood, D.M. 1990. *Soil Behaviour and Critical State Soil Mechanics*. Cambridge Univ. Press, UK: 462 p.

Yu, H.S. & Mitchell, J.K. 1998. Analysis of cone resistance: review of methods. *J. Geotechnical & Geoenvironmental Engineering* 124 (2): 140-149.

Geotechnical and Geophysical Site Characterisation 5 – Lehane, Acosta-Martínez & Kelly (Eds)
 ISBN 978-0-9946261-1-0

Characterizing mine tailings for geotechnical design

K. Been
Golder Associates, Canada

ABSTRACT: Mine tailings are ground up rock and generally consist of sand and silt size particles, without clay minerals. Tailings "storage" (actually disposal) facilities are some of the largest constructed works, with seismic design an integral component. High value mines are frequently in earthquake prone areas and tailings liquefaction is an ever-present concern. A screening level liquefaction assessment based on the CPTu is a needed first step, but cannot be accurate because the fines content of tailings can be high, and engineering behaviour is only loosely related to fines content. An engineering mechanics based procedure is laid out in this paper which is applicable regardless of the fines content. It is anchored to the eighty year old principles of critical state soil mechanics originated by the Corp of Engineers. The state parameter provides the practical engineer an entry to this framework, as well as insight into a simple stability principle that sets the strategy for a tailings characterization project aimed at the analyses that a tailings engineer needs. The approach requires systematic *in situ* and laboratory testing to determine the soil mechanics properties of the tailings.

1 INTRODUCTION

Characterization of mine tailings is a difficult and underestimated problem in geotechnical engineering (even neglecting geochemical aspects, with acid drainage a pervasive and real issue). Much of the difficulty arises because tailings are ground up rock waste from the mineral extraction process and generally consist of sand and silt size particles, without clay minerals although cohesion may be present. They often fall into a "transitional material" category, somewhere between idealized sand-like or clay-like behaviour (idealizations controlled by void ratio or overconsolidation respectively). The pressure to minimize costs of investigation without a coherent approach to evaluate transitional materials means that empirical methods derived from research work on sands or clays is often applied inappropriately (or at least with a significant uncertainty).

Tailings deposits need to be characterized for many reasons: centerline or upstream dyke raises may be built on recent tailings, sometimes facility expansion occurs over historical tailings deposits and there is a need to confirm the design assumptions for new facilities. This latter requirement is particularly important for thickened tailings where the final geometry includes a slope of weak silts extending above the crest of containment structures.

Characterization is influenced by "what has failed and why", as there are no industry-standard or internationally-recognized codes of practice for tailings impoundment engineering. Earthquake resistant design, largely driven by the significance of damage in the Niigata and Lower San Fernando events, became a focus of what were the appropriate procedures after 1965. But static failure has actually been one of the most damaging failure modes for tailings facilities: Aberfan (1968, UK), 144 dead from static liquefaction caused by rising ground water pressure; Aznalcollar (1998, Spain), brittle foundation failure causing dam breach and wide-spread contamination downstream; Kingston fly ash (2008, USA), undrained static failure of fine-grained fly ash, causing significant environmental contamination; Mt Polley (2014, Canada), rapid foundation failure resulting in dam breach and one of the biggest environmental disasters in modern Canadian history; and, Fundao (2015, Brazil) static liquefaction with at least 17 dead and estimated damages of billions of dollars (*www.fundaoinvestigation.com*). A guide to what needs considering is the ICOLD bulletin on dam failures. This paper focuses on the subset of geotechnical considerations including both static and earthquake-induced liquefaction.

A good practice approach, based on engineering mechanics, is laid out in this paper. This means measuring the engineering parameters needed for design/assessment: soil strength (drained and undrained), soil stiffness, and cyclic softening. Assumptions that engineering behaviour can be satisfactorily related to fines content are avoided as tailings may consist of 100% fines. Underlying the

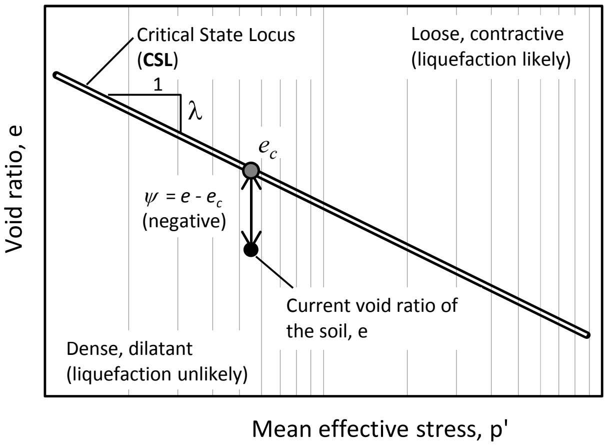

Figure 1. Definition of state parameter

approach in this paper is generalized critical state soil mechanics (CSSM), implemented through the state parameter ψ (defined on Figure 1). In many ways, this is the thread of characterizing soil behaviour that started in 1935 with the world's first liquefaction-resistant dam (Franklin Falls, NH) and with contributions by various workers over the past 80 years now making it the dominant framework for understanding all soil stress-strain behaviour (drained or undrained, and all stress paths). It is not difficult to use, as will be shown in this paper.

2 PARTICULAR ASPECTS OF SILTS

Tailings start as a slurry of sand and silt particles, which are discharged into an impoundment to sediment and accumulate – almost a perfect example of 'normally consolidated' geology. If simply spigoted, the tailings hydraulically segregate. In any particular tailings storage facility (TSF), you should anticipate at least two material types with the sand fraction dropping out quickly to form beaches or similar features with sandy silts and pure silts (slimes) moving further down the impoundment and usually accumulating underwater. These silt-dominated soils comprise a large portion of the impoundment, so tailings characterization becomes "how do we determine silt behavior"?

A recent trend in the mining industry has been to increase the slurry density (and recover more water) before discharge, referred to as thickening. Thickened tailings do not segregate, so in this instance the material being dealt with is commonly a silt containing around 10-15% sand size particles and the characterization question remains the same. Tailings silts are also not that different from rock-flour derived natural silts found in western Canada. The same testing issues arise.

Silts, whether tailings or natural rock flour soils, can be sampled successfully using a thin-wall un-

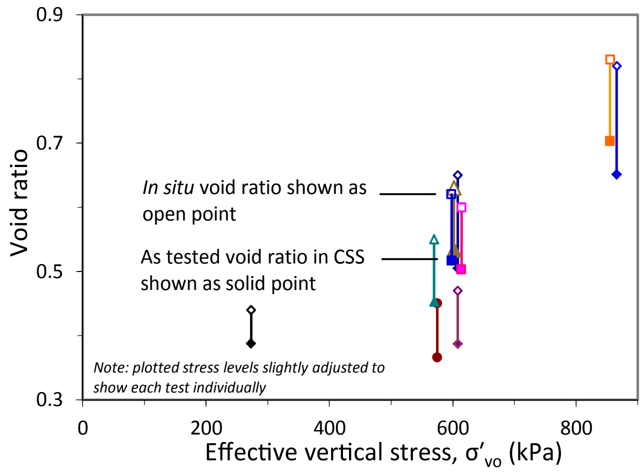

swaged Shelby tube, much like clays are sampled. Often, it is also possible to recover sandy silts using

Figure 2. Effect of post sampling process on void ratio of undisturbed silt samples

similar samplers. But, in either case, subsequent processes, i.e sample transportation, extrusion, trimming, and setting up in the laboratory apparatus (e.g. reconsolidation to the *in situ* stress level in a triaxial cell prior to loading), cause substantial densification between the as recovered void ratio in the sample tube and the as tested void ratio. The effect of these post-sampling processes is illustrated on Figure 2 for a natural silt (from Vancouver Island, Canada) that was sampled and handled with extreme care (Mohajeri & Ghafghazi, 2012). A densification of about $\Delta e \approx 0.15$ was found, which is about a third of the void ratio range between the loosest possible soil and the densest possible soil (analogous to e_{max} and e_{min}, although of course the ASTM procedure does not apply to silt-dominated soils).

This densification means what is tested is much stronger than what is *in situ*. For perspective, testing of a natural silt using careful reconstitution found that the number of cycles to liquefaction doubles for Δe = 0.05 densification. This densification of silts from *in situ* to laboratory is a serious engineering challenge, making it dangerous to use a clay-like approach where laboratory strengths are taken at face value. What to do ?

There are two alternative, and complementary, approaches to characterizing silts: a) measure strengths in the laboratory and correct the results for the known densification; and/or b) treat silts as sand-like, measuring ψ *in situ* and using that to compute *in situ* strengths from appropriate test results.

In either approach, how silt behaviour changes with void ratio must be quantified and, today, that requires critical state soil mechanics.

3 CRITICAL STATE SOIL MECHANICS

The critical void ratio was identified from the practical concern of avoiding static liquefaction failures of hydraulic fill dams in the late 19th and early 20th centuries. "Critical" really meant what it said – it was the criterion of a safe density in constructed engineering work, with the practical concern to avoid sudden transitioning of drained construction with no excess pore pressure, into an undrained liquefaction failure. The critical void ratio developed from engineering by the Corps of Engineers for Franklin Falls dam, with Casagrande's famous experiments at Harvard. This was rapidly followed by Taylor at MIT (in connection with the Fort Peck dam failure) who showed that the critical void ratio depended on confining stress, or what is today called the critical state line (CSL).

Theoretical soil mechanics has always sought to explain observed soil behaviour in terms of simple physical principles and corresponding mathematics. Since particulate materials can exist over a range of void ratios at any confining stress, depending on the packing of the particles, the key challenge has always been to understand (and quantify) how void ratio affects soil strength and stiffness. The stress-strain behaviour of all engineering materials is dominated by the theory of plasticity, and for various theoretical reasons the CSL was adopted as a central idealization in the Original Cam Clay and Modified Cam Clay models. Seemingly because of the title of the Schofield & Wroth (1968) book setting out these ideas, critical state soil mechanics (CSSM) became (erroneously) synonymous with Cam Clay.

Cam Clay is both simple and mathematically elegant, theoretically quantifying how void ratio affects soil stiffness and strength. Some (i.e. the British) view these models as "the greatest 20th century contribution to soil mechanics". Others view Cam Clay (either variant) as excessively idealized and utterly useless for real soils in engineering practice (delightfully summed up in the *critique* of CSSM on Wikipedia). The problem has become the linkage of Cam Clay with CSSM because of the book's title, with the inadequacies of Cam Clay being used to throw out the real engineering value of the thread that started with the Corps of Engineers in 1935.

A key contribution in returning to the value of CSSM was Been & Jefferies (1985). This was driven, much like the original work at Franklin Falls, with concerns about static liquefaction of hydraulically placed sand. It was found that a large number of drained strength tests on various sands, with fines contents ranging from 0 to 18%, showed a simple and systematic trend:

$$\phi = \phi_c - 45\,\psi \qquad (1)$$

where the coefficient 45 in (1) appeared constant from one soil to another. An updated version of this trend is shown on Figure 3.

The trends in sand behaviour reported by Been & Jefferies resurrected CSSM. The basic theoretical insight that followed from Figure 3 was that yield surfaces (the limits of elastic behaviour) in general do not lie on the CSL but rather evolve to the CSL with shear strain. This insight produced two strands of

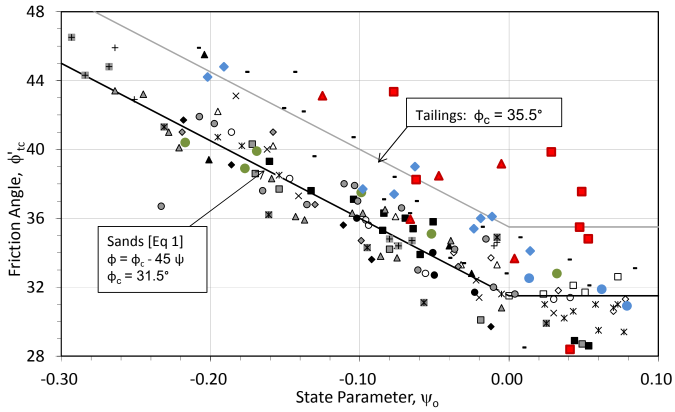

Figure 3: Friction angle as a function of state parameter. Original data for sands (Jefferies & Been, 2015) updated with tailings, shown as coloured symbols

constitutive models: those strictly following the Drucker at al. (1957) framework (e.g. Jefferies, 1993) and developments of bounding surface plasticity (e.g. Manzari & Dafalias, 1997). These models are "good" in the sense that they closely predict the effect of void ratio and confining stress on soil behaviour and only use a few (generally familiar) soil properties. There are now about a dozen good models, and they extend past their origins in triaxial *p,q* space to general stress states and all loading paths. These models all have common features:

1 a CSL (not necessarily the familiar semi-log idealization);
2 a critical friction ratio (or angle);
3 dilation and strength controlled by ψ;
4 plastic hardening that partially scales with the slope of the CSL; and,
5 isotropic elasticity with stress-level dependence.

The models differ in rather small details, and it is largely a matter of taste as to which is used. They all give comparable stress-strain behaviour and show how void ratio affects that behaviour. Figure 4 illustrates the match between one of these good models (NorSand) and test data. An excellent fit to a spectrum of drained and undrained soil behaviour is apparent. The test data shown is a construction sand used in a large hydraulic fill that suddenly failed near full-height (Nerlerk).

A recurrent critique of CSSM has been that the CSL is not unique and changes with stress path to reach CSL. This critique was thoroughly addressed for laboratory tests on sands in Been et al. (1991) while Jefferies & Shuttle (2005) showed that NorSand, which has an explicit unique CSL, captured

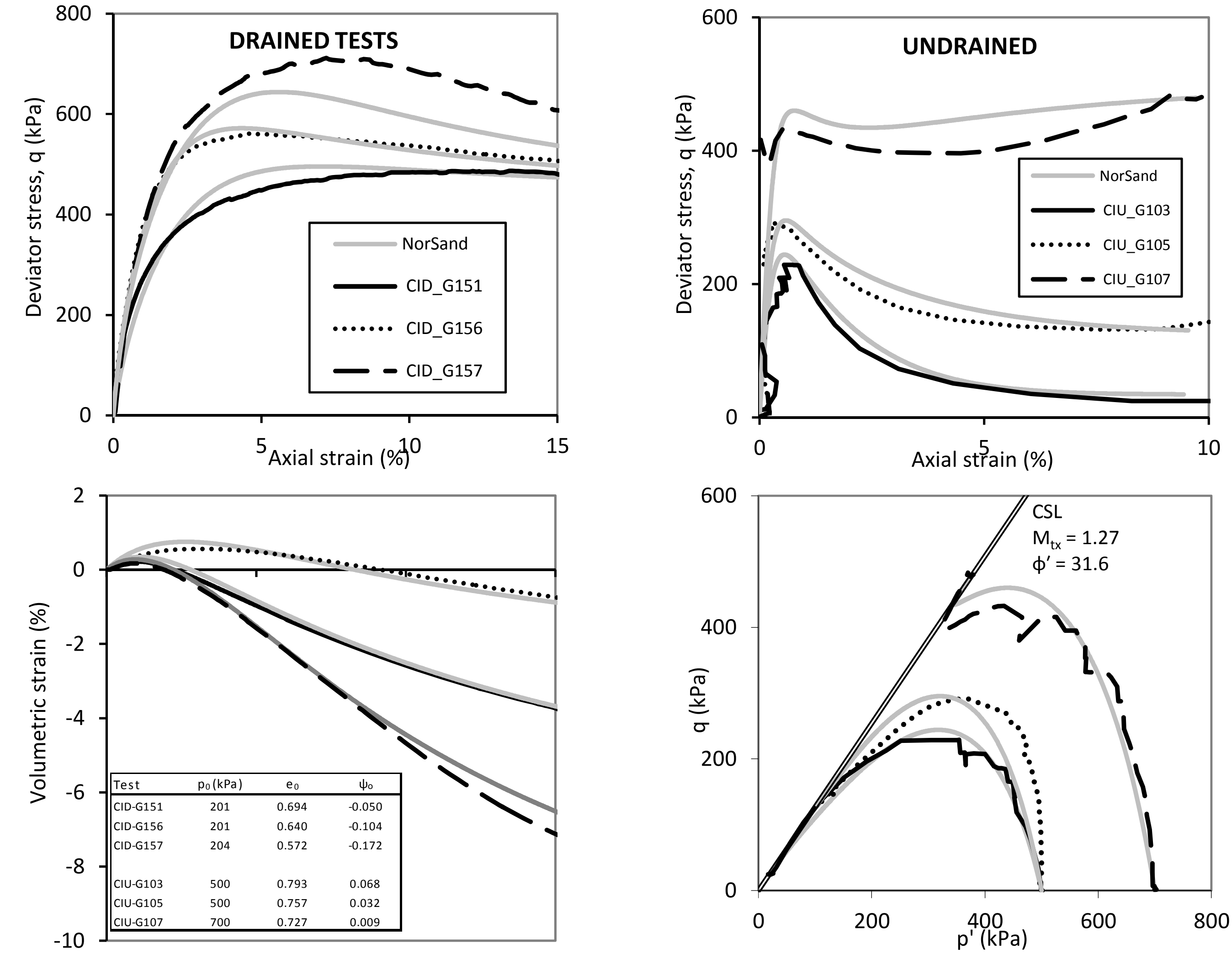

Figure 4. Match between CSSM model for sand (NorSand) and triaxial test data from Nerlerk hydraulic fill. Results are compared at a range of ψ for drained (dense) and undrained (loose) specimens.

the range of soil behaviour used to assert non-uniqueness.

Using CSSM in engineering practice is simple and involves just three steps which are always part of the geotechnical engineering process:

- determine the state of the soil (tailings) *in situ*;
- measure the engineering parameters as a function of state, and;
- carry out the appropriate analyses.

These steps are discussed shortly, but first we need to return to 1935 and the concerns about hydraulic fill construction to identify the key problem.

4 A BASIC STABILITY PRINCIPLE

A feature of staged construction of earthworks is that it is done slowly to allow consolidation during fill placement. This aspect is often formalized in upstream construction of tailings dams with piezometric measurement to confirm drained or consolidated conditions. Yet, these dams can fail suddenly and not only during construction. This was the concern of the Corps of Engineers in 1935, and it is a concern that ought to have applied at Fundao eighty years later. What is the soil behaviour causing the rapid instability and transition from drained to undrained behaviour?

Figure 5 shows some soil stress-strain curves and the associated stress paths under constant horizontal plane-strain compression. The data annotated as A is a purely undrained test of loose soil, with the familiar associated static liquefaction once the undrained-strength is reached. The curve annotated as B comprises soil with the same ψ, but now first loaded to point B1 drained. The soil is then subject to change to undrained loading, but this change is not dramatic as the stress at the change to undrained loading is less that its undrained strength (B2). The data shown as ‘C’ is a further progression of drained loading of soil at the same ψ but now with the drained loading exceeding the undrained strength at B2 before switching to undrained conditions. As can be seen on the figure, instant brittle liquefaction develops despite there being zero excess pore pressure at the instant of liquefaction. The reason for the instantaneous transition is that the potential rate of excess pore pressure generation is infinite under load-controlled situations if the current undrained strength of the soil is exceeded even though the loading path to that limit is perfectly drained. This undrained strength is called the "instability limit" in effective stress terms.

The path from point B1 to point B2 on Figure 5 corresponds to a rapid loading event, which could be a quickly placed berm raise, an earthquake, or even simply an increase in phreatic level within the tail-

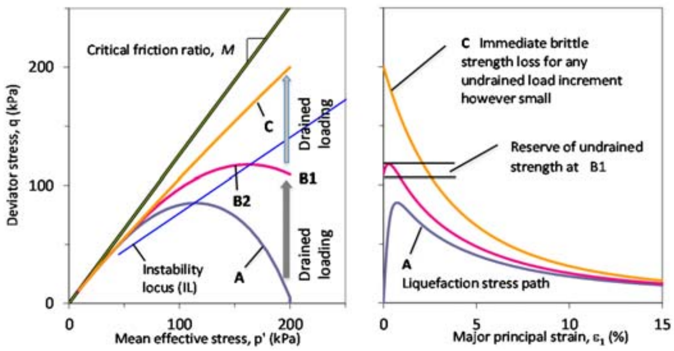

Figure 5: Transition from drained to undrained behaviour leading to potential rapid liquefaction after undrained perturbation

ings unrelated to construction processes. Provided the stresses are less than the instability limit, the soil has sufficient strength reserve to withstand the perturbation and the expected consolidation can develop. But, if the perturbation stresses exceed the instability limit then monitoring construction and/or onset of failure with piezometers in conjunction with drained shear strengths is an unsafe engineering approach. There will be no warning of the liquefaction failure, apparently the situation at Fundao and a century earlier at other hydraulic fill dams. Let us now consider this instability limit a little further.

Figure 3 showed a large data base of drained triaxial tests, and there is a comparable data base of undrained tests (that is how the various CSLs were measured to determine the ψ plotted on Figure 3). So that we compare like with like, the peak undrained strength can be reduced to a mobilized effective stress ratio $\eta_L = q/p'$ and the peak strength in drained compression likewise to an effective mobilized stress ratio. Figure 6 plots the η_L at peak undrained strength versus ψ at that peak strength for the undrained tests. A comparable trend to Figure 3 is observed, with an interesting feature. The top trend line annotated on Figure 6 is the average trend for the drained tests of Figure 3 (but extrapolated to positive state parameters from the dense states of Figure 3). This is sensibly an upper bound to the undrained data. However, the best-fit trend through the undrained data is parallel to the drained trendline and the two are offset by $\Delta\psi = 0.06$ as indicated. This offset develops because the conditions are different. In drained loading, the mean effective stress is constant (temporarily) at peak strength. In undrained loading of loose soils, the mean effective stress is changing at its greatest rate because of pore pressure changes at peak strength. This effect of rapidly changing mean effective stress on soil behaviour is intrinsic to the good soil models mentioned earlier, with good models accurately capturing both drained and undrained soil behaviour using the same properties.

The idea of triggering undrained instability is sometimes difficult to appreciate as it involves the balance between drainage time and strain rates, with

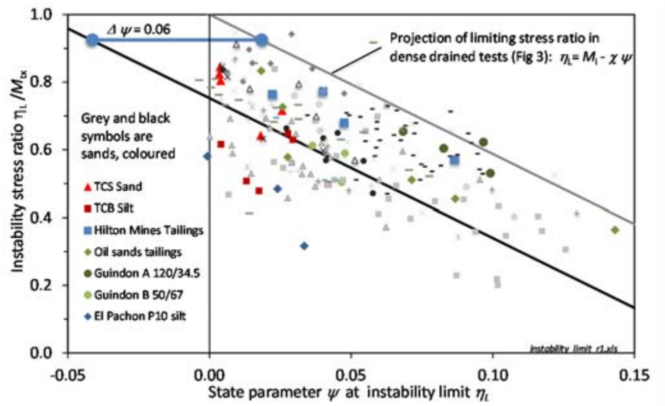

Figure 6: Instability limit (effective stress ratio at peak undrained strength) in relation to projected limiting stress ratio from drained tests on dense specimens (from Figure 3)

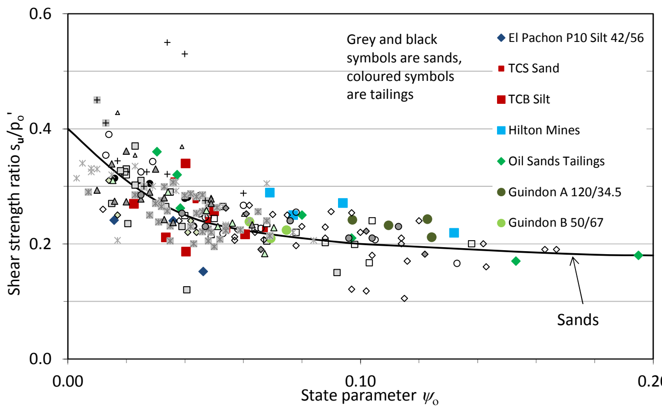

Figure 7: Undrained shear strength ratio for sands and silts (a total stress version of the instability limit on Figure 6)

internal load transfers also affecting the mechanics. It may be simpler to think in the same way as stageloading on soft clays and always keep the embank-ment stable using undrained strengths in analyses. Thus, rather than use Figure 6, the same data is shown on Figure 7 as a familiar undrained strength ratio. Both the effective instability limit and the undrained shear show the same thing in a different way but neither is fundamental. The instability depends on the soil properties, such as the ratio of elastic and plastic modulus, critical friction ratio, compressibility and loading path. The scatter in Figures 6 & 7 reflect these unreported factors, not testing errors.

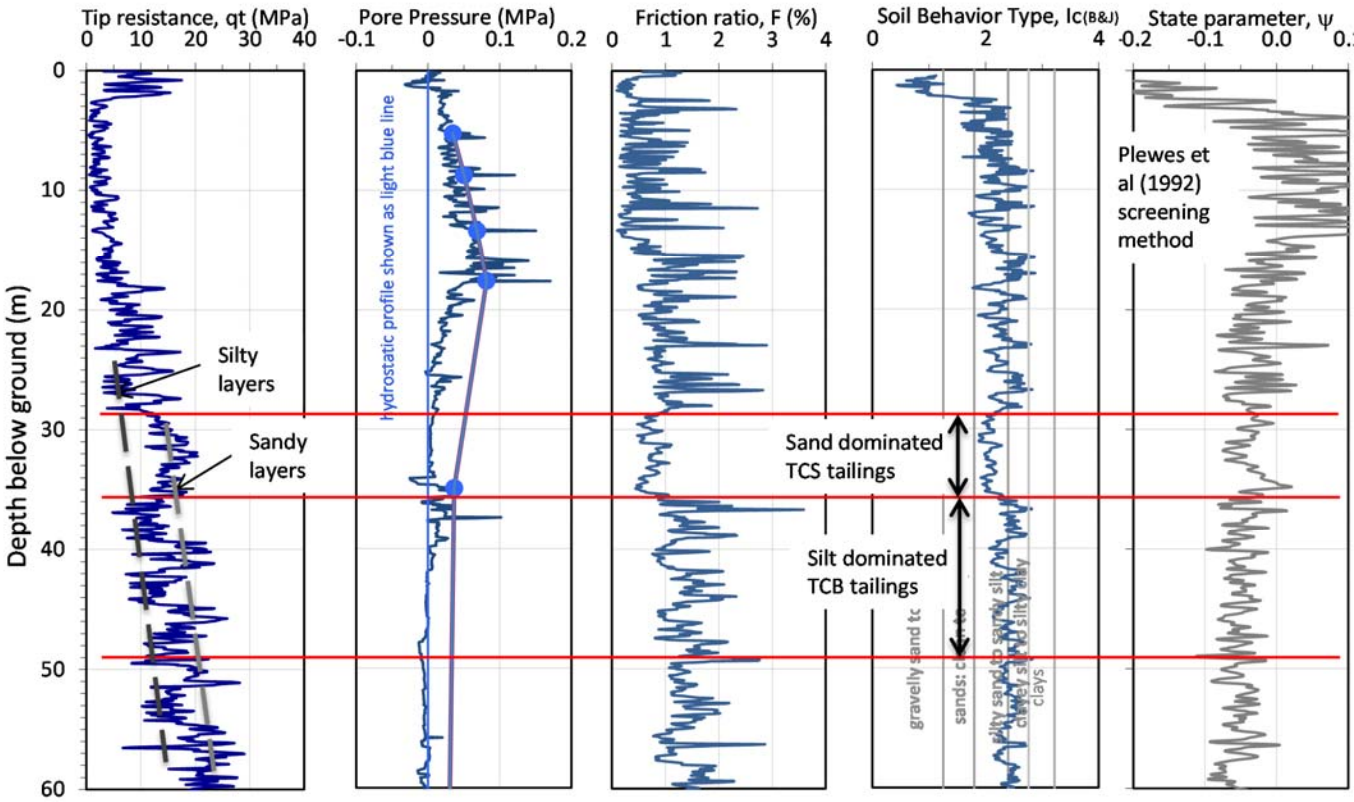

Figure 8: Example CPTu in a TSF showing segregation of coarse and fine layers. The tailings are TCS and TCB materials used for illustration of the CSSM techniques in the paper

Practically, it may be simpler to appreciate that the "critical" decision point that concerned the Corps of Engineers 80 years ago is the offset $\psi < -0.06$. This -0.06 in void ratio or ψ is a generally conservative number, as can be seen on Figure 6, where some soils are systematically better since undrained behaviour depends on soil compressibility as well as intrinsic frictional properties.

What should a practical engineer take away from these considerations? The basic instability principle is this:

- if $\psi < -0.06$ then undrained strengths will be greater than drained;
- if ψ is looser, then stability depends on the available undrained strength even though current loading may be drained

There is a corollary to this principle if the second situation prevails, and that invariably arises with thickened tailings, which is whether to use peak undrained strength with a decent factor of safety (to allow for brittle load transfer of overstressed soil) or to use residual undrained (minimum assured) strength with a much lower factor of safety. There are various views on this issue, with a preference for the second approach in the Author's company.

So, with this principle established as a background to engineering at a TSF site, let us turn our attention to characterizing the *in situ* state of the tailings and the associated strengths to use for engineering.

5 MEASURING *IN SITU* STATE OF TAILINGS

Geotechnical engineers have several options for a parameter to characterize the *in situ* state of tailings. Amongst them are void ratio, relative density, dilatancy index, gamma ray absorption from downhole logging, etc. All of these methods are technically challenging and really require an accurate calibration to what actually occurs *in situ*.

What we should be measuring is the *in situ* state parameter (ψ) with a CPTu, as rigorously as possible. The degree of rigour will determine the cost of the investigation. Firstly, we recognize that we cannot easily obtain undisturbed samples of tailings materials, but the CPTu gives us an accurate profile through our deposit. Second, we know that the value of ψ is the major control on behaviour of soils, and this applies to the CPTu resistance, friction angle and cyclic stress (although each behaviour has other factors that are also important). Third, if we could accurately measure void ratio or density, we would still be left with a problem of converting the void ratio back to ψ and the engineering behaviour because of the range of CSLs of the soil *in situ*.

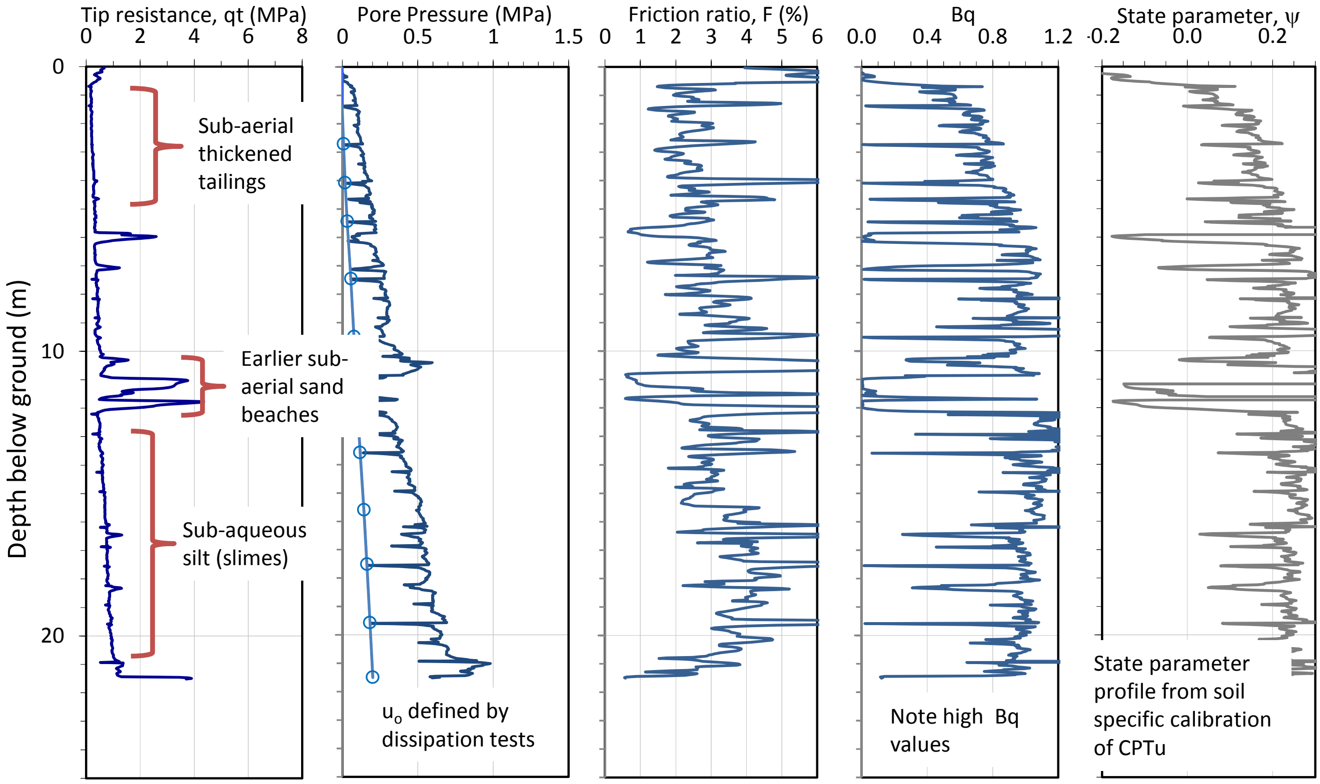

5.1 *Examples of CPTu in tailings*

Variations of material type in the TSF will show up on the CPTu and it is important to recognize them. However, the differences in *ψ in situ* affect the CPTu measurements in approximately the same way for most materials and we are able to deal with that if we know the properties of each material.

This aspect is illustrated in Figure 8, a CPTu showing there are two interbedded materials within the tailings storage facility (TSF). One material is a coarser silty sand tailings (which we will call TCS sand) deposited near the spigots as it drops out first from the slurry, while the second is a finer (sandy) silt tailings (TCB silt) deposited when the spigot was further away from the location. The TCB silt tailings have a soil behaviour type index of $I_c \sim 2.7$ while TCS sand shows $I_c \sim 2.0$. Interpretation of the CPTu for tailings will be addressed using these tailings for illustration, but first we will examine another example and useful screening tool.

Figure 9: Example CPTu in copper-zinc tailings. It is a massive silt tion and more recent thickened tailings.

Figure 9 shows conditions in a different TSF with massive sub- aqueous silt (slimes) deposits, some relict sandy beach features and more recent thickened tailings deposited sub-aerially. There is clearly a very wide range of CPTu signatures that occur in tailings facilities. Some insight is gained by viewing the data on a soil behaviour type chart rather than a plot with depth, Figure 10. This chart was contoured

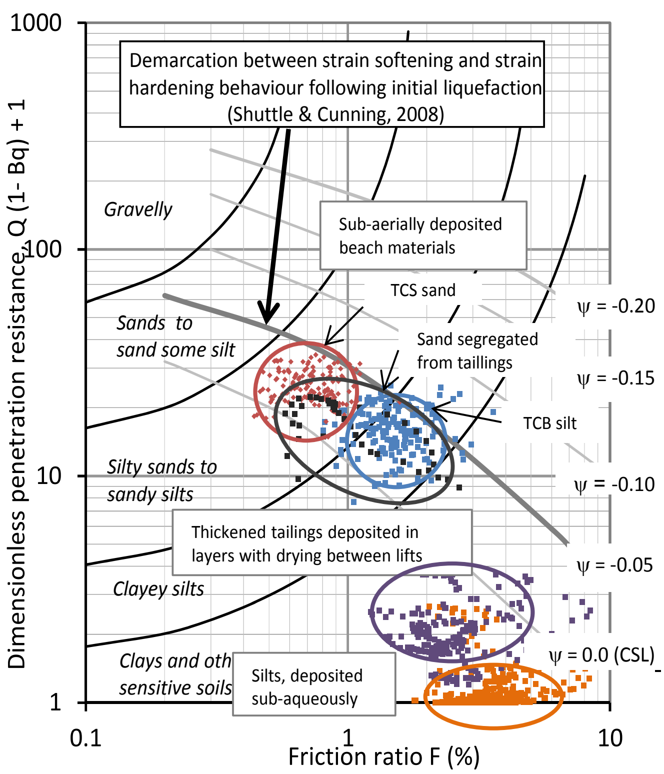

Figure 10: Dimensionless classification chart for soil behaviour type for identified materials on CPTu examples in Figure 8 and Figure 9.

for the state parameter by Shuttle & Cunning (2008) using their effective stress cavity expansion simulations, discussion with Robertson (2008) and the Plewes et al. (1992) equations, which give a guide to soil state as well as the soil behaviour type. The example sounding has the beached sands plotting only slightly contractive ($-0.05 < \psi < 0.0$) and thus prone to liquefaction. The sub-aqeous silts ($\psi > +0.05$, and very low CPTu resistance) are exceedingly loose and raise interesting questions about their potential strength loss following liquefaction. Thickened tailings in this instance ($0.0 < \psi < +0.05$) would require careful engineering to avoid liquefaction flow failures on slopes.

For comparison, TCS sand (from 28.5 to 36m depth) and TCB silt strata (36 to 49.5 m depth) are also shown on Figure 10, and maybe not surprisingly the three sub-aerially deposited tailings show up as the same soil behaviour type and *in situ* state.

5.2 *Interpreting in situ ψ for tailings*

Interpretation of ψ from CPTu data has been in the geotechnical literature for almost 30 years now, starting with Been et al. (1986 & 1987). A more recent publication specifically for tailings deposits is in Been et al. (2012). However, there are numerous references leading from 1986 to the present. An issue was that the early work was based on large calibration chamber tests of the CPTu in sand, and Sladen (1989) identified a potentially significant stress-level bias. Shuttle & Jefferies (1998) eventually modeled this bias and showed how the elastic zone outside of the plastic zone caused this effect. Evaluation of CPTu data needs to include the *in situ* G_{max}. In the meantime, various engineers had been working on other ways to progress the understanding and the methods adopted are rather varied. Some of the main contributions and their features are:

- Been et al. (1987) methods are appropriate if there is indeed a calibration chamber test program, for which there is good data. This is not common.
- Plewes et at. (1992) developed a screening level method to provide the *in situ* state of tailings, in which λ (the slope of the CSL) is related to the CPTu friction ratio F%. This method is still fairly robust, as expounded by Reid (2015) showing how λ_{10} and F compare on Figure 11.
- Shuttle & Jefferies (1998) carried out detailed, large strain, numerical analyses of the CPTu in sand. They identified both the elastic and plastic components of the resistance, and identified a simplified method to determine ψ (of course, only after knowing the CSL and the complete set of soil properties including G_{max})
- Shuttle & Cunning (2007) next examined what would happen with undrained behaviour in tailings, bringing in the effective stress dimensionless parameter grouping to tip resistance introduced by Houlsby (1988). Besides their method of analysis, they entered a discussion (Shuttle & Cunning, 2008) with Robertson (2008) and identified the contractive/dilatant boundary for all soils ($\psi = -0.05$, which is essentially equivalent to offset between drained behaviour and the instability limit shown on Figure 6; see Figure 10).
- Robertson (2009, 2010, 2012) has continued to publish more information, pulling together what he sees as the state-of-the-practice.

5.2.1 *Data reduction in sand*

In the case of sands, which are fully drained soundings, the relationship between ψ and the CPTu resistance was originally determined from calibration chamber tests. Such tests, which are in effect a giant triaxial cell, involve pushing a CPTu into a sand of known void ratio and under known stress. Repeating the procedure with many samples provides a mapping between tip resistance, soil state, and stress level. Most in the *in situ* testing community regard chamber calibration of the CPTu as the gold standard to be used. The only catch in this is that each chamber test involves careful placement of 2 tonnes of sand so is not commercially viable for most projects. Chamber tests tend to be research programs by universities.

The starting point for determining the state parameter from the CPTu was this worldwide set of chamber tests, with samples of the sands then tested to determine their CSL. This process showed that (Been et al, 1986):

$Q_p = k \exp(-m\,\psi)$ or in its correct inverted form

$$\psi = -\ln(Q_p / k) / m \qquad (2)$$

where $Q_p = (q_t - p)/p'$ and is the dimensionless CPTu resistance (note use of mean, not vertical, stress). The coefficients *k, m* are soil-specific, depending on the soil properties. It was acknowledged that the CPTu resistance depended on soil compressibility, which Been et al. (1987) formalized by relating *k, m* to λ_{10} (the slope of the CSL). The method recovers ψ with a precision ±0.05 across the range of available calibration chamber results at the time. They were mainly clean sands, and nearly all quartz sands, which is a big limitation for tailings.

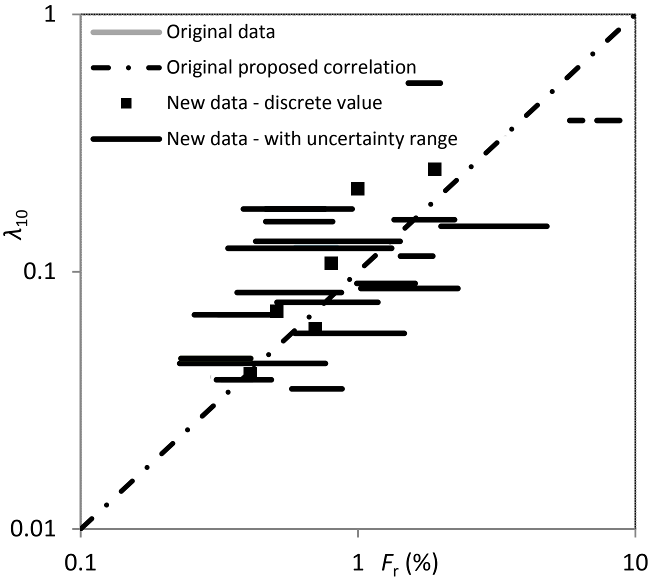

Figure 11: Slope of λ_{10} as a function of F% (after Reid 2015, Reid 2012 and Plewes et al 1992)

Strictly, the coefficients *k, m* depend on all the soil properties and also on the *in situ* G_{max}. This was explored using the familiar cavity-expansion analogue for the CPT, scaled to the chamber calibration data, using large-displacement finite element simulations with NorSand (Shuttle & Jefferies, 1998). The extensive parametric simulations were fitted using simple functions relating *k,m* to the soil properties discussed earlier. This is easy enough to use in practice and recovers ψ with a precision ±0.02. The method explicitly considers aspects like the critical stress ratio M_{tx} (or constant volume friction angle) being quite different in tailings compared to natural soils, for example.

Of course, many practical engineers still prefer a physical calibration, and it is a little surprising that one sees so few calibration chamber studies in the context of billion dollar liabilities for many projects. Lower cost physical calibrations have been achieved by doing CPTu tests in a centrifuge (Bolton et al., 1999), with the advantage of a smaller sample and the fact that each test covers a range of effective stresses at the same void ratio. Scaling of the soil to the CPTu diameter is a complication and it is typical to check the five or so centrifuge tests with a couple of full scale calibration chamber tests.

Other researchers are investigating whether an even smaller CPTu test in a triaxial specimen with good control of boundary stresses might be an alternative, but this is a relatively recent development (Damavandi-Monfared & Sadrekarimi, 2015).

5.2.2 *Data reduction in silt*

Although sands are encountered in tailings, nearly all TSF will have some silts and, possibly, even be dominated by silts. However there are no properly carried out calibration chamber studies for the CPTu in silt. CPTu soundings in silts are undrained, often with rather large excess pore pressures (Figure 9). What should be done?

In the case of clays, undrained CPTu are evaluated on the basis of total, not effective, stress by comparing the undrained strength s_u inferred from the CPTu to some reference strength to establish the calibration (commonly a triaxial strength using one of several testing protocols or *in situ* vane shear). But silts offer a challenge as their densification from an as sampled void ratio to the tested void ratio precludes a sensible reference laboratory procedure. It is not evident what might form a reference *in situ* test.

On the other hand, good models using CSSM have no trouble capturing the stress-strain behaviour of silts, drained and undrained. Thus the state parameter must be the basis for characterizing silt-dominated soils. It then follows (Been et al, 1988) that the framework for evaluating CPTu in undrained soundings should be analogous to (2):

$$\psi = - \ln (Q' / k') / m' \tag{3}$$

where $Q' = Q(1\text{-}B_q)+1$ with k', m' being the soil-specific coefficients for undrained soundings. The Shuttle & Cunning (2007) work determined these coefficients k', m' using the same cavity expansion approach of the Shuttle & Jefferies (1998) study by simply switching the analysis to undrained conditions. This is reasonable as the NorSand constitutive model fits silts, drained or undrained, just as well as it fits sands and the numerical procedures do not depend on the boundary conditions. The soil properties (e.g. M_{tx}, λ) remain identical although obviously the numerical values change from one soil to another, but Shuttle & Cunning did not report extensive parametric studies, and there are no convenient expressions for engineering practice to compute the state parameter in undrained soundings. What is available is their public-domain finite element code, downloadable at *www.crcpress.com/Soil-Liquefaction*.

One further step in using (3) is that it is based on the cavity expansion analogue for the CPT, which then suggests that it should use the pore pressure at the u_1 location, not the accepted standard procedure of measuring at the shoulder u_2 location. Thus, a mapping needs to be introduced for u_1/u_2. At present the Peuchen et al. (2010) relationship is used.

5.2.3 *Improved precision: pore pressure and shear modulus*

Tailings may be under-consolidated because of the placement rate. It is also common to find the TSF to be under-drained with a consequent downward hydraulic gradient (at least in the longer term). These two factors dictate that the piezometric regime must be measured during any field investigation. A convenient way of doing this is to carry out dissipation tests at a few rod-changes for each CPTu sounding, in

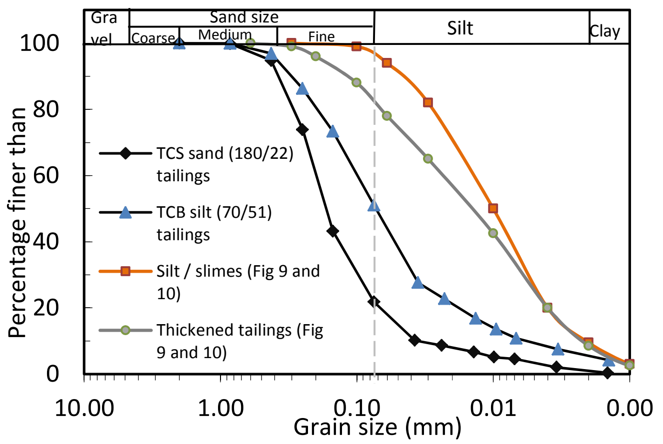

Figure 12: Grain size distributions of TCS Sand (180/22) tailings and TCB silt (70/51) tailings, as well as thickened tailings and slimes on Figure 10.

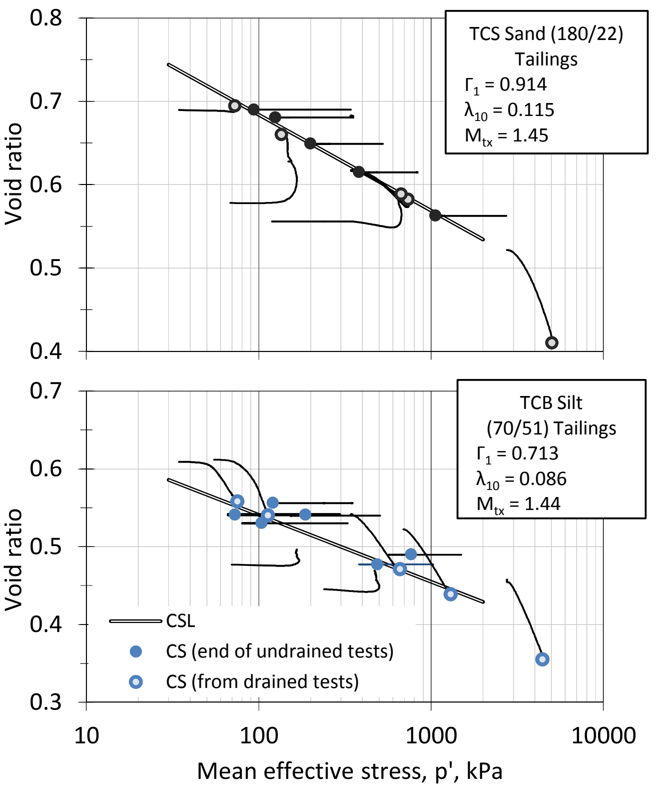

Figure 13: Critical state lines for TCS sand (180/22) and TCB sandy silt (70/51) tailings. Black lines represent state paths – horizontal lines are undrained tests while hooked lines are drained tests.

essence measuring both horizontal coefficient of consolidation (c_h) *in situ* and the current pore pressure (u_o) using the CPTu pore pressure sensor.

The elastic shear modulus G_{max} was discussed earlier in the context of *k, m* values in (2) but it is also a sensitive indicator of fabric as it captures how the particle contacts can transmit elastic shear waves. We should always include at least some seismic CPTu soundings in any field program; about 1 test in 5 seems sufficient to greatly add to the understanding of any site. A G_{max} profile is, of course, the starting point for any earthquake ground response study as well.

5.3 *Application to TCS sand and TCB silt*

Representative samples of both of the tailings materials were tested to determine their properties for the CPTu interpretation, essentially *k, m* or *k′, m′*. The general scope and procedures for laboratory testing are left to the following section. Figure 12 shows that TCS sand is indeed a silty sand with a D_{50} of 180µm and 22% fines, while TCB silt contains more than 50% silt (D_{50} = 70µm and 51% fines). There is excellent definition of the CSL in both cases (Figure 13), with the usual semi-log idealization being adequate for confining stresses less than about 2 MPa.

An interesting aspect of these tests is the properties of these CSL, with λ_{10}=0.115 for TCS sand (22% fines) and λ_{10}=0.086 for TCB silty sample (51% fines). The CSL slope λ_{10} is directly comparable to the familiar compression index C_c used with clays. It then follows that the higher-fines TCB silt is actually less compressible than the TCS sand, in the case of these two tailings gradations. This is an important observation that illustrates the significant limitations of relying on fines content as a proxy for compressibility in the interpretation of CPTu results. The additional fines content fills up more of the pore space providing less opportunity for particle movement during shear (note that the CSL of the TCB silt is also at a lower void ratio than the TCS sand with 22% fines).

Table 2 summarizes the parameters developed for the full interpretation of the *in situ* state. The average *in situ* state of both materials based on the CPTu turns out to be about ψ = –0.02. Now we have measured the *in situ* ψ we only need the soil behaviour at that state.

Figure 14 shows the corresponding stress-strain behaviour of the drained and undrained specimens closest to this state for each material. Their behaviour is comparable, as it should be at the same ψ. There is some strain softening, and large strains, but maybe not the very brittle behaviour that may be expected in sands without fines.

5.4 *Soil samples and laboratory testing*

Moving ahead to a full assessment of the behaviour of the soil for both static and earthquake loading needs samples in addition to those needed for soil index testing and CSL determination. These do not have to be undisturbed as soil properties can be measured on reconstituted samples. Tests on undisturbed would be misleading as to *in situ* behaviour because they are practically impossible with silts (see Figure 2).

Most CPTu equipment is now available with a form of piston sampler (MOSTAP or similar) that is deployed using the CPTu system itself. The sampler

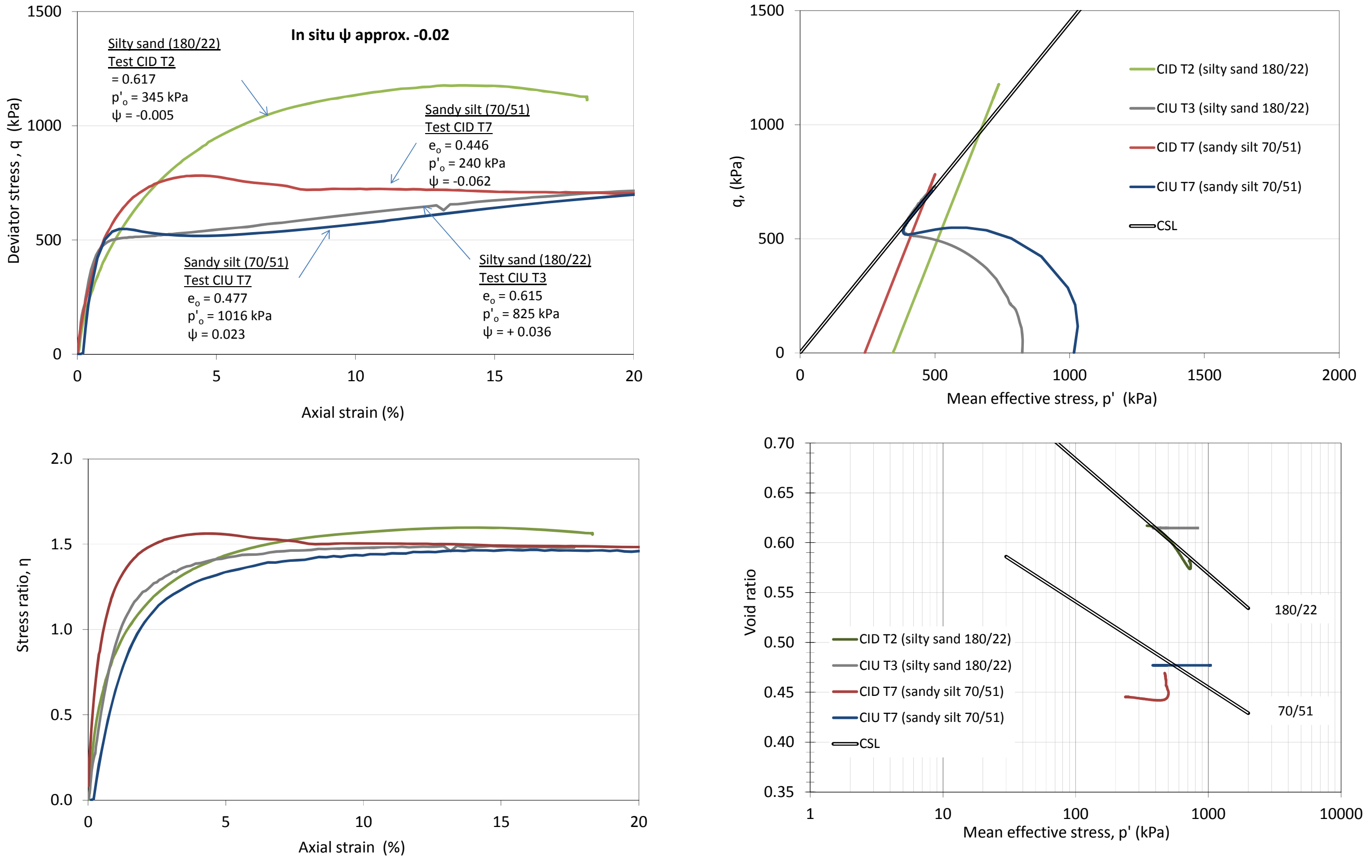

Figure 14: Stress strain curves for drained and undrained triaxial tests on TCS sand and TCB silt tailings at the estimated average in situ state $\psi \sim -0.02$

is pushed to the test depth and then opened to recover the soil in the target zone. Sampling does not need to be at every CPTu sounding, but once the characteristic soils have been identified, sufficient samples need to be recovered to characterize the variability of the materials (grain size). Then you need to look at CPTu in conjunction with the grain sizes. How many materials do you really have? Often you can boil it down to just two or three characteristic gradations.

This provides the basis for laboratory testing on disturbed, blended samples that provide a base of measuring engineering properties that support the *in situ* test interpretation of the CPTu, with distinction between different material types.

So, what testing is needed to support the characterization of tailings behaviour?

6 ENGINEERING PROPERTIES

6.1 *Laboratory test program*

Characterizing the soils in a TSF requires enough testing on each representative material. Table 1 provides a basic minimum set of tests with the purpose of measuring:

1 Static strengths, brittleness and so forth and with sufficient data to calibrate any of the good soil models;
2 Data on the cyclic behaviour as it seems inevitable that high-value mines will be in earthquake prone area; and,
3 Index tests to document the soils tested.

This testing is really quite modest (and certainly in the context of the recent tailings failures) but is sufficient to allow us to define the material behaviour as a function of the *in situ* state ψ.

Assuming a semi-log CSL is used (and this will often be adequate) there are only five soil properties: Γ, λ which define the CSL; M, N, which define the stress-dilatancy behaviour; and χ which defines the effect of ψ on strength. (χ defines the slope of the trend line in Figure 3, which varies slightly from one soil to another. This was not considered in 1985). These properties are simply obtained by plotting test data in the appropriate form. The properties are all dimensionless (although Γ has a convention of being defined at 1 kPa) and do not imply any particular constitutive model. They capture the fundamental behaviour of any particulate material. Table 1 indicates which tests provide which properties.

The discussion so far has been directed to strength, but generally we will need to know tailings consolidation behaviour. First, consolidation affects the capacity of the TSF, a business consideration. Second, because mine life is commonly about 25 years there

Table 1. Suggested laboratory testing program per representative sample of tailings

Test type	No of Tests	Purpose
Particle size distribution	20	Define heterogeneity of material, identify representative materials
Specific gravity	2	Basic property to calculate void ratio
Max. & min. density	2	Not part of CSL framework, but helpful to laboratory technicians for sample preparation
Triaxial consolidated undrained	5 - 8	Define CSL, undrained strength, brittleness (Γ, λ, M)
Triaxial consolidated drained	5 – 8	Define CSL, stress-dilatancy,, state-dilatancy (M, N, χ). Also provide the basic stress-strain data for calibrating constitutive models.
Oedometer/Rowe Cell	3-5	Consolidation behaviour (C_c, c_v)
Bender element tests	2 sets of 8	Measure G_{max} as function of stress level at 2 initial void ratios. Measure consolidation curves
Cyclic simple shear tests	8	Two sets of 4 tests. Each set at same ψ. Include post-liquefaction settlement if possible.
Resonant column testing	2	Optional, but avoids reliance on published curves for G and D_r

will be substantial strength gain in this time. Thus some oedometer or Rowe Cell tests are needed.

The elastic soil stiffness is also important, both for improved precision in determining ψ from CPTu and for seismic response assessments. We have found it is helpful to use bender elements within a set of triaxial consolidation tests. This defines the relationship between G_{max}, void ratio and stress level better than the field measurement of G_{max}, since we have a better measurement of void ratio in the laboratory sample than in the field. It also defines consolidation properties of the tailings.

In the case of static strength and stiffness there are several good models that will closely predict the soil's behaviour from the tests discussed. This is, as yet, not true for cyclic softening during earthquakes, thus cyclic simple shear tests are needed for seismic work on tailings, and these are discussed in more detail in Section 6.4.

6.2 *Accurate void ratio measurement*

Geotechnical laboratories are familiar with accurate measurement of stress and strain. However, the essence of CSSM is quantifying the effect of void ratio on that stress-strain behaviour, which requires accurate measurement of void ratio during laboratory triaxial testing. And this causes a problem as the standard procedures of most laboratories are inadequate for accurate void ratio measurement despite ISO 9000 accreditation. The problem is that samples densify during the saturation step and that densification is difficult to measure accurately. This issue of accurate void ratio measurement has plagued CSSM since the early work of Casagrande in 1935 until it was resolved in the mid 1980s during work in the Canadian Arctic.

The required technique for accurate void ratio measurement is to shut the drainage and pore pressure measurement lines on the specimen immediately shearing is terminated. The cell is then depressurized before moving the entire specimen at its end-of-test water content to a freezer. A few hours of freezing is sufficient to allow the specimen to be demounted from the test equipment which had to be frozen (mainly the platens) without loss of any water. The water content of the entire sample is then measured by standard oven drying, and converted to void ratio using the measured G_s (the void ratio is accurate, since the test procedure was to saturate the sample with back pressure at the start of the test).

The costs and effort of this freezing technique is minimal. It is simply a question of taking care to make sure it is done.

6.3 *Soil properties from laboratory tests*

The soil properties Γ, λ, M, N, χ are independent of any constitutive model but, on their own, will usually not be quite sufficient to capture soil behaviour. The missing property is some measure of plastic shear stiffness analogous to G_{max} for elasticity. The concept of plastic shear hardening may be common, but there is no agreed standard soil property for plastic modulus and each constitutive model generally defines its own property. The approach we use to determine plastic modulus from the triaxial testing is *Iterative Forward Modelling* (IFM) in which the soil behaviour in a test is computed using the chosen constitutive model and estimated properties, with the computed behaviour being visually compared to that measured. Then, the plastic hardening is revised to improve the fit and the process repeats until a good fit is obtained. This can all be done in Excel as any good model is readily programmed using the VBA environment that is included with Excel. The modelling also has the advantage of rapidly showing up questionable laboratory results as well as confirming the appropriate plastic hardening. The earlier Figure 4 was developed just this way.

In the case of the NorSand model, plastic hardening is represented by the dimensionless modulus H. This modulus is proportional to the plastic hardening of Cam Clay with $H \sim 1/(\lambda - \kappa)$. The IFM procedure generates the best-value of H for the entire test, and it is common to find an effect of ψ so that $H = a + b\psi$ where a, b become the true soil properties. It is also common to find that H scales with G_{max}/p, which is analogous to a constant λ/κ ratio often used in Cam Clay.

Table 2. Results of laboratory testing for CPTu interpretation and soil behaviour

	TCS sand	TCB silt
D_{50} (mm)	180	70
Fines (%)	22	51
Γ_1	0.914	0.713
λ_{10}	0.115	0.086
M_{tx}	1.45	1.44
χ_{tc}	3.5	3.5
N	0.2	0.2
H	50	140
G_{max}	50	32
S	160	160
n	0.65	0.65
v	0.25	0.25
H/I_r ($I_r = G/p'$)	0.74	3.22

Note: K_o = 0.7 assumed for calculation of mean effective stress

it is common to find an effect of ψ so that $H = a + b\psi$ where *a, b* become the true soil properties. It is also common to find that H scales with G_{max}/p, which is analogous to a constant λ/κ ratio often used in Cam Clay.

Table 2 shows a full set of properties measured on TCS sand and TCB silt materials identified from the CPTu sounding.

6.4 *Cyclic Resistance Curves*

A cyclic shear resistance curve is needed for a total stress analysis of seismic loading (whereas a pore pressure generation function is needed for an effective stress analysis, which is not covered here). For a cyclic resistance curve, the engineer needs data over the range of *in situ* states encountered for each identified material. This likely means at least two curves of cyclic shear stress ratio (τ/σ'_v) versus number of cycles to liquefaction (N_L). A liquefaction strength (stress ratio) can be picked for a number of cycles of loading from each curve to provide a "strength vs state" relationship.

Cyclic simple shear tests are preferred, as they are most representative of seismic loading. (If only cyclic triaxial testing is available, a reduction of about 0.65 on the cyclic shear stress ratio may be needed to "correct" for simple shear conditions.) Figure 15 shows cyclic resistance data for five tailings materials, including TCS sand, TCB silt and a couple of pure silts. The results cover a wide range of conditions, but interestingly fall within a rather narrow band, which at this stage is likely coincidental rather than a reliable trend.

The key to cyclic simple shear testing is to have tests at the *in situ* state, or at least to be able to adjust the cyclic resistance to the *in situ* state. We have been able to achieve something close to undisturbed simple shear specimens of tailings silts in Shelby tubes, including TCS sand and TCB silt data shown

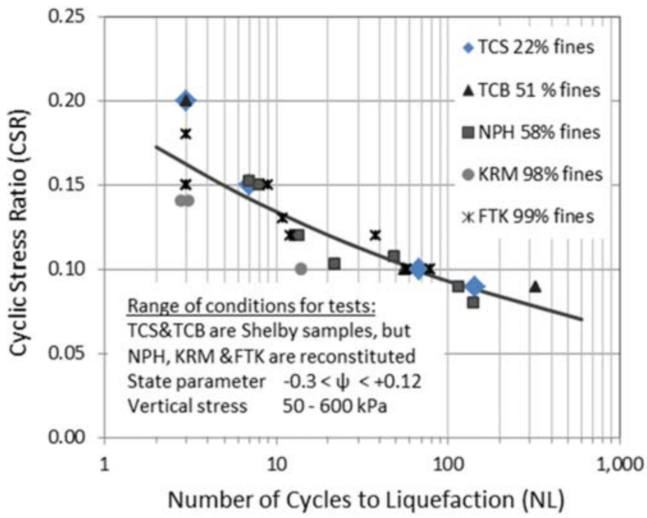

Figure 15: Cyclic resistance ratio in simple shear for tailings

on Figure 15. Once we get these samples into a laboratory, extruded and reconsolidated, we like to think we have a sample at the *in situ* state with a semblance of *in situ* fabric. However, the void ratio will likely be rather different, and we cannot assume the laboratory sample will be the same as *in situ*, because that would tend to overestimate the cyclic strength. We therefore have two options:

1. Do not try to obtain undisturbed samples, and produce strength curves from reconstituted samples at the correct range of *in situ* states. This will likely be a low estimate of the cyclic strength because field fabric would be lost.
2. Test the undisturbed samples consolidated back to the *in situ* stress level, but then make an adjustment to account for the post-sampling void ratio change.

In order to make the correction to the strength of the undisturbed sample, you need two pieces of information. First information is an estimate of the reduction in void ratio during sample handling and consolidation. The second piece of information is how much this void ratio reduction affects the value of ψ and how this change in ψ affects the cyclic resistance. The actual procedure used is not important, but it does need to be done.

The approach used for TCS sand and TCS silt is illustrated on Figure 16. We first used the available data to show CSR_{10} (τ/σ'_v at which liquefaction occurs in 10 cycles) variation with ψ. This needed cyclic triaxial data from earlier work, adjusted to simple shear conditions. Our simple shear tests on undisturbed samples were at ψ = -0.06 with CSR_{10} of 0.145. The characteristic *in situ* state to use for liquefaction is ψ = 0 (this is looser than the average *in situ*

ψ) so the adjusted CSR_{10} is 0.125, as illustrated on Figure 16.

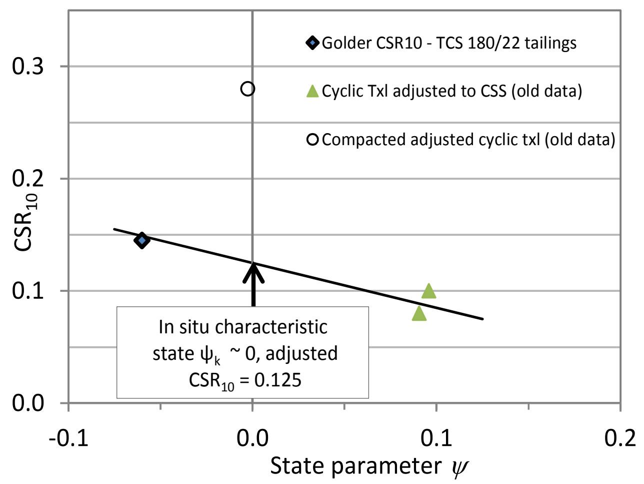

Figure 16: Correction to cyclic stress ratio for difference between state in laboratory tests and estimated characteristic in situ state.

7 ANALYSES

This paper is not about the analyses, except to make the point that the groundwork has been laid for whatever analyses you want to do. You have done a thorough investigation of the TSF, and based on the CPTu and index testing have a sound knowledge of how many different materials there are. Thereafter, you carried out a series of laboratory tests (mainly testing to determine the CSL and other properties) on each material type so that you can determine the *in situ* ψ of your key materials. You may also have measured the *in situ* G_{max} to enhance the CPTu analysis.

Once you have characterized the *in situ* ψ, your laboratory testing then focused on the engineering behaviour you need. This is generally the static strength and the cyclic resistance ratio curve, in simple shear, over the range of ψ (meaning density and stress level) expected *in situ*. One warning, though, is that you need to consider the effects of fabric and/or sample disturbance on your results. Supplementary approaches may include pore pressure models, shear modulus reduction and post-liquefaction settlements.

8 CLOSURE

The paper has briefly overviewed determining the *in situ* state of the TSF with a CPTu, recognizing that there is often more than one way to make the interpretation. We also need to think carefully how many material types there are for us to consider. Once we have the mechanical parameters for the TSF, in this case for two materials, we carry out the careful analyses for the whole facility. That includes the overall cyclic behaviour and stability of the existing and future geometries.

All of the above looks satisfactory. Yet, as an industry, we have seen three tailings dam failures in the last decade each with huge environmental and human consequences. The news media likes to portray these dam failures as careless (verging on negligent) management or shareholder greed. But, each of the three big failures had geotechnical engineers involved and at least two of the three had engineering review. How is a mine manager supposed to know who is competent? Each firm proposing on a TSF design or assessment will claim to be “world class”. The problem is not the mine manager or shareholders. The problem is the standard of engineering.

An issue is the continued propagation of ideas based on “fines content corrections”. It should be self-evident that fines content is nonsense when dealing with tailings, as pretty much every TSF will have fines content higher than found in research sand, and many of the tailings may comprise just fines. The properties used for engineering could be entirely “the correction” rather than “the data”. Further, it will become quickly apparent when tailings are tested, as illustrated with the example of this paper, that mechanical properties do not correlate well with “fines”. No such trouble exists at all if the tailings behaviour is viewed within the framework of CSSM. The CSLs are measurable, other properties are familiar, and the details of the stress-strain behaviour can be modelled in a spreadsheet. The required *in situ* ψ can be reliably computed from CPTu data. All the aspects for sound engineering exist.

We have already drawn attention to the parallels of Fundao with the concerns of the Corps of Engineers eighty years earlier. It is the lack of teaching of critical state concepts to geotechnical engineers and application of rigorous mechanical approaches that has caused this problem. If you look at the Wikipedia critique of CSSM you will find the statement “Prof. Alan Bishop at Imperial College used to routinely demonstrate the inability of these theories to match the stress-strain curves of real soils”. This is a true statement, but what is not stated is that Bishop brought Prof. Peter Wroth to Imperial College to ensure each M.Sc. course gained a thorough grounding in the principles of CSSM. Bishop was well-aware that CSSM was the only coherent framework for soil behaviour (and indeed CSSM is based on work at Imperial College as much as Cambridge and elsewhere). The objections summarized on Wikipedia reflect 1975 and they have since faded into the background, as can be seen by the excellent match of critical state theory to the spectrum of real soil shown on Figure 4.

What remains a concern is that the situation stated in Wikipedia probably does reflect current geo-technical teaching attitudes in North America and elsewhere. It is why instances such as Fundao will continue to occur. On the bright side, Hugh Golder, who was one of the founders of *Geotechnique,* instilled strong values of sharing within Golder Associates. The Golder Foundation has been established to reach outside the company as well. We make our data and models freely available under the GNU Open Software license. Do visit *www.golderfoundation.org/* and then do get up to speed with CSSM. Of course reading "Soil Liquefaction: a critical state approach" may also help.

9 ACKNOWLEDGEMENT

Mike Jefferies has been a tremendous help in pulling this paper together with me. Many of our colleagues at Golder Associates have used Mike and my brain waves on CSSM, the state parameter and tailings behaviour over the years. The engineers we have worked with, and who have contributed significantly in their own right, are too numerous to recognize individually but I acknowledgement all their input. David Reid specifically has carried out good research on the issues and provided input and review of this paper.

10 REFERENCES

Been, K. & Jefferies, M.G. (1985). A state parameter for sands. *Géotechnique*, 35, 2, 99-112.

Been, K, Crooks, J.H.A., Becker, D.E & Jefferies M.G. (1986). The cone penetration test in sands: Part 1, State parameter interpretation. *Géotechnique*, 36, 2, 239-249.

Been K., Jefferies M.G., Crooks J.H.A. & Rothenberg L. (1987). The cone penetration test in sands: Part II, general inference of state. *Géotechnique*, 37, 3, 285-299.

Been K., Crooks J.H.A. & Jefferies M.G. (1988). Interpretation of material state from CPT in sands and clays. Proc. Conf. *Penetration Testing*, 215-218. ISBN 0 7277 1377 9, pbl Thomas Telford.

Been, K., Jefferies, M.G. & Hachey, J.E. (1991). The critical state of sands. *Géotechnique*, 41, 3, 365-381.

Been, K, Romero, S., Obermeyer, J and Hebeler, G. (2012). Determining the in situ state of silt and sand tailings with the CPT. Proc. Tailings and Mine Waste '12, 14–17 October, Keystone, Co., USA. pp. 325-333

Bolton, M.D., Gui, M. W., Garnier, J., Corte, J. F., Bagge, G., Laue, J. & Renzi, R. (1999). Centrifuge cone penetration tests in sand. *Geotechnique*, 49, 4, 543-552.

Damavandi-Monfared, S. & Sadrekarimi, A. (2015). Development of a miniature cone penetrometer for calibration chamber testing. *Geotechnical Testing Journal*, 38, 6, 878-892.

Drucker, D.C., Gibson, R.E. & Henkel, D.J. (1957). Soil mechanics and work hardening theories of plasticity. *Transactions American Society of Civil Engineers*, 122, 338-346.

Houlsby, G.T. (1988). Session Leader's Introduction, *Proc. Conference on Penetration Testing in the U.K.*, Birmingham, Thomas Telford, 141-146.

Jefferies, M.G. (1993). NorSand: a simple critical state model for sand. *Géotechnique* 43, 91-103.

Jefferies, M.G. & D.A. Shuttle (2005). NorSand: features, calibration and use. *ASCE Geotechnical Special Publication No. 128, Soil Constitutive Models: Evaluation, Selection, and Calibration*, 204-236, eds. J.A. Yamamuro and V.N. Kaliakin.

Jefferies, M. & Been, K. (2015). *Soil liquefaction: a critical state approach*, 2nd ed. CRC Press.

Manzari, M.T., & Dafalias, Y.F. (1997). A critical state two-surface plasticity model for sands. *Géotechnique* 47, 255-272.

Mohajeri, M. & Ghafghazi, M. (2012). Ground sampling and laboratory testing on low plasticity clays. Proc. 15th World Conference on Earthquake Engineering, Lisbon.

Plewes H.D., Davies M.P., & Jefferies M.G. (1992). CPT based screening procedure for evaluating liquefaction susceptibility. *Proc 45th Canadian Geotechnical Conference*, Toronto.

Peuchen, J, Vanden Berghe, J.F, & Coulais, C. (2010). Estimation of u1/u2 conversion factor for piezocone. *CPT'10, 2nd International Symposium on Cone Penetration Testing*, Paper 1-03.

Reid, D. (2015). Estimating slope of critical state line from cone penetration test – an update. *Canadian Geotechnical Journal*, 52, 46 - 57

Robertson, P.K. (2008). Discussion: Liquefaction potential of silts from CPTu. *Canadian Geotechnical Journal*, 45, 1, 140-141.

Robertson, P.K. (2009). Interpretation of cone penetration tests – a unified approach. *Canadian Geotechnical Journal*, 46, 1337-1355

Robertson, P.K. (2010). Evaluation of flow liquefaction and liquefied strength using the cone penetration test. *Journal of Geotechnical and Geoenvironmental Engineering*, *ASCE*, 136, 6, 842-853.

Robertson, P.K. (2012). Evaluating flow (static) liquefaction using the CPT: an update. *Proceedings Tailings and Mine Waste '12*, 14–17 October, Keystone, Co., USA.

Schofield, A. & Wroth, C.P. (1968). *Critical State Soil Mechanics*. London, McGraw-Hill.

Shuttle, D.A., and Jefferies, M.G (1998). Dimensionless and unbiased CPT interpretation in sand. *International Journal of Numerical and Analytical Methods in Geomechanics*, 22, 351-391.

Shuttle, D.A. & Cunning, J. (2007). Liquefaction Potential of Silts from CPTu. *Canadian Geotechnical Journal,* 44, 1, 1-19.

Shuttle, D.A. & Cunning, J. (2008). Reply to discussion: Liquefaction Potential of Silts from CPTu. *Canadian Geotechnical Journal,* 45, 1, 142-145.

Sladen, J.A. (1989). Problems with interpretation of sand state from cone penetration test. *Géotechnique*, 39, 2, 323-332.

Geotechnical and Geophysical Site Characterisation 5 – Lehane, Acosta-Martínez & Kelly (Eds)
 ISBN 978-0-9946261-1-0

New tools and directions in offshore site investigation

M.F. Randolph
Centre for Offshore Foundation Systems, The University of Western Australia

ABSTRACT: The offshore environment provides a number of challenges for geotechnical site investigation, among which are the high costs associated with vessel day-rates and an associated need for equipment reliability. New oil and gas developments are increasingly remote, in terms of distance from land and water depths, and seabed conditions often comprise extremely soft sediments within the depth range relevant for infrastructure such as pipelines, subsea foundations and anchoring systems. These factors have combined to provide a gradual shift away from ship-based drilling tools towards seabed-based robotic equipment for drilling, sampling and in situ penetrometer testing. In parallel, a variety of free-fall samplers and penetrometers have been developed, particularly for preliminary investigations to characterise the seabed sediments. An important aspect of the soil response is the extent to which it may be considered drained or undrained during particular operational events. For example, design calculations for the stability and operational movements of pipelines are relatively sensitive to the consolidation response of the soil. Even interpretation of penetrometer data requires an assumption with respect to the degree of consolidation occurring during penetration. The paper provides an overview of recent developments in offshore site investigation equipment, and then focuses on evaluation of consolidation properties.

1 INTRODUCTION

Over the last couple of decades there have been major advances in robotic seabed-based geotechnical site investigation tool, driven partly by the high day-rate costs of traditional site investigation vessels and also by the need for greater control and hence quality of seabed sampling or penetrometer data. In moderate water depths and beyond, seabed sediments may be relatively low strength, for example lightly overconsolidated clays or fine grained carbonate silts, particularly in the depth zones of interest for the design of pipelines, subsea foundations and even certain types of anchor. In soft sediments, free-fall piston samplers and penetrometers offer an alternative low-cost approach, especially during the early stages of a project, allowing geophysical data to be ‘ground-truthed’ by means of physical samples and quantitative penetrometer data.

The sophistication and required robustness of modern offshore site investigation equipment demand significant investment in order to take conceptual ideas through to implementation. The offshore environment is much harsher than in a laboratory or even typical onshore site conditions and as much attention may need to be paid to launch and recovery systems as to the equipment itself. The scientific benefits of a given tool must be balanced against development costs relative to the expected pay-back period, and the potential to persuade operators to adopt the technology. It is necessary to consider the performance of the equipment, or methods of interpretation, in complex layered seabed conditions in addition to more idealised single layer profiles. Maximum advantage can be gained from small lightweight devices that can provide relatively undisturbed samples or data of reasonable accuracy early in a project.

Operational conditions offshore encompass significant components of cyclic or periodic loading, generally at time scales that lead to undrained response in the short term, with consequential softening and pore pressure generation, but with continuous consolidation occurring over a longer time scale. Accurate assessment of the consolidation characteristics of seabed sediments is therefore important within the design process. In the calcareous silts and sands that predominate off the coast of Australia (among many other sub-equatorial regions of the world), penetrometer testing may well occur under partially consolidated conditions. Interpretation of penetrometer data must then take account of the degree of partial consolation, with appropriate adjustments made in order to assess equivalent undrained penetration resistance and shear strengths. Measurement of the consolidation coefficient from dissipation tests may also be affected by partial consolidation occurring during the penetration phase.

The paper summarise some recent developments in offshore site investigation, and also methods to assess consolidation properties from different in situ tests. New tools to explore very shallow seabed properties for pipeline design are also introduced; these are in the process of development as part of a current joint industry project.

2 SEABED-BASED DRILLUNG AND IN SITU TESTING

Modern advances in robotic control have been exploited in full measure in a number of commercial seabed-based robotic drilling, sampling and testing systems. The pioneer amongst these was the portable remotely operated drill (PROD), developed by Benthic Geotech. Figure shows the second generation device. The landing legs close up to allow the equipment to fit within a standard shipping container for transport. A purpose-designed launch and recovery system allows efficient and safe operation offshore. A full-length electrical umbilical cable provides power, with operational water depths of up to 3000 m. The specification allows drilling and 75 mm diameter sample recovery, or alternatively cone or ball penetration testing, to a depth of 125 mm below the seabed, gradually extending the drill or cone rods to reach successive depths.

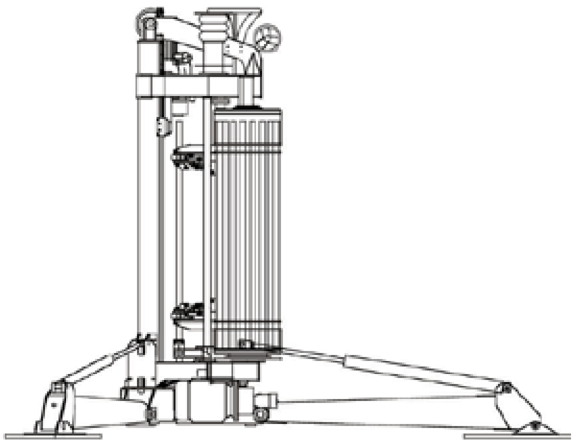

(a)

(b)

Figure 1. Portable remotely operated drill (PROD - Benthic Geotech) (a)Schematic with landing legs extended (b) During land-based trials

(a)

(b)

Figure 2. Seabed-based robotic drilling and sampling equipment from Fugro and Canyon-Geomarine (a) Fugro Seafloor Drill and (b) Canyon-Geomarine ROVDrill

Two other seabed-based drills are shown in Figure 2, both of which are designed to be powered through standard work-class remotely operated vehicles (ROVs). By contrast with PROD, the Fugro Seafloor Drill uses wireline tools, allowing more efficient sampling and penetrometer testing at increasing depths below the seabed. Specifications include water depths of up to 4000 m, sampling (73 mm diameter) and penetrometer testing to 150 m below the seabed or alternatively penetrometer testing directly from the seabed down to 30 m depth. The smaller ROVDrill (Figure 2b) allows sampling and penetrometer testing to 40 m below the seabed, or rock-coring to 20 m depth.

(a)

(b)

Figure 3. Equipment for near seabed investigation (a) Fugro Smartsurf seabed unit and (b) Varieties of penetrometers

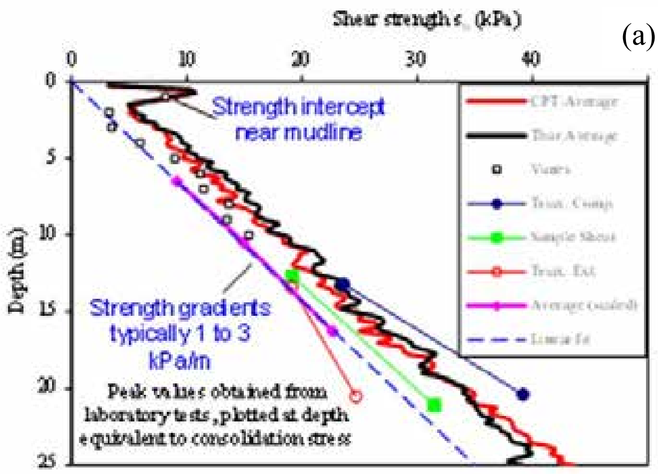

(a)

Figure 4a Strength profiles in deep water sediments at two different scales: general profile in upper 25 m

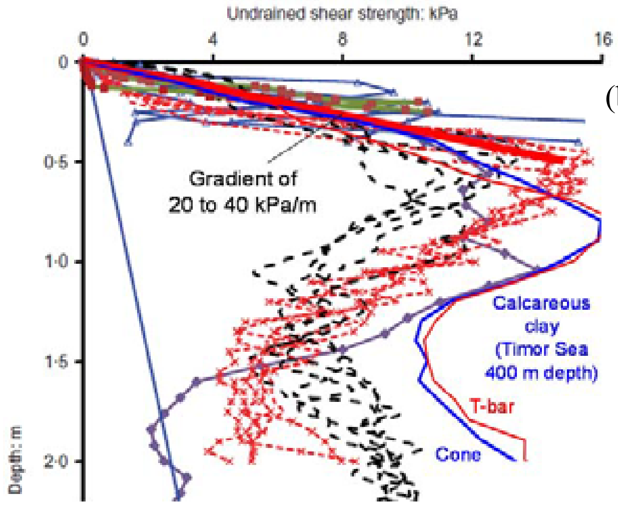

(b)

Figure 4b Strength profiles in deep water sediments at two different scales: near seabed strength profiles

Deep water sediments are generally fine grained and lightly overconsolidated due to aging processes. The low near-surface strengths require lightweight equipment (to minimise selfweight penetration) and accurate penetrometer tools. For very shallow depths, units such as the Fugro Smartsurf (Figure 3a) offer capabilities of taking samples of up to 2 m length, or carrying out penetrometer testing to 3 m depth. Often, penetrometers with greater cross-sectional area than a standard 10 cm^2 cone are used, in particular full-flow penetrometers such as T-bar or balls that have projected areas an order of magnitude greater than that of the shaft (Figure 4b).

Over a depth scale of 20 to 30 m, the shear strength profile may increase essentially proportionally with depth, with strength gradients ranging from as low as 1 kPa/m in high liquidity index clays, to around 3 kPa/m in fine-grained carbonate material. As shown in Figure 4, however, the strength profile very close to the surface can exhibit a form of crust. The majority of the data in Figure 4b are from offshore West Africa (assembled by DeJong et al., 2013), but interestingly a strength profile in calcareous 'clay' from the Timor Sea off the north coast of Australia shows a similar feature. From a design perspective for risers or pipelines, the very high strength gradients of 20 to 40 kPa/m are an important consideration, as is the potentially high sensitivity of the sediments forming the crust. Detailed studies of the nature of these sediments have been undertaken by Kuo and Bolton (2013), who identified the presence of a high proportion of faecal pellets from invertebrate worms living in the benthic zone. The sensitivity of such material can be quantified in situ using cyclic penetration and extraction of T-bar and ball penetrometers.

3 FREE-FALL SAMPLING AND PENETRATION TESTING

Free-fall approaches for piston sampling or penetration testing inevitably offer less control than static pushes from a fixed base. However, the significant savings in set-up and execution times are a strong incentive, trading off a measure of quality (of samples or interpreted strength data) for the much lower costs. Favourable site conditions are necessary, since sand layers will tend to give very high dynamic penetration resistance. However, modern equipment has demonstrated potential to retrieve large diameter (e.g. ~100 mm) piston cores of up to 30 m length in soft clays.

The basic technology of a free-fall piston sampler was established by Kullenberg in the 1940s, but recent advances have led to highly efficient containerized equipment, with much improved control on triggering of the piston (Figure 5). The piston-corer and associated triggering system is lowered to close to the seabed before releasing the entire unit. A key consideration is accurate detection of the seabed, so that the internal piston within the sampler is 'locked' in absolute position at the right moment. Early or later triggering would either reduced the length of the recovered sample, or cause the sampler to plunge through the upper 1 or 2 m of the seabed before soil starts to enter.

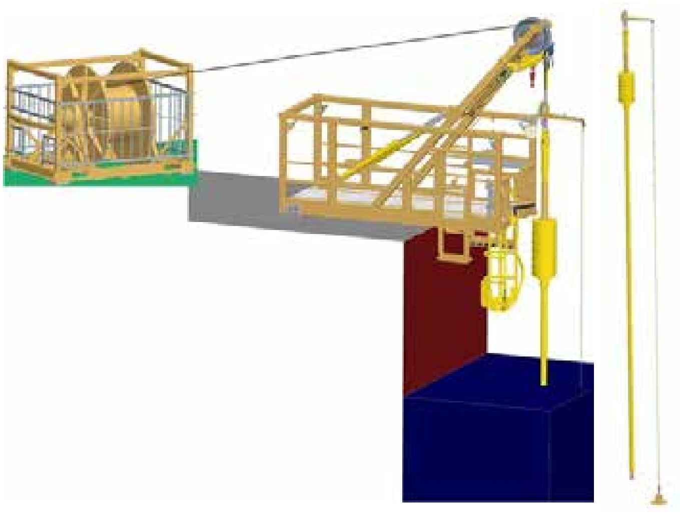

Figure 5 Self-contained launch and recovery system with Kullenberg-style free-fall piston sampler (courtesy Fugro)

Free-fall penetrometers have also had wide application for assessing shallow seabed conditions, at least semi-quantitatively. Early instruments merely recorded the acceleration-time history, enabling a simple assessment of soil resistance as a function of penetration depth. However, advances in miniaturised electronics, such as miniature MEMS accelerometers and on-board signal conditioning and acquisition, now allow fully instrumented piezocones to obtain much more reliable data.

Field and model scale devices are shown in Figure 6. Interpretation of data is aimed at deducing equivalent 'static' values of penetration resistance, ideally including tip resistance, sleeve friction and (excess) pore pressure. That requires correction of the dynamic data to eliminate the effects of the much higher strain rates that occur during dynamic penetration compared with static penetration. The importance of measuring the tip resistance directly has been underlined by increasing evidence of the much greater strain rate corrections required for the shaft friction than for the tip resistance (Steiner et al., 2014; Chow et al., 2014, 2016).

Uncorrected data from recent centrifuge model tests of a free-fall piezocone penetrometer are shown in Figure 7, comparing the tip resistance and sleeve friction with equivalent data from static penetration tests. The data are taken from a recently submitted paper (Chow et al., 2016) and form part of the work being conducted for the RIGSS (Remote intelligent geotechnical seabed surveys) JIP. While the dynamic tip resistance is 20 to 50 % greater than the static tip resistance, the dynamic sleeve friction is 2 or 3 times the equivalent static values.

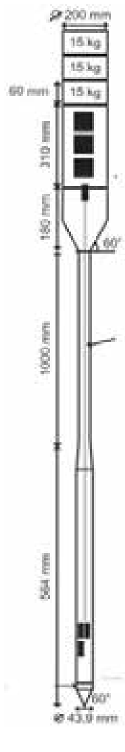

(a)

(b)

Figure 6. Free-fall cone penetrometers (a) Field scale (Stegmann et al., 2006), *(b)* Centrifuge model scale (Chow et al., 2014)

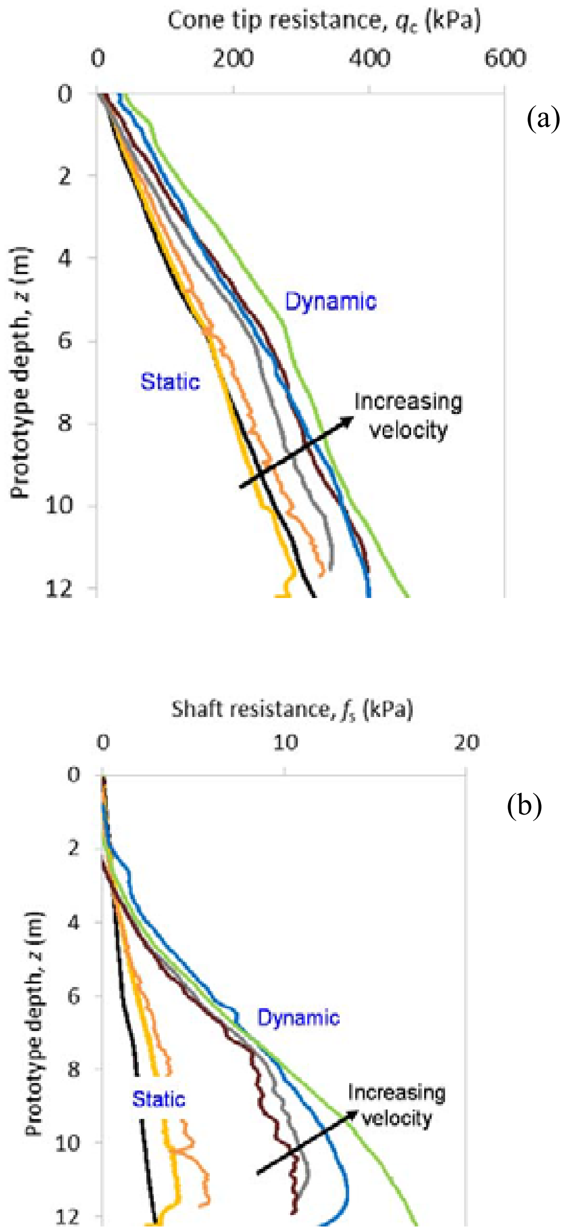

Figure 7 Comparison of uncorrected static and dynamic penetration resistance (Chow et al., 2016), (a) Tip resistance and (b) Friction sleeve resistance

The form of rate correction may be expressed (using a power law) as

$$\mathrm{Q}_{corrected} = \frac{Q_{dynamic}}{\mathrm{R}_f} = \left(\frac{\dot{\gamma}_{ref}}{\dot{\gamma}}\right)^{\beta} Q_{dynamic}$$
$$= \left(\frac{(v/D)_{ref}}{v/D}\right)^{\beta} Q_{dynamic} \tag{1}$$

where Q is a relevant measurement, such as tip resistance, $\dot{\gamma}$ is the shear strain rate and R_f the rate correction. In absolute terms, the operational shear strain rates affecting the tip resistance have been shown to be of the same order of magnitude as the ratio of penetration velocity, v, to the device diameter, D, hence

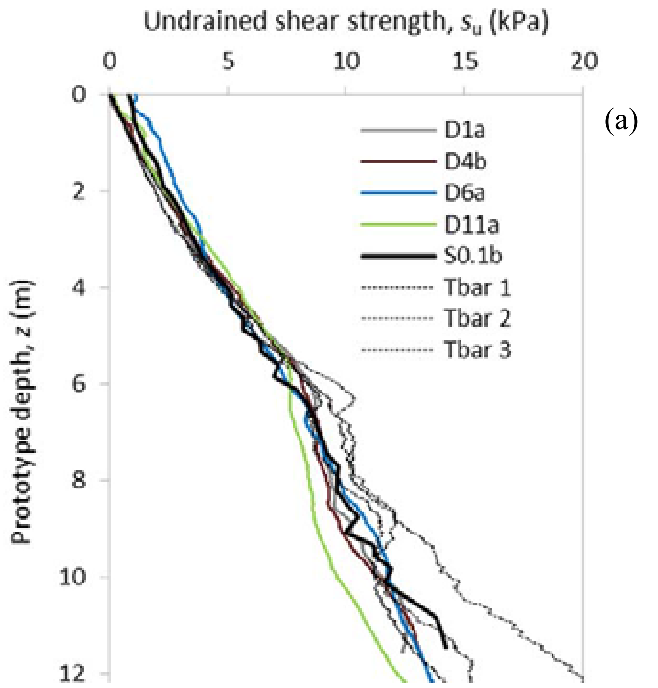

Figure 8a Comparison of uncorrected static and dynamic penetration resistance (Chow et al., 2016): Static and rate-corrected dynamic tip resistance

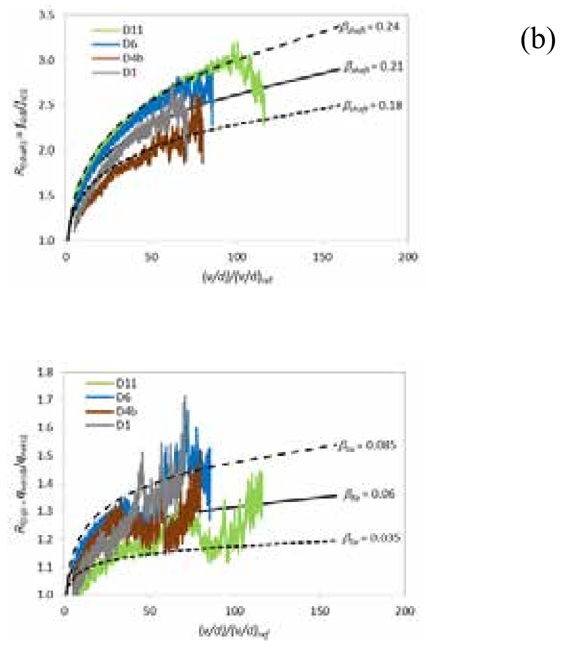

Figure 8b Comparison of uncorrected static and dynamic penetration resistance (Chow et al., 2016): Tip (upper) and shaft (lower) rate correction

allowing the substitution in the final form of the equation. While the relevant shear strain rates around the shaft are more than an order of magnitude greater than v/D (Einav and Randolph, 2006), the strain rates relative to those at the reference (i.e. static) penetration rate would be expected to be in the same ratio for tip and shaft. However, it is clear from the data that a much greater correction for rate effects is necessary for the shaft friction than for the tip resistance. Figure 8 illustrates this, showing corrected profiles of tip resistance (obtained using β = 0.85), and ranges of rate correction factors required to match 'static' values for tip and shaft. The range of β values is 0.035 to 0.085 for the tip resistance, but 0.18 to 0.24 for the sleeve friction. Reasons for this difference are yet to be determined and indeed are an area of active research, with application not only to the interpretation of free-fall penetrometer data, but also for accurate prediction of embedment depths (and hence capacity) for gravity-installed offshore anchors such as torpedo anchors or Delmar's OmniMax anchor.

An exciting new development in free-fall technology is the idea of combining dynamic penetration in the upper seabed sediments, with a static cone penetration to greater depth. The concept was pioneered by TDI-Brooks with their CPT Stinger (see Figure 9a), with similar equipment now available in the form of Fugro's SeaDart. The operating sequence for these devices comprises:

a) Lowering through the water until the penetrometer tip is in the vicinity of the seabed, with the cone in 'retracted' position, protruding 1 m or so beyond the barrel of the instrument.
b) Triggering of the release mechanism using a Kullenberg sensor weight, just as for a free-fall piston sampler.
c) Dynamic penetration into the seabed, acquiring relevant data (accelerometer, inclination, and all usual CPT data) at high sampling rates.
d) Static penetration of the cone to the limit of the hydraulic jacking system contained within the barrel.
e) Retrieval back to deck.

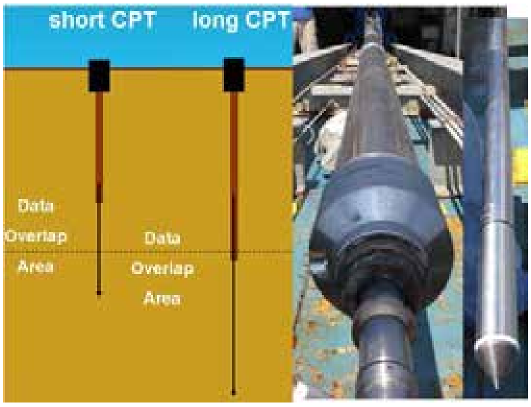

(a)

Figure 9a CPT Stinger developed by TDI-Brooks (Young et al., 2011): Concept and actual field device

The combination of both dynamic and static cone penetration allows calibration of the dynamic rate effects. Using two different configurations, with short and long barrels or alternatively by varying the instrument weight to achieve different dynamic penetrations, it is possible to achieve overlap of the dynamic and static zones, as illustrated in Figure 9b. In soft clays, overall penetration depths of up to 50 m are achievable.

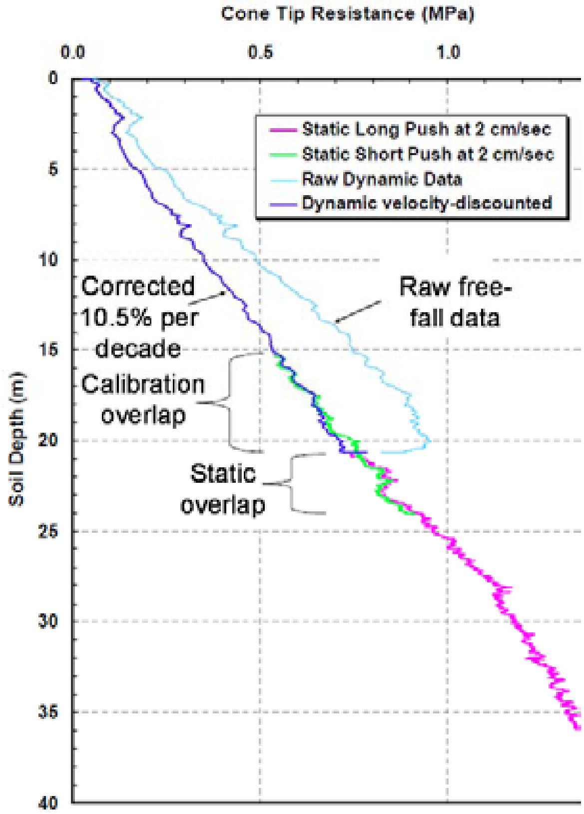

(b)

Figure 9b. CPT Stinger developed by TDI-Brooks (Young et al., 2011): Example data showing overlaps for calibration

4 EVALUATING CONSOLIDATION PROPETIES

The consolidation properties of seabed sediments have an important influence in design calculations and yet are extremely difficult to quantify accurately. Typically field and laboratory data may span two or three orders of magnitude, with laboratory oedometer tests generally giving values that are significantly higher than those from field dissipation testing. In many stratigraphies, though, natural layering of sediments compounds the degree of scatter.

The coefficient of consolidation is not an intrinsic soil property but proportional to the product of appropriate values of stiffness (associated with either reloading or normal compression) and permeability (vertical, horizontal or a combination). Although it has become customary to use nomenclature c_v for consolidation coefficients from laboratory oedometer testing and c_h for those from field dissipation tests, the subscript 'h' for the latter should not be associated with purely horizontal drainage. Recent numerical studies have demonstrated that, even for isotropic permeability, c_h from a piezocone dissipation test is some 3 to 5 times an equivalent c_v from oedometric normal compression.

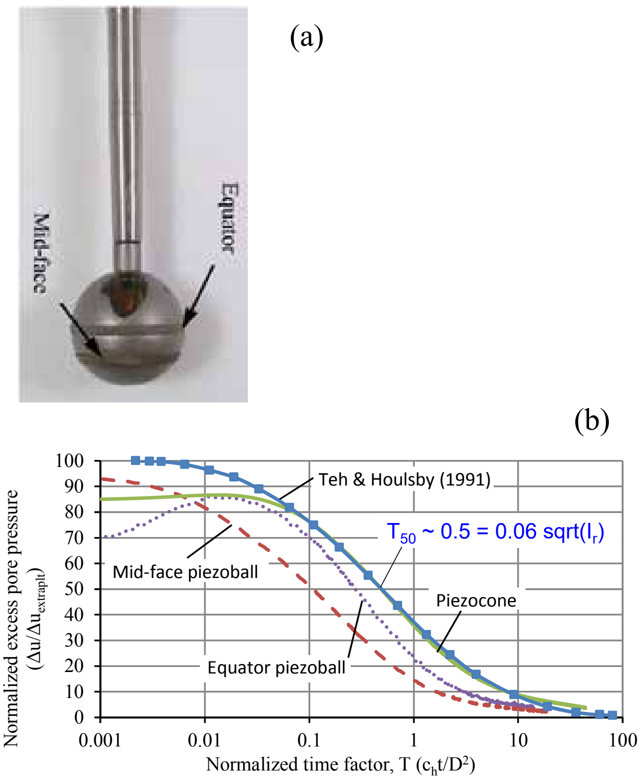

Figure 10. Model dual filter piezoball and comparative dissipation curves from piezocone and piezoball (a) model scale piezoball and b) normalised dissipation curves

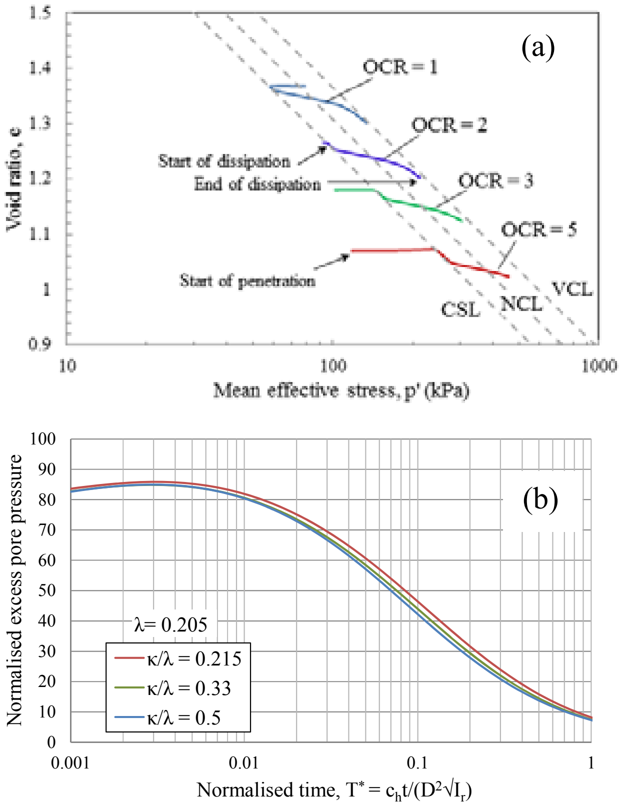

Figure 11. Numerical modelling of piezocone dissipation responses (Mahmoodzadeh et al., 2014), (a) Paths in e-p' space during consolidation (b) Effect of κ/λ ratio (isotropic permeability).

Recent numerical and experimental research on piezocone and piezoball have provided a framework to link c_v and c_h, separating out the effects of differences in (a) stiffness, and (b) operational permeability, between field dissipation tests and oedometric response for normally or lightly over-consolidated clays (Mahmoodzadeh and Randolph, 2014; Mahmoodzadeh et al. 2014). Modern ball penetrometers accommodate two different locations for pore pressure measurement, one (equator) at the largest horizontal cross-section of the ball and the other (mid-face) midway between the equator and the tip. At model scale, full annular filters are used (Figure 10a, Colreavy et al., 2016a), while at field scale button filters are used (Colreavy et al., 2016b). Interestingly, as shown in Figure 10b, both normalized and absolute dissipation times for the mid-face piezoball position are shorter than for the piezocone.

Figures 11 and 12 show results from finite element modelling, using a Modified Cam Clay soil model based on kaolin properties (Mahmoodzadeh et al., 2014). The paths followed in void ratio-mean effective stress space during dissipation are much closer to reloading (κ) gradients than normally consolidated (λ) gradients. Artificially varying input values of κ and λ allowed synthesis of the dissipation curves (for isotropic permeability) by using a stiffness based on a weighted geometric mean of $\kappa^{0.75}\lambda^{0.25}$. This allows the dissipation coefficient of consolidation to be expressed as:

$$c_h = \frac{\beta k_v}{\gamma_w}\frac{(1+e)p'}{\kappa^{0.75}\lambda^{0.25}} = \beta\frac{3(1-\nu)}{(1+\nu)}\left(\frac{\lambda}{\kappa}\right)^{0.75} c_v \quad (2)$$

where β quantifies the operational permeability as a ratio of the vertical permeability. For the piezocone, the best synthesis of analyses with different k_h/k_v ratios was for a 2:1 weighting between horizontal (k_h) and vertical (k_v) permeabilities (Figure 12). For the mid-face piezoball, the corresponding weighting is 1:1 (so $\beta = (k_h/k_v + 1)/2$).

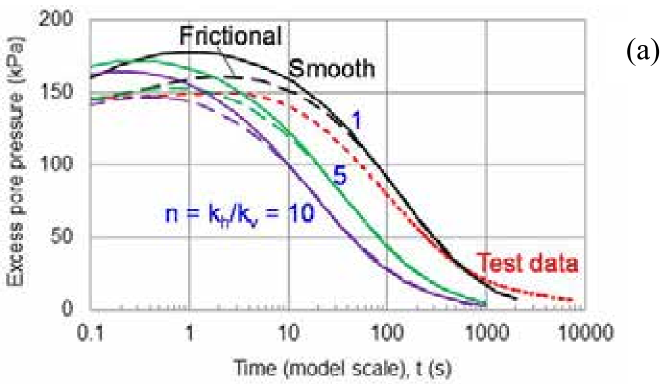

Figure 12a. Effect of permeability anisotropy on piezocone dissipation: Experimental and LDFE raw data

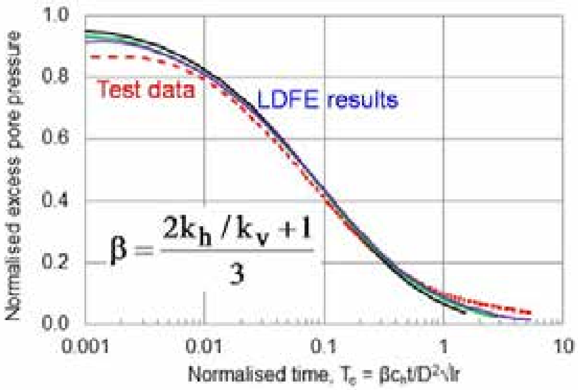

Figure 12b. Effect of permeability anisotropy on piezocone dissipation: Normalised responses

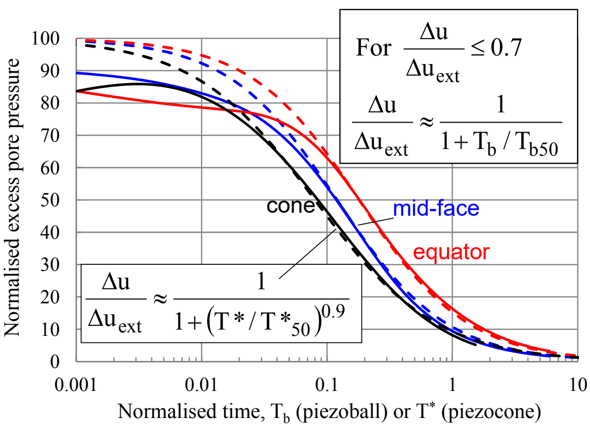

(b)

$$c_h = \beta \frac{3(1-\nu)}{(1+\nu)} \left(\frac{\lambda}{\kappa}\right)^{0.75} c_v$$

$$T_b = \frac{c_h t}{D_{ball} d_{shaft} I_r^{0.25}}$$

$$T^* = \frac{c_h t}{D_c^2 I_r^{0.5}}$$

Figure 13. Generalised relationships for piezocone and piezoball dissipation responses (Mahmoodzadeh et al., 2015), (a) LDFE and fitted dissipation curves, (b) Relationships

Values of normalised times for a given degree of dissipation from piezocone tests have been found to be proportional to the square root of the rigidity index I_r (Teh and Houlsby, 1991). For the piezoball, it recommended to normalise dissipation times by the geometric mean of shaft (d_{shaft}) and ball (D_{ball}) diameters, with the dependency on the rigidity index reduced to the power of 1/4. Figure 13 shows normalised dissipation responses for piezocone and piezoball dissipation, together with the relevant relationships. For typical cone and ball diameters of 36 mm and 60 mm respectively, and assuming a 20 mm diameter shaft in the vicinity of the ball attachment, absolute 50 % dissipation times t_{50} for the piezoball mid-face position is approximately half that for the piezocone (Mahmoodzadeh et al., 2015).

4.1 *Effects of partial consolidation*

In intermediate 'silty' sediments, for example the calcareous silts encountered offshore Australia, field penetrometer tests may occur under partially consolidated conditions, resulting increased penetration resistance and reduced excess pore pressures compared with fully undrained penetration. By contrast, operational response such as spudcan penetration or environmental loading transmitted to an anchor will generally be fully undrained. Such differences need to be taken into account in design calculations, as also do potential differences due to rate effects (Erbrich, 2005).

A first priority is assessment of the coefficient of consolidation, in order to evaluate whether a penetrometer test occurs under drained ($vD/c_h < 0.1$), undrained ($vD/c_h > 10$) or partially drained conditions. Dissipation tests are an obvious solution, although care is needed since partial drainage during penetration may alter the form of the dissipation response, potentially increasing T_{50} times (DeJong and Randolph, 2012). To explore the effect of cone penetration under partially consolidated conditions, centrifuge model tests were carried out in kaolin at different penetration rates, hence gradually reducing vD/c_h values (Colreavy et al., 2016a). The dissipation responses are shown in Figure 14. The maximum excess pore pressures reduce with decreasing penetration rate, with a gradually increasing delay in the time at which the maximum pore pressure is reached. When normalised by an extrapolated excess pore pressure corresponding to zero time (using a root time plot), the normalised decay curves shows a similar pattern. For values of vD/c_h greater than about 1 (which corresponds approximately to a penetration rate mid-way between undrained and drained conditions) there is no appreciable effect on the time scale of pore pressure dissipation, e.g. in respect of T^*_{50} values. However, for slower penetration rates the T^*_{50} values increase significantly, eventually by a factor between 2 and 3.

Once the likely degree of partial consolidation has been established, it is useful to be able to adjust the cone resistance to a corresponding 'undrained' value from which to deduce an undrained shear strength for design. In addition to the effects of partial consolidation, the cone resistance will also be affected by penetration rate due to viscous effects. Figure 15 shows theoretical curves that combine the effects of partial consolidation (first part of the relationship shown) and strain rate effects (second part of the relationship

– also shown as the dashed curves). The strain rate effect has been modelled using a Herschel-Bulkley approach, with t_{ref} representing a reference time; alternatively, a reference velocity v_{ref} may be used, for example representing the velocity for which penetration of one diameter occurs in time t_{ref}. The curves are for $q_{drained}/q_{u,ref} = 4$, $V'_{50} = 1$, $c = 1.2$, $\mu = 0.5$ and $\beta = 0.12$. The lowest two curves might represent those relevant for a standard piezocone (or piezoball) test in a soft clay with $c_h \sim 3$ to $30\ m^2/yr$. Interestingly, for c_h of $3000\ m^2yr$ or higher, the minimum penetration resistance remains above the notional reference undrained value.

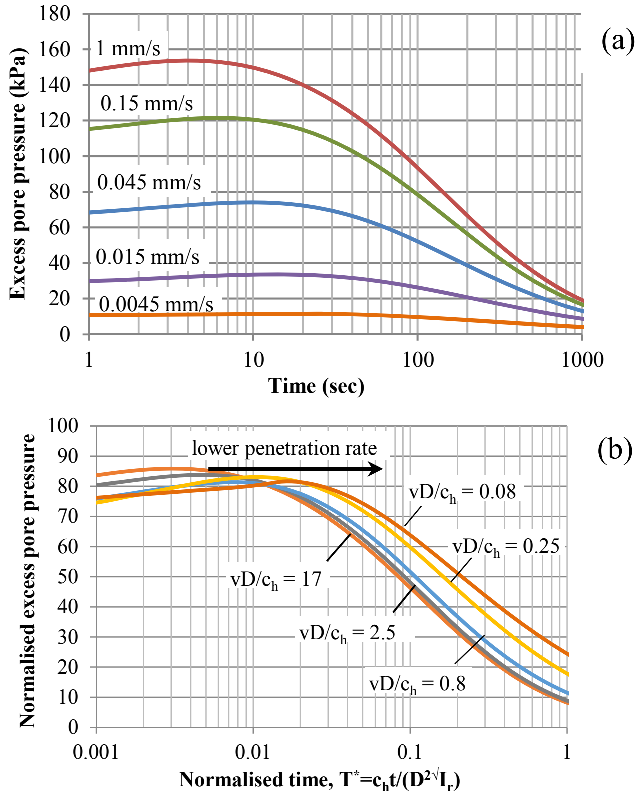

Figure 14. Effect of permeability anisotropy on piezocone dissipation (a) Experimental and LDFE raw data and (b) Normalised responses

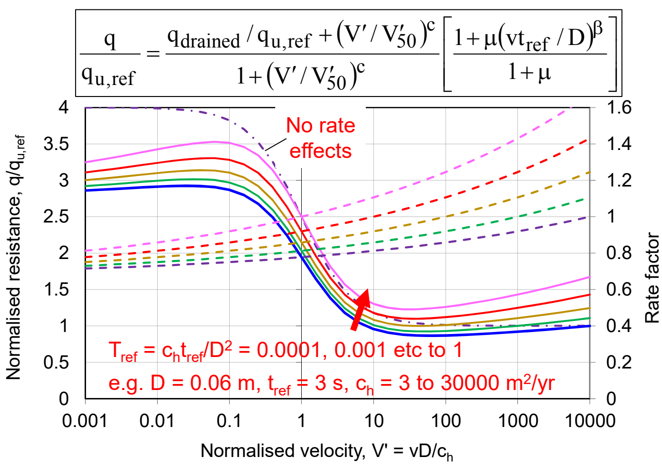

Figure 15. Modelling combined effects on penetration resistance of partial consolidation and strain rate effects

5 NOVEL TOOLS FOR QUANTIFYING PIPELINE-SOIL AXIAL FRICTION

A current joint industry project (RIGSS JIP), based at the Centre for Offshore Foundation Systems at the University of Western Australia, and led by Professor David White, is developing novel tools for exploring the near-surface properties of seabed sediments. A primary focus has been to improve methods to quantify the time-dependency of pipeline-soil interface friction. Consolidation of the soil immediately beneath a pipeline can change the interface friction by a factor of 3 or more, and that can have significant repercussions for design against lateral buckling and pipeline walking (Carr et al., 2003). As noted by Randolph et al. (2012), monotonic axial displacement of a pipe partially embedded in the seabed at different rates leads to a similar S-shaped variation of resistance from undrained (low friction) at high velocities to drained (high friction) at low velocities. Equally, if the pipe is displaced sufficiently far, for example in excess of 1 diameter, even relatively high velocities will eventually give rise to high friction as consolidation proceeds.

Cycles of forward and backward motion of the pipe, especially with intervening periods for consolidation such as would occur during normal operating conditions, will show similar trends of gradually increasing interface friction (Figure 16, after Smith and White, 2014). Novel torsional penetrometers are being developed as part of the RIGSS JIP in order to quantify time dependent pipe-soil axial friction. The penetrometers (see Figure 17) allow assessment of the shallow seabed strength during penetration, and then monotonic and cyclic torsional tests conducted under constant vertical load provide data on interface friction. Devices in the shape of a toroid or hemi-ball have been fabricated, aimed at testing either in box-cores, or directly on the seabed. Data from torsional tests carried out in a simulated box-core are shown in Figure 18, together with predictive models that are under development as part of the JIP.

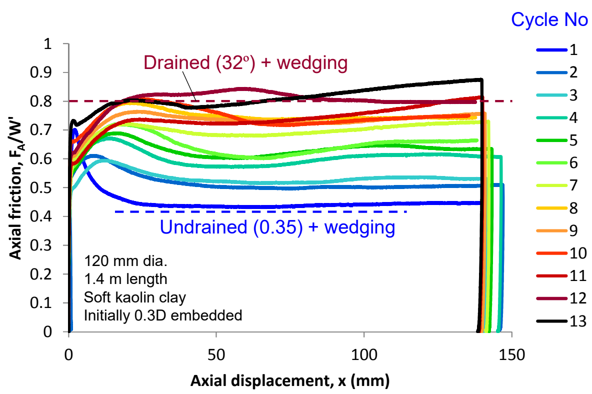

Figure 16. Modelling combined effects on penetration resistance of partial consolidation and strain rate effects

(a)

(b)

Figure 17. Box-core and seabed scales of toroidal and hemi-ball penetrometers (a) Toroidal penetrometer (top 2), (b) Hemi-ball penetrometer (bottom 2)

6 CONCLUSIONS

This paper has reviewed some of the recent developments in offshore site investigation equipment, with particular emphasis on seabed-based robotic drilling systems and free-fall samplers and penetrometers. Accurate characterisation of the very shallow seabed sediments is essential for design of pipelines and subsea foundations and, in turn, that has led to modern lightweight units that can explore the upper 1 or 2 m of the seabed in a cost-effective manner. In an effort to improve understanding of factors that affect values of coefficient of consolidation, recent work has been summarised that relates values of c_h deduced from field dissipation tests to c_v values from laboratory oedometer tests, separating out effects of stiffness and of potentially anisotropic permeability. Simplified dissipation responses are presented for piezocone and piezoball penetrometers and the effects of partial consolidation during penetration are discussed. Novel torsional penetrometers being developed under a current joint industry project are introduced.

7 ACKNOWLEDGEMENTS

This work forms part of the activities of the Centre for Offshore Foundation Systems (COFS), currently supported as a node of the Australian Research Council Centre of Excellence for Geotechnical Science and Engineering and through the Fugro Chair in Geotechnics, the Lloyd's Register Foundation Chair and Centre of Excellence in Offshore Foundations and the Shell EMI Chair in Offshore Engineering. Grateful acknowledgement is made to the many colleagues on whose research the author has drawn.

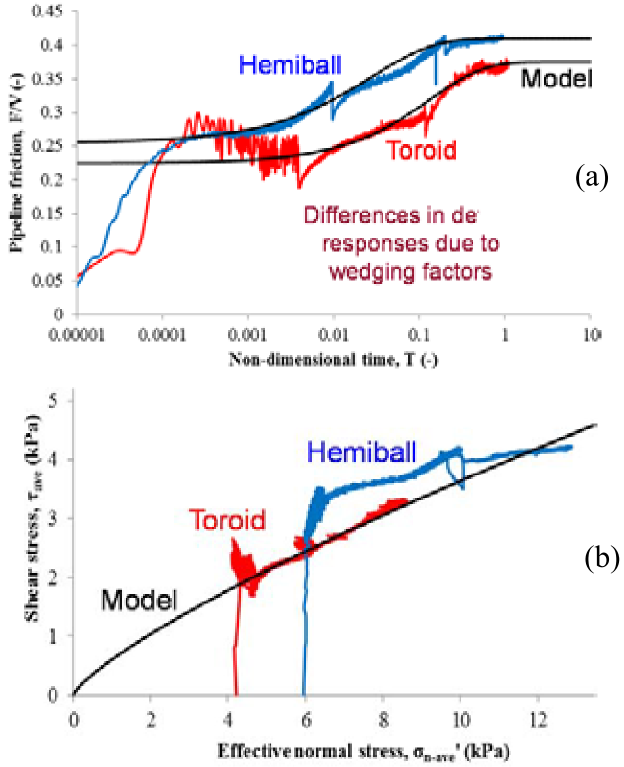

Figure 18. Torsional response of toroidal and hemi-ball penetrometers (courtesy RIGSS JIP): (a) Total stress interface friction response and (b) Effective stress interface friction

8 REFERENCES

DeJong, J. and Randolph, M.F. (2012). Influence of partial consolidation during cone penetration on estimated soil behavior type and pore pressure dissipation measurements. *J. Geotech. and Geoenv. Eng.*, ASCE, 138(7), 777–788.

DeJong, J. et al. (34 authors) (2013). Biogeochemical processes and geotechnical applications: progress, opportunities and challenges. *Géotechnique* 63(4), 287-301.

Carr, M., Bruton, D.A.S. & Leslie, D. (2003). Lateral buckling and pipeline walking, a challenge for hot pipelines. *Proc. Offshore Pipeline Technology Conf.*, Amsterdam.

Chow, S.H., O'Loughlin, C.D. and Randolph, M.F. (2014). A centrifuge investigation of free-fall piezocone in clay. Géotechnique, 64(10), 817-827.

Chow, S.H., O'Loughlin, C.D. and Randolph, M.F. (2014). An extended interpretation of the free-fall piezocone test in clay. Under review.

Colreavy, C., O'Loughlin, C. and Randolph, M.F. (2016a). A new dual pore pressure element piezoball for measuring strength and consolidation characteristics of soft clay. *Int. J. of Physical Modelling in Geomech.*, 16(3), 101-118.

Colreavy, C., O'Loughlin, C. and Randolph, M.F. (2016b). Estimating consolidation parameters from field piezoball tests. *Géotechnique*, 66(4), 333-343.

Einav, I. and Randolph, M.F. (2006). Effect of strain rate on mobilised strength and thickness of curved shear bands. *Géotechnique*, 56(7), 501-504.

Erbrich, C.T. (2005). Australian frontiers – spudcans on the edge. *Int. Symp. on Frontiers in Offshore Geotechnics: ISFOG*, Taylor & Francis, 49-74.

Kuo, M. and Bolton, M.D. (2013). The nature and origin of deep ocean clay crust from the Gulf of Guinea. *Géotechnique*, 63(6), 500-509.

Mahmoodzadeh, H. and Randolph, M.F. (2014). Penetrometer testing - the effect of partial consolidation on subsequent dissipation response. *J. of Geotechnical and Geoenvironmental Engineering*, ASCE, 140(6), 04014022(12).

Mahmoodzadeh, H., Randolph, M.F. and Wang, D. (2014). Numerical simulation of piezocone dissipation test in clays. *Géotechnique*, 64(8), 657–666, 680, corrigenda (10), 848-850.

Mahmoodzadeh, H., Wang, D. and Randolph, M.F. (2015). Interpretation of piezoball dissipation testing in clay. *Géotechnique*, 65(10), 831-842.

Randolph, M.F., White, D.J. and Yan, Y. (2012). Modelling the axial soil resistance on deep water pipelines. *Géotechnique*, 62(9), 837-846.

Smith, V.B. and White, D.J. (2014). Volumetric hardening in axial pipe soil interaction. *Proc. Offshore Technology Conf.*, Kuala Lumpur, Malaysia. Paper OTC24856.

Stegmann, S., Morz, T. and Kopf, A. (2006). Initial results of a new free fall-cone penetrometer (FF-CPT) for geotechnical in situ characterisation of soft marine sediments. *Norsk Geologisk Tidsskrift* 86(3), 199-208.

Steiner, A., Kopf, A. J., L'Heureux, J.-S., Kreiter, S., Stegmann, S., Haflidason, H. and Moerz, T. (2014). In situ dynamic piezocone penetrometer tests in natural clayey soils. *Can. Geotech. J.* 51(3), 272–288.

Teh, C.I. and Houlsby, G.T. (1991). An analytical study of the cone penetration test in clay. *Géotechnique*, 41 (1), 17-34.

Wang, D., Randolph, M.F. and Gourvenec, S. (2015). Coefficient of consolidation for soil – that elusive quantity. *Proc. VI Int. Conf. on Comp. Methods for Coupled Problems in Science and Eng.*, Coupled Problems 2015, Venice.

Young, A.G., Bernard, B.B., Remmes, B.D., Babb, L.V. and Brooks, J.M. (2011). "CPT Stinger" – an innovative method to obtain CPT data. *Proc. Offshore Technology Conf.*, Houston, USA. Paper OTC21569.

Geotechnical and Geophysical Site Characterisation 5 – Lehane, Acosta-Martínez & Kelly (Eds)
 ISBN 978-0-9946261-1-0

Geotechnical site investigation in energetic nearshore zones: opportunities & challenges

N. Stark
Charles E. Via, Jr. Department of Civil and Environmental Engineering, Virginia Tech, Blacksburg, USA

ABSTRACT: Coastal erosion and scour around structures in the nearshore zone represent major societal challenges with regard to coastline conservation, the protection of coastal communities and eco-systems, as well as the development of coastal structures or renewable energy projects. Despite rapidly advancing sediment erosion, scour and morphodynamics prediction tools, the models still struggle to correctly simulate the impact of severe storm events and storm event clusters, particularly regarding long-term projections considering sea level rise and climate change. Scour prediction models still struggle to accurately predict the depth and extent of the scour around a structure, and often rely on significant overpredictions which impact the cost-efficiency of the structural foundation design. A review of common erosion and scour prediction models reveals that particularly sediment characteristics appear underrepresented. This results from challenges to derive these information in the field. Areas of active sediment remobilization processes, such as the nearshore zone, are characterized by energetic hydrodynamics (waves, tides and currents), and morphodynamics (migrating bars, etc.) representing challenges and risks to people, vessels and instrumentation. Most geotechnical field instrumentation to-date are not designed or suitable for measurements in such conditions, and new devices are needed to fill this gap. This paper presents results (i) using a portable free fall penetrometer of projectile-like shape to investigate in-situ characteristics and stratification of sediment surface sediments in the nearshore zone under hydrodynamic forcing, and (ii) preliminary data using embedded pressure sensors to investigate the pore pressure response to irregular wave forcing in the nearshore zone and its potential impact on sediment erosion. The devices proved to be suitable for the deployment in energetic nearshore conditions. The data emphasize the potential regarding deriving novel information about in-situ sediment characteristics, such as changes in sediment strength under the active sediment dynamics, as well as an increase of erodibility through the development of excess pore pressures on different time scales. However, the data also reveal challenges related to calibration of the instrumentation and data processing, particularly with limited additional information about the sediment.

1 INTRODUCTION

Coastal erosion, coastal land loss and scour around structures in the nearshore zone represent major societal challenges with regard to coastline conservation, the protection of coastal communities and eco-systems, as well as the development of ocean renewable energy projects (Zhang et al. 2004; NAS 2010; Hinkel et al. 2014). Despite the rapid advancement in predicting sediment erosion, scour and morphodynamics, the models still struggle to correctly simulate the impacts of severe storm events and storm event clusters, particularly regarding long-term projections considering sea level rise and climate change (e.g., Coco et al. 2014). This issue becomes especially dramatic for locations at which coastal erosion rates have reached values in the order of meters per year, or the Arctic where the additional impact of permafrost is increasing erosion rates to more than ten meters per year (Dolan et al. 1979; Jones et al. 2008; Obu et al. 2016).

Similar problems can be identified for scour prediction models which often struggle to accurately predict the depth and extent of the scour around a structure (Falcone and Stark 2016). Currently, the most commonly applied prediction models rely on significant overpredictions of scour depth, resulting in safe, but often expensive foundation designs. Particularly in energetic areas, such as proposed bottom-mounted wave energy converter sites, this may even lead to a conflict between the costs of a safe design, and the available budget.

An analysis of common erosion and scour prediction models reveals that particularly sediment characteristics appear underrepresented. Often only the median grain size is considered, although the impacts of particle shapes, packing, bulk density, friction angles, and pore pressure behavior have been acknowledged (see section 2). A main reason for this is the lack of field investigation methods to derive these information in a safe, time- and cost-effective manner.

Areas of active sediment remobilization processes in the nearshore zone are characterized by energetic hydrodynamics (waves, tides and currents), and morphodynamics (migrating bars, etc.) representing challenges and risks to people, vessels and instrumentation. Most geotechnical in-situ instrumentation to-date are not designed or suitable for measurements in such conditions, and new devices are needed to fill this gap. The deployment under energetic conditions is thereby of highest interest to actually monitor the soil behavior with respect to active sediment dynamics.

In the following chapters, representative sediment remobilization models will be reviewed regarding the implementation of sediment characteristics. This will be followed by a discussion of potential impacts of sediment properties on sediment transport, and vice versa, variations in sediment properties with sediment dynamics. Then, two survey methods will be presented, including data examples: (i) the use of portable free fall penetrometers for the geotechnical characterization of seafloor surface sediments in areas of energetic hydrodynamics, and (ii) opportunities of long-term pore pressure monitoring using embedded pressure transducers.

2 PREDICTING THE INITIATION OF SEDIMENT TRANSPORT

2.1 *Non-cohesive sediments*

A most common method to determine the initiation of sediment remobilization is the approach by Shields (1936). Here, the critical Shields parameter, θ_{cr}, is calculated, representing a threshold value at which sediment mobilizing forces overcome sediment stabilizing forces:

$$\theta = \tau_{cr,0}/[(\rho_s - \rho_w)gd_{50}] \tag{1}$$

with $\tau_{cr,0}$ representing the critical bed shear stress for cohesionless particles, ρ_s being the sediment density, ρ_w being the water density, the gravitational acceleration g, and application of the median grain size d_{50}. θ_{cr} depends on the hydraulic conditions at the bed, particle shape, and particle packing, and thus, also on the friction angle (Kirchner et al. 1990; Van Rijn 2007). These properties are reflected in the respective $\tau_{cr,0}$. Hydraulic conditions can be estimated using the Reynolds number, and viscous effects can be assessed using a dimensionless particle size, D_*, depending on the d_{50}, relative density, and the kinematic viscosity coefficient. Van Rijn (2007) argues that the critical shear stress can be represented best in relation to D_*.

In an approach to address the sediment transport problem from general physics, Bagnold (1966) highlights the work that has to be conducted by a fluid to transport sediment as bedload. He states that the bedload work is directly dependent on the friction coefficient $\tan\phi$, representing the ratio of the shear stress over the normal stress. However, only an approximate of $\phi \approx 33°$ is provided for sands. Hsu et al. (2006) presented a model for wave-induced sediment transport and onshore sandbar migration including the friction angle, but also these authors applied the same approximated value as Bagnold (1966). This approximated value of the friction angle is challenged by the fact that friction angles depend on density, packing, particle shape and size distribution. Kirchner et al. (1990) documented the strong variations of the friction angle of water worked sediments, and measured friction angles more than twice as high for sandy sediments. These authors suggested to estimate the median friction angle from grain sizes of the abundant sediments using

$$\phi_{50} = \alpha(D/D_{50})^{-\beta} \tag{2}$$

with D being the test grain size, D_{50} being the median bed grain diameter, and α and β being empirical factors. This approach was successful when different empirical factors were applied depending on grain shape and packing. This is also supported by Stark et al. (2014) who found surprisingly high friction angles for sandy beach sediments with flat elliptic shape which proved to have a significant impact on the local beach dynamics.

It follows that sandy sediment transport prediction models would benefit significantly from a method to derive *in situ* friction angles.

2.2 *Cohesive sediments*

A number of physical, geochemical and biological properties influence the erodibility of fine, cohesive sediments, such as d_{50}, particle size distribution, bulk density, water content, temperature, mineralogy, salinity, organic content, biogenic structures and more. Grabowski et al. (2011) showed relationships to τ_{cr} of many of these properties. Amos et al. (2004) suggested the following relationship with regard to wet bulk density ρ_b:

$$\tau_{cr} = 5.44 \times 10^{-4}(\rho_b) - 0.28 \tag{3}$$

for lacustrine, estuarine, and marine muds. However, this disregards many of the other impacting factors. Many of those can be determined from sediment cores, and laboratory tests. However, the risk of sample disturbance, the difficulty of retrieving undisturbed sediment surface sediments, and the effort associated to these laboratory experiments are often hampering such detailed site investigations.

In potentially cohesive sediment mixtures of grain sizes ranging from 62-200 µm, Van Rijn (2007) suggested as a rough estimate

$$\tau_{cr} = (1 + p_{cs})^3 \tau_{cr,0} \quad (4)$$

using the proportion of the clay content in the sediment p_{cs}. While this allows a quick estimate of the critical shear stress, and thus, erodibility of mixed sediments, variations in above mentioned impacting factors may lead to significant variations of this relationship.

An assessment of critical shear stress from *in situ* measured properties, such as shear strength, would be attractive to simplify and speed up investigations of erodibility, but also to allow validation of derived sediment characteristics based on extracted sediment samples using *in situ* data.

2.3 *The impact of pore pressure with wave action*

The impact of excess pore pressures, p, on marine sediment stability has been acknowledged since the 1970s when Bjerrum (1973) associated the failure of offshore oil platforms in the North Sea to liquefaction of marine sands under storm wave action. Different processes may lead to sediment liquefaction or fluidization under ocean wave forcing:

(i) Pore pressure build-up. The hydrostatic pressure fluctuations resulting from the passing of wave crests and troughs lead to a cyclic deformation of the seabed surface, and shear forces. Resulting sediment particle rearrangement at the expense of pore space, can create excess pore pressures that exceed the effective stress (Nataraja and Gill 1983; Lin and Jeng 2000; Sassa and Sekiguchi 2001; Sumer et al. 2006). Sumer (2014) suggests to relate the excess pore pressure averaged per wave period $\bar{p}$ to the initial mean normal effective stress σ'_0 to assess the risk of liquefaction due to pore pressure build-up under ocean wave forcing, based on sand liquefaction experiments in a wave flume (Sumer et al. 2006, 2012). This means that liquefaction occurs when $\bar{p} > \sigma'_0$, and the critical excess pore pressure averaged per wave period can be estimated using

$$\bar{p}_{cr} = \sigma'_0 = \gamma' z[(1 + 2k_0)/3] \quad (5)$$

using the submerged specific weight of the soil γ', the sediment depth z, and the coefficient of lateral earth pressure k_0 which can be estimated using the friction angle and the Jaky equation (Lambe and Whitman 1969).

In most recent field experiments, Stark and Hay (2014) observed pore pressure build-up over multiple wave periods in mixed sand gravel beach sediments, and Stark and Quinn (2015) documented pore pressure build-up over short wave groups in the intertidal zone of a sandy beach. While in both cases, no full residual liquefaction like described by Sumer (2014) was observed, high excess pore pressures in the upper tens of centimeters of the beachface can likely increase sediment erodibility through lift of the particles, or even by a resulting upward flow.

(ii) Momentary sediment liquefaction may occur in response to vertical directed pressure gradients within one wave period. Turner and Nielsen (1997) expressed the impact of vertical pore pressure gradients in vertical velocities of pore water flow. The observations showed that periods of rapid water infiltration/exfiltration were commensurate with rapid pore pressure changes and upflow/downflow. Turner and Nielsen (1997) estimated that velocities ≥ 0.042 m/s are sufficient for fluidization of a bed with particles ranging from 0.1 mm to 2 mm in diameter. The subject was also investigated by Yeh and Mason (2014) for the case of a tsunami. The authors stated that the soil potentially liquefies when the vertical upward gradient of the excess pore pressure exceeds the buoyant specific weight, and proposed a modified Shields parameter to account for this effect by introducing the critical pore pressure gradient:

$$-\partial p/\partial z > \gamma' \quad (6)$$

(iii) Strong horizontal pressure gradients, p_x, induced by the passage of skewed or breaking waves can destabilize the sediment bed (Sleath 1999; Foster et al. 2006). Sleath (1999) defined the role of the horizontal pressure gradient for momentary liquefaction of some sediment layer of thickness h, expressed as the Sleath parameter, S, with a ratio between the destabilizing force p_x relative to the stabilizing force applied by gravity, similarly to the structure of the Shields parameter.

Foster et al. (2006) provided the first field evidence of the momentary liquefaction of 100s of grain thicknesses in response to large horizontal pressure gradients present in a shallow water wave environment. They defined the instantaneous Sleath parameter as:

$$S(t) = -p_x(t)/(\rho_s - \rho_w)g, \quad (7)$$

and proposed a generalized incipient motion formulation for a thickness h of sediment due to both the pressure gradient and shear stress.

The impact of pore pressure on sediment erodibility in the nearshore zone is unquestioned. However, the interaction between the above described processes, and the integration into sediment transport models is still limited. There is an urgent need for field data sets that test, validate, and advance the proposed approaches.

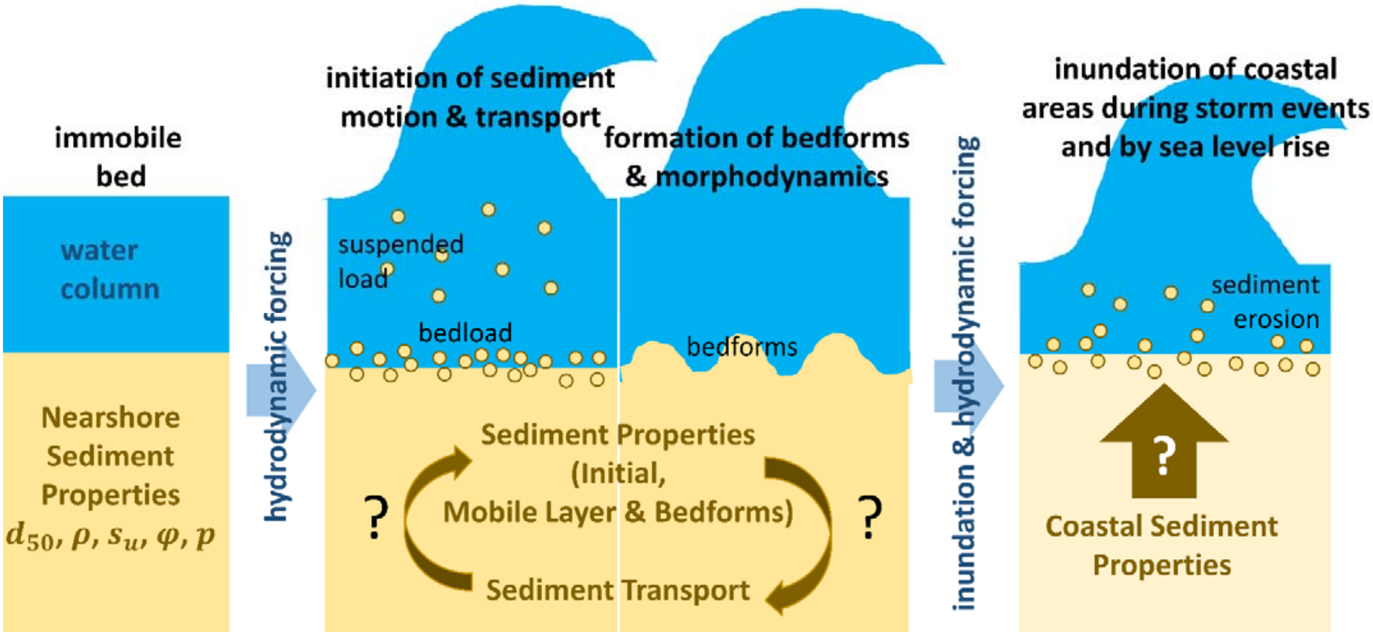

Figure 1. The impact of sediment properties such as median grain size d_{50}, bulk density ρ_b, undrained shear strength s_u, friction angle ϕ, and excess pore pressure p, on sediment transport and erosion has been acknowledged, but for most of these properties rarely been quantified. Vice versa, sediment properties change with the formation of a mobile sediment layer and bedforms, however to what extent is still rarely documented. Coastal sediments in potential inundation zones are characterized by different sediment properties than the current nearshore zone, and have experienced a different exposure history to saturation and sediment transport processes. This impacts the sediment erodibility in these areas. However, predictions still suffer from limitations in understanding between the interaction of sediment properties, hydrodynamic forcing, and geomorphodynamics.

3 THE ROLE OF SEDIMENT PROPERTIES IN AREAS OF ACTIVE SEDIMENT DYNAMICS

3.1 *Subaqueous sediment dynamics*

The initiation of sediment transport is an important problem, and has been reviewed briefly in section 2. It has been emphasized that sediment properties such particle size distribution, packing, strength, and pore pressures play an important role for the onset of sediment erosion. In areas of active sediment dynamics, this problem must even be considered in a larger spatial and temporal context. After the entrainment of particles, sediment will be transported as bedload (rolling, saltating, and sliding close to the immobile seabed), or as suspended load in the water column (Fig. 1). The transport mode has a significant impact on transport rates and volumes (Bagnold 1966). With the ongoing sediment transport, bedforms (such as ripples, bars, dunes) can be formed, destroyed, reshaped, or shifted, and a mobile sediment layer representing sediment impacted by sediment transport can be defined (Fig. 1). Sediment properties of this mobile layer as well as of the bedforms can be expected to differ from the initial sediment properties of the immobile bed. Particle size and shape distributions may change through selective sediment transport. Here, sediment size or shape fractions can vary in transport mode and rate, or some large particles, or sediment of large friction angles may not be entrained under moderate forcing conditions. Such selective sediment transport is reflected in sediment sorting along bedforms, for example (Fig. 2).

With the deposition of sediment, possible remobilization, and re-deposition on different temporal scales from single waves over tidal cycles to the reoccurrence of extreme events, also significant variations in sediment settling, consolidation, and thus, packing, density, friction angle, and shear strength must also be expected (Fig. 1).

Figure 2. Sediment sorting along large ripples in Grand Passage, Bay of Fundy, Nova Scotia. Grand Passage is characterized by maximum tidal current velocities in excess of 4 m/s, and is a proposed site for the harvesting of tidal energy. Ongoing sediment transport is clearly documented in the existence of bedforms, as well as sediment sorting.

Figure 3. Thaw mud slump at the coastline of Herschel Island, Yukon.

In some areas new and varying sediment inputs must be considered. That applies to, e.g., river outflow areas impacted by river diversion, dredging or dams, as well as large sediment input by thawing of glaciers or permafrost coastlines. For example, Herschel Island, Yukon, in the Canadian Beaufort Sea features some of the largest thaw mud slumps in the world, delivering significant amounts of fine to mixed sediments into the nearshore zone (Fig. 3).

With climate change, and the associated sea level rise, retreat of permafrost and glaciers, and increase of the storm intensities and frequencies, the erodibility of onshore areas under inundation and nearshore forcing becomes important. From above discussed processes, it follows that sediments exposed to hydrodynamic forcing in the nearshore zone will potentially exhibit different sediment properties than sediments that are usually located onshore, and do not experience hydrodynamic forcing. A more detailed understanding of the differences in *in situ* sediment characteristics, and the response to hydrodynamic forcing and morphodynamics, is crucial to predict long-term coastline evolution, erosion, and erodibility during extreme events, and thus, for coastal management and planning.

3.2 *Beach dynamics*

Beaches represent in many locations the natural border between the nearshore zone and the onshore coastal zone which are both exposed to significantly different processes and forcing conditions (see section 3.1). Resulting from water level fluctuations on temporal scales of waves, semidiurnal to lunar tidal cycles, and events, beaches are impacted by additional effects of changing water levels, ground water dynamics, water infiltration and exfiltration (Fig. 4). This leads to the fact that beaches are highly dynamic environments, while they represent at the same time recreational hot spots, and a natural barrier against ocean forcing.

Examples of significant beach dynamics can be found worldwide. Figure 5 shows traces of erosion at the high water edge at a sandy beach on the Outer Banks, USA. Figure 6 depicts the change of grain size distribution along a cross-shore profile at a steep, mixed sand-gravel megatidal beach in Advocate, Nova Scotia. Here, zones of offshore directed sediment fining, or coarsening, a fine sand zone, and a coarse mixed sediment zone can be identified, and the position of the fine sand zone is shifting in the cross-shore direction, apparently in correspondence to the lunar tidal cycle, while a storm event leads to an overall fining of the central and lower intertidal zone. Due

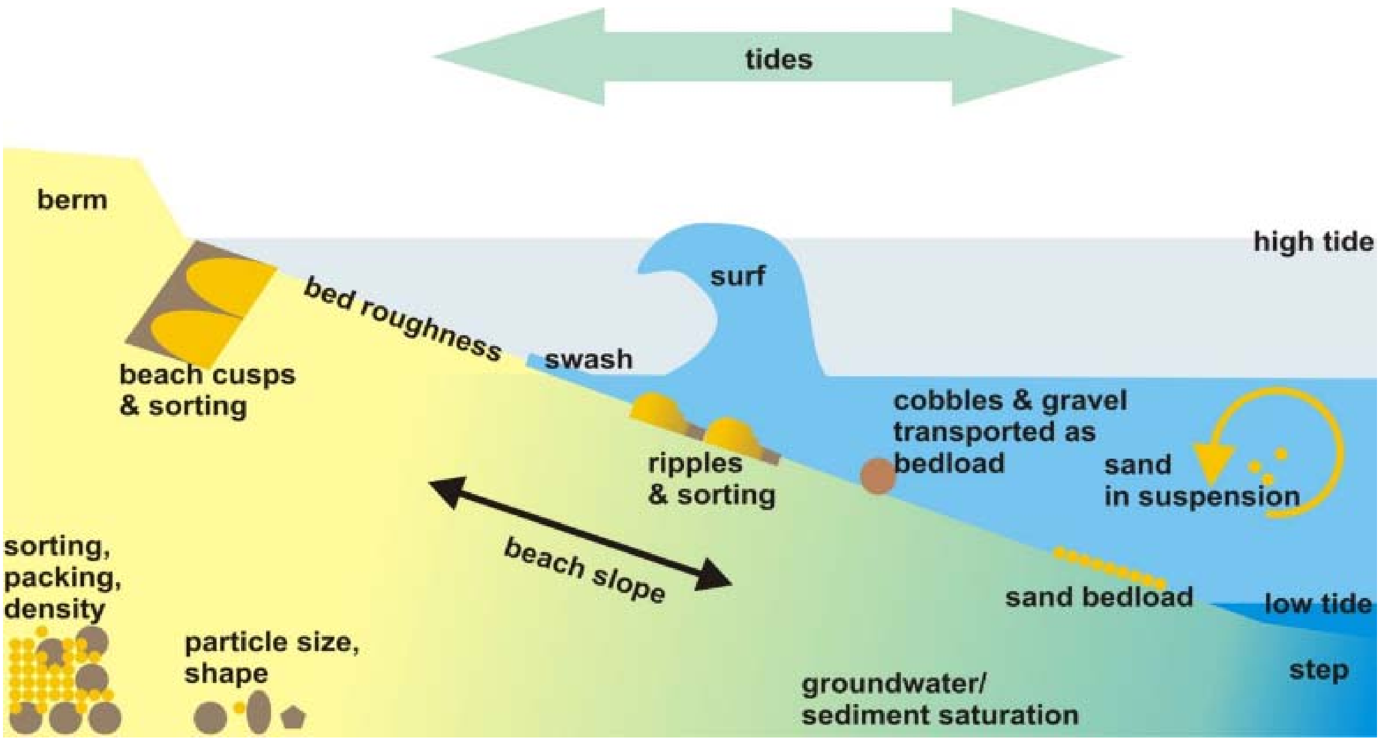

Figure 4. Concept sketch of aspects of sediment properties, sediment transport, morphology and hydrodynamics influencing beach dynamics.

Figure 5. Traces of significant erosion at a beach in Nags Head, NC, in the direct vicinity of beach properties after a moderate wind event in June 2016.

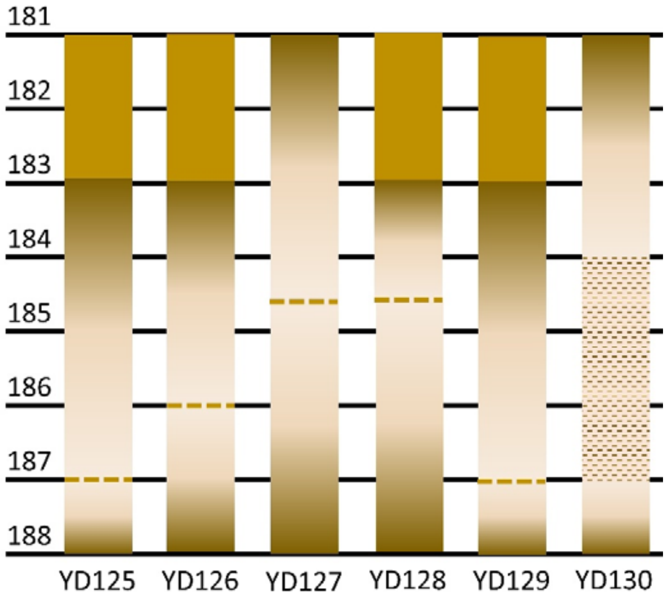

Figure 6. Conceptual representation of grain size distributions along a cross-shore transect (188 low tide water line; 181 close to the berm) at Advocate Beach, Nova Scotia, a steep, mixed sand-gravel, megatidal beach, from yeardays 125-130 in 2012. Ungraded brown indicates mixed coarse sediment, graded brown shading indicates fining towards the lighter shading. The dashed lines indicate the fine sand zone. A storm event hit the site starting in the night of yearday 129.

to the extreme tidal range at this location (~ 12 meters), the beach undergoes full saturation and drainage twice per day. The observations cannot currently be fully simulated in beach sediment transport models. Particularly, the wide distribution of fine sediment at the beachface after the storm event seems puzzling, considering an expected sediment armoring with coarse sediments prevailing under storm conditions. Hay et al. (2014) and Stark et al. (2014) found that the surprising presence of fine sediments can be associated to the creation and destruction of sorted ripples in the swash and surf zone, and large friction angles of the sandy size fraction.

Such observations and studies highlight the need for more field data sets, particularly in the framework of multidisciplinary research programs. However, *in situ* measurements during hydrodynamic forcing are difficult, and novel methods and tools are needed to obtain the desired data sets.

4 USING PORTABLE FREE FALL PENETROMETERS TO INVESTIGATE SEDIMENT TRANSPORT PROCESSES

Free fall penetrometers have been introduced to offshore geotechnical site characterization in the 1970s by researchers such as Dayal and Allen (1973) who already recognized the potential, as well as associated challenges, particularly in the data analysis. Later, Stoll and Akal (1999) presented the expendable bottom penetrometer, being a lightweight, fish-like shaped device suitable for a rapid investigation of the uppermost seafloor surface layers. Different data analysis approaches were tested for this device, including a correlation of the deceleration record directly to sediment types, or estimating undrained shear strength (Aubeny and Shi 2006; Stoll et al. 2007; Stark and Wever 2009). Motivated by these results, the ease of deployment, and the wish to design a non-expendable probe with similar capabilities, but particularly for deployments in areas of active sediment dynamics, a torpedo-shaped probe was developed, *Nimrod*, targeting specifically surficial seabed characterization with regard to geotechnical site characterization of sediment remobilization processes (Stark 2011).

Some representative results of *in situ* geotechnical investigations of sediment remobilization processes are shown in figure 7. The main findings can be summed up as follows: The sediment type was correctly identified from the deceleration values, and an equivalent of quasi-static bearing capacity can roughly be estimated (Stark et al. 2012). The evolution of a loose sediment top layer can be associated to a mobile sediment layer, and be quantified in vertical thickness with a resolution in the order of ~1 cm (Stark and Kopf 2011). Variations of this mobile top layer can be correlated to the sediment deposition and remobilization with tidal, and wave forcing (Stark et al. 2010, 2011). Areas of sediment erosion and deposition can be identified (Stark et al. 2010).

The results confirmed that portable free fall penetrometers deliver complementary information for the investigation of sediment remobilization processes. However, some questions remained unsolved, or were even raised by the results. A loose sediment top layer was clearly identified, and associated to sediment transport processes. However, the evolution of such a layer can express reworking of native surface

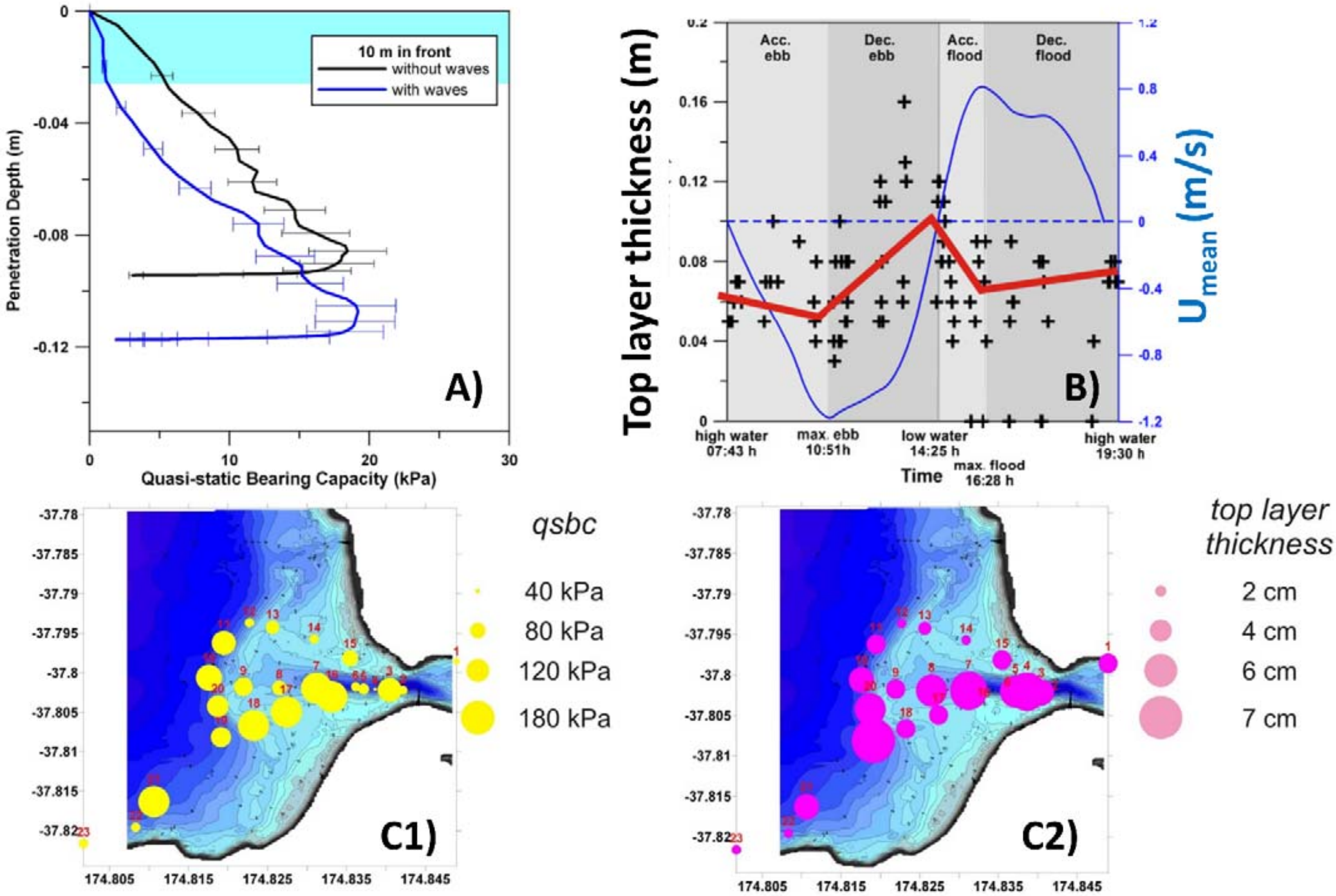

Figure 7. A) Estimates of quasi-static bearing capacity (*qsbc*) of a sandy soil under no-current-no-waves conditions (black line), and with wave action (blue line) versus penetration depth, measured in the large wave channel in Hannover, Germany. The evolution of a loose top sand layer is clearly indicated by low sediment strength in the upper 3 cm (mint shading). Figure modified from Stark and Kopf (2011). B) Thickness of a loose sediment top layer measured over one tidal cycle along subaqueous dunes in the Knudedyb tidal channel in the Danish Wadden Sea (black crosses; trend outlined in red). The mean flow velocity is indicated in blue. Scatter in top layer thickness can be associated to different locations along the dunes. The figure is modified after Stark et al. (2011). C1-2) Estimates of quasi-static bearing capacity (C1) and loose top layer thickness (C2) over an active sand bar in front of Whaingaroa Harbour, Raglan, New Zealand. Areas of low *qsbc* and high top layer thickness were associated to areas of fresh sediment deposition, while areas of high *qsbc* and low top layer thickness suggested ongoing erosion (modified after Stark et al. 2010). This allowed the prediction of the offshore migration of the southern arm of the bar which was confirmed later from aerial images. All measurements were obtained using the portable free fall penetrometer *Nimrod*.

sediments, as well as the deposition of sediment entrained at a different location and deposited here. The governing process cannot be inferred from the penetrometer data alone, but usually, information about the local hydrodynamic forcing and morphodynamics allow to derive a conclusion in this matter. Nevertheless, it would be an important step forward if more details about this mobile layer could be derived, such as bulk density or concentration, sediment grain size distribution, or if sediments behave cohesive. If such properties would be derived in a vertical profile for the mobile layer as well as its underlying substratum, this would also enable to derive conclusions regarding selective sediment transport. These information would be directly applicable to sediment transport models, and would improve the prediction of sediment erosion, transport, and deposition, and thus, potential bathymetric change. This is of high importance for addressing issues such as coastal erosion, sediment dredging and disposal projects, navigation in shallow nearshore, estuarine and riverine environments, as well as scour and seabed stability around coastal structures.

Portable free fall penetrometers have the potential to contribute further to address these issues. One consideration is to add a sampling device that would allow to retrieve a sediment sample of the penetrated layers. If such samples would be similar to mini sediment cores, stratification would be represented, and differences in sediment type, and size distribution could be assessed. Dependent on the level of disturbance, *in situ* density may be estimated. For very fine sediments, subsamples could be extracted using a syringe. For coarse sediments, high resolution images of the mini-core could be a potential method to assess particle packing and density. From this information

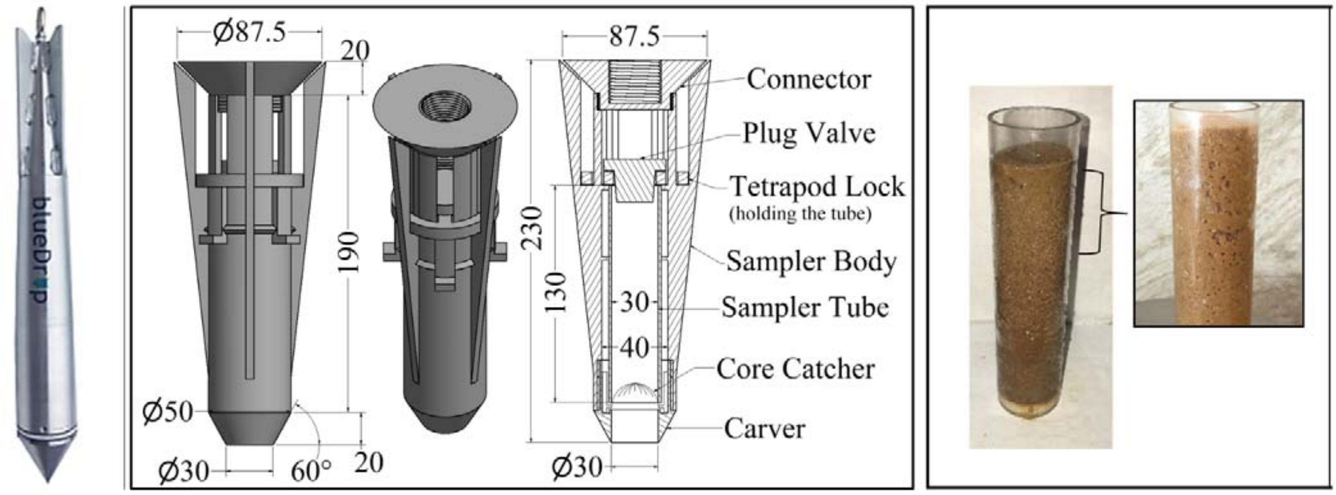

Figure 8. Left) *BlueDrop* portable free fall penetrometer (63 cm in length; approx. 8 kg). Center) Design of one of three prototype add-on samplers. Right) Representative sand sample obtained during preliminary tests. The figure is modified after Bilici and Stark (2017).

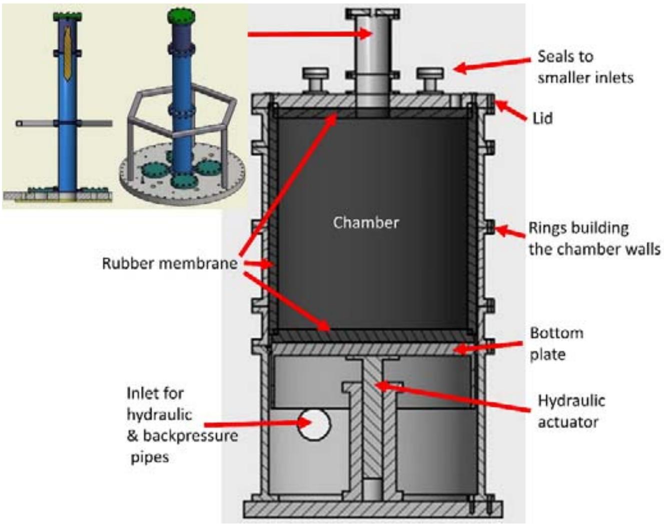

Figure 9. Concept sketch of large-scale CPT calibration chamber and modified free fall tower.

and with enough sample material, a sample could even be reconstructed for further testing in the laboratory. Bilici and Stark (2017) have developed three different prototypes of sampler add-on units for the portable free fall penetrometer *BlueDrop*, including the design of a novel core catcher mechanism, and have initiated preliminary laboratory experiments to evaluate the performance of the samplers and sample quality (Fig. 8). More tests are currently ongoing to improve sample quality, and to investigate the impact of penetration speed on the sample.

In addition to *in situ* sampling, calibration of the penetrometer acceleration/deceleration records under controlled conditions, and specifically targeting soft and loose surface sediments will advance research in this field. This is particularly important if the rapid deployment process, allowing to deploy under energetic conditions, and to cover a large number of locations in a short time, should be preserved. This has been attempted by Dayal and Allen (1973) and Stoll et al. (2007) using a large sediment sample in the laboratory, and most recently, authors such as Chow et al. (2014) and O'Loughlin et al. (2014) conducted centrifuge tests with small-sized free fall penetrometers. Another potential route to calibrate small-scale, but prototype size portable free fall penetrometers is a modified large-scale Cone Penetration Test calibration chamber (Fig. 9). A large-scale chamber with a diameter and height of ~1.5 m, and a water backpressure system would allow to simulate different seabed conditions, and to calibrate a small-scale portable free fall penetrometer with small impact of the confinement. This would enable a calibration of the penetrometer's deceleration records to different sediment types, shear strength, and bulk density, as well as to investigate the strain rate effect for high velocity impact penetrometers of different shapes in more detail.

Another potential route of seabed surface characterization using portable free fall penetrometers is the measurement of pore pressure. Stegmann et al. (2006), Seifert et al. (2008) and Chow et al. (2014) have indicated the potential of using pore pressure measurements of impact penetrometers to derive information about shear strength as well as hydraulic conductivity. The *BlueDrop* penetrometer is equipped with a 300 psi pressure gauge at the u_2 position. Stark et al. (2015) found that the pore pressure recordings during penetration reflected the sediment stratification that was identified from the deceleration and estimated strength profiles. However, the pore pressure behavior deviates significantly from documented standard Cone Penetration Test records. This can be explained with a different soil and pore pressure behavior, as well as influences of the Bernoulli effect at the often more than 200-times higher impact velocities. More research is required to investigate the specific mechanisms in more detail to potential derive information of *in situ* hydraulic conductivity and relative density directly from the penetrometer pressure recordings.

5 *PORE PRESSURE MONITORING NEARSHORE* & AT THE BEACH

Section 2.3 discusses different concepts of the impact of pore water pressure under wave forcing on sediment dynamics. Most of these concepts are based on theoretical approaches, and laboratory experiments. Few data sets from the field are available to-date. Data loggers which are smaller in size, larger in memory, and faster in sampling rate are enabling new measurement approaches. Stark and Hay (2014) embedded a wave gauge at a sediment depth of 50 cm at a mixed sand gravel megatidal beach in Advocate, Nova Scotia, and found that pore pressure build-up occurred over multiple wave cycles despite the sediment coarseness. Stark and Quinn (2015) observed excess pore pressure peaks under irregular wave forcing at a sandy beach in Yakutat, Alaska. Stark (2017) applied the approaches to assess the risk for residual liquefaction by Sumer (2014), and for momentary liquefaction by Yeh and Mason (2014) and Foster et al. (2006) on the same data set, and derived that critical values were frequently exceeded for the upper 20 cm of the beachface (Fig. 10). During the field experiment active sediment transport was observed. However, differently than these calculations may suggest, no significant erosion was observed. Thus, processes investigated in a controlled manner in the laboratory may underestimate the actual complexness of field conditions.

More field data is necessary to understand the interplay of different processes, and to potentially integrate them into a larger sediment erosion prediction scheme. Novel field instrumentation can help to make data more accessible, and field measurements more feasible. Small-scale wave gauges such as *RBR SoloD* have most recently been applied for pore pressure monitoring in different beach and nearshore environments (Fig. 11). The ease of deployment, sampling rates of 10 Hz and faster, and a continuous monitoring duration in excess of 28 days allow new data acquisition strategies in vertical, cross-shore or long-shore arrangements.

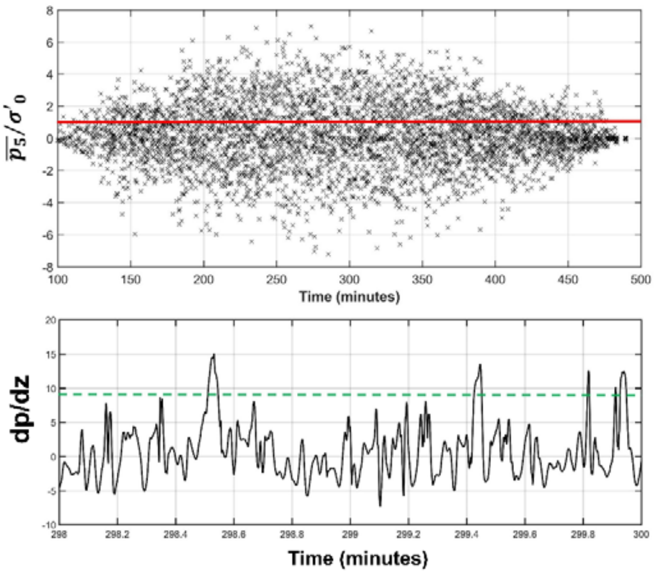

Figure 10. Upper panel) Wave-period average of excess pore pressure over initial mean normal effective stress at a sediment depth of 5 cm versus time measured at a sandy beach in Yakutat, AK. The red line indicates when theoretically residual liquefaction may be achieved under wave forcing. Lower panel) Upward directed vertical pressure gradients between a sediment depth of 25 cm and 5 cm for an excerpt of the above shown data set. The dashed green line indicates when momentary liquefaction may occur. Figure modified after Stark (2017).

Figure 11. Deployment of *RBR Solo* pressure transducers during an undergraduate research field experiment in a sandy nearshore zone in the Punta Cana, Dominican Republic.

6 CONCLUSIONS

The reliable and accurate prediction of sediment erosion, scour and deposition processes is of high importance for issues related to coastal erosion and coastline evolution, the maintenance of navigation channels, and the stability of coastal and offshore structures. The relocation and movement of significant sediment volumes occur particularly in the energetic nearshore zone where water depths are shallow, waves undergo shoaling and breaking, and tidal cycles can play an important role. The same area is the connection between offshore and onshore environments. The sediment behavior in these areas governs coastline evolution, represents important habitats, and is of increasing interest for wave energy conversion, and coastal protection structures.

Geotechnical sediment properties such as shear strength, friction angles and cohesion, as well as pore pressure behavior have been recognized as potentially important factors for improving the prediction of sediment erosion. Portable free fall penetrometers have successfully displayed variations between seabed surface top layers associated to active and most recent sediment transport processes. Preliminary pore pressure monitoring revealed that the pore pressure behavior under active wave forcing should be considered when assessing sediment erodibility, particularly under energetic wave forcing. It also indicated that some processes and their interaction may not be fully understood yet. The current gaps in understanding regarding the correlation between geotechnical soil characteristics and behavior and subaqueous sediment transport processes, and the associated limited integration into erosion or scour prediction schemes likely contributes significantly to the still existing model and prediction limitations.

To address this issue, more field investigations and data are required, highlighting the need for novel instrumentation and measurement strategies suitable for deployment in these energetic hydrodynamics or active sediment transport processes, and with limited impact on the native sediment processes.

Portable free fall penetrometer have proven to be suitable for the deployment in energetic hydrodynamics, for the classification of sediment type, estimating sediment strength, and to quantify sediment stratification. Most recently, pore pressure measurements during penetration and at rest in the sediment promise additional information about the sediment's hydraulic conductivity and density. However, more research is needed to derive geotechnical parameters directly comparable to other standard in-situ methods such as Cone Penetration Testing, and deliver more information about mobile seafloor surface layers. There is particularly a need for calibration facilities and experiments.

Pore pressure gauges embedded in beach and nearshore sediments over periods of hours to weeks indicated that the role of sediment pore pressures for sediment erosion is more important than currently considered, and that the processes are complex. The presented and similar measurement concepts may drive this field of research forward, and allow to obtain statistically valid amounts of data sets.

In summary, the coastal and nearshore zone still holds many open questions, challenges, and opportunities for researchers in the field of geotechnical engineering. At the same time, the collaboration with colleagues from different disciplines such as coastal sciences and engineering, oceanography, geology, geophysics, and sedimentology is crucial to fully understand the processes, and implement them into tools and prediction schemes important to coastal managers and communities.

7. ACKNOWLEDGMENTS

This paper presents data and information from a number of different projects. Funding was provided for these projects by (in random order) the National Sciences Foundation through grants NSF-IIA-142661 and NSF-OCE-1434938, the Offshore Energy Research Association of Nova Scotia, the Natural Sciences and Engineering Research Council of Canada, the Atlantic Innovation Fund, the German Research Association (via MARUM), the German Federal Ministry for the Environment, Nature Conservation and Nuclear Safety (via the German Federal Maritime and Hydrographic Agency), the German Academic Exchange Service, Virginia Tech and the Institute for Critical Technology and Applied Science at Virginia Tech.

Numerous people contributed to the acquisition of the presented data. The following individuals played a crucial role in making the data acquisition possible: Alex E. Hay (Dalhousie University, Halifax, Canada), Hugues Lantuit (Alfred-Wegener-Institute, Potsdam, Germany), Achim Kopf, Christian Winter, Christian Zoellner, Hendrik Hanff, and Matthias Lange (all MARUM, Bremen, Germany), Maria Lambers-Huesmann (BSH, Hamburg, Germany), Arne Stahlmann (Franzius Institute, Hannover, Germany), Jose Borrero (eCoast, Raglan, New Zealand), Shawn Harrison (University of Waikato, Hamilton, New Zealand), Tom Brandon and Lindy Cranwell (Virginia Tech), Rhonda Coston (City and Borough of Yakutat, AK), Bill Staby (Resolute Marine Energy, Boston), Stephen Smyth (Blue C Design, Dartmouth, Canada), and Doug Schillinger (RBR, Ottawa, Canada). Former or current students who have made a significant contribution to the presented data are Boris Radosavljevic (Alfred-Wegener-Institute, Postdam, Germany), Matthew Hatcher (Dalhousie University, Halifax, Canada), Ali Albatal, Cagdas Bilici, Freddie Falcone, Greg Lucking, Brandon Quinn and Jared Dorvinen (all current or former Virginia Tech students).

8. REFERENCES

Amos, C. L., Bergamasco, A., Umgiesser, G., Cappucci, S., Cloutier, D., DeNat, L., Flindt, M., Bonardi, M. & Cristante, S. 2004. The stability of tidal flats in Venice Lagoon—the results of in-situ measurements using two benthic, annular flumes. *Journal of Marine Systems* 51(1): 211-241.

Aubeny, C. P., & Shi, H. 2006. Interpretation of impact penetration measurements in soft clays. *Journal of Geotechnical and Geoenvironmental Engineering* 132(6): 770-777.

Bagnold, R. A. 1966. *An approach to the sediment transport problem from general physics.* Geological Survey Professional Paper 422-1.

Bilici, C., & Stark, N. 2017. Design and preliminary tests of mobile seafloor layer sampler prototypes as an add-on unit for portable free-fall penetrometers. Accepted for *Geotechnical Frontiers 2017*, Orlando, FL.

Bjerrum, L. 1973. Geotechnical problems involved in foundations of structures in the North Sea. *Geotechnique* 23(3): 319-358.

Chow, S. H., O'Loughlin, C. D., & Randolph, M. F. 2014. Soil strength estimation and pore pressure dissipation for free-fall piezocone in soft clay. *Géotechnique* 64(10): 817-827.

Coco, G., Senechal, N., Rejas, A., Bryan, K. R., Capo, S., Parisot, J. P., Brown, J.A., & MacMahan, J. H. 2014. Beach response to a sequence of extreme storms. *Geomorphology* 204: 493-501.

Dayal, U., & Allen, J. H. 1973. Instrumented impact cone penetrometer. *Canadian Geotechnical Journal* 10(3): 397-409.

Dolan, R., Hayden, B., Rea, C., & Heywood, J. 1979. Shoreline erosion rates along the middle Atlantic coast of the United States. *Geology* 7(12): 602-606.

Falcone, F.T., & Stark, N. 2016. Evaluation of the performance of scour prediction equations with regards to flow and sediment characteristics. *ASCE Geo-Chicago 2016*, Chicago, IL.

Foster, D. L., Bowen, A. J., Holman, R. A., & Natoo, P. 2006. Field evidence of pressure gradient induced incipient motion. *Journal of Geophysical Research: Oceans* 111(C5): 1-8.

Grabowski, R. C., Droppo, I. G. & Wharton, G. (2011). Erodibility of cohesive sediment: the importance of sediment properties. *Earth-Science Reviews* 105(3): 101-120.

Hay, A. E., Zedel, L., & Stark, N. 2014. Sediment dynamics on a steep, megatidal, mixed sand-gravel-cobble beach. *Earth Surface Dynamics* 2(2): 443-453.

Hinkel, J., Lincke, D., Vafeidis, A. T., Perrette, M., Nicholls, R. J., Tol, R. S., Marzeion, B., Fettweis, X., Ionescu, C., & Levermann, A. 2014. Coastal flood damage and adaptation costs under 21st century sea-level rise. *Proceedings of the National Academy of Sciences* 111(9): 3292-3297.

Hsu, T. J., Elgar, S. & Guza, R. T. 2006. Wave-induced sediment transport and onshore sandbar migration. *Coastal Engineering* 53(10): 817-824.

Jones, B. M., Hinkel, K. M., Arp, C. D., & Eisner, W. R. 2008. Modern erosion rates and loss of coastal features and sites, Beaufort Sea coastline, Alaska. *Arctic*: 361-372.

Kirchner, J. W., Dietrich, W. E., Iseya, F. & Ikeda, H. 1990. The variability of critical shear stress, friction angle, and grain protrusion in water-worked sediments. *Sedimentology* 37(4): 647-672.

Lambe, T. W., & Whitman, R. V. 1969. *Soil mechanics*. John Willey & Sons. Inc., NY.

Lin, Y. S. & Jeng, D. S. 2000. Short-crested wave-induced liquefaction in porous seabed. *Journal of geotechnical and geoenvironmental engineering* 126(5): 481-494.

Nataraja, M. S. & Gill, H. S. 1983. Ocean wave-induced liquefaction analysis. *Journal of Geotechnical Engineering* 109(4): 573-590.

National Academy of Sciences (2010). *Advancing the Science of Climate Change*. The National Academies Press, DOI 10.17226/12782.

Obu, J., Lantuit, H., Grosse, G., Günther, F., Sachs, T., Helm, V., & Fritz, M. 2016. Coastal erosion and mass wasting along the Canadian Beaufort Sea based on annual airborne LiDAR elevation data. *Geomorphology*. DOI:10.1016/j.geomorph.2016.02.014

O'Loughlin, C. D., Gaudin, C., Morton, J. P., & White, D. J. 2014. MEMS accelerometers for measuring dynamic penetration events in geotechnical centrifuge tests. *International Journal* 14(2): 31-39.

Sassa, S. & Sekiguchi, H. 2001. Analysis of wave-induced liquefaction of sand beds. *Geotechnique* 51(2): 115-126.

Seifert, A., Stegmann, S., Mörz, T., Lange, M., Wever, T., & Kopf, A. 2008. In situ pore-pressure evolution during dynamic CPT measurements in soft sediments of the western Baltic Sea. *Geo-Marine Letters* 28(4): 213-227.

Shields, A. 1936. *Anwendung der Aehnlichkeitsmechanik und der Turbulenzforschung auf die Geschiebebewegung.* Dissertation submitted to Preussischen Versuchsanstalt für Wasserbau.

Sleath, J. F. A. 1999. Conditions for plug formation in oscillatory flow. *Continental Shelf Research* 19(13): 1643-1664.

Stark, N., & Wever, T. F. 2009. Unraveling subtle details of expendable bottom penetrometer (XBP) deceleration profiles. *Geo-Marine Letters* 29(1): 39-45.

Stark, N. 2011. *Geotechnical investigation of sediment remobilization processes using a dynamic penetrometer.* PhD thesis submitted to the University of Bremen, Germany.

Stark, N., Hanff, H., Svenson, C., Ernstsen, V. B., Lefebvre, A., Winter, C., & Kopf, A. 2011. Coupled penetrometer, MBES and ADCP assessments of tidal variations in surface sediment layer characteristics along active subaqueous dunes, Danish Wadden Sea. *Geo-Marine Letters* 31(4): 249-258.

Stark, N., & Kopf, A. 2011. Detection and quantification of sediment remobilization processes using a dynamic penetrometer. *MTS/IEEE OCEANS'11*, Kona, HI: 1-9.

Stark, N., Greer, D., Phillips, D., Borrero, J., Harrison, S., Kopf, A. 2010. In-situ geotechnical investigation of sediment dynamics over 'The Bar', Raglan, New Zealand. *AGU 2010*, San Francisco.

Stark, N., Wilkens, R., Ernstsen, V. B., Lambers-Huesmann, M., Stegmann, S., & Kopf, A. 2012. Geotechnical properties of sandy seafloors and the consequences for dynamic penetrometer interpretations: quartz sand versus carbonate sand. *Geotechnical and Geological Engineering* 30(1): 1-14.

Stark, N., & Hay, A. E. 2014. Pore water infiltration and drainage on a megatidal beach in relation to tide-and wave-forcing. *Coastal Engineering Proceedings* 1(34): 25.

Stark, N., Hay, A. E., Cheel, R. & Lake, C. B. 2014. The impact of particle shape on the angle of internal friction and the implications for sediment dynamics at a steep, mixed sand-gravel beach. *Earth Surface Dynamics* 2(2): 469-480.

Stark, N., & Quinn, B. 2015. Pore pressure monitoring of surficial coastal sediments on wave-resolving scale with outlook on liquefaction risk prediction at offshore wind and marine hydrokinetic energy converters. *MTS/IEEE OCEANS 2015*, Washington, DC: 1-7.

Stark, N., Quinn, B., Ziotopoulou, K., & Lantuit, H. 2015. Geotechnical Investigation of Pore Pressure Behavior of Muddy Seafloor Sediments in an Arctic Permafrost Environment. *ASME 2015 34th International Conference on Ocean, Offshore and Arctic Engineering*: V001T10A017.

Stark, N. 2017. Pore pressure response to irregular waves at a sandy beach. Submitted to *Geotechnical Frontiers 2017*, Orlando, FL.

Stegmann, S., Morz, T., & Kopf, A. 2006. Initial Results of a new Free Fall-Cone Penetrometer (FF-CPT) for geotechnical in situ characterisation of soft marine sediments. *Norsk Geologisk Tidsskrift* 86(3): 199-208.

Stoll, R. D., & Akal, T. 1999. XBP- Tool for Rapid Assessment of Seabed Sediment Properties. *Sea technology* 40(2): 47-52.

Stoll, R. D., Sun, Y. F., & Bitte, I. 2007. Seafloor properties from penetrometer tests. *IEEE Journal of Oceanic Engineering* 32(1): 57-63.

Sumer, B. M., Hatipoglu, F., Fredsøe, J. & Kaan Sumer, S. 2006. The sequence of sediment behaviour during wave-induced liquefaction. *Sedimentology* 53(3): 611-629.

Sumer, B. M., Kirca, O. V. S. & Fredsøe, J. 2012. Experimental validation of a mathematical model for seabed liquefaction under waves. *International Journal of Offshore and Polar Engineering* 22(02): 1-9.

Sumer, B. M. 2014. *Liquefaction Around Marine Structures*. World Scientific.

Turner, I. L., & Nielsen, P. 1997. Rapid water table fluctuations within the beach face: Implications for swash zone sediment mobility? *Coastal Engineering* 32(1): 45-59.

Van Rijn, L. C. 2007. Unified view of sediment transport by currents and waves. I: Initiation of motion, bed roughness, and bed-load transport. *Journal of Hydraulic Engineering* 133(6): 649-667.

Yeh, H., & Mason, H. B. 2014. Sediment response to tsunami loading: mechanisms and estimates. *Geotechnique* 64(2): 131-143.

Zhang, K., Douglas, B. C., & Leatherman, S. P. (2004). Global warming and coastal erosion. *Climatic Change*, 64(1-2), 41-58.

Geotechnical and Geophysical Site Characterisation 5 – Lehane, Acosta-Martínez & Kelly (Eds)

Evaluating liquefaction and lateral spreading in interbedded sand, silt, and clay deposits using the cone penetrometer

R. W. Boulanger, D. M. Moug, S. K. Munter, A. B. Price, and J. T. DeJong
Department of Civil and Environmental Engineering, University of California, Davis, CA, USA

ABSTRACT: Current procedures for evaluating potential earthquake-induced liquefaction and lateral spreading appear to have a tendency to over-predict liquefaction effects in interbedded sand, silt, and clay deposits. Possible reasons for over-prediction of liquefaction effects are discussed, and investigations regarding some factors pertinent to use of the cone penetrometer are described. An axisymmetric direct cone penetration model is presented for use with the MIT-S1 constitutive model to explore cone penetration processes in a range of soil types; current efforts are focused on validating this new direct cone penetration model, beginning with simulations of cone penetration in soft clay. The relationship between cyclic strength and cone penetration resistance in non-plastic and low-plasticity fine-grained soils is examined by relating cyclic strengths from laboratory tests to cone penetration resistances from simulations. The performance of a site underlain by interbedded soils along the Çark canal during the 1999 M=7.5 Kocaeli earthquake is analyzed using one-dimensional lateral displacement index procedures and two-dimensional nonlinear deformation analyses with spatially correlated stochastic models to illustrate how several factors can contribute to an over-prediction of liquefaction effects. Future research needs and directions for improving the ability to evaluate liquefaction effects in interbedded sand, silt, and clay deposits are discussed.

1 INTRODUCTION

Case histories have shown that the engineering procedures currently used in the US and other countries to evaluate potential earthquake-induced liquefaction and lateral spreading appear to have a tendency to over-predict liquefaction effects in interbedded sand, silt, and clay deposits. For example, this was observed in the Gainsborough Reserve and Riccarton areas of Christchurch, New Zealand, where minimal damage occurred but various engineering analyses predict that at least one of the earthquakes in the 2010-2011 Canterbury Earthquake Sequence (CES) should have caused significant ground surface damage due to liquefaction (e.g., Beyzaei et al. 2015, Stringer et al. 2015, van Ballegooy et al. 2014, 2015). Other examples include a site along the Çark Canal in Turkey during the 1999 M=7.5 Kocaeli earthquake (Youd et al. 2009) and sites in Taiwan during the 1999 M=7.6 Chi-Chi earthquake (e.g., Chu et al. 2007 and 2008).

The apparent tendency of current liquefaction evaluation procedures to over-predict liquefaction effects for interbedded sand, silt, and clay deposits, while conservative, can have large economic implications. For example, it is common to compute a potential for tens of cm of lateral displacement or a few cm of settlement in such deposits, which may lead to potentially unnecessary and expensive ground improvement or structural strengthening efforts.

The purpose of this paper is to discuss possible reasons for over-prediction of earthquake-induced liquefaction effects in interbedded sand, silt and clay deposits and describe results from three research projects regarding factors pertinent to use of the cone penetrometer for liquefaction evaluations. Possible factors contributing to an over-prediction of liquefaction effects in different situations are reviewed first. An axisymmetric direct cone penetration model is presented for use with the MIT-S1 constitutive model to explore cone penetration processes in a range of soil types, including intermediate soils (e.g., silty/clayey sands or sandy/clayey silts) which are often present in interbedded soil deposits. Current work toward validating this direct cone penetration model is illustrated by simulations of penetration resistance in Boston Blue clay. The relationship between cyclic strength and cone penetration resistance in non-plastic and low-plasticity fine-grained soils is then examined by relating cyclic strengths from laboratory tests to cone penetration resistances from simulations. Lastly, the performance of a site underlain by interbedded soils along the Çark canal during the 1999 M=7.5 Kocaeli

Table 1. Factors affecting prediction of liquefaction effects in interbedded soil deposits

Factor	Role
Limitations in site characterization tools and procedures	
Interface transitions	Penetration resistance (e.g., q_t) in sand is reduced near interfaces with clays or silts. I_c values increase in the sandy soils and decrease in the clays/silts near the interface.
Thin layer effects	Penetration resistance (e.g., q_t) reduced throughout sand layers less than about 1 m thick (with clays/silts on either side of the layer).
Graded bedding	In-situ tests measurements may not differentiate between material transitions that occur across distinct interfaces (e.g., erosional contacts) and material transitions that are gradual (e.g., beds with normal or reverse grading, or bed series in fining-upward or coarsening-upward patterns). Transition and thin layer effects in interbedded soils with graded bedding are not well understood.
Continuity of lenses	Large horizontal spacing of explorations may not enable the lateral continuity of weak or liquefiable layers to be evaluated or quantified.
Saturation	Presumption of 100% saturation below the groundwater table may underestimate cyclic strengths for partially saturated zones.
Limitations in correlations for liquefaction triggering or consequences	
Triggering correlations	Triggering correlations are not well constrained for intermediate soils with certain FC and PI combinations; CRR likely underestimated if treated as sand-like, and overestimated if treated as clay-like. Effects of age, stress & strain history, K_o, and cementation not explicitly accounted for.
Strain correlations	Correlations for estimating shear and volumetric strains have been developed primarily from data for sands or clays; the applicability of these correlations for intermediate soils is uncertain.
Limitations from analysis approaches and neglected mechanisms	
Spatial variability	The assumption that liquefiable layers are laterally continuous can contribute to over-estimation of potential liquefaction effects. Composite strength from nonliquefied and liquefied zones may limit deformations.
Thick crust layers	Thick crust layers can reduce surface manifestations of liquefaction at depth in areas without lateral spreading.
Dynamic response	Liquefaction of loose layers in one depth interval may reduce seismic demand on soils in other depth intervals.
Geometry & scale	The 2D or 3D scale of a deformation mechanism affects the dynamic response and role of spatial variability.
Diffusion	Seepage driven by excess pore pressures may increase or decrease ground deformations depending on stratigraphy, permeability contrasts, geometry, seismic loading, and other factors.

earthquake is analyzed using one-dimensional (1-D) lateral displacement index (LDI) procedures and nonlinear deformation analyses (NDAs) with spatially correlated stochastic profiles to illustrate how several factors contributed to over-prediction of liquefaction effects at the site. Future research needs and directions for improving the ability to evaluate liquefaction effects in interbedded sand, silt, and clay deposits are discussed.

2 REVIEW OF CONTRIBUTING FACTORS

The potential for current liquefaction evaluation procedures to over-predict liquefaction effects in interbedded sand, silt and clay deposits stems from several contributing factors, each of which can be important in different situations and depend on the type of analysis method employed. Possible factors contributing to over-predictions in different situations are listed in Table 1 and grouped into those factors associated with: (1) limitations in site characterization tools and procedures, (2) limitations in liquefaction triggering or consequence correlations, and (3) limitations from analysis approaches and neglected mechanisms. The first three factors listed under site characterization tools in Table 1 are described in relation to the cone penetrometer, but analogous issues exist with all in situ testing methods. The next three subsections focus on a subset of factors that are related to use of the cone penetrometer or important to the Çark canal case history. The last subsection provides a more concise review of the other contributing factors.

2.1 *Spatial resolution of cone measurements*

The spatial resolution of cone tip resistance (q_t) and sleeve friction (f_s) measurements as indicators of soil properties is limited by the physical volume of soil around a cone tip that influences these measurements. Measurements of q_t are generally influenced by soils within about 10 to 30 cone diameters around the cone tip, which corresponds to influence zones ranging from about 35 to 130 cm thick for standard 10 cm^2 and 15 cm^2 cones. Measurements of f_s have similar zones of influence because they are influenced by the normal stresses on the friction sleeve (which are related to q_t) and represent an integration of shear stress along the typically 13.4 to 16.4 cm long sleeve. Values of q_t and f_s therefore depend on the sequence and properties of all soils within the zone of influence, which can greatly complicate (and often obscure) the ability to relate q_t and f_s to soil properties at a specific point.

The zone of physical influence around a cone tip is essentially a spatial low-pass variable filter on the q_t and f_s measurements that would have been obtained if they were true point measurements (i.e., a negligible zone of influence). This spatial filtering limits the resolution with which sharp transitions in soil properties can be determined or distinguished from gradual transitions in soil properties (e.g., Frost et al. 2006). For example, the values of q_t and f_s measured near a clay-sand interface will smoothly transition from values representative of those for the clay to those for the sand, as illustrated schematically by case 1 in Figure 1. This smooth transition in q_t and f_s values, if interpreted literally on a point-by-point basis, leads to erroneous soil classifications and property estimates in the transition zone. For thin sand seams embedded in clay or plastic silt deposits, the transition zones for the upper and lower interfaces can overlap, which results in q_t values at the middle of the sand seam [$(q_t)_{thin}$ in Fig. 1] that under-predict the sand's true relative density [i.e., as represented by q_t^* in Fig. 1]. The difference between $(q_t)_{thin}$ and q_t^* increases as the sand layer thickness decreases, as illustrated by cases 2 and 3 in Figure 1.

Limitations in the spatial resolution of property estimates from cone penetrometer data in thin lenses or at interfaces between soils of strongly different properties is well recognized in the literature (e.g., Mayne 2007). Thin-layer correction procedures have been developed to adjust q_t values from the middle of a thin layer to those that would be measured in a thick layer of the same sand; i.e., $q_t^* = K_H\ (q_t)_{thin}$, where K_H is a thin-layer correction factor. The thin-layer correction factors shown in Figure 2, for example, include the relationship recommended for liquefaction evaluations at a 1997/98 NCEER workshop (Youd et al. 2001). In addition, procedures to account for transition effects at sand-clay interfaces have been developed and implemented in commercially available software for evaluating liquefaction effects (e.g., GeoLogismiki 2016).

A consistent theoretical and empirical understanding of cone penetration across interfaces or thin layers is lacking, however. For example, the thin-layer correction relationship recommended by Youd et al. (2001) based on limited field data falls below those produced by elastic solutions (Vreugdenhil et al. 1994, Robertson & Fear 1995), as shown in Fig-

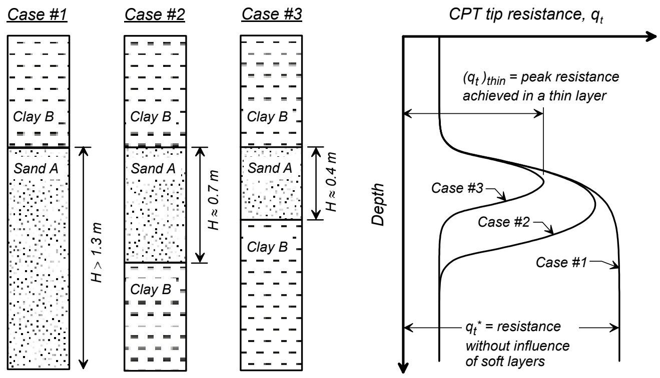

Figure 1. Influence of clay-sand interfaces and sand layer thickness on cone penetration resistance (modified from Robertson and Fear 1995; after Idriss and Boulanger 2008)

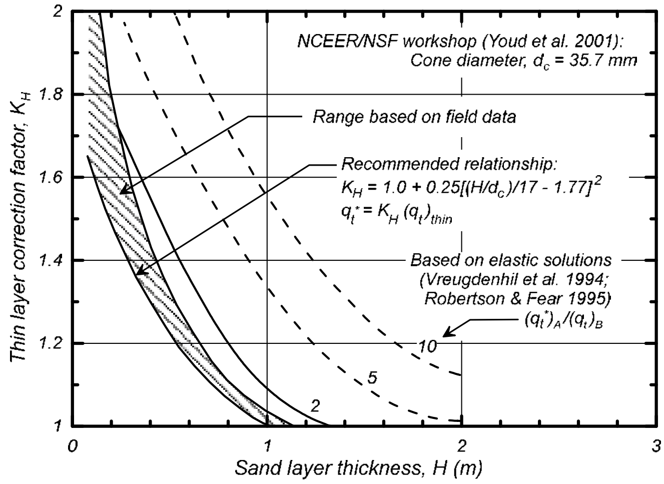

Figure 2. Thin layer correction factors for determining equivalent thick-layer cone tip resistance (modified from Youd et al. 2001; after Idriss and Boulanger 2008)

ure 2. Past experimental studies of cone penetration in layered soils have included tests with sands of different types and relative densities (e.g., Mo et al. 2013, 2015; Silva & Bolton 2004; Canou 1989 and Foray & Pautre 1988 as reported in Vreugdenhil et al. 1994). The results show transitions in q_t values over intervals of about 4 to 5 cone diameters, depending on the layer sequence and strength contrasts. Simulations of cone penetration in two layer systems by Van den Berg et al. (1996) indicate that when a cone passes from sand into soft clay, the q_t in the sand is influenced when the cone is within about 3 cone diameters of the interface, and when a cone passes from soft clay into sand, it takes about 4 cone diameters of penetration into the sand for the full q_t to develop. Simulations of cone penetration in multi-layered clays by Walker & Yu (2010) show that when a cone passes from a stronger layer to a weaker layer, the q_t is significantly influenced to a distance of about 2 or 3 cone diameters on either side of the interface, whereas when the cone passes from a weaker layer to a stronger layer, the q_t rises more abruptly. The transition interval thicknesses obtained in the above experiments and simulations would suggest that thin-layer effects should be smaller than indicated by the empirical thin-layer correction factors recommended in Youd et al. (2001) (Fig. 2). It is likely that additional experimental data, numerical simulations and field studies will be required to develop a consistent understanding of thin-layer effects for sand lenses interbedded with softer fine-grained sediments.

The influence of graded bedding on interface transition and thin-layer effects is another issue that needs to be addressed (Table 1). Individual beds of sand may exhibit normal grading (upward decrease in grain size) or reverse grading (upward increase in grain size), and series of beds can be arranged in fining-upward or coarsening-upward sequences (Nichols 2009). Current procedures for evaluating interface transition and thin-layer effects lack guidance on how one should distinguish between interfaces where soil properties transition gradually (e.g., a fining-upward sequence) versus sharply (e.g., an abrupt transition from sand to clay at an erosional contact). Measurements of q_t and f_s cannot be expected to differentiate between a sharp transition and a gradual transition that occurs over a length scale that is similar to, or smaller than, the zone of physical influence around the cone tip. Characterizing graded bedding at these smaller scales may instead require supplemental information, such as continuous core samples from the same deposit. Regardless, the currently available transition and thin-layer correction procedures were developed for abrupt soil transitions and the potential impacts of applying them to deposits with gradual transitions have not been adequately examined.

The problem in practice is that using cone penetrometer data in interbedded deposits without transition and thin-layer corrections has the potential to significantly under-estimate the available resistance to liquefaction triggering or deformation. These effects are illustrated in Figure 3 for an idealized analysis of a thin clean sand layer embedded in a clay deposit at a depth where the initial vertical effective stress (σ'_{vo}) is 100 kPa. The normalized tip resistance ($q_{tN} = q_t/P_a$ where P_a = atmospheric pressure) in the clay is 20. The sand layer is characterized by the "true" value of q_{tN} that it would have had if the layer were thick. The value of q_{tN} "measured" at the middle of the sand layer is the "true" q_{tN} divided by the thin-layer correction factor K_H based on field data from Youd et al. (2001), as shown in Figure 2. The "measured" q_{tN} is assumed to transition linearly from the clay value to the mid-sand-layer value over a transition interval of either 15 cm (blue lines) or 30 cm (red lines), or just half the sand layer thickness if the sand layer is thinner than twice the transition interval thickness. The "measured" sleeve friction is assumed to produce normalized tip resistance (Q) and sleeve friction ratio (F) values that

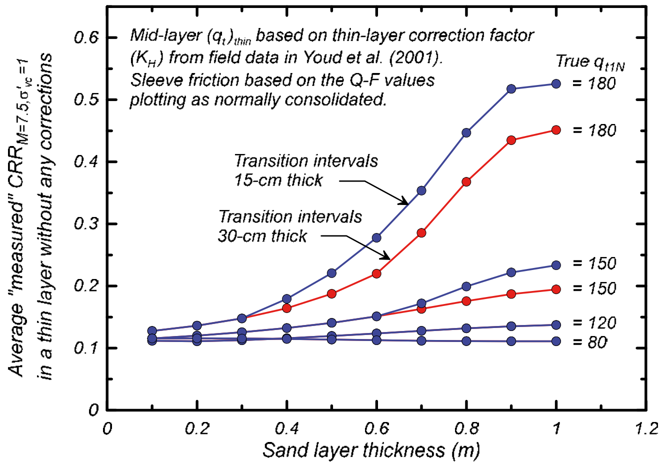

Figure 3. Idealized example illustrating the underestimation of CRR for a thin sand layer embedded between clay layers if transition and thin-layer corrections are not applied

plot in the middle of the normally consolidated zone on the soil behavior type chart by Robertson (1990). The cyclic resistance ratio (CRR) for M=7.5 and σ'_{vo} = 1 atm was computed using the liquefaction triggering correlation by Boulanger & Idriss (2015); this calculation based on the "measured" CPT data includes the apparent increase in fines content as the sand layer thickness decreases (i.e., Q decreases and the soil behavior type index I_c increases). Lastly, the average CRR across the sand layer was computed and plotted versus the sand layer thickness in Figure 3 for various "true" q_{t1N} values. The results in Figure 3 illustrate how the use of CPT data without transition and thin-layer corrections can significantly under-predict the CRR of dense sand lenses less than about 1 m thick and cannot distinguish between loose or dense conditions for sand lenses less than about 0.3 m thick. Ideally, transition and thin-layer corrections would remove this source of potential bias, but the details of their application are subjective in practice (e.g., the issue of graded bedding) and difficult to automate. For this reason, these corrections are not uniformly applied or relied upon.

2.2 *Intermediate soil types*

Current liquefaction triggering correlations (e.g., Robertson & Wride 1998, Moss et al. 2006, Boulanger & Idriss 2015) have some of their greatest differences in silty sands, sandy silts and silts of low-plasticity. These differences are not surprising because the triggering correlations are not well constrained by the limited number of case histories involving intermediate soil types and thus their differences also stem from differences in their functional forms. Recent research has shown that q_t in low-plasticity fine-grained soils can vary strongly with small changes in clay content [or plasticity index (PI)], and this has a strong effect on the correlation to cyclic strength for soils with high percentages of fines that are either non-plastic or of low plasticity (say PI < ~ 5). Current liquefaction triggering procedures do not have theoretical bases or sufficient field data for confidently constraining these correlations across the full range of possible fines content (FC) and PI combinations.

Procedures for evaluating cyclic strengths have tended to be either well suited for sand-like soils or well suited for clay-like soils. For sand-like soils, concerns with the effects of sampling disturbance have led to an emphasis on case history based liquefaction triggering correlations using CPT, SPT or shear wave velocity (V_s) data. For clay-like soils, the ability to sample and test with reasonable confidence has led to procedures that are similar to those used to evaluate monotonic undrained shear strengths. An artifact of these two different approaches has been sharp jumps in the estimated cyclic strength when the soil classification toggles across a classification of clay-like versus sand-like. These sharp jumps in CRR values were illustrated by Robertson (2009) as contours on a soil behavior type chart (Fig. 4).

Similarly, correlations for estimating earthquake-induced shear strains or post-shaking reconsolidation strains have been developed primarily from laboratory test data for either sands or clays. The extension of these correlations to intermediate soils has not been systematically examined, and is another source of potential bias in evaluating liquefaction consequences (Table 1).

The fundamental basis for cone penetration resistance to correlate with cyclic strengths also warrants discussion. Consider the schematic in Figure 5 showing critical state lines, initial conditions, and stress paths for a point near the cone tip as it penetrates either medium-dense sand or normally consolidated clay. The monotonic loading imposed by cone penetration produces an undrained stress path that moves to the left in the normally consolidated clay and a drained path that moves to the right in the medium-dense sand. The path for the medium-dense sand moves down and to the right because the sand is much less compressible under monotonic loading (as represented by a flatter critical state line at lower stresses) and is initially dense of critical state, which together lead to large mean stresses near the cone tip during drained penetration. The path for the medium-dense sand under seismic loading, however, would potentially be to the left if saturated and largely undrained during the seismic loading. The path for seismic loading may move to the left because the sand can accumulate net plastic volumetric contractive strains during reversed cyclic loading, which causes a loss of effective stress for undrained conditions. Thus, the stress path followed by sand during cone penetration is not the same as that for seismic loading. The greater compressibility of clay relative to sand and the undrained conditions during cone penetration in clay (versus drained in sand) result in much lower cone penetration resistances, even if the clay is heavily over-consolidated and has a large cyclic strength. For sand or clay, cyclic strength correlates with cone penetration resistance because variations in fundamental properties or soil characteristics that tend to increase cone penetration resistance also tend to increase cyclic strength, and vice versa (e.g., state, compressibility, stress history, age, and cementation). The effects of variations in the fundamental properties or soil characteristics on cyclic strength and cone penetration resistance are nonetheless unlikely to be identical, which is one source of dispersion in the resulting correlations for either sand or clay. At the same time, the general

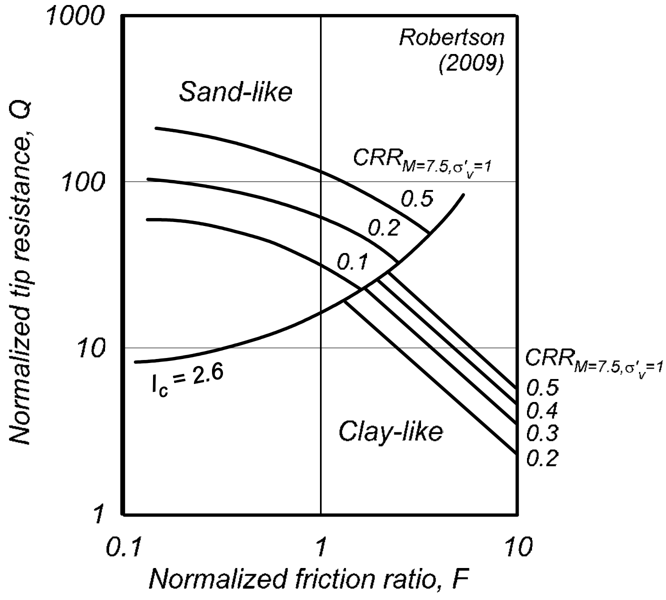

Figure 4. Contours of $CRR_{M=7.5,\sigma'=1}$ for sand-like and clay-like soils based on the procedures by Robertson and Wride (1998) for sand-like soils and by Boulanger and Idriss (2007) for clay-like soils (after Robertson 2009)

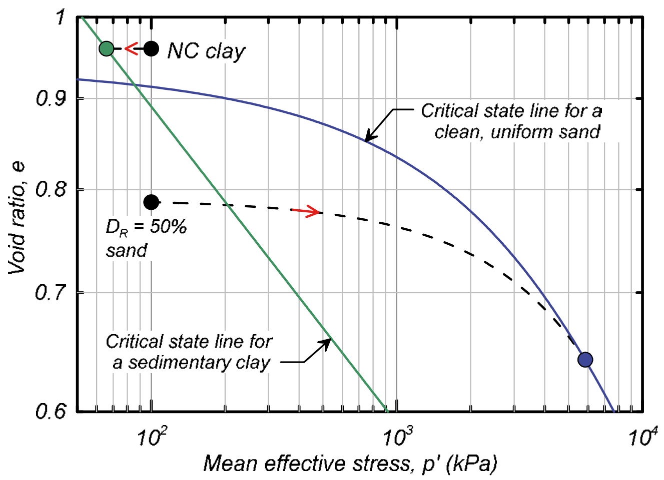

Figure 5. Schematic of loading paths near a penetrating cone in normally consolidated clay (an undrained path) or medium dense sand (a drained path)

differences in fundamental properties for sand versus clay are sufficiently large that distinctly different cyclic strength correlations have been developed for these two soil types. The subsequent application of these correlations therefore depends strongly on soil characteristics that are currently only accounted for by broad categorizations such as clay-like or sand-like. The generalization of cyclic strength correlations across intermediate soil types (i.e., from sand to clay) would benefit from a more generalized theoretical framework and may also benefit from independent measures or indices of other soil attributes, such as shear wave velocity, compressibility, and permeability.

2.3 *Spatial variability*

Simplifying and ultimately conservative assumptions regarding the lateral continuity and extent of liquefiable lenses within interbedded deposits are explicitly incorporated in some liquefaction evaluation methods and often implicitly invoked in the application of other liquefaction evaluation methods. For example, liquefaction vulnerability indices (LVIs) such as the lateral displacement index (LDI), liquefaction potential index (LPI), liquefaction severity number (LSN), or post-liquefaction reconsolidation settlement ($S_{v\text{-}1D}$) are all commonly computed using data from individual borings or CPT soundings. These calculations are therefore based on the assumption of horizontal layering with infinite lateral extent, such that the results are referred to as 1-D LVIs. Other liquefaction evaluation methods include empirical regression models (e.g., the multiple linear regression models by Youd et al. 2002) and Newmark sliding block methods (e.g., Olson & Johnson 2008). In applying these methods, it is common in practice to conservatively assume lateral continuity or connectivity of liquefiable layers across borings and soundings that are often spaced too far apart for the lateral continuity to be properly evaluated.

Limited lateral continuity of liquefiable lenses in interbedded sand, silt and clay deposits has been hypothesized as a possible factor when ground deformations are over-predicted by current liquefaction evaluation procedures. In these cases, it is possible that any potential failure or shear deformation mechanisms must engage both liquefiable and nonliquefiable soils, and that the shear strengths of the nonliquefiable soils are sufficient to reduce ground deformations. Youd et al. (2009) concluded this was the case at Çark Canal during the 1999 M=7.5 Kocaeli earthquake, for example. NDAs using stochastic models of interbedded sands and clays in mildly sloping ground demonstrated this is potentially a major factor controlling lateral spreading displacements (Munter et al. 2016). More generally, Cubrinovski & Robinson (2015) examined characteristics of lateral spreads in the 2010-11 CES and concluded that small-displacement lateral spreads were associated with thin critical layers that were discontinuous along and away from the river, and that large-displacement lateral spreads of narrow extent were associated with critical layers confined within narrow zones along riverbanks. Their findings illustrate the importance of the scale of the critical layers relative to the scale of the deformation mechanisms.

Methods for systematically evaluating spatial variability in interbedded deposits and accounting for it in liquefaction evaluation procedures are not well developed. Improved guidance on how to systematically account for the influence of spatial variability in estimating vertical settlements and/or lateral spreading in naturally variable deposits is needed.

2.4 *Other contributing factors*

Several other factors, in addition to those discussed above, are considered as likely contributing to why current liquefaction evaluation procedures can sometimes over-predict liquefaction effects in interbedded sand, silt and clay deposits (Table 1). The significance of each factor depends, in part, on the analysis approach being used to evaluate liquefaction effects: e.g., empirical regression models, 1-D LVIs, Newmark sliding block models, or NDAs.

One factor is the role of thick crust layers in reducing surface manifestations of liquefaction in areas without lateral spreading (e.g., Ishihara 1985). A crust layer that is sufficiently thick relative to the extent and thickness of any liquefied zone can reduce differential surface settlements, ground cracking, and emergence of soil ejecta. This effect can also complicate case history interpretations, especially in distinguishing cases of non-manifestation from cases of non-liquefaction triggering.

Another possible factor is partial saturation of soils within some depth interval below the ground water table, with the partially saturated soils having a greater cyclic resistance than otherwise expected. Soils may be partially saturated because of past water table fluctuations or chemical and biological activity. The greater cyclic strength of a partially saturated zone could result in a thicker crust of nonliquefied materials that could help reduce surface manifestations of liquefaction, as discussed above.

Another possible factor is the influence of liquefaction on the dynamic response of a site, such that liquefaction of looser soils within one depth interval may reduce the dynamic stresses and strains imposed on soils in other depth intervals. Simplified 1-D LVI procedures do not account for these effects and thus will over-predict the potential for lateral displacements in situations where they are significant.

Another factor is that the inter-bedding of sand, silt and clay impedes the diffusion of excess pore water pressures that develop within the liquefiable lenses. In some cases, this impeding of diffusion may reduce deformations relative to those that can develop in thick layers of liquefiable sands where a steady upward flow of pore water may weaken soils near the surface and contribute to deformations. In other cases, this impeding of diffusion may increase deformations if it leads to sufficiently extensive water film formation or localized strength loss (e.g., Kokusho 2003, Boulanger et al. 2014). The potential for impeded diffusion to increase or decrease deformations depends on the stratigraphy, permeability contrasts, geometry, seismic loading, and other factors. It is difficult to predict diffusion effects during and after seismic loading even with advanced NDAs, and the empirical data are still insufficient to propose accounting for these effects in any simplified method.

In most cases, it is likely that several of the factors listed in Table 1 will contribute to any observed bias in liquefaction evaluations for interbedded sand, silt and clay deposits. The degree to which each factor contributes will depend on the specific situation and the analysis method employed. For this reason, the systematic evaluation of case histories with due consideration to all contributing factors will be important for developing improved guidance for practice.

3 DIRECT CONE PENETRATION MODEL

Numerical simulations for cone penetration have been performed for sand or clay using direct and indirect axisymmetric models. Direct models simulate penetration with the full cone geometry, whereas indirect models simulate cylindrical or spherical cavity expansion. Indirect models require converting the cavity expansion limit pressure to a cone tip resistance using relationships or procedures that are significantly different for sand versus clay. A direct model is preferable for studying intermediate soils (e.g., silty and clayey sands) because indirect conversion procedures are not available for these soil types.

A direct axisymmetric model for cone penetration in intermediate soils requires a constitutive model that can reasonably approximate a broad range of soil behaviors. A review of the literature (Moug et al. 2016) found that direct penetration models have primarily used relatively simple elastic-plastic constitutive models, such as Mohr-Coulomb (e.g., Huang et al. 2004, Chai et al. 2012), von-Mises (e.g., Walker & Yu 2006, Liyanapathirana 2009, Wang et al. 2015), Drucker-Prager (e.g., Yi et al. 2012) and modified Cam Clay models (e.g., Yu et al. 2000, Chai et al. 2012, Mahmoodzadeh et al. 2014). These types of constitutive models are not general enough to simulate the full range of intermediate soil behaviors.

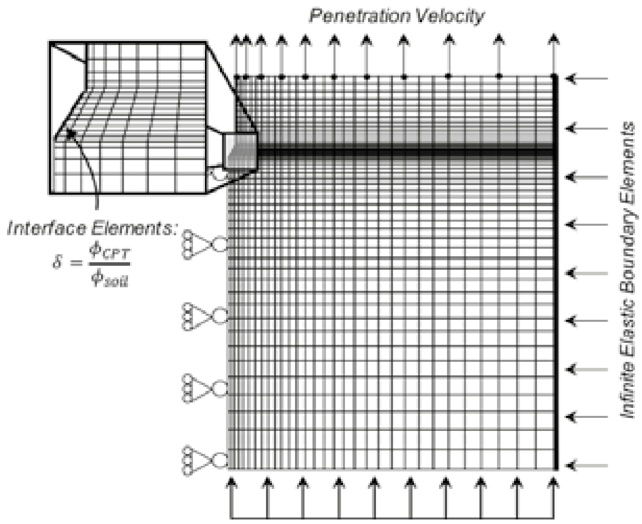

Figure 6. Boundary conditions and mesh for direct axisymmetric penetration model (Moug et al. 2016)

A direct axisymmetric model for steady state cone penetration using the MIT-S1 constitutive model was therefore developed by Moug et al. (2016). The MIT-S1 constitutive model (Pestana & Whittle 1999), with its generalized, bounding surface formulation, is able to approximate the stress-strain responses of a broad range of soil types. The MIT-S1 model was implemented in the finite difference platform FLAC 7.0 (Itasca 2011) by Jaeger (2012). The penetration model implemented by Moug et al. (2016) uses an Arbitrary Lagrangian Eulerian (ALE) algorithm that couples the large deformation Lagrangian formulation in FLAC with a user-written rezoning algorithm and a user-written second-order Eulerian advection remapping algorithm after Colella (1990). Interface elements between the soil and cone enable the specification of interface friction angles, as opposed to assuming purely rough or purely smooth interfaces. An example mesh for the axisymmetric model and its boundary conditions are shown in Figure 6.

The first application of this direct penetration model was an examination of cone penetration in Boston Blue Clay (BBC) using the Mohr-Coulomb (MC), Modified Cam Clay (MCC), and MIT-SI constitutive models. Details are in Moug et al. (2016).

Laboratory test results on intact samples (Landon 2007) and re-sedimented specimens (Ladd & Varallyay 1965) show that BBC has significant strength anisotropy. The undrained shear strength ratio (s_u/σ'_{vo}) for $CK_{ONC}UC$ loading is about 0.28 and 0.33 for intact and resedimented specimens, respectively. The s_u/σ'_{vo} for $CK_{ONC}UDSS$ and $CK_{ONC}UE$

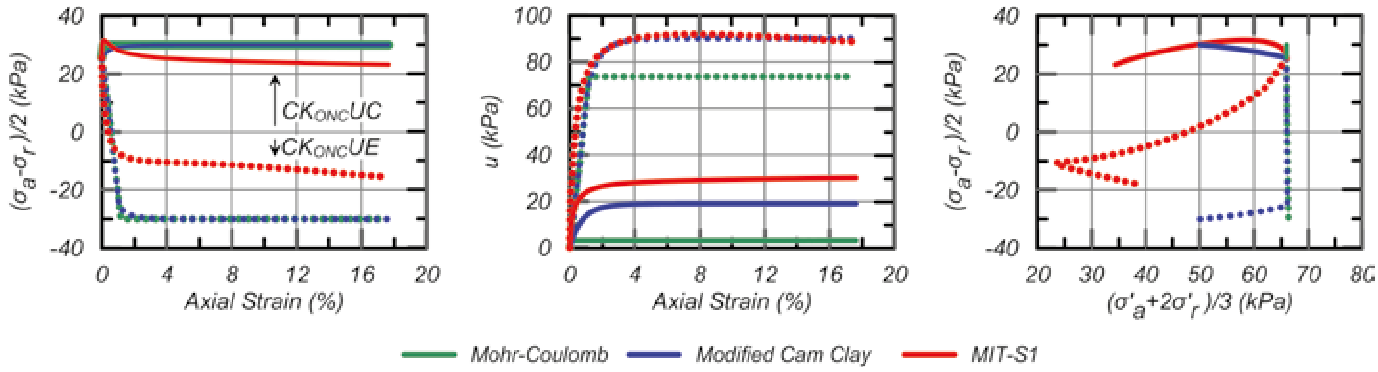

Figure 7. Single element simulations of BBC response in CK$_{ONC}$UC and CK$_{ONC}$UE loading using the MC, MCC and MIT-SI constitutive models calibrated to the same CK$_{ONC}$UC strength (after Moug et al. 2016)

loading of resedimented specimens decreases to 0.20 and 0.14, respectively.

Only the MIT-S1 model is able to approximate the BBC's strength anisotropy, as illustrated in Figure 7 showing single-element simulations for CK$_{ONC}$UC and CK$_{ONC}$UE loading with the three constitutive models calibrated to the same CK$_{ONC}$UC strength. The MC and MCC models produce the same s_u in extension and compression, whereas the MIT-S1 model is able to simulate a much lower s_u in extension than in compression. The MIT-S1 calibration is presented in Jaeger (2012), which was updated from the calibration in Pestana et al. (2002).

The pore pressure and stress path responses for the single-element simulations in Figure 7 illustrate the significant differences in shear-induced pore pressure for the three constitutive models. The MC model, with a friction angle of zero and associative flow, does not develop plastic volumetric strains during deviatoric loading and thus only develops excess pore pressure in response to changes in mean total stress. The MCC model generates greater pore pressures than the MC model for either loading condition because the MCC model does develop plastic volumetric strains once the yield surface has been reached. The MIT-S1 model generates even greater pore pressure for either loading path because its more flexible formulation enabled a calibration that could approximate pore pressures associated with the BBC strength anisotropy.

Cone penetration at a BBC site in Newbury, Massachusetts was then simulated for a depth of 9.6 m where the vertical total stress was 175 kPa, vertical effective stress was 100 kPa, and the overconsolidation ratio (OCR) was about 2.2 (Landon 2007). The measured q_t at this depth range from 530 to 730 kPa (Landon 2007). The simulated cone penetration resistances (q_t) were reached by about 5 cone diameters of penetration for all three soil models (Fig. 8). Cone tip resistances with the MC and MCC soil models are both about 750 kPa, which is consistent with both models producing essentially the same s_u of 59 kPa for either CK$_0$UC or CK$_0$UE

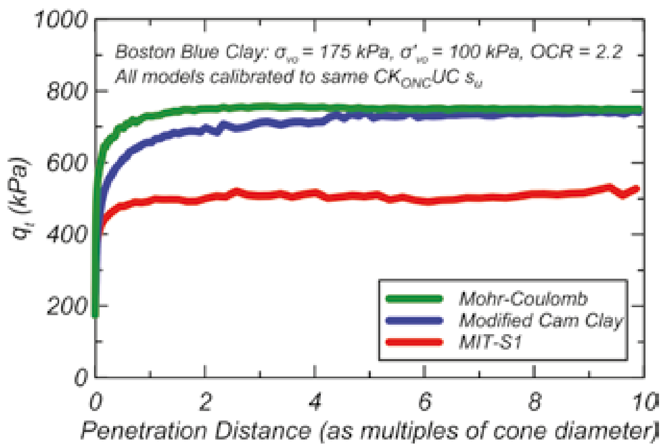

Figure 8. Simulated tip resistance versus penetration distance from wished in-place initial condition (after Moug et al. 2016)

loading conditions. The cone bearing factor N_{kt} from these simulations, with their essentially isotropic s_u values, correspond to an $N_{kt,iso}$ of about 9.7.

Cone tip resistance with the MIT-S1 model was about 515 kPa, or 31% smaller than with the MC and MCC models. The MIT-S1 model produces a smaller q_t value because its calibration produces smaller s_u values for all but the CK$_0$UC loading condition; i.e., MIT-S1 with OCR of 2.2 and σ'_{vc} = 100 kPa produces s_u of 54, 36 and 38 kPa for CK$_0$UC, CK$_0$DSS and CK$_0$UE loading conditions respectively. This simulation result thus corresponds to $N_{kt,C}$, $N_{kt,DSS}$ and $N_{kt,E}$ values of 6.3, 9.4 and 8.9, respectively. The cone tip resistance could alternatively be related to the average s_u for these three test types (i.e., 43 kPa for this example) which would correspond to an $N_{kt,ave}$ of 8.0.

The simulated total vertical stress fields around the penetrating cone at 25 cone diameters of penetration are shown in Figure 9 for each soil model. The steady state stress distributions show similar stress values in the cone tip area for MC and MCC models, while total vertical stress is less for the MIT-S1 model. The differences in total vertical

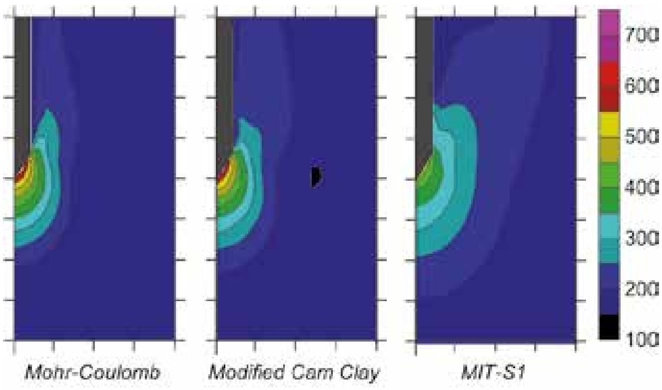

Figure 9. Total vertical stress at 25 cone diameters of penetration in Boston Blue Clay; σ_{vo} =175 kPa prior to penetration (after Moug et al. 2016)

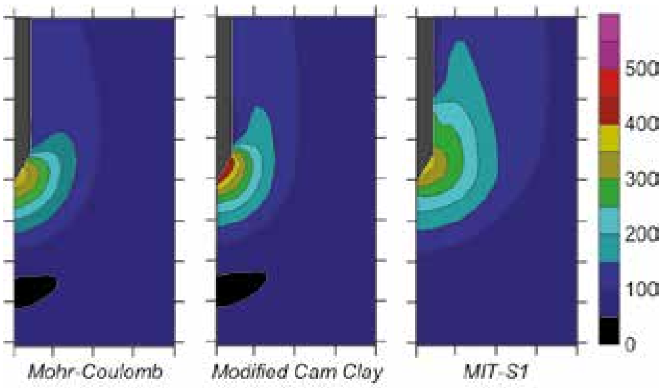

Figure 10. Pore water pressure at 25 cone diameters of penetration in Boston Blue Clay; u_o = 75 kPa prior to penetration (after Moug et al. 2016)

stress are consistent with the differences in cone tip resistance for the three models.

Steady state pore pressure fields are presented in Figure 10 for the three constitutive models. There are two components to the pore pressures generated during undrained cone penetration: (1) pore pressure due to a change in total mean stress, and (2) pore pressure due to deviatoric loading. Pore pressures induced by the cone penetration with the MCC model are slightly greater than with the MC model. The total stress fields are similar for the two models because they have similar strengths and therefore produce similar cone tip resistances. The MCC model, however, produces more pore pressure during deviatoric loading as illustrated by the single element simulations in Figure 7.

The steady state pore pressure for the MIT-S1 model shows smaller pore pressures near the cone face, but greater pore pressures for some zones near the cone shaft above the tip. The smaller pore pressures near the cone face are attributed to the MIT-S1 model producing smaller mean total stresses and smaller cone tip resistance because of its lower average strength. The pore pressures near the cone shaft above the tip are larger with MIT-S1 because it produces more pore pressure during deviatoric shearing (as shown by the single element simulations in Fig. 7) and the mean total stresses for the three models are not as different in this area.

The cone tip resistances for the Newbury site were slightly over-estimated with the MCC and MC models and slightly under-estimated with the MIT-S1 model. The analyses with the MCC and MC models over-predicted q_t because they were calibrated to the stronger $CK_{ONC}UC$ loading condition. The under-prediction obtained with the MIT-S1 model suggests that calibration to resedimented BBC data may have underestimated in-situ s_u values for some of the loading conditions that develop around the cone. Overall, the reasonable agreement between simulated and measured tip resistances provides a measure of validation for the cone penetration model.

The development of a direct cone penetration model with the MIT-S1 constitutive model was considered an important step for supporting studies of some factors contributing to over-predictions of liquefaction effects in interbedded sand, silt and clay deposits (Table 1). One objective is developing a mechanistic framework for relating CPT data to cyclic behaviors of intermediate soils. Another objective is examining the influence of interface transitions, thin layers, and graded bedding on cone penetrometer measurements. For these objectives, the simulation of cone penetration with realistic constitutive responses is expected to provide improved insights and capabilities.

4 LIQUEFACTION TRIGGERING CORRELATION FOR INTERMEDIATE SOILS

Advancement of CPT based methods for estimating cyclic strengths of intermediate soils requires improvements in our understanding of the properties influencing cone penetration and cyclic loading behaviors. For example, insights have been obtained from studies examining cyclic strength and cone tip resistance in intermediate soils through cyclic lab tests, cone penetration tests in calibration chambers, and numerical simulations of cone penetration (Salgado et al. 1997, Carraro et al. 2003, Cubrinovski et al. 2010, Jaeger 2012, Kokusho et al. 2012, Park & Kim 2013, DeJong et al. 2013).

In this section, initial results are presented for a study relating laboratory measured cyclic strengths to simulated cone tip resistances in mixtures of non-plastic silt and kaolin (Price et al. 2015). Non-plastic silica silt and kaolin clay were blended to create soil mixtures with PIs of 0, 6, and 20. The PI = 0 mixture was 100% silica silt, the PI = 6 mixture was 80% silica silt and 20% kaolin clay by dry mass, and the PI

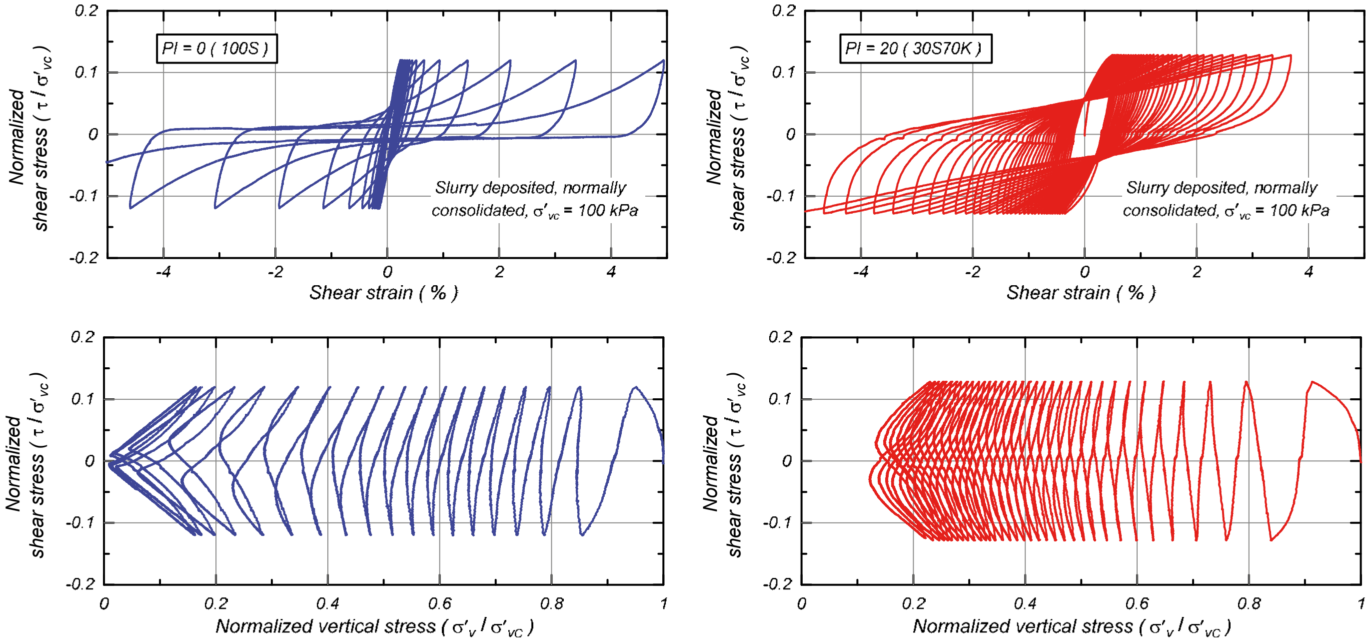

Figure 11. Undrained cyclic direct simple shear test results for normally consolidated, slurry sedimented specimens of PI=0 silt (left side) and PI=20 clayey silt (right side)

= 20 mixture was 30% silica silt and 70% kaolin clay.

The monotonic and cyclic loading responses of slurry deposited specimens at different overconsolidation ratios were characterized by undrained monotonic and cyclic direct simple shear (DSS) tests and one-dimensional consolidation tests. The cyclic loading response of normally consolidated specimens of the PI = 0 and PI = 20 mixtures are shown in Figure 11. The cyclic stress ratios required to cause single-amplitude peak shear strains of 3% are plotted versus number of loading cycles in Figure 12 for all three mixtures and OCRs of 1 and 4. Overconsolidation increased the CRR values for all three mixtures, although the increase was greater for the PI = 6 and 20 mixtures than for the PI = 0 soil. The CRR values ranged from 0.10 to 0.14 for the NC specimens and from 0.21 to 0.29 for the OCR = 4 specimens. The observed variation in CRR with mixture PI and OCR is conditional on the three mixtures having been placed by a similar depositional process, while recognizing that they are unavoidably different in all other key characteristics (e.g., initial void ratio, critical state line, compressibility). Comparisons of laboratory strengths obtained on soil mixtures with different characteristics (e.g., fines contents, PIs, OCRs, fabrics) become more valuable if they can instead be expressed conditional on independent test measurements available in practice, such as data from a cone penetrometer.

Indirect cone penetration analyses were performed in this preliminary work because the direct penetration model described in the previous section was still under development. Cylindrical cavity expansion simulations were performed in FLAC using the MIT-S1 model. The calibrated response of the MIT-S1 model for the three soil mixtures is illustrated in Figure 13 for undrained monotonic DSS loading of normally consolidated specimens. The limit pressures from the cavity expansion analyses were converted to cone tip resistances using the procedure by Leblanc & Randolph (2008), although the appropriateness of this or other conversion procedures for nonplastic and low plasticity silts has not yet been established.

The laboratory measured cyclic strengths are related to the simulated cone tip resistances in Figure 14 for the three mixtures and σ'_{vc} = 100 kPa. The

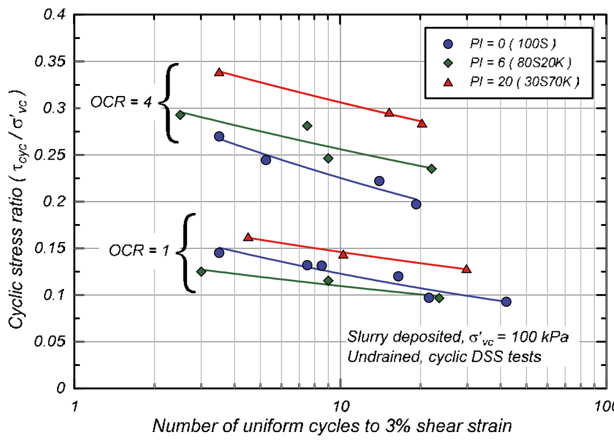

Figure 12. Cyclic stress ratio to 3% single amplitude peak shear strain in undrained cyclic DSS tests on slurry sedimented specimens of PI = 0, 6, and 20 soils at OCRs of 1 and 4 (after Price et al. 2015)

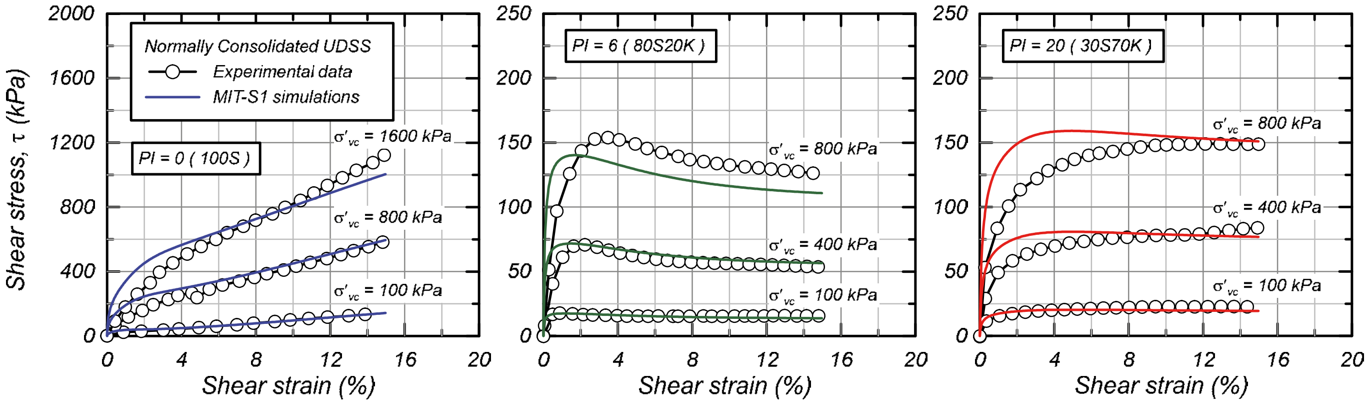

Figure 13. Simulation of undrained monotonic DSS responses for normally consolidated, slurry sedimented specimens of the PI = 0, 6, and 20 soils at different initial consolidation stresses (Price et al. 2015)

shaded regions for each mixture indicate the range of tip resistances for drained and undrained conditions. Cone penetration in the field would be expected to range from partially drained for the PI = 0 and 6 soils to largely undrained for the PI = 20 soil based on their measured coefficients of consolidation and established relationships for drainage during cone penetration (e.g., DeJong & Randolph 2012). The curves relating CRR to tip resistance for the PI = 6 and 20 soils are located much further to the left than the curves for the PI = 0 soil. This leftward shift with a small amount of plasticity is primarily due to the order-of-magnitude smaller tip resistances for the PI = 6 and 20 soils, whereas the CRR values for all three mixtures at any given OCR varied to a lesser extent (Fig. 12). The order-of-magnitude smaller tip resistances for the PI = 6 and 20 soils relative to the PI = 0 soil are consistent with their differences in compressibility and initial states (Price et al. 2015), as schematically illustrated previously in Figure 5. The results in Figure 14 are consistent with studies showing that the leftward shift in SPT liquefaction triggering correlations with increasing fines content is largely attributable to the effects of the fines on the SPT penetration resistance (e.g., Cubrinovski et al. 2010).

Empirical curves of CRR versus tip resistance are also shown in Figure 14 for clays and nonplastic silts at a σ'_{vc} of 100 kPa. The relationships between CRR and undrained tip resistance for the PI = 6 and 20 soils are in reasonable agreement with the empirical curve for ordinary sedimentary clays. The range of CRR versus tip resistance curves for the PI = 0 soil is also in reasonable agreement with its corresponding empirical correlation for nonplastic liquefiable soils (Boulanger & Idriss 2015). The general agreement between the relationships developed for these PI = 0, 6, and 20 soils and their applicable empirical counterparts is promising in suggesting that the present approach can be used to further examine the use of CPT tests for estimating cyclic strengths

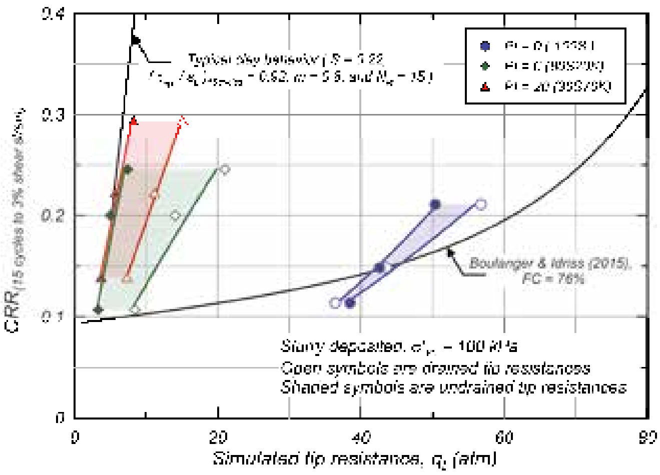

Figure 14. Measured cyclic strength versus simulated cone tip resistance for slurry sedimented PI = 0, 6, and 20 soils at OCR of 1, 2, and 4 (Price et al. 2015)

of intermediate soils across a broader range of in-situ conditions.

Results from this project are expected to support the refinement of triggering correlations for intermediate soils, which is one potential factor contributing to over-prediction of liquefaction effects in interbedded sand, silt, and clay deposits (Table 1). Future work will include examining additional intermediate soil mixtures, repeating the cone penetration simulations with the direct penetration model described in the previous section, and validating select cases with centrifuge model tests. Interpretation of these results will also examine how CPT based relationships may be augmented by independent measurements of the soil's mechanical properties, such as small-strain shear wave velocity or limiting compression behavior.

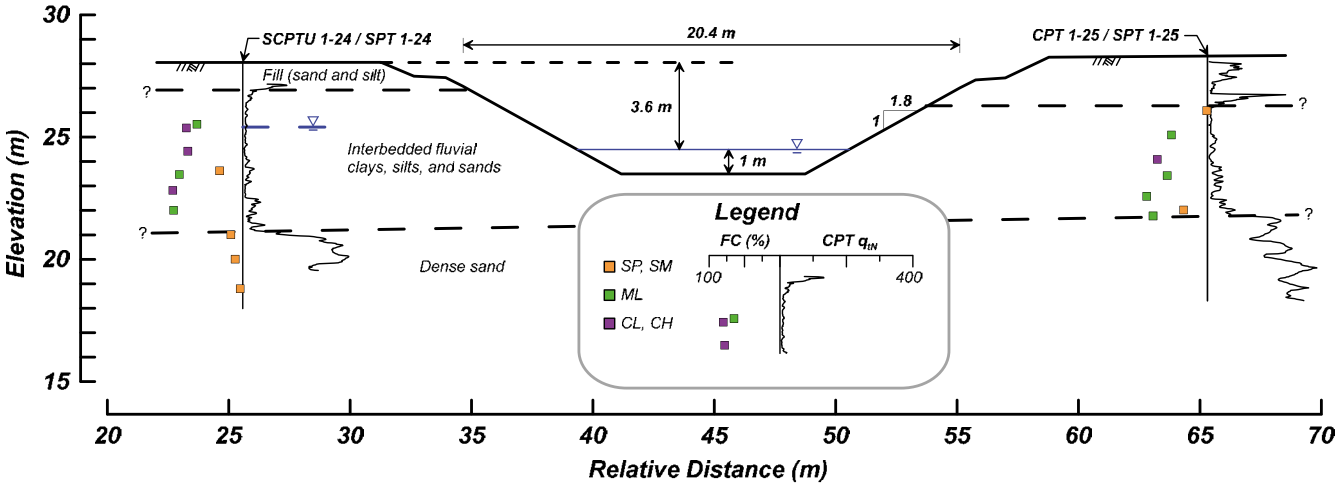

Figure 15. Cross-section of Çark Canal with CPT and borehole data near the channel (modified from Youd et al. 2009)

5 EVALUATION OF LIQUEFACTION EFFECTS AT ÇARK CANAL

The performance of a site underlain by interbedded soils along the Çark canal in the 1999 M=7.5 Kocaeli earthquake is reexamined to evaluate how different factors can contribute to an over-prediction of liquefaction effects. Lateral spreading displacements are estimated using 1-D LDI procedures and 2-D NDAs with spatially correlated stochastic models. The results of the LDI analyses illustrate the potential importance of transition and thin-layer corrections in CPT based evaluations of liquefaction effects for interbedded sand, silt, and clay deposits. The results of the NDA analyses illustrate the additional roles of spatial variability, geometry and nonlinear dynamic response.

The characterization of a section of Çark canal and its performance during the 1999 M=7.5 Kocaeli earthquake was presented by Youd et al. (2009). The canal is a channelized segment of the meandering Çark River. The critical stratum for evaluating ground deformations is a fluvial deposit of predominantly clay-like fine-grained sediments with interbedded silty sands, as shown on the cross-section in Figure 15. Five CPT soundings and two borings with SPTs were performed at the site and documented in Youd et al. (2000). No lateral spreading damage was observed at the site after the Kocaeli earthquake despite an estimated peak ground acceleration of 0.4 g. Youd et al. (2009) showed that current liquefaction susceptibility criteria in combination with a multiple linear regression model greatly overpredicted lateral spreading displacements for this site. They concluded that the sand lenses were likely not horizontally continuous and that the strength of the clays between the liquefiable lenses must have been sufficient to limit ground deformations.

Lateral displacement indices (LDIs) were computed for the five CPT soundings using two different procedures and a sequence of refinements to evaluate their impacts on the results. One set of LDIs was computed using the liquefaction triggering correlation by Boulanger & Idriss (2015) with strains estimated using the procedures in Idriss & Boulanger (2008) based on Ishihara & Yoshimine (1992). The second set of LDIs was computed using the liquefaction triggering correlation by Robertson & Wride (1998) with the procedure by Zhang et al. (2004) to arrive at the lateral displacement (LD) values that might be expected for a point located about 6 m back from the canal edge. Both procedures were first applied using the common practice of point-by-point calculations without transition or thin-layer corrections and using all applicable default parameters. The default parameters include using $I_c \leq 2.6$ for identification of sand-like (or liquefiable) soils and using $C_{FC} = 0$ for estimating FC in the Boulanger & Idriss (2015) liquefaction triggering procedure. The LDs ranged from 176 to 313 cm (median of 230 cm) and the LDIs ranged from 56 to 123 cm (median of 76 cm) for the five CPT soundings. The LDs are greater than the LDIs primarily because the Zhang et al. (2004) procedure includes a multiplier of 2.4 on displacements for the chosen point 6 m back from the canal edge. Regardless, the application of either procedure without transition or thin-layer corrections greatly over-predicts the potential for liquefaction effects at this site.

The LDI procedure using Boulanger & Idriss (2015) was then used to compute LDI values with the progressive addition of transition corrections, thin-layer corrections, and a site specific calibration to the FC data (i.e., the C_{FC} parameter). The median LDI for the five CPT soundings reduced to 67 cm with transition corrections, to 53 cm with transition and thin-layer corrections, and to 36 cm with both corrections and the site-specific C_{FC} calibration (C_{FC}

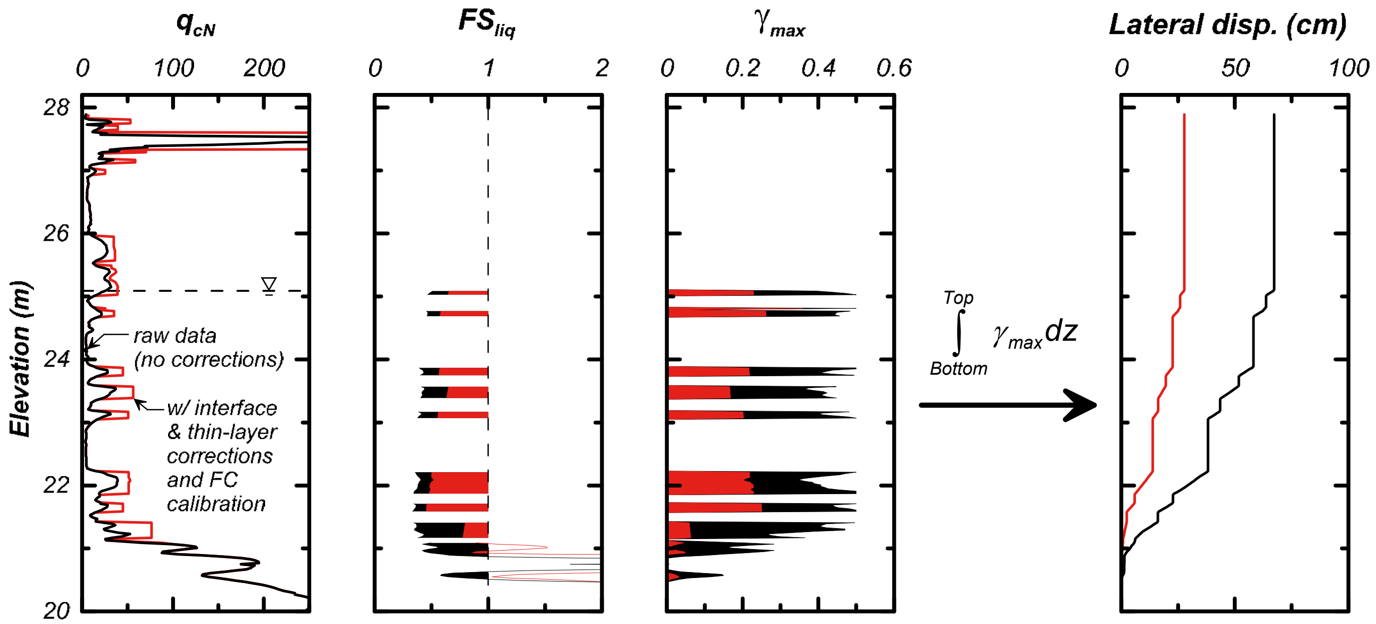

Figure 16. LDI results for CPT 1-23 without any adjustments (black lines) and with application of transition and thin-layer corrections and a site-specific fines content calibration (red lines).

= 0.27). The cumulative effect of these refinements are illustrated for CPT 1-23 in Figure 16, showing the cone tip resistance, factor of safety against liquefaction triggering, the maximum potential shear strain, and the integrated LDI profile for the first analysis case (no corrections; black lines) and last analysis case (all refinements combined; red lines). Each of the above refinements contributed to a progressive reduction in the estimated LDIs, but the last analysis case with all refinements combined still over-predicts the potential for liquefaction effects at this site.

The sensitivity of these LDI results to the I_c cutoff was also examined. If liquefiable soils are instead identified using $I_c \leq 2.4$, the median LDI is further reduced to 10 cm using both corrections and the revised site-specific C_{FC} value of 0.41. The site characterization data do not indicate that a lower I_c cutoff is justifiable for this site, but these sensitivity results do illustrate the potential value in detailed site-specific field sampling and laboratory testing to refine the I_c cutoff used in these analyses.

NDAs of this site were performed using stochastic realizations of the interbedded sand and clay stratigraphy to assess the impact of spatial variability on the potential deformations. The realizations were produced using a transition probability geostatistical approach (Carle 1999, Weissmann et al. 1999) with parameters determined from analysis of the CPT data, supplemented by estimates based on the depositional environment. Realizations conditional on the CPTs on either side of the canal were produced using different estimates for the horizontal mean lengths and percent sand-like materials in the critical stratum. The realization shown in Figure 17 is for a case with 40% sand with horizontal and vertical mean lengths for the sand lenses of 10 m and 26 cm, respectively.

Representative properties for the sand and clay portions of the critical stratum were selected by binning the data for the sand-like and clay-like portions of the stratum and examining the data for spatial patterns separately. The sand-like materials were characterized using q_{c1Ncs} = 115 which is approximately the median value after applying transition and thin-layer corrections and the site-specific C_{FC} calibration. The clay-like materials were characterized using an undrained shear strength (s_u) of 50 kPa, which is approximately the median value based on an N_{kt} of 15. The fill layer and underlying dense sands layers were also characterized using median properties estimated from the CPT data.

The sand-like sediment in the critical stratum and underlying dense sand layer were modeled using the user-defined PM4Sand constitutive model (Boulanger & Ziotopoulou 2015; Ziotopoulou & Boulanger 2016). The constitutive model parameters were calibrated to the cyclic resistance ratios estimated from the CPT based liquefaction triggering correlation of Boulanger & Idriss (2015).

The clay-like sediment in the critical stratum and the overlying fill layer were modeled using the Mohr Coulomb constitutive model in FLAC.

The input motion was the E-W component of the recording from Sakarya scaled to a peak ground acceleration of 0.4 g. The motion was specified as an outcrop motion for the underlying dense sand. The base of the model was a compliant boundary and the opposing side boundaries were attached.

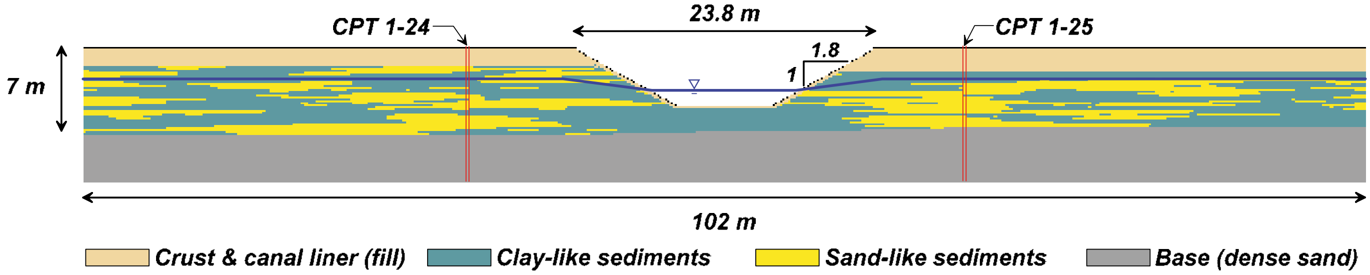

Figure 17. Realization B10-3 based on sand with sill = 40%, l_y = 10 m, and l_z = 0.26 m

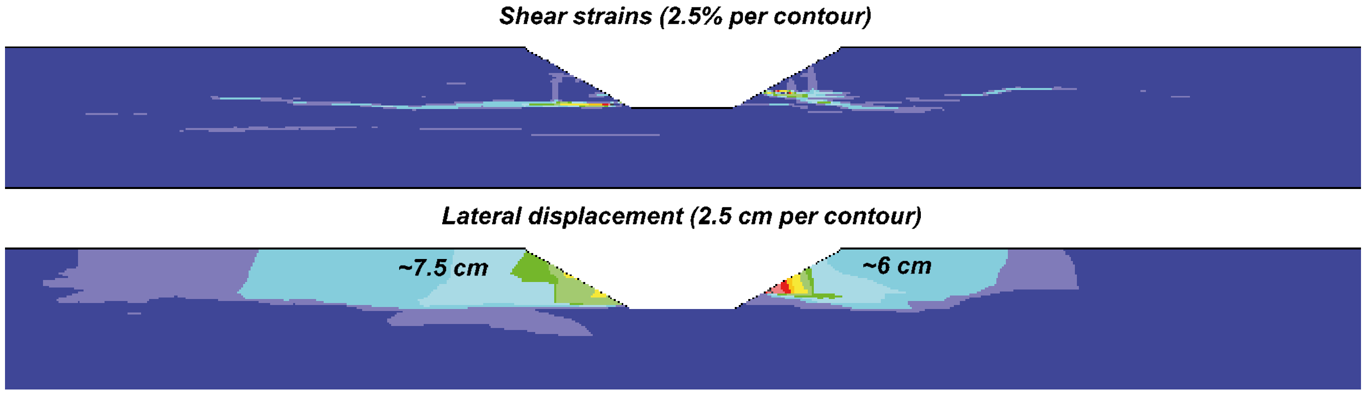

Figure 18. Contours of peak shear strain and lateral displacements toward the canal after earthquake shaking for realization B10-3

Contours of peak shear strain and lateral displacement after strong shaking are shown in Figure 18 for realization B10-3 (Fig. 17). Shear strains in the sand lenses are greatest where the lenses are thickest and closest to the canal face, and smallest when the lenses are thinner and isolated. The banks of the canal have maximum lateral displacements of about 6 to 8 cm toward the canal for this realization. The results from other realizations gave maximum lateral displacements of about 2 to 10 cm depending on the parameters used to generate the realizations. Overall, the lateral displacements from the NDAs are in the range of what might reasonably have developed at this site without causing damage or cracking that would be visible during post-earthquake inspections.

Sensitivity analyses included examining the effect of uncertainty in the input ground motion on the LDI and NDA results. For example, reducing the peak ground acceleration to 0.3 g reduces the estimated ground displacements for both analysis methods, but the LDI results still significantly over-predict the potential for liquefaction effects at this site.

These comparisons illustrate that the discontinuous nature of sand lenses in interbedded sand, silt, and clay deposits can be an important factor influencing the potential for lateral spreading displacements. Simplified analysis procedures that assume horizontal continuity of sand lenses can be expected to over-predict liquefaction effects if the sand lenses are, in fact, not horizontally continuous over the length scale of potential deformation mechanisms. Improvements in our ability to account for these effects will require better guidance on geologic modeling, stochastic procedures, and site investigation practices. The results of this case study illustrate how several factors from Table 1 can contribute to over-prediction of liquefaction effects at a specific site. Analyses were able to predict the absence of significant ground deformations at this site only after the CPT soundings were corrected for transition and thin-layer effects, the spatial variability of the interbedded deposits was accounted for, and the analysis method was upgraded to a 2-D NDA. Stochastic realizations for representing spatial variability in NDAs offer the potential for significant insights on field behaviors, although they are not currently practicable for routine applications. Thus, future work is needed for providing guidance on how the effects of spatial variability can be incorporated into simplified analysis procedures.

6 CONCLUDING REMARKS

Case histories have shown that current liquefaction evaluation procedures and practices can have a tendency to over-predict liquefaction effects in interbedded sand, silt, and clay deposits. This tendency is attributed to several contributing factors as summarized in Table 1, with the importance of each factor depending on site-specific conditions and the analysis method employed.

The correction of CPT data for transition and thin-layer effects can be important for interbedded deposits. Incorporating these corrections reduced the degree to which 1-D LDIs over-predicted lateral spreading displacements at the Çark canal site and were important for the calibration of the constitutive model used in the NDAs. Additional work is needed to develop improved tools and guidance for applying these corrections in practice, including distinguishing between distinct interfaces (e.g., erosional contacts) and gradual transitions in soil characteristics (e.g., graded bedding).

The further development of CPT-based procedures for evaluating liquefaction or cyclic softening effects in intermediate soils is expected to benefit from mechanistic models for relating cone penetration and cyclic loading responses. The direct axisymmetric cone penetration model developed for use with the MIT-S1 constitutive model provides a means for relating cone penetration resistances to the constitutive properties of intermediate soils. The initial results obtained using laboratory-measured cyclic strengths with simulated cone penetration resistances for silt and clay mixtures suggest this approach is promising.

Reexamination of the performance of a site underlain by interbedded soils along the Çark canal in the 1999 M=7.5 Kocaeli earthquake illustrated how several factors can contribute to an over-prediction of liquefaction effects. Analyses were able to predict the absence of significant ground deformations at this site only after the CPT soundings were corrected for transition and thin-layer effects, the spatial variability of the interbedded deposits was accounted for, and the analysis approach was upgraded to a 2-D nonlinear deformation analysis. Other factors may have contributed to the good performance of this site during the Kocaeli earthquake, but their potential contributions are difficult to assess based on the existing data.

The advancement of liquefaction evaluation procedures for interbedded sand, silt, and clay deposits will require a systematic examination of the various contributing factors listed in Table 1. The ability to address these factors will require improvements in experimental, theoretical and site characterization methods. Reevaluation of case histories involving interbedded deposits, with due consideration to all contributing factors, will be important for developing improved procedures and advancing practice.

7 ACKNOWLEDGMENTS

The authors appreciate the financial support of the National Science Foundation (awards CMMI-1300518 and 1547846), California Department of Water Resources (contract 4600009751), and California Division of Safety of Dams (contract 4600009523) for different aspects of the work described in the paper. Any opinions, findings, and conclusions or recommendations expressed in this material are those of the authors and do not necessarily reflect the views of either agency. The review of potential sources of bias in liquefaction evaluations for interbedded deposits benefited from discussions with Jonathan Bray, Brady Cox, Misko Cubrinovski, Kenneth Stokoe, Sjoerd van Ballegooy and others as part of collaborative studies examining sites in the Christchurch area. The review of fundamental aspects of relating cone penetrometer data to cyclic resistance ratios for different soil types draws from discussions with B. L. Kutter. Chris Krage helped prepare the stochastic realizations for Çark Canal and Ana Maria Parra Bastidas provided 1D limiting compression test data on the silt-kaolin mixtures for calibration of the MIT-S1 constitutive model. The research projects described herein have benefited from discussions with, and comments from, I. M. Idriss and B. L. Kutter. Additional comments on a draft of this paper were provided by Misko Cubrinovski and I. M. Idriss. The authors appreciate the above support and interactions.

8 REFERENCES

Beyzaei, C. Z., Bray, J. D., Cubrinovski, M., Riemer, M., Stringer, M. E., Jacka, M. & Wentz, F. J. 2015. Liquefaction resistance of silty soils at the Riccarton Road site, Christchurch, New Zealand. 6th International Conference on Earthquake Geotechnical Engineering, November 1 4, Christchurch, New Zealand.

Boulanger, R. W. & Idriss, I. M. 2007. Evaluation of cyclic softening in silts and clays. Journal of Geotechnical and Geoenvironmental Engineering, ASCE, 133(6), 641-652.

Boulanger, R. W. & Idriss, I. M. 2015. CPT-based liquefaction triggering procedure. Journal of Geotechnical and Geoenvironmental Engineering, ASCE, 142(2): 04015065, 10.1061/(ASCE)GT.1943-5606.0001388.

Boulanger, R. W., Kamai, R., & Ziotopoulou, K. 2014. Liquefaction induced strength loss and deformation: Simulation and design. Bulletin of Earthquake Engineering, Springer, 12: 1107-1128, 10.1007/s10518-013-9549-x.

Boulanger, R. W. & Ziotopoulou, K. 2015. PM4Sand (Version 3): A sand plasticity model for earthquake engineering applications. Report No. UCD/CGM-15/01. Center for Geotechnical Modeling, Department of Civil and Environmental Engineering, University of California, Davis, CA.

Canou, J. 1989. Piezocone et liquefaction des sables. Rapport de synthese des travaux realizes au CERMES, Research Report CERMES/ENPC, Paris, 176 p.

Carle, S. F. 1999. T-PROGS: Transition probability geostatistical software. University of California, Davis, CA.

Carraro, J. A. H., Bandini, P. & Salgado, R. 2003. Liquefaction resistance of clean and nonplastic silty sands based on cone penetration resistance. J. Geotechnical and Geoenvironmental Engineering, 129(11), 965-976.

Chai, J., Sheng, D., Carter, J.P. & Zhu, H. 2012. Coefficient of consolidation from non-standard piezocone dissipation curves. Computers and Geotechnics 41: 13-22.

Chu, D. B., Stewart, J. P., Boulanger, R. W. & Lin, P. S. 2008. Cyclic softening of low-plasticity clay and its effect on seismic foundation performance. Journal of Geotechnical and Geoenvironmental Engineering, ASCE, 134(11), 1595-1608.

Chu, D. B., Stewart, J. P., Youd, T. L. & Chu, B. L. 2007. Liquefaction-induced lateral spreading in near-fault regions during the 1999 Chi-Chi, Taiwan Earthquake. J. Geotechnical and Geoenvironmental Engineering, ASCE, 132(12), 1549-1565.

Colella, P. 1990. Multidimensional upwind methods for hyperbolic conservation laws. Journal of Computational Physics, 87: 171-200.

Cubrinovski, M., Rees, S. & Bowman, E. 2010. Effects of non-plastic fines on liquefaction resistance of sandy soils. 17, 125-144.

Cubrinovski, M. & Robinson, K. 2015. Lateral spreading: evidence and interpretation from the 2010-11 Christchurch earthquakes. 6th International Conference on Earthquake Geotechnical Engineering, November 1 4, Christchurch, New Zealand.

DeJong, J. T. & Randolph, M. 2012. Influence of partial consolidation during cone penetration on estimated soil behavior type and pore pressure dissipation measurements. JGGE, ASCE, 138(7), 777-788.

DeJong, J. T., Jaeger, R. A., Randolph, M. F., Boulanger, R. W., & Wahl, D. 2012. Variable penetration rate cone testing for characterization of intermediate soils. Geotechnical and Geophysical Site Characterization 4 (ISC'4), Coutinho and Mayne, eds., Taylor and Francis Group, London, 25-42.

Foray, P. & Pautre, J-L. 1988. Piezocone et liquefaction des sables: synthese des essais sur sites en Nouvelle-Zelande et des essais en Chambre de Calibration a l'IMG, Research Report, IMG, Grenoble, 70 p.

Frost, J. D., DeJong, J. T. & Saussus, D. R. 2006. Analytical investigation of friction sleeve length effects on stratigraphic interpretation. Intl. J. of Geomechanics, 6(1), 11-29.

GeoLogismiki 2016. CLiq v.2.0 – CPT liquefaction software. http://www.geologismiki.gr/products/cliq/, accessed 7/2016.

Huang, W., Sheng, D., Sloan, S.W. & Yu, H.S. 2004. Finite element analysis of cone penetration in cohesionless soil. Computers and Geotechnics, 31:517-528.

Idriss, I. M. & Boulanger, R. W. 2008. Soil liquefaction during earthquakes. Earthquake Engineering Research Institute.

Ishihara K. 1985. 'Stability of natural deposits during earthquakes.' Proceedings, 11th International Conference on Soil Mechanics and Foundation Engineering, San Francisco. Vol. 1, p. 321-376.

Ishihara, K. & Yoshimine, M., 1992. Evaluation of settlements in sand deposits following liquefaction during earthquakes. Soils and Foundations 32, 173–188.

Itasca 2011. FLAC, Fast Lagrangian Analysis of Continua, User's Guide, Version 7.0. Itasca Consulting Group, Inc., Minneapolis, MN.

Jaeger, R.A. 2012. Numerical and experimental study of cone penetration in sands and intermediate soils. Doctoral Dissertation, University of California, Davis.

Kokusho, T. 2003. Current state of research on flow failure considering void redistribution in liquefied deposits. Soil Dynamics and Earthquake Engineering, 23(7):585–603.

Kokusho, T., Ito, F., Nagao, Y. & Green, A. R. 2012. Influence of non/low-plastic fines and associated aging effects on liquefaction resistance. J. Geotechnical and Geoenvironmental Engineering, 138(6), 747-756.

Ladd, C.C. & Varallyay, J. 1965. The influence of stress system on the behavior of saturated clays during undrained shear. No. RR-R65-11. Massachusetts Institute of Technology Cambridge Soil Mechanics Division.

Landon, M.M. 2007. Development of a non-destructive sample quality assessment method for soft clays. Doctoral Dissertation, University of Massachusetts, Amherst.

LeBlanc, C., and Randolph, M. F. 2008. Interpretation of piezocones in silt, using cavity expansion and critical state methods. Proc. 12th International Conference of IACMAG, 822-829.

Liyanapathirana, D.S. 2009. Arbitrary Lagrangian Eulerian based finite element analysis of cone penetration in soft clay. Computers and Geotechnics 36: 851-860.

Mahmoodzadeh, H., Randolph, M.F. & Wang, D. 2014. Numerical simulation of piezocone dissipation test in clays. Geotechnique 64(8): 657-666.

Mayne, P. 2007. Cone Penetration Testing – A synthesis of highway practice. NCHRP Synthesis 268, Transportation Research Board, Washington, D.C.

Mo, P.Q., Marshall, A. M., & Yu, H.S. 2013. Centrifuge modeling of CPT in layered soils. Geotechnical and Geophysical Site Characterization 4 – Coutinho and Mayne (eds), Taylor and Francis Group, 219-225.

Mo, P.-Q., Marshall, A. M., & Yu, H.S. 2015. Centrifuge modelling of cone penetration tests in layered soils. Géotechnique 65, No. 6, 468–481.

Moss, R., Seed, R., Kayen, R., Stewart, J., Der Kiureghian, A. & Cetin, K. 2006. CPT-based probabilistic and deterministic assessment of in situ seismic soil liquefaction potential. Journal of Geotechnical and Geoenvironmental Engineering, 132(8), pp.1032-1051.

Moug, D. M., Boulanger, R. W., DeJong, J. T. & Jaeger, R. W. 2016. Simulation of cone penetration in anisotropic clay. Proc., GeoVancouver 2016, Canadian Geotechnical Society, Vancouver, Oct. 2-5.

Munter, S. K., Krage, C. P., Boulanger, R. W., DeJong, J. T. & Montgomery, J. 2016. Potential for liquefaction-induced lateral spreading in interbedded deposits considering spatial variability. Proceedings, Geotechnical and Structural Engineering Congress, Phoenix, AZ, Feb. 14-17, ASCE.

Nichols, G. 2009. Sedimentology and stratigraphy. Second edition, Wiley-Blackwell, John Wiley & Sons Ltd., West Sussex, UK.

Olson, S. M. & Johnson, C. I. 2008. Analyzing liquefaction-induced lateral spreads using strength ratios. J. Geotechnical and Geoenvironmental Engineering, ASCE, 134(8), 1035-1049.

Park, S.-S. & Kim, Y.-S. 2013. Liquefaction resistance of sands containing plastic fines with different plasticity. Journal of Geotechnical and Geoenvironmental Engineering, 139(5), 825-830.

Pestana, J.M. and Whittle, A. J. 1999. Formulation of a unified constitutive model for clays and sands. International Journal for Numerical and Analytical Methods in Geomechanics, 23: 125-1243.

Pestana, J.M., Whittle, A.J. & Gens, A. 2002. Evaluation of a constitutive model for clays and sands: Part II – Clay behaviour. International Journal for Numerical and Analytical Methods in Geomechanics, 26:1123-1146.

Price, A. B., Boulanger, R. W., DeJong, J. T., Parra Bastidas, A. M. & Moug, D. 2015. Cyclic strengths and simulated CPT penetration resistances in intermediate soils. 6th International Conference on Earthquake Geotechnical Engineering, November 1 4, Christchurch, New Zealand.

Robertson, P.K. 1990. Soil classification using the cone penetration test, Canadian Geotechnical J. 27(1), 151–58.

Robertson, P. K. 2009. Discussion of "Evaluation of Cyclic Softening in Silts and Clays" by Ross W. Boulanger and I. M. Idriss. J. Geotechnical and Geoenvironmental Engineering, 135:2(306), 306-307.

Robertson, P. K. & Fear, C. E. 1995. ''Liquefaction of sands and its evaluation.'' Proc., 1st Int. Conf. on Earthquake Geotechnical Engineering.

Robertson, P. & Wride, C., 1998. Evaluating cyclic liquefaction potential using the cone penetration test. Canadian Geotechnical Journal, 35(3), pp.442--459.

Salgado, R., Mitchell, J. K. & Jamiolkowski, M. 1997. Cavity expansion and penetration resistance in sand. Journal of Geotechnical and Geoenvironmental Engineering, 123(4), 344-354.

Silva, M. F., & Bolton, M. D. 2004. Centrifuge penetration tests in saturated layered sands. Proc. ISC-2 on Geotechnical and Geophysical Site Characterization, Viana da Fonseca and Mayne (eds), 377-384.

Stringer, M., Beyzaei, C., Cubrinovski, M., Bray, J. D., Riemer, M., Jacka, M. & Wentz, F. 2015. Liquefaction characteristics of Christchurch silty soils: Gainsborough Reserve. 6th International Conference on Earthquake Geotechnical Engineering, November 1 4, Christchurch, New Zealand.

Van Ballegooy, S., Malan, P., Lacrosse, V., Jacka, M. E., Cubrinovski, M., Bray, J. D., O'Rourke, T. D. O., Crawford, S. A. & Cowan, H. 2014. Assessment of liquefaction-induced land damage for residential Christchurch. Earthquake Spectra, EERI, 30(1), 31-55.

Van Ballegooy, S., Wentz, F. & Boulanger, R. W. 2015. Evaluation of CPT-based liquefaction procedures at regional scale. Soil Dynamics and Earthquake Engineering, 10.1016/j.soildyn.2015.09.016.

Van den Berg, P., deBorst, R. & Huetink, H. 1996. An Eulerian finite element model for penetration in layered soil. International Journal for Numerical and Analytical Methods in Geomechanics, 20(12): 865–86.

Vreugdenhil, R., Davis, R. & Berrill, J. 1994. Interpretation of cone penetration results in multilayered soils. Intl. J. Numerical and Analytical Methods in Geomechanics, 18: 585-599.

Walker, J. & Yu, H.S. 2006. Adaptive finite element analysis of cone penetration in clay. Acta Geotechnica 1: 43-57.

Walker, J. and Yu, H.S. 2010. Analysis of the cone penetration test in layered clay. Geotechnique, 60(12): 939-948.

Wang, D., Bienen, B., Nazem, M., Tian, Y., Zheng, J., Pucker, T., Randolph, M.F. 2015. Large deformation finite element analysis in geotechnical engineering. Computers and Geotechnics 65: 104-114.

Weissmann, G. S., Carle, S. F. & Fogg, G. E. 1999. Three-dimensional hydrofacies modeling based on soil surveys and transition probability geostatistics. Water Resources Research, 35(6), 1761-1770.

Yi, J.T., Goh, S.H., Lee, F.H. & Randolph, M.F. 2012. A numerical study of cone penetration in fine-grained soils allowing for consolidation effects. Geotechnique 62(8): 707-719.

Youd, T. L., Cetin, K. O., Bray, J. D., Seed, R. B., Durgunoglu, H. T. & Onalp, A. 2000. Geotechnical site investigation at lateral sites. *spread http://peer.berkeley.edu/publications/* turkey/adapazari/index.html, last accessed 7/2016.

Youd, T. L., DeDen, D. W., Bray, J. D., Sancio, R., Cetin, K. O. & Gerber, T. M. 2009. Zero-displacement lateral spreads, 1999 Kocaeli, Turkey, earthquake. Journal of Geotechnical and Geoenvironmental engineering, 135(1), 46-61.

Youd, T. L., Hansen, C. M. & Bartlett, S. F. 2002. Revised multilinear regression equations for prediction of lateral spread displacement. Journal of Geotechnical and Geoenvironmental Engineering, 128(12), 1007-1017.

Youd, T. L., Idriss, I. M., Andrus, R. D., Arango, I., Castro, G., Christian, J. T., Dobry, R., Finn, W. D. L., Harder, L. F., Hynes, M. E., Ishihara, K., Koester, J. P., Liao, S. S. C., Marcuson, W. F., Martin, G. R., Mitchell, J. K., Moriwaki, Y., Power, M. S., Robertson, P. K., Seed, R. B. & Stokoe, K. H. 2001. Liquefaction resistance of soils: summary report from the 1996 NCEER and 1998 NCEER/NSF workshops on evaluation of liquefaction resistance of soils. Journal of Geotechnical and Geoenvironmental Engineering, American Society of Civil Engineers, 127(10): 817-833.

Yu, H. S., Herrmann, L. R., & Boulanger, R. W. 2000. Analysis of steady cone penetration in clay. Journal of Geotechnical and Geoenvironmental Engineering, ASCE, 126(7), 594-605.

Zhang, G., Robertson, P. K. & Brachman, R. W. I. 2004. Estimating liquefaction-induced lateral displacements using the standard penetration test or cone penetration test. Journal of Geotechnical and Geoenvironmental Engineering, 130(8), 861-871.

Ziotopoulou , K. & Boulanger, R. W. 2016. Plasticity modeling of liquefaction effects under sloping ground and irregular cyclic loading conditions. Soil Dynamics and Earthquake Engineering, 84 (2016), 269-283.

Geotechnical and Geophysical Site Characterisation 5 – Lehane, Acosta-Martínez & Kelly (Eds)

The GP sampler: a new innovation in core sampling

K. Mori
Special Adviser, Raito Kogyo Co., Ltd.
Former Chairman and President, Kiso-Jiban Consultants Co., Ltd.

K. Sakai
Kiso-Jiban Consultants Co., Ltd.

ABSTRACT: This paper introduces a new type of sampler called the GP sampler. It was designed to sample gravelly soils, but has proven to be successful in sampling soils ranging from dense sand, to gravel, as well as sedimentary rocks. The sampler is constructed of a single core barrel and uses a viscous polymer gel as its drilling fluid. The polymer plays a key role in obtaining high-quality samples, helping to preserve the soil structure. The polymer gel was also employed in more traditional style samplers, in an effort to improve the quality of samples obtained from silt, silty sand, and sand. In the field, GP samplers have been successful where other conventional methods have experienced difficulties or failed altogether. Although the GP sampler is not a perfect sampler, it is beginning to make a qualitative difference in the sampling of granular soils for engineering analyses.

1 INTRODUCTION

In geotechnical site investigation, obtaining a high quality sample of granular soils is one the most difficult tasks, principally because the very process of sampling can easily disturb the soil. During the late 1990s, the Japanese geotechnical consulting company, Kiso-Jiban Consultants, developed a new type of sampler called the GP sampler. This innovative sampler was designed specifically to overcome the limitations of prevailing sampler methods: to obtain high-quality samples of sands and gravels, without freezing and without the typical disruptive impact to the integrity of the sample.

The name GP is an abbreviation for Gel Push. The sampler uses a very thick polymer gel or solution as its drilling fluid, as well as for a lubricant. Unlike conventional drilling fluid, the polymer solution is not circulated; it is simply pushed out of the sampler tube or barrel to remove the cuttings, cooling the bit and protecting the sample as it enters into the sampler. Thus, the name Gel Push or GP has been adopted.

The sampler design was completed in 2010. This produced four variations of GP samplers, each specifically useful for a particular sampling requirement: GP-Rotary, GP-Drilling, GP-Triple, and GP-Static. They will be referred to as GP-R, GP-D, GP-Tr, and GP-S in the rest of the text. Table 1 summarizes the principal features of each one of the GP samplers.

The GP-R sampler is a single core barrel sampler

Table 1. Summary of GP samplers.

	GP-R	GP-D	GP-Tr	GP-S
Sampler configuration	single core barrel	single core barrel	modified triple tube sampler	modified Osterberg sampler
Bit type or shoe	impregnated diamond bit	impregnated diamond bit	shoe with metal bit for overcoring	shoe
Function of polymer	Non-circulating drilling fluid for carrying cuttings, cooling the bit and protecting the cored sample.	Non-circulating drilling fluid for carrying cuttings, cooling the bit and protecting the cored sample.	Reducing friction between the cored sample and sampler wall.	Reducing friction between the cored sample and sampler wall.
Special features	Electric motor is used for coring.	Electric motor is used for coring. Fitted with core lifter.	Polymer dispensing ring is fitted.	Core catcher dispenses the polymer and retains cored sample.
Ground suited for sampling	dense sand, gravel, and sedimentary rock.	dense sand, gravel, and sedimentary rock.	medium to dense sand and sand with gravel.	silt, silty sand, and loose sand.
Typical core diameter (mm)	100, 150, 200, and 300	100, 150, and 200	83	75
Maximum sample length	1 m	1 m	1 m	1 m

with very simple construction. It has proven successful in obtaining high-quality samples of sands, gravels, and sedimentary rocks. The sampler's flexibility in accommodating a wide range of formations is one of its attractive features.

While the GP-R sampler was designed for sampling at the ground surface, or from an excavated trench, the GP-D sampler was developed in order to conduct equally high-quality sampling in boreholes. It has the same basic construction as the GP-R, but is fitted with a special "catcher" mechanism that enables it to retain the core inside the sampler during retraction from the ground and borehole.

The GP-Tr and GP-S samplers were designed around a rotational triple tube sampler and the Osterberg sampler, respectively. They both use the highly viscous polymer solution to reduce friction between the cored sample and sampler tube wall, minimizing one of the primary causes of sample disturbance.

The basic design of the four GP samplers, their operating procedures, and several case records of actual site investigations are described in this paper. GP samplers have proven to be successful in obtaining samples at formations where sampling had previously not been possible, or was otherwise difficult to accomplish through conventional means. Furthermore, this paper illustrates the impact and contributions these innovative samplers have made in site investigation.

2 THE GP-R SAMPLER

The GP-R sampler was originally designed for sampling gravel formations at the ground surface. It was the first GP sampler built and its successful use of the GP technology made it the archetype of the line of GP samplers that followed. Foundational to this technology is the more than 30 years of experience in sampling held by the engineers responsible for its development. In this section, the design and operation of the GP-R sampler, the behavior characteristics of the polymer solution, and two case records of site investigations are included.

2.1 *The design and operation of GP-R sampler*

The GP-R sampler is a single core barrel sampler, available in barrel diameters of 100 mm, 150 mm, 200 mm, and 300 mm. Figure 1 depicts a GP-R sampler with the sample having entered about one-third of the way into the core barrel. Prior to drilling, the ground surface is prepared by the addition of a thin layer of cement mortar, which is shown in Figure 1. This layer assures the smooth start of the drilling and minimizes disturbance to the ground below. The sampler barrel is filled with a thick polymer solution and placed at the ground surface. As the barrel is turned and pushed downward, an impregnated diamond bit cuts into the ground. This specific bit is smooth to the touch and grinds through granular soils and other ground formations with minimum disturbance. The sample core, with its mortar cap, is forced into the barrel as the sample cuts it from the surrounding soil, pushing the stored polymer solution up, and squeezing it over and around the core into an annular space of about 1 mm between the core and the barrel wall.

The polymer utilized in this process is a commercially available product, and is commonly added to traditional drilling fluid to increase its viscosity. Unlike the prevailing drilling fluid, the polymer solution used in all the GP sampling is highly concentrated with a 2.5 to 4 % ratio of polymer to water. This creates a fluid whose viscosity is more than ten times thicker than the industry norm of 0.1 to 0.4 % concentration and takes full advantage of the polymer's non-Newtonian fluid characteristics. The polymer solution is very thick and viscous when it is still, but becomes more fluid-like when it is sheared. This behavior is known as "shear-thinning".

During the sampling process, the barrel rotates at 300 to 800 rpm depending on the size of the barrel. Smaller barrels need to rotate faster to attain the desired linear cutting speed. The polymer solution flowing alongside the barrel wall in the annular space is sheared by the high rotational speed and loses viscosity. This zone of low viscosity polymer solution acts like a protective membrane, isolating the cored sample from the barrel's rotational motion.

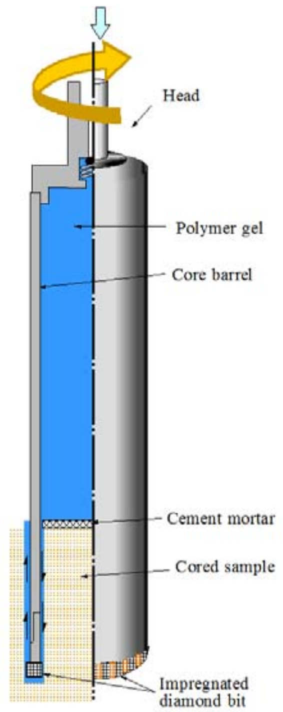

Figure 1. Cross-section of GP-R sampler with cored sample entering into the sampler barrel.

Unlike conventional drilling fluid, which tends to wash out fine particles, the polymer solution's high viscosity and slow flow rate leave the fines undisturbed. Since the fines act as a matrix material, holding the coarser particles or gravels in place, sample disturbance during the polymer gel sampler coring is kept to a minimum. The sheared solution essentially seals the cored sample as it flows downward to exit the barrel at and around the bit, cooling the bit and carrying away the cuttings as it passes out of the barrel into the borehole. Further details of the polymer characteristics are discussed in sub-section, 2.2.

Figure 2 shows the operating sequence of GP-R sampling from start to finish. When the coring is completed the excess polymer gel is extracted, the ground adjacent to the barrel is excavated, and a wedge is then driven under the barrel to separate the core sample from the ground. It is then a simple procedure to obtain the sample. Figure 3 shows the photos of a coring operation at a pit, driving a wedge, and trimming the ends of the sample which is at the laboratory for testing. The circular saw in the photo has an impregnated diamond cutting edge and is lubricated by the GP formulated polymer solution.

A beneficial feature of both the GP-R and GP-D samplers is their use of an electrically powered motor for coring. The motor can be preprogrammed to precisely control the sampler's rotational speed and penetration rate. In stark contrast to the oscillation caused by diesel motors, the electric motor produces very little vibration and consequently, significantly less disturbance to the sample and the subject soil.

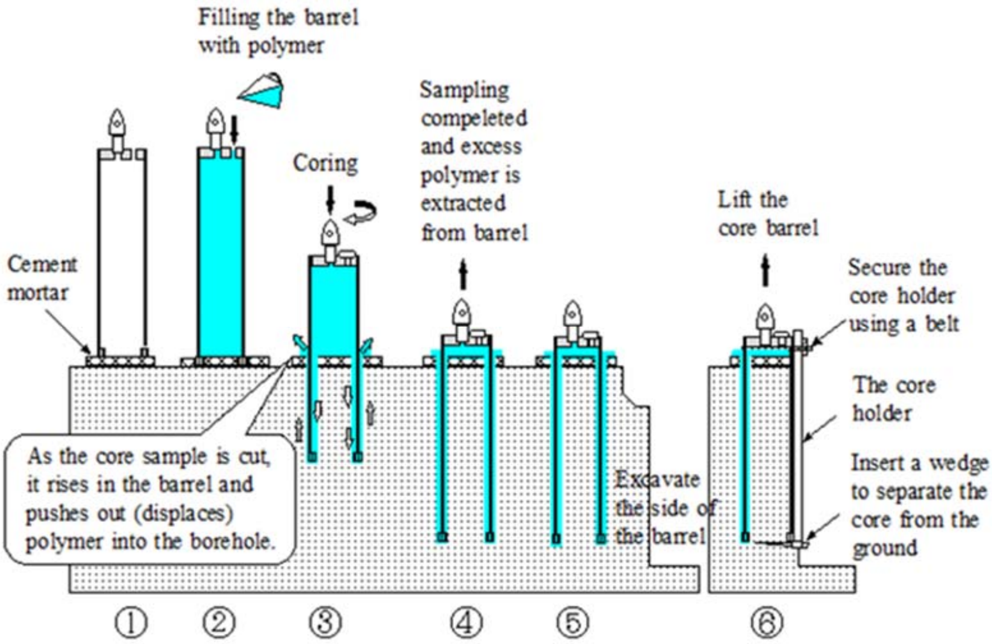

Figure 2. Operating sequence of GP-R sampling on the ground surface.

(a) Coring using electric motor. (b) Inserting a wedge. (c) Trimming the ends.

Figure 3. GP-R sampling on the ground surface at a trench pit, and trimming the ends in the laboratory.

This results in a smoother core sample, leaving a cleaner cut face and allowing for multiple samples to be extracted in close proximity, increasing sampling efficiency. Because of the relative ease and compactness of the GP-R's operation, sampling may be conducted in trenches, excavation pits, inside tunnels, or at the bottom of deep wells. Additionally, as many samples as are needed may be economically obtained from the same location.

Figure 4 shows the first GP-R sample obtained from the commercial use of a GP sampler. The site was an artificially compacted fill for the construction of highway facilities. All the gradation curves obtained at the site are shown in Figure 5, and reveal a ground consisting mostly of gravel with the maximum size ranging from 50 to 100 mm. The seismic stability of the fill was under investigation, and due to the maximum size of the gravel at the site investigated being around 50 mm, the 300 mm diameter

Figure 4. The first GP-R sample obtained.

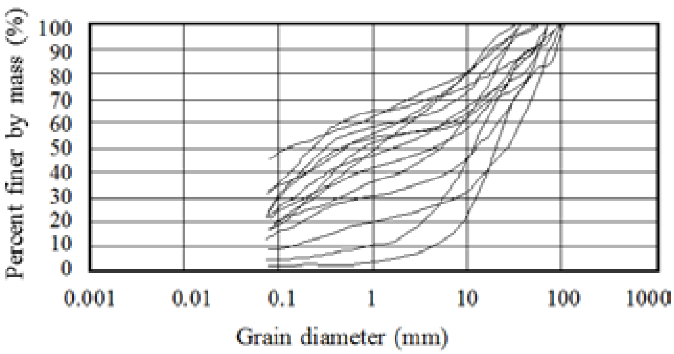

Figure 5. All the gradation curves obtained at the site (Abe et al. 2002).

GP-R sampler barrel was used. In line with the industry practice of a particle size to core diameter ratio of five to one, the choice of the 300 mm barrel to obtain samples was appropriate to ensure accurate testing of the fill.

The GP-R sampler was initially developed for sampling gravelly soils, but it can accommodate a broad range of soils from sands to gravels, and even soft rocks. Figure 6 shows examples of a variety of cored samples obtained by GP samplers.

Sample core of mudstone (GP-R: 200 mm).

Sample core of gravels suspended in a matrix of dense sand (GP-R: 300 mm).

Dense sand sample core (GP-D: 200 mm).

.

Sample core of fragmented shell in dense sand (GP-D: 200 mm).

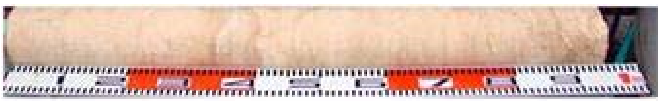

Sample core of coral limestone (GP-D: 100mm).

Figure 6. Wide range of rocks and soils sampled by GP samplers.

2.2 *Polymer characteristics and its functions*

Since the polymer solution plays a vital role in GP sampling, a description of the general characteristics of the polymer is given in this sub-section. Some characteristics unique to the polymer solution used in GP sampling are also addressed. The basic polymer is a partially hydrolyzed polyacrylamide and is commonly called PHP polymer. It is readily available throughout the world, but the viscosity characteristics vary depending on the manufacturer.

The polymer characteristics discussed here are those of a product locally available in Japan and may not apply to PHP polymers produced elsewhere. The polymer is sold in liquid form dissolved in mineral oil. The concentration of polymer solution referred to in this text is measured in the weight percentage of commercially sold polymer to the water it is mixed with.

Figure 7 shows the viscosity of the polymer solution having concentrations ranging from 0.1 to 5.0 %. Viscosity is measured by a viscometer, which rotates at different speeds. It is clear from Figure 7 that the higher the concentration and slower the rotation of the viscometer, the higher the viscosity, and vice versa.

GP sampler barrels typically rotate at a viscometer rotation equivalent of 8000 rpm, or the zone indicated by the letter A in Figure 7. Thus, from still to the barrel's full rotational speed, the polymer's viscosity drops to about one ten-thousandths of still state. Since the viscosity of water is about 1.0 mPa・s, the polymer is still viscous enough to maintain laminar flow, even when the barrel is rotating at full speed, yet fluid enough to isolate the barrel's rotational motion, preventing it from being transmitted to the cored sample. To achieve these favorable conditions, there is a delicate balance that must be maintained between the concentration of the polymer solution and the speed at which the barrel rotates.

Figure 8 illustrates the different behaviors of drilling solutions. Presented are three buckets, each containing one of these solutions, respectively, being mixed with an electric blender; 3.0 % polymer concentration, 0.3 % polymer concentration, and conventional drilling fluid. The polymer solution of 3.0 % climbs up along the mixing rod as if long polymer chains are being curled up. The effect of the polymer solution rising up, as shown in Figure 8 is called the Weissenberg effect. This effect is known to generate inward normal stress, which can act to hold the cored sample together inside the GP

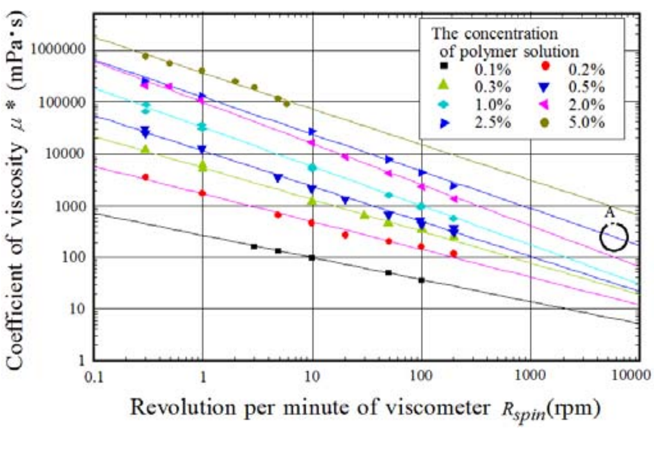

Figure 7. Viscosity of polymer solution at different concentrations (Yanagisawa et al. 2003).

(a) 3.0 % polymer (b) 0.3 % polymer (c) drilling fluid

Figure 8. Polymer behavior at different concentrations and conventional drilling fluid.

barrel. The bucket filled with a 0.3 % solution shows only a very faint rise, indicating a thin polymer solution will be much less effective at protecting the cored sample. The bucket with the conventional drilling fluid shows it behaving like an ordinary fluid, displaying none of the advantageous characteristics of the GP polymer solution.

Figure 9 shows an apparatus built to simulate the GP-R and GP-D coring samplers. A stationary metal tube representing the cored sample, being 100 mm in diameter, with load cells mounted on its sides to measure shear and normal stresses, was placed at the center of the apparatus. A slightly larger tube, representing the barrel, and having a diameter 2 mm wider than the first, was placed over the stationary tube. The annular space was then filled with a 2.5% concentration polymer solution and confining pressures of 100 and 149 kPa were applied. The outer tube was rotated from still to 400 rpm and then returned to still. Figure 10 shows the normal and shear stresses

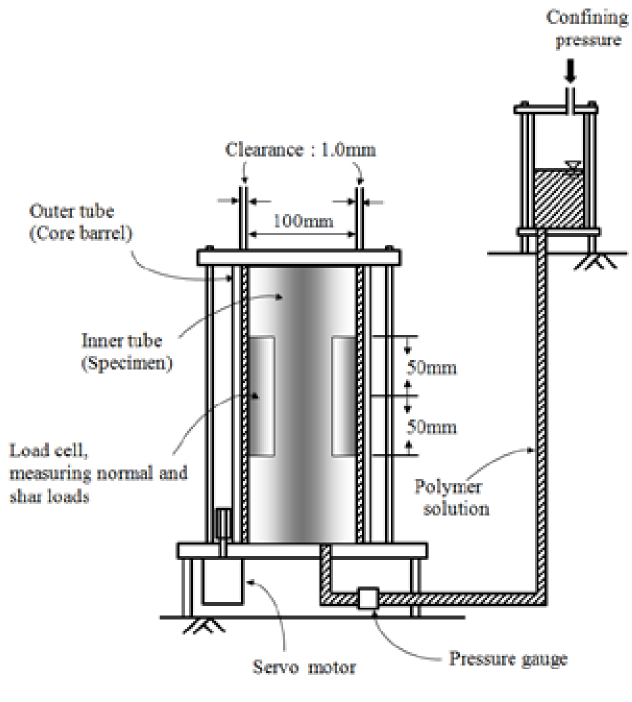

Figure 9. An apparatus simulating GP-R and GP-D coring (Yanagisawa et al. 2004).

measured at different rotational speeds. As is evident from Figure 10, normal stress builds up steadily until the revolutions reach 100 rpm, and then the stress becomes stable. Interestingly, a small normal stress remains even after the barrel comes to a stop. This is likely to be the normal stress generated by the Weissenberg effect. On the other hand, the shear stress measurements showed no increase at all during the entire test, indicating that a very narrow annular space of 1mm, filled with the polymer solution, is enough to isolate the cored sample from the rotational motion of the barrel.

With the GP-Tr and GP-S samplers, the polymer solution is used differently from the GP-R and GP-D samplers. As will be discussed in Sections 4 and 5, these samplers behave very much like conventional samplers, with the sample coming into direct contact with the sampler wall. However, the same thick polymer solution is employed to decrease the resulting friction, which is a major cause of sample disturbance in conventional methods.

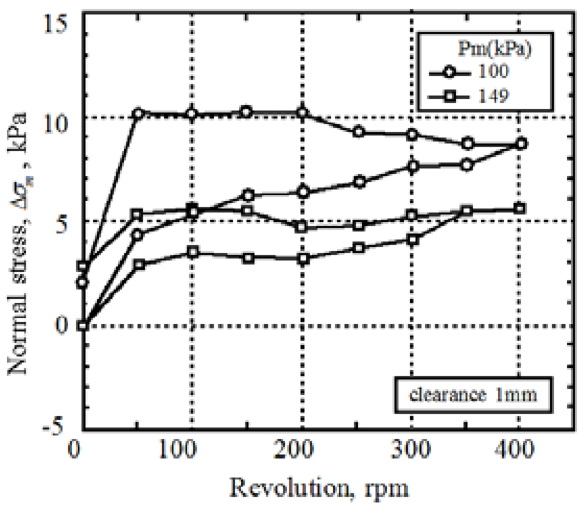

(a) Normal stress vs. revolution.

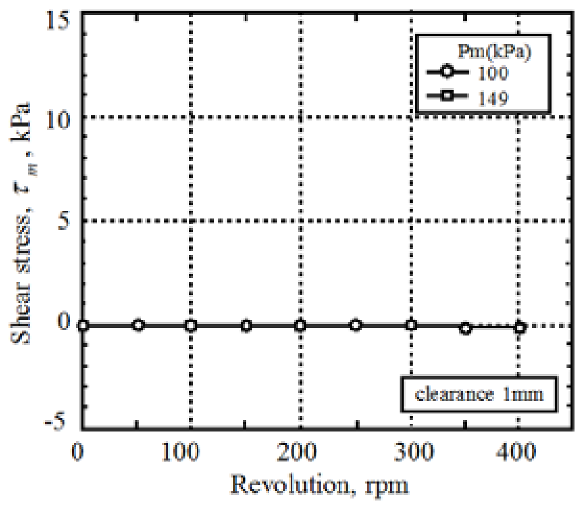

(b) Shear stress vs. revolution.

Figure 10. Normal and shear stresses measured on a tube simulating cored sample (Yanagisawa et al. 2004).

In order to estimate the effectiveness of the polymer as a lubricant, a series of tests were carried out. River sand was compacted inside test tubes, forming samples each 30 cm in length, with a density of 14 kN/m^3 and having a moisture content of 14 %. A hydraulic piston was used to push the compacted soil out of the tubes. Figure 11 shows the thrust force needed to extrude each sample.

Both thin wall stainless steel and PVC tubes were used for this test; their inside diameters being 70 mm and 83 mm, respectively. It is clear that the stainless steel tubes exhibited significantly more friction as compared to the PVC tubes. The lower friction of the PVC tubes may be attributable to the material's smooth surface and flexibility to expand, both of which reduce stress build-up.

Figure 11 also shows the thrust force needed to eject soil samples from the stainless steel tubes, each of which had been either coated with polymer or lined with Teflon. Both surface treatments were equally effective in significantly reducing the friction between the sample and the sampler wall. This property lends further support to the use of the polymer enhanced samplers, as it produces a very low friction environment for the sample to enter into the collection tube. It also significantly reduces the force needed to extrude a cored sample out of the tube, whether in situ or in the laboratory.

It should be noted that in the course of the design of the GP Sampler, Professor Tani, of Yokohama National University, along with his research group, conducted extensive studies on the polymer behavior. Their work made a significant contribution to the development of the GP samplers and the unique use of the high viscosity polymer to obtain a reliably superior core sample (Tani et al. 2004, 2006, Yanagisawa et al. 2003, 2004, Kaneko et al. 2005, Shirai et al. 2004, Ishizuka et al. 2010).

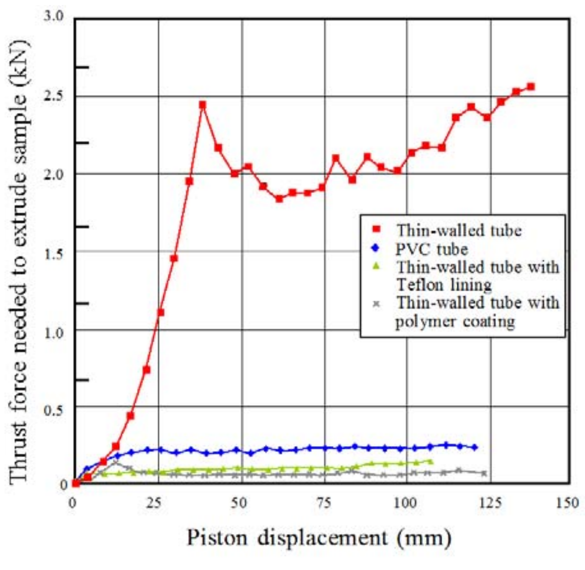

Figure 11. Thrust force needed to extrude soil sample out of various sampler tube configurations.

2.3 *A site investigation at Yui landslide site*

Yui is located along the Pacific coast of Shizuoka Prefecture, between Tokyo and Nagoya, and situated south-southwest of Mount Fuji. The hillside of Yui hangs over the narrow coastline making the area picturesque. However, the hillside presents a serious landslide hazard to three of Japan's major transportation arteries: the Tomei Expressway; the Tokaido Line of Japan Rail; and the National Route One. They are all located just underneath the hill as shown in Figures 12(a) and (b).

The hillside experienced a number of slides in the past which negatively affected the traffic flow of the three arteries. Specific slides were caused by either heavy precipitation or by earthquake activity. The site is located along the coast of the Suruga Bay where the Sagami Trough runs north to south. The trough, which is capable of generating an earthquake with a magnitude in excess of 8, makes the area's seismic stability of principal concern.

(a) Yui site overview.

(b) Yui site looking from south.

Figure 12. Photos of Yui site (Mt. Fuji Sabo Office Homepage).

Figure 13 shows four potential landslide zones at the Yui site. These zones are referred to as Blocks. They include the Yamanaka Block, the Hachigasawa Block, the Ohkubo Block and the Ooshi Block. All the data presented in this section was made possible with the consent of Mt. Fuji Sabo Office, Chubu Regional Bureau of the Ministry of Land, Infrastructure, Transport, and Tourism.

In 2005, a comprehensive investigation was conducted at the site, followed by the necessary mitigation work. GP-R sampling was carried out as a part of the geotechnical site investigation. Sampler barrels 200 mm in diameter were used at the Yui site. At the time of the GP-R sampling work, some of the deep drainage wells for groundwater were still under construction. Using these wells, GP-R sampling was conducted at various depths, ranging from the ground surface to a depth in excess of 50 m underground.

Figure 14 shows a cross section of Ohkubo Block. It indicates that several slip surfaces have been identified from previous investigations. GP-R sampling was carried out at one of the drainage wells in the center of the slope, near the location shown as site in Figure 14. At the actual drainage well site, the slip surfaced appeared closer to the ground surface than shown in Figure 14. Figure 15 is a photo of GP-R sampling work being done inside the well. Figure 16 shows the photos of the GP-R samples obtained at Ohkubo Block at the ground surface, as well as depths of 18.5 m, 27 m, and 29.5 m. Also seen in the figure, is a photo taken of the grounds after the samples were removed. One of the amazing features of the sampler is that it not only obtains high-quality samples, but the precision of the coring method leaves behind a beautifully excavated

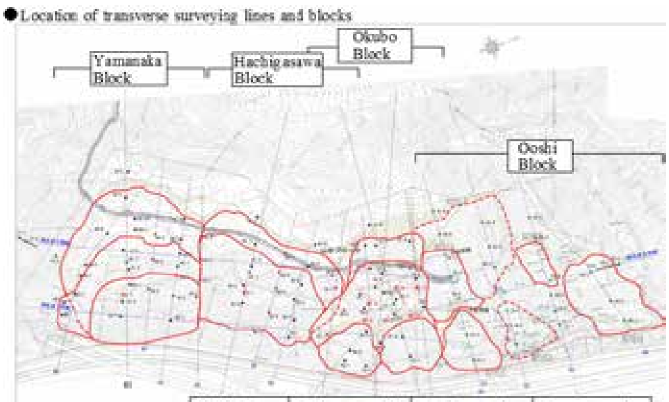

Block Name	Maximum width	Maximum slope length	Maximum slip surface depth
Yamanaka Block	360m	440m	65m
Hachigasawa Block	380m	300m	59m
Okubo Block	300m	380m	47m

Figure 13. Four slide blocks at Yui site (Mt. Fuji Sabo Office Homepage).

surface, which facilitates the visualization of the site soil formation. Here, it can clearly be seen that below the depth of 27 m, the formation changes to more solid sedimentary rocks.

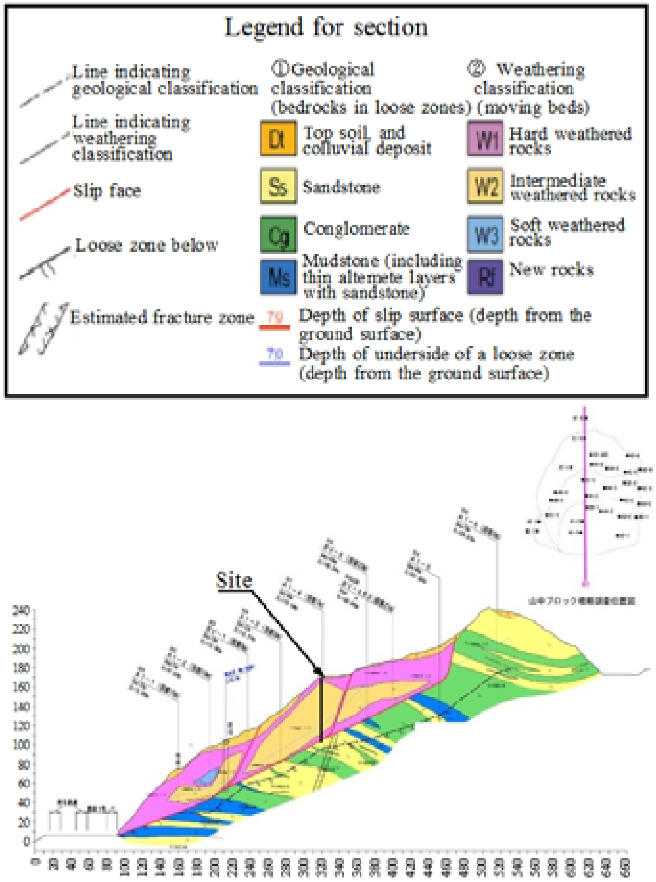

Figure 14. Cross-section at Ohkubo Block, Yui (Site location is marked on a cross-section made available in Mt. Fuji Sabo Office Homepage).

Figure 15. Photo of GP-R sampling inside the deep well at Ohkubo Block (Supplied by Mt. Fuji Sabo Office).

(a) Ground surface.

(b) At depth of 18.5 m.

(c) At depth of 27 m.

(d) At depth of 29.5 m.

Figure 16. Photos of GP-R samples obtained at Ohkubo site at four depths and the excavated surfaces (Supplied by Mt. Fuji Sabo Office).

At Hachigasawa Block, the GP-R sampler captured a slip surface in a core sample taken at a depth of 42 m, as shown in Figure 17. It is quite rare to be accorded the opportunity to view a slip surface, captured in a core obtained at depth, at such close proximity.

At the Yui site, the shear wave velocities measured in situ were compared with those of the GP-R samples in the laboratory. Figure 18 shows the ratio of the two shear wave velocities in the ordinate and the laboratory measured shear wave velocities in the abscissa for the samples obtained at depths of: 2.0 m, 13.0 m, 31.0 m, 46.5 m, and 52.0 m at Yamanaka Block. Judging from the shear wave velocities, the overall quality of the samples appeared very good, except for one data point having the shear velocity ratio falling below 0.8, which was considered too low for a high-quality sample. There seems to be a tendency for the quality of the sample to improve with increasing depth, as well as with increasing shear velocity.

Figure 17. A photo of suspected slip surface at Hachigasawa Block at a depth of 42 m (Supplied by Mt. Fuji Sabo Office).

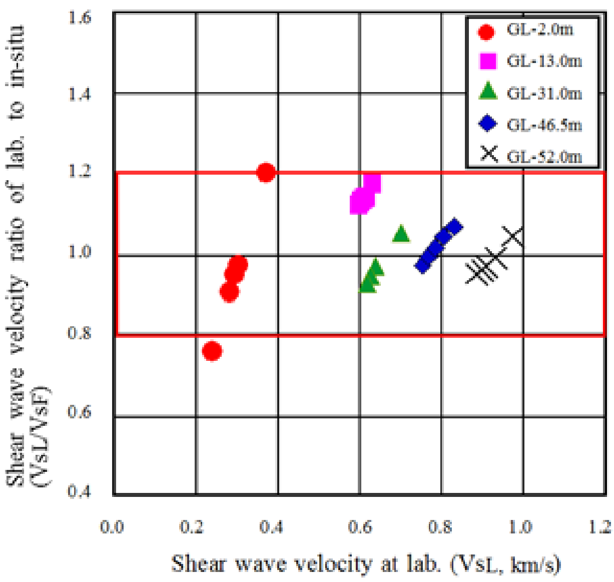

Figure 18. Shear wave velocity ratio of laboratory to in-situ vs. shear wave velocity at laboratory (Supplied by Mt. Fuji Sabo Office).

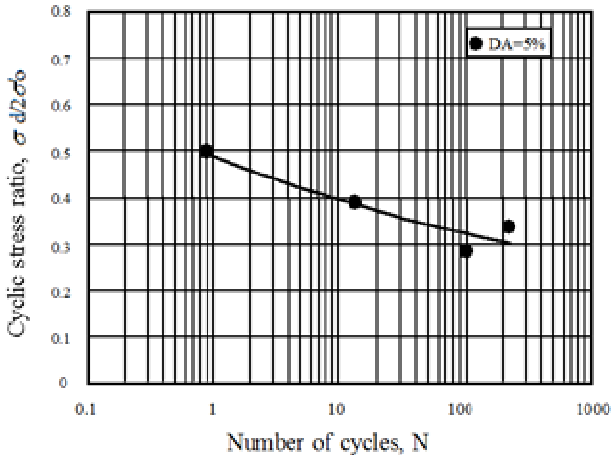

Figure 19. Relationship between cyclic stress ratio and number of cycles to cause DA=5% at Yamanaka Block (Supplied Mt. Fuji Sabo Office).

Undrained cyclic triaxial tests were carried out on GP-R samples obtained above the slip surface at Yamanaka Block to determine the liquefaction potential and deformation characteristics of the ground. Figure 19 shows the results of the test using the criteria of a double amplitude of 5 %, as the pore water pressures never reached the confining pressures.

The GP-R sampler performed admirably at the Yui site. High-quality samples were obtained and provided to the laboratory for testing to determine the seismic stability of the slope. Though not included in this report, static triaxial tests were also performed using GP-R samples. Furthermore, because 200 mm diameter samples were obtained, smaller specimens 80 mm in diameter were carved out from them, so that the general alignment of the formation coincided with the shear plane of the triaxial tests, to more accurately determine the strength of the formation. Last but not least, the samples provided incredible visual images of the site, contributing to a better understanding of its geology.

3 THE GP-D SAMPLER

The GP-D sampler is a single core barrel sampler that has been specifically engineered to operate in boreholes. The design of the sampler, operational procedures, and two cases of site investigation, carried out using the sampler, will be discussed in this section.

3.1 *Design and operation of the GP-D sampler*

The GP-D sampler has essentially the same construction as the GP-R sampler, as shown in Figure

20. Three features have been added to the GP-R so that it can operate in a borehole. These features are as follows: the introduction of a free piston, a core lifter, and a polymer solution supply connection at the sampler head.

The free piston serves as a plug at the bottom end of the barrel, and prevents the polymer solution from leaking out of the barrel while the sampler is being lowered down the borehole. Once the sampler is positioned on the bottom of the borehole, the barrel begins to rotate, cutting the sample. The free piston is pushed upwards by the entering core, forcing the polymer to flow into the annular space between the core and the barrel. Finally, it exits the barrel in the same way as in the GP-R sampling process, cooling the bit and carrying away the cuttings.

Since a wedge cannot be driven in the borehole to separate the core from the ground, a core lifter is fitted just above the bit to squeeze the core sample, holding it in the barrel as the sampler is raised from the borehole. The lifter mechanism is a circular band as shown in Figure 21(a). When the coring is completed, the sampler barrel is nominally lifted, still attached to the formation site, the core sample resists the pull, slumping down slightly, and dragging the core lifter with it. This triggers the core lifter mechanism, causing it to tighten around the cored sample, and enabling the sample to break free from the ground. Finally, with the sample secured, the GP-D barrel is raised to the surface for sample extraction.

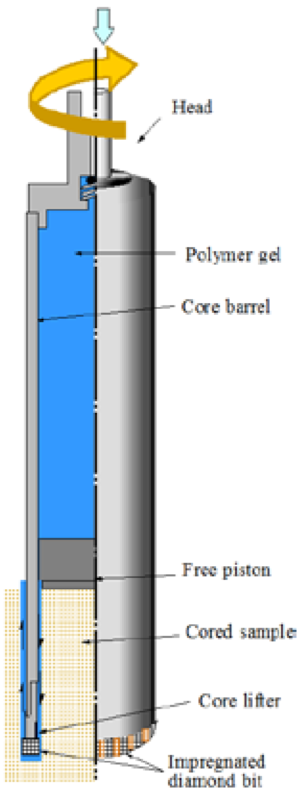

Figure 20. Cross-section of GP-D sampler with cored sample entering into the sampler barrel.

(a) Photo of core lifter.

(b) Photo of 200 mm GP-D sampler.

(c) Photo of GP-D sampling using an electric motor.

Figure 21. Photos of GP-D core lifer and sampling work.

The GP-D sampler barrel is available in diameters of 100 mm, 150 mm and 200 mm. The larger, 300 mm diameter sampler was not chosen for GP-D production as it would be excessively heavy to handle in borehole applications. Since the diameter of the sampler barrel is only 200 mm or less, the polymer stored in the barrel at the beginning of the sampling is not adequate to complete the drilling of a 1 meter long sample. Instead, the design of the GP-D sampler provides for the polymer solution to be continuously supplied through drill strings connected to the top of the sampler.

Figure 21(b) shows a 200 mm diameter GP-D sampler being lowered down into a casing for sampling. Figure 21(c) shows a foreman operating the 200 mm diameter barrel employing the same style electric motor as used with GP-R samplers. Since the GP-D sampler rotates at a very high speed, multiple centralizers are placed on the drill strings to ensure smooth, vibration free coring.

GP-D samplers are not bulky. As an example of the versatility of the GP-D sampler design, a very modest 100 mm diameter barrel sampler may be used inside a building as shown in Figure 22, where coring work is being carried out on the floor of a convenience store.

3.2 *A case of GP-D sampling at Site K*

One of the quandaries of sampling, especially with large diameter samples containing gravels or any other granular material, is the difficulty in verifying the quality of the samples obtained. It is extremely rare to know all the relevant parameters such as: in-situ density; the degree of cementation or aging; the way the granular particles are packed; past stress

Figure 22. Photo of GP-D sampling at a shop floor.

histories the ground has been subjected to; etc. It is generally accepted that if shear modulus or shear wave velocities in situ agree reasonably well with those measured in the laboratory, then the samples are considered to be of good quality. Another parameter that can be used to evaluate the sample quality is void ratio.

In the 1980s, the Central Research Institute of Electric Power Industry conducted extensive studies on Pleistocene gravel formations at four locations identified as Sites A, K, T, and KJ. At all four sites, very extensive geotechnical investigation and testing programs were carried out. These included: SPT; seismic survey; conventional sampling; freezing sampling; static; and cyclic laboratory tests. Since the gravels at the four sites contained very little fines, the freezing method was well suited for obtaining high quality samples.

Kokusho et al. (1994), Tanaka et al. (1989), Kudo et al. (1991), and others have reported the details of these investigations. About a quarter century later, an occasion arose to conduct GP-D sampling at Site K. This presented a very rare opportunity to check the quality of GP sampling against the results of the freezing method.

Figure 23(a) shows the photo of freezing sampling performed over twenty-five years ago at Site K. The sampler used then was a specially designed, 300 mm diameter, triple tube sampler. Figure 23(b) is a photo of the GP-D sampling carried out in 2006. Figure 24(a) shows one of the frozen core samples obtained during the Central Research Institute of Electric Power Industry study in the 1980s. The drill bit used for the freezing sampling was an impregnated diamond bit. Figure 24(b) shows a photo taken in 2006 of the GP-D sampler's barrel, with its impregnated diamond bit, with the cored sample inside. The figure also shows the cored sample after it has been extracted from the barrel.

Figures 25(1), (2) shows the soil profile at the four original sites, including SPT N-values, and the locations where the frozen samples were obtained. Also shown in the figure, are the results of a large penetration test or LPT, this is a heavyweight version of SPT, which has been designed for gravel formations. It uses a hammer weighing 980 N, instead of the SPT's 622.3 N, and has a drop height of 150 cm instead of the SPT's 75 cm. Figure 26 shows the gradation curves of the gravels at the four sites resulting from these tests.

From the results of seismic surveys carried out at all four locations, shear modulus at small-strain were calculated and compared with the shear modulus determined in the laboratory using the frozen samples, as shown in Figure 27. It is clear from the figure that the shear modulus determined in the laboratory measured about 40 % less than those measured in situ. The reason for the laboratory determined small-strain shear modulus being consistently lower than

(a) Photo of freezing sampling.

(b) Photo of GP-D sampling

Figure 23. Photos of freezing and GP-D samplings at Site K.

the in-situ measurements may be attributed to some or all of the following causes: 1) freezing method can disturb the cored sample; 2) bedding error in laboratory testing; 3) small-strain shear modulus in the laboratory is not the same as in-situ determined modulus; and 4) anisotropy in the ground (Tanaka et al. 1998). At that time, conventional sampling without freezing was carried out at Site A, and the small-

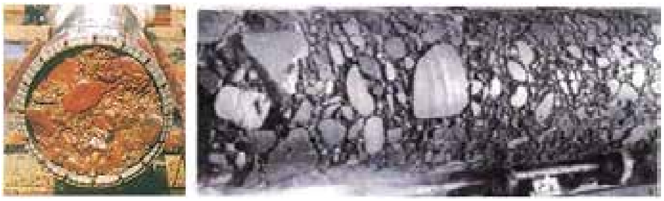

(a) Photos of frozen core sample.

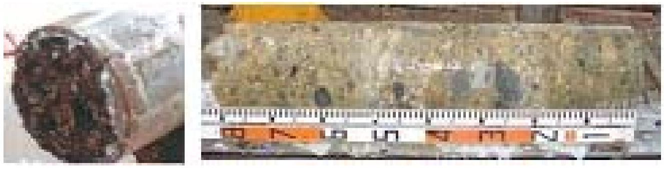

(b) Photos of GP-D sample.

Figure 24. Photos of frozen and GP-D samples obtained at Site K.

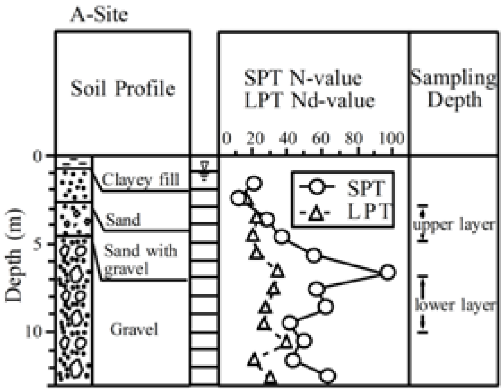

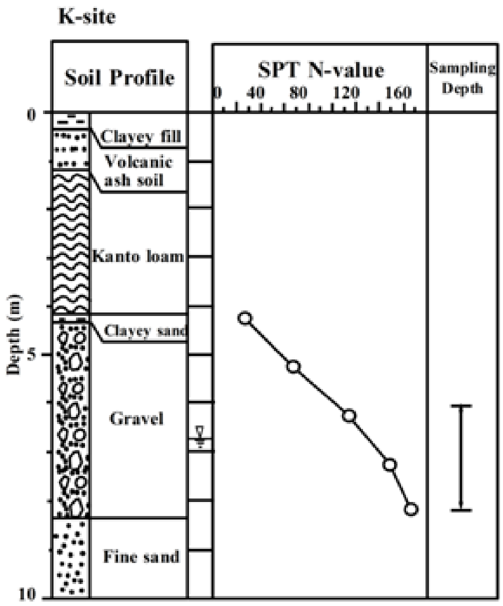

Figure 25(1). Soil profiles at A-site and K-site of four gravelly sites (Kokusho et al. 1994).

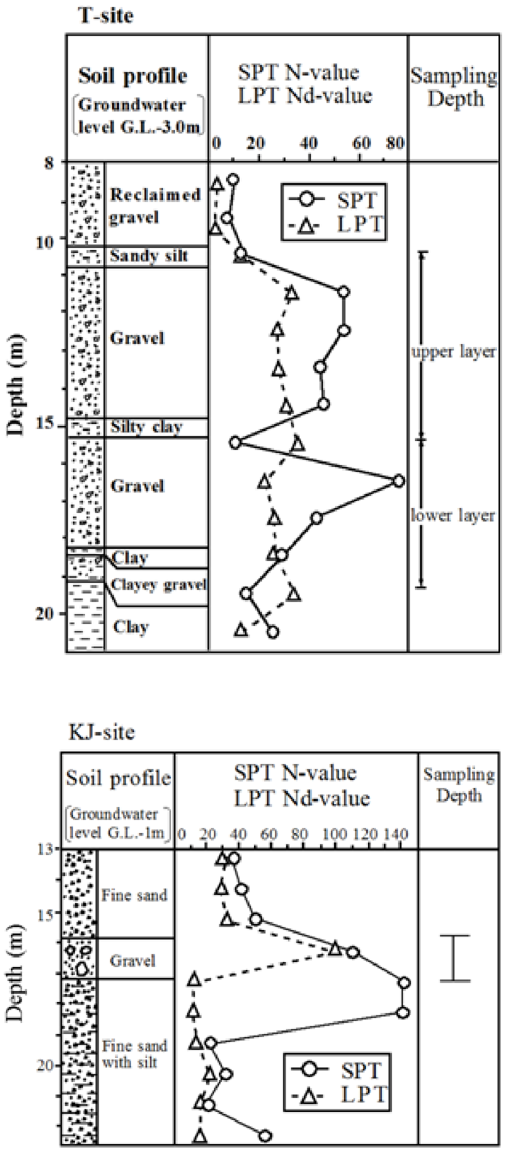

Figure 25(2). Soil profiles at T-site and KJ-site of four gravelly sites (Kokusho et al. 1994).

strain shear modulus determined from these samples showed even smaller values. The disturbance caused by sampling without the benefit of freezing was suspected to have severely loosened the pack of the cored samples.

In 2006, small-strain shear modulus of GP-D samples obtained at Site K were determined in the laboratory and compared with those of the frozen samples as shown in Figure 28. It is clear that the GP-D sample results align with those from the frozen samples, an indication that the GP-D samples are equal in quality to the frozen ones.

To further investigate the quality of GP-D samples, undrained cyclic triaxial tests were carried out to compare with the frozen samples, see Figure 29. Again, GP-D samples were in good agreement with the frozen samples. The average dry densities of the frozen and GP-D samples were 21.33 kN/m^3 and 21.51 kN/m^3, respectively. In the graph, one of the data points of the frozen sample plotted well below the others, indicating that the sample was very weak. The co-author of this paper was present on site for both the freezing and GP-D samplings and noticed the presence of underground water flow channels in some of the samples. These channels had formed where the fine particles, including sands, were carried away leaving only skeletal structures made of gravels. The weak sample contained such a zone. When tested in the laboratory, this type of zone breaks down easily under cyclic loading and falls low on the graph, as was suspected in this case. The average dry density of the frozen samples, excluding the weak sample was 21.53 kN/m^3, which is very close to that of GP-D samples, indicating the two sampling methods obtained samples with equivalent density.

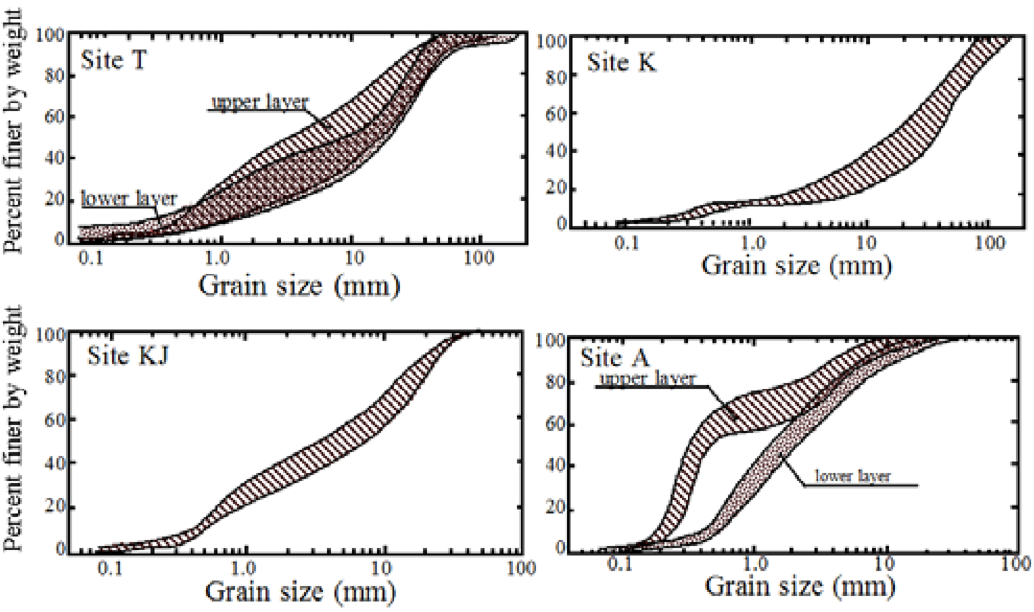

Figure 26. Grain size distributions of gravels at Sites T, K, KJ, and A (Kokusho et al. 1994).

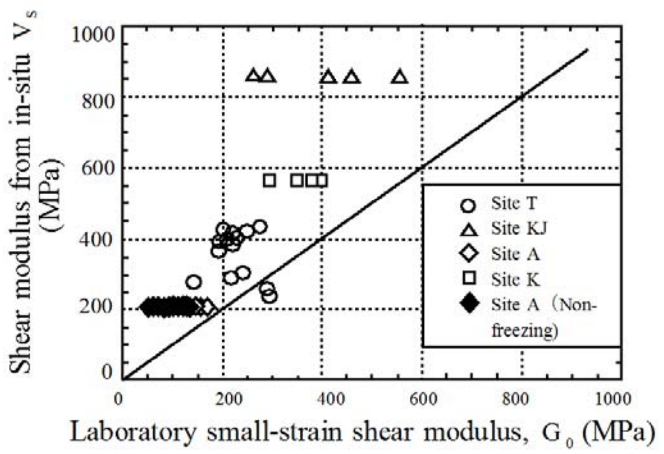

Figure 27. Comparison of small-strain shear modulus between in-situ and laboratory (Kokusho et al. 1994).

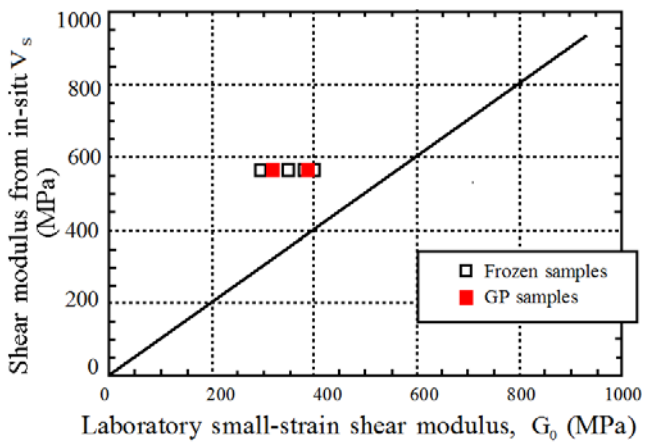

Figure 28. Comparison on small-strain shear modulus between in-situ and laboratory at Site K (GP-D data added to Kokusho et al. 1994).

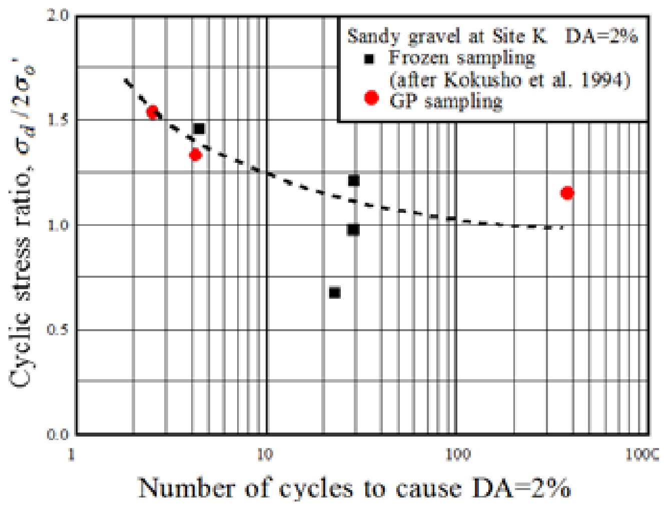

Figure 29. Cyclic stress ratio vs. number of cycles to cause DA=2 % for frozen and GP-D samples obtained at Site K.

From the results of shear modulus tests at small-strain, and undrained cyclic triaxial tests, it is justifiable to state that for the gravels at Site K, the GP-D sampling performed equally to that of the freezing method. It may not be appropriate to generalize the capability of the GP-D sampler with just one case record, but it seems reasonable to state that the sampler obtains high-quality samples of gravels.

3.3 *A case of sampling limestone and coral mixed gravel soils*

A limestone formation called Ryukyu Limestone is found in one of Japan's southernmost chains of islands, known internationally as the Ryukyu Arc. Okinawa Island is the largest in this chain and serves as its political and economic center. Ryukyu Limestone was formed in the Pleistocene Epoch, from the sedimentation of coral in the warm waters of the area, and widely distributed throughout the region. The formation is known for its wide variations in strengths and solidness, ranging from the solidified state by recrystallization, to cemented but unsolidified state. Cavities are also found in these limestone formations.

A cross-section of the Ryukyu Limestone formation, found in Okinawa is shown in Figure 30 (Arikawa & Sasaki 2008). The limestone formation is designated by Ls-1, Ls-2, and Ls-3, and the red zone in the center, with the SPT N-values showing large scatters. Conventional sampling produced very poor core recovery, as shown in Figure 31(a). Many of the structures built over the formation have had to be supported by piles, penetrating through the limestone to rest on the sounder mudstone formations found underneath.

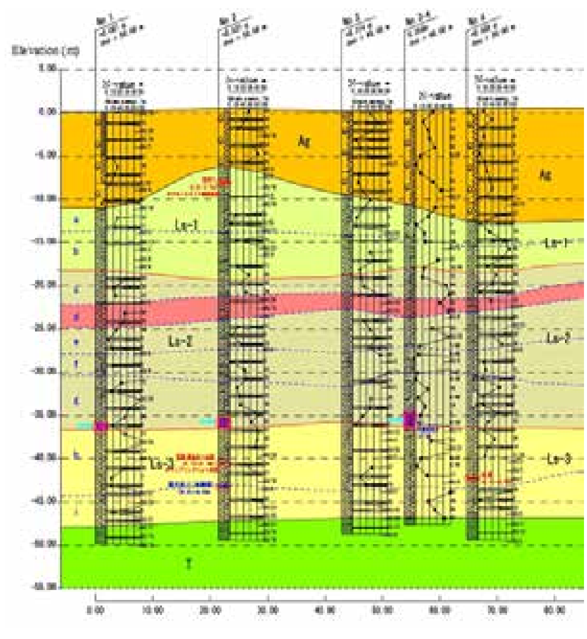

Figure 30. A cross-section of Ryukyu Limestone formation in Okinawa (Arikawa et al. 2008).

(a) Core samples obtained by conventional sampler (b) GP-D samples

Figure 31. Photos of Ryukyu Limestone core samples obtained by conventional sampling and GP-D sampler (Arikawa et al. 2008)

Since the thickness of Ryukyu Limestone often reaches 40 to 50 m on the shore, driving piles through the formation can become difficult and uneconomical. An attempt was made to obtain high-quality samples employing the GP-D sampler in order to more accurately ascertain the engineering properties of the limestone formation. Figure 31(b) shows two GP-D core samples obtained at depths of 23.0 m and 25.0 m. Contrary to the images of fractured cores and widely scattered N-values obtained through conventional sampling methods, the formation appeared to be more intact than previously thought.

Consolidated-drained triaxial compression tests were carried out on GP-D samples of the limestone obtained at depths of 26.7 m, 29.7 m, and 35.45 m as shown in Table 2 (Kokai et al. 2014). The SPT N-values, measured 1 m below the sampling depths, are also given. The samples at 26.7 m and 35.45 m came from relatively soft zones, but the laboratory tests showed reasonable soil strengths. The sampler core obtained at 29.7 m exhibited the strength of soft rock.

In the Ryukyu Islands, a more recent geological deposit called coral mixed gravelly soils, is found overlaying the Ryukyu Limestone. These soils are also difficult to sample with conventional samplers. Here, the GP-D sampler once again proved successful in obtaining high-quality samples. Figure 32 shows a photo of one such sample, and the CT scanning images taken of that sample. It is remarkable that the core scans reveal signs of past biological activity without disruption, indicating the superlative quality of the GP-D samples.

Consolidated-drained triaxial tests carried out on the GP-D samples obtained from the coral mixed gravel formation at Miyako-Jima, one of the Ryukyu Islands, showed an angle of internal friction higher than those estimated by empirical equations using N-values (Ogawa et al. 2013). Similarly, the actual undrained cyclic strengths of the samples were stronger than the undrained cyclic strengths estimated using the SPT N-value based empirical equation. This equation is taken from the *Specification for Highway Bridges*, published by the Japan Road Association.

Upon reviewing the GP-D sampler data from the Ryukyu Limestone and coral mixed gravelly soil, it is evident that the GP-D sampler demonstrated its ability to successfully sample very brittle soils that conventional samplers had previously failed to do. These quality samples enabled engineers to observe and test cores that accurately represented the strength and deformation characteristics of the Ryu-

Table 2. Consolidated-drained traiaxial test results of Ryukyu Limestone (Kokai et al. 2014).

Sampled depth	GL-26.7m	GL-29.7m	GL-35.45m
Avg. N-value, 1m below	11	78	18
GP samples			
Moist density ρ_t (g/cm^3)	1.895	2.172	1.804
Fines content Fc (%)	37.3	31.8	22.2
Angle of int. fric. ϕ (°)	38.9	0	30.3
Cohesion c (kN/m^2)	0	1,270	0
Def. modulus E_{50}(MN/m^2)	37	459	22
Def. modulus $E_{(0.1\%)}$(MN/m^2)	101	862	82

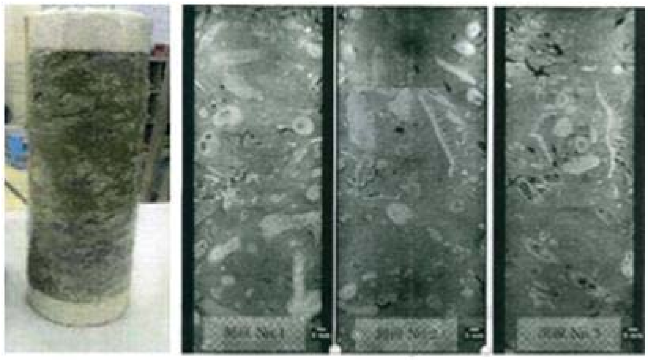

Figure 32. A GP-D sample of coral gravel mixed soil, and CT scanning images (Courtesy of the Port and Airport Research Institute, Japan).

kyu Limestone formations and coral mixed gravelly soil.

The GP-D sampler was the first sampler to succeed at obtaining intact samples of Ryukyu Limestone. This made thorough testing of the core samples in the laboratory feasible and ushered in a breakthrough in how limestone is analyzed

4 THE GP-TR SAMPLER

The GP-Tr sampler is designed for sampling medium to dense sandy soils. It can sample sand containing some gravel, but not gravelly soil. As with all GP samplers, the GP-Tr uses the polymer solution in a unique way: relying on it as a lubricant to reduce the friction between the sample and the sampler tube. In this section, the design of the sampler, its operating procedures, and three case records of site investigations using the sampler, are discussed.

4.1 *The design of GP-Tr sampler and its operations*

As shown in Figure 33(a), the GP-Tr sampler's construction is based upon a conventional rotary triple tube sampler, retaining the triple tube's basic features, including: self-adjusting shoe penetration; stationary liner and inner tubes; and an outer tube, tipped with a bit, that is employed to rotate and drill the soil above the shoe. Figure 33(b) shows a photo of the sampler. Unlike the GP-R and GP-D samplers, the GP-Tr utilizes ordinary drilling fluid to remove the cuttings and cool the bit.

Differentiating the GP-Tr design from common triple tube samplers, is its exclusive use of polymer solution to lubricate the core sample as it enters the liner tube. This is accomplished as a small volume of polymer solution is dispensed just above the shoe through a dispenser ring. The ring is attached to the bottom end of the PVC liner tube, as shown in Figure 33(c). The polymer flows through 45 degree cuts in the dispenser ring and comes into contact with the entering core, after it passes through the shoe, coating the sample surface with polymer solution. This significantly reduces the friction between the sample and the liner tube, which is one of the most serious causes of sample disturbance.

Another unique component of the GP-Tr is the free piston. The piston is designed with a ridge which catches on a lip inside of the shoe. This prevents the piston from falling out, and allows it to act as a stopper; storing the polymer solution inside the liner tube of the sampler. Once the sampling starts, the cored sample moves through the shoe, pushing the free piston up along the liner tube. In turn, the piston squeezes the polymer solution, forcing it to flow out of the liner tube chamber into an annular space between the liner and inner tubes. Once there, some of the polymer flows downward and is delivered to the dispenser ring to coat the sample.

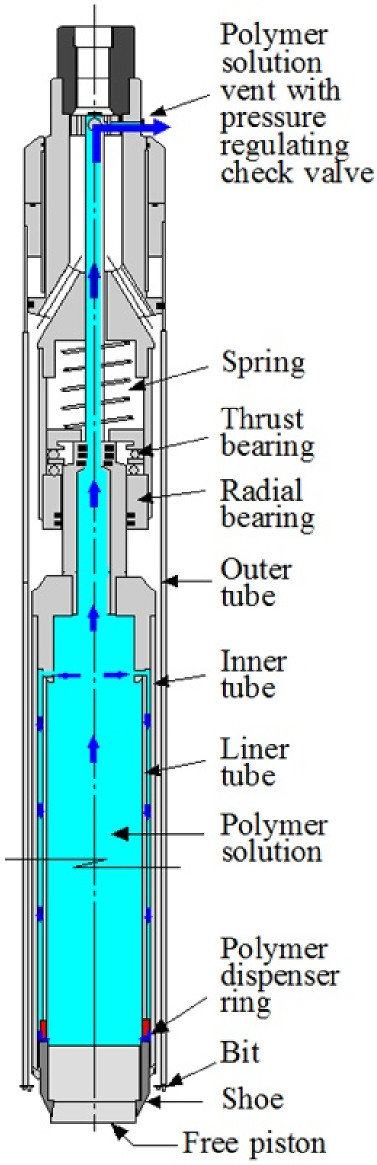

(a) Cross section

(b) Photo of sampler

(c) Photo of polymer dispenser rinng

Figure 33. Schematic illustration and photo of GP-Tr sampler.

A very small percentage of the polymer solution which originally filled the liner tube is actually used for this coating. The excess is vented out through a check valve located at the top of the sampler. The check valve has two functions: first, it blocks the ordinary drilling fluid used from entering into the liner chamber, contaminating the polymer solution; second, it protects the core sample by preventing the polymer pressure from building up above a few kPa. A higher pressure would result in the polymer penetrating into the cored sample, which is a very undesirable condition. To help avert the possibility of this event, it is imperative to carry out the coring slowly, and avoid applying any abrupt thrust force to the sampler.

Figure 34 is a schematic illustration of the GP-Tr sampling process: first depicted is the positioning of the sampler at the floor of the borehole; next is the coring process nearing midpoint, with the sampler half way into the ground; finally, a drawing of the retraction of the sampler, with the sample core captured inside. Figure 35(a) shows a photo of the sampler with the piston and polymer solution in place, ready to be lowered into the borehole. As seen in Figure 35(a), the shoe is retaining the free piston prior to drilling.

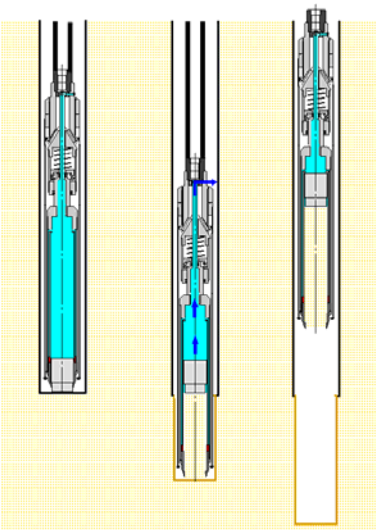

Figure 34. Schematic illustration of GP-Tr sampling.

(a) Photo of free piston (b) After sampling (c) Bit and shoe removed

Figure 35. Photos of GP-Tr sampler before and after sampling.

Figure 36. Photos of GP-Tr sample extruded out of the liner tube (above) and polymer solution wiped off (below).

The sampler is designed to obtain a sample length of up to 1 m. The shoe's tapering angle is set at 14 degrees in order to form the lip that serves to retain the free piston, preventing it from falling out. The inside diameter of the shoe is set between 80 mm and 83 mm to have an inside clearance ratio of 0.6 % to a maximum of 3.6 %. The area ratio ranges from 12 % to 21%. It is customary for a drilling operator to carry several sets of shoes for the best sampling results. The operator typically sizes the shoe, starting with the shoe having the least inside clearance and sizes up if necessary.

Figure 35(b) shows the sampler with a sample inside, while (c) shows the sample with the bit and shoe removed. Figure 36 shows the sample extruded out of the liner tube, still coated in polymer (above); and with the polymer removed (below). GP-Tr samples are usually kept upright in the liner tube overnight in order to facilitate the drainage of water. This ensures that the samples regain strength and stability before being sealed for shipment to the laboratory.

4.2 *A case of sampling at Zelazny Most, Poland, copper tailings disposal depository*

Jamiolkowski et al. (2015) report on comprehensive geotechnical site investigations, carried out over a period of two decades, at one of the world's largest copper tailings disposal reservoirs, located in Zelazny Most, Poland. In view of the difficulties associated with obtaining undisturbed samples of silt and silty sand at the tailings depository, the investigation relied primarily on in-situ tests including: S-CPTU; S-DMT; cross-hole tests; and block sampling. In 2013, a GP-Tr sampler was brought in and succeeded in obtaining quality samples.

Figure 37 shows the zone of gradation curves of the tailings disposal at location 7E-8E, close to where the GP-Tr samples were obtained. One of the gradation curves of the GP-Tr samples, taken at the site, is also shown. The specific GP-Tr sample used appears to be sandier than the surrounding area. Figure 38 shows the shear wave velocities determined by cross-hole tests at location 7E-8E, and the shear wave velocities measured in the laboratory using GP-Tr samples. The figure also shows the measurements normalized at 98 kN/m^2 in order to remove the effect of overburden pressures on the shear wave velocities. A good overall agreement seems to exist between the in-situ and laboratory measurements.

The normalized shear wave velocities were replotted to show the ratio of the velocities in the laboratory to in situ, against the normalized in-situ velocities, see Figure 39. This figure clearly demonstrates the relative difference between the two normalized velocities. All the data lie between normalized in-situ velocities of 200 and 300 m/s. However, the ratios of normalized shear velocities show a wide scat-

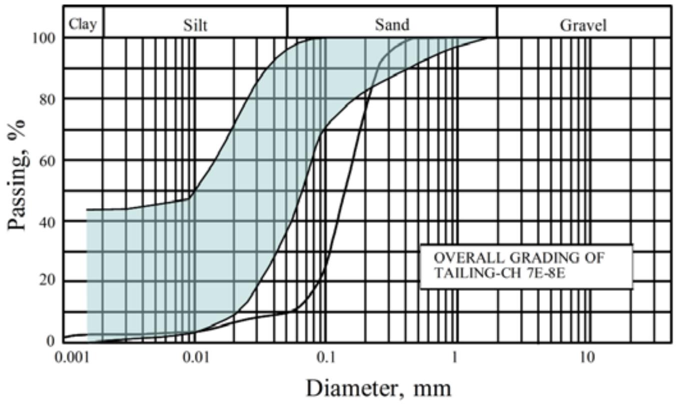

Figure 37. Gradation curves of tailings at 7E-8E and GP-Tr sample (Jamiolkowski et al. 2015).

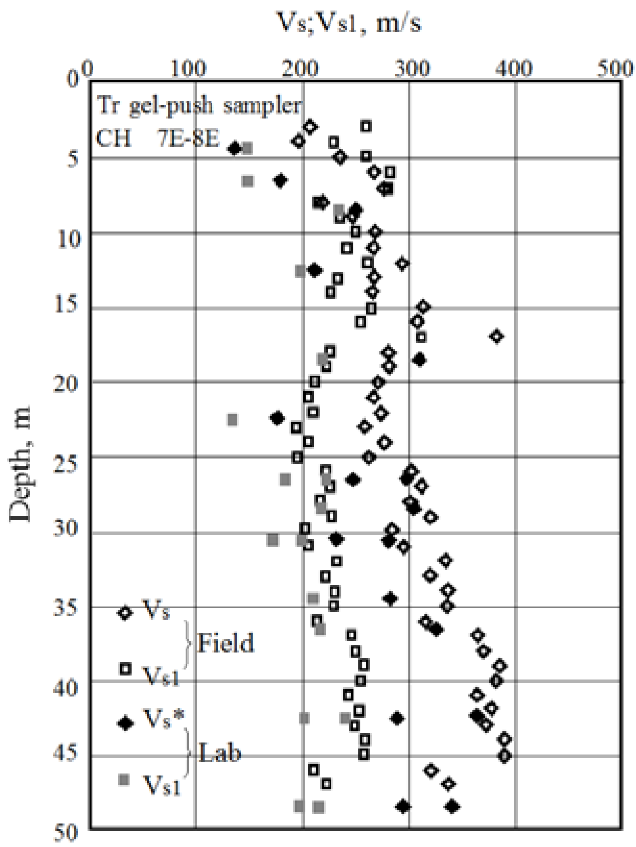

Figure 38. East dam-Comparison Vs1(F) vs. Vs1(L).(*) Bender element test. Geoteko (2014) (after Jamiolkowski et al. 2015).

ter, falling between 0.5 to 1.3, and indicating a possible divergence in the sample quality. In general, samples having shear wave velocity ratios close to unity are considered high-quality. It is however noticeable that many of the data points lie between 0.8 and 1.0, indicating these samples retained high-quality. It may be of value to compare the stress paths of static and cyclic loading tests using the samples having the ratios close to unity, with those having very large or small values to examine the possibility of sample disturbance. Since block sampling has been conducted on the site, it may also be

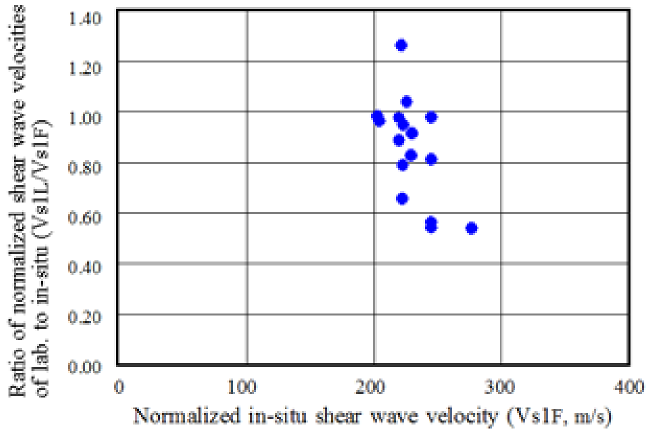

Figure 39. Ratio of normalized shear wave velocities of laboratory to in-situ vs. normalized in-situ shear wave velocity.

of interest to compare the strength and stress paths of the GP-Tr and block samples, as block sampling can preserve soil characteristics in situ (Mori et al. 1979).

4.3 *A case of sampling at Padma Bridge Project in Bangladesh*

Padma Bridge is located about 30 km southwest of Dhaka, crossing the Padma River in the district of Mawa on the left bank; and in the district on Janjira on the right bank. The bridge is under construction. When completed, it will become one of the longest bridges in Bangladesh, having a total span of 6.15 km.

The Padma River occasionally becomes turbulent, and is known to scour the riverbed to a depth in excess of 60 m. Thus, the piles supporting the bridge have to be primarily supported by the soil below the scour level. The soil formation at the site is predominately sand, with some gravel layers appearing. Layers of mica are also found. Seismicity of the area is moderate. However, for the stability analysis of the bridge structure, liquefaction susceptibility of the shallow sand formation was investigated.

A very comprehensive geotechnical investigation program was carried out as reported by De Silva et al. (2010): SPT; CTP; seismic survey; Dilatometer; pressuremeter tests; SB-IFT (self-boring in-situ shearing apparatus); and GP-Tr sampling. SB-IFT equipment and GP-Tr samplers were brought in from Japan and used at three locations, reaching to depths of about 100 m. To date, this is the deepest the GP-Tr samplers have been used.

Figure 40 shows: SPT N-values; sample recovery ratio; dry density; void ratio; the maximum and minimum void ratios at one of the boreholes. From the SPT N-values and the void ratios, the soil at Padma seems relatively dense. The gradation curves of the samples indicate the soil to be uniformly graded

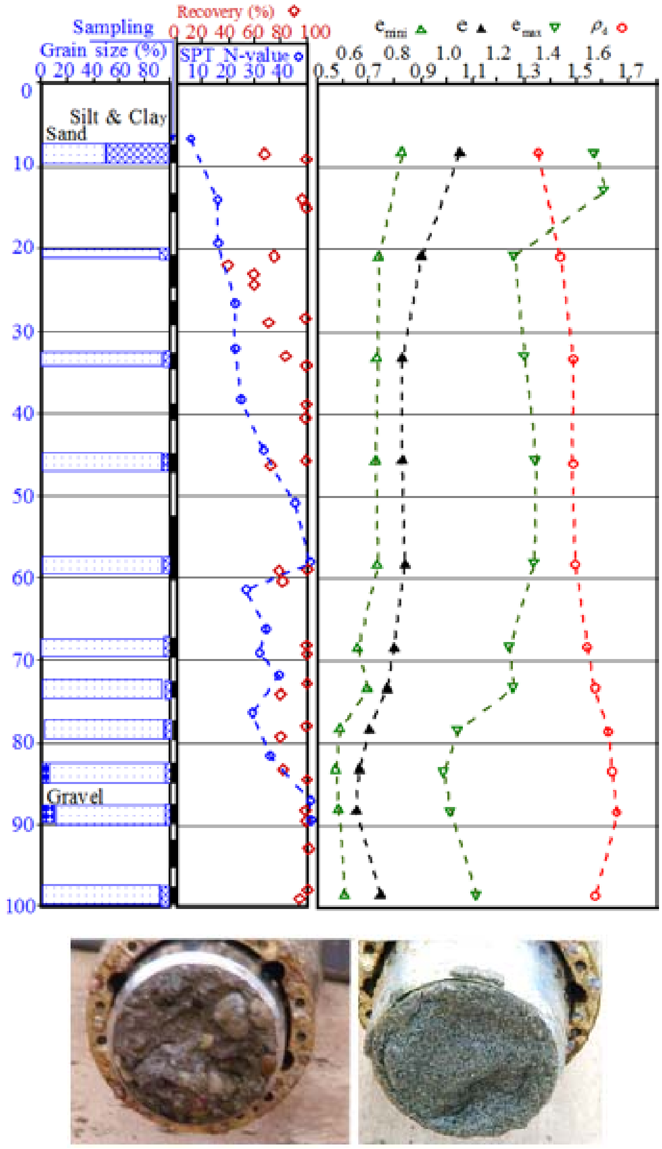

Figure 40. Soil profile at Padma site, and samples obtained at 58 m (left) and at 84 m (right).

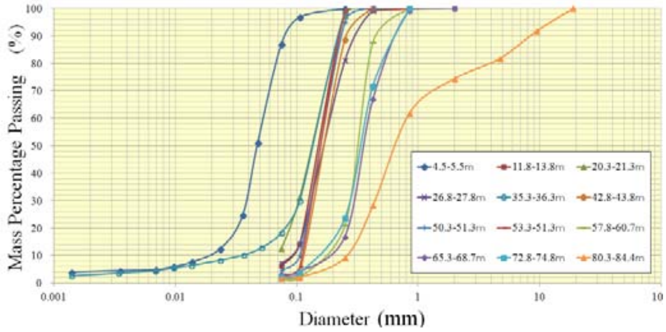

Figure 41. Gradation curves at Padma site.

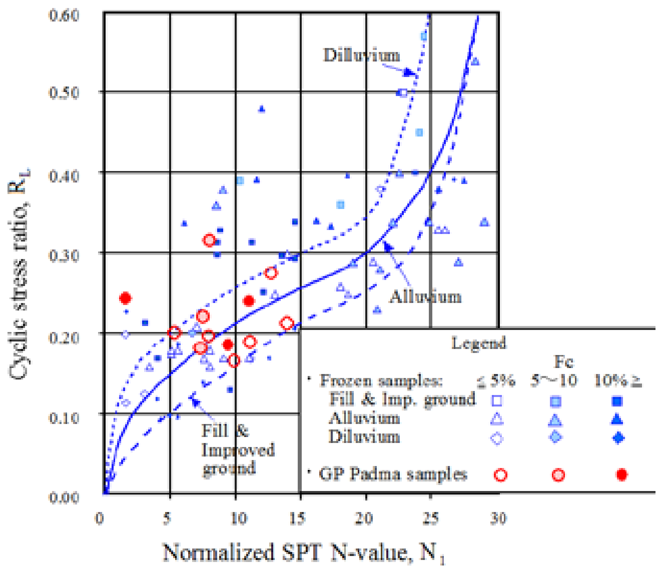

Figure 42. Cyclic stress ratio vs. normalized SPT value for frozen samples (Matsuo 2004), and GP samples obtained at Padma.

clean sand, as shown in Figure 41. Since the seismic survey data is not yet available, the comparison of the laboratory determined shear wave velocities of the GP-Tr samples to those measured in situ, to assess sample quality, is not possible at this time.

However, with the results of undrained cyclic triaxial tests carried out on the samples, and using SPT N-values, an attempt was made to compare the Padma data with the data compiled by Matsuo (2004), on Japanese sandy soils obtained by the freezing method, as shown in Figure 42. The SPT N-values were normalized at 98 kN/m^2. The Padma data seems to agree overall with the general trend of the Japanese sandy soils. When the results of seismic and other in-situ tests, listed above, become available the quality of the GP-Tr samples obtained at Padma bridge project may be revisited.

4.4 *A case of sampling of Jurong Formation*

The Jurong formation is a sedimentary rock formed from the late Triassic to the early Jurassic eras, and found in the western part of Singapore. It consists of conglomerate, sandstone, shale, mudstone, limestone, and dolomite. It has been severely folded, and the weathered section has become a residual soil.

This formation is known for its slaking characteristic. Slaking occurs when overburden pressures are lifted and the soil comes into contact with a fluid, including drilling fluid. In Singapore, the Mazier sampler, which is very similar in construction to the rotary triple tube sampler, is commonly used for sampling the formation. A sample taken from the formation utilizing this method exhibiting slaking is shown in Figure 43(a).

In an attempt to obtain higher quality samples of the Jurong formation, GP-Tr sampling was carried out at the same location and depth where the Mazier sample shown in Figure 43(a) was obtained (Yokoi et al. 2015). Figure 43(b) shows the GP-Tr sample. Both the Mazier and GP-Tr samples were obtained at a depth of 50.5 m. It is clear that the GP-Tr sample shows no trace of slaking. A total of seven samples, including the core sample shown in Figure 43(c), were obtained by the GP-Tr sampler along the depth of the borehole, none of which showed slaking. The gradation curves of two of the GP-Tr samples are shown in Figure 44.

Figure 45 depicts the undrained shear strengths of the GP-Tr and Mazier samples, which have been plotted against SPT N-values. Due to the limited amount of test data nothing conclusive can be stated, but it appears that the GP-Tr samples give somewhat higher strengths. When more data becomes available, it may prove the GP-Tr sampler to be a beneficial tool for assessing the engineering properties of the Jurong formation.

The GP-Tr's success in sampling the slaking-prone Jurong formation is attributable to its use of a thick polymer solution in the sampling process. The PHP polymer chain is negatively charged (anion), and attracted to the clay mineral's positively charged side (cation). Since clay mineral has a negatively charged side as well, the polymer chain is repelled at the same time. The combination of attraction and repulsion between the clay mineral and polymer strings forms a quasi-membrane, isolating the slaking-prone clay mineral and preventing it from being exposed to the drilling fluid. A polymer identical to the one used in GP polymer solutions is being marketed as an additive for drilling in slaking-prone formations. It has been demonstrated that using the polymer at high concentration makes it even more effective at preventing slaking.

(a) Mazier sample exhibiting slaking.

(b) GP-Tr sampled obtained at 50.5 m.

(c) GP-Tr sample obtained at 58.5 m.

Figure 43. Photos of Jurong formation samples obtained by Mazier and GP-Tr samplers (Yokoi et al. 2015).

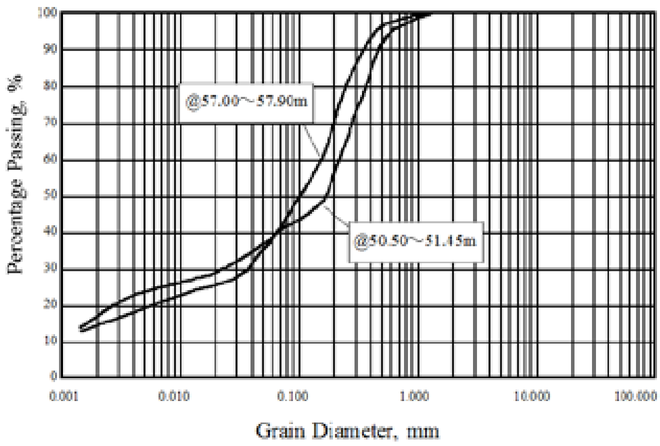

Figure 44. Gradation curves of two GP-Tr samples.

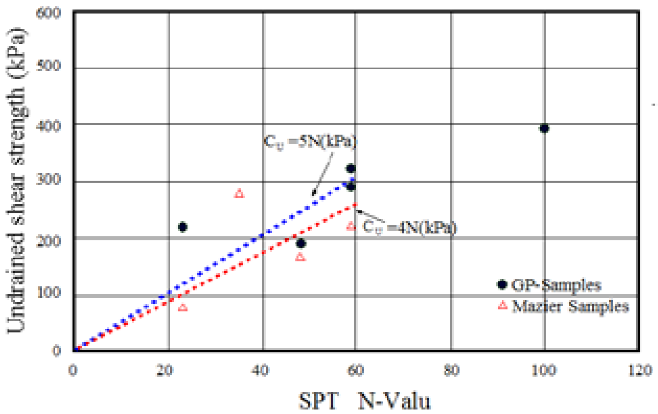

Figure 45. Relationship between undrained shear strengths and SPT N-Values of Jurong formation estimated from the samples obtained by GP-Tr and Mazier samplers.

5 THE GP-S SAMPLER

The GP-S sampler is designed to obtain high-quality samples of silt, silty sand, and loose sand. Unlike the other GP samplers, the GP-S does not use the rotational motion of a drill bit to obtain a sample. Instead, the sampler tube penetrates the ground statically. The design of the sampler, operating procedures, and actual case records, are discussed in this section.

5.1 *The design of GP-S sampler and its operations*

The GP-S sampler was developed as a joint project in 2006, between Kiso-Jiban Consultants and the Chinese Research Institute of Taiwan, led by Professor Lee. It is built around the Osterberg sampler design, with a fixed piston, and using hydraulic pressure to push the sampler tube into the ground.

The GP-S sampler has three pistons: the stationary piston, the sampling tube advancing piston, and the core-catcher activating piston. The stationary piston remains at the bottom of the borehole during the sampling. The sampling tube advancing piston pushes the shoe, the sampling tube, and the liner tube into the ground simultaneously.

As a major modification to the conventional Osterberg model, the GP-S sampler has a core catcher that is extended into position by a hydraulically activated piston. The core catcher acts to retain the cored sample, preventing it from falling out of the sample tube as it is retracted from the ground. The core catcher also dispenses a coating of thick polymer solution onto the surface of the cored sample, in a way similar to that of the dispenser ring in the GP-Tr sampler.

Figure 46 shows a cross-section of the sampler at three stages of sampling operation. Figure 46(a) shows the sampler at the bottom of the borehole. Figure 46(b) shows the shoe and sampler being pushed into the ground. Figure 46(c) shows the core catcher being activated and holding the core at the base of the shoe.

With the GP-R, GP-D and GP-Tr samplers, the cored sample entering into the liner tube, squeezes the polymer solution to flow up out of the barrel or liner tube, but with the GP-S, the sampling tube advancing piston squeezes the polymer solution down to flow out. Care must be exercised not to apply excessively high hydraulic pressure on the sampling tube advancing piston, which may cause the polymer pressure to rise too rapidly. A penetration rate of 1m/min is recommended. The polymer solution flows through the annular space between the sampling and liner tubes. Upon reaching the core catcher, the polymer solution seeps through the slight gaps between the diagonal fins of the core catcher to coat the sample, see Figure 47(a).

The sampling starts with the hydraulic pressure pushing the sampling tube advancing piston and forcing the entire sampling mechanism to move downward, see Figure 46(b). At this stage the polymer solution is being dispensed to coat the sample. Additionally, the polymer solution is being released to the outside of the sampler just above the shoe, to coat the exterior wall of the sampling tube, lubricating it to reduce the penetration resistance. As in the case of the GP-Tr sampler, the volume of polymer solution needed to accomplish these two tasks is limited and the bulk of the solution is vented out through a check valve at the top.

When the sampling tube is pushed down fully to

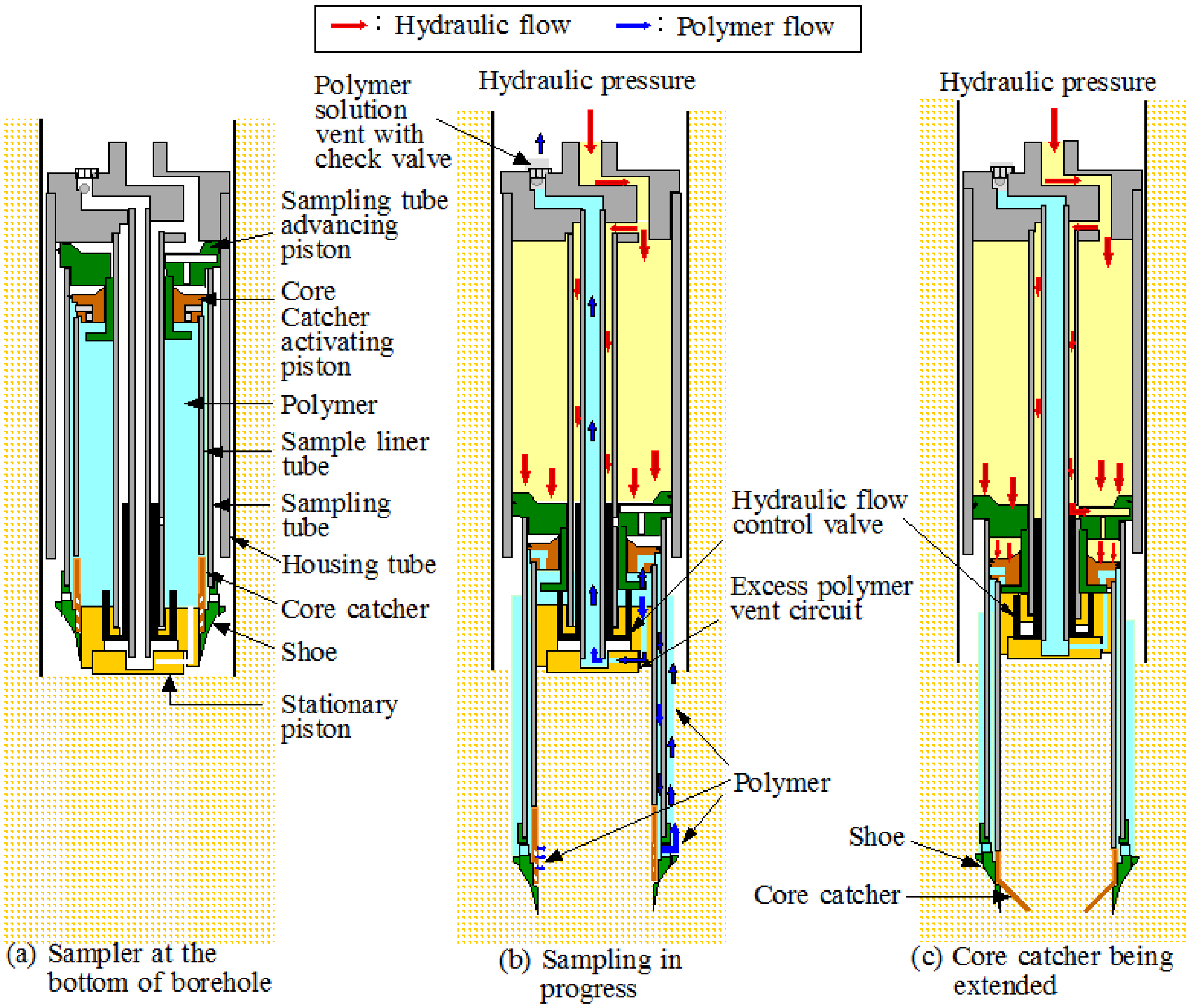

Figure 46. Schematic illustration of GP-S sampler in operation.

(a) Shoe and core catcher with piston removed.

(b) Activated core catcher with sample inside.

Figure 47. Photos of GP-S sampler.

a length of 1 m, it locks itself and shifts the position of the hydraulic flow control valve, shown in Figure 46(b). This diverts the hydraulic flow and triggers the core catcher activating piston. The piston forces the liner tube to move down, causing the core catcher to slide out of its resting position, extending its fins, as shown in Figures 46(c) and 47(b).

The fins ride over the inside wall of the shoe and extend out to constrict the cored sample at the shoe. The inside diameter of the shoe is made to be anywhere between 71 mm and 74 mm, while the inside clearance ratio is selected to be anywhere from 0.0 % to a maximum of 3.6 %. The shoe's tapering angle is set at 6.6 degrees, and the area ratio is set between 9 % to 18 %. Drilling operators usually carry several sets of shoes, and try to obtain quality samples using the shoe with the least inside clearance ratio.

Figure 48(a) shows a sand sample after having been removed from the liner tube with some polymer still visible. Figure 48(b) shows the sample with the polymer removed and the surface soil trimmed off to show the layering of the sample. As with the GP-Tr samples, GP-S samples are usually kept overnight upright in the liner tubes. This drains excess water from the sample, allowing the soil to reestablish stability before being sealed for shipment to the laboratory.

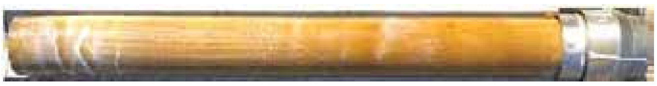

(a) Sample extruded out of liner tube.

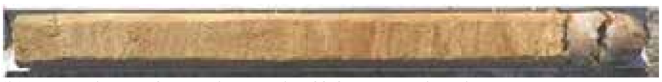

(b) Sample surface trimmed off for examination.

Figure 48. Photos of GP-S sample.

5.2 *A case of site investigation at Muya coastal dyke, Japan*

The port of Muya is located in Tokushima Prefecture on the Island of Shikoku, as shown in Figure 49. The coastal area in western Japan expects to be subjected to an earthquake having a magnitude in excess of 8, with accompanying subsequent tsunami waves. An investigation has been carried out to study the seismic stability of soils at Muya port coastal dike.

In the course of the geotechnical investigation suspension type seismic survey, GP-S, thin walled tube, and triple tube samplings were carried out. Per the consent of the Komatsujima Port & Airport Construction Office, Shikoku Regional Development Bureau of the Ministry of Land, Infrastructure, Transport and Tourism, the following data and information is made possible.

Figure 50 shows the cross-section of the dike at Muya port. As the gradation curves shown in Figure 51 indicate, all the soil layers except the clay layer Ac2, fall in the zone of very likely to liquefy. GP-S samples were obtained at Layers B, Asc1, and Asc2. The fill material used behind the dike consists of coal cinders and some gravel, having SPT N-values between 5 and 10. A thin walled tube sampler was used for Layer Asc1, and a triple tube sampler for Layers B and Asc2. Figure 52 shows the photo of a GP-S sample obtained from Layer B containing coal cinders. It is evident the material is loosely packed.

In order to evaluate the sample quality, shear modulus determined in the laboratory using wave propagation method were compared with those determined from the in-situ seismic survey, as shown in Figure 53. The ordinate shows the ratio of shear modulus determined in the laboratory to the in-situ, and the abscissa shows the in-situ shear modulus. Most of the shear modulus ratios of the GP-S samples lie close to the axis of unity, indicating the samples were likely to have retained their high-quality.

The shear modulus ratios of the samples obtained

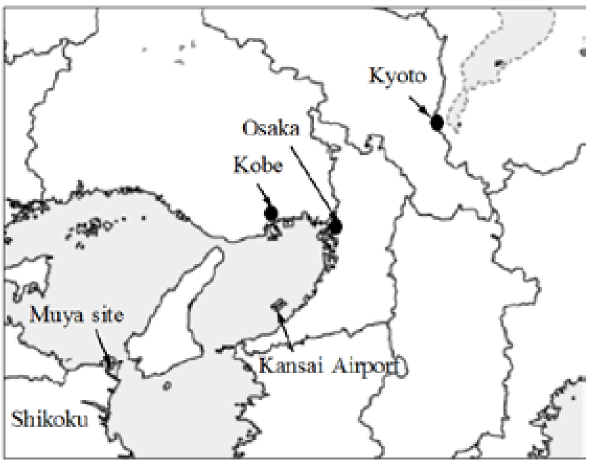

Figure 49. Location of Muya site.

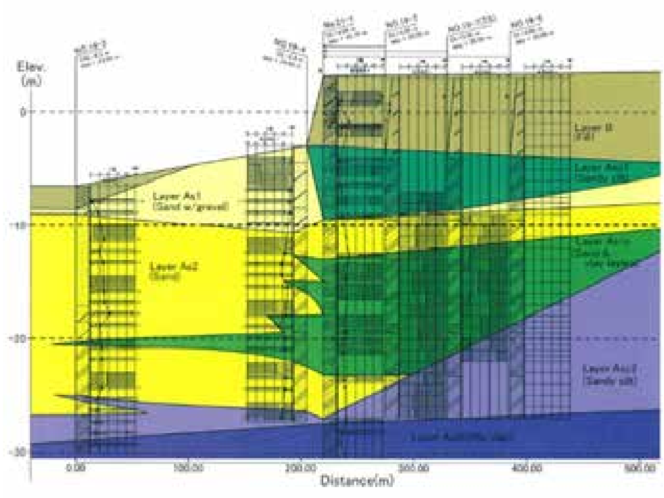

Figure 50. Cross-section of Muya Port coastal dyke.

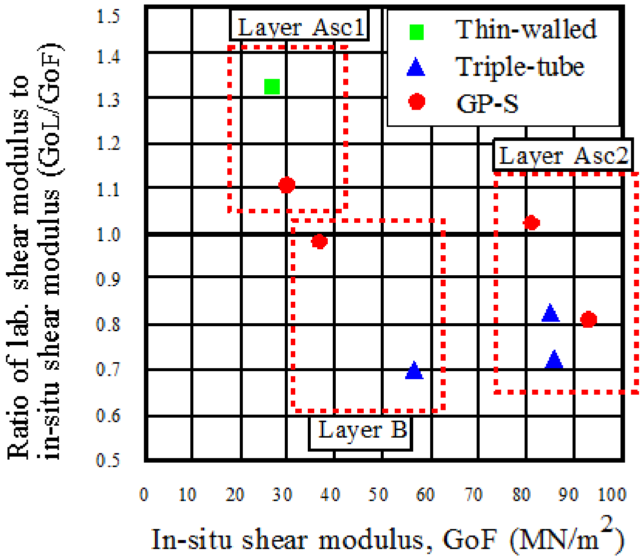

Figure 53. Ratio of shear modulus in the laboratory to in-situ vs. in-situ shear modulus (revisions made to Sunakawa et al. 2010).

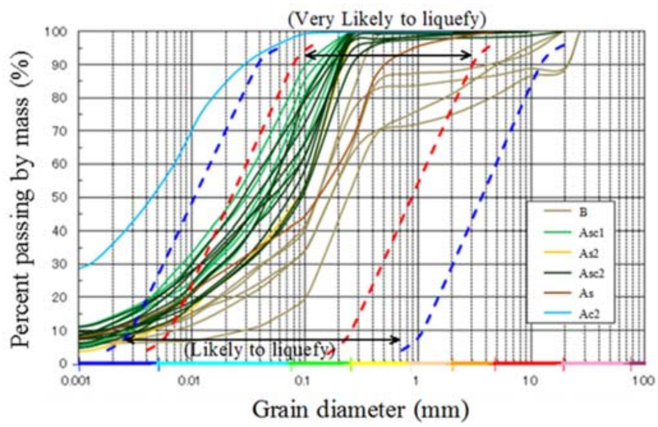

Figure 51. Gradation curves of soils at Muya Port.

Figure 52. Photo of Layer B sample.

by the thin walled tube and the triple tube samplers show a wide scatter, possibly indicating disturbance due to the sampling. At the Muya site, soil composition varies even within the same layer, and the samples obtained by the GP-S and thin walled tube or triple tube samplers for each layer may not necessarily have the same or similar soils. Consequently, the direct comparison of the GP-S samples with samples obtained by other samplers, for each of the three layers, is not possible. However, the polymer coating system of the GP-S sampler appears to be effective in reducing friction between the cored sample and the sampler wall, obtaining high-quality samples regardless of the variation in soil compositions.

5.3 *Cases of New Zealand and Taiwan*

Outside Japan, the GP-S sampler has been used in New Zealand and Taiwan for sampling of silt and silty sands. Stringer et al. (2015a, b), Taylor et al. (2012), and others have reported the site investigation and liquefaction analyses carried out at Christchurch, subsequent to the 2010-2011 Canterbury Earthquake Sequence.

At Christchurch, extensive seismic surveys were carried out. One such set of data collected at Gainsborough Reserve site was used to compare with shear wave velocities measured in the laboratory using GP-S samples obtained at the same location, as shown in Figure 54. In-situ shear wave velocity was measured by the cross-hole method. The in-situ and laboratory shear wave velocities seem to agree very well, except for one GP-S data plotted at a shallow depth, where the sample was reported to have contained some organic fibers, causing the quality of sample to be suspect.

The shear wave velocity data was replotted, as shown in Figure 55, to compare the ratio of shear wave velocities of laboratory to in-situ, against the in-situ velocity. Since most of the data plots around the ratio of 1.0, the samples are considered high-quality.

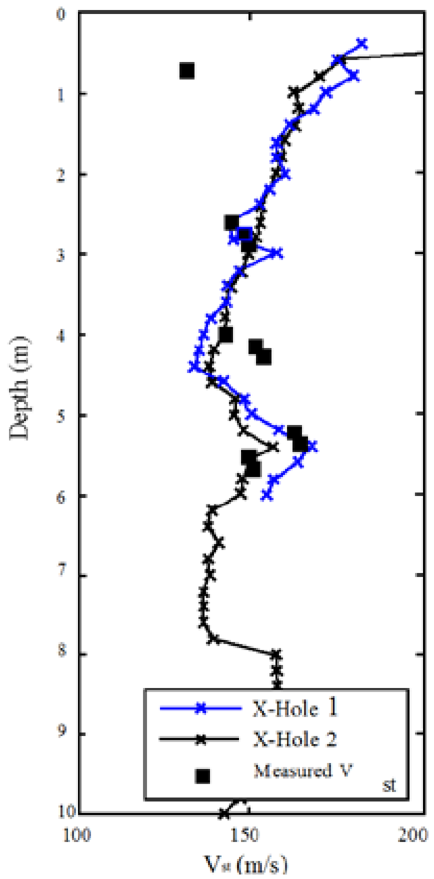

Figure 54. Comparison of shear wave velocity measured by the cross-hole at Gainsborough Reserve to the same determined using GP-S sample (Stringer et al. 2015b).

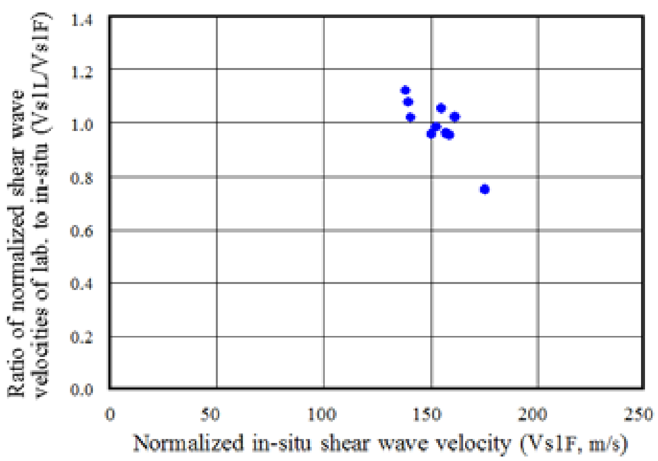

Figure 55. Ratio of normalized shear wave velocities of laboratory to in-situ vs. normalized in-situ velocity at Gainsborough Reserve.

In Taiwan, Lee et al. (2012), also carried out sampling of silty sand containing a high percentage of fines. They used the conventional tube, as well as GP-S samplers. Table 3 shows the sample recovery ratio and the fines content of the samples obtained. The recovery ratios for the GP-S sampler are consistently higher than those of the tube sampler. Although the recovery ratio does not necessarily assure

Table 3. Comparison of sampling results between conventional tube sampler and Gel-Push sampler (Lee et al. 2012).

	Depth (m)	4.0-4.9	5.0-5.9	6.0-6.9	7.0-7.9	8.0-8.9	avg. of sample length (cm)
Tube sampler	No.	T2	T3	T4	T5	T6	54.6
	Sample length	64/80	50/80	55/80	58/80	46/80	
	Sampling ratio	80.0%	62.5%	68.5%	72.5%	57.5%	
	Fines content	24.0%	9.0%	-	20.3%	15.0%	
Gel Push sampler	No.	BT1	BT2	BT3	BT4	BT5	81.8
	Sample length	83/90	81/90	82/90	77/90	86/90	
	Sampling ratio	92.2%	90.0%	91.1%	85.5%	95.6%	
	Fines content	27.5%	24.3%	9.5%	14.5%	9.0%	

the quality of samples, it may be considered a positive indication of quality.

In Taiwan, the GP-S sampler performed satisfactorily. In New Zealand, sample quality evaluation using shear wave velocities measured in situ and in the laboratory proved favorable. In both Taiwan and New Zealand, local drilling foremen operated the samplers and obtained satisfactory results. However, due to the differences in drilling machines and sampling practices, it takes considerable time and care to make a mechanically complex sampler such as the GP-S operationally stable. The design of the sampler is under continuous review to ensure that it becomes simpler to operate.

6 CONCLUSIONS

GP samplers are relatively new entrants to geological site investigation. They have been in use primarily for sampling granular soils for the last fifteen years, during which time, the four GP sampler types have successfully obtained over 1000 core samples in Japan alone.

The use of a thick polymer gel or solution as a drilling fluid is a major departure from the concept of conventional drilling. Polymer solutions have been used as an additive to soil and rock coring, slurry wall construction, etc., but not at the high concentration levels used by the GP samplers. The polymer's non-Newtonian behavior, when used appropriately, delivers remarkable results.

The GP-R and GP-D samplers have proven their remarkable capabilities in obtaining high-quality samples of dense sand, gravel, and even sedimentary rock. These versatile samplers perform well beyond what would be expected from such seemingly simple construction. They employ a combination of thick polymer gel, an impregnated diamond bit, and an electric motor to obtain granular soils without freezing. With these samplers, the presence of fines has a nominal effect on sampling.

The sample quality of the GP-R and GP-D samples may be examined visually as these samples reveal a remarkable surface appearance, but for more qualitative evaluation, shear wave velocities or shear modulus are better indicators. In this paper, some of the in situ vs laboratory comparison cases are reported, with data indicating the overall good quality of the samples. An effort needs to be made to continue to collect these data to further confirm the samples' high-quality.

The GP-Tr and GP-S samplers are the latest additions to the GP family and have shown remarkable capability in sampling hard to obtain silt, silty sand, and sand. The polymer coating mechanism is innovative, but makes the design of the samplers complex and delicate to operate, which may need further refinement. However, the GP-Tr's success in sampling clean sand at a depth close to 100 m shows its high potential.

The GP-Tr and GP-S have been used outside Japan mostly with success, but some problems have been reported. The use of different types of drilling machines and sampling procedures seems to have contributed to these difficulties. Input from the experiences of overseas users will be most valuable for the next round of improvements on these two samplers.

The GP samplers have accomplished a great deal, obtaining samples that had previously been impossible or very difficult to collect with conventional methods. However, there is no end to the improvement of sampling technology, and the entire profession will benefit from the emergence of more innovative samplers.

7 ACKNOWLEDGMENTS

The authors gratefully acknowledge the consent given by the Mt. Fuji Sabo Office of Chubu Regional Bureau, as well as the Komatsujima Port & Airport Construction Office of Shikoku Regional Development Bureau of the Ministry of Land, Infrastructure, Transport and Tourism to publish the data presented in this paper. Special gratitude is expressed to the former Japan Highway Corporation, currently Central Nippon Expressway Company Limited, for permission to release the relevant data. The authors express their sincere gratitude to Professor Kenji Ishihara for his helpful and constructive suggestions in preparation of the text. The authors also acknowledge the contributions made by Professor Kazuo Tani and his graduate research group at Yokohama National University for their studies of polymer behavior. Special thanks are also due to Director Md. Shafiqul Islam; Supervising Engineer Mr. Muhammad Kamaruzzaman of Padma Multipurpose Bridge Project, Bangladesh Bridge and Road Authority; and Professor Dr. A. M. M. Safiullah of Ahsanullah University of Science for permission to release the information presented in this paper. The authors also wish to express their special appreciation to Mr. Susumu Kaneko and Mr. Hironori Yukawa of Kiso-Jiban Consultants for their dedication in the development and execution of the GP sampling method. Last but not least, the authors wish to express their sincere gratitude to Ms. Shizyo Yamada for her careful drafting work and Mrs. Mary Meyer for her excellent editing of the text.

8 REFERENCES

Abe, H., Yokota, S., Kawasaki, H. & Kubo, M. 2002. Evaluation of various in-situ density measurements carried out on test fill made of gravel. 57th Japanese Society of Civil Engineering Annual Conference: 1621-1623. (in Japanese.)

Arikawa, T. & Sasaki, N. 2008. A study of design methodology for port facility using Ryukyu limestone as its bearing strata. Proceedings of 2008 National Technical Conference, Ministry of Land, Infrastructure, Transport and Tourism. (in Japanese.)

De Silva, S., Wightman, E.N.R. & Kamruzzaman, M. 2010. Geotechnical ground investigation for the Padma Main Bridge. IABSE-JSCE Joint Conference on Advances in Bridge Engineering-II: 427-436. Dhaka, Bangladesh.

Ishizaki, T. & Tani, K. 2010. Experimental study on film forming effect for polymer sampling considering roughness of drilled-core. 45th Geotechnical Engineering Conference, Matsuyama: Japanese Geotechnical Society: 39-40. (in Japanese).

Jamiolkowski, M. & Masella, A. 2015. Geotechnical characterization of copper tailings at Zelazny Most Site. Proceedings of DMT'15 The 3rd Int. Conf. on the Flat Dilatometer: 25-42. Rome, Italy.

Kaneko, S. & Tani, K. 2005. Application of sampling method using high-concentration water-soluble polymer to deep ground. 40th Geotechnical Engineering Conference, Hakodate: Japanese Geotechnical Society: 183-184. (in Japanese.)

Kokai, H., Yonamine, K. & Ikeda, A. 2014. Geotechnical investigation at a Ryukyu Limestone site for the design and construction. Kisoko. Vol. 12: 84-87. (in Japanese.)

Kokusho, T. & Tanaka, Y. 1994. Dynamic properties of gravel layers investigated by in-situ freezing sampling, Ground Failures under Seismic Conditions. ASCE National Convention: 121-140. Atlanta, Georgia.

Kudo, K., Nishi, K. & Tanaka, Y. 1991. Static mechanical properties of gravel ground (Part 2 Properties of diluvial gravel procured by freezing sampling and its evaluation method). Central Research Institute of Electric Power Industries, Abiko Research Laboratory Rep. No. U90062. (in Japanese.)

Lee, W. F., Ishihara, K., & Chen, C. 2012. Liquefaction of silty sand-preliminary studies from recent Taiwan, New Zealand, and Japan earthquakes. Proceedings of the International Symposium on Engineering Lessons Learned from the 2011 Great East Japan Earthquake, March 1-4, 2012. Tokyo, Japan.

Matsuo, O. 2004. Simplified procedure for assessing liquefaction potential of soils in the specifications for highway bridges, Technical Journal of Japan Society of Civil Engineers, No.757/III-66:1-20 (in Japanese).

Mori, K. & Ishihara, K. 1979. Undisturbed block sampling of Niigata sand, Proc. of 6th Asian Regional Conference on Soil Mechanics and Foundation Engineering, Vo. 1:39-42, Singapore.

Mt. Fuji Sabo Office Homepage 2016. Mt. Fuji Sabo Office, Chubu Regional Bureau of the Ministry of Land, Infrastructure, Transport and Tourism.

Mt. Fuji Sabo Office, supplied 2016. Supplied by Mr. Fuji Sabo Office, Chubu Regional Bureau of the Ministry of Land, Infrastructure, Transport and Tourism.

Ogawa, Y., Ogi, S., Takaishi, M. & Nose, H. 2013. High quality undisturbed soil sampling for Young Limestone. 7th International Joint Symposium on Problematic Soils and Geoenvironment in Asia: 151-154. Japan.

Shirai, M., Tani, K. & Kaneko, S. 2004. Comparison between sampling using high-concentration water-soluble polymer and sampling using drilling mud; coefficient of viscosity. 33rd Symposium on Rock Mechanics: Japan Society of Civil Engineering: 319-324. (in Japanese.)

Stringer, M., Beyzaei, C., Cubrinovski, M., Bray, J., Riemer, M., Jacka, M. & Wentz, F. 2015a. Liquefaction characteristics of Christchurch silty soils: Gainsborough Reserve, Proceedings of 6th International Conference on Earthquake Geotechnical Engineering, Christchurch, New Zealand.

Stringer, M., Taylor, M.L. & Cubrinovski, M. 2015b. Advanced soil sampling of silty sands in Christchurch, Research Report 2015-06, Civil & Natural Resources Engineering, University of Canterbury.

Sunakawa, N., Shimada, T., Kai, H., Koizumi, K., Hamada, K. & Mochizuki, A. 2010. A new sampling method of potential liquefaction skill agess and evaluation of liquefaction strengths. 45th Geotechnical Engineering Conference, Matsuyama: the Japanese Geotechnical Society: 53-54. (in Japanese.)

Tanaka, Y., Kokusho, T., Yoshida, Y. & Kudo, K. 1989. Dynamic strength evaluation of gravelly soils. 12th International Conference on SMFE, Proceedings of Discussion Session on Influence of Local Condition on Seismic Response: 113-120, Rio de Janeiro, Brazil.

Tanaka, Y., Kudo, K., Nishi, K. & Suzuki, H. 1998. Properties and quality assessment of gravelly soil samples obtained by the conventional tube sampling method and the in-situ freezing method. Soils and Foundations. Vol 46. No. 5: 37-39. (in Japanese.)

Tani, K., Shirai, M. & Kaneko, S. 2004. Consideration on sampling method using high-concentration water-soluble polymer. 39th Geotechnical Engineering Conference, Niigata: Japanese Geotechnical Society: 145-146. (in Japanese.)

Tani, K., & Kaneko, S. 2006. Undisturbed sampling method using thick water-soluble polymer solution. Tsuchi-to-Kiso (Soils and Foundations), Vol. 54-4: 19-21. (in Japanese.)

Taylor, M.L., Cubrinovski, M. & Haycock, I. 2012. Application of new “Gel-push” sampling procedure to obtain high quality laboratory test data for advanced geotechnical analyses, Proceedings 2012 New Zealand Society for Earthquake Engineering Conference: Paper number 123, Christchurch, NZSEE.

Yanagisawa, N., Kaneko, S., Tani, K. & Sakai, K., 2003. Experimental study on a new method of undisturbed sampling using high-concentration water-soluble polymer. 32nd Symposium on Rock Mechanics: Japanese Society of Civil Engineering: 311-316. (in Japanese.)

Yanagisawa, N., Tani, K., Kaneko, S., & Sakai, K. 2004. Mechanism of undisturbed sampling using high-concentration water-soluble polymer. 33th Symposium on Rock Mechanics: Japanese Society of Civil Engineering: 49-56. (in Japanese.)

Yokoi, Y., Sakai, K., Yukawa, H. & Orihara, K. 2015. Application of Gel-Push (GP) sampling method to slaking prone residual soil and reclaimed sand in Singapore. Proceedings of International Conference on Soft Ground Engineering, Singapore.

Geotechnical and Geophysical Site Characterisation 5 – Lehane, Acosta-Martínez & Kelly (Eds)

Simulation of the cone penetration test: discrete and continuum approaches

A. Gens, M. Arroyo, J. Butlanska & L. Monforte
Department of Civil and Environmental Engineering, Universitat Politècnica de Catalunya, Barcelona, Spain

J.M. Carbonell
International Centre for Numerical Methods in Engineering (CIMNE), Barcelona, Spain

M. Ciantia, C. O'Sullivan
Department of Civil and Environmental Engineering, Imperial College, London, UK

ABSTRACT: The paper presents the modelling of the cone penetration test using two procedures: a discrete approach and a continuum approach. The discrete approach is based on the Discrete Element Method where a granular material is represented by an assembly of separate particles. Cone penetration has been simulated for both uncrushable and crushable sands. For the continuum approach, the Particle Finite Element Method has been adapted in order to overcome the difficulties posed by the occurrence of large displacements as well as by the geometrical, material and contact nonlinearities of the problem. Both single phase and two-phase (coupled hydromechanical) formulations have been developed and applied. Although not exempt of problems, both approaches yield realistic results leading to the possibility of a closer examination and an enhanced understanding of the mechanisms underlying cone penetration.

1 INTRODUCTION

Penetration problems are widespread in geotechnical engineering. Among them, cone penetration is one the prime means of soil investigation but its interpretation remains largely empirical especially for sands (Mayne 2007, Schnaid 2009); theoretical approaches are more advanced for clays (e.g. Randolph 2004). A more rational interpretation may benefit from appropriate modelling although it must be recognized that significant challenges arise when numerical analyses of penetration problems are undertaken. Those types of problems involve large deformations as well as geometrical and contact nonlinearities. Also, complex constitutive laws are generally required to represent adequately the mechanical behaviour of geotechnical materials.

The paper presents a brief summary of some recent work carried out by our group concerning the modelling of penetration problems and, more specifically, the simulation of cone penetration tests. Two approaches have been pursued: discrete modelling and continuum modelling. Granular soils have been modelled by an assembly of distinct particles using the Discrete Element Modelling (DEM). This approach is not practicable in the case of fine-grained materials where a continuum analysis has been favoured. The Particle Finite Element Method (PFEM) has been employed as the preferred numerical technique for this approach.

2 DISCRETE MODELLING

2.1 *General*

The use of the Discrete Element Method (DEM) to model the mechanical behaviour of granular materials has certainly important limitations bus also a considerable number of advantages (O'Sullivan, 2011). Among the limitations are the generally oversimplified geometrical representation of the particles (often assumed to be spheres) and the need to scale up their size, especially in boundary value problems such as the cone penetration analyses. In spite of this scaling, the resulting calculations are computationally intensive if a sufficiently representative number of particles are considered.

The main advantage is that large strains, displacements and rotations are readily accommodated in the analyses. Also, it is possible to bypass the need for quite sophisticated constitutive models for sands; instead only the contact law between pairs of individual particles are usually required. It should be noted, however, that there is considerable uncertainty over the precise form of those contact laws and their parameters are generally calibrated comparing the macroscopic response of a DEM model and the results of analogous laboratory tests.

First attempts to use DEM to simulate cone penetration tests (Huang & Ma 1994, Calvetti & Nova 2005, Jiang et al. 2006) used 2D elements (i.e. disks). Although undoubtedly useful, they fail however to provide a realistic representation of the kinematics of granular deformation. More representative results are obtained using 3D analyses although, so far, they have been limited to spherical shapes (Butlanska et al. 2010a, 2010b, Arroyo et al. 2011, Mcdowell et al. 2012, Lin &Wu 2012, Butlanska et al. 2013).

2.2 *Cone penetration modelling in crushable sands*

A strong motivation for this modelling work has been to explore the possibility to develop virtual calibration chambers, VCC (Arroyo et al. 2011). Analyses have been performed with the PFC3D code (Itasca 2010); the rotation of spheres has been inhibited in order to capture the limited rotation observed when non-spherical particles are involved. The necessary limitation of the number of particles employed in the analyses has required the adoption of results' filtering (to smooth the oscillation of cone resistance) and to account for chamber size effects, a requirement also necessary in the interpretation of the results form physical calibration chambers. Another importance difference with the physical system lies in the fact that the way of forming the specimens is quite different in the virtual and in the physical calibration chambers, leading to differences in initial fabric.

In spite of those difficulties, it has been possible to obtain good quantitative agreement between the results of the DEM analyses and the extensive set of data reported by Jamiolkowski et al. (2003). The tests were performed on Ticino sand, a medium-size silica sand with mostly sub-rounded grains. Because of the strength of the basic particle material, it was not necessary to account for grain crushing in the analyses. Figure 1 (Arroyo et al. 2011) shows the comparison for a number of tests covering relative densities form 60% to 90% and confining pressures from 40 to 400 kPa.

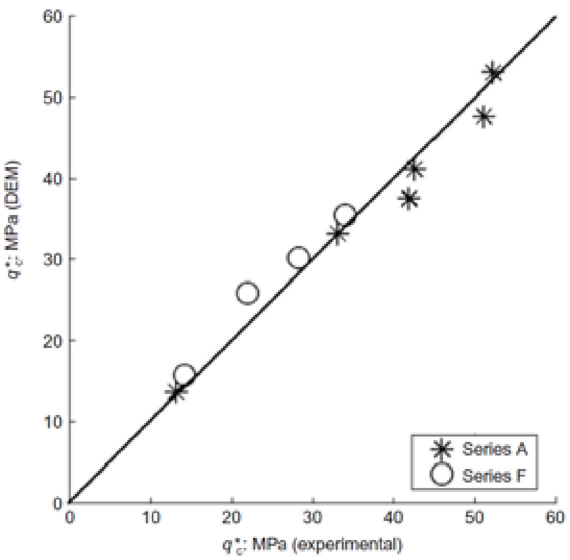

Figure 1. Comparison between corrected cone resistance from DEM and corrected cone resistance values from physical tests on Ticino sand.

One of the important advantages of using DEM is the possibility to perform observations not only at the microscale (individual particles and contacts) but also at the mesoscale (continuum stress-strain). The mesoscale is particularly useful as the observations have direct counterparts in continuum analysis (Butlanska et al., 2011, 2014).

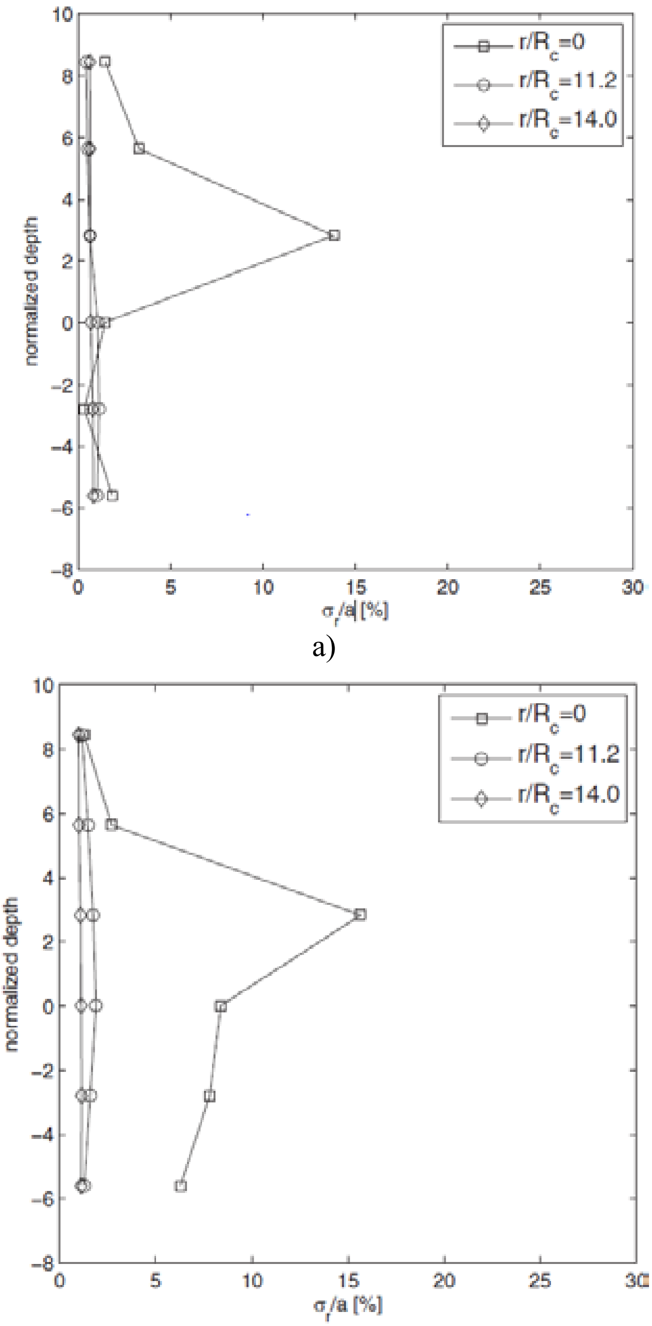

a)

b)

Figure 2. Distribution of radial stresses at different radial distances, r, normalized by cone radius, R_c. Stresses are normalized by cone resistance, a. Normalized depth 0 corresponds to the cone tip position. a) No lateral displacement condition (BC3). b) Constant radial stress condition (BC1)

As an example, Figure 2 shows the computed distribution of radial stress at different radial distances for a dense granular assembly under two different boundary conditions. The distributions close to the axis of the cone closely resemble the experimental observations obtained by Jardine et al. (2013) in a physical chamber. Indeed, as shown in Figure 3, the peak values computed from the DEM analyses follow the same quantitative trend as those obtained in the physical chamber tests.

It appears therefore, that in spite of its limitations, DEM analysis is capable to simulate satisfactorily many of the physical features of cone penetration in granular materials. In addition, it is possible to achieve an enhanced understanding of the underlying mechanisms when examining the results at the microscale and at the mesoscale.

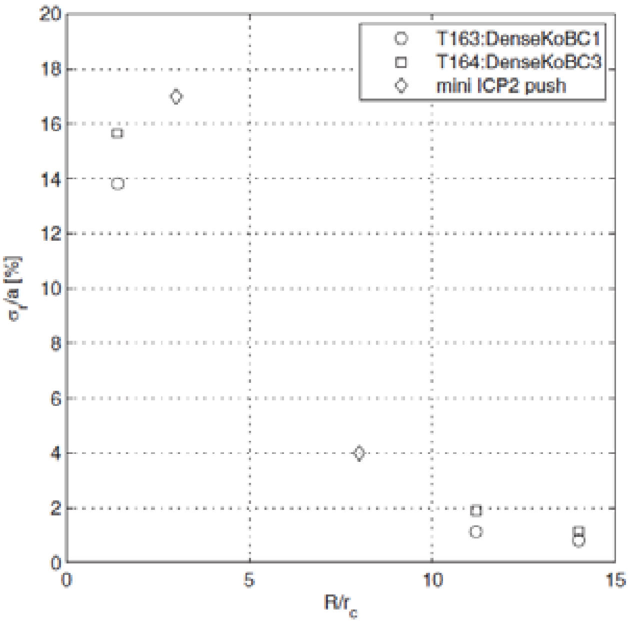

Figure 3. Peak values of normalized radial stress versus normalized radial distance (see caption of Figure 2). DEM results and physical chamber observations from Jardine et al. (2013).

2.3 *Cone penetration modelling in crushable sands*

Granular materials made up of weaker grains, such as calcareous sands, often exhibit significant particle crushing when subjected to high or even moderate stresses. It has been observed (e.g. Almeida et al. 1991) that the pattern of cone resistance increase with relative density is notably different in calcareous crushable sand compared to non-crushable silica sand. This difference results in difficulties when correlations developed for silica sands are applied to materials with crushable grains (Ahmed et al. 2014, Moss 2014). In this context, the application of DEM analysis is appealing because it allows isolating the effects of grain strength and crushability. It will be applied to an extreme case, reported by Wesley (2007), where the cone resistance was insensitive to relative density (Figure 4). The material is a volcanic pumice sand the grains of which are porous themselves.

To performed those analyses, it is necessary to extend the DEM formulation to account for the possibility of grain crushing. Two different approaches have been proposed: the use of multigrain aggregates (Cheng et al. 2003, Bolton et al. 2008) or a multigenerational approach (Marketos & Bolton 2009, Ben-Nun & Einav 2010, Bruchmüller et al. 2011) in which a single element breaks and it is replaced by a new generation of smaller grains.

Recently, an efficient formulation has been proposed, using the latter approach, that allows the performance of DEM analyses of boundary value problems in a reasonably economical manner (Ciantia et al. 2014, 2015). The main features of this approach can be summarized as follows: a particle failure criterion inspired by the analytical work of Russell & Muir Wood (2009) and Russell et al. (2009), a particle spawning procedure based on Apollonian packing and upscaling rules for particle strength and contact constant stiffness parameters for both linear and Hertzian contact laws. As in many multigenerational approaches, mass is not conserved after particle splitting but the missing mass of broken particles is allocated, during post-processing, to finer fractions according to a fractal distribution. In this way, it is possible to track evolving porosity and grain size distribution (GSD). Figure 5 shows the configuration of the spawned particles after the breakage of a single sphere. It has been shown (Ciantia et al. 2015) that this DEM formulation readily captures the macroscopic behaviour of highly crushable granular materials.

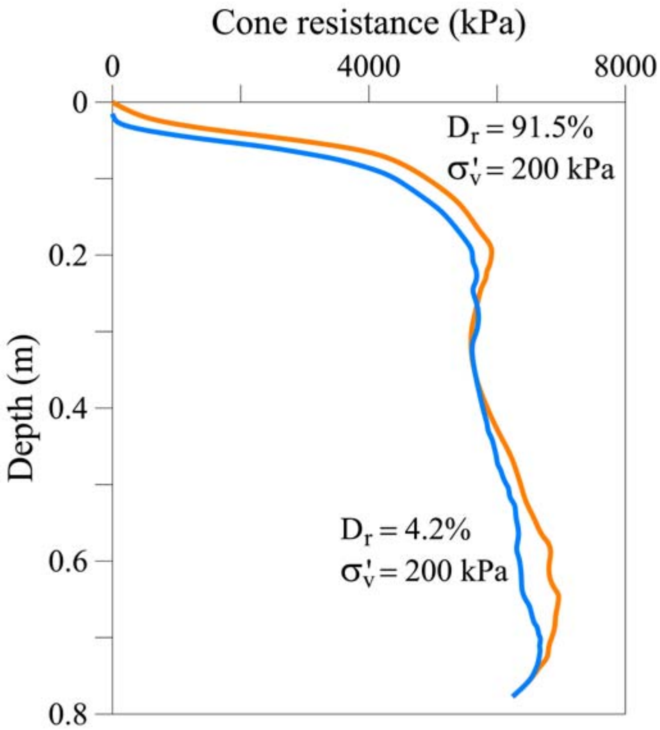

Figure 4. CPT results observed in cone penetration tests on pumice sand performed in a calibration chamber. (Wesley 2007).

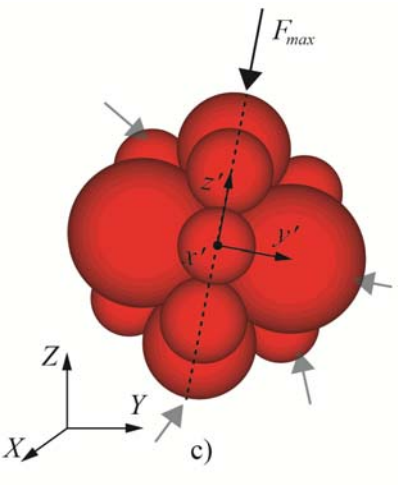

Figure 5. Apollonian configuration of the spawned particles after the breakage of a single sphere

The DEM model has been calibrated against oedometer and triaxial tests on the pumice sand used in the calibration chamber tests (Wesley 2007). For instance, Figure 6 shows the comparison with two oedometer tests performed at different densities. Grain size distributions were determined at various values of vertical stress. Figure 7 shows that the grain fragmentation procedure is able to follow successfully the evolution of the GSD during tests reaching a vertical stress of 8 MPa.

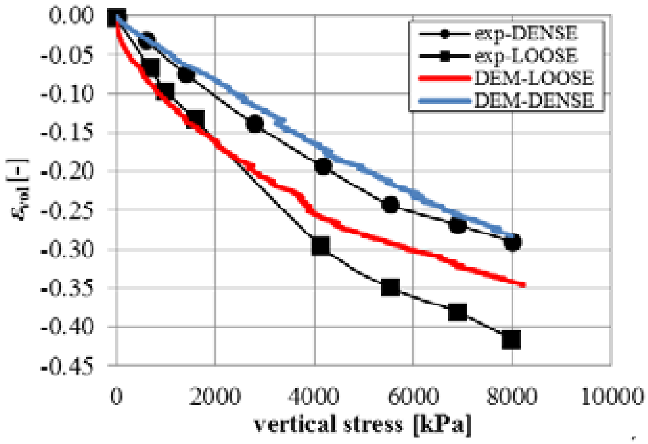

Figure 6. Observed and computed volumetric strain in oedometer tests on pumice sands.

The virtual calibration chamber (Figure 8) has been constructed with the same procedure employed for silica uncrushed sand (Arroyo et al. 2011) and a similar upscaling procedure for grains and cone has been used. The zero-strain radial lateral condition of the physical chamber was replicated by the model. Selected results of the DEM analyses are presented in Figure 9 where it is apparent that the cone penetration values are quite insensitive to the density of the sand, as observed in the physical experiments.

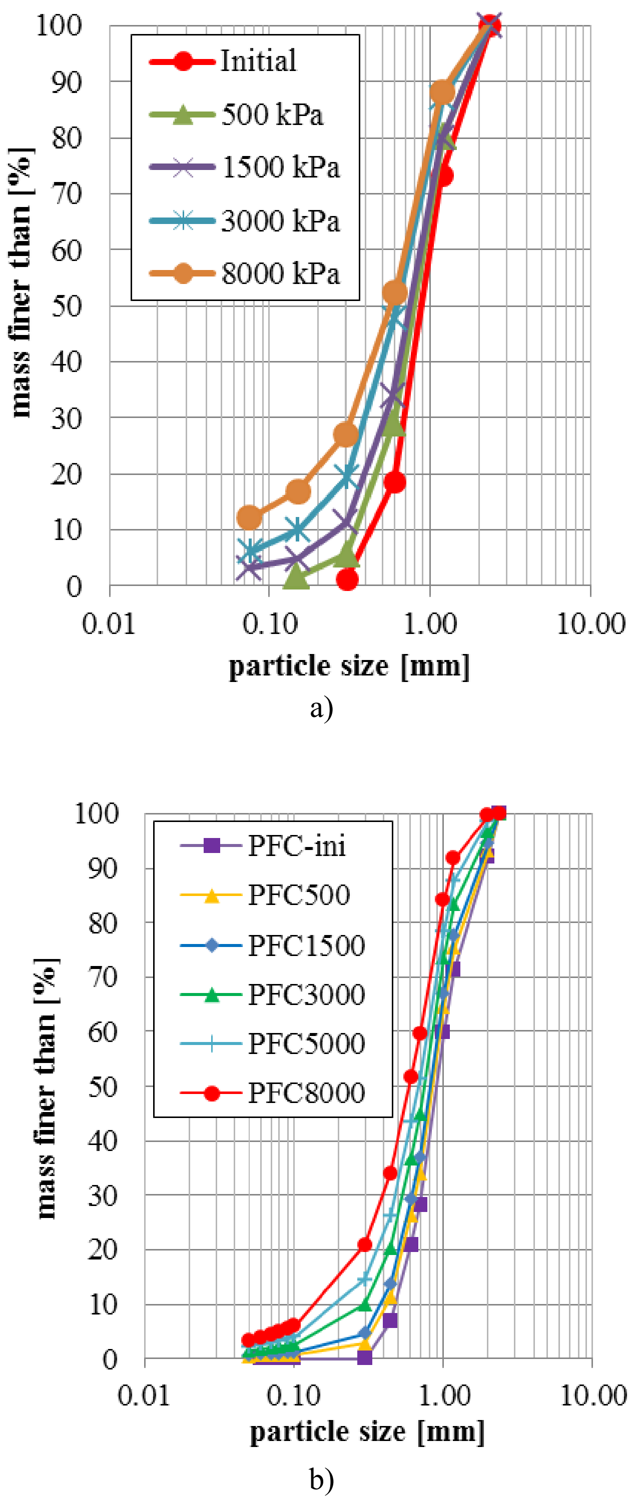

Figure 7. Evolution of grain size distribution in oedometer tests on pumice sand. a) Experimental observations, b) Computations

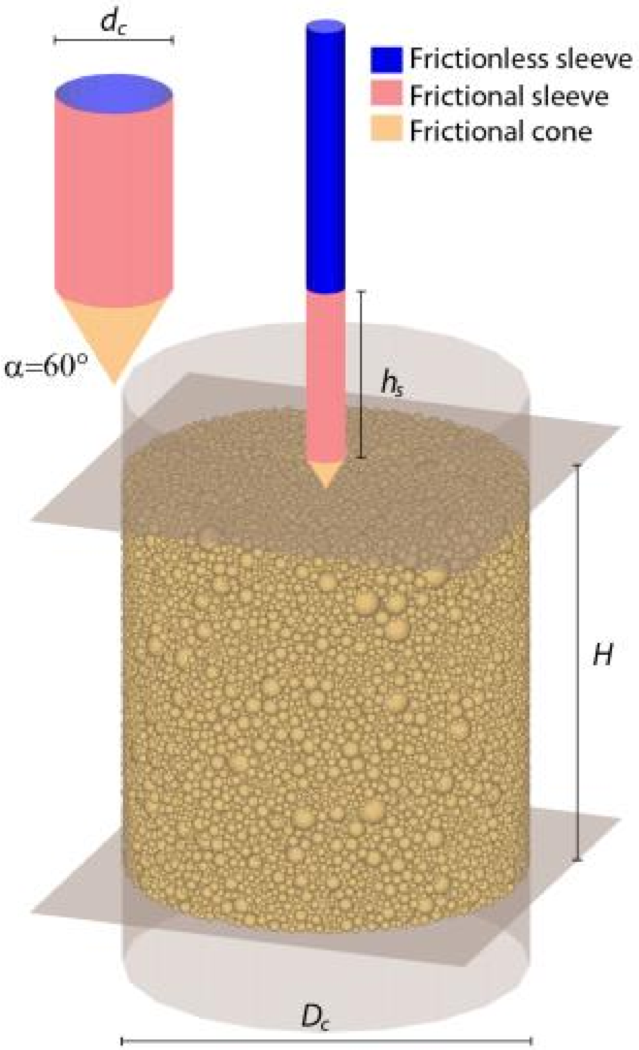

Figure 8. Virtual calibration chamber and cone

Parallel DEM calculations assuming uncrushable grains were also performed so that the effects of particle crushability could be readily identified. Results in terms of ratio of cone penetration resistance of uncrushable and crushable granular materials are collected in Figure 10. It can be noted that the pattern of variation with relative density agrees well with reported experimental results. No DEM results are available for densities below about 40% due to the difficulty of constructing very loose virtual specimens. In any case, it appears that the use of the new DEM formulation for crushable materials provides a good tool to further explore penetration problems in this type of materials. More information on this study is given in Ciantia et al. (2016).

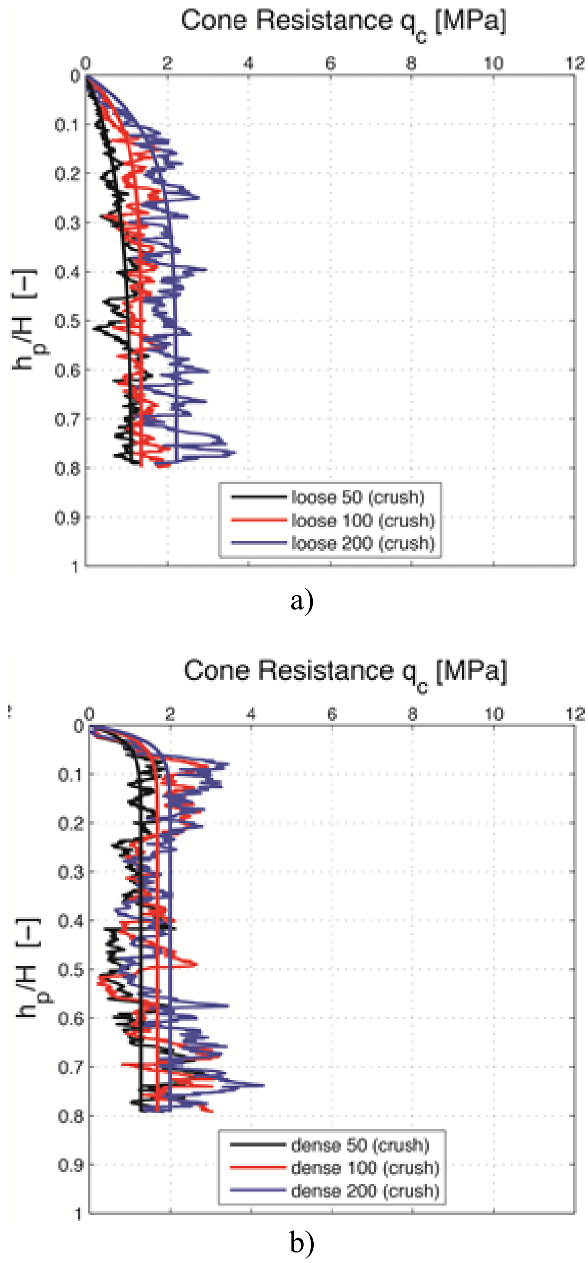

Figure 9. Computed cone resistance of simulated cone penetration tests on pumice sand at different stress values. a) Loose specimen, b) Dense specimen.

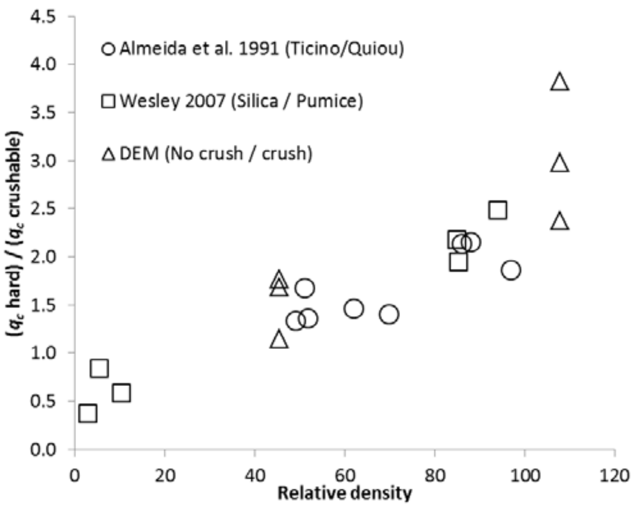

Figure 10. Effect of crushability on cone resistance for different relative densities. Experimental and DEM results.

3 CONTINUUM MODELLING

3.1 *General*

The continuum modelling of the cone penetration test has been performed using the Particle Finite Element Method, PFEM (Idelshon et al. 2004, Onate et al. 2004, Carbonell 2009).

The PFEM uses a Finite Element approximation to compute the movement of the particles within an updated Lagrangian framework. In this method particles and nodes coincide and the mesh is updated when required to prevent excessive distortions; Delaunay tessellation is used for this purpose. The mesh nodes are considered particles that carry mass and the state variables and, being particles, they can separate from the main domain giving rise to new boundaries. For this reasin, the Alpha Shape technique (Edelsbrunner & Mucke 1994) is used to identify the boundaries at every step of the analysis. Further refinements involve the addition/removing of particles depending on a characteristic distance and the formulation of the contact conditions via a penalty method. Although the method was initially developed for fluid-solid interaction problems, there have already been some applications to geotechnical problems (Carbonell et al. 2010, Zhang et al. 2013, 2015).

Figure 11 shows a scheme of the method that can be summarised in the following steps: i) A cloud of particles, C_n, is defined at a time $t=t_n$, ii) identify the boundaries defining the analysis domain, iii) discretize the domain with a finite element mesh, iv) solve the governing equations within a Lagrangian formulation and compute the state variables at the next updated configuration at t_{n+1}, v) move the nodes to the new position C_{n+1}, vi) go back to step i).

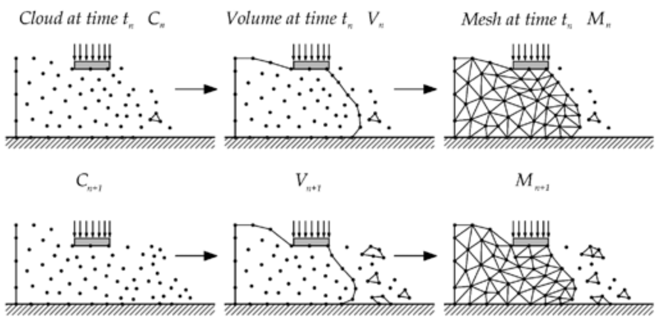

Figure 11. Scheme of a PFEM computation step

3.2 *Single phase formulation*

In a purely undrained case the soil can be considered as a single phase medium and only the linear momentum balance equation (equilibrium) needs to be solved. Accordingly, a total-stress Tresca constitutive model has been adopted to represent the soil whereas the tangential contact with the rigid cone has been simulated with a von Mises yield criterion. The analyses presented here have been performed with a rigidly index, $I_r = 100$. The geometry of the problem and the computation domain are shown in Figure 12.

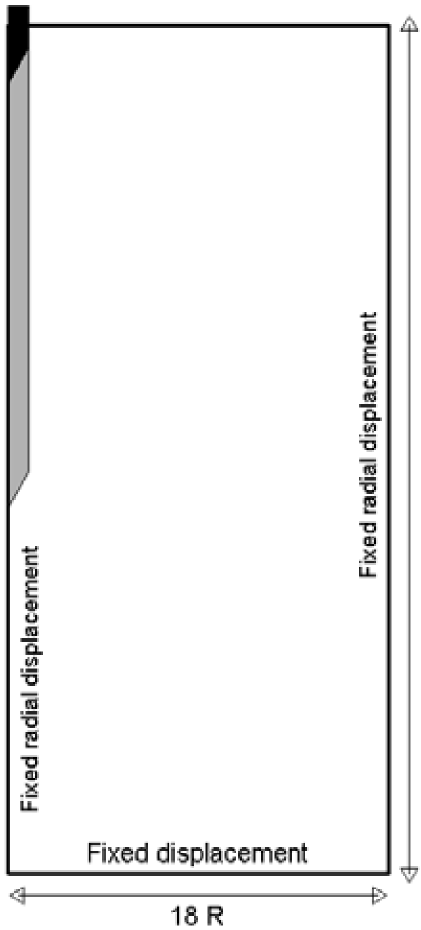

Figure 12. Geometry and computational domain of the PFEM analysis of cone penetration

The cone penetration analyses have been carried out using values of cone-soil adhesion ratio (α=adhesion/undrained shear strength) ranging from 0 to 0.7. The results in terms of cone penetration (normalized as cone factor N_{kt}) and friction sleeve resistance are plotted in Figure 13. As expected, the friction sleeve resistance coincides with the specified adhesion and the cone resistance increases modestly with the value of adhesion. Figure 14 shows more explicitly the variation of cone factor with the value of adhesion

3.3 *Two-phase formulation*

The PFEM formulation has been extended to deal with coupled hydromechanical problems so that the full range of partially drained conditions and consolidation problems for saturated soils can be examined. Consequently, the formulation requires the simultaneous solution of the equilibrium equation and of the water mass conservation. Now, the soil constitutive models can be expressed in terms of effective stresses.

Using this formulation, the problem of cone penetration has been analysed adopting Modified Cam clay as the constitutive model for the soil. An explicit finite deformation integration of the constitutive law is used following the procedure outlined in Monforte et al. (2015). Figure 15 shows the contours of total displacements at three stages of penetration: initial and at normalised penetration ratios (z/R) of 6 and 10. z is the penetration depth and R the cone radius. z/R= 10 corresponds to a steady state condition. The progress of the PFEM analysis is illustrated in Figure 16 where the evolution of the mesh during the calculation is presented. The refinement of the mesh of the soil domain directly affected by the penetration is apparent.

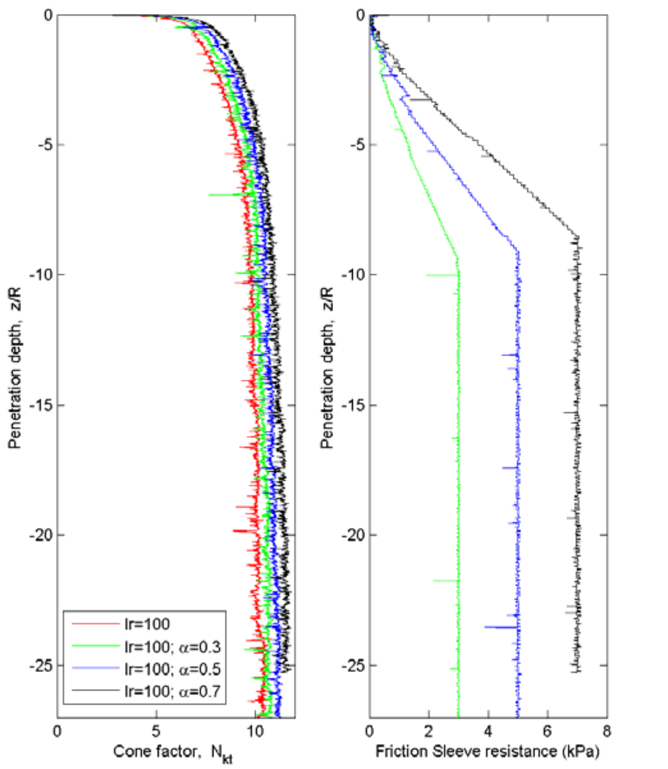

Figure 13. Cone factor and friction sleeve resistance for different values of adhesion computed with PFEM

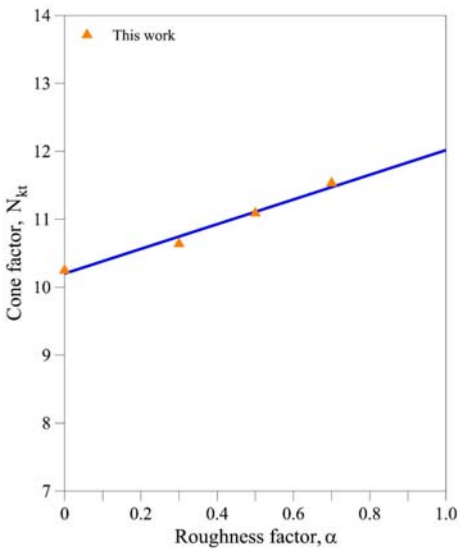

Figure 14. Variation of cone factor with adhesion, α

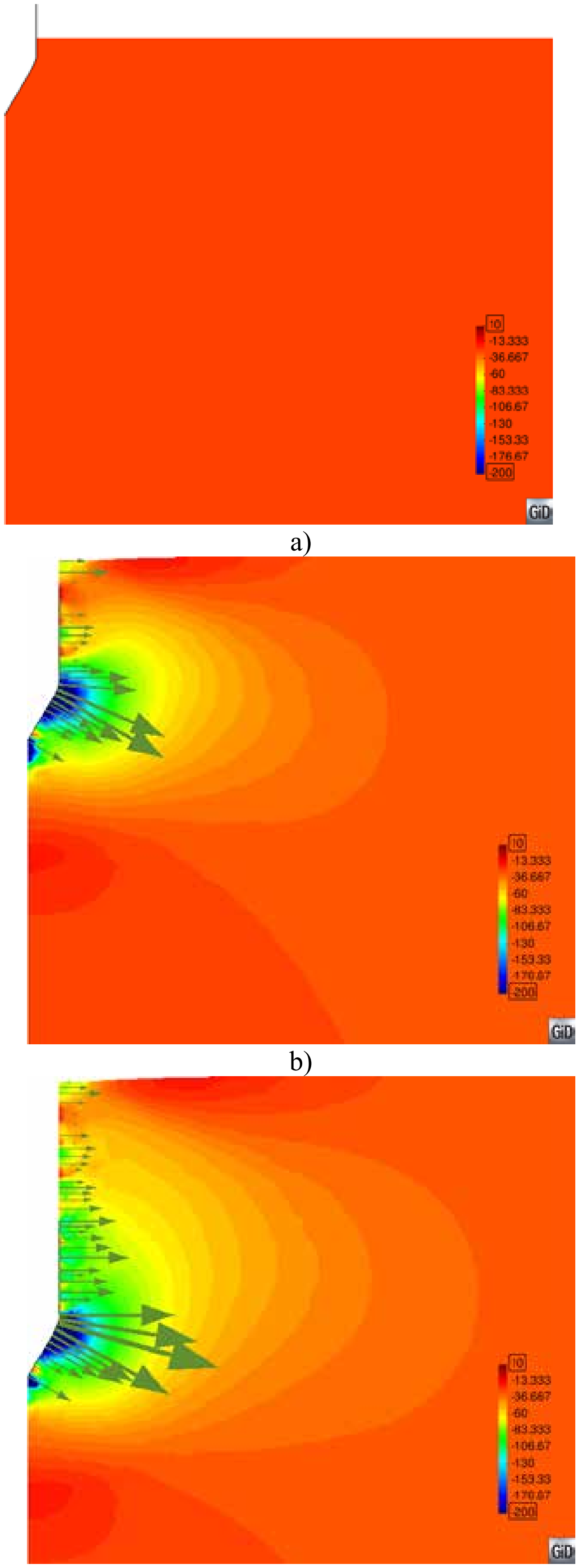

Figure 15. Total displacements during cone penetration. a) Initial, b) z/R=6, c) z/R=10. z: penetration depth and R: cone radius.

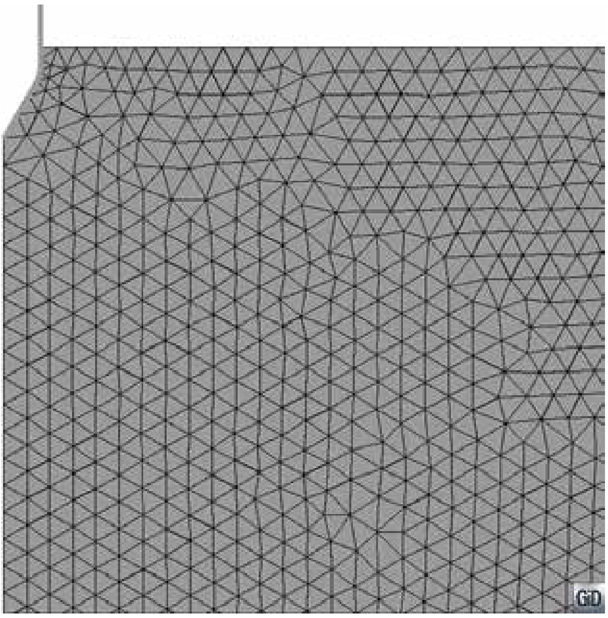

a)

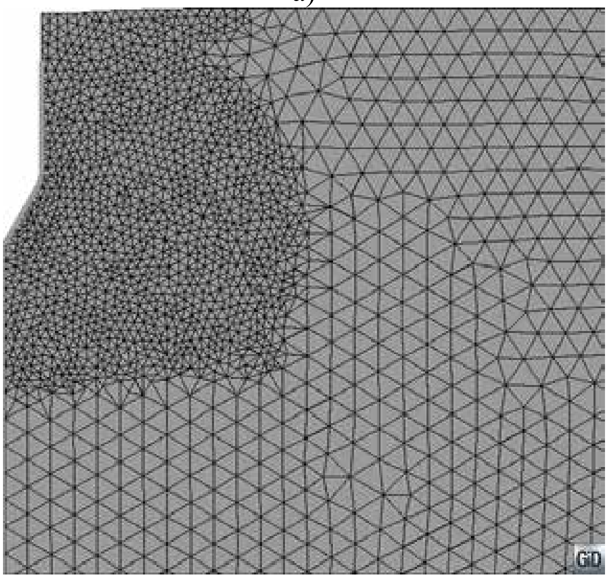

b)

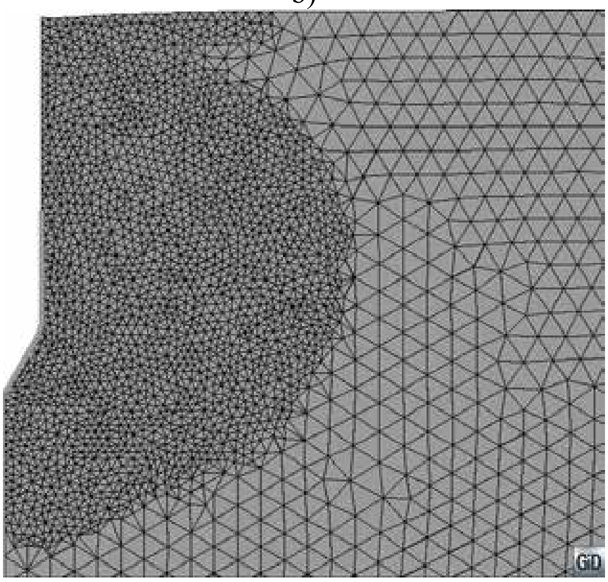

c)

Figure 16. Evolution of the PFEM mesh during cone penetration. a) Initial, b) z/R=6, c) z/R=10. z: penetration depth and R: cone radius.

Figure 17 presents the variation of cone resistance with penetration depth showing that a steady state condition has been reached. Some oscillations in the solution can be noted; they result from the incompressibility of the soil at critical state combined with the use of low-order elements in the mesh. To address this issue, mixed formulations have been recently developed (Monforte et al. 2016) that have proved very successful in overcoming this problem.

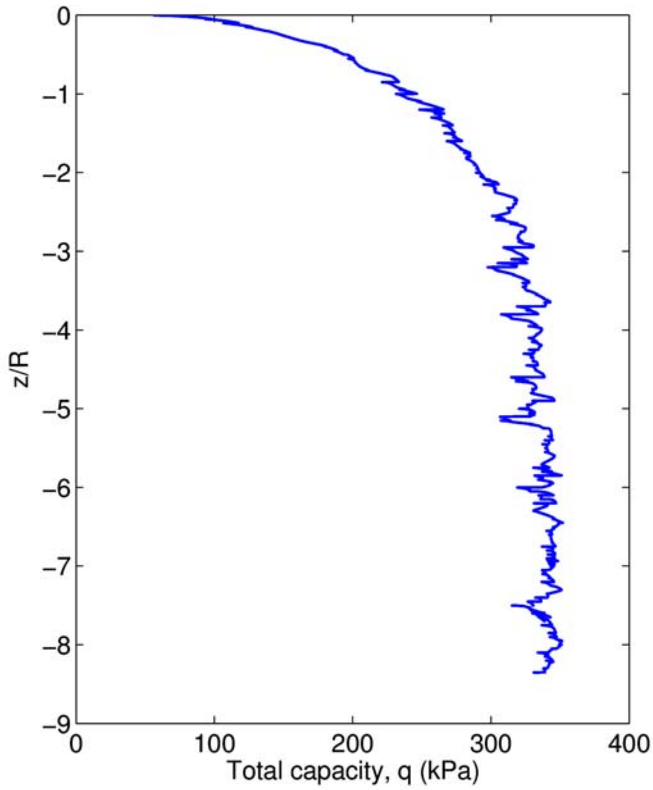

Figure 17. Variation of penetration resistance with depth. z: penetration depth and R: cone radius

4 CONCLUSIONS

Two different approaches have been presented for the modelling of the cone penetration test that attempt to overcome the considerable difficulties associated with the simulation of penetration problems, i.e. large displacements, large strains and rotations, severe domain distortion as well as geometrical, material and contact nonlinearities. Both the DEM and PFEM procedures have shown their capabilities in this context although some significant challenges and shortcomings remain. They constitute, however, areas of intense development and research that should lead to an increasingly realistic description of the process of cone penetration in all its complexity. Consequently, it can be envisaged that more rational-based procedures for the interpretation of the test should ensue or, at least, a better understanding of the mechanisms underlying cone penetration should be achieved.

5. ACKNOWLEDGEMENTS

The support of the Ministerio de Economía y Competividad of Spain through research grants BIA2011-27217 and BIA2014-59467-R is gratefully acknowledged.

6. REFERENCES

Ahmed, S. M., Agaiby, S. W. & Abdel-Rahman, A. H. 2014. A unified CPT–SPT correlation for non-crushable and crushable cohesionless soils. *Ain Shams Engineering Journal* 5: 63-73

Almeida, M., Jamiolkowski, M., & Peterson, R. 1991. Preliminary result of CPT tests in calcareous Quiou sand. *Proceedings of the International Symposium on Calibration Chamber Testing*: 41-53. New York: Elsevier.

Arroyo, M., Butlanska, J., Gens, A., Calvetti, F., & Jamiolkowski, M. 2011. Cone penetration tests in a virtual calibration chamber. *Géotechnique*, 61: 525-531.

Ben-Nun, O. & Einav, I. 2010. The role of self-organization during confined comminution of granular materials. *Phil. Trans. R. Soc.* A 368, No. 1910: 231–247.

Bolton, M. D., Nakata, Y. & Cheng, Y. P. 2008. Micro- and macro-mechanical behaviour of DEM crushable materials. *Géotechnique* 58 : 471–480.

Bruchmüller, J., Van Wachem, B. G. M., Gua, S. & Luo, K. H. 2011. Modelling discrete fragmentation of brittle particles. *Powder Technol.* 208: 731–739.

Butlanska, J., Arroyo, M., & Gens, A. 2010a. Size effects on a virtual calibration chamber. In T. Benz and S. Nordal (eds.), *Numerical methods in geotechnical engineering*: 225-230. CRC Press, Balkema.

Butlanska, J., Arroyo, M., & Gens, A. 2010b. Virtual calibration chamber CPT tests on Ticino sand. *Proceedings of the 2nd International Symposium on Cone Penetration Testing, CPT'10*: 217–224.

Butlanska, J., Arroyo, M., & Gens, A. 2013. 3D DEM simulations in sand. In Coutinho & Mayne (eds.), *Geotechnical and Geophysical Site Characterization*. 817- 824. London: Taylor & Francis.

Butlanska, J., Arroyo, M., Gens, A. & OSullivan, C. 2014. Multi-scale analysis of cone penetration (CPT) in a virtual calibration chamber. *Canadian Geotechnical Journal*. 51: 51-66.

Butlanska, J., OSullivan, C., Arroyo, M., & Gens, A. 2011. Mapping deformation during CPT in a virtual calibration chamber. *Proceedings of the International Symposium on Geomechanics and Geotechnics: From Micro to Macro*: 559–564. London: Taylor & Francis..

Calvetti, F., & Nova, R. 2005. Micro-macro relationships from DEM simulated element and in-situ tests. *Proc. 5th Int. Conf. Micromechanics of Granular Media: Powders and Grains 2005, Stuttgart*: 245–250.

Carbonell, J.M. 2009. *Modeling of ground excavation with the Particle Finite Element Method.* Ph.D. Thesis. Universitat Politècnica de Catalunya, Barcelona.

Carbonell J.M., Onate, E. & Suarez, B. 2010. Modeling of ground excavation with the Particle Finite Element Method. *Journal of Engineering Mechanics, ASCE*. 136: 455-463.

Cheng, Y. P., Nakata, Y. & Bolton, M. D. 2003. Discrete element simulation of crushable soil. *Géotechnique* 53: 633–641.

Ciantia, M. O., Arroyo, M., Butlanska, J. & Gens, A. 2014. DEM modelling of a double-porosity crushable granular material. In K. Soga et al. (Ed.), *Proc. Int. Symp. on Geomechanics from Micro to Macro*: 269-274. London: Taylor & Francis.

Ciantia, M. O., Arroyo, M., Butlanska, J. & Gens, A. 2016. DEM modelling of cone penetration test in a double-porosity crushable granular material. *Computers and Geotechnics*. 2016:109-127.

Ciantia, M. O., Arroyo, M., Calvetti, F. & Gens, A. 2015. An approach to enhance efficiency of DEM modelling of soils with crushable grains. *Géotechnique*. 65: 91–110.

Edelsbrunner, H. & Mucke, E.P. 1994. Three dimensional alpha shapes. *ACM Transaction on Graphics*, 13. 43-72.

Huang, A.-B. & Ma, M.Y. 1994. An analytical study of cone penetration tests in granular material. *Canadian Geotechnical Journal*,. 31: 91–103.

Idelsohn, S.R., Onate, E., Del Pin, F. 2004. The particle finite element method: a powerful tool to solve incompressible flows with free-surfaces and breaking waves. *Int J Numer Meth Eng.* 61:964–89.

Itasca. 2010. *Particle flow code in three dimensions: software manual.* Minnesota, USA.

Jamiolkowski, M., Lo Presti, D.C.F., & Manassero, M. 2003. Evaluation of relative density and shear strength of sands from CPT and DMT. *Soil behavior and soft ground construction. American Society of Civil Engineers*: 201–238.

Jardine, R.J., Zhu, B.T., Foray, P., & Yang, Z.X. 2013. Measurement of stresses around closed-ended displacement piles in sand. *Géotechnique*, 63: 1–17.

Jiang, M.J., Yu, H.-S., & Harris, D. 2006. Discrete element modelling of Deep penetration in granular soils. *International Journal for Numerical and Analytical Methods in Geomechanics*, 30: 335–361.

Lin, J., & Wu, W. 2012. Numerical study of miniature penetrometer in granular material by discrete element method. *Philosophical Magazine*. 92(28–30): 3474–3482.

Marketos, G., & Bolton, M. D. 2010. Flat boundaries and their effect on sand testing. *International Journal for numerical and analytical methods in geomechanics*, 34: 821-837

Mayne, P. W. 2007. In-situ test calibrations for evaluating soil parameters. In Tan et al. (ed.) *Characterisation and Engineering properties of Natural Soils*. 3: 1601–1652. London: Taylor & Francis.

Mcdowell, G.R., Falagush, O., & Yu, H.-S. 2012. A particle refinement method for simulating DEM of cone penetration testing in granular materials. *Géotechnique Letters*, 2: 141–147.

Monforte, L., Arroyo, M., Gens, A. & Carbonell, J.M., 2015. Explicit finite deformation stress integration of the elastoplastic constitutive equations. In Oka et al. (eds.), Computer Methods and Advances in Geomechanics: 267-272. London: Taylor & Francis.

Monforte, L., Carbonell, J.M., Arroyo, M. & Gens, A. 2016. Performance of mixed formulations for the Particle Element Method in soil mechanics problems. *Computational Particle Mechanics* (in press).

Moss, R.E.S. 2014. A Critical State framework for seismic soil liquefaction triggering using CPT, *3rd International Symposium on Cone Penetration Testing, CPT14*, Las Vegas, Nevada, Paper 2#20.

Onate, E., Idelsohn, S.R., Del Pin, F. & Aubry, R. 2004. The particle finite element method an overview. *Int J Comput Meth*. 1:267–307.

O'Sullivan, C. 2011 *Particle-Based Discrete Element Modeling: A geomechanics perspective*. Hoboken, NJ: Taylor & Francis.

Randolph, M. F. 2004. Characterisation of soft sediments for offshore applications. *Proc. 2nd Int. Conf. Site Characterisation*, Porto 1: 209–232

Russell, A. R. & Muir Wood, D. 2009. Point load tests and strength measurments for brittle spheres. *I. J. of Rock Mech. and Mining Sciences*. 46: 272–280

Russell, A. R., Muir Wood, D. & Kikumoto, M. 2009. Crushing of particles in idealised granular assemblies. *J. Mech. Phys. Solids* 57: 1293–1313.
Schnaid, F. 2009. *In situ testing in geomechanics: the main tests*. London: Taylor & Francis.
Wesley L. D. 2007. Geotechnical characteristics of a pumice sand. In Tan et al. (ed.) *Characterisation and Engineering properties of Natural Soils*: 2449-2473. London: Taylor & Francis.
Zhang, X., Krabbenhoft, K., Pedroso D.M., Lyamin, A.V., Sheng, D., da Silva, M.V. & Wang, D. 2013. Particle finite element analysis of large deformation and granular flow problems. *Computers and Geotechnics*, 54: 133-142.
Zhang, X., Krabbenhoft, K., Sheng, D. & Li., W. 2015. Numerical simulation of a flow-like landslide using the particle finite element method. *Computational Mechanics*, 55: 167-177.

.

Geotechnical and Geophysical Site Characterisation 5 – Lehane, Acosta-Martínez & Kelly (Eds)

Geophysical properties of soils

J. C. Santamarina and J. Park
Earth Science & Engineering, King Abdullah University of Science and Technology (KAUST)

ABSTRACT: Low energy perturbations used in geophysical methods provide insightful information about constant-fabric soil properties and their spatial variability. There are causal links between soil type, index properties, elastic wave velocity, electromagnetic wave parameters and thermal properties. Soil type relates to the stress-dependent S-wave velocity, thermal and electrical conductivity and permittivity. The small strain stiffness reflects the state of stress, the extent of diagenetic cementation and/or freezing. Pore fluid chemistry, fluid phase and changes in either fluid chemistry or phase manifest through electromagnetic measurements. The volumetric water content measured with electromagnetic techniques is the best predictor of porosity if the water saturation is 100%. Changes in water saturation alter the P-wave velocity when $S_r \rightarrow 100\%$, the S-wave velocity at intermediate saturations, and the thermal conductivity when the saturation is low $S_r \rightarrow 0\%$. Finally, tabulated values suffice to estimate heat capacity and latent heat for engineering design, however thermal conductivity requires measurements under proper field conditions.

1 INTRODUCTION

Geophysical methods have played a crucial role in subsurface characterization, in the detection of hydrocarbon and mineral resources, and in monitoring a wide range of subsurface processes. Geophysical surveys are minimally invasive and involve low-energy stimuli, thus, they are inherently non-destructive constant-fabric measurements. In addition, the same geophysical assessment takes place in laboratory studies as in field surveys (Note: laboratory measurements may require careful analysis prior to the interpretation of field data due to frequency-dependent wave dispersion and scattering).
Geophysical parameters are most relevant to engineering design. This manuscript presents a concise yet practical summary of the geophysical properties of soils. The four central themes include: soil classification, characterization with elastic waves, characterization with electromagnetic waves and thermal properties.

2 SOIL CLASSIFICATION

Step 1: Coarse or fine? Let's accept the general definition of gravel (retained on sieve #4), sand (passing through sieve #4 and retained on sieve #200) and fines (passing through sieve #200). Any one of these soil components can control the mechanical and hydraulic behaviour of a soil mixture. For example, a densely packed sand near e_S^{min} will carry the load and control the mechanical behaviour of a sand-gravel mixture when the gravel is looser than e_G^{max}. Similar analyses define the 13 notable mixtures listed in Table 1. The gravimetric-volume equations presented in this table compute the corresponding fractions for gravel, sand and fines. Specific factors included in the definition of these mixtures reflect an extensive database of soil properties (details in Park & Santamarina 2016). These notable mixtures determine classification boundaries in the triangular RSCS classification chart. Analyses and experimental data demonstrate that mixture thresholds are different for flow and mechanical control. Table 1 presents the classification procedure:

- Input the coefficient of uniformity C_u and the mean particle roundness R, of gravel and sand fractions (or their values of e^{max} and e^{min}).
- Input the liquid limit LL of fines (or the void ratio of fines at σ'=10 kPa, σ'=1 MPa, and at the liquid limit LL).
- Compute notable mixtures ①-through-⑨ for mechanical-control and ⑩-through-⑬ for flow control; plot the 13 notable mixtures on the triangular chart and draw the classification boundaries. Note: the Excel file available on the authors' websites simultaneously draws the chart, classification boundaries and plots the point that represents the soil under consideration.
- Classify the soil under consideration. The double letter nomenclature recognizes: first, the soil fraction that controls the mechanical behaviour and second, the soil fraction that controls flow (in parenthesis).

Table 1. Revised Soil Classification System RSCS.

Background:

Physics-based: gravimetric-volumetric analysis

Data-driven: takes into consideration extensive databases of soil behaviour

Input:

Gravel G (> 4.75mm)	F_G	e_G^{max} and e_G^{min}	or roundness R and uniformity C_u
Sand S (0.075~4.75mm)	F_S	e_S^{max} and e_S^{min}	or roundness R and uniformity C_u
Fines F (< 0.075mm)	F_F	$e_F\|^{10kPa}$, $e_F\|^{1MPa}$, and $e_F\|^{LL}$	or liquid limit LL

Compute Threshold Fractions

Gravel fraction $F_G=M_G/M_T$ Sand fraction $F_S=M_S/M_T$ Fines fraction $F_F=M_F/M_T$

$$F_G=\left(1+\frac{e_G}{1+e_S}+\frac{e_S}{1+e_F}\frac{e_G}{1+e_S}\right)^{-1} \quad F_S=\left(\frac{1+e_S}{e_G}+1+\frac{e_S}{1+e_F}\right)^{-1} \quad F_F=\left(\frac{1+e_S}{e_G}\frac{1+e_F}{e_S}+\frac{1+e_F}{e_S}+1\right)^{-1}$$

Support information & Correlations:

Fines: Fluid flow $e_F|^{flow}=0.05LL\log(LL-25)$

Fines: Load carrying $e_F|^{10kPa}=e_F|^{1kPa}-C_c=0.026LL+0.07$ $\quad e_F|^{1MPa}=e_F|^{1kPa}-3C_c=0.011LL+0.21$

Gravel and sand: $e_C^{\max}=0.032+\dfrac{0.154}{R}+\dfrac{0.522}{C_u}$, $\quad e_C^{\min}=-0.012+\dfrac{0.082}{R}+\dfrac{0.371}{C_u}$

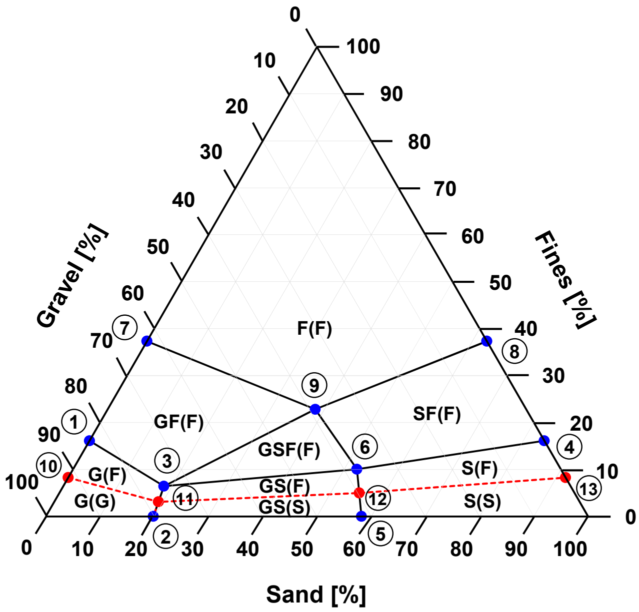

	No.	Notable Mixtures		
		Gravel	Sand	Fines
(a) Load carrying	1	e_G^{min}	-	$e_F\|^{10kPa}$
	2	e_G^{min}	e_S^{max}	-
	3	e_G^{min}	e_S^{max}	$e_F\|^{10kPa}$
	4	-	e_S^{min}	$e_F\|^{10kPa}$
	5	$2.5e_G^{max}$	e_S^{min}	-
	6	$2.5e_G^{max}$	e_S^{min}	$e_F\|^{10kPa}$
	7	$1.3e_G^{max}$	-	$e_F\|^{1MPa}$
	8	-	$1.3e_S^{max}$	$e_F\|^{1MPa}$
	9	$2.5e_G^{max}$	$1.3e_S^{max}$	$e_F\|^{1MPa}$
(b) Flow	10	e_G^{min}	-	$\lambda e_F\|^{LL}$
	11	e_G^{min}	e_S^{max}	$\lambda e_F\|^{LL}$
	12	$2.5e_G^{max}$	e_S^{min}	$\lambda e_F\|^{LL}$
	13	-	e_S^{min}	$\lambda e_F\|^{LL}$

Classify the soil. Report the two-name nomenclature: first letter/letters indicate the load-carrying fraction the second letter indicates the flow-controlling fraction. If either letter is F ➔ proceed to classify the fines - Table 2.

Sources: Park and Santamarina (2016).

Step 2: Fines classification. Soils that are fines-controlled -either in their mechanical and/or flow response- require further analysis to determine that type of fines. The most salient characteristics of fines are (1) their specific surface, assessed by the liquid limit, and (2) their sensitivity to pore fluid chemistry. We determine fluid sensitivity by running liquid limits with deionized water LL_{DW}, brine LL_{brine} to collapse the double layer (2 M NaCl solution), and kerosene LL_{ker} to explore the effect of van der Waals forces. Measured liquid limits are corrected for specific gravity and precipitated salts. Then two ratios LL_{ker}/LL_{brine} and LL_{DW}/LL_{brine} combine the corrected values as demonstrated in Table 2. The electrical sensitivity S_E captures the distance between measured values and the absolute "non-sensitive" soil response at LL_{ker}/LL_{brine}=1 and LL_{DW}/LL_{brine}=1. The two-letter pair classification of a fine soil recognizes its plasticity and its electrical sensitivity (Table 2).

Table 2. Fines Classification based on Plasticity and Sensitivity to Pore-Fluid Chemistry.

Background:
Specific surface and sensitivity to pore fluid chemistry are the salient characteristics of fines.

Input: Three liquid limits (soil fraction passes sieve #200 - fall cone method BSI 1990)
Sediment mixed with deionized water LL_{DW}, kerosene LL_{ker}, and 2-M NaCl brine LL_{brine}.

Compute corrected liquid limit ratios

$$\left.\frac{LL_{\ker}}{LL_{brine}}\right|_{corr} = \frac{LL_{\ker}}{LL_{brine}} \frac{1 - c_{brine}\dfrac{LL_{brine}}{100}}{G_{\ker}} \quad \text{and} \quad \left.\frac{LL_{DW}}{LL_{brine}}\right|_{corr} = \frac{LL_{DW}}{LL_{brine}}\left(1 - c_{brine}\frac{LL_{brine}}{100}\right)$$

where G_{ker} is the specific gravity of kerosene; c_{brine}=concentration of NaCl brine [mol/L]

Calculate the electrical sensitivity S_E (use ratios above, or their inverse such that they are ≥1)

$$S_E^{\,left} = \sqrt{\left(\frac{LL_{\ker}}{LL_{brine}} - 1\right)^2 + \left(\frac{LL_{DW}}{LL_{brine}} - 1\right)^2} \quad \text{or} \quad S_E^{\,(right)} = \sqrt{\left(\frac{LL_{brine}}{LL_{\ker}} - 1\right)^2 + \left(\frac{LL_{DW}}{LL_{brine}} - 1\right)^2}$$

Classify the soil

Report the two-letter pair for
- Plasticity
- Electrical sensitivity

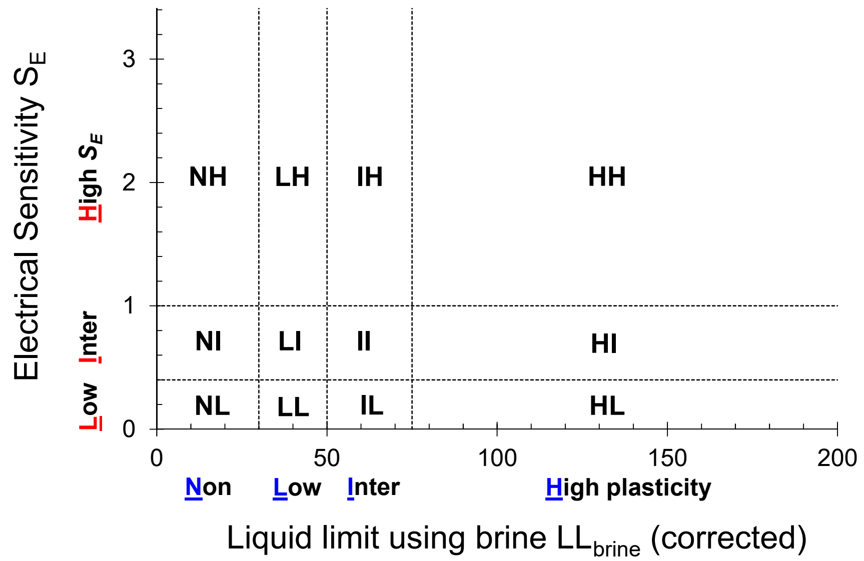

Sources: Jang and Santamarina (2016a); Jang and Santamarina (2016b)

3 ELASTIC WAVES

A small-strain mechanical perturbation propagates through the soil mass as an elastic wave. The wave equation for mechanical wave propagation combines Newton's law F=m·a=m·d²u/dt², dynamic force equilibrium, constitutive equations (Hooke's law σ=Eε), and compatibility of deformations. The resulting wave equation anticipates two modes of propagation in a linear-elastic, homogeneous, isotropic, single-phase and infinite continuum: (1) S-waves where the particle motion is normal to the direction of propagation, and (2) P-waves where the particle motion is in the direction of wave propagation. New forms of wave propagation emerge anytime the above assumptions are relaxed, for example: shock waves (large strain); reflection, refraction and scatter (heterogeneous); S-wave splitting (anisotropy); slow & fast waves (mixed phase); Rayleigh, Love, and tube waves (bounded media).

Wave velocity The shear stiffness of the granular skeleton G_{sk} defines the S-wave velocity V_S. Therefore, V_S increases with effective stress, diagenesis (e.g., cementation, creep, and salt precipitation), and suction (Table 3).

The P-wave velocity V_P depends on the constrained modulus of the soil M_{soil}, which is a function of the shear stiffness of the skeleton G_{sk} (see above) and the bulk stiffness of the soil B_{soil}. The bulk stiffness of the soil can be computed by successive substitutions to capture (Table 3): the skeleton stiffness B_{sk} and porosity n, the stiffness of water and air B_w and B_a, and the degree of saturation S_r as presented in Table 3.

V_P/V_S - Poisson's ratio. Theory of elasticity anticipates that the ratio V_P/V_S is a function of Poisson's ratio ν (Table 3). For small-strain wave propagation, Poisson's ratio is ν=0.15±0.05 for dry or unsaturated soils, but it tends to $\nu\rightarrow 0.5$ for well saturated soils; for example, Poisson's ratio can be ν=0.485 for a saturated sand 20m deep and exceed ν=0.499 for a saturated soft clay.

Attenuation. The wave amplitude decreases with distance due to (Table 4): geometric spreading of the propagating spherical or cylindrical front (i.e., same energy across a larger area), reflection and backscatter at interfaces (lower transmitted energy), and unrecovered energy consumed while deforming the material as the wave propagates (viscous, thermoelastic and/or frictional losses). Geometric spreading vanishes in plane waves.

Table 3. Elastic Waves: Velocity.

S-wave V_S		
saturated or dry soils; uncemented	$V_S = \sqrt{\frac{G_{sk}}{\rho}} = \alpha\left(\frac{\sigma'_{mean}}{1kPa}\right)^{\beta}$	where $\beta = 0.73 - 0.27\log\left(\frac{\alpha}{m/s}\right)$
	σ'_{mean} mean effective stress on the polarization plane	
unsaturated soils	$V_S \approx V_{S(for\ S_r=1.0)}\left[1+\frac{suction \cdot S_r}{0.75\sigma'_v}\right]^{\beta}$	
P-wave V_P	$V_P = \sqrt{\frac{M_{soil}}{\rho_{soil}}} = \sqrt{\frac{B_{soil}+4/3G_{sk}}{\rho_{soil}}}$	water V_P=1482 m/s air V_P= 343 m/s
Bulk modulus and mass density (Assumes $B_{sk}/B_g \approx 0$ and low frequency limit)		
Skeleton	$B_{sk} = \frac{2(1+\nu)}{3(1-2\nu)}G_{sk}$	G_{sk} from $G_{sk} = V_S^2\rho$
Soil (fluid + skeleton)	$B_{soil} = B_{sus} + B_{sk}$	$\rho_{soil} = \rho_{sus} = (1-n)\rho_g + n\rho_{fl}$
Suspension (fluid + particles)	$B_{sus} = \left(\frac{1-n}{B_g}+\frac{n}{B_{fl}}\right)^{-1}$	$\rho_{sus} = (1-n)\rho_g + n\rho_{fl}$
Fluid Mixture	$B_{fl} = \left(\frac{S_r}{B_w}+\frac{1-S_r}{B_a}\right)^{-1}$	$\rho_{fl} = (1-S_r)\rho_a + S_r\rho_w$ $\rho_{fl} = S_r\rho_w$ in case a≡air
V_P/V_S – Poisson's ratio	$\frac{V_P}{V_P} = \sqrt{\frac{M_{soil}}{G_{sk}}} = \sqrt{\frac{2(1-\nu)}{(1-2\nu)}}$	unsaturated soils ν=0.15±0.05 well saturated soils $\nu\rightarrow 0.5$

Sources: Richart *et al.* (1970); Hardin and Drnevich (1972); Reynolds (1997); Santamarina *et al.* (2001); Cho and Santamarina (2001). Based on an earlier compendium by Santamarina *et al.* 2005.

4 ELECTROMAGNETIC WAVES

An electrical or magnetic transient propagates through the soil mass as an electromagnetic wave. The wave equation for electromagnetic waves results from Maxwell's equations. The electrical field and the magnetic field oscillate transversely to the direction of propagation and to each other.

There are three electromagnetic material parameters: magnetic permeability μ, electrical conductivity σ_{el}, permittivity κ. Permittivity and permeability are complex quantities because they represent both in-and-out of phase responses. The three material parameters combine to determine the propagation velocity V and the material attenuation coefficient α or skin depth $S_d = 1/\alpha$ i.e., is the distance travelled by a plane wave when its amplitude decreases to $1/e$ of the initial amplitude. Table 5 summarizes equations for wave velocity and skin depth. Typically, most fluids and solids in the subsurface are either paramagnetic or diamagnetic; then, velocity and skin depth equations become those listed in the second half of Table 5.

Magnetization and polarization losses add to Ohmic conduction to render an effective conductivity. When the effective conductivity is high, the first term of the wave equation prevails and the electromagnetic transient propagates in diffusional mode.

Table 4. Elastic Waves: Attenuation

1 *Attenuation* $\frac{A_2}{A_1} = \left(\frac{r_1}{r_2}\right)^{\varsigma} T\, e^{-\alpha(r_2 - r_1)}$

2 Ratio between the amplitude of particle motion A at radial distances r_1 and r_2 [m]

3 Transmission coefficient T across an interface: a function of relative impedance

4 Exponent: plane wave ς=0; cylindrical front ς=0.5; spherical front ς=1

5 Relationship between linear attenuation coefficient α [1/m], skin depth *Sd* [m], and damping ratio *D*:

6 $\alpha = \frac{1}{S_d} = \frac{2\pi D}{\lambda}$ Note: the skin depth in terms of wavelengths is $\frac{S_d}{\lambda} = \frac{1}{2\pi D}$

7 *Physical processes in material attenuation*

Dry - small strain: thermo-elastic relaxation

Moist/wet - small strain: viscous loss prevails

Large strain: frictional loss

Typical damping values at small strain for P- and S- waves

Material		Damping D	Comments
Air		2×10^{-4}	Changes with relative humidity
Water		2×10^{-6}	Increases with dissolved gas
Coarse soils	*dry*	0.002~0.008	Increases when wet
	saturated	0.005~0.02	
Fine soils	*saturated*	0.01~0.05	
Organic soils	*saturated*	0.01~0.05	
Rocks	*dry*	0.002~0.004	
	wet	0.006~0.025	

Notes: γ is the strain, σ_0' is the effective confinement, w_g is the gravimetric water content. Sources: Johnston and Toksoz 1980; Yasuda and Matsumoto (1993); Kim *et al*. (1991); Laird and Stokoe (1993); Santamarina and Cascante (1996); Li *et al.* (1998); Kokusho (1980); Kokusho *et al.* (1982); Cascante and Santamarina (1996); Diaz-Rodriguez and Santamarina (2001); Kim and Novak (1981).

Table 5. Electromagnetic Waves: Velocity and Attenuation.

Electromagnetic wave propagation

Maxwell's Equations $\frac{\partial^2 E}{\partial x^2} = \mu\sigma \frac{\partial E}{\partial t} + \mu\varepsilon \frac{\partial^2 E}{\partial t^2}$

Electromagnetic properties

Permeability	μ^*	Relative $\mu_r=\mu^*/\mu_0$	free space $\mu_0 = 4\pi\cdot10^7$ H/m
Permittivity	ε^*	Relative $\kappa=\varepsilon^*/\varepsilon_0$	free space $\varepsilon_0 = 8.85\times10^{-12}$ $C^2N^{-1}m^{-2}$
Conductivity	σ_{el}		

Velocity (*non-ferromagnetic*)

$$V = c_0 \frac{1}{\sqrt{\frac{1}{2}\left[\sqrt{\kappa^2 + \left(\frac{\sigma}{\varepsilon_0\omega}\right)^2} + \kappa\right]}}$$

In free space $c_0 = 1/\sqrt{\varepsilon_0\mu_0}$ =3×10^8 m/s

Attenuation (*non-ferromagnetic*)

Linear attenuation $\alpha=1/S_d$

$$S_d = \frac{c_0}{\omega} \frac{1}{\sqrt{\frac{1}{2}\left[\sqrt{\kappa^2 + \left(\frac{\sigma}{\varepsilon_0\omega}\right)^2} - \kappa\right]}}$$

Table 6. Electrical Conductivity.

Availability and mobility of hydrated ions

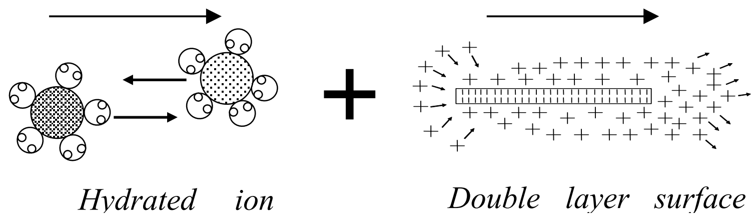

Note: The effective conductivity rises as the frequency increases

Conductivity of single-phase soil components (σ in S/m)

de-ionized water	10^{-6}	organic fluids	$\sim 10^{-11}$
fresh water	10^{-3}	most soil-forming minerals	10^{-15}-10^{-7}
sea water	4	(Note: some minerals are conductive)	

9 Conductivity of mixtures

water + salt = electrolyte	$\sigma_{el} = 0.15\,TDS$	σ_{el} in mS/m (Annan, 1992) TDS: total dissolved salts in mg/L
wet soils	$\sigma_{soil} = n\sigma_{el} + (1-n)\Theta\rho_g S_s$	Water saturation S_r= 100% Θ surface conduction. Needs correction for tortuosity
	$\sigma_{soil} = a\sigma_{el}\, S_r^c\, n^m$	(Archie, 1942) a≈1, m~1-2.4, c~4-5

Trend for soils (σ in S/m)

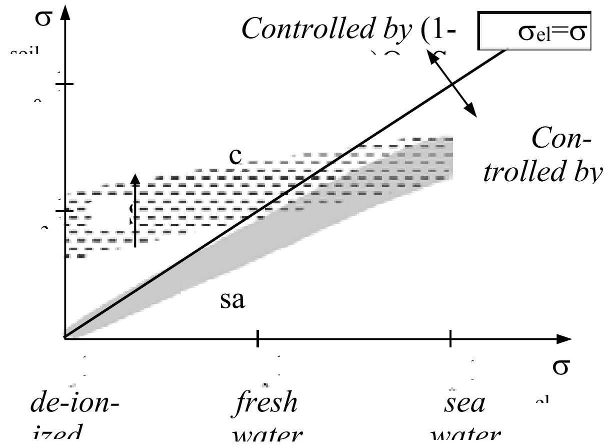

Notes: The surface conduction for kaolinite is about Θ ≈ 10^{-9} Siemens. Tortuosity may reduce the electrical conductivity in clays more than in sands. Hence, the conductivity of marine clays may be lower than the conductivity of marine sands, at the same void ratio.

Sources: Annan (1992); Reynolds (1997); Santamarina *et al*. (2001). Based on an earlier compendium by Santamarina *et al*. (2005).

Electrical conductivity. The movement of hydrated ions is responsible for electrical conduction in geomaterials. Hydrated ions imply the presence of water, dissolved salts (both cations and anions), and hydrated counter-ions next to charged mineral surfaces (diffuse double layer). Therefore, the electrical conductivity of soils is proportional to the volumetric water content, the conductivity of the pore fluid which increases linearly with salt concentration *c* (for low *c*<~0.2M), and the specific surface of the soil; Table 6 lists convenient semi-empirical models. Pore fluid conductivity prevails in sands and silts, while surface conduction gains relevance in low porosity, high specific surface clayey sediments saturated with low salt concentration water (Table 6).

Permittivity. Permittivity is a measure of polarizability. Free water molecules control the permittivity of soils and rocks in the MHz-to-GHz frequency range; therefore, the permittivity of wet soils is proportional to the volumetric water content $\theta_v = S_r n$. By contrast, the orientational polarization of water is hindered when water is frozen, in adsorbed layers close to mineral surfaces and when water molecules hydrate ions. Table 7 summarizes semi-empirical models.

Permeability. We can assume that soils are non-ferromagnetic in the absence of ferromagnetic inclusions. Otherwise, the volume fraction of ferromagnetic inclusions determines the magnetic permeability of the soil (Table 8).

Table 7. Permittivity (Relevant frequency range 1 MHz-1 GHz).

Polarization

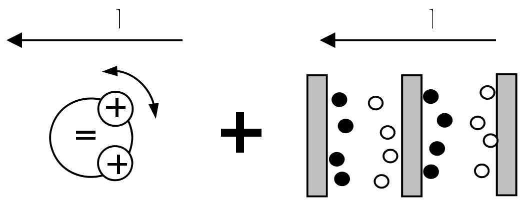

orientation of polar molecules — *interfacial polarization*

Note: Permittivity increases as frequency decreases

Permittivity of single-phase soil components (radio frequencies)

water	78.5	quartz	4.2 - 5
methanol	32.6	calcite	7.7 - 8.5
most organic fluids	2 - 6	most minerals	6 - 10

Permittivity of wet soils ($\theta_v = S_r \cdot n$)

$\kappa' = 1.40 + 87.6\,\theta_v - 18.7\,\theta_v^2$	50 MHz	Wensink (1993)
$\kappa' = 3.03 + 9.3\,\theta_v + 146.0\,\theta_v^2 - 76.7\,\theta_v^3$	MHz to GHz	Topp et al. (1980)
$\kappa' = 3.3 + 41.4\theta_v + 16.0\theta_v^2$	~ 1GHz	Wensink (1993)
$\kappa' = 3.14 + 23.8\theta_v + 16.0\theta_v^2$		Wang (1980)
$\kappa' = 40\theta_v - 3.9 + \sqrt{44.8 - 392\theta_v + 1600\theta_v^2}$		Selig and Mansukhani (1975)
$\kappa' = \left(2.6 - 1.6\,n + 7.9\,\theta_v\right)^2$		Based on CRI mixture model

Table 8: Magnetic Permeability.

Magnetization

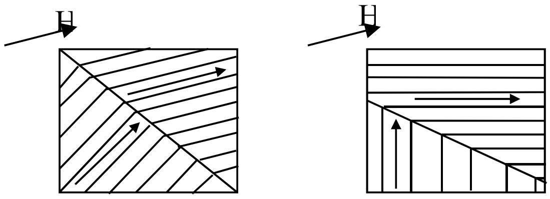

(a) (b) (c)

Magnetization mechanisms in ferromagnetic materials: (a) no magnetic field H=0; (b) rotation of spins within domains H>0; and (c) translation of domain walls H>0.

Single materials

water, quartz, kaolinite	~0.9999 (diamagnetic)
montmorillonite, illite, granite, hematite	1.00002-1.0005 (paramagnetic)
nickel, iron	> 300 (ferromagnetic)

Predictive relations

Wagner's model for spherical particles (1)	$\mu' = 1 + 3v_{Fe}$	for $v_{Fe}<0.2$
Kaolinite with iron filings (at 10 kHz) (2)	$\mu' = 1 + 4v_{Fe} + 7v_{Fe}^2$	for $v_{Fe}<0.3$

Sources: (1) Göktürk *et al*. (1993); (2) Klein and Santamarina (2000)
Note: v_{Fe} is the volume fraction of ferromagnetic inclusions

5 THERMAL PROPERTIES

Table 9 schematically summarizes thermal conduction phenomena.

Table 9: Thermal Phenomena in Soils.

Parameters

<u>*Latent heat L*</u> [kJ/kg]: Heat required for phase transformation at constant temperature.
<u>*Specific heat c_p*</u> [$Jkg^{-1}K^{-1}$]: Heat required to increase the temperature of 1 kg by 1 K.
<u>*Thermal conductivity k_T*</u> [$Wm^{-1}K^{-1}$]: relates the heat flux density q [$J/sec/m^2$] to the thermal gradient
$q = k_T \, \Delta T/\Delta x$ (Fourier's heat law)
<u>*Thermal diffusivity*</u>: $D_T = k_T/\rho c_p$.
<u>*Volumetric expansion coeff*</u> α_T [K^{-1}]: Relates temperature change to strain $\varepsilon = \alpha \Delta T$

Typical values

Material	Latent heat [kJ/kg]	Specific heat c_p [$Jkg^{-1}K^{-1}$]	Thermal conduct. k_T [$Wm^{-1}K^{-1}$]	Thermal diffusivity D_T [$m^2sec^{-1} \times 10^{-7}$]	Volumetric thermal expansion coefficient α_T [$10^{-6}\,K^{-1}$]
Quartz (single crystal)		750	12 (‖) - 6.8 (⊥)	45	800 (‖)-1400 (⊥)
Shale		630	1.56	31	
Limestone		900	1.3	27	3.3
Sand, dry		800	0.15 - 0.33		
Sand, water sat		2200	2 - 4		
Water	334	4200	0.6	1.4	200 (at 293K)
Ice (0 °C)	334	2040	2.2	11.2	51 (at 273K)
Air		1000	0.024	0.21	3400 (at 293K)

Trends: *General* $k_T^{\text{dry soil}} < k_T^{\text{wet soil}} < k_T^{\text{mineral}}$

Dry soils $$k_{T,dry} = \frac{0.135\rho_{dry} + 64.7}{\rho_g - 0.947\rho_{dry}}$$ (Johansen 1975)

Wet soils $$k_{T,wet} = k_{T,dry} + (1 - e^{-0.89 S_r})(k_{T,sat} - k_{T,dry})$$ (Ewen and Thomas 1987)

Thermal conduction: Grain and pore-scale processes

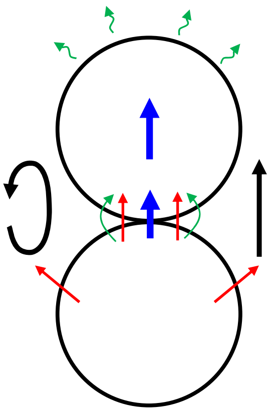

Particle conduction
Contact conduction

Radiation
Particle-particle radiation

Particle-fluid conduction
Particle-fluid-part conduction

Pore fluid conduction
Pore fluid convection

<u>*k_T increase with*</u>:

- porosity n ↓
- effective stress σ' ↑ (heat transfer at contacts ↑)
- water content ↑
- quartz content ↑
- frozen water
- coarser grains

A change in temperature propagates as a diffusion front through the soil mass, facilitated by the thermal conductivity of the soil yet hindered by the heat consumed in changing the temperature of the soil mass. The propagating thermal front causes volume strains, and phase changes may take place (vapour↔liquid↔solid). Consequently, the thermal properties of soils include: thermal diffusivity D_T, thermal conductivity k_T, specific heat c_p, latent heat L, and volumetric thermal expansion coefficient α_T. Table 9 presents definitions and typical values.

In general, we can use tabulated values and gravimetric or volumetric averages to estimate thermal properties for engineering analyses, except for the thermal conductivity (and hence diffusivity). Thermal conduction depends on:

- The type of mineral: quartz exhibits particularly high thermal conductivity
- The coordination number between grains: denser soils exhibit higher k_T
- The quality of contacts: contact resistance decreases as stress increases (it follows a power

function that resembles Hertzian contact behaviour), and in cemented soils
- The presence of water: while the thermal conductivity of water is lower than that of most minerals, the presence of water at contacts has a pronounced effect on the thermal conduction across contacts and the conductivity of the soil.

6 CLOSING THOUGHTS: GEOPHYSICS AND ENGINEERING

The previous sections identify various causal links between geophysical properties, soil type, index properties and soil behaviour. Salient causal relations follow:

- Soil type: related to stress-dependent changes in the S-wave velocity, thermal conductivity, electrical conductivity and permittivity.
- Small strain shear stiffness (for deformation-based design): it is computed from S-wave velocity V_s measurements using cross-hole downhole and surface wave methods. Shear stiffness and V_s reflect effective stress –including suction, extent of diagenetic cementation and/or freezing. Exercise caution when soils are unsaturated as variation in saturation levels will result in changes in the shear stiffness.
- Porosity: from the volumetric water content calculated with electromagnetic measurements using ground penetrating radar, electrical resistivity or time domain reflectometry. In addition, electromagnetic parameters can be used to detect time-varying water saturation, pore fluid chemistry, and fluid phase (e.g., freezing).
- Other geophysical parameters mirror time varying water saturation, including P-wave velocity when $S_r \rightarrow 100\%$, S-wave velocity for intermediate saturations, and thermal conductivity when $S_r \rightarrow 0\%$.
- Thermal properties are needed for the design of systems such as buried cable installations and thermal piles. Specific and latent heats are gravimetric or volumetric averages of tabulated values for the individual soil components. The thermal conductivity (and hence diffusivity) can be measured in the lab under proper field stress and moisture conditions.

7 ACKNOWLEDGEMENTS

This research is supported by the KAUST endowment. G. Abelskamp edited the manuscript. The authors are grateful to the organizers of the 5th International Conference on Geotechnical and Geophysical Site Characterization.

8 LIST OF SYMBOLS

α attenuation coefficient
α_T volumetric thermal expansion coefficient
α, β fitting parameters in velocity-stress relation
Δ energy loss/cycle
ε strain
ε^* complex permittivity
ε_0 permittivity of free space, $\varepsilon_0 = 8.85 \times 10^{-12}$ $C^2/(N{\cdot}m^2)$ = 8.85×10^{-12} F/m
γ shear strain (γ_{elas} elastic threshold strain)
κ relative permittivity
λ wavelength
μ^* magnetic permeability (subscript r: relative permeability)
μ_0 magnetic permeability of free space, $\mu_0 = 4\pi \times 10^7$ H/m
ν Poisson's ratio
θ_v volumetric water content
Θ surface conduction
ρ mass density (fl: fluid; g: mineral that makes the grains; sus: suspension; dry: bulk dry)
ς exponent in geometric attenuation that depends on wave front
σ_{el} electrical conductivity (el: electrolyte; fl: fluid)
σ stress (σ': effective stress; v: vertical; h: horizontal; mean: mean in polarization plane)
ω angular frequency
A amplitude
a, c, m constants used in Archie's equation
B bulk stiffness (sk: soil skeleton; g: mineral that makes grains; sus: suspension; fl: fluid)
C_c compression index
C_u coefficient of uniformity
c_{brine} concentration of NaCl brine [mol/L]
c_o speed of light in free space, $c_o = 3\times10^8$ m/s
c_p specific heat [$Jkg^{-1}K^{-1}$]
D damping ratio
D_T thermal diffusivity
E electric field
E Young's modulus
F soil fraction (G: gravel; S: sand; F: fines)
e void ratio (subscripts G and S denote the gravel and sand, respectively)
f frequency (r: resonant frequency)
G shear modulus (sk: soil skeleton)
G_{ker} specific gravity of kerosene
H magnetic field
k_T thermal conductivity (sat: saturated)
L latent heat
LL liquid limit (ker: kerosene; DW: de-ionized water)
M constraint modulus
n porosity
R roundness
r distance from source
S_d skin depth
S_E electrical sensitivity
S_r degree of saturation
S_s specific surface
T transmission coefficient
TDS total dissolved salts in mg/L
V wave velocity (ph: phase; P: P-wave; S: S-wave; R: Rayleigh wave)
v_{Fe} volume fraction of ferromagnetic inclusions
w_g gravimetric water content

9 REFERENCES

Annan, A. P. (1992). Ground penetrating radar, Workshop Notes, Sensors and Software, Mississauga.

Archie, G. E. (1942). The electrical resistivity log as an aid in determining some reservoir characteristics: Transactions of the American Institute of Mining, *Metallurgical and Petroleum Engineers*, 146, 54-62.

Cascante, G. and Santamarina, J. C. (1996). Interparticle contact behavior and wave propagation. *Journal of Geotechnical Engineering*, ASCE, 122(10), 831-839.

Cho, G. C. and Santamarina, J. C. (2001). Unsaturated particulate materials - particle level studies. *Journal of Geotechnical Geoenvironmental Engineering*, ASCE, 127, 84-96.

Dìaz-Rodrìguez, J.A. and Santamarina, J.C. (2001), Mexico city soil behavior at different strains: observations and physical interpretation. *Journal of Geotechnical and Geoenvironmental Engineering*, ASCE, 127, 783-789.

Ewen, J., and Thomas, H. R. (1987). The thermal probe - a new method and its use on an unsaturated sand. *Geotechnique*, 37(1), 91-105.

Göktürk, H. S., Fiske, T. J. and Kalyon, D. M. (1993). Electric and magnetic properties of a thermoplastic elastomer incorporated with ferromagnetic powders. IEEE Transactions on Magnetics, 29, 4170-4176.

Hardin, B. O. and Drnevich, V. P. (1972). Shear modulus and damping in soils: measurement and parameter effects. *Journal of Soil Mechanics Foundation Division*, ASCE, 98, 603-624.

Jang, J. and Santamarina, J. C. (2016a). Fines classification based on sensitivity to pore-fluid chemistry. *Journal of Geotechnical and Geoenvironmental Engineering*, ASCE, 142 (4), p.06015018.

Jang, J. and Santamarina, J. C. (2016b). Closure of "Fines classification based on sensitivity to pore-fluid chemistry". *Journal of Geotechnical and Geoenvironmental Engineering*, ASCE (in progress).

Johansen, T. A. (1975). Thermal conductivity of soils. US Army Corps of Engineers, Trondheim, Hanover, New Hampshire.

Johnston, D.H. and Toksöz, M.N. (1980). Ultrasonic P and S wave attenuation in dry and saturated rocks under pressure. *Journal of Geophysical Research: Solid Earth*, *85*(B2), 925-936.

Kim, T.C. and Novak, M. (1981). Dynamic properties of some cohesive soils of Ontario. *Canadian Geotechnical Journal*, 18, 371-389.

Kim, D. S., Stokoe, K. H. and Hudson, W. R. (1991). Deformational characteristics of soils at small to intermediate strains from cyclic tests. Report 1177-3, Center for Transportation Research, Bureau of Engineering Research, the University of Texas Austin, 142 pages.

Klein, K. and J. C. Santamarina. (2000). Ferromagnetic inclusions in geomaterials – implications. *Geotechnical Journal*, ASCE, 162, 167-179.

Kokusho, T. (1980). Cyclic triaxial test of dynamic soil properties for wide strain range. *Soils and Foundations*, 20, 45-60.

Kokusho, T., Yoshida, Y. and Esashi, Y. (1982). Dynamic properties of soft clay for wide strain range. *Soils and Foundations*, 22, 1-18.

Laird, J. P. and Stokoe, K. H. (1993). Dynamic properties of remolded and undisturbed soil samples tested at high confining pressures. Geotechnical Engineering Report GR93-6, Electrical Power Research Institute, Palo Alto, Calif.

Li, X. S., Yang, W. L., Shen, C. K., and Wang, W. C. (1998). Energy-injecting virtual mass resonant column system. *Journal of Geotechnical and Geoenvironmental Engineering*, ASCE, 124, 428-438.

O'Konski, C. T. (1960). Electrical properties of macromolecules V. Theory of ionic polarization in polyelectrolytes. *Journal of Physical Chemistry*, 64, 605-618.

Park, J and Santamarina, J. C. (2016). Revised soil classification system for coarse-fine mixtures. *Journal of Geotechnical and Geoenvironmental Engineering*, ASCE (Under review).

Reynolds, J.M. (1997). An introduction to applied and environmental geophysics. John Wiley and Sons, Chichester, U.K., 796 pages.

Richart, F. E., Hall, J. R., and Woods, R. D. (1970). Vibrations of soils and foundations, Prentice Hall, Englewood Cliffs, 414 pages.

Santamarina, J. C. and Cascante, G. (1996). Stress anisotropy and wave propagation: a micromechanical view. *Canadian Geotechnical Journal*, 33, 770-782.

Santamarina, J. C., Klein, K. A., and Fam, M. A. (2001). Soils and waves. John Wiley & Sons, LTD. New York, 488 pages.

Selig, E. T. and Mansukhani, S. (1975). Relationship of soil moisture to the dielectric property. *Journal of the Geotechnical Engineering Division*, 101, 757-770.

Topp, G. C., Davis, J. L., Bailey, W. G. and Zebchuk, W. D. (1980). The measurement of soil water content using a portable TDR hand probe. *Canadian Journal of Soil Science*, 64, 313-321.

Wang, J. R. (1980). The dielectric properties of soil-water mixtures at microwave frequencies. *Radio Science*, 15, 977-985.

Wensink, W. A. (1993). Dielectric properties of wet soils in the frequency range 1-3000 MHz. *Geophysical Prospecting*, 41, 671-696.

Yasuda, N. and Matsumoto, N. (1993). Dynamic deformation characteristics of sand and rockfill materials. *Canadian Geotechnical Journal*, 30, 747-757.

Session Reports

Geotechnical and Geophysical Site Characterisation 5 – Lehane, Acosta-Martínez & Kelly (Eds)
 ISBN 978-0-9946261-1-0

Session Report: Geophysics,1

S. Foti
Politecnico di Torino, Turin, Italy

ABSTRACT: A large number of papers has been presented in the session devoted to geophysical methods, confirming their consolidated role in site characterization. Different applications and a wide variety of techniques are covered in the contributions with several case histories and some developments on new tools. Crucial issues are also discussed in the present report. For one the reliability, which can be improved with advanced interpretation strategies based on joint inversion of multiple geophysical datasets. The role of guidelines for the execution and interpretation in improving the standard of practice is finally commented.

1 INTRODUCTION

The role of geophysical surveys in site characterization has been growing in the past decades thanks to the relevant improvements in the interpretation processes and to the availability of increasingly powerful hardware at cheaper and cheaper prices. Nevertheless great attention has to be posed as diffusion of geophysical surveys is not always taking place with sufficient quality in the professional practice. A deeper insight on geophysical methods is required not only to service providers but also to the end users, e.g. the professionals making use of the results of geophysical tests for the conception of the geological and the geotechnical model.

The relevance of geophysical methods for site characterization is associated to two different objectives of the investigation:

- Reconstruction of subsurface geometries (layering, inclusions, lateral variability);
- Direct or indirect estimate of physical and mechanical parameters of interest for the geotechnical model.

As the first point is concerned a very wide variety of geophysical methods can provide useful information for the construction of 2D-3D subsurface models. A recent overview is provided by Malehmir et al. (2016). Crucial points are the sensitivity of the specific geophysical parameter to the expected variation in the subsoil and the resolution with depth, considering that most geophysical tests are run from the ground surface.

As for the second objective, seismic methods traditionally play a major role as the geophysical parameters (i.e. the seismic velocities) are directly related to elastic parameters, which are of direct use in geotechnical models as they represent the mechanical response of the medium in the low strain region. Other geophysical parameters can be related to parameters of interest for the geotechnical model (e.g. the soil porosity), but only with the adoption of empirical rock physic relations.

The growing interest in geophysical prospecting for near-surface geotechnical and geoenvironmental applications is testified by the number of papers presented in the different editions of this series of International conferences on Site Characterization (ISC), which has been initiated in 1998 in Atlanta (USA) and has now reached its 5th edition in Gold Coast (Australia).

The large number of papers submitted for the ISC'5 conference has led to the decision of splitting the theme of Geophysical Methods in two different sessions, one of which is reviewed and commented in the present contribution. Most papers in this session are related to non-seismic methods, nevertheless to account for the importance of seismic methods in geotechnical site characterization, part of the paper will be devoted to the latter.

The paper is organized as follows, after a general overview of the topics covered by the papers presented in the session, some issue related to reliability of geophysical methods and a review of existing guidelines are reported.

2 GENERAL OVERVIEW

Most papers in the session are devoted to the identification of stratigraphic features, which is attempted with a variety of techniques. In some situations different techniques are used at the same site (e.g. Pfaffhuber et al. 2016, Bazin et al. 2016), but the level of coupling between different methods is usually weak: the final results are compared in order to assess from a qualitative/quantitative point of view the reliability of the results. Joint inversion schemes could provide a much significant synergy between different methods, as discussed in the next section. Similarly, stratigraphic information from boreholes and direct push methods could be used as additional constraints in the inversion process in order to get robust estimates and reliable soil models. In fact, in most projects the stratigraphic information is just used a posteriori for double-checking the results obtained with geophysical test or for calibration (e.g. to identify the stratigraphic features associated to the estimated geophysical model).

When dealing with the identification of the stratigraphic sequence, it is important to recognize the inherent nature of the data that are presented. 2D models are most often reconstructed with tomographic techniques (Reynolds 1997), in which a single inversion problem is solved using all the available experimental data. A notable exception is constituted by MASW profiling (e.g. Cox 2016) in which the 2D distribution of the geophysical parameter (V_S) is obtained from a collection of 1D profiles that are interpolated to provide a pseudo-2D section. The main implication is that with this approach the inverse problem is typically solved as a collection of individual 1D inversions. Considering the ill-posedness of inverse problems (see next section), such an approach may lead to instabilities of the results. A possible countermeasure is to impose a lateral constraint on each 1D profile (Figure 1) in order to solve a single better-posed inverse problem (Auken and Christiansen 2004, Wisen and Christiansen 2005, Socco et al. 2009).

Several papers in the session deal with the identification of underground voids, which is a typical application of geophysical tests in engineering projects. In particular, ERT (Abduljauwad et al. 2016, Porres-Benito et al. 2016), GPR (Hughes et al. 2016) or a combination of the two (Jafarzadeh et al. 2016) are adopted.

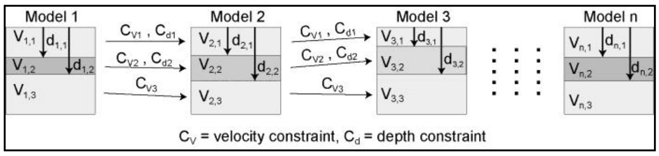

Figure 1. Laterally Constrained Inversion (LCI) scheme: adjacent 1D model are linked by constraints on the model parameters to be resolved (velocity of each layer and interface depths in this example) (modified after Wisen and Christiansen, 2004)

GPR is also proposed as a tool for the evaluation of lateral variability in the context of foundation engineering (Hebsur et al. 2016) and of slope stability (Bednarczyk 2016). Although some features are identified, the interpretation is not always straightforward and the association of the observed discontinuities in radargrams to specific stratigraphic conditions requires an expert interpretation procedure.

A few papers are dealing with penetrating probes equipped for geophysical measurements, either of electrical resistivity (Bazin et al. 2016, Fuiji et al. 2016) or seismic velocities (Amoroso et al. 2016). These approaches are very promising as they provide improved capabilities for the identifications of layers with respect to conventional penetration testing. Apart for being used as standalone tools, such probes could provide very useful information for the calibration and verification of ground surface geophysical measurements. A significant advancement would be gained by including these data in joint inversion algorithms to constrain the solution of tomographic 2D reconstructions.

Two papers in the session are focused on the comparison of laboratory and field data (Bazin et al. 2016, Campbell 2016). This aspect is very relevant and more and more studies should be devoted to it in the future. Indeed the investigation of geophysical properties of soils and rocks under controlled conditions in the lab may help in the definition of general and site-specific correlations with geotechnical parameters. These are the prerequisite for a quantitative use of geophysical parameters for the conception of the geotechnical model.

Campbell (2016) presented a statistical analysis of shear wave velocities measured in soils and rocks to assess the influence of different material parameters. Several other authors have dealt in the past with the relationship between in situ and laboratory measurements of seismic wave velocity. Indeed two counteracting main factors have to be taken into account: namely sampling disturbance and scale effects. The effect of the former is typically a reduction of the measured shear wave velocity on laboratory sample as the original fabric and the structure of the material are damaged by sampling operation, even in virtually undisturbed sampling. This effect is typically prevalent in soils.

Stokoe and Santamarina (2000) showed that the effect of sample disturbance is more important for stiffer soils. The comparison of laboratory and in situ shear wave velocity can hence be used as a proxy for the evaluation of sample quality (Jamiolkowski, 2012). In rocks, the scale effect is usually prevalent as laboratory measurements are conducted on intact cores and not affected by the fractures of the rock mass. Therefore typically a higher velocity is obtained on laboratory samples than on site. Musso et al. (2015) exploited this property to develop a procedure aimed at quantitatively define the representativeness of rock samples for the construction of the geomechanical model.

Bazin et al. (2016) deal with the comparison of in situ and laboratory values of both seismic velocities and electrical resistivity in soils. In particular they have used the combination of the different parameters in order to identify quick clay layers. Combination of seismic and electrical measurements could indeed be pursued at higher levels of integration by using seismo-electrical models (e.g. Mota and Monteiro Santos, 2010). Cosentini and Foti (2014) reported an example of the combined use of measured seismic wave velocities and electrical resistivity in unsaturated soils to infer soil porosity and degree of saturation.

3 RELIABILITY OF GEOPHYSICAL SURVEYS

A crucial issue in geophysical methods is related to the reliability of the reconstruction of the ground model. Indeed most geophysical tests are based on the solution of inverse problems which are inherently ill-posed and ill-conditioned, according to the Hadamard (1902) definition. The main consequence is solution non-uniqueness, i.e. several different geophysical models may honour equally well the available experimental data that are used to constrain the solution. Possible countermeasures to mitigate solution non-uniqueness are:

a) the inclusion of a-priori information on the ground model to better constrain the solution (Tarantola, 1987);
b) the adoption of joint inversion schemes in which different experimental datasets are simultaneously inverted (Vozoff and Jupp 1975).

Several examples are reported in the literature where different geophysical dataset are jointly inverted with a significant improvement in the reliability when compared to individual inversion of each dataset (Dobroka et al. 1991, Comina et al. 2002, Dal Moro 2008, Doetsch et al. 2010, Gao et al. 2010, Piatti et al. 2013). Typically the combination of the datasets is obtained with a structural merging of the different geophysical model, i.e. by assuming the same geometry for the subsoil models (Haber and Oldenburg 1997, Hu et al. 2009). A stronger link can be devised by adding a link between geophysical parameters (Eberhart-Phillips et al. 1989, Dell'Aversana et al. 2011, Gao et al. 2011). For example, Garofalo (2014) proposed a joint inversion scheme in which the soil porosity links the geo-electrical model to the seismic model. In particular Archie's relation (Archie 1942) is used to express the soil resistivity as a function of porosity, whereas the formula proposed by Foti et al. (2002) on the basis of Biot's theory (Biot, 1956a-b) for wave propagation in saturated porous media is used to express soil porosity as a function of wave velocities. Considering that the two models (seismic and electrical) are expected to share the same porosities, a further constraint is introduced in the inversion process (Figure 2).

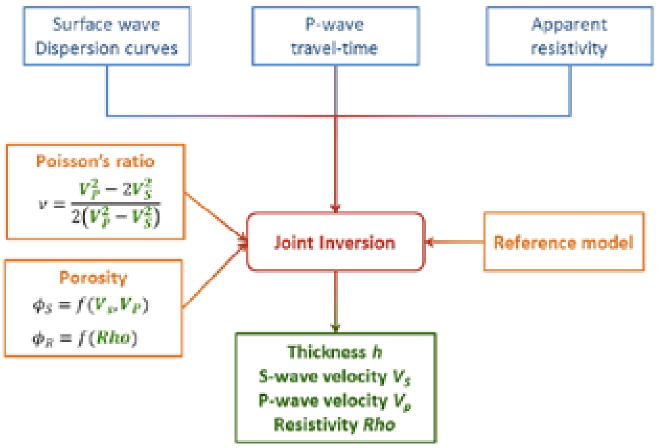

Figure 2. Example of joint inversion scheme in which the experimental data from different geophysical datasets (surface wave analysis, P-wave refraction and vertical electrical soundings) are simultaneous inverted with the addition of physical constraint between model parameter to retrieve a robust seismo-electrical model of the site (Garofalo, 2014)

However it is observed that in the case histories presented at the ISC'5 conference little attention has been posed to this aspect. Indeed most of the interpretations are based on the use of available commercial software, which are typically specialized on the processing and interpretation of a single technique dataset. The use of multiple methods is confined to a low level of integration in which the final results are visually compared to check the consistency of observed features in geophysical models from different techniques.

In this respect, the state of the practice of geophysical applications, as demonstrate by the contributions presented in the geophysical session at ISC'5, is a step behind the state of the art of the research in geophysics.

For the future it is desirable that this gap is filled. The technical community should adopt joint inversion schemes more frequently as they offer the possibility to improve significantly the reliability of the ground models retrieved by geophysical methods. In this respect, it is necessary that commercial codes are expanded and improved to allow the analysis of multiple datasets from a variety of methods.

Another relevant issue for the reliability of geophysical tests is related to the repeatability and reproducibility of the results. Indeed the reliability can be described as the combination of accuracy (i.e. the ability to get the true value of the parameter) and precision (i.e. the ability to get the same result when repeating the measurement).

Attempt to study accuracy of the solution typically faces the difficulty of dealing with unknown targets, as the focus of the characterization is indeed on natural materials (soils and rocks). For this reason, quite often synthetic datasets obtained from numerical simulations are used to check the accuracy of inversion algorithms. Such approach is obviously limited in scope as it is not able to account for the inherent uncertainties associated to the measurement process. Other possible approaches are based on small scale experiments on physical models. For example the paper by Porres-Benito et al. (2016) at ISC'5 reports an experiment on scaled model aimed at representing the presence of voids. In this case the potential of ERT are clearly shown. Nevertheless, as in several similar applications, the performance are not explicitly quantified and the accuracy is only estimated from visual inspection. A typical limitation in terms of the capability of reconstructing sharp boundaries is observed. This is common to most tomographic inversion process as regularization criteria are imposed to improve the stability of the solution (e.g Tikhonov and Arsenin, 1977). Borsic et al. (2005) and Comina et al. (2008) report experiments at laboratory scale, showing that under controlled boundary conditions it is possible to reach a good accuracy. As for seismic techniques, experiments on scaled model are reported by Bodet et al. (2005) and Bergamo et al. (2014), showing the possibility to obtain not only geometrical features of the deposit, but also quantitative information of the 2D shear wave velocity model.

As mentioned above the other side of reliability is represented by the precision. An assessment of the repeatability requires repeated of measurements in the same configuration. Examples for cross-hole tests are reported in Callerio et al. (2013), whose results have been subsequently used by Passeri and Foti (2016) to assess the reliability of porosity estimate from seismic wave velocities. The observed uncertainty on the field data can be projected into an estimate of uncertainties on the estimated model parameters, by using error propagation techniques (Tarantola 1987, Taylor 1997). Examples for shear wave velocity obtained from surface wave inversion are reported by Lai et al., 2005.

In more general terms, the whole chain of experimental data collection and interpretation affects precision and accuracy. In this respect the results obtained in round robin tests in which different operators are asked to perform measurements at the same test site may provide valuable information on reliability. Several blind tests have been performed in the past, especially with respect to seismic methods (e.g. Brown et al. 2002, Xia et al. 2002, Jung et al. 2012). Kim et al. (2013) report a comparison at a shallow bedrock site where several in-hole and surface measurements where adopted for the characterization of the shallow sediments. More recently, during the Interpacific Project the performance of different seismic techniques have been compared at three test sites in France and Italy (Garofalo et al., 2016a,b). The sites cover a variety of geological conditions ranging from rock outcrop to soft alluvial sediments. In particular, the focus was on the evaluation of the shear wave velocity profile under the assumption of horizontally layered media. Results from surface wave methods (with active and passive measurements) have been compared to different invasive methods (Cross-Hole Test, Down Hole Test, P-S suspension logging, Seismic dilatometer SDMT). The main findings can be summarized as follows:

- invasive methods provide an higher vertical resolution, with the possibility to identify stratigraphical details also at large depth;
- although invasive methods are often considered more reliable than surface methods, the observed variability in the results is comparable. This uncertainty should therefore be taken into account when the results are used for modeling;
- for average parameters, such as the $V_{S,30}$ often adopted for site classification in seismic codes, very similar results are obtained from surface wave analysis and invasive methods, both in terms of mean values and of associated variability;
- observed variability in surface wave test results is mainly due to non-uniqueness of the solution of the problem, whereas the estimated experimental dispersion curves show very limited variability. This variability could be reduced with the inclusion of a-priori information, often available from other surveys (e.g. stratigraphic information from boreholes).

4 TESTING STANDARDS AND GUIDELINES

The fast and wide diffusion of geophysical tests has lead to the necessity of technical references that can help in homogenizing the quality and the significance of these surveys. Testing standards (e.g. by ASTM, American Society of Testing Materials) are available for several geophysical methods. They can be imposed for quality assurance. However, for some geophysical methods the interpretation process is hard to standardize as it can be successfully performed with different strategies. This is for example the case for surface wave analysis, which can be implemented with a large variety of tools (see Socco et al. 2010 and Foti et al 2011 for literature reviews). Moreover, testing standards are of little help for a full understanding of potentiality and limitations of each technique.

For a correct planning of a geophysical survey, the first essential step is the choice of the right technique according to the target of the project. Multidisciplinary cooperation is therefore necessary since the first stages of the project.

Recently the technical community has developed some guidelines for geophysical testing (e.g. Butcher et al., 2005 for down-hole tests). These may fill the gap between textbooks and testing standards or replace the latter, when they are not available for a given method.

The Geological Survey of Canada, issued a guideline for site characterization in terms of shear wave velocity, covering most invasive and non-invasive seismic tests (Hunter and Crow 2012). The Canadian guidelines also include brief coverage of other geophysical techniques that provide complementary information to improve the characterization and the interpretation of seismic tests (Electromagnetic methods, Resistivity methods, Ground penetrating radar, Micro-gravimetric surveys).

Guidelines for the execution and interpretation of single-station passive measurements with the Horizontal-to-Vertical Spectral Ratio (HVSR) technique, also known as Nakamura method, are provided by SESAME (2004).

Guidelines for 1D V_S profiling with surface wave analysis have been developed within the previously mentioned Interpacific project (Foti et al., 2016). These guidelines cover both active (MASW – Multistation Analysis of Surface Waves) and passive (AVA – Ambient Vibration Analysis) methods providing the key elements for the planning and interpretation. The guidelines are addressed specifically to non-expert users, but may constitute a reference for professionals and researchers involved in the field at different levels. The theoretical background is reported in textbooks (Okada 2003, Foti et al. 2014).

Recently COSMOS (Consortium of Organizations for Strong-Motion Observation Systems) has launched an international effort for the development of thorough guidelines covering a variety of seismic methods for site characterization (Yong et al., 2016), focusing on methods from the ground surface.

5 CONCLUSIONS

The role of geophysical tests in site characterization is progressively increasing in the years, as reflected in the proceedings of the series of International Conferences on Geotechnical and Geophysical Site Characterization. Several issues deserve further efforts in research and development:

- Reliability, with the quantification of expected accuracy and precision. Model tests and blind tests are desirable to collect more data on these two issues respectively;
- interaction with lab tests can provide significant synergies that are worth to be exploited more systematically;
- development of joint interpretation at the highest possible level to improve the reliability of the geophysical model that is then reflected on the geotechnical model of the site;
- formulation of shared guidelines that can help in improving the quality of geophysical services.

6 REFERENCES

Abduljauwad, S.N., Ahmed, H.R., Shafiq, M.A. & Abdul-Waheed, M. 2016. Multi-dimensional Electrical Resistivity Tomography (ERT) for the mapping of the cavitated zones in Hofuf KSA. Proc. of 5th Int. Conf. on Geotechnical and Geophysical Site Characterization ISC-5, Gold Coast, Australia, 5-9 september 2016

Amoroso, S., Comina, C., Foti, S. & Marchetti, D. 2016. Preliminary results of P-wave and S-wave measurements by seismic dilatometer test (SPDMT) in Mirandola (Italy). Proc. of 5th Int. Conf. on Geotechnical and Geophysical Site Characterization ISC-5, Gold Coast, Australia, 5-9 september 2016

Archie, G. E., 1942, The electrical resistivity log as an aid in determining some reservoir characteristics: Trans. Am. Inst. Min. Metall. Pet. Eng. 146: 54-62.

Auken, E., & Christiansen A. V. 2004. Layered and laterally constrained 2D inversion of resistivity data: Geophysics, 69, 752–761.

Bazin, S., Anschütz, H., Sauvin, G., Helle, T.E., Gribben, S., Donohue, S. & Long, M. 2016. Geophysical characterisation of clay sites: field and laboratory tests. Proc. of 5th Int. Conf. on Geotechnical and Geophysical Site Characterization ISC-5, Gold Coast, Australia, 5-9 september 2016

Bednarczyk, Z. 2016. Near-surface geophysical scanning for exemplar landslide projects in Poland. Proc. of 5th Int. Conf. on Geotechnical and Geophysical Site Characterization ISC-5, Gold Coast, Australia, 5-9 september 2016

Bergamo, P., Bodet, L., Socco, L.V., Mourgues, R. & Tournat, V. 2014. Physical modelling of a surface-wave survey over a laterally varying granular medium with property contrasts and velocity gradients. Geophysical Journal International 197 (1), 233-247

Biot, M. A. 1956a. Theory of propagation of elastic waves in a fluid-saturated porous solid I. Lower frequency range. J. Acoust. Soc. Am. 28: 168-178.

Biot, M. A. 1956b. Theory of propagation of elastic waves in a fluid-saturated porous solid. II. Higher frequency range. J. Acoust. Soc. Am. 28: 179-191.

Bodet, L., van Wijk, K., Bitri, A., Abraham, O., Côte, P., Grandjean, G., & Leparoux D. 2005. Surface-wave Inversion Limitations from Laser-Doppler Physical Modeling. JEEG, 10(2), 151-162.

Borsic, A., Comina, C., Foti, S., Lancellotta, R. & Musso, G. 2005. Imaging heterogeneities with Electrical Impedance Tomography: laboratory results. Geotechnique, vol. 55 (7), 539-547

Brown, L.T., Boore, D.M. & Stoke, K.H. II, 2002. Comparison of shear-wave slowness profiles at 10 strong-motion sites from noninvasive SASW measurements and measurements made in boreholes. Bulletin of Seismological Society of America, 92 (8), 3116-3133.

Butcher, A., Campanella, R., Kaynia, A., & Massarsch, K, 2005. Seismic cone downhole procedure to measure shear wave velocity - a guideline prepared by ISSMGE TC10. Geophysical Testing in Geotechnical Engineering, Osaka, Japan, XVI Internl. Conference on Soil Mechanics and Geotechnical Engineering.

Callerio, A., Janicki, K., Milani, D., Priano, S. & Signori, M. 2013. Cross-Hole Tests at Zelazny Most Tailings Pond, Poland–Highlights and Statistical Interpretation of Results. Near Surface Geoscience 2013, 19th European Meeting of Environmental and Engineering Geophysics, Bochum, Germany, 9-11 September 2013.

Campbell, N. 2016. An Investigation into the Effects of Material Properties on Shear Wave Velocity in Rocks/Soils. Proc. of 5th Int. Conf. on Geotechnical and Geophysical Site Characterization ISC-5, Gold Coast, Australia, 5-9 september 2016

Castellaro, S. 2016. The complementarity of H/V and dispersion curves. Proc. of 5th Int. Conf. on Geotechnical and Geophysical Site Characterization ISC-5, Gold Coast, Australia, 5-9 september 2016

Comina, C., Foti, S., Musso, G., & Romero, E. 2008. EIT oedometer - an advanced cell to monitor spatial and time variability in soil. Geotechnical Testing Journal, ASTM, vol. 31 (5), DOI: 10.1520/GTJ101367

Comina, C., Cosentini, R. M., Foti, S. & Musso, G., 2010, Electrical Tomography as laboratory monitoring tool. Rivista Italiana di Geotecnica, 44, 15-26.

Comina, C., Foti, S., Sambuelli, L., Socco, L. V., & Strobbia, C., 2002, Joint inversion of VES and Surface Wave data: Proceedings of the SAGEEP, Las Vegas.

Comina, C., Foti, S., Boiero, D., & Socco, L.V., 2011. Reliability of $V_{S,30}$ evaluation from Surface Waves Tests: Journal of Geotechnical and Geoenvironmental Engineering: 137, 6, 579-588.

Cosentini, R. & Foti, S. 2014. Evaluation of porosity and degree of saturation from seismic and electrical data. Geotechnique, ICE, 64 (4), 278-286

Cox, J. 2016. MASW – Filling in the gaps. Proc. of 5th Int. Conf. on Geotechnical and Geophysical Site Characterization ISC-5, Gold Coast, Australia, 5-9 september 2016

Dal Moro, G., 2008, VS and VP Vertical Profiling via Joint Inversion of Rayleigh Waves and Refraction Travel Times by means of Bi-Objective Evolutionary Algorithm: Journal of Applied Geophysics, 66, 15-24.

Dell'Aversana, P., Bernasconi, G., Miotti, F. & Rovetta, D., 2011, Joint inversion of rock properties from sonic, resistivity and density well-log measurements: Geophysical Prospecting, 59, 1144-1154.

Dobróka, M., Gyulai, Á., Ormos, T., Csókás, J. & Dresen, L., 1991, Joint inversion of seismic and geoelectric data recorded in an underground coal mine. Geophyisical Prospecting, 39, 643-665.

Doetsch, J., Linde, N. & Binley, A., 2010. Structural joint inversion of time-lapse crosshole ERT and GPR traveltime data. Geophysical Research letters, 37, L24404.

Eberhart-Phillips, D., Han, D.-H. & Zoback, M. D., 1989, Empirical relationships among seismic velocity, effective pressure, porosity and clay content in sandstone: Geophysics, 54(1), 82-89.

Foti, S., Comina, C., Boiero, D. & Socco, L.V. 2009. Non-uniqueness in surface wave inversion and consequences on seismic site response analyses, Soil Dynamics and Earthquake Engineering, 29(6), 982-993

Foti, S., Hollender, F., Garofalo, F., Albarello, D., Asten, M., Bard, P.Y., Comina, C., Cornou, C., Cox, B.R., Di Giulio, G., Forbriger, T., Hayashi, K., Lunedei, E., Martin, A., Mercerat, D., Ohrnberger M., Poggi, V., Renalier, F., Sicilia, D. & Socco, V. 2016. Guidelines for the good practice of surface wave analysis: a product of the Interpacific project. Submitted to Bulletin of Earthquake Engineering

Foti, S., Lai, C.G., Rix, G.J. & Strobbia C., 2014, Surface Wave Methods for Near-Surface Site Characterization, CRC Press.

Foti, S. & Passeri, F. 2016. Reliability of soil porosity estimation from seismic wave velocities. Proc. of 5th Int. Conf. on Geotechnical and Geophysical Site Characterization ISC-5, Gold Coast, Australia, 5-9 september 2016

Foti, S., Parolai, S., Albarello, D. & Picozzi, M. 2011. Application of Surface Wave Methods for Seismic site characterization, Survey in Geophysics, 32(6), 777-825.

Foti, S., Lai, C.G. & Lancellotta, R. 2002. Porosity of fluid saturated porous media from measured seismic wave velocities. Géotechnique 52(5): 359-373.

Gao, G., Abubakar, A. & Habashy, T. M., 2011. Inversion of porosity and fluid saturations from joint electromagnetic and elastic full-waveform data: 81th SEG annual meeting, Expanded Abstract: 660-665.

Gao, G., Abubakar, A. & Habashy, T., 2010. Simultaneous joint inversion of electromagnetic and seismic measurements: Denver, USA, 80th SEG annual meeting, Expanded Abstract: 2799-2804.

Garofalo, F. 2014. Physically constrained joint inversionof seismic and electrical data for near-surface applications. PhD Dissertation. Politecnico di Torino, Italy.

Garofalo, F., Foti, S., Hollender, F., Bard, P.Y., Cornou, C., Cox, B.R., Ohrnberger, M., Sicilia, D., Asten, M., Di Giulio, G., Forbriger, T., Guillier, B., Hayashi, K., Martin, A., Matsushima, S., Mercerat, D., Poggi, V. & Yamanaka, H. 2016a. InterPACIFIC project: Comparison of invasive and non-invasive methods for seismic site characterization. Part I: Intra-comparison of surface wave methods. Soil Dynamics and Earthquake Engineering, 82: 222-240.

Garofalo, F., Foti, S., Hollender, F., Bard, P.Y., Cornou, C., Cox, B.R., Dechamp, A., Ohrnberger, M., Perron, V., Sicilia, D., Teague, D. & Vergniault, C. 2016. InterPACIFIC project: Comparison of invasive and non-invasive methods for seismic site characterization. Part II: Inter-comparison between surface-wave and borehole methods, Soil Dynamics and Earthquake Engineering, 82: 241-254.

Haber, E. & Oldenburg, D., 1997, Joint inversion: a structural approach: Inverse Problems, 13: 63-77.

Hadamard, J. 1902. Sur les problèmes aux dérivées partielles et leur signification physique. Princeton University Bulletin: 49–52.

Hu, W., Abubakar, A. & Habashy, T. M., 2009, Joint electromagnetic and seismic inversion using structural constraints: Geophysics, 74(6): R99-R109.

Hughes, C.G.C., Watson, M. & Read, K. 2016. Use Of GPR On Two Sites With Voids To Enable Safer Work And Targeted Probing. Proc. of 5th Int. Conf. on Geotechnical and Geophysical Site Characterization ISC-5, Gold Coast, Australia, 5-9 september 2016

Hunter, J.A. & Crow, H.L. (ed.), 2012. Shear Wave Velocity Measurement Guidelines for Canadian Seismic Site Characterization in Soil and Rock; Geological Survey of Canada, Open File 7078, 227 p., doi:10.4095/291753

Jafarzadeh, F., Banikheir, M., Shahrabi, M.M., Garakani, A.A., & Eskandari, N. 2016. Assessment of Underground Karst Caves Using Geophysical Tests (Case Study: Lajamgir Dam Site, Iran). Proc. of 5th Int. Conf. on Geotechnical and Geophysical Site Characterization ISC-5, Gold Coast, Australia, 5-9 september 2016

Jamiolkowski, M. 2012. Role of Geophysical Testing in Geotechnical Site Characterization. *Soils and Rocks* 35(2): 117-137.

Jung, J.S., Sim, Y., Park, J.B. & Park, Y.B., 2012. A comparative study on borehole seismic test methods for site classification. LHI Journal, 3 (4), 389-397.

Kim, D.S., Park. H.J., Bang. E.S., 2012. Round Robin Test for Comparative Study of In-Situ Seismic Tests. In: Geotechnical and Geophysical site Characterization, 4, 1427-1434, Leiden (NL), CRC Press, Mayne R. Q., Coutinho P. W.

Lai, C.G., Foti. S., & Rix, G.J. 2005. Propagation of data uncertainty in surface wave inversion. Journal of Environmental and Engineering Geophysics 10(2): 219-228.

Malehmir, A., Socco, L.V., Bastani, M., Krawczyk, C.M., Pfaffhuber, A.A., Miller, R.D., Maurer, H., Frauenfelder, R., Suto, K., Bazin, S., Merz, K. & Dahlin, T. 2016. Near-Surface Geophysical Characterization of Areas Prone to Natural Hazards: A Review of the Current and Perspective on the Future. In L. Nielsen (Ed.) Advances in Geophysics, 51–146.

Fuiji, M., Watanabe, K., Fukaya, T. & Takechi, K. 2016. Soil discrimination using an electrical logging method. Proc. of 5th Int. Conf. on Geotechnical and Geophysical Site Characterization ISC-5, Gold Coast, Australia, 5-9 september 2016

Mota, R. & Monteiro Santos, F. A. 2010. 2D sections of porosity and water saturation from integrated resistivity and seismic survey: Near Surface Geophysics, 8: 575-584.

Musso, G., Cosentini, R. M., Foti, S., Comina, C. & Capasso, G. 2015. Assessment of the structural representativeness of sample data sets for the mechanical characterization of deep formations. Geophysics 80(5): D441-D457.

Okada, H., 2003. The microtremor survey method. Geophysical Monograph series, 12, Society of Exploration Geophysics.

Pfaffhuber A.A., Anschütz, H., Ørbech, T., Bazin, S., Lysdahl, A.O.K., Vöge, M., Sauvin, G., Waarum, I.-K., Smebye, H. C., Kåsin, K., Grøneng, G., Berggren, A.-L., Pedersen, J. B. & Foged, N. 2016. In-situ detection of sensitive clays from a geophysical perspective. Proc. of 5th Int. Conf. on Geotechnical and Geophysical Site Characterization ISC-5, Gold Coast, Australia, 5-9 september 2016

Piatti, C., Socco, L. V., Boiero, D. & Foti, S., 2013, Constrained 1D joint inversion of seismic surface waves and P-refraction travel times: Geophysical Prospecting, 61 (1): 77-93.

Porres-Benito, J.A., Ibanez, S.J., Ortiz-Palacio, S. & López-Ausín, V. 2016. Fractures location on karstified limestone surfaces by Electrical Resistivity Tomography Characterization. Proc. of 5th Int. Conf. on Geotechnical and Geophysical Site Characterization ISC-5, Gold Coast, Australia, 5-9 september 2016

Reynolds, J.M. 1997. An introduction to applied and environmental geophysics, Wiley.

SESAME team, 2004. Guidelines for the implementation of the H/V spectral ratio technique on ambient vibrations: measurements, processing and interpretation (Deliverable No. D23.12), WP12. SESAME European research project.

Socco L.V., Boiero D., Foti S., Wìsén R. 2009. Laterally constrained inversion of ground roll from seismic reflection records. Geophysics, SEG, 74, G35-G45

Socco, L., S. Foti and D. Boiero, 2010. Surface wave analysis for building near surface velocity models: established approaches and new prospectives, Geophysics, 75(5), A83-A102.

Stokoe, K.H. II & Santamarina, J.C. 2000. Seismic-wave-based testing in geotechnical engineering, GEOENG 2000, Melbourne, Australia, 19-24 Nov., CD-Rom

Tarantola, A., 1987, Inverse Problem Theory: Methods for data fitting and model parameter estimation. Elsevier Science Publisher.

Tikhonov, A.N. & Arsenin, V.Y. (1977). Solutions of Ill-Posed Problems. New York: Winston. ISBN 0-470-99124-0.

Vozoff, K. & Jupp, D.L.B., 1975. Joint inversion of geophysical data. Geophysical Journal of the Royal Astronomical Society, Volume 42, pp. 977-991.

Wisén, R. & A. V. Christiansen, 2005, Laterally and mutually constrained inversion of surface wave seismic data and resistivity data: JEEG, 10, 251-262.

Xia, J., Miller, R.D., Park, C.B., Hunter, J.A., Harris, J.B. & Ivanov, J, 2002. Comparing shear-wave velocity profiles inverted from multichannel surface wave with borehole measurements. Soil Dynamics and Earthquake Engineering, 22, 181-19.

Yong A. et al. 2016. A progress report on the development of the COSMOS International Guidelines for Applying Noninvasive Geophysical Techniques to Characterize Seismic Site Conditions. Proc. of American Geophysical Union (AGU) Fall Meeting, San Francisco.

Geotechnical and Geophysical Site Characterisation 5 – Lehane, Acosta-Martínez & Kelly (Eds)

Session Report: Geophysics, 2

Koya Suto
Terra Australis Geophysica Pty Ltd, Brisbane, Queensland, Australia

ABSTRACT: This report outlines seven papers presented in the geophysics sessions in the Fifth International Conference on Geotechnical Site Characterisation (ISC'5) held in Gold Coast, Australia on 5 to 9 September 2016. Twenty-five papers were presented in the geophysics sessions and the eight papers selected for this report are in application of the seismic and airborne electromagnetic methods, and development of new equipments. These research, case history and development papers represent recent effort of site characterization using the geophysical methods.

1 INTRODUCTION

The geophysical techniques are applied to all scales of investigation of the earth from large scale such as the interior of the earth and earth's crust to small scale like surface rocks and soil. They are primarily developed for petroleum and minerals exploration because of its economic interest. They are also applied to geotechnical and environmental problems. This engineering geophysics is perhaps the smallest in scale of the geophysical applications (Table 1).

Table 1 Category of Geophysics by scale

Geophysics	Scale	Range
Solid Earth Geophysics	Huge	<6400 km
Crustal Geophysics	Large	10-50 km
Exploration Geophysics	Medium	<10 km
Engineering Geophysics	Small	<100m

Geotechnical engineers often address these techniques collectively as "geophysics", in such a phrase as "we applied geophysics". Such an expression is vague and it is best to avoid. Geophysics is indeed a group of physical survey techniques to investigate a variety of physical properties of the earth. For example, the magnetic survey investigates distribution of magnetic properties such as magnetic susceptibility and magnetic permeability; the gravity survey for distribution of mass; and seismic survey for velocity of various seismic waves.

A comprehensive manual of geophysics for engineering application by Society of Exploration Geophysicists of Japan (2014) explains twenty geophysical methods for engineering application including ground, offshore, airborne and downhole surveys.

The geophysical parameters obtained from geophysical surveys are physical properties of the ground. They have physical dimensions and they are analytically interrelated through physical observations and mathematical manipulation. On the other hand, geotechnical parameters are often stand alone, and relationships among them are generally derived empirically. Relationship between the engineering parameters and physical parameters are also deduced empirically, and there are always discrepancy between the parameters inferred from an empirical formula and values from actual measurement. This is because the geotechnical engineering deals with the parameters influenced by multitude of factors, some can be physically quantified and others are impossible to quantify. Therefore an attempt to relate a physical parameter to a geotechnical parameter is like looking at two-dimensional cross section of multi-dimensional space. Yet, geophysics can contribute to geotechnical site characterisation through physical properties.

In the Fifth International Conference on Geotechnical and Geophysical Site Characterisation (ISC'5), twenty-five papers were selected for presentation. Eight of the presentations are accepted to present. However one presenter failed to appear at the conference and it is omitted from the review in this report. The majority of the papers reviewed are on the seismic methods, with which the present author is familiar (Table 2).

Table 2. Papers reviewed in this report by classification of techniques.

Seismic	Surface	onshore	Sathwik, et al.	MASW Parameter study
			Heymann et al.	New inversion algorithm of MASW data - model test
			Lin & Lin	Proposal of data acquisition method for MASW
		offshore	McGrath et al.	Case study of offshore application of MASW
	Crosshole		Sylvain, et al.	Hardware development / test
			von Ketelhodt et al.	development / experiment
	Lab measurement		Look et al.	Testing new equipment
Electro-magnetic	Airborne		Pfaffhuber et al.	Application case history

2 SUMMARY OF PAPERS

2.1 Onshore MASW

Heymann, *et al.* (2016) points out inversion of dispersion of surface waves is an ill-posed problem, as is geophysical inversion generally is. In attempt to circumvent the problem and to reach an accurate inversion result the authors proposes a procedure called "partial least squares regression". They

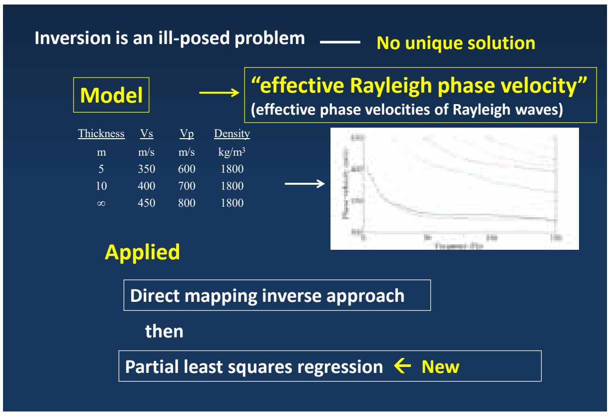

Figure 1. Modelling procedure of Heymann (2016).

examined the process by applying it to a three-layer model using the "direct mapping inverse approach" first, which saves computation time (Figure 1). Their result showed: a) if the thicknesses of the layers of the model is known *a priori*, the S-wave velocities (Vs) of the three layers are predicted within 1% accuracy; b) If the Vs of the layers of the model are known *a priori*, the thicknesses are also predicted to about 5-8% accuracy; while c) both Vs and thicknesses are to be predicted the inversion result presents errors around 5% in Vs and 10% in thickness with right set of inversion parameters.

Lin & Lin (2016) tackles the aliasing problem in SASW data by using the MASW method (Figure 2).

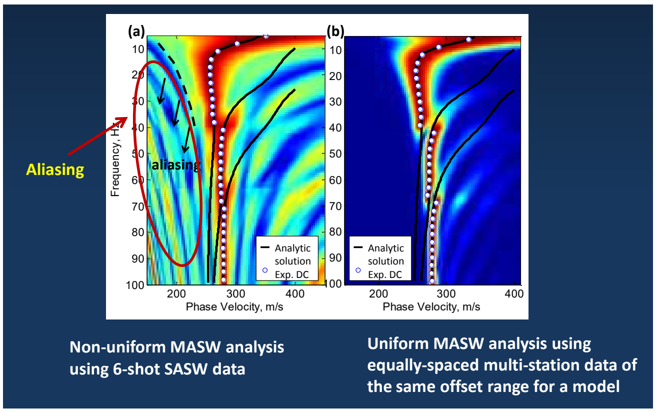

Figure 2. Aliasing problem in SASW in comparison with uniform MASW display in the frequency-velocity domain

This method, while reduces aliasing, trades off the spatial resolution by using a long geophone array. To achieve a good spatial resolution, it is necessary to increase offset range. Their solution is to use multiple shots to a geophone array (Figure 3). This achieves a wide bandwidth necessary to improve probe depth while not compromising the aliasing problem.

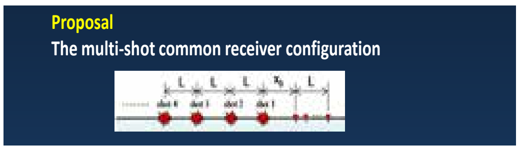

Figure 3. Proposed configuration of multi-shot common receiver survey

2.2 Offshore MASW

McGrath *et al.* (2016) is a case history of an offshore MASW survey near Dublin, Ireland. It deployed a water bottom cable and airgun on the floor (Figure 4).

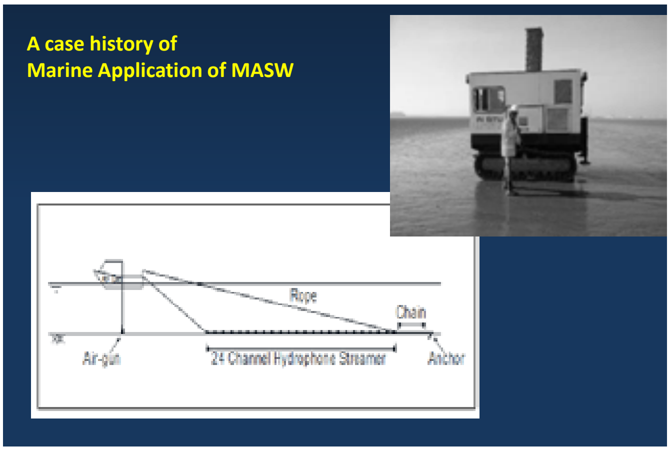

Figure 4. Schematic diagram of marine MASW configuration and field photo

The subsurface is made of 3 to 9.5 metres of alluvium clay, gravels, sands and marine deposits overlying glacial till and bedrock. The result was compared with the CPT and SCPT (Figure 5) and found good correlation with MASW's ability to probe deeper than SCPT can in this situation. The MASW could profile deeper than SCPT. This case study demonstrated validity of MASW survey and repeatability of the results.

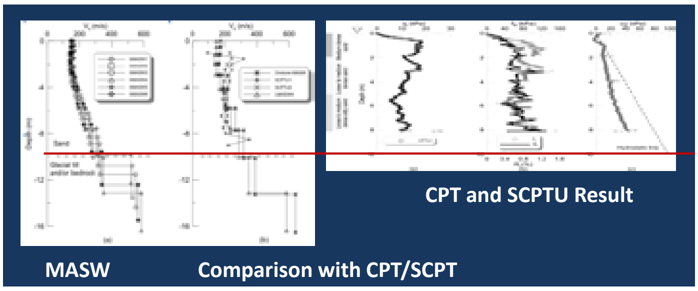

Figure 5. Comparison between under-water MASW and CPT and SCPT

2.3 Crosshole Tomography

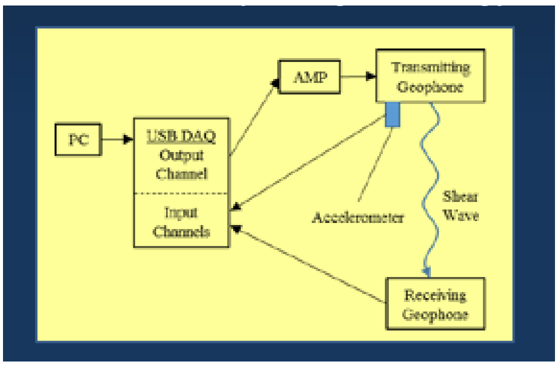

Figure 6. Components of crosshole testing system

Sylvain *et al.* (2016) created a new tool for crosshole tomography (Figure 6). Using the 3D printing technology for its housing of transmitter and receiver and selection of material resulted in a low-cost but reliable system. They tested the system in a backfilled sand pit (Figure 7) and compared with MASW, SCPT and DMT. The result was presented in detail in their extended abstract in this volume (McGrath *et al.*, 2016).


Figure 7. Backfilled test pit 3m x 3m x 3m

An experiment on crosshole tomography using both P- and S-waves was carried out by von Ketelhodt, *et al.* (2016). They also developed a new three-component data acquisition system. With the velocity data of both P- and S-waves, shear modulus, Young's modulus, bulk modulus and Poisson's ratio can be calculated in the two-dimensional plane between the boreholes. The experiment revealed that S-wave tomography has a better resolution than P-wave tomography.

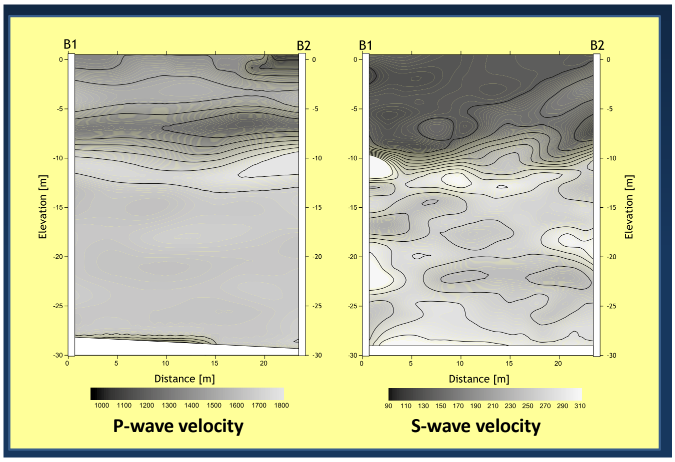

Figure 8. Comparison between P- and S-wave tomography

2.4 Laboratory Measurement

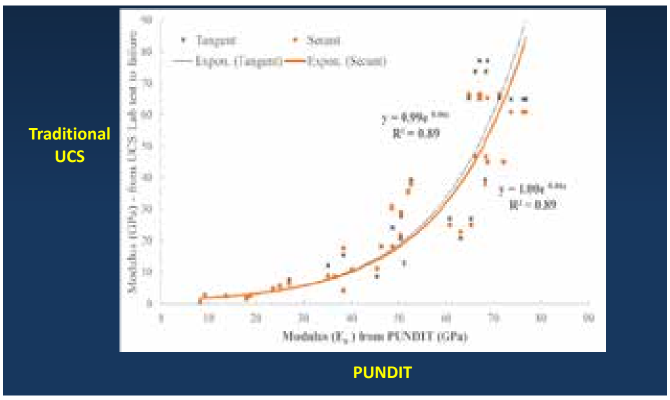

Figure 9. Comparison between results by "traditional" UCS and by PUNDIT.

Look, *et al.* (2016) attempted to improve the conventional method of measuring uniaxial compressive rock strength (UCS) and Young's modulus (E), which is time-consuming and expensive, by devising ultrasonic pulse velocity testing technique (PUNDIT). This is a non-destructive testing method. They found a significant correlation between the results of this new method and "traditional" UCS testing (Figure 9).

2.5 Application of Airborne Electromagnetic Survey

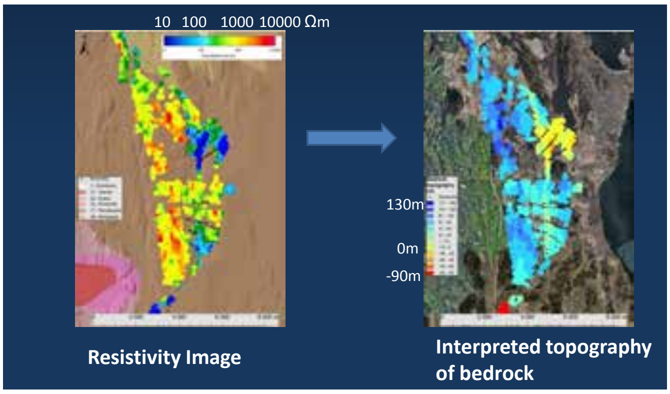

Figure 10. Map image of electric resistivity from AEM and its interpretation to depth of bedrock.

Pfaffhuber *et al.* (2016) presented a case history of application of airborne electromagnetic (AEM) survey to planned railway alignment in Norway. The area is known to have problem of quick clay. As well as relief of the bedrock from AEM data (Figure 10), they managed to detect and map the quick clay (Figure 11).

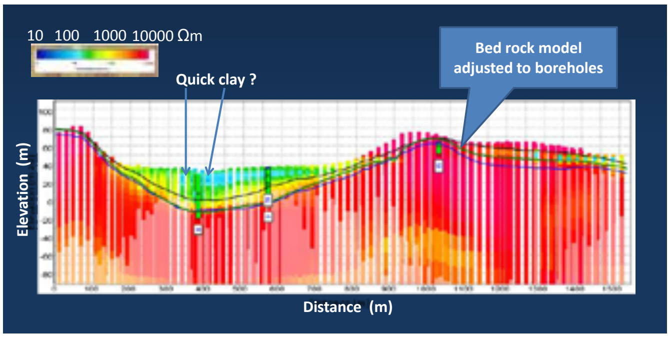

Figure 11. Resistivity cross section along the railway alignment.

3 CONCLUSION

Seven papers presented in geophysics sessions at the Fifth International Conference on Geotechnical Site Characterisation are reviewed. These represent recent efforts all over the world to apply geophysical methods to geotechnical characterization. They include development of algorithm and software, making new hardware, and application case history. These made a significant contribution to site characterisation using geophysical techniques.

4 REFERENCES

Heymann G., Wilke D.N. & Kok S., 2016, Inversion of Effective Phase Velocity Seismic Surface Wave Data by Partial Least Squares Regression, *Proc Fifth International Conference on Geotechnical Site Characterisation (ISC'5), Gold Coast, Australia, 5-9 September 2016.*

Lin, C.P. & Lin, C.H., 2016, Generalization and Standardization of Multi-station Surface Wave Method for Site Investigation. *Proc Fifth International Conference on Geotechnical Site Characterisation (ISC'5), Gold Coast, Australia, 5-9 September 2016.*

Look, B., Schneider, S. & Chaminda Gallage, C, 2016, Characterisation of Small Strain Rock Modulus From Ultrasonic Pulse Velocity Testing. *Proc Fifth International Conference on Geotechnical Site Characterisation (ISC'5), Gold Coast, Australia, 5-9 September 2016.*

McGrath T., Long M., O'Connor, P., Trafford, A. & Ward D., 2016, Multichannel Analysis of Surface Waves (MASW) for Offshore Geotechnical Investigations. *Proc Fifth International Conference on Geotechnical Site Characterisation (ISC'5), Gold Coast, Australia, 5-9 September 2016.*

Pfaffhuber, A. A., Anschütz, H., Ørbech, T., S. Bazin, A. Lysdahl, O. K., Vöge, M., Sauvin, G., Waarum, I.-K., Smebye, H. C., Kåsin, K., G. Grøneng, Berggren, A.-L., Pedersen J. B. & Foged, N., 2016, Regional Geotechnical Railway Corridor Mapping Using Airborne Electromagnetics. *Proc Fifth International Conference on Geotechnical Site Characterisation (ISC'5), Gold Coast, Australia, 5-9 September 2016.*

Society of Exploration Geophysicists of Japan (*ed.*), 2014, Application manual of geophysical methods to engineering and environmental problems. *661pp.* European Association of Geoscientists and Engineers, Houten, Netherlands

Sylvain, M.B., Pando, M.A., Whelan, M.J., Ogunro, V.O. & Park, Y. 2016, Design and application of a low-cost, 3D printed crosshole seismic system- Preliminary assessment. *Proc Fifth International Conference on Geotechnical Site Characterisation (ISC'5), Gold Coast, Australia, 5-9 September 2016.*

von Ketelhodt, J.K. Fechner, T. & de Kleine, M.P.E., 2016. S-wave borehole tomography for geotechnical site characterization. *Proc Fifth International Conference on Geotechnical Site Characterisation (ISC'5), Gold Coast, Australia, 5-9 September.*

Geotechnical and Geophysical Site Characterisation 5 – Lehane, Acosta-Martínez & Kelly (Eds)
© 2016 Australian Geomechanics Society, Sydney, Australia, ISBN 978-0-9946261-1-0

Session Report: Case Histories, 1

S. Buttling
National Geotechnical Consulting, PO Box 6342, Yatala, Queensland 4207

ABSTRACT: This session report covers three sessions all of which are described as Case Histories, with one session covering Foundations, one on Ground Improvement, and one on Settlement. In total 10 papers are covered by this report but, since the basic theme of the conference is Site Characterisation, they have been grouped by the reporter in order of how much emphasis has been placed on, and how much relevance attaches to, site characterisation.

1 PAPER REVIEWS

The first paper considered is the one by *Premstaller*, describing a project in Austria on the shores of the Zell am See. A deep basement was required to be constructed right next to an existing hotel to create underground car parking, and initial conventional thoughts were that 10 boreholes would be necessary. However the author carried out a desk study which showed that the site was contained within an alluvial fan, shown in Figure 1, and also produced may previous borehole logs. This allowed the author to characterise the site based ion that pre-existing data, and have a very good idea of the nature of the soils to be expected which, in turn, meant that he could reduce the new investigation to only two CPT profiles.

Figure 1. Alluvial delta with existing investigations from *Premstaller*

This would appear to be a very efficient way of characterising this particular site. The CPT profiles were processed through commercial interpretation software, and showed very uniform conditions over the 25 m depth, which must have contributed to the successful use of jet grouted columns to create retaining walls and to underpin adjacent structures.

The second paper, by *Failmezger, Sedran and Marchetti*, demonstrates the advances that have been made in site characterisation in the last 75 years although, unfortunately, many sites do not take advantage of them as much as this one. The work was done for a replacement highway bridge and, when the original bridge was constructed in 1939, the soil was tested in situ by driving a 25 mm diameter steel pipe with a 68 kg drop hammer, obviously predating the SPT. The river bed conditions being investigated for the foundations of the new bridge comprised about 15 m of mud and very soft to soft clay overlying stiff to hard clay, and this time appropriate techniques were used for the varying soil conditions.

Conventional drilling with telescopic casing was used to deal with issues from the floating barge, the depth of water, and the very soft seabed, and SPT tests were carried out. IN addition a fixed piston sampler was used to retrieve samples of the very soft and soft clays, with a Denison piston sampler used for the stiff to hard clays. Within the standard boreholes pressuremeter testing (PMT) was also carried out, with a monocell pressuremeter, which was calibrated for both membrane resistance and system compressibility. Vane shear testing was also carried out, with a large vane in the very soft to soft clays, but even the smallest vane exceeded the available torque in the stiff to hard clays.

A direct push seafloor system was used to push CPT cones and DMT probes, without needing to worry about buckling in the string through the water. However, the mud and soft clay provided so little resistance that the cone had to be supported in order to penetrate at 20 mm/s, and the limited lateral restraint was generally a constraint on the testing, which reached depths of 30 to 41 m against a target of 55 m. DMT testing was also carried out, and a lot of details are provided of the special drilling techniques used to reach the required depths.

Seismic tests were also carried out with the DMT seismic module, determining the shear wave velocity profile, from which shear modulus could be calculated for comparison with the empirical relationships with DMT pressures and cone resistances, and also the results of the PMT tests, as shown in Figure 2.

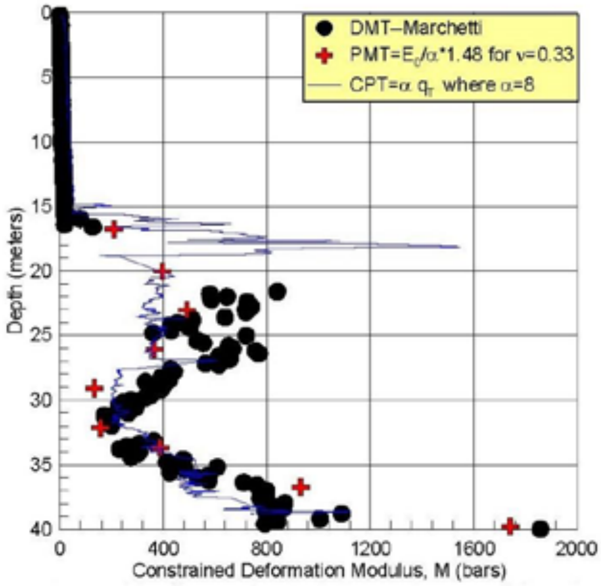

Figure 2. Constrained modulus determined by various methods, from *Failmezger et al*.

Another of the more detailed papers with regard to site characterisation is that by *Schofield*, who was involved with a housing development over a brownfield site in Melbourne. The profile consisted of demolition debris, some of which was contaminated from the previous industrial use, over compressible soils including recent deposits and the infamous Coode Island Silt. This was carefully investigated with CPTu and DMT testing (see Figure 3), together with some rapid dissipation tests to examine permeability. The proposed treatment to allow construction of 3 storey housing without the need for piled foundations included High Energy Impact Compaction for the demolition fill and Port of Melbourne Sands, where present, and surcharge loading to consolidate the softer sediments.

Obstructions within the site formed by old piled foundations were a potential problem, also dealt with by surcharge loading. A trial was carried out on a test pad, which confirmed the rates of consolidation predicted from the rapid dissipation tests, which in any event covered a range of three orders of magnitude.
To check the success of the HEIC method, post treatment CPT cone tip resistances were compared with pre-treatment values, and in addition geophysical testing was carried out both before and after treatment using the MASW signal processing technique.

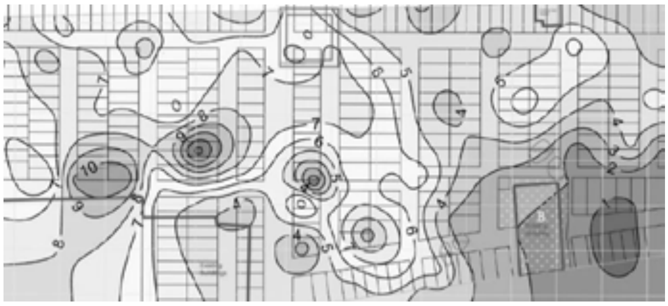

Figure 3. Thickness (m) of CIS with CPT qt < 1 MPa, from *Schofield*

Although this is an interesting paper, and a saving of about $10 million in foundation costs is claimed by avoiding piles for the 300 townhouses, there remain some questions about the surcharge loading. OCR values were derived from the CPT testing and from the DMT testing, and gave values of about 2. It is not clear whether this applies to the upper compressible layer of Unnamed Recent Alluvium, which appears to be between 2.5 and 3.5 m below the site surface, or to the Coode Island Silt which was deeper but up to 13 m in thickness. The author also states that the test pad applied a surcharge pressure of 50 kPa, which is on the low side for surcharges but plausible. However, it is then stated twice in the paper that the actual surcharge was originally planned at 7.5 kPa for a period of 9 months, which does not seem to be reasonable, as this is unlikely to have exceeded the pre-consolidation pressure with an OCR = 2. It was later stated that the surcharge pressure was increased to 20 kPa and then to 45 kPa, which would have a better chance of exceeding the p'_c, although surcharge periods were correspondingly reduced to only 1 month, which could be possible with high horizontal permeability. The suggestion that exceeding p'_c will lead to an increase in t90 also indicates some confusion since , generally, exceeding p'_c will lead to a change from C_s to C_c which will influence the magnitude of the consolidation, but will not automatically affect c_v and c_h which control the rate of consolidation and the time factor.

Although all four papers reported on here deal with case histories of foundations, they are very different from each other in so far as one deals with micro-piles, one with a deep excavation, one with design of bored and driven piles, and one with foundations on rock. This last, by *da Silva and Coutinho*, also looks at site characterisation by both geophysical and mechanical methods, in order to build geological and geophysical models, in some complex geological conditions in Brazil where tropical weathering can extend to depths of 50 m below the "top of rock". It is noted that this is not within the experience of engineers working in temperate climates, but can have a profound effect on the performance of deep foundations in tropically weathered zones, such as South America, Australia, southern Africa and South East Asia. The paper points out that classification of weathering alone is necessary but not sufficient as it oversimplifies the relevant factors.

On the site which is the subject of the paper, investigative holes were drilled using conventional techniques, and also with "a rock drill, normally deployed for rock blasting". This is taken to mean a rotary percussive drill, typically mounted on an air driven tracked rig. This sort of drilling is especially useful in weathered rock profiles, where the presence of boulders formed as corestones can be very misleading, especially with regard to the founding level of bored piles. In previous times, before they were outlawed by health and safety regulations, the toe level of hand dug caissons was generally confirmed by rotary percussive drilling through the base to confirm that the exposed rock was massive, and not a floating corestone.

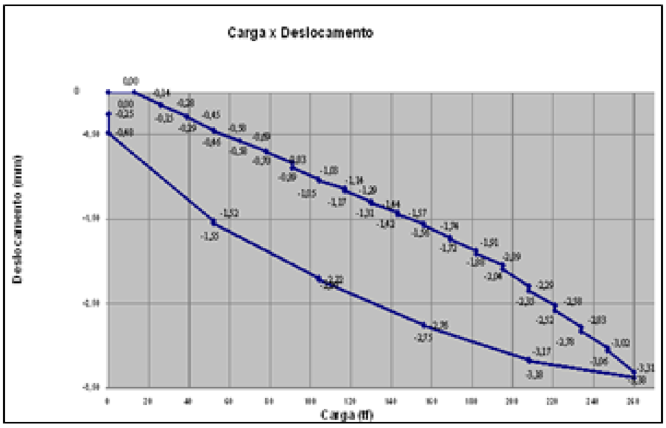

Figure 4. Load settlement curve for rock socket from *Silva et al*.

From the laboratory test results it is inferred that there is a relationship between porosity and strength, suggesting that porosity is an indicator of weathering, while absorption is an indicator of the variability of the rock mass. The results of the "rock drilling" are also compared with the conventional drilling, and found to have a reasonable correlation.

These results were then considered in relation to the design of rock socketed piles, and compared with the results of a static load test and also a dynamic load test. The working load of the pile was 130 tonnes, with a length of 10 m of which half was the rock socket, and two diameters were given, 410 and 300 mm, the latter assumed to apply to the rock socket.

The test load was taken up to twice the working load and, as might be expected for a rock socketed pile, there was no indication of reaching failure or even yield, with a final pile head displacement of only 3.38 mm, and a residual settlement after all load had been removed of only 0.25 mm, as seen in Figure 4. If half of the load were carried in the soil and the other half at the base of the rock socket, the elastic shortening alone might be expected to be about 6 mm.

The dynamic load test verified an ultimate capacity in excess of 350 tonnes, but this was still at a theoretical displacement of only 9 mm, which could not be considered a true ultimate capacity for a 410 mm diameter pile. The test had to be stopped because of excessive compressive stress on the pile from the 3780 kg drop weight causing damage. It would appear that more dynamic tests were carried out, but these were not reported other than saying that 86% of those tested showed an ultimate capacity of twice the working load, with the remaining 14% close to this value, and all at relatively small displacements. Reference is made to possible savings in piling cost by reducing rock socket penetration, but these are not quantified or applied, nor is it explained how these may be related to the "rock drilling".

The paper by *Buttling* looks at pile design using two limit state design standards, the European Standard often known as EC7, and the Australian Standard AS 2159-2009. It does so though examining two separate case histories, one in Bangkok using a lot of deep bored piles under a common mat foundation for three high-rise towers, and one in Queensland using driven precast piles for structures within a water treatment plant. Because these are past projects, and because there is a reasonable amount of soil and pile testing data available for both, it has been possible to "wind the clock back" and carry out the design according to several of the available methods within each standard, and thereby to compare the outcomes.

OneOne of the aspects that makes this difficult with regard to EC7 is that it is, in effect, an incomplete code since, in order to deal with conflicting requirements from different nation states within Europe, it requires a number of matters to be dealt with in National Annexes, which makes the standard, in effect, unique to each country. The author, not practising in any of these countries, was not experienced in the use of any National Annex, so opted to apply the blanket requirements of the base document.

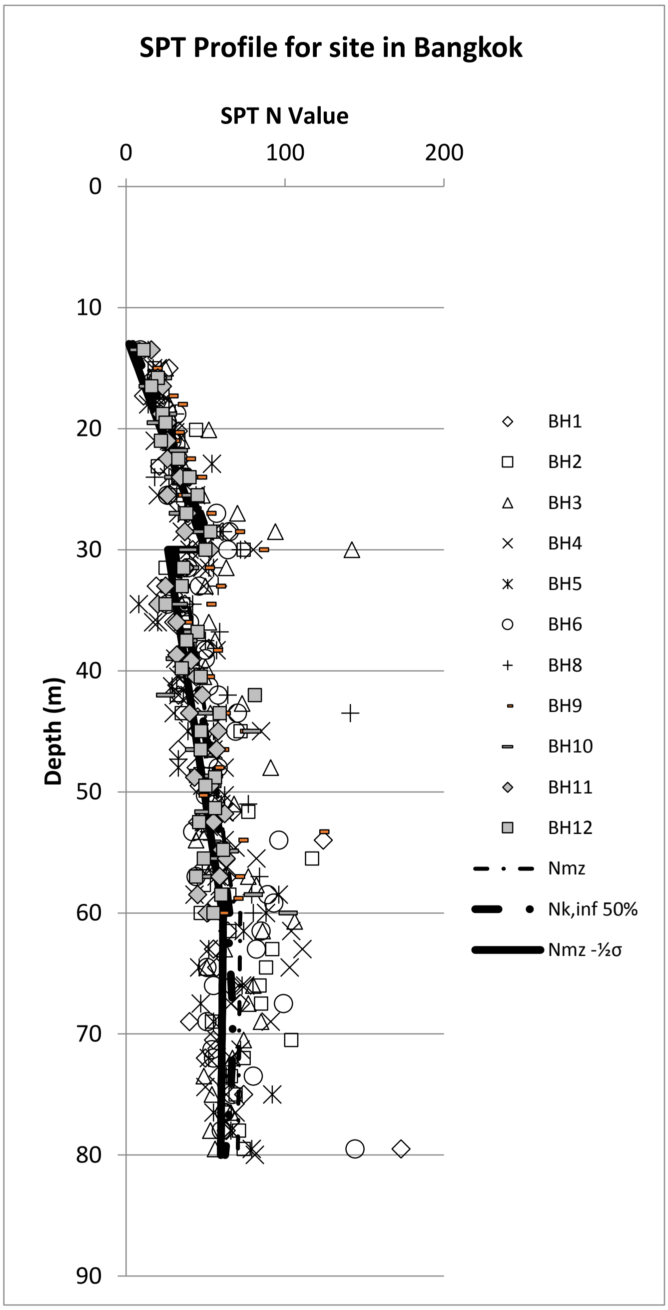

Figure 5. SPT profile for Bangkok site from *Buttling*.

The site in Bangkok was characterised with SPT N values, which seems to be unfortunately common in everyday practice, in spite of the excellent advanced methods being discussed at this conference. CPTu testing was also available, but could not penetrate to the depths required for large diameter bored piles. Since Bangkok has been subject to a lot of major development in the last 40 years, not only of high-rise buildings but also significant amounts of infrastructure, especially elevated expressways, there has been a very useful amount of soil investigation and pile testing carried out, and a lot has been published in regional conferences and by the Asian Institute of Technology. This has allowed the development of local empirical rules relating shaft friction to SPT N value, for example, based on a significant database of experience.
Comparisons are made between the use of individual boreholes in design, the "model pile method", and the use of borehole data to determine design lines which are then applied across the site. They are also made for design using static load tests, since several were available. It is found that all methods gave very comparable results, with appropriate cognisance being given to increased uncertainty.
The EC7 methods were then also applied to the project from Queensland. In this CPT testing was also available from the site, but not over the depth required to provide founding support for driven piles. There was also no static load testing, although there were 15 dynamic load tests, 5 of which were subject to signal matching (CAPWAP) analysis. Again the results of different methods were found to be reasonably comparable.
AS 2159-2009 was then applied to the same two projects, although strict comparisons are difficult because of the differing load factors used associated with the two standards. The Australian Standard appeared to give higher design resistances, as shown by Table 1:

The next paper in this group is quite unusual with regard to site characterisation, since it does not relate to any particular site, but rather to the characterisation of sites in general. It is the paper by *Barvashov and Boldyrev*, which makes strong reference to the limited volume of soil affected by a foundation which is normally sampled, suggested at less than 10^{-6}, and also to the small fees typically paid for soil investigation, which, it is suggested, are between 5 x 10^{-4} and 1 x 10^{-3} of the construction cost. While the reporter acknowledges that these sort of proportions may well be applicable to projects in Russia, and notes that he has been admonished for suggesting a spending of 1.7 x 10^{-3} on site investigation for a capital infrastructure project here in Australia was excessive, and that 5 x 10^{-4} should have been enough, he also believes that interpolation between investigation points is a perfectly acceptable and recognised international practice, and does not justify description as "inflation".

Table 1: Comparison of the results from the two codes

Site	With or without testing	Code	
		EC7 – $R_{c,k}$ (kN)	AS2159 – $R_{d,ug}$ (kN)
Bangkok	No testing	11,526	12,464
	With static load testing	11,434	15,277
	With dynamic testing	14,736	20,630
Queensland	No testing	2,121	2,379
	With dynamic testing	2,017	2,017

In relation to the prediction of settlement of structures, the paper goes on to suggest a statistical approach to building on a heterogeneous soil. The profiles of E, c' and φ' proposed are as shown in Figure 6, but it is noted that, while the profile of E seems to be similar to some real data from DMT testing, included in the data to show heterogeneity, the other data has been randomly generated because "real data" was not available.

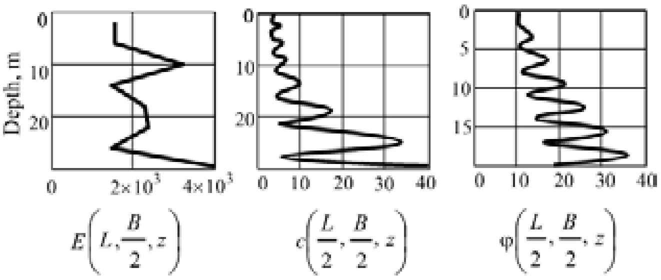

Figure 6. Vertical profiles of E, c' and φ' used in *Barvashov et al.*

A number of problems seem to exist with this concept. One is that it is based on Winkler springs, as commonly used by structural engineers in conjunction with structural models, but which fail to take account of the continuum which is soil. Another is that, in the random generation of data, no account has been taken of correlation distance so that both c' and φ' are seen to oscillate about their mean values in an unrealistic manner.

It is also worthy of note that, while the authors are scathing of geologists and geotechnical engineers who interpolate between measured points, referring to it as inflation, they seem quite happy to accept extrapolation in values of subgrade modulus, a process generally regarded as much less safe than interpolation. They apply their method to the determination of tilt along two axes of a theoretical 20 x 40 m structure creating a load of 300 kPa, with either 5 boreholes (one at each corner and one in the centre) or 9 boreholes (3 x 3), but appear to show that, while the predicted tilt in the X-direction for 9 boreholes is about 2/3 of that for 5 boreholes, in the Y-direction it is 5 times greater. This defies logic and, while the application of statistical methods to geotechnical engineering in general and site characterisation in particular is to be applauded, there seems to be quite a lot of additional work required before this method could be applied in practice.

A form of ground improvement using granular inclusion is described in the paper by *Unver*, based on a conceptual design for a proposed project in Turkey. The shopping centre is planned to have 12 separate blocks of varying proportions but only a single storey. Unfortunately the site characterisation in this case must be considered below standard. The main issue has been the very soft nature of a layer of clay between 4 and 9 m in thickness beneath the site. Unfortunately, as too often happens in these situations, the site investigation appears to have been carried out with more consideration of cost than of the value of the data obtained. As a result the Standard Penetration Test was used, with 18 out of 25 test results giving an N value of zero, which is also equal to the value of the information. It is worthy of note that the weight of one standard rod, together with the anvil and a split spoon, even without the hammer placed on the anvil, will produce an end-bearing pressure of nearly 350 kPa, which will require an undrained shear strength of between about 35 and 65 kPa to resist penetration, depending on whether the bearing capacity is nearer to 5 or 9. As soon as the hammer is placed on the anvil, prior to lifting, the required undrained shear strength increases to between 75 and 125 kPa. It is therefore clearly not possible to estimate the undrained shear strength of very soft and soft soils using this test, so it is also not possible to presume an undrained shear strength of "5 – 10 kPa at most". Many of the in situ tests to be discussed at this conference will give much more meaningful results, and it is to be hoped that, in the further investigation "using more advanced site investigation techniques" proposed for the final design stage, such test methods will be employed.

Given the very low presumption of undrained shear strength, it is not surprising that conventional stone columns, which rely on some confining pressure coming from the surrounding soil (Greenwood and Kirsch, 1983), were found to provide insufficient bearing capacity even for the single storey buildings. Unver has therefore proposed to post-grout the columns to create a form of pile, about 60 cm in diameter, and relying upon the end-bearing on the underlying stiff strata for support.

The layer of soft clay will also be subject to considerable settlement under both the building load and also the weight of about 2 m of fill to be placed over surrounding areas to raise the ground levels. *Unver* has calculated these at between about 250 and 350 mm, which are considered unacceptable. While the grouting of the columns may reduce the settlement under the buildings, it is also proposed to use geogrid reinforced fill over the same columns under filled areas to reduce their settlement.

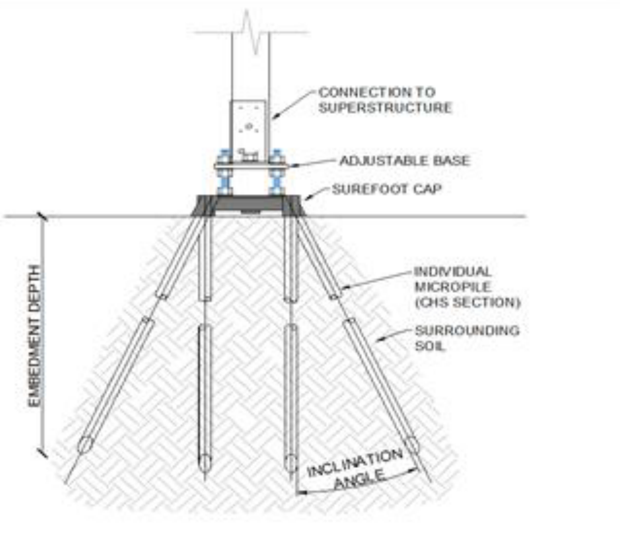

Figure 7. A cross section through the Surefoot micropile foundation from *Mehdizadeh*

No mention has been made of any trials, so it is not known how the grout will be introduced into the columns. Typically, even though clean granular material is used to form columns, by the time they are installed in soft soils the voids are all filled, which will make it difficult for grout to permeate in a post-grouting process. This will also need to be considered in the final design stage, and load testing of trial columns must be recommended before committing to construction.

The paper by *Mehdizadeh* is an unusual paper on some load testing on small groups of micropiles. This is a special technique on which raking galvanised steel pipes 40 mm in diameter are driven into the ground at an unspecified rake that looks to be about 3 (V) to 1(H), to depths of between 1200 and 2000 mm. Because the tops of the pipes are located by and guided through a steel pile cap, the whole procedure is claimed to be very quick, with no concrete required, as illustrated in Figure 7.

It must be said that this arrangement is unusual, since it is more common for raking piles to be used to minimise pile moments in favour of axial forces, whereas the opposite is happening here, with vertical loads being turned into moments in the piles. Since they are steel tubes their moment capacity is probably adequate, but some special study is probably warranted to measure how the bending in the piles varies with applied load and how the soil supports those non-axial forces.

A total of four tests were carried out, each being in both tension and compression, and the reaction was provided by a further four similar pile groups of a larger size. The tests were carried out in Victoria, about 1,700 km south west of here and, although the reference to site characterisation was very limited, the soil conditions were described as between 300 and 700 mm of fill over a high plasticity clay which was soft at its upper surface but was claimed to become very stiff at 5 m depth. Pile depths were limited to 2 m. Some soil properties were provided.

Load/settlement curves were provided for each test, which clearly show a stiffer response for the tension loads than for the compression loads, apart from the first test on the pile denoted as SF100-1200, where the compression test was carried out first. It is perhaps unfortunate that the influence of a test in one direction on a subsequent test in the opposite direction, even after a delay of 2-3 days, has not been considered in the analysis, since the results clearly seem to indicate this. It may also explain the note that SF300-1200 did not follow the pattern of increasing capacity with increasing length and number of piles, since its ultimate tension load does appear to exceed the ultimate tension load of SF100-1500.

Attempts have been made to determine the ultimate capacity in compression, based on extrapolation of load settlement curves on tests not taken to failure by a number of authors. Since these were based on the assumption of a single vertical pile, it is not clear why any of them should apply to a group of slender raking micropiles, so that requires some further explanation. It would also be interesting to note if any tendency was observed for the pile cap to rotate under axial load, as a result of the raking piles applying a torque. It is also noted that theoretical bearing capacity in compression, and pullout capacity in tension, have been determined, the latter including a contribution from passive resistance, although no detail has been provided as to how these were calculated. It is further agreed that some numerical modelling, which can be calibrated by these static load tests, would be very useful in examining the influence of various parameters.

In the Ground Improvement Case Histories section, the paper by *Du and Shahin* is unusual, since it has no mention of site characterisation, and does not seem to relate to any particular site or case history. It describes a method for compacting a layer of liquefiable soil, at some depth below the surface, to form a raft which, it is claimed, allows construction of a variety of structures over the raft while avoiding liquefaction. The compaction is achieved by driving construction debris out from the bottom of a steel tube, in a manner similar to a Franki pile, although it does not use fresh concrete. The compacted bulbs are claimed to compact the surrounding soil, reducing its liquefaction potential in the process, and to link up to form a raft.

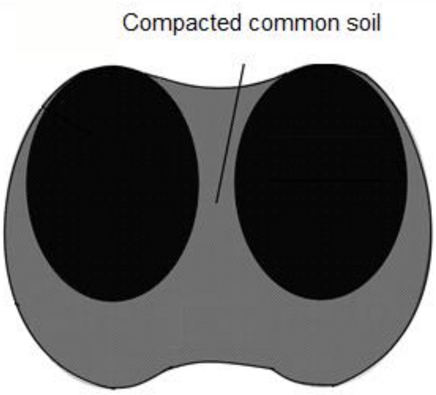

Figure 8. Cross section of two bulbs with compacted soil zone, from *Du and Shahin*.

Although it is claimed that there is a patent application out on this process, it is not at all clear what novelty has been introduced, since it has long been known that compaction reduces the potential for liquefaction, and this can be achieved by a variety of dynamic techniques, such as vibrocompaction or vibroflotation, and dynamic compaction or dynamic replacement, as well as the Franki pile technique referred to. No actual case histories are reported, but it is suggested that the penetration of the hammer over the last three blows can be used as a form of quality control, even though the hammer may be out of sight inside the steel casing.

The last paper in this summary report also makes no reference to site characterisation, being related only to some 1g model tests in a laboratory in relation to the response of a piled raft system. Some physical properties of the marine clay used in the tests are provided but, since it appears to be a natural marine clay from a site at Dahej in Gujarat, it is not clear how relevant they are after the clay has been remixed at its Liquid Limit, and then consolidated under 80 kPa for an unspecified length of time.

An illustration is shown of a single pile and a small *square of four piles under a 160 mm square model raft, and it appears that loads have been placed on (i) an unpiled raft, (ii) a piled raft with one or four piles, and (iii) something called a pile group with one or four piles, although it is not clear what this looks like.*

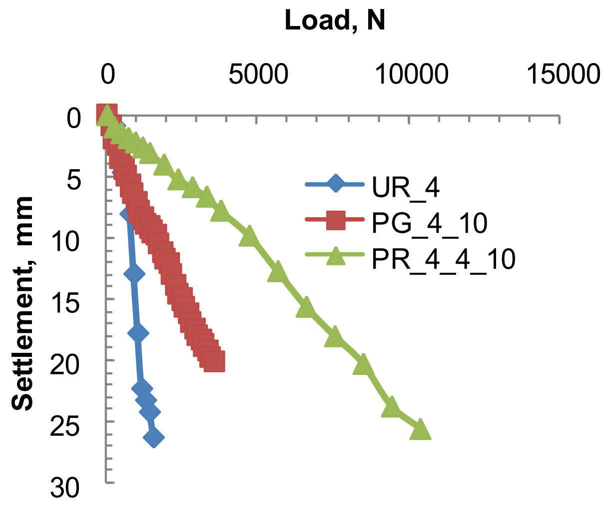

Figure 9. Load vs Settlement for a raft, a group of four piles, and a raft with four piles, from *Shah et al.*

Although reference is made to the use of piles in piled rafts as settlement reducers, that principle does not appear to have been used here. An essential feature of settlement reducing piles in piled rafts is that the raft on its own has sufficient bearing capacity, allowing the piles to be designed only as settlement reducers, and with an appropriately low factor of safety (Poulos 2001). As clearly seen in Figure 9 that is not the case with these model piled rafts, since the unpiled raft, shown by the blue line, has an ultimate capacity about 10 times less than the piled raft.

2 REFERENCES

Greenwood, D.A.G. and Kirsch, K. 1983. Specialist ground treatment by vibratory and dynamic methods. *Proc. International Conference on Advances in Piling and Ground Treatment for Foundations, ICE, London.* 17-46.

Poulos H.G. 2001. Piled raft foundations: design and applications. *Geotechnique,* 51, 2, 95-113.

Geotechnical and Geophysical Site Characterisation 5 – Lehane, Acosta-Martínez & Kelly (Eds)

Session Report: Case Histories, 2

M. Arroyo
Department of Civil and Environmental Engineering, UPC, Barcelona, Spain

ABSTRACT: The papers submitted to this session are varied in their methods, scope and in the characterization techniques described or applied. They have in common the need to cope with practical engineering problems and varied ground conditions which is characteristic of geotechnical case histories. There are always interesting lessons to be learned by examining well-documented cases. Sometimes the analogy with other cases makes them directly useful. Sometimes details that may appear secondary to the authors are revealing if considered from a wider, comparative perspective.

1 INTRODUCTION

A total of 9 papers were contributed to this session. While all of them are of high technical quality they lack an obviously unifying subject. Therefore this report will first describe in parallel some the most relevant traits of the different contributions and would then highlight the results that have seemed more relevant from the point of view of the equipment used or the geotechnical property discussed.

2 OVERVIEW

2.1 *Geographical origin*

The majority of the contributors were based in Europe, with a large presence of Italian researchers. As might be expected there was also a large contribution from Oceania. (Figure 1).

2.2 *Characterization techniques*

A fair variety of site investigation techniques are discussed in the contributions to the session (Table 1). The dominant characterization strategy in these cases appears to be based on boreholes and subsequent laboratory testing. Some of the laboratory testing reported was unconventional, for instance the large triaxial tests reported by Pérez & Ale. It is also interesting to note that in two thirds of the papers field monitoring in one guise or another was employed for characterization. There is a significant presence of the (seismic) Marchetti dilatometer, (S)DMT. A variety of geophysical techniques is also employed –apart that is from the seismic measurements that are associated with SDMT.

It is remarkable that, despite its general preeminence in geotechnical site characterization, the cone penetration test (CPT) and its derived techniques (e.g. CPTu, Seismic CPT) feature in only one of the papers contributed to the session. The absence of CPTu may be particularly striking for the Port investigation reported by Jaditager & Sivakugan (2016); this is the kind of job that CPTu seems well adapted to. However the surprise may diminish when it is noted that the investigation reported was conducted almost 25 years ago. At that time there was less availability of CPTu deployment tools for nearshore jobs. This report is thus a useful reminder of the relatively recent maturity of site investigation tools that now seem present everywhere.

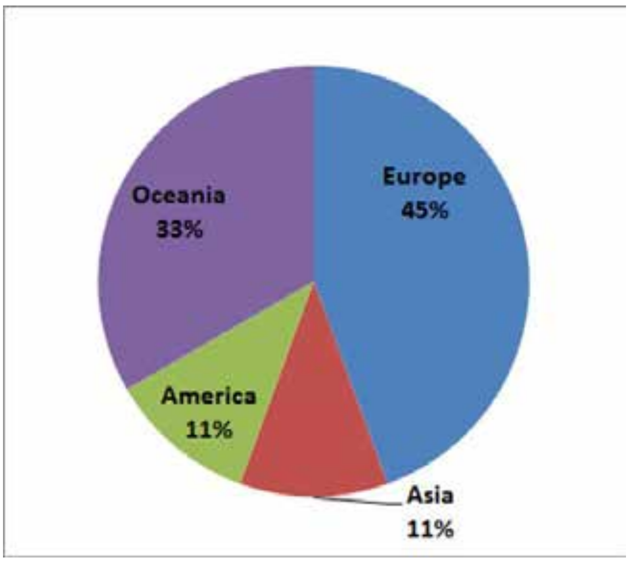

Figure 1 Geographic origin of the session contributions

2.3 *Problem related traits*

By problem related traits (**Error! Reference source not found.**) we make reference to those aspects of the session contributions that were dictated by the nature of the problem discussed by the authors. One first such trait is given by the nature of the driving application. All the papers presented were dealing with some specific application -a case history- rather than with methodological issues. But the driving application differed in nature. Four cases were related with the development of one kind or another of classic civil engineering infrastructures (railways, roads, ports). Three papers dealt with the analysis of different geotechnical related natural risks, seismic in two cases and slope stability in another. Finally two papers were motivated by mining applications, one of them with the post-closure phase of a conventional open pit another with the exploitation phase of a relatively newer mining technique (heap pad leaching).

Another problem-related trait is the nature of the geotechnical materials that are dealt with. In most contributions (6) fine-grained materials are dominant, two deal with granular materials and one (Castellaro, 2016) is surprisingly unspecific in this respect. Of those dealing with fine grained soils, four are about soft clays and silts, and two with stiff overconsolidated clays. Granular soils are also varied, featuring both conventional quartz sand and run-of-mine ore.

Table 1 Characterization techniques employed by the session contributors. CPT(+): CPT and derived techniques. BH+LAB: laboratory tests on recovered soil samples. DMT/SDMT: Flat dilatometer / Seismic flat dilatometer GPHY: geophysical techniques. RC: resonant column

	Characterization techniques					
Authors	CPT(+)	BH + LAB	DMT / SDMT	GPHY	monitoring	other
Castellaro				Y	y	passive seismic survey
Cavallaro et al		Y	Y			RC
Harianto et al.		Y			y	
Iftekhar		Y			Y	physical model
Jaditager & Sivakugan		Y				
Karim & Rahman					Y	
Pérez & Ale		Y		Y		MASW, large TX
Peiffer	Y		Y		Y	
Totani		Y	Y		Y	torpedo DMT

Most contributions describe several properties of the soils under study. However, in many cases it is easy to identify one geotechnical property where the characterization emphasis lies. As can be seen, in a relative majority of contributions (3) the main issue was that of dynamic characterization, with two more contributions dominated other by stiffness-related properties, either operative stiffness or resilient modulus. In the two contributions related with OC clays the issue was one of surface failure detection. One contribution dealt mostly with permeability and, finally, another presented a general stratigraphic picture of a site.

Table 2 Problem-related traits of the different session contributions. OC: over consolidated

Authors	Driving application	Materials	Characterization emphasis
Castellaro	seismic risk	not specified	structural dynamics
Cavallaro et al	seismic risk	OC silty clay	Gmax, damping
Harianto et al.	road embankment	soft clay	settlement
Iftekhar et al.	railtrack	sand	Settlement under cyclyc loading
Jaditager & Sivakugan	dredging	soft soils	Profiling
Karim & Rahman	road embankment /rail cutting	soft clay /glacial till	permeability
Pérez & Ale	heap leach mining	Run-of-mine ore (sandstone)	Gmax, friction
Peiffer	opencast mining	OC clay	failure surface detection
Totani et al.	forensic slope analysis	OC clay	failure surface detection

2.4 *Method related traits*

Several traits of the scientific methodologies employed by the different authors are collected in **Error! Reference source not found.**. The scientific emphasis of the different contributions is quite varied. Groundwater effects are dominant in the cases reported by Totani et al., Karin & Rahman and Jaditager & Sivakukan, generally through its effect on failure properties, although with very different scales at play -from slope stability to dredging. Different aspects of soil-structure interaction are dealt with by Castellaro, whereas Cavallaro and Pérez y Ale deal with seismic site response either of natural soils or of man-made fills.

In three cases there was use of large scale in situ tests or of physical models to aid in the characterization problem. Some are particularly interesting because they represent unique data sources in relatively unexplored corners of geotechnics. This is the case, for instance, of the paper by Iftekhar et al (2016), who present five large scale fatigue model tests on a model railway infrastructure with geogrid reinforcement. The tests reported include careful observations of settlement and stress evolution during hold periods in between cyclic load sequences.

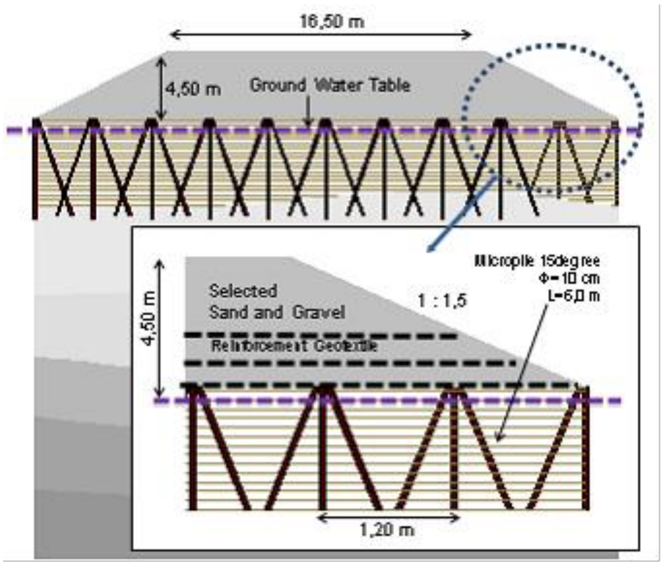

Figure 2 Cross section of wooden pile reinforced embankment tested by Harianto et al. (2016)

Another test, this time full scale, is reported by Harianto et al (2016). They test different configurations of wooden piles for embankment foundation reinforcement (Figure 2). The use of wooden piles for soil reinforcement purposes is a technique that has very ancient precedents. It is infrequent to see reports documenting in detail their benefits for large scale civil engineering projects such as the one presented here.

It is also interesting that in most cases the characterization was linked with numerical analysis of different kinds (Finite Elements, Finite Differences, Limit Equilibrium…). In most cases it was through a direct route in which the geotechnical site investigation produced parameters that were later applied to make different numerical predictions. However there were examples of inverse analysis, in which the numerical tool itself was a key part of the characterization effort. This was particularly the case of the contribution by Karin & Rahman (Figure 3).

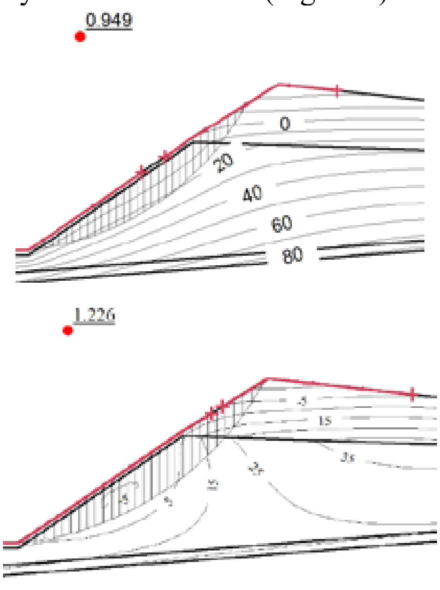

Figure 3 Computed pwp profiles and FoS for slope failure in two hydraulic characterization scenarios (Karin & Rahman, 2016)

Table 3 Method-related traits of the different session contributions. N: no. Y: yes. NE: not explicit. EA: explicitly acknowledged. F: formal treatment. NA: not applicable

Authors	Scientific emphasis	Test site	Analysis method
Castellaro	soil-structure interaction	Y	NA
Cavallaro et al	ground response analysis		Elastic multi-layer transfer function
Harianto et al.	timber piles	Y	NA
Iftekhar et al.	fatigue (cumulative settlement)	Y (scaled)	NA
Jaditager & Sivakugan	dredgeability	N	NA
Karim & Rahman	backanalysis; effects of saturation	N	FEM
Pérez & Ale	stress dependency of properties	N	FDM
Peiffer	Re-consolidation detected via DMT KD	N	FEM
Totani et al.	groundwater controls on slope stability	N	LEQ

3 SOME HIGHLIGHTS

Many lessons may be extracted from reading the papers presented to the session. What follows are some reflections based on the reporter subjective interests.

3.1 *Shear wave profile: how distinctive?*

Several papers submitted to the session present profiles of shear wave velocity against depth. It is somewhat surprising to note how very different geotechnical materials may result in similar shear wave velocity profiles. In Figure 4 the profile obtained by Pérez & Ale (2016) on the crushed sandstone that constitutes the heap leach pad they describe is presented side by side with that obtained by Cavallaro et al (2016) in the overconsolidated clay underneath the Bellini gardens in Catania. The medium grain size of these two materials is in a ratio of 2000. The frictional strength is almost in a ratio of 2. The shear wave velocity is roughly within 0.2 of their average.

Even if the comparison between these two profiles may be somewhat distorted by the different technique employed to obtain them, (spectral analysis of surface waves in the pad, downhole SDMT in Catania), it seems that the possibilities of identifying the soil type by its shear wave profile are small. Indeed, the reader is invited to reflect for a second on the profile presented in another session paper by Castellaro (2016). Perhaps inadvertently the type of soil was not precisely identified, although an indication of the location was given (Po river plain). However, that is somewhat too broad: within the Po river plain one may found both profiles dominated by coarse gravels and by clays (Amorosi & Colalongo, 2005). If only the shear wave velocity profile was provided (Figure 5) and the previous examples from the session, it would be hard to decide if that was a gravel or a clay site. In this respect it is instructive the comparison with the work -presented in a different session of the conference- by Sastre et al (2016). There the authors present an -apparently successful- automated method of grain size class soil classification based on the results of a dynamic hand- held probe. Perhaps the success is due to it being a failure test? The reader is left wondering if attempts to relate shear wave stiffness to failure related soil properties (e.g. liquefaction susceptibility) may not be more based in convenience of measurement than in predictive capability

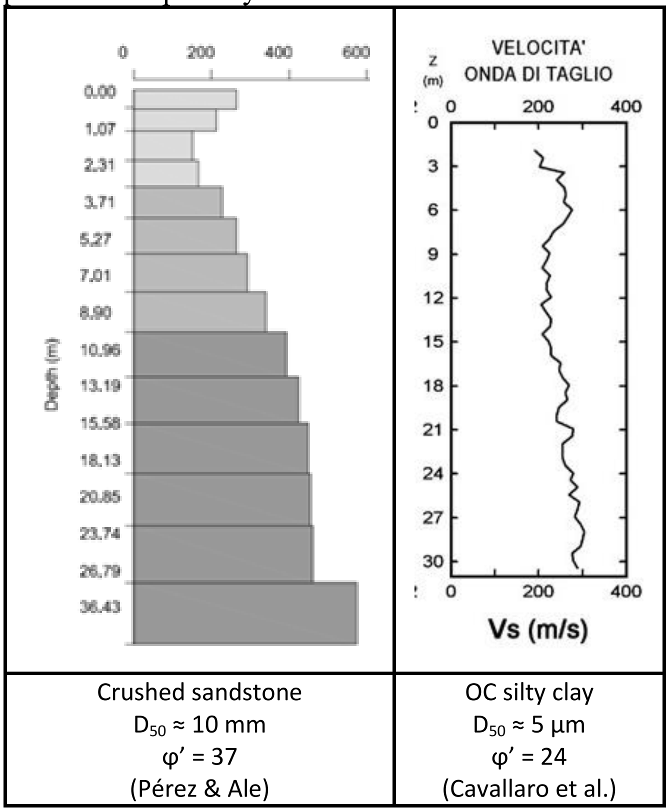

Figure 4 Profiles of shear wave velocity against depth for two cases described in the session: very different soils result in quite similar profiles

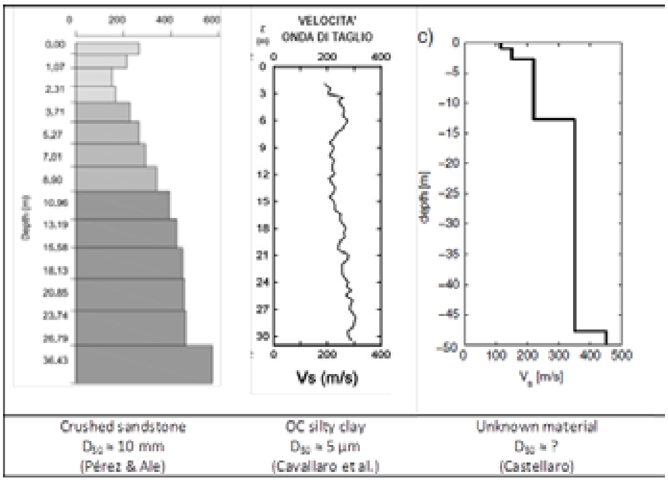

Figure 5 Profiles of shear wave velocity against depth for the two cases above plus one extra profile from a site with unspecified soil type.

3.2 *Dynamic properties: how precise?*

Perhaps the dynamic properties of soils reflect too many factors of soil composition and state to be useful as a stand-alone classificatory. On the other hand enhanced precision in measurement may allow refined discrimination. The need for precision in dynamic property measurement is also well illustrated by the results presented in the paper by Castellaro (2016).

In that paper an interesting case is presented in which two apparently identical buildings, located on the same site responded differently to an earthquake excitation. One of them suffered significant damage, whereas the other did not. Modal analysis based on passive excitation of the buildings is presented revealing some differences in their dynamical response, that are attributed to modest changes in internal structural details. The author rightly emphasizes the importance of soil-structure interaction studies for risk analysis, but, apart from that it is also significant that the back-analyzed eigenfrequencies of the two buildings differ by less than 20% This is a level of precision that is not often requested in other areas of geotechnical analysis.

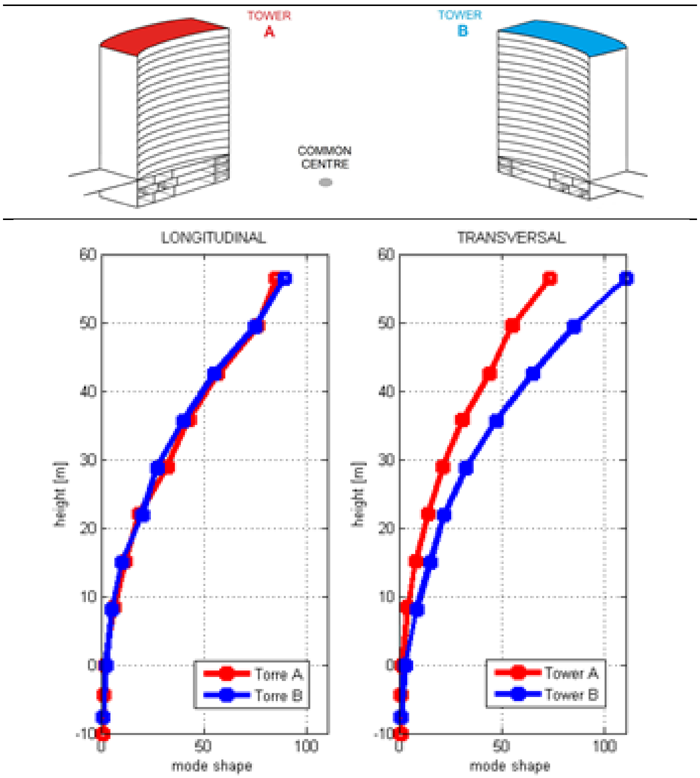

Figure 6 Dynamic response of two apparently identical buildings that responded differently to an earthquake (Castellaro, 2016)

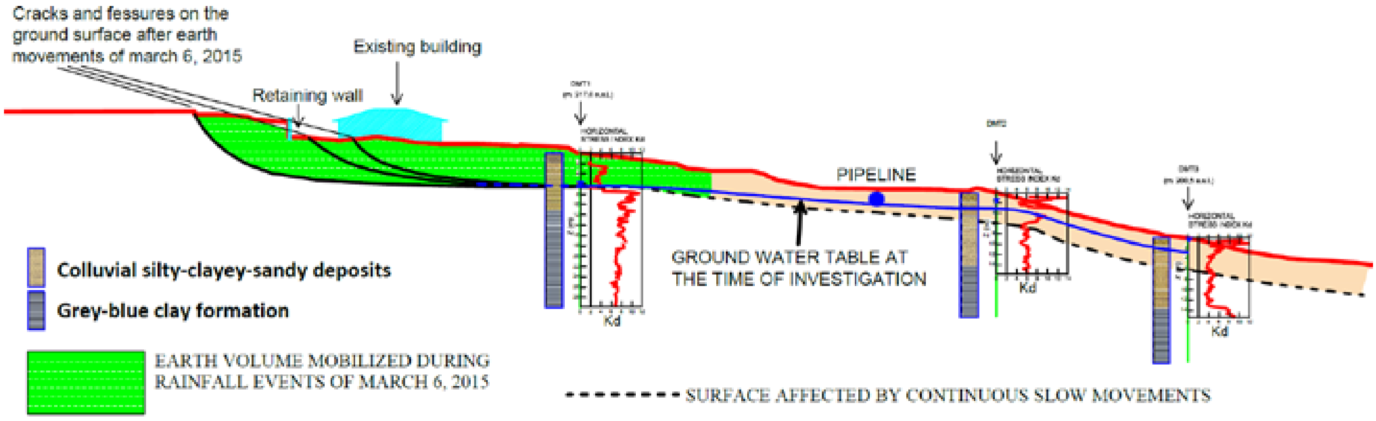

Figure 7 Use of DMT Kd profiles to detect sliding surface location (Totani et al. 2016)

3.3 *SDMT: the multitasking instrument*

It is not always appreciated the variety of purposes that a SDMT profile might serve. We have already mentioned the example in this session in which the instrument is used to obtain a shear wave velocity profile. The other two examples coincide in illustrating a very different application (Figure 5) that of detecting failure shear surfaces, much faster than what is generally possible with inclinometers.

4 FINAL COMMENTS

A large deal of ingenuity is shown in the papers contributed to this session to illustrate, advance and extend the techniques of geotechnical characterisation. The variety of purpose and geotechnical setting of the case histories reported will surely help the readers to extract individual or collective lessons from them.

5 REFERENCES

Amorosi, A., & Colalongo, M. L. (2005). The linkage between alluvial and coeval nearshore marine successions: evidence from the Late Quaternary record of the Po River Plain, Italy. Fluvial Sedimentology VII, 255-275.

Castellaro, S. (2016) Different Response of Apparently Identical Structures: A Far-Field Lesson From the Mirandola (Italy) 2012 Earthquake Fifth International Conference on Site Characterization, ISC'5. Gold Coast, Australia, September 2016.

Cavallaro, A., Grasso, S. & Ferraro, A. (2016) Study on Seismic Response Analysis in "Vincenzo Bellini" Garden Area by Seismic Dilatometer Marchetti Tests Fifth International Conference on Site Characterization, ISC'5. Gold Coast, Australia, September 2016.

Harianto, A.T., Samang, L., Suheriyatna, B. & Sandyutama, Y. (2016) Field Investigation of the Performance of Soft Soil Reinforcement with Inclined Pile Fifth International Conference on Site Characterization, ISC'5. Gold Coast, Australia, September 2016.

Iftekhar Alam, M., Gnanendran, C.T. & Lo, S.R. (2016) Behaviour of Reinforced Shallow Foundation on Sandy Sloped Fill Under Cyclic Loading Fifth International Conference on Site Characterization, ISC'5. Gold Coast, Australia, September 2016.

Jaditager, M. & Sivakugan, N. (2016) Geotechnical Site Investigations for Dredging Works - Port Of Townsville Fifth International Conference on Site Characterization, ISC'5. Gold Coast, Australia, September 2016.

Karim, M.R. & Mizanur Rahman, M. (2016) Estimation of soil hydraulic conductivity assisted by numerical tools – two case studies, Fifth International Conference on Site Characterization, ISC'5. Gold Coast, Australia, September 2016.

Pérez, F.C. & Ale, J.D. (2016) Two-Dimensional Non-Linear Dynamic Response of a Heap Leach Pad Located in Peru, Fifth International Conference on Site Characterization, ISC'5. Gold Coast, Australia, September 2016.

Peiffer, H. (2016) Analysis of Slope Stability in Overconsolidated Clay Based on CPT & DMT Measurements, Fifth International Conference on Site Characterization, ISC'5. Gold Coast, Australia, September 2016.

Sastre, C., Benz, M., Gourvès,R., Breul, P. & Bacconnet, C. (2016) Automatic methodology to predict grain size class from dynamic penetration test using neural networks, Fifth International Conference on Site Characterization, ISC'5. Gold Coast, Australia, September 2016.

Totani, G., Totatni, F., Monaco, P.. & Simeoni, L. (2016) Site Investigation, Monitoring & Stability Analysis of a Built-Up Slope Involved By Gas Pipeline Explosion, Fifth International Conference on Site Characterization, ISC'5. Gold Coast, Australia, September 2016.

Geotechnical and Geophysical Site Characterisation 5 – Lehane, Acosta-Martínez & Kelly (Eds)
© 2016 Australian Geomechanics Society, Sydney, Australia, ISBN 978-0-9946261-1-0

Session report – General site characterisation

J. Wierzbicki
Institute of Geology, Adam Mickiewicz University, Poznań, Poland

ABSTRACT: This paper presents highlights from 8 papers submitted to the General Site Characterisation session of the ISC'5 Conference. The general findings of all papers are presented and these are subsequently compared with experience from previous research.

1 INTRODUCTION

The General Site Characterization session (GSC), as its title itself indicates, refers to a very wide range of issues. It applies to both the scope of the research methods used, as well as the subject of research itself, that is soil. The expression "General" can be understood in two ways; it can refer to a general view on a research issue, but it can also specify versatility of identification of a given matter. It also applies to 8 articles submitted for this session. This, perhaps, a small number of works does not, in any way, affect limitation of research topics covered by the authors. Most of the works address a few significant research themes which are often mutually permeant. Therefore, this paper identifies five main research areas on the basis of which the results obtained by particular authors have been discussed.

As Figure 1 shows, the most common theme addressed in the GSC session works is research on soft and organic soils. Most of the research focused on reference test sites, thus its objective was to characterise typical in some respects soils in a given area and it did not refer to specific project cases. In case of three papers, a crucial element of the research problem was accessibility difficulties of the studied area, which, in turn, did not necessarily mean the presence of soft and organic soils. The subject of seismic areas was also clearly addressed, although it was not always the focus of the paper. Unlike previous, intersecting research themes, identification of the subsoil within non-standard investments presented in the one work, formed a slightly different problem.

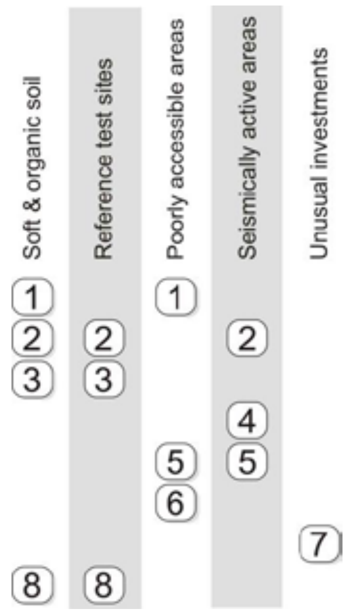

Figure 1. Main research topics addressed in the GSC session works: [1] Geophysical and Geotechnical Characterisation of the Saltwater Creek Bridge Site, Morten Bay Rail Link, Queensland, Australia -. Purwodiharjo A., Rahiman T., Parsons M., Kruger J.; [2] The Phase of Geotechnical Study for a new construction in Albania - Allkja S., Bozo L., Malaj A., Harizaj L., Kosho A., Xhagolli B.; [3] Geotechnical characterization of Ballina clay – Pineda J.A., Kelly R.B., Suwal L., Bates L. & Solan S.W.; [4] Site characterization and seismic response analysis in the area of Collemaggio, L'Aquila (Italy) - Totani G., Monaco P., Totani F., lanzo G., Pagliaroli A., Amoroso S., Marchetti D.; [5] Using Multi-Channel Analysis of Surface Waves and Cone Penetrometer Tests to delineate an in-filled palaeochannel during routine investigations – A Christchurch Earthquake Case Study - Kaumuhangire R., Plunket T., Ruegg C.; [6] Geophysical and in situ testing applied to site characterisation for non-engineered structures in developing regions - Ortiz-Palacio S.; [7] Geotechnical and geophysical site characterization of a nuclear power plant site in United Arab Emirates - Parashar S., Rice R., Asprouda P., Al Hammadi H.; [8] Characterisation of Halden silt - Blaker Ø.

2 SOFT AND ORGANIC SOILS

Studies conducted on soft and organic soils are an integral part of contemporary geotechnics. The intense development of infrastructure is increasingly creating a need for investments in areas with problematical soils in terms of foundation of buildings. The need to utilise soft and organic soils as construction grounds usually poses two kinds of problems. One of them is a difficulty in obtaining a valuable outcome of in situ (Long, 2008) or laboratory (de Groot & Landon, 2007) studies. Another one, related to design itself, is narrowing the absolute margin of error in the assessment of geotechnical parameter value, which derives from numerically low parameter values with standard measurement accuracy. For obvious reasons, works presented within the GSC session mainly refer to the first issue. In this case, due to technical and economic difficulties in obtaining high-quality undisturbed samples, in situ studies dominate in identification of geotechnical conditions. In typical, commercial studies [1] sampling is mainly limited to enable assessment of fundamental physical properties. It is even worse if such a situation applies to areas considered to be reference test sites [2]. The need for calibration of in situ test results to local conditions is particularly important in the case of soft and organic soils, where the aforementioned margin of error gradually narrows (e.g., Młynarek et al., 2014). It is finely proven by test results of [3] which show how a specific structure of soft marine illitic clays affect strong non-linearity of deformation characteristics of such soils (Fig. 2). High values of peak friction angle reaching up to 42 degrees may be somewhat perplexing in case of sediments with high plasticity (PI > 34%) and presence of organic matter reaching 3%. In the context of strong non-linearity of deformation characteristic of these soils it can be assumed that, in this case, its cause may be preliminary sediment cementation. A similar effect of disproportionately high values of peak friction angle and constrained moduli caused by carbonate cementation of alluvial soils was identified e.g., by Stefaniak (2014).

Domination of in situ methods in identifying soft and organic soils, as it has already been mentioned, is in some ways understandable. However, very economical use of penetration techniques dedicated, in a sense, to the soft and organic soils testing, such as the Field Vane Test, the T-bar or Ball penetrometer (Colreavy et al. 2010) is puzzling. Only in the case of tests carried out by [3] the FVT was used, confirming that undrained shear strength measured in situ conditions is higher than the one specified in the triaxial compression test, even on samples of a documented high quality. In this context, correlation attempts of simple methods based on dynamic penetration with advanced techniques of surface wave measurement can be explained by being accustomed to typical test methods. Nonetheless, it is difficult to expect in this case satisfactory results of such analyses (Fig. 3) [1], which has been already indicated by, inter alia, Schnaid 2010.

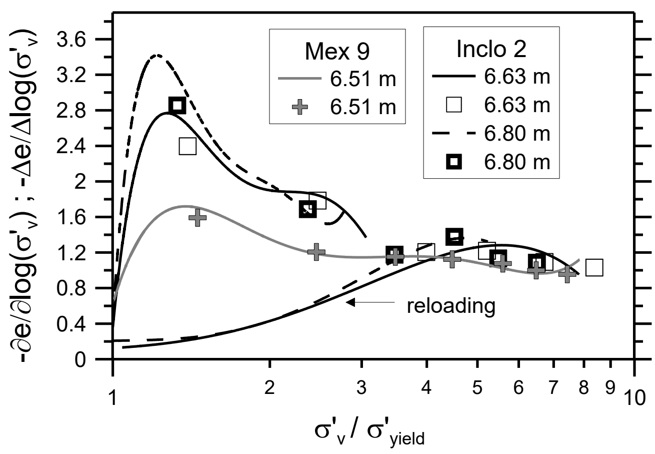

Figure 2. Variation of C_c with the stress level in the case of Balina clay (Pineda et al.).

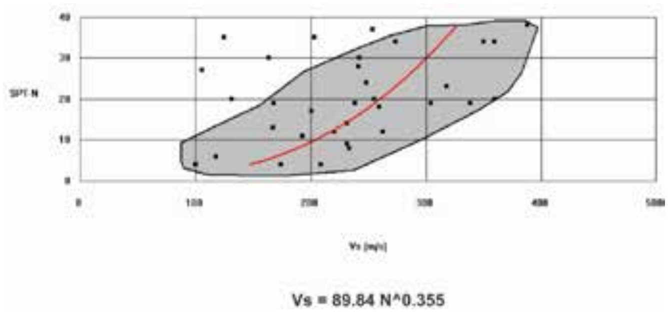

Figure 3. Regression analysis of SPT data and V_s measurements for the Saltwater Creek Bridges sediments (Puwodihardjo et al.).

3 REFERENCE TEST SITES

The location of reference test sites is usually decided, on one hand, by typicality of soils tested for a given area and by geotechnical "problematic nature" of these soils on the other. The same applies to the works presented in the GSC session which mainly analyse intermediate soils deposited in offshore and alluvial environment and organic soils. A common feature of tests conducted on test sites is a comprehensive identification of soil, often far beyond the scope of typical commercial research. Tests conducted by NGI can be a good role model leading to a comprehensive characteristic of the tested sediments and examining correlations between the results obtained using different test methods (Lunne et al. 2003). In general, however, these results are not the effect of a one-time research campaign, but rather the sum of perennial, complementary studies conducted even in the span of 30 years (Wierzbicki & Lunne 1999). In this context, among the works presented in the GSC session one can underline both the ones that are more signal in nature [2] and referring to an almost full characteristic of soils [3] and [8]. Multi-faceted substrate studies, mainly in terms of in situ tests, were conducted notably by [3]. A rather rarely found in practice push-in pressure cells and direct assessment of horizontal stress values are noteworthy. The obtained results remind us how different they can be if they are obtained using different methods, (up to 30-70% reassessment of K_0value specified in the DMT study). As it was noted by [3], in this case dissipation of horizontal stress was not analysed after installation of the device in the soil. Such phenomenon takes place, however, its time depends on the local soil conditions and installation method. In this context, it would be useful to include information about details of the performed measurements with the help of the PIPC. Studies conducted on reference test sites also reflect an increased interest in surface wave measurement methods. As it was earlier noticed by different authors (inter alia, Foti 2013, Vanneste et al. 2014) this method provides a very valuable complement to penetration testing and facilitates creating geotechnical models of substrate structure. [3] and [1] used the results of the MASW test to identify the position of a boundary between the soft and organic soils and the bearing subsoil. In both cases, the criteria value of V_s wave was adopted following the correlation between the CPTU tests results (Fig. 4). As a complement to this theme one can indicate opportunities offered by the use of statistical methods, cluster analysis in particular, in a complementary use of various geotechnical data (Smaga 2014). On the other hand, [8] drew attention to the problem of identification of geotechnical layers in intermediate soils. In terms of lithology, a seemingly homogeneous substrate may often require a more detailed breakdown into layers resulting from significant differences in strength properties. As one of the explanations for this state of affairs, the author provides small, but statistically significant, differences in the content of organic parts. Although the difference of the content of organic parts expressed in per milles seems to be almost imperceptible, in this particular case it may have a decisive impact on the increase of moisture and simultaneously decrease of soil strength parameters. An interesting and important observation of [8] is the need for a cautious approach to the interpretation of intermediate soils using common CPTU classification charts. These conclusions are confirmed by works of other authors (inter alia, Stefaniak 2014) is to draw attention to the opportunities offered by the combination of two classification charts - SBT Robertson (1990) and Schneider et al. (2008) (Fig. 5).

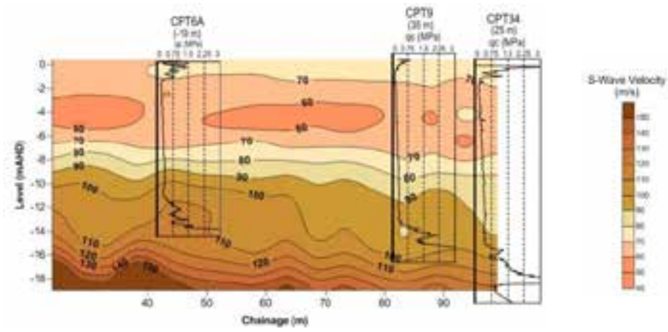

Figure 4. Shear wave velocity profiles obtained from MASW1 alongside East-West direction on the Balina Clay test site (Pineda et al.).

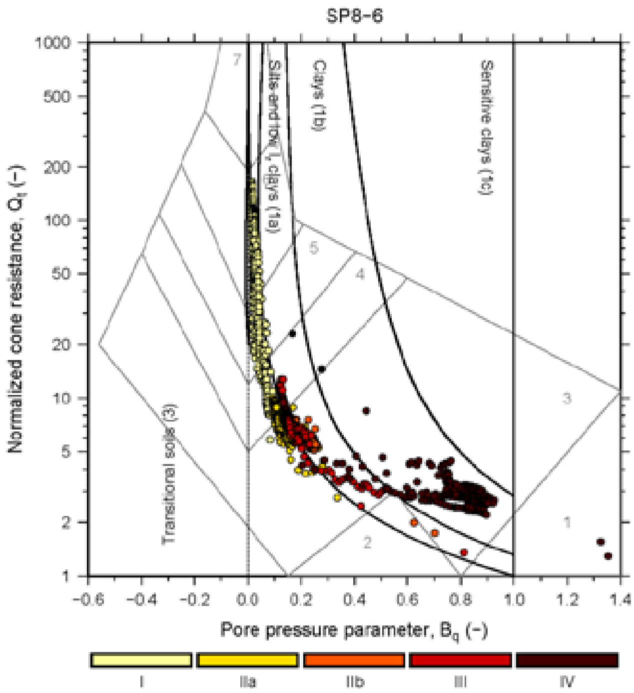

Figure 5. Robertson (1990) soil behaviour type chart combined with the Schneider et al. (2008) classification chart for the Halden silt deposits (Blaker Ø.).

A frequent lack of information on the soil sample quality, unfortunately, leaves a deficiency in the description of the laboratory tests of reference test sites. Sample quality, especially in cases of soft and organic soils, can have a significant impact on the results obtained (Lacasse et al. 2008). It seems that sample quality assessment should be a certain standard in case of reference tests e.g., the one accomplished by [8] based on the criteria of Lunne et al. (1997).

4 POORLY ACCESSIBLE AREAS

It is not always that a geotechnical engineer can have full access to the area of research to conduct all theoretically appropriate tests of the substrate. These restrictions may occur as a result of economic and timely pressures of an investor, but also their more common reason is concern for the natural environment. The first possibility is generally associated with local investments and developing countries and is also well known in the Eastern European countries (Młynarek 2008). An interesting article of [6], on one hand, refers to the well-known pattern that indicates the validity of investing funds in soil research in the pre-project phase (Fig. 6), on the other hand, it indicates possible solutions in terms of economically weaker areas. According to [6], economic-technological constraints around the world cause a dynamic penetration tests to be commonly used. Nonetheless, the author does not see a special alternative to this fact in the case of the less developed world party. It correctly assumes that information about a limited credibility is better than its complete absence, which cannot always be agreed upon. Leaving aside the dubious idea of correlation of simple geotechnical tests with the results of the more advanced ones, such as geophysical tests (Schnaid 2010), this approach may be a significant temptation to conduct "shortcut" tests, even when there are possibilities of a complete analysis of the substrate. This situation occurs e.g., in Poland, where after World War II simple rules of evaluating substrate bearing capacity were developed. Over the years, these rules were complemented and developed resulting in the creation of a set of nomograms in the 80s of the 20th century which allowed the assessment of strength and deformation properties of all soils only on the basis of knowledge of the type of soil along with its relative density or liquidity index (PN-82/03020). In spite of technological and economic development of the country, the vast majority of commercial geotechnical analyses uses these simple and not always justified correlations up to this day. It even leads to peculiar situations when according to the current Eurocode more advanced geotechnical research is performed, but the values of geotechnical parameters are determined on the basis of the old rules (Lipiński et al. 2016).

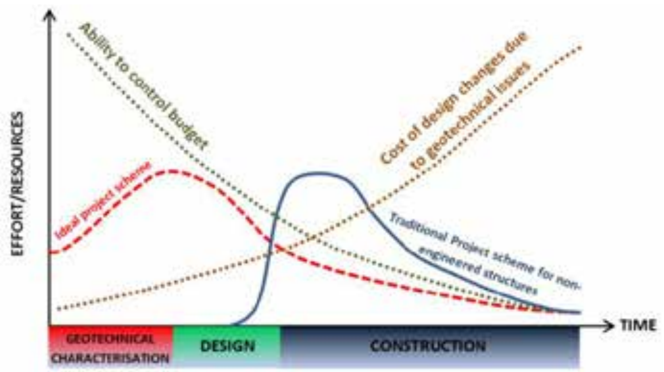

Figure 6. Effort curves in non-engineered buildings projects, adapted from MacLeamy (2004) (Ortiz-Palacio S.).

Another problem is conducting substrate research in areas that are partially protected or densely built-up. In such cases, reducing the number of penetration tests and possibilities of sampling can be successfully compensated with performing surface wave measurements. As shown by the results obtained by [1] and [5], an important part of planned works is a skillful use of penetration test findings and of non-standard measurement techniques, such as Seismic Refraction and LIDAR. Particular attention deserves the result of a joint analysis of geotechnical, geological and geodetic data in the work of [5]. As it emerges, only a summary of these data allowed to present a valid hypothesis for the observed phenomena essential to the building of similar areas (Fig. 7).

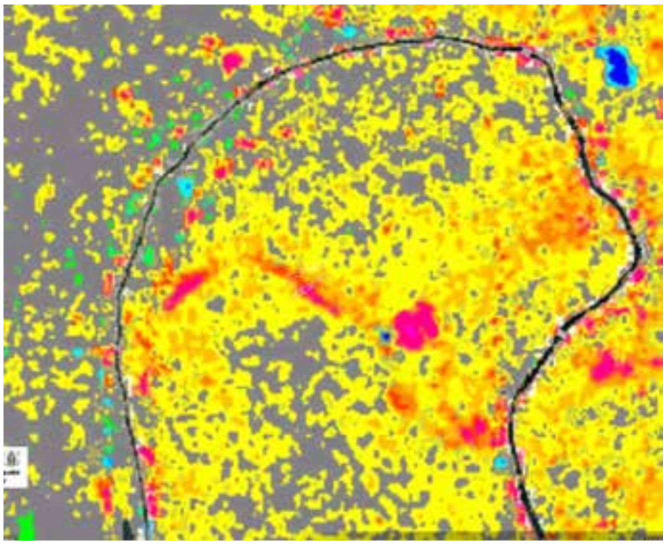

Figure 7. LiDAR vertical movement at the Cresselly Place, St Martins Christchurch test site (Kaumuhangire R. et al.).

5 SEISMICALLY ACTIVE AREAS

Research conducted on seismically active areas pose a separate challenge in geotechnics. Soils that under static load are a stable construction ground, in the case of dynamic loads (e.g. caused by seismic wave propagation) lose their bearing capacity.

For non-lithificated soils, the primary task is to determine liquefaction potential and the extent of occurrence of soils susceptible to this phenomenon. Both penetration (Zhang et al. 2002) and seismic methods are used for this purpose (Andrus et al. 2000). Universality of the results obtained with different methods is obviously a debatable issue. [2] suggest that the correct way in this case is correlation of penetration tests results with a direct shear wave velocity measurement. The differences obtained, however, indicate caution when using these dependents and the need for their calibration to local conditions (Fig. 8). On the other hand, [5] stress commonly observed restrictions in the use of surface wave measurements for a reliable assessment of substrate properties. Ambiguous results derive from geophysical surface prospecting due to the effect of "shadowing" with rigid structures and discontinuities of lower lying layers of the substrate (Godlewski & Szczepański 2015), which is an inherent feature of these studies. As rightly observed by [5], this creates a need for parallel penetration tests, which significantly complement assessment potential of substrate liquefaction (fig. 9).

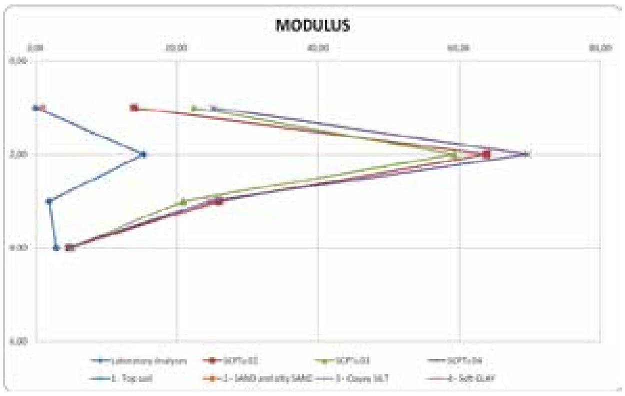

Figure 8. Comparison of constrained modulus obtained from field and laboratory tests for the Fier in Albania test site (Allkja S. et al.).

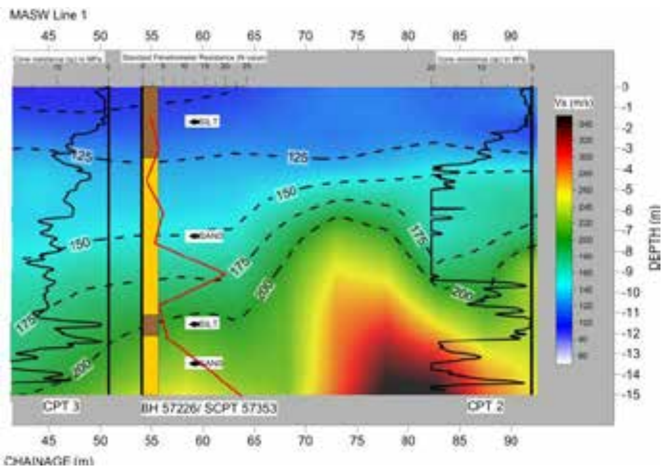

Figure 9. MASW plot superimposed with results of intrusive investigations at the Cresselly Place test site (Kaumuhangire R. et al.).

In turn, [4] represent a very interesting problem of adequacy of modelling subsoil performance wherein the layer susceptible to liquefaction is located between two layers of greater stiffness. Proper restoration of destruction causes and mechanisms caused by an earthquake required in this case employing non-standard SDMT investigations, precise determination of geological structure and topography of the area, but also a detailed analysis of characteristics of historical seismic activity. An important result of the model studies, explaining surprising destruction in the area of the basilica in L'Aquila, as it turns out, is a confirmation of underestimation of seismic action in the range of 2.5-10 Hz (0.1-0.4 s) using data provided by the Italian National Seismic Code (fig. 10).

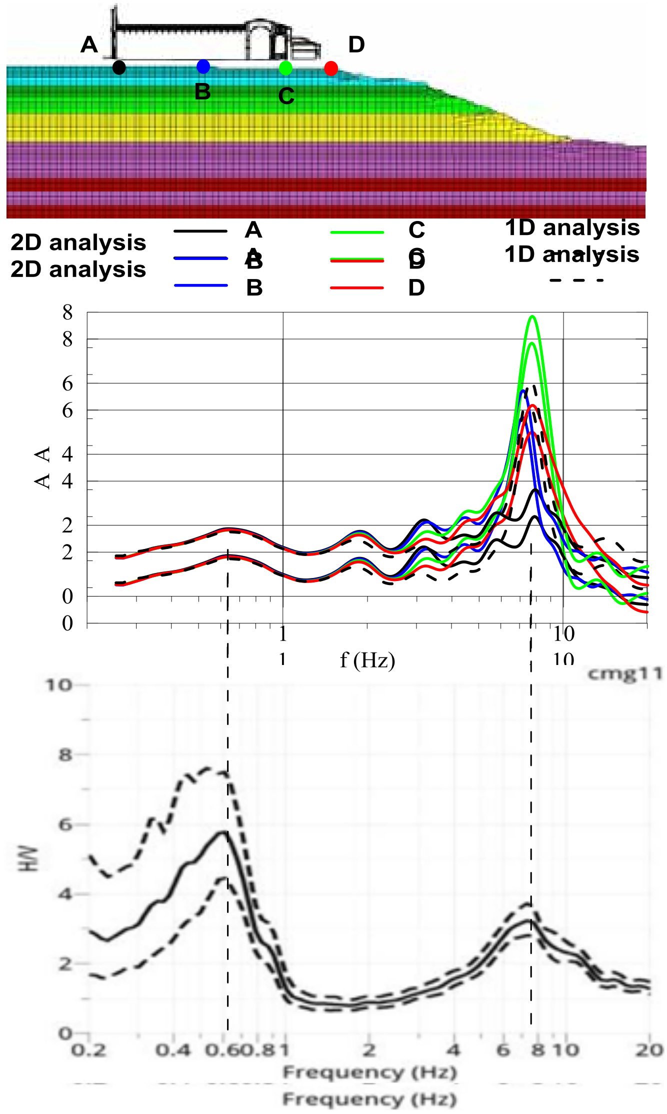

Figure 10. Comparison between transfer functions computed by 1D and 2D visco-elastic linear analyses and representative H/V ratio from noise measurements carried out in the Basilica area (Monaco et al.).

6 UNUSUAL INVESTMENTS

Identifying subsoil for structures such as a nuclear power plant, many problems covered by [6] will not be encountered. The scale of such investment and its significance cause virtual disappearance of economic restrictions in conducting substrate tests resulting in hundreds of test holes, dozens of attempts with undisturbed samples, a full range of in situ and laboratory tests [7]. Against this background, a tenfold reassessment of subsidence calculated based on the results of oedometric tests looks baffling (Tab. 1). Taking into account soils found in the substrate, insufficient quality of samples may have affected such result. As showed by, among others, Landon et al. (2007), the impact of sampling methods may be of critical importance for the results of the analysis of soil compressibility. This hypothesis can also confirm observed by [7] significant differences between the results of geophysical, pressuremeter and laboratory tests.

Table 1. Average Elastic Modulus Values Based on Pressuremeter and Consolidation Tests (Units MPa) for the power plant test site in United Arab Emirates (Parashar S. et al.)

Layer	E (from Pressuremeter Tests)			Ec	Erm, (recommended)
	Initial, Ei	Unload/ Reload E_{ur}	E_{ur} / E_i	(from Consolidation Test)	
2	398	1235	3.1	58	500
3	646	1600	2.5	65	1046
4	2876	3089	1.1	-	1852
5	794	1989	2.5	54	1075
6	1892	4211	2.2	-	1633
7	1599	2567	1.6	107	1580

The importance of non-standard analysis of the subsoil in the case of unusual investments can be well illustrated by the example presented by Jamiolkowski (2014). In that case the large structure of Zelazny Most tailings reservoir, weighted of over 1 giga tons, influences the subsoil much more deeper than was previously expected. The specific geological structure and the enormous load causes that even 80 m below the ground level the horizontal movement can be detected. In such a cases the biggest challenge is to identify such areas in the pre-operational phase.

7 SUMMARY

Review of the works presented in this conference session allows some observations to be made concerning both the current research issues, as well as their likely future in terms of general site characterisation.

Reference test sites are becoming a more and more common practice in geotechnical studies. They provide reference data, allow calibration of commonly used interpretation dependents and understand local specificities of certain soil types. One can wonder whether the right direction would not be a creation of a worldwide register of typical and specific soils and conducting their more coordinated research. A step in this direction could be, for example, adoption of one research standard concerning both the scope and quality control of the conducted research.

Without a doubt, surface wave measurements, especially MASW, are becoming an increasingly more common tool. Results of these studies are an important complement of an image obtained on the basis of penetration tests, however, they require awareness of limitations of physical properties of wave propagation in the subsoil. In this context, parallel use of different tests to create a geotechnical model of ground structure should also be considered. It seems that some of the new possibilities in this regard can provide a wider use of statistical methods e.g., the use of cluster analysis and Bayes' theory.

8 REFERENCES

Andrus, R.D. & Stokoe, K.H. 2000. Liquefaction resistance of soils from shear-wave velocity. *J. Geotech. Geoenviron. Eng.*, ASCE, 126(11): 1015-1025.

Colreavy, C., O'Loughlin, C. D., Long, M., Boylan, N., Ward, D. 2010. Field experience of the piezoball in soft clay. *Proceedings of 2nd International Symposium on Cone Penetration Testing, Huntington Beach, CA, USA, May 2010*.

DeGroot, D.J. & Landon, M.M. 2007. Laboratory Testing of Undisturbed Soft Clay Samples to Determine Engineering Design Parameters. *Studia Geotechnica et Mechanica*. No. 1-2: 23-37.

Foti, S. 2013. Combined use of geophysical methods in site characterization. *Geotechnical and Geophysical Site Characterization 4*, Coutinho & Mayne (eds), Taylor & Francis Group, London: 43–61.

Godlewski, T., Szczepański, T. 2015. Measurement of soil shear wave velocity using in situ and laboratory seismic methods – some methodological aspects. *Geological Quarterly* Vol 59, No 2 (2015): 358-366.

Jamiolkowski, M. 2014. Soil mechanics and the observational method: challenges at the Zelazny Most cooper tailings disposal facility. *Geotechnique*, 64, No. 8: 590-619.

Lacasse, S., Lunne, T., Sjursen M.A. & Dyvik R. 2008. Laboratory testing for soils in maritime environment. *Proceedings of the 11th Baltic Sea Geotechnical Conference, Gdansk, Poland*.

Landon, M.M., DeGroot, D.J. & Sheahan, T.C. 2007. Nondestructive sample quality assessment of a soft clay using shear wave velocity. *Journal of Geotechnical and Geoenvironmental Engineering*, ASCE. 133 (4): 424-432.

Lipiński, M., Wdowska, M. & Michalczuk, K. 2016. Geotechnical parameters from Polish Standard PN-81/B-03020 – the present perspective. *Inżynieria i budownictwo* 4/2016: 212-216.

Long, M. 2008. Design parameters from in situ tests in soft ground – recent developments. *Proceedings 3rd International Conference on Geotechnical and Geophysical Site Characterisation (ISC'3),* Taipei, Huang and Mayne (eds.), Taylor and Francis, April, Vol 1: 89 –116.

Long, M., Boylan, N. & O'Connor, S. 2007. The application of CPTU to soft soils and alternative techniques. In *Proceedings SGE – 2007, Soft Ground Engineering Conference, Athlone, Ireland, February 2007*, ISBN 1 898 012 83 0, paper 1.1.

Lunne, T., Berre, T. and Strandvik, S. 1997. Sample disturbance in soft low plastic Norwegian clay. M. Almeida (Ed.), *Recent Developments in Soil and Pavement Mechanics*, Balkema, Rotterdam, pp. 81–102.

Lunne, T., Long, M. & Forsberg, C.F. 2003. Characterization and engineering properties of Onsoy clay. *Characterisation & Engineering Properties of Natural Soils, Singapore*, Vol. 2, Swets & Zeitlinger, Lisse: 395-427.

MacLeamy, P. 2004. The future of the building industry: The effort curve. *HOK Network, www.youtube.com/watch* vol.9.
Młynarek, Z. 2010. Quality of in-situ and laboratory tests contribution to risk management. In: *Proc. of 14th Danube European Conference on Geotechnical Engineering*, Bratislava, Slovakia.
Młynarek, Z., Wierzbicki, J., Gogolik, S. & Bogucki M. 2014. Shear strength and deformation parameters of peat and gyttja from CPTU, SDMT and VT tests. In: *CPTU and DMT in soft clays and organic soils*, Młynarek Z., Wierzbicki J. (eds.). ISBN: 978-83-62690-19-0 , Exemplum, Poznań: 193-210.
Robertson, P. K. 1990. Soil classification using the cone penetration test. *Canadian Geotechnical Journal* 27(1): 151–158.
Schnaid, F. 2010. Session Report 3: CPT Applications. *Proceedings of 2nd International Symposium on Cone Penetration Testing, Huntington Beach, CA, USA, May 2010*.
Schneider, J. A., Randolph, M. F., Mayne, P. W. & Ramsey, N. R. 2008. Analysis of factors influencing soil classification using normalized piezocone tip resistance and pore pressure parameters. *Journal of Geotechnical and Geoenvironmental Engineering* 134(11): 1569–1586.
Smaga, A. 2014. Analysis of spatial variability of relative density values in the Warta River alluvial. In: *Interdisciplinary issues in mining and geology*, Drzymała J. (ed.), Faculty of Geoengineering, Mining and Geology Wrocław University of Technology, ISBN 978-83-937788-5-0, Wrocław: 197 – 201,
Stefaniak, K. 2013. Wybrane osady aluwialne jako podłoże budowlane i materiał do budowli ziemnych (Selected alluvial deposits as a subsoil and material for earthen structures). PhD Thesis, Poznań University of Life Sciences.
Vanneste, M., Sultan, N., Garziglia, S., Forsberg, C.F. & L'heureux, J.-S. 2014. Seafloor instabilities and sediment deformation processes: The need for integrated, multidisciplinary investigations. *Marine Geology*, 352: 183–214.
Wierzbicki, J. & Lunne ,T. 1999. NGI's Research Site at Holmen, Drammen. *Norwegian Geotechnical Institute Report No. 972508-1*, Oslo 1999.
Zhang, G., Robertson, P.K. & Brachman, R.W.I. 2002. Estimating liquefaction-induced ground settlements from CPT for level ground. *NRC Research Press J*:19: 1168-1180.

Geotechnical and Geophysical Site Characterisation 5 – Lehane, Acosta-Martínez & Kelly (Eds)

Session Report: Pavements and Fills

Burt G. Look
Foundation Specialists Pty, Brisbane, Australia

ABSTRACT: This report provides an overview of the reviewed papers presented in the Conference under the Theme of Pavements and Fills. The papers cover a breadth of topics which encompass both the old and new. Pavements cover both road and rail, while fill includes subgrades, embankment fills and mining stockpiles. The reader should refer to those papers for more details. This report is meant to encourage both discussion of those papers, highlight areas where further explanation is required and/or opportunity for further research. Quality control processes with simple testing and low cost procedures dominate. A move away from the traditional density testing to other approaches is also apparent. Modulus has a greater importance than strength in QC.

1 INTRODUCTION

This review discusses each of the 11 papers initially before providing an overview in aggregate. This report reflects both areas of interest for the reviewer and where some clarification or discussion is useful during the paper presentation.

This is not a paper review, as that had been carried out prior to this session report. Readers are encouraged to attend the presentations if the discussions on a particular paper herein is of interest and also to refer to the papers for specific details.

2 INDIVIDUAL PAPER DISCUSSION

2.1 *Verification of impact rolling compaction using various in situ testing methods (Scott et al.,2016)*

This paper uses a field based study to compare before and after compaction test results when an impact (non-circular) roller is used on trial. Various in situ testing methods, as well as instrumentation is used to measure the ground response and surface settlement measurements.

This trial is for a limited 1.5m depth and using a homogeneous material. The authors have carried out previous work in this area of using rolling dynamic compaction (RDC) and should have referenced more of their earlier work which covers other aspects (I am obviously following their research work). For example in Scott & Jaksa (2015), the authors show an average peak pressure of 120 kPa at 2m depth (Figure 1), yet this paper uses only 1.5m trial. Given this RDC approach has already been shown (by the authors) to extend to greater depths, then a question for the authors is the use of a lesser depth for this paper. Is this suggesting a target 200kPa pressure or does different depths apply to different materials?

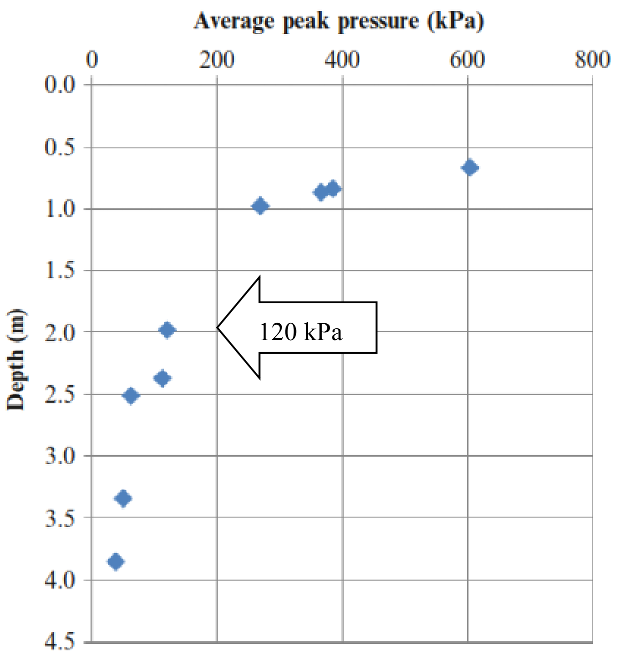

Figure 1. Average peak pressure vs depth ground (Scott and Jaksa, 2015).

The paper contributes to our understanding that deep lift compactions are achievable using RDC. No doubt this is just part of an ongoing research program. The benefits of deep lift compactions using modern equipment needs even more research before industry can promote its benefits on a wider basis rather than a project specific basis. Issues that still need to be addressed include.

(i) For traditional lifts, testing and reinstatement typically represent 15% of the compaction activity of placing, testing and re-instatement (Look, 2013). Deep lift compaction using RDC or heavy vibratory rollers have been possible for some time now, and this paper provides further proof of its effectiveness. However in practice the limitation is being able to provide quality control to that depth. Various techniques were used in the paper but industry needs verification processes which balances the benefit from deep lift compaction with not having increased testing + reinstatement offsetting the time benefit. (Figure 2).

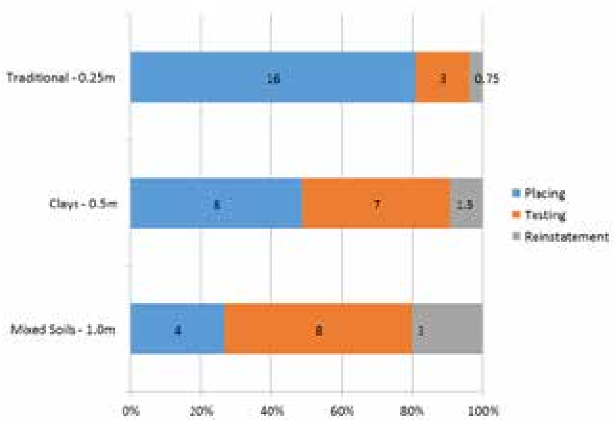

Figure 2. Typical Time (hrs) of various compaction activities for 4,000m^3 with 8 sand replacement tests (Look, 2012).

(ii) The paper shows 70 passes to achieve no further settlement. Although at a higher speed this is still a significant number as compared to traditional means of compaction (a factor of approximately 10). It would be informative for their further research to provide a cost and energy comparison as compared with other methods. For example a vibratory roller may not be able to achieve such a depth of compaction, but if 750mm (½ depth say) were achieved with 20 (say) passes, this may be a better production rate overall with less of an energy foot print. These equipment have a significant petrol consumption operational cost.

(iii) This paper supports the findings of Briaud and Saez (2012) who show the depth of influence from theoretical studies for various shape rollers (Figure 3). A match of that theory and this field practice does provide credence to the 1.5m depth. However in practice the more non round a roller, the less uniform for a given pass, which affects the quality control. This now leads to a similar question as 2) above, but for different reason. What is the *minimum* number of passes to achieve a similar "uniformity" of compaction similar to a round roller?

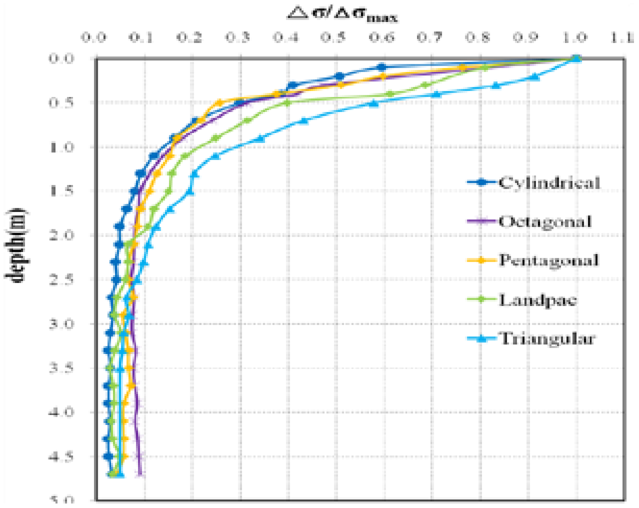

Figure 3. Depth of Influence for various shape rollers based on finite element analysis (Briaud & Saez, 2012).

2.2 *Suggested QC criteria for deep compaction using the CPT (Robertson, 2016)*

This paper is by one of the leaders in CPT use. This application is for quality control (QC) in deep compaction. However, while the CPT is popular in this application due to its low cost, the current methods of using CPT measurements for QC for deep compaction often apply only to clean silica sands and are not effective in soils with higher fines. This has frequently resulted in uncertainty on the effectiveness of the deep compaction. A suggested approach for QC for deep compaction is described based on the normalized equivalent clean sand cone resistance. There is also an associated webinar with more details freely down loaded at:- *www.greggdrilling.com/webinars/DwIgW/cpt-for-quality-control-of-ground-improvement-deep-compaction*

This is highly recommended reading as it answered some of the questions I had when writing this report. My first question was "what was a clean sand" as mentioned in the paper. The webinar provided the answer, and this is defined as $F_r < 0.5\%$. This also shows data from Kirsch and Kirsch (2010) with sandy soils with high fines content (> ~40%) and high CPT ($I_c < 2.6$) are generally not / less compactable (Figure 4). While ~40% is mentioned, this seems as an upper bound. Soils with 35% fines is considered "clays" in British Standards and would have been a closer match to the data of Figure 4.

My second question is on the clean sands at $F_r < 0.5\%$. Figure 5 shows soils as compactable and marginally compactible up to 1% and 1.5% friction ratio, respectively, then some discussion between these 2 different values would be helpful.

clarify why the 150mm gauge length has such a disproportionate change for the c_g and d_g constants.

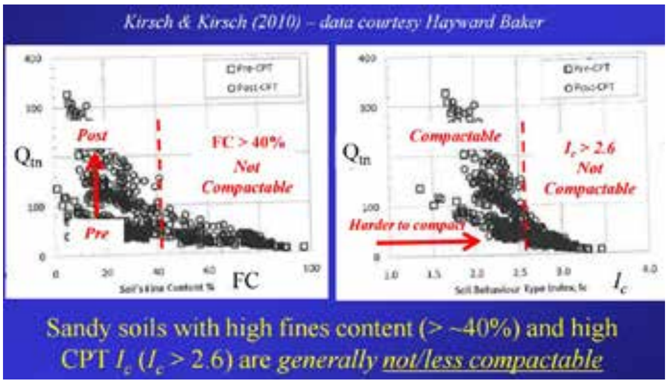

Figure 4. Compactibility slide (Robertson, 2015).

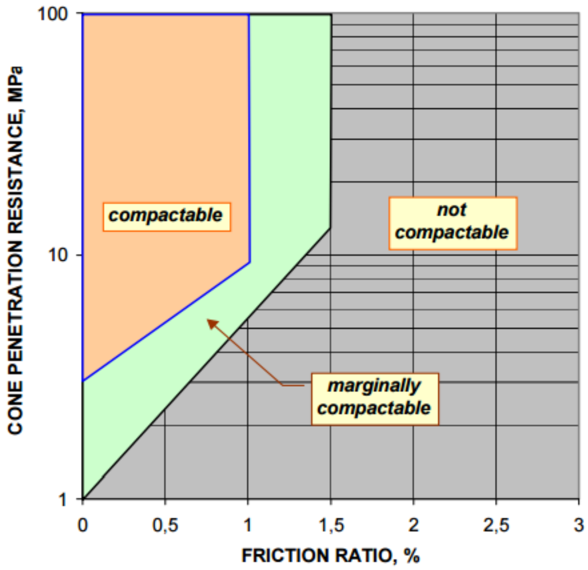

Figure 5. Soil classification for deep compaction based on CPT (Massarsch, 1998).

My final question is on time effects. Again the webinar provides some insights, but no recent data. Assuming there is less time effects with "clean" sands, then as the percentage fine increases, then some time effect is likely. Observing Pore Water Pressure dissipation is one approach, but further guidance on this aspect of likely increase in his future research would be appreciated.

2.3 *A new indirect tensile testing setup to determine stiffness properties of lightly stabilised granular materials (Gnanendran and Alam, 2016)*

A new IDT testing setup was developed in this study to determine deformations along the horizontal and vertical diameters of a cylindrical IDT specimen. The experimental program included the determination of IDT strength, stiffness modulus and Poisson's ratio for a lightly stabilized granular base material.

Table 1 provided the constants to be used in the equations provided in the paper. The authors should clarify why the 150mm gauge length has such a disproportionate change for the c_g and d_g constants.

Table 1: Values of constants for determination of elastic modulus and Poisson's ratio

Gauge length, g	a_g	b_g	c_g	d_g
37.5 mm (= D/4)	0.146	0.451	0.490	0.157
75 mm (= D/2)	0.236	0.780	1.075	0.314
100 mm (= 2D/3)	0.262	0.911	1.609	0.413
112.5 mm (= 3D/4)	0.268	0.952	1.970	0.457
150 mm (= D)	0.272	0.999	4.13	-0.04

The paper states "… an inaccurate Poisson's ratio with a difference of 0.1 from the actual value may increase/decrease the stiffness modulus by up to 25% resulting in an uneconomical and conservative pavement design". This is interesting as Poisson Ratio (in general geotechnical work) is not usually considered a governing parameter as compared to other material variables. The Poisson's ratios ranged from 0.18 to 0.26 for binder content variations of 1% to 3%

The IDT strength and modulus varied by a factor of 3.4 to 4, respectively for the 1% to 3% Binder content (Figure 6). The modulus was derived from both the IDT strength and Poisson ratio with the constants of Table 1. The assertion that the modulus is highly dependent on Poisson ratio is not immediately apparent from these figures. Showing the sensitivity by changing the values from 0.2 to 0.3 (say) would help illustrate the assertion of "being highly dependent on Poisson Ratio" to the reader.

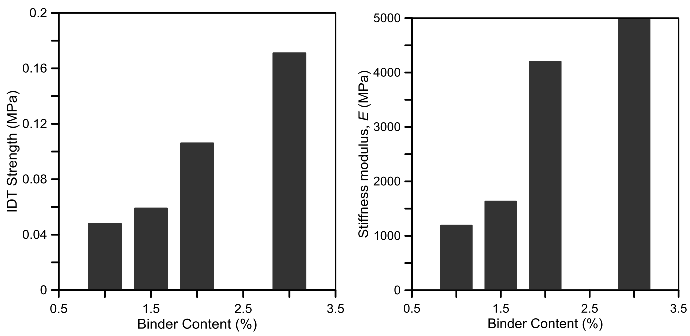

Figure 6. Variation of IDT strength and stiffness modulus with binder content.

2.4 *Geotechnical characterization of a heterogeneous unsuitable stockpile (Rengifo et al., 2016)*

This paper presents the geotechnical characterization of a heterogeneous stockpile in order verify the physical stability of the deposit and to optimize the closure configuration. This characterization was based on test pits, CPTU, MASW, field and laboratory tests. Based on the analysis of that information, strength parameters were proposed for slope stability analysis.

The amount of data provided by the CPTU tests, allowed statistical analysis for precise strength parameters for the different strata.

CPTU with dissipation tests were done, but the latter was not discussed. Given the phreatic level is shown at some depth the authors should describe its usefulness and rationale.

Laboratory tests were divide into coarse and fine materials. These 2 geotechnical units would have been clear enough to warrant that differentiation. This explanation would be useful as the reader is unclear if this was because of a clear differentiation in material stratigraphy, or is this location dependent, or simply for testing purposes. The UU triaxial and Atterberg limits are very similar with a very similar range for cohesion whether classified as coarse (35% average fines) or fine (64% average fines content). Which leads to the other consideration below.

Given the nature of mine waste stockpiles with a large quantity of coarse materials and with over 20% average material greater than 20mm fines (Figure 7) then an explanation on if large size samples were tested to derive the strength parameters, as scale effects may be different as compared to the fine samples tested.

The coarse material has friction angle of 32° to 34° based on field tests. Yet the fine material has an effective friction angle of 34° to 39° based on laboratory results. This is reverse of what one would expect but is a "normal" conundrum faced when correlations are adopted.

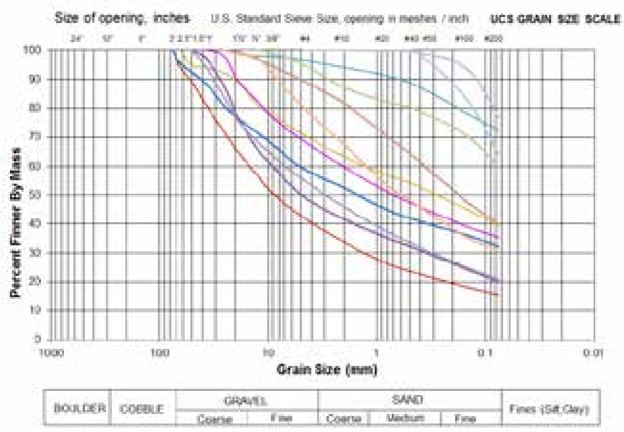

Figure 7. Grain size distribution of representative samples.

Equation 1 in the paper uses the exiting correlation for the N_{kt} value and even uses a conservative value in that range. Using a generic correlation seems out-of-place given the quantum of testing available to provide a site specific correlation. Correlations are used in the absence of site specific other testing, so some explanation is warranted.

2.5 *Control of soil compaction in pavement layers: A new approach using the dynamic cone penetrometer (DCP), (Belincanta et al. 2016)*

Compaction is widely used for the improvement of soil behavior. This paper presents field penetration tests data for compaction control and comparative laboratory testing for calibration of the penetration index (PI), the dry unit weight and the soil moisture content. In this way, the control can be performed in situ by measuring the PI and soil moisture content, as they are directly related to the degree of compaction of the layer. The results indicate that the PI value is inversely proportional to the degree of compaction and that it is strongly influenced by the soil moisture content.

A site specific relationship was developed for obtaining the degree of compaction at a given moisture content. This is not a universal equation as it is referenced to a poorly graded gravel with a soil of unit weight of 16.3 kN/m^3. The moisture content tested seems high at 20% to 32% for a gravelly material, and with CBR_{max} above 20%, but 10% to 13% at the optimum moisture content (Figure 8).

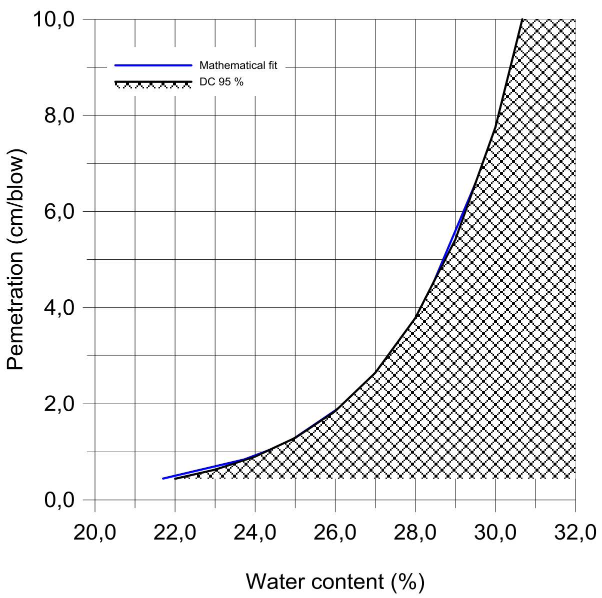

Figure 8. Compaction control as a function of the PI and moisture content, considering a degree of compaction greater than 95%.

The paper title is for soil compaction of pavement layers, but such a low CBR and high moisture content is inconsistent with the CBR required for pavement layers. These properties are more consistent with the subgrade material. Some clarification would be useful here.

In contrast, Burnham et al. (1997) provides the application of the DCP to pavement assessment procedures, with typical limit values of

- Silty clay material PI < 25 mm/ blow
- Select Granular material < 7mm/blow
- Special Gradation materials < 5mm / blow

These values are used when rehabilitation is required, but does not account for moisture variability which can be significant. Similar criteria can be found in various reports in the technical literature.

Some discussion on such an alternative approach which has a wider application and easier criteria as compared to this more refined criteria in the paper that accounts for moisture content but is very site specific.

The DCP can have a significant coefficient of variation (COV > 30%) as compared to density tests COV = 4%). While the DCP is certainly a more expedient tool, a discussion on how that greater variability accounted for in any assessment of compactions control would be useful.

2.6 *Use of the Light Falling Weight Deflectometer as a site investigation tool (Lacey et al., 2016)*

The Light Falling Weight Deflectometer (LFWD) is a surface based, dynamic plate load test that provides quick and direct measurement of the insitu modulus parameter of the near-surface. To demonstrate the potential use of the LFWD as an effective site investigation tool, two brands of LFWD were used to assess the insitu modulus of a residual soil and weak sedimentary rock profile. The performance of both LFWDs are compared to other 'traditional' site Characterisation techniques including DCP profiling and laboratory (soaked) CBR testing. Although strongly correlated, the two LFWD instruments will routinely produce different deflections.

I have been associated with the principal author for many years during his PhD studies where he used this tool demonstrating its usefulness. I would also refer the reader to Lacey et al (2015) which has a methodology using the LFWD to directly assess the improved modulus with geotextile inclusions rather than relying on manufacturer's values.

Over the past 50 years the construction industry has used density as the quality control test, yet in analysis and design the strength or modulus is used. The assumption is that the density controls relates to the strength and modulus values used. While that is the traditional approach the LFWD can provide a direct measurement of modulus and a better assessment of strength than a density inference can provide. Yet tradition rather than technology seems to govern.

Another barrier is that different LFWDs can provide different modulus This aspect is examined in this paper for 2 different LFWDs with one equipment giving approximately half the value of other although a strong correlation exists between the two and both instruments were consistent (Table 2).

Additionally, the limitations of the laboratory soaked CBR was discussed. That test does not apply for oversize a particles which are discarded during the test. Thus that test would incorrectly plateau at CBR 13% due to discarding the "rock" sizes.

Table 2. Typical DCP and insitu modulus material properties

	Insitu Modulus, $E_{LFWD\text{-}100kPa}$ (MPa)		
Blows / 100mm	Prima 100 LFWD	ZFG-2000 LFWD	Material Unit / Weathering State
3	16	8	SOIL (Fill / Residual Soil)
4	20	10	
5	24	12	
	43	21	Residual Soil to XW/HW Rock
10			
20	76	36	XW / HW Rock
25	92	42	
33	116	53	HW Rock

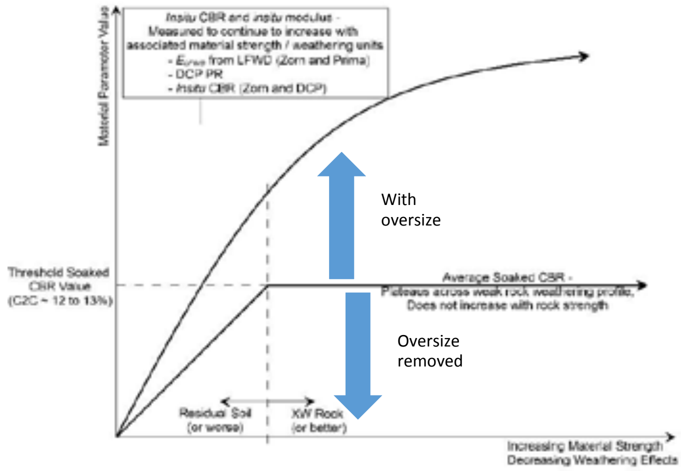

Figure 9. Comparisons between in-situ modulus and soaked CBR tests.

2.7 *Correlation between the results of the PLT and CBR tests to determine the elasticity modulus (Hajiannia et al., 2016)*

The CBR test is usually used to determine the relative strength of the subgrade soil and compacted layers. The Plate Load Test (PLT) yields more realistic soil elastic parameters, but it is costly. This paper presents a correlation between PLT and CBR test. Numerical modelling in ABAQUS and PLTs were used to develop a relation for determining the elasticity modulus using CBR test results. The relation was then checked through some PLTs in the site and CBR tests on the rebuilt specimens. The PLT was also used for the determination of the deflections due to loading, bearing capacity of foundations, and the soil elastic parameters. The modulus of elasticity yields an approximate estimation of the bed reaction coefficient (K_s). The related PLT load-deflection curves were predicted.

The CBR is a pseudo bearing failure test used to correlate to resilient modulus (M_r) and at a high strain of 2.5mm and 5.0mm. This does not occur in the linear elastic phase. A PLT load is a low strain for modulus test for measuring E in the linear elastic range. In fills and or to correlate to M_r the second cycle of PLT loading is typically used (not the first cycle). Hence the 2 tests are not directly comparable. However $E_{v2} \sim 2.3\ E_{v1}$ for comparison of 2^{nd} and first cycle of loading.

Thus, the paper attempts to correlate with the linear elastic first cycle of loading of a PLT field test with a laboratory parameter (CBR) in the high plastic strain range. The PLT is a relatively low strain hence comparisons are being made between low and high strain tests. Figure 10 illustrates a few of these differences. The authors should clarify these considerations or mention the limitations of this approach in the paper.

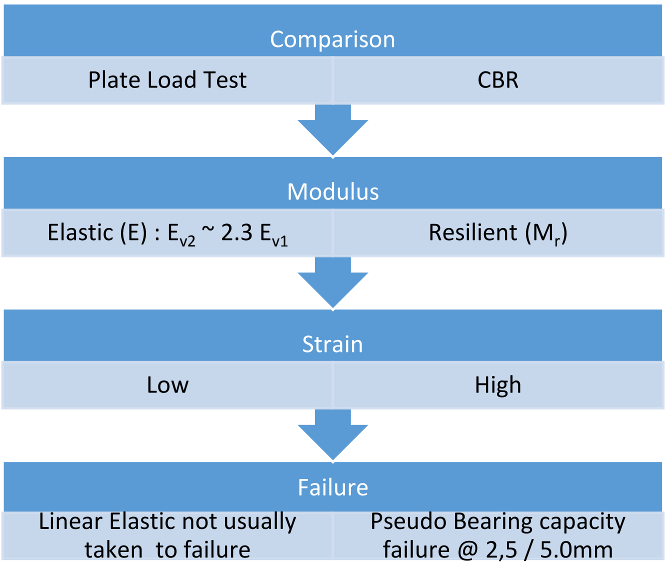

Figure 10. Comparisons between PLT and CBR tests.

This difference needs to be recognized in the FE analysis as a high strain modulus (lab) test is compared with a low strain modulus (field) test. The authors should clarify the rationale accordingly.

E/M_r ratios are material dependent (for example $E/M_r = 1.4$ to 0.3 for granular bases with stabilized layers and embankments below a granular base, respectively). Hence, while the procedure is interesting, any resulting relationship should not be applied outside of this case study due to that material dependency.

2.8 *Characterization of Railroad Track Substructures using Dynamic and Static Cone Penetrometer (Hong et al., 2016)*

A dynamic and static cone penetrometer (DSCP) is developed for characterization of rail-road track substructures. The DSCP consists of an outer rod for dynamic penetration in the ballast and sub-ballast layer and is an extendable inner rod for static penetration in the subgrade.

The DSCP is dynamically penetrated into the ballast and sub-ballast. In the subgrade, the inner rod with the mini cone is pushed. A dynamic cone penetration index is measured in the ballast and sub-ballast layer, and cone tip and friction resistances are obtained in the subgrade with a high resolution.

This is a hybrid of the cone penetrometer tests for penetrating ballast material. The dynamic component has a DSCP index associated. The standard DCP has an energy of 45J with a drop height of 575mm / 510mm and hammer weight of 8kg / 9kg. The drop height corresponds to the DCP but with no weight equivalent. The DCPI index is therefore new, and a discussion on why the index did not adopt the DCP standard would be useful as many existing correlations exist for the standard DCP.

The example experimental result (Figure 11) has 2 measurements (DCPI and cone tip resistance). As the main aim was for penetrating the ballast, the usefulness of the DSCP index needs further discussion.

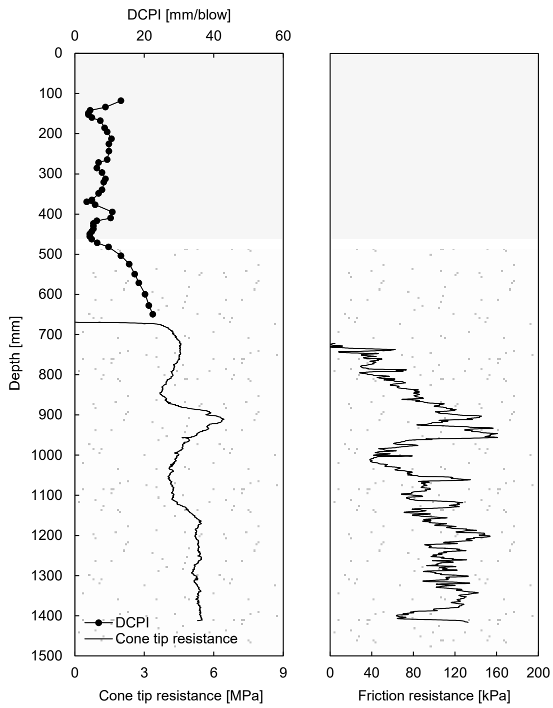

Figure 11. Experimental Results.

2.9 *Remedial measures to facilitate the construction of stable bridge approach fills-a case study (Diyaljee, 2016)*

This paper deals primarily with stability issues associated with the proposed 20 m high bridge approach fill. In November 1988 deep seated movements were noted at a depth of 22 m below the original ground from monitoring of slope indicators on the north approach. Remedial measures consisting of wick drains, stone columns, flatter approach fill head and side-slopes, and interceptor drains were then implemented.

The implementation of the remedial measures did not fully arrest the ground movements. As a result, the fill slope was modified. As the movements were taking place at depth it was decided to abandon the proposed 3-span bridge and construct a one-span Bailey bridge. This paper addresses the geotechnical investigation, evaluation and assessment of the bridge approach fills and the remedial measures implemented to minimize the movements

This is case study which is a bit dated except for a recent site observation in August 2013 which showed that the bridge is still serviceable after 23 years.

This provides an interesting reference case study to now assess if more recent understandings and/or design and construction techniques would have affected the decisions at the time. This would be in hindsight wisdom of course.

Monitoring of this bridge by survey hubs between June 2 and October 11, 1990 showed initial movements of 7 mm per day to July 4 and thereafter 1.2 mm per day. The bridge is still serviceable, but at 1.2mm / day, then over 100 mm had occurred in that period. One assumes that rate stopped over the next 23 years (or it would be over 10m movement). What was the final movement and hence tolerable movement for this type of bridge would be a key learning for industry.

Moulton et al. (1985) use intolerable movements of 100mm and 50mm for vertical and horizontal movements – but these were not for Bailey Bridges. These movements were significantly exceeded during the initial monitoring phase, and this case study shows the flexibility of Bailey Bridges.

2.10 *New and Innovative Approach to Ensuring Quality of Quarry Source Materials in Queensland Road Infrastructure Construction (Dissanayake and Evans, 2016)*

This paper discusses an approach that the Department of Queensland Transport and Main Roads (QTMR) adopts to manage the quality of road construction quarry products. A Quarry Registration System (QRS) was developed between QTMR and the Quarry Industry to address concerns that excessive testing was resulting in increased costs which were being passed on to the Department's construction projects. Guidelines allows the quarry management to self-assess their own testing frequencies and allows the Department as well as Quarry Industry to concentrate testing resources to where risks are highest. Testing frequency reductions of 90% have been realized in some cases with well managed quarries.

This paper is essentially about a management system for assessing quarries. Quality Assurance requires establishing the material variability (such as the coefficient of variation - COV). Each test listed would have a different COV (homogeneous vs heterogeneous) and the tests with the largest COV would represent the greatest quality "risk". Testing frequency is really only a subset of that risk profile (Figure 12). That level of technical detail would be useful to benefit the technical community. Reference to an associated paper Dissanayake & Evans (2015) provided no further detail, and with modest differences between the 2 papers.

.

Figure 12. Frequency of Testing.

The list of tests required has been extended from the 2015 paper, but excluding 2 tests shown. Table 3 compares between the 2015 and 2016 papers. The rationale for this change would be useful. A ranking order (not shown), where some tests are mandatory, some are secondary and others as required would be useful discussion, as each test would not be given the same weighting by QTMR.

Table 3. Relevant source material Tests.

Source Rock Property Test ISC5 (2016)	Dissanayake & Evans (2015)
Petrographic Analysis	√
Wet 10% Fines Value	√
Wet/Dry Strength Variation	√
Degradation Factor	√
Particle Density (SSD)	√
Water Absorption	√
Bulk Density of Aggregate	--
Soundness (Sodium Sulfate)	--
Polish Aggregate Friction value	√
Weak Particles	--
Crushed Particles	--
Methylene Blue Value (MBV)	--
Sand equivalent	√
Light Particles	--
Particle Size Distribution	--
Material Passing 75µm	--
Material Passing 2µm	--
Organic Impurities	--
Sugar Presence	--
Sulfate Content	--
Chloride Content	--
	Alkali Silica Reactivity
	Alkali Carbonate Reaction

The original cost of testing was 1.5% of the road quarry materials. That testing has now been reduced in half with this QMS system.

The paper contributes to our understanding of the requirements for this quality management system, but gives little detail in terms of the quality control testing requirements, by only listing the type of test rather than acceptable, uncertain and unacceptable test boundaries. A few such indicators during the presentation would enhance our understanding of the QRS. Reference to specification and quality control details would also be required to be implemented and understood (Figure 13).

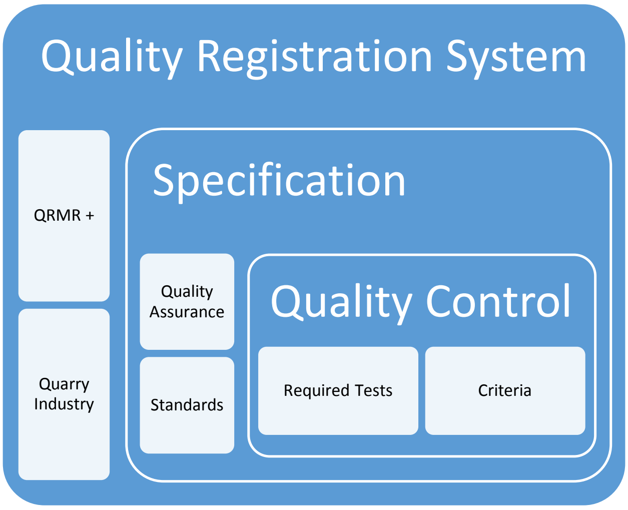

Figure 13. QRS and supporting documents.

2.11 *Evaluation of rockfill embankments by field tests in Siraf Refinery Complex site, Iran (Asghari-Kaljahi et al., 2016)*

Rock fill was used to fill valleys with up to 35m height required in some places. Trial embankments were used with lift thickness of 30, 45 and 60 cm and with 3 different compaction efforts. Differences between compaction percentages of 45cm and 60cm lift thickness showed the vibratory 15 ton roller compaction rate would be more effective in 45cm lifts. Various test were used to determine the compaction requirements. These tests consisted of field grading, large density, plate load test and surface seismic tests.

Constructing to "standard" maximum loose lift thickness of 300mm with heavy plant and 95% Standard compaction may be adequate for small to medium size project. But with large quantities of fill, a trial should be used to evaluate a best for project specification. The methodology and testing associated with development of such a specification is what is presented in this paper. This is a sound approach with some interesting insights.

The grading curve (Figure 14) should always be sue with caution in rock fill as soil testers sample a shovel into their sample bag. Hence, these curves show 200 to 300mm maximum. Clearly these are larger sizes (Figure 15). This highlights a common failure in industry (and this reporter has noted this in Australia on many projects) where soil testers do not place large sizes into their sample bag. Hence grading curves may be misleading with rock fills.

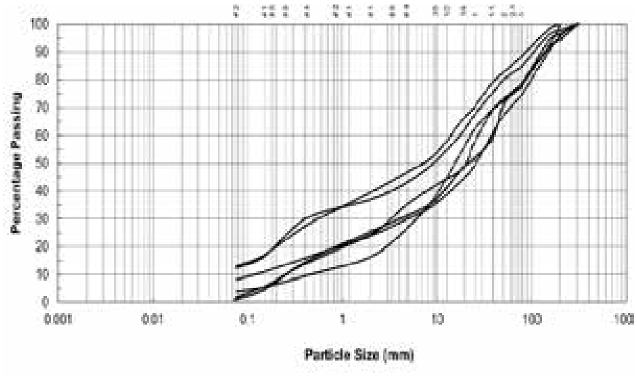

Figure 14. Particle size distribution curves rock-fill materials

Figure 15. Spreading of rock fill material.

At 8 passes, there was a reduced density as compared to 4 and 6 passes. The authors suggests it would be the result of particle breakage and loosening below the roller. This is an interesting result.

Both large in place density tests (water replacement) and the usual compaction test were carried out with 75mm and 20mm maximum sizes, respectively.

For the 20mm maximum size test, the maximum dry density was 21.6 kN/m^3 and 22.8 kN/m^3 for the uncorrected and corrected tests, respectively. A density change of 5.5% due to oversize. Even the large scale water replacement requires correction for oversize and that data would also be useful.

The modulus values seem high. Perhaps this was the first cycle of loading. For placed fill the second cycle of loading would be more relevant if that parameter was used in design. That said, the test as used is more as a comparative number to evaluate between passes / thickness rather than as a design value.

3 OVERVIEW

All of the papers in this session on "Pavements and Fills" could be in an alternative session heading, e.g. Sessions on "Case Histories", "Interpretation of in – situ tests", etc. Categorizing papers therefore ends in the trap of placing in another session heading. There are also associated papers in other sessions that could just as easily have been categorized into this session.

Readers interested in this topic areas should therefore look more bodily at other papers as well.

These discussions points are meant to be a prompt for possible discussion during the presentations, however the scheduling of this session report means that some presentations may have already occurred.

Quality Control (compaction) issues governs. Most are still wrestling with the basics of:-

- Density
- DCPs
- CBRs
- Gradings
- Oversize affects lab values

These simple issues affect our results. Standard CBRs, compactions and many lab testing cannot use large sizes and this is often over looked in our use of laboratory results. Issues that are trending in earthworks control are:-

- Light Falling weight Deflectometers
- Shear wave velocity
- Modulus Measurements
- Penetration testing
- Deeper Lifts

A clear shift to in situ testing is evident. Our comfort with the past approaches seem to hamper the progression and application of these tests. They provide a more direct measurement rather than density which "assumes" a permeability, strength or modulus has also improved without directly knowing by how much. A shift in quality control to these modern tools can be expected in time.

4 CONCLUSIONS

"Pavements and Fills" papers remain dominated by quality control processes with simple testing and low cost procedures a major consideration. A move away from the traditional density testing to other approaches is also apparent. Modulus has greater importance than strength.

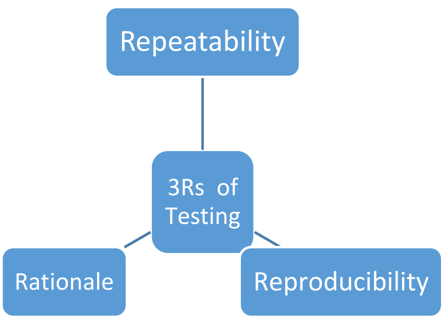

Figure 16. The 3Rs of Testing

Provided we confirm the 3Rs of testing (Figure 16), the traditional (and often outdated) approaches will continue to give way to the technology shown at this 5th International conference on Geotechnical and Geophysical Characterisation. "In Pursuit of best practice" is not just a conference theme, but an obligation we must continue with - forever.

5 REFEREENCES

Briaud J.L. & Saez D. (2012). Soil compaction: Recent Developments. International Conference on Ground Improvement and Ground Control, Wollongong, Proceedings of the International Conference on Ground Improvement and Ground Control, Edited by Buddhima Indraratna, Cholachat Rujikiatkamjorn & Jayan S. Vinod, pp 3 – 30.

Burnham T. R. (1997). Application of dynamic cone penetrometer to Minnesota Department of Transportation Pavement Assessment Procedures. Report MN/RC – 97/19.

Dissanayake, A. & Evans, P.A. 2015. Queensland Transport and Main Roads Department Quarry Registration System 511-514, Geotechnics for Sustainable Development; Proc. intern. Conference on Geotechnical Engineering, ICGE-Colombo-2015, 10-11 August 2015.

Lacey D, Look B and Williams D (2015). Relative Modulus Improvement due to inclusion of geo-reinforcement within a gravel material. 12th Australia New Zealand Conference in Geomechanics, Wellington, N.Z., p123.

Look B (2012). Quality control specifications for large earthworks projects. International Conference on Ground Improvement and Ground Control, Wollongong, Proceedings of the International Conference on Ground Improvement and Ground Control, Edited by Buddhima Indraratna, Cholachat Rujikiatkamjorn & Jayan S. Vinod, pp 1113 – 1118.

Massarsch, K. R. 1999. Dynamic compaction of granular soils. State-of-the art report, Lecture Series: A Look Back for the Future, Lecture Series, University of Zejiang, China, pp. 181 - 223.

Moulton L.K., Gangarao, H.V.S. and Halvorsen G.T. (1985), "Tolerable movement criteria for highway bridges" Report No. FHRA / RD – 85 / 107, Federal Highway Administration, Washington

Robertson P.K. (2015). CPT for quality control of ground improvement (deep compaction). Webinar #13: www.greggdrilling.com/webinars/DwIgW/cpt-for-quality-control-of-ground-improvement-deep-compaction

Scott Brendan T. & Jaksa Mark B. (2015). A field based study of the effectiveness of roiling dynamic compaction. Ground Improvement Case Histories: Compaction, Grouting and Geosynthetics, Edited by Buddhima Indraratna, Jian Chu & Cholachat Rujikiatkamjorn.

Geotechnical and Geophysical Site Characterisation 5 – Lehane, Acosta-Martínez & Kelly (Eds)
© 2016 Australian Geomechanics Society, Sydney, Australia, ISBN 978-0-9946261-1-0

Session Report on Sampling and Laboratory Testing

J.A. Pineda
ARC Centre of Excellence for Geotechnical Sciences and Engineering, The University of Newcastle Australia

ABSTRACT: This report provides an overview of the reviewed papers presented at the Conference under the theme of sampling and laboratory testing. Two key themes namely 'sampling and sample quality assessment' and 'Testing' are reviewed.

1 INTRODUCTION

This Session Report reviews the topic of Sampling and Laboratory Testing based on 11 papers submitted to the 5th International Conference on Geotechnical and Geophysical Site Characterization, Gold Coast, Australia. The papers presented to this session describe a wide range of natural as well as artificial geomaterials, varying from sands to highly plastic clays and mudstone. The majority of the natural soils correspond to high plasticity clays and silts whereas artificial soil specimens (silica silt-kaolin mixtures) are used to represent the behaviour of the so-called *intermediate soils* (e.g., silty clays, clayey silts with PI typically between 0-10) (Figure 1). Two key themes, *Sampling and Sample Quality Assessment* as well as *Laboratory Testing*, are reviewed in the report, identifying the main findings of the studies reported.

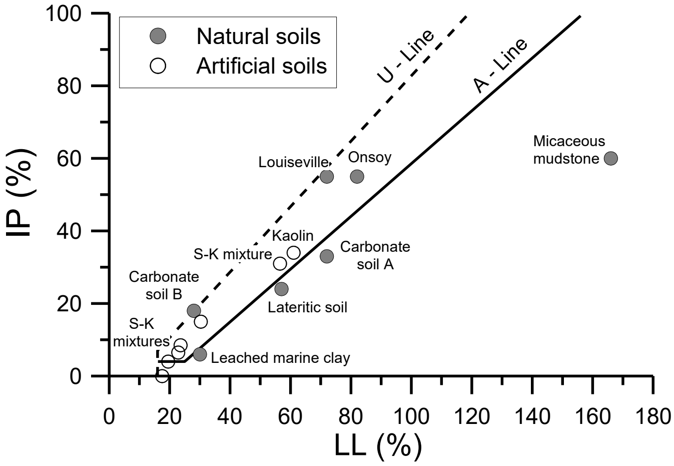

Figure 1.Plasticity of soils tested.

2 SAMPLING AND SAMPLE QUALITY ASSESSMENT

Available criteria for assessing sample quality in soils have been developed using laboratory results obtained primarily for marine clays (PI between 6 and 43) retrieved from relatively shallow depths (5-25 m). Sample quality is estimated in terms of the volumetric strain change (SQD, Andresen and Kolstad, 1979; Terzaghi et al., 1996) or the normalized voids ratio change ($\Delta e/e_0$, Lunne et al., 1997) caused during recompression to the *in situ* effective stress in laboratory tests. These methods are currently used to evaluate sample quality in a wide variety of natural soils without additional considerations. Although the influence of OCR is accounted for, no correction is considered for recompression to *in situ* stress in specimens with high overburden stresses which have been subjected to large stress relief due to sampling. The paper by *Krage et al.* explores this topic by using artificial silica silt-kaolin mixtures to prepare reconstituted specimens with PI ranging from 0 to 31. Specimens are subjected to a wide range of overburden stresses ($20 < \sigma'_{v0} < 500$ kPa) to establish depositional stress history. Two levels of disturbance are then induced as follows: 1D 'perfect sampling' (1DPS) and highly disturbed (HD) state. 1D 'Perfect sampling' condition is achieved via removal of deviatoric stress until reach K_0 of 1 whereas highly disturbed specimens are obtained by applying a freezing-thawing cycle under unstressed conditions. HD samples are then loaded beyond the preconsolidation stress followed by unloading until achieve K_0=1, as imposed to 1DPS specimens. Finally, both 1DPS and HD samples are loaded further to a vertical effective stress of 2500 kPa. Figure 2 shows HD specimens range from very good to excellent to poor sample quality. These results are inconsistent with level of disturbance induced to each specimen. There, the influence of the stress relief (overburden stress) on $\Delta e/e_0$ in HD specimens should be considered. *Krage et al.* suggest that the incorporation of the unloading-reloading stiffness would be useful to improve the assessment of sample quality in low plasticity soils subjected to large stress relief.

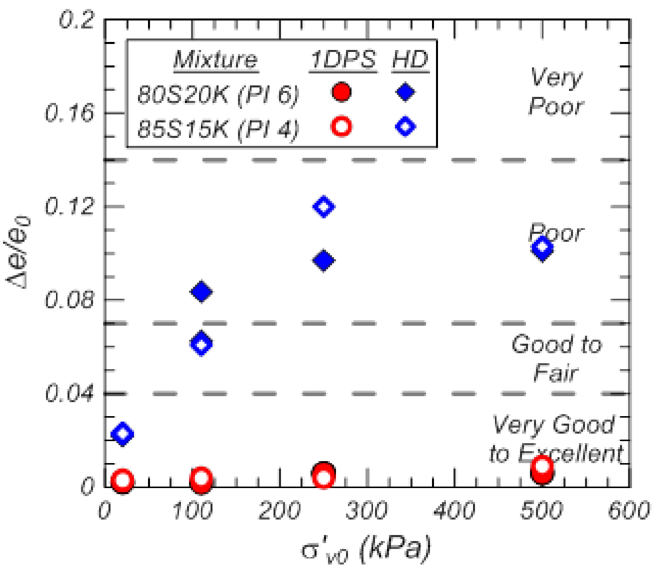

Figure 2. Sample quality assessment for 1DPS and HD specimens (4 in-situ stress levels and 2 mixtures: PI=7 and PI=4) (from *Krage et al.*).

Emerging tube sampling techniques are nowadays getting attention from practitioners due to the well-recognized issues of standard sampling techniques for obtaining undisturbed specimens in granular soils (e.g., clean and silty sands) as well as the cost-prohibitive use of the freezing technique. This is the case of geotechnical projects where the liquefaction potential has to be evaluated. There, high-quality soil specimens are required to carry out laboratory tests. *Stringer et al.* describe the use of the Gel-Push tube sampling technique for obtaining undisturbed specimens of silty soils, micaceous silts and clean sands in New Zealand. The Gel-Push (GP) sampling technique (e.g., Lee et al., 2012), which keeps the same operational principle as the Osterberg fixed-piston sampler, assumes that the main source of soil disturbance is due to sidewall friction as the soil enters the tube sampler. To overcome this problem, a low friction polymer gel is injected which acts as lubricant. Three different versions of Gel-Push sampler are available (GP-S, GP-Tr and GP-D) depending on the system employed to deliver the gel to the base of the sampler. *Stringer et al.* used the GP-S sampler in silty soils and silts whereas an attempt was made with the GP-Tr version in clean sands (Figure 3). Sample quality is assessed by visual inspection after soil extrusion as well as from the comparison between in situ and laboratory shear wave velocity measurements. *Stringer et al.* report a successful trial using the GP-S sampler in silty clays and silty sands. They also provide some comments about particular operational aspects for further application of the sampler in similar soils. Large amount of swelling, which led to poor sample quality, is reported for the GP-S in micaceous silts. The trials using the GP-Tr sampler indicate that further improvements are required to obtain undisturbed specimens, at least in the case of clean sands. Overall, the GP sampling technique appears to be very promising for obtaining high-quality specimens in complex natural soils deposits.

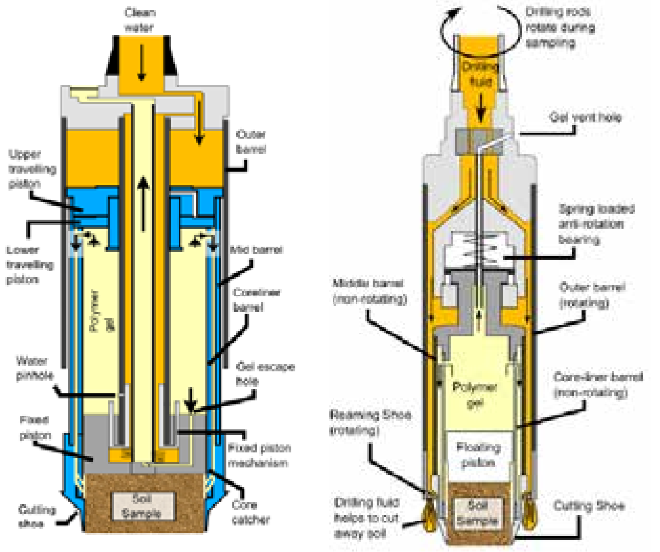

Figure 3.Schematic view of the GP sampler. (a) GP-S sampler. (b) GP-Tr sampler (from Stringer et al.)

Soil sampling in offshore projects put forward additional challenges which make difficult to obtain undisturbed specimens for laboratory testing. Gravity samplers are commonly employed in offshore geotechnics, mainly for characterization purposes, due to its operational simplicity and economical cost. A common observation is the larger sampler penetration regarding to sampler recovery. The contribution by *Ramsey* proposes an approach for predicting sampler penetration and sample recovery by using CPT data. It is assumed that the soil recovery is less than the sampler penetration due to a temporary tube ‘plugging’ at one or more elevations during penetration. The phenomenon of tube ‘plugging’ occurs when the friction resistance exceeds the bearing capacity of the soil. Analytical expressions are provided in the paper to estimate ‘plug’ as well as ‘unplug’ resistances (F_{plug} and F_{unplug}) used to predict the elevations at which tube ‘plugging’ may occur: $F_{unplug}/F_{plug}>1$.

The applicability of the proposed methodology is demonstrated by using a case study where CPT data are available (Figure 4). Tube ‘plugging’ is predicted to occur at three different levels which is in agreement with the sampler inspection. Maximum variations of -15% in tube penetration and +/- 10% in sample recovery are reported by *Ramsey* for the case study described in the paper. Further improvements to the proposed technique are discussed by the Author in order to minimize uncertainty of the predicted sample recovery.

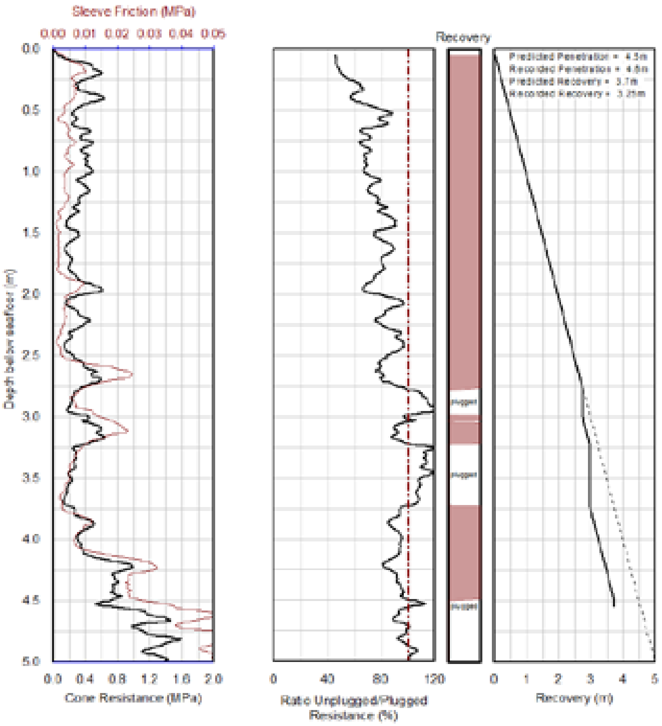

Figure 4.Assessment of sampler recovery (from *Ramsey*).

3 LABORATORY TESTING

3.1 *Undrained shear strength and soil sensitivity*

Amundsen et al. describe the geotechnical characterization of Rissa clay, a lightly overconsolidated low plasticity (OCR≈2; PI≈8.5) leached marine clay from Norway. The soil profile at Rissa site, estimated using electrical resistivity tomography (ERT), shows a complex geological environment formed by the indentation between two mountain ridges filled with marine clay as well as sand and gravel deposits (see Figure 5a). The shallow upper 9 m correspond to leached marine clay with salt content ranging between 2.0 to 9.5 g/l. High-quality block specimens, retrieved from 4 m depth using the Sherbrooke sampler, are used to characterize the mechanical behaviour of the clay. Additional specimens retrieved using piston samplers (54 mm and 73 mm in diameter) allow the Authors to assess sample quality based on the results from one-dimensional and triaxial compression tests. The comparison shows that, as would be expected, block specimens produce the highest sample quality followed by the 73 mm piston sampler. *Amundsen et al.* explores the rate dependency of the undrained shear strength in Rissa clay by means of CAUC triaxial tests. The undrained shear strength increases around 20% with the strain rate from 0.1%/h to 4.5%/h (typical strain rates in Norway varies from 0.7%/h to 3.0%/h). This behaviour is in agreement with the results presented by Lunne and Andersen (2007) for NC and OC Norwegian clays (Figure 5b). It is shown that the failure envelope of Rissa clay is not affected by rate effects. It means that the shear strain rate only affects the induced excess pore pressure without modifying the effective cohesion or the friction angle of the soil. The influence of the strain rate on the preconsolidation stress of Rissa clay (one-dimensional loading) is also explored by comparing estimations of σ'_{prec} obtained from Incremental Loading (24h load steps) and Constant Rate of Strain (1.5%/h) tests. An increase in σ'_{prec} of 16 % is reported for the case of the CRS test. Overall, the mechanical behaviour of Rissa clay is consistent with the response of other Norwegian low plasticity clays previously reported in the literature.

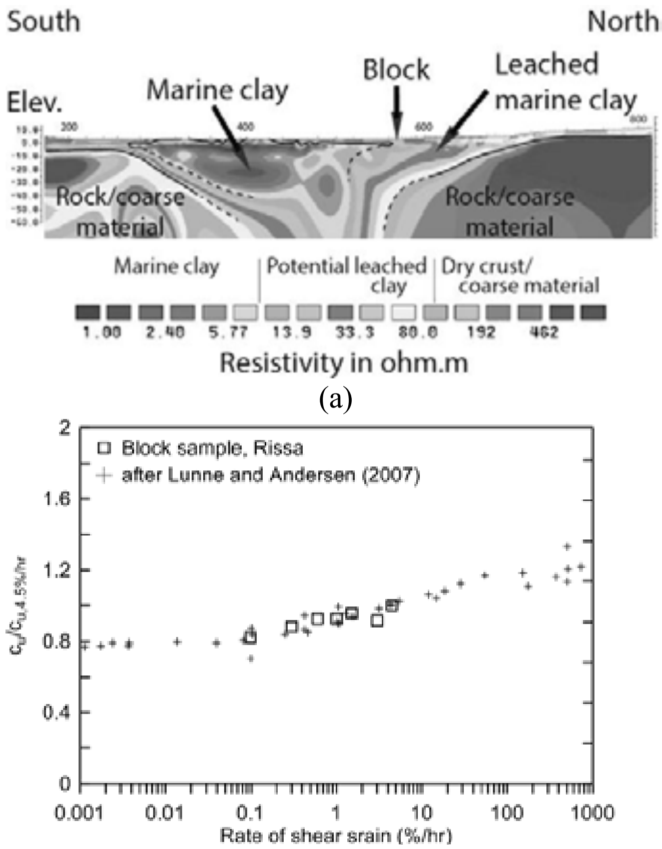

Figure 5.(a) Geophysical profile at Rissa site. (b) Normalized undrained shear strength of Rissa clay as a function of the strain rate (from *Amundsen et al.*).

The paper by *Hirabayashi et al.* describes the engineering properties of three natural high-plasticity soft clays estimated from in situ and laboratory tests: Onsoy clay (Norway), Louisville clay (EEUU) and Mexico City clay (Mexico). Particular emphasis is given here to the estimation of the cone factor N_{kt}, required to compute the undrained shear strength, by comparing CPTu data against in situ (Field Vane

Test, FVT) as well as laboratory tests results (constant-volume Direct Shear Tests, DST, and Unconfirmed Compression Test, UCT). As would be expected, N_{kt} varies depending on the testing method with no appreciable influence of the soil type. The cone factor N_{kt} seems insensitive to changes in plasticity index irrespective of the clay type (see Figure 6). Mean values of N_{kt} are: 12.5 (FVT), 13.4 (UCT_ and 11.5 (DST). *Hirabayashi et al.* claim further clarification in the Standards to select the testing technique for estimating the undrained shear strength (and therefore N_{kt}) in soft clays.

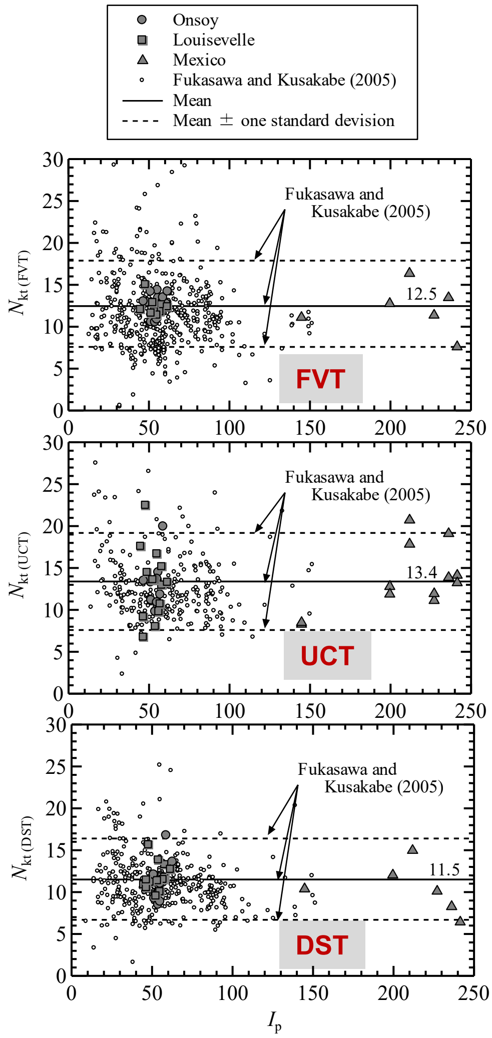

Figure 6.Estimated values of N_{kt} as a function of PI (from *Hirabayashi et al.*).

The contribution by *Arsalan et al.* reports a laboratory investigation carried out to estimate the undrained shear strength as well as the anisotropic yield surface of a natural diatomaceous mudstone from Japan. A comprehensive experimental program that included CID as well as CK_0U triaxial tests is used to study the yielding behaviour of this complex naturally cemented soft rock. CID tests results are used to map the initial yield surface of the mudstone which seems to be well-represented by the Original Cam Clay (OCC) model (see Figure 7a). The stress-strain response observed in CK_0U compression tests shows an increase in rock brittleness with overconsolidation state: from 25% in NC samples up to 40% in OC specimens. Anisotropic consolidation leads to the enlargement of the yield locus with a variation in shape so that the effective stress ratio at maximum deviatoric stress differs from the stress ratio at critical state (see Figure 7b). The OCC model is therefore unable to represent the new yield locus. *Arsaland et al.* propose a modification of an existing yield function to properly capture the (macroscopic) anisotropic response of the mudstone. As indicated by a solid black line in Figure 7b, good agreement between the experimental results and the model simulations is achieved by using the modified anisotropic yield locus.

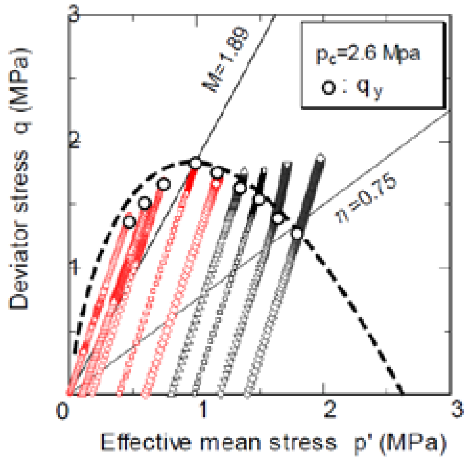

(a)

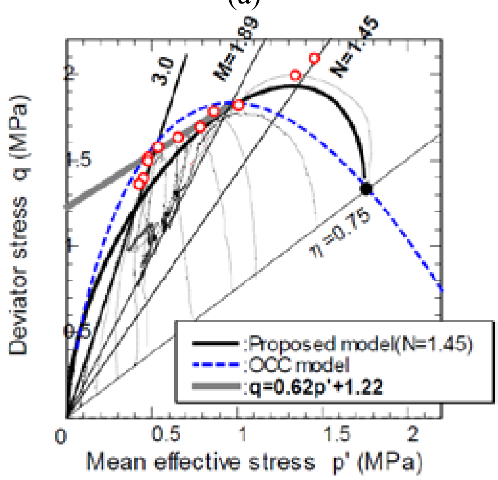

(b)

Figure 7. (a) Stress paths and yield surface from CID triaxial tests. (b) Stress paths and anisotropic yield surface from CK_0U triaxial tests (from *Arsalan et al.*)

The paper by *Boukpeti and Lehane* explores the use of simple laboratory techniques for the estimation of the soil sensitivity in two natural carbonate soils (Soil A and Soil B) retrieved using Shelby tubes from the North West Shelf in Australia. Although both soils display similar mineralogical compositions (mainly calcite and aragonite) Soil A classifies as a well-graded clayey silt whereas Soil B is a well-graded silty sand. Fines content/clay fraction are equal to 85/28 and 35/10 for Soil A and Soil B, respectively. Soil sensitivity (S_t) is evaluated by means of three different laboratory tests as follows: fall cone (apex angle of 30, cone mass of 80g and cone factor K=2), hand vane (rotation speed of 1 r.p.m) as well as miniature T-bar penetrometer (resistance factor N_p=10.5). Values of soil sensitivity show important differences depending on the testing method. In Soil A, S_t increases with depth for the fall cone (4-33) and T-bar (9-18) but it remains approximately constant for the hand vane (~ 4) (see Figure 8a). Soil B shows lower soil sensitivity than Soil A which is indicative of differences in soil structure. S_t ranges around 4-18 for the fall cone and remains almost uniform for the hand vane (~ 6) (T-bar was not used in Soil B). Tests carried out on reconstituted Soil A show that St reduced, around 2 times less the value measured in undisturbed specimens. This behaviour remarks the importance of the natural soil structure which may not be created by reconstitution methods. The use of available correlations for soil sensitivity and liquidity index (LI) predict large variation in S_t for specimens with similar liquidity indices (LI). *Boukpeti and Lehane* conclude that LI is not an adequate parameter to assess the sensitivity of carbonate soils. The Authors use results obtained from one-dimensional compression tests carried out on Soil A to estimate soil sensitivity following the sensitivity framework proposed by Cotecchia and Chandler (2000). There, sensitivity prediction is based on the distance of the yield point in compression to the Intrinsic Compression Line, ICL: $S_t = \sigma'_{vy} / \sigma'_{ey}$ (Figure 8b). Estimated values of St are slightly lower than sensitivities measured on specimens of similar depths. This discrepancy is attributed partly to disturbance caused by tube sampling.

3.2 *Cyclic undrained shear strength*

The common assumption in offshore design of a unified failure criterion for normally consolidated clays under symmetrical and non-symmetrical undrained cyclic loading conditions is studied in the paper by *Zografou et al.* The results of symmetrical and non-symmetrical Cyclic Direct Simple Shear (CDSS) tests carried out on normally consolidated kaolin are discussed. The CDSS tests were carried using stacked rings to restrict the lateral deformation. The vertical load was adjusted during the cyclic shearing stage in order to ensure constant volume conditions. Samples used in symmetrical cyclic loading tests were incrementally consolidated to a maximum vertical effective stress of 150 kPa. This value reduced to 70 kPa in non-symmetrical tests. The cyclic loading was applied at a frequency of 0.1 Hz and it was maintained for N=1000 cycles unless failure was achieved earlier. Low stress levels were used by *Zografou et al.* during CDSS tests in order to simulate similar conditions to those occurring in offshore subsea structures. Results from symmetrical loading tests show that failure is achieved by cyclic degradation at a maximum shear strain of 4-5% (vertical dashed line in Figure 9a). On the other hand, shear strain accumulation is the failure mechanism observed in non-symmetrical tests (Figure 9b). The maximum shear strain is in this case much higher than achieved in symmetrical tests. It means that independent failure criteria should be used in design depending on the loading type. Shear strain contour diagram for symmetrical cyclic loading (only) is provided in the paper which could be used in design. In the case of non-symmetrical tests, high tolerances to movements (larges shear strains) should be considered for the definition of the failure criterion.

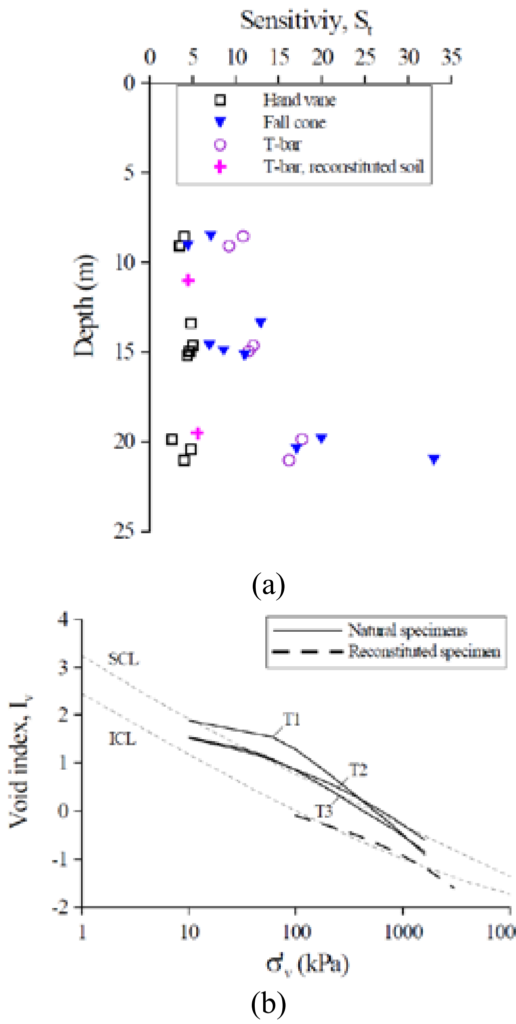

Figure 8.(a) Variation of St with depth for Soil A. (b) Estimation of St from oedometer test results (from *Boukpeti and Lehane*).

A simple methodology for the assessment of the cyclic softening in clays from Matsyapuri (India) is described by *Raskar-Phule et al.* The term ‘cyclic softening’ refers to the temporal reduction in clay strength due to the increase in excess pore pressure during undrained cyclic loading (e.g. earthquakes). The soil profile under study is composed by an upper zone fill layer (clayey sand + gravel) overlaying high plasticity cohesive layer of around 6.7 m thickness. The cyclic softening is assessed at five locations by evaluating the cyclic resistance ratio (CRR) and the cyclic stress ratio (CSR). A factor of safety (FoS=CRR/CSR) of 1.3 is adopted as threshold value to establish the occurrence of cyclic softening of Matsyapuri clays. CSR and $CRR_{7.5}$ are estimated following the proposals by Idriss and Boulanger (2008) and Idriss and Boulanger (2007). In the absence of laboratory as well as in situ estimations, values of undrained shear strength are computed using an empirical correlation expressed in terms of N_{SPT}, water content, liquid limit and plasticity index. Earthquakes of moment magnitudes 6.5 and 7.5 are considered in combination with maximum accelerations of 0.16 g and 0.3 g. For such scenarios, the results of this rather simple methodology show that clays at depths between 3.75 m to 12 m may be subjected to cyclic softening.

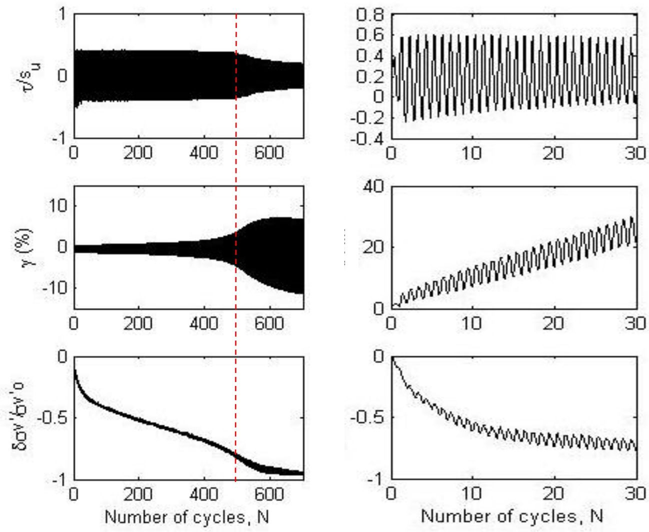

(a) (b)

Figure 9.(a) Symmetrical CDSS test results for τ_{max}/s_u=0.40. (b) Non-symmetrical CDSS test results for τ_{max}/s_u=0.60 and τ_{ave}/τ_{cyc}=0.5) (from *Zografou et al.*)

3.3 *Small strain stiffness*

The contribution by *Décourt et al.* compares estimates of small-strain shear modulus (G_0) from *in situ* and laboratory tests for a Brazilian lateritic soil. As expected, very good agreement is observed between *in situ* seismic tests (cross-hole and SDMT). *Décourt et al.* correlate values of G_0 (cross-hole) with N_{SPT} values obtained from SPT tests and compare them against available relationships from the literature for non-cemented soils. Site-dependent empirical correlations for lateritic soil deposits are also considered. It is shown the relationship between G_0 and N_{SPT}, q_c, p' (and e) is not properly captured by using general expressions for non-cemented soils (including temperate zone soils). Lateritic soils display a much higher small strain stiffness than the predicted by using expressions for non-cemented soils. The reason for such higher soil stiffness in lateritic soils is attributed by the Authors to chemical bonding.

3.4 *K_0 estimation in granular materials*

Lee et al. revisit the expression proposed by Jaky (1944) for the estimation of the coefficient of earth pressure at rest (K_0=1-sinφ′) in granular materials. By using oedometer tests results carried out on sand, glass beads and etched glass beads it is shown that the use of the critical state friction angle ϕ'_c in the original Jaky's equation is not able to capture both the behaviour of uniform and irregularly angular particles. Good agreement is only obtained in the former case. By adopting an inter-particle strength model, the following modified expression for K_0 is proposed in terms of the critical state friction angle ϕ'_c which incorporates a new parameter β to account for the particle interlocking:

$$K_0 = \frac{1-\sin(\beta \cdot \phi'_c)}{1+\sin(\beta \cdot \phi'_c)} \quad (1)$$

Equation (1) is expanded further to consider the influence of relative density (D_R) on particle interlocking by incorporating an experimentally-based relationship between β and D_R, given by: $\beta=a[D_R(\%)]^b$, where a and b are correlation parameters.

4 CONCLUDING REMARKS

The papers submitted to the technical session on *Sampling and Laboratory Testing* at the 5th International Conference on Geotechnical and Geophysical Site Characterization provide a useful snapshot of the current state of practice. The following general observations can be inferred.

The effects of sampling depth on sample quality are not well quantified using current clay-based quality criteria. Consideration of overburden stress and stress history is crucial for the correct assessment of sample quality in intermediate soils.

Emerging sampling technologies like the GP sampler are currently getting attention due to their potential use in complex soil deposits to provide high-quality specimens for geotechnical characterization. Despite being a global problem, the answers to the sampling issues are local, because they need to be grounded in the local practice of drilling and sounding and be adapted to suit the local geological and geochemical conditions. Further research should be devoted to understand the effects of tube sampling on the soil fabric as it controls the mechanical behaviour of the soil.

The estimation of the static but also cyclic undrained shear strength has been the main topic of the papers devoted to Laboratory Testing. Aspects like the failure criteria for symmetrical and non-symmetrical undrained cyclic loading conditions (crucial in offshore design), the strain rate dependency of the undrained shear strength and preconsolidation pressure as well as the effects of natural leaching in sensitive clays have been discussed in some detail. However, in the Reporter´s opinion, little attention is given in current practice to the presence of cations/ions in natural soils and the application and/or control of geochemical variables (e.g. pore fluid conductivity) during index and mechanical tests.

5 REFERENCES

Amundsen H.A., Emdal A. and Thakur V. (2016). "Engineering characterization of a leached marine clay using SHerbrooke block samples" *Proc. 5th International Conference in Geotechnical and Geophysical Site Characterization, ISC'5 (this issue)*.

Andresen A, Kolstad P. The NGI 54-mm samplers for undisturbed sampling of clays and representative sampling of coarser materials. *Proceedings of the International Symposium of Soil Sampling, State of the Art on Current Practice of Soil Sampling*, Singapore 1979: 13-23.

Arsalan N., Akaishi M. and Sugiyama M. (2016). "Undrained shear strength and anisotropic yield surface of diatomaceous mudstone" *Proc. 5th International Conference in Geotechnical and Geophysical Site Characterization, ISC'5 (this issue)*.

Boukpeti N. and Lehane B. (2016). "Laboratory measurement of sensitivity of carbonate soils" *Proc. 5th International Conference in Geotechnical and Geophysical Site Characterization, ISC'5 (this issue)*.

Cotecchia, F. & Chandler, R.J. 2000. A general framework for the mechanical behaviour of clays. Géotechnique 50(4): 431-447

Décourt L., de Campos Barros J.M., Coaracy O., Quaresma Filho A.R. and Damasco Penna F. (2016) "Maximum shear modulus of a Brazilian lateritic soil from in situ and laboratory tests" *Proc. 5th International Conference in Geotechnical and Geophysical Site Characterization, ISC'5 (this issue)*.

Hirabayashi H., Tanaka M., Fukasawa T., Saegusa H. and Tomita R. (2016) "Engineering properties and cone factor of Onsoy clay, Louiseville clay and Mexico City clay" *Proc. 5th International Conference in Geotechnical and Geophysical Site Characterization, ISC'5 (this issue)*.

Idriss, I.M. & Boulanger, R.W. 2007. SPT- and CPT-based relationships for the residual shear strength of liquefied soils, Earthquake Geotechnical Engineering. In Invited Lectures, K. D. Pitilakis, (ed); Proc., 4th Intl. Conf. on Earthq. Geotech. Engrg., Springer: The Netherlands

Idriss, I.M. & Boulanger, R.W. 2008. Soil Liquefaction during Earthquakes. MNO-12, Earthquake Engineering Research Institute, Oakland: CA.

Jaky, J. (1944). "The coefficient of earth pressure at rest. In Hungarian (A nyugalmi nyomas tenyezoje)." *Journal of the Society of Hungarian Architects and Engineering*, 355–358.

Krage, C., Albin, B.M., DeJong, and DeGroot, D. (2016). "The influence of in situ effective stress on sample quality for intermediate soils" Proc. 5th International Conference in *Geotechnical and Geophysical Site Characterization, ISC'5 (this issue)*.

Lee, W.F., Ishihara, K. & Chen, C.C. (2012) "Liquefaction of silty sand – preliminary studies from recent Taiwan, New Zealand and Japan earthquakes". *In Proc. Int. Symp. Engineering lessons learned from the 2011 Great East Japan Earthquake. Tokyo.*

Lee J., Kim G., Kim I., Kim D. and Byun B. (2016) "Effect of inter-particle strength on K0 correlation for granular materials" *Proc. 5th International Conference in Geotechnical and Geophysical Site Characterization, ISC'5 (this issue)*.

Lunne T, Berre T, Strandvik S. (1997) Sample disturbance effects in soft low plastic Norwegian clay. *Symposium on Recent Developments in Soil and Pavement Mechanics* 1997: 81-103.

Lunne, T. and K. H. Andersen (2007). Soft clay shear strength parameters for deepwater geotechnical design. *6th Int. Offshore Site Investigation and Geotech. Conf.*, *London*, 151-176.

Ramsey N. (2016) "Offshore prediction of sampler penetrateon and recovery using CPTs" *Proc. 5th International Conference in Geotechnical and Geophysical Site Characterization, ISC'5 (this issue)*.

Raskar-Phule R., Nilesh P., Prajas K., Rashmi A. Vaibhav, G. (2016) "Estimating the cyclic softening of clayey soils at Matsyapuri site, Cochin, India" *Proc. 5th International Conference in Geotechnical and Geophysical Site Characterization, ISC'5 (this issue)*.

Stringer M.E., Cubrinovski M. and Haycock I. (2016) "Experience with Gel-Push sampling in New Zealand" *Proc. 5th International Conference in Geotechnical and Geophysical Site Characterization, ISC'5 (this issue)*.

Terzaghi K, Peck R, Mesri G. (1996) *Soil Mechanics in Engineering Practice.* Wiley: New York.

Zografou D., Boukpeti N., Gouvernec S. & O'Loughlin C. (2016) "Shear strain contour diagram for normally consolidated kaolin clay under cyclic loading" *Proc. 5th International Conference in Geotechnical and Geophysical Site Characterization, ISC'5 (this issue)*.

Geotechnical and Geophysical Site Characterisation 5 – Lehane, Acosta-Martínez & Kelly (Eds)

Session Report: Rock and residual soil characterisation

E.A.G. Marques
Universidade Federal de Viçosa, Viçosa, Brazil

ABSTRACT: This report provides a short overview of the topics covered in eight papers submitted to the ISC´5 session on rock and residual soils characterisationon penetration testing.

1 INTRODUCTION

This report presents an evaluation and an overview of the eight manuscripts presented to the Rock and Soil Characterisation Technical Session. The themes were divided in only three papers focus on soils, while the other five presents results on characterisation of rocks. Papers were based on studies developed on five different countries (Australia, Brazil, Iran, Portugal, Singapore). Papers dealing with soils were mainly focused on in situ tests such as CPT, CPTu, SDMT, Seismic (Cross-hole tests), SPT, SPT-T and were applied to a wide range of soil types, including residual (from granite), stiff clays and lateritic soils developed under different climate conditions. The main purpose was, in general, to obtain geotechnical parameters, some of them for design.

For the manuscripts dealing with rock characterisation, two have used Schmidt hammer to characterise rock mechanical properties (one trying to determine strength loss with weathering and the other one its relationship with rock excavability). A third one deals with rock mass strength parameters obtained from rock mass classifications methods and a fourth presents results from plate loading tests used to determine deformability parameters of weak rock masses. The last paper focusing on rock presents the results of hydraulic fracturing test used for the determination of stress behaviour on two rock formations from Singapore.

2 SOIL CHARACTERISATION

The paper by *Shi et al.* entitled “Characterisation of a lateritic soil using laboratory and in-situ tests” deals with the characterisation of residual soils based on field (CPT) (Figure 1) and laboratory investigation of a laterite soil from the Millstream Dam site, southern West Australia (WA). Laboratory tests were performed on intact and reconstituted samples in order to evaluate the influence of soil structure on mechanical and general geotechnical characteristics: hydrometer and sieve particle size distribution, Atterberg limits, mean bulk density, specific gravity, degree of saturation, in situ water content and void ratio, X-ray diffraction, 1D compression (oedometer test) and triaxial tests. Some conclusions from the research were that

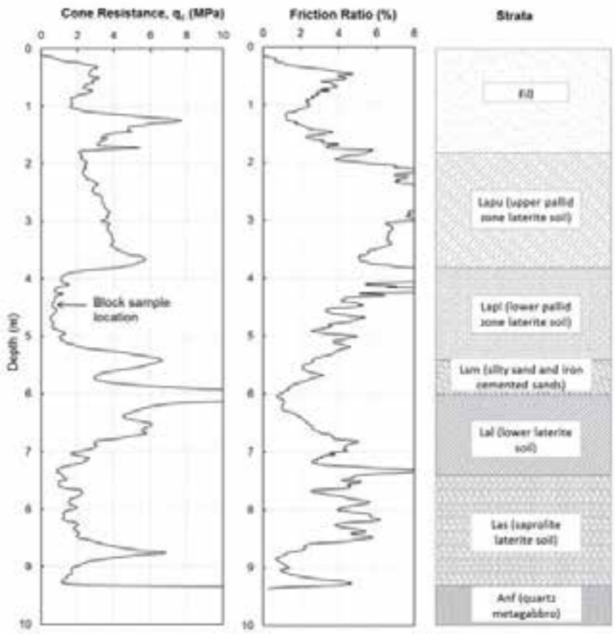

Figure 1 – The in situ CPT test results and soil profile.

Triaxial tests on high quality block samples from the lower pallid zone of a lateritic profile have shown a relatively low level of structure (consistent with a c' value of about 20 kPa) and a comparable friction angle to reconstituted material, as shown on Figure 2. The void ratio of the in-situ material is higher than equivalent reconstituted samples consolidated to the same effective stress level and that the CPT is show to provide reasonable means of assessing the in-situ undrained strength of the type of laterite encountered at the Millstream site.

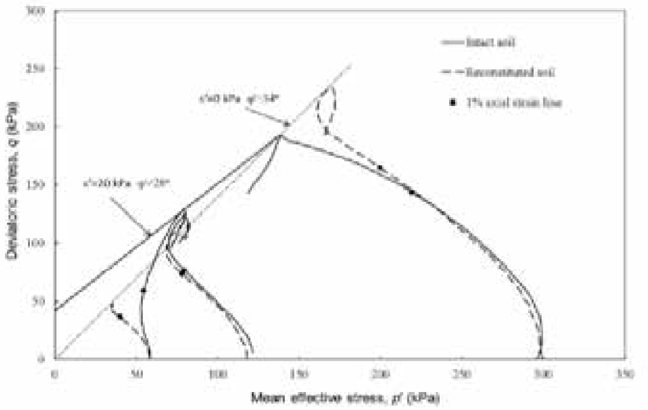

Figure 2 – Stress path in q-p’ space during undrained triaxial compression both in intact and reconstituted (normally consolidated) samples from Shi et al.

Cruz et al. have presented an interesting manuscript, which is entitled “Piezocone tests in residual soils. A Portuguese experience in granitic soils”. The authors state that Residual soils strength characterization it is not an easy task, due to its cohesive-frictional nature as well as disturbance effects related with both sampling and installation of in-situ devices. So, it is fundamental to be sure that any correlations with in-situ test parameters respond properly in these soils. The study presented aims to contribute to the evaluation of adequacy of CPTu current correlations to determine the geotechnical design parameters, in a similar way that was developed by one of the authors (Cruz, 2010) for DMT tests. The study was developed on Porto (North) and Guarda (Centre) regions of Portugal in granitic residual environments, where pairs of tests CPTu+DMT were available. One of the findings is that of strength behaviour, in the context of the range of NSPT deduced from CPTu (Robertson & Cabal, 2010) match perfectly with the results obtained in the field, indicating that the established correlation between the two tests is also valid in residual soils, at least in this specific environment.” Part of the results show that CPT data revealed not strongly structured soils, lying near the lower bound line for cemented materials and converging to the previous findings (Figure 3). Also, the obtained results prove that CPTu tests correctly predict most part of the main geotechnical parameter ranges, with the exception of the deduction of cohesive strength (a correlation has to be settled) and the angle of shear strength that is over predicted when sedimentary approaches are followed. There is a specific research program is under development in IPG experimental site to try to solve this problem.

The paper named “Predicted and measured behaviour of a tall building in a lateritic clay” by Décourt et al. presents the results of a foundation design and the comparison between the predicted and the actual behaviour of this foundation. The study was performed in São Paulo city, Southeast Brazil. Foundation design was based on SPT-T results. Also Cross Hole and SDMT tests have also been carried out and the correlation between G0 and NSPT was used for identifying the lateritic soil type occurring within the area. .

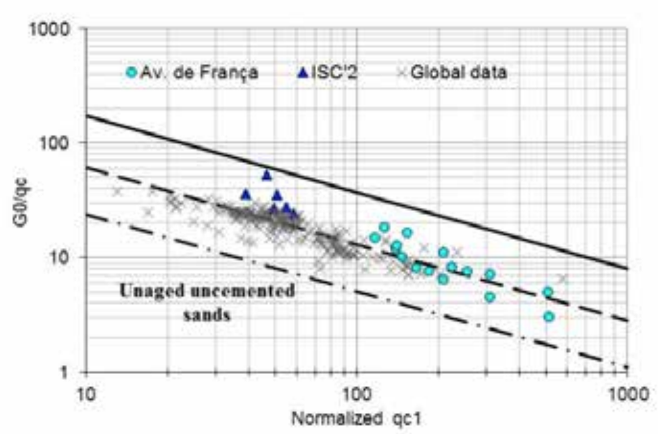

Figure 3 - Cemented/no cemented plot (adapted by the authors from Viana da Fonseca et al., 2007).

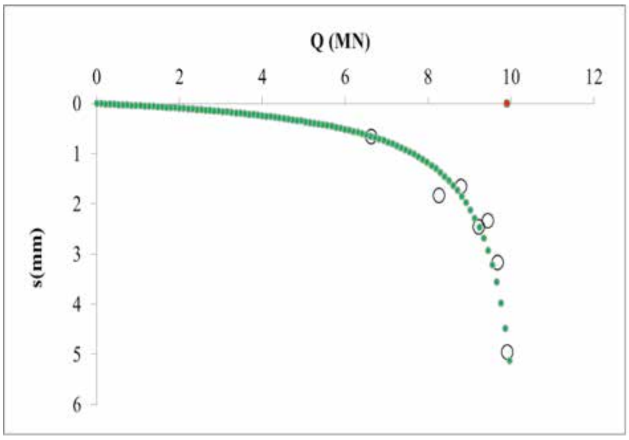

Figure 4 - Example of a corrected load-settlement curve for column P13-B/P15-B.

Later, with the building already under construction, other tests have been performed, exclusively for research purposes. Based on the results, predictions of capacity and deformations of the foundations have been made (as the example showed on Figure 3). Concluding, the authors have mentioned that the initial investigations (SPT-T, Cross-Hole and SDMT) allowed correct assessments of capacity and confirmed the lateritic characteristics of the upper clay layer. But these tests provided no information on the compressibility of this clay, which is fundamental for correct predictions of settlements and was latter obtained from a load test on a square block, which has confirmed the predicted capacity of shallow footings on this clay. Also of paramount importance, the test has shown that the average coefficient of intrinsic compressibility, C, were half of the estimated value used in design and was not constant, as it usually happens with most of the soils, but decreases as the applied stresses increase. So, the study shows the importance of recognizing lateritic clays, as it can present lower settlements.

3 ROCK CHARACTERISATION

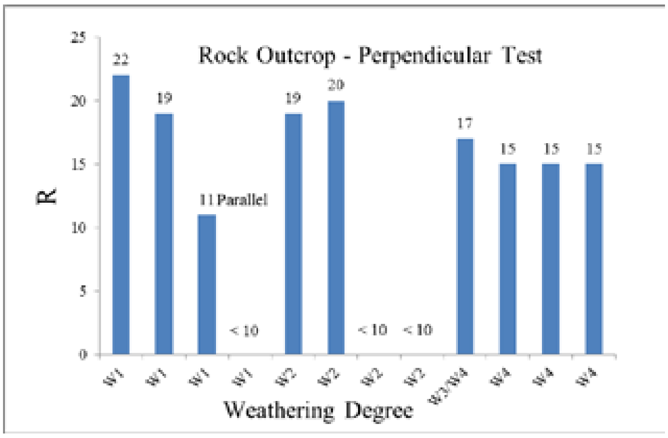

Figure 5 - Results from in situ Schmidt hammer rebound test for one phyllite from Iron Quadrangle.

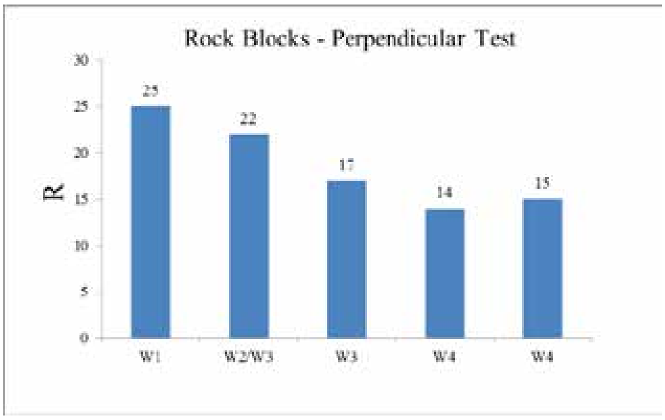

Figure 6 – Results from laboratory Schmidt hammer rebound for one phyllite from Iron Quadrangle.

Leão et al presented some initial results from a study on the "Morphology and geotechnical characterization of a phyllite weathering profile developed under tropical climate" developed in Iron Quadrangle Region, southeast Brazil. The study comprises a complete geotechnical characterization of rock material present in a phyllite weathering profile but the paper only presents the results from a detailed morphological description and Schmidt Hammer tests performed on those materials, both in situ and on lab. Five weathering materials - W1 to W5 (based on ISRM classification) were found. Contacts between different rock weathering materials are sharp and controlled by foliation. Characterization was performed throughout macroscopic analysis of mineralogy and mineralogical changes, evaluation of degree of coherence, fracture characteristics, RQD (from JV ratio) and Schmidt hammer in situ tests. JV, coherence and Schmidt rebound results, specially the last two, shows good correlation with weathering classes. Schmidt rebound has varied from 25 to 14 for W1 to W4 (Figures 5 and 6) and was also able to detect some strength anisotropy as for W1 materials results parallel to foliation the results were equal to 11 while in the direction perpendicular to this structure, the average values were equal to 21.5. The main conclusion is that the morphological description of weathering materials in the filed was in accordance to Schmidt hammer test results and from other authors (Marques & Williams, 2015) as differences on rebound could be observed for more sound materials in comparison to more weathered ones.

The paper Li et al. entitled "Impact of Rock Mass Strength Parameters on Lowwall Stability Assessment Outcomes in Open-cut Coal Mines" presents a rock mass strength estimation process (trough equations 1, by Hoek and Brown, 1997; equation 2, by Hoek, 1998; and Figure 7) applied to underground stope stability assessment and its application to an open cut coal mine over a two year period. The rock mass parameters were obtained from rock mass classifications – RMR, Q-system and GSI. The authors provide no information regarding the localization of the mine and according to them, they have started applying these rock mass strength estimation techniques to open cut coal mining in the last two years (2014?). The main conclusion of the study is that "understanding pit floor rock mass characterisation is the most critical and challenging step for rock mass strength estimation. Identification of floor shear and weak ground can be easily missed due to sparsely spaced exploration holes and limited floor trenches in coal mines." And, because of that "the default material strength values should not be blindly applied to any rock mass condition from aspects of either safety or cost reduction and productivity increase".

$$\sigma_{cm} = 0.5 \times \frac{RMR_{89} - 15}{85} \sigma_{ci} \quad (1)$$

$$\sigma_{cm} = 0.022 \sigma_{ci} e^{0.038 GSI} \quad (2)$$

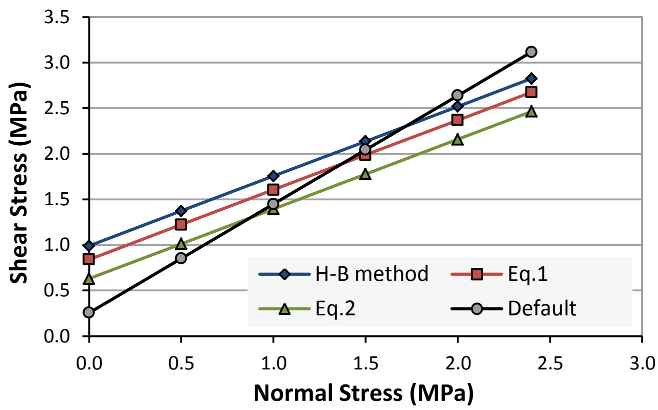

Figure 7 - Using the Mohr-Coulomb criterion to fit the Hoek-Brown criterion – the Hoek-Brown method.

The manuscript entitled "Investigation on the results of Plate Load tests using rigid plates in weak rock masses (case study)" was presented by Abrah et al. The paper presents and discusses the results of plate loading tests used to determine the deformability modulus of low quality rocks occurring under the left abutment of Karun 2 dam site. The tests results (Figure 8) were analysed through three methods: ASTM (2008), ISRM (1981) and UNAL (1997) and the last one has show significant differences with the first two, especially for higher anchor depths. The authors have performed tests for checking the results for the three methods but no explanation of the discrepancies between ASTM and ISRM methods to UNAL method was presented.

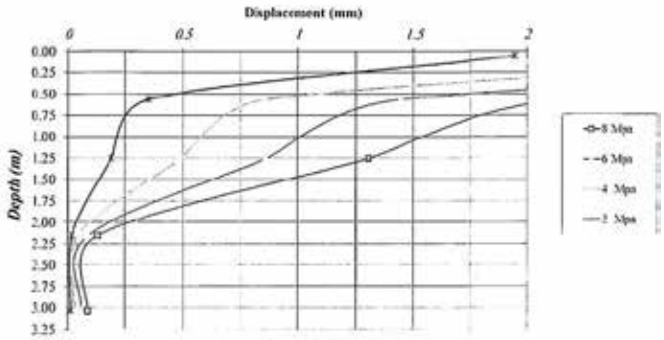

Figure 8 – Displacements measured for left plate.

The study by Elbaz et al. is entitled "Assessing rock strength and excavatability of diamondiferous kimberlite ore through in situ rock testing". The investigation have considered "the excavatability of diamondiferous kimberlite pipes of the Merlin field in the Northern Territory, Australia", through the use of in situ rock testing to "assess hardness and subsequently excavatability and have provided a relationship that can be used to relate field testing of rock hardness with rock strength. The results of the hardness (based on Schmidt hammer tests) to strength relationship (Figure 9) were used in established empirical equations to confirm excavatability of the kimberlite ore. The median of the twenty Q-values (Schmidt hammer rebound) for each core sample was taken prior to destructive UCS testing of the same samples in the laboratory. As a final conclusion, the authors states that the Schmidt Hammer rock strength (Q-value) showed a near direct relationship "to the UCS where UCS = 1.04 Q – 5.31. The results confirm the use of the Schmidt Hammer as a suitable device for in situ measuring of kimberlite and UCS estimation".

Finally, the last manuscript is the one from Kimura et al. entitled "In Situ Rock Stress Determined by Hydraulic Fracturing Test in Singapore" and presents the results of a series of hydraulic fracturing tests conducted in the Bukit Timah Granite and in the Jurong Formation, performed in vertical boreholes ranging in depth from 90 to 170 m mostly in Classes I and II of Rock Mass Rating (RMR).

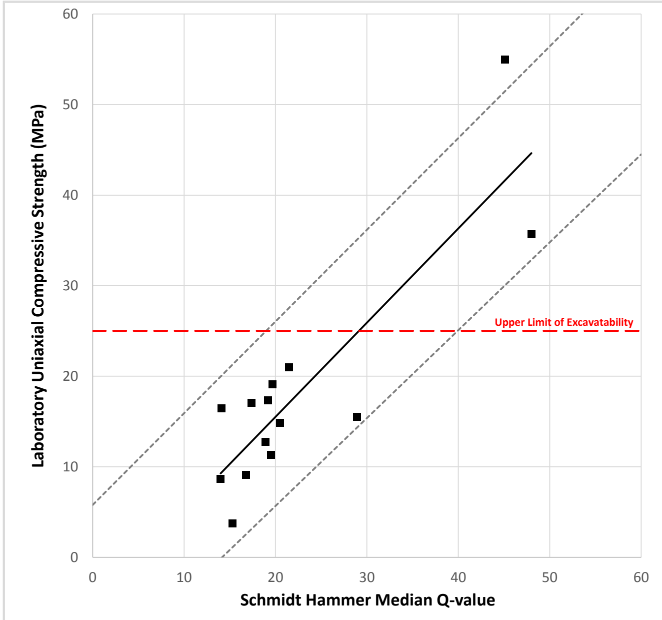

Figure 9 - Schmidt hammer test results relative to UCS (measured on lab).

The Bukit Timah Granite is located in the centre of Singapore Island and the outcrops are exposed on the ground surface on the hills and lies underneath recent deposits in valleys, while the Jurong Formation is distributed in the western part of the Island and is normally composed of series of sedimentary rocks such as sandstone, mudstone, shale, tuff, conglomerate, limestone etc. The hydraulic fracturing tests had been conducted in six different boreholes. The main conclusions were: the ratios of maximum horizontal stress to vertical stress are approximately 3 and 2 (Figure 8), in the Bukit Timah Granite and the Jurong Formation, respectively; the maximum and minimum horizontal stresses were higher than the vertical stress and indicates a thrust faulting stress regime that is characteristic of a compressional tectonic environment; and, finally, the orientations of the maximum horizontal stresses, generally N-S to NE-SW, are consistent with the general compressive stress in the region.

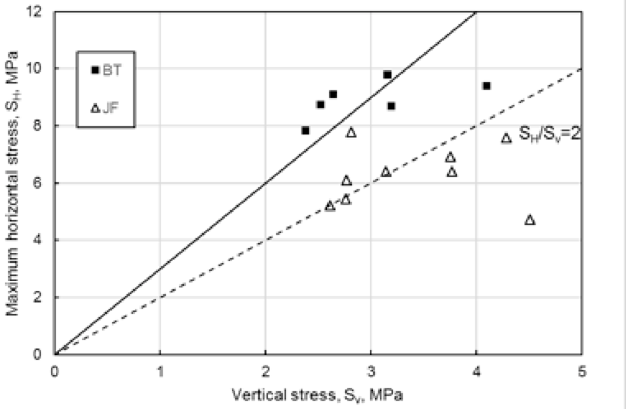

Figure 10 - Stress ratios of S_H (maximum horizontal stress)/S_V (vertical stress) in Bukit Timah Granite (BT) and Jurong Formation (JF).

4 CONCLUSIONS

Papers related to residual soil studies were, all, mainly focused on determining geotechnical parameters to provide data for engineering design. The most used test on the presented papers was CPT and event those that focused on other field tests, such as SPT, SPT, crosshole seismic and DMT, the main purpose was to correlate those results with CPT results. The only exception to this general trend was the paper by Décourt et al., which was mainly based on SPT-T results.

Based on this, the main contribution that can be withdraw from these contributions to the current state-of-the-art is the application of in situ tests to some unusual soil types and the proposition of new correlations for these materials to support design.

On the other hand, papers based on rock characterisation have presented a more wide variety of approaches, but again, the main purpose was to determine geotechnical parameters for engineering design and mainly by using already well established in situ and lab tests.

One final comment is related to the small amount of rock characterisation studies presented to the Symposium, which makes me suggest that authors should be encourage to present more studies on rock characterisation on future ISC symposia.

5 REFERENCES

ASTM D4394 – 08 2008. *Standard Test Method for Determining In Situ Modulus of Deformation of Rock Mass Using Rigid Plate Loading Method*. 10 p.

Begemann, H.K.S.P. 1965. The friction Jacket Cone as an aid in determining the soil profile. *6th International Conference of Soil Mechanics and Foundation Engineering, Proc., Montreal, Quebec, Canada*, v.1, 17-20.

Cruz, N. 2010. *Modelling geomechanics of residual Soils with DMT Tests*. Ph.D. thesis. Porto: Porto University.

Douglas, B.J. & Olsen, R.S. 1981. Soil classification using electric cone penetrometer. *Symposium of Cone Penetration Testing and Experience, Proc., ASCE. New York*, 209-227.

Eslami, A. & Fellenius, B. H. 1997. Pile capacity by direct CPT and CPTu methods applied to 102 case histories. *Canadian Geotechnical Journal*, 34 (6), 880 - 898.

Hoek, E. 1998. *Practical Rock Engineering. http://www.rocscience.com/roc/Hoek/Hoek.htm*

Hoek, E. and Brown, E. T. 1997. Practical estimates of rock mass strength. In Int. *Journal of Rock Mechanics & Mining Sciences,* 34 (8):1165–1186.

ISRM 1981. *The complete ISRM suggested methods for characterization, testing and monitoring*. 628 p.

Marques, E.A.G. and Williams, D.J. 2015. Weathering of Bunya phyllites in Southwest Brisbane – a geotechnical approach. In: *ANZ 2015 – 12th Australia New Zealand Conference on Geomechanics. Proc.,* New Zealand Geotechnical Society Inc., Wellington, p 1-8.

Robertson, P.K. 1990. Soil classification using the cone penetration test. *Canadian Geotechnical Journal*, 27: 151-158.

Robertson, P.K, Campanella, R.G., Gillespie. D. & Greig, J. 1986. Use of piezometer cone data". *In-Situ 86, Specialty Conference, Proc., ASCE, Blacksburg*, 1263-1280.

Robertson, P. K. & Cabal, K.L. 2010. *Guide to Cone Penetration Test*. Gregg Drilling and testing, Inc. 4th edition.

Schnaid, F., Lehane, B. M. & Fahey, M. 2004. In situ test characterization of unusual geomaterials. In: Viana da Fonseca e Mayne (eds.) *2º Geotechnical and Geophysical Site Characterization*. *Proceedings, Porto, Portugal.* 49-74. Rotterdam, Balkema.

Schmertmann J. H. 1969. *Dutch Friction Cone Penetration Exploration of Research Area at Field 5, Eglin Air Force Base, Florida, US Army Waterways Experimental Station*, *Vicksburg, Mississippi*, Contract Report S-69-4.

Unal, E. 1997. Determination of in situ deformation modulus: New approaches for Plate-loading Tests. *Int. J. Rock. Mech. Min. Sci*, 34: 897-915.

Geotechnical and Geophysical Site Characterisation 5 – Lehane, Acosta-Martínez & Kelly (Eds)
© 2016 Australian Geomechanics Society, Sydney, Australia, ISBN 978-0-9946261-1-0

Session Report: Interpretation & Design of In Situ Tests

J.T. DeJong
School of Civil & Environmental Engineering, University of California, Davis, CA 95616, USA

ABSTRACT: This paper presents an overview of eight of the papers submitted and published in the ISC'5 conference proceedings in the area of interpretation and design of in situ tests. Herein an overview of the process of site characterization process is briefly covered in order to place each paper with the broader context. The general paper focus, scope of work, and observations/conclusions of each paper are highlighted. While each paper is summarized herein, readers are strongly encouraged to read the original manuscripts presented in the proceedings by the authors.

1 INTEGRATED SITE CHARACTERIZATION

An integrated perspective of the process of site characterization, as detailed by DeJong et al. (2015) and Krage et al. (2016), spans from the desk study to site investigation to design to long term performance observations. This occurs through a series of stages as shown in Figure 1: inductive reasoning, scenario assessment, site investigation, site idealization, analysis and design, and the observational method. This perspective encompasses the entire geotechnical engineering process, and as such extends beyond the single task of site investigation wherein in situ and laboratory techniques are used to obtain measurements of the soil conditions. It expands and builds upon work by others which was largely focused on the site investigation stage.

The overall scope of the ISC conference series ideally covers much of this spectrum, but in general is weighted towards the site investigation stage. Herein eight papers are summarized, with one paper addressing experimental/operational issues, two papers exploring Soil Behavior Type chart applications, two papers using shear wave velocity measurements to estimate soil properties, one method developing a correlation for modulus, one exploring the use of field vane for undrained strength determination, and the last one using an inverse numerical simulation of CPT to estimate soil properties.

2 SUMMARY OF PAPERS

2.1 *CPTU Crossing Existing Boreholes in the Soil – Kasin*

Over the past 15 to 20 years anomalies in CPT profiles, wherein the tip measurement values are exceedingly low for short depth intervals, have been observed in soft clay deposits. An example of this is presented in Figure 2. As evident, the tip resistance is very low, producing estimated undrained strength values significantly less than that predicted by a lower bound normalized strength ratio values. This paper sought to identify the source/reason for these anomalies. The authors identified five different possible causes for this anomaly, ranging from equipment performance, to unique soil conditions, to influence of adjacent soundings/borings that were performed previously. The authors logically conclude that the low CPT tip resistance values obtained were likely due to the CPT being penetrated in soil that had been softened due to disturbance caused by a prior boring performed in close proximity to the CPT sounding. The author estimated that the disturbed zone around a boring is about 10 times the drill bit diameter. This study highlights the importance of considering the influence of prior field borings/soundings on data obtained at project sites.

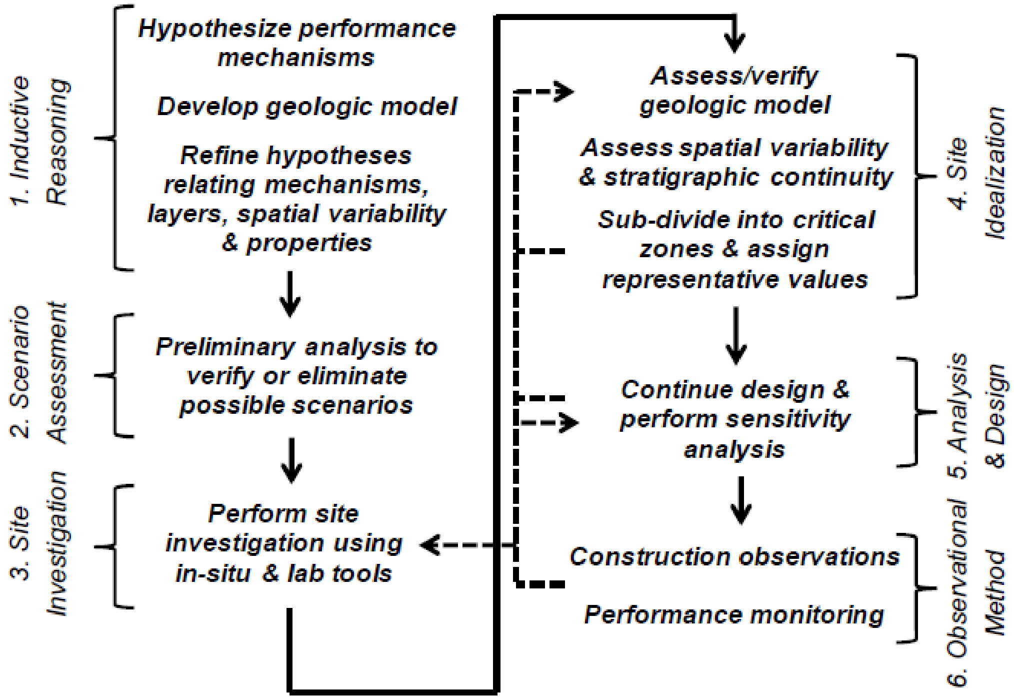

Figure 1. Schematic of the integrated site characterization framework.

2.2 *Soil Behaviour Type of the Sarapui II Test Site – Nejaim, Jannuzzi, & Danziger*

The general utility of the Soil Behavior Type (SBT) charts was applied and evaluated to two lightly over-consolidated soft clay layers present at the Sarapui II test site near Rio de Janeiro, Brazil. Detailed laboratory and CPT testing and data analysis re-confirmed the general applicability of Robertson's (1990, 2009) SBT charts with the data overall showing good agreements with the empirically type bins. Robertson's (2009) further suggestion of the approximate delineation between dilative and contractive materials, however, did not agree with the experimental data as well. The authors recommend a slight shift in this delineating line for a site-specific fit. This is presented in Figure 3. The observations in this paper overall highlight the importance of remembering that the SBT chart as well as the various delineations suggested are intended for general guidance; they should be considered indicators of transition zones and not definitive boundaries.

2.3 *Application and Tentative Validation of Soil Behavior Classification Chart Based on Drilling Parameters – Reiffsteck, Benoir, Hamel, & Vaillant*

The demonstrated effectiveness of the CPT Soil Behavior Type (SBT) chart for estimation of soil type by Robertson (1990) inspired Reiffsteck et al. to modify the framework for use with Menard pressuremeter test drilling data. Specifically, they introduce Q_t and F_r terms defined based on a range of drilling parameters. These two parameters are inputs into an I_c functional equation, producing contours in log-log space similar to the CPT SBT charts. Figure 4 presents the contours of the classification chart overlaid by a portion of the database available. Trends in the data are present, but significant scatter remains; the performance level currently is not comparable to the CPT SBT chart performance. As the authors acknowledge, further development is necessary and is currently underway.

2.4 *Empirical Estimation of Soil Unit Weight and Undrained Shear Strength from Shear Wave Velocity Measurements – Moon & Ku*

The increased use of seismic CPT on projects now provides an opportunity to use shear wave velocity, V_s, based empirical correlations to estimate different soil properties and parameters. Moon and Ku, building on the extensive database by Prof. Paul Mayne (Georgia Institute of Technology), produced a suite of new empirical correlations that provide estimates of totally unit weight as a function of normalized shear wave velocity, V_{s1}, and plasticity index, PI, and undrained strength as a function of Vs and either PI or over consolidation ratio (OCR). Figure 5 presents the undrained strength correlation as a function of OCR. As evident, the correlation functions provide a reasonable fit to the database. The application of these new correlations and comparison against measured values at two different research project sites, Burswood, Australia, and Huaiyan, China, indicate that the correlations perform reasonably. Further use will determine whether these correlations, which appear reasonable, will performed better than CPT tip measurement based correlations.

2.5 *Relative Density Prediction Based on In Situ and Laboratory Measurements of Shear Wave Velocity – Biryaltseva, Lunne, Kreiter & Morz*

Biraltseva et al. utilized a similar research approach to the prior paper to refine an empirical correlation to estimate the relative density of granular soils. The functional equation form adopted from Schmertmann (1978) was $D_r = (1/C_2) \cdot ln[V_S/(C_0 \cdot (\sigma'_m)^{C_1})]$. Calibration to site specific in situ and laboratory data led to setting the constants to values of $C_0 = 34.2$, $C_1 = 0.30$, and $C_2 = 0.64$. Figure 6 presents the fit of the empirical correlation with the laboratory data. As with the prior paper, further development and evaluation will provide insight as to whether this approach is more reliable than cone tip measurement based correlations.

2.6 *Identification of the Influence of Overconsolidation Effect on Subsoil's Stiffness by a CPTU Method – Mlynarek, Wierzbicki, & Lunne*

Mlynarek et al. focused on developing empirical correlations to estimate the constrained modulus for normally and over consolidated glacial till deposits using CPT data. Twelve CPT soundings and complimentary oedometric laboratory tests were performed across a couple different sites. The authors identified the unique and important properties of glacial tills relative to more conventional geomaterials. They concluded that the constrained modulus, M, for normally consolidated cohesive soils can be estimated based on CPT data using $M_{CPTU} = 8.25\ (q_t\text{-}\sigma_{vo})$. The empirical factor for over consolidated soils was observed to increase to 13.13. Given the importance of the constrained modulus value for design and the preliminary nature of this study, additional work is needed to verify the applicability of this correlation to other till deposits around the world.

2.7 *On the Determination of the Undrained Shear Strength from Vane Shear Testing in Soft Clays – Wilson*

The field vane test, FVT, considered the most direct method available to obtain a measure of undrained strength, is frequently used in field programs to characterize soft clays. This study focused on the effects of insertion disturbance, vane rotation rate, soil anisotropy and structure, and failure mechanisms shape on the characterization of Ballina clay, a sensitive and structured marine clay. An example result from this study showing the evolution of normalized pore pressure during the vane shearing and insertion process in a laboratory tests is shown in Figure 7. As evident, the generation of pore pressure during vane insertion, the subsequent dissipation, the regeneration during the start of shearing, and the gradual decay during shearing are well defined. Similar types of observations were made for rotation rate and strength variation with continued rotation. The research program is still underway, and while unique observations do exist, alternative guidance that deviates from standard-of-practice have not been developed.

2.8 *Interpretation of CPT Data for Pile Loading Behaviour – Inverse Estimation of Void Ratio Over Depth – Seitz, Heins, Carstensen & Grabe*

CPT measurements can be used directly to estimate base and shaft capacity or can be used indirectly to estimate soil properties and conditions, which are in turn used to estimate based and shaft capacity. The authors present an inverse solution approach using an evolutionary algorithm to estimate the initial void ratio and initial stress conditions based on minimizing the difference between CPT field data and a FEM simulation of cone penetration resistance. From this they intend for the estimated parameters to be used for pile design. The FEM model allows for large strain deformations and utilizes a hypoplastic constitutive model that is defined with parameter variables defined previously for Cuxhavener Sand. The initial analysis presented indicates that potential for this approach. However, the reliability of the prediction is not compared against more direct empirical estimation methods.

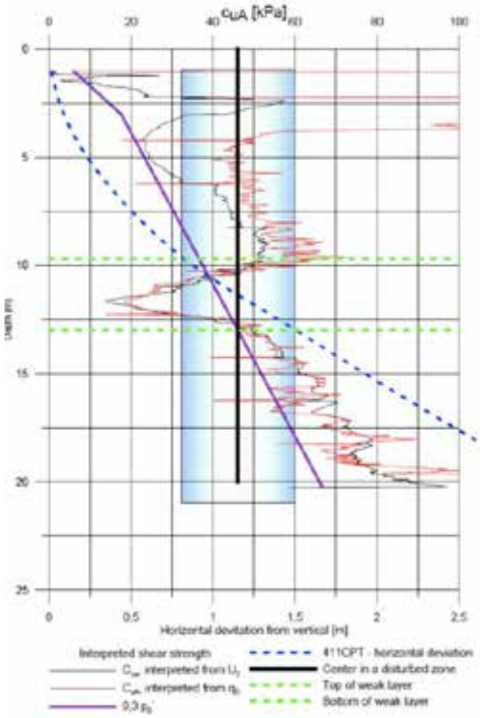

.

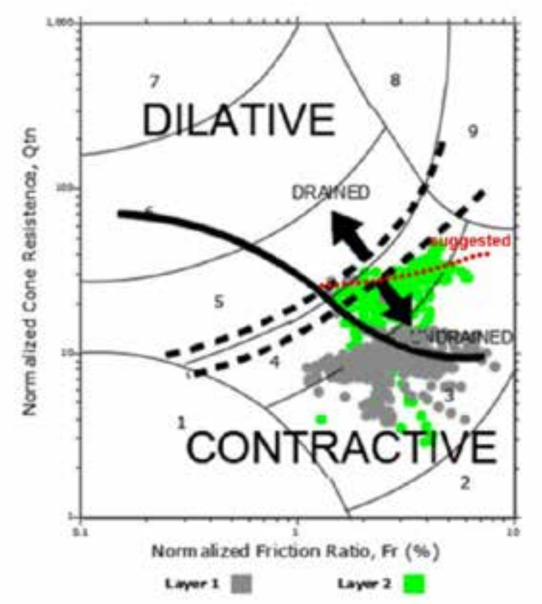

Figure 3. Nejiam et al. (2016). Results from two lightly overconsolidated soil layers with dashed line indicating trend for site-specific delineation of contractive versus dilative behavior.

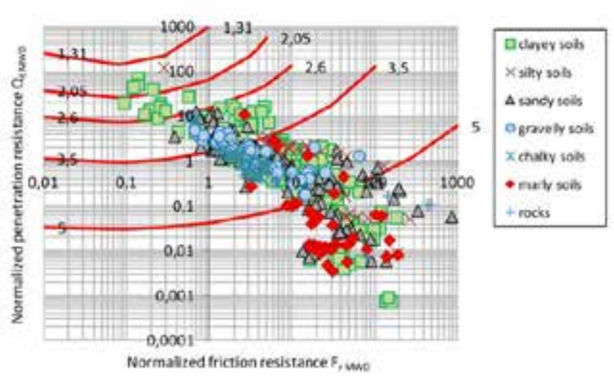

Figure 4. Reiffsteck et al. (2016) Ic-type chart developed for drilling parameters with field data from a range of soil types.

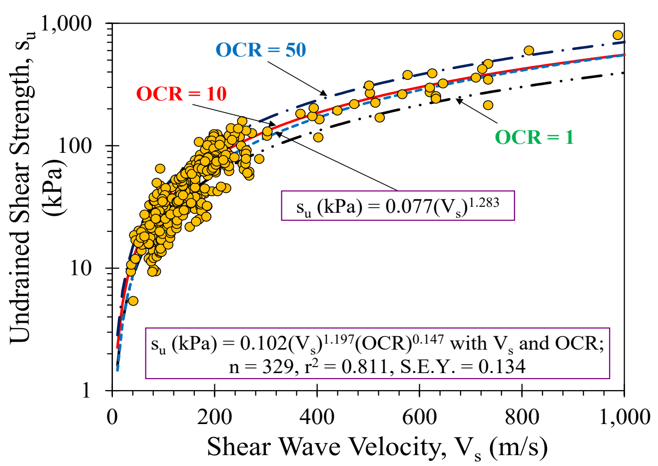

Figure 5. Moon and Ku (2016). Developed correlation of undrained shear strength as a function of V_s and OCR.

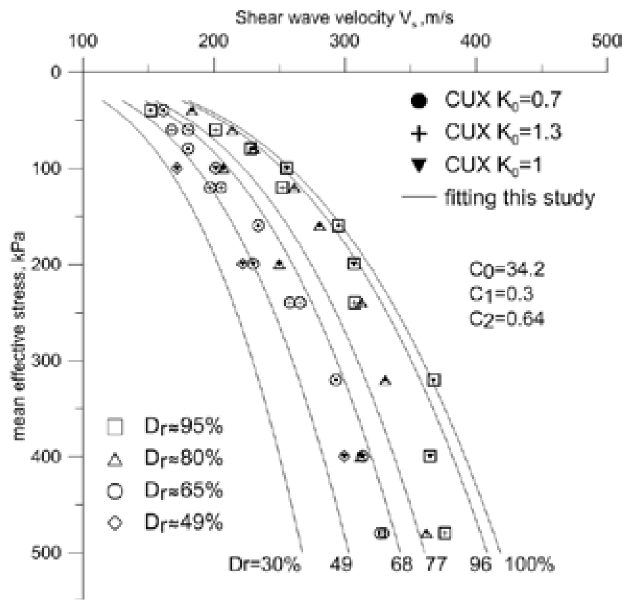

Figure 6. Biraltseva et al. (2016). Developed correlation for relative density and stress conditions based on V_s measurements.

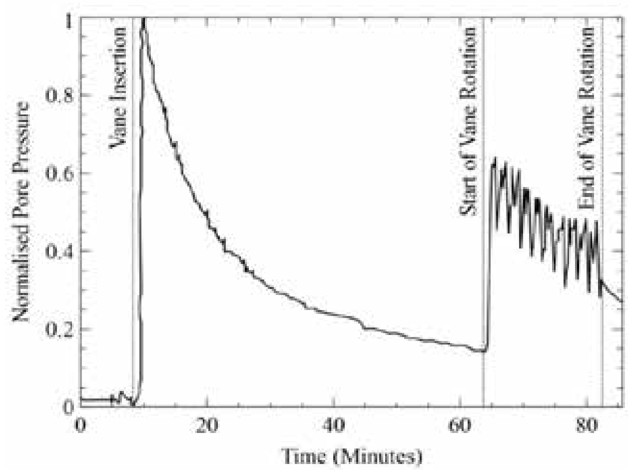

Figure 7. Wilson (2016). Normalized excess pore pressure generation measured during select stages of a laboratory vane test performed in Ballina clay.

3 SUMMARY

The high level overview of papers provides a snapshot of the detailed work that was performed. Readers are encouraged to retrieve and read the original manuscripts as the contain more detailed information. Overall, the body of work reviewed demonstrates a continued, steady evaluation and refinement of previously developed methods, with far fewer containing significant innovation advances.

4 REFERENCES

Biryaltseva, T., Lunne, T., Kreiter, S., and Morz, T. 2016. Relative Density Prediction Based on In Situ and Laboratory Measurements of Shear Wave Velocity, *Proceedings of ISC'5*, Gold Coast, Australia, 7 pp.

DeJong, J.T., Sturm, A.P. and Ghafgazhi, M. 2015. Characterization of gravelly alluvium. *Proceedings of 6ICEGE,* Christchurch, New Zealand, 20 pp.
Kasin, Kristoffer 2016. CPTU Crossing Existing Boreholes in the Soil, *Proceedings of ISC'5*, Gold Coast, Australia, 6 pp.
Krage, C.P., DeJong, J.T., and Boulanger, R.W. 2016. Identification of Geologic Depositional Variations using CPT-based Conditional Probability Mapping. *Proceedings of ISC'5*, Gold Coast, Australia, 7 pp.
Mlynarek, Z., Wierzbicki, J., and Lunne, T. 2016. Identification of the Influence of Overconsolidation Effect on Subsoil's Stiffness by a CPTU Method, *Proceedings of ISC'5*, Gold Coast, Australia, 7 pp.
Moon, S.W. and Ku, T. 2016. Empirical Estimation of Soil Unit Weight and Undrained Shear Strength from Shear Wave Velocity Measurements, *Proceedings of ISC'5*, Gold Coast, Australia, 7 pp.
Nejaim, P.F., Jannuzzi, G.M.F., and Danziger, F.A.B. 2016. Soil Behaviour Type of the Sarapui II Test Site – Nejaim, Jannuzzi, & Danziger, *Proceedings of ISC'5*, Gold Coast, Australia, 6 pp.
Reiffsteck, P., Benoit, J., Hamel, M., and Vaillant, J.M. 2016. Application and Tentative Validation of Soil Behavior Classification Chart Based on Drilling Parameters, *Proceedings of ISC'5*, Gold Coast, Australia, 7 pp.
Robertson, P.K. 1990. "Soil classification using the cone penetration test". Canadian Geotechnical Journal, 27(1): 151-158.
Robertson, P.K. 2009. "Interpretation of cone penetration tests – a unified approach." Canadian Geotechnical Journal, 46: 1337-1355.
Schmertmann, J. H. 1978. *Guidelines for cone penetration test, performance and design.* Report FHWA-TS-78-209, U.S. Department of Transportation. Federal Highway Administration.
Seitz, K.F., Heins, E., Carstensen, A., and Grabe, J. 2016. Interpretation of CPT Data for Pile Loading Behaviour – Inverse Estimation of Void Ratio Over Depth, *Proceedings of ISC'5*, Gold Coast, Australia, 5 pp.
Wilson, L. 2016. On the Determination of the Undrained Shear Strength from Vane Shear Testing in Soft Clays, *Proceedings of ISC'5*, Gold Coast, Australia, 6 pp.

Geotechnical and Geophysical Site Characterisation 5 – Lehane, Acosta-Martínez & Kelly (Eds)

Session Report on Design Using In-Situ Tests

A. Klar
Faculty of Civil and Environmental Engineering, Technion – Israel Institute of Technology, Haifa, Israel

ABSTRACT: This report provides an overview of the reviewed papers presented at the Conference under the theme of design using in-situ tests. The papers cover a breadth of topics spanning from estimation of specific soil properties through determination of their spatial distribution, and up to global direct design which encompass both the old and new.

1 INTRODUCTION

This report overviews 13 papers related to the theme of "design using in-situ tests" of the 5th international conference on geotechnical and geophysical site characterization.

In-situ testing is a prerequisite for a successful site investigation program that leads to a reliable design. The contribution of in-situ testing to the design process may take various forms, spanning from estimation of specific soil properties, through determination of their spatial distribution, and up to global direct design (see later the concept of "data driven design" proposed by *Doherty & Lehane*). This broad range of topics was clearly felt in the different contributions to the session. In the report, the papers are categorized as follows:

(i) Studies towards new correlations.
(ii) Approaches for determination of constitutive parameters.
(iii) Direct use of in-situ test results for design.
(iv) Reports of site investigations in specific projects.

The first category focuses on papers dealing with the development of new correlations for certain parameters, without a specific engineering use for design. The second category focuses on papers suggesting various approaches to establish the non-linear stress-strain response for numerical simulations. The third category focuses on papers suggesting direct utilization of in-situ tests for design. The fourth category focuses on papers reporting specific projects and their site investigation programs.

The majority of the papers (10 of 13) focused on the use of CPT/CPTu/SCPT. 3 out of the 13 papers, considered also the DMT and SDMT. SPT, DCP, PMT, and FVT have received lower attention in this session.

2 STUDIES TOWARDS NEW CORRELATIONS

Engineering correlations are among the essential tools of design. They enable quick and affordable determination of soil properties based on in-situ tests. 5 out of the 13 papers presented in the session focused on the formulation of new correlations.

Agaiby & Mayne focused on the formulation of a new correlation between the shear wave velocity and the preconsolidation stress. They have compiled an extensive database, representing 64 sites around the world, with 790 samples (and test results) of one-dimensional consolidation with their corresponding downhole shear wave velocity V_{sVH} (evaluated using either by SCPTu or SDMT). Their database contained 8 sites of normally consolidated clay ($OCR \approx 1$) with a total of 94 preconsolidation stress, σ'_p, measurements, 28 sites of lightly overconsolidated clay (OCR=1-2) with a total of 392 σ'_p test values, 19 test sites of overconsolidated clay (OCR=2-5) with 204 σ'_p values, and 9 sites of highly overconsolidated (OCR>5) fissured clay (mainly stiff London clay) with 100 σ'_p values. Excluding the fissured clays from the database, their regression analysis inferred on a unique relation between V_{sVH}, σ'_p, and σ'_{v0} (the effective vertical overburden stress):

$$\sigma'_p\,[kPa] = 0.18\left(V_{sVH}\,[m/s]\right)^{1.14}\left(\sigma'_{v0}\,[kPa]\right)^{0.26} \quad (1)$$

One can rewrite this newly suggested correlation in terms of the overconsolidation ratio (*OCR*) and the small strain shear stiffness, $G_{\max}$. This results in:

$$\frac{G_{\max}}{p_a}=80\frac{G_s+e}{1+e}OCR^{1.754}\left(\frac{\sigma'_{v0}}{p_a}\right)^{1.298} \tag{2}$$

where p_a is the atmospheric pressure (≈100kPa), G_s is the specific weight, and e is the void ratio. Note that an assumption of fully saturated soil is involved in the above alternative form (required for determination of the density for the relation $G_{\max}=\rho\cdot V_s^2$).

As can be seen the exponents of the *OCR* is quite high relatively to that commonly used for clays (e.g. Hardin, 1978; Vucetic & Dobry, 1991). This may infer that the regression analysis was governed by the low *OCR* samples, and that the correlation should be used with caution for high *OCR* values, without further research and support.

Agaiby & Mayne applied their new correlation for the estimation of the undrained shear strength, using the well-accepted relation of $s_u = S\cdot\sigma'_{v0}\cdot OCR^m$. Their undrained shear strength predictions are found to be in excellent agreement with those determined from field and laboratory tests. One can establish an expression of the undrained shear strength based on the above equations:

$$\frac{G_{\max}}{s_u}=80\frac{G_s+e}{1+e}\frac{OCR^{1.754-m}}{S}\left(\frac{\sigma'_{v0}}{p_a}\right)^{0.3} \tag{3}$$

where S and m may be determined by the shearing mode and rate. For triaxial compression test, S and m are usually taken as 0.3 and 0.8, respectively. Considering that $(G_s+e)/(1+e)$ is found in a narrow range of about 1.6 to 1.9, one can present a simple expression for the ratio of $G_{\max}/s_{uTC}$:

$$\frac{G_{\max}}{s_{uTC}}\approx 450\cdot OCR^{0.95}\left(\frac{\sigma'_{v0}}{p_a}\right)^{0.3} \tag{4}$$

Strictly speaking, the above equation is not a correlation, but a combination of the new correlation with a well-accepted expression. As such, it requires further validation before it can be used in design.

Yi & Yi commented on the fact that correlations between SPT and shear wave velocity are commonly separated into groups of different soils, such as sands, silts, clays and gravels. They suggested that the division may be avoided by including the fines content (*FC*) in the correlation. Using a total of 188 data sets, collected by a specially designed field investigation program of Yi (2014), they developed a new correlation to estimate V_s based on three parameters: N_{60} (SPT blow count for 60% energy), *FC* and the mean effective confining stress, σ'_m:

$$V_s=210.4\cdot N_{60}^{0.0195}\cdot FC^{0.0272}\cdot\left(\frac{\sigma'_m}{p_a}\right)^{0.3846} \tag{5}$$

A less successful, yet convenient, correlation was suggested based on the effective overburden pressure:

$$V_s=157\cdot N_{60}^{0.0831}\cdot FC^{0.0579}\cdot\left(\frac{\sigma'_v}{p_a}\right)^{0.2385} \tag{6}$$

Note that while the correlation is stated to be valid also for clean sands, a value of $FC = 0$ would lead to zero shear wave velocity. It is presumed that *Yi & Yi* have associated a value of *FC*=1% for clean sands (based on their Fig.4b lower values).

It is of interest to compare the newly suggested expression with those of Wair et al. (2012) who performed an extensive investigation using existing databases. The expressions of Wair et al. (2012) are of the following form:

$$V_s=a\cdot N_{60}^{b}\cdot\sigma'^{c}_v \tag{7}$$

where the values of a, b and c depend on the soil type and geological era. Table 1 shows a comparison between the expressions (in terms of a, b and c) for soils with a Holocene geologic epoch. As be seen from the table, V_s values based on Wair et al. (2012)'s expression will increase by 12% when the SPT value is doubled, while values based on the *Yi & Yi's* expression will increase by merely 5%. The *Yi & Yi* new expression appears to provide higher shear wave velocities than those of Wair et al. (2012) for silty sand. For N_{60} of 15 and effective overburden of 100kPa V_s is in the range of 227 to 255 m/s (*FC*=12-90%), whereas for the same condition Wair et al.'s expression yields a shear wave velocity of 160 m/s.

Table 1. Comparison of *Yi & Yi* values to those of Wair et al. (2012).

Soil Type	*a*	*b*	*c*
Wair et al. (2012)			
Silts and Clays	23	0.17	0.32
Sands	27	0.23	0.25
All Soils	26	0.215	0.275
Yi & Yin			
FC=1%	52.34	0.0831	0.2385
FC=12%	60.44	0.0831	0.2385
FC=50%	65.65	0.0831	0.2385
FC=90%	67.92	0.0831	0.2385

Godlewski presented regional correlations suitable for the soil conditions in Poland, to be used together with their national annex to Eurocode 7. The main objective of the work was to relate between the DMT and CPT results for Polish soils.

Li et al. examined and developed relation between *OCR* and CPTu test results for cutoff walls made of bentonite and natural soil mixtures, as part of an engineering project in Jiangsu, China. A ratio of 0.32

was found to exist between normalized cone resistance and laboratory *OCR* values. The authors also evaluated the hydraulic permeability based the CPTu dissipation data.

Mlynarek et al. presented statistical analyses to define the spatial distribution of soil stiffness using constrained moduli values estimated by CPTu test results. They used 9 soil profiles to define a set of coefficients, that are estimated by a least squares method and a clustering approach, for the spatial variation between points.

3 APPROACHES FOR DETERMINATION OF CONSTITUTIVE PARAMETERS

Fig. 1 shows typical degradation (or stiffness reduction) curves and the strain range for various geotechnical problems. This section provides an overview of two papers, presented in the session, aiming to resolve the overall (from small to large strains) behavior of the soil using in-situ tests.

Bosco & Monaco suggested to construct the degradation curve using a few working strain values. In specific, the small strain value based on the shear wave velocity, and another point, based on the constrained modulus at strain levels of the DMT. The DMT working strain value is typically in the range of 0.015-0.3% in sand and 0.23-1.75% in silt. *Bosco & Monaco* utilized Amoroso et al. (2014) hyperbolic stress-strain relation for the determination of the shape of the degradation curve. They were able to obtain a very good fit with the resonant column test with γ_{DMT} of 0.65%, which is higher than the 0.3% value recommended by Amoroso et al. This has led *Bosco & Monaco* to the conclusion that further work, aiming at better defining γ_{DMT} values for different soil, is in order.

Bahar aimed at establishing the complete strain-range soil response using Menard pressuremeter test, for a later numerical determination of the bearing capacity and settlement of bored piles. The approach taken by *Bahar* involved fitting the test data with a numerical analysis (inverse problem solution) involving the Duncan Chang (1970) model. The approach was demonstrated using pressuremeter test results from Annaba at east Algeria. Since both cohesion and friction were back calculated in the process, their values had to be evaluated by performing tests at different depths. The values defined by this approach were used for the design of the El-Djaziar Mosque.

4 DIRECT USE OF IN-SITU TEST RESULTS FOR DESIGN

More often than not, the process of estimating soil properties for design from in-situ tests involves an "engineering judgment". This engineering judgment may lead to significant variations in the final design output, as was demonstrated in the design competition reported by Lehane et al. (2008). *Doherty & Lehane* presented a vision in which the subjectivity is removed from the design process. Their vision relies on a process named "*data driven design*" in which in-situ data is directly used for the design process, skipping the stage of subjective selection of soil parameters. As a proof of concept, *Doherty & Lehane* developed the approach for the problem of laterally loaded piles.

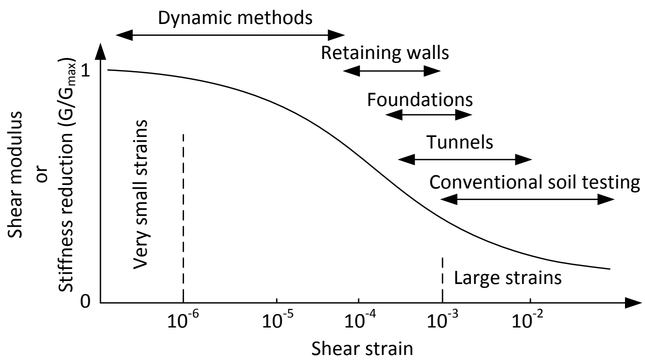

Figure 1. Typical degradation curve and strain ranges for various geotechnical problems, after Atkinson & Sallfors (1991) and Mair (1993).

The outcome is an easy-to-use web application (Doherty, 2016), which uses CPT data to generate *p-y* load transfer function for a Winkler model of laterally loaded piles. The *p-y* functions used in the software are those of Suryasentana & Lehane (2014). The approach was demonstrated for the pile load test of Robertson et al. (1985) with a reasonable success. The approach is certainly a first step towards automation in engineering analysis and design.

On the same topic, of utilizing CPT results for laterally loaded piles, *Qin & Guo* investigated the relation between the cone resistance and the soil lateral capacity (p_u), aiming to formulate a q_c-p_u relation. They have compared 8, previously conducted, tests of laterally loaded piles against the closed form solution of Guo (2008) for laterally loaded rigid piles. Their investigation resulted in a value of A_rD/q_c in the range of 1.8% to 8.8% (A_r being the gradient of lateral soil resistance = dp_u/dz). The ultimate lateral soil capacity based on the above range falls significantly below that based on the expressions of Suryasentana & Lehane (2014) (also used in the data driven model presented earlier). It is possible that this result is limited to short (rigid) piles. However, it should be recognized that the analytical model used by *Qin & Guo* was quite constrained; it involved elastic perfectly plastic Winkler springs, with linearly increasing resistance with depth. As such, an average value (with depth) of q_c was used for the investigation. Moreover, the model did not consider any potential yielding (or deformation) along the pile. The discrepancy between the aforementioned q_c-p_u relations may well be explained by these factors.

Yoon et al. suggested using the Dynamic Cone Penetrometer (DCP) for identification of the active layer in the regions of freezing and thawing soils. Their approach involves evaluation of the differential penetration with depth, recognizing the lower boundary of the active layer by a constant and low differential penetration. Field trials were performed in Svalbard Norway, and the results of layer thickness were compared with those based on the variation of temperature profile with changing seasons. While the approach appears to be promising, further research is required to develop clear guidelines for the routine use of DCP for active layer identification. For example, research focusing on the dependency of DCP differential penetration on the temperature and/or season.

Boldyrev & Novichkov suggested using the auger drilling resistance to evaluate soil properties, in a similar manner to other penetration tests. For this aim, they have presented an analytical solution for the auger resistance to drilling, in terms of torque and axial force, considering various input parameters, such as rotation speed, linear velocity and soil strength parameters. However, the solution is based on interface strength parameters between the soil and the steel, and does not consider aspects of soil volume increase or decrease (due to lack of rotation, or excessive rotation, with penetration). The idea requires further development before it could generally be used for evaluation of soil properties.

6 REPORTS OF SITE INVESTIGATIONS IN SPECIFIC PROJECTS

Two papers in the session detailed specific projects in which in-situ testing altered the design details or allowed educated design decisions.

The details of the site investigation program of the Smithfield Bypass project, in Queensland Australia, were reported by *Ezeajugh*. In the project, a 2-stage site investigation plan was carried out, involving CPTu soundings and DCP probing. The second stage was performed due to poorly executed dissipation tests, which led to an alternation of the design.

Williams presented two case studies in which geotechnical investigations were performed to evaluate the strength of desiccated tailings in Queensland, Australia. The CPTu and vane shear tests were used in the investigation of both sites. Using trend lines and evaluating their intersection with the surface, following Schmertmann (1978) method *Williams* classified the state of the material as underconsolidated, normally consolidated or overconsolidated. The author derived a ratio of 0.17 for $s_u/\sigma'_{v0,nc}$, a somewhat lower value than the expected 0.25. However, for the shear strength value from the CPTu a ratio of 0.25 was obtained.

3 SUMMARY

From the selection of papers submitted to the session, it appears that the CPT and DMT have been attracting greater interest than other in-situ tests. This is probably the case because SPT, FVT and pressuremeter, are so well accepted in routine design that little advancement can be made with respect to their use. It is clear that CPT and DMT have the advantage of supplying spatially continuous data, and hence facilitate better understanding of the soil profile, as was demonstrated in the session by *Mlynarek et al.* They can also be used for the creation of automatic engineering analysis and design processes as suggested in the session by *Doherty & Lehane*. SCPT and SDMT have a clear advantage over other test devices, as they provide valuable information both in the small strain and large strain ranges. The papers of *Agaiby & Mayne* and *Bosco & Monaco* are good examples of how in-situ small strain and large strain measurements can be combined to result in better estimation of soil properties over the complete non-linear stress-strain range.

Since FVT, SPT, DCP and pressuremeter tests will remain a vital part of the design process, for years to come, improvements in their use are welcome. The attempt of *Yi & Yi* to develop fines content based correlation for the shear wave velocity is a good example. The new use of the SPT to identify active layers in permafrost regions is another good example.

While the ideas and results presented in the session appear to be very promising, some of them require further support and validation.

7 REFRENCES

Amoroso, S., Monaco, P., Lehane, B.M. & Marchetti, D. 2014. Examination of the Potential of the Seismic Dilatometer (SDMT) to Estimate In Situ Stiffness Decay Curves in Various Soil Types. *Soils and Rocks*, 37(3): 177-194.

Atkinson, J.H., Sallfors, G. (1991). Experimental determination of soil properties. Proc. 10th ECSMFE, vol. 3, 915–956.

Doherty, J. (2016). User manual for LAP, Laterally loaded pile analysis. School of Civil, Environmental & Mining Engineering, University of Western Australia, Perth WA 6009. www.geocalcs.com/lap

Duncan, J. M., and C. Y. Chang. (1970). Nonlinear Analysis of Stress and Strain in Soils. Soil Mechanics 96(SM5), 1629-1653.

Guo, W. D. (2008). Laterally loaded rigid piles in cohesionless soil. Canadian Geotechnical Journal, 45 (5), 676-697.

Hardin, B. O. (1978). The nature of stress-strain behavior for soils. Proc. ASCE Geotechnical Engineering Division. Specialty Conference on Earthquakes Engineering and Soil Dynamic, Vol. 1, 3-90.

Lehane B.M., Doherty J.P. and Schneider J.A. (2008). Settlement prediction for footings on sand. Keynote Lecture, Proc. 4th International Symposium on deformation characteristics of Geomaterials, Atlanta, 1, 133-152, IOS press, The Netherlands.

Mair, R. J. (1993). Development in geotechnical engineering research: application to tunnels and deep excavation. Proc. Instn. Civ. Engng., 93, 27–41.
Schmertmann, J.H. 1978. *Guidelines for cone penetration test, performance and design*. Federal Highway Administration, Report FHWA-TS-78-209, Washington, July 1978.
Suryasentana, S. K., & Lehane, B. M. (2014). Numerical derivation of CPT-based p-y curves for piles in sand. Géotechnique, 64(3), 186-194.
Vucetic, M., & Dobry, R. (1991). Effect of soil plasticity on cyclic response. Journal of Geotechnical Engineering, 117(1), 89–107.
Wair, B. R., Dejong, J. T., & Shantz, T. (2012). Guidelines for Estimation of Shear Wave Velocity Profiles. PEER Report 2012/08.
Yi, F. (2014). Estimating soil fines contents from CPT data. *3rd International Symposium on Cone Penetration Testing,* May 12-14, 2014 - Las Vegas, Nevada.

Geotechnical and Geophysical Site Characterisation 5 – Lehane, Acosta-Martínez & Kelly (Eds)

Session Report: Liquefaction Assessment

A. Viana da Fonseca & C. Ramos
CONSTRUCT-GEO, Faculty of Engineering (FEUP), University of Porto, Portugal

M. Cubrinovski
Civil & Natural Resources Engineering, University of Canterbury, Christchurch, New Zealand

ABSTRACT: This session report provides an overview of papers the presented at the conference that were related to liquefaction assessment. Aspects related to the current research and practice are also addressed by the reporters to provide an indication of the current state-of-the-art and of areas requiring further investigation.

1 INTRODUCTION

The use of in situ tests for evaluating soil liquefaction potential in the engineering design and in performing case history analysis where soil liquefaction did occur during an earthquake event has increased significantly, particularly with respect to the cone penetrometer, as is illustrated by the papers submitted to this Section of ICS5 and summarized in this Report. There is a clear recognition that evaluation of soil liquefaction is a challenging task in all steps of the process including liquefaction triggering, liquefaction-induced ground deformation and impacts on buildings and infrastructure. This has been well illustrated in the experiences from recent earthquakes in New Zealand, Japan and Italy which have highlighted some of the complexities of liquefaction phenomena, and have demonstrated the inter-related effects of various influencing factors. These case history evidence together with the continuing research efforts using in situ testing, experimental and numerical studies have driven the development and further evolution of liquefaction evaluation procedures.

In addition to these well established penetration tests, there are attempts to develop new devices addressing the evaluation of particular soils. Importantly, there are significant efforts to make use of multiple parameters and testing approaches in order to combine different facets of stress-strain characteristics of soils and hence improve the predictive capacity of models. There is an increased confidence on the use of dilatometer and pressuremeter devices, as well as an increase use of geophysical approaches in support of liquefaction evaluation, with emphasis to surface seismic techniques or passive interpretation of ambient seismic noise wavefield (natural and human), which are particularly appealing for use in urban areas and offer the advantages of non-destructive testing. Besides this very qualitative information, little information is available on the quantitative proportions between body and surface waves, and within the different kinds of surface waves that may contribute to vibrations (Rayleigh/Love waves, fundamental/higher modes). The few available results, reviewed in Bonnefoy-Claudet et al. (2006), report that low frequency micro-tremors predominantly consist of fundamental Rayleigh waves, while there is no real consensus for higher frequencies ($f > 1$Hz). Different approaches were followed to reach these results, including analysis of seismic noise at depth and array analysis to measure the phase velocity.

The recent experiences in New Zealand, Japan and Italy have allowed new developments in Earthquake Induced Liquefaction Damage (EILD), where large geotechnical groups worked and are still working together in developing design guidelines for the application of soil characterization and liquefaction risk assessment protocols (e.g. Cubrinovski et al. 2011a, b, c, Bray et al. 2014 – for the 22 February 2011 Christchurch Earthquake; Boulanger 2012 – for the 2011 Great East Japan Earthquake, Fioravante et al. 2013 – for the 2012 Emilia-Romagna Earthquake). Key elements in these developments have been the extensive in situ and laboratory characterization of sites and soils that provide the basis for further advances in the liquefaction assessment.

The papers overviewed in this Report are examples of some case histories (Rodrigues et al. 2016, Bahadori & Hasheminezhad 2016, Castellaro 2016 and Klibbe 2016), application of newly developed techniques to assess soil susceptibility to liquefaction

(Mirjafari et al. 2016, Sawada 2016, Roberts et al. 2016 and Rollins et al. 2016), combination of results from different in situ tests (Monaco et al. 2016) and relationships between different parameters to study liquefaction susceptibility (Fioravante & Giretti 2016, Bán et al. 2016, Mengé et al.2016).

2 EVALUATING SANDS CYCLIC LIQUEFACTION TRIGGERING

A subject addressed recently is the incorporation of two important factors in liquefaction assessments from in situ tests: (i) Stress History - overconsolidation and any other aging agents; and, (ii) cementation, which can also be related to time, therefore aging, but not only. In fact, natural and anthropic agents can generate inter-particle bonding that can largely change CRR estimates and therefore the risk indices commonly used in practice such as "Liquefaction Factor of Safety" (LFS), "Liquefaction Potential Index" (LPI) and "Liquefaction Severity Number" (LSN) (van Ballegooy 2014) The possibility of reducing the uncertainty of the liquefaction resistance CRR estimates, by incorporating Stress History into the liquefaction correlations, is therefore one of the current aims for research (Marchetti 2015, Robertson 2015, etc.). This is also discussed by Monaco et al. (2016), as they try to relate the CPTu results with the SDMT results and incorporate the information of the K_D (related with stress history/OCR). Some disagreements seem to arise due to different interpretations of the consequences of aging on the unstable behaviour of soils under cyclic/seismic actions, specifically in relation to the more or less sensitivity of flat dilatometer (DMT) tests results (K_D) to stress-history and Shear Waves velocities (V_s measurements obtained from geophysical seismic tests, from surface or in hole, some complementing static cone and piezocone tests – SCPT and SCPTu) to cementation.

Liquefaction methods based on V_s analysis have had significant developments over the last years since they have the advantage to be essentially independent of soil characteristics, such as fines content (this however can be identified by the stratigraphy obtained using the CPT, for instance). Relations between normalized V_s values to clean sands $[(V_{s1})_{cs}]$ and $Q_{tn,cs}$ for Holocene-age were proposed by Andrus et al. (2004), but there is little difference observed between $[(V_{s1})_{cs}]$ and V_{s1}, as pointed out by Robertson (2009) in a summary of SCPT data obtained in Holocene-age uncemented deposits from California comparing V_{s1} with $Q_{tn,cs}$.

As remarked by Robertson (2015), the most recent Vs-based method with a CPT-based method provides an independent evaluation of the associated corrections applied to the CPT-based method. The method was essentially applied to case histories comprised of soils that are essentially normally consolidated with in situ stress ratio (K_0) likely in the range $0.4 < K_0 < 0.7$. For soils where K_0 is significantly larger than around 0.5 it can introduce uncertainty, but Robertson suggests that a correction for K_0 should be applied (e.g. Maki et al. 2014).

But, comparing the current Vs-based method with a specific CPT-based method from the literature to evaluate the associated CPT-based corrections, it is decisive to combine CPT and V_s measurements to evaluate Liquefaction Triggering in sands that are not clean and/or un-cemented. Being certain that "V_{s1}–liquefaction correlations require the cautionary understanding that some soils with unusual soil-specific void ratio–relative density characteristics or bonding may exhibit liquefaction behaviour that differs from the generalized proposed relationships" (quoting Kayen et al. 2013), due to microstructure in soils, such as: aging, cementation, cold welding, etc., increasing a soil strength, but even more stiffness, and specifically the very small stiffness (G_0 determined from V_s measurements). The small strain shear modulus (G_0 or G_{max}), if properly normalised with respect to void ratio and/or effective stress, is in practical terms independent of the type of loading, number of loading cycles, strain rate, and stress/strain history (as described by Viana da Fonseca et al. 2011). So, it is a fundamental parameter of the ground, considered as a benchmark value, revealing its true elastic behaviour. This small-strain shear stiffness of a soil reflects the nature of interparticle contacts, such as the Hertzian deformation of contacting smooth spherical particles; the resulting nonlinear load-deformation response determines the stress-dependent shear wave velocity (Cho et al. 2006). This is consistent with the general pattern of relations between shear wave (V_s) and effective stress state (p'/p_a), as suggested by Santamarina (2005). This is why, the CPT tip resistance (q_t) being predominately a large-strain measure of soil strength, tends to be less influenced by the strength of the bonds than G_0 (and V_s), especially in lightly bonded soils.

Quoting Eslaamizaad & Robertson (1996), the SCPT can therefore be helpful in identifying soils with "unusual" characteristics (i.e., soils with microstructure) based on a link between G_0/q_t and Q_{tn}, since both aging and bonding tend to increase the small-strain stiffness (G_0) significantly more than they increase the large-strain strength of a soil (reflected in Q_{tn}, the normalized value proposed by Robertson 2009). Schneider & Moss (2011) extended the link between CPT and V_s to establish a method to evaluate the threshold to trigger liquefaction in sandy soils with microstructure, suggesting the use of an empirical parameter, K_G, which was slightly modified by Robertson (2015) to use q_t instead of q_c and Q_{tn} instead of q_{c1N} : $K_G = (G_0/q_t)\, Q_{tn}^{0.75}$. Soils with little or no microstructure (i.e., young Holocene-age, sandy soils with no bonding), will have $110 < K_G < 330$, with an average of 215, which allows easily to evaluate if a soil with $K_G > 330$ can be considered to have "unusual" characteristics (i.e., microstructure) in terms of the application of the liquefaction triggering correlations. Then, the author considers that the lower limits of liquefaction resistance can be defined where induced cyclic strains are less than the elastic threshold shear strain, γ^{th}, this being independent of the number of cycles of typical earthquakes (<30 cycles) and has a value of about 1×10^{-4}. A cyclic stress ratio at the threshold strain (CSRth) for a normalized small strain shear module, G_{01}, is proposed by Robertson (2015), which is essentially independent of earthquake magnitude, since any cyclic stress ratio less that CSRth will not exceed the elastic threshold strain and liquefaction will not result, since excess pore pressures will not develop. It has been suggested while at low values of Q_{tn}, small-strain stiffness controls liquefaction resistance (Schneider & Moss 2011), at higher values of Q_{tn} the consequences of liquefaction are limited by soil dilation, being correlations based on CPT Q_{tn} more applicable. Robertson (2015), in view of previous work associate these two behaviours to: $Q_{tn,cs} < 70$, where shear strains quickly become very large (>20%) when liquefaction is triggered and $Q_{tn,cs} > 70$, for which when the threshold strain is exceeded, strains tend to accumulate more slowly and dilation tends to play an increasing role, respectively.

Finally, to account for soil aging on the resistance to cyclic loading based on CPT and V_s results, an approach considers a correction to cyclic resistance ratio (K_{DR}) which involves a ratio between values of V_{s1} measured in situ and V_{s1}, estimated for a very young unbounded soil, namely in reconstituted soils (Andrus et al. 2009, and Hayati & Andrus 2009). An alternative and simpler approach suggested by Schneider & Moss (2011) has the advantage that a generalized value for K_{GE} (~200) can be assumed that does not require selection of a specific relationship between CPT and V_s with the associated uncertainty.

Some references are due to articles that have addressed the topic of the use of DMT to assess liquefaction. One of the most interesting is the one recently published in ASCE J. Geotech. Geoenviron. Engng., where the authors study how the overconsolidation in sand affects the behaviour of granular soils in the research site of Treporti, Venice Lagoon (Monaco et al. 2014). A trial embankment was built and removed after 5 years, while SDMTs and SCPTu were performed before and after the construction and after the removal of the embankment. The overconsolidation of the deposits was estimated and an OCR-K_D graph was produced, comparing CPT (in terms of q_c) and DMT (in terms of M_{DMT} or K_D) interpretation. They conclude that DMT appears to be more sensitive than CPT to the OCR. Other studies, very recent and still under publishing processes, have been developed in real earthquake areas (L'Aquila and Emilia Romagna, in Italy), and where CPT and SDMT data in sands and silty sands where extensively performed, showed that there is a good agreement between CPT and DMT liquefiability estimation (discussed by Monaco et al. 2016), while Vs seems to underestimate the liquefaction potential.

Analyses have to be carried out to produce a good framework and establish sound basis for these approaches, but some doubts remain, particularly for silts or silty-sands, which can be less sensitive to K_D. This seems to be the case of the preliminary DMT results analyses of the evidences of large liquefied areas in one of the more extensive known database of recent seismic events (the 2010-11 Canterbury-New Zealand earthquakes).

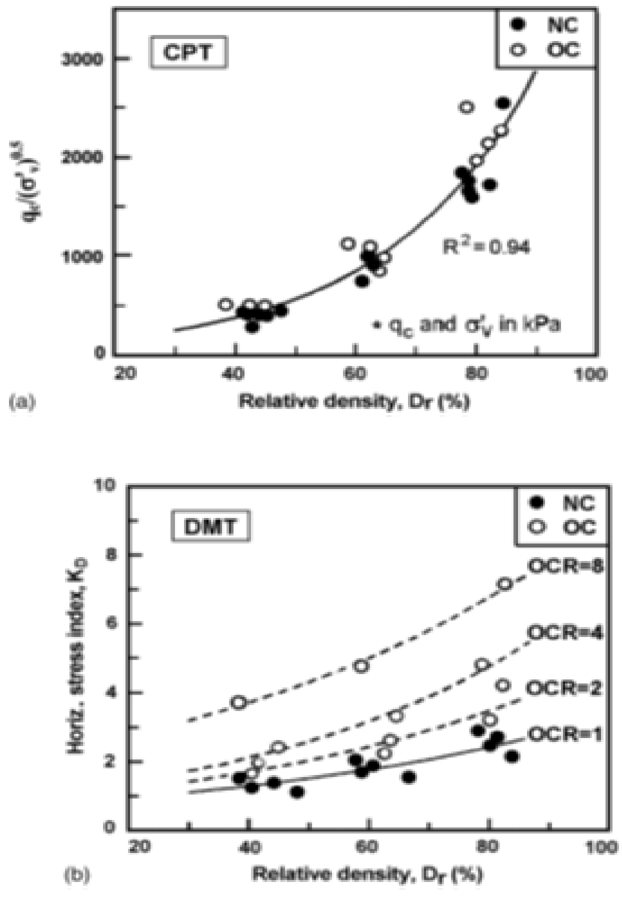

Figure 1. Sensitivity of CPT and DMT to stress history: (a) CPT; (b) DMT (Marchetti, 2015)

Still, mostly in sandy soils, Marchetti (2015) proves that the Flat Dilatometer (DMT) Horizontal Stress Index, K_D, is very sensitive to Stress History (as it is mostly revealing indirect overconsolidation by the detection of high value of horizontal stress state –see Fig. 1). Because of this, K_D is equally sensitive to liquefaction assessment in low as in high penetration resistances, that is, for soils that resist to liquefaction in conditions where the instability is triggered with the increase of pore pressure to annul the effective stress (pure concept of liquefaction collapse) or when the liquefaction is due to excessive strain accumulation.

CRR estimation is hereby based not on the one-to-one correlations CRR- Q_{cn} or CRR- K_D, but on a correlation based at the same time on both Q_{cn} and K_D. A Q_{cn} - K_D –CRR correlation has been constructed by combining the current CRR- Q_{cn} and CRR- K_D correlations. Monaco et al. (2016) use this combination of methods to perform a liquefaction analyses at a site in Bondeno, near the region where the May 2012 Emilia- Romagna (Italy) seismic sequence struck. It is expectable that an estimate based at the same time on two measured parameters would be more accurate than estimates based on just one parameter (Marchetti 2016). Figure 3 is a framework for initiating the accumulation of co-located Q_{cn} - K_D -CRR datapoints.

In view of that, the known CRR - Q_{cn} (similar to Q_{tn}) correlation, based on results of a large number of documented earthquake case histories data proposed by Idriss and Boulanger (2006), which is slightly more conservative than the previous Robertson and Wride (1998):

$$CRR = \exp\left[\left(Q_{cn}/540\right)+\left(Q_{cn}/67\right)^2-\left(Q_{cn}/80\right)^3+\left(Q_{cn}/114\right)^4-3\right] \quad (1)$$

which was integrated with the CRR - K_D correlation based on the above CRR - Q_{cn} combining it with Q_{cn} =25 K_D, following a procedure suggested by Robertson (2012). According to Marchetti (2015), this ratio Q_{cn} / K_D =25, is highly approximate, since it was obtained by interpolating a straight line through the Tsai et al. (2009) data – Figure 2 a) -, but complemented by the author with new data points (Fig. 2 a), b), c)).

The data are for a DMT material index $I_d > 3$, i.e., for clean sand. The high dispersion in the K_D-Q_{cn} relation is, to a large extent, the consequence of the higher reactivity of K_D to stress history (Fig. 1). As stated by Marchetti (2015), if the scatter were small, it would mean that Q_{cn} and K_D contain equivalent information, which is negated by Fig. 2c). The high scatter indicates that K_D contributes fresh collateral independent information to the characterization of the sand. So, a key factor that can differentiate the highest applicability of V_s (G_0) – q_c approaches versus K_D in different soils can be the presence of fines or/and the type of aging that was developed in the history of the ground.

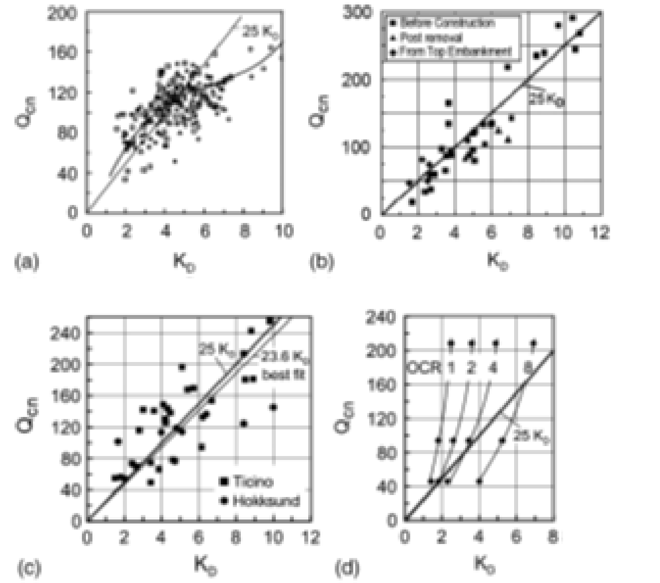

Figure 2. K_D-Q_{cn} relations: (a) from five Taiwan sand sites; (b) from Treporti research site; (c) from calibration chamber results (data from Baldi et al. 1986); (d) derived from Figure 1

The author presents an approach that combines the CRR-Q_{cn} correlation and the CRR-K_D correlation adopting as CRR the geometric average between a first CRR estimate obtained from Q_{cn} (Equation (2)) and a second CRR estimate obtained from K_D:

$$AverageCRR = \left[\left(CRRfromQ_{cn}\right)\left(CRRfromK_D\right)\right]^{0.5} \quad (2)$$

This solution is plotted in Figure 3 as a function of Q_{cn}.

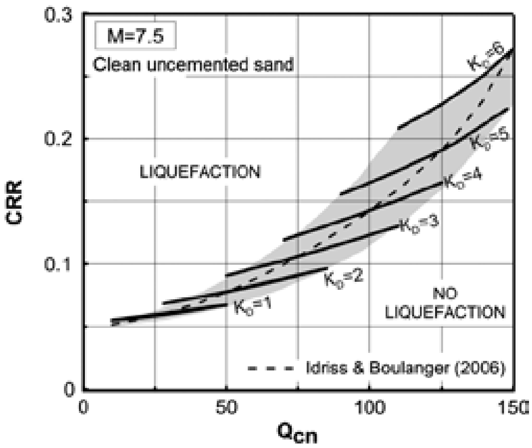

Figure 3. Chart for estimating CRR in clean uncemented sand based on Q_{cn} and K_D (Marchetti, 2016)

This figure was constructed with clean un-cemented sand in mind. But as Marchetti (2015) refers, if the sand contains fines or is cemented, estimating CRR is much more complex. Transcribing his final remarks, the cementation can be ductile (toothpaste like) or fragile (glasslike), a quality that affects either Q_{cn} or K_D and the sand liquefaction behaviour. And also, fine content may possibly have effects similar to a ductile cementation. Clearly the unknowns are too many and it may not be sufficient to add the K_D information to Q_{cn}. The knowledge of G_0 (small strain shear modulus) could help, because high G_0=q_c and/or high G_0=MDMT (Schnaid et al. 2004; Cruz et al. 2012) are also indicators of cementation. Even the dilatometer modulus E_D from DMT could possibly help.

In conclusion, the authors emphasise the need for considerable additional study in case of sands that are not clean and/or un-cemented.

3 COMMENTARY ON THE LIQUEFACTION EVALUATION

The 2010-2011 earthquakes that struck the region of Canterbury and the city of Christchurch (New Zealand), in particular, provided abundance of liquefaction observations and a large number of well documented case histories that captured important details on the liquefaction manifestation and its impacts on land, buildings and infrastructure. A comprehensive field investigations including thousands of CPTs and extensive V_s profiling were performed to characterise the sites and soils of Christchurch. In addition, a number of research-led studies provided detailed site and soil characterization using closely spaced CPTs, V_s measurements through cross-hole testing, and laboratory tests on undisturbed samples recovered from critical soil layers. Some comments from these observations and ongoing studies are provided below which directly link to or address issues discussed in papers presented in this session.

One may argue that, by and large, three group of factors have to be addressed in the liquefaction assessment related to the:

a) Material characteristics of the soil
b) In situ state of the soil, and
c) Site response of the soil deposit specific to earthquake induced liquefaction

Material characteristics would include grain-size composition (across all fractions), soil plasticity, and particle shape, to mention few properties of particular significance. The in situ state of the soil would incorporate the soil density, effective overburden stresses, fabric (related to the depositional environment), and aging and overconsolidation effects (discussed in the previous section). Finally, when considering the site response relevant for the liquefaction evaluation, interaction between different layers within the soil profile (including effects on the dynamic response, development and dissipation of excess pore pressures, and consequent water flow), partial saturation in parts of the deposit, presence of strong and competent crust layer at the ground surface (in relative terms, for the soils at the site and structure considered), and micro- and macro-structures in the stratification of interbedded deposits all contribute to the complexities in the evolution and manifestation of liquefaction in the field. Boulanger et al. (2016) provide an excellent summary of factors affecting prediction of liquefaction effects in interbedded soil deposits, and discuss some of the challenges in the characterization of spatially heterogeneous deposits.

For clean sands and uniform deposits, many of the above factors (e.g. grain-size composition, plasticity, interaction between layers) are either not critically important or their effects can be estimated reasonably well, and the effects of others (e.g. density, overburden stress) are reasonably well defined in the current state-of-the-art methodology. In addition to the above, the empirical relationships specific to particular penetration tests (CPT, SPT) are well calibrated. However, the above is certainly not the case once sands with fines of different content and plasticity are discussed. For example, one source of uncertainty in the liquefaction triggering estimates based on penetration tests, in which clean sand is used as a reference, is that the addition of fines in a given sand would change the density of the soil and would also change its liquefaction resistance as well as its penetration resistance. In the well-known NCEER approach, Youd et al. (2001) state: *"In the original development, Seed et al. (1985) noted an apparent increase of CRR with increased fines content. Whether this increase is caused by an increase of liquefaction resistance or a decrease of penetration resistance is not clear."* Some recent studies have shown that the effects of fines on the penetration resistance are significant, and that the leftward shift in SPT (CPT) liquefaction triggering correlations with increasing fines content is largely attributable to the effects of the fines on the penetration resistance (Cubrinovski et al. 2010; Price et al. 2015). This suggests that quantifying the effects of particle sizes, grain-size composition and soil plasticity on specific penetration tests is needed in order to provide better estimates for the effects of fines and their plasticity on the SPT- or CPT-based liquefaction triggering correlations. In this context, approaches based on the soil behaviour type index I_c (e.g. Robertson & Wride 1998 and updated versions) or fines content (e.g. Boulanger & Idriss 2015) will be subject to further improvement as some of the above effects are better quantified.

When evaluating the appropriateness of specific testing procedures for liquefaction evaluation, we need to recognize the significant differences in soil profiles and geotechnical conditions that may be encountered in the evaluation. To illustrate this, CPT data for two sites in Christchurch are shown in Figure 4 using cone tip resistance (q_c) and soil behaviour type index (I_c) throughout the depth of the deposits. They represent typical but dramatically different soil profiles of Christchurch soils which in the top 10 m consist of: (a) predominantly uniform fine sands with relatively low penetration resistance or high liquefaction potential, with a 2-3 meters thick silty sand layers of high liquefaction potential near the surface (Fig. 4(a)), and (b) highly stratified deposits of silty sand and silt layers interbedded with non-liquefiable soils (I_c > 2.6). Undisturbed soil samples recovered from these sites (Beyzaei et al. 2015; Stringer et al. 2015) showed clear micro-structure or well-defined layers of different grains sizes in millimetres and centimetres scales in addition to the macro-structure and layering clearly depicted by the CPT traces. Boulanger et al. (2016) discuss the limitations in the spatial resolution of property estimates from CPT data in such deposits. Needless to say, surface waves approaches, as demonstrated in the presented papers, would have very severe limitations in this context and would not be applicable even to deposits with significantly coarser stratification.

By and large, penetration based methods performed better in uniform sand deposits and showed poorer predictive capacity in highly stratified soils consisting of silty sands, sands and non-liquefiable soils. The simplified methods were generally conservative and over-predicted occurrence and consequences of liquefaction in such deposits. With all of the above in mind, it is not surprising that Vs-based approaches were less successful in predicting liquefaction occurrence for the soils in Christchurch. The previous section highlights, however, that different parameters have different contributions in the liquefaction evaluation, and in this context it is encouraging to see a number of studies presented in this session in which multi-parameter approaches have been used in an attempt to exploit particular beneficial contributions of a given parameter in the liquefaction prediction. Given the complexities of the liquefaction phenomena mentioned above, it is anticipated that integrated approaches including not only different types of in situ tests but also laboratory testing and numerical analyses would provide means for further advancements of liquefaction assessment procedures.

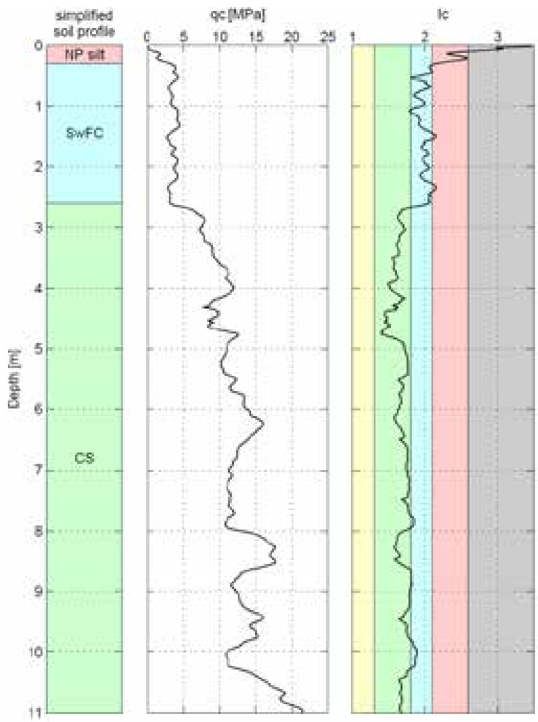

(a) Uniform fine sand deposit

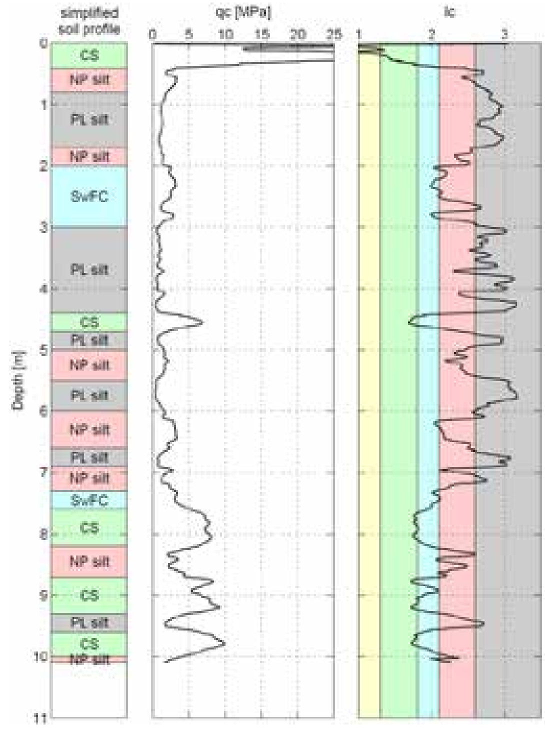

b) Highly stratified deposit of silty sand and sand layers interbedded with non-liquefiable soils

Figure 4. Characteristic CPT profiles of Christchurch Soils

4 COMMENTARY ON PAPERS ON EARTHQUAKE INDUCED LIQUEFACTION DAMAGE (EILD)

In this session distinct and complementary approaches are presented covering a wide range of issues in the evaluation of liquefaction. These include advances in the development of in situ testing equipment, combined use of different (complementary) in situ tests, interpretation of measured in situ data for evaluation of liquefaction potential, and liquefaction assessment of crushable calcareous sands that cannot be evaluated based on the empirical database for quartz and feldspar sands. In the following sections, a brief outline of the papers and summary of key findings are presented, while readers are referred to the papers for details.

5 LIQUEFACTION EVALUATION BASED ON SHEAR WAVE VELOCITY

Castellaro, Panzeri: A surface seismic approach to liquefaction

The paper focuses on surface seismic approaches to liquefaction evaluation based on SASW. The authors specifically explore the use of active and passive seismic techniques based on the measurement of surface waves and explore their performance in liquefaction evaluation of soils.

The authors classified 84 sites, in the area struck by the 2012 Emilia Earthquake (Italy), into four classes (A, B, C, D) and employed the V_s-based method proposed by Kayen et al. (2013) to predict liquefaction triggering (and surface manifestation) at the 84 case history sites. They found that 'global' V_s values derived based on the surface-wave methods could not discriminate between the sites at which liquefaction was manifested at the ground surface (A) and those with generally similar conditions that did not manifest liquefaction (B). The limitations of this method can be linked to the insensitivity of the seismic surface-wave based measurements to identify details of stratigraphy required in the identification of liquefiable horizons. For the particular depositional environment considered, the authors discuss that a simple analysis of the Rayleigh wave phase velocity spectra (in the frequency domain, with no inversion) could be useful in preliminary liquefaction evaluation. It is concluded that measuring V_S in boreholes or in the laboratory (when the collection of undisturbed samples is possible) has the advantage of providing more accurate values at the specific depth of interest but at the expense of higher costs and invasiveness compared to the geotechnical methods and of the same point validity. They have verified the applicability of seismic active and passive multichannel modern surface wave techniques in the prediction of liquefaction potential, using data from two earthquakes that occurred in Po Plain (Northern Italy) in 2012, causing extensive liquefaction. The geophysical surveys showed that the Rayleigh wave phase velocity spectra were clustered into three groups only: classes A and B were found to be indistinguishable from a seismic point of view, being this limitation due to the resolution of the adopted seismic methods, a function of the 'exploring wavelength', making seismic layers such as the sands under investigation – which are just 2–4 m thick and have V_S just a few ten of meters higher than the surrounding clay-silt – practically invisible at depths greater than 4–5 m. Even the probabilistic and deterministic methods to assess the liquefaction potential of sands through the V_S measurement failed in the case of the present study since classes A and B soils were found to be randomly distributed between the liquefaction and non-liquefaction zones, while predictive power exists for class C soils, which, as they represent deep sands, fall in the non-liquefaction zone. However, the geotechnical approach based on the tip resistance of the CPT to assess the liquefaction potential was found to be more successful. The reason for the failure of the surface geophysical method seems to be linked, therefore, not to specific features of the sands in this area, but to the insensitivity of the seismic surface-wave based methods (MASW, ReMi, ESAC, SPAC, and many others) used to the details of stratigraphy for this specific goal. However, it seems that the simple analysis of the Rayleigh wave phase velocity spectra, before any inversion procedure, can be used as it suggests the presence of sand or clay. It was possible to build a 'caution against liquefaction' graph that can – after specific extra studies in different geological settings – also be applied.

6 PENETRATION TESTS AND DEVICES

Rollins, Youd, Talbot: Liquefaction Resistance of Gravelly Soil from Becker Penetrometer (BPT) and Chinese Dynamic Cone Penetrometer (DPT)

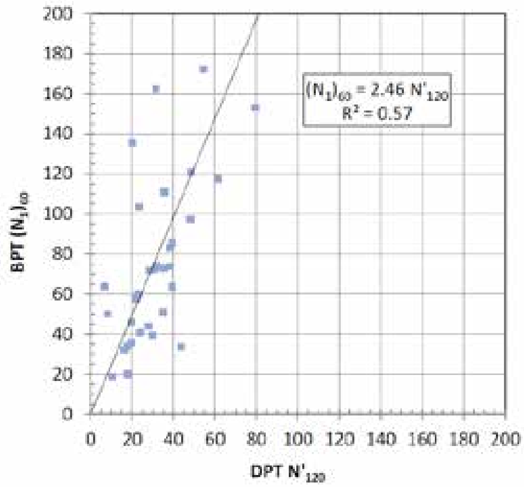

Figure 5. BPT $(N_1)_{60}$ vs. DPT N'_{120} for gravel, automatic hammer with best-fit correlation line (Rollins et al. 2016)

Liquefaction assessment of gravelly soils has been one of the challenging topics in this area, because the principal penetration tests used in the liquefaction evaluation (CPT and SPT) are not generally useful in gravelly soils. The large particle size of gravels (relative to the penetration probe) results either in a refusal or inconsistent correlations for CPT and SPT. Hence, the paper focuses on a comparison between the BPT and the Chinese DPT, two tests specifically developed for evaluation of gravelly soils. The motivation of the study is to explore the potential use of a DPT as a simpler and more economical test. The authors used two hammers in the DPT, one donut hammer and one automatic hammer. The blow counts from the

BPT and DPT correlated reasonably well when using the automatic hammer, but poor correlation was obtained with the donut hammer. Figure 5 shows the correlation between the BPT and DPT blow counts with automatic hammer.
The authors conclude that: (i) CRR curves from DPT (for PL30%) are generally consistent with results from BPT; (ii) In contrast to the gravels, the agreement between the CRRs obtained from DPT and BPT was rather poor for sand layers; hence, the DPT liquefaction resistance curves at gravel sites are not appropriate for evaluation of liquefaction in sands; (iii) DPT identified a thin potentially liquefiable layer not resolved by the BPT (Fig. 6).

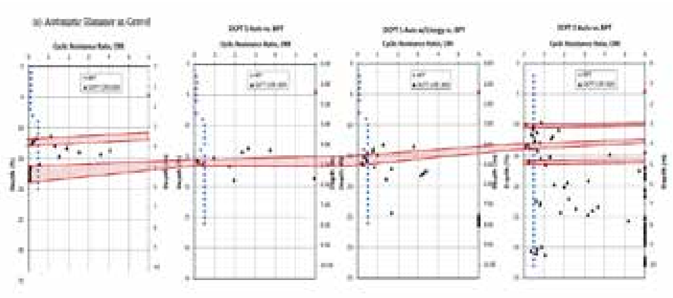

Figure 6 - Plot of cyclic resistance ratio causing liquefaction in gravel layers at Millsite dam based on BPT $(N_1)_{60}$ and DPT N'_{120} with the automatic hammer (Rollins et al. 2016)

Mirjafari, Orense, Suemasa: Soil classification and liquefaction evaluation using Screw Driving Sounding

The motivation behind this study is to use a more economical and practical device for liquefaction assessment of residential properties, for which conventional CPTs cannot be accommodated due to space (Fig. 7) or cost limitations. In this context, the authors explore the use of the Screw Driving Sounding (SDS) method, as an improved version of the Swedish Weight Sounding (SWS) technique, commonly used in Japan. In the SDS test, the required torque, load, speed of penetration and rod friction are measured thus allowing the user to not only measure the penetration resistance but also discriminate between different soil types.

Figure 7. SDS equipment

The authors show on one example that the variation of the specific energy with depth obtained in SDS is similar to the variation of the CPT tip resistance with depth. Based on the NZ soil database, two parameters were obtained, the average of the change in torque and the modified coefficient of plastic potential, to develop a soil classification chart (Fig. 8).

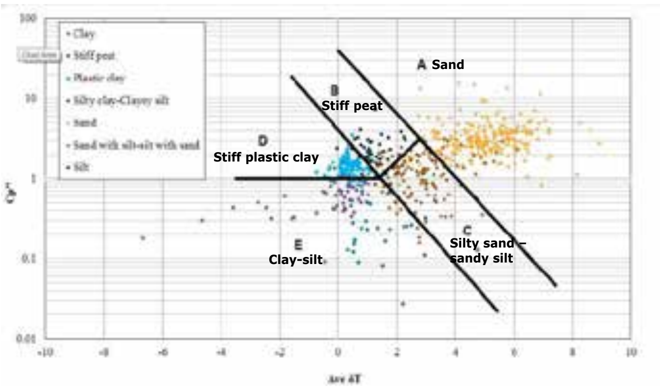

Figure 8. Soil classification chart based on SDS data (Mirjafari et al. 2016)

Using the data obtained following the Christchurch Earthquake Sequence, empirical relationships (equivalent to those for CPT) were developed for liquefaction potential assessment using SDS data (Fig. 9).

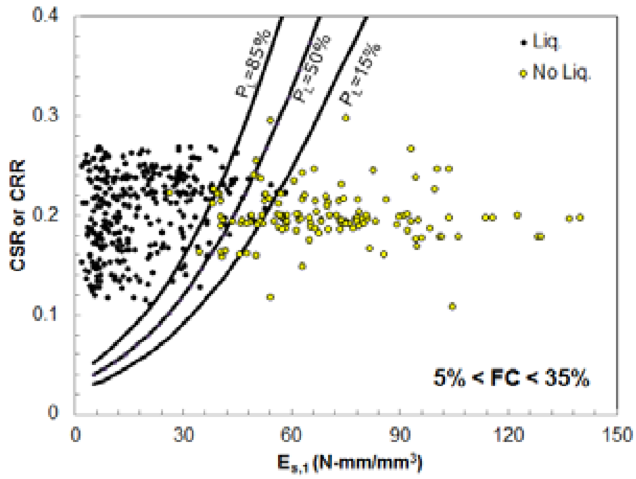

Figure 9. Proposed empirical chart for estimating CRR based on Es,1 from SDS test (Mirjafari et al. 2016)

Sawada: New developed soundings to assess liquefaction potential of soils

This paper presents three newly developed types of sounding equipment for evaluating the liquefaction susceptibility of soils.

The validation test results indicate that PDC (Piezo Drive Cone), PPT (Penetration & Pull-out Test) and DWS (Dynamic Weight Sounding) are highly useful for evaluation of liquefaction-induced problems due to earthquakes. In addition, liquefaction risks assessment in terms of the factor of safety can be evaluated in a short time. Therefore, liquefaction risks for a large area can be evaluated in a relatively short period.The authors give examples of the results obtained with these new equipment but they do not specify where they were done and in which conditions (Figs 10, 11, 12).

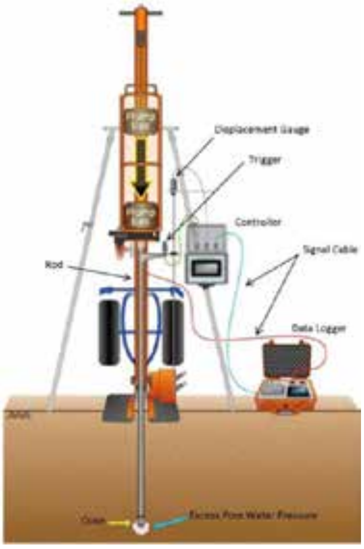

Figure 10. Schematic illustration of PDC

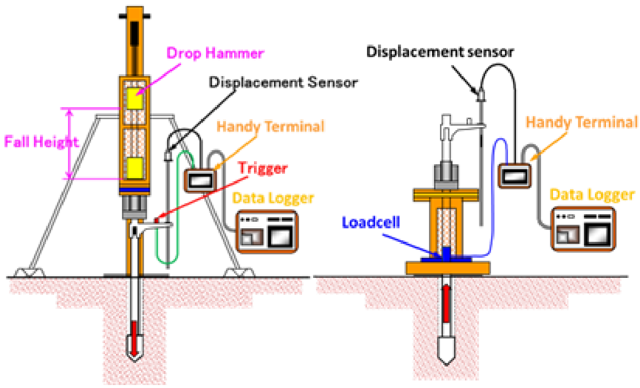

Figure 11. Schematic illustration of PPT

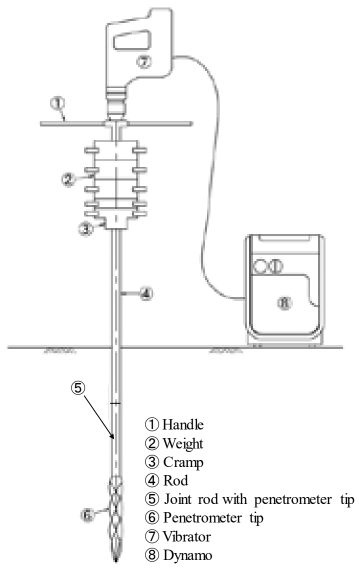

Figure 12. Schematic illustration of DWS

The authors emphasize that "degree of accuracy" is direct in trade-off with economy. The material for reclamation becomes inhomogeneous by the reclaimed method. It is essential for the high-resolute information (advancement of the spatial resolution) on performing the evaluation of soil liquefaction.

The most suitable solution which balances degree of accuracy (reliability of the ground information) with economy depends on field conditions. The agenda that is the most important for us is to take care of the field engineer who can select the most suitable technique of the ground investigation technique.

7 COMBINED USE OF DIFFERENT (COMPLEMENTARY) TESTS

Recognizing the limitations of any given test, several authors explored the combined use of complementary in situ tests to combine strengths of different tests or parameters for an enhanced liquefaction evaluation. This approach is strongly encouraged because it allows refinement and further evolution of single-test (parameter) approaches that are inherently limited in their capacity to address all complexities in the liquefaction evaluation.

Bán, Mahler, Katona, Győri: Liquefaction Assessment Based on Combined Use of CPT and Shear Wave Velocity Measurement

The goal of this research was to develop an empirical method where the result of CPT and V_s measurement are used in parallel and can supplement each other. This subject has been studied by other authors (e.g. Robertson 2015). After confirming the independence of q_c and V_s for the subset of case histories considered, the authors performed a logistic regression to obtain the probability contours of liquefaction occurrence. The graphical representation of the cyclic resistance ratio 'curve' for a given probability is a surface (Fig. 13).

$$CRR_{M=7.5\sigma'v=1atm}$$

$$= \exp\left(\frac{0.080Vs1 + 0.177qc1Ncs - 46.04 + 3.46\phi^{-1}(PL)}{8.40}\right) \quad (3)$$

Equation (3) expresses the cyclic resistance ratio for a given probability of liquefaction. A problem of the equation is that it does not include the variation (uncertainties) of the parameters, but just takes into account model uncertainties. In this context, a significant uncertainty was introduced in the method through the use of an I_c-FC correlation for estimating the fines content and then the normalized clean-sand equivalent cone tip resistance (q_{1Ncs}).

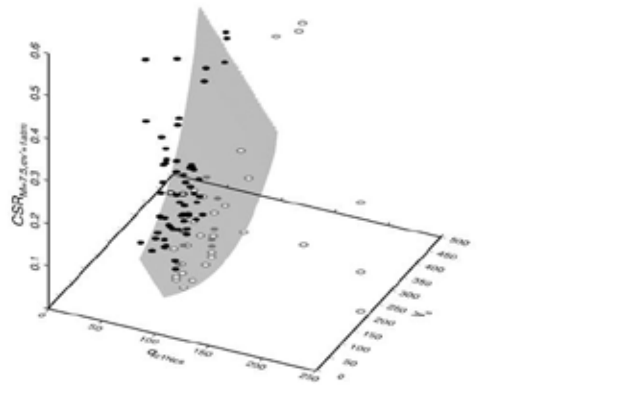

Figure 13. Cyclic resistance ratio surface corresponding to 50% of liquefaction probability (Bán et al. 2016)

It is an interesting approach along the idea of combining two measurements that complement each other, and provide small-strain and large-strain properties respectively, as has been suggested by Robertson (2015) and Schneider & Moss (2011).

Monaco, Tonni, Gottardi, Marchi, Martelli, Amoroso, Simeoni: Combined use of SDMT-CPTU results for site characterization and liquefaction analysis of canal levees

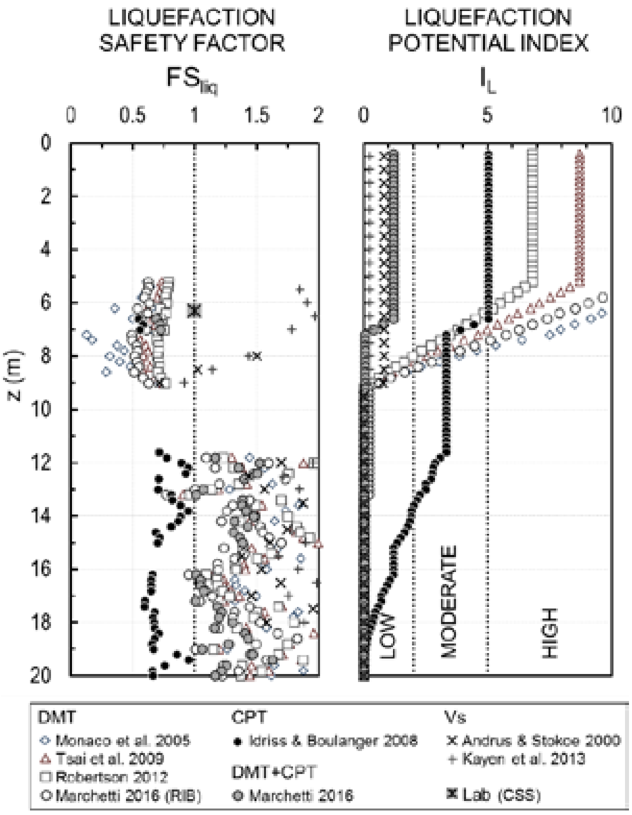

Figure 14. Results of liquefaction analyses based on the horizontal stress index K_D (SDMT), on the cone penetration resistance q_t (CPTU) and on the combination K_D (SDMT) & q_t (CPTU): results obtained by methods based on shear wave velocity V_S and by laboratory cyclic simple shear tests (CSS) are compared (Monaco et al. 2016)

This paper focuses on the comparison of results obtained by SDMT vs. CPTU test interpretation, and liquefaction analysis using a recent simplified method (Marchetti 2016) based on the combined use of the horizontal stress index K_D provided by SDMT and the cone penetration resistance q_t provided by CPTU.

The results obtained by this method are compared with the results obtained by existing methods based on q_t (CPT) and K_D (DMT) alone, as well as with the results obtained by methods based on the shear wave velocity V_S and by laboratory cyclic tests.

Tonni et al. (2015a, b) presented the results of the evaluation of CRR from K_D (SDMT) and CRR from q_t (CPTU). The correlation proposed by Marchetti (2016) was defined by combining the Idriss & Boulanger (2004, 2006) CRR-Q_{cn} correlation with the Robertson (2012) average Q_{cn}-K_D interrelationship and is the geometric average between a first *CRR* estimate obtained from Q_{cn} and a second *CRR* estimate obtained from K_D (Eq. (2)).

In the case illustrated in the paper, the use of a combined correlation for estimating CRR based at the same time on CPT-q_t and DMT-K_D (Marchetti 2016) has confirmed the probable occurrence of liquefaction. However, the estimated overall liquefaction susceptibility, represented by the liquefaction potential index I_L, is lower than indicated by methods based both on K_D alone and q_t alone. This results in reasonable agreement with field observations. As noted by Marchetti (2016), it is expectable that an estimate based at the same time on two measured parameters is more accurate than estimates based on just one parameter, and incorporating the DMT stress history parameter K_D into the liquefaction correlations should possibly reduce the uncertainty in estimating CRR. Considerable additional research is obviously necessary, especially if the sand is not clean and uncemented.

The analyses based on V_S generally indicate minor liquefaction. The results from DMT parameter show a layer between 5-9m susceptible to liquefaction and no significant liquefaction in deeper sands. The results from CPTU suggest generalized liquefaction in the deeper sands (Fig. 14). The results of liquefaction analyses carried out using simplified methods based on the DMT horizontal stress index K_D, in agreement with well-established methods based on the CPT cone penetration resistance q_t, suggest that plausibly local liquefaction phenomena, of variable extent, may have been induced by the May 20, 2012 earthquake in the sandy-silty soils below the Scortichino canal levee.

Fioravante. Giretti: CRR from CPT via state parameter

The paper proposes a methodology to evaluate the undrained cyclic resistance of clean, uncemented, normally consolidated, young sands from cone penetration tests through the state parameter. A comprehensive experimental study on an Italian sandy deposit (San Carlo Sand, SCS) and two well-known standard silica sands, Ticino and Toyoura (TS4 and TOS), involves the determination of liquefaction resistance curves using cyclic triaxial tests, and a series of model cone penetration tests using a seismic centrifuge. In both series a range of void ratios and overburden stresses states (state parameter values) were taken. The tip resistance–state parameter relationships used the results of CPT performed in a centrifuge with a miniaturized piezocone on homogeneous reconstituted sand models. On this basis an expression for q_c* was defined as a function of the state parameter. The liquefaction resistance curves (*CRR-N_c* relationship) derived from the cyclic test results were also expressed through the state parameter. By combing these expressions, a direct correlation between q_c* and the cyclic resistance ratio at N cycles was derived. The experimental q_c* - state parameter relationships for the three sands are shown in Figure 15.

The authors propose an exponential equation to obtain a direct correlation between q_c* and the cyclic resistance ratio at N cycles for simple shear condition, CRRNSS, relying in five fitting parameters of SCS. The correlations to compute CRRNSS profiles from in situ CPTs for the sand considered the number of equivalent cycles associable to an earthquake of moment magnitude M = 5.8 (as the 20 May earthquake), according to the Idriss (1999) approach. From the five q_c profiles the average profile was computed, taking into account the slightly different altitude of the ground level at each test site. The computed CRR profile is represented in Figure 16, where it is compared with the cyclic earthquake-induced stresses CSR, computed according to Seed & Idriss (1971), which is consistent with the liquefaction phenomena occurred at the reference site in San Carlo, affected by the 2012 Emilia earthquake.

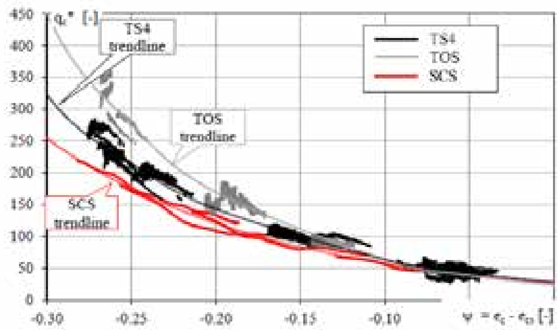

Figure 15. Normalized q_c* vs. ψ for all tested sands (Fioravante & Giretti 2016)

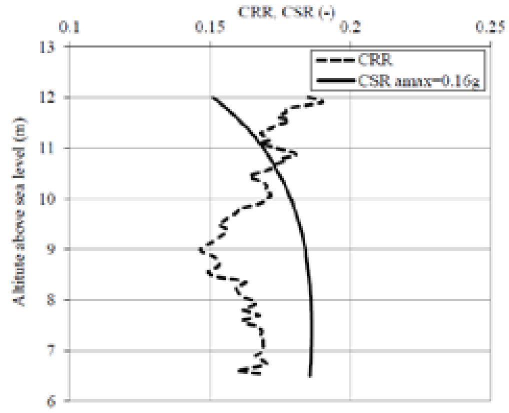

Figure 16. CRR and CSR profile (Fioravante & Giretti 2016)

Roberts, Stokoe, Hwang, Cox, Wang, Menq, van Ballegooy: Field Measurements of the Variability in Shear Strain and Pore Pressure Generation in Christchurch Soils

A direct, in-situ test method has been developed to investigate the shear strain at which pore pressure generation begins, the combined effects of shear strain amplitude and number of loading cycles on pore pressure generation, and estimate the point at which liquefaction "triggering" occurs. r_u is the excess pore pressure.

The dynamic performance was evaluated at three test panels, two natural soil test panels (6-NS-1 and 6-NS-2) and one test panel improved by the Rapid Impact Compaction method (6-RIC-1). A significant variability arose in the r_u-logγ relationships due to degree of saturation, density (reflected in the V_S values), and fines content (SP versus SM soils) –Figure 17. From this figure it can be concluded that loose, clean sand with FC ≤ 5%, SP and D_r ~40 to 55% (samples 6-NS-1 and 6-NS-2) generated a positive r_u-logγ relationship that would predict liquefaction; the threshold strain at which pore pressure generation began, γ_t^{pp}, for the loose, clean sands was in the range of 0.01 to 0.02 %; denser, clean sand with FC ≤ 5 %, SP and D_r ~ 80% (6-RIC-1) generated a negative r_u-logγ relationship that would predict no liquefaction. As for the influence of fines content, loose, silty sand with FC = 15 – 30 % (SM) generated little to no r_u even at a relatively high level of shear strain γ ≃ 0.12 %, as can be verified in Figure 18.

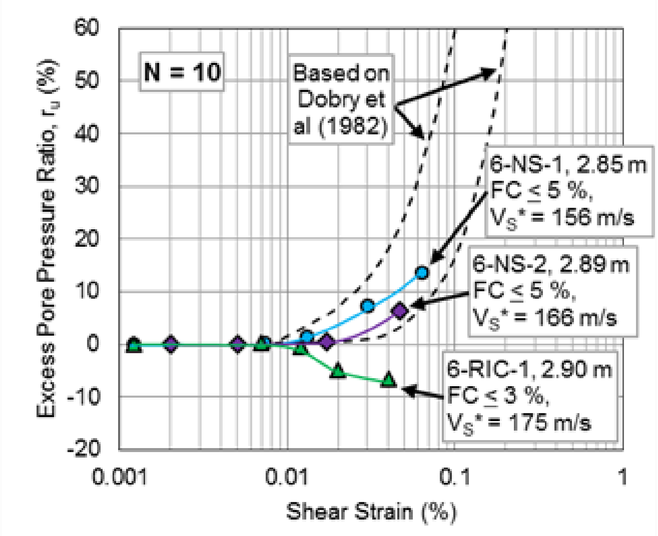

Figure 17. Variation in r_u with γ and Vs at N=10 cycles for SP material (Roberts et al. 2016)

Figure 19 shows the normalized shear modulus reduction curve from RC testing for a reconstituted specimen taken from 6-NS-2 at a depth of 2.0 m. The value of γ_t^e marks the boundary between the linear and nonlinear-elastic shear strain ranges and the range of γ_t^{pp} (~0.01-0.02%) of the loose, clean sands was about 25 to 50 times the γ_t^e (0.0004%). The range in values of γ_t^{pp} corresponds to strains at which values of G/G_{max} are in the range of 0.7 to 0.6 for this sand, indicating that the soil has already lost 30 to 40 % of its initial stiffness before volume change, hence r_u begins to occur.

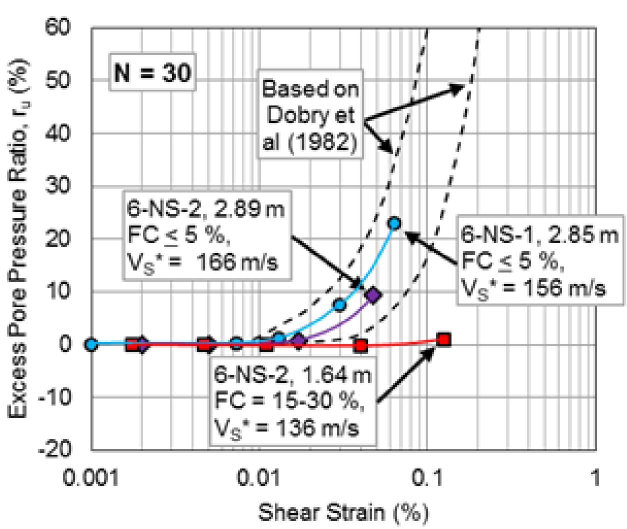

Figure 18. Effect of fines content on r_u-logγ relationships (Roberts et al. 2016)

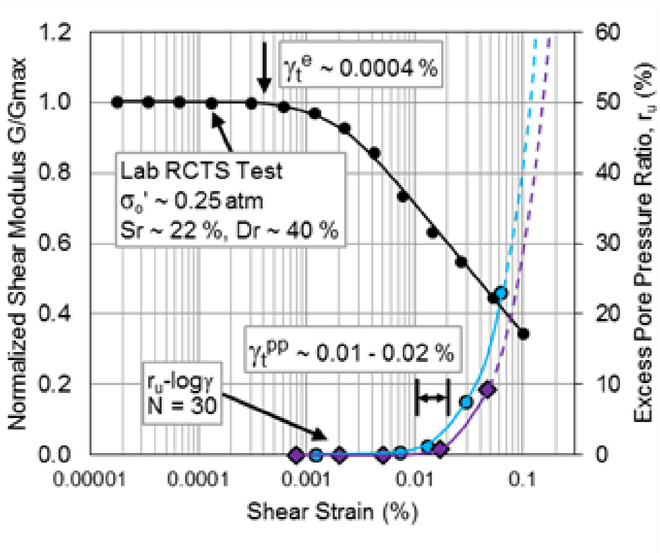

Figure 19. Comparison between the G/G_{max}-logγ curve from RC testing ant the r_u-logγ relationships at test panel 6-NS-1 and 6-NS-2 (Roberts et al. 2016)

Mengé, Vinck, Van Den Broeck, Van Impe, Van Impe: Evaluation of relative density and liquefaction potential with CPT in reclaimed calcareous sand

The paper discusses the quality control of the compaction of large land reclamation works with calcareous sands. With Centrifuge chamber tests, it is possible to have an undisputable correlation between q_c, D_r and σ'_v. Liquefaction assessment is often performed according to the NCEER (National Center for Earthquake Engineering Research) method, based on corrected CPT results.

The results of the centrifuge tests (Fig. 20) show that a significant impact of the presence of water was found, leading to much lower values of $q_{c,wet}$ compared to $q_{c,dry}$ at similar relative density and stress level. It is also shown that Particle Size Distribution has less impact on the behavior of the material than its mineralogy.

Because of the heterogeneity of the compacted fill, a specific approach was followed when evaluating the CPT's in calcareous materials (this "Shell Correction Factor", SCF, is illustrated in Fig. 21). Correlations between q_c and D_r were found, and compared with Wehr (2009) and Mayne (2014) proposals. The SCF which was proposed by Wehr perfectly matches the SCF derived here for a stress level of 100kPa The SCF as suggested by Mayne seems not to correspond well and may be valid for other types of calcareous sands. Nevertheless the findings with regard to SCF and its ease of use, authors prefer the more accurate scientific approach using the results of CC-tests to define the relative density of calcareous sands from CPT.

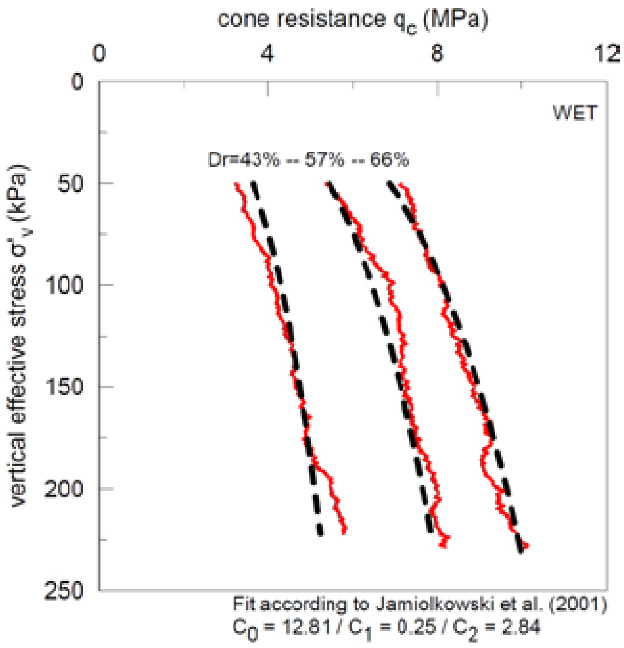

Figure 20. Results of the centrifuge CC tests on wet BAW material (Mengé et al. 2016)

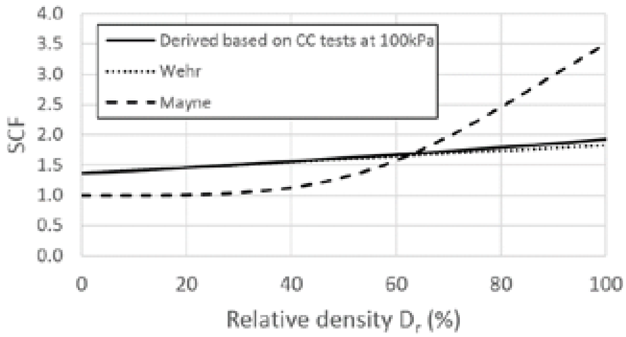

Figure 21. SCF in function of relative density (Mengé et al. 2016)

The authors conclude that the problem of quality control of the compaction of large land reclamation works with calcareous sands can be addressed by an approach that relies performing CC tests at an early stage of the project. This allows to have an undisputable correlation between q_c, D_r and σ'v, particularly when compacted fill is highly heterogeneous. Liquefaction assessment is often performed according to the NCEER method, based on corrected CPT results.

8 CASE-HISTORIES: 2 EXAMPLES OF APPLICATIONS

Klibbe: The Determination of Factor of Safety against Liquefaction and Post-Liquefaction Settlement

In this paper, the calculation of factor of safety against liquefaction and post-liquefaction settlement has been determined using CPTu and shear wave velocity records. This data was obtained and recorded across an entire project site at centimetre depth increments, being this interpreted in dedicated spreadsheets elaborated to allow both profiling and contouring of the factor of safety and settlement (Fig. 22).

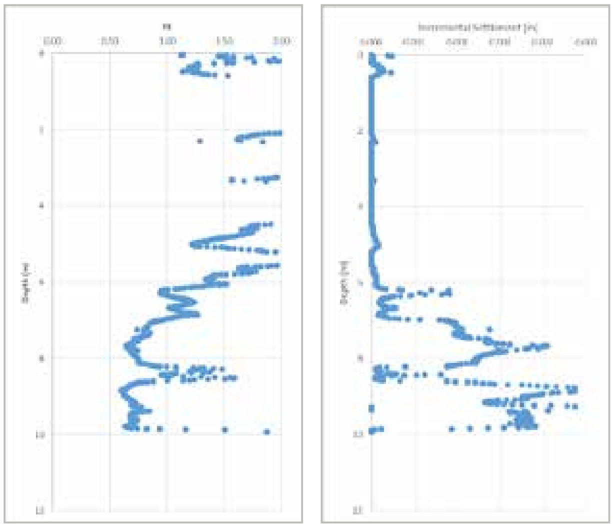

Figure 22 - Calculated factor of safety against liquefaction and incremental settlement (Klibbe 2016)

This has allowed each facility to be assigned the appropriate seismic site class. Appropriate foundation system based on conventional bearing capacity and settlement as well as liquefaction affects were suggested. Due to the high carbonate content of the sands, a correction of penetration resistance, q_{t1}, conversion from normalized tip resistance in calcareous-carbonate sands to an equivalent normalized tip resistance in silica-quartz sands, was implemented. Due to the carbonate nature of the sands, the generic fines content correlations do not perform well at this site. Therefore, a site specific fines content correlation was adopted (as suggested by Mayne 2014).

Rodrigues, Amoroso, Cruz, Viana da Fonseca, A. Liquefaction assessment from CPTu tests in a site in South of Portugal.

This paper focuses on the assessment of the liquefaction potential of the site. The liquefaction potential index, as well as the liquefaction severity number, recognizes high liquefaction damage for Seismic Action 1 and low to high for Seismic Action 2. The critical conditions are concentrated in the most superficial layers, evidencing very high lateral spreading risk. It was decided to improve the ground by densification through vibration techniques, in order to mitigate possible damage in the water distribution net that runs mainly near the surface, thus preventing cuts in the water supply post-seismic events.

The authors concluded that: (i) Liquefaction assessment from CPTu results revealed a high superficial liquefaction vulnerability for the new water supply reservoir in Monte Gordo, Algarve, in the South of Portugal; (ii) the respective liquefaction vulnerability has shown that the condition is critical for the reference action associated to the Atlantic Ocean far distance seismic action. As a consequence, it was decided to improve the ground by densification through vibration techniques, in order to mitigate possible damage in the water distribution net that runs mainly near the surface, thus preventing cuts in the water supply post-seismic events.

9 CONCLUSIONS

The use of combined CPT test results with the measurements of shear wave velocity, Vs is increasing, as the shear wave velocity are independent of soil characteristics but lack the stratigraphic detail of CPT (Robertson 2015). Shear wave (Vs) is more sensitive to factors such as age and cementation. Robertson (2015) proposes a modification CPT "fines" correction to improve the agreement between the two methods. A comprehensive study for a combined or parallel use of CPT and Vs/Vp measurements in liquefaction evaluation is currently under way for Christchurch (New Zealand) soils.

The identification of soils with microstructure (aging and/or cementation) is important in a way that for unusual soils traditional cyclic liquefaction trigger methods can be uncertain. According to Robertson (2015), the combination of CPT with V_s (SCPT) and geologic age can be useful to separate the effects of age or cementation. For uncemented aged soils, V_s-based methods provide better of CRR than CPT methods. For light cemented soils, the approach of Schneider and Moss (2011) can be used to estimate if the design earthquake loading (CSR*) exceeds CSR to reach the threshold strain (CSR*th). If so, the benefits of cementation may be lost. It appears that the benefits of bonding can end when CSR*>CSR*th.

A discussion about the difference between aging and cementation benefits is initiated, but further research is needed. According to Robertson (2015) aging may have little influence on the threshold strain whereas bonding may increase the threshold strain depending on its nature and degree.

10 ACKNOWLEDGEMENTS

The authors would like to acknowledge the to the Portuguese Science and Technology Foundation for their financial support through the Investigation Scholarship part of the project PTDC/ECM-GEO/1780/2014): *"Liquefaction Assessment Protocols to Protect Critical Infrastructures Against Earthquake Damage (LIQ2PROEARTH)"* financed by the European Communion Operational Program for Competitive Factors, COMPETE.

11 REFERENCES

Andrus, R.D., Piratheepan, P., Ellis, B.S., Zhang, J. and Juang, C.H. (2004). Comparing liquefaction evaluation methods using penetration-Vs relationships. Soil Dyn. Earthquake Eng., 24(9-10), 713-721

Andrus, R. D., Hayati, H., and Mohanan, N. P. (2009). "Correcting liquefaction resistance of aged sands using measured to estimated velocity ratio." J. Geotech. Geoenviron. Eng., 10.1061/(ASCE)GT.1943-5606.0000025, 735–744.

Bahadori, H. and Hasheminezhad, A. (2016). Standard Penetration Test-Based Assessment of Seismic Soil Liquefaction Potential of Urmia, Iran. Proc., 5th Int. Conf. on Geotechnical and Geophysical Site Characterisation ICS'5

Baldi G., Bellotti R., Ghionna N., Jamiolkowski M., Pasqualini E. (1986) Interpretation of CPTs and CPTU's, 2nd Part. In: Proceedings of the 4th international geotechnical seminar, Nanyang Technological Institute. Singapore, pp 143–156

Bán, Z., Mahler, A., Katona, T.J. and Györi, E. (2016). Liquefaction assessment based on combined use of CPT and shear wave velocity measurement. Proc., 5th Int. Conf. on Geotechnical and Geophysical Site Characterisation ICS'5

Beyzaei, C.Z., Bray J.D., Cubrinovski M., Riemer M., Stringer M.E., Jacka M., Wentz F.J. (2015). Liquefaction resistance of silty soils at the Riccarton road site, Christchurch, New Zealand. Proc. 6th Int. Conf. Earthquake Geotech. Eng., Christchurch, New Zealand. Paper No. 616

Boulanger R.W. (2012). Liquefaction in the 2011 Great East Japan Earthquake: lessons for U.S. practice, Proceedings of the International Symposium on Engineering Lessons Learned from the 2011 Great East Japan Earthquake, Tokyo, Japan, 655–664

Boulanger, R.W, Moug, D. M. Munter, S. K. Price, A. B. and. DeJong J. T (2016) Evaluating liquefaction in interbedded sand, silt, and clay deposits using the cone penetrometer. Keynote Lecture, *ISC'5*, 5-8 September, Gold Coast, Australia.

Boulanger, R. W. & Idriss, I. M. 2015. CPT-based liquefaction triggering procedure. Journal of Geotechnical and Geoenvironmental Engineering, ASCE, 142(2): 04015065, 10.1061/(ASCE)GT.1943-5606.0001388.

Bonnefoy-Claudet, S., Cotton, F. and Bard, P.Y. (2006). The nature of noise wavefield and its applications for site effects studies. A literature review. Earth-Science Reviews, 79, 205-227

Bray, J.D., Zupan, J.D., Cubrinovski, M. and Taylor, M. (2014). CPT-based liquefaction assessments in Christchurch, New Zealand. Keynote Lecture in CPT'14, Las Vegas, Ne. Available in: *http://www.cpt14.com*

Castellaro, S. and Panzeri, R. (2016). A surface seismic approach to liquefaction. Proc., 5th Int. Conf. on Geotechnical and Geophysical Site Characterisation ICS'5

Cho, G–C., Dodds, J. & Santamarina, J. C. (2006). "Particle Shape Effects on Packing Density, Stiffness, and Strength: Natural and Crushed Sands", J. Geotech. Geoenviron. Eng., ASCE, 132(5), 591–602.

Cruz, N., Rodrigues, C., and Viana da Fonseca, A. (2012). "Detecting the presence of cementation structures in soils, based in DMT interpreted charts." Proc., 4th Int. Conf. on Site Characterization ISC-4, Vol. 2, Balkema, Rotterdam, Netherlands, 1723–1728.

Cubrinovski, M., Rees, S. & Bowman, E. (2010). Effects of non-plastic fines on liquefaction resistance of sandy soils. 17, 125-144.

Cubrinovski, M., Bray, J.D., Taylor, M., Giorgini, S., Bradley B.A., Wotherspoon, L., and Zupan, J. (2011a). Soil Liquefaction Effects in the Central Business District during the February 2011 Christchurch Earthquake. *Seismological Research Letters,* Vol. 82: 893-904.

Cubrinovski, M., Bradley, B., Wotherspoon, L., Green, R., Bray, J., Wood, C., Pender, M., Allen, J., Bradshaw, A., Rix, G., Taylor, M., Robinson, K., Henderson, D., Giorgini, S., Ma, K., Winkley, A., Zupan, J., O'Rourke, T., DePascale, G. and Wells, D. (2011b). Geotechnical Aspects of the 22 February 2011 Christchurch Earthquake. *Bulletin of the New Zealand Society of Earthquake Engineering*, Vol. 44(4): 205-226.

Cubrinovski, M., Green, R.A. and Wotherspoon, L. [Eds] (2011c). Geotechnical Reconnaissance of the 2011 Christchurch Earthquake. *Technical Report*, retrieved from *http://geerassociation.org/GEER_Post%20EQ%20Reports/Christchurch_2011/Index_Christchurch_2011.html*

*E*slaamizaad, S. and Robertson, P.K. (1996). Seismic cone penetration test to identify cemented sands. Proc. 49th Canadian Geotechnical Conf., St. John's, Newfoundland, Canadian Geotechnical Society (CGS), 1, 352-360

Fioravante, V. and Giretti, D. (2016). CRR from CPT via state parameter. Proc., 5th Int. Conf. on Geotechnical and Geophysical Site Characterisation ICS'5

Fioravante V, Giretti D, Abate G, Aversa S, Boldini D, Capilleri PP, Cavallaro A, Chamlagain D, Crespellani T, Dezi F, Facciorusso J, Ghinelli A, Grasso S, Lanzo G, Madiai C, Massimino MR, Maugeri M, Pagliaroli A, Rainieri C, Tropeano G, Santucci De Magistris F, Sica S, Silvestri F, Vannucchi G, (2013). Earthquake Geotechnical Engineering Aspects of the 2012 Emilia-Romagna Earthquake (Italy). Proc. 7th Int. Conf. on Case Histories in Geotech.Eng., Paper EQ-5, 34 pp.

Green, R.A., and Cubrinovski, M. [Eds] (2010). Geotechnical Reconnaissance of the 2010 Darfield (New Zealand) Earthquake. *Technical Report,* retrieved from *http://www.geerassociation.org/GEER_Post%20EQ%20Reports/Darfield%20New%20Zealand_2010/Darfield_New%20Zealand_2010_index.html*

Hayati, H., and Andrus, R. D. (2009). "Updated liquefaction resistance correction factors for aged sands." J. Geotech. Geoenviron. Eng., 10.1061/ (ASCE)GT.1943-5606.0000118, 1683–1692.

Idriss, I.M. (1999). "An update to the Seed-Idriss simplified procedure for evaluating liquefaction potential." Proc. TRB Workshop on New Approaches to Liquefaction, Publ. No. FHWA-RD-99-165, Federal Highway Administration.

Idriss, I.M. & Boulanger, R.W. (2004). Semi-empirical procedures for evaluating liquefaction potential during earthquakes. *Proc. 11th Int. Conf. on Soil Dyn. and Earthquake Eng. & 33rd Int. Conf. on Earthquake Geotech. Eng., Univ. of California, Berkeley*, 1: 32-56.

Idriss, I.M. and Boulanger, R.W. (2006). Semi-empirical procedures for evaluating liquefaction potential during earthquakes. *Soil Dyn. and Earthquake Eng.*, 26: 115-130.

Kayen, R., et al. (2013). "Shear-wave velocity-based probabilistic and deterministic assessment of seismic soil liquefaction potential." J. Geotech. Geoenviron. Eng., 10.1061/(ASCE)GT.1943-5606.0000743, 407–419.

Klibbe, P.R. (2016). The Determinations of Factor of Safety against Liquefaction and Post-Liquefaction Settlement. Proc., 5th Int. Conf. on Geotechnical and Geophysical Site Characterisation ICS'5

Mayne, P.W. (2014). Interpretation of geotechnical parameters from seismic piezocone tests. *3rd Int. Symp. on Cone Penetration Testing*, Las Vegas, Nevada, USA: 47-73.

Maki, I. P., Boulanger, R.W., DeJong, M., and Jaeger, R. A. (2014). "Statebased overburden normalization of cone penetration resistance in clean sand." J. Geotech. Geoenviron. Eng., 10.1061/(ASCE)GT.1943-5606.0001020, 04013006.

Marchetti, S. (2015). Incorporating the Stress-History Parameter KD of DMT into the Liquefaction Correlations in Clean Uncemented Sands. J. Geotech. Geoenviron. Eng., ASCE, 142(2)

Marchetti, S. (2016). Incorporating the Stress History Parameter K_D of DMT into the Liquefaction Correlations in Clean Uncemented Sands. *J. Geotech. Geoenviron. Eng.*, 142(2): 04015072

Mengé, P., Vinck, K., Van den Broeck, M., Van Impe, P.O. and Van Impe, W.F. (2016). Evaluation of relative density and liquefaction potential with CPT in reclaimed calcareous sand. Proc., 5th Int. Conf. on Geotechnical and Geophysical Site Characterisation ICS'5

Mirjafari, S.Y., Orense, R.P., ASCE, M. and Suemase, N. (2016). Soil classification and liquefaction evaluation using Screw Driving Sounding. Proc., 5th Int. Conf. on Geotechnical and Geophysical Site Characterisation ICS'5

Monaco, P., Amoroso, S., Marchetti, S., Marchetti, D., Totani, G., Cola, S. and Simonini, P. (2014). Overconsolidation and stiffness of Venice Lagoon Sands and Silts from SDMT and CPTU. J. Geotech. Geoenviron. Engng 140, No. 1, 215-227

Monaco, P., Tonni, L., Gottardi, G., Marchi, M., Martelli, L., Amoroso, S. and Simeoni, L. (2016). Combined use of SDMT-CPTU results for site characterization and liquefaction analysis of canal levees. Proc., 5th Int. Conf. on Geotechnical and Geophysical Site Characterisation ICS'5

Roberts, J.N., Stokoe, K.H., Hwang, S., Cox, B.R., Wang, Y., Menq, F.M. and van Ballegooy, S. (2016). Field measurements of the variability in shear strain and pore pressure generation in Christchurch soils. Proc., 5th Int. Conf. on Geotechnical and Geophysical Site Characterisation ICS'5

Robertson P.K. & Wride C.E. (1998). "Evaluating cyclic liquefaction potential using the cone penetration test." Canadian Geotechnical Journal, 35(3): 442-459

Robertson, P. K. (2009). "Interpretation of Cone Penetration Tests—A unified approach." Can. Geotech. J., 46(11), 1337–1355.

Robertson, P.K. (2012). The James K. Mitchell Lecture: Interpretation of in-situ tests – some insights. *Proc. 4th Int. Conf. on Geotechnical and Geophysical Site Characterization, Porto de Galinhas*, 1: 3-24

Robertson, P. K. (2015). Comparing CPT and Vs Liquefaction Triggering Methods. J. Geotech. Geoenviron. Eng., 141 (9) 04015037 (doi: 10.1061/(ASCE)GT.1943-5606.0001338)

Rodrigues, C., Amoroso, S., Cruz, N. and Viana da Fonseca, A. (2016). Liquefaction assessment from CPTu tests in a site in South of Portugal. Proc., 5th Int. Conf. on Geotechnical and Geophysical Site Characterisation ICS'5

Rollins, K.M., Youd, T.L. and Talbot, M. (2016). Liquefaction Resistance of Gravelly Soil from Becker Penetrometer (BPT) and Chinese Dynamic Cone Penetrometer (DPT). Proc., 5th Int. Conf. on Geotechnical and Geophysical Site Characterisation ICS'5

Santamarina, J.C. (2005). "The role of geophysics in geotechnical engineering", Presentation in Microscale: Particle Forces. SAGEEP, 2005 – Symp. on the Applic.of Geophysics to Eng. and Environmental Problems (http://pmrl.ce.gatech.edu/presentations.html).

Sawada, S. (2016). New developed soundings to assess liquefaction potential of soils. Proc., 5th Int. Conf. on Geotechnical and Geophysical Site Characterisation ICS'5

Schnaid, F., Lehane, B.M., and Fahey, M. (2004). "In situ test characterization of unusual geomaterials." Proc., 2nd Int. Conf. on Site Characterization ISC-2, Porto, Vol. 1, Millpress, Rotterdam, 49–73.

Schneider, J. A. and Moss, R. E. S. (2011). Linking cyclic stress and cyclic strain based methods for assessment of cyclic liquefaction triggering in sands. Géotechnique Letters (doi: 10.1680/geolett.11.00021)

Seed, H.B. and Idriss, I.M. (1971). "Simplified procedure for evaluating soil liquefaction potential." J. Geotech. Engrg. Div., ASCE, 97(9), 1249–1273

Stringer, M., Beyzaei, C., Cubrinovski, M., Bray, J., Riemer, M., Jacka, M., Wentz, F. (2015). Liquefaction Characteristics of Christchurch Silty Soils: Gainsborough Reserve. Proc. 6th Int. Conf. Earthquake Geotech. Eng., Christchurch, New Zealand. Paper No. 726.

Tonni, L., Gottardi, G., Amoroso, S., Bardotti, R., Bonzi, L., Chiaradonna, A., d'Onofrio, A., Fioravante, V., Ghinelli, A., Giretti, D., Lanzo, G., Madiai, C., Marchi, M., Martelli, L., Monaco, P., Porcino, D., Razzano, R., Rosselli, S., Severi, P., Silvestri, F., Simeoni, L., Vannucchi, G. & Aversa, S. 2015a. Interpreting the deformation phenomena triggered by the 2012 Emilia seismic sequence on the Canale Diversivo di Burana banks. *Rivista Italiana di Geotecnica,* XLIX(2): 28-58 (in Italian).

Tonni, L., Gottardi, G., Marchi, M., Martelli, L., Monaco, P., Simeoni, L. & Amoroso, S. 2015b. SDMT-based Site Characterization and Liquefaction Analysis of Canal Levees Damaged by the 2012 Emilia (Italy) Seismic Sequence. *Proc. 3rd International Conference on the Flat Dilatometer DMT'15, Rome, Italy*, 341-348.

Tsai, P., Lee, D., Kung, G. T. and Juang, C.H. (2009). "Simplified DMT-based methods for evaluating Liquefaction Resistance of Soils". *J . Engrg.Geology, Elsevier*, 103, 13-22.

van Ballegooy, S., Malan, P., Lacrosse, V., Jacka, M.E., Cubrinovski, M., Bray, J.D., O'Rourke, T.D., Crawford, S.A. and Cowan, H. (2014) Assessment of Liquefaction-Induced Land Damage for Residential Christchurch. Earthquake Spectra: February 2014, Vol. 30, No. 1, pp. 31-55.

Viana da Fonseca, A., Coop, M.R., Fahey, M. & Consoli, N. (2011). "The interpretation of conventional and non-conventional laboratory tests for challenging geotechnical problems". 'Deformation Characteristics of Geomaterials', Vol. 1, pp. 84-119. IOS Press, Amsterdam.

Wehr, W.J. 2005. Influence of the carbonate content of sand on vibrocompaction. *Proc. 6th Int. conf. on Ground Improvement techniques*, Coimbra, Portugal: 525-632

Youd T. L. (1984). Recurrence of liquefaction at the same site. Proc. 8th World Conf. on Earthquake Engng, San Francisco, CA, III, 231–238.

Youd, T. L., Idriss, I. M., Andrus, R. D., Arango, I., Castro, G., Christian, J. T., Dobry, R., Finn, W. D. L., Harder, L. F., Hynes, M. E., Ishihara, K., Koester, J. P., Liao, S. S. C., Marcuson, W. F., Martin, G. R., Mitchell, J. K., Moriwaki, Y., Power, M. S., Robertson, P. K., Seed, R. B. & Stokoe, K. H. (2001). Liquefaction resistance of soils: summary report from the 1996 NCEER and 1998 NCEER/NSF workshops on evaluation of liquefaction resistance of soils. *Journal of Geotechnical and Geoenvironmental Engineering, ASCE*, 127(10): 817-833.

Geotechnical and Geophysical Site Characterisation 5 – Lehane, Acosta-Martínez & Kelly (Eds)
© 2016 Australian Geomechanics Society, Sydney, Australia, ISBN 978-0-9946261-1-0

Session Report: Application of Statistical Techniques

M.B. Jaksa
School of Civil, Environmental and Mining Engineering, University of Adelaide, Australia

ABSTRACT: This report presents an overview of the aims, key aspects and conclusions associated with the 10 papers submitted to the conference relating to the application of statistical techniques, as well as some areas that the authors may wish to consider in future work. The papers are divided into 3 sections dealing with statistics and probability, spatial variability and artificial intelligence. The papers demonstrate the broad application of the statistics and probability methods to geotechnical site characterization and underline the important role these techniques play in, and value they deliver to, geotechnical engineering.

1 INTRODUCTION

It is well appreciated that, because they are natural, geotechnical materials are inherently variable and their behavior is complex. As such, stochastic methods have been shown, since the mid-1960s, to be of great benefit in geotechnical engineering. In particular, the application of statistical and probabilistic methods to geotechnical engineering can provide valuable insights into the nature of uncertainties in site characterization and geotechnical design and the influence of spatial variability on the behavior of geotechnical systems. In addition, these methods are essential for providing a framework for understanding and quantifying risk and reliability and also in facilitating accurate geotechnical predictions.

This report presents an overview of the aims, key aspects and conclusions associated with the 10 papers assigned to the *Application of Statistical Techniques* session, as well as some suggestions that the authors may wish to consider in future work. The papers are divided into 3 categories: *Statistics and Reliability*, with 4 papers (Baziw & Verbeek 2016, Foti & Passeri 2016, Huang et al. 2016, Styler & Weemees 2016); *Spatial Variability* incorporating 5 papers (Lehane et al. 2016, Krage et al. 2016, Parida et al. 2016, Wierzbicki et al. 2016, Zho et al. 2016); and *Artificial Intelligence* which includes a single paper dealing with an artificial neural networks model (Sastre et al. 2016). The papers are arranged in alphabetical order of the first author.

2 STATISTICS AND RELIABILITY

2.1 *Gaussian distribution fitting for reliability of shear wave velocity*

Baziw & Verbeek (2016) present an extension to their interval velocity classification (IVC) technique, which they originally proposed in 2015. The IVC method utilizes linearity estimates from polarization analysis, in conjunction with cross correlation coefficient calculations of the full waveforms obtained from the seismic cone penetration test (SCPT). The paper outlines details of the mathematics and implementation of a new parameter, termed spectrum rank (*SR*), which is introduced into the IVC technique. The spectrum rank quantifies the deviation of the source wave frequency spectrum from a desirable Gaussian-shaped curve. The seismic traces from the SCPT, with high signal-to-noise ratios, were observed to exhibit a similar shape to that of a Gaussian (i.e. normal) distribution.

The authors show that, when applied to actual SCPT data, the *SR* value is strongly correlated to the signal-to-noise ratio (SNR) of the acquired trace. In addition, for seismic traces with a low SNR, the authors recommend that batch or automated processing should be avoided and arrival times should be obtained visually from vertical seismic profiles in order to identify first breaks or dominant peaks or troughs.

2.2 *Reliability of soil porosity estimation*

Foti & Passeri (2016) present a research study investigating the reliability of porosity estimation from shear wave velocities using error propagation theory. They make use of the relationship in Equation (1) that was developed by the authors in an earlier study where the porosity, n, is expressed as a function of: ρ^s and ρ^w, which are, respectively, the mass densities of the soil particles and pore water; K^w is the bulk modulus of the pore water; V_p and V_s are the velocities of propagation of the dilatational and shear waves, respectively; and ν_{sk} is the Poisson's ratio of the soil skeleton.

$$n = \frac{\rho^s - \sqrt{(\rho^s)^2 - \dfrac{4\,(\rho^s - \rho^w)\,K^w}{V_p^{\,2} - 2\left(\dfrac{1-\nu_{sk}}{1-2\,\nu_{sk}}\right)V_s^{\,2}}}}{2\,(\rho^s - \rho^w)} \quad (1)$$

The authors consider n as a function of ρ^s, ρ^w, K^w, $V_p = d/t_p$, $V_s = d/t_s$ and ν_{sk}, where d is the travel distance and t_i the travel times for each seismic wave (with $i = p, s$).

Error propagation theory is used to characterize the influence of each parameter that appears in the porosity formulation in (1), in this example specialized for a cross-hole test configuration. In their study, the authors assume that each variable is normally and randomly distributed and independent. In addition, the analyses assume $\nu_{sk} = 0.25 \pm 0.1$, $\rho^s = 2.7$ g/cm^3 and $\rho^w = 1$ g/cm^3.

The authors present data from two case studies, one from the site of the Zelazny Most tailings dam in Poland and the second from a site in the Italian town of Mirandola. From their analyses, the authors conclude that, for cross-hole tests, the distance between boreholes has the most significant influence on soil porosity estimation, whereas travel times have a modest effect. The influence of the velocity of compressional waves in water and the Poisson's ratio of the soil skeleton also affect the estimate of n. The effect of P-waves is also found to be significant.

2.3 *Bayesian updating using in situ test data*

The study by Huang et al. (2016) seeks to apply Bayesian updating to include laboratory testing and associated uncertainties to enhance the accuracy of seismic measurements. Their work involves the measurement of shear wave velocity, V_s, using the seismic dilatometer test (SDMT), supplemented with laboratory determined preconsolidation pressure data from constant rate of strain oedometer tests.

The authors adopt the Markov Chain Monte Carlo sampling method to sample the posterior distribution. Empirical relationships are then derived between the preconsolidation pressure, σ', and V_s. A prior distribution of preconsolidation pressures is obtained assuming a log-normal distribution, and using a linear trend and the geostatistical technique of kriging.

The posterior mean preconsolidation pressure is then used to update the SDMT data such that its trend and magnitude more closely approximates the laboratory values. The authors observe that the posterior prediction is a better fit to the laboratory test data and the use of a scale of fluctuation with the kriged prior also provides greater accuracy when interpolating between data points.

The authors conclude that the uncertainties associated with preconsolidation pressure can be significantly reduced by incorporating shear wave velocity measurements. In addition, whilst the paper presents a 1D example, the authors suggest that the technique is equally relevant to 2D and 3D situations.

2.4 *Quantifying and reducing uncertainty in down-hole shear wave velocities using signal stacking*

The research study presented by Styler & Weemees (2016) seeks to quantify the improvement in the interpreted shear wave propagation time, in down-hole seismic testing using a seismic piezocone (SCPTU), that can be realized through signal stacking of multiple traces. The extensive paper demonstrates how to: calculate the noise in a set of down-hole seismic traces; quantify the signal-to-noise ratio (SNR) for a trace and for stacked signals; and evaluate the error in the propagation time when comparing two seismic traces.

The authors found that the SNR increases with signal stacking, the error in the propagation time decreases with higher SNR, and the decrease in SNR with depth can be overcome by signal stacking.

In addition, the authors presented interpretation methods that can be used to: quantify signal noise through signal-subtraction; quantify SNR in down-hole seismic signals; and calculate the error in the shear wave propagation time using the cross-correlation function. The authors state that, while the techniques outlined in the paper are applicable to the SCPTU, they can also be applied to any SCPTU that recorded more than one trace per seismic test.

3 SPATIAL VARIABILITY

3.1 *Probabilistic assessment of laterally loaded pile performance in sand*

Lehane et al. (2016) present a probabilistic assessment of the lateral response of a pile in a uniformly graded dune sand using cone penetration test (CPT) and load test data. The paper examines the effects of the spatial variability of the ground parameters using a large series of CPTs performed at the site of the lateral pile tests. The authors use a direct CPT approach developed by Suryasentana & Lehane [S&L] (2014, 2016) to predict the sand's lateral load-displacement (*p-y*) curves and these are compared with the measurements of the test piles. A Monte Carlo simulation is performed which involves the generation of a series of random q_c profiles consistent with the assessed site variability and their combination with the *LAP* program to generate probability density functions for the load that would cause a 1% rotation gradient (=0.57°) at the pile head.

The paper examines the sensitivity of variations in q_c to the performance of two laterally loaded test piles conducted at the Shenton Park site in Perth, Western Australia. The stratigraphy at the Shenton Park site consists of a 5–7 m thick deposit of siliceous dune sand overlying weakly cemented limestone. A total of 12 CPTs were performed on the site. Two 225 mm diameter x 3.5 m long grout piles, constructed using the continuous flight auger technique, were adopted in the study and pushed laterally apart.

The lateral load-displacement relationship is predicted using the *LAP* program incorporating the S&L Method. Good agreement is observed between the predicted and measured behaviours.

A total of 50 CPTs were randomly generated, using *Microsoft Excel* and a vertical scale of fluctuation of 0.5 m, which was estimated from the CPTs performed on site.

The authors observed that the lateral load range likely to induce a given level of head rotation for a pile in sand is significantly lower than the range anticipated from the q_c variability and the CPT-based S&L Method provides good predictions for the lateral response of a test pile in a medium dense sand site. The authors also observed that the predictions using the S&L and the API sand methods have a low sensitivity to randomly generated q_c or ϕ' profiles that are normally distributed at any given depth.

3.2 *Identification of geological depositional variations using CPT-based conditional probability mapping*

Krage et al. (2016) present research aimed at improving the characterization and understanding of subsurface stratigraphy at a project site using transition probability geostatistics conditioned to CPT soundings and combined with geological information.

The authors use geostatistics in two ways to augment site investigations to: (1) identify or estimate the soil type at unknown locations; and (2) estimate the engineering properties at these unknown spatial locations. Their integrated site characterization framework is summarized in Figure 1.

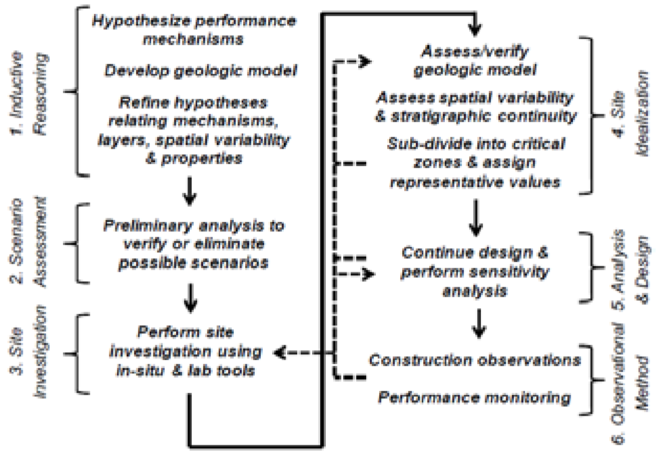

Figure 1. Flowchart of the integrated site characterization framework.

The authors incorporate the transition probability in their analyses, which describes the likelihood of transitioning from one category (where categories are user defined, such as soil type or engineering property based) to another over some separation distance. The main advantage of this approach is the ability to model ordered systems, such as geological facies environments.

The authors present an example case of a site for a new 11 m high embankment dam with respect to liquefaction assessment to which they applied their framework. Geostatistical simulation was performed conditioned to the CPTs taken along the dam wall alignment.

The authors concluded that the simulations indicate liquefaction is expected to be most prevalent at shallow depths: 1–2 m deep on the west side and to 4–6 m deep on the east side. Liquefaction is also expected at greater depths.

3.3 *Stochastic waveform inversion for probabilistic geotechnical site characterization*

Parida et al. (2016) propose a stochastic inverse analysis methodology to estimate probabilistically the Young's modulus from geophysical test measurements by accounting for uncertainties from spatial variability, measurement errors and limited data. They focus on the spectral analysis of surface waves (SASW) seismic geophysical test and adopt Monte Carlo simulation.

The authors simulate a 3D virtual site of soil moduli using an anisotropic random field. The methodology employs the finite element method with the stochastic collocation approach to solve probabilistically the forward problem for the SASW test. The virtual site is then excited using a chirp signal and the ground is assumed to be linear-elastic.

From the simulations performed the authors observe that the amount of information gained decreases with depth, implying that the sensors towards the bottom contribute modestly to the inverse estimation process. The authors suggest that the developed methodology is mathematically rigorous and computationally efficient, and is general enough to be extended widely, including inverse estimation of additional elastic, as well as elastoplastic, soil parameters.

3.4 *3D mapping of organic layers by means of CPTU and statistical data analysis*

Wierzbicki et al. (2016) present a research study which seeks to examine selected methods of statistical data analysis to determine the spatial extent of organic soil layers using piezocone (CPTU) data. Geotechnical characterization is undertaken for a site located 50 km from Poznań, Poland. The ground at the study area consists of glacial clay, layered sands and gravels, silts and organic soils.

CPTU data are subjected to clustering analysis using the *k*-means method and the inverse distance weighting (IDW) method is used to develop 2D and 3D models. The authors conclude that only simultaneous use of all available data result in accurate identification of the organic soil layer. The complete 3D IDW model, however, yields unsatisfactory results.

3.5 *Assessment of ground improvement on silt based on spatial variability analysis of CPTU data*

The research study undertaken by Zho et al. (2016) seeks to examine the difference in spatial variability characteristics of silt before and after compaction. A silt site located in the Jiangsu province, China, was improved using a new deep resonance compaction technique to increase the liquefaction resistance of the silt. A total of 17 CPTUs were performed prior to compaction and 26 after ground improvement (9 after 14 days, 7 after 54 days and 10 after 60 days) to assess the efficacy of the technique.

The study undertakes spatial variability analyses on the CPTU data before and after compaction. In particular, random field theory is used to examine cone tip resistance, q_t. The mean, coefficient of variation, *COV*, and the vertical scale of fluctuation, δ_v, of q_t are examined prior to and after compaction.

The results show that both the mean and δ_v decreased immediately after compaction, but gradually increased with the strength and density recovery; and the *COV* consistently decreased after compaction. The authors also suggest that the variation in the spatial variability of q_t could possibly be explained by the actions of the CPTU test and resonance compaction, their effect on the structure of the silt and the increase in soil strength with time.

4 ARTIFICIAL INTELLIGENCE

In the final paper in this session, Sastre et al. (2016), using data from the Panda2 variable energy dynamic cone penetrometer, develop an artificial intelligence-based model to predict the grain size class of the subsurface profile. The Panda is a lightweight dynamic cone penetrometer that is used to investigate ground profiles to depths of up to 5 m. It uses variable energy which is delivered manually by repeated blows of a standardized hammer. After each blow, the dynamic cone resistance, q_d, is calculated at the current depth using the Dutch formula (Cassan 1988):

$$q_d = \frac{\frac{1}{2}MV^2}{A(1 + P/M)x_{90^\circ}} \tag{2}$$

where: M is the weight of the striking mass; V is the speed of impact of the hammer; A is the area of the cone; P is the weight of the struck mass; and x_{90° is the penetration due to a single blow of the hammer (for a 90° cone).

The authors develop an artificial neural networks (ANNs) model using a database consisting of 218 Panda2 penetrograms (soundings), incorporating 149 tests performed in a laboratory-based calibration chamber (370 mm in diameter and 800 mm in depth) and 69 in situ tests from various locations in France. The tests were undertaken on relatively homogeneous soils containing particles with a grain size smaller than 50 mm, and the nature and geotechnical properties of the soils were characterized using standard laboratory classification tests.

In order to determine the appropriate set of ANN input parameters, the authors used a technique inspired by speech recognition, termed the ‘4 signal analysis’ approach, which the authors state incorporates a statistical, nonlinear, morphological and spectral, and pattern vector of 26 parameters for each penetrogram. Using a ‘one-at-a-time approach’ the authors examined the sensitivity of each of the 26 parameters and reduced the number of inputs to the following 17: (1) q_d mean; (2) q_d median; (3) q_d standard deviation; (4) q_d coefficient of variation; (5) q_d variance; (6) q_d range; (7) q_d interquartile range; (8) q_d skewness; (9) q_d kurtosis; (10) q_d Shannon entropy; (11) q_d logarithm entropy range; (12) q_d skewness; (13) q_d slope changes; (14) q_d waveform; (15) linear coefficient of linear trend; (16) independent coefficient of linear trend; and (17) maximum spectral power. The sole

ANN output is termed by the authors *GTR classification*, which is essentially a soil type classification into one of the following 4 classes: Class 1: fine-grained soils; Class 2: fine sands; Class 3: sands/gravels; and Class 4: gravels.

Between 2 and 25 hidden nodes are examined, as well as one and two hidden layers. The final, optimal ANN model consists of 17 input nodes, 12 nodes in a single hidden layer, and a single output node. The authors observe that the optimal ANN model assigned the correct class to of 97% of the samples (212 out of 218). The authors also report an accuracy of 94% and 97% for the testing and validation and sets, respectively.

In the interests of progressing and improving the work in the future, that authors may wish to consider the following comments. Closer examination of the 17 input nodes shows some degree of redundancy and potential inefficiency. For example, inputs (8) and (12) appear to be identical and it is difficult, from the description provided in the paper, to appreciate parameters (15) and (16). Furthermore, parameter (4), the coefficient of variation, is simply the ratio of the standard deviation [parameter (3)] to the mean [parameter (1)]. Hence, the inclusion of parameter (4) adds no new information to the model. Furthermore, parameter (5), the variance, is simply the square of the standard deviation [parameter (3)]. In addition, it is likely that other statistical parameters, such as (2), (6)–(9), (12), may also provide marginal value. If so, one would need to question the validity of the 'one-at-a-time' approach, which is used to assess the sensitivity of the individual input parameters.

In order to develop a parsimonious model, and one that perhaps yields an equation which is suitable for simple hand calculation [see Shahin et al. (2002); Shahin & Jaksa (2005), for example], the authors are encouraged to explore redeveloping the ANN with the following input parameters: (1) q_d mean; (3) q_d standard deviation; (8) q_d skewness; (9) q_d kurtosis; (10) q_d Shannon entropy; (11) q_d logarithm entropy range; (13) q_d slope changes; (14) q_d waveform; (15) linear coefficient of linear trend; (16) independent coefficient of linear trend; and (17) maximum spectral power.

Finally, it is unclear from the paper how the authors plan to disseminate the model that it can be used in practice. The development of a parsimonious model and an equation would certainly assist in this endeavor.

5 CONCLUSION

The 10 papers presented in this session demonstrate the wide range of geotechnical site characterization problems that can be successfully addressed using statistical and probabilistic methods.

6 REFERENCES

Baziw, E. & Verbeek, G. 2016. Frequency spectrum "bell-curve" fitting as a component of SCPT interval velocity accuracy assessment. In Editor (ed.) *5th International Conference on Geotechnical and Geophysical Site Characterisation*; *Proc. intern. conf., Gold Coast, 3-4 September 2016*. Rotterdam: Balkema.

Cassan, M. 1988. Les essais in situ en mechanique des sols. Volume I realisation et interpretation, Eyrolles, 146-151.

Foti, S. & Passeri, F. 2016. Reliability of soil porosity estimation from seismic wave velocities. In Editor (ed.) *5th International Conference on Geotechnical and Geophysical Site Characterisation*; *Proc. intern. conf., Gold Coast, 3-4 September 2016*. Rotterdam: Balkema.

Huang, J., Kelly, R. & Sloan, S.W. 2016. Enhanced data interpretation: combining in-situ test data by Bayesian updating. In Editor (ed.) *5th International Conference on Geotechnical and Geophysical Site Characterisation*; *Proc. intern. conf., Gold Coast, 3-4 September 2016*. Rotterdam: Balkema.

Krage, C., DeJong, J.T. & Boulanger, R.W. 2016. Identification of geological depositional variations using CPT-based conditional probability mapping. In Editor (ed.) *5th International Conference on Geotechnical and Geophysical Site Characterisation*; *Proc. intern. conf., Gold Coast, 3-4 September 2016*. Rotterdam: Balkema.

Lehane, B.M., Glisic, F. & Doherty J.P. 2016. Probabilistic assessment of laterally loaded pile performance in sand. In Editor (ed.) *5th International Conference on Geotechnical and Geophysical Site Characterisation*; *Proc. intern. conf., Gold Coast, 3-4 September 2016*. Rotterdam: Balkema.

Parida, S.S., Sett, K. & Singla, P. 2016. Stochastic waveform inversion for probabilistic geotechnical site characterization. In Editor (ed.) *5th International Conference on Geotechnical and Geophysical Site Characterisation*; *Proc. intern. conf., Gold Coast, 3-4 September 2016*. Rotterdam: Balkema.

Sastre, C., Benz, M., Gourvès, R., Breul, P. & Bacconnet, C. 2016. Automatic methodology to predict grain size class from dynamic penetration test using neural networks. In Editor (ed.) *5th International Conference on Geotechnical and Geophysical Site Characterisation*; *Proc. intern. conf., Gold Coast, 3-4 September 2016*. Rotterdam: Balkema.

Shahin, M.A., Jaksa, M.B. & Maier, H.R. 2002. Artificial neural network–based settlement prediction formula for shallow foundations on granular soils. *Australian Geomechanics* 37(4): 45-52.

Shahin, M.A. & Jaksa, M.B. 2005. Neural network prediction of pullout capacity of marquee ground anchors. *Computers and Geotechnics* 32(3): 153-163.

Styler, M.A. & Weemees, I. 2016. Quantifying and reducing uncertainty in down-hole shear wave velocities using signal stacking. In Editor (ed.) *5th International Conference on Geotechnical and Geophysical Site Characterisation*; *Proc. intern. conf., Gold Coast, 3-4 September 2016*. Rotterdam: Balkema.

Suryasentana, S.K. & Lehane, B.M. 2014. Numerical derivation of CPT-based p–y curves for piles in sand. *Géotechnique* 64(3): 186-194.

Suryasentana, S.K. & Lehane, B.M. 2016. Updated CPT-based p-y formulation for laterally loaded piles in cohesionless soil under static loading. *Géotechnique*, dx.doi.org/10.1680/ jgeot.14.P.156.

Wierzbicki, J., Smaga, A., Stefaniak, K., Wołyński, W. 2016. 3D mapping of organic layers by means of CPTU and statistical data analysis. In Editor (ed.) *5th International Conference on Geotechnical and Geophysical Site Characterisation*; *Proc. intern. conf., Gold Coast, 3-4 September 2016*. Rotterdam: Balkema.

Zou, H.F., Cai, G.J., Liu, S.Y., Lin, J., Bheemasetti, T.V. & Puppala, A.J. 2016. Assessment of ground improvement on silt based on spatial variability analysis of CPTU data. In Editor (ed.) *5th International Conference on Geotechnical and Geophysical Site Characterisation*; *Proc. intern. conf., Gold Coast, 3-4 September 2016*. Rotterdam: Balkema.

Geotechnical and Geophysical Site Characterisation 5 – Lehane, Acosta-Martínez & Kelly (Eds)
 ISBN 978-0-9946261-1-0

Session Report on Non-standard materials and tailings

F. Schnaid
Federal University of Rio Grande do Sul, Brazil

ABSTRACT: This Report provides a short overview of the themes covered by ISC´5 Session "*Non-standard materials and Tailings*". This very broad subject, by its very *n*ature, comprises both natural soil deposits and man-made materials under a wide range of conditions, characteristics and properties. Yet coverage of research on non-standard materials is very limited and only 4 papers have been presented on this theme at ISC´5. Consequences are that site characterization is supported primarily by a framework based on idealized soil conditions applied to sand and clay which can only be extended to other geomaterials under a number of limiting factors and considerable uncertainty. This Report not only examines the papers presented on this theme but includes some general comments which are used as basis for addressing questions about what are the main recent contributions in this area.

1 INTRODUCTION

Non-standard geomaterials are defined as those that possess one or more of the following criteria:

(a) Classical constitutive models do not necessarily offer a close approximation of the soil true nature due to bonding, soil structure, anisotropy, unsaturated soil conditions, among other factors.
(b) The soil state is variable due to complex geological processes and depositional conditions.
(c) These soils are difficult to sample and the soil structure cannot be reproduced in the laboratory.
(d) Little systematic experience has been gathered and reported, and values of parameters are outside the range that would be expected for more commonly encountered soils such as sand and clay formations of sedimentary deposits.

Table 1 gives an overview of the essential features associated to natural soils and man-made geomaterials. Regarding type of soil properties covered, there is scope to evaluate the cohesive-frictional nature of soils (hard soils and soft rocks, residual soil formations), the susceptibility to mineral crushing and to the breakage of natural cementation (calcareous sand, volcanic soil formations), high compressibility (very soft clays, volcanic soils, tailings), susceptibility to flow instability and dynamic liquefaction (sand, tailings), rheological effects due to physical and chemical alterations (waste repositories).

Based on the general picture provided in this introduction and the review of the papers, it was decided to use this session report to discuss the following selected topics:

a) Residual soil formations
b) Difficult soft soils
c) Permafrost conditions
d) Tailings

2 RESIDUAL SOIL FORMATIONS

Characterization and assessment of geotechnical properties of residual soils is a complex subject given the fact that these soil formations are a product of the physical, chemical and biological weathering processes of the rock. This *in situ* decomposition of the parent rock and rock minerals produces characteristic features of mechanical behavior that cannot be necessarily approached by conventional geotechnical design methods (Schnaid et al, 2004; Schnaid & Huat, 2012).

For example, one could consider the evaluation of the peak friction angle from standard interpretation methods developed for cohesionless soils from CPT measurements (e.g. Lunne et al, 1997; Mayne, 2005; Schnaid & Huat, 2012). Since one measured parameter (q_t) cannot be associate to the 2 shear strength components (c' and ϕ'), in bonded soils the contribution of the cohesive component linking particles is disregarded, which impacts the predicted shear strength: by ignoring the soil cohesion intercept (c'=0) the predicted friction angle ϕ' is crudely overestimated (up to 5 degrees).

Table 1. Non-standard materials (modified from Schnaid et al, 2004)

Natural deposits	Main Features of behaviour
Hard soils, soft rocks, residual soils	Bonding and structured Cohesive-frictional nature Anisotropy derived from relic structures Unsaturated soil conditions
Calcareous sand	Susceptible to post-depositional physical and chemical alterations, Fairly compressible Crushability and interparticle cementation
Transitional soils	Conditions of drainage are difficult to determine
Coarse-grained cemented aged materials	Sufficient high permeability to ensure drained conditions Important influence of aging and cementation Susceptible to erosion and liquefaction
Volcanic soils	Low specific gravity and angular crushable grains Often high compressibility Susceptible to liquefaction
Difficult soft soil conditions	Peat layers impart considerable spatial variations in water content and index properties Organic content has a strong impact on soil fabric and mechanical proper Extremely soft and compressible ties
Permafrost	Fine to coarse-grained materials Low water content
Man-made materials	**Main characteristics**
Earth-fills and improved ground	Void ratio and structure controlled by the mode of placement and/or by compaction Anisotropy and stress history
Tailings	Stratified and layered, the particle size ranging from coarse rock to clay size Mechanical properties vary with ore type, method of placement, location, exposure to evaporation, ageing Susceptible to flow and dynamic liquefaction
Waste repositories	Rheological effects due to physical and chemical alterations

Under unsaturated soil conditions, penetration tests offer no more than some crude information of soil behaviour since the role of matrix suction is not (and cannot) be accounted for. Pressuremeter and plate loading tests combined to suction measurements become the only viable means of assessing soil parameters (e.g. Schnaid et al, 2004). Thus, local validation of interpretation methods developed for textbook approaches is an essential recommendation in these soil formations.

Ground investigation of residual soils often reveals weathered profiles exhibiting high heterogeneity on both vertical and horizontal directions, complex structural arrangements, expectancy of pronounced metastability due to decomposition and lixiviation processes, presence of rock block, *boulders*, among others (e.g. Novais Ferreira, 1985; Vargas, 1974). Factors affecting swelling and shrinking of soils in relation to soil properties, environmental effects and state of stress are complex and damage losses attributed to these problems demand continuous research on soil-structure interactions.

Expansive soils are those which swell considerably on absorption of water and shrink on the removal of water. The seasonal moisture variation in such soil deposits around and beneath the structure results into subsequent upward and downward movements of structures leading to structural damage, in the form of wide cracks in the wall and distortion of floors. The work by *Denis, Fabre & Lataste* presents the results of in situ monitoring of the behavior of the Brach clay geological formation over six consecutive years, using various instruments such as borehole extensometers, hygrometers and a meteorological station. Displacement measurements (shrinkage and swelling) recorded at the experimental site were then related to soil moisture and temperature variations, which were in turn related to climatic variations observed at the site. The clay content in this formation ranges from 10% to 83% and consists essentially of kaolinite [60; 88%], and illite (muscovite) [9; 20%] with very few smectites [2; 10%]. The variation in water content between wet and dry periods was of the order of 20% at a depth of 1.5m, reducing with depth to value of the order of 6% to 12% at 3m (see Figure 1). These water content variations, along the first 3m, are reported to contribute to 50% of the overall measured displacements of up to 8mm, undergoing several cycles of swelling and shrinkage. The accumulated hydrical condition, defined as a function of rain fall and potential evapotransportation over a period of time, was found to be a good indicator of the behaviour of soil. Figure 1. Soil moisture profiles from 2009, 2010, 2011 and 2015 (*Denis, Fabre & Lataste*)

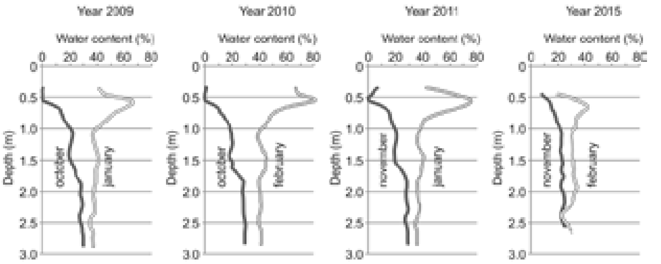

Figure 1. Soil moisture profiles from 2009, 2010, 2011 and 2015 (*Denis, Fabre & Lataste*)

We recall that accurate determination of the particle size distribution is an essential step towards the assessment of the geotechnical performance of buildings in clay, as the clay content of the soil is used to determine the activity of a soil. *Kaur & Fanourakis* present a discussion on the influence of phosphate dispersing agents on particle size distribution of soil fines. Dispersants de-flocculate solids and thus significantly reduce the viscosity of the dispersion paste. In the study, the authors mixed different quantities of dispersing agents with about 400 ml of distilled water to evaluate the effect of volume and concentration of calgon, sodium pyrophosphate decahydrate and sodium tetra pyrophosphate on hydrometer readings. Results such as those illustrate in Figure 2 demonstrate that with the increase in the concentration and volume of the dispersing agents, there is increase in the hydrometer readings. With calgon the hydrometer readings varied from 5 to 47 *g/litre*, which is attributed to the increase is the aggregation of uniformed sized solid particles of dispersing agent in the hydrometer cylinder, increasing the density of the solution in the zones measured by the hydrometer. The use of dispersants in higher concentrations thus produced anomalous increases in the hydrometer readings, affecting the fine soil particle size distribution analyses.

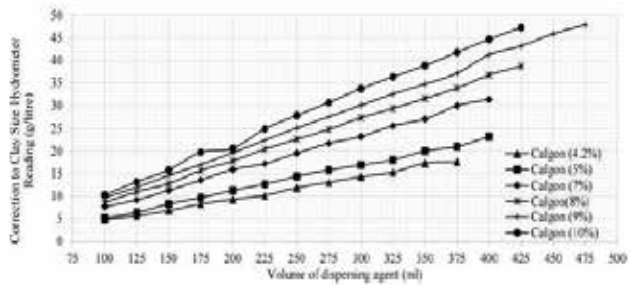

Figure 2. Effect of volume and concentration of calgon on clay size period readings (*Kaur & Fanourakis)*

Continuous research is necessary to identify index properties, structure and mineralogy criteria for identification and behaviour of clay under shrinkage, swelling, or soil collapsibility.

3 DIFFICULT SOFT SOIL CONDITIONS

Very soft and extremely compressible clay deposits present very special problems of engineering design, where the construction of different structures has always been associated with stability problems and settlements. The presence of organic matter can have undesirable effects: the bearing capacity is reduced, the compressibility is increased, swelling and shrinkage potential is increased due to organic content.

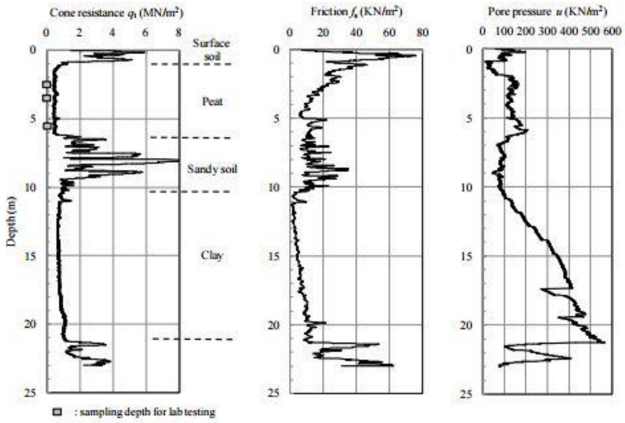

Figure 3. Typical CPTU profile (Hayashi & Hayashi)

An interesting case study is reported by *Hayashi & Hayashi* on 4 different peat sites in Hokkaido, Japan, where CPTu data are analyzed against K_0 consolidated-undrained triaxial compression tests to determine the undrained shear strength s_u. The undisturbed samples were collected using a thin-wall sampler with a fixed piston. The engineering properties of soils at the investigation sites reveal water contents ranging typically between 300 and 900%, in situ void ratios from 8 to 15 and compression index C_c from 5 to 10. Figure 3 shows the depth distribution results of a typical CPT profile (qt, fs and u). Large excess pore water pressures were generated in both the peat and clay layers, yielding B_q values tipically in the 0.3 to 0.4 range. The q_t in the peat layer (q_t = 0.33-0.71 MPa) was lower than values usually reported for clay, which indicates that the peat layer is very soft. In this study, an average N_{kt}=21 of peat was used to calculate the undrained shear strength s_u.

In contrast to previous reported data, N_{kt} values exhibited little scatter. Take for example the results from Almeida el al (2010) for the cone factor obtained using corrected tip resistance and s_u from vane tests in the soft to very soft soils from the Brazilian coast (Figure 4). In peat soils, N_{kt} can be either very low (~3, due to the contribution of entrapped gas bubbles to the soil coming from the organic matter) or relatively high (16 or more, which is often attributed to partial drained effects when the vane undrained shear strength is used as reference).

4 PERMAFROST CONDITIONS

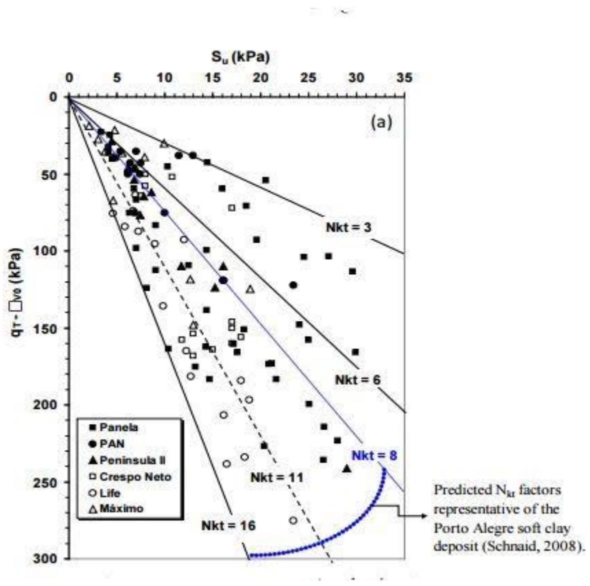

Figure 4. Calculated N_{kt} factors for soft clay deposits (*Almeida et al, 2010*)

The potential reserve of oil and gas resources in the Arctic regions has led to increased attention from oil companies in the site characterization of permafrost. Continuous efforts have been placed on sampling and testing to determining index and geotechnical properties of these soil formations, especially in fine-grained soils. Yet, few studies have reported developments in drilling equipment that can handle coarse-grained soils.

Le presents an interesting case from a project performed in coarse-grained permafrost on Svalbard, an island north of mainland Europe, midway between continental Norway and the North Pole. The site consists of well-graded materials with particles varying between gravel and silts. The investigation described in the paper was conducted using four different techniques comprising a permafrost corer, the *Atlas Copco* core barrel, the Moraine percussion sampler and a conventional auger sampler. The permafrost corer used in the investigation is illustrated in Figure 5, showing a cutting tool with a wall thickness of 15mm that has the ability to cut cores with a diameter of 45mm. The authors reports that none of the methods tested were able to cut or retrieve undisturbed cores in the low water/ice content and coarse-grained permafrost in Svalbard. Under low water content, the few frozen bonds cannot hold the soil particles together during the drilling process. The permafrost corer and the *Atlas Copco* core could not cut through coarse-grained loose permafrost, whereas the Moraine percussion sampler and a conventional auger sampler retrieved highly remolded samples.

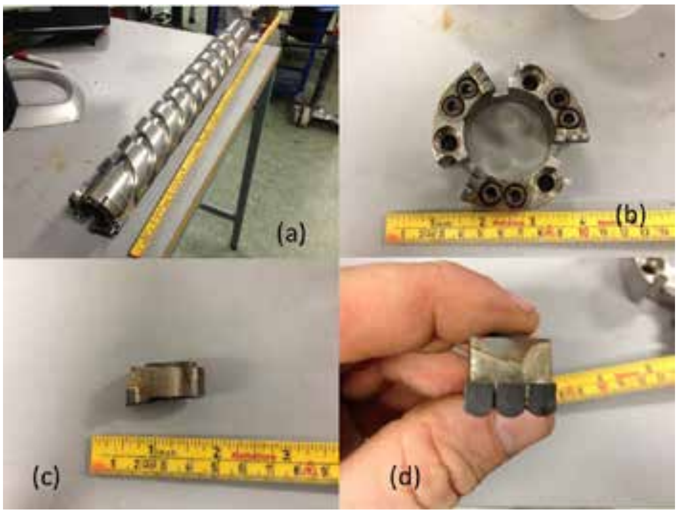

Figure 5. Permafrost corer (a) assembled (b) drill bit (c) cutting tool (d) poly-crystalline diamond composite inserts (*Le*)

5 TAILINGS

The disposal of large volumes of waste produced in mining operations and metal processing industries is increasing the demand for larger and higher storage facilities, which as a consequence increases the environmental risk of contamination of the surrounding natural ground and groundwater. There are no papers under review in this subject, but some comments are made to contextualize the topic in the overall theme of this Report.

In tailings spatial variability, rate of penetration and influence of fine contests are among the most important factors affecting cone (and SPT) penetration and pore pressure measurements. These aspects are often neglected in data interpretation, inducing errors in the analysis of test results when estimating the coefficient of consolidation, the undrained shear strength, and the characterization of soil conditions and potential to liquefaction. Among major concerns is the flow instability and dynamic liquefaction of tailing deposits that has been reported to produce devastating environmental effects due to partial or overall failure of the perimeter dike or dike foundation. During the past decade, several simplified procedures have been proposed for assessing soil liquefaction in granular deposits. Methods are based on indices or non-dimensional parameters based on strength (e.g. Seed, 1979; Tokimatsu, 1988; Seed et al, 1985; Robertson & Wride, 1997) and dynamic shear stiffness (e.g. Stokoe et al, 1988; Tokimatsu et al, 1995; Robertson et al, 1992), as well as on the combined values of strength and stiffness measurements (Schnaid, 2005; Schnaid and Yu, 2007; Roy, 2008). These approaches were developed for clean sands and the influence of fine contents has to be empirically addressed (bear in mind that liquefaction is covered in another Session Report of this Conference).

As for the drainage conditions, previous research has identified the need to account for the effects of probe size, testing rates and soil consolidation characteristics when evaluating the response of piezocone penetration (Randolph and Hope, 2004), vane rotation (Blight, 1968) and dilatometer expansion (Schnaid et al, 2016). For the CPTU, normalization of penetration results can be represented by an analytical curve of either penetration resistance or penetration pore pressures plotted against normalized penetration velocity V defined as (Randolph and Hope, 2004):

$$V_v = \frac{vd}{c_v} \quad \text{or} \quad V_h = \frac{vd}{c_h} \tag{1}$$

where v is the penetrometer velocity, d is the probe diameter and c_h (or c_v) is the coefficient of consolidation. This normalized penetration rate V has been successfully used for the data analysis of various penetration tests, indicating that fully undrained penetration typically occurs when V_v is larger than about 30 to100 and fully drained penetration occurs when V_v is less than about 0.03–0.01 (e.g. Randolph, 2004). Although equation (1) captures the key elements which needed to be considered for in situ testing interpretation in transient soils, uncertainties on how to apply the method in tailings have been recognized. An operative coefficient of consolidation for the soil adjacent to the cone has to be arbitrarily selected, but an average vertical coefficient of consolidation c_v measured from laboratory one-dimensional (1D) consolidation data cannot be used: the shortcomings of sampling tailings are well recognized. An average c_h measured in a piezocone dissipation test is inaccurate due to partial consolidation taking place during cone penetration. Finally, the determination of phreatic surface location for tailings and tailing-retention structures is not always precise, being influenced by pond location, anisotropic permeability of deposits, boundary flow conditions including the presence of permeable layers and drains, among other factors.

6 CONCLUDING REMARKS

The conclusions drawn at the ISC´2 Keynote Lecture by Schnaid et al (2004) remain to a large extent still valid: "Although we believe we are making steady progress in our ability to measure properties in a wide range of geomaterials, interpretation of in situ tests is still very problematic…. In the light of recent recognition of aspects such as structural effects, soil non-linearity and unsaturated soil conditions, there is a new opportunity to make significant improvement in methods for predicting behaviour from in situ tests. This is of fundamental importance in soils where constitutive parameters cannot be measured from laboratory tests in routine site investigation practice".

Twelve years later, there is still a clear need to extend the current interpretation methods developed for sand and clay to other geomaterials to enhance our ability in assessing soil type and estimating geotechnical design parameters. Compared with transported cemented soils, the knowledge and understanding of the engineering behaviour of many natural soils and man-made materials is not as comprehensive. Yet relatively few contributions have been made at ISC´5 to this field and it is not possible to draw general conclusions from the submitted papers.

In general*, non-standard geomaterials* are difficult to sample, the soil structure cannot be easily reproduced in the laboratory and our ability in characterizing the mechanical behaviour and geotechnical properties from *in situ* testing is limited.

7 REFERENCES

Almeida, M.S.S. Marques, M.E.S. & Baroni, M. 2010. Geotechnical parameters of very soft clays from CPTu compared with other site investigation tools. *2nd Int. Symp. Cone Penetration Testing*, CPT10, USA

Blight, G. E. 1968. A note on field vane testing of silty soils. *Can.Geotech. J.* 5, 142-149.

Lunne, T. Robertson, P.K. & Powell, J.J.M. 1997. Cone penetration testing in geotechnical practice, *Blackie Academic & Professional*, 312p.

Mayne, P.W. 2005. Keynote: Integrated ground behavior: in-situ and lab tests. *Deformation Characteristics of Geomaterials*, Taylor and Francis Group, London, 2: 155-177

Novais Ferreira, H. 1985. Characterization, identification and classification of tropical lateritic and saprolitic soils for geotechnical purposes. *General Report, Int. Conf. Geomech. in Tropical Lateritic and Saprolitic Soils*, Brasília, 3:139-170.

Randolph, M. F. 2004. Characterisation of soft sediments for offshore applications. *2nd Int. Conf. on Site Charact.*, Milpress, Porto, 1: 209-232.

Randolph, M. F. & Hope, S. 2004. Effect of cone velocity on cone resistance and excess pore pressures. *Proc. Int. Symp. on Engng. Practice and Performance of Soft Deposits*. Osaka.

Robertson, P.K. & Wride, C.E. 1997. Cyclic liquefaction and its evaluation based on the SPT and CPT. Evaluation of liquefaction resistance in soils. *National Center for Earthquake Engineering and Research Technical Report*, 97-0022, 41-89.

Robertson, P.K. Sully, J.P. Woeller, D.J. Lunne, T. Powell, J.J.M. & Gillespie, D.G. 1992. Estimating coefficient of consolidation from piezocone tests. *Can. Geotech. J.*, 29(4):551-557.

Schnaid, F. 2005. Geocharacterisation and properties of natural soils by *in situ* tests. State-of-the-Art Report. *16th International Conference on Soil Mechanics and Geotechnical Engineering (ICSMGE)*, Osaka, 1: 3-46.

Schnaid, F. & Yu, H.S., 2007. Theoretical interpretation of the seismic cone test in granular soils. *Geotechnique*, 57(3), 265-272.

Schnaid, F. & Huat, B.B.K. 2012. *Handbook of Tropical Residual Soils Engineering*, Chapter 3, CRC Press. 536p.

Schnaid, F.; Lehane, B.M. & Fahey. M. 2004. *In situ* test characterisation of unusual geomaterials. *2nd Int. Conf. on Site Charact.*, Milpress, Porto, 1: 49-74.

Schnaid, F.; Oliveira, L.A.K. & Geling, W.Y.Y. 2004. Unsaturated constitutive surfaces from pressuremeter tests. . *J. Geotech. and Geoenvironmental Engineering*. 130(2): 1-12.

Schnaid, E.; Odebrecht, J.; Sosnoski, & P.K. Robertson. 2016. Effects of test procedure on flat dilatometer test (DMT) results in intermediate soils. *Can. Geotech. J*. 2016, 53(8): 1270-1280.
Seed, H.B. 1979 Soil liquefaction and cyclic mobility evaluation for level ground during earthquakes. *J. Geotch. Engng.*, 105(2): 201-255.
Seed, H.B. Tokimatsu, K. Harder, L.F. & Chung, R. 1985. Influence of SPT procedures in soil liquefaction resistance evaluations. *ASCE J. of Geotech. Engineering*, 111(12):1425-1445.
Stokoe, K.H. Roeset, J.M. Bierschwalle, J.G. & Aouad, M. 1988. Liquefaction potantial of sands from shear wave velocity, *Proc. 9nd World Conf. on Earthquake*. 13: 213-218.
Tokimatsu, K. 1988. Penetration tests fro dynamic problems. *Int. Symp. Penetration Testing, ISOPT-1,* Orlando, 1: 117-136, Balkema Publishing, Rotterdam.
Tokimatsu, K. Suzuki, Y. Taya, Y. & Kubota, Y. 1995. Correlation of CPT data with static and dynamic properties of insitu frozen sands. *Proc. CPT'95*, Vol. 2, Swedish Geotechnical Society: 323-328.
Vargas, M. 1974. Engineering properties of residual soils from southern-central region of Brazl. *Proc. 2nd Int. Cong. IAEG*, São Paulo, 1:5.1-5.26.

Geotechnical and Geophysical Site Characterisation 5 – Lehane, Acosta-Martínez & Kelly (Eds)

Session Report: Developments in Technology and Standards

Fernando A. B. Danziger
Federal University of Rio de Janeiro, Brazil

Tom Lunne
Norwegian Geotechnical Institute, Norway

ABSTRACT: The paper presents a review and discussion of the eight papers presented in the Technical Session, entitled, 'Developments in Technology and Standards'. The papers cover a wide range of topics. Some experience of the reporters related to errors in friction sleeve measurements is provided to supplement findings from one of the papers presented at this session.

1 INTRODUCTION

Thirteen papers have been reviewed by the reporters, however only eight out of the papers have been included in the Proceedings, and six presented in Technical Session 1. Table 1 presents the origin of the papers.

Table 1. Papers from countries.

Country	Number of papers
Australia	3
New Zealand	1
Netherlands/Finland	1
France	1
Belgium	1
Croatia	1

A wide range of topics were covered by the papers, as shown in Table 2.

Due to the specific experience of the reporters of the present Session Report, the paper presented by Holtrigter and Thorp on a correction for CPT f_s errors due to variation in sleeve diameter will be discussed in more detail in this report.

Table 2. Topics covered.

Authors	Title	Technique
Woolard et al.	Additional parameters in CPT	CPT
Ekanayake et al.	Integration of invasive and non-evasive technologies	CPT/PS/HVSR
Escobar et al.	Deform. Modulus and wave velocity parameters using Panda	DynPen
Holtrigter and Thorp	Correction for CPT f_s errors due to sleeve diameter effects	CPT
Iskander	Reduced pressuremeter test time procedure and new anal meth	PM
Kovacevic et al.	Comparison of Unified and European Soil Class systems	N/A
Look	SPT N-value errors examined with digital technology	SPT
McKenna and Roberts-Kelly	Televiewer imaging of boreholes in rock	Televiewer

2 COMMENTS ON THE PAPERS

2.1 *Additional parameters measured in a single CPT, by Woolard, Storteboom, Länsivaara and Selänpää*

The authors describe a CPT system which allows the use of different devices without the need of changing cones, cables and data loggers. Seismic, conductivity, magneto and vane modules have been presented. The practical significance of this system is significant.

The main advantage of the vane device is measuring the torque close to the blade. Tests have been performed in a very soft clay site in Finland, to compare the undrained shear strength, s_u, from CPTU (from the cone factors N_{KT} and $N_{\Delta u}$) and vane test. Good results have been obtained.

2.2 *Integration of invasive and non-invasive techniques in ground characterization, by Ekanayake, Leo, Liyanapathirana and Harutoonian*

The authors present a case study where non-invasive Horizontal-to-Vertical Spectral Ratio (HVSR) of micro tremors was used to assess the compaction of a large compacted site.

The HVSR technique uses ambient vibrations in soil to determine the V_s profile rather than an artificial source, and can survey large areas.

Results are less reliable than invasive techniques, thus a methodology was developed to calibrate and verify the V_s profile against the data obtained from CPTs. The results were compared to the V_s profile from P-S logging technique (Figure 1). Reasonable match between P-S and HVSR has been obtained, except close to the surface. V_s gradients from HVSR are less pronounced than from P-S logging.

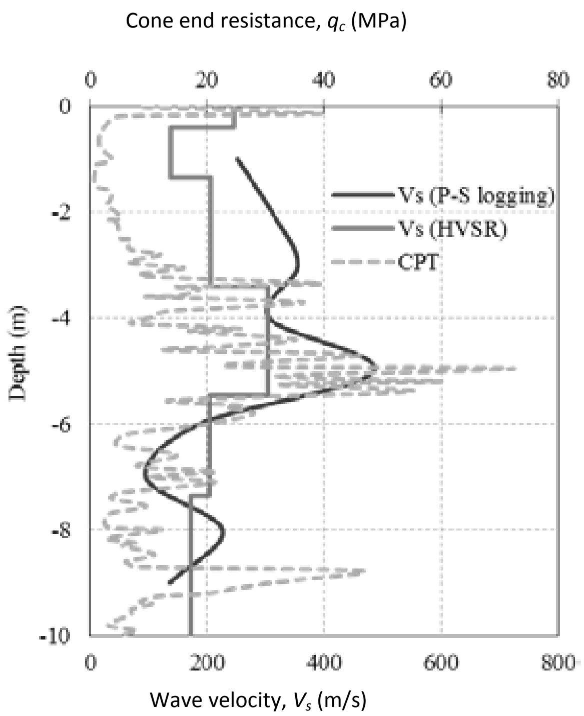

Figure 1. V_s from HVSR and P-S logging.

2.3 *In-situ determination of soil deformation modulus and the wave velocity parameters using the Panda 3®, by Escobar, Benz Navarrete, Gourvès, Breul and Chevalier*

The authors present the results of in situ tests performed with the Panda 3 penetrometer (Figure 2), which is similar to a monitored dynamic load test performed in a pile, where strain (force) and acceleration is measured just below the top of the pile. It is also based on wave equation analysis. From some hypotheses and simplifications, a number of parameters can be obtained.

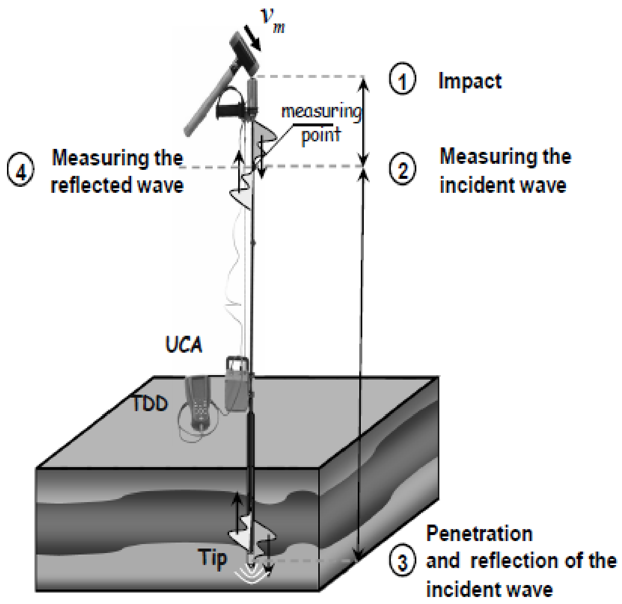

Figure 2. Panda 3 penetrometer.

A comparison with established in situ tests (CPT, PMT and MASW) was carried out. Reasonable match was obtained between q_c (CPT) and q_d (Panda), E_m (PMT) and E_{kd} (Panda), however not as good in V_s (MASW) versus V_s (Panda).

Although in the paper it is mentioned that it is presently limited to 6 – 7 m depth, in their presentation the authors mentioned that the penetration was also carried out to 18 m depth.

2.4 *Reduced pressumeter test time procedure and new analysis method, by Iskander*

The author suggests a new definition for pressure limit in pressuremeter testing, which is determined in only three loading step procedure, thus reducing the time for running the test.

The new pressure limit is defined by the applied pressure at the start of the radial cracks at the cavity surface around the probe.

2.5 *Comparison of Unified and European Soil Classification Systems, by Kovacevic, Juric-Kacunic, Libric*

An interesting historical review on the development of soil classification systems has been presented in the introduction.

A comparison between Unified (USCS) and European (ESCS) Soil Classification System showed that procedures for soil classification are very similar; names of soil groups are relatively similar, whereas the symbols of soil groups are completely different.

A program (CLASSIF) was developed that allows classification from both systems using same input data.

It is a useful tool if a comparison between the Unified (USCS) and European (ESCS) Soil Classification System is needed.

2.6 *The SPT N-value errors examined with digital technology, by Look*

The Pile Driving Monitoring (PDM) device – which remotely measures set, temporary compression and velocity of piles using optically safe infrared laser technology – was used to measure the true increment in each step of the test (nominal value 150 mm). A quite interesting picture was obtained, as can be seen in Figure 3.

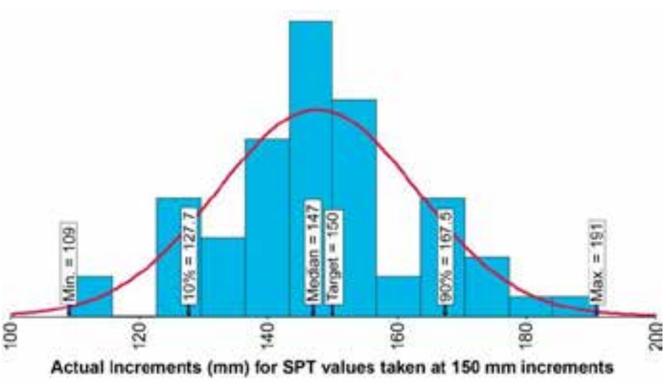

Figure 3 PDM Digital Measurements of 150mm increments Site 1 (54 No.)

The reporters would like to point out that the difference would probably be even more significant in the case of low N-values than high N-values.

Using the results of site 2 and the measured energy by the PDA analyser (also used in the investigation), the correction (efficiency) factors have been determined.

The reporters would like to point out that measured energy losses are essential in using the N-value as a design value. The errors are amplified when multiple drill rigs are used on the same project.

2.7 *Televiewer imaging of boreholes; benefits and some considerations for its interpretation in the absence of physical rock core, by McKenna and Roberts-Kelly*

The paper aims to provide a comparison of televiewer data against rock cores, borehole logs and core photographs so the reader can make an educated assessment of the likely defect conditions in the absence of rock cores during the design period.

Two case studies have been presented in paper. In the Southeast Queensland case Sedimentary Optical and acoustic televiewer have been compared with log and core photographs (Figure 5).

It was emphasized that calibration with physical rock core by experienced personnel is vital in interpreting televiewer data accurately. Televiewer data are a powerful tool for understanding the ground conditions and structural geology data, however understanding the limitations of televiewer imaging is critical.

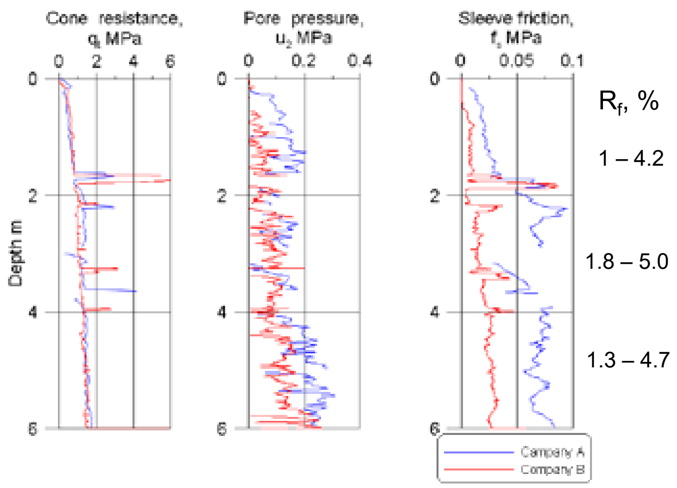

Figure 4. Piezocone tests from two companies in an offshore clay

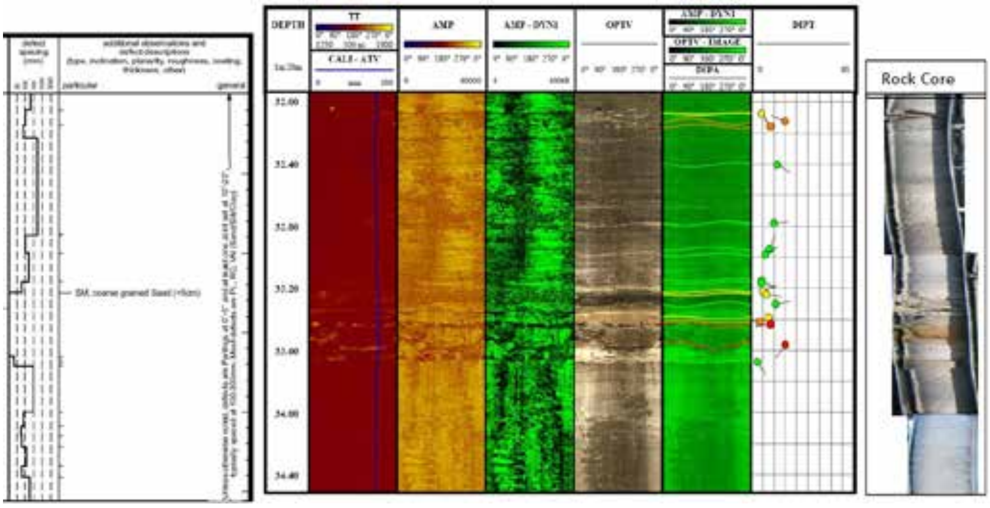

Figure 5. Case Study information; borehole log, optical and acoustic televiewer and rock core photograph.

2.8 *Correction for CPT f_s errors due to variation in sleeve diameter, by Holtrigter and Thorp*

Since the subject of the paper has been a major concern for the reporters for many years, the comments about the reviewed paper will follow some initial thoughts.

NGI and other consultants frequently receive CPT data on projects where two or more soil investigation contractors have done the testing.

The general experience in soft clays is that:

i) *Corrected cone resistance q_t*: Good repeatability from one cone type to another.

ii) *Pore pressure at cone shoulder u_2*: Best repeatability.

iii) *Uncorrected sleeve friction f_s*: Not good repeatability – less reliable of all piezocone measurements.

Some examples from recent projects are presented below. The first one refers to CPTU profiles from two companies in 300 m water depth in Norwegian Sea, carried out in 2008 and 2009 (Figure 4).

The second example (Figure 6) is from tests performed by four companies at NGI´s soft clay test site in Onsøy, where all cones are used in offshore soil investigations.

Correcting for unequal end areas reduce differences, as shown in Figure 8. However different pore pressures at each end of sleeve can also cause some differences. The reporters think that the status on sleeve friction readings is that reliability has improved due to more cone types now having equal end areas and efforts in more detailed calibrations. However more research is needed on this subject.

The third example (Figure 7) is from offshore tests performed by two companies, with very dense sand overlaying stiff OC clay.

From the reasons above, due to less reliable f_s results this measurement is not used so much in interpretation. Fortunately, due to log scale some variation in F_r is not so critical for Soil Behaviour Type (SBT) when used is classification charts, like the one presented by Robertson (1990).

According to Lunne and Andersen (2007), reasons for lack of accuracy in f_s are: (i) pore pressure effects on ends of the sleeve; (ii) tolerance in dimensions between the cone and the sleeve; (iii) surface roughness of the sleeve; (iv) load cell design and calibration.

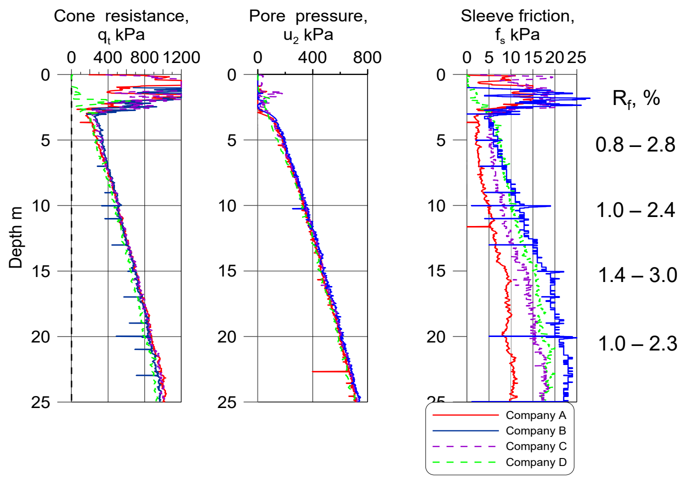

Figure 6. Results of CPTU profiles from four cone penetrometers at NGI's soft clay test site in Onsøy

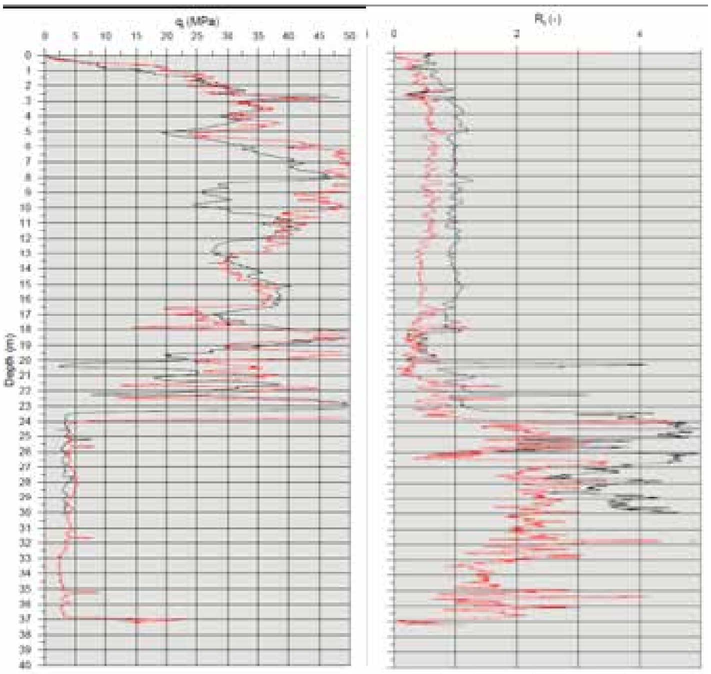

Figure 7. Results of CPTU profiles by two contractors in North Sea, with very dense sand overlaying stiff OC clay.

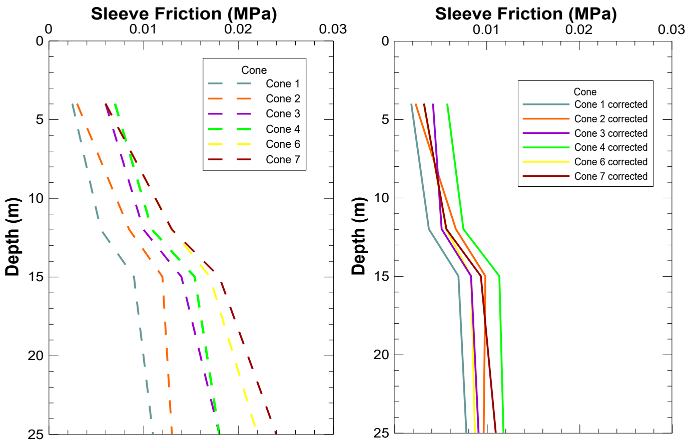

Figure 8. Pore pressure correction for unequal end areas, results from Onsøy soft clay test site.

In this context the study by Holtrigter and Thorp represents an important contribution. They studied four diameters, 35.70 (nominal value), 35.85, 36.05 and 36.15 mm, representing increases of 0.15, 0.35, 0.45 mm with respect to the nominal value. Test results in clay indicate that the cone resistance is not much affected by the increase in sleeve diameter, but the sleeve friction increases with the sleeve diameter increase (Figure 9).

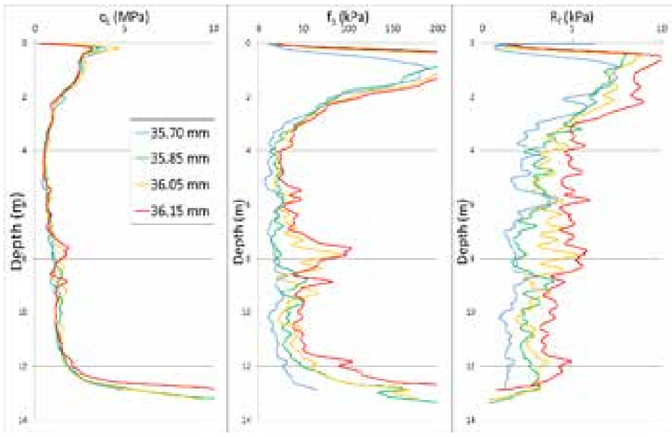

Figure 9. Results of CPTU profiles in clay with four sleeve diameters, tests performed by Holtrigter and Thorp.

Test results in sand show the same trend, although not as clear as in the case of clay (Figure 10). An empirical correlation was proposed by the authors to account for the difference in friction sleeve diameter (which, however, depends on the "correct" value).An important conclusion is that tighter tolerances in standards will very likely reduce differences in f_s readings.

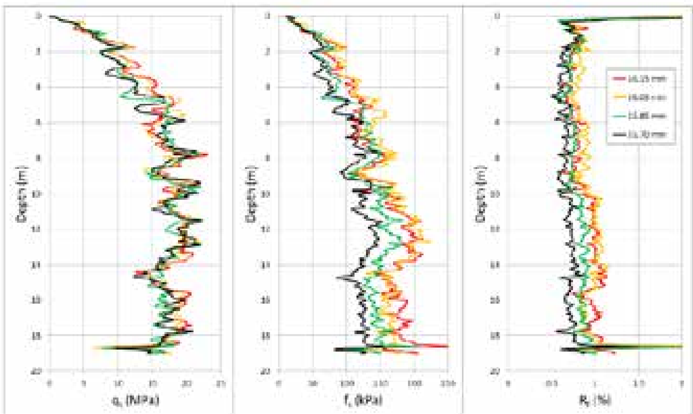

Figure 10. Results of CPTU profiles in sand with four sleeve diameters, tests performed by Holtrigter and Thorp.

It is hoped that the reliability of f_s readings can be further increased to be at same level as q_c and u. This will potentially open up for a new range of correlations and interpretation methods.

3 REFERENCES

Lunne, T., Andersen, K.H. 2007. "Soft clay shear strength parameters for deepwater geotechnical design". Keynote Lecture, International Offshore Site Investigation and Geotechnics Conference, 6. London 2007. Proceedings, 151-176.

Robertson, P.K. 1990. "Soil classification using the cone penetration test". Canadian Geotechnical Journal, 27(1): 151-158.

Geotechnical and Geophysical Site Characterisation 5 – Lehane, Acosta-Martínez & Kelly (Eds)

Session Report: Penetration Testing

J. Peuchen
Fugro, Netherlands

ABSTRACT: This Report provides a short overview of the topics covered in nine papers submitted to one of the ISC´5 sessions on penetration testing. The reporter provides comments on each of these papers and these should be regarded as representing the opinion/interpretation of the reporter.

1 INTRODUCTION

This session report summarises 9 papers on a range of penetration tests. The groupings given in Table 1 can be considered, where the values indicate the number of papers covering the particular topic.

Table 1 Groupings of papers at session

Discontinuous penetration test	5
pore pressure dissipation	2
seismic downhole for shear wave velocity	1
torque/ rotation resistance	3
Monotonic push/ extraction	6
cone penetration test	6
T-bar penetration test	1
ball penetration test	2
sharp cone test	1
Free fall penetration test	2
Impact penetration test	2
Equipment hardware and data acquisition	3
Data processing/ interpretation model(s)	8
Field experience	6
Unconventional soils	3

General review comments are follows.

(a) All session papers show incremental developments for existing test systems, i.e. no breakthrough innovations.

(b) All papers aim at getting cost down for geotechnical design, by adding geotechnical value and/or by equipment optimisation.

(c) Several papers consider additional measurements for existing test systems, adding geotechnical value at relatively low cost. This is no surprise, considering the increasingly lower threshold for adding electronics and associated processing techniques.

(d) Many papers consider distinct applications, particularly soil response of low-permeability normally consolidated and slightly overconsolidated soils.

(e) The cone penetration test continues to dominate as benchmark for in situ penetration testing.

The sections below summarise the papers assigned to the conference session. Note that this session report relies on draft versions of the papers, as submitted by their authors. Final submissions may have included comments from the conference review committee.

The selected sequence is according to last name of the first author. The selected figures are copies from the papers. Each section includes comments from the session reporter, below "Comments are as follows".

The opinions expressed in this session report are those of the session reporter. They are not necessarily shared by Fugro.

2 CONTINUOUS-INTERVAL SEISMIC PIEZOCONE TESTING IN PIEDMONT RESIDUUM

Agaiby et al. describe a comparison of measured in situ shear wave velocities v_s derived from seismic cone penetration tests (SCPT) for continuous-push and discontinuous-push. Results from multi-channel analyses of surface waves MASW are also available. The test site comprises residual soils from in-place weathering of metamorphic and igneous bedrock. The soils range from micaceous fine sandy silts to silty fine sands. They are uniform to the investigated depth of 12 m; refer to Figure 1. The spread in v_s in the upper few metres is attributed to testing having been conducted at various times. This allowed changes in pore water saturation and water level fluctuations.

The continuous-push SCPT system uses an electromechanical gear system as seismic source, generating uni-directional acoustic impact every 5 seconds. Acquisition of seismic signals takes place during cone penetration, thereby providing v_s resolution in the order of 0.1 m depth intervals. The discontinuous-push SCPT system requires a penetration interruption for acquisition of seismic signals. This allows left and right strikes and signal stacking.

The authors focus on signal processing for the continuous-push SCPT system, according to the following steps:

(a) Detrending of time series, i.e. a statistical operation for removing abnormal unexpected trends or any signal distortion such that the detrended raw data signals approach a baseline value
(b) Filtering for noise and wavelet interference; the settings for bandpass filtering were applied on the basis of visual examinations of fluctuations in signals
(c) Windowing to capture the zone of interest for shear wave velocity
(d) Cross correlation in the time domain; this evaluates time shift between to independent wavelets by finding the lag time corresponding to the maximum covariance or maximum cross correlation in the time domain
(e) Cross-spectral analysis in the frequency domain, identifying correlation between two time series at given frequencies; the analysis provides a phase spectrum in the frequency domain allowing the calculation of time shifts and phase velocities between two different wavelets
(f) Application of a 10th order running-mean filter for reduction of scatter, particularly zero-phase forward and reverse digital filtering techniques.

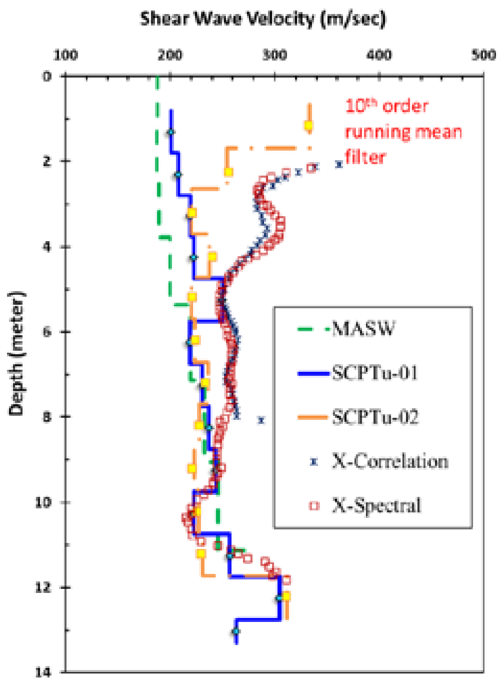

Figure 1. Comparison of derived shear wave velocities, where SCPTu refers to discontinuous-push and X to continuous-push testing.

Comments are follows:
(a) The continuous-push SCPT system offers opportunities for v_s resolution in the order of 0.1 m depth intervals in a shorter time on site, compared to a discontinuous-push SCPT system. Reduction in on-site time can reduce overall cost of v_s data.
(b) Soil conditions for the test site are uniform. This is favourable for consistent derivation of shear wave velocities. It would be of interest to consider non-uniform soil conditions. Unfortunately, this is not practicable for interpretation of any comparisons.
(c) SCPT systems introduce steel "rod" into soil, for which the stiffness and velocity properties differ inevitably from those of the surrounding soil. The geophones are inside the rod. The precise travel path of acoustic waves in vicinity of the geophones remains unclear. Particularly, it may vary for non-uniform soil conditions.
(d) The authors claim that signals generated by the continuous-push SCPT are "more accurate with lower scatter" compared to the discontinuous-push SCPT. Presumably, this claim is guessed from the comparisons. The session reporter is not aware of published uncertainty analyses for v_s from SCPT, regardless of system type.
(e) It should be remembered that derivation of small-strain shear modulus G_{max} from v_s includes a quadratic relationship. Uncertainties in v_s will be propagated accordingly.

2 CHARACTERISATION OF A NORWEGIAN QUICK CLAY USING A PIEZOBALL PENETROMETER

Boylan et al. compare results from ball penetration testing BPT and cone penetration testing CPT in quick clay. The ball penetrometer has a diameter of 60 mm or a projected cross sectional area $A = 2830\ mm^2$. The push rod is step-tapered with $A = 1000\ mm^2$ and $A = 314\ mm^2$. The ball includes button filters and pressure sensors for pore pressure measurement at the ball equator u_m and ball tip u_{tip}. The piezocone penetrometer has a cross sectional area of 1000 mm^2 and includes a cylindrical filter and pressure sensor for pore pressure measurement u_2 at the shoulder of the cone tip.

Figure 2 presents BPT results. Quick clay is present below a depth of about 8 m. It is defined by a remoulded undrained shear strength $s_{u\text{-}rem}$ of less than 0.5 kPa, i.e. almost liquid. Strength index tests indicate a laboratory strength sensitivity S_t in the order of 150 to 350. The water content, plasticity index and liquidity index are about 38%, 6% and 4 respectively.

Ball resistance q_{ball} and net cone resistance q_n in the quick clay increase with depth at average rates of about 15 kPa/m and 40 kPa/m respectively. The ratio of q_{ball}/q_n is between 0.3 and 0.5. This low ratio is attributed to a greater degree of soil remoulding for a ball penetrometer compared with a cone penetrometer. The BPT ratio $\Delta u_m/\Delta u_{tip}$ is in the range 0.6 to 0.7. At the ball tip position, the soil is in compression at all times and positive pore pressures Δu_{tip} are measured. At the equator position, the soil is subjected to shear stresses and the response in normally consolidated to lightly overconsolidated clay results in positive excess pore pressures Δu_m during penetration.

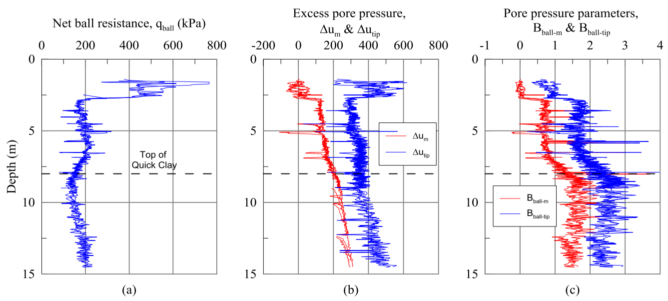

Figure 2. BPT results (a) net ball resistance (b) excess pore pressures (c) pore pressure parameters.

Figure 3 compares interpretation of pore pressure dissipation test results for BPTs and CPTs, in terms of coefficient of consolidation c_h. The comparison includes interpretative results for c_v derived from laboratory oedometer tests.

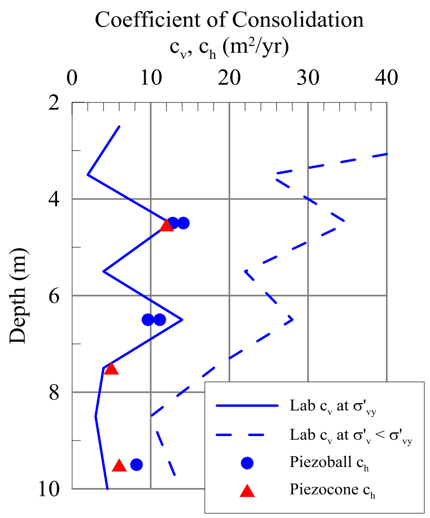

Figure 3. Comparison of consolidation properties derived from BPT, CPT and laboratory oedometer; quick clay is below 8 m depth.

Comments are follows:

(a) The authors add to experience with ball penetration testing in unconventional soft clays, i.e. quick clays.

(b) The presented test results may assist in future standardisation of BPT pore pressure measurements. BPTs are standardised by ISO 19901-8 “marine soil investigation”. This standard mentions BPT pore pressure measurement but provides no requirements for pore pressure measurement including location(s) of measurement.

(c) The authors mention that at least one cyclic BPT was carried out “to evaluate the symmetry of penetration and extraction resistance and allow the data to be re-zeroed if necessary”. No results are presented. Clarification would be of interest about why/how symmetry would be obtained for penetration and extraction resistance of a ball+push rod with limited symmetry in terms of soil flow.

3 SOIL STRENGTH IN THE MURRAY RIVER DETERMINED FROM A FREE FALLING PENETROMETER

Fawaz et al. describe design and application of a low-cost free-fall penetrometer that allows manual operation in shallow water depth. The penetrometer has a mass of about 12 kg. The penetration part of the penetrometer consists of circular disc as tip, with diameter options in the range of 30 mm to 50 mm. Disc size affects penetration (Figure 4). The straight shaft is about 1.9 m long, with a diameter of 20 mm. The instrumentation is at the top of the penetrometer and consists of an IMU (inertial measuring unit) that incorporates a triple axis gyroscope, a triple axis accelerometer and a triple axis magnetometer producing 9 degrees of inertial measurement. Logging rates of up to 750 Hz are feasible if vertical acceleration is recorded only. The penetrometer was trialled in a river setting, using a small vessel and a hand-held rope. Achieved penetrations depend on size of tip selected and strength of the river sediments. Acceleration data are correlated to undrained shear strength using conventional bearing capacity theory and allowances for rate effects and drag forces. Estimation of drag forces on the penetrometer and the rope is based on data acquired just before the tip impacting the soil surface. Test results suggest a penetration limit equivalent to undrained shear strength of about 5 kPa to 10 kPa at a minimum water depth of about 5 m.

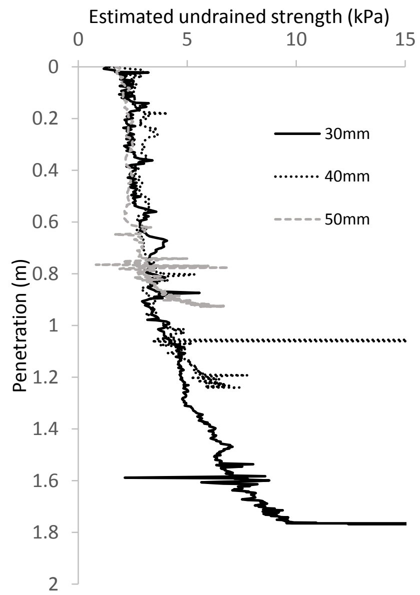

Figure 4. Effect of disc diameter on penetration into soil.

Comments are as follows.

(a) Portability of the test equipment is an important advantage. The presented system has a total mass of about 12 kg. The authors report no information on required forces for recovery of the tool from the soil. Special measures may possibly be required.

(b) The relatively large area of the penetrometer tip allows easier detection of the interface between water and extremely soft soil, compared to a free fall penetrometer with a tip diameter equal to the shaft. Interface detection is a common issue with free fall penetrometers relying on acceleration measurements only.
(c) The time required for soil penetration was about 0.5 s to 1 s. The authors report issues with low logging frequencies. Tool modification for a logging frequency of 1500 Hz will probably be adequate.
(d) The authors provide no information on data filtering for ambient noise, e.g. noise arising from soil penetration and retrieval rope.

4 STRENGTH ASSESSMENT OF FROZEN SOILS BY INSTRUMENTED DYNAMIC CONE PENETROMETER

Kim et al. summarise results of laboratory experiments with a portable dynamic penetrometer that is instrumented near its conical tip of 24 mm diameter as shown in Figure 5. The weight of the hammer is 118 N and the drop height is 383 mm. The experiments are conducted in a calibration chamber of 0.5 m diameter and 0.4 m height. The calibration chamber contains a sample composed of 70% sand and 30% silt, compacted to an initial relative density of 60% and an initial degree of saturation of 10%. The chamber including its sample was subsequently frozen to -5°C. Vertical stresses of 5, 10, and 25 kPa were applied during the freezing and penetrating phases.

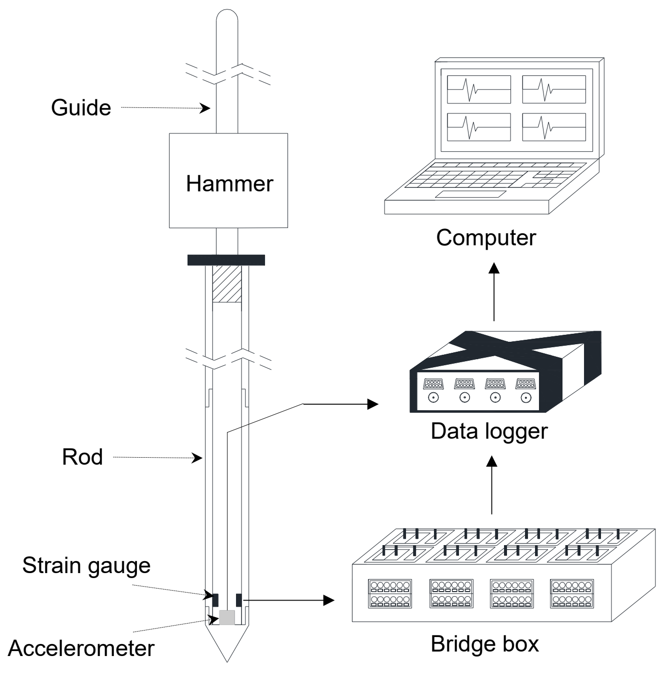

Figure 5. Instrumented dynamic penetrometer.

The presented test results show penetration resistance expressed as 30.5 mm/blow, 2.0 mm/blow and 1.4 mm/blow for the vertical stresses of 5 kPa, 10 kPa and 25 kPa respectively. The data acquired from the sensors allow derivation of force-time diagrams. These data provide further input for estimation of frozen soil resistance.

Comments are as follows.
(a) Portability of the test equipment is an important advantage. The presented system has a total mass of probably less than 20 kg and can probably be manually operated by 2 persons.
(b) The proposed system will probably require modification before use in practice. The blowcounts observed in the laboratory indicate limited penetration capability, i.e. early penetrometer refusal in real-world frozen soils can be expected. Also, penetrometer recovery should be considered for penetrations in the order of metres. Modification may compromise portability.
(c) Consideration may be given to an additional set of instrumentation near the top of the penetrometer.
(d) Further laboratory experiments covering a wide range of frozen soil conditions may eventually make instrumentation redundant. Correlations with blowcount may then be adequate for practice.

5 ROTATION SPEED ANALYSIS IN SPT-T TEST BY TYPE OF SOIL

Nuñez et al. present results of standard penetration tests (SPT) with an additional measurement of rotational resistance expressed as maximum torque T_{max} and residual torque T_{res}. Torque is applied to the SPT rods and sampler immediately after completion of the penetration phase of the SPT (Figure 6). The presented work focuses on the influence of rotational speed v_T on T_{max} and T_{res}. Results can be normalised to SPT N-value in blows/300 mm, i.e. T_{max}/N.

Test results are presented for 7 sites in Southeast Brazil, to depths ranging between 11 m and 27 m below ground surface. One site shows marine organic clay. It shows N-values of 0 and 1 to a depth of 20 m below ground surface. This site is not considered further in this session report. Residual soil conditions apply to 6 sites. N-values typically range between 2 and 15. T_{max}/N values are typically in the range 1 to 2 for T_{max} expressed in kilogram-force-metre (kfgm) or 10 to 20 when expressed in Nm. No information is presented on groundwater levels. Figure 7 presents selected results including rotational speed.

Rotational speeds were typically between 3 rpm and 9 rpm for N-values of less than 20. The test equipment approached practical torque limits for N-values exceeding 20. The authors concluded no significant influence of rotational speed on test results.

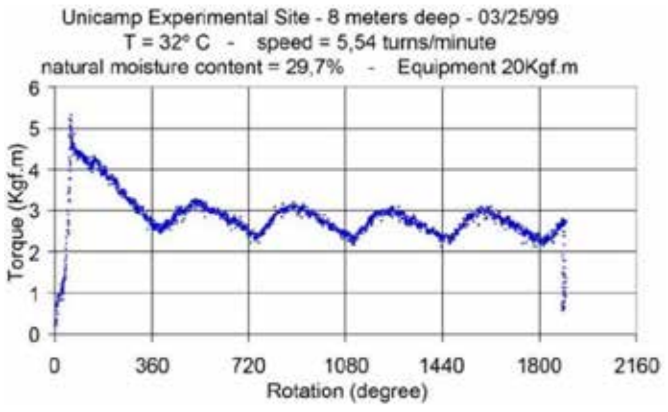

Figure 6. Example of SPT torque measurement.

Comments are as follows:

(a) The SPT is a crude tool for estimation of soil strength and acquisition of SPT data points is time consuming compared to cone penetration testing. It is therefore commendable to conduct supplementary measurements within a period of minutes, i.e. rotational resistance T_{max} and T_{res}.

(b) Measurement of rotational resistance T_{max} and T_{res} requires a torque or force sensor. This introduces novelty for common SPT practice, namely requirements for metrological confirmation of measuring equipment according to ISO 10012 (measurement management systems) or equivalent.

(c) An axial downward force applies to the sampler at the time of rotation. This force depends on groundwater level and on the SPT assembly, including depth-dependent mass of rods. It may be of interest to consider the combined torsional and axial forces in interpretation of test results.

6 CRITICAL APPRAISAL OF T-BAR PENETRATION TESTS

Peuchen & Terwindt compare T-bar penetration tests (TBT), ball penetration tests (BPT) and cone drift and associated bending influence on measurements, (2) sensitivity to torsional forces acting on T-bar, giving undetectable measurement error, (3) limited opportunity for enhanced test interpretation from pore pressure data.

Items (1) and (2) are supported by uncertainty analyses in accordance with ISO standard 19901-8 "Marine Soil Investigations". The uncertainty analyses are for T-bar penetration resistance q_m $|U_{qm}|$ and CPT cone resistance q_c $|U_{qc}|$. Figure 8 shows uncertainties for T-bar results to be slightly better than for CPTs.

The presented values for $|U_{qm}|$ possibly represent first-ever calculation results.

The authors suggest quantification of combined measurement data and interpretation uncertainties for TBTs, BPTs and CPTs, rather than comparing test results against a test standard designed for practice. "Analytic tests", with idealised test conditions and geometry, can serve as a reference.

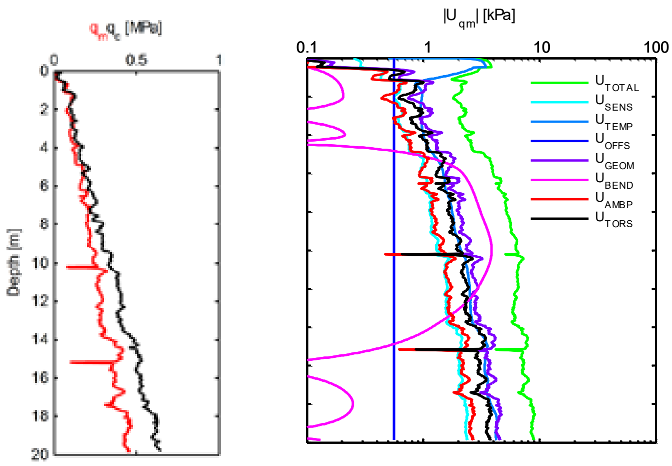

Figure 8. Examples of uncertainty estimates for high-quality TBT and CPT systems and practices, non-drilling deployment and water depth of 1500 m.

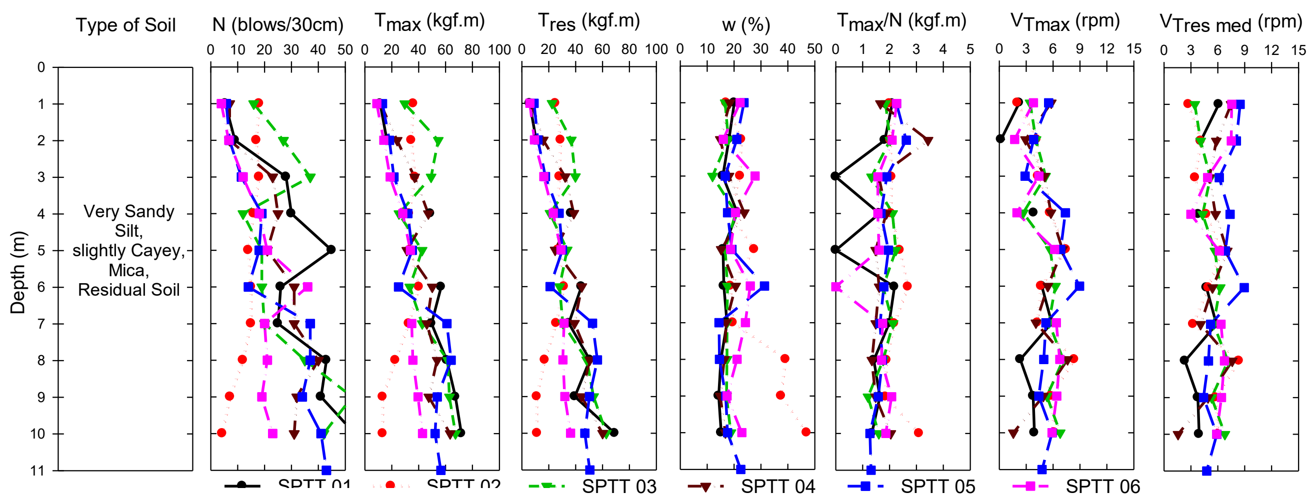

Figure 7. Results for Site E

Comments are follows:

(a) There appears to be good reason for replacing TBTs with BPTs. The reason for a high ratio of TBTs to BPTs in offshore practice is a mystery.

(b) The presented uncertainty analysis depends significantly on the seven component uncertainties, as shown in Figure 8. Particularly, limited knowledge is available for estimates of transient temperature influence U_{TEMP}, bending moment and axial torsion acting on the penetrometer U_{BEND} and U_{TORS}. A change of these input parameters will significantly affect total uncertainty U_{TOTAL} for T-bar penetration resistance q_m. Further research is recommended.

(c) The session reporter is one of the authors of the paper considered here. Inevitable bias applies to the above comments.

7 FREE-FALLING FULL-FLOW PENETROMETER FOR MARINE MATERIAL CHARACTERIZATION

Pinkert presents an analytical approach to interpretation of free fall penetration tests in soft clays. Specifically, the approach applies to a penetrometer equipped with a T-bar or ball. The T-bar or ball is instrumented to measure penetration resistance and extraction resistance. The target parameter is undrained shear strength of very soft clays. This target is expressed as reference undrained shear strength s_{u0} that applies to 1%/h axial strain rate in a laboratory monotonic triaxial test. Values for s_u inferred from a free fall penetration test are expressed as $s_u = f_r f_{ss} s_{u0}$, where f_r and f_{ss} account for shear rate and strain softening effects. The paper focusses on soil viscosity μ* which is part of the calculation framework for f_r and on strength sensitivity S_T used for estimation of f_{ss}. The proposed analytical approach considers (1) s_{u0} as either linearly increasing with depth with $s_{u0} = 0$ at seafloor or a constant value for s_{u0}, as illustrated in Figure 9, (2) μ* as constant with depth and (3) S_T as constant with depth. A value for μ* is first estimated from two data points with a significant difference in velocity values. A constant value for S_T requires measurement of monotonic extraction resistance of the ball or T-bar. The author recommends further verification.

Comments are follows:

(a) Free-fall penetrometers offer opportunities for reduced deployment/ handling equipment and deck space, compared to the offshore benchmark, i.e. the cone penetration test CPT. The applicability of free-fall penetration tests is limited to soft clays and the target geotechnical parameter is typically undrained shear strength.

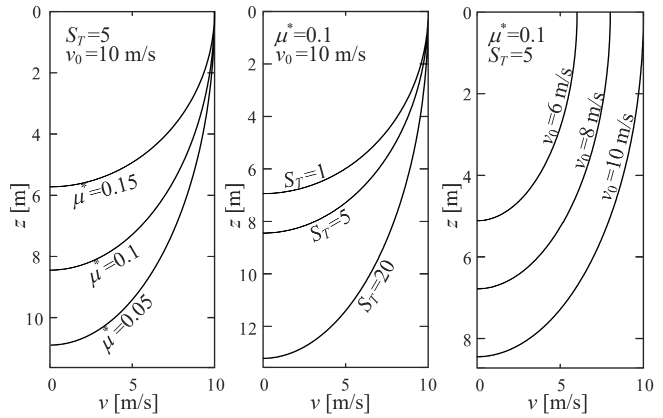

Figure 9. Calculated velocity profiles of a free-fall ball penetrometer, with mass of 400 kg, ball cross sectional area A = 10 000 mm^2, s_{u0} = 1.5 z(m) kPa, and a range of m*, S_T and initial velocity v_0 values.

(b) The author expands on existing calculation approaches for an equivalent laboratory undrained shear strength derived from free fall penetration tests.

(c) The term "full flow" is used for the high-velocity penetration phase. Full flow does not apply in practice because of the inevitable presence of the shaft. The effect of such simplification is generally perceived as small. However, consideration should be also given to conditions of gap/cavity formation around the penetrometer at high velocity and associated loss of tool robustness. Even at low velocity, gap/cavity formation will take place at shallow penetration.

(d) The author recommends measurement of ball resistance upon monotonic extraction. The measurement of ball resistance upon extraction should be feasible if the system includes an accurate depth measurement system, for example relative to deepest penetration. It is not clear how a monotonic rate can be maintained in practice, i.e. for tool deployment from a heaving vessel. It may be possible to develop a calculation framework that allows variable rates for tool extraction.

8 EFFECT OF ROTATION RATE ON SHEAR VANE RESULTS IN A SILTY TAILINGS

Reid highlights interpretation issues with vane shear tests (VST) for tailings consisting of sandy silts with up to 40% sand-sized particles (>75 μm), and finer zones with up to 30% clay-sized particles (<2 μm). Overestimates of undrained shear strengths are up to about a factor of two. The overestimates are attributed to partially drained soil response during vane rotation.

The presented confirmatory work included direct simple shear (DSS) testing on specimen trimmed from piston samples, cone penetration testing (CPT) and ball penetration testing (BPT). The author provides evidence for the DSS test results having been substantially affected by sample disturbance. The CPT results are generally presented as "reference". It is implied that penetration of the cone penetrometer generated undrained soil response, using $N_{kt} = q_n/s_u = 10$ and $N_u = \Delta u/s_u = 5$ (Figure 10). CPT pore pressure dissipation tests showed derived values for coefficient of consolidation c_h in the range 130 m^2/year to 500 m^2/year. Penetration results were obtained for BPTs at parts of the site that allowed penetration of the ball penetrometer with the equipment as mobilised. The ball penetrometer had no pore pressure sensors.

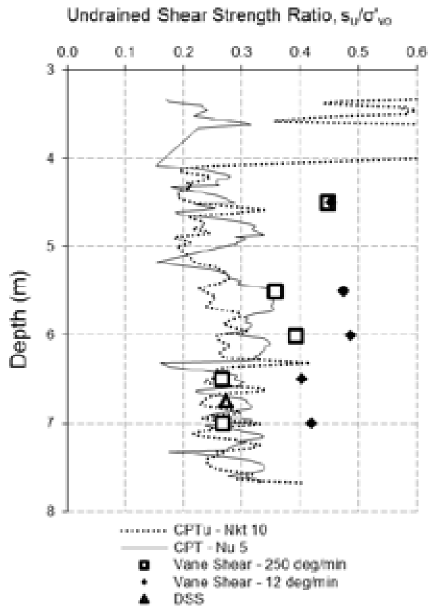

Figure 10. Summary of shear strength results (Reid)

Comments are follows:

(a) The reason for conducting VSTs in tailings probably relates to attempts at cost savings for site investigation, i.e. use of hand-held VST equipment versus operation of vehicle-mounted CPT equipment.

(b) The author confirms recommendations by other researchers, i.e. conducting VSTs at multiple rotation rates when in doubt about undrained soil response.

(c) The presented challenges in integration of the various data sets illustrate common real-world practice. The engineer applies judgement for site variability, uncertainties in measurements, limited data sets and simplifications in models for derivation of parameter values. For example, the indications for substantial DSS sample disturbance are assessed according to expectations for the type of material tested. The actual results for intended undisturbed soil may approach those for reconstituted specimen conditions. This means that in situ structure/ cementation and soil unit weight may not be adequately represented. The reliability of the presented DSS undrained strength ratios (s_u/σ'_{vo} in range 0.20 to 0.27) remains thus unclear, yet appears to fall within the expected range. Supplementary laboratory measurements could be considered for undisturbed sample quality assessment, for example volume change during initial oedometer loading.

9 ANALYSIS OF INSTRUMENTED SHARP CONE TESTS IN A SENSITIVE CLAY OF QUEBEC

Silvestri & Tabib derive in situ undrained shear strength and shear modulus from instrumented sharp cone tests (ISCTs) pushed into a pilot hole. The ISCT data (Figure 11) are compared with values derived from vane shear tests (VSTs), pre-bored and self-bored pressuremeter tests (PMTs and SBPMTs), and cone penetration tests. The principal conclusion is that no reliable ISCT results can be obtained using a pre-drilling procedure. A self-boring device is recommended.

The setting for the comparison is an overconsolidated stiff sensitive clay with VST undrained strength ratios s_u/σ'_{vo} in the order 1.3 to 1.5 for the depth range of interest, 2 m to 6 m. The reported water content is about 70 % and the plasticity index is about 40 %. The water table is reported at 2.2 m.

The penetrometer used for the ISCTs has a length of 86 mm + 340 mm, where the 86 mm lower section has a blunt tip and a constant diameter of 73 mm. The 340 mm section has a low-angle taper. The lower diameter is 73 mm and the upper diameter is 92 mm. The tapered section has 5 lateral pressure transducers (Figure 12). The penetration rate is 3.3 mm/s. This provides strain rates that are approximately equivalent to pressuremeter testing.

Derivation of ISCT undrained shear strength and shear modulus is similar to PMT and SBPMT interpretation, e.g. use of a Tresca soil model. Two ratios are presented for s_{uISCT} / s_{uVST}: 2.6 and 3.7. A single comparison is presented for shear modulus at in situ stress conditions: $G_{ISCT} / G_{SBPMT} = 0.2$. Speculation about reasons for these large difference includes (1) disturbance from pilot hole activities, (2) further damage to the pilot hole by push of ISCT penetrometer with a blunt tip equal to the nominal size of pilot hole, (3) cemented and brittle soil at high lateral in situ stress (K_o >3.5), and (4) partially drained soil response where undrained is assumed.

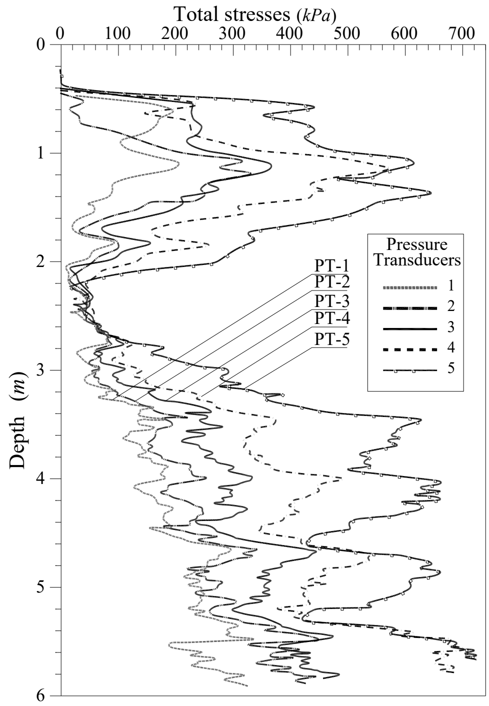

Figure 11. ISCP results, where pressure transducer 1 has the lowest position in the penetrometer.

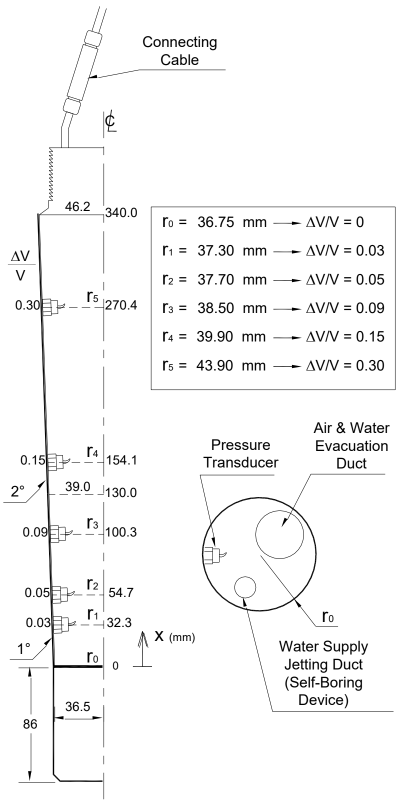

Figure 12. Penetrometer used for ISCT.

Comments are as follows.

(a) The ISCP in pilot hole mode aims at deriving soil parameters similar to the PMT in pilot hole mode. For clays, the ISCP provides fast and continuous data compared to discontinuous PMT results.

(b) Data confidence for the ISCT is low compared to SBPMT results. Development of a self-boring ISCT device may be of interest. Results may possibly approach those of SBPMTs, at (much) lower cost per data set per test depth.

(c) The ISCP requires consistently reliable measurement of total stress in penetration mode. This is a major challenge for tool designers. It will require consideration of a complex range of instrument issues that can affect test results.

10 CONCLUSIONS

Comments reflecting the session reporters interpretation on each of the papers are provided individually in preceding sessions.

Geotechnical and Geophysical Site Characterisation 5 – Lehane, Acosta-Martínez & Kelly (Eds)
© 2016 Australian Geomechanics Society, Sydney, Australia, ISBN 978-0-9946261-1-0

Session report: Pressuremeter and Dilatometer

S. Burlon
Université Paris-Est, ISFTTAR, Marne La Vallée, France

W. Frikha
ENIT, Tunis, Tunisia

P. Monaco
University of L'Aquila, Italy

ABSTRACT: The present report provides an overview of 14 papers dealing with pressuremeter tests (PMTs) and dilatometer tests (DMTs). These papers include many subjects in relation with geotechnical engineering, soil and rock mechanics and engineering geology. Pressuremeter tests and dilatometer tests are used for the assessment of site stratigraphy and ground type (soils and rocks), the derivation of geotechnical design parameters, the calibration of constitutive laws for numerical modelling and the design of geotechnical structures, especially deep foundations with a direct use of measured data. This report presents the application fields of these two materials.

1 INTRODUCTION

The present report shows the various subjects dealt with by the papers accepted for the ISC'5 Conference. Two main parts are presented: the first one dealing with pressuremeter test and the second one treating dilatometer test.

Table 1. Articles received at the ISC'5 Conference (Session Pressuremeter/Dilatometer) for pressuremeter tests.

Papers	References
1	Gaone, F.M., Doherty, J., & Gourvenec, S. (2016) self boring pressuremeter tests at the national field testing facility, Ballina.
2	Kaljahi, Asghari E. (2016) Pressuremeter in the hard soils and rocks of arak aluminum plant site, Iran.
3	Bagbag, A.A., Doherty, J.P., & Lehane, B.M. (2016) Stress-strain response of fine silica sand using a miniature pressuremeter.
4	Ho, C.E. (2016) In situ characteristics of manhattan glacial deposits from pressuremeter tests.
5	Monnet, J., Mahmutovic, D., Boutonnier, L. (2016) Membrane correction for pressuremeter test.
6	Silva, T.Q.. Câdido, E.S., Marques E.A.G., & Minette, E. (2016) Determination of em from pressuremeter insitu tests in gneiss residual soils under tropical conditions.
7	Baud, J.P. (2016) soil and rock classification by pressuremeter data. New developments and applications.
8	Oztoprak, S., Uyar, H.K., & Sargin, S. (2016) Modelling pressuremeter test in sand.
9	Reiffsteck, S.Fanelli & G. Desanneaux (2016) Evolution of deformation parameters during cyclic expansion tests at several experimental test sites.

Regarding the pressuremeter test, 9 papers have been received and the following aspects are considered: materials and *in situ* procedures, test programs and interpretation, soil classifications and correlations, constitutive laws and numerical modelling and foundation design. The list of papers is presented in Table 1.

Regarding the dilatometer test, 5 papers have been received and the following aspects are mostly considered: updates on test interpretation, combination/comparisons with other in situ tests, liquefaction assessment, upgrade of testing equipment. The papers on DMT (initially) included in the Session Pressuremeter/Dilatometer, specifically addressed in this report, are listed in Table 2.

Table 2. Articles received at the ISC'5 Conference (Session Pressuremeter/Dilatometer) for dilatometer tests

Papers	References
1	Cao, L.F., Peaker, S.M. & Ahmad, S. (2016) Use of Flat Dilatometer in Ontario.
2	Ouyang, Z. & Mayne, P.W. (2016) New DMT method for evaluating soil unit weight in soft to firm clays.
3	Rodrigues, C., Amoroso, S., Cruz, N. & Cruz, J. (2016) *G*-γ Decay curves in granitic residual soils by seismic dilatometer.
4	Rollins, K.M., Remund, T.K. & Amoroso, S. (2016) Evaluation of DMT-Based Liquefaction Triggering Curves Based on Field Case Histories.
5	Shen, H., Haegeman, W. & Peiffer, H. (2016) Interpretation of the instrumented DMT (iDMT): a more accurate estimation of p_0.

1 PRESSUREMETER TESTS

1.1 *History, current status, and updates*

Louis Ménard, undergraduate student at the Ecole Nationale des Ponts et Chaussées, deposited on January 1955, via his alumnus P. Regimbeau, a patent on the pressuremeter. This apparatus resulted from Menard's fruitful thoughts when, as a trainee student, he was handling soil samples at a job site. He then submitted his idea in his graduation project in the form of a theory and a first prototype. The following year, at the University of Illinois in cooperation with Professor Peck, within the four semesters he spent at the Talbot Laboratory, Ménard built a second pressuremeter prototype and started his tests. He understood that he had to develop a new approach too for the design of foundations where by the pressuremeter will play a central role.

With such a new vision of geotechnical engineering, from the late sixties up to his untimely death in 1978, Louis Ménard could become the pioneer in the ground improvement field. With pressuremeter tests he perfectly demonstrated the soil improvement rate in terms of expected settlements before and after treatment.

From this first idea, several developments were made in many countries to develop alternative approaches to pressuremeter Ménard procedure, especially the self-boring procedures. Now, many standards describe the use of pressuremeter tests: ISO 22476-4, EN 22476-4, ASTM D4719, etc.

In parallel, a pressuremeter engineering has emerged considering this tool as useful (Briaud 1992), on the one hand, for the ground investigations with the measurement of deformation and strength parameters and, on the other hand, for the calculation of geotechnical structures with many methods dealing with bearing capacity and settlements of shallow foundations, deep foundations or displacements of retaining walls, etc. (Baguelin et al. 1978, Baker 2005).

2.2 Materials and in situ procedures

The papers received for the ISC'5 Conference show the diversity of materials and *in situ* procedures: Ménard procedure (Kaljahi, Silva et al.) and self-boring procedure (Gaone et al., Ho et al.). All types of ground (soft soils, soft rocks, etc.) can be investigated with these two procedures and a large range of values can be measured in terms of modulus and limit pressure. The choice between the two procedures depends on the ground type since, in very stiff ground where pre-boring is required only Ménard procedure is appropriate. In soft soils, self-boring pressuremeter is able to provide more reliable measures. Comparisons between the two procedures show the effects of the borehole as underlined by Ho et al. with an example in varved silts and clays. Another interesting development ~~is~~ related to the present limitation of the pressuremeter Ménard tests is due to the difficulty of reaching large expansion volumes and high pressures without any significant risks of bursting of the probe. A new probe has been developed (Jacquard et al. 2013) allowing the volume of the hole to be doubled, even under high pressures: the conventional limit pressure can then be directly measured. Technological innovations increasing the capability and the reliability of pressuremeter probes are described.

The complexity of the project and the quality of the measured data are other aspects to consider. For projects of major importance where the behaviour of the ground has to be characterized in detail and where the prediction of displacements is of a major issue, more complex procedures can be used: self-boring pressuremeter, procedures including unloading and reloading loop, cyclic procedures, etc. It seems important to have a clear and precise ground investigation strategy in order to choose the most appropriate procedure for pressuremeter tests. This strategy must have the ambition to ensure quality ground investigation and cost management.

The present report shows the various subjects dealt with by the papers accepted for the ISC'5 Conference. Two main parts are presented: the first one dealing with pressuremeter test and the second one treating dilatometer test.

Regarding the pressuremeter test, 9 papers have been received and the following aspects are considered: materials and *in situ* procedures, test programs and interpretation, soil classifications and correlations, constitutive laws and numerical modelling and foundation design. The list of papers is presented in Table 1.

1.2 *Test programmes and interpretation*

The test programs and its interpretation ~~is~~ are another important topics for ~~of~~ pressuremeter tests. Monnet et al. propose a new approach to analyze the influence of the membrane rigidity on the measured limit pressures. The aim is to consider the pressuremeter probe in expansion as a shearing test where the measured parameters could be considered as "real" elastic and plastic parameters and compared to those measured in laboratory by means of triaxial tests. This paper raises the problem of the use of the measured parameters by pressuremeter tests and the need to have either direct methods of correlation, for example between the limit pressure and the axial shaft friction, or indirect methods of correlation, for example between the limit pressure and the undrained cohesion and then between the undrained cohesion and the axial shaft friction.

Pressuremeter tests with Ménard procedure are often used to provide the shear modulus G and the Ménard modulus E_M while self-boring pressuremeter tests are better used to assess the earth pressure coefficient at rest K_0 and the variation of shear modulus G with the strain level (Gaone et al.). In this paper from Gaone et al., the procedure to assess the horizontal pressure based on the lift-off pressure concept is discussed (Figure 1). This type of application can be very interesting for the use of numerical modeling where the influence of the initial earth pressure coefficient at rest can be very significant and really affect the numerical results. The analysis of the pressure-volume curve gives the reduction of the shear modulus with the strain level, which allows as mentioned later in this paper to deal with the calibration of constitutive laws.

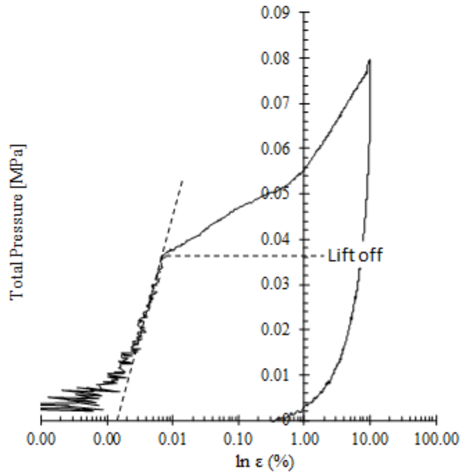

Figure 1. Assessment of the lift-off pressure with self-boring pressuremeter test (Gaone et al.).

Nevertheless, Ménard pressuremeter test equipment allows operators to achieve not only monotonic expansion tests (EN ISO 22476-4 similar to NF P94-110-1 ASTM D4719) but also cyclic tests (NF P94-110-2) (AFNOR, 1999 and 2000). These tests include an unload-reload cycle performed in steps, in the same conditions as the Ménard pressuremeter test described in the EN ISO 22476-4 standard. The conventional expansion test using the drilling conditions recommended by the EN ISO 22476-4 standard and with the proposed loading program, does not give directly available results for deformability prediction of geotechnical structures especially when the modulus in the small strain range is required (Combarieu & Canépa 2001). Therefore, cyclic procedures are developed (Reiffsteck et al.) to assess the accumulation of displacements and strains, the variations of shear stiffness with cyclic loadings and the soil layer sensitivity to liquefaction (Figure 2). The procedure is based on the pressure control and a cyclic loading between two limit pressures is applied.

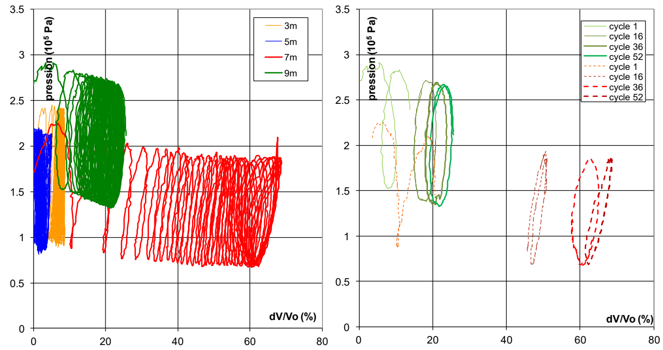

Figure 2. PMT cyclic expansion tests at the Gosier site (Reiffsteck et al.)

Quality control for soil improvement such as stone columns addresses the problem of the inclusion continuity into the ground and their mechanical properties and thus relies on in-situ testing. Interpretation of pressuremeter tests can provide very interesting information related to this topic.

1.3 *Ground classifications and correlation*

Results from pressuremeter tests allow to classify the ground types since the nature of the ground can be defined by the analysis of the bored ground sampling and assess its mechanical properties in terms of deformation and resistance. Many proposed papers confirm this approach and explain how the use of pressuremeter tests can be gainful for the understanding of a site (Gaone et al. 2016, Kaljahi 2016, Ho et al. 2016, Silva et al. 2016). For example, undrained cohesions are usually derived from limit pressures (Figure 3).

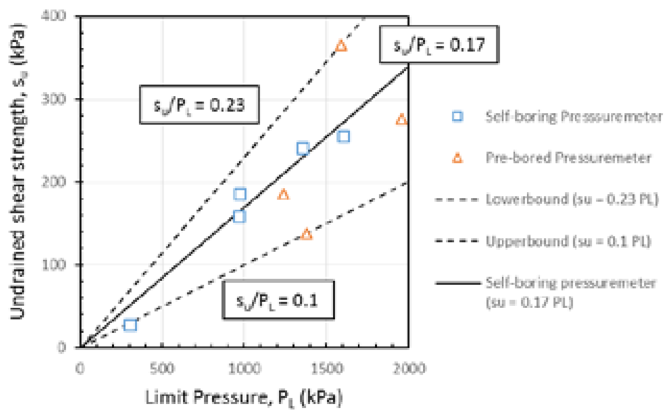

Figure 3. Correlation between undrained cohesion and limit pressure (Ho)

Comparisons with shear vane tests and cone penetration tests show good agreements. In complex grounds, for example, in gneiss residual soils (Brazil), pressuremeter tests provide very interesting information related to the variation of the stiffness with the depth. Data from pressuremeter both Ménard modulus and limit pressure can be used to appreciate the ground heterongeneity by analyzing their scatter. Several comparisons with plasticity index, N_{SPT} or uniaxial compression strength show that the heterogenity is more or less the same. Variations according to the horizontal plane and the depth can be highlighted in a homogenous ground layer with pressuremeter tests showing variations of stiffness and strength resistance.

Soil profiling chart based on SPT and CPT results have a great success among practitioners. One resistance parameter is figured versus another one dimensional or normalized (by the first one) and zones of specific behavior are delimitated by curves. As these parameters do not vary linearly between each other, logarithmic scales are often used to linearize non linear trends. Recently the same development was initiated for pressuremeter tests results.

Baud gives in his paper an update of previous development of their soil behavior chart called Pressiorama (figure 4). This tool defines soil classes or mechanical properties, in a plane constructed with the normalized limit pressure versus the ratio of the Ménard modulus to the limit pressure. The new version presented skip from limit pressure to rheological factor α invented by Louis Ménard. In order to complete the Pressiorama diagram with an α values axis, the authors used a calibration mostly based on PMT performed in various soil types from soft clay to rock.

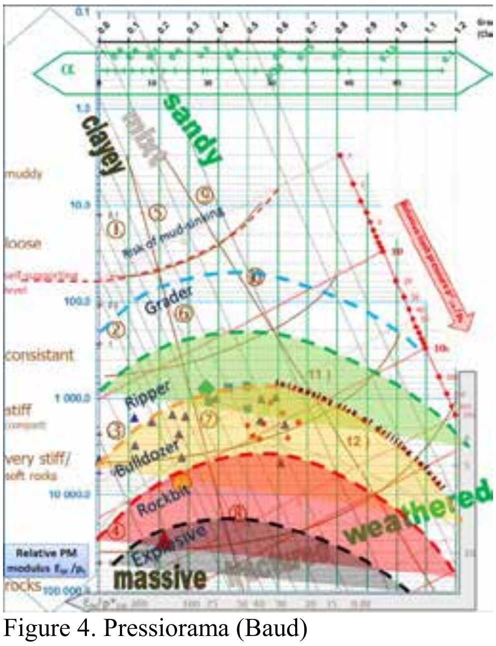

Figure 4. Pressiorama (Baud)

1.4 *Constitutive laws and numerical modeling*

The analysis of the pressure-volume curve can be very interesting for the calibration of constitutive laws. A numerical procedure is developed in laboratory with a miniature pressuremeter to calibrate a complex constitutive law called Hardening Soil Small model using Plaxis finite element code (Plaxis 2015, Bagbag). The model provides a very good simulation of the measured pressuremeter response at small and medium cavity strains. It is also noticed that the parameters determined from triaxial tests provide a reliable simulation of the pressuremeter tests. Another paper proposed by Oztoprak et al. deals with the same issue. Small strain considerations are coupled with the strain-hardening/softening Mohr-Coulomb (SHS-MC) criterion to better capture the soil behaviour in the small strain range. The SHS-MC model allows the representation of nonlinear material softening and hardening behaviour based on prescribed variations of the MC criterion properties as functions of the plastic shear strain which are not an output in the MC model. Oztoprak et al. show that a pressuremeter test can successfully be modelled through the proposed hyperbolic model. To model the small strain behavior and therefore to obtain the corresponding shear modulus and index properties of the tested soils, loops are of crucial importance. The size and the inclination of loops are completely related to the degradation behavior of shear modulus.

This topic is very interesting for pressuremeter engineering since it allows to clearly assess parameters that are usually measured in laboratory: for example, E and ν for elastic parameters and c, φ and ψ for plastic parameters. Nevertheless, the pressure-volume curve can provide additional elements to take into account non-linear elasticity with for example the reduction of the shear modulus with strain level, plastic volumetric strains with contraction or dilation, hardening mechanisms, etc. It avoids the discussion about the difference between Ménard modulus and Young modulus.

The main barrier remains the measure of pore pressures that would allow to perform analysis according to the effective stresses framework. It can be interesting to note that very few works try to account for creep effects based on pressuremeter tests whereas the maintained load procedure should allow to study this topic. Creep pressure is rarely considered whereas this parameter could be viewed as the ground reaction compatible with very low strains. For example, this idea leads to limit p-y curves to creep pressure in order to limit the pile displacements submitted to transversal loads. The creep pressure can be considered as the lower bound of the limit pressure when the ground is submitted to many cyclic loadings.

1.5 *Geotechnical design*

The use of pressuremeter tests for the geotechnical design has not been addressed by the papers of this conference. Nevertheless, pressuremeter test provides both a failure parameter, the limit pressure, and a deformation parameter, the Ménard modulus, which enables to tackle with the same *in situ* test the problems of bearing capacity of foundations (using the limit pressure p_{LM}), as well as the problems of displacements of foundations (using the pressuremeter modulus E_M). In France, design codes for shallow and deep foundations are based on the use of pressuremeter parameters. Recent developments and new experiments have been performed and show that improvements are possible.

The calculation model based on pressuremeter data for the assessment of pile bearing capacity has been recently improved to take into account new pile techniques and be compatible with Eurocode 7 approach (Burlon et al. 2014). Based on 174 full-scale static pile load tests (IFSTTAR pile database), this work includes a comparison between measured values of pile bearing capacity and calculated values by an improved calculation model ‘PMT2012’ (figure 5).

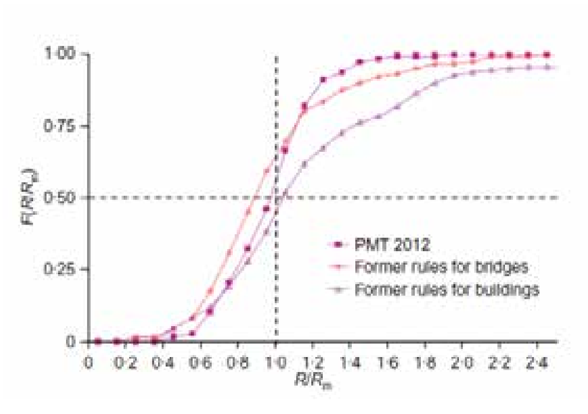

Figure 5. Scatter of different calculation models for pile bearing capacity based on pressuremeter data – Comparison of distribution functions (R-calculated values ; R_m-measured values) (from Burlon et al. 2014)

Pressuremeter data can be used to propose t-z curves (Frank et al. 1981) or p-y curves both for static and cyclic applications (Burlon et al. 2013). Regarding *t-z* curves, from IFSTTAR pile database, new calculation models have been proposed (Abchir et al.). For cyclic applications, the use of the cyclic pressuremeter test can provide relevant data for the calibration of *t-z* and *p-y* curves.

2 DILATOMETER TESTS

2.1 *Current status, background and updates*

The flat dilatometer test (DMT), introduced by Marchetti (1980), is increasingly used in the last years, also stimulated by the diffusion of its efficient "All-in-One" seismic version (SDMT). The DMT is standardized by ASTM (D6635-15). ISO/TC 182/SC1 is currently converting the DMT Technical Specification into a Standard (ISO/DIS 22476-11:2015(E)). The state-of-the-art of DMT/SDMT was recently overviewed in the 3rd International Conference on the Flat Dilatometer DMT'15 (Rome, Italy, June 2015). A basic reference document (Marchetti et al. 2001), including detailed information on DMT equipment, test procedure, interpretation and applications, was released in 2001 by the ISSMGE Technical Committee TC16 (now TC102) – In-Situ Testing. In his DMT'15 keynote, Marchetti (2015) presented some updates to the 2001 TC16 Report, as well as new developments and clarifications on specific aspects on use and interpretation of the DMT. Key papers on DMT/SDMT, including the DMT'15 Proceedings, can be downloaded from the recently restyled website *www.marchetti-dmt.it*.

Major distinctive contributions that the DMT can provide in a *routine* site investigation are: (1) information on stress history, which has a dominant influence on soil behaviour; (2) being a load-displacement test, DMT results are more closely related to soil stiffness than other in situ penetration tests (e.g. CPT). As to the SDMT, the add-on module has added to the parameters measurable by DMT the shear wave velocity V_S, hence information on small strain stiffness.

In most cases the DMT is utilized in site investigations to obtain information and soil parameters (stratigraphy/soil type, undrained shear strength, constrained modulus, etc.) to be used with common geotechnical engineering design methods. Most frequent DMT applications include: prediction of settlements of shallow foundations, compaction control, liquefaction assessment, design of laterally loaded piles, detecting slip surfaces in OC clay. Recently, researchers have also focused on: correlations and comparisons with other in situ (or laboratory) tests, theoretical and numerical modelling of the test, applications in difficult geomaterials (e.g. tailings, residual soils), new developments and improvement of testing equipment (seismic/other instrumentation, nearshore/seafloor test setup), seismic site characterization (SDMT). The papers on DMT submitted to this conference are mostly focused on: updates on interpretation of soil parameters; combination/comparisons with other in-situ tests (mostly CPT); liquefaction assessment; technological innovation of testing equipment (instrumented DMT, upgrade of seismic probe). The main findings revealed by the papers on DMT included in the Session Pressuremeter/Dilatometer are briefly discussed in the following. Comments to these papers are tentatively outlined in a more general framework of current trends and ongoing developments of DMT research and practice.

2.2 *Sensitivity of DMT to stress history*

Research carried out over the years has pointed out the centrality of the horizontal stress index K_D, a key parameter obtained from DMT and one of the few in situ parameters able to provide information on stress history (especially in sand). Knowledge of stress history is fundamental for obtaining realistic predictions, e.g. of settlements and liquefaction behaviour. Numerous researchers have observed that K_D from DMT is considerably more sensitive to stress history than the cone penetration resistance q_c from CPT, either in monitoring compaction in the field and in calibration chamber (see Marchetti 2015 for details and references). K_D reflects cumulatively various stress history effects, such as aging, in situ horizontal earth pressure (K_0), structure and cementation.

2.3 *In-situ multi-parameter/multi-test approach*

Most in situ tests are only able to measure "mixed" soil responses that depend at the same time on strength, stiffness, stress history, etc. Hence "pure" soil properties are determined by solving an inverse problem, based on multiple independent in situ responses. Mayne et al. (2009) emphasized the use of direct-push in situ tests providing multi-measurements, in particular "hybrid" tests that combine the advantages of full-displacement penetrometer probes with downhole geophysics (such as seismic piezocone SCPTU and SDMT), as a more efficient approach to geotechnical site characterization. While in simple problems one in situ technique could be sufficient, in general an adequate number of responses from different in situ tests should be available to define a soil model. Moving towards an in-situ multi-parameter/multi-test approach appears a logical trend. In this respect, the availability of the DMT stress history parameter K_D is important not only "per se", but also in combination with parameters obtained from other in situ tests less sensitive to stress history (e.g. CPT).

An example of in-situ multi-parameter/multi-test approach is the estimation of the overconsolidation ratio *OCR* in sand based on both DMT and CPT. The 2001 TC16 DMT Report (Marchetti et al. 2001) indicated semi-quantitative guidelines of the ratio between the constrained modulus M_{DMT} estimated from DMT and the CPT cone resistance q_c in NC and OC sands. The potential use of the ratio M_{DMT}/q_c as a broad indicator of *OCR* in sands descended from field observations before/after compaction of sandfills, where M_{DMT}/q_c was found to increase with compaction (a way of imposing stress history) due to the fact that compaction increases both M_{DMT} and q_c, but M_{DMT} at a faster rate. Monaco et al. (2014) also combined DMT and CPTU to derive a general correlation for estimating *OCR* in sand from the ratio M_{DMT}/q_t. This correlation was constructed using the results of an experimental study at the research site of Treporti, Venice (Italy), where a full-scale trial embankment was built and then removed four years later, permitting to calculate *OCR* at each depth (by its simple definition), and paired values of M_{DMT} and q_t in sand layers were available.

Other examples of multi-parameter/multi-test approach, based on the combined use of DMT and CPT, are the methods for estimating K_0 in sand (see Marchetti 2015) and the method for estimating liquefaction resistance proposed by Marchetti (2016).

Several papers presented in different Sessions of this conference show comparisons of DMT and CPT results. This interest indicates the trend of increasing diffusion of a combined multi-parameter/ multi-test approach in site investigation practice.

2.4 *Updates on DMT interpretation*

2.4.1 *In situ G-γ decay curves from SDMT*

Predicting settlements of shallow foundations is often considered the No. 1 DMT application. A large number of comparisons collected over the years has indicated, in general, reasonable agreement between measured and DMT-predicted settlements (Monaco et al. 2006). The accumulated experience indicates that the constrained modulus M_{DMT} (Marchetti 1980) can be assumed as an adequate "operative" or "working strain" modulus for most practical purposes.

A distinctive feature of the SDMT is its ability to provide routinely, besides the *working strain* modulus M_{DMT}, also the *small strain* shear modulus G_0 (obtained as $G_0 = \rho V_S^2$, where ρ is the soil density).

The potential of obtaining stiffness decay curves in situ is of considerable interest, since such curves are difficult and expensive to achieve in the laboratory. A procedure to derive in situ curves depicting elemental soil stiffness variations with strain level from SDMT was outlined by Marchetti et al. (2008). Such decay curves could be constructed by fitting "reference typical-shape" laboratory G/G_0-γ curves through two points, both provided by SDMT: (1) the *small strain* shear modulus G_0 from V_S; (2) a *working strain* shear modulus G_{DMT} derived from M_{DMT} (using linear elasticity formulae, as a first approximation). To locate the second point on the curve it is necessary to know, at least approximately, the elemental shear strain γ_{DMT} corresponding to G_{DMT} along the G/G_0-γ curve. Typical ranges of γ_{DMT} in different soil types (0.015-0.30% in sand, 0.23-1.75% in silt and clay) were inferred by Amoroso et al. (2014) based on comparisons of SDMT data with reference stiffness decay curves from laboratory tests or back-calculated from full-scale tests. Amoroso et al. (2014) also proposed a hyperbolic stress-strain formulation for estimating G/G_0-γ decay curves from SDMT, which require to input the ratio G_{DMT}/G_0 obtained from SDMT at a given site and a "typical" shear strain γ_{DMT} estimated for the given soil type.

Rodrigues et al. present an interesting application of the Amoroso et al. (2014) procedure for estimating G/G_0-γ decay curve from SDMT in granitic residual soils in the area of Guarda (Portugal). The behaviour of these structured soils, often classified as "problematic", is strongly influenced by bonding and fabric. The investigated soils are characterized by very high values of K_D and M_{DMT}, which suggest significant cementation. Rodrigues et al. applied the Amoroso et al. (2014) procedure by comparing SDMT data with stiffness decay curves obtained by triaxial tests (CID) with internal instrumentation executed on samples retrieved at the same depth and subjected to the same confinement stress. The comparisons (Figure 6) indicate that in these residual soils γ_{DMT} falls in the range 0.0025-0.003%, i.e. one order of magnitude lower than γ_{DMT} proposed by Amoroso et al. (2014) for sedimentary soils of similar grain size (0.015-0.30%). This finding clearly reflects the influence of cementation/fabric on the mechanical behaviour of these soils and points out the necessity of specific calibration of methods developed for "textbook" soils.

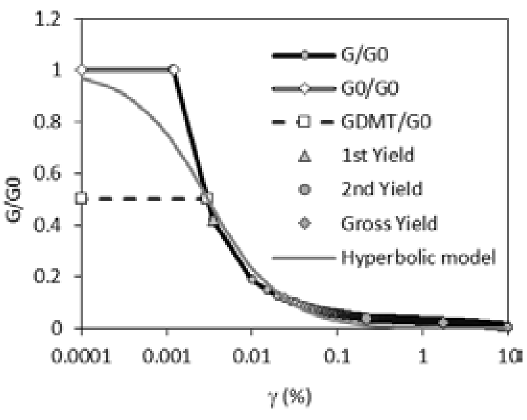

Figure 6. Laboratory G/G_0-γ curve, superimposed G_{DMT}/G_0 data points and hyperbolic G/G_0-γ curve (Amoroso et al. 2014) in granitic residual soils at Guarda, Portugal (Rodrigues et al.)

2.4.2 *OCR, c_u and γ in clays*

Cao et al. present the results of DMTs conducted in silty clay and silty clay till at two sites in Ontario, Canada. They used semi-theoretical formulas developed from cavity expansion theory in the Modified Cam Clay (MCC) model to estimate *OCR* and c_u from the DMT measurements p_0 and p_1 (also requiring additional information, e.g. the friction angle ϕ'). The profiles of *OCR* and c_u obtained by these formulas were compared with those interpreted from DMT using the original Marchetti (1980) correlations and with corresponding results from field vane, triaxial and oedometer tests. Cao et al. found in general good agreement between *OCR* and c_u obtained by their semi-theoretical formulas and determined by other reference tests (Figure 7), while the Marchetti (1980) correlations provided higher *OCR* and c_u estimates at both sites. It is noted that at the first site various indicators (very low in situ void ratio, very high p_0) suggest significant stress history of the till deposit, denoted as very stiff to hard, while based on oedometer test the deposit is defined NC to slightly OC. At the second site (Figure 7) very low values of the DMT material index I_D suggest that the silty clay deposit is a so-called "niche silt" (Marchetti 2015), where the difference $(p_1 - p_0)$ is "too low" and so are the derived parameters.

As pointed out by Marchetti (2015), the original Marchetti (1980) *OCR*-K_D correlation in clay (origin of many derived correlations, including c_u-K_D by SHANSEP) was later confirmed by experimental and theoretical research work. The Marchetti (1980) *OCR* and c_u correlations can be considered roughly as "median" correlations for "average" soils, able to provide reasonable estimates in many "textbook" clays. It is not surprising that the till deposits investigated by Cao et al. present some deviation compared with the generality of "textbook" clays.

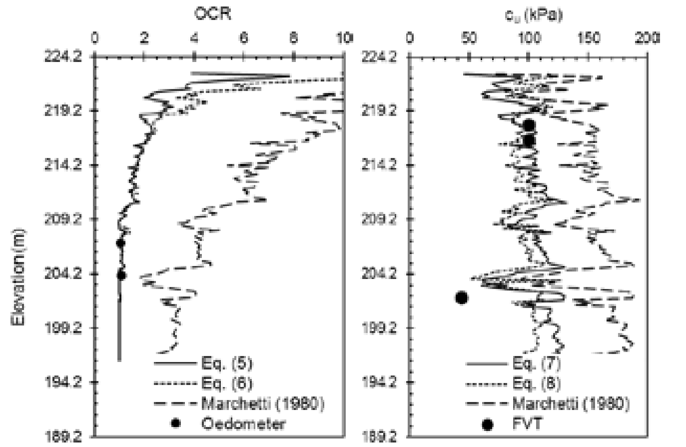

Figure 7. Comparison of *OCR* and c_u obtained from DMT and from other tests at Bradford West Gwillimbury, Ontario, Canada (Cao et al.)

Ouyang & Mayne present a new method for estimating the total soil unit weight γ_t from DMT in soft to firm clays. The study is based on a re-interpretation of DMT results from 31 NC to lightly OC ($OCR \approx$ 1-2) clay deposits in different countries, mostly homogeneous and having a shallow groundwater table (≈ 1-3 m depth). The database comprises laboratory data from undisturbed samples, including γ_t determinations. In these clays, as commonly observed in NC clays, the DMT contact pressure p_0 increases almost linearly with depth z. Using a regression analysis, Ouyang & Mayne defined a new slope parameter $m_{p0} = \Delta p_0/\Delta z$.

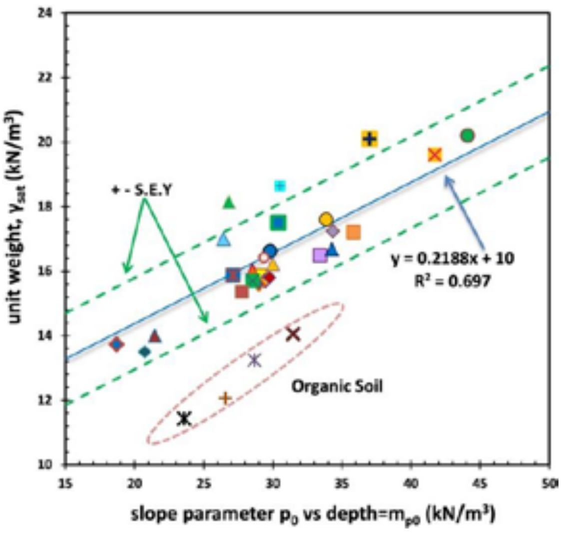

Figure 8. Total unit weight versus slope parameter m_{p0} (Ouyang & Mayne)

The comparison with laboratory γ_t values (Figure 8) indicated a correlation between γ_t and m_{p0} in most inorganic clays, while a few organic clays showed different trends. Based on this finding, Ouyang & Mayne proposed an approximate expression for deriving γ_t from m_{p0}. Compared statistically with the earlier Marchetti & Crapps (1981) chart, the new correlation was found to give a better estimate of γ_t in the tested clays. However Ouyang & Mayne note that the proposed m_{p0} approach is not applicable to stiff and hard clays, nor to silts and sands, thus it appears to be specific only for soft to firm inorganic clays.

2.5 *Liquefaction assessment based on DMT-K_D*

The use of the DMT for liquefaction assessment has received increasing attention in the last years and is a central topic in recent DMT research. Simplified methods for estimating the cyclic resistance ratio (CRR) based on the horizontal stress index K_D have recently been proposed by Monaco et al. (2005), Tsai et al. (2009), Robertson (2012). The CRR-K_D correlation has potentially the advantage of incorporating the high sensitivity of K_D to stress history, besides to other factors that increase liquefaction resistance (relative density, in situ horizontal earth pressure, aging, cementation). Recently Marchetti (2016) proposed a method to estimate CRR based on the combined use of CPT-DMT results, in the form $CRR = f(Q_{cn}, K_D)$, where Q_{cn} (or q_{c1N}) is the normalized cone resistance. The interest in combining the information obtainable from both tests is in that the commonly used CPT-based liquefaction curves are based on a vast field performance experience, but stress history, which has a primary influence on CRR, is modestly reflected by Q_{cn}, while K_D is a sensitive indicator of stress history. This is a remarkable example of multi-parameter/multi-test approach. It is expectable that an estimate based at the same time on two measured parameters could be more accurate than an estimate based on just one parameter. Another useful multi-parameter approach facility when using the SDMT is the possibility to obtain two independent estimates of CRR, one from K_D and another from V_S using existing CRR-V_S correlations.

The major obstacle to the diffusion of DMT-based liquefaction triggering methods today is their limited experimental validation based on field performance data from real earthquakes, in contrast to methods based on CPT, SPT or V_S. The paper presented in this conference by Rollins et al. is a valuable attempt to fill this gap. The Authors note that, despite the availability of liquefaction triggering curves based on CPT and SPT, a DMT-based liquefaction triggering curve is highly desirable because it is more sensitive to factors, such as aging, stress history and horizontal earth pressure, which are particularly important when evaluating increased liquefaction resistance produced by ground improvement techniques that increase both the density and lateral pressure. Rollins et al. assessed comparatively the accuracy of three available K_D-based methods (Monaco et al. 2005, Tsai et al. 2009, Robertson 2012) built on DMT data collected at sites where liquefaction did or did not occur in various earthquakes (California, Taiwan, New Zealand, Italy). They found that the DMT-based field performance data provide reasonable discrimination between liquefaction and no liquefaction for $K_D < 4$ (Figure 9). Both the Tsai et al. (2009) and Robertson (2012) curves provide reasonable triggering boundaries within this range, while the Monaco et al. (2005) curve is somewhat unconservative. In the region where $K_D > 4$ and the cyclic stress ratio $CSR > 0.20$, there is currently insufficient data to constrain the triggering boundary curve and additional testing is necessary. It is noted that, as today, fines content corrections are not accounted for by existing DMT liquefaction triggering curves, valid only for clean sand. Rollins et al. included also silty sand and sandy silt data points, regardless of fines content, in their DMT data collection. However they observe that the implementation of the DMT case history database could support the introduction of a more consistent liquefaction curve that could also consider the fines content influence using the material index I_D.

The construction of an adequate field performance database for the validation of DMT-based liquefaction triggering curves, including information on fines content and/or cementation, is a strong address for future research. The inclusion of data points from sites affected by severe lateral spreading, which may influence to a significant extent the post-liquefaction K_D, requires caution and further investigation.

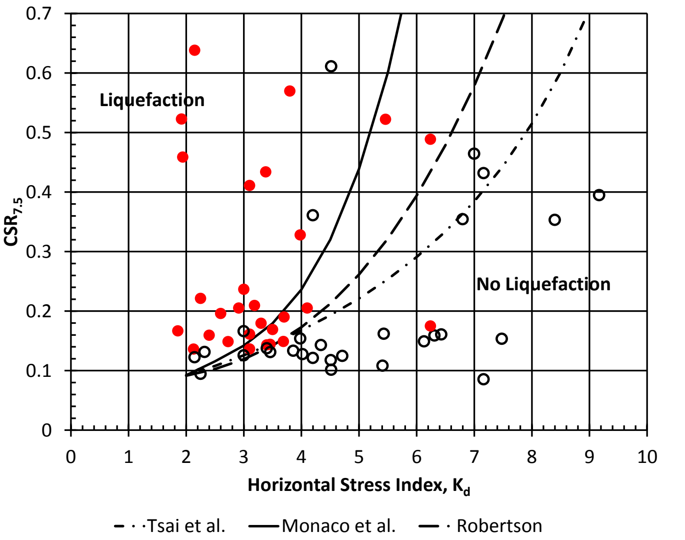

Figure 9. Comparison of DMT-based liquefaction triggering curves with field performance data points using the Boulanger & Idriss (2016) approach for *CSR* (Rollins et al.)

2.6 *Modified instrumented DMT*

A number of modified instrumented DMT (iDMT) have been prototyped in the years by various researchers. Some of these modified probes incorporate a pressure sensor and a displacement sensor, able to produce a full pressure-displacement curve instead of the standard DMT pressure readings at two fixed displacements.

Shen et al. present a novel method for determining the "lift-off" pressure p_0 from interpretation of the full pressure-displacement curve provided by iDMTs. The difference with the standard DMT interpretation is in that the original formulation for p_0 (Marchetti 1980) derives from the assumption of a linear pressure-displacement relation; actually p_0 (corrected pressure at zero displacement) is not measured directly, but is back-extrapolated from the pressure readings at 0.05 mm and 1.10 mm displacements. Shen et al. observe that the standard method can provide accurate and repeatable p_0 as long as the pressure-displacement relation is nearly linear, while a biased estimation of p_0 is obtained in case of high non-linearity, which could only be evidenced if a full pressure-displacement curve is available. The analytical procedure proposed by Shen et al. involves the identification of a yield point and then the back-extrapolation of p_0 at zero displacement from a regression model fitting the post-yield curve. The yield point is identified by use of a graphical method, implemented in Matlab, resembling the Casagrande method for estimating the preconsolidation pressure in the oedometer test. Shen et al. present examples of application of their p_0 interpretation method to available iDMT pressure-displacement curves obtained by various researchers both in the field and in calibration chamber, in different soil types (Figure 10). Comparisons with p_0 estimated by the standard Marchetti (1980) formulation show a variable trend, depending on the non-linearity of the pressure-displacement curve. In most cases the p_0 estimated by Shen et al. from iDMT were larger than the standard DMT p_0, with a percentage increase from 6% in sand to a large 43% in soft varved clay. A decrease (24%) was observed for calibration chamber data on Toyoura sand.

The reliable determination of p_0 is a central issue in DMT interpretation, since p_0 is a necessary input for all three intermediate DMT parameters (I_D, K_D, E_D) which are used to derive common soil parameters. In particular, the p_0-derived stress history parameter K_D has a dominant role. At present, the new interpretation technique for p_0 proposed by Shen et al. appears to need further validation. It should also be considered that existing correlations for determining a variety of soil parameters from DMT are based on the "conventional" determination of p_0.

Future developments of iDMTs should eventually tend toward standardization of probes and procedures, in order to translate cautiously the available experience into new interpretation models. The development of modified iDMTs providing full pressure-displacement curves has the undeniable merit of permitting a deeper insight into the non-linear soil response and is a potential opportunity to improve the interpretation of soil properties. Notably the same Authors (Shen et al. 2016) are involved in an ongoing project using the 3D printing technology for manufacturing an iDMT probe, an innovative frontier application of this technology in the field of geotechnical testing.

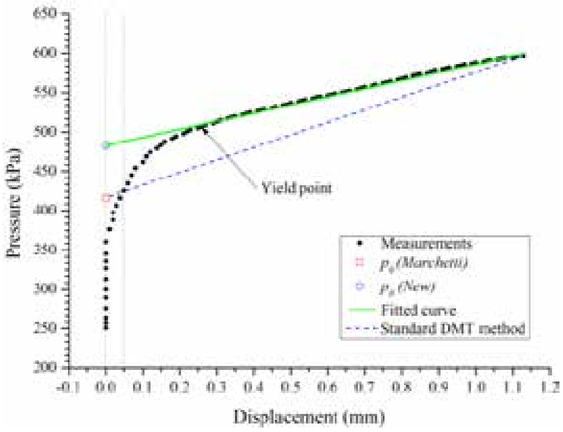

Figure 10. Application of the proposed p_0 interpretation technique to test data from Akbar et al. (2005) (Shen et al.)

3 DISCUSSION AND FURTHER DEVELOPMENTS (FOR PMT AND DMT)

Regarding PMT, all papers presented in this symposium show that pressuremeter has still a great interest for practice in basic application such as classification of ground mass or quality control but also for deriving parameters or to develop and fit behavior law needed for finite element modeling. For this purpose as pointed out by Briaud (2013) in his Ménard lecture, simple techniques can be used to recreate the small strain early part of the curve lost by the decompression-recompression process associated with the preparation of the Ménard pressuremeter borehole. The use of the Ménard pressuremeter test unload-reload modulus can be also a reliable way to derive small strain modulus.

In order to continue the development of the pressuremeter, the National Project ARSCOP initiated in France aims to provide on the one hand, test procedures and tools for a better ground investigation and, on the other hand, values of soil and rock properties and calculation methods ensuring more reliable geotechnical design. Concerning test procedures and tools, the main issues are: the measurement of the pore pressures around the probe in order to perform total and effective stress analysis, the development of cyclic procedures for off-shore applications especially with the implementation of cyclic *p-y* curves, the development of procedures to quantify liquefaction susceptibility, etc.

As to the DMT, many papers presented in this conference confirm its utility as a fast, simple to operate and repeatable in situ test, which provides estimates of a variety of soil parameters for design. Major distinctive contributions that the DMT can offer in a routine site investigation are information on stress history and on "working strain" stiffness. In addition the SDMT provides also measurements of V_S, hence information on small strain stiffness.

Current trends and ongoing developments of DMT research and practice addressed in this conference include:

– increasing application of a multi-parameter/multi-test approach, with combination/comparisons of DMT/SDMT and other in situ tests (mostly CPT);
– increasing interest in methods for deriving in situ G-γ decay curves from SDMT;
– updates in the interpretation of geotechnical parameters, particularly in "non-textbook" soils;
– validation of methods for liquefaction assessment based on DMT/SDMT;
– technological innovation of the testing equipment (instrumented DMT, upgrade of seismic probe).

4 CONCLUSIONS

This report includes a brief summary of the papers received for the ISC'5 Conference for pressuremeter and dilatometer tests. Some of the more interesting topics covered are presented and discussed in order to give an overview of the current practice of pressuremeter and dilatometer tests. These two expansion tests can provide very detailed information about the soil behavior especially in terms of stiffness. They seem to be complementary to penetration tests that can provide strength parameters.

5 REFERENCES

Abchir, Z., Burlon, S., Frank, R., Habert, J. & Legrand, S. (2016) t-z curves for piles from pressuremeter test results. *Géotechnique*, 66(2): 137-148.

Akbar, A., Kibria, S. & Clarke, B.G. (2005) The Newcastle Dilatometer testing in Lahore cohesive soils. *Proc. XVI ICSMGE, Osaka*, 2: 651-654.

Amoroso, S., Monaco, P., Lehane, B.M. & Marchetti, D. (2014) Examination of the Potential of the Seismic Dilatometer (SDMT) to Estimate *In Situ* Stiffness Decay Curves in Various Soil Types. *Soils and Rocks*, 37(3): 177-194.

Baguelin, F., Jézéquel, J.F. & Shields, D.H. (1978) The Pressuremeter and Foundation Engineering. Transtech Publications, pp. 618.

Baker, C.N. (2005) The use of the Menard pressuremeter in innovative foundation design from Chicago to Kuala Lumpur. *2nd Menard Lecture, Proceedings of the 5th Int. Symp. on the Pressuremeter – ISP5, Paris, France*, Presses de l'ENPC.

Boulanger, R.W. & Idriss, I.M. (2016) CPT-Based Liquefaction Triggering Procedure. *J. Geotech. Geoenviron. Eng.*, 142(2): 04015065.

Briaud, J.L. (1992) The Pressuremeter. Taylor and Francis, London, pp. 422.

Briaud, J.L. (2013) The pressuremeter test: expanding its use. *Ménard Lecture, 18th ISSMGE, Paris*.

Burlon, S., Roger, F., Baguelin, F., Habert, J. & Legrand,S. (2014) Model factor for the bearing capacity of piles from pressuremeter test results. A Eurocode 7 approach. *Géotechnique*, 64(7): 513-525.

Combarieu, O. & Canépa, Y. (2001) L'essai cyclique au pressiomètre. *BLPC*, 233: 37-65.

Frank, R. & Zhao, S.R. (1982) Estimation par les paramètres pressiométriques de l'enfoncement sous charge axiale de pieux forés dans des sols fins. *Bull. Liaison Labo P. et Ch.*, 119: 17 - 24.

Marchetti, S. (1980) In Situ Tests by Flat Dilatometer. *J. Geotech. Eng. Div.*, 106(GT3): 299-321.

Marchetti, S. (2015) Some 2015 Updates to the TC16 DMT Report 2001. *Proc. 3rd International Conference on the Flat Dilatometer DMT'15, Rome, Italy*, 43-65.

Marchetti, S. (2016) Incorporating the Stress History Parameter K_D of DMT into the Liquefaction Correlations in Clean Uncemented Sands. *J. Geotech. Geoenviron. Eng.*, 142(2): 04015072.

Marchetti, S. & Crapps, D.K. (1981) Flat Dilatometer Manual. *Internal Report of G.P.E. Inc., Gainesville, Florida*.

Marchetti, S., Monaco, P., Totani, G. & Calabrese, M. (2001) The Flat Dilatometer Test (DMT) in Soil Investigations – A Report by the ISSMGE Committee TC16. Official version approved by TC16 reprinted in *Flat Dilatometer Testing*, *Proc. 2nd Int. Conf. on the Flat Dilatometer, Washington DC*, 2006, Failmezger R.A. & Anderson J.B. (eds), 7-48.

Marchetti, S., Monaco, P., Totani, G. & Marchetti, D. (2008) In Situ Tests by Seismic Dilatometer (SDMT). *From Research to Practice in Geotechnical Engineering*, *Geotech. Spec. Publ. No. 180*, ASCE, 292-311.

Mayne, P.W., Coop, M.R., Springman, S.M., Huang, A.B. & Zornberg, J.G. (2009) Geomaterial behavior and testing. *Proc. XVII ICSMGE, Alexandria*, 4: 2777-2872.

Monaco, P., Amoroso, S., Marchetti, S., Marchetti, D., Totani, G., Cola, S. & Simonini, P. (2014) Overconsolidation and Stiffness of Venice Lagoon Sands and Silts from SDMT and CPTU. *J. Geotech. Geoenviron. Eng.*, 140(1): 215-227.

Monaco, P., Marchetti, S., Totani, G. & Calabrese, M. (2005) Sand liquefiability assessment by Flat Dilatometer Test (DMT). *Proc. XVI ICSMGE, Osaka*, 4: 2693-2697.

Monaco, P., Totani, G. & Calabrese, M. (2006) DMT-predicted vs observed settlements: a review of the available experience. *Proc. 2nd International Conference on the Flat Dilatometer, Washington D.C.*, 244-252.

Robertson, P.K. (2012) The James K. Mitchell Lecture: Interpretation of in-situ tests – some insights. *Proc. 4th Int. Conf. on Geotechnical and Geophysical Site Characterization, Porto de Galinhas*, 1: 3-24.

Shen, H., Haegeman, W. & Peiffer, H. (2016) 3D Printing of an Instrumented DMT: Design, Development, and Initial Testing. *Geotechnical Testing Journal*, 39(3): 1-8.

Tsai, P., Lee, D., Kung, G.T. & Juang, C.H. (2009) Simplified DMT-based methods for evaluating liquefaction resistance of soils. *Engineering Geology*, 103: 13-22.

Theme 1. Developments in Technology & Standards

Geotechnical and Geophysical Site Characterisation 5 – Lehane, Acosta-Martínez & Kelly (Eds)

Integration of invasive and non-invasive techniques in ground characterisation

S. D. Ekanayake
Coffey Corporate Services, Chatswood, NSW, Australia.

C. J. Leo & D. S. Liyanapathirana
School of Computing, Engineering and Mathematics, Western Sydney University, Penrith, NSW, Australia.

P. Harutoonian
Citilink Piling, Quantum Corporate Park, Rydalmere, NSW, Australia.

ABSTRACT: This paper presents a case study, where non-invasive Horizontal-to-Vertical Spectral Ratio (HVSR) of microtremors was used to assess the compaction of a large site located in Western Sydney area in NSW. The integration of measurements of non-invasive microtremors, with invasive CPT and PS-logging techniques were investigated aiming to optimise the characterisation of the compacted ground. The invasive CPT and PS-logging tests were carried out sparsely at the compacted site due to the cost and they would only give spot-wise soil information at the test location. Hence there were many areas at the compacted site, where the quality of the compaction cannot be ascertained based on the invasive techniques. On the other hand, the low cost non-invasive HVSR technique is well suited for areal-wise site characterization in terms of the shear wave velocity, although not with the same reliability, detail and accuracy as the invasive methods. Integrating the two forms of techniques can thus help to exploit the respective strengths of invasive and non-invasive methods and optimize site characterization in terms of resources, cost and reliability. The study presented in this paper measured vertical and horizontal components of microtremors at regularly spaced stations across the site. The measured HVSR curves were then interpreted to obtain the shear wave velocity profile of the ground. Results show that the non-invasive HVSR technique can be successfully integrated with invasive techniques such as CPT and PS-logging to characterise large compacted areas.

1 INTRODUCTION

The invasive site investigation methods such as boreholes, standard penetration tests (SPTs), cone penetration tests (CPTs), flat plate dilatometer tests (DMTs), P-S well logging and density tests are well known techniques for site characterization, which are widely accepted by practicing geotechnical engineers. These techniques generally provide accurate and detailed characterisation of the soil but the results are localised to the points being tested. Hence, in order to provide a reasonable assessment of the site, a sufficient number of invasive tests must be conducted, which can be a costly and time consuming exercise for a large site.

Alternatively, the non-invasive site characterisation techniques incorporating seismic surface waves such as Multichannel Analysis of Surface Waves (MASW), Spectral Analysis of Surface Waves (SASW), Multichannel Simulation with One Receiver (MSOR) and Horizontal-to-Vertical Spectral Ratio (HVSR) have gained popularity among geotechnical practitioners due to the reduced costs and simplicity of the testing methods (Harutoonian et al., 2010; Tokeshi et al., 2013). In these methods, the shear wave velocity (V_s) of the soil profile is determined. V_s is influenced by the density of the soil medium (Kim et al., 2001); it can be appropriately used to estimate the properties of the soil layers underneath. Theoretically, V_s is defined as

$$V_S = \sqrt{\frac{G}{\rho_b}} \tag{1}$$

where G is the shear modulus and ρ_b is the bulk density of the soil. This shows that V_s is a geotechnical property and it supports the concept of using V_s to investigate the stiffness of soil.

These non-invasive techniques can survey deep soil profiles over large areas more expeditiously when compared to traditional invasive site investigation techniques. The HVSR technique uses ambient vibrations in soil to determine the Vs profile while the other active techniques require an artificial excitation to infer the *Vs* profile of the soil domain. Empirical experimental evidence and theoretical modelling results reveal that the shape and peaks of the HVSR curves are mainly governed by the geology of the site (Fah et al. 2003, Nakamura 1989).

Understandably, the shortcoming of these techniques is that the results may not be as reliable when compared to invasive site investigation techniques as they rely on inversion of the theoretical model to infer the V_s profile. Hence if the more reliable invasive techniques can be used to calibrate and validate the inversion, then the integration of the invasive and non-invasive techniques will provide an efficient and cost effective means of assessing large sites. However, caution is necessary because invasive techniques such as CPT are large strain measurements while the V_s is obtained from small strain dynamic tests. Moreover the CPT measures the cone resistance and not the *Vs* of the ground, though some investigators have established empirical relationships between the two (e.g. Robertson, 2009). For this reason an attempt was made to use a second invasive technique, the PS logging as an additional tool to directly validate the HVSR inversion.

In this paper, a case study is presented where HVSR of microtremors was used to obtain the V_s profile of a large compacted site in order to assess the compaction. A methodology was developed to calibrate and verify the V_s profile against the data obtained from CPTs. The results are later also compared with the V_s profile obtained from P-S logging technique. This will improve the reliability of incorporating HVSR technique to conduct site characterisation, without significantly increasing the operational costs as well as the time.

2 SITE CONDITIONS AND TEST PROCEDURES

The test site is located in a sand and gravel quarry on the Hawkesbury-Nepean River flood plain west of Sydney at the edge of the Blue Mountains region. The site consists of Bringelly shale of the Wianamatta group. The subject area of this study, Dynamic Compaction Prototype Trial Area 7 (DCPT-7), has been dynamically compacted with a 20 tonne weight free falling about 20 m, providing approximately 400 tonne-m energy with each drop. Each dynamic compaction station, 4.2 m apart from each other, was compacted using 32 drops. The craters created by the compaction were then backfilled and re-levelled with ground surface. The fill consists of a mixture of clayey, silty and sandy soil, which extends over an area of 9,500 m^2. The bedrock can be found approximately 12 – 13 m below the surface and the ground water level is approximately 10 m below the surface. The stratification of the ground was examined by the following methods: HVSR technique, Cone Penetration Test (CPT) and P-S logging.

2.1 *Determining V_s using HVSR technique*

The HVSR technique relies on the measurement of the horizontal and vertical spectra of the ambient vibrations (the microtremors and microseisms) which are ubiquitous in the Earth surface. Microseisms and microtremors, strictly speaking, refer to ambient vibrations attributed to the natural atmospheric phenomena (e.g. ocean current, wind, strong meteorological conditions) and cultural sources (e.g. anthropic activities such as traffic, construction and plant operations) respectively. However, both have been loosely lumped as ‘microtremor’ to the extent that the distinction between the two terms ‘microtremors’ and ‘microseisms’ have often become blurred in the literature. The components of ambient vibrations linked to natural atmospheric sources generally occur in the low frequency range (less than 1 Hz) while the cultural noises (traffic, machinery etc) will generally include components of higher frequencies (greater than 1 Hz). HVSR technique has been widely used in the past to identify the fundamental resonance frequency of a site at the observation point (e.g. Nakamura, 2008). The horizontal to vertical ratio (H/V) of the Fourier amplitude spectra of the microtremors is defined as:

$$HVSR(\omega) = \frac{|F_H(\omega)|}{|F_V(\omega)|} \tag{2}$$

where $|F_H(\omega)|$ and $|F_V(\omega)|$ are horizontal and vertical Fourier amplitude spectra, respectively. The HVSR curve is thought to be mainly constituted of fundamental and higher modes of surface waves (both Rayleigh and Love waves, and the proportion varies with frequency and location of sensor). HVSR curves are derived in this study by analysing data recorded using a single station with three sensor components (North-South, East-West and Vertical). Since the time and effort required in setting up a single station for HVSR technique is much less than that for setting up other types of surface wave techniques, the HVSR technique is much preferred for its ease of use in site investigations. Figure 1 shows the velocimeter (Tromino^{TM}) used by the authors to record the surface waves generated by microtremors.

HVSR was measured using a regularly spaced grid of observation points, as described in Figure 2. The squares represent the HVSR observation points spread across an area of 95 x 100 m while the circles represent the locations of invasive tests (CPT and P-S logging). A commercially available software Grilla, was used to transfer the recorded data from the velocimeter to a computer.

Adequate statistical sampling for the frequency range used in this investigation: 1-50 Hz; was achieved by sampling the ground vibrations at a rate of 512 Hz. Vibrations were sampled for 16 minutes at each station. An in-house program developed using MATLAB language was utilised to analyse the recorded data and optimize the misfit between the measured and theoretical HVSR curves.

Figure 1. Tromino™ velocimeter used for HVSR technique.

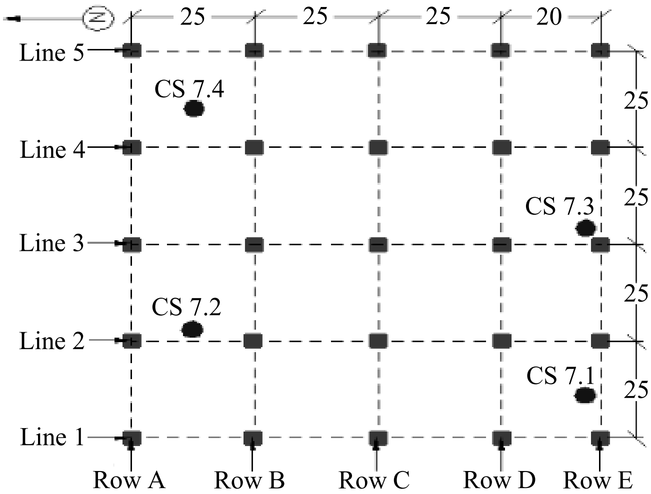

Figure 2. Observation stations of the compacted area (dimensions are in metres).

The H/V curves were calculated by averaging the H/V data obtained by dividing the recorded signal into non-overlapping time windows. The geometric average was used to combine the North-South (H_{NS}) and East-West (H_{EW}) components in the single horizontal spectrum. It was then divided by the vertical component (V) to obtain the measured HVSR curves. Equation 3 shows the calculation of measured HVSR curves.

$$HVSR_m = \frac{\sqrt{H_{NS} \times H_{EW}}}{V} \tag{3}$$

Once the measured HVSR curve is obtained for a given location, a theoretical HVSR curve is derived by forward modelling (Lunedei & Albarello 2009) of the measured data. This incorporates a layered soil model (Figure 3) with assumed soil parameters: shear wave velocity (V_s), primary wave velocity (V_p), soil layer thickness (y), bulk density (ρ) and quality factors (Q_s, Q_p). The inversion is a process to minimise the misfit between the theoretical and the measured HVSR curves. The errors between the measured and theoretical HVSR curves are minimised with each iteration using optimisation techniques based on the Covariance Matrix Adaptation - Evolutionary Strategy (CMA-ES) (Young et al. 2013). The final values of the soil model used in the forward modelling are considered as the estimated soil properties. Care should be taken not to result in unrealistic soil properties when the errors are being minimized by modifying the initial soil properties. Figure 4 presents the process of forward modelling in a flow chart.

Layer 1	$\boldsymbol{V_{s1}}, V_{p1}, \boldsymbol{y_1}, \rho_1, Q_{s1}, Q_{p1}$
Layer 2	$\boldsymbol{V_{s2}}, V_{p2}, \boldsymbol{y_2}, \rho_2, Q_{s2}, Q_{p2}$
Layer 3	$\boldsymbol{V_{s3}}, V_{p3}, \boldsymbol{y_3}, \rho_3, Q_{s3}, Q_{p3}$
Layer 4	$\boldsymbol{V_{s4}}, V_{p4}, \boldsymbol{y_4}, \rho_4, Q_{s4}, Q_{p4}$
⋮	⋮
Layer *n*	$\boldsymbol{V_{sn}}, V_{pn}, \boldsymbol{y_\infty}, \rho_n, Q_{sn}, Q_{pn}$

Figure 3. Layered soil model for forward modelling.

2.2 *Determining the soil layering using CPT*

CPT involves continuously pushing a cone tip to the soil medium at a constant rate, reflecting soil properties at large strains. Interconnected cylindrical steel rods are used to push the cone tip deep in to soil, enabling investigation of soil layers at greater depths. As the cone is pushed to the ground, the resistance at the tip and the surface friction along the outer sleeve of the rod are measured.

CPT tests were conducted at 4 locations at the DCPT-7 site (denoted by “CS” symbol in Figure 2). The CPT data were used to assist in providing an initial guess of the material layering information including the stiffness contrast between layers. One set of CPT data (CS 7.2) was also used to “calibrate” the soil model during the forward modelling procedure in HVSR technique. The “calibration” methodology is a process, where the peaks in the HVSR curve were studied from right to left, from high to low frequency (i.e. from shallow to deep soil). The amplitude and frequency of the predominant and secondary peaks of the HVSR curves were thus identified. These features represent possible impedance contrasts identifying significant material changes picked up by the ambient vibration recordings, as well as giving an indication of the number and the likely depth of the soil layering. The thicknesses of the soil layers revealed by the CPT were used to

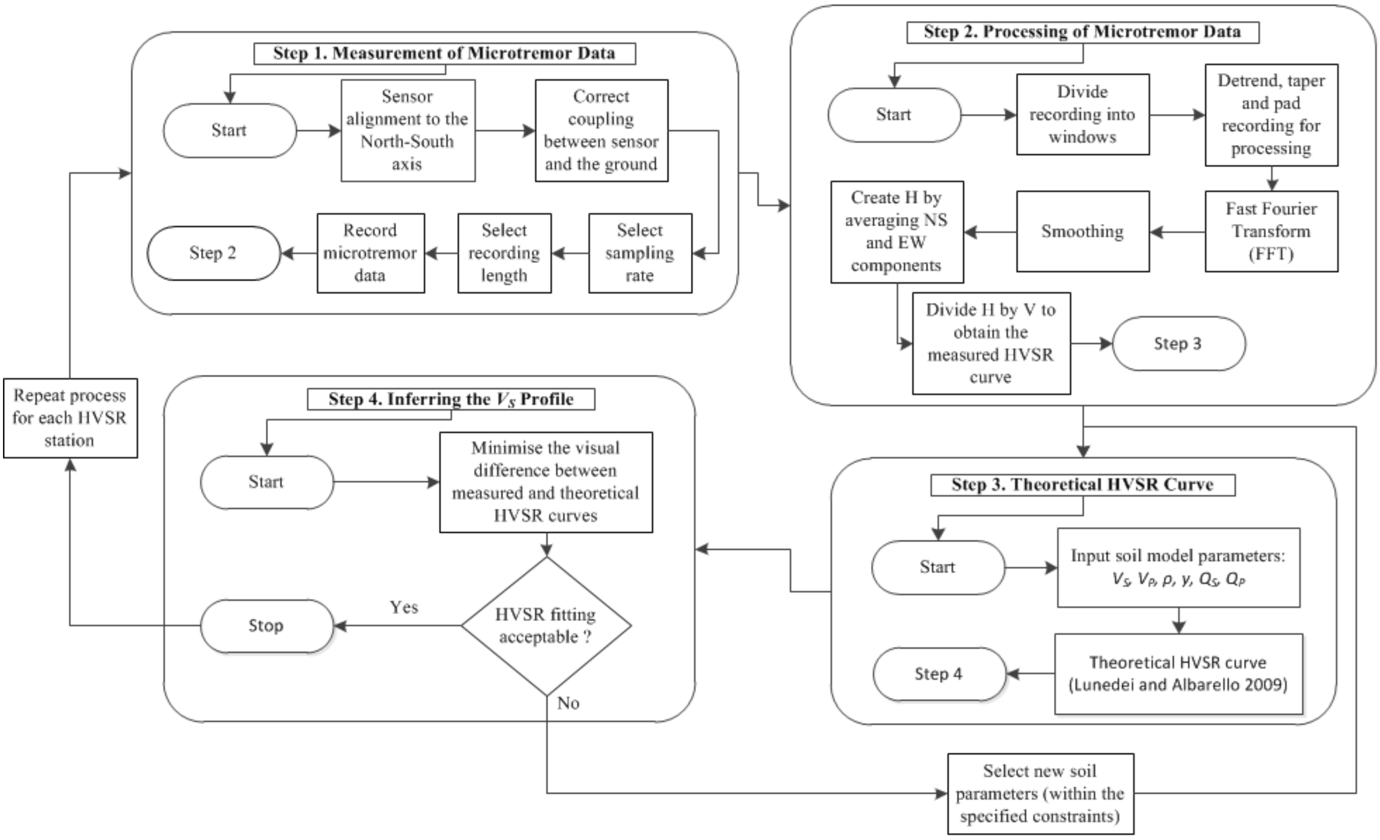

Figure 4. Flow chart for the forward modelling of HVSR technique (Harutoonian et al. 2012)

provide a reliable guide to constrain the layering thickness of the soil model applied in the forward modelling. The soil type, the CPT data and depth of the water table moreover provide feasible constraining ranges for the V_s and V_p values of the soil layers. These constraining data were used to formulate an "initial guess" of the soil model while taking cognizance of the identified features from the HVSR curve. After this, iteration of the layered soil properties of the soil model was undertaken with due regard for the constraints and the identified features of the HVSR curve to seek an improved fit between measured and theoretical curves at each successive iteration, until the best possible fit was achieved. It is noted that during this process, some of the secondary peaks could be fitted (i.e. the theoretical and measured HVSR curves are in agreement at those points in the curves). These secondary peaks are kept while the ones that did not fit were ruled out as reflecting the impedance contrasts within the surface layers. After a satisfactory calibration had been achieved, the "calibrated" soil model was used as an initial guess to derive the Vs profiles for the rest of the site. Independent validations of the HVSR inversions were also made against CPT data at the remaining locations where CPT data are available (CS 7.1, 7.3 and 7.4). This is done by confirming that the impedance contrasts of the inferred Vs profiles produced by the HVSR techniques were consistent with those obtained from the CPT data. Figure 5 shows the validated profile for HVSR 'V_s' against CPT data for borehole CS 7.2).

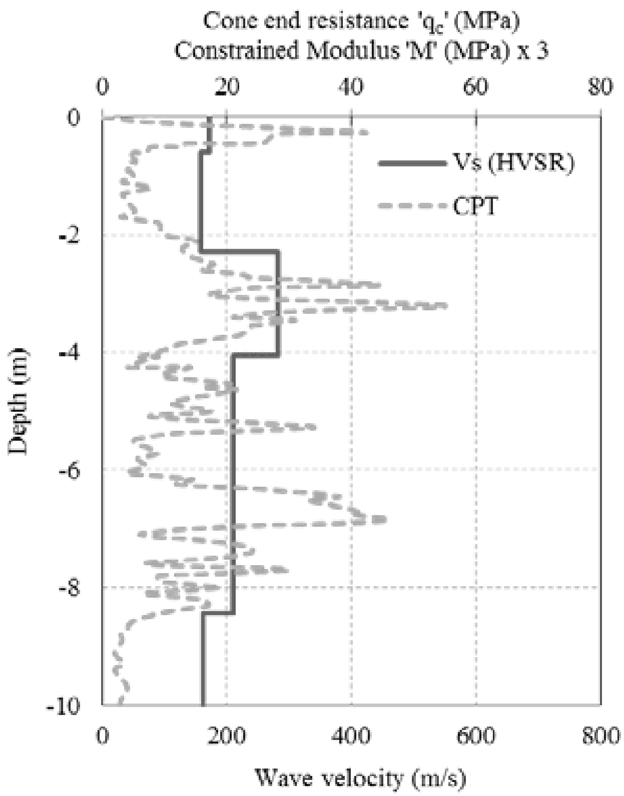

Figure 5. Validated HVSR 'V_s' profile for borehole CS 7.2.

2.3 *Determining V_s using P-S logging*

One of the limitations in using the CPT data for calibration and validation of the HVSR results is that it can only confirm the relative impedance contrasts of the V_s profiles but not the absolute values of the V_s. The P-S logging on the other hand is considered to be the gold standard for measuring the in-situ V_s of the ground. However, conducting a P-S logging test is an invasive, expensive and time consuming task. Nevertheless, for a large site, integration of an invasive technique such as P-S logging with a non-invasive technique such as HVSR technique would facilitate determining the stratification with higher accuracy when compared to the use of surface wave techniques alone. Moreover, with integration a lesser number of invasive tests is required, thus it is less expensive to investigate large sites using this method.

The borehole CS7.1 was used to conduct a P-S logging test to determine the stratification of the site. The P-S logging probe, with geophone receivers inside, is suspended inside the borehole by pneumatic clamping. A vibration source is stationed at the surface and generates excitations as necessary. In this test, the time it takes for a wave to travel from the source to the receiver suspended in the borehole is used to determine the wave velocity of the soil medium. The P-S logging equipment used in this test was a single receiver system with two horizontal geophones and one vertical geophone placed inside. The horizontal geophones record the arrival of the shear wave while the vertical geophone records the arrival of the primary wave. Figure 6 shows the Geotomographie™ borehole equipment used for the P-S logging during this study.

Figure 6. Geotomographie™ borehole geophone and other equipment used for P-S logging in DCPT-7.

The probe is 50 mm in diameter and the borehole used for P-S logging was 90 mm in diameter. The drum, which holds the cable of the probe, has a control unit for the operator to supply air to clamp the probe pneumatically and also to record the readings by connecting a personal computer to the drum.

The source was located 2.5 m away from the borehole. The travel times of the ground waves from the source to the receiver were recorded at each 1 m depth down to 10 m. Commercially available software SoilSpy Rosina™ was used to record the travel times for shear (V_s) and primary (V_p) waves. The system has one channel recording movements at the impact source and another three channels recording the readings from three geophones in the borehole probe. Once the system senses the impact at the source, rest of the channels connected to the probe start recording data from the geophones. This allows the operator to measure the travel times correctly as the ground waves arrive at the probe. Recordings from the horizontal geophones are considered to calculate the arrival of shear waves. The velocity was calculated considering soil layers with a 1 m depth.

3 RESULTS AND DATA INTEPRETATION

The results obtained from each technique for the location CS 7.1 are plotted in Figure 7. The estimated V_s values in this study are normalised to avoid the influence of the confining pressure using the equation

$$V_{sn} = V_{sm}\left(\frac{P_a}{\sigma'_v}\right)^{0.25} \tag{4}$$

where V_{sn} is the normalised shear wave velocity, V_{sm} is the measured shear wave velocity, P_a is the atmospheric pressure and σ'_v is the vertical effective stress (Robertson et al 1992). The unit weight of soil obtained from borehole logs was used to determine the effective stress.

The mechanical data obtained from CPTs have also been normalised to eliminate the influence of confining pressure as

$$q_{cn} = q_{cm}\left(\frac{P_a}{\sigma'_v}\right)^{0.5} \tag{5}$$

where q_{cn} is the normalised end resistance of the cone and q_{cm} is the measured end resistance of the cone (Robertson et al 1992).

The V_s profile derived from inversion of the HVSR curves, as described in Section 2.2, shows a good agreement with the CPT data in Figure 7. Hence, the methodology described may also be applied with some confidence to the rest of the HVSR measurements which are not adjacent to invasive test locations. However, as mentioned before, the CPT data can only be used to confirm the relative stiffness contrast between layers but not the absolute values of the V_s.

An attempt was therefore made here to compare the V_s profile from P-S logging with that of the HVSR technique. According to Figure 5, a reasonable match between the two profiles can be surmised. However, a slight discrepancy in the two profiles closer to the surface of the soil medium is apparent. This can be attributed to the smaller travel times between the source and the receiver at those levels.

Since the travel time is quite small closer to the surface, even a slight error in picking the travel time will result in significant changes to the V_s profile. Perhaps this can be eliminated by placing the wave source sufficiently away from the borehole. Further studies will be conducted to eliminate these issues and to integrate P-S logging with HVSR technique, providing reliable and cost effective technique of investigating large sites.

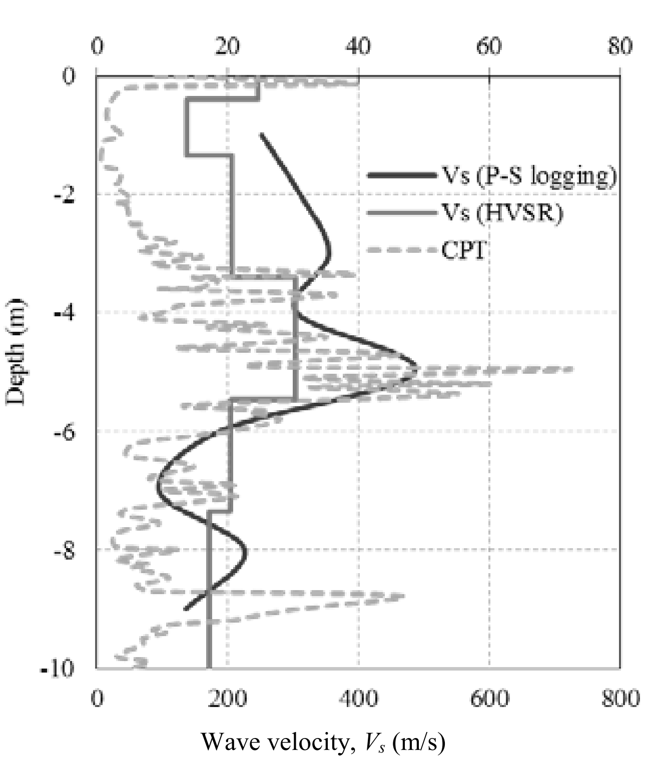

Figure 7. Normalised HVSR V_s versus normalised CPT q_c versus normalised P-S logging V_s.

4 CONCLUSION

A case study on integration of invasive and non-invasive techniques for geotechnical site investigations is presented. Non-invasive HVSR technique is integrated with invasive CPT to determine the shear wave velocity profile of the site. The V_s profiles obtained by inversion of the HVSR curves are found to be in agreement with the CPT data extracted at the same location, in terms of the relative impedance contrasts of the soil layers. Hence, it can be concluded that the HVSR technique can successfully be used for site investigation by integrating with an invasive testing procedure such as CPT. This provides a significantly better coverage in determining the stratification of soil, without restricting the judgement to few control stations of mechanical tests.

These data are then compared with the V_s profile obtained from another invasive technique: P-S logging. The two V_s profiles are a reasonable match, however, discrepancies in picking the travel times closer to the surface challenges the validity of the system. However, once improved, P-S logging technique will offer a better calibration and validation of the measured HVSR data, providing enhanced insight to the stratification of the soil medium. This will be the direction of this study in future.

5 ACKNOWLEDGEMENTS

The authors would like to acknowledge the Western Sydney University, Australian Research Council, Penrith Lakes Development Corporation and Coffey Geotechnics for facilitating this research.

6 REFERENCES

Harutoonian, P., Chapman, B., Yong, C. N., Leo, C. J. and Zou, J. J. (2010) “Near surface soil characterisation by passive ambient noise HVSR method.” GeoShanghai, GSP 201, eds M. Huang, X. Yu & Y. Huang, ASCE, Shanghai, China. 288-293.

Harutoonian, P., Leo, C. J., Liyanapathirana, S. and Wong, H. (2012) “Site characterisation by the HVSR technique.” Australian Geomechanics, 47(3):101-110.

Fah D, Kind F, Giardini D. (2003) “Inversion of local S-wave velocity structures from average H/V ratios, and their use for the estimation of site-effects.” Journal of Seismology, 7: 449–67.

Kim, D. S., Shin, M. K., and Park, H. C. (2001) “Evaluation of density in layer compaction using SASW method.” Soil Dynamics and Earthquake Engineering, 21(1): 39-46.

Lunedei, E. & Albarello, D. (2009) “On the seismic noise wavefield in a weakly dissipative layered earth.” Geophysical Journal International, 177(3): 1001 - 1014.

Nakamura, Y (1989). A method for dynamic characteristics estimation of subsurface using microtremor on the ground surface. Quarterly Report of Railway Technical Research Institute (RTRI), 30 (1989): 25–33.

Nakamura, Y. (2008). 'On the H/V spectrum', paper presented to the The 14th World Conference on Earthquake Engineering, Beijing, China. Paper ID: 07-0033, 12 - 17 October 2008.

Robertson, P.K., Woeller, D.J. & Finn, W.D.L. (1992) “Seismic cone penetration test for evaluating liquefaction potential under cyclic loading.” Canadian Geotechnical Journal, 29(4): 686-695.

Robertson, P.K. (2009), Interpretation of cone penetration tests – a unified approach. Canadian Geotechnical Journal, 46: 1337-1355.

Tokeshi, K., Harutoonian, P., Leo, C. J. and Liyanapathirana, . (2013) “Use of surface waves for geotechnical engineering applications in Western Sydney.” Advances in Geosciences, 35: 37-44.

Young, C., Le Brese, C., Zou, J. and Leo, C.J. (2013) A Robust Search Paradigm with Enhanced Vine Creeping Optimisation, Engineering Optimisation. 45(2),pp225-244. ISSN: 0305-215X (Print), 1029-0273.

Geotechnical and Geophysical Site Characterisation 5 – Lehane, Acosta-Martínez & Kelly (Eds)
 ISBN 978-0-9946261-1-0

In-situ determination of soil deformation modulus and the wave velocity parameters using the Panda 3®

E. Escobar, M. A. Benz Navarrete & R. Gourvès
Sol-Solution Géotechnique Réseaux, Riom, France

P. Breul & B. Chevalier
Institut Pascal, Université Blaise Pascal, Clermont Ferrand, France

ABSTRACT: This article, after a brief reminder of the principle and the interpretation of Panda 3®, present the results of a test campaign on an experimental field. The aim is to achieve in-situ comparative tests to study the relationship between the results obtained with this new measurement technique (elastic modulus, wave velocity, dynamic cone resistance) and those proposed by other classical geotechnical techniques (CPTu, PMT, MASW ...). The results show the potential and interest of this new investigation technique for the characterization of surface soil (depth less than 7 m). Likewise, we find that the response of the load-penetration curve may vary depending on the conditions of the inspected ground (nature, compactness ...). The test allows a more refined geomechanical characterization of the stratigraphy of the soil.

1 INTRODUCTION

Predicting the pre-failure behavior of soils plays an important role in geotechnical studies. This requires a reliable estimation of the deformation characteristics of geomaterials. The determination of the elastic parameters, including the deformation modulus and the wave velocity is extremely important. Currently the in-situ techniques allowing to obtain these parameters are the pressuremeter test (PMT), the flat dilatometer test (DMT), the surface wave method (SWM)… However, these methods only provide discontinuous soil profile. This considered, it seems important to develop ad hoc measurement techniques allowing a continuous study of these parameters according to depth. Furthermore, recent research work on the Panda 3 investigation technique allowed obtaining, for each impact, a load-penetration curve of the inspected soil. The interpretation of this curve allows estimation of the deformation parameters and the wave velocity in the soil.

This article, after a brief reminder of the principle and the interpretation method of Panda 3, present the results of a test campaign on an experimental field. The aim is to achieve in-situ comparative tests to study the relationship between the results obtained with this new measurement technique (elastic modulus, wave velocity, dynamic cone resistance) and those proposed by other classical geotechnical techniques (CPTu, PMT, MASW ...).

2 THE INSTRUMENTED DYNAMIC PENETROMETER PANDA 3®

The Panda 3 penetrometer has been designed based on the penetrometer Panda® (Gourvès, 1991). The principle of the test is simple (Fig. 1): during driving, we measure on the rods, near the anvil, the variation of the deformation $\varepsilon(x,t)$ and/or acceleration $a(x,t)$ caused by the compressional wave created by the impact. For each impact, after decoupling descending ε_d and ascending wave ε_r it is possible to calculate the penetration $s_p(t)$ and the resulting force $F_p(t)$ at the tip during penetration of the cone. By making some simplifying assumptions (Escobar, 2015), it is also possible to plot the dynamic load-penetration curve σ_p-s_p for each hammer impact (Fig. 1c).

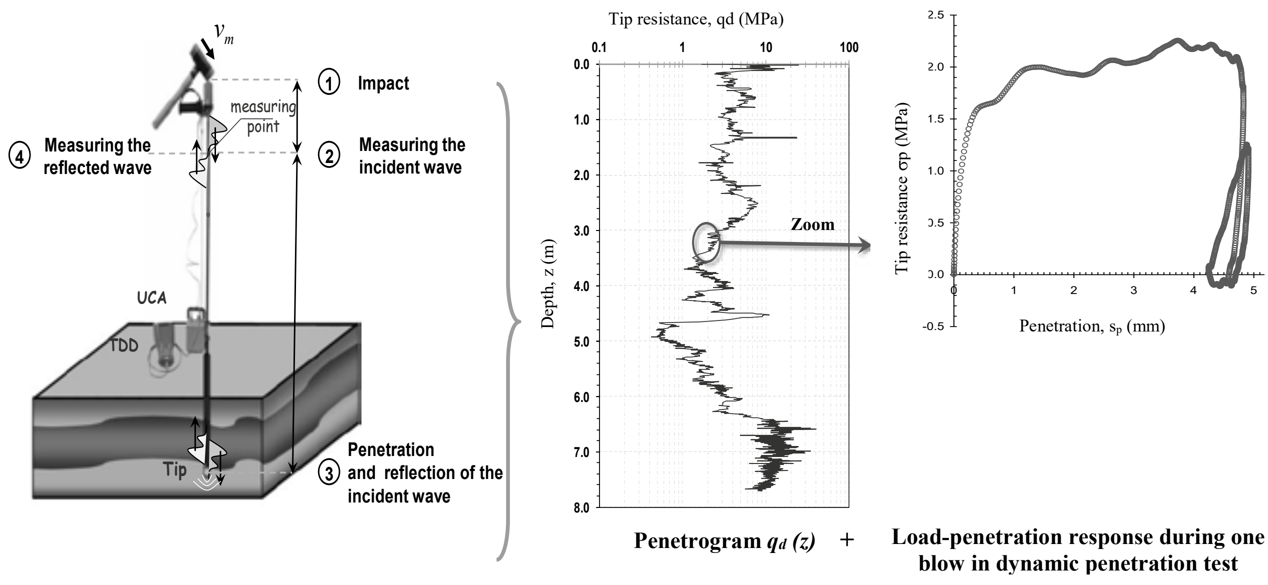

Figure 1. Principle of the Panda 3®: (a) wave propagation, (b) the penetrogram of tip resistance qd and (c) load-penetration curve at the tip σ_p-s_p.

An analytical methodology permits to exploit this curve to determine different soil parameters such as: penetration resistance q_d and q_c, the dynamic stiffness E_{kd}^{P3}, the deformation modulus E_d^{P3} and the wave velocity in the soil V_p^{P3} (Benz et al, 2013). A summary of the operating parameters from the time and frequency analysis of the signals recorded during driving is presented in the following chapter.

2.1 *Strength parameters*

An analytical methodology for the interpretation of the σ_p-s_p curve was proposed by Smith (1960). Assuming that the tip resistance $q_d(t)$ is the resultant of:

static component R_s, which obeys an elastic-perfectly plastic law, and

dynamic component $R_d(t)$,which is proportional to the velocity of the penetration $v_p(t)$;

We determine the value of R_s supposing that when $v_p(t)$ equals zero the dynamic component $R_d(t)$ cancels itself out and R_s is then equal to $q_d(t)$. The values of $R_d(t)$ and the dampening ratio of Smith J_s are determined in the penetration interval [s_e; s_{max}], with s_e and s_{max} being the elastic and maximum penetration and writing that $R_d(t) = q_d(t)-R_s$ and $J_s=R_d(t)/(R_s v_p(t))$ (Fig. 2.a).

2.2 *Deformation parameters*

Once the maximum penetration s_{max} is reached, we assumed that soil and the penetrometer vibrate together in a pseudo-elastic regime. In this part of the σ_p-s_p, curve, two modules are defined as: an unloading module E_d^{P3} (line AB) and a reloading module E_r^{P3} (line BC) (Fig.2.a). Supposing that the cone is a small plate embedded in a semi-infinite elastic solid we can calculate the value of $E_{d,r}^{P3}$ by applying the equation of Boussinesq (1) proposed by Arbaoui, (2006).

$$E_{d'r}^{p3} = (1-\mu^2)\frac{\Delta q_d}{\Delta s_p}\frac{\pi d_p}{4}\frac{1}{k_M} \tag{1}$$

With μ the Poisson's ratio supposed equal to 0,33, d_p the diameter of the cone and k_M the coefficient of embedding of Mindlin (Arbaoui, 2006).

2.3 *Dynamic stiffness*

Another method to exploit the signals recorded during driving of Panda 3 penetrometer is one proposed by Paquet (1968). In fact, the shock wave caused by the impact of the hammer and vibration of system penetrometer/soil can be described by determining the impedance. This is obtained by conventional methods of the Fourier transform to obtain the transfer functions, and thus drawing the mobility curve (Fig.2.b). Moreover, according to Caballero (2007) it is possible to estimate the dynamic stiffness K_d^{P3} for the frequency range between 0 and 100 Hz. Similarly, assuming the cone penetrometer is a small plate in a semi-infinite elastic medium, it is possible; through the expression proposed by Boussinesq to calculate the deformation module E_{kd}^{P3} at low-frequency according to the expressions (2) and (3).

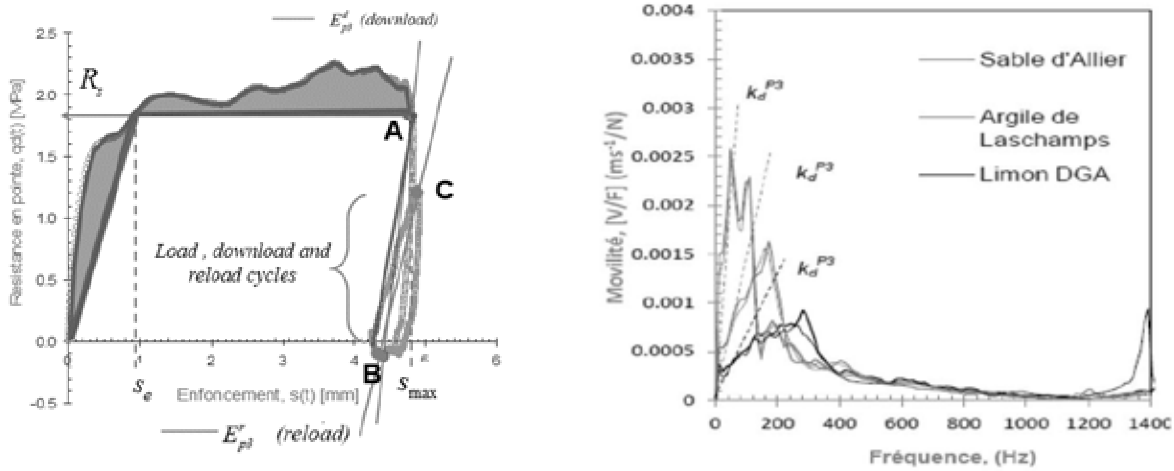

Figure 2. Interpretation of the signals recorded during the driving from the time and frequency analysis: (a) analytical model of interaction cone/soil [4] and (b) mobility curves obtained in the laboratory for different materials (Allier sand, Laschamps clay and DGA Silt)

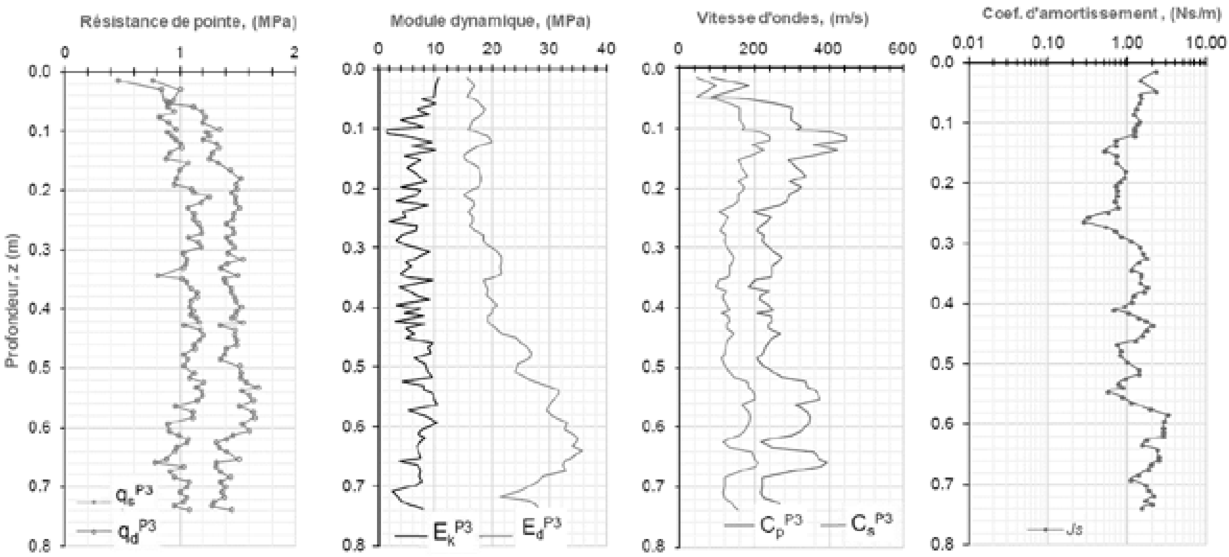

Figure 3. Panda 3® results obtained in a calibration chamber for Laschamps clay. Penetrogram of: (a) tip resistance q_d et q_c, (b) dynamic stiffness E_{kd}^{P3} and deformation modulus E_d^{P3}, (c) the shear and compressional waves celerity V_s^{P3} et V_p^{P3} and (d) damping coefficient J_s.

$$K_d^{P3} = 2\pi \frac{\Delta\omega}{\Delta M} \qquad (2)$$

$$E_{Kd}^{P3} = \frac{\left(1-\mu^2\right)}{\phi_p} K_d^{P3} \qquad (3)$$

With K_d^{P3} the dynamic stiffness determined from the transfer curves, $\Delta\omega$ the frequency variation and ΔM variation of mobility in the frequency range between 0 and 100 Hz, μ Poisson's ratio (0,33) and the ϕ_p the diameter of the cone.

2.4 *Waves velocity*

The compressional wave velocity V_p^{P3} in the soil is calculated through polar shock suggested by Aussedat (1970). For each impact we measure the peaks of the descending and ascending waves in a time t_o+2L_t/c_t. The value of the shear wave celerity c_s^{P3} is calculated according to the expression (4) assuming that the value of μ equals 0,45 at dynamic compression conditions.

$$V_s^{P3} = \sqrt{\frac{1-2\mu}{2(1-\mu)}} V_p^{P3} \qquad (4)$$

In the practice, at the end of one penetration test, we obtained the penetrograms curves of the dynamic q_d and pseudo-static q_s resistance, dynamic stiffness E_{kd}^{P3}, deformation modulus E_d^{P3}, the shear and compressional waves velocity (V_p^{P3} and V_s^{P3}) and a damping coefficient J_s (Fig. 3). Numerous tests were conducted in a calibration chamber to validate the feasibility of this technique (Benz et al. 2013), as well as a numerical model of dynamic cone penetration test in granular media (Escobar et al. 2013).

To show the interest of this new auscultation technique, one experimental champagne is submitted to tests. Those tests are briefly described in the following chapter.

3 EXERIMENTAL CAMPAIGN

The tests were realized on an experimental site in the commune of Gerzat (Puy-de-Dôme, France). The soil has mainly clay-marl formation. This site was subjected to the geotechnical survey by different techniques (CPTu, MASW, Pressiometer PMT, Panda 2…).

The interest of performing tests with Panda 3 on these sites, in addition to validate the obtained results, is to study the repeatability and measurement sensitivity subjected to variations related to the characteristics of the soil mentioned above. Indeed, the soil in the commune of Gerzat as an embankment has a rather great heterogeneity regarding the nature and condition of these soils.

3.1 *Panda 3 results*

In these experiments we studied the feasibility of field tests which allow validating the repeatability and quality of measurements with the Panda 3. Among the results obtained from analysing the signals and load-penetration curves which are previously presented, the characterization of the failure behaviour and stiffness using the dynamic resistance measures of the tip q_d, and dynamic stiffness E_{Kd}^{P3}, as well as the shear waves velocity V_s^{P3} are of particular interest. The experiments shown that the value of the shaft friction on the cone rod mobilized during driving was negligible. This was estimated qualitatively rotating the rod every meter.

Figure 4 presents the results obtained with Panda 3 plotted in function of the depth of tip resistance, the deformation modulus and shear wave velocity. Similarly, a graphical representation of various soil layers is shown on the right of Figure 4. Two surveys were conducted using Panda 3 where reached depth was approximately 6.50 m. It is possible to notice the sensitivity of the measurements obtained according to encountered ground.

Figure 5 presents some examples of load-penetration curves σ_p-s_p obtained for different impacts and different layers of auscultated soil. In order to facilitate understanding and comparison of these curves, values of tip resistance σ_p and the penetration s_p were normalized by their maximum values σ_{max} and s_{max}. It is observed that the shape of σ_p-s_p curve is very repetitive for the same material and is different for the other soil layers. Similarly, the shape of these curves varies with changes in soil conditions (density, moisture...), thereby identifying stress-strain behavior of different soil.

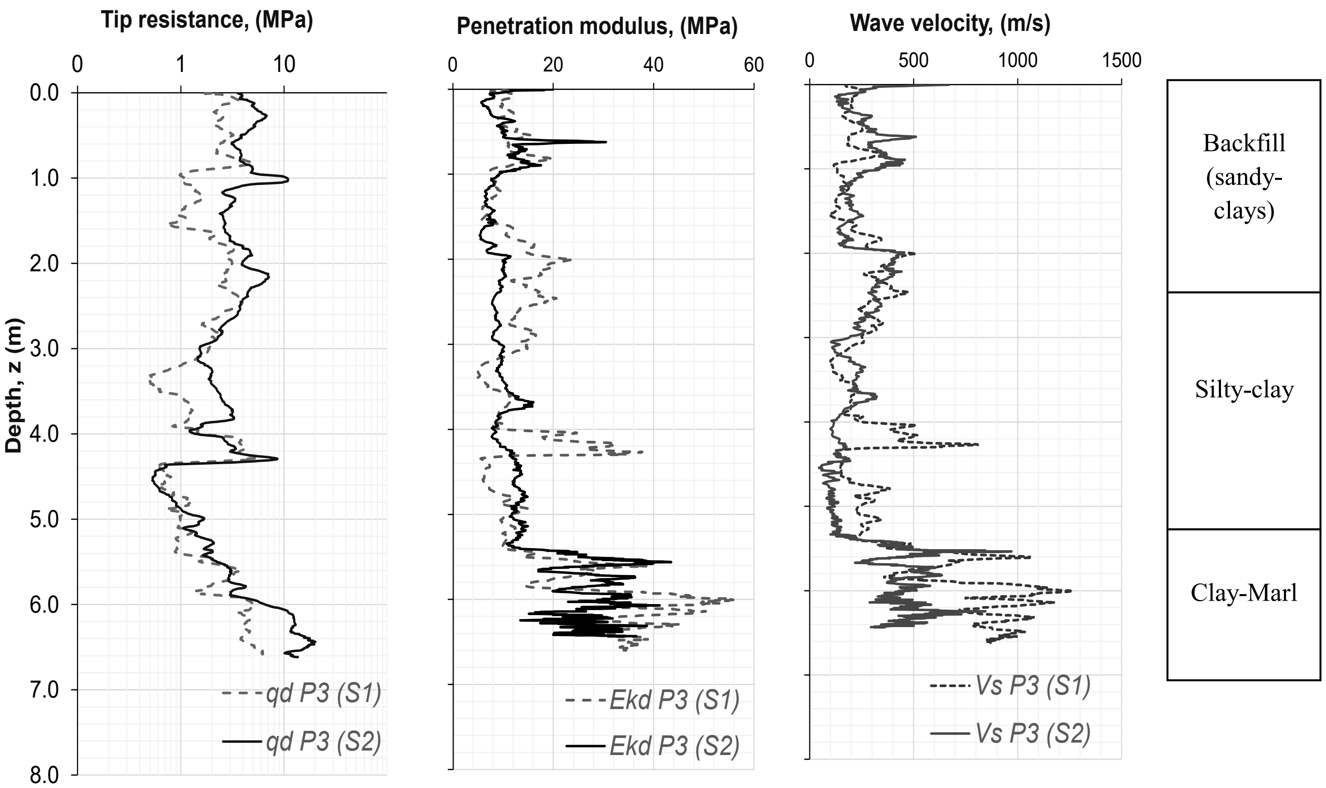

Figure 4. Repeatability of measurements: (a) dynamic tip resistance q_d^{P3}, (b) penetrometer modulus Ek_d^{P3}, (c) shear waves velocity V_s^{P3} – (Gerzat site).

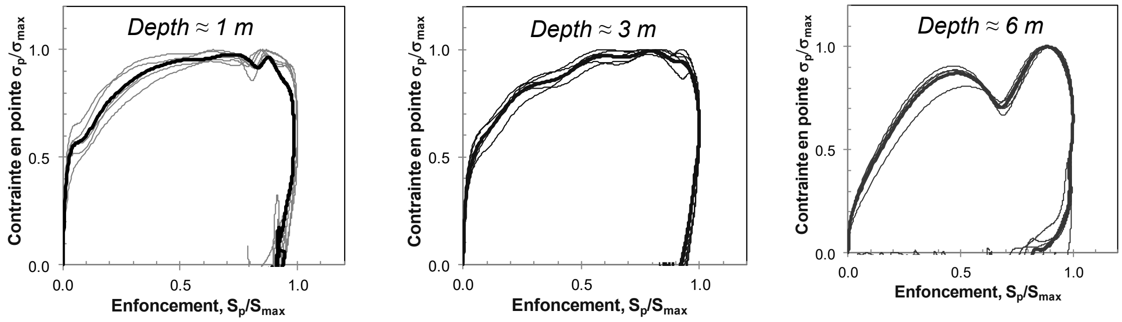

Figure 5. Standardized load penetration curves obtained in Gerzat for different soil layers: (a) Sandy clay, (b) Silty clay and (c) Marl clay (compact). Panda 3 survey.

3.2 *Comparison results*

In the following is provided the comparison of results obtained with the Panda 3 (strength, modulus, wave velocity) with those obtained by using other techniques (geophysical MASW, penetrometer CPTu, Panda 2 and Pressuremeter PMT).

Figure 6.a presents the superposition of penetrograms *qd* (Panda 2), *qd* (Panda 3) and *qc* (CPTu). Despite the high variability in the first auscultated meter on this experimental site it is possible to observe a very good reproducibility between the obtained signals.

Figure 6.b shows the superposition of two tests conducted with Panda 3 and one pressuremeter test. It is possible to notice that the values of the pressuremeter modulus are naturally smoother than those obtained with the penetrometer Panda 3. Indeed, Pressuremeter tests were carried out by steps of 1m and the results obtained for each measurement level, incorporate a soil volume much greater. However, measurements with Panda 3, are carried out ad hoc, with average penetration of 10mm, allowing to highlight the variability of soil and to identify either the singular points or passage of different layers.

Despite the effects of discreet character of the measurement that Panda 3 may have on the comparison of data, it is possible to notice the good match between these values.

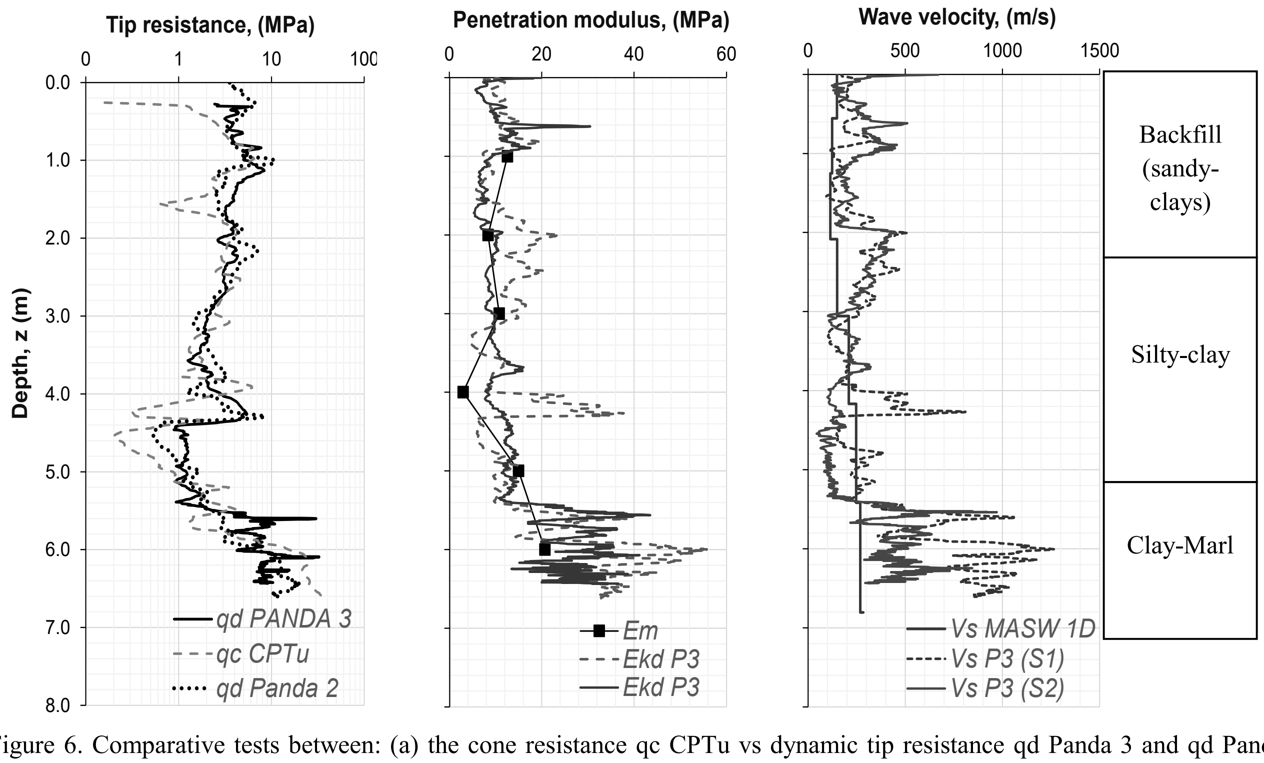

Figure 6. Comparative tests between: (a) the cone resistance qc CPTu vs dynamic tip resistance qd Panda 3 and qd Panda 2, (b) penetrometer modulus Ek_d^{P3} vs pressuremeter modulus Em et (c) shear wave velocity V_s^{P3} vs the shear wave velocity of the seismic method MASW 1D.

Figure 6.c shows the results obtained in terms of shear wave velocity. It is observed that superposition of obtained curves follows the same velocity as the shear wave velocity of the seismic method V_s. However there are occasional passages where the results obtained using Panda 3 and seismic measurement MASW 1D are less compatible. This could be explained by the integrative character of the seismic method which takes into account a large volume of soil and tends to homogenize the results

Table 1 presents a summary overview of the results for each auscultated soil layer presented in the preceding paragraphs. The results thus presented correspond to the average values for each parameter and for each soil layer.

Table 1. Summary of Panda 3® results for each soil layer identified along the survey

	Layer 1	Layer 2	Layer 3
Nature	Backfill (sandy clays)	silty clay	Clay Marl
deep, z (m)	(0,0 – 2,4)	(2,4 – 5,2)	(z > 5,2)
qd P3 (MPa)	2,6	2,5	9,4
qd P2(MPa)	3,5	2,7	10,5
qc CPTu(MPa)	3,1	2,1	17,0
EkdP3 (MPa)	9,2	11,0	27,0
Em PMT(MPa)	10,2	9,6	20,7
Vs P3 (m/s)	235	231	421
Vs MASW (m/s)	132	212	308

4 CONCLUSION

This article presents the recent developments made on the Panda 3 penetrometer in order to characterize the geomechanical behaviour of the soil auscultated. The test allows, from the measurement and the decoupling of waves created by the impact, to obtain for each impact a load-penetration σ_p-s_p curve of the tested soil. The exploitation of this curve permits to determine the resistance parameters (cone resistance q_d and q_c), deformation (E_{kd}^{P3} and E_d^{P3}), damping characteristics (J_s) and wave velocity of soils (V_p^{P3} and V_s^{P3}) inspected in function of the depth throughout the survey.

The realization of these experimental campaign allowed us to demonstrate their feasibility and identify different usage limitations in the current state of development (maximum auscultation depth 6,0m for compact soils). Similarly, we could identify the richness of continuous information on each load-penetration curve obtained during penetrometer driving. Indeed, the Panda 3 tests were able to provide measurements up to 6-7 m depth in most cases and identify singularities and transitions layers that other techniques fail to highlight. The results are highly satisfactory both qualitatively and quantitatively.

Furthermore, regarding the results provided by the test, it is observed that there is good correspondence between the results (tip resistance, deformation modulus and shear wave velocity) with those obtained using "conventional" tests, namely MASW method, pressuremeter PMT, Panda 2® and the piezocone test CPTu. This technique would allow engineers to provide satisfactory data for predicting the pre-failure behavior of soils for geotechnical studies.

5 REFERENCES

Arbaoui, Gourvès R., Bressolette Ph., Bodé L. 2006. *Mesure de la déformabilité des sols in situ à l'aide d'un essai de chargement statique d'une pointe pénétromètrique*, Revue Canadienne de géotechnique 43(4), pp. 355-369.

Aussedat, G. 1970, *Sollicitations rapides des sols*, Phd Thesis, Faculté de sciences de l'Université de Grenoble, Grenoble, France.

Benz Navarrete M. A. 2009. *Mesures dynamiques lors du battage du pénétromètre Panda 2*. Thèse de doctorat de l'Université Blaise Pascal, Clermont-Ferrand, France.

Benz Navarrete M.A., Escobar E., Gourvès R., Haddani Y., Breul P., Bacconnet. C. 2013. *Mesures dynamiques lors du battage pénétromètrique – Détermination de la courbe charge-enfoncement dynamique en pointe*. In Proceedings of the 18th International Conférence on Soil Mechanics and Geotechnical Engineering, Paris, France, pp 409-503.

Benz-Navarrete M.A., Gourvès R., Escobar E., Haddani Y., Calon N., Costa D'Aguiar S. et Robinet A. 2014. *Détermination de la raideur dynamique des plateformes ferroviaires à l'aide de l'essai pénétrométrique Panda 3®*, 2ème Symposium International en Géotechnique Ferroviaire, Marne la Vallée, France.

Caballero, C.R. 2007. *Evaluación Numérico Experimental del comportamiento bajo carga axial de Pilotes*. Tesis Doctoral. Facultad de Ciencias Exactas, Fisicas y Naturales de la Universidad Nacional de Cordoba, Argentina.

Escobar E., Benz-Navarrete M.A., Gourvès R. 2013. *Dynamic cone penetration tests in granular media: determination of the tip's dynamic load-penetration curve*. Powder and Grains, Sydney.

Escobar E. 2015. *Mise au point et exploitation d'une nouvelle technique pour la reconnaissance des sols : le Panda 3*. Thèse de doctorat de l'Université Blaise Pascal, Clermont-Ferrand, France.

Gourvès, R. 1991. *Le PANDA - Pénétromètre dynamique léger à énergie variable LERMES CUST*. Université Blaise Pascal Clermont-Ferrand, France.

Paquet J. 1968. *Etude vibratoire des pieux en béton, réponse harmonique et impulsionnelle. Application au contrôle*. Annales de l'ITBTP, n°245.

Smith, E. 1960. *Pile driving analysis by wave equation*. Soil Mech. ASCE. Paper No. 3306, Volume 127, Partie I, pp 1145-1193.

Geotechnical and Geophysical Site Characterisation 5 – Lehane, Acosta-Martínez & Kelly (Eds)

Comparison of Unified and European Soil Classification Systems

M.S. Kovacevic, D. Juric-Kacunic, L. Libric
Faculty of Civil Engineering, University of Zagreb, Zagreb, Croatia

ABSTRACT: Soil classification for engineering purposes is a set of procedures which enables engineers all over the world to separate different soil types into groups of similar mechanical properties. It also enables them to compare results obtained in different laboratories, communicate with one another, and understand soil test results more easily. This paper presents a comparison of two soil classification systems using computer program Classif, developed by the authors. CLASSIF is a spreadsheet solution based on Microsoft Excel and VBA. It enables performing both the USCS and ESCS using the same input data. The examples presented in the paper show that the symbols are completely different, soil group names are relatively different, while the soil classification procedures are pretty similar.

1 INTRODUCTION

For engineers around the globe, soil description and classification for engineering purposes is a basis for ensuring mutual communication as well as studying and understanding soil test results. Soil description and classification enable rough identification of the type of material at hand and definition of the range within which its mechanical properties are expected to vary. What is more, types of soil with the same description and classified into the same category share similar mechanical characteristics and behave similarly under the influence of load.

Traditionally, soil belongs to one of the 4 major groups: gravel, sand, silt or clay. Initial efforts to classify soil were strictly related to the classification according to the size of grains, i.e. particle size distribution of soil (Child 1986). Such divisions were based on soil texture, i.e. relative proportions of sand, silt and clay in the total mass of soil tested. The best known texture-based classification is the classification by the US Department of Agriculture (USDA). Developed in 1938, this classification has been modified on several occasions since its initial appearance (Soil Survey Staff 1951). It is based on the use of a triangular classification chart proposed by Davis & Bennet 1927. This classification is nowadays used mostly in agriculture and hardly ever in geotechnical engineering.

Textural classifications were first researched in detail by Atterberg, at the beginning of the 20th century (Atterberg 1905, Atterberg 1912). In his work, he pointed to the fact that textural classifications of soil can successfully be used in agriculture, but that clay and silt parameters also have to be considered when this classification is used for geotechnical applications. In line with his conclusions, in 1929, the AASHTO (American Association of State Highway and Transportation Officials) classification was developed, which, apart from the particle size distribution, considered also the consistency limits of coherent soil particles (AASHTO, 1978). For the most part it is used for designing roads.

In 1942, Arthur Casagrande developed the Airfield Classification System (ACS) for the design of the US airfields during the Second World War, which considered particle size distribution and consistency limits of coherent soil particles, as did the AASHTO (Casagrande 1947, Casagrande 1948). A modification of the ACS in 1952 resulted in the creation of the Unified Soil Classification System (USCS), which is an integral part of the US standard (ASTM D 2487-11). Adjustment of the ACS to the mechanical properties of soil prevailing in the UK gave rise in 1981 to the British Soil Classification System (BSCS) (Dumbleton 1968, Dumbleton 1981), which makes an integral part of the British standard (BS 5930:1999). The DIN (*Deutsches Institut für Normun*) soil classification was developed in a similar way in 1988, and makes an integral part of German standards (DIN 18196:2011-05).

In order to improve the quality, safety, reliability, efficiency, compatibility, and communication among experts in the field of geotechnics, the ISO (International Standards Organisation) and CEN (Comité Européen de Normalisation) developed the standards for the identification and description of soil and defined the principles of soil classification, with their soil marking methods differing greatly from the formerly used national classification systems. In 2002, the ISO/TC 182 "Geotechnics" Technical Committee, in cooperation with the CEN/TC 341 "Geotechnical Investigation and Testing" Technical Committee, prepared the soil description standard entitled: Geotechnical investigation and testing – Identification and classification of soil – Part 1: Identification and description (EN ISO 14688-1:2002). In 2004, the relevant committee prepared the standard on soil classification principles entitled: Geotechnical investigation and testing – Identification and classification of soil – Part 2: Principles for a classification (EN ISO 14688-2:2004).

European countries that have undertaken, as CEN members, to adopt and implement European standards through their national standardisation bodies are: Austria, Belgium, Bulgaria, Cyprus, the Czech Republic, Denmark, Estonia, Finland, France, Greece, Croatia, Ireland, Iceland, Italy, Latvia, Lithuania, Luxembourg, Hungary, Macedonia, Malta, the Netherlands, Norway, Germany, Poland, Portugal, Romania, Slovakia, Slovenia, Spain, Sweden, Switzerland, Turkey, and the UK.

The acceptance of European standards did not result in transition to the new way of describing, identifying, and classifying soil in most European countries. Objective reasons for this lie in the fact that European standards merely describe classification principles. There is room to develop a more comprehensive classification using the relevant principles on a national or project level. Kovacevic and Juric-Kacunic (2014) developed the European Soil Classification System (ESCS), which makes use of soil descriptions and symbols in line with the European standard EN ISO 14688-1 and is based on soil classification principles prescribed in EN ISO 14688-2.

2 CLASSIF PROGRAM - IT SUPPORT FOR USCS AND ESCS SOIL CLASSIFICATIONS

CLASSIF computer program was developed at the Department of Geotechnical Engineering, Faculty of Civil Engineering in Zagreb to facilitate the adaptation to the new manner of marking and classifying soils further to European guidelines. The program provides IT support for implementing the bothUSCS and ESCS classifications and facilitates their parallel use (Fig. 1).

CLASSIF was developed using the Microsoft Excel program and Visual Basic for Applications (VBA) integrated programming language, which enables programming of special functions, not included in Microsoft Excel by default. The program is available for free download from the link: http://www.grad.unizg.hr/download/repositorij/classif.

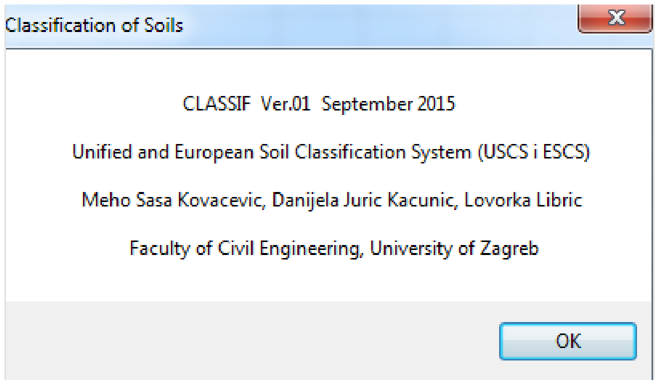

Figure 1. Initial user interface in CLASSIF

Input data for both classifications are the same, which enables simple comparison of the results.

The total number of input parameters that can be set or changed is 8. Not every change in every parameter will affect the final results. For example, changing the liquid limit will not affect the result of both soil classifications if the percentage of fine grains in the soil is below 5%.

The first parameter is textural one-letter information which answers the question whether the sample of the soil being tested contains organic matter. The second and third parameters are numeric data on the percentage of gravel and sand in the total mass of soil tested. The program automatically calculates the percentage of fine grains (silt + clay) so that the total sum equals 100%. The fourth, fifth and sixth parameters are numeric data on characteristic diameters of grains D_{60}, D_{30} and D_{10}, expressed in mm. The program automatically calculates the coefficient of uniformity (c_u) and the coefficient of curvature (c_c). The seventh and eighth parameters are numeric data on liquid limit w_L and plasticity w_P. The program automatically calculates the index of plasticity I_P.

CLASSIF continuously controls data input so as not to allow the input of unrealistic values of parameters (Fig. 2).

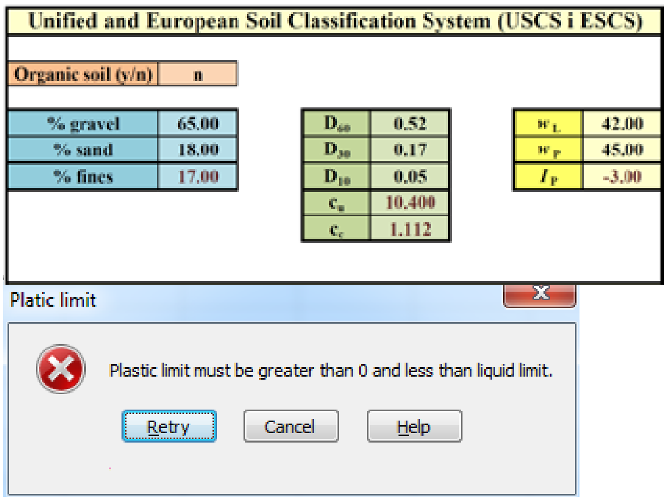

Figure 2. The value entered for plastic limit is not valid

3 SOIL GROUP SYMBOLS

According to both classifications, soils are divided into coarse-grained and fine-grained soils, whereas the latter may contain organic matter. Both classifications also identify highly organic soils (peat), for which no classification procedures are carried out. Soil grading and consistency limits are both used when classifying soils. According to the ESCS, a soil is classified as coarse-grained if more than 50% of the total quantity of a dry sample is retained on a 0.063 mm sieve, and according to the USCS, if more than 50% of the total quantity of a dry sample is retained on a 0.075 mm sieve.

The main idea behind soil classification is to mark the soils using symbols that represent the principal and secondary fractions which make up the soil. The principal fraction of the soil determines engineering properties of the soil. Secondary fractions do not determine, but rather influence, the engineering properties of the soil.

According to the ESCS, the principal fraction of the soil, that which determines its engineering properties, is marked with a symbol consisting of the first two letters of the name of the fraction, the first of which is written in capital letters:

Gr – gravel, Sa – sand,
Si – silt, Cl – clay.

According to the USCS, the principal fraction of the soil is marked with a symbol consisting of a single capital letter:

G – gravel, S – sand,
M – silt, C – clay.

According to the ESCS, the first secondary fraction, which has the most influence on the engineering properties of the soil, is that which, in a coarse-grained soil sample, contains more than 5% of fine grains. It is marked with a symbol consisting of the first two letters of the fraction name, which are written in lowercase in front of the principal fraction:

siGr – silty gravel, clGr – clayey gravel,
siSa – silty sand, clSa – clayey sand.

With fine-grained soils, the ESCS defines the first secondary fraction as the one which contains more than 15% of coarse grains. It is marked with a symbol which consists of the first two letters of the fraction name, written in lowercase in front of the principal fraction:

grSi – gravelly silt, saSi – sandy silt,
grCl – gravelly clay, saCl – sandy clay,

According to the USCS, the first secondary fraction, which has the most influence on the engineering properties of the soil, is that which, in a course-grained soil sample, contains between 5% and 12% of fine grains. It is marked using a two-part symbol comprising of 4 capital letters, the first two of which refer to the grading level of the soil, and the fraction is marked with the last capital letter:

GW-GM – well graded gravel with silt,
GW-GC – well graded gravel with clay,
GP-GM – poorly graded gravel with silt,
GP-GC – poorly graded gravel with clay,
SW-SM – well graded sand with silt,
SW-SC – well graded sand with clay,
SP-SM – poorly graded sand with silt,
SP-SC – poorly graded sand with clay.

According to the USCS, the first secondary fraction is the one that, in a course-grained soil sample, contains more than 12% of fine grains. It is marked using a symbol that consists of 2 or 4 capital letters, depending on whether the fine grains are silt, clay, silty clay:

GM – silty gravel, GC – clayey gravel,
SM – silty sand, SC – clayey sand,
GC-GM – silty, clayey gravel,
SC-SM – silty, clayey sand.

With fine-grained soils, the USCS defines the first secondary fraction as the one which contains more than 30% of coarse grains. In this classification the fraction is not marked, rather the word "sandy" or "gravelly" is added before the group name.

According to the ESCS, the second secondary fraction, which influences the engineering properties of the soil, is that which, in a coarse-grained soil sample, contains more than 15% of other coarse-grained fractions. It is marked with a symbol consisting of the first two letters of the fraction name, in lowercase, before the secondary fraction, or before the primary fraction if there is no first secondary fraction:

sasiGr – sandy, silty gravel,
saclGr – sandy, clayey gravel,
grsiSa – gravelly, silty sand,
grclSa – gravelly, clayey sand,
saGr – sandy gravel,
grSa – gravelly sand.

When it comes to fine-grained soils, according to the ESCS, the second secondary fraction does not exist.

According to the USCS, the second secondary fraction, is that which, in a coarse-grained soil sample, contains more than 15% of other coarse-grained fractions. In this classification the fraction is not marked, rather the words "with sand" or "with gravel" are added after the group name.

With fine-grained soils, the USCS defines the second secondary fraction as the one which contains between 15% and 30% of coarse grains. In this classification the fraction is not marked, rather the words "with sand" or "with gravel" are added after the group name.

Coarse-grained soils are additionally marked with respect to their grading level. According to the ESCS, symbols of coarse-grained soils with less than 15% of fine grains are supplemented with the following capital letters:

W – well graded sand or gravel,
M – medium-graded sand or gravel,

P – poorly graded sand or gravel.

According to the USCS, symbols of coarse-grained soils with less than 12% of fine grains are supplemented with the following capital letters:

W – well graded sand or gravel,

P – poorly graded sand or gravel.

Fine-grained soils are additionally marked with respect to their plasticity. According to the ESCS, symbols of fine-grained soils are supplemented with the following capital letters:

L – low plasticity,

I – intermediate plasticity,

H – high plasticity.

According to the USCS, symbols of fine-grained soils are supplemented with the following capital letters:

L – low plasticity,

H – high plasticity.

According to the ESCS, presence of organic matter in coarse-grained or fine-grained soil samples is marked by adding the small letters "or" in front of the symbol.

According to the USCS, presence of organic matter in a sample of coarse-grained soil is not marked by a symbol, but rather by adding the words "with organic fines" before the group name.

In line with the USCS, presence of organic matter in a sample of fine-grained soils is marked by substituting the symbol of the principal fraction (C or M) with a capital "O".

4 SOIL GROUP NAME

According to the ESCS, names of soil groups are consistent with the symbols of soil groups, so that every symbol represents a soil group. Examples of group symbols and names:

SaP – poorly graded sand,

SiI – intermediate plasticity silt,

grSaM – medium graded gravelly sand,

sasiGrW – well graded sandy, silty gravel,

grSiL – low plasticity gravelly silt,

orsaClH – high plasticity organic sandy clay.

According to the USCS, one soil group symbol can represent several soil group names. Examples of group symbols and names:

CL – lean clay,
– lean clay with sand,
– lean clay with gravel,
– sandy lean clay,
– sandy lean clay with gravel,
– gravelly lean clay,
– gravelly lean clay with sand.

SM – silty sand,
– silty sand with organic fines,
– silty sand with gravel,
– silty sand with gravel and organic fines.

5 CLASSIFICATION PROCEDURES

Procedures for the ESCS and USCS are fairly similar. They are carried out in five steps for coarse-grained and fine-grained soils.

Step one is determining, based on the results of a sieving experiment, whether the principal fraction of the soil is coarse-grained or fine-grained soil.

Step two is determining, for coarse-grained soils, based on percentage, whether the principal fraction is sand or gravel. According to the ESCS, with fine-grained soils the liquid limit w_L determines whether the principal fraction is soil of low, intermediate or high plasticity. According to the USCS, it determines whether the principal fraction is soil of low or high plasticity.

Step three is determining, for coarse-grained soils, based on percentage, whether there is a first secondary fraction of fine-grained soil. According to the ESCS, with fine-grained soils, the liquid limit w_L and the plasticity index I_P determine whether the principal fraction is clay or silt. According to the USCS, they determine whether the principal fraction is clay, silt or silty clay.

Step four is determining, for coarse-grained soils, the grading level of the principal fraction, except when there is a first secondary fraction of fine-grained soil whose fines percentage is higher than 15% (ESCS) or 12% (USCS). According to the ESCS, if there is a first secondary fraction of fine-grained soil, the liquid limit w_L and the plasticity index I_P are used to determine whether the principal fraction is clay or silt. According to the USCS, they determine whether the principal fraction is clay, silt or silty clay. With fine-grained soils, the percentages are used to determine whether there is a first secondary fraction of coarse-grained soil.

Step five is determining, for coarse-grained soils, based on percentage, whether there is a second secondary fraction of coarse-grained soil. With fine-grained soils, according to the ESCS, if there is a first secondary fraction, it determines which coarse-grained fraction is the dominant one. According to the USCS, with fine-grained soils, if there is a first secondary fraction of coarse-grained soil, it determines whether there is a second secondary fraction of coarse-grained soil.

Having carried out all five steps, a decision is made regarding the symbol and name of soil group.

6 EXAMPLES OF COMPARISON OF USCS AND ESCS USING CLASSIF

Both classifications use the same input data, which enables simple comparison of obtained results. Below are some examples illustrating the similarities and differences between the USCS and ESCS.

Unified and European Soil Classification System (USCS i ESCS)

Organic soil (y/n)	n

% gravel	72.00
% sand	10.00
% fines	18.00

D_{60}	0.52
D_{30}	0.17
D_{10}	0.08
c_u	6.500
c_c	0.695

w_L	42.00
w_P	22.00
I_P	20.00

Unified Soil Classification System (USCS)

Coarse-grained soil (less than 50% fines)
Gravel (percent of gravel is greater than percent of sand)
Gravel with more than 12% fines
fines are clay
Percent of sand less than 15% doesn't have influence on group name

Group Name	Symbol
Clayey gravel	**GC**

European Soil Classification System (ESCS)

Coarse-grained soil (less than 50% fines)
Gravel (percent of gravel is greater than percent of sand)
Gravel with more than 15% fines
fines are clay
Percent of sand less than 15% doesn't have influence on group name

Group Name	Symbol
Clayey gravel	**clGr**

References

ASTM D 2487-11: Standard Practice for Classification of Soils for Engineering Purposes (Unified Soil Classification System) ASTM International, West Conshohocken, PA, 2011.

EN ISO 14688-2:2004: Geotechnical investigation and testing – Identification and classification of soil – Part 2: Principles for a classification. CEN, 2004.

Kovacevic, M. S., Juric-Kacunic, D.: European soil classification system for engineering purposes, GRAĐEVINAR 66 (2014) 9, pp. 801-810, doi: 10.14256/JCE.1077.2014.

Figure 3. Soil Classification using CLASSIF - example 1

Unified and European Soil Classification System (USCS i ESCS)

Organic soil (y/n)	n

% gravel	8.00
% sand	88.00
% fines	4.00

D_{60}	0.52
D_{30}	0.17
D_{10}	0.08
c_u	6.500
c_c	0.695

w_L	42.00
w_P	32.00
I_P	10.00

Unified Soil Classification System (USCS)

Coarse-grained soil (less than 50% fines)
Sand (percent of gravel is less than or equal to percent of sand)
Sand with less than 5% fines
Poorly graded sand
Percent of gravel less than 15% doesn't have influence on group name

Group Name	Symbol
Poorly graded sand	**SP**

European Soil Classification System (ESCS)

Coarse-grained soil (less than 50% fines)
Sand (percent of gravel is greater thanpercent of sand)
Sand with less than 5% fines
Poorly graded sand
Percent of gravel less than 15% doesn't have influence on group name

Group Name	Symbol
Poorly graded sand	**SaP**

References

ASTM D 2487-11: Standard Practice for Classification of Soils for Engineering Purposes (Unified Soil Classification System) ASTM International, West Conshohocken, PA, 2011.

EN ISO 14688-2:2004: Geotechnical investigation and testing – Identification and classification of soil – Part 2: Principles for a classification. CEN, 2004.

Kovacevic, M. S., Juric-Kacunic, D.: European soil classification system for engineering purposes, GRAĐEVINAR 66 (2014) 9, pp. 801-810, doi: 10.14256/JCE.1077.2014.

Figure 4. Soil Classification using CLASSIF - example 2

Unified and European Soil Classification System (USCS i ESCS)

Organic soil (y/n)	n

% gravel	20.00
% sand	25.00
% fines	55.00

D_{60}	0.52
D_{30}	0.17
D_{10}	0.08
c_u	6.500
c_c	0.695

w_L	42.00
w_P	22.00
I_P	20.00

Unified Soil Classification System (USCS)

Fine-grained soil (more than or equal to 50% fines)
Liquid limit less than 50%
Lean clay
Percent of coarse greater than or equal to 30% (% sand >= % gravel)
Percent of gravel equal to or greater than 15% have influence on group name

Group Name	Symbol
Sandy lean clay with gravel	**CL**

European Soil Classification System (ESCS)

Fine-grained soil (more than or equal to 50% fines)
Liquid between 35% and 50%
Clay
Percent of coarse greater than or equal to 15%
% sand >= % gravel

Group Name	Symbol
Sandy intermediate plasticity clay	**saCI**

References

ASTM D 2487-11: Standard Practice for Classification of Soils for Engineering Purposes (Unified Soil Classification System) ASTM International, West Conshohocken, PA, 2011.

EN ISO 14688-2:2004: Geotechnical investigation and testing – Identification and classification of soil – Part 2: Principles for a classification. CEN, 2004.

Kovacevic, M. S., Juric-Kacunic, D.: European soil classification system for engineering purposes, GRAĐEVINAR 66 (2014) 9, pp. 801-810, doi: 10.14256/JCE.1077.2014.

Figure 5. Soil Classification using CLASSIF - example 3

Unified and European Soil Classification System (USCS i ESCS)

Organic soil (y/n)	y

% gravel	12.00
% sand	25.00
% fines	63.00

D_{60}	0.52
D_{30}	0.17
D_{10}	0.08
c_u	6.500
c_c	0.695

w_L	55.00
w_P	22.00
I_P	33.00

Unified Soil Classification System (USCS)

Fine-grained soil (more than or equal to 50% fines)
Liquid limit greater than or equal to 50%
Organic clay
Percent of coarse greater than or equal to 30% (% sand >= % gravel)
Percent of gravel less than 15% doesn't have influence on group name

Group Name	Symbol
Sandy organic clay	**OH**

European Soil Classification System (ESCS)

Fine-grained soil (more than or equal to 50% fines)
Liquid limit greater than or equal to 50%
Organic clay
Percent of coarse greater than or equal to 15%
% sand >= % gravel

Group Name	Symbol
Organic sandy high plasticity clay	**orsaCIH**

References

ASTM D 2487-11: Standard Practice for Classification of Soils for Engineering Purposes (Unified Soil Classification System) ASTM International, West Conshohocken, PA, 2011.

EN ISO 14688-2:2004: Geotechnical investigation and testing – Identification and classification of soil – Part 2: Principles for a classification. CEN, 2004.

Kovacevic, M. S., Juric-Kacunic, D.: European soil classification system for engineering purposes, GRAĐEVINAR 66 (2014) 9, pp. 801-810, doi: 10.14256/JCE.1077.2014.

Figure 6. Soil Classification using CLASSIF - example 4

7 CONCLUSIONS

The following systems can be used to classify soils: the Unified Soil Classification System (USCS), in line with US standard ASTM D 2487-11, and the European Soil Classification System (ESCS), which uses soil descriptions and symbols in line with European standard EN ISO 14688-1 and is based on the principles of soil classification in line with European standard EN ISO 14688-2. Procedures for soil classification are very similar; names of soil groups are relatively similar, whereas the symbols of soil groups are completely different. Simple and fast classification of soil in line with the USCS and ESCS can be done by using the CLASSIF program.

8 REFERENCES

Child, G.H. 1986. Soil descriptions - Quo Vadis?. in A.B. Hawkins (ed) *Site Investigation Practice: Assessing BS 5930*: 73-81. English Geological Society.

Soil Survey Staff 1951. *Soil Survey Manual*, U.S. Department of Agriculture, Washington, D.C.

Davis, R.O.E. & Bennet, H.H. 1927. *Grouping of soils on the basis of mechanical analysis*, U.S. Department of Agriculture, Washington, D.C.

Atterberg, A. 1905. Die rationale Klassifikation der Sande und Kiese, *Chem. Ztg.* 29: 195-198.

Atterberg, A. 1912. Die Konsistenz und die Bindigheit der Boden, *Int. Mitt. Bodenkunde* 2: 148-189.

AASHTO 1978. *Standard specifications for transportation materials and methods of sampling and testing*, AASHTO Designation: M 145-73, 12th ed. Washington, D.C.

Casagrande, A. 1947. Classification and identification of soils, *Proc. ASCE* 73(6): 783-810.

Casagrande, A. 1948. Classification and identification of soils, *Trans. ASCE* 113: 901-992; reprint of Casagrande (1947) including discussion.

ASTM D2487-11 2011. *Standard Practice for Classification of Soils for Engineering Purposes (Unified Soil Classification System)*. ASTM International, West Conshohocken, PA.

Dumbleton, M.J. 1968. *The classification and description of soils for engineering purposes: a suggested revision of the British system*, Ministry of Transport, RRL Report LR 182, Road Research Laboratory, Crowthorne, Berks.

Dumbleton, M.J. 1981. *The British soil classification system for engineering purposes: its development and relation to other comparable systems*, TRRL Report LR 1030, Transport and Road Research Laboratory, Crowthorne, Berks.

BS 5930:1990. *British Standard. Code of practice for site investigations*. British Standards Institute, London.

DIN 18196:2011-05. *Erd-und Grundbau-Bodenklassifikation für bautechnishe Zwecke*, Beuth Verlag GmbH, Berlin.

EN ISO 14688-1:2002: *Geotechnical investigation and testing – Identification and classification of soil – Part 1: Identification and description*. Comité Européen de Normalisation. Brussels.

EN ISO 14688-2:2004: *Geotechnical investigation and testing – Identification and classification of soil – Part 2: Principles for a classification*. Comité Européen de Normalisation.Brussels.

Kovačević, M.S., Jurić-Kaćunić, D. 2014. European Soil Classification System for Engineering Purposes, *GRAĐEVINAR*, 66(9): 801-810.

Geotechnical and Geophysical Site Characterisation 5 – Lehane, Acosta-Martínez & Kelly (Eds)
© 2016 Australian Geomechanics Society, Sydney, Australia, ISBN 978-0-9946261-1-0

Televiewer imaging of boreholes; benefits and considerations for interpretation in the absence of physical rock core

G.T.C.McKenna & S.L.Roberts-Kelly
Coffey Corporate Services Pty Ltd: A Tetratech Company, Australia

ABSTRACT: A common occurrence in geotechnical assessment during geological and geotechnical modelling is the lack of readily accessible physical core. Defect characterisation can therefore be based only on borehole logs, core photographs and remote imaging data (if available). Previous experience indicates that interpretation of remote imaging data by data acquisition companies can differ from the actual rock core. This paper highlights that remote imaging data can be a useful resource especially where access to the physical core is limited or not possible. Two Australian cases are considered, where remote imaging data show discrepancies in ground conditions to those apparent in the rock core; these discrepancies were subsequently exposed during construction. A final recommendation interpretation of Televiewer data be reviewed by trained geotechnical professionals for consistency with core photographs and other sources, as data acquisition companies may not have access to all sources for correlation during their interpretation.

1 INTRODUCTION

All civil engineering projects benefit from an accurate geotechnical ground model, typically conceived from desk study assessment supported with a targeted site investigation and engineering geological review. Projects with deep or long cuttings in rock require a thorough understanding of the materials that are to be excavated to allow accurate estimation of rippability, support requirements and (if applicable) material reuse characteristics. Cored boreholes are the most common intrusive form of deep geotechnical investigation, but due to the staged procurement process on many larger projects the core may not be readily accessible during- or may have deteriorated prior to- the design period, and geotechnical design may have to rely on logs, photographs and Televiewer data.

In the authors' experience Televiewer data is beneficial but, as with most sources of data, requires careful analysis to ensure consistency with other available sources and the actual ground conditions, otherwise additional design and construction costs can result. This paper aims to provide a comparison of Televiewer data against the rock core, borehole logs and core photographs so the reader can make an educated assessment of the likely defect conditions in the absence of rock core during the design period.

It is noted that in some cases the Televiewer data can actually provide better information than the rock core, if the core has been mistreated, poorly handled or is damaged due to drilling. For an extensive bibliography regarding use of Televiewers the reader is referred to Prensky (1999).

2 BRIEF OVERVIEW OF GEOTECHNICAL CUTTING DESIGN

2.1 *Components of geotechnical cutting design*

Geotechnical design of cuttings involves assessment of:

Rippability – specifically what method is required to remove the material with minimal disturbance to the final cut slopes?

Support requirements – what will be required to maintain the final cut slopes at a required factor of safety for the design life?

Material reuse – is the excavated material suitable for reuse elsewhere on the project? What processing will be required so that it can be placed in accordance with the construction specification?

3 HISTORICAL/TYPICAL SOURCES OF GEOTECHNICAL INFORMATION

A good understanding of rock defects and strength is vital for every component of design. Rock defects or structural geology can be assessed using mapping of surface rock outcrops but will typically be supported by intrusive investigation in the form of cored boreholes. The strength of in situ materials can be assessed based on seismic studies, but is typically (and arguably more accurately) ascertained from point load or uniaxial compression testing of recovered rock core. Therefore cuttings usually have a number of cored boreholes that extend beyond the final cutting design depth. Variation of the orientation of the boreholes increases both the likelihood of encountering variably orientated strata, and recording of their structural geology data accurately (Versteeg & Morris, 1994).

Information from the boreholes is presented as a borehole log and core photograph. During logging a trained geotechnical professional will measure the structural geology data for each defect observable in the recovered core. If there are areas of core loss or core samples are disturbed during drilling and acquisition, then gaps or errors in the geological profile can occur.

Other sources of data that can corroborate Televiewer findings include published geological maps (and associated publications), local knowledge, past experience and a thorough understanding of geological processes.

Partially due to the receptiveness of the petroleum industry, there has been a rise in the use of borehole geophysical logging methods since the 1960's (Prensky 1999), specifically down the hole viewers or 'Televiewers' being used for geotechnical data acquisition. Televiewers used for geotechnical applications are separated into two types: optical and acoustic. Optical viewers take a 360° continuous 'true colour' image using a rotating prism and onboard light of the entire inner borehole wall. Acoustic Televiewers operate by firing ultrasound beams at the borehole walls and record the resultant travel time and amplitude. Both methods record inclination and magnetic orientation so that images can be located in three dimensional space for quantification and calibration of the structural geology data.

3.1 *Types of geotechnical information*

Table 1 provides a summary of the sources outlined in Section 3.

Table 1. Sources of geotechnical information for cutting design.

Source	Factual / Interpretation	Ease of reinterpretation
Rock core	Factual	Quality and access dependent, source for reinterpretation of other sources listed in this table
Laboratory results	Factual	-
Core photographs	Factual	Quality dependent, source for reinterpretation of other sources listed in this table.
Optical Televiewer	Factual and Interpretation	Images can be reinterpreted easily, particularly if compared with other sources. Reinterpretation can be undertaken (Li et al. 2013).
Acoustic Televiewer	Interpretation	Specific software used to assess raw input is typically not available during reassessment. Reinterpretation of outputs typically not reliable unless undertaken by specialists (Li et al. 2013).
Borehole log	Interpretation	Trained geotechnical professionals are able to assess interpreted information, correlate with other sources listed in this table and make educated reinterpretation if required.
Professional Knowledge	Factual and Interpretation	Can be difficult due to professionals having different experience levels.
Published Geological Maps	Factual and Interpretation	Maps may have additional notes or prior revisions which can be assessed and reinterpreted if required.

4 CASE STUDIES

Literature confirms that Televiewer data should be validated or calibrated with rock core (de Frederick et al. 2014). This section illustrates two examples of Televiewer data compared with data sources for the same borehole. The examples have been selected to highlight potential issues that should be considered when assessing Televiewer data. Note that rock core photographs in the figures have been scaled for ease of comparison and correlation has been undertaken based on the original photographs. The rock core was logged to AS1726-1993 standard; in which an extremely weathered material (XW) is defined as a rock weathered to such an extent that it has soil properties (ie, it either disintegrates or can be remoulded in air or water).

4.1 *Case Study One – optical Televiewer*

Case Study One is from an igneous source located in Queensland, Australia. Figure 1 illustrates a section where the defects identified in the interpreted Televiewer data do not align wholly with the other data sources. This can be seen immediately as defect 333/70 is absent from the Televiewer result.

The borehole log shows two defects with a 20° and 35° dip at 15.45m and 15.65m respectively and a drill break at 15.38m; aligning exactly with the rock core photograph. Optical output from the Televiewer shows two defects in this area; the first is a clearly visible open defect interpreted with the dip direction and dip of 114/24, the second is closed and less obvious in Figure 1 but it aligns with the interpreted

100/29 defect. The latter two interpreted defects (333/70 and 094/31) are not visible in the optical output or other data sources. The depth of Televiewer data also appears to be slightly inconsistent, as the 114/24 defect is shown at the same depth as the drill break. Depth data can be amended easily in this borehole; note however that in heavily fractured boreholes or where strata are more homogeneous this process can be quite difficult.

Close examination of the optical output indicates that there are artefacts on the image. Misinterpretation of the artefacts may account for the anomalous defects. [Artefacts are non-geological features that can blur, distort or otherwise reduce the quality and accuracy of the Televiewer output. Sources of artefacts are numerous and varied; for more information the reader is referred to Lofts & Bourke (1999) who provide a comprehensive review.] For example, the presentation of the Televiewer data can also create issues due to scaling exaggeration; the unfolded sine traces for the defects are horizontally exaggerated due to the relatively skinny core circumference versus the borehole depth; the sine trace can therefore vary significantly during interpretation and this can significantly affect the final dip direction and dip.

In this case the two anomalous defects appear to be due to misinterpretation of the optical output due to artefacts. It is noted that the data acquisition company did not have access to borehole logs or rock core at the time of their interpretation, highlighting the requirement for independent geotechnical review and correlation between data sources.

Although Figure 1 shows only two metres of the entire borehole the errors constitutes half of the defects in this area and if unchecked these errors can accumulate, creating enough scatter on summary stereonet plots to affect design.

During the construction of this project the igneous rocks displayed a preferential orientation that aligned with other data sources (including field mapping and the other defects shown on Figure 1). The structural geology data imported directly from the Televiewers contained a wide spread of data that did not readily align with other data sources. It was only after significant reinterpretation and correlation with the rock core, core photographs and borehole logs that an accurate structural geology representation was achieved.

4.2 *Case Study Two – acoustic and optical Televiewer*

Case study two is from a sedimentary source, located in Queensland, Australia. Figure 2 illustrates a section where the defects again do not wholly correlate between the data sources.

The borehole log shows defects that align with interpreted Televiewer data (DIPA and DIPT column on Figure 2) between 32.00m and 33.25m. The generalised defect description in the borehole log also correlates with the findings of the Televiewer. The borehole log indicates an XW zone between 33.25m and 33.65m which aligns with the Televiewer imagery and rock core. However the defects within the XW zone have been interpreted as open/partially open/closed fractures and foliation/banding/bedding in the Televiewer data and, arguably, should be classified as a weak zone. The defect description is critical when assessing design parameters and directly affects design.

Televiewer data here confirms the XW description in the log (possibly indicating a larger grain size for the gravel component) and provides structural information that is not measurable in the rock core. The representation of the core photograph on Figure 2 is distorted but original photographs correlate with the borehole log well. Bedding within the sedimentary rocks has been identified in the interpreted Televiewer data but not overrepresented (noting that overrepresentation of bedding can be a concern when stereographic modelling if not identified and considered probabilistically by the geotechnical professional).

A major omission from the Televiewer data occurs below the XW zone where an artefact precludes the observation of the defects shown between 34.00m and 34.50m depth in the borehole log.

5 ADVANTAGES AND LIMITATIONS OF TELEVIEWER DATA

5.1 *Advantages of Televiewers*

In the authors' experience the main advantages of Televiewers are:

Continuous measurement of the ground.

Invaluable in 'filling the gaps' where core loss or core disturbance has occurred. The in situ nature of data acquisition means that even the weakest and hardest to recover geological units can be accurately assessed.

When rock core is not available for physical assessment, it provides a valuable resource for correlation against borehole logs and core photographs.

Provides oriented defects; this can be achieved with inclined and/or oriented drilling methods but is typically quite time consuming and requires an appropriately skilled geotechnical professional.

Provides an additional visual record that can be relied upon if core is misplaced or damaged.

Is a valuable tool even if not correlated but offers a more accurate ground model when calibrated.

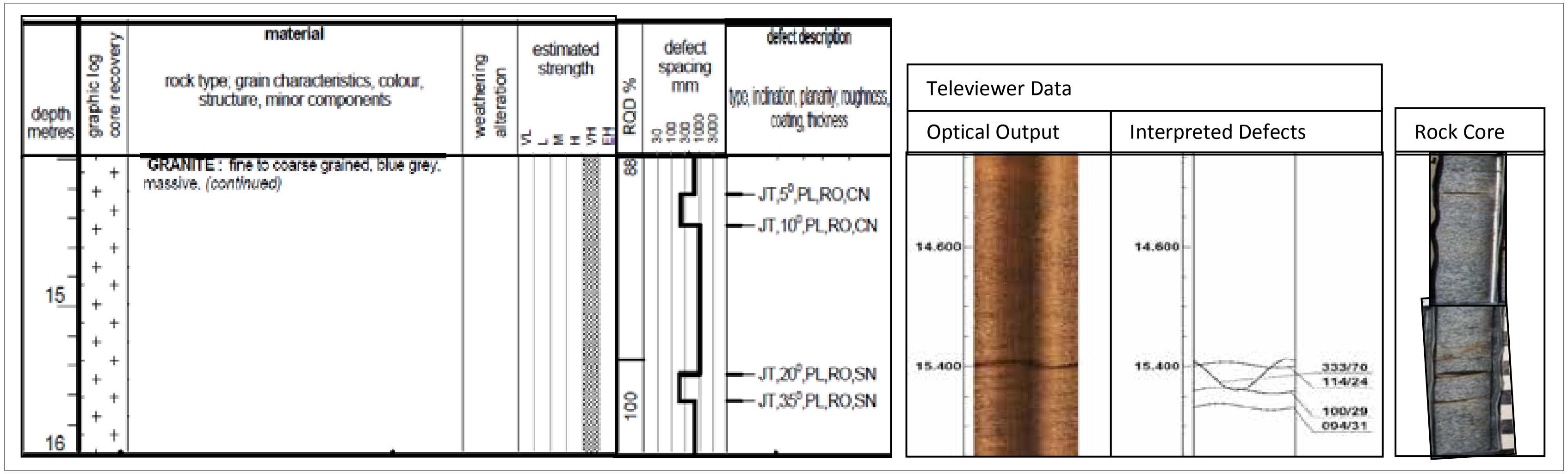

Figure 1 – Case Study 1 information; borehole log, optical Televiewer and rock core photograph. Refer Appendix A for definitions of abbreviations.

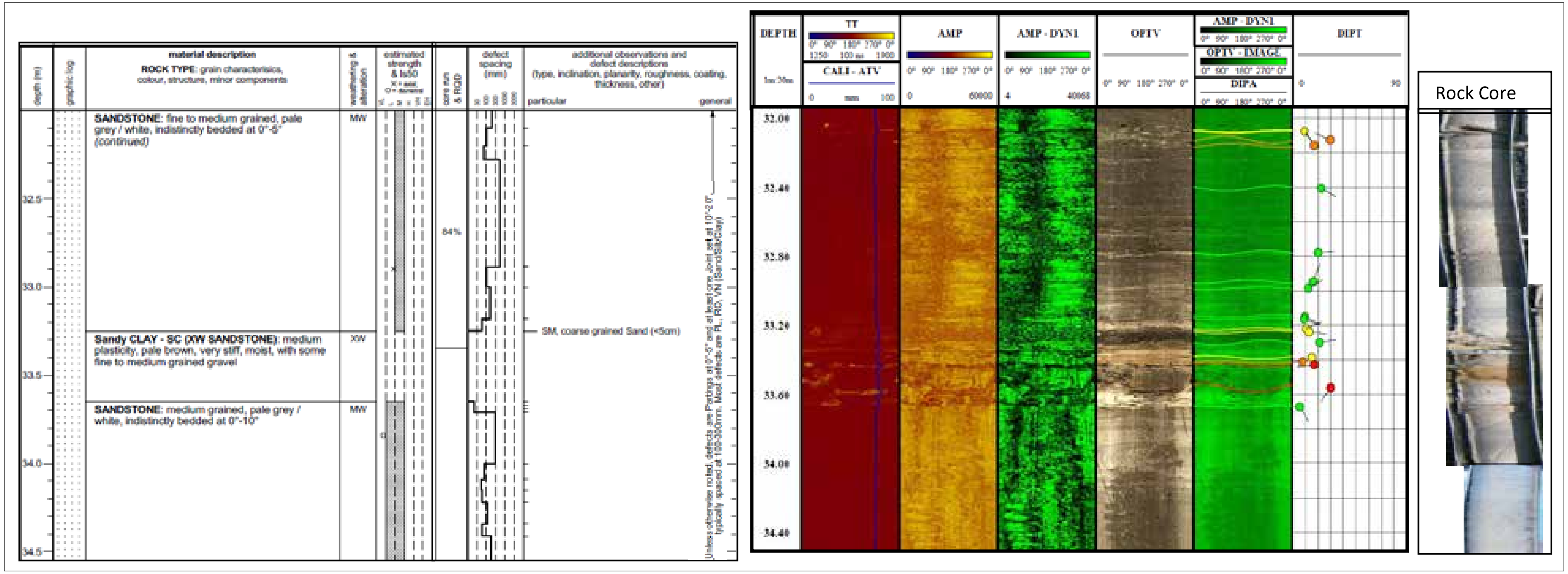

Figure 2 – Case Study 2 information; borehole log, optical and acoustic Televiewer and rock core photograph. Refer Appendix A for definitions of abbreviations

5.2 *Potential issues/limitations with Televiewers*

The main questions that should be considered by a geologist (as highlighted in the case studies) are therefore:

Are defects shown on the interpreted Televiewer artefacts or genuine defects?

The strength of materials. As these are not quantitatively assessed this can affect defect characterisation and description. Are the defects correctly classified in the Televiewer interpretation?

Statistical representation of the data. Are more visible defects such as bedding overrepresented?

Scaling issues. Is the data distorted or stretched? Are the sine waves correctly located or is there additional variance in the dip direction and dip?

Do the depths between the different sources align? Other considerations include:

Closed vs. open defects, although these are sometimes correctly separated in interpreted Televiewer data, open defects are easily identified when logging physical rock core and may be missed in Televiewer data. Due to this these defects may be overrepresented in the borehole logs and closed defects may be missed. For engineering however, open defects are more relevant than closed defects.

Similar to borehole logs, Televiewer data is provided to the geotechnical professional as an interpreted source; the main difference between the sources is the ease of re-interpretation. Most geotechnical professionals will have experience logging boreholes and reviewing and interpreting borehole logs and can therefore make informed judgements as to the validity of provided data. Fewer geotechnical professionals have formal training in understanding Televiewer outputs and therefore the accuracy of the data is harder to validate. This is not the subject of this paper but the authors believe it is of note.

Televiewer data is typically provided as a visual output (pdf) and the defects listed in a spreadsheet. This allows easy input in stereographic modelling software and with tight time constraints correlation of data between sources does not always occur. Unfortunately when the data is in the software it can be even harder to identify errors (due to natural variation in structural geology measurements) and may jeopardise the evaluation of preferential defect orientations. The sheer quantity of data provided for assessment can also be an issue, if bedding is dominant then it can easily be overrepresented in the data set and if not clearly understood or misinterpreted then may be presented as a dominant joint set.

Smearing of the lens or suspended particles in the groundwater can create artefacts or reduce the visual acuity and the acoustic accuracy of the data. Therefore flocculating the borehole prior to carrying out Televiewer investigation is critical.

Some of the interpretation by the data acquisition company can be automated (Al-Sit et al. 2015) and may have systematic errors. Also the background knowledge in engineering geology of the data acquisition company can be unknown.

For the reasons listed above, reinterpretation of Televiewer should be undertaken by sufficiently trained professionals.

6 CONCLUSION

Our experience indicates that calibration with physical rock core is vital in interpreting Televiewer data accurately. It is noted that defects in the rock core can be drilling induced, so it is also vital to use the logs as personnel in the field have assessed whether the fractures are in situ or just drilling induced. In the absence of physical rock core, logs and photographs have to be used extensively to corroborate the Televiewer interpretation, and this can be successful. Televiewer data provides a powerful tool for understanding ground conditions and structural geology data. Understanding the limitations of Televiewer imaging is critical and reliance on the information without geotechnical interpretation can cause inaccuracies in the geological model and additional design and construction costs.

The advantage of undertaking optical and acoustic Televiewer on the same hole allows for better interpretation even in the absence of borehole logs and rock core.

7 ACKNOWLEDGEMENTS

The issues outlined in this paper have been identified by the authors through professional exposure with Coffey Corporate Services Pty Ltd: A Tetratech Company. Thanks to Dr C. Bridges for his helpful suggestions during the review of this manuscript.

8 REFERENCES

Al-Sit, W., Al-Nuaimy, W., Marelli, M., & Al-Ataby, A. (2015). Visual texture for automated characterisation of geological features in borehole Televiewer imagery. *Journal of Applied Geophysics*, 139-146.

de Frederick, F., Nguyen, T., Seymour, C., & Dempers, G. (2014, Oct). *Geotechnical data from optical and acoustic Televiewer surveys*. AusIMM Bulletin, pp. 62-66.

Li, S. J., Feng, X.-T., Wang, C. Y., & Hudson, J. A. (2013). ISRM Suggested Method for Rock Fractures Observations Using a Borehole Digital Optical Televiewer. *Rock Mechanics Rock Engineering*, 635-644.

Lofts, J. C., & Bourke, L. T. (1999). The recognition of artefacts from acoustic and resisitivity borehole imaging devices. In M. A. Lovell, G. Williamson, & P. K. Harvey, *Borehole Imaging: Applications and Case Histories* (pp. 59-76). Geological Society London: Special Publications 159.

Prensky, S. E. (1999). Advances in borehole imaging technology and applications. In M. A. Lovell, G. Williamson, & P. K. Harvey, *Borehole Imaging: Applications and Case Histories* (pp. 1-43). Geological Society London: Special Publications 159.

Versteeg, J. K., & Morris, W. A. (1994). Pitfalls and procedures for determining fabric orientations in non-oriented bore core. *Journal of Structural Geology*, 283-286.

Geotechnical and Geophysical Site Characterisation 5 – Lehane, Acosta-Martínez & Kelly (Eds)

Additional parameters measured in a single CPT, click-on modules for the digital cone

M. Woollard & O. Storteboom
A.P. van den Berg, Heerenveen, The Netherlands

T. Länsivaara & J. Selänpää
Tampere University of Technology, Tampere, Finland

ABSTRACT: The paper describes a new CPT system that consists of a digital data logger "Icontrol" and a digital cone "Icone". The Icone is easily extendable by click-on modules to measure additional parameters and any module is automatically recognized by the Icontrol, thus creating a true plug & play system. This paper describes how, by moving to smart digital communication, sufficient bandwidth over a thin flexible measuring cable was created to accommodate additional parameters, without the need for changing cones, ca-bles or data loggers. The following modules are described: seismic, conductivity, magneto and vane. Feed-back from fieldwork with the Icone and a selection of click-on modules highlights the user experience with this new approach

1 INTRODUCTION

Due to its benefits, digital technology is used in many applications and is now also available to support efficient soil investigation. The possibilities of this technology have led to the development of the digital cone, the digital data logger and digital click-on modules.

2 DIGITAL CONE

The digital cone or Icone has been available since 2006. The integration of intelligent electronics provides a range of possibilities in order to make further improvements to the electrical cone and to simplify its use. In addition, the Icone is stronger due to mechanical adjustments.

The Icone basically uses the same measuring sensors as applied in the analog cone. The difference however is that the analog signals are being digitized and multiplexed already inside the cone.

Digitizing means that the analog signals are being sampled with a certain frequency and converted into a digital data stream. This digital data stream is more robust, and therefore less sensitive to distortion and loss of accuracy in comparison with the analog signals.

By multiplexing, an almost unlimited amount of sensor signals can be combined into one digital data stream and transmitted through a simple 4-wired cable.

Figure 1. Icone 10 cm^2 and 15 cm^2 area with Icontrol data logger.

A built-in memory capacity increases the user friendliness of the Icone system. For example:

- the Icone number and calibration data are stored inside and are exchanged automatically with the Icontrol data logger.
- Extreme sensor values are stored in memory and can be read for evaluation purposes.
- The memory capacity allows the data storage of a full working day.

The Icontrol data logger provides power to the Icone and synchronizes the Icone signals with the depth signal, recorded from the pushing device. The Icontrol transmits the signals to a computer system, where the CPT-parameters are shown on real time graphs.

The use of smart electronics for the Icone system has provided the following benefits:

- The accuracy of the total data acquisition system is determined only by the accuracy of the Icone.
- Interchangeable click-on modules with specific sensors can be easily added to the Icone without the need of changing cables and data loggers.
- These modules are automatically recognized by the Icontrol and the corresponding display is automatically shown on the screen.
- The Icone is able to recognize surges in measured parameters and overrule system control if needed.
- Several mechanical improvements have led to a stronger design.
- An Icone can be combined with one or more (different) modules.

3 ICONE AND CLICK-ON MODULES

In the past five years several click-on modules for the Icone were developed. In this chapter the following three are described: the seismic module, the conductivity module and the magneto module. A fourth application for vane testing is described in chapter 4. All modules can be used with a 10 cm^2 and a 15 cm^2 Icone. When CPT-data is not required, the click-on modules can also be used with a dummy tip instead.

3.1 *Seismic module*

Seismic tests are performed to investigate the elastic properties of the soil. For this purpose a shear wave (S) or a compression wave (P) is guided into the soil. Elastic soil properties are essential input for prediction of ground-surface motions related to earthquake excitation and for assessment of: foundation design for vibrating equipment, offshore structure behavior during wave loading and deformations around excavations.

Figure 2. Seismic module with 10 cm^2 Icone.

3.2 *Conductivity module*

The measurement of electrical conductivity in the subsoil is a function of the conductivity of the pore water and of the soil particles, the first being the dominant factor. With the conductivity module, changes in the concentration of (dissolved) electrolytes are determined without specifying the exact nature of these electrolytes. Therefore the module facilitates separation of zones with differentiated water content, including determining the water table depth and the thickness of the capillary ascent zone or separation of fresh and salt water carrying soil layers. Another very important application of the conductivity module is detection of (the degree of) contamination in the soil. Further soil investigation should provide details on the actual contaminants.

Figure 3. Conductivity module with 10 cm^2 Icone.

3.3 *Magneto module*

Unknown structures and obstacles, like unex-ploded ordnance (UXO), are a risk factor in the execution of earthworks. To avoid risks of damage and interruptions of work, these underground elements must be identified and mapped. Most underground structures contain metal such as sheet-piles, ground anchors and pipe lines or a combination of metal and concrete, such as reinforced foundation piles. Power supply cables and above structures have in common that they affect the earth's magnetic field.

Using the magneto module, metal objects in the underground can be detected by interpreting anomalies of the earth's magnetic field.

Figure 4. Magneto module with 10 cm^2 Icone.

4 ICONE VANE

The vane test is primarily used to determine the undrained shear strength s_u of saturated clay layers. The test can also be used in fine-grained soils such as silts, organic peat, tailings and other geomaterials where a prediction of the undrained shear strength is required.

4.1 *Principles*

The field vane test consists of four rectangular blades fixed at 90° angels to each other, that are pushed into the ground to the desired depth. This is followed by the measurement of the torque required to produce rotation of the blades and hence the shearing of the soil. The chosen blade size depends on the stiffness of the soil in order to perform an accurate measurement; the stiffer the soil, the smaller the blades of the vane.

Figure 5. Icone vane (without protection tube).

The Icone vane has many features that facilitate an accurate vane test. In the past the torque was measured at the surface. Now the actuator is integrated in the same compact housing, enabling easier, faster and more accurate operation. The vane is pushed out of its protection tube and retracted again after the test. This advantage allows more vane tests at different depths without the need of retrieving the tool to surface level. The vane rotation speed is adjustable from 0.1 °/s for performing very accurate shear tests, up to 12 °/s for fast remoulding.

The vane tool is pushed into the soil by means of standard casing tubes and CPT-rods. Depth is measured on the pushing device and added to the field data by the Icontrol data logger. The Icone vane tester can be used for onshore as well as offshore applications.

4.2 *Data processing and visualizing*

During a vane test, the vane is being rotated with a very low constant speed, while the required torque is measured with respect to the angel of rotation. This measured torque is analytically converted to the shearing resistance of the cylindrical failure surface of the vane used, and expressed in kPa. A typical shear curve is shown in figure 6.

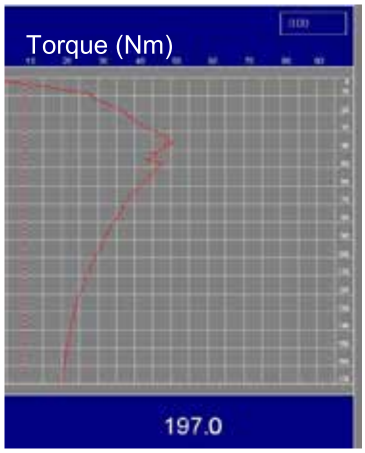

Figure 6. Results of an Icone vane test.

The highest value of this curve is a measure for the undrained shear strength of the soil material that is being investigated. A repetition of this test, after thorough remoulding of the soil, provides a uniform curve of which the highest value is a measure of the remoulded shear strength.

5 PRACTICAL EXPERIENCES ICONE VANE

5.1 *Background*

In Finland the field vane test is still the most used method to determine undrained shear strength (s_u). Nevertheless the equipment generally in use faces several shortcomings. (Ukonjärvi 2015):

- Spring elements used for propulsion are nonlinear, but the calibration factor is usually constant (Nilcon system).
- Zero shifts occur when rotating is performed from ground level.
- Some slip-coupling models don´t have constant inner friction.
- Errors and different phases of the Vane test are not that obvious in graphs using the circular coordinate system (Nilcon system).
- Rotation speed may vary when using different vane sizes.

The most common impact of these errors is an overestimation of the friction between the vane rod and the surrounding soil. Consequently this causes an underestimation of strength that may lead to expensive and uneconomic solutions.

The Icone Vane meets the requirements of application Class 1 according to the EN-ISO 22476-9 standard. By measuring torque and rotation right above the vane, the above mentioned shortcomings with the existing vane measuring tools can be avoided.

Although a correctly performed field vane test can be regarded as a very reliable way to measure the average undrained shear strength, the test procedure is rather time-consuming. The values are obtained at multiple depths, often with 0.5 or 1.0 m intervals. To shorten this procedure, a sensitive Icone CPTu has been taken into use in parallel with the Icone Vane. As Finnish clays can be very soft with undrained shear strengths as low as 5 kPa, the requirements for accuracy of the equipment and measurements are very high.

The accuracy of the torque measurement of the Icone Vane is very good. However to transform the torque into shear stress, some assumptions have to be made. Usually it is assumed that soil shears as a cylinder and shear stress is distributed uniformly across the horizontal area at the top and bottom of the vane. These assumptions could cause a bit error to the interpretation of the undrained shear strength (Wroth 1984). However, if the torque measurement was accurately determined, this error can be neglected.

5.2 *Aim of the study*

The aim of the ongoing study at the Tampere University is to determine reliable cone factors with which the undrained shear strength can be determined by using a sensitive Icone. The Icone Vane is used as one of the reference methods to calibrate the undrained shear strength. In addition, laboratory tests will be performed on high quality undisturbed samples.

The key goal is to find the best practice for the determination of the undrained shear strength in very soft soils. The future practice could well be that the investigation plans contain one Icone Vane field test with torque and rotation measurements just above the vane, supplemented by several CPTu tests with a sensitive Icone.

5.3 *Equipment used*

In-situ soil investigations were made by a CPT Crawler with a hydraulic cone penetrometer (100 kN max. pushing load), an Icone Vane and a sensitive Icone (7.5 kN max. tip load), see Figure 7.

Figure 7. 12 ton CPT rig in Perniö (Salo).

5.4 *Test site*

The test site is located in Perniö, directly next to the coastal railway track between Helsinki and Turku on the edge of a marine clay area. A full scale embankment failure test was conducted in 2009 in this area (Mansikkamäki and Länsivaara 2010). The present study includes investigations outside the failure test area on natural ground. The subsoil comprises the following layers (from top to bottom):

- Organic material 0.0 - 0.3 m
- Dry crust 0.3 - 1.4 m
- Stiff clay 1.4 - 1.8 m
- Soft clay 1.8 - 11.7 m
- Silt 11.7 - 12.8 m

The soft clay has a very high water content varying generally between 70 and 110%, which is above the liquid limit. Previous investigations on the test site indicate a very high sensitivity with an average value of around 40. The sensitivity is the relation between the undisturbed and fully remoulded undrained shear strength. With the field vane test the remoulded strength is determined after the vane is turned 20 full rotations with higher speed than the undisturbed test. The clay is just slightly over consolidated.

5.5 *Test results*

In the preliminary interpretation of the CPTu tests existing formulas and cone factors that have proven to perform well in similar conditions have been used.

To determine the undrained shear strength by measuring the tip resistance, the standard formula $s_u = (q_T-\sigma_{vo})/N_{kT}$ has been used. Because the undrained shear strength is anisotropic, i.e. its values depend on the mode of shearing, the value of N_{kT} depends on which test the results are compared to. It is common to compare results to either direct shear tests (DSS) or triaxial compression tests (UC). DSS strength is generally close to the average strength and comparable to field vane, while the triaxial compression corresponds to the active strength. As the triaxial compression strength is higher than the direct shear strength, the value for N_{kT} should be higher when comparing to DSS strength. Larsson and Åhneberg (2003) recommend to use the tip resistance factor $N_{kT} = 16.3$ to rough estimation for the average undrained shear strength for normally consolidated inorganic clays. Another method that was used herein is the one by Larsson & Mulabdic (1991) where the cone factor is estimated, based on the liquid limit as $N_{kT} = 13.4 + 6.65 * w_L$. The ground conditions are very similar in Finland and Sweden, so these interpretation methods were considered to provide a good first estimate.

Using only the pore pressure measurements for the interpretation of the undrained shear strength, the formula $s_u = (q_T-\sigma_{vo})/N_{\Delta u}$ was used. The value of the $N_{\Delta u}$-factor given in the literature varies quite much. Based on cavity expansion theory the value of $N_{\Delta u}$-factor varies between 2 and 20 (on a global basis for any comparison test). La Rochelle et al. (1988) found that $N_{\Delta u}$ varied between 7 and 9 for three Canadian clays using uncorrected field vane measurements as reference strength when OCR ranged between 1.2 and 50. The over consolidation ratio (OCR) is the ratio between the highest stress experienced divided by the current stress.

Larsson suggested to determine the pore pressure factor as a function of liquid limit by equation $N_{\Delta u} = 14.1 - 2.8*w_L$ (Larsson 2007). Values of liquid limit are between 55 and 79. The liquid limit is an index property of fine-grained soils. The liquid limit is defined as the moisture content where soil behaves as liquid. According to the mentioned range for the liquid limit, the value of $N_{\Delta u}$ is between 11.3 and 12.4 when comparing to corrected field vane values. In figure 8 profiles of corrected field vane results and undrained shear strength evaluated from CPTu are presented.

Although there is some scatter in the results, the different interpretation methods show quite good correlation and consistency to the Icone vane tester results. In the future the scatter will be narrowed by developing the methods to evaluate the cone factors for Finnish clays.

The difference between interpreted undrained shear strength and corrected field vane results at depth 5 – 6 m could be the result of silty inclusions like previous study has shown (Mataic 2016).

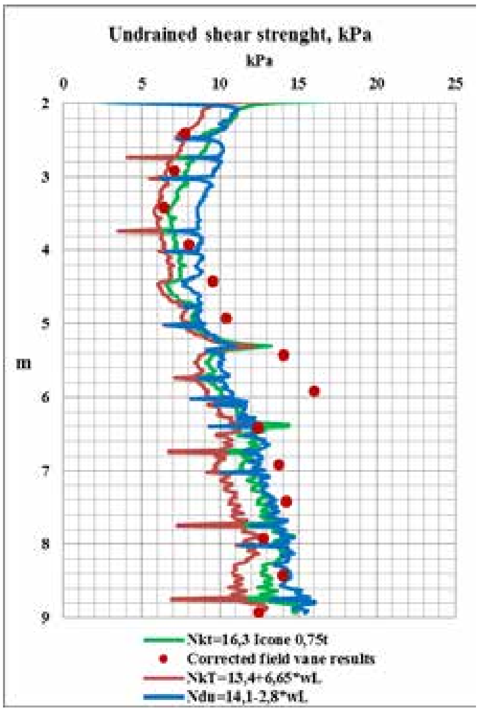

Figure 8. Interpretations of CPTu tests and corrected field vane results.

In figure 9 the shear stress-deformation behavior with the Icone Vane in Perniö is shown. The torque (T) is measured every 0.1° of rotation and the torque is converted to shear stress with equation $\tau_{fv} = 273*T/D^3$ where D is the diameter of the vane. A very illustrative strength profile with softening can be seen for the sensitive structured Perniö clay. In some of the results small steps can be seen at the start of the rotation indicating that rods have not been tightened well enough.

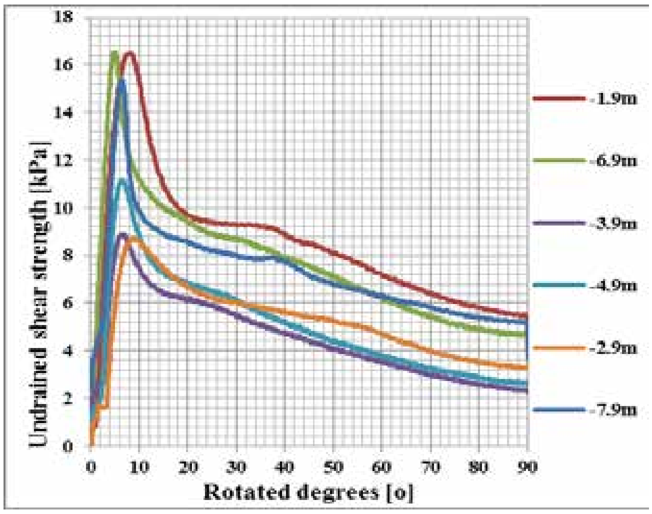

Figure 9. Shear stress-deformation behavior with field vane test in Perniö.

The study will be continued by doing laboratory tests for further verification of data. Several test sites will be studied to create a reliable data base for the study. Finally recommendations will be given for the most suitable interpretation methods and cone factors for the Finnish soft clay conditions.

6 CONCLUSIONS

Cone Penetration Testing (CPT), as a technique for in-situ soil investigation, is a recognized and widespread method for efficiently performing soil surveys. In the course of time CPT is continuously improved by the effective use of the latest state of the art. Recent developments, concerning the application of digital electronics inside the cone, offer a range of new features and benefits. The most prominant of these is the ability to easily extend the digital Icone by click-on modules to measure additional parameters. Any module is automatically recognized by the Icontrol data logger, creating a true plug & play system.

The new Icone Vane with rotation and torque measurement right above the vane gives an accurate direct measurement of the average undrained shear strength of soft soils. In addition, it provides valuable data on the strength deformation behavior of soils. It still takes time to do the testing and the results are given only for certain depths.

CPTu with the sensitive Icone has proven to give very reliable and repeatable results from soft Finnish clays. For the determination of the undrained shear strength, the accuracy is very much dependent on the cone factors used to convert the CPTu measurements into undrained shear strength.

By combining these two pieces of equipment as in the A.P. van den Berg system, the redeeming features for both can fully be utilized. CPTu testing provides a fast way to versatile continuous data, which among many other things can be used for the determination of the undrained shear strength. With the aid of the accurate new Icone Vane, the cone factors used can be adjusted to correspond to the local soil conditions. The authors strongly believe that this combination can significantly reduce the uncertainties in relation to the undrained shear strength.

7 REFERENCES

EN-ISO 22476-9:2009 *Ground investigation and testing – Field testing – part 9: Field vane test.*

Ukonjärvi, P., 2016. On the reliability of undrained shear strength in railway environment (in Finnish). Master thesis. Tampere University of technology.

Mansikkamäki, J., Länsivaara, T. 2010 Analysis of a full scale failure test on old railway embankment. In Thomas Benz (ed.), *Numerical Methods in Geotechnical Engineering; Proc. euro. conf,. Trondheim, 2-4 June 2010*. Abingdon: Taylor & Francis.

Mataić, I. 2016. *On structure and rate dependence of Perniö clay.* PhD Thesis, Aalto University, Helsinki, Finland

Larsson, R., Åhnberg, H., 2003. *Long-term effects of excavations at crests of slopes.* Swedish geotechnical institute. Linköping 2003. Report 61. s.130

Larsson, R., 2007 *CPT-sondering utrustning – utförande – utvärdering En in-situ me-tod för bestämning av jordlagerföljd och egenskaper i jord.* Swedish geotechnical institute. Linköping 2007. Information 15. s.71

La Rochelle, P., Zebdi, P.M., Leroueil, S., Tavenas, F. and Virely, D., 1988. *Piezocone Tests in Sensitive Clays of Eastern Canada. Proceedings of the International Symposium on Penetration Testing,* ISOPT-1, Orlando, 2, Balkema Pub., Rotterdam., 831-841.

Wroth, C. P. 1984 The interpretation of in situ soil tests. Geotechnique, 34(4) 449-488.

Vesic. A. S. 1972 Expansion of cavities in infinite soil mass. *Journal of the Soil Mechanics and Foundation Division, Proc. of the ASCE, Vol. 98, No. SM3., 265- 290.*

Woollard, M., Storteboom, O., and Coto Loria M. 2013 Additional Parameters Measured in a Single CPT, Cick-on Modules for the Digital Cone. In *Proc., Geotechnics for sustainable developments*: *Geotec Hanoi 2013, Hanoi, Vietnam, 899-908.*

Geotechnical and Geophysical Site Characterisation 5 – Lehane, Acosta-Martínez & Kelly (Eds)
© 2016 Australian Geomechanics Society, Sydney, Australia, ISBN 978-0-9946261-1-0

Correction for CPT f_s errors due to variation in sleeve diameter

M. Holtrigter & A. Thorp
Ground Investigation Ltd, Auckland, New Zealand

ABSTRACT: The sleeve friction measurement, f_s, is considered to be the least reliable of the three measurements in piezocone testing. It has been shown that the diameter of the friction sleeve in relation to the cone tip diameter has an effect on the sleeve friction measurements (f_s). Testing standards (e.g. ASTM D 5778-12) allow a tolerance range such that the friction sleeve can be equal to, or up to 0.35 mm greater than the cone tip diameter. Cone penetrometers with larger friction sleeve diameters show higher f_s measurements (Holtrigter, et al. 2014). The most accurate results are generally considered to be when the friction sleeve and cone tip are of the same diameter (Cabal and Robertson 2014). In this study, friction sleeves of different diameter have been used in side-by-side piezocone testing on two test sites in New Zealand to investigation the variation to sleeve friction measurements with sleeve diameter. By empirical correlation of these tests the equation to allow correction for this effect (Holtrigter et al. 2014) has been further developed.

1 INTRODUCTION

It is widely considered that the sleeve friction measurement, f_s, is the least reliable of the three measurements provided by the piezocone. In comparative studies of side-by-side piezocone tests performed by different contractors, the f_s measurements show the most variation (Tigglemann & Beukema 2008, Lunne 2010). Lunne and Andersen (2007) suggest that the lack of accuracy in f_s measurement is primarily due to the following factors:

- Pore pressure effects on the ends of the sleeve
- Tolerance in dimensions between the cone and sleeve
- Surface roughness of the sleeve
- Load cell design and calibration

In side-by-side piezocone testing at three sites in New Zealand, Holtrigter et al. (2014) showed that the comparative diameter of the cone tip and the friction sleeve affected the f_s measurements. In that study four or five different diameter friction sleeves were used in the side-by-side tests, with the same diameter cone tip. The same piezocone by the same manufacturer was used in the side-by-side tests so that the only variable of the four listed above was the size difference between the sleeve and cone tip diameters.

In the side-by-side tests, the cone tip diameter was kept constant at 35.7 mm. Friction sleeve diameters of 35.6 mm, 35.7 mm, 35.85 mm, 36.05 mm and 36.15 mm were used, corresponding to -0.1 mm, 0.0 mm, +0.15 mm, +0.35 mm and +0.45 mm greater than the cone diameter, respectively. It should be noted that ASTM D 5778-12 allows a tolerance between sleeve and cone tip diameters of between 0.0 mm and 0.35 mm.

The results of the side-by-side tests showed that the f_s measurements (and friction ratio, R_f) increased with increasing difference between sleeve and cone diameters, as illustrated in Figure 1.

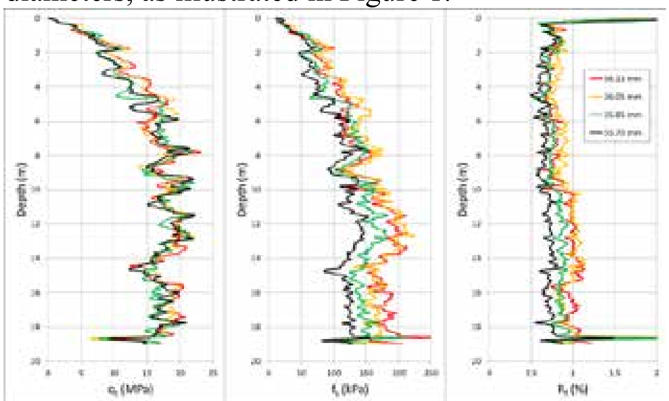

Figure 1. Illustration of increasing f_s and R_f with increasing sleeve diameters (Holtrigter et al. 2014)

As a reference, it was suggested that the f_s measurements relating to the test results where the sleeve diameter was equal to the cone tip diameter presents the 'correct' result for f_s. Cabal and Robertson (2014) showed that the f_s measurements relating to a sleeve diameter equal to the cone tip diameter more precisely related to the results of residual undrained shear strengths measured by adjacent field vane tests (Figure 2). A further adjacent CPT test using a larger diameter sleeve showed higher f_s measurements.

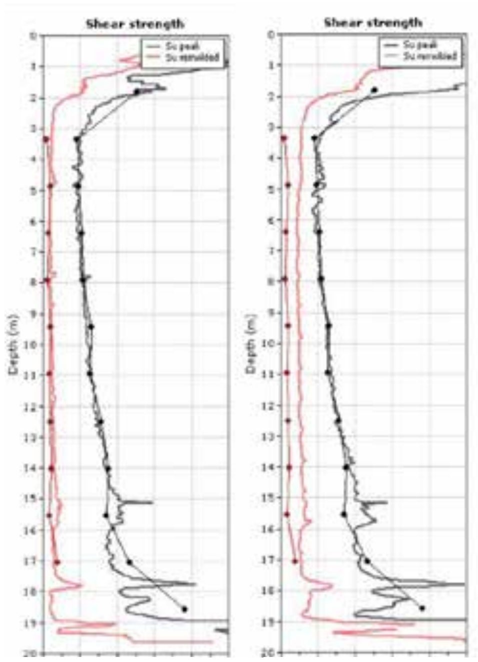

Figure 2a Figure 2b

Figure 2. Comparison of fs measurements of differing sleeve diameter and field vane tests (Cabal and Robertson 2014). Figure 2a. Equal size cone & sleeve. Figure 2b. Over size sleeve.

Holtrigter et al. (2014) suggested that the variation in f_s measurements between cones with equal sleeve and tip diameter and those with larger diameter sleeves was due to:

- End resistance (=q_t) on the edge of the sleeve that protrudes from the cone tip
- Increased friction along the sides of the sleeve due to increased volume of displacement

A correction (Equation 1, below) was suggested for adjusting the f_s measurements of oversized cones to 'corrected' values relating to sleeves of equal diameter to the cone diameter. Please note that Equation 1 has been corrected for a typo that appeared in the original paper.

$$f_{s(0)} = \left[f_s - \left(\frac{\pi q_t(d_s^2 - d_c^2)}{60}\right)\right] \times [1 - 0.0084(d_s^2 - d_c^2)] \quad (1)$$

The first factor in the equation relates to correcting for end resistance on the edge of the sleeve and the second factor is an empirically derived correction for the additional friction due to volume expansion of the sleeve.

In this paper the results of two further sites are discussed.

2 EQUIPMENT AND PROCEEDURES

For this study, a piezocone manufactured by Pagani Geotechnical Equipment from Italy has been used. The same piezocone was used at each test site. The piezocone has a 50 MPa capacity load cell for end resistance and 1,600 kPa capacity sleeve friction load cell. The friction sleeve has equal end areas. The pore water pressure element is at the u_2 position.

A cone tip diameter, d_c = 35.7 mm was used for all testing. Friction sleeves of different diameters were supplied by Pagani Geotechnical Equipment for this study. Friction sleeve diameters of 35.7 mm, 35.85 mm, 36.05 mm and 36.15 mm have been used. These correspond to differences to cone diameter (d_s – d_c) of -0.1 mm, 0.0 mm, 0.15 mm, 0.35 mm and 0.45 mm, respectively.

For the purposes of this study, a grease filled slot filter that has been machined to the exact size of the cone diameter has been used so as to eliminate the effect of a slightly smaller or larger diameter filter element.

At each of the two test sites CPTs were performed with different friction sleeves as side-by-side tests approximately 1.0 m in horizontal distance apart.

3 TEST SITES AND RESULTS

Two test sites were selected. Both are clay sites in Auckland, New Zealand. The sites are:

- Huapai (Pleisocene alluvium)
- Herald Island (residual soil)

The results of the measured data from each of the sites are shown in Figures 3 and 4. The results show reasonable agreement between the end resistance, q_t, but a noticeable visual difference in the friction sleeve values, f_s. This difference also translates to the friction ratio values, R_f.

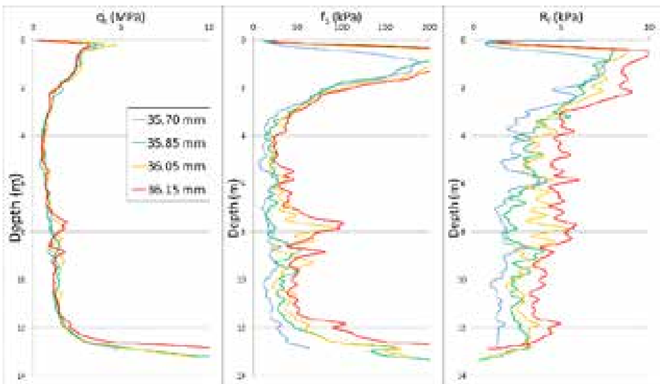

Figure 3. Raw data from Huapai site.

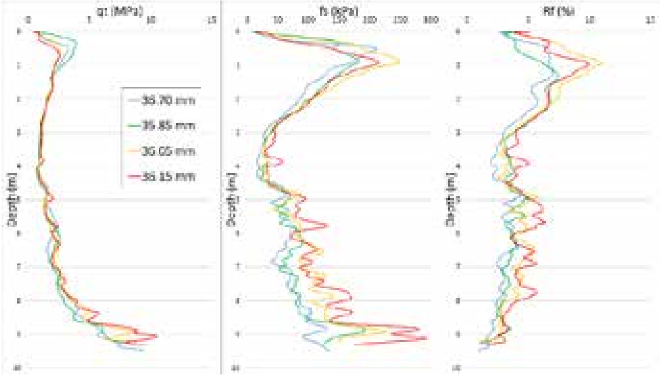

Figure 4 Raw data from Herald Island site.

4 INTERPRETATION OF RESULTS

It is clear from the results of the side-by-side tests that the sleeve friction values, f_s, (and the friction ratio values, R_f), progressively increase with increasing sleeve diameter. This is considered to be due to two effects:

1. End resistance on the edge of the sleeve that protrudes from the cone tip
2. Increased friction along the sides of the sleeve due to increased volume of displacement

Figure 5 illustrates how the end resistance can develop on the edge of the friction sleeve. Thus the measured sleeve friction, f_s, can be considered to have two components, as per Equation 2:

$$fs = fs(qt) + fs(f) \tag{2}$$

where f_s = measured sleeve friction; $f_{s(qt)}$ = component of measured sleeve friction due to end resistance on sleeve edge; and $f_{s(f)}$ = component of measured sleeve friction due to true friction on the sleeve.

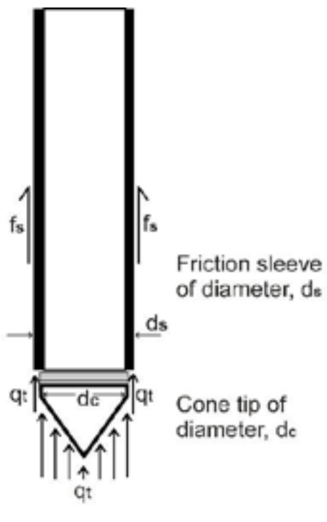

Figure 5. End resistance effect on oversize friction sleeve

4.1 *End Resistance on Friction Sleeve*

The component $f_{s(qt)}$ can be calculated by assuming that the same end resistance measured by the cone tip, q_t, also applies to the oversize edge of the sleeve, as illustrated on Figure 5. The force thus measured by the friction sleeve load cell will be equal to the area of the sleeve end that protrudes over the cone tip multiplied by q_t. This is then divided by the cone sleeve surface area (150 cm^2) to give an equivalent sleeve friction value. In this way, Equation 3 below is derived.

$$f_{s(qt)} = \frac{\pi q_t(d_s^2 - d_c^2)}{60} \tag{3}$$

Where q_t = total cone resistance in MPa; and d_s & d_c in mm

By combining Equations 1 and 2, the measured f_s data can then be corrected for this end resistance effect to give $f_{s(f)}$.

$$f_{s(f)} = f_s - f_{s(qt)} = f_s - \left[\frac{\pi q_t(d_s^2 - d_c^2)}{60}\right] \tag{4}$$

4.2 *Relationship between end-resistance corrected $f_{s(f)}$ values and reference f_s values*

The correction given in Equation 4 accounts for the end resistance effect. Holtrigter et al. (2014) found that his correction does not fully account for the difference in measured f_s values for the various size sleeves. The further effect is considered to be a function of the volume change between sleeves of increasing diameter (i.e. a function of $d_s^2 - d_c^2$).

To investigate this relationship, a comparison has been made between the $f_{s(f)}$ values corresponding to each of the various sized sleeves and the sleeve friction measured for the cone with the same size cone tip and sleeve diameter.

For the case of same sized cone and sleeve diameters, $d_s^2 - d_c^2 = 0$ and so no correction is required and $f_{s(f)} = f_s$, the measured sleeve friction. For the purposes of this study the measured sleeve friction values resulting from same size sleeve and cone are considered to represent the correct data for comparison purposes.

The graph in Figure 6 shows the average results of the comparative study. In this graph, the average values of $f_{s(0)}/f_{s(f)}$ are plotted against $d_s^2 - d_c^2$. The results of this study and also those of the previous study (Holtrigter et al. 2014) are shown. In the previous study, the points for the three sites tested in that study

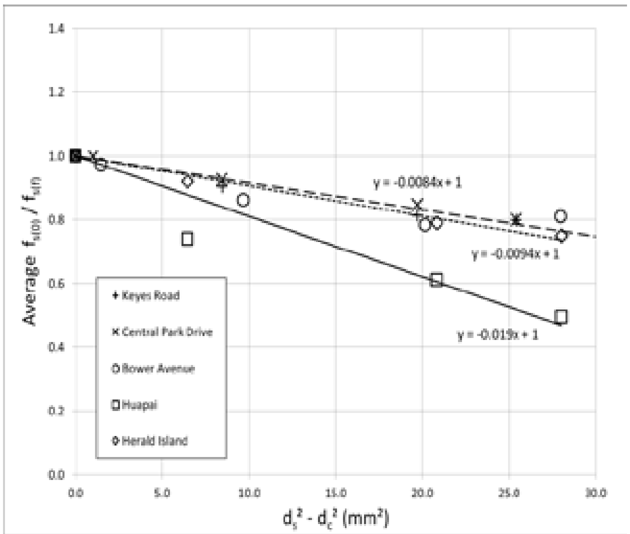

Figure 6. Plot of $f_{s(0)}/f_{s(f)}$ vs $d_s^2 - d_c^2$

showed a linear relationship with a gradient of -0.0084 giving Equation 5, below.

$$f_{s(0)} = f_{s(f)} \times [1 - 0.0084(d_s^2 - d_c^2)] \tag{5}$$

Where $f_{s(0)}$ = sleeve friction equivalent to that of an equal diameter cone and sleeve

In the current study, the two sites show different linear relationships, with gradients of -0.0094 and -0.019, as shown in Figure 6. This suggests that the relationship may be site or soil specific and that the equation is best presented with a variable component, m_{fs}, being the gradient of the linear relationship shown in Figure 6. Thus Equation 5 becomes:

$$f_{s(0)} = f_{s(f)} \times [1 - m_{fs}(d_s^2 - d_c^2) \tag{6}$$

By combining Equations 4 and 6, an overall correction direct from the raw sleeve friction values, f_s, can be obtained, as shown in Equation 7 below:

$$f_{s(0)} = \left[f_s - \left(\frac{\pi q_t(d_s^2 - d_c^2)}{60}\right)\right] \times [1 - m_{fs}(d_s^2 - d_c^2)] \tag{7}$$

This equation was then applied to the data at both sites, with m_{sf} = 0.0094 for the Huapai site and msf = 0.012 for the Herald Island site. The resulting measured and corrected fs and R_f values are shown in Figures 7 and 8.

5 DISCUSSION

The results of this study and that of the previous studies (Holtrigter et al. 2014, Cabal and Robertson 2014) confirm that the effect on f_s measurements is sensitive to the tolerance between the cone and sleeve diameters. The effect appears to occur in both sands and clays and in soft/loose as well as stiff/dense soils.

The suggested correlation (Equation 7) appears to provide a reasonable correction. However, there is a variable (m_{fs}) that is an unknown factor without the benefit of a reference test (with equal sleeve and tip diameters). This makes Equation 7 difficult to apply in practice. Further research is required to better understand this effect, possibly with the application of cavity expansion theory. In the meantime, it is suggested that if corrections are to be made to f_s data, a first order approximation could be made using Equation 7 with m_{fs} = 0.0084. This may not provide a complete correction, but may be more accurate than the measured f_s values for oversized friction sleeves.

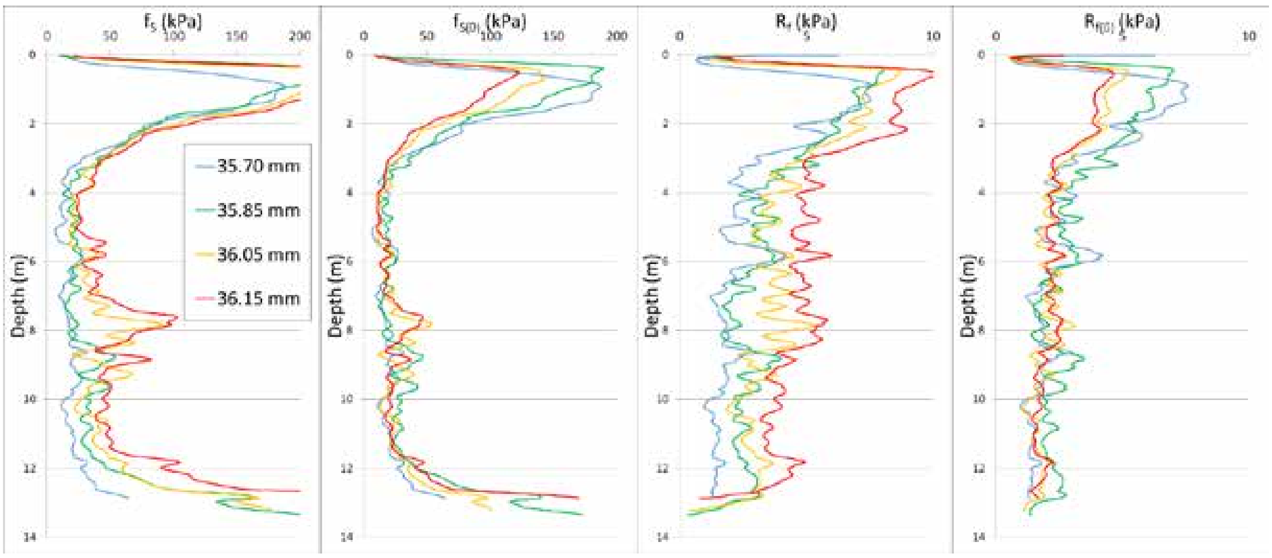

Figure 7. Huapai f_s, $f_{s(0)}$, R_f and $R_{f(0)}$.

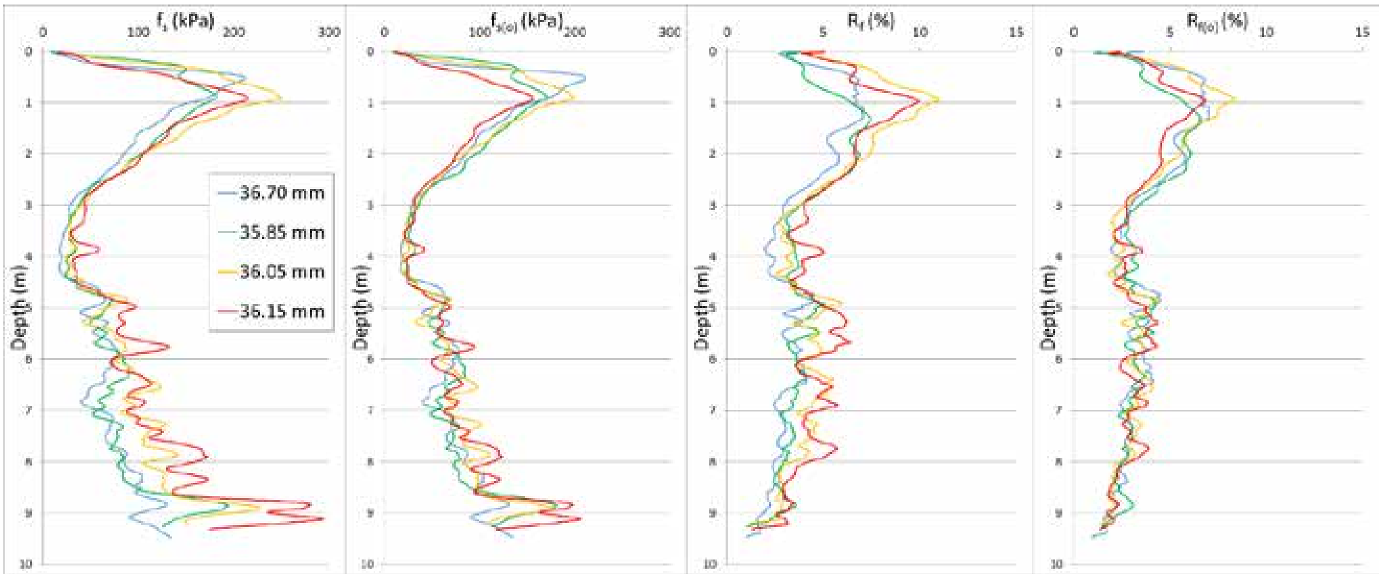

Figure 8. Herald Island f_s, $f_{s(0)}$, R_f and $R_{f(0)}$.

The sensitivity of this effect on f_s measurements puts greater reliance on regular checking of cone and sleeve dimensions as wear on these components will have an effect. ASTM D 5778-12 allows a tolerance of up to 0.35 mm between the cone and sleeve, but within this tolerance there is a significant difference in the effect on f_s. Even differences as little as 0.1 mm can have an appreciable effect. In sandy or gravely soils, wear can occur rapidly. As little as one day's wear in such soils could result in significant error is f_s measurement.

It is considered that cones and sleeves manufactured to the same diameter (ideally 35.7 mm) would be preferable. For friction sleeves that have diameters greater than the cone tip, either due to wear or by manufacture, a correction such as that suggested by Equation 7 (with $m_{fs} = 0.0084$) should be applied. In abrasive soils, it is suggested that cone and sleeve measurements be recorded daily and corrected accordingly.

6 CONCLUSIONS

From the side-by-side tests undertaken in this study and previous studies it has been shown that different f_s measurements are obtained with piezocones of different sleeve and cone diameters. Piezocones with sleeve diameters larger than the cone tip result in larger f_s measurements than those obtained using a piezocone with equal diameter sleeve and cone. Increasingly larger sleeves (in relation to cone size) create increasingly larger f_s measurements. The increased f_s measurements are thought to be due to a combination of end-resistance on the edge of the oversized sleeve plus increased friction due to the displacement volume increase of the larger sleeve.

The f_s measurements appear to be sensitive to these effects
and significant error can arise, particularly in stiff/dense soils.

From empirical correlation between the side-by-side tests, Equation 7, below has been derived to allow correction of this effect.

$$f_{s(0)} = f_s - \left[\frac{\pi q_t (d_s^2 - d_c^2)}{60}\right] \times \left[1 - m_{fs}(d_s^2 - d_c^2)\right] \qquad (7)$$

This equation has been found to provide a reasonable correction to the f_s values measured in the test sites in this study. The correction appears to work for both sands and clays and for soft/loose soils as well as stiff/dense soils. As a first order approximation a value of $m_{fs} = 0.0084$ can be used.

Further research will be required to confirm or refine this correlation for other sites and using piezocones from different manufacturers. It is considered preferable for piezocones to be manufactured with equal diameter sleeve and cone tips to minimize this effect. This may also lead to more consistent measurements between cones from different manufacturers. Tighter tolerances in standards may also be required.

7 REFERENCES

ASTM D5778-12. 2012. Standard Test Method for Performing Electronic Friction Cone and Piezocone Penetration Testing of Soils. *ASTM International*. West Conshohocken, PA.

Cabal, K. & Robertson, P.K. 2014. Accuracy and Repeatability of CPT Sleeve Friction Measurements. *Proc. CPT'14*, Las Vegas, Nevada, USA.

Holtrigter, M., Thorp, A. & Hoskin, P. The Effect of Sleeve Diameter of f_s Measurements. . *Proc. CPT'14,* Las Vegas, Nevada, USA.

Lunne, T. & Andersen, K.H. 2007. Soft Clay Shear Strength Parameters for Deepwater Geotechnical Design. *Proc. 6th Int. Conf. Society for Underwater Technology, Offshore Site Investigation and Geotechnics*, London.151-176

Lunne, T. 2010. The CPT in Offshore Soil Investigation – a historic perspective. *Proc. CPT'10*, Los Angeles, May 2010. 71-113

Robertson, P.K. 2009. Interpretation of Cone Penetration Tests – a unified approach. *Canadian Geotechnical Journal*, 46. 1337-1355

Tigglemann, L. & Beukema, H.J. 2008. Sounding Ring Investigation. *Proc. ISC-3*, Taiwan. 757-762

Geotechnical and Geophysical Site Characterisation 5 – Lehane, Acosta-Martínez & Kelly (Eds)
 ISBN 978-0-9946261-1-0

Reduced pressuremeter test time procedure and new analysis method

K. Iskander
Free University of Brussels ULB, Brussels, BEGIUM.

ABSTRACT: This paper presents solutions for the drawbacks of Pressuremeter Test (PMT) concerning the long time duration in site in comparison to the other in situ tests and the use of empirical rules to express the medium behavior. A new definition for pressure limit is adopted. It is determined within the first few loading steps. The proposed analysis accounts for: test rate, PMT size, volume of clay influenced by the test, heterogeneity of strain distribution around cavity. The medium behavior is being examined by the modified Cam Clay criterion. The medium octahedral shear stress strain relationship at the level of testing can be deduced. An overall clay medium shear modulus at some depth underground can be estimated. The present analysis method can be adopted for the design of tunnels and for modeling pile shaft clay medium interaction.

1 INTRODUCTION

Pressuremeter test requires long time duration in site compared to the necessary time to carry out the other in situ tests such as CPT and SPT. At any level underground, to determine the pressure limit that would be attained at infinite expansion of the cavity during testing, PMT requires at least twelve minutes. This duration differ from one test to another according to the considered code of practice. So for ten levels underground, PMT requires at least two hour time, while, for example CPT requires few minutes for testing along the same depth underground.

The reason for PMT long duration in site is the necessary time to determine the pressure limit ψ_L. Following French Standards NF P 94-110 (2000), P94-250-I (1996) and the ASTM D47 (1987), this conventional limit is defined by the pressure required to double the initial volume of the membrane cell. This limit has no solid theoretical bases and is assumed to express the clay failure state without defining a failure criterion. J.J. Powell (1990) and other authors separately reported the uncertainties in the methods of assessing and the applicability of pressure limit as well.

To avoid the drawbacks encountered in the analysis methods, Iskander (2013 &2015) adopted an energy concept taking into account: 1) Test rate: the developed excess pore pressure is sensitive to testing rate. Thus, the developed excess pore pressure during the test has to be measured to estimate the effective stress and introduce it in the analysis. 2) PMT size and type: the input energy is a function of the applied pressure and membrane volume. 3) Reliable analysis method: pressure limit ψ_L is newly defined by the applied pressure by PMT at the initiation of radial cracks at cavity surface that occur during the first few loading steps. These cracks are due to the negative stress development thereof. 4) The influenced clay volume during the test is obtained from the equality condition of input energy - work done across the influenced cylinder around PMT cavity. 5) Heterogeneity of strain distribution: to estimate the strains at any radius across the thickness of the influenced clay cylinder, that models the medium around the cavity, the plastic strain increment can be estimated by normality rule. These increments are assumed normal to the modified cam clay criterion (MCC) yield surface.

2 APPLICATION AND ANALYSIS

In two and three dimensional analysis for clay hollow cylinder that is assumed to simulate the clay medium around PMT probe. Iskander (2013& 2015) showed that at some pressure within the first three loading steps, during PMT, the developed excess pore water pressure at the inner radius surface became greater than the created increase in the compressive hoop stress. And, further loading increase by the probe results in further increase in the developed excess pore water pressure.

Moreover, it was shown that the effective octahedral stress path at the inner radius of hollow cylinder, that is the cavity radius, crosses the critical state boundary surface at this state of stress as well. This indicates that at this state of stress the clay fails thereof. Further, (Thevayanagam et al. 1994) and other authors observed the creation of radial cracks at the cavity surface during PMT which agrees with the results of the proposed analysis method. Thus, further loading results in increase in the developed negative stresses at the cavity surface and the corresponding strain increase is being due to the increase in the developed excess pore water pressure thereof.

In conclusion, cracks started to occur during the first three loading steps. It depends on test rate. The faster the test rate, the sooner the clay fails at the cavity surface. Further loading is time waste in site and more cost for nothing. Therefore, it is suggested to limit testing procedure to few loading steps.

The classical interpretation methods assume that the evolution of the strain of the perimeter of PMT cavity expresses the medium strains. But the heterogeneity of strain distribution around the cavity across the medium makes this assumption questionable. Iskander (2015) adopted the Modified Cam Clay criterion MCC (Roscoe & Burland 1968) and the variation energy principle Washizu (1975) to analyze the clay medium behavior due to cylindrical cavity expansion in three dimensions during PMT. Following MCC, the mean strains across the medium that correspond to the calculated average effective stresses can be estimated by normality rule (Equations are written in Appendix). So the increase in the work done by the developed average effective stresses increase and mean strains across the hollow cylinder must be equal to the input complementary energy by the probe so that:

$$V\Delta\psi/A = \tfrac{1}{2}\sum_{i=r}^{z} \bar{\epsilon}_i \times \Delta\bar{\sigma}'_i \qquad (1)$$

Where V= current membrane volume during an applied pressure increase of $\Delta\psi$; ψ = applied pressure by the probe; A = area of the hollow cylinder $\bar{\epsilon}'_{i,}$ $\Delta\bar{\sigma}'_i$ = mean strains, the increase in average effective stresses $\Delta\bar{\sigma}'_\theta$, $\Delta\,\bar{\sigma}'_R$ and $\Delta\bar{\sigma}'_z$ in hoop, radial and vertical directions across the influenced hollow cylinder.

2.1 Hollow cylinder test

Anderson & Pyrah (1987) performed tests on clay hollow cylinder of outer and inner radii of 7.5 and 1.25 cm and it was 15 cm high. This cylinder was provided by three piezometers at its mid height at 1.25, 3 and 5.5 cm measured from the axis of the cylinder. Clay Index properties were W_L = 42%, W_p = 23%, I_p= 19%, Activity = 0.63, Specific volume v = 1.85. Critical State parameters $\lambda = 0.136$ and $\kappa = 0.033$. The reported test results are summarized in Tables 1& 2. for loading rates 30 kPa/minute and 10 kPa/minute respectively.

Figs 1-2 show that, during PMT, the developed excess pore water pressure increases as the test proceeds and the faster the test rate, the greater is the developed excess pore water pressure. But the developed excess pore water pressure decreases with distance from the axis of the cylinder.

Table 1 Experimental Test results, 30 kPa per minute

Applied pressure	Cavity radius	Developed excess pore water pressure at		
		Cavity	3 cm	5.5 cm
ψ kPa	a cm	u_a kPa	u_b kPa	u_c kPa
(1)	(2)	(3)	(4)	(5)
190	1.257	20	18	.1
220	1.27	40	36	4
250	1.29	80	58	10
280	1.32	120	76	16
310	1.37	140	87	23
340	1.41	160	96	30
370	1.45	180	102.	40

Table 2. Experimental Test results, 10 kPa per minute

Applied pressure	Cavity radius	Developed excess pore water pressure at		
		Cavity	3 cm	5.5 cm
ψ kPa	a cm	u_a kPa	u_b kPa	u_c kPa
(6)	(7)	(8)	(9)	(10)
160	1.252	15	10	5
210	1.261	35	18.9	9
240	1.282	60	31	10
260	1.299	75	37.8	16
290	1.317	95	52	19
320	1.37	110	63	27
360	1.454	120	68	40

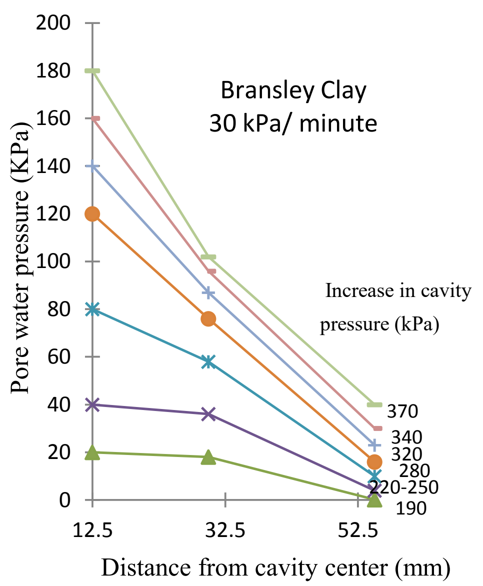

Fig 1. Pore pressure gradients across cylinder, 30 kPa / minute.

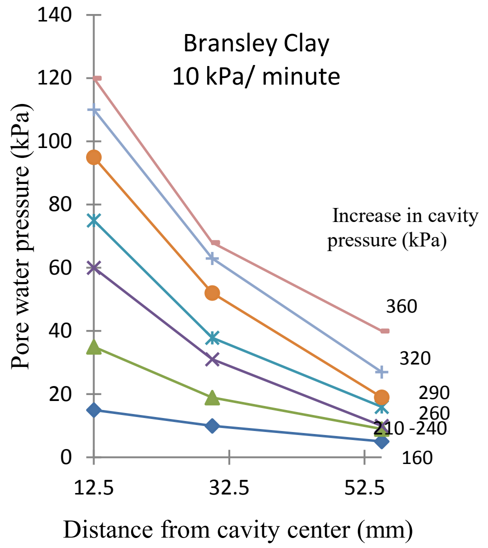

Fig 2. Pore pressure gradients across cylinder, 10 kPa/minute

2.2. *Pressure limit* ψ_L:

The average radial and hoop total stresses across the hollow cylinder at the PMT membrane mid height can be obtained by integrating the equations of Lamé (1852). To estimate the average effective stresses subtract the average measured developed excess pore water pressure. The vertical effective stress is equal to overburden pressure minus the average pore pressure. From equation (1), the deduced outer radii of the hollow cylinders that model the clay medium around the cavity during PMT and reported by Iskander (2015) are written in Tables 3 - 4 for the fast and slow testing rates respectively. Following Lamé (1852), the hoop stress at the inner radius of hollow cylinder is obtained as follows:

$$\sigma_{\theta a} = ((\psi - \sigma_h)R^2 + \psi\, a^2 - \sigma_h R^2)/(R^2 - a^2) \qquad (2)$$

Where σ_h= lateral stress at rest; R, a = outer and inner radii of hollow cylinder.

Table 3 shows for the faster test at the second loading step, the developed excess pore water pressure written in column (4) is equal to 40 kPa and is greater than the created compressive hoop stress at the cavity surface that is written in column (5). So, the total pressure limit = 220 then the effective pressure limit ψ'_L is equal to 180 kPa. The same analysis for the slower test rate showed that at the third loading step ψ_L= 240 kPa then ψ'_L= 180 kPa.

In the present work the deduced pressure limit is attained at the second and the third loading steps for fast and slow tests respectively and its effective value is independent of test rate.

Note the effective ψ'_L is more reliable than the total pressure limit for comparisons because the developed excess pore water pressure is sensitive to testing rate such as stated by Powell (1990).

Table 3 Hoop stress at cylinder inner radius 30 kPa/minute.

Applied pressure	Hollow cylinder radius		pore pressure at cavity	Hoop Stress
	inner	outer		
ψ kPa	a cm	R cm	u_a kPa	$\sigma_{\theta a}$ kPa
(1)	(2)	(3)	(4)	(5)
190	1.257	21.39	20	69.58
220	1.27	38.19	40	39.8
250	1.29	51.09	80	9.84
280	1.316	51.29	120	-20.26
310	1.368	60.69	140	-50.83
340	1.41	70.09	160	-80.17
370	1.45	79.89	180	-110.2

Table 4 Hoop stress at cylinder inner radius,10 kPa/minute.

Applied pressure	Hollow cylinder radius		pore pressure at cavity	Hoop Stress
	inner	outer		
ψ kPa	a cm	R cm	u_a kPa	$\sigma_{\theta a}$ kPa
(1)	(2)	(3)	(4)	(5)
160	1.252	18.96	15	99.74
210	1.261	26.66	35	49.64
240	1.282	41.76	60	19.79
260	1.299	43.86	75	-.228
290	1.317	48.56	95	-30.09
320	1.370	56.46	110	-60.22
360	1.454	73.66	120	-100.2

2.3. *Octahedral shear stress* $\bar{G}_{oct}$:

The geostatic stresses are the initial state of stress. The average effective stress in radial, in hoop and in vertical directions are written in Tables 5 – 6 for the fast and slow test rates respectively. The changes in octahedral stress deviators are estimated by Equation (3) so that:

$$\Delta\bar{\tau}_{oct} = \tfrac{1}{3}\left((\Delta\bar{\sigma}'_R - \Delta\bar{\sigma}'_\theta)^2 + (\Delta\bar{\sigma}'_\theta - \Delta\bar{\sigma}'_Z)^2 + (\Delta\bar{\sigma}'_Z - \Delta\bar{\sigma}'_R)^2\right)^{1/2} \qquad (3)$$

Where $\Delta\bar{\sigma}'_\theta$, $\Delta\,\bar{\sigma}'_R$ *and* $\Delta\bar{\sigma}'_z$: The change in average effective stresses in hoop, radial and vertical directions across the thickness of the hollow cylinder.

And, the corresponding change in strains are estimated following MCC from Equations (13-17) in Appendix. The octahedral change in strain deviator is estimated as follows:

$$\Delta\,\bar{\gamma}_{oct} = \tfrac{2}{3}\left((\Delta\bar{\epsilon}_R - \Delta\bar{\epsilon}_\theta)^2 + (\Delta\bar{\epsilon}_\theta - \Delta\bar{\epsilon}_z)^2 + (\Delta\bar{\epsilon}_z - \Delta\bar{\epsilon}_R)^2\right)^{1/2} \qquad (4)$$

Where $\Delta\bar{\epsilon}_\theta, \Delta\bar{\epsilon}_R$ *and* $\Delta\bar{\epsilon}_z$: The change in average radial, hoop and vertical strains across the thickness of the hollow cylinder respectively.

Accumulate the octahedral stress and strain change values for the successive hollow cylinders that model the whole medium. The medium average shear modulus at the level of the test is defined by $\bar{\tau}_{oct}/\bar{\gamma}_{oct}$. (5)

Table 5. Octahedral effective stress strain relationship, 30 kPa per minute.

Hollow Cylinder radius		Average Effective Stress			Average Octahedral	
Outer R cm	Inner a cm	Radial $\bar{\sigma}'_R$ kPa	Hoop $\bar{\sigma}'_\theta$ kPa	Vertical $\bar{\sigma}'_Z$ kPa	Stress $\bar{\tau}_{oct}$ kPa	Strain $\bar{\gamma}_{oct}$ %
(1)	(2)	(3)	(4)	(5)	(6)	(7)
24.29	1.257	1.90	4.33	1.05	2.57	0.10
42.29	1.270	1.64	0.82	1.31	0.33	0.01
48.29	1.290	2.60	3.61	03.1	0.41	0.02
54.29	1.316	2.60	3.46	3.03	0.35	0.01
60.29	1.368	3.02	3.91	3.46	0.36	0.01
62.29	1.410	2.97	4.02	3.49	0.43	0.02
66.29	1.450	4.37	5.65	5.00	0.52	0.02

Table 6. Octahedral effective stress strain relationship 10 kPa per minute.

Hollow Cylinder radius		Average Effective Stress			Average Octahedral	
Outer R cm	Inner a cm	Radial $\Delta\bar{\sigma}'_R$ kPa	Hoop $\Delta\bar{\sigma}'_\theta$ kPa	Vertical $\Delta\bar{\sigma}'_Z$ kPa	Stress $\bar{\tau}_{oct}$ kPa	Strain $\bar{\gamma}_{oct}$ %
(1)	(2)	(3)	(4)	(5)	(6)	(7)
20.26	1.252	1.2	4.92	2.95	1.52	0.06
36.26	1.2614	0.89	2.73	1.82	0.75	0.03
40.26	1.282	- 0.09	1.35	0.61	0.59	0.02
42.26	1.299	2.55	3.55	3.04	0.41	0.02
58.26	1.317	1.71	0.95	1.38	1.18	0.05
62.26	1.37	3.34	4.75	4.03	0.58	0.02
66.26	1.454	5.40	7.67	6.50	0.93	0.03

The results are plotted in Fig 3 for fast and slow test rates. It shows the evolution of medium octahedral shear stress and strain until failure following MCC criterion. In the present work, the medium shear modulus value is found independent of test rate. The value of average octahedral shear modulus $\bar{G}_{oct}$ is found = 2640 and 2600 kPa for the fast and slow test rates. Note the present analysis method is valid for linear and nonlinear stress strain relationships as well.
Applying the present analysis method at different depths under the ground, the shear modulus variation with depth can be found and an overall shear modulus across some depth in question can be estimated.

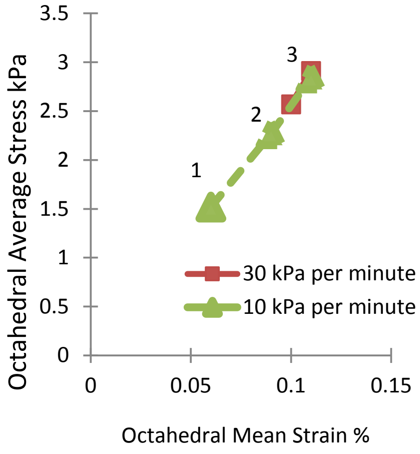

Fig 3. Octahedral Stress Strain Relationship

3 SUMMARY AND CONCLUSIONS

a) MCC and the variation energy principal are adopted to examine the clay medium behavior due to cavity expansion during the PMT.
b) The outer radius of clay hollow cylinder influenced and models the medium around PMT cavity can be deduced.
c) A proposed new pressure limit is defined by the applied pressure that initiate radial cracks at the cavity surface during PMT.
d) The analysis of the hollow cylinder test results showed that the deduced effective limit pressure is independent of test rate and the medium average octahedral shear modulus at the level of testing as well.
e) The present analysis method is devoted to analyze the normally consolidated clay under undrained conditions. It can be adopted to analyze soil behavior under drained conditions.
f) The present analysis method is applicable for the design of tunnels and piles.
g) It is suggested to provide PMT probe by two piezometers, one at the membrane cell, the other in the soil against the first one at short distance far from it but both at the membrane cell mid height.
h) More test data is required to confirm the conclusions and to analyze other applications in geotechnical design.

4 APPENDIX

4.1 The derived equations to calculate the strains

The average values of the total hoop and radial stresses across the thickness of hollow cylinder of outer and inner radii R and a are expressed as follows:

$$\bar{\sigma}_\theta = \frac{(\psi a - \sigma_h R)}{(R-a)} \tag{6}$$

$$\bar{\sigma}_R = -\frac{(\psi a + \sigma_h R)}{(R+a)} \tag{7}$$

$\bar{\sigma}_Z = \gamma z$, the overburden pressure (8)

Where ψ = the applied pressure by the probe, R = outer radius of clay hollow cylinder, a = radius of the cavity radius that is the radius of membrane cell at its mid height,

The corresponding average effective stresses are:

$$\bar{\sigma}'_\theta = \bar{\sigma}_\theta - \bar{u} \tag{9}$$

$$\bar{\sigma}'_R = \bar{\sigma}_R - \bar{u} \tag{10}$$

$$\bar{\sigma}'_Z = \bar{\sigma}_Z - \bar{u} \tag{11}$$

Where $\bar{u}$ the average developed excess pore water pressure across the thickness of hollow cylinder.

The modified Cam Clay (MCC) expressed in terms of *(p′, J,* θ_L) so that:

$$F = \frac{J^2}{\left(p' g(\theta_L)\right)^2} - \frac{p'_0}{p'} + 1 = 0 \tag{12}$$

Where p' = the current mean effective stress; p'_0 = the initial mean effective stress and $=(\sigma'_h + \sigma'_z)/3$; $J = \sqrt{J_2}$; J_2= second deviator stress invariant defined by $\left(\bar{S}^2_R + \bar{S}^2_\theta + \bar{S}^2_Z\right)/2$; $\bar{S}'_R$,$\bar{S}'_\theta$and $\bar{S}'_z$ are the three deviator normal stresses $\bar{S}'_R = (\bar{\sigma}'_R - p')$,
$\bar{S}'_\theta = (\bar{\sigma}'_\theta - p')$ and $\bar{S}'_Z = (\bar{\sigma}'_Z - p')$; Lode angle $\theta_L = \frac{1}{3}\sin^{-1} - \frac{J_3}{2}\left(\frac{3}{J_2}\right)^{1.5}$; J_3 = third deviator of stress = $\left(\bar{S}^3_R + \bar{S}^3_\theta + \bar{S}'^3_Z\right)/3$ and,

$$g(\theta_L) = \frac{\sin\phi'_{cs}}{\cos\theta_L + \frac{(\sin\phi'_{cs}\sin\theta_L)}{\sqrt{3}}} \tag{13}$$

Where ϕ'_{cs}= the critical state angle of shearing resistance.

From normality in the π plane the strain increase is given by the chain rule so that;

$$\bar{\epsilon}_i = \frac{\partial F}{\partial J}\frac{\partial J}{\partial \bar{\sigma}_i} + \frac{\partial F}{\partial \theta_L}\frac{\partial \theta_L}{\partial \bar{\sigma}_i} \tag{14}$$

$$Where\colon \frac{\partial F}{\partial J} = \frac{2J}{\left(p' g(\theta_L)\right)^2} \tag{15}$$

$$\frac{\partial F}{\partial \theta_L} = \frac{2J^2}{p'^2 g(\theta_L)}\frac{\left(\cos\theta_L \sin\phi'_{cs}\right)/\sqrt{3} - \sin 3\theta_L}{\sin\phi'_{cs}} \tag{16}$$

Hereafter the stress partial differentials for $\bar{\sigma}'_R$ and the others by cyclic rotation

$$\frac{\partial J}{\partial \bar{\sigma}'_R} = \frac{\bar{S}'_R}{2\sqrt{2}J} \tag{17}$$

$$\frac{\partial \theta_L}{\partial \bar{\sigma}'_R} = \frac{-\sqrt{3}(2\bar{S}'^2_R - \bar{S}'^2_\theta - \bar{S}'^2_z) + 3\sqrt{J_2}\bar{S}'_R \sin 3\theta_L}{3\sqrt{4J_2^3 - 27J_3^2}} \tag{18}$$

4.2 The proposed two piezometer pressuremeter test device (PCT/BE2011/000026; EP 0705941A1):

Description

The two piezometer PMT consists of two separate parts: (1) the standard PMT probe equipped by a piezometer at its membrane cell mid height; and (2) a separate and movable part that is a short tube of smaller diameter than the intermediary between the ground surface and the probe membrane cell. This tube contains an inclined gun. The ball of this gun is a hypodermic needle that measures pore water pressure.

Device installation

After installing the standard PMT under the ground, the tube of the second movable part is to be introduced. The hypodermic needle is inserted by shooting it into the ground in inclined direction, almost 35 cm to reach from just above the expanding membrane to a point opposite the present piezometer in the membrane cell but at short distance far from it.

After carrying out the test, the hypodermic needle is to be pulled back to its initial position in the gun. Then the tube that contains the gun is pulled up to the ground surface. This procedure is to be repeated at each level of testing.

5 REFERENCES

AFNOR. (1996).”French Standard NF P 94-250-1”, Eurocode 7 Calcul géotechnique.

AFNOR. (2000). ”French Standard NF P 94-110”, Essai pressiométrique Ménard.

Anderson, W., Pyrah, I.C., and Ali, F. (1987). “Rate Effects in Pressuremeter test in Clays.” Journal of geotechnical Engineering. ASCE. 113(11), 1348-1358.

ASTM standard D4719-87, “Standard test method for Pressuremeter testing in soils”, Annual book of ASTM standards, vol. 04.08 American Society for testing materials.

Iskander, K. (2013). “New Pressuremeter test analysis based on critical state mechanics.” International journal of geomechanics, 10.1061 (ASCE) , GM.1943-5622.0000257.

Iskander, K. (2015). “Three Dimensional Cavity expansion analysis for strain heterogeneity in clay medium by Pressuremeter test results,” ISP7-Pressio, International symposium 60 years of pressuremeters in Tunisia, pp 121-135.

Lamé, G. (1852). ”Leçons sur la théorie mathématique de l’élasticité des corps solides” Bachelier, Paris.

Powel, J. J. M. (1990). “A comparison of four different PMTs and their methods of interpretation in a stiff heavily overconsolidated clay.” Proceedings of the Third International Symposium on Pressuremeters, Oxford.

Roscoe, K.H., and Burland, J.B. (1968). “On the generalized stress strain behavior of wet clays Engineering plasticity.” (Ets. J Heyman and F. Leckie) 535-609 Cambridge University Press.

Thevayanagam, S.L., Chameau, J.L., and Altschaeffl, A.G. (1994). “Some Aspects of Pressuremeter test interpretation in clay” Géotechnique vol. 44 (2),319-334.

Washizu, K. (1975). “Variational Methods in Elasticity and Plasticity”. Publisher Pergamon Press.

Geotechnical and Geophysical Site Characterisation 5 – Lehane, Acosta-Martínez & Kelly (Eds)
© 2016 Australian Geomechanics Society, Sydney, Australia, ISBN 978-0-9946261-1-0

Earth pressure evaluation and safety assessment employing a novel measurement device – The Inclinodeformeter

G. M. Ausweger & F. Tschuchnigg
Computational Geotechnics Group, Institute for Soil Mechanics and Foundation Engineering, Graz University of Technology, Austria

ABSTRACT: The measurement of earth pressure changes in the subsoil due to construction works is a challenging task. The installation of standard measurement devices for earth pressure measurement is relatively complex and in many cases the measured data is influenced by installation effects. These problems led researchers of ETH Zurich to develop a novel measurement device for determining earth pressure changes in the subsoil – the Inclinodeformeter (IDM). The IDM probe is lowered into a classical inclinometer casing to determine the diameters of the inclinometer casing in two perpendicular directions. Based on this deformation measurement a back calculation of the earth pressure changes between subsequent measurements is possible. A combination of IDM measurements with conventional measurements allows an evaluation of the earth pressure changes and enables the assessment of safety levels of such complex structures. The paper introduces briefly the inclinodeformeter and the method for the back analysis of earth pressure changes. In the following an application of the new device and a numerical back analysis of the boundary value problem are presented. Based on a comparison of IDM data with the numerical analysis, possible improvements with respect to the back calculation of earth pressure changes are given.

1 INTRODUCTION TO INCLINODEFORMETER

1.1 *Equipment*

The Inclinodeformeter (IDM) is a novel measurement device for measuring earth pressure changes, which was developed at the ETH Zurich (Schwager 2013). Figure 1a shows the IDM probe. The measurement system consists of the probe, a winch with a positioning system (shown in Figure 1b), a converter, a connecting cable between converter and laptop, a cable and a transition piece between inclinometer casing and winch. The different components of an inclinometer are shown in Figure 2.

The probe is lowered down into the inclinometer casing, where the upper and the lower wheel are guided in one groove of the inclinometer casing. These two wheels are firmly connected with the probe. The middle wheel is pushed by means of a spring into the opposite groove and is equipped with a tilt sensor. Based on the inclination of the middle wheel the distance between two opposite grooves, i.e. the diameter of the inclinometer casing, can be measured. The measurements of the diameter are performed in two perpendicular directions.

Two additional tilt sensors at the top of the probe enable the measurement of the inclination of the inclinometer casing, i.e. a conventional inclinometer measurement. Furthermore, the IDM probe is equipped with a pressure sensor and a temperature sensor for measuring the water pressure in the inclinometer casing, and the temperature for a temperature correction respectively.

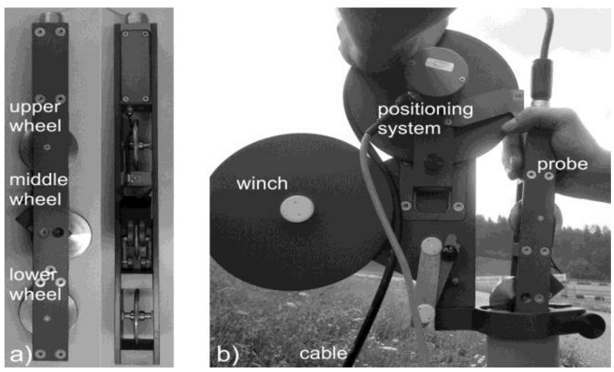

Figure 1. Inclinodeformeter: a) IDM probe, b) winch with IDM probe

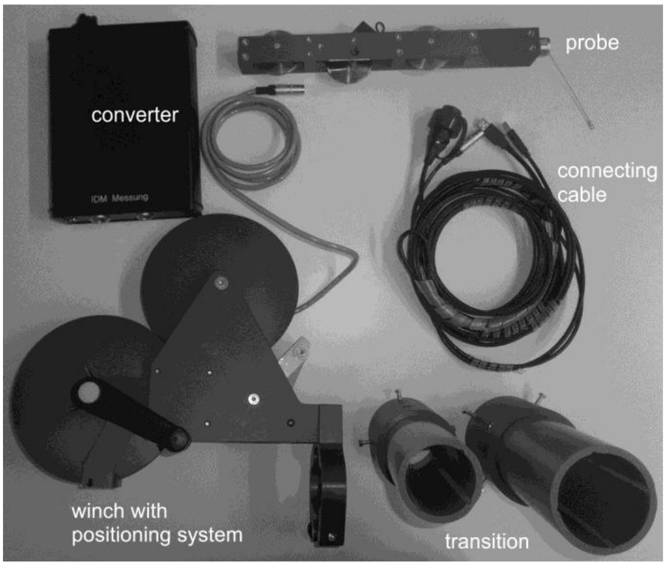

Figure 2. Inclinodeformeter: components of measurement system.

The position of the probe in the inclinometer casing is determined with a rotation sensor on the winch. The measurements are taken continuously.

1.2 *Determination of earth pressure changes*

The model for determining earth pressure changes with the IDM probe, based on diameter measurements was also developed at ETH Zurich (Schwager 2013). The basic idea is that changes in the earth pressure lead to a change in two perpendicular diameters of the inclinometer casing, i.e. the circular cross section of the inclinometer casing is deformed to an elliptical cross section.

The cross section of the inclinometer casing is described by an ovalization value Ω on the basis of the measured diameters D_A and D_B and the initial radius of the inclinometer casing R (see Figure 3).

$$\Omega = \left(D_B - D_A\right)/R \qquad (1)$$

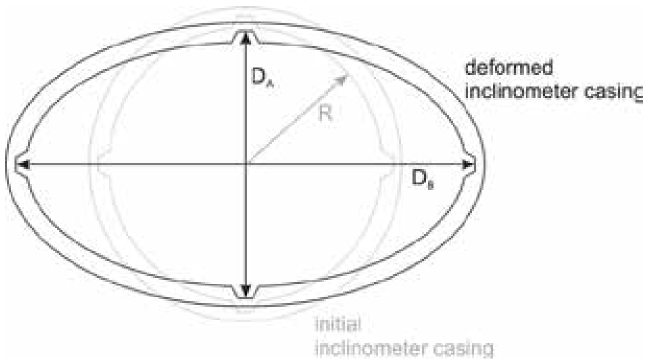

Figure 3. Cross section of inclinometer casing

The change in the cross section of the inclinometer casing due to a change in the earth pressure is described by the difference in the ovalization value between two sequential measurements.

$$\Delta\Omega = \Omega_{(t=t1)} - \Omega_{(t=t0)} \qquad (2)$$

The earth pressure increment, which caused the deformation of the cross section of the inclinometer casing in a certain depth, is back calculated on the basis of the corresponding boundary value problem (Schwager 2013), which is explained briefly in the following. Therefore, the stiffness of the inclinometer casing, of the grout and of the soil must be known. The time-dependent stiffness of the inclinometer casing was determined by Schwager (2013) in laboratory tests. The grout stiffness is assumed equal to the soil stiffness as the back calculation is not very sensitive to the grout stiffness. The soil stiffness can be determined on core samples in the laboratory or estimated with in situ tests. The vertical direction is assumed as principal stress direction with a constant normal stress at a certain depth due to the overburden. Thus, the horizontal cross section is under plane stress conditions. The two remaining principal stress increments, which represent the change in the earth pressure, are back calculated. A schematic layout of the boundary value problem is shown in Figure 4. The direction of the major principal stress increment is another important parameter for the back calculation and is indicated in Figure 4 with δ. This direction of the major stress increment, i.e. the rotation of the ellipse axis with respect to the measured diameters of the inclinometer casing, cannot be determined from the measurements as only two diameters are measured. Meanwhile an inclinometer casing with 8 grooves has been developed to overcome this problem (Wachter 2016). Thus, in a first step the direction of the major principal stress increment is assumed equal to the resulting displacement vector of the inclinometer casing, which can be determined by conventional inclinometer measurements. In some cases this assumption could lead to mistakes in the back calculation as shown in chapter 3.

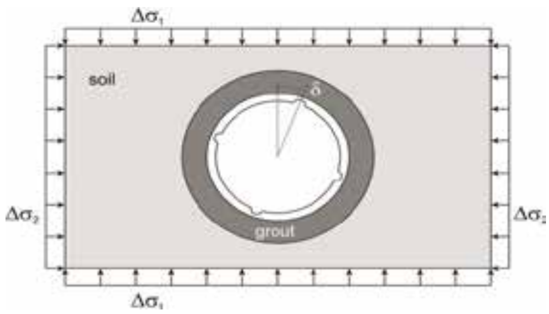

Figure 4. Layout of boundary value problem adapted according to Schwager (2013)

The mathematical procedure for the back calculation of the changes in earth pressure is comprehensive but consists of the parameters described before. Thus, the authors refer to the research work at ETH Zurich (Schwager 2013) concerning the equation for determining the changes in earth pressure based on IDM measurements.

2 PRACITCAL APPLICATION OF THE IDM PROBE

The Inclinodeformeter has already been used on different sites, including the stabilization of slow moving landslides, bridge abutments and retaining walls (Marte & Ausweger 2014, Ausweger 2014).

In this chapter the application of the Inclinodeformeter for the strengthening of an existing retaining wall in Austria is presented.

1.3 *Presentation of the site*

The measurements at an already existing cantilever wall, which stabilizes a cutting for a highway showed high horizontal deformations of the retaining wall. To avoid a collapse of the retaining wall, a stabilization measure with pre-stressed grouted anchors was designed and executed. The height of the cantilever retaining wall is about 12.9 m with an inside stem at the bottom and a reverse stem at a height of about 7.5 m from the bottom. The additional anchors were installed at three different levels. At about 3.9 m, 5.1 m and 8.4 m measured from the bottom of the retaining wall. The pre-stress load of the anchors is between 50 kN for the upper anchor level and 340 kN for the lower anchor level. The grouted anchors are inclined with 10°, the anchor length is between 15 m and 18 m and the anchor bond length is 10 m.

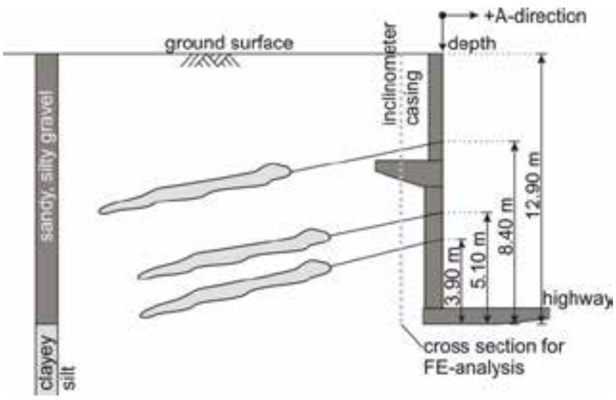

Figure 5. Schematic layout of the boundary value problem including the position of the inclinometer casing

Table 1. Material parameters Hardening Soil model

Parameter	Unit	Gravel	Silt
γ_{unsat}	kN/m³	21.0	20.0
γ_{sat}	kN/m³	22.0	20.0
$E_{50,ref}$	kN/m²	40 000	20 000
$E_{oed,ref}$	kN/m²	40 000	20 000
$E_{ur,ref}$	kN/m²	120 000	50 000
ν'_{ur}	-	0.2	0.2
p_{ref}	kN/m²	100	100
m	-	0.5	0.8
φ'	°	39.5	20.0
c'	kN/m²	3.5	14.0
ψ	°	9.5	0.0
K_{0nc}	-	1-sinφ′	1-sinφ′

A schematic representation of the retaining wall and the ground profile is shown in Figure 5. Additionally the position of the inclinometer casing for the Inclinodeformeter measurements is given.

The soil behind the retaining wall consists mainly of sandy, silty gravel. Below the retaining wall the subsurface explorations identified clayey silt. The soil parameters were determined on the basis of laboratory tests. Together with the input parameters for the FE-calculation, they are summarized in Table 1.

As the retaining wall was close to the ultimate limit state, before the stabilization work started, the increased earth pressure due to the pre-stressing of the anchors was of high interest. For this reason, measurements with the IDM probe were conducted before and after the remediation work. The inclinometer casing was measured also one year after the stabilization work has been finished. This was done to evaluate the changes in earth pressure with time.

1.4 *Measurement results*

As mentioned in chapter 1 the IDM probe enables conventional inclinometer measurements and diameter measurements of the inclinometer casing. In the following the results of the conventional inclinometer measurements, which means the displacements of the inclinometer casing, and the results of the IDM measurements (diameters), i.e. the earth pressure changes are shown.

The zero measurement was taken on the 16th January 2014, before the pre-stressed anchors were installed. Further measurements were taken on the 2nd April 2014 (after the installation of the anchors) and on the 16th April 2015.

The measurement results are shown in Figure 6 and Figure 7. The conventional inclinometer measurements show the displacements perpendicular to the retaining wall. Positive displacements represent a deformation of the retaining wall in direction of the highway (see Figure 5). The magnitude of the displacements is very small.

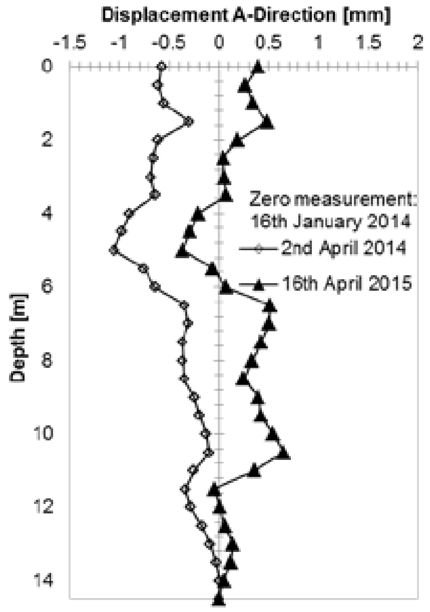

Figure 6. Results IDM measurements: displacements A-direction

However, after the installation of the pre-stressed anchors a deformation in the negative direction occurred. After one year the retaining wall is roughly at the same position as it was before the anchors were installed.

Figure 7a and 7b show the earth pressure changes for a major principal stress increment direction δ of 0° and 30°, respectively. A positive value means an increase of earth pressure. The measurement data is averaged over one inclinometer casing with a length of 3.0 m and the data in the area of couplings between two inclinometer casings is not taken into account. For the back calculation of the earth pressure changes the unloading / reloading stiffness of E = 120 MPa for the gravel and E = 50 MPa for the silt was chosen. These values are based on the site investigations and lab tests. The measurement results show a continuous increase of earth pressure over depth due to the installation of the anchors (measurement on the 2nd April 2014). The measurement one year after the remediation work shows a further increase of the earth pressure.

As mentioned in chapter 1.2, is the direction of the major principal stress increment δ (see Figure 4) generally assumed equal to the resulting displacement vector of the inclinometer casing. Due to the fact that the displacements in this boundary value problem are very small it is very difficult to determine the resulting displacement vector in this case. In principle a deformation perpendicular to the retaining wall (due to the pre-stressing of the anchors) can be assumed. In this case the direction of the major principal stress increment would be δ = 0° (Figure 7a).

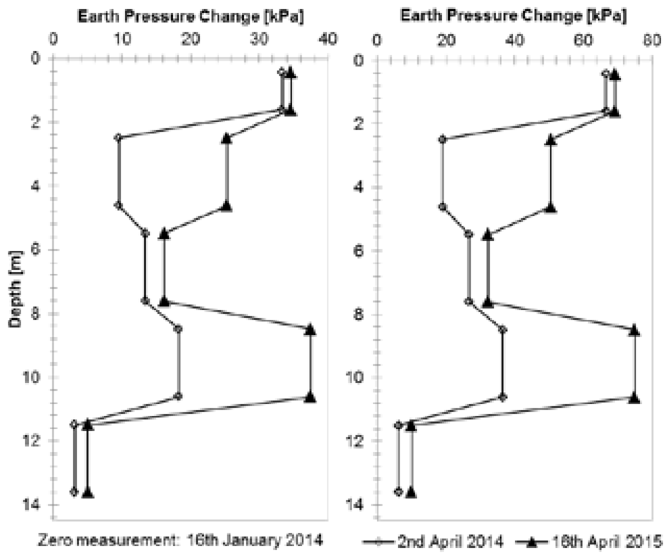

Figure 7. Results IDM measurements: a) earth pressure changes with δ = 0°; b) earth pressure changes with δ = 30°

Figure 7b shows the results of the analysis of the measurement data, considering a direction of the principal stress increment of δ = 30°. These different directions of the major principal stress increment are considered for the following reasons: firstly, to show the significant influence of the direction of δ, the major principal stress increment and secondly, the comparison with the FE-analysis, as presented in chapter 3, which shows that the value for δ cannot be equal to 0° over the entire depth.

The comparison of Figure 7a and Figure 7b shows the big influence of the major principal stress increment direction on the earth pressure changes. From that follows, that it is important to improve the determination of the parameter δ in future. In general the earth pressure changes show an expected result, which is an increase of the earth pressure due to the anchor installation, but measurements also indicate an increase of the earth pressure with time.

2 COMPARISON OF MEASUREMENT RESULTS WITH FE-ANALYSIS

To validate the measurement results of the Inclinodeformeter the remediation work of the retaining wall was analysed by means of a FE-analysis. Therefore, the software PLAXIS 2D 2012 (Brinkgreve et al. 2012) was used.

For the sandy, silty gravel and the clayey silt the Hardening Soil model was used. The material parameters are summarized in Table 1. The unloading/reloading stiffness E_{ur} for the Hardening Soil model is the same as the stiffness for the back calculation of earth pressure changes.

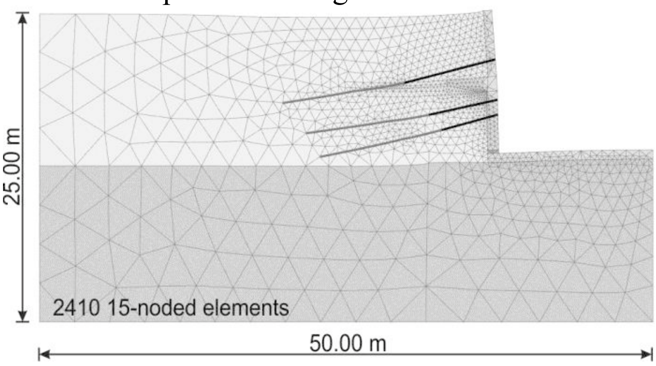

Figure 8. FE-model: deformed mesh after pre-stressing of anchors

Other parameters are determined based on laboratory tests or estimated from the results of the site investigations. The (deformed) FE-mesh after the calculation phase of "anchor pre-stressing" is shown in Figure 8. The used model consists of about 2400 15-noded elements with a shape function of 4th order.

Figure 9 shows the comparison between the measured earth pressure changes and the calculated earth pressure changes obtained with the FE-analysis. In the FE-analysis the change in earth pressure due to anchor installation is evaluated 2.5 m behind the retaining wall, which is the position of the inclinometer casing (Figure 5). The measured earth pressure changes are in a good agreement with the results obtained with FE-analysis, with the exception of the area from 0.0 to 2.0 m. In this area the measurement results are distorted due to a concrete pavement of an adjacent street behind the retaining wall. However, this good agreement can only be achieved if the direction of the major principal stress increment is changed with depth in the back calculation of the earth pressure changes based on the measurements with the IDM probe. Above the reverse stem $\delta = 0°$ and below the reverse stem $\delta = 30°$ was used for the direction of the major principal stress increment. This difference is most probably due to torsion of the inclinometer casing with depth, and maybe also a real change in the direction of the major principal stress increment (e.g. due to the reverse stem). However, the change in the direction of the major principal stress increment seems to be very large and the reason for that has not been clarified so far.

The change with depth might also indicate a mistake in the assumption of a rotated ellipse for the deformed inclinometer casing. This problem with respect to the direction of the major principal stress increment shows, that improvements for an easy and correct determination of the major principal stress increment direction are necessary. Thus, an inclinometer casing with 8 grooves was developed (Wachter, 2016).

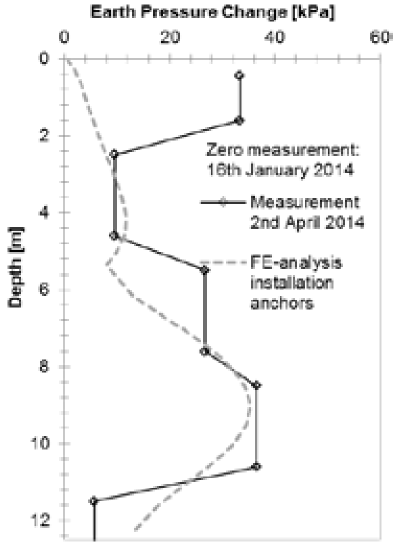

Figure 9. Comparison measurements and FE-analysis

During the investigation of the deformed retaining wall, cracks at the transition between the inside stem and the wall were detected. In order to investigate whether these cracks also develop in the FE-model, a novel constitutive model for shotcrete was used for the cantilever retaining wall. This model enables to calculate the crack propagation in concrete structures. The model is briefly described in chapter 4.

3 CONCRETE CONSTITUTIVE MODEL

The constitutive model is explained in detail in Schaedlich & Schweiger (2014), therefore only a brief summary is given here. The model has been implemented in the finite element software PLAXIS 2D and PLAXIS 3D 2013 (Brinkgreve et al. 2013).

A compression negative notation is employed throughout this chapter of the paper.

3.1 *Yield surfaces and strain hardening/softening*

Plastic strains are calculated according to strain hardening/softening elastoplasticity. The model employs a Mohr-Coulomb yield surface F_c for deviatoric loading and a Rankine yield surface F_t in the tensile regime. Strain hardening in compression follows a quadratic function up to the peak strength f_c, governed by $H_c = \varepsilon_3^p / \varepsilon_{cp}^p$ (ε_3^p = minor plastic strain, ε_{cp}^p = minor plastic strain at peak in uniaxial compression). Strain softening in compression is available in the model, but has not been employed in this study. The model behaviour in tension is linear elastic until the tensile strength f_t is reached. Linear strain softening follows, governed by the major principal plastic strain

ε_1^p and the fracture energy G_t. L_{eq} is the equivalent length of the current stress point, which is derived automatically from the size of the finite element.

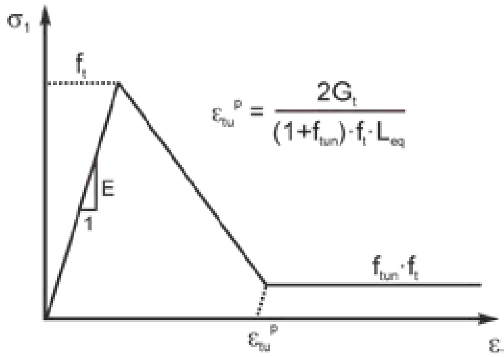

Figure 10. Stress - strain curve in tension

3.2 *Time dependent stiffness, time dependent strength, creep and shrinkage*

Young's modulus E increases with time t following the recommendation of CEB-FIP model code (1990). The same approach is followed for the evolution of concrete strength with time. The ratio of f_t / f_c is assumed to be constant. Creep strains $\boldsymbol{\varepsilon}^{cr}$ increase linearly with stress $\boldsymbol{\sigma}$ and are related to elastic strains via the creep factor φ^{cr}. For concrete utilization above 45% of f_c, non-linear creep effects are accounted for according to EC 2 (2004).

Shrinkage strains ε^{shr} are calculated as:

$$\varepsilon^{shr}(t) = \varepsilon_\infty^{shr} \cdot \frac{t}{t + t_{50}^{shr}} \tag{3}$$

with ε_∞^{shr} being the final shrinkage strain and t_{50}^{shr} the time when 50% of shrinkage has occurred.

4 BACK ANALYSIS OF CRACK PROPAGATION

As time effects of stiffness and strength, creep and shrinkage are of minor importance in this example, only strain softening in tension was considered for the cantilever retaining wall. This feature of the constitutive model enables to investigate the crack propagation in concrete structures due to high tensile stresses.

In Figure 11 the normalized tension softening parameter H_t is shown for the cantilever retaining wall before the pre-stressing of the anchors. H_t is plotted from 0 (dark) to 1 (light), while H_t of 0 means no strain softening in tension, H_t = 0-1 means strain softening in tension and H_t > 1 would show regions with the residual tensile strength.

The results of the FE-analysis show strain softening in tension at the transition between the inside stem and the wall, i.e. according to the FE-analysis in this area the crack propagation starts. This is exactly the same position where the cracks were observed at the real cantilever retaining wall.

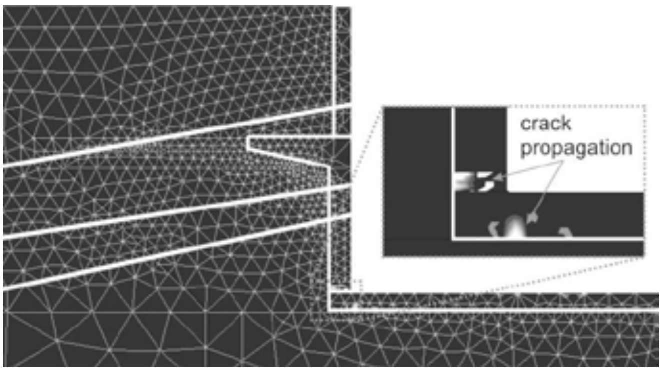

Figure 11. FE-analysis: crack propagation in cantilever retaining wall bevor pre-stressing of anchors

5 CONCLUSION

The paper shows the successful application of the Inclinodeformeter for measuring the earth pressure changes behind a retaining wall due to the pre-stressing of anchors. The comparison with FE-analyses confirms the measurement results, but shows also that that the current approach used for the back analysis of earth pressure changes needs some improvements concerning the definition of the major principal stress increment.

Finally, for the retaining wall a novel constitutive model for concrete was used. With that advanced model it is possible to calculate the crack propagation. In the performed analysis the position of the calculated tensile cracks show a very good agreement with the cracks observed at the real cantilever wall.

6 REFERENCES

Ausweger, G. M. 2014. Earth pressure on retaining walls in slopes. *Proceedings European Young Geotechnical Engineers' Conference, 23 (2014)*, 181-184.

Brinkgreve, R. B. J., Engin, E., Swolfs, W. M. 2012. *PLAXIS 2D 2012 - User Manual*. Plaxis bv, Delft.

Brinkgreve, R. B. J., Engin, E., Swolfs, W. M. 2013. *PLAXIS 3D 2013 - User Manual*. Plaxis bv, Delft.

Marte, R. and Ausweger, G. M. 2014. Monitoring of landslides with a novel device for measuring earth pressures - Inclinodeformeter. *Proceedings Danube-European Conference on Geotechnical Engineering,* 465-470.

Schwager, M. V. 2013. Development, analysis and applications of an 'inclinodeformeter' device for earth pressure measurements. *PhD-thesis* ETH Zurich.

Schaedlich, B. and Schweiger, H. F. 2014. A new constitutive model for shotcrete. *Proc. 8th Eur. Conf. Num. Meth. Geot. Eng.,* 103-108.

Wachter, B. 2016. Untersuchungen zur Meßgenauigkeit und Weiterentwicklung der IDM-Sonde. *Master thesis* Graz University of Technology.

Theme 2. Penetration Testing

Geotechnical and Geophysical Site Characterisation 5 – Lehane, Acosta-Martínez & Kelly (Eds)

Correlation of p-wave velocity and SPT-N on volcanic soils in Costa Rica

Ibanez, S.J., Ortiz-Palacio, S., Lopez-Ausin, V. & Porres-Benito, J.A.
INGITER S.L.-University of Burgos, Burgos, Spain

ABSTRACT: The prediction of the Standard Penetration Test (SPT-N) blow count using p-wave velocities (V_p) has been barely studied. Traditionally, the field s-wave velocities (V_s) have been the aim of the most of the efforts to correlate seismic behavior and penetration resistance properties of soils. Nevertheless, this new approach will expand the correlation to the field of primary waves. The potential use of this correlation will be useful in the search for new easy, non-invasive and non-expensive methods to probe soil properties in underdeveloped and developing countries, in which deep-boring machinery is hard to find or too expensive to use. After a large soil testing program in Costa Rica, in volcanic soils, p-waves were used to develop a correlation between p-wave velocity and N_{SPT} in the investigated soils.

1 INTRODUCTION

So far, there are many empirical studies getting a correlation between the shear wave velocity and the blow count from Standard Penetration Tests (V_s-N_{SPT}). This is a logical correlation because these magnitudes mainly depend on the shear strength of the soil skeleton.

The quantity of pore water only slightly changes the soil density (Qiu & Fox 2008) and has little influence on the V_s (Foti 2012).

The shear modulus of a soil (G) does not depend on the water content of a soil, but does depend on the effective stress, which in turn is affected by the pore pressure. This way, the aforementioned correlations are different for saturated and non-saturated soils.

Thaker & Rao (2011) calculated several correlations between V_s and N_{SPT} (see Table 1). It is interesting to note that they found better correlations for non-energy corrected values of N_{SPT}.

In practice, it is easier to perform p-wave testing than s-wave testing. So, even though there is much less done research about this issue, in this paper a correlation between V_p and N_{SPT} will be tried to find out.

Although it is relatively easy to get V_p, these dilatational wave velocities are more difficult to study because of the more complex multivariable mechanism around the propagation of these waves.

Table 1. Correlations between the shear wave velocity and the blow count from SPT tests.

Soil type	Correlation m/s	Correlation factor (R^2)
All soils	$V_s=59.72 \cdot N_{SPT}^{0.42}$	0.77
Sandy soils	$V_s=51.21 \cdot N_{SPT}^{0.42}$	0.78
Clayed soils	$V_s=62.41 \cdot N_{SPT}^{0.42}$	0.78

Studies from Foti (2012) state that V_s depends mainly on G, but V_p depends also on the soil particle bulk modulus (K^{SK}) and water bulk modulus (K^F). This way, assuming complete saturation and solid incompressibility, we have the following dependencies (Equations 1 and 2):

$$V_s = f(G, n, \rho_s, \rho_F) \tag{1}$$

where n = porosity; ρ_s = solid particle density; and ρ_F = water density.

$$V_p = f(G, n, \rho_s, \rho_F, K^{SK}, K^F) \tag{2}$$

For unsaturated soils, Conte et al. (2009) introduced more new variables, as we can see in Equations 3 and 4:

$$V_s = f(G, n, \rho_s, \rho_F, S_r) \tag{3}$$

$$V_p = f(G, n, \rho_s, \rho_F, S_r, K^{SK}, K^F, K^a, \rho_a, \nu^{SK}, m_2^W) \tag{4}$$

where S_r=degree of saturation, K^a=air bulk modulus, ρ_a=air density, ν^{SK}=Poisson´s ratio, $m^w{}_2$=coefficient of water volume change due to matric suction variations.

V_p is affected by more variables than V_s is, so it is would seem reasonable to assume that a correlation between V_p and N_{SPT} is presumed to be affected by more parameters than the correlation between V_s and N_{SPT}.

There are several approaches to this issue. Ulugergerli & Uyanik (2007) proposed a range of possible values between an upper and a lower bound for clay-silt-sand-gravel deposits in western Turkey.

Bery & Saad (2012) also proposed a correlation for soils in Malaysia (sedimentary sands and clays over igneous rocks).

2 GEOTECHNICAL SURVEYING

2.1 *Site*

The field work was conducted at four different locations in Costa Rica (four different projected wind farms). One is called "Campos Azules" wind farm, another one is called "Altamira". Both of them are located in Liberia, Guanacaste region. The third and the fourth wind farms are called "Vientos de Miramar" and "Vientos de la Perla", and are situated close to Santa Rosa de Tilarán, also in the Guanacaste region (see Figure 1).

Figure 1. Research field site (from Código Sísmico de Costa Rica (2010)).

2.2 *Geological environment*

As this is a volcanic area, the geomorphology is a typical volcanic kind. At these four locations the geology is not quite different. At the surface there are volcanic ashes that mostly have turned into silty-clayed soil, because of weathering and alteration. These materials overlie a layer composed of volcanic rock fragments and blocks, that came from old lahar flows. Underlying these above mentioned layers there is a soft volcanic tuff layer. The latter layer is usually so deep that the tests analyzed in this research were not be carried out so deep to reach this tuff layer (in Santa Rosa de Tilarán zone, this tuff layer is even deeper than in Liberia zone).

2.3 *Tests performed*

The SPT tests were performed by Insuma Company with an old, but typical equipment in Costa Rica, as shown in Figure 2. The V_p were obtained using seismic refraction tests. These tests were carried out with a modern Pasi seismograph (Mod. 16S24-P) owned by INGITER, a university company. Twenty four geophones with a natural frequency of 10 Hz and 5 m span were used and a 6 kg sledge hammer was used to produce the seismic excitation.

The tests were performed at every location of a wind turbine mill. So, at some locations, there were directly comparable SPT and p-wave measurements. During this research, 61 data pairs were used to develop a new correlation between N_{SPT} and V_p that works in this type of volcanic soils in Costa Rica.

Figure 2. Equipment and tests carried out: SPT and seismic refraction tests.

3 RESULTS

In order to get the best possible correlation between N_{SPT} and V_p, the authors interpreted data pairs (N_{SPT}-V_p) in clearly comparable layers. If there was any doubt, the data were discarded.

Before researching and analyzing data, it was very difficult to predict which value of N_{SPT} would provide the best correlation with V_p, so several different N_{SPT} values were considered. First, the characteristic value with a 95% confidence interval ($N_{60,k}$), then the mean value of N_{SPT} in that layer (N_{60}). Then, the SPT results were corrected using the depth correction factor (Liao & Whitman 1986). So, in summary, the following two values of N_{SPT}: $(N_1)_{60,k}$ and $(N_1)_{60}$ were investigated.

No energy correction was used for two main reasons. The first one is because Thaker & Rao (2011) found the uncorrected values produced better correlations. The second reason is that, because of the kind of SPT drill used, and the age of the equipment, the energy efficiency will be around 60%.

Figures 3, 4, 5, 6 present V_p vs. $N_{60,k}$, N_{60}, $(N_1)_{60,k}$ and $(N_1)_{60}$ respectively. Best fit lines are presented on these figures, together with the Pearson´s correlation factors.

As we can see from those figures, the correlations are slightly better for average values rather than for characteristic values, but are much lower than might be expected for a V_s vs. N_{SPT} correlation.

It is interesting to note that the correlations without the Liao & Whitman (1986) depth correction are better than with the depth correction – possibly because the Liao & Whitman (1986) correction is intended for sand, rather than volcanic clays.

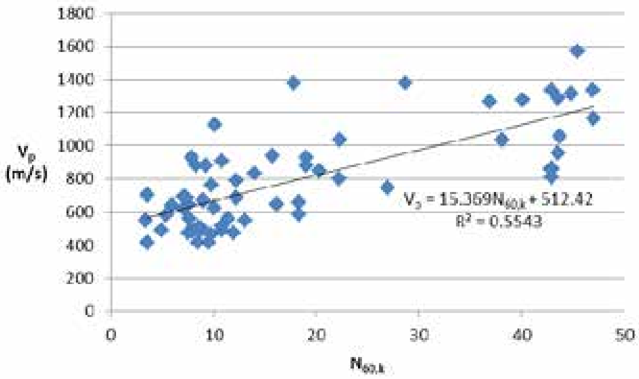

Figure 3. Correlation between characteristic value of N_{SPT} and V_p.

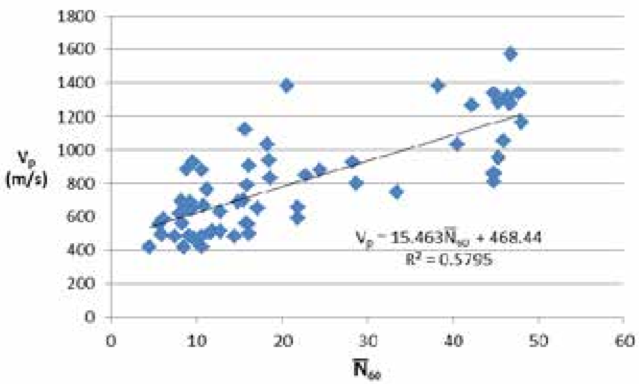

Figure 4. Correlation between mean value of N_{SPT} and V_p.

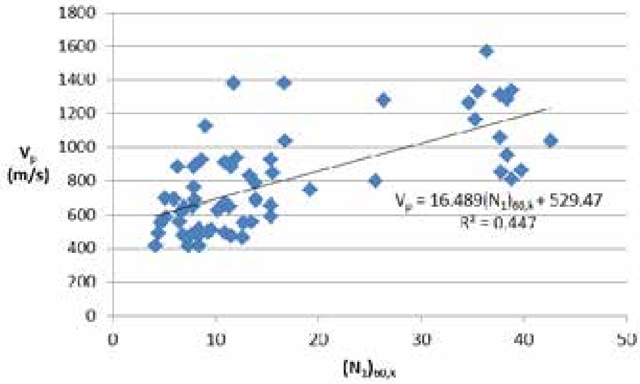

Figure 5. Correlation between characteristic value of N_{SPT} with depth correction and V_p.

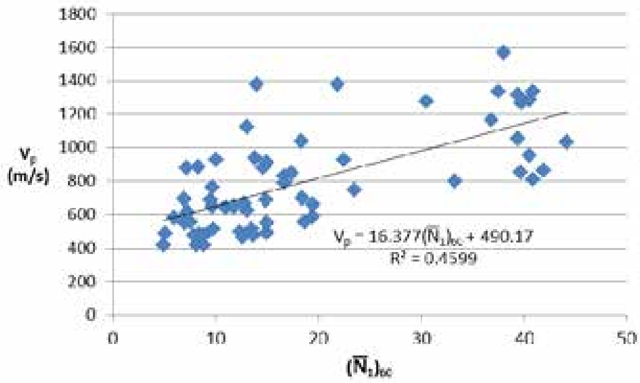

Figure 6. Correlation between mean value of N_{SPT} with depth correction and V_p.

4 DISCUSSION

The average value of N_{SPT}, without depth correction, provides the highest Pearson´s correlation factor, even though it is not as high as would be desirable. As explained during the introduction, there are many variables that affect dilatational wave velocities, so in the future a multivariable analysis would be required to improve these correlations.

In Figures 7, 8, 9, 10, these results are compared with the studies of Ulugergerli & Uyanik (2007) and Bery & Saad (2012). The Bery & Saad (2012) correlation can be seen to form a lower bound to the data presented in this paper, so using this correlation would result in overestimates of N_{SPT} at the sites investigated in this study

The data also fit within the wide-ranging Ulugergerli & Uyanik (2007) upper and lower bound correlations for volcanic soils. It may be seen that, for the data presented in this study, the Ulugergerli & Uyanik (2007) upper bound is much more conservative than the lower bound.

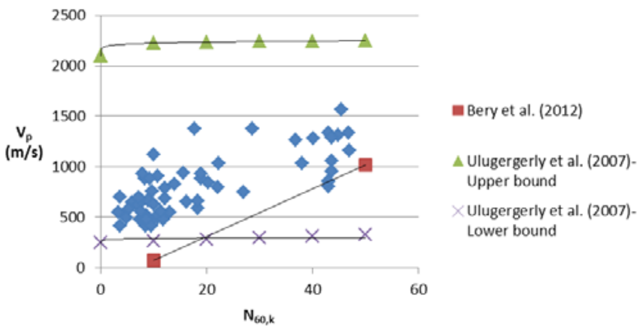

Figure 7. Analysis of Ulugergerli & Uyanik (2007) upper and lower bound and Bery & Saad (2012) correlation, in case of characteristic values of N_{SPT}.

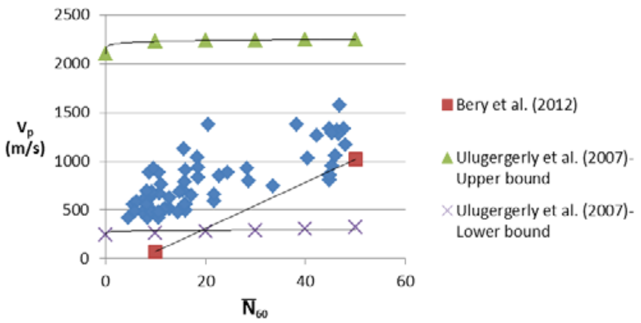

Figure 8. Analysis of Ulugergerli & Uyanik (2007) upper and lower bound and Bery and Saad (2012) correlation, in case of mean values of N_{SPT}.

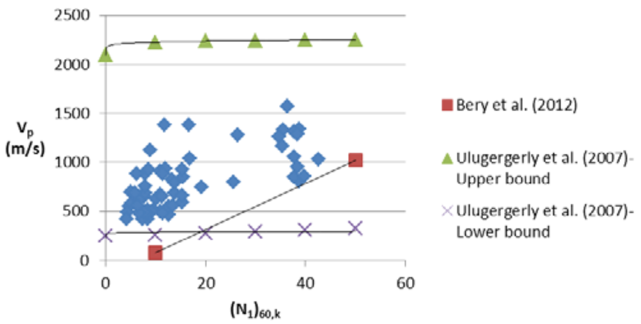

Figure 9. Analysis of Ulugergerli & Uyanik (2007) upper and lower bound and Bery & Saad (2012) correlation, in case of characteristic values of depth corrected N_{SPT}.

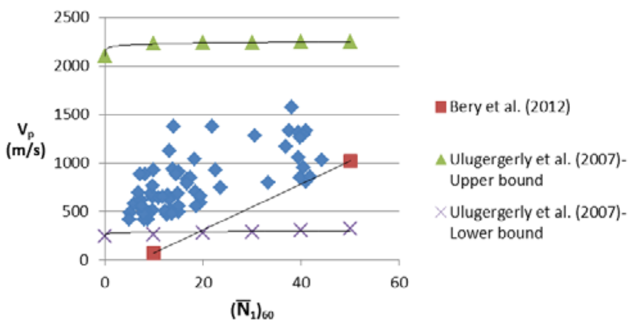

Figure 10. Analysis of Ulugergerli & Uyanik (2007) upper and lower bound and Bery & Saad (2012) correlation, in case of mean values of depth corrected N_{SPT}.

5 CONCLUSIONS

The best correlation for N_{SPT}-V_p is when using mean values of uncorrected (depth correction) values of N_{SPT}.

The results from this research lie within the wide-ranging correlation bounds proposed by Ulugergerli & Uyanik (2007) for volcanic soils.

The correlation proposed by Bery & Saad (2012) forms a lower bound to the data presented in this research, so using this correlation would result in overestimates of N_{SPT} at the sites investigated in this study .

Although there are clear trends in the measured data, the Pearson's correlation is lower than would be considered desirable. Therefore, a multivariable study would be needed to try and improve the reliability of these correlations.

As V_p depends on soil characteristics that will, vary between sites, it is likely that site-specific correlations will always be required at new sites – however, even in this situation, the site investigation cost might be reduced by performing a suitable combination of boreholes and p-wave tests.

6 ACKNOWLEDGEMENTS

We wish to thank MS ENERTECH S.L., the University of Burgos and INGITER S.L. for their support and funding in this research.

7 REFERENCES

ASTM 2010. D 4633-10, "Standard Test Method for Energy Measurement for Dynamic Penetrometers". ASTM International, West Conshohocken, PA.

ASTM 2011. D 1586-11 "Standard Test Method for Standard Penetration Test (SPT) and Split-Barrel Sampling of Soils". ASTM International, West Conshohocken, P.

Bery, A.A. & Saad, R. 2012. Correlation of Seismic P-Wave Velocities with Engineering Parameters (NValue and Rock Quality) for Tropical Environmental Study. International Journal of Geosciences 2012; 3: 749-757.

Buzzi, O. 2010. On the use of dimensional analysis to predict swelling strain. Engineering Geology 2010; 116: 149-156.

CEN 2005. EN ISO 22476-2, Geotechnical investigation and testing - Field testing - Part 2: Dynamic probing. European Committee for Standardisation: Brussels, Belgium.

Colegio Federado de Ingenieros y de Arquitectos de Costa Rica 2011. Código sísmico de Costa Rica 2010. Editorial Tecnológica de Costa Rica: San José, Costa Rica.

Conte, E.A. et al. 2009. Shear and dilatational wave velocities for unsaturated soils. Soil Dynamics and Earthquake Engineering 2009; 29: 946-952.

Foti, S. 2012. Combined use of geophysical methods in site characterization, Geotechnical and Geophysical Site Characterization 4. CRC Press 2012; 43-61.

Liao, S.S. & Whitman, R.V. 1986. Overburden correction factors for sand. Journal of the Geotechnical Engineering Division, ASCE 1986; Vol. 112, No. 3: 373-377.

Maheshwari, B.K. et al. 2013. Relationship between Shear Wave Velocity and SPT Resistance for Sandy Soils in the Ganga Basin. International Journal of Geotechnical Engineering 2013; 7: 60-66.
Peck, R.B. et al. 1953. Foundation Engineering. John Wiley & Sons: New York, 1953.
Qiu, T. & Fox, P. 2008. Effective Soil Density for Small Strain Shear Wave Propagation, Geotechnical Earthquake Engineering and Soil Dynamics IV 2008; 1-9.
Sanglerat, G. 1972. The penetrometer and soil exploration: Interpretation of penetration diagrams - theory and practice. Elsevier Pub. Co.
Stroud, M.A. 1974. The Standard Penetration Test in insensitive clays and soft rocks, Proceedings of the 1st European Symposium on Penetration Testing 1974; Stockholm, Sweden: 367-375.
Terzaghi, K. & Peck, R.B. 1967. Soil mechanics in engineering practice. Wiley.
Thaker, T.P. & Rao, K.S. 2011. Development of statistical correlations between shear wave velocity and penetration resistance using MASW technique, 2011 Pan-Am CGS Geotechnical Conference: Toronto, Ontario, Canada.
Ulugergerli, E.U. & Uyanik, O. 2007. Statistical correlations between seismic wave velocities and SPT blow counts and the relative density of soils. Journal of Testing and Evaluation 2007; 35: 187-191.

Geotechnical and Geophysical Site Characterisation 5 – Lehane, Acosta-Martínez & Kelly (Eds)

Strength Assessment of Frozen Soils by Instrumented Dynamic Cone Penetrometer

S.Y. Kim, W-T. Hong & J-S. Lee
School of Civil, Environmental and Architectural Engineering, Korea University, Seoul, Republic of Korea

Y. Kim
Geotechnical Engineering Research Institute, Korea Institute of Civil Engineering and Building Technology, Goyang, Republic of Korea

ABSTRACT: As an interest in cold region resource development increases, infrastructure constructions on frozen soils have been actively conducted. Thus, the investigation of the frozen soils is fundamental and essential to ensure the stability of frozen ground. The goal of this study is to estimate the strength of the frozen soils by the instrumented dynamic cone penetrometer. The dynamic cone penetrometer is incorporated with strain gauges and accelerometer at the cone tip to figure out transferred energy through rods. During dynamic penetration phase, a rod guide is located on the frozen soils to prevent eccentricity of impact. Specimens are prepared with sand-silt mixture at the silt fraction of 30 % in weight. The relative density and the degree of saturation are of the soils is 60 % and 10 %, respectively. The specimens are located in the freezing chamber at sub-zero temperature to freeze under the specified vertical stresses for simulating frozen ground. The dynamic penetration tests are conducted after freezing phase. Experimental results show that as the vertical stress increases, the dynamic cone penetration index which represents the strength of the frozen soils decreases. The force signal increases and the velocity estimated by accelerometer decreases as the vertical stress during freezing and penetrating phases increases. This study suggests that instrumented dynamic cone penetration test may be suitable for the investigation of the strength of the frozen soils.

1 INTRODUCTION

The characteristics of soils rapidly change when the soils are frozen at sub-zero temperature. Especially, the strength of the frozen soils significantly increases compare to unfrozen soils due to ice bonding between soil particles. A number of studies related to the strength evaluation of the frozen soils have been conducted (Zhu et al. 1988; Fitzsimons et al. 2001; Yasufuku et al. 2003). Furthermore, the characterization of the frozen soils is important factor for the safety design in cold regions. Linell and Lobacz (1980) studied the design and construction of foundations in the frost and permafrost ground. In addition, numerous researchers have been studied pile design in cold region to ensure the stability of infrastructures on the frozen ground (Weaver and Morgenstrern 1981; Landanyi and Theriault 1990).

For the characterization of the strength of the frozen ground, experimental device which could be applied directly to the field has been required. Several devices are developed to perform field tests such as standard penetration test (SPT), cone penetration test (CPT), and dynamic cone penetration test (DCPT). In the cold regions, the accessibility is relatively low because the area is unexplored due to barren surrounding condition. For this reason, dynamic cone penetrometer which is more portable compare to the other devices is applicable. The dynamic cone penetration tests have been frequently carried out to investigate the strength of the ground (Rahim and George 2002; Abu-Farsakh et al. 2004; Chen et al. 2005). Salgado and Yoon (2003) showed result of the dynamic cone penetration test is related to other engineering properties.

In this study, dynamic cone penetration tests are conducted to characterize frozen soils. Specimens are prepared with the relative density of 60 % and the degree of saturation of 10 %. The specimens are located into the ice chamber to freeze at -5 ºC. Vertical stresses of 5, 10, and 25 kPa are applied during freezing and penetrating phases using air pressure. The dynamic cone penetration tests are conducted after the freezing phase. Dynamic cone penetration index (DCPI) and signals through instrumented sensors are measured to characterize the frozen soils with different vertical stress. This paper describes experimental setup including preparing specimens, results of the dynamic cone penetration tests, analyses, and conclusions of this study.

2 EXPERIMENTAL SETUP

2.1 *Preparing specimens*

Specimens are prepared with sand and silt mixture to simulate actual ground state in the field. The silt fraction, which is the ratio of silt weight to sand weight, is fixed at 30%. The prepared specimens are put into mixer with distilled water. The amount of water is determined to be 10 % in degree of saturation during mixing.

The mixture of sand, silt and water is set into calibration chamber whose size is 500 mm in diameter and 400 mm in height. Compaction number with same energy is applied to each 5 layers, respectively. All cases of the specimens are equally compacted to be 60 % in relative density. After the compaction, the top plate of the chamber is bolted to prevent movement or deformation of the plate. Note that, the hole with 50 mm diameter is prepared in the middle of the top plate which will be a path of the dynamic cone penetrometer.

The calibration chamber is located in ice chamber. Temperature is set into -5 ºC for 48 hours to freeze specimens. During freezing phase, air pressure is injected to underneath the calibration chamber, and then bottom plate moves up to prepared specimens to apply vertical stress. The applied vertical stresses are 5, 10, and 25 kPa to figure out the influence of the confining stress on the strength of the frozen soils. The target vertical stresses are maintained during whole procedure by using regulator.

2.2 *Instrumented dynamic cone penetrometer*

The instrumented dynamic cone penetrometer is developed to characterize the strength parameter of the frozen soils as shown in Figure 1. Rods are manufactured with 24 mm in a diameter. The angle of the cone tip is 60º. Note that the cone tip is reinforced to minimize wear and tear due to the hardness of the frozen specimens.

Strain gauges and accelerometer are instrumented at the cone tip to measure dynamic responses. The strain gauges are attached symmetrically to compensate an effect of eccentricity, and arranged by the full bridge of wheatstone circuit to minimize a temperature influence. The strain gauges sense physical deformation of the cone penetrometer from changed electrical resistance of the circuit. For the estimation of applied force to cone penetrometer, load calibration tests are conducted as show in Figure 2. The accelerometer is equipped at the same location with the strain gauges to figure out dynamic response. Furthermore, the results of the dynamic response which is get from accelerometer can be used to estimate the strength of the frozen soils.

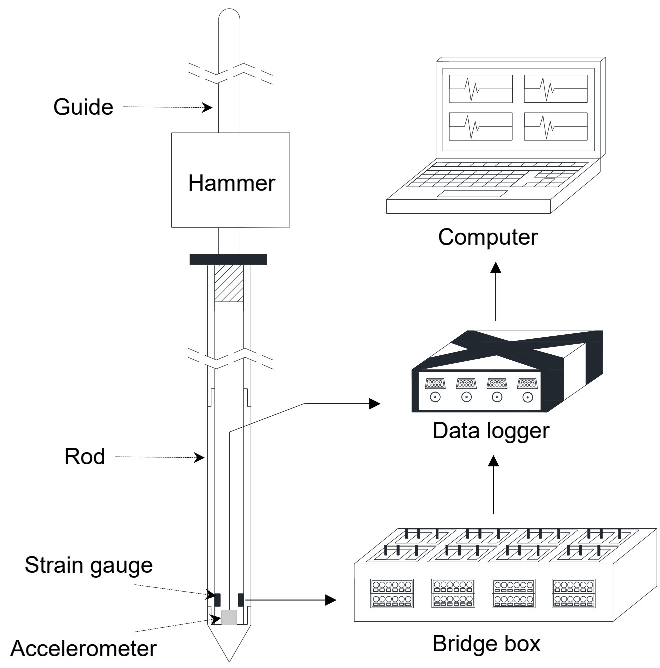

Figure 1. Measurement system of dynamic cone penetration test.

The hammer and hammer guide are manufactured to impact cone penetrometer dynamically. The weight of the cylindrical hammer is 117.6 N. The hammer falls down freely from 383 mm of the height through hammer guide to impact with 46 N·m in potential energy. Furthermore, the guide of the cone penetrometer is manufactured to make sure of straightness when the rods are being penetrated. The level of cone penetrometer guide can be controlled according to process of the cone penetration test.

The signals of each blow are measured through bridge box and data logger. The output voltage from strain gauges is amplified and filtered through the bridge box, and acquired at the data logger. The accelerometer signal is captured at the data logger directly. Both of the signals are monitored through computer, and can be stored automatically.

3 RESULTS AND ANALYSES

3.1 *Dynamic cone penetration index*

The dynamic cone penetration tests are carried out to estimate the strength parameter of the frozen soils. The vertical stresses for setting up different confining conditions are applied during penetration tests. The dynamic cone penetration indices (DCPI) are plotted from 100 mm to 300 mm in depth to minimize boundary effect as shown in Figure 3.

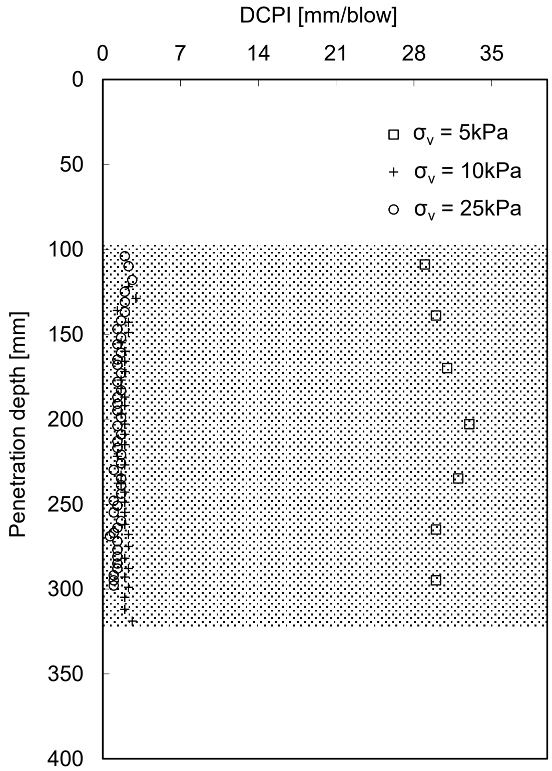

Figure 2. Results of dynamic cone penetration index.

The measured dynamic cone penetration indices are averaged at the penetration depth of 100 ~ 300 mm to find out representative set value for each condition of the frozen soils. The averaged DCPI of 30.5, 2.0, and 1.4 mm/blow are calculated for the vertical stresses of 5, 10, and 25 kPa, respectivly. The dynamic cone penetration index decrease significantly as the vertical stress increases from 5 kPa to 10 kPa. However, the index slightly decreases from 10 kPa to 25 kPa. The result shows that the effect of the vertical stress on the strength of the frozen soils decreases with an increase in the confining stress.

3.2 *Dynamic responses*

Force and velocity signals are measured during penetration phase. The signals of force and velocity multiplied by impedence (Z) are captured at the penetration depth of 200 mm under different confining stresses are plotted in Figure 4. Figure 4(a) shows the response with the vertical stress of 5 kPa, and Figure 4(b) expresses with the vertical stress of 25 kPa. In the case of the vertical stress of 5 kPa, the duration of the signals is longer than the vertical stress of 25 kPa. As the strength of the frozen soils increases, the force signal from strain gauges increases due to the greater deformation of the rods. However, the velocity integrated from the measured acceleration shows higher value for the specimen prepared under the higher vertical stress. The dynamic responses show that the strength of the frozen soils can be evaluated from the force and velocity signals. Furthermore, transferred energy at the cone tip can be obtained by integrating force and velocity values. The transferred energy can improve the accuracy of estimating the strength of the soils by dividing DCPI.

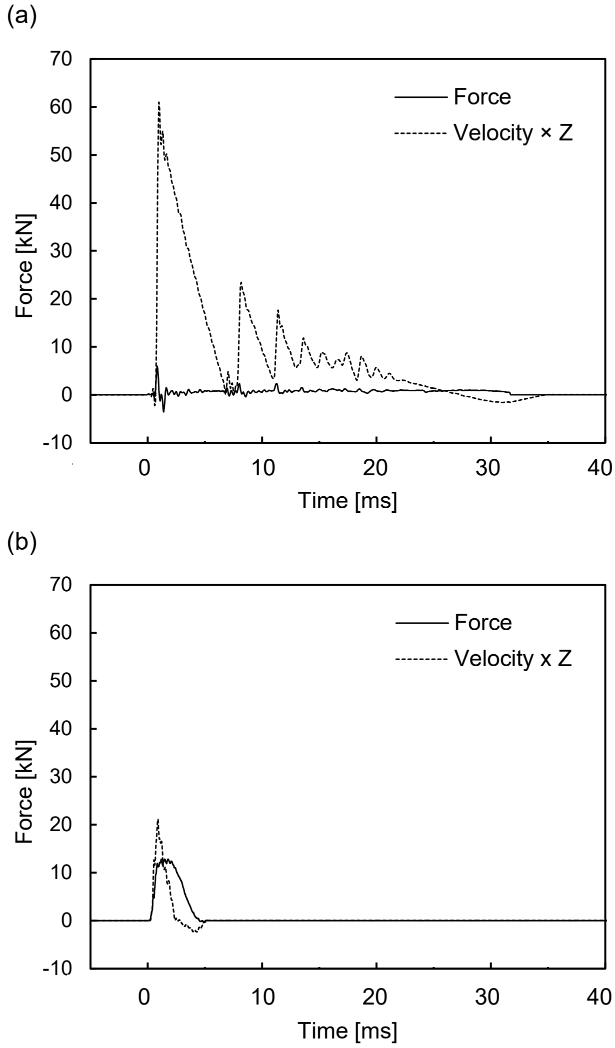

Figure 3. Signals of dynamic responses: (a) 5kPa of vertical stress; (b) 25kPa of vertical stress.

4 SUMMARY AND CONCLUSIONS

The goal of this study is to characterize the strength of the frozen soils by using instrumented dynamic cone penetrometer. The specimens with the degree of saturation of 10 % and the relative density of 60 % are prepared in the freezing chamber. The applied vertical stresses during freezing and penetrating phases are 5, 10, and 25 kPa. The dynamic cone penetration tests are conducted after freezing phase to measure dynamic cone penetration indices. Furthermore, the force and velocity signals are acquired using instrumented strain gauges and accelerometer at the cone tip. The observations of the study are as follows at 200 mm in depth:

(a) The dynamic cone penetration index decreases as the strength of the frozen soils increases. The difference of the strength which can be evaluated by dynamic cone penetration indices decreases with an increase in the vertical stress.

(b) As the vertical stress increases during freezing and penetrating phases, the force measured by strain gauges increases and the velocity estimated by the accelerometer decreases because the strength of frozen soils increases.

5 ACKNOWLEDGEMENTS

This research was supported by a grant(13IFIP-B06700801) from Plant Research Program funded by Korea Agency for Infrastructure Technology Advancement.

6 REFERENCES

Abu-Farsakh, M.Y., Alshibli, K., Nazzal, M. & Seyman, E. 2004. Assessment of in-situ test technology for construction control of base courses and embankment. *Louisiana Transportation Research Center.*

Chen, D.H., Lin, D.F., Liau, P.H. & Bilyeu, J. 2005. A correlation between dynamic cone penetrometer values and pavement layer moduli. *Geotechnical Testing Journal* ASTM 28(1): 42-49.

Fitzsimons, S.J., McManus, K.J., Sirota, P. & Lorrain, R.D. 2001. Direct shear tests of materials from a cold glacier: implications for landform development. *Quaternary international* 86(1): 129-137.

Ladanyi, B. & Theriault, A. 1990. A study of some factors affecting the adfreeze bond of piles in permafrost. *In Proc. of Geotechnical Engineering Congress GSP* 27: 213-224.

Linell, K.A. & Lobacz, E.F. 1980. Design and Construction of Foundations in Areas of Deep Seasonal Frost and Permafrost. *Report of Cold Regions Research Engineering Laboratory* U.S. Army: 80-134.

Rahim, A. & George, K. 2002. Automated dynamic cone penetrometer for subgrade resilient modulus characterization. *Journal of the Transportation Research Board* 1896: 70-77.

Salgado, R. & Yoon, S. 2003. Dynamic cone penetration test (DCPT) for subgrade assessment. *Joint Transportation Research Program*. West Lafayette.

Weaver, J.S. & Morgenstern, N.R. 1981. Pile design in permafrost. *Canadian geotechnical journal* 18(3): 357-370.

Yasufuku, N., Springman, S.M., Arenson, L.U. & Ramholt, T. 2003. Stress-dilatancy behaviour of frozen sand in direct shear. *In 8th International Conference on Permafrost*. Rotterdam: 1253-1258.

Zhu, Y.L., Zhang, J.Y. & Shen, Z.Y. 1988. Uniaxial compressive strength of frozen medium sand under constant deformation rates. *In 5th International Symposium on Ground Freezing*. Rotterdam: 225-232.

Geotechnical and Geophysical Site Characterisation 5 – Lehane, Acosta-Martínez & Kelly (Eds)
© 2016 Australian Geomechanics Society, Sydney, Australia, ISBN 978-0-9946261-1-0

The SPT N-value errors examined with digital technology

Burt Look
Foundation Specialists Pty Ltd, Brisbane Queensland Australia

ABSTRACT: The Standard Penetration Test (SPT) has the simplicity of only counting the number of blows over 3 penetration increments. The blow counts are taken as close as possible to 150mm, based on the supervisor's judgement. Digital measurements show the "standard" 150mm increments varied considerably. These digital measurements were obtained using a Pile Driving Monitoring (PDM) – a device which remotely measures set, temporary compression and velocity using optically safe infrared laser technology. This technology was applied to SPT measurements in a similar way to observe the set and energy. The 3 data points for the N - value are measured as 30,000 data points. The energy corrections are required with the in situ N – values to be effectively used as a design value. These energy values on the hammer and below the anvil was different even for a specified hammer and is dependent on both soil type and rod length.

1 INTRODUCTION

The Standard Penetration test (SPT) is one of the common in situ tests used in geotechnical engineering to determine properties of subsurface soils. The SPT requires 3 data points - the seating drive and 2 test drives to 150mm penetration each. The N-value is used to estimate the approximate shear strength properties of the soils (Clayton, 1995). Various corrections should then be made to the in- situ value to allow for type of hammer, energy corrections, etc. (Skempton, 1986).

Different types of hammers used influence the N-value, with different energy efficiencies. The failings of the SPT was revealed in Look and Seidel (2015). These include

1. Counting of integer values over 150mm increment is inexact
2. A seating drive is a constant 150mm yet seating varies significantly (Figure 1)
3. Energy transfer which (even for given drill rig) depends on the soil type and the variability in each blow energy transfer from the hammer to the anvil to the rod.

Thus the SPT is far from "standard" as the name implies, despite a standard hammer weight and drop height. Energy and other corrections are required to effectively use the SPT value in design. The SPT is analogous with pile driving, with an energy transfer between blows, dependent on the drill string location, rod length and material stiffness.

Thus a Pile Driving Monitoring (PDM) device was used with the SPT to digitally measure blow counts in terms of set and temporary compression, similar to pile driving. At the same time energy ratio is also measured. Digital measurements provide an improved accuracy which the current "visual" measurements using chalk mark references cannot provide.

The PDM can also measure energy transfer. However the energy transfer of the hammer at impact is different to the energy below the anvil (Figure 1). The energy ratio also varies with each blow (Figure 2) and is discussed further in Look et al. (2015). This data is apparent only with digital measurements and cannot be seen by eye.

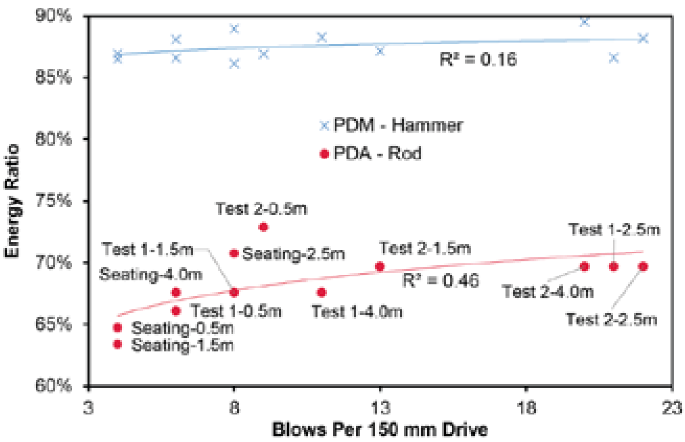

Figure 1. Energy transfer between hammer and below anvil.

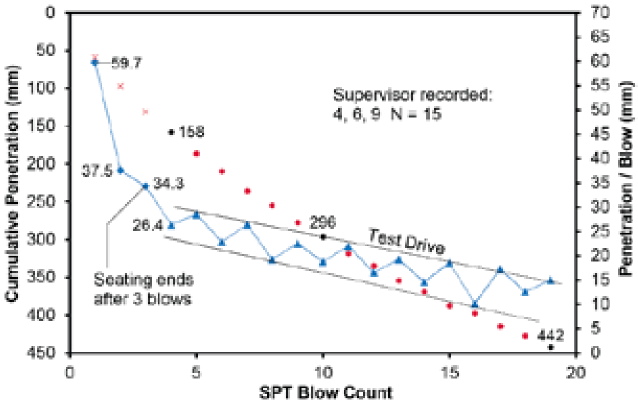

Figure 2. Seating complete before the 150mm seating drive (but measured as 158mm).

2 BACKGROUND

2.1 *Applicable Standards*

Australian Standards (AS 1289.6.3.1-2004) for the Standard Penetration Test (SPT) does not require energy measurements to be made, while the British and ASTM standards require energy measurements.

Testing was performed in accordance with ASTM D4633 – Standard Test Method for Energy Measurement for Dynamic Penetrometers. This method involves inserting an instrumented rod at the top of the drill rod string directly below the hammer-anvil system so that the hammer impact is transmitted through the anvil, into the instrumented rod and then into the drill rods. The instrumented rod contains two strain transducers and two accelerometers such that measurements of time varying force and acceleration can be made during hammer impact.

The force and acceleration signals are transmitted by connecting the gauges to a Pile Driving Analyser (PDA) computer which then enables recording, processing and displaying of the data to allow determination of force and velocity versus time. This in turn provides a measurement of the energy transferred to the instrumented rod as a result of the impact from the hammer. However accelerometers cannot reliably determine final displacement and as such unadjusted PDA data may lead to an overestimation of the energy transfer.

The above is the usual approach as per the British or American Standards. A Pile Driving Monitor (PDM) test was used in parallel with the PDA in order to accurately determine the vertical displacement of the rod after each blow. The PDM measures the vertical displacement of a target reflector which is attached to the drill rod. Look and Seidel (2015), Look et al. (2015a and 2015b) has consistently shown, the digitally measured N - values are not the same as the supervisor N-value measured by eye referenced to the chalk or paint marks on the rod.

The PDA and PDM data obtained was downloaded from the devices and processed to determine the energy delivered to the rods for each blow and from a hammer efficiency relationship was determined.

2.2 *PDM Device*

The PDM uses LED to track the movement of a reflector attached to the moving object, safely placed about 10-15m from the pile and accurate to better than 0.1mm at 10m range. There are no connections required. Thus the device is first and foremost a safety device to avoid operators measuring with a ruler below a pile driving hammer with falling parts above. The device is also a quality measuring device to measure pile set and energy.

Pile driving is similar to the SPT, when a hammer is used to drive an object into the ground. The PDM measures set and temporary compression and the peak velocity (energy) can also be determined.

Figure 3 shows the SPT on the hammer only, while Figure 4 shows measurement where 2 PDMs were used with one on the hammer, and the other below the anvil. An SPT analyser placed below the anvil is also shown in Figure 4.

Figure 3. PDM measurement with reflector on SPT hammer.

Figure 4. Two PDMs used with SPT analyser.

The PDM was used both for accurate displacements to be recorded for each blow and for estimating energy transfer as well as using the PDA. The energy mass is not the hammer only, but the combined effect of hammer, anvil, rod and soil being penetrated. Research is ongoing to assess that mass more accurately.

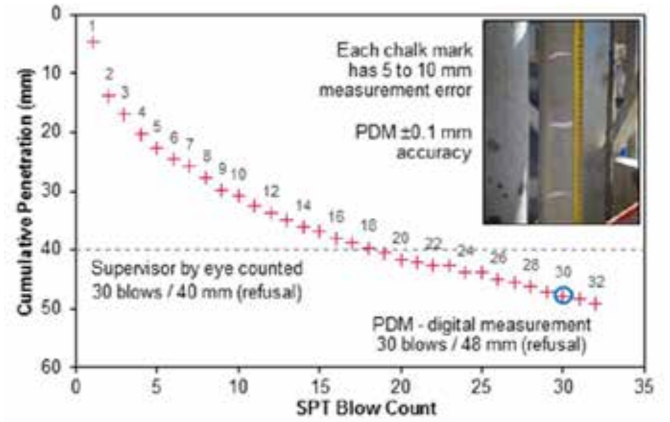

Figure 5. PDM measurements compared with counting between chalk marks.

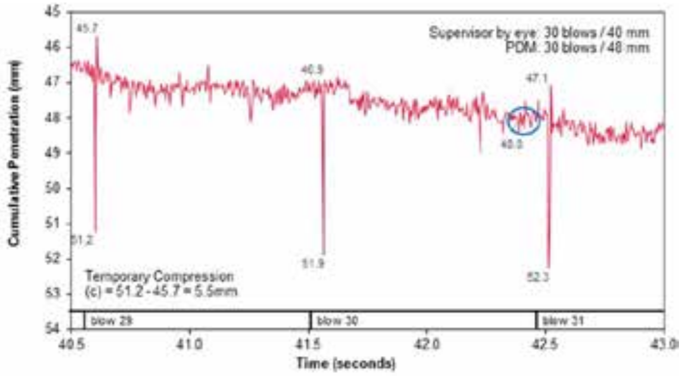

Figure 6. Digital Trace of blow No. 30.

Figures 5 and 6 show the measurement process and compares with the supervisor's blow count. In this case driving to refusal occurred in 42 seconds with an automatic trip hammer. The experienced supervisor measured 30 blows in the 48mm refusal while the digital measurements show 30 blows occurred within 40mm. This is a 20% counting error.

2.3 *Counting Accuracy*

Industry Standards state an SPT N – value is "factual". Yet it is only possible to count whole blows between increments. The supervisor must decide which of the 150mm increment to assign a blow which overlaps. The actual blows are NOT @ 150mm but the nearest which is before or after the 150mm chalk mark. This "error" is then transferred to the next 150mm increment.

In carrying out the SPT, the time is typically

- 0.2 seconds for the hammer falling
- < 0.05 second to come to a standstill (temporary compression occurs here),
- < 5 seconds before the next below is delivered
- With some automatic hammers the time can be less than 1 second between blows

The accuracy of the drilling supervisor's assessment in that time frame is required, while standing at a safe distance. A chalk mark reference is also 5mm to 10mm wide, which accounts for a reliable reading error range of 2 X 5mm to 2 X 10mm (7% to 13% error / 150mm).

Look et al. (2015) show the counting variation for 54 digitally measured increments (Figure 7). The target of 150mm had a mean and standard deviation of 147mm and 16mm, respectively. The lowest and highest values recorded was 109mm and 191mm. Because two 150mm increments are used for the N-value, compensating errors occur. The error transfer between the seating and test drive is the greater concern.

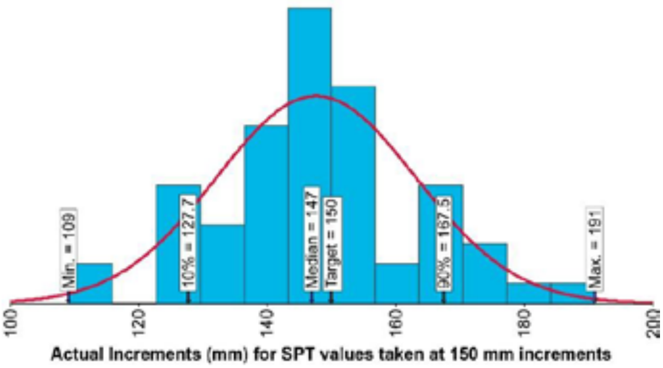

Figure 7. Digital Measurements at Site 1 (54 No.)

Figure 8. compares the visual measurements at another site with similar results. This data shows counting blows is not a "standard" value as implied by the test.

These sites have a coefficient of variation (COV) of 11% and 15% for the 150mm increments. Phoon and Kulhawy (1999) show the variability of in situ tests with a COV of 15% to 45% for the SPT. The counting errors alone would account for 15% COV.

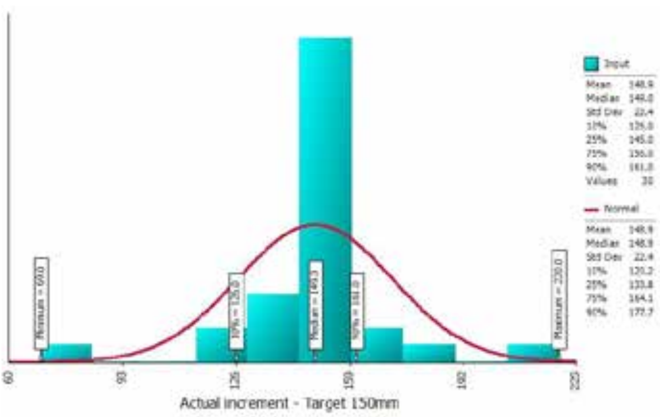

Figure 8. Digital Measurements at Site 2 (30 No.).

2.4 *SPT Correction Factors*

The insitu SPT N - value provides an indicator of relative change. However, correction factors are required for design. Typically "text book" correction values are used but these vary widely between references. These correction factors include:-

- Overburden correction factor - C_N
- Energy correction factor (C_{ER}) to account for
    - Hammer - C_H
    - Rod Length (depth) - C_R
    - Sampler - C_s ; Borehole diameter - C_B ; Anvil – C_A

The design value $(N_o)_{60}$ is then used, when also corrected for overburden.

$$(N_o)_{60} = C_N C_{ER} N. \tag{1}$$

Aggour and Radding (2001) summarise the SPT correction factors applied by the various researchers and conclude that the most significant factor affecting the measured N values is the amount of energy delivered to the drill rods. Yet Skempton (1986) uses an anvil correction factor of 0.6 to 0.8, while this is not included in the correction factors by others. This significant factor warrants further research.

Australian Standards do not currently specify energy requirements in the SPT procedure, thus energy is rarely measured. Any correction (if applied) is based on the international literature. There is a wide range of energy correction factors described in the technical literature (Table 1). The SPT energy correction for a trip hammer is therefore 80% to 172% depending on one's favourite reference. Thus only actual energy measurements would provide confidence of an appropriate correction factor.

Table 1: Energy Correction Factors for trip or Automatic Hammers

Reference	Energy ratio
Bowles (1996)	1.14 – 1.72 (N_{70} used)
Skempton (1986)	None Listed
Robertson and Wide (1997)	0.8 – 1.5
Seed (1984)	1.67

While correction factors are emphasised for liquefaction studies, many design correlations for strength and settlements also rely on an energy correction (Equations 2 and 3, respectively from Stroud, 1989)

$$\text{Undrained Cohesion } (C_u) \sim 5\, N_{60} \text{ (kPa)} \tag{2}$$

$$\text{Modulus } (E') \sim N_{60} \text{ (MPa) for a factor of safety of 3} \tag{3}$$

3 FIELD RESULTS

Using the results of site 2 (refer

Figure 8. for set variation) and the measured energy by the PDA analyser, the correction factors were determined. Figure 9 summarises the appropriate correction factors required for correcting the measured SPT N-value to a design N-value and considers both rig hammer and rod length. This assumes similar energy efficiency applies for a given drill rig throughout the project and in the various materials.

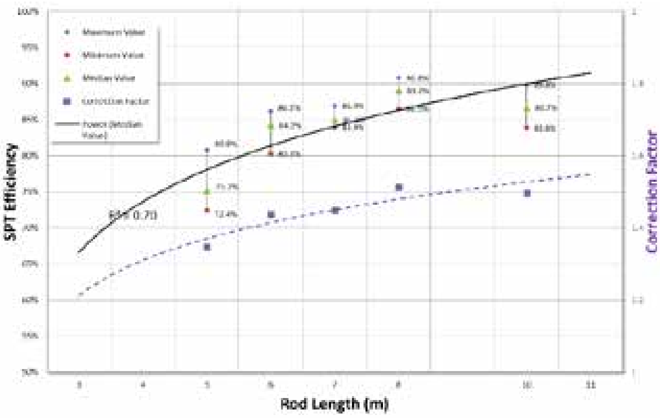

Figure 9. SPT Energy Efficiency Measurements with correction factors - Site 2.

This was for a large site investigation where 3 drilling rigs were operational. The energy associated with the hammer and rod length have been measured for only 2 of the 3 rigs used at this site. These 2 factors (energy and rod length) are known to be the main variables for energy correction factors. The energy ratio is then normalized to 60% of total energy.

As rig No. 3 was not measured for its energy, then the energy correction factor is unknown and a value of 1.0 is shown in Figure 10. With a correction factor of 1.5 for rig 1, and using equations 2 and 3, then the design strength and modulus would proportionally increase by 50%.

For this site, there was 1120 SPTs carried out. With one rig having no correction applied, another with a negligible correction and the third with a significant change, then 18% of the N- values required a classification adjustment. No classification correction applies to an N-Value > 50, although the value itself changed.

4 CONCLUSIONS

Integer values are measured for each 150mm increment in the SPT. PDM measurements show that integer values required by the test means that blow counts are taken as close as possible to 150mm which may be more or less based on the supervisor's judgement. The "standard" 150mm increments has a counting measurement coefficient of variation of 15%.

The PDM provides both a true count of the SPT set values and the energy for the various elements. The digital measurements expose the inaccuracy for N - values measured visually.

Measured energy losses are essential in using the N-value as a design value. The errors are amplified when multiple drill rigs are used on the same project.

This case study shows that the same SPT value obtained with the 2 drill rigs on this one site can have its design value (N_{60}) vary by a factor of 1.5/1.1 ~1.4. Even more concerning was that the energy of the 3rd drilling rig was not measured. And yet the variation of 140% is superior to using a value from a reference which can vary from 80% to 172% for the hammer being used.

Perhaps it is time for the ubiquitous SPT (1940s procedure) to enter the 21st Century digital age.

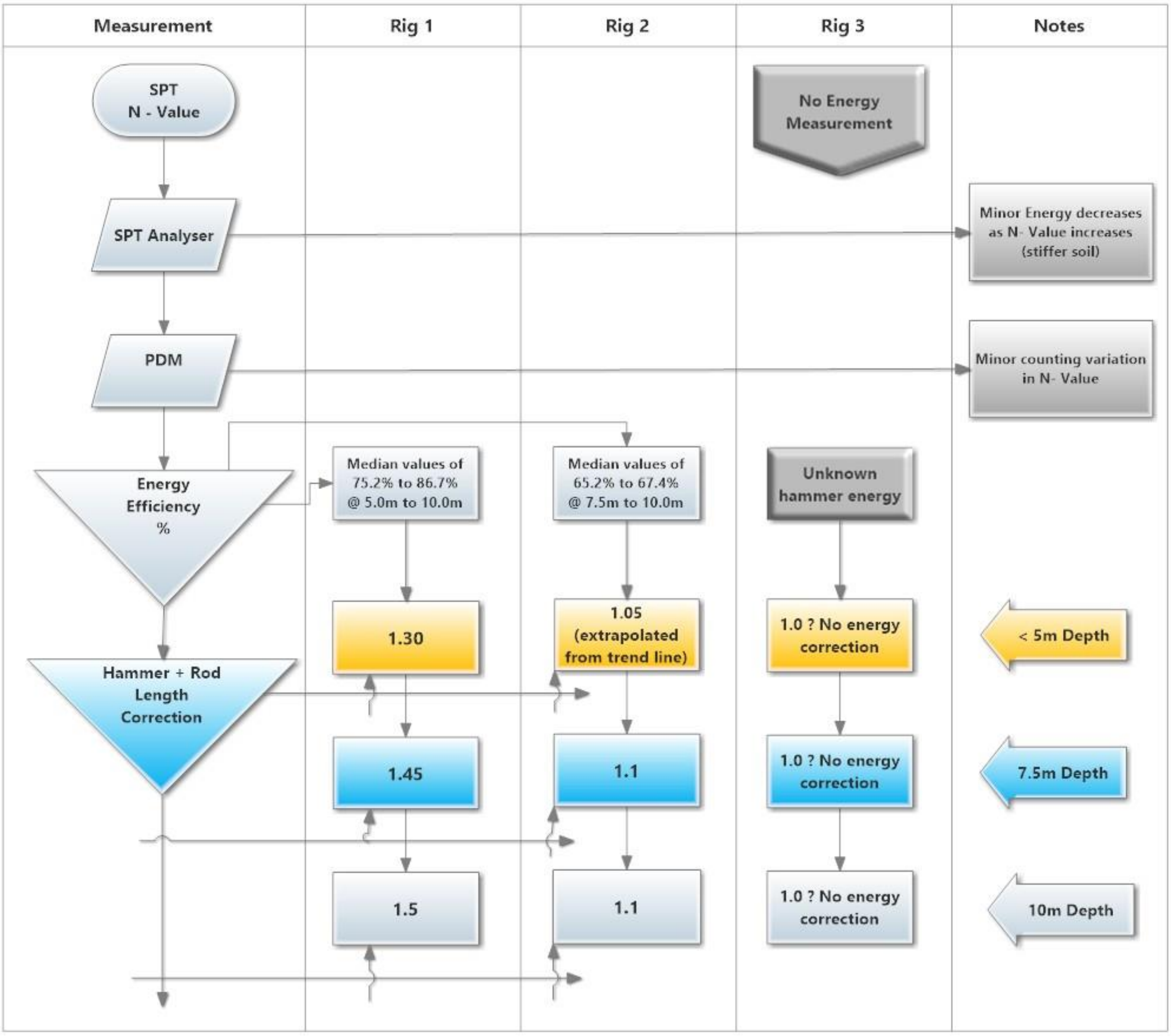

Figure 2. Summary of Procedure and Correction Factors for each rig at Site 2

5 REFERENCES

Aggour, M. & Radding, W.R. 2001. Standard Penetration Test Correction. Maryland State Highway Administration, Report No. MD02-007B48.

Australian Standards. 2004. Soil Strength and Consolidatyion Tests – determination of the penetration resistance of a soil – Standrad PenetrationTest (SPT). *AS1289.6.3.1 Methods of tesing soils for engineering purposes.*

ASTM D4633-10. 2010. Standard Test Method for Energy Measurement for Dynamic Penetrometers. *American Society for Testing and Methods.*

British Standards. 2012. Geotechnical investigation and testing - Field testing - Part 3: Standard Penetration Tests. *BS EN ISO 22476-3:2005+A1: 2011.*

Clayton C.R.I. 1995. The Standard Penetration Test (SPT): Methods and Use. *CIRIA Report 143*

Look, B. & Seidel, J. 2015. SPT and PDM – Macro vs micro measurements. *12th Australia New Zealand Conference in Geomechanics,* Wellington, New Zealand, P015.

Look, B.G., Seidel, J.P., Sivakumar, S.T & Welikala, D.L.C. 2015. Real time monitoring of SPT using a PDM device – The Failings of our Standard Test revealed. *International Conference on Geotechnical Engineering*, Colombo, Sri Lanka. 435 – 438.

Look, B.G., Seidel, J.P., Sivakumar S.T & Welikala, D.L.C. 2015. Standard Penetration Test measurement exposed using a Digital PDM device. *International Conference on Geotechnical Engineering*, Colombo, Sri Lanka. 451 – 454.

Phoon, K. & Kulhawy, F.H. 1999. Characterization of geotechnical variability. *Canadian Geotechnical Journal*. 36: 612 – 624.

Skempton, A.W. 1986. Standard Penetration Test Procedures and the Effects in Sands of Overburden Pressure, Relative Density, Particle Size, Ageing and Over-consolidation. *Geotechnique*, 36 (Sept): 425 – 47.

Stroud, M.A. 1989. The Standard Penetration Test – its application and interpretation. *Proceedings ICE Conference on Penetration Testing in the UK,* London: Thomas Telford.

Geotechnical and Geophysical Site Characterisation 5 – Lehane, Acosta-Martínez & Kelly (Eds)

SPT test: An approach to predicting undrained shear strength based on energy concepts

J. A. Lukiantchuki
Department of Civil Engineering, State University of Maringá, Maringá, Brazil

ABSTRACT: The Standard Penetration Test (SPT) is used for geotechnical subsurface investigation. It is intended to provide soil properties and foundation design parameters. Recently, new approaches that use rational methods to assess the static and dynamic soil reaction force have been proposed. These approaches were developed based on the amount of energy delivered to the sampler. This paper presents an approach to predict undrained shear strength (Su) based on energy concepts. Soil reaction force values were used to estimate the undrained shear strength using the adhesion factor, which relates the lateral skin friction mobilized during sampler penetration and the undrained shear strength. The proposed approach was used to estimate the undrained shear strength for two sites: the Sepetiba region, located in the state of Rio de Janeiro (Brazil) and the Porto Velho region located in the state of Roraima (Brazil). The suitability of this method was evaluated by comparing undrained shear strength estimated by both vane shear test (VST) and SPT. Theoretical values are significant lower than experimental results. The proposed method can be useful in estimating Su values during preliminary design.

1 INTRODUCTION

Based on energy concepts introduced by Aoki and Cintra (2000), to improve SPT test interpretation, new methods have been proposed to estimate soil parameters and contribute to pile design (Schnaid et al., 2009; Hettiarachchi and Brown, 2009). These methods were developed based on energy balance, which is represented by the work done by the sampler to penetrate the soil. The mechanical energy conservation, known as Hamilton's Principle can be expressed by the following equation (Clough and Penzien, 1975) (Eq. 1):

$$\int_{t_1}^{t_2} \delta[\,T(t) - V(t)]\,dt + \int_{t_1}^{t_2} \delta[\,W_s(t) + W_{nc}(t)]\,dt = 0 \quad (1)$$

where: δ = variation in the time interval (t_2-t_1); T(t) = total kinetic energy in the system; V(t) = potential energy in the system; W_s (t) = work done by non-conservative forces acting on the sampler-soil system and W_{nc} (t) = work done by other non-conservative forces related to energy losses.

Schnaid et al (2009), based on previous results (Odebrecht et al., 2005), proposed an equation to estimate soil dynamic force (Fd), that was used to equalize soil properties of sand (internal friction angle) and clay (undrained shear strength). The method was developed through limit equilibrium and cavity expansion theory concepts. Results showed a correlation when compared with other methods or experimental tests.

The method proposed by Hettiarachchi and Brown (2009) is based on two basic assumptions: (1) the resistive force mobilized on the sampler inside surface is negligible (2) no plugging occurs during sampler penetration. The first assumption is due to the variation in the inside diameter of the sampler which is enlarged above the open end to allow for a liner (which is rarely used). Consequently, when no liner is used, this difference in diameters reduces friction on the inside surface of the sampler (Hettiarachchi and Brown, 2009 and Schmertmann, 1979). The second assumption is based on experimental observations of Schmertmann (1979), who noted a lower probability of soil plugging in samplers without liners.

To propose a method for assessing soil shear strength parameters, Hettiarachchi and Brown (2009) assumed that the energy loss in the string of rods is negligible. Consequently, the amount of energy delivered to the string of rods was set to equal the amount of energy that reaches the sampler. However, other research (Odebrecht et al., 2005; Cavalcanti et al., 2008; Lukiantchuki, 2012) demonstrated that the energy loss in the string of rod is significant and contributes to a rational interpretation of SPT test results.

This paper presents an approach to predicting undrained shear strength based on the amount of energy that reaches the sampler during wave propagation. Soil reaction force was used to estimate the lateral skin friction in the soil-sampler interface. The undrained shear strength (Su) was calculated using the adhesion factor. The suitability of this method was evaluated by comparing undrained shear strength estimated by both vane shear test (VST) and standard penetration test (SPT) for two Brazilian sites. Despite the variability, results demonstrate a good correlation between Su experimental and theoretical values. This approach can be useful in estimating Su values during preliminary design.

2 SOIL REACTION FORCE

Soil reaction forces that are developed during sampler penetration in SPT has been broadly investigated (Schmertmann, 1979; Aoki et al., 2007; Schnaid et al., 2009; Lukiantchuki et al., 2012; Restrepo et al., 2012). The forces developed during the sampler penetration can be very useful for interpreting the soil behavior and the observations can be extrapolated to pile designs.

Based on this, Schnaid et al (2009) proposed a method to estimate the dynamic soil reaction force (Fd) based on the amount of energy that reaches the sampler (Eq. 2). Lukiantchuki (2012) compared theoretical and experimental dynamic reaction force, and showed that this equation is suitable for estimating Fd values. Therefore, the following equation can be used to in the development of undrained shear strength estimates.

$$Fd = \frac{[(H + \Delta\rho) \times M_H \times g + \Delta\rho \times M_R \times g]}{\Delta\rho} \qquad (2)$$

where $\Delta\rho$ is the average sampler permanent penetration (=30/N_{SPT}), M_H is the hammer mass, H is the height of fall, M_R is the total mass of the string of rods and g is the acceleration of gravity.

2.1 *Soil reaction force interpretation*

Soil reaction force values were used to estimate the undrained shear strength (Su) using the lateral skin friction ($f\ell$) in the soil sampler interface (Eq.3).

$$f\ell = \alpha \times Su \qquad (3)$$

where $f\ell$ is the lateral skin friction, mobilized during sampler penetration, in the soil sampler interface, α is the adhesion factor which relates the lateral skin friction to undrained shear strength (Su).

The dynamic force (Fd) can be converted to static force (Fs) using a load increase factor (ν) (Hermansson and Gravare, 1978; Schnaid et al., 2009) (Eq. 4).

$$Fs = \frac{Fd}{\nu} = \frac{Fd}{1.70} \qquad (4)$$

For soft clay it was adopted 1.70 (Hermansson and Gravare, 1978; Bernardes et al., 2010) (Eq. 4).

The static force (Fs) is composed of the point resistance (Rp) and the result of lateral skin friction ($F\ell$) (Eq. 5). However, in the present paper, only was taken into account the lateral skin friction and the point resistance was negligible (Eq. 6). The undrained shear strength can be estimated using Equation 7.

$$Fs = \frac{Fd}{1.70} = Rp + F\ell \qquad (5)$$

$$Fs = \frac{Fd}{1.70} = (\alpha \times Su) \times (A\ell_o + A\ell_i) \qquad (6)$$

$$Su = \frac{[(H + \Delta\rho) \times M_H \times g + \Delta\rho \times M_R \times g]}{(A\ell_o + A\ell_i) \times (\alpha \times \Delta\rho) \times 1.70} \qquad (7)$$

where $A\ell_o$ and $A\ell_i$ are the outside and inside shaft surface area, respectively.

The adhesion factor (α) shows a general trend higher than unit for very soft clays and to decrease to values as low as 0.2 for very stiff clays (Tomlinson, 1994). In this paper, the SPT sampler was studied as a mini-pile, which according to Brazilian Standard (ABNT, 2001) shows sampler penetration (L) approximately equal to ten times outside sampler diameter (Do) (L≅10Do) (Fig. 1).

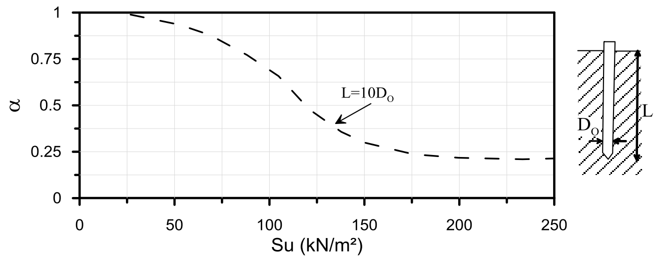

Figure 1. Curves for adhesion factors for piles driven into clay soils (adapted from Tomlinson, 1994).

Undrained shear strength values (Su) were ascertained through Vane Shear Tests (VST), which allowed for estimating adhesion factors. In this work α was assumed to equal 1 for very soft clays and α was set to equal 0.21 for stiff clay. (Figure 1).

3 UNDRAINED SHEAR STRENGTH

Undrained shear strength values were estimated (Eq. 7) for two case studies: 1) Sepetiba region site located in the state of Rio de Janeiro, Brazil and 2) Porto Velho region site located in the state of Roraima, Brazil.

3.1 *Case study*

A case study describing the site of the Porto Velho soft clay deposit in North region of Brazil is useful for illustrating the suitability of Eqs. (4), (5) and (6). Geotechnical investigation comprising in situ tests (SPT and VST) and laboratory tests (oedometer and triaxial) has been carried out (Marques et al., 2008). Figure 2 shows a typical SPT profile, describing the soft clay layers, and the comparison between Su estimated by vane shear test (VST) and SPT, which demonstrates a very good agreement between Su values. There is consensus that SPT is not suitable to estimate soft clay parameters due to soil remolding. However, since SPT is widely used in some countries for preliminary geotechnical site investigation, the method presented in this work can be useful for estimating Su values during preliminary design.

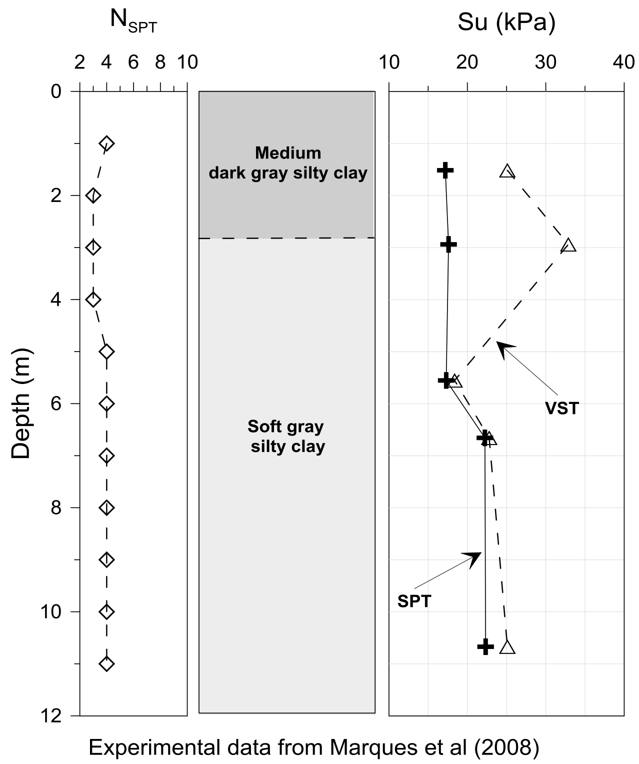

Figure 2. Prediction of Su for soft clay (Porto Velho Site).

Table 1 shows the step by step method proposed for estimating undrained shear strength from SPT results. Results show that the proposed method provides a preliminary estimation of Su values. Dispersions were observed for shallow depths, where it is more difficult to estimate the amount of energy of the SPT.

Table 1. Estimation of Su from the shear strength mobilized during sampler penetration.

Depth (m)	N_{SPT}	$\rho_{average}$ (m)	$E_{sampler}$ (J)	Fd (kN)	α	SPT Su (kPa)	VST Su (kPa)
1.5	3.0	0.100	416.1	4.16	1	19.27	25.10
3.0	3.0	0.100	417.4	4.17	1	19.33	32.88
5.5	3.0	0.100	418.7	4.19	1	24.96	18.38
6.5	4.0	0.075	403.6	5.38	1	24.99	22.78
10.5	4.0	0.075	405.3	5.40	1	25.09	25.10

In order to confirm this behavior another case study was evaluated. The investigation site in the city of Sepetiba is composed of a very soft silty clay deposit in the Southeast of Brazil. Geotechnical in situ investigation (SPT and VST) has been carried out. Figure 3 shows the comparison between experimental and estimated results and Table 2 shows the results from SPT and VST. Large dispersions were observed for borehole 614, the VST values were about 4 or 5 times larger than SPT values. However, for borehole 328 the comparison showed closer values.

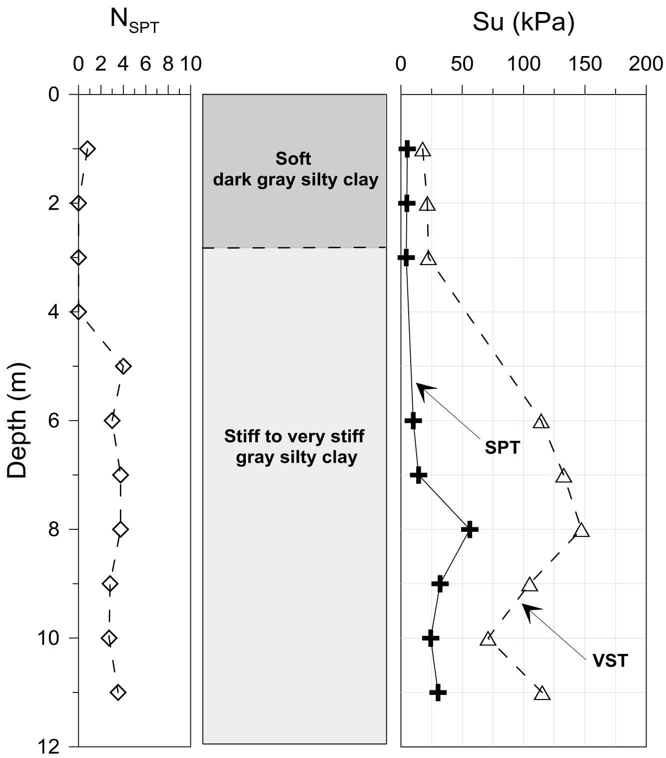

(a) Borehole 614

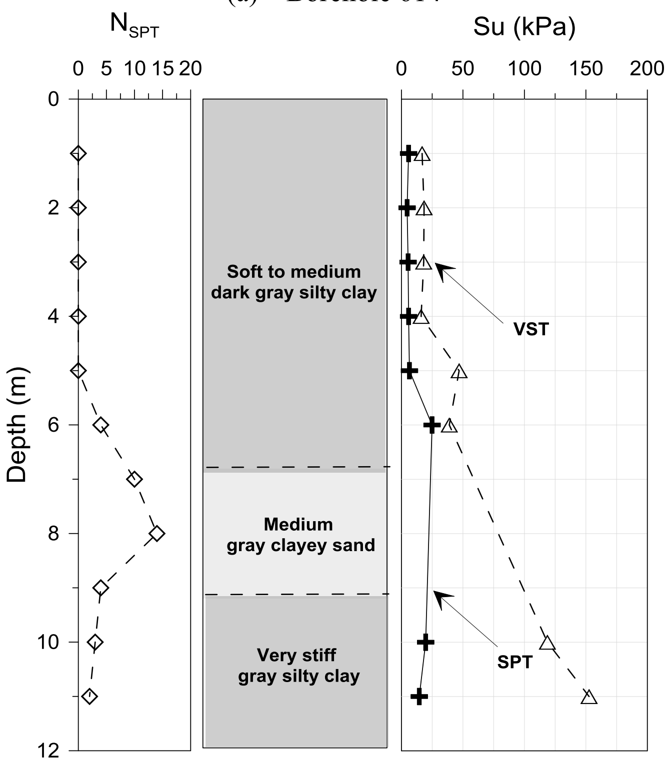

(b) Borehole 328

Figure 3. Prediction of Su for soft clay (Sepetiba Site).

Table 2. Estimation of Su from the shear strength mobilized during sampler penetration.

Depth (m)	N_{SPT}	$\rho_{average}$ (m)	$E_{sampler}$ (J)	Fd (kN)	α	SPT Su (kPa)	VST Su (kPa)
BOREHOLE 614							
1.0	0.8	0.510	636.9	1.25	1	5.8	17.7
2.0	0.0	0.600	701.6	1.17	1	5.4	21.5
3.0	0.0	0.800	837.2	1.05	1	4.9	22.4
6.0	3.0	0.100	421.3	4.21	1	19.5	114.3
7.0	3.75	0.080	408.3	5.10	1	23.6	132.7
8.0	3.75	0.080	408.9	5.11	1	23.7	147.1
9.0	2.80	0.107	430.0	4.03	1	18.7	104.9
10.0	2.73	0.110	434.0	3.95	1	18.3	71.02
11.0	3.53	0.085	414.2	4.88	1	22.6	115.2
BOREHOLE 328							
1.0	0.0	0.510	636.9	1.25	1	5.8	16.8
2.0	0.0	0.860	849.9	0.99	1	4.6	18.4
3.0	0.0	0.640	741.2	1.16	1	5.4	18.1
4.0	0.0	0.580	720.2	1.24	1	5.8	16.0
5.0	0.0	0.480	669.4	1.39	1	6.5	46.9
6.0	4.0	0.075	404.2	5.39	1	24.9	38.9
10.0	3.0	0.100	426.1	4.26	1	19.7	118.7
11.0	2.0	0.150	468.2	3.12	1	14.5	152.6

Figure 6 shows the comparison between experimental and theoretical Su values, which demonstrate that there is a large dispersion between values. In general, Su estimated using SPT energy approach is significant lower than VST results.

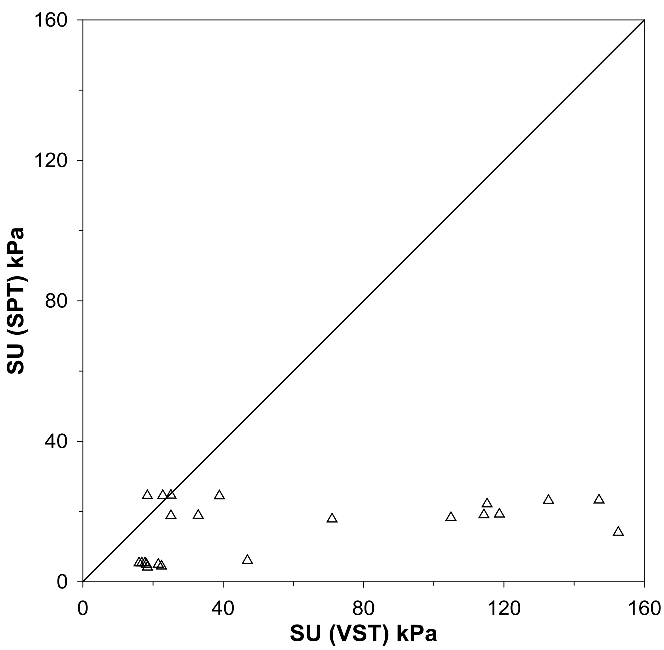

Figure 4. Comparison between experimental and theoretical Su values.

4 CONCLUSIONS

The suitability of a simple procedure to estimate undrained shear strength was evaluated by comparing experimental and theoretical values. Since SPT is widely used in Brazil and other countries, the purpose of this work is to estimate undrained shear strength using energy concepts. For this, the lateral skin friction mobilized during sampler penetration was calculated through the dynamic soil reaction force. The undrained shear strength was estimated based on the lateral skin friction and the adhesion factor. Theoretical values, for two experimental sites, were compared with vane shear test values. Results show that the theoretical method allows for estimating Su values for preliminary design. However, for both sites, the theoretical values were lower than experimental values. SPT energy interpretation is an important improvement in the analysis of SPT test results, allowing a rational interpretation instead of an empirical interpretation. The current method needs to be improved through other parameters which can influence the results.

5 REFERENCES

ABNT. (2001). "Standard penetration test (SPT)". NBR 6484, Rio de Janeiro, 17p. (In Portuguese).

Aoki, N; Cintra, J. C. A. 2000. The application of energy conservation Hamilton's principle to the determination of energy efficiency in SPT test. *Proc. 6th International Conference on the Application of Stress-Wave Theory to Piles*, S. Niyama, and J. Bein, eds., Balkema, São Paulo, Brazil, 457-460.

Aoki, N; Esquivel, E. R.; Neves, L. F. S.; Cintra, J. C. A. 2007. The impact efficiency obtained from static load test performed on the SPT sampler. *Soils and Foundations*, 47 (6), 1045–1052.

Clough, R. W; Penzien, J. 1975. *Dynamics of structures*. New York: McGraw-Hill.

Hettiarachchi, H.; Brown, T. (2009). Use of SPT blow counts to estimate shear strength properties of soils: energy balance approach. *Journal of Geotechnical and Geoenvironmental engineering*, ASCE, 135 (6), 830-834.

Lukiantchuki, J. A. 2012. *Interpretation of SPT test results based on dynamic instrumentation*. Doctoral thesis, University of Sao Paulo, Sao Carlos, Brazil, 326p. (in Portuguese).

Lukiantchuki, J. A; Esquivel, E. R; Bernardes, G. P. 2012. Experimental soil dynamic force: An improvement of Standard Penetration Test (SPT) interpretation. *14th International Conference on Geotechnical and Geophysical Site Characterization*, Porto de Galinhas/Brasil.

Marques, M. E. S.; Oliveira, J. R. M. S.; Souza, A. I. 2008. Characterization of a soft sedimentar deposit in the region of Porto Velho. *Proc. Brazilian Conference on Soil Mechanics and Geotechnical Engineering*, Buzios, Rio de Janeiro (in Portuguese).

Odebrecht, E; Schnaid, F.; Rocha, M. M.; Bernardes, G. 2005. Energy efficiency for standard penetration tests. *Journal of Geotechnical and Geoenvironmental Engineering*, 131 (10), 1252-1263.

Schmertmann, J. H.; Palacios, A. 1979. Energy dynamics of SPT. *Journal of the Geotechnical Engineering Division*, ASCE, 105 (GT8), 909-926.

Schnaid, F.; Odebrecht, E.; Rocha, M. M.; Bernardes, G. 2009. Prediction of soil properties from the concepts of energy transfer in dynamics penetration test. *Journal of Geotechnical and Geoenvironmental Engineering*, 135 (8), 1092-1100.

Tomlinson, M. J. 1994. Pile design and construction practice. E & FN SPON, 411p.

Geotechnical and Geophysical Site Characterisation 5 – Lehane, Acosta-Martínez & Kelly (Eds)

Rotation Speed Analysis in SPT-T Test by Type of Soil

R.R. Nuñez, T.T.C. Piovan & A.S.P. Peixoto
Univ. Estadual Paulista. Depart. of Civil and Environmental Engineering, Bauru, SP, Brazil

ABSTRACT: One of the main purposes of the Standard Penetration Test (SPT) is related to prediction of load capacity of foundations. In addition, the SPT-T was proposed using a torquemeter device in order to break the adhesion of soil sampler after the end of each SPT. This measurement can be used to calculate the amount of lateral friction improving foundations design. The rotation speed is analyzed to set its variation range and its influence on the torque measurement is assessed based on soil type. First, a theoretical study was conducted. Secondly, analysis were performed with data obtained from a system that simultaneously enabled the acquisition of torque measurement and its corresponding rotation speed resulting in 426 curves in seven sites with different geotechnical characteristics. The analysis of rotation degrees had considered the geotechnical profile of each site and then they were faced with N; maximum torque (T_{max}); residual torque (T_{res}); T_{max}/N ratio; and finally type of soil. A statistical analysis was done and then in conclusion this study will improve the SPT-T implementation procedure.

1 INTRODUCTION

The Standard Penetration Test with Torque Measurements, SPT-T, was proposed by Ranzini (1988) in order to measure the friction-adhesion developed in the soil sampler interface. After each penetration test, i.e. SPT, a torque wrench is used to break the adhesion between the ground and the sampler thus facilitating its removal from the hole.

Peixoto & Carvalho (2014) recommended the following procedure: immediately after driving the sampler, attach the torque meter with an adapter on the anvil. In order to prevent the rod's shifting while the torque is applied, a centralizing device should be placed, either on the mouth of the hole or on the pipe. The rotation needs to be carried without interruption and after maximum torque is obtained continued until its value becomes constant, when the residual torque is obtained. It provides a "static" component for a "dynamic" test.

According to Ranzini (1994), the maximum torque could be used to calculate the lateral skin friction of piles, Equation 1.

$$fT = (T_{max}) / (41.336h - 0.032) \qquad (1)$$

where: fT= sampler-soil adhesion, kPa; T_{max}= maximum torque measurement, m.kN; h = depth of penetration of the sampler, m.

Lutenegger & Kelley (1998) corroborated the use of fT for predicting lateral skin friction of piles. Nevertheless, Decourt (1998) implied the torque assesses the skin friction in an area partially disturbed but, despite that, Tmax/N tends to be larger in structured soils (Figure 1). However, Peixoto & Carvalho (1999) also demonstrated the great variability of the T_{max}/N ratio. In spite of that, it was verified that medium values show some tendencies. For instance: for T_{max}/N minor than value one, the soil is always collapsible. But, there are collapsible soils with T_{max}/N ratio greater than value one.

On the other hand, Peixoto et al. (2004) concluded that the T_{max}/N ratio can be used as a parameter to predict the behaviour of the soil, for example, when implanting a foundation element. Here, the T_{max}/N ratio is not used as a correlation yet as a correction factor leading to an index, F1, in the bearing capacity prediction considering foundation type, Equation 2 and Table 1.

$$qs = F_1.fT \qquad (2)$$

where: qs = shaft resistance; fT = sampler-soil adhesion (kPa); F_1= Correction value function of pile type and T_{max}(kgf.m)/N ratio, (Table 1)

Although the applicability of torque measurement in foundation's design is stimulated by various authors, the device used to obtain the rotation speed has to be normalized before the equipment is actually used in engineering practice. This paper aims to analyse the variation of the rotational speed considering the type of soil, the N, the maximum torque

T_{max}, the residual torque, T_{res}, the moisture content, w and the T_{max}/N ratio.

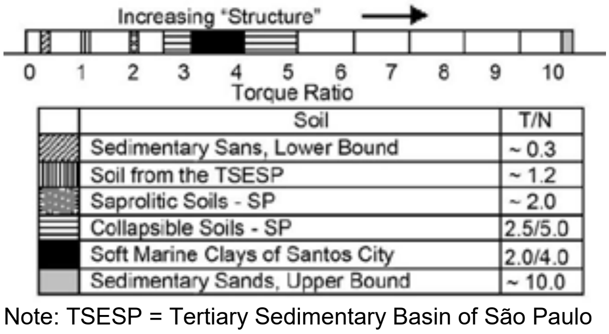

Figure 1. Soil Classification based on torque ratio (Tmax/N) *apud* Decourt (1998)

Table 1. F1 coefficients.

Pile Type	F_1	
	$T_{max}/N < 1$	$T_{max}/N>1$
Precast concrete	1.0	1.0
Omega	1.0	1.0
Steel	1.0	1.0
Small Diameter Injected	1.0	1.0
Root	1.0	1.0
Strauss	1.3	0.7
Franki	0.7	0.5
Socketed	0.7	0.5
Continuous-Flight-Auger	1.0*	0.3*
Auger and Bored	1.3	0.7
Diaphragm Panel Bored	1.0	1.0

Note: when fT> 80kPa, use F_1=0.3 to any T_{max}/N

2 METHODS AND MATERIALS

The statistical study was based on data from seven places of Southeast Brazil with different geotechnical characteristics, Figure 2. The soils of Paraná Basin (Ilha Solteira, São Carlos and Bauru) have a first layer of clayey sand (depth between 7m and 13m), porous, of lateritic behaviour; the second layer depends on the geological formation. Campinas is a transition site with a 6m depth sandy clay layer porous and lateritic with a residual soil diabase below it. The soil from São Paulo site is residual of Migmatitte.

Figure 2. Places where the research were carried out. Modified of Peixoto et al. (2004)

The tests carried out on the seven sites, using Peixoto (2001) data, resulted in 426 curves, shown on Figure 3, possible by the development of a system that simultaneously enabled the acquisition of torque measurement and its corresponding rotation speed. Each curve provided the corresponding rotation speed to the maximum and residual torque. The findings were separated by site and borehole to be confronted with soil type, N, moisture content and T_{max}/N ratio.

To calculate the speed corresponding to maximum torque, V_{Tmax}, the average of a range of 1 sec (0.5" before and 0.5" later) and acquisition frequency were taken as regarded. The medium velocity of residual torque, $V_{Tres\ med}$, was obtained by the medium value between the first minimum value and the last value of the curve.

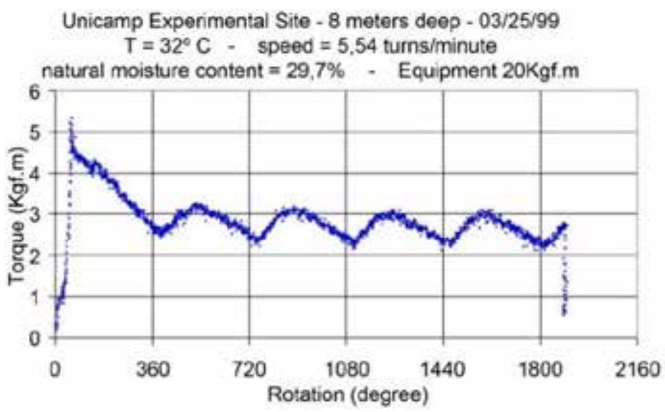

Figure 3. Typical Curves. Modified of Peixoto et al. (2004)

3 RESULTS AND DISCUSSION

Figures 4 to 10 show borehole profiles of the seven analysed fields. In general, the soil sites A, B and C are compounds of clayey sand. In these places, the values of N, T_{max} and T_{res} increased with depth.

On Figures 4 to 6, the medium velocity of residual torque, $V_{Tres\ med}$, is greater than the one responsible for breaking the soil-sampler adhesion V_{max}. Also, considering same depth, the higher the values of N and T_{max} are, the lower the V_{max} is.

Site D is composed of a first layer of porous sandy clay and below that, a Diabase residual soil. Here the values of V_{Tmax} have a wide variability between boreholes for the same depth. Although this variation seems to be a reflection of the difficulty of breaking the adhesion soil-sampler due to soil anisotropy, it does not reflect in the results of torque, as shown in Figure 7.

The site E, Figure 8, with Migmatite residual soil showed the same behaviour, i.e. N values ranging between 10 and 40 blows to the same depth, and again different torque values. These characteristics are due to the soil heterogeneity and not due to the speed of rotation, which intensity is also affected by the same factor.

Few data of organic clay at site F, Figure 9, do not permit a conclusion about the influence of rotation speed, but it is possible to highlight the small values observed for V_{Tmax} compared with other sites and in contrast the $V_{Tres\ med}$ values corroborating the other sites. Again in Figure 10 can be noticed that the variation of the rotation speed within the analysis range, i.e. between 3 and 10 rpm, do not affect on the value of the maximum and residual torques.

To enhance discussion, Table 2 shows the statistical analysis where can be noticed a higher coefficient of variation for the speeds that lead to maximum torque, with an overall average of 5.3 rpm. Moreover, regarding the speed range which measures the residual torque it can be obtained an overall average of 6.85 and low coefficient of variation.

In all figures can be noticed no interference of rotation speed in T_{max}/N ratio. The interference of moisture content can be noted only in the site F where there was a greater variation of this parameter.

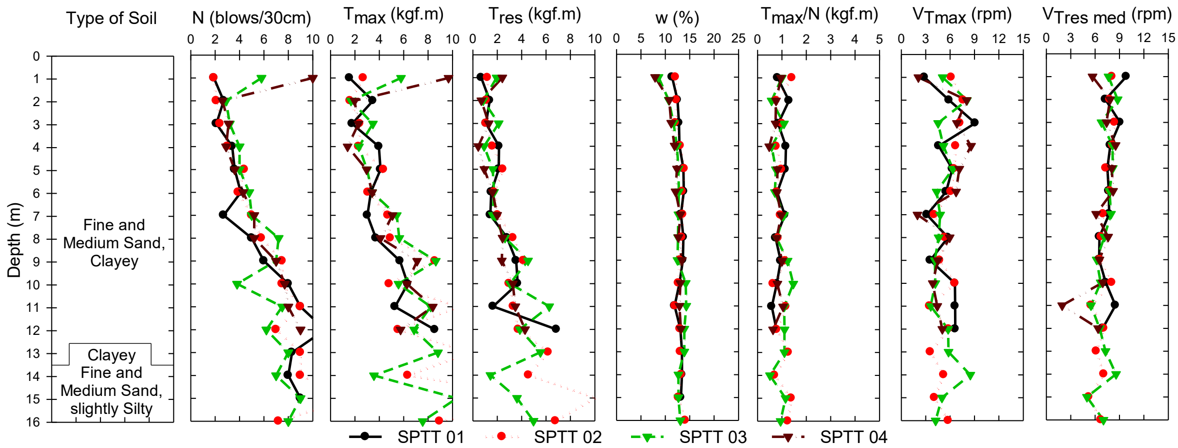

Figure 4. Borehole profiles of Site A

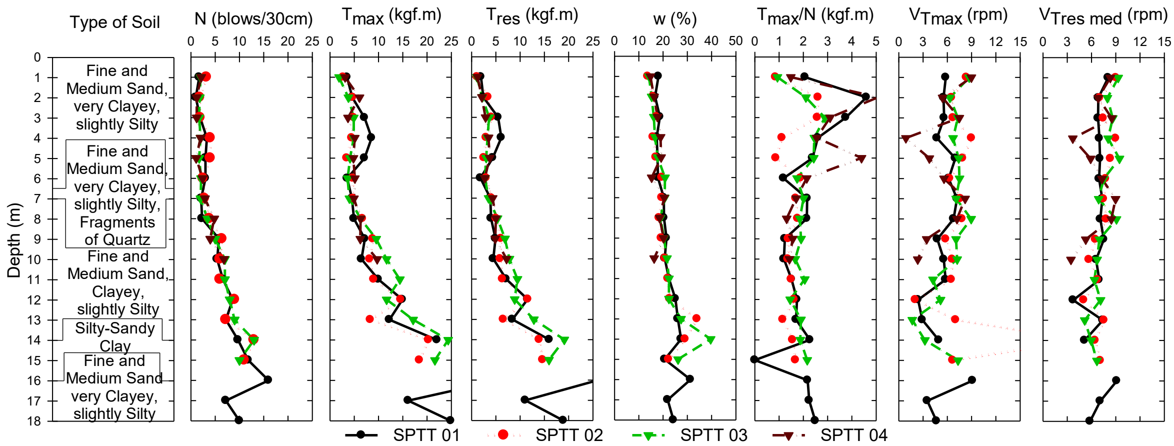

Figure 5. Borehole profiles of Site B

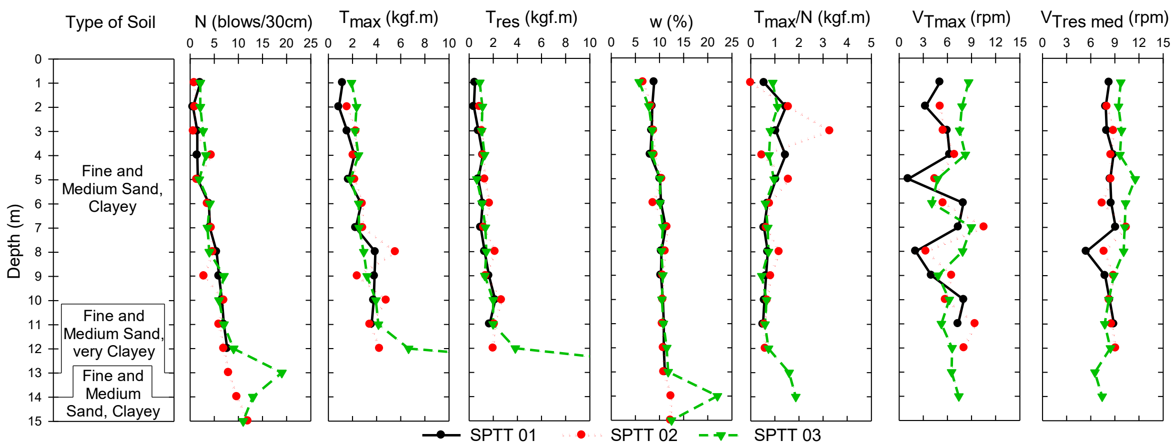

Figure 6. Borehole profiles of Site C

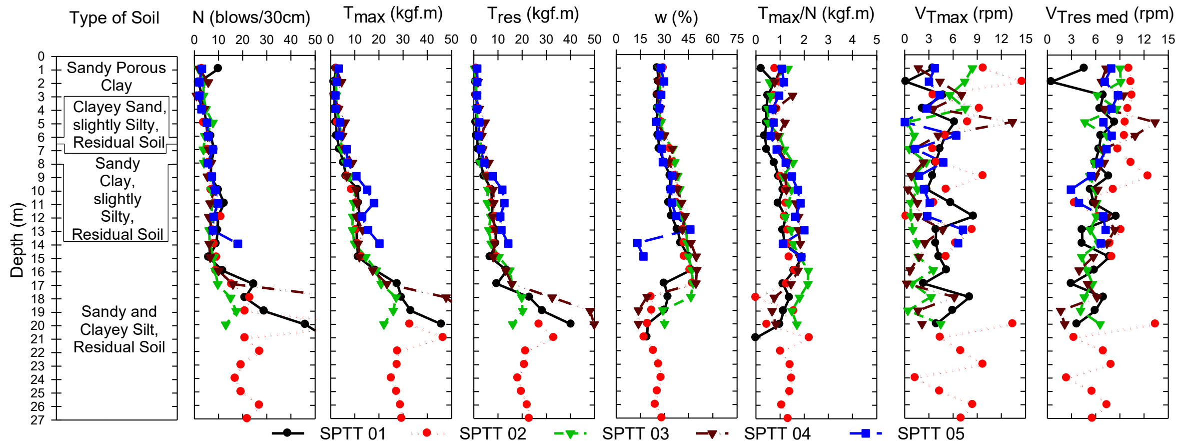

Figure 7. Borehole profiles of Site D

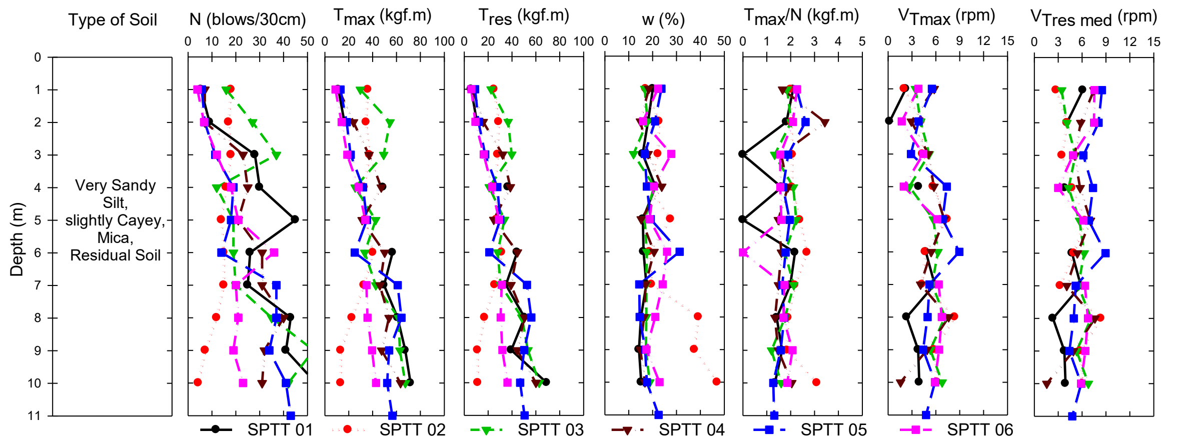

Figure 8. Borehole profiles of Site E

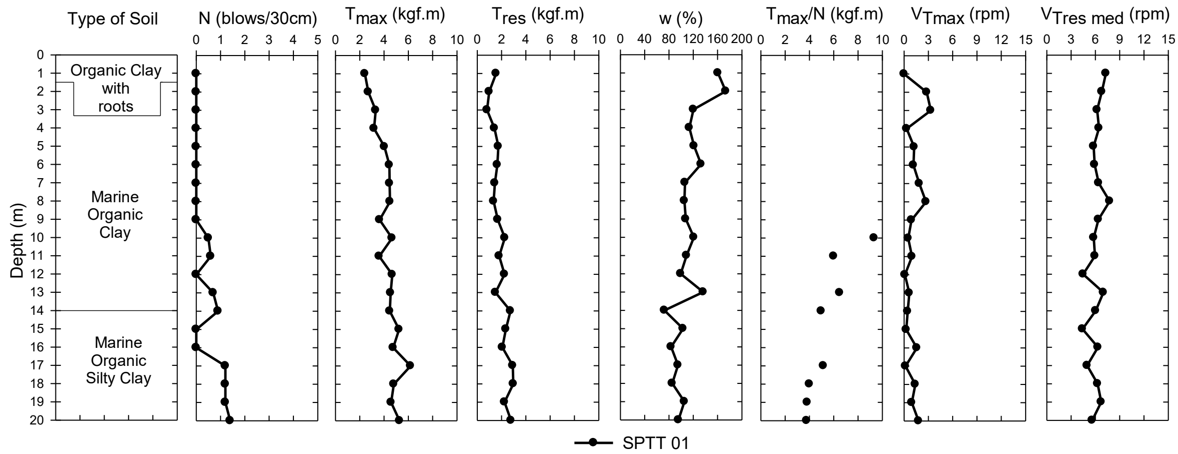

Figure 9. Borehole profiles of Site F

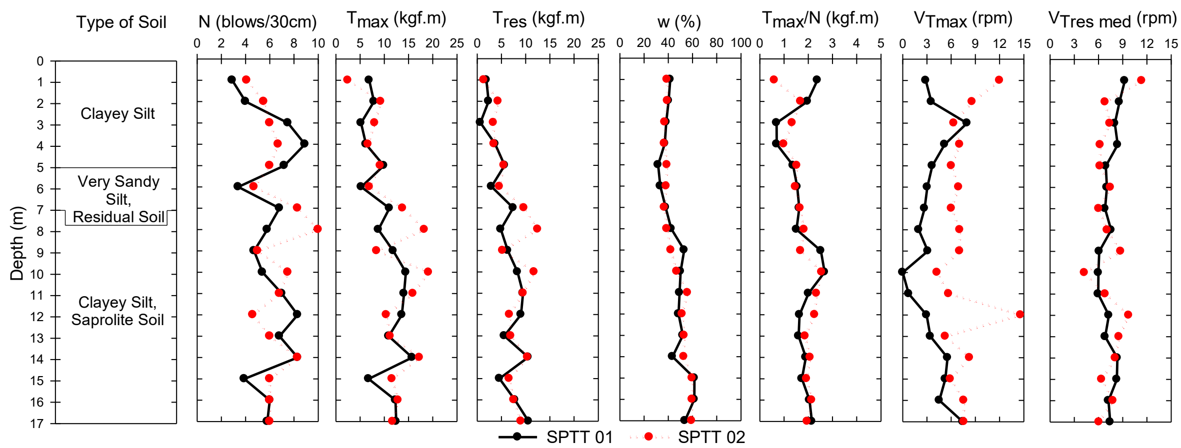

Figure 10. Borehole profiles of Site G

Table 2. Statistical analysis

site	layer	V_{Tmax} (rpm)	sd cv (%)	$V_{Tres\ med}$ (rpm)	sd cv (%)	Δ
A	In general way, clayey sand	5.44	1.606 29.5	7.20	1.218 16.9	24.4
B	In general way, silty clayey sand	6.30	2.933 46.5	7.09	1.275 18.0	11.1
C	In general way, clayey sand	6.24	2.071 33.4	8.67	1.146 13.2	28.0
D	Porous sandy clay	5.01	3.302 64.5	7.88	2.291 29.0	36.4
	Clayey sandy silt, Diabase residual soil	3.89	2.291 75.4	5.98	2.173 36.3	34.9
E	In general little clayey, very sandy	4.93	1.797 36.4	5.49	1.601 29.1	10.2
F	Sea organic clay	1.22	0.949 77.6	6.07	0.841 13.9	79.9
G	Clayey silt	6.32	2.766 43.7	7.92	1.589 20.1	20.2
	Clayey silt, Residual Soil	6.71	6.526 97.3	7.17	1.163 16.2	6.6
	All data	5.13	3.147 61.3	6.85	1.869 27.2	25.1

Note: sd = standard deviation; cv = coefficient of variation; $\Delta=(V_{Tres\ med} - V_{Tmax})/ V_{Tres\ med}$

Piovan and Peixoto (2015) studied the influence of angular thrust in the measurement of torque in the SPT-T. Those authors highlighted the maximum angular thrust does not happen at the same instant as the maximum torque, but prior to this. This is explained as the initial force applied by the torquemeter is absorbed by the set of rods before it reaches the sampler and then breaks the soil-sampler adhesion. In fact, this justifies the interval up to the maximum torque ending in low values of angular thrust, that is, slow rotational speed. In addition, due to this breakdown, the velocity increases after the maximum torque occurs, defining a residual angular thrust. This explains the difference between V_{Tmax} and $V_{Tres\ med}$.

In this way, N with values greater than 20, as site E of Figure 8, have shown high difficulties in test procedure due to high challenge to completely break the adhesion soil-sampler leading to a variability of V_{Tmax}.

4 CONCLUSIONS

After analysing the seven sites, it was concluded the velocity variation was due to soil type and N, but this range did not interfere in the torque values.

Considering the rotation speed range between 3 and 9 rpm, which results in a comfortable conduction led by the operator, there is no influence in the maximum and residual torques.

Finally, the Brazilian Association for Technical Standards has been drawing the revision of Standard Penetration Test since 2013 and the commission is supposed to include the measurement of torque as a not mandatory complementation to the SPT procedure. It is not appropriate to suggest a fixed value for the rotation speed since it is closely linked to soil type and angular thrust that will lead to the breakdown of the soil-sampler adhesion after the maximum torque. In this way, here is recommended a rotation speed between 5 and 8 rpm.

5 ACKNOWLEDGEMENTS

The authors would like to thank the two grants 13/26750-6 and 05/01953-5, São Paulo Research Foundation (FAPESP) and CNPq for the scientific initiation scholarship of first author.

6 REFERENCES

ABNT NBR 6484. 2001. Execução de Sondagens de Simples Reconhecimento dos Solos.

Decourt, L. 1998. A more rational utilization of some old in situ tests. *Proc. Geotechnical Site Characterization.* Balkema. Atlanta. USA, 913-918.

Lutenegger, A.J. & Kelley, S.P. 1998. Standard Penetretion Test with torque measuremen*". Proc. Geotechnical Site Characterization.* Balkema. Atlanta. USA, 939-945.

Peixoto, A. S .P. & Carvalho, D. 1999. Standard penetration test with torque measurement (SPT-T) and some factors that affect the T/N ratio. *Proc. XI Panamerican Conference on Soil Mechanics and Geotechnical Engineering.* Foz do Iguaçu. ISSMGE/ABMS/SAMS/SPG. V. 3,1605-1612.

Peixoto, A. S .P. & Carvalho, D. 2014. Determination of soil properties from standard penetration test complemented by torque measurement (SPT-T). *Acta Scientiarium. Technology*. 36: 617-621, 2014.

Peixoto, A. S .P.; Carvalho, D. & Giacheti, H. L. 2004. SPT-T: Test Procedure and applications. *Proc. International Site Characterization - ISC'2.* Porto. Roterdam: Millpress. 1: 359-366.

Piovan, T. T. C. & Peixoto, A. S. P. Influence of Angular Thrust in the Measurement of Torque in the SPT-T. *Proc. 15th Pan-American Conference on Soil Mechanics and Geotechnical Engineering (XV PCSMGE)* Buenos Aires. *From Fundamentals to Applications in Geotecnics*. Amsterdan: IOS Press BV, 2015. 1: 430-437.

Ranzini, S.M.T. 1988. SPTF. *Solos e Rocha*. 11, 29-30.

Geotechnical and Geophysical Site Characterisation 5 – Lehane, Acosta-Martínez & Kelly (Eds)

Critical appraisal of T-bar penetration tests

J. Peuchen & J. Terwindt
Fugro, the Netherlands

ABSTRACT: Deployment experience and metrological assessment indicate an overvalued applicability of the T-bar penetration test (TBT) as an offshore in situ test. More attention should be given to a combination of ball penetration tests (BPT) and cone penetration tests (CPT). Reasons for reducing TBT preference include: (1) no axial symmetry of T-bar, which promotes unwanted directional drift and associated bending influence on measurements, (2) sensitivity to torsional forces acting on T-bar, giving undetectable measurement error, (3) limited opportunity for enhanced test interpretation from pore pressure data. The current ratio of offshore TBTs to BPTs is about 10:1 to 100:1 when expressed in metres penetration. A reversal of the TBT:BPT ratio would be prudent, as BPTs rate better. This is supported by uncertainty analysis for penetration resistance q_m according to ISO 19901-8, possibly representing a first-ever calculation.

1 INTRODUCTION

This paper focuses on the T-bar penetration test (TBT) as in situ test. It excludes miniature versions of the TBT used for testing of soil samples on site or in a geotechnical laboratory.

The TBT involves measurement of the resistance of ground to continuous penetration at a steady slow rate of a cylindrical rod (T-bar penetrometer) positioned perpendicular to the lower end of push rods (Figure 1). A T-bar penetrometer is equipped with internal sensors, the output of which is recorded at least every second, at a nominal penetration rate of 20 mm/s ± 5 mm/s. The measurements comprise penetration length, penetration resistance and inclination from vertical. Optional measurements can include penetration resistance during retraction, cyclic penetration resistance and pore pressure. The ball penetration test (BPT) is equivalent to the TBT except that the T-bar is replaced by a sphere. Figure 1 shows T-bar and ball penetrometers with optional button filters for pore pressure measurement. A cone penetrometer with a cross sectional area of 1000 mm^2 is shown for comparison of scale.

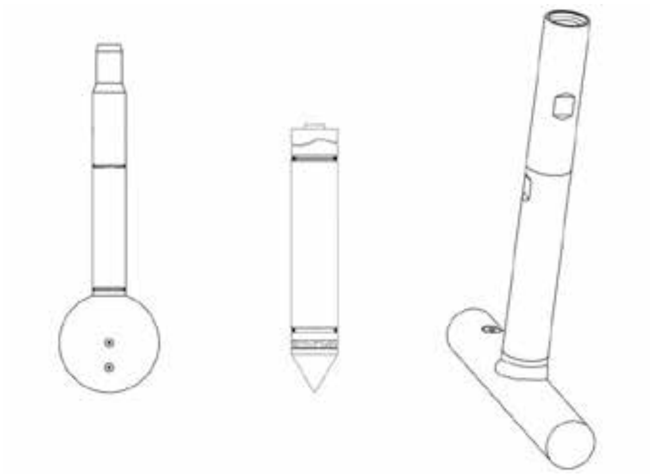

Figure 1 Fugro T-bar, cone and ball penetrometers.

In practice, TBT and BPT systems are comparable to cone penetration test (CPT) systems. The T-bar or ball is in place of the cone part of the cone penetrometer. The geometry differences lead to differences in characterisation of soil behaviour, primarily related to displacement and flow of soil around a cone with the same cross sectional area as the shaft and push rods versus flow of soil around a T-bar+shaft or ball+shaft.

The in situ version of the TBT was first used in Australia during 1996 (Randolph et al. 1998). It quickly gained offshore industry recognition as a profiling tool for deepwater soft clays. Its offshore use has been fairly steady over the past 10 years, with an annual guestimate in the order of 2 km total penetration. The ratio of TBT to CPT is in the order of 0.03 in terms of penetration metres, considering offshore use. Onshore use of the TBT is almost entirely for research purposes. This ratio for combined onshore and offshore penetration metres is possibly in the order of 0.002. The current ratio of offshore TBTs to BPTs is about 10:1 to 100:1

2 INTERNATIONAL STANDARDISATION

ISO 19901-8 (2014) and EN (2015) provide requirements and recommendations for offshore TBTs and BPTs. EN (2015) is a copy of ISO 19901-8. This paper will further refer to ISO 19901-8.

ISO 19901-8 considers TBTs and BPTs to be "particularly suitable for characterizing very soft to soft clays and clayey silts with an undrained shear strength < 50 kPa". In practice, this suitability or applicability corresponds to normally consolidated profiles of fine grained soils to depths in the order of 35 m below seafloor, or shallower for overconsolidated profiles.

The allowable minimum accuracy for measurement of penetration resistance q_m is 5% or 20 kPa, whichever is larger. This means that the changeover from 20 kPa to 5% is at $q_m = 400$ kPa, which corresponds with an undrained shear strength of about 40 kPa. Note that minimum accuracy is a *requirement* of ISO 19901-8, i.e. mandatory for compliance. Metrological confirmation should be done according to ISO (2003). This is a *recommendation*, i.e. not mandatory. The following comments are offered.

1 To the knowledge of the authors, the requirements for accuracy of q_m were set based on a general uncertainty estimate. No uncertainty estimate according to ISO (2003) was published prior to first issue of ISO 19901-8 and, probably, this paper.
2 The accuracy requirements for q_m apply to downward penetration. ISO 19901-8 considers upward retraction and cyclic test phases as optional possibilities.
3 The parameter q_m is uncoupled from depth below seafloor. ISO 19901-8 considers depth accuracy classes Z1 to Z5, with allowable accuracy values ranging between 0.1 m and >2 m. Z4 (2 m) is the default accuracy class.
4 The terms error and accuracy are used. These terms can lead to interpretative differences in practice. Error implies a reference quantity value. This probably refers to a value determined in a calibration laboratory or similar, as it is generally impossible to obtain an in situ reference value. Accuracy assumes knowledge of a true value, i.e. what should be regarded as true value.
5 True values depend on permissible equipment-specific and procedure-specific features. This means that compliance with ISO 19901-8 only provides a first indication of accuracy required for geotechnical practice. Further processing can be necessary to obtain fit-for-purpose accuracy, i.e. accuracy that is independent of equipment and procedures. To the knowledge of the authors, such benchmarking is yet to be demonstrated.

Further requirements of ISO 19901-8 include a nominal penetration rate of 20 mm/s ± 5 mm/s and data recording at 1 Hz or more. Further recommendations of ISO 19901-8 include a "standard" T-bar with a length of 250 mm and diameter of 40 mm and a minimum ratio of 7:1 for the projected cross sectional area of the T-bar to the cross sectional area of the push rod. This ratio suits use of a modified CPT cone penetrometer for TBTs. BPT recommendations are equivalent to those for the TBT. ISO 19901-8 gives no requirements for pore pressure measurement.

3 UNCERTAINTY ESTIMATION FOR PENETRATION RESISTANCE

Figure 2 shows example results of uncertainty $|U_{qm}|$ analysis for q_m according to ISO 19901-8, possibly representing a first-ever calculation. The figure includes a comparison with CPT cone resistance q_c $|U_{qc}|$. The results confirm TBT and BPT benefits in accuracy when considering the upper few metres below seafloor. The benefits primarily relate to sensitivity of a penetrometer load cell to transient temperature change. The example calculations consider uncertainties from 2 °C initial temperature difference between seabed temperature and seawater temperature just above seafloor as well as additional heat generated by frictional work. The larger area of a T-bar or ball, compared to a cone, mitigates such uncertainties. The benefits reduce with increasing penetration resistance and penetration depth, particularly after a penetrometer has acquired a stable temperature environment.

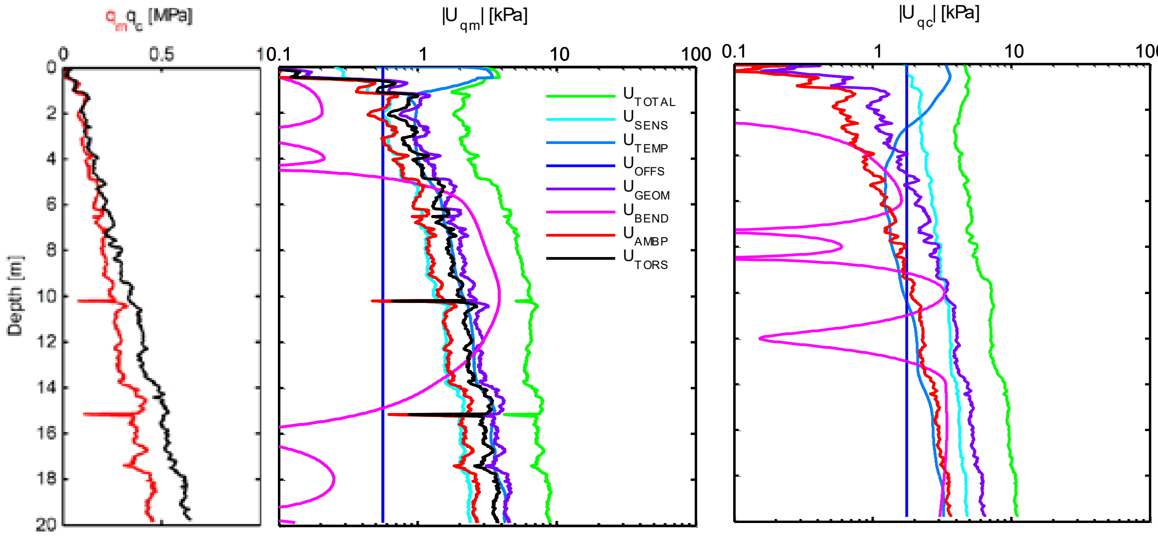

Figure 2 Examples of uncertainty estimates for high-quality TBT and CPT systems and practices, non-drilling deployment and water depth of 1500 m.

The selected approach is according to a published method for CPT cone resistance q_c (Peuchen & Terwindt 2015):

$$U_{TOTAL} = k \cdot \sqrt{\left(c_1 \frac{U_1}{d_1}\right)^2 + \left(c_2 \frac{U_2}{d_2}\right)^2 + \ldots + \left(c_i \frac{U_i}{d_i}\right)^2}$$

where U_{TOTAL} is parameter value uncertainty, k is a coverage factor, U_1 to U_i are estimated standard uncertainties, c_1 to c_i are sensitivity coefficients and d_1 to d_i are distribution coefficients. The selected value for k is 2, which corresponds to a 95% confidence interval. The selected value for the c-coefficients is 1, applicable to a linear relationship. The selected value for the d-coefficients is √3, which corresponds to an extreme value approach and a rectangular distribution. The component uncertainties cover sensor for force measurement U_{SENS}, geometry and dimensional errors of penetrometer U_{GEOM}, ambient and transient temperature influence U_{TEMP}, bending moment acting on penetrometer U_{BEND}, influence of water pressures acting on penetrometer U_{AMBP}, offset of measurements to seafloor as reference U_{OFFS}.

A CPT approach for TBTs and TBTs requires consideration of additional factors: definition of q_m and estimated uncertainty for axial torsion U_{TORS} affecting q_m.

The parameter q_m is partially defined by ISO 19901-8. In practice, q_m is assumed as the measured axial force divided by the maximum cross sectional area of the penetrometer. This assumption implies that (1) the cross sectional area for upward retraction is equal to the downward push and (2) q_m includes axial soil resistance on the fixed portion of the vertical connection between the horizontal part of the T-bar and the vertical part of the T-bar that has no effect on force measurement. The influence of these assumptions can be ignored for uncertainty estimates according to ISO 19901-8.

Laboratory calibrations of penetrometers are generally for compressive loading. Limited experiments indicate that linearity of high quality load cells for cone penetrometers differ by up to a few percent when comparing compressive and tensile loading. Note that the load cell of a T-bar penetrometer often remains in compression during offshore retraction and cycling. For example, a T-bar would be just in compression for q_m = -250 kPa and a water depth in the order of 350 m.

U_{TORS} can be estimated according to $U_{TORS} = a \cdot b \cdot q_m$. The presented example results for U_{TORS} consider $a = 0.3\ \text{kPa}\cdot\text{N}^{-1}\cdot\text{m}^{-1}$ and $b = 2.75\cdot10^{-5}\ \text{m}^3$. The coefficient a represents laboratory experiments at $q_m = 0$, showing a linear response of apparent q_m to torsional load. The coefficient b represents an example proportion of axial force transferred to torsional load. Note that torsional measurement error remains undetectable during TBTs, when applying CPT load cell technology. The T-bar geometry contributes to torsional influence, as the penetrometer shape has no axial symmetry. This implies sensitivity to (1) development of torsion compared to CPTs and to a lesser extent BPTs, (2) non-vertical penetration and (3) cork-screw rotation in case of incomplete fixity to axial rotation of the push rods. Note that (3) can possibly imply that penetrometer retraction will be (partially) in undisturbed soil and that the number of cycles for obtaining nearly constant cyclic penetration resistance will increase.

It may be expected that U_{TORS} correlates significantly to bending U_{BEND}. Such correlation is currently not accounted for. U_{BEND} correlates to inclination of a penetrometer (Peuchen and Terwindt 2014). Figure 3 illustrates results of a brief review of inclination measurements. This brief review generally showed (1) comparable penetrometer inclination for normally consolidated clays to 20 m below seafloor and (2) potential for reducing bending forces during a cyclic TBT phase. The change in inclination (i) of Fig. 3 is shown by some but not all tests.

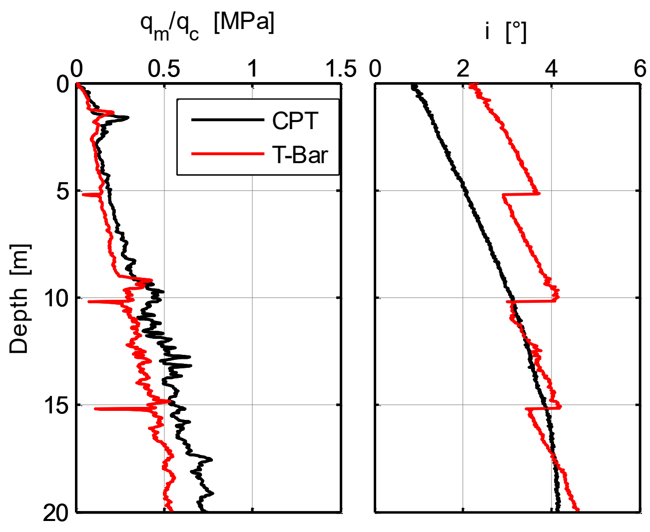

Figure 3 T-bar inclination changes during cyclic test stages compared to a cone penetration test; cyclic test stages are evident from low-value spikes in q_m profile.

4 ANALYTIC TBT AND BPT

It can be convenient to compare results against an Analytic test, rather than a test standard designed for practice (Peuchen and Terwindt 2014). The Analytic TBT would include a 250 mm long bar of 40 mm diameter with a "push rod of zero cross-sectional area". Similarly, the Analytic BPT would have a sphere of 113 mm diameter. The Analytic versions exist in computer models. They allow true full-flow of soil around a deeply embedded object, i.e. no material volume (e.g. push rod or soil) is introduced or withdrawn from the soil body during penetration. Similarly, modelling of shallow embedment is simplified when considering (1) formation of a cavity in soil during penetration and (2) "excavation" of soil during retraction (Fig. 4).

The Analytic TBT would render:

$$q_m = Q_p/A_1 = q_{T\text{-bar}} = q_T.$$

The parameter $q_{T\text{-bar}}$ (q_{ball}) is given by ISO 19901-8 as:

$$q_{T\text{-bar}} = Q_p/A_1 - (A_2/A_1)u_0 - (A_3/A_1)(\sigma_{vo} - u_0),$$

where:

A_1 = maximum cross sectional area of the penetrometer perpendicular to the axis of the push rod
A_2 = cross-sectional (steel) area at the push rod / penetrometer connection
A_3 = cross-sectional area of the push rod immediately above the penetrometer
Q_p = axially measured force on the penetrometer, positive for downward push
$q_{T\text{-bar}}$ = net penetration resistance for T-bar
u_o = hydrostatic pore pressure calculated for penetration depth z, relative to seafloor
σ_{vo} = total in situ vertical stress calculated for the horizontal axis of the T-bar, relative to seafloor.

Figure 4 Soil adhering to mini T-bar penetrometer after retraction from offshore box core sample.

The equation for $q_{T\text{-bar}}$ is a simplification, in that pore pressure in the gap at the level of A_2 is replaced with u_0. The equation for $q_{T\text{-bar}}$ is based on Senneset et al. (1982), who relate net penetration resistance of a (cone) penetrometer to classical bearing capacity theory for a wished-in-place penetrometer in undrained soil. Robertson and Campanella (1983) added a correction for pore pressures that depends on (cone) penetrometer design, particularly net area ratio $a = A_2/A_1$.

5 COMPARATIVE COMMENTS FOR TBT, BPT AND CPT

TBT / BPT applicability applies to a narrow range of soil conditions compared to a wide range of soil conditions for CPTs. In practice, the range of soil conditions may be expressed in terms of q_m and q_c. Values for q_m are typically limited to 0.5 MPa to 1 MPa and values for q_c to 50 MPa to 100 MPa. These limits vary in practice, based on assessment of value of higher limits versus risk of loss or damage of equipment. The differences in limits to penetration resistance relate to push forces in kN required to penetrate a relatively large T-bar (ball) penetrometer plus push rods versus a relatively small cone penetrometer plus push rods. Risk of equipment damage and loss in heterogeneous soil also contributes to practical limits. The cone penetrometer has a favourable geometry for heterogeneous soil. The ball penetrometer is axi-symmetric, with a weak point at the connection with the vertical shaft. The T-bar penetrometer has no axial symmetry, as discussed above. It is less robust than the ball penetrometer.

TBT deployment is limited to non-drilling mode, whereby T-bar push and retraction are from a seafloor-based template. The 250 mm width of a T-bar precludes drilling mode. A miniature TBT for drilling mode deployment (i.e. through the drill string) was trialled and found to lack the robustness required for the typically onerous offshore operating conditions (Peuchen et al. 2005). The geometries of ball penetrometers and cone penetrometers allow both non-drilling and drilling modes, including wireline deployment down a borehole. Drilling mode enhances flexibility for testing as-found, heterogeneous soil conditions. Drilling modes include floating vessel, stable-non floating platform and seafloor drilling.

The above section on Uncertainty Estimation for Penetration Resistance illustrates that TBT/ BPT accuracy for penetration resistance is *slightly better* than for CPTs. This is contrary to popular beliefs: *much better*, *superior*. The halo effect for TBT and BPT accuracy is probably related to misunderstanding of metrology of load cells, particularly confusion between load cell range and hysteresis within the measuring range of interest rather than full scale output (Peuchen & Terwindt 2014).

Conventional CPT measurements (cone resistance, sleeve friction and pore pressure) allow excellent profiling for soil behaviour types. The TBT and BPT also allow for profiling for soil behaviour type if pore pressure sensors are incorporated. However, this is of limited interest because tests are generally done only in clays and clayey silts with undrained shear strengths of less than 50 kPa. Pore pressure measurements can be of interest for optional pore pressure dissipation and twitch testing. The ball penetrometer has the better qualifications compared to the T-bar (e.g. Mahmoodzadeh et al. 2015).

Interpretation of upward TBT results and cyclic test results should consider possible axial rotation of the T-bar relative to the downward push. Penetrometer retraction may be (partially) in undisturbed soil. Axial rotation may imply an increase in number of cycles for obtaining nearly constant cyclic penetration resistance. A ball penetrometer has axial symmetry. Any axial rotation is of little concern.

Interpretation of TBTs, BPTs and CPTs for undrained shear strength is empirical. Interpretation is similar in that it requires a range of considerations to account for equipment-specific differences and soil behaviour around complex penetrometer geometry. Correlation with undrained shear strength with T-bar or ball penetration resistance has a reduced influence of in situ effective stresses, in comparison with CPTs. This benefit appears to be obscured by other correlation issues, as indicated by a Joint Industry Project (NGI 2006) showing very close statistical comparison of TBT and CPT results in soft clays. It may be of interest to explore accuracy of undrained shear strength by comparing uncertainty estimates based on the Analytic versions of the TBT, BPT and CPT.

A particular consideration for TBT and BPT interpretation is partial flow of soil around the penetrometer, i.e. soil closure around the penetrometer except for the shaft. A gap in soil applies close to seafloor. The length of the zone with gap formation depends on soil strength and overconsolidation ratio. It can possibly exceed 1 m. The authors are not aware of specific measurements. A cone penetrometer requires an initial embedment for achieving full displacement conditions. This initial embedment is typically less than 0.2 m for cone resistance and pore pressure in very soft to soft clays and clayey silts.

TBTs and BPTs offer improved opportunity for characterising strength degradation upon soil disturbance compared to CPTs, if cyclic test phases are implemented. A cyclic test phase provides information for a single test zone. It requires interruption of downward penetration. Vessel time requirements are about 15 minutes per cyclic test. Selective, site-specific TBT or BPT cyclic test phases allow fine tuning of generalised correlations of remoulded undrained shear strength with continuous CPT profiling of sleeve friction f_s or corrected sleeve friction f_t. Note that ISO-type accuracy of f_s of a high quality cone penetrometer is in the order of ± 3 kPa (Peuchen and Terwindt 2015) for offshore non-drilling deployment in very soft to soft clays and clayey silts. These soil conditions are particularly suitable for accurate f_s profiling.

6 REFERENCES

ISO. 2003. “Measurement management systems - requirements for measurement processes and measuring equipment, International Standard ISO 10012” Geneva: International Organization for Standardization.

ISO 19901-8:2014 “Petroleum and natural gas industries - Specific requirements for offshore structures – Part 8: Marine soil investigations”. Geneva: ISO.

EN ISO 19901-8:2015 “Petroleum and natural gas industries - Specific requirements for offshore structures - Part 8: Marine soil investigations (ISO 19901-8:2014)”. Brussels: CEN

Lunne, T., Randolph, M.F., Andersen, K.H. and Low, H.E. (2006), "Shear strength parameters determined by in situ tests for deep water soft soils : summary report/manual", Norwegian Geotechnical Institute (NGI), Oslo, 77 p. (NGI Report ; 20041618-6).

Mahmoodzadeh, H., Wang, D. and Randolph, M.F. “Interpretation of Piezoball Dissipation Testing in Clay “Géotechnique 65, No. 10, pp. 831-842

Peuchen, J., Adrichem, J. and Hefer, P.A. 2005. “Practice notes on push-in penetrometers for offshore geotechnical investigation”. In Gourvenec, S. and Cassidy, M. Eds., Frontiers in Offshore Geotechnics ISFOG 2005: Proceedings of the First International Symposium on Frontiers in Offshore Geotechnics, University of Western Australia, Perth, 19-21 September 2005, London: Taylor & Francis, pp. 973-979.

Peuchen, J. and Terwindt, J. 2014. "Introduction to CPT accuracy". Keynote in 3rd International Symposium on Cone Penetration Testing CPT14: May 12-14, 2014 - Las Vegas, Nevada, 45 p.

Peuchen, J. and Terwindt, J. 2015. Measurement uncertainty of offshore cone penetration tests. In Meyer, V. ed. Frontiers in Offshore Geotechnics III: proceedings of the Third International Symposium on Frontiers in Offshore Geotechnics ISFOG 2015, Oslo, Norway, 10-12 June 2015, Boca Raton: CRC Press, pp. 1209-1214.

Randolph, M.F., Hefer, P.A., Geise, J.M. & Watson, P.G. 1998., Improved Seabed Strength Profiling using T-bar Penetrometer, Proceedings International Conference Offshore Site Investigation and Foundation Behaviour – "New Frontiers", Society for Underwater Technology, London, pp. 221-235.

Senneset, K., Janbu, N. and Svanø, G. 1982. Strength and Deformation Parameters from Cone Penetration Tests. In Leeuw, E.H. de, Beringen, F.L. and Verruijt, A. Eds., *Proceedings of the second European Symposium on Penetration Testing, ESOPT II, Amsterdam, 24-27 May, 1982*. Rotterdam: Balkema, pp. 863-870.

Geotechnical and Geophysical Site Characterisation 5 – Lehane, Acosta-Martínez & Kelly (Eds)

Free-falling full-flow penetrometer for marine material characterization – analytical solution.

S. Pinkert
Civil and Environmental Engineering Faculty, Technion-IIT, Haifa, Israel.

ABSTRACT: This paper presents a conceptual testing procedure and analytical development of a free-falling full-flow penetrometer. In a free-fall penetration test, the velocity changes with depth and the soil is inherently softened throughout the testing process. Investigation of the undisturbed soil properties, thus, requires a thorough large-displacement rate-dependent analysis. This paper uses previous work's analysis for constant-rate full-flow penetration with strain-softening and rate-effect treatment, implemented in a penetrometer's equation of motion, to evaluate a continuous profile of the undisturbed undrained shear strength throughout the free-falling penetration, until a full stop. A conceptual testing procedure is presented in light of the required penetration depth, device weight and falling height, with a reference to the developed analysis and correlations.

1 INTRODUCTION

Offshore geotechnical site investigation is commonly performed by in-situ penetration tests. In these tests, soil properties are evaluated using a correlation between the penetration resistance and the developed failure mechanism around the probe. The main challenge in analyzing test results, is to determine the soil undisturbed undrained shear strength, since the soil is been disturbed during the penetration process and since the strength is affected by a hardening rate effect. In attempt to evaluate strain softening and rate-effect parameters, a typical testing procedure may include cyclic penetration, inward/upward until the soil reaches its residual strength, and penetration in different velocities or different device geometries.

Throughout recent decades, there is an increasing use in "full-flow" penetrometers, as T-bar and ball (Fig. 1a). In these penetrometers, the leading shaft area is significantly smaller than the tip area and may be ignored in the calculation. Under this simplification, the failure mechanism does not include volume change but a purely plastic flow mechanism around the tip, associate with the undrained shear strength (Randolph, 2004). Because of a coupling between the failure mechanism and soil strength effects (strain softening and rate effects) and since the penetration process is involved with large-strains, the problem has been studied numerically, either by penetration through a re-meshed grid (Zhou and Randolph, 2007) or as a steady state problem, in which the frame of reference is fixed on the pene trometer and cumulative soil characteristics are calculated along soil streamlines (Klar and Pinkert, 2010).

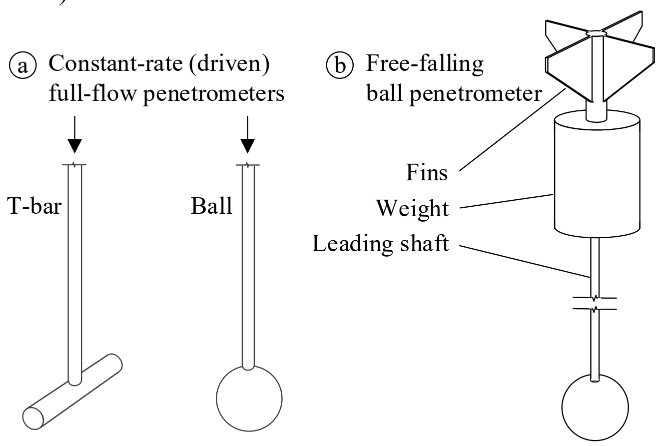

Figure 1. Illustration of (a) T-bar and ball penetration devices and (b) free falling ball penetrometer.

These offshore in-situ testing devices require the use of heavy equipment and large vessels, and thus associate with a high cost. Alternatively, in recent years there is an increasing interest in free-falling penetration tests, in which the device is released from a certain depth above seafloor, then penetrates the upper the soil layer. A qualitative illustration of the free-falling test device is presented in Fig. 1b, which is composed of a ball, leading shaft, weight and fins, similarly as shown in Chow and Airey (2014). This test allows a cost effective evaluation of soil properties for such engineering problems which require a geotechnical characterization of seafloor surface (for example, pipelines routes alternatives examination). Laboratory small-scale simulations of free-fall tests were compared with a constant-rate penetration tests through a similar soil medium, tested under different impact velocities and different penetrometer masses and geometries (Chow and Airey, 2014). Although an empirical correlations have been suggested between soil properties, resistance force profiles and testing conditions, a thorough calculation framework of all soil strength parameters, including strain softening and rate effects, has not been presented.

This paper presents a full investigation of the undisturbed undrained shear strength of the upper seabed layer using free-falling full-flow penetrometers, including a suggestion of an additional testing component for the evaluation of soil sensitivity.

2 SOIL STRENGTH

2.1 *Fundamental strength properties*

In this work, the undrained shear strength, s_u, is expressed by a multiplication of the laboratory-measured undrained shear strength, s_{u0}, with the shear rate effect, f_r, and the strain softening effect, f_{ss}:

$$s_u = f_r f_{ss} s_{u0} \tag{1}$$

f_r is expressed using a logarithmic strength law, which has been widely used in previous works (e.g., Randolph, 2004, Einav and Randolph, 2005, Yafrate and DeJong, 2007, Klar and Osman, 2008, Klar and Pinkert, 2010, Zhou and Randolph, 2007&2009, Pinkert and Klar, 2014), given by:

$$f_r = 1 + \mu \log\left[\max\left(\frac{\dot{\gamma}}{\dot{\gamma}_{ref}}, 1\right)\right] \tag{2}$$

where μ is a soil viscosity parameter, $\dot{\gamma}$ is the maximum engineering shear strain rate and $\dot{\gamma}_{ref}$ is the reference shear rate associated with s_{u0} (1%/h for triaxial test). In an attempt to evaluate μ, a link between the fundamental rate-effect (between strain-rates; Eq. 2) and a global effect, which may express a difference in penetration resistance for different penetration velocities, was suggested by Klar et al. (2013), based on Yafrate et al. (2009)'s analogy, given by:

$$\mu = \frac{\mu^*}{1 - 5\mu^*} \quad ; \quad \mu^* = \frac{q/q_{ref} - 1}{\log\left[\dfrac{(v/d)}{(v/d)_{ref}}\right]} \tag{3}$$

where μ^* is a global viscosity parameter, q is penetration resistance (stress units), v is penetration velocity, d is shortest lateral length of the penetrometer tip, and the subscript *ref* refers to a reference penetrometer velocity (0.02 m/s) and diameter (4 and 11.3 cm for T-bar and ball, respectively).

The strain softening factor, f_{ss}, is a modification of an exponential strain softening model (e.g., Randolph, 2004, Einav and Randolph, 2005, Yafrate and DeJong, 2007, Klar and Osman, 2008, Klar and Pinkert, 2010, Zhou and Randolph, 2007&2009), which was developed and calibrated with cyclic penetration field test results by Pinkert and Klar (2015), given by:

$$f_{ss} = \frac{1}{S_T} + \left(1 - \frac{1}{S_T}\right) e^{-3(\xi/\xi_{95})^\beta} \tag{4}$$

where S_T is soil sensitivity ($=s_{u0}/s_{u,\mathrm{residual}}$), β=2/3, ξ is the cumulative engineering strain rate and ξ_{95} is the ξ required for 95% remolding, given by:

$$\xi_{95} = 2\xi_p \left(4.52 S_T^{-0.18} - 0.5^{2/3}\right)^{3/2}$$
$$\xi_p = \begin{cases} 0.83\log(S_T) + 3.09 & T-bar \\ 1.1\log(S_T) + 2.62 & ball \end{cases} \tag{5}$$

where ξ_p is the average magnitude of shear strain undergone by soil elements passing through the failure mechanism in individual penetration, evaluated by curve fitting of Zhou and Randolph (2009)'s results.

2.2 *Evaluation of soil strength from a penetration test*

In this paper, the evaluation of undisturbed undrained shear strength from full-flow penetration tests is based on Pinkert and Klar (2013)'s engineering-use expressions, based on a steady state solution for cylindrical and sphere penetrometers of a constant-rate penetration, in a sensitive viscous soil medium (Klar and Pinkert, 2010), based on Eqs. 1-5, given by:

$$s_{u0} = \frac{P/A}{N} = \frac{P/A}{\alpha_1 \alpha_2 N_{ref}} \tag{6}$$

where P is the resistance force, A is the penetrometer tip projected area and N is a resistance factor, which expressed by the three factors: N_{ref}, a reference value related to a conventional penetration velocity and geometry in a non-viscous non-soften soil, α_1, which refer to the effect of soil sensitivity on the global penetration resistance, and α_2, which refer to the effect of soil viscosity under a penetration velocity v. These three factors were developed in Pinkert and Klar (2013), given by:

$$N_{ref} = \begin{cases} 11.98 & T-bar \\ 15.23 & ball \end{cases} \tag{7}$$

$$\alpha_1 = \begin{cases} 1 - 0.22\log(S_T) - \dfrac{0.114}{1+\left(\frac{S_T}{15}\right)^{-7}} & T-bar \\ 1 - 0.55\log(S_T) + \dfrac{0.438}{1+\left(\frac{S_T}{11}\right)^{-1.8}} & ball \end{cases} \tag{8}$$

$$\alpha_2 = \begin{cases} \left(1+\dfrac{4.5\mu^*}{1-5\mu^*}\right)\left(1+\mu^*\log\dfrac{v/d}{(v/d)_{ref}}\right) & T-bar \\ \left(1+\dfrac{4.2\mu^*}{1-5\mu^*}\right)\left(1+\mu^*\log\dfrac{v/d}{(v/d)_{ref}}\right) & ball \end{cases} \tag{9}$$

The factor α_2 expresses the effect of different constant penetration velocities on the penetration resistance. This factor is utilized in this work in a reversed analysis for the evaluation of μ^*, through a correlation between $P(z)$ profile (z = depth below seafloor) and a non-constant velocity profile $v(z)$ in a free-falling penetration test. The calculation procedure of both μ^* and S_T, together with s_{u0} will be described in the next section.

3 DATA ANALYSIS OF A FREE-FALLING PENETRATION TEST

Although soil viscosity and sensitivity parameters may vary with depth, this work assumes both (μ^* and S_T, respectively) as constants with depth. The undisturbed undrained shear strength is assumed to vary linearly with depth, given by:

$$s_{u0}(z) = a + bz \tag{10}$$

where a and b are constants. Although Eq. 10 involves two constants, only one is considered in the analysis, in which either a=0 (refers to zero strength at the soil surface) or b=0 (refers to a constant s_{u0}; practical for laboratory simulations). Thus, this paper focuses on the evaluation of the three strength parameters; s_{u0}, μ^* and S_T, according to three calculation steps:

3.1 *Equation of motion:*

The velocity profile in a free-falling penetration is determined using the equation of motion:

$$m\ddot{z} + P\left(s_{u0}, S_T, \mu^*, \dot{z}, A\right) + R = W \tag{11}$$

in which the penetrometer weight, W, equals to the static soil reaction, R. m is the penetrometer mass and P the penetration resistance force (Eq. 6). Figs. 2 and 3 show velocity profiles for different S_T, μ^* and v_0 (impact velocity; $v(z=0)$) values, for a constant or linear s_{u0} variation, respectively. As can be seen from these figure, the penetration (final) depth, z_f, increases with the increase in S_T and v_0, and the decrease in μ^*. This parameter (z_f) can be determined by comparing the initial kinetic energy with the work done by the penetrometer,

$$\int_0^{z_f} P(z)dz = \frac{1}{2}mv_0^2 \tag{12}$$

and thus may be appropriate as a test output parameter for data analysis. Fig. 4 presents the velocity profiles from Figs. 2 and 3, normalized by z_f and v_0 values (z and v axes, respectively). As can be seen, the non-dimensional velocity function $v(z/z_f)/v_0$ shows a same shape function for all strength parameters and impact velocities, for a given s_{u0} variation with depth (regardless of a and b vales).

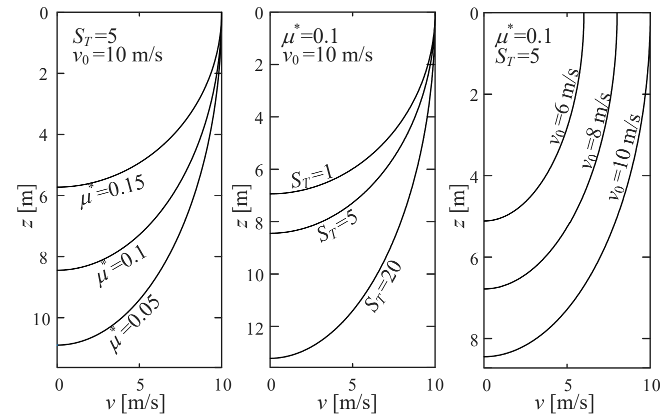

Figure 2. Calculated velocity profiles of a free-falling ball penetrometer in a linear strength variation field; s_{u0}=1.5z(m) kPa. Simulations for m=400 kg, A=100 cm^2, and different μ^*, S_T and v_0 values.

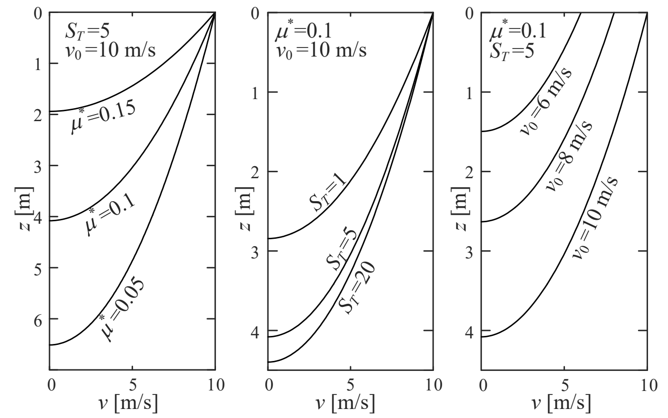

Figure 3. Calculated velocity profiles of a free-falling ball penetrometer in a constant strength field; s_{u0}=20 kPa. Simulations for m=400 kg, A=100 cm^2, and different μ^*, S_T and v_0 values.

3.2 *Rate effect analysis:*

Theoretically, μ^* can be determined for every nearby points in depth, with a given pair of P and v values, using an extension of Eq. 3:

$$\mu^* = \frac{\dfrac{P_1}{P_2} - 1}{\log\left(\dfrac{(v_1/d)}{(v/d)_{ref}}\right) - \dfrac{P_1}{P_2}\log\left(\dfrac{(v_2/d)}{(v/d)_{ref}}\right)} \tag{13}$$

However, Eq. 13's sensitivity for close v values is not sufficient, since they are applied in a logarithm scale. Thus, μ^* may be determined using points 1 and 2 (in Eq. 13) with a significant difference in v values. In this case, the extracted μ^* may only function as a representative average value for the entire penetration depth (i.e., assumed as constant).

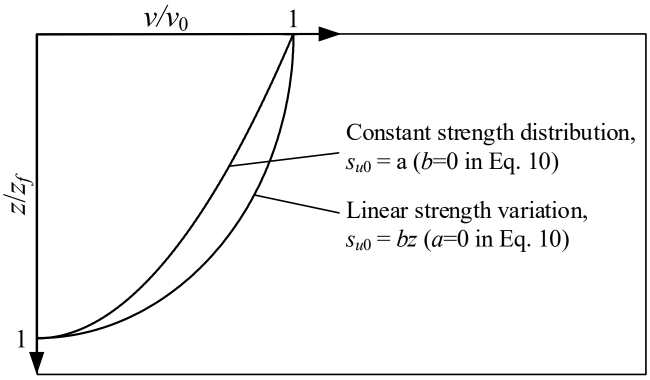

Figure 4. Normalized calculated velocity profiles of a free-falling ball penetration for different s_{u0} distributions.

3.3 *Soil sensitivity analysis:*

With lack of information on soil sensitivity, S_T, it is not clear weather an obtained low P value denotes a low s_{u0} value or on a high S_T (reflects a lower α_1 value; in Eq. 8). Therefore an additional testing procedure is suggested, in which the penetrometer is extracted upward in a constant rate after the free-fall stage is completed. If both insertion and extraction stages would have been triggered in a same penetration rate, S_T would have been calculated using DeJong et al. (2011)'s empirical correlation; $S_T=(q_{in}/q_{out})^{3.7}$. However, using Eq. 3, q_{in} (which is obtained at a non-constant (free-fall) penetration rate) can be calibrated to an equivalent $q_{in,ref}$ value as if it was inserted in a same reference rate (refers to $q_{out,ref}$), for S_T calculation:

$$S_T = \left(\frac{q_{in,ref}}{q_{out,ref}}\right)^{3.7} = \left(\frac{q_{in}(z)/q_{out,ref}}{1+\mu^*\log\left[\dfrac{v(z)/d}{(v/d)_{ref}}\right]}\right)^{3.7} \tag{14}$$

in which the penetrometer weight has to be subtracted from the extraction force at $q_{out,ref}$ calculation:

$$q_{out} = \frac{P_{out} - W}{A} \tag{15}$$

The three equalities in Eqs. 12, 13 and 14 are used for the evaluation of the three unknown soil strength parameters, in which μ^* is first to be calculated using Eq. 13, S_T is secondly calculated using Eq. 14, and finally s_{u0} (i.e., a or b) is calculated from Eq. 12.

4 DISCUSSION AND CONCLUSIONS

This paper presents an advanced calculation frameworks for the evaluation of soil strength parameters using free-falling full-flow penetration test. In a free-falling penetration, the penetrometer velocity changes with depth, affecting the soil resistance through a rate effect on the undrained shear strength. The evaluation of the rate-effect parameter (assumed constant) is determined using an equivalence to an already published solution for constant-rate penetration problems with different penetration rates. The effect of soil sensitivity is evaluated using an additional testing procedure, in which the penetrometer is pulled out in a constant rate at the end of the free-fall stage, and the soil sensitivity is calculated based on the ratio between the inward and the outward penetration resistances together P/v data from the free-fall stage. Using the calculated viscosity (hardening) and soil sensitivity (softening) strength parameters, the undisturbed undrained shear strength can in turn be evaluated based on the obtained penetration resistance profile and the final penetration depth.

Taking into account the limited output data in a free-falling penetration test, the author suggested some simplification to ensure sufficient understanding of test results; (1) soil sensitivity is constant with depth, (2) the viscosity parameter is constant with depth, and (3) soil strength profile is either linearly changes from zero at seafloor or a constant with depth (for laboratory simulation).

As part of a penetrometer designing procedure, this paper gives an analytical tool for selecting penetrometer mass and falling height (which can be correlated with the intact velocity) to match the desirable investigated (penetrated) soil depth. The practical application of the pullout procedure should be further discussed, in which the pullout path has to be lined at the same inward free-falling penetration path. In addition, the suggested calculation framework should be further verified against laboratory test simulation of free-falling and constant-rate penetration, together with standard laboratory testing of the undisturbed (intact) undrained shear strength, soil sensitivity and rate-effect parameters.

As this work is based on a steady state analytical approach, it cannot be used for interpretation of high velocity penetration problems (e.g., Morton et al. (2015)), since it may involve turbulent flow (of soil).

Therefore, instead of increasing the penetration velocity for deeper penetration, the additional weight is suggested (Fig. 1b).

5 REFERENCES

Chow, S. & Airey, D. 2014. Free-falling penetrometers: a laboratory investigation in clay. *J. Geotech. Geoenviron. Eng. ASCE* 140 (1): 201-214.

DeJong, J. T., Yafrate, N. J., & DeGroot, D. J. 2011. Evaluation of undrained shear strength using full-flow penetrometers. *J. Geotech. Geoenviron. Eng. ASCE* 137(14): 14–26.

Einav, I. & Randolph, M. 2005. Combining upper bound and strain path methods for evaluating penetration resistance. *International Journal for Numerical Methods in Engineering* 63 (14): 1991-2016.

Klar, A. & Osman, A. S. 2008. Continuous velocity fields for the T-bar problem. *International Journal for Numerical and Analytical Methods in Geomechanics* 32(8): 949–963.

Klar, A. & Pinkert, S. 2010. Steady state solution for cylindrical penetrometers. *International Journal for Numerical and Analytical Method in Geomechanics* 34(6): 645-659.

Klar, A., Pinkert, S. & DeJong, J. T. 2013. Evaluation of a logarithmic-law strength rate parameter using full-flow penetrometers. *ICE Geotechnical Research* 1(2): 53-59.

Morton, J. P., O'Loughlin, C. D. & White D. J. 2015. Centrifuge modelling of an instrumented free-fall sphere for measurement of undrained strength in fine-grained soils. *Canadian Geotechnical Journal*, 2016, 53: 918-929Pinkert, S. & Klar, A. 2013. Analytically and experimentally based resistance factors for "full-flow" penetrometers, *The 18th International Conference on Soil Mechanics and Geotechnical Engineering*, Paris, 781-784.

Pinkert, S. & Klar, A. 2015. Enhanced strain-softening model from cyclic full-flow penetration tests. *J. Geotech. Geoenviron. Eng. ASCE* 142(3): 04015087.

Randolph, M. F. 2004. Characterisation of soft sediments for offshore applications. *In Proc. 2nd Int. Conf. on Site Characterisation*, Porto, 1: 209–231.

Yafrate, N. J. & DeJong, J. T. 2007. Influence of penetration rate on measured resistance with full-flow penetrometers in soft clay. *In New Peaks in Geotechnique, GeoDenver*. Denver. US.

Yafrate, N. J., DeJong, J. T., Degroot, D. & Randolph, M. F. 2009. Evaluation of remolded shear strength and sensitivity of soft clay using full flow penetrometers. *J. Geotech. Geoenviron. Eng. ASCE* 135 (9): 1179-1189.

Zhou, H. & Randolph, M. F. 2007. Computational techniques and shear band development for cylindrical and spherical penetrometers in strain-softening clay. International journal of Geomechanics, ASCE, 7(4), 287–295.

Zhou, H. & Randolph, M. F. 2009. Numerical investigations into cycling of full-flow penetrometers in soft clay. *Geotechnique* 59(10): 801–812.

Geotechnical and Geophysical Site Characterisation 5 – Lehane, Acosta-Martínez & Kelly (Eds)
© 2016 Australian Geomechanics Society, Sydney, Australia, ISBN 978-0-9946261-1-0

CPTu in Consolidating Soils

Rahardjo, P. P.
Professor, Department of Civil Engineering, Universitas Katolik Parahyangan, Bandung, Indonesia

Anggoro, B. W.
Geotechnical Engineer, PT. Geotechnical Engineering Consultant, Bandung, Indonesia

Wirawan, A.
Geotechnical Engineer, PT. Geotechnical Engineering Consultant, Bandung, Indonesia

ABSTRACT: The interpretation of CPTu for normally consolidated clay soils and slightly, or, strongly overconsolidated soils have been published in many papers (Chen and Mayne, 1995, Lunne et al. 1997). For both conditions of soils (normally consolidated and overconsolidated clay), there is hydrostatic pore water pressure, however no initial excess pore water pressure exists. Hence the assumption that excess pore water pressure due to cone penetration only is valid. In soils where consolidation is still ongoing which could be due to natural deposition of the soils or soft soils under reclamation fill material, the excess pore pressure still exists, which means that prior to penetration testing, the initial excess pore pressure has not completely diminished. In this case, the measured excess pore water pressure shall be interpreted as combined existing pore water pressures and the additional excess pore water pressure due to cone penetration. In case of testings conducted at certain interval time such as during the course of consolidation in reclamation area, then the excess pore pressure response as well as the tip resistance and the friction ratio will change toward a normally consolidated condition. This paper represents research results of CPTu in reclaimed soils and naturally deposited mud resulted from eruption. The authors have developed methods for interpretation of these combined excess pore water pressures. In the end, the methods can separate between the excess pore water pressure due to penetration and the prior existing pore water pressure. The tip resistance in under-consolidating soft soils subjected to fill placement will not form a linear tip resistance (not straight line) when carefully examined and hence the interpretation were done considering the initial (remaining) excess pore pressure or the effective stress at certain time. The methods have been proved to be consistent and has the potential for prospective future interpretation.

1 INTRODUCTION

1.1 *Jakarta Bay Reclamation*

The reclamation works now being actively conducted are located in the Jakarta bay as shown on Figure 1. There will be a number of islands to be proposed and implemented for the development of the Jakarta Megapolitan City. Currently three projects are ongoing, the first one is north of Pluit area (called Pluit City) with 2 islands (E and F) of about 500 hectares of land reclamation, the Kapuk Naga reclamation works which is on the west side of the development consists of 3 islands each of about 300 hectares (C, D and E) and the New Priok Port (N). The research is mainly conducted at the first island (island D) of Kapuk Naga which has been completed. On this reclamation works, the use of CPTu for quality control has been very extensively before and during reclamation.

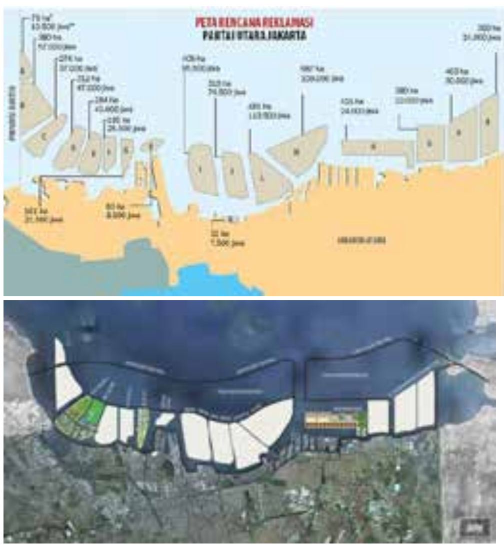

Figure 1. Reclamation Plan at Jakarta Bay (www.tempo.co, 2015)

1.2 *Mud Deposit from Eruption in East Java*

Mud eruption in East Java occurred on May 29, 2006 has been well known. The mechanism of the causes of the eruptions are still in debate, whether triggered by the drilling or pressurised fluid reactivated by the Jogyakarta quake on May 27, 2006. The debate is more from the geological point of view, and is not the main issue in this report. Instead, the main objective of this paper is to discuss mainly on the results of CPTu tests recently conducted and discuss mitigation and risk reduction.

In the early days of eruption, as much as 150,000 cubic meters discharge per day was reported, although presently only less than 5000 cubic meters of the discharge is estimated. Due to unknown characteristics of the mud, dykes were constructed to contain the mud and the areas reaching 650 hectares (Sofyan, 2015, “Recent investigation of Lumpur Sidoardjo”, internal report (unpublished) delivered during the International Conference on Landslide and Slope Stability, Bali). The location of the disaster is just in the middle of the town of Porong in the district of Sidoardjo, East Java.

The soil condition of the site is deep soft clays which causes instability of the dykes. Some dyke failures occurred which endangered the residential areas due to the flow of the mud (Rahardjo, 2015). This paper discusses the characteristics of the soil conditions from a number of drillings and CPTu tests conducted by the authors for design of the replacement of the arterial road, west of the site and for the dyke reinforcement and also in the middle of the mud. Figure 2 shows the effect of mud eruption in 2006.

Figure 2. Mud Eruption in East Java – causing thousands of houses flooded

2 PRINCIPLE OF CPTu AND THE USE OF CPTU FOR SOFT SOILS

The use of CPTu (Cone Penetration Test with pore pressure measurement) has been popular in Indonesia since 1990, specially for soft soils. The increasing use of the CPTu is due to a number of factors, such as:

- It is handy, fast and accurate for soil profiling and not depending on operators
- It can distinguish the soil resistance and the pore pressure, hence the effective reaction of the soils being measured and it can recognize drained or undrained response of the soils
- The interpretation of soil properties, although heavily relying on empirical correlations, are accurate due to many available data for comparison and justification
- Dissipation tests can be conducted to measure the permeability and consolidation characteristics of the soils, which give more reliable data

The authors have gained a lot of experience in many projects throughout the northern coast of Jakarta and also in many places where soft soil deposit create instability during construction and the problems of long term settlement.

3 DETERMINATION OF THE DEGREE OF CONSOLIDATION FROM CPTu

Degrees of consolidation are very important in reclamation projects to determine the readiness of the reclaimed land. When conducting CPTu at reclamation works, there are possibilities that the underlying soft soils are still consolidating and residual excess pore pressure still exists. Method for Interpretation of degree of consolidation may be determined by:

1. Schmertmann Method (1978)
2. B_q vs OCR Correlation (Rahardjo et al. 2015)

Schmertmann method is a method to interpret the degree of consolidation for clay layer. The method is very simple by using the cone resistance (q_c) from CPTu Data. Figure 3 illustrates the interpretation of the degree of consolidation based on Schmertmann Method (1978).

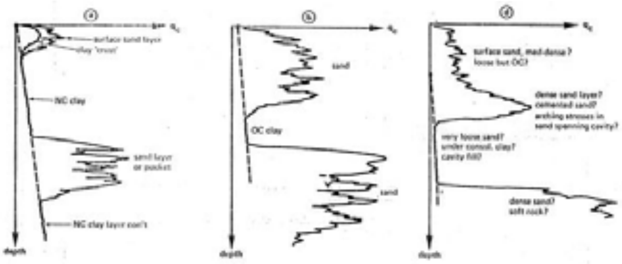

Figure 3. Interpretation of the Degree of Consolidation by Schmertmann Method (1978)

Degree of consolidation can also be interpreted by using pore pressure ratio (B_q). The correlation between B_q vs OCR was already researched by Setionegoro (2013). The OCR value lower than 1.0 basically represent the degree of consolidation. The following equation shows the correlation between B_q vs OCR.

CPTu result can be used to obtained the B_q value. Then the OCR value can be obtained for every data B_q value by using the correlation (Rahardjo et al. 2015). To make the calculation easier the equation of the correlation is interpreted using curve expert program. The equation that represents the correlation between B_q and OCR (modified from the results of Setionegoro, 2013) is:

$$OCR = \frac{1}{(1.2B_q + 0.1)}$$

Figure 4 shows this correlation collected from several data in Indonesia.

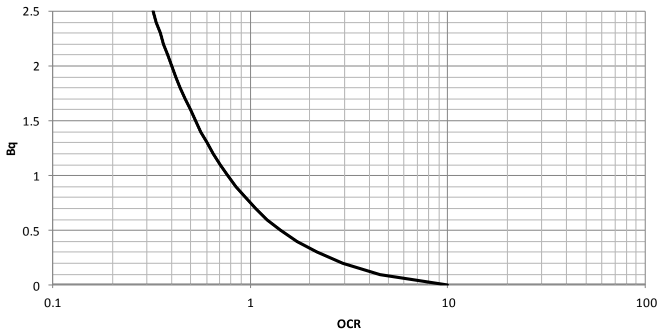

Figure 4. Correlation of the degree of consolidation and OCR from B_q values of CPTu

4 CPTu AND DISSIPATION TEST IN CONSOLIDATING SOILS

In soils where consolidation is still progressing which could be due to natural deposition of the soils or soft soils under reclamation fill material, the excess pore pressure still exists, which means that prior to penetration testing, the initial excess pore pressure has not completely diminished. In this case, the measured excess pore water pressure shall be interpreted as combined existing pore water pressure and the additional excess pore water pressure due to cone penetration.

The excess pore pressure is substantially higher. This could be due to three factors, the existence of the residual excess pore pressure which has not dissipated, the behavior of the soil which could be in the state of being more sensitive, and higher overburden. The value of B_q ratio could be much higher than 0.75 as indicated by Tanaka and Sakagami (1989) as boundary of normally consolidated soil. When the dissipation test is carried out ultimately, the pore pressure measured shall be the hydrostatic pressure related to the ground water table, u_0, however, this is not possible due to limited time during the test. The authors recommend to approximate the dissipation curves using hyperbolic function to obtain the final pore pressure u_f. Figure 5(a) shows the meaning of u_f. The difference between this value and the hydrostatic pressure is called the residual excess pore pressure which can be used to calculate the degree of consolidation. Figure 5(b) illustrates the method and the difference of ultimate pore pressure, u_f to the hydrostatic pressure is residual excess pore pressure due to the load. This can be used for the calculation of the degree of consolidation using the expression $u_z = 1 - \frac{\Delta u_t}{\Delta \sigma}$ where $\Delta u_t = u_f - u_0$ and $\Delta\sigma$ = overburden pressure.

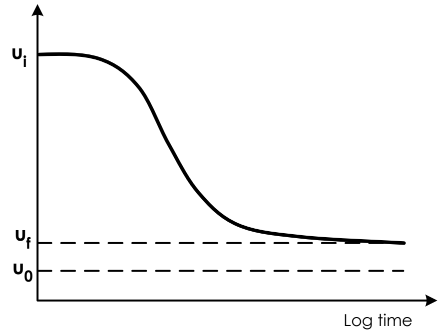

Figure 5(a) Extrapolation of dissipation test results

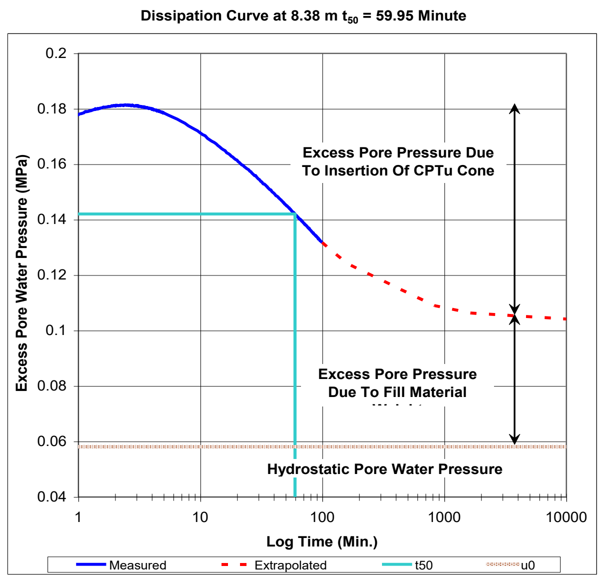

Figure 5(b) Example of the determination of the residual excess pore pressure

5 CPTu IN CONSOLIDATING SOILS UNDER RECLAMATION IN JAKARTA BAY

The CPTu used for illustration in this paper is at island D. 2A island project (island D) is a reclamation project near shore at Pantai Indah Kapuk, North Jakarta. The reclamation project purpose is for land development for housing, apartments and golf. Total area of the reclamation is 312 Hectares. Depth of seabed at the project site is about 3.7 to 8.7 m bellow main sea level (MSL). The elevation of MSL is 1.2 m pp* and the final level of the area is 0.5 m pp*. The 2A island is planned to be a polder area with dyke elevation at 6 m pp* to 9.6 m pp*. Soil condition at the project site is very soft soil with thickness of about 5 – 12 m. These conditions cause a settlement due to a fill of sand material. The reclamation was started in 2012 until 2015 and the soft soil is still consolidating. This section discusses the interpretation of degree of consolidation of 2A Island at the polder area. The location of the test sites is shown in Figure 6(a). The area has been divided into grid with 50 m intervals. There are too many data, and for this purpose only selected positions are discussed. The results of the tests are shown on Figure 6(b) and Figure 6(c).

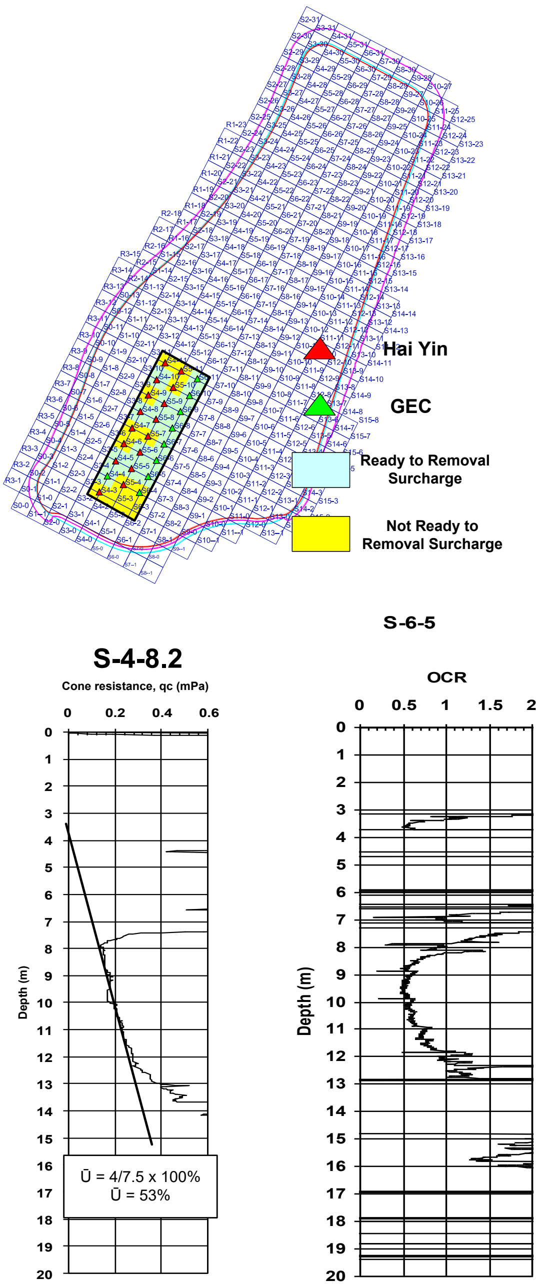

Figure 6(a) Hundreds of CPTu tests at grid of 50 m
Figure 6(b) Interpretation of the degree of consolidation based on Schmertmann Method
Figure 6(c) interpretation of the degree of consolidation based on B_q

Using the method by Schmertmann, apparently is not easy due to the fact that the shape of the q_c resistances of the soils are not the same then as assumed by Schmertmann. In fact, the straight line as expected can not be found, instead a curved such as an isochrone was seen. This is understood to be due to the fact that the middle of the soil is in a very low degree of consolidation due to its distance from the top and bottom of the soft clay. A method is being proposed based on the fact that the curved shape of the CPTu test results are more rational. It thus represents the state of the effective stress. Near the drainage boundary the degree of consolidation should be much higher due to its proximity to the drainage layer. However, this also shows the possibility the Prefabricated Vertical Drain (PVD) might not work very well.

Using the B_q method, it can be seen that the degree of consolidation of the soft clay layer varies from 50% at the middle to about 100% at the boundary of the drainage layer. This is logical as q_c represents the effective stress which in turn also related to the soil shear strength.

6 CPTu IN MUD DEPOSIT RESULTED FROM MUD ERUPTION DISASTER IN EAST JAVA

Based on laboratory tests west of this area, the soils are highly plastic materials, the natural water content ranges from 40 – 100 %. Generally, the upper part is slightly stronger showing slight overconsolidation. However, the void ratio could be as high as 1.5 – 3.0. Laboratory consolidation tests also show that the soft soils are still consolidating. Compressibility of the soils as measured from its compression index is very high with a range of 0.5 – 1.5. This explains why settlement is large (Soleman, 2012).

Figure 7. Situation at the Mud Center where CPTu were conducted

CPTu tests are also conducted in the mud area. Location of CPTu tests are just at the dykes and in the middle of the mud as shown on Figure 8. Based on insitu tests (CPTu and SPT), the soil upper layers are very soft with thickness of 15 – 25 m dominated by clays to silts and silty sands. The silty sands are mixed with clay. This soil condition has very low bearing capacity and may cause very large settlement upon loading. The possibility of squeezing of lower soil layers are among the problems that need to be considered. Typical CPTu test results are shown in Figure 9 for the result of CPTu at the center of the mud.

Based on the results of the CPTu test in the mud area, it is concluded that the mud is very deep and still consolidating as shown from the low tip resistance and high value of B_q. It is also shown from the results of the dissipation tests, the excess pore pressure is still high consisting of residual excess pore pressure due to its own weight. A separate plot of the excess pore pressure is recommended by the authors to using $B_q^{**} = u_2 / q_t$ which is more representative because it shows the proportion of the excess pore pressure response compared to its corresponding tip resistance. For this case, the ratio of $B_q^{**} = 0.9$ in the middle of the mud which shows that 90% of the measured resistance was practically by water. In soft soils, sleeve friction is practically the undrained shear strength of the soils. Figure 9 shows the friction is very low. The interpreted shear strength is in the range of 2 – 10 kPa.

Figure 8. Location of CPTu tests in the Mud Area

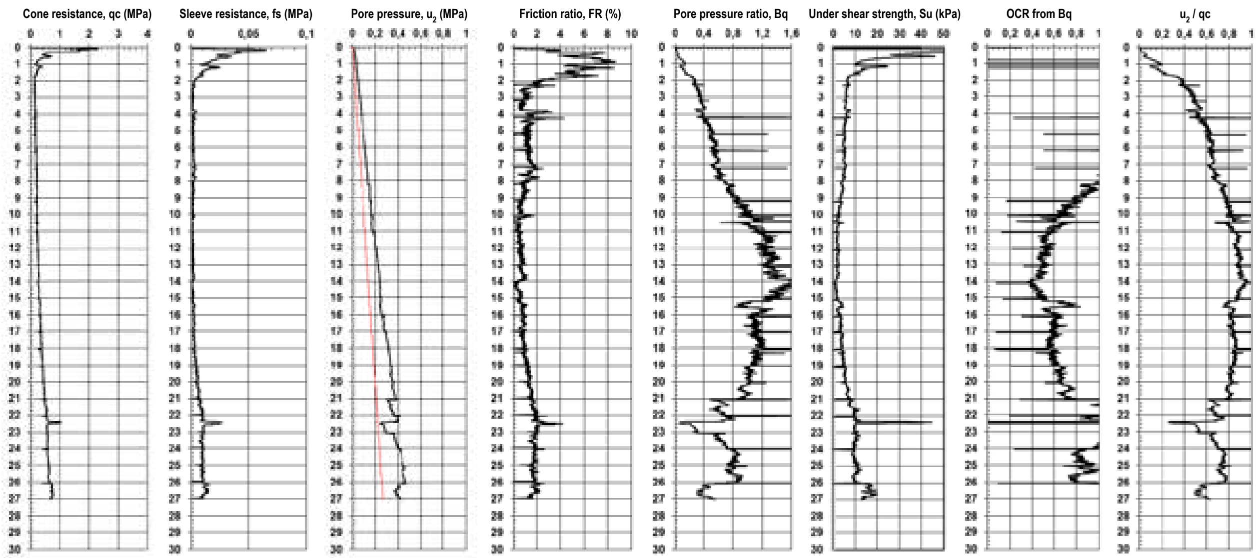

Figure 9. Results and Interpretation of CPTu-10 at the center of the Mud

Another interesting fact is that, the initial elevation of the site before mud eruption was +5.00 above sea level, and the CPTu was conducted at mud top elevation +14.00 m. Assuming that there was no settlement, the depth of the mud should be 9.00 m. However, down to 30 m, the CPTu shows that all penetration is in the mud, which means that the center of the eruption might have settle down more than 21 m.

7 CONCLUSIONS

Based on the data of CPTu, it is concluded :

- The use of CPTu for investigation of the degree of consolidation and the investigation of residual pore pressure is very effective and prospective for future use and application.
- The use of empirical correlation for degree of consolidation (OCR < 1.0) as well as the overconsolidation ratio using B_q value is very usefull.
- To obtain information on the proportion of soil resistance and pore pressure, $B_q^{**} = u_2 / q_t$, is prospective.

8 REFERENCES

Chen, B. S., Mayne, P. W., (1995), “Type 1 and 2 Piezocone Evaluations of Overconsolidation Ratio in Clays”, Proceeding International Symposium on Cone Penetration Testing, Linkoping Sweden.

Lunne, T., Robertson, P. K. and Powel, J. J. M., (1997), “Cone Penetration Testing in Geotechnical Practice”, Blackie Academic & Professional.

Rahardjo, P.P., Anggoro, B.W., Yakin Y.A., Darmawan, H., (2008). “Determination of the Degree of Consolidation of Reclaimed Site on Deep Soft Mahakam Deltaic Soils using CPTu", Proceeding of the Fourth International Symposium in Deformation Characteristics of Geomaterials, IS Atlanta, 22-24 September 2008, Atlanta Georgia, 883-889.

Rahardjo, P.P. (2015). "Mitigation and Risk Reduction for Mud Eruption Disaster in East Java", First Year Report, ICL-IPL Project 195, International Consortium on Landslides.

Setionegoro, N. (2015). "Research on the Characterization of Consolidating Soils (in Indonesian)", Ph.D. Dissertation submitted to the Graduate School, Universitas Katolik Parahyangan, Bandung Indonesia.

Tanaka, Y and Sakagami, T., (1989), "Piezocone Testing in Underconsolidated Clay", Canadian Geotechnical Journal, 26(4), 563 – 567.

Geotechnical and Geophysical Site Characterisation 5 – Lehane, Acosta-Martínez & Kelly (Eds)
ISBN 978-0-9946261-1-0

Effect of rotation rate on shear vane results in a silty tailings

D. Reid
Golder Associates Pty Ltd, Perth, Australia
University of Western Australia, Perth, Australia

ABSTRACT: Undrained strength is a key parameter in assessing the stability of a tailings facility. However, the available methods to assess undrained strength directly from piezocone penetration test (CPTu) results suffer inherent uncertainty. Therefore, when practical, shear vane testing is often used to enable site-specific correlations between CPTu results and undrained strength to be developed. While the shear vane is recognised to provide excellent estimates of undrained shear strength, it can be effected by drainage during shear for intermediate soils, including many silt tailings. To assess the effects of drainage conditions on shear vane results, a series of tests at different rotation rates were undertaken within a silty tailings. Corresponding dissipation tests were undertaken to assess consolidation behaviour, along with CPTu, piston sample collection for laboratory testing, and ball penetrometer tests. The results indicated that for the silty tailings investigated, "standard" shear vane rotation rates overestimated undrained shear strength owing to drainage effects during vane rotation. The rotation rates required to produce undrained shearing were consistent with some of the typically-applied methods for assessing the effect of drainage, when based on estimates of consolidation behaviour from dissipation tests.

1 INTRODUCTION

1.1 *General*

The importance of achieving undrained conditions for vane shear testing in silts and "intermediate" soils has been long understood (Blight 1968, Chandler 1988, Castro and Troncoso 1989, Morris and Williams 2000, Fell et al. 2014, ASTM 2015). However, despite this recognition, the author is aware of frequent uses of the vane shear test in tailings investigations in Western Australia (WA), and elsewhere, where insufficient recognition of partial drainage on inferred undrained strengths has been applied. Such results have then led to difficulties in developing site-specific correlations of undrained shear strength in general, and specifically with respect to Piezocone Penetration Test (CPTu) results. As tailings often consist of a large proportion of silt-sized particles and frequently exhibit significant layering and hence hydraulic anisotropy, they are a material that is particularly prone to the effects of drainage during vane shear. As the peak undrained strength is possibly the single-most important strength parameter for many tailings facilities, it is of importance that where vane shear testing is used to supplement other assessment methods, the potential for overestimation of strengths through partial drainage is accounted for and avoided where possible.

1.2 *Purpose of this paper*

The purpose of this paper is to present results of in situ and laboratory testing of a moderate plasticity tailings in WA, including vane shear testing undertaken at different rotation rates at the same test locations and depth. These vane shear results, referenced to other measures of undrained shear strength and horizontal coefficient of consolidation (c_h) enable an assessment of the performance of available methods to assess drainage around the vane

2 IN SITU AND LABORATORY TESTING

2.1 *General*

The tailings facility investigated is upstream-raised and hence the undrained strength of the tailings are of critical importance to stability of the perimeter embankments. The tailings are of moderate plasticity, with plasticity indices (PI) ranging from 10 to 33% for recovered samples from the beach and at depth. The material is predominately silt, ranging from sandy silts with up to 40% sand-sized particles (>75 μm), and finer zones with up to 30% clay-sized particles (<2 μm). Surficial and piston tube samples from depth indicated an average bulk density of 1.8 t/m^3. The material is cyclically deposited across the tailings cell, meaning that significant solar drying and densification of the material typically occurs prior to placement of additional tailings. Additional information regarding the mine site and location cannot be provided, in order to maintain anonymity for the site.

The site investigation undertaken consisted of CPTu probing with regular dissipation testing, with vane shear testing, ball penetrometer, and piston sampling at key locations. Three test locations are relevant to this study, as outlined in Table 1. It is noted that ball penetrometer testing was only possible for locations on the tailings beach, as this device was unable to penetrate the stiff compacted crest of the embankment.

Table 1. Test location summary

Test Information	CPT1	CPT2	CPT3
Location	Crest	Crest	Beach
Dissipation Depths (m)	5	3.5, 7.5	4, 9
Piston Samples	Y	N	Y
Vane Testing Rates (°/min)	12, 240	12, 90	240
Ball Testing	N	N	Y

2.2 *Methods – CPTu, ball, piston sampling*

CPTu probing was undertaken with a 10 cm^2 cone, with pore pressure recorded at the u_2 shoulder location. Cone resistance was corrected for the unequal area effect. The cone had an equal end area friction sleeve. The ball penetrometer used was 80 mm in diameter, and did not include a piezometer. Piston samples were taken using a "Gouda-type" sampling system, in 63.5 mm internal diameter tubes with an outside cutting edge angle of 10º and with no inside clearance. CPTu probes were conducted first at each location to provide stratigraphy information to assess suitability and target zones for other tests. Other tests were undertaken within a 3 m radius from the initial CPTu.

2.3 *Vane shear testing*

The system used was a GeoMil FFL 100 vane shear, with a rectangular vane 100 mm in length and 50 mm in diameter. The vane shear rods were inserted within larger-diameter casing, and a slip coupling was used to estimate, and correct for, rod friction on each test prior to commencing shear of the tailings. Shaft rotation commenced approximately 60 seconds following insertion of the vane into a new depth of soil. This was the fastest practical time in which the torque application and measurement system could be fitted to the rods and activated after advancing the vane to a new depth. The rods typically required rotation of between 10 and 20º before rotation of the vane and hence shearing of the soil commenced. Tests were undertaken generally at 0.5 or 1.0 m depth intervals.

Tests were initially conducted at a rotation rate of 12º/min. However, initial assessment of the strength results obtained from these tests on-site indicated they were likely erroneously high. Partial drainage was suspected as the cause. Initial screening assessment of dissipation test results suggested that at 12º/min, partial drainage was likely. Therefore, higher rates of both 90 and 240º/min were attempted. Comparison of these results is the primary purpose of this paper.

Electronic data collection was employed during vane shear rotation, with the system as used at the time of the investigation only able to record data at 4 second intervals. Owing to this minimum save interval, the results for tests with higher rotation rates are somewhat sparse. As a result of the limitations of the system seen during the investigation outlined here, the contractor subsequently had the data recording system modified to enable smaller data recording time intervals in future investigations.

2.4 *Laboratory test methods*

Samples extruded and trimmed from piston tubes were used to undertake direct simple shear (DSS) tests. The DSS system used was of the Swedish Geotechnical Institute-type, where the sample was laterally restrained by a membrane and Teflon rings, and sheared under constant volume conditions at 5% strain per hour. Samples were consolidated in increments to their estimated in situ vertical effective stress, to assess sample disturbance prior to selection of a vertical effective stress for testing. Significant vertical strain was observed in reconsolidated the specimens to their in situ vertical effective stress, indicating sample disturbance. This is likely a result of the long distances required to transport the samples from site to the testing laboratory in Perth (>400 km). Owing to the likely sample disturbance, some of the samples were consolidated to vertical stresses higher than in situ values to attempt to provide more relevant normally consolidated strength ratios.

3 ASSESSING VANE SHEAR DRAINAGE CONDITIONS

Literature review undertaken as part of this study suggests there currently exists two different approaches to assessing whether a vane shear test has occurred under undrained conditions:

- The method of Blight (1968), as updated by Chandler (1988). This method assumes the primary excess pore pressure generation relevant to drainage during shear occurs during vane rotation. Further, this method assumes that drainage path length is equal to the diameter of the vane. Therefore, time factor T can be directly related to degree of drainage U.
- The method of Morris and Williams (2000). This method assumes that the primary excess pore pressure generation relevant to drainage during shear occurs during vane insertion. Further, the drainage path length relevant to application of

this method is not generally known a priori, and hence directly relating T and U is more difficult.

The two methods outlined approach the vane shear assessment problem in considerably different frameworks. Both have been used to interpret the data presented in this paper, to assess their respective performance.

4 RESULTS AND INTERPRETATION

4.1 *Laboratory undrained strength*

The results of four DSS tests undertaken are presented in Table 2. The results indicate peak undrained strengths ranging from 0.20 to 0.27, which are reasonable values for a normally consolidated, moderate plasticity material loaded in the simple shear direction (for example, Ladd 1991). Rigidity index (I_r) calculated for each test are included, as these values were used to assist in inferring c_h from dissipation tests. I_r was calculated based on stresses and strains recorded at 50% of the failure shear stress, i.e. G_{50}. As discussed previously, the vertical effective stresses selected for the tests are higher than the estimated preconsolidation pressures that are likely to have occurred owing to air drying on the tailings beach.

Table 2. DSS test summary

CPTu No.	DSS Test No.	Sampled Depth (m)	s_u / σ'_v (-)	I_r (-)
1	1	6.5-7.0	0.27	70
3	2	7.5-8.0	0.24	100
3	3	7.5-8.0	0.20	135
3	4	7.5-8.0	0.22	98

4.2 *Phreatic conditions and dissipation tests*

Horizontal coefficient of consolidation c_h was inferred based on Teh and Houlsby's (1991) solution, assuming an average I_r as indicated from the DSS tests undertaken. Dissipations tests undertaken at locations relevant to this study are summarized in Table 3. The values are seen to range from approximately 100 to 500 m^2/year. These values are in excess of that suggested to provide undrained shearing at "typical" vane rotation rates (Chandler 1988).

Table 3. Dissipation test summary

CPTu No.	Depth (m)	c_h (m^2/year)
1	5.0	132
2	3.5	348
2	7.5	505
4	4.0	334
4	9.0	311

Dissipations tests indicated approximately hydrostatic pore pressure profiles with depth. Evidence of small amounts of base drainage were observed at test locations other than those assessed in this study.

4.3 *Undrained strength synthesis*

In situ peak undrained strengths were assessed through CPTu, ball penetrometer, vane shear, and comparison to DSS tests previously outlined. A comparison of results at CPTu 1 (crest location) is made in Figure 1. The compacted crest material in this area was estimated to be between 3 – 4 m in depth from the surface. Peak undrained strengths are inferred from the CPTu based on an N_{kt} of 10 and an N_u of 5, based on peak undrained strength ratios obtained from the DSS across the sampled depth interval. The vane results are shown for rotation rates of 12 and 240 degrees per minute. The vane shear results indicate that at 12°/min, the results appear to significantly overestimate undrained strengths compared to other techniques. When the rate is increased, the resulting undrained strengths align more favourably to those from other tests.

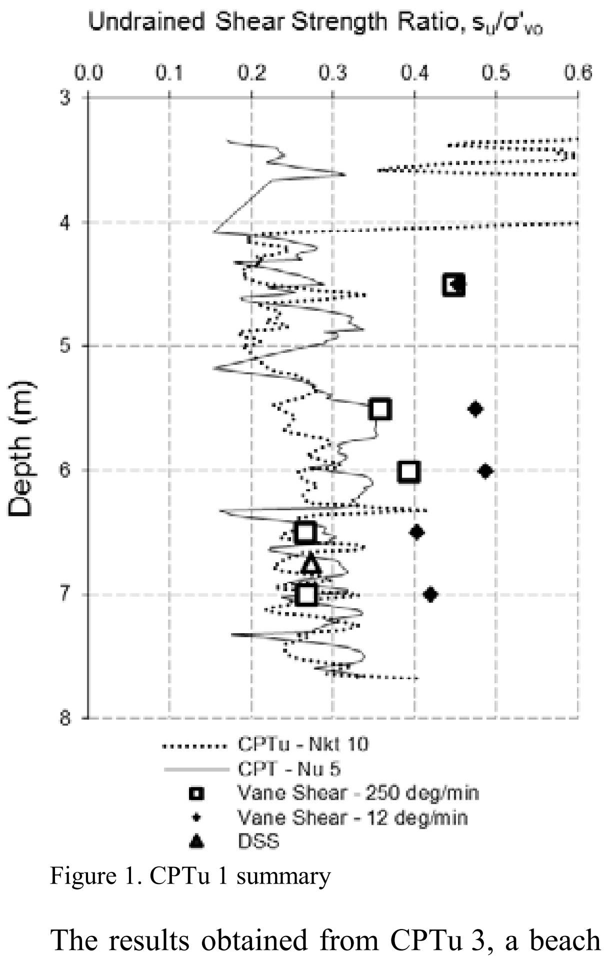

Figure 1. CPTu 1 summary

The results obtained from CPTu 3, a beach location, are presented in Figure 2. At this beach location ball penetrometer testing was undertaken adjacent to the initial CPTu, to provide another assessment of peak undrained shear strengths. The ball penetrometer was inferred based on the methods of Randolph (2004) and DeJong et al. (2011), with an assumed N_{ball} of 11. The results suggest that for this test location, solar drying processes following deposition result in overconsolidated tailings to a depth of approximately 5 m. This suggests a preconsolidation pressure imparted by solar drying of approximately 70 kPa, which seems reasonable in the context of the typically observed beach condition in fallow areas.

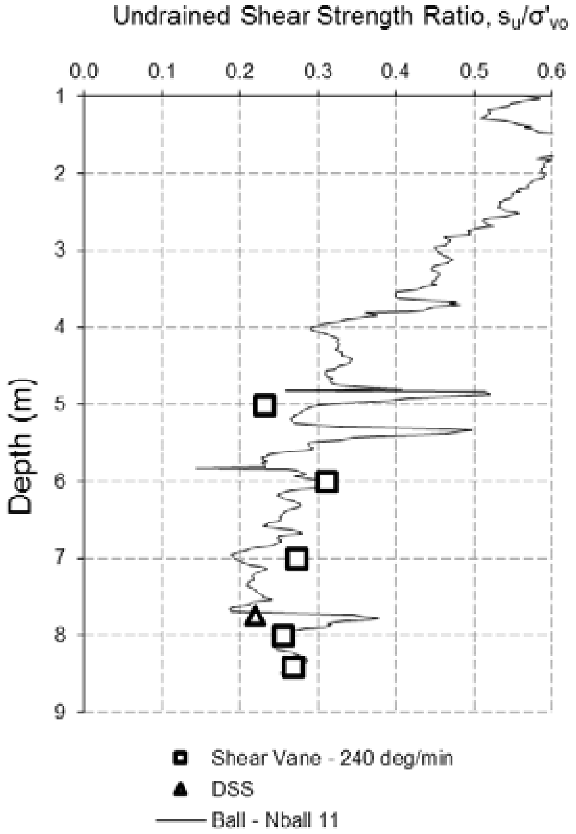

Figure 2. CPTu 3 summary

4.4 *Vane shear interpretation (Chandler 1988)*

The peak undrained strength ratio results of all of the vane shear tests undertaken at CPTu 1, 2 and 3 locations are presented in Figure 3, with reference to the inferred time factor *T*, based on the start of shearing. Time factor was calculated from the start of rotation of the vane (not the rods, owing to slip coupling), assuming drainage path length is equivalent to the diameter of the vane (Chandler 1988), and applying a c_h value from the nearest dissipation test. A time factor of 0.05 is also indicated on Figure 3, which represents the approximate threshold suggested by Chandler between drained and undrained shearing. For results at CPT 1, where vane shear tests were undertaken at the same depths at 12 and 240 degree/min., the paired results for each depth are connected for clarity.

The results indicate a weak trend between peak undrained strength ratio and time factor. However, the results where partial drainage is likely are all in excess of the expected normally consolidation undrained strength ratio range of 0.20 – 0.30 for this material. This suggests that the effects of partial drainage are providing overestimates of undrained strength when low rotation rates are used. While a number of tests with $T<0.05$ still indicate peak undrained strength ratios exceeding 0.3 this may be a result of sandy seams of material in these areas. Importantly, the linked tests for CPT 1 undertaken at rates giving time factors higher and lower than Chandler's theorized drained/undrained threshold appear to support that proposed drainage criterion.

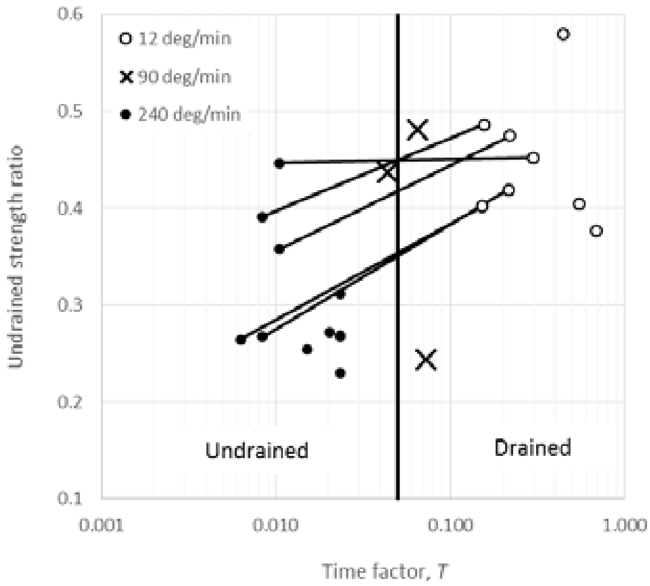

Figure 3. Vane summary, based on Chandler (1988)

4.5 *Vane shear interpretation (Morris and Williams 2000)*

The peak undrained strength ratios results are plotted again on Figure 4, where *T* is now based on the methods suggested by Morris and Williams (2000), where time to failure is taken from insertion of the vane. The relevant *T* below which undrained conditions would prevail cannot be definitely estimated for the data in this study based on the method of Morris and Williams, as their method requires additional information to directly link *T* to degree of drainage *U*, which varies for different materials. However, based on the data they present, the lowest required *T* value relevant to their method to define undrained conditions would be approximately 1.3. This value is indicated on Figure 4. The test results undertaken at CPT 1 at the same depths, but with different rotation rates, are again linked for clarity.

The summary of the results as shown in Figure 4 does not, in general, support the interpretation method of Williams and Morris. Where tests were undertaken at the same depth, at different rates, the resulting calculated change in *T* are such that either rate is suggested to be essentially undrained. This appears to be contradictory to the strength results, which indicate significantly lower strengths in many case at the higher shear rate. The reasons for this lack of agreement are unclear. However, it is noted that application of the Morris and Williams method is based, by current necessity, on the assumption that T of 1.3 be taken as potential limit on undrained behavior, from a limited number of data points. Additional data to refine this criterion may be useful (as was pointed out by the authors of this method in their publication).

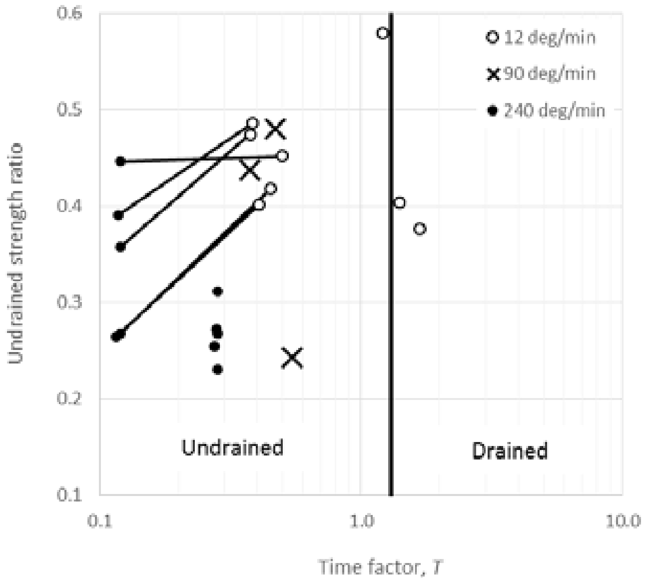

Figure 4. Vane summary, based on Morris and Williams (2000)

5 DISCUSSION AND LIMITATIONS

The results obtained in this study provide greater support to the methods of Blight (1968) and Chandler (1988) compared to that of Morris and Williams (2000). However, it must be acknowledged that the site procedures, while undertaken in a manner that controlled for the effects of vane rotation rate, were not adequately planned to fully assess the effect of time from vane insertion. Therefore, the available data is insufficient to directly relate time factor to drainage coefficient as proposed by Morris and Williams (2000). Further, a relatively small number of tests are available at similar depths to enable direct comparison.

It is noted that the results of the current study, in the context of the above comparison, suffer a number of relevant limitations, including *(i)* reliance in some cases upon dissipation test data from different depths to that of the vane shear tests interpreted, and, *(ii)* the potential that "paired" vane tests at the same depth, yet 1 to 3 m apart laterally, may not test identical material owing to the inherent variability within a typical tailings deposit. Despite these uncertainties, it is observed that application of the vast majority of the range of c_h values typical of the results obtained in the investigation would not materially affect the results of the comparisons made. Further, where c_h values from adjacent depths were applied to the interpreted vane shear results, soil behaviour type index (SBT) inferred from the CPTu did not vary significantly. The highest c_h value, at CPT 2, was undertaken in a location that may have included sandier material, as there is a local drop in SBT around this location.

It is interesting to note the effect of rotation rate on the time to commencement of shearing when using a slip coupling. For example, when using a rotation rate of 12°/min, it can take up to two minutes of shaft rotation prior to the commencement of vane rotation. This is an important consideration if assessing the potential for partially drained conditions in the context of Morris and Williams' (2000) method, where time to failure commences from vane insertion.

It is noted that in parallel to the effect of rotation rate on potential drainage around the vane, rotation rate also effects shear rate. This can itself affect undrained shear strengths, with faster shear rates leading to higher measures of shear strength. Indeed, much of the typically-applied vane correction factors are suggested to be a result of such rate effects, and their increase with increasing plasticity (for example, Ladd and DeGroot 2003). Fortuitously, the index properties of the material considered in this study suggest that rheological rate-effects may be low, when viewed in the context of Bjerrum's (1972) vane correction method. Alternatively, laboratory-based studies have suggested that variation in shear rate is likely to have significant effect on resulting undrained shear strengths for a material with the index properties relevant in this study (for example, Sheahan et al. 1996). This is an area of ongoing uncertainty and research in geotechnical practice.

6 CONCLUSIONS

A series of shear vane tests were undertaken adjacent to CPTu and ball penetrometer tests within a silty, moderate plasticity tailings. Dissipation tests within the tailing suggested that vane shear testing may not achieved undrained conditions without consideration of the time to failure and/or rate of shear. Vane shear tests were therefore conducted at different shear rates to assess their effect on the results obtained. In general, rapid shear rates resulted in closer agreement with other available estimates of undrained shear strengths. This result enabled an assessment of two current methods for assessing the drainage behaviour of vane shear tests.

7 REFERENCES

ASTM D2573 / D2573M-15. 2015. Standard Test Method for Field Vane Shear Test in Saturated Fine-Grained Soils. West Conshohocken , ASTM International.

Bjerrum, L. 1972. Embankments on soft ground: SOA Report. *Proceedings Specialty Conference on Performance of Earth and Earth-Supported Structures*: 1 – 54. Purdue, ASCE.

Blight, G.E. 1968. A note on field vane testing of silty soils. *Canadian Geotechnical Journal* 5: 142-149.

Castro, G. and Troncoso, J.H. 1989. Effects of 1985 Chilean earthquake on three tailings dams. *Fifth Chilean Conference on Seismology and Earthquake Engineering*. Santiago.

Chandler, R. 1988. The in situ measurement of the undrained shear strength of clays using the field vane. In A. Richards (ed) *Vane shear testing in soils: field and laboratory studies*, Tampa, Florida, January 1987 .Baltimore: ASTM.

DeJong, J.T., Yafrate, N..J, and DeGroot, D.J. 2011. Evaluation of undrained shear strength using full-flow penetrometers. *Journal of Geotechnical and Geoenvironmental Engineering* 137(1): 14 – 26.

Fell, R., MacGregor, P., Stapledon, D., Bell, G. and Foster, M. 2014. Geotechnical Engineering of Dams. Boca Raton: CRC Press.

Ladd, C.C. 1991. Stability evaluation during staged construction (22nd Terzaghi Lecture). *Journal of Geotechnical Engineering* 117(4): 540-615.

Ladd, C.C. and DeGroot, D.J. 2003. Recommended practice for soft ground characterisation – The Arthur Casagrande Lecture. Proceedings of the 12th Panamerican Conference on Soil Mechanics and Geotechnical Engineering: 3-57.

Morris, P.H., and Williams, D.J. 2000. A revision of Blight's model of field vane testing. *Canadian Geotechnical Journal* 37(5): 1089-1098.

Randolph, M.F. 2004. Characterisation of soft sediments for offshore applications. In V. da Foneseca and P. Mayne (eds.), *Proceedings ICS-2, 2nd International conference on site characterization:* 209-232. Rotterdam: Millpress.

Sheahan, T., Ladd, C., Germaine, J. 1996. Rate-dependent undrained shear behaviour of saturated clay. *Journal of Geotechnical Engineering* 122(2): 99-108.

Teh, C.I. and Houlsby, G.T. 1991. An analytical study of the cone penetration test in clay. *Géotechnique* 41(1): 17-34.

Geotechnical and Geophysical Site Characterisation 5 – Lehane, Acosta-Martínez & Kelly (Eds)

Analysis of instrumented sharp cone tests performed in a sensitive clay of Quebec

V. Silvestri
Ecole Polytechnique, Montreal , Quebec, Canada. E-mail : vincenzo.silvestri@polymtl.ca
C. Tabib
Consultant, Montreal, Quebec, Canada

ABSTRACT: The objective of this paper is to compare field test results obtained in a stiff sensitive clay of Quebec using prebored sharp cone tests (ISCTs) with data obtained from prebored and self-bored pressuremeter tests (PMTs and SBPMTs), and vane shear tests (VSTs). Results are interpreted using both the elastic-plastic Tresca model and Palmer's approach. It is shown that while ISCTs and PMTs greatly overestimate the undrained shear strength compared to the SBPMTs and VSTs, the opposite trend is found for the shear modulus. It is thought that such behaviour is due to remoulding and unloading of the clay caused by drilling of the pilot holes for the ISCTs and PMTs. In addition, it has been found that the in situ coefficient of lateral pressure at rest, K_o, deduced from the SBPMTs is abnormally high. The primary cause has been attributed to the cemented nature of the clay.

1. INTRODUCTION

The most useful field tests in clay are the vane shear test (VST), the cone and the piezocone penetration tests (CPT and CPTu), the prebored and self-bored pressuremeter tests (PMT and SBPMT), and the flat dilatometer test (DMT). Although in each of these tests the soil undergoes different stress and strain paths, it is possible, by means of appropriate interpretation methods, to deduce soil parameters for design purposes.

The instrumented sharp cone test (ISCT) is a recent addition to the arsenal of in situ testing methods. The test consists in driving an instrumented low-angle truncated sharp cone (ISC) at a constant penetration rate in a prebored vertical pilot hole or a self-bored hole. The purpose of the test is to produce in the soil a quasi-cylindrical cavity expansion similar to that in a PMT or a SBPMT. The ISCT is thus intended to provide soil parameters like those obtained in a PMT or a SBPMT, but in the continuous manner of the CTP or the CPTu. Soil and water pressures generated by the steady penetration of the probe are measured by means of pressure transducers mounted on the wall of the cone. On account of the small apical angles (i.e., 1°-2°) of the ISC, pressuremeter interpretation methods are currently employed to analyse ISCT data for the determination of soil properties.

The objective of the present paper is to compare field test results obtained in a stiff sensitive clay of eastern Canada by means of prebored ISCTs with results deduced from PMTs, SBPMTs, and VSTs. It is shown that while both PMTs and ISCTs yield very similar results, they nonetheless lead to undrained shear strengths that are much higher than those deduced from SBPMTs and VSTs. The opposite trend is found to occur with the values of the shear modulus. Reasons are given for the observed response.

2. FIELD TEST RESULTS

ISCT

The instrumented sharp cone (ISC) used in the present investigation is shown in Fig.1. The device is equipped with five total pressure transducers installed at the positions indicated in the same figure. Because a plane strain undrained cylindrical cavity expansion is considered to take place during the steady penetration of the device, the total pressure recorded by each transducer corresponds to a volumetric strain $(\Delta V/V)_i$, which is defined as follows (Ladanyi and Longtin 2005):

$$\left(\frac{\Delta V}{V}\right)_i = \frac{V_i - V_o}{V_i} = \frac{r_i^2 - r_o^2}{r_i^2} = 1 - \left(\frac{r_o}{r_i}\right)^2 \tag{1}$$

where V_i, V_o = expanded and initial volumes of the pilot hole. If there are n lateral pressure transducers mounted on the ISC, there will be n points on the equivalent pressuremeter expansion curve, or n points, including the origin, on the deduced stress-strain curve. The volumetric strains which correspond to the positions of the pressure transducers range between 3 and 30%. Volumetric strains are equal to shear strains generated in the horizontal plane surrounding the ISC.

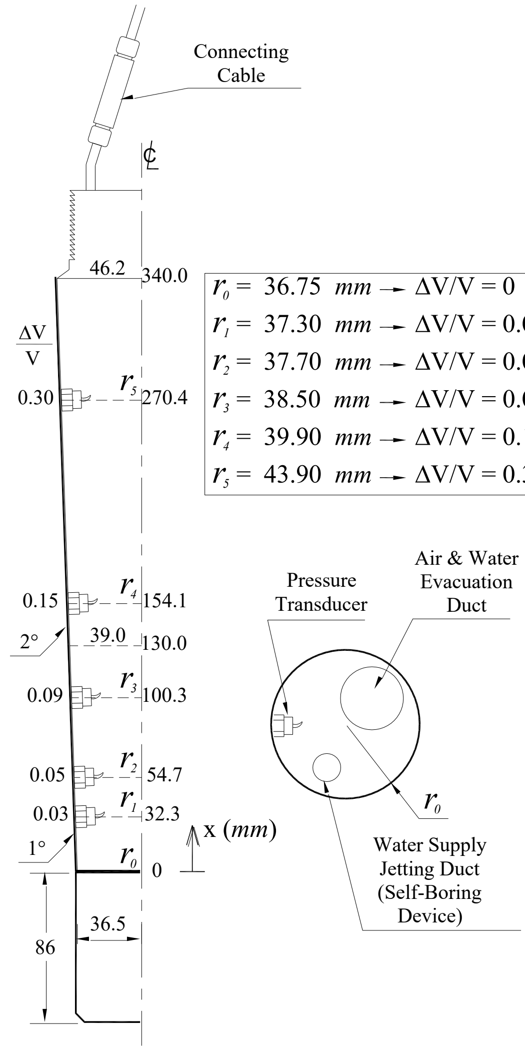

Fig. 1: Instrumented sharp cone. r_0, r_1, r_2, r_3, r_4, r_5, borehole radii; x, distance from the tip of the cone to the centre of a pressure gauge; $\Delta V/V$, current volumetric strain (Adapted from Longtin 2004).

ISCTs were carried out in 73 mm diameter vertical pilot holes which were bored by using the technique of retrieving continuous samples of clay by means of 73 mm diameter, 710 mm long Shelby tubes. ISCTs were performed immediately after completion of the pilot holes. The ISC was driven at a constant vertical penetration rate of 20 cm/min, which corresponds to the strain rate produced in a pressuremeter test in clay.

PMTs and SBPMTs

PMTs were carried out in pilot holes which were bored using the technique employed for the ISCTs. The tests were conducted with a 70 mm diameter, Texam NX probe (Felio and Briaud 1986) of length-to-diameter ratio, *L/D*, of 5.1, which was expanded at a rate of 1%/min. SBPMTs were performed using a Mark VIII, Cambridge In situ, instrument, equipped with two pore pressure gauges, and expanded at a rate of 1.09%/min.

3. INTERPRETATION METHODS

PMTs, SBPMT, and ISCT results were first analysed by assuming that the clay obeyed an ideally elastic perfectly plastic (Tresca) soil model (Gibson and Anderson 1961). For small strains, the constitutive relations are:

$$\tau = \begin{cases} \gamma G \quad , \quad \gamma \le \dfrac{S_u}{G} \\ S_u \quad , \quad \gamma > \dfrac{S_u}{G} \end{cases} \tag{2}$$

where τ = shear stress, γ = shear strain, G = shear modulus, and S_u = undrained shear strength. The corresponding radial stress-shear strain relationships are the following:

$$\sigma_r = p = \begin{cases} p_o + \gamma G \quad , \quad \gamma \le \dfrac{S_u}{G} \\ p_o + S_u\left(1 + \ln\left(\dfrac{G\gamma}{S_u}\right)\right) \quad , \quad \gamma > \dfrac{S_u}{G} \end{cases} \tag{3}$$

where $\sigma_r = p$ = applied or generated radial pressure, $p_o = \sigma_{ho}$ = initial horizontal geostatic stress, and G/S_u = rigidity index. Eq. 3 indicates that if the pressure p is drawn as a function of lnγ, the undrained shear strength S_u equals the constant slope of the resulting curve in the plastic phase of the expansion (See, also, Whittle and Wroth 1977). In addition, the shear modulus G may be found from the value of the shear strain γ recorded at the end of the elastic phase of the expansion, because $G = (p - p_o)/\gamma$.

PMTs and SBPMT data were also interpreted using Palmer's approach (Palmer 1972), which allows the determination of the shear stress τ from the pressure-expansion curve, by means of the following expression:

$$\tau = \gamma \frac{dp}{d\gamma} \tag{4}$$

where $dp/d\gamma$ represents the slope of the experimental curve. Eq. 4 is only valid for small strains.

4. SOIL DEPOSIT

PMTs, ISCTs, and VSTs were completed at an experimental site located 25 km northeast of Montreal in Quebec. The soil stratigraphy is shown in Fig. 2. It consists of a 2.2 m thick crust of oxidized clay which overlies a deposit of firm to medium stiff sensitive clay of high plasticity. Below the crust, the moisture content is about 70% and the plasticity index averages 40%. The overconsolidation ratio, *OCR*, ranges between 4 and 7. The undrained shear strength, S_u, measured with a Nilcon vane, increases from 50 kPa at 2 m to just over 100 kPa at 6 m.

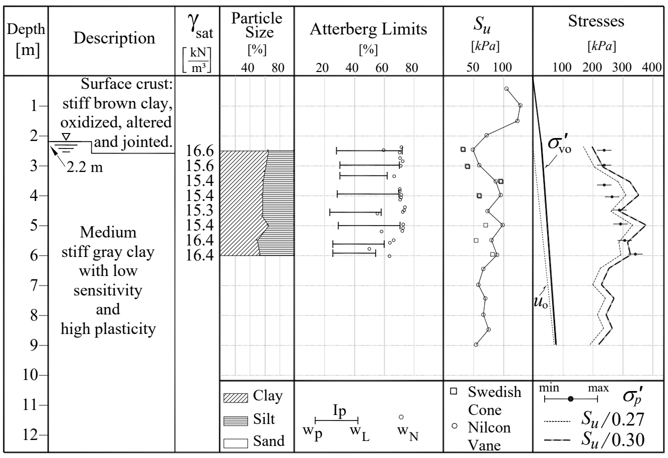

Fig. 2: Soil stratigraphy at Mascouche. S_u, undrained shear strength; w_L, liquid limit; w_N, natural water content; w_P, plastic limit; γ_{sat}, saturated unit weight; σ'_p, vertical preconsolidation pressure.

While most ISCTs were carried out in the depth interval from 0.5 to 6 m, PMTs were completed at three distinct depths of 2.5, 4.5, and 6.0 m. Typical PMT and ISCT results are shown in Figs. 3 and 4. The ISCT data reported in the latter figure clearly indicate the existence of a softer clay layer between 2.1 and 2.7 m depth. Palmer's approach was not used to interpret ISCT results because of the small number of experimental points on the expansion curve.

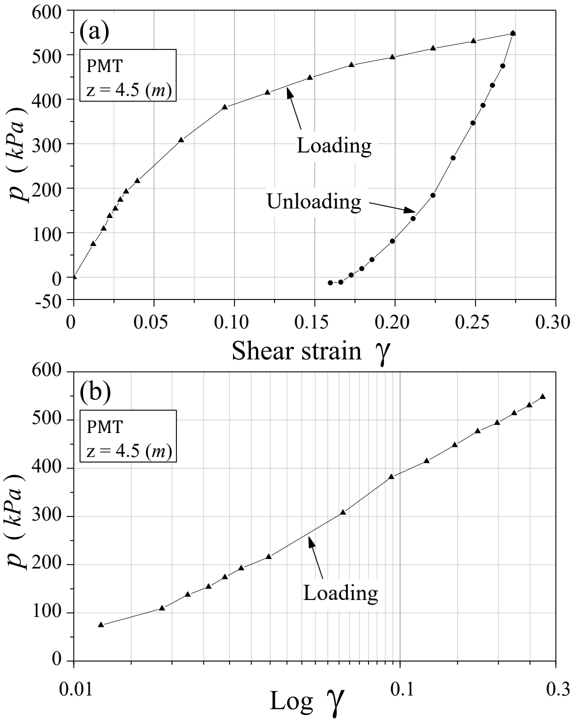

Fig. 3: a) Applied pressure versus shear strain, b) Applied pressure (loading) versus natural logarithm of shear strain.

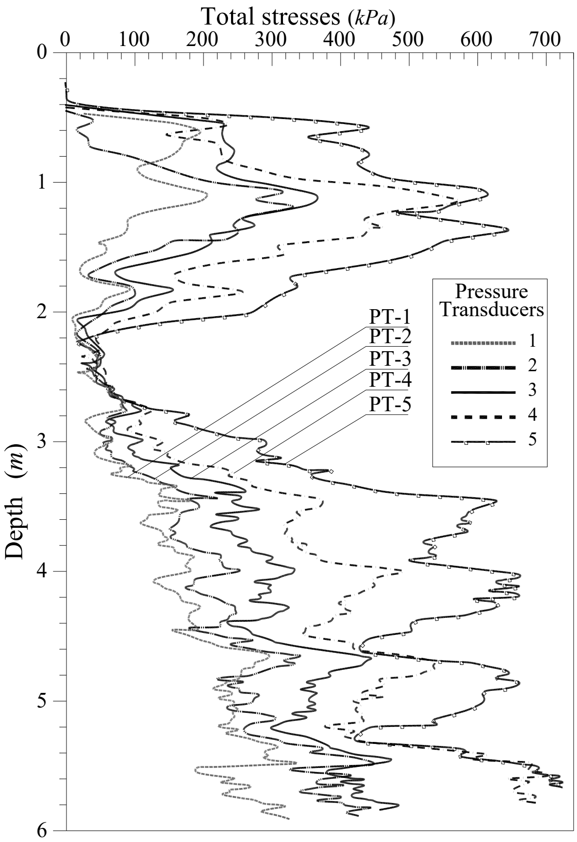

Fig. 4: ISCT profile at Mascouche (adapted from Longtin 2004)

SBPMTs, CPTus, and VSTs were performed at a nearby site by a team from Laval University of

Quebec City. Typical SBPMT and CPTu data are reported in Figs. 5 and 6. Comparison between the CPTu and VST results showed that the cone factor N_{kt} varies between 14.3 and 12.8 in the depth interval from 4.5 to 7.9 m. The cone factor $N_{kt} = (q_t - \sigma_{vo})/S_{uVST}$, where q_t = measured cone tip resistance, σ_{vo}= total vertical stress, and S_{uVST}= undrained shear strength by vane shear test.

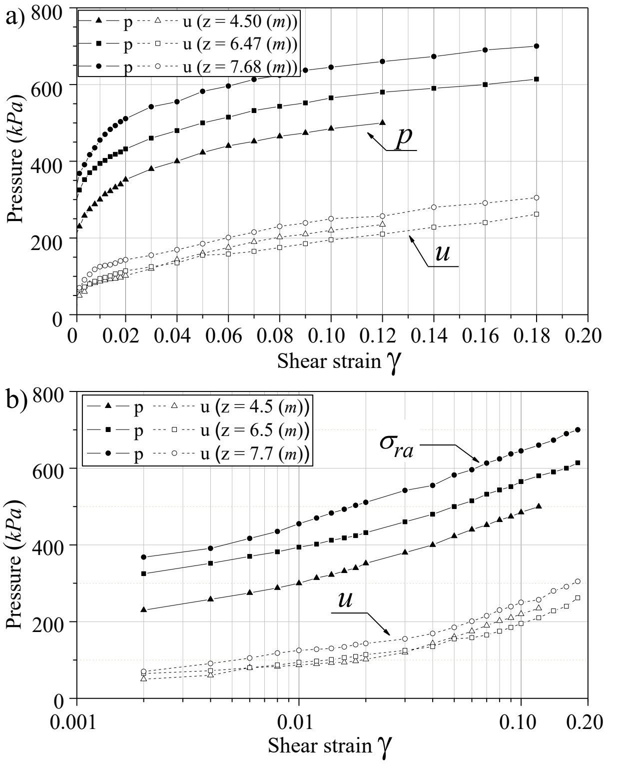

Fig. 5: SBPMT expansion tests. p, applied pressure; u, pore pressure; z, depth.

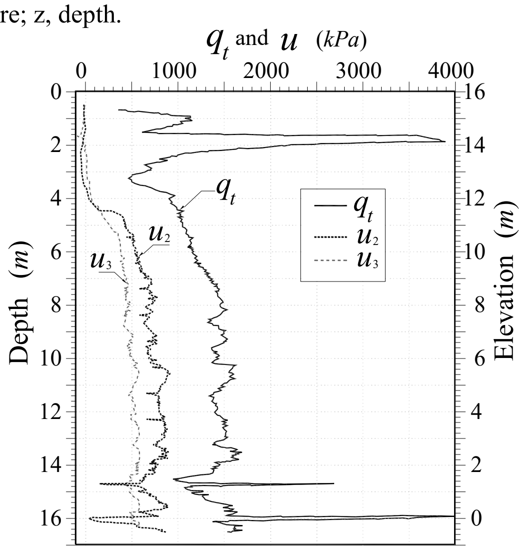

Fig. 6: CPTU data at Mascouche B. q_t, cone resistance; u, pore pressure; u_2, pore pressure above the cone tip; u_3, pore pressure at five diameters above the shoulder of the piezocone shaft (adapted from D. Demers, personal communication, 2001)

5. DISCUSSION OF TEST RESULTS

In situ Coefficient of Lateral Earth Pressure at Rest

Table 1 presents the initial stress states in the clay deposit, as deduced from SBPMTs. The horizontal geostatic stress, p_o or σ_{ho}, was found from the average lift-off pressure registered by the three feeler arms of the pressuremeter. The initial pore water pressure, u_o, was measured in standard Geonor piezometers. The in situ coefficient of lateral earth at rest, K_o, was deduced from the ratio $\sigma'_{ho}/\sigma'_{vo}$ or $(\sigma_{ho} - u_o)/(\sigma_{vo} - u_o)$, where σ'_{ho}, σ'_{vo} = effective lateral and vertical pressures, and σ_{vo} = calculated total vertical overburden pressure. K_o values which vary between 3.9 at 4.50 m and 3.6 at 6.5 m, are much higher than the corresponding ones obtained from application of the well-known relationship:

$$K_o = (1 - \sin\phi'_{nc})\, OCR^{\sin\phi'_{nc}} \tag{5}$$

where ϕ'_{nc} = friction angle of destructured clay. For the sensitive clay at study, ϕ'_{nc} = 33°. High lateral pressures similar to those deduced from the SBPMTs were also obtained from hydraulic fracture tests and flat dilatometers tests carried out at the same site, as reported by Hamouche at al. (1995). According to these investigators, the causes of the very high values of K_o are related primarily to the cemented nature of the sensitive clay and unloading due to past erosion, and to a lesser extent to delayed consolidation.

Table 1 Initial stress states of clay deposit

Depth (m)	u_o (kPa)	σ'_{ho} (kPa)	σ'_{vo} (kPa)	OCR	K_o $\sigma'_{ho}/\sigma'_{vo}$	K_o Eq.5
4.5	30	165	42	6.4	3.9	1.25
6.5	44	232	60	5.1	3.9	1.11
7.7	55	255	70	5.9	3.6	1.20

Undrained Shear Strength and Shear Modulus

PMTs were carried out first by loading the soil to a maximum predetermined radial strain of 10%, and then by unloading to zero radial pressure. However, because only loading phases were completed in the SBPMTs and necessarily so in the ISCTs, the discussion will be restricted to soil strength parameters deduced from the loading test results. Table 2 presents a comparison between the undrained shear strengths and shear moduli which were determined based on the Tresca model. Examination of the data immediately shows that both the PMTs and ISCTs greatly overestimate the undrained shear strength compared to SBPMTs and VSTs. In addition, SBPMTs overestimate by 10 to 25% the undrained shear strength deduced from VSTs. The existence of such differences between PMT, SBPMT, and VST data has been known for several decades (See, for example, Roy et al. 1975 and Lacasse et al. 1981). The cause has been attributed to a) the existence of a remoulded annulus of soil at the wall of the pilot holes due to the boring technique, b) unloading of the soil resulting from drilling of the pilot holes, and c) the possibility that the PMT tests were carried out under partially drained conditions. While factors a) and b) are considered to lead to overestimation of the undrained shear strength (Baguelin at al. 1978; Prévost 1979; Eden and Law 1980; Law and Eden 1982; Benoît and Clough 1986; Prapaharan et al. 1990), the last factor c) is less important because the tests were carried out quite rapidly. There is, however an additional factor which is believed to have considerable impact on the experimental data obtained from the ISCTs. Indeed, after completion of these tests, the boreholes were examined for possible damage resulting from the sharp tip of the probe. It was discovered that the interior surface of 20 to 40% of the pilot holes was not as smooth as at the beginning of the tests. The steady penetration of ISC caused spalling of the clay ahead of the advancing conical probe. There were fragments and chunks of soil on the bottom of the pilot holes. Such a phenomenon which is thought to especially occur in fragile materials like the sensitive clays of eastern Canada, may be eliminated by conducting ISCTs using a self-boring device.

Concerning the shear modulus G deduced from the data, Table 2 indicates that while the highest values are obtained from the SBPMTs, the lowest values are deduced from the ISCTs. Borehole disturbance and unloading are thought to be responsible for the poor performance of the PMTs and ISCTs, as also discussed by Silvestri and Abou-Samra (2008).

Table 2 Soil strength parameters

Depth	PMT		ISCT		SBPMT		VST
	S_u	G	S_u	G	S_u	G	S_u
(m)	(kPa)	(kPa)	(kPa)	(kPa)	(kPa)	(kPa)	(kPa)
2.5	100	1000	184	1050	91	--	50
4.5	180	4540	189	1550	91	8190	72
6.0	260	5100	--	--	91	8190	80

Stress Paths

Total and effective stress paths, followed by the clay during the expansion process, could only be deduced from SBPMT data, because only this test allowed determination of the initial stress state. For discussion purposes, only the test completed at the depth of 4.5 m will be analysed in the present study. Total stress paths were obtained from both the Tresca model and Palmer's approach. The stress parameters, s and t are given by $s = (\sigma_r + \sigma_t)/2$ and $t = (\sigma_r - \sigma_t)/2$, where σ_t = tangential stress, and become $s = \sigma_r - \tau$ and $t = \tau$, because $\sigma_t = \sigma_r - 2\tau$. The total stress paths are shown in Fig. 7. For the Tresca model, the initial phase of the expansion is elastic for $t \leq S_u$ and, therefore, s is constant, equal to p_o or σ_{ho}. Once the shear stress reaches the shear strength S_u, the soil becomes plastic, and the stress path turns to the right and remains horizontal until the radial pressure σ_r attains its ultimate value, $p_{ult} = p_o + S_u\,[1+\ln(G/S_u)]$, as shown by Gibson and Anderson (1961).

For Palmer's approach, the resulting stress path is curved, as shown in Fig. 7. At large strain, the stress path converges with that deduced from the Tresca model, because the shear strength S_u is the same in both cases. The effective stress path, which is also shown in Fig. 7, was obtained by subtracting the pore water pressure measured during the expansion test from the curved Palmer's total stress path.

Because the effective stress path is almost vertical throughout the deformation process, the increase in total radial pressure during the plastic phase of the expansion is practically equivalent to the excess pore water pressure generated in the clay. Such behaviour is clearly indicated in Fig. 5 where the curves of radial pressure are almost parallel to those of pore water pressure.

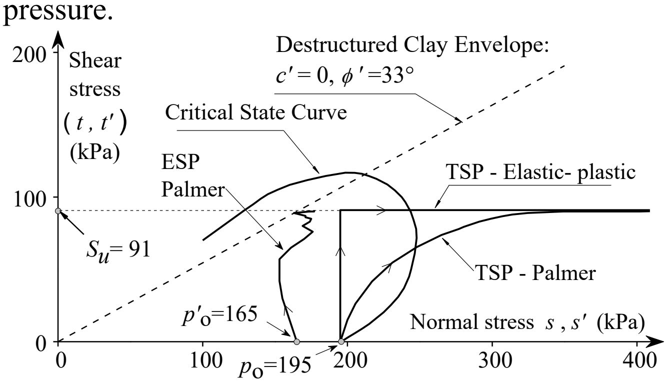

Fig. 7: Stress paths from SBPTM. c', effective cohesion; ESP, effective stress path; p', effective pressure; p_o, initial horizontal total pressure; p'_o, initial horizontal effective pressure; S_u, undrained shear strength; TSP, total stress path; ϕ', effective friction angle.

6. CONCLUSIONS

The following conclusions ensue from the results reported in the paper:

a) Both the PMTs and ISCTs considerably overestimate the undrained shear strength of the clay, as compared to VSTs. The cause is attributed to borehole disturbance and unloading.
b) SBPT-deduced S_u values are from 10 to 25% higher than VST-derived parameters.
c) Shear moduli derived from PMTs and ISCTs are much lower than values deduced from SBPMTs. Again, the cause is probably related to borehole disturbance and unloading.
d) Initial horizontal geostatic stresses were found to be much higher than expected using a well-known correlation.
e) Because of the spalling phenomenon of the pilot holes ahead of the advancing ISC, it is recommended that ISCTs be performed using a self-boring device. This will also avoid unloading and will minimize remoulding of the soil around the boreholes.

7. ACKNOWLEDGEMENTS

The senior author expresses his gratitude to the late Professor Marius Roy of Laval University for making available the SBPMT test data. The authors are grateful to the Natural Sciences and Engineering Research Council of Canada for the financial support received in the course of the present investigation.

8. REFERENCES

Baguelin, F., Jézéquel, J.F., and Shields, D.H. 1978. "The pressuremeter and foundation engineering". *Trans Tech Publications*, Clausthal, Germany.

Benoît, J., and Clough, G.W.1986. "Self-boring pressuremeter tests in clay". *Journal of the Geotechnical Engineering Division, ASCE*, 112:60-78.

Demers, D. 2001. "Personal communication". *Department of Transport of Quebec*, Quebec City, Quebec, Canada.

Eden, W.J., and Law, K.T. 1980. "Comparison of undrained shear strength results obtained by different test methods". *Canadian Geotechnical Journal*, 17:369-381.doi:10.1139/t80-044.

Felio, G.Y., and Briaud, J.L. 1986. "Conventional parameters from pressuremeter tes data: review of existing methods". Proceedings of the 2nd International Symposium on the Pressuremeter and its Marine Applications, College Station, TX., 2-3 May 1986, ASTM STP 950, pp. 265-282.

Gibson, R.E., and Anderson, W.F. 1961. "In situ measurements of soil properties with the pressuremeter". *Civil Engineering and Public Works Review*, 56:615-618.

Hamouche, K.K., Leroueil, S., Roy, M., and Lutenegger, A.J. 1995. "In situ evaluation of K_0 in eastern Canada clays." *Canadian Geotechnical Journal*. 32(4):677-688.

Lacasse, S., Jamiolkowski, M. Lancellotta, R., and Lunne, T. 1981. "In situ characteristics of two Norwegian clays". *Proceedings of the 10th International Conference on Soil Mechanics and Foundation Engineering*, 15-19 June 1981, Stockholm, Vol. 2, pp.507-511.

Ladanyi, B., and Longtin, H. 2005. "Short- and long-term sharp cone tests in clay". Canadian Geotechnical Journal, 42:136-146.

Law, K.T., and Eden, W.J. 1982. "Effects of soil disturbance in pressuremeter test". *Proceedings of the Conference on Updating Subsurface Sampling of Soils and Rocks and their In-Situ Testing.* Santa Barbara, Calif., 3-8 January 1982, pp. 291-303.

Longtin, H. 2004. "Characteristics of clayey soils by instrumented sharp cone" (In French). *Master's Thesis, Department of Civil, Geological, and Mining Engineering, Ecole Polytechnique of Montreal*, Montreal, Quebec, Canada.

Palmer, A. C. 1972. "Undrained plane strain expansion of a cylindrical cavity in clays: a simple interpretation of the pressuremeter test". Geotechnique, 22:451-457.

Prapaharan, S., Chameau, J.L., Altschaeffl, A.G., and Holtz, R.D. 1990. "Effect of disturbance on pressuremeter results in clays". *Journal of Geotechnical Engineering, ASCE*, 116:35-53.

Prévost, J.H. 1979. "Undrained shear tests on clay". *Journal of the Geotechnical Engineering Division, ASCE*, 105(GT1):49-64.

Roy, M. Juneau, R. La Rochelle, P., and Tavenas, F.A. 1975. "In situ measurements of the properties of sensitive clays by pressuremeter tests". *Proceedings of the Conference on In-situ Measurement of Soil Properties*, Raleigh, N.C., 1-4 June 1975, Geotechnical Engineering Division, ASCE, New York. Vol. 1, pp. 350-372.

Silvestri, V., and Abou-Samra, G. 2008. "Analysis of instrumented sharp cone and pressuremeter tests in stiff sensitive clay". *Canadian Geotechnical Journal*, 45:957-972.

Whittle, D., and Wroth, C.P. 1977. "Use of self-boring pressuremeter to determine the undrained properties of clays". *Ground Engineering*, 10:37-46.

Theme 3. Interpretation of In-Situ Testing

Geotechnical and Geophysical Site Characterisation 5 – Lehane, Acosta-Martínez & Kelly (Eds)
© 2016 Australian Geomechanics Society, Sydney, Australia, ISBN 978-0-9946261-1-0

Relative densities and void ratios derived from CPT data using in situ field calibration

T. Biryaltseva & T. Mörz
Fraunhofer Institute for Wind Energy and Energy System Technology, Bremerhaven, Germany

S. Brandt & S. Kreiter
MARUM Center for marine and environmental science, Bremen University, Bremen, Germany

U. Gerdes & B. Ossig
Geo-Engineering.org GmbH, Bremen, Germany

ABSTRACT: This study shows the results of an attempt to develop a transfer function of cone resistance measured in medium over-consolidated sands (< 2 MPa) toward relative soil density and absolute porosity solely based on in-situ testing. In a sand pit, a water saturated, Late Pleistocene fluvial section of 15 m thickness with homogeneous grain size distribution and comparable e_{max} and e_{min} values, but highly variable cone resistance was selected for testing. Two ~25 m deep sampling holes, 6 CPTs and two approximately 40 m deep neighboring flush drilled holes for downhole logging with a horizontal distance of 2.5 m to the CPTs were used in this study. Relevant downhole logging parameters are wet bulk density derived from active gamma logs and porosities derived from neutron-neutron logs. The results show a straightforward stratigraphic picture with clear soil package boundaries. However, within the sand formation of interest fluvial foresets bars, top sets and incised channels with local unconformities lead to changes of stratigraphic height over short horizontal distances challenging in turn the correlation of logging and CPT data. Despite these difficulties, the project resulted in a new transfer function for glacially overconsolidated sands not only linking tip values to relative density but also directly to porosity, making sampling at least for stratigraphic equivalent sands no longer a requirement.

1 INTRODUCTION

Obtaining undisturbed sand samples in non-cohesive soils could require expensive ground freezing while conventional sampling with pushed thin walled tubes or hammered thick wall tubes usually causes densification of looser layers and loosening of densely packed layers (e.g. Fig. 1, line A). The reconstruction of the sand sample in the laboratory therefore has to rely on in-situ test results. The most common technique to estimate the relative in-situ density of sands is the application of recognized empirical correlations for cone penetration tests based on large calibration chamber tests (e.g. Baldi et al. (1986), Bolton & Gui (1993), Jamiolkowski et al. (2001), Kulhawy & Mayne (1990) see Fig. 1).

However, these correlations based on specific local test sands can provide deviant results when applied to sands of different origin, composition, grain texture, age or consolidation state.

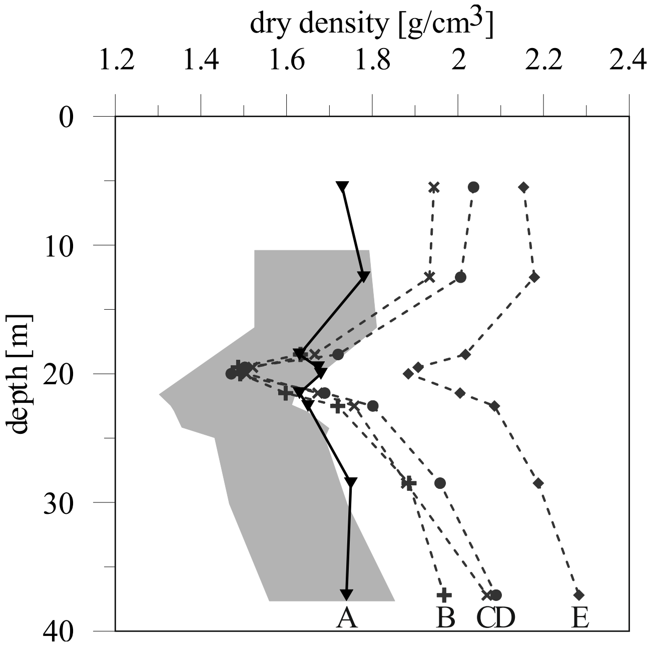

Figure 1. Offshore profile over a looser packed sand layer at around 20 m depth. Showing laboratory derived dry bulk densities from offshore taken push core samples (line A), as well as estimated dry densities using empirical CPT correlations after Bolton & Gui (1993) (B), Jamiolkowski et al. (2001) (C), Baldi et al. (1986) (D), Kulhawy & Mayne (1990) (E).
Minimum and maximum compactness (according to DIN 18126) are indicated by grey shading.

So far no transfer function exists for dense, often over-consolidated Pleistocene sands of the North Sea. Establishing a new correlation in the laboratory requires comprehensive and time consuming testing and correction for equipment effects such as chamber and cone sizes. In addition freshly prepared samples in the laboratory cannot provide information on ageing or other diagenetic longer term effects.

In-situ testing and down hole logging has the advantage to account for most of the soil conditions (stress state, temperature etc..) although limitations and calibrations of the testing equipment have to be considered. In this study, a correlation among cone resistance and relative density based on in-situ CPT and gamma density measurements in dense, slightly over-consolidated Late Pleistocene sand is proposed and compared with internationally recognized correlations.

2 STUDY AREA

The study area is located south of the town Cuxhaven in Northern Germany, close to the North Sea coast (Fig. 2). The site exhibits the same sand dominated stratigraphy and related geotechnical properties as found in many offshore wind farm areas within the Danish, German and Dutch sector of the southern North Sea.

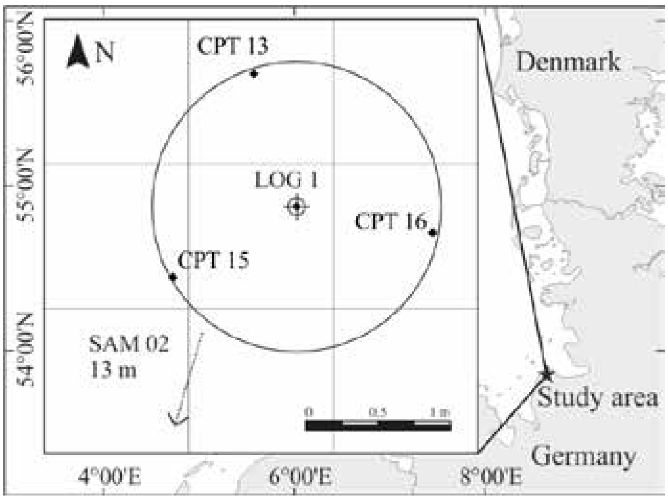

Figure 2. Study area and example of the spatial configuration of CPT, downhole logging and sampling boreholes.

In general the following requirements to the soil have to be fulfilled to consider an area suitable for in situ correlations: (i) full saturation, (ii) close to no variability in the grain size distribution and index densities ρ_{min} and ρ_{max} (iii) high variability in tip resistance and (iv) a simple horizontally layered stratigraphy with homogenous lateral soil properties.

3 METHODS

3.1 *Sampling*

A dry drilling Nordmeyer DSB 1/6 percussion hammer sampling unit has been used at the two sampling sites with a cumulative core length of 30.0 and 21.0 m respectively. A total of 41 samples have been investigated with regard to water content (DIN 18121) and soil bulk density (DIN 18125). Grain size analyses were performed according to DIN 18123, Fig. 3. Minimum and maximum void ratios (e_{min}, e_{max}) were measured according to DIN 18126 under the assumption of a grain density of ρ=2,675 g/cm^3 see Fig. 4. The derived data shows a uniformly graded deposit with consistent grain size distributions and near uniform index void ratios approximately between 6.5 and ~15 m depth. Appreciable variation in cone resistance throughout this section (Fig. 4) are ideal prerequisites in establishing an in-situ correlation function.

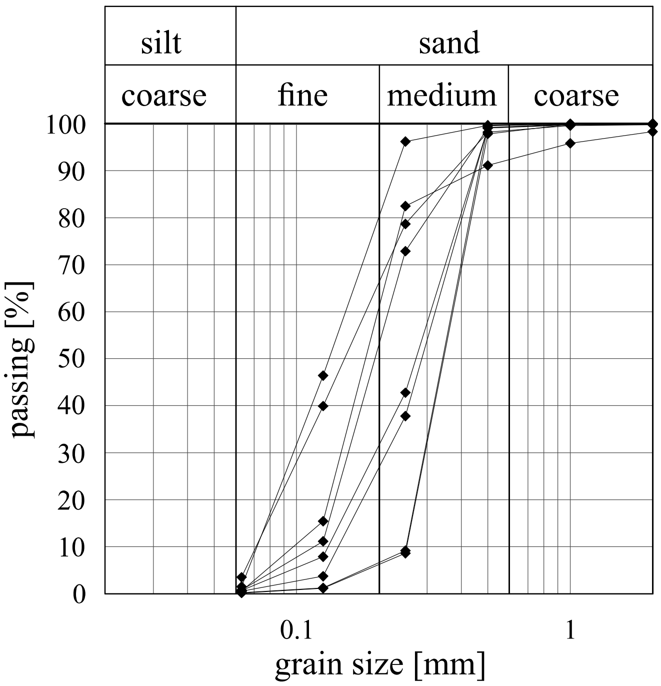

Figure 3. Fine to medium sand size grain distribution curves from the investigated sand section (6.5-15 m).

3.2 *Downhole logging*

The active gamma density with two receivers and neutron logging were carried out in uncased, open polymer mud-supported boreholes with straight bore hole geometry. More details of the logging methodology can be found in Biryaltseva et al. (2016).

The quality of the active gamma calibration, which was based on sand and water standards was tested with wet bulk densities derived from undisturbed samples of cohesive layers from the same borehole. The maximum deviation in wet bulk densities of this test is 4.5 %, proving that the gamma probe has been well calibrated delivering data well

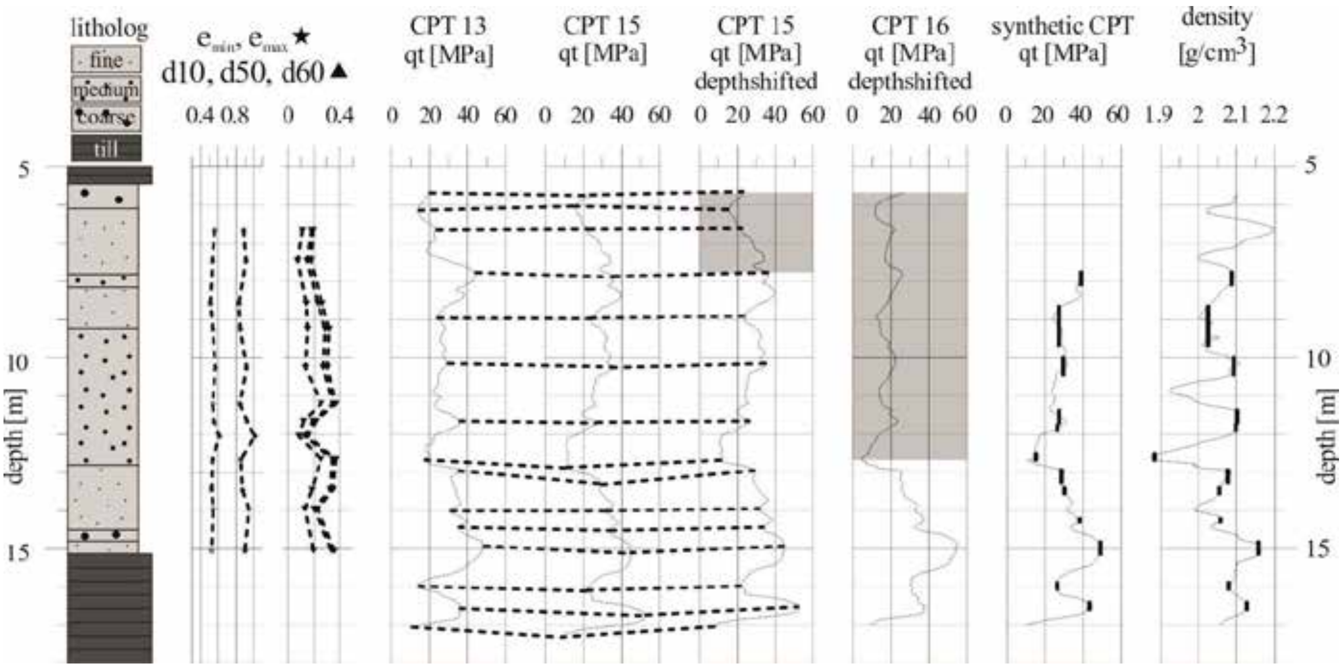

Figure 4. Data example of the investigation site LOG 1. The sequence of processing steps, correlation, depth shifting, data exclusion, establishment of a representative synthetic CPT profile and final extraction of matching averaged data pair intervals, is illustrated.

within its tool specifications. Derived wet bulk densities from the neutron porosity log showed to be less accurate and therefore were excluded from the further investigation. Averaged e_{min} and e_{max} values were used to convert wet bulk density values to relative densities (D_r).

3.3 *CPTu*

A total of 16 CPT each approximately 45 meter deep were carried out to identify and locate the soil section best suited for the study. Tests followed DIN EN ISO 22476-1, using a top driven 35 tons CPT unit and a Van den Berg 15 cm², fully digital 24 bit compression ICONE delivering data every 1 cm. Nine CPTs (including three repetitions) were carried out along a 2 m radius circle around the central logging boreholes, (Fig. 2). Two data sets of 3 CPTs and one downhole logging site each were selected and used for the further correlation process.

4 EXISTING EMPIRICAL RELATION

Equation (1) has been initially proposed by Schmertmann (1976).

$$D_r = (1/C_2) \cdot ln[q_c/(C_0 \cdot (\sigma')^{C_1})] \quad (1)$$

With σ' being effective vertical or mean stress [kPa], q_c - cone resistance [kPa] and C_0, C_1 and C_2 are empirical soil constants.

Baldi et al. (1986) established empirical constants for normally consolidated and over-consolidated sand using Ticino sand applying index densities according to ASTM. According to this formulation, an estimation of the relative density in normally consolidated sand requires only the knowledge of the vertical effective stress and the cone resistance. Soil constants are in this case given as: C_0= 157, C_1= 0.55, C_2= 2.41.Jamiolkowski et al. (2001) (cited in Mayne, 2007) proposed a correlation involving normalized cone resistance q_{t1} in in form:

$$D_r = 100 \cdot [A \ln q_{t1} - B] \quad (2)$$

With A=0.268, B= 0.675, where

$$\mathrm{q_{t1}} = \mathrm{q_t}/\sqrt{\sigma'_{\mathrm{vo}} \cdot \sigma_{\mathrm{atm}}} \quad (3)$$

In this case q_{t1} and σ_{atm} atmospheric pressure are measured in [bar], while q_t denotes cone resistance corrected for fluid pressure effects and is defined as

$$q_t = q_c + (1 - a)u_2 - \quad (4)$$

5 DEPTH CORRELATION

Due to local small scale lateral heterogeneities, e.g. dipping beds of fluvial bars, CPT data around the central logging locations were depth correlated using one of the circumference CPTs as a depth reference. The correlation made use of recognizable key points recognized in all 3 CPT profiles of each site (Fig. 4).

Afterwards, the three circumferential CPTs were combined to one depth shifted synthetic CPT profile with averaged tip values between correlation points (Fig. 4).

Intervals of strong inconsistent lateral variation marked with grey shadowed areas in Fig. 4 were excluded from the synthetic CPT forming procedure.

The density curve was smoothed and interpolated with moving average to achieve the same spatial frequency as the CPT profile. In a final step the density profile was correlated with the representative CPT profile using the same key point approach. Average values at plateaus and local maxima of q_c and ρ were calculated to form averaged matching pairs of cone resistance and density.

The final correlation step between averaged matching pairs of cone resistance and density focused on plateaus and trough to exclude the transitions zones which a higher margin of error in depth matching. The general sequence of processing steps is illustrated in Fig. 4.

6 RESULTS

The last two columns of Fig. 4 show the data intervals selected for the correlation approach, in the following referred to as the training data. The measured gamma-gamma density was converted to the relative density using averaged e_{min} and e_{max} values. In total 18 data pairs were established.

The training data were fitted to Equation (1) to determine new constants C_0, C_1, C_2. Since the horizontal stress in-situ is difficult to estimate only the vertical effective stress was used as a variable in the resulting function. The resulting relative density to cone resistance function is shown in Fig. 5.

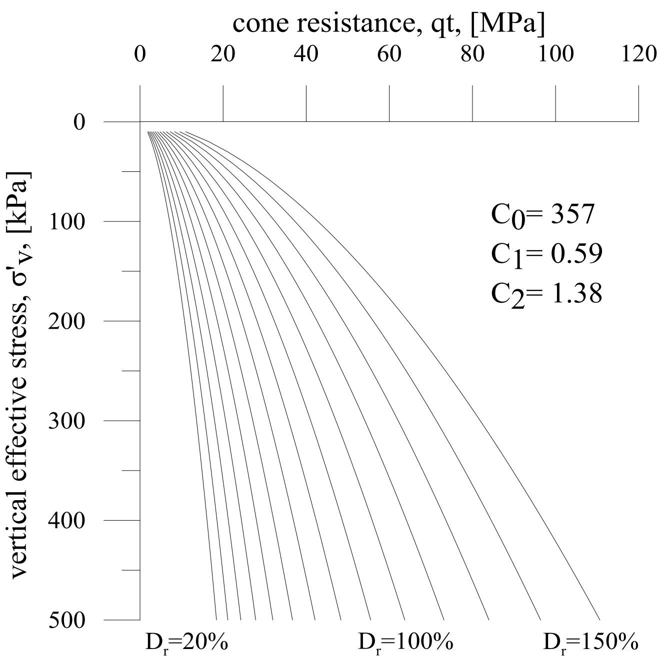

Figure 5. Relative densities as a function of vertical effective stress and cone resistance.

7 DISCUSSION

To evaluate the newly formulated relationship Fig. 6 shows established empirical relations applied to the training data. The relation by Jamiolkowski et al. (2001) seems to constantly underestimate the measured relative density values. The relation proposed in this study as well as the one by Baldi et al. (1986) provide comparable results with the new relation being more progressive in having a tendency to produce comparable higher relative densities per interval tip resistance increase.

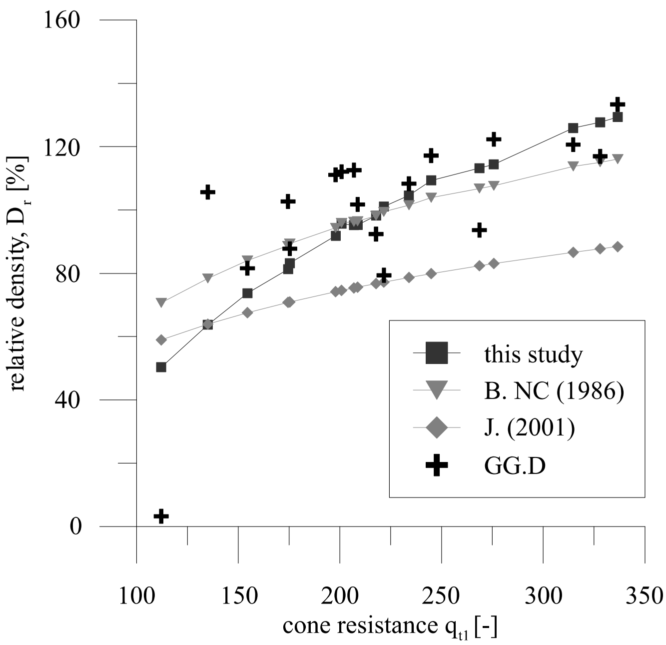

Figure 6. Relative density estimated from the measured gamma-gamma density (GG.D) (crosses) and comparison of literature transfer functions with results of this study (squares). The cone resistance is given as dimensionless q_{t1} to simplify the visual comparison. Existing empirical relations proposed by B. NC (1986) – Baldi et al. (1986) for normally consolidated sand; J. (2001) – Jamiolkowski et al. (2001).

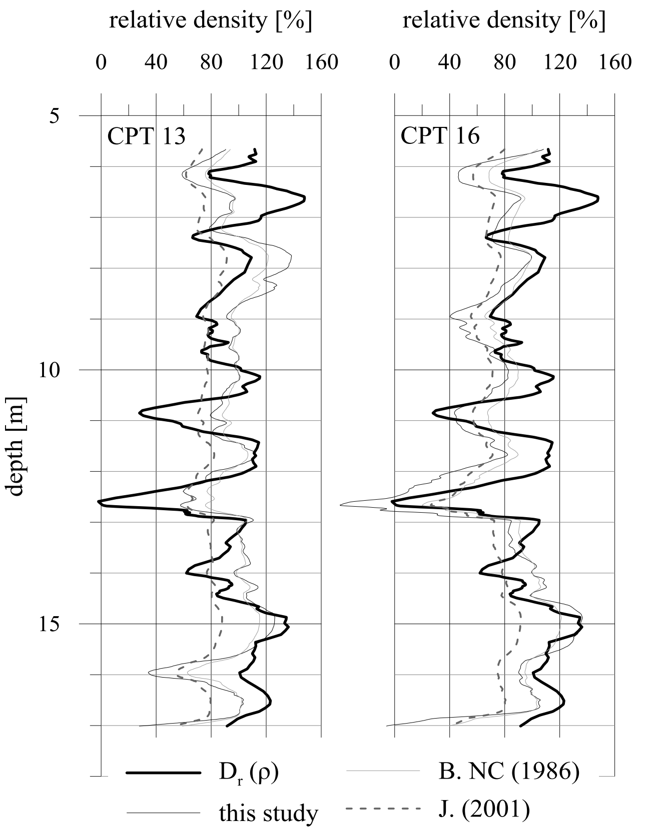

Figure 7. Application of the proposed and existing empirical relations to CPT data in comparison to logging derived relative densities D_r. B. NC – Baldi et al. (1986) for normally consolidated sand; J – Jamiolkowski et al. (2001)

The correlation by Baldi et al. (1986) seems to fit the training data better for low normalized stresses while the proposed new correlation seems to better capture the data with $q_{t1} > 200$.

Fig. 7 shows relative densities estimated from measured cone resistance profiles of the same overconsolidated strata using existing empirical relations and the empirical relation proposed in this study. Again the correlation by Jamiolkowski et al. (2001) mainly underestimates the measured values. The proposed correlation is in a good agreement with the correlation for normally consolidated sand after Baldi et al. (1986). Both correlations show a slight tendency toward a D_r - overestimation but provide an overall fairly acceptable averaged representation of the measured relative in situ densities. Local heterogeneities (extreme values) are not captured by either correlation. Both Figures (6 and 7) demonstrate that high relative densities can occur in the shallow subsurface under moderate stresses and intermediate tip resistances.

The application of this function and strictly speaking all CPT transfer functions of course are limited to the sand material used for the development of the correlation.

Blaker et al. (2015) showed that the method for determining maximum and minimum dry unit weight influences the results of laboratory testing and therefore also causes the inconsistencies when determining relative density in-situ. DIN standard may provide a broader range of possible packing densities in comparison to ASTM. In the case of the same cone resistance, this would lead to lower relative densities for loose sands and higher relative densities for dense sands when calculated according to empirical relations based on ASTM. However even in this case the ASTM-based empirical relations provide more slowly increase in relative densities per interval cone resistance increase then the new proposed correlation.

Accuracy of the density logging may strongly affect the correlation results. According to information from the subcontractor conducted the density logging the difference between two consequently repeated measurements along the same profile, may be as big as 0.05 g/cm^3. For the considered site, this would lead to the differences of about 20% of the relative density. Moreover while using the correlations the influence of the disturbed zone around the borehole should be noted. Even in case of carefully prepared boreholes density changes in the surrounding soil can be expected. In contrast the CPT method is fully non-destructive in the sense that no changes of the soil structure occur prior measurement. However as noted by e.g. Lunne et al. (1997) the soil area beneath the cone influencing the results may be as large as several cone diameters in dense soils. Therefore none of the methods provide the punctual information about the soil and the results should be considered as an averaged value around the point of interest.

The modern trend toward ground investigations with no or only a reduced numbers of sample holes results in a dilemma when it comes to complex static or cyclic soil modelling. Especially in cyclic models when using the for instance the hypoplastic soil law introduced by Kolymbas (2000) the initial void ratio e_0 is of great importance. A back calculation from CPT data is often ambiguous when no matching sample material for e_{min} and e_{max} determination was collected. By using the data of our in-situ transfer approach the latter disadvantage is overcome as it enables the direct expression of the tip resistance of CPT in terms of porosities and vertical stress. (Fig. 8).

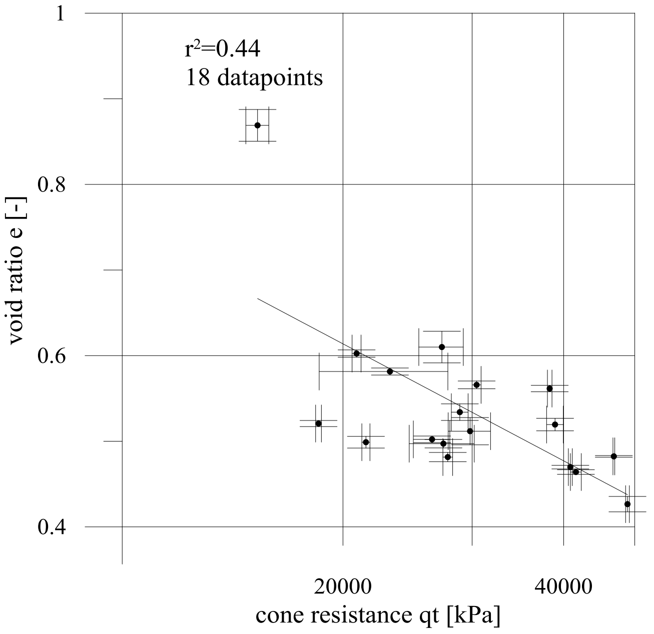

Figure 8. Measured void ratios as a function of measured cone resistance.

8 CONCLUSIONS

High variation in the relative density were measured using geophysical logging in an interval of well sorted, overconsolidated Pleistocene North Sea equivalent sands with constant relative density boundaries ($e_{\min}$-$e_{\max}$). An empirical relation among relative density, vertical effective stress and cone resistance was proposed based on in-situ cone resistance, gamma densities and laboratory estimations of minimum and maximum void ratios. Since in this new formulation D_r is solely related to the vertical effective stress no estimation of the horizontal stress is required. Development of the correlation based on in-situ data is an alternative and fast approach independent of boundary effects and stress state reproduction limits found in CPT test chamber studies. The relatively fast and economic approach is universal and may be applied to all sorts of settings and granular materials. The study was finished in approximately two month of work, which is way faster and more economic compared to year long experiments using CPT test chambers data to fill the D_r/stress matrix with sufficient data. However this study also shows that the complex soil physics during signal formation of cone resistance measurements is never a sole function of only packing density of the grains and construction projects with high stakes and risks should consider direct measurements using e.g. active gamma density logging giving likely far superior results in carefully prepared holes. Up to now the correlation was applied merely on the data from the same area where it was established. Application on further areas and comparison with additional density measurements will show the validity or usefulness of the newly found correlation.

9 REFERENCES

Baldi, G., R. Belotti, N. Ghionna, M. Jamiolkowski, & E. Pasqualini. 1986. Interpretation of CPT and CPTU; 2nd part: drained penetration of sands. In *Fourth International Geotechnical Seminar*: *143–156.* Singapour.

Biryaltseva, T., Lunne, T Kreiter, S., Moerz, T., Relative density prediction based on in-situ laboratory measurements of shear wave velocity. Submitted. *International conference of geotechnical and geophysical site characterization ISC'5.*

Blaker, O., T. Lunne, T. Vestgarden, L. Krogh, N. V. Thomsen, J. J. M. Powell, & C. F. Wallance. 2015. Method dependency for determining maximum and minimum dry unit weights of sands.

Bolton, M.D. and M.W. Gui. 1993. The study of relative density and boundary effects for cone penetration tests in centrifuge. *CUED/D-Soils/TR256*

Kolymbas, D. 2000. *Introduction to hypoplasticity*. Rotterdam: Balkema.

Kulhawy, F.H. and Mayne, P.W. 1990. Estimating Soil Properties for Foundation Design. *EPRI Report EL-6800, Electric Power Research Institute,* Palo Alto.

Lunne, T., Robertson, P.K., Powell, J.J.M. (1997). *Cone penetration testing in geotechnical practice.* Oxon: Spon Press.

Mayne, P. W. (2007*). NCHRP synthesis 368. Cone Penetration Testing. A synthesis of highway practice.* Washington, D.C.: Transportation research board.

Robertson, P., R. Campanella, D. Gillespie, & A. Rice. 1986. Seismic CPT to measure in-situ shear wave velocity. *J. of Geotechnical Engineering Division*, ASCE 112(8), 791–803.

Robertson, P. & K. Cabal. 2012. *Guide to cone penetration testing for geotechnical engineering*. Signal Hill: Gregg Drilling and Testing, Inc.

Schmertmann, J. H. 1978. *Guidelines for cone penetration test, performance and design.* Report FHWA-TS-78-209, U.S. Department of Transportation. Federal Highway Administration.

Geotechnical and Geophysical Site Characterisation 5 – Lehane, Acosta-Martínez & Kelly (Eds)

Relative density prediction based on in-situ and laboratory measurements of shear wave velocity

T. Biryaltseva
Fraunhofer Institute for Wind Energy and Energy System Technology, Bremerhaven, Germany

T. Lunne
Norwegian Geotechnical Institute, Oslo, Norway

S. Kreiter & T. Mörz
MARUM Center for marine and environmental science, Bremen University, Bremen, Germany

ABSTRACT: Extensive laboratory and in-situ testing has been carried out in an onshore test site on the North Sea Coast near Cuxhaven, Germany. The test site was chosen due to initially high cone resistance (>30 MPa) in sand and close stratigraphic links to North Sea offshore wind soil conditions. The in-situ program included cone penetration testing, geophysical downhole logging and sampling. A correlation between relative density, shear wave velocity and mean effective stress is proposed based on laboratory measurements with bender elements under anisotropic stress conditions. The proposed correlation is applied on in-situ shear wave velocity data and compared with relative density estimated over density logs and recognized empirical CPT correlations. Taking the density logging as a reference, the new correlation provides comparable accuracy range as the existing empirical CPT-based relations although with a slight tendency to underestimation. This novel correlation could be used as an alternative and conservative verification procedure for the relative density of sands.

1 INTRODUCTION

In geotechnical practice it is very difficult and frequently impossible to obtain undisturbed sand samples. As the geotechnical design parameters rely on laboratory tests, sand specimens have to be reconstituted in the laboratory to an estimated in-situ relative density. Reconstitution of the samples has in turn to be based on interpretation of in-situ tests. The most common technique to estimate the in-situ relative density (D_r) is to interpret the cone penetration test results using internationally recognized empirical correlations based on large calibration chamber tests (e.g Jamiolkowski et al. 2003, Baldi et al. 1986). Uncertainties in the D_r -estimation cause a wide variation of expected in-situ soil behavior, which can lead to a conservative and uneconomic foundation design.

Research is being carried out for establishing reliable methods for estimating relative density from other in-situ tests. One approach is the measurements of in-situ shear wave velocities. Such measurements can be made using suspension logging (P-S-logging) which provide velocities of compressional (V_p) and shear (V_s) waves, other techniques include seismic cone penetration test (SCPT) (e.g. Robertson et al. 1986) and measurement of surface wave velocities (e.g. MASW) (Long and Donohue 2007). Wave propagation velocities depend on the mechanical properties of the media and therefore are intrinsic soil parameters.

In this study a correlation developed among D_r, V_s and effective stresses in laboratory is applied and validated at a location with available P-S-logging, CPT and density log data. The question whether cone resistance (q_t)-based and the V_s-based correlations provide comparable results and the reasons in case of discrepancies are discussed.

2 STUDY AREA

The study area is a sand pit in operation located south of the town Cuxhaven in Northern Germany, close to the North Sea coast. (Fig. 1). Prior to the testing described here initial CPT screening was performed to identify sand layers with cone resistance values over 30 MPa. During further sand recovery in the pit 18 m of sand were excavated and the described work was carried out from the floor of the excavated area, in the following referred to here as the ground level.

In order to verify a laboratory-based correlation with in-situ data the chosen field site has to fulfill the following criteria: i) grain size distribution and grain shape and void ratios comparable to laboratory samples ii) water-saturation iii) bulk density variations over depth as a function of packing.

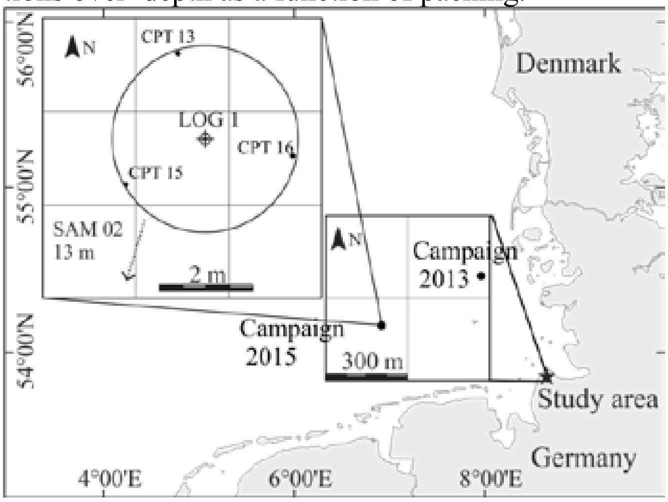

Figure 1. Study area, locations investigated in 2013 and 2015 with an example of the spatial configuration of CPT, downhole logging and sampling boreholes. Campaign 2013 included first screening CPTs and sampling of 2 m^3 of sand for additional Bender Element investigation. Campaign 2015 included CPT, downhole velocity and density logging, as well as sampling for application of the new proposed correlation.

3 METHODS

3.1 *Sampling*

Two sampling campaigns were carried out in the sand pit. During the Campaign 2013 (see Fig. 1) 2 m^3 of sand were recovered from an outcrop in the sand pit corresponding to the layer with initial q_t=40 MPa. After sand excavation this layer can be seen between 0 and 4 m below ground level (mbgl) in Fig. 3. The sand was carefully mixed and two batches were taken for subsequent laboratory testing. Grain size distributions (Fig. 2) and minimum and maximum void ratios (e_{min}, e_{max}) were measured according to NGI and DIN procedures. (Table 1)

Table 1. Grain size properties of CUX sand. * marked samples were used for V_s measurements (Campaign 2013). Parameters according to NGI procedures are used for establishing the correlation. Grain density was measured to ρ = 2,675 g/cm^3 (2013). DIN values are given for comparison.

Sample, Method	d_{10} mm	d_{50} mm	d_{60} mm	C_u /	e_{min} /	e_{max} /
CUX, DIN*	0.125	0.23	0.26	2.08	0.55	0.84
CUX, NGI*	0.12	0.255	0.26	2.17	0.55	0.81
5-17 m, DIN	0.15	0.25	0.28	1.79	0.54	0.89
22-30m , DIN	0.37	0.93	1.12	2.96	0.37	0.67
30-38m, DIN	0.25	0.37	0.4	1.57	0.5	0.88

Campaign 2015 included grain size analyses and e_{min}, e_{max} measurements according to DIN. The data shows three uniformly graded deposits with consistent grain size distributions and near uniform index void ratios. (see Table 1).

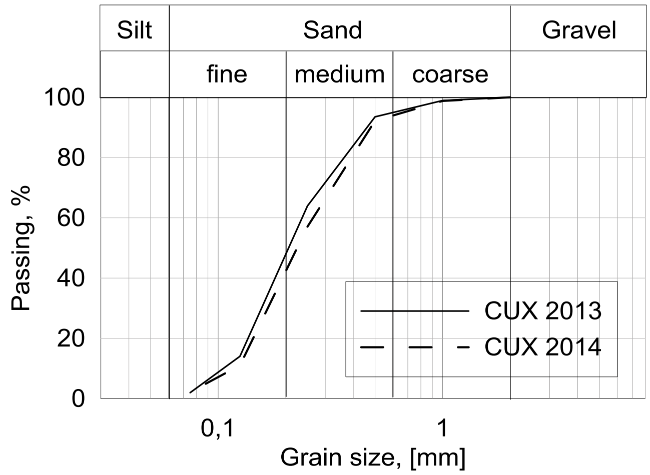

Figure 2. CUX. Grain size distributions of samples used for laboratory testing. Testing was carried out in two rounds in 2013 and 2014.

3.2 *Downhole logging*

The 40 m deep flush drilled borehole for geophysical logging was surrounded by three CPTs carried out at a distance of 2 m (Fig. 1). The sampling borehole was situated 13 m from the logging borehole. Downhole logging in the open, mud-supported boreholes included caliper, natural and active gamma as well as neutron porosity measurements and velocity logging.

3.2.1 *Density logging*

The applied active gamma logging probe utilizes a Cesium-137 source emitting gamma rays of about 0.66 MeV. Two scintillation crystal detectors are situated at distances of 15 and 35 cm from the source, which sets the vertical resolution to 20 cm. A shield prevents source photons from reaching the detectors without scattering. The depth of investigation is considered to be up to 15 cm behind the borehole wall. The in-situ data were captured every 5 cm. Prior testing the tool was calibrated with two known bulk densities of fresh water $\rho = 1.0\ g/cm^3$ and a sand $\rho = 2.05\ g/cm^3$. The quality of the calibration of the active gamma probe was tested with wet bulk densities derived from samples of cohesive layers from the same borehole. The maximum deviation in wet bulk densities of this test is 4.5 %. Derived wet bulk densities from the neutron porosity log showed to be less accurate and therefore were excluded from the further investigation.

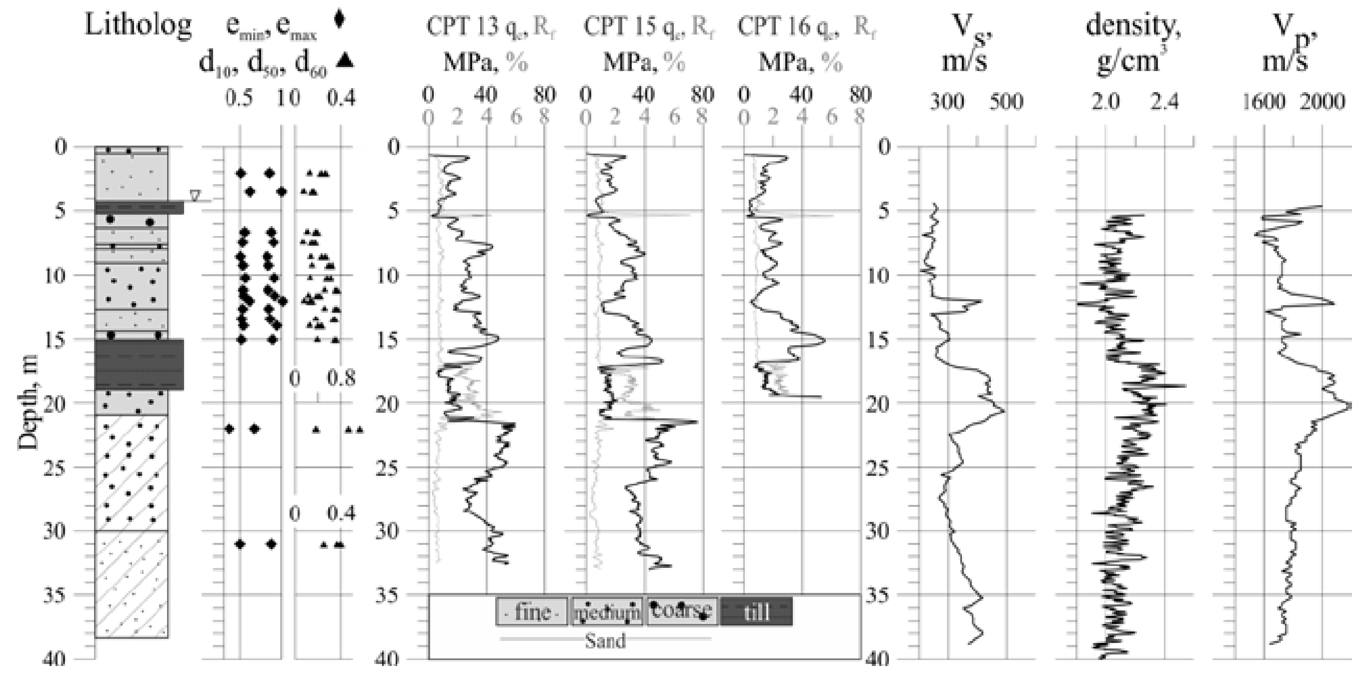

Figure 3. LOG1. Core description, index void ratios, in-situ CPT, P-S-logging and density log. Ground water level corresponds to the upper boundary of first till unit (approx. 4 mbgl) but may vary with precipitation. The till layers in the depth 4-5 mbgl and 15-19 mbgl are related to the older Saalian and Elsterian glaciation respectively.

3.2.2 *Velocity logging*

The downhole P-S-tool of Robertson Geologging Ltd contains a directional seismic source and two seismo-acoustic receivers separated by acoustic damping tubes. The seismic source produces a tube wave at the borehole wall with velocity close to the shear velocity of the formation together with a compressional wave. The waves are recorded with two 2D hydrophones spaced 1 m apart from each other. Sonic data were captured every 20 cm. (See Fig. 3.)

3.3 *CPTu*

The CPT readings were recorded every 1 cm with a 15 cm² van den Berg fully digital 24 bit compression ICONE. Details of the CPT campaign are described in the companion paper by Biryaltseva et al. (2016). The data are shown on Fig. 3. CPT, P-S-log and the density log were depth correlated with the core description. The depth velocity logging profile was taken as a reference.

4 ESTIMATION OF FIELD *OCR*

CPTu and cores reveal two till layers which are related to the older Saalian (Drenthe stadium) and Elsterian glaciation (Sindowski, 1965). Due to high sand content in the till material oedometer testing could not be applied to estimate the overconsolidation ratio (OCR). Therefore the minimum ice shield thickness during these glaciations was estimated as by Otto et al. (2011) to 150-180 m and 350-400 m respectively based on oedometer lab tests on stratigraphic equivalent material. The assumed ice shield thickness and the weight of original overlaying strata were applied to estimate the OCR. Further the coefficient of the earth pressure at rest (K_0) was calculated according to Mayne (2007):

$$K_0 = 0.192 \left({}^{q_t}/_{\sigma_{atm}} \right)^{0.22} \left({}^{\sigma_{atm}}/_{\sigma'_{v0}} \right)^{0.31} OCR^{0.27} \qquad (1)$$

Exemplary results are shown in Table 2.

Table 2. Estimation of OCR. p'_c – preconsolidation stress, σ'_{v0} – vertical effective stress. Ground water level is given in Fig.3.

depth	p'_c	σ'_v	OCR	q_t	K_0
mbgl	kPa	kPa	/	MPa	/
10	1700	160	11	28	1.08
15	1700	210	8	49	1.05
23	3500	306	11	47	1.02
27	3500	352	10	34	0.87
30	3500	384	9	40	0.86
32.5	3500	412	9	53	0.88

5 LABORATORY CORRELATIONS BETWEEN V_S, D_R AND σ'_v

5.1 *Triaxial testing*

The laboratory program was carried out at NGI and consisted of four static isotropically consolidated and six static anisotropically consolidated drained triaxial tests. Specimens for isotropic consolidation were prepared loose (D_r = 50 %), medium dense

(65 %), dense (80 %) and very dense (95 %) using the moist tamping (MT) technique (Ladd, 1978). Specimens for anisotropic testing were prepared at $D_r = 65$ %, $D_r = 80$ % and $D_r = 95$ %.

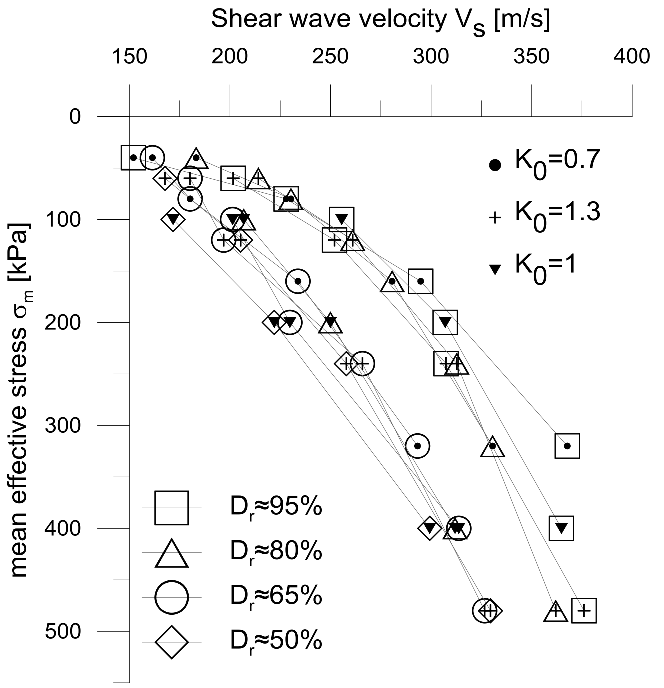

Figure 4. Laboratory test results. Measured shear wave velocity as a function of relative density and mean effective stress for isotropic and anisotropic consolidation. Two groups: dense (square and triangle) and medium dense (circle and diamond) can be identified.

A shear wave was triggered and received using piezoceramic bender elements (BE) placed at the top and bottom of the specimens. Detailed description of the bender element technique is given in Dyvik & Madshus (1985). V_s measurements were performed during consolidation at effective vertical stress of 50, 100, 200 and 400 kPa. To account for in-situ overconsolidation anisotropic consolidation in the laboratory was achieved with K_0=0.7 and K_0=1.3.

5.2 *Data fitting*

Analogous to the empirical formulation between cone resistance and relative density proposed by Schmertmann (1976) the dependency of the relative density on the shear wave velocity was assumed to be governed by the same structural type of equations:

$$D_r = \frac{1}{C_2} ln\left[\frac{V_S}{C_0 \cdot (\sigma_m')^{C_1}}\right] \tag{2}$$

With V_S shear wave velocity [m/s], σ_m' mean effective stress [kPa], D_r relative density in decimal representation.

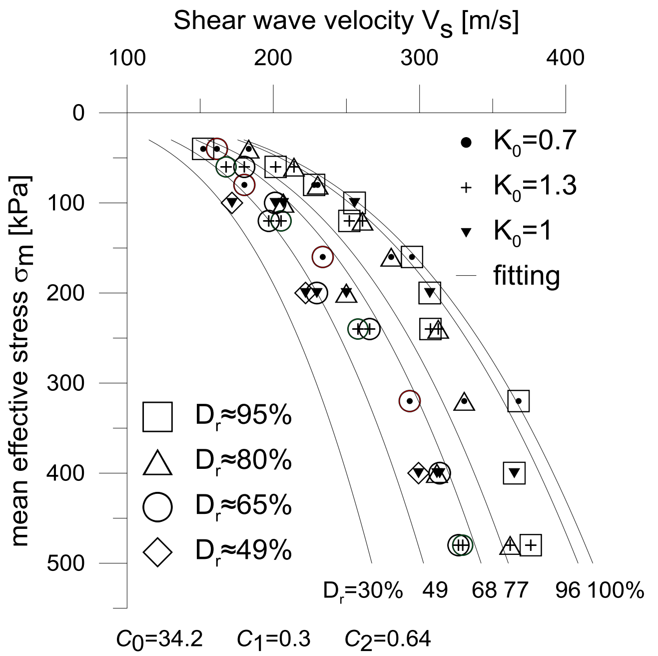

Figure 5. Proposed correlation among relative density, shear wave velocity and mean effective stress based on laboratory data. The derived empirical constants C_0, C_1 and C_2 are given.

The empirical constants were found as a solution of the optimization problem for the equation:

$$V_S = C_0 \cdot (\sigma_m')^{C_1} \exp(C_2 D_r) \tag{3}$$

At three relative densities ($D_r \approx$ 95, 78 and 68 %) eight measurements were selected for data fitting. The lowest density (approx. D_r = 49%) was not used due to small number of measurements. Measured data and fits are shown in Fig. 5.

6 APPLICATION TO IN-SITU DATA

The proposed $D_r(V_s)$ correlation as well as the $D_r(q_t)$ correlation after Baldi et al. (1986) for overconsolidated sand with C_0=181, C_1=0.55, C_2=2.61 were applied to the in-situ shear wave velocity and the cone resistance data respectively (Fig. 5). K_0=1 and K_0=0.85 were assumed for the upper and lower part of the profile. Averaged e_{min} and e_{max} values (Table 1) were used to convert measured wet bulk density values to relative densities.

Pairwise comparison of the measured and predicted data over the profile is summarized in Fig. 6. Very high in-situ measured relative density values and an overall large variability in the data should be noted. At 5-17 mbgl depth the predicted q_t-based and measured relative density are in good agreement. The $D_r(V_s)$ slightly underestimates the measured values.

In the depth 22-30 mbgl both empirical relations show comparable deviations against the in situ data. In the depth below 30 m both correlations underestimate the measured values. However the V_s measurements below 33mbgl show a tendency towards overestimation.

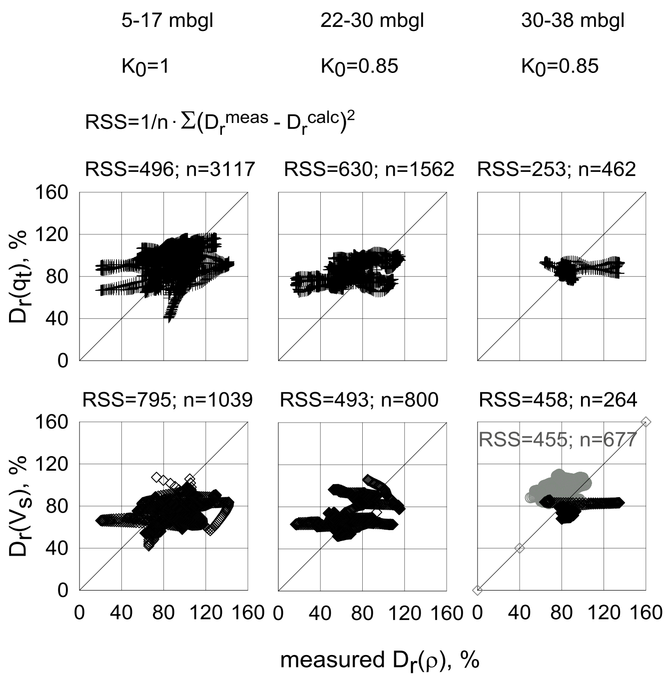

Figure 6. Comparison of measured (X-axis) and predicted (Y-axis) relative densities by Baldi et al. (1986) (above) and this study (below) for different sand layers throughout the profile with assumed K_0 values. Grey symbols represent the depth below 33 mbgl at which V_S but no q_t data are available. The derived relative density from gamma-gamma logging is based on assumption of fully saturated sand with grain density of ρ=2,675 g/cm^3. Residual sum of squares (RSS) is shown for every data set.

7 DISCUSSION

The discrepancies between the results of the $D_r(V_s)$ correlations with the measured data in the upper part of the profile may be explained with the stress dependency of the empirical relations. The partial derivative of Eq. (2) with respect to σ'_m is equal to:

$$\frac{\partial D_r}{\partial \sigma'_m} = -\frac{C_1}{C_2 \cdot \sigma'_m} \tag{4}$$

The derivative is inversely proportional to stress, meaning that the dependency decreases with increasing stress. Since the derivative also depends on the empirical constants the stress dependency of the proposed velocity correlation is higher compared to q_t-based correlation after Baldi et al. (1986). This can be explained with the different mechanisms of the cone penetration and V_s propagation. The cone penetration includes the stages of punching at shallow depth and extrusion at greater depth according to Emerson et al. (2008). These mechanisms provoke volume as well as shape changes in the surrounding soil. The shear wave velocity in turn depends on the grain-to-grain configuration.

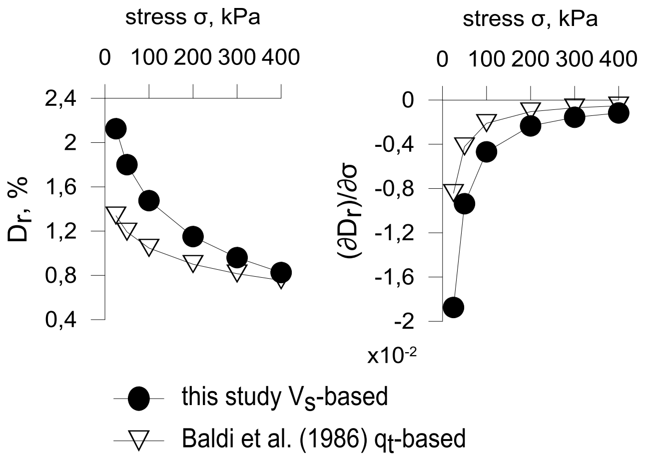

Figure 7. Left: Stress dependency of the proposed correlation (circle) and the CPT-based after Baldi et al. (1986). Right: Derivative of the relative density with respect to stress for both correlations.

For the proposed V_s-based correlation the choice of the K_0 is therefore shown to be more important than for q_t-based one, especially for low stresses under 100 kPa. The assumption about the coefficient of earth pressure at rest was made in this study based on Mayne (2007). This empirical relation was established using calibration chamber measurements on freshly pluviated sands and is considered to be a first estimate. K_0=1 leads to a good agreement among measured data and $D_r(q_t)$ in the pre-Saalian deposit. However the $D_r(V_s)$ underestimates the measured data. As discussed earlier this can be associated with different test mechanisms especially at shallow depth. Furthermore the form of the equation may also be not fully suitable for describing the $D_r(V_s)$ dependency.

Accuracy of the gamma density measurements in situ is found to highly influence the results. According to information from the subcontractor the difference between two consequently repeated measurements along the same profile, may be as high as 0.05 g/cm^3. For this sand this would lead to the differences of 20 percentage points in D_r. As the investigation depth is considered to be up to 15 cm behind the borehole wall even in a carefully prepared borehole the drilling can influence the density of the surrounding soil. Mud-cake and tool standoff are compensated using short and long transmitter receiver spacing but larger drilling induced irregularities may still have local effects on the measurement. Furthermore the void ratios calculated from the geophysical logging are sensitive to the specific gravity. Increase in specific gravity leads at constant bulk density to an increase in the void ratio and therefore to a decrease in the relative density.

Blaker et al. (2015) showed that the method for determining index void ratios influences the results of laboratory testing and therefore also causes the inconsistencies when determining relative density in-situ. In this study DIN standard provides a broader range of possible void ratios in comparison to NGI method. In the case of the same void ratio the correlation based on NGI method provides lower relative densities for loose sands and slightly higher relative densities for dense sands than a correlation based on DIN method. The ASTM method used for establishing the q_t-based laboratory correlations may also provide a narrower void ratio range than the DIN. However no measurements according to ASTM methods were carried out in this study, therefore no quantitative assessment is possible here.

The proposed V_s-based correlation was established on a medium-to-fine poorly graded sand. As a V_s-dependency on the C_u and the amount of angular particles was shown by Shin & Santamarina (2013), this correlation can strictly speaking be applied on the comparable soils only. Like any laboratory correlation the new relationship does not account for cementation and ageing effects. As discussed in Robertson and Cabal (2012) the shear wave velocity increases with age and cementation. Consequently the relative density of older deposits can be overestimated.

Due to probe configuration the shear wave velocity provides an average value over 1 m soil column, the cone resistance is measured every 2 cm. However as mentioned by Lunne et al. (1997) underlying layers may influence the cone resistance. Therefore none of the methods provide the punctual information about the soil and the results should be considered as an averaged value around the point of interest. In the investigated area neither CPT nor P-S-logging fully reflects thin loose layers.

8 CONCLUSIONS

A correlation among V_s, mean effective stress and D_r in form of an empirical equation based on laboratory bender element tests is proposed here for a medium-to-fine Cuxhaven sand. The correlation is found to be sensitive to the stress state, but an application of K_0 estimations provides a fairly acceptable slightly conservative estimation of the relative density in-situ. Compared to recognized CPT-based empirical relations applied to the same site the new found correlation is on the safe side.

The estimation of the site specific V_s-D_r correlations can be integrated into the laboratory program without high additional effort. The proposed correlation can easily be rewritten in terms of the small strain shear modulus G_{max} to provide an estimation of the G_{max} changes with relative density. Although some shortcomings such as not accounting for the ageing effects and dependency of the predicted relative density on the stress state have to be mentioned, a potential of using the shear wave velocity as a backup procedure for estimating the relative density is shown. The significance and applicability of the proposed correlation has to be further investigated on more data with comparable sets of in-situ measurements.

9 REFERENCES

Baldi, G., R. Belotti, N. Ghionna, M. Jamiolkowski, & E. Pasqualini . 1986. Interpretation of CPT and CPTU; 2nd part: drained penetration of sands. In *Fourth International Geotechnical Seminar*: *143–156.* Singapore.

Biryaltseva, T., T. Moerz, S. Brandt, S. Kreiter, U. Gerdes & B. Ossig. 2016. Relative densities and void ratios derived from CPT data using in situ field calibration. *ISC'5. In Press.*

Blaker, O., T. Lunne, T. Vestgarden, L. Krogh, N. V. Thomsen, J. J. M. Powell, & C. F. Wallance. 2015. Method dependency for determining maximum and minimum dry unit weights of sands.

Dyvik, R. & Madshus, C. 1985. Lab measurements of G_{max} using bender elements. *Advances in Art of Testing: soils under cyclic conditions, ASCE Annual Convention*: *186-196.* Detroit, Michigan.

Emerson. M., Foray, P., Puech, A. & Palix, E. 2008. A global model for accurately interpreting CPT data in sands from shallow to greater depth. In Huang & Mayne(eds.) *Geotechnical and Geophysical Site Characterization.:687-694* London: Taylor & Francis Group

Ladd, R.S. 1978. Preparing specimens using undercompaction; *GTJOAD*, 1(1), 16-23.

Lunne, T., Robertson, P.K., Powell, J.J.M. (1997). *Cone penetration testing in geotechnical practice.* Oxon: Spon Press.

Mayne, P. W. (2007*). NCHRP synthesis 368. Cone Penetration Testing. A synthesis of highway practice.* Washington, D.C.: Transportation research board.

Otto, D., Kreiter, S., Fan, W., Hepp, D.A., Mörz, T., 2011. Estimation of minimum Quarternary ice sheet thicknesses and relative chronology of intersecting buried valleys in the Southern North Sea. *XVIII. INQUA-Congress Quaternary sciences: the view from the mountains*, July 20-27, 2011, Bern.

Robertson, P., R. Campanella, D. Gillespie, & A. Rice. 1986. Seismic CPT to measure in-situ shear wave velocity. *J. of Geotechnical Engineering Division*, ASCE 112(8), 791–803.

Robertson Geologging. *PS Logger Operational Manual.* Robertson Geologging Ltd.

Robertson, P. & K. Cabal. 2012. *Guide to cone penetration testing for geotechnical engineering*. Signal Hill: Gregg Drilling and Testing, Inc.

Shin, H. & Santamarina, J.C. 2013. The role of particle angularity on the mechanical behavior of granular mixtures. *J. Geotech. Geoinviron. Eng*., ASCE, 139(2);353-355

Sindowski, K.-H., (1965). Die drenthestadiale Altenwalder Stauchmoräne südlich Cuxhaven. *Zeitschr. Dt. Ges. Geowiss.* 115, 158-162.

Schmertmann, J. H. 1978. *Guidelines for cone penetration test, performance and design.* Report FHWA-TS-78-209, U.S. Department of Transportation. Federal Highway Administration.

Geotechnical and Geophysical Site Characterisation 5 – Lehane, Acosta-Martínez & Kelly (Eds)
 ISBN 978-0-9946261-1-0

Strain moduli of alluvial soils from CPT, DMT, Vs, and lab tests

G. Bosco & P. Monaco
University of L'Aquila, L'Aquila, Italy

ABSTRACT: In situ and laboratory test data from normally consolidated alluvial soils, deposited along the Tevere River about 15 km from the coastline, are analyzed and compared. Attention is focused on the sandy and silty layers, for which CPTU, SCPTU, SDMT, Cross-Hole, identification and resonant column data are available. The aim is to search strain levels associated to DMT and CPT tests and also to derive moduli decay curves for practical use in soil-structure interaction analyses.

1 INTRODUCTION

A variety of geotechnical problems, such as settlement calculations and soil-structure interaction analyses under static and dynamic loading conditions, require adequate knowledge of the stiffness properties of each interacting soil layer. Because the response of soils to loading-unloading is markedly non linear, constitutive models must include decay curves in order to follow the variation of stiffness with varying strain beyond a nearly elastic state.

Following initial studies on the evaluation of soil stiffness and damping properties for use in dynamic analyses, several procedures have been proposed to derive moduli decay curves from in situ test data. To this aim, it has proven quite effective to combine laboratory results, even from few samples, with extensive seismic dilatometer and cone (SDMT, SCPTU) profiling, supplemented by Cross-Hole and Down-Hole inside the boreholes. Laboratory tests should cover identification and cyclic loading, as in triaxial, simple shear, torsional and resonant column.

In this paper only data on well graded sandy and silty soils are analysed. They are part of investigation results from two sites, North and South of the right and left banks of the Tevere River, in the outskirts of Rome. Data include SDMT, SCPTU, CPTU, Cross-Hole measures, a large set of index properties, and the results of one resonant column test.

Test results have been analysed in pursue of various objectives. These include a comparison of soil stiffness from DMT and CPT; a comparison of shear wave velocity data from the down-hole measurements in SDMT and SCPTU and from the Cross-Hole results; an evaluation of the strain levels associated to DMT and CPT; the reconstruction of moduli decay curves for sandy soils from SDMT and Vs test data.

2 INVESTIGATION AND SUBSOIL PROFILE

The results of the in situ and lab tests used in this study are a fraction of the data retrieved during an extensive investigation program performed throughout the second half of last year. As shown in Figure 1, the investigated areas extend on both sides of the river. The southern area is enclosed within a hairpin bend of the stream; the northern one is split into four smaller sites, generally close to the right bank.

The investigation completed to date includes a total of 59 boreholes extended to maximum depth of 120 m, with core recovery by rotary drilling and casing, the retrieval of several samples, the execution of some SPT tests, of 13 SDMT and 30 SCPTU-CPTU tests, and 4 Cross-Hole to maximum depth of 120 m.

The piezocone was equipped with a porous stone inside the cylindrical part of the tip, above the cone, to measure u_2. A cylindrical module equipped with two receivers, to detect arrival of shear and compression waves, was also installed above the friction sleeve. An analogous module was installed above the blade to perform SDMT tests.

Samples for laboratory tests were retrieved using thin tube sampling in boreholes (intact) and by cutting portions of the cores extracted from the subsoil (disturbed); these disturbed samples were used to implement data on index properties and prepare reconstituted samples for drained direct shear tests.

Within the investigated area the elevation of the ground surface varies between 7.0 and 10.0 m a.s.l.

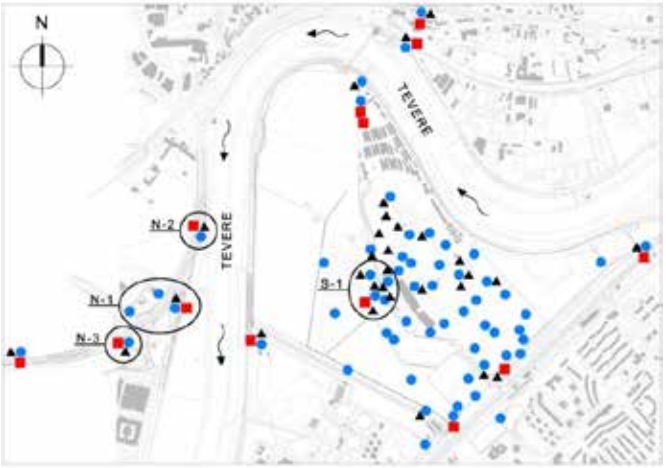

Figure 1. Investigation area and test sites used in this study

with minimal changes from the North to the South side of the river; thus the surface is essentially flat.

Data from boreholes and in situ tests reveal a thick alluvial deposit extending to depths of 55 m (North-East) and 65 m (South-West). It consists of layers of fine to medium coarse soils, silty clays and clayey silts, often mixed with organic matter, sandy silts and silty sands. In the top 20-30 m the predominantly clayey and silty soils are often mixed with organic clays and peat. At greater depths fine soils consist of horizontally layered silty clays and clayey silts containing fine sand; instead coarser strata are often interbedded with finer materials; the grain size spans from clayey silts with traces of sand to silty sands with moderate clay, and from silty sands with minor clay to slightly silty and slightly clayey sands.

The alluvial deposit covers a sandy gravel layer with thickness between 6-12 m on the northern side of the river and between 11 m (North-East) and 3 m (South-West) on the southern side. These coarse soils were deposited during the plio-pleistocene age atop a silty clay formation of comparable age; this fine soils deposit extends to great depths and includes thin layers of sandy and clayey silt.

At ground surface a thin layer of rubble, 1-2 m thick, and a layer of redeposited fine soils, 5-8 m thick, are encountered atop the alluvial deposit. The fine soils are highly overconsolidated as a result of desiccation and high suctions.

The distribution of pore water pressures with depth has been determined from measurements in standpipe and Casagrande piezometers and from recorded readings in electrical piezometers at four depths. Data agree well with the results of dissipation tests executed in the sandy layers during CPTU and SCPTU profiling. In essence a hydrostatic distribution can be assumed with a water table at an average depth of 7 m below surface.

This linear pore pressures increase and a constant unit weight of 19 kN/m^3 for soils above and below water table were used to analyse all test data.

The numerous lab tests provide a detailed identification of the different soils, with data on physical properties and also on the shear strength of the clayey and sandy soils. Combined information from borehole logs and in situ tests, allow detailed profiling and determination of shear strength and stiffness.

3 STUDY AREA NORTH OF THE RIVER

The investigation within this study area comprised a total of five boreholes, 4 of which drilled to 75 m and 1 to 85 m, the retrieval of 23 thin-tube and 16 disturbed samples from the sandy strata, three SCPTU to depths of 46, 48, 51 m, three SDMT to depths of 41, 46, 49 m, one Cross-Hole to 75 m.

One of the thin-tube samples was used for a resonant column test, to obtain a stiffness decay curve and values of damping with increasing shear strain.

Logs of boreholes show two stratigraphic conditions. At two locations (N-1, N-2) the alluvial deposit is entirely composed of sandy soils, including thin layers of fine materials and becoming finer at depths greater than about 35 m; at the third location (N-3) the top 16 m and the lower 20 m of the deposit consist of soft clayey silts and silty clays, while the central part (16-39 m) is essentially sandy in nature.

The grain size distributions of the 39 samples retrieved from the sandy layers are plotted in Figure 2. Despite the variability of the soil composition, it can be recognized that samples come from essentially sandy and silty layers with interbedded silty clays and clayey silts. In detail 11 samples contained less than 20% sand (d > 75 μm, retained by #200), 18 samples contained less than 50% silt and clay (d < 75 μm, passing #200), the remaining 10 samples are relatively well graded with a 50-70% content of particles finer than 75 μm. Accordingly 8 samples were non plastic, 6 samples had PI = 7-13%, 12 had PI = 15-24%, and 3 had PI = 29-34%.

The sample used for the resonant column contained 74% sand particles, 21% silt and 5% clay (d < 2μm), and was non plastic.

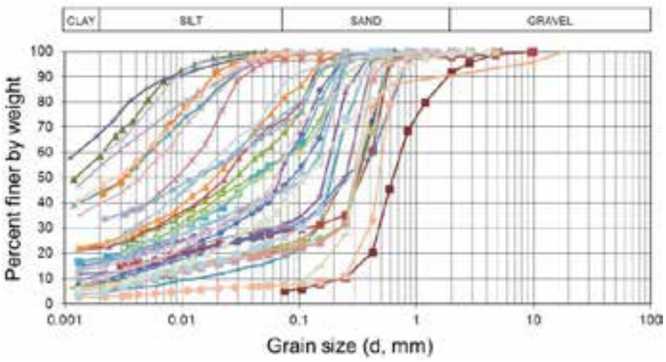

Figure 2. Grain size distributions of samples retrieved from sandy layers at the test sites on the North side of the river

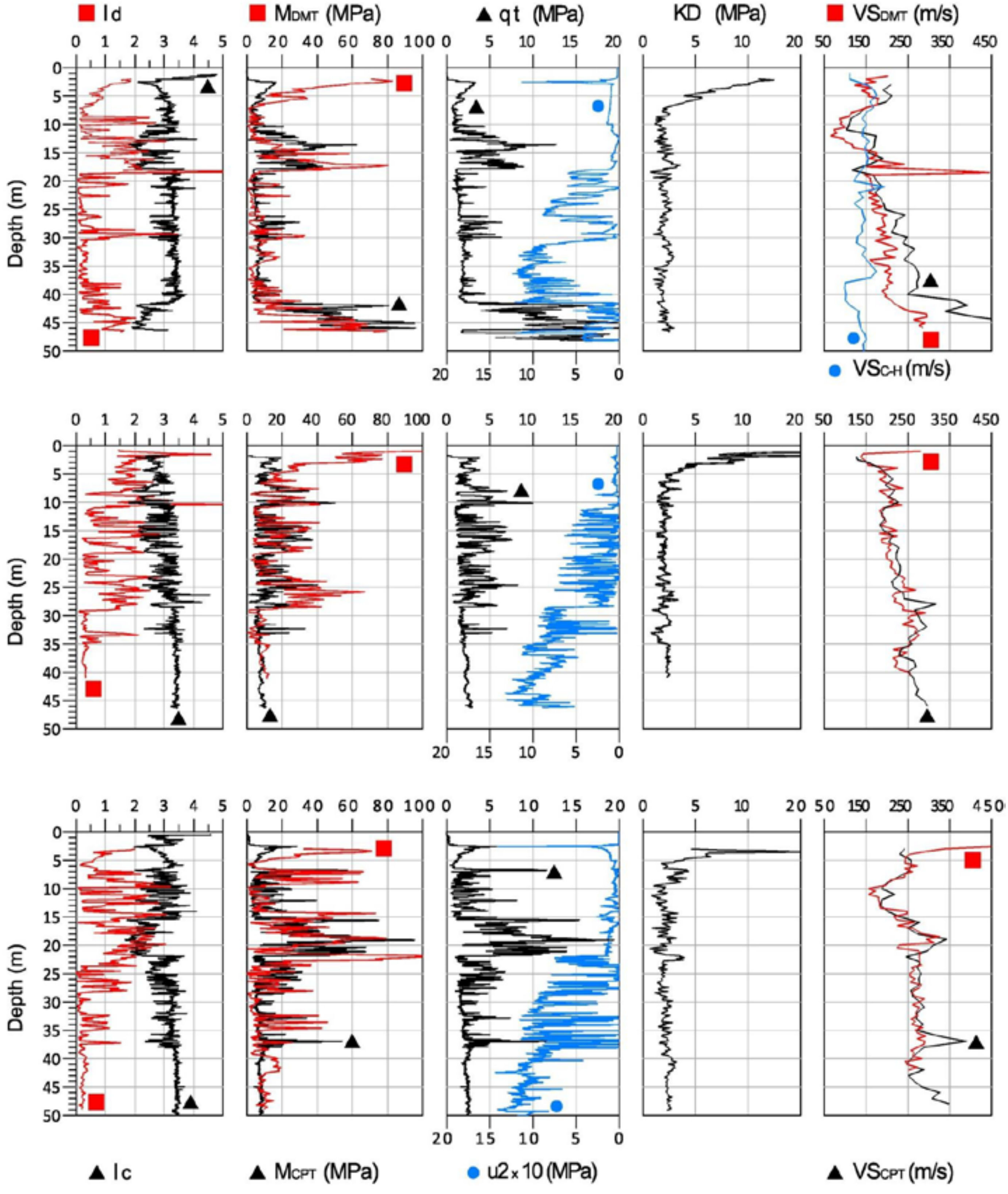

Figure 3. Comparison between values of measurements and of calculated parameters from SDMT, SCPTU, Cross-Hole tests from the three study sites on the North side of the river (N-1 top; N-2 centre; N-3 bottom)

Results of SCPTU, SDMT, Cross-Hole tests and values of calculated parameter are presented versus depth in Figure 3. The five plots of each row were drawn using data from each one of the three locations (N-1 top, N-2 centre, N-3 bottom). In each row these plots show the calculated values of I_c (Soil Behaviour Type Index from CPT-CPTU) and I_D (material index from SDMT), the constrained moduli (M_{CPT} and M_{DMT}), the data from SCPTU or CPTU (total cone tip resistance q_t, measured pore water pressure u_2 plotted by a factor of ten), the values of K_D (horizontal stress index from SDMT), and the velocities of shear waves (Vs) measured in the SCPTU, in the SDMT, and in the Cross-Hole test (only N-1). Calculations were performed using procedures described in the literature (Marchetti 1980; Robertson 1990); values of M_{CPT} have been determined using the relationship $M_{CPT} = 5\ (q_t - \sigma_{v0})$ with σ_{v0} total overburden at test depth (Mayne 2006).

The information on the type of soil, namely its behaviour with respect to drainage obtained from Ic and from Id is quite similar.

At the same time, values of the constrained modulus calculated from the cone (M_{CPT}) appear in good agreement with those obtained from the dilatometer (M_{DMT}), both in the fine and the coarse grained soils in the alluvial deposit.

A remarkably good agreement is noted between values of Vs measured along the SCPT and SDMT profiles. Instead both sets of values tend to diverge from the data obtained with the Cross-Hole test (location N-1). In this respect it shall be noted that in general the distance between the SCPT and SDMT profiles was less than 10 m; in addition, at location N-1 the two profiles are close to the borehole used for Cross-Hole testing. Thus, deviations between values of Vs measured with the two Down-Hole profiles and with the Cross-Hole test may originate from local variations in soil composition, density and resulting stiffness. It shall be noted, in fact, that in the upper 35 m all measurements agree quite well; visible minor differences may be due to local soil conditions.

4 STUDY AREA SOUTH OF THE RIVER

The investigation in the area on the South side of the river that was selected for this study (S-1) included the execution of three boreholes, 2 drilled to 60 m and 1 to 75 m, the retrieval of 21 samples from the sandy strata, 10 thin-tube and 11 disturbed samples, the execution of 4 CPTU to depths of 47, 55, 56, 59 m and 1 SDMT to a depth of 53 m.

The 3 boreholes and the 5 test profiles are enclosed within a limited area, in a radius of about 80 m. Data on shear wave velocities have been obtained from measurements along the dilatometer profile and from a Cross-Hole test; this test was performed in a borehole about 500 m away from the SDMT profile, but located within the same geological formation.

Logs of the four boreholes, including the one used for the Cross-Hole test, show similar stratigraphic conditions. The alluvial deposit comprises a top layer of soft silty clays, peaty clays, and clayey silts, extending to depths ranging from 17 m to 22 m, followed by a thick layer of sandy soils reaching an essentially constant depth of 60 m; at this depth the gravelly and sandy stratum is reached.

The grain size distributions of the 21 samples retrieved from the sandy layers are plotted in Figure 4. Once again the composition of the sampled material varies within a large interval, even if samples were retrieved from essentially sandy and silty soils. In essence, three types of material can be distinguished; in fact, 5 samples contained less than 20% sand (d > 75 μm), 10 samples contained less than 50% silt and clay (d < 75 μm), the remaining 6 samples are relatively well graded with a 50-70% content of particles finer than 75 μm. Accordingly 13 samples were non plastic, 4 had PI = 10-15%, 4 had PI = 15-24%.

In Figure 5 the results of the SDMT test are plotted versus depth and compared with data from one of the four CPTU located within the study area and with values of Vs. Shear wave velocity were obtained from the nearby Cross-Hole test.

As in the case of the three other study areas, values of I_c and I_D lead to essentially the same information with respect to soil type.

Instead, values of constrained modulus from the SDMT profile (M_{DMT}) tend to be smaller than those calculated from cone resistance (M_{CPT}), at least for the coarser portion of the sandy alluvium (depths 20 to 40 m). A better agreement is observed where the silty and clayey fractions become predominant, in the upper and lower layers of the deposit.

Values of M_{DMT} are aligned with similarly low values of K_D, comprised in the range 1-2 at depths greater than 20 m. Nonetheless, it shall be noted that K_D reflects the NC condition of the alluvial soils below the water table.

To a certain extent the differences between values of M_{CPT} and M_{DMT} may originate from thin layering and local variations of soil composition; these may produce the observed variability of q_t that shows high peaks and almost continuous oscillation between the lowest and highest range.

Such localized variations of stratigraphy and stiffness are not traced with the shear wave velocity measurements. In fact, values of Vs from SDMT and from the Cross-Hole test show a remarkably good agreement, despite the 500 m distance between the borehole and the dilatometer profile.

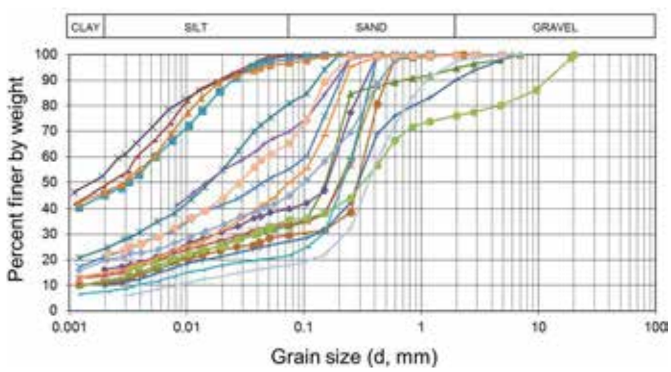

Figure 4. Grain size distributions of samples retrieved from sandy layers at the test site on the South side of the river

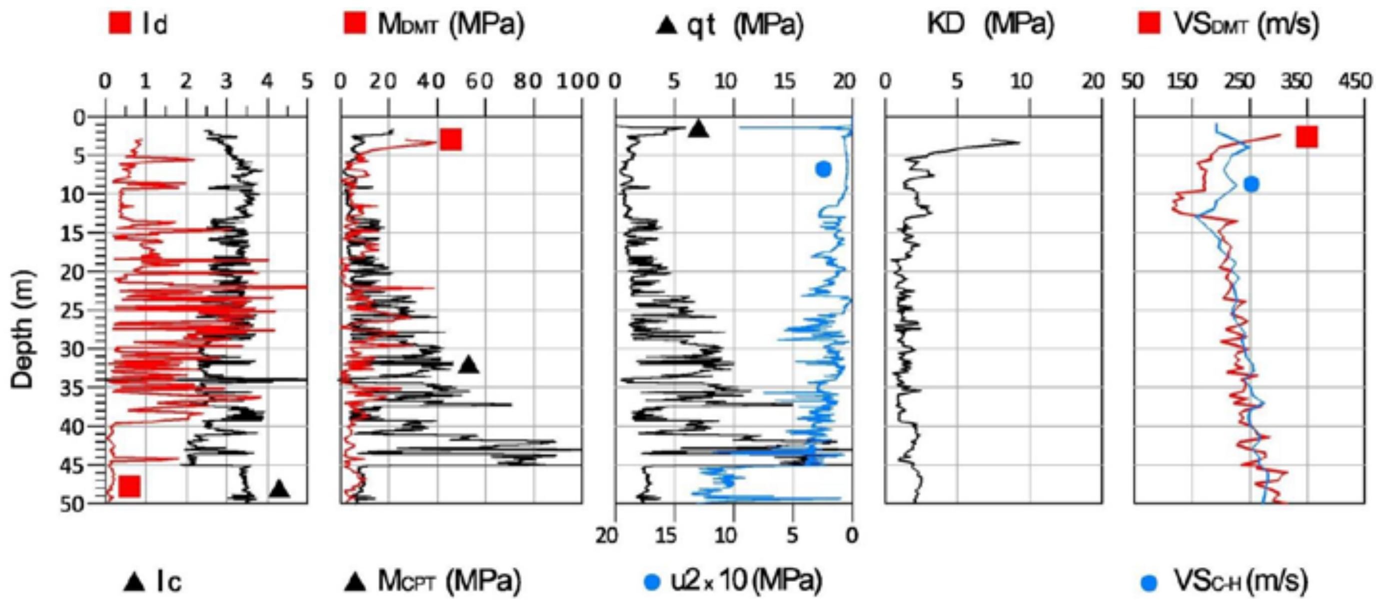

Figure 4. Comparison between values of measurements and of calculated parameters from SDMT, CPTU, Cross-Hole tests from the study site on the South side of the river

5 IN SITU G/G_0-γ DECAY CURVES FROM SDMT

A procedure to derive in situ curves depicting elemental soil stiffness variations with strain level from SDMT was originally outlined by Marchetti et al. (2008). Such decay curves could be tentatively constructed by fitting "reference typical-shape" laboratory G/G_0-γ curves through two points, both provided routinely by SDMT: (1) the initial *small strain* shear modulus G_0, obtained as $G_0 = \rho\ V_S^2$; (2) a *working strain* shear modulus G_{DMT} derived from the constrained modulus M_{DMT} obtained by the usual DMT interpretation. As a first approximation, the two moduli may be linked using linear elasticity formulae.

The effectiveness of the M_{DMT} estimation relies on a large number of well documented comparisons between measured and DMT-predicted settlements or moduli (Monaco et al. 2006).

To locate the second point on the curve it is necessary to know, at least approximately, the elemental shear strain corresponding to G_{DMT} (hereafter denoted as γ_{DMT}) along the G/G_0-γ curve.

Indications of values of γ_{DMT} in different soil types were presented by Amoroso et al. (2014); the Authors compared SDMT data with reference stiffness decay curves, from lab tests or back-calculated from real scale tests. The γ_{DMT} shear strains associated to the working strain moduli G_{DMT} typically range between 0.015-0.30 % in sand and 0.23-1.75 % in silt and clay.

Amoroso et al. (2014) proposed a hyperbolic stress-strain formulation (Eq. 1) for estimating the G/G_0-γ decay curve from SDMT data:

$$\frac{G}{G_0} = \frac{1}{1+\left(\frac{G_0}{G_{DMT}}-1\right)\frac{\gamma}{\gamma_{DMT}}} \quad (1)$$

At a given site, by introducing into Eq. (1) the ratio G_{DMT}/G_0 obtained from SDMT results and a "typical" shear strain γ_{DMT} estimated for the given soil type, it is possible to plot the corresponding G/G_0-γ curve.

Figure 6 shows the comparison between the G/G_0-γ curve obtained in the laboratory by resonant column (RC) test on the silty sand sample from study area N-1 and the G/G_0-γ curve obtained by Eq. (1) using data from the SDMT (N-1) at the same depth.

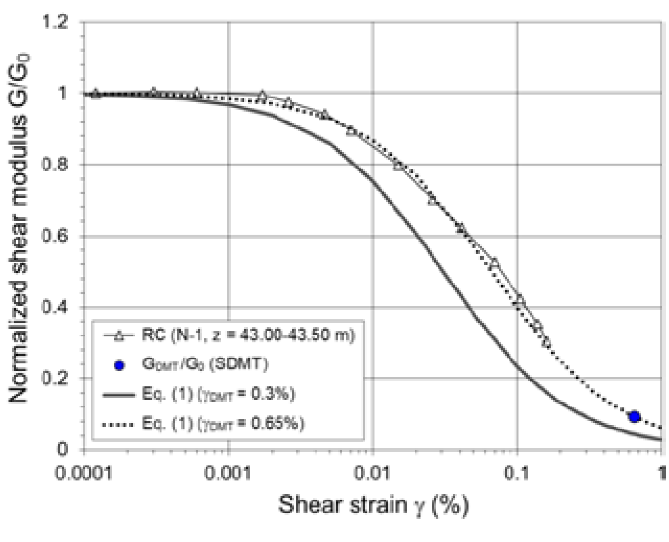

Figure 6. Comparison between G/G_0-γ decay curves obtained in the laboratory by resonant column test and estimated from SDMT by Eq. (1)

G_{DMT} was calculated from M_{DMT} assuming a Poisson's ratio $\nu = 0.2$. As indicated by Amoroso et al. (2014) for sands it was assumed $\gamma_{DMT} = 0.30\%$.

It can be observed that the hyperbolic G/G_0 -γ curve does not fit the laboratory RC curve. Instead a much better agreement is found by introducing $\gamma_{DMT} = 0.65\%$ into Eq. (1).

6 CONCLUSIONS

An analysis and interpretation of results from an extensive investigation performed through an alluvial plain, along the Tevere River is presented herein. The examined data were obtained from SDMT, SCPTU, CPTU, Cross-Hole and laboratory tests.

With the attention focused on the sandy soils encountered within the 60-70 m thick deposit originated by the river, one of the main objectives of this study was to compare SDMT, SCPTU, and Cross-Hole test results. Test results have been analysed to check the potential of the two procedures in reconstructing the stratigraphy of the site, determining stiffness properties of well graded silty and sandy soils for small and working level strains, reconstruct stiffness decay curve for use in practical problems, such as soil-structure interaction analyses.

Based on the analyses performed herein, it can be concluded that both SDMT and SCPTU are a reliable mean of investigation, even in largely variable soil conditions, typically occurring in thinly bedded alluvial deposits. In fact, the results of the two procedures appear well aligned and coherent with respect to soil identification and evaluation of stiffness at small strains; some discrepancies have been noted, however, with respect to the constrained modulus M, which corresponds to the higher strain levels that are reached in most geotechnical problems under working conditions. Based on the information available herein, it could not be understood, however, if the observed differences (M_{DMT} vs M_{CPT}) depended on the type of relationship adopted to calculate M, on differences in soil conditions between the two test profiles, on a specific layering of fine and coarse materials, on possible errors during testing, or a combination of such factors.

With respect to reconstructing moduli decay curves from in situ tests, it appears that further studies are required; these should be aimed at defining values of γ_{DMT} related to specific and well identified soil types, to reduce the ranges in which γ_{DMT} may vary, and to provide a firm link between one soil type and corresponding narrow range of γ_{DMT} values.

7 REFERENCES

Amoroso, S., Monaco, P., Lehane, B.M. & Marchetti, D. 2014. Examination of the Potential of the Seismic Dilatometer (SDMT) to Estimate In Situ Stiffness Decay Curves in Various Soil Types. *Soils and Rocks*, 37(3): 177-194.

Marchetti, S. 1980. In Situ Tests by Flat Dilatometer. *J. Geotech. Engrg. Div.*, 106(GT3): 299-321.

Marchetti, S., Monaco, P., Totani, G. & Marchetti, D. 2008. In Situ Tests by Seismic Dilatometer (SDMT). *From Research to Practice in Geotechnical Engineering*, ASCE Geotech. Spec. Pub. No. 180: 292-311.

Mayne, P.W. 2006. In-Situ Test Calibrations for Evaluating Soil Parameters. Invited overview paper, *Characterization and Engineering Properties of Natural Soils*, 3: 1602-1652. Taylor & Francis Group, London.

Monaco, P., Totani, G. & Calabrese, M. 2006. DMT-predicted vs observed settlements: a review of the available experience. *Proc. 2nd Int. Conf. on the Flat Dilatometer, Washington D.C.*, 244-252. R.A. Failmezger & J.B. Anderson (eds).

Robertson, P.K. 2009. Interpretation of cone penetration tests. A unified approach. *Canadian Geotech. J.*, 46(11): 1337-1355.

Geotechnical and Geophysical Site Characterisation 5 – Lehane, Acosta-Martínez & Kelly (Eds)
© 2016 Australian Geomechanics Society, Sydney, Australia, ISBN 978-0-9946261-1-0

Virtual T-bar penetrometer tests using Discrete Element Method

L.S. Carvalho, J.R.M.S. Oliveira, C.A.B. Vasconcellos & M.E.S Marques
Military Institute of Engineering, Rio de Janeiro, Brazil

M.G. Teixeira
Federal University of Rio de Janeiro, Rio de Janeiro, Brazil

J.A. Lukiantchuki
State University of Maringá, Maringá, Paraná

ABSTRACT: The Discrete Element Method (DEM) is an important tool to investigate soil-structure interaction problems involving dynamics and large strains. This technique can be applied to reproduce the behaviour of granular soils but can also be used to simulate the behaviour of very soft clay, where the material performs as a viscous fluid. Unlike the Finite Element Method (FEM), in the DEM the elements are discontinuous, allowing large strain simulations with no need for remeshing, which is a complex and time spending technique. In that way, a DEM software so-called VISED, was developed based on principles of equilibrium and interaction between the elements. The program algorithm is an adapted version of the software Munjiza-NBS and uses the following chain of processes: calculation of velocities and positions, contacts checking, calculation of contact forces and calculation of external forces and links. VISED takes into account two forces of contact between the elements: normal and tangential. The normal force uses as parameters: stiffness, damping, interpenetration between particles and velocity. On the other hand, the tangential force uses as parameters: stiffness, damping, velocity and dynamic friction. The links are calculated using an elastic perfectly plastic model, where an elasticity modulus, a yield stress and a limit strain are needed. The aim of this paper is to present a series of T-bar penetrometer virtual tests in order to evaluate the performance of the program. Thus, input parameters such as dynamic friction and damping were changed in a specific range to evaluate the influence of this variation in the final results. The final T-bar penetration test in the soil was compared with data from real tests in clays.

1 INTRODUCTION

The numerical modelling of soil behaviour is a very important tool to solve engineering problems, although quite challenging regarding some types of soils and loading conditions. That is the case of dry non-cohesive soils, where the material is clearly discontinuous and constituted of independent particles. Another example is the case of very soft clays, where regular loadings are associated with large deformations.

The Finite Element Method (FEM) is by far the most frequent numerical method applied for soil simulation in academy and industry. However, there are some restrictions associated with the simulation of problems involving discontinuous materials and large deformations.

In that way, the Discrete Element Method (DEM) shows up as a very promising tool due to some particular characteristics. The method is based on a number of non-deformable elements that constitute the material and these elements interact with each other through predefined bond conditions. When a limit condition is reached, the bond is broken and the elements are disconnected.

Thus, regarding situations where large deformations are expected, the numerical simulation is feasible with no need of any remeshing technique or equivalent procedure, once the elements are naturally rearranged in a new configuration.

The aim of this paper is to present a series of T-bar penetrometer virtual tests in order to evaluate the performance of the program. Thus, input parameters such as dynamic friction and damping were changed in a specific range to evaluate the influence of this variation in the final results. The final T-bar penetration test in the soil was compared with data from real tests in clays.

2 THE T-BAR PENETRATION TEST

The T-Bar penetration test was first developed as a mini tool to assess the undrained shear strength in reduced models in geotechnical centrifuge tests (Stewart & Randolph 1991). After a considerable number of modellings, a real size tool was developed and used in field tests (Stewart & Randolph 1994).

Academic applications of the T-bar penetrometer in Brazil were conducted by Macedo (2004) in a series of field tests in the very soft grey clay of Rio de Janeiro. The results were compared with piezocone and vane tests carried out at the same place, as well as triaxial tests with samples taken from the same site with very good agreement.

Jannuzi (2009) also conducted T-bar field tests in Sarapuí II site in Rio de Janeiro, which is a very well known deposit, also with very good agreement. The author concluded that the T-bar test is an important tool to assess the undrained shear strength continuous profile of very soft clay layers.

As far as the Brazilian centrifuge modeling scenario is concerned, Oliveira & Almeida (2010) conducted a series of centrifuge tests to evaluate the pore-pressure generation around the bar in cyclic T-bar tests on clayey soil. Oliveira et al. (2010) also investigated the influence of the T-bar penetration rate on the penetrometer resistance. Finally, Almeida et al. (2013) studied the variation of the bearing capacity factor of T-bar penetration tests at shallow depths in clayey soils.

The T-Bar tool itself is a 50 mm diameter and 200 mm length bar which is attached to an adapted piezocone rod as presented in Figure 1. The bar is pushed against the soil at a 2 cm/s rate and the soil resistance is measured through a load cell positioned at the rod just above the bar.

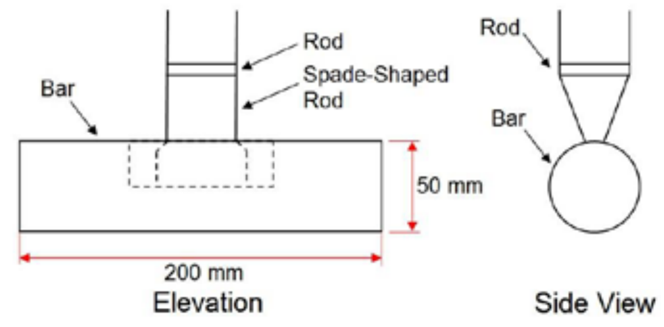

Figure 1. Field T-bar penetrometer (adapted from Stewart & Randolph 1994).

The undrained shear strength (S_u) is calculated using the limiting pressure on a circular surface in cohesive soil as proposed by Randolph & Houlsby (1984) in Equation (1), where P is the limit force acting on the bar, D is the bar diameter and N_b is the loading factor.

$$P = S_u \cdot D \cdot N_b \quad (1)$$

3 THE GEOTECHNICAL MODEL

The natural water content Brazilian coastal very soft clays are sometimes higher than its liquid limit, thus these soils behave as a fluid when remolded. When in fluid state the behavior of the Clay is mainly due to electrochemical forces between clay particles, water and ions that compose the soil. Mitchell (2005) proposes that the determination of these forces is very complex due to soil composition and the high variation of environmental factors that act during soil formation. However, Mitchell (2005) presented a qualitative analysis of the attraction and repulsive forces showing that when the particles interact, there is an attraction force increasing to a maximum value and then decreasing until changing to repulsive force, as seen in Figure 2.

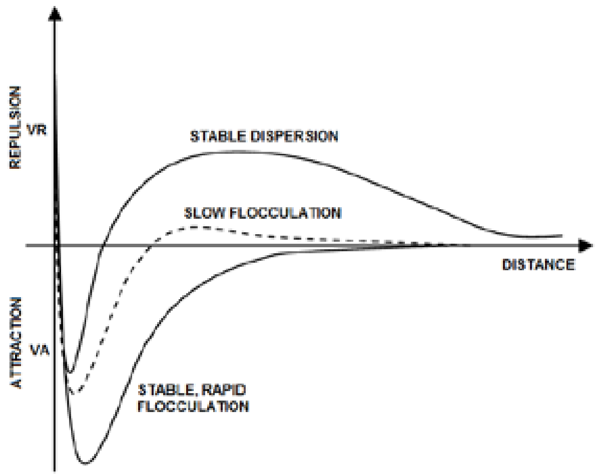

Figure 2. Interaction electrochemical forces between clay particles (after Mitchell, 2005).

From the numerical model point of view, it is not possible to consider the individual clay particles due to time processing. Therefore, an arrangement, where each discrete element is considered as a soil agglomerate composed by clay particles, water and ions, is proposed for the numerical model. The physical characteristics of the soil, as liquidity and cohesiveness are represented in the numerical model as field forces which will be discussed later.

4 THE VISED PROGRAM

4.1 *Introduction*

The Discrete Element Method visualization software – VISED 3.7, developed in C++ by Minato et al. (2009), uses the graphic library OpenGL© capable of generating graphics in real time with many effects such as texture and animation. The OpenGL Utility Tools (GLUT) is used to create special input and output features.

The software was initially developed to simulate materials that behave as discontinuous matter such as non-cohesive soils, but is also being used to emulate very soft soils in large strain conditions.

The numerical method adopted for the VISED 3.7 software is the discrete element method, which deals with each element as a rigid and independent particle. The elements interact with each other through predefined bond conditions.

Silva et al. (2011) presents a DEM simulation of the fall cone test using the VISED 3.7 software with good agreement.

4.2 *The Algorithm Procedure*

The software uses the interaction between particles and equilibrium principles to calculate the numerical solution. The developed algorithm combines four main processes: collision detection between particles; analysis of interaction forces between particles; fixations and external forces calculation; and new velocities and position calculation.

The collision detection between particles uses the Munjiza-NBS (No Binary Search) algorithm, described on Munjiza (2004), which employs direct mapping to detect contact between elements and thus compute the collision forces.

The interaction forces between particles can be divided in two components: contact forces and field forces. In this work, the field forces are modelled based on the Morse potential and will be discussed later.

The contact forces between particles have a normal and a tangential component. The normal component (F_n) uses as parameters the normal stiffness (k_n) associated with the elements interpenetration (u_n), and the normal dumping (c_n) associated with the normal component of the relative velocity between elements (v_n) as shown in Equation (2).

$$F_n = k_n \cdot u_n + c_n \cdot v_n \tag{2}$$

The tangential component (F_t) uses as parameters the minimum value of the force, calculated based on the tangential stiffness (k_t), and the force calculated based on the dynamic friction (μ), as shown in Equation (3). The tangential stiffness is associated with the tangential damping (c_t) and the tangential component of the relative velocity (v_t), while the dynamic friction is associated with the normal force (F_n),

$$F_t = \min\left[k_t \int v_t \cdot dt + v_t \cdot c_t ; F_n \cdot \mu\right] \tag{3}$$

The bond forces are generated by the deformations between the virtual bond elements which have an elasto-plastic behaviour. Therefore, the forces are calculated using the following parameters: the Young modulus (E), yield stress (σ_E) and the strain at rupture (ε_r). These parameters are input data for the program. In the case of the simulations presented in this work, the bond elements are not used and therefore not considered in the calculations.

The velocities and position calculations of each element are processed as solutions of the differential equilibrium equations $F = md^2u/dt^2$, based on the initial pre-established conditions. The algorithm uses the Central Differences Method (Krysyl & Belytschko 1998) to solve the equations numerically.

4.3 *Field Forces*

The program allows the implementation of many different ways of interaction forces between the elements, with intensity, direction and signal determined by the programmer.

This work adopted forces with intermolecular interaction characteristics, considering an attraction between the elements for distances greater than a minimum value and repulsion for distances smaller than the same minimum value. This behaviour is very similar to the one described by Mitchell (2005) and presented in Section 3.

The formulation of this interaction is based on the interaction force due to Morse potential which is an interatomic interaction model. The intensity of the force is obtained taking the derivative of the potential with respect to the distance between the elements. Equation (4) and Equation (5) show, respectively, the Morse potential and the interaction force between the elements, where: d is the depth of the potential and represents the dissociation energy (necessary energy to break the link between the elements); k is related with the width of the potential and has the dimension of m^{-1}; x is the distance between the centers of the elements; and $dist$ is the equilibrium distance, i.e., the distance between the elements where the force is zero.

$$E_p(x) = -d + d\left(1 - e^{-k(x - dist)}\right)^2 \tag{4}$$

$$E_p(x) = \frac{-dE_p(x)}{dx} = -2dk\left(1 - e^{-k(x-dist)}\right)e^{-k(x-dist)} \tag{5}$$

The force F_p acts in the direction of the vector that links the centers of the elements and might be positive, when the elements are being attracted, or negative, when they are being repulsed.

Figure 3 shows the intensity of the field force as a function of the distance between the elements. In this work, this force aims to emulate the interaction between the clay particles. The behaviour shown in Figure 3 is similar to the one shown in Figure 2. In that way, the field forces role the play of the clay particles electrochemical interaction forces as the main link between the clay particles.

The output of the VISED program is the frames sequence of the simulation and a text file, both saved in a rate predefined by the user. With the DAT file the program can shows an animation of the simulation.

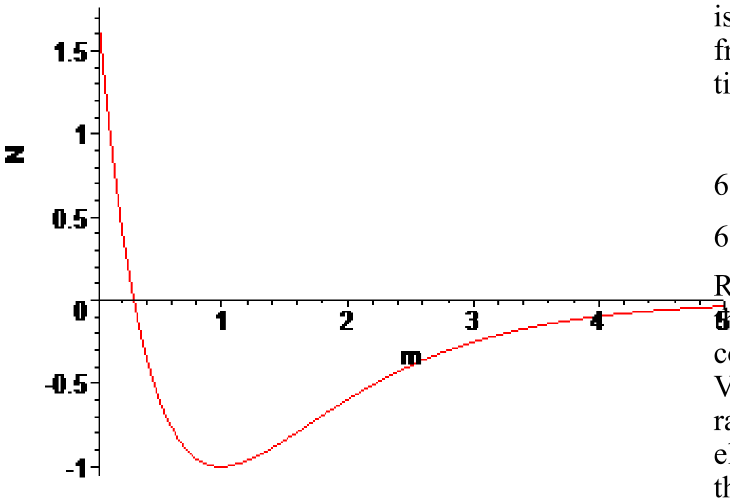

Figure 3. Field force with $dist = 0.3$, $k = 1$, $d = 2$ and $x = 5$.

5 SOFT SOIL CHARACTERISTICS

Brazilian coastal soft soils are very compressible, organic and with very low S_u values. The soil used for comparison with the simulations in this work is a very soft clay from Guanabara Bay, Rio de Janeiro State. Table 1 shows the soft clay parameters from several field and laboratory tests.

Table 1. Soft soil parameters.

Soil Parameter	Values
Plasticity Index (*PI*)	90% – 120%
Liquid Limit (w_L)	140% – 180%
Plastic Limit (w_P)	50%
Void Ratio (*e*)	3.6 – 4.5
Density of Grains (G_S)	2.49 – 2.68 kN/m^3
Specific Submerged Weight (γ')	2.5 – 4.5 kN/m^3
Coefficient of Consolidation (c_v)	3x10^{-8} – 5x10^{-9} m^2/s

Figure 4 shows the average S_u prototype profile for this clay from T-bar centrifuge tests carried out by Oliveira et al. (2010).

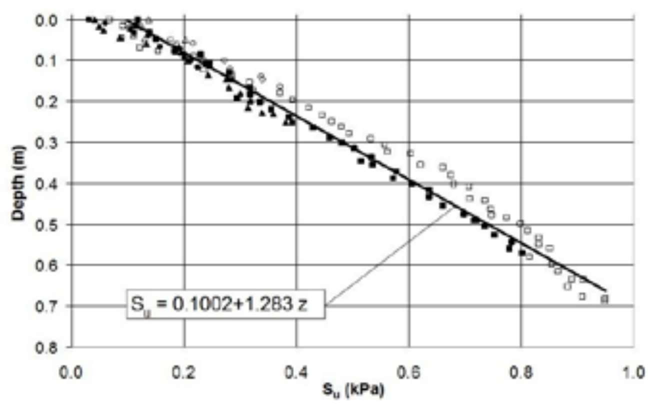

Figure 4. Prototype undrained shear strength profile from centrifuge tests (after Oliveira et al. 2010).

These soft soils are very heterogeneous and there is a scatter of the Young Modulus values obtained from several triaxial tests, thus the *E* values were estimated as $E = 300S_u$ (Oliveira et al., 2010).

6 DEM SIMULATION OF T-BAR TEST

6.1 *Model Dimensions*

Regarding the determination of the dimensions of the virtual model, it was necessary to take into account the time to achieve convergence when running VISED. This time of processing is function of the radius of the discrete elements as well as how many elements were used to represent the soil domain. In this particular case of study, a scale factor of N = 0.25 was found to be more appropriate once it would reduce processing time.

Thus, for a 4.4 m high by 1.0 m width soil domain, 5,920 discrete elements were used with a 10 mm radius each. The T-Bar (prototype diameter of 50 mm) was modeled as a sole discrete element with a 100 mm radius. All modeling relationships were considered when calculating results back from model to prototype scale.

6.2 *Contact Forces Input Parameters*

Table 2 presents the parameters VISED used to obtain the contact forces. The damping ($c_{n,t}$) value was adopted as proposed by Silva et al. (2011) and the Young modulus (*E*) was considered as function of the S_u value at 0.5m.

Table 2. Contact forces input parameters.

Parameter	Values
Submerged Specific Weight (γ')	3.5 kN/m^3
Young Modulus (*E*)	222 kPa
Yield Stress (σ_R)	4.94 kPa
Deformation at Rupture (ε_R)	0.022
Friction (μ)	0.05
Specific Submerged Weight (γ')	2.5 – 4.5 kN/m^3
Damping ($c_{n,t}$)	3.5 kg/s

6.3 *Field Forces Input Parameters*

The parameter *dist* was considered constant and equal to 4x10^{-2} m. This value, kept the elements, when subjected to a contact force, under space equilibrium, thus decreasing the number of elements necessary to occupy the same area of domain and decreasing processing time.

It was also considered for the computation of field forces a dumping parameter, proportional to the component of relative velocity between elements at the direction of the vector that connects the centers of these elements. This parameter (*h*), which is associated to relative velocity, is also called damping and has the same physical meaning as the damping used for computation of the contact forces.

Three different series of simulations were carried out varying *d*, *k* and *h* as shown in Table 3. The 36 tests were conducted with 5,920 discrete elements, and a single element representing the T-bar. The simulation time was 60 s and processing time was average 15h for the following computer configuration: Intel® Core ™ Quad CPU Q9550 @ 2.83 GHz, 3.24 GB RAM.

Table 3. Field force parameters.

Range = 0.1m k = 60 m^{-1} h = 500 kg/s *Dist* = 4 x 10^{-2} m		*Range = 0.1m* d = 5.2 x 10^{-2} J h = 500 kg/s *Dist* = 4 x 10^{-2} m		*Range = 0.1m* d = 5.2 x 10^{-2} J k = 60 m^{-1} *Dist* = 4 x 10^{-2} m	
Model	d (J)	Model	k (m^{-1})	Model	h (kg/s)
1.1	5.2 x 10^{-2}	2.1	30	3.1	1
1.2	5.4 x 10^{-2}	2.2	35	3.2	10
1.3	5.6 x 10^{-2}	2.3	65	3.3	50
1.4	5.8 x 10^{-2}	2.4	70	3.4	100
1.5	6.0 x 10^{-2}	-	-	3.5	550
1.6	6.2 x 10^{-2}	-	-	3.6	600
1.7	6.4 x 10^{-2}	-	-	3.7	650
1.8	6.6 x 10^{-2}	-	-	3.8	700
1.9	7.0 x 10^{-2}	-	-	3.9	750
1.10	7.5 x 10^{-2}	-	-	3.10	1000
1.11	8.0 x 10^{-2}	-	-	3.11	1250
1.12	8.5 x 10^{-2}	-	-	3.12	1500
1.13	9.0 x 10^{-2}	-	-	3.13	1750
1.14	9.7 x 10^{-2}	-	-	3.14	2000
1.15	10.5 x 10^{-2}	-	-	-	-
1.16	11.5 x 10^{-2}	-	-	-	-
1.17	30.0 x 10^{-2}	-	-	-	-
1.18	40.0 x 10^{-2}	-	-	-	-

7 RESULTS AND DISCUSSION

Figure 5 shows the discrete elements set for the T-bar depth ratios H/D = 50%, 75%, 100% and 125%. It was observed that the elements flowed around the bar as expected for a very soft clay soil.

For each virtual test a S_u profile was obtained and the tendency line for the computed data was compared with the expected profile line from Figure 4. Virtual tests and real tests were then compared by analyzing the angular coefficient (a) and the linear coefficient (b) of these profiles ($S_u = a.z + b$). Table 4 presents the angular and linear coefficients of the virtual tests for each model presented in Table 3.

Series 1 results show that the variation of the parameter d did not affect significantly the inclination of the S_u profile, i.e., the angular coefficient of the tendency line. However, model 1.18 was an exception with values much lower than the other ones. It was also observed that the increase of d parameter increased the dispersion of the S_u values, increasing the line R^2.

Regarding Series 2, the k values adopted for the tests 2.1 and 2.2 conducted to repulsion values lower than expected, causing superposition of the elements at the bottom of the domain.

Series 3 show that the increase in h caused an increase of the inclination of the S_u profile, as well as the R^2 of the tendency line, i.e., the dispersion of the data.

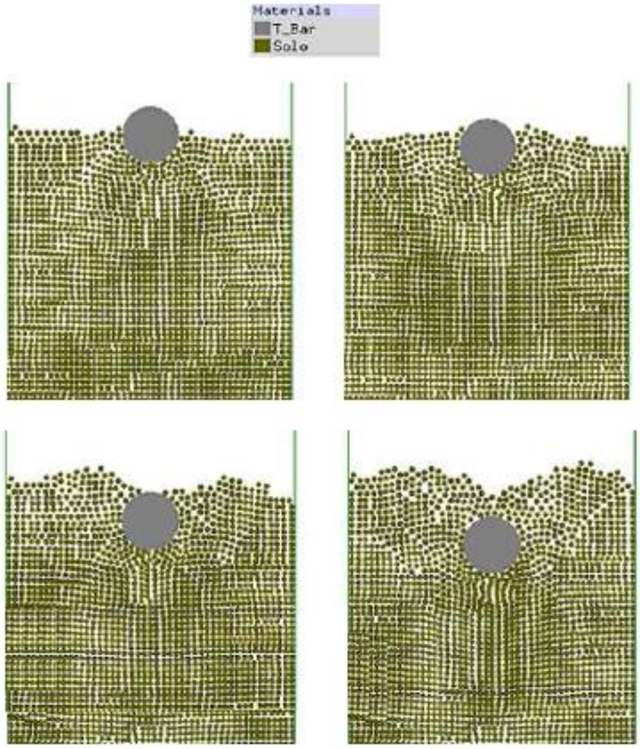

Figure 5. Visualization of a T-bar virtual test with depth ratios H/D = 50%, 75%, 100% and 125%.

Table 4. Results of the angular and linear coefficients for the virtual T-bar tests profiles.

Range = 0.1m k = 60 m^{-1} h = 500 kg/s *Dist* = 4 x 10^{-2} m			*Range = 0.1m* d = 5.2 x 10^{-2} J h = 500 kg/s *Dist* = 4 x 10^{-2} m			*Range = 0.1m* d = 5.2 x 10^{-2} J k = 60 m^{-1} *Dist* = 4 x 10^{-2} m		
Model	a	b	Model	a	b	Model	a	b
1.1	-0.71	0.12	3.1	-0.08	0.44	3.1	0.00	-0.11
1.2	-0.68	0.10	2.2	-3.44	-0.29	3.2	0.02	0.07
1.3	-0.75	0.14	2.3	-0.66	0.12	3.3	-0.02	0.09
1.4	-0.67	0.14	2.4	-0.66	0.09	3.4	-0.24	0.09
1.5	-0.64	0.14	-	-	-	3.5	-0.72	0.11
1.6	-0.71	0.08	-	-	-	3.6	-0.77	0.13
1.7	-0.73	0.14	-	-	-	3.7	-0.81	0.13
1.8	-0.76	0.10	-	-	-	3.8	-0.88	0.12
1.9	-0.69	0.14	-	-	-	3.9	-0.94	0.10
1.10	-0.66	0.12	-	-	-	3.10	-1.07	0.13
1.11	-0.64	0.13	-	-	-	3.11	-1.23	0.14
1.12	-0.64	0.11	-	-	-	3.12	-1.32	0.20
1.13	-0.70	0.13	-	-	-	3.13	-1.51	0.17
1.14	-0.64	0.14	-	-	-	3.14	-1.45	0.26
1.15	-0.64	0.11	-	-	-	-	-	-
1.16	-0.76	0.14	-	-	-	-	-	-
1.17	-0.70	0.15	-	-	-	-	-	-
1.18	-0.37	0.15	-	-	-	-	-	-

Figure 6 shows the output of the virtual test 3.11, which was the best result, along with its tendency line and the real test line, as shown in Figure 4. The tendency lines are almost coincident, although dispersion seems to be greater in the virtual data than in the real data.

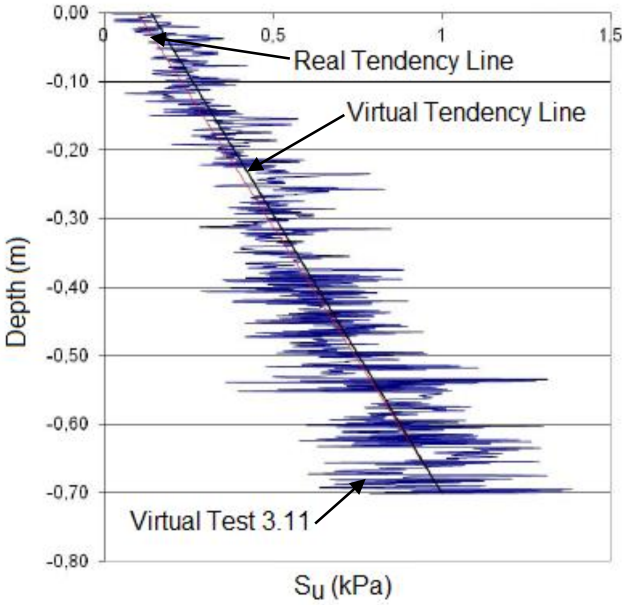

Figure 6. Result of the virtual test 3.11 along with its tendency line and the real test tendency line.

Graphic output files from VISED allow observation of the behaviour of the elements during the test. Figure 7 shows the formation of a triangle below the bar which stays in the same relative position while the other elements seem to flow around the pipe, as expected.

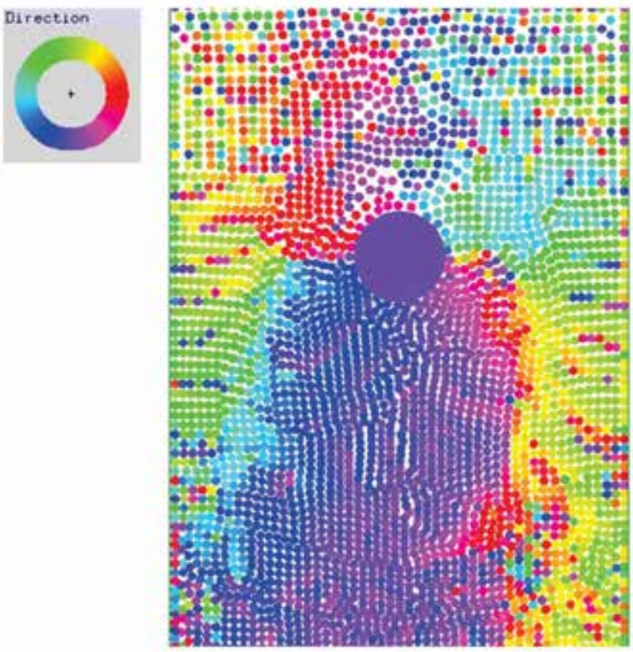

Figure 7. Visualization of the directions of the elements during a T-bar virtual test.

8 CONCLUSIONS

The use of field forces was fundamental to give the model soil cohesion characteristics which allowed virtual tests closer to real results. Although some data dispersion was expected, the virtual values show to be fairly more dispersive than the real ones. The parameters used in the analysis stays as the major problem once they are not classical geotechnical parameters and can be hard to evaluate.

The DEM method dealt with the large deformations problem without any difficulties and show to be a promising tool for geotechnical simulation of very soft soils, although further investigations are needed.

9 REFERENCES

Almeida, M.S.S., Oliveira, J.R.M.S., Rammah, K.I. & Trejo, P.C. 2013. Investigation of bearing capacity factor of T-bar penetrometer. Journal of Geo-Engineering Sciences 1, No. 1, 1–12, DOI 10.3233/JGS-13005.

Jannuzi, G.M.F. 2009. Characterization of the Sarapuí II soft soil deposit through field tests (in Portuguese). Federal University of Rio de Janeiro: M.Sc. Thesis.

Krysyl, P. & Belytschko, T. 1998. Object-Oriented Parallelization of Explicit Structural Dynamics with PVM. Pennsylvania: Computers & Structures, v. 66.

Macedo, E.O. 2004. Investigations of the in-situ undrained shear strength through cylinder penetration tests (in Portuguese). Federal University of Rio de Janeiro: M.Sc. Thesis.

Minato, K.K., Cantini, C.V. & Teixeira, M.G. 2009. Study and implementation of the Discrete Element Method. XXX Ibero-Latin-American Conference in Computational Methods in Engineering, Rio de Janeiro.

Munjiza, A. 2004 The Combined Finite-Discrete Element Method. London: John Wiley & Sons. ISBN 0-470-84199-0.

Oliveira, J.R.M.S. & Almeida, M.S.S. 2010. Pore-pressure generation in cyclic T-bar tests on clayey soil. International Journal of Physical Modelling in Geotechnics 10, No. 1, 19–24. DOI 10.1680/ijpmg.2010.10.1.19.

Oliveira, J.R.M.S., Almeida, M.S.S., Almeida, M.C.F. & Borges, R.G. 2010. Physical Modeling of Lateral Clay-Pipe Interaction. J. Geotech. Geoenviron. Eng. 136, No. 7, 950-956, DOI 10.1061/(ASCE)GT.1943-5606.0000311.

Oliveira, J.R.M.S., Almeida, M.S.S., Motta, H.P.G., & Almeida, M.C.F. 2011. Influence of Penetration Rate on Penetrometer Resistance. J. Geotech. Geoenviron. Eng. 137, No. 7, 695-703, DOI 10.1061/(ASCE)GT.1943-5606.0000480.

Randolph, M.F. & Houlsby, G.T. 1984. The limiting pressure on a circular pile loaded laterally in cohesive soil. Géotechnique 34, No. 4, 613–623.

Silva, V.M., Carvalho, L.S., Oliveira, J.R.M.S. & Marques, M.E.S. 2011 Virtual fall cone tests using Discrete Element Method. 14th Pan-American Conference on Soil Mechanics and Geotechnical Engineering, Toronto.

Stewart, D.P. & Randolph, M.F. 1991. A new site investigation tool for the centrifuge. Colorado: International Conference on Centrifuge Modeling. p. 531-538.

Stewart, D.P. & Randolph, M.F. 1994. T-Bar Penetration Testing in Soft Clay. Journal of Geotechnical Engineering 120, No. 12, p. 2230-2235.

Geotechnical and Geophysical Site Characterisation 5 – Lehane, Acosta-Martínez & Kelly (Eds)
© 2016 Australian Geomechanics Society, Sydney, Australia, ISBN 978-0-9946261-1-0

Correlations between SPT and CPT data for a sedimentary tropical silty sand deposit in Brazil

Y.D. Costa, E.S. Cunha & C.L. Costa
Federal University of Rio Grande do Norte, Natal, Brazil.

A. C. Pereira
Federal Institute of Education, Science & Tecnology of Rio Grande do Norte, Natal, Brazil.

ABSTRACT: This study aims at presenting correlations between the SPT blow count number (N_{SPT}) and results of CPT tests (tip resistance, q_c, and sleeve friction resistance, f_s) for a sedimentary silty sand deposit. Correlations were obtained for 88 SPT tests and eight CPT tests carried out in the construction site of the new football stadium of the City of Natal, situated on the Northeast region of Brazil. Field test data were analyzed using a simplified geostatistic approach. Correlations between SPT and CPT data were developed using semivariograms for defining influence zones at the site. The range calculated with the semivariograms was used in the selection of appropriate SPT boreholes to correlate with a specific CPT borehole. SPT data outside this range were discarded. Correlations between q_c and N_{60} with coefficients of determination larger than 0.7 were obtained following this methodology. A representative ratio q_c/N_{60} of 0.39 MPa was found for the investigated soil.

1 INTRODUCTION

The standard penetration test (SPT) is still the most commonly used in situ test for obtaining the required geotechnical parameters for foundation analysis and design in Brazil. A reason for that may be because of the lack of local availability of other better tests. Geotechnical engineers in Brazil are likely to request CPT tests only for moderate to high-risk projects. Because CPT tests are seldom requested in ordinary practice, local contractors do not offer them, and vice-versa. Robertson (2012) highlights the need of breaking such a cycle. Moreover, the low cost is also taken as another strong argument for choosing the SPT test.

Since in most situations only SPT data is available, the search for new SPT-CPT correlations is necessary. However, most of the available SPT-CPT correlations in Brazil have been established for soils of southern regions of the country. New local correlations for other soil types are therefore necessary.

This paper aims at presenting correlations between the SPT resistance number (N_{SPT}), cone tip resistance (q_c) and sleeve friction resistance (f_s) for a sedimentary tropical silty sand deposit in the Northeast Region of Brazil. The correlations were devised from the results of 88 SPT tests and eight CPT tests, which reached a maximum depth of 35 m in the subsoil.

2 CPT-SPT CORRELATIONS

Studies on correlations for estimating cone tip resistance (q_c) and sleeve friction resistance (f_s) from SPT data using statistical approaches have been conducted for a large variety of soil types (Schmertmann & Palacios 1979, Robertson & Campanella 1983, Kasim et al. 1986, Chan et al. 1988, Danziger & Velloso 1995, Politano 1999, Akca 2003, Kara & Gündüz 2010, Shahri et al. 2014). Statistical correlations based on linear regressions have been widely used, particularly for granular materials (Alonso 1980).

Table 1 presents a compilation of values of $k = q_c/N_{SPT}$ proposed for soils of southern regions of Brazil. It should be noted that some correlations in Table 1 were proposed using non-corrected N_{SPT} values for 60% energy.

Amongst the available correlations published in the literature, very few studies attempt to describe the statistical methods used for developing their proposed SPT-CPT correlations. Geostatistical concepts have been incorporated in more recent investigations. For instance, Akca (2003) presents a study conducted in the United Arab Emirates, which included results from 65 SPT borings and 101 CPT borings. SPT data were divided into two large groups according to their proximity from the CPT boreholes. For those SPT boreholes within a distance of 30 m from a specific CPT borehole, representative N_{60} values were calculated from the arithmetic mean of the data. The inverse distance weighting (IDW) method was employed in the analysis of the data from the SPT boreholes beyond this range.

Table 1. Values of k for Brazilian soils.

Reference	Soil	k (MPa)
Aoki & Velloso (1975)*	Sand	1.00
	Silty sand	0.80
	Clayey sand	0.60
	Silt	0.40
	Sandy silt	0.55
	Sandy clay	0.35
	Clayey silt	0.23
	Clay	0.20
Barata et al. (1978)*	Sandy silty clay	0.15 – 0.25
	Clayey silty sand	0.20 – 0.35
Danziger & Velloso (1986, 1995) Danziger et al. (1998)	Silt, sandy silt, sandy clay Sandy-clayey silt, clayey-sandy silt, silty-sandy clay,	0.48
	sandy-silty clay	0.38
	Clayey silt	0.30
	Clay, silty clay	0.25
	Sand	0.57
	Silty sand, silty clay	0.5 – 0.64
	Clayey silt	0.31
	Sandy clay	0.18 – 0.35
	Clay	0.45

*N_{SPT} not corrected for 60% efficiency

3 METHODOLOGY

3.1 *Site location and Geology*

The field data used as part of this research were collected from standard penetration tests (SPT) and cone penetration tests (CPT) conducted to investigate the subsoil for the project of the new football stadium of the City of Natal, Brazil. Situated in the Northeast Region of Brazil, Natal was one of the 12 host cities of the 2014 Football World Championship. Figure 1 shows the location of the investigated site.

Figure 1. Location of the investigated site.

The subsoil of Natal and neighboring areas is composed of colluvium and alluvial tertiary deposits of unconsolidated sand, clayey sand, and silty sand sediments with some laterization. Overlying the tertiary deposits are quaternary deposits of eolian sediments composed of quartz sands with fine to coarse grain sizes (Angelim 2006).

3.2 *Site investigation*

Eighty-eight SPT borings and eight CPT borings were carried out in an area of 45,100 m^2 where the stadium was constructed. Figure 2 shows the distribution of the CPT boreholes on the site within the limits of the stadium. The SPT borings are also distributed within the limits of the stadium.

The SPT boreholes reached maximum depths ranging from 15 m to 26 m. The N_{SPT} blow count number was collected within each meter below ground surface, and corresponds to the number of blows required to drive in the soil the last 300 mm of a 450-mm-long sampler. The SPT tests were performed in accordance with Brazilian Standard NBR 6484. SPT blow count numbers were corrected for 60% efficiency (N_{60}).

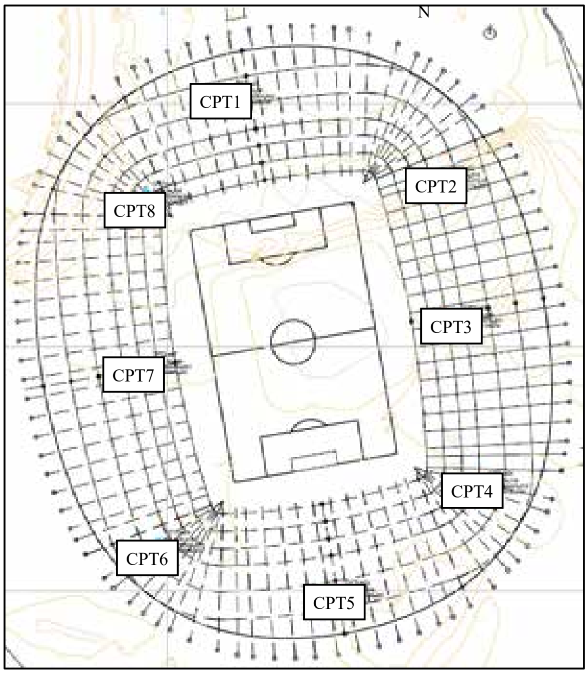

Figure 2. Location of the CPT boreholes.

The CPT boreholes reached maximum depths between 22 m to 35 m. In order to allow comparisons with the SPT results, average cone tip resistance (q_c) and average sleeve friction resistance (f_s) were calculated from the CPT profiles at the same depth interval of determination of the N_{SPT} number within the soil. The CPT tests were carried out following Brazilian Standard NBR 12069.

3.3 *Subsoil characteristics*

Figure 3 shows a simplified profile of the experimental site as well as the results of the eight CPT tests. Measurements of the cone tip resistance, q_c, and sleeve friction, f_s, obtained with the CPT tests, are plotted with depth. The subsoil is composed of a surficial layer of pure sand with thickness of about 3 m. This is a medium uniformly graded quartz silica sand that classifies as SP according to the Unified Soil Classification System. Underneath the sand layer is a silty sand deposit with non-plastic fines. CPT based soil behavior type (SBT) charts were used to classify the soil (Robertson, 2010). The soil layers in the profile were classified into SBT zone 6 (clean sand to silty sand).

Figure 4 shows the plots of N_{SPT} number with depth for all 88 boreholes. The mean N_{SPT} and the range of deviation of N_{SPT} from the mean are also shown in Figure 4 (thick line and dashed lines, respectively). Figure 4 provides a good indication of the large spatial variability of the investigated subsoil. The large dispersion of the data shows the need of portioning the subsoil into zones of influence for the SPT tests, in order to derive consistent correlations with the CPT results, instead of using all SPT results at once.

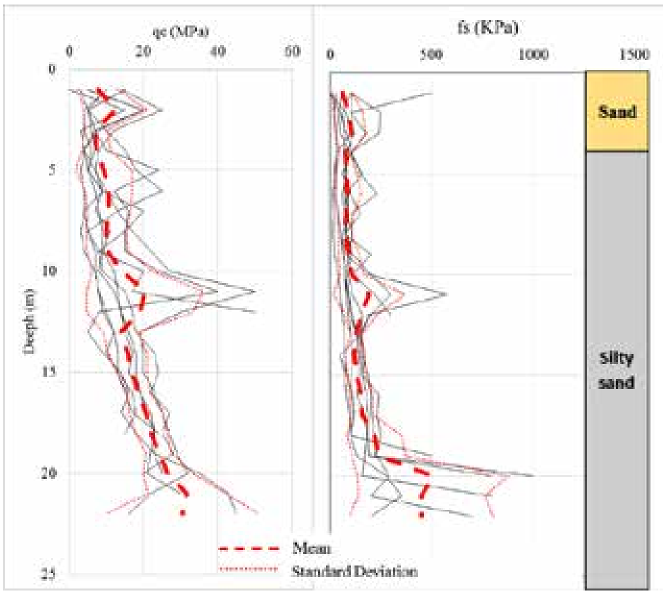

Figure 3. Soil profile at the experimental site and results of CPT tests.

4 VARIOGRAPHIC ANALYSIS

The zones of influence of the sampled values (zones with non-zero correlation) were determined using a semivariogram-based approach using data from CPT boreholes 1 to 8. Data from CPT 4 were excluded from this analysis due to lack of correspondence of soil type with the SPT data within its zone of influence. Semivariograms of the samples were calculated using Equation 1 for the field data collected in the ground at the following selected depths (z): 1 m, 5 m, 10 m, and 15 m.

$$\gamma(h) = (1/2N(h)) \sum_{i=1}^{N(h)} [Z(x+h) - Z(x)]^2 \qquad (1)$$

where: h = distance vector between observed pairs; n = number of pairs; Z(x+h) and Z(x) = random variables at locations x+h and x, respectively.

The empirical semivariogram was fitted with a theoretical semivariogram of a spherical semivariance model, according to Equation 2:

$$\gamma(h) = \begin{cases} C_0 + C\left[1.5\frac{h}{a} - 0.5\left(\frac{h}{a}\right)^3\right], h < a \\ C_0 + C \qquad , h \geq a \end{cases} \qquad (2)$$

where: a = range; C_0 = nugget effect; C = spatial variance.

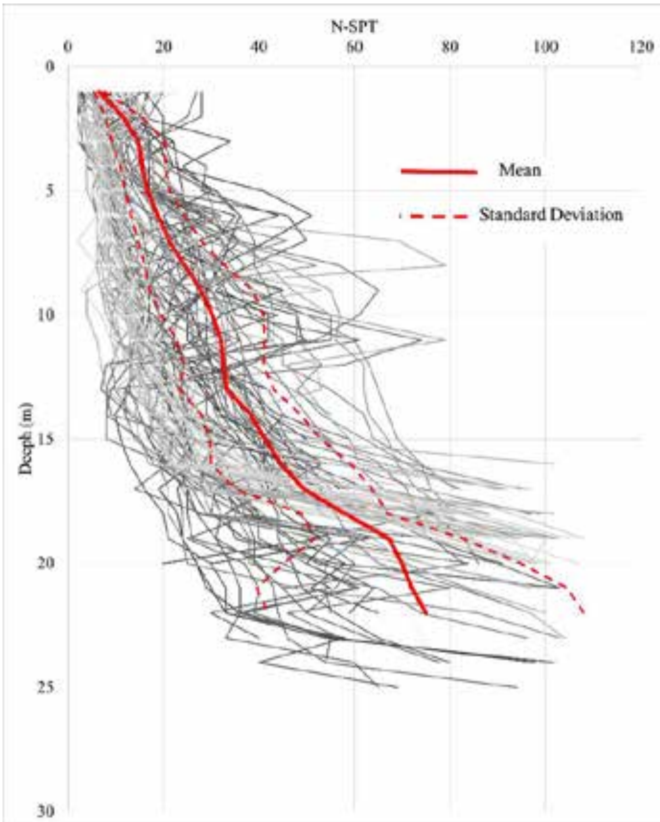

Figure 4. Variation of N_{SPT} with depth.

As an example, Figure 5 presents the empirical semivariogram and the corresponding theoretical fitting (dashed line) obtained for the data collected at depth z = 1 m. The range *a* of the variogram, i.e., the distance beyond which the SPT data fail to correlate adequately, was obtained from the fitted curve. In the semivariogram, this range was assumed as the lag distance for which the fitted curve begins to divert from its initial trend of linear increase of the semivariance with distance.

Among all investigated depths, the shortest range was found for z = 1 m, and measured 32 m. This distance was therefore used to limit the influence zone around the CPT boreholes. In other words, only SPT boreholes within a distance of 32 m were used for a given a CPT borehole.

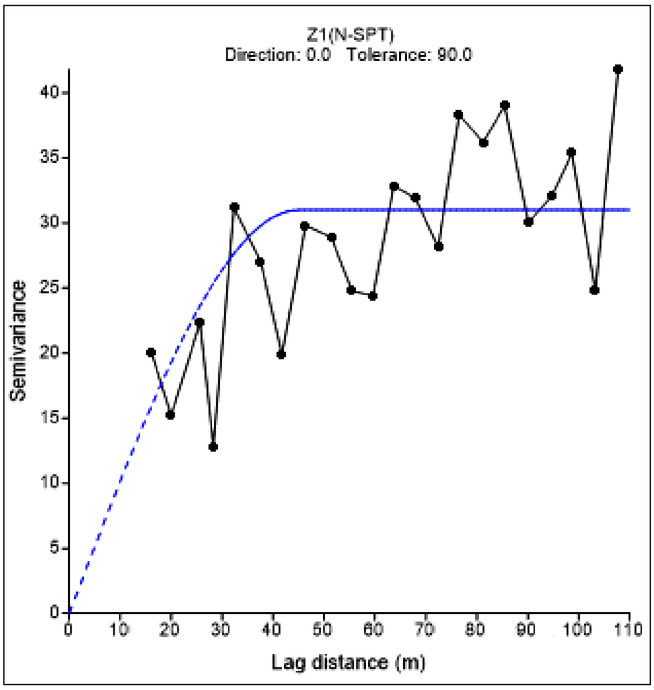

Figure 5. Semivariogram for depth z = 1 m.

5 RESULTS AND DISCUSSION

5.1 *Arithmetic mean approach*

In a first approach, a correlation between SPT and CPT results was achieved by calculating the arithmetic mean of the values. In this simple approach, all data were used regardless the distance from the CPT boreholes. No attempt was made to pick specific SPT data. 402 pairs of q_c – N_{60} values were combined, resulting in an average q_c/N_{60} ratio (k) of 0.6 (with standard deviation of 0.4) for the silty sand deposit. No correlation between q_c and N_{60} was found with this methodology.

5.2 *Correlations of q_c and N_{60}*

In an attempt to reduce the influence of soil spatial variability, the CPT results were correlated with N_{60} values collected within the zone of influence of each CPT borehole, defined by a circle with ray equal to the smallest range found in the variographic analysis, i.e. 32 m (see Section 4). Soil mass was thus divided into eight distinct zones of influence, and eight different CPT-SPT correlations were established for those zones.

Figure 6 shows the relationship between q_c and N_{60} for Zones 1 to 8. The experimental data points of each influence zone were adjusted using a linear fitting passing through the origin. Table 2 presents k = q_c/N_{60} ratios found from the linear fittings for Zones 1 to 8. The found coefficients of determination (R^2), as indicated in Table 2, show the good agreement achieved between the correlated variables.

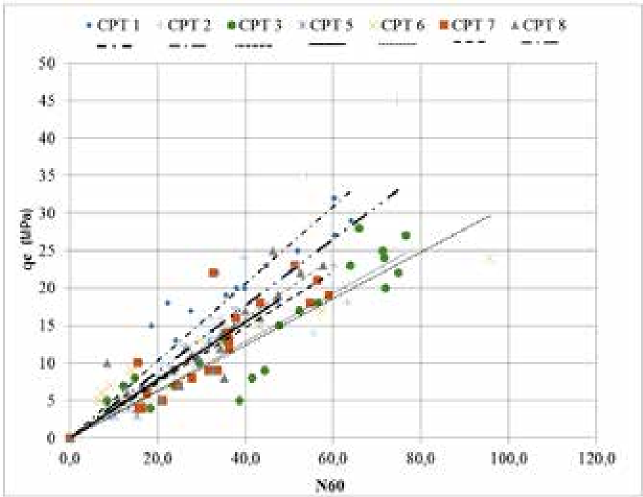

Figure 6. Correlations between q_c and N_{60} assuming distinct zones of influence for the SPT boreholes at the site.

Table 2. Values of k for the influence zones.

CPT Zone	k (MPa)	R^2
1	0.51	0.863
2	0.44	0.701
3	0.32	0.848
5	0.39	0.919
6	0.31	0.761
7	0.37	0.766
8	0.40	0.822

Figure 7 shows the correlation of q_c and N_{60} obtained using the data points from all eight zones, and selected according to the variogram-based approach previously described. A k ratio of 0.39 MPa was obtained for the soil according to this analysis. This value is lower than the range reported by Danziger et al. (1998) for residual silty sand deposits in Brazil, which is in the range of 0.5 – 0.64.

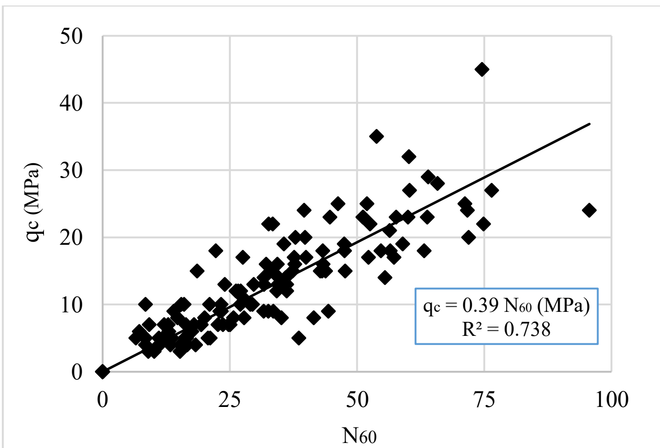

Figure 7. General correlation between qc and N_{60} for the investigated soil.

5.3 *Correlations of f_s and q_c/N_{60}*

Figure 8 shows the sleeve friction f_s as a function of $(q_c/p_a)/N_{60}$ for Zones of influence 1 to 8. The cone tip resistance q_c is normalized by the atmospheric pressure p_a (p_a = 100 kPa). A linear regression passing through the origin was fitted to the experimental data points. Table 3 presents the ratio $fs{\cdot}N_{60}/(q_c/p_a)$ found with the linear fittings, for Zones 1 to 8. Except for Zones 1 and 6, the coefficients of determination (R^2) found according to this analysis are relatively high.

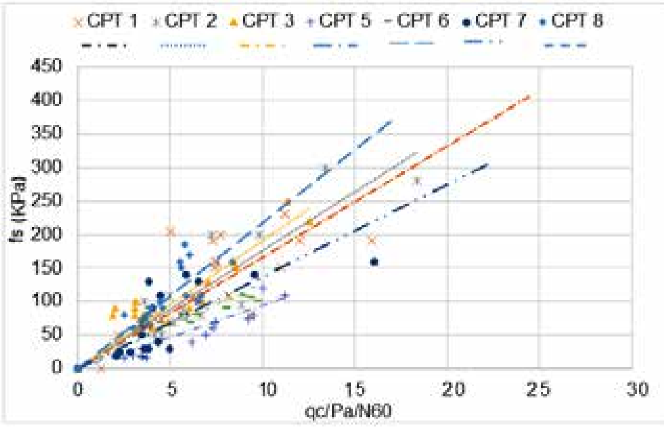

Figure 8. Correlations between f_s and $(q_c/p_a)/N_{60}$ assuming distinct zones of influence for the SPT boreholes at the site.

Table 3. Values of $fs{\cdot}N_{60}/(q_c/p_a)$ for the influence Zones.

CPT Zone	$fs{\cdot}N_{60}/(q_c/p_a)$	R^2
1	16.63	0.468
2	17.61	0.807
3	19.03	0.795
5	9.40	0.790
6	12.79	0.441
7	13.75	0.507
8	21.81	0.658

Figure 9 shows the correlation between f_s and $(q_c/p_a)/N_{60}$ obtained using the data points from all zones, selected according to the variogram-based approach previously described. A value of 16.01 found for the ratio $fs{\cdot}N_{60}/(q_c/p_a)$ for the investigated soil.

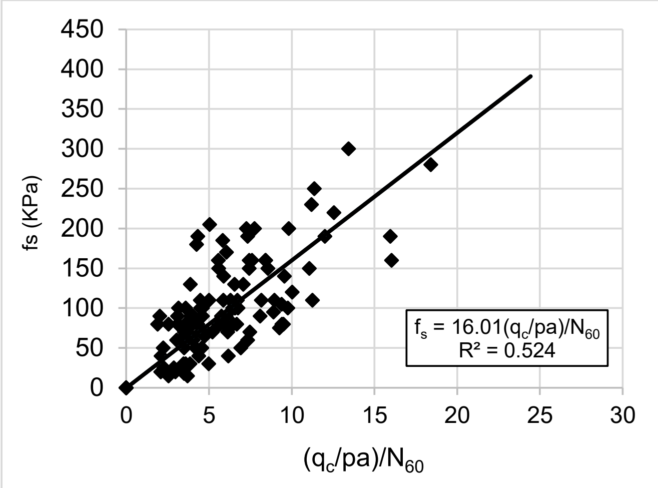

Figure 9. General correlation between f_s and $(q_c/p_a/N_{60})$ for the investigated soil.

6 SUMMARY AND CONCLUSIONS

Analyses on correlations between SPT and CPT data for a sedimentary silty sand deposit in the Northeast Region of Brazil were presented in this paper. The investigation included results of 88 SPT borings and eight CPT borings. Data were selected using a variogram-based approach.

A preliminary analysis consisted of finding a relation between cone tip resistance (q_c) and the N_{SPT} blow count number corrected for 60% efficiency (N_{60}) by calculating the arithmetic mean of the variables. Because of the large dispersion of the values caused by soil spatial variability, no correlation between q_c and f_s was found with this approach.

In an attempt to reduce the effect of soil spatial variability, a zone of influence for each CPT borehole was defined using a variographic-based approach. Only N_{60} values within a range of 32 m were picked to correlate with data from a specific CPT borehole. This approach led to good correlations with comparatively high coefficients of determination. A representative ratio k = q_c/N_{60} of 0.39 MPa was found for the silty sand deposit. This ratio is below the range reported in the literature for silty sand deposits of residual origin in Brazil.

Geostatistics is an essential tool for the achievement of more refined SPT-CPT correlations, and its use should be more disseminated.

7 ACKNOWLEDGEMENTS

The authors are thankful to the Government of Rio Grande do Norte State for the permission to publish the field test data.

8 REFERENCES

Akca, N. 2003. Correlation of spt-cpt data from the United Arab Emirates. *Engineering Geology*. 67: 219-231.

Alonso, U. R. 1980. Correlations between results of static and dynamic penetration tests for the City of São Paulo. *Solos e Rochas*. 3(3): 19-25. *[in Portuguese]*

Angelim, L. A. A.; Nesi, J. R.; Torres, H. H. F.; Medeiros, V. C.; Santos, C. A.; Junior, J. P. V.; Mendes, V. A. (1ª ed.) 2006. *Geologia e Recursos Minerais do Estado do Rio Grande do Norte*.. Recife. CPRM. *[in Portuguese]*

Aoki, N.; Velloso, D.A. 1978. An approximate method to estimate the bearing capacity of piles. In: Panamerican Conf. Soil Mech. Found. Eng., 5, Buenos Aires, 1975. Proc., Buenos Aires, Huella Estudio Grafico, 1975. 1: 367-376.

Barata E., et al. 1978. Uplift Tests on Drilled Piers and Footings Built in Residual Soil. *In: VI Congresso Brasileiro de Mecânica dos Solos e Engenharia de Fundações*. Proc., Rio de Janeiro. 3: 1-37. *[in Portuguese]*

Brazilian Association of Technical Standards. 1991. *NBR 12069: Soil - Cone penetration test - CPT in situ - Test method.* 10p. [*in Portuguese*]

Brazilian Association of Technical Standards. 2001. *NBR 6484: Soil - Standard penetration test - SPT - Soil sampling and classification - Test method.* 17p. [*in Portuguese*]

Chan, C.T; Duan, S.W; Kao, T.C. 1988. SPT-CPT coerrelations for granular soils. In: *1st International Symposium on Penetration Testing*, Orlando, Florida. 1: 335-339, USA.

Danziger, B.R.; Velloso, D.A. 1986. Study on correlations between SPT and the result of continuous penetration tests. In: *VIII Congresso Brasileiro de Mecânica dos Solos e Engenharia de Fundações*. Proc., Porto Alegre. 6: 103-113. *[in Portuguese]*

Danziger, B.R.; Velloso, D.A. 1995. Correlation between the CPT and the SPT for some Brazilian soils. *In: International Symposium on Penetration Testing*, Proc., Linkoping, Sweden. 155-160.

Danziger, F. A. B.; Politano, C. F. & Danziger, B. R. 1998. CPT - SPT correlations for some Brazilian residual soils. *In: Geotechnical Site Characterization.* Proc. 1st Int. Conf. on Site Characterization, ISC'98, Atlanta, USA, Balkema, 2: 907-912.

Jesus, A.P. 2002. Geological and Geomorphological characterization of a sand dune deposit at the City of Natal, Brazil. M.Sc. Dissertation, Federal University of Rio Grande do Norte, Geodynamics and Geophysics Graduate Program. *[in Portuguese]*

Kara, O.; Gündüz, Z. 2010. Correlation between cpt and spt in adapazari, turkey. *In: 2nd international symposium on cone penetration test.* Huntington Beach, California. Proceedings. California.

Kasim, A. G.; Chu, M.; Jensen, C. N. 1986. Field correlation of cone and standard penetration tests. *Jornal of Geotechnical Engineering Division, ASCE.* 112: 368- 372.

Politano, C. F. 1999. *Correlations between results of CPT and SPT in residual soils.* 210 p. M.Sc. Dissertation – Federal University of Rio de Janeiro – COPPE. Rio de Janeiro. *[in Portuguese]*

Robertson, P.K. 2012. Interpretation of in-situ tests – some insights. *In: Geotechnical and Geophisical site characterization 4*. Coutinho & Mayne, eds. 1: 3-24. 2013. Taylor & Francis: London.

Robertson, P.K.; Campanella, R.G.; Wightman, A. 1983. SPT-CPT Correlations. *Jornal of Geotechnical Engineering Division, ASCE*. 109(111): 1449- 1459.

Schmertmann, J.H.; Palacios, A. 1979. Energy dynamics of spt. *Journal of soil mechanics and foundation division – ASCE*. 105: 909-926.

Shahri, A.A, Juhlin, C. and Malemir A. 2014. "A reliable correlation of SPT-CPT data for southwest of Sweden", *Electronic Journal of Geotechnical Engineering*. 19: 1013-1032.

Geotechnical and Geophysical Site Characterisation 5 – Lehane, Acosta-Martínez & Kelly (Eds)

Finite element modeling of cone penetration test in weakly cemented sand

R. Debasis, S. Digvijay Kumar, D. Arghya & G. Saswati
Department of Civil Engineering, IIT Kharagpur, India

ABSTRACT: A stress-strain model has been developed for weakly cemented sand using Drucker-Prager yield and failure criteria modified to account for the strain dependencies of friction angle, dilation angle and cohesion. The model was calibrated against drained triaxial compression test data obtained from laboratory tests of water pluviated weakly cemented sand samples. Miniature cone penetration tests were conducted in the laboratory to check the performance of the calibrated model. Weak cementation for performing miniature cone test samples were introduced in an identical process that used for introducing cementation in triaxial sand samples. The 2.75-mm diameter model cone used in these tests had a non-standard apex angle 18°. The model cone was pushed through samples of weakly cemented sand prepared within a steel cylinder with 200 mm diameter and 170 mm height. Miniature cone resistances were calculated numerically using ABAQUS/EXPLICIT version 6.11 which showed good agreement with experimental test data.

1 INTRODUCTION

Weakly cemented sands and silts widely occur in nature. In general, cementation typically develops due to either chemical precipitation of calcium carbonate, microbial metabolic products or dissolution and deposition of soluble salts from groundwater (van Paasen LA, 2009). Natural cementation creates bonds between soils grains due to various geological processes such as chemical precipitation, weathering by-products and welding effect (Clough et al., 1981). Naturally cemented materials typically have variable densities and degrees of cementation. Characterization of cemented sand in the laboratory is often difficult due to sampling difficulties. Disturbance during sampling damages or breaks intergranular cementation render the soil weak. To overcome these difficulties, artificially cemented sand has been investigated via laboratory tests that simulate the cemented sand present in natural soil deposit.

In this study, weak cementation was introduced by pluviating sand particles in an aqueous medium reflecting typical groundwater mineral salt contents inoculating with a strain of calcifying bacteria obtained from a cemented sand site on the east coast of India. Isotropically consolidated drained triaxial tests were conducted on these weakly cemented sand samples in the laboratory. A stress-strain model was then developed and calibrated using ABAQUS (version 6.11) for the drained response of the artificially prepared weakly cemented sands. Subsequently, a miniature cone penetration test (MCPT) model was developed using the calibrated stress-strain model and then compared with the results of MCPT conducted in the laboratory.

2 DRAINED TRIAXIAL TEST

A series of isotropically consolidated drained triaxial tests were conducted on water pluviated sand samples. Triaxial samples, approximately 37 mm in diameter and 74 mm in height, were prepared by pouring poorly-graded siliceous sand within a mixture of mineral salt media and EPS (Extracellular polymeric substances), calcite producing bacteria obtained from a cemented sand site on the east coast of India. Specimens were prepared for introducing microbially induced cementation through three different bio-processes namely non-ureolytic calcifying, ureolytic calcifying and EPS only. Microbe produces EPS along with calcite in non-ureolytic and ureolytic calcifying processes in the absence and presence of urea in the nutrient media respectively. On the other hand, in "EPS only" process microbe produces only EPS as extracellular metabolic products leads to cementation. Specimens were prepared in such a manner that the post consolidation relative density was approximately 40 %. Bacteria-inoculated samples were sheared under a constant strain rate of 0.012 mm/min.

3 STRESS-STRAIN MODEL

A stress-strain model has been developed by modifying the Drucker-Prager model implemented in the general purpose continuum mechanics software package in ABAQUS 6.11 to account for the mobilization of friction angle, dilation angle and cohesion as the material hardens/softens. The model was used via explicit finite element algorithm incorporated in ABAQUS/explicit together with arbitrary Lagrangian Eulerian (ALE) approach to accommodate very large distortion. The model was first calibrated using drained stress-strain and volumetric behaviour of weakly cemented soil sample obtained from three processes non-urelolytic, urelolytic and EPS for isotropic confining pressures of 100 kPa and 300 kPa. Soil was modeled as elastic-plastic material. The Young's modulus, which controls the elastic behaviour, was estimated from small strain shear modulus, G_0, using

$$G_0 = \rho \times v_s^2 \qquad (2.1)$$

Where, ρ is the total mass density and V_S is the shear wave velocity. Shear wave velocities used in the model were estimated following Baxter and Sharma (2012). In Drucker-Prager constitutive model, the ratio of flow stress in triaxial tension to flow stress in triaxial compression was assumed to be 0.778 (Abaqus keyword reference manual).

A cylindrical assemblage comprised of 952 eight-noded elements with one reduced integration point (C3D8R), 76 mm in height and 38 mm in diameter, was used in these simulations. The bottom plate of Specimen was restrained in vertical and horizontal directions. Equal radial and axial pressures were applied in the next step. In the subsequent step, the axial pressure was removed, a rigid surface was placed on the top surface and a velocity was applied so as to deform the sample at a compressive axial deformation of 0.12 mm. Triaxial model was initialized to isotropic states of stress of 100 kPa and 300 kPa.

The peak friction and dilation angles and peak cohesion for cemented specimens as well as the manner in which these parameters depend on plastic strain were obtained by fitting the computed stress-strain response to laboratory test data by trial and error. The observed and simulated deformation behavior of weakly cemented sand samples in drained triaxial compression at 100 kPa and 300 kPa are presented in figures 3.1, 3.2 and 3.3. The results indicate that the stress-strain model developed in this study captures soil behavior reasonably. Friction angles, cohesion and dilation angles back figured from calibrated model are presented in Figure 3.4, 3.5 and 3.6 respectively. The parameters thus obtained indicated that the mobilized friction angle is an increasing function of plastic strain of approximately hyperbolic nature. The variation in friction angle and dilation angle with plastic strain is accommodated in this study through a user-defined subroutine. The cohesion, on the other hand, increases at small strain and found to decrease at larger strain.

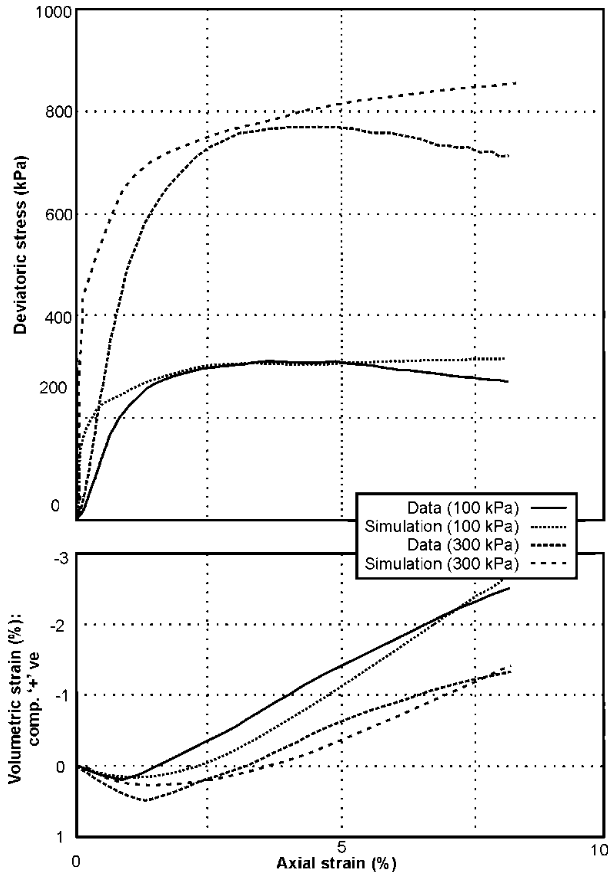

Figure 3.1: Observed and simulated triaxial compression behaviour of non-urelolytic soil sample at 100kPa and 300kPa cell pressure

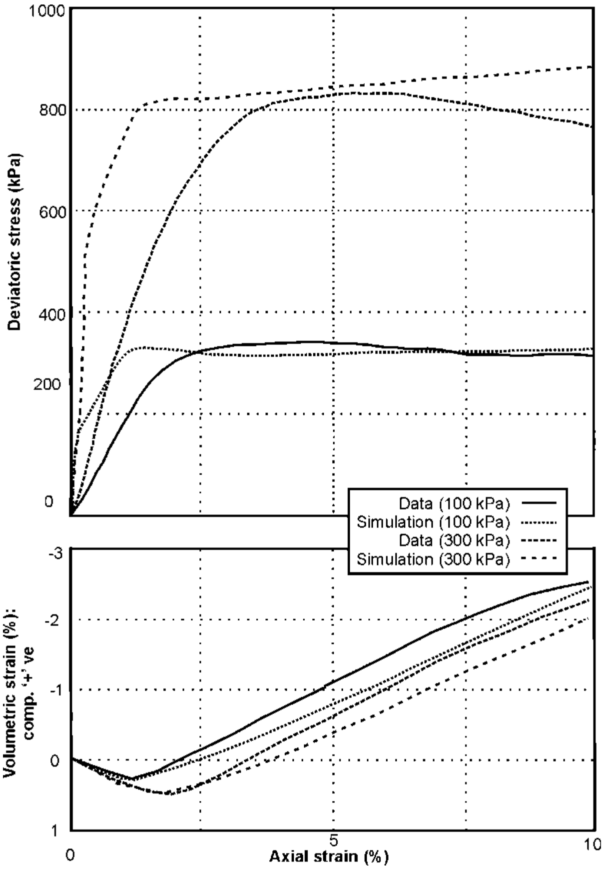

Figure 3.2: Observed and simulated triaxial compression behaviour of ureolytic soil sample at 100kPa and 300kPa cell pressure

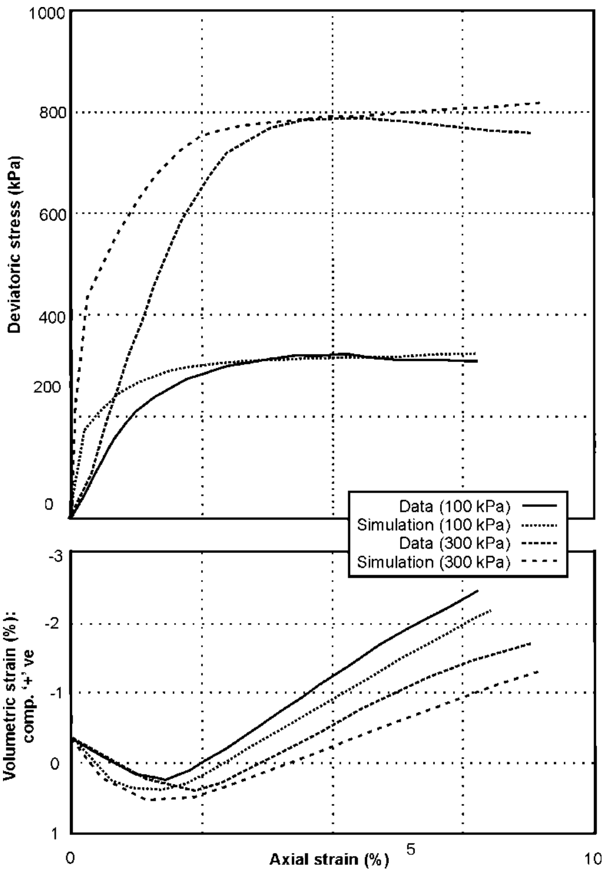

Figure 3.3: Observed and simulated triaxial compression behaviour of an EPS soil sample at 100kPa and 300kPa cell pressure

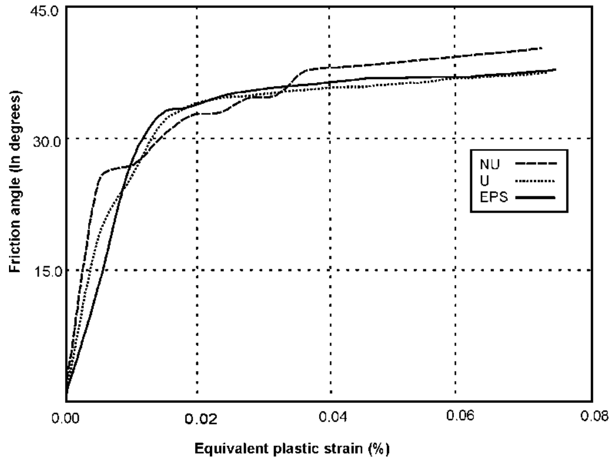

Figure 3.4: Variation of friction angle with equivalent plastic strain

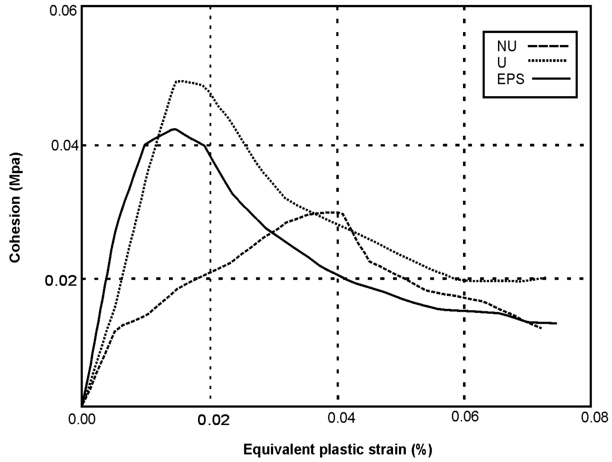

Figure 3.5: Variation of Cohesion with equivalent plastic strain

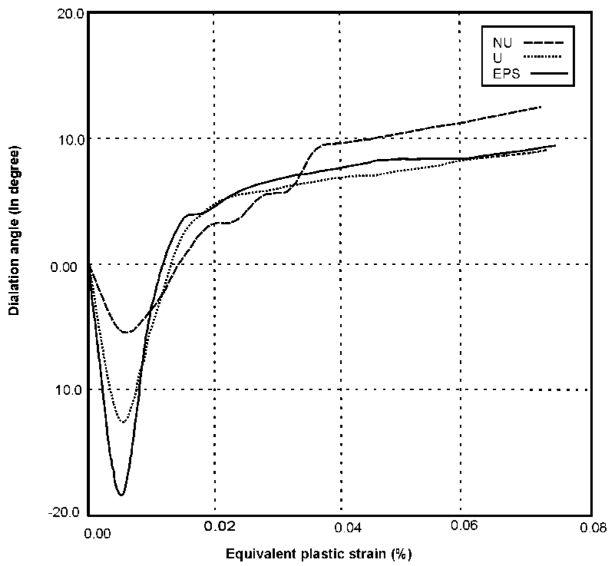

Figure 3.6: Variation of dilation angle with equivalent plastic strain

4 MINIATURE CONE PENETRATION TEST

The sample preparation procedure for miniature cone penetration test in laboratory was similar to drained triaxial test. Special precautions were made to maintain the relative density and biomass concentration to achieve certain degree of cementation. The sample is kept in a cylindrical container having diameter 200 mm and height 200 mm. An instrument similar to cone penetrometer was designed to measure tip resistance in penetrating the soil sample. The instrument was calibrated. The diameter of the needle was chosen in such a manner that ratio of the diameter of needle to that of sand sample remained less than 1:40 to minimize the effect of boundary on the result.

A 2.75-mm diameter cone used in these tests had an apex angle 18°. The diameter ratio was 36.5. The length of miniature cone was 238mm. The sleeve length was set to 1.25 times the diameter of cone. The soil sample was placed on triaxial frame and loaded at a penetration rate of 3mm/min. Load was measured from modified load cell ring at every 5 sec interval or 0.25mm penetration depth.

5 MINIATURE CONE MODEL

An axisymmetric model was created, the outer boundary of soil was 100mm from centerline and soil thickness was 170mm. In this study a diameter ratio of 72.73 was used which is more than the standard diameter ratio of 50 suggested by Lee et al. (2010) required to minimize boundary effects. An Elasto-plastic stress-strain model was used for soil with linear Drucker-Prager model defining the plastic behaviour. The cone was modeled as rigid body and soil as deformable. Initially, the cone was placed in a conical notch in the soil domain and was penetrated to a depth of 80mm at a rate of 3 mm/min. The bottom and side boundaries were restrained from moving vertically and horizontally, respectively. Adaptive Lagrangian Eulerian meshing is used to control element distortion in cases where large deformation or loss of material occurs. A master-slave relationship was used to model the penetrometer-soil contact, where the nodes of the master surface capable of penetrating through slave surface. The penetrometer was considered to be the master surface and soil as slave surface. The interface friction angle was chosen in accordance with Dietz and Lings (2006). The cone penetration resistance was calculated at an interval of 0.25mm numerically which shows good agreement with experimental test data. The comparisons of test data and simulated data were shown in Fig. 5.1, Fig. 5.2 and Fig. 5.3 for non-urelolytic, urelolytic and EPS respectively.

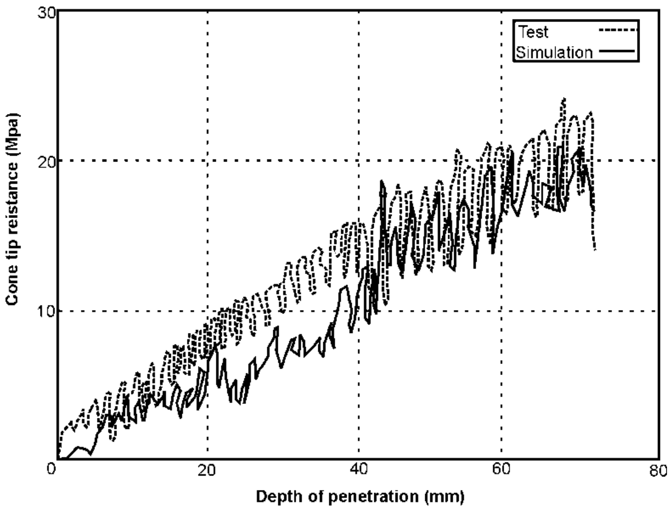

Figure 5.1: Observed and simulated cone tip resistance of non-urelolytic soil sample.

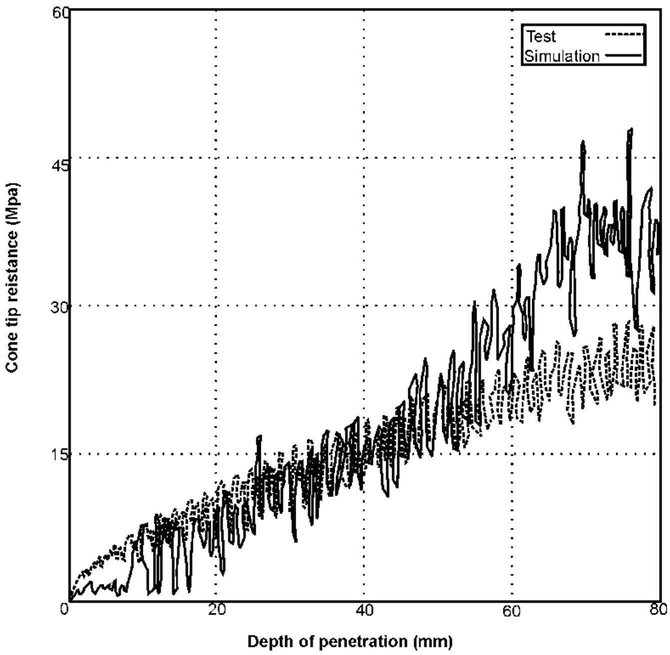

Figure 5.2: Observed and simulated cone tip resistance of urelolytic soil sample

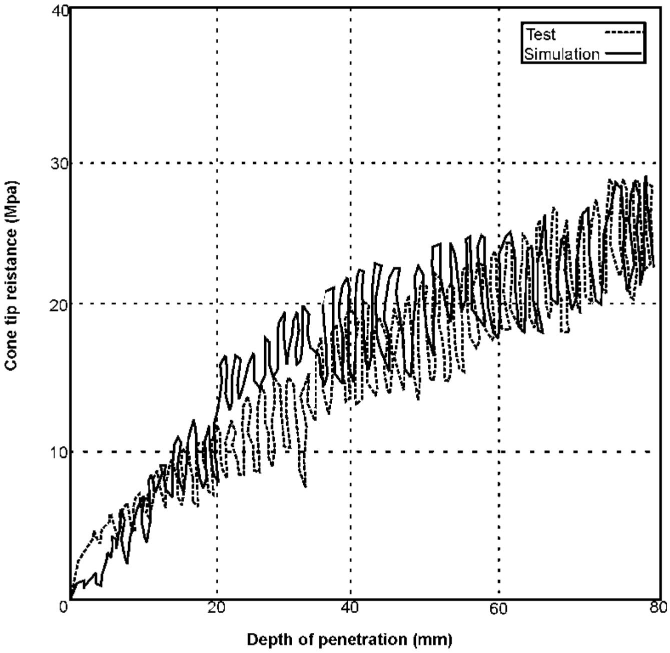

Figure 5.3: Observed and simulated cone tip resistance of EPS soil sample

6 CONCLUSIONS

It was observed that the drained triaxial compression test data and numerically simulated data shows good agreement for isotropically consolidated weakly cemented soil samples. The test data conducted in laboratory on miniature cone and simulated data from finite element analysis shows good agreement between them. The cone penetration resistance obtained in the case of EPS sample is greater in comparison with non-urelolytic and urelolytic samples due to high cementation bonding between particles.

7 REFERENCES

Ahmadi, M.M., Byrne, P.M. & Campanella, R.G 1999. Numerical Simulation of CPT Tip Resistance in Layered Soil, Asia Inst. Of Tech., 40th Year Conference, New Frontier sand Challenges.

Baxter, C.D.P & Sharma, M.S.R. 2012. Shear wave velocity of weakly cemented silty sand during drained and undrained triaxial compression, GeoCongress: 890-899.

Clough, G.W., Sitar, N., Bachus, R.C., & Rad, N.S. 1981. Cemented sands under static loading. Journal of Geotechnical Engineering, 107(6), 799-817.

Dietz, M.S. & Lings, L. 2006. Postpeak strength of interfaces in a Stress-Dilatancy framework. Journal of Geotechnical and Geoenvironmental Engineering, 132(11), 1474-1484.

Lee, M.J., Choo, H., Kim, J. & Lee, W 2010. Effect of artificial cementation on cone tip resistance and small strain shear modulus of sand. Bulletin of Engineering Geology and the Environment, 70, 193-201.

Puppala, A. J., Acar, Y. B. & Tumay, M.T 1995. Cone penetration in very weakly cemented sand. Journal of Geotechnical Engineering, 121, 589-600.

Rad, N. S. & Tumay, M. T. 1986. Effect of cementation on the Cone Penetration Resistance of Sand: A Model Study, Geotechnical Testing Journal, 9 (3), 117-125

Simulia, Inc. 2008. *ABAQUS Analysis Keywordreference Manual, Version 6.11*. Providence, RI, USA

Van Paassen, L. A. 2009. Biogrout, ground improvement by microbially induced carbonate precipitation. Doctoral dissertation, Department of Biotechnology, Delft University of Technology, the Netherlands

Geotechnical and Geophysical Site Characterisation 5 – Lehane, Acosta-Martínez & Kelly (Eds)

Cylindrical cavity expansion analysis applied to the interpretation of variable rate cone penetration in tailings

G. Dienstmann, F. Schnaid & S. Maghous
Dept. of Civil Engineering, Federal University of Rio Grande do Sul, Brazil

ABSTRACT: The assessment of rate effects on piezocone test in tailings is a necessary step in the design of tailings storage facilities, since these geomaterials often exhibit coefficients of hydraulic conductivity in the range of transitional soils. The present paper describes the application of a non-linear poroelastic model conceived to capture the transient flow effects of the soil around an expanding cylinder (Dienstmann et al, 2015), to the interpretation of piezocone tests in gold tailings. Tests carried out at constant penetration rates ranging from 0.3mm/s to 57 mm/s are used in the analysis. Results are interpreted in a space that correlates dimensionless velocity V_h to cone resistance Q and degree of drainage U showing that penetration is essentially drained at normalized velocities less than about 0.1 and essentially undrained at normalized velocities greater than 10.

1 INTRODUCTION

The design of tailings storage facilities (TSF) is still a challenge to geotechnical engineers because of the high complexity involving the tailings geotechnical behavior coming from the heterogeneous nature of waste products, the hydraulic depositional processes and the change in the constitutive parameters during the lifetime of deposits. The experience gathered in the last 20 years (e.g. Schnaid et al. 2013 Jamiolkowsky & Masella, 2014) shows that the depositional process often produces tailings in the so-called intermediate permeability range of 10^{-5} to 10^{-8} m/s. In intermediate soils including natural clayey and sandy–silts, tailing and others geomaterials, a partially drainage behavior is likely to occur when insitu tests as cone penetration are performed at the standardized velocity (20mm/s), introducing errors in interpretation.

In this context, theoretical solutions can be an essential tool helping understanding what controls the drainage behavior taking place during cone penetration tests executed in silty materials. Among the existing methods, cavity expansion approach is extensively used and accepted for modeling the cone penetration (e.g. Gibson and Anderson, 1961; Baligh, 1985; Teh and Houlsby, 1991; Salgado et al., 1997; Yu and Mitchell, 1998; Burns and Mayne, 2000; Chang et al. 2001; Cao et al., 2001; Chen and Abousleiman, 2012, 2013; Zhang et al., 2016), with a variety of soil stress–strain models. Although, there is an extensively literature on cavity expansion solutions applied to the interpretation of piezocone tests, there is not a complete understanding of what controls the transient behavior during penetration. The present paper describes the use of a cylindrical cavity solution proposed by Dienstmann et al. (2015), to assist the drainage behavior interpretation of experimental data from a gold TSF.

2 BRIEF DESCRIPTION OF THE MODEL

The analytical cylindrical cavity expansion solution proposed in Dienstmann et al. (2015) is structured as a consolidation analysis of a rigid cylinder deeply embedded within an isotropic fully saturated poroelastic medium of infinite extent. The analysis is based on the assumption of plane strain conditions in the cross-section of a system defined by the cylinder and surrounding porous medium, restricting displacements and flow to two dimensions. The soil surrounding the cylinder is model as a fully saturated poroelastic material undergoing infinitesimal strains.

The problem of consolidation around infinite expanding cylinder is idealized in Figure 1. Starting from an initial stress and pore pressure states (σ_0, p_0), a prescribed radial displacement of magnitude $\alpha(t)R$ is applied at the cylinder wall $r = R$. The concept of influence zone $R \geq r \geq a$ is also introduced in this analysis to characterize the extent of the region whose poromechanical state is no longer affected by cylinder installation and subsequent expansion (e.g. Blight, 1968; Randolph and Wroth, 1979; Osman and Randolph, 2012). This means in particular that displacement and pore pressure vanish at r = a.

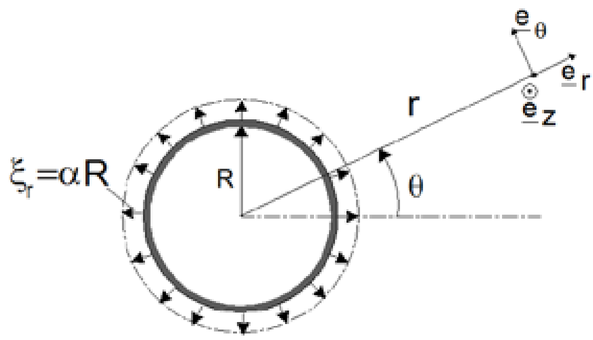

Figure 1. Idealized geometry and loading conditions for consolidation around infinite expanding cylinder.

2.1 *Constitutive formulation*

A non-linear poroelastic model is adopted for the problem of the cylindrical cavity solution. The model assumes the local equivalence between the response of a perfectly plastic behavior to monotonic loading and an appropriate fictitious non-linear poroelastic behavior.

The non-linear poroleastic behavior is conceived as an asymptotic representation of the plastic yielding of the material. Adopting a Drucker-Prager yield condition for the material strength, Equation 1 describes the non-linear shear modulus as a function of both volumetric and equivalent deviatoric strains (ε_v and ε_d, respectively) and pore pressure p.

$$G(\varepsilon_d, \varepsilon_v, p) = \frac{1}{2}\left[T(h - K\varepsilon_v - (1-b)\ p)\right]\ \frac{1/\varepsilon_{ref}}{1+\varepsilon_d/\varepsilon_{ref}} \tag{1}$$

where $\varepsilon_{ref} \ll 1$ is a reference strain that physically represents the order of magnitude of the shear strain mobilized at yielding, parameters h and T respectively characterize the tensile strength and the friction coefficient of the medium, and K is a constant value for the bulk modulus.

The pore flow problem is solved observing first that the combination of the fluid mass balance equation, the second poroelastic state equation and Darcy's law yields:

$$b\frac{\partial \varepsilon_v}{\partial t} + \frac{1}{M}\frac{\partial p}{\partial t} = k\nabla^2 p \tag{2}$$

where M is the material Biot modulus, and k is the permeability coefficient. Considering the non-linear poroelastic medium the following generalized Navier equation can be derived (assuming irrotational displacement field).

$$\left[K + \tfrac{4}{3}G\right]\nabla\varepsilon_v + 2\,\nabla G\cdot(\boldsymbol{\varepsilon} - \tfrac{1}{3}\varepsilon_v \mathbf{1}) = b\nabla p \tag{3}$$

The above equation emphasizes the coupling between skeleton strains and pore-fluid pressure. The formulation differs from the classical formulations in which only the volumetric part ε_v of skeleton strains affects pore-fluid pressure. In the present case, pore pressure is also related to the deviatoric part ε_d of skeleton strains through the shear modulus $G(\varepsilon_d,\varepsilon_v,p)$. In classical formulations considering a constant shear modulus, the volume strain ε_v is eliminated between Equations (2) and (3) to get an uncoupled pressure diffusion equation governing the evolution of pore pressure, what is not possible on the derived formulation. A time incremental procedure has been elaborated and implemented in Dienstmann et al. (2015) to handle semi-analytically this problem, making use of a specific iterative algorithm within each time step. The incremental procedure determines the pore pressure distribution p(r,t) and displacement function f(r,t) for each time increment by solving the coupled system defined by the set of non-linear partial differential equations (2) and (3), together with associated boundary and initial conditions.

2.2 *Initial excess pore-fluid pressure distribution*

The solution of equations (2) and (3) requires the initial field of pore pressure to be determined to represent the initial excess of pore pressure u_0 (or equivalently p_0) generated by insertion of a rigid cylinder within the medium. Observing that none of the expressions proposed in literature (e.g. Randolph and Wroth, 1979, Morris and Williams, 2000), complies with the condition of null fluid flow through the cylinder wall a new expression shall be proposed. It extends classical expressions to account for the flow restriction at cylinder wall:

$$u_0(r) = u_{0,\max}\frac{\mathfrak{F}(r)}{\mathfrak{F}(R)} \tag{4}$$

$$\textit{with}\quad \mathfrak{F}(r) = 1 - \frac{a}{r} + \frac{a}{R}\ln\frac{a}{r} \qquad \text{for } R \le r \le a$$

where $u_{0,\max}$ refers to the maximum value of pore pressure generated by cylinder insertion. In the present paper $u_{0,\max}$ is estimated by the pore pressure generated during the consolidation phase in an undrained triaxial test

$$u_{0,\max} = \frac{p_{c0}}{2}\left(1 + M_{cs}\right) \tag{5}$$

where p_{c0} denotes a reference initial consolidation pressure, and M_{cs} is the critical state line inclination.

2.3 *Cone resistance estimation from the cavity approach*

The conversion of the cavity expansion results into cone resistance values was defined according the approach formulated by Rohani & Baladi (1981) and adopted by Silva (2005) and LeBlanc & Randolph (2008). The approach estimates the cone tip resistance from the vertical projections of all forces acting on the cone. Equation 6 presents the general estimation of q_c, which is derived considering that constant values of σ and τ act over the whole length of the cone.

$$q_c = \sigma + \tau \cot\ (\alpha) \tag{6}$$

For cylindrical cavity expansion is more convenient to write Expression 6 in terms of the radial stresses:

$$q_c = \sigma_r'(1+\tan(\delta)/\tan(\alpha))/(1-\tan(\delta)\tan(\alpha))+u \tag{7}$$

Equation 7 is obtained by the application of the equilibrium condition in a point along the cone, in which α is half of the angle of the cone tip (60°/2), δ is the interface friction taken as ϕ' and σ_r' is the radial stress at the expanding cylinder radius.

3 GOLD TAILINGS DEPOSIT

The *Fazenda Brasileiro* disposal plant from Bahia State, located in northeast Brazil is being a subject of research for the past 10 years, as reported by a series of papers (Bedin et al., 2012, Schnaid et al., 2013) and MSc and PhD thesis (Bedin, 2010; Klahold 2013, Nierwinski 2013, Dienstmann, 2015). This set of studies indicates that the material disposed in ponds is predominantly silty sand (see Figure 2) with an average in situ solids content (in weight) of about 30%, in situ water content of 35%, low to non plastic and high specific gravity (2.89<Gs<3.2 g/cm3).

To evaluate drainage effects during piezocone penetration test a total of 14 variable penetration rate cone tests in the 0.3mm/s to 57mm/s range was performed at the *Fazenda Brasileiro* testing site (see Table 1).

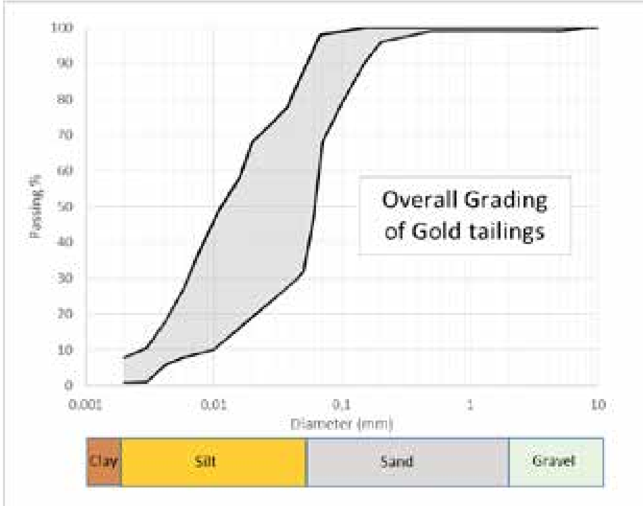

Figure 2. Grain size distribution

Table 1. Piezocone penetration rate

Study	Location	Penetration rate (mm/s)	Distance between tests (m)
Bedin (2006)	PZC 03	1; 20; 35	2
	PZC 07	20; 45	
	PZC 08	1,5; 10; 20	
Klahold (2012)	Island 01	0.3 to 0.7 (*); 20; 57	1.5
	Island 02	0.3 to 0.7 (*); 20; 57	

(*) test only executed between 3 to 5m

Figure 3 presents the gold tailings variable rate piezocone database interpreted in terms of a normalized resistance $Q=q_{cnet}/\sigma'_{v0}$ with $q_{cnet}=q_c - \sigma_{v0}$, and normalized pore pressure $U=\Delta u_2/\sigma'_{v0}$ plotted against the dimensionless velocities V_h, where q_c is the cone tip resistance and u_2 is the pore pressure. The normalized velocity V_h is defined according Equation 8, where d is the cone diameter, v the velocity of penetration and c_h the horizontal coefficient of consolidation.

$$V_h = \frac{v \times d}{c_h} \tag{8}$$

In the Q×V_h space it is possible to identify a region characterized by normalized velocities V_h in the range of about 0.01 to 10 where partial drainage appears to occur during CPTu penetration. The lowest (undrained) penetration resistance (Q_{UD}) is of the order of 2.0. The drained penetration resistance (Q_D) of 22.0 yields a drained to undrained ratio Q_D/Q_{UD} of about 11, which is consistent to previously reported data (Jager et al. 2010 and Lehane et al. 2010).

From the results in the U×V_h space a slightly larger scatter is observed, but some conclusions can be drawn from the CPTu response. Partial drainage takes place for V_h values in the 0.01 to 10 range, which is in agreement with the interpretation of cone penetration data. At fully undrained conditions the normalized pore pressure $\Delta u_2/\sigma'_{v0}$ ratio is of the order of 1.5 reducing to zero for drained penetration.

The adjusting curves presented in Figure 3 were constructed using the hyperbolic cosine function suggested by Schnaid (2005) in the form of:

$$Q = Q_{\min} + \left(a + (1-a)\frac{1}{\cosh(bV^c)} \right) \times (Q_{\max} - Q_{\min}) \quad (9)$$

$$\frac{\Delta u}{\sigma'_{v0}} = \frac{\Delta u_{\max}}{\sigma'_{v0}} - \left(a + (1-a)\frac{1}{\cosh(bV^c)} \right) \times \left(\frac{\Delta u_{\max}}{\sigma'_{v0}} - \frac{\Delta u_{\min}}{\sigma'_{v0}} \right) \quad (10)$$

Curve fitting coefficients for gold tailings are shown in Table 2.

Table 2. Curve fitting parameters

Curve fitting coefficients gold tailings			
	a	b	c
Lower Boundary	0.025	4	0.7
Upper Boundary	0.025	1	0.7

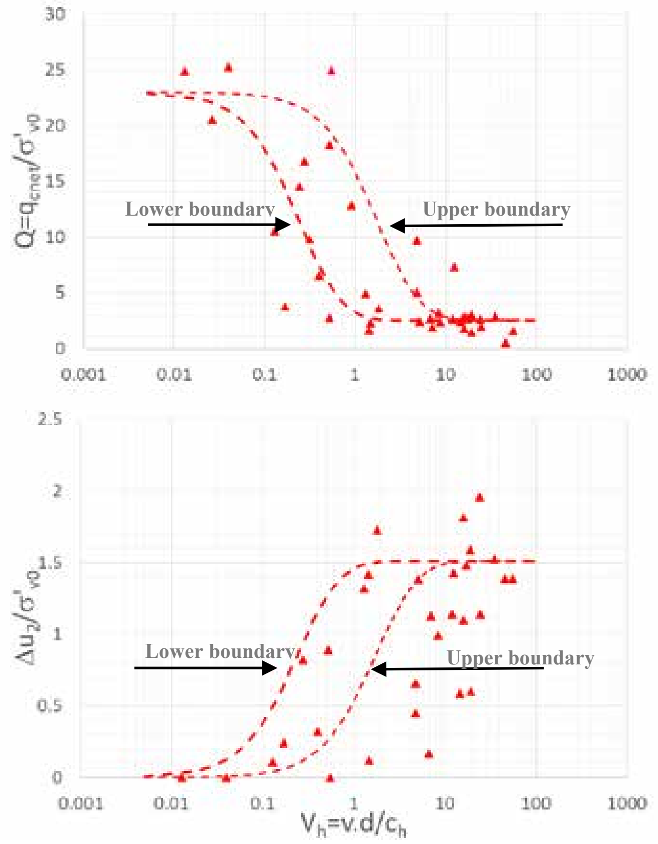

Figure 3. Rate effects in the (a) Q versus V_h space and (b) U versus V_h space

4 MODELING THE GOLD TAILINGS

The gold tailings average properties were used for modeling analytically and numerically the cylinder expansion problem with the aim of helping on assess rate effects on piezocone tests. The properties used in the analyses are summarized in Table 3. The parameters h and T from the Drucker Prager criteria are defined according to an inner Mohr Coulomb yield surface condition, with a friction angle $\phi' = 32°$.

Results of a cavity expansion modeled using a finite element software ABAQUS@ (Abaqus, 2009) are also introduced for analysis. The cavity expansion simulated in Abaqus was defined according an axisymmetric model, with unit weight and infinite extend (classical approach). The same initial and boundary conditions used in the analytical model were adopted in the finite element approach. For the constitutive model, the Drucker Prager combined with linear elasticity was considered. Elements used are 8-node axyssimetric quadrilateral, biquadratic displacement, bilinear pore pressure and reduced integration (CAX8RP).

Two radius of influence were considered for analysis:

- a = $(I_r)^{1/2}$×R with I_r=874 (defined from triaxial results, Bedin et al. 2012)), corresponding to a radius of influence of about 30 times the cylinder radius (a=30×R).
- and a=10×R to examine the possibility of better prediction of measured data and to comply with previous studies (Vesic, 1972; Randolph & Wroth, 1979; Osman & Randolph, 2010, 2012).

Maximum displacements were defined by limiting the local strains to 10% to try to comply with the model assumptions (infinitesimal strains). From a practical engineering perspective, strain levels as high as 10% are often admitted for geotechnical testing interpretation. It is therefore implicitly assumed that predictions obtained from both the simplified model and numerical approach are reasonable approximations for cylinder expansion, although a large strain formulation would be more appropriate.

The measured piezocone data are compared to analytical and numerical (finite element) predictions in Figures 4 and 5. The results presented in the present paper are focused on the interpretation of drainage effects in the normalized velocity space (for simplicity only V_h) combined with normalized cone tip resistance Q/Q_{ref} and normalized pore pressure $\Delta u/\Delta u_{ref}$, where Q_{ref} is the maximum value of Q (Q_{ref}=Q_{max}) corresponding to the drained penetration, and Δu_{ref} is the maximum value of mobilized pore pressure (Δu_{ref} =Δu_{max}), corresponding to undrained penetration.

From Figures 4 and 5 is possible to observe that predictions are generally able to capture the experimental trends shown in the Q×V_h and U×V_h spaces, but with some discrepancies. In terms of resistance (Q×V_h) both the analytical and numerical models underestimate the Q_D/Q_{UD} measured ratio of 11, but the models somehow capture the transitions from drained to partial drained to undrained. In the normalized pore pressure space U×V_h the models underestimate the drained normalized velocity. Transition from undrained to partial drainage is typically in the range of 1 to 10, but the onset of drainage is underestimated by at least one log-cycle.

The reduction proposed in the zone of influence (a=10×R instead of a=30×R) has a significant effect on the variation of pore fluid pressure with time. Adopting a zone of influence of 10 times the cavity radius produces a better approximation of the velocity V_h that characterized the transition for partially drained to drained behavior.

Table 3. Gold Tailings constitutive parameters

Constitutive parameters	
p_{c0}(kPa)	100
p_0' (kPa)	50
u_{max}	$p_{c0}(1+M_{cs})/2$
p_0 (kPa)	$p_0' + u_{max}$
γ_w (kPa)	10
k (m/s)	1.00E-08
K (KPa)	5814
ε_{ref}	0.01
e_0	1.34
K_s (GPa)	0.1
ϕ	32
ν	0.30
R (cm)	2.5
a (cm)	10R 30R

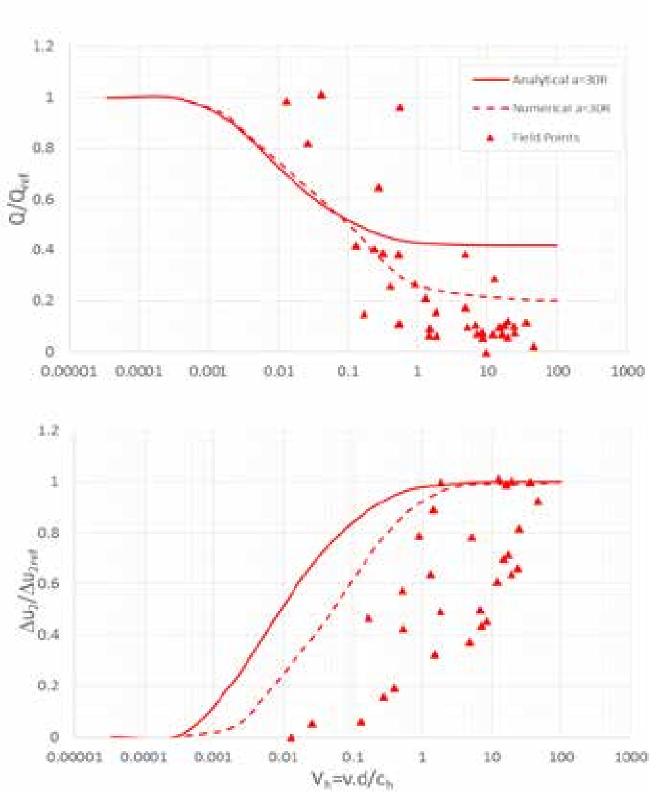

Figure 4. Comparisons between analytical and numerical predictions to field data in tailings for a/R=30

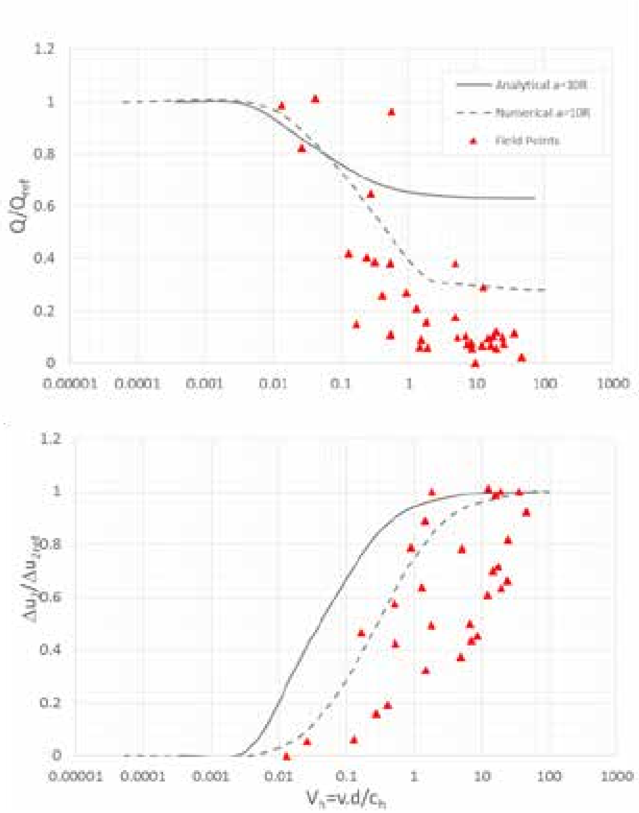

Figure 5. Comparisons between analytical and numerical predictions to field data in tailings for a/R=10

5 CONCLUSION

A non-linear poroelastic analytical solution for a cylindrical cavity expansion analysis developed in Dienstmann et al. (2015) is briefly described and applied to the investigation of rate effects into piezocone tests executed in a gold tailings deposit. Numerical simulations using finite elements are also used to enforce the validity of the analysis. The derived limit pressure (associated to q_c by the method of Rohani & Baladi, 1981) together with the pore pressure u_2 obtained from the analytical and numerical formulations are directly compared to field data. Results are shown to capture the experimental trends in the Q×V_h and U×V_h spaces: the ratio of drained to undrained resistance Q_D/Q_{UD} is underestimated in both models, and the velocity that defines the transition from drained to partially drained response is also under-predicted. Partially drained behavior occurs at a normalized velocities V_h in the range of 0.01 to 10. The practical recommendation is to perform tests at different penetration rates in the same location to establish the characteristic drainage curve of the soil to guide interpretation.

6 ACKNOWLEDGMENTS

The writers wish to express their gratitude to the Brazilian agency CNPq for the financial support to the research group. We are particularly grateful to YAMANA for the permission to assess their operational facilities and GEOFORMA for the collaboration during the field tests.

7 REFERENCES

ABAQUS *User's Manual*. Dassault Systèmes, Simulia Corp. ABAQUS© vs. 6.9, Providence, Rohde Island, USA.

Baligh M.M. (1985). Strain path method. *Journal of Soil Mechanics and Foundation engineering Division*, ASCE, 11(7):1108-1136.

Bedin, J. (2010). Study of the geomechanical behavior of tailings. PhD thesis, Federal University of Rio Grande do Sul, Brazil, Graduate Course in Civil Engineering (in Portuguese).

Bedin, J.; Schnaid, F.; Fonseca, A. J. P. V.; Costa Filho, L. M. (2012). Gold tailings liquefaction under critical state soil mechanics. *Geotechnique*, v. 62, p. 263-267.

Biot, M.A. (1941).General theory of three-dimensional consolidation, *Journal of Applied Physics*, 12:155-164.

Blight, G.E. (1968). A note on field vane testing of silty soils. *Canadian Geotechnical Journal*, 5: 142–149.

Burns, S.E., Mayne, P.W. (2002). Analytical Cavity Expansion – Critical State Model for Dissipation in Fine-Grained Soils. *Soils and Foundations*, 42(2):131-137.

Cao, L.F., TEH, C.I., Chang, M.F. (2001) Undrained cavity expansion in modified Cam clay. I: Theoretical analysis. *Geotechnique* 51(4):323–334

Chang, M.F., Cao, L.F., Teh, C.I. (2001) Undrained cavity expansion in modified Cam clay. II: Application to the interpretation of cone penetration tests. *Geotechnique* 51(4):331–346

Chen, S.L., Abousleiman, N.Y. (2012) Exact undrained elastoplastic solution for cylindrical cavity expansion in modified Cam Clay soil. *Geotechnique* 62(5):447–456

Chen, S.L., Abousleiman, N.Y. (2013) Exact drained solution for cylindrical cavity expansion in modified Cam Clay soil. *Geotechnique* 63(6):510–517

Dienstman, G. (2015). Analysis of in situ test in transient flow. PhD thesis, Federal University of Rio Grande do Sul, Brazil, Graduate Course in Civil Engineering (in Portuguese).

Dientsman, G., Maghous, S. and Schnaid, F. (2015). Theoretical analysis and finite element simulation for non-linear poroelastic behavior of cylinder expansion in infinite media under transient pore-fluid flow conditions. *International Journal of Geomechanics*. Submitted for publication.

Gibson, R.E., Anderson, W.F. (1961). In situ measurement of soil properties with the pressuremeter. *Civil Engineering and Public Works Review*, 56: 615-618.

Jaeger, R. A., DeJong, J. T., Boulanger, R. W., Low, H. E., and Randolph, M. F. (2010). Variable penetration rate CPT in an intermediate soil. *Proceedings of International Symposium of Cone Penetration Testing*, Huntington Beach, CA.

Jamiolkowski, M. Masella, A., (2015) Geotechnical Characterization of Copper Tailings at Zelazny Most Site. *DMT'15 The 3rd Int. Conf. on the Flat Dilatometer*, Rome, Italy, 25-42.

Klahold P.A. (2013). Interpretation of field tests on soils with intermediate permeability. MSc Thesis, Federal University of Rio Grande do Sul, Brazil, Graduate Course in Civil Engineering (in Portuguese).

LeBlanc, C. & Randolph, M.F. (2008). Interpretation of piezocones in silt, using cavity expansion and critical state methods. *Proceedings of the 12th International Conference of International Association for Computer Methods and Advances in Geomechanics* (IACMAG), pp. 822-829.

Lehane, B.M., O'Loughlin, C.D., Gaudin, C., Randolph, M.F. (2010). Rate effects on penetrometer resistance in kaolin. *Géotechnique*, 59(1): 41–52.

Morris, P.H., Williams, D.J. (2000). A revision of Blight's model of field vane testing. *Canadian Geotechnical Journal*, 37: 1089–1098.

Nierwinski, H.,P. (2013). Liquefaction potential of mining tailings estimated by field tests. MsC thesis, Federal University of Rio Grande do Sul, Brazil, Graduate Course in Civil Engineering (in Portuguese).

Osman, A. (2010). Comparison between Coupled and Uncoupled Consolidation Analysis of a Rigid Sphere in a Porous Elastic Infinite Space. *Journal of Engineering Mechanics,* ASCE, 136(8):1059–1064.

Osman, A. S., Randolph (2012) Analytical solution for the consolidation around a laterally loaded pile. *International Journal of Geomechanics*, 12:199–208.

Randolph, M.F., Wroth, C.P. (1979). An analytical solution for the consolidation around a driven pile. *International Journal for Numerical and Analytical Methods in Geomechanics,* 3(2): 217-229.

Rohani, B. & G. Y. Baladi. (1981). Correlation of mobility cone index with fundamental engineering properties of soil. *International Society for Terrain-Vehicle Systems.* Vol 3:959-990. Alberta, Canada.

Salgado R., Mitchell, J.K., Jamiolkowski, M. (1997) Cavity expansion and penetration resistance in sand. *J Geotech Geoenviron Eng.* ASCE 123(4):344–354

Schnaid, F. (2005). Geo-Characterization and Properties of Natural Soils by In Situ Tests. *Proceedings of the International Conference on Soil Mechanics and Geotechnical Engineering*, Osaka, Vol. 1, 3–47.

Schnaid, F. , Bedin, J., Viana da Fonseca, A. J. P. , De Moura Cista Filho, L. (2013). Stiffness and Strength Governing the Static Liquefaction of Tailings. *Journal of Geotechnical and Geoenvironmental Engineering*, v. 139, p. 2136-2144.

Silva, M. F. (2005). Numerical and physical models of rate effects in soil penetration. Ph.D. thesis, Cambridge University, Cambridge, UK.

Silva, M.F., White, D.J., Bolton, M.D. (2006). An analytical study of the effect of penetration rate on piezocone tests in clays. *International Journal for Analytical and Numerical Methods in Geomechanics*, 30(6):501-527.

Teh, C.I., Houlsby, G.T. (1991). An analytical study of the cone penetration test in clay. *Geotechnique*, 41(1): 17-34.

Vesic, A.S. (1972). Expansion of cavities in infinite soil mass. Journal of the Soil Mechanics and Foundations Division (JSMFD), *Proceedings of the American Society of Civil Engineers* (ASCE), 98:265-290.

Yu, H.S. & Mitchell, J.K. (1998). Analysis of cone resistance: a brief review of methods. *Journal of Geotechnical and Geoenvironmental Engineering*, ASCE, 124(2):140-149.

Zhang, Y., Jingpei, L., Liang, F., Tang, J. (2016). Interpretation of cone resistance and pore-water pressure in clay with a modified spherical cavity expansion solution. *Bull Eng Geol Environ* 75:391–399

Geotechnical and Geophysical Site Characterisation 5 – Lehane, Acosta-Martínez & Kelly (Eds)
© 2016 Australian Geomechanics Society, Sydney, Australia, ISBN 978-0-9946261-1-0

Reliability of soil porosity estimation from seismic wave velocities

S. Foti & F. Passeri
Politecnico di Torino, Turin, Italy

ABSTRACT: Soil porosity is a state parameter of fundamental importance for several geotechnical problems. Geophysical testing provides appealing strategies for the determination of soil porosity, as several geophysical parameters are directly related to soil porosity. In particular the theory of wave propagation in saturated porous media, developed by Biot in the 1950s, allows the determination of soil porosity from the measured velocity of propagation of compressional and shear waves. A formal assessment of the reliability of the estimated porosity values is of primary importance to evaluate the applicability of this approach to solve practical geotechnical problems. In this paper the propagation of measurement uncertainties on the estimated values of soil porosity is theoretically evaluated. Moreover, experimental data of multiple acquisitions of cross-hole tests are considered. Data collected by different operators are also used to assess the confidence interval associated to different equipment, acquisition practices and testing methodology.

1 INTRODUCTION

Porosity is widely recognised as a key parameter as it affects the mechanical and hydraulic response of soils. A crucial issue in its determination is typically represented by the difficulties in collecting high quality undisturbed samples for coarse-grained soils (Jamiolkowski 2012) or for deep formations (Musso et al. 2015). Usually in geotechnical engineering, the relative density of sands is obtained through empirical correlations with in situ tests, whose reliability is not easily assessed.

In geomechanics of reservoirs and rock physics, porosity is commonly derived through analytical and/or (semi-)empirical formulations from geophysical parameters measured in wells (e.g. Mavko et al. 1998).

Foti et al. (2002) proposed an approach for porosity assessment on the basis of measured seismic wave velocity by adopting the formulation by Biot (1956a, 1956b) for linear elastic, isotropic and fully saturated porous media. In the Biot theory linear poroelasticity is applied with simultaneous superposition of fluid and solid phases in the same region of space.

Under the assumption of undeformable solid grains, the non-linear functional relationship to evaluate soil porosity n can be written as (Foti et al. 2002):

$$n = \frac{\rho^s - \sqrt{(\rho^s)^2 - \dfrac{4\,(\rho^s - \rho^w)\,K^w}{V_p^{\,2} - 2\left(\dfrac{1-\nu_{sk}}{1-2\,\nu_{sk}}\right)V_s^{\,2}}}}{2\,(\rho^s - \rho^w)} \tag{1}$$

where: ρ^s and ρ^w are respectively the mass densities of the soil particles and pore water; K^w is the bulk modulus of the pore water; V_p and V_s are the velocities of propagation of the dilatational and shear waves, respectively; ν_{sk} is the Poisson's ratio of the (evacuated) soil skeleton.

The equation (1) was also validated in several case studies (Foti et al. 2002, Foti & Lancellotta 2004, Lai & Crempien 2012, Jamiolkowski 2012, Callerio et al. 2013). The stability of the inversion procedure and the problem well-posedness were established by exploring the connection with ν_{sk} at different V_p-V_s couples (Lai & Crempien 2012). Results proved a general low-dependence on the parameter, except for high velocities (stiff soils), whereas the study offers a useful guide in adopting the simplified formulation.

In the present paper an analysis of the uncertainties is conducted, making use of the basic tools of the error propagation theory (Taylor 1997). The final aim is to reveal the influence of the parameters involved in the porosity equation (1). A particular attention is paid to the role of the Poisson's ratio of the evacuated soil skeleton and to the velocity of compressional waves in water, which appear to be the most influent a-priori parameters on the final estimate.

Finally, two case studies are reported, with experimental data from Zelazny Most (Poland) and Mirandola (Italy). The first example regards an ad-hoc geophysical survey in which repeated travel times and inclinations measures were carried out for a cross-hole experiment, aiming at reaching a well-defined statistical population. The latter includes data from different companies, operators and field techniques to investigate the soil using cross-hole and suspension loggings tests.

2 PARAMETRIC UNCERTANTIES ANALYSES

In physics, there are two kinds of measurements: direct and indirect. Uncertainties are related to experimental errors (systematic or random) during the measuring stage or introduced in the subsequent interpretation process that provides a derivative physical quantity.

The error propagation theory can be used to characterise the influence of each parameter that appears in the porosity formulation in (1), in this example specialized for a cross-hole test configuration.

The starting point is to consider all uncertainties involved in the direct measures as randomly distributed and independent. These hypotheses enable us to assume each parameter as normally distributed (following a Gaussian probability distribution). We consider $n = n\ (\rho^s, \rho^w, K^w, V_p = d/t_p, V_s = d/t_s, \nu_{sk})$ as a several variable function, where d is the travel distance and t_i the travel times for each seismic wave (with $i = p, s$). Supposing that ρ^s, …, ν_{sk} are measured with fractional uncertainties $\varepsilon_{\rho s}$, …, $\varepsilon_{\nu sk}$ and the measured values are used to compute the function n, the uncertainties in porosity are never larger than the ordinary sum:

$$\varepsilon_n n = \left|\frac{\partial n}{\partial V_p}\right| V_p(\varepsilon_{t_p} + \varepsilon_d) + \left|\frac{\partial n}{\partial V_s}\right| V_s(\varepsilon_{t_s} + \varepsilon_d) + \\ + \left|\frac{\partial n}{\partial K^w}\right| \left(2\rho^w {V_w}^2 \varepsilon_{V_w}\right) + \left|\frac{\partial n}{\partial \nu_{sk}}\right| \nu_{sk}\varepsilon_{\nu_{sk}} + \\ + \left|\frac{\partial n}{\partial \rho_w}\right| \rho_w \varepsilon_{\rho_w} + \left|\frac{\partial n}{\partial \rho_s}\right| \rho_s \varepsilon_{\rho_s} \qquad (2)$$

In (2) $V_p = d/t_p$ and $V_s = d/t_s$ are associated to the fractional uncertainties on distance and travel-times, as they are the actual measured quantities in cross-hole tests. Moreover the bulk modulus of the fluid is defined as $K^w = \rho^w {V_w}^2$, whereas $\partial/\partial n$ are partial derivatives.

It is essential to emphasise that quantities ν_{sk} and V_w are not typically evaluated through an experimental procedure on site (as for d or t_i). In the following they have been defined by a presumptive best value and an associated own uncertainty.

Many authors examined the typical Poisson's ratio for sands and its dependence on other parameters of the soil. For example, Nakagawa et al. (1997) and Bates (1989) illustrated the connection between ν_{sk} and effective confining pressure for different example of sands. Wichtmann & Triantafyllidis (2010) analysed the link between ν_{sk} and size distribution characteristics, whereas they are in accordance with Xiaoquiang et al. (2013), which stated the dependence on confining pressure and void ratio. An additional study is reported by Kumar & Madhusadhan (2010), where the Poisson ratio is also analysed changing the relative density of the sand. Taking into account this literature, it has been assumed $\nu_{sk} = 0.25 \pm 0.1$.

As for the velocity of compressional waves in water, in accordance with Lubbers & Graaff (1998), it is calculated by a formula considering temperature-dependence in the 10°C - 20°C range, determining the reference value and dispersion as $V_w = 1464.8 \pm 17.4$ m/s. In this context our aim was to identify a realistic situation of underground fluctuating temperature, for the illustration of the proposed approach. However it is evident that a more precise evaluation of the water temperature allows minimising the contribution of this physic parameter to the uncertainty on the porosity evaluation.

In this study other ancillary parameters are always assumed as $\rho^s = 2.7$ g/cm^3 and $\rho^w = 1$ g/cm^3.

Figure 1 shows the percentage fractional error propagated on n due to 1% error on t_p, d, V_w and ν_{sk}, respectively. It is worth to mention that the percentage fractional error is convenient as a comparison tool, however each parameter has a typical uncertainty range (e.g. 0.1% for d and 40% ν_{sk}). The distance (Fig. 1b) is the most influent parameter involved, with highest percentage fractional errors propagated on n. Following the propagation theory, its influence is the sum of the t_p (Fig. 1a) and t_s contributes, i.e. slightly more than t_p, since t_s has minor importance. A mass density change achieves a small oscillation in the porosity and uncertainties in these two parameters are negligible. The velocity of sound in water shows a marked effect on the calculated porosity (Fig. 1c). Finally, Figure 1d regards the Poisson's ratio of the evacuated soil skeleton. In this case, percentage fractional errors propagated on n are very limited, but the uncertainty associated to this parameter is substantial, so it actually has a large influence on the estimate of porosity.

In Figure 1, the white curves delimitate the most significant area with respect to natural sand deposits. Indeed several couples of V_s-V_p values in Figure 1 are unrealistic for two main causes: the typical porosities of sands and the physical relationships between the variables. In particular high V_p values are not realistic if associated to low V_s values (area above the top white line), whereas couples below the lower white line represent unrealistic values of porosity for a typical coarse grained soil.

Considering the area between the two white curves in Figure 1, it is possible to draw the following conclusions of the parametric analysis for an uncemented sand ($V_s < 500$m/s):

- Uncertainties on the arrival time of P-wave (t_p) are amplified with a factor 3.5 to 5;
- Uncertainties on the distance between the two holes (d) are amplified with a factor 3.5 to 6;
- Uncertainties on compressional wave velocity in the pore fluid (V_w) are amplified with a factor 2.5 to 4;
- Uncertainties on the Poisson's ratio of the (evacuated) solid skeleton are factored with a weight 0.2 to 0.45
- Uncertainties on the other parameters (t_s, ρ^s and ρ^w) are negligible (the corresponding graphs are not reported).

3 CASE STUDIES

3.1 *Zelazny Most*

Repeated measurements of cross-hole experimental data were collected at the site of Zelazny Most tailing dam in two different campaigns in 2011 and 2014 (Callerio et al. 2013, Jamiolkowski 2012-2014, Jamiolkowski & Masella 2015). Measurements of P and S seismic wave propagation were constantly repeated to form a statistical population. Specifically, travel time measurements and deviation surveys were repeated to statistically evaluate average values and related uncertainties.

A statistical assessment of the test repeatability was obtained and 50th, 85th and 95th percentiles have been calculated.

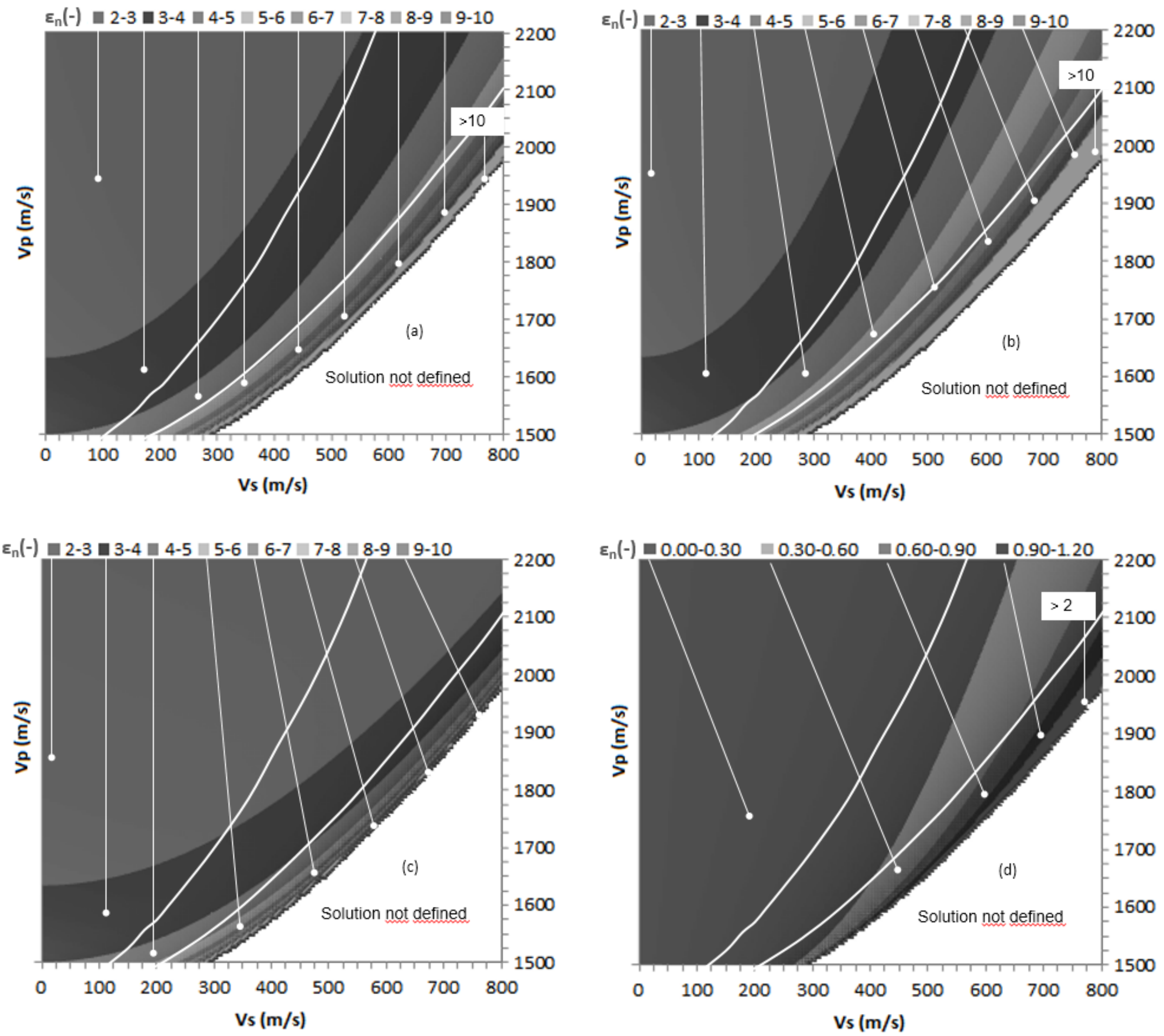

Figure 1. Induced fractional uncertainties on n by: (a) t_p, (b) d, (c) V_w, (d) ν_{sk}.

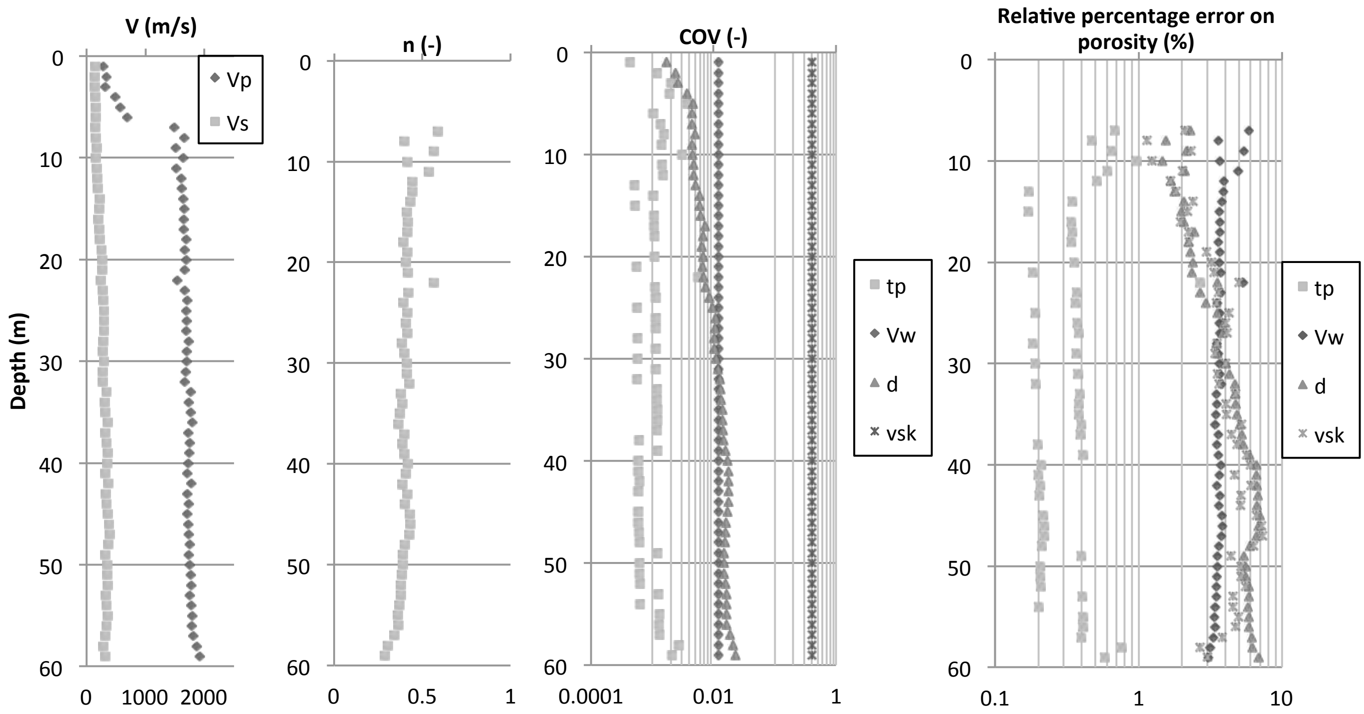

Figure 2. (a) Velocities profiles, (b) estimated porosities, (c) coefficients of variation, (d) relative percentage errors on porosity (XIX 4E-5E).

Evidences for a single borehole (XIX 4E-5E) are illustrated in Figure 2, with the velocity profiles (Figure 2a) and the estimated porosity according to equation 1 (Figure 2b). In Figure 2c and 2d the coefficients of variation and the calculated percentage uncertainty propagated on n are proposed for each parameter involved. Figure 2d shows that the propagated percentage error on n due to t_p is one order lower than the uncertainty due to d, V_w or ν_{sk}. In any case the uncertainty associated to each parameter is limited to values lower than 7%.

In this case Poisson ratio of the solid skeleton was set to a standard range according to literature ($\nu_{sk} = 0.25 \pm 0.1$).

As no information was available of the actual temperature in the subsoil, the mean value and the associated standard deviation of V_w have been assumed as in Section 2.

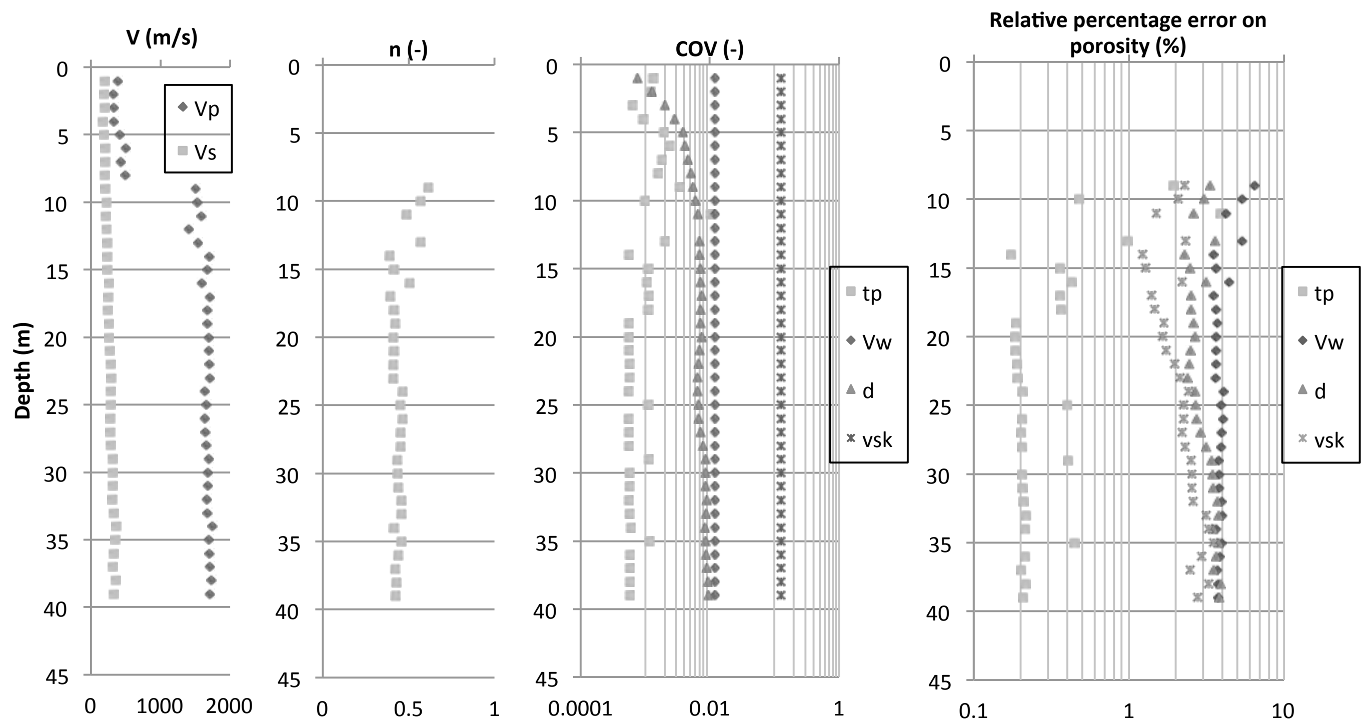

Figure 3. (a) Velocities profiles, (b) estimated porosities, (c) coefficients of variation, (d) relative percentage errors on porosity (VIII 7W-8W).

Figure 3 illustrates another example. For this borehole (VIII 7W-8W) the Poisson's ratio of the evacuated soil skeleton was assessed using data above the water table and the elastic formulations of wave propagation. The mean value of the Poisson's ratio of the evacuated soil skeleton is then 0.29, with a standard deviation of 0.04. Comparing Figure 2d and 3d, it is evident the lower impact of uncertainties from ν_{sk} on porosity assessments. Moreover uncertainties from a single parameter do not exceed 4-5%.

Figures 2 and 3 also show a relevant importance of the velocity of compressional waves in water propagated in the general formula. In both cases, its contribution is always ranging from 3% to 6% and it is often the most influent uncertainty on the calculated porosity. However, these uncertainties could be mitigated by restricting the temperature reference values, if reliable experimental measures are available. Finally, in this particular case, great care was adopted in the travel time and distance measurements, nevertheless clearly the uncertainty on distance evaluation plays a greater role than the uncertainty on travel time estimation (see also Callerio et al. 2013).

3.2 *Mirandola*

The second case study regards a site in the town of Mirandola (Italy), where extensive experimental data were gathered for the InterPACIFIC project (Garofalo et al. 2015), that aimed at assessing the reliability of different geophysical methods for seismic response analyses. In Mirandola several teams used different invasive methods at the same boreholes, carefully collecting information on accuracy (ability to obtain the ideal true value) and repeatability (precision) of each test.

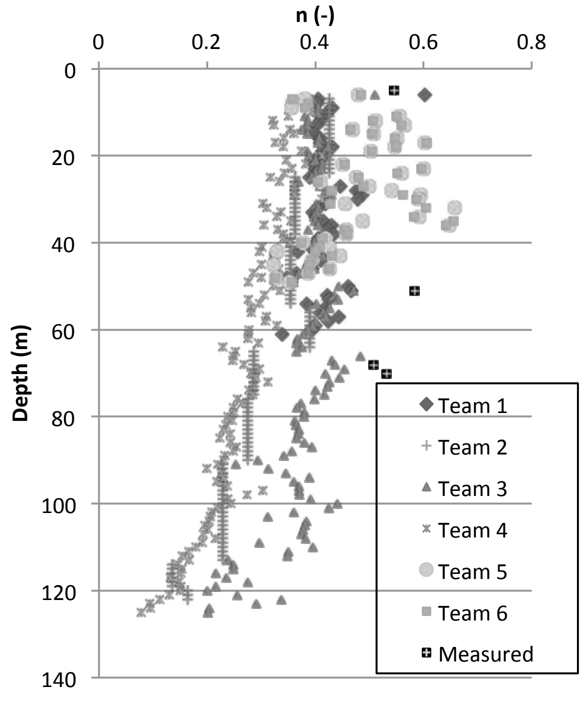

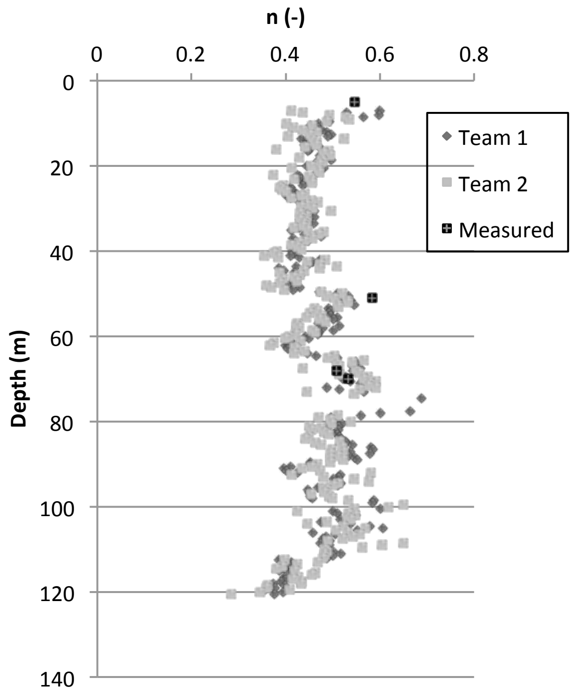

Figure 4. (a) Estimated porosities by different cross-hole tests, (b) estimated porosities by suspension loggings.

In the present study, porosity has been estimated with the seismic velocities measured by each team in cross-hole tests (Fig. 4a) and with P-S suspension logging measurements (Fig. 4b). Values of soil porosities from direct estimates on laboratory samples are also reported as a reference.

Figure 4a shows a very large variability on the results from cross-hole tests. Moreover apparently most of the estimates leads to underestimated values with respect to laboratory values. Apparently, more consistent results are obtained with the values of the P-S suspension logging (Fig. 4b).

4 CONCLUSIONS

In the present study, the uncertainties associated to porosity estimation with the approach proposed by Foti et al. (2002) have been considered. Results of the error propagation procedure show different relevance of the parameters, which appear in the formula. In particular, for a cross-hole test, the care in measuring the distance between the boreholes has huge importance, whereas the travel times revealed minor influence. The S-waves travel times have a very low incidence, especially for realistic V_p-V_s couples, whereas major attention should be paid on P-waves. On the other hand the velocity of compressional waves in water and the Poisson's ratio of the evacuated soil skeleton, which are usually assumed a-priori, are to be estimated with extreme care, since they present relevant effects on the estimate of n. As reported in the case studies these two parameters are the most important together with the distance, and future researches should be conducted in order to evaluate some mitigation possibilities. For example a more accurate investigation of the underground temperature oscillations could lead to narrower V_w uncertainty bounds. Moreover calculation of the Poisson ratio from unsaturated and homogeneous shallow layers can help in the evaluation of a site specific value of ν_{sk}, lowering the uncertainty on this parameter.

In the Mirandola case study the porosities estimations represented a useful tool to verify the results from cross-hole and suspension logging tests. In this case reliable laboratory porosities measurements are compared to estimates from seismic wave velocities to assess the reliability of the latter. Following this approach, the most reliable cross-hole result has been identified. An impressive match between porosities estimated by the suspension logging tests and the laboratory direct evaluation has also been found.

5 ACKNOWLEDGMENTS

The Authors are grateful to prof. Michele Jamiolkowski for making available the experimental data for the Zelasny Most case study and for the highly valuable discussions on the topic of this paper. The Mirandola data were collected for the InterPACIFIC project financed by the Research & Development Program SIGMA funded by EdF, Areva, CEA and ENEL and by CASHIMA project, funded by CEA, ILL and ITER. Regione Emilia Romagna made available additional borehole data and laboratory test results.

REFERENCES

Bates, C. R. 1989. Dynamic soil property measurements during triaxial testing. *Géotechnique* 39(4): 721-726.

Biot, M. A. 1956a. Theory of propagation of elastic waves in a fluid-saturated porous solid I. Lower frequency range. *J. Acoust. Soc. Am.* 28: 168-178.

Biot, M. A. 1956b. Theory of propagation of elastic waves in a fluid-saturated porous solid. II. Higher frequency range. *J. Acoust. Soc. Am*. 28: 179-191.

Callerio, A., Janicki, K., Milani, D., Priano, S. & Signori, M. 2013. Cross-Hole Tests at Zelazny Most Tailings Pond, Poland–Highlights and Statistical Interpretation of Results. *Near Surface Geoscience 2013, 19th European Meeting of Environmental and Engineering Geophysics*, *Bochum, Germany, 9-11 September 2013.*

Foti, S. & Lancellotta, R. 2004. Soil porosity from seismic velocities. *Géotechnique* 54(8): 551-554.

Foti, S., Lai, C. G. & Lancellotta, R. 2002. Porosity of fluid saturated porous media from measured seismic wave velocities. *Géotechnique* 52(5): 359-373.

Garofalo, F., Foti, S., Hollender, F., Bard, P.Y., Corno, C., Cox, B.R., Dechamp, A., Ohrnberger, M., Perron, V., Sicilia, D., Teague, D. & Vergniault, C. 2015. InterPACIFIC project: Comparison of invasive and non-invasive methods for seismic site characterization. Part II: Inter-comparison between surface-wave and borehole methods. *Soil Dynamics and Earthquake Engineering* 82: 241-254.

Jamiolkowski, M. 2012. Role of Geophysical Testing in Geotechnical Site Characterization. *Soils and Rocks* 35(2): 117-137.

Jamiolkowski, M. 2014. Soil mechanics and the observational method: challenges at the Zelazny Most copper tailings disposal facility. *Géotechnique* 64 (8): 590-618

Jamiolkowski, M. & Masella, A. 2015. Geotechnical Characterization of Copper Tailings at Zelazny Most Site. *3rd International Conference on the Flat Dilatometer*: 25-42

Kumar, J. & Madhusudhan, B. N. 2010. Effect of relative density and confining pressure on Poisson ratio from bender and extender element tests. *Géotechnique* 60(7): 561-567.

Lai, C. G. & Crempien de la Carrera, J. G. F. 2012. Stable inversion of measured V_P and V_S to estimate porosity in fluid-saturated soils. *Géotechnique* 62(4): 359-364.

Lubbers, J. & Graaff, R. 1998. A simple and accurate formula for the sound velocity in water. *Ultrasound Med. Biol.* 24(7): 1065-1068.

Mavko, G.M., Mukerji, T. & Dvorkin, J. 1998. *The Rock Physics Handbook.* New York: Cambridge University Press.

Musso, G., Cosentini, R. M., Foti, S., Comina, C. & Capasso, G. 2015. Assessment of the structural representativeness of sample data sets for the mechanical characterization of deep formations. *Geophysics* 80(5): D441-D457.

Nakagawa, K., Soga, K. & Mitchell, J. K. 1997. Observation of Biot compressional wave of the second kind in granular soils. *Géotechnique* 47(1): 133-147.

Taylor, J. R. 1997. *An introduction to error analysis, the study of uncertainties in physical measurements*. University Science Books Sausalito, California.

Wichtmann, T. & Triantafyllidis, T. 2010. On the influence of the grain size distribution curve on P-wave velocity, constrained elastic modulus M_{max} and Poisson's ratio of quartz sands. *Soil Dynamics and Earthquake Engineering* 30: 757-766.

Xiaoqiang, G., Jun, Y. & Maosong, H. 2013. Laboratory measurements of small strain properties of dry sands by bender element. *Soils and Foundations* 53(5): 735-745.

Geotechnical and Geophysical Site Characterisation 5 – Lehane, Acosta-Martínez & Kelly (Eds)

Discrete Element Method Modeling Studies of the Interactions between Soils and In-Situ Testing Devices

J. D. Frost, A. Martinez, J. Su and T. Xu
Georgia Institute of Technology, Atlanta, United States of America

ABSTRACT: This paper presents the results of a series of Discrete Element Modeling (DEM) studies that focus on the soil-device interactions that take place during in-situ testing with the Cone Penetration Test (CPT), the Dilatometer Test (DMT) and the K_0 Stepped Blade (KSB). Results from two-dimensional (2D) and three-dimensional (3D) simulations give insights regarding the induced soil deformations, loading conditions and soil fabric, which influence the measured soil response and should be accounted for in the interpretation of results from in-situ tests. The results highlight the relative importance of insertion disturbance effects on the induced stress conditions and measured soil response, as well as the effect of tool and push-rod rod geometry. Detailed results on the effect of sleeve surface roughness on the response of CPT friction sleeve measurements provides insights into potential modifications to the existing testing devices and procedures, as well as modified and new testing procedures and tools that would allow for a "more undisturbed" measurement of the soil response. The results presented in this paper illustrate the usefulness of DEM methods to study the processes involved in in-situ testing, as well as to assess their limitations.

1 INTRODUCTION

Discrete Element Method (DEM) modeling provides a valuable technique to compare various in-situ testing devices and the manner in which they interact with the surrounding soil either during insertion or in subsequent test phases as relevant. For example, in contrast to Cone Penetration Test (CPT) soundings where, in general, soil-instrument interaction is predominantly measured during actual device insertion using load and pressure sensors, other test techniques including the Dilatometer Test (DMT) and the K_0 Stepped Blade (KSB) rely on the measurement of soil-device interactions that occur at sequential stationary steps during insertion with pressure or displacement transducers. Empirical correlations developed over several decades using both calibration chamber and field data have yielded robust relationships that are used to predict soil properties.

During the development of the various test devices noted above, efforts have been expended to assess and account for the degree to which unavoidable effects are imparted to the soil due to the invasive nature of all these tests. In particular, disturbance effects due to the insertion of the physical devices into the ground are unavoidable but can be accounted for to varying degrees either through the incorporation of empirical correction factors based on experimental observations or numerical simulations. These simulations to date have largely used continuum based approaches such as the Finite Element or Finite Difference Methods.

The DEM method is a more recently developed simulation approach that is now being increasingly used to evaluate soil-device interactions and in particular to assess how a range of factors including device geometry, soil characteristics and test methodology can be accounted for in test interpretation. This paper follows this latter approach and uses the results of several different studies to isolate differences in the manner in which various devices interact with the surrounding soil. Specifically, these studies include:

- A comparison of the insertion stages of CPT, DMT and KSB devices in terms of total insertion force, contact force distribution and induced horizontal stresses using a 2D DEM model.
- A comparison of the response, particle displacements and normal and shear stresses during insertion of smooth and textured CPT friction sleeves using a 2D DEM model.
- A comparison of the response, shear zones, and void ratio evolution during insertion of smooth and textured CPT friction sleeves using a 3D DEM model.

Individually, and collectively, the results presented herein illustrate the valuable insight that can be gained from DEM model simulations of device insertion including device-soil interface interactions.

2 INSERTION OF CPT, DMT AND KSB

2.1 *Device Insertion DEM Model*

A model to evaluate the insertion of various devices was built using the PFC^{2D} software. The model consisted of a chamber whose boundaries were made of rigid walls containing circular particles (Figure 1). The simulations involved inserting the testing devices vertically from the top to the bottom of the chamber. During the insertion of each device, the contact force between any two particles at any testing stage was recorded as well as the local stress responses of soil at some locations (using the measurement circles, indicated in Figure 1). The total vertical forces required to insert the devices were also recorded. The linear elastic contact model without cohesion was used for all simulations.

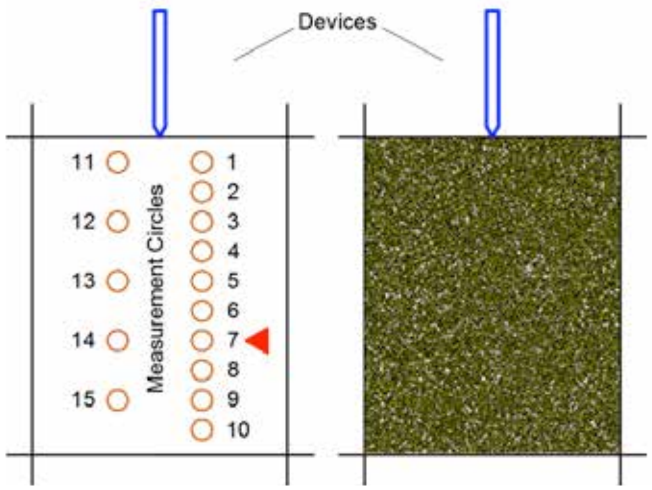

Figure 1. DEM model and location of measurement circle #7.

The devices in the DEM models were created with the wall function. The surface of the devices was set to be smooth and rigid. The relative sizes of the three devices (ASTM Standard D 6635-01, D 5778-95, D 3451-05 and Handy et al. 1990) are shown in Figure 2. The curves in light gray represent the membranes of the DMT and KSB devices.

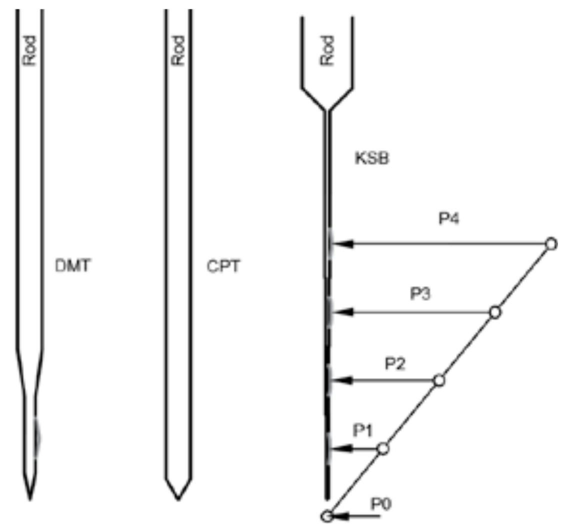

Figure 2. Relative sizes of the three devices

2.2 *Device insertion*

Contact forces between particles change during the insertion process. As a result, the particles adjacent to the penetration path are either displaced horizontally, accompanied by some slight rotation, or displaced vertically down. Porosities near the devices evolve, which results in stress redistribution in neighboring regions (Figure 3). This effect decreases to a negligible magnitude in the far field. Greater contact forces (reflected by the density of force chains in black) are observed for device elements with larger dimensions (e.g. CPT). Higher stress concentrations are also observed around irregular shaped regions of the devices (joint connecting DMT blade and rod, joints connecting KSB blades, etc.). As for insertion effects, thinner devices primarily displace the particles horizontally while thicker shaped devices result in both lateral displacement and vertical compaction effects on the particles (e.g. lower regions of the DMT and CPT plots, Figure 3).

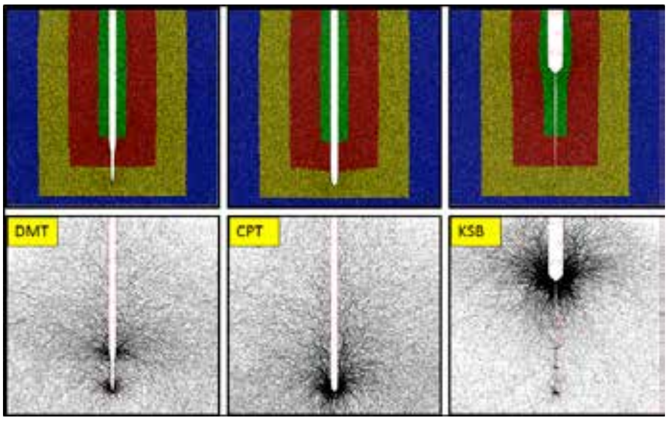

Figure 3. Close-up of sample deformation and contact force chain distribution during insertion of the three devices.

2.3 *Insertion forces and induced changes in stress*

The upper plot in Figure 4 shows the horizontal stress history during the insertion of the three devices. Specifically, the magnitude of stress plotted as a function of time step when the tips of the devices approach and pass measurement circle #7 (highlighted in Figure 1), shows that the stress magnitudes increase and then decrease back to a smaller value as the soil adjusts to the insertion of the device. For all devices, the initial increase is observed to be greater than any later increases. The later increases are due to either the DMT push-rod or the thicker KSB blades approaching the measurement circle.

The lower plot in Figure 4 shows the total force required to insert the device into the model. The result presented herein were obtained from simulations performed with the soil properties presented in Xu & Frost (2015). The devices with larger cross sectional areas require greater insertion force than those with smaller sizes during insertion (CPT > DMT > KSB). It is noted that the large increase in the KSB plot midway through the simulation reflects the larger diameter upper portion of the KSB contacting the soil and not the KSB blade itself.

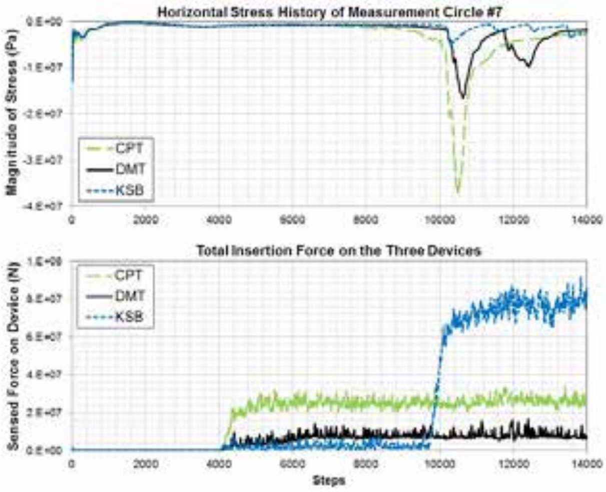

Figure 4. Vertical resistance and horizontal stress history of measurement circle #7 during the simulations.

3 2D SIMULATIONS OF CPT SLEEVE INSERTION

3.1 *Sleeve Displacement DEM Model*

A model to evaluate CPT friction sleeve insertion was built using the PFC^{2D} software. This model consisted of a two-sided shear box with the granular assembly and the friction sleeve inside it, as shown in Figure 5a. Constant lateral stress boundary conditions of 50 kPa were imposed on both sides of the shear box by means of a servo-control algorithm. The assembly consisted of 9000 two-particle clumps with an aspect ratio of 1.5. This particle shape was selected because it resembles the shape of Ottawa 20-30 sand. The linear elastic contact model without cohesion was used for all simulations. The virtual friction sleeves were modeled after conventional CPT sleeves (Figure 5b) and textured sleeves (Figure 5c) utilized by Frost & DeJong (2005) and Frost et al. (2012) in field testing with their multi-sleeve friction attachments. The smooth sleeve represented conventional CPT sleeves, while the textured sleeves had a maximum roughness of 1.00 mm and an average roughness of 0.185 mm. Detailed information regarding the calibration procedure and modeling parameters can be found in Martinez 2015.

3.2 *Response of CPT f_s reading*

Simulations against smooth and textured CPT sleeves allowed for study of the effect of sleeve surface roughness on the f_s reading, which captures the interface response of the sleeve-soil system. Figure 6 presents the f_s measurements, in terms of stress ratio, obtained from tests with smooth and textured friction sleeves. As shown, the test performed against

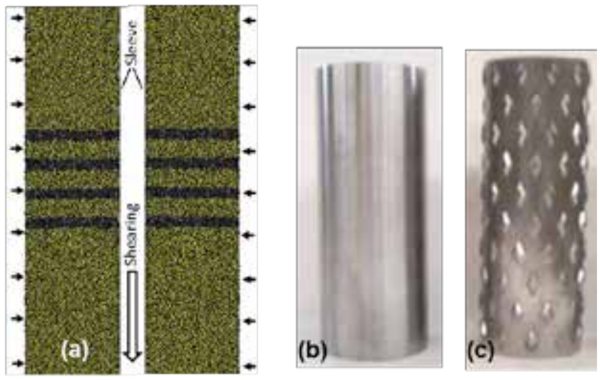

Figure 5. (a) DEM model. Photograph of (b) smooth and (c) textured sleeves.

the textured sleeve mobilized f_s readings that were on average 250% larger than those obtained from the test with a smooth sleeve. These results agree with the trends reported by Uesugi & Kishida (1986) for interface behavior and highlight the strong effect that the surface roughness of the friction sleeves has on the magnitude of the f_s measurements.

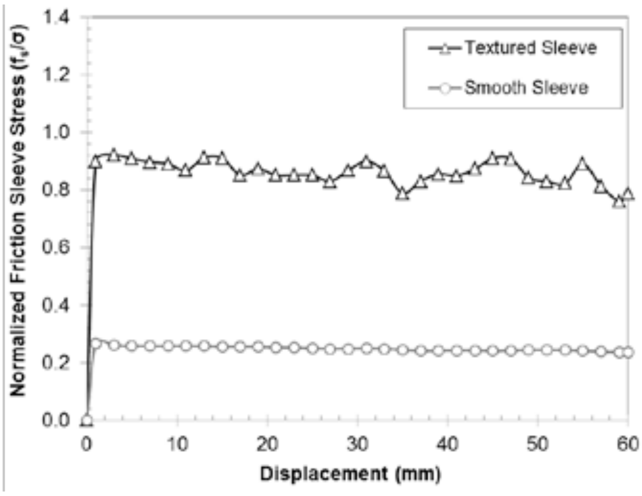

Figure 6. Normalized friction sleeve stress, f_s/σ, for tests against smooth and textured sleeves in 2D simulations.

3.3 *Induced soil deformations and loading conditions*

One of the principal advantages of DEM modeling is the ability to monitor particle-scale soil response, such as particle displacements and induced loading conditions. This allows for insight into the micro-mechanisms that govern the global response of the assembly. Figures 7a and 7b present soil deformations in the vicinity of smooth and textured sleeves, respectively, after 30 mm of sleeve displacement. It can be observed that negligible particle displacements were induced by shearing against the smooth sleeve, indicating that sliding between the sleeve and the particles was the principal interaction mechanism at the interface. On the other hand, shearing against the textured sleeve resulted in a well-defined shear zone where particle displacements are evident. These results clearly show the greater ability of the textured sleeves to engage the contacting soil.

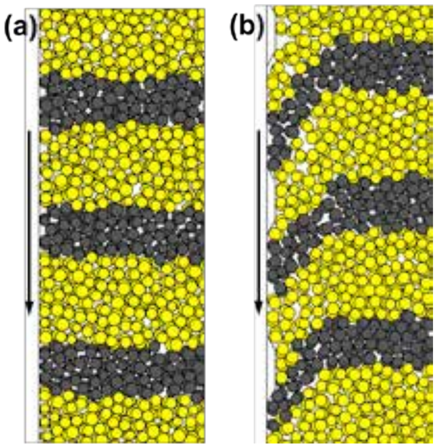

Figure 7. Soil deformations in the vicinity of (a) smooth and (b) textured sleeves.

The loading conditions induced during the insertion of smooth and textured sleeves are presented in Figures 8a and 8b, respectively. It can be observed that shearing against the smooth sleeve resulted in negligible increases in stress, while shearing against the textured sleeve resulted in large increases in both normal and shear stresses. These results further indicate that the textured sleeves were significantly more efficient at transferring load to the contacting soil, resulting in the larger friction sleeve readings presented in Figure 6.

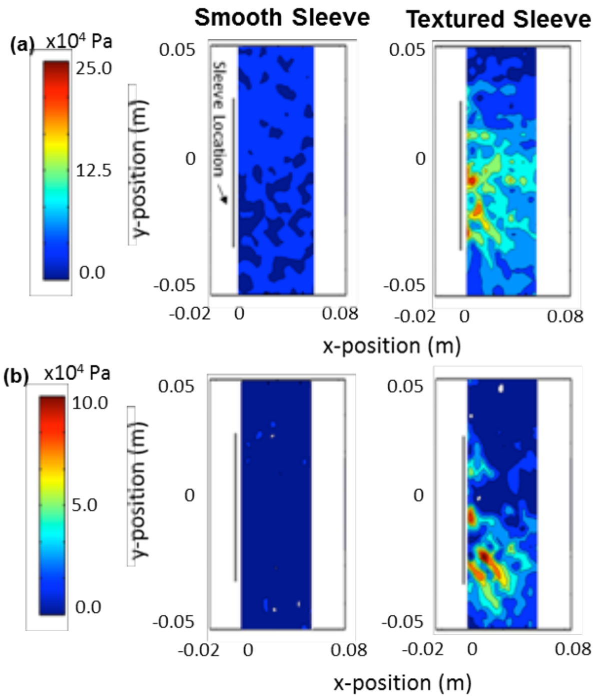

Figure 8. (a) Normal and (b) shear stresses in the vicinity of smooth and textured sleeves during shearing.

The results presented in this section clearly show the differences in global and local responses during insertion of smooth and textured CPT friction sleeves. It can be concluded that the friction sleeve measurements obtained from soundings with textured sleeves will be more representative of the soil response. The reasons are that soil shearing is effectively induced at the interface and loads are transferred from the friction sleeves to locations within the soil. Frost & DeJong (2005) have presented field data that support the numerical results presented herein. In contrast, the measurements from soundings with conventional smooth CPT sleeves only capture the resistance to sliding at the interface.

4 3D SIMULATIONS OF CPT SLEEVE INSERTION

4.1 *Sleeve Displacement DEM Model*

In order to better simulate the real experimental environment, the two dimensional study presented in the previous section was extended to a corresponding three dimensional model using the PFC^{3D} software. The computational requirements of the 3D model increase significantly faster because the number of particles in 3D increases more rapidly than for the corresponding 2D simulations. Certain simplifications such as scaling up particle size are a viable approach to reduce the number of particles (Butlanska et al. 2013). For simplicity, the soil particles were simulated as spherical particles, although more complex particle shapes are being evaluated in ongoing studies. In the current model (shown in Figures 9a and 9b), the soil parameters and testing environment are similar to the previous 2D simulations, with the exception that the mean particle size was chosen as six times larger than the 2D particle size in order to keep the relative roughness as well as the total number of particles in an acceptable range. The sleeve lengths and chamber heights in the model were also shortened to further decrease the computational demands. Even with all these simplifications applied, the number of particles in the model is still more than five times of that in the 2D model.

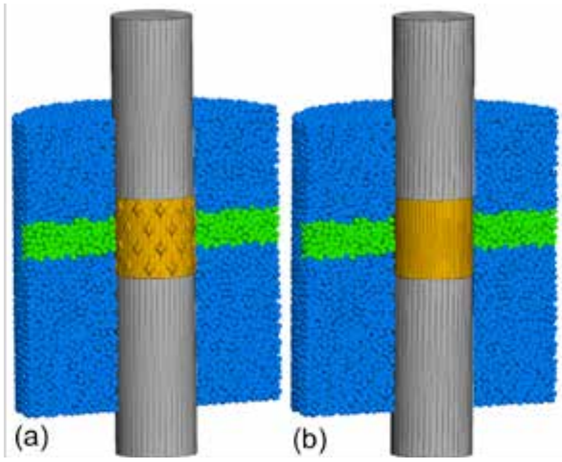

Figure 9. (a) 3D model with textured and (b) smooth sleeves

4.2 *Response of CPT f_s reading*

The responses of tests against a friction sleeve with a maximum roughness of 1 mm and against a smooth sleeve are shown in Figure 10. The normalized friction sleeve stress is lower than that in the corresponding 2D case due to the lack of particle angularity; however, the trend is similar with the peak shear stress of the textured sleeve-soil interface being about two times higher than that of the smooth sleeve interface.

The residual f_s values, which exhibit greater strain softening behavior in the 3D model than the corresponding 2D model, are also larger for the textured sleeve test than for the smooth sleeve test. These trends result from the fact that interfaces with a rougher surface are able to transfer more force from the device into the soil. Further, the 3D model has an additional degree of freedom that allows for the rearrangement of soil particles in space, and as a result, a larger number of soil particles is displaced.

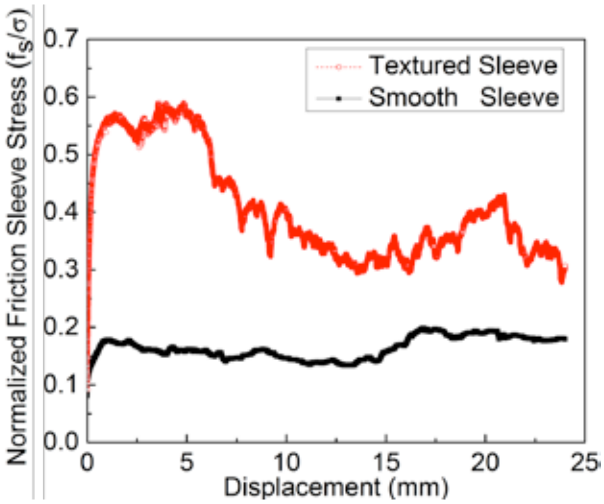

Figure 10. Normalized friction sleeve stress, f_s/σ, for tests against smooth and textured sleeves in 3D simulations.

4.3 *Induced soil deformations and loading conditions*

Based on the 3D model simulations, Figures 11a and 11b show the void ratio within the vicinity of textured and conventional smooth sleeves, respectively, after 24 mm of shearing. Larger void ratios are formed at the rough interface as a result of soil dilation. This is in contrast to the negligible void ratio changes following shearing against the smooth sleeve, which as previously noted only induces particle sliding against the sleeve surface.

These results visually assist in quantifying the size of the shear zone which evolves during friction sleeve insertion. In the 3D simulations presented herein, it is about 5 time the D_{50} of the particles, which matches the findings of others including Hebeler et al. (2015) from physical experiments.

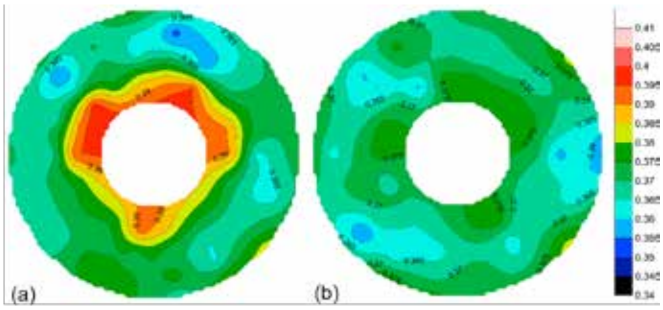

Figure 11. Local void ratio map after shearing against (a) textured and (b) smooth sleeves.

The induced particle displacements observed in the 3D simulations shown in Figure 12 confirm the different particle-sleeve interaction mechanisms that occur during shearing against textured and smooth sleeves. The force at the rough interface is transferred into the soil mass and more particles are mobilized. For smooth interfaces, only negligible shearing occurs at the interface. The limited soil displacements agree with the pure sliding mechanism described by Frost & DeJong (2005).

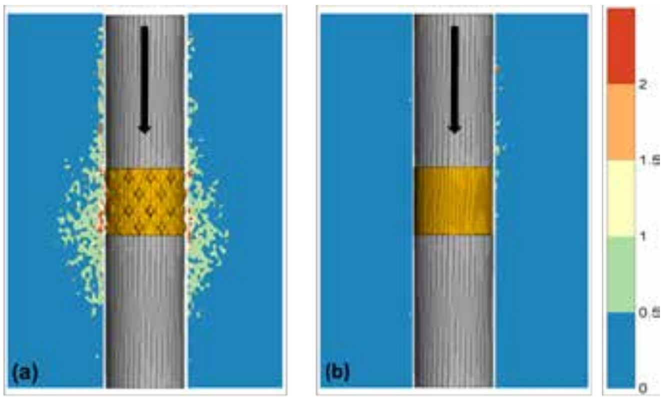

Figure 12. Particle displacement after shear for (a) textured and (b) smooth sleeves.

5 DISCUSSION

The preceding sections have presented the results of a series of DEM model simulation studies into the manner in which in-situ testing devices interact with the surrounding soil either during insertion or in subsequent test phases. Based on these studies, the following preliminary observations are made. It is noted that ongoing studies are continuing to further quantify the implications of these findings and propose interpretation enhancements to support the utilization of these well-established in-situ test devices.

The 2D DEM model simulation studies of device insertion showed the following:

• Changes in cross section, either as part of the actual device or where the device connects to the push-rod system, can lead to significant increases in interparticle contact force magnitude and distribution that may produce unintended "foreshadow" consequences that affect the measurements made with the test device. Such effects were previously reported based on physical experiments when texture was added to the sleeve of a conventional CPT device (DeJong et al. 2001). Similar "foreshadow" issues were shown to be present with the current design of the KSB that impact the upper portion of the blade but can be resolved with geometric modifications.

• The model simulations reported herein showed that consistent with the device cross sectional areas, KSB requires less total insertion force that the DMT which in turn requires less than the CPT for a given soil type. A sharp increase in the required KSB insertion force is attributable to the change in the device cross-section and any potential impacts of this can be readily addressed as noted above.

• The change in horizontal stresses as the devices approach and pass a "measurement zone" are also related to device cross-sectional area with the CPT producing larger increases than the DMT and the KSB, respectively. Stress changes due to the upper portion of the KSB blade are comparable to those for the DMT.

The 2D and 3D DEM model studies of device-soil interactions showed similar behaviors as follows:

• Textured sleeves induced larger shear stresses than smooth sleeves as a result of greater engagement of soil with the sleeve during insertion. Particle sliding dominated the smooth sleeve response whereas particle shearing dominated that of the textured sleeve.

• Void ratio changes and particle displacements were negligible for shearing against smooth sleeves while those for textured sleeves showed well-defined shear zones with significant increase in local void ratio due to dilation and concomitant particle displacements.

• The results obtained from the 2D and 3D simulations agree with each other, a fact that provides confidence in the validity of the insights obtained during this study.

6 CONCLUSIONS

Simulations of the type presented herein illustrate the ability of DEM modeling to provide valuable complimentary insight into physical experiments and their interpretation. Not only can the approach yield useful macro-scale simulations of the device insertion but it can also provide useful micro-scale insights into the manner in which devices interact with the soil either during insertion or in subsequent test phases as appropriate. While physical experiments can generally allow for useful boundary measurements of responses of a soil mass (force, displacement) to be determined, the ability of techniques such as DEM to allow individual particle displacements, rotations and contact forces and their distributions to be quantified and visualized, significantly expands our ability to understand the degree to which the interpreted soil properties are representative of in-situ conditions.

7 REFERENCES

ASTM Standards: D 6635-01. (2007) "Standard Test Method for Performing the Flat Dilatometer Test." ASTM International, West Conshohocken, PA.

ASTM Standards: D 5778-95. (2000) "Standard Test Method for Performing Electronic Friction Cone and Piezocone Penetration Testing of Soils." ASTM International, West Conshohocken, PA.

ASTM Standards: D 3451-05. (2005) "Standard Test Method for Mechanical Cone Penetration Tests of Soil." ASTM International, West Conshohocken, PA.

Butlanska, J., Arroyo, M., Gens, A. & O'Sullivan, C. 2013. Multi-scale analysis of cone penetration test (CPT) in a virtual calibration chamber. *Canadian Geotechnical Journal* 51: 51-66.

DeJong, J.T., Frost, J.D, and Cargill, P.E., (2001), "Effect of Surface Texturing on CPT Friction Sleeve Measurements", ASCE Journal of Geotechnical and Geoenvironmental Engineering, Vol. 127, No. 2, pp. 158-168.

Handy, R. L., Mings, C., Retz, D., and Eichner, D. (1990). Field Experience with the K_0 Stepped Blade. *Transportation Research Record.* 1278: 125-134.

Hebeler, G.L., Martinez, A. & Frost, J.D. 2015. Shear zone evolution of granular soils in contact with conventional and textured CPT friction sleeves. *KSCE Journal of Civil Engineering*. (Available online).

Frost, J.D. and DeJong, J.T. 2005. In-situ assessment of the role of surface roughness on interface response. *Journal of Geotechnical and Geoenvironmental Engineering,* 131(4): 498-511.

Frost, J.D., Hebeler, G.L. and Martinez, A. 2012. Cyclic multi-piezo-friction sleeve penetrometer testing for liquefaction assessment. *Proc. 4th International Conference on Geotechnical and Geophysical Site Characterization (ISC'4).* Pernambuco, *Brazil*, CRC Press, Boca Raton, pp. 629-636.

Martinez, A. 2015. Multi-scale studies of particulate-continuum interface systems under axial and torsional loading conditions. Ph.D. Dissertation, *Georgia Institute of Technology*, Atlanta, US. 246 pp.

Uesugi, M. and Kishida, H. 1986. Frictional resistance at yield between dry sand and mild steel. *Soils and Foundations*, 26(4): 139-149.

Xu, T., & Frost, J. D. (2015). "DEM Modeling of Insertion and Expansion during Flat Dilatometer Testing." Proc. *3rd International Conference on the Flat Dilatometer.* June 14-16, 2015. Rome.

Geotechnical and Geophysical Site Characterisation 5 – Lehane, Acosta-Martínez & Kelly (Eds)

Identification of the influence of overconsolidation effect on subsoil's stiffness by a CPTU method

Z. Młynarek
Poznań University of Life Sciences, Poznań, Poland

J. Wierzbicki
Institute of Geology, Adam Mickiewicz University, Poznań, Poland

T. Lunne
Norwegian Geotechnical Institute, Oslo, Norway

ABSTRACT: The paper contains the analysis of the influence of overconsolidation effect on the constrained moduli. The tested soils included soils from the area of Poland of similar grain size distribution that belong to two geological formations: normally consolidated tills of the Pomeranian Phase and overconsolidated tills of the Posnanian Phase. The overconsolidation ratio (OCR) was obtained with CPTU and oedometric tests. The tests revealed that for the assessment of changes in constrained modulus in the subsoil with CPTU tests, the formula determining the relationship between cone resistance and constrained moduli requires empirical coefficient different for soils of varied genesis. These coefficients were calculated from the relationship between cone resistance and constrained moduli from oedometric tests.

1 INTRODUCTION

The preconsolidation effect, which occurs in overconsolidated soils, entails the change in mechanical properties of the subsoil in relation to deposits undergoing the process of normal consolidation. This change can be explained with the analysis of the subsoil's behavior according to the "modified Cam-Clay" elastic-plastic model (Burland 1967). Worth & Houlsby (1985) demonstrated that subsoil overload, and subsequent unloading, modifies the position of the envelope elastic state for a given soil. Within the "Cam-Clay" model, the point that can be actually observed while testing subsoil's behavior under the re-load, is the point defining the so called plasticization stress σ'_y, and not the overconsolidation stress in the geological sense. In this approach, the change in mechanical parameters of soils does not necessarily have to be connected with historical overload. The necessity to include this fact in the interpretation of the test results was underscored by, among others, Jamiolkowski et al. (1985) and Izbicki & Stróżycki (2006).

Following this way of thinking, it can be assumed that, in the geological process, the series of post-sedimentation changes, which are part of generally understood diagenesis, begin with the deposition of sediment (Bolewski and Parachoniak 1988). The beginnings of the early diagenesis, in turn, (Pettijohn et al. 1987) are connected with the process of consolidation. Natural consolidation may be both syngenetic and post-genetic. The major interaction that triggers post-genetic consolidation of soil is the force of gravity, and the crucial mechanisms included are related to geological and engineering regimes (Powell 2005). Phenomena that support consolidation included also desiccation and the influence of hydrodynamic pressure (Jamiolkowski et al. 1985, Młynarek & Wierzbicki 2012, 2015). Therefore, it should be assumed that soils are formations at one of early stages of diagenesis. Overconsolidated soils, understood within the geotechnical meaning, may be then at the same stage of diagenesis as normally consolidated soils, i.e. the degree of diagenesis of both kinds of soil may be similar. Hence, as far as geological processes are concerned, the difference between overconsolidated and normally consolidated soils is relative, visible only in the context of the current state of geological environment. These processes are well represented by subsoils found in Poland.

In this view it becomes crucial not only to determine the general genetic type of soil (e.g. glacial till), but also to consider differences in sedimentary facies (e.g. melt-out till or lodgement till) and the stratigraphic position of the deposits (different phases of glaciation). The present paper aims at identification of these factors and their influence on constrained moduli obtained with CPTU.

2 CHARACTERISTICS OF THE TESTED SOILS

Soils selected for tests were the popularly characterized by homogenous genesis and lithology glacial tills. However, these formations fundamentally differ between one another in facies (hence, in more broadly understood genesis as well) (Stankowski 1996), which, in turn, leads to substantial differences in geotechnical properties (Wierzbicki 2009). The tests involved glacial tills of the Weichselian glaciation, which constitute a typical for Central European lowlands subsoil for foundation of constructions. Two groups of these soils were separated. The first group included glacial tills of the older stage, connected with transgression and retreat of Posnanian phase; the second group comprised of younger soils, connected with transgression and retreat of the so called Parsęta lobe of the Pomeranian phase. The important geological fact is that the growing Parsęta lobe trespassed on the earlier deposits of Posnanian phase, and then relatively soon retreated by melting of the so called dead-ice (Maksiak & Mróz 1978, Wierzbicki 2010). Grain size of the tills of both phases is similar, and the only difference is the smaller amount of sand fraction in the older tills (Fig. 1). Plasticity index of both deposits ranges from 11 to 18 per cent, and the $CaCO_3$ content from 3 to 8 per cent. Therefore, these are the deposits typically occurring in the Central European lowlands (Krygowski 1961). However, noticeable differences do occur in the facial of the sediments. These differences result mainly from the influence of geological processes that lead to the presence of overconsolidation effect in the tills of Posnanian phase, i.e. the lodgement type of deposits, additionally overconsolidated by the transgressing Parsęta lobe. In turn, deposits of the Pomeranian phase belong to the group of melt-out tills, which remained after the rapidly retreating ice sheet. Such a genesis of the tested soils allows for the assumption that the decisive factor influencing geotechnical properties of these soils, including compressibility, would be the variation of the degree of overconsolidation.

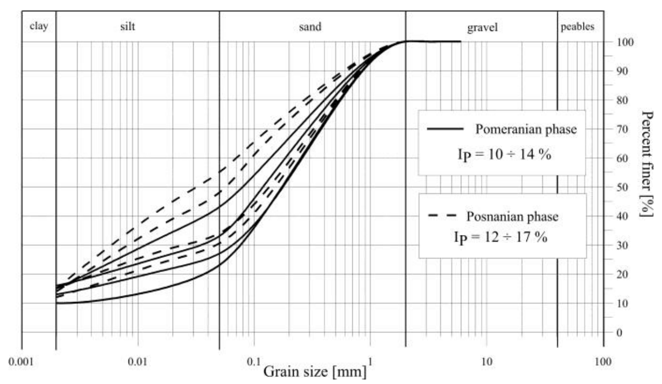

Figure 1. Standard grain size distribution of the tested soils.

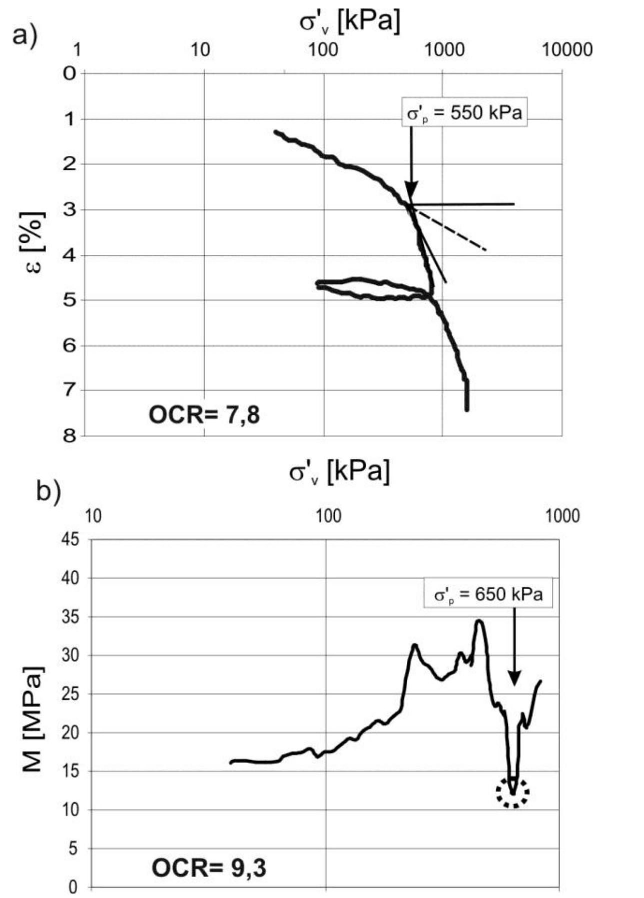

Figure 2. Results of oedometric tests of glacial tills of Posnanian phase and the values of preconsolidation stress, determined via Casagrande (a) and Janbu's (b) methods.

3 RESULTS OF LABORATORY TESTS ON OEDOMETRIC MODULI

The tests for determination of constrained moduli by means of CRS oedometric method were conducted with the Geonor device in compliance with guidelines introduced by Sandbaeken (1986). In the CRS test, a sample was being variably loaded with constant value of gradient of relative sample deformation in-situ. Initially, the sample was consolidated to the σ_{v0} value, and the actual test was initiated after the value of consolidation stress had been obtained. The test was carried out up to a stress value of 900 kPa. The sample was and then unloaded and reloaded to a stress value of 1.1 MPa. The CRS test provided constrained modulus distribution and graphs of changes in the values of oedometric constrained modulus - M_{0ed} in the function of stress changes (Fig. 2). Overconsolidation stress was determined with use of Casagrande graphic procedure (Fig. 2a) and Janbu et al. (1981) method (Fig. 2b). The soil samples, for which sample results are provided by Fig. 2, were block samples extracted from the depth range of 3,0 to 3,5 m of the tested profile.

The sample of Pomeranian phase till was extracted from the bottom layer of the profile, whereas the sample of Posnanian phase till from the top of the profile. The obtained results support the hypothesis of the differences in geotechnical properties between both sets of glacial till differ. Noticeably higher values of overconsolidation stress were received for tills of the Posnanian phase, hence the higher OCR values and twofold higher values of constrained modulus of these deposits in comparison to the Pomeranian phase.

4 IN SITU TESTS RESULTS

Twelve piezocone static penetration (CPTU) were conducted with the Hyson 20Tf penetrometer in the area of occurrence of the analyzed soils. As a complementation of these tests, samples for analysis of physical properties of the soil were extracted from boreholes. Based on this analysis, grain size distribution and liquidity index were determined. Fig. 3 presents results of the tested soils against the lithological profile.

For CPTU test, overconsolidation ratio (OCR) was determined using Wierzbicki (2010) nomograms for Polish soils (Fig. 4). Obtained results were compared with OCR values from oedometric tests, from an open pit in the direct vicinity of the CPTU (Fig. 5). Figure 5 indicates that CPTU yield results concerning the change pattern of OCR with depth and the actual values of the parameter. The Pomeranian phase tills are characterized by sharp decrease of OCR with depth, to the value of 2 at 5 m, and they are visibly separated from the lower tills of the Posnanian phase.

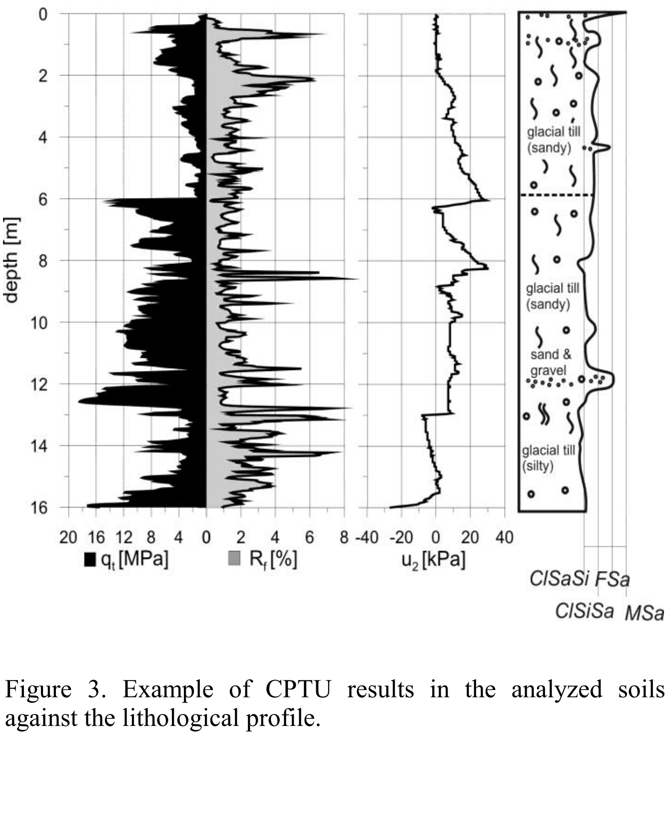

Figure 3. Example of CPTU results in the analyzed soils against the lithological profile.

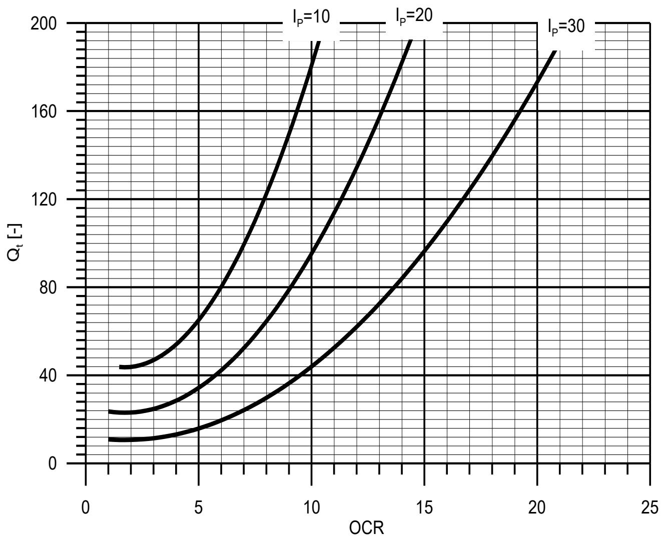

Figure 4. A nomogram for calculating the OCR values of cohesive soils with plasticity index I_P<30%, based on the Q_t parameter and the I_P value (Wierzbicki 2010).

On the border between the two sets a clear increase in the OCR values to about 12 can be observed. Further decline of the OCR values with depth is no more as pronounced as in the younger tills. The results of the in situ tests interpretation have been confirmed by the laboratory tests results.

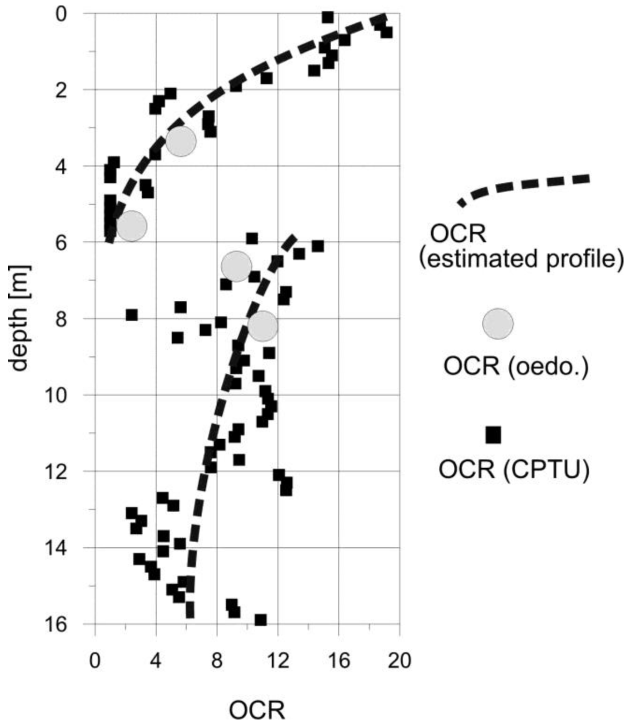

Figure 5. Changes in OCR values in the glacial tills profile.

5 INFLUENCE OF OVERCONSOLIDATION ON THE VALUES OF CONSTRAINED MODULUS

Values of the constrained modulus of tested soils were calculated with formula (1), commonly used for cohesive soils in Poland, for CPTU (Młynarek et al. 2003).

$$M_{CPTU} = 8{,}25\ (q_t - \sigma_{v0}) \qquad (1)$$

where: q_t – corrected total cone resistance.
This formula constituted a starting point for the further analyses aimed at clarification of the relationship between moduli from oedometric tests and from CPTU tests. To this end, values of the constrained modulus were determined also from the CRS tests. As a reference value, the σ_{v0} value determined for stresses occurring at the depth of soil samples extraction. CPTU and laboratory tests results were compared with the σ'_{v0} and σ'_p values. Figure 6 show two distinct trends of changes in the M_{oed} value depending on σ'_{v0} – for normally consolidated and overconsolidated soils (Fig. 6, 7). The values of M_{oed} moduli are similar to M_{CPTU} moduli in overconsolidated tills, but not in the case of normally consolidated soils.

The influence of overconsolidation and effective geostatic stress σ'_{v0} on the constrained moduli calculated from CPTU are shown in Figure 6 and 7. It is a generally known principle that in the subsoil composed of lithologically homogenous soils of a nearly constant value of liquidity index, a linear trend of constrained modulus with depth can be observed.

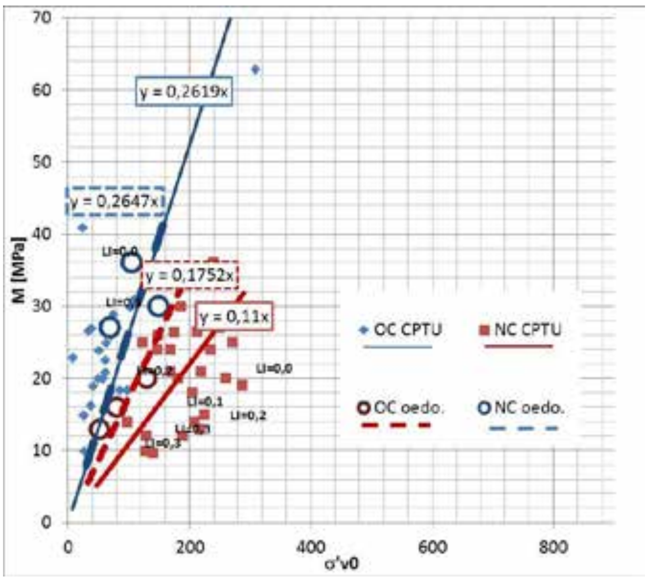

Figure 6. M_{CPTU} and M_{oed} moduli variation in comparison to σ'_{v0}.

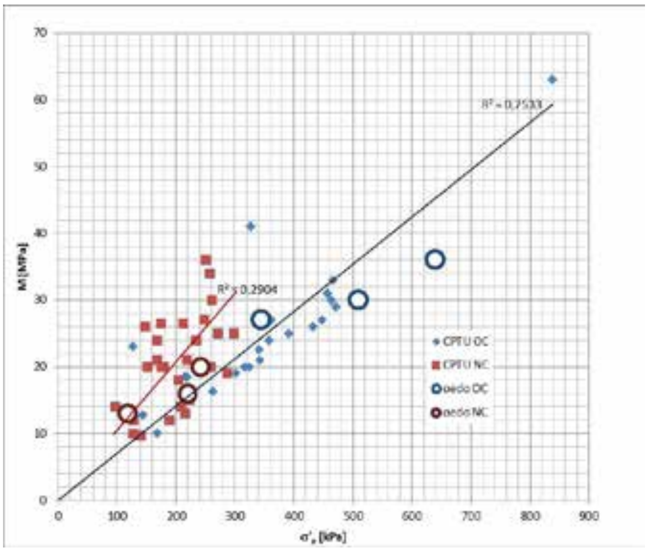

Figure 7. M_{CPTU} and M_{oed} moduli variation in comparison to σ'_p.

In the case of the tested deposits, the constrained modulus is a random variable, which depends on stress variability σ'_{v0}, OCR and liquidity index LI or sensitivity (Karlsrud et al. 2005). This fact is well illustrated by Figure 6. The obtained linear trendlines for relationship between constrained moduli M_{oed} and M_{CPTU} are characterized by relatively low values of correlation coefficient (R^2~0,3), because the other two variables, σ'_p i LI, not included in this assumption, also affect the correlation. At the same time in the discussed correlation the decrease of the difference between normally consolidated and overconsolidated tills is observed with the increase of liquidity index. Following this, Figure 7 demostrates the effect of σ'_p on M_{CPTU} modulus variability. Unambiguity and statistical significance of the influence of this variable are confirmed by high values of correlation coefficient which reached 0,75 for overconsolidated soils.

Figure 6 leads to two crucial conclusions that should be included in the assessment of the constrained modulus values from CPTU:

– Straight trendlines of M_{CPTU} and M_{oed} moduli variablity clearly separate normally consolidated tills from the overconsolidated ones. This fact substantiates the indication that the formula (1) cannot be treated as universal and has to be adjusted by inclusion of the overconsolidation effect.
– An important element of the analysis is the fact that the impact of overconsolidation effect vanishes in the plastic states of both kinds of till (LI > 0,3), and the predicted values of moduli yield in this area similar results for all CPTU and oedometric tests.

In the overconsolidated tills, the application of the formula (1) allows for fair estimation of the M_{CPTU} value in comparison to oedometric test. Results obtained in normally consolidated tills, in turn, seem to be underestimated compared to the laboratory values. The corrected value of coefficient in CPTU formula for normally consolidated tills can be calculated on the basis of data shown on the Figure 6 and is given in the equation 2.

$$M_{CPTU} = 13{,}13\ (q_t - \sigma_{v0}) \qquad (2)$$

The coefficient values exceeding 13 were also determined by Robertson for fine-grained soils with $I_c > 2{,}2$ and $Q_t > 14$ (coefficient equal to 14).

6 CONCLUSIONS

The conducted tests confirmed two general and essential hypotheses. The first hypothesis was that CPTU allow for identification of subsoil's overconsolidation effect that is connected with soil genesis. The second one stated that the overconsolidation effect influences the values of constrained moduli clearly and unambiguously. Inclusion of the influence of overconsolidation effect on the values of constrained moduli variation is made possible with introduction of such variables as OCR coefficient and plasticity index into the formula for the relationship between cone resistance (CPTU test) and constrained modulus (M_{oed}). This way of deformation moduli assessment has been known for shear modulus G_0 (e.g. Hardin 1978, Godlewski & Szczepański 2013, Młynarek et al. 2013). However, such a solution requires a great number of tests in soils of varied genesis and grain size. Another way is the proposed method of separating normally consolidated from overconsolidated soils that occur in the subsoil. A preliminary method of classification of soils into one of these categories may be classification charts for CPTU (Lunne et al. 1997). At the second stage, OCR or σ'_p values need to be determined for each group. For overconsolidated deposits, the formula (1) can be recognized as satisfactory for determination of changes of constrained moduli in the subsoil. In the case of normally consolidated tills, the modified formula with the 13.13 coefficient can be used. It has to be remembered that in soils of massive macrostructure, e.g. alluvial soils and loess, values of this coefficient may be different.

7 REFERENCES

Bolewski A. & Parachoniak W. 1988. Petrografia. Wydawnictwa Geologiczne. Warszawa.

Burland J.B. 1967. Deformation of soft clay. *Ph.D. Thesis*. University of Cambridge, UK.

Godlewski T. & Szczepański T. 2013. Determination of soil stiffness parameters using in-situ seismic methods-insight in repeatability and methodological aspects. R. Q. Coutinho& P.W. Mayne (eds.) *Geotechnical and Geophysical Site Characterization 4,. Proc. of 4th International Conference on Geotechnical and Geophisical Site Investigations:* 441-446. Taylor & Francis Group, London

Hardin B.O. 1978. The nature of stress-strain behavior for soils. *Proc. ASCE Geotechnical Div. Specialty Conf. on Earthquake Engng and Soil Dynamics*: 3-90, Pasadena.

Izbicki R. & Stróżyk J. 2006. Stopień YSR miarą prekonsolidacji iłów formacji poznańskiej. Zeszyty Naukowe Politechniki Białostockiej – Budownictwo. Z. 28, T. 1: 117-126.

Jamiolkowski M., Ladd C.C., Germaine J.T. & Lancellotta R. 1985. New developments in field and laboratory testing of soils. *Proc. 11th ICSMFE*, Vol. 1: 57-154. San Francisco.

Janbu, N., Tokheim, O. & Senneset, K. 1981. Consolidation Tests with Continuous Loading. *Proc. 10th ICSMFE*, Vol. 1: 645-654. Stockholm.

Karlsrud K., Lunne T., Kort D.A. & Strandvik S. 2005. CPTU correlations for clays. *Proc. of 14th International Conference on Soil Mechanics and Geotechnical Engineering:* 693-702. Millpress, Rotterdam.

Krygowski B. 1961. Geografia fizyczna Niziny Wielkopolskiej: Geomorfologia, Część 1. Państwowe Wydawnictwo Naukowe, Warszawa.

Lunne T., Robertson P. K. & Powell J. 1997. Cone penetration testing in geotechnical practice. E&FN Spon, London.

Maksiak S. & Mróz W. J. 1978. Czwartorzęd środkowej części Pojezierza Pomorskiego. *Z badań czwartorzędu w Polsce*, t.19: 97-146.

Młynarek Z., Tschuschke W. & Gogolik S. 2003. W sprawie wyznaczania modułów odkształcenia podłoża budowlanego metodą statycznego sondowania i dylatometrem Marchettiego. *Inżynieria Morska i Geotechnika*, nr 3: 135-139.

Młynarek Z., Wierzbicki J. & Mańka M. 2015. Geotechnical parameters of loess soils from CPTU and SDMT. Marchetti S., Monaco P., Viana da Fonseca A. (eds.) *International Conference on the Flat Dilatometer DMT'15:* 481-489. Rome.

Młynarek Z., Wierzbicki J. & Stefaniak K. 2013. Deformation characteristics of overconsolidated subsoil from CPTU and SDMT tests. R. Q. Coutinho & P.W. Mayne (eds.) *Geotechnical and Geophysical Site Characterization 4,. Proc. of 4th International Conference on Geotechnical and Geophisical Site Investigations:* 1189-1193.Taylor & Francis Group, London.

Pettijohn F. J., Potter P. E. & Siever R. 1987. Sand and sandstone. Springer-Verlag.

Powell J.M. 2005. In situ testing. General report. *Proc. of 14th International Conference on Soil Mechanics and Geotechnical Engineering*:729-734. Millpress.

Stankowski W. 1996. Podstawowe facje glin morenowych oraz kryteria ich wyróżniania. *Geologos* 1, UAM Poznań: 150-157.

Wierzbicki J. 2009. Analysis of changes in overconsoildation ratio in selected profiles of non-lithified deposits. *ACEE Journal*. V.2 No. 3/2009: 77-84.

Wierzbicki J. 2010. Evaluation of subsoil overconsolidation by means of in situ tests at the aspect of its origin. *Rozprawy Naukowe nr 410.* Wydawnictwo Uniwersytetu Przyrodniczego w Poznaniu.

Wierzbicki J. & Młynarek Z. 2012. Identification of overconsoildation effect by means of in situ tests. *Inżynieria Morska i Geotechnika*, nr 4/2012: 277-285.

Worth C.P. & Houlsby G.T. 1985. Soil mechanics – property characterization and analysis procedures. *Proc. of 11th ICSMFE*, Vol. 1: 1-56. San Francisco.

Geotechnical and Geophysical Site Characterisation 5 – Lehane, Acosta-Martínez & Kelly (Eds)

Application and tentative validation of soil behavior classification chart based on drilling parameter measurements

P. Reiffsteck
IFSTTAR, Marne la Vallée, Ile-de-France, France

J. Benoît
University of New Hampshire, Durham, New Hampshire, USA

M. Hamel
Fondasol, Cesson, Ile-de-France, France

J.-M. Vaillant
Fondasol, Enghein, Hainaut, Belgique

ABSTRACT: This paper presents an approach for developing a soil classification chart based on drilling parameters. Tentative validation by comparison with a database of these tests leads to conclude on the reliability of the chart and proposes some suggestions for its practical use. A newer and preliminary version taking into account initial stress state of the ground is also presented.

1 INTRODUCTION

Correlations of in situ test results with results obtained in the laboratory on test specimens from disturbed and intact samples has helped improving various empirical relationships between field and laboratory properties. However, it would be misleading to say that values derived from in situ testing can fully substitute values from laboratory tests. It is difficult to integrate certain aspects of soil behavior such as overconsolidation and effect of fines into these field correlations. However, it has become an increasingly important tool for the practitioner to check the consistency and variability of results in the field.

Recently, the French national applications documents of Eurocode 7 for the design of shallow and deep foundations proposed using a classification chart based on the results of pressuremeter tests: limit pressure and Menard modulus. Similar to the soil classification developed by Robertson (1990) for the static cone penetration test, this tool defines soil classes in a log-log plot using the normalized limit pressure versus the ratio of limit pressure to pressuremeter modulus. A similar approach has been taken and is presented in this paper whereas different drilling parameters are combined and normalized to define similar graphs to those proposed by Robertson (1990) in an effort to develop classification charts based on drilling measurements.

1.1 *Classification and CPT*

Following Schmertmann (1978), Douglas and Olsen (1981) and Parez and Fauriel (1988), Robertson suggested in 1990, a chart based on the normalized cone penetration resistance, Q_t, and the normalized friction ratio, F_r. These charts have been adopted by practitioners as they provide a "reliable" soil classification using the CPT and minimizes the need for sampling. The graph shown in Figure 1 is divided into zones that allow soil classification according to particle size. The zones reflect the expected behavior of the soils within each zone rather than strictly based on grain size. The zones show a gradual transition from fine soil behavior to that of coarse soil. These two CPT normalized parameters are in fact compounds parameters specific to cone penetration.

The 1990 chart from Robertson is an improved version of the initial chart because of the normalization to in situ vertical stresses.

$$Q_t == \frac{q_t - \sigma_v}{\sigma'_v} \quad (1)$$

$$F_r = \left[\frac{f_s}{q_t - \sigma_v}\right] \cdot 100\% \quad (2)$$

considering that $q_t = q_c + (1-a) \cdot u_2$ where a is the area ratio correction.

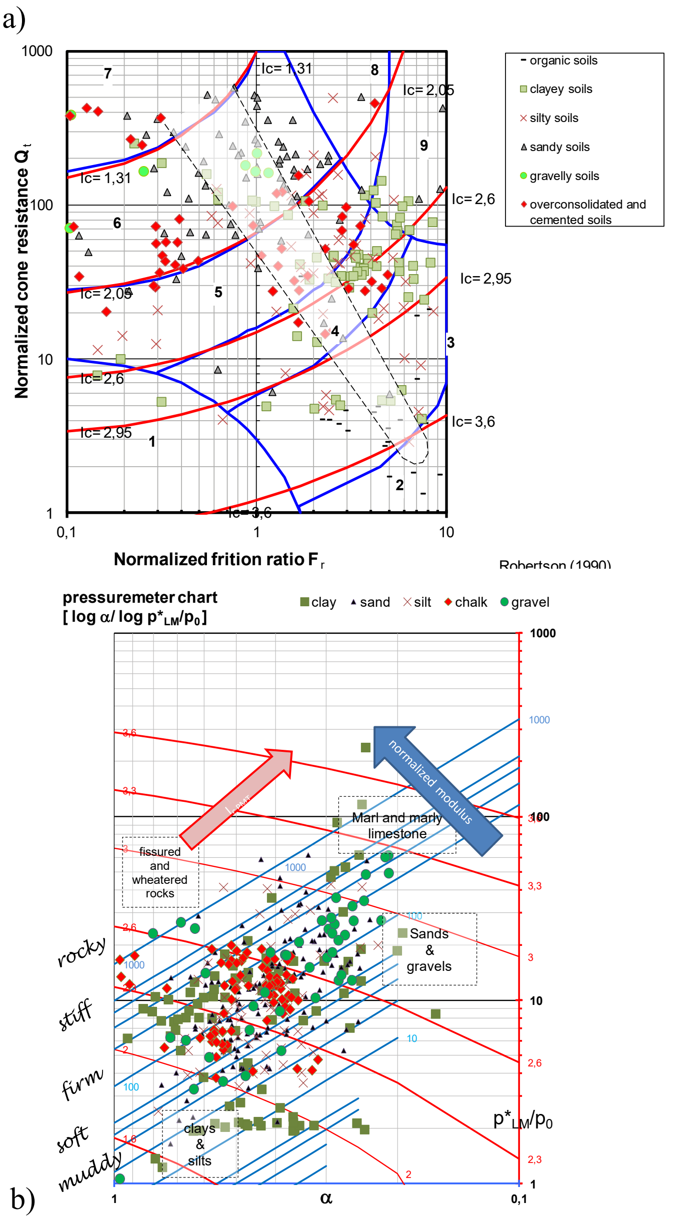

Figure 1. Classification charts (according to Robertson, 1990 and 2009) and chart based on pressuremeter results from current data sets

With

1. Sensitive fine-grained;
2. Clay - organic soil;
3. Clays: clay to silty clay;
4. Silt mixtures: clayey silt & silty clay;
5. Sand mixtures: silty sand to sandy silt;
6. Sands: clean sands to silty sands;
7. Dense sand to gravelly sand;
8. Stiff sand to clayey sand;
9. Stiff fine-grained.

In 2009, Robertson included the index I_c proposed by Jefferies and Been (2006), which resulted in the circular arcs shown as thick lines in Figure 1a. The index Ic is defined as follows:

$$I_c = \left[(3.47 + \log(Q_t))^2 + (1.22 - \log(F_r))^2\right]^{0,5} \qquad (3)$$

The limit between the clayey behavior and sandy behavior is given for $I_c = 2.60$.

Figure 1 also shows a dataset from experimental sites where quality PMT, CPT, SPT, FVT tests were conducted but in different geological and geographical conditions and locations. The classifications were done using soil descriptions from core drilling and laboratory test specimens.

1.2 *Classification using Ménard pressuremeter test*

Similar to the classification of soils developed from the results of static cone penetration tests, we can envision creating a chart based on soil types and sizes on a graph of standardized limit pressure and the ratio of limit pressure to pressuremeter modulus. The log-log chart proposed by Baud (2005) and Baud and Gambin (2011, 2012), looks promising although the comparison of different classifications does not allow to define clear disjointed unique areas (Reiffsteck et al., 2013). These same authors proposed a more elaborate version taking into account the initial state of the soil, whose importance is known, but it did not solve the problems of inadequate discrimination between soils inherent in this chart. The normalized pressuremeter based chart is shown in Figure 1b and compared to Figure 1a. It shows an average sensitivity of the five soil classes based on data from the experimental sites database. Fine soils are located at the bottom left of the graph and granular soils in the upper right, with the intermediate soils in a central position.
Consequently, the use of curves defining a classification index I_c seems suitable for delimiting these areas. This index could have the same threshold value of 2.6, separating the granular and coherent behavior as proposed by Jefferies and Been (2006), but with an opposite development (1.3 for clays and 3.6 gravel).

$$I_{c\,PMT} = \left[\left(1 + \log\left(\frac{p^*_{LM}}{p_0}\right)\right)^2 + (1{,}22 - \log(\alpha))^2\right]^{0,5} \qquad (4)$$

This chart shows promises in its ability to classify soils where soils are firm (stiff soil, soft rock) and when having tests with Ménard modulus measured with minimal remoulding of borehole walls and unrestricted by the artificial limit of 5 MPa as defined in the test standard.

2 CLASSIFICATION BASED ON MWD

Conception of a soil classification based on parameters recorded during drilling (V_A: penetration rate; P_E: net thrust pressure; P_i: injection pressure; Q_i: *Drilling* *fluid flow;* C_r: torque; *V_r: rotation speed* - italicized are those which are not usually measured) was attempted by many authors (Girard, 1985; Bourget and Rat, 1995; Ferry, 1996; Colosimo, 1998; Gui et al, 1999; Moussoutheguy, 2002). However, the combination of several compounds parameters with weighting methods and thresholds have not led to a fully reliable method of identification.

Figure 2 shows a graph of penetration resistance (R_p) and modified Somerton index (S_d) for different soil types and rock. It can be seen that compact clay and marl give large range of values of penetration resistance and does not allow discriminating between the two materials without direct identification of the cuttings. The distinction between clays and marl is mainly based on the content of $CaCO^3$.

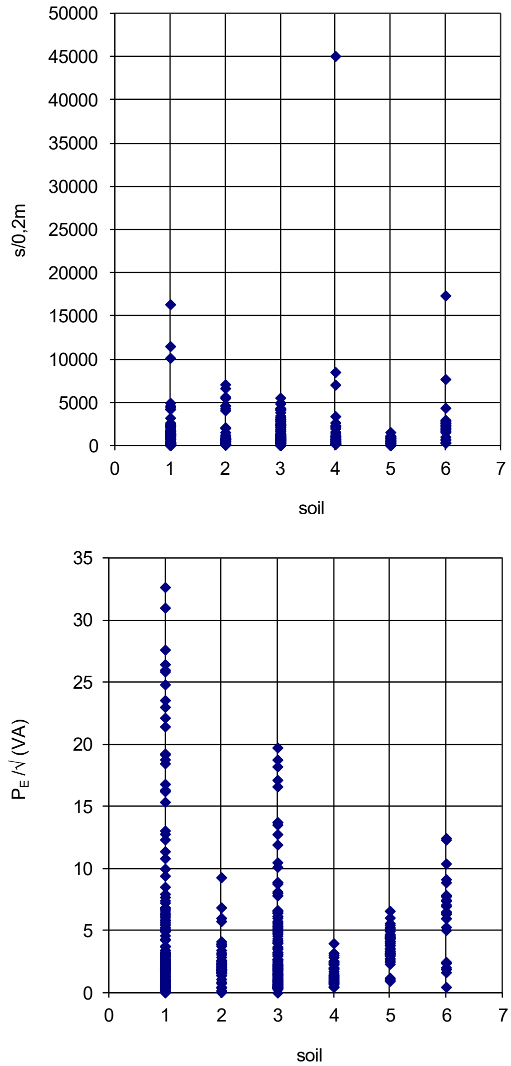

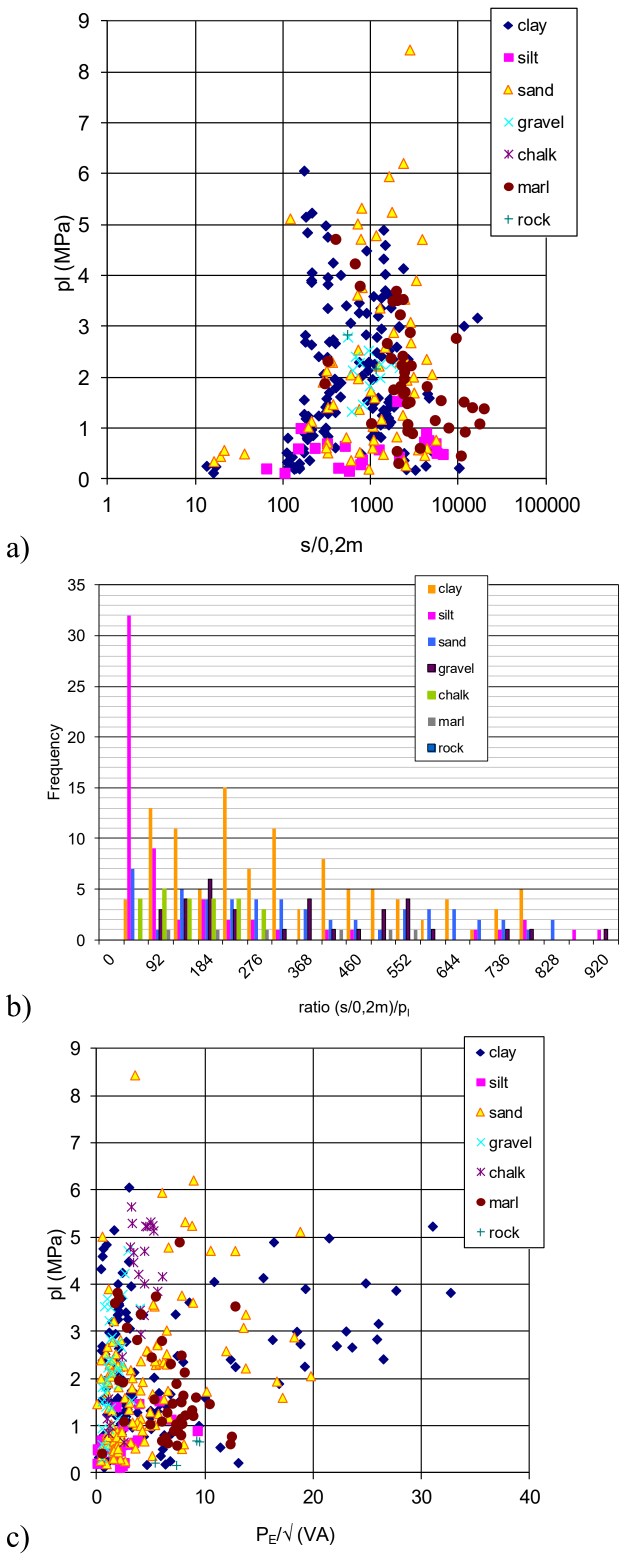

Figure 2. Relationship between the classification and the penetration resistance or modified Somerton index (clay = 1, silt = 2, sand = 3, gravel = 4, chalk = 5, marl = 6, rock = 7)

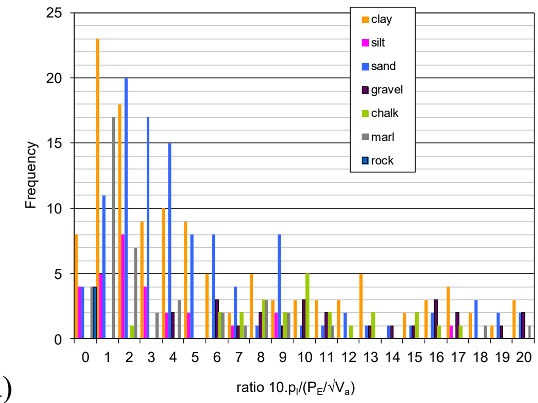

d)

Figure 3. Relationship and histograms of relations between the pressuremeter limit pressure and various compounds parameters

The French national application document of Eurocode 7 for design of shallow foundation NF P94-261 provides in its Appendix A a preliminary soil classification based on ranges of values from two drilling parameters, the penetration resistance Rp and modified Somerton index Sd (Figure 3) which consistently show good differentiation between soil and rock types. These two parameters are defined as follows:

$$R_p = {}^{s}\!/_{0.2\,m} \quad \text{and} \quad S_d = {}^{P_E}\!/_{\sqrt{V_A}} \ (\text{bar}/(\text{m/h})^{-0.5}) \qquad (5)$$

Table 1 — classification of soils according to in situ testing and R_p and S_d

soil classes		p_l* (MPa)	q_c (MPa)	$N_{(1,60)}$	Su (kPa)	R_p	S_d
clays and silts	very soft to soft	< 0.4	< 1.0		< 75	< 45	< 2.5
	firm	0.4 - 1.2	1.0 - 2.5		75 - 150	45 -138	2.5 - 8
	stiff	1.2 - 2	2.5 - 4.0		150 - 300	138 -230	8 - 13
	very stiff	≥ 2	≥ 4.0		≥ 300	≥ 230	≥ 13
intermediate soils (silty sands, clayey sands, sandy clay)	Classification according to figure 1						
sands and gravels	very loose	< 0.2	< 1.5	< 3		< 27	< 1.3
	loose	0.2 - 0.5	1.5 - 4	3 - 8		27 - 70	1.3 - 3.3
	medium dense	0.5 - 1	4 - 10	8 - 25		70 - 140	3.3 - 6.6
	dense	1 - 2	10 - 20	25 - 42		140 - 277	6.6 - 13
	very dense	> 2	> 20	42 - 58		> 277	> 13
chalks	soft	< 0.7	< 5			< 64	< 7
	weathered	0.7 - 3	5 - 15			64 - 272	7 - 30
	sound	≥ 3	≥15			> 272	> 30
marls & limestones	soft	< 1	< 5			< 1100	< 6
	stiff	1 - 4	5 - 15			1100 - 4400	6 - 26
	very stiff	> 4	>15			> 4400	>26
rocks	weathered	2.5 - 4				4750-7600	50-80
	Fragmented	> 4				>7600	>80

Similar relationships to those proposed by Robertson (1990) can be developed for characterizing soils and rocks from the information obtained during the penetration of a drilling tool. However, in order to normalize the net thrust pressure it must be divided by the penetration rate (speed) in order to be constant as during penetration in CPT testing. The units have also been modified to be in meters per second for penetration and rotational speed.

$$Q_{t\,MWD} = \frac{(P_E - \sigma_v)/V_A}{\sigma'_v} \qquad (6)$$

$$F_{r\,MWD} = \left[\frac{\text{torque/rotation speed}}{(P_E - \sigma_v)/V_A}\right]\cdot 100\% = \left[\frac{C_R/V_R}{(P_E - \sigma_v)/V_A}\right]\cdot 100\% \qquad (7)$$

To use the expression in Equation 7, the rotation pressure must be converted into torque. This requires knowing the capacity of the machine rotary motor (cm^3/rev).

$$C_R = {}^{P_{CR}\cdot \text{cylinder capacity}}\!/_{2\cdot\pi} \qquad (8)$$

Similarly the rotational speed which is an angular velocity must be expressed in linear speed at the periphery of the tool.

$$V_R = \omega\cdot r\cdot {}^{\pi}\!/_{30} \qquad (9)$$

A first calibration was performed on the IFSTTAR database (Figure 4) which unfortunately does not completely cover the experimental sites used on the two graphs in Figure 1.

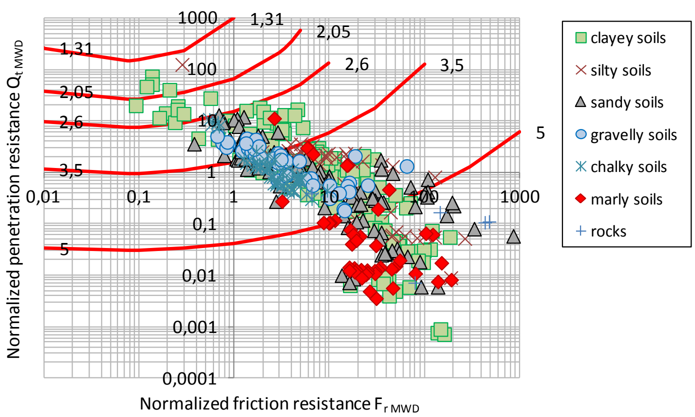

Figure 4. Classification chart based on the proposed drilling parameters with sites data set

Figure 4 shows that stiff soils and rocks are located in the lower right part, granular soils are in an approximate central position and clay soils are spread over the entire range. At this time, the influence of overconsolidation or cementation of clays has not been completed. Similarly, soils classified as clayey or sandy are mostly intermediate soils with this second classification not yet defined.

An attempt to introduce a classification index to refine the soil classes is shown in Equation 10 and represented in the graphs of Figures 4 and 5.

$$I_{c\,MWD} = \left[(3.47 + \log(Q_{t\,MWD}))^2 + (1.22 + \log(F_{r\,MWD}))^2\right]^{0,5} \quad (10)$$

The chart has been tested with a database collected by Fondasol using their project data (Hamel and Vaillant, 2014). It has 18 sites mainly in the Paris region and around 100 boreholes from 15 to 30 m deep, leading to 121,730 values (Figure 5).

It can be observed, in spite of the dispersion associated with the inherent variability of tested geologic materials, the test procedures and the potential classification errors or other approximations, a fair positioning of classes of soils on parallel axes going from (1; 10) to (1000 ; 0.01).

The clay materials are situated on an $F_{r\,MWD}$ zone = 10 and $Q_{t\,MWD}$ ranging from 0.1 to 1. The marly clays are found closer to hard soils as they are similar to calcareous marl. The percentage of limestone is indeed not defined ($I_{c\,MWD} > 5$).

Granular materials are along high values of $F_{r\,MWD}$ for $Q_{t\,MWD}$ close to unity. Some of the silt is also located on this part of the diagram ($I_{c\,MWD} \cong 5$).

Indurated materials such as limestone, calcareous marl and marl are positioned on two lines: a high line ((1; 10) (1000, 0.01)) and a low line ((1; 0.02) (100; 0.001)). The cluster of points for calcareous marl, marly clay and limestone are located in an area where $F_{r\,MWD}$ = 1 and $Q_{t\,MWD}$ varying between 1 and 10 ($I_{c\,MWD}$ <3.5).

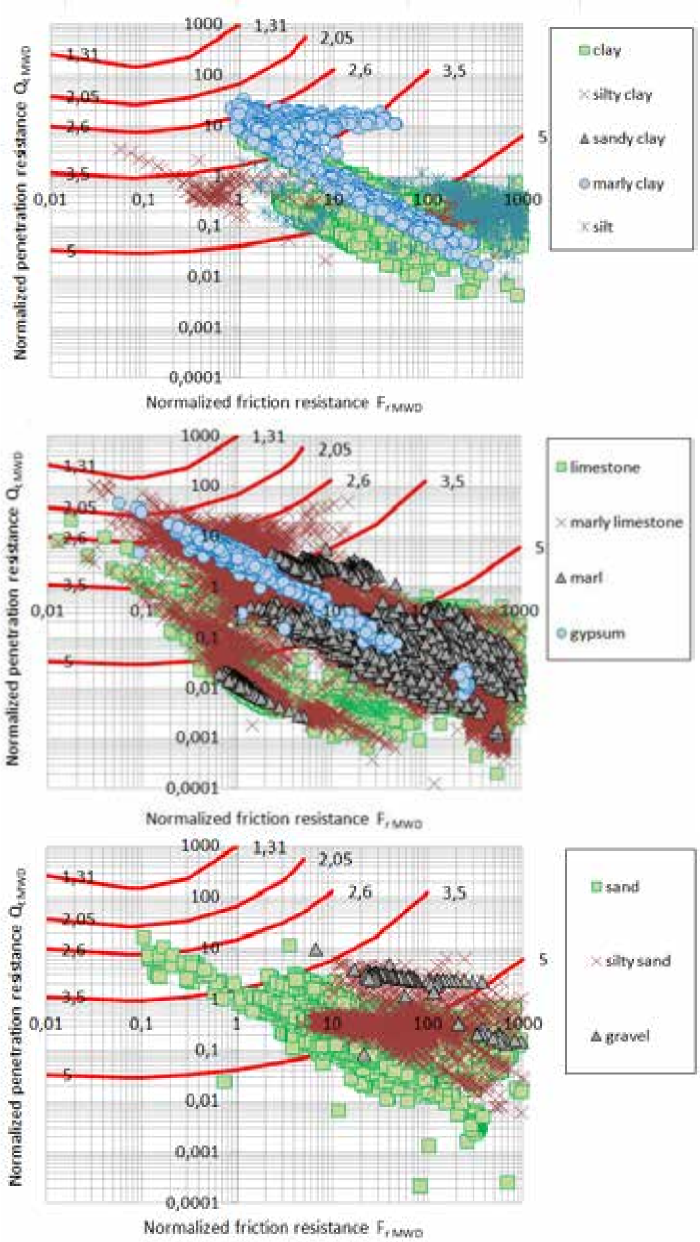

Figure 5. Classification chart based on the proposed drilling parameters with the dataset of sites provided by Fondasol

3 CONCLUSIONS

Drilling parameters measurements or instant logging parameters have greatly improved the quality of drilling. The use of the recorded drilling parameters has been used in this paper to suggest a new application to classify soil using a classification chart similar to what Robertson proposed for the CPT. However, the results obtained to date can not be used as is for the following reasons:

- Greater data variation than for the CPT and the pressuremeter,
- Heterogeneity of the drilling machines used to develop the database,

- Possible interrelationship of the various parameters and factors influencing the recorded responses.

Identification and classification of soil and rock is normally a matter of EN ISO 14688-1 and EN 14688-2 and also the 14689-1 standards. The idea is to use in combination the information from these techniques with those of conventional reconnaissance (sampling, penetration or expansion tests), to improve the image of the subsurface and better manage the overall risk generating a geotechnical model of the site richer qualitatively and quantitatively.

4 ACKNOWLEDGEMENTS

The authors thank P. Sauvage and B. Tcherniawsky for the information they were able to provide them on the drilling machines used in this study.

5 REFERENCES

Baud J.P. (2005) ISP5 Analyse des résultats pressiométriques Ménard dans un diagramme spectral [log(pLM), log(EM /pLM)] et utilisation des regroupements statistiques dans la modélisation d'un site, 50 ans de pressiomètres. Vol. 1. Gambin, Magnan et Mestat (ed.), Presses de l'ENPC/LCPC, Paris, 167-174

Baud, J.-P, Gambin, M. (2011), Classification des sols et des roches à partir d'essais d'expansion cylindrique en haute pression, C. R. du 15ème Congrès Européen de Mécanique des Sols et de Géotechnique, edited by A. Anagnostopoulos, M. Patchakis, C.Tsatsanifos, ISO Press, Amsterdam .

Baud, J.-P, Gambin, M. (2012). 50 MPa Ménard PMTs help linking Soil and Rock Classifications. in A. Anagnostopoulos, ed., Geotechnical & Geological Engineering Journal, Special Issue on Hard Soils and Weak Rocks, Springer Verlag, Berlin.

Bourget M., Rat M. (1995) Interprétation semi-automatique des enregistrements Des paramètres de forage (sondeuses hydrauliques en rotation), Rev. Franç. Géotech., 73 : 3-14.

Colosimo (1998) On the use of drilling parameters in rock foundations, Geotechnical site characterisation, Robertson et Mayne Eds, 347-352

Douglas, B. J., and Olsen, R. S., (1981). Soil classification using electric cone penetrometer. American Society of Civil Engineers, ASCE, Proceedings of Conference on Cone Penetration Testing and Experience, St. Louis, October 26 - 30, pp. 209 - 227.

Ferry S. (1996) Traitement automatique des diagraphie instantanées de forage en Génie Civil, Thèse de doctorat de l'université Bordeaux I, 99 p.

Girard H. (1985) Contribution à l'exploitation des paramètres de forage en génie civil. Thèse d'Etat - Université Bordeaux I. 161 p.

Gui, M W, Bolton, M D, Soga, K, Hamelin, J P, Hass, G, Burgess, N and Butler, A P (1999). Instrumented borehole drilling using ENPASOL system. 5th Int. Symp. on Field Measurements in Geomechanics, Singapore.

Hamel M., Vaillant J.-M., (2014) Utilisation des paramètres combinés dans des études géotechniques à Vitry sur seine (F) et Charleroi (B), JNGG Beauvais, 10 pages

Jefferies M.G., Been, K., (2006). Soil liquefaction – A critical state approach. Taylor & Francis Group, London and New York. ISBN 0-419-16170-8, 479 p.

Robertson, P. K., (1990). Soil classification using the cone penetration test. Canadian Geotechnical Journal, 27(1): 151 - 158.

Moussouteguy N. (2002) Utilisation combinée des essais pressiométriques et diagraphie instantanée pour mieux évaluer le risque, Thèse de doctorat de l'université Bordeaux I, 417 p.

Parez L., Fauriel R., (1988) Le piézocône : améliorations apportées à la reconnaissance des sols. Rev. Franç. Géotech., 44, 13-27

Reiffsteck P., Martin A. & Perini T. (2013) Application et validation d'abaques pour la classification des sols à partir des résultats pressiométriques, Symposium International ISP6/PRESSIO 2013, Paris, 6 pages

Robertson, P. K., (1990). Soil classification using the cone penetration test. Canadian Geotechnical Journal, 27(1): 151 - 158.

Robertson, P. K., (2009). Interpretation of cone penetration test – a unified approach, Canadian Geotechnical Journal, 46(1): 1337 - 1355.

Schmertmann, J. H., (1978). Guidelines for cone test, performance and design. Federal Highway Administration, Report FHWA-TS-78209, Washington, 145 p.

Geotechnical and Geophysical Site Characterisation 5 – Lehane, Acosta-Martínez & Kelly (Eds)

Calibrating CPT relative density and strength correlations for a laboratory fine sand

J.A. Schneider
NAVFAC EXWC, Port Hueneme, CA, USA

J. R. Giampa & A.S. Bradshaw
University of Rhode Island, Kingston, RI, USA

J.T. Newgard
MAR Range Services, Ventura, CA, USA

ABSTRACT: Interpretation of drained loading of foundations and anchors requires knowledge of peak and critical state friction angles, as well as the peak dilation angle. Correlations to relative density are typically used to assess these parameters, however, these correlations are not unique, particularly when dealing with low effective stresses that are encountered during model testing or for shallow seabed interactions. Results from a series of cone penetrations tests with inferred relative density profiles are presented to develop a sand specific relative density correlation. The results from laboratory triaxial tests at representative densities and stress levels are compared to cone tip resistance to discuss friction and dilation angle correlations.

1 INTRODUCTION

When attempting to use model tests to characterize the static and cyclic response of footings or anchors, the uniformity of prepared samples needs verification such that inferred differences in foundation response due to changes in load or object geometry are not a result of differences in soil conditions. The cone penetration test (CPT) is ideal for assessing intra- and inter- sample variability.

For more detailed interpretation of drained loading of objects, accurate interpretation of peak and critical state friction angles, as well as the relationship between the difference in peak (ϕ'_{pk}) and critical state friction angle (ϕ'_{cv}) and the dilation angle (ψ'_{pk}) are needed. It is common to use Bolton's stress dilatancy theory (Bolton 1986) to estimate ϕ'_{pk} and ψ'_{pk} as a function of relative density (D_r) and mean effective stress at failure (p'_f). However, the correlation between CPT tip resistance (q_t) and relative density is not unique (e.g., Baldi et al. 1986), and requires calibration for specific sand types. Additionally, 'Bolton' parameters have been shown to be strongly influenced by particle roundness and sphericity (e.g., Liu & Lehane 2012), and thus also require specific calibration for various sand types.

This paper presents results of a testing series in fine 'Golden Flint' sand that are intended to:

- calibrate a correlation between CPT q_t and D_r.
- evaluate correlations between CPT q_t and ϕ'_{pk} for various engineering applications.
- calibrate a correlation between (ϕ'_{pk}-ϕ'_{cv}) and ψ'_{pk} for laboratory triaxial tests.

It is noted that in this paper CPTs are limited to the upper meter of soil, which is applicable to interpretation of model test results or performance of objects interacting with the shallow seabed (e.g., shallow anchors, pipelines and related infrastructure).

2 RELATIVE DENSITY CORRELATION FORMAT

For the assessment of relative density from (normalized) cone tip resistance, the format of Baldi et al. (1986) has been adopted for use herein:

$$D_r = \frac{1}{C_1} \cdot \ln\left[\frac{\left(q_c / p_{ref}\right)}{\left(\sigma'_v / p_{ref}\right)^n} \cdot \frac{1}{C_2}\right] = \frac{1}{C_1} \cdot \ln\left[\frac{Q_{tn}}{C_2}\right] \qquad (1)$$

The parameter Q_{tn} will be used to discuss normalized cone tip resistance in sands with an unknown stress exponent (Robertson 2009). The stress exponent (n) tends to vary from 0.35 to 0.75 in sands, and will be fit for this sand as part of data analysis. Normalization exponents of 0.5., 0.7, and 1 are used in this paper, and referred to as $Q_{t0.5}$, $Q_{t0.7}$, and Q_{t1}. Use of vertical effective stress within Equation 1 implies that the soil is not overconsolidated.

The format of Equation 1 gives a physical meaning to the parameter C_2, which is the normalized cone tip resistance for a soil with a relative density of zero (zero dilation). This parameter would therefore increase with critical state friction angle.

In general, normalized cone tip resistance approximately doubles for each relative density class (i.e., very loose to loose, loose to medium dense, etc), such that a sand with a 100 percent relative density would have a normalized cone tip resistance that is 32 times (2^5) higher than that for a relative density of zero. C_1 is therefore approximately equal to ln(32) = 3.46. If a soils tends to crush rather than dilate at high stresses induced by cone penetration, C_1 will decrease, reducing the ratio of Q_{tn} at a relative density of 100 percent compared to that at $D_r = 0$.

3 SAND PROPERTIES

Testing was performed on fine uniformly graded Golden Flint Sand. Characterization of the sand included standard index testing, as well as 28 triaxial tests performed among three laboratories (Tufenkjian & Yee 2006, Giampa 2014, Alshibli 2015, Giampa et al. 2016). Sand properties are summarized in Table 1.

Table 1. Properties of Golden Flint sand from laboratory tests

Property	Value
γ_{max} (kN/m^3)	17.68
γ_{min} (kN/m^3)	14.24
e_{max}	0.847
e_{min}	0.487
G_s	2.68
D_{50} (mm)	0.25
C_u	1.61
C_c	1.13
ϕ'_c (deg)	33.9
$\beta = (\phi'_{pk}-\phi'_{cv})/\psi'_{pk}$	0.64
A_f (see Bolton 1986)	3.6
Q (see Bolton 1986)	9.5
R (see Bolton 1986)	-0.68

4 SAMPLE PREPARATION METHODS

Sand samples were prepared in a 1.5 m x 1.5 m x 21 m long reinforced concrete trench filled with 60 tons of fine uniformly graded Golden Flint sand. Three different sample preparation methods were used:

- Method 1: A customized sand dispensing system (Tufenkjian & Yee, 2006) was used to air pluviate the sand into the test trench (Fig. 1).
- Method 2: Sand was pluviated through water (Fig. 2).
- Method 3: Sand was placed moist in 225 mm height lifts and vibrocompacted (Fig. 3). After the sand was placed to the final height, it was bottom saturated at a slow rate over a period of approximately 5 days.

Figure 1. Sand placement by air pluviation

Figure 2. Sand placement by water pluviation

Figure 3. Sand placement by vibrocompaction

5 CALIBRATION OF RELATIVE DENSITY CORRELATIONS

The air pluviation method (Method 1), described in more detail by Giampa et al. (2016), allowed for accurate estimation of as placed density through correlations to fall height and pluviator opening size. These as placed density estimations were then used to develop a sand specific correlation between normalized CPT cone tip resistance and relative density by modifying parameters in Equation 1. Relative density estimated from Q_{tn} in saturated deposits (Methods 2 and 3) are then presented for discussion purposes.

In a manner simulating Method 1 sample preparation, measurements of (dry) density were recoded as a function of (i) pluviator opening size; (ii) pluviator ramp angle; and (iii) fall height (h_{fall}), for a constant pluviator rate of movement along the trench. Sample tins were placed at heights of 100 mm, 225 mm, 425 mm, and 825 mm, and filled by passes of the pluviator over the test trench. Relationships between fall height and D_r are summarized for three pluviator gap opening sizes in Figures 4, 5, and 6. Parameters tested are summarized in Table 2.

Table 2. Parameters explored for pluviator – relative density calibrations

Case	Opening (mm)	Ramp Angle (deg)	Inferred $D_{r,max}$
1	3	40	0.80
2	6	40	0.60
3	6	55	0.45
4	13	40	0.30
5	19	40	0.10

A relationship was developed based on fall height (h_{fall}) and tray gap size (g) for a constant ramp angle, and took the form:

$$D_r = D_{r,\max}\left[1-\exp\left(\frac{h_{fall}}{-225mm}\right)\right] \quad (2)$$

$$D_{r,\max} = \left(1-\frac{g}{28mm}\right)^2 \quad (3)$$

The term '$D_{r,max}$' implies that once a certain fall height is reached, the pluviated relative density for the combination gap size and ramp angle is constant and at a maximum for that configuration.

Figures 7 through 10 present data used for the procedure of calibrating the relative density correlation. The best direct comparison of profiles comes from Figures 7 and 9, which show estimates of relative density and measurements of normalized cone tip resistance, $Q_{t0.7}$.

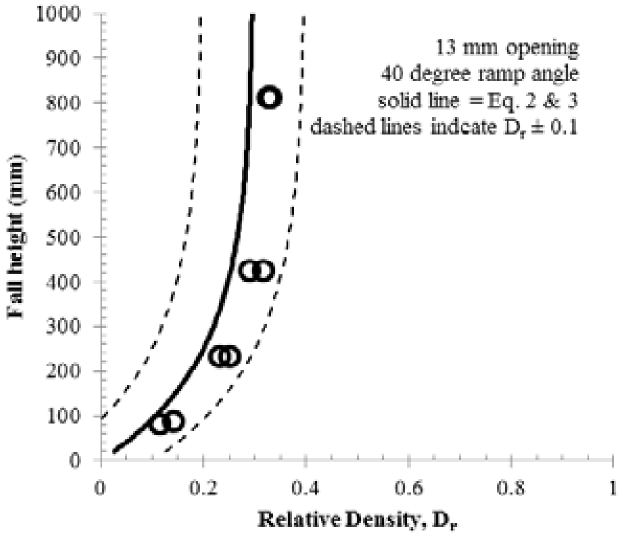

Figure 4. Relationship between fall height and relative density for 13 mm gap and 40 degree ramp angle

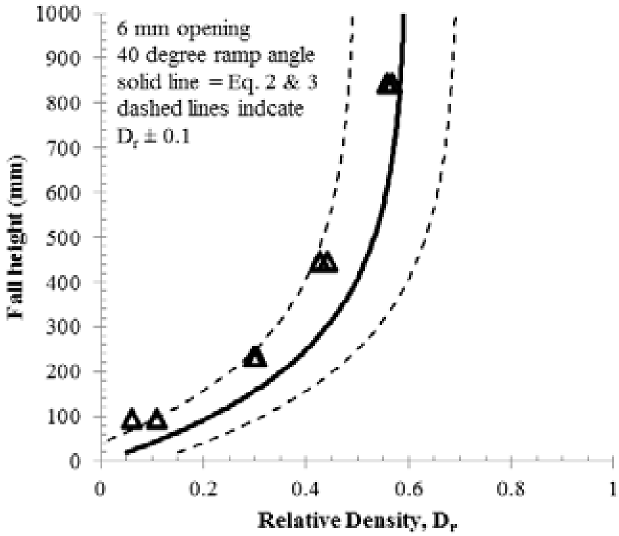

Figure 5. Relationship between fall height and relative density for 6 mm gap and 40 degree ramp angle

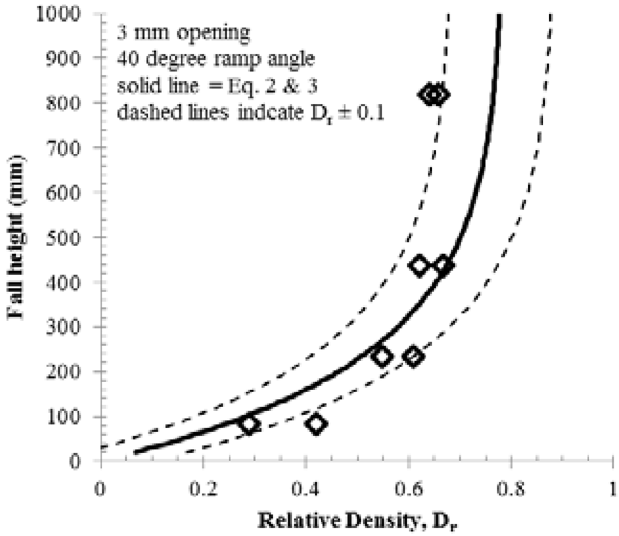

Figure 6. Relationship between fall height and relative density for 3 mm gap and 40 degree ramp angle

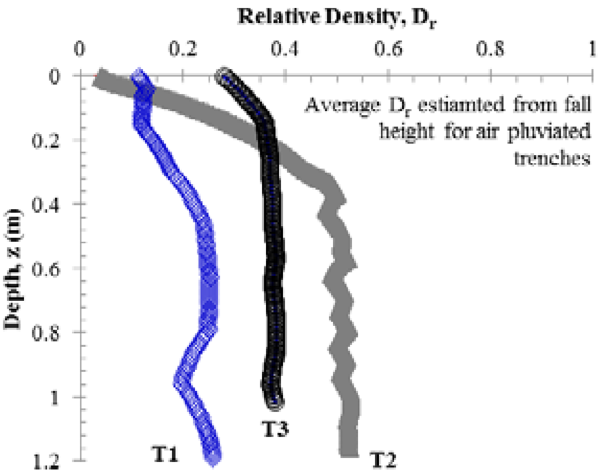

Figure 7. Relative density estimated from fall height for three air pluviated trenches

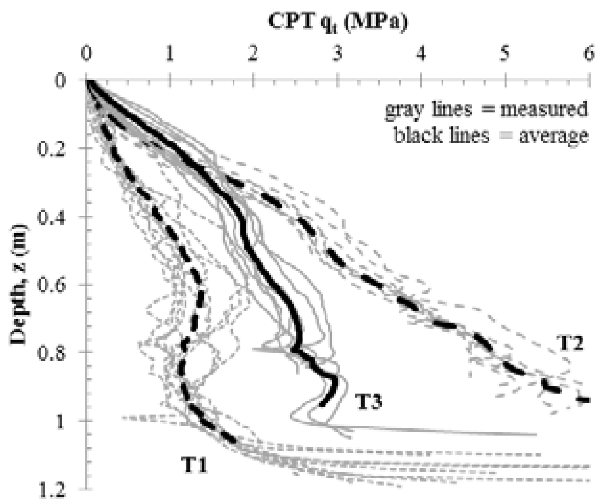

Figure 8. Cone Penetration Test results in air pluviated trenches

Steps used for calibration of relative density correlations were followed:

1 Performed fall height – D_r calibration for pluviator opening sizes and ramp angle (Figures 4 – 6).
2 Measured fall height periodically during sand placement (data not shown).
3 Converted fall height measurements to relative density profiles (Eq. 2 & 3, Figure 7).
4 Performed approximately 10 CPTs within each trench and average data to create a single CPT profile for each trench (Figure 8).
5 Plotted normalized cone tip resistance (log scale) against relative density (linear scale) (Figure 10). Adjust stress exponent n (Equation 1) to reduce coefficient in variation of normalized cone tip resistance for a given relative density.
6 Coefficient C_2 for Equation 1 is the intercept of the best fit line through the data at a D_r equal to zero (Figure 10).
7 Adjust coefficient C_1 from Equation 1 to change the slope of the D_r-Q_{tn} correlation.

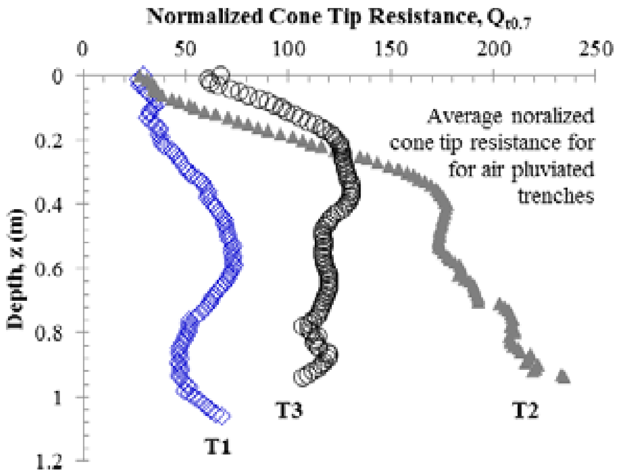

Figure 9. Normalized CPT tip resistance in air pluviated trenches

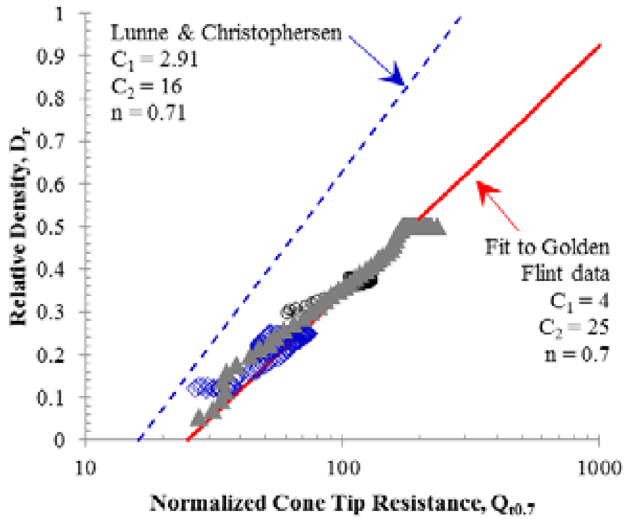

Figure 10. Calibrating relative density correlation parameters for Eq. 1

The resulting correlation matches measured data well, and is significantly different from typical relative density correlations of, for example, Lunne & Christoffersen (1983). The Lunne & Christoffersen (1983) correlation is shown since it uses essentially the same stress exponent, n.

Further performance of the relative density correlation can be assessed from profiles created using water pluviation (Method 2) and vibrocompaction (Method 3). Relative density inferred from average CPT q_t profiles in 5 different trenches are shown in Figure 11. Average CPT data are consistent and the relative density results in general agree with expectations in that:

- Water pluviation (T9, T10) produces very loose samples (e.g. Sladen and Hewitt 1989).
- Vibrocompaction (T11, T12, T13) produces samples with D_r between 0.5 and 0.65 (e.g., Schuettpelz et al. 2010). It is noted that vibrocompacted samples are overconsolidated, and therefore the correlation would slightly overpredict D_r.

The increase in apparent relative density with depth is not unexpected for a prepared sample, however, warrants additional investigation in future trenches.

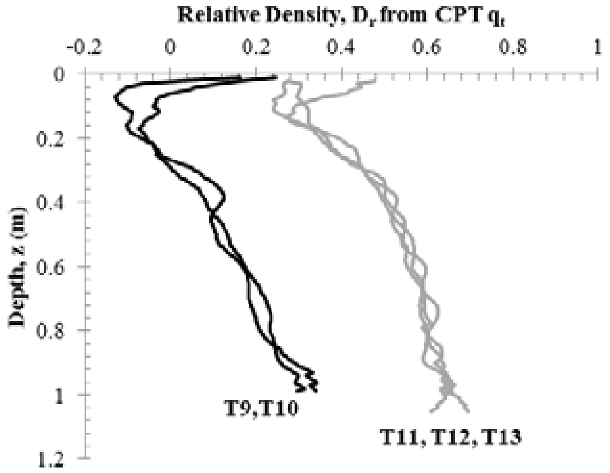

Figure 11. Estimates of relative density from average cone tip resistance in water pluviated (T9, T10, Method 2) and saturated vibrocompacted (T11, T12, T13, Method 3) sand

6 PEAK FRICTION ANGLE

While the drained peak friction angle of sands (ϕ'_{pk}) has a relatively narrow range from about 30 degrees to 50 degrees, the appropriate operational level of friction angle is difficult to evaluate. This results from the peak frictional resistance being a combination of particle friction without volume change (ϕ'_{cv}) as well as additional apparent frictional resistance that results from the dilation of particles during shear (e.g., Bolton 1986).

For evaluation of friction angle within this study for comparison to CPT tip resistance based correlations, sand specific Bolton stress dilatancy parameters were calibrated (see Giampa et al. 2016), as summarized in Table 1. Relative density within the calibration was estimated from fall height measurements, as shown in Figure 7. Two values of mean effective stress at failure (p'_f) are explored; (i) the in-situ vertical effective stress (Figure 12) which is appropriate for problems such as shallow pipes and helical anchors (White et al. 2008, Giampa et al. 2016); and (ii) $\sqrt{(q_n \cdot \sigma'_{v0})}$ (Figure 13) which is more appropriate for interpretation of pile end bearing, cone penetration tests (e.g., Flemming et al. 2009, Liu & Lehane 2012).

Estimated values of friction angle are compared to two CPT cone tip resistance correlations from the literature. The standard correlation of Kulhawy & Mayne (1990) is expressed in Equation 4 and compared to data at σ'_{v0} in Figure 12.

$$\phi'_{pk} = 17.6 + 11 \cdot \log Q_{t0.5} \quad (4)$$

The estimated friction angle compares favorably to the shape of the correlation, however, is approximately 10 degrees higher than that suggested by Equation 4. This is primarily attributed to the stress level effects on ϕ'_{pk} for a constant packing of particles. In the upper meter of the soil deposits p'_f analyzed is between zero and 15 kPa, while the stress level at failure in triaxial tests used to calibrate the Kulhawy & Mayne (1990) correlation were typically in excess of 200 kPa.

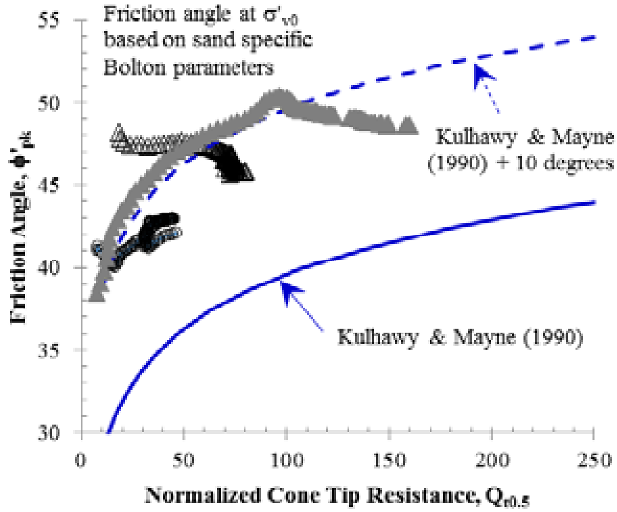

Figure 12. Comparison of peak friction angle based on Bolton's stress dilatancy theory at in situ vertical effective stress to cone tip resistance normalized to $\sqrt{\sigma'_{v0}}$ ($Q_{t0.5}$) for air pluviated sands

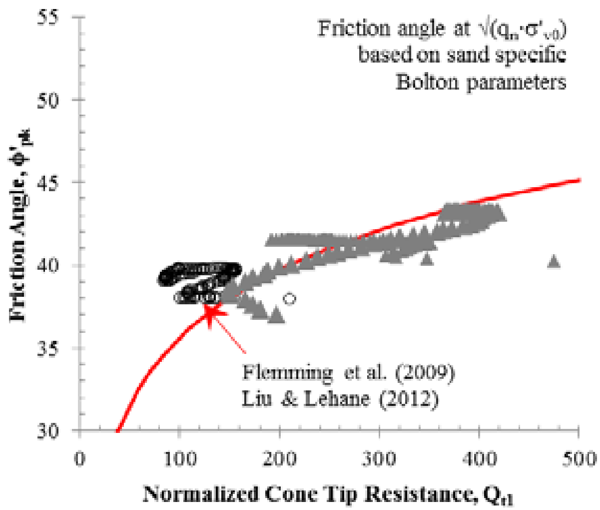

Figure 13. Comparison of peak friction angle based on Bolton's stress dilatancy theory at representative mean effective stress for cone penetration testing to cone tip resistance normalized to σ'_{v0} (Q_{t1}) for air pluviated sands

The second friction angle correlation explored was proposed in Flemming et al. (2009) for evaluation of pile based capacity.

$$\phi'_{pk} = 8.2 + 13.7 \cdot \log Q_{t1} \quad (5)$$

When estimating ϕ'_{pk} using Bolton's equation at p'_f equal to $\sqrt{(q_n \cdot \sigma'_{v0})}$, the correlation in Equation 5 showed good agreement for cone penetration testing in a number of sands tested in the centrifuge (Liu & Lehane 2012). Friction angle estimated in the same way for CPTs in Golden Flint sand, using relative density from fall height measurements, are compared to cone tip resistance normalized to vertical effective stress (Q_{t1}) in Figure 13. While the correlation from Equation 5 was a good agreement to ϕ'_{pk} estimates for the Golden Flint sand, the main point of interest that comes from Figure 13 is that the peak friction angle at stress levels appropriate for interpretation of cone penetration tests in the upper meter, tends to range from 38 to 44 degrees for these densities. The friction angle appropriate to analyzing shallow anchors and pipelines can be much higher, on the order of 38 to 50 degrees, depending upon density.

7 PEAK DILATION ANGLE

For numerical analysis of anchor or foundation response an estimate of dilation angle is necessary. If the critical state friction angle (ϕ'_{cv}) is known, the dilation angle can be estimated from peak friction angle as:

$$\psi'_{pk} = \frac{\phi'_{pk} - \phi'_{cv}}{\beta} \tag{6}$$

Bolton (1986) suggests that 0.8 is a reasonable first order estimate, but when dilation angle is critical to interpretation of results, for example for anchor uplift (e.g., Giampa et al. 2016), sand specific calibrations are recommended. Figure 14 shows the relationship between peak friction and dilation angles for Golden Flint sand. The value of β (Eq. 6) is closer to 0.64 than recommendations of 0.8 by Bolton (1986). Values of β near 0.6 have been discussed by Chakraborty & Salgado (2010), among others.

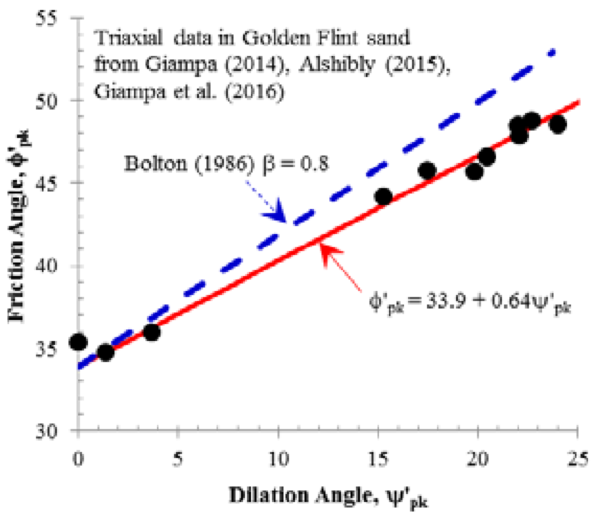

Figure 14. Relationship between peak friction and dilation angle for Golden Flint sand

8 CONCLUSIONS

Data from a laboratory fine sand have been presented such that relative density and friction angle correlations for a specific laboratory fine sand were calibrated. The Q_{tn}-D_r correlation format of Baldi et al. (1986) was appropriate, however, sand specific parameters were needed. Friction angle based on relative density and mean effective stress at failure per Bolton (1986) were found to be most reliable when assessing ϕ'_{pk} for various engineering applications. The range of peak friction angle varied from 38 to 50 degrees at low stress levels but 38 to 44 degrees for stress levels related to interpretation of CPT data. Use of σ'_{v0} as p'_f within Bolton equations was appropriate for shallow anchors and pipeline response, while use of $\sqrt{(q_n \cdot \sigma'_{v0})}$ for p'_f was more appropriate for interpretation of cone penetration results. Laboratory specific measurements are recommended for assessing $(\phi'_{pk}-\phi'_{cv})/\psi'_{pk}$.

9 REFERENCES

Alshibli, K.A. 2015. Stress-Dilatancy Response of Fine Golden Flint Sand. 15 April 2015.

Baldi, G., Bellotti, R., Ghionna, V., Jamiolkowski, M., and Pasqualini, E. 1986. Interpretation of CPTs and CPTUs; 2nd part: drained penetration of sands. Proc., 4th Int. Geotech. Seminar, Singapore: 143-156.

Bolton, M. 1986. The strength and dilatancy of sands. Géotechnique, 36(1): 65–78.

Chakraborty, T. and Salgado, R. 2010. Dilatancy and Shear Strength of Sand at Low Confining Pressures. ASCE J. of Geotech. and Geoenv. Eng., 136(3): 527-532.

Fleming, W. G. K., Weltman, A. J., Randolph, M. F. & Elson, W.K. 2009. Piling engineering, 3rd edn, Taylor & Francis, New York, NY, USA/London, UK.

Giampa, J.R. 2014. Interpretation of shallow helical anchor capacity in sand. MS Thesis, University of Rhode Island, July.

Giampa, J.R., Bradshaw, A.S., and Schneider, J.A. 2016. Influence of dilation angle on drained shallow circular anchor uplift capacity, Int. J. of Geomech., accepted.

Kulhawy, F.H. & Mayne, P.W. 1990. Manual on Estimating Soil Properties for Foundation Design, Report EL-6800, EPRI, Palo Alto, CA, August.

Liu, Q.B., and Lehane, B.M. 2012. The influence of particle shape on the (centrifuge) cone penetration test (CPT) end resistance in uniformly graded granular soils. Géotechnique: 62(11): 973-984.

Lunne, T., and Christoffersen, H.P. 1983. Interpretation of cone penetrometer data for offshore sands. Proceedings, 15th Annual OTC, OTC 4464: 181-188.

Robertson, P.K. 2009. Interpretation of cone penetration tests – a unified approach, Can. Geotech. J., 46: 1-19.

Schuettpelz, C. C., Fratta, D., and Edil, T. B. 2010. Mechanistic method for determining the resilient modulus of base course materials based on elastic wave measurements. ASCE J. of Geotech. & Geoenvir. Eng. 136 (8): 1086-1094.

Sladen, J.A., and Hewitt, K.J. 1989. Influence of placement method on the in situ density of hydraulic sand fills. Can. Geotech. J., 26(3): 453-466.

Tufenkjian, M., & Yee, E. 2006. Soil friction angle and relative density of sand from minicone penetration tests at shallow depth. Report prepared for Ocean Engineering Division, NAVFAC ESC, Port Hueneme, California.

White, D.J, Cheuk, C.Y, Bolton, M. 2008. The uplift resistance of pipes and plate anchors buried in sand." Géotechnique, 58(10): 771–779.

Geotechnical and Geophysical Site Characterisation 5 – Lehane, Acosta-Martínez & Kelly (Eds)

On the determination of the undrained shear strength from vane shear testing in soft clays

L. J. Wilson, G. P. Kouretzis & J. A. Pineda
ARC Centre for Geotechnical Science and Engineering, The University of Newcastle, Australia

R. B. Kelly
Chief Technical Principal Geotechnical, SMEC Australia; Hon Prof Fellow, University of Wollongong; ARC Centre for Geotechnical Science and Engineering, The University of Newcastle,Australia

ABSTRACT: The vane shear test is one of the most common techniques for estimating the *in situ* undrained shear strength of clay deposits. Despite its simple operational principle, interpretation of test results is inherently based on several assumptions regarding the interaction between the rotating blades and the deforming soil, which have not been adequately validated for soft marine clays of variable geotechnical and geochemical prop-erties. This paper provides a brief review on the background of current interpretation methods, followed by a critical discussion of their key simplifying assumptions in the light of new experimental data from undisturbed and remoulded samples.

1 INTRODUCTION

The vane shear test is widely used for determining the undrained shear strength and sensitivity of soft clays, yet interpretation of its results is based on certain key assumptions, the validity of which is questioned by several researchers. The aim of this paper is to shed some light on the effects of insertion disturbance; vane rotation rate; soil anisotropy and structure; shape of the failure mechanism on the interpretation of the vane shear test in soft clays. A critical review of current methods and findings from the literature is presented alongside preliminary experimental results that demonstrate the influence of each one of the above parameters on the vane-measured strength. Directions for future research and opportunities for improvement of the vane shear test are identified, aimed at enhancing the accuracy of shear strength measurements, and potentially retrieving more information about the mechanical properties of the soil from vane shear tests.

2 FACTORS AFFECTING THE INTERPRETATION OF VANE TESTS

2.1 *Soil disturbance during vane insertion*

Strength measured via vane tests can be significantly affected by localized soil destructuration and pore pressure generation following vane insertion, with the resultant influence on the results dependent on soil and blade properties (Chandler 1988). Insertion disturbance is correlated to the perimeter ratio, defined as the ratio of the blade thickness over the vane circumference. Chandler (1988) reports that disturbance due to typical blades may result in strength degradation between 10% - 25% of the undisturbed strength. While there is a positive correlation between strength loss due to insertion disturbance and soil structure/sensitivity (Chandler 1988), insertion disturbance can variably affect both the peak and residual strength (Cerato & Lutenegger 2004), limiting the accuracy by which soil sensitivity can be measured with the vane test. Vane insertion can further result in development of a disturbed zone of uniform thickness around the perimeter of the vane (Morgenstern & Tchalenko 1967). The influence of soil structure and sensitivity on the thickness of this zone has been noted in the literature (Juneja et al. 2013), however its effect on strength measurements remains unquantified. As the disturbed zone can transect the vane failure surface with a thickness exceeding that currently considered in interpretation methods (Chandler 1988), the resultant contribution to soil resistance may vary in highly structured or sensitive soils. To depict the potential effect of soil structure on insertion disturbance, Figure 1 compares the microstructure of a typical soft marine clay against the microstructure of a consolidated kaolin sample, pre- and post- shearing. As soil destructuration and particle realignment resulted in 25% strength decrease for the artificial clay (Juneja et al. 2013), the potential influence of insertion disturbance may be extrapolated to the weakly cemented and sensitive microstructure of natural soft marine clays.

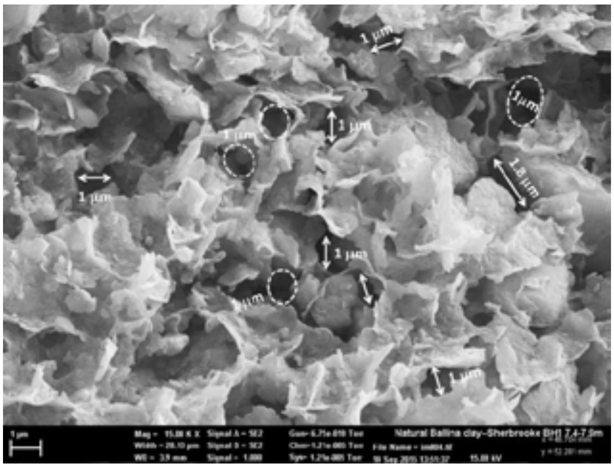

(a)

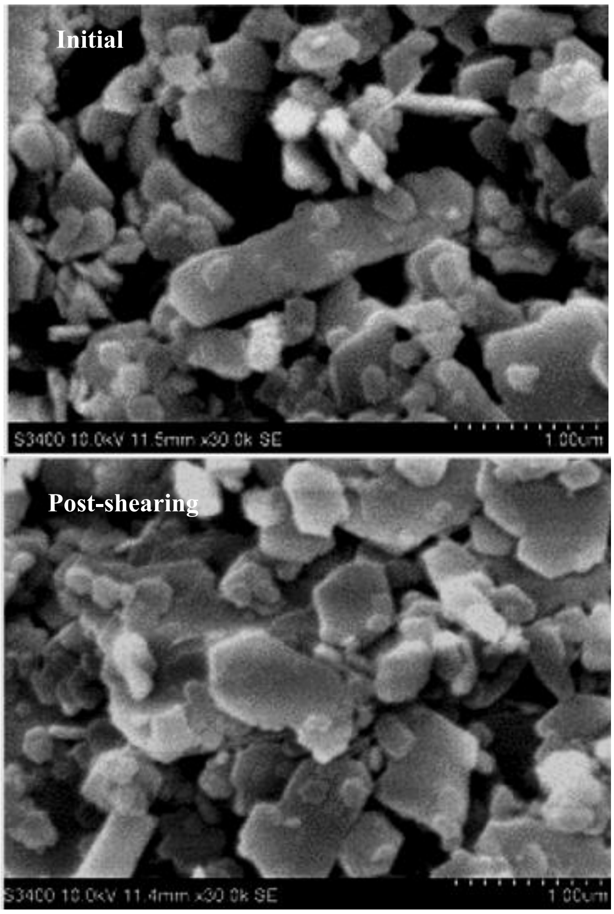

(b)

Figure 1. Comparison of soil fabric for (a) natural Ballina clay (after Pineda et al. 2016), and (b) Pre- and post- shear 50kPa-consolidated kaolin (after Juneja et al. 2013), as viewed through scanning electron microscope (SEM) photomicrography.

Quantitative information regarding the influence of microstructural and compositional variation on the measured soil strength is provided in Figure 2, which presents laboratory mini vane shear test results performed at 6 deg/min with a 20mm square vane in soft marine Ballina clay (from the east coast of Australia) and remoulded kaolin. The plasticity index for the Ballina clay and kaolin used is 86.3 and 20.7 respectively. A clear reduction in stiffness and strength is evident between the structured (undisturbed) and remoulded Ballina clay samples, but also between the remoulded Ballina and kaolin samples.

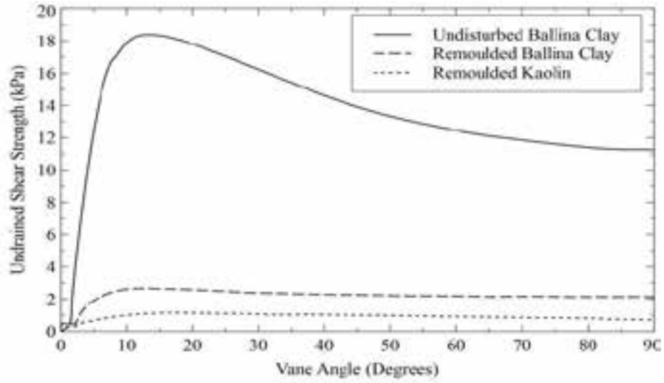

Figure 2. Comparison of resistance to vane shearing of undisturbed Ballina clay, remoulded Ballina clay and remoulded kaolin, measured during laboratory mini vane shear tests. Undisturbed Ballina clay block samples were retrieved with a Sherbrooke sampler from the National Field Test Facility at Ballina, New South Wales, Australia (Kelly et al. 2014).

Vane insertion is associated with the generation of excess pore pressures, that can reach up to 75% of vertical effective stress (Morris & Williams 1993). These exceed by far excess pore pressures generated during the rotation of the vane (Kimura & Saitoh 1983). As the former dissipate, consolidation of the soil may compensate for the decrease in its strength due to disturbance effects (Chandler 1988). This process is illustrated in Figure 3, which presents the evolution of normalised pore pressure during insertion of a 20mm square laboratory vane, partial dissipation of insertion excess pore pressure, and subsequent undrained rotation at 200 deg/min. For regular *in situ* vane testing, the required time to achieve full dissipation of excess pore pressures may vary between 4 hours and 7 days, while full strength recovery can vary between 20% to 50% of the initial undisturbed strength, depending on the soil coefficient of consolidation (c_v) and sensitivity respectively (Chandler 1988). As full drainage conditions are difficult to assess or achieve during regular *in situ* vane testing, this introduces a potentially un-conservative ambiguity to the interpretation. To avoid this, a delay time no longer than 1 minute (Morris & Williams 2000) is required to ensure undrained conditions; this is in contrast to the standard delay time of 5 minutes (Chandler 1988; Morris & Williams 2000; ASTM D2573 2008).

Recent developments in numerical and analytical methods may also provide significant insight into pore pressure generation and dissipation during insertion (Kouretzis et al. 2015) and vane rotation (Puzrin & Randolph 2015). Combined with experimental results, they can lead to the proposal of a framework for quantifying disturbance and pore pressure generation effects on the interpreted value of undrained strength from vane tests.

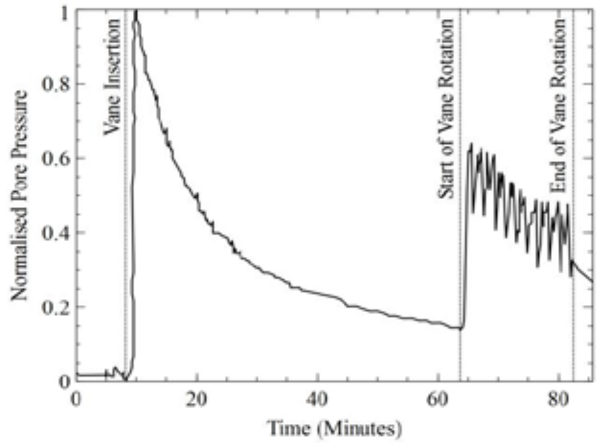

Figure 3. Evolution of normalised pore pressure in Ballina clay due to vane insertion and delayed vane rotation, measured experimentally in the laboratory using a 20mm square blade at 200 deg/min rotation rate.

2.2 *Shearing rate effects*

The resistance to vane shearing is a function of the testing rate. There is no unique correlation between these two quantities, as it depends on soil properties and composition, shearing mechanism, and rate range under consideration. This is due to the simultaneous mechanisms of pore pressure dissipation and soil viscosity influencing the measured strength, with the conceptual diagram of Figure 4 indicating the relative rate regions in which each mechanism typically governs soil response. While standardization of the testing procedure and interpretation methodology are designed to minimize strength variation by achieving "reference" conditions, comparison between tests performed at varied strain rates requires quantification of strength dependency on shearing rate. This is necessary when comparing strength measured via alternate test procedures or alternate blade shapes and sizes, as commonly done for calibration and verification purposes respectively.

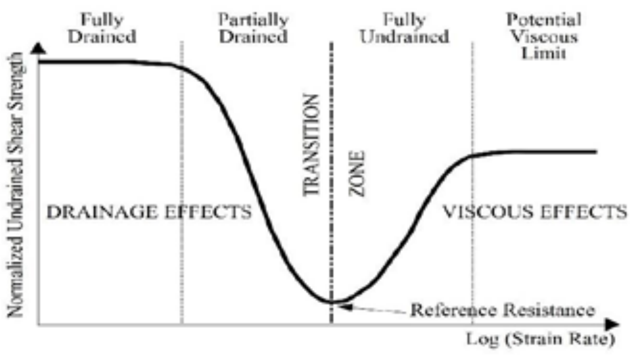

Figure 4. Conceptual "backbone" rate response model presenting the variation of measured strength with the rate of testing (after Quinn & Brown 2011).

Rate effects in vane testing are commonly quantified via the comparison of normalised vane strength to the logarithm of rotation rate or time to failure. For the common range of field vane rotation rates (6 deg/min to 60 deg/min), the strength increase per log cycle increase in rotation rate is in the range of: 1% - 2% for disturbed, remoulded or partially drained soils; 10% for typical *in situ* soil conditions; and up to 20% - 30% for sensitive, structured or cemented soils (Chandler 1988; Biscontin & Pestana 2001). Variation in vane size and shape can alter the rate of soil shearing at constant rotation rate, which has resulted in analysis methods being generalized to consider shear rate in terms of vane peripheral velocity (Biscontin & Pestana 2001) or c_v-normalised peripheral velocity (Quinn & Brown 2011). These methods account for variation in shear surface and soil drainage velocity respectively.

The use of peripheral velocity based semi-logarithmic or power law models for vane rate effects is common, with empirical fitting parameters documented for a range of soil types (Biscontin & Pestana 2001). Figure 5a presents power law fits from mini vane tests in kaolin and bentonite, in comparison with published data for a similar bentonite-kaolin mixture tested with a full-size vane (Biscontin & Pestana 2001). Reasonable agreement is observed for tests in bentonite, despite using vanes of different size. The influence of soil structure on rate is demonstrated using mini vanes in Figure 5b, which compares rate effects from high quality, undisturbed Ballina clay to that of remoulded Ballina clay. In contrast with *in situ* vane results (Chandler 1988), a decrease in rate effect is evident between the remoulded and undisturbed Ballina clay samples when interpreted using peripheral velocity. This may be due to the influence of c_v between soil states. As the reduced diameter and drainage path of laboratory miniature vanes can result in partially drained test conditions (Biscontin & Pestana 2001), and a reduced c_v may be expected following remoulding (Hamblin 1985) or disturbance (Kelly 2008) of structured soils, c_v and reference rate variation due to soil state may influence measured strength significantly. This can be modelled using c_v-normalised peripheral velocity.

While the peripheral velocity and c_v can be used to normalise measurements obtained with similarly shaped blades, further research is required on modelling rate effects on measurements obtained with vane blades of varied length (Chandler 1988), a non-zero taper angle (ASTM D2573 2008) or variably inclined or elliptical edges (Menzies & Mailey 1976; Selvadurai 1979; Silvestri & Aubertin 1988). Models that can describe the variation of the shear strength with the strain rate (e.g. Quinn and Brown, 2011) can be valuable for comparison/calibration between alternate test techniques, or for the estimation of design strength parameters in soils subjected to diverse loading rates. However, calibration of such multi-parameter models requires extensive experimental testing and parameters that cannot be readily obtained from common vane tests.

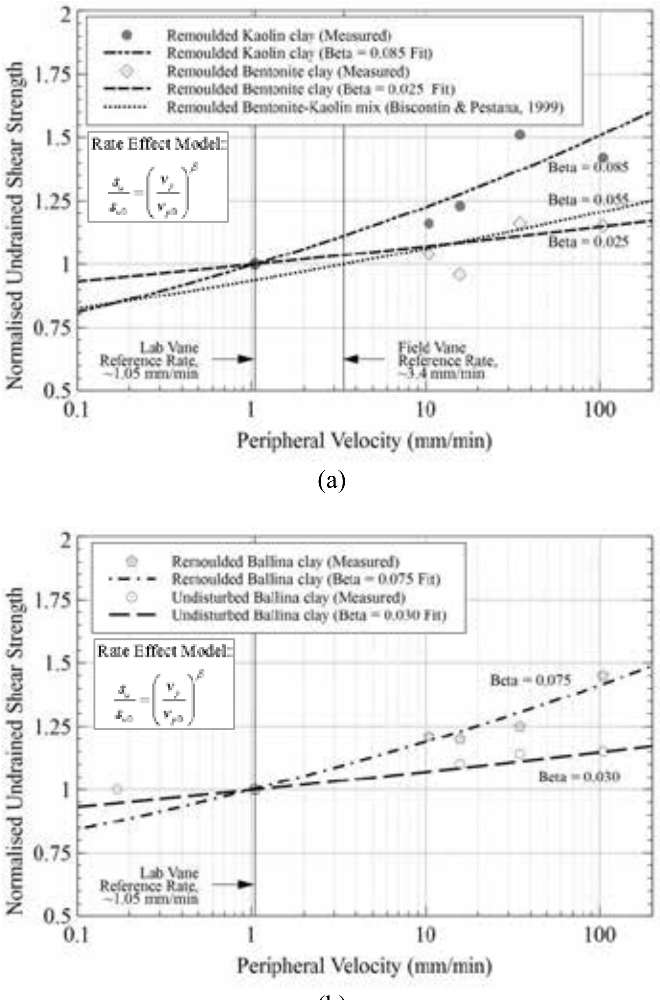

Figure 5. Shear strength dependency on the rotation rate for (a) Remoulded kaolin and bentonite, and (b) Structured and remoulded Ballina clay.

Numerical investigations exploring the influence of rate effects on measured strength have combined semi-logarithmic rate law and strength degradation models to describe localized soil softening in both pre- and post-peak failure regimes (Zhu & Randolph 2007). More recent studies (Zhu & Randolph 2011; Puzrin & Randolph 2015) consider the influence of soil rheological characteristics and pore pressure development inside shear bands with varied rotation rate. Good agreement between the abovementioned solutions and experimental results suggests that they can provide a framework for the quantification of soil parameter influence on rate effects.

2.3 *Soil anisotropy and stress distribution effects*

Both soil anisotropy and the distribution of stresses around the blade during shearing failure can significantly affect the estimation of soil strength from torque measurements. As these factors cannot be quantified with standard testing procedures, they are ignored in current interpretation methods: soil is assumed to be isotropic, and a simplified stress distribution along the edges of the blade is assumed.

However, various techniques are described in the literature to infer strength anisotropy from the vane test. Strength measurements from vanes of varied height or inclination angle are reported by Silvestri & Aubertin (1988), who proposed a method to obtain the contribution of each shear plane to the torsional resistance. As anisotropic soil strength can result in different rotation angle at failure between vanes featuring edges of non-standard taper angle (Morris & Williams 1993), stress conditions at failure may also vary as a function of soil softening on tapered edges (Silvestri & Aubertin 1988). These factors are ignored in practical interpretation methods. Specific to the standard blade (zero taper angle), the state-of-practice formula for deriving the undrained strength from torque measurements is based on the (conservative) assumption of uniform shear stress distribution at the edges of the blade and isotropic soil (equal horizontal to vertical stress ratio, $b = 1$ in Figure 6). A sensitivity study by Chandler (1988) suggests that considering the maximum “likely” anisotropic strength ratio of $b = 0.6$ and a more realistic polynomial stress distribution (n = 6, Figure 6) at the top and bottom edges will result in a variation of the calculated soil strength of the order of 6%, compared to the standard method. As the assumption of strength anisotropy results in lower strength predictions (Chandler 1988), and a polynomial stress distribution may be likely in anisotropic soils (Wroth 1984; Pérez Foguet et al. 1999), adoption of $b = 0.6$ and a polynomial stress distribution of degree $n = 5$ at the top and bottom edges may provide a more reasonable interpretation model for structured soils.

The use of blades with non-zero taper angle is not excluded from current standards (ASTM D2573 2008). However, in anisotropic soils the strength estimated with "standard" and tapered vanes under the same test conditions will vary, depending on the anisotropic strength ratio and the taper angle. Various models that can introduce the effect of soil anisotropy and taper angle in the interpretation formulas are summarized by Silvestri & Aubertin (1988), which model strength variation with shearing angle. These formulas were derived by considering anisotropic elasticity and require empirical fitting at intermediary shearing angles.

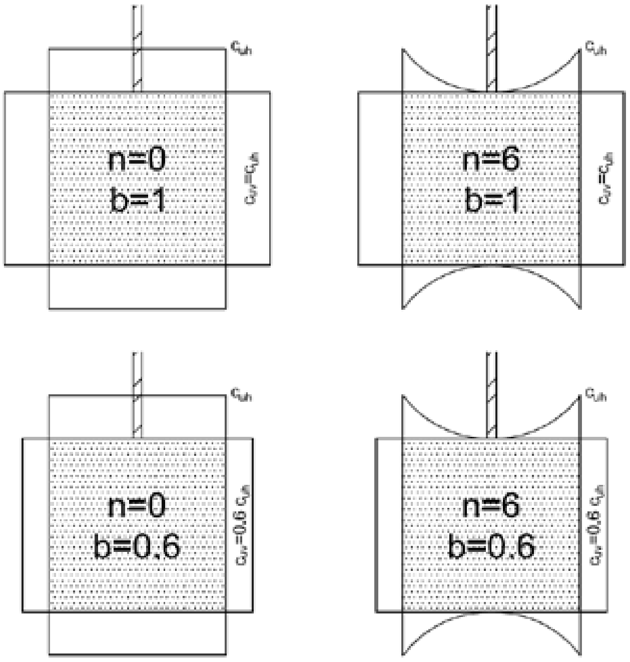

Figure 6. Schematic representation of commonly adopted shear stress distributions (after Chandler 1988)

A more elaborate approach on the effect of soil anisotropy on the measured torque and stress distribution at failure is presented by Morris & Williams (1993), who proposed an effective stress framework based on the Modified Cam Clay soil model. By considering the soil effective stress state and the critical state friction angle, prediction of torque contributions from varied shear plane inclinations is made possible, facilitating the independent analysis of failure evolution with rotation angle at the horizontal and vertical shearing surfaces. While the model cannot delineate between the influence of soil anisotropy and stress distribution on the resistance torque, a modification of the method to account for varying vane geometry will enable the quantification of the contribution of soil anisotropy. Morris & Williams (1993) further demonstrate that assuming a polynomial stress distribution at the top and bottom edges of the blade may result in overestimating the available strength by up to 30% in normally and isotropically consolidated soils. This highlights the significant influence of soil anisotropy on the relative contribution of the resistance developing at the horizontal and vertical edges of the blade to the measured torque. This framework can be further evolved to consider vanes (and thus failure surfaces) of different shapes, and provide the theoretical background for obtaining additional soil properties from the vane test through measurements with diverse blade configurations.

2.4 *Shape of the failure surface*

The shape of the failure surface that develops in the soil as a result of vane rotation, and thus the total resistance to shearing translated to torque, depends on the shape of the vane but also on soil properties. A simplified cylindrical shear surface is assumed in current normative interpretation methods. In reality, the failure surface that develops around the vane features a square shape during the initial stages of shearing, with increased vane rotation resulting in rounding and smoothing of the shear band (Veneman & Edil 1988). In some cases, a circular failure surface may not develop until full remoulding takes place. Interpreting vane failure by assuming a simple cylindrical failure surface may result in error of up to 16% according to Veneman & Edil (1988), depending on the blade geometry, rotation rate and soil properties.

Oscillatory resistance behaviour in the post-peak region has been documented for the vane when the standard test procedure is followed (McConnell 2014), which may influence the measured residual strength considerably. McConnell (2014) attributes this effect to soil remoulding. Similar behaviour has been observed and modelled numerically for penetration-based methods of strength determination, with resistance oscillation attributed to evolving shear bands at large strains (Zhu & Randolph 2007). An example of post-peak normalised oscillatory behaviour is shown in Figure 7, which compares the resistance up to large rotations of a remoulded and a high quality block sample of Ballina clay, measured experimentally using laboratory vanes rotated at 200 deg/min.

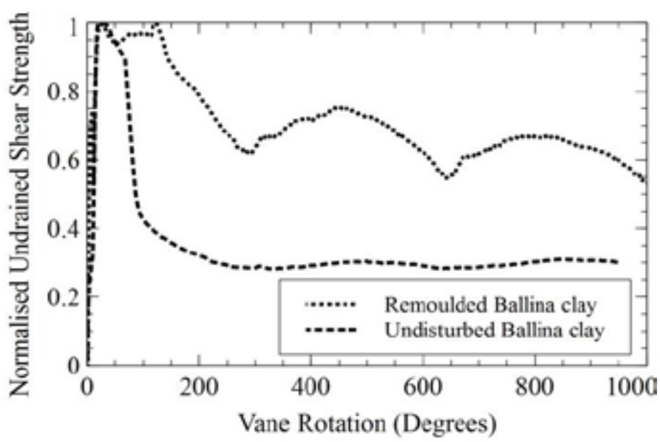

Figure 7. Comparison of post-peak strength oscillation with rotation rate for remoulded and undisturbed Ballina clay.

While mechanical influences related to the vane test setup cannot be excluded at this stage, evolving shear bands due to quick remoulding may also provide explanation. Due to the widespread observation of this post-peak behaviour in both experimental and numerical studies from a range of large-strain test methods, further research is required to ascertain the conditions influencing the existence of this mechanism. The theoretical background for evolving shear band behaviour can be found in analytical and numerical models proposed for the analysis of shear band propagation and localized pore pressure development and dissipation (Puzrin & Germanovich 2005).

3 CONCLUDING REMARKS

The presented preliminary experimental results and theoretical concepts highlight the mechanisms that influence the resistance developing during vane shear tests in soft marine clays, and how this can be correlated to the *in situ* undrained strength. Further research currently underway aims to collate experimental, theoretical and numerical results into a robust framework for the interpretation of vane shear tests, and for retrieving more information about the mechanical properties of the soil through vane tests.

4 REFERENCES

ASTM D2573. (2008). Standard Test Method for Field Vane Shear Test in Cohesive Soil *D2573* (pp. 8). United States of America: ASTM International.

Biscontin, G. & Pestana, J. M. (2001). Influence of peripheral velocity on vane shear strength of an artificial clay. *ASTM geotechnical testing journal, 24*(4), 423-429.

Cerato, A. & Lutenegger, A. (2004). *Disturbance effects of field vane tests in a varved clay.* In Proc. of the 2nd International Conference on Site Characterisation, Porto, Portugal. Millpress, Rotterdam, the Netherlands, 861-867.

Chandler, R. J. (1988). The in-situ measurement of the undrained shear strength of clays using the field vane. *Vane shear strength testing in soils: field and laboratory studies*, 13-44.

Hamblin, A. P. (1985). The influence of soil structure on water movement, crop root growth and water uptake. *Advances in Agronomy, 38*(95), 155.

Juneja, A. & Mir, B. & Roshan, N. (2013). Effect of the Smear Zone around SCP Improved Composite Samples Tested in the Laboratory. *International Journal of Geomechanics, 13*(1), 16-25.

Kelly, R. & O'Loughlin, C. & Bates, L. & Gourvenec, S. & Colreavy, C. & White, D. & Gaone, F. & Doherty, J. & Randolph, M. (2014). In situ testing at the National Soft Soil Field Testing Facility, Ballina. *New South Wales. Australian Geomechanics, 49*(4), 15-26.

Kelly, R. B. (2008). Back analysis of the Cumbalum trial embankment. *Aust Geomech, 43*(1), 47-54.

Kimura, T. & Saitoh, K. (1983). Effect of disturbance due to insertion on vane shear strength of normally consolidated cohesive soils. *Soils and Foundations, 23*(2), 113-124.

Kouretzis, G. P. & Ansari, Y. & Pineda, J. & Kelly, R. & Sheng, D. (2015). Numerical evaluation of clay disturbance during blade penetration in the flat dilatometer test. *Géotechnique Letters, 5*(3), 91-95.

McConnell, A. (2014). *An Update on Vane Shear Testing by IGS*. IGS. Australia.

Menzies, B. & Mailey, L. (1976). Some measurements of strength anisotropy in soft clays using diamond-shaped shear vanes. *Geotechnique, 26*(3).

Morgenstern, N. & Tchalenko, J. (1967). Microscopic structures in kaolin subjected to direct shear. *Geotechnique, 17*(4), 309-328.

Morris, P. & Williams, D. (1993). A new model of vane shear strength testing in soils. *Geotechnique, 43*(3), 489-500.

Morris, P. & Williams, D. (2000). A revision of Blight's model of field vane testing. *Canadian Geotechnical Journal, 37*(5), 1089-1098.

Pérez Foguet, A. & Ledesma Villalba, A. & Huerta, A. (1999). Analysis of the vane test considering size and time effects. *International Journal for Numerical and Analytical Methods in Geomechanics, 23*(5), 383-412.

Pineda, J. A. & Liu, X.-F. & Sloan, S. W. (2016). Tube sampling in soft clay: a microstructural insight. *Geotechnique (in print)*.

Puzrin, A. & Germanovich, L. (2005). *The growth of shear bands in the catastrophic failure of soils.* In Proc. of the Royal Society of London A: Mathematical, Physical and Engineering Sciences, 1199-1228.

Puzrin, A. M. & Randolph, M. F. (2015). Effects of pore water pressure dissipation on rate dependency of shear strength in localised failure of soils. *International Journal for Numerical and Analytical Methods in Geomechanics, 39*(10), 1045-1062.

Quinn, T. A. C. & Brown, M. J. (2011). *Effect of strain rate on isotropically consolidated kaolin over a wide range of strain rates in the triaxial apparatus.* In Proc. of the 5th International Symposium on Deformation Characteristics of Geomaterials, Chung, Kim, Lee, Jung, & Kim (Eds.), 607-613.

Selvadurai, A. P. S. (1979). On the estimation of the deformability characteristics of an isotropic elastic soil medium by means of a vane test. *International Journal for Numerical and Analytical Methods in Geomechanics, 3*(3), 231-243.

Silvestri, V. & Aubertin, M. (1988). Anisotropy and in-situ vane tests. *Vane shear strength testing in soils. STP, 1014*, 88-103.

Veneman, P. L. & Edil, T. B. (1988). Micromorphological aspects of the vane shear test *Vane shear strength testing in soils: field and laboratory studies*: ASTM International.

Wroth, C. (1984). The Interpretation of In Situ Soil Tests. *Geotechnique, 34*(4), 449-489.

Zhu, H. & Randolph, M. (2007). Computational techniques and shear band development for cylindrical and spherical penetrometers in strain-softening clay. *International Journal of Geomechanics, 7*(4), 287-295.

Zhu, H. & Randolph, M. F. (2011). Numerical analysis of a cylinder moving through rate-dependent undrained soil. *Ocean Engineering, 38*(7), 943-953.

Geotechnical and Geophysical Site Characterisation 5 – Lehane, Acosta-Martínez & Kelly (Eds)

Use of shear wave velocity to estimate stress history and undrained shear strength of clays

S.S. Agaiby & P.W. Mayne
Geosystems Engineering, Georgia Institute of Technology, Atlanta, GA, USA

ABSTRACT: A quality database of downhole shear wave velocity profiles (V_{sVH}) from 64 worldwide well-documented clay sites has been compiled to provide a first-order estimate of stress history of clays. The database primarily includes soft-to-firm normally consolidated (NC) to lightly overconsolidated where OCR < 2, as well as some stiff to hard overconsolidated (OC) and fissured clays. The stress history is expressed in terms of effective yield or preconsolidation stress (σ_p') which was measured in the laboratory by oedometer and/or consolidation tests on undisturbed samples. The in-situ V_{sVH} were measured by downhole tests (DHT), mostly using seismic piezocones (SCPTu) or seismic dilatometers (SDMT). The estimated stress history is applied to provide an evaluation of undrained shear strength (s_u) of intact clays using a SHANSEP type approach which considers different shearing modes. The suggested approach can be used as an independent estimate of stress history and undrained shear strength of clays reliant on only the in-situ measured shear wave velocity.

1 INTRODUCTION

1.1 *Stress History*

The stress history of a soil can be used to delineate the geological processes which have occurred over the many years and can be considered the focal point for soil behavior in terms of strength, flow, and compressibility. The preconsolidation stress (σ_p') can be defined as the maximum effective overburden stress experienced by the soil during its stress history. The overconsolidation ratio (OCR) is a convenient normalized and dimensionless parameter based on σ_p' and current effective vertical stress (σ_{v0}') such that: OCR = σ_p'/σ_{v0}'. More recently, the terms yield stress (σ_{vy}') and yield stress ratio (YSR = σ_{vy}'/σ_{vo}') are used to also include effects of diagenesis, bonding, and ageing.

1.2 *Stress History Evaluation Methods*

The most basic and conventional means to determine stress history is a laboratory one-dimensional consolidation test using a consolidometer (ASTM D2435). The specimen is subjected to constrained compression in either a mechanical oedometer, pneumatic or hydraulic consolidometer, or automated constant rate of strain (CRS) device. On the basis of the oedometer test, many methods have been proposed to evaluate σ_p' from the compression measurements. However, the results are dependent on the plotting methods and curve-fitting procedures. Casagrande analyzed the stress history and established the first and most common method to obtain σ_p' using a graphical method. Afterwards, others attempted to improve and develop new methods in order to determine the preconsolidation stress more definitively such as the Schmertmann (1955) reconstruction method, Janbu (1969) stress-strain and modulus-strain method, Butterfield (1979) approach with a bilogarithmic representation, and Becker et al. (1987) work-energy method. At least 28 methods are available for these purposes (Ku and Mayne 2013).

1.3 *Stress History Evaluation Problems*

Laboratory based techniques are associated with many issues: disturbance which can be attributed to sampling process, specimen handling, disturbance, and stress relief due to bringing the sample from depths to the ground surface with possible swelling. Other issues include: lack of information on sampling effective stress before testing, specimen trimming method, load application duration, secondary consolidation consideration, temperature, salt concentration in pore fluid, friction between specimen ring and the soil, load increment ratio and schedule, lack of proper saturation, specimen slenderness, and capacity of loading frame (Germaine & Germaine, 2009).

To overcome issues associated with the laboratory methods, σ_p' can be estimated using empirical correlations or analytical solutions with in-situ test measurements that avert the issues of sample disturbance and these are also faster and more economical than laboratory tests. Many relationships for stress history evaluation have been proposed for various in-situ tests such as cone penetration test (CPT), flat dilatometer test (DMT), standard penetration test (SPT), vane shear test (VST) and pressuremeter test (PMT), as discussed for instance by Mayne (1995).

Herein, a direct relationship between σ_p' and V_s was sought following the concepts and logic previously established by Mayne et al. (1998) and Mayne (2005) on smaller datasets.

2 SHEAR WAVE VELOCITY

Shear wave velocity (V_s) can be measured using either invasive and/or non-invasive geophysics, as well as obtained on small lab specimens. Shear waves can be measured in all geomaterials where it serves as an excellent reference benchmark in comparing stiffness and stress states. The measured V_s profile is fundamentally applicable to both static and dynamic geotechnical analyses as it provides the small-strain shear modulus.

The magnitude of shear modulus can be measured from small specimens in the laboratory using resonant column, ultrasonics, bender elements, and/or triaxial tests with local strain sensors, however, these methods have several issues: sampling disturbance difficulties, loss of ageing and diagenesis effects in addition to stress relief. Hence, V_s is best measured in-situ rather than in the laboratory.

Field methods for V_s measurement can be either invasive or non-invasive. Invasive methods include cased borehole methods such as: crosshole test (CHT), downhole test (DHT), uphole test (UHT), and P-S suspension logger, as well as direct push methods: seismic cone penetration test (SCPT) and seismic flat dilatometer test (SDMT) which are efficient versions of the DHT mode that measures a vertically-propagating horizontally-polarized shear wave velocity, or V_{sVH} mode. Non-invasive methods include refraction survey, reflection survey, and surface wave methods using either active sources to measure Rayleigh waves: spectral analyses of surface waves (SASW), multi-channel analyses of surface waves (MASW), and continuous surface wave method (CSW), or passive source techniques, such as passive surface waves (PSW) or reflection microseism (ReMi).

3 COMPILED DATABASE

A comprehensive database was prepared from a total of 64 well-documented worldwide geotechnical test sites. The sites primarily include soft to firm normally-consolidated young to aged clays, as well as a few sites from stiff to hard overconsolidated clays and fissured fine-grained soils. Only high-end laboratory tests were included with a focus on one-dimension consolidation tests for stress history profiles measured using standard 1D consolidation tests with a constant load increment duration of 24 hr (IL_{24}) and successive load increments applied at end-of-primary consolidation tests (IL_{EOP}), and constant rate of strain (CRS) consolidation tests.

Regarding V_s data, only in-situ results were compiled from downhole shear wave velocity (V_{sVH}) which can be measured using DHT, SCPT, and SDMT. At each of the studied sites, complementary field and lab data were also often available such as: Atterberg limits and unit weight for evaluating the effective vertical overburden pressure.

In the events where no undisturbed samples or natural water contents were available, unit weight was estimated using indirect methods such (Mayne 2005):

$$\gamma_t\,(\mathrm{kN/m^3}) = 8.63\log(V_s) - 1.18\log(z) - 0.53 \quad (1)$$

where V_s (m/s) and depth z reported in meters.

The compiled database has a total pairing of 790 one-dimension consolidation tests along with their corresponding V_{sVH} values which can be classified into 3 main groups: (a) normally consolidated (NC) intact to lightly overconsolidated (LOC) intact clays; (b) overconsolidated (OC) intact clays; and (c) highly overconsolidated (HOC) fissured clays.

A total of 36 different NC-LOC intact clays with a total of 486 preconsolidation effective stress (σ_p') measurements were collected, as presented in Table 1. Whereas, the OC clays generally exhibit 2 < OCRs < 5 and include intact and lightly cemented clays from 19 test sites with a total of 204 σ_p' measurements, as presented in Table 2. Finally, the HOC clays group includes fine-grained soils with OCRs > 5 and a total of 9 hard to fissured clay sites with 100 σ_p' measurements, as listed in Table 3. The reference sources of data and information in the presented tables are given in an abbreviated form (i.e., CEPNS = Characterization & Engineering Properties of Natural Soils, Taylor & Francis, London) due to the need to conserve space in allocated pages.

Table 1. Soft/firm clays (1<OCRs < 2) with paired σ_p' and V_{sVH}

Site	Location	Reference(s)
AIT	Bangkok	Watabe et al. (2004), 2nd ISC (2), Porto: 1765-1772.
Amherst, MA	USA	DeGroot & Lutenegger (2003), CEPNS (1): 695 - 724.
Ariake	Japan	Tanaka et al. (2001), Canadian Geot. J. 38 (2): 378-400.
Bäckebol	Sweden	Larsson & Mulabdić (1991), SGI (40)
Belfast	Ireland	Lehane (2003), Geot. Engrg. 156 (1) ICE, London: 17-26.
Bothkennar	UK	Hight et al. (1992) Géotechnique Vol. 42 (2): 303-347
Burswood	Australia	Low et al (2011) Géotechnique Vol. 61(7): 575-591

Busan	Korea	Chung et al. (2012), KSCE J. Civil Engrg. 16(3): 341-50
Drammen	Norway	Long & Donohue (2007), Canadian Geotechnical J. 44 (5): 533 – 544.
Evanston, IL	USA	Finno et al. (2000), National Geotech Sites, ASCE GSP 93: 130-159
Fucino	Italy	Burghignoli et al. (1991), 10th ECSMFE (1), Florence: 27-40.
Hachirougata	Japan	Tanaka (2006), CEPNS (3): 1831-1852
Higashi	Japan	Shibuya et al. (1995), Earthquake Geotechnical Eng. (1): 77-82
Kobe	Japan	Nakase et al. (1988), J. Geotech. Eng. 114(7): 844-858.
Kurihama	Japan	Shibuya & Tanaka (1996), Soils & Foundations 36(4): 45-55.
Lianyungang	China	Liu (2008), Marine Georesources & Geotechnology 26(3): 189-210.
Lierstranda	Norway	Long & Donohue (2007), Canadian Geotechnical J. 44 (5): 533 – 544.
Lilla Mellösa	Sweden	Larsson & Mulabdić (1991), Swedish Geot. Institute Report 42.
Munkedal	Sweden	Larsson & Mulabdić (1991), Swedish Geot. Inst. Report 42.
Museumpark	Norway	Long & Donohue (2007), Canadian Geot. J. 44(5): 533-544.
Norrköping	Sweden	Larsson & Mulabdić (1991), Swedish Geot. Institute Report 42.
Onsøy	Norway	Lunne et al. (2003), CEPNS (1): 395-428
Pentre	UK	Lambson et al. (1992), Large-scale Pile Tests in Clay, ICE:134-196
Perniö	Finland	Lehtonen (2015), PhD Thesis, Tampere University: 213 p
Sarapui	Brazil	Almeida & Marques (2003), CEPN (1): 477-504.
Sarapui II	Brazil	Jannuzzi et al. (2015), Eng. Geology (190): 77-86.
Saro Rd 6-900	Sweden	Larsson & Mulabdić (1991) Swedish Geot. Institute Report 42.
Saro Rd 7-600	Sweden	Larsson & Mulabdić (1991) Swedish Geot. Institute Report 42.
Singapore	Singapore	Tanaka et al. (2001), Canadian Geot. J. 38(2): 378-400
Skä Edeby	Sweden	Larsson & Mulabdić (1991) Swedish Geot. Institute Report 42.
S. Gloucester ON	Canada	Bozozuk (1972), PhD Thesis, Purdue Univ.: 208p.
Sutthisan	Bangkok	Shibuya & Tamrakar (2003), CEPNS, (2): 645-692.
Taipei	Taiwan	Chin et al. (2007), CEPNS (4): 1755-1803
Troll Upper	North Sea	Lunne et al. (2007), CEPNS (4): 1939-1972
Tuve	Sweden	Larsson & Mulabdić (1991) Swedish Geot. Institute Report 42.
Valen	Sweden	Larsson & Mulabdić (1991) Swedish Geot. Institute Report 42.

Table 2. Overconsolidated Clays with 2.0 < OCR < 5.0

Site	Location	Reference(s)
Beaumont, TX	USA	Mahar & O'Neill (1983), J. Geotech Engrg. 109(1): 56 -71.
Bonneville, UT	USA	Gardner (2007) MS Thesis, Brigham Young Univ: 142p.
Cooper Marl, SC	USA	Camp (2004), *GeoSupport* GSP 124, ASCE Reston VA: 1-18.
Hai-Phong	Vietnam	Watabe et al. (2004), 2nd ISC (2), Porto.
Hamilton, CA	USA	Nguyen (2007) MS Thesis, MIT: 366p.
Hilleren	Norway	Long et al. (2009), J. Geotech. and Geoenvir. Engrg. 135(2): 185-198.
I-395, ME	USA	Hardison (2013) MS Thesis. Univ. Maine
Louiseville, Quebec	Canada	Leroueil & Hamouche (2003), CEPNS (2): 363-393.
Montalto di Castro	Italy	Jamiolkowski & LoPresti (1994), 13th ICSMGE, (5):51-55.
Newbury, MA	USA	Landon (2007), PhD Thesis, U.Mass. Amherst: 701p.
Newport, OR	USA	Ferguson (2015), Seismic Evaluation Big Creek Dams: 561p.
Oseberg	North Sea	Rutledal et al. (2000), SEG: 570-573
Pisa	Italy	LoPresti et al. (2003), CEPNS (2): 909-946.
Port of Anchorage, AK	USA	Mayne & Pearce (2005), Frontiers Offshore Geot, Perth: 951-955.
Route 197 Bridge, ME	USA	Hardison (2013) MS Thesis, Univ. Maine: 394p.
Saint Alban, Quebec	Canada	Levesque et al. (2007), CEPNS (4): 2645-2677.
Troll Lower	North Sea	Lunne et al. (2007), CEPNS (4).
Lower 232 St., BC	Canada	Sully (1991) PhD Thesis, Univ. British Columbia: 485p.
200th St., BC	Canada	Sully (1991) PhD Thesis, UBC: 485p

Table 3. HOC and Fissured Clays with OCRs > 5

Site	Country	Reference(s)
AGS, NJ	USA	Stoll et al. (1988), J. Acoustical Society of America 83(1): 93-102.
Brent Cross	UK	Hight et al.(2003),CEPNS(2):851–907
Chattenden	UK	Butcher & Powell (1995), 11th ECSMFE (1), Copenhagen: 27-36
Cowden	UK	Hight et al.(2003),CEPNS(2):851–907
Heathrow	UK	Hight et al.(2003),CEPNS(2):851–907
Madingley	UK	Butcher & Powell(1995),11thECSMFE, Copenhagen
Martin's Point Bridge, ME	USA	Hardison (2013) M.Sc. Thesis Univ. Maine: 394p.
Oxford	UK	Bates & Phillips (2000), J. Applied Geophysics (44): 257-273
Tornhill	Sweden	Larsson (1991), SGI Rept 59: 169p.

4 ESTIMATING STRESS HISTORY FROM SHEAR WAVE VELOCITY

Using multiple regression analyses and investigating the compiled database from 64 clay sites given in Tables 1 to 3, a relationship between the preconsolidation stress, σ_p' (measured in kPa), the downhole shear wave velocity, V_{sVH} (measured in m/sec), and the effective vertical overburden stress, σ_{v0}' (measured in kPa) was developed, as shown in Figure 1, andcan be expressed:

$$\sigma_P' = 0.18 \cdot (V_{sVH})^{1.14} \cdot (\sigma_{vo}')^{0.26} \tag{2}$$

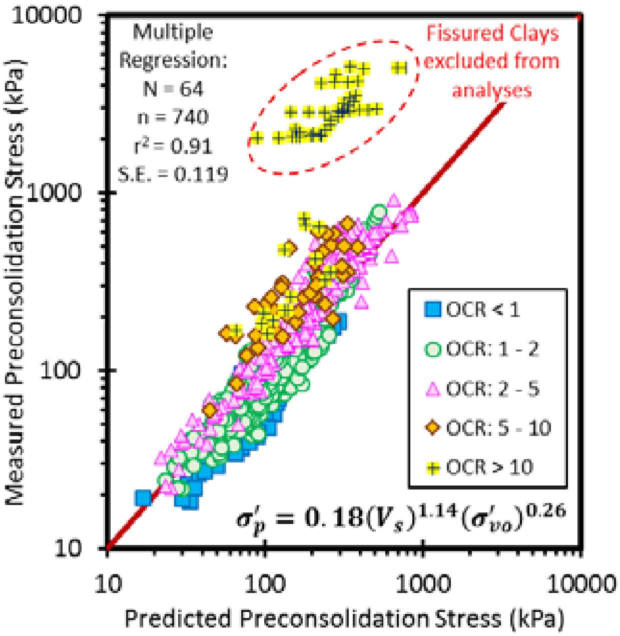

Figure 1. Measured versus predicted preconsolidation stress in terms of downhole shear wave velocity and effective vertical overburden stress for different OCR ranges.

Notably, the highly overconsolidated and fissured clays were found to behave differently and did not fit any of the developed expressions, therefore were excluded from the regression analyses.

By considering the results plotted in Figure 1, an good agreement between the measured and the predicted σ_p' values is achieved for intact clays. Hence, the proposed expression can be used as a first order estimate of stress history where only shear wave velocity data are available prior any other geotechnical investigations. Exception is again noted to the data from fissured overconsolidated clays that have discontinuities and joints. By considering the complementary compiled data, it was interesting to investigate the effect of the plasticity characteristics of the studied clays expressed in terms of plasticity index (PI), as shown in Figure 2. The clays can be divided into 4 subgroups based on their plasticity ranges where the higher the plasticity the lower the preconsolidation stress. Note here that the majority of data are from low OCR clays in the NC-LOC range.

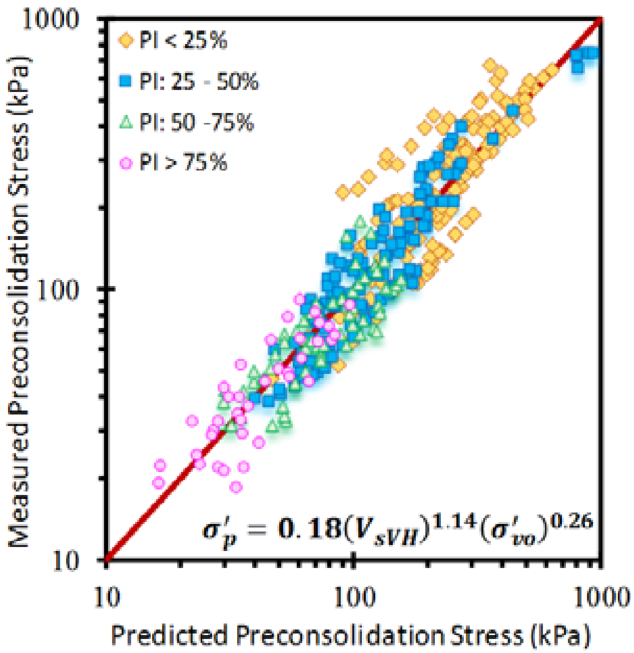

Figure 2. Measured versus predicted preconsolidation stress in terms of downhole shear wave velocity and effective vertical overburden stress for different PI values.

5 UNDRAINED SHEAR STRENGTH AND CASE STUDY APPLICATIONS

Different lab and field testing techniques can be used to measure undrained shear strength and provide a reference profile of s_u with depth. An alternate means to directly evaluating the magnitude of s_u in clays involves the utilization of stress history (i.e., OCR) of the clay deposit to profile a family of undrained strength ratios:

$$(s_u/\sigma_{vo}') = S \cdot OCR^m \tag{3}$$

where the coefficient S and exponent m can be found using SHANSEP (Stress History And Normalized Soil Engineering Parameters), as detailed by Ladd (1991) and Ladd & DeGroot (2003). The value of $S = (s_u/\sigma_{vo}')_{NC}$ is found experimentally by extensive laboratory testing with companion series of plane strain compression (PSC), simple shear (SS), and plane strain extension (PSE) tests on the soils at varied OCRs, or by series of triaxial compression (TC), simple shear (DSS), and triaxial extension (TE) tests. Representative S values as suggested by Ladd (1991) are 0.30 for TC, 0.21 for DSS, and 0.15 for TE. The exponent *m* can be determined experimentally and has been generally found to be on the order of 0.8 ± 0.1.

5.1 *Bothkennar Clay*

Bothkennar is a soft silty estuarine clay that is located on the south side of the River Forth, between Edinburgh and Glasgow in Scotland (Hight et al., 2003). The clay has the following average index parameters and soil properties: e_0 = 1.69, w_n = 61%, LL = 72.6%, PI = 41.8%, clay fraction of 30%, G_s = 2.65, and bulk density (ρ) = 1.607 Mg/m^3. The behavior in one-dimensional compression was investigated by Hight et al. (1992) using three types of consolidation tests: conventional incremental load tests, continuous load tests, and restricted flow tests as presented in Figure 3b. These give an average OCR = 1.54 with depth. Results of downhole V_{sVH} profiles from SCPT were measured by Hepton (1988) and presented in Figure 3a. These data along with the profile of the effective vertical stress are used to provide an estimate for σ_p' using Equation (2) showing a good agreement as shown in Figure 3b.

The evaluated stress history profile is used to estimate s_{uDSS}, s_{uTC}, and s_{uTE} profiles for Bothkennar clay via Equation (3), with adopted S values of 0.3 for TC, 0.21 for DSS, and 0.15 for TE and an exponent of m = 0.8, as presented in Figure 3c. Laboratory CK_0UC, DSS, and CK_0UE tests on undisturbed samples from the site are reported by Hight et al. (2003). Comparison of results show good agreement between measured and estimated profiles.

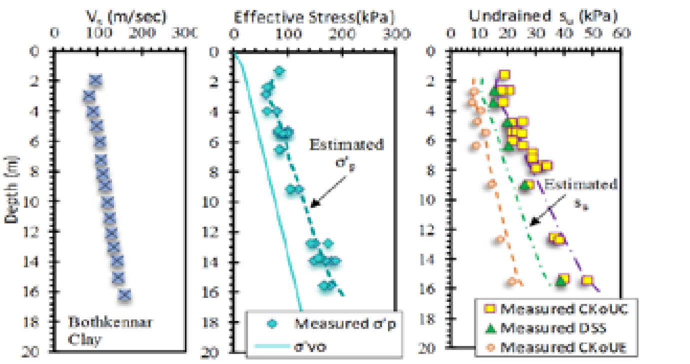

Figure 3. Profiles at Bothkennar soft clay: (a) Measured downhole shear wave velocity profile; (b) Estimated preconsolidation stress compared to lab-measured values; (c) Lab-measured and V_s-estimated TC, DSS, and TE strengths.

5.2 *Busan Clay*

Busan (or Pusan) is a soft clay that covers the Nakdong River delta in South Korea (Locat and Tanaka 1999). The clay has the following average index parameters and soil properties: e_0 = 1.59, w_n = 58.4%, LL = 61.5 %, PI = 27.2%, clay fraction of 27%, G_s = 2.71, and bulk density (ρ) = 1.60 Mg/m^3 (Chung et al., 2011). The behavior in one-dimensional compression was investigated by Singh & Chung (2015) using three test types: standard 1D consolidation tests with a constant load increment duration of 24 h (IL_{24}) and a successive load increments applied after 100% primary consolidation (end-of-primary consolidation, IL_{EOP}); and a constant rate of strain (CRS) consolidation test.

Results of downhole V_{sVH} profiles from SCPT are reported by Chung and Kweon (2013) and presented in Figure 4a. These data along with the profile of the effective vertical stress are used to provide an estimate for σ_p' using Equation (2) showing a good agreement as shown in Figure 4b. The estimated stress history profile is used to evaluate the OCR profile to estimate s_{uDSS}, s_{uTC}, and s_{uTE} with adopted S values of 0.30 for TC, 0.21 for DSS, and 0.15 for TE and an exponent m = 0.8 using Equation (3) as presented in Figure 4c. Laboratory CK_0UC and CK_0UE tests on undisturbed samples are reported by Chung et al. (2012). By comparing the undrained shear strength profiles, the estimated values compare well with lab data.

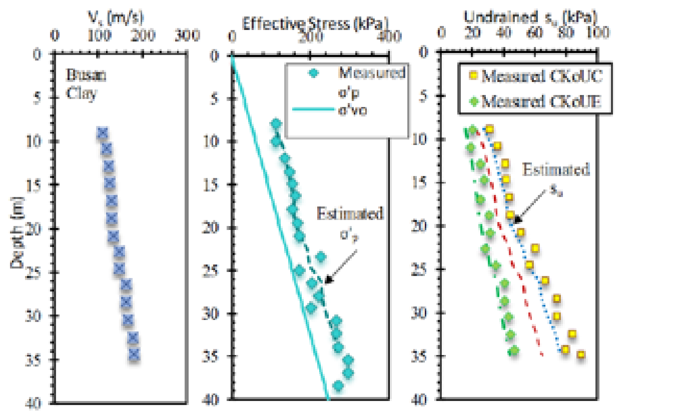

Figure 4. Profiles in soft Busan clay: (a) Measured downhole shear wave velocity; (b) Estimated preconsolidation stress compared to lab-measured stress history profile; (c) Lab-measured and V_s-estimated TC, DSS, and TE strengths.

5.3 *Onsøy Clay*

Onsøy is a soft marine clay that is located in Norway, southeast of Oslo (Lunne et al., 2003). The soil profile at Onsøy consists of a one meter thick weathered crust followed by an 8-m thick soft clay layer underlain by a soft medium plastic clay layer over the remaining thickness of 36 m over bedrock. The clay has the following average index parameters and soil properties: clay fraction of 53 %, e_0 = 1.75, w_n= 64%, LL= 68%, PI= 35%, G_s= 2.71, and bulk density (ρ) = 1.587 Mg/m^3. The profile of preconsolidation stress from one-dimensional oedometer tests has been measured in several investigations (e.g. Lunne et al., 2001). These give an average OCR = 1.69. The profile of the field measured V_{sVH} from seismic cone test is presented in Figure 5a. These data along with the profile of the effective vertical stress are used to provide an estimate for σ_p' using Equation (2) showing a good agreement as shown in Figure 5b.

The estimated stress history profile is used to evaluate the OCR profile to estimate s_{uDSS}, s_{uTC}, and s_{uTE} for Onsøy clay with typical S and m values as in Bothkennar and Busan clays as presented in Figure 5c. Laboratory s_u from DSS, CK_0UC, and CK_0UE tests have been obtained and reported by Lunne et al. (2006). Reasonable agreement is evident between measured and estimated values.

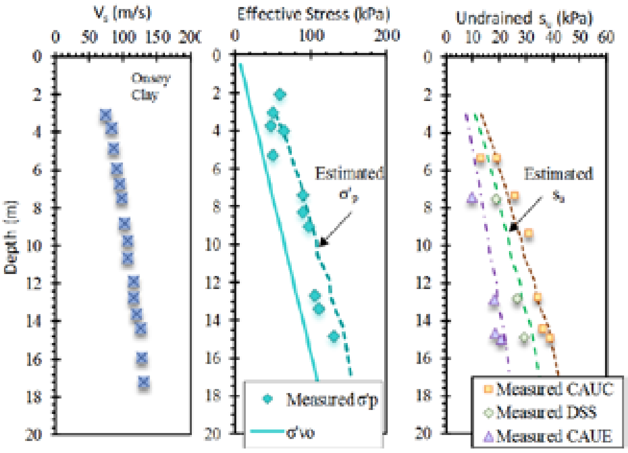

Figure 5. Profiles in soft clay at Onsøy, Norway: (a) Measured downhole shear wave velocity; (b) Estimated preconsolidation stress compared to lab measured stress history profile; (c) Measured and estimated DSS, TC, and TE strengths.

6 SUMMARY AND CONCLUSIONS

A compiled database study was statistically analyzed to produce a general expression for σ_p' from downhole shear wave velocity (V_{sVH}) and effective vertical overburden stress (σ_{v0}'). The data were collected from 64 worldwide well-documented natural soils primarily covering primarily NC to LOC clays, as well as some OC and HOC fissured clays. Case studies were used to verify the ability of the proposed expression in estimating stress history in comparison with reference values from consolidation tests on undisturbed samples.

The derived stress history profiles were used to estimate the undrained shear strengths under three different shearing modes: triaxial compression, direct simple shear, and triaxial extension using the SHANSEP approach.

7 ACKNOWLEDGMENTS

The authors appreciate the support of ConeTec Investigations of Richmond, BC and Design House Engineering Consultancy of New York, NY in support of this research effort.

8 REFERENCES

Becker D.E., Crooks J.H., Been K., Jefferies M.G. 1987. Work as a criterion for determining in situ and yield stresses in clays. *Canadian Geotechnical Journal*, Vol.24: 549-564.

Butterfield (1979). A natural compression law for soils, *Geotechnique*, Vol. 29, No. 4, pp. 468-480.

Chung, S.G., & Kweon, H.J., 2013. Oil-operated fixed-piston sampler and its applicability. *Journal of Geotechnical and Geoenvironmental Engineering*, 139(1), 134-142.

Chung, S.G., Hong, Y.P., Lee, J.M., & Min, S.C. 2012. Evaluation of the undrained shear strength of Busan clay. *KSCE Journal of Civil Engineering*, 16(5), 733-741.

Chung, S.G., Ryu, C.K., Min, S.C., Lee, J.M., Hong, Y.P., & Odgerel, E. 2011. Geotechnical characterization of Busan clay. *KSCE Journal of Civil Engineering*, 16(2), 341-350.

Germaine, J.T. & Germaine, A.V. 2009. *Geotechnical Laboratory Measurements for Engineers*. Wiley & Sons: 359p

Hepton, P. 1988. Shear wave velocity measurements during penetration testing. *Penetration Testing in the UK*. Thomas Telford, London: 275–278.

Hight, D.W., Bond, A.J., & Legge, J.D. 1992. Characterization of the Bothkennaar clay. *Géotechnique*, 42(2), 303-347.

Hight, D.W., Paul, M.A., Barras, B.F., Powell, J.M., Nash, D.T., Smith, P.R., Jardine, R.J., & Edwards, D.H., 2003. The characterization of the Bothkennar clay. *Characterization and Engineering Properties of Natural Soils*, Balkema, Rotterdam, Vol. 1: 543-597.

Janbu, N. (1969), The resistance concept applied to deforma-tion of soils, *Proc. 7th ICSMFE*, Mexico, Vol. 1: 191-196.

Ku, T. and Mayne, P.W. (2013). Yield stress history evaluated from paired in-situ shear moduli of different modes. *Engineering Geology* 152, Elsevier: 122-132.

Ladd, C.C. & DeGroot, D.J. 2003. Recommended practice for soft ground site characterization. *Soils and Rock America 2003*, Vol. 1, (Proc. 12th PCSMGE, MIT), Verlag Gluckauf Publishing, Essen: 3-57.

Locat, J. & Tanaka, H. 1999. Microstructure, mineralogy and physical properties; Techniques and application to the Busan clays. *Proc. KSG'99 Dredging and Geoenvironmental Conference*, Seoul: 15-31.

Lunne, T., Berre, T., Andersen, K.H., Strandvik, S. & Sjursen, M., 2006. Effects of sample disturbance and consolidation procedures on measured shear strength of soft marine Norwegian clays. *Canadian Geotechnical J.* 43(7), 726-50.

Lunne, T., Long, M., & Forsberg, C.F., 2003. Characterization and engineering properties of Onsøy clay. *Characterization and Engineering Properties of Natural Soils*, Vol. 1, Singapore, Balkema / Swets & Zeitlinger, Lisse: 395-428.

Lunne, T., Nerland, Ø. & Solhell, E. 2001. Quality of CPTU. Factual report, field tests at Onsøy. *NGI report No. 20011099-1*, 16/7/01, Oslo.

Mayne, P.W., (1995). Profiling yield stress in clays by in-situ tests, *Transportation Research Record* 1479, National Academy Press, Washington, DC: 43-50.

Mayne, P.W. 2005. Invited Keynote: Integrated Ground Behavior: In-Situ and Lab Tests, *Deformation Characteristics of Geomaterials*, Vol. 2 (Proc. IS Lyon'03), Taylor & Francis Group, London: 155-177.

Schmertmann, J.H. 1955, The undisturbed consolidation behavior of clay, *Transactions, ASCE*, Vol. 120, p. 1201.

Singh, V.K., & Chung, S.G. 2015. Evaluation of overconsolidation ratios from laboratory and in situ tests on Busan clay. *Engineering Geology*, 199: 38-47.

Geotechnical and Geophysical Site Characterisation 5 – Lehane, Acosta-Martínez & Kelly (Eds)
 ISBN 978-0-9946261-1-0

Permeability profile of a planosol based on in situ falling head permeability tests

C.A.B. Bastos & D.F. Fagundes
School of Engineering, Rio Grande Federal University, Rio Grande/RS, Brazil

ABSTRACT: The present paper show the results of in situ falling head permeability tests conducted in a planosol formed above the coastal quaternary deposits in south of Brazil. An excavation was planned to be performed to drainage of a road constructed nearby. The influence of this excavation on the seepage behavior of the marshy ground of this region was important to be considered in order to protect the habitat of endangered fish species. Results showed that for the depth up to 2.0 m, the value of permeability coefficient decreased (from 2.4×10^{-5} to 4.1×10^{-6} cm/s) and then it increased to 4.4×10^{-5} cm/s. The results are in agreement with the concentration of clay in subsurface, resultant of the pedogenesis of the planosol. This study will subsidize a numerical analysis of the flow resulting from excavation and therefore an indication of the best solution to minimize the project impacts on the surrounding environment.

1 INTRODUCTION

The water behavior of the land has great relevance in environmental studies, particularly in assessing the impact caused by engineering works. In roadworks, drainage structures and the highway embankment itself modify the water surface behavior and seepage characteristics in adjacent land.

The area of the study are located in southern Brazil, between the cities of Pelotas and Turuçu in the state of Rio Grande do Sul, where road works on the BR 116 highway doubling are being carried out. In this area, close to the km 510 + 500, will be performed a drainage gallery that crossing the road under the pavement (Figure 1).

The excavation works, required for the gallery construction, are located around 70 m of a marshy ground with a 230 m length that is a habitat of a fish specimen called Rivulideos. The rivulideos fish or annual fish (Figure 2) has the characteristic to be a small fish and lives in shallow water environments or temporary ponds. The fish lay eggs in the substrate of ponds, where they remain inactive during the dry phase and return to develop after the flooding. The Chico Mendes Institute for Biodiversity Conservation (ICMBio) approved on 20 June 2013, the National Action Plan for the Conservation of Rivulideos Fish Threatened with Extinction. One of the actions of this Plan, it is to protect the remaining habitat of these animals, preventing them from being deleted, impacted or handled incorrectly (DNIT 2013).

Aiming at the fulfillment of that plan within the environmental management goals of the roadworks, it was necessary to assess the impact of the gallery excavations in the seepage behavior in this marshy ground. For this purpose, it was necessary to assess the parameters of this site in terms of the geotechnical characterization and the permeability profile of the soil with depth.

This paper presents the procedures and results of the geotechnical characterization and determination of the permeability profile using a series of in situ falling head tests.

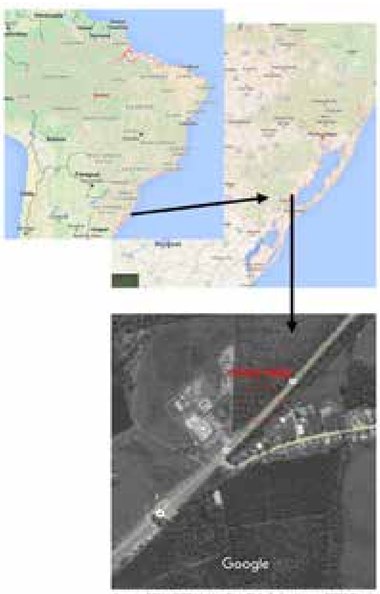

Figure 1. Location of the study area (Google Maps 2016).

Figure 2. Rivulídeos or annual fish found in highway work (DNIT 2013)

2 MATERIALS AND METHODS

2.1 *Characterization of the study area*

The study was conducted in the marginal area on the left side of the highway BR116 between Pelotas - Turuçu. The excavation of drainage gallery will be executed between the km 510 + 500 (Figure 1) in the transverse direction of the highway axis.

The area investigated has a square area of 5x5 m, where five points were located (with a minimum spacing between points of 3 m). In each point, was performed an auger drilling and collecting samples of the different soil horizons for geotechnical characterization. These holes were used to the falling head tests. The depths of the holes were 0.5, 1.0, 2.0, 3.0 and 4.0 m (Figure 3).

The geology and pedology of the study area have great importance to the interpretation of the geotechnical characterization and the permeability profile. According to segment of the Geological Map of the Sheet Pelotas/Mostardas - SH.22-Y-D / Z-C (IBGE 2003) presented in Figure 4, the study area has the geological substrate TQPg unit, characterized by arkose sandstones weakly consolidated that constitute alluvial fans deposits. The soil formed from this substrate belongs to the class of eutrophic Planosols with texture medium/clay (unit PLe3 in Figure 5) or Subdystric Paraquic Ochric Planosol obtained by the Soil Taxonomy American System. The soil profile is inserted in the geomorphologic unit Lagoon High Plain (Cunha & Silveira 1996).

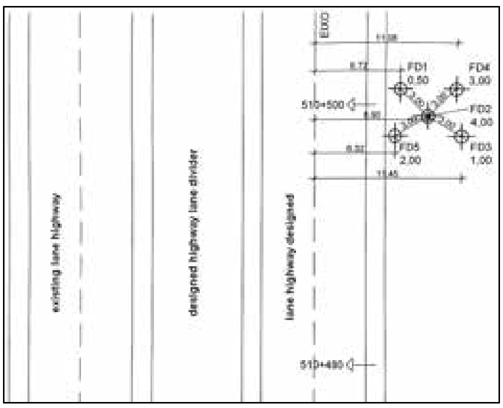

Figure 3. Design of the experimental area with collection points samples and testing

Figure 4. Geological map of the study area

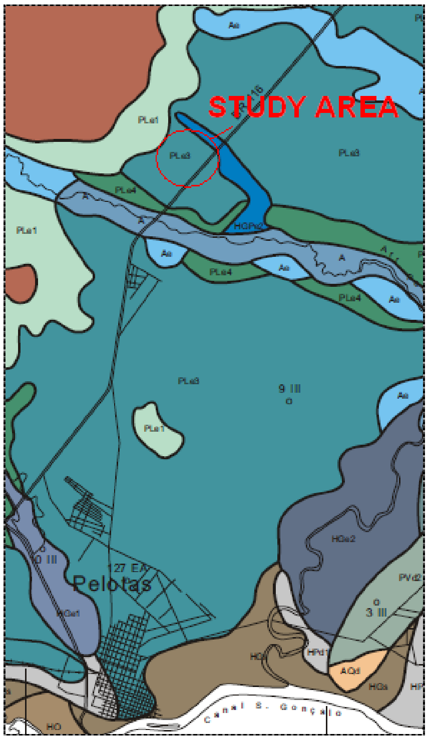

Figure 5: Soil map of the study area

Cunha & Silveira (1996) describe this planosol as a deep soil with imperfect drainage. The superficial horizon has 30-80 cm thick, texture medium (with 6-10% clay), poor structure (massive), strong acidity, color brown to dark grayish. The profile shows an abrupt and flat textural transition to the subsuperficial horizon B, with texture clay (25-40% clay), weak structure (angular or prismatic blocks) and consistency very firm when moist and very hard when dry. The authors indicate in this horizon the presence of a clay-pan, which difficult water penetration, and also reddish and yellowish brown mottled, indicating imperfect drainage. Therefore, the pedological records already indicate poor drainage and water retention by the textural gradient (increase in the clay content) of the horizon B.

2.2 *Geotechnical characterization*

For geotechnical characterization of the soils with depth, the auger samples were collected (Figure 6) at five different depths around 0.5, 1.0, 2.0, 3.0 and 4.0 m (in an amount sufficient for geotechnical characterization in the laboratory tests). The samples packaged and identified were sent to the Laboratory of the Geotechnics and Concrete of the Federal University of Rio Grande - FURG to the geotechnical characterization according the Brazilian standards: NBR 6457/1986 (Soil Samples - Preparation for Compaction and Characterization Tests); NBR 7181/1984 (Soil - Grain Size Analysis); NBR 6459/84 (Soil -Determination of Liquid Limit); NBR 7180/84 (Soil - Determination of Plastic Limit). These results allowed obtain the HRB-AASHTO and USCS classifications.

2.3 *Permeability profile*

The measures of the coefficient of permeability of soil in different depths were performed by a series of in situ falling head permeability tests. The falling head permeability tests followed the procedure indicated in the publication of ABGE (Brazilian Association of Engineering and Environmental Geology) - *Permeability Testing in Soils - guidance for its implementation in the field* - 4th edition (ABGE 2013). This test is considered a variable level test executed in the borehole. In the beginning of the procedure the water level inside the tube is elevated until the initial position of the test. During the test, the downward of the water level is monitored with time. In other words, a PVC tube is positioned in the depth of the test, filled with water until the initial level and then measures of the downgrade speed are performed. Figure 7 shows the test setup.

Before the measures, it was allowed percolation to ensure the saturation condition surrounding the borehole bottom. Furthermore, as the tip of the tube inserted coincides with the bottom of the borehole, the hypothesis adopted was that the water infiltrates the ground through spherical surfaces (Figure 8). In this case the ground permeability coefficient (k) can be estimated by equation 1.

$$k = \left[\frac{D}{8(h1 + h2)} \right] \cdot \left[\frac{\Delta h}{\Delta t} \right] \tag{1}$$

where: D = internal diameter of the tube; $h1$ = height between initial water level and soil surface e $h2$ = height between soil surface and borehole bottom; $\Delta h/\Delta t$ = falling head speed measured.

Figure 9 illustrates the sequence of operations in the assembly and executing the tests on each of the depths.

Figure 6. Sampling auger for geotechnical characterization of materials

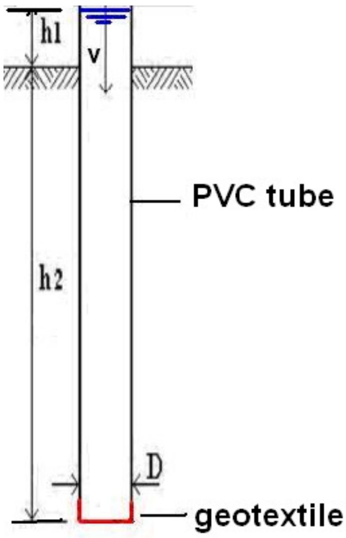

Figure 7. Test setup

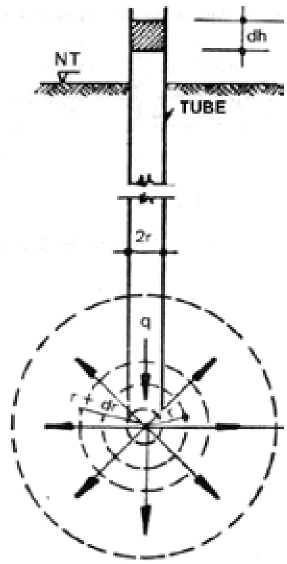

Figure 8. Flow hypothesis by circular concentric surfaces

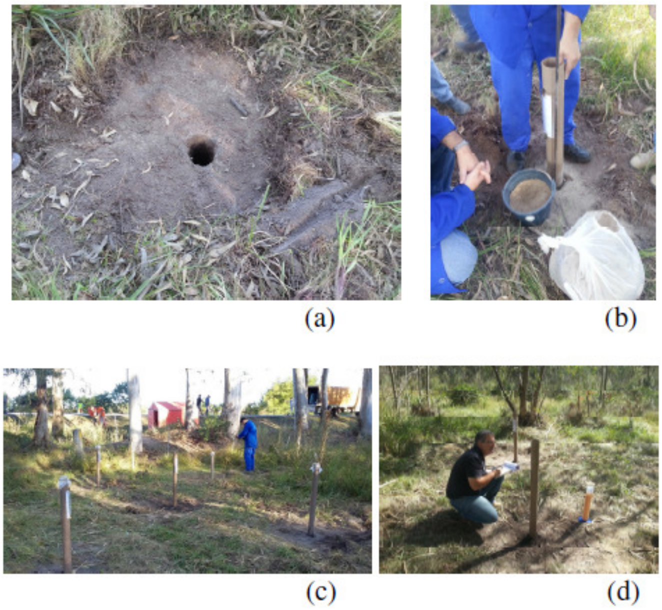

Figure 9: Sequence of operations in the falling head permeability tests. (a) opening borehole; (b) tube installation; (c) tubes installed at different depths; (d) taking measurements

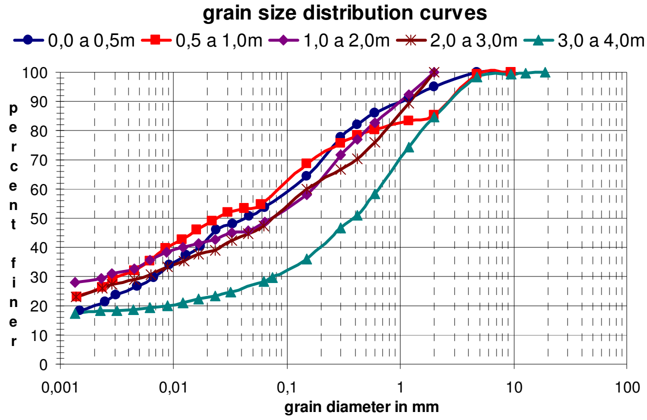

Figure 10. Grain size distribution curves

Table 3. Results of falling head permeability tests

depth test (m)	*D* (cm)	*h1 + h2* (cm)	$\Delta h / \Delta t$ (cm/s)	*k* (cm/s)
0.5	7.45	111	0.0029	$2.43.10^{-5}$
1.0	6.60	186	0.0053	$2.35.10^{-5}$
2.0	6.60	285	0.0017	$4.92.10^{-6}$
3.0	6.60	384	0.0019	$4.08.10^{-6}$
4.0	6.60	485	0.0257	$4.37.10^{-5}$

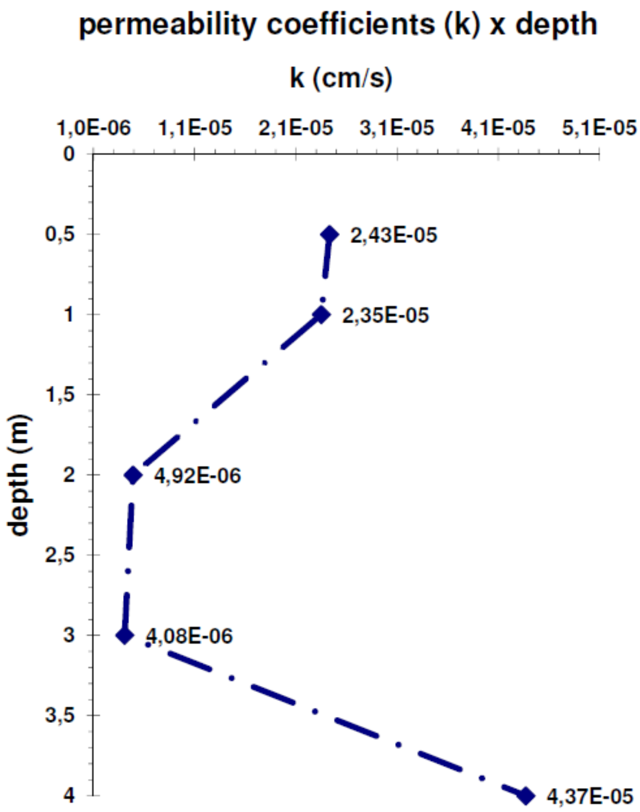

Figure 11. Permeability profile

3 RESULTS

The parameters obtained from the grain size analysis tests and Atterberg limits are show in Table 1. The consequent geotechnical classification of the soils is presented in Table 2. The grain size distribution curves are shown in Figure 10.

Table 3 shows the results obtained for the soil permeability coefficients at different depths tested. Figure 11 illustrates the permeability coefficient values along the depth. It is observed that the soil permeability significantly decreased in the depths 2.0 and 3.0 m and returns to reach a much higher value in the depth 4.0 m.

Table 1. Results of characterization tests

sample depth (m)	gravel (%)	sand (%)	silt (%)	clay (%)	wl (%)	Ip (%)
0 - 0,5	5	52	23	20	27	10
0.5 – 1.0	15	30	30	25	33	13
1.0 – 2.0	-	56	15	29	40	24
2.0 – 3.0	-	52	23	25	38	24
3.0 – 4.0	15	57	10	18	26	14

wl – liquid limit; Ip – plasticity index

Table 2. Geotechnical classification

sample depth (m)	HRB-AASHTO geotechnical classification	USCS geotechnical classification
0 - 0,5	A4(4)	CL
0.5 – 1.0	A6(6)	CL
1.0 – 2.0	A6(8)	CL
2.0 – 3.0	A6(8)	CL
3.0 – 4.0	A2-6(1)	SC

4 CONCLUSIONS

The in situ falling head permeability tests performed show that the soil profile in the study area has permeability coefficient values consistent with the range between silty clayey sand and sand in agreement with the particle size observed in the geotechnical characterization tests.

According the results presented in Table 3 and illustrated in Figure 11, the permeability (or hydraulic conductivity) of the ground decreases in the clayey subsuperficial horizon (25% to 29% clay between depths 1.0 to 3.0 m) with values of k between $4.0x10^{-6}$ and $5.0x10^{-6}$ cm/s and tendency to increase to have high values in the depth 4.0 m ($k = 4.37x10^{-5}$ cm/s), where terrain profile becomes more sandy (72% gravel + sand between depths of 3.0 to 4.0 m).

The results are in agreement with the pedogenesis of planosol profile and confirm the importance of water retention by subsuperficial horizon in the seepage of the marshy ground (ruvilideos fish habitat). This study will subsidize a numerical analysis of the flow resulting from the excavation to be performed and therefore an indication of the best project solution to minimize the environmental impacts.

5 ACKNOWLEDGEMENTS

The authors are grateful to the staff of the Laboratory of the Geotechnics and Concrete of Federal University of Rio Grande - FURG, and also thanks to MAC Engineering and Enecon Engineers and Consultants Economists S.A. for the study opportunity.

6 REFERENCES

Brazilian Association of Engineering and Environmental Geology - ABGE 2013. *Permeability tests on soil: guidelines for its implementation in the field*. São Paulo/Brazil: ABGE (in portuguese).

Cunha, N. G. & Silveira, R. J. C. 1996. *Study of Pelotas city soils*. Documentos CPACT 12/96, Pelotas/Brazil: EMBRAPA/CPACT, Ed. UFPel. (in portuguese)

National Department of Transport Infrastructure – DNIT 2013. BR-392: The DNIT care with annual fish. *Boletim BR-116/392 Gestão Ambiental*, n.19: 2-2 (in Portuguese)

Brazilian Institute of Geography and Statistics – IBGE 2003. *Geological Map Sheet Pelotas/Mostardas - SH.22-Y-D / Z-C*. Florianópolis/Brazil: IBGE (in portuguese)

Google 2016. *BR 116, 510 – Sítio Floresta*. Images CNES/Astrium, Digital Globe, https://www.google.com.br/maps/place/BR-116,+510+-+Sítio+Floresta

Geotechnical and Geophysical Site Characterisation 5 – Lehane, Acosta-Martínez & Kelly (Eds)
© 2016 Australian Geomechanics Society, Sydney, Australia, ISBN 978-0-9946261-1-0

Influence of penetration rate on CPTU measurements in saturated silty soils

M.F. García Martínez, L. Tonni, G. Gottardi & I. Rocchi
Dept. DICAM, University of Bologna, Italy

ABSTRACT: Drainage behaviour of intermediate soils (e.g. silts, sandy silts, clayey silts) during standard cone penetration rate (20 mm/s) typically falls between that of sand and clay, for which fully drained and fully undrained conditions are expected to apply, respectively. Partial drainage phenomena may be evaluated by varying the penetration rate within a range which depends on the consolidation characteristics of the soil to be tested. This paper presents the results of a variable rate piezocone test (CPTU) campaign carried out in a clayey silt deposit of the southern margin of the Po river valley (Forlì, Italy). In order to assess the in situ drainage conditions, normalized piezocone measurements have been interpreted in terms of a non-dimensional penetration rate. In this way, it is potentially possible to detect the transition point from undrained to partially drained and drained responses. Results have been compared to previously reported data on both natural deposits and laboratory reconstituted soils.

1 INTRODUCTION

From the time of the first use of cone penetration test, over four decades ago, CPT (and its variation CPTU) has become the most popular in situ testing technique worldwide. CPT/CPTU results may be used for detailed stratigraphic profiling as well as for estimating geotechnical parameters, allowing cheap and fast interpretation of data compared to sampling and laboratory testing.

At ASTM standard cone velocity (20 mm/s), soil response typically turns out to be fully drained in sands and fully undrained in clays; by contrast, partially drained conditions may pertain to silts and other naturally soil deposits at such penetration rate. This implies evident limitations on the applicability of well-established empirical correlations, developed for sands or clays, to intermediate soils for the estimate of their geotechnical parameters (Gottardi & Tonni 2009).

A proper interpretation of CPT/CPTU in silts and other naturally mixed soil deposits is generally difficult to achieve and should be based on the preliminary assessment of drainage conditions during the test. As shown in a number of research contributions (e.g. Randolph 2004; Schneider et al. 2007), an effective procedure for identifying drainage degree around the advancing cone consists in performing CPTU tests at variable penetration rates, which result in different tip resistance and pore pressure measurements. In order to assess the drainage degree, Finnie and Randolph (1994) proposed the use of a normalized velocity, V, defined as:

$$V = \frac{v \cdot d}{c_v} \tag{1}$$

where v is the penetration rate, d is the cone diameter and c_v is the vertical coefficient of consolidation. According to the experimental data collected from centrifuge CPTU in kaolin clay, Randolph (2004) stated that drained penetration would occur at V less than about 0.03-0.01 whilst undrained penetration occurs at V larger than 30-100.

Compared to the relatively large amount of data collected in recent years from non-standard rate CPTU in physical models, a rather limited database from field scale tests on natural deposits is at present available (Kim et al. 2008; Suzuki et al. 2013; García et al. 2014, Krage et al. 2014). According to the experience so far collected, interpretation of field tests is not always straightforward due to soil heterogeneity and equipment capability to embrace a sufficiently wide range of penetration rates.

This paper aims at providing some insight into the interpretation of CPTU measurements in intermediate soils, by presenting results from a piezocone campaign recently performed in a silty deposit located in the southern margin of the river Po valley (Forlì, Italy). The research programme included CPTUs carried out at different rates, ranging from about 0.9 to 61.7 mm/s, combined with laboratory tests per-

Figure 1. Location of the test site.

formed on undisturbed samples. Rate effects on normalized CPTU measurements are investigated and compared with results reported by other authors.

2 FIELD TESTING

2.1 *Overview*

The variable rate CPTUs were conducted in an industrial area (Figure 1) located in the surroundings of the city of Forlì (Emilia-Romagna, Northern Italy). The experimental programme included No. 8 adjacent piezocone tests, all pushed over 15 m in depth, carried out by the Soil Mechanics Laboratory of the University of Bologna (Italy) using an integrated Delft Geotechnics piezocone equipment, with a hydraulic system having a pushing capacity of 200 kN. A standard cone was employed, with a diameter of 35.7 mm and a section area of 10 cm^2.

The pore pressure was recorded at the shoulder position (u_2). Special attention was paid to the saturation procedure in order to achieve a fully saturated pore pressure system before penetration. It is worth observing that insufficient saturation may be caused by either an inadequate choice of saturation methods or by penetration of unsaturated zones or dilative soils (Sandven 2010).

2.2 *Site details and CPTU campaign*

The city of Forlì is located along the Romagna Apennines-Po Plain margin, in a foreland basin in which Plio-Quaternary deposits built up.

During Late Quaternary, erosion phenomena induced the current mountain relief. As a consequence of the deposition of the erosional sediments in the Po plain, a thick alluvial deposit was formed in this area. The thickness of such sediments underneath the city is over 200 m.

The deposits are referable to the Ravenna AS8 Subsystem, consisting of clayey-sandy silts, and to the Unit of Modena AS8a, consisting of silty-clayey sands.

Such stratigraphic condition was confirmed by a 32 m-deep borehole, as well as by standard CPTU results, which revealed that the upper 29 m basically consist of silty-clayey sediments, with local interbedded silty sand levels from 8 to 9 m, 12 to 16 m and 19 to 21 m in depth. Below such macro-unit, gravels were encountered. The water table was located at about 2 m in depth.

Laboratory tests were also performed on samples extracted from the borehole in order to determine physical and mechanical properties of the soils under investigation. Table 1 shows the basic physical soil properties; particle size distribution curves are depicted in Figure 2.

Table 1. Basic physical soil properties.

Depth (m)	γ_n (kN/m^3)	w_n (%)	w_L (%)	w_P (%)
6.2-6.7	19.8	25	57.6	21
12.2-12.5	19.2	31.3	25	17
15.0-15.5	20.6	22.2	-	-
18.0-18.5	19.2	31.5	50.8	23.1

Figure 3 shows the corrected tip resistance, q_t, and the pore pressure, u_2, measurements from the test performed at the standard penetration rate (CPTU 1) as well as the Soil Behaviour Type (SBT) profile according to the well-known CPTU-based classification system proposed by Robertson (2009), providing a very detailed description of stratigraphy. As it can be observed, the upper 4 meters mainly consist of silt mixtures (*SBT* = 4) with occasional presence of silty sands/sandy silts (*SBT* = 5); below 4 m in depth sediments consist of an alternation of silt mixtures (*SBT* = 4) and clays (*SBT* = 3) with interbedded sand mixtures (*SBT* = 5 and *SBT* = 6). The soil lithology detected by an adjacent borehole, also

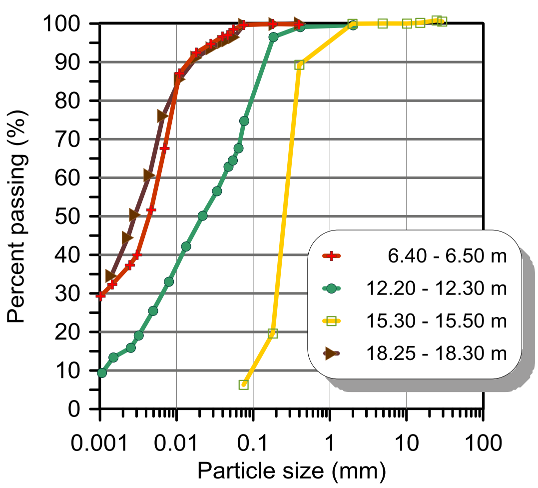

Figure 2. Grain size distribution of representative soil samples.

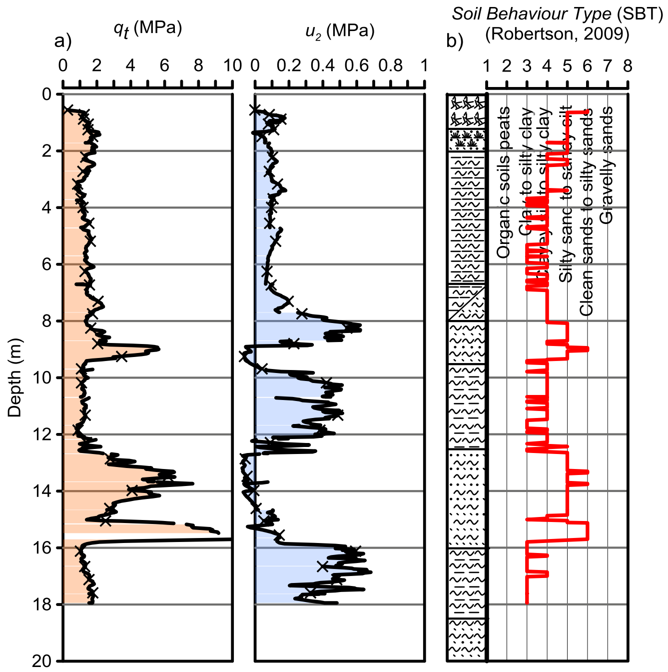

Figure 3. a) CPTU 1 log profiles and b) SBT profile according to Robertson (2009).

reported in Figure 3, is in substantial agreement with the SBT-profile, hence confirming the effectiveness of the approach to predict soil behaviour.

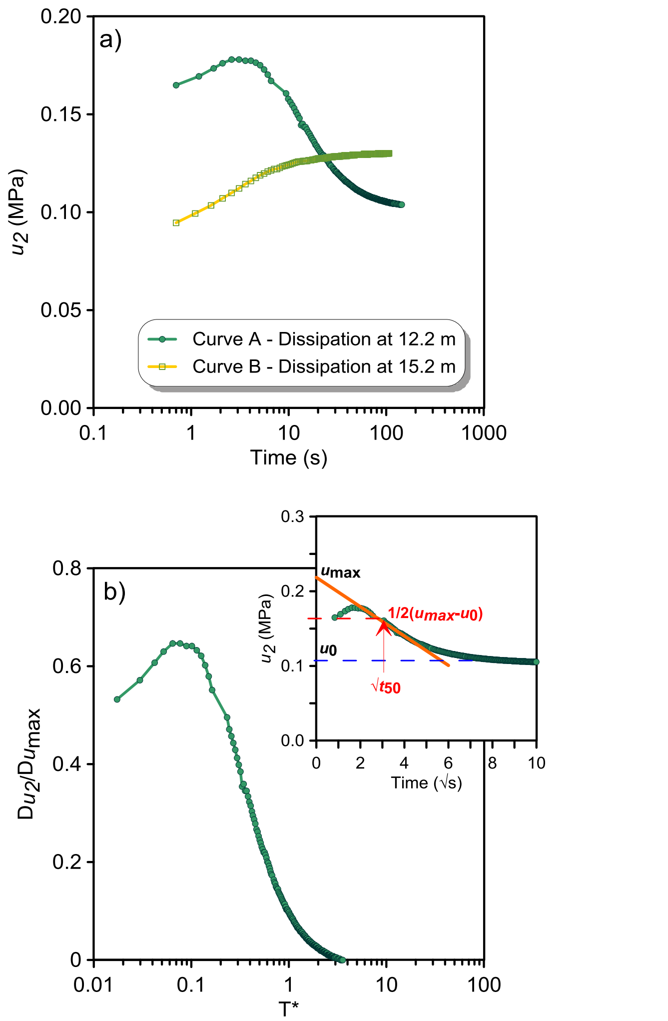

Figure 4. a) Dissipation tests and b) Normalized dissipation curve and root-square method.

Dissipation tests were also carried out at the site in order to measure the piezometric head and to evaluate the coefficient of consolidation. Figure 4a shows the dissipation curves at a depth of 12.2 m and 15.2 m (curves A and B hereafter), corresponding to clayey silt and silty sand level respectively. The pore pressures in curve A is always greater than hydrostatic, but show a short (~5 seconds) initial rise before dissipating probably owed to a redistribution of pore pressures around the tip in such slightly overconsolidated soil (Sully et al. 1999). Besides, the negative excess pore pressures that occur in the silty sand (curve B) are probably due to the contribution of the shear component (Wroth, 1984) of pore pressure.

The well-known method proposed by Teh & Houlsby (1991) was used to estimate the value of c_h in the clayey silt. Figure 4b shows the normalized excess pore pressures, $\Delta u/\Delta u_{max}$, plotted against the time factor T^*, defined as:

$$T^* = \frac{c_h \cdot t}{r^2 \sqrt{I_r}} \tag{2}$$

where t is the time, r is the cone radius and I_r is the rigidity index. The initial maximum excess pore pressures, Δu_{max}, were found by back-extrapolating to t=0 the straight-line part of the u_2-$\sqrt{t}$ curve (square root method) and an estimate of t_{50} was directly derived. Then, assuming $I_r \approx 22$, c_h turned out to be equal to $3.7 \cdot 10^{-5}$ m^2/s. Compared to experimental data from laboratory results, it turns out that the c_h-value derived from the dissipation test is one order of magnitude higher than the vertical coefficient of consolidation c_v deduced from the oedometer test. Moreover, it must be emphasized that the method used for interpreting dissipation tests is based on the assumption of fully undrained response during cone penetration at standard rate, which may be not obvious in silts.

The adjacent CPTUs were performed at eight different penetration rates, ranging from about 0.9 mm/s to 61.7 mm/s. Lower and upper values of test velocity were established on the basis of the equipment capability to vary the penetration rate.

Figure 5 shows the q_t and u_2 profiles obtained from tests CPTU 1 to CPTU 8. Although tests were performed along close verticals, a certain horizontal spatial variability can be appreciated.

Tip resistance and pore pressures were approximately equal up to 8 m thus indicating that penetration remained undrained within the entire range of penetration rates performed. In the interbedded silty sand levels, from 8 to about 9.5 m and from about 12.7 to 16 m, q_t increases and u_2 generally decreases as cone penetration rate is reduced; it is worth observing that within the latter depth interval, the u_2 profile at 1 mm/s follows the hydrostratic pressure

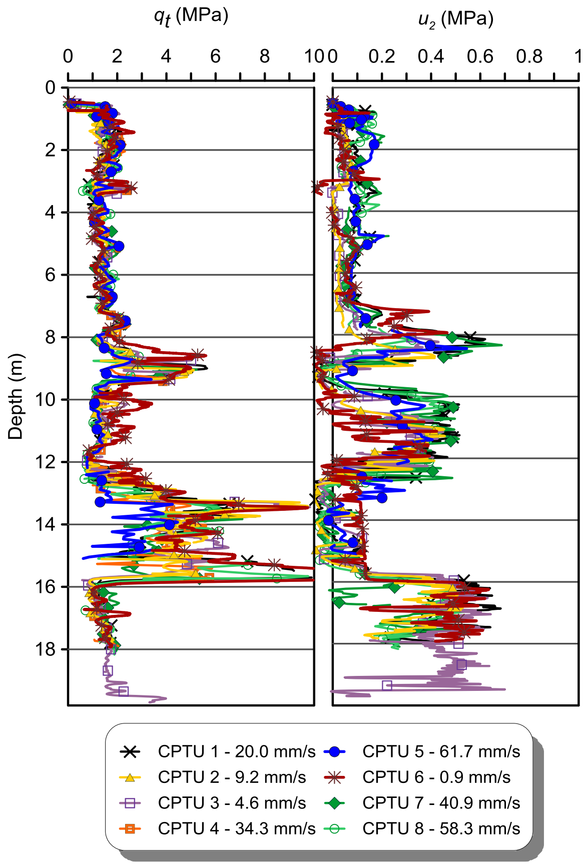

Figure 5. CPTU profiles from adjacent tests at variable rate.

distribution, thus indicating that the penetration is fully drained. From 9.5 to 12.7 m and from 16 m up to the end of the probes, the q_t profiles are almost coincident whereas the pore pressures seem to be more sensitive to different testing conditions.

3 PENETRATION RATE EFFECTS

Figure 6 shows averaged values of q_t and u_2 within thin homogeneous clayey silt layers from 10.0 to 10.3 m and from 11.8 to 12.2 m, for each penetration rate (v) performed. As shown in the figure, the q_t values between 10.0 to 10.3 m were almost constant from 61.7 mm/s to 40.9 mm/s; for v < 40.9 mm/s cone resistance increases due to partial consolidation. However, for the clayey silt between 11.8 to 12.2 m, q_t remains almost constant from 61.7 mm/s to 9.2 mm/s (around 1 MPa) and slightly increases as penetration rate is reduced up to 0.9 mm/s.

The trend behaviour of u_2 with penetration velocity is similar at both range of depths. As evident from Figure 6, the pore pressure increases as penetration is reduced from 61.7 mms/s up to around 40.9 mm/s, due to viscous effects. On the other hand, as cone velocity keeps reducing below 40.9 mm/s, u_2 decreases due to partial consolidation occurrence around the cone.

Despite a certain difficulty in correlating the variation of u_2 with the variation of q_t as penetration rate changes in such sediments, it seems reasonable to assume that the transition point from undrained to partially drained response occurs at around v = 40.9 mm/s.

3.1 *Normalized variable rate CPTU results*

In recent years, emphasis has been put on the normalization of variable rate CPTU measurements, by representing a curve that relates the normalized tip resistance (or normalized excess pore pressure) versus the normalized cone velocity (e.g. Randolph & Hope 2004, Kim et al. 2008, Jaeger et al. 2010, Schnaid et al. 2010, Suzuki et al. 2013).

DeJong & Randolph (2012) presented consolidation trends obtained by processing variable penetration rate data referred to both field and laboratory measurements on soft soils as well as numerical results. Measurements were analysed in terms of the normalized variable Q/Q_{ref} as a function of the dimensionless cone velocity V according to Equation (1), in which $Q = (q_t - \sigma_{v0})/\sigma'_{v0}$ whereas Q_{ref} is the reference values the normalized cone resistance in fully undrained conditions. The following equation to capture the overall trend was proposed:

$$\frac{Q}{Q_{ref}} \approx 1 + \left(\frac{Q_{drained}/Q_{ref} - 1}{1 + \left(V/V_{50}\right)^c} \right) \quad (3)$$

where V_{50} is the normalized velocity corresponding to the penetration velocity at which 50% of the excess pore pressure for fully undrained penetration is mobilized, c is the maximum rate of change of Q/Q_{ref} with V and $Q_{drained}/Q_{ref}$ is the normalized

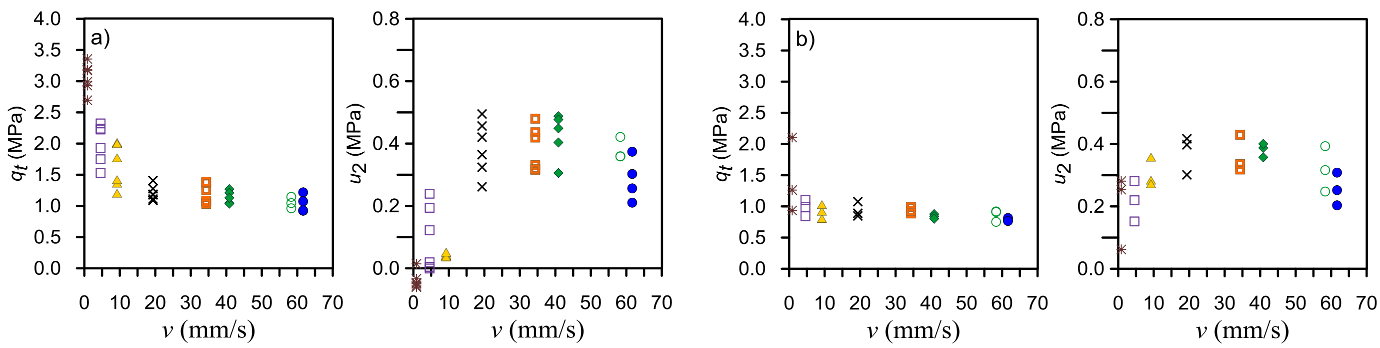

Figure 6. Variation of q_t and u_2 with penetration rate within clayey silt layers from a) 10 to 10.3 m and from b) 11.8 to 12.2 m.

drained resistance. For all the examined data, they obtained V_{50} values varying from about 0.3 to 8, and c varying from 0.5 to 1.5. However, due to insufficient site specific data, they finally suggested to use V_{50}, c and $Q_{drained}/\ Q_{ref}$ equal to 3, 1 and 2.5 respectively (DeJong & Randolph 2012).

On the other hand, Oliveira et al. (2011) presented an analytical approach to the backbone-shaped curve equation to fit test data:

$$\frac{q}{q_{und}} = 1 + \left(\frac{b-1}{1+\left(\frac{V}{n}\right)^{\frac{4c}{b-1}}} \right) \tag{4}$$

in which b is the ratio between the fully drained and the fully undrained tip resistance, c is a coefficient that describes the probe-soil interaction and n is the normalized velocity associated with the maximum rate of increase in resistance. Their work presented centrifuge tests with variable rate CPTU performed on a silty tailing. Furthermore, they compared the respective backbone curve to those already published by other researchers (e.g. Randolph & Hope 2004, Schneider et al. 2007). Table 2 shows the constants from centrifuge penetration tests based on Equation (4).

Table 2. Constants based on Equation (4).

Data	soil	b	c	n
Randolph & Hope (2004)	UWA[(1)] kaolin	3.65	0.55	0.61
Schneider et al. (2007)	SFB[(2)]	3.57	4.45	0.92
Oliveira et al. (2011)	Silty tailings	3.40	1.00	15.00
Chung et al. (2006)[*]	Burswood Clay	3.77	1.00	1.75

[(1)] University of Western Australia.

[(2)] Silica Flour and Bentonite.

[*] Data modified from Poulsen et al. 2011.

Figure 7 represents the data on Figure 6 in terms of Q/Q_{ref} as a function of V, using the horizontal coefficient of consolidation obtained from dissipation tests in the clayey silt layer. The plot in Figure 7 suggests that the transition point from partially drained to fully undrained penetration occurs at $V \approx 30$. On the other hand, the transition from partially drained to fully drained response can not be clearly identified due to the lack of slow rate CPTU data. However, it still may be related to $V < 1$.

From the above-mentioned, it is reasonable to assume that for a CPTU performed at 20 mm/s with a standard cone (d = 35.7 mm), undrained penetration is very likely to occur when $c_h < 2.4 \cdot 10^{-5}$ m^2/s.

Based on Equation (3), the span of experimental data in Figure 7 can be captured for V_{50} ranging between 0.01 and 4.14 and for c varying between 0.76 and 1.80. Best fit-values were achieved, however,

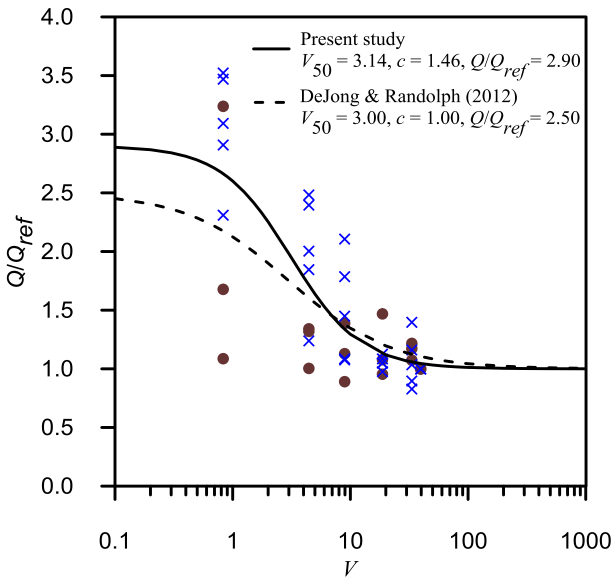

Figure 7. Normalized cone resistance versus V.

for V_{50} = 3.14, c = 1.46 and $Q_{drained}/\ Q_{ref}$ = 2.90. It should be noticed that the ratio $Q_{drained}/\ Q_{ref}$ is difficult to be retrieved from field. As evident, these constants turn out to be close to those proposed by DeJong & Randolph (2012).

The data in Figure 8 are now fitted by the expression given in Equation (4). The figure also plots the backbone curve equation using the constants presented in Table 2. As can be observed, the comparison between the field data and the centrifuge test results shows that the b value turns out to be lower in the field (b = 2.52). Regarding the field value of c (= 0.57), it falls between that obtained from Randolph

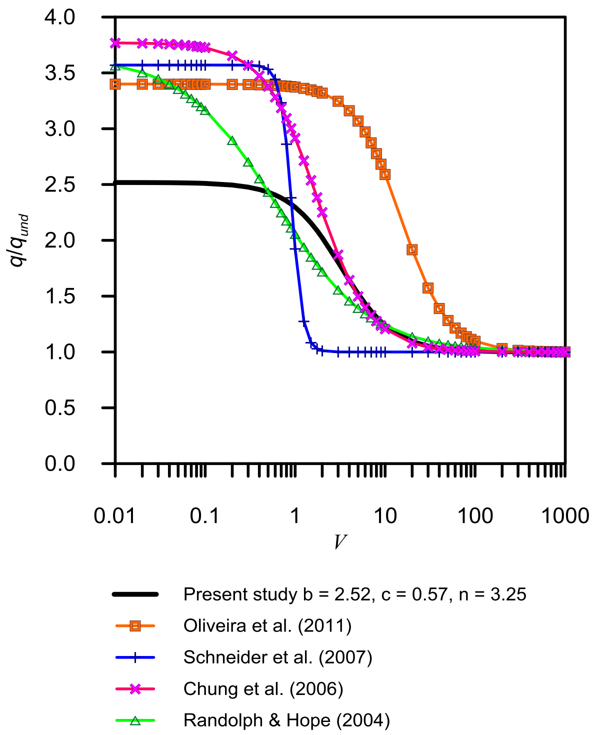

Figure 8. Backbone curves from centrifuge tests and present (field) study.

& Hope (2004) and from Oliveira et al. (2011). On the other hand, the *n* value obtained for the field data is almost twice the value associated to the Chung et al. (2006) curve, remaining at the same time below the value determined by Oliveira et al. (2011).

4 CONCLUSIONS

This paper presents results from field CPTU performed at various rates in a saturated clayey silt deposit, with the aim of providing some fundamental insights into the consolidation pattern during cone penetration and thus identifying drainage conditions in standard tests. Previous experiences in the context of variable rate CPTU tests have mainly dealt with centrifuge physical models and predominantly fine sediments, whereas this study presents a contribution, though preliminary, in the analysis of the rate effects on natural silt mixtures using a full size penetrometer.

From the accurate analysis of CPTU measurements, it turned out that in these soils, the transition point from undrained to partially drained conditions corresponds to a normalized velocity $V \approx 30$. The effects of penetration rate on CPTU measurements in the fully drained region could not be investigated due to the difficulty of achieving in the field very low cone penetration rates, but a preliminary estimate of the velocity at which drained conditions apply, could be proposed by applying some recently developed interpretation procedures to the available data.

The drainage trend curves of the normalized cone resistance as a function of the normalized velocity have been presented and compared to those obtained by previous researchers from field and centrifuge CPTU. Despite a certain difficulty in interpreting field data in intermediate soils compared to centrifuge, a substantial agreement in the overall response could be observed.

5 ACKNOWLEDGMENTS

The authors would like to thank SOLES S.r.l. for providing the access to the site and Gianfranco Marchi for his valuable information and advice.

6 REFERENCES

Chung, S.F., Randolph, M.F. and Schneider, J.A. 2006. Effect of cone penetration rate on penetrometer resistance in clay. *J. Geotech. Geoenviron. Eng.* 132(9): 1188-1196.

DeJong, J.T. and Randolph, M. 2012. Influence of partial consolidation during cone penetration on estimated soil behaviour type and pore pressure dissipation measurements. *J. Geotechnical and Geoenvironmental. Eng.* 138(7): 777-788.

Finnie, I. and Randolph, M.F. 1994. Punch-through and liquefaction induced failure of shallow foundations on calcareous sediments. Proc. Int. Conf. on Behavior of Offshore Structures, Boston (USA): 217-230.

García Martínez, M.F., Tonni, L. and Romagnoli, F. 2014. Variable rate CPTU in liquefaction-prone silty sand deposits of the Emilia-Romagna Region (Italy). *3rd International Symposium on Cone Penetration Testing*, Las Vegas (USA): 737-744.

Jaeger, R.A., DeJong, J.T., Boulanger, R.W., Low, H.E. and Randolph, M.F. 2010. Variable penetration rate CPT in an intermediate soil. *Proc. Int. Symp. on Cone Penetration Testing*, Huntington Beach (USA).

Kim, K., Prezzi, M., Salgado, R. and Lee, W. 2008. Effect of penetration rate on cone penetration resistance in saturated clayey soils. *J. Geotechnical and Geoenvironmental Eng.* 134(8): 1142-1153.

Krage, C.P., DeJong, J.T. and Wilson, D.W. 2014. Variable Penetration Rate Cone Testing in Sands with Fines. *Geo-Congress* 2014, GSP 234: 170-179.

Oliveira, J.R.M.S., Almeida, M.S.S., Motta, H.P.G. and Almeida, M.C.F. 2011. Influence of penetration rate on penetrometer resistance. *J. Geotechnical and Geoenvironmental Eng.,*137(7): 695-703.

Poulsen, R., Nielsen, B.N. and Ibsen, L.B. 2011. Effect of Drainage Conditions on Cone Penetration Testing in Silty Soils. *Proc. 64th Canadian Geotechnical Conference and 14th Pan-American Conference on Soil Mechanics and Engineering*, Toronto (Canada).

Randolph, M.F. and Hope, S. 2004. Effect of cone velocity on cone resistance and excess pore pressures. *Proc. Int. Symp. on engineering practice and performance of soft deposits,* Osaka (Japan): 147-152.

Randolph, M. 2004. Characterisation of soft sediments for offshore applications. *Proc. Int. Conf. Geotechnical and Geophysical Site Characterization*, *ISC-2,* Porto (Portugal) 1: 209-232. Millpress, The Netherlands.

Robertson, P.K. 2009. Interpretation of cone penetration tests – a unified approach. *Can. Geotechnical J.* 46 (11): 1337 – 1355.

Sandven, R. 2010. Influence of test equipment and procedures on obtained accuracy in CPTU. *2nd International Symposium on Cone Penetration Testing*, Huntington Beach (USA).

Schnaid, F., Bedin, J. and Costa Filho, L.M. 2010. Drainage characterization of tailings from in situ tests. Proc. 2nd Int. Symp. Cone Penetration Testing, Huntington Beach (USA).

Schneider, J.A., Lehane, B.M. and Schnaid, F. 2007. Velocity effects on piezocone measurements in normally and overconsolidated clays. *Int. J. Physical Modelling in Geotechnics* 2: 23-34.

Sully, J.P., Robertson, P.K.,Campanella, R.G. and Woeller, D.J. 1999. An approach to evaluation of field CPTU dissipation data in overconsolidated fine-grained soils. Canadian Geotechnical Journal 36(2): 369-381.

Suzuki, Y., Lehane, B.M. and Fourie, A. 2013. Effect of penetration rate on piezocone parameters in two silty deposits. *Proc. ISC'4 – Geotechnical and Geophysical Site Characterization*: 809-815.

Teh, C.I. & Houlsby, G.T. 1991. An analytical study of cone penetration test in clay. *Geotechnique* 41(1): 17-34.

Tonni, L. and Gottardi G., 2009. Partial drainage effects in the interpretation of piezocone tests in Venetian silty soils. Proceedings of the 17th International Conference on Soil Mechanics and Geotechnical Engineering, Alexandria (Egypt) 2: 1004-1007. Amsterdam: IOS Press.

Wroth, C.P. 1984. The interpretation of in situ soil tests. *Géotechnique*, 34(4): 449-489.

Geotechnical and Geophysical Site Characterisation 5 – Lehane, Acosta-Martínez & Kelly (Eds)

Dissipation tests in saline environment

E. Imre
Obuda University BMF, Bp., Hungary,

D. Bishop, L. Bates, S. Fityus
University of Newcastle, Newcastle, Australia,

Z. Bakacsi, K. Rajkai
MTA ATK TAKI, Budapest, Hungary

M. Juhász
Taupe Kft Budapest, Hungary

ABSTRACT: The results of two research projects are presented here. The first is based on soil exploration down to 20 m indicating that a difference exist horizontally in Szeged City, Hungary, possibly due to the variation of saline and non-saline soils in depth. The geotechnical laboratory and in situ data are treated by some statistical tests. In addition, chemical and some special, new tests (simple local side friction and cone resistance dissipation tests and multistage oedometric relaxation tests) are mentioned to characterize the fabric instability and composition of the saline layers. The second is based on the results of some geotechnical laboratory and in situ dissipation tests related to a saline spot up a depth down to 66 m.

1 INTRODUCTION

1.1 *The aim of research*

There is a hilly area with a divider between the Duna and the Tisza Rivers in Hungary, where the groundwater moves downwards, in the low areas along the two large rivers the soil water is moving upwards (Figs 1, 2, Arany, 1956; Bakacsi and Kuti, 1998, Simon et al. 2011). A statistical study made by Réthá-ti and Ungár (1978), based on soil physical parameters of 11000 laboratory tests determined from 2600 soil samples taken in the western side of Szeged (Figs 1 to 3) revealed that the layering is the same, however, the soil conditions are worse on part C in comparison with parts A and B. The aim of the research is to explain this difference, based on existing data.

1.2 *Content of paper*

In this work it is assumed that in area C some saline groundwater may move upwards in some spots from a very deep, old clay marine deposit, and, as a result, the soil may be altered in a different degree at various depths and locations.

Concerning this, the results of two research projects are presented. In the first borings, laboratory and CPT data were produced in Szeged down to 20 m depth, which was completed by chemical and special dissipation tests.

In the second one, a site in area C was investigated down to 70 m depth using conventional laboratory tests and CPTu u_2 dissipation tests.

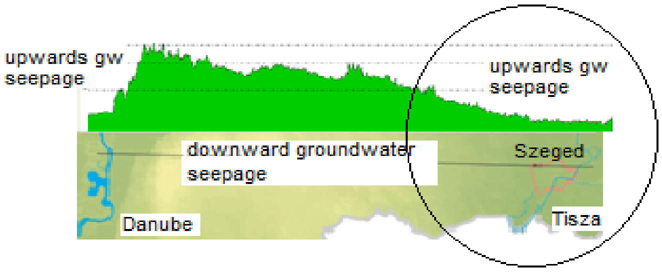

Figure 1. The Duna -Tisza Rivers section

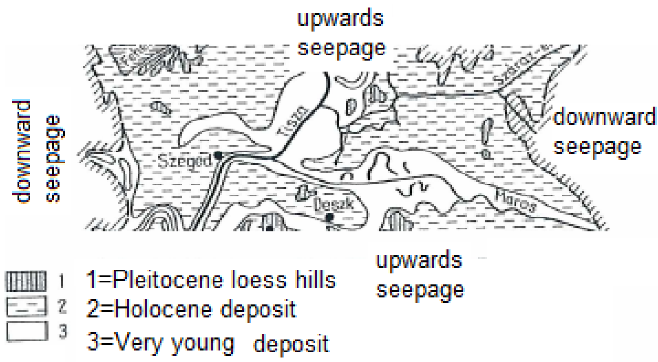

Figure 2. The Szeged environment of the section

2 METHODS

2.1 *Analysis in large area down to 20 m*

2.1.1 *Statistical and soil science tests*

In the frame of the OTKA research on in situ test modelling seven, approximately 15 to 20 m deep borings with undisturbed samples and CPT's with simple dissipation tests were made at locations indicated in Figure 1 (Imre, 1995). All geotechnical data (classification tests, chemistry tests, continuous or dissipation type CPT) were separated into horizontal and vertical groups on the basis of soil classification and area (i.e. area A, B and C). The data sets were statistically compared. Chemical tests and double compression tests were made on a few samples. The less usual dissipation type CPT and the double compression tests can be described as follows.

2.1.2 *Simple (rheological) dissipation test*

The CPT can be used in a logging and a rheological testing mode. In the ‘‘simple rheological test” the time variation of the local side friction and the cone resistance are measured for a few minutes.

135 simple rheological type CPT were made with the CPT Sz832 (with a shaft sensor of 350 cm^2) in Szeged. These were divided into 10 groups on the basis of soil classification and site A, B and C. Tests made in the vicinity of layer boundaries were not included into these groups. Tests made in an eolian sand layer 6 in Debrecen city were used as a reference with two groups on the basis of the d<0.1 mm grain content (Tables 1a and b).

2.1.3 *Double oedometer tests*

In the multistage oedometric relaxation test the displacement load is increased with 0.1 mm, the rate of strain is 1e-3 to 5e-2 %/s during the load imposition. This rate is slightly greater than the laboratory testing rates and may cause some load reversal due to the error of the control system.

The non-monotonic loading at the beginning of the stage changes the soil response (which will depend on the energy stored in the solid phase). As a results, the compression curve point changes.

It can be noted that oedometric relaxation test and the simple CPT dissipation tests are similar in terms of boundary conditions, similar models can be used for the modelling (Imre et al, 2010).

It can also be noted that there is a partial unloading effect along the shaft surface when the penetration stops due to the stress release of the equipment entailing a decrease in the penetrometer diameter.

The double compression test results were the by-product of the basic research on the similarity. Both conventional multistage compression tests (MCT) and multistage oedometer relaxation tests (MRT) were made on all soil samples.

2.2 *Analysis of a saline spot down to 66 m*

2.2.1 *Dissipation test*

The pore water pressure dissipation tests were evaluated using three methods. Methods I and II (slow and fast methods) were precise Least Squares fittings of a 1D consolidation model. Method I was numerically more expensive than II. Method III – the one of Teh and Houlsby (1988) - was based on a two-dimensional model and a one-point-fitting at the t_{50} determined according to Sully et al. (1999).

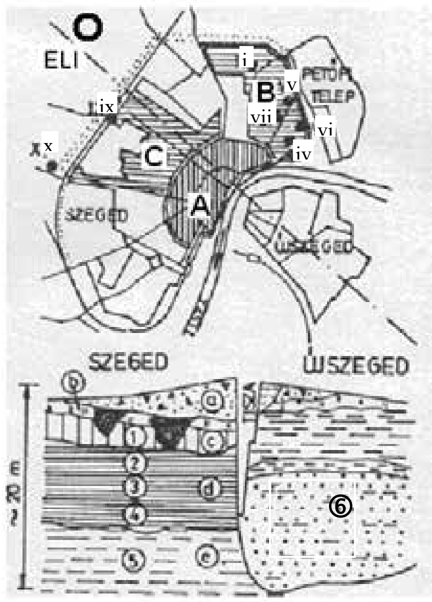

Figure 3. Site plan with explorations of OTKA (closed symbols) and the saline spot denoted by ELI. Layers 1 to 5 (or a to e) are shown in Table 1 (or Réthári and Ungár, 1978).

Table 1a. Layers in the OTKA research.

Notation	soil
1	Loess
2	Upper yellow lacustrine clay
3	Silty inclusion
4	Lower yellow lacustrine clay
5	Blueish fresh-water deposit
6	Sand

Table 1b. Category limits and notations OTKA research

Notation	Category limits
a	> 25 I_p [%]
b	15-25 I_p [%]
c	10-15 I_p, [%]
d	5-10 I_p, [%]
e	d_{30}>0.1mm
f	d_{30}<0.1mm

Table 2. Soil chemistry tests (Site X is at part C, site VI is at part B.)

Site,depth	pH(H_2O)	Electric conductivity mS/cm	ESP	Salt %
X-12,3m	8.02	0.66	3.94	0.15
VI-12,5m	8.29	0.30	1.536	0.06
X-10,0m	7.96	0.86	5.142	0.17
VI-5,0m	8.46	0.36	3.117	0.06
VI-6,5m	8.53	0.34	1.93	0.05

2.2.2 *Conventional oedometer tests*

The conventional oedometric compression tests was evaluated with the modified Terzaghi and Bjerrum models (a constant term for the immediate compression was added, Imre et al, 2013, 2014). The immediate, primary and secondary consolidation settlements were separated.

3 RESULTS

3.1 *Analysis in large area down to 20 m*

3.1.1 *Rheological dissipation test*

The mean simple CPT dissipation test records shown in Figure 4 generally show an immediate stress drop (or discontinuity) at the stop of the steady penetration, possibly since the loading type changes from basically dynamic to quasi-static.

After the stress drop, the rate of the cone resistance dissipation is larger in sand and is smaller in clay, it can be related to soil plasticity. The sign of the shaft resistance change during dissipation, in the first two minutes (measured with a 350 cm2 element for the shaft) is strongly dependent on the soil type. For sands the local side resistance increases with time and for clays it decreases with time in the first two minutes.

Concerning the horizontal inhomogenity (Fig 4), the stress decrease after 2 minutes was larger in part C than in parts A or B possibly since the normalization unit was less in area C than in area A and B. In addition, a non-zero final tangent was observed in area C which may indicate an unstable fabric.

It can be noted that the plasticity dependent results of the mean simple CPT dissipation test records were qualitatively reproduced by some multistage oedometric relaxation test both experimentally and in terms of modelling (Imre, 1985, Imre et al, 2010).

3.1.2 *Double oedometer tests*

By plotting the MCT and MRT compression curves together, some difference, reflecting the fabric and plasticity, was observed (Imre at al, 2015, Imre and Singh, 2012).

No deviation occurred for soft, intact, plastic clays. For small plasticity soils there was an increasing difference. For saline silts, zero MRT compression curve was measured (Imre et al., 2013) indicating the collapse lack of the fabric structure (Fig 5).

3.1.3 *Statistics and soil science*

The bluish-grey deposit has lower plasticity index I_P at C than at A and B. The montmorillonite + illite content of the lower yellow clay layer was less on unit C than A and B. According to the results of the chemistry tests (see Table 2) saline soil with high salt content was found at various depths in part C.

The lower yellow clay and the bluish-grey deposit has considerably less undrained shear strength c_u, and ultimate cone resistance q_{cu}, on area C than on areas A, B (see Table 3). This result supported the result of the statistical study made by Rétháti and Ungár (1978).

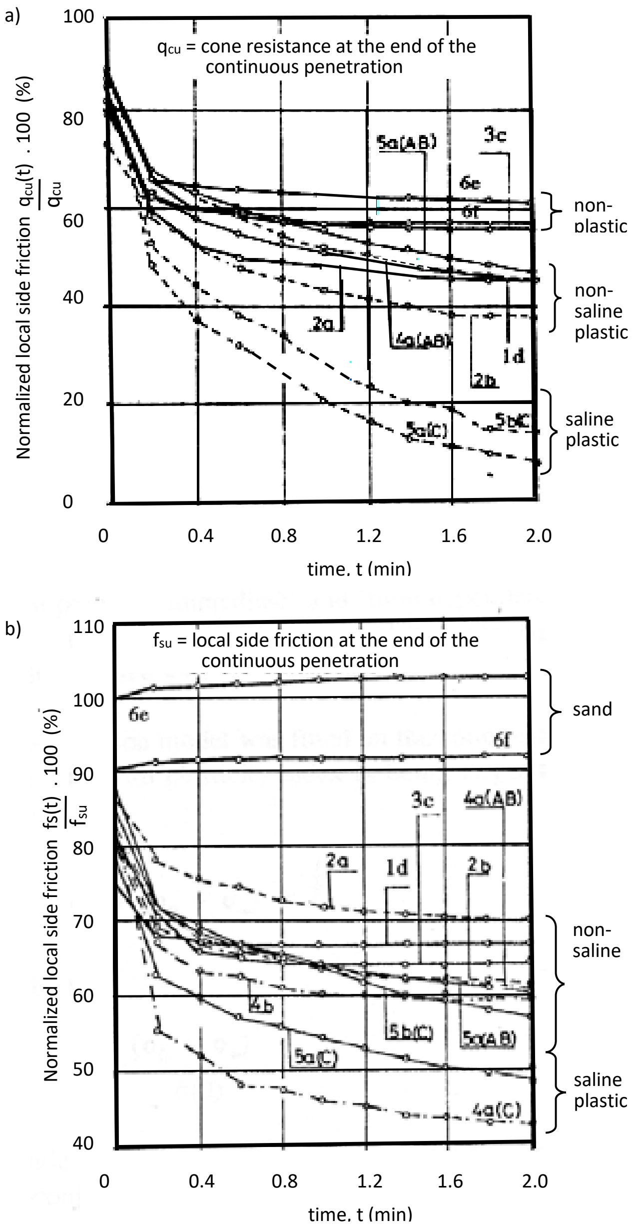

Figure 4. Average dissipation test records (OTKA research) a) cone resistance b) local side friction (on the basis of CPTs I to X shown in Fig 3) Area A, B or C is indicated in bracket. (The sand shows f_s increase, the saline soils show the largest stress drops.)

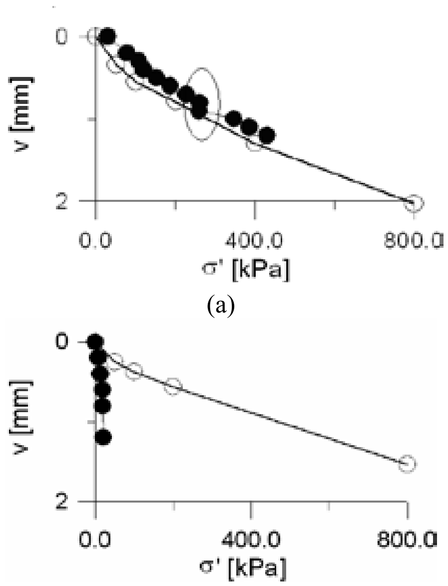

Figure 5 OTKA research, the usual and the relaxation test compression curves determined with a slight partial unloading (MRT: full circle, MCT: open circle). (a) Ip =23%, area A. (b) Ip =10%, saline, area C

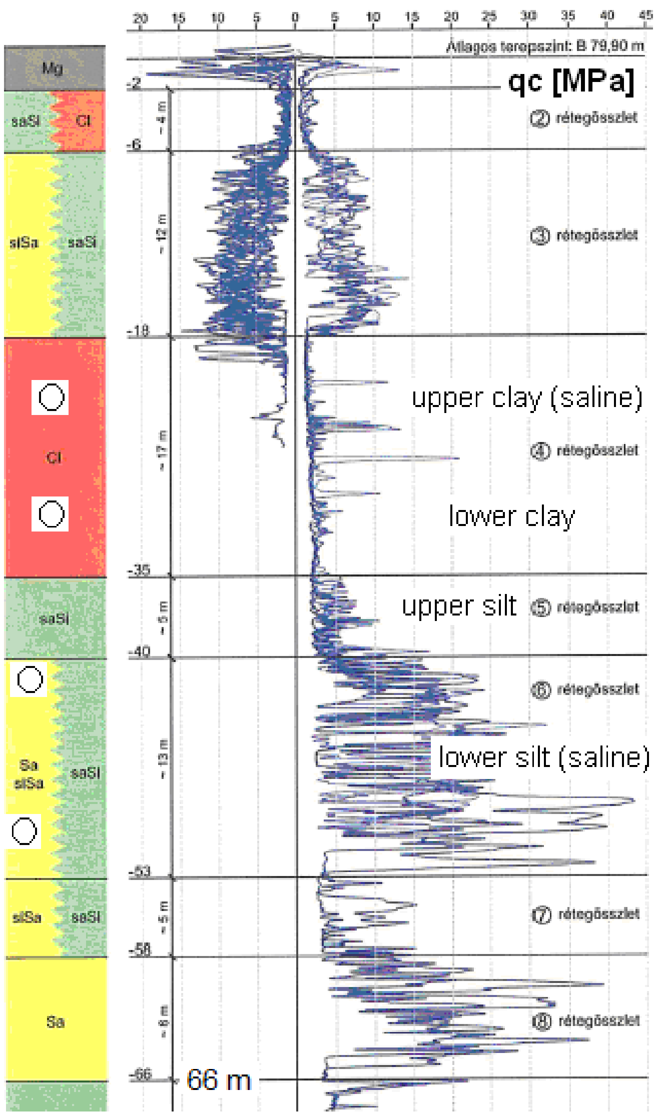

Figure 6. Mean profile indicating location of the dissipation tests.

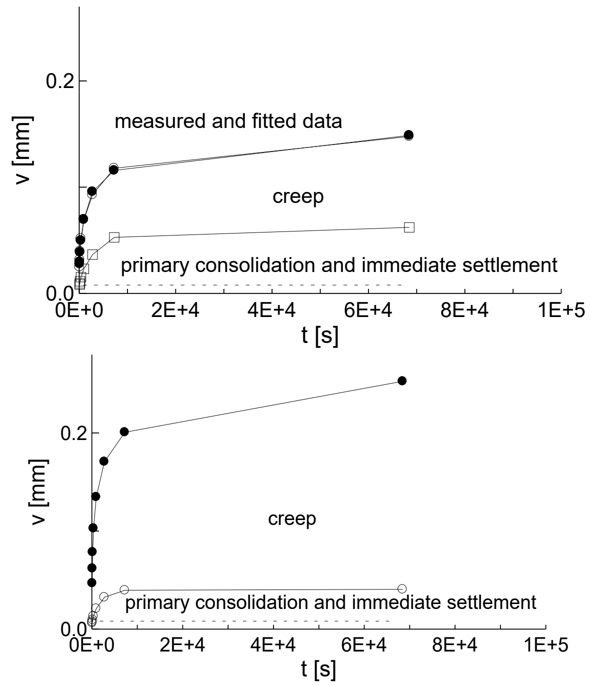

Figure 7. ELI-site, Compression test evaluation for non-saline and saline Szeged soils, upper: Non-saline clay e = 0,74, lower: Saline clay e = 1.06.

Table 3. OTKA; mean of relative shear strength parameters.

Layer Group	s_u [%]	q_c [%l	f_s [%l
4AB	100	100	100
4C	88	67	62
2	80	68	71
5AB	79	91	91
3	58	51	53
5C	32	31	51

3.2 *Analysis a saline spot down to 66 m*

The results are shown in Figs 6 to 10, Tables 4 and 5 which can be summarized as follows.

3.2.1 *Oedometer tests*

The coefficient of consolidation *c* identified from oedometer test data was considerably smaller than the dissipation test values, as expected. By evaluating the stages of the compression tests with the modified Bjerrum (1967) model, the ratio of the primary consolidation settlement was smaller and the creep settlement was larger for the saline soils than for the non-saline soils at the end of the stages (Fig 7). The immediate compression was zero for the sand-silt.

3.2.2 *Measured dissipation test data*

The upward flow was proven by the 100% long, measured dissipation curve data which resulted in various groundwater levels on the same location. An approximate equilibrium groundwater level was also defined for each location, the evaluation of measured data was made for both the approximate equilibrium and the actual non-equilibrium groundwater levels.

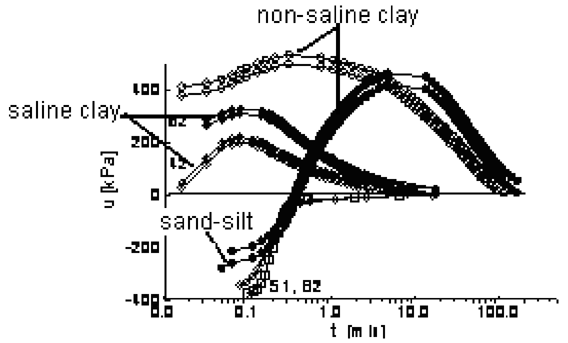

Figure 8. Pore water pressure dissipation curves at ELI-site

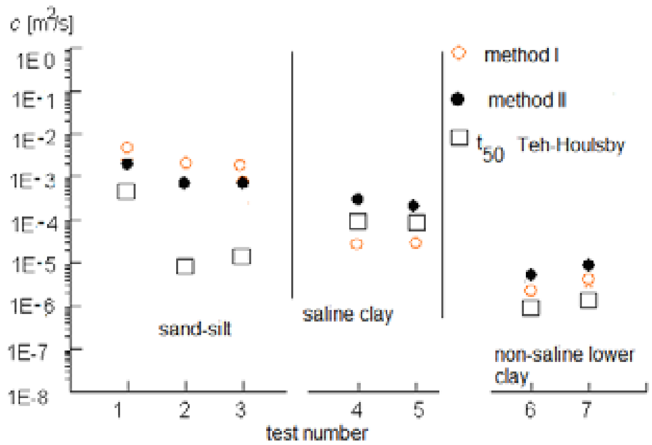

Figure 9. The coefficient of consolidation c values identified from dissipation tests, with correction factors.

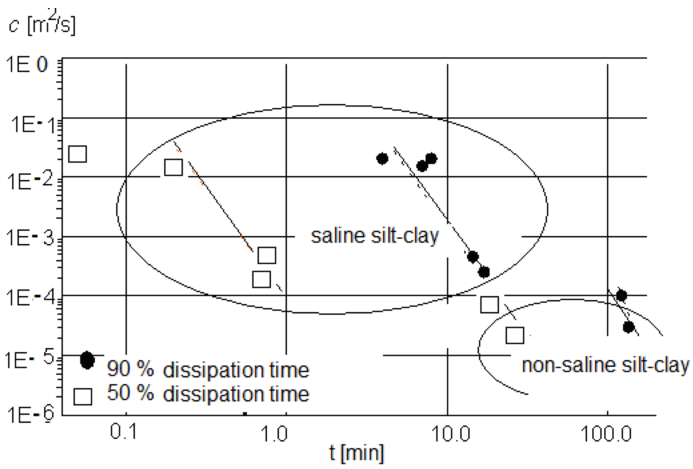

Figure 10. The relation between c and time (with t50 or t90), with correction factors, method I.

Table 4. Dissipation testing time

Site/ depth m	Test id	Test id for Fig 9	t_{50}[min]	t_{90}[min]
52/22	41/42/5	4	0,62	14,5
53/22	61/62/6	5	0,78	22,5
52/30	91/92/8	6	27,73	135
53/30	71/72/9	7	20,05	122
51/50	33/1	1	0,05	4
52/40	51/2	2	1,97	7
53/40	82/3	3	2,37	8,5

Table 5. The identified *c* without correction factors (*c* in m^2/s)

Test id for Fig 9	Compression test	Method III	Method I	Method II
4	5E-8	7,00E-05	6,00E-05	6,00E-04
5	5E-8	5,00E-05	9,00E-05	4,00E-04
6	3E-8	1,00E-06	4,00E-06	7,00E-06
7	3E-8	2,00E-06	1,00E-05	2,00E-05
1		5,00E-04	1,00E-02	8,00E-03
2		1,00E-05	4,00E-03	2,00E-03
3	1E-7	1,00E-05	3,00E-03	3,00E-03

The dissipation curves were non-monotonic in the NC clays (type III and IV), similarly to the case of quick clays in Australia.

The dissipation curves were negative, monotonic in the silty sand (type V). This result can be explained by the small compressibility of the particles and, the nearly drained penetration around the tip. At the shaft the sand layer becomes highly overconsolidated due to the effect of the compression made by the penetrometers tip.

The incompressibility of the sand grains can be linked with the results of the evaluation of the oedometer test: the immediate compression was zero for the sand-silt in each case.

3.2.3 *Dissipation test evaluation*

The u_2 data were evaluated using three methods. The first and second methods were Least Squares fittings of a coupled consolidation model using two initial conditions. The third method was suggested by Teh and Houlsby (1988) as a one-point-fitting-method based on the t_{50} determined according to Sully et al, 1999 being valid for undrained penetration.

The results are shown in Figs 9 to 10, Tables 4 and 5. The method I gave better fit than method II but the solution was not unique (double, larger the c-valued solution was accepted). The solution of the methods I and II needed to be corrected with a factor of 0.49 to 0.86 for the clays and silts (see e.g. in Imre and Bates, 2015).

For clays, the c solution of method II was larger than the one of method I. The solution of method I was close to the one of method III if a correction factor of 0.5 was used.

In silts and sands the *c* values determined by method III seemed to be too large since method is not precise in partly drained case. The *c* values identified from oedometer tests were smaller than the dissipation test values, as expected (Table 4, Bjerrum, 1967).

4 DISCUSSION, CONCLUSION

4.1 *Analyses in large area down to 20 m*

The results of the statistical analyses showed a considerable reduction in the CPT data in area C with respect to areas A and B. The chemical tests showed saline soils at various depth in area C.

The simple CPT dissipation tests results showed dependence on soil plasticity on the one side which can be explained as follows. The simple CPT dissipation tests (and the oedometer relaxation tests) can be modelled in terms of c and the relaxation coefficient s both determined by soil plasticity.

The simple CPT dissipation tests (and the oedometer relaxation tests) revealed some fabric instability tests in area C.

4.2 *Analysis of a saline spot down to 66 m*

The u_2 dissipation tests were evaluated by methods I and II (slow and fast methods) which were precise, automatic methods and by method III which was a one-point-fitting method valid for undrained penetration. The c values identified by these methods were similar in clays and were different in silts-sands possibly due to error of method III in case of partly drained of penetration.

The conventional oedometric compression tests was evaluated with the modified Terzaghi and Bjerrum model (a constant term for the immediate compression was added). The c identified from compression tests was considerably smaller than the in situ test values. The salinity caused an increase in the compressibility and creep as follows. The compression tests showed smaller primary consolidation, larger creep settlements for saline-like than non-saline-like soils. The void ratio was larger for the saline-like soils than for the non-saline-like soils. The immediate compression was zero for silts which can be linked with the incompressibility of the grains. This result may explain that the dissipation curves were negative, monotonic in the silty sand (type V).

Different c - t_{50} or t_{90} relations were obtained for saline-like and non-saline-like clays in both the in situ and the laboratory tests, reflecting larger permeability for the saline-like soils.

The presence of upward flow was proven by both the 100% long, measured dissipation curve data which resulted in various groundwater levels on the same location and by the compression test data which resulted under-consolidated state otherwise.

4.3 *Summary*

The effect of the upwards groundwater flow with saline content in spots causes a change in the chemistry of the soils leading to unstable fabric, larger void ratio, less clay content, a reduction in shear strength, an increase in the compressibility and creep. It can be noted that similar results can be found in quick clay deposits (Bates et al, 2012, Bishop, 2009).

REFERENCES

Arany, S. 1956. Salt-affected Soils and Their Reclamation. In Hungarian Mezőgazd. Kiadó. Budapest.

Bakacsi, Zs. & Kuti, I., 1998. Agrogeological investigation on a salt affected landscape in the Danube Valley, Hungary. Agrokémia és Talajtan. 47**.** 129–138.

Bates L. Bishop D., Fityus S.. Hegedüs T M, Imre E. 2012 The evaluation of some dissipation test records and of the initial part of some simple rheological CPT records. These proceedings.

Bishop, D. 2009. Eng. Geol. Of Richmond River Estuary. PhD Thesis, The University of Newcastle.

Bjerrum, L. 1967. Engineering geology of normally consolidated marine clays as related to settlements of buildings. Seventh Rankine Lecture. *Geotechnique*, 162: 83-118.

Brand, E.W. and Brenner, R.P. 1981: Soft Clay Engineering. Elsevier.

Imre, E. 1995: Statistical evaluation of simple rheological CPT data. *Proc. of XI. ECSMFE,* 1. 155-161.

Imre E., Singh V.P. 2012: The oedometric relaxation test. Proc. of 12th ISEG, pp. 38-47.

Imre, E., Rózsa, P., Bates, L., Fityus, S. 2010: Evaluation of monotonous and non-monotonous dissipation test results. *COGE.* 37: 885-904.

Imre, E, Schanz, T, Hegedűs, Cs. 2013. Some thoughts in non-linear inverse problem solution. EURO:TUN 2013. Bochum, Németország, 2013.04.17-04.19. pp. 357-365.

Imre E., Juhász M., Józsa V., Hegedûs M., Bíró B., Singh V. G. 2014 CPTu tests and CPT simple dissipation tests in saline environnent. In: 3rd International Symposium on Cone Penetration Testing Las Vegas, pp. 683-690.

Imre E, Firgi T, Juhász M, Hazay M, Hegedűs M, Bakacsi Zs, Singh V 2014b CPTu pore water pressure dissipation tests in saline environment In: 3rd International Symposium on Cone Penetration Testing: Las Vegas, pp. 675-682.

Réthági, L., Ungár, T. 1978: Large settlement's soil physical data – statistical analyses. *Építés, Építészettudomány*, X. 1-2 In Hungarian.

Lunne, T., Robertson, P.K. and Powell, J.J.M. 1997. Cone Penetration Testing in Geotechnical Practice, London: Taylor & Francis. ISBN 9780419237501, pp. 60-61.

Simon, Sz. Mádl-Szőny, Müller, I., Pogácsás, Gy. 2011. Conceptual model for surface salinization in an overpressured and a superimposed gravity-flow field, Lake Kelemenszék area, Hungary Hydrogeology Journal (2011) 19: 701–717.

Sully, J.P., Robertson, P.K., Campanella, R.G., Woeller, D.J. 1999. An approach to evaluation of field CPTU dissipation data in overconsolidated fine-grained soils. Can. Geotech. J. 36: 369–381.

Teh, C.I. and Houlsby, G.T. 1988. Analysis of the cone penetration test by the strain path method. Proc. 6th Int. Conf. on Num. Meth. in Geomechanics, Innsbruck.

Geotechnical and Geophysical Site Characterisation 5 – Lehane, Acosta-Martínez & Kelly (Eds)

Some comments on the CPTu and DMT dissipation tests

E. Imre
Obuda University BMF, Bp., Hungary,

D. Bishop, L. Bates, S. Fityus
University of Newcastle, Newcastle, Australia

Z. Hortobagyi
BME, Budapest, Hungary

M. Juhasz
Taupe Kft Budapest, Hungary

ABSTRACT: Some u_2 and some DMT dissipation test data, measured at the Ballina soft clay test site, are compared. The DMT tests are evaluated using the Flex method which is based on the assumption that the t_{50} is related to the inflexion point of the total stress-time curve. The u_2 dissipation tests are evaluated by two previously suggested, mathematically-precise methods and by the Teh-Houlsby method. Results show that the testing time can be considerably reduced by applying the mathematically-precise methods.

1 INTRODUCTION

The cone penetrometer test can be made either in continuous or in rheological testing modes. In the rheological or dissipation tests (Table 1) the time variation of a stress variable is measured on the penetrometer, after steady penetration is stopped. These tests can be used to assess the in situ permeability of soils if a suitable evaluation method is available.
The goal of the research is to get more information from shorter dissipation tests using optimal measuring system and proper evaluation methods. The research plan includes the following general steps.
(i) Selection of in situ test sites with known properties: soft soil sites in Australia and Hungary (Szeged) are used. (ii) some preliminary tests are undertaken. (iii) possible modifications in the measuring and evaluation system are considered.

In this work some new u_2 and DMT dissipation tests were performed, at a soft clay test site in an Australian estuary, according to the present standards. The long u_2 data were evaluated with the one-point fitting method of Teh-Houlsby and two precise evaluation methods, a slow (A) and a fast (B) method. Some truncated short u_2 data were evaluated with the precise methods. The long DMT tests were evaluated with the Flex method (Totani, et al. (1998)).

First results show that the t_{50} dissipation time is longer for the DMT than for the CPTu for low permeability soils. The necessary testing time is considerably shorter than the t_{50} time if mathematically-precise – several point-fitting type – evaluation methods are used.

2 METHODS

2.1 *One-point fitting evaluation of dissipation*

At present, the measured and the theoretical dissipation curves are fitted in one point. For example, the coefficient of consolidation c_{T-H} is determined by Teh and Houlsby (1991) as follows:

$$c_{T-H} = \frac{T_{50}^{T-H}}{t_{50}} r_0^2 \ I_r^{\ 1/2} \tag{1}$$

where r_0 is radius of the rod, t_{50} is measured time for 50% dissipation, I_r is rigidity index, $T^{T\text{-}H}_{50}$ is an approximate time factor based on the observation that the dissipation curves can approximately be normalized.

Using total stress data measured in DMT, the coefficient of consolidation c is determined with the following one-point fitting equation:

$$c_{DMT} = \frac{F}{t_{50}} \tag{2}$$

Table 1 Measured variables of some dissipation tests

CPTu dissipation test*	CPT Piezo-lateral stress cell test, DMT dissipation test**	CPT dissipation test***
pore water pressure on the shaft or the tip	total stress on the shaft	local side friction and the cone resistance on the usual shaft and tip position

*Lunne et al (1992) ** Totani, et al. (1998), *** Imre et al (2014, 2014b) where F is between 7 and 12 cm^2 (Totani et al, (1998)). It is assumed that the t_{50} dissipation time of the pore water pressure and the inflexion point of the total normal stress dissipation curve coincide.

2.2 *Model for the precise CPTu evaluation*

2.2.1 *Differential Equation*

The pore water pressure variation with time is either monotonic or non-monotonic, determined by the initial pore water pressure distribution u_o.

In this work, the solution of a coupled model was used with a fixed r_1 (influence radius), as follows, for the pore water pressure (Imre et al, 2010):

$$u(t,r)= \sum_{k=0}^{\infty} \lambda_k C_k e^{-\gamma_k^2 \cdot c_h \cdot t} \left\{ \begin{matrix} [I_0(\lambda_k r)+\mu_k Y_0(\lambda_k r)] \\ -[I_0(\lambda_k r_1)+\mu_k Y_0(\lambda_k r_1)] \end{matrix} \right\} \quad (3)$$

where J_p and Y_p are Bessel functions of first and second kind, order of p, λ_k, μ_k are roots of the boundary condition equations depending on r_1; C_k (k=1...∞) are Bessel coefficients and $c(= k\ E_{oed}/\gamma_v)$ is coefficient of consolidation.

2.2.2 *The initial condition, boundary condition*

The C_k (k=1...∞) were determined from the initial condition in two different ways. In one approach, a few C_k (k=1...n) were identified during the inverse problem solution (fast model). If the value of n was 1, the initial condition was monotonic, valid after undrained penetration. If the value of n was greater than 1, the initial condition was non-monotonic but not necessarily realistic.

Alternatively, the parameters C_k were determined beforehand for various shape functions, and the shape functions were identified (slow method). This resulted in some additional non-linearly dependent parameters, the model fitting was very slow.

The shape functions were defined as follows. The initial pore water pressure distribution u_o may monotonically decrease with distance away from the shaft or it may increase initially over a short distance, (possibly from a negative value) due to interface shear in a thin shear zone of thickness t_s, between radii of r_o and r_s.

Within the shear zone ($r_o \leq r \leq r_s$), the increasing initial pore water pressure function was assumed to be linear, having one of five prescribed values at r_o, called relative negativities, denoted by n_1 ($0 \leq n_1 \leq 4$) corresponding in Figure 1 to the distributions I to V.

The pore pressure decreasing part of the initial condition is a curve denoted by an integer parameter n_2 ($0 \leq n_2 \leq 9$) with an increasing mean ordinate, shown in Figure 1 as distributions 1 to 10.

The two parts of the initial condition (n_1, n_2) were combined to give $n = n_1 n_2$ ($0 \leq n \leq 49$), there were 50 different initial conditions (shown in Figure 1). A variable, the relative thickness of the interface shear zone s, was defined as t_s/r_o. was also used. The possible range of s was covered by seven different values ($0.05r_o < t_s < 1.92r_o$), denoted by s in Table 2.

In the evaluation method r_1 = 37 r_0 (valid in filter position E; Imre et al, 2010) is used. The identified c values are greater by a factor of 4.5-6.5 if the measured data are related to other filter positions. A correction factor can be determined by using the model law (see Section 4). In this work 0.5 was used.

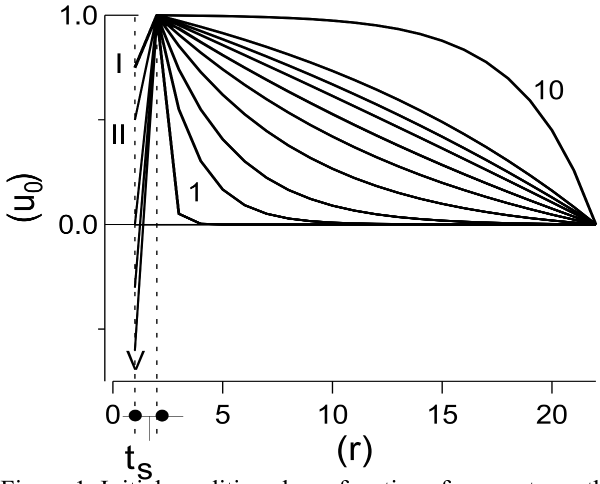

Figure 1. Initial condition shape functions from r_o to r_1, the sheared zone extends from r_o to $r_s = r_o + t_s$ where lines are labelled I to V, outside the curves are labelled 1 to 10.

Table 2 Specified thickness values of the interface shear zone (r_o and r_s is the radius of the CPT and the sheared zone, resp.)

s number [-]	t_s [cm]	$r_s = r_o + t_s$ [cm]	t_s/r_o [-]
1	0.1	1.85	0.05
2	0.21	1.96	0.12
3	0.42	2.17	0.24
4	0.84	2.59	0.48
5	1.89	3.64	1.08
6	2.94	4.69	1.68
7	3.36	5.11	1.92

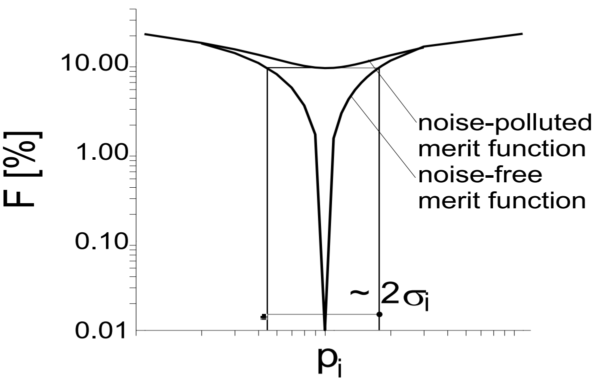

Figure 2. The clever section of the merit function and the geometrical concept of the parameter error domain for p_i.

2.3 *The inverse problem solution, precise evaluation*

Concerning the minimisation of the least squares objective function, the following concepts were used (Imre et al, 2010 and 2013): (i) the elimination of the linearly dependent parameters by sub-minimisation, (ii) the closest noise-free merit function (called follower function), (iii) the “deepest” or “clever section” section of the merit function, with respect to a parameter. The clever section contains the global minimum and gives information on the maximum error of the respective parameter (Figure 2).

The merit function was minimised such that a convex sublevel set - called an error domain – of the follower merit function was bracketed with a predetermined mesh generated in the subspace of the non-linearly dependent parameters, the linearly dependent parameters were eliminated. The clever sections for each non-linearly dependent parameter were determined on the basis of grid computations.

3 RESULTS

3.1 *CPTu and DMT measurements*

The soft clays associated sediments in the coastal estuaries has been extensively investigated in the Richmond River estuary (Bishop, 2009).

The Upper Clay is sensitive, has a liquid limit of around 100%, a plastic limit of 40% and a natural water content of 80%, with a unit weight of around 14.2 kN/m^3. The shear vane strength is low; around 25kPa. CPTu u_2 dissipation curves made in this layer are generally non-monotonic (Bates et al, 2014). From a geotechnical perspective, in the highly sensitive clays the organic substances lead to some physical stabilization in “normally consolidated” clays at high void ratio. This clay has a metastable structure.

The Lower Clay is not sensitive, has a liquid limit of around 80%, a plastic limit of 25% and a natural water content of 60% with a unit weight of around 16.4 kN/m^3. The shear vane strengths are higher; around 70kPa. The dissipation curves made in this layer are generally monotonic (Bates et al, 2014).

The site from which the data presented in this paper has been obtained is located on the Ballina coastal plain of eastern Australia (Figs 3 to 5). The main feature of the profile is the 3-4m thick sand layer that separates the upper Holocene estuarine clays from the lower Pleistocene estuarine and deeper clays. Two test -pairs are presented in this paper.

The CPTu tests were undertaken by the “NEWSYD” 200kN truck-mounted penetrometer facility using a 50MPa compression cone with the filter in the u_2 position. The same facility also performed the DMT tests.

The dissipation tests were conducted in the two clay layers (Fig. 5). According to the expectations, the lower clay has monotonic behavior while the upper clay has a non-monotonic response.

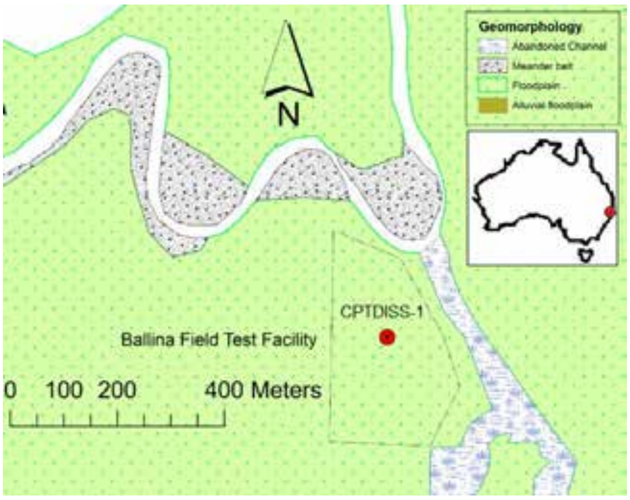

Figure 3. CPTDISS-1 at Ballina soft soils test site.

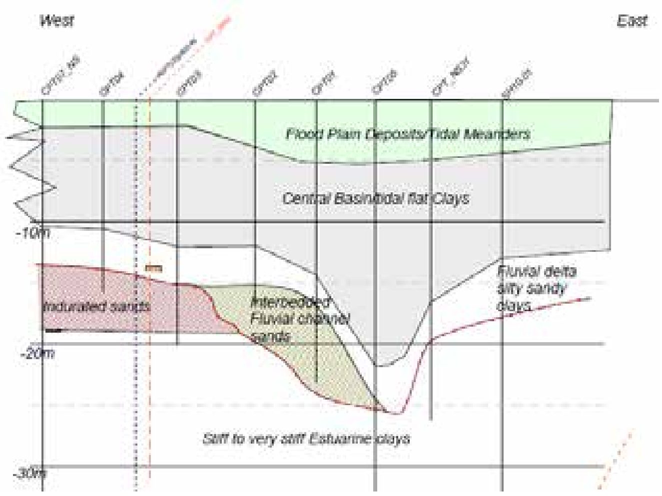

Figure 4. Section at Ballina soft soils test site.

Table 3 Identified c [cm^2/s] (uncorrected/corrected values)

Test Depth [m]	5	23
Method A (c_A)	5E-3/2.5E-3	0.4/0.2
Method B (c_B)	2E-2/1E-2	0.4/0.2
DMT (c_{DMT})	3E-04	1.8E-01
Teh-Houlsby (c_{T-H})	4E-04	3E-02

Table 4 Test duration data [min]

Test Depth [m]	5	23
CPTu duration	218	14.5
CPTu t_{50}	120	4.16
DMT t_{50}	340	0.65
DMT duration	450	240
Method A minimum*	5	4
Method B minimum*	20	2

* minimum test length from truncated tests

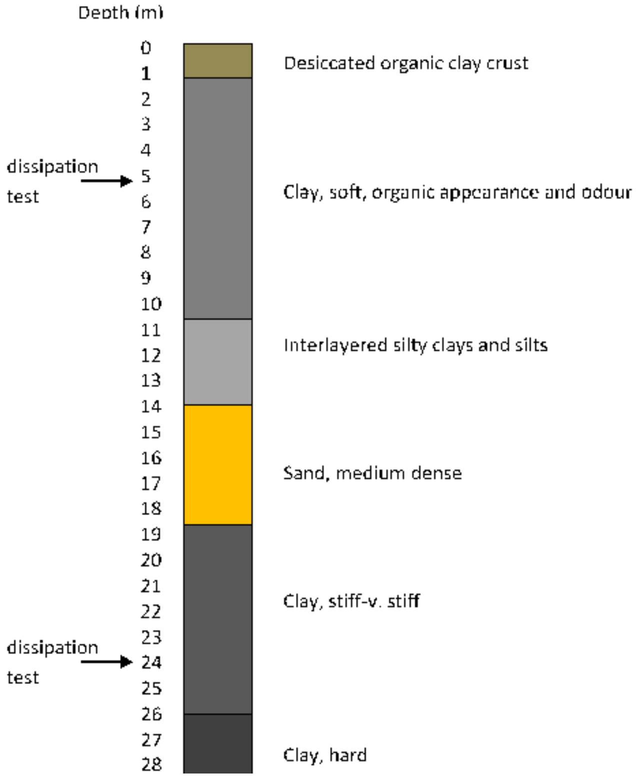

Figure 5. CPT profile showing dissipation tests: 5m, 7m and 23 m in estuarine clay from the Holocene and Pleistocene, resp.

3.2 *Evaluation results*

The results are shown in Figures 6 to 10 in Tables 3 to 4. Measured and fitted data in Figure 6 show good agreement. The identified coefficient of consolidation c can be characterized as follows.

In the upper clay where the CPTu t_{50} was 120 min and the DMT t_{50} was 340 min, the coefficient of consolidation c identified with the Flex method was close to the one identified with the Teh-Houlsby method $c_{DMT} \approx c_{T\text{-}H}$ and $c_{T\text{-}H} < c_A < c_B$ was observed which is a previously observed experience (see e.g. Imre et al, 2014 and 2014b).

In the lower clay where the CPTu t_{50} was 4.16 min and the DMT t_{50} was 0.65 min, the coefficient of consolidation c identified with the Flex method was close to the precise method value $c_{DMT} \approx c_A \approx c_B$ and was larger than the one identified with the Teh-Houlsby method $c_{T\text{-}H} < c_{DMT} \approx c_A \approx c_B$.

According to the clever sections of the merit functions for parameter c (Figures 7 and 8), the results of the precise method indicate reliable solutions in each case for the long tests. This is because the solution was unique, since the global minimum of the clever section was single, non-degenerated and the local minima were not 'too deep' (e.g. not deeper than global minimum of the real-life merit function).

The solution of the inverse problem was acceptably precise since the error domain of the solution on the clever sections was situated within the physically admissible parameter domain.

The evaluation of the short tests was made with methods A and B for each test, and the variation in the determined c values is shown in Figure 9. It is apparent that consistent values of c can be obtained as the data record is shortened by a great amount.

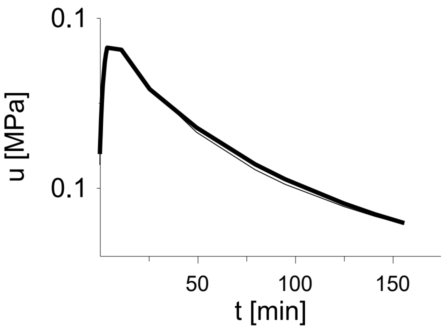

(a) CPTu test 5m

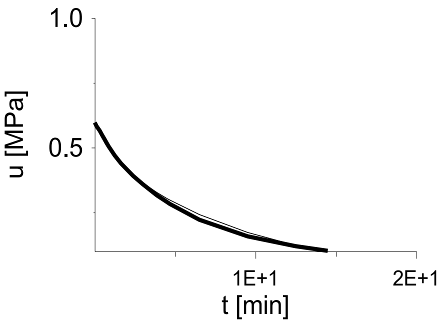

(b) CPTu test 23m

Figure 6. Measured – fitted data, slow method A

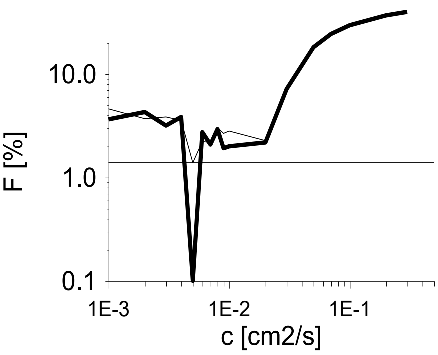

(a) CPTu test 5m

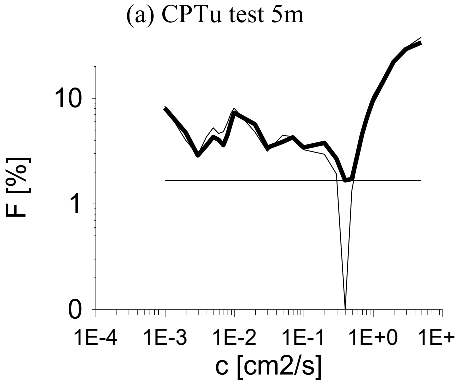

(b) CPTu test 23m

Figure 7. Clever section of the merit functions of c, method A.

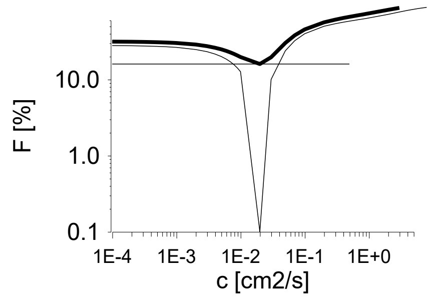

(a) CPTu test 5m

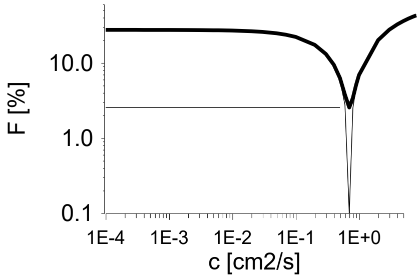

(b) CPTu test 23m

Figure 8. Clever section of the merit functions of c, method B.

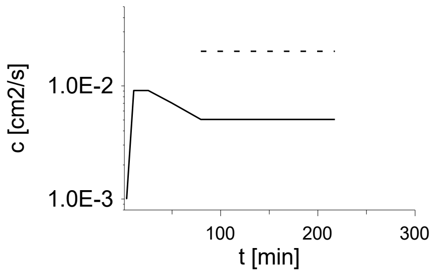

(a) CPTu test 5m

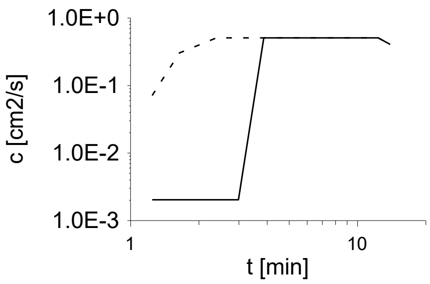

(b) CPTu test 23m

Figure 9. Identified c and testing time (method A and B are indicated in solid and dashed lines, resp.)

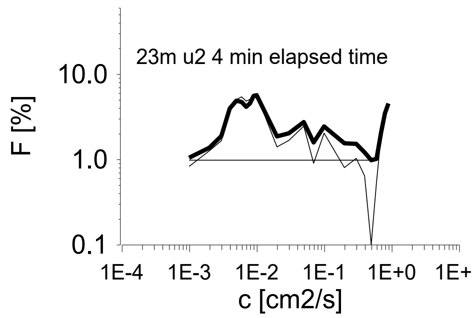

Figure 10. CPTu 23 m, method A, too short data (4 min elapsed time, see Fig. 7 for long test with unique solution).

By representing the clever sections of the short data series (Fig. 10), it can be seen that in the initial, inconsistent part of the c-t diagrams the solution is not unique. The value of c is only consistent for data longer than 20 minutes elapsed time for the upper clay where the solution of the inverse problem became unique.

4 DISCUSSION

4.1 *Time factor concept*

4.1.1 *The t_{50} relationship*

The relation of the t_{50} of CPT and DMT can be expressed by combining Equations (1) and (2):

$$\frac{t_{50,CPT}}{t_{50,DMT}} = \frac{T_{50}^{T-H}}{F} r_0^2 \; I_r^{1/2} \tag{4}$$

It is clear from approximate Equation (3) that the t_{50} dissipation time ration for the DMT and CPT may be dependent on the rigidity index I_r.

4.1.2 *The use of rigidity index*

An approximate time factor can be derived from the analytical solution (3) (Imre et al., 2014 and 2014b):

$$T = \frac{ct}{(r_1 - r_o)^2} \tag{5}$$

Combining Equations (1) and (5) gives:

$$r_1 - r_0 = r_0 \left(T^{T-H} / T^1\right)^{1/2} I_r^{1/4} \tag{6}$$

It follows that some information can be collected for the value of r_1 using the rigidity index I_r. As the rigidity index I_r is smaller, the value of r_1 - r_0 is less for sands and silts than for clays.

4.1.3 *The model law*

The approximate time factor (5) can be used to derive various model laws (Imre et al, 2010) just as in the case Terzaghi's model law. One possibility is shown here as follows.

The differences in the dissipation time can be explained by the size of the displacement domain r_1 where the in which dissipation extends. This depends on filter position and drainage condition.

Assuming that the same linear model applies for every filter position and the soil is isotropic, the following ‘‘c formula” can be derived from the time factor. The ratio of the c values from the filter position A and position D depends on the size of the displacement domains:

$$\sqrt{c_E/c_D} = \frac{(r_{D1} - r_{D0})}{(r_{E1} - r_{E0})} \qquad (7)$$

using the r_1 value valid for filter position E and D and one corresponding identified c.

4.2 *Precise method for DMT*

The evaluation of the DMTA dilatometer dissipation test - based on the inflexion point of the measured stress curve (Flex method) -, may not work if no inflexion point can be found.

In this case the dilatometer dissipation test data can be evaluated in the frame of a double parameter sensitivity analysis including not only the Flex method but also the precise pore water pressure dissipation test evaluation method A (Imre et al, 2011).

The double parameter sensitivity analysis can also be used to validate the constant of the DMTA dilatometer dissipation test evaluation (Flex) method.

5 CONCLUSIONS

The preliminary results of the evaluation of two test - pairs of CPTu u_2 and DMT dissipation tests data, compared in this paper - show some differences in terms of the identified c and the t_{50} dissipation time.

The c values determined by the one-point fitting method (Teh-Houlsby method) in the upper clay, was smaller than the ones determined by the mathematically precise fitting methods A and B. The difference decreased if a correction factor of 0.5 was used to account for the u_2 filter position. The DMT value was the same as the Teh-Houlsby value. Method A gave smaller values than method B. In the lower, assumingly low plasticity soil the opposite was true in the sense that the DMT and the precise methods gave basically the same result, but the Teh-Houlsby value was smaller.

It can be concluded that the c values identified with the various u_2 methods showed a similar picture – depending on soil plasticity - as in earlier works, e.g. in the case of the Hungarian soft clay site (Imre et al, 2014, 2014a) which need some further research using additional information.

No unique rule was found for the relation of the t_{50} dissipation time of CPT and DMT. The t_{50} in the upper clay was shorter for the CPT than for the DMT (the t_{50} was longer than 100 min for the CPTu and longer than 300 min for the DMT). In the less plastic, lower soil the opposite was true. The difference may be dependent on rigidity index, as derived in this paper and may be influenced by the fact that the dilatometer blade has a different geometry than the CPT cone.

The necessary testing time of the one-point fitting methods (i.e. for the Flex and The-Houlsby method) is equal to the t_{50} time at present. The evaluation results of a series of truncated u_2 dissipation test data indicated unique solution for shorter data series even by an order of magnitude.

It follows that the necessary testing time can be decreased with the precise method in plastic clays. The same can probably be true for the DMT if evaluated with the precise method.

Further research is suggested on the t_{50} dissipation time and on the possible decrease in the testing time by using precise – several point-fitting – evaluation methods. In the subsequent, detailed analyses of the data, the laboratory test results, for example rigidity index information is suggested to be included.

6 REFERENCES

Bates L., Bishop D., Fityus S., Hegedüs M., Imre E. 2012. "The joint evaluation of some pore water pressure and cone resistance dissipation test records." Proceedings of ISC-4: the 4th International Site Characterisation Conference 1, 881-890.

Baligh, M. M. 1986. Undrained deep penetration, II. pore pressures. Geotechnique, 364: 487-503.

Bishop, D. 2009. Eng. Geol. Of Richmond River Estuary. PhD Thesis, The University of Newcastle.

Imre E. and Bates L. 2015 Some comments on dissipation testing of the soils, 3rd Int. DMT Conf. Rome 2015: 415-422.

Imre E., Juhász M., Józsa V., Hegedûs M., Bíró B., Singh V. G. 2014 CPTu tests and CPT simple dissipation tests in saline environnent. In: 3rd International Symposium on Cone Penetration Testing Las Vegas, pp. 683-690.

Imre E , Firgi T , Juhász M , Hazay M , Hegedűs M , Bakacsi Zs, Singh V 2014b CPTu pore water pressure dissipation tests in saline environment In: 3rd International Symposium on Cone Penetration Testing: Las Vegas, pp. 675-682.

Imre, E, Rózsa, P, Bates, L, Fityus, S 2010" Evaluation of monotonous and non-monotonous dissipation test results". COGE Computers and Geotechnics. 37: 885-904.

Imre E., Trang P.Q., Fityus S., Telekes G. A 2011 "Geomeric parameter error estimation method for inverse prolems." Proceedings of the Second International Symposium on Computational Geomechanics ComGeo II, Cavtat, Croatia, 27-29 April, 2011.

Imre E , Bates L. , Fityus S. 2011. Evaluation of dilatometer dissipation test data with no inflexion point. In: 13th International Conference of the International Association for Computer Methods and Advances in Geomechanics, Melbourne, Australia , 2011.09.09 -2011.09.11. Melbourne: pp. 495-502.

Lunne, T; Robertson, P.K.; Powell, J.J.M. 1992. Cone Penetration testing. Blackie Academic & Professional.

Totani, G Clabrese, M; and Monaco, P 1998. In situ determination of ch by fl at plate dilatometer. *Proceedings of ISC-1, Atlanta, Georgia,* 883–888.

Geotechnical and Geophysical Site Characterisation 5 – Lehane, Acosta-Martínez & Kelly (Eds)
© 2016 Australian Geomechanics Society, Sydney, Australia, ISBN 978-0-9946261-1-0

Estimation of soil hydraulic conductivity assisted by numerical tools – two case studies

R. Karim
Lecturer, School of Natural and Built Environments, University of South Australia, Australia

M. Rahman
Senior Lecturer, School of Natural and Built Environments, University of South Australia, Australia

D. Hughes
Senior Lecturer, School of Planning Architecture and Civil engineering, Queen's University Belfast, UK

ABSTRACT: Hydraulic conductivity of soil is one of most difficult parameter to deduce with high degree of certainty. Its value from field and laboratory tests are often very different. The implicit assumptions made in the interpretation of the test data may also influence the results. This paper presents 2 case studies where numerical tools have been used to estimate the hydraulic conductivity (for saturated and unsaturated soils). The first case involves a prefabricated vertical drain improved embankment foundation where, in addition to the above mentioned issues, the smearing due to the installation of vertical drains further complicates the situation. In the second case study, the method have been extended to estimate the hydraulic conductivity of unsaturated soils. The effectiveness of the method have been demonstrated by comparing numerical analysis results with field measurements for both cases.

1 GENERAL INSTRUCTIONS

One of the most important input parameter used in a seepage analysis (for both saturated and unsaturated soils) is the hydraulic conductivity (K). However, objective estimating an appropriate value of K even for saturated soils (K_{sat}) can be difficult.

The value of K_{sat} deduced from field and laboratory tests are often different - sometimes by orders of magnitudes. Furthermore, K_{sat} deduced from field tests can be affected by the presence of hidden cracks or fissures in the soil and local heterogeneity. The implicit assumptions in the interpretation of test data also influences the result- which is often overlooked.

Soils in many geotechnical structures often remain in unsaturated states (e.g., cutting or embankments). K in unsaturated soil (K_{unsat}) varies with soil suction and requires specialized skills and test equipment to deduce even in a controlled laboratory environment. The difference between the field and laboratory condition also needs consideration. Correlations (Green and Corey 1971, Van-Genuchten 1980, Fredlund and Xing 1994) are often used to deduce K_{unsat} as a function of K_{sat} and soil water characteristics curve (SWCC).

Thus, in many cases, it may be very difficult to have an objective estimation of K_{sat} and therefore also K_{unsat}. In this paper, an objective and observational approach is presented. The effectiveness of the approach has been demonstrated using 2 case studies (the first one for saturated soil and the second one for unsaturated soils).

2 CASE 1 – LENEGHANS EMBANKMENT

This case study demonstrates the effectiveness of the approach to deduce K_{sat} for the case of a prefabricated vertical drain (PVD) improved soil. This approach can easily be extended to suit other situations. The

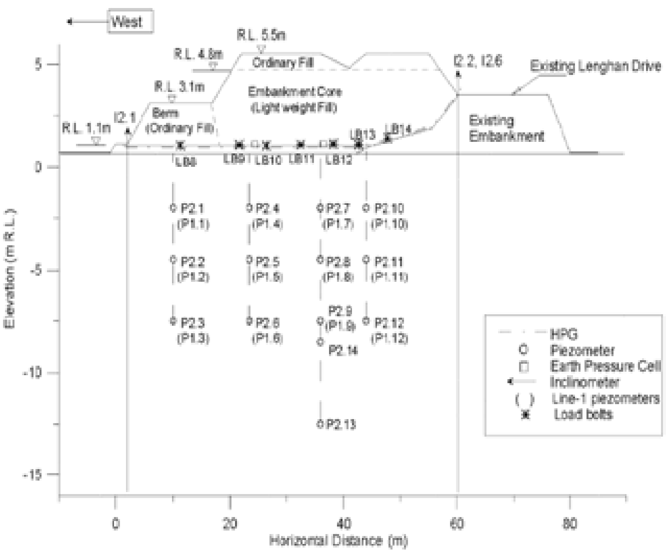

Figure 1: Cross-section of Leneghans embankment and instrumentation details (Lo, Mak et al. 2008)

embankment (Leneghans embankment) is located about 150 km north of Sydney, Australia and was constructed in 1990s and is about 300 m long with base and top width of 60 m and 32 m respectively. The fill height of the embankment was approximately 5m.

The foundation soil was very soft to soft clay (about 16.5m thick) and showed significant creep behavior (Lo, Mak et al. 2008, Karim, Gnanendran et al. 2010, Karim, Manivannan et al. 2011, Manivannan, Karim et al. 2011). To enhance the foundation stability PVDs and geogrid reinforcement were installed; construction was done in 3 stages; an observational approach with extensive instrumentation was adapted. Figure 1 shows a cross section and instrumentation details of the embankment.

2.1 Numerical analysis

To calculate the settlement and excess pore water pressure (U) due to the presence of a single PVD, an axisymmetric analysis was conducted using a finite element program AFENA (Carter and Ballam 1995). The idealized geometry is presented in Figure 2. The outer and bottom boundary of the geometry was modelled as impermeable. The inner boundary represented the vertical drain and was modelled using zero U.

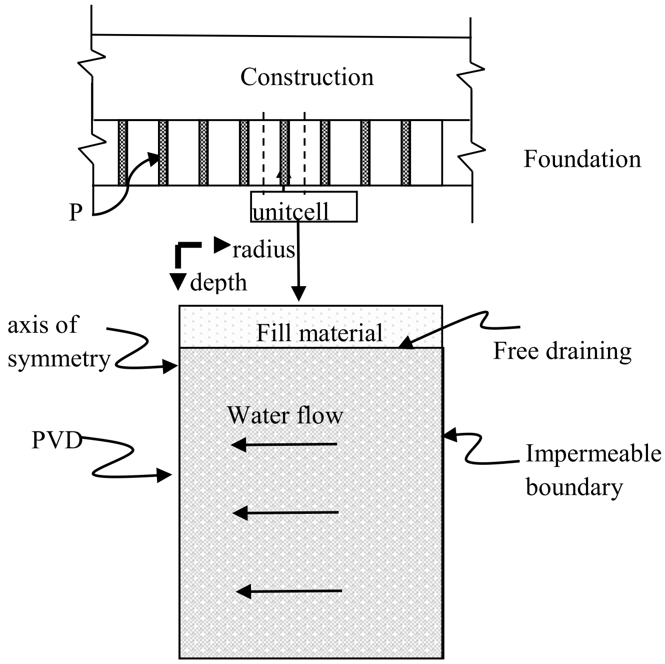

Figure 2: Geometry idealization (not drawn to scale)

An elastic-viscoplastic constitutive model proposed by Karim (2011) was used to model the soft clay since it showed significant creep behavior. The model uses 7 material parameters (M – slope of critical state line; λ and κ the compression and recompression indices; e_N – void ration on normal consolidation line at unit mean normal pressure; P_c- preconsolidation stress; Poisson's ratio and a creep coefficient C_α) along with K for a consolidation analysis. The parameters are presented in Table 1. More details on the constitutive model and unit cell idealization can be found in Karim, Gnanendran et al. (2010) and Karim, Manivannan et al. (2011).

RL	M	λ	κ	e_N	p_c (kPa) Layer top	C_α
+0.3 to -2.8 m	1.113	0.33	0.066	2.87	152.9	0.14
-2.8 to -7.8 m		0.38	0.076	3.29	122.48	
-7.8 to -10m		0.38	0.076	3.29	52.99	
-10 to -16 m		0.33	0.066	2.88	57.68*	

TABLE 1. Foundation soil parameters of Leneghans embankment (Karim et al. 2010)

2.2 Estimation of K_{sat} for PVD improved soils

In the numerical analysis K will be allowed to vary with void ratio (e). In this particular case, variation of vertical K with e were available. A semi-log function (Taylor 1948) presented in eq. (1) was fitted to these data (see Figure 3).

$$\log K = \log K_r - \frac{e_r - e}{c_k} \quad (1)$$

where, K is related to void ratio e, K_r is hydraulic conductivity at e_r and c_k is a constant. Fitting gave the coefficients for eq. (1) as follows, K_r= 1.5×10^{-5} m/day (1.74 m/s), e_r =1.78 and C_k = 0.83.

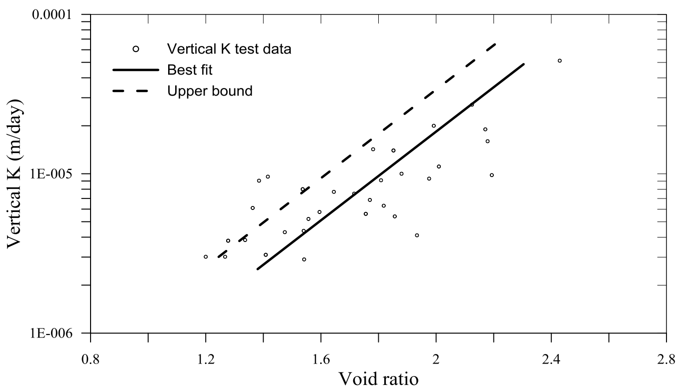

Figure 3: Vertical K plotted against e (Manivannan, Karim et al. 2011)

It is to be noted that, the dominant flow in a PVD improved soil is radial and K in the horizontal direction (K_h) dominates the process. If it is assumed that K_h follows the same functional form as eq. (1) then K_h can be treated as a constant multiple of the vertical K. The multiplier can be deduced via trials using the early period of settlement or U data. In this case the first 3 months of settlement data was used and the estimated multiplier was 1.55.

A second set of analysis was conducted to show the effectiveness of the current technique for a hypothetical situations where no K data are available. A constant K_h value was estimated from back analyzing using the first 3 months of field settlement data. The constant K_h obtained was 1.334×10^{-5} m/day. The back estimation plots are presented in Figure 4.

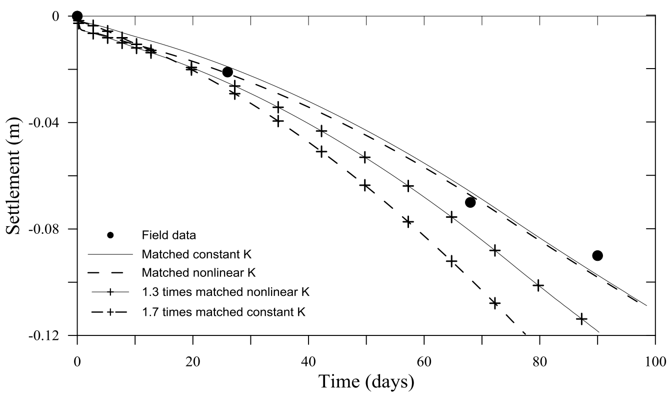

Figure 4: Back estimation of hydraulic conductivity using 3 months of field settlement data

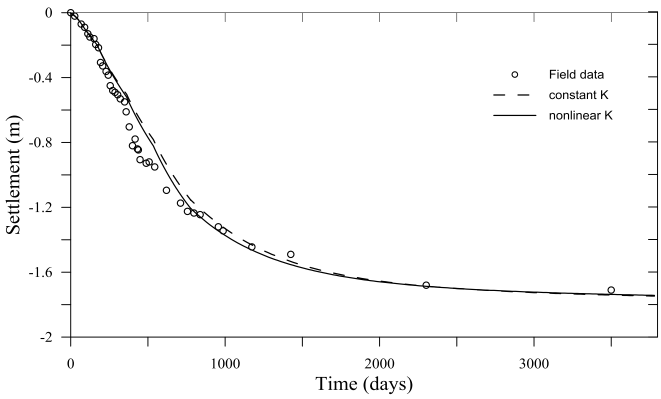

Figure 5: Calculated and observed settlement near the centerline of the embankment

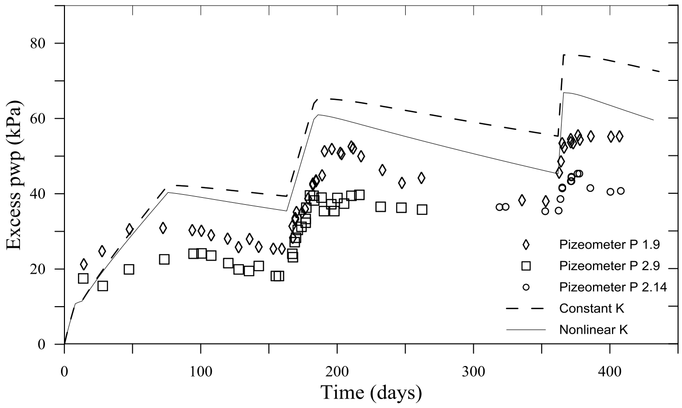

Figure 6: Calculated and observed U at 4.5m depth

2.3 Results and discussion

Calculated and measured settlement (for more than 9 years) along the center-line of the embankment are presented in Figure 5. There are little differences between the results from the two analyses and both were able to capture the field settlement behavior with very high accuracy.

In Figure 6, the measured and calculated U at 4.5m depth (between two PVDs- at the outer boundary in the numerical analyses) are presented. The analysis conducted with nonlinear K traces the upper bound of the field measured values. The analysis with constant K calculates slightly higher U. The results from the constant K analysis was with reasonable accuracy and as expected the analysis with nonlinear K performed better as better input K data were used.

3 CASE 2 – CRAIGMORE CUTTING

This case study extends the process of estimation of K into the unsaturated domain and analyses the interaction between atmospheric boundary and soil in a cut slope. The research site is located near Craigmore, Norther Ireland. Details of the site (including geometry, geology, meteorology, instrumentation and monitoring) can be found in McLernon et al. (2015). A brief description is presented here.

The slope is 17 m high (slope angle 36°) cutting made in heavily over-consolidated glacial till constructed in 1850s. Fig. 7 presents a cross section of the slope along with instrumentation.

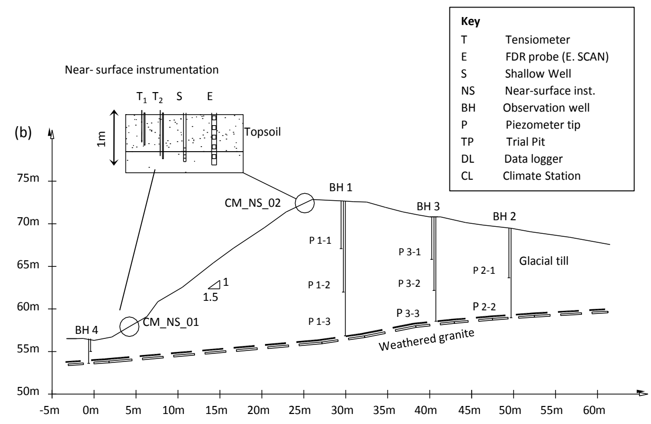

Figure 7: Craigmore cutting cross-section and instrumentation

The slope has been a concern for the Northern Ireland railway authorities due to evidence of shallow surface failures, bent tree trunks and seepage on the face of the slope. A large number of insitu and laboratory tests including moisture content test, particle size analysis, insitu K_{sat} tests (mostly using Guelph permeameter), index tests and strength tests were conducted. Fig. 8 presents the deduced K_{sat} values at different depths. Up to 4 orders of magnitude differences were observed in the tests results. The vegetation at the site consisted mostly of grass and herbs with a few mature trees.

A range of instruments, including near surface moisture probes to measure soil moisture changes above the phreatic surface, standard water filled tensiometers to measure the soil suction, piezometers to measure U at greater depths, and a weather station to record local meteorological parameters, were installed at the site.

a. *Numerical modelling*

The modelling was carried out with a finite element program SEEP/W (Geo-Slope 2013). It is capable of analyzing groundwater seepage and U distribution within porous media such as soil in saturated or unsaturated state. The U distribution from such analysis can be used as input for a stability analysis or in a stress-strain analysis.

For a complete description of soil U behavior, SEEP/W requires the knowledge of Soil water characteristics curve (SWCC) and a K function (i.e., variation of K with soil suction).

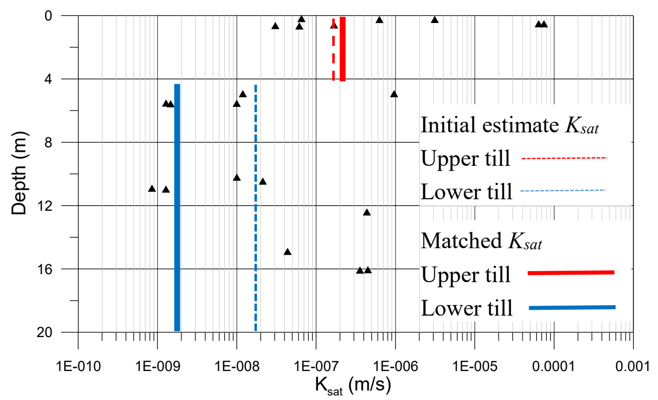

Figure 8: Saturated hydraulic conductivity determined from different field tests (Carse, 2014)

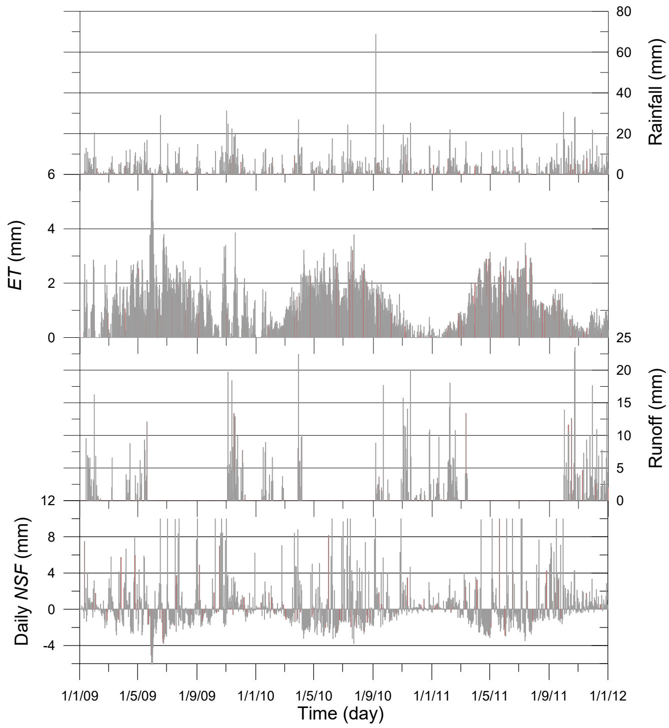

Figure 9: Rainfall, calculated *ET*, *RO* and *NSF*

It is to be noted that, SEEP/W does not have the capability of directly modelling the effect of meteorological parameters and vegetation in a seepage analysis. An equivalent flux boundary condition (Karim et al. 2015) that can represents the combined effect of meteorological parameters and vegetation was calculated and was used as an input boundary condition. The flux boundary condition (net surface flux - *NSF*) is presented below,

$$\sum R - RO - ET = NSF \qquad (2)$$

Where, R is the rainfall, RO is the runoff and ET is the evapotranspiration - can be calculated using the Penman-Monteith equation.

Figure 9 presents the rainfall, calculated *ET, RO* (estimated using McLernon (2014) soil water storage model) and *NSF.*

Parameters (specific to Craigmore) needed to calculate *ET* are presented in Table 2. The meteorological data needed i.e., temperature, dew point, wind speed were collected from the site weather station and are presented elsewhere (McLernon 2014).

Table 2: Parameters used for the calculation of evapotranspiration

Parameter	Value
Psychrometric constant (kPa/0C)	0.000665×atm. pressure
Solar constant	0.082
Latitude (rad)	0.946614
Albido or canopy reflection coefficient	0.23
Stefan-Boltzman constant (Mj/K4/M2/day)	4.903×10-9
Elevation above sea level (m)	70

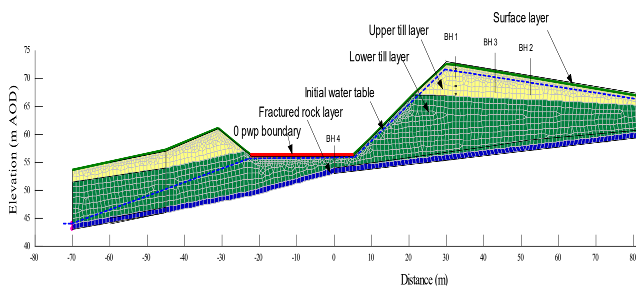

Fig. 10: Discretized geometry used for the analyses.

The discretized geometry used for the analyses is presented in Figure 10. A total of 5118 nodes and 4859 elements were used. As found during the site investigation, the soil in the slope showed 5 distinct subdivisions, namely, weathered upper till layer, lower till layers, surface layers for the upper and lower till layers and a weathered bedrock layer showing by significantly higher K than the layers above. They were modelled using 5 different materials. The material parameters are discussed in a later section.

Two different analysis were conducted the first one using a best guess K_{sat} value from the field test results (i.e., Figure 8) and the second one with estimated value using the current approach (discussed in a later section). The analyses are referred to as Analysis 1 and 2 respectively.

b. SWCC

The SWCCs for the upper and lower till layers and the weathered bedrock layer was taken from McLernon (2014). There was inadequate information available on the soil-water behavior of the surface layers. Thus, the surface layers were modelled using the same SWCC as of the layers below. The SWCCs for different soil layers are presented in Fig. 11.

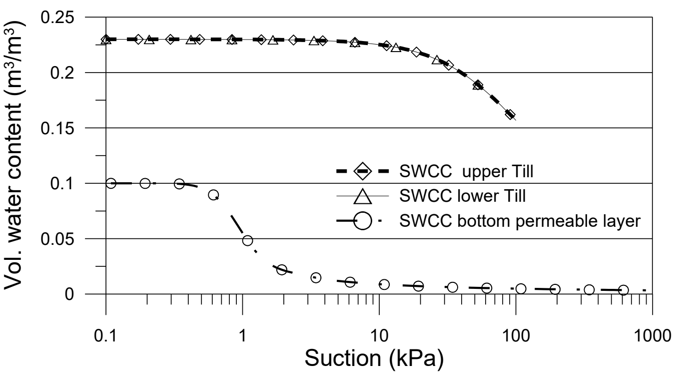

Fig. 11: SWCCs used for modelling different material (McLernon, 2014).

c. Estimation of K_{unsat}

For K_{unsat} calculation, SEEP/W (Geo-Slope 2013a) allows the choice different functions that uses correlations with K_{sat} and SWCC. The functions available are Fredlund and Xing (1994), Green and Corey (1971) and Van-Genuchten (1980). In this investigation, the Van-Genuchten (1980) function (as below) was used.

$$k_{unsat} = k_{sat} \frac{\left[\left(1-(a\Psi^{n-1})(1+(a\Psi^{n})^{-m}\right)\right]^2}{(1+(a\Psi)^n)^{\frac{m}{2}}} \qquad (3)$$

Where, a, n and m are curve fitting parameters and Ψ is the suction range.

Figure 8 presents the K_{sat} values deduced from field tests at different depths. It can be seen from the figure that, the K_{sat} values between the depths of 4 and 8 m varies by as much as 3 orders of magnitude. The variations between test results for shallower depths are even greater. This makes an objective estimation of K_{sat} very difficult. Instead K_{sat} has been estimated by numerically analyzing the first 6 months of field measured U data. Piezometer readings from 2 locations, i.e., BH1.1 (5.6m below ground level - BGL) and BH1.3 (16.0m BGL) were used for this purpose. Few trial analyses were conducted with K_{sat} being systematically varied until a good match was found. The best match K_{sat} were used for further analysis of the problem.

d. Results and discussion

In Fig. 12, the measured and calculated pressure heads are presented for BH1.3 which is located at a depth of 16.0m BGL in crest area. At this location, Analysis 2 (matched K) was able to calculate the U variations very high accuracy. Analysis 1 (with K estimated from field tests results), on the contrary, over estimated it by a very high margin. The magnitude of overestimation more than 6m during more than two thirds of the analysis period.

It is clear from here that, the K_{sat} and thus K_{unsat} plays a very important role in predicting the U distribution in of a soil slope. Error in estimating K_{sat} can lead to erroneous results.

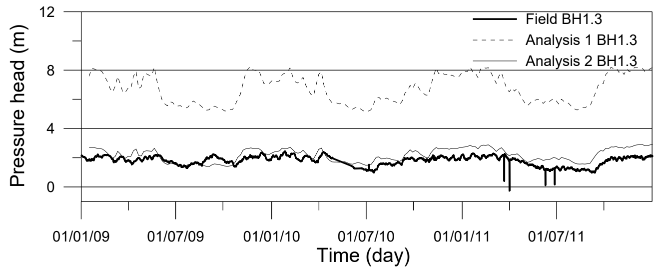

Fig. 12: Measured and calculated U head for BH1.3 from two different analyses

In Fig 13 measured and calculated suctions at 0.8m BGL at the toe location is presented. At this location, Analysis 2 overestimated the suction response by up to 15 kPa. Whereas, analysis 1 underestimates during most of the monitoring period. One hypothesis behind this over estimation can be, the modelling of the area near the toe of the slope (ballasted rail track) as zero U boundary. This might have contributed to quicker draining of the toe and resulted in higher suction in the analysis.

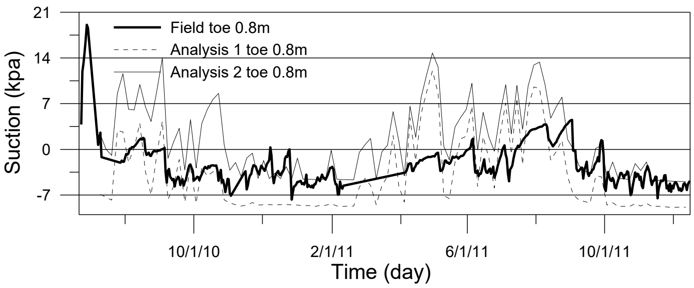

Fig. 13: Measured and calculated suctions at the toe location 0.8m BGL

Fig. 14 presents the calculated and measured volumetric water content at two different depths. At 0.3m BGL both the analyses traced the upper bounds of the field response. At a greater depth (0.9m), both analyses traced the average values of the field measurements. The difference between the calculations from the 2 analyses was minimal.

U contours for the slope are presented in Figs. 15 (a) and (b) for Analyses 1 and 2 respectively for a selected date of 1 January 2010 (mid-Winter). Significant differences can be observed between the 2 contour plots. Analysis conducted with an initial estimate of K_{sat} calculated significantly higher *U*. There was a suction bulb formed (maximum suction -28 kPa) near the crest of the slope. There was no or insignificant amount of suction was calculated near or below the sloping face. In analysis 2, the magnitude of *U* was much smaller than the case of Analysis 1. There was a suction bulb (approximately 8 kPa) generated and was carried through the winter.

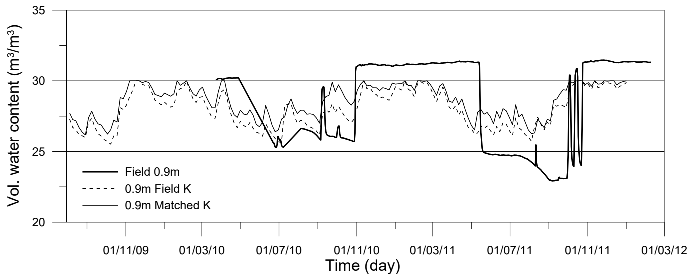

Fig. 14: Measured and calculated VWC at 0.9m depth at the crest location

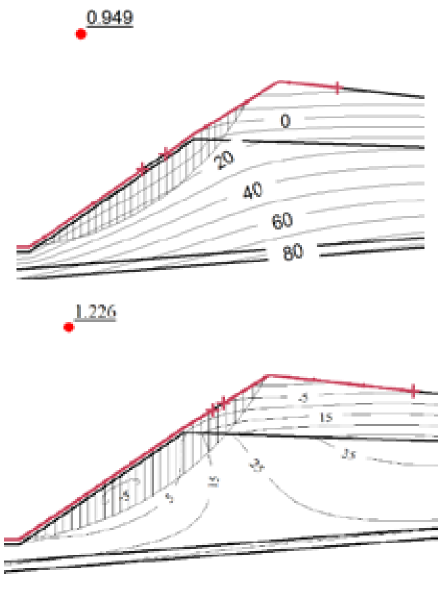

Fig. 15: *U* distribution in on 1 January 2014 Analysis 1 (top) and Analysis 2 (bottom)

Using the calculated *U* distributions, 2 limit equilibrium (Morgenstern-Price) analyses ware conducted using a numerical program SLOPE/W (Geo-Slope 2013b) to assess the factor of safety of the slope. Analysis 1 calculated a factor of safety of 0.95 which can be treated as unrealistic considering the fact that the slope has been in service for more than 150 years and has only shown some small and shallow failures on the surface. For the case of Analysis 2 the calculated factor of safety was around 1.2. This can be treated as a more acceptable/realistic number.

4 CONCLUSIONS

The paper discusses the use of numerical tools to estimate *K* for saturated and unsaturated soils. The two case studies discussed show that the technique works well and can capture the field behavior with reasonable accuracy. Incorrect estimation of *K* can lead to erroneous result. It is very difficult to objectively estimate *K* from field or laboratory test results. The numerical tools discussed here can overcome these difficulties.

5 ACKNOWLEDGEMENTS

Part of the research discussed here was conducted while the first author was working in Queen's University Belfast, UK as a part of iSMART project (an EPSRC funded project in UK).

6 REFERENCES

Carter, J. P. and N. P. Ballam (1995). AFENA Users' Manual Version 5.0 [computer program], Center for Geotechnical Research, University of Sydney, Sydney-2006, Australia.
Fredlund, D. G. and A. Xing (1994). "Equations for the soil-water characteristic curve." Canadian Geotechnical Journal 31(3): 521-532.
Geo-Slope (2013). Seepage Modeling with SEEP / W An Engineering Methodology, Geo-slope international limited.
Green, R. E. and J. C. Corey (1971). "Calculation of hydraulic concuctivity: a further evaluation of some predictive methods." Soil science society of America journal 35: 3-8.
Karim, M. R. (2011). Modeling the long term behaviour of soft soils. PhD, University of New South Wales Canberra.
Karim, M. R., C. T. Gnanendran, S.-C. R. Lo and J. Mak (2010). "Predicting the long-term performance of a wide embankment on soft soil using an elastic-visco-plastic model." Canadian Geotechnical Journal 47: 244-257.
Karim, M. R., G. Manivannan, C. T. Gnanendran and S.-C. R. Lo (2011). "Predicting the long-term performance of a geogrid-reinforced embankment on soft soil using two-dimensional finite element analysis." Canadian Geotechnical Journal 48(5): 741-753.
Lo, S. R., J. Mak, C. T. Gnanendran, R. Zhang and G. Manivannan (2008). "Long-term performance of a wide embankment on soft clay improved with prefabricated vertical drains." Canadian Geotechnical Journal 45: 1073-1091.
Manivannan, G., M. R. Karim, C. T. Gnanendran and S.-C. R. Lo (2011). "Calculated and observed long term performance of Leneghans embankment." Geomechanics and Geoengineering 6(3): 195-207.
McLernon, M. (2014). Climate driven pore awter pressure dynamics and slope stability within glacial till drumlins in Northern Ireland, Queen's Unvieristy, Belfast.
Taylor, D. W. (1948). Fundamentals of soil mechanics. New York, John Wiley & Sons.
Van-Genuchten, M. T. (1980). "A Closed-form Equation for Predicting the Hydraulic Conductivity of Unsaturated Soils." Soil science society of America journal 44: 892-898.

Geotechnical and Geophysical Site Characterisation 5 – Lehane, Acosta-Martínez & Kelly (Eds)

Effect of soil stiffness on cone penetration response in soft-stiff-soft clays

H. Ma, Y. Hu & M. Zhou
School of Civil, Environmental and Mining Engineering, The University of Western Australia, Perth, WA, Australia

M.S. Hossain
Centre for Offshore Foundation Systems, The University of Western Australia, Perth, WA, Australia

ABSTRACT: This paper describes the results from large deformation FE (LDFE) analysis undertaken to provide insight into the influence of soil stiffness, or rigidity index, on cone penetration resistance in three-layer soft-stiff-soft clays. A range of soil stiffnesses were selected encompassing practical interest. A correction factor is proposed for interpreting the actual undrained shear strength of the interbedded stiff layer. The results can assist foundation design in offshore practice.

1 INTRODUCTION

Depletion of known reserves in the shallow waters of traditional hydrocarbon regions is resulting in exploration in deeper, unexplored and undeveloped environments. These are exhibiting more complex soil conditions at the seabed. In emerging provinces and fields, highly layered soils are prevalent. The Sunda Shelf, offshore Malaysia, Australia's Bass Strait and North-West Shelf, Gulf of Thailand, South China Sea, offshore India and Arabian Gulf are particularly problematic in terms of stratigraphy and soil types (InSafeJIP 2010). The difficulty of obtaining high-quality soil samples from these problematic offshore sites has placed increasing reliance on *in situ* testing results.

Currently, the most commonly adopted *in situ* test in offshore site investigations is cone penetration test (CPT). The standard cone penetrometer is cylindrical in shape with a conical tip that has a base area of 10 cm^2 (diameter D = 35.7 mm) and a 60° tip-apex angle, as shown schematically in Figure 1. Parameters measured during a piezocone test include (a) cone tip resistance, q_c; (b) sleeve friction, f_s; and (c) pore water pressure, u_2. This paper considers only cone tip resistance.

The penetration tests are carried out at a rate of v = 20 mm/s. For clay deposits, the velocity is fast enough to ensure undrained conditions. As such, the cone factor N_{kt} is used to relate the net cone tip resistance q_{net} to the intact undrained shear strength s_u as

$$N_{kt} = \frac{q_{net}}{s_u} = \frac{q_t - \sigma_{v0}}{s_u} \tag{1}$$

where q_t is the total cone tip resistance and σ_{v0} is the total overburden stress at the level of the cone shoulder, d (Fig. 1). For this study, the correction for the effect of unequal pore pressure was not necessary as the cone was simulated as a solid shaft (see Fig. 1; i.e. q_t = measured tip resistance q_c).

For stratified seabed sediments, the undrained shear strength for each layer, in particular for the interbedded stiff layer, deduced using Equation 1 may not represent the actual value as the layer thickness may not be sufficient to mobilize the stable (full) penetration resistance for that layer. A corresponding adjustment is required to interpret the actual shear strength. It is also well established that cone penetration resistance is strongly influenced by soil stiffness or rigidity index, which should be taken into account. These are addressed in this paper.

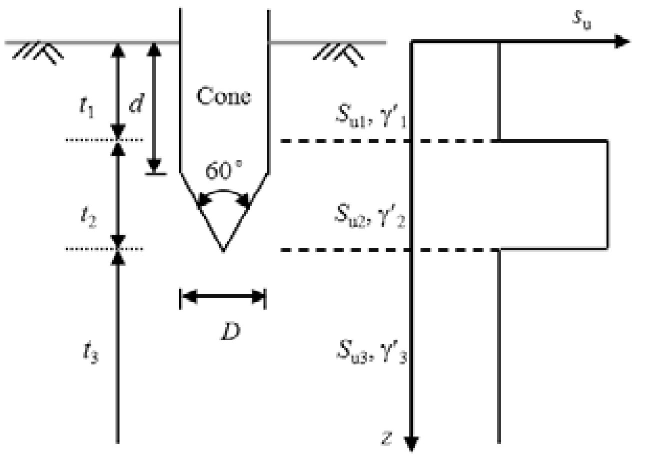

Figure 1. Schematic diagram of cone penetration in soft-stiff-soft clay

For piezocone penetration in single layer clay, the effect of soil rigidity index I_r was quantified through various solutions. These include strain path method (Baligh 1985), hybrid strain path method (Teh & Houlsby 1991), and FE analysis (Yu 2000), large deformation finite element analysis (van den Berg 1994; Lu et al. 2004; Walker & Yu 2006; Liyanapathirana 2009). Recently, Low et al. (2010) assesmbled a worldwide high quality database of lightly overconsolidated clays and used to evaluate the sensitivity of various factors on penetration resistance factors of various penetrometers. It was indicated that I_r has the most significant effect on the cone bearing capacity factor N_{kt}.

Piezocone penetration in layered clays has attracted less attention from researchers. Walker & Yu (2010) carried out analysis for two-layer stiff-soft and three-layer uniform stiff-soft-stiff clays, adopting the linear elastic-perfectly plastic von Mises soil model. The rigidity index of the 1st-2nd-3rd layers were considered as 100-300-100 and 100-500-100, keeping the shear modulus constant (G = 1 MPa) throughout the model. The effects of soil stiffness as well as shear strength have been investigated qualitatively, but no quantitative solutions were given.

Cone penetration in soft-stiff-soft clays has been extensively investigated by Ma et al. (2015) through large deformation finite element (LDFE) analyses. A new design framework was proposed for interpreting the layer boundaries and undrained shear strength of each identified layer. The framework includes a correction factor for interpreting the shear strength of the interbedded stiff layer. The soil rigidity index was considered as constant with I_r =167. In this study, the effect of soil stiffness was particularly explored. The robustness of the correction factor proposed by Ma et al. (2015) was further improved by incorporating the influence of I_r in this paper.

2 NUMERICAL ANALYSES

2.1 *Geometry and parameters*

This study has considered a cylindrical cone penetrometer of diameter D, penetrating into a three-layer deposit as illustrated schematically in Figure 1, where a stiff clay layer with undrained shear strength s_{u2}, effective unit weight γ'_2, and thickness t_2 is sandwiched by two soft layers with identical undrained shear strength $s_{u1} = s_{u3}$ and effective unit weight $\gamma'_1 = \gamma'_3$. The thickness of the top (1st) soft layer is t_1 and that of the bottom (3rd) soft layer is (nominally) infinite. Analyses were undertaken for the standard cone penetrometer of D = 0.0357 m with a 60° tip angle. The soil-cone shaft and soil-cone tip interfaces were modelled as fully smooth (α = 0), using nodal joint elements (Herrmann 1978). From a separate study (Ma et al. 2014), it was found that a smooth cone penetration in non-homogeneous clays resulted insignificant effect of soil strength non-homogeneity on cone penetration resistance. As such, uniform strength was considered for all three layers.

A survey was carried out through offshore geotechnical characterization reports to select realistic soil parameters for parametric study. The three-layer geometries considered here are commonly encountered in the Gulf of Thailand and Sunda Shelf, including Java Sea, as reported by Castleberry and Prebaharan (1985); Handidjaja et al. (2004); Kostelnik et al. (2007); Chan et al. (2008); Osborne et al. (2009). For uniform three-layer clay sediments, the undrained shear strength of stiff clay ranges from 40 to 120 kPa, while that of soft clay varies between 10 and 40 kPa.

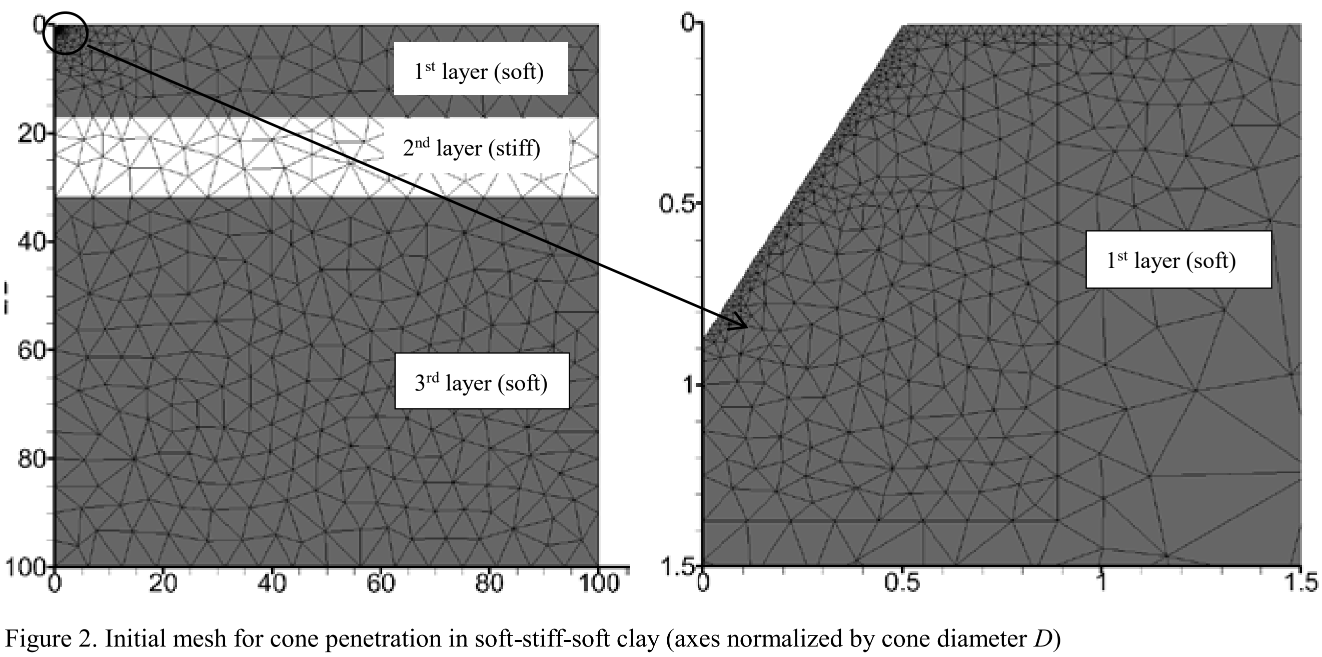

Figure 2. Initial mesh for cone penetration in soft-stiff-soft clay (axes normalized by cone diameter D)

2.2 *Analysis details*

Finite element analyses were performed using the finite element package AFENA (Carter & Balaam 1995) developed at the University of Sydney. *H*-adaptive mesh refinement cycles (Hu & Randolph 1998b) were implemented to optimize the mesh, minimizing discretization errors, concentrating in the most highly stressed zones. Large deformation FE (LDFE) analyses were undertaken using RITSS (Remeshing and Interpolation Technique with Small Strain; Hu & Randolph 1998a). This method falls within what are known as arbitrary Lagrangian-Eulerian (ALE) finite element methods (Ponthot & Belytschko 1998). The details of the LDFE/RITSS approach can be found in Hu & Randolph 1998a. The displacement increment size and the number of steps of small strain analysis between each re-meshing were chosen such that the cumulative penetration between re-meshing stages remained in the small strain range and was less than half the minimum element size.

The axisymmetric soil domain was chosen as 100D in radius and 100D in depth to ensure that the boundaries were well outside the plastic zone. Hinge and roller conditions were applied along the base and vertical sides of the soil domain respectively. Six-noded triangular elements with three internal Gauss points were used in all the FE analyses. A typical initial mesh for the cone penetration in a three-layer soft-stiff-soft clay deposit is shown in Figure 2, with the cone tip just penetrated into the ground. A fine mesh was considered around the cone tip to ensure the accuracy of the computed results.

The soil was modelled as a linear elastic-perfectly plastic material obeying a Tresca yield criterion. A uniform stiffness ratio of E/s_u = 500 (Zhou et al., 2013) was taken throughout the stratified profiles, except in the exploration of the effect of soil rigidity (I_r), where variation was set up accordingly. Considering the relatively fast penetration of the field cone penetrometer (v = 20 mm/s), all the analyses simulated undrained conditions and adopted a Poisson's ratio ν = 0.49 (sufficiently high to give minimal volumetric strains, while maintaining numerical stability) and friction and dilation angles $\phi = \psi = 0$ in total stress analysis. The geostatic stress conditions were modelled using K_0 = 1, as the stable penetration resistance has been found to be unaffected by the value of K_0 (Zhou & Randolph 2009; Low et al. 2010).

3 RESULTS AND DISCUSSION

LDFE analyses were first carried out for three-layer clays with equal strength i.e. $s_{u1} = s_{u2} = s_{u3}$, but varying rigidity index I_r as 50, 150, 300 and 500. Deep bearing capacity factor N_{kt} was calculated according

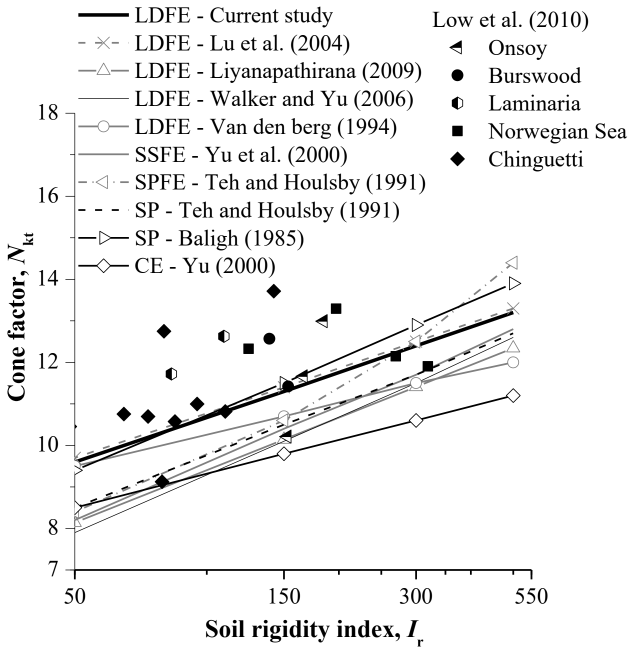

Figure 3. Effect of soil rigidity index on piezocone deep bearing capacity factor N_{kt}

to Equation 1. Figure 3 shows a comparison between the results from this study and existing solutions and laboratory test data of lightly overconsolidated clays in single layer uniform clays (as noted previously). It can be seen that, for the considered smooth cone (α = 0), the cone factors derived from the current work agree well with the LDFE results by Lu et al. (2004), lower than the strain path solutions by Baligh (1985) and higher than all other results. The factors lie below the laboratory test data, which may be due to the consideration of fully smooth interface. Generally, bearing capacity factor increases as the soil rigidity index increases, the values from this study can be approximated as

$$N_{kt} = 3.47 + 1.56 I_r \tag{2}$$

For investigation on three-layer deposits, the relative thickness of the top layer t_1/D was deliberately kept constant as 16.8 so that all penetration resistance profiles attain its steady state response in the top layer prior to be influenced by the underlying stiff layer. A typical profile is illustrated in Figure 4 to define the steady state response for each layer and correction factor *k*. As discussed previously, the measured resistance profile in the 2nd (stiff) layer may not reach the steady state prior to dropping its value by sensing the bottom soft layer. This means full resistance of the layer may not be achieved. The strength interpreted using the measured value will then provide a misleading value – lower than the true value.

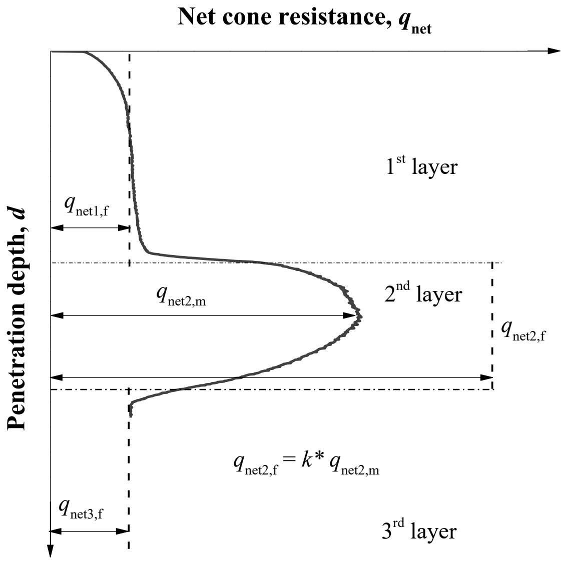

Figure 4. Typical penetration resistance profile in soft-stiff-soft clay and thin-layer correction factor k for 2nd layer

Therefore, following Robertson & Fear's (1995) suggestion, a correction factor k (as described in Fig. 4) is introduced defining as the ratio of the actual full net resistance to measured peak net resistance

$$k = \frac{q_{\text{net2,f}}}{q_{\text{net2,m}}} \tag{3}$$

where $q_{\text{net2,f}}$ and $q_{\text{net2,m}}$ are the actual full and measured peak/maximum net resistance in the 2nd layer respectively. It is found that k is a function of t_2/D, s_{u2}/s_{u3}, and I_{r2}/I_{r3} with the effect of former two dimensionless factors were discussed by Ma et al. (2015).

In order to systematically investigate the effect of soil rigidity index, analyses have been carried out, considering different combinations of soil rigidity indices. Figure 5a plots the values of k for $I_{r3} = I_{r1} = 50$, $I_{r2}/I_{r3} = 1$, 2, 3.34, and 6.68, while the 2nd layer thickness ratio t_2/D ranges from 2 to 20 and strength ratio s_{u2}/s_{u3} varies between 2 and 8. The horizontal axis x_1 is defined as a combined variable of strength ratio s_{u2}/s_{u3} and 2nd layer thickness ratio t_2/D

$$x_1 = \frac{\left(s_{\text{u2}} / s_{\text{u3}}\right)^{0.5}}{\left(t_2 / D\right)} \tag{4}$$

From Figure 5a, it is seen that the value of correction factor k increases with increasing stiffness ratio I_{r2}/I_{r3} and strength ratio s_{u2}/s_{u3}, and decreases with increasing thickness ratio t_2/D. For each I_{r2}/I_{r3}, the values of k form a linear distribution. When $x_1 = 1$, k equals to 1.53, 1.66, 1.75 and 1.88 for $I_{r2}/I_{r3} = 1$, 2, 3.34, 6.68.

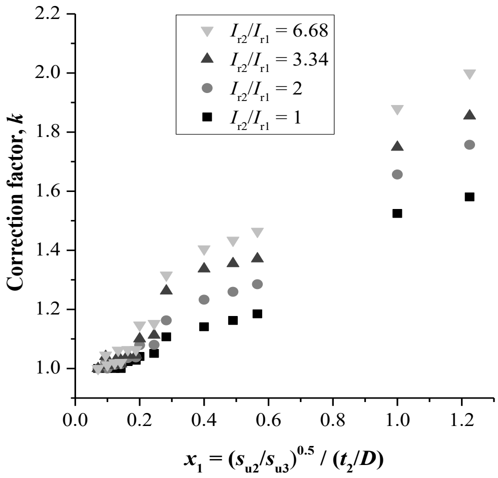

(a) $I_{r1} = I_{r3} = 50$

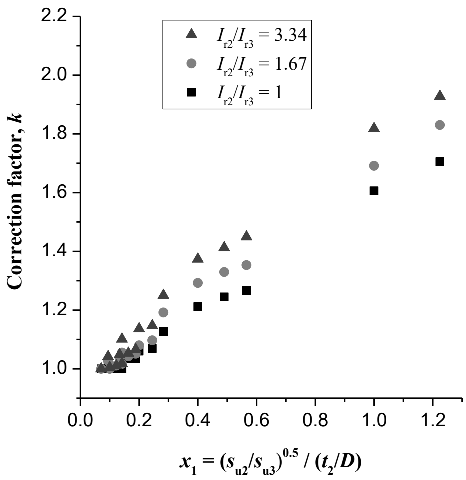

(b) $I_{r1} = I_{r3} = 100$

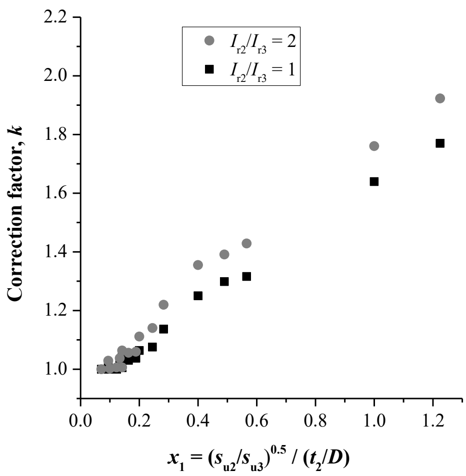

(c) $I_{r1} = I_{r3} = 167$

Figure 5. Values of correction factor k for 2nd layer

Similarly, Figures 5b and c plot the values of k for $I_{r3} = I_{r1} = 100$ and $I_{r2} = 167$. By comparing Figures 5a, b and c, it is seen that the values of k increase with increasing I_{r3}, and the gap gradually reduces with increasing rigidity index ratio I_{r2}/I_{r3}. For instance, for $I_{r2}/I_{r3} = 1$, 3.34 and $x_1 = 1$, the lowest correction factor $k = 1.53$, 1.75 for $I_{r3} = I_{r1} = 50$, which are respectively about 5.0%, 3.8% lower than those for $I_{r3} = I_{r1} = 100$ (see Figs 5a and b). The rate of increasing k with I_{r3} also reduces for higher I_{r3}. For instance, for $I_{r2}/I_{r3} = 1$ and $x_1 = 1$, $k = 1.53$, for $I_{r3} = I_{r1} = 50$, which is increased by 5.2% for $I_{r3} = I_{r1} = 100$ and 7.5% for $I_{r3} = I_{r1} = 167$ (see Figs 5a~c). In short, k is a function of I_{r2}/I_{r3} as well as I_{r3}.

To propose a general expression for k taking the influencing factors into account, all values of k plotted in Figure 6 incorporating I_{r2}/I_{r3} and I_{r3} in the horizontal axis. This gives a unique relationship for the correction factor k. A best fit through the data allows k to be approximated as (see Fig. 6)

$$k = \begin{cases} 0.909 + 0.305x_2 - 0.016x_2^{\ 2} & \text{for } x_2 \geq 0.35 \\ 1 & \text{for } x_2 < 0.35 \end{cases}$$
$$x_2 = I_{r3}^{\ 0.2} \times \left(I_{r2} / I_{r3}\right)^{0.3} \frac{\left(s_{u2} / s_{u3}\right)^{0.5}}{\left(t_2 / D\right)} \tag{5}$$

As s_{u2} is an input parameter for calculating k, and some iteration is necessary between Equation 3 and 5. An initial value of s_{u2} can be calculated using measured $q_{net2,m}$ and bearing factor N_{kt} (from Equation 2). Then Equations 5, 3 and 2 should be used to calculate k and $q_{net2,f}$ and s_{u2}. Iteration should be continued until the difference between initial and updated s_{u2} becomes less than 3% (Ma et al. 2015).

4 CONCLUDING REMARKS

This paper reports the results from an extensive numerical investigation on soft-stiff-soft clay deposits, simulating continuous penetration of the standard cone penetrometer from the seabed surface. For interpreting the actual undrained shear strength of the interbedded stiff layer, a robust design chart, along with an expression, is proposed incorporating the effects of the interbedded stiff layer strength ratio, thickness ratio and rigidity index ratio.

5 ACKNOWLEDGEMENTS

The research presented here was undertaken with support from the Australian Research Council (ARC) Discovery Grant DP140103997. The fourth author is an ARC Discovery Early Career Researcher Award (DECRA) Fellow and is supported by the ARC Project DE140100903. The work forms part of the activities of the Centre for Offshore Foundation Systems (COFS), currently supported as a node of the Australian Research Council Centre of Excellence for Geotechnical Science and Engineering and as a Centre of Excellence by the Lloyd's Register Foundation. This support is gratefully acknowledged.

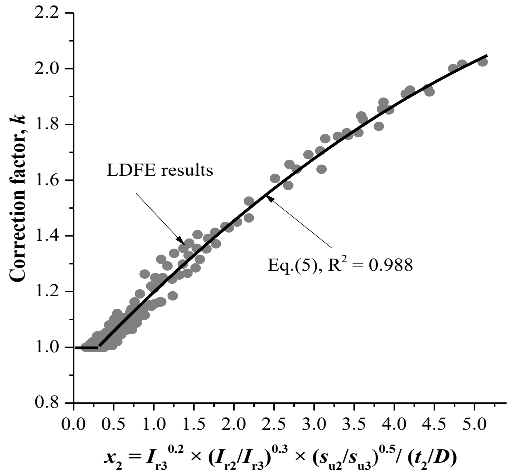

Figure 6. Design chart for correction factor k accounting for effect of soil stiffness

6 REFERENCES

Baligh, M. M. 1985. Strain path method. *Journal of Geotechnical Engineering*, 111(9), 1108-1136.

Carter, J. P. & Balaam, N. P. 1995. *AFENA users' manual*. Centre for Geotechnical Research, Department of Civil Engineering, University of Sydney, Australia.

Castleberry II, J. P. & Prebaharan, N. 1985. Clay crusts of the Sunda Shelf: a hazard to jack-up operations. *Proc. 8th Southeast Asian geotechnical conference*, Kuala Lumpur, 40-48.

Chan, N., Paisley, J. & Holloway, G. 2008. Characterization of soils affected by rig emplacement and Swiss cheese operations-Natuna Sea, Indonesia, a case study. *Proc. 2nd Jack-up Asia Conference and Exhibition*, Singapore.

Handidjaja, P., Somehsa, P. & Manoj, M. 2004. "Swiss-cheese" – A method of degrading soil crust and minimizing risk to punch through problem on the installation of mobile offshore drilling unit (MODU). *Proc. 15th Southeast Asian Geotechnical Society Conference*, Bangkok, Thailand, 303-306.

Herrmann, L. R. 1978. Finite element analysis of contact problems. *Journal of the Engineering Mechanics Division*, 104(5), 1043-1057.

Hu, Y. & Randolph, M. F. 1998a. A practical numerical approach for large deformation problems in soil. *International Journal for Numerical and Analytical Methods in Geomechanics*, 22(5), 327-350.

Hu, Y. & Randolph, M. F. 1998b. H-adaptive FE analysis of elasto-plastic non-homogeneous soil with large deformation. *Computers and Geotechnics*, 23(1-2), 61-83.

InSafeJIP (2010). *Improved guidelines for the prediction of geotechnical performance of spudcan foundations during installation and removal of jack-up units*. RPS Energy, Abingdon, Oxfordshire, UK.

Kostelnik, A., Guerra, M., Alford, J., Vazquez, J. & Zhong, J. (2007). Jackup mobilization in hazardous soils. *SPE Drilling & Completion*, 22(1), 4-15.

Liyanapathirana, D. S. 2009. Arbitrary Lagrangian Eulerian based finite element analysis of cone penetration in soft clay. *Computers and Geotechnics*, 36(5), 851-860.

Low, H. E., Lunne, T., Randolph, M. F., Li, X., Andersen, K. H. & Sjursen, M. A. 2010. Estimation of intact and remoulded undrained shear strengths from penetration tests in soft clays. *Géotechnique*, 60(11), 843-859.
Lu, Q., Randolph, M. F., Hu, Y. & Bugarski, I. 2004. A numerical study of cone penetration in clay. *Géotechnique*, 54(4), 257-267.
Ma, H., Zhou, M., Hu, Y. & Hossain, M. S. 2014. Large deformation FE analyses of cone penetration in single layer non-homogeneous and three-layer soft-stiff-soft clays. *Proc. 33rd Int. conf. on Ocean, Offshore and Arctic Engineering* (OMAE), San Francisco, 23709.
Ma, H., Zhou, M., Hu, Y. & Hossain, M. S. 2015. Interpretation of layer boundaries and shear strengths for soft-stiff-soft clays using CPT data: LDFE analyses. *Journal of Geotecnical and Geoenvironmental Engineering*, DOI: 10.1061/(ASCE)GT.1943-5606.0001370.
Osborne, J. J., Houlsby, G. T., Teh, K. L., Bienen, B., Cassidy, M. J., Randolph, M. F. & Leung, C. F. 2009. Improved guidelines for the prediction of geotechnical performance of spudcan foundations during installation and removal of jack-up units. *Proc. 41st Offshore Technology Conference*, Houston, OTC20291.
Ponthot, J.-P. & Belytschko, T. 1998. Arbitrary Lagrangian-Eulerian formulation for element-free Galerkin method. *Computer methods in applied mechanics and engineering*, 152(1-2), 19-46.
Robertson, P. K. & Fear, C. E. 1995. Liquefaction of sands and its evaluation. *Proc., 1st Int. Conf. on Earthquake Geotechnical Engineering*, Tokyo, 3, K. Ishihara, ed., A. A. Balkema, Rotterdam, the Nederlands, 1253-1289.
Teh, C. I. & Houlsby, G. T. 1991. An analytical study of the cone penetration test in clay. *Géotechnique*, 41(1), 17-34.
van den Berg, P. 1994. *Analysis of soil penetration*. Ph.D. thesis, Delft University, the Netherlands.
Walker, J. & Yu, H. S. 2006. Adaptive finite element analysis of cone penetration in clay. *Acta Geotech.*, 1(1), 43-57.
Walker, J. & Yu, H. S. 2010. Analysis of the cone penetration test in layered clay. *Géotechnique*, 60(12), 939-948.
Yu, H. S. 2000. *Cavity expansion methods in geomechanics*. Kluwer Academic, Dordrecht, the Netherlands.
Zhou, H. & Randolph, M. F. 2009. Numerical investigations into cycling of full-flow penetrometers in soft clay. *Géotechnique*, 59(10), 801-812.
Zhou, M., Hossain, M.S., Hu, Y. & Liu, H. 2013. Behaviour of ball penetrometer in uniform single- and double-layer clays. *Géotechnique*, 63(8), 682-694.

Geotechnical and Geophysical Site Characterisation 5 – Lehane, Acosta-Martínez & Kelly (Eds)
© 2016 Australian Geomechanics Society, Sydney, Australia, ISBN 978-0-9946261-1-0

A method for predicting the undrained shear strength from piezocone dissipation tests: case studies

E. Odebrecht
UDSC, Joinville, Brazil

F. Mantaras
Geoforma Engenharia Ltda, Joinvile, Brazil

F. Schnaid
UFRGS, Porto Alegre, Brazil

ABSTRACT: Case studies in clay deposits are presented to evaluate the applicability of the method developed by Mantaras et al (2015) to estimate the soil undrained shear strength (s_u) from the measured piezocone dissipation excess pore-water pressure (Δu). Three testing sites located along the Brazilian coast are presented and discussed. The predicted s_u values obtained from the proposed approach are show to be consistent and encourage the use of the method in engineering practice.

1 INTRODUCTION

The piezocone is instrumented with pressure transducers located at the tip or shoulder of the cone to measure pore water pressures generated during penetration. Pore pressures in excess of hydrostatic values allow the evaluation of geoenvironmental parameters including the coefficient of consolidation and the permeability of a soil deposit. This is achieved by interpreting dissipation test response using cavity expansion or strain path methods (Torstensson, 1977; Randolph & Wroth, 1979; Baligh & Levadoux, 1986; Teh & Houlsby, 1991; Burns & Mayne, 1998). The mathematical solution proposed by Burns & Mayne (1998), based on the cavity expansion-critical state, can model the monotonic and dilatory pore pressure responses with regard to time, allowing both the octahedral and shear-induced components during penetration to be calculated as a function of OCR, ϕ' and I_r (=G/s_u). Incidentally, the undrained shear strength ratio s_u/σ'_{vo} is also a function of the same variables (e.g. Wroth, 1984; Jamiolkowski et al., 1985; Ladd, 1991). By combining these concepts, Mantaras et al (2015) demonstrated the possibility to define the ratio of the maximum pore water pressure Δu_{max} and the undrained shear strength s_u. The derived formulation shows little sensitivity to variations on OCR and ϕ', and for typical soil parameters can be reduced to a relatively simple expression expressed as:

$$S_u = \frac{\Delta u_{max}}{4.2(\pm 0.2)\cdot \log(I_r)} \tag{1}$$

where I_r is the rigidity index, $I_r = G/s_u$.

This approach offers major advantage with respect to s_u and q_t type correlations that have to rely on the N_{kt} factor which is known to range from 10 to 20 and are influenced by soil plasticity, overconsolidation ratio, sample disturbance, strain rate and scale effects (Aas et al, 1986; Mesri, 1989; Lunne et al, 1997).

The present paper presents a series of well reported case studies that are analysed to demonstrate the applicability of the proposed approach. It includes evaluation of data from three (3) sites were comprehensive geotechnical data is available: the Tubarão experimental testing site, the Athletic Village for the Olympic games in Rio de Janeiro and a motorway in Florianópolis, all distributed along the Brazilian coast.

2 CASE STUDIES

2.1 *Olympic Villa: Rio de Janeiro*

The city of Rio de Janeiro has been selected to host the Games of the XXXI Olympiad in 2016. In the Olympic Villa, athletes will be housed in thirty-one storey buildings, which make up seven compounds. In all, there will be 3,604 flats and over 18 thousand beds. With a total of 200,000m², it will also have a 72,000m² park with green areas, 4.5 km of cycle lane and a 5,500 m² reflecting pool. For the Paralympic Games, 21 buildings and 5 compounds will be used. There will be 800 accessible flats and over 8 thousand beds. The longest distance to the Villa's main restaurant will be of 800m.

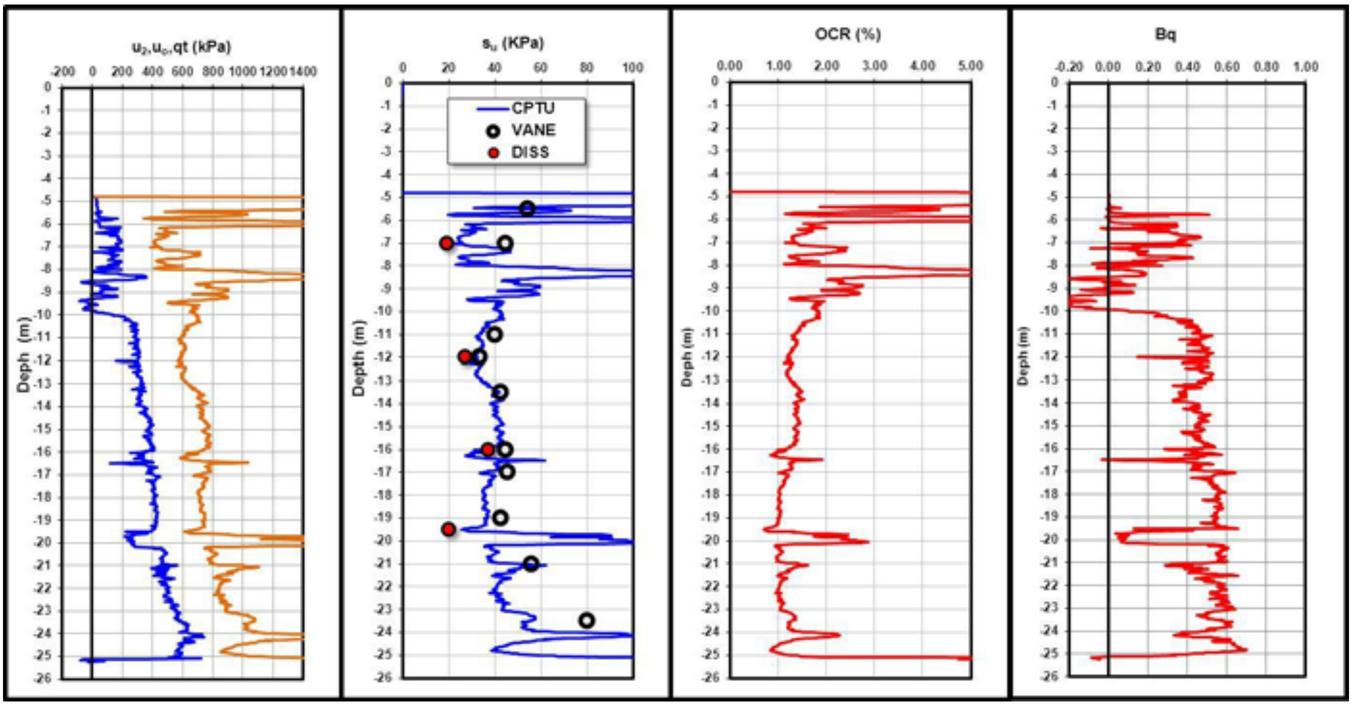

Figure 1. Olympic Villa at Rio de Janeiro, Brazil.

A typical soil profile is shown in Figure 1. The profile shows a normally consolidated Holocene deposit, recently formed (last 10 thousand years) with an overconsolidation ratio close to unity in the deeper layers. The undrained shear strength was estimated from vane, piezocone tip resistance and dissipation pore pressure. The 3 different procedures yield s_u values in close agreement along the soft clay layer. It is interesting to note that some scatter is observed when tests are performed near sand layers (at 7m and 20m depth) where the vane strength is higher than values estimated by dissipation tests.

Figure 2 shows the results of the four dissipation tests carried out the site. These examples of the recorded data are representative of normally to lightly overconsolidated clay, indicating large excess pore pressures generated during penetration, followed by an initial dilatant response during dissipation that, after 10s to 50s turn into monotonic dissipation. The maximum measured pore pressure in each dissipation test is used to derived the undrained shear strength at each depth.

2.2 *Motorway at Florianópolis, Southen Brazil*

The second case describes a profile located 35 kilometers northern from the city of Florianópolis, at the BR101 motorway. This profile is also characteristic of a Quaternary deposit from the Holocene period, formed in the last twelve to eight thousand years (Figure 3). It a relatively homogenous clay profile with a number of sand lenses. The vane test was used to calibrate the undrained shear strength near the surface, yielding a cone factor (N_{KT}) of 13. Along depth the consistency of predictions is evaluated by comparing values estimated from q_t and Δu_{max}. The agreement between the predicted and experimental values is reasonably accurate and encourages the use of the proposed methodology.

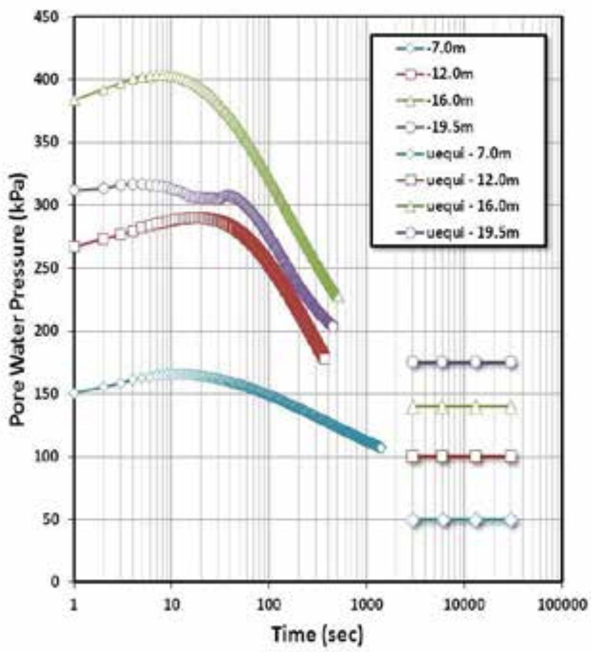

Figure 2. Dissipation test at the Olympic Villa.

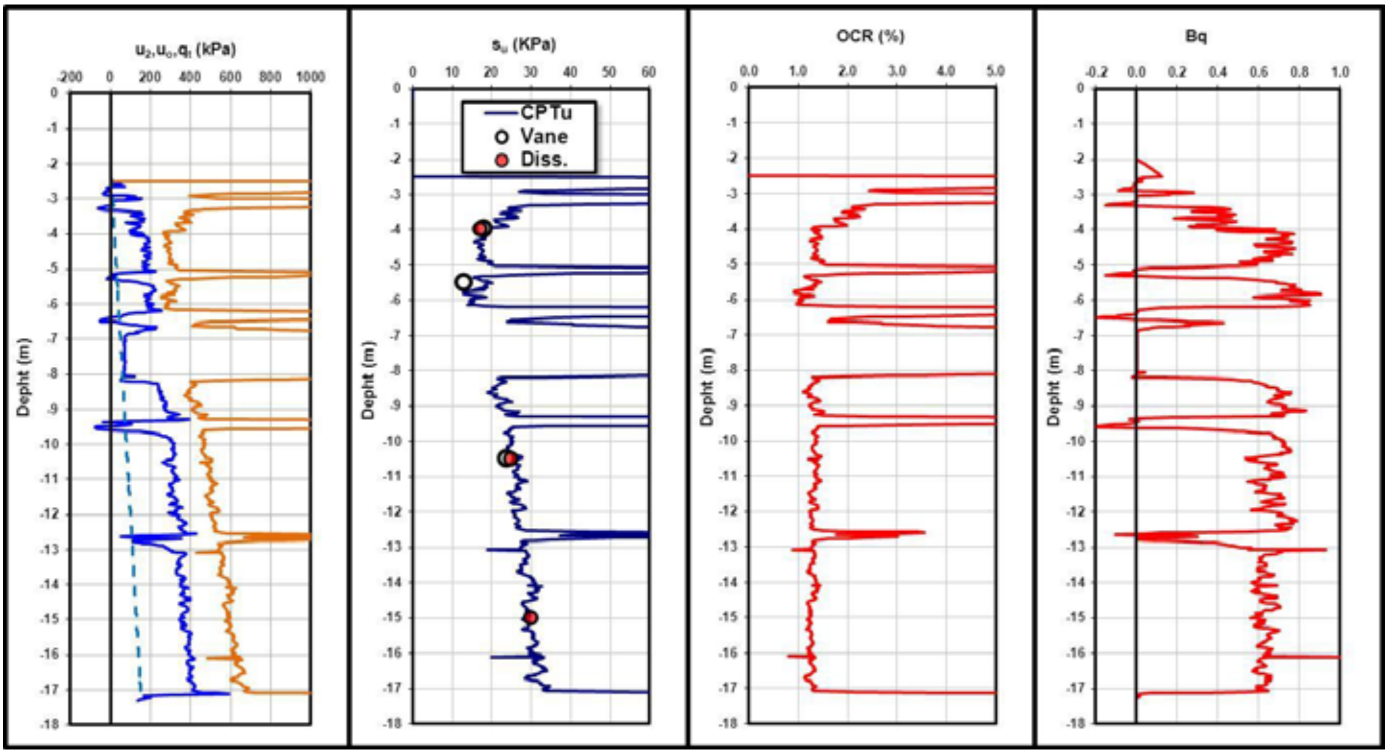

Figure 3. BR101 motorway near Florianópolis, Northern Brazil.

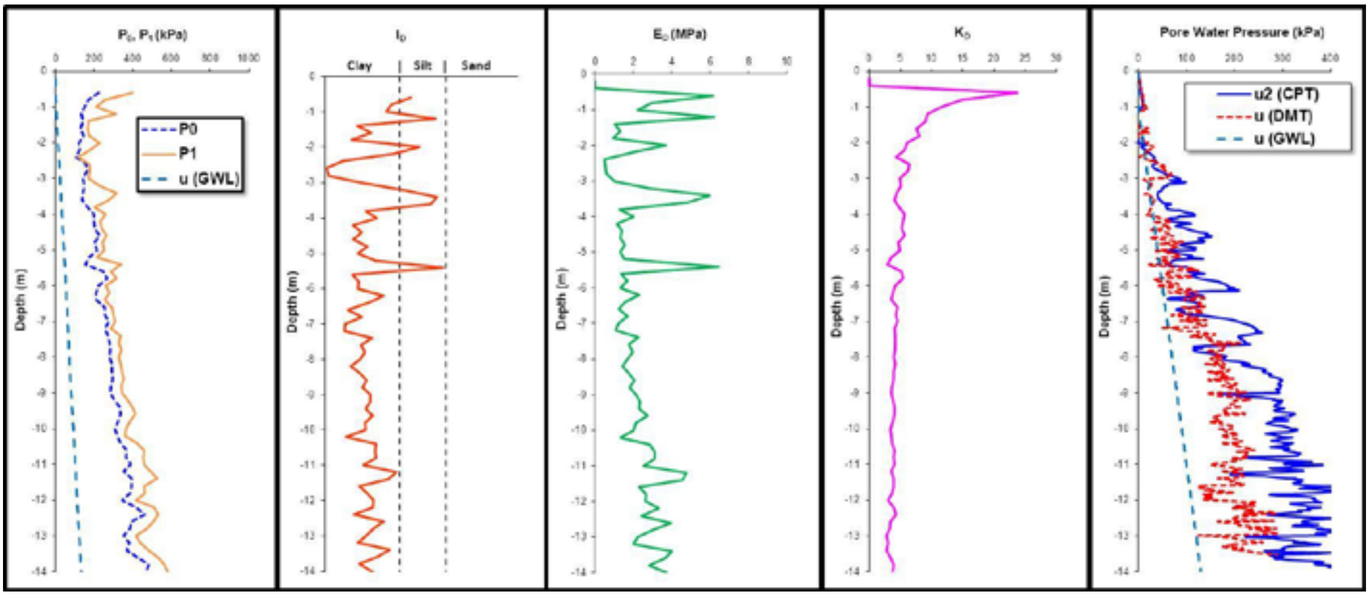

Figure 4. Typical soil profile at the Tubarão experimental testing site (Schnaid et al, 2016).

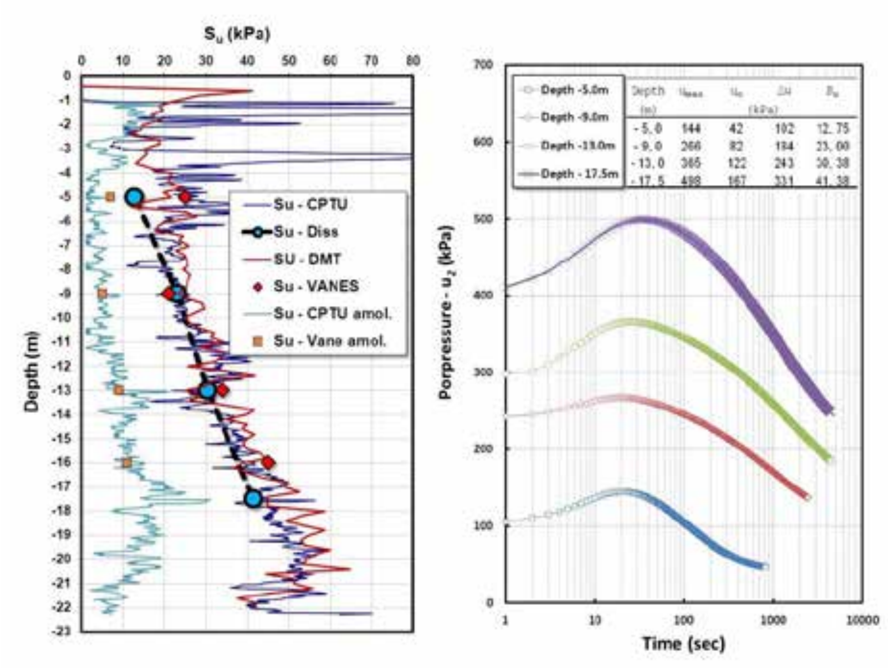

Figure 5. The Tubarão testing site undrained shear strength.

2.3 *Tubarão Experimental Testing Site*

Comprehensive site investigation carried out in clay at the Tubarão experimental testing site in Brazil comprises SDMT, CPTU, vane, shear wave velocity and SPT performed to identify soil type and stratigraphy (e.g. Mantaras et al, 2014, Schnaid et al, 2016). A typical profile, including pore pressure measurements is presented in Figure 4, revealing essentially a 15 m thick, very soft, essentially normally consolidated clay. In the Tubarão profile, the DMT pore pressures acting on the membrane during and immediately after penetration are high and comparable (slightly lower) to those measured behind the friction sleeve in the CPTU.

The database presented in the below figure is used to estimate variation of the undrained shear strength with depth, comparing data from vane, CPTU, DMT and dissipation tests.

3 CONCLUSIONS

The paper describes three case studies reporting in situ tests in soft clay deposits with the aim of evaluating the applicability of the method developed by Mantaras et al (2015) to estimate the undrained shear strength from CPTU dissipation tests. In the method, stress history, shear strength and compressibility are the critical factors affecting the accuracy of predictions. Reported case studies encourage the use of the method in engineering practice.

4 REFERENCES

Aas, G., Lacasse, S., Lunne, T. & Hoeg, K. 1986. Use of in situ test for foundation design on clay. *Proc. of the ASCE Specialty Conf. In Situ'86: Use of In Situ Tests in Geotech. Engineering (GSP 6)*, Blacksburg, 1-30 (American Society of Engineers (ASCE).

Baligh, M.M.1985. Strain path method. *J. Soil Mech. Found. Engng. Div., ASCE*. 11(7):1108-1136.

Baligh, M.M.; Levadox, J.N. 1986. Consolidation after undrained piezocone penetration. II: Interpretation. *J. Soil Mech. Found. Engng. Div., ASCE*. 11(7), 727-745.

Burns, S.E. & Mayne, P.W. 1998. Monotonic and dilatory pore-pressure decay during piezocone tests in clay. *Can. Geotech. J.*, 35(6): 1063-1073.

Ladd, C.C. 1991. Stability evaluation during staged construction (22nd Terzaghi Lecture). *Journal of Geotechnical Engineering*, 117(4): 540-615.

Jamiolkowski, M., Ladd, C.C., Germaine, J. and Lancellotta, R. 1985. "New developments in field and lab testing of soils", Proceedings, 11th International Conference on Soil Mechanics and Foundations Engineering, Vol. 1, San Francisco, 57-154.

Lunne, T.; Robertson, P.K. & Powell, J.J.M. 1997. Cone penetration testing in geotechnical practice, *Blackie Academic & Professional*, 312p.

Mantaras, F.M.B; Odebrecht, E.; Schnaid, F. 2014. Using piezocone dissipation test to estimate the undrained shear strength in cohesive soil. *CPT'14; 3rd International Symposium on Cone Penetration Testing,* Las Vegas.

Mantaras, F.M.B; Odebrecht, E.; Schnaid, F. 2014. Using piezocone dissipation test to estimate the undrained shear strength in cohesive soil. *CPT'14; 3rd International Symposium on Cone Penetration Testing,* Las Vegas.

Mantaras, F.M.B; Odebrecht, E.; Schnaid, F. 2015. Using piezocone dissipation test to estimate the undrained shear strength in cohesive soil. *Canadiam Geotechnical Journal*, 52(3): 318-325.

Mantaras, F.M.B; Odebrecht, E.; Schnaid, F. 2015. Using piezocone dissipation test to estimate the undrained shear strength in cohesive soil. *CPT'14; 3rd International Symposium on Cone Penetration Testing,* Las Vegas.

Mesri, G. 1975. Discussion: on new design procedure for stability of soft clays by Ladd and Foott. *Joumal of the Geotechnical Engineering Dision*, ASCE, (101) 4: 409-412.
Randolph, M.F. & Wroth, C.P. 1979. An analytical solution for the consolidation around a driven pile. *Int. J. for Numerical and Analytical Methods in Geomech.*, 3: 217- 229.
Teh, C.I. & Houlsby, G.T. 1991. An analytical study of the cone penetration test in clay. *Geotechnique*, 41(1): 17-34.
Torstensson, B.A. 1977. The pore pressure probe. Nordiske Geotekniske Mte, Oslo. Paper 34: 34.1- 34.15.
Wroth, C.P. 1984 The interpretation of in situ soil test. 24th Rankine Lecture. *Geotechnique*, 34 (4): 449-489.

Geotechnical and Geophysical Site Characterisation 5 – Lehane, Acosta-Martínez & Kelly (Eds)

Monotonic and dilatory excess pore water dissipations in silt following CPTU at variable penetration rate

P. Paniagua, R. Carroll, J.-S. L'heureux
Norwegian Geotechnical Institute, Trondheim & Oslo, Norway

S. Nordal
Norwegian University of Science and Technology, Trondheim, Norway

ABSTRACT: The relationship between cone penetration rate and pore pressure decay is investigated through dissipation tests following penetration at different rates. Field tests and model scale tests in the laboratory are performed. The rates of penetration in situ were 2, 20 (standard) and 250 mm/s while the model scale tests had rates of 0.06, 6 and 50 mm/s. The in situ tests were carried out in a silt with clay content of 11.8 % and the model scale tests were conducted in a silt with 2.5 % clay. Both materials are natural Norwegian silts. The fast penetration rate tests show high pore pressure gradients as soon as the penetration stops and a dilatory response during dissipation. The tests conducted at the slowest penetration rate show monotonic decay. The standard and medium rates show smaller gradients and a dilatory response during dissipation. The results are compared with representative solutions for monotonic and dilatory dissipation responses for determination of t_{50}.

1 INTRODUCTION

Cone penetration tests (CPTU) in saturated intermediate materials such as silty soils typically occur under partial drainage at the standard rate of penetration. Undrained and drained soil responses can be induced by changing the penetration rate (v). High v are typically associated to undrained behavior and slow v are typically associated to drained behavior. The undrained or drained response can be contractive or dilative. A contractive response shows an increase in pore pressure (u_2) and a decrease in cone resistance (q_t) with an increase in v. Recent studies have focused on investigation of effect of increase and decrease of rate in contractive silty intermediate soils (DeJong et al. 2012, Schneider et al. 2008, Randolph & Hope, 2004). Opposite trends have been observed by Silva (2005), Schneider et al. (2007) and Paniagua (2014) which are typical of a dilative response. The contractive or dilative responses can either generate large, zero or negative excess pore water pressures (Δu). Regardless of rate, once cone penetration stops for a dissipation test, Δu will vary with time and eventually reach equilibrium conditions towards in situ u_o values. This variation with time can be either monotonic (i.e. the initial pore water pressure u_i is greater than u_o and u_i is the maximum pore water pressure measured) or dilatory (i.e. u_i rises with time, reaches a peak value u_{max}, and then decreases with time towards u_o). Such variations are generally affected by the permeability (k) and coefficient of consolidation (c_h).

The work presented in this study shows results of pore pressure dissipation tests following cone penetration at different rates (i.e. slow, medium/standard and fast) carried out in the field and in the laboratory. Two Norwegian silts with contrasting percentages of clay, 2.5 % and 11.8 % have been tested. Monotonic and dilatory dissipation responses have been recorded. The scope of work is to compare the monotonic and dilatory responses from in situ and laboratory dissipation tests, and assess the influence of the penetration rate on the time for 50% dissipation (t_{50}) for further interpretation of c_h.

2 ANALYSIS OF CPTU DISSIPATIONS TESTS

Evaluation of c_h is based on the change in Δu with time (t), see Equation 1, where u_t is the measured pore pressure (in this case at the u_2 position) at the time t:

$$\Delta u = u_t - u_0 \tag{1}$$

The initial pore pressure (u_i) has a major influence on the dissipation process and its definition is used to select the time for 50% dissipation which is used to calculate c_h. Lunne et al. (1997) highlighted complications encountered for analysis of c_h which include; estimation of u_i, disturbance effects, anisotropy and preferential flow. Carroll & Long (2015) discussed that the estimation of u_i is critical for further analysis of dissipation tests results. The normalized excess pore pressure ratio (U) is used to plot dissipation test results (Equation 2).

$$U = \frac{u_t - u_o}{u_i - u_o} \tag{2}$$

Interpretation of a dissipation tests can be made by taking the time to 50% dissipation from shoulder pore water (u_2) decay if one is certain that u_o has been reached at the end of the dissipation. A theoretical solution to a monotonic response of Δu with time has been proposed by Teh & Houlsby (1991) based on the strain path method. This method requires the use of a time factor T* (Equation 3), where a is the cone radius and I_r is the rigidity index. The theoretical solution plots T* for different degrees of consolidation (1-U) and a value of $T_{50}^* = 0.245$ for u_2 is defined for a 50% consolidation.

$$T^* = \frac{c_h t}{a^2\sqrt{I_r}} \tag{3}$$

A dilatory response may be due to high vertically oriented pore pressure gradients of different magnitudes at various distances from the u_2 filter (Davidson, 1985, Burns and Mayne, 1998) or pore pressure redistribution that may be associated with partial drainage and pore pressures in gaps between the cone and sleeve. In the case of silts, changes in the soil fabric caused by grain reorientation around the cone create contractive and dilative zones that modify the drainage pattern that at the same time can be modified by the penetration rate (Paniagua et al. 2015). Such behavior complicates interpretation of dissipation tests. Different approaches, for example Burns & Mayne (1998), Sully et al. (1999), Mantaras et al. (2014) and Chai et al. (2012), have been proposed to account for non-standard dissipation behavior. These approaches are applied to results in this study.

2.1.1 *Burns & Mayne (1998)*

This mathematical solution is based on the cavity expansion-critical state. The excess pore water pressure is generated due to changes in the mean octahedral normal stress (u_{oct}, Equation 4) and in the octahedral shear stress (u_{shear}, Equation 5). The excess pore water pressures, Δu_t, at any time (t) can be compared with the initial values during penetration, $\Delta u_i = (\Delta u_{oct})_i + (\Delta u_{shear})_i$, and are represented by Equation 6 where T' is a modified time factor defined in Equation 7. OCR is the overconsolidation ratio, σ'_{vo} is the effective stress in situ, Λ is the plastic volumetric strain ratio and φ' is the friction angle. The procedure requires curve fitting to provide the best overall value of c_h.

$$\Delta u_{oct} = \sigma'_{vo}\frac{2}{3}\left(\frac{6\sin\varphi'}{3-\sin\varphi'}\right)\left(\frac{OCR}{2}\right)^{\Lambda}\ln(I_R) \tag{4}$$

$$\Delta u_{shear} = \sigma'_{vo}\left(1-\left(\frac{OCR}{2}\right)^{\Lambda}\right) \tag{5}$$

$$\Delta u_t = \frac{(\Delta u_{oct})_i}{1+50T'} + \frac{(\Delta u_{shear})_i}{1+5000T'} \tag{6}$$

$$T' = \frac{c_h t}{a^2 I_R^{0,75}} \tag{7}$$

2.1.2 *Sully et al. (1999)*

A dilatory response is transferred to a monotonic dissipation case by correcting the dissipation curve. One method is the logarithm of time plot correction and the other method is square root of time plot correction. In the square root of time plot, the dissipation after the peak is back extrapolated to t = 0 in order to obtain the modified maximum initial value of pore pressure. This value is then used to calculate the normalized dissipation curve. These methods were noted to only show a significant difference in time for short dissipation periods (Sully et al., 1999). One should notice that these methods do not account for the initial part of the dissipation curve since the shift in time does not account for effect of redistribution of Δu before u_{max} resulting in a possible overestimation of t_{50} thus underestimation of c_h (Chai et al., 2004).

2.1.3 *Chai et al. (2012)*

This method (Equation 8) uses time to u_{max} and t_{50} interpreted using u_{max} and u_o to establish an empirical correction to give a time for 50% dissipation of a non-standard curve. The empirically corrected value for 50% dissipation is referred to as t_{50c}. Chai et al. (2004) noted that the magnitude of the correction was dependent on the ratio $t_{u\text{-}max}/t_{50}$, where $t_{u\text{-}max}$ is time to u_{max}.

$$t_{50c} = \frac{t_{50}}{1+18{,}5\left(\frac{t_{u,max}}{t_{50}}\right)^{0,67}\left(\frac{I_r}{200}\right)^{0,3}} \tag{8}$$

2.1.4 *Mantaras et al. (2014)*

This procedure determines t_{50} by finding the best fit expression for the measured data and using the first and second derivate without any consideration regarding u_o. The approach lacks of a physical basis. The minimum point of the first derivate and the point when the second derivate is zero correspond to t_{50}. The accuracy of the proposed solution depends mainly on how well the theoretical idealization such as Teh & Houlsby (1991) or Burns & Mayne (1998) describes the pore pressure distribution around the cone.

3 SOIL DESCRIPTION

Two natural silt materials were tested in this study: Vassfjellet silt in the laboratory and Halden silt in the field. Vassfjellet silt is a non-plastic uniform silt.

Its grain size distribution is shown in Figure 1a. The clay, silt and sand contents are 2.5%, 90% and ~7%, respectively. High dilatant behavior is observed in samples tested in undrained triaxial tests at maximum density. Electron probe micro analysis (EPMA, Figure 1b) shows two main grain classes: bulky (AR > 0.5) and flaky grains (AR < 0.5). AR or aspect ratio is the ratio between the minor and the major axis lengths, (e.g., AR_{sphere} = 1). High quartz (27%) and low feldspar (15%) are found in this material.

Halden silt is a low plasticity silt. The water table is 2.5 m below ground level. It has an average I_P of 10.8% between 6.3 m and 6.8 m .The clay, silt and sand content are 12%, 67% and 20% respectively, see Figure 1a. Under anisotropic consolidation, a piston sample from 5.3 m had a dilatant response with and 'S' shaped stress path, indicating some contraction before dilation. A scanning electron microscope (SEM) image of material from 6.4 m shows a majority of bulky grains (Figure 1c). There is high quartz (41%) and feldspar (42%) in the Halden sample and the feldspar grains of are considered to be angular and of various shapes.

Table 1 presents a summary of the index properties for Vassfjellet and Halden where it is possible to compare the two silts. For example, Vassfjellet silt had high muscovite (35%) compared to Halden silt (8%). The muscovite flaky shapes will infer a stronger anisotropy in the deposit.

Table 1: Comparison of soil parameters

Parameter	Vassfjellet silt	Halden silt at 6.5 m or 6-7 m
Water content, w (%)	21-23	27-33
Total unit weight, γ (kN/m³)	19-19.3	18.9-19.0
Density of solids, γ_s (kN/m³)	24.6	26.3-26.5
Organic content,	< 2%	< 0.5%
Friction angle, φ (o)	32	35
c_v* cm²/s	0.063	0.055
k* at 0% strain m/s	---	$1.5x10^{-8}$
CPTU	6 mm/s	20 mm/s
q_t (MPa)	0.75-1.75	0.8-1.0
B_q	-0.01-0.04	0.1-0.14

*Measured in CRS tests, k at 0% axial strain, c_v at in situ effective vertical stress.

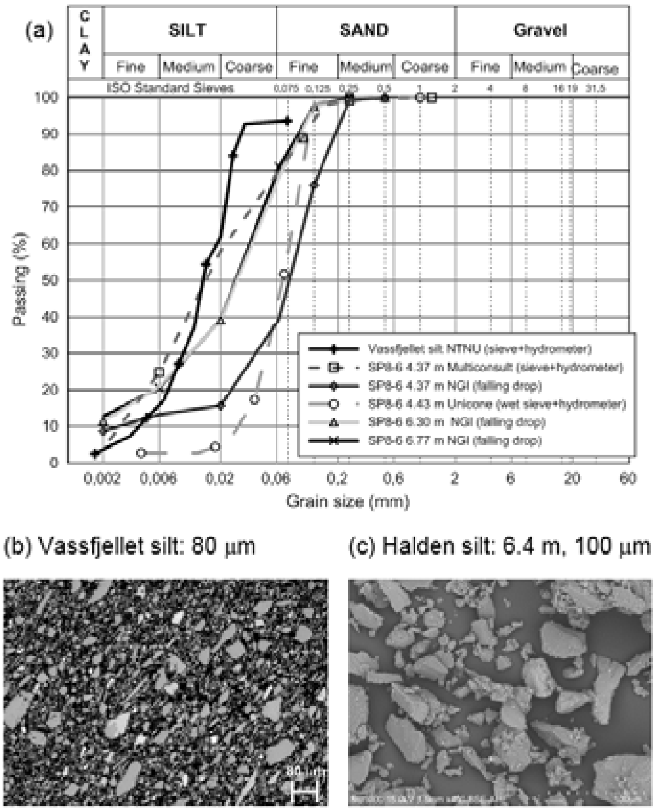

Figure 1: (a) Grain size distribution, (b) backscattered EPMA scan and (c) SEM

4 CPTU DISSIPATION TESTS

4.1 *CPTU dissipation tests in model scale*

Vassfjellet silt specimens were built inside a Plexiglas cylinder of 100 mm inner diameter internally padded with a 6 mm layer of neoprene selected to compensate for the effect of boundary closeness and to simulate a compressible surrounding soil. Saturated specimens of 180 mm height were consolidated from slurry deposition. An overburden pressure of 80 kPa was applied during testing. During sample preparation and cone penetration, pore pressure is monitored in the sample specimens. Laboratory CPTU tests were performed with an F0.5CKEW2 Fugro miniature cone, 11.28 mm diameter, owned by University of Colorado. The rates of v were selected according to the ranges of non-dimensional velocity, V, observed by DeJong & Randolph (2012) corresponding to V = 0.15, 15 and 126, for drained, partially drained and undrained conditions, respectively. The cone stopped at 100-110 mm depth and dissipations of u_2 were immediately recorded.

4.2 *CPTU dissipation tests in the field*

In situ penetration tests at Halden were carried out using NGI's standard rig setup. The penetration rate was constant for 1.2 - 1.5 m before the target depth of the dissipation tests. The penetration occurred at three different rates: 2 mm/s (slow), 20 mm/s (standard) and 320 mm/s (fast). The mechanical operation for a test comprised of stopping penetration at the target depth (i.e. 6,5 m for the slow, 6,51 m for the standard and 6,62 m fast tests) and start logging by manual trigger by the operator. The base clamps are then engaged and the top hydraulic clamps are disengaged to avoid possible movement of the hydraulic system with time and applying pressure on the cone. In essence there can be a short time laps of a couple of seconds between end of penetration and start of logging and some change in stress

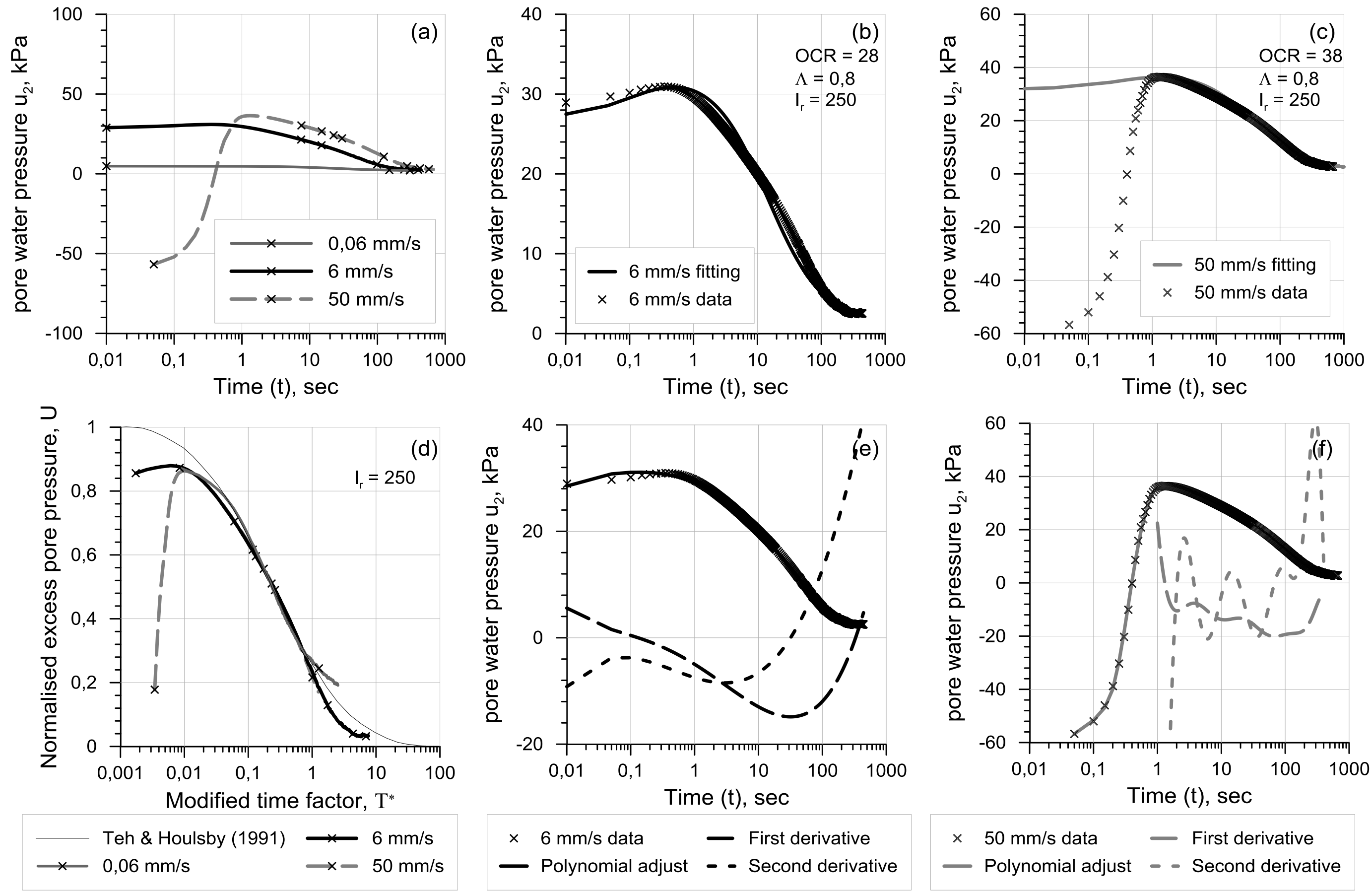

Figure 2. Vassfjellet silt: (a) measured u_2 with time. Burns & Mayne (1998) solution (b) medium v (c) fast v. (d) U with Teh & Houlsby (1991) using square root time method. Mantaras et al. (2014) (e) medium v and (f) fast v.

conditions due to movement of the clamps engaging and disengaging. However care and attention to these processes was made during testing to minimize possible effects on measurements.

5 TEST RESULTS

Results of model scale dissipation tests in Vassfjellet silt are shown in Figure 2. A monotonic decay is observed after the slow tests where low u_2 values, u_{max} ~ 5 kPa, are reached. A dilatory response during dissipation is observed for the tests conducted at medium and fast v. This dilatory response is more accentuated

for the fast test where the dissipation starts at negative pore pressures (due to suction and the dilatant behavior of the soil) and increases to positive values. The fastest test has the highest u_2 value, 36 kPa, compared to the medium v, 31 kPa. Data was continuously recorded between penetration and start of dissipation hence final u_2 penetration is equal to the u_i.

The Halden dissipation test results are presented in Figure 3a. A monotonic decay is observed in the slow test despite the sharp reduction in u_2 after 3 s. This may be due to the clamping arrangement. Values recover to the previous state within 5 s. The medium and fast tests both show a dilatory response. There is an increase in u_2 after 4 s for the standard test while the fastest v shows a steady rapid build up to u_{max}. A sudden small reduction in u_2 post u_{max} is recorded in the fast test. Overall the sharp reductions in u_2 are likely to be linked to rig operation while the increases in u_2 are thought to be linked to natural soil behavior around the cone tip and shoulder. In these tests measured u_i agrees well with the final u_2 measurements before stopping penetration (Figure 3a). This is a simple check which provides reliable background information on conditions just before the dissipation starts. The fastest test generated the highest u_2 value, 193 kPa, compared to the standard and slow v, ~158 kPa. A degree of consolidation higher than 50% was reached in the laboratory (values between 81-97%) and in the field (values between 69-77%).

6 DISCUSSION

The dissipation results in Vassfjellet silt have been interpreted following the procedures described in the analysis section to estimate t_{50}. The u_2 decay method assumed that $u_i = u_{max}$ and therefore there is some account of the time for pore pressure redistribution at the start of the test. The square root method (Sully et al. 1999) was applied in order to further analyze the data with Teh & Houlsby (1991) solution. Figure

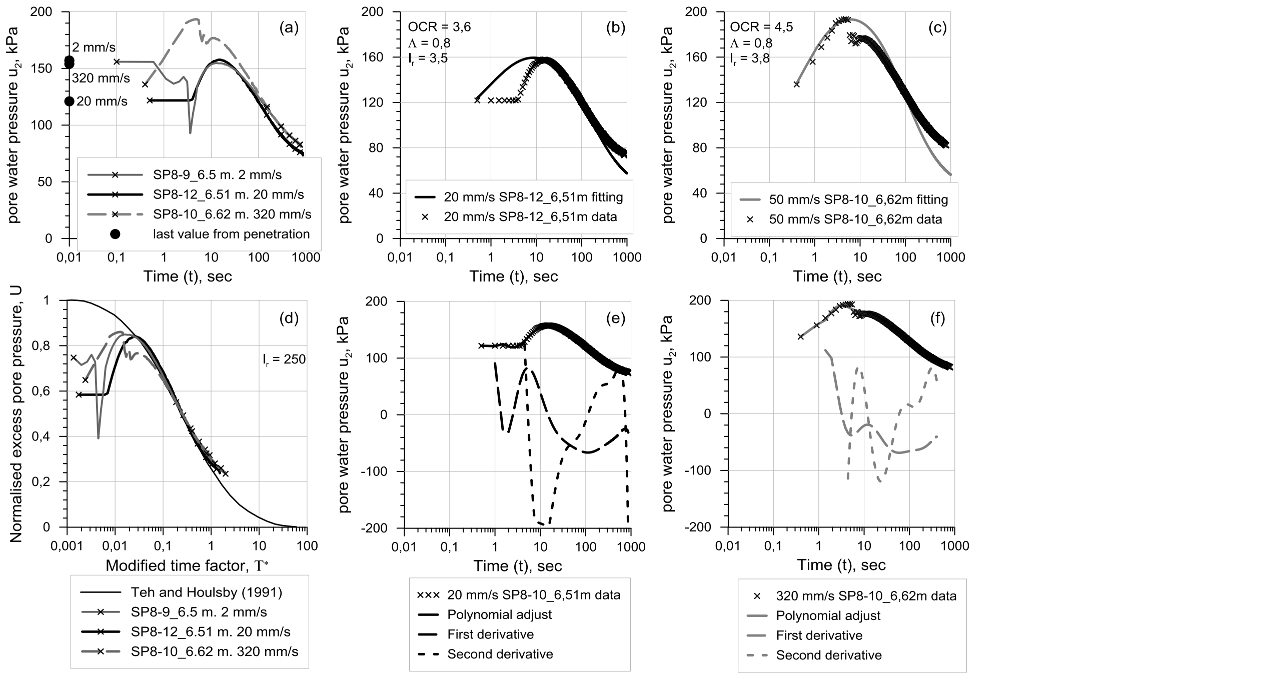

Figure 3. Halden silt: (a) measured u_2 with time. Burns & Mayne (1998) solution (b) standard v (c) fast v. (d) U with Teh & Houlsby (1991) using square root time method. Mantaras et al. (2014) (e) standard v and (f) fast v.

2d shows that for short dissipation times, all dissipation tests are about 15% below the theoretical Teh & Houlsby (1991) solution while at 80 % dissipation the measured data for slow v is above the solution and the medium and fast test are below the solution.

The curve fitting proposed by Burns & Mayne (1998) appears to give satisfactory results for the dissipation data after slow and medium tests (Figure 2b). It was not possible to fully fit the fast test results due to the negative pore pressures which are not captured by the analysis (Figure 2c). In order to fit these transition from negative to positive values, Δu_{shear} must be much larger than Δu_{oct}. Burns & Mayne (1998) theory assumed that Δu_{oct} is due to an increase in pore pressure for changes in the octahedral stress. However, investigation of the zone around the cone in Vassfjellet silt tests identified compaction and dilation (Paniagua et al. 2015). Hence a dilation (i.e. suction) zone might reduce the expected Δu_{oct}.

Mantaras et al. (2014) (Figure 2e, 2f) and Chai et al. (2012) procedures were relatively simple to apply. The estimated t_{50} values obtained with these methods show high contrast with each other (Figure 4). The interpretation for t_{50} from Halden silt was similar to that for Vassfjellet silt. The dissipation data is 15-20% below Teh & Houlsby (1991) solution at the beginning of the test while at 80% dissipation the measured data are above the solution (Figure 3d). Hence suggesting that dissipation is slower than estimated based on the u_i and u_o conditions applied in the analysis. The trend of agreement is opposite to Vassfjellet silt for the medium and fast test.

Application of Burns & Mayne (1998) procedure was challenging for all tests due to reductions in u_2

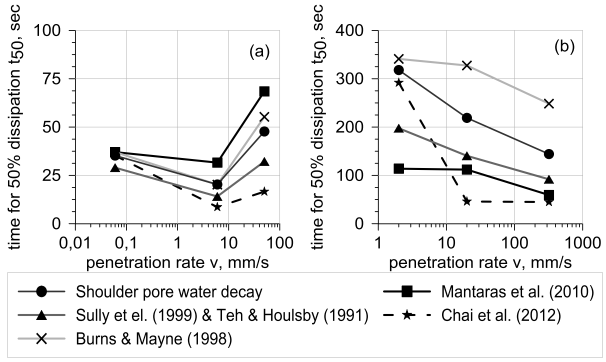

Figure 4: t_{50} and v for (a) Vassfjellet silt and (b) Halden silt

and the sudden increase in u_2 for the standard test (Figure 3b, 3c). The fitting process could not capture these features. Some unrealistic parameters have to be used for fitting. Hence it is challenging to apply this theory to the Halden data set. It is also noted that the fitting vas sensitive to small changes in the parameters. As experienced with Vassfjellet silt data, Mantaras et al. (2014) (Figure 2e, 2f) and Chai et al. (2012) analyses are simpler to apply. Results from Chai et al. (2012) method estimated the shortest t_{50} times at standard and fast v while there is scatter in the trend for the slowest v, see Figure 4. This was also the case for results from Vassfjellet silt tests with this method. Conditions of testing are under greater control for the model scale tests compared to field tests, in terms of soil uniformity and cone set up. In situ tests are reliant on consistent controlled operation of the CPTU rig, stress conditions at start of dissipation, similar soil conditions between tests at the required depths and correct u_o estimation. The challenges in applying the theories have been greatest for the field data set, due to a combination of the conditions discussed above and the material dilatory response.

6.1 *Rate effects on t_{50} times*

The t_{50} values obtained from the different theories are shown in Figure 4 for Vassfjellet and Halden silt. For the model scale tests, the range of scatter at the slow and medium v is relatively low while at fast v (associated with $u_2 < 0$s and pore pressure migration from adjacent soil) there is greater scatter. There is a similar trend of reducing t_{50} with increased v for the two data sets if the fastest v with negative u_2 is omitted. In both data sets, the shoulder u_2 decay and Burns and Mayne (1998) estimated high t_{50} times compared to the Sully et al. (1999) square root time method with Teh and Houlsby (1991). However, Mantaras et al. (2014) show the highest t_{50} values in Vassfjellet silt and the lowest t_{50} values for Halden silt, see Figure 4.

7 CONCLUSIONS

Results show that model scale dissipation tests give short t_{50} values due to the smaller cone size and therefore a smaller cone influence area. The negative pore pressures in Vassfjellet silt may be due to the low clay (2.5%) content and proportion of flaky grains which have a tendency to create dilatancy during penetration at high penetration rates. Once penetration stops, pore pressure redistribution occurs between zones further away from the cone and the zone adjacent to the cone shoulder as also observed by Silva (2005). Halden silt has a coarser silt and sand content compared to Vassfjellet silt although the 12% clay content may be a controlling factor on the extent to which u_i and u_{max} vary for these tests. However, no negative u_2 values are recorded at the fastest rate.

The scatter in the in situ data leads to uncertainty as to which method is most appropriate to evaluate a dilatory test. It is noted that irrespective of v, the scatter in t_{50} does not reduce for in situ tests while the model scale tests show greater agreement at the slowest v. Both silts have a monotonic response at slowest v. The Burns & Mayne (1998) method proved unrealistic parameters for fitting that did not reflect expected material parameters, particularly in situ.

With the exception of the fastest v (expected to be undrained), these tests are carried out under partially drained conditions. The theories used are designed for fully undrained conditions tests and leads to challenges for interpretation. Future testing to investigate the usefulness and practical conditions required to obtain fully undrained penetration should be carried out. Corrections for partial drainage proposed by DeJong et al. (2012) may also be considered in analysis since t_{50} value increases with the increase in the degree of partial consolidation during penetration. However, the correction applies to contractive materials and monotonic dissipation curves. The measurement of u_i during a dissipation test, good quality data recording and holding the CPTU-rods fixed are factors of critical importance for subsequent analysis with theoretical solutions.

8 ACKNOWLEDGEMENTS

The Vassfjellet testing was funded by NTNU. Professors Stein Sture and John S. McCartney (University of Colorado) are greatly acknowledged for lending the miniature CPTU. Halden testing was funded by the Norwegian Research Council through the strategic research project SP8- GEODIP at NGI.

9 REFERENCES

Burns, S.E., Mayne, P.W. 1998. Monotonic and dilatory pore pressure decay during piezocone tests in clay. *Can Geotech J* 35: 1063–1073.

Carroll, R. & Long, M. 2015. Assessment of dissipation tests in silty soils with standard and non-standard decay. *Frontiers in Offshore Geotechnics III.* 1173–1178, CRC Press.

Chai, J., Sheng, D., Carter, J.P. & Zhu, H. 2012. Coefficient of consolidation from non-standard piezocone dissipation curves. *Computers and Geotechnics* 41: 13-22.

Chai, J.C., Carter, J.P., Miura, N. & Hino, T. 2004. Coefficient of consolidation from piezocone dissipation tests. *International Symposium on Lowland Technology*. Bangkok.

Davidson, J. L. (1985) Pore pressures generated during cone penetration testing in heavily overconsolidated clays. In discussion to session 2d: field instrumentation and field measurements. *Proc 11th ICSMFE.* San Francisco, 5, 2699.

DeJong, J., Jaeger, R.A., Boulanger, R.W., Randolph, M.F. & Wahl, D.A.J. 2012. Variable penetration rate cone testing for characterization of intermediate soils. *Geotechnical Site Characterization 4*. 25-42- London: Taylor & Francis.

Lunne, T., Robertson, P. K. & Powell, J. J. M. 1997. *Cone penetration testing in geotechnical practice.* Glasgow: Blackie Educational & Professional.

Mantaras, F.M., Odebrecht, E. & Schnaid, F. 2014. On the interpretation pf piezocone dissipation testing data. *Proc 3rd International Symposium on CPT*, Las Vegas, US.

Paniagua, P. 2014. *Model testing of cone penetration in silt with numerical simulations*. PhD. thesis, NTNU, Norway.

Paniagua, P., Fonseca, J., Gylland, A.S. & Nordal, S. (2015). Microstructural study of deformation zones during cone penetration in silt at variable penetration rates. *Can Geotech J* 52: 2088–2098.

Randolph, M.F. & Hope, S. 2004. Effect of cone velocity on cone resistance and excess pore pressures, *Proc., IS Osaka-Engineering Practice and Performance of Soft Deposits*, Osaka, Japan, 147–152.

Schneider, J.A., Lehane, B.M. & Schnaid, F. 2007. Velocity effects on piezocone tests in normally and overconsolidated clays, *Int. J. Phys. Modell. Geotech.*7 (2): 23–34.

Schneider, J.A., Randolph, M.F., Mayne, P.W. & Ramsey, N.R. 2008. Analysis of factors influencing soil classification using normalized piezocone tip resistance and pore pressure parameters. *J Geotech Geoenviron Eng* 134: 1569-1586.

Silva, M.F. 2005. *Numerical and Physical Models of Rate Effects in Soil Penetration,* PhD. thesis, Cambridge University.

Sully, J.P., Robertson, P.K., Campanella, R.G. & Woeller, D.J. 1999. An approach to evaluation of field CPTU dissipation data in overconsolidated fine grained soils. *Can Geotech J* 36: 369-381.

Teh, C.-I. & Houlsby, G. T. 1991. An analytical study of cone penetration test in clay. *Géotechnique* 41: 17-34.

Geotechnical and Geophysical Site Characterisation 5 – Lehane, Acosta-Martínez & Kelly (Eds)

Estimating K_o in sandy soils using the CPT

P.K. Robertson
Gregg Drilling & Testing, Inc., 2726 Walnut Ave., Signal Hill, CA, USA

ABSTRACT: One of the more challenging geotechnical parameters to estimate using in-situ tests is K_o in sandy soils. Re-search has shown that K_o can have a significant effect on soil behavior and that it can be helpful to estimate a reasonable value using in-situ tests. Marchetti (2015) has shown that ideally this requires two independent measurements and has suggested that a combination of the CPT and DMT can achieve this goal. However, this increases the cost of the site investigation, since two in-situ tests are required at one location and the in-terpretation is not always straight forward since each test collects measurements at different locations and at different depth intervals. The CPT already provides two independent measurements in the cone resistance, q_c and the sleeve resistance, f_s. This paper will present similarities between DMT and CPT data and show that the normalized CPT sleeve resistance (f_s/σ'_{vo}) can be used to estimate both DMT K_D and, when combined with the normalized cone resistance (Q_{tn}), can estimate the in-situ K_o in young, uncemented sandy soils. Background research will be presented to explain the logic and combined CPT and DMT data from several sites around the world will be presented to support the proposed correlation. The paper will also include a short discussion regarding repeatability of the CPT sleeve resistance (f_s) and how this affects the proposed ap-proach.

1 INTRODUCTION

One of the more challenging geotechnical parameters to estimate using in-situ tests is K_o in sandy soils. Research has shown that K_o can have a significant effect on soil behavior and that it can be helpful to estimate a reasonable value using in-situ tests. Marchetti (2015) has shown that ideally this requires two independent measurements and has suggested that a combination of the CPT and DMT can achieve this goal. However, this increases the cost of the site investigation, since two in-situ tests are required at one location and the interpretation is not always straight forward sine each test collects measurements at different locations and at different depth intervals.

This paper presents similarities between DMT and CPT data and show that the normalized CPT sleeve resistance (f_s/σ'_{vo}) can be used to estimate both DMT K_D and, when combined with the normalized cone resistance (Q_{tn}), can estimate the in-situ K_o in young, uncemented sandy soils.

2 CPT-DMT RELATIONSHIPS

Robertson (2009) suggested a preliminary set of average correlations that link the main DMT parameters (I_D, K_D) to normalized CPT parameters (Q_t, F_r). The proposed correlations are approximate and influenced by variations in in-situ stress state, soil density, stress and strain history, age, cementation and soil sensitivity. The correlations are unlikely to be unique for all soils but the suggested relationships form a framework for possible future refinements. The resulting correlations are shown in Figure 1, in the form of contours of I_D, K_D on the CPT normalized SBT chart. Included in Figure 1 are contours (in red) of the normalized sleeve resistance, F = f_s/σ'_{vo}.

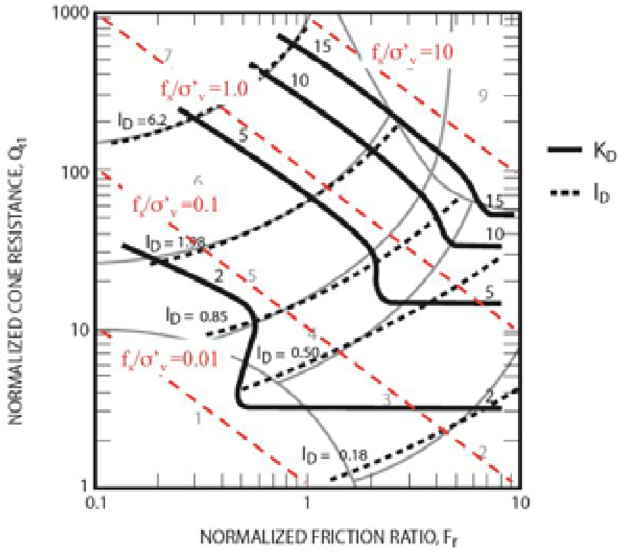

Figure 1. Approximate correlation between DMT K_D and I_D andCPT normalized parameters for soils with little or no microstructure (After Robertson, 2015)

Figure 1 shows that in the region dominated by sandy soils (SBT zones 5, 6 and 7; $I_c < 2.5$; $I_D > 1.0$) there appears to be a clear link between DMT K_D and CPT f_s/σ'_{vo}. Figure 1 shows that f_s/σ'_{vo} ranges over 3 orders of magnitude, with f_s/σ'_{vo} = 0.01 representing the typical limit of accuracy in the measurement and f_s/σ'_{vo} = 10 representing the typical limit of capacity of the cone. This matches a similar range for the DMT K_D from a low of about 1.0, based on accuracy, to high of around 50 based on capacity.

To illustrate this link, a comparison is shown in Figure 2 between DMT and CPT data at a sand site in Western Australia (Shenton Park). This site is composed of siliceous wind-blown, dune sand (Amoroso, 2011). Figure 2 shows that K_D and f_s/σ'_{vo} have a very similar variation with depth (note that both K_D and f_s/σ'_{vo} are plotted on a log scale). Figure 3 shows a similar comparison between DMT and CPT data from another sand site (Ledge Point) in Western Australia. This site is composed of slightly cemented calcareous sand, with 90% carbonate (Amoroso, 2011). Figure 3 also shows how both K_D and f_s/σ'_{vo} vary in a similar manner, with larger changes of f_s/σ'_{vo} in fine-grained soils.

Based on companion DMT and CPT data from 10 sites around the world, Figure 4 shows an approximate relationship between K_D and f_s/σ'_{vo} in sandy soils ($I_c < 2.5$; $I_D > 1.0$). The data shown on Figure 4 has been averaged to remove isolated points due to soil variability, since the DMT and CPT were not at the exact same location but within a few meters. Ranges are shown to reflect the variation of each measurement within a given relatively uniform sand zone.

An average relationship can be represented by:

$$\text{Log } F = \log K_D - 0.85$$
for sandy soils where $I_c < 2.5$ or $I_D > 1.0$ (1)

Where $F = f_s/\sigma'_{vo}$

Equation 1 and the data in Figure 3 indicate that the CPT normalized sleeve friction, F, is essentially similar to the DMT K_D in sandy soils, both with similar sensitivity.

3 ESTIMATING K_o IN SANDY SOILS

Hughes and Robertson (1985) discussed the changes in stresses around a cone and showed that there is significant stress relief as soil elements travel pass the shoulder of the cone. However, cavity expansion suggests that although the soil around the friction sleeve has experience a significant stress relief, the final horizontal stress around the sleeve is linked to the original horizontal stress prior to cone penetration and that the measured sleeve friction is strongly influenced by the horizontal effective stress around the sleeve. The data shown in Figures 2, 3 and 4 appear to support that concept. Marchetti (1985) suggested that it was possible to estimate K_o in sandy soils from a combination of both DMT and CPT data, as shown on Figure 5.

Using the link between DMT and CPT in sandy soils, it's possible to estimate K_o directly from CPT data, by combining normalized cone resistance, Q_t and normalized sleeve friction, F. In fine-grained soils ($I_c > 2.6$; $I_D < 0.8$) the in-situ K_o is more closely linked to OCR. Combining these two observations it is possible to represented contours of K_o on the CPT-based normalized soil behavior type chart (Robertson, 2009), as shown in Figure 6. The contours of K_o have been extended into the region of I_c > 2.5 based on the link between OCR and K_o in clay-like soils.

In the original SBT chart presented by Robertson (1990) there was a zone shown down the center of the chart that represented approximately normally consolidated soils that is also shown on Figure 6, where $K_o \sim 1 - \sin\phi' \sim 0.5$. This zone matches quite well the proposed contour of $K_o \sim 0.5$. The region to the left of the K_o = 0.5 contour can be assumed to be predominately normally consolidated with $K_o \sim 0.5$, as shown on Figure 6.

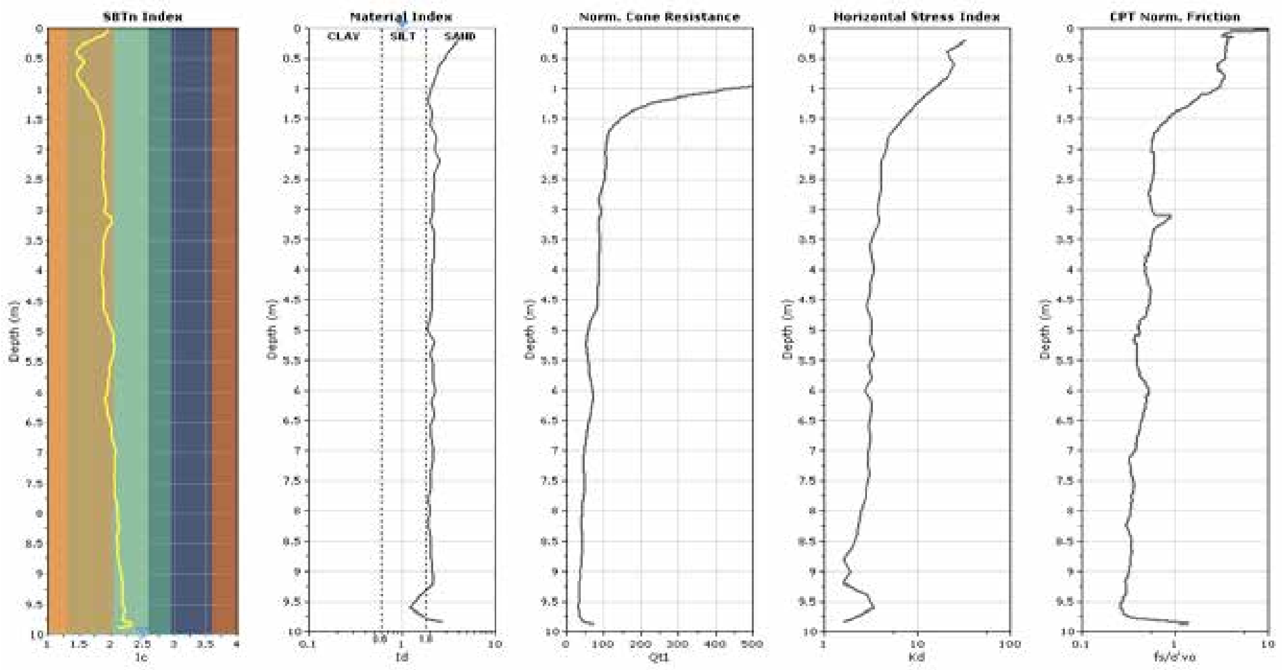

Figure 2. Comparison between CPT and DMT data in a sand site (Shenton Park) in Western Australia (data from Amoroso, 2011)

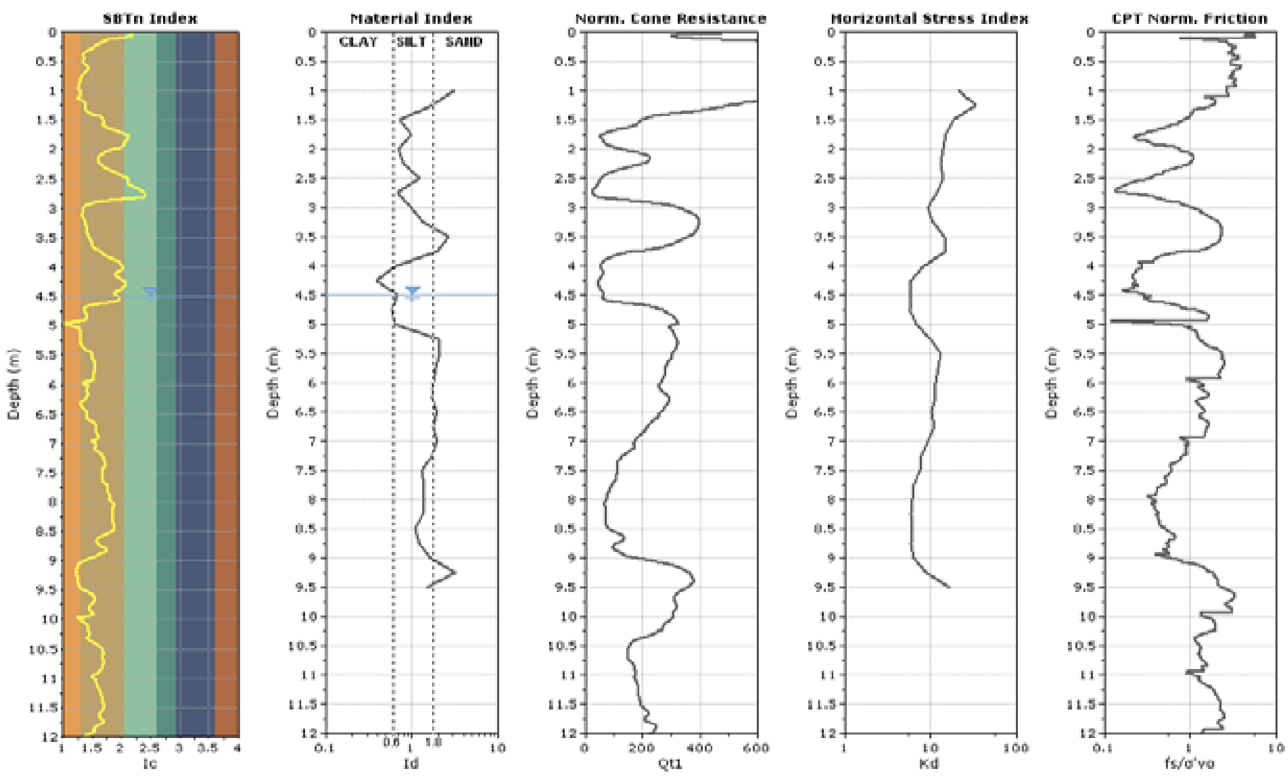

Figure 3. Comparison between CPT and DMT data in a sand site (Ledge Point) in Western Australia (data from Amoroso, 2011)

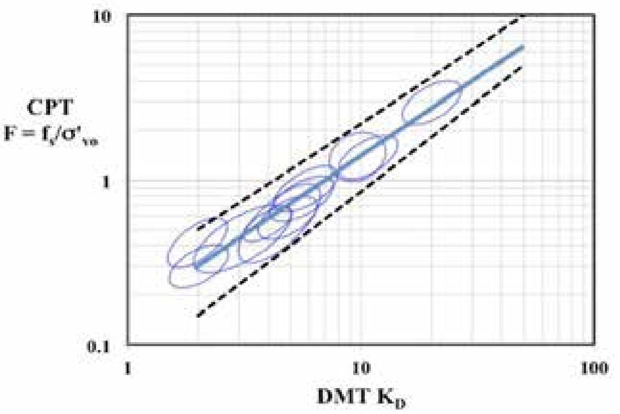

Figure 4. Relationship between DMT K_D and CPT normalized sleeve friction $F = f_s/\sigma'_{vo}$ based on 10 sandy soil ($I_c < 2.5$; $I_D > 1.0$) around the world

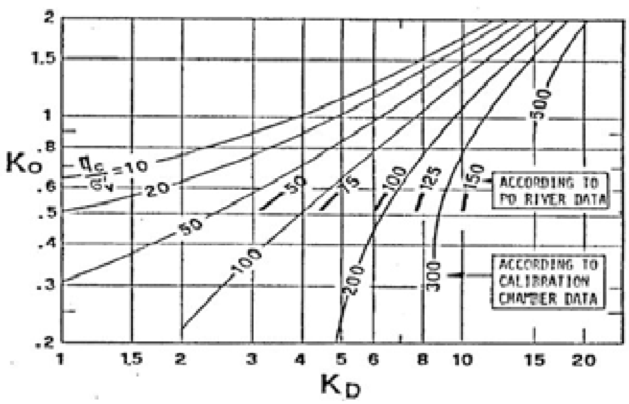

Figure 5. Chart for estimating K_o in sands as a function of DMT K_D and CPT q_c/σ'_{vo} (After Marchetti, 1985)

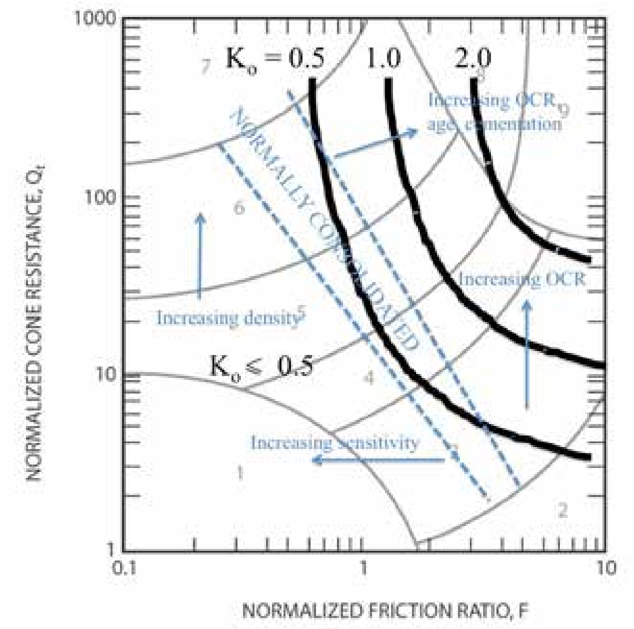

Figure 6. Suggested approximate contours of in-situ K_o on the CPT-based soil behavior type chart by Robertson (2009)

Also shown on Figure 6 are the trends suggested by Robertson (1990) for increasing sensitivity and increasing OCR for fine-grained soils and increasing density and increasing OCR, age and cementation for coarse-grained soils. These trends are consistent with the proposed approximate contours for K_o. In fine-grained soils (SBT zones 1, 2, 3 and 4), the measured sleeve friction tends to become dominated by the remolded shear strength of the soil and hence, can be a less accurate estimate of K_o.

The contours shown on Figure 6 are approximate, since there are many variables that influence K_o in soils. However, the trends are consistent with past experience, where stiff overconsolidated soils tend to plot toward the top right-hand portion of the chart (high Q_t and high F_r) and normally consolidated soils tend to plot in the central and lower left portion of the chart. In fine-grained soil, sensitivity tends to dominate and influence the measured sleeve friction values, since the measured sleeve resistance is often close to the remolded shear strength. Hence, fine-grained soils with high sensitivity tend to plot toward the lower left portion of the chart, regardless of in-situ K_o.

The CPT sleeve friction is often considered an unreliable measurement (e.g. Lunne et al 1986). Most modern electric cones have an accuracy/repeatability of the sleeve friction of between 1 to 5 kPa (e.g. separate load cells and equal-end area friction sleeves). Based on the contours of f_s/σ'_{vo} shown on Figure 1, the sleeve friction is less reliable when $f_s/\sigma'_{vo} < 0.1$, that represents predominately soft sensitive fine-grained soils and some very loose sands close to the ground surface (where σ'_{vo} is small).

4 SUMMARY AND RECOMENDATIONS

One of the more challenging geotechnical parameters to estimate using in-situ tests is K_o in sandy soils. Research has shown that K_o can have a significant effect on soil behavior and that it can be helpful to estimate a reasonable value using in-situ tests. Marchetti (2015) has shown that ideally this requires two independent measurements and has suggested that a combination of the CPT and DMT can achieve this goal. However, this increases the cost of the site investigation, since two in-situ tests are required at one location and the interpretation is not always straight forward since each test collects measurements at different locations and at different depth intervals.

The CPT already provides two independent measurements in the cone resistance, q_c and the sleeve resistance, f_s. Similarities between DMT and CPT data have been presented and show that the normalized

CPT sleeve resistance ($F = f_s/\sigma'_{vo}$) can be used to estimate both DMT K_D and, when combined with the normalized cone resistance (Q_t), can estimate the in-situ K_o in sandy soils.

The CPT and DMT are the most promising in-situ penetration tests currently used in practice. Each test has advantages and limitations. Relationships between the two in-situ tests can be used to expand and improve correlations and applications using experience and databases from one test and extrapolating to the other test. Since the CPT is faster, less expensive and provides a near continuous profile, it is often used more than the DMT, especially for smaller, low risk projects. The correlations presented in this paper provide some insight into how the links between the CPT and DMT can be used to expand our understanding of each test.

5 ACKNOWLEGEMENTS

This work was supported by Gregg Drilling & Testing, Inc. The author would also like to thank several researchers/users from around the world for sharing their DMT-CPT data sets, such as, S. Amoroso, S. Marchetti, G. Togliani, W. Steiner, F. Schnaid and A. McConnell.

REFERENCES

Amoroso, S., 2011. G decay curves by seismic dilatometer (SDMT). PhD thesis, Universita' Degli Studi Dell'Aquila, Departimento di Ingegneria della Strutture, delle Acque e del Terreno, Italy.

Hughes, J.M.O. & Robertson, P.K., 1985. Full displacement pressuremeter testing in sand. Canadian Geotechnical Journal, 22, 3 : 298-307.

Lunne, T., Eidsmoen, T., Gillespie, D., and Howland, J.D., 1986. Laboratory and field evaluation on cone penetrometers. Proceedings of ASCE Specialty Conference In Situ'86: Use of In Situ Tests in Geotechnical Engineering. Blacksburg, ASCE, 714-729

Marchetti, S., 1985. On the Field Determination of K_o in Sand. Proceeding XI ICSMFE, S. Francisco, Vol. 5: 2667-2672.

Marchetti, S., 2015. Some 2015 Updates to the TC 16 DMT Report of 2001. Proceedings of 3rd International Conference on the Flat Dilatometer, DMT'15, Roma, Italy

Robertson, P.K., 2009. Interpretation of Cone Penetration Tests – a unified approach. Canadian Geotechnical Journal, 46: 1337-1355

Robertson, P.K., 2015. Soil Behavior Type using the DMT. Proceedings of 3rd International Conference on the Flat Dilatometer, DMT'15, Roma, Italy

Geotechnical and Geophysical Site Characterisation 5 – Lehane, Acosta-Martínez & Kelly (Eds)
 ISBN 978-0-9946261-1-0

Effects of suction on CPT results and soil classification

A. R. Russell
Centre for Infrastructure Engineering and Safety, School of Civil and Environmental Engineering, The University of New South Wales, Australia

D. Reid
Senior Tailings Engineer, Golder Associates Pty Ltd, West Perth, Australia

ABSTRACT: Laboratory-controlled CPT results for an unsaturated sand and silty sand show suction has a pronounced influence. The penetration resistances increase significantly due to the presence of suction when compared to those for saturated or dry states, for a given relative density and net confining stress. Also, for unsaturated sands, when suction is included in the effective stress, the same semi-empirical expressions used for saturated conditions are found to link penetration resistance to the relative density and effective confining stress. However, the same is not true for unsaturated silty sands, as saturated and unsaturated silty sands behave very differently around a penetrating cone. Suction also has implications when using classification charts. CPT results from a range of soils for both saturated and unsaturated conditions are plotted in one type of chart. Suction induced increases in penetration resistances, and changes of the soil behaviours from partially drained/undrained to drained, cause incorrect soil classifications and assessments that soils are dilative.

1 INTRODUCTION

Unsaturated soils are widely encountered and need to be dealt with in many engineering problems (e.g. foundations, fills, embankment dams, pavements and slopes). Their behaviour is complex and influenced by many factors including externally applied stresses, soil type, structure, density and suction. Suction, in particular, increases the shear strength and may contribute to the stiffening of the soil.

The characterisation of unsaturated soils may involve expensive and time-consuming investigations including soil borings and undisturbed sampling for laboratory testing. Performing the cone penetration test (CPT), a widely used in situ test, in an unsaturated soil may enable less costly and more rapid characterisation of the unsaturated soil properties.

The evaluation of soil properties from CPT results has been an area of intense practical interest. For both coarse- and fine-grained saturated soils, many correlations have been developed that link cone penetration resistance (q_c) to in situ state and shear strength (e.g. Baldi et al. 1982, Robertson & Campanella 1983a, b, Jamiolkowski et al. 2003).

However, it is only in the past few years that correlations have emerged for the CPT that take into account the effects of unsaturation (Pournaghiazar et al, 2013, Yang & Russell, 2016). So far these have been limited to a clean quartz sand and a silty sand (decomposed granite). These and other studies (Lehane et al. 2004, Collins & Miller 2014) show that suction significantly increases q_c.

Most notably, Pournaghiazar et al. (2013) showed for the unsaturated sand, as long as suction is correctly incorporated in the effective stress, correlations developed for the sand when saturated/dry to establish the peak friction angle and relative density from the measured q_c are equally applicable to the sand when unsaturated. This is because the sand when unsaturated did not exhibit suction hardening (where suction hardening only exists if the yield surface size and isotropic normal consolidation line location depend on suction (Russell & Khalili 2006a)), and the sand behaved like a drained material during cone penetration irrespective of whether it was dry, saturated and unsaturated.

The same was not true for the unsaturated silty sand. Yang & Russell (2015, 2016) showed that the unsaturated silty sand behaved like a drained material. This is because the air in the pore space permitted volumetric compression to take place around a penetrating cone. Furthermore, since the silty sand exhibited suction hardening, the relationships which link penetration resistance to effective stress and relative density for drained saturated conditions would not apply to drained unsaturated conditions. These are a highly significant features to note and are the main reasons why CPT charts and relationships developed for saturated silty sands (or any soil with say more than 5% fines (i.e. sub 75 micron in size)) have no applicability to unsaturated silty sands. Any correlations for CPTs in a saturated silty sands, where undrained or partially drained conditions prevail around the penetrometer, are inapplicable to the interpretation of the CPT in the same soil when unsaturated.

This paper summaries the laboratory-controlled CPT results for the two unsaturated soils obtained. The effects of suction are highlighted.

The paper goes on to demonstrate how not accounting for suction can lead to incorrect soil classifications and incorrect estimates of a soil's tendency to dilate or contract. This may lead to unsafe consequences, for example when using the CPT to assess a soil's potential for liquefaction.

2 EFFECTIVE STRESS

Following the work of Bishop (1959) the effective stress σ' is defined as:

$$\sigma' = \sigma + \chi s \tag{1}$$

where a prime symbol denotes the stress invariant to be effective, σ is the total stress in excess of pore-air pressure (u_a) also referred to as the net stress, s is the suction, being the difference between pore-air and pore-water pressure ($u_a - u_w$), and χ is the effective stress parameter, having a value of 1 for saturated soils and 0 for dry soils.

3 CPT RESULTS IN UNSATURATED SYDNEY SAND AND LYELL SILTY SAND

The calibration chamber used was detailed by Pourhangiazar et al. (2011). The testing was conducted using a constant stress boundary condition.

The chamber accommodated cylindrical specimens with a height of 840 mm and diameter of 460 mm. The chamber has high–air entry ceramics embedded in the base plate for imposing suction in a specimen using the axis translation technique (i.e. imposing suction by elevating the pore air pressure above a positive pore water pressure). The axis translation technique was used for some specimens, while others were tested with suction being measured using vibrating wire piezometers.

CPTs were conducted using a miniature electrical cone with a diameter of 16 mm and cone tip area of 2 cm^2. The cone was pushed into the soil at constant rate of 2 cm/s. The miniature cone was used to increase the chamber to cone diameter ratio (R_D), which has a value of 29 in this study.

Sydney sand is a predominantly quartz sand sourced from the dunes around Kurnell, Sydney, Australia. An extensive experimental program was conducted by Russell & Khalili (2006a) to characterise saturated and unsaturated Sydney sand including the soil-water characteristic curves and mechanical behaviour. Index properties of the soil include a particle density of $\rho_s = 2.65$ g/cm^3, a minimum dry density of $\rho_{min} = 1.38$ g/cm^3 corresponding to the maximum voids ratio $e_{max} = 0.92$, and a maximum dry density $\rho_{max} = 1.66$ g/cm^3 corresponding to the minimum voids ratio $e_{min} = 0.60$. Peak friction angles φ' observed in drained triaxial compression, for both constant cell pressure and constant p' load paths, may be estimated using:

$$\varphi' - \varphi'_{cs} = 3\left[D_r\left(3.7 - \ln\left(\frac{p'_i}{p_a}\right)\right) - 0.9\right] \tag{2}$$

in which $D_r = (e_{max} - e)/(e_{max} - e_{min})$ is the relative density, φ'_{cs}=36.3° is the critical state friction angle and p'_i the mean effective stress at the beginning of shear. Russell & Khalili (2006a) found for Sydney sand that:

$$\chi = \begin{cases} 1 & \text{for} \quad \frac{s}{s_e} \le 1 \\ \left(\frac{s}{s_e}\right)^{-0.55} & \text{for} \quad 1 < \frac{s}{s_e} \le 25 \\ 25^{0.45}\left(\frac{s}{s_e}\right)^{-1} & \text{for} \quad 25 < \frac{s}{s_e} \end{cases} \tag{3}$$

where s_e is the suction value separating saturated from unsaturated states.

Lyell silty sand is a decomposed granite from the catchment area of Lyell dam, NSW, Australia. It contains 27% fines, including 4% clay (sub 2 micron). Index properties of the soil include ρ_s = 2.55 g/cm^3, ρ_{min} = 1.51 g/cm^3 corresponding to $e_{max} = 0.69$, and ρ_{max} = 2.02 g/cm^3 corresponding to $e_{min} = 0.29$. φ' observed in the triaxial compression tests on unsaturated samples with constant suctions may be estimated using:

$$\varphi' - \varphi'_{cs} = 3\left[D_r\left(4.9 - \ln\left(\frac{p'_i}{p_a}\right)\right) - 1.0\right] \tag{4}$$

where φ'_{cs}=35.7° and p'_i is the mean effective stress at the start of shearing. χ may be expressed as:

$$\chi = \begin{cases} 1 & \text{for} \quad \frac{s}{s_e} \le 1 \\ \left(\frac{s}{s_e}\right)^{-0.55} & \text{for} \quad 1 < \frac{s}{s_e} \end{cases} \tag{5}$$

Numerous CPTs were conducted on saturated and unsaturated Sydney sand within the calibration chamber (Pournaghiazar et al. 2013). Dry sand specimens were prepared by the pluvial deposition technique. Unsaturated specimens were formed by first saturating the specimens and then letting the moisture content reduce and then the applying axis translation technique to achieve a target suction.

Two initial relative densities ($D_r = 0.61$ and 0.33) and five net confining stresses (25 kPa, 30 kPa, 50 kPa, 100 kPa and 150 kPa, each applied isotropically) were used to test specimens. For a given relative density and confining stress combination, a test on a saturated specimen was performed, along with a number of tests on unsaturated specimens with initial suction measurements ranging from slightly larger than s_e to 200 kPa. It is noted that unsaturated Sydney sand specimens prepared in this way do not exhibit suction hardening (Russell & Khalili 2006a).

Samples of Lyell silty sand were prepared using static compaction of soil cured at certain moisture contents. After compaction of some samples a CPT was conducted immediately so that the sample suction was equal to the as-compacted value. For other samples the axis translation technique was used to reduce moisture content and increase suction. The axis translation technique enables more direct control of the suction applied. But the test soil had a low hydraulic conductivity (around 3×10^{-7} m/s for saturated conditions, and much lower for unsaturated conditions), which prevented uniform moisture and suction profiles from being achieved in reasonable time frames (Yang et al. 2014). Therefore, the moisture contents of the samples measured after a CPT was conducted were used to infer suctions. In samples in which CPTs were conducted without use of axis translation, the suction values were measured by three vibrating wire piezometers. Before inserting the piezometers their tips comprising high air-entry-value disks were carefully saturated.

For Sydney sand Pournaghiazar et al. (2013) presents the plots of q_c versus depth for saturated and unsaturated specimens. Suction has a significant influence on q_c. In all cases, suction causes the q_c to increase above the value measured in a saturated specimen for a given combination of relative density and net confining stress. For loose specimens, suctions of 25 kPa and 200 kPa increased q_c by 24% and 50% when the net confining stress was 50 kPa, and by 14% and 31% when the net confining stress was 100 kPa. For medium-dense specimens, the suction-induced increase of q_c was less than that for loose specimens for all the net confining stresses considered.

To interpret the Sydney sand results further it may be assumed that cone penetration in Sydney sand occurs under drained conditions; that is, when suction is constant, even though a constant moisture content condition actually exists. The differences in Sydney sand's stress-strain behaviour for constant suction and constant moisture content conditions are negligible, as long as the degree of saturation is less than about 10% (which is almost always the case in unsaturated sands) (Russell & Khalili 2006b). The constant suction assumption in Sydney sand means that the suction around the cone tip can be assumed equal to the initial or far-field value. Also, as s_e in the χ relationship does not vary significantly with sand deformation it can also be assumed that χs around the cone tip is also equal to the initial or far-field value. This greatly simplifies interpretation of the results. A plot of q_c versus imposed mean effective stress p' is presented in Figure 1, where $p' = p - u_w$ for saturated sands (u_w is the pore-water pressure), $p' = p + \chi s$ for unsaturated sands, and p is the mean net stress. An air entry value of $s_e = 7$ kPa was used in the calculations of χ. The data can be reasonably well fitted by the power law expression in the figure caption.

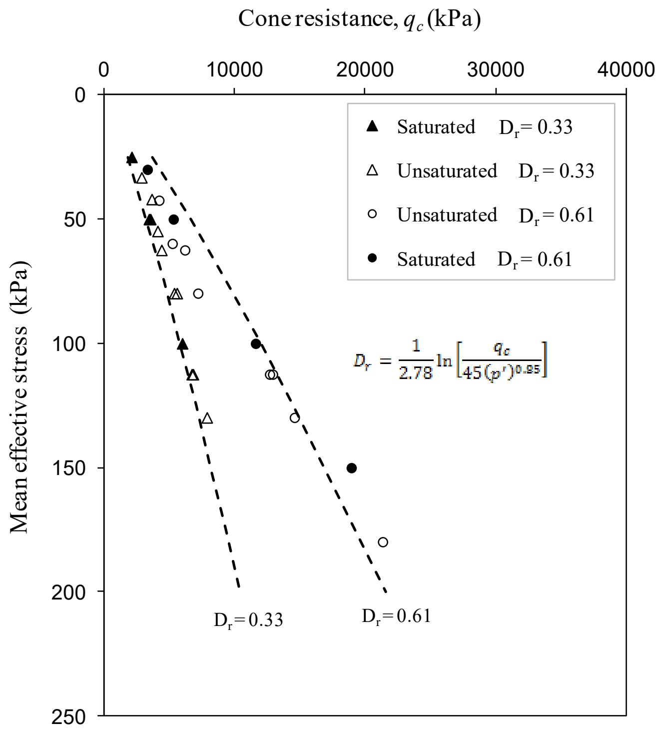

Figure 1. Comparison of CPT results for Sydney sand and estimations using the power law relationship $q_c = 45(p')^{0.85}\exp(2.78D_r)$.

Lyell silty samples were subjected to a range of isotropic net confining stresses. Yang & Russell (2016) presents plots of q_c versus depth for CPTs performed in unsaturated samples. Larger suctions caused larger cone penetration resistances. A suction of 37 kPa is associated with a q_c that is 50 % larger than the value for a suction of 24 kPa. A suction of 72 kPa is associated with a q_c that is 55 % larger than the value for a suction of 24 kPa.

Saturated CPTs in samples at void ratios comparable to those used in unsaturated CPTs were not conducted. However, insight in to the differences that would exist in CPT results from saturated and unsaturated Lyell silty sand can be obtained from cavity expansion analysis - an analog to the CPT. The pressure at the wall of an expanding spherical cavity (σ_L) is related to q_c. The most relevant findings of Yang & Russell (2015) who studied cavity expansions in unsaturated Lyell silty sand are summarised here. They studied the effects of three different drainage conditions (constant suction, constant moisture content and constant χs) on σ_L. For each drainage condition they observed that a significant change of void ratio occurs around an expanding cavity in the unsaturated soil, and analogously occurs around the tip of a penetrating cone. They found that, for a constant moisture content condition and full hydro-mechanical coupling, the changes to χ and s mostly counteract each other and constant χs may be assumed to give a reasonable approximation. The assumption of χs being a constant may be used to simplify interpretation of the CPT results.

Yang & Russell (2015) explained that the unsaturated silty sand around a cavity behaves more like a saturated drained soil than a saturated undrained soil as the air in the pore space permits volumetric compression. However, as Lyell silty sand exhibits suction hardening, there is not a 1:1 correlation between saturated drained behaviour and unsaturated drained behaviour. This is in contrast to unsaturated Sydney sand, which did not exhibit suction hardening, meaning unsaturated drained and saturated drained behaviours were virtually identical. This is a significant feature to note and the main reason why CPT charts and relationships developed for saturated silty sands (or any soil with, say, more than 5% fines) have no applicability to unsaturated silty sands. The saturated soil is partially drained or undrained, whereas the unsaturated soil behaves like it is drained causing very different stress-strain behaviours.

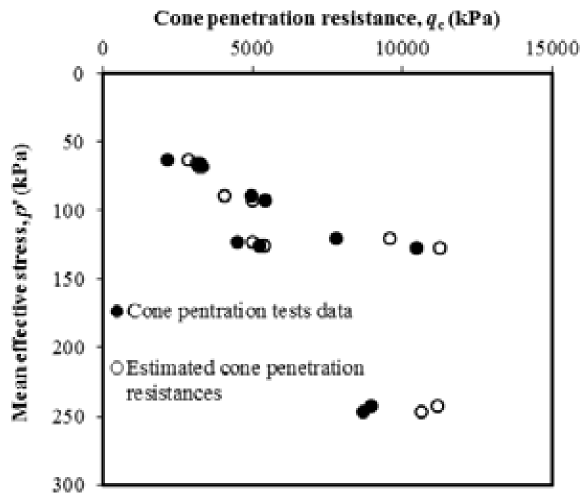

Figure 2. Comparison of CPT results for Lyell silty sand and estimations using the power law relationship $q_c = 162(p')^{0.65}\exp(2.6D_r)$.

The CPT results are presented in Figure 2 in the q_c versus p' plane using solid symbols. The initial χs was used in the computation of p'. The data can be reasonably well fitted by the power law expression in the caption of Figure 2 in which q_c and p' have units of kPa. The predicted q_c values from this expression are shown using hollow symbols. The error associated with the expression to obtain q_c is less than 30%.

4 SUCTION INFLUENCES ON SOIL CLASSIFICATION

A chart for classifying soil type and assessing whether a soil being tested is contractive or dilative has been proposed by Robertson (2010). Only that chart will be focussed on here, although many others exist in the literature. The findings made here would also be evident in other interpretation frameworks, if they were put under the same scrutiny.

In using the chart the normalised cone resistance, Q_{tn}, is plotted against the normalised friction ratio, F_r, where each is defined as:

$$Q_{tn} = \frac{q_c - \sigma_v}{p_a}\left(\frac{p_a}{\sigma'_v}\right)^n \tag{6}$$

$$F_r(\%) = \frac{f_s}{q_c - \sigma_v} \times 100 \tag{7}$$

The exponent n is the exponent that relates q_c to σ'_v or p' in power law relationships, thus n = 0.85 for Sydney sand while saturated and unsaturated and n = 0.65 for Lyell silty sand while unsaturated. f_s denotes the sleeve friction. The chart is plotted as Figure 3, and it can be seen that the location of the Q_{tn}, F_r coordinate enables estimation of soil type and whether it is contractive or dilative.

Figure 3 also shows the Sydney sand data with the effects of suction correctly incorporated in to σ'_v, with solid circular symbols representing saturated or dry tests and hollow circular symbols the unsaturated tests. Also shown is the Sydney sand data when the effects of suction are ignored, that is when σ'_v is taken to be equal to σ_v for the unsaturated tests, with cross symbols representing the unsaturated tests. It can be seen that the circular symbols, hollow and solid, are located in region 6 belonging to clean sands. Correct interpretation of the CPT results using the effective stress concept results in the correct soil classification. The crosses, representing data when suction is ignored, plot a little higher than the hollow circular symbols, indicating the soil is more dilative than it actually is, although not to the extent that an incorrect soil classification would result. Care should be taken and account given to χs in the effective stress before charts like this are used, even for clean sands.

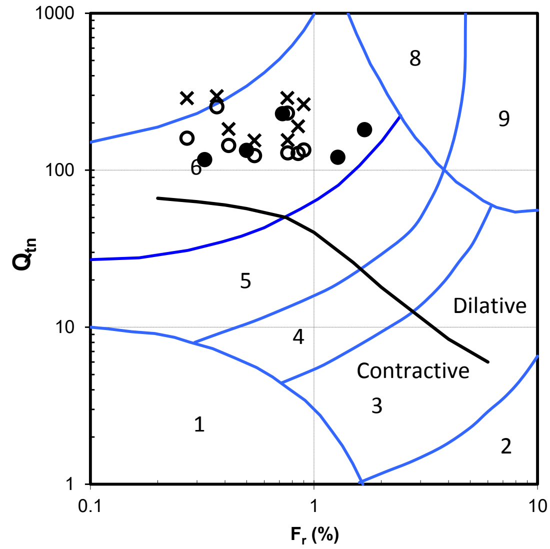

Figure 3. CPT data for Sydney sand with the effects of suction correctly incorporated in the circular symbols (solid symbols representing saturated or dry tests and hollow symbols representing the unsaturated tests). Also shown is data when the effects of suction are ignored in the unsaturated tests using the cross symbols. (Key: 1. Sensitive, fine grained, 2. Organic soils – peats, 3. Clays – clay to silty clay, 4. Silt mixtures – clayey silt to silty clay, 5. Sand mixtures – silty sand to sandy silt, 6. Sands – clean sand to silty sand, 7. Gravelly sand to sand, 8. Very stiff sand to clayey sand*, 9. Very stiff, fine grained*; where (*) indicates heavily overconsolidated or cemented.)

Figure 4 shows data for a quartz marine sand, including up to 8% fines, taken from a reclaimed land site in Hong Kong (Lee et al. 1999). It was not possible to incorporate the effects of suction correctly into σ'_V. Calibration chamber tests on that soil enabled the exponent n = 0.8 to be determined. Solid circular symbols represent saturated test data and cross symbols the unsaturated test data (where σ'_V is taken to be equal to σ_V). It can be seen that the solid circular symbols are located across regions 4 and 5, belonging to silt and sand mixtures, and all but one data point indicate that the soil is slightly dilative. The cross symbols are located in region 6, incorrectly implying that the soil is a clean sand and very dilative. The drastic shift of the unsaturated data for this soil most probably comes from the pronounced affect suction has on the effective stress, arising from the significant fines content, and also from the sand behaving more like a partially drained/ undrained material when saturated as penetration occurs compared to it behaving more like a drained material when unsaturated as penetration occurs.

Figure 5 shows data for a gold tailings. For this material, CPT probing was undertaken in the same location on a tailings facility at regular intervals, across which the phreatic surface (inferred through dissipation tests) was seen to vary. Again it was not possible to incorporate the effects of suction correctly in to σ'_V. Solid circular symbols represent saturated test data and cross symbols the unsaturated test data (where σ'_V is taken to be equal to σ_V). It can be seen that the solid circular symbols are located across regions 3 and 4, belonging to clays and silt mixtures, and all data points indicate that the tailings is highly contractive and susceptible to liquefaction. The cross symbols locate in region 4, incorrectly implying that the tailings is a silt mixture that is slightly contractive or slightly dilative. Again suction causes a drastic shift of the unsaturated data for this tailings, and can give an unsafe and false indication of the tailings' susceptibility to contractive behaviour and liquefaction if not accounted for.

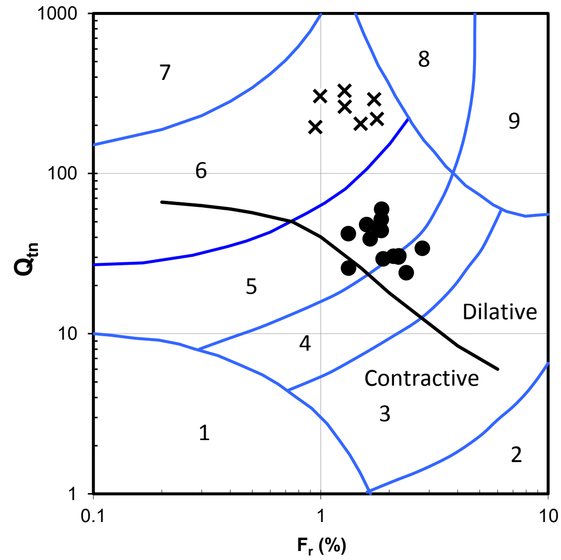

Figure 4. CPT data for marine sand with up to 8% fines. Solid circular symbols represent saturated test data and the cross symbols represent the unsaturated test data. The effects of suction were not incorporated.

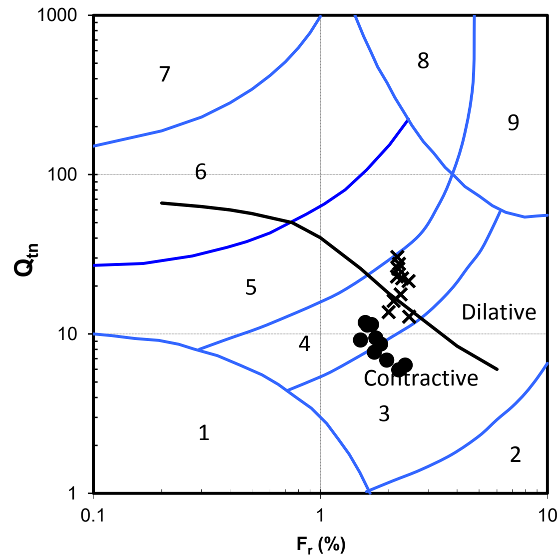

Figure 5. CPT data for a gold tailings. Solid circular symbols represent saturated test data and the cross symbols represent the unsaturated test data. The effects of suction were not incorporated.

5 CONCLUSION

CPTs conducted in saturated and unsaturated Sydney sand and unsaturated Lyell silty sand highlight the effects of suction on cone penetration resistance. In general the effects of suction were most pronounced for the lowest relative densities considered. Also, the effects of suction became more significant as the applied net confining stress decreased, and thus the effects of suction in field testing are most important for shallow penetrations (up to 5 m) where a soil is most likely to be unsaturated.

The unsaturated Sydney sand around a penetrating cone behaves just like the saturated Sydney sand. The same empirical power law relationship linking D_r, q_c, and p' holds for saturated and unsaturated conditions, because unsaturated Sydney sand does not exhibit suction hardening.

Conversely, the unsaturated silty sand around a penetrating cone behaves more like a saturated drained soil than a saturated undrained soil as the air in the pore space permits volumetric compression. However, as Lyell silty sand exhibits suction hardening, there is not a 1:1 correlation between saturated drained behaviour and unsaturated drained behaviour. This is a highly significant feature to note and is the main reason why CPT charts and relationships developed for saturated silty sands (or any soil with say more than 5% fines) have no applicability to unsaturated silty sands.

This is also evident when CPT data from a range of soils for both saturated and unsaturated conditions are plotted in soil classification charts. For unsaturated soils having a significant amount of fines (say more than 5%) the suction induced increase in cone resistance, and the change of the soil behaviour from partially drained/undrained to more like drained, causes incorrect soil classification and an incorrect assessment that the soil is dilative.

6 ACKNOWLEDEMENTS

Thanks goes to UNSW's Industry Research Fellowship scheme for DR to visit AR, and to the Australian Research Council for funding (DP0667260).

7 REFERENCES

Baldi, G., Bellotti, R., Ghionna, V., Jamiolkowski, M. & Pasqualini, E. 1982. Design parameters for sands from CPT. *In Proceedings of the Second Euro Symposium on Penetration Test,* Balkema, Rotterdam, The Netherlands, Vol. 2, 425-432.

Bishop, A.W. 1959. The principle of effective stress. *Teknisk Ukeblad* 106: 859-863

Collins, R., & Miller, G.A. 2014. Cone penetration testing in unsaturated soils at two Instrumented test sites. *In Proceedings of the 6th international conference on unsaturated soils*, UNSAT, Sydney, Australia, Balkema, Lisse, Vol. 2, 1489-1494.

Jamiolkowski, M., Lo Presti, D.C.F. & Manassero, M. 2003. Evaluation of relative density and shear strength of sands from CPT and DMT, Soil behavior and soft ground construction, *ASCE Geotechnical Special Publication 119* (eds. Germaine, J.T., Sheahan, T.C. & Whitman, R.V.) 201-238.

Lee, K.M., Shen, C.K., Leung, D.H.K. & Mitchell, J.K. 1999. Effects of placement method on geotechnical behaviour of hydraulic fill sands. *Journal of Geotechnical and Geoenvironmental Engineering* 125(10): 832-846.

Lehane, B., Ismail, M.A., & Fahey, M. 2004. Seasonal dependence of in situ testparameters in sand above the water table. *Geotechnique* 54(3): 215-218.

Pournaghiazar, M., Russell, A.R., & Khalili, N. 2011. Development of a new calibration chamber for conducting cone penetration tests in unsaturated soils. *Canadian Geotechnical Journal* 48(2): 314-321.

Pournaghiazar, M., Russell, A.R., & Khalili, N. 2013. The cone penetration test in unsaturated sands. *Geotechnique* 63(14): 1209-1220.

Robertson, P.K. 2010. Evaluation of flow liquefaction and liquefied strength using the cone penetration test. *Journal of Geotechnical and Geoenvironmental Engineering* 136(6): 846–853.

Robertson, P.K. & Campanella, R.G. 1983a. Interpretation of cone penetration tests, Part I: Sand. *Canadian Geotechnical Journal* 20(4) 718–733.

Robertson, P.K., & Campanella, R.G. 1983b. Interpretation of cone penetration tests. Part II: Clay. *Canadian Geotechnical Journal* 20(4): 734-745.

Russell, A.R. & Khalili, N. 2006a. A unified bounding surface plasticity model for unsaturated soils. *International Journal for Numerical and Analytical Methods in Geomechanics* 30(3): 181-212.

Russell, A.R., & Khalili, N. 2006b. On the problem of cavity expansion in unsaturated soils. *Computational Mechanics* 37(4): 311-330.

Yang, H., Khoshghalb, A., & Russell, A.R. 2014. Fractal-based estimation of hydraulic conductivity from soil-water characteristic curves considering hysteresis. *Geotechnique Letters* 4: 1-10.

Yang, H., & Russell, A.R. 2015. Cavity expansion in unsaturated soils exhibiting hydraulic hysteresis considering three drainage conditions. *International Journal for Numerical and Analytical Methods in Geomechanics.* 39: 1975-2016.

Yang, H. & Russell, A.R. 2016. The cone penetration test in an unsaturated silty sand. *Canadian Geotechnical Journal.* 53(3): 431-444.

Theme 4. Laboratory Testing and Sampling

Geotechnical and Geophysical Site Characterisation 5 – Lehane, Acosta-Martínez & Kelly (Eds)
 ISBN 978-0-9946261-1-0

Engineering characterization of a leached marine clay using Sherbrooke block samples

H.A. Amundsen, A. Emdal & V. Thakur
Norwegian University of Science and Technology (NTNU), Trondheim, Norway

ABSTRACT: A detailed characterization of the leached marine clay at Rissa, North-West of Trondheim in Norway, is presented. The site lies just a few hundred meters away from the location where the well-known Rissa slide occurred in 1978. Geotechnical investigations were carried out in connection with the planning of a new road. Norwegian University of Science and Technology (NTNU) has done extensive work related to the geotechnical characterization of the site over several years, using 54 mm and 73 mm diameter tube sampling. High quality block samples were extracted using a Sherbrooke block sampler. This paper aims to characterize the material in view of results from block samples and study the effect of sample disturbance on the soil properties.

1 INTRODUCTION

Marine clay deposits in Norway have been subjected to leaching by a flow of fresh water. As a result to this, their salt ion concentration in the pore water is reduced to as low as 3-5 g/l. Such clays, termed leached marine clays in this paper, are characterized using its sensitivity (S_t), which is the ratio between undrained shear strength (c_u) and remoulded shear strength (c_{ur}). The engineering characterization of leached marine clays is a challenging task because this type of material changes character upon the slightest disturbance. Because of this, undrained shear strength, stiffness and preconsolidation stress is often underestimated. Hence, high quality sampling is essential to get a proper understanding of the engineering behavior of such clays (e.g. Hvorslev, 1949; Noorany & Seed, 1965; Berre et al., 1969; La Rochelle & Lefebvre, 1971; Bjerrum, 1973; Baligh et al., 1987; Hight et al., 1992; Lunne et al., 1997a; 2006; Ladd & DeGroot, 2003; Long, 2006; Karlsrud & Hernandez-Martinez, 2013; Amundsen et al., 2015a; 2015b). This issue is addressed in this paper using the laboratory test results from two types of piston samplers and a Sherbrooke sampler (Lefebvre & Poulin, 1979). The results are compared with piezocone tests and geophysical investigations.

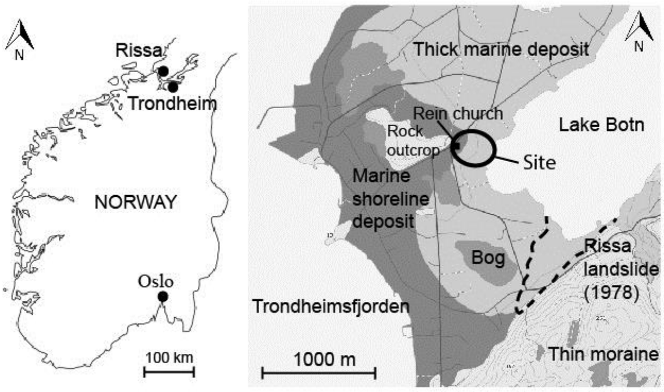

Figure 1. The Rissa site (map: www.ngu.no).

Table 1. Summary of investigations at Rissa site.

Date of work	Description	Reference and companies
1974-80	Conventional investigation – development of a new road	NPRA*
1978-81	Geotechnical investigation in connection with Rissa landslide that occurred in 1979	NPRA*, NGI*, NTNU(NTH)*, SINTEF(IKU)*
1981-90	Evaluation of slope stability near Lake Botn	NGI*
2008-10	Detailed geotechnical investigation – CPTU, sampling and hazard mapping	NGI (2009a), (2009b)
2009-12	Resistivity measurements and the sea floor mapping of Lake Botn (NGU)	L'Heureux et al. (2012), Solberg et al. (2012), (2014)
2010	2D resistivity and RCPT measurements (NTNU and NGU)	Aasland (2010), Solberg et al. (2012), (2014)
2010	Steel tube sampling, 54 mm and 73 mm, and CPTU (NTNU)	Kåsin (2010)
2011	High quality CPTU tests and 54 mm tube sampling	Multiconsult AS*
2011-12	High quality Sherbrooke block sampling and testing (NTNU)	Amundsen (2012)

*Several reports

2 GEOLOGICAL CHARACTERIZATION OF THE RISSA CLAY

The Rissa site is located North-West of Trondheim in Norway, shown in Figure 1. The site slopes slightly from Rein church to the shoreline of Lake Botn, which is brackish. The length of the slope is about 200 m and the inclination is 6°. The site lies just a few hundred meters away from the location where the Rissa landslide occurred in 1978 (Gregersen, 1981). The landscape around Lake Botn is formed by erosion and landslides, and is now mainly used as farmland.

The groundwater flow in the upper part of slope is seasonal, while at the bottom the groundwater level located about one meter below the ground surface. The elevation of the site is 3 m above the mean sea level. The typical temperature at the site is 4-6°C.

The geology of the Rissa site is shown as a geological map in Figure 1. The marine limit from the glacial period was elevated - at the highest to approximately 158 m above the current sea level (Reite, 1987). The main ice movement was directed northeast in this part of Norway, until the ice became so thin that its direction was determined by the topography (Reite, 1996). At the Rissa site however, the ice moved to the southeast (Reite, 1996), resulting in large deposits of thick marine sediments on the uneven rock surface surrounding Lake Botn, shown in Figure 1.

The Rissa site was characterized using electrical resistivty tomography (ERT), which produces resistivity profiles of the soil (see Figure 2). The profiles were interpreted based on the following classification (e.g. Solberg et al., 2011, 2014; Donohue et al., 2014): Unleached clay deposits: 1–10 Ωm; Leached clay deposits, possibly quick: 10–100 Ωm; Dry crust clay deposits and coarse sediments: >100Ωm.

Geophysical investigations showed an indentation between two mountain ridges filled with marine clay deposits (15-70 m) that is covered with sand and gravel (1-5 m). Based on the geophysical profiles (Solberg et al., 2012) a sketch of underground topography has been developed to illustrate the complexity of the site, shown in Figure 4. On the geological

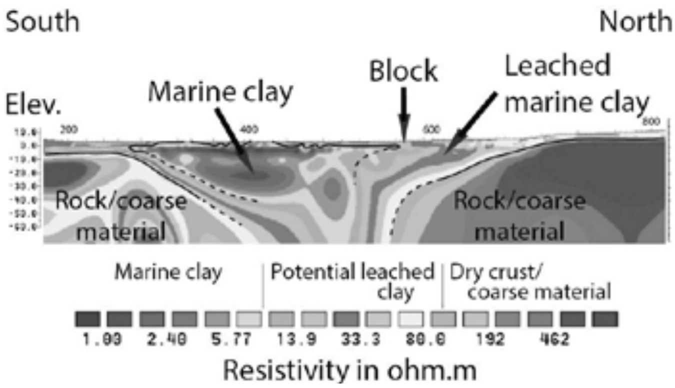

Figure 2. Geophysical profile - Rissa site (Solberg et al., 2012).

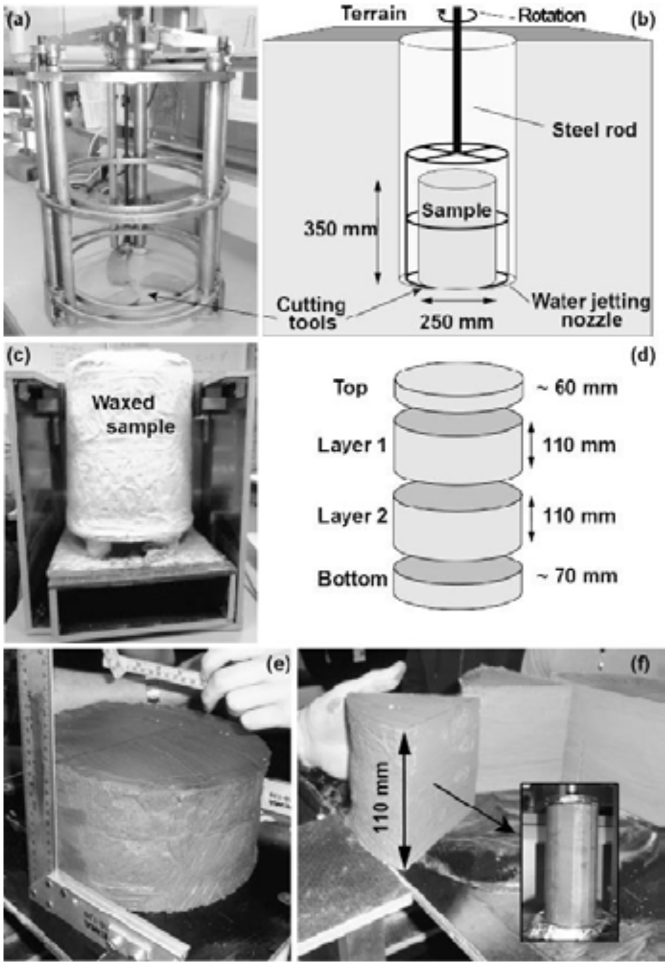

Figure 3. (a) Sherbrooke block sampler at NTNU, (b) schematic view of a block sample being carved, (c) waxed sample, (d) schematic view of a sliced sample, (e) a block sample slice and (f) a piece of clay from a block sample (after Amundsen et al., 2016).

map in Figure 1, these mountains ridges are visible as rock outcrops. The Sherbrooke block samples were taken from the leached marine clay deposit, as indicated in Figure 2.

3 GEOTECHNICAL INVESTIGATIONS

The Rissa site was extensively studied between 1974 and 2011 using a variety of investigation techniques. A brief summary of the geotechnical investigations

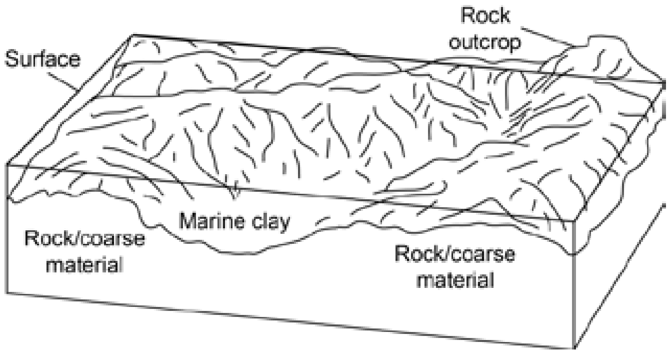

Figure 4. Sketch of underground topography at Rissa, based on geophysical profiles carried out by Solberg et al. (2012).

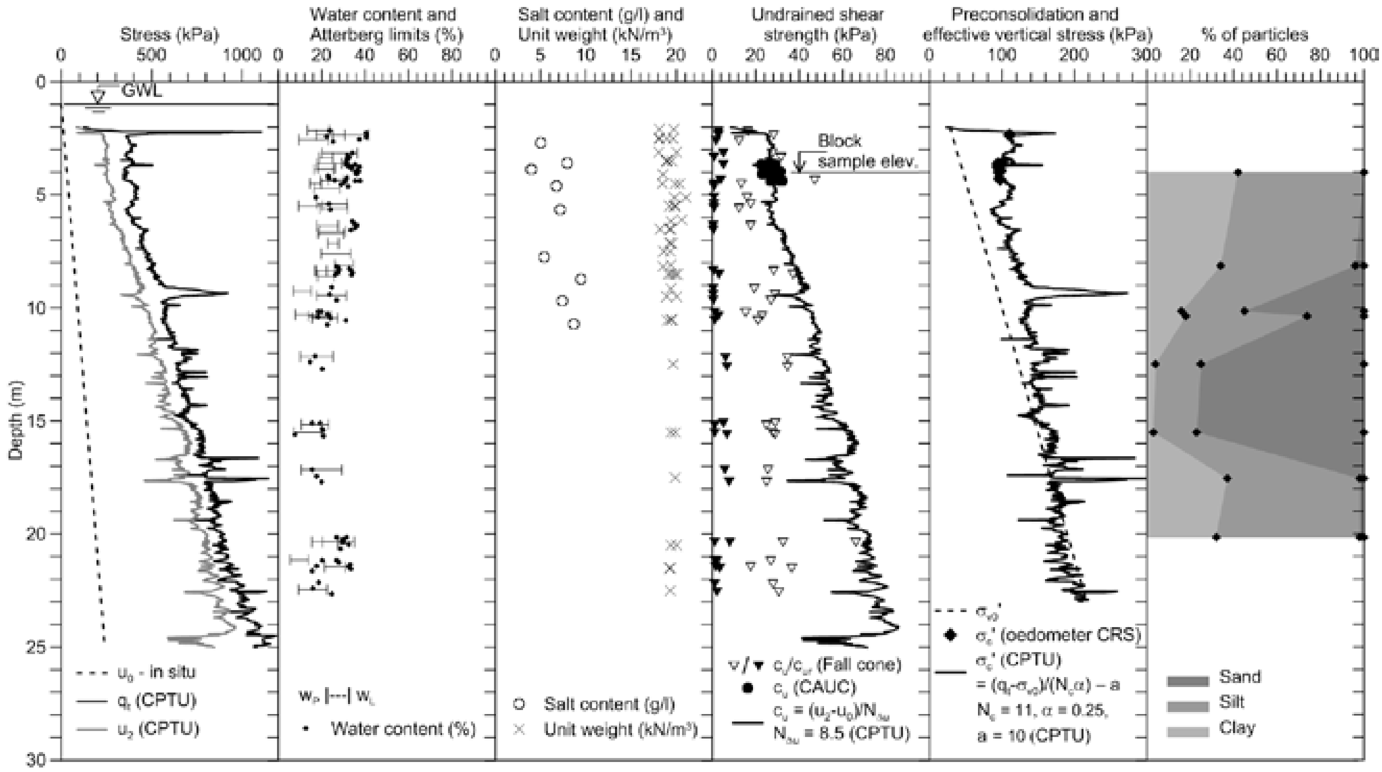

Figure 5. Geotechnical profile of Rissa site. CPTU correlations of the undrained shear strength and preconsolidation stress are based on work of Lunne et al. (1997b) and Sandven (1990).

is presented in Table 1. The marked area in Figure 1, enclosing about 0.05 km^2, was heavily investigated. A total of 2 soundings, 21 rotary pressure soundings, 13 piezometers, 9 CPTU soundings, 4 RCPTU soundings, 11 boreholes with tube sampling (54 mm and 73 mm) and one borehole with five Sherbrooke block samples were conducted. The block samples were taken by the Norwegian University of Science and Technology (NTNU) in order to study the effect of sample disturbance.

The Sherbrooke sampler, sampling process and the laboratory handling is illustrated in Figure 3. The obtained block samples had a diameter of 250 mm and a height of 350 mm.

The laboratory testing at NTNU included a study of the effect of shear strain rate (0.1-4.5%/hr) on peak undrained shear strength in triaxial tests. The study included 18 triaxial tests. In addition, 20 constant rate of strain (CRS) oedometer tests and 5 incremental loading (IL) oedometer tests were carried out on the block samples.

4 RESULTS

The soil profile of the Rissa clay, Figure 5, indicates that the shallow upper 9 m of the deposit is covered by leached marine clay with the unit weight of 18-20 kN/m^3 the salt content varied between 2.0 and 9.5 g/l. The remoulded shear strength is between 0.2 to 6 kPa and the sensitivity is in the range of 2 to 94.

The test site is also underlain by lower (> 9 m) non-sensitive clay with silt, sand and gravel. The ERT geophysical investigations verifies the interpretation of the layering at the site.

Anisotropically consolidated triaxial undrained compression tests (CAUC) and oedometer tests were performed on 54 mm and 73 mm diameter tube samples of the Rissa clay, and the results are compared with those obtained from block samples, as shown in Figure 6. The triaxial test results are normalized with vertical effective in situ stress ($\sigma`_{v0}$). The presented samples in Figure 6 were retrieved from a depth of 3.6 to 5.4 meters and have an estimated preconsolidation stress of 94 to 103 kPa and an OCR of 1.8-2.2.

The effect of sample disturbance on the stress and the deformation properties of Rissa clay is investigated using the triaxial and odometer results. The quality of the samples was determined by its compressibility during reconsolidation to the in situ stresses. Lunne et al. (1997a) proposed a sample assessment criterion on a normalized change in void ratio, $\Delta e/e_0$, where e_0 is the initial void ratio.

5 DISCUSSION

5.1 *Conventional tube versus block samples*

In the case of soft low plastic clay, such as Rissa clay, it was found that the block samples results in better quality that the tube samples, see Figure 6. The tests conducted on block samples yield higher peak undrained shear strength, stiffness and preconsolidation stress. The reason for the discrepancies is a well-known tube sampler disturbance (e.g. Baligh

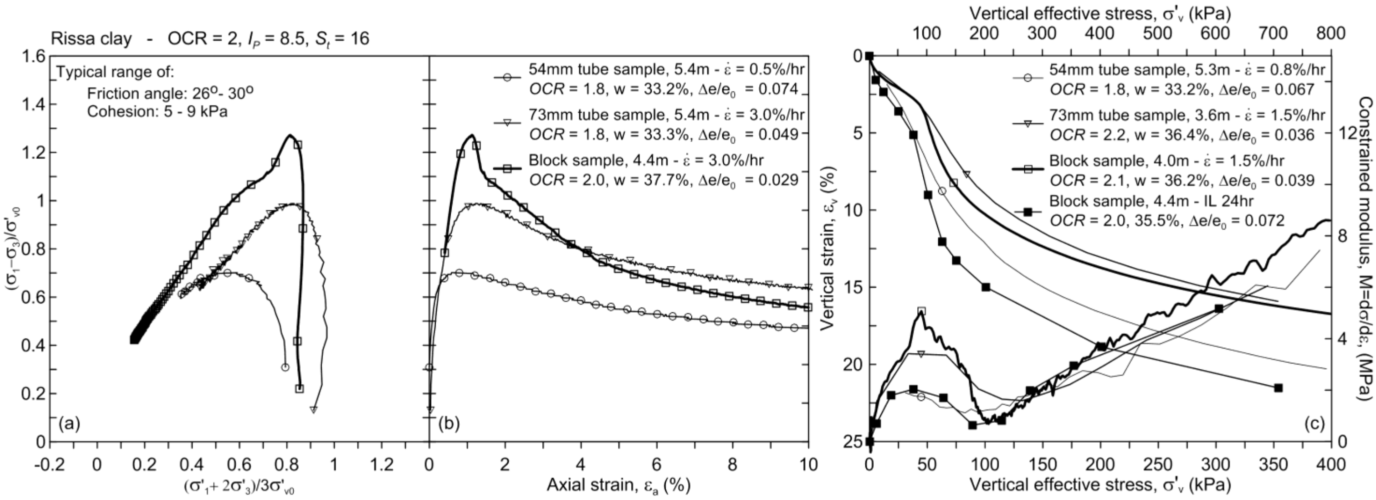

Figure 6. Typical (a)-(b) CAUC triaxial test results and (b) CRS oedometer tests results from Rissa.

et al., 1987). Block sampling avoids this type of disturbance; however stress relief may become an issue if the sample is extracted from a great depth (Amundsen et al., 2016). A careful handling of the block sample is essential to obtain high quality results. Therefore, sealing techniques, transport and storage methods are important factors to consider in preventing sample disturbance.

Even though the advantages of block sampling are well known, the conventional 54 mm diameter tube sampler is still used in Norway as a part of routine sampling. Block sampling is done only for selected cases.

5.2 *Strength behavior*

The normalized undrained peak shear strength (c_u/σ'_{v0}) obtained from CAUC triaxial test results were expressed by the "Stress History And Normalized Soil Engineering Properties" (SHANSEP) concept, developed by Ladd & Foott (1974). The concept was developed to study the c_u of artificially overconsolidated clays, but it is also useful for comparing c_u of block samples (Karlsrud & Hernandez-Martinez, 2013). The results in Figure 7 show that Rissa clay fits well between the average and upper limit of the proposed correlation values, which are based on empirical data from Norwegian clays (Karlsrud & Hernandez-Martinez, 2013).

As in the oedometer tests, the results of a triaxial test depend on the strain rate. An increase in the strain rate generally results in an increased c_u and brittle behavior. Lunne & Andersen (2007) showed that there is a factor of approximately 1.5 in the estimate of c_u in a triaxial compression test for strain rates from 0.01%/hr to 100%/hr. The strain rate sensitivity of a soil varies with soil type and its stress history. Lightly overconsolidated clays, such as the Rissa clay, are more sensitive to the rate of shear strain than highly overconsolidated clays (Ladd & DeGroot, 2003). Both normally consolidated and overconsolidated Norwegian clays (Lunne & Andersen, 2007) are presented in Figure 8, with the test carried out on the Rissa clay. The c_u is normalized with a value from a test carried out with a shear strain rate of 4.5%/hr, after a study conducted by Lunne & Andersen (2007).

A distinct increase in the shear strength with increasing rate of strain is observed in Figure 8. A triaxial test carried out at 4.5%/hr has 20% higher normalized undrained shear strength than a test sheared with 0.1%/hr. Commonly used strain rates in Norway have been between 0.7% and 3.0% per hour.

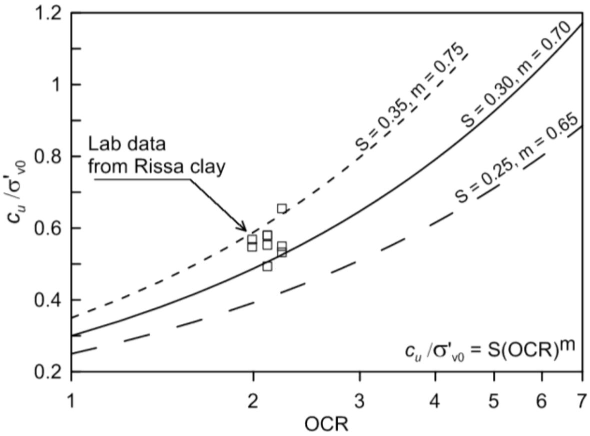

Figure 7. Normalized undrained shear strength vs. OCR from block samples from Rissa. Compared with SHANSEP correlations (Karlsrud & Hernandez-Martinez, 2013).

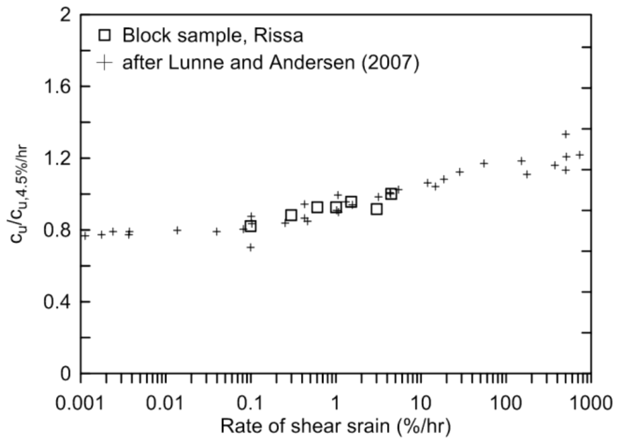

Figure 8. Normalized undrained shear strength as a function of rate of shear strain in strain-controlled laboratory tests from Rissa and data from Lunne & Andersen (2007).

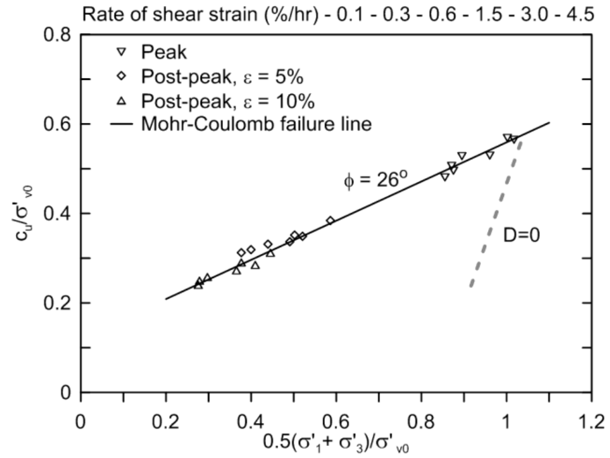

Figure 9. Normalized undrained shear strength from CAUC triaxial tests on block samples from Rissa.

In practice, this has a minimal effect on the strength and the strain softening behavior (Thakur et al., 2016).

The effect of shear strain rate influences the peak undrained shear strength, however, based on the presented results in Figure 9; it does not influence the failure line or the friction angle of the Rissa clay. In other words, the strain softening at the laboratory strain levels in such material is due to shear induced excess pore pressure not because of the reduction in the cohesion or the friction angle. The concept of cohesion and friction softening is more applicable to overconsolidated clays than to soft sensitive clays at laboratory strain levels under undrained conditions. However, for very large strain levels cohesion and friction softening may also be observed for soft sensitive clays, such as Rissa clay. This observation is in line with the work done by Thakur et al. (2014).

5.3 *Preconsolidation pressure*

For the block samples, oedometer tests clearly indicate the preconsolidation pressure compared to the tube samples, see Figure 6c. The effects of sample disturbance is also evident in the reduction of stiffness in the overconsolidated range. Some discrepancies in the results are expected due to the comparison of samples from different depths and overconsolidation. However, the reduction in stiffness of the 54 mm tube sample is greater than what one may expect.

An incremental loading (IL with 24 hr load steps) oedometer test and a constant rate of strain (CRS – 1.5%/hr) odometer test from the same block sample are compared in Figure 6c. The preconsolidation stress is 95 kPa for the CRS test and 80 kPa for the IL test, which corresponds to a 16% decrease. The preconsolidation stress from CRS oedometer tests is rate dependent and may result in a high preconsolidation stress at high strain rates (e.g. Leroueil et al., 1983, 1985; Nash et al., 1992). On the other hand, the 24hr load duration in IL tests causes creep deformations in the soil and therefore contributes to a large change in void ratio. In return, a lower preconsolidation pressure results.

In practice, one should consider carefully which material parameters one should use. An oedometer test conducted on a block sample may give a higher stiffness than a tube sample; however, it will reduce dramatically when the stresses exceed the preconsolidation. It is especially important to consider this in the settlement analysis.

6 CONCLUDING REMARKS

This paper details the characteristics and engineering properties of the Rissa clay, a thick deposit of leached marine clay in Central Norway. The soil layering interpreted using ERT is in good agreement with the conventional geotechnical investigations.

Laboratory results indicate that the block sampler, compared with tube samplers, obtained less disturbed samples. However, the 73 mm sampler can provide high quality results similar to those of block samples. Poor quality samples can provide non-representative and even non-conservative design parameters.

The Rissa clay is a low plastic soft clay with a plasticity index of 5-8%. The typical range of c_u/σ'_{v0} from CAUC triaxial tests conducted on block samples is between 0.49 and 0.65. From the oedometer CRS tests, the overconsolidation ratio was estimated to be from 1.99 to 2.23.

The behavior of the Rissa clay is similar to other Norwegian clays regarding the effect of the rate of shear strain. The correlation between the undrained shear strength in triaxial tests and the overconsolidated ratio is also as expected.

7 ACKNOWLEDGEMENTS

Engineers J. Jønland, G. Winther, E. Husby and P. Østensen at NTNU are gratefully acknowledged for their skills and knowledge that made the experimental work possible. The authors are also grateful for a collaboration with Multiconsult AS and NPRA.

The authors wish to acknowledge support from the intergovernmental program “NIFS” (2012-15), funded by the NPRA, Norwegian Water Resources and Energy Directorate, and Norwegian National Rail Administration. The authors gratefully acknowledge the OFFPHD, a program by the Research Council of Norway their financial support.

8 REFERENCES

Aasland, R. (2010). Kartlegging av kvikkleire med 2D resistivitet og RCPT i Rissa (in Norwegian). MSc thesis, NTNU.

Amundsen, H. A. (2012). (prev. Kornbrekke) Slope stability at Rein Kirke based on results from Sherbrooke block samples (in Norwegian). MSc thesis, NTNU.

Amundsen, H. A., A. Emdal, R. Sandven and V. Thakur (2015a). On engineering characterisation of a low plastic sensitive soft clay. GeoQuébec2015 - Challenges from North to South. Québec, Canada.

Amundsen, H. A., V. Thakur and A. Emdal (2015b). Comparison of Two Sample Quality Assessment Methods Applied to Oedometer Test Results. *Proc. of the 6th Int. Symp. on Deform. Charact. of Geomat.*, Vol. 6, 923-930.

Amundsen, H. A., V. Thakur and A. Emdal (2016). Sample disturbances in block samples of low plastic soft clays. *Proc. of the 17th Nordic Geotechnical Meeting*, *Reykjavik, Iceland*, 159-168.

Baligh, M., A. Azzouz and C. Chin (1987). Disturbances Due to "Ideal" Tube Sampling. *Journal of Geotechnical Engineering* 113(7): 739-757.

Berre, T., K. Schjetne and S. Sollie (1969). Sampling disturbance of soft marine clays. *Proc. of the 7th ICSMFE, Special Session*, *Mexico*, Vol. 1, 21-24.

Bjerrum, L. (1973). Problems of Soil Mechanics and Construction on Soft Clays. State-of-the-art report. *Proc. of the 8th ICSMFE*, *Moscow*, Vol. 3, 111-159.

Donohue, S., M. Long, J.-S. L'Heureux, et al. (2014). The Use of Geophysics for Sensitive Clay Investigations. *Landslides in Sensitive Clays: From Geosciences to Risk Management*. Springer Netherlands, 159-178.

Gregersen, O. (1981). The Quick Clay Landslide in Rissa, Norway. NGI-Publications. 135.

Hight, D. W., R. Böese, A. P. Butcher, et al. (1992). Disturbance of the Bothkennar clay prior to laboratory testing. *Géotechnique* 42(2): 199-217.

Hvorslev, M. J. (1949). *Subsurface exploration and sampling of soils for civil engineering purposes. Report on soil sampling.* Vicksburg, U.S. waterways experiment station.

Karlsrud, K. and F. G. Hernandez-Martinez (2013). Strength and deformation properties of Norwegian clays from laboratory tests on high-quality block samples. *Canadian Geotechnical Journal* 50(12): 1273-1293.

Kåsin, K. (2010). CPTU i kvikkleire i Rissa (in Norwegian). MSc thesis, NTNU.

L'Heureux, J.-S., R. S. Eilertsen, S. Glimsdal, et al. (2012). The 1978 Quick Clay Landslide at Rissa, Mid Norway: Subaqueous Morphology and Tsunami Simulations. *Submarine Mass Movement and Their Consequences: 5th Int. Symp.* Springer Netherlands, 507-516.

La Rochelle, P. and G. Lefebvre (1971). Sampling disturbance in Champlain clays. *Sampling of Soil and rock, ASTM STP 483*, 143-163.

Ladd, C. C. and D. J. DeGroot (2003). Recommended practice for soft ground site characterization: Arthur Casagrande Lecture. *12th PCSMGE*, *MIT, Cambridge, Massachusetts*.

Ladd, C. C. and R. Foott (1974). New design procedure for stability of soft clays. *Journal of the Geotechnical Engineering Division* 100(GT7): 763-786.

Lefebvre, G. and C. Poulin (1979). A new method of sampling in sensitive clay. *Canadian Geotechnical Journal* 16(1): 226-233.

Leroueil, S., M. Kabbaj, F. Tavenas and R. Bouchard (1985). Stress-strain-strain rate relation for the compressibility of sensitive natural clays. *Géotechnique* 35(2): 159-180.

Leroueil, S., F. Tavenas, L. Samson and P. Morin (1983). Preconsolidation pressure of Champlain clays. Part II. Laboratory determination. *Canadian Geotechnical Journal* 20(4): 803-816.

Long, M. (2006). Sample disturbance effects on medium plasticity clay/silt. *Proceedings of the Institution of Civil Engineers - Geotechnical Engineering* 159(2): 99-111.

Lunne, T. and K. H. Andersen (2007). Soft clay shear strength parameters for deepwater geotechnical design. *6th Int. Offshore Site Investigation and Geotech. Conf.*, *London*, 151-176.

Lunne, T., T. Berre, K. H. Andersen, et al. (2006). Effects of sample disturbance and consolidation procedures on measured shear strength of soft marine Norwegian clays. *Canadian Geotechnical Journal* 43(7): 726-750.

Lunne, T., T. Berre and S. Strandvik (1997a). Sample disturbance effects in soft low plastic Norwegian clay. *Proc. of the Symp. on Recent Develop. in Soil and Pavement Mech.*, *Rio de Janeiro, Brazil*, 81-102.

Lunne, T., P. K. Robertson and J. J. M. Powell (1997b). *Cone penetration testing in geotechnical practice*. London, Spon Press.

Nash, D. F. T., G. C. Sills and L. R. Davison (1992). One-dimensional consolidation testing of soft clay from Bothkennar. *Géotechnique* 42(2): 241-256.

NGI (2009a). Grunnundersøkelse, Datarapport. Rv. 717 Sund-Bradden (in Norwegian), NGI.

NGI (2009b). Stabilitetsberegning, Rv. 717 Sund-Bradden (in Norwegian), NGI.

Noorany, I. and H. B. Seed (1965). In-Situ Strength Characteristics of Soft Clays. *Journal of the Soil Mechanics and Foundations Division* 91(2): 49-80.

Reite, A. J. (1987). Rissa. Kvartærgeologisk kart 1522 II - M 1:50 000. Beskrivelse (in Norwegian). *NGU Skrifter* 82.

Reite, A. J. (1996). Sør-Trøndelag fylke, Kvartærgeologisk kart M 1:250 000, Veiledning til kartet (in Norwegian). *NGU Skrifter* 96.

Sandven, R. (1990). Strength and deformation properties of fine grained soils obtained from piezocone tests Ph.D. thesis, Norges tekniske høgskole (now NTNU).

Solberg, I.-L., E. Dalsegg and J.-S. L'Heureux (2012). Resistivitetsmålinger for løsmassekartlegging ved Rein kirke i Rissa, Sør-Trøndelag. Data og tolkninger. (in Norwegian), NGU Report 2012.018.

Solberg, I.-L., L. Hansen, J. S. Rønning and E. Dalsegg (2014). Applications of 2D Resistivity Measurements for Quick-Clay Mapping in Mid Norway. *Landslides in Sensitive Clays: From Geosciences to Risk Management*. Springer Netherlands, 179-191.

Solberg, I.-L., L. Hansen, J. S. Rønning, et al. (2011). Combined geophysical and geotechnical approach to ground investigations and hazard zonation of a quick clay area, mid Norway. *Bulletin of Eng. Geology and the Environment* 71(1): 119-133.

Thakur, V., O. A. Fauskerud, V. Gjelsvik, et al. (2016). A procedure for the assessment of the undrained shear strength profile of soft clays. *Proc. of the 17th Nordic Geotechnical Meeting*, *Reykjavik, Iceland*.

Thakur, V., H. P. Jostad, H. A. Kornbrekke and S. A. Degago (2014). How Well Do We Understand the Undrained Strain Softening Response in Soft Sensitive Clays? *Landslides in Sensitive Clays - From Geosciences to Risk Management*. Springer, Vol. 36, 291-303.

Geotechnical and Geophysical Site Characterisation 5 – Lehane, Acosta-Martínez & Kelly (Eds)

Undrained shear strength and anisotropic yield surface of diatomaceous mudstone

N. Arsalan
Bakhtar University, Kabul, Afghanistan

M. Akaishi
PEC Co.,Ltd, Tokyo, Japan

M. Sugiyama
Tokai University, Kanagawa, Japan

ABSTRACT: With the increase of the size of foundations of civil engineering structures and the underground development at great depth, studies have been conducted to investigate the mechanical properties of sedimentary soft rock. Stress-strain and effective stress path of a soft rock (diatomaceous mudstone) have been examined by triaxial compression tests using anisotropically consolidated samples and its results have been compared with Cam-Clay model. Finally, an anisotropic yield surface that suits the experimental results has been introduced.

1 INTRODUCTION

When constructing a structure on soft rock, adequate research and study are required concerning the shear behavior in the over-consolidation region because soft rock is considered to be in a heavily over-consolidated state. Sedimentary soft rock that was studied in this research shows the strain softening behavior significantly in normally and over-consolidated conditions. For evaluating the influences of the residual strength of strain softening materials through numerical analysis, constitutive equations for evaluating strain softening behavior are required.

In many of the existing studies concerning the strength of soft rock, triaxial compression tests are conducted using isotropically consolidated samples. In this study, undrained triaxial compression tests are conducted using diatomaceous mudstone (Maekawa et al.1989, Nishi et al.1983, Liao et al.1995, Shigematsu et al.2001) that is anisotropically consolidated under varying pressures to examine the ratio of residual strength to peak strength and changes in effective stress during the period between the peak and residual strengths.

The effective stress path in the over-consolidated condition that was obtained in the tests reached the maximum deviator stress q_p and immediately lowered to critical state line (CLS) while the mean effective stress p' remained constant. The finite element (FE) analysis program incorporating the anisotropic yield function (Akaishi et al.2007) was modified to reflect the test results. Furthermore, the yield function that has been modified to fit well with the experimental result of over-consolidated condition has been proposed.

Table 1. Chemical composition of diatomaceous mudstone (Kaseno, 1984)

SiO_2	66 - 75 %
Al_2O_3	6.2 - 10.5 %
Fe_2O_3	3.4 - 5.8 %
CaO	0.82 - 1.26 %
Na_2O	0.73 - 1.24 %
K_2O	0.71 - 1.94 %

Table 2. Physical properties of material

Density: ρ_s	2.153 (g/cm^3)
Natural water content: w_n	126.2 (%)
Wet unit density of soil: ρ_t	1.35 (g/cm^3)
Dry unit density of soil: ρ_d	1.60 (g/cm^3)
Natural voild ratio: e_n	2.62
Liquid limit: w_L	166.0 (%)
Plastic limit: w_p	105.5 (%)

2 SAMPLES AND TEST METHOD

2.1 *Samples*

Diatomaceous mudstone sampled in Suzu City, Ishikawa Prefecture was used in the test. The chemical composition of the mudstone is reported by Kaseno (1984) as shown in Table 1. The high percentage of SiO_2 indicates that the mudstone is made from the dead body of diatom. A specimen 5 cm in diameter and 10 cm in height was made from a mudstone mass, a cube approximately 40 cm on a side that was free from cracks or discontinuities. Table 2 shows the results of physical tests using crushed fine particles not exceeding 0.0042 mm. The samples have low gravity and high natural water content. Samples with an initial natural water content of 120 % ± 5 % were used in consolidated-undrained and consolidated-drained triaxial compression tests. Maekawa et al.(1989) conducted numerous laboratory tests using similar diatomaceous mudstone and provided numerous pieces of information. As one of those outcomes is that the initial yield surface of this mudstone can be expressed by original Cam-clay model.

The mudstone used in this study was sampled at the same site as Maekawa used, but at a different time. Then, a consolidated-drained test was also conducted to obtain the initial yield surface of the sample and to identify the shear behavior in the over-consolidated condition.

2.2 *Consolidated-drained (CD) triaxial compression test*

The sample was isotropically consolidated under nine levels of consolidation pressure between 0.01 and 1.4 MPa using a triaxial compression test apparatus (a maximum lateral pressure of 4.92 MPa) and then subjected to shear at a strain rate of 0.005%/min until the axial strain reached 15%.

2.3 *Consolidated-undrained (CU) triaxial compression test*

The sample was subjected to anisotropic consolidation under a designated consolidation pressure *p'* and then to shear at a strain rate of 0.1 %/min. Consolidation pressure varied at 14 levels from 0.08 to 2.5 MPa. For anisotropic consolidation, the sample was subjected to isotropic consolidation and then only axial pressure was applied so as to achieve an effective stress ratio η (= q / p') of 0.75 while confirming in stages the dissipation of water pressure. Water pressure was dissipated in 24 hours or less in isotropic consolidation and in anisotropic consolidation under a consolidation pressure *p'* of 1.5 MPa or lower. Water pressure dissipation, however, took one week in anisotropic consolidation under *p'* of 2.0 MPa or higher. In both tests, a back pressure of 0.5 MPa was applied.

3 TEST RESULTS AND DISCUSSIONS

3.1 *Stress-strain relationship and initial yield surface in consolidated-drained compression test*

Figure 1 shows *e*-log σ_v curves obtained in the triaxial anisotropic and one-dimensional consolidation test in which the loading was possible up to 20 MPa. It is worthy of notice that the consolidation yield

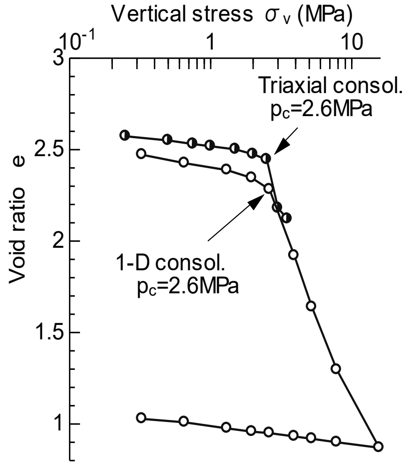

Figure1. *e*-log σ_v relationship in one-dimensional consolidation and triaxial anisotropic consolidation

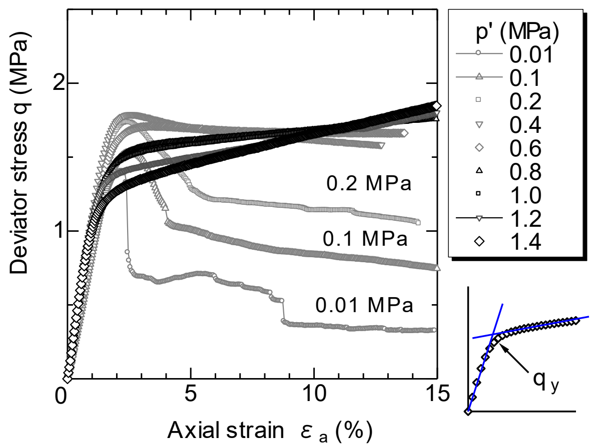

Figure 2. Stress-strain relationships in CD test

stress p_c obtained from two tests shows 2.6 MPa of the approximately equal.

The relationship between deviator stress *q* and axial strain ε_a obtained in the consolidated-drained compression test is shown in Figure 2. Strain softening occurred after the maximum deviator stress q_p was reached. As for the *q* and axial strain ε_a curves shown in gray by which consolidation pressure is less than 0.6, axial strains indicate the maximum of the deviator stress at 2.5% from 2%. After that, the deviator stress suddenly decreases to a residual state.

The degree of softening was remarkable under a lower consolidation pressure. It is evident that strain hardening occurred under an isotropic consolidation pressure of 0.8 MPa or higher and that yield stress q_y decreased as consolidation pressure increased. Yield stress q_y was obtained by the method shown at the right bottom corner of Figure 2 (intersection of two straight lines with different inclinations). The yield stress q_y of the sample that experienced strain softening was specified as the maximum deviator stress q_p.

In Figure 3, the yield stresses q_y obtained are plotted on the effective stress paths in respective tests using white circles. The broken curve indicates the yield surface of original Cam-clay (OCC) model calculated using p_c of 2.6 MPa and parameter M of 1.89.

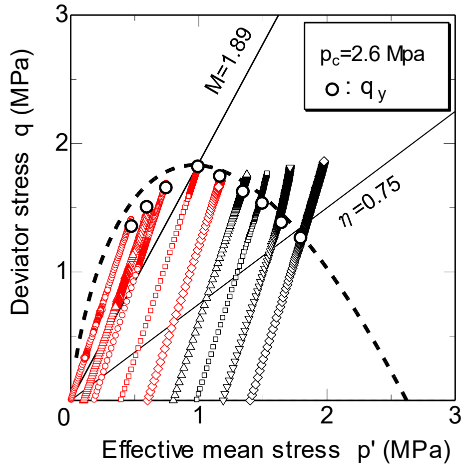

Figure 3. Effective stress paths of CD test

The figure, like the results of Maekawa's study, shows that the initial yield surface of the mudstone used in the study can be well expressed by the OCC model. Yield stress in the over-consolidation region, however, exists further inside the yield surface. The inclination M of the critical state line in the figure was obtained by averaging the effective stress ratios η when the axial strain was 15 % in the consolidated-undrained test.

3.2 *Results of Consolidated-undrained (CU) test*

Effective stress paths and stress-strain relationships for all the samples that were anisotropically consolidated at an effective stress ratio η of 0.75 are shown in Figures 4 (a) and (b). The results in the normally and over-consolidated conditions are indicated in small circle symbol and black solid line, respectively. The results of shearing from the black circle at (p', q) = (1.75, 1.31) on the initial yield surface represented by a broken curve are shown thick line in Figure 3 (a). Effective stress paths shows that in the sample in the normal consolidation region, positive pore water pressure occurred in the initial stages of shear and strain softening occurred after the maximum deviator stress q_p was reached (large circles in the figure) with the pore water pressure increasing. The maximum effective stress ratio $\eta_{\max}$ is therefore different from η when the maximum deviator stress q_p was reached. The path varies in the ten specimens in the over-consolidated condition according to the consolidation pressure or over-consolidation ratio. The path to the maximum deviator stress q_p varies with the decrease of consolidation pressure, or increase of over-consolidation ratio, from leftward to upward and rightward with the changes in dilatancy. Subsequently, drastic strain softening occurred in all the specimens (Figure 4 (b)). The stress paths under a consolidation pressure of 0.5 MPa or lower show that stress continuously increased along the $q = 3p'$ line until q_p, and strain softening occurred subsequently while p' was nearly constant. It is worth

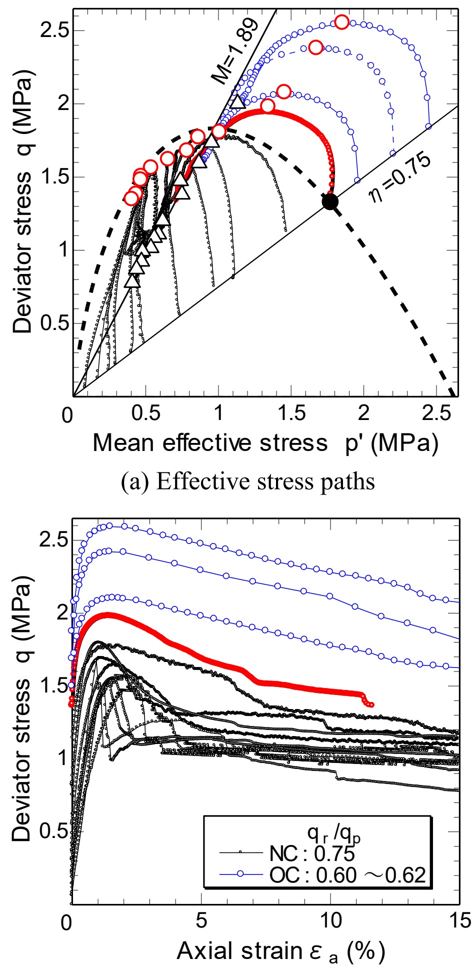

(a) Effective stress paths

(b) Stress-strain relationship

Figure 4. Results of anisotropic consolidated-undrained test

noting that the points of residual stress q_r at a post-softening axial strain of 15% in all the tests (represented by black circles) are located on a straight line that passes the point of origin. The inclination of the line obtained by the least square method is 1.89. In this study, the line is referred to as the critical state line (CSL). The points of maximum deviator stress indicated by large circles may be represented by two lines separately in the normal and over-consolidated conditions. Discussions will be made concerning the matter in the following chapter.

The stress-strain relationships in Figure 4 (b) indicate strain hardening and softening behavior. The rate of reduction of deviator stress after q_p was reached varies according to the consolidation pressure or over-consolidation ratio. Residual strength in the over-consolidated condition is 0.8 to 1.2 MN/m^2, nearly 60% of q_p. In the normal consolidation region on the other hand, residual strength increased to nearly 75%. Axial strain when q_p was reached is 1.5 to 2% regardless of stress condition.

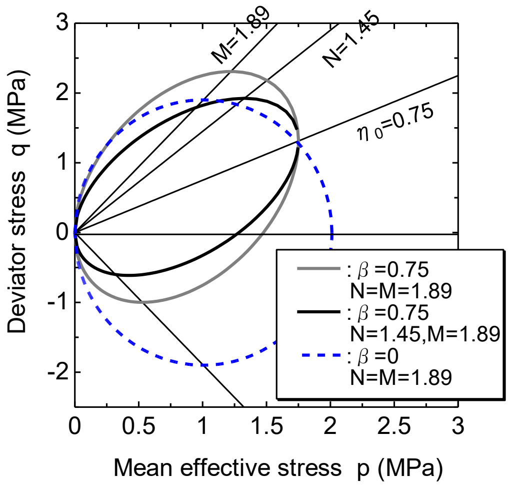

Figure 5. Shape of anisotropic yield function

4 MAXIMUM DEVIATOR STRESS AND ANISOTROPIC YIELD SURFACE

4.1 *Anisotropic yield function*

Akaishi et al. (2002) proposed equation (1) as an anisotropic yield function, and examined its applicability to clay or soft rock in a normally consolidated state.

$$F = q^2 - 2\beta pq + \beta^2 pp_0 + N^2(p^2 - pp_0) = 0 \qquad (1)$$

where, N and β are empirical constants. It was assumed that N was equal to the effective stress ratio at the maximum deviator stress and that β was equal to the initial stress ratio η_0 at the time of anisotropic normal consolidation. If it is assumed that N is equal to M and β is zero, equation (1) is identical to the yield function of a modified Cam-clay (MCC) model. Figure 5 shows an example of an anisotropic yield function calculated by combining N and β. The behavior of normally consolidated soil represented by a MCC model is the strain-hardening type. No strain-softening behavior can be calculated. The anisotropic yield function expressed by equation (1) can reproduce strain softening behavior if N is assumed to be lower than M (Imai et al. 2007).

4.2 *Results of calculation*

Figure 6 shows the yield surface of the proposed model and the effective stress paths in the normally and over-consolidated conditions using the material parameters listed in Table 3 Calculations were made using an FE analysis program incorporating the anisotropic model. For comparison, the results of calculation using the MCC model are also shown in the Figure 6 using broken lines. The results of calculation indicate that the stress path in the normally -

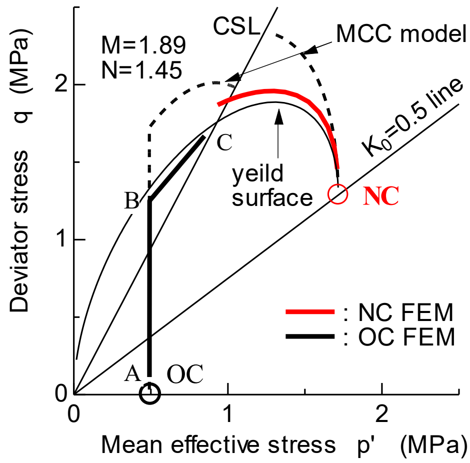

Figure 6. Results of calculation of effective stress paths

Table 3 Soil parameters used for the calculation

λ	κ	e_0	ν	M	N
0.642	0.071	2.40	0.3	1.89	1.45

-consolidated area calculated on the assumption of M = 1.89 and N = 1.45 is slightly outside the yield surface and exhibits strain softening after the maximum deviator stress q was reached. The stress paths calculated from point A in the over-consolidated condition (p = 0.5 MPa) obtained by conducting FE analysis reached point B on the yield surface and moved toward point C on the critical state line (CSL) with strain hardening, resulting in an increase in deviator stress.

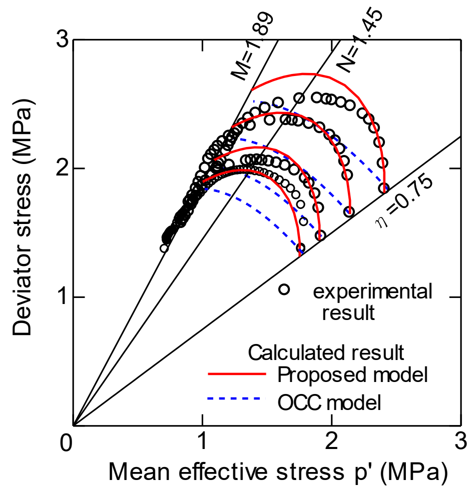

Figure 7. Results of calculation of effective stress path of normally consolidated soft rock using an anisotropic yield function

Figure 7 shows the experimental and calculated results of effective stress paths of normally consolidated soil. It is evident that the results of calculation using the anisotropic yield function based on the assumption that N was smaller than M is much more in agreement with test results than the results using a OCC model (represented by broken lines).

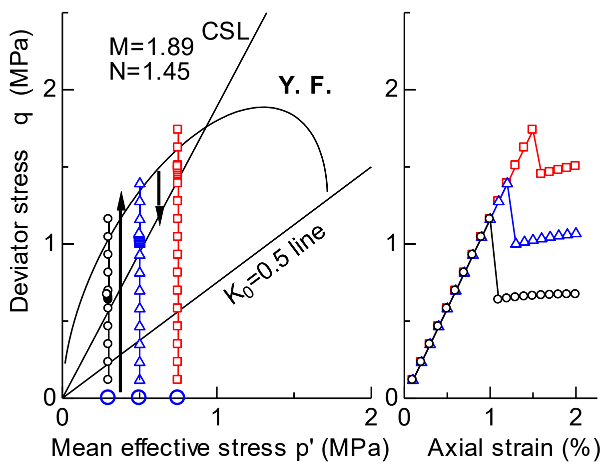

Figure 8. Calculations of strain softening in over-consolidated condition

As a result of calculations, it was found that the strain softening behavior in the normally consolidated condition properly reproduced the triaxial test results, but no strain softening behavior was reproduced that occurred more remarkably in the over-consolidated condition in Figure 6. The effective stress path in the over-consolidated condition that was obtained in the tests reached the maximum deviator stress q_p (point B in Figure 6) and immediately lowered to the CSL while the mean effective stress p' remained constant. Then, the FE analysis program incorporating the proposed model was modified to reflect the test results.

Figures 8 shows the effective stress paths and stress-strain relationship in an over-consolidated state calculated at three different consolidation pressures after modifying the FE program. Different from the stress path in Figure 4, the stress path lowered to CSL right after the deviator stress q exceeded the yield surface. This is more evident from the stress-strain relationship.

4.3 *Yield surface in dry side*)

In order to examine the applicability of anisotropic yield function (N = 1.45, M = 1.89) to over-consolidated condition, the yield function was plotted on Figure 6 and was represent as Figure 9. The anisotropic yield function that well captured the normal consolidation region and is shown as proposed model is slightly smaller than the test result on the left (dry side) of the intersection with the CSL. The yield surface of the original Cam-clay model on the dry side is generally larger than the test result. Then, a gray solid line with a series of q_p that crosses CSL was proposed as the yield surface on the dry side. In triaxial compression tests in which axial loading is applied, it is impossible to reach a space upper left of $q = 3p'$ (Atkinson et al.1978). The red solid line in Figure 10 was then proposed as the state boundary surface (yield surface) of anisotropically consolidated diatomaceous mudstone.

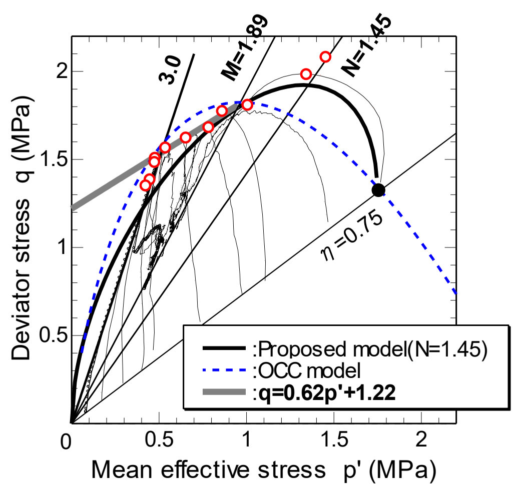

Fig.9 Yield surface in the over-consolidation region

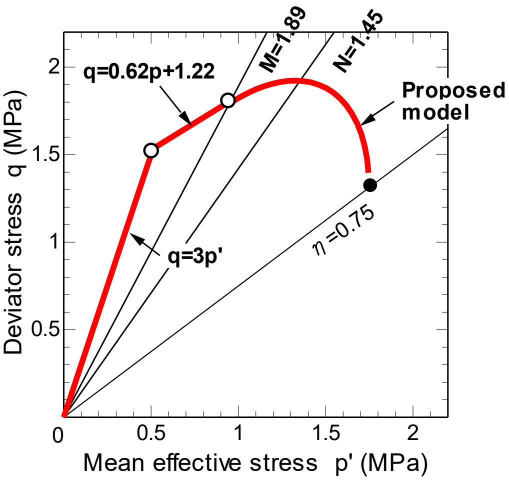

Figure 10. Anisotropic yield surface of diatomaceous mudstone

5 CLOSING REMARKS

Triaxial compression tests were conducted on diatomaceous mudstone subjected to anisotropic normal consolidation and over-consolidation, and the maximum deviator stress q_p and residual stress q_r were examined. The effective stress path in the over-consolidated condition that was obtained in the tests reached the maximum deviator stress q_p and immediately lowered to the CLS while the mean effective stress p' remained constant. The FE analysis program incorporating the anisotropic yield function was modified to reflect the test results. Furthermore, the yield function that has been modified to fit well with the experimental result of over-consolidated condition has been proposed.

6 REFERENCES

Akaishi, M. et al. 2002. A simple anisotropic clay plasticity model. *Mechanics Research Communications* 29: 241-245.

Atkinson, J. H. & Bransby 1978. The Mechanics of Soils, McGraw-Hill, London.

Imai, Y., Sugiyama, M. Tonosaki, A. and Akaishi, M. 2007. Yield function for anisotropically consolidated clays. *Pro-*

Liao, H.,Akaishi, M. Hayashi, M. 1995. Residual strength characteristics of soft rocks with a discontinuous plane, *Journal of Geotechnical Engineering, JSCE*. 529: 103-111.

Maekawa, H., Miyakita, K. 1983. Mechanical characteristics of diatomaceous soft rock, *Proceedings of the Japan Society of Civil Engineers*. 334: 135-143.

ceedings of the 41th Japan National Conference on Geotechnical Engineering. 287-291.

Liao, H.,Akaishi, M. Hayashi, M. 1995. Residual strength characteristics of soft rocks with a discontinuous plane, *Journal of Geotechnical Engineering, JSCE*. 529: 103-111.

Maekawa, H., Miyakita, K. 1983. Mechanical characteristics of diatomaceous soft rock, *Proceedings of the Japan Society of Civil Engineers*. 334: 135-143.

Nishi, K., Okamoto, T and Esashi, Y. 1983. Strength-deformation characteristics of mudstone under some kinds of loading conditions and its unificative interpretation, *Proceedings of the Japan Society of Civil Engineers*. 338: 149-158.

Shigematsu, H., Yashima, et al 2001. Geotechnical properties of Diatomaceous earth in northern Gifu prefecture and cut slope stability. *Journal of Geotechnical Engineering*, JSCE. 687(56): 139-154.

Imai, Y., Sugiyama, M. Tonosaki, A. and Akaishi, M. 2007. Yield function for anisotropically consolidated clays. *Proceedings of the 41th Japan National Conference on Geotechnical Engineering*. 287-291.

Geotechnical and Geophysical Site Characterisation 5 – Lehane, Acosta-Martínez & Kelly (Eds)
© 2016 Australian Geomechanics Society, Sydney, Australia, ISBN 978-0-9946261-1-0

Laboratory measurement of sensitivity of carbonate soils

N. Boukpeti & B.M. Lehane
School of Civil, Environmental & Mining Engineering, The University of Western Australia

ABSTRACT: Design of geotechnical structures such as piles and offshore pipelines requires knowledge of the soil's sensitivity to account for the effect of remoulding on the soil's strength. This effect of remoulding is particularly significant for soils exhibiting post-depositional structure, such as carbonate fine-grained soils. This paper investigates laboratory measurement of sensitivity using three different methods: fall cone, hand vane and mini T-bar penetrometer. Tests were conducted on two carbonate soils from offshore Western Australia, with different grain size distributions. Additional T-bar tests were performed on two reconstituted specimens of one of the soils that was consolidated from a slurry, to evaluate the influence of the method of reconstitution on the soil structure and sensitivity. The results for the more fine grained soil show that the fall cone and T-bar measurements of sensitivity are similar, whereas the hand vane yields much lower values, in particular for deeper samples; the sensitivity of reconstituted samples of this soil is approximately half that of the intact soil. The hand vane and fall cone data for the sandier soil investigated show a significant amount of scatter, with the average value of sensitivity being similar. The results are analysed in the light of existing frameworks for clays, investigating how soil sensitivity can be related to liquidity index and soil structure.

1 INTRODUCTION

Fine-grained soils are prone to various degrees of loss of strength upon remoulding. For example, some carbonate sediments offshore Australia exhibit sensitivities in the range 2 to 50. Knowledge of the degree of strength reduction due to remoulding is essential for the design of structures such as piles, suction caissons or pipelines, which subject the soil to intense remoulding during installation or in service. The soil's sensitivity can be measured either in situ, using vane shear tests or full-flow penetrometer tests (e.g., Yafrate et al. 2009), or in the laboratory using fall cone tests, vane shear tests, unconfined compression tests or miniature full-flow penetrometer tests (e.g., DeGroot et al. 2012, Tanaka et al. 2012, Hodder et al. 2010).

Previous studies on a variety of clays have shown that significant variation in sensitivity measurements is generally obtained depending on the method used for testing (e.g., DeGroot et al. 2012, Tanaka et al. 2012). These studies have demonstrated that one of the main factors affecting the measurement of remoulded strength (and thus sensitivity) is the mode of remoulding. Specimens remoulded by hand have a much lower strength than those remoulded with the vane, resulting in higher sensitivity. The wide variety of ways in which the undrained strength can be assessed (e.g. empirical correlations with the fall cone or direct strength measurement with the vane) causes variability in the assessed sensitivity- as does variations in the rate of shearing applied in any given test and the soil anisotropy.

This paper extends previous studies on the sensitivity of clays to carbonate soils, which are prevalent offshore Australia. The present study aims at quantifying the difference in sensitivity measurements obtained with three different methods, namely, the fall cone test, hand vane test and miniature T-bar penetrometer test. The two soils tested are a clayey silt (Soil A) and a silty sand (Soil B). Tube samples up to a depth of about 20 m were tested and profiles of intact strength, remoulded strength and sensitivity were determined using the different methods. The sensitivity of two reconstituted specimens of Soil A was also measured using T-bar test. The differences in measurements of intact strength, remoulded strength and sensitivity obtained with the three methods are discussed. The results are analysed in the light of existing frameworks for clays, investigating how soil sensitivity can be related to liquidity index and soil structure.

2 MATERIALS AND PROCEDURES

2.1 *Soils tested*

Soils A and B are from different regions of the Northern Carnavon Basin, on the North West Shelf (NWS) of Australia. Soil A lies in a deep water region, past the continental slope, with water depth of ~1100 m, whereas Soil B is located on the outer continental shelf, in water depth of ~100 m. Their mineral composition is very similar, dominated by carbonate minerals (mainly calcite and aragonite), whereas their particle size distribution differs significantly, as shown by the envelopes in Figure 1. General classification data were summarized by Lehane et al. (2014) and the average values are reproduced in Table 1. Soil A is classified as a well-graded clayey silt (muddy silt), whereas Soil B is a well-graded silty sand.

Table 1. Classification data for Soils A and B

Property	Soil A	Soil B
D_{50} (mm)	0.0065	0.065
Fines content (%)	85	35
Clay fraction (%)	28	10
Clay minerals (%)	1.7	4.5
Organic content (%)	1.6	N/A
Carbonate content (%)	84	89
Water content (%)	84	41
Liquid limit (%)	72	28
Plasticity index (%)	33	18
Liquidity index	1.6	1.7
Specific gravity	2.71	2.75
Estimated void ratio	2.3	1.1
Sensitivity	11.6	10

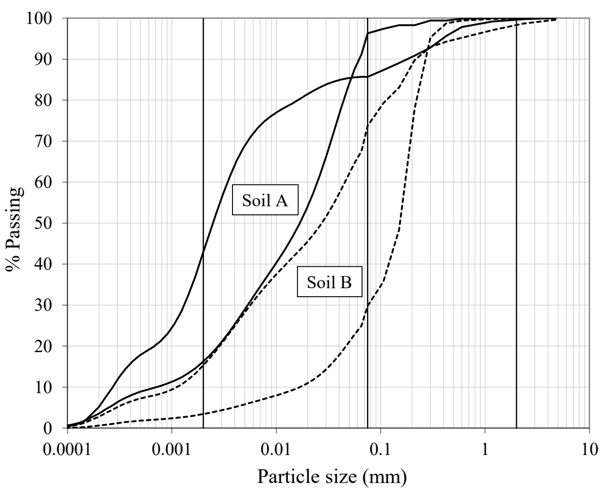

Figure 1. Particle size distribution envelopes for Soils A and B

2.2 *Experimental methods*

2.2.1 *Sample preparation*

Samples were provided in Shelby tubes with inner diameter of 60 mm and wall thickness of 1.6 mm. The tubes were X-rayed and sections showing significant disturbance were disregarded. In particular, samples of Soil B showed a relatively low quality with disturbance along entire tube lengths for multiple tubes. Each sampling tube selected for testing was cut into five sections as follows: two sections of length 45 mm for fall cone tests, two sections of length 110 mm for hand vane tests and one section of length 120 mm for T-bar tests. For some tubes with disturbed zones, only one test for each method could be performed.

Two reconstituted specimens of Soil A were prepared by consolidating a slurry at a water content of ~1.5 times the liquid limit (LL). The specimens were loaded incrementally over 7 days up to their final effective vertical stress, namely 55 kPa and 96 kPa, to represent samples from depths of 11 m and 19.5 m, respectively. The specimens were left to consolidate for a further 7 days, after which the recorded vertical displacement became negligible.

2.2.2 *Fall cone tests*

Fall cone tests were carried out using a cone with an apex angle of 30° and a mass of 80g, which was allowed to fall freely and penetrate into the sample under its own weight for 5 s. Measurement of cone penetration was carried out on the top and bottom side of each specimen. With two specimens tested for each tube (when sample quality permitted), this lead to four measurements, which were averaged to compute the intact undrained shear strength for the tube (using Equation (1) below). After extrusion from the tube and selection of a small fraction for water content measurement, each specimen was remoulded on a glass plate using a spatula and then filled into a cup 56 mm in diameter and 42 mm high. The cone penetration was measured for the remoulded sample. After remoulding the sample again a second measurement was performed. The remoulded undrained shear strength for the tube was determined using the average of four measurements (two for each specimen).

The undrained shear strength was interpreted from the cone penetration using the formulation proposed by Hansbo (1957)

$$s_u = \frac{KQ}{h^2} \tag{1}$$

where Q is the cone weight, h is the penetrated depth and K is a correlation parameter. In this paper, the theoretical value, K = 2.0, determined by Koumoto and Houlsby (2001) for a cone with a smooth surface was adopted. Using Equation (1), the intact (s_{ui}) and remoulded (s_{ur}) undrained shear strength were determined for each tube. The sensitivity was calculated as $S_t = s_{ui}/s_{ur}$ for each specimen and then averaged to obtain a value for each tube. Thus, the choice of the parameter K does not influence the value of sensitivity.

2.2.3 *Hand vane tests*

Hand vane tests were performed using a four-bladed Pilcon Hand vane 19 mm in diameter and 28 mm in height. The vane was initially pushed into the specimen up to a depth of 68 mm (referred to the tip of the vane) and then rotated clockwise at a rate of ~1 revolution per minute until a peak strength value was recorded. Remoulding of the soil was performed by applying 10 clockwise rotations at a faster rate, while maintaining the axis of the vane vertical. After remoulding, a second strength measurement was carried out by again rotating the vane at a rate of ~1 revolution per minute until a maximum value was reached. The soil's undrained shear strength is read directly on the vane dial. The method of calibration of the vane, which uses undrained triaxial tests results, is described by Serota and Jangle (1972). Hand vane tests were performed on two specimens for each tube. The intact strength (s_{ui}), remoulded strength (s_{ur}) and sensitivity for each tube were obtained by averaging the measurements obtained for the two specimens.

2.2.4 *T-bar penetrometer tests*

Miniature T-bar penetrometer tests were carried out using a T-bar of size 20 mm × 5 mm. A penetration rate of 1 mm/s was adopted. The tests consisted of penetrating the T-bar up to a depth of 75 mm, followed by 10 remoulding cycles of 30 mm amplitude (between depths of 75 mm and 45 mm), before extraction of the T-bar. The undrained shear strength s_u was determined by dividing the measured penetration resistance q by the resistance factor N_p = 10.5 (Randolph & Houlsby 1984, Stewart& Randolph 1994). The intact strength was obtained by averaging the penetration resistance between 30 mm and 60 mm depth during the initial penetration. The remoulded strength was determined from the average resistance measured between 65 mm and 50 mm depth, during the extraction phase of the last remoulding cycle. These values were then used to calculate the sensitivity.

2.3 *Testing programme*

The testing programme for Soil A consisted of a series of 15 hand vane tests, 21 fall cone tests and 6 T-bar tests carried out on 9 tubes retrieved from two boreholes between the depths of 8.5 m and 20 m. In addition, 2 T-bar tests were carried out on reconstituted specimens. For Soil B, 9 tubes were also tested, which were obtained from 5 boreholes between the depths of 2 m and 20 m. Due to the sandy nature of Soil B and to the low stress level, the flow around mechanism could not develop around the T-bar and for this reason T-bar tests were not conducted in this soil. A total of 12 hand vane tests and 12 fall cone tests were performed on Soil B.

3 RESULTS AND DISCUSSION

3.1 *Comparison of the different laboratory testing methods*

The intact strength, remoulded strength and sensitivity obtained with the three different methods are shown in Figures 2 to 4 for Soil A, whereas Figures 5 to 6 show the intact strength and sensitivity measured with the fall cone and hand vane for Soil B. Figure 2 indicates some significant variations in intact strength data obtained with the three methods for Soil A. These variations may reflect differences in sample quality as well as the difference in mode of shearing for the three methods. The fall cone and T-bar strength data increase with depth, whereas the hand vane data are approximately uniform.

When compared with the strength profile determined from consolidated undrained simple shear tests, all the measurements yield lower intact strength, with the T-bar giving the best estimate within the 25% range (Figure 2). The lower measured strengths are likely to reflect lower effective stresses in the tube samples which were not re-consolidated to in-situ stress levels (lower effective stresses are a typical consequence of sampling disturbance for lightly overconsolidated soils). It is interesting to note that the hand vane measurements of intact strength at ~20 m depth are almost 4 times less than the estimated in-situ simple shear strengths. The process of inserting the hand vane prior to shearing causes some disturbance and destructuration, which could partly explain the inability of the vane to capture the intact strength reliably.

There is more consistency in the remoulded strength values, which fall approximately within the 1 to 3 kPa range, with lowest values obtained with the fall cone, intermediate values obtained with the T-bar and highest values obtained with the hand vane (Figure 3). This is consistent with the mode of remoulding, which is more intense when using the fall cone method (remoulding by hand), less intense when using the hand vane (remoulding with the vane rotation) and intermediate when using the T-bar. In case of the fall cone, however, the remoulded strength value depends on the choice of cone factor K. On average, the remoulded strength is slightly lower than 2, which is consistent with a water content slightly above the liquid limit.

The sensitivity results plotted in Figure 4 show an increasing trend with depth for the fall cone and T-bar (as observed for the intact strength), with sensitivity values in the range 4 to 33 for the fall cone and 9 to 18 for the T-bar. Lower values of sensitivity are obtained with the hand vane, which are approximately uniform with depth, with an average of $S_t \sim 4$.

As for Soil A, the intact strength measurements for Soil B obtained with the fall cone and the hand vane show significant variations (Figure 5). Both methods fail to capture the increase of strength with depth, which is apparent in the strength profile determined from consolidated undrained simple shear tests, as shown in Figure 5. In general, fall cone and hand vane strength measurements are lower than the simple shear strength. Loss of suction (effective stress) in the samples is the most likely explanation for this trend.

Fall cone and hand vane measurements on Soil B yield similar average remoulded strength, s_{ur} ~ 2.5, and sensitivity, S_t~10 (Figure 6). The fall cone data show significant variability, which may be related to variability in fines content (and hence suction) of the silty sand samples.

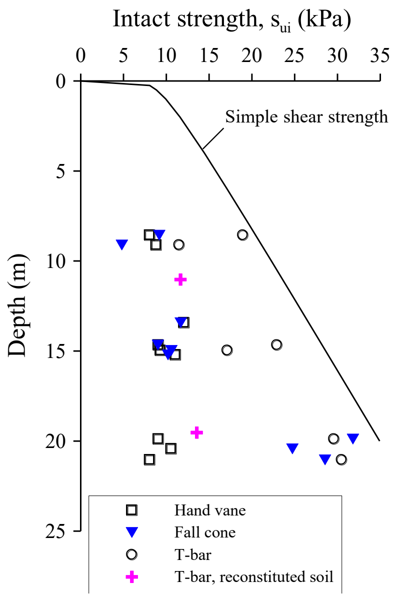

Figure 2. Intact strength measured with different laboratory testing methods for Soil A

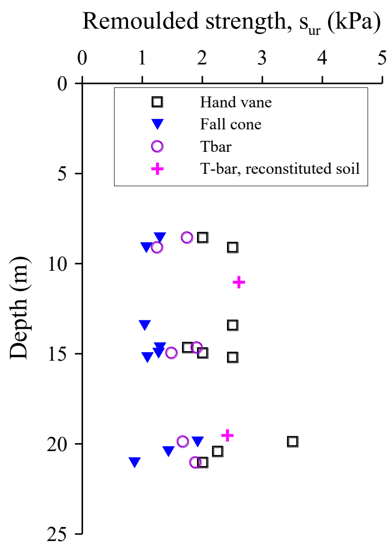

Figure 3. Remoulded strength measured with different laboratory testing methods for Soil A

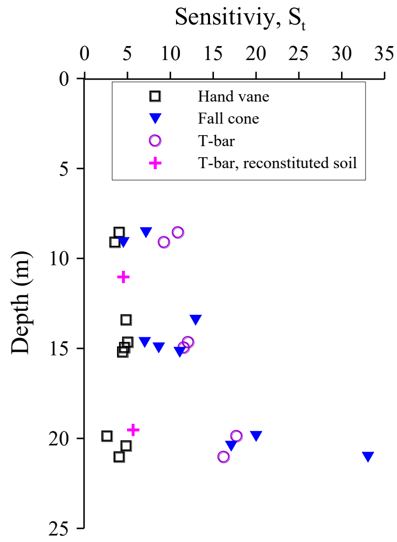

Figure 4. Sensitivity measured with different laboratory testing methods for Soil A

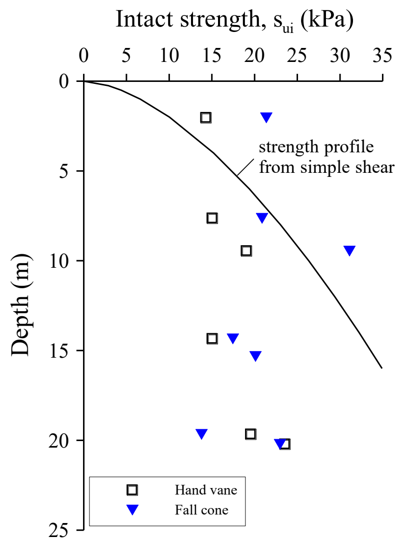

Figure 5. Intact strength measured with different laboratory testing methods for Soil B

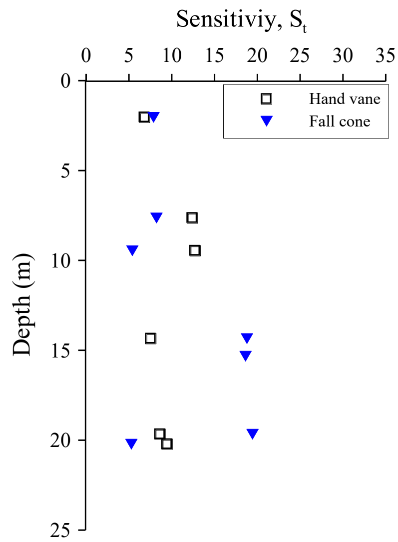

Figure 6. Sensitivity measured with different laboratory testing methods for Soil B

3.2 *Effect of sample reconstitution*

The two reconstituted specimens of Soil A exhibited similar intact (in this case 'intact' means during initial penetration of the T-bar) and remoulded strengths when tested with the T-bar, irrespective of the pre-consolidated stress (55 kPa and 96 kPa). The value s_{ui} ~12.5 kPa is consistent with the intact strength measured for specimens at ~10 m depth, but is much lower than the strength measured at ~20 m depth (Figure 2). When compared with the remoulded strength measured with the T-bar on the original specimens, the value of s_{ur} for the reconstituted specimens is slightly higher (Figure 3). The sensitivity of the reconstituted specimens is S_t~5, which is 2.0 times less than the sensitivity of the undisturbed samples at ~10 m depth measured with the T-bar. Evidently, the intact soil can exist at a higher void ratio and has a more sensitive structure than that created by the reconstitution process.

3.3 *Comparison with sensitivity of marine clays*

The sensitivity measurements for Soil A obtained with the three different methods are plotted as a function of the liquidity index (LI) in Figure 7. LI was determined from the water content measured on each specimen tested and using average values of liquid limit (LL) and plastic limit (PL) obtained from a previous study on the same soil (see Table 1). The data in Figure 7 are compared with the following relationship

$$S_t = \exp(kI_L) \tag{2}$$

which was used by Muir Wood (1990), with k in the range 1 to 3, to fit data obtained for various natural clays. For example, data from Bjerrum (1954) were reasonably well fitted with k = 2. The data for Soil A shown in Figure 7 also fall within the k range of 1 and 3. However, for the narrow range of liquidity indices of the specimens tested (1<LI<1.6), a wide range of sensitivity values were measured (from fall cone data, $4<S_t<33$ and from T-bar data $9<S_t<18$). As discussed earlier, soil structure is a key variable influencing soil sensitivity and the LI may not be adequate to capture this influence.

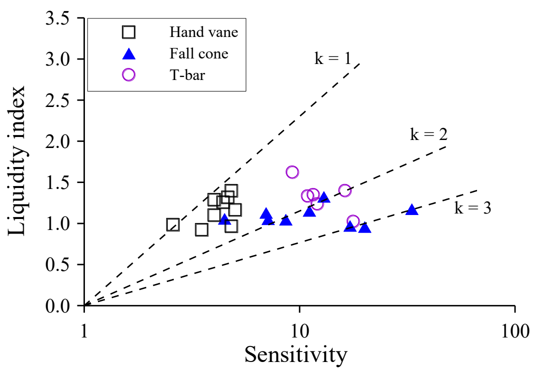

Figure 7. Liquidity index vs sensitivity for Soil A

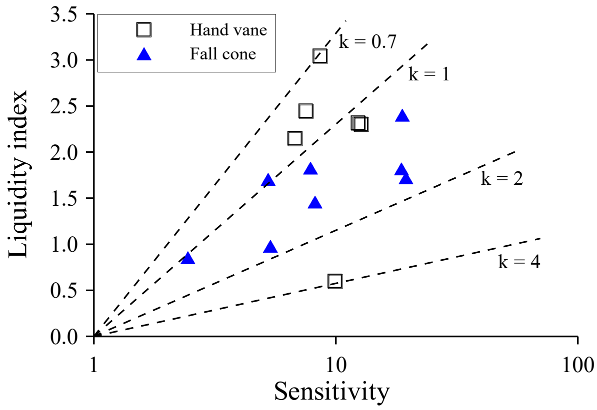

Figure 8. Liquidity index vs sensitivity for Soil B

Figure 8 shows the data of sensitivity versus LI for Soil B. The data exhibit a greater variability in LI and the fall cone data indicate an increasing trend of sensitivity with LI. However, the data should be regarded with caution as average values of LL and PL were used to compute LI, whereas a previous study indicated significant variations in these parameters, correlating with variations in fines content.

3.4 *Comparison with prediction using the idealized sensitivity framework*

Cotecchia & Chandler (2000) have proposed a sensitivity framework based on the observation that clays with similar sensitivity follow similar curves during one-dimensional compression. These curves can be plotted in terms of the void index, $I_v = (e - e^*_{100})/(e^*_{100} - e^*_{1000})$, where e^*_{100} and e^*_{1000} are the void ratios of the clay reconstituted and compressed one-dimensionally to 100 kPa and 1000 kPa respectively (Burland, 1990). The compression curves of the reconstituted clays are intrinsic compression curves (ICL) and can be approximated by a unique line in the normalized space $I_v - \log \sigma'_v$. The compression curves for the natural clays with their natural structure plot above the ICL, with the horizontal distance between the yield point (σ'_{vy}) and the ICL (σ'_{ey}) being related to the sensitivity, $S_t = \sigma'_{vy} / \sigma'_{ey}$.

Figure 9 shows the ICL for soil A obtained from an oedometer test conducted on a reconstituted specimen (from a slurry with water content w ~ 1.5 LL pre-consolidated to 50 kPa), together with the ICL predicted using Burland's correlations for e^*_{100} and $C_c^* = e^*_{100} - e^*_{1000}$. The correlations, which were derived for clays, give a reasonable estimate of C_c^* (C_c^* = 0.46 from correlations and C_c^* = 0.39 from compression of reconstituted sample), but underestimate the void ratio in the intrinsic state. However, void ratio was derived from water content measurements and this may not be adequate for calcareous soils having hollow particles which can trap water.

Figure 10 shows three compression curves obtained from oedometer tests conducted on tube specimens of Soil A plotted in terms of I_v, together with the ICL. Tests T1, T2 and T3 were conducted on specimens from depth 11.5 m, 5.5 m and 5.9 m, respectively. Using the relation, $S_t = \sigma'_{vy} / \sigma'_{ey}$, sensitivity values of 11.5, 5.5 and 5.0 are estimated for T1, T2 and T3 specimens, respectively. These values are slightly lower than sensitivities measured on specimens of similar depth of 15.5, 10.5 and 7.5, respectively. The lower sensitivity prediction may be attributed partly to disturbance caused by tube sampling, which results in a decrease in yield stress σ'_{vy}.

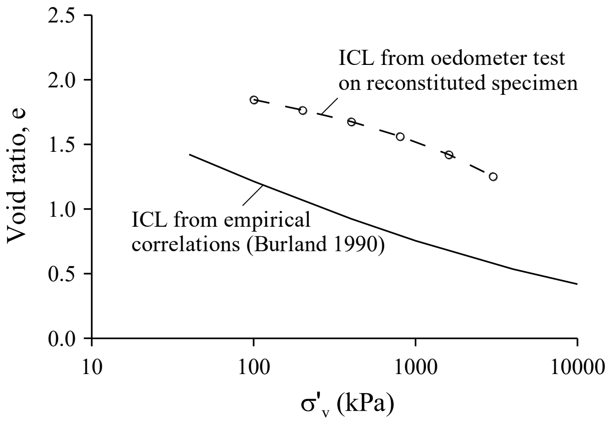

Figure 9. ICL for Soil A

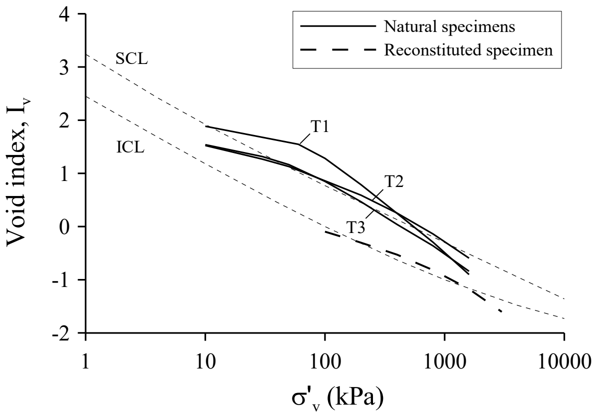

Figure 10. Oedometer results for Soil A in terms of I_v

4 CONCLUDING REMARKS

Three laboratory methods have been used to measure the sensitivity of two calcareous soils from offshore Australia, namely the fall cone, vane shear and T-bar penetrometer. For Soil A, the fall cone and T-bar lead to similar values of intact and remouled undrained strength (s_{ui} and s_{ur}), whereas the hand vane yields lower s_{ui} and slightly higher s_{ur}, resulting in lower sensitivity. The sensitivity of reconstituted specimens is approximately half that of the intact specimens. For Soil B, the hand vane and fall cone yield similar sensitivity on average. Large variation in sensitivity is observed in specimens having similar liquidity indices (LI), indicating that LI is not an adequate parameter to predict sensitivity. This may be related to the fact that water content measurement in calcareous soil is not indicative of the particle packing due to the presence of trapped water in hollow particles. Applying the idealized sensitivity framework (Cotecchia & Chandler, 2000), which predicts sensitivity based on the distance of the yield point in compression to the ICL, yielded slightly lower sensitivity compared with measured values. This preliminary finding needs to be investigated further with additional testing.

5 ACKNOWLEDGEMENTS

This work forms part of the activities of the Centre for Offshore Foundation Systems, currently supported as a node of the Australian Research Council Centre of Excellence for Geotechnical Science and Engineering. The authors would like to thank J. V. Cheng and C. Watt for conducting the tests.

6 REFERENCES

Bjerrum, L. 1954. Geotechnical properties of Norwegian marine clays. *Géotechnique* 4(2): 49-69.

Burland, J.B. 1990. On the compressibility and shear strength of natural clays. *Géotechnique* 40(3): 49-69.

Cotecchia, F. & Chandler, R.J. 2000. A general framework for the mechanical behaviour of clays. *Géotechnique* 50(4): 431-447.

DeGroot, D.J.., Lunne, T., Andersen, K.H. & Boscardin, A.G. 2012. Laboratory measurement of the remoulded shear strength of clays with application to design of offshore infrastructure. In, , *Offshore Site Investigation and Geotechnics, London, 12-14 September 2012*. Society of Underwater Technology.

Hansbo, S. 1957. A new approach to the determination of the shear strength of clay by the fall cone test. *Proc. R. Swedish Geotechnol. Inst.* 14: 1-49.

Hodder, M.S., White, D.J. & Cassidy, M.J. 2010. Analysis of soil strength degradation during episodes of cyclic loading, illustrated by the T-bar penetration test. *Int. J. Geomech* 10(3): 117-123.

Koumoto, T. & Houlsby, G.T. 2001. Theory and practice of the fall cone test. *Géotechnique* 51(8): 701-712.

Lehane, B., Carraro, A., Boukpeti, N. & Elkhatib, S. 2014. Mechanical response of two carbonate sediments from Australia's north west shelf. *Proc. Int. conf. Ocean Offshore Arctic Engnr. (OMAE), San Francicsco, USA*.

Muir Wood, D. 1990. *Soil behaviour and critical state soil mechanics*. Cambridge: Cambridge University Press.

Randolph, M.F. & Houlsby, G.T. 1984. The limiting pressure on a circular pile loaded laterally in cohesive soil. *Géotechnique* 34(4): 613-623.

Serota, S. & Jangle, A. 1972. A direct reading pocket shear vane. *Civil Engineering – American Society of Civil Engineers*.

Stewart, D.P. & Randolph, M. F. 1994. T-bar penetration testing in soft clay. *J. Geotech. Engng* ASCE 120(12): 2230-2235.

Tanaka, H., Hirabayshi, H., Matsuoka, T. & Kaneko H. 2012. Use of fall cone test as measurement of shear strength for soft clay materials. *Soils and Foundations* 52(4): 590-599.

Yafrate, N., DeJong, J. DeGroot, D. & Randolph, M. 2009. Evaluation of remolded shear strength and sensitiveity of soft clay using full-flow penetrometers. *Journal of Geotechnical and Geoenvironmental Engineering.* 135: 1179-1189.

Geotechnical and Geophysical Site Characterisation 5 – Lehane, Acosta-Martínez & Kelly (Eds)

Maximum shear modulus of a Brazilian lateritic soil from in situ and laboratory tests

L. Décourt
Luciano Décourt Consulting Engineers, São Paulo, SP, Brazil

J.M. de Camargo Barros, O.C.B. Gandolfo
Institute for Technological Research of the State of São Paulo, Brazil

A.R. Q. Filho
Engesolos Soil and Foundation Engineering, São Paulo, SP, Brazil

F.D. Penna
Damasco Penna Associate Engineers, São Paulo, SP, Brazil

ABSTRACT: This paper presents the results of the in-situ tests (SPTT, crosshole, SDMT and CPTU) and laboratory tests (characterization, compaction, MCT classification, consolidation, UU triaxial and resonant column) to investigate the properties of a lateritic soil from Santo André, metropolitan region of São Paulo, Brazil, for purposes of foundations of a building. Lateritic soils are frequently found in tropical regions and present a peculiar behavior compared to temperate zone soils. It was possible to obtain the maximum shear modulus from different tests and could be verified that lateritic soils present stiffness significantly higher than that derived from empirical correlations obtained for temperate zone soils.

1 INTRODUCTION

Lateritic soils are formed by the process of laterization in hot and wet tropical regions and present high iron and aluminum oxide and hydroxide concentration. They can be either residual or transported, generally present red or yellow coloration and the clay fraction is compound mainly of kaolinite.

The oxides involve the surface of the individual clay particles producing a cementation between adjacent particles. As a result, lateritic soils exhibit a peculiar behavior, showing a more rigid behavior than non-lateritic soils.

Nogami and Villibor (1981) developed the MCT classification system of tropical soils and Ignatius (1991), based on the inclination of dry side of the Standard Proctor compaction curve, proposed a Laterization Index L to identify lateritic soils.

An opportunity for improving the knowledge of engineering properties of this type of soil occurred a few years ago when the first author was engaged in the design of footing foundations for a twenty five-story building.

For design purposes, standard penetration tests complemented by torque measurement (SPTT), crosshole (CH) and seismic dilatometer test (SDMT) have been performed. After that, during the construction of the building, it was decided to carry out others in situ tests, to better understand the behavior of this type of soil. Piezocone tests (CPTU), load test on a block foundation and many other SPTTs and laboratory tests have been performed.

2 IN SITU AND LABORATORY TESTS

The in situ investigation was conducted in three distinct areas at the site, named Site I, II and III (Figure 1). A total of eight SPTT were carried out in the three sites.

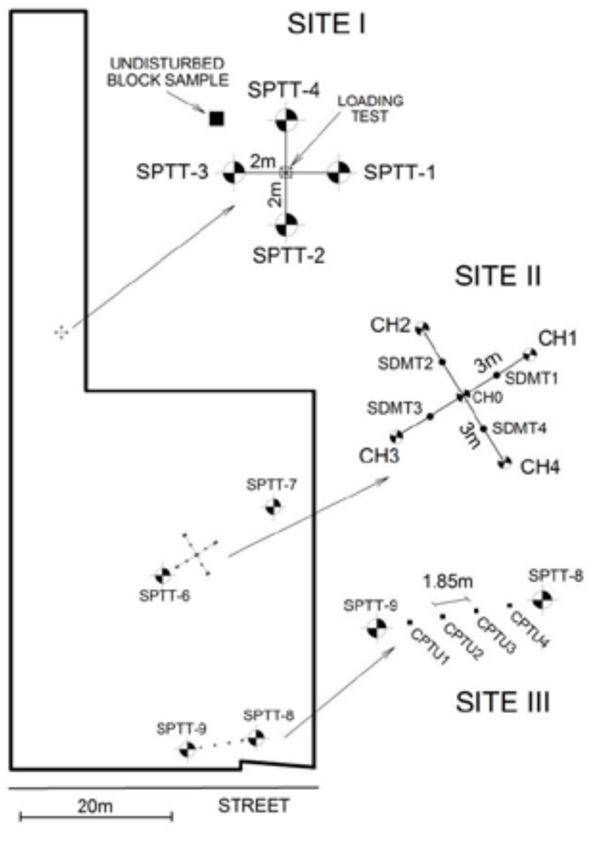

Figure 1. Site test layout.

For design purposes two tests were performed before the building at the Site II: crosshole (CH) and SDMT, which are based on the propagation of elastic waves through the ground. As seismic waves impose strains smaller than 10^{-4}% on the media, the maximum modulus is developed where seismic field tests are used. Equation (1) shows the relationships for the maximum shear modulus (G_0) and shear wave velocity (V_S).

$$G_0 = \rho \cdot V_S^2 \tag{1}$$

The CH is a well-established geophysical method that allows for the direct measurements of V_S using cased boreholes. The SDMT is the combination of the mechanical flat dilatometer (DMT), introduced by Marchetti, with a seismic module for measuring V_S.

Four crosshole tests were performed, in accordance with ASTM D4428 (2007), using five boreholes (20m depth, source at CH0 and receiver at CH1 to CH4). Each test was carried out using two boreholes. As shown in Figure 1, SDMT tests were performed down to 13 meters depth at the middle of the two boreholes used for each crosshole test. Figure 2 shows the typical soil profile of the investigated site, namely SPTT-6, beside the CH and SDMT tests. Six layers of soil were clearly identified.

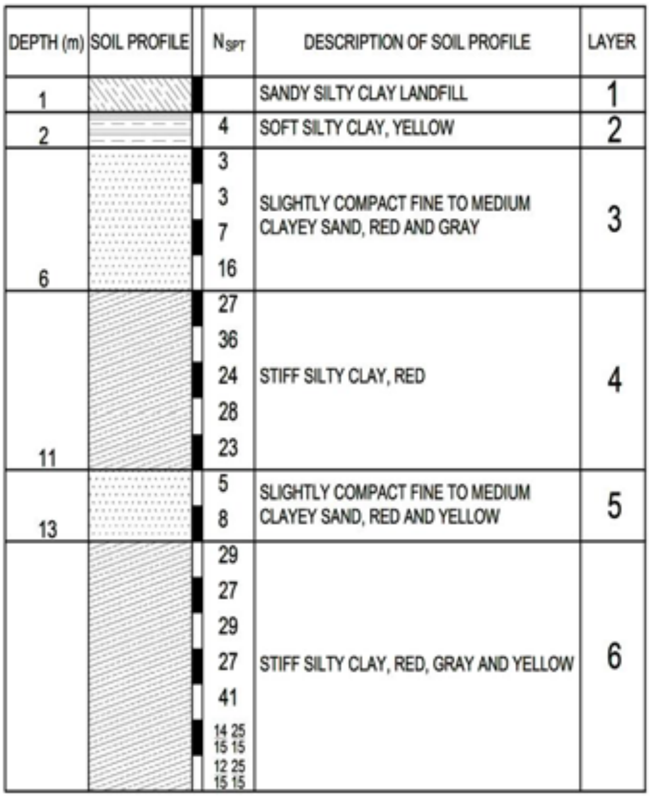

Figure 2. Soil profile (SPTT-6).

After that, during the construction of the building, it was decided to carry out other in situ and laboratory tests.

At the Site I a loading test was performed on a block foundation. The results of this test are presented by Décourt et al. in this same conference. Two blocks were extracted from upper clay layer (Layer 4 in Figure 2) and the following laboratory tests were carried out: characterization, MCT classification, determination of the Laterization Index using Proctor compaction test, one-dimensional consolidation, UU triaxial and resonant column.

Finally, at the Site III piezocone tests (CPTU) were performed adjacent to two SPT-T tests. The CPTU provides a continuous measurement of tip resistance, sleeve friction and pore pressure.

Four CPTU, going down around 19.5 meter deep, were executed in the same line of the SPT-Ts.

The site investigation presented in this paper focuses on the maximum shear modulus of Layers 2 to 5, which present lateritic characteristics.

3 RESULTS AND ANALYSIS

3.1 *In situ tests*

Figure 3 show the maximum shear modulus (G_0) determined by crosshole and SDMT tests at the Site II (average of the four tests). As can be seen, the data showed excellent agreement. The greatest values of G_0 were observed within the stiff silty clay layer (Layer 4) with an average value of 418 MPa.

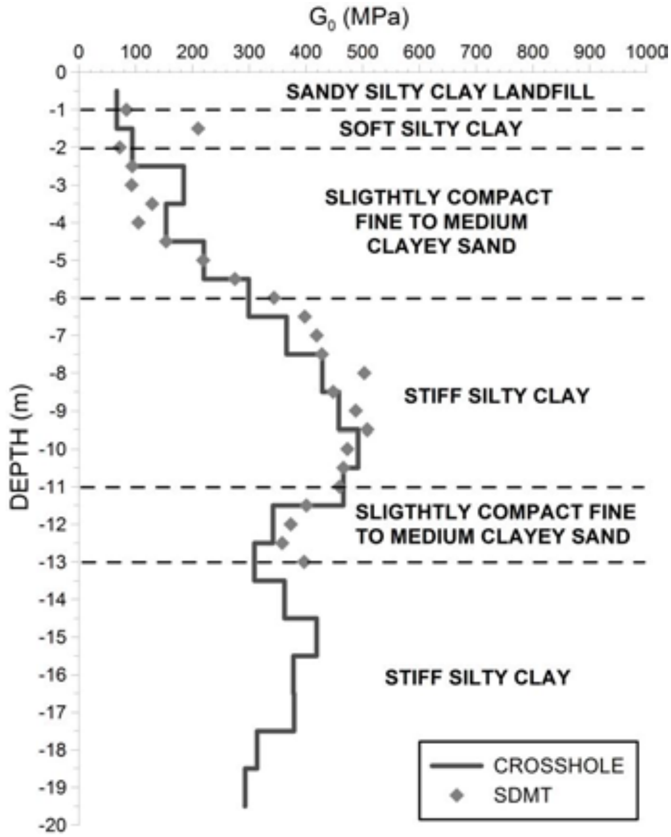

Figure 3. Crosshole and SDMT tests results.

Figure 4 shows the variation of G_0 from crosshole test with N_{SPT} for the lateritic layers (Layers 2 to 5). As the energy level in typical tests performed in Brazil is 72% (Décourt et al., 1989), the N_{SPT} values in this figure were converted to N_{60}.

The following relationship (Imai & Tonouchi, 1982) obtained from Japanese soils is considered in this paper as representative of non-lateritic soils:

$$G_0 = 11.96\ N_{60}^{0.68} \quad (2)$$

The original relationship was modified to N_{60} considering energy level in SPT performed in Japan equal to 76% (Décourt et al., 1989).

This expression underestimates in a significant way the G_0 values of the lateritic soils at this site. The relationship between measured values and estimated by Imai and Tonouchi relationship is greater than 2.5 times.

In the same figure the two forms of regression proposed by Barros & Pinto (1997) for Brazilian lateritic soils are also presented, according to the following relationships, also converted to N_{60}:

$$G_0 = 48.9\ N_{60}^{0.665} \quad (3)$$

$$G_0 = 56 + 16.9 N_{60} \quad (4)$$

The measured values show a much better adjust with Barros & Pinto expressions, manly with the non-linear equation.

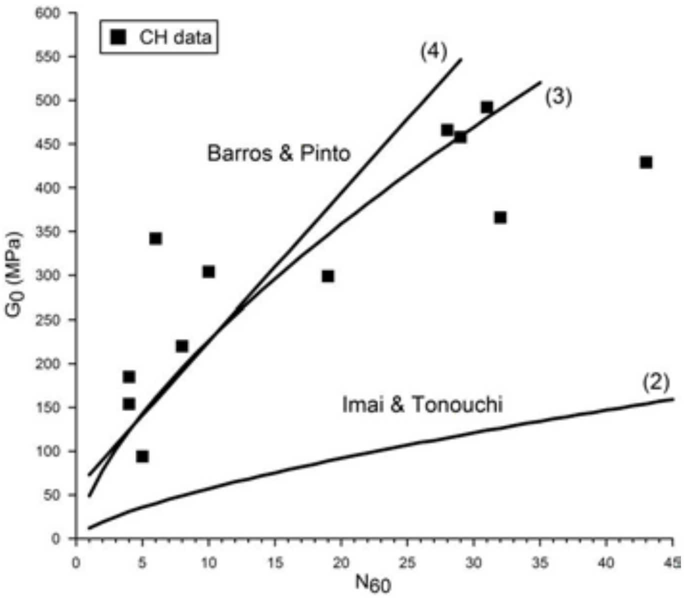

Figure 4. G_0 x N_{60} (SPTT-6).

Figure 5 shows G_0 profile obtained from CPTU data, based on Robertson & Cabal expression (2010). For the investigated soil, the moduli determined by CH and SDMT are higher than those from CPTU (average of the four CPTU tests values performed at the Site III).

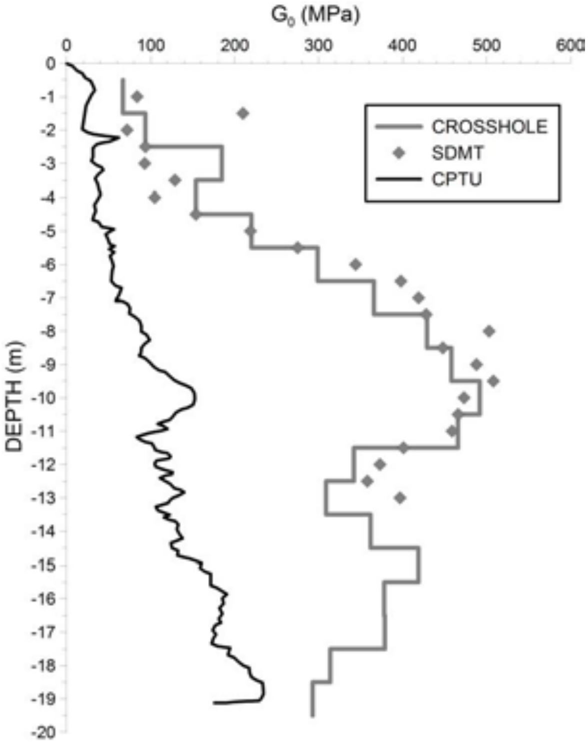

Figure 5. G_0 obtained from CPTU compared with CH and SDMT results.

3.2 *Laboratory tests*

The laboratory tests were carried out on the blocks extracted from upper clay layer (Layer 4) at Site I. The particle size distribution curve of the soil is shown in Figure 6. The Atterberg Limits and the average mass-volume relationships are presented in Table 1.

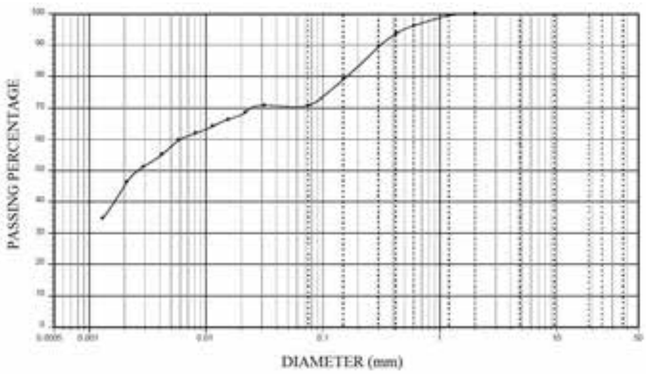

Figure 6. Particle size distribution curve.

Table 1. Atterberg limits and average mass-volume relationships

LL (%)	PI (%)	w (%)	ρ (kg/m³)	e	Sr (%)
57	24	16,4	2081	0,589	79,4

In the MCT Classification the soil was classified in the LG´ group (lateritic clay) and the Laterization Index obtained was 0.43, corresponding to lateritic soils.

Two consolidation tests were performed. As can be seen in Figure 7, although the maximum vertical stress applied has reached 2500 kPa, the virgin curve could not be well defined. However, it is possible to conclude that the maximum past vertical consolidation stress is higher than 300 kPa and probably about 500 kPa.

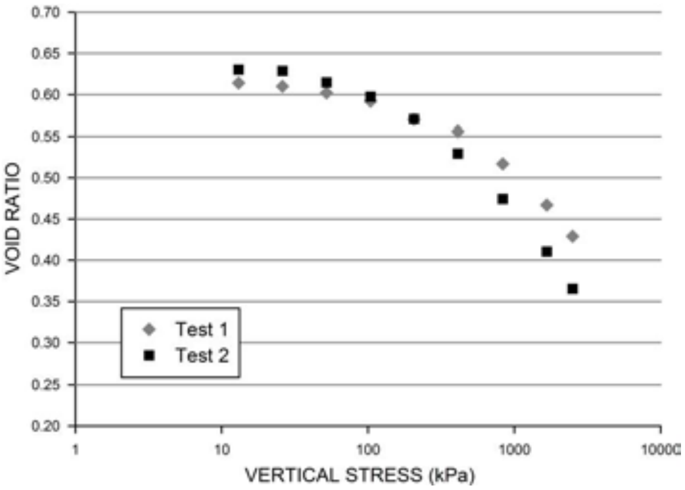

Figure 7. Consolidation test results.

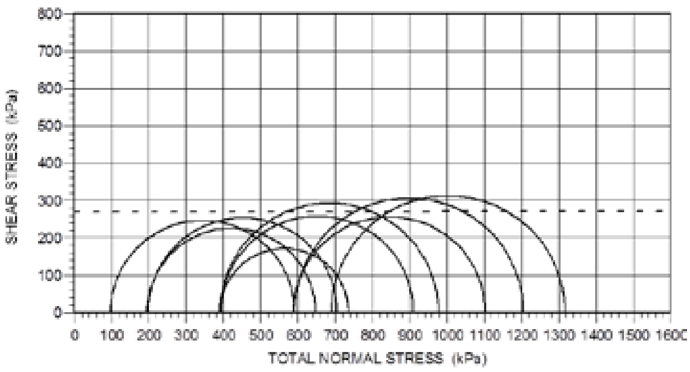

Figure 8 shows the results of the UU triaxial tests. As can be seen, the average value of the undrained cohesion was 270 kPa.

The obtained G_0/S_u ratio was 1550, with G_0 and S_u determined from CH and UU triaxial tests, respectively. Several linear correlations between G_0 and S_u are presented in the technical literature. However, it is difficult to compare the results since both S_u and G_0 values are obtained from different laboratory and field tests. Values from 488 (Hara et al., 1974) to 1800 (Bouckovalas et al., 1989) are encountered in the literature.

Resonant column test was performed in four different levels of confining pressure. Figure 9 shows the G_0 values as a function of the confining pressure. In the same figure is presented the well-known equation proposed by Hardin (1978):

$$G_0 = 625\ OCR^K (p_a\sigma_0)^{0.5}/(0{,}3+0{,}7e^2) \qquad (5)$$

where: OCR = overconsolidation ratio; p_a = atmospheric pressure; σ_0 = confining pressure; e = void ratio and K = parameter that depends on Plasticity Index of the soil. The OCR value was computed adopting the maximum past vertical consolidation stress equal to 500 kPa.

It can be seen that Hardin's equation, obtained from data of temperate zone soils, underestimates significantly the G_0 value of the soil investigated in this study.

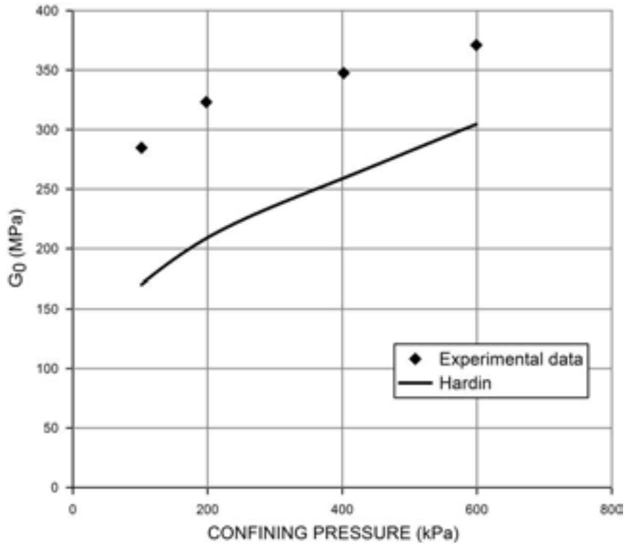

Figure 9. Variation of G_0 with confining pressure obtained in resonant column tests.

4 CONCLUSIONS

G_0 values of the lateritic soil investigated in this study were obtained from different in situ and laboratory tests.

The results of both seismic techniques performed (crosshole and SDMT) showed a very good agreement.

The well-known relationships between G_0 and N_{SPT} (Imai & Tonouchi) and G_0 and q_c (Robertson & Cabal), both representative of non-lateritic soils, underestimated in a significant way the G_0 values of the lateritic soils at the site investigated. By using the relationships proposed by Barros & Pinto for lateritic soils, a much better match was observed.

MCT Classification and the Laterization Index determined in laboratory confirmed lateritic behavior of the soil block extracted from the stiff silty clay (Layer 4). The Hardin expression also underestimated the G_0 values obtained by resonant column tests in laboratory.

Different tests performed in this study showed that lateritic soils present stiffness significantly higher than temperate zone soils. This high rigidity is resultant of the cementation that occurs between adjacent particles.

Empirical correlations commonly used for G_0 estimation for temperate zone soils are not adequate and should not be used for lateritic soils.

5 REFERENCES

ASTM D4428. 2007. Standard test methods for crosshole seismic testing.

Barros, J.M.C. & Pinto, C.S. 1997. Estimation of maximum shear modulus of Brazilian tropical soils from standard penetration test. In: International Conference on Soil Mechanics and Foundation Engineering, 14, Hamburgo, 1: 29-30.

Bouckovalas, G.; Kalteziotis, N.; Sabatakakis, N. & Zervogiannis, 1989. C. Shear wave velocity in a very soft clay – Measurement and correlations. In: International Conf. on Soil Mechanics and Foundation Engineering, 12, Rio de Janeiro. 191-194.

Décourt, L.; Belincanta, A. & Quaresma Filho, A.R. 1989. Brazilian Experience on SPT, Supplementary Contributions by the Brazilian Society of Soil Mechanics, XII ICSMFE, Rio de Janeiro: 49-54.

Hara, A; Ohta, T. Niwam M; Tanaka, S. & Banno, T. 1974. Shear modulus and shear strength of coesive soils. Soils and Foundations, JSSMFE, 14: 3, 1-24.

Hardin, B.O. 1978. The nature of stress-strain behavior for soils. In: Earthquake Engineering and Soil Dynamics, Proceedings of the ASCE Geotechnical Engineering Division Specialty Conference, Pasadena, 1: 3-90.

Ignatius, S.G. 1991. Tropical Soils: proposal of a classificatory index. Solos e Rochas, São Paulo, 14(2): 89-93. (in Portuguese).

Imai, T. & Tonouchi, K. 1982. Correlation of N-value with S-wave velocity and shear modulus. Proceedings of the 2nd European Symposium on Penetrating Testing, Amsterdam, 67-72.

Nogami, J.S. & Villibor, D.F. 1981. A new soil classification for highway purposes. In: Brazilian Symposium of Tropical Soils in Engineering, Rio de Janeiro, COPPE/UFRJ, CNPq, ABMS, 1: 30-41. (in Portuguese).

Robertson, P.K & Cabal, K.L. 2010. Guide to cone penetration Testing for geotechnical engineering. Gregg Drilling and Testing, Inc. 4th Ed.

Geotechnical and Geophysical Site Characterisation 5 – Lehane, Acosta-Martínez & Kelly (Eds)
© 2016 Australian Geomechanics Society, Sydney, Australia, ISBN 978-0-9946261-1-0

Engineering properties and cone factor of Onsøy Clay, Louiseville Clay and Mexico City Clay

H. Hirabayashi & H. Saegusa
TOA CORPORATION, Research and Development Centre, Yokohama, Japan

M. Tanaka
Port and Airport Research Institute, Yokosuka, Japan

T. Fukasawa
JGC CORPORATION, Yokohama, Japan

R. Tomita
KOA KAIHATSU Co., Ltd, Chiba, Japan

ABSTRACT: Site investigations such as electrical piezocone penetration test, field vane shear test and undisturbed soil sampling were carried out at Onsøy in Norway, Louiseville in eastern Canada and Mexico City. Push-in typed vane with protective casing was used to conduct field vane shear tests so that rod friction was minimized and influence of stress release caused by predrilling was discounted. All undisturbed samples were taken by Japanese type sampler with fixed piston to remove technical effects of the local sampling method. Subsequently, laboratory tests including physical properties tests, direct shear tests and unconfined compression tests were carried out using the undisturbed samples. In this paper, engineering properties of three clays are presented and cone factor obtained from each shear test are compared. Correlation of cone factor with plasticity index is also explained.

1 INTRODUCTION

Electrical piezocone penetration test (CPTU) has become widely used for soil investigations. However, in-situ undrained shear strength su of clay cannot be determined directly from its results. Empirical approaches for interpretation of su from CPTU results have been reported using cone factor N_{kt}, corrected cone resistance qt and overburden pressure in total stress σ_v (Aas et al. 1986; La Rochelle et al. 1988; Rad & Lunne 1988; Powell & Quarterman 1988; Tanaka & Tanaka 2004; Fukasawa & Kusakabe 2005).

The authors have carried out a series of general site investigations such as undisturbed sampling, CPTUs and field vane shear tests on cohesive soils at Onsøy in Norway, Louiseville in eastern Canada and Mexico City. This paper describes engineering properties of three sensitive clays and cone factors computed from the data of field vane shear tests, direct shear tests and unconfined compression tests using the undisturbed samples.

2 TESTING PROCEDURE

2.1 *Field vane shear test*

Push-in type filed vane shear test (FVT) apparatus which consists of a rectangular vane blade, protective shoe, sleeved torque rods, and outer rods was used to obtain field vane shear strength s_{fv} at each location. Centre sustainment supports are attached to minimize the friction between torque rods and outer rods. The dimensions of the vane blade are 20 mm in width, 80 mm in height and 1.5 mm in thickness. In order to minimize the effect of disturbance caused by penetration of the vane, after the vane attached to the bottom of rods is penetrated into the ground up to 250 mm above a depth of testing, the vane blade is pushed out from the protective shoe to carry out testing. Torque is applied to the vane through torque rods from the ground surface at a constant rotation rate of 0.1 deg/s in accordance with Japanese Geotechnical Society Standards JGS1411: Method for field vane shear test.

2.2 *Direct shear test*

The dimensions of the cylindrical specimen for direct shear test (DST) are 60 mm in diameter and 20 mm in height. Recompression method is adopted to obtain in-situ undrained shear strength $s_{u(DST)}$. The specimen is consolidated under the effective overburden stress until end of primary consolidation is confirmed. After completion of consolidation, it is sheared at a displacement ratio of 0.25 mm/min, under constant volume condition during shearing period, in order to achieve undrained shear condition, in accordance with JGS 0560: Method for consolidated constant volume direct box shear test on soils.

2.3 *Unconfined compression test*

The dimensions of the cylindrical specimen for unconfined compression test (UCT) are 35 mm in diameter and 80 mm in height. The specimen is compressed at a strain rate of 1 %/min. Undrained shear strength s_u obtained from UCT is defined as a half of the unconfined compression strength:

$$s_u = q_u/2 \quad (1)$$

where s_u = undrained shear strength; and q_u = unconfined compression strength.

3 RESULTS OF SITE INVESTIGATION

3.1 *Onsøy*

The site is located at about 100 km southeast side from Oslo in Norway, where Norwegian Geotechnical Institute (NGI) has carried out a series of soil investigations (Bjerrum 1954; Lunne et al. 2003). Onsøy clay is marine clay deposited during the postglacial period, and consists of thick and homogeneous very soft soils. Figure 1 shows the results of soil property tests, CPTU, FVTs, DSTs and UCTs at the Onsøy site. At depths of 7 m to 15 m, values of liquid limits w_L are relatively constant ranging from 76 to 88% and show a tendency of increasing with the depth, meanwhile values of w_L decrease with increasing depth at depths greater than 15 m. The values of plasticity index I_p range from 47 to 62. The values of soil grain density ρ_s range from 2.76 to 2.79, which are larger than the values of marine cohesive soils investigated in Japan. At depths between 10 m and 15 m, a change of tendency on increment of su is observed for each test.

3.2 *Louiseville*

The site is located halfway between Montreal and Québec in east Canada, on the north shore of the St. Lawrence River, where studies were conducted by Université Laval from the late 70s to the late 90s (Leroueil et al. 2003). Louiseville clay is marine clay deposited during the postglacial period and consists of thick and homogeneous sediments. Figure 2 shows the results of soil property tests, CPTU, FVTs, DSTs and UCTs at the Louiseville site. Values of w_L are relatively constant ranging from 65 to 80%. Values of natural water content w_n drop from 85% at 3 m depth, to 63% at 20 m depth and are very close to the value of w_L. The values of I_p range from 45 to 62. The values of ρ_s range from 2.76 to 2.82, which are larger than the values of marine cohesive soils investigated in Japan. Below the depth of 10 m, values of s_u obtained from UCT are about 30% smaller than those from FVT and DST.

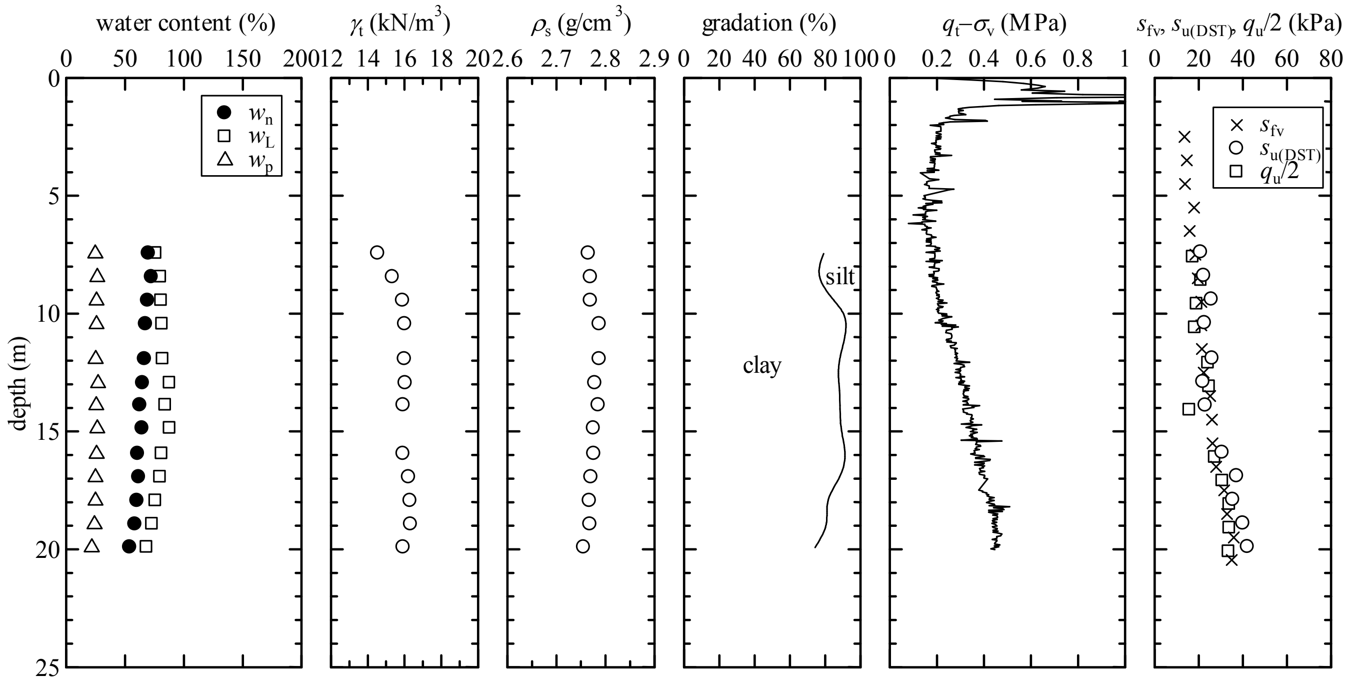

Figure 1. Profiles of engineering properties at Onsøy

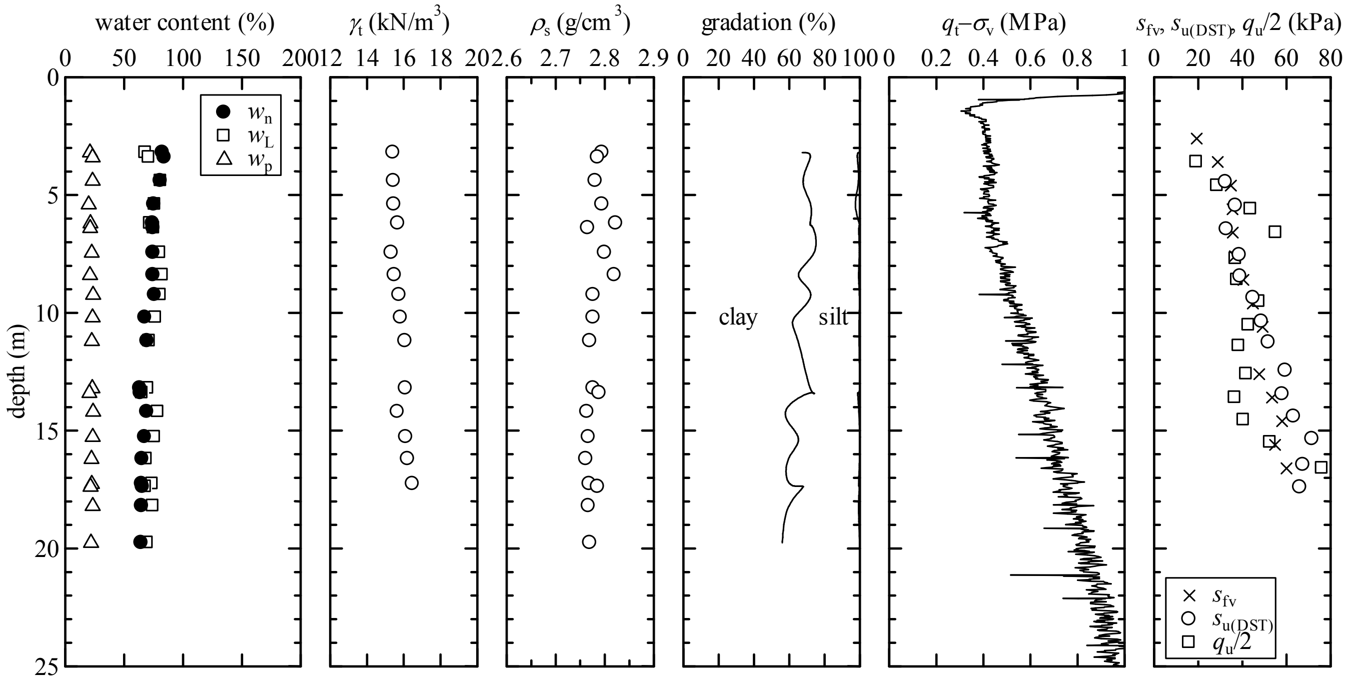

Figure 2. Profiles of engineering properties at Louiseville

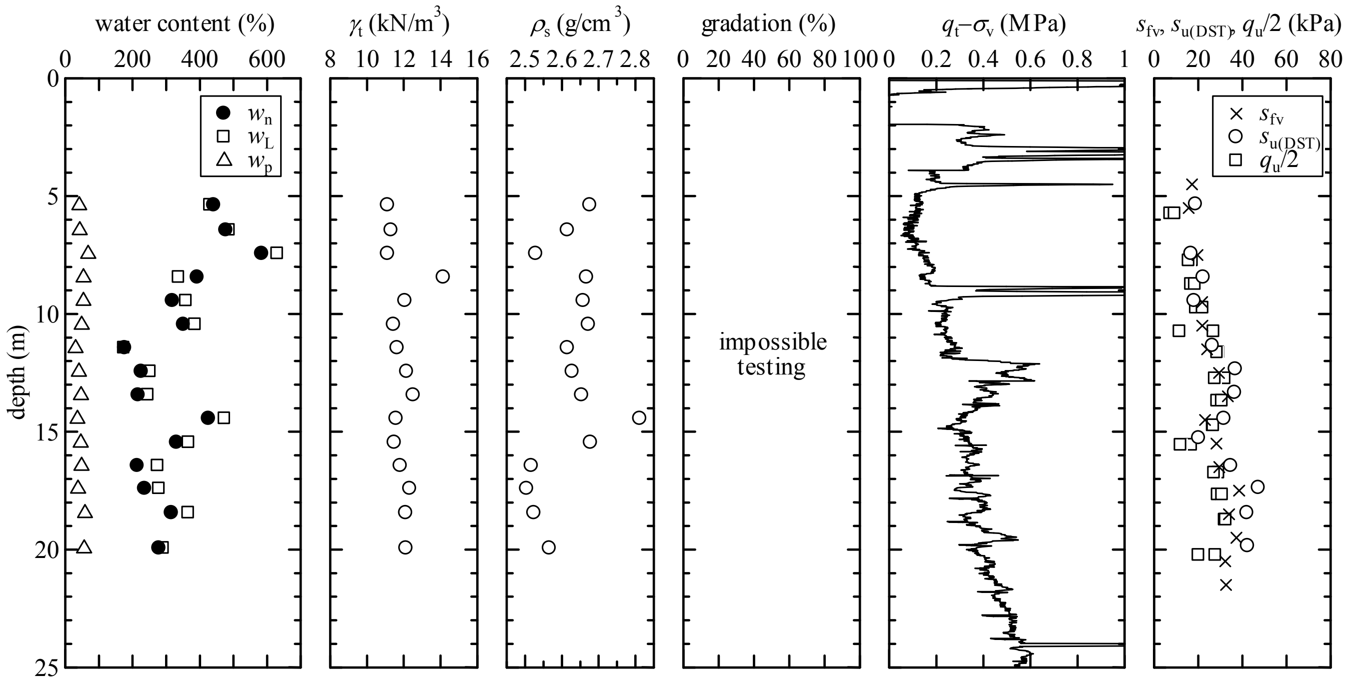

Figure 3. Profiles of engineering properties at Mexico

3.3 *Mexico*

The site is located at the urban district of Mexico City. Mexico City clay composed of volcanic and lacustrine sediments was deposited in a lake which has been desiccated progressively over the last 400 years. Figure 3 shows the results of soil property tests, CPTU, FVTs, DSTs and UCTs at the Mexico site. Fill material was encountered from ground surface to about 5m depth. Values of w_L ranging from 430 to 630% are generally similar to the values of w_n encountered above depth of 7m. Below this depth w_L ranging from 175 to 474% exceeds wn by about 50%. w_L and w_n vary considerably with depth. The values of Ip range from 145 to 564. The values of ρ_s range from 2.51 to 2.81. ρ_s values below 16 m depth are quite smaller than the values of marine cohesive soils investigated in Japan.

4 DISCUSSION

4.1 *Cone factor*

The cone factor N_{kt} is required to estimate s_u of clay from the results of CPTU. The shear strength of the soils in undrained condition and N_{kt} are empirically correlated by the following equation:

$$s_u = (q_t - \sigma_v)/N_{kt} \quad (2)$$

where s_u = undrained shear strength from CPTU; q_t = corrected cone resistance; σ_v = overburden pressure, in total stress; and N_{kt} = cone factor.

Figure 4 shows cone factors obtained from FVT, DST and UCT. For Onsøy clay the values of N_{kt} from FVT, DST and UCT are 12.7, 11.3 and 13.2, respectively. The values of N_{kt} for Louiseville clay

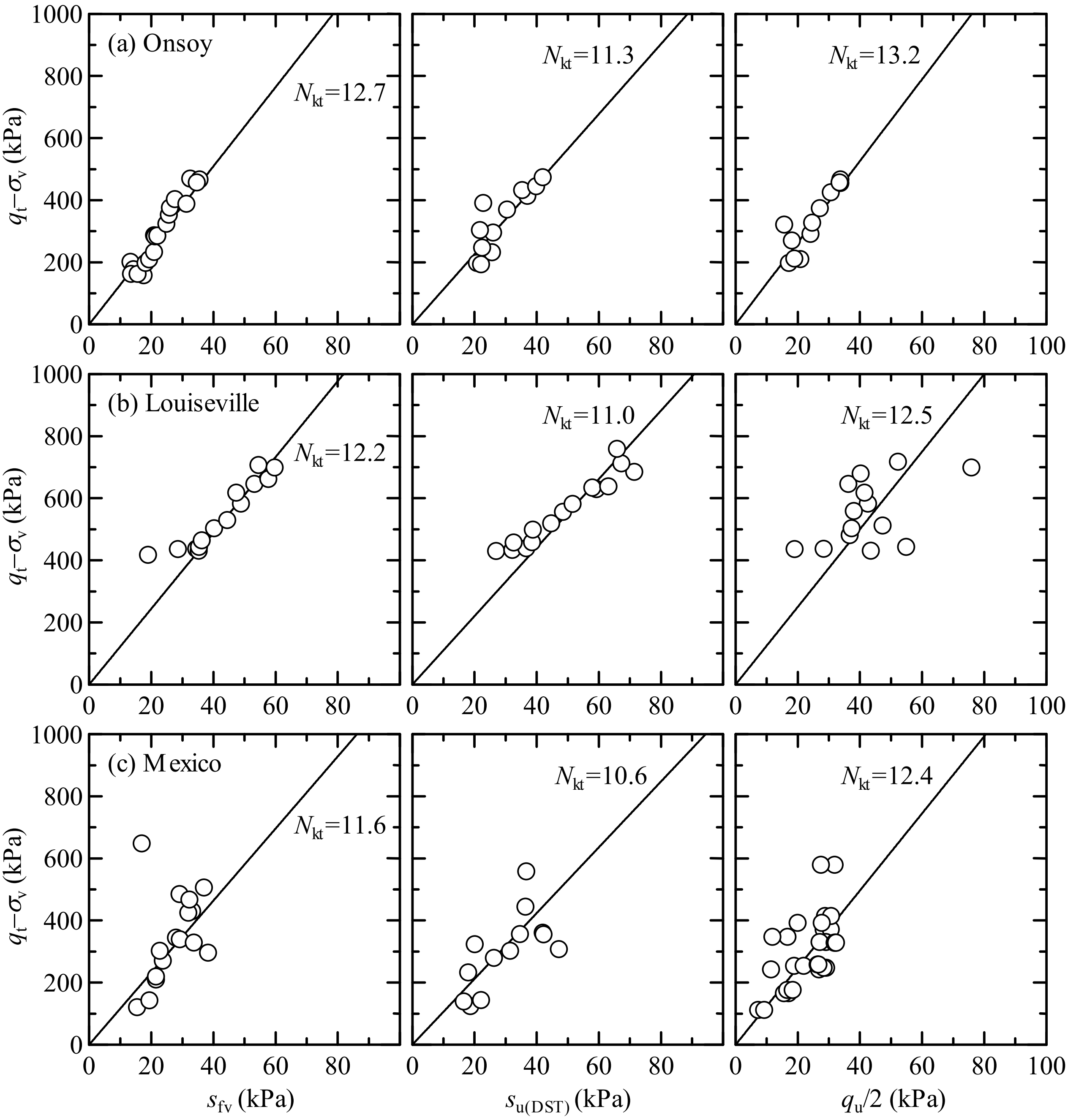

Figure 4. Cone factors

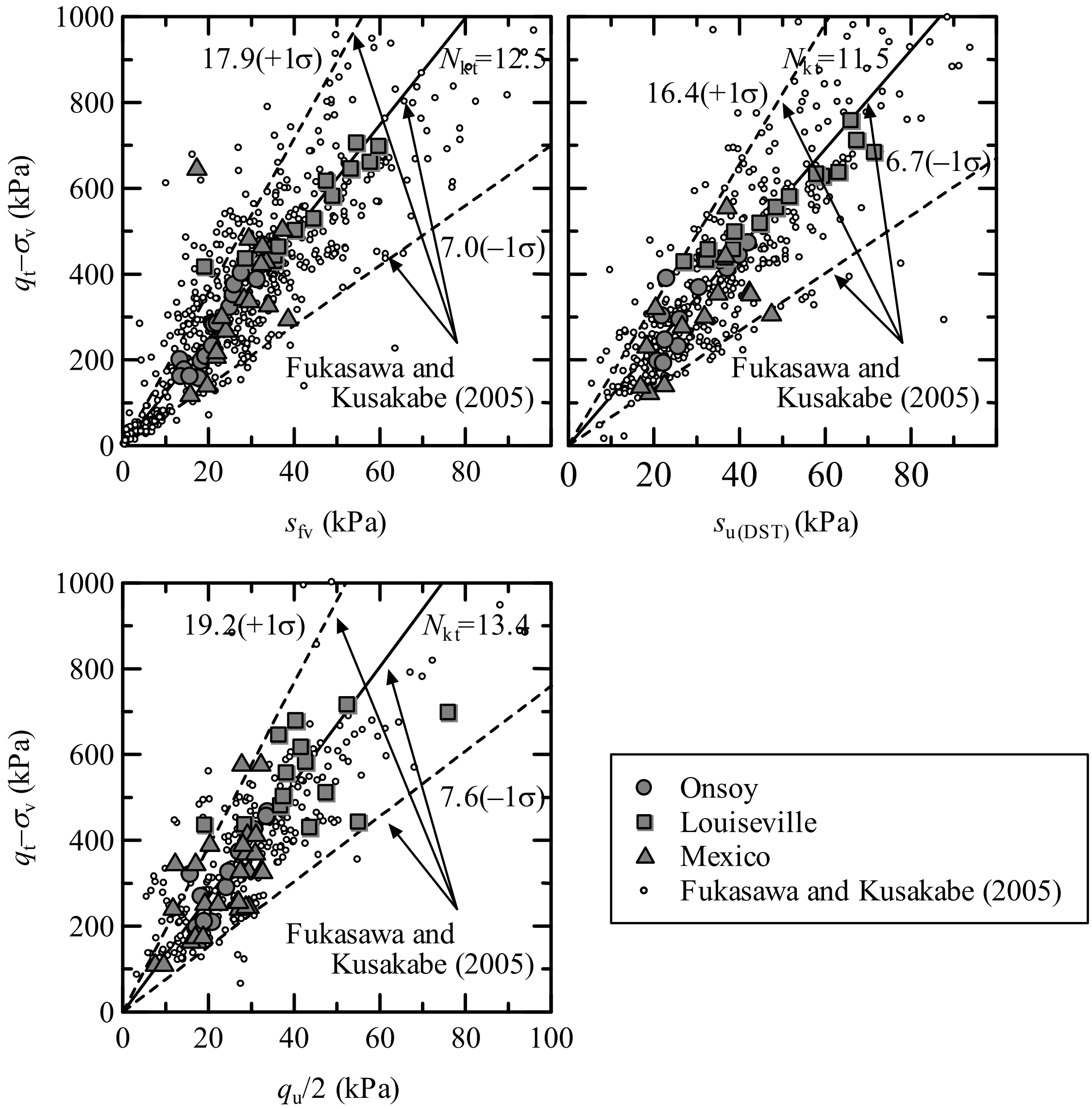

Figure 5. Relationships between s_{fv}, $s_{u(DST)}$, $q_u/2$ and q_t-σ_v

are 12.2, 11.0 and 12.5, respectively. The values of N_{kt} for Mexico clay are 11.6, 10.6 and 12.4, respectively. These results indicate that the values of N_{kt} depend on the method for determination of s_u. Accordingly, it is suggested that adopted test method for obtaining s_u to calculate N_{kt} should be made clear, considering the strength anisotropy and the rate effect.

Figure 5 shows a comparison between the data of three sites and the data of Holocene clays in Japan and South East Asia by Fukasawa & Kusakabe (2005). Data of N_{kt} obtained from Onsøy, Louiseville and Mexico clay correlate well with the result of Japanese and South East Asian clays. In addition, N_{kt} values are also plotted in the range of one standard deviation from the mean value. It appears that regional characteristics cannot be found on N_{kt}.

4.2 *$N_{kt} - I_p$ relationships*

Relationships between N_{kt} and I_p are shown in Figure 6. Regardless of variations per region and sedimental condition, the values of N_{kt} measured on these three sites are not influenced by I_p in the same way as experimental results of La Rochelle et al. (1988), Tanaka & Tanaka (2004) and Fukasawa & Kusakabe (2005), contrary to the results of Aas et al. (1986) and Powell & Quarterman (1988).

In former times, it was said that the value of N_{kt} is dependent of I_p. This is probably due to the reliability of the sampling procedure and results of laboratory and in-situ tests for lean clay. Hence, the values of N_{kt} based on results using the latest techniques could be constant without regard to the change of I_p.

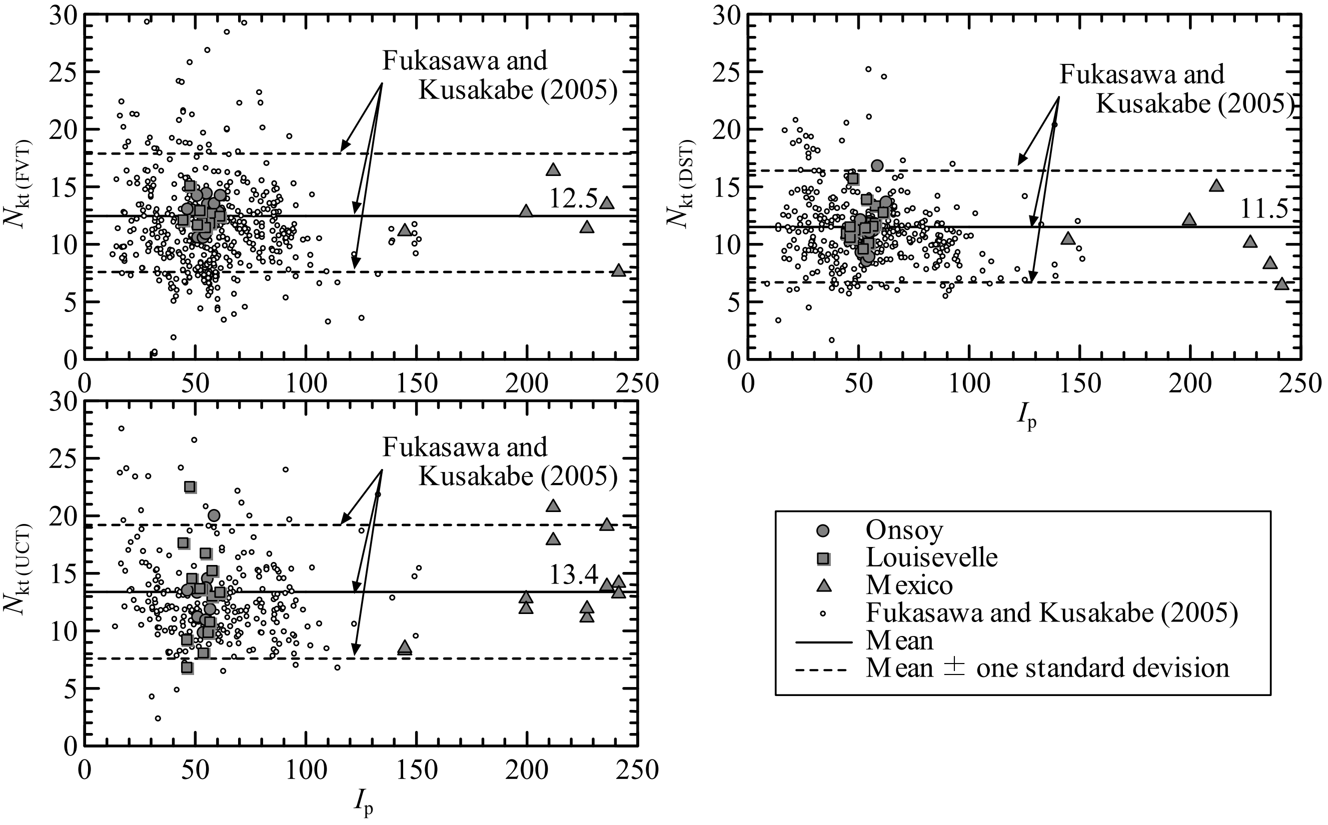

Figure 6. $N_{kt} - I_p$ relationships

5 CONCLUSION

The studies on cone factors of three sensitive clays at Onsøy, Louiseville and Mexico were carried out. The conclusions of this investigation are as follows:

1. The value of the cone factor N_{kt} of Onsøy, Louiseville and Mexico clays is approximately 12 and correlate well with the value obtained from Holocene clays in Japan and South East Asia.
2. The values of N_{kt} are not influenced by variation of the plasticity index of clay.
3. The adopted test method for obtaining undrained shear strength to calculate N_{kt} should be made clear.

6 ACHKNOWLEDGEMENTS

This work was supported by KAKENHI 15H04041.

REFERENCES

Aas, G., Lacasse, S., Lunne, T., & Hoeg, K. 1986. Use of in situ tests for foundation design on clay. *Proceedings of ASCE Specialty Conference, In-situ '86, Use of in Situ Tests in Geotechnical Engineering*: 1-30.

Bjerrum, L. 1954. Geotechnical properties of Norwegian marine clays. *Géotechnique* 4: 49-69.

Fukasawa, T. & Kusakabe, O. 2005. Applicability of Cone Penetration Test to Cohesive Soils. *Journal of Japan Society of Civil Engineering* 779(III-72): 153-170. (in Japanese).

Japanese Geotechnical Society Standard JGS 0560 2000. Method for consolidated constant volume direct box shear test on soils. Japanese Geotechnical Society. (in Japanese).

Japanese Geotechnical Society Standard JGS 1411 2003. Method for field vane shear test. Japanese Geotechnical Society. (in Japanese).

La Rochelle, P. Zebdi, M., Leroueil, S., Tavenas, F., & Virely, D. 1988. Piezocone tests in sensitive clays of eastern Canada. *Proceedings of Penetration Testing 1988, ISOPT-1*: 831-841.

Leroueil, S., Hamouche, K., Tavenas, F., Boudali, M., Locat, J., Virely, D., Roy, M., La Rochelle, P., & Leblond, P. 2003. Geotechnical characterization and properties of sensitive clay from Québec. *Proceedings of Characterisation and Engineering Properties of Natural Soils* 1: 363-394.

Lunne, T., Long, M., & Forsberg, C.F. 2003. Characterisation and engineering properties of Onsøy clay. *Proceedings of Characterisation and Engineering Properties of natural Soils* 1: 395-427.

Powell, J.J.M. & Quarterman, R.S.T. 1988. The interpretation of cone penetration tests in clays, with particular reference to rate effect. *Proceedings of Penetration Testing 1988, ISOPT-1*: 903-909.

Rad, N.S. & Lunne, T. 1988. Direct correlations between piezocone test results and undrained shear strength of clay. *Proceedings of Penetration Testing 1988, ISOPT-1:* 911-917.

Tanaka, M. & Tanaka, H. 2004. An examination of the engineering properties and the cone factor of soils from East Asia. *Proceedings of ISC-2 on Geotechnical and Geophysical Site Characterization*: 1019-1024.

Geotechnical and Geophysical Site Characterisation 5 – Lehane, Acosta-Martínez & Kelly (Eds)

Influence of phosphate dispersing agents on particle size distribution of soil fines

A. Kaur & G.C. Fanourakis
University of Johannesburg, Johannesburg, South Africa

ABSTRACT: The particle size distribution of the fine portion of soils is usually determined using sedimentation principles and the hydrometer method. Some hydrometer test methods, such as the South African Standard (SANS3001, 2014) and Guidelines laid by International Soil Reference and Information Centre (ISRIC, 2002) make provision for the effect of the dispersing agent in the solution on readings recorded during the test. Test methods that do not make such provision may be incorrectly yielding inflated fines (including clay) contents. This paper discusses the results of an investigation into the effect of dispersants when applying the TMH1 (1986) test method. The results have been compared using phosphate dispersants such as Calgon, sodium pyrophosphate decahydrate and sodium tetra pyrophosphate in various concentrations. The use of dispersants in higher concentrations produced anomalous increases in the hydrometer readings and the results indicated the importance of understanding the effect of dispersants on the fine soil particle size distribution analyses.

1 INTRODUCTION

The accurate determination of the particle size distribution of a soil is of utmost importance in the field of geotechnical engineering, as the clay content of the soil is used to determine the activity of a soil, which in turn is used for design purposes. Inaccurate clay content determinations have resulted in inappropriate design solutions which have even led to unacceptable damage to the structures. In South Africa, there is a problem with the accurate determination of the clay content of soils, basically due to the differences in the laboratory results (Jacobsz and Day, 2008). Therefore, there is a need for research into all the variables of the hydrometer test, with a view to improve its accuracy and thus standardize the test nationally and possibly, in future, internationally.

In the hydrometer analysis, an additive known as a dispersing agent or chemical dispersant is usually added to make the dispersion process more effective. Dispersants deflocculate solids and thus significantly reduce the viscosity of the dispersion paste. A variety of dispersing agents are used in different parts of the world for the sedimentation analysis. According to Lambe 1951, two commonly used deflocculants are sodium silicate and Daxad No. 23 (polymerized sodium salts of substituted benzoid alkyl sulfonic acid). Sodium hexametaphosphate (Lambe, 1951 and ASTM D422-63, 1965), sodium silicate (TMH1, 1986), sodium oxalate (TMH1, 1986), sodium pyrophosphate (Schuurman & Goedewaagen, 1971), sodium tetra pyrophosphate (Yoo & Boyd, 1994) and Disodium Dihydrogen pyrophosphate (formerly used by the Soils Testing Laboratory of Department of Water Affairs of South Africa) have also been successfully used. Calgon which is a combination of sodium hexametaphosphate and sodium carbonate is one of the popular and considered to be the best dispersing agent. All over the world, Calgon has been used as a dispersing agent in varying concentrations (BS 1377 Part 2, 1990, IS 2720 Part IV, 1985 and International Soil Reference and Information Centre (ISRIC, 2002)). As mentioned earlier TMH1 (1986) uses a combination of sodium silicate and sodium oxalate as the dispersing agent. However, the dispersing agents prescribed in TMH1 (1986) do not yield the maximum clay percentage (Kaur & Fanourakis, 2016 (a) and (b)). For this reason, many national laboratories have adopted the TMH1 (1986) test method, with a deviation in the dispersing agent type, with the objective of obtaining more accurate results reflected by higher clay percentages. However, it has been observed that altering the dispersing agent and following the TMH1 (1986) method gives inaccurately inflated results, especially with higher concentrations and volume in the case of certain dispersing agents (Kaur & Fanourakis, 2016 (a) and (b)). This is because of the aggregation of uniformed sized particles of dispersing agent (solids) in the hydrometer cylinder, which increases the density in the zones measured by the hydrometer. Some hydrometer test methods, such as the South African Standard (SANS 3001, 2014) and the guidelines laid by International Soil Reference and Information Centre (ISRIC, 2002) make provision for a correction for the effect of the dispersing agent in the solution on the readings recorded during the test. As TMH1 (1986) does not make provision for such a correction, it yields incorrectly inflated fines contents with dispersing agents other than the one recommended by the TMH1 (1986) method. Hydrometer test readings should be corrected by subtracting the readings obtained on companion "blank" solutions containing only water and dispersing agent (no soil), at the relevant time period, from the reading taken on the solution containing water, soil and dispersing agent.

In the current investigation, the effect of various dispersing agents on the hydrometer test results was considered, while following the TMH1 (1986) test method. The results were compared using phosphate dispersants such as Calgon (a combination of sodium hexametaphosphate and sodium carbonate), sodium pyrophosphate decahydrate and sodium tetra pyrophosphate in various concentrations.

2 TESTING PROGRAM

2.1 *Tests Performed*

A total of 155 hydrometer tests were conducted to explore the effects of using a high concentration and volume of the generally accepted most effective dispersing agents (Sridharan et al, 1991, Bindu & Ramabhadran, 2010 and Kaur & Fanourakis, 2016 (a) and (b)) on the hydrometer readings of water solutions (blank) containing no soil. The solutions comprised Calgon in concentrations of 35:7, 40:10, 60:10, 70:10, 80:10 and 90:10 and in the case of both sodium pyrophosphate decahydrate and sodium tetra pyrophosphate in the concentrations of 3.6%, 5%, 6%, and 7%.

The quantities of chemicals added for preparation of one litre of stock solution are given in Table 1.

When using Calgon as a dispersing agent, the minimum volume used was 100 ml and for both sodium pyrophosphate decahydrate and sodium tetra pyrophosphate, the minimum volume used was 20 ml. The justification for these quantities is that many methods (BS 1377 Part 2, 1990 and IS 2720 Part IV, 1985) recommend 125 ml of Calgon solution, so 100 ml volume was tried to confirm the recommended volume, whereas many national laboratories use 20 ml of sodium pyrophosphate decahydrate.

Table 1. Quantity of chemicals added for preparation of Calgon, sodium pyrophosphate decahydrate, and sodium tetra pyrophosphate solution

Solution of Concentration (%)	Calgon Quantity of NaHMP Added (g)	Calgon Quantity of Na_2CO_3 Added (g)	NaPP Quantity of NaPP Added (g)	NaTPP Quantity of NaTPP Added (g)
3.6	-	-	36	36
4.2	35	7	-	-
5	40	10	50	50
6	-	-	60	60
7	60	10	70	70
8	70	10	-	-
9	80	10	-	-
10	90	10	-	-

When using Calgon as a dispersing agent, the minimum volume used was 100 ml and for both sodium pyrophosphate decahydrate and sodium tetra pyrophosphate, the minimum volume used was 20 ml. The justification for these quantities is that many methods (BS 1377 Part 2, 1990 and IS 2720 Part IV, 1985) recommend 125 ml of Calgon solution, hence 100 ml volume was tried to confirm the recommended volume, whereas many national laboratories use 20 ml of sodium pyrophosphate decahydrate.

TMH1 (1986) recommended the use of 5ml of sodium silicate and 5 ml of sodium oxalate.

The stock solution of sodium silicate was prepared by dissolving sodium silicate in distilled water until the solution yielded a reading of 36 at a temperature of 20°C on the standard soil hydrometer and the stock solution of sodium oxalate consisted of a filtered saturated solution of sodium oxalate ($Na_2C_2O_4$).

2.2 *Testing procedure*

For all the tests performed, the desired quantity of dispersing agent was mixed with about 400 ml of distilled water in a canning jar. This dispersing agent – water mixture was allowed to stand overnight. After the mixture had been allowed to stand, it was dispersed for 15 minutes with a standard paddle. The paddle was washed clean with distilled water allowing the wash water to run into the container. This mixture was then poured into the Bouyoucos cylinder and the canning jar was rinsed with distilled water from the wash bottle. The cylinder was then filled with distilled water to 1130 ml mark with the hydrometer (152H) inside. Thereafter, the hydrometer was removed and the cylinder was inverted a few times, using the palm of one hand as a stopper over the mouth of the cylinder to ensure that the temperature was uniform throughout. After bringing the cylinder to a vertical position, the stopwatch was started. The hydrometer was inserted and the readings were taken at 18 seconds and 40 seconds without removing the hydrometer from the cylinder. The hydrometer was then taken out and rinsed with water and it was again inserted into the suspension when the elapsed time was 2 minutes. This reading was noted and the hydrometer was removed and placed in distilled water. This procedure was repeated for the 5 minutes, 15 minutes, 30 minutes, 1 hour, 4 hour and 24-hour readings. After taking each hydrometer reading, the temperature of the liquid was also recorded. Temperature corrections were appropriately applied to the readings.

For any soil sample, the percentages finer than 0.075 mm, 0.05 mm, 0.04 mm, 0.026 mm, 0.015 mm, 0.01 mm, 0.0074 mm, 0.0036 mm and 0.0015 mm were respectively calculated by the readings taken at 18 sec, 40 sec, 2 min, 5 min, 15 min, 30 min, 1 hour, 4 hours and 24 hours, by means by Equation 1.

$$P=\frac{C\times Sf}{Sm} \tag{1}$$

Where, P = Percentage finer than relevant size,
S_m = Mass of soil fines used in analysis (50 grams),
S_f = Percentage soil fines in total sample (<0.425 mm),
C = Corrected hydrometer reading
The percentage clay content present in each sample (fraction finer than 0.002 mm) was obtained from the relevant particle size distribution curve. As, in the current study the hydrometer analysis was done on blank solutions (no soil), Equation 1 was not applicable.

3 RESULTS AND DISCUSSION

Semi-logarithmic graphs were plotted with grain size on the x-axis (log scale) and correction to be applied to (subtracted from) hydrometer readings (in tests where the soil is included) on the y-axis. Figure 1 shows the effect of the dispersing agent on hydrometer readings while following TMH1 (1986) guidelines.

It is clear from Figure 1 that in the case of all the dispersing agents except the Calgon, the corrections to be applied to hydrometer readings would be less than 1 g/litre. In the case of Calgon, the correction ranged from 5.3 to 5.8 g/litre (average 5.6 g/ litre).

Most of the national laboratories (in South Africa) are using 125 ml of Calgon (35:7) and TMH1 (1986). However, the hydrometer test results are not appropriately corrected (reduced) to allow for the above-mentioned contribution of the dispersing agent to the test readings.

In addition, hydrometer test analyses were conducted using Calgon, sodium pyrophosphate decahydrate and sodium tetra pyrophosphate in different concentrations and volumes to establish the effect of the increase in the volume and concentration of the solution on the hydrometer readings.

It is clearly seen from Figure 2, which is a plot between correction to the hydrometer reading and grain size for 9% Calgon (80:10) that, an increase in the volume of the dispersing agent used resulted in a concomitant increase in the hydrometer reading. Also, it is evident from the figure that there is almost no difference between the18 sec reading and 24 hour reading which shows that the amount of dispersing agent particles in suspension remained almost constant with the time. A dispersing agent volume of up to 475 ml was included in the test program.

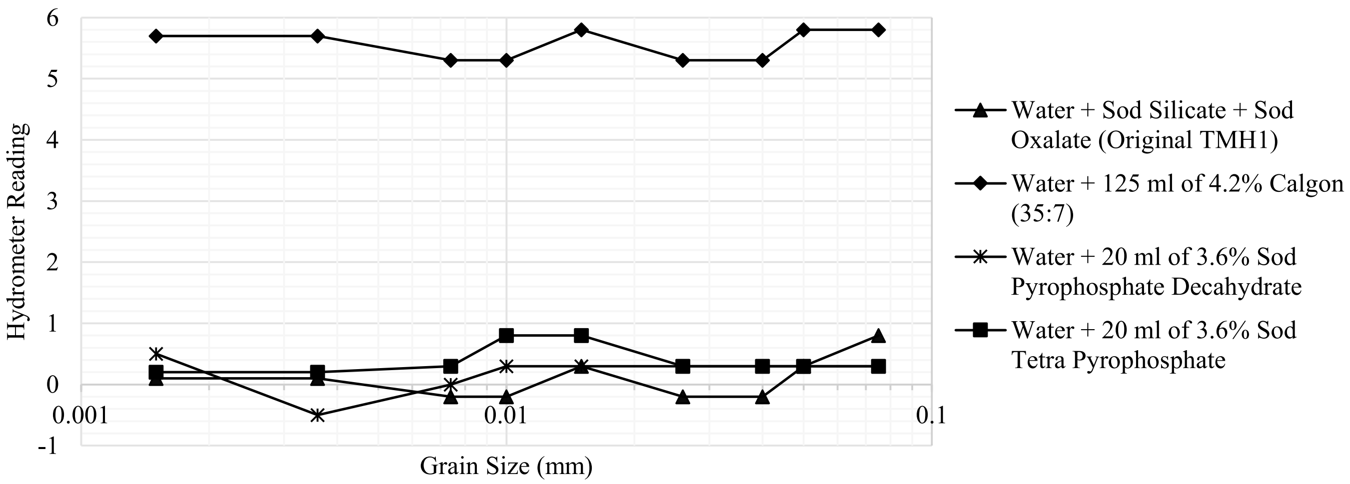

Figure 1. Effect of dispersing agent types on hydrometer readings.

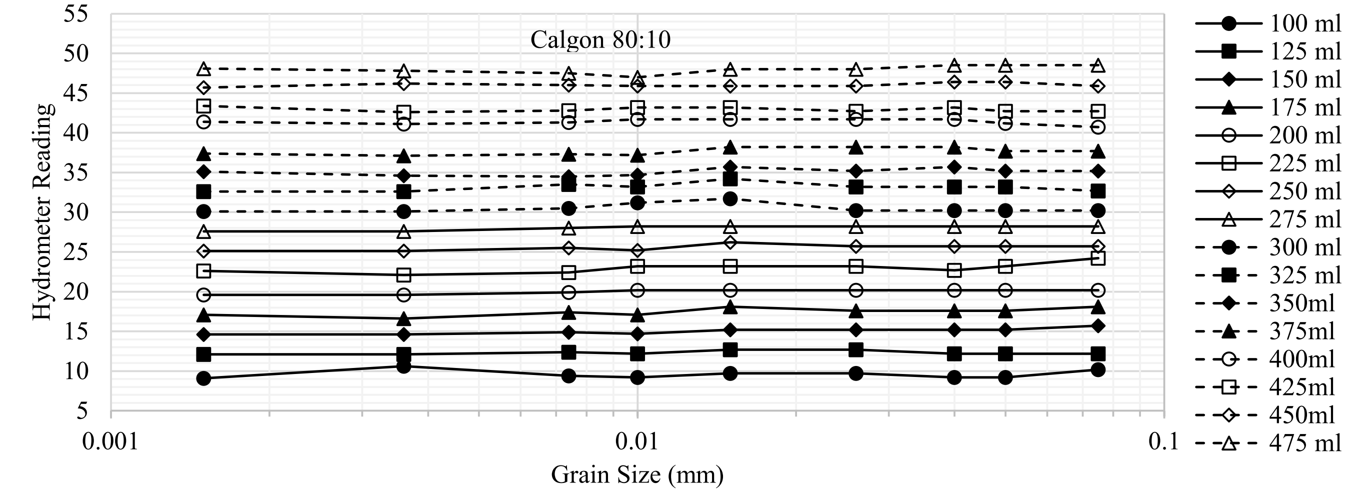

Figure 2. Hydrometer reading corrections for different grain sizes for Calgon (80:10).

Figures 3, 4 and 5 show the effect of volume and concentration of Calgon, sodium pyrophosphate decahydrate and sodium tetra pyrophosphate, respectively, on the hydrometer readings pertaining to the time at which the clay size (0,002 mm) reading would be taken. From all three figures it is clear that, with the increase in the concentration and volume of the dispersing agents, there is an increase in the hydrometer readings. With Calgon as a dispersing agent, the hydrometer readings varied from 5 to 47 with an increase in volume and concentration while with sodium pyrophosphate decahydrate and sodium tetra pyrophosphate they varied from 0 to 20 and 0 to 9, respectively. The reason behind this increase is the aggregation of uniformed sized solid particles of dispersing agent in the hydrometer cylinder, increasing the density of the solution in the zones measured by the hydrometer.

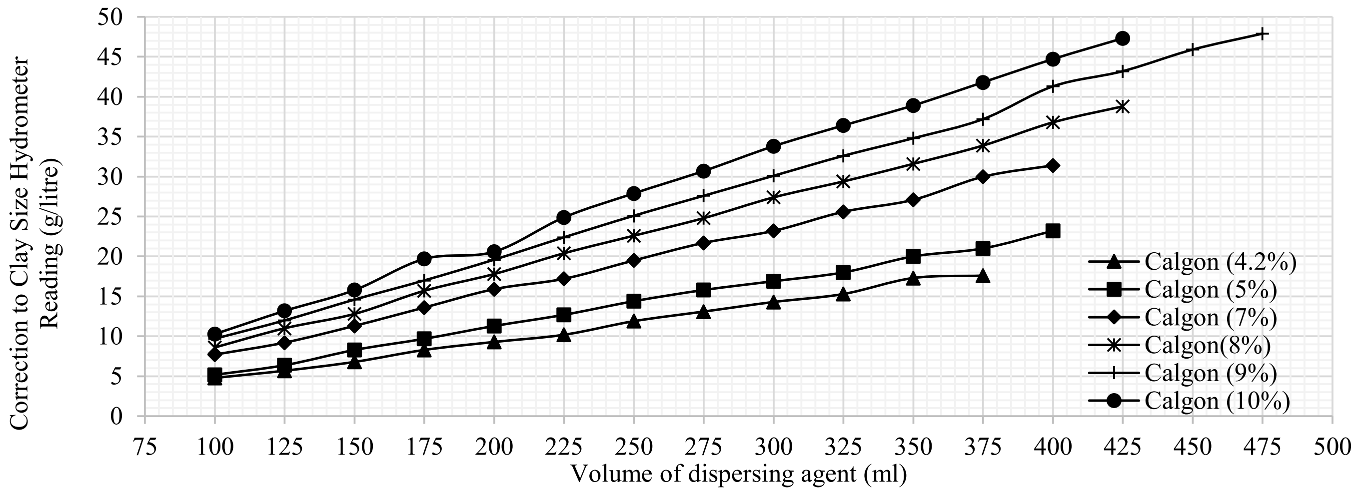

Figure 3. Effect of volume and concentration of Calgon on clay-sized period readings.

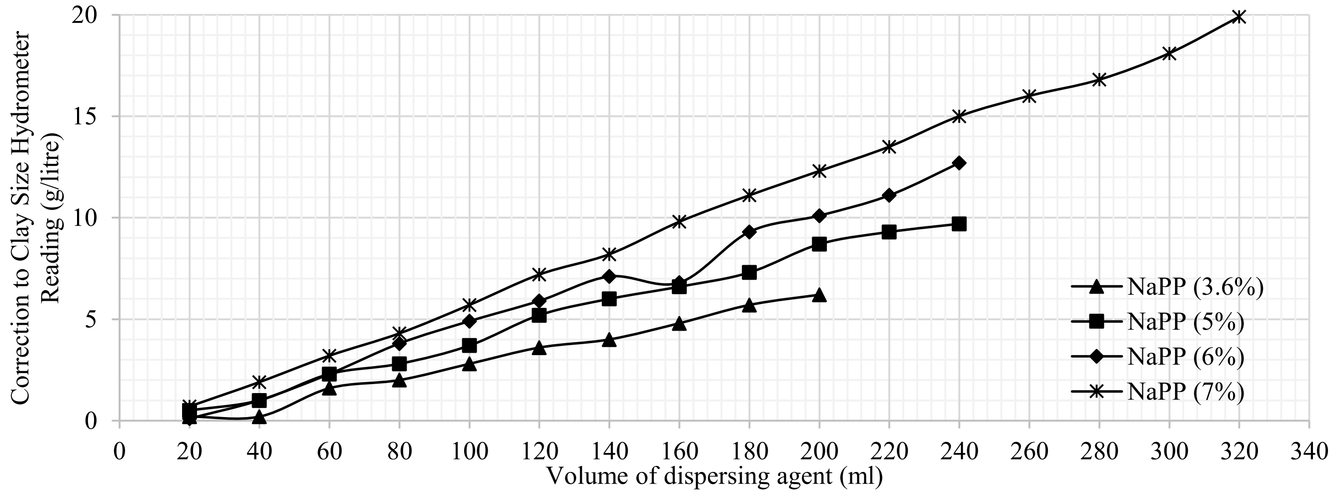

Figure 4. Effect of volume and concentration of sodium pyrophosphate decahydrate on clay-sized period readings.

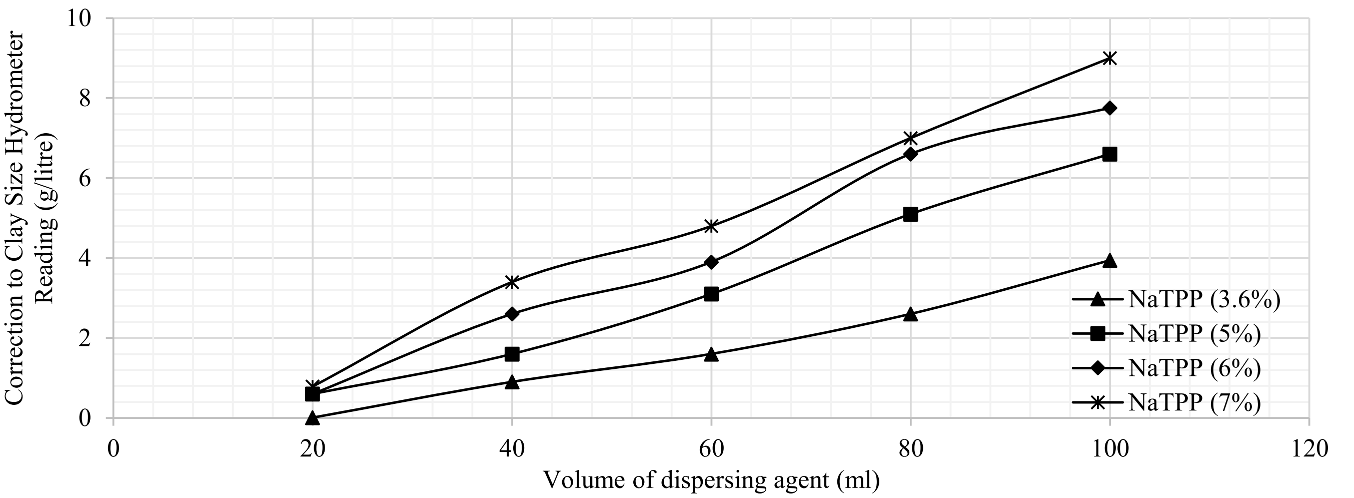

Figure 5. Effect of volume and concentration of sodium tetra pyrophosphate on clay-sized period readings.

In addition, the calculated soil activity is strongly affected if the dispersing agent corrections are not applied to the hydrometer readings. Table 2 shows the Atterberg's limits, activities and clay contents of the four soil samples used by Kaur and Fanourakis, 2016 (a) and (b). The activities tabulated in Table 2 were computed with and without applying the dispersing agent corrections and are referred to as A and A', respectively. The clay contents determined with and without the dispersing agent corrections are referred to as C and C', respectively.

Table 2. Activities of the soil samples with and without dispersing agent corrections

Properties	Light Yellow Soil	Black Soil	Light Brown Soil	Red Soil
Liquid limit (LL)	32	56	33	28
Plastic Limit (PL)	16	22	24	15
Plasticity Index (PI)	16	34	9	13
C	21.5	32	5.7	29
A	0.74	1.06	1.58	0.45
C'	32.4	44	11.8	40
A'	0.49	0.77	0.76	0.33
Δ % Activity	33.8	27.4	51.9	26.7

It is observed that as the blank readings are not subtracted from the hydrometer readings of the suspension thus yielding more clay content there is about 34 %, 27 %, 52 % and 27 % decrease (Δ %) in the activity of light yellow soil, black soil, light brown soil, and red soil, respectively (Table 2). Therefore, the results discussed in this study indicate the importance of understanding the effect of dispersing agents in the water on the hydrometer test readings. Thus, hydrometer test readings should be corrected (reduced) to account for the contribution made by the type, concentration and volume of dispersing agent used in the test.

4 CONCLUSIONS

The following conclusions were drawn from the study conducted:

- Tests with different dispersing agents clearly indicated that the hydrometer readings of blank solutions vary significantly depending upon the type of dispersing agent.
- The hydrometer readings for blank solutions increased with an increase in the concentration and volume of a dispersing agent. For Calgon, the hydrometer readings varied from 5 to 47 (g/litre) while for sodium pyrophosphate decahydrate and sodium tetra pyrophosphate, they varied from 0 to 20 (g/litre) and 0 to 9 (g/litre), respectively.
- The increase was attributed to the aggregation of uniformed sized solid particles of dispersing agent in the hydrometer cylinder, increasing the density of the solution in the zones measured by the hydrometer.
- There is an average decrease ranging from approximately 27 % to 52 % (average of 36 %) in the activities of soils computed with the clay content determined without dispersing agent corrections.
- Readings of hydrometer tests where deviations from the prescribed type, volume, and concentration of the dispersing agent occur should be appropriately corrected.

5 REFERENCES

ASTM, 1965. *Grain size analysis of soils*. ASTM Designation D422-63, ASTM, Philadelphia.

British Standard, BS, 1990. *Methods of test for soils for civil engineering purposes*. BS Designation 1377 Part 2, BSI, London.

Bindu, J & Ramabhadran, A 2010. Effect of concentration of dispersing agent on the grain size distribution of fine-grained soil. *Proceedings, Indian Geotechnical Conference,* Mumbai, India pp 275-278.

Indian Standard, IS, 1985. *Methods of tests for soils*. IS Designation 2720 Part IV, BIS, New Delhi.

International Soil Reference and Information Centre, ISRIC 2002. *Procedures for soil analysis*. Technical paper 9, The Netherlands.

Jacobsz, S W & Day, P 2008. Are we getting what we pay for from geotechnical laboratories? *Journal of South African Institution of Civil Engineering*, 16(4):8-11.

Kaur, A & Fanourakis, G C 2016 (a). The effect of type, concentration and volume of dispersing agent on the magnitude of the clay content determined by the hydrometer analysis. *Journal of South African Institution of Civil Engineers* (Accepted for publication).

Kaur, A & Fanourakis, G C 2016 (b). A further investigation of the effect of type, concentration and volume of dispersing agent on the magnitude of the clay content determined by the hydrometer analysis. *Journal of South African Institution of Civil Engineers*. (Under review)

Lambe, T W 1951. *Soil testing for engineers*, New York: John Wiley & Sons, Inc.

SANS, 2014. *Civil Engineering test methods*. SABS Standard Division Designation 3001 Part GR3, SABS, Pretoria.

Schuurman, J J & Goedewaagen, M A J 1971. *Methods for the examination of root systems and roots*, Wageningen, The Netherlands: Pudoc.

Sridharan, A., Jose, B.T. & Abraham, B.M. 1991. Determination of clay size fraction of marine clays. *Geotechnical Testing Journal*, 14(1): 103-107.

TMH1:1986. *Standard methods of testing road construction materials*. Method A6. Pretoria: National Transport Commission.

Yoo, K H & Boyd, C E 1994. *Hydrology and water supply for pond aquaculture*, USA: Springer.

Geotechnical and Geophysical Site Characterisation 5 – Lehane, Acosta-Martínez & Kelly (Eds)

The Influence of In-situ Effective Stress on Sample Quality for Intermediate Soils

C.P. Krage, B.M. Albin, & J.T. DeJong
University of California - Davis, Davis CA, USA

D.J. DeGroot
University of Massachusetts - Amherst, Amherst MA, USA

ABSTRACT: The role of overburden stress on sample quality for synthetic mixtures of silica silt and kaolin clay across a range of plasticity and silt content was investigated using oedometer tests. Existing clay-based sample quality criteria ($\Delta e/e_0$ and SQD) were developed from datasets obtained on samples of plastic clays obtained from 5 to 25 m depth, which indicate a trend of decrease in sample quality with depth. Measurements from oedometer specimens subjected to various simulated levels of overburden stress are used to quantify the sensitivity of current sample disturbance criteria to overburden stress. Low overburden stress specimens (i.e. shallow depths) undergo little total stress relief, requiring less volumetric recompression to in-situ stress, which results in an apparent higher sample quality regardless of the disturbance level. High overburden stress specimens (i.e. deep depths) undergo greater total stress relief during the sampling and specimen preparation process, which often results in a higher level of disturbance. The laboratory results show that SQD and $\Delta e/e_0$ are overburden stress level dependent for the PI 4 and 6 intermediate soil mixtures tested.

1 INTRODUCTION

Characterization of in-situ soil behavior requires soil sampling and laboratory testing where in-situ testing cannot be reliably performed. Sampling of clay soils is widespread in practice and has resulted in the development of sample quality criteria to assess the effectiveness of sampling techniques in obtaining undisturbed samples for laboratory testing. In sandy soils, where permeability is greater and suction is less effective at preserving the soil specimen, in-situ testing techniques are the preferred approach. Soils between plastic clays and clean sands, termed intermediate soils herein, can often be sampled using clay-based techniques, but the quality of the sample obtained as well as the applicability of the sample quality indices is not well understood.

Laboratory testing of soil specimens requires quantification of sample quality to assess the effectiveness of test results in representing in-situ soil properties. Empirically developed quality indices, based mostly on marine clays, are used in practice to evaluate the quality of specimens obtained by sampling. In practice these methods are often applied to soils that lie outside of the empirical database, with an implicit assumption that they are applicable. However, the broader applicability of these methods for intermediate soils is poorly understood.

This paper presents results from a continuing study investigating the behavior of intermediate soils (i.e. silty clays, clayey silts) when subjected to different levels of sample disturbance. Synthetic silt-kaolin specimens, which span a range of plasticity, are subjected to various stress paths that represent different levels of disturbance. The effect of simulated in-situ overburden stress level on the stress-strain responses during sampling and recompression is investigated using constant rate of strain consolidation tests, and the effectiveness of clay based sample quality criteria to capture this response is investigated.

2 CURRENT PRACTICE EVALUATING SAMPLE QUALITY

Sampling techniques typically used in practice are robust for clayey soils. The low permeability and high suction of clayey soils assists in maintaining the in-situ effective stresses during the drilling, sampling, and handling process, resulting in intact specimens that largely retain their in-situ stress-strain behavior.

Sampling of cohesionless soils is possible via ground freezing techniques, but is often cost prohibitive to implement on typical projects. Engineers are left with the choice between in-situ tests, sampling and laboratory testing, or a combination of the two to obtain soil properties at the site.

Sample quality criteria is used in practice to evaluate the effectiveness of sampling techniques in obtaining soil samples that will produce representative engineering properties when tested in the laboratory.

2.1 *Overview of Clay Criteria*

Efforts to obtain high quality samples of clay soils occur in geotechnical practice, particularly on larger scale projects. Reliable and practical sampling equipment and procedures to obtain high quality samples have developed over the last several decades. The tube sampler is the most common in practice, though use of a thin walled fixed piston sampler provides a practical high quality alternative to the tube sampler (Tanaka et al. 1996), while the Sherbrooke block sampler (Lacasse et al. 1985) is considered the highest quality sampler developed (and mostly limited to research projects).

The primary metrics used to indicate sample quality are ε_{vol} and $\Delta e/e_0$, which were developed by the Norwegian Geotechnical Institute (NGI) in the late 1970s and early 1990s, respectively (Andresen and Kolstad 1979, Lunne et al. 1997, Lunne et al 2006). Measuring recompression strain to in-situ stress levels during 1D (odometer) or triaxial consolidation tests is used to indicate changes in specimen effective stress and destructuring during the drilling, sampling, and handling procedures. Terzaghi et al. (1996) defined the Specimen Quality Designation (SQD) as a rating index for the value of volumetric strain, ε_{vol}, necessary to re-establish the in-situ effective stress. In a similar manner, $\Delta e/e_0$ tracks changes in void space during recompression to in-situ effective stress, normalized by the initial void ratio.

These methods to evaluate sample quality are empirically derived based on comparisons between how different quality samplers induce sample disturbance. The database used to derive the recommendations in Table 1 consists primarily of marine clays with PI values of 6-43, OCR values of 1-4, obtained from depths of 5-25m, and are moderate to highly sensitive (measured from fall cone tests, Lunne et al. 2006).

2.2 *Influence of Overburden Stress*

The influence of overburden stress, or the magnitude of stress relief that occurs when a soil is removed from its in situ stress condition and prepared for laboratory testing, is not explicitly accounted for in the clay-based sample quality metrics, since samples were obtained from a limited depth range (5-25m). Some attempt was made, however, to account for trends in over consolidation ratio (OCR).

Table 1. Quantification of sample disturbance based on specimen volume change during laboratory reconsolidation to σ'_{v0}.

Specimen Quality Designation (SQD) (Terzaghi et al. 1996)		$\Delta e/e_0$ Criteria (Lunne et al. 1997)		
Volumetric Strain (%)	SQD	OCR = 1 – 2 $\Delta e/e_0$	OCR = 2 – 4 $\Delta e/e_0$	Rating*
< 1	A	< 0.04	< 0.03	Very good to excellent
1 – 2	B	0.04 – 0.07	0.03 – 0.05	Good to fair
2 – 4	C	0.07 – 0.14	0.05 – 0.10	Poor
4 – 8	D	> 0.14	> 0.10	Very poor
> 8	E			

* Refers to use of samples for measurement of mechanical properties.

Lunne et al. (1997) defined $\Delta e/e_0$ threshold values for sample quality for OCR ranges of 1-2 and 2-4 specimens to account for the greater stiffness and strength of higher OCR soils (Table 1). However, no correction was developed to account for increased strain during laboratory recompression to the in-situ state for samples with high overburden stresses. Trends in $\Delta e/e_0$ with depth from the Lunne et al. (1997) dataset for three different sampling techniques presented in Figure 1 shows that $\Delta e/e_0$ increases with sampling depth, or overburden stress.

Though not sampling the same soils as Lunne et al., Tanaka et al. (2002) obtained samples of marine clay from depths up to 400 m for design of a port facility in Japan. They initially hypothesized that there

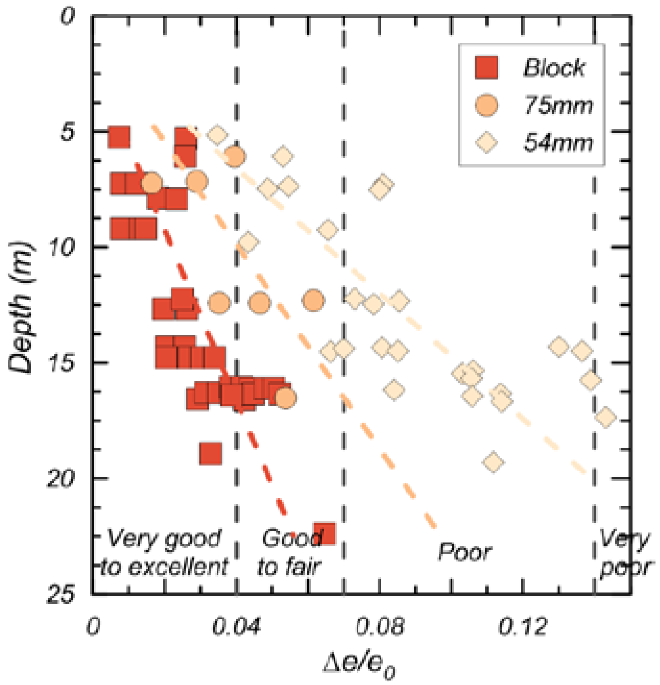

Figure 1 – Sample quality for different sampling methods: Sherbrooke Block, 75mm piston, and 54mm piston samplers. Dashed lines are added to indicate trend with depth (overburden stress) for each sampling method. Note that each sampling method was performed on three different clay soils.

would be a degradation of sample quality with increasing sampling depth due to the significant increase in recompression strains necessary to reestablish in-situ stresses as well as the increased stress relief from these significant depths. Their observations indicate that the sample quality of these soils is independent of sampling depth (Tanaka et al. 2002).

2.3 *Application to Intermediate Soils*

The clay-based sample disturbance criteria may not be applicable to intermediate soils even if they can be successfully sampled. The transition from a conventional clayey soil to a more sand-like material typically corresponds to an increase in the soil permeability, resulting in loss of the ability to maintain suction and constant volume during the sampling process. These changes affect the sample's ability to maintain in-situ effective stress and state, resulting in a laboratory specimen that is dissimilar to its in-situ counterpart. In addition, the decrease in clay fraction and/or fines content (and the corresponding increase in silt and/or sand content) results in increasing soil stiffness as silica particles have a higher material stiffness than the overall clay fabric, which has significant effect on measured stiffness during recompression in the laboratory. Fundamental differences in drainage, particle scale, soil fabric and sampling stress paths highlight some of the difficulties in applying clay-based criteria to intermediate soils.

Krage et al. (2015) demonstrated that clay based sample criteria do not track with the sample disturbance level for soils with a PI less than about 10. Further, the clay-based indices incorrectly indicated that the sample quality increased as the PI value decreased for a given level of disturbance; this could mislead engineers to interpret samples to be of higher quality than they actually are. The study compared a suite of mixtures across a range of plasticity subjected to differing levels of simulated sample disturbance. Heavily disturbed tests, obtained via a freezing and thawing cycle, show trends of increasing sample quality with decreasing PI (Figure 2) despite similar levels of extreme disturbance. Freezing and thawing of a non-plastic silica silt resulted in complete degradation of soil fabric, though recompression strains indicate a very good to excellent sample quality ($\Delta e/e_0 < 0.04$) that cannot be corroborated via laboratory observations of the mixture. This research highlighted the need for an improved sample quality metric for soils that accounts for effects of material stiffness and overburden stress.

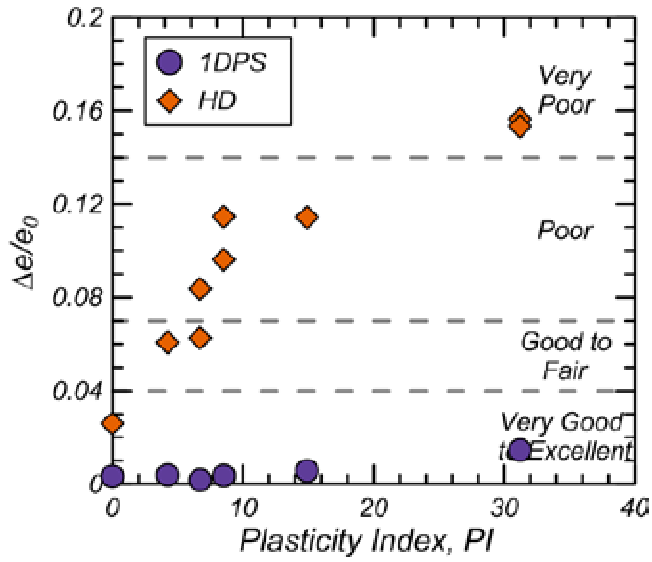

Figure 2. Results from a study using synthetic intermediate soil mixtures indicate a strong trend of increasing sample quality with decreasing PI for heavily disturbed mixtures.

3 MATERIALS AND METHODS FOR STUDY WITH SYNTHETIC INTERMEDIATE SOILS

Synthetic intermediate soil mixtures were prepared in the laboratory using varying proportions of silica silt (US-Sil-Co-Sil 250) and kaolin clay (Old Hickory, No. 1 Glaze) (Figure 3, e.g. 80S20K indicates 80% silica silt and 20% kaolin clay by mass). Each soil mixture was obtained by mixing dry soils and deionized water to hydrate at 1.5-2 times liquid limit of the mixture for a minimum of 24 hours. Following dry mixing and hydration, the slurry was mixed with a 1390 rpm mixing blade under vacuum pressures exceeding 68 kPa to thoroughly mix, de-air, and promote saturation of the initially dry soil particles prior to slurry deposition into 71.1 mm (2.8 inch) diameter oedometer cells for initial consolidation. Rotation was allowed as needed to prevent par-

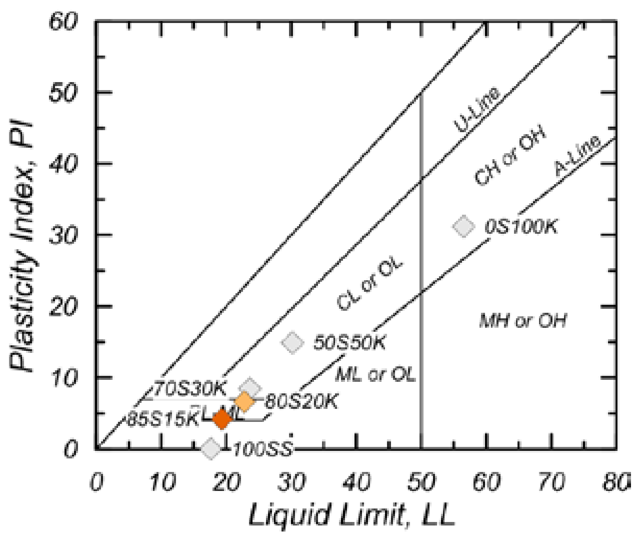

Figure 3. Atterberg limits for the synthetic intermediate soils where colored symbols indicate mixtures used in this study and gray symbols indicate mixtures used in Krage et al. (2015).

ticle segregation during deposition. This approached enabled preparation of replicable specimens with a consistent deposition method across the range of soil mixtures presented in Figure 3 (PI ranging from 0 to 31). Artificial specimens were prepared in the laboratory to capture behavioral trends in a controlled environment, therefore the structure inherent to natural intermediate soils is not captured in this study.

The processes used to induce two levels of disturbance, from an ideal best case “perfect sample” to a highly disturbed sample, were developed to examine the effects of sample disturbance on consolidation behavior. The development of each type of disturbance and the loading conditions necessary to establish consistent mechanical loading stress history between these cases are presented in the following section. The three distinct phases were: (1) initial preloading to establish stress history for simulating depositional processes, (2) inducing disturbance to each specimen to simulate disturbance during drilling, sampling, and handling, and (3) re-consolidating the specimen to evaluate recompression trends as performed in the laboratory.

3.1 *1D Perfect Sample*

1D perfect sampling (1DPS) was defined as the removal of deviatoric stress for an oedometer specimen to obtain K_0 of 1 ($\sigma'_v = \sigma'_h$). Under internal isotropic effective stresses, the removal of total stress results in an equal and opposite application of an isotropic suction stress that maintains effective stresses estimated to be equal to σ'_{h0} (per Jamiolkowski et al. 1985). The amount of unloading necessary to achieve K_0 of 1 was estimated using Equation 1 (Mesri and Hyatt 1993).

$$K_{0,OC} = (1 - \sin\varphi'_{cv})OCR^{\sin\varphi'_{cv}} \qquad (1)$$

where OCR was controlled with consolidation loading and φ'_{cv} was either obtained using monotonic direct simple shear (DSS) tests or estimated using DSS results from similar mixtures.

The 1DPS, in principle, is the best possible condition the sample could experience and therefore provides the baseline “perfect” sample quality in this study. The vertical total stress was not further relieved beyond what was necessary to obtain K_0=1 such that existing effective stresses remained constant. Removal of total stress would inevitably disturb the specimen, changing the actual stress conditions within the specimen (due to handling, exposure to moisture/air, etc.).

3.2 *Highly Disturbed Sample*

Highly disturbed (HD) conditions were established using the following procedure. Specimens were first loaded from slurry deposition in the same manner as 1DPS. Specimens were then removed from the IL oedometer (in the same 71.1 mm ring) and CRS loaded to establish the desired σ'_p, simulated in-situ stress σ'_{v0}, and estimated K_0 of 1 stress (as discussed in the following section). At this point, the HD specimens were immediately unloaded to zero vertical stress and extruded from the 71.1 mm oedometer cell. To create the HD condition, the unconfined specimen was then placed in a freezer for a minimum of 24 hours at -12ºC, allowed to thaw in a constant temperature, constant humidity chamber for a minimum of 24 hours, and then trimmed into a 63.5 mm oedometer cell. The specimen was then CRS tested following the remainder of the loading schedule for each in-situ stress level. This procedure was used to breakdown the structure of the specimen through the expansion of saturated void space during freezing.

3.3 *Loading Conditions*

Though the loading path is unique for each simulated in-situ stress, the stages of loading are consistent across all simulated in-situ stress levels (Table 2). Loading of the specimen is achieved using the following steps.

(1) Specimens were first loaded from slurry deposition to approximately 50% of the target σ'_p (Table 2) by incrementally doubling the load (load increment ratio of 1) in a 71.1 mm diameter oedometer cell. This process eliminated excess water from the slurry and established material stiffness. 1DPS specimens were then trimmed into a 63.5 mm oedometer cell *prior* to CRS loading to establish simulated in-situ stress history while HD specimens are trimmed *after* establishing simulated in-situ stress history and induced disturbance. This ensures the 1DPS specimen will not be further removed from the oedometer cell, ensuring the specimen maintains perfect sampling conditions previously discussed. Additionally, trimming the HD specimen following application of stress history and disturbance simulates the trimming process of the typical field sample.

(2) In order to simulate the desired in-situ stress history, specimens were loaded via constant rate of strain consolidation (CRS) to establish the desired σ'_p (Table 2), then unloaded to desired simulated “in-situ” stress, σ'_{v0}. Specimens were further unloaded to vertical stress corresponding to estimated

Table 2. Loading stress derived from in-situ effective stress

σ'_{v0} (kPa)	OCR	σ'_p (kPa)	$\sigma'_{v,unload}$ (kPa)	$\sigma'_{v,reload}$ (kPa)	σ'_{final} (kPa)
20	1.8	36	90	23	2500
110	1.8	200	500	128	2500
250	1.8	450	1125	292	2500
500	1.8	900	2250	583	2500

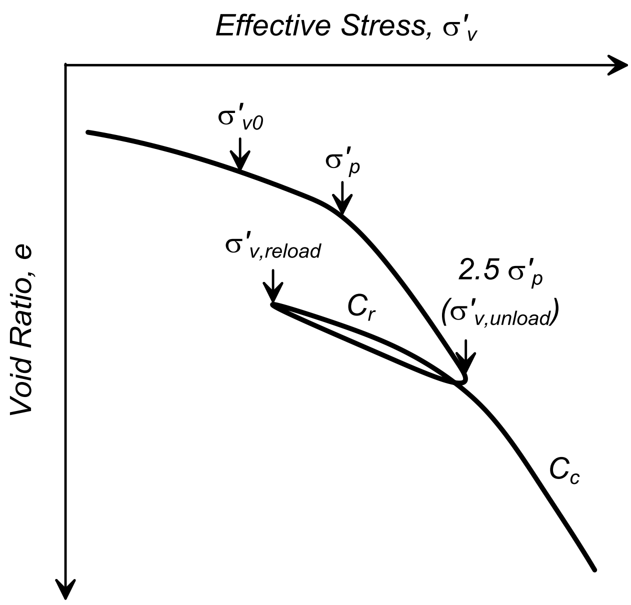

Figure 4. Conceptual loading path for phase 3 loading.

K_0=1 conditions using Equation 1 (OCR of approximately 4). Up until this point the stress history for 1DPS and HD specimens are identical. While the loading conditions will remain identical for both levels of simulated sampling, significant disturbance is induced to the HD specimen via a freezing and thawing cycle where the specimen was removed from the ring, sealed, frozen, thawed, and retrimmed into a 63 mm oedometer cell.

(3) Following induced disturbance for the HD sample (whereas no unloading removal of total stress beyond $\sigma'_{v,K0=1}$ for 1DPS), specimens are reloaded following the conceptual stress path in Figure 4. First, they were loaded to 2.5 times the corresponding σ'_p (=$\sigma'_{v,unload}$) followed by unloading at this stress level to K_0 of 1 (=$\sigma'_{v,reload}$), then reloaded to 2500 kPa (capacity of the consolidation device).

4 RESULTS OF EXPERIMENTAL STUDY

The consolidation response of specimens shows varying amounts of recompression strain for different σ'_{v0}. Figure 5 shows the response of one mixture to four in-situ stresses for both 1DPS and HD cases. There are systematic trends in the observed consolidation behavior for both 1DPS and HD specimens. 1DPS specimens have a well-defined yield stress (σ'_p) and virgin compression line while HD specimens exhibit a less defined response with no apparent yield stress. The trend is consistent across a range of in-situ stress levels for 1DPS and HD specimens. Additionally, specimens initially loaded to higher σ'_{v0} require more recompression strain to reestablish σ'_{v0} for both 1DPS and HD specimens. Albeit the 1DPS specimens only require less than 1% strain to reestablish σ'_{v0}, while HD specimens

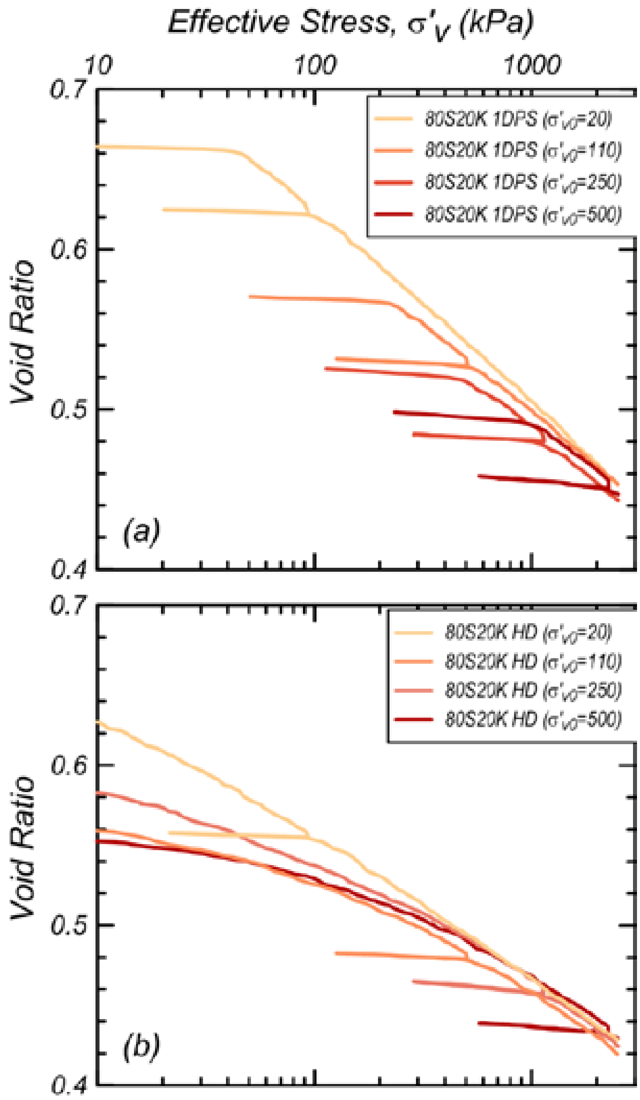

Figure 5. Plots of void ratio versus effective stress for (a) 1DPS and (b) HD loading of 80S20K for 4 simulated in-situ stress levels.

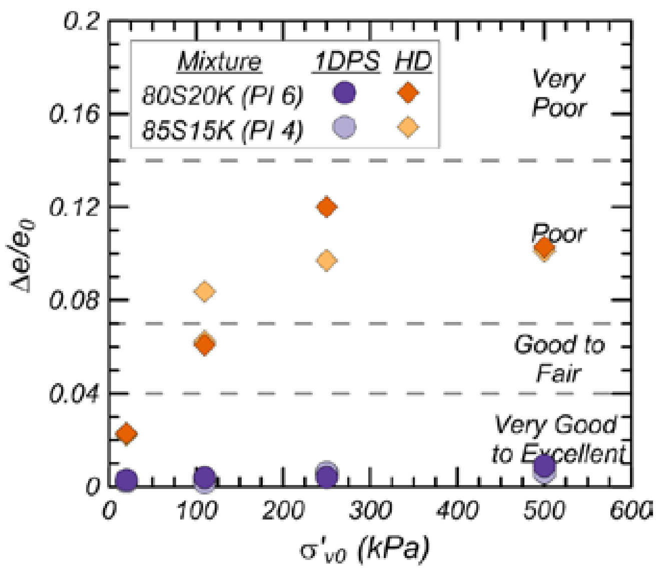

Figure 6. $\Delta e/e_0$ sample quality rating for 1DPS and HD specimens for 4 different simulated in-situ stress levels and two different mixtures: 80S20K (PI 7) and 85S15K (PI 4).

require 1-4% strain. Further scrutiny of the compression curves reveals a small increase in the unload-reload stiffness from low to high σ'_{v0} for both levels of disturbance.

There is a strong trend of decreasing sample quality with increasing simulated in-situ effective stress for HD mixtures. Figure 6 shows that all 1DPS specimens are of very good to excellent sample quality, while HD specimens range from very good to excellent to poor sample quality. These observations are inconsistent with level of disturbance induced to each specimen. HD specimens with low σ'_{v0} undergo less recompression strain (or Δe) to reestablish σ'_{v0}, while specimens with high σ'_{v0} undergo more recompression strain to reestablish σ'_{v0}. This reflects the greater overall stress relief of the high σ'_{v0} specimens during the simulated disturbance procedure.

The magnitude of quality rating ($\Delta e/e_0$) of the PI 4 (85S15K) and PI 7 (80S20K) mixtures shown in Figure 6 appears to be consistent for a given σ'_{v0}. This observation is consistent with the observations from Krage et al. (2015) where decreasing PI resulted in an improved quality rating for a given simulated in-situ effective stress.

These observations further highlight the limitations of clay-based sample quality indices for tracking sample quality in intermediate soils with different simulated in-situ effective stress. Further research is necessary to successfully account for trends with σ'_{v0} identified in this paper.

5 CONCLUSIONS

This paper examined the adequacy of existing clay-based sample quality criteria for evaluating the influence of in-situ overburden effective stress on synthetic intermediate soil mixtures. The effects of sampling depth on sample quality are not well quantified within current clay-based quality criteria with samples obtained from 5-25 meters and depth effects not discussed in detail.

In this study, synthetic intermediate soil specimens subjected to 1D perfect sampling have a clearly defined yield stress (σ'_p) and produce a well-defined virgin compression line, while highly disturbed specimens exhibit a less defined response with no apparent yield stress. These trends are consistent across a range of simulated in-situ stress levels for the 1DPS and HD specimens.

There is an apparent trend of decreasing quality rating ($\Delta e/e_0$) with increasing simulated in-situ effective stress for the HD samples. Current recompression based quality rating methods do not account for this observed trend. Shallow samples are likely to undergo less recompression strain (or Δe) while deep samples are more likely to undergo greater recompression strain to in-situ stresses.

6 ACKNOWLEDGMENTS

This work was completed with funding from the National Science Foundation under grant CMMI-1436617. Any opinions, findings, and conclusions or recommendations expressed in this paper are those of the authors and do not necessarily reflect the views of the National Science Foundation.

7 REFERENCES

Andresen A, Kolstad P. The NGI 54-mm samplers for undisturbed sampling of clays and representative sampling of coarser materials. *Proceedings of the International Symposium of Soil Sampling, State of the Art on Current Practice of Soil Sampling*, Singapore 1979: 13-21.

Jamiolkowski M, Ladd CC, Germaine JT, Lancellotta R. New developments in field and laboratory testing of soils. *Proc. 11th Int. Conf. on SMFE* 1985; 1:57-153.

Krage, C.P., DeJong, J.T., DeGroot, D.J., Dyer, A.M., & Lukas, W.G. 2015. Applicability of clay-based sample disturbance criteria to intermediate soils. *6th International Conference on Earthquake Geotechnical Engineering*.

Lacasse, S., Berre, T., & Lefebvre, G. 1985. Block sampling of sensitive clay. *Proceedings of the 11th International Conference on Soil Mechanics and Foundation Engineering*, San Francisco, CA pp 887-892.

Lunne T, Berre T, Strandvik S. 1997. Sample disturbance effects in soft low plastic Norwegian clay. *Symposium on Recent Developments in Soil and Pavement Mechanics*: 81-103.

Lunne T, Berre T, Andresen K, Strandvik S, Sjursen M. 2006. Effects of sample disturbance and consolidation procedures on measured shear strength of soft marine Norwegian clays. *Canadian Geotechnical Journal* 43 (7): 726-750.

Mesri, G., and Hayat, T.M. 1993. The coefficient of earth pressure at rest. *Canadian Geotech. Journal* 30 (4), 647-666.

Tanaka, H. Sharma, P., Tsuchida, T. and Tanaka, M. 1996. Comparative study on sample quality using several types of samplers. *Soils and Foundations* 36(2) pp 57-68.

Tanaka, H., Ritoh, F., Omukai, N. 2002. Quality of samples retrieved from great depth and its influence on consolidation properties. *Canadian Geotechnical Journal* 39(6): 1288-1301.

Terzaghi, K., Peck, R., Mesri, G. *Soil Mechanics in Engineering Practice.* Wiley: New York, 1996.

Geotechnical and Geophysical Site Characterisation 5 – Lehane, Acosta-Martínez & Kelly (Eds)

Offshore prediction of sampler penetration and recovery using CPTs

N. Ramsey
Fugro AG Pty Ltd

ABSTRACT: Gravity-sampling provides a relatively quick and economical method of sampling soils, typically within 6m of seafloor, during offshore projects. This paper presents a proposed approach for predicting gravity-sampler penetration and sample recovery, when nearby Cone Penetration Test (CPT) data are available. The CPT data are used to predict the resistance to gravity-sampler penetration, and the relationship between the internal friction in the sampling tube and the plugged end-bearing of the sampler, which is an important predictor for whether or not soil enters the sampling tube, i.e. whether the soil sampler will behave "unplugged" or "plugged". Knowledge of the unplugged-plugged behaviour of the gravity-sampler is necessary, for more reliable assessments of geotechnical boundary elevations and for some types of geohazard assessments.

1 INTRODUCTION

Gravity-sampling provides a relatively quick and economical method of obtaining samples of surficial soils during offshore projects. Figure 1 presents a photograph of a typical gravity sampler, showing the top-weight and sampler barrel. It is often observed that gravity-sampler (sampler) penetration exceeds sampler recovery. This discrepancy is typically attributed to poor equipment performance or unsuitable testing procedures, or because soil has fallen from the base of the sampler during retrieval. Another possibility, however, is that the soil recovery is less than the sampler recovery because the sampler-tube has temporarily "plugged" at one of more elevations during penetration as a consequence of the soil characteristics, rather than any problems with the gravity-sampling equipment or sampling procedure – this possibility is the primary subject of this paper.

2 SCOPE OF PAPER

The scope of this paper encompasses:

- Estimating the velocity of the sampler at seafloor.
- Predicting the penetration of the sampler, i.e. the penetration at which the resistance to sampler penetration equals the effective weight of the sampler.
- Predicting unplugged-plugged behaviour and total sample recovery.
- Presenting an example illustrating predicted and actual penetrations and recoveries at an offshore site.
- Discussing the results and presenting recommendations on how the approach might be improved on future projects.

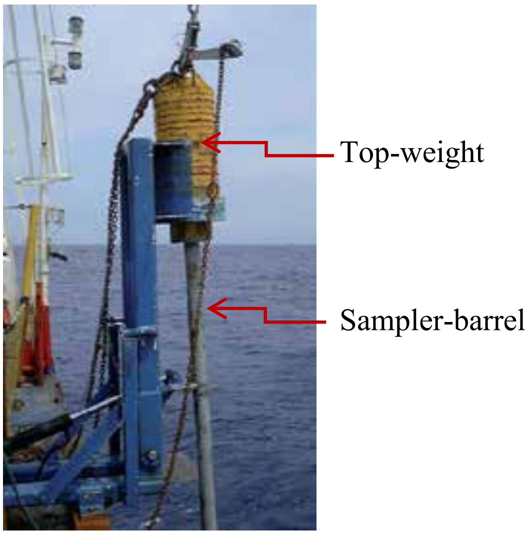

Figure 1: Generic gravity-sampler

3 THEORY

3.1 *Estimating the velocity of a gravity-sampler at seafloor*

The drag, F, on a sampler with projected top-weight area, A_p, passing at velocity, v, through seawater can be calculated as:

$$F = C_d * s_w * v^2 * A_p / 2 \quad (1)$$

where C_d is the drag-coefficient and ρ_{sw} is the density of seawater.

The terminal velocity, v_{term}, is the limiting velocity of the sampler. It occurs when the induced drag equals the submerged static weight of the sampler, F_s, as shown in Equation 2.

$$v_{term} = [(2 * F_s) / (C_d * \rho_{sw} * A_p)]^{0.5} \quad (2)$$

The key unknown parameter in Equation 2 is the drag-coefficient, C_d. In the absence of specific measurements, it is considered likely that the C_d of a typical gravity sampler is likely to be in the range 0.4 to 0.8.

3.2 *Predicting the soil resistance to sampler penetration*

Soil resistance to sampler penetration can be estimated using adjacent CPT data – with cone resistance, q_c, used to calculate end bearing, and sleeve friction, f_s, used to calculate friction inside and outside the sampler.

Total soil resistance to sampler penetration, F_r, can be calculated using Equation 3.

$$F_r = [F_{unplug}, F_{plug}]_{min} \quad (3)$$

where

$$F_{unplug} = A_{ann} * q_c + D_{int} * \alpha * \pi * f_s * (z - z_{plug}) + D_{ext} * \pi * f_s * (z - z_{dead}) \quad (4)$$

and

$$F_{plug} = A_{ext} * q_c + D_{ext} * \pi * f_s * (z - z_{dead}) \quad (5)$$

Key parameters to note in Equations 4 and 5 are:

- z_{dead}, the "dead zone" behind the sampler tip, where external friction is not mobilised during plugged penetration,
- α a factor to account for the reduced friction between the soil and the inside of the sampler-barrel.
- z_{plug}, the accumulated length of plugged penetration at any elevation – z_{plug} is used to ensure the internal friction is calculated taking account of any ranges of plugged penetration.

Experience suggests that typically z_{dead} would be expected to be between three and five diameters behind the sampler-barrel tip during plugged penetration, and α would be expected to vary between 0.05 and 0.2 depending on the geometry of the shoe of the sampler-barrel.

3.3 *Predicting the effective weight of the gravity-sampler*

A simple method for assessing the gravity-sampler penetration is to assume that the gravity-sampler will stop when the soil resistance is equal to the effective weight of the sampler, where the effective weight of the sampler is equal to its static weight, plus a dynamic component induced by the deceleration of the sampler from its velocity at mudline to zero at the final penetration. The average dynamic component of deceleration, a_d, for any penetration below seafloor, can be calculated using Equation 6:

$$a_d = v_s^2 / (2 * z) \quad (6)$$

Consequently, the effective dynamic weight of the sampler, F_d, for any final penetration below seafloor can be calculated as:

$$F_d = m_s * (a_d + g - 1) \quad (7)$$

where m_s is the mass of the sampler.

3.4 *Predicting unplugged-plugged behaviour and total sample recovery*

By calculating the unplugged and plugged resistances, F_{unplug} and F_{plug} throughout the cone profile (using Equations 4 and 5) it is possible to predict the ranges of elevation over which plugging is predicted to occur, i.e. where F_{plug} is less than F_{unplug}. The total recovery is then calculated by accumulating ranges of elevation where unplugged penetration. As for predicting the sampler penetration, key parameters in the assessment of unplugged-plugged behaviour are z_{dead}, α and z_{plug}.

4 EXAMPLE

Figures 2 to 4 present comparisons of predicted and actual penetrations and recoveries at an offshore site in more than 1,000 metres of water. Figure 5 presents more detailed results at one of the locations, and illustrates how temporary plugging can occur at more than one range of elevations during sampler penetration.

For this example, the following supporting inputs were used.

- Mass of gravity-sampler = 550kg (exception Location 9 {330kg} – shown with open symbols on Figures 2 and 3).
- Projected area of sampler top-weight = 0.2m^2

- Height of gravity-sampler top-weight above seafloor when sampler released = 9m
- External diameter of sampler = 0.105m
- Internal diameter of sampler = 0.086m
- Assumptions:
  - Drag coefficient, C_d = 0.4
  - Sampler velocity at mudline = 12m/s (except Location 9 {8m/s} due to lower top-weight and reduced drop height – shown with open symbols on Figures 2 and 3)
  - Dead-zone, z_{dead} = 4 core-barrel diameters
  - α = 0.05

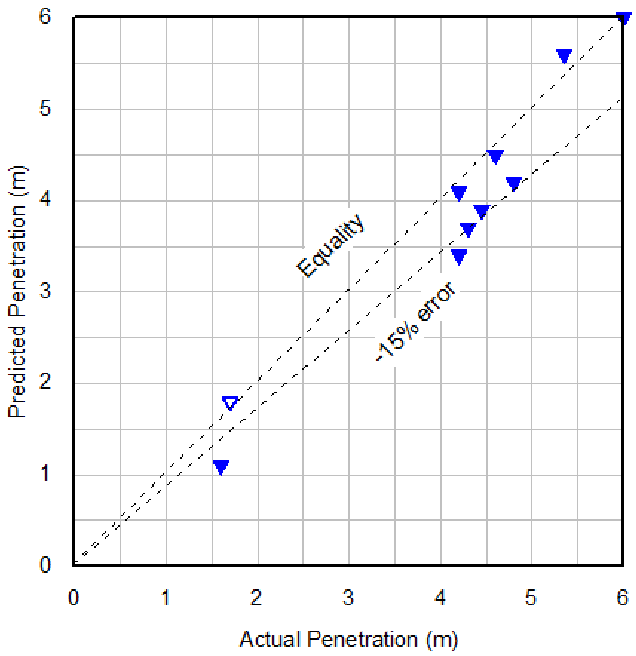

Figure 2: Actual versus predicted penetration

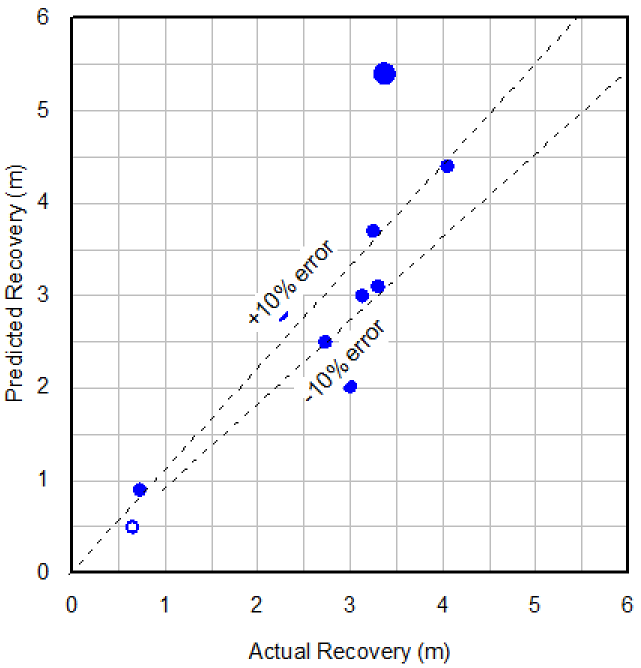

Figure 3: Actual versus predicted recovery

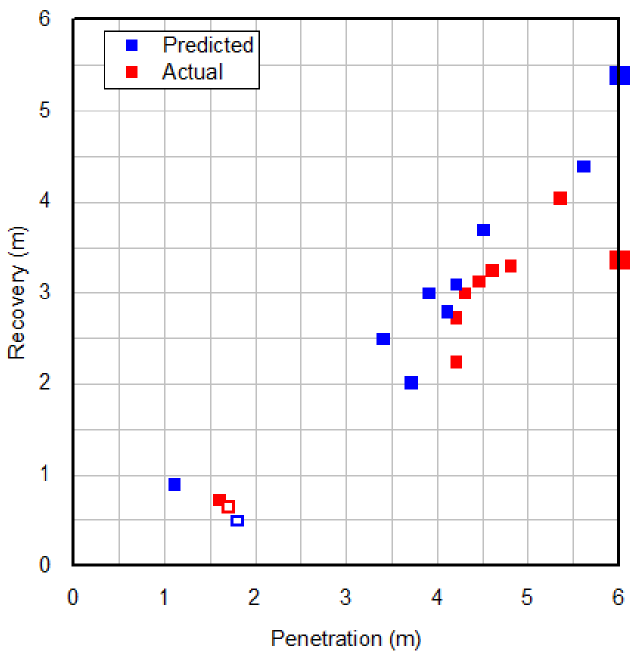

Figure 4: Summary of penetrations and recoveries

5 DISCUSSION

Comparisons between the predicted and actual sampler penetrations are encouraging, with predicted penetrations generally within -15% of the actual penetrations and sample recoveries generally within +/-10% actual recoveries.

It is notable that the predicted penetrations tend to be less than the actual penetrations. This is considered to be because average decelerations have been used for predictions, whereas decelerations will be lower in the softer soils close to seafloor and higher as the sampler reaches its final penetration, thus increasing the effective weight of the sampler, and thus its final penetration.

It is interesting to note that the data suggest that at one location, the sampler was not working properly. The results at this location, which are shown with larger symbols on Figures 3 and 4, indicate that the actual recovery is much lower than the predicted recovery, and not consistent with the performance of the gravity-sampler at other project locations.

At this site, "typical" values of C_d, z_{dead}, α and v_s yielded reasonable estimates of sampler penetration and sample recovery. However, it is possible that at other sites, better agreement would be obtained with other combinations of values.

In order to improve the reliability of the approach:

- An accelerometer could be attached to the top-weight, thus enabling v_s and a_d to be measured, rather than assumed.
- Earth pressure sensors could be attached to the external and internal surfaces of the sampler-barrel, thus enabling the internal and external unit frictions to be measured rather than assumed.

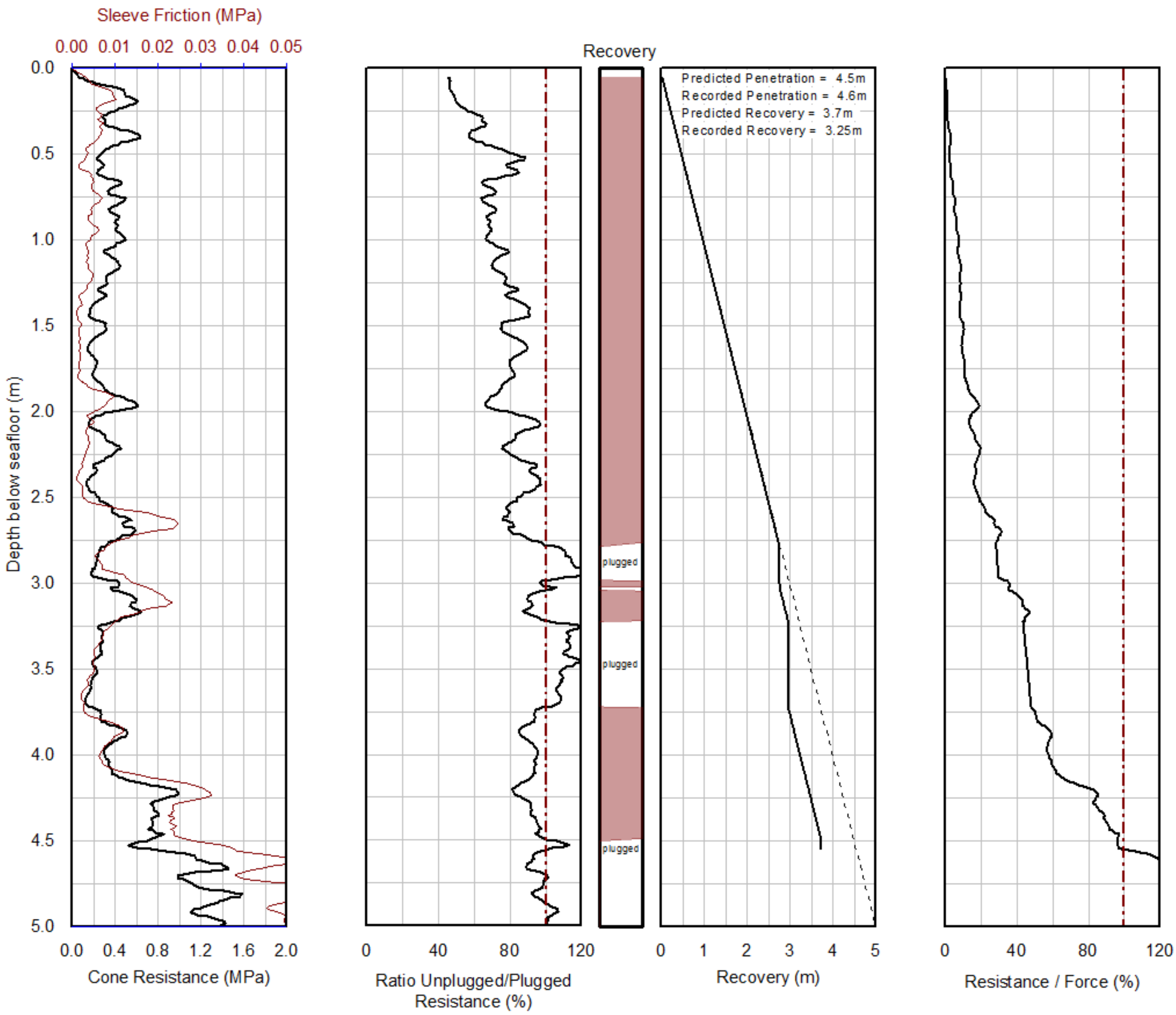

Figure 5: Example of more detailed results

6 CONCLUSIONS AND RECOMMENDATIONS

1. A proposed approach for predicting gravity-sampler penetration and sample recovery, when nearby CPT data are available, has been presented.
2. The approach can be used to assess ranges of penetration where plugging is likely to have occurred. This information could be critical for reliable assessments of geotechnical boundary elevations and for some types of geohazard evaluations.
3. The approach results in slight underestimates of predicted penetrations, probably due to the assumption that deceleration of the sampler is constant over the penetration length, whereas it is likely that decelerations will be greater as the sampler reaches its final penetration.
4. Predicted sample recoveries at an example deep-water site, are typically within +/-10% of the actual recoveries.
5. The approach might be used to identify locations at which the sampler may not have been working properly.
6. The reliability of the approach could be ratified and/or improved by adding an accelerometer to the top-weight and earth-pressure sensors to the sampler-barrel.

7 SYMBOLS AND TERMS

A_{ext} Base area of sampler-barrel (m^2)
A_{ann} Annulus area of sampler-barrel (m^2)
a_d average dynamic deceleration for a given final depth below seafloor (m/s^2).
A_{tw} Projected area of sampler top-weight (m^2)
C_d Drag coefficient (-)
CPT Cone Penetration Test
D_{ext} External diameter of sampler-barrel
D_{int} Internal diameter of sampler-barrel
f_s CPT unit skin friction (kPa)
g acceleration due to gravity
m_s total mass of gravity sampler (kg)
q_c CPT cone resistance (kPa)
v_s velocity of gravity sampler at seafloor (m/s).
F_d Effective dynamic weight of sampler for a given z (kN)
F_s static weight of sampler (kN)
F_{ext} external unit skin friction (kN)
F_r = Total soil resistance to sampler penetration (kN)
z penetration below seafloor (m)
z_{dead} the "dead zone" behind the sampler tip, where external friction is not mobilised during plugged penetration (m)
z_{plug} the accumulated length of plugged penetration (m)
α factor to account for reduced friction inside of sampler-barrel (-)
ρ_{sw} density of seawater (Mg/m^3)

8 REFERENCES

Holt, J.R. and Ims, B.W. 1985. The Phenomenon of Sample Tube Plugging, In Chaney and Demars (eds) *Strength Testing of Marine Sediments: Laboratory and In-situ measurements:* 166-177*:* ASTM ST

Geotechnical and Geophysical Site Characterisation 5 – Lehane, Acosta-Martínez & Kelly (Eds)

Experience with gel-push sampling in New Zealand

M.E. Stringer & M. Cubrinovski
Department of Civil and Natural Resources Engineering, University of Canterbury, New Zealand

I. Haycock
McMillan Drilling, New Zealand

ABSTRACT: The gel-push sampling technique was developed to try to provide an economic technique capable of obtaining high quality specimens of silty sands and sands. This paper describes two of the gel-push samplers which are now commercially available and describes their performance on recent projects carried out on soils in New Zealand with reference to field measurements of shear wave velocity.

1 INTRODUCTION

High quality soil sampling is well established, and many tools and techniques have been developed over the years to obtain samples of different types of soils. Of particular relevance to the earthquake engineering community is the ability to obtain undisturbed samples of sands and silty sands, so that their behaviour during the cyclic loading of an earthquake can be better understood. Yoshimi et al (1994) showed that it is very difficult to obtain high quality specimens of these soils using downhole samplers. To date, freeze sampling remains the "gold standard" for obtaining sand samples, though the associated costs make it unfeasible for most projects.

2 GEL-PUSH SAMPLING

The gel-push sampling methodology was developed by Kiso-Jiban Consultants (Japan) with the aim of retrieving undisturbed specimens of silty and clean sands at reasonable cost. The technique has been used by a number of researchers in locations around the world including Japan, Taiwan, Poland, Bangladesh and New Zealand (e.g. Lee et al. 2012, Taylor et al. 2012, Jamiolkowski 2014).

It is assumed that the main source of disturbance associated with conventional downhole tools is due to friction which is mobilised on the sides of the soil sample as it enters the core-liner barrel. Gel-push sampling removes this friction by coating the outer surface of the soil (as it enters the sampler) with a low-friction polymer gel.

Gel-push sampling is typically carried out with one of three types of sampler: GP-S, GP-Tr and GP-D. These three samplers are conceptually similar to existing techniques, with some modification to allow the delivery of gel to the base of the sampler.

It is important to note that gel-push sampling is still developing, and small changes to the samplers are occasionally made by the designers to address specific issues which are reported by end users.

While all three tools are available in New Zealand, experience to date is limited to the GP-S and GP-Tr samplers. A brief description of these samplers is given in the following section, while more details concerning the samplers and field procedures are given in Stringer et al. (2015b).

2.1 *GP-S Sampling*

The GP-S sampler is similar to the improved Osterberg sampler (Osterberg 1973), comprising three barrels, one fixed and two travelling pistons, as shown in Figure 1**Error! Reference source not found.**. Samples are captured inside a PVC core-liner barrel, with approximate inner/outer diameters of 71/76 mm and 99 cm length. Holes near the top of the core-liner barrel allow the polymer gel to flow during sampling. Prior to inserting the core-liner barrel into the sampler, the middle barrel is filled with polymer gel. This ensures gel coats both sides of the core-liner barrel when it is inserted.

The fixed piston of the sampler is fitted to the end of the fixed piston shaft, and features an internal mechanism to enable the core-catcher activation process. Finally, a cutting shoe (with an inner diameter slightly smaller than the core-liner barrel) is attached to the bottom end of the middle barrel.

During sampling, clean water is pumped into the sampler through the drilling rods. The hydraulic pressure acting on the upper travelling piston advances the middle and core-liner barrels. The reduction in the

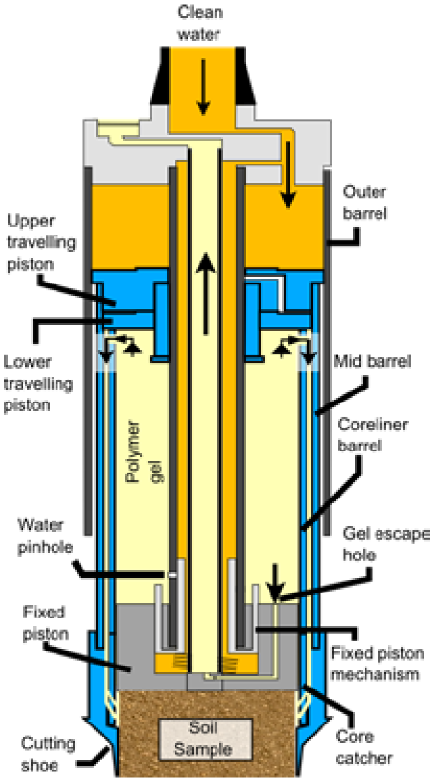

Figure 1:Schematic of GP-S type sampler

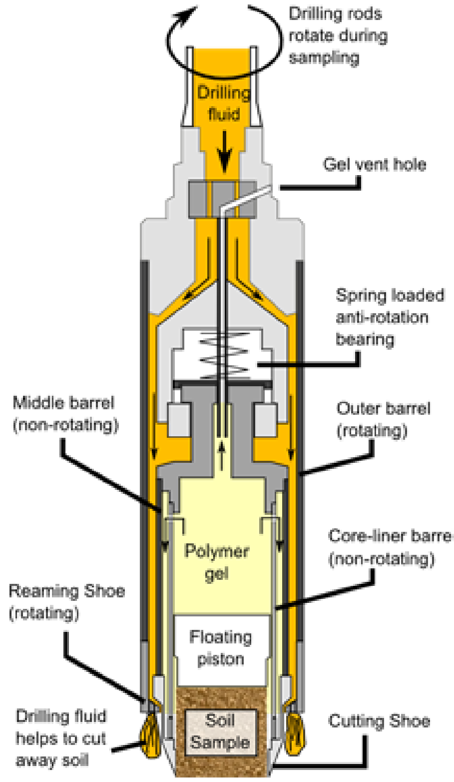

Figure 2: Schematic of GP-TR type sampler

volume between the travelling and fixed pistons forces some of the polymer gel to pass through the holes in the top of the core-liner barrel and travel down the annulus between the inner and middle barrel. The gel passes through the fins of the core catcher, and coats the outer edge of the soil sample as it is captured in the sampler. The remaining polymer gel is vented through "gel-escape holes" in the fixed piston, travelling up the central shaft of the sampler and exiting into the borehole.

When the travelling pistons reach the fixed piston, the internal fixed piston mechanism is activated and hydraulic pressure is supplied between the upper and lower travelling pistons. At this point, the lower travelling piston acts on the core-liner barrel only, which advances a small distance to partially close the fins of the core catcher. In this way, the soil sample is prevented from dropping out of the sampler, and the tool can be carefully retrieved from the borehole and laid out horizontally to enable the soil sample to be retrieved. Complete recovery with this sampler results in 92cm of soil, not including any material retained in the core catcher. Typically, GP-S sampling is completed in a period of 1-2 minutes.

2.2 *GP-TR Sampling*

The GP-TR sampler is a rotary triple tube device; a sketch of key components is shown in Figure 2**Error! Reference source not found.**. Drilling mud is pumped through a rotating reaming shoe to help remove soil in the bottom of the borehole, and allow the sampler to advance. Protruding slightly ahead of the reaming shoe is a spring-loaded non-rotating cutting shoe. Soil passing through the cutting shoe is captured within a PVC core-liner barrel (outer/inner diameter = 89/83.5 mm). The floating piston moves upwards on the top of the captured soil column, and forces polymer gel to travel down the annulus between core-liner barrel and middle barrel, exiting above the cutting shoe and coating the soil sample. Excess gel is vented into the main borehole. Full recovery with this sampler is approximately 100 cm. Ideal sampling with the GP-TR is slow and steady, taking at least 10 minutes to advance the tool 100 cm.

2.3 *Choice of Sampler*

While the GP-S sampler appears a more complex tool, the physical operation of the device is much less demanding on the drilling crew than the GP-TR (the GP-TR requires manual control of the rate of advance, the flow rate of drilling mud and the rate of rotation), and as such is likely to be easier to operate to its "full" potential. Due to the thin-walled sections within the GP-S sampler, the hydraulic pressure which can be applied to the sampler is limited to 7 MPa, on the advice of the manufacturer. The ratio of piston driving area to the area of the cutting shoe shoulder is approximately 2.2, implying an upper limit of 15 MPa. However, allowing for any leaks in the drill rods, pressure required to drive the gel through the restricted passages and friction within the device, the authors recommend that an upper limit on cone tip resistance (q_c) of 5 MPa be applied when using the GP-S sampler and switching to the GP-TR sampler above this level.

3 ASSESSING "SPECIMEN QUALITY"

One of the most important things to consider when carrying out advanced laboratory tests (such as triaxial tests) on field samples is how well the in-situ density and fabric (structure) of the soil has been preserved. When evaluating the performance of the gel-push samplers in different soil types, the authors have chosen to use a number of different criteria. First, whether there is any visual disturbance to the soil specimen, or if anything has occurred during the sampling, transportation and preparation which is likely to have caused severe disturbance to the specimen. Where the specimens appear in good condition, it is desirable to compare measurable in-situ properties with values measured in the laboratory. In this paper, measurements of shear wave velocity have been used as a basis for this comparison.

Shear wave velocity (V_s) is related to small strain shear modulus (G_0) and density (ρ) by Equation 1:

$$G_0 = \rho V_s^{\,2} \tag{1}$$

The shear modulus reduces significantly on the application of even modest shear strains, hence offers a good insight into any disturbance which might affect a specimen. Soil stiffness increases with stress level in the directions both parallel and normal to the wave propagation. Hence differences between the stress level in the field and the laboratory (e.g. K_0 conditions in the field vs isotropic in the lab) must be accounted for. To account for differences in stress levels, the shear wave velocity measurements are normalised to a stress level of 1 atmosphere (V_{s1}), using Equation 2, where P_a is atmospheric pressure and p' is the mean effective stress. Given the limited number of undisturbed specimens, it was necessary to assume that the principal stress ratio doesn't affect G_0 or V_s provided p' is constant.

$$V_{s1} = V_s \left(\frac{P_a}{p'}\right)^{0.25} = V_s \left(\frac{3P_a}{\sigma_v' + 2\sigma_h'}\right)^{0.25} \tag{2}$$

3.1 *Measurement of V_s in the field*

As part of the projects described in Sections 4.1 and 5, a number of field-based tests were carried out at each research site. Among these were direct-push cross-hole measurements (described by Wotherspoon et al. 2015) of V_s and V_p, carried out every 20cm. The resulting V_s profile (vertically orientated, horizontally propagating waves) has been used to evaluate the sampling performance in this paper.

3.2 *Measurement of V_s on undisturbed specimens*

After sampling, soil samples were carefully transported back to the laboratory (in a vertical orientation) where they were extruded from their core-liner barrels. During extrusion, the samples were cut into (approximately) 15 cm lengths before being wrapped in cling film until they are tested.

The polymer gel which is used during sampling tends to penetrate a couple of millimetres into the specimen. Hence extruded specimens are carefully trimmed using a soil lathe prior to carrying out triaxial testing; the final specimen is 50 mm in diameter and 100 mm tall. Small slots are cut into the top & bottom of the specimen with a razor blade to facilitate the insertion of the bender elements when the specimen is mounted on the triaxial platens.

Specimens are saturated (typically by percolating CO_2 and then deaired water through the specimen). The back-pressure is then raised until the B-Value is at least 0.97. Saturated specimens are isotropically consolidated to a mean stress equal to 1.1 times the estimated in-situ vertical effective stress to ensure that specimens are normally consolidated.

Once consolidated, the shear wave velocity is estimated using bender elements excited at a number of discrete frequencies between 4 kHz and 8 kHz. The arrival time of the shear wave is estimated as the point just prior to the first major peak, where the receiver signal denotes that the bender element is beginning to deflect in the direction associated with the incoming wave. Travel distance is taken as the distance between the tips of the bender elements.

4 EXPERIENCE WITH THE GP-S SAMPLER

4.1 *Silty Soils and Silts*

Undisturbed sampling was carried out with the GP-S sampler in the suburban park of Gainsborough Reserve in Christchurch, New Zealand. A total of 10 samples were taken in three different boreholes at depths between 0.4 m and 9 m below the ground surface. The soil profile at this site consists of alternating layers of silts and sandy silts. The upper 6 m of CPT data is shown in Figure 3**Error! Reference source not found.**. CPT results to a depth of 10 m indicated that q_c values in the deeper silty sand layers increased with depth, reaching approximately 7 MPa in the deepest target layer for sampling. The top of the sampling intervals, average CPT values and the recovery of each sample are listed in Table 1.

The poor recovery of samples S2-GP1-1U and 3U arose from issues with the core catcher; In the case of the first sample, the sampling was prematurely stopped such that the core catcher was not activated. As a result, the recovered sample dropped out of the sampler when it was being recovered. In the second

Table 1: Samples recovered at Gainsborough Reserve

Sample	Depth (m)	q_c (MPa)	I_c	Recovery (%)
S2-GP1-1U	0.4	1.3	2.7	0
S2-GP1-2U	2.5	2.2	2.2	78
S2-GP1-3U	3.6	0.4	3.2	27
S2-GP1-4U	5.0	4	2.0	90
S2-GP1-5U	6.5	1.3	2.0/3.0	53
S2-GP1-6U	8.0	6	1.9	60
S2-GP2-1U	0.8	0.8	2.9	66
S2-GP2-2U	3.6	0.4	3.2	53
S2-GP3-1U	0.5	1.3	2.7	89
S2-GP3-2U	3.6	0.4	3.2	96

case, the core catcher was partially activated, but the fins of the core catcher locked together during sampling. When the sampler was recovered to the surface, portions of the soil sample were dropping out of the sampler; It appeared that despite the partial closure of the catcher, the silty material experienced large axial extension, and significant radial contraction, such that it was able to pass through the partially activated core catcher.

On extrusion, S2-GP1-5U, 6U and S2-GP2-1U were found to be severely cracked, with the soil sample clearly split into several pieces during sampling. Sample S2-GP2-2U was found to contain large amounts of wood.

The GP-S sampler is hydraulically advanced using clean water. Hence the drilling rods are disconnected from the rig prior to sampling. Vertical reaction loads during the initial sampling attempts at Gainsborough Reserve were mobilised using the hydraulic break-out arms of the drilling rig. While this arrangement is adequate for soils with very low penetration resistance, it was observed that the arms would lift slightly during sampling attempts. In the cases of S2-GP1-5U and 6U, noises were heard during sampling, which are now known to have been the drilling rods slipping through the clamps. These mechanisms have severe consequences for the sampling (especially the latter), since upward movement of the drilling rods (and therefore the fixed piston) can create tensile loads on the top of the specimen. If it happens slowly, and at the start of sampling (i.e. mechanism 1), it is possible that polymer gel can flow into the space between the top of the soil sample and the fixed piston. However, if the movement is rapid and occurs while sampling is underway, then a large vacuum will be created at the top of the specimen. This is assumed to be the cause of the breaks in the specimens previously mentioned.

The remaining 4 samples appeared much better when extruded, though several horizontal cracks up to 1 inch in length were observed on the outer edge of sample S2-GP3-1U, and some vertically orientated cuts were observed running the entire length of S2-GP3-2U (this sample was taken at the same depth as S2-GP2-2U and the cuts are assumed to be caused by a twig caught on the leading edge of the sampler). These four samples were deemed of sufficient quality to test in the cyclic triaxial device. Figure 4 shows an example of a specimen which was tested from sample S2-GP1-2U. The sample moved freely within the core-liner barrel and the exterior of the extruded sample appears free of defects and when the specimen was trimmed in the soil lathe, it was apparent that the finely interlayered soil structure was preserved during sampling.

The laboratory shear wave velocities (corrected for stress level) of the specimens taken from the four samples which were tested are shown in Figure 3 with black squares**Error! Reference source not found.**. Two profiles of shear wave velocity were carried out approximately 3m from the sampling boreholes and are represented by lines with cross markers. The data in this figure appears to suggest that the shear stiffness of the specimens is close to that in the field for the specimens taken between 2.5 and 5.8m below the

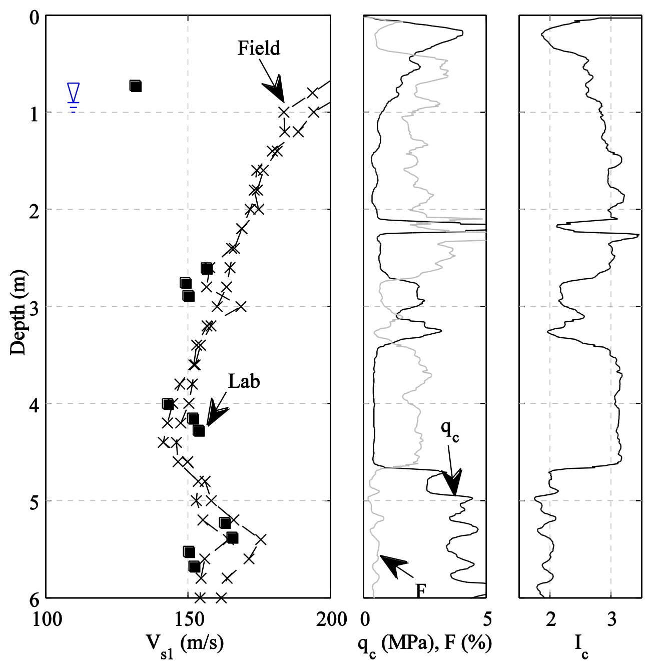

Figure 3: Comparison of lab and field shear wave velocities for samples obtained at Gainsborough Reserve

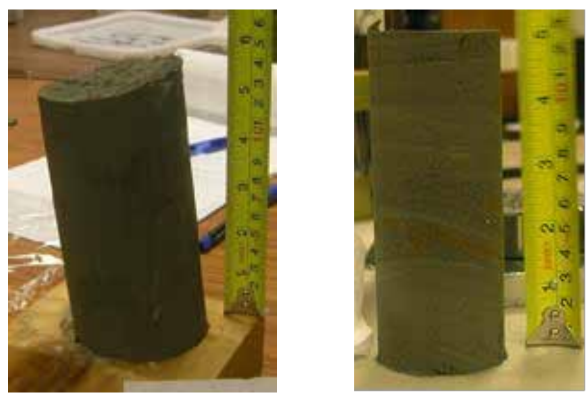

(a) As extruded (b) After trimming

Figure 4: Specimen S2-GP1-2U-C

ground surface. These specimens came from layers comprising silty sands and silt.

By contrast, the shear wave velocity from the shallowest silty sand layer (S2-GP3-1U) falls far beneath the value measured in-situ. This specimen was above the water table, and as previously described, this specimen had a number of cracks on its exterior.

4.2 *Micaceous Silts*

Gel-push sampling was attempted on soft micaceous silt, at a site in the South of New Zealand using the GP-S sampler. A total of 4 soil samples were obtained using the GP-S sampler, and 3 using a conventional push tube sampler (1m long). The soil sampling intervals were selected from a CPT log and had I_c values between 2 and 2.6, and q_c values between 2 and 5 MPa. The recoveries from the gel-push sampling ranged between 65 % and 87 % of the theoretical maximum.

Despite good recovery in some tubes, the extrusion of these samples was very difficult. When load was applied at the base of the soil sample, water would be squeezed out, and it was not possible to push the soil out of the tube. As a result, the plastic core liner barrels were cut open by hand. When opened, the soil occupied the full diameter of the core-liner barrel, and with the exception of a few small areas, no polymer gel was present on the soil surface. The conventional push tubes were cut into short sections of 15cm in length before de-bonding the soil from the tube. During the initial cutting it was observed that these soils swelled rapidly and by a large amount. Similar behaviour in the gel-push samples would have squeezed the gel out of the annular space between the soil and core-liner barrel. Given the relatively fine grained nature of these soils, it is unlikely that the gel would have been sucked into the soils. While it is unknown when the gel was squeezed out of the space between sample and core barrel, it is clear that the beneficial effects were lost by the time it came to extruding the samples. Therefore, in the case of these special soils, the friction associated with conventional sampling methods would also affect gel-push sampling. Depending how rapidly the swelling occurs it may be possible to obtain good results if the samples are extruded from the tubes almost immediately after sampling, though this approach has not been attempted.

5 EXPERIENCE WITH GP-TR SAMPLER IN CLEAN SAND

Undisturbed sampling with the GP-TR sampler was attempted in the clean sands which are found in the Eastern Suburb of Bexley in Christchurch. The testing site (18-20 Wairoa Street) has been included in many research projects (including the "Ground Improvement Trials") and as such a large amount of characterisation data was available. A selection of CPT data from the site is shown in Figure 5 and indicates some of the soil variability in this area of Christchurch. A large number of samples were obtained using both GP-S and GP-TR samplers, but a number of issues not related to the sampling were encountered. The discussion in this section therefore focusses on three samples obtained using the GP-TR sampler between 3.5 and 6.5m below the ground surface. These samples represent the best performance which has been obtained in clean sand with this sampler in New Zealand to date. It should be noted that the soils being sampled were clean sands which were likely to be uncemented. These are therefore some of the most challenging soils to attempt undisturbed sampling.

In each case, the soil sample was obtained with the drill rods rotating at approximately 80rpm, and advancing 1m over a period of 20minutes. The advance of the sampler was controlled manually and aimed to maintain a very slow, but continuous advance. Conventional mud was pumped through the drill rods throughout the sampling, with the rate being controlled by the driller who attempted to keep the flow rate low enough to prevent washing out the bottom of the hole, but high enough to provide some cutting action (via the fluid jets).

Samples were drained on-site prior to transportation back to the laboratory (in a vertical orientation). It was observed on-site that the soil specimens were very difficult to move within the tubes.

When the samples were extruded, they appeared in a good condition visually, though the sides of the

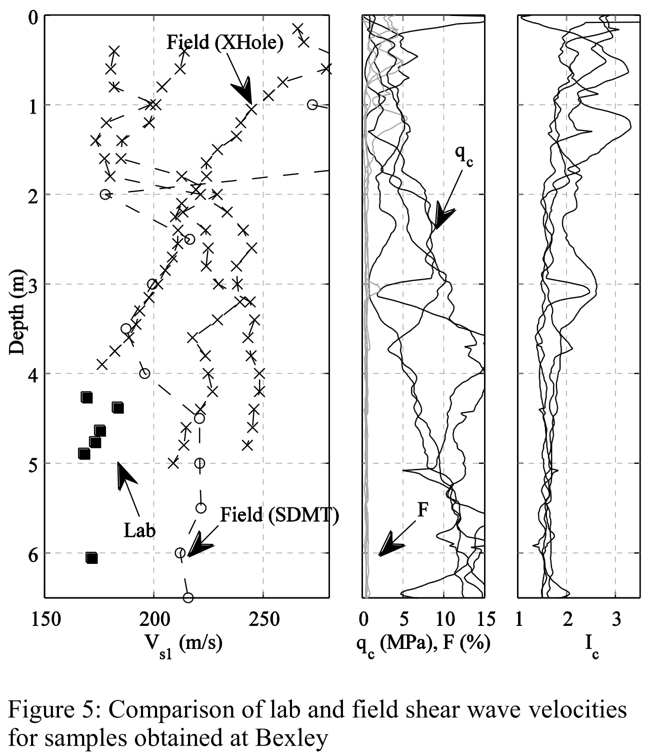

Figure 5: Comparison of lab and field shear wave velocities for samples obtained at Bexley

specimens were not coated in gel. During the trimming of the specimens, it was observed that that the polymer gel had penetrated deep inside the specimen.

In addition to the cross-hole V_s measurements, a downhole V_s profile was available from a seismic dilatometer test. This profile is shown in Figure 5 with circular markers, while the cross-hole data is shown with crosses. There is some apparent scatter in the field measurements of V_{s1}. However, the laboratory measurements of V_{s1} are significantly lower than the field measurements. The observation that the samples did not slide easily in the tube implies that some radial straining has occurred during the sampling (or when the samples are retrieved from the tool). It is thought that the coarse grained nature of these soils prevented the soils from maintaining any effective stresses once they were captured within the sample barrel, with the polymer gel solution able to flow into the sample, rather than providing a coating on the exterior. Any small vibrations, or even self weight of the sample may have led to the samples straining outwards against the walls of the core liner barrel. If this occured, the samples would be expected to rub against the side of the core-liner barrel, generating increasing amounts of sidewall friction. Fonseca & Coutinho (2008) pointed out that soil disturbance can occur in rotary triple tube sampling as a result of incorrect combinations of drilling parameters (i.e. fluid flow rate, penetration rate etc). It is therefore also possible that the disturbance of these samples was caused by inappropriate drilling settings.

6 SUMMARY AND FINAL REMARKS

The gel-push sampling methodology remains an emerging technique. The trials conducted in New Zealand have shown that there will be a range of soils for which these samplers can recover high quality soil specimens. The procedures for sampling are still evolving and it is expected that as more experience is gained, refinements will be made to the way that sampling is carried out which will improve the performance of the gel-push samplers.

The success of gel-push sampling depends as much on the treatment of the samples once the tool is recovered from the ground as the actual process of sampling. Ensuring that the drilling crews understand that the samplers must be handled with exceptional care while the core-liner barrels are recovered is fundamental to the success of the sampling.

In the trials, the GP-S sampler was successful in recovering samples of silts and silty sands with low values of cone penetration resistance (<5MPa). Key issues which require specific attention with this sampler include: ensuring that sufficient vertical reaction loads can be mobilised to prevent the drilling rods moving upwards during sampling; that the pressure and volume of water pumped during sampling is carefully monitored to confirm the **likely** activation of the core catcher; the sampler includes many seals and a test run of the sampler should be carried out prior to sampling to ensure that all seals are working correctly.

It was found that sampling micaceous silts with the GP-S sampler was unsuccessful due to the large amount of swelling which occurred after the soil was captured in the core-liner barrel.

To date, the trials of the GP-TR sampler in New Zealand have not been able to produce high quality specimens. The trials however have been limited to clean sands, and it is likely that greater success might be obtained with this sampler in different soils, or with further refinement of the drilling procedures.

7 ACKNOWLEDGEMENTS

The authors wish to acknowledge the financial support of the Earthquake Commission, New Zealand (EQC), the Ministry for Business, Innovation and Employment.

During the sampling campaigns, the authors were grateful to receive technical advice, suggestions and experience from Prof. Kenji Ishihara and Mr Katsuo Sakai of Kiso-Jiban Consultants. Ms Nicole Van De Weerd conducted much of the laboratory testing described in this paper.

8 REFERENCES

Fonseca, A.V. & Coutinho, R.Q.,(2008) Characterization of Natural Soils. In proc *Geotechnical and Geophysical Site Characterization*. 1-4 April, Taiwan. 195-248.

Lee, W.F., Ishihara, K. & Chen, C.C. (2012) Liquefaction of silty sand – preliminary studies from recent Taiwan, New Zealand and Japan earthquakes. In proc. *Int. Symp. Engineering lessons learned from the 2011 Great East Japan Earthquake*. Tokyo.

Jamiolkowski, M. (2014) Geotechnical characterization of a tailings deposit in Poland – an update. In proc. *3rd Int. Symp. Cone Penetration Testing*. Las Vegas.

Osterberg, J.O. (1973). An improved hydraulic piston sampler. Proc. *8th Int. Conf. on Soil Mechanics and Foundation Engineering*, Moscow. Vol. 1: 317—321.

Stringer, M.E., Taylor, M.L. & Cubrinovski, M. (2015b) *Advanced soil sampling of silty sands in Christchurch*, Tech Rep. University of Canterbury, ISSN: 1172-9511

Taylor, M.L., Cubrinovski, M. & Haycock, I. (2012) Application of new 'Gel-push' sampling procedure to obtain high quality laboratory test data for advanced geotechnical analyses. In proc. *2012 NZSEE Conference.* Paper No. 123

Wotherspoon, L.M., Cox, B.R., Stokoe, K.H., Ashfield, D.J. & Phillips, R.A. (2015) Utilising direct-push crosshole technology to assess the effectiveness of soil stiffening caused by installation of stone columns and rammed aggregate piers. In proc. *6ICEGE*, Christchurch, New Zealand.

Yoshimi, Y., Tokimatsu, K. & Ohara, J. (1994) In situ liquefaction resistance of clean sands over a wide range in density. *Geotechnique*. 44(3):479-494

Geotechnical and Geophysical Site Characterisation 5 – Lehane, Acosta-Martínez & Kelly (Eds)

Definition of failure in cyclic direct simple shear tests on normally consolidated kaolin clay and presentation of shear strain contour diagrams

D. Zografou, N. Boukpeti, S. M. Gourvenec & C. D. O'Loughlin
Centre for Offshore Foundation Systems, University of Western Australia

ABSTRACT: Advanced laboratory testing is the main tool currently used to characterise soil behaviour under cyclic loading and inform offshore foundation design. Laboratory tests, such as cyclic direct simple shear tests, are used to compile contour diagrams of cyclic shear strain or pore pressure from which the effect of cyclic loading is assessed based on an accumulation procedure. In this study, a practical reference for design purposes is presented in the form of a contour diagram of maximum shear strain for normally consolidated kaolin clay under symmetrical cyclic loading. The paper also attempts to define the mode of failure of normally consolidated kaolin under cyclic loading based on a series of symmetrical and non-symmetrical cyclic direct simple shear tests and the shear strain failure criterion plotted as a failure envelope on contour diagrams.

1 INTRODUCTION

The main soil characterisation technique used in the industry to inform foundation design of offshore structures under cyclic loading is advanced laboratory testing. Stress-controlled laboratory tests, such as cyclic direct simple shear (CDSS) tests, are used to produce contour diagrams and predict the displacements and capacity of foundations under cyclic loading induced by waves and wind (Andersen 2015). There is an extensive database of contour diagrams for offshore clays (Andersen 2009, Andersen et al. 2013), with the most notable being the one for Drammen clay, but it appears that there are no contour diagrams available in the public domain for kaolin clay. Previous studies on the cyclic response of kaolin have employed strain-controlled cyclic testing, such as Ohara & Matsuda (1988) and Hsu & Vucetic (2006), but there are only limited data from the stress-controlled cyclic tests (Ansal & Erken 1989) that are required to produce the contour diagrams. As geotechnical model tests are frequently carried out on kaolin clay, it is of interest to provide a means to assess model test performance against conventional predictions from a contour diagram derived from cyclic element tests. This paper presents a contour diagram for normally consolidated kaolin clay based on a series of stress-controlled symmetrical CDSS tests that can be used as a reference for assessing model test performance to inform design approaches.

In the diagram, contours of maximum shear strain, γ_{max}, are presented as a function of maximum applied shear stress, τ_{max}, and number of cycles, N. The shear stress and shear strain components during cyclic loading are illustrated in Figure 1. The maximum applied shear stress within a cycle is the sum of cyclic shear stress, τ_{cyc}, and average shear stress, τ_{ave}. The maximum shear strain within a cycle is the sum of the average value of shear strain, γ_{ave}, and the cyclic shear strain, γ_{cyc}, which is the amplitude of shear strain within a cycle.

The contour of shear strain with the maximum value on a contour diagram corresponds to the failure envelope. In the literature, there is a great range of shear strain levels used as failure criteria, usually ranging from 2% to 15%, without background information provided on why failure is defined at that particular strain level. Frequently the same failure criterion is used for both symmetrical and non-symmetrical cyclic load tests. In this paper, an attempt is made to define failure, at a soil element level, for normally consolidated kaolin under symmetrical and non-symmetrical CDSS test conditions, and the associated shear strain at failure. The paper also investigates whether the use of a common shear strain failure criterion for both symmetrical and non-symmetrical cyclic loading is appropriate.

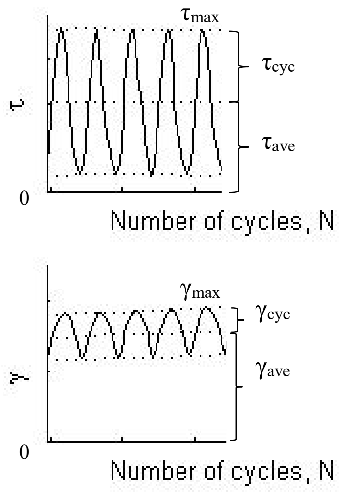

Figure 1. Shear stress and shear strain components during cyclic loading.

2 LABORATORY TESTING SET UP AND METHODOLOGY

2.1 *Laboratory equipment*

The laboratory testing programme was conducted at the Geotechnical Testing Laboratory of the Centre for Offshore Foundation Systems/University of Western Australia. The Geocomp ShearTrac-II DSS apparatus was used to perform the direct simple shear tests. The ShearTrac-II system comprises the ShearTrac-II load frame and a computer that is used to set up, monitor and control a test. In this device, the cylindrical soil specimen is enclosed in a rubber membrane and confined by a stack of rings during shearing. Two high speed, precision micro-stepper motors combined with embedded controllers are used to apply the vertical load and to move the carriage box containing the specimen horizontally.

2.2 *Kaolin sample*

Kaolin was used in the tests, with liquid limit, LL=61%, plastic limit, PL=27%, soil particle density, G_s=2.6, and plasticity index, I_p=34% (Stewart 1992, Acosta-Martinez & Gourvenec 2006). The specimens were prepared from kaolin slurry, with water content, w, equal to twice the liquid limit. The slurry was poured into a 72 mm diameter tube, and was consolidated under a vertical effective stress of 60kPa, for non-symmetrical tests, and 100kPa, for symmetrical tests, over a period of seven days. The specimens were extruded from the consolidated kaolin samples into a sample ring and after the excess material was trimmed, they were pushed gently into the shearing box. After placing a rubber membrane and Teflon coated stacked rings around the specimen, it was positioned in the carriage box and submerged in water.

2.3 *Testing procedure*

The test procedure involves initially the phase of consolidation and subsequently the phase of shearing under monotonic or cyclic loading conditions. The specimens were consolidated incrementally to the required stress, 150kPa in the symmetrical tests and 70kPa in the non-symmetrical tests, and were left to consolidate under the last increment. Shearing was performed while maintaining the specimen volume constant; radial deformation was prevented by the stacked rings while vertical deformation was prevented by adjusting the vertical load through a closed loop computer control (Geocomp Corporation 2012).

Monotonic tests were performed under strain control to assess the monotonic direct simple shear (DSS) strength, s_u, of the normally consolidated kaolin, that is equivalent to the undrained shear strength. The monotonic tests were performed at a rate of 0.1mm/min, i.e. at a shear strain rate ≈32.8%/h. The DSS strength measured in the monotonic tests was used to normalise the applied stresses in the cyclic tests.

A total of eight CDSS tests were performed under stress control, including five symmetrical tests and three non-symmetrical tests. The CDSS tests were performed at a frequency, f = 0.1Hz and were continued for N=1000 cycles, unless failure was reached earlier. In the symmetrical CDSS tests, the average stress τ_{ave}=0 and the maximum shear stress normalised by the DSS strength, $\tau_{max}/s_u=\tau_{cyc}/s_u$, varied from 0.10 to 0.47. In the non-symmetrical tests, the average stress was maintained constant at τ_{ave}/s_u=0.20 and τ_{max}/s_u varied from 0.30 to 0.60. It is noted that the applied stresses were relatively low as this study is part of an ongoing research project on offshore subsea structures subjected to low to moderate cyclic loading.

3 LABORATORY TEST RESULTS

3.1 *Definition of failure for symmetrical CDSS tests*

Typical results from the symmetrical CDSS tests with the two highest applied shear stresses, τ_{max}/s_u= 0.40 and 0.47, that reached failure, are presented in Figure 2. At the beginning of the tests, the shear strain develops symmetrically and increases at a slow rate, while after a number of cycles the rate starts increasing rapidly and shear strain develops non-symmetrically. The shear strain at this transition point is the onset of failure. Once failure begins, the target shear stress cannot be achieved by the actuator and the applied shear stress drops. The vertical effective stresses reduce during the tests and reach a plateau after failure is reached. Failure is therefore

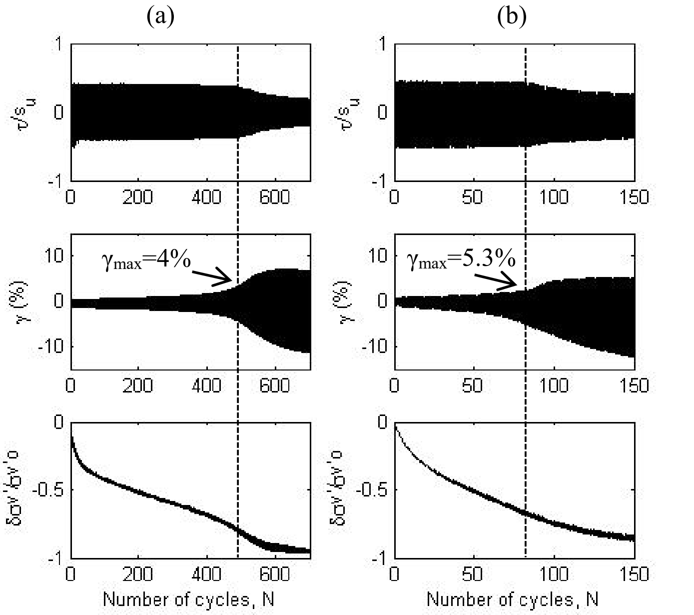

Figure 2. Typical results from symmetrical CDSS tests under shear stress (a) τ_{max}/s_u=0.40 and (b) τ_{max}/s_u=0.47, versus number of cycles: applied shear stress normalised by DSS strength, τ/s_u, measured shear strain, γ, and change in vertical effective stress, $\delta\sigma'_v$, normalised by the initial vertical effective stress, σ'_{v0}.

achieved through cyclic degradation that is the loss of strength and stiffness as the number of cycles increases (Vucetic 1990). Based on the above, the shear strain at failure is defined at the point where the rate of shear strain starts increasing rapidly after significant cyclic degradation has taken place, that is at γ_{max} = 4% and 5.3% for the particular tests with τ_{max}/s_u=0.40 and 0.47 respectively. Failure is denoted with a dashed line in Figure 2.

3.2 *Shear strain contour diagrams based on symmetrical CDSS tests*

The results from all symmetrical CDSS tests were used to construct the shear strain contour diagram shown in Figure 3. The γ_{max} contours were drawn based on the measured data also shown in Figure 3. As discussed earlier, the failure envelope is defined at γ_{max}=5%.

The contour diagram for normally consolidated kaolin clay is compared with published data of cyclic simple shear/direct simple shear tests on normally consolidated clays in Figure 4. Ansal & Erken (1989) have presented results of cyclic shear strain from symmetrical cyclic simple shear tests, on normally consolidated kaolin (LL=65%, PL=27%, w≈LL) consolidated to 100kPa as a function of normalized shear stress. The undrained shear strength used for normalising shear stresses was defined from stress-controlled monotonic tests. The cyclic tests were conducted at a frequency of

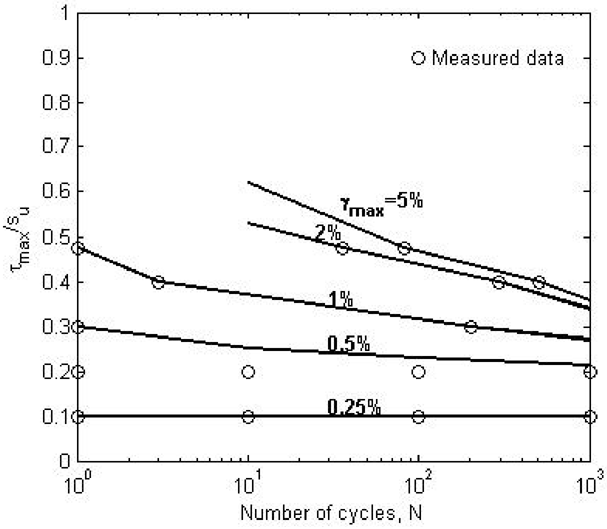

Figure 3. Maximum shear strain contour diagram as a function of normalised maximum shear stress, τ_{max}/s_u, and number of cycles from symmetrical CDSS tests on normally consolidated kaolin, f=0.1Hz.

0.1Hz, similar to the present study. It is noted that the values of cyclic shear strain in symmetrical tests are anticipated to be close to the maximum shear strains, and the comparison is therefore valid. The results are in good agreement with the contour diagram of the present study. The small differences observed may be attributed to differences in the natural properties of kaolin, in the testing method, for example the use of a reinforced membrane instead of a stack of rings as a confining method, and the consolidation stress level.

The contour diagram for normally consolidated kaolin clay is also compared in Figure 4 with the cyclic shear strain contours for normally consolidated Drammen clay (I_p=27%) from symmetrical CDSS tests (Andersen 2009). The Drammen clay samples were consolidated to 400kPa. The DSS strength used for normalising the applied stress was defined from strain-controlled monotonic tests conducted at a rate of shear strain of 4.5%/h. The cyclic tests were also conducted at a frequency of 0.1Hz. Figure 4 shows that the same shear strain levels are achieved at higher shear stress levels in Drammen clay indicating that the cyclic shear strength and stiffness of normally consolidated Drammen clay is higher than those of normally consolidated kaolin. Based on Andersen (2015), the cyclic shear strength of natural clays increases with increasing plasticity. Although kaolin has a higher plasticity, I_p=34%, it is a reconstituted clay and its strength is expected to be lower than the strength of a natural clay due to the lack of ageing. The lower cyclic shear strength observed by the present study may also be attributed to differences in the testing methods and the different

`

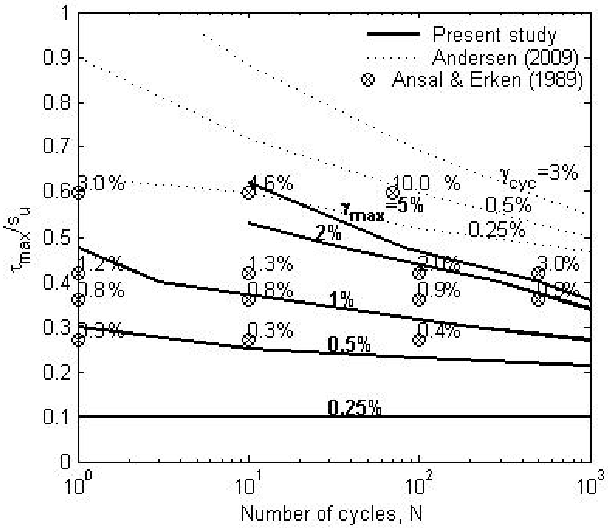

Figure 4. Comparison of maximum shear strain contour diagram for normally consolidated kaolin with published data for kaolin clay (Ansal & Erken 1989) and Drammen clay (Andersen 2009).

consolidation stress. For example, the faster shearing rate used in the monotonic tests on kaolin leads to higher values of DSS strength and therefore lower normalised shear stresses. A different confining method, a reinforced membrane instead of a stack of rings, was also used in the tests on Drammen clay.

3.3 *Definition of failure for non-symmetrical CDSS tests*

Typical results from the non-symmetrical CDSS tests conducted with τ_{ave}/s_u = 0.2 and with τ_{max}/s_u = 0.30, 0.50 and 0.60, and τ_{ave}/τ_{cyc} = 2, 0.67 and 0.5 respectively, are presented in Figure 5. The tests with the highest τ_{max}/s_u (= 0.50 and 0.60) reached very large shear strains. Contrary to the response of the symmetrical CDSS tests, shear strain develops at a relatively steady rate throughout the tests without any sudden increase. The vertical effective stresses reduce during the tests and reach a plateau at relatively high shear strains. In Figure 6, stress-strain loops are presented for the non-symmetrical tests that reached high shear strains at the beginning of each test and at a high shear strain level. No cyclic stiffness degradation is observed in the non-symmetrical test with τ_{ave}/τ_{cyc}=0.67 while some cyclic stiffness degradation is observed in the test with τ_{ave}/τ_{cyc}=0.5. These results conform to the trend of existing data (Mao & Fahey 2003) that in non-symmetrical tests, failure is achieved through accumulation of shear strains and that the failure mechanism depends on the ratio τ_{ave}/τ_{cyc}. Low ratios of τ_{ave}/τ_{cyc} appear to lead to some cyclic degradation while no degradation is caused for high to medium τ_{ave}/τ_{cyc} ratios. Failure in non-symmetrical tests can be therefore determined by shear strain reaching a specified value.

Similarly, the combination of γ_{cyc} and γ_{ave} at failure, and throughout the tests, depends on the ratio τ_{ave}/τ_{cyc}. For example, in the test with τ_{max}/s_u=0.30 and τ_{ave}/τ_{cyc}=2, the average shear strain increases and cyclic shear strain remains constant while in the test with τ_{max}/s_u=0.60 and τ_{ave}/τ_{cyc}=0.5, both average and cyclic shear strain develops rapidly. Significant increase in cyclic shear strain is therefore developed for low ratios of τ_{ave}/τ_{cyc} while no increase of cyclic shear strain is observed for high τ_{ave}/τ_{cyc}. This is in agreement with Mao & Fahey (2003) and Andersen (2015) who observed that the final combination of average and cyclic shear strain at failure depends on the ratio of the applied τ_{ave}/τ_{cyc} for calcareous soils and offshore clays respectively.

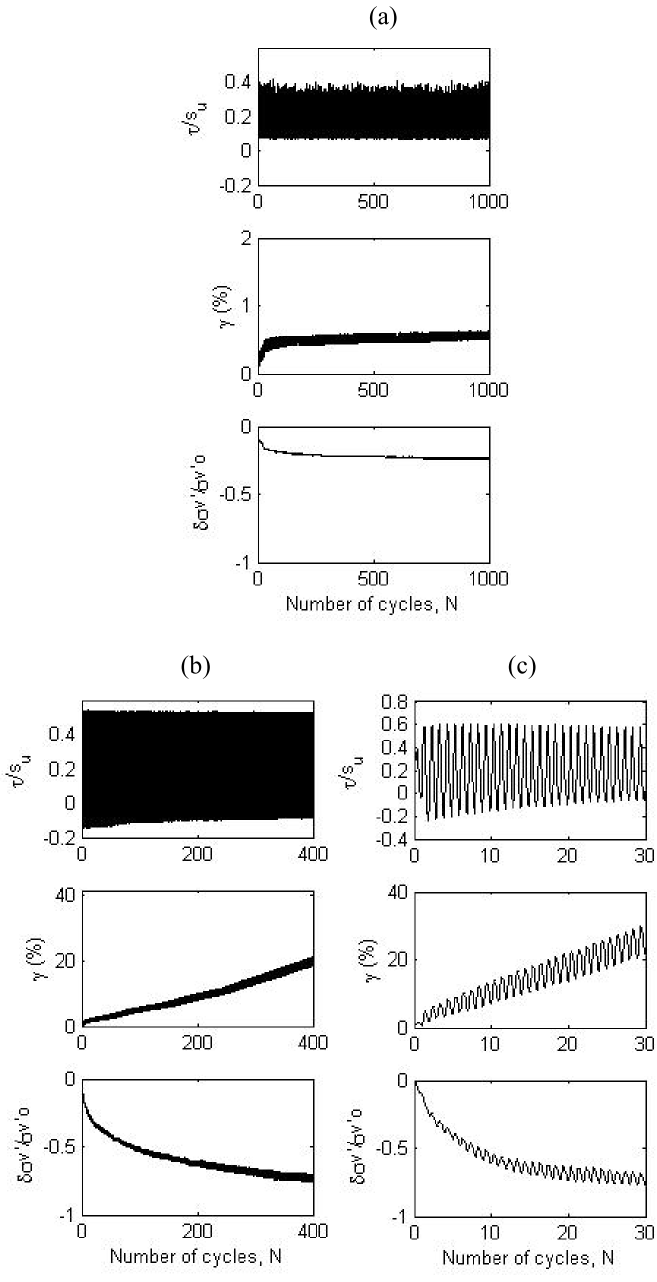

Figure 5. Data of non-symmetrical CDSS tests under (a) τ_{max}/s_u=0.30 and τ_{ave}/τ_{cyc} =2, (b) τ_{max}/s_u=0.50 and τ_{ave}/τ_{cyc} =0.67 and (c) τ_{max}/s_u=0.60 and τ_{ave}/τ_{cyc} =0.5

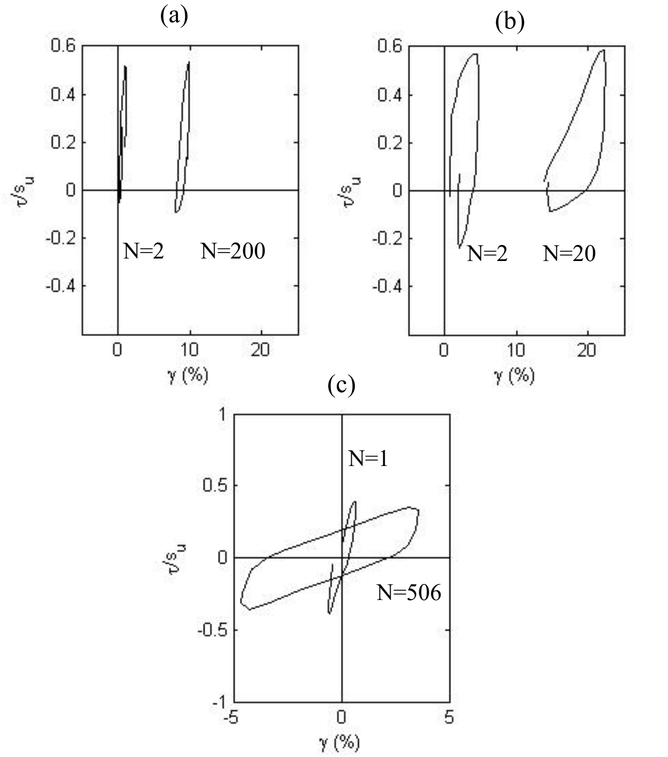

Figure 6. Comparison of normalised shear stress, τ/s_u, versus shear strain, γ, for non-symmetrical CDSS tests under (a) τ_{max}/s_u=0.50 & τ_{ave}/τ_{cyc} =0.67 and (b) τ_{max}/s_u=0.60 & τ_{ave}/τ_{cyc} =0.5 and with (c) symmetrical CDSS test under τ_{max}/s_u=0.40

3.4 *Comparison of failure in symmetrical and non-symmetrical CDSS tests*

The mode of failure in symmetrical and non-symmetrical cyclic loading on normally consolidated kaolin is very different. Failure in symmetrical tests is achieved through cyclic degradation and failure in non-symmetrical tests is achieved with shear strain accumulation. This is also evident in Figure 6, where significant stiffness degradation is shown to take place in the symmetrical tests after cyclic loading, in contrast with the non-symmetrical tests. The response of clay under non-symmetrical cyclic loading should not be predicted by contour diagrams from symmetrical CDSS tests.

The use of a common failure criterion for symmetrical and non-symmetrical tests, frequently used in the literature, may need to be revisited. The failure criterion, for both symmetrical and non-symmetrical tests, can be defined from element tests in agreement with the foundation tolerances to movement. In addition to this, the failure criterion for symmetrical CDSS tests can be defined at the point where significant cyclic degradation has taken place. For instance, γ_{max}=5% could be used as a failure criterion for normally consolidated kaolin under symmetrical cyclic loading based on the findings of this study, but a higher shear strain failure criterion could be used for normally consolidated kaolin under non-symmetrical cyclic loading. The use of a γ_{max} higher than 5% for symmetrical tests would be based on shear strain measurements after the sample has failed or ruptured internally and may not be reliable.

4 CONCLUSIONS

Results from a series of symmetrical and non-symmetrical CDSS tests on normally consolidated kaolin clay are presented. The main outcome is the compilation of a shear strain contour diagram for symmetrical cyclic loading on normally consolidated kaolin that can be used to inform design. The contour diagram is in good agreement with limited existing published data on normally consolidated kaolin. The following conclusions can also be drawn:

- Failure in the symmetrical CDSS tests on normally consolidated kaolin was achieved through cyclic degradation when maximum shear strain γ_{max} was between 4 and 5%. Based on this, the maximum strain γ_{max} contour plotted on the shear strain contour diagram was 5%.
- Failure in the non-symmetrical CDSS tests was achieved through the accumulation of shear strain and can be defined by γ_{max} reaching a specified value, much greater than the one achieved in the symmetrical tests.
- The combination of γ_{cyc} and γ_{ave} during the non-symmetrical tests depends on the ratio τ_{ave}/τ_{cyc}, with high ratios leading to increase of γ_{ave} and with low ratios leading to increase of both γ_{cyc} and γ_{ave}.
- The common use of a failure shear strain criterion for normally consolidated clays under symmetrical and non-symmetrical cyclic loading may be inappropriate. The failure criterion can be defined from element tests in agreement with the foundation tolerances to movement. In addition to this, for symmetrical tests, the failure criterion can be defined at the point where significant cyclic degradation has taken place. For non-symmetrical tests, where no or limited degradation occurs, a higher shear strain failure criterion could be used for types of foundations with high tolerances to movement.

5 ACKNOWLEDGEMENTS

This work forms part of the activities of the Centre for Offshore Foundation Systems (COFS). Established in 1997 under the Australian Research Council's Special Research Centres Program. Supported as a node of the Australian Research Council's Centre of Excellence for Geotechnical Science and Engineering, and through the Fugro Chair in Geotechnics, the Lloyd's Register Foundation Chair and Centre of Excellence in Offshore Foundations and the Shell EMI Chair in Offshore Engineering. The work presented in this paper is supported through ARC grant CE110001009. This support is gratefully acknowledged. The authors would also like to thank Mrs Behnaz Abdollahzadeh, Senior Soils Technician, for her assistance during the tests.

6 REFERENCES

Acosta-Martinez, H.E. & Gourvenec, S.M. 2006. One-dimensional consolidation tests on kaolin clay, *Research Report GEO: 06385.* Perth, Australia: Centre for Offshore Foundations Systems, School of Civil and Resource Engineering, The University of Western Australia.

Andersen, K.H. 2009. Bearing capacity under cyclic loading - offshore, along the coast, and on land, The 21st Bjerrum Lecture presented in Oslo, 23 November 2007. *Canadian Geotechnical Journal*, 46 (5): 513-535.

Andersen, K.H., Puech, A.A. & Jardine, R. J. 2013. Cyclic resistant geotechnical design and parameter selection for offshore engineering and other applications. *ISSMGE conference – TC 209 Workshop* – Design for cyclic loading: piles and other foundations - Paris, 9-44.

Andersen K.H. 2015. Cyclic soil parameters for offshore foundation design, *Proceedings Frontiers in Offshore Geotechnics III*, Oslo, 5-82.

Ansal, A. & Erken, A. 1989. Undrained Behavior of clay under cyclic shear stresses. *Journal of Geotechnical Engineering*, 115 (7): 968-983.

Hsu, C. & Vucetic, M. 2006. Threshold Shear Strain for Cyclic Pore-Water Pressure in Cohesive Soils. *Journal of Geotechnical and Geoenvironmental Engineering*, 132 (10): 1325-1335.

Geocomp Corporation 2012. Control and Report Software for Fully Automated Cyclic Direct Simple Shear Tests on ShearTrac-II DSS Systems using Windows®XP/Vista/7, Cyclic Direct Simple Shear- User's Manual.

Mao, X., & Fahey, M. 2003. Behaviour of calcareous soils in undrained cyclic simple shear. *Geotechnique*, 53 (8): 715-727.

Ohara S. & Matsuda H. 1988. Study on the settlement of saturated clay layer induced by cyclic shear. *Soils and Foundations*, 28 (3): 103-113.

Stewart, D. P. 1992. Lateral loading of piled bridge abutments due to embankment construction. PhD thesis, The University of Western Australia.

Vucetic M. 1990. Normalized behavior of clay under irregular cyclic loading. *Canadian Geotechnical Journal*, 27 (1): 29-46.

Theme 5. Liquefaction Assessments

Geotechnical and Geophysical Site Characterisation 5 – Lehane, Acosta-Martínez & Kelly (Eds)
© 2016 Australian Geomechanics Society, Sydney, Australia, ISBN 978-0-9946261-1-0

Standard Penetration Test-Based Assessment of Seismic Soil Liquefaction Potential of Urmia, Iran

H. Bahadori & A. Hasheminezhad
Department of Civil Engineering, Urmia University, Urmia, Iran

ABSTRACT: Soil liquefaction phenomenon has been observed for many years, but was brought to the attention of researches after Alaska and Niigata (Japan) earthquakes in 1964. There is no direct way to measure the liquefaction potential in soil, yet. What can be measured directly or indirectly are the various parameters that control soil's propensity to liquefy on seismic loading. For this purpose, various penetration test methods such as SPT, CPT and DMT are examined. These methods are completely empirical in nature and have worked well to date. Since Iran is located in an area with high seismic probability, there is a need for the liquefaction potential assessment in coastal areas like Urmia due to its proximity to Urmia Lake. In this paper, with the collected borehole data, an attempt was made to assess in detail the liquefaction potential of Urmia soil using SPT-based method. The Liquefaction potential was expressed in terms of the liquefaction potential index and calculated using standard penetration test profiles. Furthermore, a liquefaction hazard map of Urmia has been presented.

1 INTRODUCTION

Liquefaction is one of the most interesting but complex and controversial topics in geotechnical engineering. Soil liquefaction has been a major cause of damage to soil structure, lifelines and building foundation. It occurs when the structure of loose, saturated sand breaks down due to some rapidly applied loadings. As the structure breaks down, the loosely-packed individual soil particles attempt to move into a denser configuration. In an earthquake, however, there is not enough time for the water in the pores of the soil to be squeezed out. However, the water is trapped and prevents the soil particles from moving closer together. This is accompanied by an increase in water pressure which reduces the contact forces between the individual soil particles, thereby softening and weakening the soil deposit, results in settlement, tilting and rupture of structures in urban areas. Liquefaction potential of a soil deposit is dependent on the magnitude of a probable earthquake, grain-size distribution and soil type, relative density, earthquake loading characteristics, vertical effective stress and over-consolidation, age and origin of the soils, seismic strain history, degree of saturation and thickness of sand layer. Therefore in its assessment, these factors must be considered. However, some of the studies about these factors could not be ascertained, but their effects probably are assessed by means of cyclic loading test on undisturbed samples or in field tests such as SPT, CPT and DMT.

2 ASSESMENT OF LIQUIFICATION POTENTIAL

Several methods have been proposed to evaluate the liquefaction potential of soils due to earthquakes. The different types of methods can be classified into four groups including topographical and geological features, standard penetration test (SPT), Laboratory cyclic shear testing of undisturbed samples; and in-situ blasting or laboratory shake table testing. Nevertheless, conventional method based on the standard penetration test (SPT) has been commonly used in most countries and Iran. Seed and Idriss (1971) proposed a simplified procedure based on SPT-N values for the evaluation of liquefaction resistance of soils after two large and catastrophic earthquakes occurred in Alaska and Niigata (Japan) in 1964. The original simplified procedure based on empirical rules has been modified and improved over the years (Seed 1983).The standard penetration test is a method that can be used in the empirical correlation with liquefaction potentials of the sub-surface materials. Previous studies indicated that the liquefaction characteristic of soil is depended on a larger number of factors (Seed 1983). Although, it may not be possible at this stage to specify a single parameter, Christian and Swiger (1975) have shown that the SPT value, N, may ultimately solve this problem. Standard penetration test (SPT) is widely used as an economic, quick and convenient method to investigate the penetration resistance of non-cohesive soils. This test is an indirect means to obtain important parameters for non-cohesive soils. The cyclic stress ratio, developed at a particular depth beneath the ground surface may be estimated using the relation developed by Seed and Idriss (1971):

$$\frac{\tau_{av}}{\sigma_0'} = 0.65\frac{a_{max}}{g}\frac{\sigma_0}{\sigma_0'}r_d \quad (1)$$

Where τ_{av} is the average cyclic shear stress during a particular time history, σ_0 is the effective overburden stress at the depth in question, σ_0' is the total overburden stress at that depth, a_{max} is the peak horizontal ground acceleration generated by the earthquake at the ground surface, g is the acceleration of gravity, and r_d a stress reduction factor which is a function of depth and the rigidity of the soil column. The second part of the Seed and Idriss procedure requires the determination of the cyclic strength of the soil deposit. This is estimated either through empirical correlation with the SPT Nm value (Seed et al., 1985), or cone penetration resistance, q_c allowing the effects of soil fines content. Empirical charts have been prepared to determine the cyclic strength based on corrected SPT blow count $(N_1)_{60}$. Based on $(N_1)_{60}$ then, the cyclic stress ratio required to induce liquefaction for a magnitude 7.5 earthquake, $(\tau_{av}/\sigma_0)1, M = 7.5$ is given by several relationships. For earthquakes of other magnitudes, the appropriate cyclic strength was obtained by multiplying a magnitude scaling factor.

As an index for the assessment of liquefaction potential, the liquefaction index (P_L value) is adopted in earthquake damage assessment of many countries. The liquefaction index is calculated from the safety rate to liquefaction (F_L value) for every depth derived from drilling data, geology sections and conditions of geo-morphological unit. The possibility of liquefaction and the safety rate to liquefaction (F_L value) or a liquefaction index (P_L value) are generally connected as follows. In next two parts, these two methods are explained in detail.

- $F_L > 1.0$ -- There is little possibility of liquefaction in the depth.
- $F_L \leq 1.0$ -- There is the possibility of liquefaction in the depth.
- $P_L = 0$ -- Liquefaction potential is quite low.
- $0 < P_L \leq 5$ -- Liquefaction potential is low.
- $5 < P_L \leq 15$-- Liquefaction potential is high.
- $P_L > 15$ -- Liquefaction potential is very high.

1.1 *F_L Method*

This method was first developed by Architectural Institute of Japan in 1988. In this method input data include JMA Magnitude of the earthquake, peak ground acceleration (PGA), depth from the ground, N-value, granule part content (Clay part content, Plastic index), groundwater level, total upper load pressure (calculated from unit weight of stratum) and effective upper load pressure (calculated from the unit weight of a stratum, the unit weight of groundwater, and groundwater level). The output of the method is rate of safety to liquefaction (F_L value). Saturated soil shallower than 20m, the granule part content F_c is 35% or less of stratum. Even if F_c is 35% or more, the clay part content P is 10% or less or the plastic index I_p is a 15% or less of silt layer with low plasticity. The stratum in which clay part content exceeds 20% can be estimated from the object for an assessment. First, the ratio of equivalent cyclic shear stress generated for every depth in the ground of an examination point is calculated using Equation 1. At the last, the rate F_L of safety to liquefaction generating in every depth is calculated using Equation 2 as follows:

$$F_L = \frac{\left(\frac{\tau_{av}}{\sigma_0'}\right)_M}{\left(\frac{\tau_{av}}{\sigma_0'}\right)} \quad (2)$$

1.2 *P_L Method*

This method was first proposed by Iwasaki et al. (1978) and used for liquefaction damage assessment during earthquakes. The method is similar to the Seed and Idriss (1971) approach. The input and output of the method are the distribution of $F_L$value to a depth of 20 m and Liquefaction index, (P_L value), respectively. The liquefaction potential of the ground is not assessed with F_L method although it assesses the generating possibility of the liquefaction in a certain depth. Iwasaki et al., (1984) defined the value (a liquefaction index, P_L value) acquired from the weighted integration of F_L value for depth, and made it as the index for liquefaction potential of soil (Equations 3).

$$P_L = \int_0^{20} F.w(z)dz$$

$$F = \begin{cases} 1 - F_L & F_L < 1.0 \\ 0 & F_L \geq 1.0 \end{cases} \quad (3)$$

$$w(z) = 10 - 0.5.z$$

(z: depth from earth surface [m])

Where $w(z)$ is a weight function for the depth, and has given bigger weight to the shallow portion. The result depends on the method that derives F_L value.

The main objective of this study is to determine the areas with the greatest liquefaction potential in Urmia.

3 ASSESMENT OF LIQUIFICATION POTENTIAL OF URMIA

Figure 1. Borehole locations in the study area in Urmia

Urmia is the second largest city in the north-west of Iran and the capital of West Azerbaijan Province, Iran. The study area in this research is Urmia with an area of about 105 km^2 and Gholman Khaneh suburb of Urmia which has an area approximately 30 km^2. The location map of the study area has been illustrated in Figure 1.

Urmia Lake is one of the world's largest salt lakes, which is situated in the east of the city and the mountainous borders of Turkey are located in west. Urmia is exposed to significant seismic hazards and it is a coastal area due to the proximity to Urmia Lake. Both the high groundwater level and the grain size of the soils, along with the active seismic features of the region, result in favourable conditions for the occurrence of liquefaction in Urmia. When the surface and near surface geological conditions were taken under consideration, it became clear that due to having a moderate liquefaction susceptibility, the study area's geology is prone to liquefaction. If geologic and geomorphologic criteria are considered, it can be seen that the study area as discussed under the region's geology is susceptible to liquefaction. All the above mentioned facts are sufficient to study the liquefaction potential of sediments in Urmia to determine the zones of major risk. The determination of absolute susceptibility requires site specific geotechnical studies. Therefore, In order to increase our knowledge about the susceptibility of the region, it was necessary to use geotechnical information. This information has been acquired through Standard Penetration Tests (SPT) performed in 108 borehole data which has been drilled during Urmia seismic microzonation studies by Sahra Kav Consulting Engineers (SKCE) in 2009-2014. This research uses the database of boreholes and data from a recently completed extensive geotechnical site investigation to assess liquefaction susceptibilities of the soils in Urmia and analyzes it in the framework of GIS. Liquefaction potential of Urmia has been assessed using standard penetration test (SPT) in conjunction with established methods such as those of Seed (1979), F_L method and P_L method.

Initially, geological mapping was carried out, and based on field observations and drilled logs, soil profiles were constructed. As a part of microzonation study of Urmia, SPT was carried out according to D1586-99 ASTM and Designation E-21 User Earth manual. Grain size distribution and saturated unit weight of the sample soils were determined by means of laboratory testing. In addition, groundwater level was an important parameter in assessing regional liquefaction potential. Regarding the significant number of drilled boreholes (108 boreholes) and the adequate coverage of the Urmia, by the use of groundwater level in these boreholes, ground water situation has been determined. Based on these studies, ground water level (GWL) map has been prepared for Urmia (Figure 2). According to this map, groundwater level varies between 1 to 33 m in Urmia. This considerable difference in the groundwater level is related to sediments' thickness and materials, changes in surface topography in different parts of the city and faults probability performance that is in need of more research. Using corrected N values and adopting an average saturated unit weight at the magnitude of earthquake of M=7, the liquefaction potentials of the soils in the study area have been estimated. Finally, the potential liquefiable zone has been quantified. The data obtained have been mapped according to susceptibility, and the susceptibility maps based on the geotechnical data indicated a moderate to high susceptibility to liquefaction for the magnitude of earthquake (M=7) for Urmia.

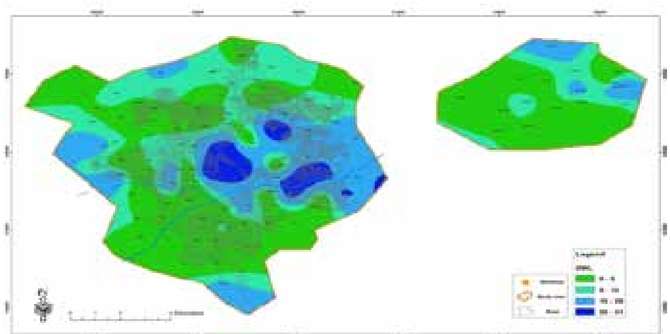

Figure 2. GWL map of the study area in Urmia

4 RESULTS AND DISCUSSIONS

The general soil profile of the study area consists of sand, silt, clay and gravel. Figure 3 indicates the typical soil profile for the borehole NO.85. Nevertheless, the main constituent is loose to medium dense sand which is a susceptible to liquefaction soil type. According to SPT results, SPT values in the most drilled boreholes in Urmia are more than 50. According to Terzaghi and peck (1967) as shown in Table 1, most of alluvial layers in points of density view in Urmia are dense to very dense and small part of those have medium dense and loose. In addition, most of the clay layers are in the very stiff and hard density and only small part of those are medium stiff and soft. According to Das, Braja M. (1941) as shown in Table 3, main parts of sands in Urmia have relative density of approximately 30-60 percent and angle of internal friction encompasses 35-42 degree. Other considerable parts of soils have relative density of approximately 95 percent and angle of internal friction is more than 42 degree.

Table 1. Urmia Soil classification based on SPT value in Boreholes (SKCE, 2013)

SPT Value	**Classification**	**Percentage of Boreholes %**
0-4	Very Loose	0
4-10	Loose	13.9
10-30	Medium	21.3
30-50	Dense	8.1
>50	Very Dense	56.7

Table 2. Urmia Fine-grained Soil classification based on SPT value in Boreholes (SKCE, 2013)

SPT Value	**Classification**	**Percentage of Fines in Boreholes %**
<2	Very Soft	2.5
2-4	Soft	4.9
4-8	Firm	7.9
8-15	Stiff	8.8
15-30	Very Stiff	11.9
>30	Hard	64

Table 3- Urmia soil classification based on SPT value In Relative density and angle of internal friction (SKCE, 2013)

Modified SPT Value	**Relative Density (D_r%)**	**Angle of Internal Friction**	**Sandy Soils in Boreholes %**
0-5	0-5	26-30	8
5-10	5-30	28-35	5.8
10-30	30-60	35-42	42.3
30-50	60-95	38-46	4.9
>50	-	-	39.1

In this part, the results of liquefaction potential analysis have been presented. In assessment of the liquefaction potential, the groundwater level in meter, peak ground acceleration for return period of 475 years in g, magnitude of region's seismicity as 7 and experimental results up to 20 m depth for each borehole have been considered. The collected data from the soil characteristics including soil grading, natural density, passing from sieve NO.200 and SPT results has been utilized in analyzing liquefaction of each borehole. In the case in which passing percent of sieve NO.200 and plastic index were more than 35 and 15 percent respectively, the soil was classified as non-liquefiable, according to seed et al., 1983. The boreholes with less than or equal 20 groundwater level can be used for liquefaction potential assessment. Rests of the boreholes due to groundwater level of more than 20 m were considered as non-liquefiable. The summary of liquefaction analysis has been presented in Table 4.

Table 4. Summary of liquefaction analysis of Urmia

Number of BH	**Criteria**	**Liquefaction Potential**
7	PL>15	Very high
5	5<PL≤15	High
7	2<PL≤5	Medium
14	0<PL≤2	low
75	PL=0	Very Low

The liquefaction potential in Urmia varies from very low to very high. Cohesive clay and hard silty soils as well as the clay sands with high plastic index have been classified as non-liquefiable soils in study area. Silty soils, silty sands with clay in high density have been classified as low to medium liquefaction potential soils. Sandy soils with silt in medium to low density had high liquefaction potential.

According to Table 4, among 108 drilled boreholes only 7 samples had very high liquefaction potential, 5 boreholes had high liquefaction potential, 7 boreholes had medium liquefaction potential, 14 boreholes had low liquefaction potential and 75 boreholes has been recognized as the lack of liquefaction potential. That is, 29 boreholes due to lack of groundwater level, 5 boreholes due to groundwater level more than 20 m and 5 boreholes due to fines percent of more than 35 percent and plastic index of more than 15 and 36 boreholes after calculating F_L and P_L which their liquefaction index was 0 and did not have any liquefaction potential.

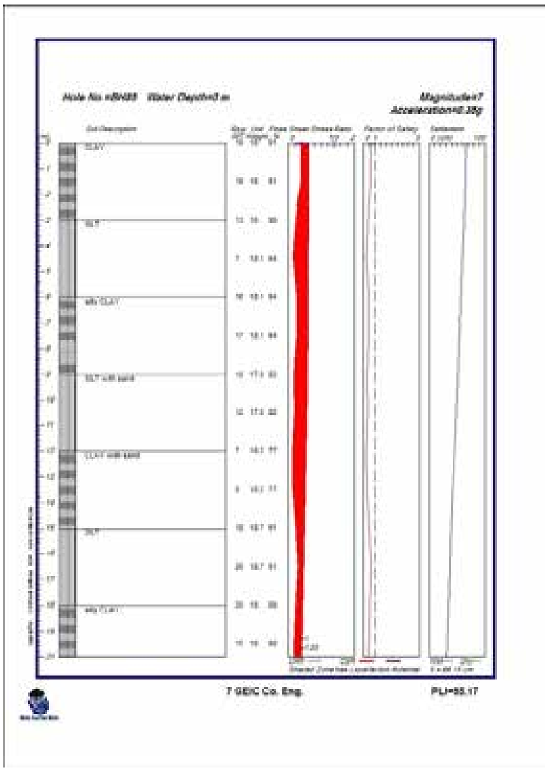

Figure 3.The soil profile for BH NO.85 (SKCE, 2013)

5 LIQUEFACTION POTENTIAL MAPPING OF URMIA

Liquefaction potential mapping of the study area was obtained by linear interpolation of the liquefaction potential index using F_L and P_L methods for probable earthquake. Liquefaction hazard map for Urmia has been presented in Figure 4. The map indicates that the boreholes which have very high liquefaction potential are mostly in the North, the Eastern-North and the Western-North and near to the center of Urmia. Other parts of the study area, including the center part and south because of low groundwater level and also existence of fine-grained soil are non-liquefiable potential soils. According to Figure 4, it's concluded that liquefaction danger in the center of Urmia to the north, the Eastern-North and the Western-North is considerable. So, in order to emphasize on dispersion of liquefaction soils in the determined limitations, the detailed and explanatory researches are essential.

6 CONCLUSIONS

Urmia is in one of the highest seismic zones of the world and due to its proximity to Urmia Lake, the evaluation of liquefaction potential is of utmost importance. In this paper, with the collected borehole data, an attempt was made to assess in detail the liquefaction potential of Urmia soil using SPT-based method. Results addressed an extensive analysis for determination of liquefaction hazard of Urmia. The Liquefaction potential was expressed in terms of the liquefaction potential index and calculated using standard penetration test profiles. Furthermore, a liquefaction hazard map of Urmia has been presented. The results indicated that the study area has highly susceptible regions to liquefaction and is in need of appropriate mitigation to reduce the risk. Thus, It is hoped that this paper will serve as a guideline for the geotechnical engineers as well as seismologists, architects and urban planners in making rational decisions while developing projects in the Urmia.

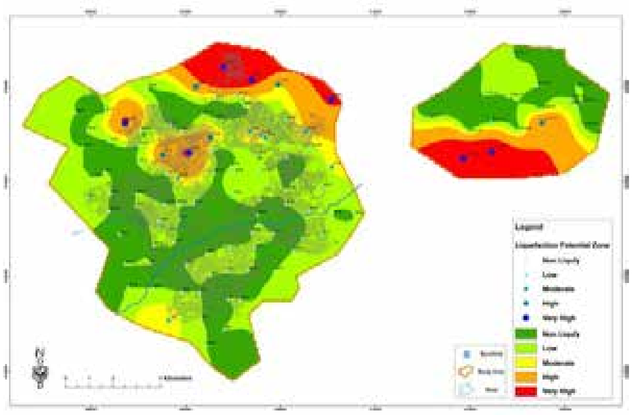

Figure 4.Urmia Liquefaction potential map

7 ACKNOWLEDGMENTS

The authors would like to thank Sahra Kav Consulting Engineers (SKCE) and khak & Rah Azma Consulting Engineers for providing the SPT data and other geotechnical properties of this study.

8 REFERENCES

Das, B. M. (2010). Geotechnical Engineering Handbook. J. Ross Publishing.

Iwasaki, T., Tatsuoka, F., Tokida, K.-I., & Yasuda, S. 1978. "A practical method for assessing soil liquefaction potential based on case studies at various sites in Japan." Proc., 2nd Int. Conf. on Microzonation, San Francisco, National Science Foundation, Washington, D.C. 885–896.

Iwasaki, T., Arakawa, T., & Tokida, K. I. (1984). Simplified procedures for assessing soil liquefaction during earthquakes. International Journal of Soil Dynamics and Earthquake Engineering, 3(1), 49-58.

Sahra Kav Consulting Engineers (SKCE).(2013), " Urmia city geology studies report", Urmia Microzonation Studies Project, Islamic Republic of Iran - Ministry of Roads & Urban Development.

Seed, H. B. and Idriss, I. M. (1971). "Simplified procedure for evaluating soil liquefaction potential." Journal of the Soil Mechanics and Foundations Division, ASCE, 97(SM9), 1249-1273.

Seed, H. B., Idriss, I. M., & Arango, I. (1983). "Evaluation of liquefaction potential using field performance data."

Journal of Geotechnical Engineering Division, ASCE, 109(3), 458-482.
Terzaghi, K. & Peck, R.B. (1967) "Soil Mechanics in Engineering Practice," John Wiley, New York. 729.

Geotechnical and Geophysical Site Characterisation 5 – Lehane, Acosta-Martínez & Kelly (Eds)
© 2016 Australian Geomechanics Society, Sydney, Australia, ISBN 978-0-9946261-1-0

Liquefaction assessment based on combined use of CPT and shear wave velocity measurement

Z. Bán & A. Mahler
Budapest University of Technology and Economics, Budapest, Hungary

T.J. Katona
MVM Nuclear Power Plant Paks Ltd., Paks, Hungary

E. Győri
MTA CSFK GGI Seismological Observatory, Budapest, Hungary

ABSTRACT: Empirical liquefaction potential assessment methods are generally based on the result of CPT, SPT or shear wave velocity measurement. In more complex or high risk projects CPT and V_S measurement are often performed at the same location commonly in the form of seismic CPT. However, combined use of both in-situ indices in one single empirical method is limited. For this reason the goal of this research was to develop such an empirical method where the result of CPT and V_S measurement are used in parallel and can supplement each other. After the accumulation of a case history database where both measurements are available and performing the necessary corrections of the variables, logistic regression was performed to obtain the probability contours of liquefaction occurrence. In this case the graphical representation of the cyclic resistance ratio curve for a given probability can be replaced by a surface.

1 INTRODUCTION

Soil liquefaction is one of the most devastating secondary effects of earthquakes and can cause significant damage in the built infrastructure. For this reason liquefaction hazard shall be considered in all regions where moderate-to-high seismic activity encounters with saturated, loose, granular soil deposits. Several approaches exist to take into account this hazard, from which the in-situ test based empirical methods are the most commonly used in practice. Traditional means of these tests are the Standard Penetration Test (SPT), Cone Penetration Test (CPT) and shear wave velocity (V_S) measurement. In routine or low-budget projects often only CPT testing is performed that will then serve as the basis of liquefaction potential assessment. In more complex or high-risk projects such as nuclear power plants, CPT and V_S measurement are often performed at the same location, commonly in the form of Seismic Cone Penetration Test (sCPT). However, even if the results of the two tests are available for the same spot, empirical liquefaction potential evaluation can be performed using either of them, but combined use of the data in one single method has been limited. In order to surmount this issue, an attempt has been made to develop an empirical method, which exploits both the results of CPT and V_S measurements. The effort is based on the assumption that these soil properties complement each other since they characterize the behavior of granular systems at different levels of strain.

2 LIQUEFACTION POTENTIAL ASSESSMENT BASED ON CPT AND V_S

2.1 *The CPT and V_S based empirical methods*

Since the introduction of cyclic shear stress approach (Seed & Idriss 1971) several empirical methods have been published by different authors that can give a relatively reliable quantification of factor of safety or probability of liquefaction. In current engineering practice the most commonly used CPT based methods are the procedures proposed by Robertson & Wride (1998), Moss et al. (2006), Idriss & Boulanger (2008) and Boulanger & Idriss (2014). As the use of CPT for ground profile characterization is very popular its application for liquefaction potential evaluation is also prevalent.

Compared with CPT and SPT based methods, the methods based on V_S tests are less widely used in practice for liquefaction susceptibility evaluation. For very long time the method of Andrus & Stokoe (2000) was used almost exclusively. Very recently the work of Kayen et al. (2013) made a huge step in the advancement of V_S based methods. Besides the advanced statistical framework adopted by the authors, the most remarkable accomplishment was the compilation of a global catalog of 422 case histories.

2.2 *Independence of CPT and V_S measurement*

Although, both V_S and CPT tip resistance (q_c) strongly depend on relative density and effective stress state, they can supply complementary information about the soil, as the former is a small strain property, while the latter is a large strain one. As discussed by Schneider et al. (2004), V_S in sands is controlled by the number and area of grain-to-grain contacts, on the other hand, penetration resistance in sands is controlled by the interaction of particles being sheared by and rotating around the penetrometer.

For the purpose of developing an empirical method exploiting both parameters a database was compiled where both measurements are available. To investigate independence of the two parameters, the correlation coefficient, R^2 between V_S and q_c (measured in the same critical layer for each case history) was determined for the dataset (Figure 1). Note that in the Figure the values of the two variables were normalized to 100 kPa effective overburden pressure to exclude the influence of different effective overburden pressure on them. The obtained correlation coefficient R^2=0.156 indicates that in their untransformed state the two parameters have poor correlation.

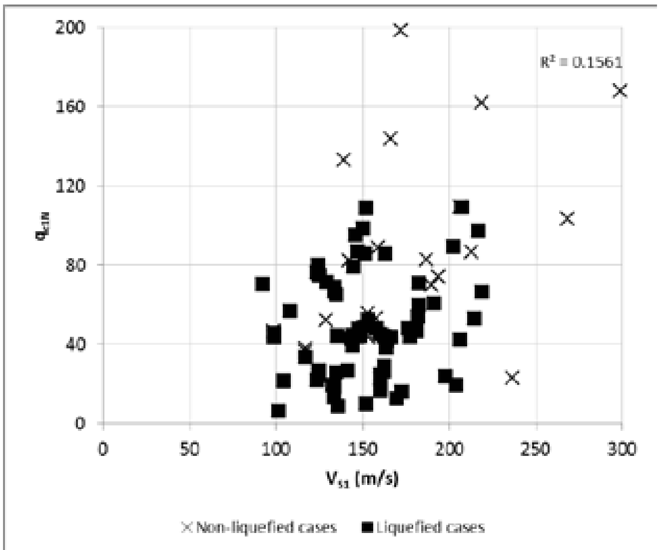

Figure 1. Correlation between V_{s1} and q_{c1N}

3 FIELD CASE HISTORY DATABASE

The first and most time consuming step of recent study was the collection of liquefaction/non-liquefaction field case history catalog. Through careful review of existing CPT and V_S databases 98 cases were found where both measurements were available. As locations where liquefaction occurred are more enticing for post-earthquake field investigators than sites where no apparent liquefaction occurred, the assembled dataset over represents liquefied sites (68 sites), relative to non-liquefied sites (30 sites).

The core of the database was assembled from the CPT case history catalog of Moss (2003) and V_S dataset of Kayen et al. (2013), from which 73 and 53 locations could be used, respectively. Additional case histories were gathered from the publications of Bay & Cox (2001), Ku et al. (2004), Moss et al. (2005), Moss et al. (2009), Cox et al. (2013) Boulanger & Idriss (2014), Batillas et al. (2014). The final database consists case histories from 12 earthquakes (1975 Haicheng, 1976 Tangshan, 1979 Imperial Valley, 1981 Westmoreland, 1983 Borah Peak, 1987 Elmore Ranch, 1987 Superstition Hills, 1989 Loma Prieta, 1999 Chi-Chi, 1999 Kocaeli, 2008 Achaia-Elia, 2011 Great Tohoku). For each case the following information was available: the triggering ground motion's moment magnitude (M_w) and maximum horizontal acceleration (a_{max}), depth of the critical layer, groundwater level, total (σ_v) and effective overburden pressure (σ'_v), stress reduction factor of the soil profile, CPT tip resistance and sleeve friction (f_s) and shear wave velocity in the critical layer. A summary of the dataset is presented in Table 1.

Table 1. Summary of the compiled case history database

	Liquefied cases		Non-liquefied cases	
	Mean	Standard deviation	Mean	Standard deviation
M_w	7.33	0.64	7.16	0.90
a_{max} (m/s^2)	0.30	0.15	0.23	0.17
σ_v (kPa)	92.73	45.43	98.13	48.80
σ'_v (kPa)	60.83	27.35	66.65	27.64
q_{c1} (MPa)	5.18	2.68	10.14	6.95
R_F (%)	0.92	0.57	1.05	0.56
V_{S1} (m/s)	152.72	29.89	181.17	67.41

4 OVERVIEW OF THE EMPIRICAL FRAMEWORK

4.1 *General approach*

In their study's Moss et al. (2006) and Kayen et al. (2013) applied Bayesian framework to quantify probability of liquefaction in which they treated the seismic demand and soil related variables separately in their logistic regression. On the other hand Idriss & Boulanger (2008) applied a semi-empirical approach in which correction and normalization of the variables were based on experimental data and theoretical considerations, and the final relationship was derived using maximum likelihood estimation treating only two variables: the magnitude and effective overburden stress corrected cyclic stress ratio ($CSR_{M=7.5,\sigma'v=1atm}$) and the equivalent clean sand value of normalized overburden corrected cone tip resistance (q_{c1Ncs}). Because the dataset for the present study was relatively small compared to the aforementioned catalogs, a wide enough range of magnitude and other variables to accurately quantify their effect on liquefaction potential was lacking. For this reason, the resistance variables (q_c and V_S) and the seismic demand were corrected and normalized before performing the logistic regression.

4.2 *Normalization of seismic demand*

According to the framework of simplified empirical procedures seismic demand induced by an earthquake can be represented by the cyclic stress ratio (CSR) at a depth z below ground surface using the following expression (Seed & Idriss 1971):

$$CSR = 0.65 \frac{a_{max}}{g} \frac{\sigma_v}{\sigma'_v} r_d \tag{1}$$

where g = gravitational acceleration; and r_d = stress reduction factor.

In order to take into account duration – or number of equivalent cycles – of different earthquakes a magnitude scaling factor (MSF) is used to adjust CSR for a duration typical of an average event of M_w=7.5. In the present study the MSF equation of Idriss (1999) was used:

$$MSF = 6.9 \exp\left(\frac{-M_w}{4}\right) - 0.058 \tag{2}$$

Previous researchers noted that susceptibility of soils to cyclic liquefaction strongly depends on effective overburden stress. This effect is often referred as K_σ effect and is generally taken into account by a multiplying factor. In this study the expression of Boulanger & Idriss (2004) developed using critical state framework was adopted:

$$K_\sigma = 1 - C_\sigma ln\left(\frac{\sigma'_v}{P_a}\right) \leq 1.1 \tag{3}$$

$$C_\sigma = \frac{1}{37.3 - 8.27(q_{c1N})^{0.264}} \leq 0.3 \tag{4}$$

where P_a = atmospheric pressure; and q_{c1N} = normalized overburden corrected cone tip resistance.

4.3 *Normalization of CPT tip resistance and shear wave velocity*

Effective overburden stress can profoundly influence CPT measurements. This effect is typically accounted for by normalizing the tip resistance measured at a given depth and vertical effective stress to a reference effective stress of 100 kPa. Boulanger & Idriss (2004) evaluated experimental and theoretical data for CPT and they obtained the following iterative formula for the effective stress normalization of q_c:

$$q_{c1N} = \frac{C_N q_c}{P_a} \tag{5}$$

$$C_N = \left(\frac{P_a}{\sigma'_v}\right)^\beta \leq 1.7 \tag{6}$$

$$\beta = 1.338 - 0.249(q_{c1N})^{0.264} \tag{7}$$

The role of fines on liquefaction susceptibility is a somewhat contentious topic. The conclusions of recent studies of the subject are rather controversial (Tan et al. 2013). Nevertheless it is agreed that if the fines content exceeds approximately 35-40% the coarser grains will "float" in the matrix of fine-size particles and the cyclic behavior of the soil will be governed by the fines. Although many researchers reported an initial increase then a decrease in liquefaction potential as fines content (FC) increases, all of the most widely used empirical methods apply monotonically increasing fines content correction. In the present study, equivalent clean sand values of the tip resistance have been determined using the updated equation of Boulanger & Idriss (2014):

$$q_{c1Ncs} = q_{c1N} + \Delta q_{c1N} \tag{8}$$

$$\Delta q_{c1N} = \left(11.9 + \frac{q_{c1N}}{14.6}\right) exp\left(1.63 - \frac{9.7}{FC+2} - \left(\frac{15.7}{FC+2}\right)^2\right) \tag{9}$$

A huge drawback of CPT compared to SPT that soil samples are not obtained during the test thus soil classification cannot be made directly. Although for many of the case histories the actual fines content were available in their source database, to keep consistency between the input data and the intended future use of the method, fines content of the critical layers were determined empirically using the soil behavior index (I_c) recommended by Robertson & Wride (1997). Boulanger & Idriss proposed the following expression:

$$FC = 80I_c - 137 \tag{10}$$

$$0\% \leq FC \leq 100\% \tag{11}$$

However, it should be noted that general correlations between FC and I_c exhibit large scatter.

As well as CPT tip resistance, V_S is also routinely normalized to an equivalent value measured at 100 kPa effective overburden stress (Robertson et al. 1992):

$$V_{S1} = V_S C_{V_S} = V_S \left(\frac{P_a}{\sigma'_v}\right)^{0.25} \quad C_{V_S} \leq 1.5 \tag{12}$$

Small strain shear modulus (G_{max}) is closely related to V_S. As the small strain stiffness of sands, silts and clays are of a similar range, V_S measurement do not allow detecting small differences in fines content, i.e.

V_S is relatively insensitive to FC. Several studies showed (Andrus & Stokoe 2000, Zhou & Chen 2007, Kayen et a. 2013) that increase in fines content to 35% has a maximum adjustment of 5 m/s. Compared to uncertainties arising from other parts of the methodology this uncertainty is fairly negligible. Thus, fines content correction of shear wave velocity has been neglected.

4.4 *Input variables for logistic regression*

After performing all of the above discussed normalization and corrections, three explanatory variables remained to participate in the logistic regression: the equivalent clean sand value of normalized overburden corrected cone tip resistance (q_{c1Ncs}), the overburden corrected shear wave velocity (V_{S1}), and the magnitude and effective stress corrected cyclic stress ratio ($CSR_{M=7.5,\sigma'v=1atm}$), which was obtained by the following formula:

$$CSR_{M=7.5,\sigma'_v=1atm} = \frac{CSR}{MSF \cdot K_\sigma} \tag{13}$$

There is no general agreement how the variables should be incorporated in the logistic regression, should they be used in their logarithmic, polynomial or untransformed form. Baecher & Christian (2003) recommended that variables should be transformed so that their frequency distribution has to be approximately normal. Following this guideline $CSR_{M=7.5,\sigma'v=1atm}$ has been included in the regression by its natural logarithm, while q_{c1Ncs} and V_{S1} remained untransformed.

5 LOGISTIC REGRESSION

Logistic regression is often used to explore the relationship between a binary response and a set of explanatory variables. The occurrence or absence of liquefaction can be considered as binary outcome and the previously summarized three parameters are the explanatory variables. Moss et al. (2006) and Kayen et al. (2013) adopted Bayesian updating technique (developed for probabilistic assessment of liquefaction initiation by Cetin et al. (2002)), while Boulanger & Idriss (2014) used maximum likelihood estimation to develop their resulting correlation.

The key components of these methods are the formulation of a limit state model that has a value of zero at the limit state and is negative and positive for liquefaction and non-liquefaction cases, respectively, and a likelihood function that is proportional to the conditional probability of observing a particular event assuming a given a set of parameters. Adopting the approach of Cetin et al. (2002) the following limit state function has been formed:

$$g = \theta_1 V_{S1} + \theta_2 q_{c1Ncs} + \theta_3 ln\left(CSR_{M=7.5,\sigma'_v=1atm}\right) + \theta_4 + \varepsilon \tag{14}$$

where $\Theta_{1...4}$ = the set of unknown parameters; and ε = model error term. The latter is introduced to account for the influences of the missing variables and the possible incorrect model form. If ε is assumed to be normally distributed with zero mean, the probability of liquefaction can be expressed as:

$$P_L = \Phi\left[-\frac{g-\varepsilon}{\sigma_\epsilon}\right] \tag{15}$$

where Φ = standard normal cumulative probability function; and σ_ε = standard deviation of the model error term.

Assuming the statistical independence of the observations compiled from different sites, the likelihood function can be written as the product of the probabilities of the observations. As it was noted in section 3 the dataset contains significantly more liquefaction cases than non-liquefaction cases; this bias is undesirable in logistic regression and can adversely affect the result. A way to address this issue is to weight each class of cases according to the proportion of the other's class population in the total database (Cetin et al. 2002, Baecher & Christian 2003) while the sum of the weights should remain 2.0 (Mayfield 2007). According to these guidelines the corresponding weight factors for liquefaction and non-liquefaction cases are 0.62 and 1.38, respectively. Then the likelihood function takes the following form:

$$L = \prod_{liq}\left[\Phi\left(-\frac{g-\varepsilon}{\sigma_\epsilon}\right)\right]^{0.62} \times \prod_{non-liq}\left[\Phi\left(\frac{g-\varepsilon}{\sigma_\epsilon}\right)\right]^{1.38} \tag{16}$$

After taking the natural logarithm of the likelihood function that is more convenient to work with, the unknown parameters were determined using maximum likelihood estimation.

6 PROBABILITY OF LIQUEFACTION

The logistic regression using the likelihood function in Equation 16 yields the following result:

$$P_L = \Phi\left[-\frac{\begin{array}{c}0.080V_{S1}+0.177q_{c1Ncs} \\ -8.40ln\left(CSR_{M=7.5,\sigma'_v=1atm}\right)-46.04\end{array}}{3.46}\right] \tag{17}$$

The denominator, that is the standard deviation of the error term, is of particular interest since it describes the efficiency of the liquefaction relationship. The regressed value is somewhat higher than that of other commonly used methods, but the method is still promising, since the method demonstrates certain refinement compared to the other methods in spite of relative small size of the dataset used. It shall be noted that the σ_E value only incorporates model uncertainty. The measurements errors or parameter uncertainty have not been taken into account in the analysis.

The cyclic resistance ratio for a given probability of liquefaction can be expressed by rearranging Equation 17:

$$CRR_{M=7.5\sigma'_v=1atm} = exp\left(\frac{0.080V_{S1}+0.177q_{c1Ncs} -46.04+3.46\Phi^{-1}(P_L)}{8.40}\right) \quad (18)$$

This can be used in deterministic analysis by selecting a probability contour to separate liquefaction and non-liquefaction states. Figure 2 shows the probability surface corresponding to P_L = 50%.

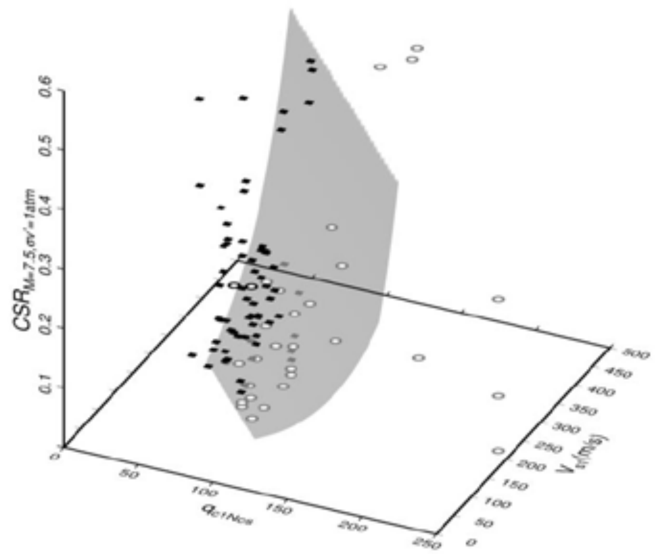

Figure 2. Cyclic resistance ratio surface corresponding to 50% of liquefaction probability (solid squares – liquefaction cases, hollow circles – non-liquefaction cases)

7 CONCLUSION

For high-risk projects CPT and V_S measurement are often performed on the same location however the possibility to characterize the soil's resistance with both indices in one single empirical liquefaction method was limited. The goal of the research was to develop such a method within the framework of simplified empirical procedures that can reduce uncertainty of empirical methods by combining two in-situ indices; a small strain property measurement with a large strain measurement. In the first step by careful reviewing of the already existing liquefaction case history databases, sites were selected where the records of both CPT and V_S measurement are available. After implementing the necessary corrections on the gathered 98 case histories with respect to fines content, overburden pressure and magnitude, a logistic regression was performed to obtain the probability contours of liquefaction occurrence. The proposed formula is an initial attempt to exploit the advantages offered by the measurements of two soil parameters instead of one.

This equation only takes into account model uncertainty but variation of the parameters has been neglected. In spite of this the proposed equation can be a useful tool in its current form (as being conditional on known values for the input parameters). To assess the probability of the phenomenon in a liquefaction hazard evaluation, the conditional probability of liquefaction provided by this equation needs to be combined with the probabilities of the q_{c1Ncs}, V_{S1} and $CSR_{M=7.5,\sigma'v=1atm}$; i.e., the parameter uncertainties.

The use of the recommended relationship is likely to be limited to high-risk projects where probabilistic seismic hazard analysis (PSHA) and detailed site characterization is required. In the sequence of hazard analysis liquefaction hazard analysis is preceded by both the PSHA (which would account for the majority of the uncertainty in the seismic demand) and the site exploration (which would account for the majority of the uncertainty in the soil resistance parameters). In that scenario, it may be reasonable to only include model uncertainty in the liquefaction triggering analysis because the parameter uncertainties were already accounted for in the previous stages of the analysis (Boulanger & Idriss 2014).

8 FUTURE WORK

This research is far from being considered as completed, there is still considerable more work to be done. As the dataset is relatively small, in the first round more emphasis was put on the quantity rather than the quality of the data. However, it is believed that if the magnitude of the database will allow proper quality assessment, omission of low quality data can improve the reliability of the methodology. This problem refers back to the most important flaw of the method that is the relatively minor number of cases included in the catalog. With the inclusion of cases from the 2010-11 Canterbury and other future earthquakes hopefully a more robust dataset will be available that will allow the separate treatment of all the independent variables and further refinement of this approach.

As it was mentioned this equation only takes into account model uncertainty but variation of the parameters were neglected. There is an intention to include measurement errors.

Although this work is only the beginning of a road, it is hoped that after more refinement and expanded dataset this approach will be able to provide answers with less degree of uncertainty that is essential for design of high-risk facilities.

9 REFERENCES

Andrus, R.D. & Stokoe, K.H., II. 2000. Liquefaction resistance of soils from shear-wave velocity. *Journal of Geotechnical and Geoenvironmental Engineering* 126(11): 1015–1025.

Batilas, A., Pelekis, P., Vlachakis, V., & Athanasopoulos, G. 2014. Soil Liquefaction/Nonliquefaction in the Achaia-Ilia (Greece) 2008 Earthquake: Field Evidence, Site Characterization and Ground Motion Assessment. *International Journal of Geoengineering Case Histories* 2(4): 270-287.

Bay, J.A., & Cox, B.R. 2001. *Shear wave velocity profiling and liquefaction assessment of sites shaken by the 1999 Kocaeli, Turkey earthquake*. PEER Project Report SA3017-18336, Pacific Earthquake Engineering Research, Berkeley.

Baecher, G.B. & Christian, J.T. 2003. *Reliability and statistics in geotechnical engineering*. Chichester: John Wiley & Sons Inc.

Boulanger, R.W. & Idriss, I.M. 2004. State normalization of penetration resistance and the effect of overburden stress on liquefaction resistance. *11th International Conf. on Soil Dynamics and Earthquake Engineering and 3rd International Conference on Earthquake Geotechnical Engineering; Proceedings, University of California, Berkeley, 7-9 January 2004*.

Boulanger, R.W. & Idriss, I.M. 2014. *CPT and SPT based Liquefaction Triggering Procedures*. Report No. UCD/CGM-14/01, University of California, Davis.

Cetin, K.O., Der Kiureghian, A. & Seed, R.B. 2002. Probabilistic models for the initiation of seismic soil liquefaction. *Structural Safety* 24(1): 67–82.

Cox, B.R., Boulanger, R.W., Tokimatsu, K., Wood, C.M., Abe, A., Ashford, S., Donahue, J., Ishihara, K., Kayen, R., Katsumata, K., Kishida, T., Kokusho, T., Mason, H.B., Moss, R.E.S., Stewart, J.P., Tohyama, K., & Zekkos, D. 2013. Liquefaction at strong motion stations and in Urayasu City during the 2011 Tohoku-Oki earthquake. *Earthquake Spectra* 29(S1): S55-S80.

Idriss, I.M. 1999. An update to the Seed-Idriss simplified procedure for evaluating liquefaction potential, *Proceedings, TRB Workshop on New Approaches to Liquefaction*, Publication No. FHWARD- 99-165, Federal Highway Administration.

Idriss, I.M. & Boulanger, R.W. 2008. *Soil Liquefaction during Earthquakes*. Monograph MNO-12, Earthquake Engineering Research Institute, Oakland.

Kayen, R., Moss, R.E.S., Thompson, E.M., Seed, R.B., Cetin, K.O., Der Kiureghian, A., Tanaka, Y. & Tokimatsu, K. 2013. Shear-Wave Velocity–Based Probabilistic and Deterministic Assessment of Seismic Soil Liquefaction Potential. *Journal of Geotechnical and Geoenvironmental Engineering* 139(3): 407-419.

Ku, C.-S., Lee, D.-H., & Wu, J.-H. 2004. Evaluation of Soil Liquefaction in the Chi-Chi, Taiwan Earthquake Using CPT. *Soil Dynamics and Earthquake Engineering* 24(9-10): 659-673.

Mayfield, R.T. 2007. *The return period of soil liquefaction*. Ph.D Dissertation, University of Washington, Seattle.

Moss, R.E.S. 2003. *CPT-based probabilistic assessment of seismic soil liquefaction initiation*. Doctor of Philosophy dissertation, University of California, Berkeley.

Moss, R.E.S., Collins, B.D. & Whang, D.H. 2005. Retesting of Liquefaction/Nonliquefaction Case Histories in the Imperial Valley. *Earthquake Spectra* 21(1): 179-196.

Moss, R.E.S., Seed, R.B., Kayen, R.E., Stewart, J.P., Der Kiureghian A. & Cetin, K.O. 2006. CPT-based probabilistic and deterministic assessment of in situ seismic soil liquefaction potential. *Journal of Geotechnical and Geoenvironmental Engineering* 132(8): 1032–1051.

Moss, R.E.S., Kayen, R.E., Tong, L., Liu, S., Cai, G. & Wu, J. 2009. *Reinvestigating liquefaction and nonliquefaction case histories from the 1976 Tangshan earthquake*. PEER Project Report 2009/102, Pacific Earthquake Engineering Center, Berkeley.

Robertson, P.K., Woeller, D.J., & Finn, W.D.L. 1992. Seismic cone penetration test for evaluating liquefaction potential under cyclic loading. *Canadian Geotechnical Journal* 29(4): 686–695.

Robertson, P.K. & Wride, C.E. 1997. Cyclic liquefaction and its evaluation based on SPT and CPT. In Youd, T.L. & Idriss, I.M. (eds.), *NCEER Workshop on Evaluation of Liquefaction Resistance of Soils, Proceedings, Salt Lake City*, Technical Report NCEER-97-0022: National Center for Earthquake Engineering Research.

Robertson, P.K. & Wride, C.E. 1998. Evaluating cyclic liquefaction potential using the cone penetration test. *Canadian Geotechnical Journal* 35(3): 442-459.

Schneider, J.A., McGillivray, A.V. & Mayne, P.W. 2004. Evaluation of SCPTU intra-correlations at sand sites in the Lower Mississippi River valley, USA. In Viana Da Fonseca, A. & Mayne, P.W. (eds), *Geotechnical & Geophysical Site Characterization; Proc. ISC-2, Porto, 19-22 September 2004*. Rotterdam: Millpress.

Seed, H.B. & Idriss, I.M. 1971. Simplified procedure for evaluating soil liquefaction potential. *Journal of the Soil Mechanics and Foundations Division* 97(SM9): 1249-1273.

Tan, C.S., Marto, A., Leong, T.K. & Teng, L.S. 2013. The Role of Fines in Liquefaction Susceptibility of Sand Matrix Soils. *Electronic Journal of Geotechnical Engineering* 18(L): 2355–2368.

Zhou, T.-G. & Chen, T.-M. 2007. Laboratory investigation on assessing liquefaction resistance of sandy soils by shear wave velocity. *Journal of Geotechnical and Geoenvironmental Engineering* 133(8): 959–972.

Geotechnical and Geophysical Site Characterisation 5 – Lehane, Acosta-Martínez & Kelly (Eds)

The Determination of Factor of Safety against Liquefaction and Post-Liquefaction Settlement

P. R. Klibbe
Bechtel Australia, Mining & Metals, Australia

ABSTRACT: This paper describes the liquefaction triggering relationships by NCEER (1997) and Youd et al. (2001, 2003), Idriss and Boulanger (2008) and Boulanger and Idriss (2014), used to assess the susceptibility of loose sands to liquefy. For the Idriss and Boulanger (2008) and Boulanger and Idriss (2014), the site-specific fines content correlation and carbonate content of the sands was incorporated in the analysis. The paper then demonstrates the use of CPTu and SCPTu soundings and shear wave velocity measurements to develop soil capacity for the site seismic input data. Factor of safety against liquefaction calculations are performed using the CPTu data and post-liquefaction settlements are calculated based on the normalized CPTu results and the factor of safety.

1 INTRODUCTION

As part of the design of the foundations and ground improvement works for a major industrial project a site specific seismic assessment was undertaken and in conjunction, a liquefaction assessment was also undertaken. The liquefaction assessment identified loose sands susceptible to liquefaction under the design seismic event. To determine the design requirements for foundations and ground improvement, the liquefaction assessment was extended to determine post-liquefaction settlements. This required calculation of the factor of safety against liquefaction, level of seismic strain and associated settlements.

The site-specific fines content correlation and carbonate content correction of the sands was incorporated in the analysis.

Post-liquefaction settlements were then calculated across the project site for the seismic inputs to identify the facilities impacted and the magnitude of post-liquefaction settlement. The results show that the post-liquefaction settlement varies from negligible in many areas to being significant in a number of facility locations. The results were used to assign the appropriate seismic site class and seismic design loads as well as appropriate foundations systems for the facilities, as determined based on the post-liquefaction settlement, as well as conventional bearing capacity and settlement basis.

2 SUBSURFACE CONDITIONS

Geotechnical investigations comprising more than 40 boreholes, 100 piezocone penetration tests (CPTu), 20 seismic piezocone penetration tests (SCPTu), 17 seismic dilatometer tests (SDMT), as well as geophysical surveys were undertaken for the design of the foundations.

The subsurface profile typically comprises compacted sandy fill over approximately 8 to 10m of natural poorly-graded silty sand, which is underlain by bedrock typically composed of calcarenite and sandstone and interbedded mudstone and gypsum to more than 70m depth.

CPTu soundings were initially terminated due to refusal in a very dense zone between 6 and 8.5m depth. Below this zone, loose sand was reported in the borehole and CPTu soundings that penetrated the very dense layer. Subsequent investigations were undertaken where the cone was withdrawn if refusal was achieved above 10m depth, and drilling was used to drill 0.5m below the depth of refusal. The CPTu was then continued until a depth of 10m was achieved.

The investigations were aimed at determining design parameters for piled foundations and ground improvement for large raft foundations, tall tank foundations, stockpile areas, reclaim tunnels, as well as a multitude of shallow raft and pad foundations.

The loose sand located from approximately 8 to 10m depth between the very dense layer and bedrock, was identified as potentially liquefiable.

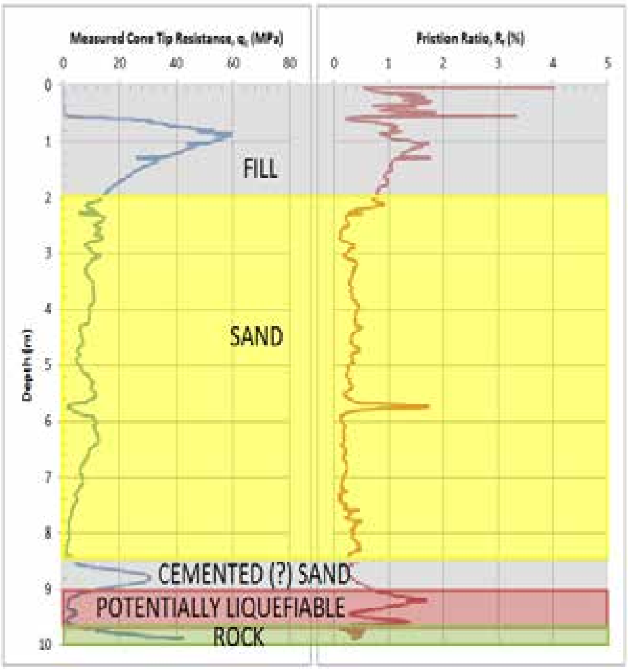

Figure 1. Subsurface profile showing typical soil conditions over the depth range of CPTu tests.

Figure 1 presents the measured cone tip resistance and friction ratio with stratigraphic interpretation of the subsurface profile and also illustrates the cemented zone, from approximately 8.5 to 9.0 metres depth, and the potentially liquefiable zone beneath from approximately 9.0 to 9.5 metres depth overlying the sedimentary rock strata.

3 SITE SPECIFIC CARBONATE CONTENT AND FINES CORRECTIONS

3.1 *Correcting Penetration Resistance for Carbonate Content*

The soils have a high carbonate content; typically, 82%. Soils with high carbonate content tend to be more compressible thereby requiring modification to typical correlations from penetration resistance to engineering parameters.

Due to the high carbonate content of the sands, a correction of penetration resistance was undertaken. Due to the carbonate nature of the sands, the generic fines content correlations do not perform well at this site. Therefore a site specific fines content correlation is constructed.

The process for use in liquefaction calculations is as follows:

- Calculate relative density using correlation for carbonate sands.
- Calculate equivalent penetration resistance for silica sand.
- Perform liquefaction calculation using input of equivalent silica sand penetration resistance.

Mayne (2014) provides a correlation from normalized cone tip resistance to relative density in carbonate sands as shown in Equation 1.

$$D_R = 0.87q_{t1} \tag{1}$$

where Dr = relative density; q_{t1} = normalized cone resistance.

Mayne (2014) provides a correction factor to be used to convert from normalized tip resistance in calcareous-carbonate sands to an equivalent normalized tip resistance in silica-quartz sands as shown in Equation 2.

$$q_{t1}(silica-quartz) = q_{t1}(calcareous-carbonate) * CF. \tag{2}$$

where CF = correction factor for calcareous sands.

The process to correct for the calcareous nature of the sands for CPTs is as follows:

- Calculate relative density based on the field measured cone resistance.
- Calculate equivalent silica-quartz cone resistance.

The equivalent quartz penetration resistances are then used in the liquefaction calculations.

3.2 *Site Specific Fines Content Correlation*

Liquefaction calculations using CPT data typically correlate CPT data in the form of the soil behavior index, Ic, to a fines content or apparent fines content. The soil behavior index is calculated using Equation 3 from Idriss and Boulanger (2008) with a stress exponent of 0.5 adopted for the sandy soil type.

$$I_c = [(3.47 - \log(Q))^2 + (\log(F) + 1.22)^2]^{0.5} \tag{3}$$

where I_c = soil behavior index; Q = normalized cone tip resistance; F = normalized friction ratio determined as follows:

$$Q = \left[\frac{q_c - \sigma_{vo}}{P_a}\right]\left[\frac{P_a}{\sigma'_{vo}}\right]^n \tag{4}$$

$$F = \frac{f_s}{(q_c - \sigma_{vo})} * 100\% \tag{5}$$

where q_c = cone tip resistance; P_a = atmospheric pressure; σ_{vo} = vertical stress; σ'_{vo} = vertical effective stress; f_s = sleeve friction.

The site-specific correlation of I_c to apparent fines content was determined based on the laboratory testing of fines content and the corresponding soil behavior index calculated from the normalized cone and friction values. A power curve as shown in Equation 6 was used to calculate the apparent fines content from the soil behavior index in the calculations.

$$AFC = 2.8{I_c}^{3.2} \tag{6}$$

4 FACTOR OF SAFETY AGAINST LIQUEFACTION

The factor of safety against liquefaction is calculated using CPTu and shear wave velocity data using CPTu results is performed using the fines content correlations.

The factor of safety against liquefaction is calculated from Youd et al. (2001), as

$$FS = \left(\frac{CRR_{7.5}}{CSR}\right) * MSF * K_\sigma * K_\alpha \tag{7}$$

where FS = factor of safety against liquefaction; $CRR_{7.5}$= cyclic resistance ratio for an equivalent magnitude 7.5 event; CSR = cyclic stress ratio for a given magnitude; MSF = magnitude scaling factor; K_σ = overburden correction factor; K_α = correction factor for sloping ground, assumed to be equal to one for level ground.

Youd et al. (2001) provides several ways of calculating the magnitude scaling factor, MSF. The overburden correction factor, K_σ is determined from the relative density and overburden stress as follows:

$$K_\sigma = \left(\frac{\sigma'_v}{P_a}\right)^{(f-1)} \tag{8}$$

where σ'_v = vertical effective stress; P_a = atmospheric pressure; f = empirical exponent; for relative density, D_r, ≤ 40% f = 0.8; 40% < D_r < 80% f = 0.7; D_r ≥ 80% f = 0.6.

4.1 *Calculation of Cyclic Resistance Ratio (CRR) using CPT Data*

The CPT tip resistance is normalized for overburden as follows:

$$q_{c1N} = C_Q\left(\frac{q_c}{P_a}\right) \tag{9}$$

$$C_Q = \left(\frac{P_a}{\sigma'_{vo}}\right)^n \tag{10}$$

where q_{c1N} = cone resistance normalized for overburden; C_Q = normalizing factor for cone resistance; q_c = cone tip resistance; P_a = atmospheric pressure; σ'_{vo} = vertical effective stress; n = stress exponent.

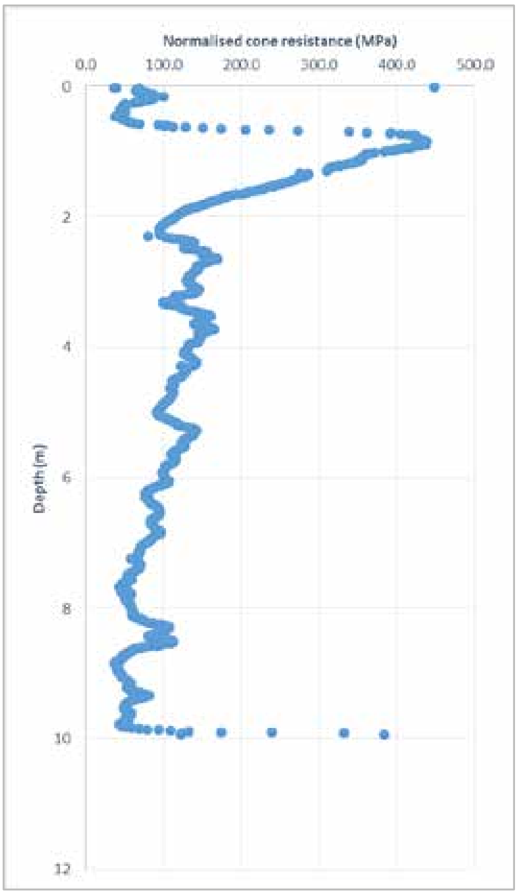

Figure 2. Normalised cone resistance.

Robertson (2009), provides a function for the stress exponent, n, as shown in Equation 11, which allows for convergence of liquefaction calculations.

$$n = 0.381(I_c) + 0.05\left(\frac{\sigma'_{vo}}{P_a}\right) - 0.15 \leq 1.0 \tag{11}$$

The $CRR_{7.5}$ is then calculated in Youd et al. (2001) dependent on the normalized cone resistance.
If $(q_{c1N})_{cs}$ < 50:

$$CRR_{7.5} = 0.833\left[\frac{(q_{c1N})_{cs}}{1000}\right] + 0.05 \tag{12}$$

If 50 < $(q_{c1N})_{cs}$ <160:

$$CRR_{7.5} = 93\left[\frac{(q_{c1N})_{cs}}{1000}\right]^3 + 0.08 \tag{13}$$

where $(q_{c1N})_{cs}$ = equivalent clean sand normalized penetration resistance; $CRR_{7.5}$ = cyclic resistance ratio for an equivalent magnitude 7.5 event.

4.2 *Calculation of Cyclic Stress Ratio (CSR) using CPT Data*

The cyclic stress ratio (CSR) is calculated using a site response analysis in which the input motion applied at rock level is propagated upward through the soil profile, as determined from the shear wave velocity profile, as shown in Figure 3.

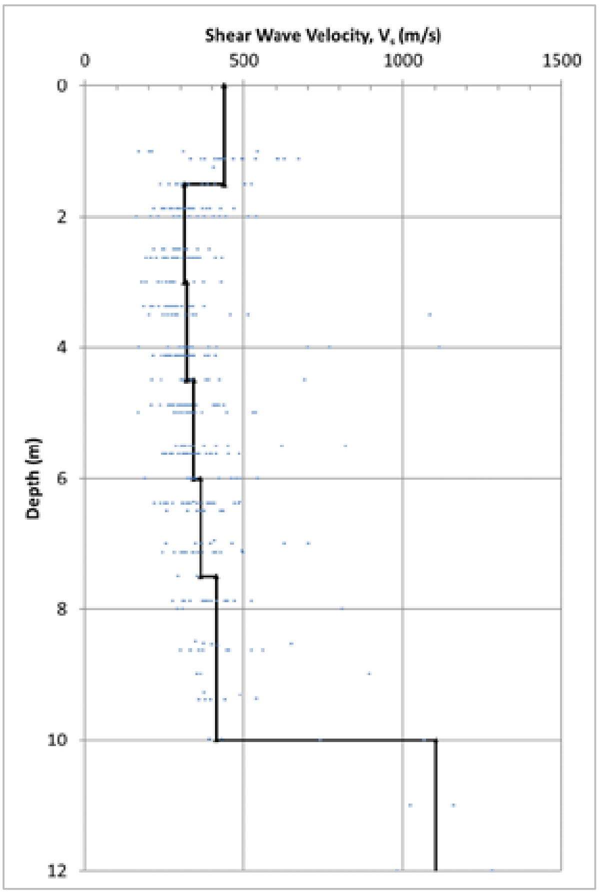

Figure 3. Profile of Shear Wave Velocities determined from SCPTu, SDMT and geophysical tests.

The input rock acceleration response spectra (ARS) and output ARS at grade are shown in Figure 4.

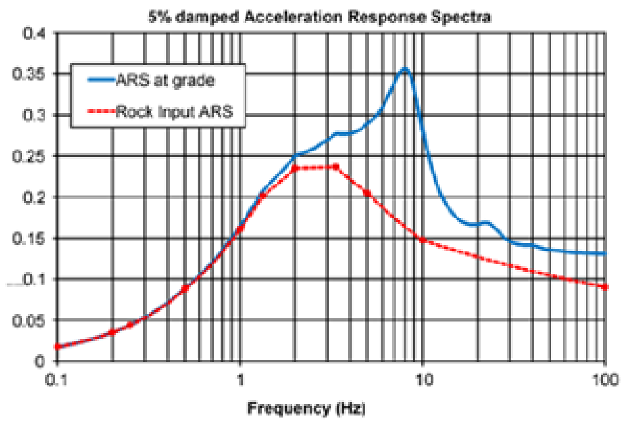

Figure 4. Acceleration response spectra at the rock level and the ground surface showing amplification in the soil profile.

The maximum shear stress is used to calculate the cyclic stress ratio (CSR) using Equation 2

$$CSR_{M,\sigma'_v} = 0.65\left(\frac{\sigma_v}{\sigma'_v}\right)\left(\frac{a_{max}}{g}\right)r_d \qquad (14)$$

where $CSR_{M,\sigma'v}$ = cyclic stress ratio for a specific earthquake magnitude and in-situ vertical effective stress; σ_v = total vertical stress; σ'_v = vertical effective stress; a_{max} = peak horizontal ground acceleration; g = gravitational acceleration; r_d = stress reduction coefficient.

Based on the calculated cyclic resistance ratio and cyclic stress ratio the factor of safety against liquefaction is calculated for each CPTu profile. The calculated factor of safety is shown in Figure 5.

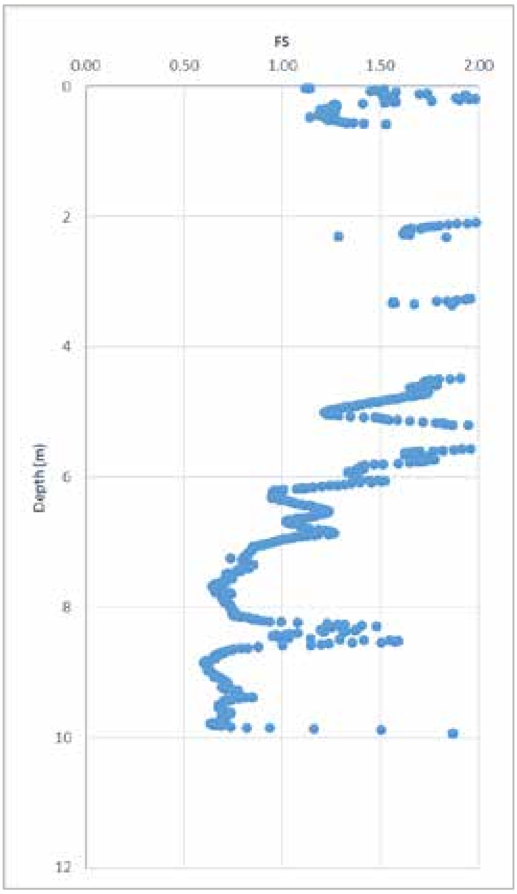

Figure 5. Calculated factor of safety against liquefaction.

5 POST-LIQUEFACTION SETTLEMENT

The calculation of post-liquefaction settlement is based on the limiting shear strain, the maximum shear strain, and the post-liquefaction strain.

The limiting shear strain is calculated from Idriss and Boulanger (2008), as follows:

$$\gamma_{lim} = 1.859(2.163 - 0.478(q_{t1Ncs})^{0.264})^3 \geq 0 \qquad (15)$$

where γ_{lim} = limiting shear strain; q_{t1Ncs} = normalized clean sand tip resistance.

The post-liquefaction strain, F_α, is calculated from Idriss and Boulanger (2008), as follows:

$$F_\alpha = -11.74 + 8.34(q_{t1Ncs})^{0.264} - 1.371(q_{t1Ncs})^{0.528} \qquad (16)$$

where F_α = post-liquefaction strain term; q_{c1Ncs} = normalized clean sand tip resistance.

The maximum shear strain is then calculated from Idriss and Boulanger (2008) as shown according to the criteria shown below and using Equation 17.

If FS ≥ 2 $\quad\quad \gamma_{max} = 0$

If 2 > FS > F_α

$$\gamma_{max} = min\left(\gamma_{lim}, 0.035(2 - FS)\left(\frac{1-F_\alpha}{FS-F_\alpha}\right)\right) \quad (17)$$

If FS < F_α $\quad\quad \gamma_{max} = \gamma_{lim}$

where FS = factor of safety against liquefaction; γ_{max} = maximum shear strain, γ_{lim} = limiting shear strain, F_α = post-liquefaction strain term.

The post-liquefaction volumetric strain is calculated from Idriss and Boulanger (2008) as follows:

$$\varepsilon_v = 1.5e^{\left(2.551-1.147(q_{t1Ncs})^{0.264}\right)} * min(0.08, \gamma_{max}) \quad (18)$$

where ε_v = post-liquefaction volumetric strain; q_{t1Ncs} = normalized clean sand tip resistance, γ_{max} = maximum shear strain.

Settlement is then calculated from strain as:

$$S = t\varepsilon_v \quad (19)$$

where S = post-liquefaction settlement, t = thickness of layer, ε_v = post-liquefaction volumetric strain.

Figure 6 shows a calculated profile of incremental settlement calculated for each depth increment in the CPTu profile.

Total settlement is then calculated as the sum of each layer incremental settlement and the post-liquefaction settlement can be plotted across the project site. Post-liquefaction settlements can then be assessed for each facility to assign the appropriate seismic site class as well as appropriate foundation systems for the facilities in addition to the requirements determined based on conventional bearing capacity and settlement basis.

6 CONCLUSIONS

The calculation of factor of safety against liquefaction and post-liquefaction settlement has been determined using CPTu and shear wave velocity data readily obtained and recorded across the entire project site at centimeter depth increments and imported and calculated in spreadsheets to allow both profiling and contouring of the factor of safety and settlement.

This has allowed each facility to be assigned the appropriate seismic site class as well as appropriate foundation system based on conventional bearing capacity and settlement as well as liquefaction affects.

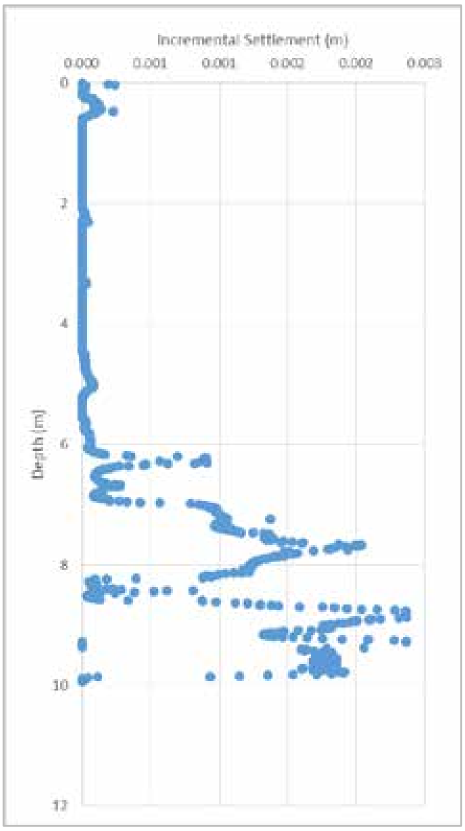

Figure 6. Incremental settlement calculated for each CPTu.

7 ACKNOWLEDGMENTS

Thanks to Michael Boone for the principles and formula and Margaret Klibbe for her support.

8 REFERENCES

Boulanger, R. W., and Idriss, I. M. (2014). "CPT and SPT based liquefaction triggering procedures." Report No. UCD/CGM-14/01, Center for Geotechnical Modeling, Department of Civil and Environmental Engineering, University of California, Davis, CA, 134 pp.

Idriss, I. M., and Boulanger, R. W., (2003). Estimating K_α for use in evaluating cyclic resistance of sloping ground, in Proceedings, 8th US-Japan Workshop on Earthquake Resistant Design of Lifeline Facilities and Countermeasures against Liquefaction, Hamada, O'Rourke, and Bardet, eds., Report MCEER-03-0003, MCEER, SUNY Buffalo, NY, pp. 449–68.

Idriss, I. M., and Boulanger, R. W. (2008). Soil liquefaction during earthquakes. Monograph MNO-12, Earthquake Engineering Research Institute, Oakland, CA, 261 pp.

Mayne, P.W. (2014) Interpretation of geotechnical parameters from seismic piezocone tests, Proc. 3nd Intl. Symposium on Cone Penetration Testing, Vol. 2 (CPT'14), www.cpt14.com.

National Center for Earthquake Engineering Research (NCEER) (1997), "Proceedings of the NCEER Workshop on Evaluation of Liquefaction Resistance of Soils," T.L. Youd and I.M. Idriss, eds., Technical Report NCEER-97-022, 302 pp.

Robertson, P.K., 2009. Interpretation of cone penetration tests – a unified approach, Can. Geotech. J. 46: 1337-1335.

Youd, T.L., Idriss, I.M., Andrus, R.D., Arango, I., Castro, G., Christian, J.T., Dobry, R., Finn, W.D.L., Harder Jr., L.F., Hynes, M.E., Ishihara, K., Koestor, J.P., Liao, S.S.C., Marcuson III, W.F., Martin, G.R., Mitchell, J.K., Moriwaki, Y., Power, M.S., Robertson, P.K., Seed, R.B., and Stokoe II, K.H. (2001), “Liquefaction Resistance of Soils: Summary Report from the 1996 NCEER and 1998 NCEER/NSF Workshops on Evaluation of Liquefaction Resistance of Soils,” Journal of Geotechnical and Geoenvironmental Engineering, ASCE, 127(10), 817-833.

Youd, T.L., Idriss, I.M., Andrus, R.D., Arango, I., Castro, G., Christian, J.T., Dobry, R., Finn, W.D.L., Harder Jr., L.F., Hynes, M.E., Ishihara, K., Koestor, J.P., Liao, S.S.C., Marcuson III, W.F., Martin, G.R., Mitchell, J.K., Moriwaki, Y., Power, M.S., Robertson, P.K., Seed, R.B., and Stokoe II, K.H. (2003), Closure to “Liquefaction Resistance of Soils: Summary Report from the 1996 NCEER and 1998 NCEER/NSF Workshops on Evaluation of Liquefaction Resistance of Soils,” Journal of Geotechnical and Geoenvironmental Engineering, ASCE, 129(3), 284-286.

Geotechnical and Geophysical Site Characterisation 5 – Lehane, Acosta-Martínez & Kelly (Eds)
© 2016 Australian Geomechanics Society, Sydney, Australia, ISBN 978-0-9946261-1-0

Soil classification and liquefaction evaluation using Screw Driving Sounding

S.Y. Mirjafari & R.P. Orense
University of Auckland, Auckland, New Zealand

N. Suemasa
Tokyo City University, Tokyo, Japan

ABSTRACT: A number of field testing techniques, such as standard penetration test (SPT), cone penetration test (CPT), and Swedish weight sounding (SWS), are popularly used for in-situ characterisation. The screw driving sounding (SDS) method, which has been recently developed in Japan, is an improved version of the SWS technique and measures more parameters, including the required torque, load, speed of penetration and rod friction; these provide more robust way of characterising soil stratigraphy. It is a cost-efficient technique which uses a machine-driven and portable device, making it ideal for testing in small-scale and confined areas. Moreover, with a testing depth of up to 10-15m, it is suitable for liquefaction assessment. Thus, the SDS method has great potential as an in-situ testing method for geotechnical site characterisation, especially for residential house construction. In this paper, the results of SDS tests performed at a variety of sites in New Zealand are presented. The soil database was employed to develop a soil classification chart based on SDS-derived parameters. Moreover, using the data obtained following the 2010-2011 Christchurch Earthquake Sequence, a methodology was established for liquefaction potential evaluation using SDS data.

1 INTRODUCTION

Soil stratigraphy in-situ is traditionally best determined through laboratory classification of samples retrieved from boreholes. However, if a continuous (or nearly continuous) subsurface profile is desired, various field investigation methods are commonly used to provide economical alternatives over the conventional methods of sampling and testing. Currently, a number of field testing techniques are being used to characterise sites, and these include standard penetration tests (SPT), cone penetration tests (CPT) and Swedish weight sounding (SWS) method. Although SPT is still popular worldwide due to its simplicity and applicability to many types of soils, it suffers from many limitations such as lack of repeatability, no continuous soil profile and the SPT blowcount is dependent on soil type, particle size, and the age and stress history of the deposit. CPT is quickly becoming popular because it is fast to perform and it provides continuous records with depth and is generally not operator-dependent; although sampling is not possible, soil type (or soil behaviour type) can be inferred from the information collected during the test. Finally, SWS is a highly portable and low-cost technique which provides a continuous profile of the soil. It is used very often in Japan to evaluate the allowable shear strength of soils for small-scale projects, and it is officially recommended as an investi gation tool by the Ministry of Land, Infrastructure and Transport (Japan).

The screw driving sounding (SDS) method, which has been recently developed in Japan, is an improved version of the SWS technique and can be used to characterise soft shallow sites, typically for residential house construction. While the SWS measures only two parameters during the test (weight during static penetration, W_{sw} and number of rotations during rotational penetration, N_{sw}), SDS measures four parameters: the required torque, load, speed of penetration and rod friction; these provide more robust way of characterising soil stratigraphy.

The SDS method was introduced in New Zealand in 2013 and a total of 164 SDS tests have been conducted at various sites to validate and/or adjust the methodologies originally developed based on Japanese soil database. Of these, a total of 74 SDS tests were conducted in Christchurch, mostly in areas which were affected by the 2010-2011 Canterbury Earthquake Sequence, with the aim of characterising various sites in the area for the on-going rebuild programme and estimating liquefaction potential considering future earthquakes. Most of the SDS tests were conducted at sites where CPT, SPT and borehole logs were available; the comparison of SDS results with existing information showed that the SDS method has great potential as an in-situ testing method for classifying the soils. Moreover, based on Christchurch data, a methodology was developed to estimate the liquefaction potential of sites using SDS-derived parameters.

2 TEST PROCEDURE

2.1 *Swedish Weight Sounding (SWS)*

Before discussing the principle and test procedure for SDS test, it is worthwhile to review the Swedish weight sounding (SWS) method, from where the SDS test has evolved. In the SWS method, which is popular in Japan and in many Nordic countries, weights (5kg clamp, two 10kg and three 25kg weights) are used together with a screw-shaped point, 22mm extension rods and a handle (or a motor) for rotating the rods. The test, which can be performed using either a machine or manually, comprises of two stages: (1) static penetration; and (2) rotational penetration. The penetration resistance of soil can be estimated either by measuring the required load or the number of half-turns that the screw point is rotated to penetrate to a specified depth. When sounding is performed in soft soil, the penetration resistance is typically measured only through the weight required for penetration of the rods. This means that the load is increased up to the weight which could penetrate the soil. The levels of static loading used in the test are: 0, 5, 25, 50, 75 and 100kg. If the penetration does not occur with 100kg weight, the rod is rotated by using a handle (or a motor). Further details of the testing procedure and the interpretation of test results are described by Tsukamoto et al. (2004) and Tsukamoto (2013). The key advantages of the SWS test are that it is highly portable, low-cost and, similar to CPT, provides a continuous profile of the soil. On the other hand, SWS has several disadvantages, such as the results being fairly influenced by rod friction. In cases when the layer contains gravel, the soil resistance tends to be over-estimated as the rod friction becomes large.

Suemasa et al. (2005) investigated the interaction between the torque and the vertical load during SWS implementation and proposed an analogy model based on plasticity theory and the results of SWS miniature test results. From the results, they noted that the coefficient of yield locus, c_y (which relates the normalised torque and normalised weight applied) and the coefficient of plastic potential, c_p (which relates the normalised half-turns and the torque on the rod), vary depending on the soil type; i.e. clay, loam, medium sand or dense sand. Consequently, they proposed that soil can be classified based on the data obtained from SWS tests if the torque can be measured. This resulted in further refinement of the SWS method in terms of operating system, which led to the development of the SDS method.

2.2 *Screw driving sounding (SDS)*

To minimize the disadvantages of the SWS as well as to incorporate a procedure to measure the rod friction, a new operating system for conducting the SWS was developed in Japan. The new system, now referred to as screw driving sounding (SDS), makes use of an improved version of the machine originally used for the SWS test. In the SDS test, monotonic loading system is used and the number of loading steps is increased to 7, while the rod is always rotated at a constant rate (25 rpm) during the test. The

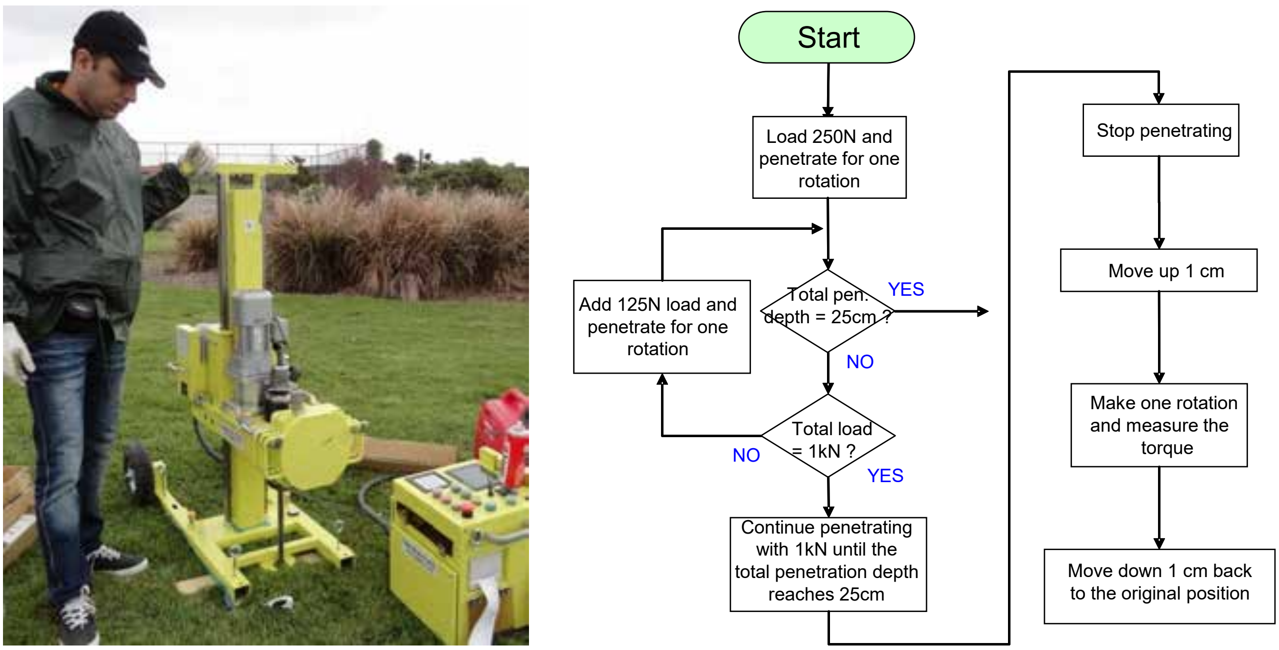

(a) (b)

Figure 1. (a) SDS equipment; and (b) SDS test procedure.

step loads are 0.25, 0.38, 0.50, 0.63, 0.75, 0.88, and 1kN and the load is increased at every complete rotation of the rod. Measured parameters in the test are: maximum torque (T_{max}), average torque (T_{avg}), minimum torque (T_{min}) on the rod, penetration length (L), penetration velocity (V) and number of rotations (N) of the rod. The parameters are measured at every complete rotation of the rod. Similar to the SWS method, a set of loading is applied in SDS test at every 25cm of penetration and after each 25cm penetration, the rod is lifted up by 1cm and then rotated to measure the rod friction. The procedure to measure the rod friction is described by Tanaka et al. (2012). Figure 1(a) illustrates the SDS test machine during operation while Figure 1(b) summarises the test procedure adopted. Further details of the SDS method are reported by Tanaka et al. (2012; 2014) and Maeda et al. (2015), while preliminary SDS results of application in New Zealand have been reported by Mirjafari et al. (2013; 2015a; 2015b) and Orense et al. (2013).

2.3 *Definition of some SDS parameters*

As discussed above, both load and torque are applied to the rod at the same time during the SDS test. The combined effect of the applied load and torque can be expressed in terms of energy, i.e., the incremental work done, δE, by the torque and vertical force for a small rotation can be calculated as (Suemasa et al. 2005):

$$\delta E = \pi T \delta n_{ht} + W \delta s_t \tag{1}$$

where T is the required torque to rotate the screw point, W is the required vertical load, δn_{ht} is the number of incremental half turns and δs_t is the incremental settlement caused by the load. The specific energy, E_s, is defined as the amount of energy for complete rotation, E, divided by the volume of penetration:

$$E_s = \frac{E}{L \cdot A} \tag{2}$$

where L is the amount of penetration per load step and A is the maximum cross-sectional area of the screw point.

Figure 2 illustrates a typical SDS result showing the variation of specific energy with depth and the tip resistance obtained by CPT test conducted at essentially the same location, (i.e. at Wordsworth Street, Christchurch). The specific energy shown is the average of the specific energies calculated at different steps of loading at each 25cm of penetration. As can be seen in the figure, the variation of the specific energy with depth is similar to the variation of the CPT tip resistance along the soil profile.

3 SOIL CLASSIFICATION CHART

Overall, SDS tests were performed at 164 sites in New Zealand (74 in Christchurch, 56 in Auckland and 34 in Wellington). These tests were conducted

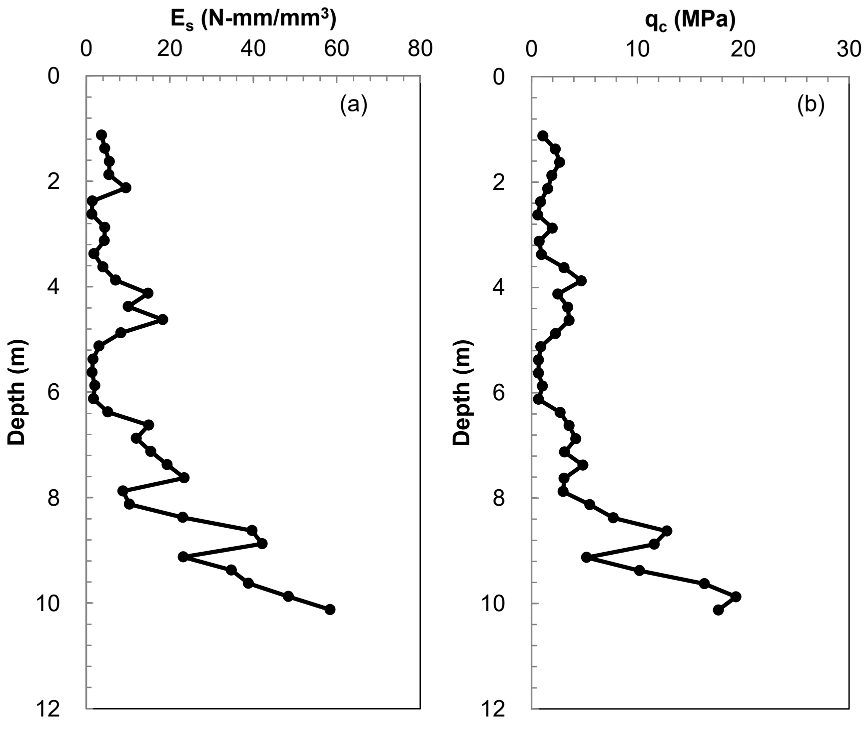

Figure 2. Variation with depth of: (a) specific energy from SDS test; and (b) cone tip resistance from CPT test conducted at a site located in Wordsworth Street, Christchurch.

adjacent to CPT sites and boreholes and therefore the soil types within a given layer are known. Various SDS parameters (expressed in terms of measured torque, load, energy, etc.) were investigated to examine which of these best correlate with the appropriate soil types. Based on the NZ soil database, the following parameters were considered:

$$\mathrm{Ave}(\delta T) = \frac{1}{n-1}\sum_{i=1}^{n-1}(T_{i+1} - T_i) \tag{3}$$

$$c_p" = \frac{1}{n}\sum_{i=1}^{n}\left(\frac{N_{SD}D}{\pi T / WD}\right)_i \tag{4}$$

where δT is the change in torque, T, at each step of loading, i; n (=7) is the number of loading; c_p" is the modified coefficient of plastic potential; N_{SD} is the number of normalised half-turns; W is the applied load; and D is the cross-sectional diameter of the screw point. The soil classification chart obtained based on the NZ soil database is shown in Figure 3.

Note that the boundary lines were drawn visually to separate data such that points representing similar soil types are grouped together. Data points in region A are sandy soils which, because of their frictional nature, are expected to have higher Ave(δT) and c_p" values compared to the other soil types. Based on borehole data analysis, sands on the left part of the region are finer than those on the right part. In addition, as c_p" is an indication of the difficulty in penetration, the upper part of region A would be denser than those on the lower part. Region B is for stiff peat, which can be found in South Auckland; peat is considered as c-ϕ soil and it is reasonable that it is positioned to the right side of Regions D and E, both of which represent cohesive soils. Region C represents sandy silt and silty sands. Soils at the bottom left of region B contain more silt than sand; therefore, this region can be considered as a transition zone from frictional behaviour to frictionless (cohesive) one. Soils in region D are highly-plastic stiff clays which have Ave(δT) values < 1 and 1 < c_p" < 2. Finally, region E belongs to clayey silt, silty-clay, silt and clay. Note that the available borehole data for clayey soils were scarce and more analysis are planned to separate clay and silt. However, it is expected that the upper part of this region would represent stiff clay or silt while the lower part would be for soft clay.

4 LIQUEFACTION POTENTIAL EVALUATION

Following the 2010-2011 Canterbury Earthquake Sequence, 74 SDS tests were conducted in Christchurch at both liquefied and non-liquefied areas. The SDS tests were conducted within 1–3 m from CPT sites, as described in the CGD (2013). For liquefaction potential evaluation, another SDS parameter, called normalised energy, $E_{s,1}$, was used:

$$E_{s,1} = E_s\left(\frac{P_a}{\sigma'_{v0}}\right)^m \tag{5}$$

where E_s represents the combined effect of the applied load and torque, as expressed by Eqtn (2), σ'_{v0} is the effective overburden pressure and P_a is the reference pressure (=100 kPa). After several anal-

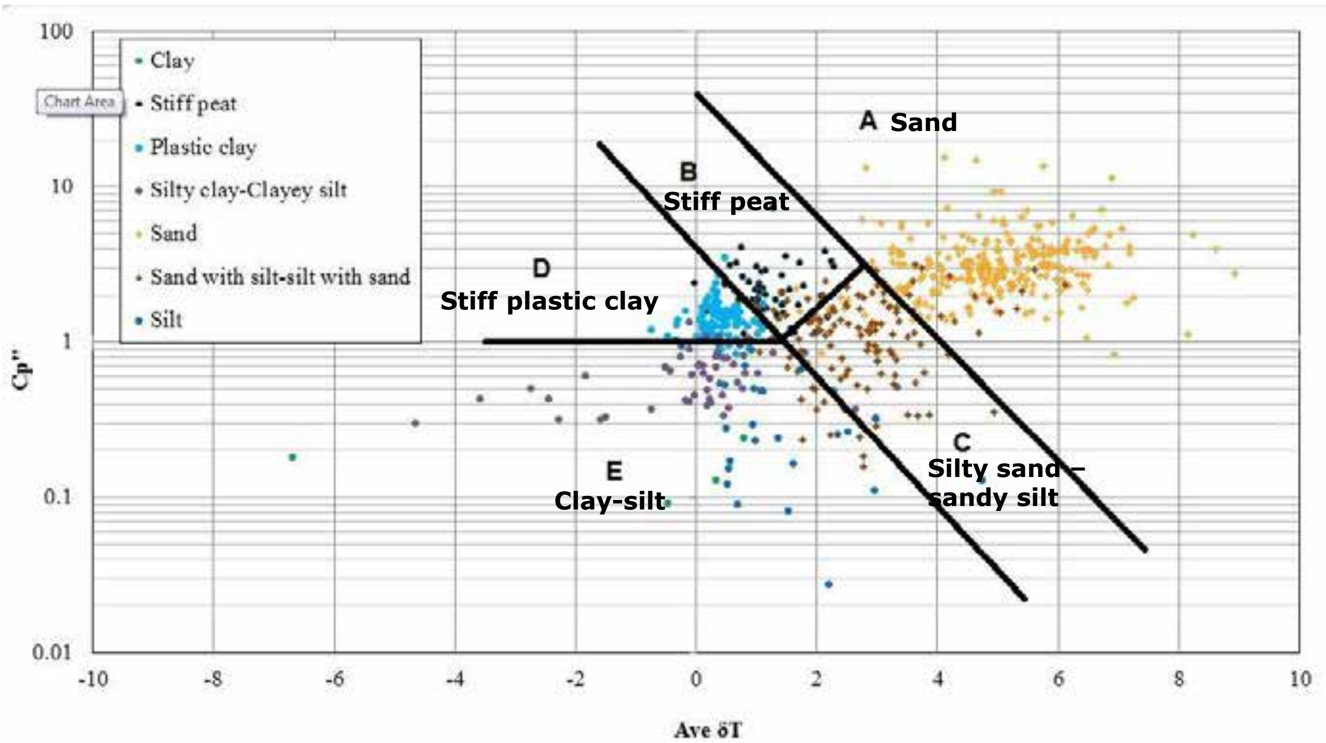

Figure 3. Soil classification chart based on SDS data.

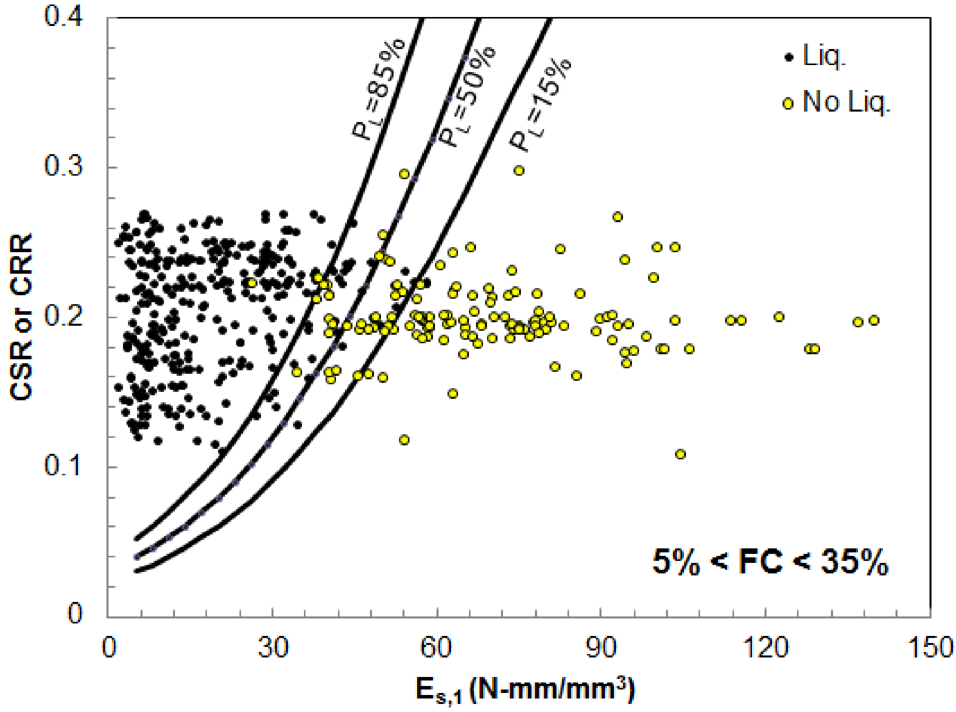

Figure 4: Proposed empirical chart for estimating CRR based on $E_{s,1}$ from SDS test (5% < F_C < 35%).

yses, it was found that m=0.5 is the best value to correlate the energy with the overburden pressure. For each data point, the cyclic shear stress ratio (CSR) and the factor of safety against liquefaction (F_L) during the 2011 Christchurch Earthquake were evaluated at adjacent CPT sites using three methods: (a) Robertson & Wride (1998); (b) Moss et al. (2006); and (c) Idriss & Boulanger (2008). If at least two of the methods indicate $F_L < 1$, the point is considered to have "liquefied". Finally, logistic regression analysis was used to define boundary curves, delineating different probabilities of liquefaction, P_L. A typical chart showing the cyclic resistance ratio (CRR) as a function of $E_{s,1}$, for soils with fines content, F_C, between 5% - 35% is presented in Figure 4.

Note that the F_C values employed in the analyses were estimated from the adjacent CPT data (excluding soil layers with F_C > 50%) using Robertson and Wride (1998) method. It is acknowledged that the applicability of this CPT-based F_C estimation for Christchurch soils is questionable (in the light of several evidence showing that the method does not work for Christchurch soils); further study is currently underway to correlate field-obtained SDS data with laboratory-derived F_C values of samples retrieved from the SDS sites.

To validate the proposed charts, liquefaction potential evaluation was conducted at several sites in Christchurch considering the 2010 Darfield earthquake (M7.1). Results indicated good correlation between estimated liquefied sites and actual/observed liquefaction. Finally, the recent M5.7 earthquake which hit Christchurch on 14 February 2016 also validated the proposed chart, with no liquefaction occurring at SDS sites near the CBD, but liquefaction observed at SDS sites in Parklands, located east of the city.

5 CONCLUDING REMARKS

The screw driving sounding method, which has been recently developed in Japan as an improved version of Swedish weight sounding test, measures more in-situ parameters and therefore provides more robust way of characterising soil profiles. It is a cost-efficient technique which uses a machine-driven screw point, making it ideal for testing in confined areas. The results of SDS testing performed at a variety of sites in New Zealand showed the method's ability to classify soils based on the measured parameters. Moreover, using the data obtained following the Christchurch Earthquake Sequence, empirical charts were developed for liquefaction potential assessment using SDS data.

6 ACKNOWLEDGEMENTS

The authors would like to acknowledge Nitto Seiko Company for providing the SDS machine and the Japan Home Shield (JHS) Corporation for providing assistance for this research. We also would like to acknowledge the Canterbury Geotechnical Database (CGD) for providing the borehole data and CPT records in Christchurch and the city councils for providing access to the test sites. Finally, the advice and

assistance of Prof Misko Cubrinovski of University of Canterbury are gratefully acknowledged.

7 REFERENCES

Canterbury Geotechnical Database, CGD (2013). https://canterburygeotechnicaldatabase.projectorbit.com/

Idriss IM & Boulanger RW. (2008). *Soil liquefaction during earthquakes*. Monograph MNO-12, Earthquake Engineering Research Institute, Oakland, CA, 261 pp.

Maeda Y, Yamato S, Sugano Y, Sakai G, Suemasa N & Tanaka T. (2015). Evaluation of soil liquefaction potential by screw driving sounding test in residential areas. *Proc. 6th International Conference on Earthquake Geotechnical Engineering*, Christchurch, New Zealand, 8p

Mirjafari SY, Orense, RP & Suemasa N. (2013). Comparison between CPT and SDS data for soil classification in Christchurch. *Proc. 10th International Conference on Urban Earthquake Engineering*, Tokyo, Japan, 561-566.

Mirjafari SY, Orense RP & Suemasa N. (2015a). "Assessment of in-situ liquefaction resistance of soils using Screw Driving Sounding." *Proc. 6th International Conference on Earthquake Geotechnical Engineering*, Christchurch, New Zealand, 8pp.

Mirjafari SY, Orense RP & Suemasa N. (2015b). Evaluation of liquefaction susceptibility of soils using Screw Driving Sounding method. *Proc. 15th Asian Regional Conference on Soil Mechanics and Geotechnical Engineering*, Fukuoka, Japan, 5pp.

Moss RES, Seed RB, Kayen RE, Stewart JP, Der Kiureghian A, & Cetin, KO. (2006). CPT- based probabilistic and deterministic assessment of in situ seismic soil liquefaction potential. *Journal of Geotechnical and Geoenvironmental Engineering*, 132(8), 1032-1051.

Orense, RP, Mirjafari SY & Suemasa N (2013). Geotechnical site characterisation using Screw Driving Sounding method. *Proc. New Zealand – Japan Workshop on Soil liquefaction during Recent Large-Scale Earthquakes*, Auckland, NZ.

Robertson PK & Wride CE (1998). Evaluating cyclic liquefaction potential using the cone penetration test. *Canadian Geotechnical Journal*, 35(3): 442-459.

Suemasa N, Shinkai K, Suzawa T & Tamura, M (2005). A plasticity model for Swedish weight sounding test. *Proc., 4th Japan – Philippines Workshop on Safety and Stability of Infrastructure*, Univ. of the Philippines, 169-177.

Tanaka T, Suemasa, N, Ikegame A & Yamato S. (2012). Classification of strata using screwdriver sounding test. *Proc. 22nd International Offshore and Polar Engineering Conference*, Rhodes, Greece.

Tanaka T, Suemasa, N, Katada T & Yamato S. (2014). Evaluation of soil liquefaction potential by screw driving sounding test. *Proc. 24th International Offshore and Polar Engineering Conference*, Busan, Korea.

Tsukamoto Y, Ishihara K & Sawada S. (2004). Correlation between penetration resistance of Swedish weight sounding tests and SPT blow counts in sandy soils. *Soils and Foundations*, 44(3):13-24.

Tsukamoto Y. (2013). Integrating the use of Swedish weight sounding tests for earthquake reconnaissance investigations. *Proc. International Conference on Earthquake Geotechnical Engineering: From Case History to Practice*, Istanbul, Turkey, 21pp.

Geotechnical and Geophysical Site Characterisation 5 – Lehane, Acosta-Martínez & Kelly (Eds)

Combined use of SDMT-CPTU results for site characterization and liquefaction analysis of canal levees

P. Monaco
University of L'Aquila – DICEAA, L'Aquila, Italy
L. Tonni, G. Gottardi & M. Marchi
University of Bologna – DICAM, Bologna, Italy
L. Martelli
Regione Emilia-Romagna, Servizio Geologico, Sismico e dei Suoli, Bologna, Italy
S. Amoroso
Istituto Nazionale di Geofisica e Vulcanologia, L'Aquila, Italy
L. Simeoni
University of Trento – DICAM, Trento, Italy

ABSTRACT: The paper illustrates the combined use of the results of seismic dilatometer tests (SDMT) and piezocone tests (CPTU), obtained as part of a comprehensive study aimed at investigating the post-earthquake stability conditions of canal levees damaged by the May 2012 Emilia (Italy) seismic sequence. The following issues are discussed: (1) Comparison of results obtained by SDMT vs. CPTU test interpretation, in particular soil type identification and ground property characterization of the embankment and the foundation soils. (2) Liquefaction analysis using a recent simplified method (Marchetti 2016) based on the combined use of the horizontal stress index K_D provided by SDMT and the cone penetration resistance q_t provided by CPTU. The results obtained by this method are compared with the results obtained by existing methods based on q_t (CPT) and K_D (DMT) alone, as well as with the results obtained by methods based on the shear wave velocity V_S and by laboratory cyclic tests.

1 INTRODUCTION

The seismic sequence which in May 2012 struck a wide area of the Po river plain (Emilia-Romagna region, Northern Italy) caused extensive damage to a number of riverbanks in the epicentral area, in the form of ground deformations, surface fractures and lateral spreading. Major damage was observed in a 3 km long segment of the embankment bordering an irrigation canal known as “Canale Diversivo di Burana” near Scortichino, Bondeno (Ferrara), hosting more than one hundred houses and productive activities. In some cases buildings and facilities built on the bank crown were found unstable or unsafe and thus declared unfit for use.

The municipality of Bondeno, supported by the Emilia-Romagna regional authority in cooperation with the Italian Geotechnical Society (AGI), promoted a Working Group of researchers from various Italian universities and experts of the Geological, Seismic and Soil Survey Regional Department, committed to analyzing the seismic response of the embankment, investigating the causes of the earthquake-induced damage, assessing the post-earthquake stability conditions and finally proposing remedial measures. A comprehensive site investigation program, including several in situ and laboratory tests, was performed for this task. The most significant results achieved by the Working Group activity were summarized by Tonni et al. (2015a). This paper is focused on the combined use of results from seismic dilatometer tests (SDMT) and piezocone tests (CPTU) for site characterization and liquefaction analysis.

2 SDMT-CPTU TESTS IN THE SCORTICHINO EMBANKMENT AREA

2.1 *Testing program and location*

The canal levee and the foundation soils were extensively investigated by in situ tests (5 boreholes, 12 CPTUs, 4 SDMTs, piezometer measurements, permeability tests) and by a large number of laboratory tests (triaxial, shearbox, resonant column and cyclic torsional shear, cyclic simple shear, double specimen direct simple shear) on undisturbed and reconstituted samples. Details on the test results and the relevant geotechnical parameters can be found in Tonni et al. (2015a,b). The site investigations were concentrated along cross-sections in four distinct areas (A, B, C, D, Fig. 1), located at about 1 km distance from each other, in which the most severe and extensive damages had been observed, particularly in the area C. In each investigated area (Fig. 2) at least three CPTU/SDMT soundings were carried out from the crest of the embankment, down to 30-35 m depth.

Figure 1. Aerial view of the damaged bank stretch and location of the investigated areas.

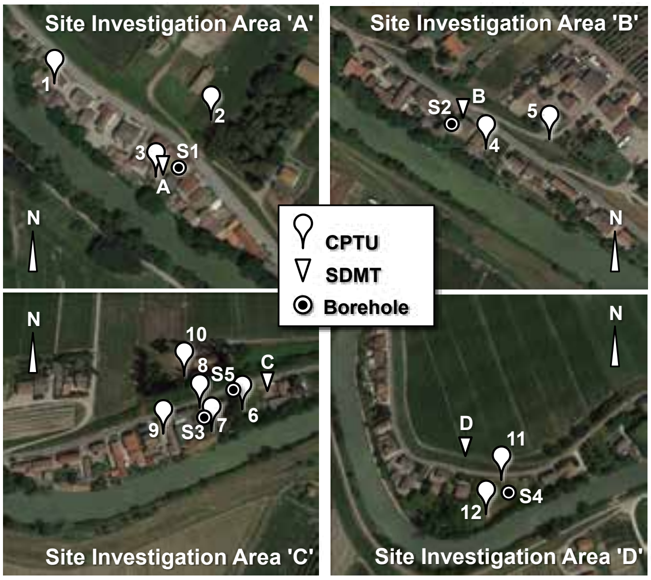

Figure 2. Location of in situ tests in the four selected areas.

2.2 *Interpretation of CPTU and SDMT results*

The borehole logs and the interpretation of CPTU and SDMT results (Tonni et al. 2015a,b) consistently allowed recognizing the following stratigraphic sequence and soil units from the crest of the embankment (see e.g. cross section c-c', area C, Fig. 3):

- an upper soil layer, about 9-10 m thick, composed of sandy silts and silty sands, corresponding to the core of the man-made embankment (Unit AR) in the topmost 6-7 m and to natural soils (Unit B) in the bottom portion;
- a clayey-silt layer with inclusions of peat and organic material (Unit C), generally ≈ 1-2 m thick;
- a medium to coarse or very coarse sand layer (Unit A) extending down to the maximum investigated depth, at least 40 m in thickness, locally including thin clayey lenses at depths between 30 and 34 m from the crest of the levee.

The above soil sequence was encountered in all the investigated areas, with minor variations in thickness of distinct soil units and/or in composition (predominantly sandy or silty) of Units AR and B. As an example, Fig. 4 shows the profiles of the corrected cone resistance q_t, the sleeve friction f_s and the pore pressure u provided by the piezocone test CPTU 6, carried out from the bank crest in area C. The plot also includes results from CPTU data interpretation, i.e. the profile of the Soil Behaviour Type (SBT), based on the Soil Behaviour Type Index I_{cn} calculated from the normalized cone resistance Q_{tn} and the normalized sleeve friction F_r (Robertson 2009), together with estimates of the friction angle φ' in each soil unit (Kulhawy & Mayne 1990 in coarse grained soil, Mayne & Campanella 2005 in fine grained soils) and of the undrained shear strength c_u in clays (Lunne et al. 1997).

Fig. 5 shows the results obtained from SDMT C, carried out from the bank crest in area C, in terms of profiles with depth of various parameters provided by usual DMT interpretation (Marchetti 1980, Marchetti et al. 2001), i.e. the material index I_D (indicating soil type), the horizontal stress index K_D (related to stress history/*OCR*), the constrained modulus M, the undrained shear strength c_u (in clay), the friction angle φ' (in sand), as well as the profiles of the measured shear wave velocity V_S and the small strain shear modulus G_0, obtained as $G_0 = \rho\, V_S^{\,2}$.

Both CPTU and SDMT profiles (Figs 4 and 5) denote rather poor mechanical properties of the soils in the upper ≈ 12 m below the crest of the embankment (Units AR, B and C). In particular the sandy-silty sediments of Unit B are characterized by low values of the horizontal stress index ($K_D \approx$ 1-2), which imply a low relative density D_R. Only the topmost 2-3 m of the embankment (Unit AR) show higher K_D values, presumably due to overconsolidation caused by desiccation-wetting cycles. The sands of Unit A, apart from sporadic thin layers having lower K_D, generally exhibit $K_D \approx$ 3-5, thus denoting a medium relative density ($D_R \approx$ 60% according to Reyna & Chameau 1991). The interpretation of DMT results in the clay layers, excluding the shallow "crusts", indicates that the deposit is normally consolidated or slightly overconsolidated. The coefficient of earth pressure at rest in the fine-grained layers is generally $K_0 \approx$ 0.6-0.7.

V_S measured by SDMT (Fig. 5) increases gradually with depth from ≈ 150-200 m/s in the topmost soil layers to ≈ 300 m/s at about 35 m depth. The profiles of the constrained modulus M (Marchetti 1980) indicate high compressibility of Units AR, B, C ($M \approx$ 5-10 MPa) as well as of the deep clay layers, while the sands of Unit A are significantly less compressible. Differently from M, which refers to a "working strain" level (Marchetti et al. 2008), the values of the small strain shear modulus G_0, obtained from V_S measured in the same SDMT sounding, gradually increase with depth, without sharp contrasts between different soil layers.

The interpolation of the p_2 values measured by SDMT indicated the presence of two distinct groundwater levels, thus confirming measurements

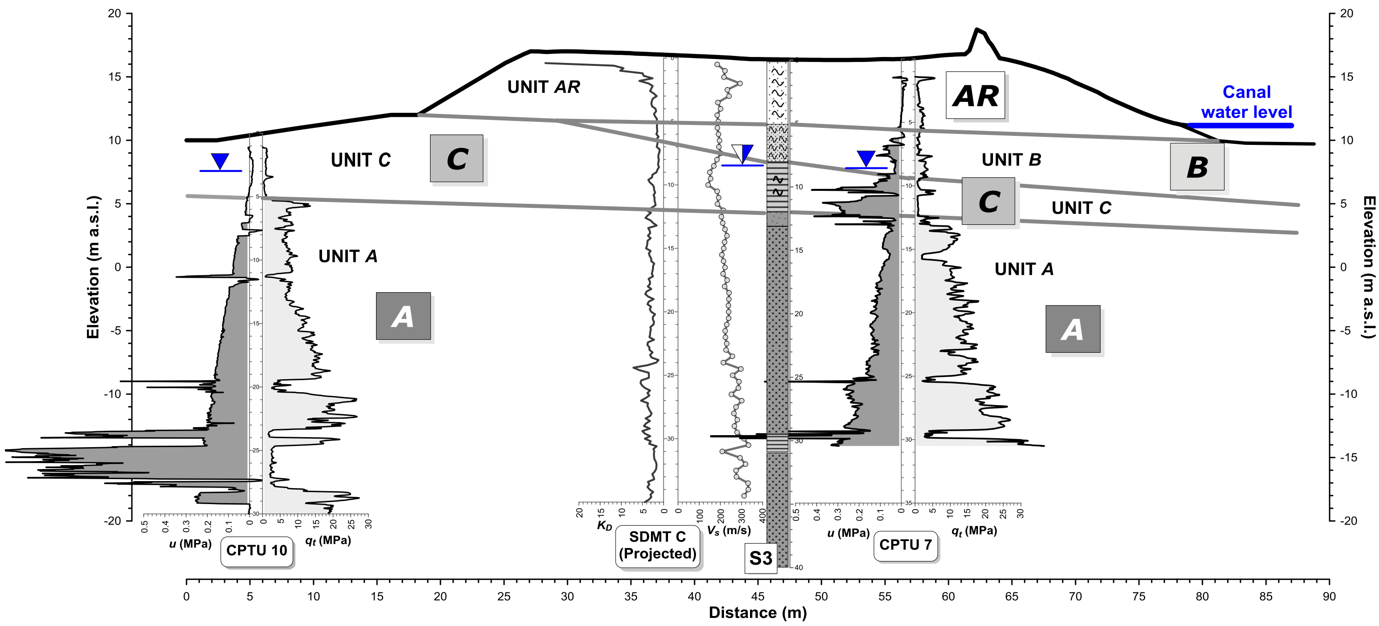

Figure 3. Stratigraphic model along the cross-section c-c', area C (Tonni et al. 2015a), including: borehole log; profiles of the corrected tip resistance q_t and the pore pressure u measured by CPTUs; profiles of the horizontal stress index K_D and the shear wave velocity V_S measured by SDMT.

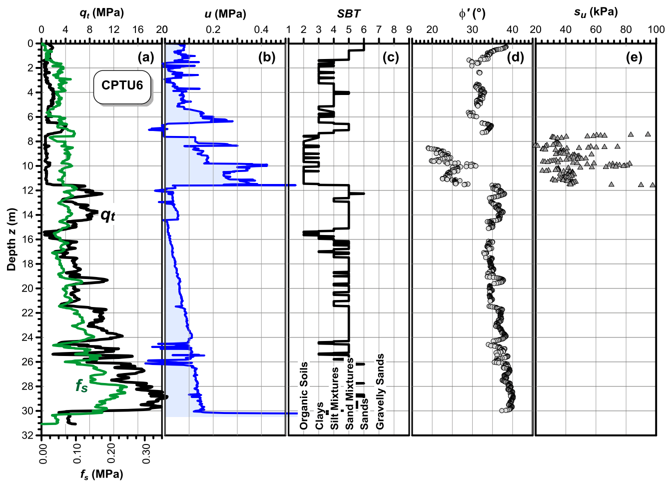

Figure 4. Interpretation of results of CPTU 6 (area C).

in open standpipe piezometers and existing wells: indeed, the upper level is located in the sandy-silty sediments of the embankment core (Unit AR) and the underlying Unit B, generally at 4-5 m depth from the crest, whilst a lower piezometric level, governing pore pressures in the confined sandy layer of Unit A (the so-called "Acquifero Padano") can be identified at about 7-8 m depth from the crest.

3 LIQUEFACTION ANALYSES

3.1 *Procedure and seismic input data*

Liquefaction analyses were carried out in each investigated area, in order to identify possible mechanisms responsible of the deformations and fractures observed on the crest of the embankment after the May 20, 2012 earthquake. The analyses were executed using a simplified dynamic approach, based on the comparison, at any depth, of the seismic demand on a soil layer generated by the earthquake (cyclic stress ratio *CSR*) and the capacity of the soil to resist liquefaction (cyclic resistance ratio *CRR*). When *CSR* is greater than *CRR* liquefaction may occur.

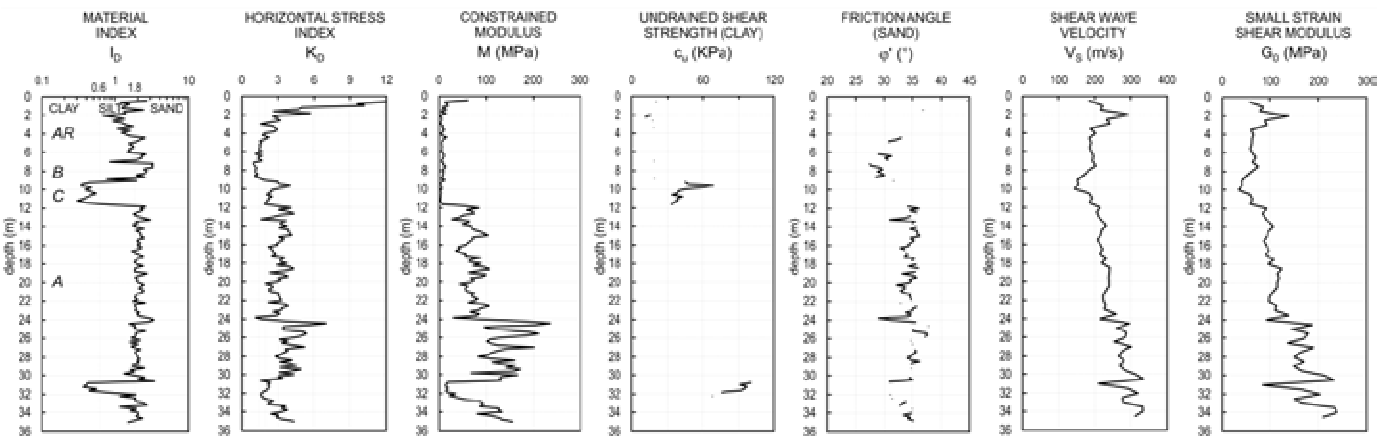

Figure 5. Interpretation of results of SDMT C (area C).

CSR was determined by 1-D ground seismic response analyses carried out using the code EERA (Bardet et al. 2000) in terms of total stresses, without taking into account the excess pore pressure build up typical of the liquefaction phenomenon. Details on the input data and results, obtained as part of the Working Group activity, can be found in Tonni et al. (2015a). The earthquake assumed as possible trigger of liquefaction was the May 20, 2012 main shock, recorded at 04:03 (local time), having local magnitude M_L = 5.9 and epicentral distance R_{epi} = 7.5 km from the Scortichino site. The main shock was followed, in about four minutes, by three aftershocks of M_L = 4.8, 4.8 and 5.0 respectively and by nine shocks having $M_L > 4$ within one hour. Since no ground motion recordings of this event were available in the area of Scortichino, the ground response analyses were carried out using four input accelerograms selected from the Italian earthquake database (ITACA 2011) by use of various search criteria (station on bedrock, moment magnitude M_w = 5.5-6.5, R_{epi} =5-10 km). In addition, a near-fault accelerogram obtained for the April 6, 2009 L'Aquila 2009 earthquake was also considered. All the input accelerograms were scaled to a peak ground acceleration *PGA* = 0.183 *g*, estimated using an attenuation law (Bindi et al. 2011).

At each depth *CSR* was evaluated as:

$$CSR = \frac{\tau_{av}}{\sigma'_{v0}} = \frac{0.65\tau_{\max}}{\sigma'_{v0}} \tag{1}$$

where τ_{max} is the maximum shear stress calculated by ground seismic response analysis (average of τ_{max} calculated using different accelerograms), τ_{av} = 0.65 τ_{max} is the amplitude of the shear stress of the equivalent regular sequence, and σ'_{v0} is the effective overburden stress at the given depth.

CSR was then compared with the cyclic resistance ratio *CRR* estimated by use of various methods based on the SDMT parameters V_S and K_D (Tonni et al. 2015b), on the cone penetration resistance q_t from CPTU and from laboratory cyclic simple shear tests (Tonni et al. 2015a). The liquefaction safety factor FS_{liq} at each depth was calculated as:

$$FS_{liq} = \frac{CRR}{CSR} = \frac{CRR_{M=7.5} \cdot MSF}{CSR} \tag{2}$$

where $CRR_{M=7.5}$ is the cyclic resistance ratio for a reference magnitude M_w = 7.5 (conventionally adopted in the simplified procedure) and *MSF* is a magnitude scaling factor. The analysis was carried out considering M_w = 6.14, equal to the maximum magnitude expected for a return period of 475 years in the seismogenetic zone in which Scortichino is located and similar to the magnitude of the May 20, 2012 main shock.

The "integral" liquefaction susceptibility at each test location was evaluated by means of the liquefaction potential index I_L (Iwasaki et al. 1982):

$$I_L = \int_{z=0}^{z_{crit}=20m} F(z) \cdot w(z)\,dz \tag{3}$$

where *w(z)* is a depth weighting factor and the function *F(z)* depends on the safety factor, according to Sonmez (2003).

3.2 *Evaluation of CRR from K_D (SDMT)*

In the last decades various *CRR*-K_D correlations have been developed, including the most recent shown in Fig. 6, which appear to converge towards a narrow central band. Results of liquefaction analyses based on K_D, with $CRR_{M=7.5}$ estimated according to Monaco et al. (2005), Tsai et al. (2009) and Robertson (2012), were presented by Tonni et al. (2015b).

3.3 *Evaluation of CRR from q_t (CPTU)*

Results of liquefaction analyses based on CPTU, with $CRR_{M=7.5}$ estimated from q_t according to Idriss & Boulanger (2004, 2006), were presented by Tonni et al. (2015a).

3.4 *Evaluation of CRR from the combination of K_D (SDMT) & q_t (CPTU)*

As noted by Marchetti (2016), much of the interest on the *CRR*-K_D correlation derives from the fact that the stress history increases significantly *CRR* and K_D, but only slightly the normalized cone resistance Q_{cn}. Hence it is possible that a correlation K_D-*CRR* will be stricter than Q_{cn}-*CRR*.

The *CRR*-K_D correlation recommended by Marchetti (2016), identified by the label "RIB" in Fig. 6, was defined by combining the Idriss & Boulanger (2004, 2006) *CRR*-Q_{cn} correlation (Eq. 4a):

$$CRR = \exp\left[(Q_{cn}/540) + (Q_{cn}/67)^2 - (Q_{cn}/80)^3 + (Q_{cn}/114)^4 - 3\right] \tag{4a}$$

and the Robertson (2012) average Q_{cn} - K_D interrelationship (Eq. 4b):

$$Q_{cn} = 25\, K_D \tag{4b}$$

A combined correlation for estimating *CRR* based at the same time on Q_{cn} and K_D (Eq. 5), plotted in the chart in Fig. 7 in the form $CRR = f(Q_{cn}, K_D)$, was obtained by Marchetti (2016) adopting as *CRR* the geometric average between a first *CRR* estimate obtained from Q_{cn} (Eq. 4a) and a second *CRR* estimate obtained from K_D (Eqs. 4a and 4b), namely:

$$\text{Average } CRR = [(CRR \text{ from } Q_{cn}) \cdot (CRR \text{ from } K_D)]^{0.5} \tag{5}$$

3.5 *Results and comments*

The results of liquefaction analyses based on different tests at the same location (area C) are compared in Fig. 8. The results provided by different methods

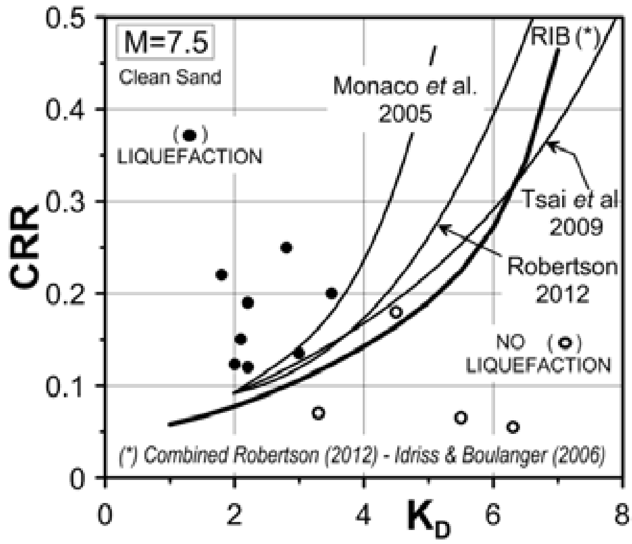

Figure 6. Recent CRR-K_D correlations (Marchetti 2016).

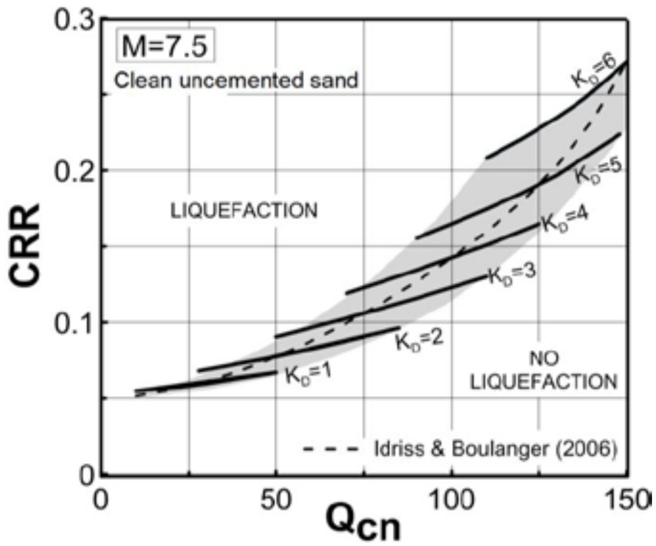

Figure 7. Correlation for estimating CRR based on both Q_{cn} and K_D, for clean uncemented sand (Marchetti 2016).

based on the DMT parameter K_D (Monaco et al. 2005, Tsai et al. 2009, Robertson 2012, Marchetti 2016 "RIB"), denoted by white symbols in Fig. 8, indicate possible occurrence of liquefaction ($FS_{liq} <$ 1) in the silty-sandy soils at the base of the embankment (Unit B), at local depths from the crest between about 5 to 9 m, while no significant liquefaction is detected in the deeper sands (Unit A). The liquefaction potential index I_L estimated from K_D by all methods is "high".

The results of the analyses based on q_t from CPTU (Idriss & Boulanger 2004, 2006), denoted by black symbols in Fig. 8, signal the presence of a liquefiable layer, having much lower thickness than indicated by K_D, within the silty sand of Unit B. Differently from K_D, the analysis based on q_t suggests generalized liquefaction in the deeper sands (Unit A). The liquefaction potential index I_L is "moderate" to "high", i.e. lower than indicated by K_D.

The results obtained by the method proposed by Marchetti (2016), based on both K_D from SDMT and q_t from CPTU (grey symbols in Fig. 8), indicate the presence of a liquefiable layer of lower thickness than indicated by K_D alone within Unit B, in agreement with the analysis based on q_t alone. At the same time, this method tends to exclude significant liquefaction in Unit A, in agreement with the analyses based on K_D alone. The liquefaction potential index I_L is "low", i.e. substantially lower than indicated by methods based on both K_D and q_t alone.

To note that all the CRR correlations based on K_D (Monaco et al. 2005, Tsai et al. 2009, Robertson 2012, Marchetti 2016) are valid for clean sand, without any correction for fines content. Hence the CRR estimated from K_D in the sandy-silty layers (Units AR and B) are probably somewhat underestimated (though the low plasticity of fines in these layers should not involve a substantial increase in CRR), while in the clean sands of Unit A the CRR estimated from K_D are presumably realistic.

In Fig. 8 the results of the analyses based on K_D and q_t – alone and combined – are compared with the results obtained by Tonni et al. (2015b) using the correlations based on V_S by Andrus & Stokoe (2000) and Kayen et al. (2013). The analyses based on V_S generally indicate minor liquefaction ("low" I_L).

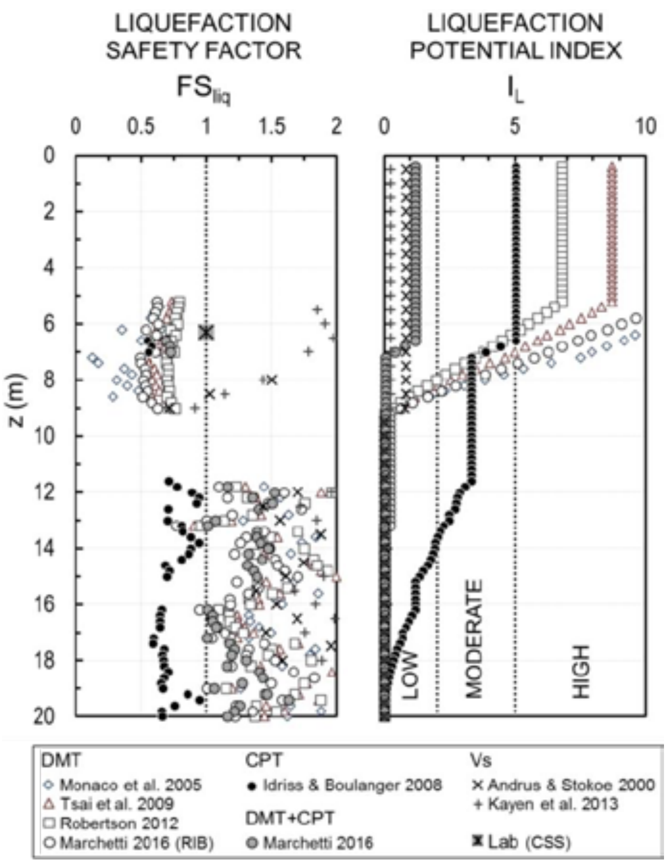

Figure 8. Area C. Results of liquefaction analyses based on the horizontal stress index K_D (SDMT), on the cone penetration resistance q_t (CPTU) and on the combination K_D (SDMT) & q_t (CPTU), compared with results obtained by methods based on the shear wave velocity V_S and by laboratory cyclic simple shear tests (CSS).

Fig. 8 also shows the value of FS_{liq} obtained by a laboratory cyclic simple shear test (CSS) performed on a silty-sandy sample taken in borehole S5 at 6.00-6.60 m depth. This result (FS_{liq} = 1) confirms the possible occurrence of liquefaction in the silty-sandy layer.

4 CONCLUSIONS

The results of liquefaction analyses carried out using simplified methods based on the DMT horizontal stress index K_D, in agreement with well-established methods based on the CPT cone penetration resistance q_t, suggest that plausibly local liquefaction phenomena, of variable extent, may have been induced by the May 20, 2012 earthquake in the sandy-silty soils below the Scortichino canal levee.

In the case illustrated in the paper, the use of a combined correlation for estimating *CRR* based at the same time on CPT-q_t and DMT-K_D (Marchetti 2016) has confirmed the probable occurrence of liquefaction. However the estimated overall liquefaction susceptibility, represented by the liquefaction potential index I_L, is lower than indicated by methods based on both K_D alone and q_t alone. This result is in reasonable agreement with field observations.

As noted by Marchetti (2016), it is expectable that an estimate based at the same time on two measured parameters is more accurate than estimates based on just one parameter, and incorporating the DMT stress history parameter K_D into the liquefaction correlations should possibly reduce the uncertainty in estimating *CRR*. Considerable additional research is obviously necessary, especially if the sand is not clean, uncemented sand.

5 REFERENCES

Andrus, R.D. & Stokoe, K.H., II. 2000. Liquefaction resistance of soils from shear-wave velocity. *J. Geotech. Geoenviron. Eng.*, 126(11): 1015-1025.

Bardet, J.P., Ichii, K. & Lin, C.H. 2000. EERA – A computer program for equivalent-linear earthquake site response analyses of layered soil deposits. Univ. Southern California.

Bindi, D., Pacor, F., Luzi, L., Puglia, R., Massa, M., Ameri, G. & Paolucci, R. 2011. Ground motion prediction equations derived from the Italian strong motion database. *Bull. Earthquake Eng.*, 9(6): 1899-1920.

Idriss, I.M. & Boulanger, R.W. 2004. Semi-empirical procedures for evaluating liquefaction potential during earthquakes. *Proc. 11th Int. Conf. on Soil Dyn. and Earthquake Eng. & 33rd Int. Conf. on Earthquake Geotech. Eng., Univ. of California, Berkeley*, 1: 32-56.

Idriss, I.M. & Boulanger, R.W. 2006. Semi-empirical procedures for evaluating liquefaction potential during earthquakes. *Soil Dyn. and Earthquake Eng.*, 26: 115-130.

ITACA 2011. ITalian ACcelerometric Archive (1972-2013), version 2.0, http://itaca.mi.ingv.it/ItacaNet/

Iwasaki, T., Tokida, K., Tatsuoka, F., Yasuda, S. & Sato, H. 1982. Microzonation for soil liquefaction potential using simplified methods. *Proc. 3rd Int. Conf. on Microzonation, Seattle*, 3: 1319-1330.

Kayen, R., Moss, R.E.S., Thompson, E.M., Seed, R.B., Cetin, K.O., Der Kiureghian, A., Tanaka, Y. & Tokimatsu, K. 2013. Shear-Wave Velocity-Based Probabilistic and Deterministic Assessment of Seismic Soil Liquefaction Potential. *J. Geotech. Geoenviron. Eng.*, 139(3): 407-419.

Kulhawy, F.H. & Mayne, P.W. 1990. Manual on estimating soil properties for foundation design. *Report EPRI EL-6800*, Electrical Power Research Institute, Palo Alto.

Lunne, T., Robertson, P.K. & Powell, J.J.M. 1997. *Cone Penetration Testing in Geotechnical Practice*. Blackie Academic & Professional, New York.

Marchetti, S. 1980. In Situ Tests by Flat Dilatometer. *J. Geotech. Eng. Div.*, 106(GT3): 299-321.

Marchetti, S. 2016. Incorporating the Stress History Parameter K_D of DMT into the Liquefaction Correlations in Clean Uncemented Sands. *J. Geotech. Geoenviron. Eng.*, 142(2): 04015072.

Marchetti, S., Monaco, P., Totani, G. & Calabrese, M. 2001. The Flat Dilatometer Test (DMT) in Soil Investigations – A Report by the ISSMGE Committee TC16. Official version approved by TC16 reprinted in *Flat Dilatometer Testing, Proc. 2nd Int. Conf. on the Flat Dilatometer, Washington D.C.*, 2006, Failmezger R.A. & Anderson J.B. (eds), 7-48.

Marchetti, S., Monaco, P., Totani, G. & Marchetti, D. 2008. In Situ Tests by Seismic Dilatometer (SDMT). *From Research to Practice in Geotechnical Engineering*, *Geotech. Spec. Publ. No. 180*, ASCE, 292-311.

Mayne, P.W. & Campanella, R.G. 2005. Versatile site characterization by seismic piezocone. *Proc. XVI ICSMGE, Osaka*, 2: 721-724.

Monaco, P., Marchetti, S., Totani, G. & Calabrese, M. 2005. Sand liquefiability assessment by Flat Dilatometer Test (DMT). *Proc. XVI ICSMGE, Osaka*, 4: 2693-2697.

Reyna, F. & Chameau, J.L. 1991. Dilatometer Based Liquefaction Potential of Sites in the Imperial Valley. *Proc. 2nd Int. Conf. on Recent Advances in Geotech. Earthquake Eng. and Soil Dyn., St. Louis*, 385-392

Robertson, P.K. 2009. Interpretation of cone penetration tests. A unified approach. *Canadian Geotech. J.*, 46(11): 1337-1355.

Robertson, P.K. 2012. The James K. Mitchell Lecture: Interpretation of in-situ tests – some insights. *Proc. 4th Int. Conf. on Geotechnical and Geophysical Site Characterization, Porto de Galinhas*, 1: 3-24.

Sonmez, H. 2003. Modification of the liquefaction potential index and liquefaction susceptibility mapping for a liquefaction-prone area (Inegol-Turkey). *Environ. Geology*, 44: 862-871.

Tonni, L., Gottardi, G., Amoroso, S., Bardotti, R., Bonzi, L., Chiaradonna, A., d'Onofrio, A., Fioravante, V., Ghinelli, A., Giretti, D., Lanzo, G., Madiai, C., Marchi, M., Martelli, L., Monaco, P., Porcino, D., Razzano, R., Rosselli, S., Severi, P., Silvestri, F., Simeoni, L., Vannucchi, G. & Aversa, S. 2015a. Interpreting the deformation phenomena triggered by the 2012 Emilia seismic sequence on the Canale Diversivo di Burana banks. *Rivista Italiana di Geotecnica,* XLIX(2): 28-58 (in Italian).

Tonni, L., Gottardi, G., Marchi, M., Martelli, L., Monaco, P., Simeoni, L. & Amoroso, S. 2015b. SDMT-based Site Characterization and Liquefaction Analysis of Canal Levees Damaged by the 2012 Emilia (Italy) Seismic Sequence. *Proc. 3rd International Conference on the Flat Dilatometer DMT'15, Rome, Italy*, 341-348.

Tsai, P., Lee, D., Kung, G.T. & Juang, C.H. 2009. Simplified DMT-based methods for evaluating liquefaction resistance of soils. *Engineering Geology*, 103: 13-22.

Geotechnical and Geophysical Site Characterisation 5 – Lehane, Acosta-Martínez & Kelly (Eds)

Estimating the Cyclic Softening of Clays of Five Different Sites at Matsyapuri, Willingdon Island, Kochin, Kerala, India

R.R. Phule, P. Kurangale, R.Alone, V.Gabhale, N.Pawar, K. Birajdar
Department of Civil Engineering, Sardar Patel College of Engineering, Andheri, Mumbai, India

ABSTRACT: This paper discusses the cyclic softening potential evaluation of clayey soils at five borehole locations at the site at Matsyapuri on Willingdon Island, in the city of Kochi, in the state of Kerala, India. The site consists loose to medium dense clayey sand overfills followed by of clayey soils at all five locations having thickness ranging from 5 to 9m. Clay behaves differently under monotonic and cyclic loading. The pore pressures produced during an earthquake reduces the effective stress of the clay thereby reducing the un-drained shear strength similar to unloading. However, after the earthquake, the pore pressure dissipates and the soil strength increases due to consolidation. This phenomenon of temporary strength loss in soft soils dur-ing an earthquake is termed as 'cyclic softening'. This paper provides a brief review of the developing new procedures for evaluating cyclic softening of clayey soils in terms of factor of safety (FoS). Established corre-lations based on in-situ testing such as Standard penetration test (SPT) and laboratory testing are adopted to estimate the undrained shear strength of the clays and to estimate the cyclic resistance ratio. It is observed that the clay deposits at all the five sites are prone to moderate cyclic softening for earthquake magnitude (M_w) of 6.5 and 7.5 at peak ground acceleration (a_{max}) of 0.3g. For practical purposes, these FoS $_{value}$ can be considered by the geotechnical engineers for design purpose.

1 INTRODUCTION

Sand and clay behave differently under earthquake loading. Majority of liquefaction related studies concentrated on relatively clean sands. It was considered that clean sandy soils only liquefy and cohesive soils are resistant to cyclic loading as these soils have high shear strength. However, earthquakes of Haicheng(1975),Tangshan(1976),Northridge(1994), Kocaeli(1999) and Chi-Chi(1999) evolved with a new study of failure of cohesive soils. The studies suggested that clay behaves quite differently. In contrast to liquefaction, cyclic mobility occurs when the static shear stress is less than the shear strength of the liquefied soil (Kramer, 1996).

Based on the cyclic behavior of clays, Boulanger & Idriss (2004) provided the first method to evaluate cyclic failure potential of soils that behave like clays. A new criterion was presented by the authors for fi-ne-grained soils that exhibit clay-like behavior dur-ing the undrained cyclic loading imposed by the earthquakes. The authors proposed plasticity index (PI) greater than 7 for cyclic mobility analysis of clay-like soils.

In this paper, all the five different borehole loca-tions of Matsyapuri site considered for the study, consist of soft clays in the second stratum having PI in the range of 21 to 58% and having SPT blow count (N-value) in the range of 1 to 5. Therefore, it is worthwhile to investigate the cyclic softening potential of these clay deposits in terms of factor of safety (FoS) and identify the nature of threat of cyclic mobility of these clay deposits. The depth of clay layer subjected to moderate to critical cyclic mobility are identified for the five locations for different earthquake magnitudes (M_w) and maximum ground acceleration (a_{max}).

2 STUDY AREA

The study area consists of five boreholes at five different locations in the plot no. 64-65-66 at Matsyapuri in Cochin. The plot is nearly trapezoidal in plan and covers an area of 4.80 acres. A canal, RCC bridge and National Highway 47A runs on the south side of the plot, a tank farm of Ruchi lies to the to the north and east and the west side of the plot is surrounded by vacant land. The depth of boreholes ranges from 20m to 40m. The upper zone fill material comprises of clayey sand with gravel upto 4m and is in loose to medium dense state with field N-value ranging from 10 to 12 whereas in the lower reaches it comprises of cobble and boulder size rock and is well compacted.

Highly cohesive soil is found below the fill at all five borehole locations. The soil material is grey and comprises of high plasticity clay mixed with little sand. This stratum is of very soft to soft consistency having most N-value between zero and 4. Thickness of this very soft cohesive layer ranges from 5.0 to 12.7m. Average thickness of this clay is 6.70 m. A typical soil profile depicting the soft clay layer is shown in Figure 1. In this paper, cyclic mobility analysis is carried out for this clay layer.

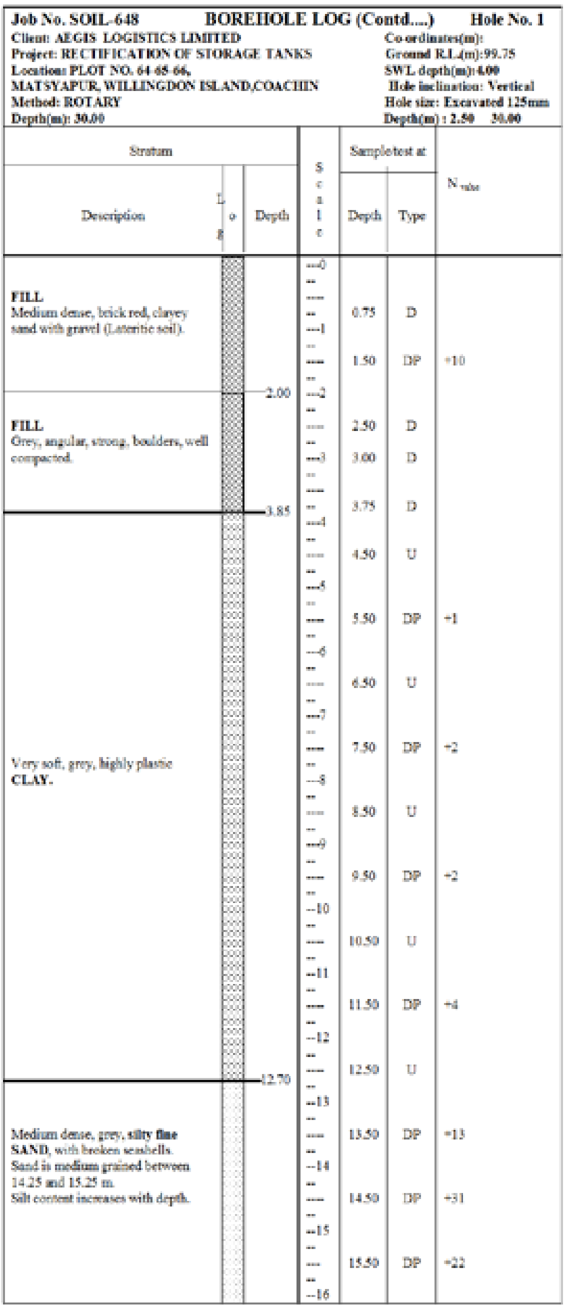

Figure 1. Typical soil profile at the sites of Matsyapuri

Next, a dominantly sandy soil layer is encountered below this clay in all boreholes and is met between 8.25 and 12.70 m. Most of the N-value are between 15 and 30 with few values lower than 10. Next, below this sand layer, cohesive soil lies at all borehole locations between 12.7 and 40m. However, the soils is of stiff to very stiff consistency with N-value vary from 20 to 35.

3 METHODOLOGY

From specified design earthquake this procedure compares the cyclic resistance ratio (CRR), which is defined as the capacity of the soil to resist cyclic mobility, and cyclic stress ratio (CSR), which is defined as the seismic demand on the soil due to earthquake, at a given depth in terms of factor of safety (FoS) as Equation1,

$$\mathrm{FoS}=\frac{\mathrm{CRR}}{\mathrm{CSR}} \tag{1}$$

This procedure is used for the classification of cyclic softening potential of clay deposits at various depths for all the five sites at Matsyapuri. The acceptable values of FoS given by various researchers or codes vary from 1.1 to 1.5. In the present study, therefore an average 1.3 is kept as the margin. The clays having FoS less than 1.3 are considered to be subjected to ground failure due to cyclic softening whereas FoS greater than 1.3 are considered to be safe.

3.1 *Evaluation of cyclic stress ratio (CSR)*

Seed & Idriss (1971) developed a procedure for the estimation of cyclic stress ratio (CSR) which was followed by Idriss & Boulanger (2008) given as Equation 2,

$$\mathrm{CSR}=0.65.\left(\frac{a_{max}}{g}\right).\left(\frac{\sigma_v}{\sigma'_v}\right).r_d \tag{2}$$

a_{max} = peak horizontal ground acceleration generated by the earthquake, g = acceleration of gravity, σ_v = initial vertical total stress, σ'_v = initial vertical effective stress, and r_d = stress reduction factor.

Seed & Idriss (1971) introduced the ratio of cyclic stresses for a flexible soil column to the cyclic stresses for a rigid column which described as stress reduction coefficient (r_d).The average curve represents all earthquake magnitude and all profiles. The r_d versus depth curve defined by Seed & Idriss (1971) and refined by Youd & Idriss (1997) with added mean value lines is shown in Figure 2.

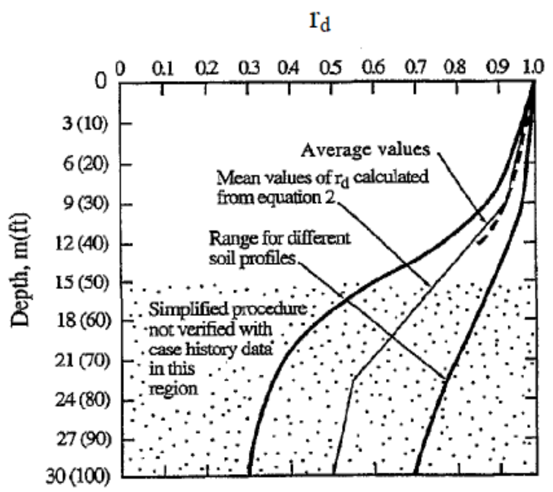

Figure 2. r_d versus depth curve (after Youd & Idriss, 1997)

3.2 *Evaluation of cyclic resistance ratio (CRR)*

CRR depends on the behavior of soils under different cyclic loading. Figure 3 shows the behavior of sandy and clay soil in terms of their cyclic strength at uniform stress cycles.

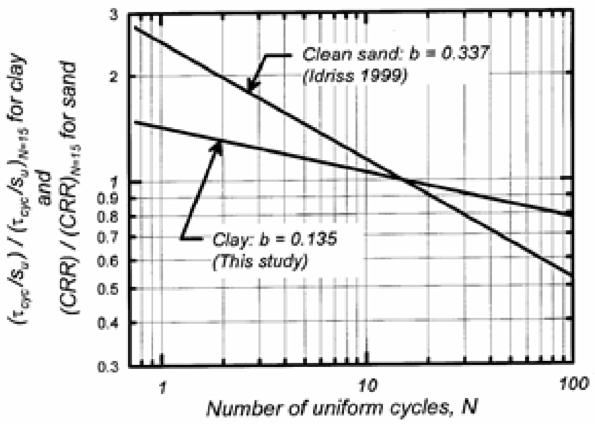

Figure 3. Variation of CRR for clay and sand (after Boulanger & Idriss, 2004)

The clay line observed in Figure 3 shows that the cyclic strength of clay is less sensitive. The cyclic strength of soil can be evaluated through direct laboratory test, S_u – CRR empirical relationship, and through empirical estimate based on stress history profile. The $CRR_{7.5}$ is then given as Equation 3 with a multiplying factor of 0.80 as suggested by Tsai et al. (2014) for OCR of 1 and cyclic shear strain of 0.03%,

$$CRR_{7.5}=0.80.\left(\frac{S_u}{\sigma'_v}\right) \tag{3}$$

where S_u = undrained shear strength.

Though, laboratory results provide high accuracy in the estimation, the CRR can be estimated using S_u estimated from previously established correlations in absence of laboratory results.

Terzaghi & Peck (1967), Sanglerat (1972), Stroud (1974), Hara et al.(1974), Sowers (1979), Nixon (1982), Ajayi & Balogun (1988), Decourt (1990), Sivrikaya & Togrol (2002), Hettiarachchi & Brown (2009), Sirvikaya (2009) proposed correlation for the estimation of S_u. These correlations are based on N-value, moisture content (w), and Atterberg's limit like liquid limit (LL) and PI of the soil deposits obtained from the laboratory.

3.3 *Magnitude Scaling Factor (MSF)*

The MSF has been used to adjust the $CRR_{7.5}$ to a site specific magnitude it provides an approximate representation of the effects of shaking duration of equivalent number stress cycle. In this paper, the MSF is calculated using Equation 4 and 5 based on the MSF relationship developed for clay by Idriss & Boulanger (2007) as shown in Figure 4.

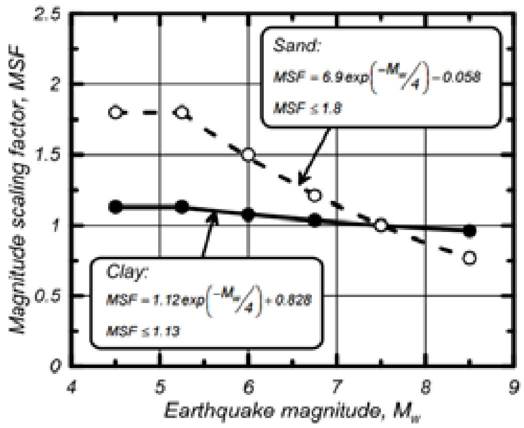

Figure 4. MSF relationships for clay (after Boulanger & Idriss, 2007)

$$MSF=1.12.\exp\left(\frac{-M_w}{4}\right)+0.828 \text{ or} \tag{4}$$

$$MSF \leq 1.13 \tag{5}$$

4 RESULTS AND DISCUSSIONS

In this research, five boreholes from the site at Matsyapuri in Kerala are analyzed. Mainly, soil layers with clay as main constituent were considered for the cyclic mobility analysis. PI of these soil layers was found to be in the range 21 to 35.

The S_u of clays is commonly determined from an unconfined compression test as Equation 6,

$$S_u=\frac{q_u}{2} \tag{6}$$

where q_u = unconfined compressive strength obtained from UCS test.

In this paper, the S_u was estimated by using all the correlation proposed by various researchers and it was found that among all the correlations, the results obtained from the correlation proposed by Sivrikaya (2009) were found to be in good agreement with the

S_u obtained from the unconfined compression test (UCS) obtained from the lab results. The correlation proposed by the author is given in Equation 7,

$$S_u = 3.33.\text{N-value} - 0.75.w + 0.20.\text{LL} + 1.67.\text{PI} \quad (7)$$

The average S_u obtained from the correlation of Sivrikaya (2009) was found to be 12.27 kPa whereas the S_u obtained from the laboratory UCS test was 15.50 kPa.

Thus, the S_u results from the correlation of Sivrikaya (2009) were considered to be most reliable as the correlation was based on the actual soil properties like N-value, *w*, LL, and PI.

Next, the FoS was computed at various depths where the N value was available for the clayey layers for different combinations of M_w of 6.5 and 7.5 with a_{max} of 0.16g and 0.3g as shown in Table 1.

It is observed from the Table 1 that clays of BH1, BH2, BH4 have varying FoS values for different combinations of M_w and a_{max}. The FoS decreases with increase in M_w and a_{max} and vice-versa. It is also observed that FoS varies with depths for each borehole. Clays at higher depths have low FoS values while clays at low depths have higher FoS values. Therefore, the FoS results for the clayey layers were analyzed for each Borehole and are shown in Figure 5-9.

Table 1. Factor of safety estimations against cyclic mobility

BH	Depth	N	Factor of safety (FoS)			
			M_w = 6.5		M_w =7.5	
			a_{max} (g)			
			0.16	0.30	0.16	0.30
BH1	5.5	1	0.609	0.325	0.657	0.350
BH1	7.5	2	0.656	0.350	0.707	0.377
BH1	9.5	2	0.490	0.261	0.528	0.281
BH1	11.5	4	0.800	0.427	0.862	0.460
BH2	4	0	0.088	0.047	0.094	0.050
BH2	6	2	1.001	0.534	1.079	0.576
BH2	8	4	1.309	0.698	1.411	0.752
BH2	9	13	3.592	1.916	3.871	2.064
BH2	10	11	2.664	1.421	2.871	1.531
BH3	3.5	7	7.267	3.876	7.832	4.177
BH3	5.5	1	0.513	0.274	0.553	0.295
BH3	7.5	0	0.050	0.027	0.054	0.029
BH3	9.5	7	1.792	0.956	1.931	1.030
BH4	6	2	0.934	0.498	1.006	0.537
BH3	8	3	0.948	0.506	1.022	0.545
BH5	3.5	2	2.325	1.240	2.505	1.336
BH3	5.5	2	1.173	0.625	1.264	0.674
BH3	7.5	4	1.454	0.775	1.567	0.835

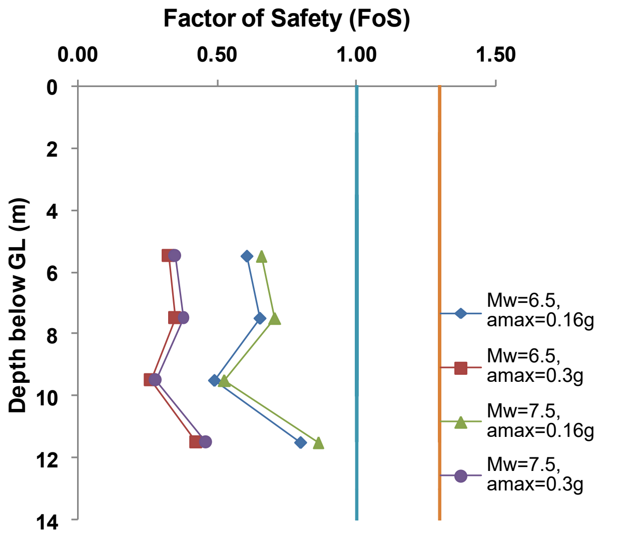

Figure 5. Factor of Safety (FoS) versus depth for borehole1

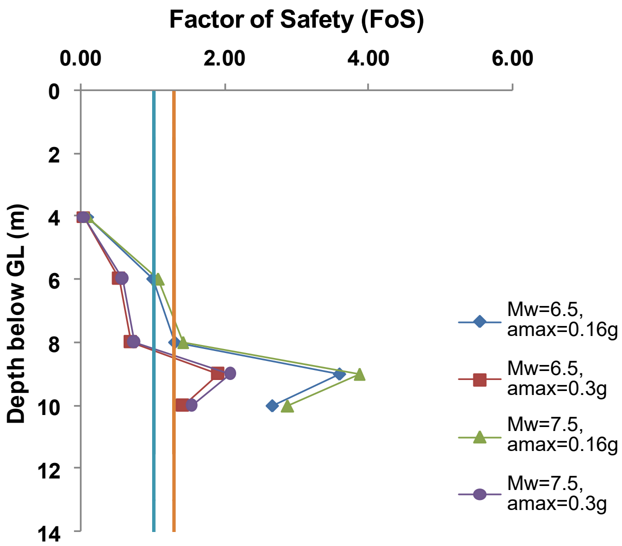

Figure 6. Factor of Safety (FoS) verses depth for borehole 2

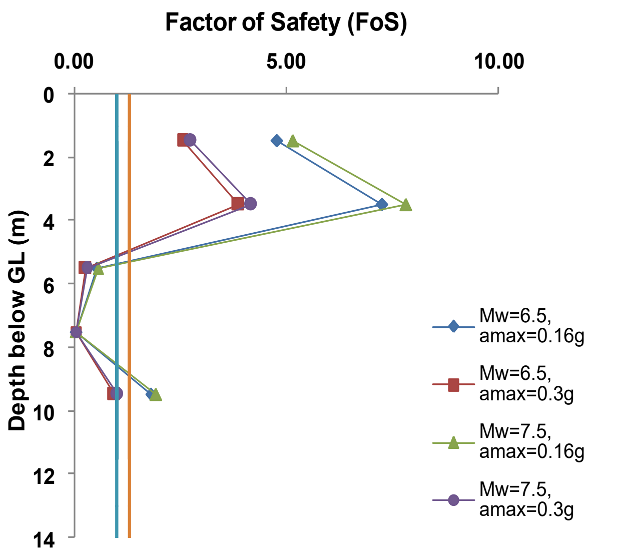

Figure 7. Factor of Safety (FoS) versus depth for borehole 3

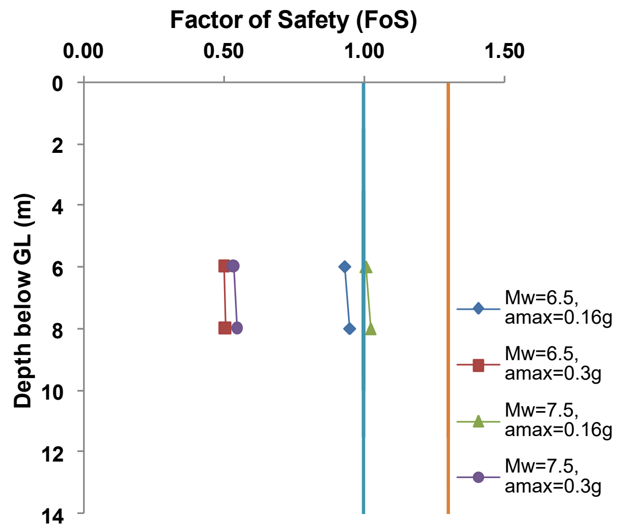

Figure 8. Factor of Safety (FoS) versus depth for borehole 4

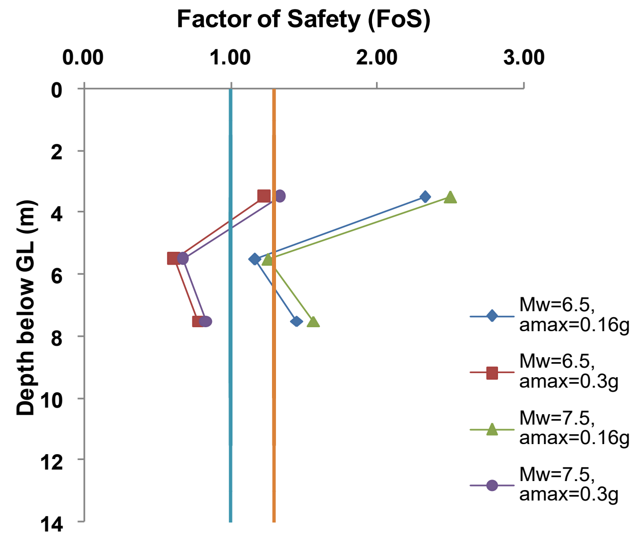

Figure 9. Factor of Safety (FoS) versus depth for borehole 5

From the above Figure 5-9 it is observed that the clay deposits have different FoS at different depths in each borehole. This indicates that the clayey deposits are not truly horizontal. Figure 4 shows that the FoS for clays in BH1 are less than even 1 for all the depths. Figure 5 for BH2 shows that clays at depths 4m to 6m have FoS less than one while clays at depths beyond 6m have FoS higher than 1.3 indicating that the BH2 consist of soft clays upto a depth of 6m and are prone to cyclic mobility. Figure 6 shows that the BH3 consist of dense clays in the upper depths, i.e from 1.5m to 4m, after which it consist of soft clays having FoS less than one. Figure 7 shows the behavior of clay deposits in BH4. The soft clays in BH4 are prone to cyclic softening at depth of 6m to 8m. Figure 8 shows that the clays between 4m to 8m depth have FoS less than 1.3 for all M_w and a_{max} combinations whereas at depth of 4m and 8m, the clays have FoS greater than 1.3 for lower M_w's and less than 1.3 for higher M_w's. Thus, the present study shows the importance and need to carry out site specific estimation of cyclic mobility of clayey soils.

5 CONCLUSIONS

It was observed from the analysis of clay deposits at the site of Matsyapuri that under existing ground water and soil conditions, clays at the depth of 3.75m to 12.5m from ground surface maybe moderately to critically subjected to cyclic mobility during high earthquakes M_w of 6.5 and 7.5. Hence, it would be suggested that the geotechnical engineers, planners should consider the aspect of cyclic mobility of clayey soils, for the construction of any structure at the given site.

6 REFERENCES

Ajayi, L.A. & Balogum, L.A. 1988. Penetration testing in tropical lateritic and residual soils – Nigerian experience, Penetration Testing, ISOPT-1:315-328. Rotterdam: Balkema.

Boulanger, R.W., & Idriss, I.M. 2004. Evaluating the liquefaction or cyclic failure of silts and clays. *Technical Report No.UCD/CGM-04/01*, Center for Geotechnical Modeling, University of California, Davis: California

Decourt, L. 1990. The Standard Penetration Test. State of the Art Report, Norwegian Geotechnical Institute Publication, Part II 179:1-12, Oslo: Norway.

Hara, A., Ohta, T., Niwa, M., Tanaka, S. & Banno, T. 1974. Shear modulus and shear strength of cohesive soils. *Soils and Foundation* 14(3):1-12.

Hettiarachchi, H., & Brown T. 2009. Use of SPT Blow Counts to Estimate Shear Strength Properties of Soils: Energy Balance Approach. *Journal of Geotechnical and Geoenvironmental Engineering* 135(6): 25-32.

Idriss, I.M. & Boulanger, R.W. 2007. SPT- and CPT-based relationships for the residual shear strength of liquefied soils, Earthquake Geotechnical Engineering. In Invited Lectures, K. D. Pitilakis, (ed); *Proc., 4th Intl. Conf. on Earthq. Geotech. Engrg.*, Springer: The Netherlands

Idriss, I.M. & Boulanger, R.W. 2008. Soil Liquefaction during Earthquakes. *MNO-12*, Earthquake Engineering Research Institute, Oakland: CA.

Kramer, S.L. 1996. *Geotechnical Earthquake Engineering*. Upper Saddle River, NJ: Prentice Hall.

Nixon, I.K. 1982. Standard penetration test: state of the art report. *Proceedings of the2nd European Symposium on Penetration Testing*, Amsterdam.

Sanglerat, G. 1972. *The Penetration and Soil Exploration; Interpretation of Penetration Diagrams — Theory and Practice*. Amsterdam: Elsevier Publishing Co.

Seed, H.B. & Idriss, I.M. 1971. Simplified procedure for evaluating soil liquefaction potential. *Journal of Soil Mechanics and Foundation Division* 97:1249–1273.

Sirvikaya, O. 2009. Comparison of artificial neural networks models with correlative works on undrained shear strength. *Eurasian Soil Science* 42(13):1487–1496.

Sivrikaya, O. & Togrol, E. 2002. Relations between SPT-N and qu. *Proceedings of 5th International Congress on Advances in Civil engineering*, Istanbul, Turkey: 943-952 .

Sowers, G.F. 1979. *Introductory Soil Mechanics and Foundations*. New York: Macmillan.

Stroud, M.A. 1974. The standard penetration test in insensitive clays and soft rock. *Proceedings of the 1st European Symposium on Penetration Testing*, Stockholm: Sweden.
Terzaghi, K. & Peck, R.B. 1967. *Soil Mechanics in Engineering Practice.* NewYork: John Wiley.
Tsaia C.C., Mejia l. H. & Meymand M. P. 2014. A strain-based procedure to estimate strength softening in saturated clays during earthquake. *Soil Dynamics and Earthquake Engineering* 66: 191-198.
Youd, T. L. & Idriss, I. M. 1997. *Proc., NCEER Workshop on Evaluation of Liquefaction Resistance of Soils*, Nat. Ctr. for Earthquake Engrg. Res., State Univ. of New York: Buffalo.

Geotechnical and Geophysical Site Characterisation 5 – Lehane, Acosta-Martínez & Kelly (Eds)

Field measurements of the variability in shear strain and pore pressure generation in Christchurch soils

J.N. Roberts, K.H. Stokoe, S. Hwang, B.R. Cox, Y. Wang, & F.M. Menq
The University of Texas at Austin, Austin, Texas, U.S.A.

S. van Ballegooy
Tonkin & Taylor Ltd, Auckland, New Zealand

ABSTRACT: A significant problem continually facing geotechnical engineers is predicting the likelihood of pore-water pressure generation leading to liquefaction triggering of soils in future earthquakes. These soils include granular soils ranging from gravels to sands to silts in saturated and nearly-saturated conditions. The problem for geotechnical engineers is that their predictions are normally based on simplified empirical correlations. A direct, in-situ test method has been developed to: (1) investigate the shear strain at which pore pressure generation begins, (2) investigate the combined effects of shear strain amplitude and number of loading cycles on pore pressure generation, and (3) estimate the point at which liquefaction "triggering" occurs. The field test involves staged, controlled shaking at the ground surface with a large vibroseis and monitoring ground motions and pore pressures over a range in depths with an embedded array of push-in sensors. In this paper, results from testing several soil types that were subjected to the 2010-2011 Canterbury Earthquake Sequence are presented. Responses to the controlled shaking vary from significant positive pore pressure generation (contraction) to negative pore pressure generation (dilation). The impacts of soil type, soil density, and saturation level on these responses are discussed and the complex field behavior is shown.

1 INTRODUCTION

The 2010-2011 Canterbury Earthquake Sequence (CES) caused repeated, widespread liquefaction of the natural soil in and around Christchurch, New Zealand. The resulting soil liquefaction was responsible for an estimated one-third of the damage to the city and its infrastructure, which is costing insurers upwards of $40 billion NZD in the effort to rebuild the city.

In an attempt to mitigate the risk of liquefaction triggering in future earthquakes, large-scale testing of various shallow ground improvement methods for residential structures and low-rise buildings was undertaken by Tonkin & Taylor Ltd on behalf of the New Zealand Earthquake Commission (EQC). Within the framework of this ground-improvement project, researchers from The University of Texas at Austin (UT) performed: (1) pre-shaking characterization of each test location with small-strain, crosshole seismic tests and (2) large-scale, staged shaking tests of the natural and ground-improved soils to study liquefaction triggering. The staged, shaking tests were performed with a large vibroseis named T-Rex as shown in Figure 1a. The objective of the shaking tests was to simulate a wide range of earthquake-loading conditions in situ while monitoring the resulting ground motions and generation of excess pore-water pressures at depth with an embedded array of push-in sensors.

The testing technique and the effectiveness of ground improvements to inhibit liquefaction triggering have been discussed in past publications (Stokoe et al, 2014, and van Ballegooy et al, 2015). The focus of this paper is on the variability in pore pressure responses measured in natural soils at Site 6, one of three test sites that were selected in the Christchurch suburbs for the liquefaction-triggering study. The observed variability at Site 6 is attributed to differences in: (1) soil type, (2) soil density, and (3) degree of saturation as discussed below.

2 OVERVIEW OF TESTING TECHNIQUES

2.1 *Small-strain crosshole testing*

Small-strain seismic testing using the crosshole method was performed to initially characterize the states of the natural soil and ground improvements prior to large-scale shake testing with T-Rex. The constrained compression wave velocity, V_P, and shear wave velocity, V_S, were measured at 20-cm depth intervals from depths of 0.6 to 5.0 m. The velocity profiles as a function of depth provided an

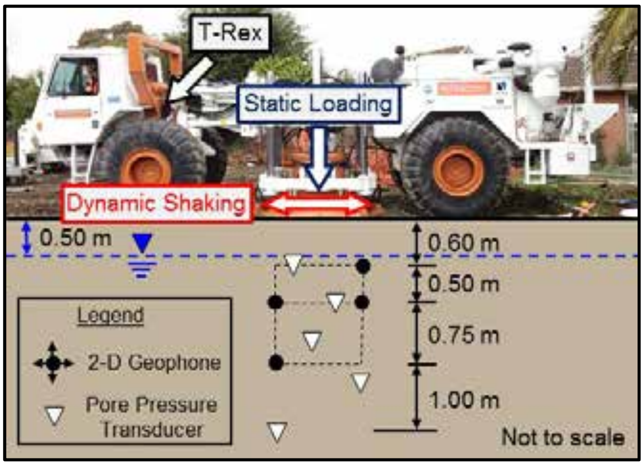

(a) Cross-sectional perspective of T-Rex and embedded array of sensors during shaking

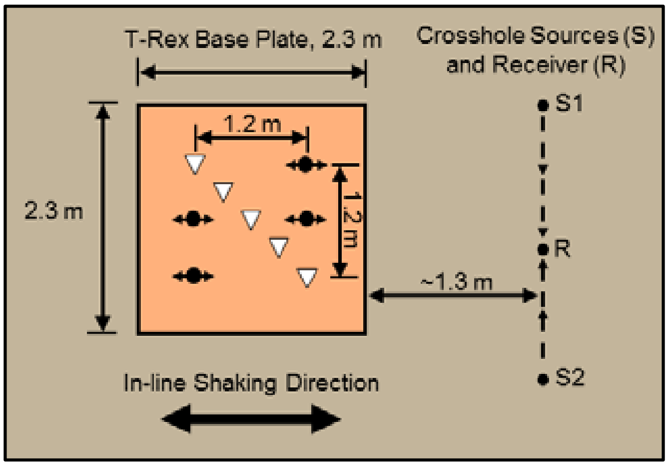

(b) Plan view of the T-Rex baseplate, embedded array of sensors, and approximate location of crosshole seismic testing

Figure 1. Cross-sectional and plan views of in-situ shaking tests with T-Rex at Site 6

initial characterization of the zone of interest. The crosshole testing was performed by pushing two source rods on either end of a linear array and a receiver rod with a bottom 3-D geophone in the middle of the array. The horizontal distance between the source rods (denoted as S1 and S2 in Figure 1b) varied somewhat but was about 2.5 m. Also, one of the two travel paths included the ground-improved zone when present. More information on this testing can be found in Stokoe et al, 2014.

The V_P measurements were used to locate the depth below the ground surface at which 100 % saturation existed. At Site 6, the ground water table was approximately 0.5 m below the ground surface. The depth to 100 % saturation varied around the site but was approximately 1.5 m for the two natural-soil sites. Complete saturation was easily identified by a high-frequency, wave arrival in the time record and a corresponding V_P ranging from about 1,450 to 1,700 m/s.

Measurement of V_S was used to evaluate the shear stiffness of the soil skeleton. The small-strain shear modulus, G_{max}, was calculated from the mass density, ρ, and V_S ($G_{max} = \rho V_S^2$). Where noted, the measured V_S was also stress-corrected to account for the increased confining pressure during shake testing that results from the distribution of the weight of T-Rex (26.7 kN (60,000 lbs)) through the baseplate.

2.2 *In-situ shake testing with T-Rex*

The coupled behavior of shear strain and generation of excess pore water pressure over a large range of strains was evaluated by controlled, horizontal shaking at the ground surface with T-Rex and monitoring the soil response at shallow depths with an embedded array of ground motion and pore pressure sensors (see Figure 1a). Besides shaking, T-Rex was also used to install all embedded sensors using the pushing mechanism at the rear of the machine. Four, 2-dimensional velocity transducers (2-D geophones) and five, pore-water pressure transducers (PPTs) were installed within the plan dimensions of the baseplate of T-Rex at depths ranging from 0.60 to 2.90 m. The location of T-Rex and the embedded sensors during shaking are shown in cross-section in Figure 1a and in plan view in Figure 1b. The relative location of the pre-shaking, crosshole testing array is also shown in Figure 1b.

2.3 *Resonant column testing of reconstituted sand specimens*

Torsional resonant column (RC) testing was performed at UT on reconstituted fine-sand specimens from one depth (1.2 m) at the first, natural-soil test panel (6-NS-1) and two depths (2.0 and 3.0 m) at the second, natural-soil test panel (6-NS-2). The RC testing was used to investigate the dynamic properties of the sand over a shear strain range of 0.00002 to 0.1 %. The RC test had a fixed-free configuration with the top of the specimen free. The top of the specimen was excited with torsional motion and a dynamic response curve was determined from which V_S, shear modulus, G, and shear strain, γ, were determined. More information on the RC testing for this project can be found in Wang (2015).

3 SUBSURFACE CONDITIONS AT THREE TEST PANELS

The dynamic performance evaluated at three test panels at Site 6 are presented below. Two natural soil test panels (6-NS-1 and 6-NS-2) and one test panel improved by the Rapid Impact Compaction method (6-RIC-1) are discussed. The 6-RIC-1 test panel is included because it provides insight into the behavior of naturally-occurring Christchurch sands in a denser state. The RIC ground improvement method is illustrated in Figure 2.

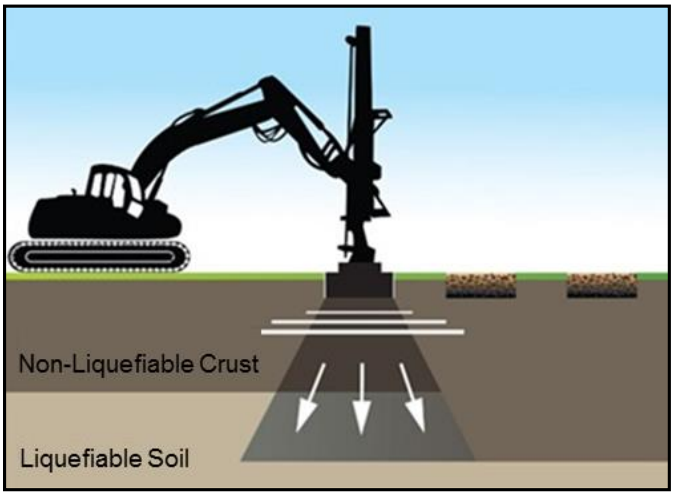

Figure 2. Rapid Impact Compaction (RIC) method used to densify natural silty sand at Site 6

A detailed soil profile at each test panel was determined after shake testing by dewatering the test panel, trenching along the centerline to a depth generally less than 3.5 m, logging and photographing the trench wall, and recovering disturbed samples for laboratory testing. The soil profile varied somewhat from panel to panel but can generally be described by a simplified, four-layer profile as:

Layer 1 – fine to medium sand with some silt and organics (thickness ~0.7 m),
Layer 2 – silt with trace organics; non-plastic, stiff (thickness ~0.45 m),
Layer 3 – sandy silt; non-plastic, stiff (thickness ~0.35 m), and
Layer 4 – silty fine sand, loose to medium dense; reducing silt component with depth (extending beyond 5 m based on borings).

4 RESULTS FROM CONTROLLED SHAKING OF THREE TEST PANELS WITH T-REX

The cyclic loading applied during shake testing at each test panel was: (1) staged, horizontal loading applied at the ground surface, (2) sinusoidal loading applied at 10 Hz for 100 cycles (N), and (3) loading performed in five distinct stages that nominally ranged from the lowest level ($\pm$ 13 kN) to the highest level ($\pm$ 107 or 133 kN).

4.1 *Excess pore pressure ratio and shear strain*

The pore pressure measured by the five PPTs is expressed in terms of an excess pore pressure ratio, r_u. This ratio is defined as the excess pore pressure, Δu, divided by the initial vertical effective stress, σ_v'. The value of σ_v' includes a component from the hold-down force applied by T-Rex. In this study, liquefaction triggering is predicted to occur by extrapolating the r_u-logγ curve to 100 %.

The four, 2-D geophones were used to measure particle velocities in the soil at various depths during cyclic loading. By integrating the velocity-time records with respect to time, displacement-time records were determined which were, in turn, used to evaluate shear strain at any location within the instrumented array using the 4-node, displacement-based, shear-strain calculation method presented by Cox et al, 2009. Example r_u-time and γ-time records for the largest level of shaking at one natural-soil test panel (6-NS-1) from depths 0.60 and 2.10 m are presented in Figures 3 and 4, respectively.

The r_u-time records from two depths show some of the natural variability in the coupled r_u-γ response of the soil. At 0.60 m, the shear strain is large (0.6 %), the soil is unsaturated (Sr < 99 %) even though it is below the water table, and r_u only increases to about 27 % after 100 cycles. However, r_u continues to increase after the end of shaking, indicating that there are areas of higher pore pressures in the vicinity that are dissipating in the direction of this shallow PPT (Figure 3a). In contrast, at 2.10 m, the shear strain is significant but smaller (0.14 %), the soil is saturated (Sr = 100 %), and r_u increases to about the same level after 100 cycles as at 0.6 m. However, r_u begins rapidly dissipating at the end of shaking (Figure 4a). Besides the complexity in pore pressure at 0.6 m, the difference in dissipation rate is related to the permeability of the soil, which is reflected in soil type. The fines content of the soil at 0.60 m ranges from 80 to 96 % while the soil at 2.10 m has a fines content ranging from 1 to 5 % based on laboratory testing. In comparison to lower-permeability silty soil, the rapid dissipation of r_u seen in Figure 4a is expected at that depth for a sand with few fines.

4.2 *Cyclic stress ratio (CSR) at a given number of cycles of loading (N)*

The cyclic stress ratio presented herein is the CSR at a given number of cycles, N, and is defined as the cyclic shear stress, τ, divided by the vertical effective stress, σ_v', at N. The vertical total stress is calculated using unit weights of 17 kN/m^3 and 19.5 kN/m^3 for soils above and below the water table, respectively. These unit weights are estimated from partially- and fully-saturated unit weights of the reconstituted laboratory specimens from the 6-NS-1 and 6-NS-2 test panels with similar laboratory and field V_S values. The vertical total stress, σ_v, also includes a component from the hold-down force applied by T-Rex, which is calculated using Poulos & Davis (1974) stress distribution equations for a square surface footing (i.e. the 2.3- by 2.3-m baseplate of T-Rex). At low levels of shaking when no excess pore-water pressure is generated, σ_v' is simply σ_v minus the static pore pressure. At larger levels of shaking when excess pore pressure is generated, the vertical effective stress

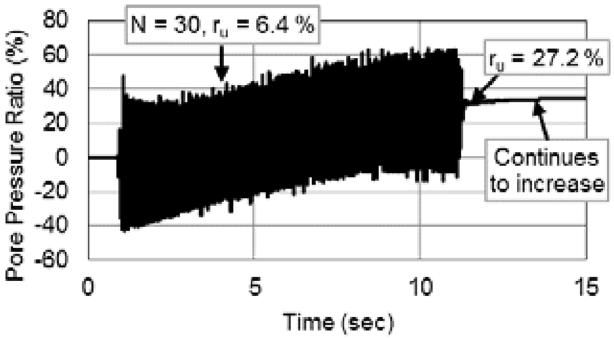

(a) Variation of excess pore pressure ratio (r_u) with time of shaking

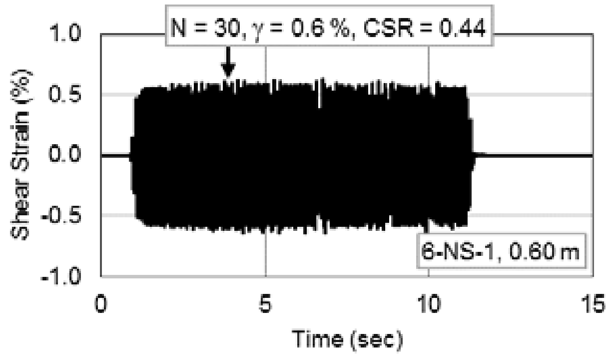

(b) Variation of shear strain (γ) with time of shaking

Figure 3. Variations in r_u and γ with time of shaking at a depth of 0.6 m at the natural soil test panel, 6-NS-1; frequency = 10 Hz; values of r_u, γ, and CSR at N = 30 cycles are identified.

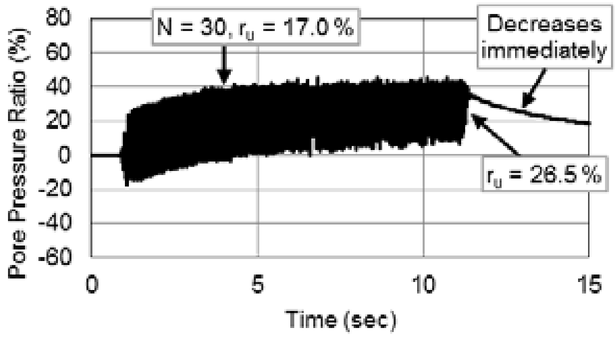

(a) Variation of excess pore pressure ratio (r_u) with time of shaking

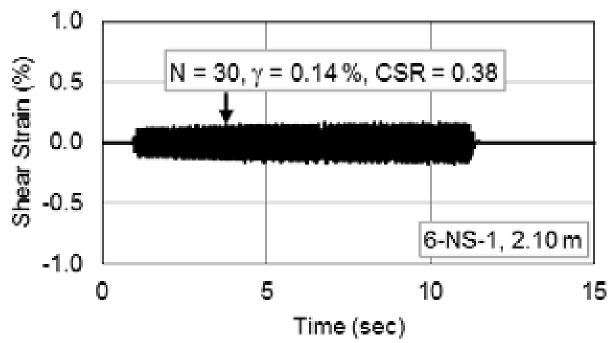

(b) Variation of shear strain (γ) with time of shaking

Figure 4. Variations in r_u and γ with time of shaking at a depth of 2.1 m at the natural soil test panel, 6-NS-1; frequency = 10 Hz; values of r_u, γ, and CSR at N = 30 cycles are identified.

is adjusted according to the excess pore pressure measured by the PPTs.

The CSR at a given N (CSR_N) is determined from the cyclic shear strain at N (γ_N calculated from shake testing), the initial shear modulus at the start of shaking (G_{max} calculated from crosshole testing and adjusted for the static load of T-Rex), the value of G_{max} adjusted for the change in σ_v' due to the generation of r_u at N (denoted as $G_{max,ru}$), and the normalized shear modulus reduction curve, G/G_{max}-logγ, determined from RC testing at the initial σ_v' that is now adjusted for σ_v' at N by using $G_{max,ru}$. By multiplying $G_{max,ru}$ times the original G/G_{max}-logγ curve, a G-logγ curve adjusted for the increased pore pressure (r_u) is constructed. The value of G at the increased pore pressure and γ_N is calculated (denoted as $G_{\gamma N,ru}$). This calculation can be expressed as:

$$CSR_N = \frac{\tau}{(\sigma_v')_N} = \frac{\gamma_N \times G_{max,ru} \times (G/G_{max})_{\gamma N}}{(\sigma_v')_N} \quad (1)$$

in which the right-hand side simply equals $\gamma_N \times G_{\gamma N,ru} / (\sigma_v')_N$. The equation for the shear modulus reduction curve from RC testing utilizes the modified hyperbolic equation as defined by:

$$\frac{G}{G_{max}} = \frac{1}{1+\left(\frac{\gamma}{\gamma_r}\right)^a} = \frac{1}{1+\left(\frac{\gamma}{0.038\ \%}\right)^{0.80}} \quad (2)$$

where "a" is the curvature coefficient and γ_r equals γ at G/G_{max} = 0.5. The values of "a" and γ_r in Equation 3 were determined with SP sand from natural soil test panel 6-NS-2 at a confining pressure of about 0.25 atmospheres (Wang, 2015). Work on determining CSR at increasing strain levels during generation of r_u is continuing.

4.3 *General trends in the r_u-logγ relationship*

4.3.1 *Variation in r_u-logγ with N, V_S, and density*

The behavior that leads to liquefaction triggering is best understood in terms of the r_u-logγ relationship at a selected number of loading cycles (N). The variation in pore pressure generation measured during shake testing can often be explained by one or more of the following: 1) degree of saturation, 2) relative density, and 3) soil type. To remove one source of variability, all soils selected for additional comparisons hereafter are 100 % saturated, with V_P > 1,450 m/s. In Table 1, the locations, characteristics, stress-corrected V_S (V_S*) for the load of T-Rex, and Unified Soil Classification System (USCS) symbol of each soil "layer" are listed.

In Figures 5 and 6, the results corresponding to the deepest PPT at the 6-NS-1, 6-NS-2, and 6-RIC-1 test panels are shown for 10 and 30 cycles, respectively. The soil at these locations have been identified as

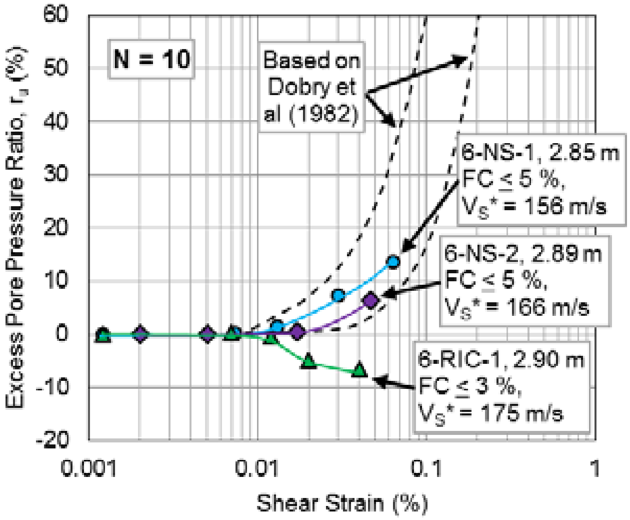

Figure 5. Variation in r_u with γ and V_S ("density") at N = 10 cycles for SP material

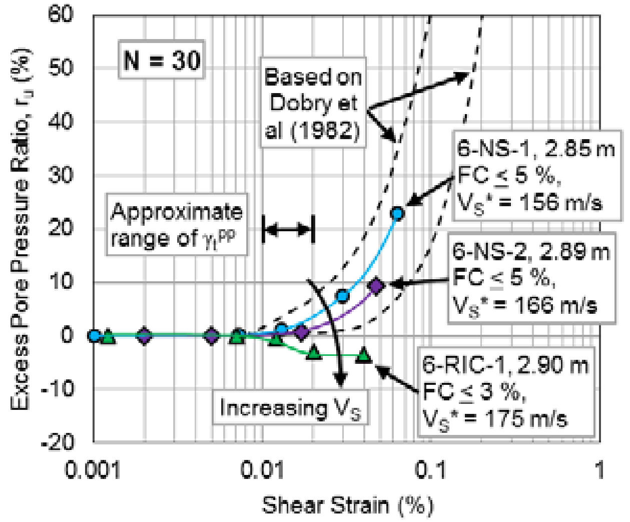

Figure 6. Variation in r_u with γ and V_S ("density") at N = 30 cycles for SP material

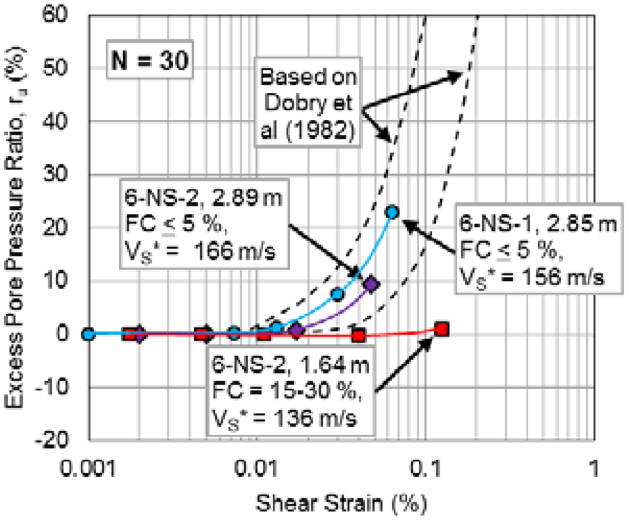

Figure 7. Effect of fines content on r_u-logγ relationships

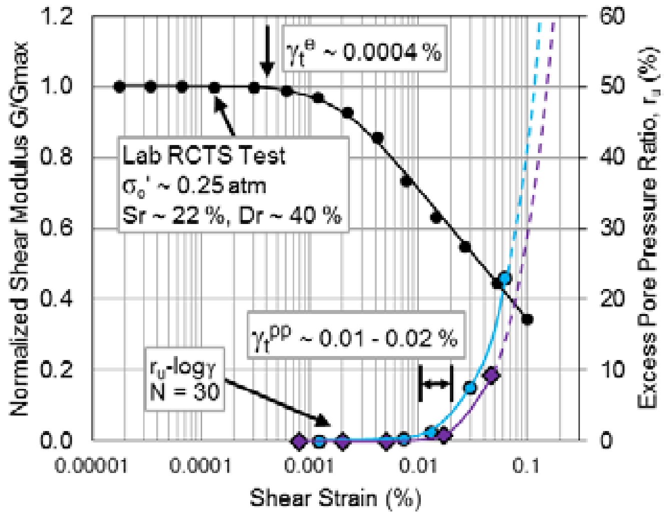

Figure 8. Comparison between the G/G_{max}-logγ curve from RC testing and the r_u-logγ relationships at test panels 6-NS-1 and 6-NS-2

poorly graded sands with less than 5 % fines content. The results for the loose, liquefiable sands from the two natural soil test panels fall within the dashed zone that designates the r_u-logγ behavior of liquefiable soils based on laboratory results analyzed by Dobry et al (1982). The denser natural soil at the 6-RIC-1 test panel, however, generates negative excess pore pressures and clearly falls outside the zone for liquefiable soils.

The number of cycles selected for this analysis has little effect on the conclusions drawn from the results. Despite the increase in pore pressure observed from 10 to 30 cycles at the two natural soil test panels, the r_u-logγ relationships still fall well within the zone for liquefiable soils. At the 6-RIC-1 test panel, the excess pore pressure is slightly less negative after 30 cycles than at 10 cycles but it is still well outside the dashed zone; hence, no liquefaction. Investigation of the effect of N is ongoing and the remainder of the discussion focuses on other effects at N = 30 cycles.

Table 1. Locations and characteristics of saturated soils compared in Figures 5 though 8

Test Panel	Depth	FC min.	FC max.	σ_v'*	V_P	V_S	V_S*	USCS
	m	%	%	(kPa)	m/s	m/s	m/s	
6-NS-1	2.85	1	5	27.0	1,728	146	156	SP
6-NS-2	1.64	15	30	27.0	1,473	113	136	SM
6-NS-2	2.89	1	5	27.2	1,676	155	166	SP
6-RIC-1	2.90	1	3	27.2	1,607	164	175	SP

*Stress-corrected for the weight of T-Rex during shake testing

It is seen in Figure 6 that, as V_S increases, the tendency to generate positive values of r_u decreases. In this case, V_S is simply a surrogate for density or relative density. Based on the RC testing of Wang (2015), the V_S values indicate relative densities are estimated to be on the order of 40, 55, and 80 % for the 6-NS-1, 6-NS-2, and 6-RIC-1 test panels, respectively, in the depth range of 2.85 to 2.90 m. Furthermore, the threshold strain at which r_u begins to be generated, γ_t^{pp}, is in the range of 0.01 to 0.02 %, with γ_t^{pp} increasing as V_S increases. However, investigation of γ_t^{pp} is readily performed in these measurements in-situ and is continuing.

4.3.2 *Variation in r_u-logγ with fines content*

The effect of soil type expressed in terms of fines content is observed in Figure 7 where the results of a silty sand with fines content ranging from 15 to 30 % from a depth 1.64 m at 6-NS- 2 is compared with the results of the clean sands from depths of 2.85 m at 6-NS-1 and 2.89 m at 6-NS-2. Despite being fully saturated and having a lower stiffness than the clean sands as indicated by the V_S (136 m/s versus 156 and 166 m/s, respectively), the silty sand generates very little excess pore pressure (r_u = 1.1 %) even at a relatively high level of shear strain ($\gamma \sim 0.12$ %).

4.3.3 *Normalized shear modulus reduction curve and threshold strains*

The elastic threshold strain, γ_t^e, the nonlinearity in the G/G_{max}-logγ relationship and the threshold strain at which excess pore pressure generation begins, γ_t^{pp}, can be compared in these liquefiable sands (SP) be combining the results of shake testing and RC testing. The normalized shear modulus reduction curve from RC testing is shown in Figure 8 for a reconstituted specimen taken from 6-NS-2 at a depth of 2.0 m. The specimen has a fines content of 2 % and a $D_r \sim 40$ %. The value of γ_t^e marks the boundary between the linear and nonlinear-elastic shear strain ranges. The r_u-logγ relationships in Figure 8 come from the shake testing results from depths 2.85 and 2.90 m at test panels 6-NS-1 and 6-NS-2, respectively. These sands have a fines content ranging from 1 to 5 %. The range in the values of γ_t^{pp} delineates the boundary between the nonlinear-inelastic strain range and the strain range where volume change begins.

The pore pressure threshold strains in the range of 0.01 to 0.02 % in Figure 8 match well with values reported in the literature for liquefiable sands from both laboratory and field testing (e.g. Dobry et al, 1982, Cox et al, 2009, Roberts, 2014). The range in values of γ_t^{pp} corresponds to strains at which values of G/Gmax are in the range of 0.7 to 0.6 for this sand, indicating that the soil has already lost 30 to 40 % of its initial stiffness before volume change, hence r_u, begins to occur.

5 CONCLUSIONS

Staged, controlled shaking with T-Rex of three, instrumented test panels of natural soils was performed to investigate in-situ the r_u-logγ relationships leading to possible liquefaction. The primary conclusions from this study are as follows.

1. Significant variability in the r_u-logγ relationships was measured due to degree of saturation, density (reflected in the V_S values), and fines content (SP versus SM soils).
2. Loose, clean sand with FC ≤ 5 % (SP and D_r ~40 to 55 %) generated a positive r_u-logγ relationship that would predict liquefaction.
3. The threshold strain at which pore pressure generation began, γ_t^{pp}, for the loose, clean sands was in the range of 0.01 to 0.02 %.
4. Denser, clean sand with FC ≤ 5 % (SP and D_r ~ 80 %) generated a negaitve r_u-logγ relationship that would predict no liquefaction.
5. Loose, silty sand with FC = 15 – 30 % (SM) generated little to no r_u at $\gamma \leq 0.12$ %.
6. The range of γ_t^{pp} of the loose, clean sands was about 25 to 50 times the γ_t^e of the G/G_{max}-logγ relationship and was in the nonlinear range where G/G_{max} was in the range of 0.7 to 0.6.

6 ACKNOWLEDGEMENTS

Financial support for this study was provided through the National Science Foundation under grants from the: RAPID Program (CMMI-0343524), NEES Program (CMMI-0927178), and Graduate Fellowship Program (DGE-1110007). Other financial support was received from the New Zealand Earthquake Commission (EQC). This support is gratefully acknowledged.

7 REFERENCES

Cox, B.R., Stokoe, K.H., and Rathje, E.M. 2009. An In Situ Test Method for Evaluating the Coupled Pore Pressure Generation and Nonlinear Shear Modulus Behavior of Liquefiable Soils. *ASTM Geotech. Testing J.*, Vol. 32(1).

Dobry, R., Ladd, R.S., Yokel, F.Y., Chung, R.M., and Powell, D. 1982. *Prediction of Pore Water Pressure Buildup and Liquefaction of Sands during Earthquakes by the Cyclic Strain Method*. Washington, D.C.: National Bureau of Standards.

Poulos, H.G., and Davis, E.H. 1974. *Elastic Solutions for Soil and Rock Mechanics*. Univ. of Sydney.

Roberts, J.N. 2014. *Direct In-Situ Evaluation of Liquefaction Suscept*. M.S. thesis. UT Austin.

Stokoe, K., Roberts, J., Hwang, S., Cox, B., Menq, F., & van Ballegooy, S. 2014. Effectiveness of Inhibiting Liquef. Triggering by Shallow Ground Imprvmnt Methods: Initial Field Shaking Trials with T-Rex. In Orense, Towhata, & Chouw (Eds.), *Soil Liquefaction During Recent Large-Scale Earthquakes* (pp. 193-202). London: Taylor & Francis Group.

van Ballegooy, S., Roberts, J.N., Stokoe, K.H., Cox, B.R., Wentz, F.J., Hwang, S. 2015. Large-Scale Testing of Shallow Ground Improvements using Controlled Staged-Loading with T-Rex. *Proc. 6th Inter. Conf. on Earthquake Geotech Engrg, November.* Christchurch, New Zealand.

Wang, Y. 2015. *Dynamic Properties of Fine Liquefiable Sand and Calcareous Sand from Resonant Col. Testing*. M.S. thesis. UT Austin.

Geotechnical and Geophysical Site Characterisation 5 – Lehane, Acosta-Martínez & Kelly (Eds)

Liquefaction assessment CPTu tests in a site in South of Portugal

C. Rodrigues
Polytechnic Institute of Guarda, Portugal; crod@ipg.pt

S. Amoroso
Istituto Nazionale di Geofisica e Vulcanologia, L'Aquila, Italy; sara.amoroso@ingv.it

N. Cruz
Direção de Coordenação Técnica Rodoviária da Mota-Engil – Engenharia e Construção, S.A. Portugal; nunocruz@mota-engil

A. Viana da Fonseca
CONSTRUCT-GEO, Faculty of Engineering (FEUP), University of Porto, Portugal; viana@fe.up.pt

ABSTRACT: The Algarve is a province in the South of Portugal located near the E-W Eurasia-Africa plate boundary and is characterized by a moderate seismicity, with some significant historical earthquakes causing important damage and economical losses. Besides the effects of large plate boundary events the region also suffers the impact of local onshore moderate-sized earthquake sources. The seismic hazard evaluation and mitigation of the area is therefore very important for the local populations and the large number of tourists that visit the region every year. This paper focuses on the assessment of the liquefaction potential of the site. The study was based on results of CPTu tests that were performed to estimate the cyclic resistance ratio (*CRR*) from in situ geotechnical investigation, and to compare it with the cyclic stress ratio (*CSR*), evaluated by considering the values proposed in the Eurocode (EC-8) for Algarve. These two parameters were used to determine the safety factor (*FSliq*) against liquefaction and the liquefaction potential index (*LPI*). In addition, the liquefaction severity number (*LSN*) was also used to quantify the effects of liquefaction and consequently the local area prospective damage estimated from the volumetric strains derived from CPTU data interpretation.

1 INTRODUCTION

The work is part of the geotechnical characterization, carried out for the design of water reservoir of the city of Monte Gordo, in Algarve (South of Portugal), inserted in the water supply system. The study is focused on the liquefiability assessment of the soils, in a region where this seismic hazard is very high and the presence of important structures require under development rigorous characterization analyses according to the Eurocode 8 criteria. Monte Gordo is located in a very touristic region in Portugal. Algarve is located near the E-W Eurasia-Africa plate boundary. It is characterized by a high seismicity, with some important historical earth-quakes causing important damage and economical losses. Not only, this region has suffered the effects of large plate boundary events but also the impact of local near distance and onshore moderate earthquake sources – similar to what has been described in Amoroso et al. (2015). The seismic hazard evaluation and mitigation of risk of the area is therefore of great importance to the local populations and to the large number of tourists that visit the region.

The liquefaction analysis was performed to estimate the cyclic resistance ratio (*CRR*) from geotechnical characterization from in situ testes, and to compare its value to that of cyclic stress ratio (*CSR*). These two parameters were used to enable the determination of the safety factor (*FSliq*) against liquefaction and the liquefaction potential index (*LPI*). In addition, the potential liquefaction-induced ground settlements index (*S*) and the lateral displacement index (*LDI*) were estimated together with the liquefaction severity number (*LSN*) in order to quantify the effects of liquefaction in the prospective damages to the local infrastructures. From the geologic point of view, the area under scope is located in the sandy coast of Algarve and is represented by a sequence of eolic (dune) sands de-posited over a silty sand unit, which in turn covers a clay/marl unit with significant thickness (Figure 1). The evaluation of liquefaction risk was a fundamental issue of the global design, once the original idea was to place the water reservoir on a mat foundation. Moreover, all the pipe system around the structure runs nearby the surface in loose soils, which normally creates severe damage in their operationally when seismic events with a certain magnitude occur.

2 SITE INVESTIGATIONS

The site investigation program comprised four Piezocone Tests, CPTu with, dissipation tests (CPTu1, CPTu2, CPTu3, CPTu4), down to 23 m depth, located as presented in Figure 2.

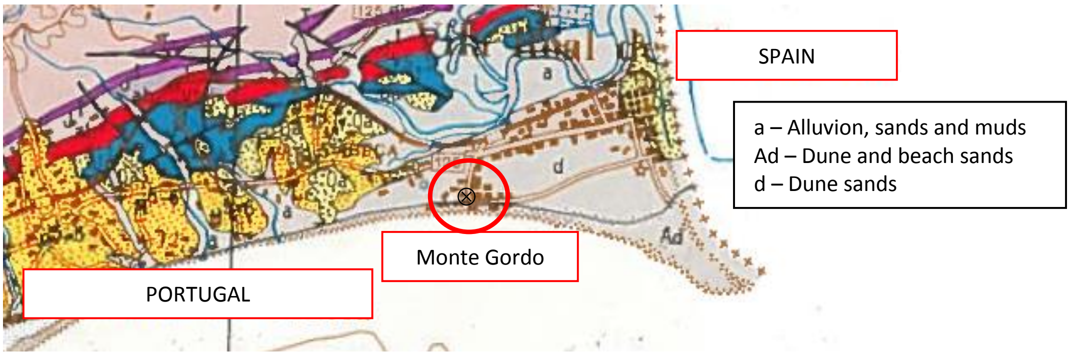

Figure 1. Geological conditions of the local under investigation.

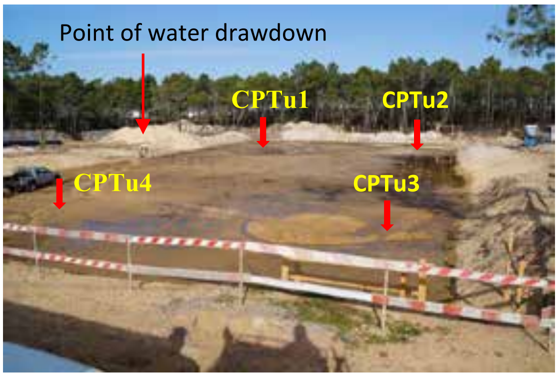

Figure 2. Site investigation program.

In Figure 3 the profiles of CPTu measured parameters are presented, namely the net cone resistance q_t, sleeve friction f_s, and pore pressure u_2, as well as the profile of the Soil Behaviour Index I_C. The ground water table is located at the surface of the excavation, as provided by the CPTu tests. It should be noted that during the execution, CPTu tests attained a very stiff layer detected at 4.5 m below the depth of excavation, which become impossible to overcome. As a consequence, the layer was drilled with an auger down to 6.5 m and then CPTu tests were conducted from that depth.

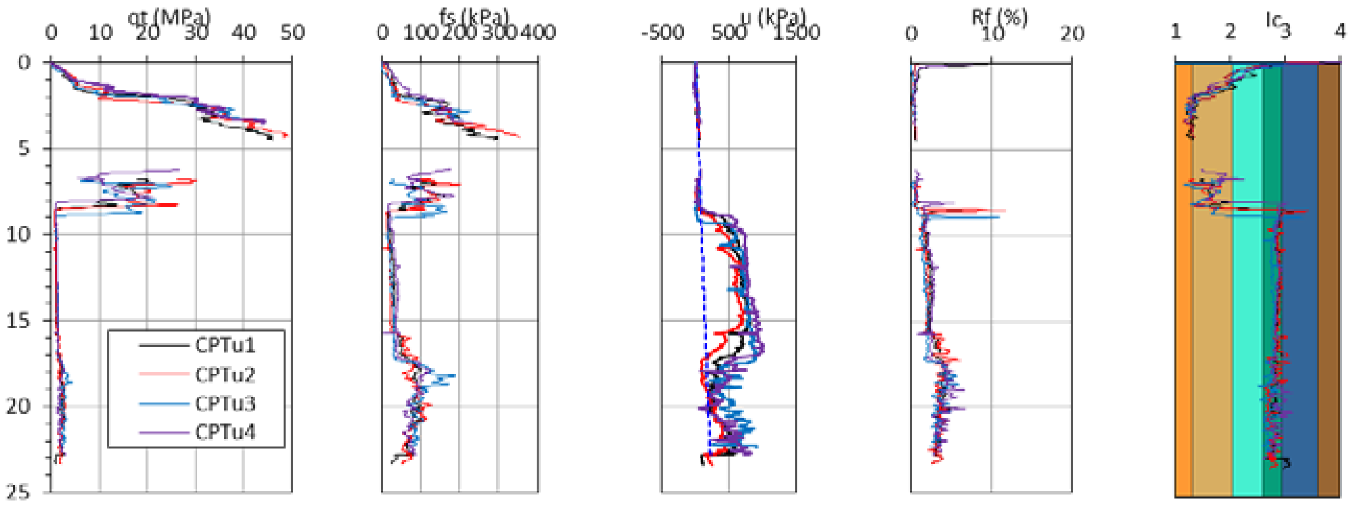

Figure 3 - CPTu results

3 LIQUEFIABILITY ASSESSMENT

3.1 *Liquefaction Safety Factor (FS_{liq})*

The liquefaction analyses were carried out according to the "simplified procedure" introduced by Seed and Idriss (1971), based on the comparison between an index of resistance of the soil in its state against liquefaction triggering, due to reference seismic action, and an index of the cyclic action, defined by the cyclic stress ratio (*CSR*). That resistance to liquefaction (cyclic resistance ratio *CRR*) can be derived by semi-empirical correlations to in situ tests results. The liquefaction safety factor *FSliq* is hereby defined as the ratio between *CRR* and *CSR*.

3.1.1 *Cyclic Stress Ratio (CSR)*

The cyclic stress ratio *CSR* was estimated by Seed and Idriss (1971) formulation, evaluating the Magnitude Scaling Factor *MSF* and the shear stress reduction coefficient r_d according to Idriss (1999).

The peak horizontal acceleration a_{max} was defined considering the two seismic reference actions considered in the Portuguese National Annex of the Eurocode 8 (NP EN 1998-1 2010, NP EN 1998-5 2010) for Monte Gordo region. The Seismic Action 1 is characterized by earthquakes with offshore epicenters (far distance source), low predominant earthquake frequency, high magnitude and long duration, while the Seismic Action 2 refers to inland epicenters (near distance source), high frequency predominant earthquake, moderate magnitude and short-duration. Table 1 summarizes the parameters that identify the two seismic actions: seismic zone, return period T_R, moment magnitude M_w, peak horizontal acceleration for stiff ground a_g, and peak horizontal acceleration at the ground surface a_{max}, estimated using a soil factor *S* based on ground type classification of Monte Gordo site.

Table 1. Seismic actions at Monte Gordo site.

	Seismic action 1	Seismic action 2
Seismic zone	1,3	2,3
Return Period, T_R (years)	475	475
Moment magnitude, M_w	7.4	5.1
Maximum acceleration of reference, a_{gR} (m/s^2)	1.5	1.7
Peak horizontal acceleration for stiff ground, a_g (m/s^2)	1.5	1.7
Amplification factor, S	1.67	1.61
Peak horizontal acceleration at the ground surface, $a_{máx}$ (g)	0.25	0.28

3.1.2 *Cyclic Resistance Ratio (CRR)*

The cyclic resistance ratio *CRR* can be evaluated using different geotechnical characterization approaches, namely from in-situ tests. From these, CPTu results have been explored with success, by well fundament approaches, such as those proposed by Robertson and Wride (1998), Youd and Idriss (2001) and Idriss and Boulanger (2004). At Monte Gordo test site *CRR* was derived from CPTu measurements, considering the relation between the normalized cone resistance $Q_{tn,cs}$ and the cyclic *CRR*-$Q_{tn,cs}$ established by Robertson (2009).

The ground water table was detected at the base of excavation at surface of the CPTu tests.

3.2 *Liquefaction Potential Index (LPI)*

According to Iwasaki et al. (1982) the Liquefaction Potential Index *LPI* was introduced to estimate the vulnerability of site to liquefaction effects, being an integral from the ground surface by 20 m depth of the following function:

$$LPI = \int_0^{20} F(z)w(z)dz \qquad (1)$$

where *z* is the depth below ground surface, *F(z)* is a linear function of the liquefaction safety factor *FSliq*, and *w(z)* is a linear function of *z*. Iwasaki et al. (1982) defined four *LPI* ranges in liquefaction damage: (i) very low for *LPI*=0; (ii) low for 0<*LPI*≤5; (iii) high for 5<*LPI*≤15; (iv) very high for *LPI*>15.

3.3 *Liquefaction Severity Number (LSN)*

The liquefaction severity number *LSN* is a parameter developed by Tonkin and Taylor (2013) for 2010-2011 Canterbury earthquakes, in New Zealand, to quantify the highest damaging effects of the loss of sustainability due to liquefaction on shallow foundations. *LSN*, as presented in Eq. (2), considers depth weighted calculated volumetric densification strain within soil layers, as a proxy for the severity of liquefaction land damage likely at the ground surface:

$$LSN = 1000\int \frac{\varepsilon_v}{z} dz \qquad (2)$$

where *z* is the depth to the layer of interest below ground surface, and ε_v is the calculated volumetric strain in the that layer. The integral is calculated, as for the LPI, for the first 20 m depth. Tonkin and

Taylor (2013) identified six *LSN* ranges for the liquefaction land effects:

(i) little to no signs of liquefaction; minor effects, for 0<LSN≤10;
(ii) minor signs of liquefaction, some sand boils, for 10<LSN≤20;
(iii) moderate signs of liquefaction, with sand boils and some structural damage, for 20<LSN≤30;
(iv) moderate to severe signs of liquefaction, settlement can cause structural damage, for 30<LSN≤40;
(v) major consequences of liquefaction, heave and collapse at the ground surface, lateral spreading, introducing differential settlement of structures, and failure of pipelines and other lines, for 40<LSN≤50;
(vi) severe damage, extensive evidence of liquefaction at surface, very high total and differential settlement affecting structures, damage to services with loss of resilience of the populations, for LSN>50.

Zhang et al. (2002) proposed that ε_v can be obtained combining $Q_{tn,cs}$ for clean sand and the liquefaction safety factor *FSliq*, when *FSliq*<2. In addition, Zhang et al. (2002) also defined the potential liquefaction induced ground settlements through the index *S*, as shown in Eq. (3), assuming that the volumetric strain is roughly equal to the vertical strain:

$$S = \sum_{i=1}^{j} \varepsilon_{vi} \Delta z_i \tag{3}$$

where ε_{vi} is the postliquefaction volumetric strain for the soil sublayer i, Δz_i is the thickness of the sublayer i, and j is the number of soil sublayers.

3.4 *Lateral Displacement Index (LDI)*

An approach for estimating liquefaction induced lateral displacement, the base of the very damaging consequences of lateral spreading was introduced by Zhang et al. (2004), defining the lateral displacement index *LDI*, as shown in Eq. (4):

$$LDI = \int_0^{z\max} \gamma_{\max} dz \tag{4}$$

where γ_{max} is maximum cyclic shear strain, z is the depth below ground surface, and z_{max} is the maximum depth to which highly liquefiable layers, which means when a calculated value of *FSliq*<2.0. According to Seed (1979) and to Ishihara and Yoshimine (1992), $\gamma_{\max}$ can be estimated in combination with the liquefaction safety factor *FSliq* and the relative density *Dr*. At Monte Gordo test site, D_r was evaluated from Robertson and Cabal (2012) for CPTu.

4 RESULTS

Table 2 summarizes the results of the liquefiability assessment performed at Monte Gordo site from the results obtained from the CPTu tests, represented in terms of *LPI*, *LSN*, *S* and *LDI*, as presented above in Eqs. (1), (2), (3) and (4), with *CRR* estimated from Robertson (2009).

The liquefaction potential index, as well as the liquefaction severity number, recognizes high liquefaction damage for Seismic Action 1 and low to high for Seismic Action 2. Postliquefaction vertical settlements at the ground surface are also confined on average within 2.5 cm and 6 cm, while the lateral displacements can reach very high values, 30 cm to 64 cm. The reason for this behaviour is mainly due to the very loose sands present in the first 2 meters below surface. *LPI* and *LSN* are in broad agreement, although *LSN* provides a higher vulnerability than *LPI*. The possibility of surface liquefaction can cause important damages to surface facilities, in the light of the reported for the Christchurch (New Zealand) earthquake of 2011, where more than 20,000 residential houses and properties were damaged by liquefaction. In this case, a clear link between the severity of liquefaction and observed damage to the potable water network with 80% pipelines losing their serviceability resulting in a serious loss of resilience of the populations, (Cubrinovki et al. 2012).

Fig. 4 shows an example of the complete analysis performed for CPTu tests considering the Seismic Action 1, the most critical. These figures provide the profiles with depth of: (1) the soil behaviour type index, *SBTn*; (2) the parameter used in each case for evaluating *CRR*:$Q_{tn,cs}$; (3) the *CSR*, divided by the *MSF*, compared to the reference value of *CRR*; (4) the liquefaction safety factor *FSliq*; and, (5) the liquefaction potential index *LPI*.

Table 2. Liquefiability assessment (Robertson 2009).

Test	Seismic Action 1				Seismic Action 2			
	LPI	*LSN*	*S* (cm)	*LDI* (cm)	*LPI*	*LSN*	*S* (cm)	*LDI*
CPTu-1	8.66	74.25	3.74	52.17	5.26	68.96	3.26	44.57
CPTu-2	7.36	69.97	3.94	43.39	4.99	68.28	3.14	30.09
CPTu-3	10.59	209.14	5.76	63.49	8.35	207.94	5.18	55.17
CPTu-4	6.58	70.47	3.40	47.36	4.10	65.65	2.48	37.14

Fig. 5 presents the interpretated values of CPTu tests considering the Seismic Action 1 for the following parameters: (1) the corrected normal cone resistance $Q_{tn,cs}$ for clean sand; (2) the relative density D_r; (3) index S for the potential liquefaction-induced ground settlements; (4) the lateral displacement index *LDI*; and, (5) the liquefaction severity number *LSN*.

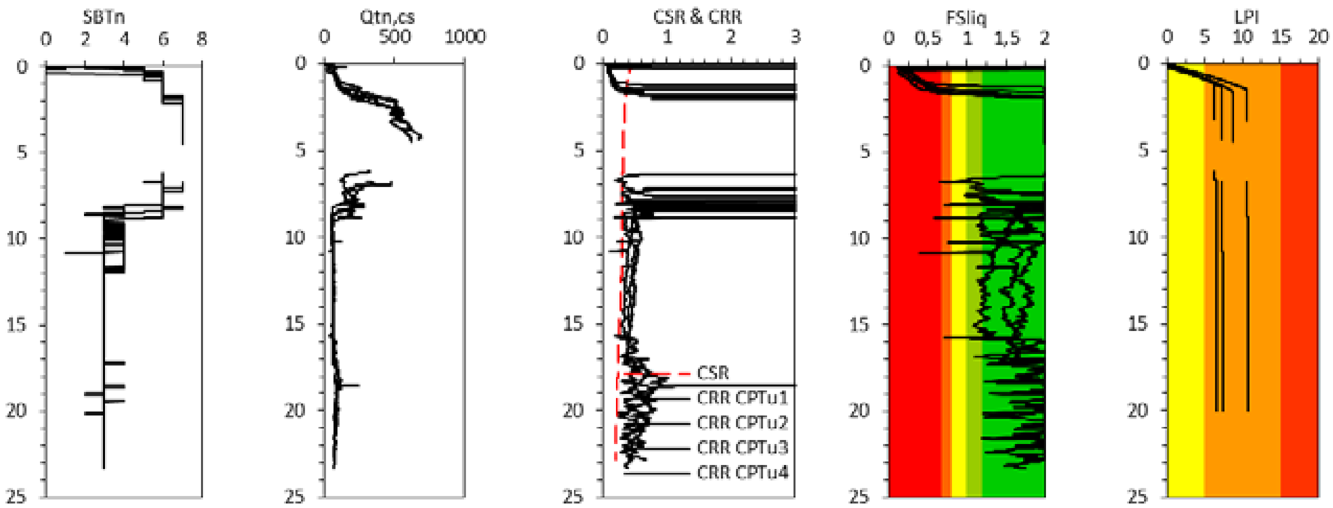

Figure 4. *LPI* estimations from CPTu tests, considering the Seismic Action 1.

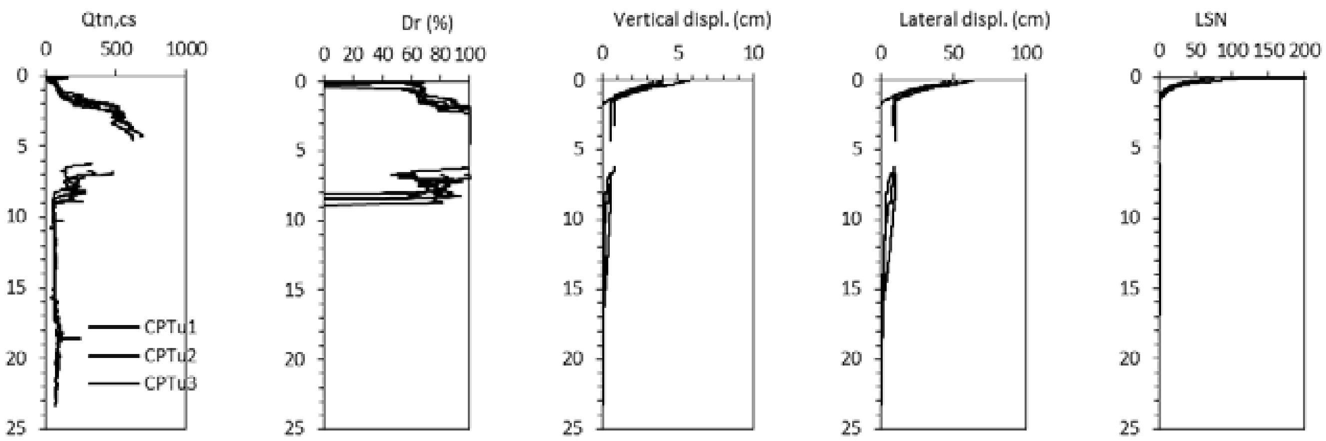

Figure 5 - S, LDI and LSN, estimations from CPTu tests, considering Seismic Action 1.

It is clear that the critical conditions are concentrated in the most superficial layers, evidencing very high lateral spreading risk. This imposes countermeasures to avoid the prospective non-acceptable damages.

5 CONCLUSIONS

a) Liquefaction assessment from CPTu results revealed a high superficial liquefaction vulnerability for the new water supply reservoir in Monte Gordo, Algarve, in the South of Portugal.
b) The respective liquefaction vulnerability has shown that the condition is critical for the reference action associated to the Atlantice Ocean far distance seismic action.
c) As a consequence, it was decided to improve the ground by densification through vibration techniques, in order to mitigate possible damage in the water distribution net that runs mainly near the surface, thus preventing cuts in the water supply post-seismic events.

6 ACKNOWLEDGEMENTS

This work is supported by FCT research project PTDC/ECM/103220/2008 "Liquefaction assessment protocols to protect critical infrasstructures against earthquake damage (LIQ2PROEARTH)", and integrated in the activities of the Institute of R&D in Structures and Construction (CONSTRUCT) in FEUP.

7 REFERENCES

Amoroso, S., Rodrigues, C., Viana da Fonseca, A., Cruz, N. 2015. “Liquefaction evaluation of Aveiro sands from SCPTU and SDMT tests”. Proc.s of the Third International

Conference on the Flat Dilatometer, 293-300. ISBN: 972-12-200-0116-8.
Cubrinovki, M., Henderson, D. and Bradley, B. 2012. “Liquefaction impacts in residential areas in the 2010-2011 Christchurch earthquakes”. Proc. Int. Symp. on Engineering Lessons Learned from the 2011 Great East Japan Earthquake, March 1-4, 2012, Tokyo, Japan.
Idriss, I.M. 1999. "An update to the Seed-Idriss simplified procedure for evaluating liquefaction potential." Proc. TRB Workshop on New Approaches to Liquefaction, Publ. No. FHWA-RD-99-165, Federal Highway Administration.
Idriss, I.M. and Boulanger, R.W. 2004. "Semi-empirical procedures for evaluating liquefaction potential during earthquakes." Proc. 11th Int. Conf. on Soil Dyn. and Earthquake Engrg. 33d. Int. Conf. on Earthquake Geotech. Engrg., Berkeley, 32-56.
Ishihara, K., and Yoshimine, M. 1992. "Evaluation of settlements in sand deposits following liquefaction during earthquakes". Soils Found., 32(1), 173–188.
Iwasaki, T., Tokida, K., Tatsuoka, F., Watanabe, S., Yasuda, S. and Sato, H. 1982. "Microzonation for soil liquefaction potential using simplified methods." Proc. of 3rd Int. Conf. on Microzonation, Seattle, 3, 1319–1330.
NP EN 1998-1 2010. "Eurocódigo 8 - Projecto de estruturas para resistência aos sismos. Parte 1: Regras gerais, acções sísmicas e regras para edifícios. " IPQ.
Robertson, P. K. 2009. "Performance based earthquake design using the CPT." Keynote Lecture at International Conference on Performance-based design in Earthquake Geotechnical Engineering, IS Tokyo, Tsukuba, Japan.
Robertson, P. K. and Wride, C. E. 1998. "Evaluating Cyclic Liquefaction Potential using the CPT." Canadian Geotechnical Journal, 35(3), 442-459.
Seed, H. B. 1979. "Soil liquefaction and cyclic mobility evaluation for level ground during earthquakes." J. Geotech. Eng. Div., Am. Soc. Civ. Eng., 105(2), 201–255.
Seed, H.B. and Idriss, I.M. 1971. "Simplified procedure for evaluating soil liquefaction potential." J. Geotech. Engrg. Div., ASCE, 97(9), 1249–1273.
Tonkin and Taylor, Ltd. 2013. "Liquefaction Vulnerability Study." Report to Earthquake Commission, Tand T ref. 52020.0200/v1.0, prepared by S. van Ballegooy and P. Malan, available at https://canterburygeotechnicaldatabase.projectorbit.com.
Youd, T.L. and Idriss, I.M. 2001. "Liquefaction Resistance of Soils: Summary Report from the 1996 NCEER and 1998 NCEER/NSF Workshops on Evaluation of Liquefaction Resistance of Soils." J. Geotech. Geoenviron. Eng., ASCE, 127(4), 297-313.
Zhang, G., Robertson, P.K. and Brachman, R.W.I. 2002. "Estimating Liquefaction induced Ground Settlements From CPT for Level Ground." Canadian Geotechnical Journal, 39(5), 1168-1180.
Zhang, G., Robertson, P.K. and Brachman, R.W.I. 2004. "Estimating Liquefaction induced Lateral Deformations From SPT and CPT." ASCE, Journal of Geotechnical and Geoenvironmental Engineering, 130 (8), 861-871.
Robertson P.K. and Cabal, K.L. 2012. "Guide to Cone Penetration Testing for geotechnical Engineering”. Gregg Driling and Testing, 5th Ed.

Geotechnical and Geophysical Site Characterisation 5 – Lehane, Acosta-Martínez & Kelly (Eds)

Evaluation of DMT-based liquefaction triggering curves based on field case histories

K.M. Rollins & T.K. Remund
Brigham Young University, Provo, Utah, U.S.A.

S. Amoroso
IstitutoNazionale di Geofisica e Vulcanologia, L'Aquila, Italy

ABSTRACT: Liquefaction is commonly evaluated using in-situ tests such as the cone penetration test (CPT) and the standard penetration test (SPT). However, these tests are relatively insensitive to a number of factors that are known to influence liquefaction resistance such as aging, stress history, overconsolidation, and horizontal earth pressure. In contrast, the flat blade dilatometer test is much more sensitive to these parameters and could potentially provide liquefaction resistance evaluations which can account for these factors. Three methods are available for predicting liquefaction resistance based on the DMT horizontal stress index K_D; however, their accuracy is poorly defined. To provide more direct evidence regarding the validity of the various approaches, DMT data has been collected at sites where liquefaction has and has not occurred in various earthquakes. The data set includes sites in California, Taiwan, New Zealand and Italy. In several cases, the sites were subjected to multiple earthquakes which did and didn't induce liquefaction. The *CRR* vs K_D curve is relatively well constrained for K_D values less than about 4. Both the Tsai et al. (2009) and Robertson (2012) curves provide reasonable triggering boundaries within this range. In contrast, the Monaco et al. (2005) curve is somewhat unconservative with liquefaction points below the curve. For K_D values greater than 4.0 there is insufficient data to determine which of the three triggering curves is most appropriate. Additional testing is necessary at sites with K_D greater than 4.0 where *CSR* is higher than 0.20 to define the triggering curve in this region.

1 INTRODUCTION

1.1 *Background*

Liquefaction is commonly evaluated using in-situ tests such as the standard penetration test (SPT) and the cone penetration test (CPT). These evaluation procedures have been developed by determining the penetration resistance at field sites which did or did not exhibit surface manifestation of liquefaction during earthquakes. The cyclic stress ratios (*CSR*), τ/σ'_o, for each of these sites were then plotted versus penetration resistance and a boundary or "triggering" curve was drawn to separate the points which liquefied from those that did not. The boundary curve then defines the cyclic resistance ratio (*CRR*), τ/σ'_o, required to induce liquefaction for that earthquake magnitude. Liquefaction triggering curves based on SPT have been developed by Youd et al. (2001), Cetin et al. (2004), and Boulanger & Idriss (2016). Curves based on the CPT have been developed by Robertson & Wride (1998), Idriss & Boulanger (2006), and Boulanger & Idriss (2016).

Unfortunately, both the SPT and CPT are relatively insensitive to a number of factors that are known to influence liquefaction resistance such as aging, stress history, overconsolidation, and horizontal earth pressure coefficient, K_o (Jamiolkowski & Lo Presti 1998, Lee et al. 2011, Marchetti 2015). In contrast, the flat blade dilatometer (DMT) test is much more sensitive to these parameters and could potentially provide liquefaction resistance evaluations that better account for these factors.

As noted by a number of researchers (e.g. Ishihara et al. 1977, Seed 1979), the liquefaction resistance of sand clearly increases as the K_o value increases. Although some researchers contend that K_o effects are reasonably considered in *CRR* vs q_{c1} evaluations (Salgado et al. 1997), other investigators have found that both the *CRR* vs q_{c1} and *CRR* vs $(N_1)_{60}$ curves were conservative without consideration of K_o effects (Harada et al. 2008). Harada et al. (2008) recommend a suite of *CRR* vs q_{c1} curves to properly account for K_o effects.

This issue is particularly important in evaluating liquefaction resistance after ground improvement because ground improvement typically increases both the soil density and K_o. If beneficial effects from increases in K_o can be relied upon, then the cost of liquefaction remediation could be reduced. Liquefaction triggering correlations based on the horizontal stress index, K_D,from the DMT (Marchetti 1980) have the potential to address this problem.

Several investigators have developed methods for predicting liquefaction resistance (*CRR*) based on the DMT K_D. In contrast to liquefaction triggering curves based on $(N_1)_{60}$, q_{c1}, orV_S,, most triggering curves based on K_D were not developed directly from field performance data owing to the paucity of data. Instead researchers developed triggering curves using indirect correlations with relative density or correlations between K_D and q_{c1}or $(N_1)_{60}$. To provide more direct evidence regarding the validity of the various approaches, DMT data has been collected at sites where liquefaction has and has not occurred in various earthquakes.

2 AVAILABLE LIQUEFACTION TRIGGERING CURVES

Correlations for predicting liquefaction resistance (*CRR*) based on the DMT K_D value have been proposed by three investigators: Monaco et al. (2005), Tsai et al. (2009), and Robertson (2012). This section summarizes the procedures used by each of these researchers and the resulting correlation equation.

2.1 *Monaco et al. (2005) Triggering Curve*

Because of the lack of$K_D$measurements at liquefaction sites, Monaco et al. (2005) used relative density as an intermediate variable to develop *CRR* vs K_D curves. For example, SPT-based liquefaction triggering curves developed by Youd et al. (2001) were used to develop a *CRR* vs. D_r curve using correlations between *SPT N* and D_r proposed by Gibbs & Holtz (1957) for a variety of vertical effective stresses. Thereafter, a correlation between K_D and D_r was used to develop the *CRR* vs K_D curve. A similar approach was used with the CPT-based liquefaction triggering curve proposed by Youd et al. (2001) and the resulting *CRR* vs K_D curve was quite similar to the curve based on the SPT-based correlation.

Finally, the following best-fit polynomial equation was developed to definean average *CRR* as a function of K_D:

$$CRR=0.0107K_D^3–0.0741K_D^2+0.2169K_D–0.1306 \quad (1)$$

This curve is plotted in Figure 1, and it is defined for clean sands and K_D > 2 considering also that Equation (1) computes negative *CRR* values for $K_D \approx 0.9$. Of course, the difficulty in using this approach is that the uncertainty associated with using two correlations with D_r would be expected to lead to greater uncertainty in the position of the *CRR* vs K_D curve.

2.2 *Tsai et al. (2009) Triggering Curve*

To avoid the problem of using an intermediate variable like D_r to develop a *CRR*-K_D correlation, Tsai et al. (2009) developed direct correlations between CPT q_{c1} and K_D as well as SPT $(N_1)_{60}$ and K_D. These correlations were developed based on companion soundings at a number of test sites in Taiwan. Based on results from both the SPT-based and CPT-based correlations in their investigations, the following equation average curve was developed defining *CRR* vs. K_D:

$$CRR = exp((K_D/8.8)^3-(K_D/6.5)^2+(K_D/2.5)-3.1) \quad (2)$$

which is also plotted in Figure 1. This curve is defined for clean sands and for K_D> 1. Although the two curves are in reasonable agreement for K_D values less than about 3, the curves diverge significantly at higher K_D values. The Monaco et al. (2005) curve yields significantly higher liquefaction resistance for a given K_D.

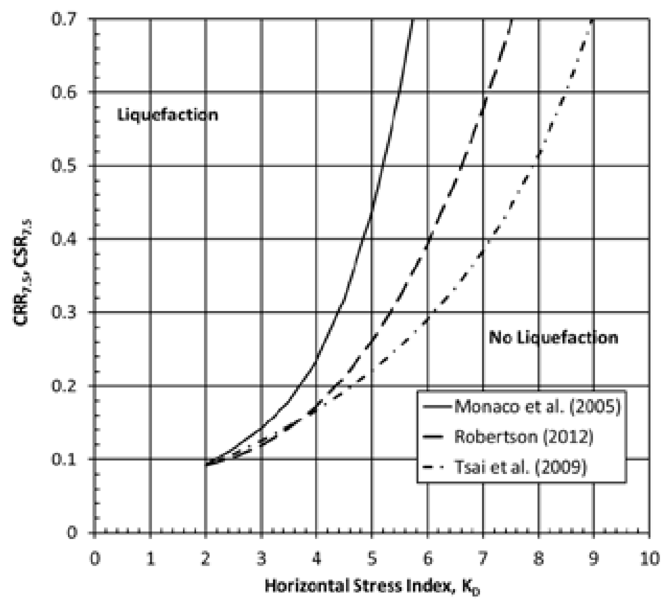

Figure 1. Comparison of DMT-based liquefaction triggering curves proposed by various researchers.

2.3 *Robertson (2012) Triggering Curve*

As part of his Mitchell lecture, Robertson (2012) proposed a third *CRR* vs K_D curve. This curve was based on a simpler correlation developed fromthe data set of companion CPT and DMT soundings developed by Tsai et al. (2009) indicating that K_D is approximately equal to $Q_{tn,cs}/25$ where $Q_{tn,cs}$ ($\approx q_{c1N,cs}$) is the clean sand equivalent cone resistance and is dimensionless. However, this correlation is highly approximate and there is significant scatter about the best-fit line.

The *CRR* vs K_D curve is defined based on the equation:

$$CRR = 93(0.025K_D)^3 + 0.08 \quad (3)$$

Equation (3) is defined for $I_D > 1.2$ and $2 < K_D < 6$. Once again, this curve is in reasonable agreement with the other two curves for K_D values less than about 3, but diverges from the other curves at higher values. Generally, the Robertson (2012) curve plots about mid-way between the Monaco et al. (2005) curve and the Tsai et al. (2009) curve.

3 COLLECTION AND PROCESSING OF AVAILABLE DATA

3.1 *Sources of Data*

Because of the significant discrepancies between the *CRR* vs. K_D curves proposed by various researchers, it will be necessary to appeal to field performance data to sort out the reliability of the various curves. Although relatively few DMT tests have been performed in post-earthquake investigations, some information is available and additional test data is being accumulated with additional earthquakes. As part of this study, a detailed literature review was undertaken to collect available DMT data. The largest data set was provided by Reyna (1991) (see also Reyna & Chameau, 1991) and included 32 tests at 5 sites in the Imperial Valley of California subjected to the the1979 M6.5 Imperial Valley earthquake, the 1981 M5.9 Westmorland earthquake, and the 1987 M6.5 Superstition Hills earthquake. These results were particularly valuable in identifying the liquefaction triggering boundary as some sites did not liquefy in the smaller event but did in the larger event. In addition, Reyna (1991) provided test data at 5 sites in the San Francisco Bay area subjected to the 1989 M6.9 Loma Prieta earthquake.

Additional DMT testing was performed by Hryciw et al. (1998) at 5 sites on Treasure Island and 5 sites in Santa Clara following the Loma Prieta Earthquake. Furthermore, Mitchell et al. (1994) report DMT test results at foursites in the SF Bay area while Rollins et al. (2015) and Faris & DeAlba (2000) each report tests for one site on Treasure Island subjected to the Loma Prieta Earthquake. An additional DMT data point was provided by Kung et al. (2011) for a site subjected to the M6.1 earthquake in Taiwan. Lastly, two data points were provided by investigations conducted by Amoroso et al. (2015) following the earthquake sequence near Christchurch, New Zealand and one from investigations at Mirabello, Italy after the M5.9 2012 Emilia-Romagna earthquake.

In many cases, CPT and V_s data has also been collected at sites where DMT testing has been performed in post-earthquake investigations. These data could be potentially useful in evaluating hybrid triggering curves which involve two in-situ measurements, such as the procedure proposed by Marchetti (2015) which uses both q_c from a CPT and K_D from the DMT. Fines contents and index tests were available in some cases along with the soil classification symbol according to the Unified Soil Classification System. Nevertheless fines content corrections are not included in DMT liquefaction triggering curves. The implementation of the *CRR*-K_D case history database could support the introduction of a more consistent liquefaction curve that could also consider the fine content influence using the material index I_D. We have included silty sand and sandy silt data points regardless of fines content to this point.

The DMT data set is clearly dominated by results from the Loma Prieta earthquake and by sites in California. Additional test data for other earthquakes and other geological settings would be very desirable. In so far as we can determine, all the sites described previously involve Holocene deposits. Some additional DMT data is available for older sediments in the New Madrid Seismic Zone and the Charleston, South Carolina area. However, these sites have been excluded at the present time as we consider how to adjust the results for aging effects. After adjustment for aging, these sites could potentially be included as data points for the same triggering curve as we routinely account for different magnitudes which are normalized to $M_w = 7.5$ using magnitude scaling factors.

3.2 *Evaluation of average values and CSR*

For each site where liquefaction occurred an average K_D value was taken from the liquefied layer. Where several depth ranges were given, the K_D value corresponding to each range was plotted throughout the liquefied layer. For sites where liquefaction did not occur average K_D values for several layers were plotted to capture the range of values involved.Fines content corrections were not taken into account in many cases owing to the lack of data in the evaluated studies.

CSR values for Figures 2, 3, and 4 were computed using the Youd et al. (2001), Idriss & Boulanger (2006), and Boulanger & Idriss(2016) methods. All methods used the *CSR* equation proposed by Seed and Idriss (1971).

$$CSR = 0.65\left(\frac{a_{max}}{g}\right)\left(\frac{\sigma_{vo}}{\sigma'_{vo}}\right)r_d/MSF \quad (4)$$

where a_{max} is the peak ground acceleration, σ_{vo} and σ'_{vo} are the total and effective vertical stresses, respectively, r_d is a stress reduction factor, and *MSF* is a magnitude scaling factor.The K_σ factor was not employed in computing *CSR* as this has not typically been done in developing the *CRR*-K_D correlations.

3.2.1 *Youd et al. (2001)Method:*

The Youdet al. (2001) method used Liao & Whitman's (1986) recommendations for stress reduction coefficients, r_d, as given by the following equations:

$$r_d = 1.0 - 0.00765z \qquad \text{for } z \leq 9.15 \text{ m} \tag{5}$$

$$r_d = 1.174 - 0.0267z \qquad \text{for } 9.15 \text{ m} < z \leq 23 \text{ m} \tag{6}$$

Magnitude scaling factors, *MSF*, were computed using the equation:

$$MSF = 10^{2.24}/M_w^{2.56} \tag{7}$$

3.2.2 *Idriss & Boulanger (2006) Method:*

Equations originally developed by Idriss (1999) were used to calculate the Boulanger & Idriss(2006) stress reduction coefficients and magnitude scaling factors. The stress reduction coefficients were computed using the equation:

$$r_d = \exp[\alpha(z) + \beta(z) \cdot M] \tag{8}$$

where:

$$\alpha(z) = -1.012 - 1.126\sin\left(\frac{z}{11.73} + 5.133\right) \tag{9}$$

$$\beta(z) = 0.106 + 0.118\sin\left(\frac{z}{11.28} + 5.142\right) \tag{10}$$

The magnitude scaling factors, *MSF*, were computed using the equation:

$$MSF = 6.9 \cdot \exp\left(\frac{-M}{4}\right) - 0.058 \leq 1.8 \tag{11}$$

3.2.3 *Boulanger & Idriss 2016 Method:*

The Idriss (1999) stress reduction coefficient equations were also used in the Boulanger and Idriss (2016) method. An overburden correction factor was first solved for to obtain MSF_{max}. $MSF_{max}$was then used to compute the overall *MSF* using the equations:

$$MSF = 1 + (MSF_{max} - 1)\left(8.64exp\left(\frac{-M}{4}\right) - 1.325\right) \tag{12}$$

where:

$$MSF_{max} = 1.09 + \left(\frac{q_{c1Ncs}}{180}\right)^3 \leq 2.2 \tag{13}$$

$$MSF_{max} = 1.09 + \left(\frac{(N_1)_{60cs}}{31.5}\right)^2 \leq 2.2 \tag{14}$$

The overburden correction factor, C_n, used in computing q_{c1} and $(N_1)_{60}$was computed using the equation:

$$C_N = \left(\frac{P_a}{\sigma'_v}\right)^m \leq 1.7 \tag{15}$$

where:

$$m = 1.338 - 0.249(q_{c1Ncs})^{0.264} \tag{16}$$

$$m = 0.784 - 0.0768\sqrt{(N_1)_{60cs}} \tag{17}$$

and

$$q_{c1N} = C_N \frac{q_c}{P_a} \tag{18}$$

4 COMPARISON OF TRIGGERING CURVES WITH FIELD PERFORMANCE DATA

As discussed in section 3, *CSR* values for each field data point were determined using the Youd et al. (2001) approach, the Idriss & Boulanger (2006) approach and the Boulanger & Idriss (2016) approach. *CSR*-K_D data pairs for these three approaches are plotted in Figures 2, 3, and 4, respectively. In these three figures, plots of the three proposed DMT-based liquefaction triggering curves are also shown along with the field performance data points.The solid red dots indicate liquefaction, while the open dots indicates no liquefaction.Generally, the Youd et al. (2001) approach gives the lowest *CSR* values, while the Idriss & Boulanger (2016) approach typically gave the highest.

For K_D values less than 4.0, where most of the data points are located, the liquefaction triggering boundary is fairly well constrained. Triggering curves proposed by Robertson (2012) and Tsai et al. (2009) seem to provide a reasonable boundary between liquefaction and no liquefaction points for most CSR assessment approaches. In contrast, the Monaco et al. (2005) curve seems to be somewhat unconservative with liquefaction points below the curve.

A review of the plots in Figures 2 through 4 indicates that there are very few data points indicating liquefaction where K_D is greater than 4. This does not necessarily mean that liquefaction will not occur at higher values, it simply means that data points have not yet been collected with high enough *CSR* values to produce liquefaction. Most of the data points with a K_D greater than 4 do not have *CSR* values above 0.175 and would not be expected to exhibit surface evidence of liquefaction based on any of the triggering curves. This observation points out the need to perform DMT tests at liquefaction sites where K_D is greater than 4 and where *CSR* is greater than 0.2 to better define the boundary of the triggering curve.

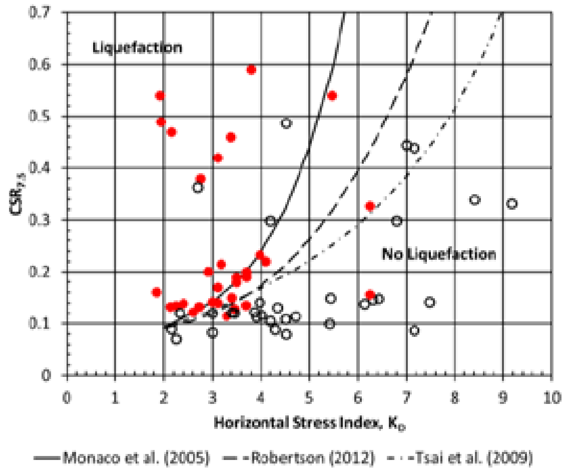

Figure 2. Comparison of proposed DMT-based liquefaction triggering curves with field performance data points using the Youd et al. (2001) approach for CSR.

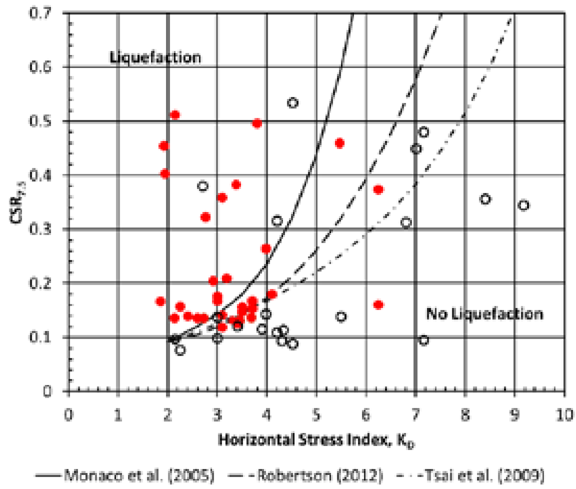

Figure 3. Comparison of proposed DMT-based liquefaction triggering curves with field performance data points using the Idriss and Boulanger (2006) approach for CSR.

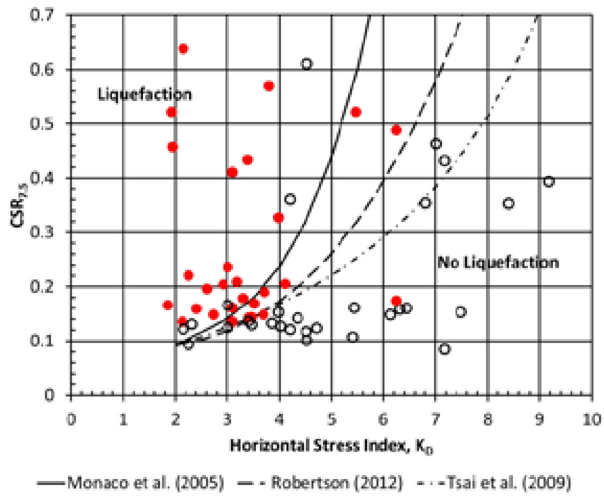

Figure 4. Comparison of proposed DMT-based liquefaction triggering curves with field performance data points using the Boulanger and Idriss (2016) approach for CSR.

There are also a few points with high *CSRs* that would be expected to liquefy based on all three DMT-based triggering curves but do not show signs of liquefaction. In some of these cases, the non-liquefiable surface layer may have been thick enough relative to the thickness of the liquefiable layer to prevent the manifestation of liquefaction effects at the surface as suggested by Ishihara (1985) and noted by Hryciw et al. (1998).

5 CONCLUSIONS

Despite the availability of liquefaction triggering curves based on CPT and SPT data, a DMT-based liquefaction triggering curve is highly desirable because it is more sensitive to aging, stress history, and horizontal earth pressure. These factors are particularly important when evaluating increased liquefaction resistance produced by ground improvement techniques when both the density and lateral pressure are increased.

The DMT-based field performance data provides reasonable discrimination between liquefaction and no liquefaction for K_D values less than 4.0. Both the Tsai et al. (2009) and Robertson (2012) curves provide reasonable triggering boundaries within this range. In contrast the Monaco et al. (2005) curve is somewhat unconservative with liquefaction points below the curve.

For K_D values greater than 4.0 there is currently insufficient data to determine which of the three triggering curves provide the most appropriate boundary. Additional testing is necessary at sites with K_D greater than 4.0 where CSR is higher than 0.20 to help define the triggering curve in this region.

6 ACKNOWLEDGEMENTS

Funding for this study was provided by US National Science Foundation grant no. CMMI-1408892. This support is gratefully acknowledged. The conclusions, interpretations, and opinions presented in this paper are those of the authors and do not necessary reflect the views of the sponsor.

7 REFERENCES

Amoroso, S., Monaco, P., Rollins, K.M., Holtrigter, M. & Thorp, A. (2015). Liquefaction assessment by seismic dilatometer test (SDMT) after 2010-2011 Canterbury earthquakes (New Zealand). *6th International Conference on Earthquake Geotechnical Engineering - 6ICEGE, 1-4 November 2015, Christchurch, New Zealand*.

Boulanger, R.W. & Idriss, I.M. 2016. CPT-Based Liquefaction Triggering Procedure. *J. Geotech. Geoenviron. Eng.*, 142(2), 11

Cetin, K.O., Seed, R.B., Der Kiureghian, A., Tokimatsu, K., Harder, L.F., Kayen, R.E. & Moss, R.E. 2004. Standard Penetration Test-Based Probabilistic and Deterministic Assessment of Seismic Soil Liquefaction Potential. *J. Geotech. Geoenviron. Eng.*, 130(12), 1314-1340.

Farris, J.R. & DeAlba, P. 2000. National Geotechnical Experimentation Site at Treasure Island, California. *National Geotechnical Experimentation Sites, GSP No. 93*, p. 52-68.

Gibbs, K.J. & Holtz, W.G. 1957. Research on determining the density ofsands by spoon penetration testing. *Proc. IV ICSMFE*, 1, 35-39.

Harada, K., Ishihara, K. Orense, R.P., & Mukai, J. 2008. Relations between penetration resistance and cyclic strength to liquefaction as affected by Kc–conditions. *Proc, Geotechnical Earthquake Engineering and Soil Dynamics IV*, Sacramento CA, Paper 111, 12pp (in CD–ROM).

Hryciw, R.D., Shewbridge, S.E., Kropp, Al, & Homolka, M. (1998). Post-earthquake investigations at liquefaction sites in Santa Cruz and on Treasure Island. *U.S. Geological Survey Prof.* Paper 1551-B, B165-B180.

Idriss, I.M. 1999. An update to the Seed-Idriss simplified procedure for evaluating liquefaction potential. *Proc. TRB Workshop on New Approaches to Liquefaction*, Publ. No. FHWA-RD-99-165, Federal Highway Administration.

Idriss, I. M., and Boulanger, R. W. (2006). Semi-empirical procedures for evaluating liquefactionpotential during earthquakes, *J. Soil Dynamics and Earthquake Eng.,* 26, 115–130.

Ishihara, K., Iwamoto, S., Yasuda, S., & Takatsu, H. 1977. Liquefaction of aniosotropically consolidated sand. *Prods. Ninth Int. Conf. on Soil Mech. and Found. Engrg.*, Japanese Society of Soil Mech. and Found. Engrg., Tokyo, Japan, Vol. 2, 261-264.

Ishihara, K. 1985. Stability of Natural deposits During Earthquakes. *Procs. 11th Intl. Conf. on Soil Mech. and Found. Engrg.*,Bakema, Rotterdam, Netherlands, Vol. 1, 321-376.

Lee, M., Choi, S., Kim, M. & Lee, W. 2011. Effect of Stress History on CPT and DMT results in Sand. *J .Engrg. Geology, Elsevier*, 117, 259-265.

Jamiolkowski, M. and Lo Presti, D.C.F. (1998). "DMT research in sand. What can be learned from calibration chamber tests".*1st Int. Conf.onSiteCharacterizationISC'98*, Atlanta. Oral presentation.

Jamiolkowski, M., Baldi, G., Bellotti, R., Ghionna, V. & Pasqualini, E. 1985. Penetration resistance and liquefaction of sands. *Proc. XI ICSMFE*, San Francisco, 4, 1891-1896.

Liao, S.S.C. & Whitman, R.V. 1986. Catalogue of liquefaction and non-liquefaction occurrences during earthquakes. *Res. Rep.*, Dept. of Civ. Engrg., Massachusetts Institute of Technology, Cambridge.

Marchetti, S. 1980. In Situ Tests by Flat Dilatometer. *J. Geotech. Engrg. Div., ASCE*, 106, No.GT3, 299-321.

Marchetti, S. 2015. Incorporating the Stress History Parameter K_D of DMT into the Liquefaction Correlations in Clean Uncemented Sands. *J. Geotech. Geoenviron. Eng.*, ASCE, 142(2).

Mitchell, J.K., Lodge, A.L., Coutinho, R.Q., Kayen, R.E., Seed, R.B.,Nishio, S. & Stokoe, K.H. 1994. Insitu test results from four LomaPrieta earthquake liquefaction sites: SPT, CPT, DMT and shearwave velocity. *Report No. UCB/EERC-94/04*, Earthquake EngineeringResearch Center, Univ. of California, Berkeley.

Monaco, P., Marchetti, S., Totani, G. & Calabrese, M. 2005. Sand liquefiability assessment by Flat Dilatometer Test (DMT). *Proc. XVI ICSMGE*, Osaka, 4, 2693-2697.

Reyna, F. & Chameau, J.L. 1991. Dilatometer Based Liquefaction Potential of Sites in the Imperial Valley. *Proc. 2nd Int. Conf. on Recent Adv. in Geot. Earthquake Engrg. and Soil Dyn.*, St. Louis, 385-392.

Reyna, F.A.M. 1991. In situ tests for liquefaction potential evaluation: Applicationto California data including data from the 1989 Loma Prietaearthquake. *Ph.D. Dissertation*, Purdue Univ. 502 p.

Robertson, P.K. 2012. Mitchell Lecture. Interpretation of in-situ tests - some insight. *Proc.4th Int. Conf. on Site Characterization ISC-4*, Porto de Galinhas - Brazil, 1, 3-24.

Robertson, P.K. & Wride, C.E. 1998. Evaluating cyclic liquefaction potential using the cone penetration test. *Canadian Geotech. J.,* 35(3), 442-459.

Rollins, K.M., Amoroso, S. & Hryciw, R. (2015). Comparison of DMT, CPT, SPT, and V_S based liquefaction assessment on Treasure Island during the Loma Prieta earthquake. *Procs. 3rd Intl. Conf. on the Flat Dilatometer, Rome, Italy*, 349-356.

Salgado, R., Boulanger, R. & Mitchell, J. 1997. Lateral Stress Effects on CPT Liquefaction Resistance Correlations. *J. Geotech. Geoenviron. Eng.*, 123(8), 726–735.

Seed, H.B., & Idriss, I.M. 1971. Simplified procedure for evaluating soil liquefaction potential. *J. Geotech. Engrg. Div.*, ASCE, 97(9),1249–1273.

Seed, H.B. 1979. Soil Liquefaction and Cyclic Mobility Evaluation for Level Ground during Earthquakes. *J. Geotech. Eng. Div., ASCE*, Vol. 105(2), 201-255.

Tsai, P., Lee, D., Kung, G. T. & Juang, C.H. 2009. Simplified DMT-based methods for evaluating Liquefaction Resistance of Soils. *J .Engrg.Geology, Elsevier*, 103, 13-22.

Kung, G. T., Lee, D. & Tsai, P. 2011. Examination of DMT-based methods for evaluating the liquefaction potential of soils. *Applied Physics & Engineering*, 12(11), 807-817.

Youd, T.L., Idriss, I.M., Andrus, R.D., Arango, I., Castro, G., Christian, J.T., Dory, R., Finn, W.D.L., Harder, L.F., Hynes, M.E., Ishihara, K., Koester, J.P., Liao, S.S.C., Marcuson, W.F., Martin, G.R., Mitchell, J.K., Moriwaki, Y., Power, M.S., Robertson, P.K., Seed, R.B., & Stokoe, K.H. 2001. Liquefaction Resistance of Soils: Summary Report from the 1996NCEER and 1998 NCEER/NSF Workshops on Evaluation of Liquefaction Resistance of Soils. *J. Geotech. Geoenviron. Eng.,* ASCE, 127(10), 817-833.

Geotechnical and Geophysical Site Characterisation 5 – Lehane, Acosta-Martínez & Kelly (Eds)

Liquefaction resistance of gravelly soil from Becker penetrometer (BPT) and Chinese dynamic cone penetrometer (DPT)

K.M. Rollins & T.L. Youd
Brigham Young University, Provo, Utah, U.S.A.

M. Talbot
U.S. Bureau of Reclamation, Provo, Utah, U.S.A.

ABSTRACT: In North American practice, the Becker Penetration Test (BPT) has become the primary field test used to measure penetration resistance of gravelly soils. However, this test is expensive and uncertainties exist regarding correlations and corrections for rod friction. As an alternative, the dynamic penetration test (DPT) developed in China has recently been correlated with liquefaction resistance. The DPT equipment consists of a 74 mm diameter cone tip driven by a 120 kg hammer with a free fall height of 100 cm using a 60 mm drill rod to reduce friction. The DPT is a very rugged, economical device, capable of penetrating dense gravel layers. During DPT field investigations following the 2008 Wenchuan earthquake in China, liquefaction resistance was correlated with DPT blow count. In this study, liquefaction resistance was evaluated using both BPT and DPT soundings in the foundation of an earth dam consisting of sand and gravel layers. Companion testing was carried out at five locations to depths of about 6 m using automatic and manual donut hammers with lower energy levels. Applied energy was measured for the DPT soundings so that energy corrections could be applied. The blow counts from the BPT and DPT correlated reasonably well for gravels using the automatic hammer, but poor correlation was obtained with the donut hammer. Liquefaction resistance for the BPT and DPT soundings were also in reasonable agreement for gravel layers suggesting that the DPT can provide liquefaction hazard evaluations more economically than the BPT using direct correlations with field performance.

1 INTRODUCTION

1.1 *Background*

One of the most challenging problems in geotechnical engineering is characterizing gravelly soils in a reliable, cost-effective manner for routine engineering projects. Even for large projects, such as dams and power projects, characterization is still expensive and problematic. Nevertheless, because liquefaction is known to have occurred in gravelly soils in a significant number of earthquakes (Sy and Campanella 1995, Cao et al 2012), engineers and geologists are frequently called upon to assess the potential for liquefaction in gravels. Therefore, innovative methods for characterizing and assessing liquefaction hazards in gravels are certainly an important objective in geotechnical engineering.

Over the past 60 years, Chinese engineers have developed a dynamic cone penetration test (DPT) which is effective in penetrating coarse or cobbly gravels and provides penetration data useful for liquefaction assessment (Chinese Design Code, 2001). This test could provide an important new procedure for characterization of gravels that fills a void in present geotechnical practice. The objective of this paper is to provide comparative evaluations of the liquefaction resistance estimated by the DPT and the BPT in the foundation of a dam with a gravel layer

1.2 *Limitations of current methods for characterizing gravels*

Owing to the difficulty of extracting undisturbed samples from gravelly soils, laboratory tests on undisturbed samples have not proven effective or reliable for measurement of shear strength or liquefaction resistance. Freezing of a gravel layer before sampling improves sample quality, but the cost is prohibitive for routine projects. Even when undisturbed samples can be extracted, changes in stress conditions between the field and laboratory can limit the usefulness of laboratory test results.

For sands and fine-grained soils, standard penetration tests (SPT) and cone penetration tests (CPT) are widely used to measure penetration resistance for applications in engineering design and for assessing liquefaction resistance. However, SPT and CPT are not generally useful in gravelly soils because of interference from large particles. Because of the large particles, the penetration resistance increases and may reach refusal even in cases when the soil is not particularly dense. This limitation makes it very difficult to obtain a consistent and reliable correlation between SPT and CPT penetration resistance and basic gravelly soil properties.

In North American practice, the Becker Penetration Test (BPT) has become the primary field test used to measure penetration resistance of gravelly soils. The BPT was developed in Canada in the late 1950s and consists of a 168-mm diameter, 3-m-long double-walled casing, whose resistance is defined as the number of blows required to drive the casing through a depth interval of 30 cm. For liquefaction resistance evaluations, closed-end casing is specified. To facilitate use of the BPT for liquefaction resistance calculations, Harder and Seed developed correlations between BPT and SPT blow counts in sand after correction for Becker bounce chamber pressure and atmospheric pressure at the elevation of testing (Harder and Seed 1986, Harder 1997) as shown in Figure 1. Despite the scatter, the correlation appears to be reasonably good.

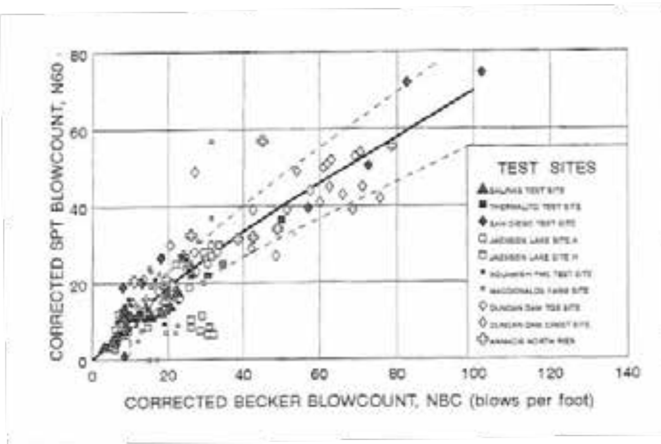

Figure 1. Correlation between corrected Becker and SPT blowcounts from Harder and Seed (1986) supplemented with data from additional test sites (Harder, 1997).

Disadvantages in applying the BPT for liquefaction hazard investigations include the high cost of mobilization, uncertainty in measuring BPT resistances, uncertainties in correlations between SPT and BPT blow counts, and friction resistance between the soil and the driven BPT casing. With respect to friction resistance, Harder (1997) states that for normally to slightly overconsolidated low plasticity soils, the effect of friction is adequately accommodated in the empirical correlations he and Prof. Seed developed.

In contrast, Sy and Campanella (1994) found that friction on the Becker penetrometer affects the measured penetration resistance. They developed a procedure for correcting BPT measurements for friction resistance by using instrumental measurements to conduct a CAPWAP analysis to quantify the effect of casing friction on BPT resistance. CAPWAP analyses, however, have not led to a significant reduction of the overall uncertainty in BPT analyses (Harder, 1997). Sy (1997) has also used mud slurry injection at the base of the Becker to reduce casing friction, with some success, but both the CAPWAP and the mud injection approaches add to the overall complexity of the test procedure.

2 DEVELOPMENT OF DYNAMIC CONE PENETRATION TEST (DPT) FOR GRAVELS

A dynamic cone penetration test (DPT) was developed in China in the early 1950s to measure penetration resistance of gravel for application in bearing capacity analyses. Based on their experience, standard test procedures and code provisions have been formulated (Chinese Specifications 1999, Chinese Design Code 2001). Because of widespread gravelly deposits beneath the Chengdu plain, the DPT is widely used in that region, particularly for the evaluation of liquefaction potential (Cao et al. 2011).

DPT equipment is relatively simple, consisting of a 120-kg (264 lb) hammer, raised to a free fall height of 100 cm (39 in), then dropped onto an anvil attached to 60-mm diameter drill rods which in turn are attached to a solid steel cone tip with a diameter of 74 mm and a cone angle of 60º as shown in Figure 2. The smaller diameter rod helps to reduce shaft friction on the rods behind the cone tip.

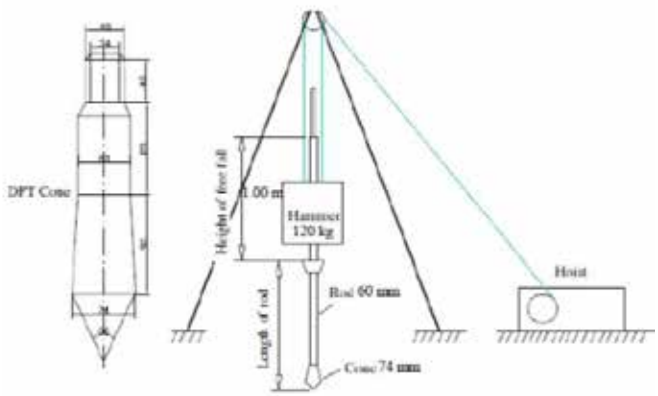

Figure 2. Component sketch of tripod and drop hammer setup for dynamic penetration tests (DPT) along with DPT cone tip. (After Cao, Youd and Yuan 2011).

Prior to testing, the drill rods are marked at 10 cm intervals and the number of blows required to penetrate each 10 cm is recorded. The raw DPT blow count is defined as the number of hammer drops required to advance the cone tip 10 cm. A second penetration resistance measure, called N_{120}, is specified in Chinese code applications where N_{120} is the number of blows required to drive the cone tip 30 cm; however, N_{120} is calculated simply by multiplying raw blow counts by a factor of three which preserves the detail of the raw blow count record.

As with the standard penetration test, a correction for overburden stress on the DPT blow count was applied using the equation

$$N'_{120} = N_{120}(100/\sigma'_v)^{0.5} \quad (1)$$

where N'_{120} is the corrected DPT resistance in blows per 30 cm, N_{120} is the measured DPT resistance in blows per 30 cm, 100 is atmospheric pressure in kN/m^2, and σ'_v is the vertical effective stress in kN/m^2 (Cao et al, 2013).

Energy transfer measurements were made for about 1200 hammer drops with the DPT in China using the conventional pulley tripod and free-fall drop weight system. These measurements indicate that on average 89% of the theoretical hammer energy was transferred to the drill rods with this system.

3 LIQUEFACTION RESISTANCE CURVE BASED ON DPT PENETRATION RESISTANCE

Following the 2008 M_w=7.9 Wenchuan earthquake in China, 47 DPT soundings were made at 19 sites with observed liquefaction effects and 28 nearby sites without liquefaction effects. Each of these sites was underlain by 2 to 4 m of clayey soils, which, in turn, were underlain by gravel beds up to 500 m thick. Looser upper layers within the gravel beds are the materials that liquefied during the Wenchuan earthquake. Because samples are not obtained with DPT, boreholes were drilled about 2 m away from most DPT soundings with nearly continuous samples retrieved using 90 to 100 mm diameter core barrels. DPT soundings reached depths as great as 15 m, readily penetrating gravelly layers that liquefied as well as many layers that were too dense to liquefy.

Layers with the lowest DPT resistance in gravelly profiles were identified as the most liquefiable. At sites with surface effects of liquefaction these penetration resistances were generally lower than those at nearby DPT sites without liquefaction effects. Thus, low DPT resistance became a reliable identifier of liquefiable layers (Cao et al. 2011).

Using the DPT data, Cao et al. (2013) plotted the cyclic stress ratio causing liquefaction against DPT blow count as shown in Figure 3. Points where liquefaction occurred are shown as solid red dots, while sites without liquefaction are shown with open circles. Cao (2013) also defined boundary curves for 15, 30, 50, 70 and 85% probability of liquefaction based on logistical regression.

4 LIQUEFACTION RESISTANCE CURVE BASED ON BPT PENETRATION RESISTANCE

Using the correlation between the corrected BPT penetration resistance, NBC, and the SPT penetration resistance corrected for hammer energy, N_{60}, shown in Figure 2, the liquefaction resistance curves for sand shown in Figure 4 can be used to evaluate liquefaction in gravelly soil. This approach assumes that the Becker hammer is relatively unaffected by the particle size of the gravel.

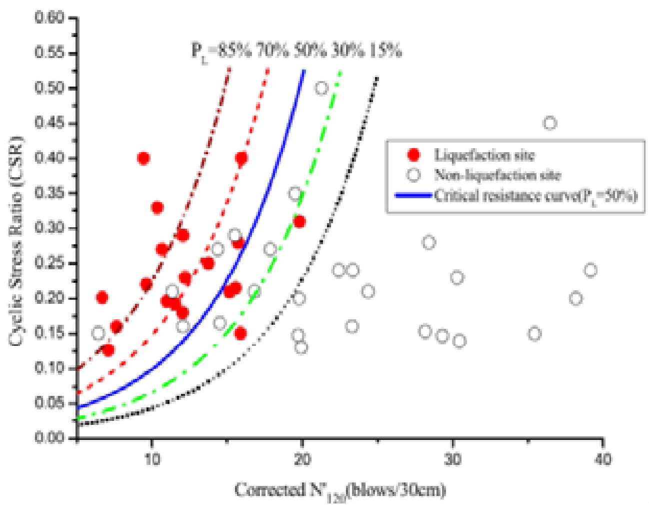

Figure 3. Liquefaction resistance curves for gravels in the Chengdu plain during the M_w=7.9 Wenchuan, China Earthquake based on DPT penetration resistance (Cao et al. 2013).

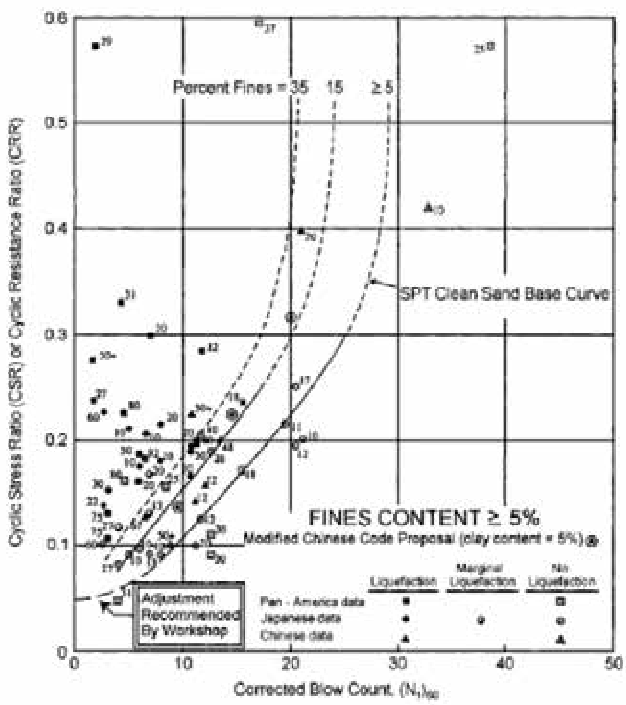

Figure 4. Correlation between cyclic resistance ratio and corrected SPT blowcount based on liquefaction case histories for M_w7.5 earthquakes (modified from Seed et al. 1985) (Youd et al. 2001).

As shown in Figure 4, the liquefaction boundary curves are essentially vertical at cyclic stress ratios greater than 0.5. For example, with a fines content less than 5%, the CRR is undefined for SPT $(N_1)_{60}$ values greater than 29, although the liquefaction resistance is clearly higher than a value of 0.50. In contrast, the CRR vs N'_{120} curves have a somewhat positive slope at their upper limits likely because of the lack of adequate field performance data.

5 COMPARISON OF BPT AND DPT EVALUATIONS OF LIQUEFACTION AT MILLSITE DAM, UTAH

Millsite dam (39.09733º, -111.1877º) is located in Ferron, Utah about 45 miles south of Price, Utah. Because the foundation soils beneath the dam contain saturated sand and gravel layers, a liquefaction evaluation was performed at the site. In particular, the Becker hammer was used to evaluate the liquefaction resistance of the gravel layers. Becker penetration tests were performed at nine locations along the downstream toe of the dam. At six of these locations, DPT soundings were also performed within about 1m of the BPT soundings using the Chinese DPT cone tip.

In contrast to the Chinese DPT where applied energy was produced by a 120-kg weight dropped from a 1-m height, DPT soundings at Millsite in this study used two different hammers: (1) a 102 kg (225 lb) donut hammer weight dropped from 0.91 m (36 in) and (2) a 64 kg (140 lbs) automatic hammer dropped from a height of 0.76 m (30 in). Energy transfer measurements were made with a PDA for each hammer at the site. The donut hammer and the automatic hammer delivered 52% and 98% of the theoretical free-fall energy, respectively. Remarkably, despite the different applied hammer energies, both hammers transferred approximately 53% of the energy transferred by the Chinese hammer.

To account for these energy differences, the measured blowcounts were corrected to obtain N'_{120} values using the equation:

$$N'_{120} = (N'_{120})_F(E_{CDPT}/E_F)$$

where $(N'_{120})_F$ is the uncorrected blowcount obtained with the hammer in the field, E_{CDPT} is the energy delivered by the Chinese DPT and E_F is the energy delivered by the hammer in the field. This linear adjustment factor is based on the energy correction approach used for the SPT hammer. In this case, the energy adjustment factor increased the measured blowcounts by a factor of 1.89.

Furthermore, to facilitate comparisons between the liquefaction resistance obtained with the DPT which is based on data from a M_w8.0 earthquake and the BPT which is based on M_w7.5 earthquake data, a magnitude scaling factor approach was used. For example, the cyclic stress ratio, CRR, obtained from a DPT-based liquefaction triggering curve in Figure 3 was adjusted using the equations below to obtain the CRR for a M_w7.5 earthquake.

$$CRR_{M7.5} = CRR_{M8.0}/MSF \quad (2)$$

where $MSF = 10^{2.24}/M_w^{2.56}$ and $M_w = 8.0$ (3)

This had the effect of increasing the CRR values obtained from the DPT correlation by a factor of about 15%.

Correlations between BPT $(N_1)_{60}$ and DPT N'_{120} were attempted for both the donut hammer and the automatic hammer data. Correlations were much improved with the automatic hammer relative to the donut hammer which was operated manually. The difficulty for the driller in consistently raising the heavier donut hammer (102 kg vs. 64 kg) led to much greater scatter in the test data relative to the automatic hammer. This finding is consistent with results obtained by Cao et al. (2013). A plot of BPT $(N_1)_{60}$ vs. DPT N'_{120} for gravel with the automatic hammer is provided in Figure 5. The best-fit equation is

$$BPT\ (N_1)_{60} = 2.46N'_{120} \quad (4)$$

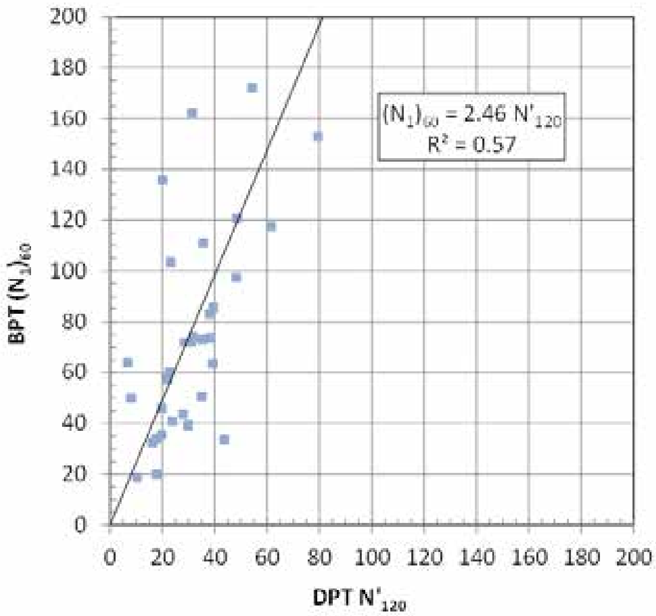

Figure 5. Plot of BPT $(N_1)_{60}$ vs. DPT N'_{120} with the automatic hammer for gravel along with best-fit correlation line.

In addition, analyses indicated that separate correlations were necessary for DPT tests in sand and in gravel layers, even with the automatic hammer. For example, for a given DPT N'_{120}, the BPT $(N_1)_{60}$ in sand was typically about 65% of the value in gravel. This result suggests that the correlation may be dependent on the maximum grain size at least for the lower energy levels used in this study. Therefore, the correlation between liquefaction resistance and DPT N'_{120} proposed by Cao et al (2013) should probably be restricted to gravel layers at present.

A comparison of liquefaction resistance obtained from the BPT and DPT evaluations within (a) gravel layers and (b) sand layers in four test holes are provided in Figure 6. In most of these holes, the BPT soundings indicated that the $(N_1)_{60}$ was higher than 29 meaning the soil is non-liquefiable. This indicates that the CRR would be greater than 0.5 as discussed

(a) Automatic Hammer in Gravel

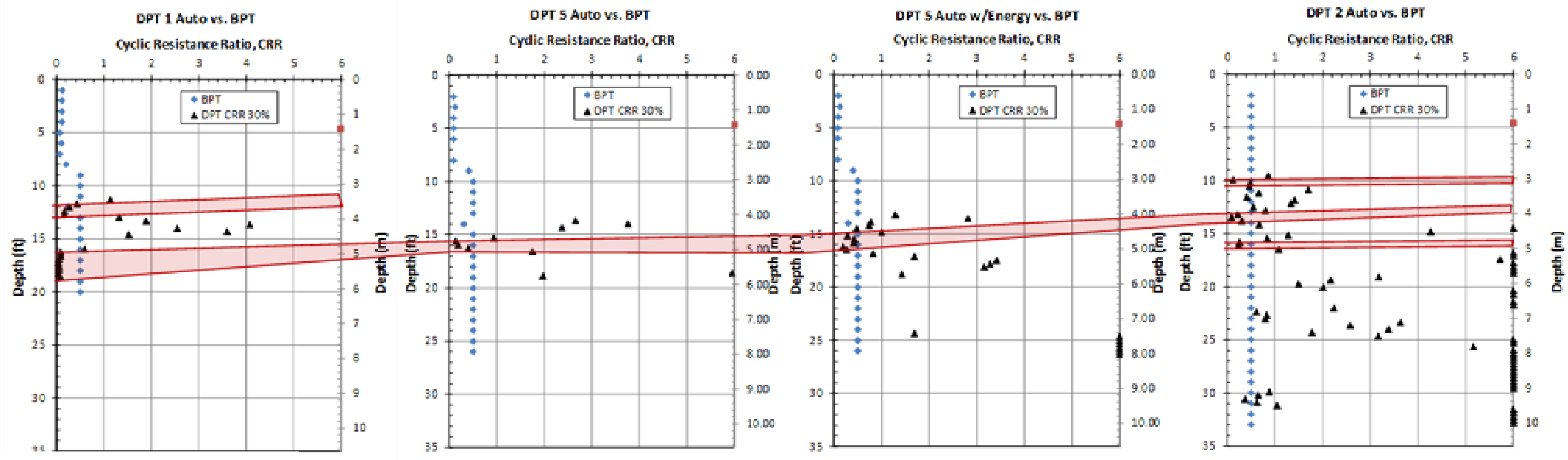

(b) Automatic Hammer in Sand

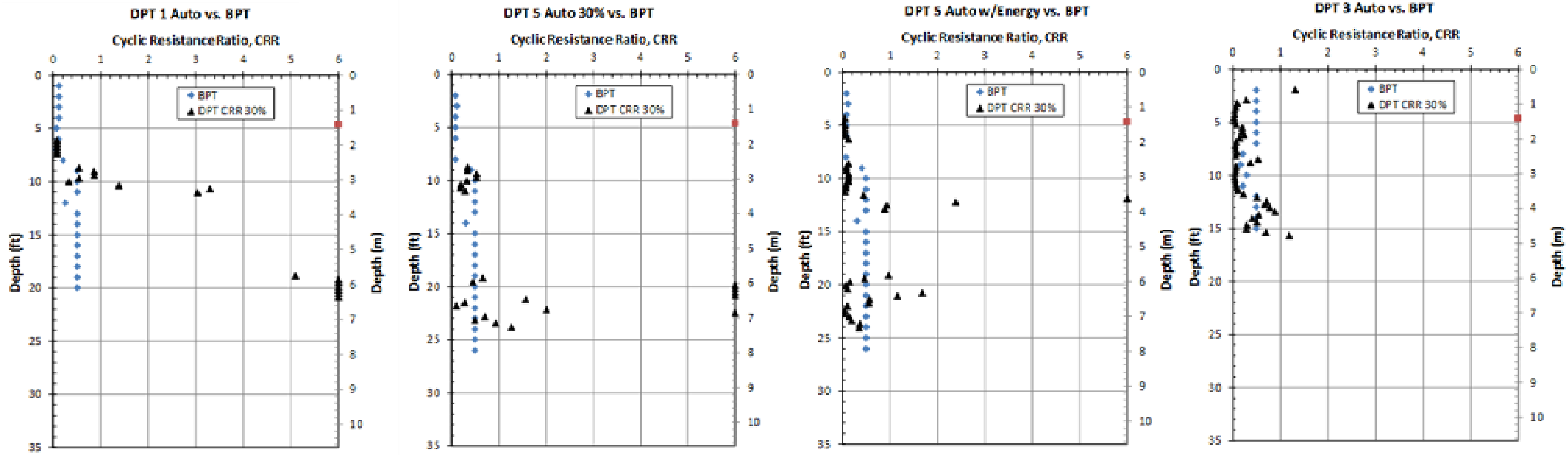

Figure 5. Plot of cyclic resistance ratio causing liquefaction in gravel layers at Millsite dam based on BPT $(N_1)_{60}$ and DPT N'_{120} with the (a) automatic hammer and (b) donut hammer.

in section 4. Therefore, the CRR is plotted as 0.5 in this figure as a reference point. It should be noted that the 30% probability DPT CRRs are generally considerably higher than the 0.5 boundary throughout the majority of the profile consistent with the BPT results in the gravel layers. However, some relatively thin (0.3-m to 0.6m-thick) potentially liquefiable layers are identified by the DPT. The consistency of the layer across the site suggests that the identification is accurate. These results also indicate that the DPT with values at 0.10 m intervals may provide better resolution for thin layers than the BPT at 0.3 m. Similar problems have been previously reported by Harder (1997) for thin silt layers.

In contrast to the gravel layers, the agreement between the CRRs obtained from the BPT and DPT soundings in the sand layers is rather poor in many cases. Typically, the CRR obtained from the DPT is lower than that from the BPT which is consistent with the lower correlation between DPT and BPT discussed previously. These results strongly suggest that the DPT based liquefaction resistance curves at gravel sites are not appropriate for evaluating liquefaction in sand.

6 CONCLUSIONS

The Chinese dynamic penetration test (DPT) provides a simpler, more economical approach for evaluating liquefaction resistance than the Becker penetration test (BPT). In addition, the DPT liquefaction resistance curves for gravel are based on direct field performance while the BPT requires an intermediate correlation to obtain an equivalent sand SPT blowcount. Correlations between DPT N'_{120} and the BPT $(N_1)_{60}$ were reasonable for gravels when using an automatic hammer to increase consistency and reduce data scatter. Regression analysis indicates that separate correlation curves would be required for sand relative to gravel.

Cyclic resistance ratio curves from the DPT for the 30% probability curve are generally consistent with results from the BPT at this field test site; however, the DPT consistently identified a thin potentially liquefiable layer that was apparently not resolved by the BPT. The DPT soundings typically underestimated the liquefaction resistance in sand layers relative to the BPT soundings. Therefore, the DPT liquefaction resistance curves should only be used to evaluate liquefaction in gravels. Additional field testing would be very desirable in understanding the performance of the DPT versus the BPT in field test sites.

7 ACKNOWLEDGEMENTS

Funding for this study was provided by a grant from the US Geological Survey. Drill rig services and hammer energy measurement were donated by the US Bureau of Reclamation. This support is gratefully acknowledged; however, the conclusions, interpretations, and opinions presented in this paper are those of the authors and do not necessary reflect the views of the sponsors.

8 REFERENCES

Cao, Z., Yuan, X., Youd, T.L., and Rollins, K.M. (2012). “Chinese Dynamic Penetration Tests (DPT) at Liquefaction Sites Following 2008 Wenchuan Earthquake.” Proc. 4th Intl. Conf. on Site Characterization, Pernambuco, Brazil.

Cao, Z. Youd, T.L., Yuan, X., (2011). “Gravelly soils that liquefied during 2008 Wenchuan, China earthquake, Ms=8.0.” Soil Dynamics and Earthquake Engineering, Elsevier, v. 31 (1132-1143).

Cao, Z., Youd, T., and Yuan, X. (2013). ”Chinese Dynamic Penetration Test for Liquefaction Evaluation in Gravelly Soils.” J. Geotech. Geoenviron. Eng., 139(8), 1320–1333.

Chinese Design Code (2001). Design code for building foundation of Chengdu region, Administration of Quality and Technology supervision of Sichuan Province PRC. (in Chinese), DB51/T5026-2001.Chinese Specifications (1999). “Specification of soil test, Ministry of Water Resources of the People’s Republic of China.” (in Chinese), SL237-1999.

Harder, L.F. (1997). “Application of the Becker Penetration Test for Evaluating the Liquefaction Potential of Gravelly Soils.” NCEER Workshop on Evaluation of Liquefaction Resistance, held in Salt Lake City, Utah.

Harder, L. F., Jr., and Seed, H. B. (1986). “Determination of penetration resistance for coarse-grained soils using the Becker hammer drill.” Report UCB/EERC-86/06, Earthquake Engrg. Res. Ctr., University of California -Berkeley

Sy, A. (1997). “Twentieth Canadian Geotechnical Colloquium: Recent developments in the Becker penetration test: 1986-1996.” Canadian Geotech. J. Vol. 34, 952-973

Sy, A. and Campanella, R.G., (1995). “Becker and Standard Penetration Tests (BPT-SPT) Correlations

Geotechnical and Geophysical Site Characterisation 5 – Lehane, Acosta-Martínez & Kelly (Eds)

New developed soundings to assess liquefaction potential of soils

S. Sawada
OYO Corporation, Saitama, Japan

ABSTRACT: This paper presents newly developed three types sounding equipment for evaluating the liquefaction susceptibility of soils. The first one is a Piezo Drive Cone (PDC) which is a dynamic penetrometer with pore pressure transducer that measures pore pressure of the ground generated during dynamic penetration at the cone tip. The second one is dynamic cone penetration test equipment with measurement of the pull-out resistance, which is named "Penetration & Pull-out Test (PPT)". The last one is a Dynamic Weight Sounding (DWS), in which an electrical hammer drill is installed at the top of Swedish weight sounding rod. The validation test results indicate that PDC, PPT and DWS are highly useful for evaluation of liquefaction-induced problems due to earthquakes. In addition, liquefaction risks assessment in teams of the factor of safety can be evaluated in a short time. Therefore, liquefaction risks for a large area can be evaluated in a relatively short period.

1 INTRODUCTION

Many case histories on earthquake disasters have been showing that significant damages due to the soil liquefaction. In particular, the liquefaction susceptibility in an area is judged based on sparse data. Therefore, a more precise evaluation is required for the reliable design against soil liquefaction. Some cost-effective methods are required from the engineering point of view.

The sounding is one of the most important and convenient tests for soil investigations. In recent decades, many efforts have been made to extend its applications to various fields in geotechnical engineering.

The present paper addresses the three types of new developed sounding equipment for evaluating the liquefaction susceptibility of soils. The first one is a Piezo Drive Cone (PDC) which is a dynamic penetrometer with pore pressure transducer that measures pore pressure of the ground generated during dynamic penetration at the cone tip. The second one is dynamic cone penetration test equipment with measurement of the pull-out resistance, which is named "Penetration & Pull-out Test (PPT)". The last one is a Dynamic Weight Sounding (DWS), in which an electrical hammer drill is installed at the top of Swedish weight sounding rod. The validation test results indicate that PDC, PPT and DWS are highly useful for evaluation of liquefaction-induced problems due to earthquakes.

2 THREE TYPES SOUNDING EQUIPMENT

2.1 *Type of evaluation related to performance grade*

Three kinds of equipment devices have different grade in terms of accuracy for the evaluation of liquefaction strength of soils.

Table 1 shows the performance grade of subject matter for evaluation. Table 2 shows the type of evaluation related to performance grade. As a matter of course, if you would like to conduct an investigation precision highly, the cost rises, and the cost is proportional to precision of the ground information.

3 PIEZO DRIVE CONE (PDC)

3.1 *Mechanism of PDC*

PDC enables evaluation of soil liquefaction strength in an in-situ test by measuring pore water pressure during the dynamic penetration test.

PDC measures at every blow not only the penetration resistance value, N_d (correlated N-value), but also the pore water pressure. The pore water pressure can be converted into fine fraction content (F_C) according to the correlation between the residual pore water pressure ratio and fine fraction content. PDC estimates liquefaction strength from the results of N_d and F_C values.

Table 1. Performance grade A, B, and C.

Performance grade	Subject matter to evaluate
Grade C	Qualitative evaluation of the subsistent of liquefiable soils.
Grade B	Qualitative evaluation of the susceptibility to liquefaction based on soil classification.
Grade A	Quantitative evaluation of liquefaction strength based on estimated to SPT *N* values and Fine contents F_C of soils.

Table 2. Type of evaluation related to performance grade.

Type of evaluation	Performance grade		
	Grade C	Grade B	Grade A
Dynamic Weight Sounding (DWS)	■		
Penetration & Pull-out Test (PPT)	□	■	
Piezo Drive Cone (PDC)		□	■

Index : ■ Standard or final investigation
□ Preliminary or roughly investigation

3.2 *Test Equipment and Data processing*

PDC is a new investigation tool that measures the pore pressure of the ground which generated at the cone tip during the dynamic penetration. Figure 1 shows the schematic figure of general PDC system. This system consists of a cone tip with an inserted pore pressure transducer, a penetration displacement sensor, a trigger, a data logger and dynamic penetration equipment.

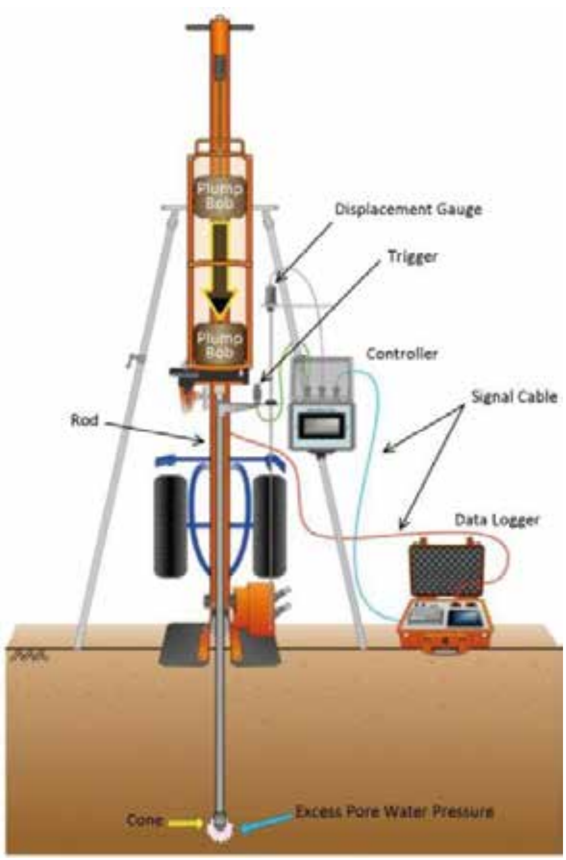

Figure 1. Schematic illustration of PDC.

In this study, we used the light weight dynamic penetration device which is a modified version of the Swedish Ram Sounding test equipment named as the Mini Ram Sounding (MRS). The penetration rods are driven down mechanically by a 30 kg hammer with free fall from the height of 35 cm. The penetration resistance is defined as the number of blow counts (N_m) required to drive the penetrometer 20 cm during which the sounded soil can be regarded as in the undrained condition. It is found *N*-value (N_{spt}) of the Standard Penetration Test (SPT) namely equals to a half of the blow counts (N_m).

$$N_{spt} \approx N_d = 1/2\ N_m \qquad (1)$$

The porous stones for measuring pore pressure are located at the cone apex as clearly shown in Figure 2. The data logger records the penetration displacement and the pore pressure response of every blow at the cone apex.

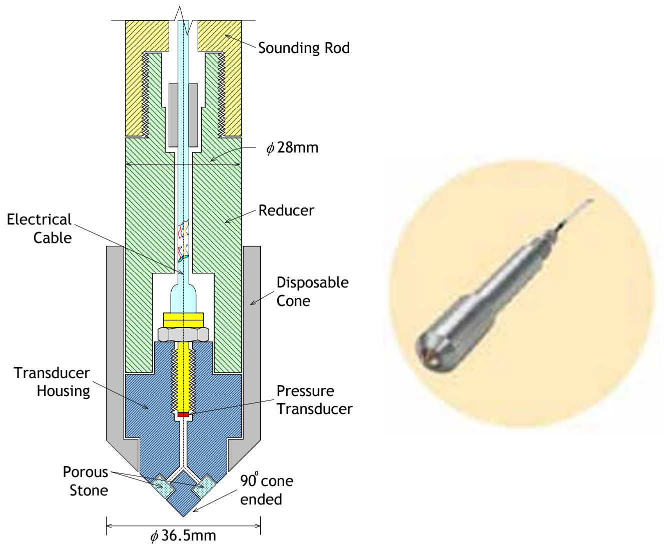

Figure 2. Detailed structure of cone apex with pore pressure transducer.

The accurate assessment of liquefaction resistance of subsoil by means of penetration resistance requires soil types to be determined. Figure 3 illustrates the typical variations of the excess pore water pressure for sandy and clayey soils. Thus, the residual cumulative pore pressure u_R is defined as the excess pore water pressure that remains at the end of the initial penetration phase of the cone tip.

In Figure 4, the residual pore water pressure ratio (u_R/σ'_v, where σ'_v : the vertical effective stress) is correlated with the fine content of tested soils.

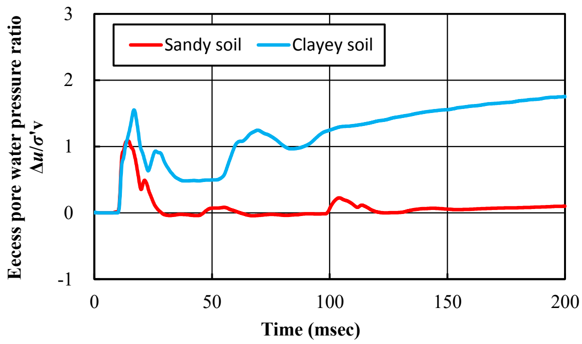

Figure 3. Typical pore water pressure change during cone penetration .

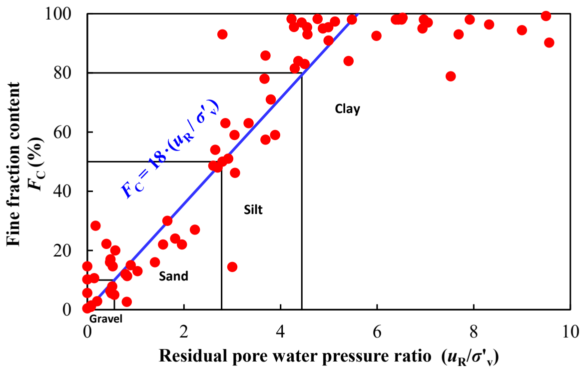

Figure 4. Determination of fine content on the basis of pore water pressure record.

Flow chart for data processing to estimate liquefaction susceptibility using PDC is shown in Figure 5. Residual cumulative pore pressure (u_R), penetration displacement and the depth of investigation without unit weight (γ_t) are able to be obtained by PDC. As far as γ_t, Ground water table (*GWT*), F_C, N value are clear, we can estimate liquefaction susceptibility which is indicated in design specifications.

3.3 *Example Data*

The liquefaction risk is assessed in two ways. First, as widely practiced, the factor of safety, F_L, is determined. As illustrated in Figure 4, the liquefaction resistance, R or otherwise called *CRR*, is determined by using the equivalent $N_{spt} \approx N_d$ together with the assessed F_C. The pore pressure record is further used to determine the level of the ground water table *GWT*. After assessing the fines content F_C, the unit weight of soil γ_t is obtained and if it is different from the initial guess, the effective vertical stress has to be modified corrected and leading to the new cumulative pore pressure ratio and F_C. Thus, there is a provision for feed-back flow in the bottom left of Figure 5. An example of assessed liquefaction risk is illustrated in Figure 6.

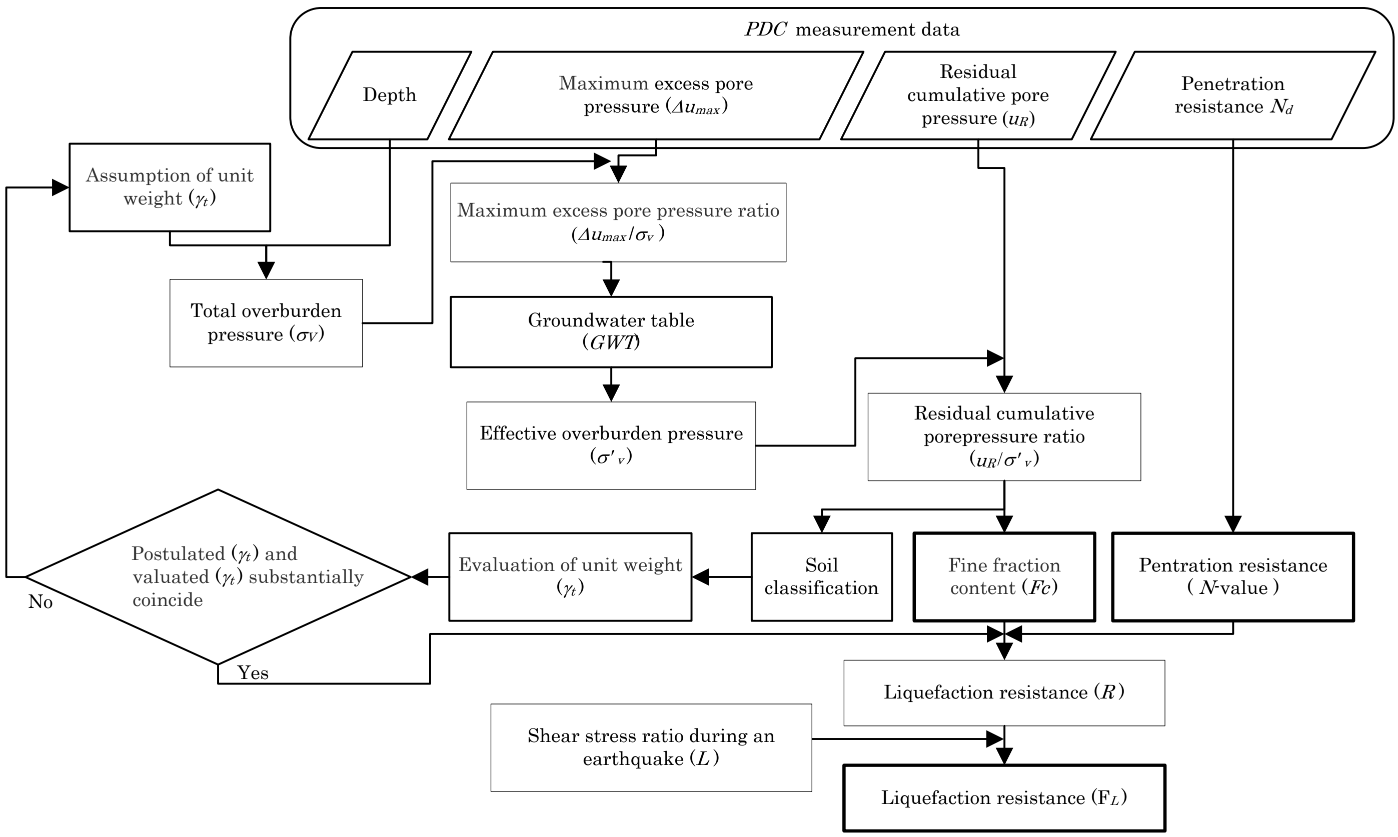

Figure 5. Flow chart to estimate settlement following liquefaction.

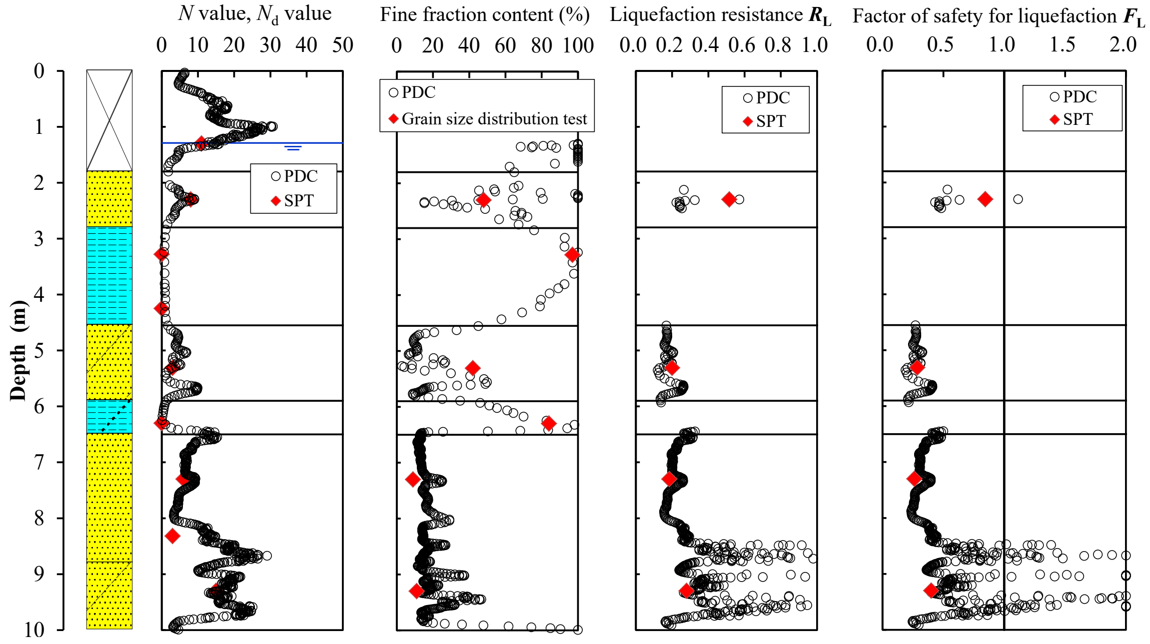

Figure 6. Example of assessed liquefaction risk.

4 PENETRATION AND PULL-OUT TEST (PPT)

4.1 *Mechanism of PPT*

Figure 7 shows a schematic figure of the dynamic penetration test with measurement of the pull-out resistance which is named “Penetration & Pull-out Test (PPT)” proposed in this paper. The test consists of two stage tests, first stage, of which the dynamic penetration test is conducted to the depth of interest; second, the pull-out test, of which the cone apex is pulled out while measuring the resistance.

A light-weight dynamic penetration device (MRS) was used.

The PPT system is equipped with the displacement sensor, triggering sensor, handy terminal and data logger. In addition, load cell is introduced to the pull-out equipment.

A view of the newly developed pull-out equipment is shown in Figure 7(b). The pull-out resistance is measured between the bottom plate and hydraulic cylinders. When the hydraulic cylinders are extending, the pull-out resistance is measured. Figure 8 shows the cone apex of PPT.

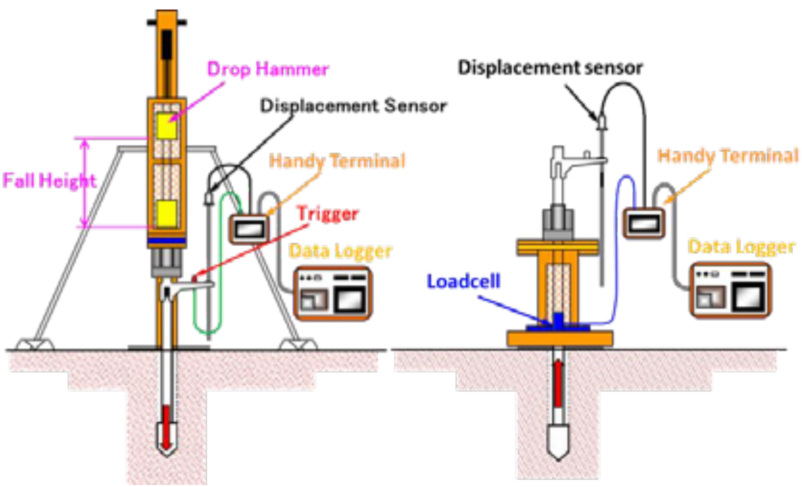

(a) Dynamic Penetration Test (b) Quasi-static Pull out Test

Figure 7. Schematic illustration of PPT.

4.2 *Test Equipment and Data Processing*

The flow chart for data processing to evaluate the liquefaction susceptibility by PPT-method is shown in Figure 9. All data except the unit weight can be obtained by PPT consisting of the dynamic penetration test and the pull-out resistance test by the quasi-static pull-out operation.

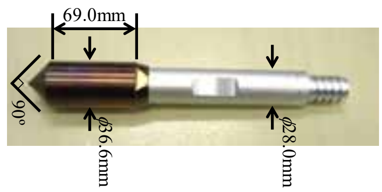

Figure 8. View of PPT cone apex.

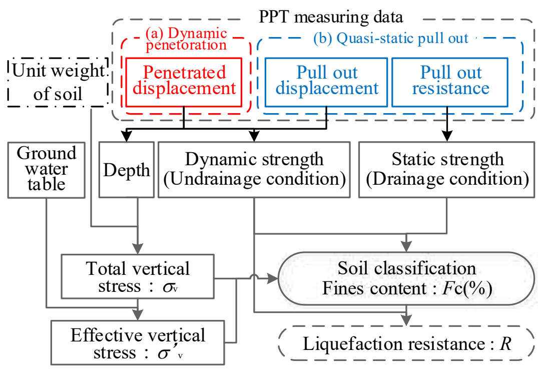

Figure 9. Flow chart to estimate settlement following liquefaction.

Wroth (1984) suggested that CPT data should be normalized as follows:

$$Q_t = \frac{q_t + \sigma_{v0}}{\sigma'_{v0}} \tag{2}$$

$$F_t = \frac{f_s}{q_t - \sigma_{v0}} \times 100 \tag{3}$$

where Q_t= normalized penetrated cone resistance

F_t= normalized pull-out resistance

q_t = cone resistance corrected for the unequal end area effect, $q_t = 392 \times N_d$ (kN/m^2)

f_s = pull-out resistance at the cone tip (kN/m^2)
σ_{v0} = total vertical stress (kN/m^2)
σ'_{v0} = effective vertical stress, $\sigma_{v0} - u_0$ (kN/m^2)

4.3 *Example Data*

Figure 10 shows the example chart for soil classification between normalized penetrated cone resistance (Q_t) and normalized pull-out resistance (F_t) based on PPT data.

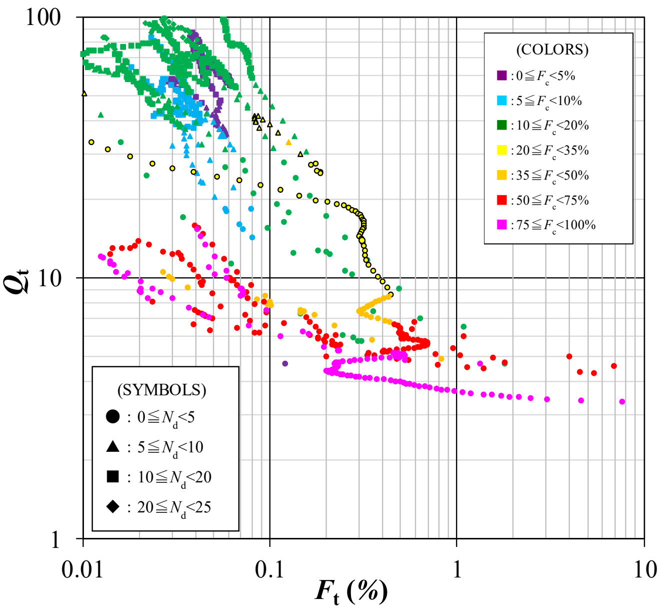

Figure 10. Example for soil classification chart based on PPT.

Colors of the legend show the range of fine contents. The warm colors, for instance from orange to red color indicate the high fine contents that is clayey soil, and cool colors, for instance from yellow to blue color indicate the low fine contents that is sandy soil. The distribution of the relationship between normalized penetrated cone resistance (Q_t) and normalized pull-out resistance (F_t) based on PPT data shows that these data can be used for the soil classification.

5 DYNAMIC WEIGHT SOUNDING (DWS)

5.1 *Mechanism of DWS*

A new index ΔN_{SW} is proposed for estimating liquefaction susceptibility of soils. The index is calculated using the results of two types of Swedish weight sounding test. One test is the traditional quasi-static weight sounding test, from which, $N_{SW\text{-}S}$ (Static), the numbers of half turns per 1 m of penetration is obtained. The other is a newly developed Dynamic Weight Sounding (DWS) in which while applying vibration generated by an electrical hammer drill installed at the top of sounding rod. The number of half turns per 1 m of penetration $N_{SW\text{-}D}$ (Dynamic) is obtained. Existing of liquefiable soils layer can be investigated by ΔN_{sw} which is the difference between $N_{SW\text{-}S}$ and $N_{SW\text{-}D}$.

5.2 *Test Equipment and Data Processing*

A schematic figure of Dynamic Weight Sounding test (DWS) proposed in this paper is shown in Figure 11. The DWS system is modified version of SWS equipment with a dynamic hammer mounted on the top of sounding rod. The system has a very simple structure and is very cheap.

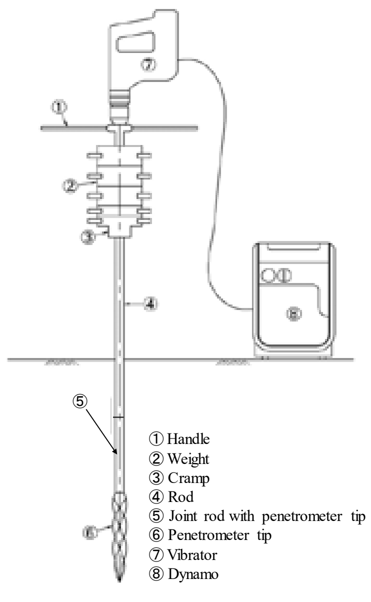

Figure 11. Schematic illustration of DWS.

$N_{SW\text{-}S}$ indicates the static resistance of SWS. On the other hand, $N_{SW\text{-}D}$ indicates the dynamic resistance of DWS. The difference at the same depth between $N_{SW\text{-}S}$ and $N_{SW\text{-}D}$ indicates the liquefaction susceptibility of soils as follows,

$$\Delta N_{SW} = N_{SW\text{-}S} - N_{SW\text{-}D} \tag{4}$$

The flow chart for data processing to estimate depths with high possibility of liquefaction by SWS & DWS-method is shown in Figure 12. All data can be obtained by SWS & DWS measurement.

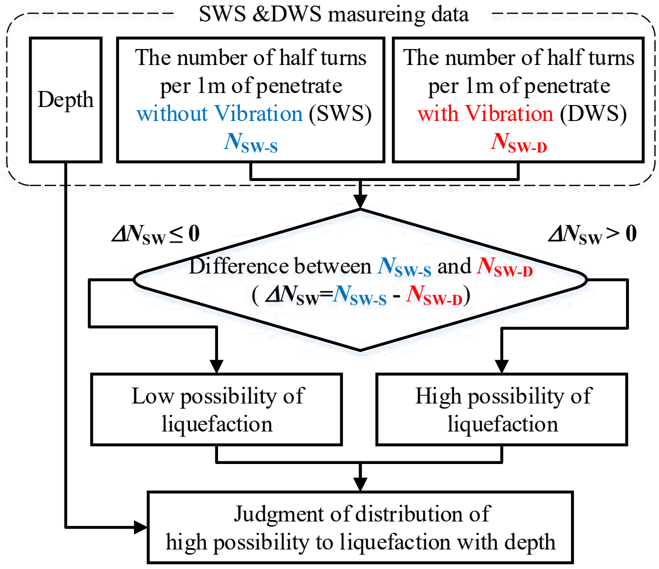

Figure 12. Fow chart of evaluating liquefaction possibility using DWS.

5.3 *Mechanism of DWS*

The soil profile and the number of half turns per 1 m penetration are shown in Figure 13. The sandy soil like an intermediate soil layer (B_{SC}) is deposited from 0.9 m to 2.3 m in depth. And the uniformed medium sand with some fine contents layer (B_S) is from 2.3 m to 3.5 m in depth. These numbers of N_{SW} observed within the sandy soil is under 100 N_{SW} ; indicating SWS results are almost greater than DWS result.

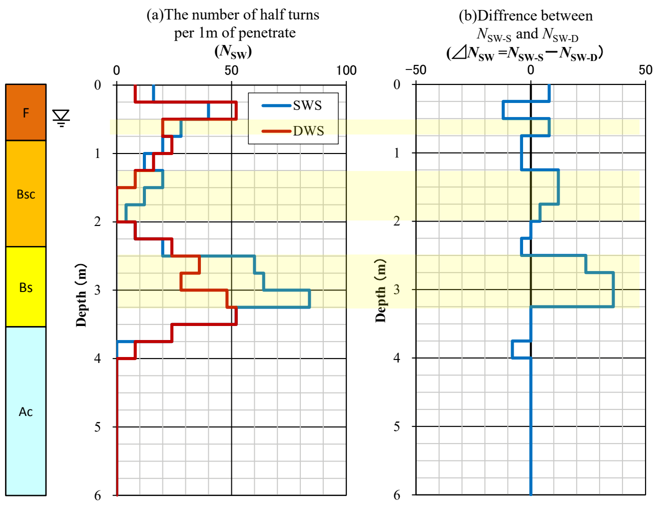

Figure 13. An example data of Dynamic Weight Sounding (DWS)

Figure 13(b) illustrates the distribution ΔN_{SW} along depth. The result of the different between the numbers of half turns DWS and SWS show locally higher value in the loose sandy soil layer rather than in the clay layer which implies that the vibration applied to DWS test affect N_{SW} for sandy soils, more significant. In order to evaluate the liquefaction potentials at each step of DWS, a new index ΔN_{SW} is now defined as equation (4). The discontinuity of ΔN_{SW} is seen in the layers between 1.2 m and 2.0 m and between 2.5 m and 3.2m below the ground surface. Therefore, the liquefaction potential index ΔN_{SW} directly indicates the degree of liquefaction susceptibility. The threshold value of this index, indicating whether the soil layers are liquefiable or not, is 0.0 in this study. An example of in-situ quasi-static and dynamic weight sounding tests was conducted in order to show the effectiveness of the new index. This DWS is an economically sounding and simple in-situ test method for estimating the liquefaction susceptibility of soils

6 CONCLUDING REMARKS

The degree of accuracy is in a relation of the trade-off with economy. The material for reclamation becomes inhomogeneous by the reclaimed method. It is essential for the high-resolute information (advancement of the spatial resolution) on performing the evaluation of soil liquefaction. The most suitable solution which balances degree of accuracy (reliability of the ground information) with economy depends on field conditions. The agenda that is the most important for us is to take care of the field engineer who can select the most suitable technique of the ground investigation technique.

7 REFERENCES

Clayton, C.R.I. & S.S. Dikran, 1982. Pore water pressure generated during dynamic penetration. *Proceedings of the Second European Symposium on Penetrating Testing,* Amsterdam, 245-250.

Janbu, N. & K. Senneset, 1974. Effective stress interpretation of in-situ static penetration test. *Proceedings European Symposium on Penetrating Testing, Stockholm,* Vol. 2.2, 181-193.

Japan Road Association, 2002. *Seismic Design Specifications for Highway Bridges*, pp.120-126, 2002 (in Japanese)

ISO/TS 22476-10, 2005. TECHNICAL SPECIFICATION, *Geotechnical investigation and testing – Field testing – Part 10: Weight sounding test.*

Sawada, S., 2009. Evaluation of differential settlement following liquefaction using. *Piezo Drive Cone, 17th International Conference on Geotechnical Engineering,* Alexandria, Egypt, 1064-1067.

Schmertmann, J.H., 1974. Penetration pore pressure effect on quasi-static cone penetration testing. *Proceedings European Symposium on Penetrating Testing,* Stockholm, Vol. 2.2, 345-352.

Terzaghi, K. & R. B. Peck, 1948. Standard penetration test method for relative density of cohensionless soils. *American Society for Testing and Materials, Philadelphia,* D2049-69.

Robertson, P.K., 1990. Soil classification using the cone penetration test. *Canadian Geotechnical Journal,* 27(1), 151-158.

Wroth, C. P., 1984. The interpretation of in situ soil test. 24th *Rankine Lecture, Geotecnique*, 34(4), pp449-489.

Geotechnical and Geophysical Site Characterisation 5 – Lehane, Acosta-Martínez & Kelly (Eds)

Comparison of liquefaction evaluation based on SPT and geophysical tests (case study: Mahabad dam, Iran)

M.M. Shahrabi
Abgeer Consulting Engineers, Tehran, Iran

F. Jafarzadeh, & A.A. Garakani
Civil Engineering Department, Sharif University of Technology, Tehran, Iran

N. Eskandari & M. Banikheir
Abgeer Consulting Engineers, Tehran, Iran

H. F. Jahromi
Civil Engineering Department, Sharif University of Technology, Tehran, Iran

ABSTRACT: Standard Penetration Test (SPT) is the most commonly used insitu test for soil characterization, including the liquefaction resistance. Many studies have sought to correlate SPT number to cyclic resistance ratio (CRR) as a frequently-used approach for assessment of liquefaction potential. However, it has been shown that SPT has major deficiencies (e.g., inaccuracy in coarse sands and clays) which have given rise to development and utilization of new characterization methods such as geophysical tests (e.g., down-hole and cross-hole). In this paper, a comparison is made between the results of SPT and geophysical tests in three boreholes through the body and foundation of Mahabad Dam (located in north-western part of Iran) and the corresponding assessment of liquefaction potential. It is shown that the cyclic resistance stresses obtained by SPT are lower than those obtained by geophysical tests. Hence, some parts of the dam body are found close to being liquefiable by means of SPT tests, whereas geophysical tests prove the dam site to be safer, indicating considerable discrepancy between the two methods. Additionally, for some parts of the dam body and especially dam foundation where confining pressures are high or the soil is very dense and SPT number (N) is not an applicable characterization measure, shear wave velocities obtained by geophysical tests provide a meaningful tool for assessment of liquefaction potential.

1 INTRODUCTION

The liquefaction potential in soils can simply be evaluated by means of semi-empirical methods by using conventional geotechnical and geophysical site characterization tests. The simplified procedure originally proposed by Seed and Idriss (1971) has been used as the main framework and takes advantage of cyclic resistance ratio (CRR) curves. Initially, this method was based on results obtained by Standard Penetration Test (SPT), however, other geotechnical and geophysical site characterization tests (e.g., cone penetration tests (CPT) and geophysical tests for small-strain shear wave velocity measurement) began to be used as alternatives.

Despite the fact that a larger database is available on real case histories to develop liquefaction potential correlations using SPT or CPT methods, some significant disadvantages make these penetration-type tests not applicable in all conditions. At large depths, such as those encountered under large embankment dams, penetration-type tests are sometimes not feasible and in addition, the available SPT and CPT data are limited to σ'_v/P_a less than about 5.5 and 7, respectively (Boulanger 2003). Penetration-type soil characterization tests are not convenient as well to be performed in some soil types, such as those with large particle size (e.g. gravels and boulders). Consequently, more attention has been drawn to shear wave velocity (V_s) of soils as a useful measure in liquefaction resistance evaluation. According to previous studies, it has been shown that a good precision exists between V_s and the resistance to liquefaction (De Alba et al. 1984; Tokimatsu et al. 1986; Tokimatsu and Uchida 1990). Although respective sensitivity to relative density, D_R, is lower in V_s compared to SPT and CPT test results (Idriss and Boulanger 2006), the fact that verifies the feasibility of V_s for liquefaction evaluation is that some important soil characteristics such as soil fabric and strains caused by past earthquakes, influence the liquefaction resistance and shear wave velocity in a comparable way (Yunmin et al. 2005).

In the present paper, results of SPT and geophysical tests (down-hole and cross-hole) conducted through the body and foundation of Mahabad Dam are presented and the liquefaction potential of the dam body and foundation is evaluated using both test types. The general guidelines provided by Yunmin et al. (2005) are implemented to assess the CRR curves by means of V_S. Lastly, a discussion is made about the obtained liquefaction evaluation curves by SPT and V_s approaches.

2 LOCATION AND GEOLOGICAL SITE CONDITIONS

2.1 *General site conditions*

Mahabad Dam is an embankment dam located about 1 km west of the City of Mahabad, in the Western Azerbaijan Province of Iran. Construction of the dam was completed in 1970; the capacity of the dam reservoir, at the normal water level (1359.1 m.a.s.l.), is about 230 million cubic meters. The dam is located on the Sanandaj-Sirjan Belt (Figure 1-a) and on an alluvial foundation of silty sand with fine-grained and coarse-grained sandy lenses. The South Mahabad Fault is situated about 3.5 km on the south of Mahabad dam and is considered as the most effective fault on the dam site (Figure 1-b). Thickness of the alluvial strata is approximately 25 meters under the right abutment and near 8 meters under the left abutment. The high reservoir capacity of the dam, being located near a large city together with being susceptible to seismic activities and a potential liquefiable foundation, necessitate a thorough liquefaction analysis for this 45-year-old embankment dam.

2.2 *Determination of the peak ground acceleration (PGA)*

For determination of the strong ground motion parameters at Mahabad Dam site, especially the peak ground acceleration (PGA) used for semi-empirical liquefaction potential assessment, different methods of deterministic and probabilistic seismic hazard analyses were applied. The probabilistic line-source method proposed by Cornell (1968) were used for evaluation of various seismic levels, including CE (Construction Earthquake), ODE (Operating Basis Earthquake), DBE (Design Basis Earthquake) and MDE (Maximum Design Earthquake) by means of the software SEISRISK-III (Bender and Perkins 1987). To obtain the Maximum Credible Earthquake (MCE), a number of attenuation relationships (Ambraseys et al 2005, Campbell and Bozorgnia 2008, Akkar and Bommer 2010), with considering different faults as the seismic source, were examined by a deterministic approach. Results indicate that the largest earthquake by the South Mahabad Fault is $Ms=6.4$, causing a maximum horizontal acceleration of about $PHA=0.50g$ at the dam site (Table 1).

Table 1. Values of maximum strong motion accelerations at the Mahabad dam site for different design earthquakes

Criteria	Return period (years)	Analysis method	Max. horizontal acceleration (g)
CE	80% of OBE	Probabilistic	0.08
OBE	145	Probabilistic	0.10
DBE	475	Probabilistic	0.16
MDE	2000	Probabilistic	0.27
MCE	Deterministic		0.50

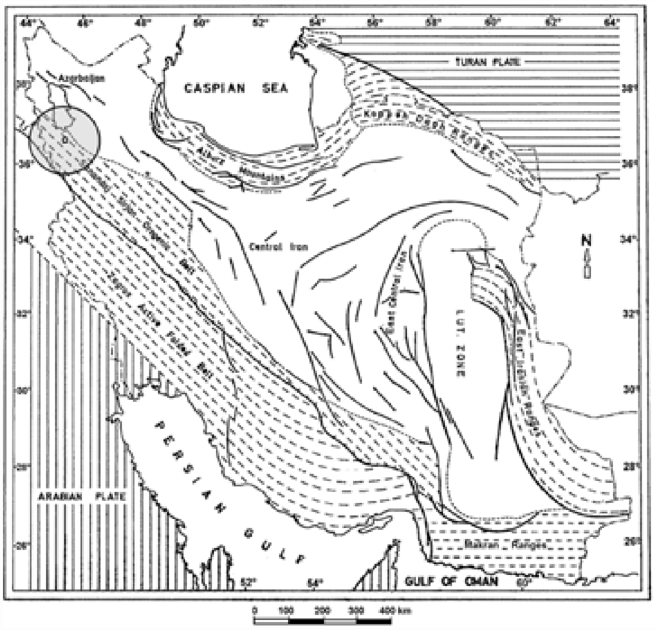

(a)

(b)

Figure 1. Mahabad Dam site; (a) location of the dam inside the Sanandaj-Sirjan Belt (b), the nearest faults (looking to west)

3 FIELD INVESTIGATIONS

Standard penetration tests (SPT) and small-strain geophysical tests (down-hole and cross-hole) were performed through the Mahabad dam body and foundation in 2013 and 2015, respectively. Three primary boreholes were drilled, topping from approximately 7 meters below the dam crest at three different sections for the purpose of carrying out the standard penetration tests (A2 at km=0+250, B2 at km=0+300, C2 at km=0+400, all distances measured from the end of the crest on the left abutment). As seen in Figure 2, A2, B2 and C2 boreholes were drilled through the downstream shell into the dam foundation at depths of 90, 85 and 85 meters, respectively. Secondary boreholes were also drilled next to each primary borehole for the purpose of cross-hole seismic tests.

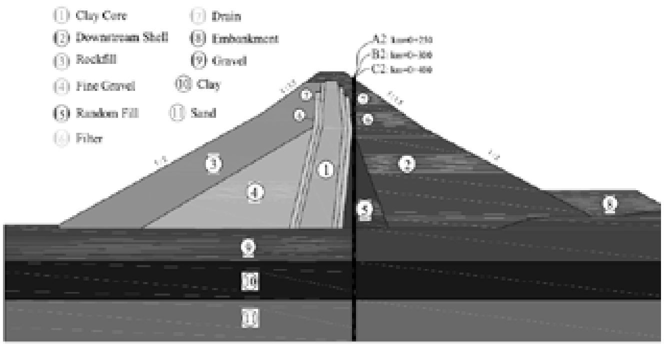

(a)

(b)

Figure 2. (a) Main section and borehole positions at Mahabad Dam (b) A view from downstream slope of the dam and placement of the drilling equipment near the crest

3.1 *Standard penetration tests (SPT)*

The liquefaction resistance evaluation of the dam body and foundation may be directly assessed by means of the SPT *N*-value (Seed and Idriss, 1971). Alternatively, correlations can be used to convert SPT *N*-values to the corresponding shear wave velocities (V_S) which are then used to evaluate the liquefaction resistance of soils. In this study, the latter approach was implemented making it possible to directly compare the results of geotechnical and geophysical tests. A total number of 121 standard penetration tests were performed inside the three boreholes at the dam. For the purpose of obtaining V_s from the SPT *N*-value, 8 correlations were used (Shibata, 1970; Ohta et al, 1972; Imai & Tonouchi, 1982; Sykora & Stokoe, 1983; Okamoto et al, 1989; Lee, 1990; Hasancebi & Ulusay, 2006; Dikemen, 2009). The average V_s (not V_{s1}) achieved by these correlations are plotted in Figure 3.

3.2 *Geophysical tests (down-hole and cross-hole)*

In the second-phase of filed investigations, geophysical tests were carried out in the form of down-hole and cross-hole tests. A secondary borehole was drilled adjacent to each primary borehole for the purpose of cross-hole tests. Geophones were placed inside the primary boreholes at every two meters and a shear wave source was placed at the top of the boreholes for down-hole tests, while in cross-hole tests, shear waves were produced in the secondary boreholes at 2-meter intervals and recorded at the primary boreholes. The shear wave velocities were calculated for the three boreholes and the results are shown in Figure 3. As observed in this figure, shear wave velocities obtained by both geophysical methods are quite the same. However, results show that at depths greater than 20 meters, the standard penetration tests, underestimate the shear wave velocities and this, in particular, is a result of inaccuracy of *N*-V_s correlations for high confining pressures at medium depths (20-50 m). Additionally, it is observed that at greater depths (e.g., >50 m), SPT tests were refused (*N*>50). As a result, the obtained V_S values based on SPT results are not useful. As previously mentioned, this is a clear example of shortcomings of penetration-type tests such as SPT at large depths.

4 LIQUEFACTION POTENTIAL ASSESSMENT

The criterion proposed by Yunmin et al. (2005) was used to estimate the liquefaction potential at the three boreholes through the body and foundation of Mahabad Dam. This method takes advantage of comparing the earthquake-induced cyclic shear stress ratio, CSR, with the cyclic resistance ratio, CRR, as a function of stress-corrected shear wave velocity (V_{s1}). The liquefaction potential based on SPT and geophysical tests is assessed and depicted in Figure 4. The figure shows that SPT results evaluate the liquefaction potential inside the non-liquefiable zone but very close to the potentially liquefiable zone. Nevertheless, the results obtained by geophysical tests demonstrate a greater liquefaction safety factor in comparison with SPT results. As discussed before, this may be attributed to the limitations of penetration-type field investigations for liquefaction evaluation at large depths (e.g., greater than 20 meters).

5 CONCLUSIONS

Mahabad Dam was constructed more than 45 years ago in the Western Azerbaijan Province, Iran. At the time it was built, the knowledge about soil liquefaction was very limited. Therefore, no reasonable investigations were carried out to evaluate the liquefaction potential of the dam body and foundation. Recently, a set of complementary geotechnical (SPT) and geophysical (down-hole and cross-hole) site investigations were conducted to characterize soil conditions and obtain the shear wave velocities at the dam site. The data were then used to assess the

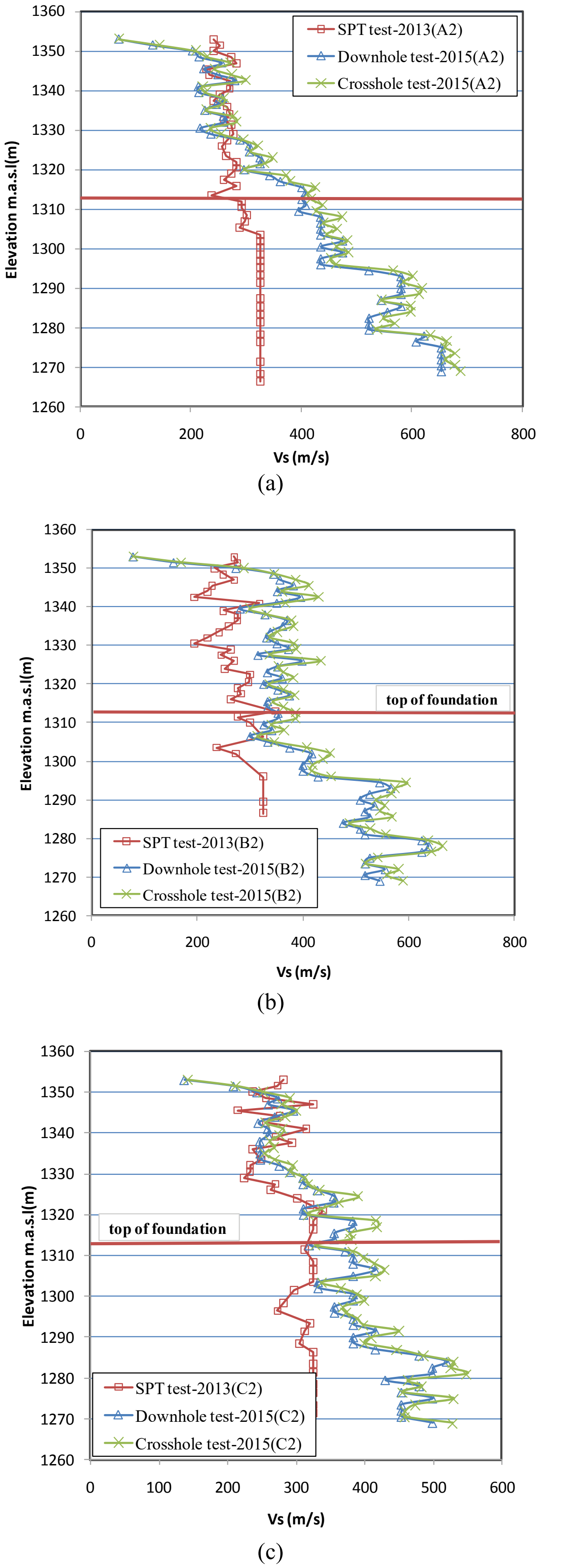

Figure 3. Shear wave velocity profiles for (a) A2, (b) B2, and (c) C2 boreholes obtained by SPT, down-hole and cross-hole tests

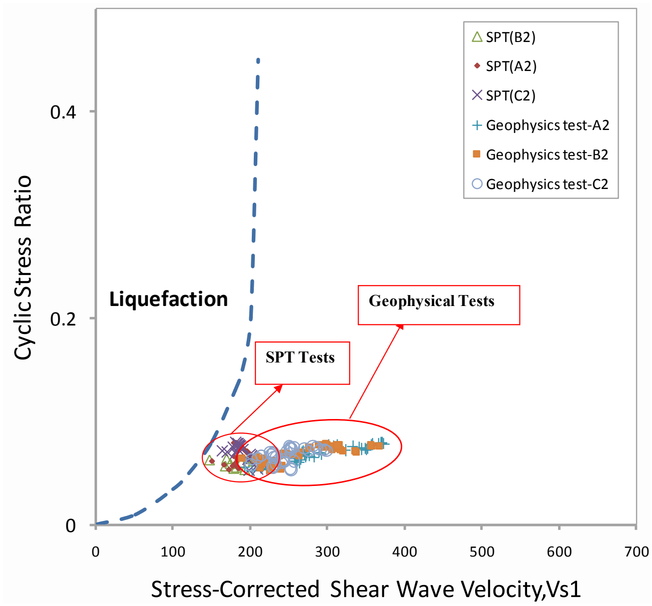

Figure 4. Liquefaction potential assessment at Mahabad Dam body and foundation, cyclic shear stress ratio (CSR) vs. stress-corrected shear wave velocity (V_{s1})

liquefaction potential of the dam body and foundation. Results indicate that the correlations used for converting the SPT *N*-Value to V_s are accurate only at small depths and should be used with caution for medium to large depths (>20 m). Although a larger database is available for liquefaction potential correlations developed by means of SPT, penetration-type tests are not feasible at large depths (> 50 m), typically encountered in large embankments such as earth dams. The geophysical values for the stress-corrected shear wave velocities (V_{s1}), as an indication of the cyclic resistance ratio (CRR), are significantly higher on average than those obtained by the SPT, and in this case seem to be more reliable, demonstrating no liquefaction exposure for the Mahabad Dam.

6 REFERENCES

Akkar, S. & Bommer, J.J. 2010. Empirical equations of the prediction of PGA, PGV, and spectral accelerations in Europe, the Mediterranean region, and the Middle East. *Seismological Research Letters* 81(2): 195-206.

Ambraseys, N.N., Douglas J., Sarma S.K. & Smit P.M. 2005. Equations for the estimation of strong ground motions from shallow crustal earthquakes using data from Europe and the Middle East: horizontal peak ground acceleration and spectral acceleration. *Bulletin of Earthquake Engineering* 3: 1-53.

Bender, B. & Perkins, D.M. 1987. SEISRISK-III, A computer program for seismic hazard estimation. *US Geological Survey*, Bulletin 1772.

Boulanger, R.W. 2003. High overburden stress effects in liquefaction analyses. *Journal of Geotechnical and Geoenvironmental Engineering* 129(12): 1071-1082.

Campbell, K.W. & Bozorgnia, Y. 2008. NGA ground motion model for the geometric mean horizontal component of PGA, PGV, PGD and 5% damped linear elastic response spectra for periods ranging from 0.01 to 10 s. *Earthquake Spectra* 24(1): 139-171.

Cornell, C.A. 1968. Engineering seismic risk analysis.” *Bulletin of the Seismological Society of America* 58(5): 1583-1606.

De Alba, P., Baldwon, K., Janoo, V., Roe, G., & Celikkol, B. 1984. Elastic-wave velocities and liquefaction potential. *Geotechnical Testing Journal* 7(2): 77-88.

Dikmen, U. 2009. Statistical correlations of shear wave velocity and penetration resistance for soils, *Journal of Geophysics and Engineering* 6: 61-72.

Hasancebi, N. & Ulusay, R. 2006. Empirical correlations between shear wave velocity and penetration resistance for ground shaking assessments. *Bulletin of Engineering Geology and the Environment* 66: 203-213.

Idriss, I.M. & Boulanger, R.W. 2006. Semi-empirical procedures for evaluating liquefaction potential during earthquakes. *Soil Dynamics and Earthquake Engineering* 26: 115-130.

Imai, T. & Tonouchi, K. 1982. Correlation of N-value with S-wave velocity and shear modulus. *Proc. 2nd European Symp. Of Penetration Testing*: 57-72.

Lee, S.H. 1990. Regression models of shear wave velocities. *Journal of Chinese Institute of Engineers* 13: 519-32.

Ohta, T., Hara, A., Niwa, M. & Sakano, T. 1972. Elastic shear moduli as estimated from N-value. *Proc. 7th Ann. Convention of Japan Society of Soil Mechanics and Foundation Engineering*: 265-268.

Okamoto, T., Kokusho, T., Yoshida, Y. & Kusuonoki, K. 1989. Comparison of surface versus subsurface wave source for P–S logging in sand layer. *Proc. 44th Annual Conference JSCE* 3: 996-997 (in Japanese).

Seed, H.B. & Idriss I.M. 1971. Simplified procedure for evaluating soil liquefaction potential. *Journal of Soil Mechanics and Foundation Division* 97(9): 1249-1273.

Shibata, T. 1970. Analysis of liquefaction of saturated sand during cyclic loading. *Disaster Prevention Resources Institute Bulletin* 13: 563–70.

Sykora, D.E. & Stokoe, K.H. 1983. Correlations of in-situ measurements in sands of shear wave velocity. *Soil Dynamics and Earthquake Engineering* 20: 125–136.

Tokimatsu, K. & Uchida, A. 1990. Correlation between liquefaction resistance and shear wave velocity. *Soils and Foundations* 30(2): 33–42.

Tokimatsu, K., Yamazaki, T. & Yoshimi, Y. 1986. Soil liquefaction evaluation by elastic shear moduli. *Soils and Foundations* 26(1): 25–35.

Yunmin, C., Han, K. & Ren-peng, C. 2005. Semi-empirical procedures for evaluating liquefaction potential during earthquakes. *Soil Dynamics and Earthquake Engineering* 25: 461–469.

Geotechnical and Geophysical Site Characterisation 5 – Lehane, Acosta-Martínez & Kelly (Eds)
© 2016 Australian Geomechanics Society, Sydney, Australia, ISBN 978-0-9946261-1-0

Fines Content Correction Factors for SPT N Values – Liquefaction Resistance Correlation

M. M. Shahien
Tanta University, Tanta, Egypt

ABSTRACT: It is common practice to evaluate liquefaction potential from correlation between liquefaction resistance as determined from field performance of soil deposits during past earthquake events and in-situ pen-etration test results. Historically, Seed and co-workers started the correlation with SPT N values. In such cor-relations, the influence of non- or low-plastic fines is taken into account by correcting SPT N values with fines content correcting factors. The correction factors are based on empirical data. The correction factors increases with the increase in fines content (FC) up to FC of about 35% and remains constant with any further increase in FC. However, laboratory investigations show a significant reduction in the cyclic resistance of sands contain-ing FC greater than 35%. Furthermore, after re-visiting of the SPT N –liquefaction case histories, Green et al. (2006) observed a trend consistent with the significant drop in the cyclic resistance of soils containing FC> 35%. This paper provides a new set of correction factors that is consistent with field and laboratory observa-tions. The correction factors are applicable to wide ranges of FC greater than 35%.

1 INTRODUCTION

1.1 *General*

The most common practice to evaluate liquefaction potential (initiation or triggering) is to use correlation between liquefaction resistance as determined from field performance of soil deposits during past earthquake events and in-situ penetration test results. Historically, Seed and co-workers started the correlation with SPT N values. Such effort started with the "simplified" procedure by Seed and Idriss (1971). Using the correlation between liquefaction resistance and penetration test results relies on an extensive database of field performance for soil deposits which did or did not liquefy during past earthquake events. Databases of such performances were developed over the years (Tokimatsu and Yoshimi, 1983; Seed et al., 1984; Jamiolkowski et al., 1985; Ambraseys, 1988; Fear and McRoberts, 1995; Cetin et al., 2000; Idriss and Boulanger, 2006; and Shahien, 2007). The developed correlation was in the form of cyclic resistance ratio (CRR) versus SPT N values corrected for both procedure and effective overburden pressure $(N_1)_{60}$. The correlation was presented for clean sand base curve and for other values of fines content as shown in Figure (1). Similar correlations were developed for other in situ tests such CPT and Vs (e.g. Youd et al., 2001).

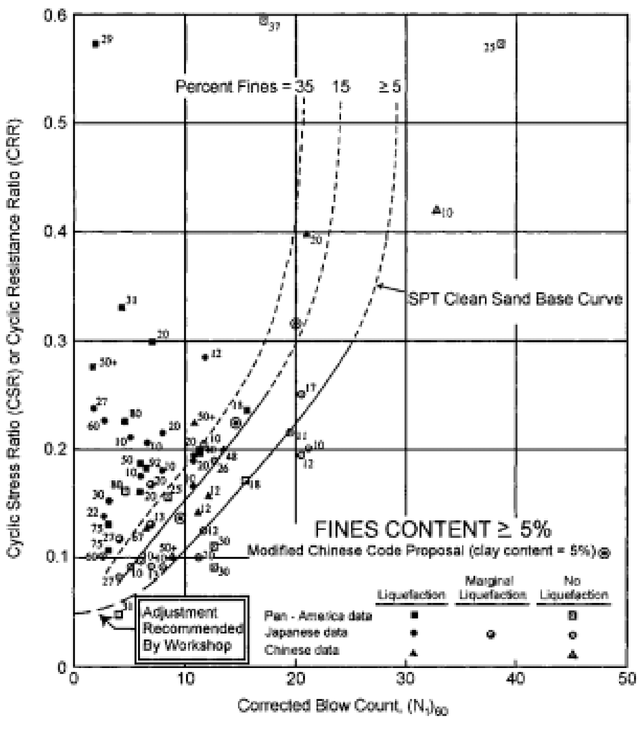

Figure 1. CRR versus $(N_1)_{60}$ curves based on case histories for various Fines Content (After Seed et al. (1984) modified by Youd et a. (2001)).

1.2 *Existing fines content correction factors*

It has been common practice to correct $(N_1)_{60}$ to equivalent clean sand $(N_1)_{60\text{-}CS}$ using the following expression:

$$\left(N_1\right)_{60-CS} = \left(N_1\right)_{60} + \Delta\left(N_1\right)_{60} \tag{1}$$

The fines content correction factors $\Delta(N_1)_{60}$ have been derived from Figure (1) by pairing the SPT $(N_1)_{60}$ value that corresponds to a certain value of CRR on the base clean sand curve with (FC≤5%) to the SPT $(N'_1)_{60}$ values corresponding to the same CRR on the other curves for sand with FC (Figure 2) (Shahien and Mesri, 1999).

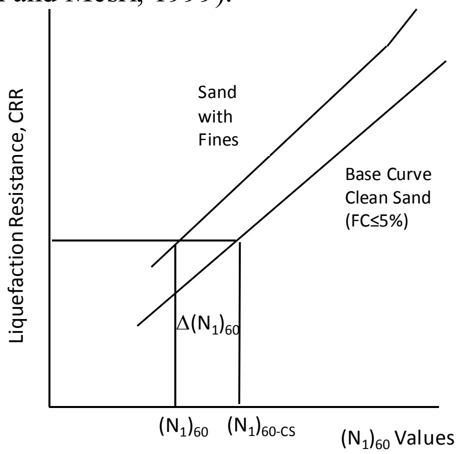

Figure 2. Schematic diagram showing the derivation of FC correction factors using base clean sand curve (Figure 1)

Table (1) lists the forms of existing correction factors available in the literature. Figure (3) shows the correction values of $\Delta(N_1)_{60}$ calculated from most of the references in Table (1). Some of the corrections were put in the form of $\Delta(N_1)_{60}$ such as Cetin et al. (2004) for sake of comparison with other corrections.

Table 1. Summary of FC correction factors in literature

Form	Reference
$(N_1)_{60\text{-}CS} = (N_1)_{60} + \Delta(N_1)_{60}$	
$\Delta(N_1)_{60}$ = constant	Seed et al. (1983)
$\Delta(N_1)_{60} = f(\text{FC})$	Tokimatsu and Yoshimi (1983)
	Seed et al.(1984) – Terzaghi et al (1996)
	Kayen and Mitchell (1997)
	Shahien and Mesri (1999)
	Youd et al. (2001)
	Idriss and Boulanger (2006)
$\Delta(N_1)_{60}=g[\text{FC},(N_1)_{60}]$	Idriss and Seed (1996)
	Robertson and Wride (1996)
$(N_1)_{60\text{-}CS} = C_{fines}(N_1)_{60}$	
$C_{fines}= k[\text{FC},(N_1)_{60}]$	Cetin et al. (2004)

It should be noted that the correction by Shahien and Mesri (1999) was based on the conventional correction by Terzaghi and Peck (1948) for SPT N values of fine and silty sands. The original correction was N_{cs}=a+0.5(N-a) with a = 15. A modification was applied using a=20 instead of 15. Such modification was based on Peck (1997). It is interesting that such correction lies within the range of the other corrections. With the exception of the Shahien and Mesri correction, all the other corrections have limiting correction value for FC ≥ 35%. Further noted is the wide range of corrections.

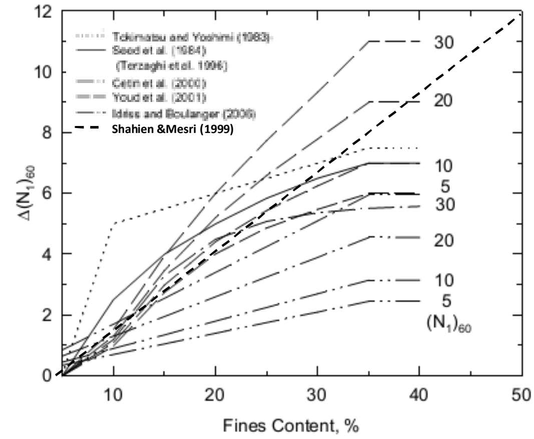

Figure 3. $\Delta(N_1)_{60}$ versus FC relationships in the literature

1.3 *Motivation and aim of this paper*

Most of the above mentioned correction factors suggest an increase in penetration resistance with the increase of FC until FC of about 35% after which no further increase in penetration resistance with increase in FC above 35%.

Green et al. (2006) used 98 case records of SPT N with liquefaction/no liquefaction from 14 earthquakes from existing databases to examine FC correction factors. The $(N_1)_{60}$ values obtained from the base curve "clean sand" with FC≤5% were corrected for FC using the correction factors of Youd et al. (2001) to produce family of curves for FC of 10%, 20%, 30% and >35%. The data records were plotted on these curves. Green et al. (2006) concluded that the Youd et al. (2001) corrected curves rationally divided the liquefaction/no liquefaction data for FC≤35%. Nevertheless, for FC>35% considerable chunk of "liquefied" number of data points fell well below the CRR curve in the "no liquefaction" zone (Figure 4). Such observation proved that the existing FC correction factors could lead to un-conservative liquefaction resistances. Green et al. (2006) suggested that no FC correction (i.e. no increase in $(N_1)_{60}$) should be applied in case of FC>35% until further investigations could better explain the concluded trend.

Idriss and Boulanger (2010) developed updated database of field liquefaction records and carried out similar exercise utilizing the Idriss and Boulanger (2006) correction factors. The conclusion of Idriss and Boulanger (2010) contradicts the conclusion of Green et al.(2006).

It should be noted that both investigation teams used filtering process to include good quality records. Green et al. (2006) used 98 cases, while Idriss and Boulanger (2010) used 230 cases. The contradiction between the two conclusions motivated the author to investigate the matter. Thus the aim of this paper is to provide a set of correction factors obtained using different approach.

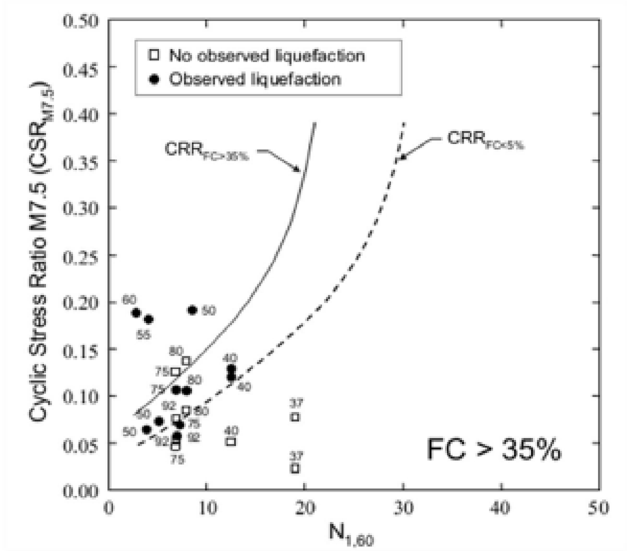

Figure 4. Results of re-analysis of SPT liquefaction case histories for FC > 35%. Numbers next to data points are the corresponding FC. (After Green et al., 2006)

1.4 *Proposed correction factors: Methodology*

As discussed earlier, most of the FC correction factors existing in the literature are derived from field performance correlation such as that in Figure 1. A different approach is followed in this paper. The proposed correction factors developed in this paper utilizes two correction factors; (1) Correction factors to correct influence of FC on penetration resistance, and (2) Correction factors to correct influence of FC on CRR. Combining both correction factors results in correction factors to correct influence of FC on CRR versus penetration resistance correlation.

2 CORRECTION FOR INFLUENCE OF FINES CONTENT ON PENETRATION RESISTANCE

2.1 *Influence of FC on penetration resistance*

Standard Penetration Test (SPT) is a dynamic test. Depending on the compressibility or contractiveness of the tested soil, a penetration induced excess porewater pressure tends to develop during penetration. The excess water pressure tends to dissipate with a rate that depends on the permeability of the soil. As non/low plastic fines content increases in the soil, the contractiveness increases thus the excess porewater pressure increases and the permeability decreases thus the dissipation of the water pressure tends to be slower. Both actions tend to decrease the measured SPT N values. Thus, as FC increases, the measured N value decreases and the deviation from representing the original state of denseness of the soil increases. Such deviation necessitates the correction of the measured N. Figure (5) shows relationship between measured N values and FC using the data from the database of Cetin et al. (2000).

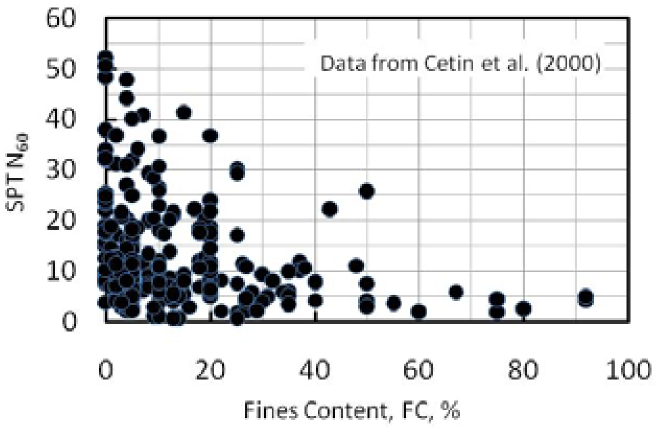

Figure 5. Relationship between SPT N_{60} versus FC.

2.2 *Penetration resistance versus Dr correlation*

Meyerhof (1957) proposed a correlation between the SPT N value and relative density, Dr, for clean sands based on chamber data in the following form:

$$\frac{N_1}{Dr^2} = a + b = 41 \tag{2}$$

Skempton (1986) collected more data of the kind for granular soils with different particle size characteristics. Skempton (1986) followed the same form and proposed that the relationship between $(N_1)_{60}$ and Dr to be in the following form:

$$\left(\frac{N_1}{Dr^2}\right) = a + b \tag{3}$$

where, a+b is constant that decreases with the increase in mean particle size of the granular soil.

Cubrinovski & Ishihara (1999), (2000) & (2001) used SPT measurements of field deposits along with data of high-quality undisturbed samples to prove that a+b defined as C_D is dependent on grain characteristics such as particle size, gradation and fines content. It was further suggested that grain characteristics can be well represented by void ratio range (e_{max}-e_{min}) or the difference in the void ratio between the loosest, e_{max}, and densest, e_{min}, packing states. The following correlation was proposed by Cubrinovski & Ishihara for gravelly, clean sand and sands with fines:

$$\frac{(N_1)_{60}}{Dr^2} = C_D = \frac{9}{\left(e_{max} - e_{max}\right)^{1.7}} \tag{4}$$

2.3 *Relationship between void ratio range and FC*

Cubrinovski & Ishihara (2002) proposed a relationship between void ratio range and FC for natural sandy and silty soils based on comprehensive data. The range of data used, as well as the average correlation by Cubrinovski & Ishihara, is shown in Figure (6). Shown also on Figure (6) back calculated values of the void ratio range based on the Youd et al (2001) correction. Figure (6) also shows the correlation peoposed ans used in this paper. The proposed relationship was influenced by the back calculated values.

Cubrinovski & Ishihara identified that the rate of increase in the void ratio range with the increase in FC changed around the FC of 30%. This is related to the difference in particle structure of sand in the two ranges separated by FC=30%. In the lower range, the particle structure is governed by coarse-grained fraction of the soil. On the other hand, in the upper range of FC, the soil structure is governed by the fine-grained fraction of the soil.

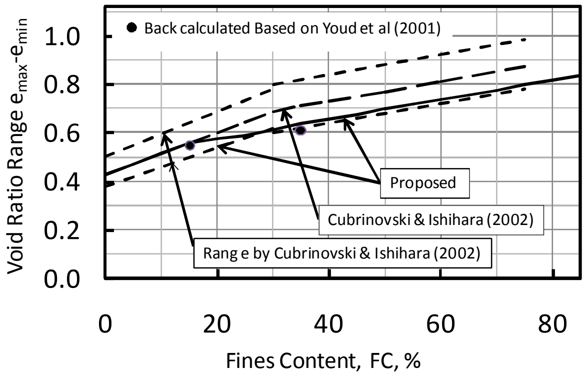

Figure 6. Relationship between e_{max}-e_{min} versus FC.

2.4 *Proposed correction for influence of FC on N*

Substituting values of the proposed correlation from Figure (6) in Equation (4), the relationship in Figure (7) is obtained between N values and FC for various relative densities.

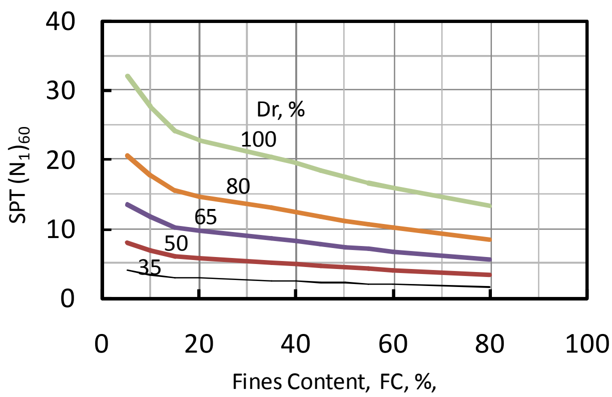

Figure 7. Correlation between $(N_1)_{60}$ versus FC for various Dr.

The range of data in Figure (7) resembles the range of data in Figure (5) taking into consideration the fact that in Figure (7) N values are corrected for the influence of effective overburden pressure, while in Figure (5) N values are not corrected for overburden pressure. The data in Figure (7) or Equation (4) is used to introduce correction factor for influence of FC on N values, RN_{FC}, that is shown in Figure (8).

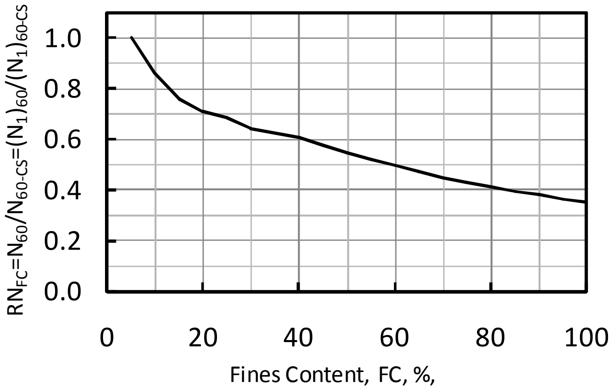

Figure 8. Correction for influence of FC on N.

3 CORRECTION FOR INFLUENCE OF FC ON CRR

Polito and Martin (2003) examined many of the laboratory parametric studies examining the influence of FC on CRR of sandy soils. Such an examination clarified the conflicting conclusions of these studies such as CRR increases, decrease and unaffected with the increase in FC. Furthermore, Polito and Martin (2001) introduced the concept of limiting fines content (LFC) showing that if the relative density of a non/low-plastic silt-sand mix is kept constant, the CRR of the mix is insensitive to FC up to the LFC, at which the CRR significantly reduces to a value that is almost unaltered by further increase in FC. Thus the LFC differentiate between two ranges of FC. The first one is the range in which the mix behaves as coarse grained soil with no significant influence of fines presence. In the second range, the mix behaves as fine grained soil with no significant influence of sand presence. Polito (1999) reported, confirmed by Cubrinovski and Ishihara (2002), that the LFC occurs in the range of 30% to 40%. Utilizing the data reported by Polito (1999) for Yatesville silt/sand mixture having Dr of 30%, The correction factor, $RCRR_{FC}$, to correct CRR for FC is introduced in Figure (9) based on Polito (1999) data. The correction factor has two values with a transition zone separating the above mentioned two ranges.

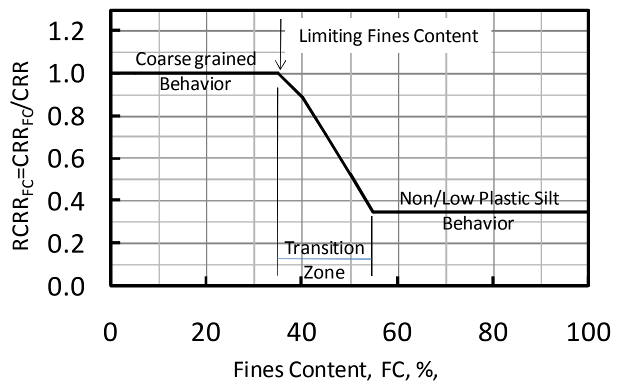

Figure 9. Correction for influence of FC on CRR (Modified after Polito, 1999)

4 COMBINED CORRECTION FOR INFLUENCE OF FC ON CRR-$(N_1)_{60}$ RELATIONSHIP

The correction factors in Figures (8) and (9) can be applied on the clean sand base curve shown in Figure (1). Figure (10) shows a clarifying sketch to explain how the CRR versus penetration resistance for silty sand with FC can be obtained. For FC ≤LFC, RN_{FC} <1 (Figure 8) and $RCRR_{FC}$=1 (Figure 9). Thus the resulting curve shall be a shift to the left reducing the penetration resistance values. On the other hand, for FC>LFC, RN_{FC}<1 (Figure 8) and $RCRR_{FC}$<1 (Figure 9). Thus the resulting curve shall reflect reduction in penetration resistance and reduction in CRR (Figure 10). Figure (11) shows the SPT clean sand base curve and CRR versus penetration resistance for various values of FC obtained using the corrections presented in this paper.

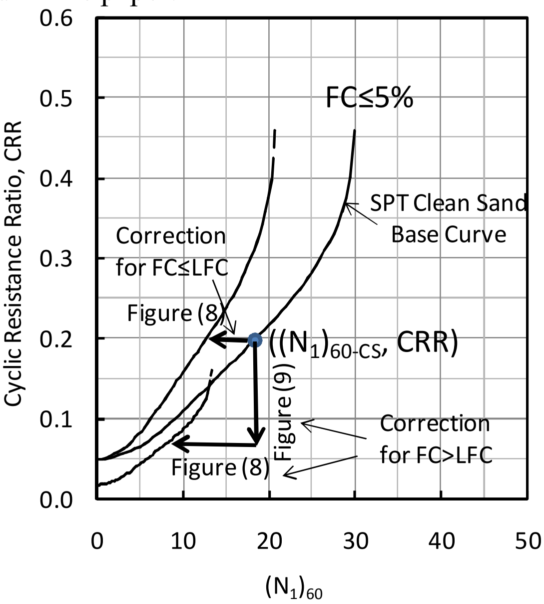

Figure 10. Combined correction for influence of FC on CRR versus $(N_1)_{60}$ relationship

It should be noted that the CRR versus $(N_1)_{60}$ curves for FC of 15% and 35% are almost identical to and confirming the curves of Youd and Idriss (2001) or youd et al (2001) showing higher cyclic re-sistance with the increase in FC. The curves for FC of 50%, 60% and 80% are different from what is currently known to be grouped with the curve of FC≥35%. The curves tend to reflect lower cyclic re-sistance close to or even lower than the curve for FC≤5%. The curves for FC of 50%, 60% and 80% tend to be close to each other to the extent that a single relationship can be proposed as shown in Fig-ure (12) in the next section.

5 FIELD CASE RECORDS CONSIDERATION AND PROPOSED RELATIONSHIP

As mentioned earlier, Green et al. (2006) used 98 case records of SPT N with liquefaction/no liquefac-tion from 14 earthquakes from existing databases to examine FC correction factors. The case records with FC>35% used by Green et al. (2006) (Figure 4) are used in this section to evaluate the curves obtained using the approach presented in this paper and shown in Figure (11). Those data are plotted in Figure (12) together with the relationships for FC of 35%, 50%, 60% and 80% from Figure (11).

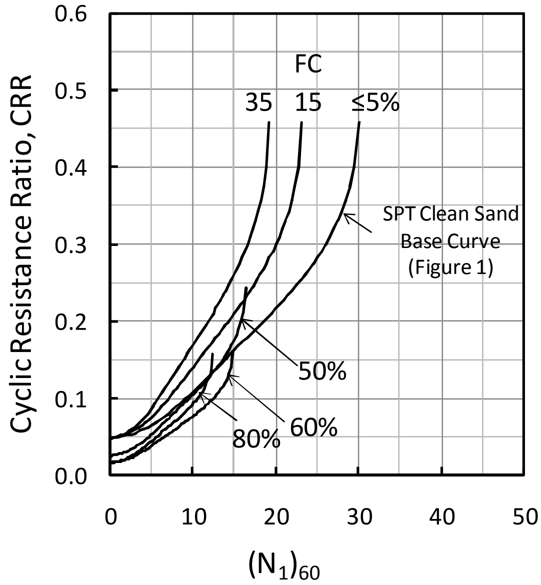

Figure 11. CRR versus $(N_1)_{60}$ for various FC

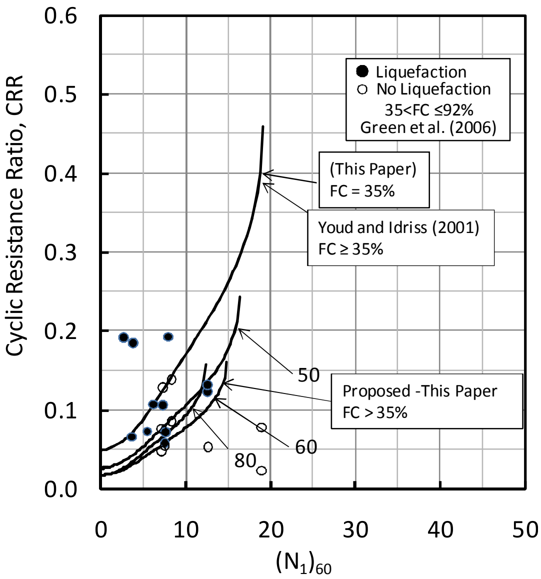

Figure 12. CRR versus $(N_1)_{60}$ for various FC and liquefaction/ no liquefaction case records for 35<FC≤92%

It is interesting to note that the liquefied case records could be well bounded by the bundle of curves for FC of 50%, 60% and 80% obtained by the approach presented in this paper. This is encouraging to the extent that a single curve can be proposed for FC>35% replacing the very close bundle of curves for FC of 50%, 60% and 80%. It should be noted that for FC in the range of 35 to 50%, there is a transition zone that can be conservatively ignored for practical purposes. Thus, based on the approach presented in this paper, the proposed CRR versus $(N_1)_{60}$ relationships for various non/low plastic FC are shown in Figure (13). The proposed curves are identical to those of Youd and Idriss (2001) for

FC≤35%. For FC≥35%, a single curve is proposed in this paper.

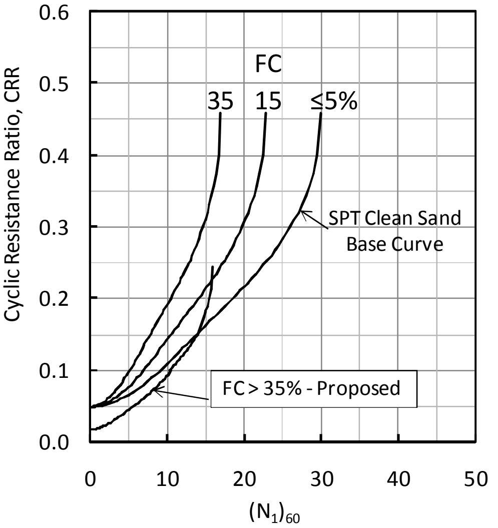

Figure 13. CRR versus $(N_1)_{60}$ for various FC and liquefaction/ no liquefaction case records for 35<FC≤92%

6 CONCLUSION

This paper presents an alternative approach to obtain fines contents correction to the liquefaction resistance versus penetration resistance relationship. The obtained correction confirmed the already existing one for fines content ≤ 35% (Youd et al., 2011). However, it provided new correction for fines content > 35% that is consistent with field case records.

7 REFERENCES

Ambraseys NN, (1988). "Engineering seismology," J of Earthquake Eng. and Structural Dynamics, 17, 1, 1-105.

Cetin, K.O. (2000). Reliability-based assessment of seismic soil liquefaction initiation hazard, PhD Thesis, Dept. of Civil and Environ. Eng. University of California at Berkeley, Berkeley, CA.

Cetin, K.O., Seed, R.B., Der Kiureghian, A., Tokimats u, K., Harder, L.F., Jr., Kayen, R.E., and Moss, R.E.S. (2004). "Standard penetration test-based probabilistic and deterministic assessment of seismic soil liquefaction potential," J. of Geotech and Geoenviron. Eng., ASCE, 130(12): 1314-1340.

Cubrinovski, M. and Ishihara, K. (1999). «Empirical correlation between SPT N-value and relative density for sandy soils, » Soils and Found. 39(5): 61-71.

Cubrinovski, M. and Ishihara, K. (2000). Flow potential of sandy soils with different grain compositions. Soils and Found., 40(4): 103-119.

Cubrinovski, M. and Ishihara, K. (2001). "Correlation between penetration resistance and relative density of sandy soils, " Proc. 15th Int. Conf. On Soil Mech. and Geotech. Eng., Istanbul.

Cubrinovski, M. and Ishihara, K. (2002). "Maximum and minimum void ratio characteristics of sands," Soils &Found., JGS, 42(6): 65-78.

Fear, C.E. and McRoberts, E.C. (1995). Report on liquefaction potential and catalogue of case records (revised March 1995), Internal Research Report, Geotech. Eng. Library, Dept. of Civil Engineering, University of Alberta, Edmonton, Alberta.

Green, R.A., Olson, S.M. and C.P. Polito (2006). "A comparative study of the influence of fines on the liquefaction susceptibility of sands: Field versus laboratory," Proc. of 8th U.S. Nat. Conf. on Earthqu. Eng. San Francisco, California, USA , Paper No. 1251.

Idriss IM and Boulanger RW. (2006). "Semi-empirical procedures for evaluating liquefaction potential during earthquakes," J. Soil Dynam. and Earthqu. Eng., 26, 115-130.

Idriss, I.M. and Boulanger, R.W. (2004). Semiempir ical procedures for evaluating liquefaction potential during earthquakes, Proc., Joint 11th Intl. Conf. on Soil Dynam and Earthqu. Eng.and the 3rd Intern. Conf. on Earthqu. Geotech. Eng. Berkeley, CA, 32-56.

Idriss, IM, and Boulanger, R.W. (2010). SPT- Based Liquefaction Triggering Procedures. Centre for Geotech. Modeling, Dep. of Civil and Environ. Eng., Univ. of California, Davis, California. .

Jamiolkowski M, Baldi G., Bellotti R., Ghionna V. and Pasqualini E. (1985)."Penetration resistance and liquefaction of sands," Proceedings of 11th Int. Conf. Soil Mech. and Geotech. Eng., San Francisco, 3, 1891-1896.

Kayen, R.E. and Mitchell, J.K. (1997). "Assessment of liquefaction potential during earthquakes by Arias intensity," J. of Geotech. and Geoenviron. Eng., ASCE, 123(12): 1162-1174.

Meyerhof, G. G. (1957) Discussion on Research on determining the density of sands by penetration testing. Proc. 4th Int. Conf. on Soil Mech. and Found. Engrg ., Vol. 1: 110.

Peck (1997) personal communication

Polito, C.P. (1999). The Effects Of Non-Plastic and Plastic Fines On The Liquefaction Of Sandy Soils. PhD Thesis, Virginia Polytechnic Institute.

Polito, C.P. and Martin, J.R., II (2001). "Effects of non- plastic fines on the liquefaction resistance of sands," J. of Geotechnical and Geoenvironmental Engineering , ASCE, 127(5): 408-415.

Polito, C.P. and Martin, J.R., II (2003). "A reconciliation of the effects of non-plastic fines on the liquefaction resistance of sands reported in the literature," Earthquake Spectra , 19(3): 635-651.

Robertson, P.K., and Wride, C.E. 1997. Cyclic liquefaction and its evaluation based on the SPT and CPT. In:Proc. of the national center for earthquake eng. research, NCEER. Report no. 970022.

Seed, HB. and Idriss, IM.(1971) "A simplified procedure for evaluating soil liquefaction potential." Journal of Soil Mechanics and Foundation Engineering, ASCE, 97, 9, 1249-1274.

Seed, H.B., Idriss, I.M., and Arango, I. (1983). "Evaluation of liquefaction potential using field performance data, J. of Geotech. Eng., ASCE, 109(3): 458-482.

Seed, H.B., Tokimatsu, K., Harder, L.F., Chung, R.M. (1984). The influence of SPT procedures in soil liquefaction resistance evaluations, EERC Report No. UCB/EERC 84/15 , Earthqu. Eng. Research Center, University of California at Berkeley, CA..

Skempton AW. (1986)."Standard penetration test procedures and the effects in sands of overburden pressure, relative density, particle size, aging and overconsolidation,"Geotechnique, 36, 3, 425-447.

Shahien, M. (2007). "New Procedure to Estimate Liquefaction Resistance from Penetration Resistance Using Field Records," 4th Int. Conf. on Earthqu. Geotech.Eng., Thessaloniki - Greece.

Shahien, M., and G. Mesri (1999). "Alternative SPT corrections for fines content in liquefaction and earthquake-induced settlement analyses," Abst. Vol. of 9th Int. Conf. on Soil Dynamics and Earthqu. Eng., Bergen, Norway.

Terzaghi, K. and Peck, R.B. (1948). Soil Mechanics in Engineering Practice. 1st. Ed., J. Wiley and Sons, New York.

Terzaghi, K, Peck, RB and Mesri, G. (1996). Soil Mechanics in Engineering Practice. Third Edition, J. Wiley and Sons, New York.

Tokimatsu, K. and Yoshimi, Y. (1983). "Empirical correlation of soil liquefaction based on SPT N-value and fines content, Soil and Foundations , JSSMFE, 23(4): 56-74.

Youd, T.L., Idriss, I.M., Andrus, R.D., Arango, I., Castro, G., Christian, J.T., Dobry , R., Finn, W.D.L., Harder, L.F., Jr., Hynes, M.E., Ishihara, K., Koester, J.P., Liao, S.S.C., Marcuson, W.F., III, Martin, G.R., Mitchell, J.K., Moriwaki, Y., Power, M.S., Robertson, P.K., Seed, R.B., and Stokoe, K.H., II (2001). "Liquefaction resistance of soils: summary report from the 1996 NCEER and 1998 NCEER/NSF Workshops on evaluation of liquefaction resistance of soils," J.of Geotechnical and Geoenvironmental Engineering, ASCE, 127(10): 817-833.

Geotechnical and Geophysical Site Characterisation 5 – Lehane, Acosta-Martínez & Kelly (Eds)
© 2016 Australian Geomechanics Society, Sydney, Australia, ISBN 978-0-9946261-1-0

A surface seismic approach to liquefaction

S. Castellaro
University of Bologna – Dep. Physics and Astronomy (Italy)

R. Panzeri
Geologist

ABSTRACT: The liquefaction potential of soils is traditionally assessed through geotechnical approaches based on the calculation of the cyclical stress ratio (CSR) induced by the expected earthquake and the 'resistance' provided by the soil, which is quantified through standard penetration (SPT), cone penetration (CPT), or similar tests. In more recent years, attempts to assess the liquefaction potential have also been made through measurement of shear wave velocity (V_S) in boreholes or from the surface. The latter approach has the advantage of being non-invasive and low cost and of surveying lines rather than single points. However, the resolution of seismic surface techniques is lower than that of borehole techniques and it is still debated whether it is sufficient to assess the liquefaction potential. In this paper we focus our attention on surface seismic techniques (specifically the popular passive and active seismic techniques based on the correlation of surface waves such as ReMi^{TM}, MASW, ESAC, SSAP, etc.) and explore their performance in assessing the liquefaction susceptibility of soils. The experimental dataset is provided by the two main seismic events of M_L = 5.9 and 5.8 (M_W = 6.1, M_W = 6.0) that struck the Emilia-Romagna region (Northern Italy) on May 20 and 29, 2012, after which extensive liquefaction phenomena were documented in an area of 1200 km^2. We found that they appear not to have sufficient resolution to address the seismic liquefaction issue. However, it also emerged that the pure observation of the surface wave dispersion curves at their simplest level (i.e. in the frequency domain, with no inversion) is still potentially informative and can be used to identify the sites where more detailed surveys to assess the liquefaction potential are recommended.

1 INTRODUCTION

Assessing the liquefaction potential at a site is a goal traditionally achieved through geotechnical approaches based on the grain size distribution or on CPT and SPT (cone penetration and standard penetration tests. These methods are based on the calculation of the cyclical stress ratio (CSR) induced by the expected earthquake at the depth of the potentially liquefiable deposit and the 'resistance' provided by the deposit, quantified through the CPT or SPT. The geotechnical approaches are certainly the most explored, used, and reliable ones since they provide direct quantitative information about some mechanical properties of the soil column. However, they have the disadvantage of providing only point information and of being invasive and inapplicable to gravelly soils, where liquefaction has sometimes been documented. Parallel to the geotechnical ones, geophysical approaches have also developed and traditionally exploited the measurement of shear wave velocity V_S (because V_S is linked to the shear modulus of the soil, $\mu = \rho V_S^2$, where ρ is the density) in boreholes or in laboratory samples but at the expense of having the same limitations as CPT and SPT, that is, providing just point information, and being more expensive.

Surface multichannel geophysical methods like those relying on the dispersion of surface waves to retrieve V_S profiles would be ideal in principle, since they are spatially distributed and not invasive and can be used on any soil type. Seismic surface methods are however much less sensitive to the stiffness variation of soil with depth compared to the classical geotechnical methods for physical reasons: first, the depth of investigation is proportional to the 'exploring' wavelength but large wavelengths (i.e. large depths of investigation) are sensitive only to reflectors of comparable size; second, while the penetration parameters (sleeve friction or tip resistance) are directly proportional to the shear modulus G, V_S is proportional to the square root of G. Additionally, deriving a V_S profile from the dispersion curve of surface waves is not an easy task and, as the method is indirect and the problem underdetermined, it does not have a unique solution.

The results of an 11-year international project to gather new V_S data and develop state-of-the-art probabilistic CSR-V_S correlations for the occurrence of seismic soil liquefaction were presented by Kayen et al. (2013). The new V_S soil profiles, mostly derived from the SASW (Spectral Analysis of Surface Waves) method (Nazarian and Stokoe, 1984), were collected mainly in Japan (213), with a minority being collected in California (39), China (24), Taiwan (14), Alaska (9), and Greece (2).

In this paper we focus on the 'descendants' of the SASW technique, exploring their applicability within the method proposed by Kayen et al. (2013) to the Italian case and examining whether different geophysical approaches are possible to assess the liquefaction susceptibility of a soil.

Our dataset is provided by the May 20 and 29, 2012 earthquakes (M_L = 5.9 and M_L = 5.8, respectively) that occurred in the Po Plain area (Northern Italy), which caused a large number of liquefaction phenomena over an area extending up to 30 km from the epicenters.

2 DATA COLLECTION

2.1 *Site selection*

In the area struck by the aforementioned seismic events, we focus on 84 sites, which we grouped into four classes (in all cases the depth of the water table was within 3 m; in the majority of cases, within 1.5 m) representative of different depositional environments. Class A and B sites include shallow (< 8 m) sandy soil with liquefaction potential. At sites labeled A, liquefaction occurred during the 2012 events while at sites labeled B there was no surface evidence of liquefaction. Class C sites are those where sand is present at large depth (> 8 m) and did not exhibit liquefaction. Class D sites are composed of clay and silt, with no liquefaction potential. A closer look to the tip resistance q_C and the sleeve friction f_S of the single penetration tests four classes (Figure 1) reveals that a geotechnical difference exists between soils A and B: in the first case a higher sand content is present between 5 and 7 m depth (which is the level that underwent liquefaction), while in the second case sand is dominant in the upper 4 m.

2.2 *Site survey*

At the 84 sites we combine the active seismic exploration approach of MASW (Multichannel Analysis of Surface Waves, Park et al., 1999) and the passive approach of ReMi^{TM}-ESAC-SSAP (Refraction Microtemor^{TM}, Louie, 2001; Extended Spatial Autocorrelation Method, Ohori, 2002; Statistical Self-Alignment Property, Mulargia and Castellaro, 2013).

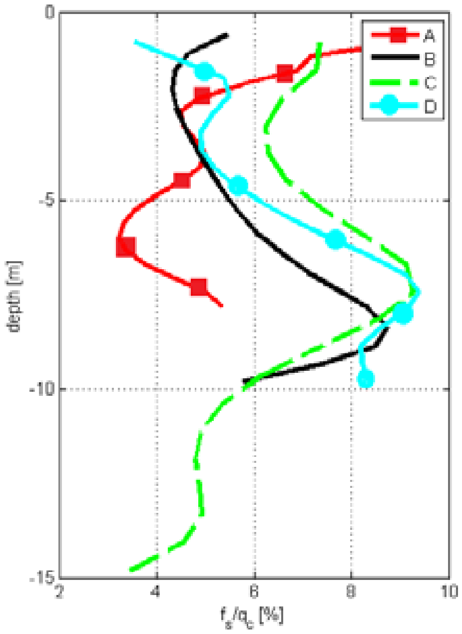

Figure 1. Average friction ratio (i.e. sleeve friction, f_S, versus tip resistance, q_C) for the four soil classes. Lower f_S/q_C ratios indicate sandy soils while ratios indicate silty-clayey soils.

This kind of survey exploits the fact that surface waves of different wavelengths, like those produced by common sources, excite the soil at different depths and travel with the specific velocity that characterizes the soil at the different depths: short wavelengths normally propagate slower (due to the low velocity of the shallow layers) while long wavelengths propagate faster. This property, called dispersion, is a phenomenon strictly related to surface waves. From the seismic signal recorded at different positions (a minimum of two) over time, slant-stack and FFT procedures produce the so-called phase/group velocity spectra, which indicate the most probable velocity of surface waves at each frequency. From this, a forward or inverse modeling procedure makes it possible to reconstruct a possible V_S model for the surveyed soil.

The 84 surveys performed in this study were conducted by using twelve 4.5 Hz, vertically polarized geophones (Geospace lp), set at intervals of 2.5 m each, connected to a SoilSpy Rosina acquisition system (MoHo srl), and data were processed by using the software Grilla, written by one of the authors (S.C.). Working with vertically polarized geophones implies that we deal with Rayleigh wave phase velocities, which are approximately 10–15% lower than V_S, depending on the Poisson's ratio of the materials.

Recalling that a Rayleigh wave induces the maximum displacement at a depth equal to 1/3 to 1/2 of its wavelength λ (e.g. Chapter 4 in Lay and Wallace, 1995), and considering that our surveys show phase velocities V_R ranging between 150 and 250 m/s at f = 4 Hz (Figure 2), we get an average wavelength of $\lambda = V_R/f = (150–250)/4 = 37–62$ m, which stands for a depth of investigation $z_{max} \approx [\lambda/3, \lambda/2] \approx [12, 32]$

m, which is adequate for our task, since liquefaction generally occurs at depths shallower than 15 m and in the present case study it was documented at a depth shallower than 8 m.

This is not always the case. We pick the dispersion curves of the fundamental mode from the phase velocity spectra at the 84 inspected sites, grouping them as per the four soil classes defined before. The average dispersion curve plus or minus the standard deviation of each group is shown in Figure 2. We immediately observe that the geophysical approach is not capable of separating the four soil classes. Class A and B sites, characterized by liquefied and non-liquefied sandy soils, have exactly the same phase velocity distributions, while the CPTs (Figure 1) suggest that some difference exists between these two classes: class A soils are richer in sand between 5 and 7 m depth. This limitation of the adopted seismic surface methods is discussed in the next section.

Class D soils, which are characterized by clay and silt in the first 10 m depth, show significantly lower phase velocity distributions compared to class A and B soils in almost the whole frequency interval considered. Class C soils, characterized by sands at depths larger than 8 m, show phase velocity distributions comparable to class D soils in the high frequency part of the spectra, increasing up to or higher than the distribution of class A and B soils in the low frequency part. This trend is somewhat expected: V_R (and V_S) normally increases from clays to silt to sand in this type of depositional environment. However, this is probably the first time that this has been well documented in this part of the Po Plain, to the point that the phase velocity distribution in this geographic area could be used as a proxy for the shallow stratigraphy.

We note that the difference in the V_S values among classes (a few tens of meters per second) appears low compared to the difference in the CPT parameters. This is not surprising if one recalls that the shear modulus G is proportional to V_S^2 (and the same relation involving an exponent 2 exists between V_P and other elastic constants and V_R is a function of both V_S and V_P).

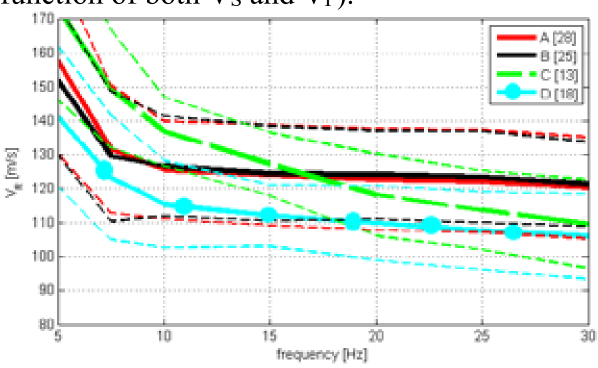

Figure 2. Dispersion curves (average ± standard deviation) grouped into the four soil classes. The number of curves used to assess the distribution of each soil group is indicated in square brackets in the legend.

3 RESULTS

The first relations between V_S values and liquefaction potential described in the literature were based on laboratory or direct (in hole) measurements. More recent attempts (Kayen et al., 2013) introduced, together with direct measurements, a number of V_S estimated from Spectral Analysis of Surface Waves (SASW), which is an ancestor of MASW. These methods consist in the calculation of the corrected seismic demand (cyclic stress ratio, CSR*) and the corrected soil capacity (V_{S1}) to be used as entry values in plots where the liquefaction and non-liquefaction areas are divided by curves representing different probability levels (Figure 3).

The critical stress ratio (CSR) is the ratio between the average shear and vertical stresses, τ_{avg}/σ_{avg}. This can be rewritten as CSR = 0.65 $a_{max}/g\ \sigma_V/\sigma'_V\ r_d$, where a_{max} is the peak ground acceleration at the surface, σ_V is the total overburden stress, σ'_V is the effective vertical overburden stress, and r_d is a non-linear mass participation factor, which depends on a number of factors including the soil depth, the average V_S of soil, the peak ground acceleration, and the earthquake magnitude. We use Eq. 4 in Kayen et al. (2013) to calculate r_d, by setting a_{max} = 0.31 g and M_W = 6.1, which are the values of the 2012 mainshock. The other parameters (depth of the sand layer on which to perform the calculations and depth of the water, average V_s of the overlying soil) are known at all sites from the penetration test, drillings, water wells, and the geophysical surveys performed *ad hoc*.

The adjustment of CSR to CSR* is done by scaling the computed CSR to compensate for the duration of shaking (duration weighting factor, DWF) relative to an equivalent M_W = 7.5 event, so that CSR* = CSR/(DWF K_σ), where K_σ = 1, following the recommendations in Kayen et al. (2013) and DWF = 15 $M_W^{-1.342}$ (Eq. 17 in *ibid.*).

The results are plotted in Figure 3 and show that our class A and B data (liquefied and non-liquefied sandy soils) are randomly distributed around the P_L = 15% line (this value is recommended in Kayen et al., 2013, and corresponds to a safety factor of 1.2), while the class C data (deep sands) are well separated and fall in the non-liquefaction zone.

We also note that if we wish to include both the A and B sites in the liquefaction area, we need to operate according to $P_L = 10^{-5}$, which represents a huge factor of safety (dashed line in Figure 3).

We observe that the phase velocity spectra/dispersion curves (Figure 2) are just experimental data with little subjective interpretation. Transforming these data into V_S profiles and calculating the CSR*-V_{S1} values requires a large number of assumptions and corrections (earthquake DWFs, adjustment for the influence of fines, calculation of effective stress, etc.) and is not a unique process (inversion of the data to get V_S profiles). All this effort does not seem to be warranted in the case of the present study and, besides the points above, there can be two further reasons for such a failure: 1) surface wave methods do not have sufficient sensitivity to characterize appropriately the V_S of the 2–4 m thick sandy layers potentially involved in the liquefaction phenomenon, and/or 2) the sandy deposits in this part of the Po Plain area have features that make them different from the sands studied worldwide by Kayen et al. (2013).

In order to better discriminate between the last two hypotheses, we calculated the liquefaction potential of the same sand layers through the fines-modified CPT tip resistance approach, $q_{c,1,mod}$ (Moss et al., 2006). Results in terms of CSR*-$q_{c,1,mod}$ are shown in Figure 4 and suggest that the geotechnical method provides a better prediction of the liquefaction potential (a failure rate of less than 20% is achieved by adopting the 20% liquefaction probability curve) compared to the seismic-surface wave based method, thus making the first hypothesis more credible.

We observe that the surface wave dispersion curves alone (Figure 2), prior to any inversion, can still be very informative. On the basis of the 84 surveys, for this area of the Po Plain we propose a soil classification scheme based on the Rayleigh wave dispersion curves (Figure 5), which indicates the degree (high, intermediate, or low) of caution recommended in assessing the liquefaction potential of the soil under the typical design earthquake ($M_W \approx 6.1$) imposed by the national building code (NTC, 2008) in this part of Italy for standard constructions. The class boundaries – high, intermediate, and low – mean that 50, 30, and <5%, respectively, of the sites presenting a dispersion curve completely falling within them experienced liquefaction during the 2012 $M_W \approx 6.1$ events (near field condition).

Generally speaking, low V_R values in this plot correspond to clays, while sand content increases the V_R values. A dispersion curve falling completely within the gray area of Figure 5 indicates with high probability a site with clays followed by sand at a depth greater than approximately 8 m. This configuration represents a low liquefaction susceptibility under a typical $M_W \approx 6.1$ earthquake.

A curve falling completely within the magenta area indicates a site with sand which can potentially undergo liquefaction. Further investigations are recommended at these sites, for example, by using CPT-STP, to better assess the liquefaction potential.

A curve falling completely within the lower yellow area (V_R < 110 m/s in the 10–30 Hz interval) indicates with high probability a clayey soil with low liquefaction potential. A curve falling completely within the upper yellow area (V_R > 150 m/s in the 10–30 Hz interval) indicates a site with dense sand in the upper 15 m, which would be less prone to liquefaction under the reference earthquake.

The above discussion applies also to the case of sites with a stiff crust, such as a dessicated clay layer or manmade fill, overlying a loose saturated sand. In these cases there would be a 'kink' in the dispersion curve (not normally dispersive) which would not closely match the dispersion curve shapes discussed above but would still represent a potentially liquefiable soil. The most part of the dispersion curve is however expected to lay within the boundaries of Figure 5, excluding the high frequency part which might lay above these limits.

Such a scheme appears to be more effective (and less demanding) in identifying the soils where further study is recommended compared to the CSR*-V_{S1} approach, in which V_{S1} is computed from surface-wave based seismic approaches. We emphasize that even though the V_R-frequency plot of Figure

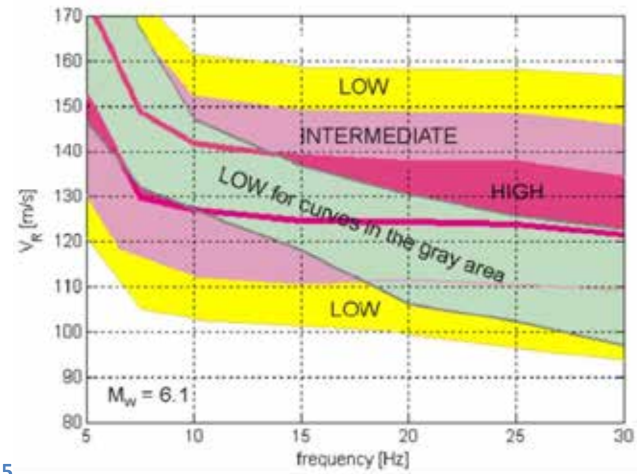

5

Figure 5. represents the result of this study, before applying it to different geographical and geological settings, specific tuning and verification are needed.

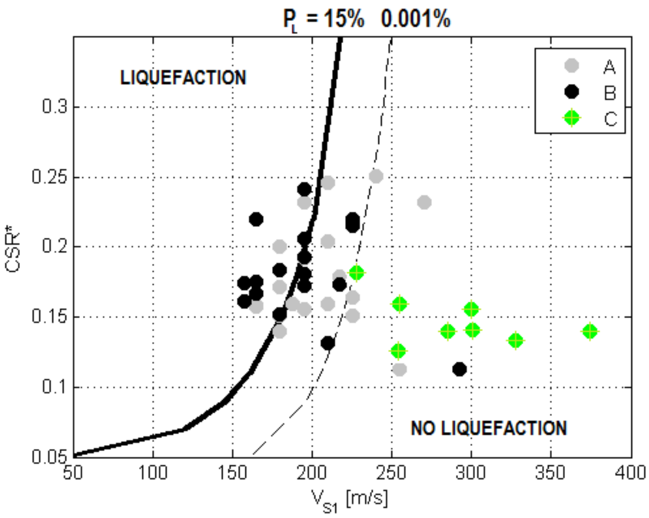

Figure 3. Corrected cyclic stress ratio (CSR*) versus corrected shear wave velocity (V_{S1}) for the sand layer at the inspected sites. The thick black line corresponds to the 15% liquefaction probability level proposed by Kayen et al. (2013).

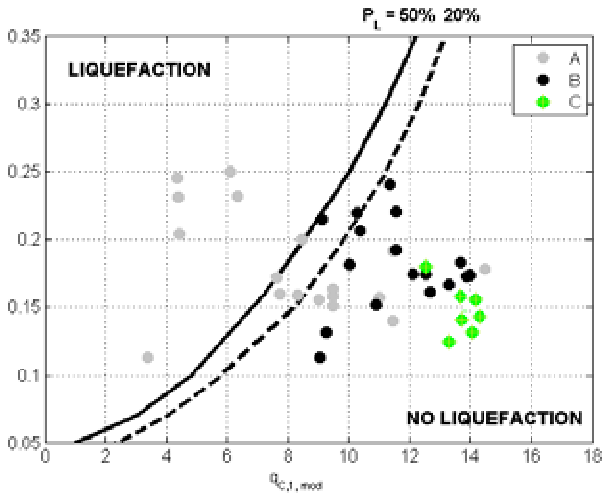

Figure 4. Corrected cyclic stress ratio (CSR*) versus corrected and fines-modified CPT tip resistance ($q_{c,1,mod}$) for the sand layer at the inspected sites. The black lines represent the contours of 50 and 20% probability of liquefaction (Moss et al., 2006). Data are normalized with respect to $M_W = 7.5$ and $\sigma'_V = 1$ atm.

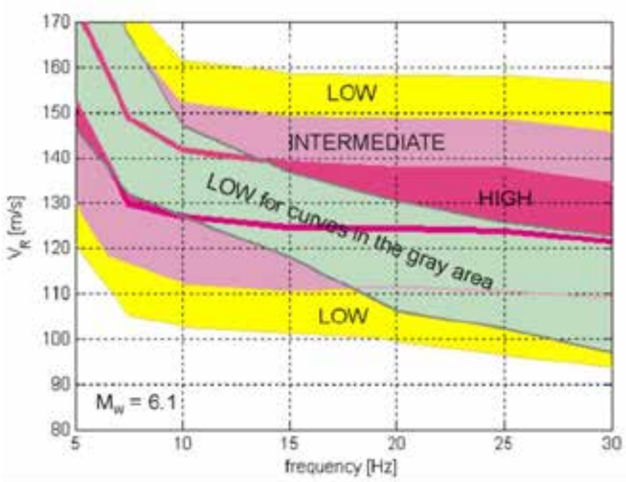

Figure 5. Soil classification scheme based on the Rayleigh wave dispersion curves for the surveyed area. The adjectives “high”, “intermediate”, and “low” indicate the degree of caution recommended in assessing the liquefaction potential of the soil. In general, low V_R values in this plot indicate clays, while the sand content increases the V_R values. A dispersion curve falling completely within the gray area indicates with high probability a site with clay at shallow depth and sand at large depth (> 8 m); this configuration represents a low liquefaction disposition under the typical $M_W \approx 6.1$ earthquakes used as design earthquakes in this area (NTC, 2008).

A curve falling completely within the magenta area indicates with high probability a site with sand which could undergo liquefaction. Further investigations are recommended at these sites, for example by using CPT-STP, to assess the liquefaction potential.

A curve falling completely within the lower yellow area indicates with high probability a clayey soil with low liquefaction potential. A curve falling completely within the upper yellow area indicates a site with dense sand in the upper 15 m, which would be less prone to liquefaction under the reference earthquake.

4 DISCUSSION AND CONCLUSIONS

The liquefaction potential of soils is commonly assessed through geotechnical methods (CPT, SPT, etc.) but some attempts to also estimate it through geophysical parameters, such as the shear wave velocity, V_S, of soils, have also been developed. Measuring V_S in boreholes or in the laboratory (when the collection of undisturbed samples is possible) has the advantage of providing more accurate values at the specific depth of interest but at the expense of higher costs and invasiveness compared to the geotechnical methods and of the same point validity. Being able to measure V_S from the surface and over wider areas therefore appears to be a desirable solution. In 2013, Kayen et al. proposed a probabilistic and deterministic method to assess the liquefaction potential of sands through V_S measurements. The dataset used also included a number of V_S estimates from surface-wave based methods, specifically SASW.

In this work we verified the applicability of seismic active and passive multichannel modern surface wave techniques in the prediction of liquefaction potential. The opportunity was provided by the two earthquakes that occurred in the Po Plain (Northern Italy) in 2012, causing extensive liquefaction. Using the abovementioned seismic surface techniques, we surveyed 84 sites where geological information was available from direct geotechnical methods (penetration test, drilling, etc.).

Based on the geotechnical information, the sites were grouped into four classes: A) liquefied sandy soils; B) non-liquefied sandy soils; C) deep sands; D) clayey-silty soils. The penetration tests suggested that on average in class A soils, sand was dominant at 5–7 m depth (and was in practice the liquefied layer) while in class B soils, sand was dominant at shallower depths. However, the geophysical surveys showed that the Rayleigh wave phase velocity spectra were clusterized into three groups only: classes A and B were found to be indistinguishable from a seismic point of view. Through a set of theoretical models, we showed that this is due to the resolution of the adopted seismic methods, which is a function of the ‘exploring wavelength’, and which makes seismic layers such as the sands under investigation – which are just 2–4 m thick and have V_S just a few ten of meters higher than the surrounding clay-silt – practically invisible at depths greater than 4–5 m.

We then applied the probabilistic and deterministic methods to assess the liquefaction potential of sands through the V_S measurement proposed by Kayen et al. (2013), but we found that this approach failed in the case of the present study since class A and B soils were found to be randomly distributed between the liquefaction and non-liquefaction zones, while predictive power exists for class C soils, which, as they represent deep sands, fall in the non-liquefaction zone.

The geotechnical approach based on the tip resistance in the CPT to assess the liquefaction potential was found to be more successful.

The reason for the failure of the surface geophysical method seems to be linked, therefore, not to the specific features of the sands in this area but to the insensitivity of the seismic surface-wave based methods used to the details of stratigraphy for this specific goal.

In conclusion, based on this study (i.e. in the region of V_{S1} = [150, 250] m/s), it seems that surface-wave methods (MASW, ReMi, ESAC, SPAC, and many others), which are extremely useful in a wide range of applications, do not have sufficient sensitivity to be used as predictors of liquefaction in the classic frame of seismic demand versus soil capacity scheme.

However, at least in this specific depositional environment, it also seems that the simple analysis of the Rayleigh wave phase velocity spectra – before any inversion procedure (Figure 2) – can be used since it suggests the presence of sand or clay. On the basis of the experimental results we built the 'caution against liquefaction' graph shown in Figure 5, which can however only be used in the studied area. Nonetheless, the procedure – after specific tuning for different geological settings – could probably also be applied at different sites.

5 REFERENCES

Kayen R., Moss R.E.S., Thompson E.M., Seed R.B., Cetin K.O., Der Kiureghian A., Tanaka Y., Tokimatsu K., 2013. Shear-wave velocity-based probabilistic and deterministic assessment of seismic soil liquefaction potential, *J. Geotech. Geoenviron. Eng.*, 139, 407-419.

Lay and Wallace, 1995. *Modern global seismology*, Academic Press, New York, 517 pp.

Louie J., 2001, Faster, better: Shear-wave velocity to 100 meters depth from refraction microtremor arrays: *Bull. Seism. Soc. Am.*, 91, 347–364.

Moss, R.E.S., Seed R.B., Kayen R.E., Stewart J.P., Der Kiureghian, Cetin, K.O., 2006. CPT-based probabilistic and deterministic Assessment of in situ seismic soil liquefaction potential, *J. Geotech. Geoenviron. Eng.*, 132, 1032-1051.

Mulargia F., Castellaro S., 2013. A seismic passive imaging step beyond SPAC and ReMi™, *Geophysics*, 78, KS63-KS72.

Nazarian S., Stokoe K.H., 1984. In situ shear wave velocities from spectral analysis of surface waves, *Proc. 8th World Conf. on Earthq. Eng.*, vol. III, Prentice-Hall, Englewood Cliffs, NJ, 31-38.

Ohori M., Nobata A., Wakamatsu K., 2002. A comparison of ESAC and FK methods of estimating phase velocity using arbitrarily shaped microtremor arrays, *Bull. Seism. Soc. Am.*, 92, 2323–2332.

Park C.B., Miller R.D., Xia J., 1999. Multichannel analysis of surface waves, *Geophysics*, 64, 800–808.

Theme 6. Pavements and Fills

Geotechnical and Geophysical Site Characterisation 5 – Lehane, Acosta-Martínez & Kelly (Eds)
© 2016 Australian Geomechanics Society, Sydney, Australia, ISBN 978-0-9946261-1-0

Evaluation of rockfill embankments by field tests in Siraf Refinery Complex site, Iran

E. Asghari-Kaljahi
Department of Earth Sciences, University of Tabriz, Tabriz, Iran

N. Nasrollahi & Z. Kheyrouri
P.O. Rahvar Consulting Engineers Company, Tehran, Iran

ABSTRACT: In Siraf Condensate Refinery Complex project in the south of Iran with about 260 hectares area, about 5 million cubic meters of fill is needed for the site rough grading because of some deep valleys. Some places need more than 35m embankment. It is decided to fill all valleys with rockfill material with lifts 45 to 60cm up to 7m below final project level and then perform embankment layers with granular soils finer than 3 inch with lifts less than 25cm.The Bakhtiari formation deposits, known weak conglomerate, have covered a vast area of project region, are consisted of coarse granular soils with many cobbles and boulders particles was the main barrow material source for rockfill. For determining of optimum lift thickness and roller passes num-ber, a trial embankment performed in a trial area and was tested with some field tests. These tests consisted of field grading, large density, plate load test and surface seismic tests.The minimum acceptable compaction rel-ative for rockfill lifts was defined 85% MDD as per ASTM D1557. For 45cm lifts with 2 passes of 15 tones vibratory roller compactors and for 60cm lifts at least 3 passes of mentioned rollers were needed. Based on refraction surface seismic tests, when the shear wave velocity of rockfill layers was more than 390m/s, the compaction ratio had been reached to more than 85% MDD.

1 INTRODUCTION

Traditional "earthfill" consist of mixtures of clay, silt, sand with fine-grained gravel sizes. With adding larger size particles, consist of coarse-grained gravel, cobble and boulder sized rocks, embankment called "rockfill". In rockfill, the predominant materials consist of coarse grained particles. In some references, rockfill is an earthfill which more than 15% of its volume is particles larger than 15cm (Iran Department of Technical Affairs, 2013)

The first use of rockfill seems to be of low level hand placed rockfill dumps with timber facing on the upstream slope in the 1850's for water storage and gold sluicing operations. During 1940's, construction water storage dams required of spreading thick dry and loose rockfill dump by trucks or draglines without compaction. Up to 1950's, High-pressure water jets and flooding techniques was used to wet and consolidate the thick loose rockfill dump lifts to achieve up to 85 percent of total dam settlement. Days after, control of lift thickness and compaction with rollers, in addition to documentation of rockfill gradation, moisture, and density large-scale test fills developed (Breitenbach, 1993).

There are two different methods for placement of rocks. First method contains of dumping and spreading a reasonably homogeneous stable horizontal layers, and second method, contains spreading dumped particles in a way that smaller rock fragments placed in the inner portion of the embankment and the larger rock fragments placed on the outer slopes (USDA and NRCS, 2009).

Three different classes of compaction exist based on the aim of embankment, compacting every lift with heave rollers, compaction each layer with light compactors and no compaction beyond spreading operations. Lift thickness is related to the volume percent of particles larger than 15 cm (USDA and NRCS, 2009).

Defining acceptable criteria for placement and compaction through the mentioned methods is one of the main objectives for rockfill structures, and mainly is related to the design and performance criteria.

The conventional earthfill test consist of field and laboratory test methods for controlling lift thickness, gradation, moisture content, and compaction are not applicable to rockfills because of large particle sizes and must be modified based on site specific compaction effort specification using large-scale test and heavy vibratory roller compactors.

Compaction percentage is one the main controlling criteria for earth structures. In some cases, to control the deformability, plate load test is defined as a controlling test of rockfill.

In this paper the site attempts and experiences for performing of rockfill layers and evaluating of them in Siraf Condensate Refinery Complex project is presented. This project is located in the south of Iran, at the coast of Persian Gulf (Fig. 1). The coordinates of site according to UTM is 619980 E, 3065485N.

Figure 1. Project location on Iran map

2 PROJECT EMBANKMENT COMPACTION PROGRAM

Siraf condensate refinery complex project site with area about 260 hectares, was divided into 23 zones. These zones will be used for construction of 8 refineries and some tanks and utilities. For rough grading of site need about 5million cubic meters rockfill embankment.

Compaction percentage is a main criterion for soil preparation below foundations. Compaction percentage was defined based on structures types, footing load and depth of embankment below the foundation. Because of wide range of elevation variations in the project site, four ranges of compaction requirement have defined for embankments, from 85% for rockfill to upper than 95% for earthfill, from bottom elevations to top.

Figures 2 and 3 show a sample area variation before grading and total depth of filling up to the project level, respectively. The minimum acceptable compaction relative for rockfill lifts was defined 85% of Modified Compaction as per ASTM D1557 test which is achievable for 45cm lift thickness with 2 passes of 15 tones vibratory roller compactors and for 60cm lift thickness, with at least 3 passes of mentioned rollers.

For more compaction density, more passes over 45 cm lift thickness required. For elevations less than 5 m below footing, the lift thickness limited to 30cm and compaction ratio limited to 90%.

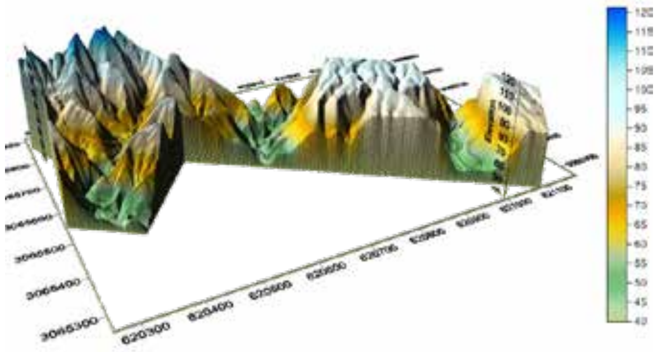

Figure 2. Topography of a zone as a sample, before rough grading (Zone No. 14)

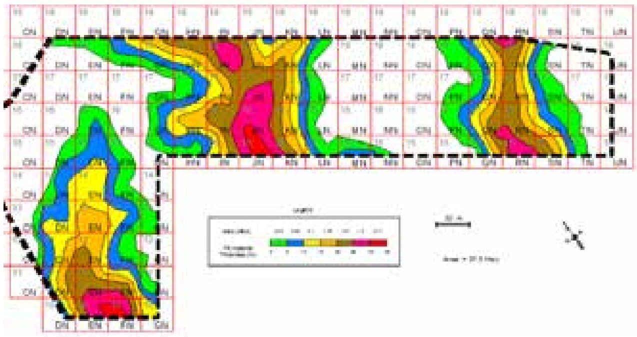

Figure 3. Need rockfill thickness in one of project zones (Zone No. 14)

3 EMBANKMENTS SPECIFICATION AND MATERIALS

Project ground form vary from hills, ridges to valleys, and about 5 million cubic meters of cut and fill is needed for the rough grading. The main borrow material for filling was obtained from Bakhtiari formation deposits that consisted of coarse granular soils with many cobbles and boulders particles as weak conglomerate. Figure 4 shows a picture of Bakhtiari formation. The stone type of Bakhtiari formation particles are limestone and sandstone. Because of the huge volume of filling and existing large size particles, using the conventional earth fill is not economic and it is rational to use rockfill layers with over 45cm lift thickness.

Determining acceptable procedures and criteria for the placement and compaction of rockfills in the site is considered using different particle size; lift thickness and compaction efforts in trial area within 9 different patterns. Maximum particle size and compaction effort were changed over the pattern to achieve the optimum compaction method. In-situ test such as large scale gradation (particle size distribution), large in-situ density, plate load test and geo-seismic tests are done for controlling quality.

Figure 4. A picture of Bakhtiari formation texture

4 TRIAL AREA SPECIFICATION

Three different rockfill with following specifications is executed at trial area. Maximum rock sizes limited to half of the lift thickness. Every part has the width of 10 m and the length of 50 m.

1- Two layers with lift thickness of 60 centimeter with 3 different compaction efforts.
2- Three layers with lift thickness of 45 centimeter with 3 different compaction efforts.
3- Four layers with lift thickness of 30 centimeter with3 different compaction efforts.

Figure 5 shows 9 different patterns for rockfill execution in trial area and Figure 6 shows spreading of rockfill materials in trial area.

	No. of Layers / Lift Thick. / No. of Passes	No. of Layers / Lift Thick. / No. of Passes	No. of Layers / Lift Thick. / No. of Passes
60 cm Lift Thickness	2/60cm/4	2/60cm/6	2/60cm/8
45 cm Lift Thickness	3/45cm/4	3/45cm/6	3/45cm/8
30 cm Lift Thickness	4/30cm/4	4/30cm/6	4/30cm/8

Figure 5. Rockfill pattern in trial area

Figure 6. Spreading of rockfill material

The roller compactor has used at the site was 15 tones vibratory steel drum rollers and the number of passes considered as 4, 6 and 8 passes.
To have the best roller pass coverage, each roller pass should overlap the edge of preceding passes.

5 CONTROLLING TESTS

5.1 *Grading Test (Particle size distribution)*

Totally 18 samples were taken from the fills, 6 of each rockfill area. Particle size distribution tests were done by taking large samples and doing in-situ grading and sieve test. Some samples particle size distribution curves are shown in Figure7.

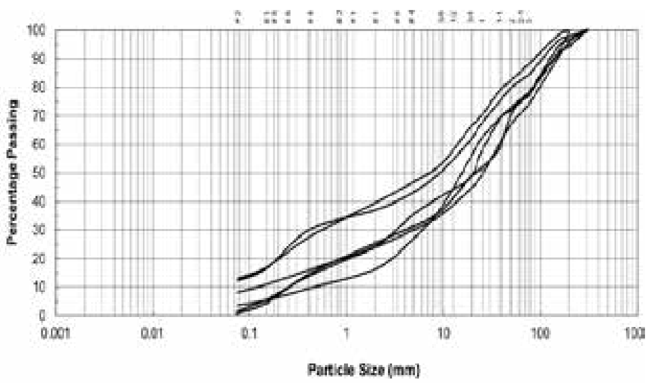

Figure 7. Particle size distribution curves rockfill materials

5.2 *Large in-place density test*

Large scale density test is done according to ASTM D5030 (ASTM, 2013) for "Density of Soil and Rock in Place by the Water Replacement Method in a Test Pit". This method contains correction for particle larger than 3 inches. Figures 8 and 9 show large in-place density test in trial area.

Table 1 shows large density tests results and Figure 10 shows the variation of dry density with lift thickness and number of roller passes. It could be seen that lift thickness 30 and 45cm lead to upper range of dry density.

The average dry density of lifts with thickness 30cm for roller pass number 4, 6 and 8 are 21.3, 21.5 and 20.4 kN/m^3 respectively. Also, the average dry density of lifts with thickness 45cm for roller pass number 4, 6 and 8 are 21.3, 21.3 and 19.6kN/m^3 respectively. The average dry densityof60 cm lifts thickness for roller pass of 4, 6 and 8 are 19.6, 19.5 and 20.0 kN/m^3 respectively.ecreasing of dry density in 8 roller passes may come back to breaking of particles and loosing of rockfill material. When there is boulder in pit, should be separate for weighting and calculating in test result.

Figure 8. Digging a pit for large in-place density test

Figure 9. A photo of trial area parts and large in-place density test holes

Table 1. Large in-place density test results

No	Lift thickness (cm)	Number of Roller Pass	Natural density (kN/m^3)	Dry density (kN/m^3)
1	30	4	21.8	21.4
2			22.2	21.2
3		6	22.2	21.2
4			22.3	21.8
5		8	21.2	20.3
6			21.2	20.4
7	45	4	22.0	21.4
8			21.9	21.3
9		6	22.4	21.8
10			21.7	20.9
11		8	19.8	19.2
12			21.9	20.8
13	60	4	19.5	18.5
14			20.1	20.8
15		6	19.3	18.8
16			20.9	20.1
17		8	18.6	19.1
18			21.4	21.0

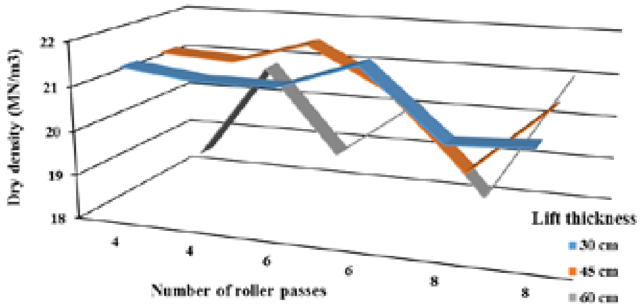

Figure 10. Variation of dry density with lift thickness and number of roller passes

5.3 *Plate Load Test*

Plate load tests done at 18 places on trial area and test results are presented at Table 2. Plate diameter was 45 cm.

Table 2. Plate load test results

No	Lift thickness	Number of Roller Pass	Ks (MN/m^3)	E (MPa)
1	30 cm	4	280	89.3
2			650	207.4
3		6	380	121.2
4			380	119.6
5		8	400	127.6
6			340	108.5
7	45 cm	4	500	159.5
8			640	204.2
9		6	450	143.5
10			320	102.1
11		8	420	134.0
12			270	86.1
13	60 cm	4	300	95.7
14			240	76.6
15		6	380	121.4
16			440	140.4
17		8	310	98.9
18			450	143.6

Subgrade modulus (Ks) calculated based on load-settlement curves. Figure 11 shows variation of subgrade modulus with lift thickness and number of passes. It could be seen than 45 cm lift thickness with 4 passes of roller compaction, have better results relative to result of 30 and 60 cm lift thickness.

A picture of plate load test performance is shown in Figure 12.

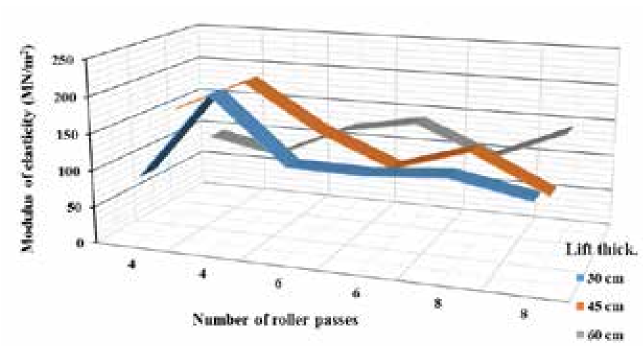

Figure 11. Variation of subgrade modulus with lift thickness and number of roller passes

Figure 12. Plate load test with track reaction load

5.4 *Compaction Test*

Compaction tests are done on particles passing sieve ¾ inches based on ASTM D1557 (ASTM, 2012) and then corrections are done based on weight percentage of particles larger than ¾ inches to 3 inches, based on ASTM D4718 (ASTM, 2001).

Three tests were done on the trial area and the results are presented on Table 3.

Table 3. Modified compaction test results

No	Maximum dry density (kN/m^3)	Optimum moisture content (%)
1	21.2	7.5
2	22.2	7.8
3	21.3	7.4

Tests results shows the maximum dry density of samples smaller than ¾ inches is about 21.6 kN/m^3 and the maximum dry density of total material is calculated as 22.8 kN/m^3.

5.5 *Seismic wave tests*

Surface seismic tests, by refraction method, are done on trial area, to see the P-wave and S-wave velocity variations in the trial area. Figure 13 shows test performance on compacted rockfill layers. The P-wave velocity (Vp) varies between 630to1050 m/s and the S-wave velocity (Vs) varies from330to460 m/s on compacted rockfill layers. A primary relation between Vs and compaction percent figure out and showed on Figure 14. Vs corresponding to compaction percent 85% is about 390 m/s. A refraction test is a non-destructive test with fast performance. Also, it could be done over a vast area for comparing the quality of compaction in different parts.

Figure 13. Seismic test performance on trial area

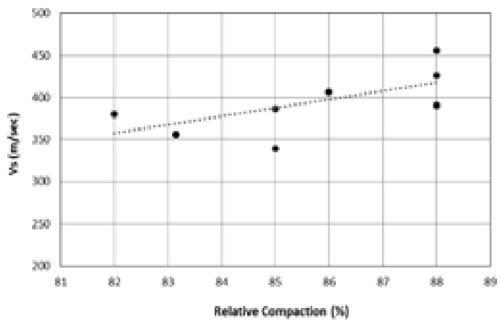

Figure 14. Relationship between shear wave velocities and compaction percent on rockfill layers

6 DISCUSSION

Performing high thickness embankment, using rockfill layers is very fast and economic. For determining the best pattern for rockfill embankment, including rockfill lift thickness and roller passes number is generally using trial embankment in a trial area. In this project, three different rockfill embankments with lift thickness of 30, 45 and 60cm had made with 3 different compaction efforts (roller passes number). Five different tests performed on trial rockfill embankment. The main object of the tests was to compare the effect of lift thickness, maximum particle size and number of roller passes on rockfills.

Figure 15. 3D chart of compaction percent and lift thickness

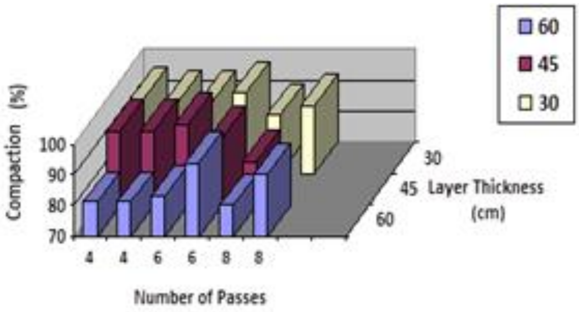

versus number of passes

The summary of tests results is presented on the Table 4. Also Figure 15 shows a 3D chart of compaction percent and lift thickness versus number of passes. It could be seen that there is a meaningful difference between compaction percentages of 45cm and 60cm lift thickness, which shows the vibratory rollers compaction rate would be more effective in 45 cm lifts.

Table 4. Summary of test results

Lift thick. cm	**No. of roller passes**	**Natural Density** kN/m^3	**Dry Density** kN/m^3	**Ks** MN/m^3	**E** MPa	**Comp.** (%)
30	4	21.8	21.4	280	89.3	94
		22.2	21.2	650	207.4	93
	6	22.2	21.2	380	121.2	93
		22.3	21.8	380	119.6	96
	8	21.2	20.3	402	127.6	89
		21.2	20.4	340	108.5	89
	Ave.	**21.8**	**21.1**	**400**	**128.9**	**92**
45	4	22.0	21.4	500	159.5	94
		21.9	21.3	640	204.2	93
	6	22.4	21.8	450	143.5	96
		21.7	20.9	320	102.1	92
	8	19.8	19.2	420	134.0	84
		21.9	20.8	270	86.1	91
	Ave.	**21.6**	**20.9**	**430**	**138.2**	**92**
60	4	19.5	18.5	300	95.7	81
		20.1	20.8	240	76.6	91
	6	19.3	18.8	380	121.4	82
		20.9	20.1	440	140.4	88
	8	18.6	18.1	310	98.9	80
		21.4	21.0	450	143.6	92
	Ave.	**20.0**	**19.4**	**350**	**112.7**	**85**

Looking at the effect of number of passes shows that 8 passes have less compaction percentage that it would be the result of particle breakage and loosing below the roller. Subgrade modulus for lift thickness 60cm is less than lift thickness 30 and 45cm.

As a main conclusion, the best rockfill compaction method for the project, proposed as using 45cm lift thickness and 6 passes of roller compactor. For zones that minimum compaction percentage was defined as 85%, the best compaction composed of 2 roller pass on 45 cm lift thickness.

Based on refraction surface seismic tests, when the shear wave velocity of rockfill layers was more than 390m/s, the compaction ratio had been reached to more than 85% MDD. Seismic methods are good methods for whole evaluation of massive rockfills.

7 CONCLUSION

Using rockfill layers for filling deep valleys in engineering embankments is prone, fast and economic. For determining the best pattern for rockfill embankment, is generally using trial embankment in a trial area. In the studied project, three different rockfill embankments with lift thickness of 30, 45 and 60 cm had made with 3 different compaction efforts. There is a meaningful difference between compaction percentages of 45cm and 60cm lift thickness, which shows the vibratory 15 tones rollers compaction rate would be more effective in 45cm lifts. Seismic wave tests are suit for evaluation rockfill layers, of course it is need to calibrate by some large density tests in trial area. In this study when the shear wave velocity of rockfill layers was over 390m/s, the compaction ratio had been passed 85% MDD.

8 ACKNOWLEDGMENTS

The authors wish to thank the SRIC Company and POR Company for supporting this research and appreciate Mr Siamak Abdolahi for valuable assistance.

9 REFERENCES

ASTM, 2001, ASTM D4718: Standard Practice for Correction of Unit Weight and Water Content for Soils Containing Oversize Particles.

ASTM, 2012, ASTM D1557: Standard Test Methods for Laboratory Compaction Characteristics of Soil Using Modified Effort.

ASTM D5030, 2013, Standard Test Methods for Density of Soil and Rock in Place by Water Replacement Method in a Test Pit.

Breitenbach, A. J. 1993, Rockfill Placement and Compaction Guidelines, Geotechnical Testing Journal, ASTM, Philadelphia, Pennsylvania, Vol. 16, No. 1, pp. 76 to 84.

Department of Technical Affairs, Office of Deputy for Strategic Supervision, Vice presidency for Strategic Planning and Supervision of Iran, 2013, Road General Technical Specification, No. 101, Second Revision.

Geotechnical and Geophysical Site Characterisation 5 – Lehane, Acosta-Martínez & Kelly (Eds)

Control of soil compaction in pavement layers: A new approach using the dynamic cone penetrometer (DCP)

A. Belincanta
Department of Civil Engineering, State University of Maringá, Maringá, Brazil
J. A. Lukiantchuki
Department of Civil Engineering, State University of Maringá, Maringá, Brazil
J. H. C. Reis
Department of Civil Engineering, State University of Maringá, Maringá, Brazil

ABSTRACT: Field control during soil compaction for pavement support layers has always been a concern for road engineers. Traditionally, the dry unit weight is measured in the field using the sand-cone method, and in some cases the drive cylinder test. An alternative to this control is the use of a dynamic cone penetrometer (DCP), which has the advantage of being fast and easy to operate. This method yields a higher number of data points, enabling better evaluation of variability and distribution of the specific gravity and ensuring that the properties of compacted soil in the field are consistent with established laboratory values. Therefore, this paper presents the results of a study on the use of DCP for soil compaction control in road pavement base and sub-base layers and proposes a mathematical equation for describing the Penetration Index (PI) behavior as a function of dry density and soil moisture content. This study was done using soils characteristic of the northwest region of Paraná and the results obtained with the proposed formula are evaluated by comparing the values of dry unit weight and soil water content. The penetration rate was observed to be inversely proportional to the degree of compaction and strongly influenced by the soil moisture content. In general, analysis of experimental results shows that the proposed use of DCP in the control of compaction in the field has great application potential.

1 INTRODUCTION

Compaction is a widely used technique for the improvement of soil behavior in the practice of pavement engineering. When a given soil does not present adequate mechanical characteristics, the compaction process is used to improve these properties by increasing compactness with a consequent reduction in soil volume and voids. From the standpoint of mechanical behavior, soil compaction is performed to achieve the desired characteristics in terms of increasing soil strength, dry density and modulus resilience. In addition, compaction enhances soil behavior in terms of reducing soil void ratio, and consequently it improves the compressibility and permeability.

In this context, the control of the degree of compaction becomes extremely important in ensuring that compacted soil in the field acquires the same properties achieved in the laboratory (Heyn, 1986; Meehan and Hertz, 2012). Usually, the compaction process in the field is monitored and controlled through in situ measurements of the density and moisture content of the compacted soil layer. These measurements are carried out with the sand-cone method (ASTM D1556-07), the rubber balloon method (ASTM D2167-08), the drive cylinder test (ASTM D2937-10), or nuclear-based test devices (ASTM D6938-10). In Brazil, compaction control is usually achieved by determining the dry unit weight in the field through the sand-cone method (NBR 7185/86) or through the California Bearing Ratio (CBR).

The employment of the compaction technique in pavement projects is achieved by determining certain parameters through the compaction test. The test lets you set the optimum moisture content and maximum dry unit weight (γ_{dmax}) for a given type of soil. With these parameters, the degree of compaction (DC) of the soil layer is defined (Eq. 1) and this value is compared to the value allowed in the project.

$$DC = \frac{\gamma_d}{\gamma_{d\,\max}} \tag{1}$$

where DC is the degree of compaction and γ_d is the field dry density.

Despite the established importance of compaction control, effective control is not always achieved. This is because cost, time and the required number of measurements are factors that can interfere with the control stage (Belincanta and Reis, 2008). Therefore, the use of the dynamic cone penetrometer (DCP) is presented as a good alternative for the indirect measurement of compaction quality. DCP equipment is portable, does not require other accessories for testing and provides a soil density estimate in less than 30 minutes. In addition, its application in pavement projects is already well established (ASTM D6951-03; Gabr et al., 2000; Salgado and Yoon, 2003; Herath et al, 2005) since this equipment has been widely used in determining the resistance to penetration in base and/or sub-base pavement layers. There are numerous empirical correlations that seek to establish a behavior between the penetration index (PI) determined in DCP testing and the California Bearing Ratio (CBR). However there are still few studies that propose the use of the DCP for the control of compaction of soil layers in the field.

This paper presents the results of a study using the dynamic cone penetrometer for the control of the execution of foundation layers in road pavements. The use of the DCP was made with the proposal of an equation that relates the penetration index as a function of the dry unit weight and the soil moisture content. This study was conducted using soil typical of the northwest region of Paraná. The results were evaluated through calibration of the proposed equation using laboratory tests and dynamic penetration tests in the field, carried out in conjunction with dry unit weight determinations and corresponding moisture content. In addition, laboratory CBR values were measured, permitting a better understanding of the results obtained in the study.

2 DYNAMIC CONE PENETROMETER (DCP) TEST

In order to contribute to the interpretation of the results of dynamic tests, the State University of Maringá (UEM) developed the design and construction of a dynamic cone penetrometer (DCP). This equipment follows the standard of the DCP developed in South Africa in 1956 (South African Penetrometer), with characteristics already commonly used in pavements. Belincanta and Reis (2008) point out that the interpretation of DCP results has changed little over time, with the most current application using correlations with CBR results. Thus, this study aims to contribute to a direct application for the control of compaction in the field.

The penetrometer used in this research is made up of a set of 16mm steel rods, 1800mm in overall length. The tip is fitted with a 60° cone, 20 mm in diameter and 45 mm in height. The penetration rod has a total length of 1000 mm, while the guide rod has a length of 575 mm (Figure 1).The penetration is performed with the free fall of an 8 kg weight, which reaches the driving head. The test consists of free fall of the weight on the driving head, providing penetration of the conical tip in the soil (Silva Junior et al., 2005). The dynamic penetration index (PI) is defined as the penetration value measured for each blow of the weight. In this study, the PI value was considered to be the average of the penetration values for 10 consecutive blows of the weight.

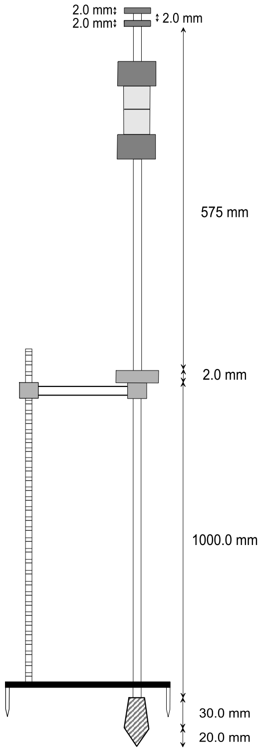

(a) DCP developed at UEM


(b) Penetration test in progress

Figure 1. Characteristics of the dynamic cone penetrometer test (Belincanta and Reis, 2008).

3 PENETRATION INDEX (PI) FOR COMPACTION CONTROL PURPOSES

The value of the penetration index (PI) is directly related to the dry unit weight γ_d), such that, the greater the dry unit weight, the denser the soil will be, and consequently the lower the penetration per blow. In addition, the PI index depends on soil moisture content, such that the higher the moisture content, the higher the value of PI. Since the technological control used in road pavement projects consists of determination in the field of the degree of compaction of the soil and the soil moisture content, the DCP should use an equation that relates the three parameters: penetration index (PI), dry unit weight γ_d) and soil moisture content (Edil et al., 2004).

Through data collection conducted with DCP, Belincanta and Reis (2008), observed that the penetration index is strongly influenced by the soil moisture content. They demonstrated that the penetration index (PI) is exponentially proportional to the soil moisture content and inversely proportional to the dry unit weight of the soil. Moreover, the greatest influence on the PI value is exerted by the soil moisture content. Thus, the authors proposed a mathematical equation that relates the penetration index (PI), the degree of soil compaction (DC) and the moisture content (Equation 2).The proposed equation also depends on the parameters of the compaction curve, such as maximum dry unit weight γ_{dmax}) and optimum water content (w_{op}.).

$$PI = C_1 \frac{\gamma_{d\max}}{\gamma_d} e^{C_2\left(\frac{w-w_{op}}{w_{op}}\right)} \tag{2}$$

where PI is the penetration index (cm/blow), γ_d is the dry unit weight of the compacted soil (kN/m^3), w is the soil water content (%); C_1 and C_2 are fit constants for the equation for determining the dynamic penetration index.

3.1 *Calibration of the proposed equation*

This study aims to employ the equation proposed by Belincanta and Reis (2008) in the interpretation of results of field tests using DCP.

The calibration of the equation was carried out through a series of field and laboratory tests performed on the soil in the city of Bandeirantes, Paraná, Brazil. The soils of the northwest of Paraná come from the decomposition of sandstone (Arenito Caiuá). Due to the hot and humid climate, the thickness of these soils can reach 30 m. Typically, these soils present two distinct layers, one being superficial, well-evolved, lateralized and approximately 10 m thick. Below this layer is the weathered soil. The location where the tests were performed presents a soil profile formed by of a top layer of lateritic silty clay, evolved from basaltic rock. It is characterized as a dark red latosol.

The results presented here were obtained from tests performed on-site (Bandeirantes) and tests carried out in the laboratory through the samples collected in the field. Thus, the testing program was developed as follows:

1. Dynamic Penetration tests using the DCP in a compacted soil layer for pavement purposes. PI values were determined from this test;
2. At the same points where the PI values were determined, tests were performed to determine the dry unit weight in situ. For this, we used the specimen method with the aid of a metal ring and the sand-cone method (NBR 7185/86);
3. Additionally, at the same points where PI values were determined, tests were conducted to determine the dry unit weight of the soil in situ. The determination of the corresponding moisture content was carried out with the oven method (NBR 6457/86). Therefore, the samples were properly packed for transport to the Soil Mechanics Laboratory of the State University of Maringa.

Besides the field tests described above, compaction tests were conducted in the laboratory using standard energy (NBR 9895/87) and tests for the determination of the California Bearing Ratio (CBR). The tests were performed for soil samples collected at three drilling sites. The results, summarized in Table 1 indicated the following behaviors:

Table 1. Summary of test results.

California Bearing Ratio		Compaction Test (Normal energy)	
CBR (%)	CBR_{max} (%)	γ_{dmax} (kN/m^3)	w_{op}(%)
10.1 - 13.2	22.2 - 24.7	16.1 - 16.5	22.2 - 24.7
Average values		16.3	23.5

1. The results of the compaction test, carried out using normal energy, indicated optimum moisture content (w_{op}) values between 25.9 and 27.0%, and maximum dry unit weight γ_{dmax}) values between 16.1 and 16.5 kN/m^3;
2. The California Bearing Ratio, conducted at normal energy and corresponding to the optimum moisture content, indicated values between 10.1 and 13.2%; and
3. The maximum California Bearing Ratio (CBR_{max}) occurred frequently in the dry branch of the compaction curve, corresponding to moisture content values between 22.2 and 24.7% for normal energy.

For the proposed equation, the average values of the maximum dry unit weight and optimum moisture content were used (Table 1). Analyses of the dynamic penetration tests, compared with the laboratory tests, indicated that the maximum value of CBR occurs in the dry branch of the compaction curve with a standard deviation of 1 to 2.5% relative to the optimum moisture content. Despite the difficulties in analyzing the PI values in these conditions, there was evidence of good resistance to dynamic penetration, with the material classified as GP (poorly graded gravel) and presenting a good bearing capacity (high CBR).

It is noteworthy that penetrometers, in terms of penetration index, are highly influenced by the moisture content relative to the influence of the dry unit weight, that is, in detriment to the influence of the actual densification conditions in the field. Experimental data conducted by Jeselay and Belicanta (2008) show the behavior of dry unit weight and moisture content in terms of penetration index.

From the results it was possible to derive the calibration for the constants C_1 and C_2 of the proposal presented by Belincanta and Reis (2008). Figure 2 shows the results of the penetration index as a function of soil moisture content. The dry unit weight values were estimated using the sand-cone method. For the analyzed soil, the PI showed a behavior exponentially proportional to the moisture content, as highlighted by the authors. The resulting fit equation indicated values of 2.10 and 9.5 for C_1 and C_2, respectively (Equation 3).

$$PI = 2.10\frac{\gamma_{d\max}}{\gamma_d}e^{9.5\left(\frac{w-w_{op}}{w_{op}}\right)} \tag{3}$$

The equation used to describe this behavior showed a good fit for the points measured in the field and compared with the laboratory results. The results indicate that the DCP has great potential for use in the control of the execution of pavement layers.

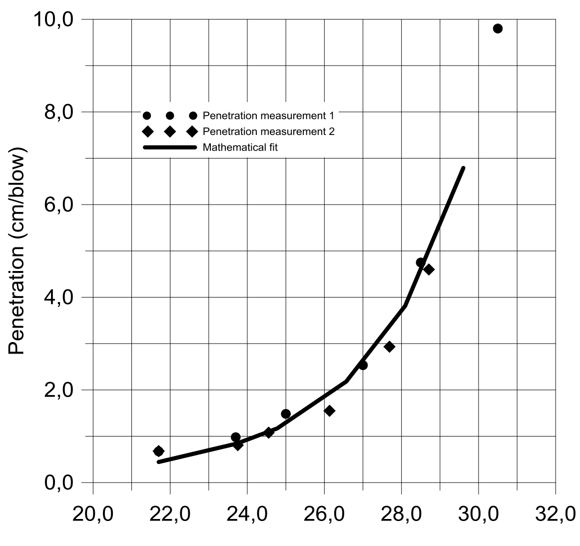

Figure 2. Penetration index versus moisture content (Calibration Equation 2).

3.2 *Control of compaction*

The results of field and laboratory tests yielded an equation for estimating the degree of compaction in the field (DC) as a function of the penetration index (PI) and the moisture content in the field (w), as presented below. Considering Equation 3 and using the average values of the results of the compaction test, such as a maximum dry unit weight of 16.3 kN/m^3 and maximum moisture content equal to 26.5% (Table 1), we have:

$$\gamma_d = 2.10\frac{16.3}{PI}e^{9.5\left(\frac{w-26.5}{26.5}\right)} \tag{4}$$

The degree of compaction can be estimated directly using the following equation:

$$DC = 100\times\frac{\gamma_d}{16.3} = \frac{210}{PI}e^{9.5\left(\frac{w-26.5}{26.5}\right)} \tag{5}$$

Equation 5 was used to graphically determine the region where the compaction conditions are acceptable considering a degree of compaction greater than 95%, as shown in Figure 3. In this way, the suitability of the compaction conditions can be achieved more quickly by directly using a measure of the penetration index relative to the moisture content in the field. This approach enables the use of dynamic penetrometer, as a quick and effective way to control the compaction of soil layers in pavement projects. However it is noted that the research carried out to date (Belincanta and Reis, 2008) were performed in soils typical of northwest Paraná, Brazil. Therefore, the use of the DCP in compaction control requires calibration tests for each type of soil to be considered.

Regarding the compaction process in the field, it is recommended that the layers should have maximum thickness of no more than 0.2 m in their final condition. The degree of compaction of basis layers should be at least 95%, with a moisture content slightly below the optimum moisture content (1% - 2%), i.e., the dry branch of the compaction curve. This is because the laboratory tests indicated that under these conditions the CBR presents above 20%, even reaching values close to 25%. .

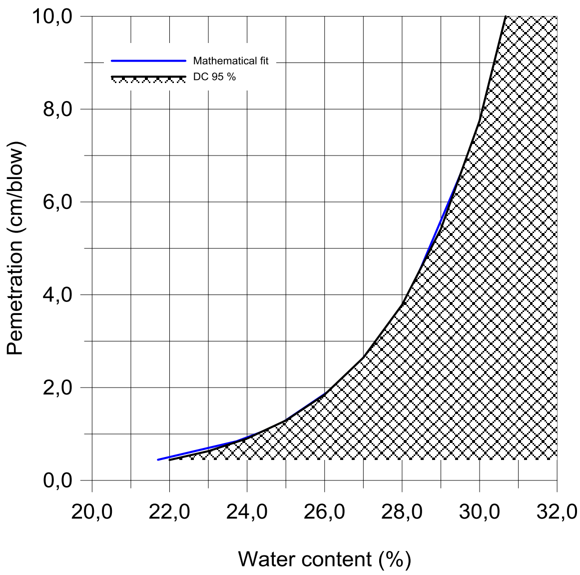

Figure 3. Compaction control as a function of the PI and moisture content, considering a degree of compaction greater than 95%.

4 CONCLUSION

This study presented the results of the calibration of dynamic penetration tests performed with the DCP penetrometer type developed at the State University of Maringá (UEM). The results obtained through field penetration tests and laboratory testing allowed for the fit and calibration of an equation relating the penetration index, the dry unit weight and the soil moisture content.

Data analysis shows that the proposal of Belincanta and Reis (2008), for the use of the DCP in control of compaction in the field, has great application potential. In this way, the control can be performed in situ by measuring the PI and soil moisture content, as they are directly related to the degree of compaction of the layer. Furthermore, the results indicate that the PI value is inversely proportional to the degree of compaction and that it is strongly influenced by the soil moisture content. The importance of the calibration of the equation parameters of the proposed equation for other types of soil was noted, since the material presented in this study represent the behavior of soils typical of the northwest of Paraná.

5 REFERENCES

ABNT (1986). Determination of in situ unit weight using sand cone method. NBR 7185, São Paulo, Brasil (in Portuguese).

ABNT (1986). Soil samples: preparing for characterization tests. NBR 6457, São Paulo, Brasil (in Portuguese).

ASTM (2003). Standard test method for use of the dynamic cone penetrometer in shallow pavement applications. D6951-03, ASTM International, West Conshohocken, PA.

ASTM (2011). Standard test method for density and unit weight of soil in place by the sand-cone method. D1556-07, V. 4.08, ASTM International, West Conshohocken, PA.

ASTM (2011). Standard test method for density and unit weight of soil in place by the rubber balloon method. D2167-08, V.4.08, ASTM International, West Conshohocken, PA.

ASTM (2011). Test method for density of soil in place by the drive-cylinder method. D2167-08, V.4.08, ASTM International, West Conshohocken, PA.

ASTM (2011). Standard test method for in-place density and water content of soil and soil-aggregate by nuclear methods (shallow depth). D6938-10, V.4.09, ASTM International, West Conshohocken, PA.

Belincanta, A.; Reis, J. H. C. (2008). Evaluation of dynamic cone penetrômetro Investigation of soils stiffness gauge and dynamic cone penetrometer for earthwork property evaluation. In: *IV Luso-Brazilian Geotechnical Conference, Coimbra, Portugal* (in Portuguese).

Edil, T. B., Benson, C. H., Sawangsuriya, A. e Allbright, R. L. (2004). *Investigation of soils stiffness gauge and dynamic cone penetrometer for earthwork property evaluation*. FINAL REPORT, Wisconsin Highway Research Program #0092-01-05, Department of Civil and Environmental Engineering, University of Wisconsin,, Madison, USA, 93 p.

Gabr, M. A., Hopkins, K., Coonse, J., Hearne, T. (2000).DCP criteria for performance evaluation of pavement layers. *Journal of performance and constructed facilities*, V. 14, N. 4, 141-148.

Heyn, A. T. (1986). Applications of dynamic penetrometer conical tip in the evaluation of pavement structures. In: *21ª. Annual Paving Conference*, Salvador, Bahia. Brasil, 139–149 (in Portuguese).

Herath, A.; Mohammad, L. N.; Gaspard, K.; Gudishala, R.; Abu-Farsakh, M. Y. (2005). The use of dynamic cone penetrometer to predict resilient modulus of subgrade soils. *Advances in pavement engineering*, 1-16.

Meehan, C. L.; Hertz, J. S. (2012). Using a complex-impedance measuring instrument to determine in situ soil unit weight and moisture content. *Geotechnical testing journal*, v. 36, n. 1, p. 1-21.

Salgado, R.; Yoon, S. (2003). *Dynamic cone penetration test (DCPT) for subgrade assessment*. Joint transportation research program, Civil engineering, Purdue University, 109 p.

Geotechnical and Geophysical Site Characterisation 5 – Lehane, Acosta-Martínez & Kelly (Eds)

A new indirect tensile testing setup to determine stiffness properties of lightly stabilised granular materials

D.K. Paul
Department of Civil & Architectural Engineering, Qatar University, Doha, Qatar.

R. Gnanendran & M. J. I. Alam
School of Engineering and Information Technology, University of New south Wales at ADFA, Canberra, ACT, Australia.

ABSTRACT: This paper presents a new indirect diametral tensile (IDT) testing setup for determining the stiffness modulus and Poisson's ratio for the characterisation of lightly stabilized granular base materials required for pavement design. The experimental program included the determination of IDT strength, stiffness modulus and Poisson's ratio for a typical freshly quarried granular base material stabilised by the addition of 1-3% cement-flyash slow-setting binder. The samples, prepared using a gyratory compactor, were cured for 28 days and then tested in the IDT testing machine. Details of the new IDT testing arrangement with on-sample deformation measurement for performing monotonic testing to obtain both the horizontal and vertical deformations along the diameters of an IDT specimen are discussed. This study indicates that the proposed IDT testing setup could be used consistently for determining the stiffness modulus and Poisson's ratio of a lightly stabilised granular material.

1 INTRODUCTION

Chemical stabilisation using cementitious binders is a low cost treatment method that is practically useful for expansive and/or weak subgrade and base materials. However a binder should be selected such that it doesn't create shrinkage cracking in the stabilized material which could otherwise affect its strength and stiffness. Small amount of slow setting general blend (GB) cement-flyash could be an option for the granular stabilization as they reduce the heat generated and have low tendency to shrink and crack upon cooling (Foley & Australian Stabilisation Group 2001a). A pavement is characterized and designed in such a way that it should withstand against rutting and fatigue failure during its span of design life. Cementitiously stabilised granular materials are generally characterised by their tensile strength, stiffness modulus and Poisson's ratio.

A number of testing methods [e.g., direct tension, flexural and Indirect Diametric Tensile (IDT) testing are generally used to characterise cementitiously stabilised materials. Flexural beam point load testing method is often preferred for characterisation due to the similarities in the stress conditions it produces with that in the stabilised base layer of a pavement structure under wheel loading. However the preparation and handling of a flexural beam of cementitiously stabilized pavement material at such low levels of binder content is quite difficult. As a consequence, IDT test method has recently been suggested as a possible alternative for economically obtaining repeatable and reliable stiffness characteristics for these materials (Foley & Australian Stabilisation Group 2001b, Gnanendran & Piratheepan 2008).

In a traditional IDT testing setup (e.g., Khattak & Alrashidi 2006, Gnanendran & Piratheepan 2009, Paul et al. 2010, Solanki & Zaman 2011), only the deformation along the horizontal diameter is measured and stiffness modulus is determined using the elastic theory equation based on an assumed value of Poisson's ratio for the tested material. However, an inaccurate Poisson's ratio with a difference of 0.1 from the actual value may increase/decrease the stiffness modulus by up to 25% resulting in an uneconomical and conservative pavement design. With the objective of addressing this limitation, a new internal test setup for measuring the deformations along both the horizontal and vertical diameters of IDT specimens is proposed in this study so that both the stiffness modulus and Poisson's ratio can be determined analytically.

2 THEORETICAL BACKGROUND

The stress-strain distributions in a specimen under IDT testing are non-uniform and complicated. The biaxial stress-strain distribution can be illustrated more clearly by Hooke's Law, the governing equation for elastic materials

$$\begin{Bmatrix} \varepsilon_x \\ \varepsilon_y \end{Bmatrix} = \frac{1}{E}\begin{bmatrix} 1 & -\nu \\ -\nu & 1 \end{bmatrix}\begin{Bmatrix} \sigma_x \\ \sigma_y \end{Bmatrix} \quad (1)$$

Where ε_x = horizontal strain, ε_y = vertical strain, σ_x = horizontal stress, σ_y = vertical stress, E = Young's (or elastic or stiffness) modulus and ν = Poisson's ratio.

Hondros (1959) formulated a complete stress solution for a disk/cylinder under loading distributed over a finite width, as shown in Figure 1, assuming the material to be homogeneous, isotropic and linear elastic. The normal strains along the vertical and horizontal diameters of a specimen derived from Hondros' stress solutions are given by the Equations 2 and 3. [It should be noted that the sign convention used in the analysis is positive (+) for tension and negative (-) for compression.]

$$\varepsilon_h = \frac{2P}{\pi a t E}\left[(1+\nu)\frac{\left(1-\frac{x^2}{R^2}\right)\sin 2\alpha}{1+2\frac{x^2}{R^2}\cos 2\alpha+\frac{x^4}{R^4}} + (\nu-1)\tan^{-1}\left(\frac{1-\frac{x^2}{R^2}}{1+\frac{x^2}{R^2}}\tan\alpha\right)\right] \quad (2)$$

$$\varepsilon_v = -\frac{2P}{\pi a t E}\left[(1+\nu)\frac{\left(1-\frac{y^2}{R^2}\right)\sin 2\alpha}{1-2\frac{y^2}{R^2}\cos 2\alpha+\frac{y^4}{R^4}} - (\nu-1)\tan^{-1}\left(\frac{1+\frac{y^2}{R^2}}{1-\frac{y^2}{R^2}}\tan\alpha\right)\right] \quad (3)$$

Where ε_h = horizontal tensile strain along the diameter normal to the loading diameter, ε_v = vertical compressive strain along the loading diameter, a = width of loading strip, t = thickness of specimen, R = $D/2$ = radius, D = diameter, α = angle at centre of specimen subtended by loading strip and P = applied vertical load.

For the strain distributions along the diameters, the total horizontal and vertical deformations may be obtained by integrating Equations 2 and 3, respectively, over the gauge length (g) of the symmetrically mounted LVDTs about the centre and shown in Equations 4 and 5.

$$\delta_h = \int_{-g/2}^{+g/2} \varepsilon_h \, dx \quad (4)$$

$$\delta_v = \int_{-g/2}^{+g/2} \varepsilon_v \, dy \quad (5)$$

Equations 4 and 5 can be simplified to a generalised form as

$$\delta_h = \frac{P}{tE}(a_g + b_g\nu) \quad (6)$$

$$\delta_v = -\frac{P}{tE}(c_g + d_g\nu) \quad (7)$$

Here a_g, b_g, c_g and d_g are the constants and their magnitudes depend on g. Their values can be obtained by performing the integrations in Equations 4 and 5. For a specimen of diameter 150 mm, strip width 12 mm and thickness 85 mm, typical values of the constants determined for different gauge lengths using the mathematical software 'MAPLE' are outlined in Table 1.

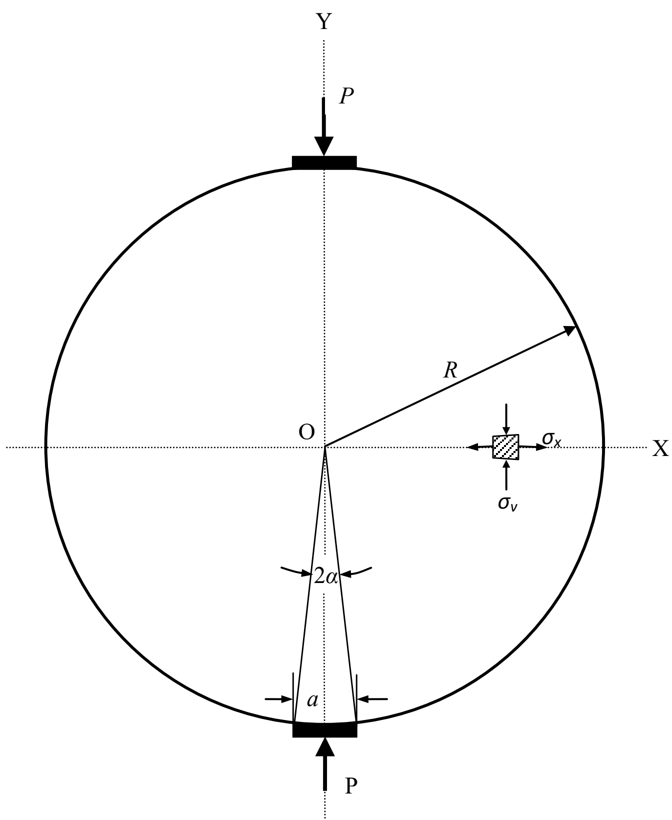

Figure 1. Schematic representation of IDT specimens subjected to strip loading

When the magnitudes of the constants for a gauge length are obtained, the values of the Poisson's ratio and stiffness modulus are calculated from Equations 8 and 9.

$$\nu = \frac{-c_g - a_g \dfrac{\delta_v}{\delta_h}}{d_g + b_g \dfrac{\delta_v}{\delta_h}} \quad (8)$$

$$E = \frac{P}{t\delta_h}(a_g + b_g \nu) \quad (9)$$

Table 1: Values of constants for determination of elastic modulus and Poisson's ratio

Gauge length, g	a_g	b_g	c_g	d_g
37.5 mm (= D/4)	0.146	0.451	0.490	0.157
75 mm (= D/2)	0.236	0.780	1.075	0.314
100 mm (= 2D/3)	0.262	0.911	1.609	0.413
112.5 mm (= 3D/4)	0.268	0.952	1.970	0.457
150 mm (= D)	0.272	0.999	4.13	-0.04

Thus by capturing deformations along the vertical and horizontal diameters (i.e., δ_h and δ_v) over specific gauge lengths, an approach for obtaining the elastic modulus and Poisson's ratio of a disk/cylinder sample of lightly stabilised granular material from IDT testing using additional strain gauges is developed in this paper.

3 IDT TEST SETUP AND EXPERIMENTAL INVESTIGATION

In this investigation, a monotonic load IDT testing program has been carried out to determine the mechanical properties of the lightly stabilized material by means of improved experimental setup. In conventional IDT testing, only deformations along the horizontal diameter are measured externally which may include some extraneous deformation. As a result, the load-deformation curve obtained may not be representative. In this study, a new and improved IDT testing setup was developed to accurately measure deformations along both the horizontal and vertical diameters with the objective of determining the values of Poisson's ratio and stiffness modulus of a lightly stabilised granular material using equations derived from the elastic analysis. Details of the development of a new IDT test setup and the experimental program is discussed in the following sections.

3.1 *Development of IDT Test Setup*

The proposed on-sample instrumentation for internal deformation measurements is shown in Figure 2. To obtain the horizontal deformation, two LVDTs were attached to two Perspex strips glued onto the diametrically opposite sides of the specimen in a symmetrical fashion. The LVDTs' tips rested against the Delran rods connected to the other sides of the strips and measured the diametrically horizontal deformation when the specimen was subjected to vertical loading.

On the other hand, vertical deformation measurement was rather complex and difficult. Initially, two small aluminium blocks were glued onto the circular faces of the specimen at distances of 55 mm from its centre. A special L-shaped frame was made, one end of which was screwed to the top aluminium block and the other held the vertical LVDT in its hole by means of another screw, as shown in Figure 2. As the tip of the LVDT rested on the bottom aluminium block, it was possible to monitor the vertical deformation along the loading diameter for a gauge length of 110 mm.

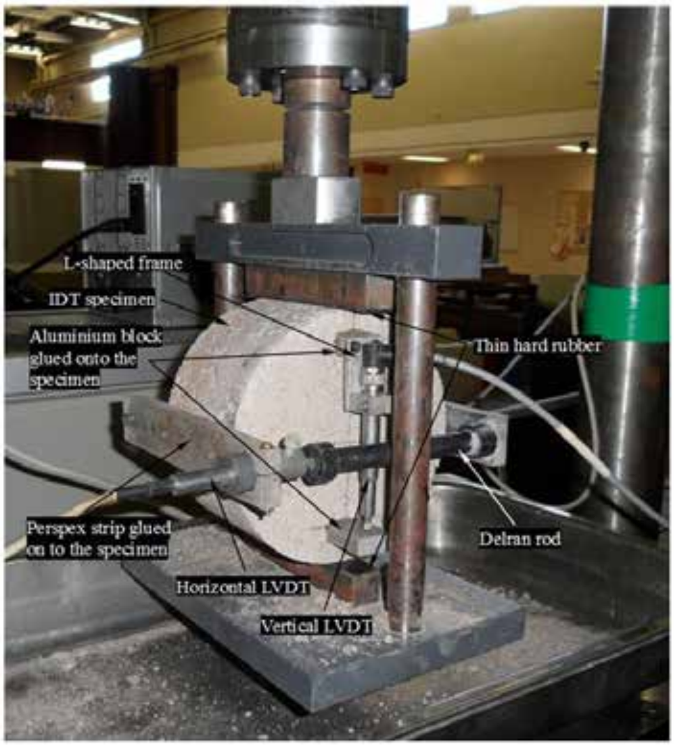

Figure 2. Photographic view of IDT test setup

3.2 *Materials and Binders*

The parent material used in this study was the freshly quarried granular base material obtained from a local query in Canberra, Australia. This was classified as well graded sandy gravel with some fines according to the Unified Soil Classification System. It is worth noting that the grading of the parent material and the grading ranges of the parent materials chosen for this investigation satisfy the guidelines for type 1 gradation C road base material according to ASTM (2005). However, to obtain representative and consistent samples, the reconstituted material with the grading shown in Figure 3 was chosen for this investigation (Paul & Gnanendran 2012; Paul & Gnanendran 2015). The adopted grading for the reconstituted sample, hereafter referred as the parent material, was essentially the same for all the samples that were tested in this experimental investigation.

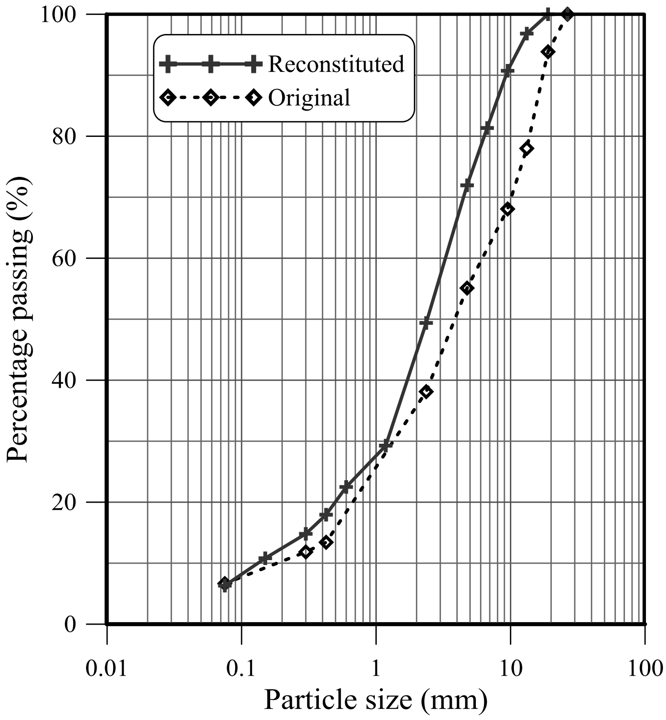

Figure 3. Original and reconstituted particle size distribution of parent material

As indicated earlier, the binder chosen for this experimental study was GB cement with flyash. GB cement-flyash blend with a ratio of 75:25 is commonly used to stabilise road pavements in Australia and therefore this blend is selected for this study. Both the cement and flyash were supplied by Blue Circle Southern Cement Company Pty. Ltd., Australia. The parent materials were stabilised by cement-flyash in the proportions of 1.0%, 1.5%, 2.0% and 3.0% by dry weight.

3.3 *Sample Preparation and Curing*

Standard Proctor Compaction test was carried out to establish the dry density-moisture content relationship according to Australian Standard (2003). The maximum dry density (MDD) of the parent material without any binder was found to be 2088 kg/m3 whereas the addition of 3% cement-flyash increased this value to 2157 kg/m3 with its optimum moisture content (OMC) remaining almost constant at 9%. Therefore, all the samples stabilized within this small binder range (1% - 3%) were prepared with a fixed moisture content of 9% throughout this study.

A total of 12 samples (i.e. 4 batches of three samples each) were prepared using the gyratory compaction method (i.e. binder contents of 1.0 %, 1.5%, 2.0%, and 3%). White & Gnanendran (2005) suggested the combination of 500 kPa pressure and 250 gyrations as the most practical gyratory compaction arrangement to achieve 95% or more density to that achieved by standard Proctor compaction. Therefore, the samples were prepared in a 150 mm diameter split mould at 500 kPa pressure and 250 gyrations. The prepared cylindrical samples of compacted thickness of around 80-85 mm were then allowed to cure in the mould for 24 hours until they gained sufficient strength. The samples, wrapped with polythene, were then put in the fog room at 23 ± 2°C and 95 ± 5% humidity for curing. After 28 days of curing, the samples were taken away from the fog room and left outside for 4 hours at room temperature before testing.

3.4 *Testing of Samples*

The monotonic load IDT testing was carried out in the displacement-control mode at a constant vertical deformation rate of 1 mm/min. Consequently, the deformations (both horizontal and vertical) and load magnitudes were saved using a data acquisition system in order to construct the load-deformation responses. Figure 4 shows a typical load-deformation diagram from the monotonic load IDT testing. As can be seen in the figure, the newly proposed IDT setup gave consistent initial linear part for the load-deformation response that enables the estimation of the stiffness modulus and Poisson's ratio of the material confidently.

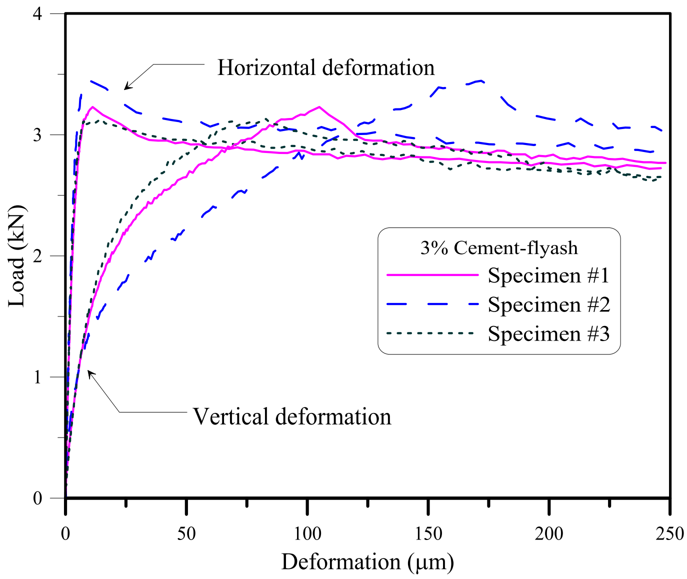

Figure 4. Typical load-deformation curve from monotonic IDT testing

4 RESULTS AND DISCUSSION

4.1 *IDT Strength*

The maximum tensile strength, known as the IDT strength, $\sigma_{t,max}$ of the stabilized material from monotonic loading is calculated from the following elastic theory solution as below:

$$\sigma_{t,\max} = \frac{2000 \times P}{\pi \times D \times t} \tag{10}$$

Figure 5 illustrates the variation of ultimate IDT strength with binder content. It is clear that the IDT strength increased almost linearly with the increase in binder content. For example, for the binder range of 1% to 3%, the average IDT strength increased from 0.048 MPa to 0.171 MPa.

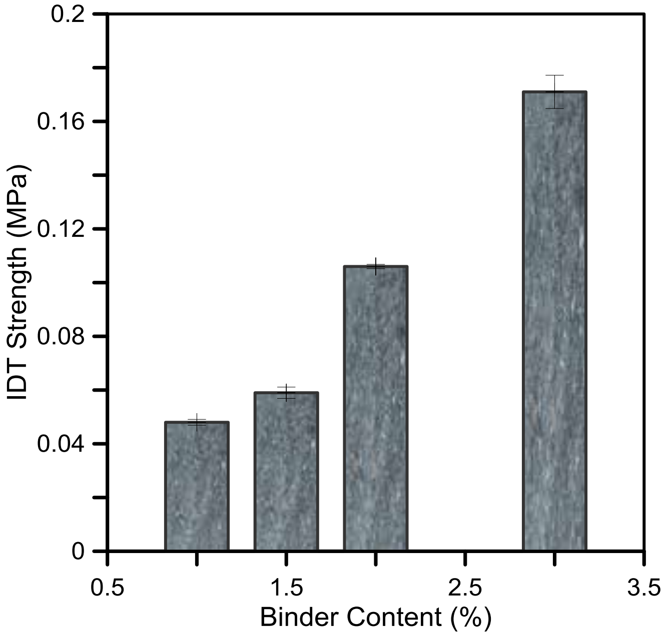

Figure 5. Variation of IDT strength with binder content

4.2 *Poisson's Ratio*

Typical load versus horizontal and vertical deformation responses obtained from the monotonic load IDT testing are shown in Figure 4. The Poisson's ratio was calculated from the initial linear part of the curves using Equation 8. The magnitudes of constants a_g and b_g were taken from Table 1 as 0.27 and 1.0, respectively, for a gauge length of D (= 150 mm) along the horizontal diameter. On the contrary, the vertical deformation was measured at a gauge length of 110 mm which gave the values of c_g and d_g as 1.90 and 0.45 respectively. Figure 6 shows the Poisson's ratios of the lightly stabilised materials determined from monotonic IDT testing. For binder content variations of 1% - 3%, the Poisson's ratios ranged from 0.18 to 0.26. The value of Poisson's ratio obtained in this study are within the range (i.e., 0.1 – 0.3) suggested by Austroads (2010) for cementitiously stabilised materials.

4.3 *Stiffness Modulus*

The static stiffness modulus was calculated from the linear portion of the load-deformation curves using Equation 9. Figure 7 shows the average static stiffness modulus obtained from a batch of three identical specimens for different binder contents. They ranged widely, from 1190 MPa to 4975 MPa, for the binder contents of 1% to 3.0% investigated in this study. In general, static stiffness modulus of both the mixes increased with increases in the binder contents.

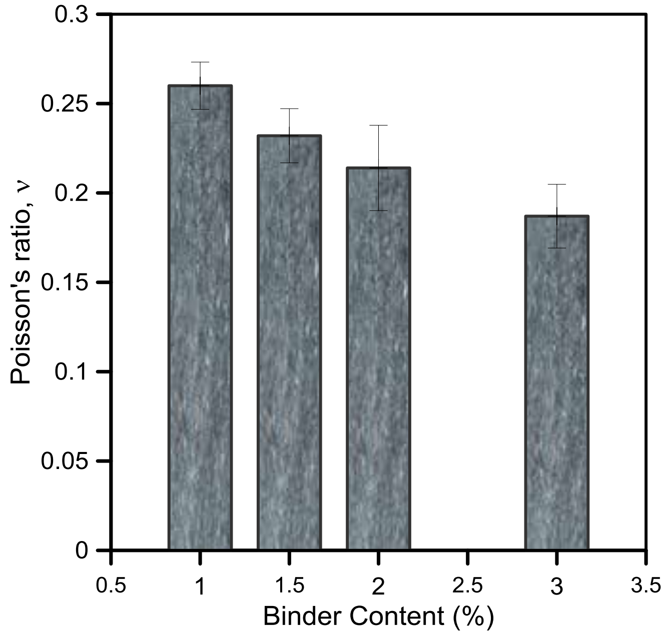

Figure 6. Variation of Poisson's ratio with binder content

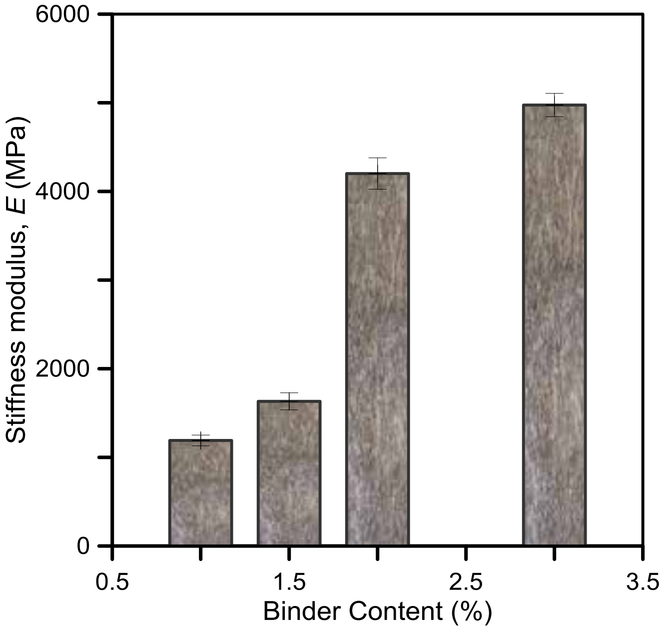

Figure 7. Variation of stiffness modulus with binder content

5 CONCLUSIONS

A new IDT testing setup was developed in this study to determine deformations along the horizontal and vertical diameters of a cylindrical IDT specimen. IDT specimens were prepared by stabilising a typical granular base material with 1% to 3% cement-flyash. Then monotonic load IDT testing was conducted on gyratory compacted specimens cured for 28 days to determine the tensile properties. Based on the test results discussed, it was concluded that the IDT strength, Poisson's ratio and the stiffness modulus of a lightly stabilized granular base material can be determined consistently and reliably from the newly developed IDT testing setup developed in this study. Almost linear increase in IDT strength and stiffness modulus was found with increasing binder contents.

6 ACKNOWLEDGEMENTS

The authors would like to thank Mr David Sharp and Mr Jim Baxter for their technical assistance during the lab work reported in this paper. The contributions of Blue Circle Southern Cement Pty Ltd for providing the binder used in the lab testing are also acknowledged and appreciated.

7 REFERENCES

Australian Standard. 2003. *Methods of testing soils for engineering purposes, Method 5.1.1: Soil compaction and density tests—Determination of the dry density/moisture content relation of a soil using standard compactive effort* (AS 1289.5.1.1.). Standards Australia, Sydney, Australia.

ASTM. 2005. *Specification for materials for soil-aggregate subbase, base and surface courses.* ASTM D1241-07, ASTM International, Conshohocken, PA, USA.

Foley, G. & Australian Stabilisation Group. 2001a. *Contract Report—Effect of Design, Construction and Environmental Factors for Long-Term Performance of Stabilised Materials*. Report No. RC91022-1, Austroads, Sydney, Australia.

Foley, G. & Australian Stabilisation Group. 2001b. *Contract report-Mechanistic Design Issues for Stabilised Pavement Materials*. Report No. RC91022-3, Austroads, Sydney, Australia.

Gnanendran, C.T. & Piratheepan, J. 2008. Characterisation of a lightly stabilised granular material by indirect diametrical tensile testing. *International Journal of Pavement Engineering* 9(6): 445-456.

Gnanendran, C.T. & Piratheepan, J. 2009. Indirect Diametrical Tensile Testing with Internal Displacement Measurement and Stiffness Determination. *Geotechnical Testing Journal* 32(1): 45-54.

Hondros, G. 1959. The evaluation of Poisson's ratio and the modulus of materials of a low tensile resistance by the Brazilian (indirect tensile) test with particular reference to concrete. *Australian Journal of Applied Science* 10: 243-268.

Khattak, M.J. & Alrashidi, M. 2006. Durability and mechanistic characteristics of fiber reinforced soil-cement mixtures. *The International Journal of Pavement Engineering* 7(7): 53-62.

Paul, D.K. & Gnanendran, C.T. 2012. Characterisation of Lightly Stabilised Granular Base Materials by Flexural Beam Testing and Effects of Loading Rate. *ASTM Geotechnical Testing Journal*, 35(5): 691-702.

Paul, D.K., Gnanendran, C.T. & Piratheepan, J. 2010. Determination of Stiffness Properties of Lightly Stabilised Granular Materials from IDT Testing using Numerical Analysis. *Proceedings of the 17th Southeast Asian Geotechnical Conference*, Taiwan Geotechnical Society & Southeast Asian Geotechnical Society, Vol 1: 75-78.

Paul, D.K. & Gnanendran, C.T. 2015. Characterization of lightly stabilized granular base materials using monotonic and cyclic load flexural testing. *Journal of Materials in Civil Engineering*, 28 (1), 04015074.

Solanki, P. & Zaman, M. 2011. Characterization of Lime- and Fly Ash-Stabilized Soil By Indirect Tensile Testing. *Geo-Frontiers 2011: Advances in Geotechnical Engineering*, American Society of Civil Engineers (ASCE), Dallas, Texas, USA: 4438-4448.

White, G.W. & Gnanendran, C.T. 2005. The influence of compaction method and density on the strength and modulus of cementitiously stabilised pavement materials. *International Journal of Pavement Engineering* 6(2): 97-110.

Geotechnical and Geophysical Site Characterisation 5 – Lehane, Acosta-Martínez & Kelly (Eds)
© 2016 Australian Geomechanics Society, Sydney, Australia, ISBN 978-0-9946261-1-0

New and Innovative Approach to Ensuring Quality of Quarry Source Materials in Queensland Road Infrastructure Construction

Ajith Dissanayake
Technical Manager (Quarries and Construction Materials), Geotechnical Unit, Engineering and Technology Branch, QLD Department of Transport & Main Roads, Brisbane, Australia.

Peter Evans
Deputy Chief Engineer (Pavements Materials and Geotechnical), Engineering & Technology Branch, QLD Department of Transport & Main Roads, Brisbane, Australia.

ABSTRACT: The Queensland Department of Transport and Main Roads (TMR) manages a road network of 33,343km. Whether constructed of concrete, asphalt, modified, stabilised or gravel base, quarry sourced materials are widely used to provide the structural strength of these pavements. Accordingly, ensuring that these quarries are providing quality materials is of vital performance to TMR. Department currently spends over $12 million annually on testing quarry material. The TMR Geotechnical Unit currently oversees 440 quarries that supply materials to TMR, Local Governments, and private industry, through its Quarry Registrations System (QRS). This paper discusses a new and innovative approach that TMR adopts to manage the quality of road construction quarry products. It also describes how test methods are applied to ensure adequate field performance, and how TMR has recently developed and implemented a sophisticated and practical system to allow quarries to self-assess their testing frequencies. QRS is already resulting in reduced testing costs for industry, which will ultimately flow on to reduce costs to government.

1 INTRODUCTION

The Queensland Department of Transport and Main Roads manages a road network of over 33,343km and associated infrastructure across the State of Queensland. The Department's heavily trafficked road pavements contain quarry-sourced materials. Quality management of construction, maintenance and rehabilitation of all pavements, and their surfacings, provides best value for the community. As the steward of this massive road network, the Department needs to ensure that these quarry materials are well managed, to avoid premature failure or reduced life of the pavements and their surfacings. Ensuring acceptable supply quality of pavement materials has always been a priority, and a major challenge, faced by State Road Authorities across Australia.

As part of Queensland's recent $6.4 billion Flood Reconstruction program, approximately $800 million worth of road construction quarry products have been produced and processed annually during that period. In Queensland, these paving materials are procured by Contractors from the 440 privately operated hard rock quarries and sand and gravel plants that produce crushed fine and coarse aggregates.

Each year it is estimated that $12 million is spent on testing road construction quarry products supplied to the Department at different stages during construction. This constitutes approximately 1.5% of the total cost of supplying these materials. Through a process of stakeholder consultation, Quarry Industry operators identified that these costs may be reduced, particularly for well managed quarries. As part its drive for aggressive cost savings and value for money (VoM), the Department had a strong incentive to work with the Quarry Industry to review the testing requirements with a goal to generating cost savings without compromising quality.

Because the type and quality of paving and concrete materials varies markedly and widely throughout Queensland due to their source rock/material and product quality variations and associated risk issues (Figures 1, 2, 3, 4, 5 & 6), a robust, source/product-specific, risk-based, effective and efficient mechanism is required by the Department to manage the material risks presented. Additionally, many local governments utilise the Department's standard specification suite in procuring local roads.

Figure 1. An example of source rock variability - Partially melted/liquefied dolomitic limestone xenoliths (white patches) embedded within andesitic intrusions resulting processing and sorting difficulties.

Figure 2. An example of product variability for the same source rock - Requirements for specific soaking & screens in production process to separate poorly cemented labile deleterious and non-durable sandstone fragments from fine to quarzitic sand.

Figure 3. An example of poor quality basaltic cover (seal) aggregate exhibiting premature break down on a newly constructed pavement overlay. In this case, the count of moisture sensitive non-durable weak particles exceeds the specification limit.

Figure 4. An example of iron sulphide bearing regional metamorphic source rock showing scattered pods and vugs of golden colour pyrite (FeS_2). Aerial oxidation of pyrite could result in adverse discoloration in aesthetic concrete & road surfaces.

Figure 5. An example of aerial oxidation of pyrite (FeS_2) bearing asphalt aggregate on a road surface showing scattered and spotted rusty red brown discoloration.

Figure 6. Formation of jarosite ($KFe_3(OH)_6(SO4)_2$) with yellow band along the moisture front due to aerial oxidation of pyrite (FeS2) in a stockpile of processed fine natural sand aggregate sourced from tidal sand deposit. This reveals the pres-

ence of potential acid sulfate condition in fine concrete aggregate.

2 MANAGEMENT OF QUARRY MATERIALS IN QLD

2.1 *Background*

The Department's specifications listed in Table 1 require that quarry products supplied to its road pavements and concrete infrastructure projects be registered in its Quarry Registration System (QRS). Registration is based on applying a well-developed process to assess the suitability of potential quarries for Departmental use. A small team of Departmental engineering geologists lead by the TMR Technical Manager (Quarries and Construction Materials) manages the QRS. To attain registration, quarries must conduct a series of laboratory tests following established TMR and Australian Standard test methods, and demonstrate that quarry materials can be produced to satisfy the material properties and engineering parameters established in TMR Technical Specifications. The respective road construction quarry products are registered in the TMR Quarry Database.

Table 1. TMR Technical Specifications impacted by TMR Quarry Registration System (QRS)

TMR Technical Specification	Technical Specification Title
MRTS05	Unbound Pavements
MRTS08	Plant-Mixed Stabilised Pavements Using Cement or Cementitious Blends
MRTS09	Plant-Mixed Pavements Layers Stabilished Using Foamed Bitumen
MRTS11	Sprayed Bituminous Surfacing
MRTS12	Sprayed Bituminous Emulsion Surfacing
MRTS13	Bituminous Slurry Surfacing
MRTS22	Supply of Cover Aggregate
MRTS30	Asphalt Pavements
MRTS39	Lean Mix Concrete Subbase for Pavements
MRTS40	Concrete Pavement Base
MRTS70	Concrete
MRTS101	Aggregates for Asphalt

2.2 *Evolution of Specified Testing Frequency*

Traditionally, contract Principals of individual road construction projects set their own testing frequencies, typically basing selection on historic practice and without up-to-date geological source or quarry production input. Consequently there were wide variations in testing frequencies between different quarries, and sometime for different projects for the same quarry. Depending on their risk appetite, some contract Principals also elected to invest heavily in testing, and others conducted minimal testing. In some cases this resulted in significantly disparate testing practices conducted in similar quarries.

The Management of the Queensland's Flood Reconstruction Program requested streamlining of testing in order to reduce the risk of delay to construction of a program within very tight delivery timelines. TMR convened a meeting of Flood Reconstruction Project Managers throughout Queensland, and negotiated a set of consistent testing frequencies for Flood Reconstruction Projects, for application across Queensland for all projects. These frequencies were then widely applied on flood recovered road construction work throughout Queensland.

However, this approach was not optimal as:

it remained discretionary within the Departments specification and contract system

it did not capture the ongoing data and analysis required to establish up-to-date testing regimes appropriate to the quarry-specific quality and risk.

the Quarry Industry identified the high financial cost of testing frequencies that were not aligned to risk and duplicated (often many times over) testing for the same material property for the same product of the same quarry.

In order to improve the specification of testing frequencies, the Department resolved to develop a system that removed these suboptimal factors from the QRS.

The Department consulted with the peak industry stakeholders representing the major quarries in Queensland throughout the review of the QRS. The Cement Concrete and Aggregates Association (CCAA) and Institute of Quarrying Australia (IQA) provided valuable input to assist the Department's geological, geotechnical, concrete and pavement materials technical experts to identify key risks and key variations, and to develop a workable system for quarry registration and utilisation of testing frequencies within TMR specifications.

2.3 *The Department's Key Challenges*

Department's fundamental challenges were as follows:

How to apply different testing frequencies for different quarries, and still manage its risk?

How to allow different frequencies fairly and with transparency, without claims of favouritism or bias?

How to incorporate the Department's existing Quarry Registration System?

How to gain Quarry Industry acceptance of the new system?

To address these challenges, collaborative consultation between the Department's technical leaders and Quarry Industry technical and operational experts commenced in mid-2013.

The Departmental and Quarry Industry working group identified the following key factors that influence the nomination of appropriate testing frequencies by individual quarries:

The type and properties of the quarry's source rocks,

The match between the source rock types and the TMR Technical Specification limits – for example some sources are in excess of required strengths,

The levels of management and technical and operational experience and expertise in managing production of quarry products, and

The robustness of the quality control measures demonstrated by the quarry in winning source rock and producing pavement products.

The agreed approach was to develop robust guidelines, which would allow the quarry's management to self-assess their own testing frequencies. The Department would retain its role to register the quarry where the TMR Manager (QRS) verifies or suggests amendments to the quarry self-assessments, and issues a QRS registration certificate accordingly. New contract provisions enable test frequencies to be applied consistently across all projects to which the quarry supplies pavement products.

2.4 *Source Rock Test Properties*

The QRS only applies to source rock/material testing, and Table 2 below summarises all relevant source rock/material property tests that are required by TMR Technical Specifications.

Table 2. All Relevant Source Rock/Material Property Tests for Coarse and Fine Aggregates in TMR Technical Specifications

Source Rock Property Test	Test Method/s
Petrographic Analysis	ASTM C295
Wet 10% Fines Value	AS1141.22 or Q205A/B
Wet/Dry Strength Variation	AS1141.22 or Q205C
Degradation Factor	Q208B
Particle Density (SSD	AS1141.5/6.1 or Q214A/B
Water Absorption	AS1141.5/6.1 or Q214A/B
Bulk Density of Aggregate	AS1141.4
Soundness (Sodium Sulfate)	AS1141.24
Polish Aggregate Friction value	Q203
Weak Particles	AS1141.32
Crushed Particles	Q215
Methylene Blue Value (MBV)	AS1141.66
Sand equivalent	AS1289.3.7.1
Light Particles*	AS1141.31
Particle Size Distribution*	AS1141.11.1
Material Passing 75μm*	AS1141.12
Material Passing 2μm*	AS1141.13
Organic Impurities*	AS1141.34
Sugar Presence*	AS1141.35
Sulfate Content*	AS1012.20
Chloride Content*	AS1012.20

* Applicable to natural fine sand aggregate only

Pavement & concrete product testing is not included in the QRS as these material products that conform at the quarry may become segregated or contaminated during subsequent handling, cartage or construction.

2.5 *Quarry Registrations System Documents*

The new QRS contains seven (7) separate documents:

QRS1 - Quarry Registration System Outline

QRS2 - Preparing a Quarry Assessment Report for a Hard Rock Quarry

QRS3 - Preparing a Quarry Assessment Report for a Natural Sand and/or Natural Gravel Quarry

QRS4 - Assigning Quarry Specific Testing Frequencies for Source Rock Tests

TMR Quarry Registration Application Form

Flowchart showing TMR Quarry Registration System

Process for assessing Quarry Specific Testing Frequencies (includes e-forms for interactive assessment spreadsheet)

These documents and a demonstration video (i.e. webinar) are all available on the TMR website at the following link:
http://www.tmr.qld.gov.au/business-industry/Business-with-us/Approved-products-and-suppliers/Pavements-materials-and-geotechnical.aspx

2.6 *Application Process*

As part of completing the application e-forms (i.e. interactive assessment spreadsheet), the Applicants address all attributes in order to satisfy the Department that they have control of their processes sufficient to allow the testing frequencies that they nominate.

The completed assessment spreadsheet, and accompanying substantiating documentation is submitted electronically to the TMR Manager (QRS) for processing. (An interactive assessment spreadsheet containing a worked example is available on the Department's website.)

2.7 *TMR Administration of QRS Process*

Upon receipt of an application, the TMR Manager (QRS) assesses the application. This includes inspecting quarry source and all nominated product stockpiles, reviewing of past performance and consulting the Department's construction project staff to obtain any updated information about recent operational and material performance.

The Manger (QRS) will either verify the submission or negotiate alternative testing frequencies with the Applicant. For successful Applicants, a QRS registration certificate is issued with an approved testing frequency schedule and the Department's website updated to include the quarry as a registered supplier.

QRS registration certificates are valid for two years, but can (upon application) be upgraded six-monthly. However TMR can still modify testing frequencies at any time based on performance.

2.8 *Future Enhancement of the QRS*

The Department is about to conduct a 12-month review of the operation of the QRS in consultation with CCAA, IQA and Departmental technical and operational staff. As more information becomes available about the quality performance of individual quarries, potential exists to even further refine the process to achieve even greater cost savings. For example, work is well underway on a new Geographical Information System (GIS) system to allow public access to quarry registration data, and also to register their approvals through the Department's interactive mapping (iMAP)

2.9 *Current Statues of the QRS*

The Department has been implementing the QRS since April 2015 and has already registered 80 quarries with approved testing frequency schedules.

4 CONCLUSIONS

The new Quarry Registration System (QRS) which was collaboratively developed between the Department and the Quarry Industry successfully delivered following main benefits:

It effectively addressed Quarry Industry concerns that excessive testing was resulting in increased costs which were being passed on to the Department's construction projects.

A set of guidelines which allows the quarry management to self-assess their own testing frequencies.

It allows the Department as well as Quarry Industry to concentrate testing resources to where risks are highest.

New contract provisions enable test frequencies to be applied consistently across all Queensland's road construction projects to which the quarry supplies pavement and concrete products.

Rewarding good performers through reduced testing costs. Testing frequency reductions of almost 90% have been realised in some cases with well managed quarries.

A preliminary estimate of cost savings is that overall quarry testing costs for Departmental projects will significantly be reduced by $6 million per year.

3 ACKNOWLEDGEMENTS

The Authors are grateful to the Engineering and Technology Branch, Department of Transport and Main Roads, Queensland for their support and assistance in the preparation of this paper.

5 REFERENCES

Cement Concrete & Aggregates Australia (2005). "Code of Practice – Testing Frequencies for Extractive Industry in Queensland", P8, September 2005.

Dissanayake, A. & Evans, P. 2015. Latest Developments on TMR Quarry Registration System (QRS) and Incorporation into TMR Standard Specification Suit; *Innovation Driving Value; 16th APPA International Flexible Pavements Conference 2015, 10-11 September 2015*.

Dissanayake, A. & Evans, P.A. 2015. Queensland Transport and Main Roads Department Quarry Registration System 511-514, *Geotechnics for Sustainable Development*; *Proc. intern. Conference on Geotechnical Engineering, ICGE-Colombo-2015, 10-11 August 2015*.

Queensland Department of Transport and Mains Roads. 2015. QRS1 - Quarry Registration System Outline, P12.

Queensland Department of Transport and Mains Roads. 2015. QRS2 - Preparing a Quarry Assessment Report for a Hard Rock Quarry, P12.

Queensland Department of Transport and Mains Roads. 2015. QRS3 - Preparing a Quarry Assessment Report for a Natural Sand and/or Natural Gravel Quarry, P8.

Queensland Department of Transport and Mains Roads. 2105. QRS4 - Assigning Quarry Specific Testing Frequencies for Source Rock Tests, P18.

Queensland Department of Transport and Mains Roads. 2013. TMR Technical Note 102: Selecting Testing Frequencies for Acceptance Sampling of Pavement Materials, P16.

Geotechnical and Geophysical Site Characterisation 5 – Lehane, Acosta-Martínez & Kelly (Eds)

Correlation between the results of the PLT and CBR tests to determine the elasticity modulus

A. Hajiannia
Department of Civil Engineering, Najafabad Branch, Islamic Azad University, Najafabad, Iran.

M. T. Dorobati
Department of Civil Engineering, Najafabad Branch, Islamic Azad University, Najafabad, Iran.

S. Kasaeian
School of Engineering, University of Queensland, Australia

S. B. Baghbadorani
Department of Civil Engineering, Najafabad Branch, Islamic Azad University, Najafabad, Iran.

ABSTRACT: Plate Load Test (PLT), among the few available field tests, is one that yields more realistic results for the determination of soil elastic parameters. Since PLT is difficult and costly, finding a correlation between this and other similar-mechanism laboratory tests can be quite beneficial. This research study is aiming at pre-senting a logical correlation between the PLT and California Bearing Ratio (CBR) test. Therefore, using the numerical modeling of the CBR test in the ABAQUS software finite element environment, and performing some PLTs in the site being studied (South Pars), we have proposed a relation for the determination of the modulus of elasticity (E) using the CBR test results in the PLT. The relation was then checked through some PLTs and Field CBR in the site and CBR tests on the rebuilt specimens. Results have revealed that the proposed relation has shown acceptable results in cases with Poisson ratio of 0.3 for the soil in the site being studied. Also, the PLT load-deflection diagram was drawn using the obtained moduli of elasticity and then compared with that of the PLT; results have shown that the PLT load- deflection curve has been predicted with a high degree of accuracy. Finally, based on the number of the PLTs performed in the site, an economic analysis was done which showed that if the results of this research are used, there will be great savings in the costs.

1 INTRODUCTION

In the design of soil foundations, the compacted layers that work as the main footing are to be designed quite accurately. The best strength evaluation, either during the construction, or during the design, is quite important. The CBR test is usually used to determine the relative strength of the bed soil and the compacted layers in the design of highways, beds of structures and so on (Eskroochi, 2011). Also, the PLT is used for the determination of the deflections due to loading, bearing capacity of foundations, and the soil elastic parameters.

The modulus of subgrade reaction, K_S is a relationship between soil pressure and deflection which is proportional to its vertical displacement as idealized in Winkler's soil model (Hetenyi, 1946; Jones, 1997). This coefficient or, in other words, the coefficient of the soil elasticity, is a parameter that affects the design of rigid (solid) and flexible pavements, continuous footings and mat foundations (Shafa Bakhsh & Kashi, 2009). This coefficient is found through PLT performed on the bed. However, not only is this test costly, but it is also quite time consuming and very difficult in different depths.

Figure 1 shows the mechanisms of the PLT and CBR test. As shown, both have load-deflection mechanisms. In the PLT, the plate is placed on the suggested level and is loaded gradually. The plate can be 300-760 mm in size, and can come in such shapes as square, circle, and rectangle (Bowles, 1997; Moayed & Janbaz, 2009).

The CBR test too can be used to draw the soil load-deflection curve. If the test is done in a semi-infinite environment, it can be considered as a small scale PLT; therefore, knowing that the two tests have similar mechanisms, we can study the correlation for the determination of some elastic parameters of the soil.

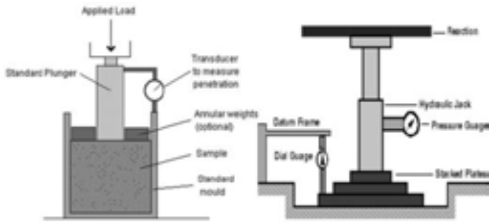

Figure. 1 Mechanisms of the PLT and CBR test

If the soil being studied is elastic or, in other words, if it can be considered as a nearly elastic mass, it is possible to use elastic or pseudo elastic parameters for estimating the load-deflection mechanism; therefore, it can be stated that in such cases, the size of the loading plate, which is an element that changesthe plastic strain in the soil, does not affect an elastic mass very much.

In this research, the soil modulus of elasticity (E) obtained by the PLT is determined through the results of the CBR tests. Then, knowing that E is a parameter that affects the determination of the modulus of the bed reaction (K_s), we can have an appropriate estimation of Ks after finding E. Finally, using the parameters thus found, we can predict the PLT load-deflection curve too.

2 LITERATURE REVIEW

So far, little research has been done on the correlation between the modulus of subgrade reaction (Ks) and the CBR test results (Elsa Eka Putri,et al. 2012). Modulus of elasticity (E) is an effective parameter in determining Ks; if E is not found correctly, Ks will not be reliable either. Many relations have been presented so far by many researchers for the determination of E from CBR values. The following are only some to mention(NAASRA, 1979):

$$E = 16.2CBR^{0.7}\left(MPa\right) \qquad \text{CBR <5} \quad (1)$$

$$E = 22.4CBR^{0.5}(MPa) \qquad \text{CBR>5} \quad (2)$$

Heukelom and Klomp, (1962) (Heukelom & Klomp, 1962) did some research on the correlation between E and CBR, and proposed a relation as follows for the determination of E in fine-grain soils with low swelling property and CBRs less than 100%:

$$E = 1500CBR(Psi) \qquad (3)$$

Powell et al. (1984) proposed another relation for determining E from CBR as follows:

$$E = 17.6CBR^{0.64}\left(MPa\right) \qquad (4)$$

Elsa Eka Putri et al. (2012) studied the CBR test numerically and proposed a relation for the determination of E as follows:

$$E = 810CBR(kPa) \qquad (5)$$

A summary of what was stated is shown in FIGURE. 2. (6)

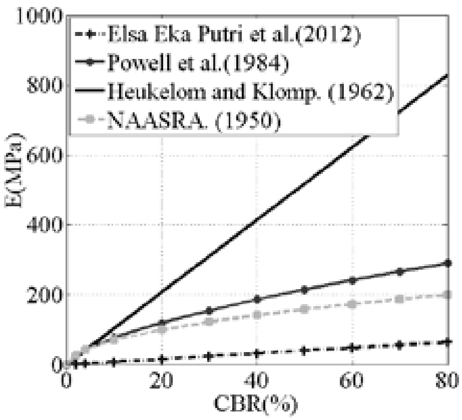

Figure. 2 CBR versus E

Opiyo (1995) (Opiyo, 1995) developed empirical equations to estimate the E-modulus through the applied stress (σo), average piston stress, and the measured vertical resilient (recoverable) deformation (u) in the final load application. He derived two methods to compute the E-modulus: an approximate solution and one based on finite element (FE) analysis. For the first solution, he made an assumption on how to spread the load over the height of the CBR sample for which an estimation of the load spreading angle (α) was necessary. It was also assumed that the elastic deformation (u) occurred in two parts of the specimen: a conical and a cylindrical part (FIGURE. 3). The total deformation was therefore taken as the sum of elastic deformations found from the two parts, (Equation 6).

$$u = \frac{\sigma_0.H.d}{E.D} + \frac{\sigma_0.d^2(L-H)}{E.D^2} \Rightarrow E = \frac{\sigma_0.d}{u.D}\left[H + \frac{d(L-H)}{D}\right] \qquad (6)$$

From the finite element (FE) analysis, Opiyo computed the magnitude of the deformations of the CBR plunger under applied load assuming linear elastic behavior of the material. His analysis covered a range of stiffness values of 50, 200, and 400 MPa, and Poisson's ratio values of 0.35, 0.45 and 0.49. These computations were performed for two extreme cases assuming no-friction and full-friction between the material and the mould. Using regression and these analyses, he developed relationships between the elastic modulus of the material and the load and elastic deformation (equations 7 and 8), (Araya, 2011).

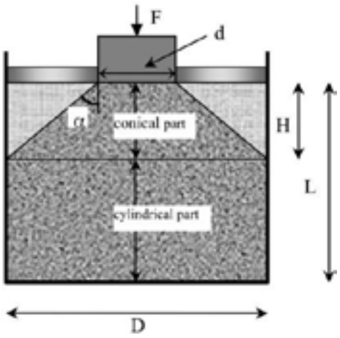

Figure. 3 Conical and cylindrical parts deformations in the approximate solution of the CBR test

$$E=\frac{1.797(1-\nu^{0.889})\sigma_0(\frac{d}{2})}{u^{1.098}}\qquad \text{No-friction (7)}$$

$$E=\frac{1.375(1-\nu^{1.286})\sigma_0(\frac{d}{2})}{u^{1.086}}\qquad \text{Full-friction (8)}$$

In all the above relations, E is found through CBR and average stress under the loading piston, but in the present research, it is directly found based on the compressive stress required for the piston to drive in as much as 2.54 mm.

3 METHODOLOGY

To find a relation that determines E from CBR test results, some PLTs were performed in the site and E was found. Then, the numerical modeling of the CBR test was done in ABAQUS Ver. 6.11 software finite element environment. The parameters required for modeling include the volumetric density (γ), soil modulus of elasticity (E), and Poisson's ratio (ν). Models were made and studied for different values of E (50-200 MPa) and Poisson's ratio (0.20-0.45) and, finally, a relation was found for the determination of E (obtained from PLTs) through CBR test results. To validate the proposed relation, some in-situ PLTs, laboratory CBR tests and in-situ CBR tests were performed on the rebuilt specimens (shown in Figure 10) and the results were compared. Figure 4 clearly shows the steps taken in the process.

4 RESULTS AND DISCUSSION

4.1 *Finite Element Model (FEM)*

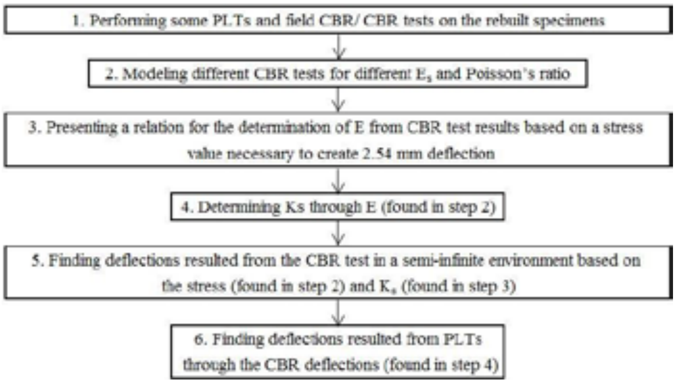

Figure. 4 Steps taken in the present research

Finite element models were made in the ABAQUS software environment according to Figure. 5 and included the soil, loading piston, and steel molds conforming to ASTM D 1883-87. Since the model structure was circular with a uniform radial transverse section, use was made of an axisymmetric model. Use has been made of the linear elastic models in our modeling.

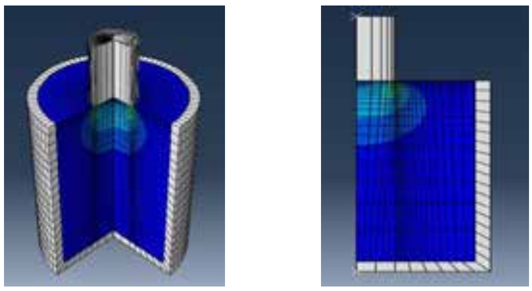

(a) (b)

Figure. 5 FEM (ABAQUS), (a) FEM mesh of the sweep model (b) FEM mesh of the axisymmetric model

To validate the software results based on the parameters obtained from the PLT site, some CBR rebuilt specimens and some models in the ABAQUS software environment were made, and the related load-displacement curves were drawn. A_s shown in Figure 6 6, the precision of the numerical modeling results is acceptable.

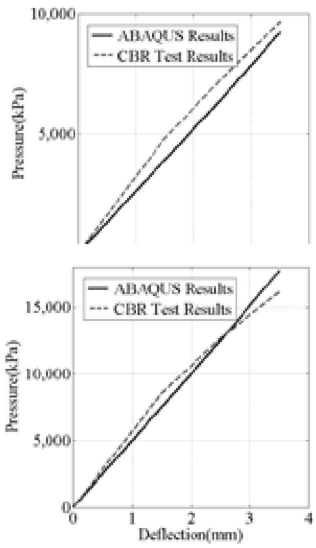

Figure. 6 Comparison of the CBR test results with those of the numerical modeling

Different models were made for different ES, and the related load-deflection curves given in Figure 7 show that for a specified load, higher deflections are for smaller E_s.

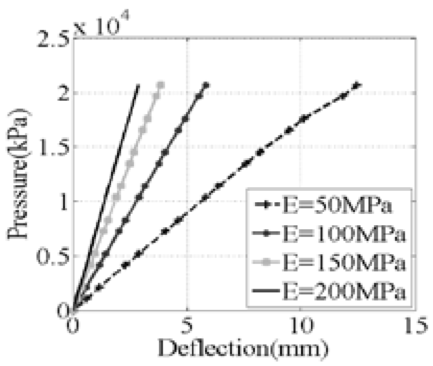

Figure. 7 Load versus deflection for different Es

4.2 *Determination of E*

According to the Elastic Theory, the amount of deflection in a semi-infinite elastic environment under an initial pseudo elastic load is found from the following relation:

$$u = \frac{f\left(1-\nu^2\right)\sigma.r}{E} \tag{9}$$

where σ is the stress at the contact surface, r is the radius of the circular loading plate, ν is the Poisson's ratio, E is the modulus of elasticity, and f is a constant equal to 2 (for uniform load distribution) and π/2 (if the load distribution is through a rigid solid plate) (Bowles, 1997). According to relation (9), if the vertical deflection (u) is known, E can be found from the following relation:

$$E = \frac{f\left(1-\nu^2\right)\sigma.r}{u} \tag{10}$$

Since relation (10) is for semi-infinite elastic environments, it can be rewritten as relation (11) for confined CBR test environments for different f coefficients and powers. It is worth mentioning that the steel mold of the CBR test fully covers the stress bubble related to the 0.1q stress ratio; therefore, confinement of the rebuilt specimens does not have much effect on the resulted deflection.

$$E = \frac{K_1\left(1-\nu^{K_2}\right)\sigma.r}{u^{K_3}} \tag{11}$$

Having found the vertical deflection u = 2.54 mm, and its corresponding σ for different values of E (50-200 MPa) and Poisson's ratio (0.20-0.45), we may now find the numerical values of K_1, K_2, and K_3, and finally propose a relation as follows to determine E from the CBR test:

$$K_1 = 1.46, K_2 = 0.983, K_3 = 1.031$$

$$E = \frac{1.46\left(1-\nu^{0.983}\right)\sigma_p.r_{CBR}}{u^{1.031}} \tag{12}$$

5 CBR TEST FOR PREDICTING PLT RESULTS

5.1 *PLT and CBR test results*

In the site being investigated, to prepare the bedding to set up the oil storage tanks, raft foundations (with layer-compacted granular material cores and crushed stone rings) were constructed according to API650/Appendix B/Section B.4.3 . The PLT was used to control the layers' compactibility/settlement and also the raft foundation bed (FIGURE. 8). The field CBR Test too was done at the PLT site and the load-displacement curve was drawn. Also, according to FIGURE. 9 the density and the local moisture were registered for reconstructing the specimens and performing CBR tests in the laboratory, and the related load-displacement curves were drawn. FIGURE. 10 shows the results of one of the tests carried out in the laboratory.

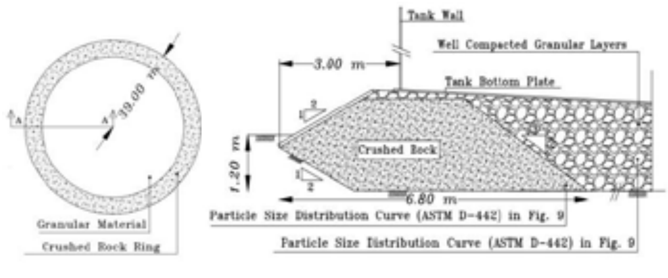

Figure. 8 Plan and transverse section of the raft foundation under investigation

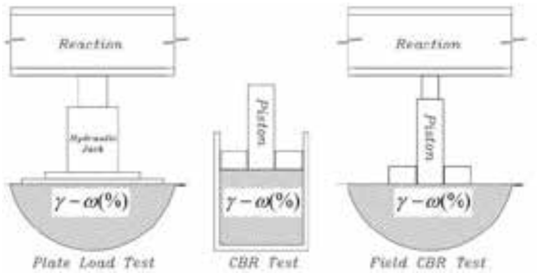

Figure. 9 Rebuilding laboratory specimens for CBR tests

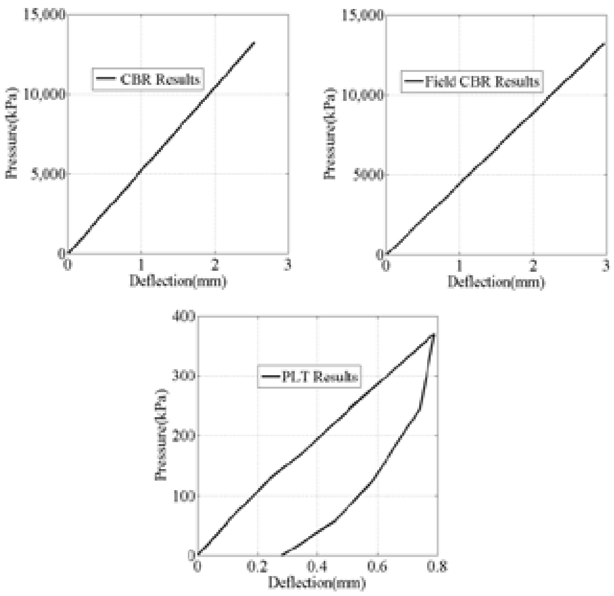

Figure. 10 PLT, Field CBR and CBR test curves

As shown, deeper infiltrations occur at heavier loads and the mechanism is somehow similar to that of the PLT results. Also, the little effects of the specimen confinement on the displacements can be observed in the CBR test.

5.2 *Determination of the modulus of subgrade reaction (K_s)*

After doing the CBR test on the rebuilt specimens according to FIGUREs. 10 and 11, we can find the required contact stress (σ_p) for an infiltration of 2.54 mm, and then find E by relation (12).

According to the Elastic Theory, we can find Ks for a rigid solid plate under a concentrated load in a semi-infinite elastic environment through relation (13) (Brown & Vinson, 2006; Harr, 1966; Kameswara Rao, 2000)

$$K_s = 1.13 \frac{E}{1-\nu^2} \frac{1}{\sqrt{A}} \tag{13}$$

where E is the modulus of elasticity, ν is the Poisson's ratio, and A is the area of the loading plate (in the PLT) or of the piston (in the CBR test).

5.3 *PLT load-deflection curves (through CBR test results)*

Using relation (13), we first find K_s for the CBR test (in a semi-infinite environment) and for the PLT, and then draw the load-deflection curve of the PLT through a correlation between them; this procedure is applicable in linear elastic or near-elastic behavior.

5.4 *Creating a correlation between the PLT and CBR test in a semi-infinite elastic environment*

According to relation (13), for the CBR test in a semi-infinite elastic environment (Field CBR) we have:

$$K_{Si} = 1.13 \frac{E}{1-\nu^2} \frac{1}{\sqrt{A_i}} = \frac{\sigma_p}{u_i} \tag{14}$$

where A_i is the piston area in the CBR test.
Similarly, for the PLT we have:

$$K_{PLT} = 1.13 \frac{E}{1-\nu^2} \frac{1}{\sqrt{A_{PLT}}} \tag{15}$$

where A_{PLT} is the plate area in the PLT.

From relations 14 and 15, we have for the circular plate:

$$\frac{\dfrac{\sigma_{P_i}}{u_i}}{\dfrac{\sigma_{PLT}}{u_{PLT}}} = \frac{K_{si}}{K_{sPLT}} = \sqrt{\frac{A_{PLT}}{A_i}} = \sqrt{\frac{\pi r_{PLT}^2}{\pi r_i^2}} = \frac{r_{PLT}}{r_i} \tag{16}$$

where u_i, r_i, and A_i are respectively the soil deflection, piston radius, and piston area in CBR test in a semi-finite elastic environment, and u_{PLT}, r_{PLT}, and A_{PLT} are respectively the soil deflection, plate radius, and plate area in the PLT. For equal stress values ($\sigma_{pi} = \sigma_{PLT}$) we have:

$$\frac{u_{PLT}}{u_i} = \sqrt{\frac{A_{PLT}}{A_i}} = \frac{r_{PLT}}{r_i} \tag{17}$$

Relation (17) shows that the deflection resulted from PLT (i.e. r_{PLT}/r_i) is equal to that from the CBR test in a semi-infinite environment and is found as follows:

$$u_{PLT} = \frac{r_{PLT}}{r_i} . u_i \tag{18}$$

Now, knowing the coordinates (σ_p,u_{PLT}), we can draw the elastic zone of the PLT load-deflection curve.

6 APPENDIX PREDICTION OF PLT DEFLECTIONS FROM CBR TEST RESULT

To control the obtained results and validate the relations, some PLTs were done with 450 mm diameter plates and field CBR and then CBR tests were performed (piston area A = 1932.2 mm^2) on the specimens rebuilt from the soil under the PLT. Next, values of E were found for ν =0.3 and then compared with those found from the PLT.

$$\nu = 0.3 \rightarrow E_{PLT} = 152.4MPa, \sigma_{p0.1} = 13.2MPa, u = 2.54mm$$

$$E_{CBR} = \frac{1.46(1-\nu^{0.983})\sigma_{\rho}.r_{CBR}}{u^{1.031}} = 157.1MPa$$

Also, considering different values, and using the obtained results, we can find different values of E from the PLTs for different specimens and predict the load-deflection curves (FIGURE. 12).

ν=0.3,E_{PLT}=152.4MPa,$\sigma_{p0.1''}$=13.5MPa,u=2.54mm (Location is layer 8)

$$E_{CBR} = \frac{1.46\left(1-\nu^{0.983}\right)\sigma_{\rho}.r_{CBR}}{u^{1.031}} = 157.1MPa \rightarrow$$

$$K_{si} = 1.13\frac{E}{1-\nu^2}\frac{1}{\sqrt{A_i}} = \frac{\sigma_{P0.1''}}{u_i} \rightarrow u_i = 2.97mm \rightarrow$$

$$u_{PLT} = \frac{r_{PLT}}{r_i}.u_i \rightarrow u_{PLT} = 26.94mm$$

It means that if a pressure of 13.5 MPa is applied on the PLT plate, it will have a settlement of 26.94 mm; therefore, we can draw the load-settlement curves based on the applied pressures according to Figure 11 using the equation of the obtained line.

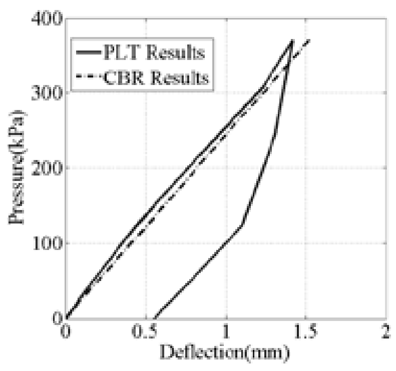

Figure 11. Comparing PLT load-settlement curve and the present study's CBR results

7 CONCLUSIONS

The relation, proposed in this research for the determination of the modulus of elasticity found from PLT through CBR test results for the soil of the site being studied, has yielded quite acceptable results.

- The modulus of elasticity thus found yields an approximate estimation of the bed reaction coefficient (K_S).
- Considering the performed PLTs and the related load-deflection curves, the results of the present research can predict such curves with a high precision and accuracy.
- The value of the Poisson's ratio (ν) affects he modulus of elasticity (E), and the results for ν values of 0.3 - 0.4 are quite acceptable.
- Based on the performed economic analysis, the results of this research study can reduce the costs considerably (more than 80%).

8 REFERENCES

API 650: Appendix-B.Tenth Edition, November 1998,Addendum 1, January 2000 Addendum 2, November 2001 (ed.

Araya A (2011) Characterization of unbound granular materials for pavements, Vol. PhD: PhD (ed. Delft University

Bowles JE (1997) Foundation Analysis and Design. McGraw-Hill, New York.

Brown DZ & Vinson RJ (2006) Stiffness parameters for a strong and colorful aeolian soil. Geomaterial Characterization (GSP 199), ASCE,Reston/VA: 12-22.

Elsa Eka P, Kameswara Rao NSV & Mannan MA (2012) Evaluation of Modulus of Elasticity and Modulus of Subgrade Reaction of Soils Using CBR Test. Journal of Civil Engineering Research 2: 34-40.

Eskroochi AM (2011) Soil Mechanics Laboratory. University Books Publications.

Harr ME (1966) Foundations of theoretical soil mechanics. McGraw-Hill, New York.

Hetenyi M (1946) Beams on elastic foundation. University of Michigan Press, Ann Arbor.

Heukelom W & Klomp AJG (1962) Dynamic Testing as a Means of Controlling Pavements During and After Construction: Proceedings International Conference on the Structural Design of Asphalt Pavements (ed., Ann Arbor, Michigan pp. 667-679.

Jones G (1997) Analysis of beams an elastic foundation Thomas Telford, United Kingdom.

Kameswara Rao NSV (2000) Dynamic soil tests and applications. A. H. Wheeler & Co. Ltd, New Delhi.

Moayed RZ & Janbaz M (2009) Effective parameters on modulus of subgrade reaction in clayey soils. J. Applied Sci 9: 4006-4012.

NAASRA (1979) Interim guide to pavement thickness design: National Association of Austrian State Road Authorities (ed., Sydney, Australia.

Opiyo TO (1995) A Mechanistic Approach to Laterite-based Pavements in Transportation and Road Engineering (TRE). International Institute for Infrastructure, Hydraulic and Environmental Engineering (IHE): Delft.

Powell WD, Potter JF, Mayhew HC & Nunn ME (1984) The structural design of bituminous roads. TRRL Report LR 1132: 62.

Shafa Bakhsh G & Kashi A (2009) A Numerical Study of the Effects of the Specifications of the Airliner Tires on the Damage Incurred by the Airport Runway. Journal of Transportation Engineering, 1st Year, 1st Edition.

Geotechnical and Geophysical Site Characterisation 5 – Lehane, Acosta-Martínez & Kelly (Eds)

Characterization of Railroad Track Substructures using Dynamic and Static Cone Penetrometer

W-T. Hong, S. Kang & J-S. Lee
School of Civil, Environmental and Architectural Engineering, Korea University, Seoul, Republic of Korea

Y-H. Byun
Department of Civil and Environmental Engineering, University of Illinois at Urbana-Champaign, Urbana, IL, USA

C-Y. Choi
High Speed Research Division, Korea Railroad Research Institute, Uiwang, Gyeonggi-do, Republic of Korea

ABSTRACT: As deteriorated track substructures cannot produce enough bearing capacity against the load of the train and may lead to serious accidents, an accurate investigation of the track substructures is necessary for proper repair and maintenance. In this study, a dynamic and static cone penetrometer (DSCP) for characterization of track substructures is developed. The DSCP is dynamically penetrated into ballast layer using a 118 N drop hammer and statically pushed into subgrade. The DSCP consists of an outer rod for the dynamic penetration into the ballast layer and inner rod for the static penetration into the subgrade. At the head of the outer rod, an energy-monitoring module is installed to obtain the transferred energy from the drop hammer and two load cells are installed to obtain the cone tip and friction resistances during the static penetration. As a pilot test, track substructures are simulated in a chamber and the DSCP penetration test is conducted and two field tests are conducted in order to investigate the applicability of the DSCP. From the DSCP tests, the energy corrected dynamic cone penetration index for the ballast layer and static penetration resistances (cone tip and friction resistances) are obtained for the subgrade. This study suggests that the DSCP may be a useful tool for the characterization of railroad track substructures.

1 INTRODUCTION

Nowadays, the railroad transportation is recognized as a future-oriented means of transportation and the railway transportation technologies have been actively advanced. Accordingly, the larger wheel load, lateral pressure, and greater starting and breaking forces are acted on the conventional lines. These problems may cause the failure of the railroad track substructures and lead to huge damages for the passengers. For the evaluation of the railroad track substructures, various subsurface investigation methods are suggested aspects on the non-destructive, static and dynamic loading tests.

As a non-destructive method, Al-Qadi et al. (2010) applied the ground penetrating radar (GPR) for the evaluation of fouling depth in the ballast layer. While the GPR is cost-effective and efficiently investigate the large area within a short time, the strength characteristics of the railroad track substructures cannot be evaluated. In addition, the light falling weight deflectometer (LFWD) and the plate bearing test (PBT) can be applied to the railroad track substructures as the static and dynamic loading tests. However, ballast layer should be removed when these methods are applied to the subgrade. In order to evaluate the strength of the railroad track substructures without large removal of ballast layer, a study on the in-situ penetration methods is required. However, the in-situ penetration methods such as cone penetration test (CPT), standard penetration test (SPT), vane shear test (VST), pressuremeter test (PMT), and flat plate dilatometer test (DMT) may cause the significant disturbance in the railroad track substructures due to the large diameter of the penetrometer and the driving rod. In addition, bore holes are necessary in some cases.

In this study, a dynamic and static cone penetrometer (DSCP) is developed for the evaluation of railroad track substructures. This paper shows the overall shape and functions of the DSCP and documents the procedure and the results of the application tests.

2 DYNAMIC AND STATIC CONE PENETROMETER (DSCP)

2.1 *Railroad track substructures*

The railroad system consists of rails, fasteners, ties, and track substructures as shown in Figure 1. Among the components of the railroad system, rails, fasteners, and ties are the parts of the track superstructures and the track substructures consists of ballast and subballast layer with a depth of 500~600 mm, and subgrade. In the ballast and subballast layer, dynamic penetration method is suitable for the characterization due to the large particle size of the gravels. In the subgrade layer, static penetration method is recommended to characterize the subgrade with a high-resolution.

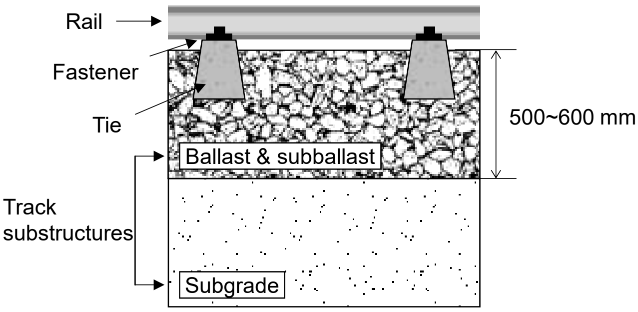

Figure 1. Cross-section of the railroad system.

2.2 *Development*

In this study, a dynamic and static cone penetrometer (DSCP) is developed for characterization of railroad track substructures. The DSCP consists of an outer rod for the dynamic penetration into the ballast and subballast layer, and extendable inner rod with a mini cone for static penetration in the subgrade. In the mini cone, two load cells are installed for measurement of cone tip and friction resistances (q_c and f_s) as shown in Figure 2.

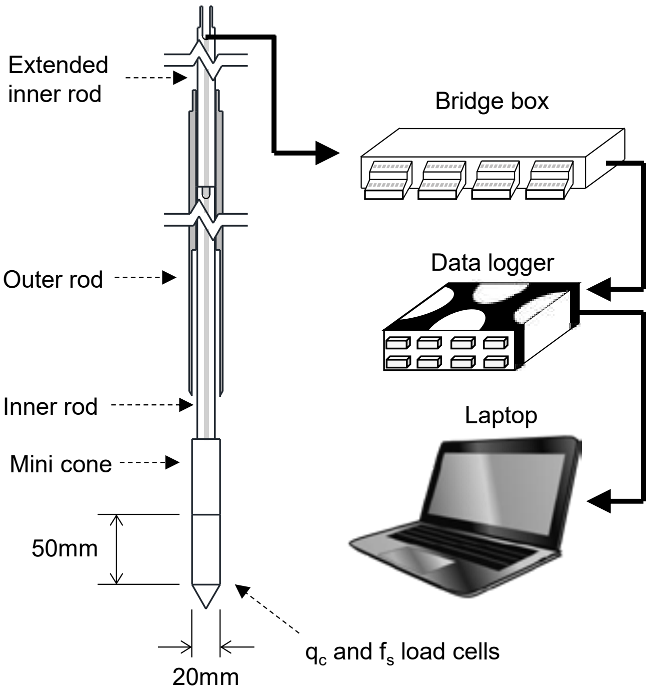

Figure 2. Schematic drawing of DSCP and the measurement system.

In the ballast and subballast layer, the DSCP is dynamically penetrated using a drop hammer with a weight of 118 N and a drop height of 575 mm as a form that the outer rod and inner rod are coupled. During the dynamic penetration, the dynamic cone penetration index (ASTM D6951) is measured along the penetration depth. In the subgrade, static penetration is conducted with a rate of 1 mm/sec as a form that the outer rod and inner rod are uncoupled. Note that the 1mm/sec penetration rate has been used for the miniaturized cone penetration test (Lee et al. 2009; Kim et al. 2010; Yoon et al. 2011). During the static penetration, the static penetration resistances (cone tip and the friction resistances) are measured using a mini cone installed at the front end of the inner rod. The cone tip and friction resistances are gathered through the bridge box and data logger, and monitored by a laptop.

2.3 *Load cells calibration*

In the q_c and f_s load cells, four strain gauges are installed at each load cell and the strain gauges at each load cell are connected as the full bridge which is a kind of Wheatstone bridge. The loads acted on the load cells cause the changes in output voltage of the full bridge circuit. Since the experimental results of the static penetration show the changes in output voltages instead of acted loads, the calibration is conducted to find the correlation factors between the output voltages and the loads acted on the each load cell.

Figure 3 shows the results of the calibration. The relationship between the output voltages (V_{out}) and loads acted on the q_c and f_s load cells show a good linearity with the coefficient of determinant (R^2) greater than 0.99. When 1.25 V is applied to the circuits, the loads acted on q_c and f_s load cells can be converted via Equation 1 and Equation 2.

$$F_{qc}[kN] = 70.3 \times V_{out}[mV] \tag{1}$$

$$F_{fs}[kN] = 84.2 \times V_{out}[mV] \tag{2}$$

where, F_{qc} and F_{fs} are the loads acted on the q_c and f_s load cells, respectively.

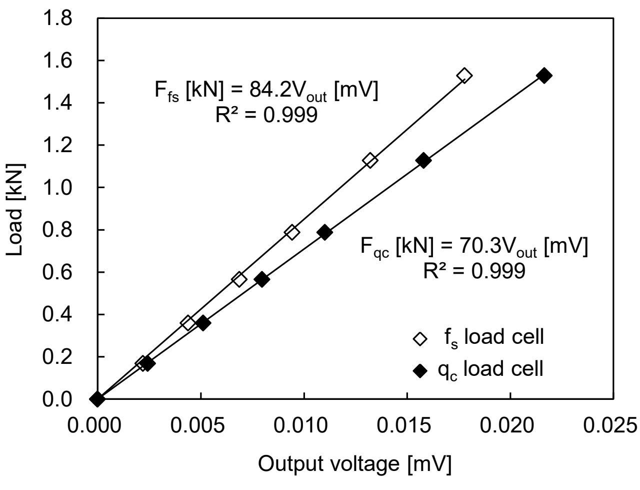

Figure 3. Relationship between the output voltages and the loads acted on the q_c and f_s load cells. F_{qc} and F_{fs} denote the loads acted on the q_c and f_s load cells, respectively.

2.4 *Test procedure*

The characterization of the railroad track substructures using the DSCP is performed as follows:

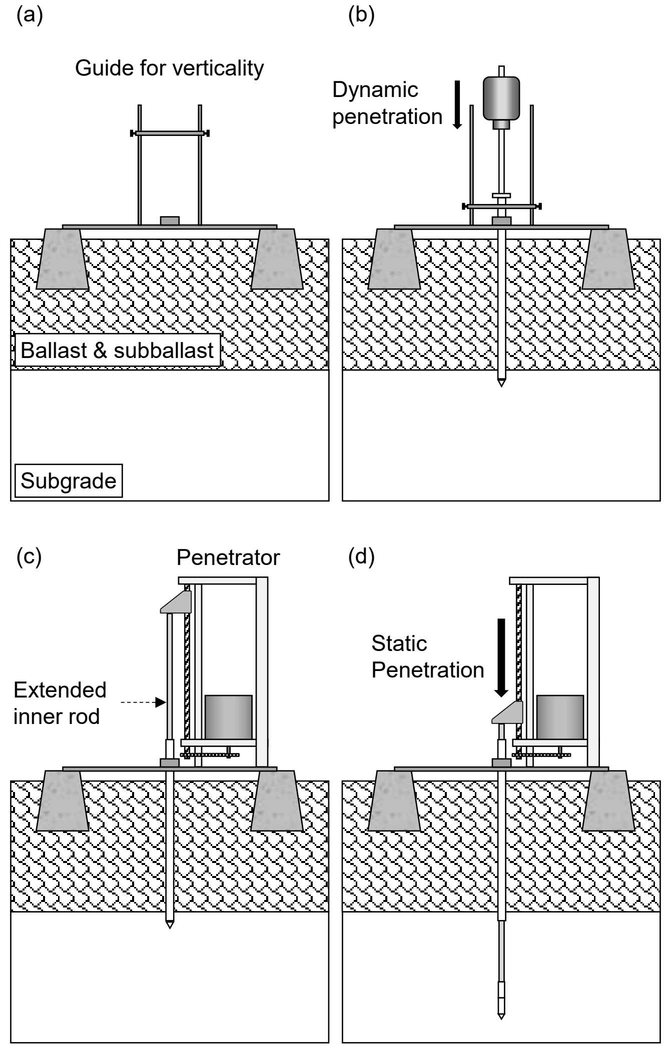

Figure 4. Test procedure of DSCP: (a) installation of a guide for verticality; (b) dynamic penetration of the DSCP; (c) installation of a penetrator; (d) static penetration of the DSCP.

(a) A guide is located on the adjacent ties to maintain the verticality of the DSCP during the dynamic penetration as shown in Figure 4(a).
(b) The DSCP is located on the guide and a hammer guide with a 118 N drop hammer is connected at the head of the DSCP; the dynamic penetration is then performed with 575 mm drop height as shown in Figure 4(b). During the dynamic penetration, the blow counts and the penetration depths are recorded to obtain the DCPI along the depth.
(c) After the completion of the dynamic penetration in the ballast and subballast layer, the hammer and hammer guide are removed, and the inner rod is extended. In addition, a penetrator is installed for static penetration as shown in Figure 4(c).
(d) The inner rod is pushed with a rate of 1mm/sec as shown in Figure 4(d). During the static penetration, static penetration resistances are measured.

3 APPLICATION TEST

3.1 *Site description*

The characterization of the railroad track substructures using the DSCP is performed at a railroad located in Seoul, Korea. Figure 5 shows the photographic image taken during the step of dynamic penetration of the DSCP (Fig. 4(b)).

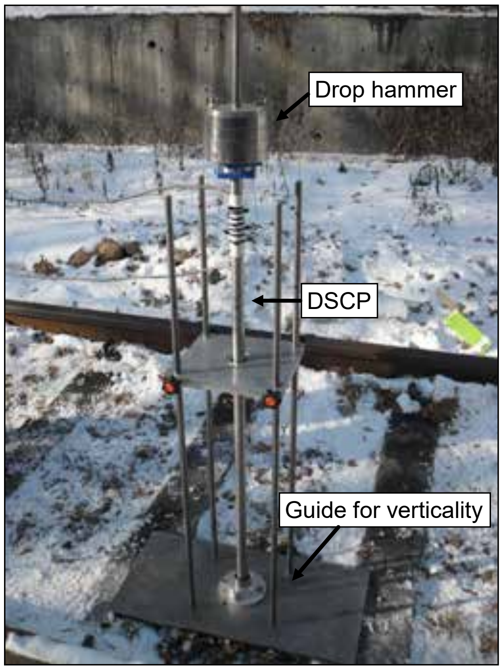

Figure 5. Photographic image of the dynamic penetration of DSCP.

The target railroad had been actually used as an urban railroad for the communication in the Seoul. As a previous study, Byun et al. (2015) investigated the railroad track substructures using a hybrid cone penetrometer and reported that the ballast and subballast layer is distributed to the depth of 400~500 mm from the top of the ties.

3.2 *Experimental results*

In this study, the dynamic penetration of the DSCP is conducted to the depth of 670 mm from the railroad surface and static penetration is performed to the depth of 1400 mm. In the ballast layer, dynamic penetration index (DCPI) is obtained along the depth. Note that the irregularity in DCPI profile may occurs according to the position between the tip of the DSCP and the particles consisting the ballast layer. In order to minimize the irregularity in the DCPI profile, the moving average for three DCPIs is computed with a higher factor in the center (Santamarina and Fratta 1998). In the subgrade, the static penetration resistances are obtained. The static penetration resistances are measured with 5 Hz sampling rate and the penetration rate is 1 mm/sec. Therefore, 5 points of cone tip resistances and friction resistance are gathered per penetration depth of 1 mm.

Figure 6 shows the experimental results of the application test.

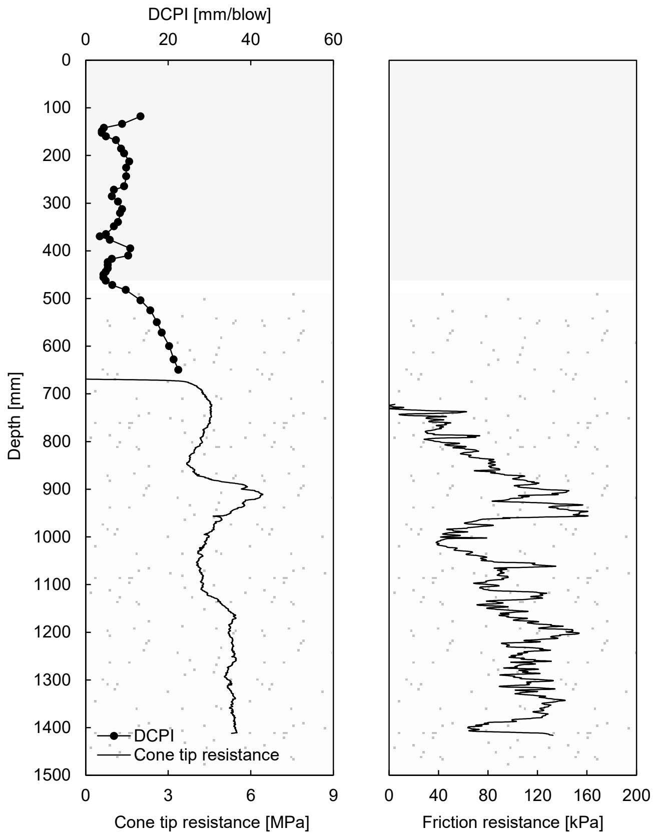

Figure 6. Experimental results.

The DCPI measured near the surface of railroad track substructures shows high values due to the effect of free stress and the DCPI is then converged to 3~10 mm/blow. At the depth of 460 mm, the DCPI rapidly increases which is considered as an interface between the ballast and subballast layer, and the subgrade. In the subgrade layer, the cone tip and friction resistances are measured at approximately 4~7 MPa and 50~150 kPa, respectively. In addition, the friction ratio is calculated as 1~3%. By using the measured cone tip resistance and the calculated friction ratio, the subgrade geo-material is classified as silty sand to sandy silt by soil classification method suggested by Lunne et al. (1997).

4 SUMMARY AND CONCLUSIONS

In this study, a dynamic and static cone penetrometer (DSCP) is developed for characterization of railroad track substructures. The DSCP consists of an outer rod for dynamic penetration in the ballast and subballast layer and an extendable inner rod for static penetration in the subgrade. In addition, a mini cone is installed at the tip of the inner rod for measurement of the cone tip and friction resistances. In order to test the applicability of the DSCP, a field test is conducted at a railroad. The DSCP is dynamically penetrated into the ballast and subballast layer using a hammer with the weight and drop height of 118 N and 575 mm, respectively. In the subgrade, the inner rod with the mini cone is pushed with a rate of 1 mm/sec. As the strength characteristics, dynamic cone penetration index is measured in the ballast and subballast layer, and cone tip and friction resistances are obtained in the subgrade with a high resolution.

The dynamic and static cone penetrometer developed in this study may be a useful tool for the characterization of the railroad track substructures.

5 ACKNOWLEDGEMENTS

This research was supported by a grant (16RTRP-B067919-04) from Railroad Technology Research Program funded by Ministry of Land, Infrastructure and Transport of Korean government.

6 REFERENCES

Al-Qadi, I.L., Xie, W., Roberts, R. & Leng, Z. 2010. Data analysis techniques for GPR used for assessing railroad ballast in high radio-frequency environment. *Journal of transportation engineering* 136(4): 392-399.

ASTM D6951. 2009. Standard test method for use of the dynamic cone penetrometer in shallow pavement applications. *Annual Book of ASTM Standard*. ASTM International: West Conshohocken, PA.

Byun, Y.H., Hong, W.T. & Lee, J.S. 2015. Characterization of railway substructure using a hybrid cone penetrometer. *Smart Structure and Systems* 15(4): 1085-1101.

Kim, R., Lee, W. & Lee, J.S. 2010. Temperature-Compensated Cone Penetration Test Mini-Cone Using Fiber Optic Sensors. *Geotechnical Testing Journal* 33(3): 243-252.

Lee, W., Shin, D.H., Yoon, H.K. & Lee, J.S. 2009. Micro-cone penetrometer for more concise subsurface layer detection. *Geotechnical Testing Journal* 32(4): 358-364.

Lunne, T., Robertson, P.K. & Powell, J.J.M. 1997. *Cone penetration testing in geotechnical practice*. Blackie Academic & Professional: London.

Santamarina, J.C. & Fratta, D. 1998. *Introduction to discrete signals and inverse problems in civil Engineering*. ASCE Press: Virginia.

Yoon, H.K., Jung, S.H. & Lee, J.S. 2011. Characterization of subsurface spatial variability by cone resistivity penetrometer. *Soil Dynamics and Earthquake Engineering* 31(7): 1064-1071.

Geotechnical and Geophysical Site Characterisation 5 – Lehane, Acosta-Martínez & Kelly (Eds)

Suggested QC criteria for deep compaction using the CPT

P.K. Robertson

Gregg Drilling & Testing, Inc., 2726 Walnut Ave., Signal Hill, CA, USA

ABSTRACT: The most common forms of deep compaction in sandy soils involve vibratory techniques, such as, vibro-compaction, vibro-replacement, dynamic compaction and rapid impact compaction. Historically, it was common to define quality control (QC) criterion for deep compaction based on a change in relative density (D_r). However, D_r cannot be directly measured in-situ at depth and does not always have well defined links with soil behavior, especially in sandy soils with high fines content. In more recent years the CPT has become popular for QC for deep compaction since it is; fast and cost effective, provides a continuous profile, gives re-liable and repeatable measurements and provides more than one measurement. Although it is possible to link CPT measurements with D_r the correlations are not unique, apply only to clean sands and can vary considera-bly with grain mineralogy and characteristics. Current methods of using CPT measurements for QC for deep compaction often apply only to clean silica sands and are not effective in soils with higher fines. This has fre-quently resulted in unnecessary disputes, delays and cost over-runs concerning the effectiveness of the deep compaction. A suggested approach for QC for deep compaction is described based on the normalized *equivalent clean sand* cone resistance ($Q_{tn,cs}$). A brief background on the development of $Q_{tn,cs}$ based on liquefaction case his-tories and how this parameter has been linked to in-situ State Parameter is provided. Hence, there is strong theoretical and experimental evidence that $Q_{tn,cs}$ is a measure of in-situ state and hence, linked to soil behavior and response over a wide range of soils from clean sand to low plastic silt.

1 INTRODUCTION

Ground improvement is often carried out for the following main reasons:

- Increase bearing capacity for shallow foundations (i.e. improve soil strength)
- Decrease settlements (i.e. improve soil stiffness)
- Increase resistance to earthquake loading (i.e. reduce soil liquefaction)

The most common forms of deep compaction in sandy soils involve vibratory techniques, such as, vibro-compaction, vibro-replacement, vibro-displacement, dynamic compaction and rapid impact compaction. These methods compact the soil through vibration that disrupts the sand structure to form denser packing. Vibratory methods also change the in-situ lateral stresses (increase K_o) but can also destroy any existing microstructure (e.g. aging, bonding, etc.).

Historically, it was common to define quality control (QC) criterion for deep compaction based on a change in relative density (D_r). However, D_r cannot be directly measured in-situ at depth and does not always have well defined links with soil behavior, especially sandy soils with high fines content.

In more recent years the CPT has become popular for QC for deep compaction since it is: fast and cost effective, provides a continuous profile, gives reliable and repeatable measurements and provides more than one measurement (e.g. cone resistance, q_c, sleeve resistance, f_s, penetration pore pressure, u_2 and sometimes shear wave velocity, V_s). Although it is possible to link CPT measurements with D_r the correlations are not unique and can vary considerably with grain mineralogy and characteristics (e.g. fines content).

Research linking either SPT (N value) or CPT penetration resistance (q_c) with D_r in clean silica sands has also shown that the penetration resistance varies with overburden stress (i.e. depth). In the past it was common to have QC criteria based on a single value of penetration resistance (either SPT N value, or CPT tip resistance q_c). Since penetration resistance varies with depth, due to increasing overburden stress, the approach of defining a single constant penetration resistance often creates problems when ground improvement cannot achieve the QC criteria at shallow depth due to the small overburden stress and hence, low penetration resistance. In more recent years it has become more common to provide QC criterion that has penetration resistance increasing with depth in an effort to capture the influence of overburden stress.

2 NORMALIZED PENETRATION RESISTANCE

In clean sands penetration resistance usually varies in a non-linear manner with depth that has resulted in the use of normalized penetration resistance, such as:

SPT $(N_1) = N\,C_N$ (1)

CPT $q_{c1} = q_c\,C_N$ (2)

Where:
(N_1) = normalized SPT blow count, corrected to an effective overburden stress of 1 atmosphere (σ'_{vo} = 1 atm. = 1bar ~ 1tsf ~ 0.1MPa = p_a). It has also become common to correct SPT N values to a 60% energy, to become $(N_1)_{60}$.

q_{c1} = normalized CPT cone resistance, corrected to an effective overburden stress of 1 atmosphere (σ'_{vo} = 1 atm. = 1bar ~ 1tsf ~ 0.1MPa = P_a). Often the normalized CPT cone resistance is made dimensionless to become:

$q_{c1N} = q_{c1}/P_a$ (3)

C_N = overburden correction factor.

Typically the correction factor (C_N) in clean sands is simplified to the following:

$C_N = (P_a/\sigma'_{vo})^{0.5}$ (4)

Hence, when $\sigma'_{vo} = P_a$ = 1 atm., C_N = 1.0.

Robertson (2009) suggested a more generalized and dimensionless form of normalized cone resistance, Q_{tn}, as follows:

$Q_{tn} = [(q_t - \sigma_v)/P_a]\,(P_a/\sigma'_{vo})^n$ (5)

Where:
q_t = cone resistance corrected for water pressure (Campanella and Robertson, 1982)
$(q_t - \sigma_v)/P_a$ = dimensionless net cone resistance
$(P_a/\sigma'_{vo})^n$ = overburden correction factor, C_N
n = stress exponent that varies with soil type.
σ_{vo} and σ'_{vo} are the total effective overburden stresses respectively;
P_a is a reference atm. pressure in the same units as σ'_{vo}, q_c and σ_{vo}.

Robertson (2009) suggested that the stress exponent (n) could be evaluated from the CPT soil behavior type (SBT) index, I_c, as follows:

$n = 0.381\,(I_c) + 0.05\,(\sigma'_{vo}/P_a) - 0.15$ (6)

Where:
$I_c = [(3.47 - \log Q_{tn})^2 + (\log F_r + 1.22)^2]^{0.5}$
F = $f_s/[(q_c - \sigma_{vo})]$ x 100% is the normalized friction ratio (in percent)
f_s is the CPT sleeve friction stress;

In most sands, n = 0.5 and q_c is large relative to σ'_{vo}, then $(q_t - \sigma_{vo}) \sim q_c$, and $Q_{tn} \sim q_{c1N}$.

3 SOIL BEHAVIOR TYPE INDEX AND COMPACTABILITY

Massarsch (1991) showed that vibratory compaction methods tend to be more effective in clean sands and Degan et al (2005) showed that vibratory compaction methods become less effective with increasing soil behavior type (SBT) index, I_c as shown in Figure 1. Hence, I_c can be used as a guide on the potential effectiveness of many vibratory compaction methods. Typically, when $I_c > 2.6$ vibratory compaction methods become less effective, in terms of improved density as measured by penetration resistance. However, soils with $I_c > 2.6$ can have improved behavior characteristics due to changes in stress history and K_o.

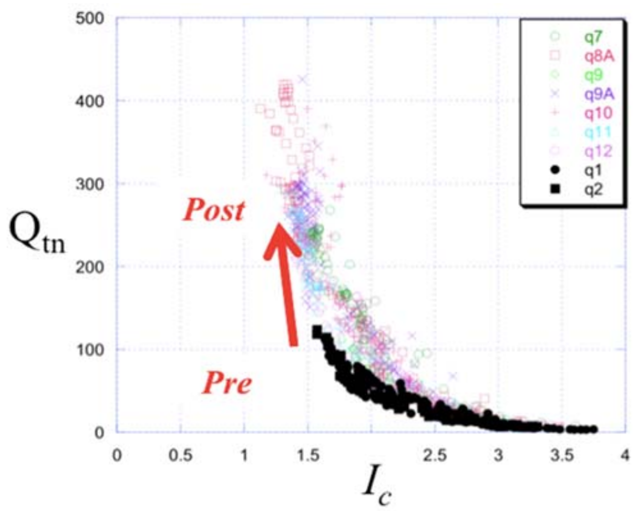

Figure 1. Change in normalized cone resistance, Q_{tn}, as a function of SBT I_c due to vibro-compaction (After Degan et al, 2005)

4 EQUIVALENT CLEAN SAND PENETRATION RESISTANCE

In clean sands a Q_C criteria based on either q_{c1N} or Q_{tn} is preferred over a simple linear variation of q_c, since it links better with relative density and soil response. Normalized values also have the advantage that they are based on vertical overburden stress (σ'_{vo}) that accounts for soil unit weight and ground water conditions at the time of the in-situ test rather than depth. Normalized penetration resistance (e.g. Q_{tn}) is preferred over a relationship of measured penetration resistance versus depth (e.g. q_c vs. depth) and can be effective in deposits of clean sand regardless of depth and groundwater level. However, not all soil profiles are composed of clean sands. Frequently, either natural soils or hydraulically placed fills are composed of varied layers of clean sand, silty sand, silt and sometimes clay. Experience and research has shown that penetration resistance is strongly influenced by the compressibility of soil. Hence, sand with high fines content have a lower penetration resistance than a similar clean sand even though both soils can have the same behavior/response under loading (e.g. similar strength and stiffness). The current practice of defining a QC criterion in terms of either a simple linear variation of q_c or normalized tip resistance (either q_{c1N} or Q_{tn}) will not be effective in the layers with higher fines content.

Experience based on many case histories, using penetration resistance to evaluate soil liquefaction has identified the benefits of correcting measured penetration resistance to an '*equivalent clean sand'* penetration resistance based on parameters such as fines content or CPT SBT index, I_c. Several methods are available to determine the '*equivalent clean sand'* normalized cone penetration resistance (e.g. Robertson and Wride, 1998; Moss et al, 2006; Idriss and Boulanger, 2008; Boulanger and Idriss, 2014). The simple method suggested by Robertson and Wride (1998) to calculate the '*equivalent clean sand'* normalized CPT cone resistance ($Q_{tn,cs}$) is based on the following:

$$(Q_{tn})_{cs} = K_c\, Q_{tn} \tag{7}$$

Where K_c is a correction factor that is a function of behavior characteristics (e.g. combined influence of fines content and plasticity) of the soil. Robertson and Wride (1998) recommended the following relationship between I_c and the correction factor K_c:

$$K_c = 1.0 \qquad \text{if } I_c \leq 1.64 \tag{8}$$

$$K_c = 5.581 I_c^3 - 0.403 I_c^4 - 21.63 I_c^2 + 33.75 I_c - 17.88 \quad \text{If } I_c > 1.64 \tag{9}$$

Robertson (2010 and 2012) showed that $Q_{tn,cs}$ can be linked to the in-situ state of a soil using the State Parameter, ψ (Been and Jefferies, 1992). Hence, there is strong theoretical and experimental evidence that $Q_{tn,cs}$ is a measure of in-situ state and hence, linked to soil behavior and response over a wide range of soils from clean sand to low plastic silt. Since $Q_{tn,cs}$ is used to evaluate the resistance of soils to cyclic loading (i.e. liquefaction resistance), it has direct application when deep compaction is used to improve ground against earthquake loading. Given the link between $Q_{tn,cs}$ and State Parameter, it also has direct application when deep compaction is used to improve both strength and stiffness of soil for either increased bearing capacity and/or reduced settlement.

Figure 2 presents an example of a CPT profile in a typical ground profile that has varied soil conditions ranging from clean sand to silty clay and Figure 3 shows the same location before and after deep compaction using vibro-compaction. Figure 3 shows that a criterion based on normalized cone resistance (Q_{tn}) is unable to capture the behavior in the fine-grained soils between depths of about 6m to 10m (20 to 31 feet), whereas the clean sand equivalent normalized cone resistance ($Q_{tn,cs}$) is better able to capture the behavior for all the soils over the full depth profile. The example shown in Figure 3 was for a project where deep compaction was used to reduce the risk of soil liquefaction. The data shown in Figure 3 after compaction produced acceptable resistance to liquefaction under the project design earthquake.

5 SUMMARY AND RECOMENDATIONS

Unless soils are clean sand, it is recommended that the QC criterion for deep compaction should be based on CPT data using '*equivalent clean sand normalized cone resistance', $Q_{tn,cs}$*. This requires a pre-agreed method to calculate $Q_{tn,cs}$, since it depends on several factors, such as effective overburden stress and fines content. A method to calculate $Q_{tn,cs}$ was suggested by Robertson and Wride (1998) that has been shown to be simple and effective. A QC criterion based on $Q_{tn,cs}$ cannot be presented as a simple plot of measured cone resistance (q_c) versus depth, since it depends on the soil characteristics (e.g. fines content) at the location of the test. Fortunately, commercial software is available (or custom software/spreadsheets) that can calculate $Q_{tn,cs}$ quickly so that it can be used efficiently to provide effective QC for deep compaction methods.

A more detailed description of the above approach is provided in a recorded webinar that can be freely downloaded at:
www.greggdrilling.com/webinars/DwIgW/cpt-for-quality-control-of-ground-improvement-deep-compaction.

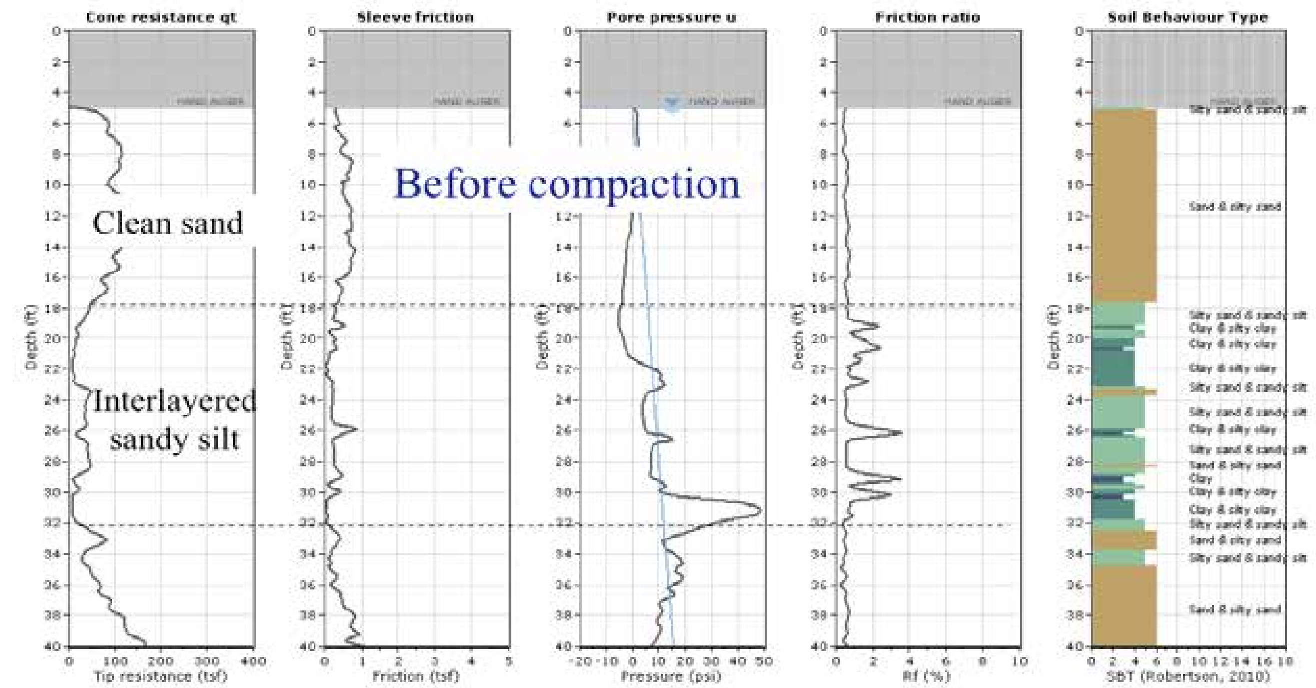

Figure 2. Example CPT profile (before compaction) in typical varied ground conditions
(note: 1 foot ~ 0.3m, 1 tsf ~ 0.1 MPa, 1psi ~ 6.7 kPa)

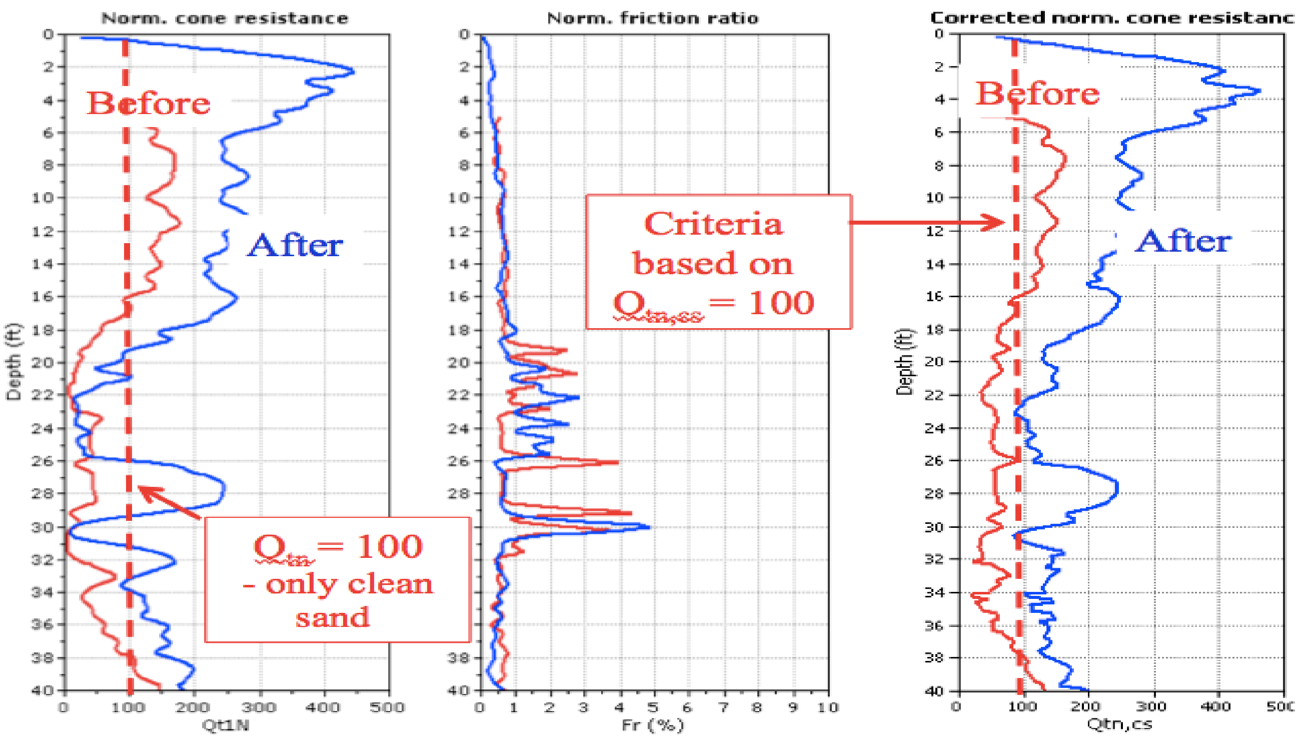

Figure 3. CPT profile at same location as data shown in Figure 2 showing before and after deep (vibro) compaction profiles in terms of normalized cone resistance (Q_{tn}) and equivalent clean sand (corrected) normalized cone resistance ($Q_{tn,cs}$) and the QC criterion of $Q_{tn,cs} > 100$.

6 ACKNOWLEDGEMENTS

This work is supported by Gregg Drilling & Testing, Inc. The author would like to thank W. Degan and S. L. Shao for their input and advice regarding ground improvement.

7 REFERENCES

Been, K. & Jefferies, M. G., 1992. "Towards systematic CPT interpretation." Proceedings of the Wroth Memorial Symposium, London, pp. 121–134.

Boulanger R.W. and Idriss, I.M., 2014. "CPT and SPT based liquefaction triggering procedures." Report No. UCD/CGM-14/01, Center for Geotechnical Modeling, Department of Civil & Environmental Engineering, College of Engineering, University of California at Davis, April 2014, 138 pages.

Campanella, R.G., and Robertson, P.K., 1982. State of the art in In-situ testing of soils: developments since 1978. *In* Proceedings of Engineering Foundation Conference on Updating Subsurface Sampling of Soils and Rocks and Their Insitu Testing. Santa Barbara, California. January 1982, pp. 245-267.

Degan, W., Baez, F. and Rose, M., 2005. Dry bottom feed stone columns at Pier 400, Phase II – An evaluation of CPT-based soil classification before and after treatment. US-Japan Workshop on 'New Applications and Challenging Soils for Ground Improvement Technologies, Sept. 8-10, Kyoto, Japan

Idriss, I. M., and Boulanger, R. W., 2008. "Soil liquefaction during earthquakes." Monograph MNO-12, Earthquake Engineering Research Institute, Oakland, CA, 261 pp.

Massarsch, K.R. 1991. Deep soil compaction using vibratory probes. In American Society for Testing and Material, ASTM, Symposium on Design, Construction, and Testing of Deep Foundation Improvement: Stone Columns and Related Techniques, Philadelphia. Edited by R. C. Bachus. ASTM Special Technical Publication, STP 1089, pp. 297–319.

Moss, R. E. S., Seed, R. B., Kayen, R. E., Stewart, J. P., Der Kiureghian, A., and Cetin, K. O., 2006. "CPT-based probabilistic and deterministic assessment of in situ seismic soil liquefaction potential." J. Geotechnical and Geoenvironmental Eng., ASCE 132(8), 1032–051.

Robertson, P.K., 2009. "Interpretation of Cone Penetration Tests – a unified approach." Canadian Geotechnical Journal, 46: 1337-1355

Robertson, P.K., and Wride C.E. 1998. "Evaluating cyclic liquefaction potential using the CPT." Canadian Geotechnical Journal, **35**(3): 442-459.

Robertson, P.K., 2010. "Estimating In-Situ State Parameter and Friction Angle in Sandy Soils from CPT." 2nd International Symposium on Cone Penetration Testing, Huntington Beach, CA, USA.

Geotechnical and Geophysical Site Characterisation 5 – Lehane, Acosta-Martínez & Kelly (Eds)

Proposed performance criteria for earthwork construction quality control

A. Sawangsuriya & S. Wachiraporn
Department of Highways, Bangkok, Thailand

S. Sirisak & W. Lawanwisut
IMMS Co., Ltd., Bangkok, Thailand

ABSTRACT: This paper proposes the performance criteria based on strength index, moisture content, and relative compaction for earthwork construction quality control. The strength index from the convenient Dynamic Cone Penetrometer (DCP) in companion with conventional moisture-density measurements were evaluated in this study. A set of data collected from both laboratory test box and field trial were evaluated for a variety of compacted unbound materials in Thailand. The strength index in term of DCP penetration index (DPI) normalized by the deviation of compaction moisture content from the optimum moisture content ranging within the constant values in companion with typical earthwork compaction acceptance criteria based on the specified target dry density of the placed unbound materials achieved through appropriate moisture content ensure proper compaction quality, structural uniformity, and aid developing a controlled design parameter during the earthwork construction.

1 INTRODUCTION

Typical earthwork compaction acceptance criteria are based on the specified target dry density of the placed earthen materials achieved through appropriate moisture content. According to this approach, by achieving a certain dry density using an acceptable level of compaction energy assures attainment of an optimum available level of structural properties and also minimizes the available pore space and thus future moisture changes. Conventional approach is also based on the premise that monitoring dry density as opposed to a structural property is relatively simple and can be applied to generate data for a statistical evaluation of compaction quality.

The difficulty and expense of acquiring quality relevant structural properties have traditionally caused engineers to rely on density tests. The relative compaction (RC) alone is not a reliable indicator of the structural properties of compacted earthen materials. In addition, the RC is only a quality index used to judge compaction acceptability and is not the most relevant property for engineering purposes. For engineered earth fills and special engineering assessment, the ultimate engineering parameters of interest are often the stiffness and strength, which are direct structural properties for determining load support capacity and deformation characteristic in engineering design (Edil & Sawangsuriya 2005).

Since the non-uniformity of structural property is directly related to progressive failures and life-cycle cost, a simple, rapid, and direct structural property testing which can be conducted independently and in companion with conventional moisture-density testing without interference with the construction process is anticipated to increase test coverage, to improve statistical evaluation, and to reduce variability, thus substantially enhance construction quality control of the entire earth fills. In-place assessment of structural properties, e.g. stiffness and strength, of earthen materials has become widely available in the transportation geotechnics (Edil & Sawangsuriya 2006). This paper presents the implementation of strength index from the dynamic cone penetrometer (DCP) in conjunction with the conventional density and moisture content measurements for construction quality control and structural performance of compacted unbound materials.

2 DCP PENETRATION INDEX FOR EARTHWORK CONSTRUCTION QUALITY CONTROL

The DCP is simple, rugged, economic, and capable of providing a rapid in-place index of strength of unbound materials during road construction in Thailand. It measures the material resistance to penetration while the cone of the device is being driven into the pavement structure. The number of blows during operation was recorded with depth of penetration. The slope of the relationship between number of blows and depth of penetration (in millimeters per blow) at a given linear depth segment was recorded as DCP penetration index (DPI) (Sawangsuriya & Edil 2005).

Since DCP testing is basically a measure of penetration resistance, expressed as DPI, the analysis of the DCP data must be interpreted to generate a representative value of penetration per blow for the material being tested. In this study, such representative value can be obtained by averaging the DPI across the penetration depth of 150 mm, i.e., a typical lift thickness during field compaction process. Two methods of calculating the representative DPI value for a penetration depth of 150 mm are: (i) arithmetic average and (ii) weighted average (Sawangsuriya & Edil 2005). Since the weighted average method yields narrower standard deviation for the representative DPI value and provided better correlations to other field tests than the arithmetic average method based on field data available, the weighted average method is therefore adopted to calculate the representative DPI value in this study. The weighted average method can be obtained as follows:

$$DPI = \frac{1}{H}\sum_{i}^{N}\left[(DPI)_i \cdot (z)_i\right] \quad (1)$$

where z is the penetration distance per blow set and H is the maximum (overall) penetration depth. According to Thailand Department of Highways (DOH)'s quality control criteria and construction specifications, Wachiraporn et al. (2010) recommended the DCP for assessing the structural uniformity of layer thickness and routine earthwork quality control evaluation in companion with the conventional moisture-density control test during pavement construction in Thailand. Wachiraporn et al. (2013) suggested an adoption of the DCP as a mechanistic quality control tool during pavement construction as well as future development for performance specifications. Based on their studies conducted in the laboratory test box and in the field trial, the DCP provided instantaneous in-place strength index monitoring in term of DCP penetration index (DPI) for construction quality control and also exhibited good potential for quality control monitoring of the earthen materials. In addition, Wachiraporn et al. (2013) studies suggested that the CBRs estimated from the DCP were considerably smaller than the field CBRs (ASTM D4429), while the laboratory unsoaked CBR (ASTM D1883) tended to give the highest value.

3 TESTING PROGRAM

3.1 *Laboratory Test Box*

A laboratory test box has a dimension of 0.60x0.60x0.25 m^3. Disturbed samples including: (1) subgrade, (2) soil-aggregate subbase, and (3) crushed rock base were collected from a pavement construction site, Highway no. 3011: Ban Rai – Ban Tai section, Uthai-thani province, Thailand. Their basic properties, classification, and compaction characteristics are summarized in Table 1. Both laboratory and field CBRs were respectively conducted in accordance with the ASTM D1883 and the ASTM D4429 and reported herein.

In this study, each sample was prepared at three varied moisture contents including one near the optimum moisture content (OMC). The sample was compacted in layers for a total of five layers (e.g. 50 mm thick per layer) using a 14-kg concrete block connected to a steel rod. The impact compaction procedure was manually and uniformly applied at 50, 100, 300, and 550 blows per layer with a drop height over 250 mm. After the compaction, four moisture-density measurements were made using the nuclear moisture-density gauge (NG) (ASTM D6938), followed by four DCP measurements. The NG measurements were made along the middle lines, while the DCP measurements were made along the diagonal lines of the test box. Both NG and DCP tests were kept at a distance of about 150 mm away from the center.

3.2 *Field Trial*

A field trial selected in this study was conducted at a pavement construction site, Highway No. 3011: Ban Rai – Ban Tai section, Uthai-thani province, Thailand. This field trial had a total length of about 30-40 m with less than 2.5 m width. The pavement structure of this highway consisted of 10-cm thick hot mixed asphalt, 20-cm thick crushed rock base, and 20-cm thick soil-aggregate subbase over the compacted subgrade. A series of tests were performed on three types of unbound materials including: (1) subgrade, (2) soil-aggregate subbase, and (3) crushed rock base. The properties of these materials are summarized in Table 1.

During the compaction procedure, the unbound material from the stockpile was first spread out by a motor grader. Loose layer with thickness of 170-180 mm was compacted to the compacted layer thickness of 150 mm. Two compaction equipment of different capacities included a vibratory roller and a pneumatic tire roller. The compactors were driven slowly forward to the end of the section and then reversed along the same track. A water tanker was used to moisten the material when necessary.

Table 1. Properties of disturbed samples for the laboratory test box and field trial.

Properties	Subgrade		Subbase		Crushed Rock Base	
	Field Trial	Test Box	Field Trial	Test Box	Field Trial	Test Box
AASHTO Classification	A-7-5	A-7-5	A-2-6	A-2-6	A-2-4	A-2-4
75.0 (3")	-	100	-	100	-	100
50.0 (2")	100	100	93.1	93.1	100	100
38.0 (1-1/2")	-	-	-	-	-	100
25.0 (1")	95.8	95.8	71.9	71.9	100	100
19.0 (3/4")	-	-	65.8	65.8	86.2	86.2
9.5 (3/8")	88.2	88.2	-	-	65.5	65.5
#4	85.2	85.2	27.5	27.2	52.4	52.4
#10	78.6	78.6	20.4	20.4	34.5	34.5
#20	-	64.9	-	15.0	-	20.0
#40	54.5	54.5	-	11.4	14.2	14.2
#60	-	50.7	-	-	-	12.7
#100	-	44.9	-	10.3	-	11.1
#200	41.3	41.3	8.9	8.9	9.8	9.8
D_{10} (mm)	4.5×10^{-4}	4.0×10^{-4}	0.1	0.1	0.1	8×10^{-2}
D_{30} (mm)	1.5×10^{-3}	1.0×10^{-2}	5.1	2.1	1.6	1.6
D_{60} (mm)	0.6	0.6	10.6	16.8	7	7.5
LL (%)	41	41	27	27	19	19
PI (%)	14	14	19	19	9	8
W_{opt} (%)	13.2	13.2	8.5	8.5	6.8	6.8
Max dry unit weight (kN/m^3)	18.6	18.6	20.6	20.6	23.5	23.5
G_s	2.65	2.65	2.68	2.68	2.77	2.77
Soaked CBR (%)	18	21	42	35	68	68
Field CBR (%)	29	27	53	37	57	41
Swell (%)	6.6	6.6	0	2.5	0.3	0.3

After the compaction procedure, the DCP and the NG were conducted instantaneously at five test locations for each material type. At most two NG measurements were made first following by a single DCP measurement per one test location. Every measurement was made at the adjacent location.

4 RESULTS AND ANALYSIS

4.1 *DCP Penetration Index and Density-Moisture Relationship*

Figure 1a shows the relationship of RC (i.e., relative compaction, RC defined as the ratio of the field dry unit weight divided by the laboratory maximum standard Proctor dry unit weight) to the deviation of moisture content from the respective optimum moisture content (w-w_{opt}) for each of the unbound materials tested in the laboratory text box. The RC of laboratory compacted samples in the test box ranged from 75 to 95% with moisture content deviation varied from -5% to 8% of the optimum moisture content, whereas those data in the dashed box indicated some subgrade data compacted at the very wet side of optimum (i.e., moisture content deviation of about 8% of the optimum moisture content). The DPI vs. RC and the DPI vs. (w-w_{opt}) plots for laboratory compacted samples in the test box are respectively illustrated in Figures 1b and 1c. Excluding those data compacted at the very wet side of optimum, DPI exhibited strong dependency on both RC and moisture content as DPI varied from 10 to 50 mm/blow for a moisture content deviation of about ±4% of the optimum moisture content and RC ranging from 75 and 95%.

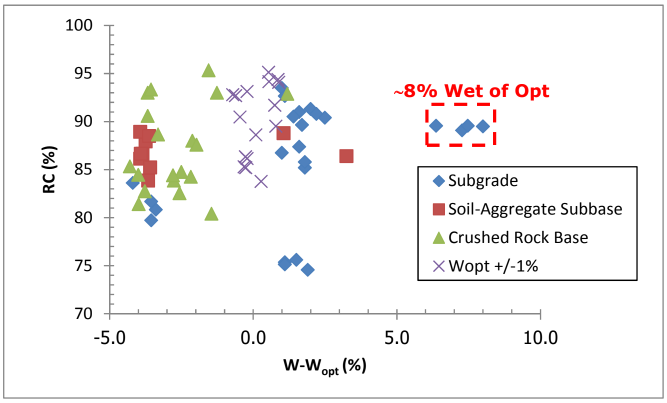

(a)

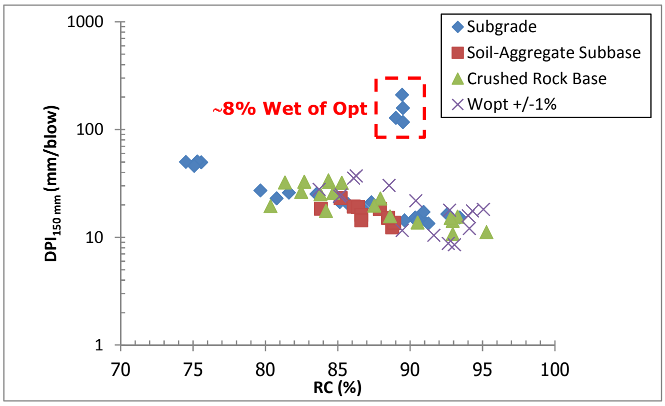

(b)

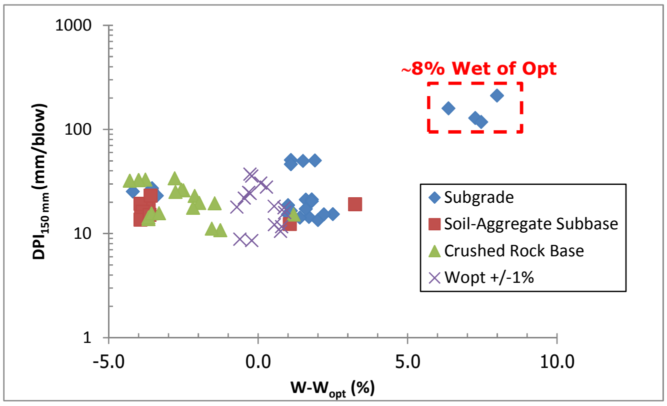

(c)

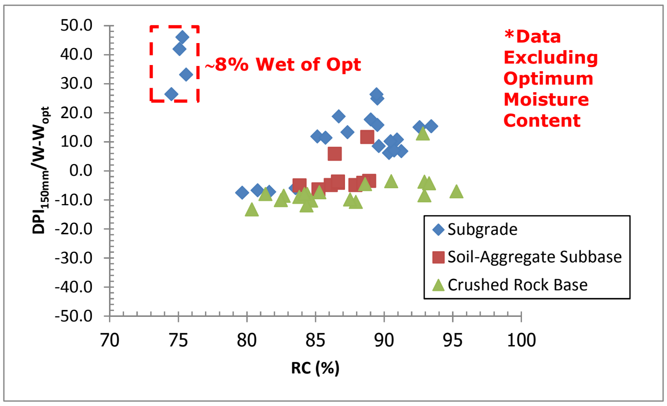

(d)

Figure 1. State of density and moisture relationship (a), DPI – state of density relationship (b), DPI – moisture relationship (c), and normalized DPI – relative compaction for laboratory test box (d).

Figure 2a shows the relationship of the RC to (w-w_{opt}) from the field trial. Most of the RC of field compacted unbound materials are ranged from 85 to 100% with moisture content deviation ranging from -3% to 7% of the optimum moisture content. Furthermore, RC decreased with increasing w-w_{opt}. Figures 2b and 2c show the variation of DPI with RC and the variation of DPI with (w-w_{opt}), respectively for the field trial. Strong dependency of DPI on both RC and (w-w_{opt}) was evident as DPI varied from 6 to 20 mm/blow for RC ranging from 85 to 100% and moisture content deviation ranging from -3% to 7% of the optimum moisture content. Of course, there are other factors that may affect DPI such as dry unit weight, microstructure, and they cause the spread in DPI for a given moisture content.

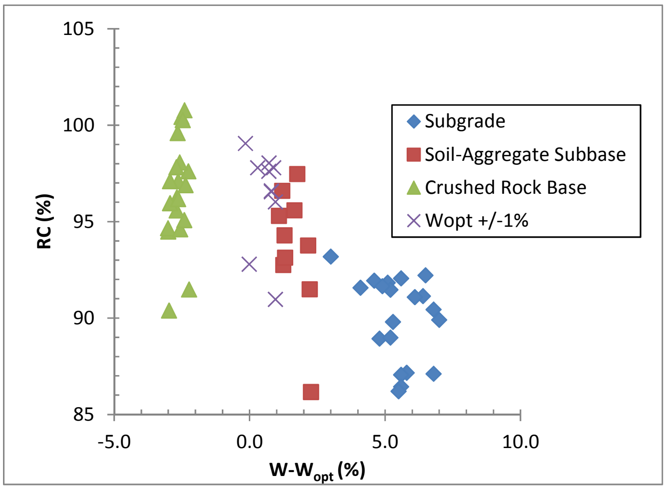

(a)

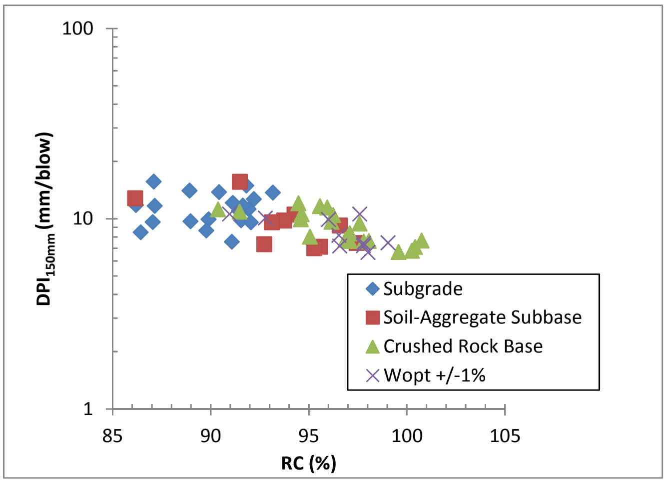

(b)

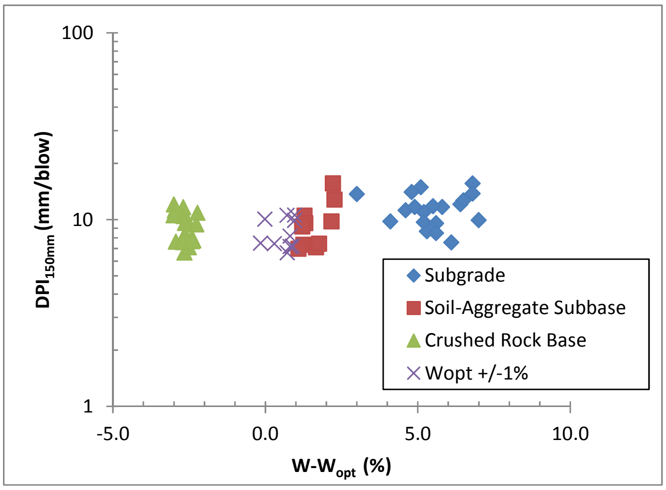

(c)

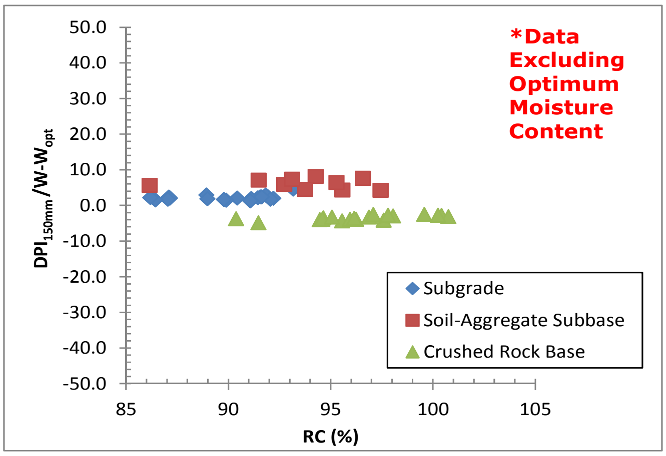

(d)

Figure 2. State of density and moisture relationship (a), DPI – state of density relationship (b), DPI – moisture relationship (c), and normalized DPI – relative compaction for field trial (d).

4.2 *Normalized DPI vs. Relative Compaction*

As aforementioned, both moisture content and dry unit weight play significant role on its DPI and their effects are hard to uncouple. To account for the effect of moisture content, DPI is divided by (w-w$_{opt}$), which is called the normalized DPI and is plotted against RC. The plot of normalized DPI vs. RC is shown in Figure 1d for the unbound materials tested in the laboratory text box. Although most of the normalized DPIs fell within the constant limits, there were some normalized DPIs falling outside the limits. These suggested that the materials compacted in the laboratory test box were subjected to either improper compaction control process or excessive moisture content used and consequently less structural uniformity and performance of compacted unbound materials.

For the field trial, it was obvious that all the normalized DPIs fell within the constant limits. These indicated the pavement construction had proper compaction control and the materials exhibited more structural uniformity as shown Figure 2d. The normalized DPIs varied fairly little with RC for the field compacted unbound materials having the constant values between -10.0 and 10.0. It should be also noted that those data set having moisture contents near the optimum moisture content (-1% < w-w$_{opt}$ < 1%) were excluded from the plot as they were theoretically in the optimum state of density and moisture. Based on the results obtained in the laboratory test box and the field trial, it is observed that the effect of dry unit weight of the compacted unbound materials on DPI is relatively minor compared to moisture content.

5 SUMMARY AND CONCLUSIONS

This paper presents the implementation of DCP in conjunction with conventional moisture-density measurements for construction quality control as well as structural performance of unbound materials. The outcome of this study can also provide a link between the construction testing and the designed pavement structural property. Use of the convenient DCP in companion with conventional moisture-density measurements enhances quality control by achieving more uniform structural property and aids developing a controlled design parameter during the construction stage. DPI normalized by the deviation of compaction moisture content from the optimum moisture content is proposed as performance criteria for a variety of compacted unbound materials. These include: (1) the normalized DPI shall be pre-specified for each compacted unbound materials tested in the field trial, (2) the relative compaction shall conform to the specified target level of compaction, and (3) the moisture content values near the optimum moisture content (i.e., $-1\% < w\text{-}w_{opt} < 1\%$) are not considered in this criteria as they are theoretically in the optimum state of density and moisture. The normalized DPI falling within the pre-specified limits ensures proper compaction quality control and consequently structural uniformity of compacted unbound materials.

6 ACKNOWLEDGEMENTS

The authors would like to express their sincere gratitude to the former director of Tak road construction and training center, Mr.Thanin Somboon, project managers, project engineers, engineers, inspectors, and other Department of Highways (DOH) personnel of the construction projects for their cooperation in arranging access to the sites and assistances during the field test. The authors acknowledge the Director Bureau of Road Research and Development, DOH for providing the laboratory facilities and test equipment. Thanks are due to Faculty of Engineering undergraduate students, Mahanakorn University of Technology for their assistances with the laboratory and field tests.

7 REFERENCES

Edil, T.B. & Sawangsuriya, A. 2005. Earthwork quality control using soil stiffness. *Proc. 16th Int. Conf. on Soil Mechanics and Geotechnical Engineering*, Osaka, Japan, 1689-1692.

Edil, T.B. & Sawangsuriya, A. 2006. Use of stiffness and strength for earthwork quality evaluation. *GeoShanghai Conference, Site and Geomaterial Characterization*, ASCE, GSP, 149, Shanghai, China, 80-87.

Sawangsuriya, A. & Edil, T.B. 2005. Evaluating Stiffness and Strength of Pavement Materials. *Proc. Inst. of Civil Engineers-Geotechnical Engineering*, 158 (4): 217-230.

Wachiraporn, S., Sawangsuriya, A., Sunitsakul, J., & Sramoon, W. 2010. Stiffness and strength based in-place evaluation of compacted unbound materials. *Proc. Sessions of GeoShanghai 2010*, GSP 203, Shanghai, China, 347-354.

Wachiraporn, S., Sawangsuriya, A., & Sramoon, W. 2013. Mechanistic based quality control during highway construction. *Proc. 18th Southeast Asian Geotech. Conf.*, Singapore, 605–610.

Geotechnical and Geophysical Site Characterisation 5 – Lehane, Acosta-Martínez & Kelly (Eds)
© 2016 Australian Geomechanics Society, Sydney, Australia, ISBN 978-0-9946261-1-0

Collapse settlement and strength characteristics of unsaturated soils with different degrees of compaction

A.M. Shahnoory & M. Sugiyama
Tokai University, Kanagawa, Japan

ABSTRACT: From a practical viewpoint, collapse settlement due to water infiltration into the soil affects fills or road bases that are developed by compacted unsaturated soils. The compacted soil is frequently assessed based on the degree of compaction (ratio of dry density to maximum dry density). Furthermore, no consideration has yet been given to the mechanical properties of compacted soils as a criterion for determining the effect of compaction, or to the condition of soil immersed in water which is the most dangerous state of soil. This paper presents the results of collapse settlement test and direct shear tests of four different types of Japanese soils. The influence of initial degree of saturation, initial dry density and overburden pressure have chosen as parameters. In addition, in this research, the influence of water content on unconfined compressive strength were investigated.

1 INTRODUCTION

In the field of geotechnical engineering, it is well known that several soil problems are caused by a surplus of water in the soil. There are various ways which soil can adsorb water such as rising of water table in the rainy seasons, reservoir in case of earth dams, leakage or damage of underground water supply system, flooding and etc. These problems generally can be caused to loss shear strength and excessive deformation, (Basma et al. 1992), therefore, it is imperative that engineers consider and control the deformation or settlement which occurs by wetting-induced (collapse) in compacted fills, including foundation of structures, embankments of transportation infrastructures such as roads, highways, railways, runways, parking-lots, and other compacted fills. The collapse can occur in engineered fills, has been demonstrated in both the field and laboratory (Booth et al. 1977).

This paper involves an extensive experimental investigation of collapse settlement and strength characteristics of unsaturated soils with different degrees of compaction. The work focuses particularly on collapse settlement and shear strength parameters to examine the influence of dry density, degree of compaction, and overburden pressures using four types of unsaturated soils (Kanto loam, DL clay, Kaolin clay and Kuroboku) which are silty loam, silt, clay and sandy loam respectively.

The work also investigated the effect of water content on unconfined compressive strength of aforementioned soils. Because the strength of fills that are constructed after compaction is considered to be reduced while the water content increases with no changes in density, especially in the rainy seasons.

2 SAMPLES AND TEST PROCEDURE OF COLLAPSE TEST

2.1 *Sample preparation*

Table 1 Physical property of the tested soils

Sample	ρ_s (g/cm^3)	WL (%)	Wp (%)	Grading (%)		
				Clay	Silt	Sand
DL clay	2.65	NP	NP	4.7	95.3	0
Kanto loam	2.65	NP	NP	4	51	45
Kaolin clay	2.67	73.1	36.7	96.8	3.2	0
Kurobuko	2.39	NP	NP	7	47	46

This research was conducted on four types of soils. Of these, Kanto loam, which was taken directly from a construction field inside Tokai University in Hiratsuka city, and the Kuroboku, collected from Ibaraki prefecture. Both soils, after being dried in an oven, were sieved by a 2 mm sieve. Thus, the maximum grain size was 2 mm. DL clay was prepared from Showa Chemical Co., Ltd and Kaolin clay was provided from Takehara Chemical Industries, Ltd.

Table 1 shows the physical properties of the tested soils and Figure 1 shows the compaction curves, tests which were obtained from the results of

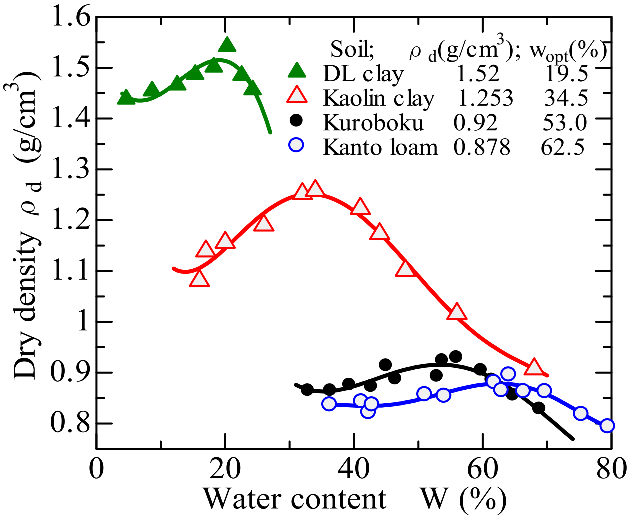

Figure 1 Compaction curves of tested soils

compaction test (JIS A1210). According to the results of compaction tests, the amount of soil and water for both collapse and shear test specimens were calculated, and after mixing the soil with water and placing it in an oedometer ring or shear box, static compaction was used to make the specimens.

2.2 *Sample preparation*

Table 2. Initial conditions of collapse tests

Type of soil	Dry density ρ_d (g/cm^3)	Degree of saturation S_r (%)	Pressure p (kPa)
DL clay	1.1, 1.2, 1.3, 1.36	20, 40	5, 10, 20, 40, 80, 160, 320, 640
Kanto loam	0.5, 0.6, 0.65	25, 40	
Kaolin clay	1, 1.1, 1.2	30, 60	
Kuroboku	0.555, 0.694, 0.74, 0.786	35, 45	

The specimens for all types of soils were developed based on the method of (Kamei et al. 1994) in order to investigate collapse settlement. The collapse settlement tests were performed using an odometer apparatus (JIS A1217). Eight different overburden pressures (p=5~640kPa) as shown in Table 2, were applied on unsaturated specimens which were 6cm in diameter and 2 cm in height. Following this, the amount of compressive deformation was measured for 24 hours. Then, keeping the same overburden pressure, water was absorbed through the bottom surface of the specimen and the influence of water on collapse settlement was monitored for another 24 hours. A total of 232 collapse tests were conducted on the four types of soils with the initial conditions shown in Table 2.

Under the same initial conditions as the collapse tests, direct shear tests (JGS 0561) were performed to investigate the shear parameters (c and ϕ). For each test condition, two specimens were tested separately to compare the results of unsubmerged specimen with submerged one. After the specimens were made, the designated vertical pressure was applied to one of them and an one hour of wait time was provisioned; while settlement occurred, the specimen was sheared. The same procedure followed for the second specimen, but after settlement, the specimen was soaked with water via its bottom surface. This soaking period depended on the permeability of each soil. Typically for clayey soils, a period of more than one hour was necessary to observe water appearing on the top surface of the ver-tical loading pedestal of the shear box. While collapse settlement occurred, shear stress was applied to compare the influence of water on shear parameters of soil.

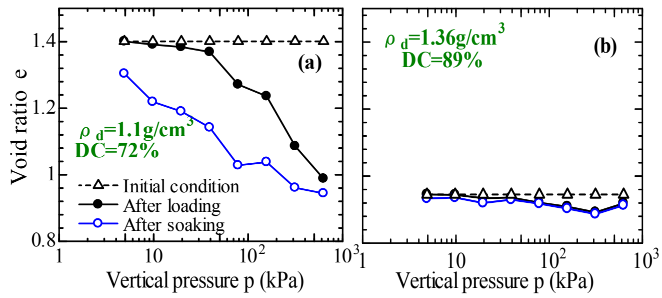

Figure 2 e– log p relation of DL clay at S_r=20%

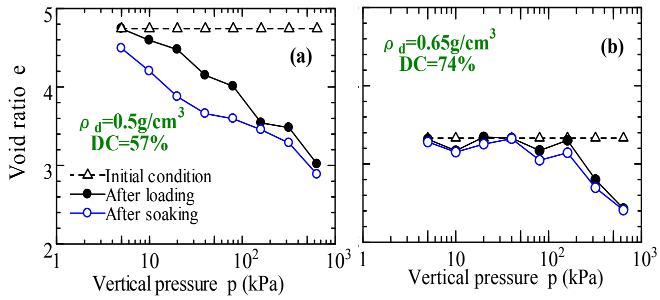

Figure 3 e– log p relation of Kanto loam at S_r=25%

3 TEST RESULTS AND DISCUSSIONS

3.1 *Result of collapse settlement test*

A literature review has shown that nearly all types of compacted soils are subjected to collapse under certain conditions (Booth A.R 1977). It is important to note that even clean sand, pure clays (including pure montmorillonite), and soils containing substantial gravel fractions can also collapse (Dakshanamurthy, V. 1979).

Figure 2 through Figure 5 show the relationships between void ratio e and overburden pressure p. For all types of soils, the filled circles indicate the deformation of specimens before soaking, and opened circles show the deformation process after specimens were soaked with water. Figure 2 indicates the result of DL clay at S_r=20 %, and ρ_{d0} =1.1 and 1.36 g/cm^3; it shows that, with increase of overburden pressure, the void ratio decreased and collapse settlement has occurred Figure 2(a). At ρ_{d0} =1.36g/cm^3 in Figure 2(b), hardly any settlement occurred. Figure 3 presents the result of Kanto loam;

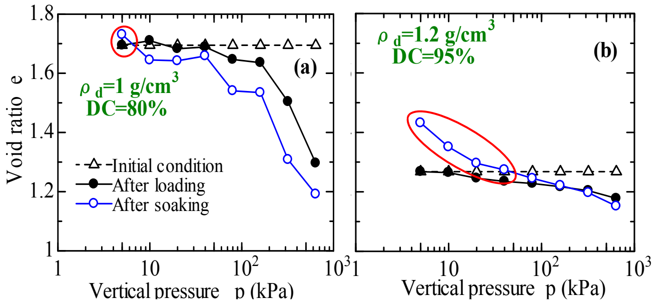

Figure 4 *e*–log *p* relation of Kaolin clay at S_r=30%

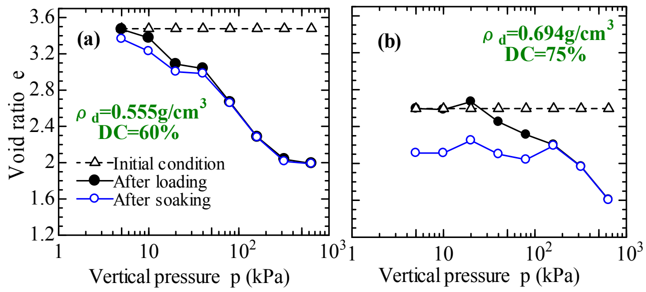

Figure 5 *e*–log *p* relation of Kuroboku at S_r=35%

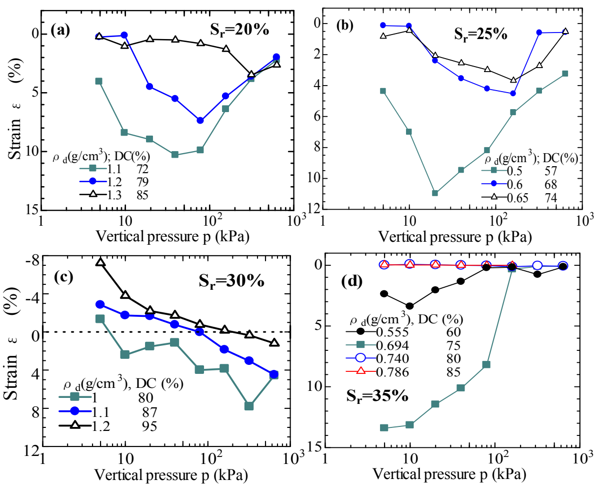

Figure 6. ε–p Relations after Soaking (a) DL clay, (b) Kanto loam, (c) Kaolin clay, (d) Kuroboku

the collapse settlement occurred immediately when water absorption started as shown in Figure 3 (a), whereas in higher dry density in Figure 3 (a), little collapse occurred.

The Kaolin clay results (Figure 4) indicated both collapse and swelling, depending on vertical pressures and dry densities. In the case of high density in Figure 4 (b), the collapse only occurred at the higher pressures, p=320 and 640 kPa. Figure 5 expresses the results of Kuroboku. Although 72 collapse tests were conducted with various initial densities, ρ_{d0}=(0.463, 0.555, 0.601, 0.694, 0.74, 0.786) g/cm^3, and initial degrees of saturation, S_r=(15, 20, 25, 35, 40, 45)%, collapsed only occurred at lower densities and pressures, (p<80kPa) at S_r=35% in Figure 5 (b). Comparing all results, except Kuroboku, at lower dry densities, the changes of void ratios after soaking are much larger than the initial condition of the tests.

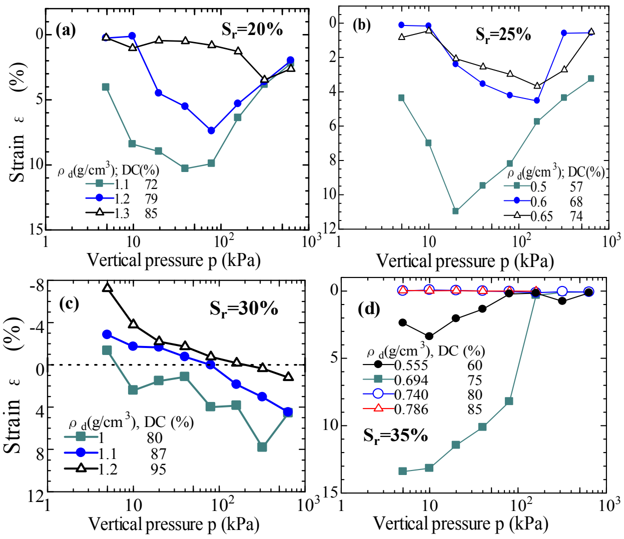

Figure 6 *ε*–*p r*elations after soaking, (a) DL clay, (b) Kanto loam, (c) Kaolin clay, (d) Kuroboku

Figure 6 shows the relations between axial strain ε and vertical pressure p. The DL clay result in Figure 6 (a) is near the result of Kanto loam in Figure 6 (b). Both results indicated that, strain increased with p peaked and then gradually decreased at lower dry densities (ρ_{d0}=1.1, and 1.2g/cm^3 for DL clay, and 0.5, and 0.6g/cm^3 for Kanto loam). Results from Kaolin clay in Figure 6 (c) show that swelling (increase in volume) gradually increased with increment of dry densities at overburden pressures lower than 320 kPa. Negative strain indicates that, after soaking, the specimen has a bigger volume than its initial volume. This result can be matched with the mechanism of collapse within which, for any given set of conditions, the amount of collapse generally decreases with increasing initial moisture content, increasing initial dry density, and decreasing overburden pressure (Lawton et al. 1991b). Figure 6 (d) shows the *ε-p* relation of Kuroboku soil. Strain constantly reduced only at ρ_{d0} = 0.555, 0.694 g/cm^3. Unlike DL Clay or Kanto loam, no increments of strain were shown.

3.2 *Result of direct shear test*

To investigate the influence of dry density and water content on shear parameters of soils (c and ϕ), the strain-controlled test method of direct shear test (JGS 0561) was performed. Therefore, shear stress was applied to one-half of the shear box, and the rate of shear displacement was measured by the horizontal dial gauge.

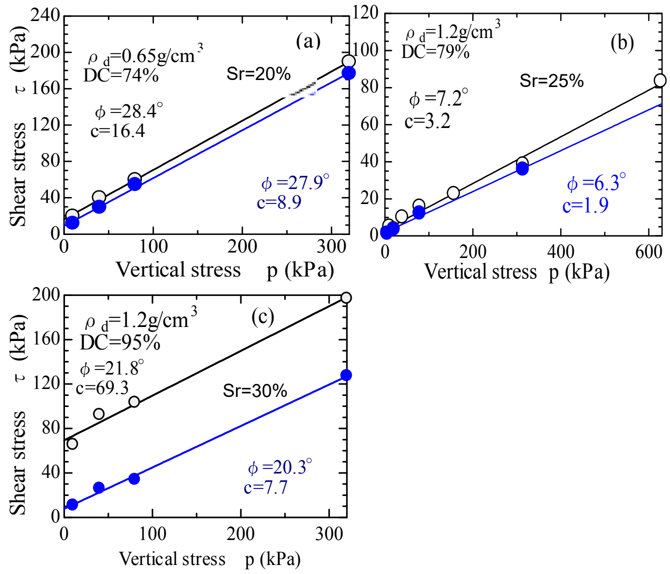

Figure 7 τ-p Relations, (a) Kanto loam, (b) DL clay and (c) Kaolin clay

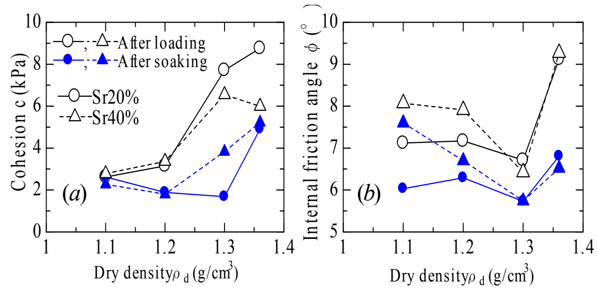

Figure 8 ρ_d-c,φ relations of DL clay

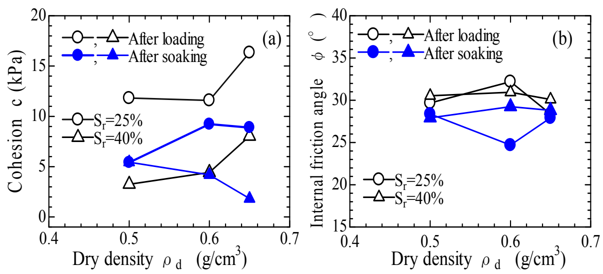

Figure 9 ρ_d-c,φ relations of Kanto loam

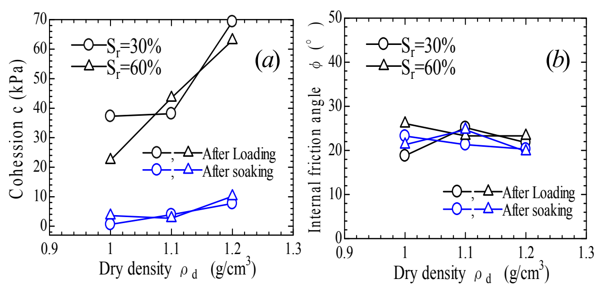

Figure 10 ρ_d-c,φ relations of Kaolin clay

Figures 7 (a) ~ (c) indicates the relationships between shear stress τ and vertical stress p of DL clay, Kanto loam and Kaolin clay at S_r=20%, 25% and 30%, respectively. The results indicated that after specimens were soaked with water, small changes occurred in ϕ (decreased), but c has significantly moved downward, especially for larger dry density condition of Kaolin clay in Figure 10 (a). Regardless of S_r, c has decreased after soaking all soils in Figure 8(a), 9 (a) and 10 (a). The results of Kanto loam show both decrease and increase of ϕ after the specimens was soaked, but the changes of ϕ in Kaolin clay is greater than the others.

The tests result shows that in the submerged specimens, the changes of cohesion c is larger than unsubmerged specimens. The changes in c of Kaolin clay are greater than Kanto loam and the changes of c in Kanto loam are greater than DL clay. The result is that whether the practical size of soil is smaller, the shear parameters will change more after the specimens are soaked. The increasing of dry density did not significantly affect the changing of cohesion c.

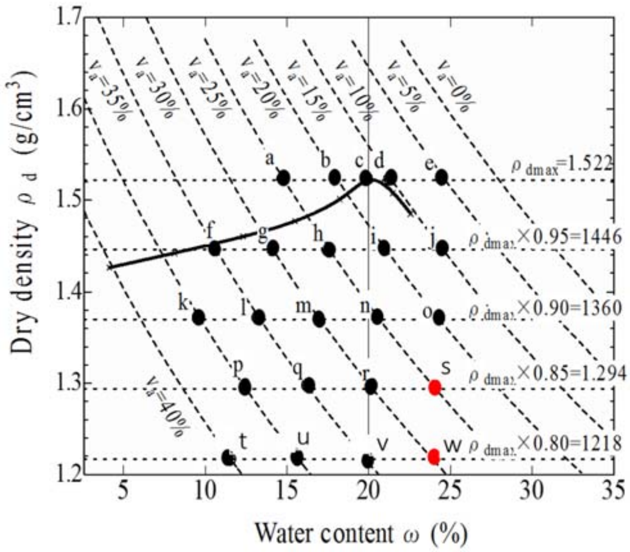

Figure 11. Initial positions of tested samples in compaction curve of DL clay

4 UNCONFINED COMPRESSION TEST

4.1 *Sample and Test Procedure*

The initial conditions of specimens were selected based on the results of compaction tests (JIS A1210). According to five different degrees of compaction (DC = 80, 85, 90, 95, 100 %), the initial densities were calculated ($\rho_d = \rho_{d\,\mathrm{dmax}} * DC$). Then the intersection points of dry densities with void ratios were selected for conducting the tests. After, based on the locations of points, the initial dry densities and water contents were measured for each specimen. A total of 21 specimens of DL clay (except point s and w, due to being so loose that they failed when they were removed from the mold), 23 specimens of Kaolin clay, 26 specimens of Kanto loam, and 24 specimens of Kuroboku were tested. Figure 11 (point a~w) is a sample of this method which belongs to the DL clay compaction result. The specimens prepared were with a height of 10 cm and a diameter of 5 cm, which was made by the static compaction method.

4.2 *Result of unconfined compression test and discussions*

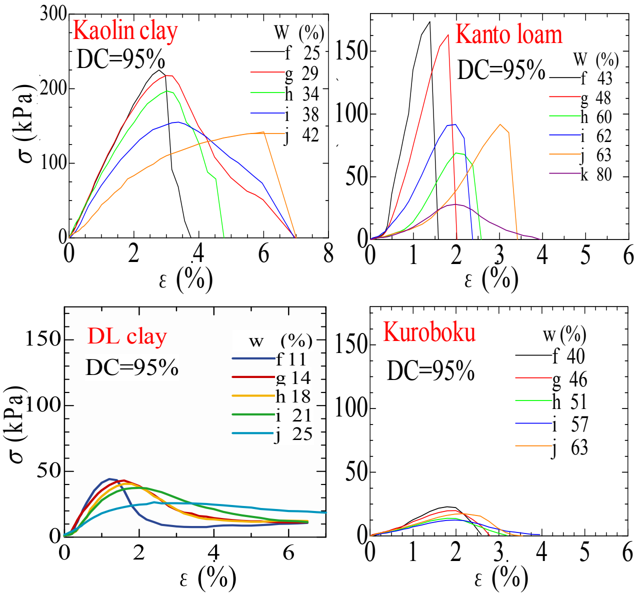

Figure 12. Stress-strain relations

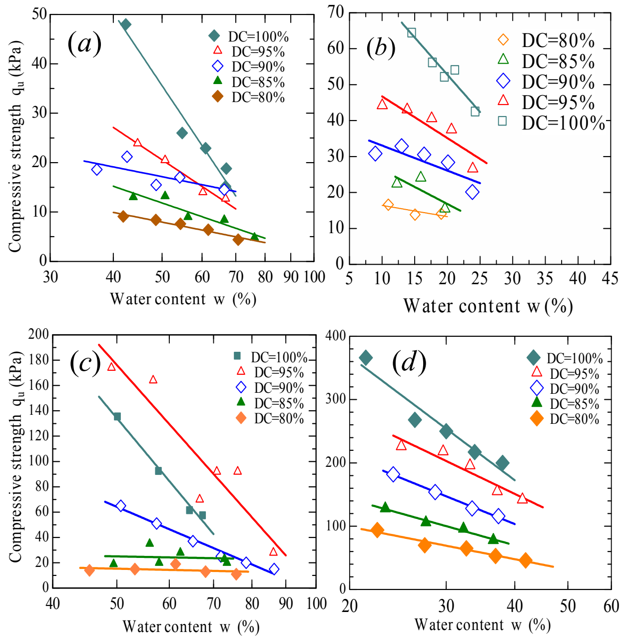

Figure 13 q_u-w relations, (a) Kuroboku, (b) DL clay, (c) Kanto loam and (d) Kaolin clay

The compressive strength of soils under embankments is one of the necessary data in embankment design. This analysis becomes increasingly important when embankments are built over weak soils, which are normally consolidated cohesive soils. The variation of this strength caused by rain can be changed in embankments when water content changes. Therefore, unconfined compression tests (JIS 1216) were conducted to investigate the effect of water contents on unconfined compressive strength q_u.

One result from each types of soil with the degree of compactions (*DC*=95%) have been shown to compare the stress-strain relations in Figure 12. The results indicated that by increasing water content, strain also increased. To compare these results, strain in Kuroboku is much less than Kaolin clay.

Generally clayey soil has shown higher strength than silty or sandy soils. Figures 13 (a)~(d) shows the relationship between water content w and compressive strength q_u, which are the results for Kuroboku, DL clay, Kanto loam and Kaolin clay, respectively. Data analysis indicated significant trends of unconfined compressive strength reduction with the increasing of water content; the degree of strength reduction is more outstanding at higher degrees of compaction. By decreasing water content, q_u has gradually increased and vice versa. Abe et al. conducted the same test using silty sand collected in the field. The test results in this study are similar to their results. In the silty sand used by Abe et al, unlike the sample in this study, q_u can be obtained even at with water content exceeding the optimum level.

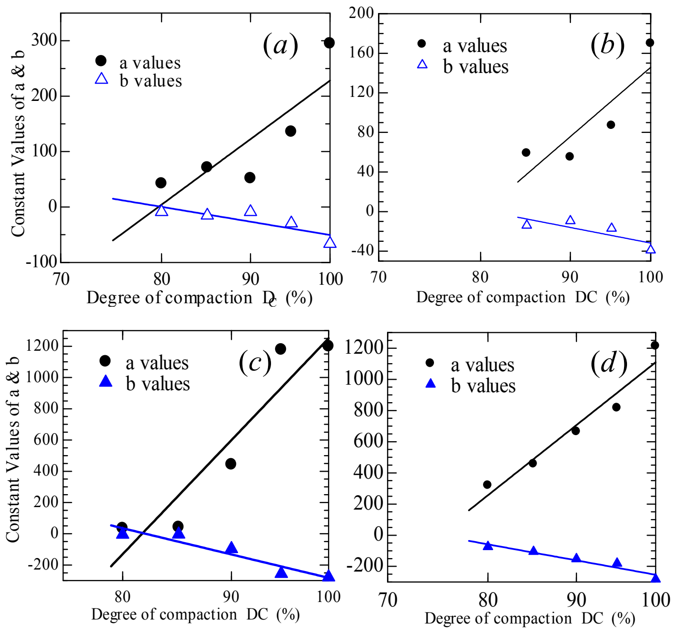

Figure 14 Constants of a and b relations with DC, (a) Kuroboku, (b) DL clay, (c) Kanto loam and (d) Kaolin clay

The strength of fills that are constructed after compaction is considered to be reduced, while there are no changes in density in the case where water content increases due to rainfall after construction (Abe et al. 2014). Therefore, it is important to prevent water from entering the fills as much as possible.

Based on the relation of q_u-w in Figure 13, and using least-square method, the following equation is proposed to determine the compressive strength of soils without performing unconfined compression test:

$$q_u = a + b \ln w \tag{1}$$

The constant a was found from the relationship of constants c and d with degree of compaction. Additionally, the coefficient. b was obtained from the relation of constants g and f with degree of compaction DC for each type of soil in Figure 14. It is worth mentioning that constant a and coefficient b have variable values according to DC.

$$a = c + d \ln DC \tag{2}$$

$$b = g + f \ln DC \tag{3}$$

It is mentionable that these equations are applicable for (JIS A 1210) standard compaction method whereas for other methods due to various compaction energies, the values of constants a, c and g and coefficients b, d and f will be varied.

5 CONCLUSION

The collapse tests results indicated that silty loam (Kanto loam) tend to collapse even at higher degree of compaction, but silty soil (DL clay) has shown no collapse at higher degree of compaction or higher density. Clayey soils (Kaolin clay) shown both collapse and swelling, depending on overburden pressures and dry densities. Mostly soils consist of montmorillonite tend to swell at higher density when the water content increase. However many experiments with various dry density and degree of saturation have been done on Kuroboku soil, but it has collapsed only at DC= 60% and 75% at lower overburden pressures. This soil which is an organic soil consist of small parts of plants and roots, difficult to determine its collapse behavior.

The result of direct shear tests indicated that changes of cohesion c are more outstanding than ϕ in submerged specimens for all types of soils. Cohesion c is willing to decrease more in clayey soils than silty or sandy soils, and the largest reduction of c appeared on the result of Kaolin clay, and this reduction has increased with increase of dry density, whereas for silty and sandy loam, the increase of dry density didn't significantly affect on cohesion.

The results of unconfined compression tests presented that, with the increasing of water content, the compressive strength of tested soils were decreased, and the degree of strength reduction is more outstanding at higher degrees of compaction. Therefore it is imperative to prevent the embankments or other compacted fill as much as possible from water infiltration. The main outcome of this part of research is the three proposed equations that in the future without conduction the unconfined compression test, the unconfined compressive strength of soils can be calculated.

6 ACKNOWLEDGEMENTS

The writer wish to express their appreciation to Mr. Yuki KAWANA and Mr. Koki HIRATA for their assistance in performing the laboratory tests.

7 REFERENCES

Basma, A.A and Tuncer, E.R 1992: Evaluation and Control of Col lapsible Soils, *Proc. ASCE*, Vol.118, No.GT 10, pp.1491-1504.

Booth, A. R 1977:Collapse settlement in compacted soils, CSIR Res. Report 324, Council for scientific and industrial Research, Pretoria, South Africa.

Cox, D.W. 1978:Volume changes of compacted clay fill Proc., Conf. on Clay fill, Inst. of Civil Ingres., London, 79-87.

Dakshanamurthy, V. 1979:A stress-controlled study of swelling characteristic of compacted expansive clays, *Geotech. Test.J.,* 2(1), 57-60.

Goro K.1985: Design and construction considerations 7. Soil compaction, *Soils and Foundations*, Vol.33, No.7, pp.57-64.

Japan Road Association: Highway Earthworks Series - Manual for Fill Works (fiscal 2010), 2010.

Kamei, T. and Enomoto, M. 1994:Wetting-induced Collapse Behavior of Compacted Silty Soil,J. of JSCE, No.505,Ⅲ-29,pp.97-103.

Lawton, E. C., Fragaszy, R J., and Hetherington, M. D. 1991: Review of wetting-induced collapse in compacted soil, Tech. Report No.9101, Univ. of Utah, Salt Lake City, Utah.

Lawton, E.C. fragaszy,r,j., and hardcastle.j,h.1989: Collapse of compacted clayey sand, *J.geotech. engrg.* ASCE. 115 (9) .1252-1267.

Tetsuo Abe et al. 2014: Strength characteristics of compacted fill dependent on changes in water content, *Proceedings of the 49th Japan National Conference on Geotechnical Engineering*, pp. 1013-1014.

Geotechnical and Geophysical Site Characterisation 5 – Lehane, Acosta-Martínez & Kelly (Eds)
© 2016 Australian Geomechanics Society, Sydney, Australia, ISBN 978-0-9946261-1-0

Geotechnical characterization of a heterogeneous unsuitable stockpile

K. Rengifo & F. Herrera
Knight Piésold Consultores, Lima, Perú

L. de la Cruz
Minera La Zanja S.R.L., Lima, Perú

ABSTRACT: Typically, stockpiled unsuitable soils from construction activities are classified as saturated soft fine soils. Nevertheless, because of some projects particularities, unsuitable materials could also present coarse soils resulting in a heterogeneous stockpile. This paper presents the geotechnical characterization of a heterogeneous stockpile in Peru in order to verify the physical stability of the disposal pile and to optimize the closure configuration. This characterization was based on a geotechnical investigation campaign that included boreholes, test pits, CPTU, MASW, field and laboratory tests. Based on the analysis of that information, strength parameters were determined for slope stability analysis. These parameters were represented by undrained shear strength lineal profile variable in depth for fine soils, and constant values of friction angle and cohesion for coarse soils. The stockpile stratigraphy was defined through the compatibility of geotechnical investigations results such as N_{SPT} blow counts, shear wave velocity (Vs), soil behavior type index (Ic), laboratory results, etc.

1 INTRODUCTION

During excavation activities for mining and civil structures construction, part of the remaining material is unsuitable, which means inappropriate for construction works and must be placed on stockpiles. Often, this material is supposed to be saturated fine soils. Nevertheless, due to the construction of different structures in diverse areas, various types of soils are found, which then conform the stockpile.

The unsuitable material stockpile studied is located in La Zanja mine, which is in the north of Peru at elevations between 2800 and 3600 m.a.s.l. La Zanja project is operated by Minera La Zanja S.R.L (MLZ) and consists on the exploitation of two open pits (San Pedro Sur and Pampa Verde), where silver and gold ore is mined and processed by heap leaching.

The need to re-assess the stability of this structure was mainly due to two reasons: in the original design, it was considered that the stored material would be saturated soft fine soils; so, the configuration of the stockpile included flat overall slopes (5H:1V). However, after the construction of the stockpile was completed, the final overall slopes were steeper in some sectors. The second reason was that MLZ wanted to evaluate the possibility to optimize the configuration of the stockpile for the closure stage.

The unsuitable material stockpile has 30 meters height and 6.9 Ha of area. The plan view of the stockpile is shown in Figure 1, while cross section A is shown in Figure 2.

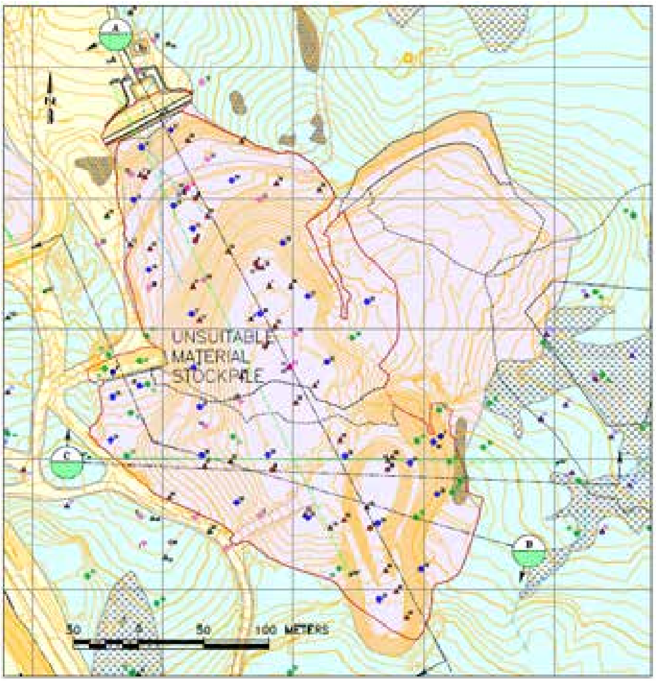

Figure 1. Plan view

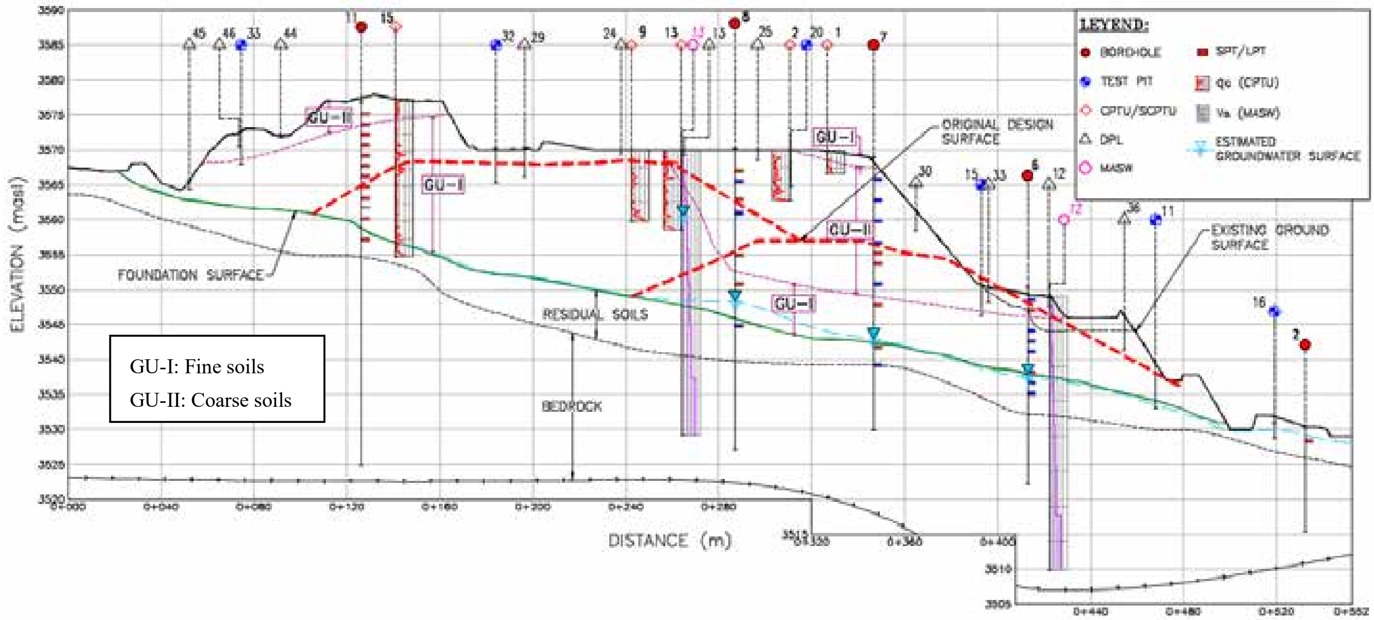

Figure 2. Cross section A

2. SUBJECT SITE

2.1 *Geological characteristics*

The unsuitable stockpile is compounded by anthropogenic deposits derived from the cut and fill materials from the earthworks. In the perimeter of the structure, quaternary deposits of the hydromorphic/colluvial /alluvial type were also found. In the same way, the stockpile foundation consisted on quaternary residual deposits or extremely to highly weathered bedrock. Beneath this layer, the highly resistant bedrock composed of porphyritic tuff of the Llama formation was located.

2.2 *Configuration of the stockpile*

As it has been previously mentioned, in the original design the overall slope to conform the stockpile was supposed to be flat (5H:1V). Nonetheless, the cut material from access roads and specific areas of the heap leach pad foundation came from residual soils or weak rock. Hence, it contained a proportion of gravels and cobbles, which increased the material's strength. For that reason, the overall slope of the unsuitable stockpile was steeper than the originally recommended.

In Table 1, the overall slope of the studied stockpile in different sectors is presented.

Table 1. Unsuitable stockpile slope angle in different sectors

Section	Slope from design	Left of section			Right of section		
		Depth	Slope		Depth	Slope	
	(H:V)	(m)	(H:V)	(°)	(m)	(H:V)	(°)
A		11	2.5:1	22	27	4.5:1	14
B	5:1	21	2:1	30	11	5.5:1	11
C		23	2:1	30	12	7.5:1	8

3 SITE- SPECIFIC INVESTIGATIONS

3.1 *Field investigations*

A summary of the field investigation program conducted is presented in Table 2.

Table 2. Field investigations summary

Description	Quantity	SPT/LPT	In situ density	
			Quantity	gr/cm^3
Boreholes	7	67	29	-
Test pits	29	-	7	1.32 – 1.68
DPL	24	-	-	-
CPTU	1	-	-	-
SCPTU	9	-	-	-
MASW	2	-	-	-
Piezometers	5	-	-	-

With the aim of obtaining referential values of the in-situ density of the different materials studied, tests were performed to obtain the in-situ density by water replacement method in some test pits.

On the other hand, 24 DPL were executed in the stockpile. The depth at which 30 blow counts were reached varied between 0.6 and 5.9 m, indicating the material compactness is not uniform.

3.1.1 *CPTU and SCPTU soundings*

Piezocone (CPTU) and seismic piezocone (SCPTU) tests were carried out at 10 positions within the subject stockpile, with the purpose of characterizing the fine soils and then stablish its strength parameters. The depth of these tests varied from 3 to 27 meters. Dissipation tests of the pore pressure were also included to verify the static pore pressure conditions.

The SCPTU tests registered shear wave velocity (V_s) data at different depth intervals in order to measure soil stiffness.

Three principal parameters were measured:

- Cone resistance q_c, (MPa).
- Sleeve friction f_s, (MPa).
- Pore pressure u_2, (MPa o m).

Figure 3 shows these three parameters registered in one SCPTU test:

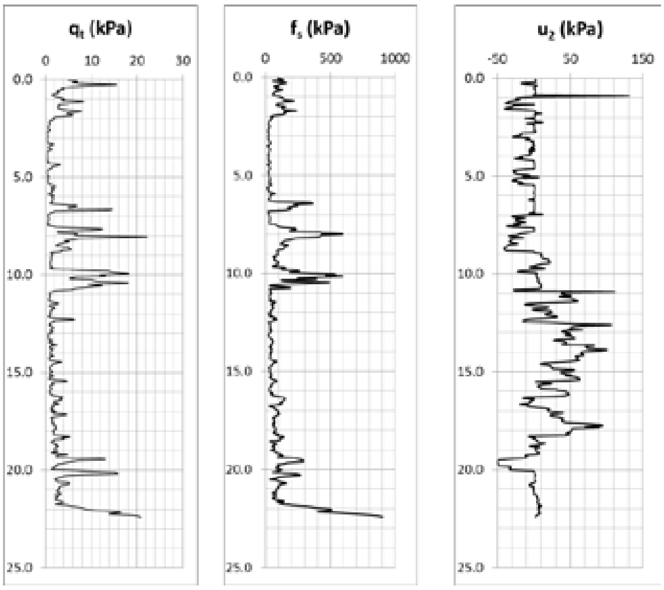

Figure 3. SCPTU profile

3.1.2 *MASW soundings*

Besides CPTU/SCPTU tests, a geophysical testing program was implemented and combined two MASW soundings with two geophysical lines of 440 and 360 m within the stockpile's footprint.

Figure 4 presents shear wave velocity (Vs) profiles of the two soundings. Moreover, Vs obtained from SCPTU tests and SPT blow counts from a near borehole are shown to compare the compactness/consistency of the material registered by each of the different tests performed. The results of shear wave velocity obtained from SCPTU and MASW adjusted to the same level of compactness/consistency according to the International Building Code (IBC 2015).

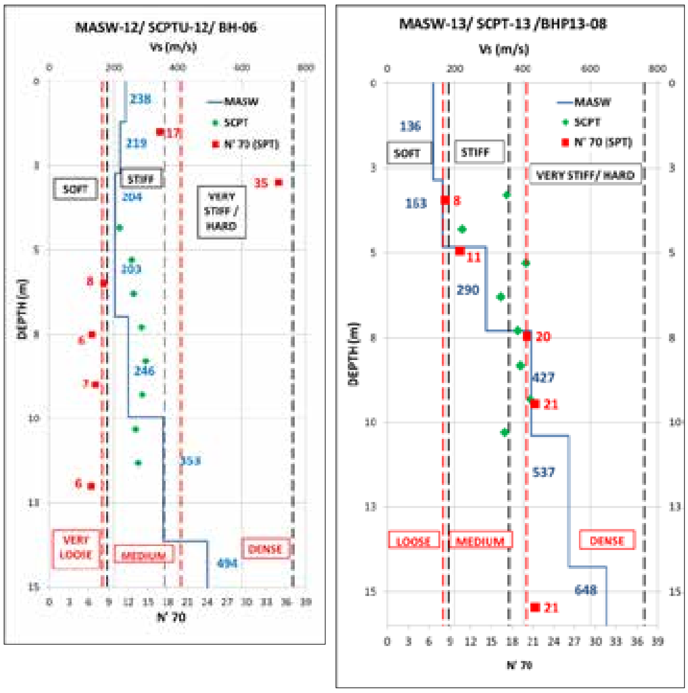

Figure 4. Shear wave velocity vs. N'_{70} (corrected SPT blow counts) profile

The intervals of compactness/consistency of soils for N'70 presented in Figure 4 were obtained from the empirical relations proposed by Bowles (Bowles 1996).

3.2 *Laboratory testing*

Concurrent with the geotechnical site investigations, the behavior of the different material types was also further evaluated by geotechnical laboratory testing. The results for fine and coarse materials are provided in Tables 3 and 4. In addition, grain size distribution curves of the most representative materials are illustrated in Figure 5.

Table 3. Laboratory results for coarse material

Coarse material	USCS	Minimum	Maximum	Average
Overall USCS classification	SM/GC/ SC/GM			
ω_0(%)		3.1	46.7	15.7
LL		36	79	53
PI		16	36	25
Fines content (%)		15.5	49.3	35.5
γ_{nat} (g/cm^3)		1.73	2.10	1.96

Table 4. Laboratory results for fine material

Fine material	USCS	Minimum	Maximum	Average
Overall USCS classification	MH/CH/ ML/CL			
ω_0(%)		6.8	55.4	31.3
LL		38	65	53
PI		16	35	24
Fines content (%)		51.9	85.5	64.3
γ_{nat} (g/cm^3)		1.61	2.10	1.88
UU triaxial:	MH			
Axial strain at failure (%)		10	Peak	
Friction angle (°)		0	5	
Cohesion (kPa)		13	40	

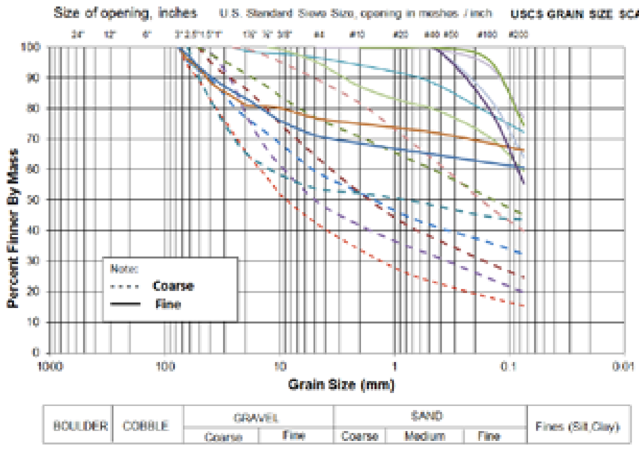

Figure 5. Grain size distribution of representative samples

Regarding the triaxial tests, UU tests were completed in undisturbed samples obtained from Shelby tubes and in remolded samples from test pits. In like manner, CU tests were completed in remolded samples obtained from test pits.

Based on the tests results, the high heterogeneity of the unsuitable material was verified. In general, there was a mixture of fine and coarse material, predominantly sands and fines.

4 GEOTECHNICAL CHARACTERIZATION AND STRENGTH PROPERTIES

After the review, processing and analysis of all the data obtained, two geotechnical units were determined according to their USCS classification and strength parameters: fine unsuitable material (GU-I) and coarse unsuitable material (GU-II). The distribution of the geotechnical units can be seen in Figure 2 for cross section A.

4.1 *Fine unsuitable material (GU-I)*

It was determined that the predominant stockpiled material was fine grained and classified as ML, MH, CL and CH, soft to very stiff consistency and wet; according to test pits and boreholes descriptions, and laboratory results.

Then, to stablish the stratigraphy of the stockpile and materials shear strength parameters, data from CPTU/SCPTU tests were analyzed, which are ideal for characterizing fine grained soils.

Again, results from the evaluation of the three measured parameters in CPTU tests (q_c, f_s, u_2) with the analytical functions developed for them (Robertson & Cabal 2012, Robertson 2010a, b, Robertson 2009); confirmed the composition of the unsuitable material consisted mainly of fine grained soils with a percentage of sands and gravels. This is also stated by the profiles of the normalized soil behavior type index (I_c). Some examples of these profiles are shown in Figure 6.

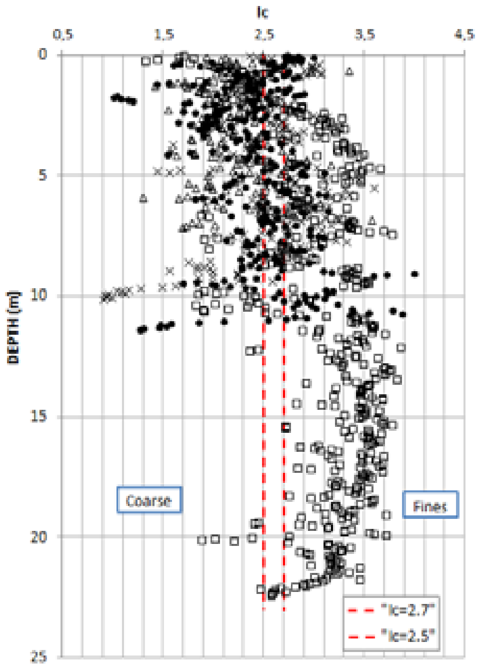

Figure 6. Ic profile

The stratigraphic profiles were stablished with the information from Ic profiles and grain size distribution tests. Then, considering the fact that perched water table conditions were identified in two CPTU tests and the stability analyses was going to be run for the short term; it was concluded that the undrained shear strength conditions resembled in a better way the actual conditions of the stockpile.

In agreement with the existing correlations in CPTU tests bibliography, the undrained shear strength

(S_u) of fine materials was determined by using the following equation:

$$S_u = \frac{(q_t - \sigma_v)}{N_{kt}} \text{ (kPa)} \qquad (1)$$

where: q_t = corrected cone resistance (kPa); σ_v = total vertical stress; and N_{kt} = cone factor $(N_{kt} = 10.5 + 7\log(F_r))$. (Robertson 2013).

Whereas the cone factor Nkt in previous publications was defined as an empiric number in the range between 10 and 20, for this study the latest correlation developed by Robertson was used and the value was limited to a minimum of 14.

Figure 7 represents the undrained shear strength profiles (S_u) of fine materials estimated from CPTU and SCPTU tests:

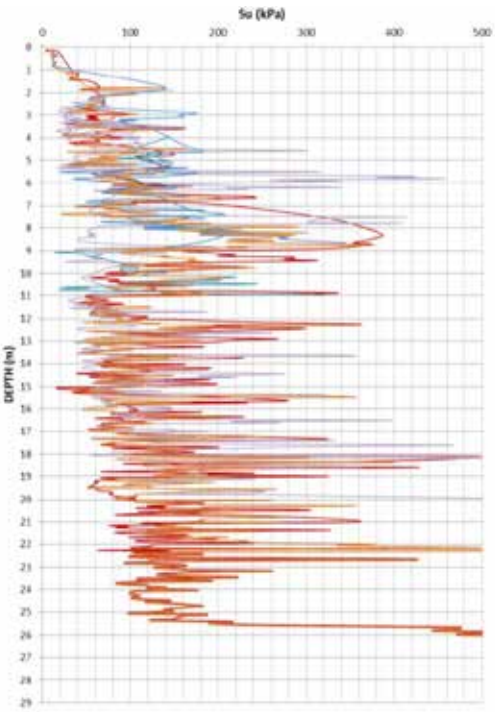

Figure 7. Undrained shear strength profiles

After obtaining the strength profile of each CPTU/SCPTU test, they were jointly processed and finally, it was decided to utilize de average values of S_u at different depths, without considering any possibly erratic or erroneous data.

Undrained shear strength estimated based on the average values of CPTU tests were more suitable for these fine grained material. Even though, these soils were predominantly cohesive, they also contained an important proportion of sands and less gravel.

Furthermore, average strength values were more representative because they complied with the back analyses done in the critical sections of the deposit, as there were not observable unstable conditions detected during neither the execution of the geotechnical investigation campaign nor latter visits to the site.

With the objective of characterizing the strength variation of fine material through the deposit, results from the CPTU data were fitted in several regressions, S_u vs. depth. Finally, based on the back analysis performed for the stockpile, the best fitting appeared as a linear regression, which is supplied in equation 2 and in Figure 8:

$$y = 4.81x + 21.3 \text{ (kPa)} \qquad (2)$$

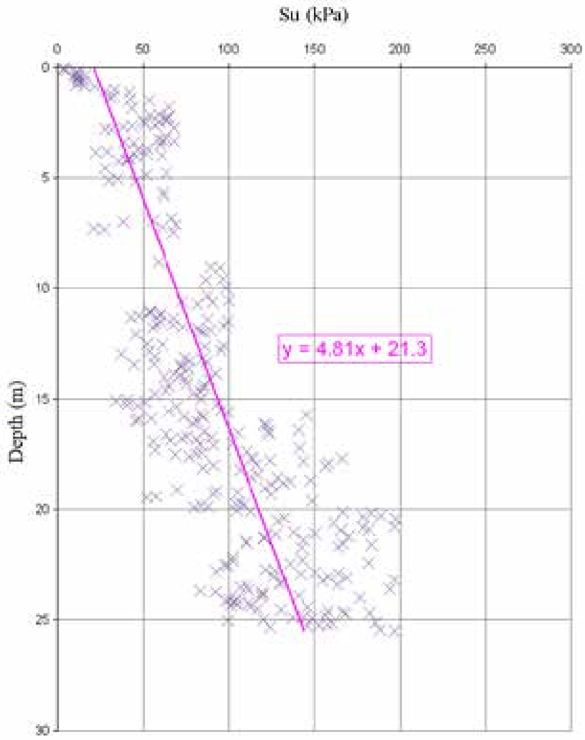

Figure 8. Final undrained shear strength profile for stability purpose

It can be observed that the lowest undrained shear strength value is 21 kPa. This value is within the range of the results of UU triaxial tests completed in this type of material.

4.2 *Coarse unsuitable material (GU-II)*

With regard to the second geotechnical unit or coarse materials, existing correlations between the SPT or LPT tests and friction angle in the soils mechanics literature were used. The analytical functions applied were from: Shioi & Fukui (1982), Kulwahy & Mayne (1990) and Hatanaka & Uchida (1996). Likewise, CPTU own formulations were used to estimate the effective friction angle for coarse materials by Jefferies & Been (2006) and Robertson (2009).

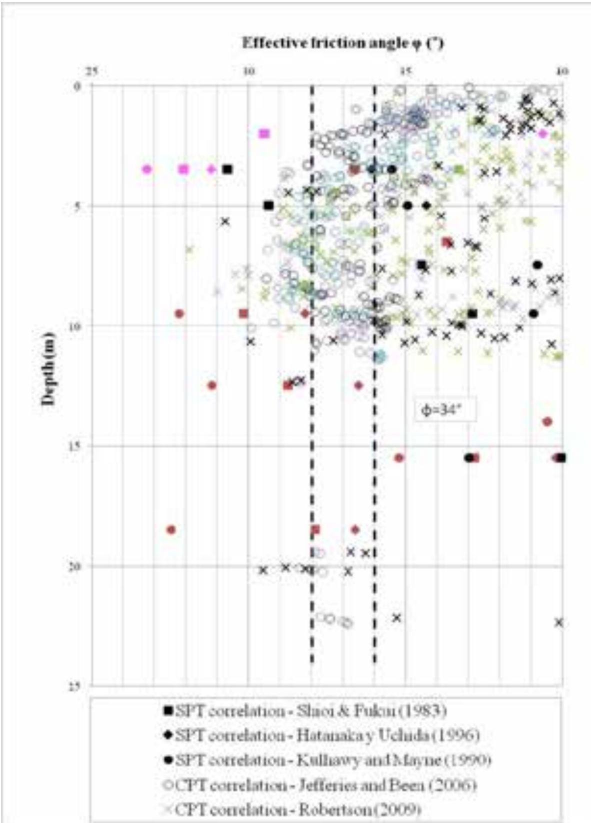

Figure 9. Effective friction angle for coarse material

In order to determine the range of values for the friction angle, back analysis of the existing conditions of the stockpile were performed. The range obtained, between 32° and 34°, was confirmed with the results of correlations with CPTU and SPT tests data.

At the end, these values were validated because they were similar to the steepest angle of repose slope found in the unsuitable stockpile.

Later, in the stability analysis it was determined that almost all the configuration of the stockpile was stable and a new configuration was proposed in the unstable sector. Also, for final closure stage, it was determined that not much earthwork was needed, influencing in the economics aspects of the project.

5 CONCLUSIONS

The case study presented has the distinction of having allowed correlating different kinds of geotechnical investigations. First, in spite of the heterogeneity of the stockpiled material, CPTU tests were successful in defining more accurate stratigraphy profiles and obtaining strength parameters for fine and coarse soils. If coarse soils are predominately sands, CPTU tests can be used in the project.

Moreover, one important parameter was Ic, which showed the heterogeneity of materials placed in the stockpile and was confirmed by the boreholes performed.

On the other hand, CPTU tests are useful to find perched water table conditions unlike the piezometers. As a result, drained and undrained behavior of different strata can be identified.

Regarding shear wave velocity results from MASW and SCPTU tests, it was observed that the values obtained from both tests adjusted to the same level of compactness/consistency. In addition, the level of compactness or consistency found with SPT blow counts was lower than the one obtained with shear wave velocity values.

Finally, because of the amount of data provided by the CPTU tests, statistical analysis could be run to get even more precise strength parameters for the different strata.

6 REFERENCES

Bowles, J. E. 1996. *Foundation Analysis and Design*. New York: Mc Graw Hill.

Hatanaka, M. & Uchida, A. 1996. Empirical correlation between penetration resistance and internal friction angle of sandy soils. *Soils & Foundations*, *Vol. 36 (4), 1-9, Japanese Geotechnical Society.*

International Code Council. 2015. *2015 International Building Code.* Country Club Hills, III: ICC.

Jefferies, M.G. and Been, K. 2006. *Soil Liquefaction – A critical state approach.* Oxon: Taylor & Francis

Kulhawy, F. H., and Mayne, P. W. 1990. *Manual on estimating soil properties for foundation design*. California: Electric Power Research Institute.

Robertson, P.K. 2013. Interpretation of in-situ tests-some insights. In Coutinho & P.W. Mayne (eds)*: The James K. Mitchell Lecture:, Geotechnical and Geophysical Site Characterization 4, 3-24*. London: Taylor and Francis Group.

Robertson, P.K. 2010a. Soil Behaviour Type from the CPT: An Update. *2nd International Symposium on Cone Penetration Testing*, *Vol. 2, 575-583*. Huntington Beach.

Robertson, P.K., 2010b. Estimating in-situ state parameter and friction angle in sandy soils from the CPT. *2nd International Symposium on Cone Penetration Testing, CPT'10*. Huntington Beach.

Robertson, P.K. 2009. Interpretation of cone penetration tests – a unified approach. *Canadian Geotechnical Journal, 46:1337-1355.*

Robertson P.K & Cabal K.L. 2012. *Guide to cone penetration testing for geotechnical engineering*. California: Greg Drilling & Testing, Inc.

Shioi, Y. and Fukui, J. 1982. Application of N-value to design of foundation in Japan. *Proceeding of the Second European Symposium on Penetration Testing, Amsterdam, Vol. 1, 159-164.*

Geotechnical and Geophysical Site Characterisation 5 – Lehane, Acosta-Martínez & Kelly (Eds)
 ISBN 978-0-9946261-1-0

Verification of an impact rolling compaction trial using various in situ testing methods

B.T. Scott, M.B. Jaksa & E. Syamsuddin
The University of Adelaide, Adelaide, South Australia, Australia

ABSTRACT: Rolling Dynamic Compaction (RDC) involves a heavy non-circular module that rotates and falls to impact the ground dynamically; it has a greater depth of influence compared to conventional circular rollers. The depth of influence to which an impact roller can compact soil is known to vary, and is dependent upon factors such as soil type, moisture content and applied input energy, thus verification of impact rolling is particularly important to quantify the extent to which soil has been improved. This paper compares before and after compaction test results using three in situ testing methods, field nuclear density, dynamic cone penetrometer (DCP) and spectral analysis of surface waves (SASW), as well as the ground response due to RDC using earth pressure cells, accelerometers and surface settlement measurements used during the compaction trial.

1 INTRODUCTION

Rolling dynamic compaction (RDC) improves ground through the use of a heavy, non-circular module that imparts energy into the soil as it falls to impact the ground. This dynamic effect results in a greater depth of influence than circular rollers, with depths of improvement found to range from more than 1 m below the ground surface to greater than 3 m in some soils (Avalle & Carter 2005) depending upon factors such as soil type, moisture content and compactive effort. RDC disturbs the ground surface leaving an undulating surface; this is a function of the surface geometry of the face of the module as it impacts the ground. As a result, whilst RDC can improve ground at depth it can make the surface soil less dense requiring a conventional circular roller to compact the near surface soil. The aim of the field trial described in this paper was to investigate the extent of ground improvement using various techniques to allow comparison between in situ testing methods undertaken before and after compaction, as well as collecting real-time data during the trial to further understand the ground response to RDC.

2 SCOPE OF COMPACTION TRIAL

In this study, a field trial was conducted using a Broons BH-1300 4-sided impact roller (Fig. 1) at Monarto Quarries, located approximately 60 km south-east of Adelaide, South Australia. The trial pad was constructed by excavating a 1.5 m depth of natural soil and replacing it with 20 mm crushed rock material. Six equal lifts of 250 mm thickness were adopted; each lift was lightly compacted in a uniform manner using a vibrating plate compactor and wheel rolling from a Volvo L150E Loader that was used to place the material.

2.1 *Soil type*

To minimize the effects of soil variability, a homogeneous soil was used for this trial; locally produced crushed rock with a maximum particle size of 20 mm; the material was classified as a well-graded Sandy Gravel (GW) in accordance with the Unified Soil Classification System.

The soil was tested for homogeneity through the use of particle size distribution testing, and both Standard and Modified Proctor compaction laboratory tests. As shown in Figure 2, the optimum moisture content for the Modified Proctor test was 11.3%, corresponding to a maximum dry density of 19.7 kN/m^3. For the Standard Proctor test, the optimum moisture content was 13.3% and the maximum dry density 18.8 kN/m^3.

2.2 *In situ testing methods*

The soil type being compacted dictates (to some extent) what in situ testing methods are appropriate. Other factors that influence the choice of testing method include, time, cost and the availability of testing equipment. Further discussion on testing methods commonly used with RDC is given by

Scott & Jaksa (2008). In this trial, field density testing using a nuclear density gauge, dynamic cone penetration (DCP) testing, and geophysical testing using the spectral analysis of surface waves (SASW) technique were undertaken before and after compaction. The aforementioned methods were chosen primarily because they were readily available given the university owns the equipment.

2.3 *Ground response*

Rinehart & Mooney (2007) successfully used Geokon 3500 earth pressure cells (EPC) in a field trial to measure the loading induced pressures due to static and vibratory circular drum rollers. Based on their success, the same cells were adopted for the present field trial to measure the pressure imparted into the soil due to RDC, as they are commercially available and capable of measuring dynamic loads.

Accelerometers have, in the past, been fixed to falling weights to monitor the deceleration upon impact with the ground surface in deep dynamic compaction applications, as reported by Mayne & Jones (1983). Clegg (1980) used the analogy of a compaction hammer, describing the peak deceleration when it is brought to rest on the soil being directly related to the resistance provided by the soil due to its stiffness and shearing resistance.

Module mounted accelerometers have also been used to measure the ground surface response from a 3-sided impact roller as reported by McCann & Schofield (2007) who stated that the magnitude of the deceleration increased with compactive effort. Whilst this technique provides useful information at the surface, there is no guarantee that measuring the ground surface response gives a true indication of what is happening at depth, especially at sites where there is inherent soil variability. For the purposes of this trial it was decided to attach accelerometers to the buried EPCs to quantify the ground deceleration produced at targeted depths within the expected depth of influence of the roller.

A custom-built accelerometer cluster was attached to each EPC consisting of ±5 g accelerometers in the X and Y planes to measure tilt, as well as the Z plane to measure vertical acceleration. An additional ±16 g accelerometer was used in the vertical plane as the magnitude of peak vertical acceleration was uncertain at the test depths of 0.7 m and 1.1 m. The EPCs and accelerometers were connected to a custom-built data acquisition system and Labview software program. The ability to capture an accurate ground response using EPCs and accelerometers relies heavily on adopting a sufficiently high sampling frequency. A sampling frequency of 4 kHz was selected for this trial to ensure that the true peak pressure and ground deceleration could be accurately captured.

3 RESULTS

3.1 *Surface settlement monitoring*

Surface settlement monitoring is a quick and simple test method that is commonly used when working with RDC to identify local soft spots that may require additional compaction, or excavation and replacement. From the authors' experience, unexpected results can be obtained with surface settlement monitoring if a grader cuts into the surface between passes (rather than just smoothing off high points of the undulating surface profile) or if targeted coordinates are blindly surveyed without taking into account the nature of the undulating surface. However, provided a consistent approach is undertaken that takes into account the undulating surface left by the impact roller, it is possible to determine how many passes are needed until effective refusal is met. In this trial, local low points from each module face that contacted the ground were surveyed, with the average surface settlement plotted every 5 passes (typically) as shown in Figure 3. A trend line fitted through the measured data indicates that effective refusal was met after approximately 70 passes. This was largely a function of the loosely placed condition of the soil, as it was subjected to minimal traffic compaction from the loader used to place the material.

3.2 *Density*

A nuclear density gauge was used to measure field density before and after compaction. The variation of dry density with depth is summarised in Figure 4, whereby it can be observed that the post compaction dry densities were greater than the pre compaction densities over the full depth of the trial pad, suggesting that the depth of influence of RDC was beyond 1.5 m. The maximum dry density achieved was measured to be 19.0 kN/m^3 at a depth of 0.55 m; corresponding to dry density ratios of 96.5% and 101%, with respect to the Modified and Standard Proctor tests, respectively.

The advantage of the nuclear density test is that it provides a measure of soil's dry density ratio, often specified in earthwork projects. The largest disadvantage is that the gauge's source rod length is limited to a maximum of 300 mm, meaning excavation of compacted material is required to test greater depths. For a dedicated trial this was not a major concern; however, for a project site the time needed for testing and the need to excavate to targeted depths and re-compact after testing can slow progress. Scott & Suto (2007) used this method to help quantify ground improvement using RDC, and cited limitations such as lengthy test durations and the difficulty with the testing process for mixed soils, particularly where oversized particles were present.

3.3 *Dynamic cone penetrometer*

DCP test results indicated a greater number of blows were required after compaction for each 100 mm increment between depths of 0.2 m to 1.8 m, as shown in Figure 5. At a depth of 0.1 m, disturbance of near surface soil due to RDC resulted in a negative improvement for reasons discussed in Section 1, as shearing of the soil had occurred as described by Clegg (1980) and discussed in Section 2.3. DCP testing was terminated at a depth of 1.8 m due to limit of equipment, with the results suggesting that the impact roller influenced the ground beyond this depth.

DCP testing is simple, low cost and uses portable equipment; however, it is a test that can be limited by the presence of large particles. This was found to be the case at this site where refusal was occasionally met on gravel-sized particles greater than the rod diameter (16 mm), in which case, the test was terminated and a substitute test performed. Whilst reasonable results from this trial were obtained due to the relatively homogeneous nature of the soil used in this trial, placing heavy reliance on DCP data without the use of other in situ testing methods is not recommended, particularly at sites containing oversized particles and heterogeneous fill. For example, Whiteley & Caffi (2014) reported difficulty in comparing pre- and post-compaction DCP test results in fill material containing crushed rock.

3.4 *SASW testing*

Non-intrusive SASW testing was undertaken before and after compaction. At this site, six receivers (geophones) were placed on the ground surface and a sledgehammer used to generate the wave energy. As shown in Figure 6, the results indicate that the 4-sided impact roller was able to improve the shear wave velocity for the full 1.5 m thickness of crushed rock material used for the trial, as well as a further 0.5 m thickness of the underlying natural soil. Below a depth of 2 m, the shear wave velocity profiles converged, suggesting this was the depth to which RDC could improve this site.

3.5 *Earth pressure cells and accelerometers*

The measured peak pressure recorded for each pass of the impact roller, 80 no. in total, is displayed in Figure 7. There is no clear relationship between number of passes and measured peak pressure, except to observe that the largest peak pressures were recorded between passes 50 to 80, suggesting that the maximum peak pressure may increase with the number of passes. The peak vertical ground deceleration for each pass is presented in Figure 8. Again, no clear trend exists between the number of passes and the peak ground deceleration measured, suggesting other factors have a greater effect, as this was an unexpected result (refer Section 2.3).

A limitation of using buried instrumentation in RDC applications is that it is not possible for the impact roller module to land in exactly the same location each time relative to the instrumentation in the ground. Avalle et al. (2009) attempted to do this by adopting the same at-rest starting location and operating speed; however it was found that the reproducibility of impacts could not be controlled due to other variables, such as the condition of the ground surface, soil moisture content, density and how quickly the operator changed through the gears and accelerated. For this trial, the same methodology undertaken by Avalle et al. (2009) was adopted, where the effects of non-direct impacts were taken into account by measuring the distance between the centre of the EPC and the centre of the module face.

A correlation between measured peak pressure and vertical ground deceleration is shown in Figure 9. At a depth of 0.7 m, greater peak pressures and vertical ground decelerations were recorded than at a depth of 1.1 m, an expected result which supports a general trend of increasing ground deceleration with increasing peak pressure.

The distribution of peak pressure with offset distance is shown in Figure 10, where it can be observed that the highest pressures corresponded to offset distances between +100 mm to +650 mm. The physical location where the module landed on the ground relative to the fixed position of the buried instrumentation was found to be critical in terms of both the peak pressure recorded and ground deceleration (Fig. 11) produced. Figure 12 summarises the same results using a heat map to illustrate which parts of the contact face of the 4-sided impact roller produced the highest peak pressures and ground decelerations. As observed in this figure, the pressure distribution beneath the contact face as it impacts the ground is non-uniform. Maximum peak pressures and ground decelerations are associated with red, intermediate values in yellow and lower values with blue colours.

The findings from this trial generally agree with Avalle et al. (2009) who found that the zone of maximum impact was located at offset distances from 0 mm to +400 mm from the centre of the roller. However, the results from this trial should be considered as being more reliable, largely due to the instrumentation used to measure load. This trial used thin EPCs that produce a much more reliable measurement of in situ soil stress than the bulky load cell used by Avalle et al. (2009) and which is significantly stiffer than the surrounding soil.

Whilst it is not possible to capture the maximum ground response from each and every impact, by burying equipment into the ground at discrete locations; this technique does provide real-time information of dynamic pressures and accelerations in the ground that other testing methods are unable to do.

Figure 1. Broons BH-1300 4-sided impact roller used in compaction trial.

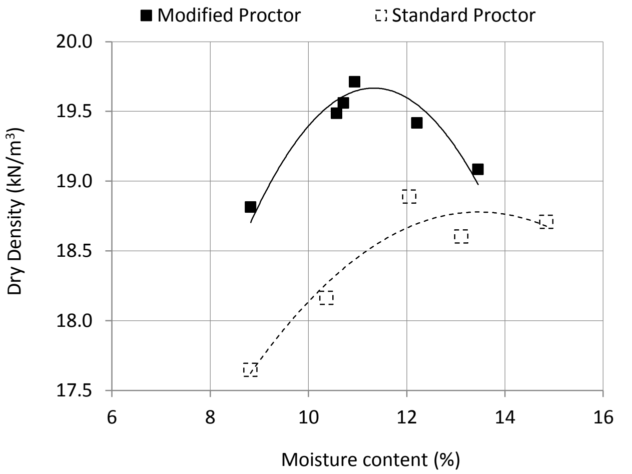

Figure 2. Modified and Standard Proctor compaction curves for 20 mm quarry material.

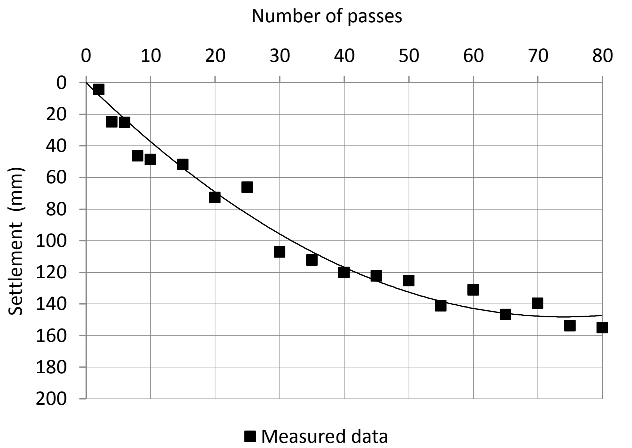

Figure 3. Summary of surface settlement with trend line through the measured data points.

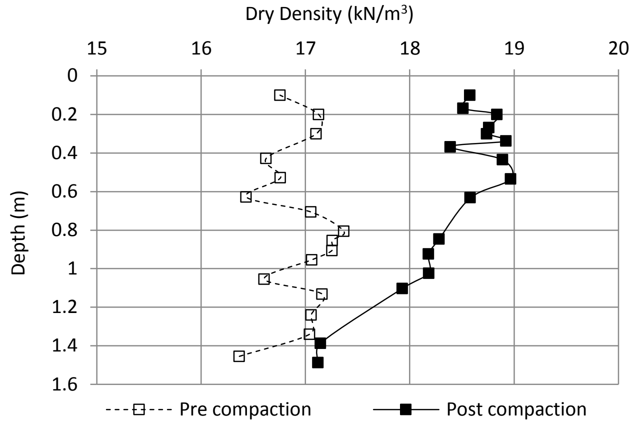

Figure 4. Dry density versus depth from field density testing.

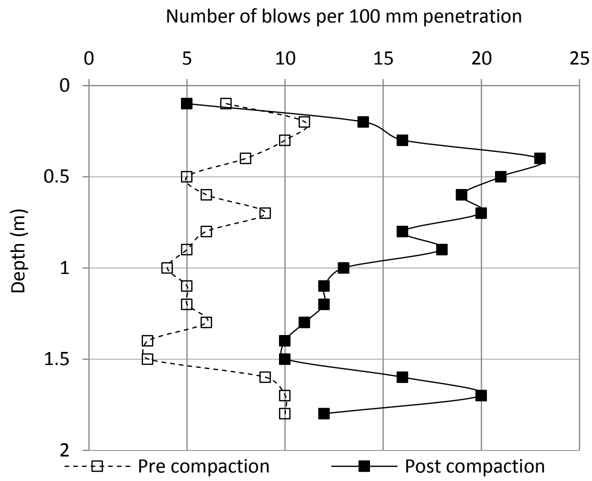

Figure 5. DCP pre and post compaction results.

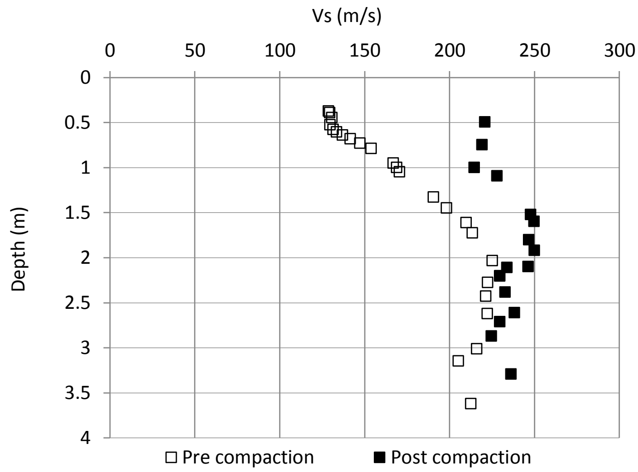

Figure 6. Shear wave velocity versus depth from SASW testing.

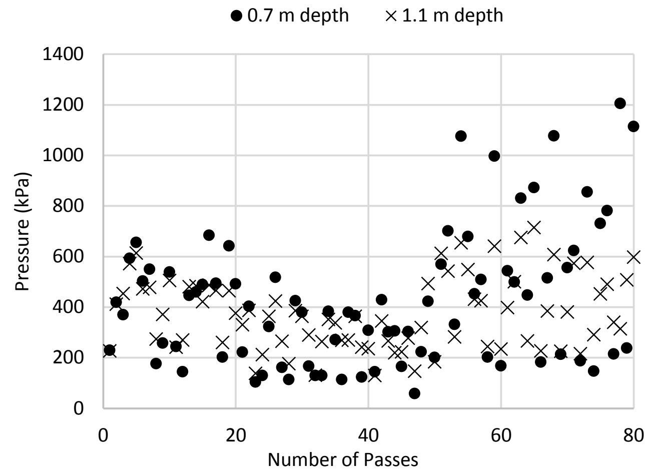

Figure 7. Measured peak pressure for each pass of the impact roller.

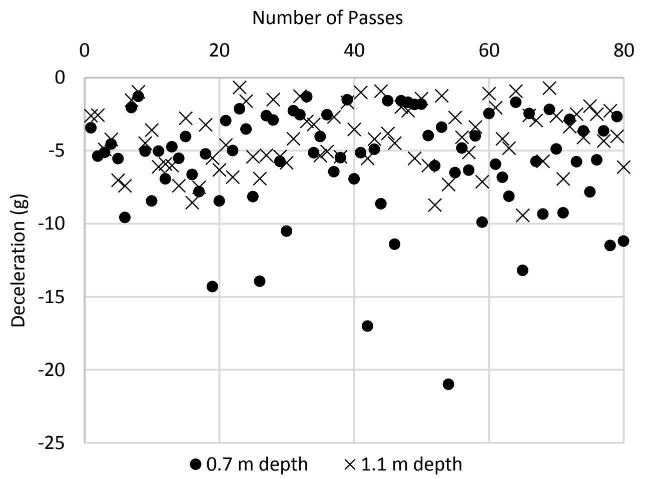

Figure 8. Measured peak deceleration for each pass of the impact roller.

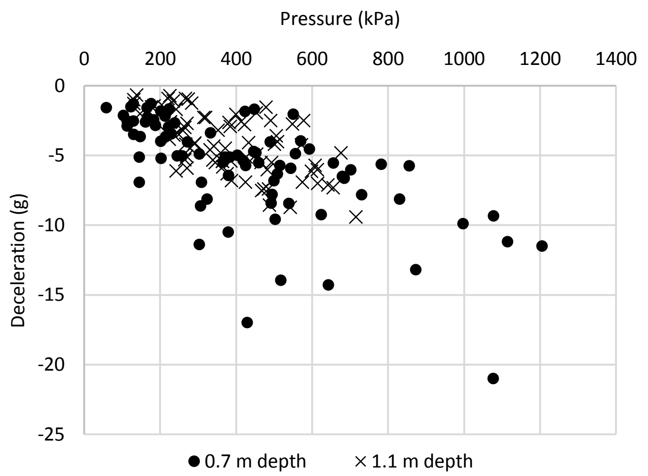

Figure 9. Correlation between measured peak pressure and deceleration.

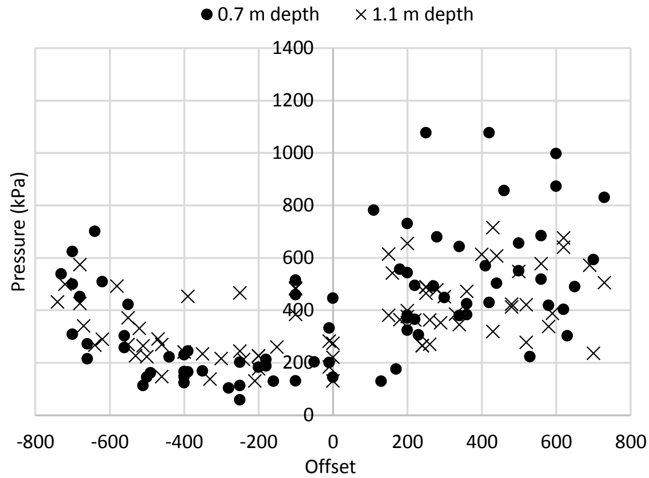

Figure 10. Distribution of peak pressure with offset distance.

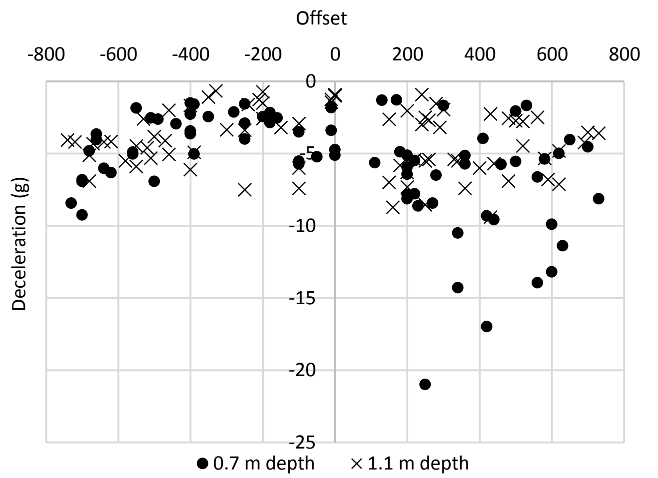

Figure 11. Distribution of peak deceleration with offset distance.

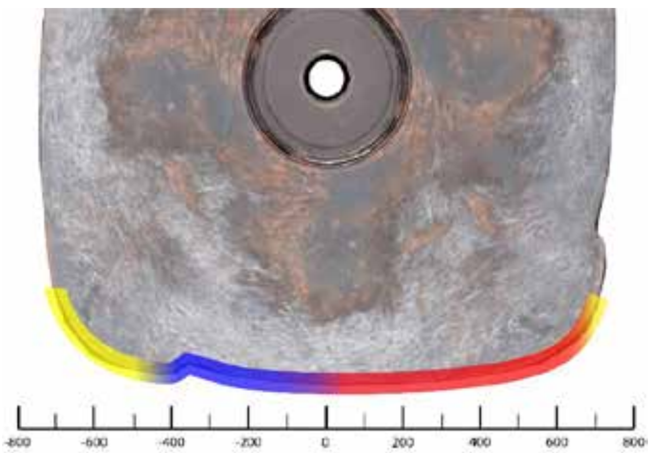

Figure 12. Heat map for 4-sided impact roller indicating the most influential parts of the contact surface that produced maximum peak pressure and peak ground deceleration.

4 CONCLUSIONS

This field based study was conducted using well-graded 20 mm quarry material to minimise the effects of soil variability. The fill material was placed to a depth of 1.5 m and compacted using a 4-sided impact roller. From testing undertaken pre- and post-compaction, ground improvement was quantified using three different in situ testing methods: DCP testing, field density testing using a nuclear density gauge and geophysical testing using the SASW method. Comparison of the three in situ testing methods adopted in this trial showed good agreement with each other.

All three in situ testing methods used in this trial indicated that the depth of influence of RDC was greater than the depth of fill material (1.5 m). As the results from field density and DCP tests were limited in depth due to limit of equipment, the SASW test method was able to provide the best estimate for the depth of improvement of RDC in this trial; approximately 2 m.

The use of earth pressure cell and accelerometers buried at depths of 0.7 m and 1.1 m, well within the depth of influence of the roller for this soil as quantified by the different in situ testing methods undertaken in this trial, found that a slight upward trend existed between the number of passes and peak pressure. There was also a weak upward trend between peak pressure and vertical deceleration. Significantly, both peak vertical deceleration and peak pressure imparted into the ground were dependent upon offset distance or, specifically, which part of the module face struck directly over the buried earth pressure cell.

Apart from a faster operating speed than circular rollers, one of the key reasons why RDC is able to improve ground to greater depths is due to the geometry of the contact face that gives rise to a non-uniform pressure distribution beneath the module. That is, there are regions on the surface of the roller that impart significantly greater pressures into the ground than other parts of the contact face. This is one of the key reasons why many passes are needed to ensure adequate coverage of a site.

Whilst the buried instrumentation used in this trial has been customised primarily for research purposes, and is unlikely to be adopted for widespread use on ground improvement projects using RDC, recent advances in technology allow the soil response subject to dynamic loading to be more accurately captured than ever before. Further analysis of real-time data and future field trials will continue to advance knowledge and understanding in this area.

5 ACKNOWLEDGEMENTS

The authors sincerely thank instrumentation staff at The University of Adelaide for their technical support with the accelerometers and earth pressure cells; the staff at Broons for their assistance with the compaction trial and supplying the 4-sided impact roller; and Monarto Quarries for making their site available and for providing quarry material and earthmoving equipment. The authors would also like to thank the following Honours Research students who have contributed to the test results referred to within this paper: Gianfranco Canala, Chris Gauro, Jackson March, Richard Strapps, Stefan Chenoweth, Jordan Colbert, Julianne Saw and Ross Vince. Without their support the work contained in this paper would not have been possible.

6 REFERENCES

Avalle, D.L. & Carter, J.P. 2005. Evaluating the improvement from impact rolling on sand, *Proc. 6th Int. Conf. on Ground Improvement Techniques,* Coimbra, Portugal, 153-160.

Avalle, D.L., Scott, B.T. & Jaksa M.B. 2009. Ground energy and impact of rolling dynamic compaction – results from research test site. *Proc. 17th Intern. Conf. Soil Mechanics and Geotechnical Engineering,* Alexandria, Egypt, Vol. 3: 2228-2231.

Clegg. B. 1980. An impact soil test as alternative to California Bearing Ratio. *Proc. 3rd Australia New Zealand Conf. on Geomechanics,* Wellington, New Zealand, 225-230

Mayne, P.W. & Jones, J. S. (1983). Impact stresses during dynamic compaction, *Journal of Geotechnical Engineering,* 109(10): 1342-1346.

McCann, K. & Schofield, N. 2007. Innovative methods in the in-situ determination of design parameters on heteregenous sites subject to ground treatment using deep impact compaction. *Proc. 10th Australia New Zealand Conf. on Geomechanics,* Brisbane, Australia, Vol. 2: 126-131.

Rinehart, R.V. & Mooney, M.A. (2009). Measurement of roller compactor induced triaxial soil stresses and strains, *Geotechnical Testing Journal,* 32(4): 347-357.

Scott, B.T & Suto, K. 2007. Case study of ground improvement at an industrial estate containing uncontrolled fill. *Proc. 10th Australia New Zealand Conf. on Geomechanics,* Brisbane, Australia, Vol. 2: 150-155.

Scott, B.T. & Jaksa, M.B. 2008. Quantifying the influence of rolling dynamic compaction, *Proc. 8th Young Geotechnical Professionals Conf.,* Wellington, New Zealand, 199-204.

Whiteley, R.J. & Caffi, P. 2014. Evaluating the effectiveness of rolling impact compaction at a brownfield site with high and low frequency seismic surface waves and geotechnical testing, *Near Surface Geophysics*, 2014(12): 405-414.

Theme 7. Pressuremeter and Dilatometer

Geotechnical and Geophysical Site Characterisation 5 – Lehane, Acosta-Martínez & Kelly (Eds)
© 2016 Australian Geomechanics Society, Sydney, Australia, ISBN 978-0-9946261-1-0

Pressuremeter tests in the hard soils and soft rocks of Arak Aluminum Plant site, Iran

E. Asghari-Kaljahi
Department of Earth Sciences, University of Tabriz, Tabriz, Iran

Z. Khalili
P.O. Rahvar Consulting Engineers Company, Tehran, Iran

S. Yasrobi
Faculty of Civil Engineering, University of Tarbiat Modarres, Tehran, Iran

ABSTRACT: The Arak Aluminum Plant site is located in the east of Meyghan Lake in the central zone of Iran. Generally, the underground layers consist of cohesive fine-grained soils at the top and weak rock layers at the bottom. From top to bottom, after silty clay layers, there are hard soils or weak rock layers with classification of Claystone and Marlstone. The depth of rock layers varies between 6 and 12 m. The dry unit weights of these layers are between 14 and 18 kN/m^3. The uniaxial compression strength of them varies between 0.1 and 1.2 MPa. For evaluating of deformation modulus and stress-strain behavior of these very weak rocks more than 70 Pressuremeter Menard test (PMT) were conducted in boreholes up to depth 30m. According to test results, PMT Modulus of hard soil and weak rock layers of this plant site vary in the range of 17 to 85 MPa. The limit pressure (P_L) of PMT tests varies between 1 and 7.7MPa.

1 INTRODUCTION

Pressuremeter Menard test (PMT) is a common in-situ test used for site investigation. It has the advantages of simplicity and if it done properly, geotechnical parameters obtained from this test can be precised. It is almost full scale loading of soils during testing and it is applicable for most soil types and soft rocks (Chiang and Ho, 1980).

Different studies about pressuremeter tests are presented in the last years. Typical Young modulus values that determined by pressuremeter for Mercia Mudstone are between 100 and 1200MPa (Cripps and Taylor, 1981). PMT were used by many researchers for hard soils and soft rocks as Marsland, and Powell (1990), Clarke and Allen (1989) Isik, et al. (2008).

Leach et al. (1976) reported in-situ pressuremeter Menard tests on Mercia Mudstone from Kilroot that gave undrained shear strength values up to 230% higher than values obtained from triaxial tests on samples from the same depth and the overall mean value was slightly more than double. Similar results were obtained for comparative elastic modulus obtained from pressuremeter, plate loading, and oedometer tests (Meigh, 1976). These showed that pressuremeter results were highly variable but generally much higher than triaxial and oedometer results. Also correlations based on many PMT tests performed at different sites in clay along with other measured soil parameters were presented by Briaud (2013). These correlations exhibit significant scatter and should be used with caution.

Nevertheless they are very useful in preliminary calculations and for estimate purposes. Table 1 gives the range of expected PMT limit pressure (P_L) and elastic modulus (E_0) in various soils.

Table 1. Expected values of E_0 and P_L in soils (Briaud, 2013)

Clay					
Soil Strength	Soft	Medium	Stiff	Very Stiff	Hard
P_L (kPa)	0-200	200-400	400-800	800-1600	>1600
E_0 (MPa)	0-2.5	2.5-5.0	5.0-12.0	12.0-25.0	>25.0

Sand				
Soil Strength	Loose	Compact	Dense	Very Dense
P_L (kPa)	0-500	500-1500	1500-2500	>2500
E_0 (MPa)	0-3.5	3.5-12	12-22.5	>22.5

The aim of this study is analysis the results of PMT tests carried out on hard soils and soft rocks in the Arak Aluminum Plant site, located in the north of Arak, Iran (Figure 1) with 49.9258E degree and 34.1656N degree.

2 PRESSUREMETER TEST THEORY

The pressuremeter is a cylindrical device that may be expanded against the walls of a borehole. There are broadly three types of pressuremeter, the self-boring type (e.g. 'Camkometer'), the push-in type (e.g. the Building Research Establishment's 'PIP'), and the original type which required a pre-formed borehole (e.g. 'Menard pressuremeter') (Mair and Wood, 1987).

These are all able to measure undrained strength and deformability simultaneously, and to determine horizontal stress (Clough et al., 1990). The method has been hampered by difficulties in interpretation due to complex boundary conditions, disturbance when cutting the hole, and the bias toward measurement of properties in a horizontal direction.

Figure 1. The vicinity of Arak Aluminum Plant

Pressuremeter test measures the strength and the deformability of soil and weak rock. The test also estimates the deformation modulus and shear modulus. The analysis is based on undrained parameters for cohesive soil and drained parameters for granular soil. The Menard probe which has been used in this research contains three flexible rubber membranes. The middle membrane provides measurements, while the outer two cells, the "guard cells," protect the measuring cell. The pressure in all cells is incrementally increased or decreased by the same amount. The measured volume change in the middle membrane is plotted against applied pressure. A typical curve is shown in Figure 2. There are three phases of the deformation curve: (1) the re-establishing phase, from the origin to point A; (2) the pseudo-elastic phase, from point A to point B; and (3) the plastic phase, from point B to point C. After the borehole is drilled and the augers are withdrawn, the borehole walls relax, thus reducing the cavity volume. As the PMT probe is initially inflated, the walls of the borehole are pushed back to their original position.

Point A marks the point at which the volume of the borehole cavity has fully returned to its initial position, and is given the coordinates, V_0, P_0. Point B is the point at which creep pressure has been reached, and is given the coordinates, V_f, P_f. The plastic phase begins at point B and extends to point C, which is asymptotic to the limit pressure. Point C, which is given the coordinates V_L, P_L, is defined as the point where the pressure remains constant despite increasing volume.

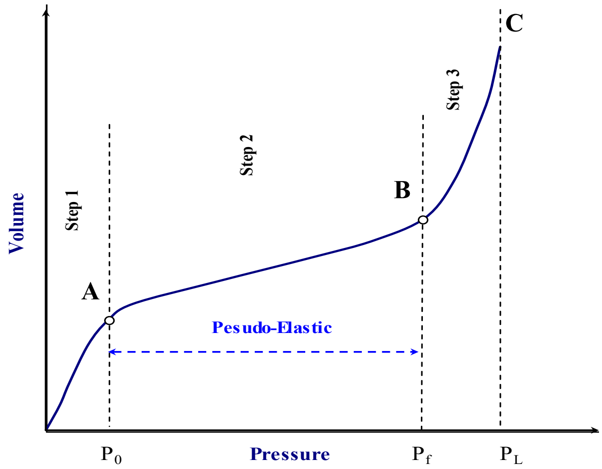

Figure 2. Typical Pressuremeter curve (Baguelin et al., 1978)

The Menard modulus or pressuremeter modulus (E_P) is an initial elastic modulus taken from the slope AB which is identified from the curve as the limits of the elastic response. The slope AB is a function of the shear modulus of the annulus and gives the modulus using the following equation;

$$E_P = 2.66[V_0+0.5(V_B-V_A)].\ (P_A-P_B)/\ (V_A-V_B) \qquad (1)$$

Where V_0 is the volume of the probe, V_A is the volume at pressure P_A and V_B is the volume at pressure P_B. The factor 2.66 is assumed based on Poisson's ratio equal 0.33.Menard shear modulus another parameter is obtained by pressuremeter coefficient (E_m) according to the equation 2.

$$G = E_m/2(1+\nu) \qquad (2)$$

3 GEOLOGY OF THE STUDY AREA

Studied project area is located in Kheir Abad industrial town, about 20km far from Arak city and about 280km far from Tehran.

According to the geological zoning of Iran (Nabavi, 1977), project area is located in the Central Iran zone.

The project site is located in the east of Meyghan Lake with a ground surface dipping towards the lake. The project area is mostly smooth and flat. The highest point of the site is located in the east with1685m, whereas the lowest point is located in the west site with 1682m above mean sea level. Based on topography map, the slope direction of the area is east to west.

According to geology map of the study region (Figure 3), all geological units belong to Quaternary. Moreover, all deposits are the subsequent of flood plain of Meyghan Lake. Underground layers consist of cohesive fine-grained soils at the top and very weak rock layers at bottom.

Groundwater depth in the site varies between 9 and 11 m.

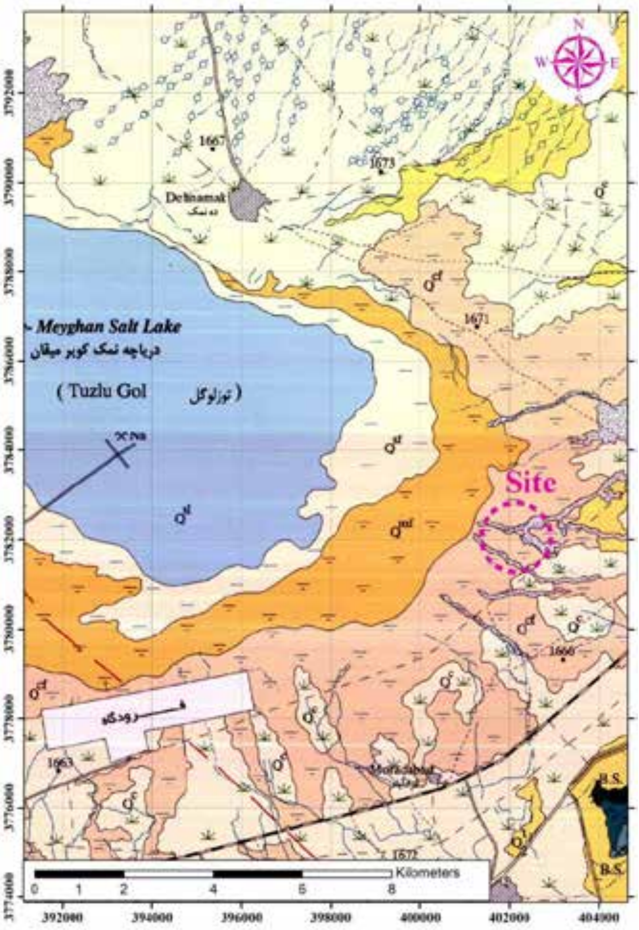

Q^{mf}: Mud flats and is formed of silt and clay soils;
Q^{cf}: Clay flats, fine clay and silt

Figure 3. Geology map of the project region (After Arak geology map; GSI, 1998)

4 GEOTECHNICAL CHARACTRIZATION OF STUDY AREA

For subsurface exploration and geotechnical investigation of the project site, 67 boreholes with depths of 15, 30, and 45 m and 6 test pits were excavated. The whole site is covered by fine-grained soils mainly formed in a flood plain.

Underground layers in the project site consist of cohesive fine-grained soils at the top and very weak rock layers at bottom. After top soil, silty clay, silty sandy clay, marl, and clayey silt are generally observed at shallow layers. This sequence of layers is followed by very weak rock layers with classification of claystone and marlstone and siltstone at lower part (Figure 4). The depth of rock layers in drilled boreholes, which are very weak, varies between 6 and 12m. A general geology profile of site is shown in Figure 5.

Based on the lab test results on undisturbed samples, dry density of soils and weak rock layers in between 15 and 19 kN/m^3. Generally the dry density of layers increase with depth (Figure 6). Plasticity index (PI) of soils and weak rocks is mostly more than 10% (Figure 7) so soils is classified as cohesive.

Figure 4. A photo of subsurface layers of site

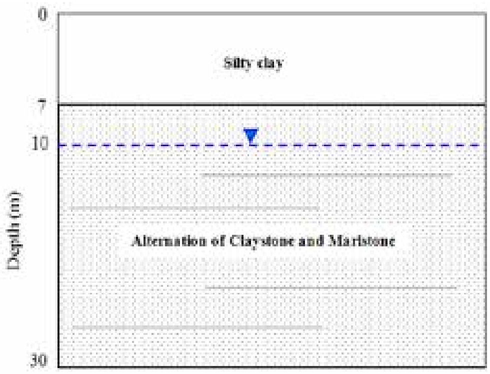

Figure 5. General geology profile of site

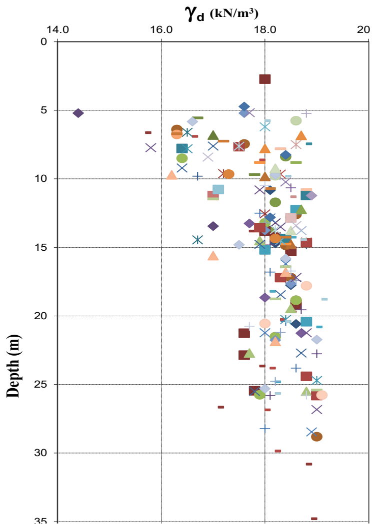

Figure 6. Variation of dry density of samples

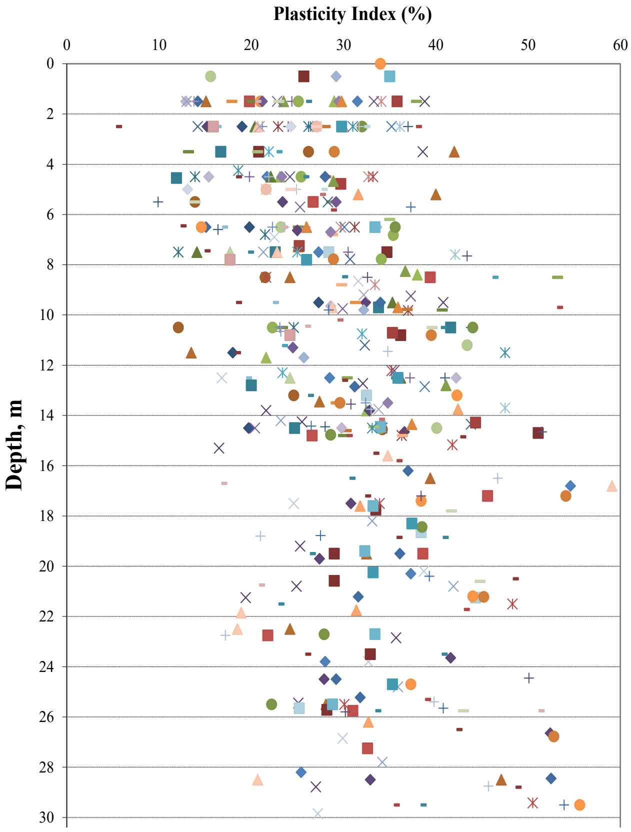

Figure 7. Variation of Plasticity Index of soils and weak rocks

Based on the SPT results, the fine-grained soils are firm to very hard (Figure 8).

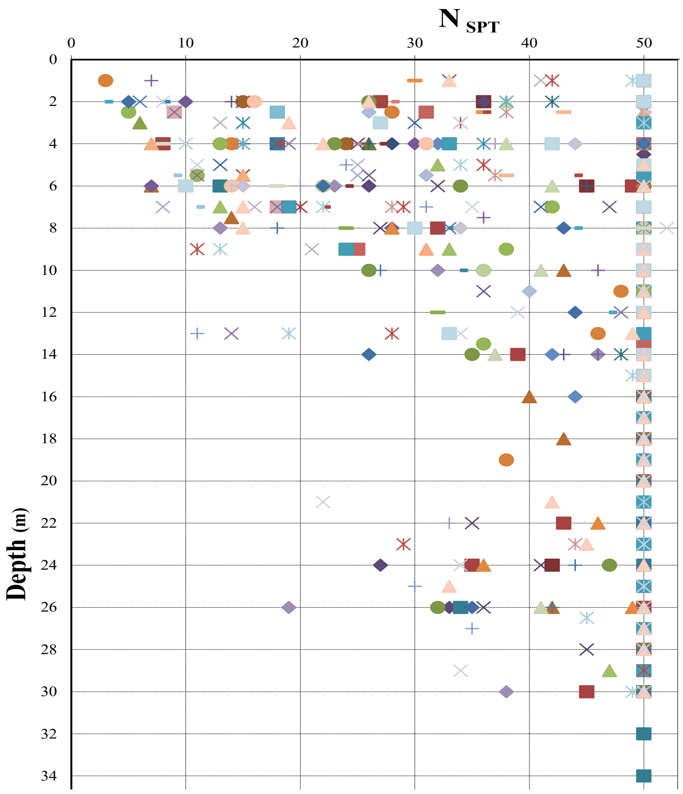

Figure 8. Variation of SPT with depth in boreholes

Uniaxial compression tests on hard soils and soft rocks samples are shown on Figure 9. The uniaxial compression strength varies between 200 and 700kPa

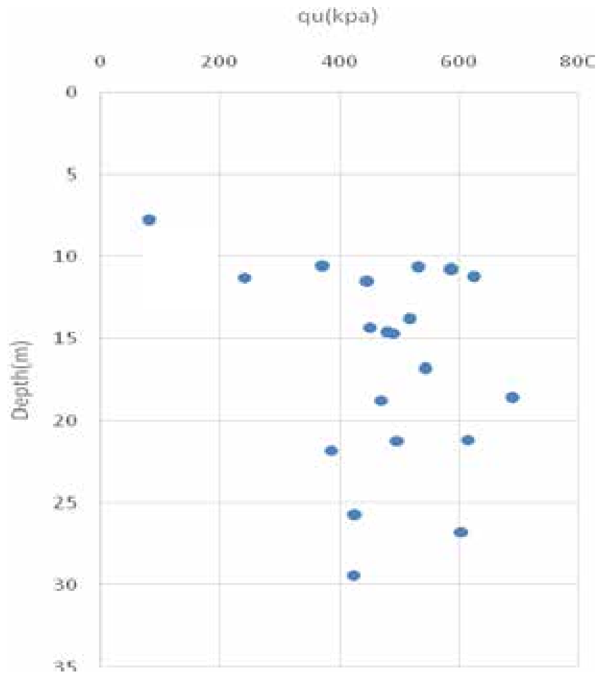

Figure 9. Uniaxial compression strength of weak rock samples vs depth

5 PRESSUREMETER TESTS RESULTS

The PMT data in this study were obtained from 75 tests that were conducted in 20 boreholes at Arak Aluminum Plant site. The depths of the drilling borehole ranged between 15 and 30m.

Based on their placement in the boreholes, three types of Pressuremeter exist:

- Pre-boring Pressuremeter (P.B.P);
- Self-boring Pressuremeter (S.B.P); and
- Push-in Pressuremeter (P.I.P)

The pre-boring Pressuremeter (P.B.P), size AX, Type GC, was used in this project (Figure 10). PMT tests are done every 5 meters on average in each borehole. Values obtained from 75 PMT tests. The variation of Pressuremeter Menard modulus (E_P) vs. depth is shown in Figure 11. E_P varies between 17 and 85MPa for very weak rock layers of this site. The limit pressure (P_L) of PMT tests varies between 1 and 7.7MPa (Figure 12).

The shear modulus (G) of these layers is determined 1 to 50MPa according to Equation 2 and also the modulus of subgrade reaction (Ks) for piles is calculated 13 to 950MN/m^3 based on the following equations:

Figure 10. A photo of PMT test in this study

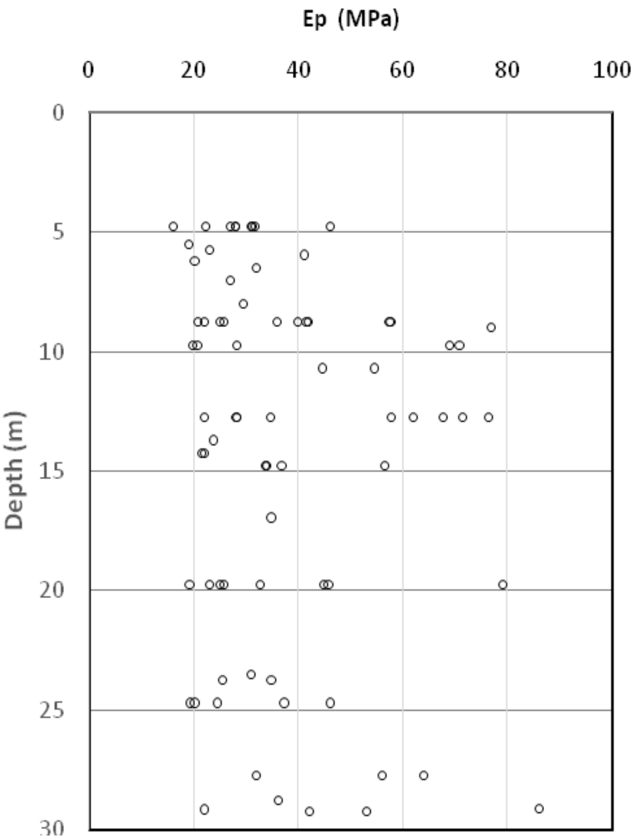

Figure 11. Pressuremeter modulus vs depth

$$K_s = \left[\frac{4R}{9E_m} (2.65)^{\alpha} + \frac{\alpha}{3E_m} R \right]^{-1} \qquad R \leq 0.3m \qquad (3)$$

$$K_s = \left[\frac{4R}{9E_m} \left(2.65 \frac{R}{R_0} \right)^{\alpha} + \frac{\alpha}{3E_m} R \right]^{-1} \qquad R>0.3m \qquad (4)$$

Where, α is selected between 0.25 and 0.5 based on practical correlations and type of soils. Also, according to Pressuremeter test manual (Bureau of technical affairs and standards of Iran, 2002), R=R0 (pile radius) was assumed as 0.3m.

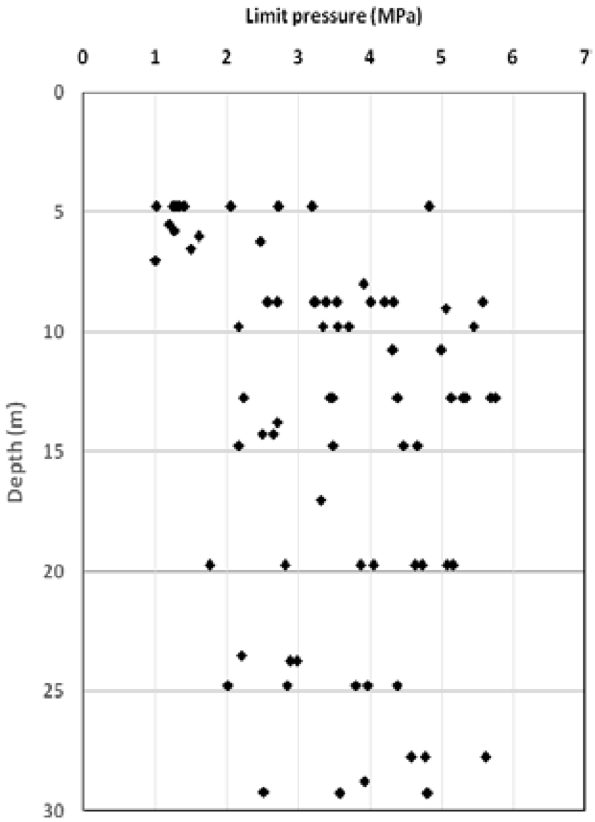

Figure 12. Limit pressuremeter of PMT tests vs depth

6 ACKNOWLEDGMENT

Wish to thank IRALCO and POR Company for assistance and preparing data.

7 REFERENCES

ASTM, 2000, Standard Test Method For Prebored Pressuremeter Testing in Soils, D 4719-00, American society for testing and materials, Philadelphia , U.S.A.

Baguelin, F, Jezequel, J. F., and shields, D.H. 1978, The Pressuremeter and Foundation Engineering, Trans. Tech. Publication.

Briaud, J. L. 2013, The pressuremeter test: Expanding its use, Ménard Lecture, Proceedings of the 18th International Conference on Soil Mechanics and Geotechnical Engineering, Paris, pp 107-126.

Bureau of technical affairs and standards of Iran, 2002, Pressuremeter test: Instruction for test and application for foundation design, No. 223, Management and planning organization of Iran.

Chiang Y.C., Ho Y.M. 1980, Pressuremeter method for foundation design in Hong. In: Proceedings of sixth Southeast Asian conference on soil engineering 1: pp 31–42.

Clarke, B. G., and Allen, P G.1989, A self-boring pressuremeter for testing weak rock, XII International Conference on Soil Mechanics and Foundation Engineering, Brazil. Vol. 1, pp 211–214.

Clough, G. W., Briaud, J.L. and Hughes, J.M.O. 1990, The development of pressuremeter testing, Third international symposium on pressuremeter, Oxford, pp 25-45.
GSI, 1998, Geology map of Arak, Scale 1:100.000, Geology survey of Iran.
Isik N.S., Doyuran V. and Ulusay R. 2008, Assessment of deformation modulus of weak rock masses from pressuremeter tests and seismic surveys. Bull Eng Geol Environ 67: pp 293–303.
Leach, B. A., Medland, J. W., and Sutherland, H. B., 1976. The ultimate bearing capacity of bored piles in weathered Keuper Marl. Proceedings of the 6th European Conference on Soil Mechanics and Foundation Engineering, Vienna, 1976, Vol. 1.2, pp 507–514.
Mair, R. J. and Wood, D. M. 1987, Pressuremeter testing method and interpretation, Construction Industry Research and Information Association Project 335. Publ. Butterworths, London. ISBN 0-408-02434-8.
Marsland, A. and Powell, J.J.M., 1990, Pressuremeter tests on stiff clays and soft rocks: factors affecting measurements and their interpretation, Field Testing m Engineering Geology, Geological Society Engineering Geology Special Publication No 6, pp 91-110.
Nabavi, 1977, Geology zoning of Iran. Geology survey of Iran.

Geotechnical and Geophysical Site Characterisation 5 – Lehane, Acosta-Martínez & Kelly (Eds)

Stress-strain response of fine silica sand using a miniature pressuremeter

A.A. Bagbag, J.P. Doherty and B.M. Lehane
School of Civil, Environmental and Mining Engineering, The University of Western Australia

ABSTRACT: The pressuremeter is a well-known geotechnical test, used to measure soil strength and stiffness. In this paper, a miniature pressuremeter device, developed at the University of Western Australia (UWA), was employed to measure the stress-strain behaviour of dense fine silica sand at a range of stress levels. The UWA miniature pressuremeter has a diameter to length ratio of unity, and its inflation after burial in a normally consolidated sand represents a well-defined boundary value problem. Back-analysis was performed using the Finite Element method and the well-known Hardening Soil-Small (HSS) model. The HSS model was found to provide a reasonable match to the measured stress-strain response using parameters derived from triaxial compression tests.

1 INTRODUCTION

Fine 'UWA sand' is a manufactured, uniformly graded silica sand used in geotechnical centrifuge testing at UWA e.g. O'Loughlin and Lehane (2003) Xu and Lehane (2008), Lee, Cassidy, and Randolph (2013). Despite its widespread use, there have been few studies that examine its mechanical properties, with O'Loughlin and Lehane (2003) one of the few studies involving triaxial testing of the sand. More recently, Bagbag et al. (2016) presented results from three anisotropically consolidated drained triaxial compression tests on UWA sand reconstituted to a relative density D_r of 70%.

This paper presents a series of laboratory scale pressuremeter tests on dense UWA sand at a range of confining stresses. The tests were conducted using the UWA miniature pressuremeter described by Johnston et al. (2013). This device is significantly different to any previously built miniature pressuremeter as it uses air as the pressurising fluid and the membrane displacement is measured using strain gauged 'feeler-arm' transducers, rather than inferring displacements from measured volume changes in the pressuring fluid. This direct method of measuring displacement is more accurate than using changes in the fluid volume (Johnston et al., 2013).

The UWA miniature pressuremeter has a diameter to length ratio of unity, and its inflation after burial in a normally consolidated sand represents a well-defined boundary value problem. Therefore, tests were interpreted using available elastic and plasticity solutions based on spherical and cylindrical cavity expansion theory, respectively. The interpreted friction angles, dilation angles and unload reload stiffnesses are presented and compared with data from other tests involving the same sand (Lehane et al. (2005), Xu and Lehane (2008), Lee et al. (2013) and Bagbag et al. (2016)).

The well-defined nature of the boundary value problem provides an opportunity to interpret the pressuremeter tests using the Finite Element (FE) method and sophisticated soil constitutive models. In this paper, the test results are compared with pressuremeter responses calculated using the FE method and the Hardening Soil Small (HSS) model; Plaxis 2D (version 2015.2) was used for the computations (Brinkgreve et al., 2014). The parameters employed for the HSS model were derived in a separate study reported by Bagbag et al. (2016). The aim of this paper is to assess the validity for application to pressuremeter loading of the HSS parameters derived from the triaxial testing.

2 LABORATORY SET-UP

2.1 *Classification data*

'UWA sand' has a minimum and maximum void ratio of 0.45 and 0.75 respectively (Bagbag et al., 2016). The material specific gravity is 2.67 and is classified as a uniform sub-rounded to sub-angular fine sand. The particle size distribution is shown in Figure 1.

2.2 *Preparing and setting-up pressuremeter tests*

A 20 mm diameter laboratory scale pressuremeter developed at UWA by Johnston et al. (2013) was used (see Figure 2a). Unlike previously developed laboratory pressuremeters, the UWA device uses air as the pressurising fluid and the membrane displacement (0.3 mm thick latex) is measured using strain-gauged “feeler-arm” transducers. The pressuremeter was built into an aluminium rod and was located 180 mm above the base of this rod. The rod was positioned at the centre of a 393 mm internal diameter, 400 mm high steel chamber (see Figure 2b, 2c). The top of aluminium rod was clamped to the top of the chamber to prevent it moving during sample preparation and testing (see Figure 2b). Sand was rained into the chamber once the pressuremeter was fixed in place (see Figure 3). The soil density was controlled using an automatic hopper with specific slot widths and heights. Dense sand was achieved by using a slot width of 1.5 mm and the height measured from the sand surface to the opening slot was held constant at 1 m. This produced sand with 70% relative density (void ratio, e = 0.54). The soil filled the chamber with an allowance for a 40 mm thick top plate through which vertical stress was applied to the sand.

A vertical load was applied to the top plate using a hydraulic jack, as shown in Figure 4. This load was applied for a minimum period of 48 hours prior to pressuremeter testing, to allow creep rates to reduce to negligible values (see Lim and Lehane 2014). In this paper, tests are presented for vertical applied pressures of 50 kPa, 60 kPa and 100 kPa.

The pressuremeter device uses a digitally controlled air compressor to expand the membrane. The feeding rate of the pressure was held constant at 50 kPa/min.

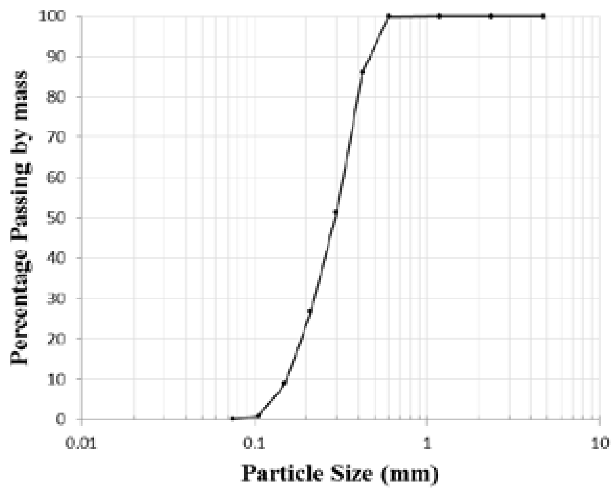

Figure 1. Particle size distribution of UWA fine silica sand

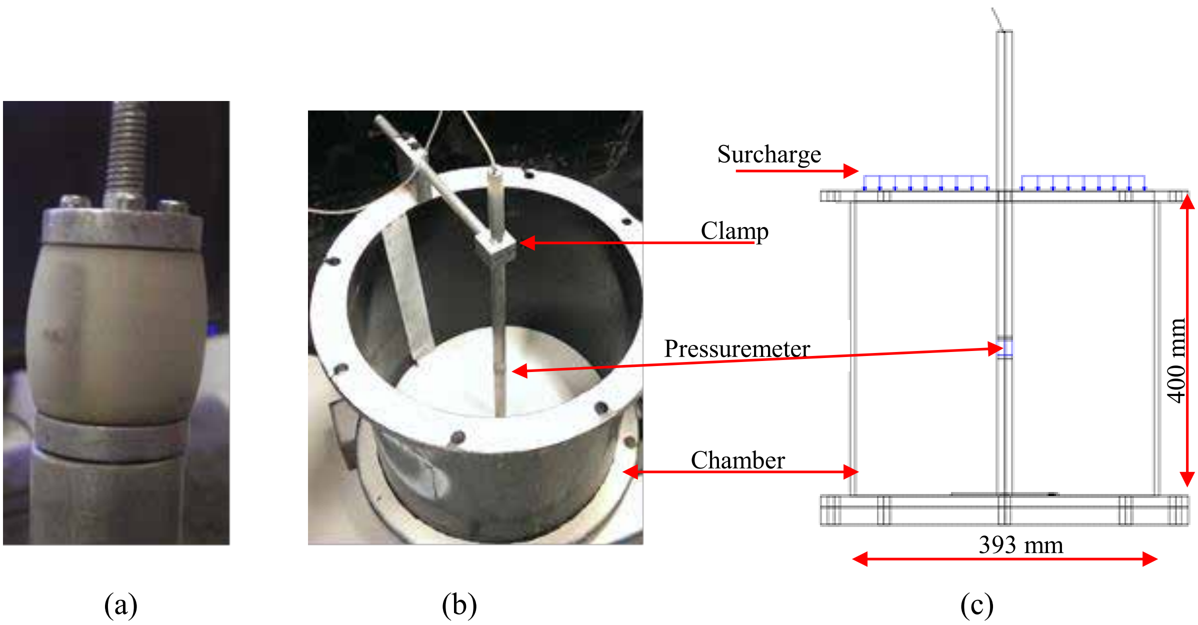

Figure 2. (a) Pressuremeter membrane, (b) pressuremeter in position prior to pouring sand (c) schematic diagram of the experimental set-up.

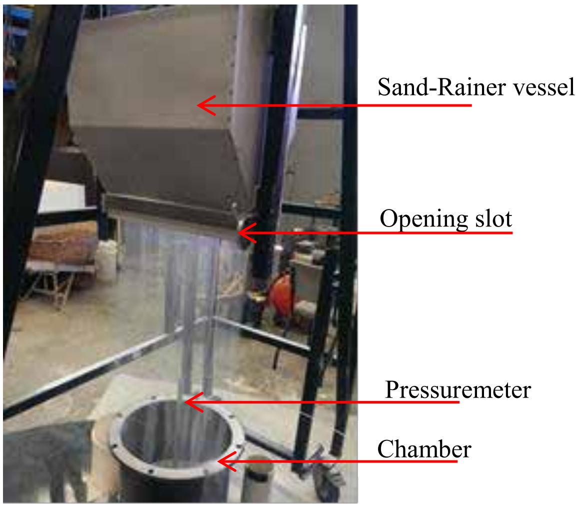

Figure 3. The automatic hopper to rain the sand into pressuremeter chamber test

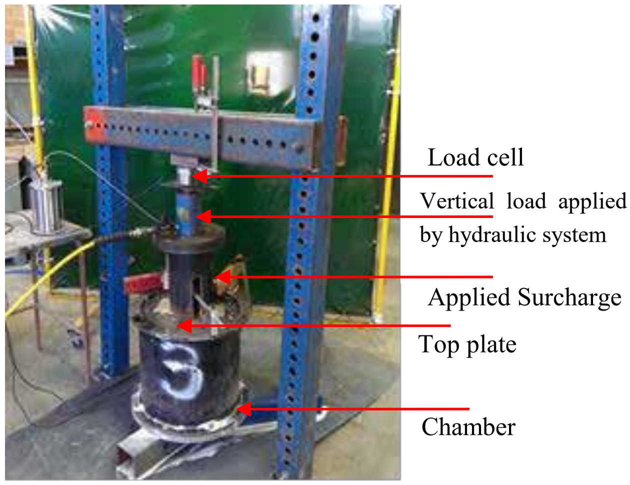

Figure 4. A typical pressuremeter test setup using a hydraulic system to apply the surcharge load

3 RESULTS AND DISCUSSION

3.1 *Experimental results*

The measured cavity pressure versus corresponding cavity strain for applied vertical stresses of 50 kPa, 60 kPa and 100 kPa are presented in Figure 5a.

Friction (ϕ') and dilation (ψ) angles were estimated using the method of Hughes et al. (1977) as presented in Table 1. This method is based on the slope (*s*) of a plot of the logarithm of the cavity pressure versus the logarithm of cavity strain (see Figure 5b). An initial estimate of the constant volume friction angle (ϕ'_{cv}) is required. Hughes et al. (1977) proposed equation (1) for friction angle and equation (2) for peak dilation angle. These equations are for cylindrical cavity expansion, which is representative of standard in-situ pressuremeters. The friction and dilation angles inferred using these equations for the three stress levels are presented in Table 1, assuming a $\phi'_{cv} = 34^{o}$ as recommended for the 'UWA sand' by O'Loughlin and Lehane (2010).

$$\sin \phi' = s/[1+(s-1) \sin \phi'_{cv}] \tag{1}$$

$$\sin \psi = s+(s-1) \sin \phi'_{cv} \tag{2}$$

Table 1. Friction and dilation angles inferred using the Hughes et al. (1977) method for cylindrical expansion.

σ'_v (kPa)	*s*	ϕ' (degs)	ψ (degs)
50	0.56	47.9	18.2
60	0.51	44.3	13.3
100	0.58	49.1	19.9

Mair and Wood (1987) mentioned that the Hughes et al. (1977) method should be considered approximate, as the friction and dilation angles derived are highly dependent on the estimated value of *s*. The method also makes the assumption of cylindrical cavity expansion, which is clearly not well suited to the UWA pressuremeter device (given the length/diameter ratio of unity). By comparison with the angles listed in Table 1, the triaxial tests reported by Bagbag et al. (2016) gave an average peak friction angle (ϕ') value of 38.5º and peak dilation angle (ψ) of 10º at the same initial stress level and same relative density of 0.7. Xu and Lehane (2008) deduced peak friction and dilation angles of 42º and 12º for a somewhat denser UWA sand sample at a in-situ stress level of 120 kPa.

Fahey (1991) proposed a method to measure the elastic shear modulus by preforming small unload-reload loops during plastic monotonic loading in pressuremeter tests. These loops exhibit a quasi-linear behaviour and it is suggested that the loop gradient may be used to determine the unload-reload shear modulus from the elastic cavity expansion solutions proposed by Yu (2000). For an assumed elastic response of the soil, the unload-reload shear moduli (G_{ur}) can be determined as:

$$G_{ur} = \Delta p_c/(2k\Delta \varepsilon_c) \tag{4}$$

where Δp_c is the difference between the cavity pressures at the start and end of the unload-reload loop and $\Delta \varepsilon_c$ is the corresponding change in cavity strain; the constant *k* is 2 for spherical expansion and unity for for cylindrical cavity expansion. As shown in Figure 5a, one test, with an applied vertical stress of 60 kPa, is included an unload-reload loop. Assuming $k = 2$ (i.e. spherical cavity expansion), the unload-reload shear modulus (G_{ur}) was found to be 25 MPa and 25.8 MPa from the first and second loops, respectively.

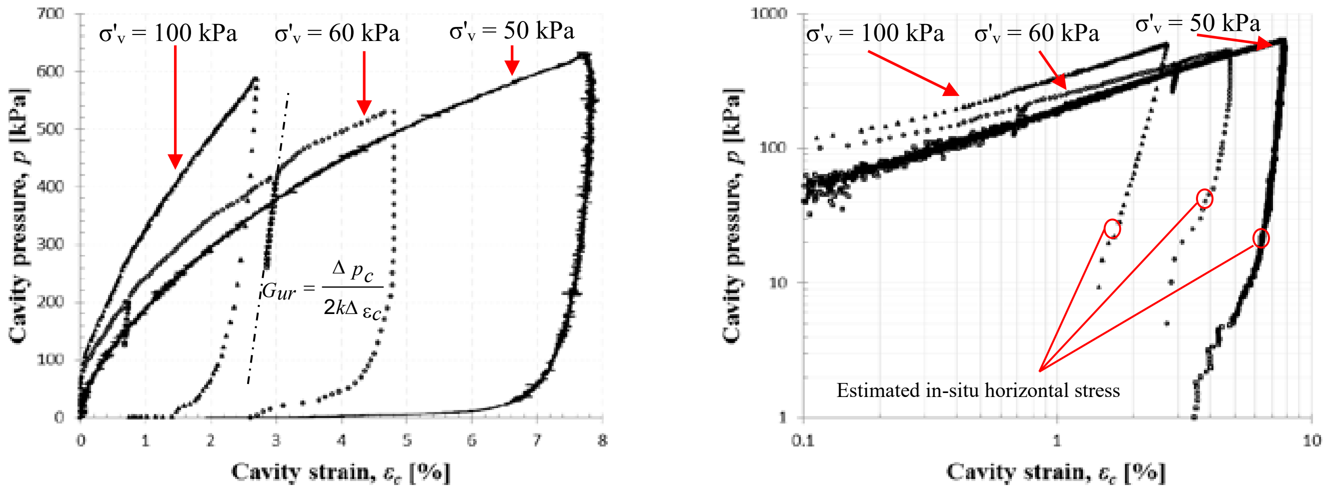

(a) (b)

Figure 5. Measured variation of cavity pressure with cavity strain (a) linear scale and (b) logarithmic axes

It is evident from Figure 5 that the lift-off pressure is not easy to distinguish at the start of the tests. However, it is apparent from the final unloading stages that there is a cavity pressure at which the cavity strain reduces rapidly while the cavity pressure remains constant i.e. the unload curve is approximately horizontal. This pressure is likely to be related strongly to the in-situ horizontal stress. The cavity stresses at which this transition occurs can be seen in Figure 5b to be at 20 kPa, 50 kPa and 25 kPa for tests with applied vertical stress of 50 kPa, 60 kPa and 100 kPa respectively, i.e. in average the cavity stresses are approximately half of the applied vertical stress, which is consistent with the expectation that K_0 is approximately 0.5 for the normally consolidated stress history of the sand (see Figure 5).

3.2 *Back analysis*

The Plaxis 2D (version 2015.2) Finite Element program, developed by Brinkgreve et al. (2014), was employed along with the small strain hardening soil model (HSS), introduced by Benz (2007), to simulate the pressuremeter tests. The HSS model soil parameters used are presented in Table 2. These were derived by Bagbag et al. (2016) from consolidated drained trixial tests on 'UWA sand' reconstituted to the same relative density of 0.7 used for the pressuremeter experiments. One of the difficulties encountered by Bagbag et al. was that the secant stiffness at 50% of the peak deviator stress (E_{50}) was found to vary with the stress level raised to the power (m) of 1.0, whereas the very small strain shear stiffness (G_0) was better represented using 'm' an exponent of 0.5. As the HSS model only allows input of a single exponent, the m value was taken equal to 0.5 for the purposes of this paper and the reference stiffness values inputted were those estimated at the average of the three initial lateral stresses in the tests (25 kPa, 30 kPa and 50 kPa). Bagbag et al. (2016) also point out that the shear strain at 70% of the maximum shear modulus ($\gamma_{0.7}$) is stress dependent. As the model does not allow for this stress dependency, the value of $\gamma_{0.7}$ assumed was also taken to be that corresponding to the average of the three initial lateral stresses in the tests.

An axisymmetric model using 687 triangular 15-noded elements was used. The mesh was refined around the membrane as shown in Figure 6. The chamber was modelled assuming a smooth inner surface. The boundary to the right (see Figure 6) was allowed to move vertically, but was fixed radially. The boundary at the base was free radially and fixed vertically. The model includes three major steps: (i) the surcharge pressure was applied in the initial step to establish the initial stresses in the soil with K_0 specified as 0.5, (ii) the pressure was applied to the vertical faces of the pressuremeter to simulate its expansion and (iii) unload-reload loops were applied, as in the physical experiments.

The Plaxis 2D HSS model simulation is presented in Figure 7. The model evidently provides a very good simulation of the measured pressuremeter response at small and medium cavity strains. It may therefore be inferred that the parameters determined from triaxial tests provide a reliable simulation of the pressuremeter tests, especially over the first 2%, which is usually most critical in geotechnical design.

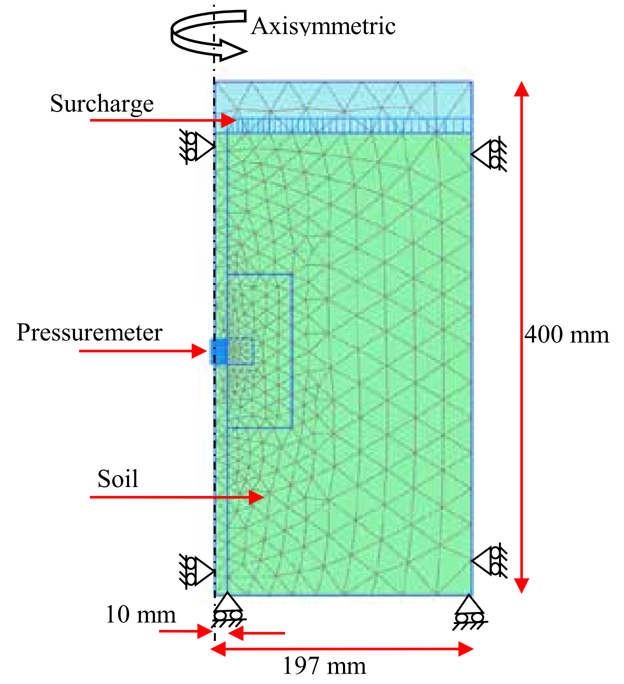

Figure 6. FE model of the experimental pressuremeter test.

Table 2. Hardening Soil Small Parameters

Parameter	Description	HSS
m	Power for stress-level dependency of stiffness	0.5
E_{50}^{ref}	Reference secant stiffness modulus at 50% of the failure load corresponding to the reference stress, p^{ref}	35 MPa
E_{oed}^{ref}	Reference tangent stiffness for oedometer loading modulus corresponding to p^{ref}	35 MPa
E_{ur}^{ref}	Reference unload-reload stiffness modulus corresponding to p^{ref}	105 MPa
c'	Cohesion	0
ϕ	Friction angle	38.5°
ψ	Dilation angle	10°
K_0^{nc}	K_0-value for normal consolidation	0.5
p^{ref}	Reference pressure at which quoted stiffness values apply (taken as atmospheric pressure)	100 kPa
R_f	Failure ratio of deviatoric stress at failure over deviatoric stress at Asymptote	0.9
ν_{ur}	Poissons ratio for unloading-reloading	0.2
$\gamma_{0.7}$	Shear-strain at 70% of small-shear modulus, G_0	2×10^{-5}
G_0^{ref}	Reference small-strain shear modulus	185 MPa

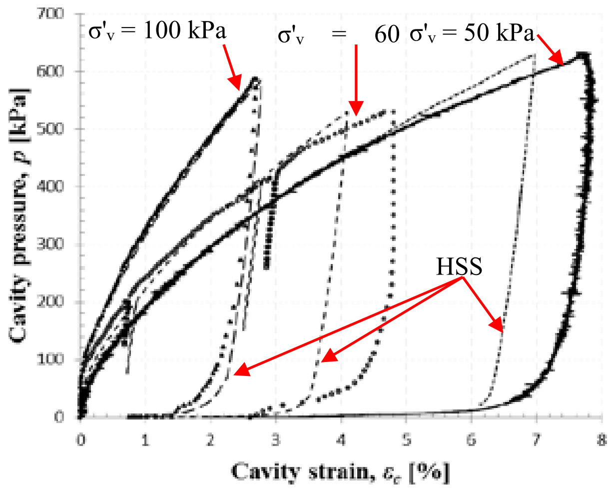

Figure 7. Hardening Soil-Small model for pressuremeter tests.

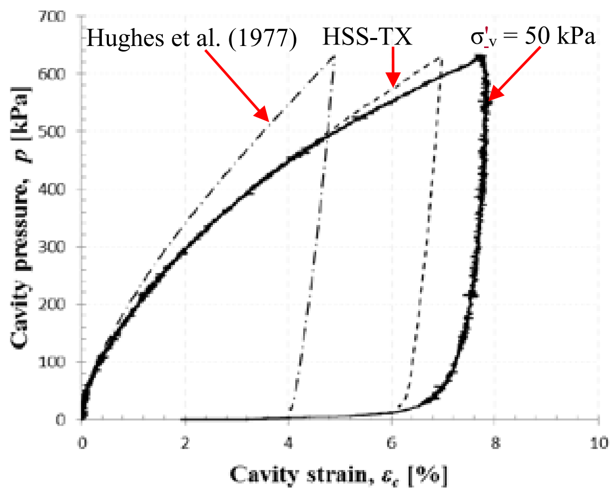

Figure 8. Comparison of measured pressuremeter response at $\sigma'_v = 50$ kPa with HSS predictions using triaxial (TX) friction angles and friction angles calculated using Hughes et al. (1977)

Figure 8 explores the sensitivity to friction and dilation angles of the HSS model predictions. All parameters in two sets of analyses (HSS-TX and Hughes et al. (1977) method) were the same except for the friction and dilation angles. The friction and dilation angles for HSS-TX model are presented in Table 2, whereas the angles for Hughes et al. (1977) method are those presented in Table 1 at σ'_v= 50 kPa. It is evident that the triaxial angles provide a better fit to the measurements, which is likely to be, at least in part, due to differences between the near spherical expansion mode in the experiments and the plane strain cylindrical expansion mode assumed in the Hughes et al. (1977) formulation.

4 CONCLUSION

This paper presents results from three laboratory-scale pressuremeter tests performed in reconstituted dense sand. It is shown that, despite its limitations, the Hardening Soil Small model provides a good match to the measured response, when parameters derived from triaxial compression tests are used in the simulations. Further studies are required to understand the differences between the operational friction angles observed in the experiments (where the mode of deformations was approximately spherical) and those back analysed using existing solutions for pressuremeter tests.

5 ACKNOWLEDGEMENTS

The first author would like to acknowledge the sponsorship provided by the King Abdullah Scholarship Program by the Ministry of Higher Education in Saudi Arabia.

6 REFERENCES

Bagbag, A. A., Lehane, B. M., & Doherty, J. P. (2016). Derivation of hardening soil model properties from triaxial tests. *Proc. 26th International Conf. Ocean and Polar Engineering*, Rhodes (Rodos), Greece, ISOPE, *2*, 848-853.

Benz, T. (2007). *Small-strain stiffness of soils and its numerical consequences*: Universität Stuttgart, Institut für Geotechnik.

Brinkgreve, R. B. J., Vermeer, P. A., & Bakker, K. J. (2014). *Material model manual*. Delft: University of Technology & Plaxis BV.

Fahey, M. (1991). Measuring shear modulus in sand with the self-boring pressuremeter. *Proc. 10th European Conference on Soil Mechanics and Foundation Engineering,* Florence, Italy, *1*, 73-76.

Hughes, J. M. O., Wroth, C. P., & Windle, D. (1977). Pressuremeter tests in sands. *Géotechnique, 27*(4), 455-477.

Johnston, G., Doherty, J., & Lehane, B. (2013). Development of a laboratory-scale pressuremeter. *Institution of Civil Engineers, 13*(1), 31-37.

Lee, K. K., Cassidy, M. J., & Randolph, M. F. (2013). Bearing capacity on sand overlying clay soils: experimental and finite-element investigation of potential punch-through failure. *Géotechnique, 63*(15), 1271-1284.

Lehane, B. M., Gaudin, C., & Schneider, J. A. (2005). Scale effects on tension capacity for rough piles buried in dense sand. *Géotechnique, 55*(10), 709-719.

Mair, R. J., & Wood, D. M. (1987). *Pressuremeter testing methods and interpretation*. London: CIRIA / Butterworths.

O'Loughlin, C. D., & Lehane, B. M. (2003). Measurement and prediction of deformation patterns beneath strip footings in sand*. Proc. International Conf. Foundations*, Dundee. British Geotechnical Association, UK, 705-714.

O'Loughlin, C. D., & Lehane, B. M. (2010). Nonlinear cone penetration test-based method for predicting footing settlements on sand. *Journal of geotechnical and geoenvironmental engineering, 136*(3), 409-416.

Xu, X., & Lehane, B. M. (2008). Pile and penetrometer end bearing resistance in two-layered soil profiles. *Géotechnique, 58*(3), 187-197.

Yu, H. S. (2000). *Cavity expansion methods in geomechanics*: Springer Science & Business Media.

Geotechnical and Geophysical Site Characterisation 5 – Lehane, Acosta-Martínez & Kelly (Eds)

Use of flat dilatometer in Ontario

L.F. Cao, S.M. Peaker & S. Ahmad
WSP Canada Inc., Toronto, Canada

ABSTRACT: This paper presents the results of the flat dilatometer test (DMT) conducted in silty clay and silty clay till at two sites in Ontario. Soil parameters included undrained shear strength and overconsolidation ratio were estimated based on published formulas using lift-off pressure p_0 or pressure for 1.1mm membrane deflection, p_1. The soil parameters estimated from the DMT are also compared with laboratory test results. It is found that some empirical correlations for the DMT overestimate the undrained shear strength and overconsolidation ratio for Ontario silty clay and silty clay till, whereas semi-theoretical formulas developed from the cavity expansion theory in modified Cam Clay (MCC) provide good estimations for these soil parameters. It is also found that some empirical correlations for DMT underestimate the unit weight and modulus for Ontario silty clay and silty clay till.

1 INTRODUCTION

Since the flat dilatometer test (DMT) was developed some 35 years (Marchetti 1980), it has been widely used to assess soil parameters. In a DMT, the DMT blade is pushed into the soil to a tested depth, and then the diaphragm is inflated and three pressure measurements (p_0, p_1, and p_2) are recorded. The p_0 is the lift-off pressure, p_1 is the pressure corresponding to 1.1 mm of membrane deflection, and p_2 is the closing pressure taken by slowly deflecting the membrane after p_1 is reached. The blade is then pushed into the ground of one depth increment (usually 0.2 m). Results of the DMT are commonly presented in three indices, the material index, I_D, the horizontal stress index, K_D and the dilatometer modulus, E_D, calculated from p_0 and p_1. These indices are used to interpret various soil parameters. Empirical correlations are often used in the interpretation.

This paper presents the DMT results conducted at two sites in Ontario, Canada: one in the City of Toronto; and another in the Town of Bradford West Gwillimbury, north of Toronto. Semi-theoretical formulas developed from the cavity expansion theory in the modified Cam clay (MCC) model are applied to estimate the undrained shear strength (c_u) and overconsolidation ratio (OCR) using p_0 and p_1. These formulas are evaluated by comparing OCR and c_u profiles interpreted from DMT measurements with corresponding direct measurements from the field vane shear tests, triaxial tests and/or the oedometer (one dimensional consolidation) tests in the silty clay and silty clay till in Ontario. The unit weight and modulus estimated from some empirical correlations using the DMT measurements are also discussed.

2 SITE CONDITION AND DMT

2.1 *A high-rise building site*

The project site is located at the north-east corner of Yonge Street and Eglinton Avenue East in the City of Toronto, Ontario. Lake Ontario is approximately 7 km south of the project site. The project is located within the physiographic region knows as the Peel Plain. Most of the tableland area consists of till partly modified by the former presence of shallow glacial lakes or post-glacial erosion features. The till in the project site is mapped as Halton Till which is generally considered as a fine-grained diamicton with minor fine-grained lacustrine sediments incorporated within the body of the unit, likely from glacial reworking of underlying lacustrine sediments. This till is typically stiff to hard in consistency, though near the ground surface, weathering can degrade it to consistencies ranging from soft to firm. The till consists of a heterogeneous mixture of gravel, sand, silt and clay size particles in varying proportions. Cobbles and boulders are common in the deposits.

Traditionally the standard penetration test (SPT), which is a rapid, simple and economical test, is widely adopted to assess the properties of glacial

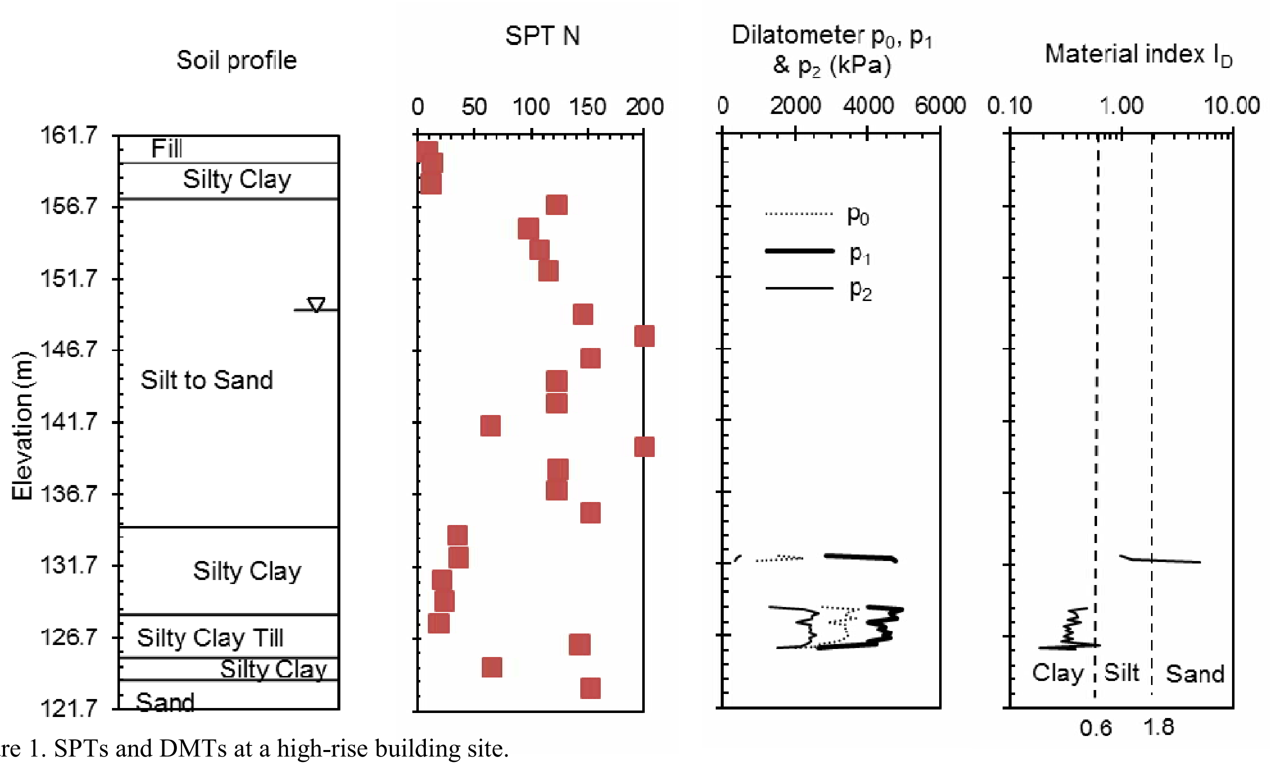

Figure 1. SPTs and DMTs at a high-rise building site.

tills in Ontario. SPTs were carried out and the number of blows was recorded for each of three 152 mm (6 in) penetrations; the first generally is considered as a seating drive and the number of blows for the final 305 mm (12 in) is reported as the standard penetration resistance or N value. When the blow number reaches 50, SPT usually stops as it is considered as actually refused and the penetration depth is roughly measured. When SPT N-value was greater than 50, the N value was generally calculated from 50 times the ratio of the 305 mm equivalent depth over the measured penetration depth in this paper for the purpose of comparison, i.e. calculated N = recorded N x (305/measured penetration depth in mm). If the calculated N-value is greater than 200, the calculated N was taken as 200. Figure 1 shows a typical profile of SPT N-values with depth at this high-rise building site.

Based on the information from boreholes and SPT N-values, the native soils below the fill material generally consist of upper very stiff to hard clayey silt till and stiff to hard silty clay, middle very dense cohesionless water bearing soil deposits (SPT N-values > 50), underlain by lower very stiff to hard silty clay and silty clay till (SPT N-values < 50). Cohesionless water bearing soils were encountered in the boreholes below depths varying from 6 to 8 m below the existing grade and continued to depths varying from 28.5 to 30.5 m. Groundwater levels in the monitoring wells were recorded at depths of 13.3 to 16.2 m below existing ground surface, corresponding to Elevations 147.3 to 149.9 m.

The differences of the lower silty clay and silty clay till are in the grain size distribution, nature water content, Atterberg limits. The silty clay till contains up to 2% gravel, 13% to 29% sand, 47% to 57% silt, and 22% to 32% clay size particles, whereas the silty clay contains generally less than 10% sand, 40% to 49% silt and 43% to 57% clay size particles. The silty clay till has liquid limits of 22 to 29, plastic limits of 15 to 18 and plasticity indices of 7 to 12, whereas the silty clay has liquid limits of 27 to 44, plastic limits of 18 to 23 and plasticity indices of 8 to 21. The natural water content of silty clay till ranges from 9% to 16%, whereas the silty clay has 12% to 29% of water content. The unit weight of silty clay till ranges from 21 to 22.5 kN/m^3, whereas the unit weight of silty clay ranges from 20 to 21 kN/m^3. The initial void ratio is 0.28 for the silty clay till and between 0.55 and 0.66 for the silty clay. The effective angle of internal friction measured from the triaxial tests ranges from 33° to 36°. The undrained shear strength obtained from triaxial test for one silty clay sample consolidated under the in-situ effective vertical stress is 320 kPa. The OCR calculated from the one dimensional consolidation tests and unit weight indicated the silty clay and silty clay till were normally consolidated to slightly overconsolidated.

As the lower silty clay and silty clay till are relatively weaker than the overlain very dense soils based on SPT N-values, the influence of the relatively weak deposits to the foundation of the high-rise building was concerned. The DMTs with shear wave measurements were carried out to evaluate the in-situ geotechnical parameters related to deformation properties of the lower silty clay and silty clay till. The DMT measurements (p_0, p_1, and p_2) at the deep silty clay and silty clay till are shown in Figure 1. The measured shear velocity, V_s ranges from 468 to

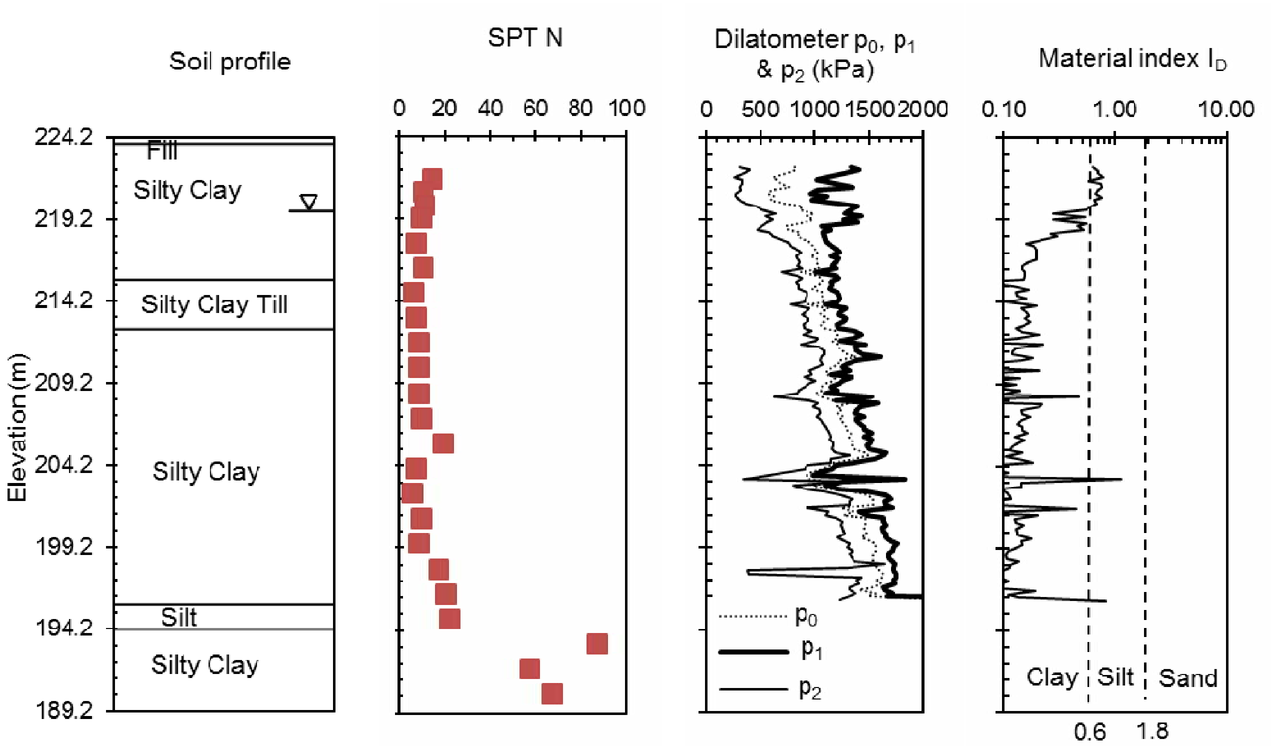

Figure 2. SPTs and DMTs at a pumping station site.

508 m/s and the maximum shear modulus, G_o calculated from the V_s ranges from 449 to 664 MPa.

In addition, preboring TEXAM pressuremeter tests and cross-hole seismic tests measurements carried out for another project located about 50 to 200 m from this site were also collected. The pressuremeter modulus for the lower silty clay ranges from 79 to 163 MPa. The shear wave velocity measured from the cross-hole seismic testing in the lower silty clay ranges from 561 to 618 m/s, generally higher than that measured by the two geophones installed in the DMT.

2.2 *A pumping station site*

The project site is located at the north-east corner of Line 5 and Highway 400 in the Town of Bradford West Gwillimbury, Ontario. Lake Ontario is approximately 60 km south of the project site. The surficial geology of the project site is relatively consistent, typically consisting of Schomberg Clay overlying Late Wisconsin Age drumlinized glacial till of brown to grey, gritty silty clay to clayey silt till. The texture of the glacial till is primarily low plasticity silty clay or less cohesive, but well-consolidated sandy silt with some rock fragments.

Based on the information from boreholes and SPT N-values, the native soils below the fill material generally consist of firm to hard silty clay embedded with stiff to hard silty clay till and compact silt at the pumping station site. Groundwater levels in the monitoring well was recorded at a depth of 4.5 m below existing ground surface, corresponding to Elevation 219.7 m. Figure 2 shows a typical profile of SPT N-values with depth at this pumping station site. The DMT measurements (p_0, p_1, and p_2) and calculated I_D are also shown in Figure 2. Marchetti (2015) indicted that the very low values of I_D suggest that the soil is a so-called "niche silt" or "very clayey" clay and difference between p_0 and p_1 is too low, from which the parameters (I_D, K_D and E_D) derived cannot be determined.

The silty clay contains generally less than 10% sand, 44% to 80% silt and 20% to 51% clay size particles, and has liquid limits of 22 to 38, plastic limits of 15 to 22 and plasticity indices of 7 to 18, with the natural water content of 11% to 33%. The unit weight of silty clay is 19.0 to 22.9 kN/m^3 with an average value of 20.6 kN/m^3. The initial void ratio ranges from 0.54 to 0.6 for the silty clay. The undrained shear strength measured from the field vane shear tests ranges from 24 to greater than 115 kPa. The overconsolidation ratio (OCR) calculated from the one dimensional consolidation tests and unit weight indicated the silty clay and silty clay till were normally consolidated to slightly overconsolidated.

The silty clay till has a similar properties with the silty clay, except that the silty clay till contains 0% to 9% gravel, 11% to 44% sand, 36% to 61% silt and 12% to 39% clay size particles, and its unit weight ranges from 20.9 to 22.9 kN/m^3 with an average value of 22.2 kN/m^3.

3 INTERPRETATION OF DMT RESULTS AND DISCUSSIONS

The DMT results have been used to estimate the OCR, c_u, unit weight and constrained modulus based on K_D and/or M_D using the methods proposed by

Marchetti (1980) and Marchetti et al. (2001). Due to the highly empirical nature, these methods of interpretation of the DMT have not been universally accepted.

Based on simplified theoretical solutions of cavity expansion in modified Cam clay, Cao (1997) and Cao et al. (2015) proposed the following semi-theoretical relationships to estimate the OCR and c_u from the DMT measurements p_0 and p_1:

$$OCR = 2\left[\frac{\sqrt{3}(p_0 - \sigma_{vo})}{1.57\sigma'_{vo}\, M(\ln I_r + 1)}\right]^{1/\Lambda} \quad (1)$$

$$OCR = 2\left[\frac{1.5(p_1 - \sigma_{vo})}{1.57\sigma'_{vo}\, M(\ln I_r + 1)}\right]^{1/\Lambda} \quad (2)$$

$$c_u = \frac{p_0 - \sigma_{vo}}{1.57(\ln I_r + 1)} \quad (3)$$

$$c_u = \frac{p_1 - \sigma_{vo}}{2.09(\ln I_r + 1)} \quad (4)$$

where σ_o = initial mean total stress; σ'_o = initial mean effective stress; M = critical state parameter or slope of critical state line and is equal to $6\sin\phi'/(3$ conventional triaxial compression tests; Λ = plastic volumetric strain ratio $\approx (C_c - C_r)/C_c$; C_c = compression index; C_r = recompression index; I_r = rigidity index = G/c_u; and G = shear modulus.

For the silty clay and silty clay till in Ontario, I_r normally ranges from 45 to 140, the effective friction angle from 30° to 36° and Λ from 0.82 to 0.86 based on limited laboratory test results. In cases where the soil properties are not available, average value of $I_r = 90$, $\phi' = 33°$ and $\Lambda = 0.84$ can be adopted in Equations (1) to (4) for approximate estimates of OCR and c_u profiles using the readings p_0 and p_1 measured from the DMT. For normally to overconsolidated clay ($OCR \geq 1$), the simplified expressions of Equations (1) to (4) become

$$OCR = 2\left(\frac{p_0 - \sigma_{vo}}{6.63\sigma'_{vo}}\right)^{1.19} \quad (5)$$

$$OCR = 2\left(\frac{p_1 - \sigma_{vo}}{7.66\sigma'_{vo}}\right)^{1.19} \quad (6)$$

$$c_u = 0.12(p_0 - \sigma_{vo}) \quad (7)$$

$$c_u = 0.09(p_1 - \sigma_{vo}) \quad (8)$$

If the OCR estimated from Equations (5) to (6) is less than 1, it should be taken as 1.

Figure 3 shows the OCR profiles developed using Equations (5) and (6) for the silty clay and silty clay till at the two sites in Ontario. At the high-rise building site in Toronto, the predicted OCR values are closed to that measured by the oedometer test for a silty clay sample taken at a location about 200 m from the DMT location. The values of the predicted OCR are also close to the oedometer measured data for the silty clay at the pumping station site. The OCR values estimated using Marchetti's (1980) correlations, $OCR = (0.5K_D)^{1.56}$ and $K_D = (p_0 - u_o)/\sigma'_{vo}$,

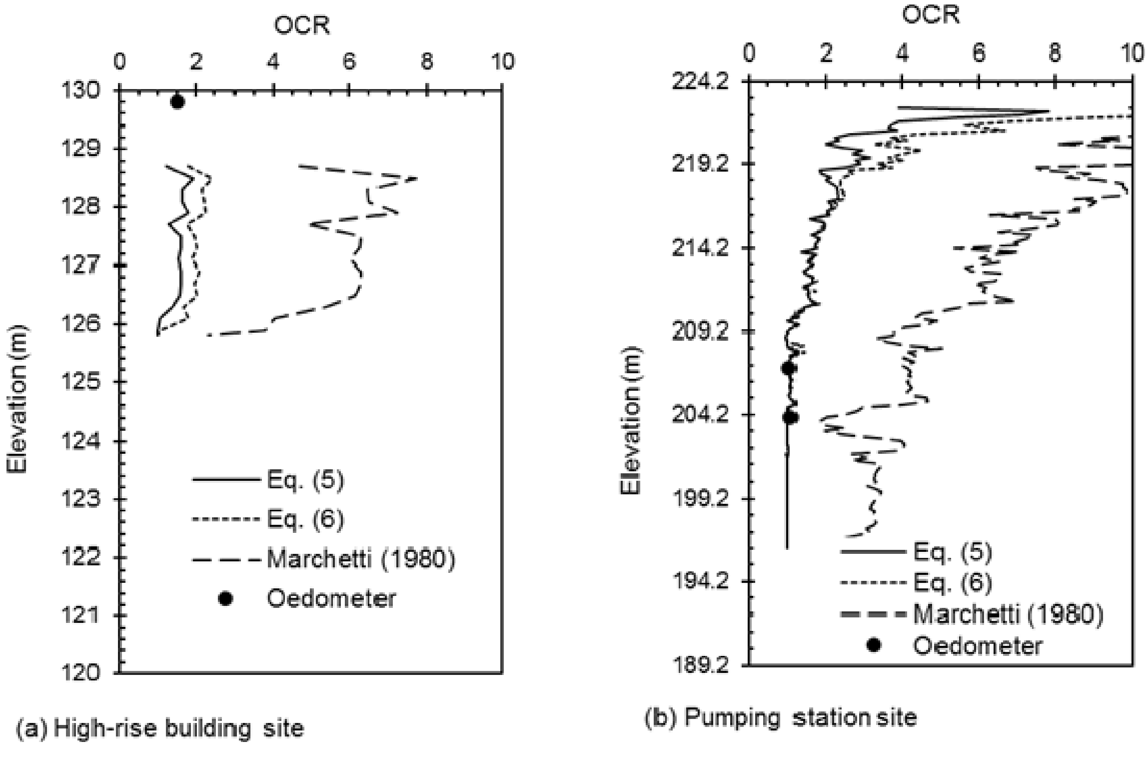

Figure 3. Predicted versus measure OCR.

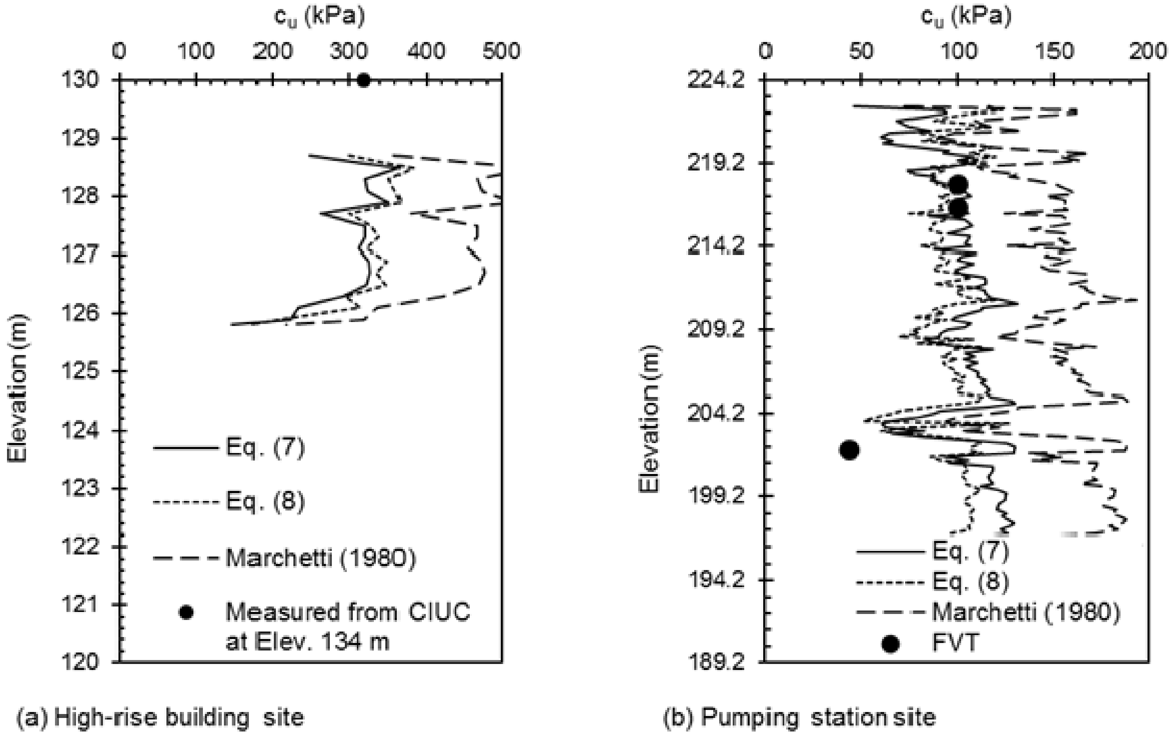

Figure 4. Predicted versus measure c_u.

are found to have overestimated the OCR values for the Ontario silty clay and silty clay till, as illustrated in Figure 3.

Figure 4 shows the c_u profiles estimated using Equations (7) and (8) for the silty cay and silty clay till at the two sites in Ontario. The predicted c_u values are generally in good agreement with those measured in the field vane test (FVT) at the pumping station site. The predicted c_u values are close to that measured from isotropic consolidated undrained triaxial test (CIUC) for a silty clay sample taken at a 5 m higher level at a location about 200 m from the DMT location at the high-rise building site. The c_u values deduced from Marchetti's (1980) correlation $c_u = 0.22\sigma'_{vo}(0.5K_D)^{1.25}$ are generally overestimated the c_u values for the Ontario silty clay and silty clay till, as shown in Figure 4.

It is noted that the unit weight based on I_D and E_D as proposed by Marchetti et al. (2001) is generally underestimated for the Ontario silty clay and silty clay till. The estimated unit weight ranges from 17 to 18 kN/m^3 based on the vales of I_D and M_D as proposed by Marchetti et al. (2001), whereas the unit weight of the silty clay and silty clay till measured from laboratory tests is generally greater than 20 kN/m^3 at the two sites.

At the high-rise building site, the constrained modulus estimated from E_D and K_D using the formula proposed by Marchetti et al. (2001) ranges from 30 to 100 MPa, corresponding to Young's modulus of 21 to 77 MPa using a Poission's ratio of 0.3. The pressuremeter modulus obtained from preboring TEXAM pressuremeter testing in the silty clay at the similar elevation at a location of about 50 m from the DMT site ranges from 79 to 162.8 MPa. It seems that the formula proposed by Marchetti et al. (2001) underestimates the modulus of the Ontario silty clay and silty clay till.

4 CONCLUSION

Semi-theoretical formulas developed from the modified Cam clay (MCC) model were used to estimate the overconsolidation ratio and undrained shear strength for the silty clay and silty clay till in Ontario. A comparison of estimated OCR and c_u values based on the proposed methods with direct measurements by other independent means indicates the validity of the proposed approach. The empirical equations proposed by Marchetti's (1980) generally overestimate the OCR and c_u for the silty clay and silty clay till in Ontario.

The unit weight and modulus using the methods proposed by Marchetti et al. (2001) are generally underestimated for the silty clay and silty clay till in Ontario.

REFERENCES

Cao, L.F. 1997. *Interpretation of In-situ Tests in Clay with Particular Reference to Reclaimed Sites*. Ph.D. Thesis. Nanyang Technological University, Singapore.

Cao, L.F., Chang, M.F. & Teh, C.I. 2015. Analysis of dilatometer in clay. *Proc. 3rd int. conf. on the flat dilatometer*, Rome, Italy.

Marchetti, S. 1980. In situ test by flat dilatometer. *Journal of Geotechnical Engineering*, ASCE, 106(3), 299-321.

Marchetti, S., Monaco P., Totani G. & Calabrese M. 2001. The flat dilatometer test (MDT) in soil investigation. A Report by the ISSMGE Committee TC16. *Proc. IN SITU 2001 int. conf. on in situ measurement of soil parameters,* Bali, Indonesia.

Marchetti, S. 2015. Some 2015 updates to the TC16 DMT report 2001. *Proc. 3rd Int. conf. on the flat dilatometer*. Roma, Italy.

Geotechnical and Geophysical Site Characterisation 5 – Lehane, Acosta-Martínez & Kelly (Eds)
© 2016 Australian Geomechanics Society, Sydney, Australia, ISBN 978-0-9946261-1-0

Self-boring pressuremeter tests at the National Field Testing Facility, Ballina NSW

F.M. Gaone
Centre for Offshore Foundation Systems, University of Western Australia, Perth, Western Australia, Australia

J. Doherty
School of Civil, Environmental and Mining Engineering, University of Western Australia, Perth, Western Australia, Australia

S. Gourvenec
Centre for Offshore Foundation Systems, University of Western Australia, Perth, Western Australia, Australia

ABSTRACT: Accurate prediction of foundation settlement is increasingly important in onshore and offshore geotechnical design. Reducing land space requires construction on non-ideal soils or above buried infrastructure onshore while offshore shallow foundations require optimization of size to facilitate installation while ensuring tolerances on attached rigid infrastructure such as pipelines are not compromised. The accuracy of settlement predictions depends on the accuracy of the measured soil stiffness, which is non-linear and dependent on stress level, stress path and stress history. Consequently, the quality of a settlement prediction is inherently tied to the relevance of the testing method that is used to derive the stiffness values. The self-boring pressuremeter (SBPM) enables the non-linear stress-strain response to be captured at different in-situ stress levels (depths) over a large range of cavity strain, and derivation of undrained strength, stiffness and creep characteristics. This paper summarizes a program of pressuremeter tests conducted in a soft clay deposit in Ballina, NSW, Australia.

1 INTRODUCTION

The University of Western Australia (UWA) self-boring pressuremeter (Fahey et al. 1988) was reconditioned for a program of testing at the National Field Testing Facility (NFTF) in Ballina, NSW (Australia). The aim of the project was to identify in-situ stiffness parameters to back analyse the undrained load-settlement response of shallow foundation field tests performed on the same site. The tests were performed in 6 different boreholes over depths between 2 m to 10 m below ground level. The program involved tests with and without unload-reload loops, tests at different stress rates and stress holding tests.

This paper presents profiles of the total horizontal stress, σ_{ho}, the undrained shear strength, s_u, and the unload/re-load shear modulus, G_{UR} of the Ballina clay at the NFTF and compares the predicted soil parameters with results from other field tests carried out at the site.

2 SITE DESCRIPTION

The Centre of Excellence for Geotechnical Science and Engineering (CGSE) has leased a 6.5 Ha soft soil site in the northwest of Ballina, NSW (Australia). The so-called National Field Testing Facility (NFTF) is being used to develop and demonstrate new and existing site investigation tools and to calibrate analytical and numerical geotechnical design methods. To date a large number of in-situ geotechnical investigations and a program of soil laboratory tests have been performed at or on samples from the NFTF site (Kelly et al. 2015; Pineda et al. 2014, Pineda et al. 2015).

The soil stratigraphy in the area of the SBPM tests is summarized in Figure 1. The site comprises a crust of alluvial clayey silty sand to a depth of 1.5 m across the area of interest, underlain by a soft estuarine clay to a depth of approximately 12 m (increasing to 22 m at other locations across the site). The soft clay overlays a transition zone of stiff clay, silt and sand. During the testing, the groundwater table was encountered at approximately 1 m below the ground surface.

3 TEST PROGRAM AND PROCEDURES

The program involved 27 SBPM tests in 6 different boreholes. A conventional drilling rig was used to predrill the first 1.5 m through the crust layer in each borehole, which was stabilized by an internal casing. After removing the drilling rod, the SBPM device was attached to the drilling rig and lowered into the borehole and self-bored continuously to the test depths. Due to the device setup, the maximum depth of self-boring was 2.65 m below the end of the bore

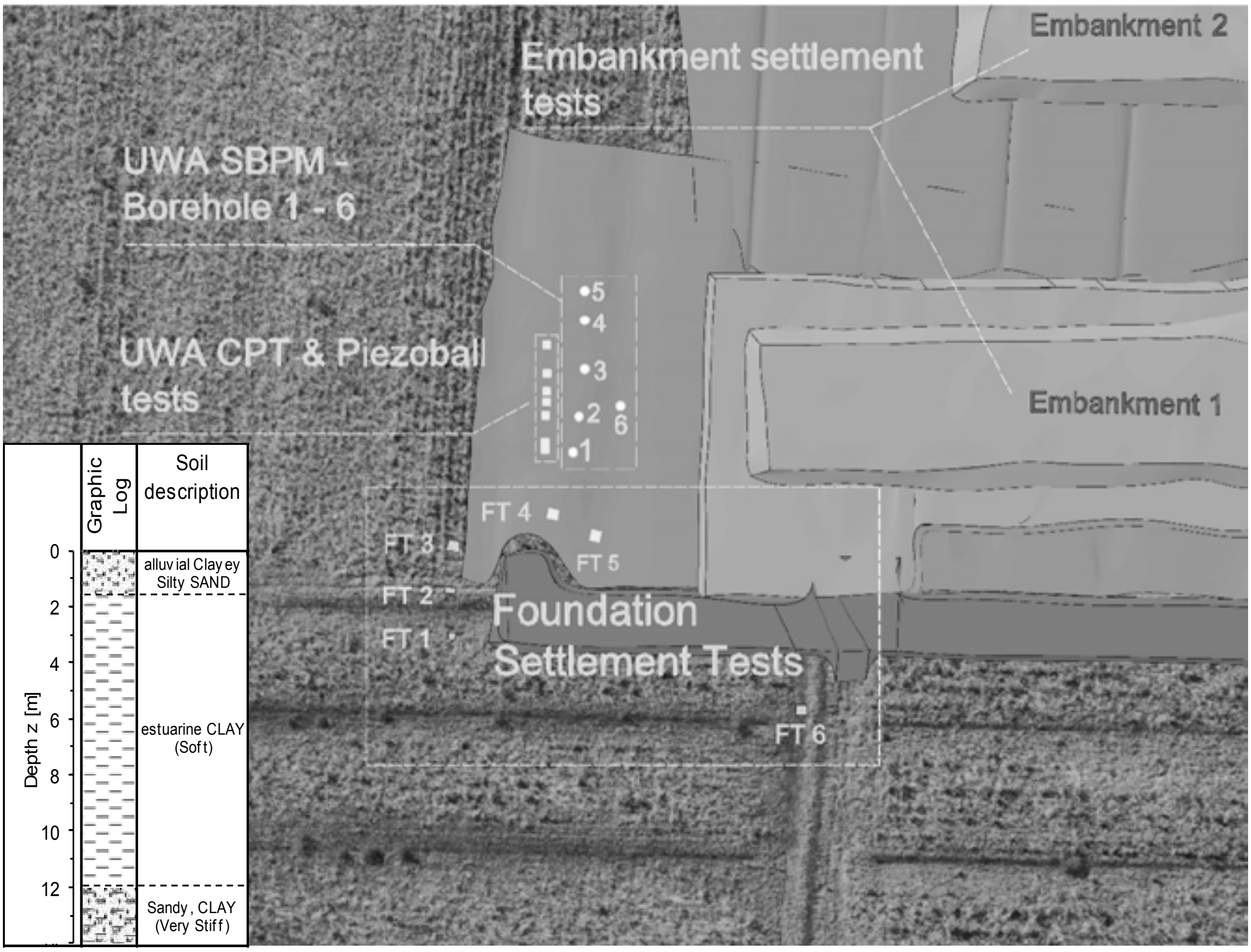

Figure 1. Aerial view of the NFTF showing the location of the SBPM tests, other in situ soil characterisation tests and foundation settlement tests.

hole casing, where tests were conducted. The SBPM was then removed and the bore hole casing advanced.

SBPM testing involves applying an internal pressure to a rubber membrane that expands radially against the soil. Steel strips (called the "Chinese lantern") are used as a protection casing for the rubber membrane. Tests were carried out under stress control at rates of 1, 10, 50 and 100 kPa/min to a limit of 10 % of the average cavity strain.

Unload/reload loops were performed in 8 of the tests at depths between 2 m and 11 m below ground level at different strain levels and strain ranges. The size of the loop (or amount of unloading Δp) was controlled by the pressure at the start of unloading (p_i) and the assumed friction angle of the soil ϕ' (Fahey 1991):

$$\Delta p = p'_i \frac{\sin\phi'}{\left(1+\sin\phi'\right)} = \left(p_i - u_0\right)\frac{\sin\phi'}{\left(1+\sin\phi'\right)} \qquad (1)$$

where u_0 is the in-situ hydrostatic water pressure. A membrane stiffness correction was applied to all 27 tests. This involved measuring the membrane stress – strain response and subtracting this from the in-situ test data.

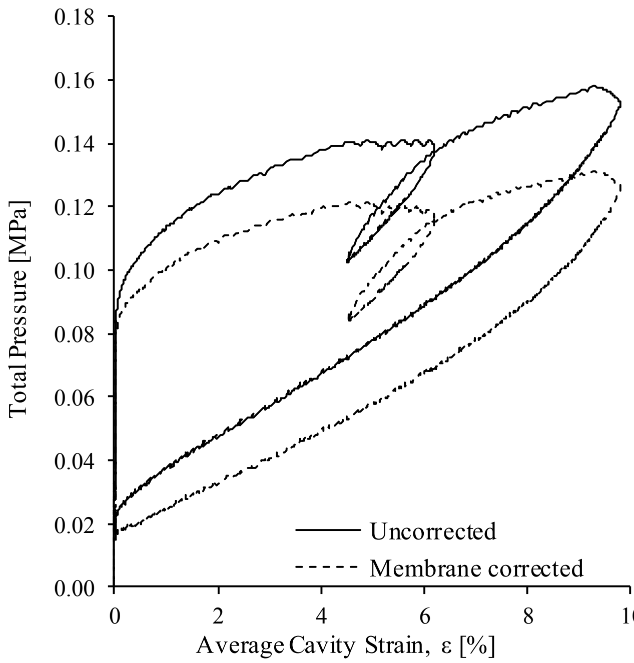

Figure 2. Typical stress-strain curve of a SBPM test

4 INTERPRETATION

Figure 2 shows a typical stress-strain response from a SBPM test involving one unload/reload loop. The stress-strain response is plotted for the uncorrected field data and the membrane corrected data. The membrane correction is strain dependent. The membrane stiffness increases with cavity strain and consequently the correction should reflect the strain level (rather than assuming a constant membrane stiffness).

The in-situ horizontal stress, undrained shear strength and unload/re-load shear modulus were determined from the SBPM data and compared with field data from independent in-situ tests where available.

4.1 *In-situ horizontal stress, σ_h*

Estimation of the in situ horizontal pressure was achieved by the visual lift-off method described by Lunne & Lacasse (1982). This method is based on close visual inspection of the initial part of the test curve. O'Brien & Newman (1990) suggested that this initial part should not exceed a strain level of 0.2%. The lift-off pressure is defined as the pressure, p_0, at which the membrane starts to deform. This deformation is identified by the displacement of the three feeler arms of the pressuremeter. The average movement of all three arms is defined as the membrane movement. The interpretation of the lift-off pressure was based on the average movement of all three feeler arms.

For the interpretation, the average strain of the arms was plotted versus the internal pressure in semi logarithmic space (see Figure 3). A straight line was fitted over the initial linear part of the curve. The point, at which the test curve deviated from the straight line was taken as the lift-off pressure.

In Figure 4, the lift-off pressures, and hence the in-situ horizontal stresses, with depth are plotted considering the average of all three feeler arms. The total horizontal stresses with depth are compared to an estimate of the vertical stress profile, which is based on measurements of the natural density obtained from laboratory tests (Pineda et al. 2015).

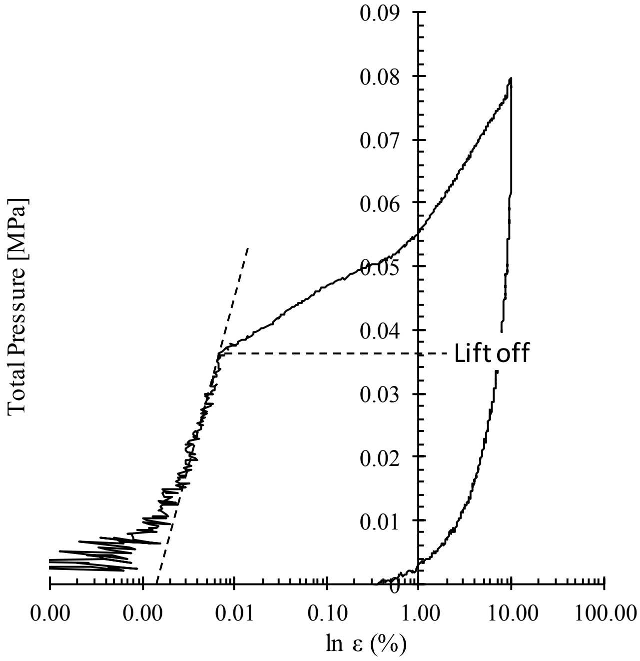

Figure 3. Example of lift-off pressure interpretation

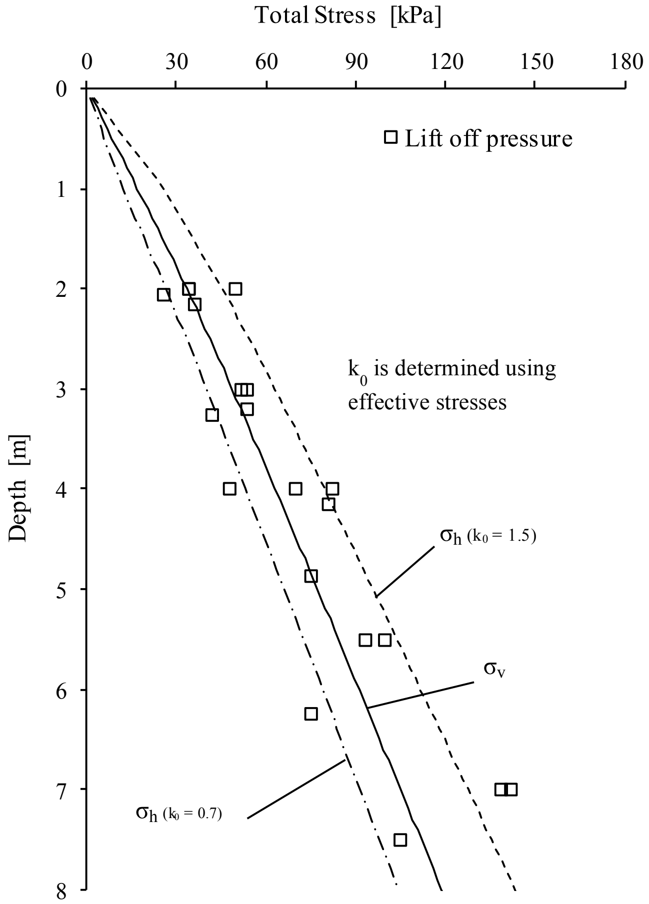

Figure 4. Interpreted lift-off pressure, equal to in situ σ_h

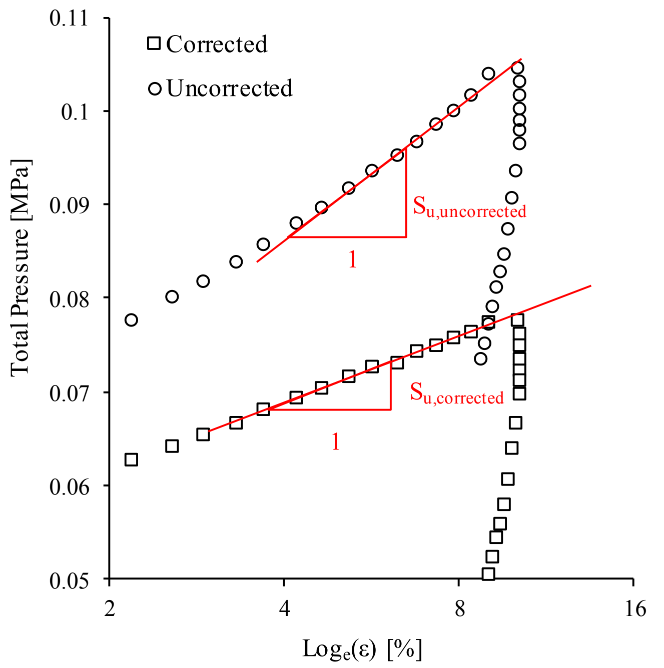

Figure 5. Example of determination of s_u from self-boring pressuremeter data

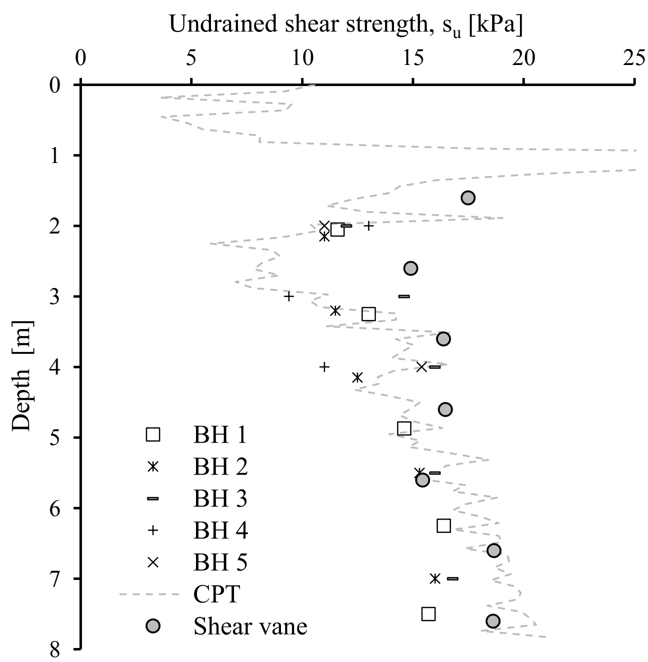

Figure 6. s_u profile with depth at NFTF

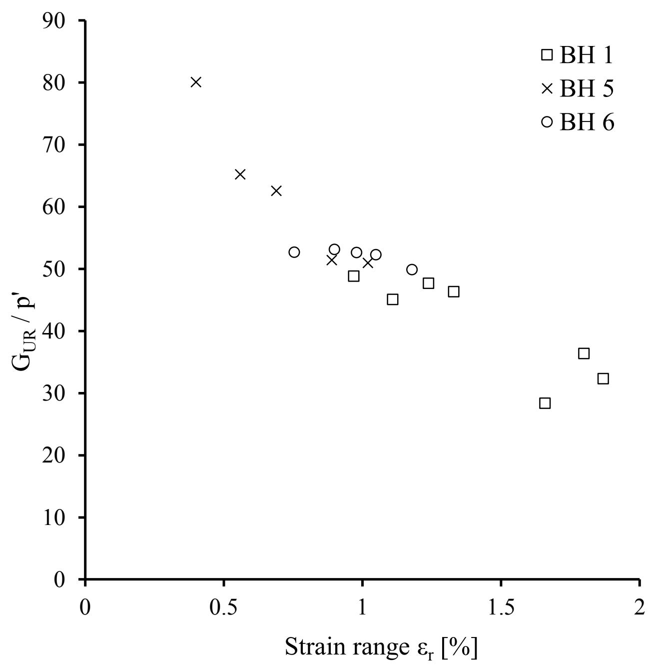

Figure 7. Normalized G_{UR} with cavity strain range, ε_r

In addition, two horizontal stress profiles are shown as an upper and lower boundary for the SBPM tests, using k_0 values of 0.7 and 1.5. The earth pressure coefficient, k_0, was determined based on the effective stress ratio ($k_0 = \sigma'_h / \sigma'_v$) using an estimated hydrostatic pore pressure profile and the water table level encountered prior to the tests in the boreholes of the SBPM. Results of SDMT and interpretations of CPT tests (Pineda et al. 2015) indicate a k_0 value in a range between 0.5 – 0.65.

4.2 *Undrained shear strength, s_u*

Various methods have been proposed for interpreting the undrained shear strength from pressuremeter tests. A commonly used method is that provided by Windle & Wroth (1977). Their interpretation method follows the Gibson & Anderson (1961) approach for the interpretation of a Menard pressuremeter test. The method is based on an elastic – perfectly plastic soil model characterized by an undrained shear strength, s_u, and a shear modulus, G. The pressuremeter is assumed to be infinitely long and following the assumptions of a cylindrical cavity expansion. These assumptions are axial symmetry, soil homogeneity and undrained behaviour.

Undrained shear strength is derived from the gradient of a plot of applied cavity pressure against the natural logarithm of the cavity strain once a plastic state has been achieved (see Figure 5).

Figure 6 shows the derived profile of the undrained shear strength obtained from the SBPM tests. This profile is compared to results from cone penetrometer tests (CPT) and shear vane tests (Kelly et al. 2015) and shows good agreement. In previous studies it was observed, that results of vane shear tests are usually lower than those from SBPM tests (Lacasse et al. 1981). In this study it was found, that the vane shear test results tend to be higher than those from the SBPM test. This difference could result due to the strain dependent membrane correction carried out in this study. In previous literature, the method used for the membrane correction is not always apparent. Benoit & Findlay (1993) pointed out, that the membrane correction method used can have a significant impact on interpreted soil values. This is illustrated in Figure 5. The effect of the membrane correction increases the softer and shallower the soil is. In the present case, the ratio between the corrected undrained shear strength and the uncorrected ($s_{u,corr}$ / $s_{u,uncorr}$) can be as high as 60%.

4.3 *Shear modulus, G*

The shear modulus can be derived either from the initial part of the test curve or from unload/reload loops conducted at various stress levels. Because the initial part of the test curve is more likely influenced by installation disturbance, the shear modulus was interpreted analysing unload/reload loops, and defined the 'unload/ reload' shear modulus, G_{UR}. The shear modulus derived from an unload/reload loop is dependent on the size of the loop. This size can be expressed by the strain range. In Figure 7, the shear modulus, G_{UR}, normalized by the mean effective stress, p′, is shown over different strain ranges. As anticipated, the shear modulus decreases with increasing strain range. This behaviour was observed and described earlier by Allan (1995) on tests performed on London Clay.

5 CONCLUDING REMARKS

Interpreted results from a programme of 27 self-boring pressuremeter tests in soft clay at the National Field Testing Facility, Ballina, NSW (Australia) have been presented.

The interpreted soil stresses, undrained strength and shear modulus are shown to compare well with results from independent tests at the same site. It was shown, that the self-boring pressuremeter is a reliable device to capture the non-linear stiffness behaviour of the clay at different in-situ stress levels (depths).

The pressuremeter results will be used to back analyse the undrained load-settlement response of shallow foundation field tests carried out at the NFTF. Results will be published at the Embankment Prediction Symposium hosted by the CGSE in September 2016.

An automated inverse analysis tool is being developed to derive optimized geotechnical properties for engineering design directly from SBPM tests (Gaone et al. in prep.).

6 ACKNOWLEDGMENT

This work forms part of the activities of the Centre for Offshore Foundation Systems (COFS). Established in 1997 under the Australian Research Council's Special Research Centres Program. Supported as a node of the Australian Research Council's Centre of Excellence for Geotechnical Science and Engineering, and through the Fugro Chair in Geotechnics, the Lloyd's Register Foundation Chair and Centre of Excellence in Offshore Foundations and the Shell EMI Chair in Offshore Engineering. The first and third authors and the work presented in this paper are supported through ARC grant CE110001009. This support is gratefully acknowledged.

7 REFERENCES

Allan, R., 1995. Assessment of in situ horizontal stress and modulus of London Clay at a site in Kent using the self-boring pressuremeter. *The Pressuremeter and Its New Avenues.*

Benoit, J. & Findlay, C., 1993. Some factors affecting in situ measurement using the Cambridge self-boring pressuremeter. , pp.188–197.

Fahey, M., 1991. Measuring shear modulus in sand with the self-boring pressuremeter. *Proceedings, 10th European Conference on SMFE, Florence, Italy. Vol. 1. 1991.*

Fahey, M., Jewell, R.J. & Brown, T. a., 1988. Self-Boring Pressuremeter System. *Geotechnical Testing Journal*, 11(3), pp.187–194.

Gaone, F.M., Doherty, J. & Gourvenec, S., in prep. Inverse Analysis of self-boring Pressuremeter data as a forecasting tool.

Gibson, R.. & Anderson, W.F., 1961. In situ measurement of soil properties with the pressuremeter. *Civil Engineering Public Works Review*, 56(May), pp.615–618.

Kelly, R.B., O'Loughlin, C.D., Bates, L., Gourvenec, S., Colreavy, C., White, D.J., Gaone, F.M. & Doherty, J., 2015. In situ testing at the National Soft Soil Field Testing Facility, Ballina, New South Wales. *Australian Geomechanics*, 50(4)(Special Edition), pp.13–26.

Lacasse, S., Jamiolkowski, M., Lancellotta, R. & Lunne, T., 1981. In situ characteristics of two Norwegian clays. *Proceedings of the 10th International Conference on Soil Mechanics and Foundation Engineering. Vol. 2.*

Lunne, T. & Lacasse, S., 1982. In situ horizontal stress from pressuremeter tests. In *Symposium on the Pressuremeter and its Marine Applications*. Editions TECHNIP, p. 187.

O'Brien, A.S. & Newman, R.L., 1990. Self-boring pressuremeter testing in London Clay. *Geological Society, London, Engineering Geology Special Publications*, 6(1), pp.39–53.

Pineda, J., McConnell, A. & Kelly, R., 2014. Performance of an innovative direct-push piston sampler in soft clay. *Proc. CPT'14*.

Pineda, J.A., Suwal, L.P., Kelly, R.B., Bates, L. & Sloan, S.W., 2015. Characterisation of Ballina clay. *Géotechnique*, p.181.

Pineda, J.A., Suwal, L.P. & Kelly, R.B., 2015. Sampling and laboratory testing of Ballina clay. *Australian Geomechanics*, 50(4)(Special Edition), pp.29–40.

Windle, D. & Wroth, C.P., 1977. The use of a self-boring pressuremeter to determine the undrained properties of clays. *Ground Engineering*, 10(6), pp.37 – 46.

Geotechnical and Geophysical Site Characterisation 5 – Lehane, Acosta-Martínez & Kelly (Eds)
© 2016 Australian Geomechanics Society, Sydney, Australia, ISBN 978-0-9946261-1-0

Practice of the PENCEL Pressuremeter in Foundations Design

F. Messaoud
University of Tebessa, Tebessa, Algeria

P.J. Cosentino
Florida Institute of Technology, Florida, USA

ABSTRACT: In all foundations design, it is necessary to know the pertinent parameters controlling the soil behavior. The aim was to reveal that Pencel pressuremeter (PPMT) pushed to the preferred test depth using the cone penetrometer equipment would produce reliable engineering parameters. The PENCEL pressuremeter is defined as a cylindrical devices designed to apply uniform pressure to walls of a borehole by means of a flexible membrane. Pressure is exerted on the borehole walls via an incompressible liquid (water). PPMT has sufficient length to diameter ratios, the soil expansion is assumed to be cylindrical allowing plain strain assumptions to be used to reduce the data. The cavity expansion and corresponding pressure increase are reduced to stress-strain, from which strength-deformation properties are determined. This study was performed to describe the standard method of PPMT testing to allow engineers to more precisely carry out the standardized tests. Comparison of typical tests from various PMT's is presented. Theoretical interpretation of PPMT results was developed. From PPMT data, which were reduced to graphs of pressure versus volume and pressure versus relative change in probe radius, soil parameters including the initial pressure, the elastic moduli, the reload moduli, and the limit pressure of the soil could be determined. Pencel pressuremeter is a suitable device to allow the rapid and reliable measurement of engineering parameters for foundations design.

1 INTRODUCTION

The Pencel pressuremeter (PPMT) consists of a cylindrical probe of 1.35-inch diameter, containing an expandable flexible membrane connected to the unit through tubing and the pressure and volume gauges for recording data (Fig. 1). PPMT Probe is lowered into the soil to produce in situ stress-strain responses. The soil response curve can be interpreted to obtain fundamental soil properties and design parameters, such as strength, stiffness and in-situ horizontal stress. PPMT probe can be connected to standard cone penetration test (CPT) rods enabling a large number of PPMT tests to be conducted within a site (Briaud & Shields 1979). Based on the proper calibration and pushing to the desired depth the test is conducted by manually recording data from analogue pressure and volume gages that can be difficult to read. The pushed-in PPMT allows engineers to efficiency use reduced stress-strain data to determine lift-off pressure (p_0) elastic moduli (E) and limit pressure (p_L) (Briaud & Shields 1979), (cosentino 1987) and (Messaoud 2008) that can be used for geotechnical analysis and design; In addition to classical geotechnical applications, Cosentino & Briaud (1989) developed procedures for using the (PPMT) in pavement design.

The current PPMT as distributed by ROCTEST® consists of three main parts, the operators control unit supported on a tripod stand and placed at the ground surface, the probe inserted into the soil and the tubing connecting the probe to the readout unit. The control unit has pressure and volume displays. A rotation of the handle by the operator moves the piston inside the control unit which forces water through the system that produces a change in the probe volume and a corresponding pressure that can be measured. This device could be enhanced by incorporating digital gages with data collection, reduction and analysis software. A strain-controlled process is typically performed requiring operators to inject equal 5 cm^3 volumes of water into the probe and wait 30 seconds (Cosentino et al. 2006) or 15 seconds (Roctest 2005) and record the corresponding pressures.

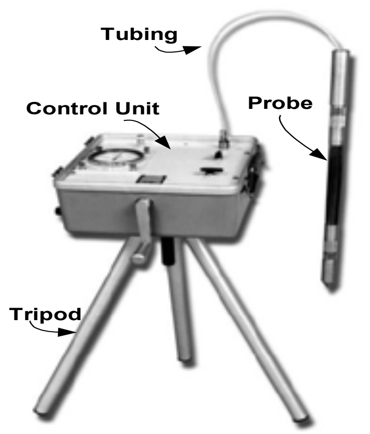

Figure 1. The PENCEL Pressuremeter

2 DATA REDUCTION AND INTERPRETATION

Following equipment saturation, the calibrations are performed. First, the membrane calibration is determined by inflating the probe in air, at the same elevation as the pressure gage while recording pressure and volume data. Second, the volume calibration is determined by inserting the probe into a 32 mm diameter steel tube and inflating it while pressures and volumes are recorded. The membrane and volume corrections are subtracted from the raw data producing a reduced curve (Fig. 2). The hydrostatic pressure developed between the control unit and the center of the probe is added to the raw pressures prior to making these corrections (Messaoud 2008).

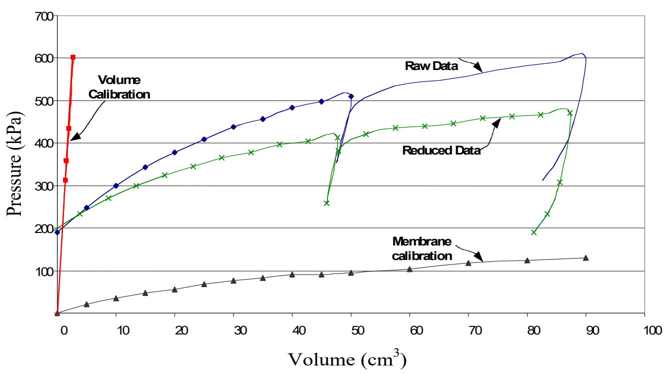

Figure 2. Raw and Reduced Data with Calibrations Applied

In order to determine the critical engineering parameters, four portions of the reduced curve are analyzed (Fig. 3). It includes an initial zone where the soil is repositioned to its original stress state, followed by an elastic zone, the rebound zone and then a plastic zone to estimate the soil limit pressure. The moduli (E) are determined from the slopes (S) while the other parameters are estimated. The PPMT limit pressure (p_L) defined as the pressure associated with doubling the initial probe volume (Messaoud et al 2011).

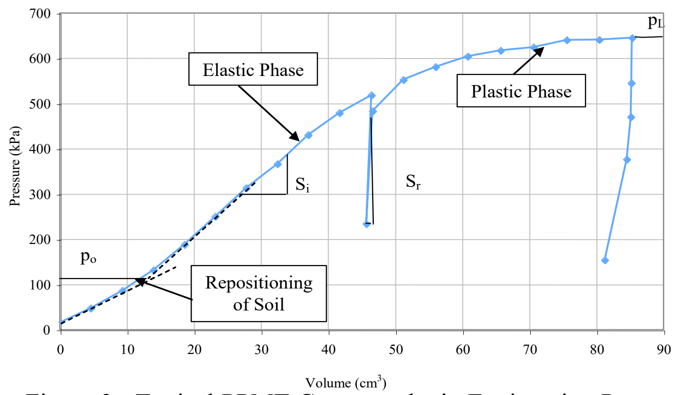

Figure 3. Typical PPMT Curve to obtain Engineering Parameters

The Following expression for determining an elastic modulus from (E) is used (Baguelin et al. 1978):

$$E = 2(1+\nu)\frac{\Delta P}{\Delta V}V_m \qquad (1)$$

Where, E = Young's modulus, ΔP = change in pressure, ($\Delta P = P_2 - P_1$),
ΔV = change in volume related to ΔP , V_m = average volume, and ν = Poisson's Ratio
Tucker (1987) & Briaud (1992) suggested using the radial strain to determine moduli. In an effort to normalize the PPMT curve it is recommended that the curve be plotted as pressure versus relative increase on probe radius (Fig. 4). Hence, Equation 1 for the initial modulus E_0 will be:

$$E_0 = (1+\nu)\left[\left(1+\frac{\Delta R_1}{R_0}\right)^2 + \left(1+\frac{\Delta R_2}{R_0}\right)^2\right]\frac{\Delta P_{2\text{-}1}}{\left[\left(1+\frac{\Delta R_2}{R_0}\right)^2 - \left(1+\frac{\Delta R_1}{R_0}\right)^2\right]} \qquad (3)$$

The value of $\left(P_1,\left(\frac{\Delta R}{R_0}\right)_1\right)$ and $\left(P_2,\left(\frac{\Delta R}{R_0}\right)_2\right)$ are taken from steepest initial linear portion of the corrected pressuremeter curve (Fig. 4).

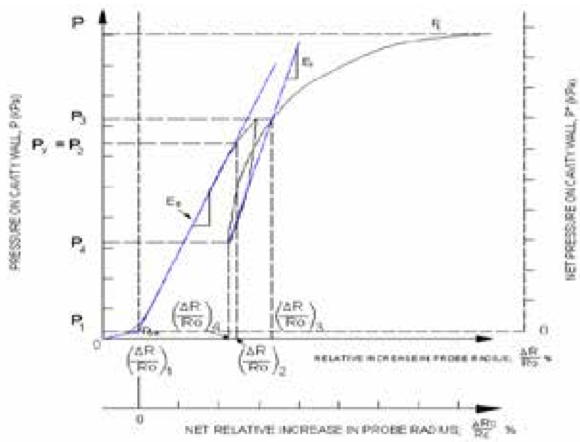

Figure 4. Typical PPMT Curve to obtain Engineering Parameters

The pressuremeter reload modulus, E_r, is calculated as the same manner (Fig. 4) as the E_0. It is calculated by using the following formula:

$$E_r = (1+\nu)\left[\left(1+\frac{\Delta R_3}{R_0}\right)^2 + \left(1+\frac{\Delta R_4}{R_0}\right)^2\right]\frac{\Delta P_{3\text{-}4}}{\left[\left(1+\frac{\Delta R_3}{R_0}\right)^2 - \left(1+\frac{\Delta R_4}{R_0}\right)^2\right]} \quad (4)$$

with $\left(P_3, \left(\frac{\Delta R}{R_0}\right)_3\right)$ and $\left(P_4, \left(\frac{\Delta R}{R_0}\right)_4\right)$ being the two data points on the reload portion of the pressuremeter test (Fig. 4).

Where:
ΔR_1 = Increase in probe radii at the beginning of the pressure increment of the initial linear portion
ΔR_2 = Increase in probe radii at the end of the pressure increment of the initial linear portion
ΔR_3 = decrease in probe radii at the beginning of the pressure increment of the reload portion
ΔR_4 = decrease in probe radii at the end of the pressure increment of the reload portion
R_0 = Initial radius of the probe.

3 DATA ACQUISITION SOFTWARE IMPROVEMENT

A stand-alone data acquisition program APMT was developed and compiled into an executable package to reduce data collection errors and simplify operator requirements during testing. Operators can use APMT to record digital pressures and volumes during all calibrations or tests, then quickly reduce test data and finally determine the engineering parameters (p_0, E_0, E_r and p_L). The reduced data is displayed on the screen during testing as either pressure versus volume, volumetric strain or radial strain. APMT records four samples per second throughout testing. This sampling rate produces sufficient data points to allow proper engineering analyses. One of the most complex operations required during testing is for the operator to wait for 30 seconds after each volume injection and then accurately record pressures as the analogue pressure gage continues to change. APMT data collection software was developed such that the display available to the operator includes a sequence of three lights; red, yellow and green that change, based on the rate of change of successive pressure readings (Fig. 5).
A red light was chosen to indicate that successive readings are within 5 kPa. It was assumed that this change was small enough to involve that the soil pressure was nearly stable. Subsequently, a yellow light would indicate that successive readings are within 1 kPa. The software would then record three successive pressures, average them and save them to a file. The green light would indicate that the data was saved and the testing could continue. Once the data has been collected for a test, a new screen becomes available to the operator. This screen allows for determining both a lift-off and limit pressure (p_0 , p_L) along with initial and reload moduli (E_0, E_r). Figure 6, shows this typical APMT screen which includes both the raw and reduced data (Cosentino et al 2006).

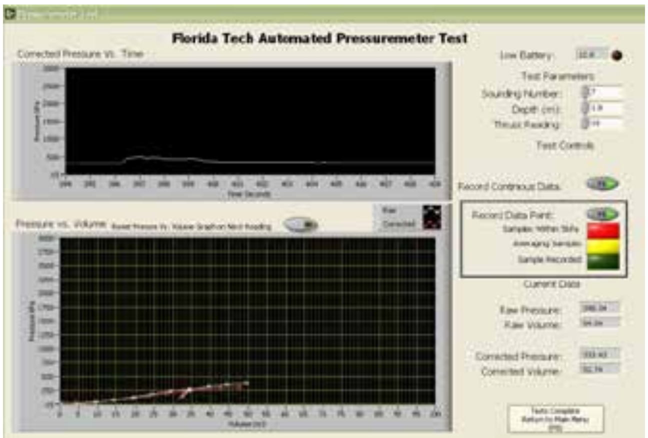

Figure 5. APMT Automatic Recording of Data Point

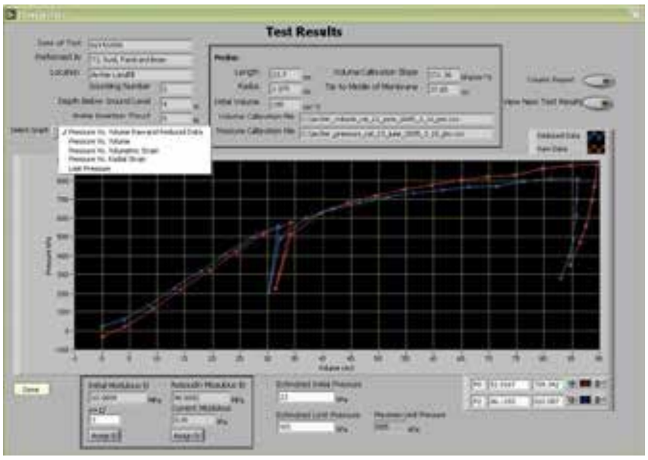

Figure 6. Typical APMT Screen

4 FIELD TESTING PROGRAM AND DATA COLLECTION

Two sites were chosen. The first site on the Florida Institute of Technology (FIT) Melbourne campus and the second site on the Archer Landfill in Gainesville, Florida, consisted predominately of sand. Testing was conducted using the FDOT SMO Cone Penetrometer rig with FDOT field technicians. To categorize the soils, Standard Penetration (SPT), CPT, Dilatometer (DMT) and PPMT tests were performed. The soil at the FIT site consisted of three sand layers. The upper medium-dense sand layer, interbedded with silt and clay lenses, varies from the surface to about 2 m. The second layer, also about 3.05 m thick, consists of very loose to loose silty sand. The third layer beginning at about 6.1 m consists of dense cemented sands. The sands at archer Landfill site displayed consistent which were divided into layers. The first layer to 2.1 m consists of loose silty sand. From 2.1 to 4.2 m, the second layer was medium dense silty sand. The third layer from 4.2 -9.1 m was predominantly medium dense sand to silty sand.

5 CORRELATION FROM PPMT ENGINEERING PARAMETERS

The initial elastic modulus was compared to the limit pressures using the engineering parameters from 96 PPMT tests in the silty sands at the FIT and Archer sites. These soils ranged from very loose to dense silty sands. An excellent correlation exists when modeled nonlinearly shown in Figure 7a. A nonlinear relationship would be expected because the limit pressure cannot increase infinitely as stiffness increases. Briaud (1992) presented linear correlations based on over 400 records, between the limit pressure and initial elastic modulus of $p_L = 0.125\ E_0$ for sands and $p_L = 0.071\ E_0$ for clays. He specifically states that the wide scatter in the data used to develop them, "makes these correlations essentially useless for design;" however, they give the engineers a relative feel for the engineering parameters (Cosentino et al 2008). When a linear regression through the origin was used to describe this data the equation becomes $p_L = 0.079\ E_0$. In conclusion, this nonlinear relationship shows that PPMT data are realistic and can be used by engineers.

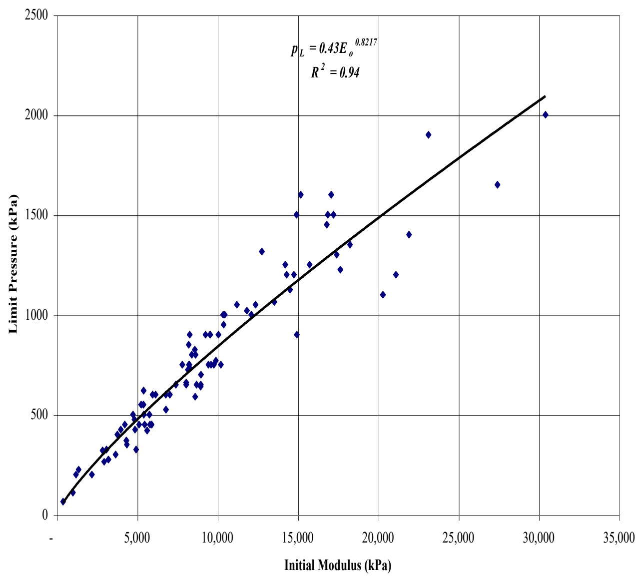

(a)

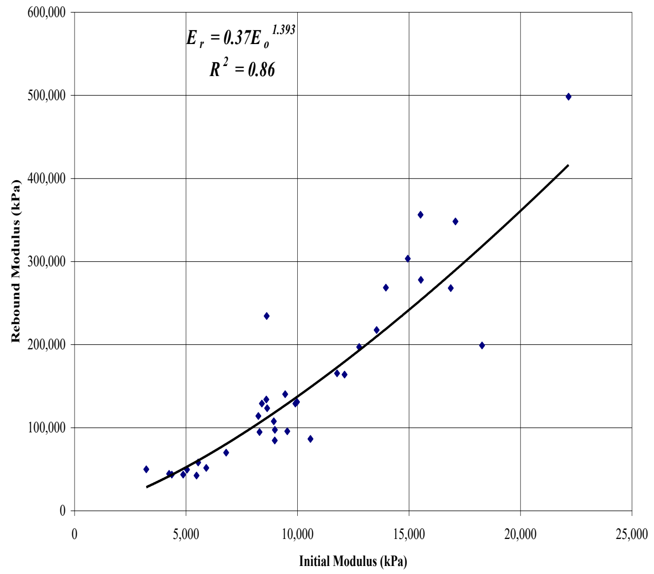

(b)

Figure 7: Correlation between Limit Pressure and Initial Elastic Modulus in Silty Sands (a), Correlation between Reload Modulus and Initial Modulus for Silty Sands (b).

A nonlinear correlation was developed between the initial elastic modulus and the reload modulus in Figure 7b. Using data from 36 tests performed in silty sands from both the FIT and Archer sites. Twenty of the 36 tests were performed and recorded using the digital system (Cosentino et al 2008). When only digital information was evaluated the regression equation became $E_r = 0.15\ E_0^{1.4864}$ and had a corresponding regression coefficient (i.e. R^2) of 0.93. This improved correlation suggests that the digital instrumentation combined with the APMT software improves the PPMT data. Briaud (1992) presents a linear correlation between these two parameters where $E_r = 8\ E_0$ in sands. If the data in Figure 7b is represented linearly a regression of $E_r = 16\ E_0$ results with an R^2 value of 0.76 and if only digital data is used the equation becomes $E_r = 21\ E_0$ results with an R^2 of 0.79. These linear results indicate that digital testing should be used to improve pressuremeter data.
Similar correlations between the lift-off or initial pressure and limit pressure were developed; however the data were not well represented statistically as shown in the equation and corresponding correlation coefficient below.

$$p_L = 24.2\ (p_0)^{0.9685} \qquad R^2 = 0.62$$

Linear correlations between the lift-off pressure and initial elastic moduli were developed from the testing in sands. The overall regression coefficient was 0.30, therefore the resulting equation is not presented. Again, limited knowledge of the stress history at these sites could be a major factor in the poor statistical fit. The data recorded by hand was compared to the digitally recorded data. The regression coefficient from the digital information was nearly 0.58 producing the equation below; while the data recorded manually was 0.36. This 60 % increase in the regression coefficient indicates that digital stress-strain data is a significant improvement over manually recorded data.

$$E_0=68\ (p_0) + 3724$$

6 CONCLUSIONS

Reliable correlations exist from the large number of PPMT test data, indicating that this device can produce useful parameters for engineers to use in geotechnical analysis and design

A precise nonlinear correlation was developed between the PPMT initial elastic modulus and the limit pressures in sands.

A reliable nonlinear correlation was developed between the PPMT initial elastic and the reload moduli in sands. This correlation improved when digital information along with the APMT software was used, indicating that the combination of digital instruments and this software will provide engineers with more reliable data than the analogue equipment alone.

The APMT software allows quick evaluations of the soil parameters, including the lift-off pressure p_0, initial modulus E_0, reload modulus E_r and limit pressure p_L.

The raw data obtained from APMT was in agreement with the data recorded using the conventional PPMT.

The pushed-in PPMT test is much faster than conventional pressuremeter testing and is recommended for use in determining the soils stress-strain response and the associated engineering parameters.

7 ACKNOWLEDGEMENTS

The authors would like to acknowledge the following people for their invaluable guidance and help in the completion of this study; John Shoucair, Brian Bixler and Todd Britton of the Florida Department of Transportation State Materials Office.

8 REFERENCES

Briaud, J.L. & Shields, D.H. 1979. A Special Pressuremeter and Pressuremeter Test for Pavement Evaluation and Design. Geotechnical Testing Journal, ASTM 2:3.

Cosentino, P.J. 1987. Pressuremeter Moduli for Airport Pavement Design. Ph.D. Dissertation, Department of Civil Engineering, Texas A&M University,

Messaoud, F. 2008. Pressuremeter Test Evaluation for Developing P-Y Curves for Driven Piles. In Proc. 11th Baltic Sea Geotechnical Conference, Geotechnic in Maritime Engineering. Gdansk, Poland, 271-278

Cosentino, P.J. & Briaud, J.L. 1989. FWD Back Calculation Moduli Compared with Pavement Pressuremeter Moduli and Cyclic Triaxial Moduli. Philadelphia, Pennsylvania: ASTM 23–340.

Cosentino, P. Kalajian, E., Stansifer, R. Anderson, J. B. Kattamuri, K. Sundaram, S. Messaoud, F. Misilo, T. & Cottingham, M. 2006. Standardizing the Pressuremeter Test for Determining p-y Curves for Laterally Loaded Piles, FDOT Research Report. Contract BD 658.

Roctest, 2005. PENCEL Pressuremeter Instruction Manual. Plattsburgh, N.Y, Roctest, Inc.

Messaoud, F. Nouaouria M.S. & Cosentino, P.J. 2011. PENCEL pressuremeter test evaluation for developing p-y curves for driven piles. ACEE International Journal on Transportation and Urban Development, v. 1:2, 14-18.

Bagueling, F. Jezequel, J.F. & Shields, D.H. 1978. The Pressuremeter and Foundation Engineering. 1st ed., trans., Tech Publications, Causthal, Germany.

Tucker, L.M. & Briaud, J.L. 1987. Laterally loaded piles and the Pressuremeter: comparison of existing methods. ASTM. 97-111.

Briaud, J.L. 1992. The Pressuremeter. A.A Balkema, Brookfield, Vermont.

Cosentino, P. Kalajian, E. Messaoud, F. Sundaram, S. Misilo, & T. David Horhota, 2008. Correlation Between PENCEL Pressuremeter, Cone Penetrometer and Dilatometer Parameters. Transportation Research Record, Soil Mechanics, Vol 2053, 65-71.

Geotechnical and Geophysical Site Characterisation 5 – Lehane, Acosta-Martínez & Kelly (Eds)

In Situ Characteristics of Manhattan Glacial Deposits from Pressuremeter Tests

C. E. Ho
Arup, New York, USA

ABSTRACT: The development of the Second Avenue Subway on the East side of Manhattan, New York City, involved a cut-and-cover section constructed in a buried valley of thick soft soil deposits. The soil stratification at the site included fill, organics, silty sands and a thick layer of glacial deposits reaching to as least 60m deep below ground surface. The glacial deposits comprised of an alternating sequence of varved silts and clays. The construction involved an 18m deep excavation supported by diaphragm walls embedded up to 12m below the base of the excavation. The excavation was carried out below the elevation of the glacial deposits. An accurate determination of the properties of the glacial deposits was therefore of utmost importance for proper design of the excavation support system. The glacial deposits were highly sensitive and prone to sample disturbance, rendering great difficulty in obtaining samples for testing the material in the laboratory. In situ testing was therefore necessary to obtain more reliable soil data. This paper presents the results of pressuremeter testing in the varved silts and clays. Practical issues that were encountered on site during drilling and testing are highlighted. The results of both self-boring and pre-bored pressuremeter tests are discussed.

1 INTRODUCTION

The development of the Second Avenue Subway on the East side of Manhattan, New York City, involved a cut-and-cover section constructed in a buried valley of thick soft soil deposits. The soil stratification at the site included fill, organics, silty sands and a thick layer of glacial deposits reaching to as least 60m deep below ground surface. The glacial deposits comprised of an alternating sequence of varved silts and clays.

The construction involved an 18m deep excavation supported by diaphragm walls embedded up to 12m below the base of the excavation. The excavation was carried out below the elevation of the glacial deposits. An accurate determination of the properties of the glacial deposits was therefore of utmost importance for proper design of the excavation support system.

The glacial deposits were highly sensitive and prone to sample disturbance, rendering great difficulty in obtaining samples for testing the material in the laboratory. In situ testing was therefore necessary to obtain more reliable soil data. This paper presents the results of pressuremeter testing in the varved silts and clays. Practical issues that were encountered on site during drilling and testing are highlighted. The results of both self-boring and pre-bored pressuremeter tests are discussed.

2 PRESSUREMETER TESTS

2.1 *Test Conditions*

Three locations were initially identified for testing using self-boring pressuremeters. Available reference borings had indicated that the ground conditions at SBP-94-5 were suitable with clays and silts having standard penetration test (SPT) blow counts less than 20 blows/0.3m. However, during actual testing operations, the soil was found to be too hard to penetrate. Three initial attempts were unsuccessful and testing was ultimately abandoned at this location.

At the second test location (SBP-97-5), four self-boring pressuremeter tests were successfully conducted.

A third location at BP96-13 was attempted. The self-boring pressuremeter test at the upper level of the test zone was successfully completed at this location, however shells and wood were found lodged in the cutting shoe. To avoid potential problems with self-boring operations at the deeper levels, it was decided to replace the subsequent testing with a pre-bored pressuremeter. The first attempt to form a pilot hole in BP96-13 was unsuccessful. The hole was over-sized and unsuitable for testing. After appropriate drilling procedures were established, there was no further difficulty in forming the pilot hole close to the correct size. However, the hole was slightly under-sized so that the soil was hard against the membrane at the start of the test. Four pre-bored pressuremeter tests were subsequently completed in BP96-13.

Table 1 summarizes the conditions under which the tests were conducted. The SPT values provide an indication of the relative density of the soils tested.

Table 1. Soil conditions at pressuremeter test locations

Location	Instrument	Depth	SPT N	Test No.
		m	blows/0.3m	
SBP-94-5	Self-boring	16.4		Abandoned
SBP-94-5	Self-boring	18.2		Abandoned
SBP-94-5	Self-boring	23.9		Abandoned
SBP-97-5	Self-boring	16.2	10	NYC1
SBP-97-5	Self-boring	19.3	7	NYC2
SBP-97-5	Self-boring	22.3	14	NYC3
SBP-97-5	Self-boring	25.3	10	NYC4
SBP-97-5	Self-boring	27.3		Abandoned
BP96-13	Self-boring	7.2	60	NYC5*
BP96-13	Pre-bored	10.5		NYC6
BP96-13	Pre-bored	12.3	36	NYC7
BP96-13	Pre-bored	18.4	45	NYC8
BP96-13	Pre-bored	20.1		NYC9
BP96-13	Pre-bored	22.9		NYC10

*Shells and wood lodged in cutting shoe of pressuremeter

2.2 *Test Procedure*

All tests were carried out in accordance with the recommendations of ASTM D4719 (1994). The readings were electronically captured in real-time and input into a computer for processing. A plot of pressure versus cavity strain, ε_c (defined as the radial deformation, Δ_r divided by the original radius of the borehole, r_o) was continuously displayed on the computer screen for control of the test (Fig. 1).

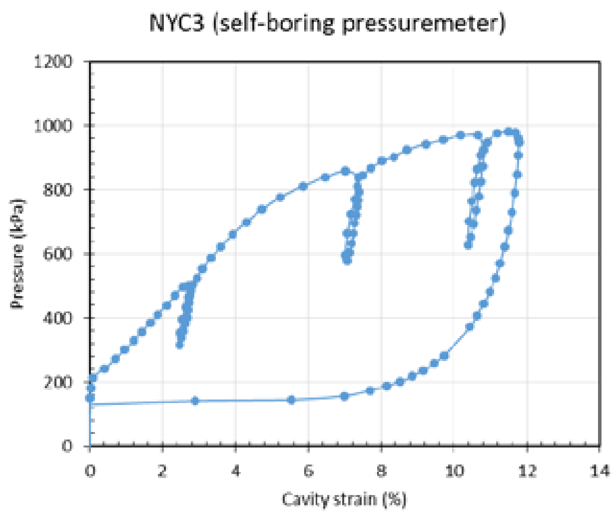

Figure 1. Typical expansion curve in pressuremeter test

Attempts were made to ensure all tests were completed in about the same time, so that influence of creep and consolidation was similar for each test. Unfortunately at this site, the strength of the tested materials varied considerably (ranging from 30 to 365 kPa). Hence, the choice of pressure increments had to be selected based on the operator's appreciation of the initial stages of the pressuremeter curve to try and determine the full pressuremeter curve as completely as possible. The maximum test pressure was usually limited by the maximum extension of one of the three electronic displacement sensors. Three unload-reload loops were conducted at each test zone to check for repeatability of the results.

3 INTERPRETATION OF SOIL PARAMETERS

3.1 *Soil shear strength and limit pressure*

Using the cavity expansion theory and assuming a linear elastic perfectly plastic soil model, Gibson and Anderson (1961) showed that the cavity pressure (P) for an undrained soil response in the plastic phase can be expressed as

$$P = P_L + s_u \ln (\Delta V/V_o) \qquad (1)$$

where P_L = limit pressure, s_u = undrained shear strength and $\Delta V/V_o$ = volumetric strain. s_u can be obtained from the slope of the plastic zone in a semi-logarithmic plot of P versus $\Delta V/V_o$. P_L is defined as the maximum cavity pressure that can be sustained at infinite expansion. For practical purposes, P_L is commonly assumed to be reached when the volumetric expansion (ΔV) is equal to the initial volume of the cavity (V_o).

The volumetric strain is related to the radial extension of the displacement sensors via the relationship $\Delta V/V_o = (r^2 - r_o^2)/r_o^2$ where r_o and r are the initial and expanded cavity radii respectively. $\Delta V/V_o = 1$ corresponds to a cavity strain $\varepsilon_c = \Delta r/r_o$ of 0.414, where $\Delta r = r - r_o$.

Figure 2 shows the semi-logarithmic plot of P vs ε_c. The pressuremeters used in this project will only expand up to about 20% of its initial volume before the displacement sensors reach their full extension. Hence P_L was obtained by extrapolating the best fit line through the data points at a cavity strain of 41%.

Table 2 summarizes the values of s_u and P_L obtained from the pressuremeter tests.

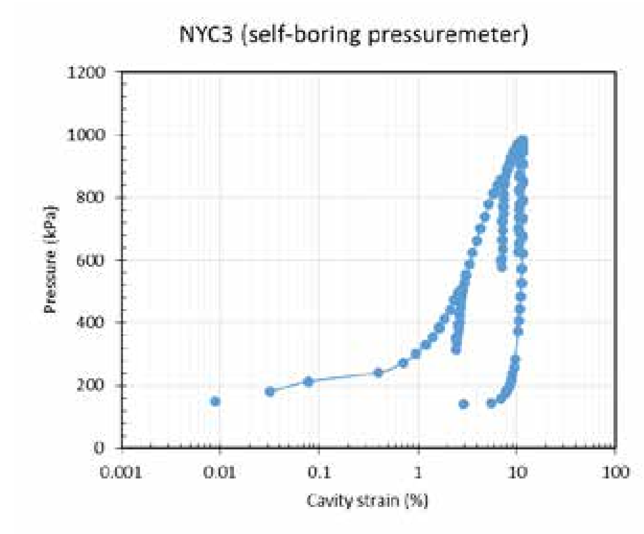

Figure 2. Semi-logarithmic plot of pressuremeter test data

Table 2. Undrained shear strength and limit pressure of soils

Test No.	Depth	Undrained Shear Strength, s_u	Limit Pressure, P_L
	m	kPa	kPa
NYC1	16.2	188.2	972.2
NYC2	19.3	162.0	965.3
NYC3	22.3	246.2	1351.4
NYC4	25.3	256.5	1606.5
NYC5	7.2	30.3	303.4
NYC7	12.3	364.1	1599.6
NYC8	18.4	275.8	1958.2
NYC9	20.1	190.3	1248.0
NYC10	22.9	137.9	1379.0

Yu and Collins (1998) indicated that the total stress approach proposed by Gibson and Anderson (1961) is reasonable for soils with low over-consolidation ratios (OCR < 2) but may under-predict s_u for higher OCRs. For comparison, s_u was also obtained using an alternate method proposed by Palmer (1972) based on the relationship between the shear stress at the cavity wall (τ) and the cavity strain (ε_c) given by Equation 2.

$$\tau = \tfrac{1}{2}(1+\varepsilon_c)\,(2+\varepsilon_c)\,dP/d\varepsilon_c \qquad (2)$$

For small strains, Equation 2 simplifies to

$$\tau = \varepsilon_c\, dP/d\varepsilon_c \qquad (3)$$

By differentiating the P versus ε_c curve, the peak shear stress (τ_{peak}) and its associated shear strain ($\gamma = 2\varepsilon_c$) can be determined. The analysis was performed only for self-boring pressuremeter test results as they were likely to be less disturbed.

Table 3 shows that τ_{peak} corresponded very closely to the values of s_u obtained from the semi-logarithmic plot in Table 2, giving confidence that the results were reliable.

Table 3. Peak shear stress (Palmer's Method)

Test No.	Depth	Peak Shear Stress, τ_{peak}	Shear Strain at Peak Stress, γ
	m	kPa	%
NYC1	16.2	179.3	4.5
NYC2	19.3	165.5	4.5
NYC3	22.3	241.3	4.0
NYC4	25.3	262.0	3.3
NYC5	7.2	27.6	1.0

Figure 3 shows that undrained shear strengths obtained from the pre-bored pressuremeter tests were significantly higher than the self-boring pressuremeter tests, with the values exhibiting a decreasing trend with depth. The strength results from self-boring pressuremeter tests however, showed an increasing trend with depth. These results suggest that the site stress history of the varved silts and clays can be significantly different between boreholes. Laboratory consolidation tests had indicated that the over-consolidation ratio (OCR) for the varved silt and clay stratum ranged from 1 to 6.4, with the mean value at about 3.

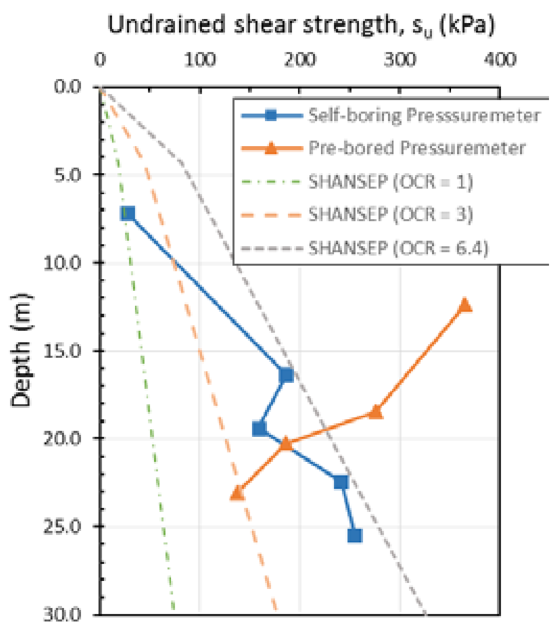

Figure 3. Shear strength profile

Alternate s_u values were computed using the SHANSHEP model for over-consolidated clays (Ladd, 1991),

$$s_u = 0.22\,\sigma_{vo}'\,(OCR)^{0.8} \qquad (4)$$

where σ_{vo}' is the effective overburden stress.

It was assumed that total unit weight of the soil was 19.6 kN/m^3 with the water table at 4.3m below ground level. The strengths obtained from the self-boring pressuremeters were in good agreement with the SHANSEP values for the range of OCRs reported by the consolidation tests. However, the pre-bored pressuremeter test results for the upper levels corresponded to OCR much greater than 6.4 and a trend suggesting a decreasing OCR with depth.

Figure 4 shows the relationship between the derived s_u and P_L values summarized in Table 2. It can be seen that the ratio of s_u/P_L varied over a narrow range between 0.1 and 0.23. The s_u/P_L ratios obtained from the pre-bored pressuremeters appear to be more scattered. The most consistent correlation was given by the self-boring pressuremeter tests with $s_u/P_L = 0.17$.

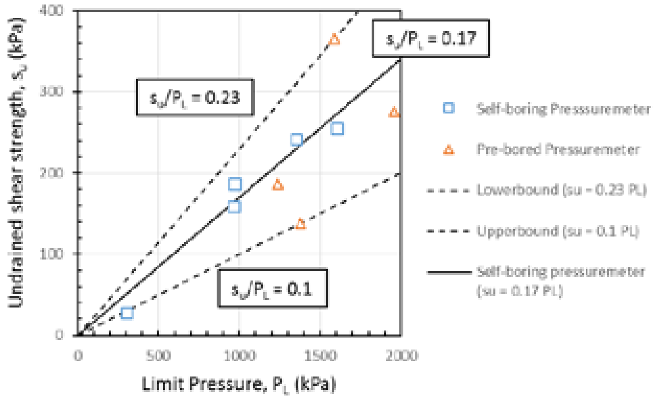

Figure 4. Shear strength – limit pressure correlation

3.2 *Small strain elastic shear modulus*

The response of a linear elastic homogeneous material subjected to cavity expansion in infinite space can be described by Equations 5 and 6:-

$$\Delta r = P\, r_o\, [(1+\mu)/E] \qquad (5)$$

$$E = 2G\,(1+\mu) \qquad (6)$$

where P = pressure at cavity wall, r_o = initial radius, Δr = radial deformation, E = Young's modulus, G = shear modulus, μ = Poisson's ratio. Combining Equations (5) and (6), and setting $\varepsilon_c = \Delta r/r_o$, we have

$$G = 0.5P/\varepsilon_c \qquad (7)$$

Hence, the small strain elastic shear modulus (G_o) can be obtained from the slope (m) of an unload-reload loop in a P versus ε_c plot, giving G_o = 0.5m. Table 4 summarizes the values of G_o obtained for each loop in the tests.

Figure 5 shows that the ratio of G_o/s_u varied over a very wide range between 100 and 350. The self-boring pressuremeter results gave lower bound G_o/s_u ratios in the majority of tests. The converse is true for the pre-bored pressuremeter tests. The spread in the data points appear to be representative of the natural variability of the varved silt and clay material as evidenced by the significant difference in the SPT blow counts given in Table 1. The large variation in shear modulus may also be in part due to the sensitivity of the soil to installation and testing disturbance, as observed from the significant differences in G_o values obtained from the three cycles in each test (Table 4).

Table 4. Elastic shear modulus of soil

Test No.	Depth	Unload-reload Shear Modulus, G_o		
		1st Cycle	2nd Cycle	3rd Cycle
	m	kPa	kPa	kPa
NYC1	16.2	12293.8	27207.7	46224.1
NYC2	19.3	19423.2	17616.7	27455.9
NYC3	22.3	27221.5	37619.1	37632.9
NYC4	25.3	74328.1	87139.0	87056.3
NYC5	7.2	2378.8	3344.1	-
NYC7	12.3	41266.6	45562.2	46224.1
NYC8	18.4	81374.8	91931.0	90427.9
NYC9	20.1	57456.0	47168.7	51429.8
NYC10	22.9	-	51133.3	48768.3

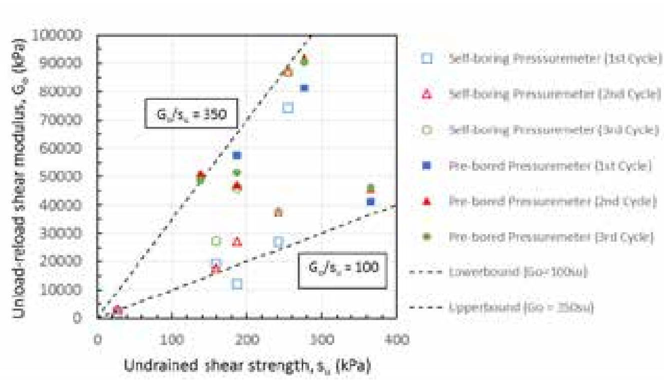

Figure 5. Elastic shear modulus – undrained shear strength relationship.

3.3 *In situ lateral earth pressure*

The in situ lateral earth pressure in the ground (σ_{ho}) can be estimated by identifying the lift-off pressure (P_o) near the starting of the pressuremeter test. This is the pressure at which the membrane first lifts off the pressuremeter body when the confining stress around it is just exceeded.

Table 5 summarizes the in situ lateral earth pressures obtained from the pressuremeter tests.

Table 5. In situ lateral earth pressures

Test No.	Depth	Lift-off Pressure, P_o	Marsland and Randolph (1977)
	m	kPa	kPa
NYC1	16.2	129.6	172.4
NYC2	19.3	168.9	303.4
NYC3	22.3	241.3	275.8
NYC4	25.3	238.6	413.7
NYC5	7.2	142.0	137.9
NYC7	12.3	416.5	-
NYC8	18.4	775.7	-
NYC9	20.1	575.7	-
NYC10	22.9	799.8	

The in situ lateral earth pressure was also estimated from the linear portion of the semi-logarithmic plot of P versus ε_c using the procedure of Marsland and Randolph, 1977 for comparison. As the pre-bored pressuremeter was inserted into a borehole with slightly smaller diameter than the instrument, the initial stresses in the soil immediately surrounding the borehole was likely to have been altered to some degree. Therefore only the data from self-boring pressuremeter tests were considered to provide a reliable basis for determining σ_{ho}. The corresponding results are tabulated in Table 5. In general, the values given by Marsland and Randolph's method were higher than the lift-off pressures. Hence, the lift-off pressures provide a lower bound estimate of the initial in situ soil stresses.

Figure 6 compares the interpreted soil pressures with the theoretical at-rest states computed from $K_o = K_{onc} (OCR)^{\sin\phi'}$ where $K_{onc} = 1-\sin\phi'$ (Mayne and Kulhawy, 1982). A total unit weight $\gamma = 19.6$ kN/m^3 and $\phi' = 32^o$ was assumed based on laboratory drained triaxial tests for the varved silt and clay stratum.

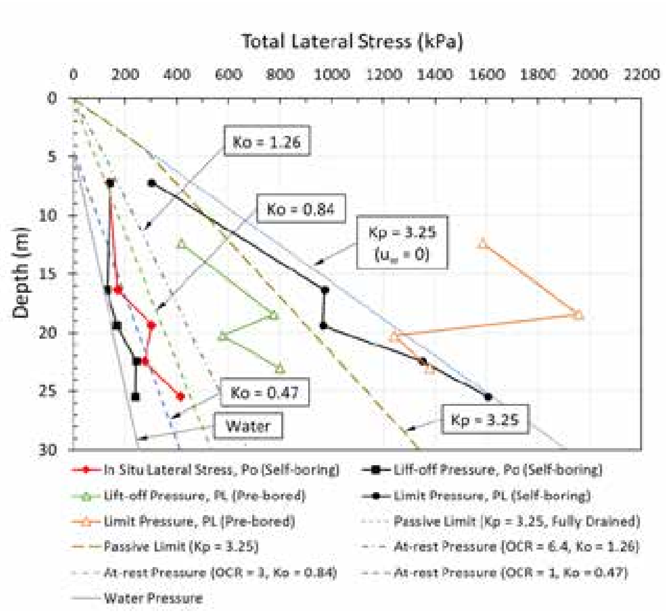

Figure 6. Lateral soil stresses interpreted from pressuremeter tests

It can be seen that lift-off pressures (P_o) obtained from the self-boring pressuremeter tests were consistent with the hydrostatic water pressure in the ground. However, P_o derived from the pre-bored pressuremeter tests were much higher than the maximum anticipated at-rest pressure for OCR = 6.4 (K_o = 1.26) for the varved silt and clay stratum. This suggests that the disturbance of the borehole walls in the pre-bored pressuremeter tests was significant. The estimated lateral stresses based on Marsland and Randolph (1977) were in general agreement with the range of at-rest earth pressures for OCR = 1 (K_o = 0.47) to 6.4 (K_o = 1.26).

The derived values of limit pressure (P_L) usually tends to be less sensitive to the initial condition at the borehole wall than the in situ lateral stress (σ_{ho}). Assuming that self-boring pressuremeter tests were reliable, it would appear that P_L for the deeper pre-bored pressuremeter tests were reasonable and consistent with the general trend of the results obtained from the self-boring pressuremeter tests. However, the pre-bored pressuremeter tests at shallower depths gave much higher P_L values, which suggests that significant disturbance was induced during insertion of the instrument into these boreholes.

It was noted that the limit pressures obtained from both the self-boring and pre-bored pressuremeter tests were higher than the plane strain passive resistance ($K_p = [1+\sin\phi']/[1-\sin\phi'] = 3.25$). This may be attributed to migration of pore water out of the soil when the volumetric cavity expansion is large, resulting in an increase in effective stress around the borehole. As can be seen, the P_L values approach the ideal fully drained K_p line, when water in soil pores have been completely expelled (i.e. when pore water pressure reduces to zero and the effective vertical stress become equal to the total overburden stress). Further investigation is needed to clarify this observation.

4 CONCLUSIONS

The glacial deposits of Manhattan, New York consists of varved silts and clays, which are highly sensitive and prone to sampling disturbance, rendering great difficulty in obtaining high quality samples for testing the material in the laboratory. In situ testing is therefore necessary for obtaining more reliable data to characterize the soil.

The total stress approach of Gibson and Anderson (1961) based on cavity expansion theory can provide reasonable results for interpreting pressuremeter tests in the glacial deposits. This paper compares the results obtained from self-boring and pre-bored pressurementer tests that were carried out as part of the Second Avenue Subway project. It was observed that self-boring pressuremeter tests gave more consistent results than pre-bored pressuremeter tests due to less soil disturbance. However, tests using self-boring pressuremeters were limited to soils with lower strength and limited obstructions.

Different methods for interpretation of soil shear strength and in situ lateral stress were used to provide guidance on the reasonableness of the results. Stress history and drainage condition of the soil deposits were considered. s_u/P_L ratios ranged from 0.1 to 0.23. The best correlation was given by self-boring pressuremeter tests with $s_u/P_L = 0.17$. G_o/s_u ratios varied between 100 and 350, with self-boring pressuremeters giving a lower bound value.

5 REFERENCES

ASTM D4719 (1994). "Standard test method for pressuremeter testing in soils".

Gibson, R.E. and Anderson, W. F. (1961). "In situ measurement of soil properties with the pressuremeter". *Civil Engineering and Public Works Review*, Vol. 56, No.658: 615-618.

Ladd, C. C. (1991). "Stability evaluation during staged construction". *J. Geot. Engg*. 117(4), ASCE: 540-615.

Mayne, P. and Kulhawy, F. H. (1982). "K_o – OCR relationships in soils". *J. Geot. Geoenv. Engg*. 108(6), ASCE: 851-872.

Marsland, A, and Randolph, M. F. (1977). "Comparison of the results from pressuremeter tests and large in situ plate tests in London Clay". *Geotechnique* 27(2): 217-243.

Palmer, A.C. (1972). "Undrained plane-strain expansion of a cylindrical cavity in clay: a simple interpretation of the pressuremeter test". *Geotechnique* 22(3): 451-457.

Yu, H.S. and Collins, I. F. (1998). "Analysis of self-boring pressuremeter tests in overconsolidated clays". *Geotechnique*, 48(5): 689-693.

Geotechnical and Geophysical Site Characterisation 5 – Lehane, Acosta-Martínez & Kelly (Eds)

Membrane correction for pressuremeter test

J. Monnet
GAIATECH, Seyssinet, France

D. Mahmutovic, L. Boutonnier
EGIS Geotechnique, Seyssins, France

ABSTRACT: The pressuremeter standards allows only two corrections: on the dilatation of the equipment; on the membrane rigidity. It assumes that the pressure applied into the probe is equal to the reaction pressure of the soil at the borehole wall. It neglects the effect of the thickness of the membrane and its defor-mation shape. This paper takes into account the effect of thickness of the membrane and its balloon shaped deformation with new corrections applied on the pressuremeter measurements. A theoretical correction is proposed and check by the results of a finite element calculation which takes into account the presence of two type of membrane: one in free ends for probe G, one with embedded ends for slotted tube probe. With these corrections, the pressuremeter test can be used as a shearing test able to measure the shearing elastic and plas-tic characteristics of the soil.

1 INTRODUCTION

The standards of the pressuremeter test (Norme NFP 94-110-1 2000, Standard D 4719-00 1994) consider that the pressuremeter probe has a membrane with no thickness so that the pressure of the water inside the probe is equal to the reaction pressure of the soil outside the probe. It consider also that the probe deforms in a cylindrical shape so that the displacement of the membrane is the same at any point along the membrane. These assumptions of Ménard can be found in Baguelin et al. (1978) Mair & Wood (1987). They are reused in the standards of the test which are described (Monnet, 2016) and in used all around the world. The effect of the ratio length over diameter (L/D) and the shape of the membrane with free ends has been studied by Houlsby & Carter (1993) with the effects on the measured modulus of the soil. They do not study the reduction of pressure linked to the shape of the deformed probe. It can be seen (Figure 1) that the pressuremeter probe G deforms as a beam on 2 free supports during the calibration. The slotted tube (Figure 2) deforms in a shape similar as an embedded beam during calibration. This paper deals with the shape of the deformed probe which is assumed to be more realistic with a parabolic shape for the probe G and a degree 4 shape for the slotted tube. These corrections has been used for the shearing interpretation of the pressuremeter test (Monnet et al.2006; Monnet 2012) and in the program Gaiapress (2014). analysis of membrane correction

2 ANALYSIS OF MEMBRANE CORRECTIONS

If we consider the probe as a tube (Figure 3) with an inner water pressure p_{yi} applied on the internal diameter Φ_i coming from the Control Pressure Volume Unit (CPV) and an outer pressure of reaction applied on the outer diameter Φ_e of the soil, there should be a difference between these two pressures. The thickness e of the membrane should decrease the value of the pressure p_{ye} applied to the soil with relation (3).

Figure 1. Deformation of the probe for the calibration of the probe for pressure losses (Baguelin et al, 1978)

Figure 2. Deformation of the probe for the calibration of the slotted tube probe for pressure losses

2.1 *Effect of the shape of the deformed probe*

2.1.1 *Case of the free end membrane*

This case is found using the E or G probe. The radius of the deformed probe is assumed to be of the quadratic form (1), where l_t is the length of the deformed probe, y is the ordinate of the point along the probe; its value is 0 at the center of the probe length and l/2 at the extremity of the probe; r_0 is the radius of the probe at its extremity and r_{max} is the radius at the center of the probe.

The value of the reaction p_y of the soil is assumed to be proportional to the deformation along the probe with relation (2) where p_0 is the pressure at the extremity of the probe and p_{max} the pressure at the center of the probe.

Taking into account the thickness e of the membrane of the probe (Figure 3) and the difference between the outer diameter Φ_e and the inner diameter Φ_i, equation (3) gives the relation between the inner pressure p_{yi} of the water inside the probe and the reaction pressure p_{ye} of the soil outside the probe. This relation shows that the pressure outside the probe is smaller than the pressure outside the probe. This phenomenon is not taken into account by the standards (Norme NFP 94-110-1, 2000; Standard D 4719-00, 1994).

$$r_y = r_{max}\left[4\left(\frac{r_0}{r_{max}} - 1\right)\left(\frac{y}{l_t}\right)^2 + 1\right] \tag{1}$$

$$p_y = p_{max}\left[4\left(\frac{p_0}{p_{max}} - 1\right)\left(\frac{y}{l_t}\right)^2 + 1\right] \tag{2}$$

$$p_{yi}.r_{yi}.d\theta = p_{ye}.(r_{yi} + e).d\theta \tag{3}$$

$$F_{react} = \int_{-l/2}^{l/2} p_y.2.\pi.r_y.dy \tag{4}$$

$$\frac{dF_{react}}{d\theta} = l_t\left\{(r_{max} - r_0)\left[\frac{(p_{max} - p_0)}{5} + \frac{p_{max}}{3} + \right] + (r_0 - r_{max})\frac{p_{max}}{3} + p_{max}.r_{max}\right\} \tag{5}$$

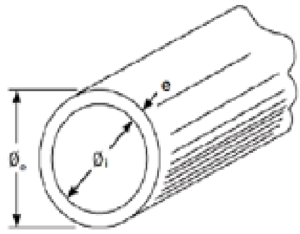

Figure 3. Influence of the thickness of the membranes

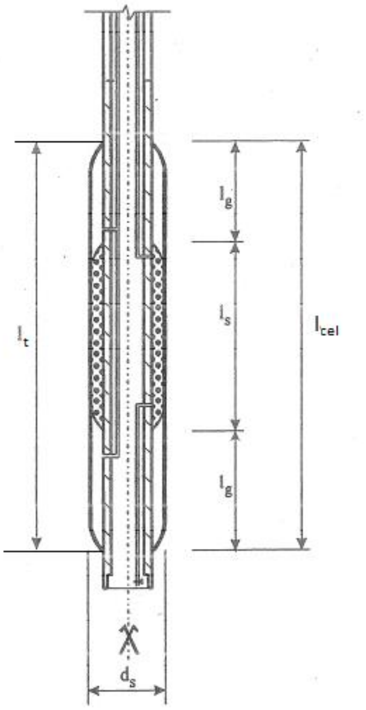

Figure 4. Scheme of the pressuremeter probe G (Standard NFP 94-110, 2000)

Outside the probe, the force of reaction of the soil is given by (4), and can be calculated per unit angle as (5). The force per unit angle gives by the water table is given by (6)

$$\frac{dF_w}{d\theta} = p_w l_t\left[\frac{(r_{max} - r_0)}{3} + r_{max}\right] \tag{6}$$

Inside the probe, the water applies a pressure of p_s (or a gaz pressure for Camkometer) along the measurement cell of length l_s. The air applies an air pressure of p_g along the two guard cells of length l_g and the total length of the loaded area is given by l_{cel} (7). There is a difference between l_{cel} the total length of the loaded aera and the total deformable lenght of the probe l_t because sometime le guard cells does not reaches the ends of the probe. The total force inside the probe is given by (8) and can be developed in (9) for a unit angle, where r_{0i} is the inner radius of the probe at its extremities, r_{maxi} is the inner radius at the center of the probe.

$$l_{cel} = l_s + 2.l_g \tag{7}$$

$$F_{cel} = 2.\int_{l_s/2}^{l_{cel}/2} p_g.dS + \int_{-l_s/2}^{l_s/2} p_s.dS \tag{8}$$

$$\frac{dF_{cel}}{d\theta} = p_g\left[(r_{maxi} - r_{0i})\frac{(l_s^3 - l_{cel}^3)}{3{l_t}^2} + r_{maxi}(l_{cel} - l_s)\right] + p_s\left[(r_{maxi} - r_{0i})\frac{l_s^3}{3{l_t}^2} + r_{maxi}l_s\right] \tag{9}$$

The equilibrium of the probe is reaches when the inner force is equal to the reaction force of the soil. This allows determining the maximum reaction pressure p_{max} of the soil (10) as a function of r_{max} the maximum radius of the probe. It is now possible to determine the mean pressure along the measurement cell by (11)

$$p_{max} = \frac{\mathrm{d}F_{cel}/\mathrm{d}\theta - \mathrm{d}F_w/\mathrm{d}\theta - l_t p_0\left(\frac{r_0}{5} - \frac{2r_{max}}{15}\right)}{\mathrm{l_t}\left(\frac{2}{15}r_0 + \frac{8}{15}r_{max}\right)} \tag{10}$$

$$p_{moy} = \mathrm{p_{max}} + (\mathrm{p_0} - \mathrm{p_{max}})\frac{\mathrm{l_s^2}}{3.\mathrm{l_t^2}} \tag{11}$$

$$V_t = \pi\left[(r_{max} - r_0)^2\frac{l_s^5}{5l_t^4} + (r_0 r_{max} - r_0 e - r_{max}^2 + r_{max}e)\frac{2l_{mes}^3}{3l_t^2} + l_s(r_{max} - e)^2\right] \tag{12}$$

$$r_{moy} = \mathrm{r_{max}} + (\mathrm{r_0} - \mathrm{r_{max}})\frac{\mathrm{l_s^2}}{3.\mathrm{l_t^2}} \tag{13}$$

$$\frac{dr}{r_0} = \frac{r_{moy} - r_0}{r_0} \tag{14}$$

The initial volume of the probe before deformation is V_s and V is the volume injected into the probe for a measurement. The total volume of the probe after deformation is V_t (12) with e the thickness of membrane. The value of r_{max} can be find solving the equation (12) and p_{max} by (10). The knowledge of r_{max}, allows determining the mean radius r_{moy} by relation (13) and the radial strain by (14)

2.1.2 *Case of the embedded membrane*

This case is found using the slotted probe. In that case the probe deforms along the relation (15),

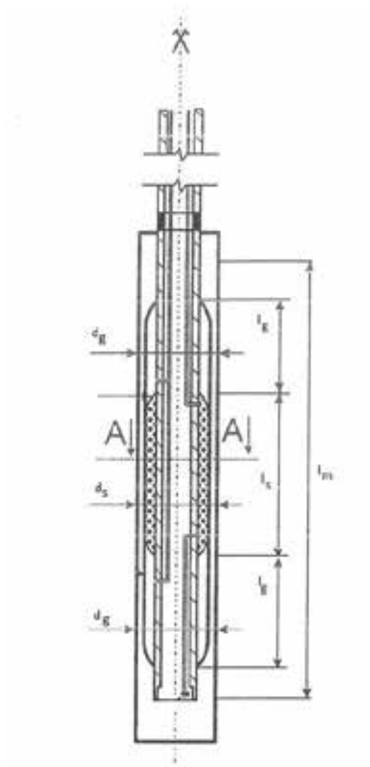

Figure 5. Scheme of the pressuremeter slotted tube (Standard NFP 94-110, 2000)

where l_m is the length of the slotted part of the tube. The pressure of reaction of the soil is given by (16).

$$r_y = 16(r_{max} - r_0)\left[\left(\frac{2y + l_m}{2l_m}\right)^2 - 2\left(\frac{2y + l_m}{2l_m}\right)^3 + \left(\frac{2y + l_m}{2l_m}\right)^4\right] + r_0 \tag{15}$$

$$p_y = 16(p_{max} - p_0)\left[\left(\frac{2y + l_m}{2l_m}\right)^2 - 2\left(\frac{2y + l_m}{2l_m}\right)^3 + \left(\frac{2y + l_m}{2l_m}\right)^4\right] + p_0 \tag{16}$$

$$\frac{dF_{react}}{d\theta} = \frac{8}{15}r_0(p_{max} - p_0)l_s + r_0 p_0 l_s \tag{17}$$

$$\frac{dF_w}{d\theta} = \frac{8}{15}p_w(r_{max} - r_0)l_t + p_w r_0 l_t \tag{18}$$

Outside the probe, the force of reaction of the soil is given by (4) and can be calculated per unit angle as (17). In (17) it is assumed that the soil has an elastic reaction to the deformation of the probe.

Outside the probe, the force per unit angle gives by the water table is given by (18).

The total force inside the probe is given by (8) and can be developed in (19) for a unit angle with the integral I_3 and I_4

$$\frac{dF_{cel}}{d\theta} = 32p_g(r_{max} - r_0)I_3 + 16p_s(r_{max} - r_0)I_4 + p_s(r_0 - e)l_s + p_g(r_0 - e)l_g \tag{19}$$

$$p_{max} = \frac{\mathrm{dF_{cel}/d\theta - dF_w/d\theta - \frac{o}{15} p_0(r_{max} - r_0) - p_0 r_0 l_t}}{\frac{128}{315}(\mathrm{r_{max} - r_0})\mathrm{l_t} + \frac{8}{15}\mathrm{r_0 l_t}} - p_0 \quad (20)$$

$$V = 256\pi(r_{max} - r_0)^2 \int_{l_s}^{l_s} r_y dy + 32\pi(r_{max} - r_0)(r_0 - e) \int_{l_s}^{l_s} r_y dy \quad (21)$$

$$r_{moy} = \sqrt{\frac{1}{l_s}\int_{-l_s/2}^{l_s/2} r_y^2 dy} \quad (22)$$

The equilibrium of the probe is reaches when the inner force is equal to the reaction force of the soil (10),. This allows determining the maximum reaction pressure p_{max} of the soil (20). The maximum radius of the probe is determined by the knowledge of the volume V injected into the probe (21), the mean radius is found by (22) and the radial strain by (14).

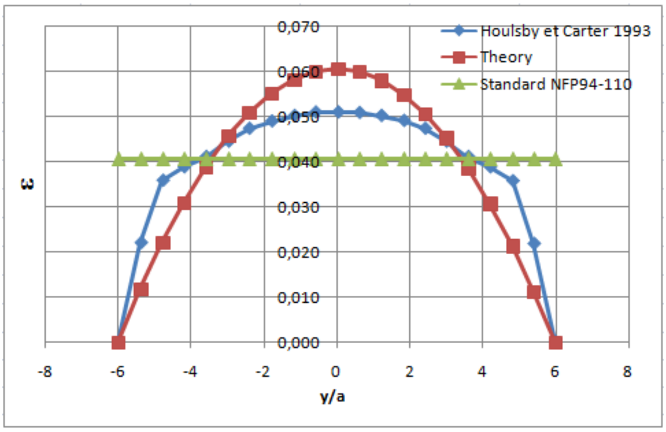

Figure 6. Comparison of the theoretical deformation of the probe and the calculated results of Houlsby and Carter (1993)

3 NUMERICAL ANALYSIS

3.1 *Case of the free end membrane, probe G*

3.1.1 *State of the art*

The state of the art shows a lot of calculation of the pressuremeter test, but no calculation of the probe with the membrane, probably because of the difficulties of meshing and computing. If we compare (Figure 6) the assumed parabolic deformation of the membrane with the calculation of Houlsby & Carter (1993) we find a good correlation with a coefficient of 0.94, where the standard cylindrical deformation is very different with no correlation with the FE results.

3.1.2 *Calculation for pressure looses*

The program Plaxis 2D (2016) was used for the simulation of a pressuremeter test with a G probe in a sand. The dimension of the probe is shown (Table 1). In colum7 the e value is the total thickness of the 2 membranes (1+5mm for G probe).

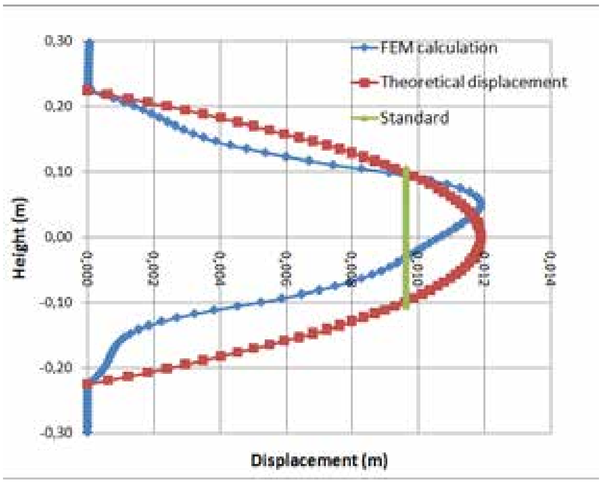

Figure 7. Comparison of the theoretical displacement of the membrane and the numerical results of Plaxis - Calibration in pressure looses of the Probe G

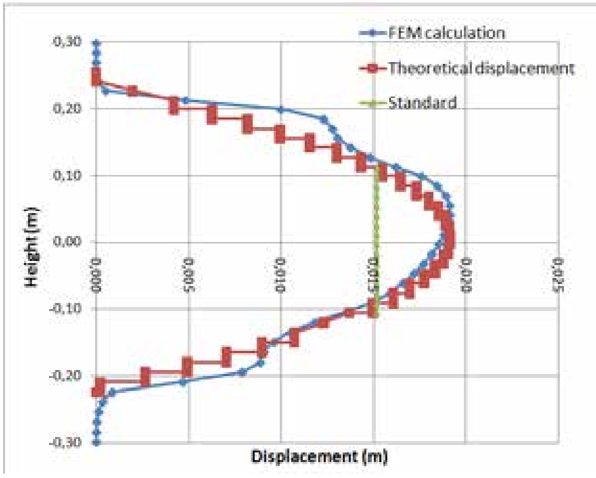

Figure 9. Comparison of the displacements of the membrane between the numerical Plaxis results, the theory and the Standard, Pressure 700kPa,

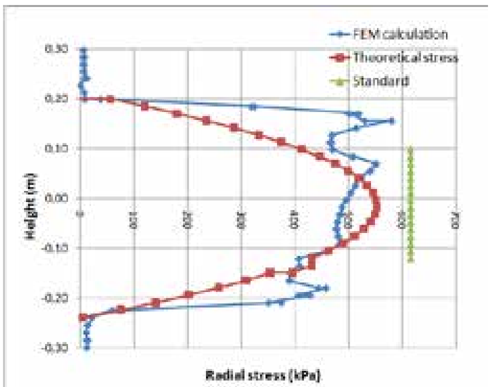

Figure 10. Comparison of the pressure applied to the membrane between the numerical Plaxis results, the theory and the standard, pressure 700kPa

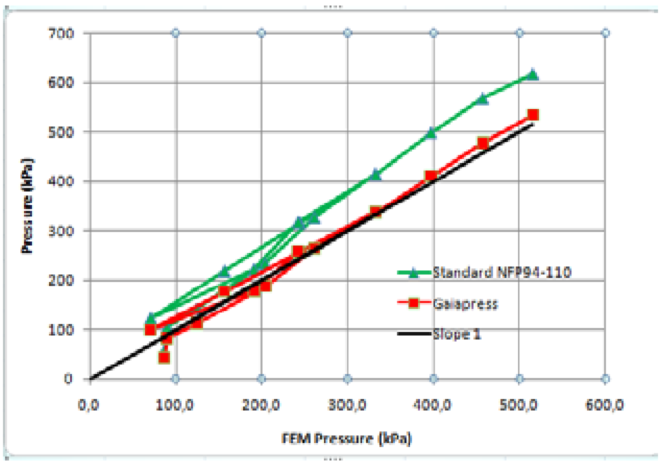

Figure 11. Comparison between the calculated pressure of the Standard, Gaiapress and Plaxis

For the self resistance of the probe (Figure 7) the radial displacement along the membrane by the theory (square points) and by the FEM calculation (diamond point) are closed together with a correlation of 0.90. Meanwhile the constant Standard displacement (triangle points) is very different of numerical results with no correlation.

Table 1. Geometry of the probes

Probe	l_t mm	l_{cel} mm	l_s mm	l_g mm	l_m mm	e mm	d_{ext} mm
G	450	450	210	120	-	6	60
Slot.Tube	-	580	360	110	870	12	60

Table 2 . Characteristic of the soil

Soil	E kPa	ν	c kPa	Φ degree	Ψ degree
Sand1	12673	0.3	0	33	5
Sand2	60000	0.3	0	32	4

3.1.3 *Calculation of the pressuremeter test with the free ends membrane*

It can be seem (Figure 9) the comparison between the calculated theoretical displacement (square points) and the FEM results (diamond points) along the vertical ordinate for a probe placed vertically. The discrepancy between theory and FEM is small, while there is a large difference between the cylindrical displacement of the Standard (triangle points) and the FEM calculation. The parameters of the Sand1 is shown (Table2)

The evolution of the stress along the verticality of the probe is shown (Figure 10). It can be seen that the theoretical stress is more or less close to the FEM contact pressure with the probe. The large variation of the FEM contact pressure seems to be proceed from the contact element between the probe and the soil. These element has a cohesion of 10kPa and a friction angle of 1° with no dilatancy, but the program exhibits some difficulties to reach the final equilibrium. It can be seen that the standard pressure (Triangle points) overestimates the FE pressure.

The comparison between the Standard pressure, the theoretical pressure found by Gaiapress (2014) and the FEM pressure from Plaxis (2016) is shown (Figure 11). It can be seen that the Gaiapress results are closed to Plaxis ones, whereas the Standard finds a pressure 24% higher.

3.2 *Case of the embedded membrane*

3.2.1 *Calculation for pressure looses*

The program Plaxis 2D (2016) was used for the simulation of a pressuremeter test with a slotted tube in a sand. The dimension of the probe is shown (Table 1). In colum7 the e value is the total thickness of the 2 membranes (1+5mm) and the slotted tube (6 mm).

The radial displacement along the membrane (Figure 12) by the theory (square points) and by the FE calculation (diamond point) are closed together with a correlation of 0.81. Meanwhile the constant Standard displacement (triangle points) is very different of numerical results with no correlation.

3.2.2 *Calculation of the pressuremeter test with the embedded membrane*

It can be seem (Figure 14) the comparison between the pressure along the probe, calculated by Plaxis (diamond points) the pressure calculated by the theory with Gaiapress (square points) and the standard (triangle points). It can be seen that the theory is closed to the Plaxis results with a correlation of 0.91, whereas the standard has no correlation with FEM results.

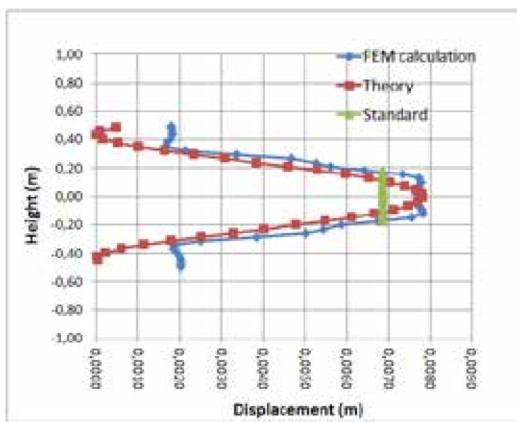

Figure 12. Comparison of the theoretical displacement of the membrane and Plaxis results - Calibration Slotted Tube Probe

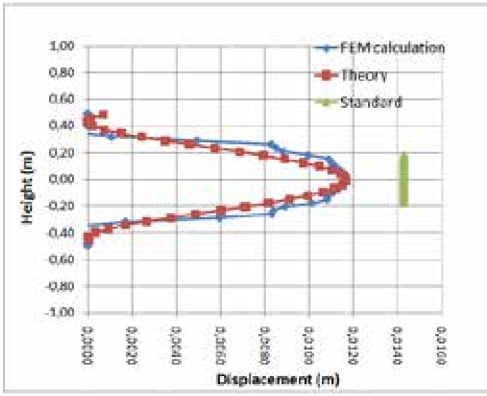

Figure 13. Comparison of the theoretical displacements of the membrane and the Standard with Plaxis results, Pressure 1697kPa

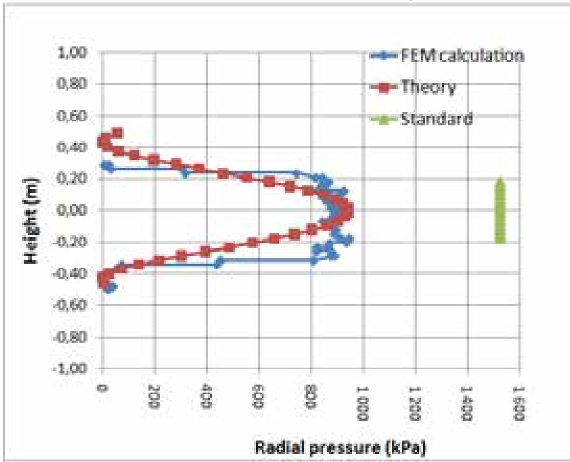

Figure 14. Comparison of the radial pressures on the membrane between the theory and the Standard with Plaxis results, , pressure applied 1697kPa

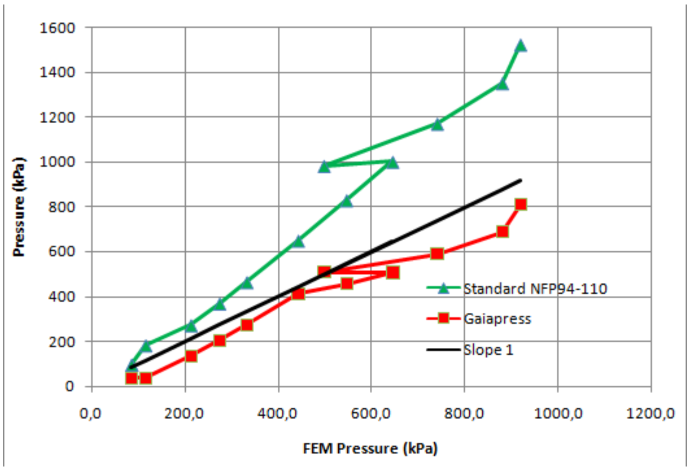

Figure 15. Comparison between the calculated pressure of the Standard, Gaiapress and Plaxis

The comparison between the Standard pressure, the theoretical pressure found by Gaiapress (2014) and the FEM pressure from Plaxis (2016) is shown (Figure 15). This figure is drawn in effective pressures. It can be seen that the Gaiapress results are a little bit under the theoretical slope 1, whereas the Standard finds a pressure 66% higher.

4 CONCLUSIONS

The standards for the pressuremeter interpretation overestimates the radial pressure at the contact with the soil of 24% for the probe G and 66% for the slotted tube.

The effect of the thickness and the shape of the deformation of the membrane must by taken into account for a better estimation of the reaction of the soil to the pressuremeter solicitation. As a consequence a coefficient of reduction of the standard limit pressure found with the slotted tube should be applied for a better uses of pressuremeter results.

A correction coefficient of 0.8 for probe G and 0.6 for slotted tube should be applied to determine the reaction pressure of the soil around the pressuremeter probe. With such correction it is possible to determine the friction angle of the soil. The program Gaiapress is adapted to this correction and this interpretation.

The FEM results should be improved using a large displacement analysis.

5 REFERENCES

Baguelin F., Jezequel J.F., Shields D.H. 1978, The pressuremeter and foundation engineering, *Trans Tech Publication*, Clausthal, Germany.

Gaiapress 2014, www.gaiatech.fr

Houlsby, G.T., Carter, J.P. 1993. The effects of pressuremeter geometry on the results of the tests in clay. *Géotechnique*, 43(4): 567–576.

Mair R.J., Wood D.M. 1987, Pressuremeter testing: Methods and interpretation, *Ciria Ground Engineering Report : In situ Testing, Butterworths*, London

Monnet J., Allagnat D, Teston J., Billet P., Baguelin F. 2006, Foundation design for a large arch bridge on alluvial soils, *Proc. Inst. Civil Eng. - Geot.Eng.* ,London,2006, vol.159(1): 19-28

Monnet J. 2012, An Elasto-Plastic analysis of the Pressuremeter Test in Granular Soil – part 1: theory, *Eur. J. of Env. and Civil Eng.*, 16(6): 699-714

Monnet J 2012, An Elasto-Plastic analysis of the Pressuremeter Test in Granular Soil – part 2: Numerical study, *Eur. J. of Env. and Civil Eng.*, 16(6): 715-729

Monnet J, 2015, In situ tests in geotechnical engineering, *ISTE John Wiley, & Sonss Inc.*, London

Norme NFP 94-110-1 2000, Essai pressiométrique Ménard, partie 1 : essai sans cycle, *AFNOR*, Paris

Norme NFP 94-110-2 1999, Essai pressiométrique Ménard, partie 1 : essai avec cycle, *AFNOR*, Paris

Plaxis 2016, www.plaxis.nl/

Standard D 4719-00 1994, Standard test method for prebored pressuremeter testing in sols, *ASTM* Vol.04.08

Geotechnical and Geophysical Site Characterisation 5 – Lehane, Acosta-Martínez & Kelly (Eds)
© 2016 Australian Geomechanics Society, Sydney, Australia, ISBN 978-0-9946261-1-0

New DMT method for evaluating soil unit weight in soft to firm clays

Z. Ouyang & P.W. Mayne
Civil & Environmental Engineering, Georgia Institute of Technology, Atlanta, Georgia USA

ABSTRACT: A set of field measurements from flat dilatometer test (DMT) and laboratory data from undisturbed samples on 31 different clays have been explored to develop an empirical expression relating soil unit weight with DMT readings. For normally-consolidated (NC) to lightly-overconsolidated (LOC) soft to firm clays under investigation, a significant trend found that the total unit weight (γ_t) tracks with the contact pressure (p_0) and depth (z). A newly defined slope parameter (designated $m_{p0} = \Delta p_0/\Delta z$ with forced intercept = 0) was established for homogenous inorganic clay deposits and found related to the soil unit weight. Results showed a more reliable prediction with improved statistical measures, when compared with other available methods.

1 INTRODUCTION

The evaluation of soil properties plays a vital role in designing geotechnical structures. A necessary first step in a proper site investigation should be the assessment of the soil unit weight, as this is needed in the calculation of total and effective stresses. Unit weights are best determined by taking undisturbed tube samples and measuring the soil mass divided by the volume. However, with in-situ tests, the unit weight is estimated from direct measurements.

The flat dilatometer test (DMT) was developed in Italy by Marchetti (1980) and gained popular acceptance since its introduction due to its simplicity, repeatability, and quick application in geotechnical explorations. The DMT produces two pressure readings (A and B) by inflating a 60 mm diameter flexible steel membrane at each test depth using nitrogen gas. The corrected A reading or contact pressure, p_0, occurs when the membrane becomes flush with the flat blade face, and p_1 is the corrected B reading or expansion pressure to reach outward 1.1 mm. The DMT results are interpreted using three indices: (a) the material index: $I_D = (p_1-p_0)/(p_0-u_0)$, (b) dilatometer modulus: $E_D = 34.7(p_1-p_0)$, and (c) horizontal stress index: $K_D = (p_0-u_0)/\sigma_{vo}'$, where u_0 is the in-situ porewater pressure and σ_{vo}' is the effective overburden stress. Although no database was presented, Marchetti and Crapps (1981) suggested estimating the soil unit weight (γ_t) as a function of the I_D and E_D values, as shown in Figure 1.

Since then, various researchers have made attempts to verify the original relationships for estimating the soil unit weight from DMT readings in site specific geologic formations (e.g., Powell & Uglow 1988; Mayne & Martin 1998) or developed new trends between unit weight and DMT indices (Ozer et al 2012). While the aforementioned address applications in a range of different soil types, the focus herein will primarily be limited to soft to firm

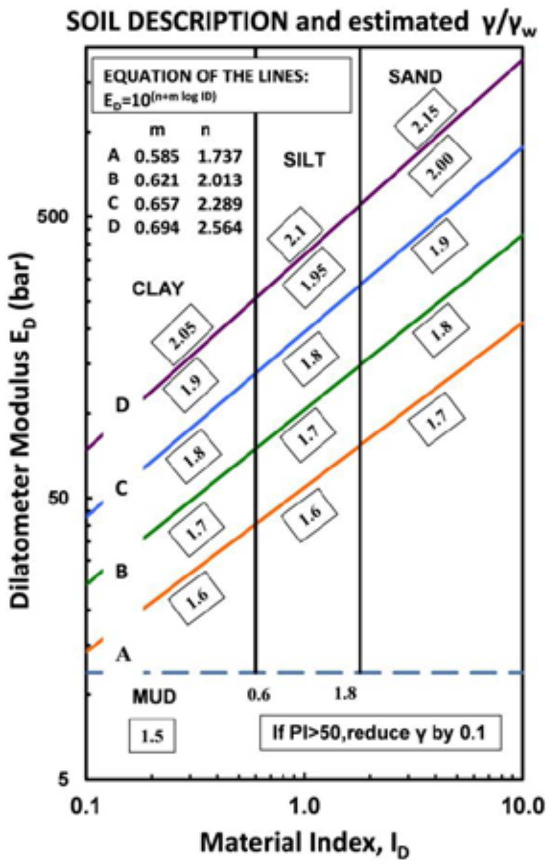

Figure 1. Unit weight estimate from DMT indices E_D and I_D (after Marchetti and Crapps, 1981)

natural clays that are relatively homogeneous and also commonly associated with a high groundwater table.

2 DATA COLLECTION

Table 1.1 Listing of soft to firm clay sites subjected to flat dilatometer tests (DMT) reviewed in this study

Site Name	Mean w_n (%)	Mean PI (%)	Mean unit weight, γ_t (kN/m^3)	Slope m_{p0} (kN/m^3)
Anacostia	65	32	15.9	29.1
Ariake	106	68	13.5	20.7
Backbol	84	56	16.0	28.5
Ballina*	107	66	14.1	31.5
Bothkennar	61	40	16.5	33.4
Colebrook Road	45	11	17.0	26.4
Drammen	52	28	16.6	29.8
Ford Design Ct	21	15	20.2	44.1
Foynes	37	23	18.6	30.5
Hamilton	95	45	13.7	18.7
Lilla Mellösa	70	54	15.7	28.6
Norrköping	76	36	15.7	29.3
NWU GSP	24	15	19.6	41.7
NWU-NGES	26	15	20.1	37.0
Onsøy	64	41	15.9	27.1
Porto Tolle	35	26	18.2	26.8
Recife	123	69	15.6	29.0
Saint Paul*	210	NA	11.4	23.6
Sarapui	139	78	14.0	21.5
Saro Rd 6/900*	160	103	12.1	26.6
Saro Rd 7/600*	150	101	13.2	28.7
Skå Edeby	74	37	15.7	28.5
South Gloucester	70	27	15.8	29.8
Strandbacken	45	13	17.2	34.3
Sundholmen	58	13	16.7	34.3
Torp	48	29	17.5	30.4
Valen	115	77	15.4	27.8
200th Street	58	27	16.2	30.0
Limerick Road	60	40	15.7	29.4
South Portland	24	44	17.2	35.8
High Prairie	38	37	17.6	33.9

* Clay site with organic content

For each site under investigation, information was compiled concerning the in-situ DMT readings, stress history, laboratory unit weight (γ_t), natural water content (w_n), and corresponding plasticity characteristics, such as the mean plasticity index (PI). The stress histories were measured from one-dimensional consolidation tests (either oedometers, automated consolidometers, and/or constant-rate-of-strain devices) and the overconsolidation ratios (OCR) generally ranged between 1 and 2 throughout much of the deposit depths. Groundwater tables are generally high in these soft clays, usually within 1 to 2 or 3 m depth.

The laboratory unit weights were measured from weighed samples of known volumes on tube samples. A variety of different samplers were used by the various researchers, including: Shelby, fixed Piston, free Piston, Laval, Sherbrooke, SGI, and Japanese type tubes. It was not possible to track all of the sample quality issues because of insufficient information, although sample disturbance may have some effects on the results.

In some cases, the unit weights were also obtained by calculation from natural water contents and specific gravity of solids (G_s). A comparison of measured γ_t and calculated unit weights from water contents, assuming fully saturated condition, is presented in Figure 2 for the Ballina site in eastern Australia (Pineda et al, 2014). The results show very good agreement.

Table 1.2 Listing of 30 soft to firm clay sites with locations and reference sources of information

Site Name & Location	Reference Source
Anacostia, DC	Mayne (1987)
Ariake, Japan	Watabe et al (2003)
Backbol, Sweden	Larsson & Mulabdic (1991)
Ballina*, Australia	Pineda et al (2014)
Bothkennar, UK	Nash et al (1992)
Colebrook Road, BC	Crawford & Campanella (1991)
Drammen, Norway	Lacasse &Lunne (1983)
Ford Center, Illinois	Mayne (2006)
Foynes, Ireland	Carroll and Long (2012)
Hamilton AFB, CA	Masood et al (1988)
Lilla Mellösa, Sweden	Larsson & Mulabdic (1991)
Norrköping, Sweden	Larsson & Mulabdic (1991)
NWU, Illinois	Finno (1989)
NWU-NGES, Illinois	Mayne (2006)
Onsøy, Norway	Lunne and Long (2003)
Porto Tolle, Italy	Marchetti (1980)
Recife, Brazil	Danziger (2007)
Saint Paul*, MN	Courtesy of MnDOT (2007)
Sarapui, Brazil	Almeida (2003), Danziger (2007)
Saro 6/900*, Sweden	Larsson & Mulabdic (1991)
Saro 7/600*, Sweden	Larsson & Mulabdic (1991)
Skå Edeby, Sweden	Larsson & Mulabdic (1991)
South Gloucester, ON	McRostie et al (2001)
Strandbacken, Sweden	Larsson and Åhnberg (2003)
Sundholmen, Sweden	Larsson and Åhnberg (2003)
Torp, Sweden	Larsson and Åhnberg (2003)
Valen, Sweden	Larsson & Mulabdic (1991)
200th Street, BC	Cruz (2009)
Limerick, Ireland	Bihs et al (2009)
South Portland, ME	Roche et al (2006)
High Prairie, AB	Cruz and Howie (2008)

* Clay site with organic content

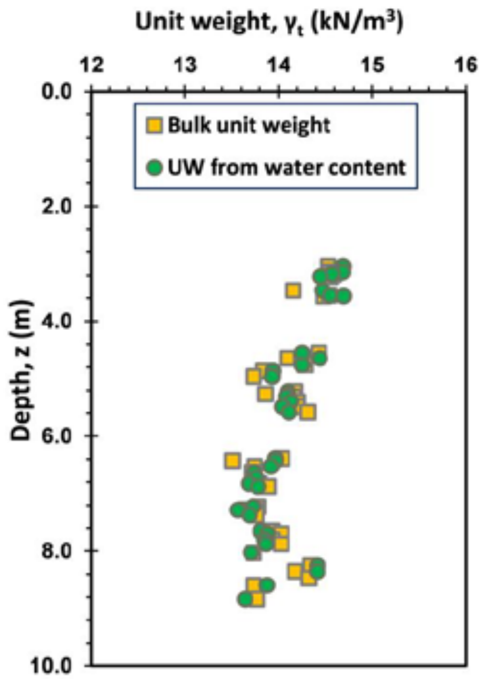

Figure 2. Unit weight profile of Ballina Clay site using mass-volume and water content data.

For the most part, all of the equipment and field procedures for DMT soundings are standardized and given by ASTM D 6635, as well as CEN and ISO standards (Marchetti et al. 2001).

During the DMT, the sharp stainless steel blade is inserted vertically at a rate of 20 mm/s and at the test depth, nitrogen gas is introduced to pressurize the inflatable circular membrane. The A-reading is captured within about 15 s after insertion and the B-reading taken about 30 s later. Thus, both A and B readings are obtained in about 1 minute. Generally, test depth intervals are every 200 mm in most of the world, excepting the USA where an approximate 300 mm interval is common (1 foot ≈ 305 mm).

3 SOIL PARAMETER TREND ANALYSIS

3.1 *Defining the DMT Parameter m_{po}*

For the series of soft to firm normally-consolidated (NC) to lightly-overconsolidate (LOC) clays under investigation, the DMT readings indicate certain trends of interest. One clear observation is that for soft clays with a high groundwater table, the corrected contact pressures (p_0) show a linear trend and increase with depth, as evidenced by four examples shown in Figure 3: (a) Anacostia Naval Air Station in Washington, DC, USA (Mayne 1987), (b) Sundholmen, Sweden (Larsson and Åhnberg 2003), (c) Ariake, Japan (Watabe et al, 2003), and (d) Onsøy, Norway (Lunne and Long 2003). The expansion pressures (p_1) in these materials also

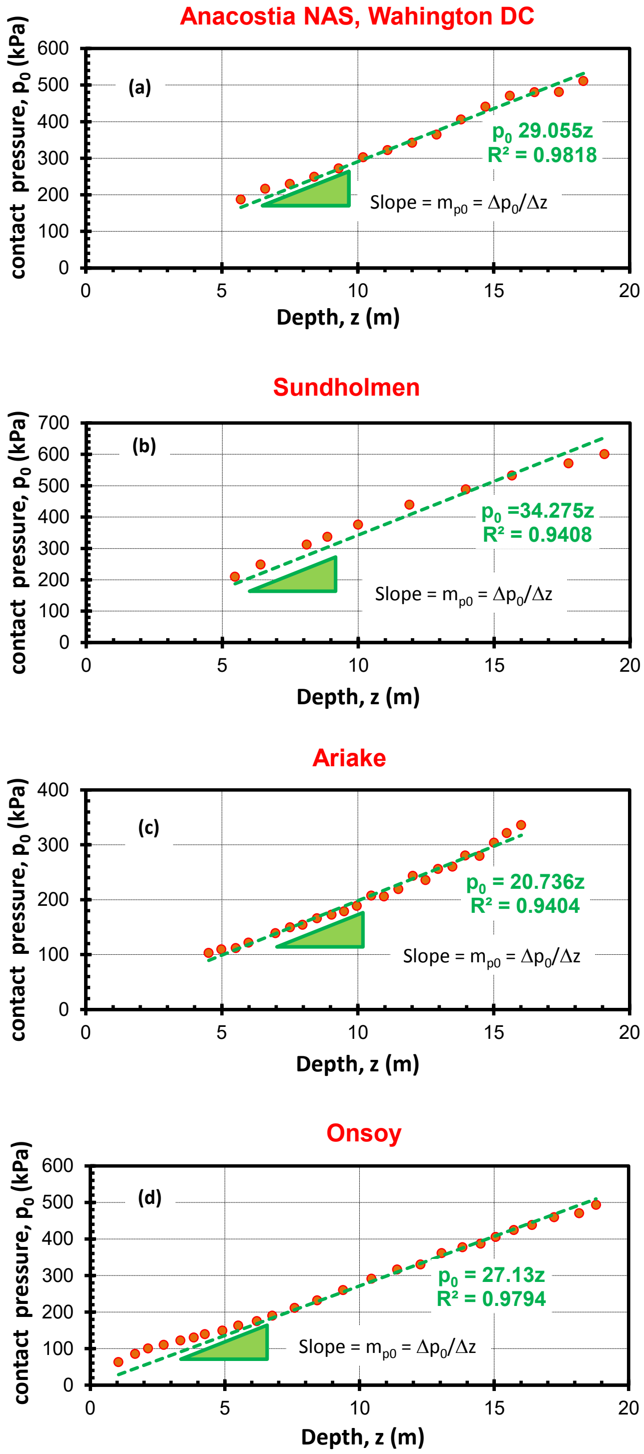

show a similar trend with depth, although not explored here.

Figure 3. Example profiles showing linear trends for contact pressure with depth and slope parameter m_{p0} for four clays: (a) Anacostia, USA, (b) Sundholmen, Sweden (c) Ariake, Japan, and (d) Onsøy, Norway

A new parameter can be defined using regression analyses to obtain a best-fit line (intercept = 0):

$$m_{po} \quad = \quad \Delta p_0 \,/\, \Delta z \qquad (1)$$

For the normally-consolidated (NC) to lightly overconsolidated (LOC) inorganic clays under investigation, the slope parameter m_{p0} ranges from a low of 18 kN/m^3 (Hamilton Air Force Base) to a high value of 44 kN/m^3 (Ford Design Center and NGES at Northwestern University). For all these soils, the total unit weights ranged from 13.5 to 20.5 kN/m^3.

An examination of the data showed that the total unit weights track with the slope parameter m_{p0} for the majority of soft to firm inorganic clay soils under investigation, as evidenced by Figure 4. A few clays with organics showed variant trends and offset to the right. These are circled together as a group.

Of additional interest, the parameter m_{p0} has the same units as soil unit weight (i.e., kN/m^3).

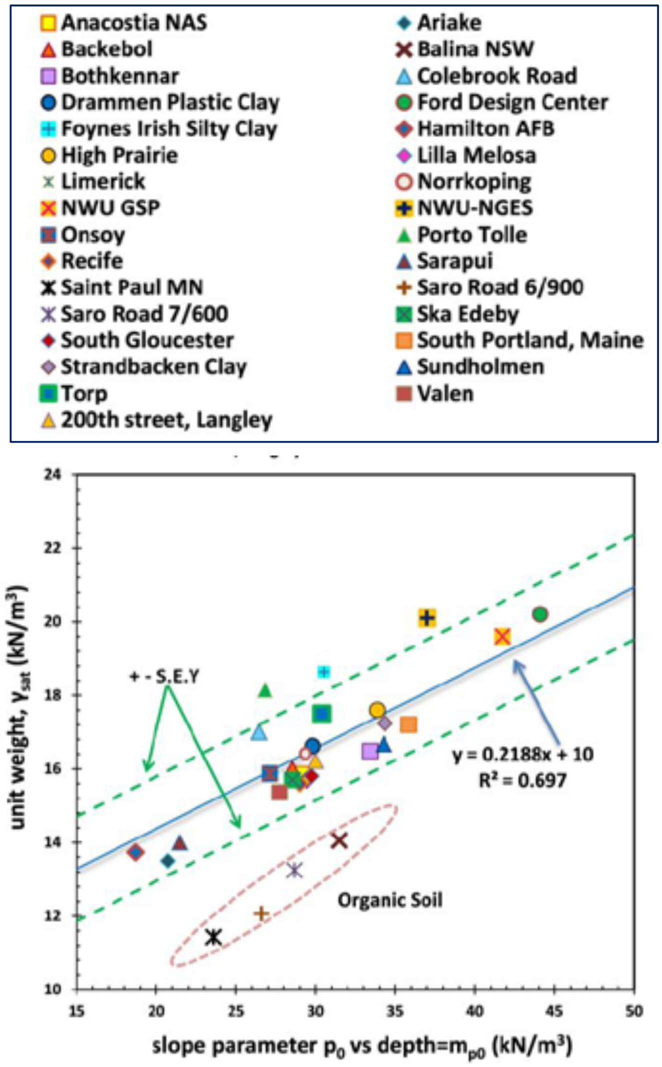

Figure 4. Total unit weight versus slope parameter m_{p0}

Based on the trend shown in Figure 4, one can establish an approximate expression between the total unit weight and slope parameter m_{p0} for soft to firm clays. Using a best fit line by forcing the trend line through intercept 10 (i.e., γ_w = unit weight of water), the relationship becomes:

$$\gamma_t = \gamma_w + 0.22 \cdot m_{po} \qquad (2)$$

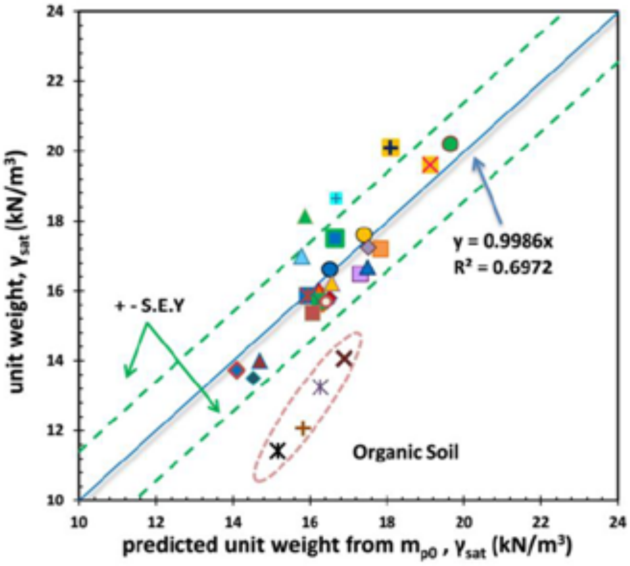

Figure 5. Lab soil unit weight versus predicted unit weight for all 31 clays

Consequently, one can apply this empirical relationship to predict the total unit weight of each of these soft clay soils. Figure 5 shows the comparison between the laboratory-measured unit weights and the predicted unit weights using the aforementioned empirical equation, and Figure 6 shows the lab unit weight profile compared to the predicted unit weight of the clay from m_{p0} of Anacostia. For stiff to hard clays with high OCRs and for fissured OC clays, an apparent value of m_{p0} is not applicable and future research is needed.

3.2 *Comparison between the Marchetti chart and this study*

Applying the DMT data from the collected sites, one can evaluate the validity of the three methods listed in the previous content. By plotting the lab unit weight against the predicted unit weight of each of the proposed approach, some statistical analyses are carried out and given in Table 2.1 for arithmetic ratio of measured-to-predicted values and Table 2.2 which considers regression fits in best fit lines between measured data and predicted results.

Table 2.1 Summary of the arithmetic statistics of Marchetti Chart and the slope parameter m_{p0} in predicting soil unit weight

Prediction Method	Number of data, n	Mean Value (Range)	Mean of Meas/Pred (Range)	COV* Meas/Pred
Marchetti-Crapps 1981 Chart	31	15.5 (14.7-16.6)	1.05 (0.82-1.28)	0.11
This study (2016)	31	16.2 (13.1-20.1)	1.01 (0.96-1.14)	0.08

Note: * COV = covariance = standard deviation/mean

Table 2.2 Summary of the regression statistics of Marchetti Chart and the slope parameter m_{p0} in predicting soil unit weight

Prediction Method	Number of data, n	Regression Slope	R^2 Meas/Pred	S.E.Y**
Marchetti-Crapps 1981 Chart	31	1.04	0.026	1.77
This study (2016)	31	1.01	0.698	1.42

Note: ** S.E.Y. = standard estimate of the Y-estimator

From Tables 2.1 and 2.2, it is observed that for the soils reviewed, the unit weights range from about 13 kN/m^3 to 20 kN/m^3 (mean γ_{sat}=16.2 kN/m^3). For the ratio of measured to predicted unit weight value, the corresponding covariance (also, called coefficient of variation, or COV=standard deviation/mean) for the two methods are 0.11 and 0.08. Thus, a better prediction is obtained for these soft clays.

The coefficient of determination (R^2) from the slope parameter regression is much larger (R^2 = 0.698) for the m_{p0} approach than that from the Marchetti chart (R^2 = 0.026). Moreover, the improvements are also drawn in terms of the standard error of the Y-estimate analysis (S.E.Y). A reduced value from 1.77 (1981) to 1.42 (2016) is obtained, indicating less variability.

4 CONCLUSIONS

This study involved a re-interpretation of in-situ DMT results from 31 soft to firm normally-consolidated to lightly overconsolidated clays worldwide where OCRs < 2. Most of these deposits were homogeneous and had a high groundwater table, generally less than 2 m. A new slope parameter (designated $m_{p0} = \Delta p_0/\Delta z$ with forced intercept = 0) was defined and found to relate to the total soil unit weight. Both m_{p0} and γ_t have units of kN/m^3.

Statistical measures are used to quantify the trends and the unit weight predicted by m_{p0} is provided and compared with the earlier Marchetti-Crapps (1981) relationship, showing an improved estimate by this new approach. However, the m_{p0} approach is not applicable to stiff and hard clays, nor silts and sands, thus specific to only to soft and firm inorganic clays. Data from a few organic clays were found to show a displaced trend.

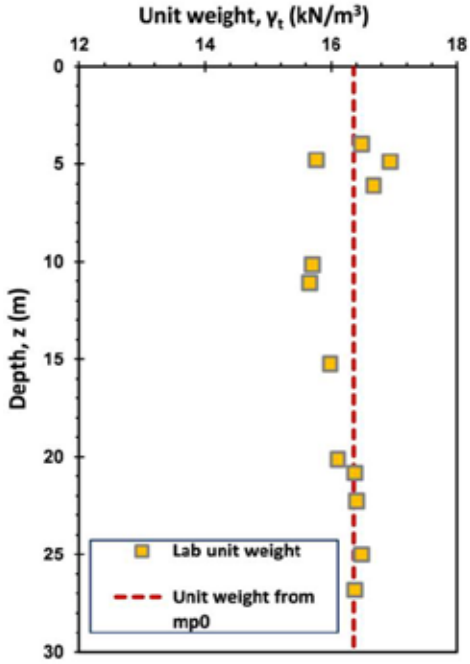

Figure 6. Profile of lab-measured unit weight and DMT-predicted unit weight from m_{p0} for Anacostia soft clay site in Washington, DC.

5 ACKNOWLEDGMENTS

The authors appreciate the continued support from ConeTec Investigations of Richmond, BC and Design House Consultancy of New York, NY.

6 REFERENCES

Almeida, M.S.S., & Marques, M.E.S. 2003. The behaviour of Sarapuí soft clay. *Characterisation & Engineering Properties of Natural Soils*, Vol. 1 (Singapore), Swets & Zeitlinger, Lisse: 395-427.

Bihs, A., Long, M., Marchetti, D., & Ward, D. 2010. Interpretation of CPTU and SDMT in organic, Irish soils. *Proceedings 2nd Intl. Symposium on Cone Penetration Testing,* (CPT'10, Huntington Beach, California), Omnipress, Vol. 2: 257-264. www.cpt10.com

Carroll, R., Long, M., & Ward, D. 2012. Use of CPTU and SDMT to characterise silty soil. *Geotechnical and Geophysical Site Characterization 4*, (ISC-4, Pernambuco), CRC Press-Taylor & Francis Group, London: 241-249.

Crawford, C.B., & Campanella, R.G. 1991. Comparison of field consolidation with laboratory and in situ tests. *Canadian Geotechnical Journal,* Vol. 28 (1), 103-112.

Cruz, I. R. 2009. An evaluation of seismic flat dilatometer and lateral seismic piezocone, *MS Thesis*, Dept. of Civil Engineering, University of British Columbia.

Cruz, I.R., Howie, J.A., Padros, G., Papanicolas, D., & Weemees, I.S. 2008. An evaluation of pile load capacity estimates using CPTu and DMT methods in silty clay in High Prairie, Alberta. *Proc. 61st Canadian Geotechnical Conference*, Edmonton, Canada.

Danziger, F. A. B. 2007. In-situ testing of soft Brazilian soils. *Studia Geotechnica et Mechanica*, *29* (1-2), 5-22.

Finno, R.J. 1989. *Predicted and Observed Axial Behavior of Piles: Results of a Pile Prediction Symposium*. GSP No. 23, ASCE, Reston, Virginia.

Lacasse, S., and Lunne, T. 1983. Dilatometer tests in two soft marine clays, *Report No. 146*, Norwegian Geotechnical Institute, Oslo.

Larsson, R. & Mulabdić, M. 1991. Shear moduli in Scandinavian clays, *Report No. 40*, Swedish Geotechnical Institute, Linköping.

Larsson, R., & Åhnberg, H. 2003. Long-term effects of excavations at crests of slopes. *Report R-61*, Swedish Geotechnical Institute, Linköping.

Lunne, T., Long, M., and Forsberg, C.F. 2003. Characterisation and engineering properties of Onsøy clay. *Characterisation & Engineering Properties of Natural Soils*, Vol. 1 (Singapore), Swets & Zeitlinger, Lisse: 395-427.

Marchetti, S. & Crapps, D.K. 1981. *Flat Dilatometer Manual.* Internal Report of G.P.E. Inc., Gainesville, Florida.

Marchetti, S. 1980. In situ tests by flat dilatometer. *Journal of the Geotechnical Engineering Division*, *106*(3), 299-321.

Marchetti, S., Monaco, P., Totani, G. & Calabrese, M. 2001. The flat dilatometer test (DMT) in soil investigations. A report by the ISSMGE Committee TC16. Reprinted in *Proc. 3rd Intl. Conf. on the Flat Dilatometer* (DMT'15), Rome: 523-565.

Masood, T., Mitchell, J.K., Lunne, T. and Hauge, E.A. 1988. In-situ testing at Hamilton Air Force Base and Day Farm Island, CA, *Joint Report*: Univ. of California, Berkeley and Norwegian Geot. Institute, Oslo, 56 p.

Mayne, P. W. 1987. Determining preconsolidation stress and penetration pore pressures from DMT contact pressures. *ASTM Geotechnical Testing Journal* Vol. 10 (3): 146-150.

Mayne, P.W. and Martin, G.K. 1998. Commentary on Marchetti flat dilatometer correlations in soils. ASTM *Geotechnical Testing Journal*, Vol. 21 (3): 222-239.

Mayne, P.W. 2006. Interrelationships of DMT and CPT readings in soft clays. *Flat Dilatometer Testing* (Proc. 2nd Intl. Conf. on DMT, Washington D.C.): 231-236.

McRostie, G.C., & Crawford, C.B. 2001. Canadian geotechnical research site no. 1 at Gloucester. *Canadian Geotechnical Journal*, 38 (5), 1134-1141.

Nash, D.F.T., Powell, J.J.M. & Lloyd, I.M. 1992. Initial investingations of the soft clay test site at Bothkennar, UK. *Geotechnique* Vol. 42 (2): 163-181.

Ozer, A. T., Bartlett, S. F., & Lawton, E. C. 2012. CPTU and DMT for estimating soil unit weight of Lake Bonneville clay. *Geotechnical and Geophysical Site Characterization 4*, (Proc. ISC-4, Pernambuco), CRC Press: 291-296

Pineda, J.A., McConnell, A., & Kelly, R.B. 2014. Performance of an innovative direct-push piston sampler in soft clay. *Proc. 3rd Intl. Symposium on Cone Penetration Testing* (CPT'14, Las Vegas): 279-288.

Powell, J.J.M. & Uglow, I.M. 1988. The interpretation of the Marchetti dilatometer test in UK clays. *Penetration Testing in the UK* (Proc. Univ. Birmingham). Institution of Civil Engineers, London, Paper 34: 269-273.

Roche, J. 2006. Modeling of a soft sensitive marine silty clay deposit for a landfill expansion study, *MS Thesis,* Dept of Civil Engineering, University of New Hampshire.

Watabe, Y., Tanaka, M., Tanaka, H., & Tsuchida, T. 2003. K_0-consolidation in a triaxial cell and evaluation of in-situ K_0 for marine clays with various characteristics. *Soils and Foundations*, Vol. 43 (1), 1-20.

Geotechnical and Geophysical Site Characterisation 5 – Lehane, Acosta-Martínez & Kelly (Eds)

Evolution of deformation parameters during cyclic expansion tests at several experimental test sites

P. Reiffsteck & S.Fanelli
Univ Paris Est IFSTTAR, Marne la Vallée, France

G. Desanneaux
CEREMA, DirTer Ouest, Saint Brieuc, France

ABSTRACT: For thirty years, cyclic pressuremeter expansion tests carried out at different experimental sites have helped develop a rich and extensive database. The results from these high quality tests allowed stress-strain parameters to be derived at low and medium strain levels. These cyclic tests were carried out using Ménard and self-boring pressuremeters. Around fifteen sites were studied covering a wide range of behavior from sandy soils to clayey materials at stress histories varying from normally consolidated to overconsolidated. This paper will present the sites and test programs with their main geotechnical characteristics. The paper will focus on the evolution of shear modulus with the number of cycles, the material type, the amplitude ratio as well as the ratio of mean expansion pressure to the at-rest horizontal stress.

1 INTRODUCTION

Ménard pressuremeter test equipment allows operators to achieve monotonic expansion tests (EN ISO 22476-4 similar to NF P94-110-1 ASTM D4719) and cyclic tests (NF P94-110-2) (AFNOR, 1999 and 2000). These tests include an unload-reload cycle performed in steps, in the same conditions as the Ménard pressuremeter test described in the EN ISO 22476-4 standard. The conventional expansion test using the drilling conditions recommended by the EN ISO 22476-4 standard and with the proposed loading program, does not give usable results directly for deformability prediction of geotechnical structures especially when the knowledge of modulus in the small strain range is required (Combarieu and Canépa, 2001).

Tests with unload-reload loops allow the determination of the cyclic deformation modulus. The values obtained are intermediate between the modulus in small strains obtained in the laboratory or with in situ wave propagation tests, and the conventional Ménard modulus (Ménard, 1960, Borel and Reiffsteck, 2006). However, a single cycle is insufficient to identify the evolution of soil characteristics under cyclic loading (Dupla and Canou, 2003). The present study, conducted as part of the national project SOLCYP (research project on the behavior of piles under cyclic loads, see the website for more information www.pnsolcyp.org) was an opportunity to perform multi-cycle tests with a probe inserted into a pre-drilled hole or by self-boring technique.

2 EXPERIMENTAL DEVICE

The principle of the test is to measure changes in the volume injected during the application of pressure cycles.

2.1 *Equipment*

The idea is to be able to perform cavity expansion cyclic tests with a pressuremeter probe inserted in the ground by self-boring or in a pre-drilled hole.The equipment used, developed by Jean Lutz SA company, is a pressure volume controller (CPV) (PREVO type), able to control solenoid valves by a PC computer via a specific application program. Measuring the change in volume during probe expansion is done either by measuring the volume of water injected or by measuring the movement of a feeler probe (Figure 1a and b).

The principle of operation is as follows. The various manual operations are carried out either directly on the CPV or by the software program. The cyclic control is performed on the basis of a test file accepting any type of signal, harmonic or multiple frequencies. The monitoring is done in real time on a datalogger.

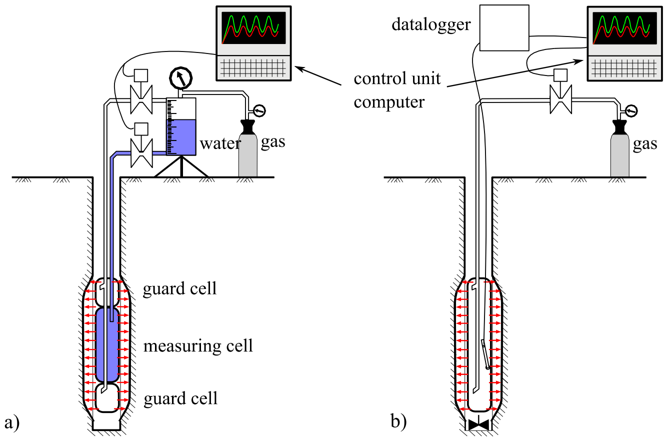

Figure 1. Architecture of the cyclic (a) Ménard pressuremeter, (b) self-boring pressuremeter

2.2 *Test Method*

During the 70s, the Association for Research in Marine Geotechnics bringing together different companies, consulting firms and research institutes in the field, coordinated numerous cyclic pressuremeter test campaigns on several sites. Details of the experiments are summarized in several reports and articles of the Symposium Pressuremeter and Offshore Applications held in Paris in 1982 (Jézéquel and Méhauté, 1982; Puech et al., 1982). Three types of tests were carried out; we present the two used in this study:

- cyclic loading test between two pressure limits p_M p_m (Figure 2 a),
- loading tests between two variable pressure limits, whose average is however constant, the lower bound kept greater than the ???earth pressure at-rest p_o (Figure 2 b).

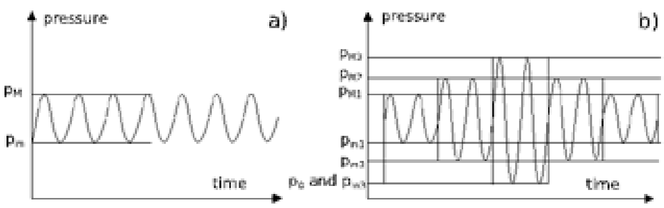

Figure 2. Different types of cyclic tests

The parameters used for the cyclic tests described above consisted in carrying out the test in pressure controlled mode and adapting the frequency to the type of soil in an attempt to remain drained using a stress level of 0.8 ($R_c = \Delta p_{cyc} / p'_0$), a frequency varying from 0.01 to 0.05 Hz and a number of cycles equal to 50.
The initial pressure p_m used to start the cyclic portion of the test is defined as the horizontal stress up to the earth pressure at-rest (effective preferably) and the maximum pressure p_M equal to (1 + 0.8) p_m (Dupla and Canou, 2003). The pressure p_m, which was taken equal to p_o, was defined from previous Ménard type expansion test results by the method proposed by Briaud (1992).

2.3 *Cyclic modulus definition*

The interest of achieving cycles with the pressuremeter to obtain small strain modulus in values appeared very early (Ménard, 1960). From the beginning, several moduli were defined from experimental curves.
In the first zone designated as "elastic", the modulus reaches a quasi-independent value of the level of deformation. It is called the "initial" G_0 (or G_{max}) module.
The curves in their monotonic part provide a "secant" modulus ($G_{s,1}$) defined by the slope of the line connecting the origin to the current point and in their cyclical part, another secant modulus ($G_{p,\,N}$) determined by the slope of the line connecting the two reversal points of the cycle N. The largest cyclic modulus is calculated using equation 1 using the notation in Figure 3:

$$G_{p,N} = \frac{\Delta p}{\Delta V / V_{mean}} \tag{1}$$

The loop in these unloading /loading sequences is elipsoidal. It represents the energy dissipated by plastic deformation. The evolution of the cycles tilt or modulus during the cycles is used to assess the soil behavior. We can evaluate the cyclic hardening or softening and accumulation of deformation, stabilization, relaxation or ratchet? effect.

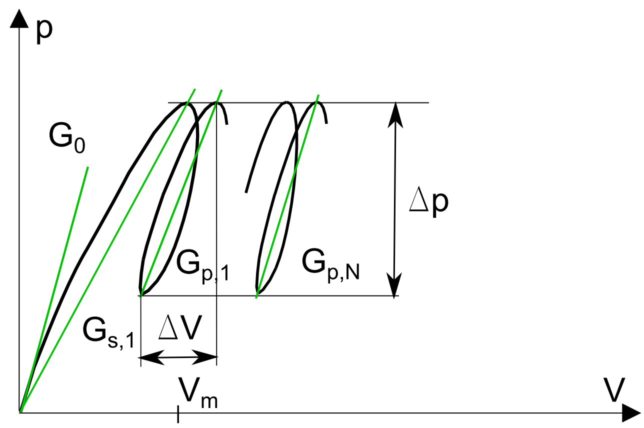

Figure 3. Calculation of cyclic modulus

The interpretation is based on the evolution of the characteristic area of the loading and unloading loops and the secant modulus of the hysteresis loops (Figure 3).

3 CYCLIC TESTS

3.1 *Saint Brieuc Regional Laboratory tests*

In the late 70s, the Laboratoire des Ponts et Chaussées of Saint Brieuc conducted several test campaigns involving the self-boring pressuremeter with cyclic expansion (132 mm diameter PAF76 model). These tests included hundreds or thousands of cycles (duration of 24 to 72 hours). They were carried out on two main sites: Cran and Plancoët (Méhauté and Jézéquel, 1980).

3.1.1 *Plancoët site*

The site consists of a flat land bordering the river Arguenon. The deposit is composed of very loose fine soils: silts at the surface (0-4 m), followed by fine sand (especially from 6 to 9 m) and clays (10 to 12 m) with some inclusions of gravel and sand. The bedrock is at 15 m. The groundwater table fluctuates depending on the season from 0.30 to 1.50 m.

3.1.2 *Cran site*

The alluvial plain of the Vilaine, downstream from Redon, is a sedimentary valley of nearly 2 km wide. A clay deposit thickness of 10 to 20 m, rests on a layer of sand and gravel that covers the bedrock. At Cran, the right bank is comprised of a soft marine clay deposit 17 m thick resting on bedrock (shale and phtanites???).

3.2 *Solcyp project tests*

Validation tests were performed on three sites: Gosier, Cran and Merville. The last two sites were the subject of numerous studies in the research project programmed by the French public road Laboratories (LCPC now IFSTTAR). The characteristics that have determined the choice, was a relatively overall homogeneity to a minimum depth of 5 to 10 m.

3.2.1 *Gosier site*

The first tests with the new equipment has been undertaken on the Gosier site in Guadeloupe (French Antilla) located in a potentially liquefiable area, instrumented and studied in the ANR project Belle Plaine. Ménard pressuremeter tests (incremental tests) were performed to complete the profiles obtained by piezocone penetration test. The tests were also used to assess the pressure p'_0 to use, then two cyclic pressuremeter soundings were conducted.
Figure 4a shows a plot of the corrected pressure using the volume variation obtained for the four tests from the MC2 series. After a first part that corresponds to the rise in the average monotonic load, the cyclic phase between p_M and p_m shows the stabilizing trend of almost all tests, even if it has never been reached. Apparently, the 7 m depth test shows a significant accumulation of volumetric strain due to the presence of a soft clay layer.

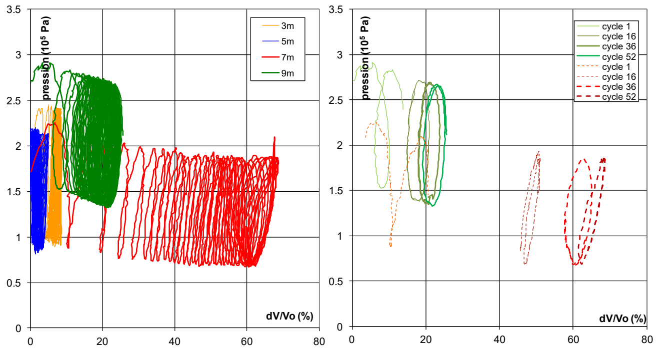

Figure 4. a et b PMT cyclic expansion tests at the Gosier site

3.2.2 *Cran site*

The tests carried out in 2011 were located close to the series made in 1979.At the 2 m depth, the test curve shown in Figure 5a shows high accumulation volume (of the order of 900 cm^3) leading to the conclusion that the test was performed in the soft layer and the initial pressure inferred from previous studies had been overestimated. The signal obtained shown in Figure 5a is rather noisy because the amplitude of the pressure range is small, and an interaction between the control of the water and air circuits could not be corrected on time during the test.

3.2.3 *Merville site*

On the experimental site of Merville (North), the top soil at 1.5 m depth has the texture of low plastic silt affected by the fluctuation of the water-table and it covers the Flanders clay (overconsolidated) of Ypresian from 1.5 to 42 m depth..

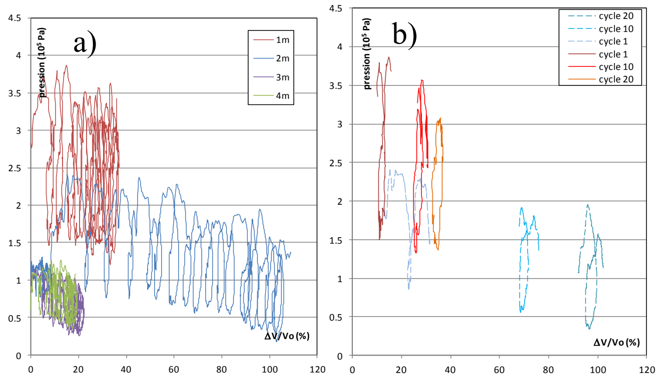

Figure 5. a et b SBP cyclic expansion tests at the Cran site

A self-boring pressuremeter sounding with cyclic tests: 6, 8, 10 and 12 m deep, alternating with monotonic expansion tests at 5, 7 and 11 m, was performed (Figure 6 and Figure 7a). The first three cyclic tests were performed with the same amplitude fixed from the monotonous expansion tests. The last test was performed with amplitude based on the 11 m test.

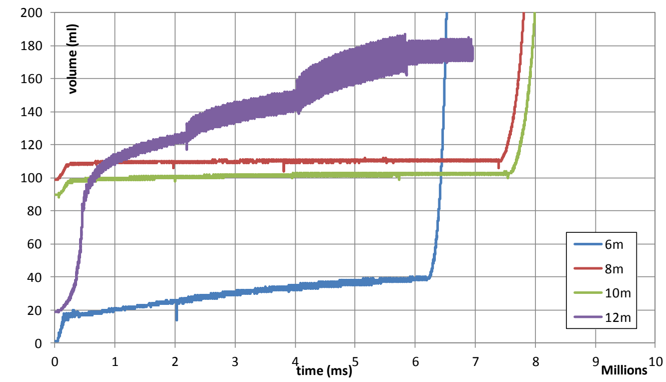

Figure 6. SBP cyclic expansion tests at the Merville site

60 kPa amplitudes have led to inaccurate results because on one hand the pressure source was set to too high pressure and therefore the solenoid valve of the buffer chamber was struggling to regulate and secondly that value is low and close to the magnitude of the precision of the servo. It is therefore necessary to adjust the amplitudes to depths and re-evaluate the method of determination thereof.

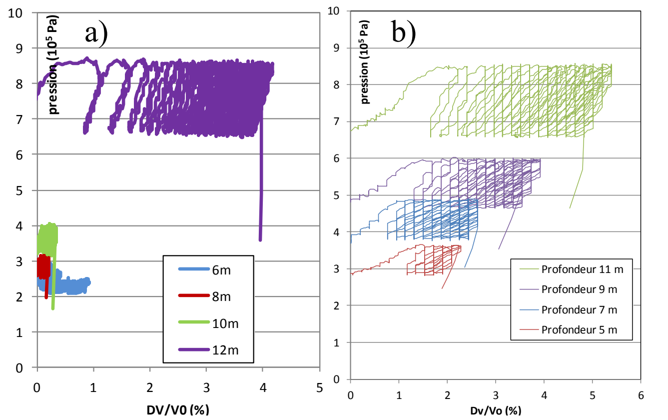

Figure 7. (a) Self boring and (b) pre-drilled cyclic expansion tests – first fifty cycles - Merville site

Right next to the self-boring tests, a Ménard pressuremeter sounding was performed in a borehole drilled meter by meter using a continuous flight auger with cyclic tests at 5, 7 and 11 m which gave comparable results (Figure 7).

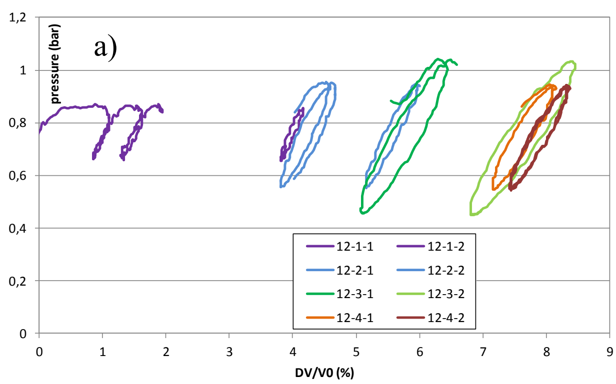

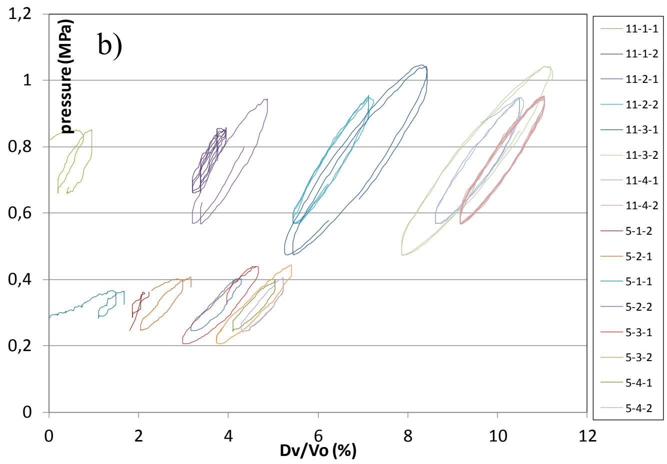

Figure 8. (a) Self boring and (b) pre-drilled cyclic expansion tests – all test sequence - Merville site

4 DISCUSSIONS

A first observation is that the signal obtained shown in Figures 4 to 7 is noisier than the one given in the articles of Jézéquel and Le Méhauté (1982) because the control of the pressure volume controller by ball screw using a volume rate of 2 % / min is more stable than a servo pressure valve. The resulting cycles have singular points with a flat part and no jog.

Various experiments have shown that a minimum of 50 cycles is required to get a clear evolution of the secant modulus and it is not possible to be limited to a few numbers of cycles – 3 to 10 for example – to obtain representative results. Note that the variation of the secant modulus of 50 to 500 cycles was 10% on average and from 500 to 5000 of 3%.

Although the protocol differences due to the development of these equipment and testing protocols do not allow a detailed comparison, the observed volume accumulations are of the same order of magnitude with various insertion modes. The quality of pre-drilling is essential for a test with a minimum initial injected volume. On two sites (Gosier and Cran) regardless of the insertion mode, the large accumulation of strain at some levels is a possible indicator to locate layers with low resistance to of cyclic loading (Figures 4 and 5).

During all tests, a stabilization of cycles means deformations relative to the number of cycles could be observed. Depending on the soil type, the cycles tend to straighten up more or less strongly, as seems to be the case for Plancoët sand and Merville clay.

According to table 2, for granular materials as silt and sand, a ratio $G_{p,50}/G_{p,1}$ close to 3 but for slightly overconsolidated clay (Plancoet, Cran at 1 m, Merville) this ratio drop to 2 and for compressible clay and loose sand (Gosier, Cran at 2 m) become close to 1.5.

Table 1. Test characteristics for first phase of 50 cycles

Site	Borehole	Soil	z (m)	$G_{p,1}$ (10^5 Pa)	a_{M0} (%)	$G_{p,50}/G_{p,1}$
Plancoët	8-3	silt	2	5,19	0,5	1,6
	16-1		3	3,46	1	1,8
	7-3		2	1,08	5	3
	8-3	sand	7	9,98	0,5	2,2
	16-1		7	6,49	1	2
	7-3		7	2,69	5	3,3
	8-3	clay	11	8,58	0,5	1,43
	16-1		11	6,47	1	1,9
	7-3		11	3,75	5	2,1
Cran 1	C1	clay	mean	29,9	1,67	1,15
	C2	clay	mean	20	0,99	1,09
Gosier	C2-PMT	sand	7	51,6	0,5	1,60
			9	13,9	3,5	1,41
Cran 2	A0-PAF	clay	1	60,8	10	2,71
			2	25,6	12	1,59
Merville	PAF	clay	6	426	0,8	2,01
			12	294	3,5	1,93
Merville	PMT	clay	5	145	0,6	1,37
			11	255	0,9	1,21

The multi-amplitude test series allow to obtain curves of cyclic modulus evolutions as a function of the depth and magnitude of the cycles for different soil conditions (Figure 8 and Table 2).

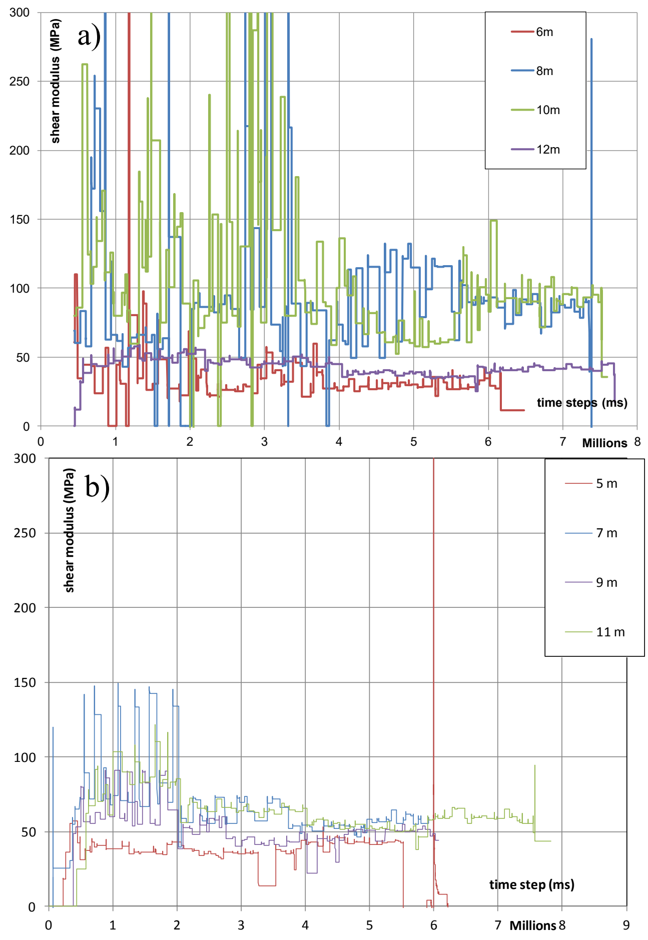

Figure 9. Evolution of loops secant modulus a SBP et b Menard expansion tests Merville site

We observe during these multi-cycle tests on clay that the moduli have changed during phases of different magnitudes but that within the same phase they remained very stable (Figure 9). In the first cycles of a constant amplitude phase, a lower value of the modulus is often observed that tends to increase quickly and to stabilize.

Unlike previous tests at low amplitude performed at the Merville site, Figure 9a shows for the 12 m test (amplitude 6 time higher) lower values of modulus and a immediate decrease of the modulus at the three first phases .

The high variability in the testing phase for the 8 and 10 m depths and the low modulus of variation is linked to the too small amplitude of the cycles. These two phenomena have disappeared for the predrilled tests.

The comparison of cyclic moduli (approximate by a simple spreadsheet function) at Merville (Figure 9) shows a factor of 1 between tests with predrilled and self-boring pressuremeters.

Table 2. Modulus evolution over several amplitudes

Site	tool	z (m)	$G_{p,50}$ / $G_{p,1}$ of phase			
			1	2	3	4
Plancoët	SBP	1	1.83	1.08	0.8	1.27
Merville	SBP	6	0,62	0,57	0,90	1,17
		8	1,23	0,98	0,82	1,12
		10	0,70	0,56	0,45	1,04
		12	4,63	0,99	0,96	1,05
Merville	PMT	5	3,16	1,38	0,91	0,99
		7	2,28	1,15	1,01	0,96
		9	1,32	1,56	1,00	1,00
		11	3,46	1,12	0,94	0,96

There is a very similar evolution in the loose soil of Plancoët site and the overconsolidated clay at the Merville site: an important development for the first amplitude and a near stabilization for other amplitudes.

5 CONCLUSION

The various campaigns, with mono or multi amplitude cyclic tests, have shown the value of this test to identify the evolution of shear modulus as a function of number of cycles and the potential of the test to locate the horizons susceptible to liquefaction.

It is better to specify the test conditions for comparability of the datasets and if possible to arrange the measurement of pore pressure at the membrane to estimate potential accumulations of pressure in clayey soils or adapt the speed of the expansion to keep the conditions drained.

6 AKNOWLEGMENT

The authors thank the national project SOLCYP and the Ministry of Environment Energy, Sustainable Development and the Sea for funding this research

project as well as their colleagues and O. Malassingne, A. le Kouby and J.-L. Tacita.

7 REFERENCES

AFNOR (1999) Essai pressiométrique Ménard – partie 2 Essai avec cycle, NF P94-110-2, Reconnaissance et essais, pp. 43.

AFNOR (2000) Essai pressiométrique Ménard – partie 1 Essai sans cycle, NF P94-110-1, Reconnaissance et essais, pp. 43.

Borel S., Reiffsteck Ph., (2006) Caractérisation de la déformabilité des sols au moyen d'essais en place. LCPC Paris, pp. 132.

Briaud, J.L., (1992). The Pressuremeter, A. A. Balkema, Rotterdam, Netherlands.

Combarieu O., Canépa Y. (2001) L'essai cyclique au pressiomètre, BLPC, 233, 37-65.

Dupla, J.C., Canou J. (2003). Cyclic pressuremeter loading and liquefaction properties of sands, Soils and Foundations, Vol. 43(2), 17-31.

Jézéquel J.F., Le Méhauté A. (1982) Essais cycliques au pressiomètre autoforeur, Symposium sur la pressiométrie et ses applications en mer, Paris, Éditions Technip, 221-233.

Le Méhauté A. Jézéquel J.F., (1980) Essais cycliques au pressiomètre autoforeur, Rapports des LPC, FAER 1-05-09-22, 29 pages

Les Pressiomètres Louis Ménard (1960) Phase de déchargement des essais pressiométriques, Etude théorique et applications, Circulaire 3 pages

Puech A., Brucy F., Ma E., (1982) Calcul de la capacité axiale des pieux de fondations marines à partir du pressiomètre autoforeur, Symposium sur la pressiométrie et ses applications en mer, Paris, Éditions Technip, 373-388..

Geotechnical and Geophysical Site Characterisation 5 – Lehane, Acosta-Martínez & Kelly (Eds)

Ground Property Characterization from In-Situ Tests: Opportunities offered by Measuring Thrust during Flat Plate Dilatometer Testing

J. H. Schmertmann & D. K. Crapps
Consulting Engineers, Gainesville, Florida, USA

ABSTRACT: This paper describes the advantages of the use of thrust measurements made during a Marchetti Flat Plate Dilatometer test sounding. They provide another method for accurate soil profiling. They may result in more accurate DMT pressure readings because thrust allows use of "advance knowledge" to estimate the change in readings at the subsequent test depth. They also provide data for protection of the equipment. The addition of thrust data provides another variable for estimating the plane strain, drained, soil friction angle using the Durgunoglu and Mitchell bearing capacity theory. Marchetti and others have recently recommended combining CPT and DMT measurements to provide data for liquefaction potential evaluations. The writers present a method to use thrust measurements for evaluations of liquefaction potential using only DMT data. This avoids the unknown, possibly serious, effects of soil variability when combining CPT and DMT data obtained in different soundings.

1 INTRODUCTION

Engineers can take better advantage of the soil properties information potential of Marchetti flat blade dilatometer test soundings (DMTs) by including measurement of the total vertical thrust, P, to advance the blade to each successive test depth. As explained subsequently in more detail, using P has some important benefits that include obtaining a stratigraphic profile, warnings of possible blade damage or loss, more accurate pressure readings, a method for calculating the blade's bearing capacity q_D and then the sand's plane strain friction angle Φ'_{ps}, and using q_D instead of q_c from an adjacent CPT sounding to evaluate a sand's liquefaction potential. Nothing in this paper applies if you advance the blade by driving it with a hammer.

2 WHERE TO MEASURE THE THRUST P

Before using P the engineer needs to decide where to measure it – above ground at the top of the string of rods going to the DMT blade or below ground directly above the blade? The argument for above ground: One can easily install, read, and maintain the load cell. The argument against: One does not measure the parasitic rod/soil side shear above the blade. The argument for directly above the blade: That eliminates the need to know the above parasitic side shear. The argument against: It creates serious equipment design and maintenance problems.

Our DMT research with load cells at both top and bottom of the rods showed bottom cells impractical for routine use and that the parasitic side shear in sands became negligible when machining a "friction reducer" 33% diameter enlargement 'ring' to the rod connector just above the blade, correcting for its additional end bearing, and testing at depths of 15m or less ASTM (2014), Schmertmann, (1982, 1984). Figure 1 shows two examples of similar (P vs z) profiles when using a friction reducer and simultaneously measuring thrust above ground (on rods) and above the blade (on DMT). Discussing Figure 1, Bullock (2015) also wrote *"Separate analyses for friction angle prepared using each thrust measurement provided almost the same values, indicating that the rod friction was not significant for these soundings."*

Figure 1 also shows, after penetrating through a strong into a weak layer, how P drops off sharply to low values and thus also indicates that the parasitic rod shear has a minor effect. However, some experience in Europe suggests that eliminating such a friction ring does not have a significant effect on the thrust required because the prior blade advance has already disturbed the soil around the overhead rods. The writers routinely use a ring but suggest trying a few soundings with and without a ring and compare how it affects the results, particularly the thrust profiling and Φ'_{ps} prediction, and choose which method seems more accurate. Eliminating the ring may reduce the thrust required to advance the blade.

3 USEFULNESS OF MEASURING THRUST

2.1 *Soil Profile of P vs. depth*

During a typical DMT sounding the engineer stops penetration at 100-300 mm depth intervals to obtain the p_0 and p_1 membrane expansion pressure data, and would measure the thrust P during every penetration interval. This provides the P vs. z (depth) points, 100-300 mm apart, for a nearly continuous profile and can detect layers as thin as 100mm. Comparing CPT q_c end bearing profiles with adjacent P profiles shows them similar to 15m depths. This suggests that most, or an important part of P, results from the DMT blade's q_D end bearing.

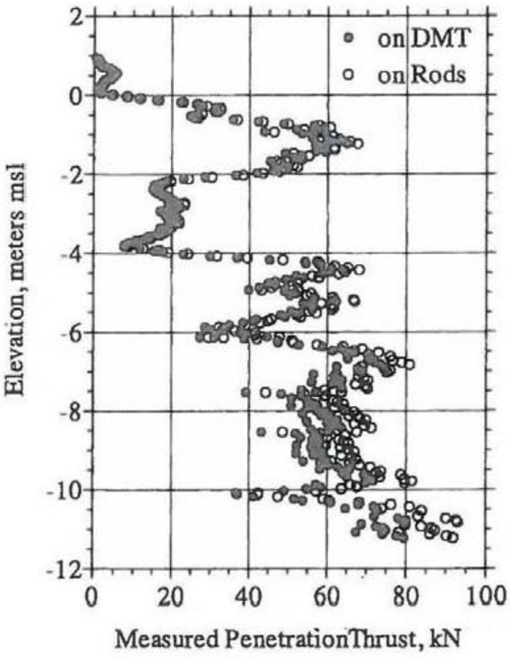

Fig. 8. VLE penetration thrust - DMT FRZ005

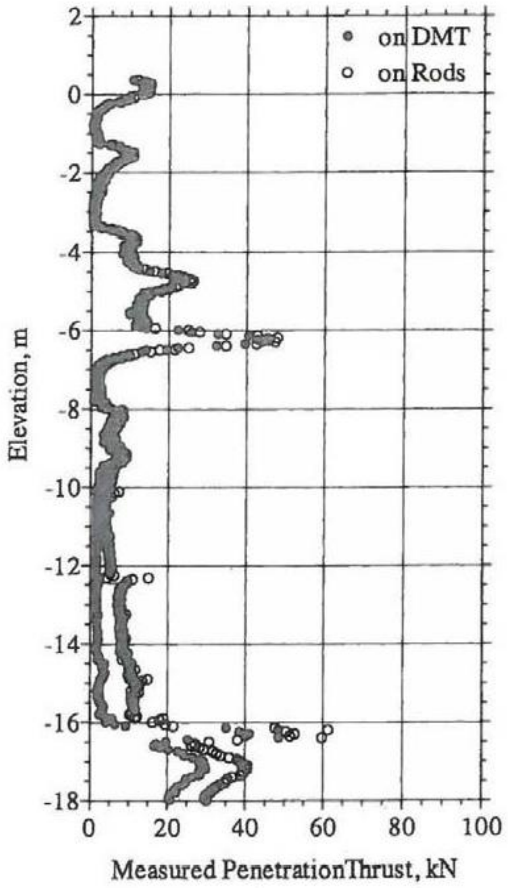

Fig. 9. VLW penetration thrust - DMT FRZ007

Figure 1. Examples of Comparative Thrust on Rods and on DMT Blade, from Bullock (2015)

2.2 *Thrust Measurements Help to Prevent Damage or Loss of the DMT Blade*

Engineers often push dilatometer (DMT) blades in the United States and Canada using SPT rigs with a typical range of maximum available thrust from about 31 to 62 kN (7 to 14 kips); and, with CPT rigs with a typical range of about 89 to 267 kN (20 to 60 kips). The potential damage or loss of the DMT blade during penetration increases as the thrust increases. However, soil type and layering can also have a dramatic effect. Most minor damage to the blade relates to pushing into sharp gravel, gravelly and shelly soils, or attempts to push into very strong soils or rock, any of which may cut the membrane or pit the cutting edge of the blade. Minor damage to the DMT blade typically occurs at thrust values less than about 62 kN (14 kips). Increased thrust, especially in sands, result in increased abrasion of the blade and membranes which decreases their useful life, especially when using thrust values over 90 kN (30 kips). A weak layer over a very strong layer may result in loss of the DMT blade when trying to push into the very strong layer when the upper weak layer lacks sufficient lateral support to prevent bucking of the rods above the blade. Loss of the blade usually occurs when the rods break at one of the joints close to the blade. One must make decisions regarding whether or not to continue penetration vs. the risk of damage or loss of the DMT blade during penetration. Previous thrust values provide information to help in these decisions and prevent serious damage to or, in the now rare case, loss of the DMT blade.

2.3 Thrust Measurements Help the Operator to Anticipate the Increase or Decrease in DMT Pressures for Subsequent Readings

The DMT data are typically considered drained for non-cohesive soils and undrained for cohesive soils. The speed of penetration and the speed of application of the pressures to the DMT membrane may have an effect upon the DMT results. The normal speed of penetration = 20mm/second. D6635-01 in ASTM (2014) standardizes the speed of application of the pressure to the membrane (within limits) to minimize differences in p_o and p_1 values by different operators. The recommended procedure: Apply the pressure quicker in the beginning and slow down when approaching the reading pressure to have a more accurate reading. Thrust measurements provide an advance warning of increasing or decreasing soil strength and the likely increase or a decrease in the next set of pressure readings and thus contribute to obtaining more accurate data.

4 OBTAINING q_D FROM P

Schmertmann (1982, 1984), describes in detail how to extract q_D from P. Figure 2, copied and annotated from Schmertmann (1984), shows the axial forces acting on the sounding rods and the DMT blade. Setting their sum = 0 gives equation (1), which one can solve for q_D. See Notation for another verbal description of each symbol.

$$P + W - F_r - F_q - F_b - q_D(bw) = 0 \qquad (1)$$

3.1 *Comments about F_q and F_b*

F_q results from parasitic end bearing loading on the additional projected bearing area $A_p = ((\pi d^2)/4 - bd)$. With 45 mm diameter AW rods this adds 885 and 1870 mm^2, without and with a ring, respectively, to the blade's end bearing area of 1440 mm^2. The addition occurs where the blade has previously passed, disturbed and then partially unloaded the soil above the top of the blade. The local bearing pressure responsible for F_q will likely fall below q_D at the bottom of the advancing blade. Using q_D when calculating $F_q = (A_p)q_D$ produces a likely too-high F_q and therefore a conservative q_D. The data reduction corrects P to that from a previous lesser depth that most closely corrects for the vertical

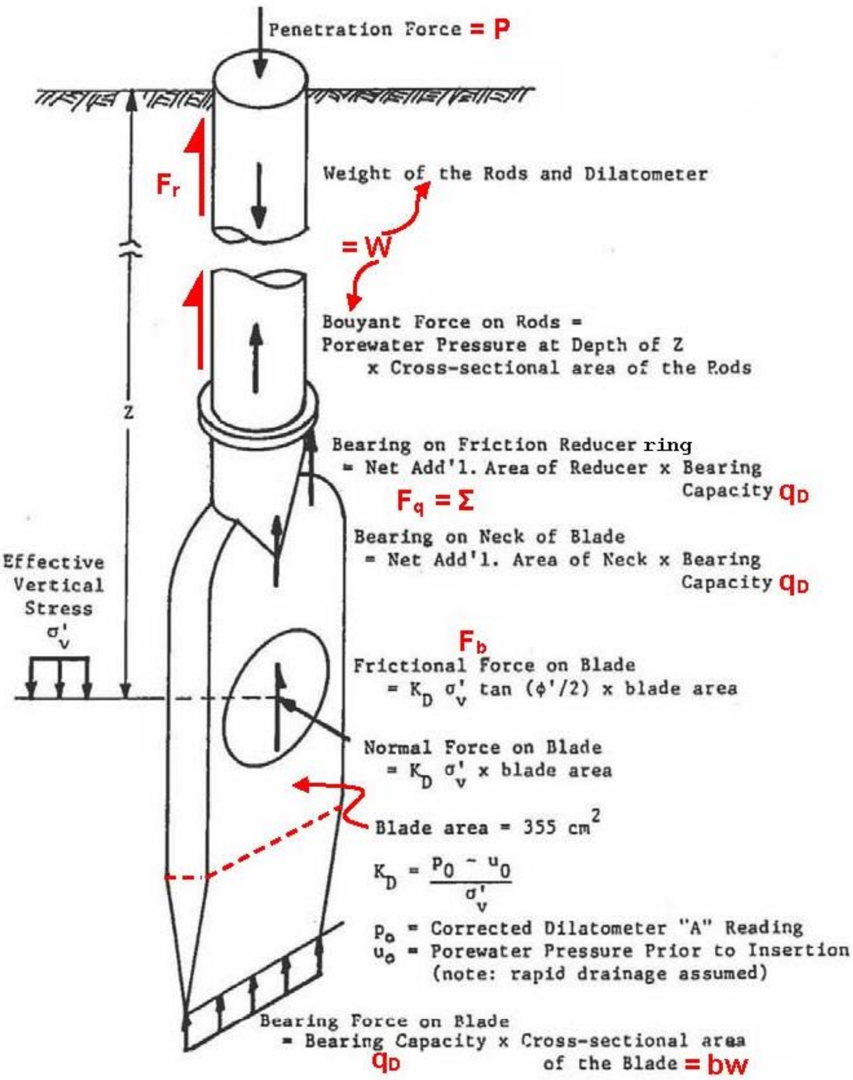

Figure 2. Vertical Forces on DMT Blade and Rods (schematic, annotated)

distance (c. 200 mm) between the ring and center of the blade's membrane.

F_b develops because of the frictional resistance to penetration along the vertical sides and edges of the blade. Because the blade has a (width/thickness) or (w/b) ratio of 7, with a penetration angle $\alpha \approx 16°$ moving the soil outward from its face with passive pressure, we assume negligible friction along the 15 mm blade edges. The two sides of the blade above the 16° bottom cutting edge have a total area, $A_s \approx 355$ cm^2. We measure $\overline{\sigma}'_n$ against the blade shortly after the operator stops penetration and reduces the thrust P to zero. The writers use the 60 mm diameter DMT membrane as both a total and effective pressure cell. This works well in rapidly draining frictional soils as described most recently by Bullock (2015). With the membrane located in the area in plane strain, and covering 8% of that area, we assume that the measured p_0, after the corrections for membrane stiffness and water pressure u, provides the average $\overline{\sigma}'_n$ against the entire 355 cm^2. We also assume a frictional soil ($c' = 0$), with an ultimate shear resistance between sand and a smooth steel blade $= \overline{\sigma}'_n \tan \delta'_{ps}$ and $\delta'_{ps} = ½\, \Phi'_{ps}$, based on experimental results by Nottingham and Schmertmann (1975) and the common use of this ½ assumption.

3.2 *Review of Conservatism*

Defining conservative as calculating a too-low q_D, Table 1 lists the writers' estimates of the conservatism of the expressed and tacit assumptions involved with calculating F_q, F_b and F_r to obtain q_D. We believe that the conservative and non-conservative assumptions tend to cancel each other. The subsequent and generally conservative Φ'_{ps} values determined from q_D suggest an overall conservatism in q_D.

Table 1. Estimates of Conservatism

	Assumption	Conservative q_D? Yes	No
F_q	Disturbed soil	✓	
	Using q_D for the unknown q above the blade	✓	
F_b	Negligible edge friction		✓
	p_0 during penetration = p_0 during DMT with penetration stopped and P = 0		✓
	Excess hydrostatic pore pressure = 0 in sands ($I_D \geq 1.8$)	✓	
F_r	Corrected p_0 gives avg. $\overline{\sigma}'_n$ over entire face area of blade	✓	
	$c' = 0$	✓	
	$\delta'_{ps} = ½\, \Phi'_{ps}$	Unknown, but a common assumption	
	$F_r = 0$		✓
Φ'	Schmertmann (1984) (see **4.**)	✓	

5 OBTAINING Φ'_{ps} FROM q_D

Schmertmann (1982, 1984) describes in detail a method to calculate Φ'_{ps} from DMT data in sands. The previous sections herein describe how to extract q_D from the thrust P to advance the DMT blade. This section summarizes the principal concepts used to determine Φ'_{ps} from q_D.

Durgunoglu and Mitchell (1973, 1975) developed a theory for calculating the bearing capacity for the near-surface penetrometers used on the moon. This theory improved on existing theories by explicitly taking into account the variables of horizontal stress, penetrometer shape, axisymmetric and plane strain penetrations, point angle, soil-friction angle and friction coefficient along the penetrometer point material surface. It seemed to produce good bearing capacity predictions in its lab verifications over $z/w \leq 30$, and reasonable results on the moon. Subsequent papers Mitchell and Lune (1978), Villet and Mitchell (1981) showed that the D&M theory also gave reasonable bearing capacity predictions for much deeper CPT and DMT soundings. Schmertmann (1982) also found that this theory produced reasonable results when compared with such soundings in soil with $I_D \geq 1.8$ (sands and silty sands). Marchetti (2015) still continues to support the validity of using the D&M theory with q_D but also notes alternate methods for obtaining Φ'_{ps} from the DMT and Φ'_{ax} from the CPT.

The D&M theory uses the Mohr-Coulomb model for soil shear strength. Therefore q_D (and q_c) also depend on plane strain (and axisymmetric) c' and Φ'. Still assuming $c' = 0$ in sands, then $q_D = f(\Phi'_{ps}$ and $K_0)$ and in principle one can calculate Φ'_{ps} from q_D. This requires an iteration procedure with K_0. Computers can now easily solve this problem during routine data reduction. Experience and research, as described in Schmertmann (1982, 1983-91, 1984) have shown that using the above D&M method produces reasonable and usually conservative values of Φ'_{ps}. It has the advantage of a partly theoretical basis vs. mostly empirical alternatives and incorporates the insitu horizontal stress in the form of K_0. The writers use a K_0 value in sands ($I_D \geq 1.8$) determined from equation (2), developed from the results from 16 DMT and CPT tests in large triaxial chambers. The unaged, uniform sands varied from fine to coarse, with OCR = 1 (mostly) to 5.6 and K_0 from 0.33 to 0.96.

$$K_0 = \frac{40+23\,K_D-86\,K_D(1-\sin\Phi'_{ax})+152(1-\sin\Phi'_{ax})-717(1-\sin\Phi'_{ax})^2}{192-717(1-\sin\Phi'_{ax})} \qquad (2)$$

The writers use equation (1) with the D&M theory and the measured K_D and thrust P as follows:

1. Use P to get q_D

2. Use the D&M theory, a 'known' q_D and K_D, plus a trial value of K_0 to calculate a Φ'_{ps}.
3. Convert to the equivalent Φ'_{ax}.
4. Put Φ'_{ax} in equation (2) and calculate a K_0.
5. Substitute this K_0 in step 2 and repeat steps 3.,4. etc. until getting an acceptable match between the trial K_0 and calculated K_0 that gives the final set of K_0 and Φ'_{ax} values.

6 CONVERTING q_D TO q_C AND Φ'_{ps} TO Φ'_{ax}

Mitchell and Lune (1978) used the D&M theory, among others, to calculate Φ'_{ax} in sands from CPT tests in lab chambers and field sites. They concluded "For the sites and chamber tests included in this paper the values of $\Phi'_{(ax)}$ found by this method agree very well with the laboratory measured values." Schmertmann (1982, 1983) found from a similar comparison that the D&M theory underpredicted Φ'_{ax} by 1° to 3.2° over the dry sand depth (z) range of 4 to 46m, and a relative density (D_r) range of 45 to 90%. Using the same theory Schmertmann (1982) calculated the ratios of (q_D/q_c) and found the ratio insensitive to depth and horizontal stress. Only Φ' mattered over a range of 25° to 45°. Actual research comparisons in large chamber tests and in the field give (q_D/q_c) ratios of about 1.1 ± 0.1.

Many researchers have clearly shown that $\Phi'_{ps} > \Phi'_{ax}$ because plane strain prevents particle movements in one dimension and axisymmetric strain does not. For example, see Terzaghi, Peck and Mesri (1996). This effect becomes negligible in loose sands with $\Phi'_{ps} \leq 32°$. The writers use and recommend equation (3) as an empirical method for converting between Φ'_{ps} and Φ'_{ax}. Use $\Phi'_{ax} = \Phi'_{ps}$ when $\Phi'_{ps} \leq 32°$. It fits conservatively with the more detailed data in Terzaghi et.al. (1996).

$$\Phi'_{ax} = \Phi'_{ps} - \frac{(\Phi'_{ps} - 32°)}{3} \tag{3}$$

7 USING q_D TO ESTIMATE LIQUEFACTION POTENTIAL (LP)

As detailed by Marchetti (2015), the writers consider it well established that LP depends importantly on the existing horizontal stress and stress history of silts and sands, and that the DMT K_D parameter increases with K_0 and aging. The risk of liquefaction decreases with increasing K_D, but not uniquely. Introducing another measurable parameter directly related to LP and sand structure, such as the local bearing capacity q_c (or potentially q_D) from insitu penetration tests, seems to improve LP predictions. The writers counted at least four papers in the DMT-2015 Conference Proceedings that proposed LP prediction methods that combine K_D and q_c, with q_c obtained from an adjacent CPT sounding at the same elevation as K_D in the DMT sounding.

Using an adjacent CPT sounding creates at least two problems, namely the cost of a possible additional CPT sounding and the uncertainty that inherently variable sand deposits may result in K_D and q_c obtained in sands with significantly different structure and LP. It seems obvious that using q_D from the same sounding, at or above and below the elevation of determining K_D greatly reduces the risk of testing significantly different sands. Furthermore, the thrust measurements from the DMT sounding itself should provide adequate profiling at its location.

The writers understand that liquefaction rarely occurs at depths of more than 15m. That means, based on the previously described experience in Section **1.**, that sounding rod side shear, F_r, has a negligible effect at most potentially liquefiable sites. Current LP correlations include q_c vs. q_D because the much more extensive use of the CPT vs. DMT sounding method has given engineers the opportunity to include q_c in LP correlations. The writers believe q_D may do equally well with an expanded correlation data base, perhaps better with the above better assurance of testing the same sand. Does an accurate q_c of adjacent sand trump a less accurate calculation of q_D on the same sand or visa-versa? More research and experience should resolve this question.

8 CONCLUSIONS

a) Profiling thrust provides a useful, real-time, measure of stratigraphy. It permits anticipating the next set of DMT p-readings and guarding against equipment damage.
b) Using a "friction ring" with a 33% increase in rod diameter above the DMT blade will reduce parasitic rod side shear to negligible values in sands at depths of less than 15m.
c) Summing thrust and the other vertical forces calculated using the ordinary DMT data permits calculating a generally conservative q_D.
d) The Durgunoglu and Mitchell bearing theory permits detaining Φ'_{ps} from q_D and Φ'_{ax} from q_c.
e) Using q_D directly with K_D from the same DMT sounding can potentially avoid using a possibly erroneous q_c from an adjacent sounding in combined (K_D-q_C) liquefaction potential correlations.
f) We find the many benefits of routinely measuring the penetration thrust P during a DMT sounding well worth the extra time and expense.

9 REFERENCES

ASTM 2014. Standard test method for performing the flat plate dilatometer, D 6635-01, Annual Book of ASTM Standards, ASTM, Philadelphia, PA, 4:09.

Bullock, P.J., 2015. "Driven Pile Setup Testing and the Dilatometer", DMT '15 The 3rd Int. Conf. on the Flat Dilatometer, Rome, Italy, June 14-16 Marchetti, Monaco & Viana da Fonseca (eds), pp. 73-74.

Durgunoglu, H.T. and Mitchell, J.K. 1975. "Static Penetration Resistance of Soils", I-Analyses, II-Evaluation of Theory and Implications for Practice, ASCE Spec. Conf. on In Situ Measurement of Soil Properties, Raleigh NC, Vol I, 1975, pp. 151-189.

Durgunoglu, H.T. and Mitchell, J.K. 1973. "Static Penetration Resistance of Soils", Research report prepared for NASA Headquarters, Washington, D.C., Univ. of California, Berkeley.

Marchetti, S. 2015. "Some 2015 Updates to the TC16 DMT Report 2001", DMT '15 The 3rd Int. Conf. on the Flat Dilatometer, Rome, Italy, June 14-16 Marchetti, Monaco & Viana da Fonseca (eds), pp.

Mitchell, J.K. and Lune, T.A. 1978. "Cone Resistance as a Measure of Sand Strength", ASCE Journal of the GED, Vol. 104, GT7, July 1978, pp. 995-1012.

Nottingham, L.C. and Schmertmann, J.H. 1975. "An Investigation of Pile Capacity Design Procedure", University of Florida, College of Engineering, EIES, Dept. of Civil Engineering, Final Report D629 to the Florida DOT, 159 pp. plus appendix.

Schmertmann, J.H. 1983-91. DMT DIGESTS, distributed by GPE Inc., Gainesville, FL, Schmertmann, J.H., Editor. Digest #1 – Apr 83.

Schmertmann, J.H. 1982. "A Method for Determining the Friction Angle in Sands from the Marchetti Dilatometer Test (DMT)", Proceedings of the 2nd European Symposium on Penetration Testing ESOPT2, Amsterdam, 24-27, pp. 853-861

Schmertmann, J.H. 1984, DMT Manual – Guidelines for using the CPT, CPTU and Marchetti DMT for Geotechnical Design, Report Number FHWA-PA-87-024+84-24, Vol. III of IV – DMT Test Methods and Data Reduction

Terzaghi, K., Peck, R.B., and Mesri, G. 1981. "Soil Mechanics in Engineering Practice", 3rd Edition, 1996, Fig. 19.3, p.149

Villet, W.C., and Mitchell, J.K. 1981. "Cone Resistance, Relative Density and Friction Angle", ASCE Cone Penetration Testing and Experience, Oct. 1981, pp. 178-208.

10 LIST of SYMBOLS

A_p	parasitic end bearing area above blade
A_S	area of blade exposed to side shear
b	blade thickness
CPT	= static cone penetration test
c'	effective cohesion strength
D_r =	Relative density (%)
DMT	Marchetti dilatometer test
d	ring, or rod diameter if no ring
F_r	side shear force along DMT rods
F_q	parasitic bearing force on ring and/or rod connector
F_b	side shear force on blade
I_D	material index = $[(p_1-p_0)/(p_0-u_0)]$
K_0	(horiz/vertical) effective stress ratio before DMT (or CPT)
K_D	horizontal stress index = $[(p_0-u_0)/(\sigma'_{vt} - u_0)$
LP	Liquefaction Potential (various definitions)
OCR	overconsolidation ratio
P	thrust force
P_z	P at depth z
p_0	corrected DMT membrane lift off pressure, movement = 0.05 mm
p_1	corrected pressure at 1.1 mm movement
q_C	CPT cone bearing capacity
q_D	DMT blade bearing capacity
SPT	Standard penetration test (dynamic)
u_0, u	total water pressure on membrane
W	buoyant weight of DMT rods and blade
w	blade width
z	depth of center of membrane below ground surface
α	angle of cutting edge of blade, 50 mm transition from edge to b
δ'_{ps}	effective blade/sand friction angle
Φ'	effective friction angle
Φ'_{ax}	axial-symmetry Φ'
Φ'_{ps}	plane strain Φ'
Σ =	sum of
$\overline{\sigma}'_n$ =	effective avg. normal stress on blade
σ'_v =	estimated effective vertical stress at depth z

Geotechnical and Geophysical Site Characterisation 5 – Lehane, Acosta-Martínez & Kelly (Eds)

Interpretation of the instrumented DMT (iDMT): a more accurate estimation of p_0

H. Shen, W. Haegeman, H. Peiffer
Laboratory of Geotechnics, Department of Civil Engineering, Ghent University, Ghent, Belgium

ABSTRACT: Based on the pioneering conceptual framework of the Marchetti DMT, a number of iDMTs have been developed to produce a full pressure-displacement curve, giving the opportunities to improve interpretation techniques such as the determination of the corrected first pressure reading p_0 (contact pressure at zero displacement). A novel p_0 interpretation technique is thus presented in this paper to reduce the potential errors caused by an invalid assumption of the linear pressure-displacement relation. The analytical procedure involves the determination of the yield point and then the estimation of p_0 from the post-yield curve. With the algorithm programmed in Matlab, the procedure is applied to field data and calibration chamber data, showing better estimated p_0 values using this new technique.

1 INTRODUCTION

The flat dilatometer (DMT) invented by Marchetti more than 30 years ago has been widely used as a routine site characterization device. It provides geotechnical engineers a simple, effective tool to get accurate, reliable soil properties such as operative moduli and stress history (Marchetti et al. 2001, Marchetti 2015). Following the global popularity of the DMT use, various modified DMTs have been developed for different purposes, these modifications have been reviewed by Shen et al. (2015). Among these modified apparatuses, iDMTs capable of producing a full pressure-displacement curve have been prototyped and investigated by a number of researchers (Akbar & Clarke 2001, Bellotti et al. 1997, Benoit & Stetson 2003, Campanella & Robertson 1991, Colcott & Lehane 2012, Fretti et al. 1992, Stetson et al. 2003, Shen et al. 2016). Compared to pressure readings at two displacements in the standard DMT, a full pressure-displacement curve in the iDMT can not only provide a better understanding of the standard DMT but also shows promising improvements in the estimation of the soil properties. An ongoing iDMT project using 3D (metal) printing technology for the probe fabrication has been carried out at UGent and Gesound.be with the following objectives: to consider non-linear soil behaviour by a sufficient large expansion of a loading piston; to perform an effective stress analysis by an additional pore-pressure sensor (Shen et al. 2016).

The corrected first reading p_0 is of importance in the DMT, since it is a necessary input for all three "intermediate" DMT parameters I_D, K_D, and E_D which are then used to derive common soil parameters. Therefore, any error in the determination of p_0 can lead to the misinterpretation of soil properties.

This paper aims to improve the determination of p_0 when a full pressure-displacement curve of the iDMT is available. The p_0 determination technique in the standard DMT is firstly reviewed along with the analysis of its possible errors. Then, to reduce these errors, a new p_0 interpretation technique is presented and applied to various types of iDMT pressure-displacement curves.

2 ESTIMATION OF p_0 IN THE DMT

In the standard DMT, p_0 derives from the assumption of a linear pressure-displacement relation and is back-extrapolated from the pressure readings at 0.05 mm and 1.10 mm, as shown in the following formula:

$$p_0 = 1.05(A - Z_M + \Delta A) - 0.05(B - Z_M - \Delta B) \qquad (1)$$

where ΔA, ΔB = corrections determined by membrane calibration, Z_M = gage zero offset.

According to this definition, p_0 cannot be measured directly but is de facto a corrected pressure value at zero displacement. This method can provide accurate and repeatable p_0 as long as a linear relation of pressure-displacement is appropriate. However, it will definitely be a biased estimation if a highly non-linear pressure-displacement relation is presented in a soil. This can only be checked by evaluating the full pressure-displacement curve from iDMT data.

3 PRESSURE-DISPLACEMENT CURVE IN THE iDMT

Using an iDMT incorporated with a pressure sensor and a displacement sensor, a full pressure-displacement curve can be obtained. However, various shapes of the curves are produced in different soils based on a review in the literature. In Figure 1, there are 4 types of typical loading curves illustrated and the common feature is that an initial stiff response occurs at the start of the membrane expansion. Specifically, in the first three sub-figures, Figure 1 (a)-(c), an abrupt change in slope is seen in most of the calibration chamber tests (Bellotti et al. 1997, Fretti et al. 1992) and in a few in-situ tests (Akbar & Clarke 2001, Akbar et al. 2005; Benoit & Stetson 2003, Campanella & Robertson 1991, Stetson et al. 2003). Also, there is a fourth type of curve which does not show an apparent abrupt change in slope, as demonstrated in Figure 1 (d). This type of curve has not yet been observed in any calibration chamber test but only in in-situ tests (Benoit & Stetson 2003, Campanella & Robertson 1991, Stetson et al. 2003). It is likely due to the lack of excess pore-water pressure during the tests in sands, while the presence of high pore-water pressure in clays and the dissipation of pore-water pressure in silts may both present difficulties to see the abrupt change in slope.

This initial stiff response shown in the data of iDMT is an unload-reload effect: soil elements are unloaded in a wedge cavity expansion by the blade tip during the probe installation; then these soil elements are reloaded as the membrane expands during the test. The soil unloading has been quantitatively evaluated in the three-dimensional numerical solutions presented by Finno (1993) and Kouretzis et al. (2015) in saturated cohesive soils. A decline in strain levels of soil elements from the blade shoulder to the membrane during the blade penetration is observed. So it is reasonable to assume the occurrence of a reloading phase for the membrane expansion during the test.

A schematic pressure-displacement curve along with an initial stiff soil response on the loading curve is illustrated in Figure 2. There are several important points to consider during the loading phase: O, the lift-off point where the membrane starts to move; Y, the onset of yield; A, the pressure reading at the displacement of 0.05 mm; B, the pressure reading at the displacement of 1.10 mm.

As pressure readings at point A and B are obtained in the standard DMT, p_0 is derived via Equation 1 based on the assumption of a linear relationship, as illustrated by the dashed line in Figure 2. In other words, the post-yield curve is assumed to be linear from A to B in the standard DMT interpretation technique. So in case of a non-linear post yield curve or/and a large initial stiff response beyond the displacement of 0.05 mm, the estimation of p_0 can be erratic using this standard method.

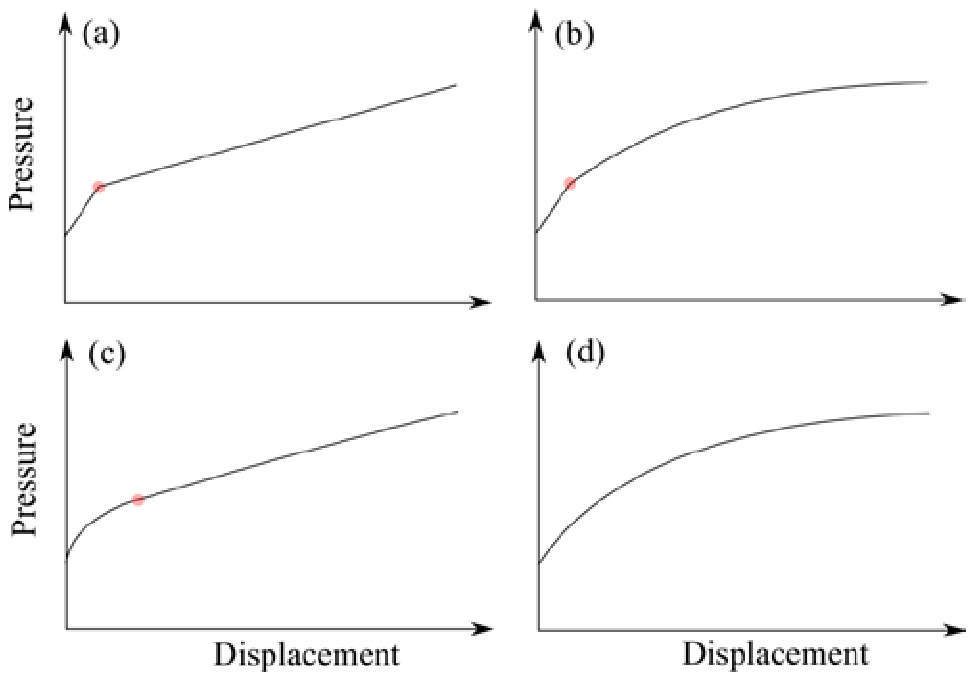

Figure 1. Schematic diagrams of typical pressure-displacement curves

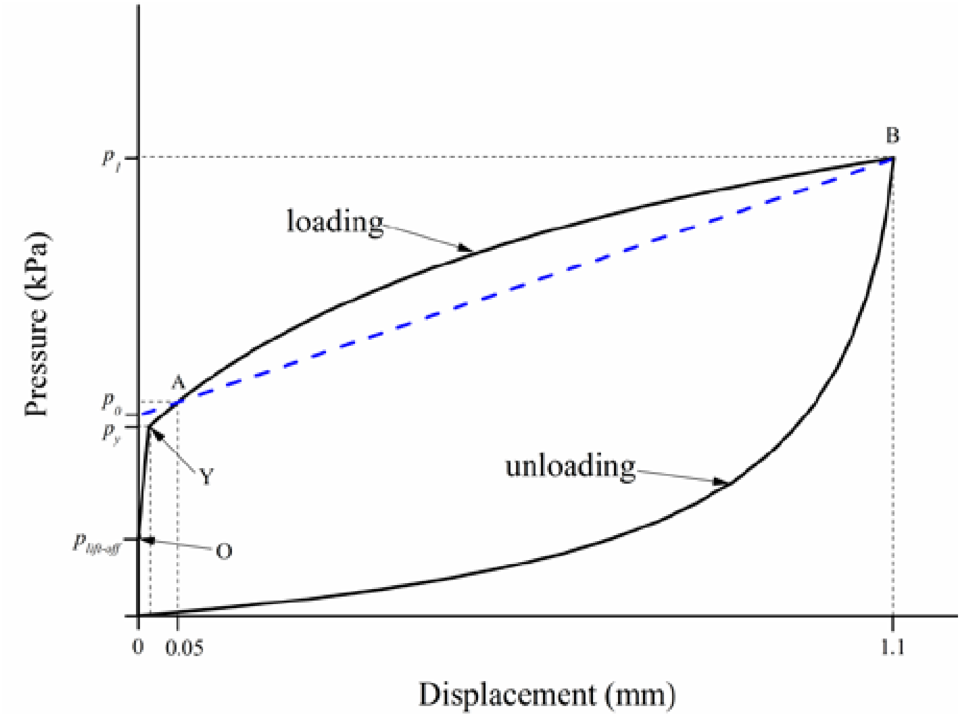

Figure 2. Schematic diagram of a full pressure-displacement curve

p_0 has been determined in different ways when a full pressure-displacement curve is available. Bellotti et al. (1997) and Fretti et al. (1992) use the pressure p_y at the onset of yield while Campanella & Robertson (1991) and Colcott & Lehane (2012) use the pressure $p_{lift\text{-}off}$ when the membrane starts to move. These methods chose specific points on the loading curve but can still bring errors.

4 A NEW INTERPRETATION TECHNIQUE

A new interpretation technique for p_0 is thus proposed to reduce the aforementioned errors. The technique finds the corrected pressure at zero displacement from the full pressure-displacement curve.

To deal with the four types of loading curves shown in Figure 1, the newly proposed solution involves two steps: (1) The determination of the yield point Y to distinguish the reloading phase O-Y from the post-yield phase Y-A-B, as shown in Figure 2; (2) The estimation of p_0 based on the post-yield phase of the loading curve.

4.1 *Determination of the point of yield*

In Figure 1(a, b, c), the point of yield is clearly identified by the circles. These results are found in calibration chamber tests with clean and uniform sand being tested as well as in a few in-situ tests. Then, this point of abrupt change in slope is readily determined as the onset point of yield Y. In most cases of in-situ testing results, a clear yield point Y cannot be found since a smoothed curve is observed, as shown in Figure 1(d).

In the one-dimensional consolidation test, the preconsolidation pressure cannot be measured directly, but can be estimated with a satisfactory degree of accuracy by means of the empirical graphical methods such as the widely used method proposed by Casagrande (1936). Likewise, in the DMT tests, an unloading phase during the blade penetration precedes an initial reloading phase during the membrane/piston expansion. Considering the similarity of the reloading process, a resemblant graphical method may also be of use in the determination of the yield point in the iDMT pressure-displacement curve, despite the fact that sufficient experience is still needed for the validation.

In addition, implementation of a manual graphical method is time consuming and inconvenient. Therefore, an algorithm has been developed and programmed in Matlab to automate the procedure. The specific steps are as follows: (One may refer to Figure 4 of an example, for better understanding of this technique)

1. Arrangement of the iDMT data on a semi-log plot of the displacement with a linear scale for the *x*-axis and the pressure with a logarithmic scale for the *y*-axis. Note that this presentation is typical in iDMT curves for a clear demonstration of the stress-strain relation.
2. Curve fitting of the data points from the lift-off point till the end of loading to a power function:

$$y = ax^b + c \quad (2)$$

3. Estimation of the point of maximum curvature on the fitted curve. Using the mathematical definition of the radius of curvature R, as shown in the Equation 3, the R determination for a power function is obtained in the Equation 4. As the curvature is the reciprocal of the radius of curvature, the point of maximum curvature is given by the minimum value of the radius.

$$R = (1+(dy/dx)^2)^{3/2}/(d^2y/dx^2) \quad (3)$$

$$R = x^{2-b}[(a^2b^2x^{(2b-2)}+1)^{3/2}]/[ab(b-1)] \quad (4)$$

4. Determination of the bisector line from the vertical line and tangent line at the point of maximum curvature.
5. Linear fitting of the straight portion of the post-yield curve.
6. The point where the lines in part 4 and part 5 intersect is used to obtain the displacement of the yield point.

In the last step, the displacement of the intersection is used to deduce the yield point, which is different from the Casagrande's method using the pressure of the intersection as the preconsolidation pressure. The rationale of this is that the DMT test can be regarded as a displacement-controlled test as the soil elements are loaded by an expansion of the membrane until a displacement of 1.1 mm is attained. So the pressure required to achieve this displacement varies in different soils. A one-dimensional consolidation test is a pressure-controlled test as the specimen is subjected to increments of pressure until the final pressure being equal to or greater than four times the preconsolidation pressure. Therefore, a large enough pressure in the DMT test is not likely to be attained in some soils but the final maximum displacement of 1.10 mm is normally higher than multiple times the displacement of the intersection.

4.2 *Back-extrapolation of p_0*

Once the yield point Y is identified, the start of the post-yield loading curve is determined. Then, p_0 at zero displacement can be back-extrapolated from a regression model fitting the post-yield loading curve.

Concerning the characteristics of the post-yield loading curve, a limit pressure p_L may be approached with increasing displacement, which has been found in some iDMT curves (Benoit & Stetson 2003, Colcott & Lehane 2012). However, this is not valid in every iDMT curve since a fixed displacement level, such as 1.1 mm in the standard DMT, may correspond to different strain levels in different soils. Therefore, a regression model which can take into account possible non-linear, asymptotic behaviours is proposed:

$$Y = c' + a'X - b'd'^X \quad (5)$$

where a' and c' are the parameters for a linear asymptote line representing a potential boundary associated with the limit pressure p_L, b' indicates the range of the non-linear part and d' is the rate of the non-linearity. It is noted that the model is valid when $b' \geq 0$ and $0 < d' < 1$.

5 EXAMPLES

An iDMT test was performed at a depth of 13.72 m in soft varved clay by Benoit & Stetson (2003). Note that the test is carried out after the full pore-pressure dissipation so the curve is not influenced by the dissipation of pore-pressure generated by probe installation. This issue is important since the performance of an unload-reload loop may require a longer time than in the standard DMT test. The partial drainage condition, which is more difficult to interpret, rather than the undrained condition may be met if the excess pore-pressure is not fully dissipated. The digitalized data points of the loading curve are shown in Figure 3.

For the standard Marchetti method, the point at the maximum displacement of 1.04 mm and the linear interpolated point at the displacement of 0.05 mm are used to obtain a p_0 value of 194 kPa. However, as shown in the graphical illustration of this method in Figure 3, the straight line linking the two points is significantly biased from the real measurements, with only an R-squared value of 0.45. This is due to the large initial stiff response in the curve which covers a range beyond the displacement of 0.05 mm.

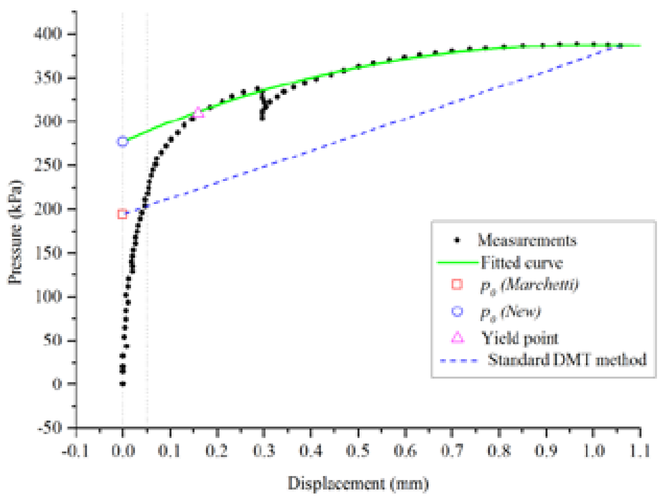

Figure 3. Test data of Benoit & Stetson (2003): application of the new p_0 interpretation technique in comparison with the Marchetti method

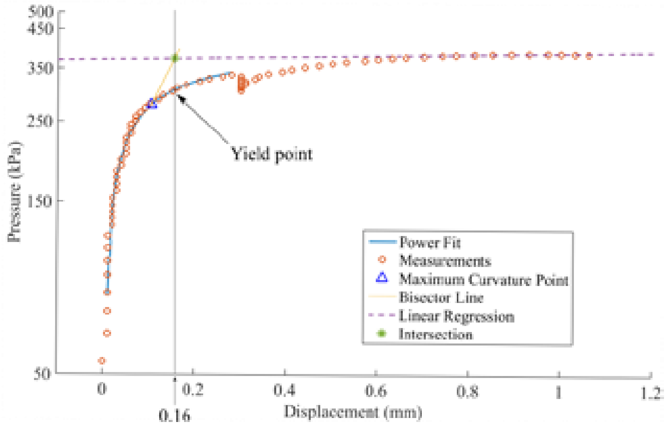

Figure 4. Determination of the yield point

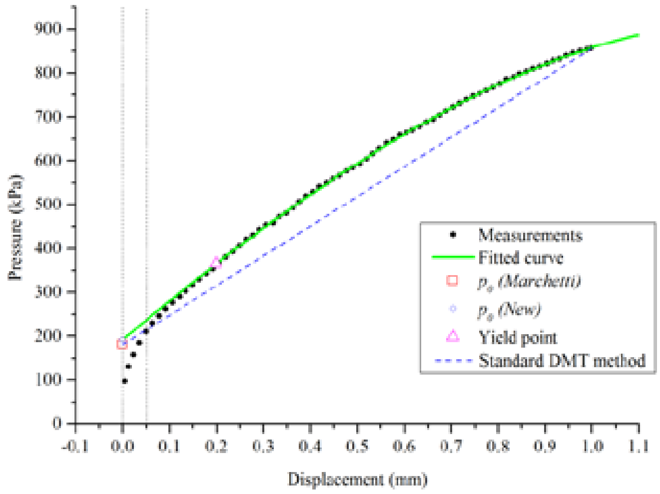

Figure 5. Test data of Campanella & Robertson (1991): application of the new p_0 interpretation technique in comparison with the Marchetti method

Therefore, the use of the standard DMT method is inappropriate in this case. To address this issue, the newly proposed interpretation technique is applied accordingly.

As a smoothed curve is seen in this data rather than an abrupt change in slope, the aforementioned algorithm based on the graphical method for the determination of the yield point is applied in Matlab, and the analytical procedure is illustrated in Figure 4. Given the location of the intersection point, the yield point on the curve is positioned at a displacement of 0.16 mm and a pressure of 309.4 kPa. Note that this displacement value is much higher than the predefined value of 0.05 mm in the standard DMT. Then, with the yield point determined, the post-yield data points (with the unload-reload loop omitted) are selected to carry out the curve fitting based on the regression model of Equation 5, estimating a p_0 of 277 kPa in Figure 3.

Following the first example, there are more measured curves analysed and discussed. The main difference is the determination of the yield point. The smoothed curve in Figure 5 requires the application of the newly developed algorithm. The yield point in Figure 6 and Figure 7 can be directly determined by the abrupt changes in slope.

In Figure 5, the results of an iDMT test performed at a depth of 9 m in sand by Campanella & Robertson (1991) are shown. Compared to the foregoing example also with a smoothed curve, a smaller difference is found between p_0 of 181 kPa using the standard DMT method and p_0 of 192 kPa using the new technique. It is due to a smaller non-linearity of the curve and the fact that the initial stiff range is lower than the displacement of 0.05 mm.

The iDMT developed by Akbar & Clarke (2001) is featured by using a rigid piston instead of a flexible membrane as loading element. In Figure 6, the testing result of this iDMT in a cohesive soil is shown (Akbar et al. 2005). It is interesting to point out that the post-yield curve is linear while the initial stiff phase covers a large range of displacement till around 0.3 mm. Thus the standard DMT method is invalid because of the large initial stiff response. The assessment based on the full pressure-displacement curve is therefore necessary to obtain a reasonable p_0. The p_0 estimated by the standard Marchetti method and the newly proposed method is 416 kPa and 483 kPa, respectively.

In Figure 7, the results of an iDMT test carried out at a depth of 70 cm in a calibration chamber on Toyoura sand by Bellotti et al. (1997) are illustrated. An initial stiff response occurs at the displacement lower than 0.05 mm, however, the standard Marchetti method is still invalid due to the non-linearity of the post-yield curve. This is also illustrated by the difference between the dashed line of the standard DMT method and the measured post-yield data points. The p_0 estimated by the standard Marchetti method and the new technique is 857 kPa and 694 kPa, respectively.

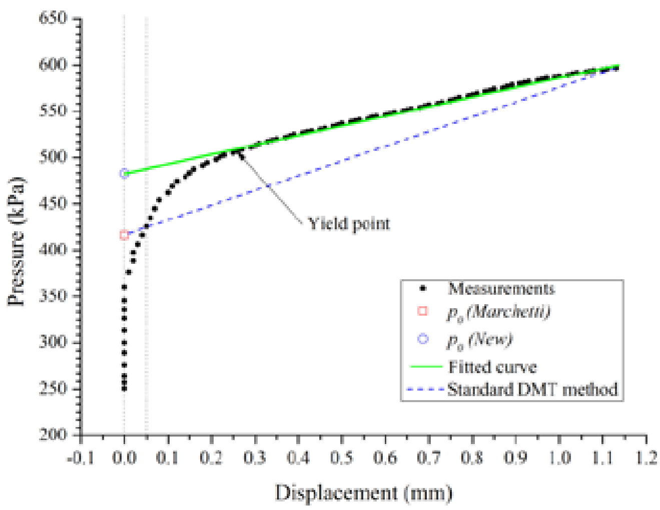

Figure 6. Test data of Akbar et al. (2005): application of the new p_0 interpretation technique in comparison with the Marchetti method

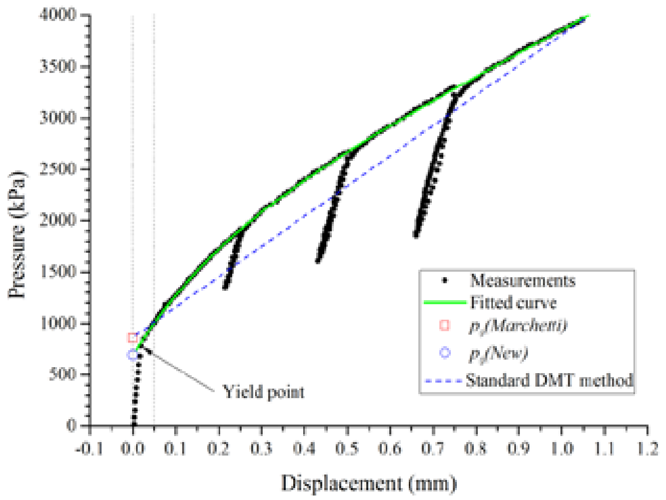

Figure 7. Test data of Bellotti et al. (1997): application of the new p_0 interpretation technique in comparison with the Marchetti method

6 CONCLUSION

A full pressure-displacement curve using an iDMT can provide a number of opportunities to improve the interpretation of soil properties. This paper specifically addresses the errors in the p_0 interpretation as non-linear measured curves may be found and so the standard DMT method, with the assumption of a linear pressure-displacement relation, is by no means sufficiently accurate. Then a new interpretation technique with the determination of the yield point and the estimation of p_0 from the post-yield curve is presented to reduce these errors. The corresponding algorithm is programmed in Matlab to automate the analytical procedure.

The application of the new p_0 interpretation technique on non-linear measured curves shows more reasonable estimation, compared to the use of the standard DMT method. Furthermore, it is the first time in the DMT/iDMT interpretation to address the soil unload-reload effects upon the estimation of p_0.

However, further research is still necessary and currently underway on validating this new technique by comparing with other in-situ data and theoretical back analysis of p_0.

A useful guideline based on this research is that p_0 obtained by the standard DMT method can be up to 30% lower or 23% higher than those using the new p_0 interpretation technique. This does not indicate a compulsory correction to apply but gives rise to awareness of possible inaccuracy in case of non-linear pressure-displacement curves. To eliminate these uncertainties, the performance of iDMT tests for a full pressure-displacement curve along with the use of this newly proposed p_0 interpretation technique are suggested.

7 AKNOWLEDGEMENTS

H. Shen acknowledges the financial support from the China Scholarships Council (No. 201306320157).

8 REFERENCES

Akbar, A., and Clarke, B. G. (2001). “A flat dilatometer to operate in glacial tills.” *Geotechnical Testing Journal*, 24(1), 51–60.

Akbar, A., Kibria, S., and Clarke, B. G. (2005). “The Newcastle Dilatorneter testing in Lahore cohesive soils.” *Proceedings of the 16th International Conference on Soil Mechanics and Geotechnical Engineering*, Rotterdam, 651–654.

Bellotti, R., Benoît, J., Fretti, C., and Jamiolkowski, M. (1997). “Stiffness of Toyoura sand from dilatometer tests.” *Journal of geotechnical and geoenvironmental engineering*, 123(9), 836–846.

Benoit, J., and Stetson, K. P. (2003). “Use of an instrumented flat dilatometer in soft varved clay.” *Journal of geotechnical and geoenvironmental engineering*, 129(12), 1159–1167.

Campanella, R. G., and Robertson, P. K. (1991). “Use and interpretation of a research dilatometer.” *Canadian Geotechnical Journal*, 28(1), 113–126.

Casagrande, A. (1936). “The determination of the preconsolidation load and its practical significance.” *Proceedings of the 1st International Conference on Soil Mechanics and Foundation Engineering*, Harvard, 60–64.

Colcott, R., and Lehane, B. M. (2012). “The design, development and application of a new DMT.” *Geotechnical and Geophysical Site Characterization 4*, Pernambuco, 565–570.

Finno, R. J. (1993). “Analytical interpretation of dilatometer penetration through saturated cohesive soils.” *Geotechnique*, 43(2), 241–254.

Fretti, C., Presti, D. LO, and Salgado, R. (1992). “The research dilatometer: in-situ and calibration chamber test results.” *Riv. Italiana di Geotecnica*, 26(4), 237–242.

Kouretzis, G. P., Ansari, Y., Pineda, J., Kelly, R., and Sheng, D. (2015). “Numerical evaluation of clay disturbance during blade penetration in the flat dilatometer test.” *Géotechnique Letters*, 5, 91–95.

Marchetti, S. (1980). “In-situ tests by flat dilatometer.” *Journal of the Geotechnical Engineering Division*, 106(3), 299–321.

Marchetti, S. (2015). “Some 2015 Updates to the TC16 DMT Report 2001.” *The 3rd International Conference on the Flat Dilatometer*, Rome, 43–65.

Marchetti, S., Monaco, P., Totani, G., and Calabrese, M. (2001). “The flat dilatometer test (DMT) in soil investigations.” *International Conference on In-situ Measurement of Soil Properties*, Bali, 95–131.

Shen, H., Haegeman, W., and Peiffer, H. (2015). “Instrumented DMT: Review and Analysis.” *The 3rd International Conference on the Flat Dilatometer*, Rome, 377–384.

Shen, H., Haegeman, W., and Peiffer, H. (2016). “3D Printing of an Instrumented DMT: Design, Development, and Initial Testing.” *Geotechnical Testing Journal*, 39(3), 492–499.

Stetson, K. P., Benoit, J., and Carter, M. J. (2003). “Design of an instrumented flat dilatometer.” *Geotechnical Testing Journal*, 26(3), 302–309.

Geotechnical and Geophysical Site Characterisation 5 – Lehane, Acosta-Martínez & Kelly (Eds)
© 2016 Australian Geomechanics Society, Sydney, Australia, ISBN 978-0-9946261-1-0

Determination of Em from Ménard pressuremeter tests for gneiss residual soils

T. Q. Silva & E. S. Cândido
Civil Engineering Department, Universidade Federal de Viçosa, Viçosa, Brazil

E. A. G. Marques & E. Minette
Civil Engineering Department, Universidade Federal de Viçosa, Viçosa, Brazil

ABSTRACT: This manuscript presents the results of some Ménard Pressuremeter tests performed in gneiss residual soils from Southeast Brazil, developed under tropical conditions. These tests are useful to determine stress-strain behavior of soils and, so, can be used on Civil Engineering applications. Amid the parameters that can be determined throughout this type of tests is Ménard Pressuremeter Modulus (E_m), which represents the deformability of a soil under external loads. Four boreholes were executed on gneisses residual soils, in which a total of 11 (eleven) pressuremeter tests were performed on mature residual soils and 18 (eighteen) on young residual soils. Results have shown that E_m for both soils increase with depth, as expected. Nevertheless, for young residual this behavior is not obvious, as a small reduction on E_m values can be noted for deeper young residual soil layers, as these present textural and structural heterogeneities – given by mica (biotite) oriented layers, that can control this behavior. In general, deformability values were higher for young residual soils than in mature residual ones.

1 INTRODUCTION

The Ménard pressuremeter prototype was developed by Ménard on 1955 to determine stress-strain soil parameters, and is composed by three overlaid chambers, one for measurements, and two safe cells, one inferior and the other superior, which protect the central chamber from the effects caused by the finite length of the equipment, by confining and inducing it to expand only in radial direction.

The interpretation of pressure x volume curves from the tests allows the acquisition of a deformability characteristic and a strength characteristic of the soil under test, known as pressiometer modulus and limit pressure, respectively. Moreover, other soil parameters, such as cyclic modulus and shear modulus, creep pressure and horizontal stress, can also be obtained.

However, those parameters do not correspond to the soil inherent mechanical characteristics as they rely not only on the material type as well as on the equipment type used, on the way the test hole is dug and on the operator experience.

Currently, the Ménard pressuremeter is recognized and used as a routine tool on geotechnical investigation, being particularly useful on the determination of stress-strain behavior of in situ soils (Schnaid, 2000).

This manuscript presents the results of an in situ testing campaign performed on gneiss residual soils from Southeast Brazil.

2 MATERIALS AND METHODS

Ménard pressuremeter tests were performed on three selected sites (High geological-geotechnical risk areas numbered 1, 2 and 3 on Figure 1). Four boreholes (one at area 1, one at area 2 and two at area 3) were excavated throughout Auger drilling (Silva, 2016; Roque et al., 2014).

Pressuremeter tests were performed at each borehole at every meter, in order to verify the stress-strain behavior for each soil layer previously identified during geological-geotechnical mapping previously executed in the study areas - mature and young residual soils. A Ménard pressuremeter, Type GC (Figure 2), belonging to Civil Engineering Department, Universidade Federal de Viçosa (DEC/UFV) was used. Previously to the tests, the equipment was calibrated by volume and pressure loss.

Test procedures followed ASTM D4719-87 e AFN P94-110-91 recommendations. Basically, tests were performed throughout the following phases: equipment saturation, pressure and volume loss calibration, borehole execution, probe insertion and expansion on desired depth up to the achievement of a good pressuremeter curve

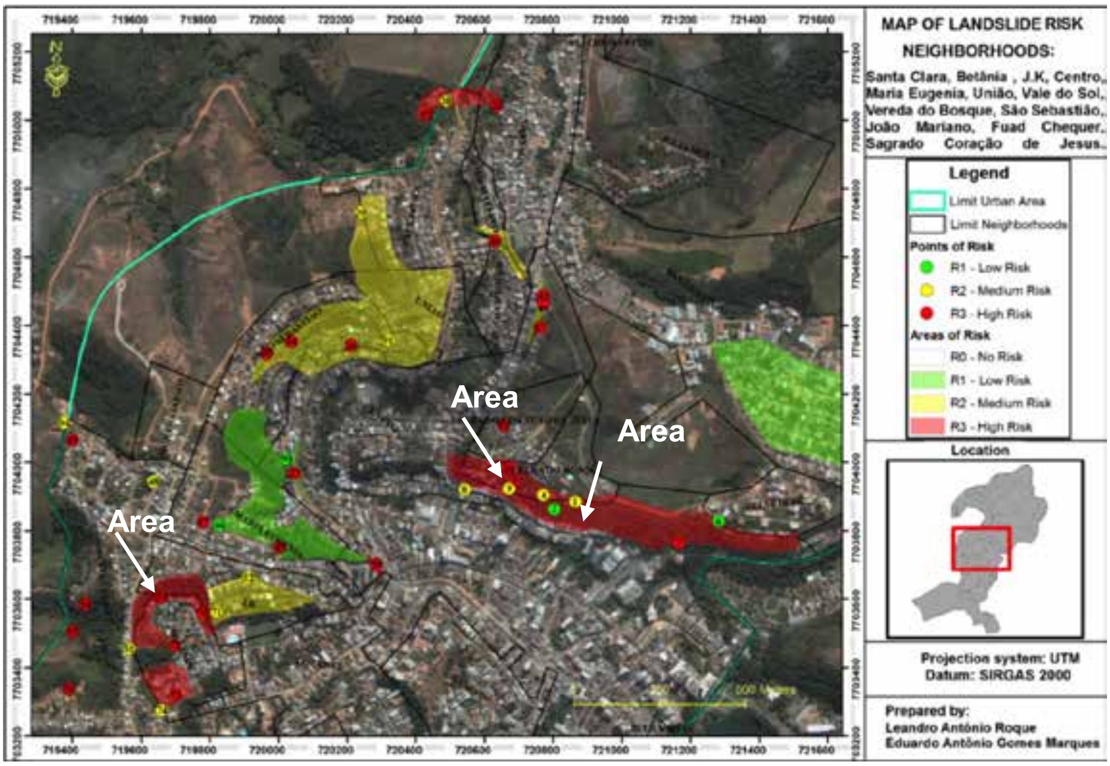

Figure 1: High landslide risk areas selected for in situ testing (Roque, 2013).

Figure 2: Ménard pressiometer equipment used in the tests (Silva, 2016).

3 RESULTS AND DISCUSSION

In Table 1 it is presented a summary of all values obtained for Ménard pressuremeter modulus (E_m) for each performed test. In Figure 3 results for each soil type are presented, allowing a better comparison. All studied soils are residual soils from high-grade metamorphic rocks (gneiss) and no lithological differences could be noted in the material present on the selected sites. Mature residual soil is a clay sandy material, with plasticity index (PI) varying from 25 to 36. Young residual soils are predominately sandy silty clayey materials, and with PI varying from 25 to 29. Figure 4 and Figure 5 presents some examples of typical soils tested.

Table 1: Results of limit pressure and Ménard pressuremeter modulus.

Depth	Area 1 - Borehole 1		Area 2 - Borehole 2	
	Soil	E_m (MPa)	Soil	E_m
0	Mature Residual Soil	0	Young Residual Soil	0
1		2.63		3.52
2		1.63		5.69
3		6.24		3.91
4		13.62		6.11
5	Young Residual Soil	6.51		3.13
6		8.35		6.43
7		5.73		5.46
8		10.75		13.11
Depth	Area 3 - Borehole 3		Area 3 - Borehole 4	
	Soil	E_m (MPa)	Soil	E_m
0	Soil	0	Young Residual Soil	0
1	Mature Residual Soil	2.00		6.76
2		2.06		7.19
3		2.41		6.05
4		3.12		6.24
5		7.23		8.88
6		12.18		14.17
7		13.49	-	-

By definition, Em usually increases with depth. This happens primarily because, among several other causes, an increase on geostatic pressure, which leads to higher pressure variations for lower volume variations of the probe, so generating higher Em values.

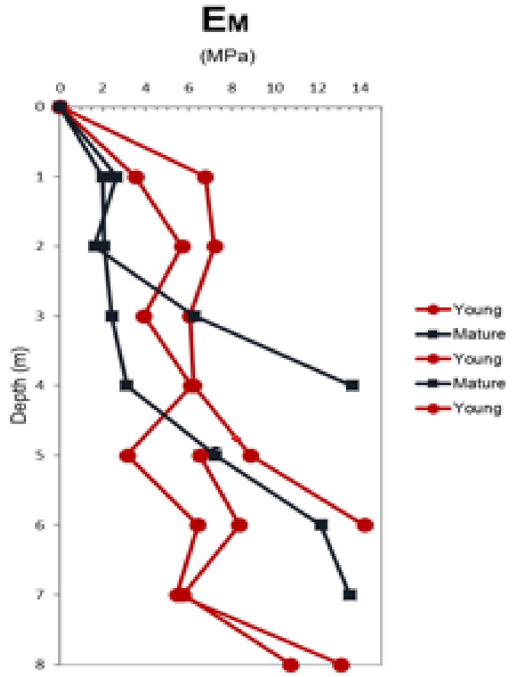

Figure 3: Results of Ménard pressuremeter modulus (Em) with depth.

The results observed on Figure 3 shows that, in general, a constant increase could be observed for gneiss mature residual soils (black lines). For young residual soils a different behavior can be observed, as only for more deep layers an increase in pressuremeter modulus can be noted. Up to a depth equal to 6 m there is no considerable variation on these parameter on some tests. Authors believe that this different behavior is mainly due to the high heterogeneity observed on these soils due to the presence of preserved foliation and high biotite rich layers.

Figure 4 – Typical mature residual soils observed in the study area.

In general, Ménard pressuremeter modulus (Em) values are higher for young residual soils than for mature residual soils.

Figure 5 – Typical young residual soil observed in the study area.

Gambim & Rosseou (1975) and Clarke (1995) have suggested some correlations between pressuremeter tests and soils types. Based on such proposals and considering the results from pressuremeter tests performed for the soils under study, the resulting soil classification are presented on Tables 2, 3, 4 and 5.

Table 2: Soil classification for borehole 1according to Gambim & Rosseou, 1975).

Area 1 – Borehole 1		
Depth	Soil Type	Soil Classification
0	Mature residual soil	---
1		Soft clay
2		Soft clay
3		Medium clay
4		Medium clay
5	Young residual soil	Medium clay
6		Medium clay
7		Silt
8		Silt

Table 3: Soil classification for borehole 2according to Gambim & Rosseou, 1975).

Area 2 – Borehole 2		
Depth	Soil Type	Soil Classification
0	Young residual soil	---
1		Soft clay
2		Soft Clay
3		Medium Clay
4		Medium Clay
5		Medium Clay
6		Medium Clay
7		Silt
8		Silt

Table 4: Soil classification for borehole 3 according to Gambim & Rosseou, 1975).

Area 3 – Borehole 3		
Depth	Soil Type	Soil Classification
0	Young residual soil	---
1		Soft clay
2		Soft clay
3		Soft clay
4		Soft clay
5		Medium clay
6		Stiff clay
7		Stiff clay

Table 5: Soil classification for borehole 4 according to Gambim & Rosseou, 1975).

Area 3 – Borehole 4		
Depth	Soil Type	Soil Classification
0	Young residual soil	---
1		Silt
2		Silt
3		Silt
4		Silt
5		Silt
6		Stiff clay

The classification based on Gambim & Rosseou (1975) however, did not correlate well with grain size distribution curves obtained from samples collected in the same area.

4 CONCLUSIONS

Results have shown that it is possible to predict an increment in pressuremeter modulus (Em) with depth for gneiss mature residual soils like the ones occurring in the studied sites. Nevertheless, for young residual soils the Em is more constant along the profile.

Based on the results, it become clear that the determination of deformability on gneiss residual soils should for use in geotechnical projects should be based on site-specific studies.

There is also a need for more detailed studies on determination of Em for metamorphic residual soils such the ones tested on the study, in order to try to establish reliable range of values for this parameter.

5 ACKNOWLEDGMENTS

The authors thank the CAPES Foundation, Ministry of Education of Brazil for the student grant, to FAPEMIG for the financial support to attend the conference and to the Universidade Federal de Viçosa, Brazil, for funding and providing laboratory support.

6 REFERENCES

American Society for Testing of Materials. (1987). D4719: *Standard Test Method for Prebored Pressuremeter Testing in Soils*. West Conshohocken, Pennsylvania.

Araújo, P. S. M. (2001). *O Ensaio Pressiométrico de Ménard e sua Utilização na Estimativa da Capacidade de Carga e Recalques de Fundações Assentes em Solo Residual de Gnaisse*. Dissertação de Mestrado, Departamento de Engenharia Civil, Universidade Federal de Viçosa, Viçosa, MG, 156 p. (In Portuguese).

Association Française de Normalisation. (1991). NF P 94-110: *Sols: reconnaissance et essais. Essai pressiométrique Ménard*. 32 p.

Clarke, B. G. (1995). *Pressuremeter in Geotechnical Design*. Cambridge, Great Britain, 364 p.

Ianelli, L. A. R., Villar, L. F. S. (2012). *Utilização do Pressiômetro de Ménard (PMT) para Determinação do Comportamento Geotécnico de Solos de Fundação e sua Aplicação nos Estudos Tensão – Deformação*. COBRAMSEG, 8 p. (In Portuguese).

Roque, L. A. (2013). *Mapeamento das áreas de risco geológico-geotécnicos associados a movimentos de massas na área urbana de Viçosa-MG*. Dissertação de Mestrado, Departamento de Engenharia Civil, Universidade Federal de Viçosa, Viçosa, MG, 86 p. (In Portuguese)

Roque, L. A.; Marques, E. A. G.; Gripp Jr. J. (2014). Risk Mapping Associated With Mass Movements in Viçosa (MG) Urban Area. *Brazilian Geographical Journal*, v.5, n.2, p.533-555, nov./2014.

Schnaid, F. (2000). *Ensaios de Campo e suas Aplicações à Engenharia de Fundações*. São Paulo: Oficina de Textos. 189 p. (In Portuguese).

Silva, T. Q. (2016). *Análise de risco geológico-geotécnico em áreas sujeitas à movimentos de massa*. Dissertação de Mestrado, Departamento de Engenharia Civil, Universidade Federal de Viçosa, Viçosa, MG, 116 p. (In Portuguese)

Author index

Aagaard, P. 1501
Abduljauwad, S.N. 819
Abdul-Waheed, M. 819
Abrah, B. 1123
Addai-Mensah, J. 1507
Agaiby, S.S. 461, 1065
Ahmad, S. 755
Ahmed, H.R. 819
Airey, D.W. 1217
Akaishi, M. 535
Al Hammadi, H. 1057
Alam, M.J.I. 689, 1423
Albin, B.M. 565
Albuquerque, P.J.R. 1071
Ale, J.D. 1291
Alimrina, N. 1297
Alone, R. 621
Amoroso, S. 615, 633, 639, 825, 1051, 1137
Amundsen, H.A. 529
Anggoro, B.W. 363
Anschütz, H. 831, 917, 923
Anzoras, C. 1547
Árabe, B.L.C.G. 1303
Arghya, D. 413
Arroyo, M. 125, 167
Arsalan, N. 535
Ascari, P. 1529
Asghari-Kaljahi, E. 677, 743
Asprouda, P. 1057
Ausweger, G.M. 315

Bacconnet, C. 1465
Bærverfjord, M.G. 1167
Bagbag, A.A. 749
Baghbadorani, S.B. 701, 1343
Bahadori, H. 591
Bahar, R. 1297
Bakacsi, Z. 479
Balasubramaniam, A.S. 1087
Balks, M. 1327
Bán, Z. 597
Banikheir, M. 657, 879
Barreto, A.W.R. 1303
Bastos C.A.B. 467
Bates, L. 479, 485, 1021
Bazin, S. 831, 917, 923
Baziw, E. 1431
Bednarczyk, Z. 837
Beecham, S. 1161
Been, K. 41
Belincanta, A. 683
Benoît, J. 443
Benz-Navarrete, M.A. 279, 1465
Berggren, A.-L. 923
Bezerra, R.C. 1129
Bheemasetti, T.V. 1487
Bihs, A. 1193
Birajdar, K. 621
Biryaltseva, T. 383, 389
Bishop, D. 479, 485
Blaker, Ø. 975
Boldyrev, G.G. 1187
Bonilla-Hidalgo, L.-F. 843
Bosco, G. 395
Boukpeti, N. 541, 583
Boulanger, R.W. 81, 1447
Boutonnier, L. 779
Boylan, N. 1193
Bradshaw, A.S. 449
Brandt, S. 383
Breul, P. 279, 1465
Burke, R.W. 1039
Burlon, S. 259
Butcher, A.P. 1253
Butlanska, J. 125
Buttling, S. 159, 1393
Byun, B. 1003
Byun, Y-H. 707, 1287

Cai, G.J. 1229, 1487
Çami, K. 843
Campbell, N. 849
Campos, G.C. 1315
Cândido, E.S. 809
Cao, L.F. 755
Carbonell, J.M. 125
Cargill, E. 1065
Carroll, R. 509, 975
Carstensen, A. 1271
Carvalho, L.S. 401
Castellaro, S. 669, 963, 967, 1405
Cavallaro, A. 1309
Chevalier, B. 279
Chiam, S. L. 1093
Choi, C-Y. 707
Chokhawala, H.C. 1535
Chung, C. 1111
Ciantia, M. 125
Coggan, J.S. 855
Colls, S. 1495
Comina, C. 825
Cosentino, P.J. 767
Costa, C.L. 407
Costa, Y.D. 407
Cox, B.R. 627
Crapps, D.K. 797
Crawford, D. 1083
Cruz, J. 1077, 1137
Cruz, M. 1077
Cruz, N. 633, 1077, 1137
Cubrinovski, M. 217, 577
Cunha, E.S. 407
Cunningham, L. 1327

Danziger, F.A.B. 245, 1009
de Camargo Barros, J.M. 547
de Kleine, M.P.E. 947
de la Cruz, L. 729
Debasis, R. 413
Décourt, L. 547, 1315
DeGroot, D.J. 565
DeJong, J.T. 81, 205, 565, 1447
Denes, D. 1199
Denis, A. 981
Desanneaux, G. 791
Dey, A. 951
Dhimitri, L. 1253
Dienstmann, G. 419
Disfani, M.M. 1353
Dissanayake, A. 695
Diyaljee, V. 1321
Djerbal, L. 1297
Doherty, J.P. 749, 761, 1205, 1453
Donohue, S. 831
Dorobati, M.T. 701, 1343
dos Santos, R.A. 1129
Du, Z. 1327, 1331

Ekanayake, S.D. 273
Elbaz, S. 1083
Emdal, A. 529, 1501
Escobar, A. 1353
Escobar, E. 279
Eskandari, N. 657, 879
Evans, P. 695
Evans, R. 1353
Eyre, M.L. 855
Ezeajugh, L.E. 1211

Fabre, R. 981
Fagundes, D.F. 467

Failmezger, R. 1417
Fanelli, S. 791
Fanourakis, G.C. 559
Fawaz, A. 1217
Fechner, T. 947
Fenton, C. 849
Ferraro, A. 1309
Filho, A.R.Q. 547
Fitter, J.F. 957
Fityus, S. 479, 485
Foged, N. 923
Foti, S. 147, 425, 825
Frikha, W. 259
Frost, J.D. 431
Fujii, M. 861
Fukasawa, T. 553
Fukaya, T. 861

Gad, E. 1353
Gabhale, V. 621
Galbiati, R. 1529
Gallage, C. 899
Gandhi, A.R. 1369
Gandolfo, O.C.B. 547
Gaone, F.M. 761
Garakani, A.A. 657, 879
García Martínez, M.F. 473
Garcia, J. 843
Gens, A. 125
Gerdes, U. 383
Giacheti, H.L. 1129
Giampa, J.R. 449
Glisic, F. 1453
Gnanendran, C.T. 1423
Gnanendran, R. 689
Goay, K. H. 1093
Godlewski, T. 1223
Gottardi, G. 473, 615
Gourvenec, S.M. 583, 761
Gourvès, R. 279, 1465
Gower, A. 1149
Grabe, J. 1271
Grasso, S. 1309
Gratchev, I. 1087
Gribben, S. 831
Grøneng, G. 923
Grotta, C. Jr. 1315
Grygierek, M. 1337
Guo, W.D. 1265
Gylland, A.S. 917
Győri, E. 597

Haegeman, W. 803
Hajiannia, A. 701, 1343
Hamel, M. 443
Harianto, A.T. 1349
Harutoonian, P. 273
Hasheminezhad, A. 591
Hayashi, H. 1157
Hayashi, T. 1157
Haycock, I. 577
Heins, E. 1271
Helle, T.E. 831, 1501
Herrera, F. 729
Heymann, G. 867
Hirabayashi, H. 553
Ho, C.E. 773
Holtrigter, M. 303
Hong, S.S. 1287
Hong, W-T. 329, 707
Hora, R.N. 1161
Hortobagyi, Z. 485
Hossain, M.S. 497
Howe, J.H. 855
Hu, Y. 497
Huang, A-B. 3
Huang, J. 1437
Hubble, T. 1217
Hughes, C.G.C. 873
Hughes, D. 491
Hwang, S. 627

Ibáñez García, S. 1015
Ibanez, S.J. 323, 929
Ichola, I.A. 1547
Imre, E. 479. 485
Indraratna, B. 1411
Iskander, K. 309

Jaditager, M. 987
Jafarzadeh, F. 657, 879
Jahromi, H.F. 657, 879
Jakhodiya, D.V. 1369
Jaksa, M.B. 233, 735
Jang, I.S. 935
Jannuzzi, G.M.F. 1009
Jennings, W. 1353
Jeong, J.M. 935
Jo, B.H. 1111
Juhász, M. 479, 485
Juric-Kacunic, D. 285

Kamuhangire, R. 991
Kang, S. 707
Karikari-Yeboah, O. 1507
Karim, R. 491, 1161
Kasaeian, S. 701, 1343
Kashyap, S.S. 951
Kåsin, K. 917, 923, 997
Katona, T.J. 597
Kaur, A. 559
Kawalec, J. 1337
Kelly, R.B. 455, 883, 1021, 1437
Khalili, Z. 743
Kheyrouri, Z. 677
Kim, D. 1003
Kim, D.H. 1087
Kim, G. 1003
Kim, I. 1003
Kim, K.S. 935
Kim, S-Y. 329
Kim, Y. 329
Kim, Y.S. 1287
Kim, Y.S. 1513
Kimura, K. 1093
Kishida, T. 1443
Klar, A. 211
Klibbe, P.R. 603
Klug, M. 975
Kok, S. 867
Kouretzis, G.P. 455
Kovacevic, M.S. 285
Krage, C.P. 565, 1447
Kreiter, S. 383, 389
Krishna, A.M. 951
Kruger, J. 1033
Ku, T. 1065, 1247
Kumar, S.D. 413
Kurangale, P. 621

Lacey, D. 1099
Langley, D.S. 1517, 1523
Länsivaara, T. 297
Lanzo, G. 1051
Lataste, J.F. 981
Lawanwisut, W. 717
Le, T.M.H. 1167
Lean, J. 887
Leão, M.F. 1105
Lee, J. 1003
Lee, J.D. 1057
Lee, J-S. 329, 707, 1287
Lee, S.H. 1111
Lehane, B.M. 541, 749, 1149, 1205, 1453
Leo, C.J. 273
Leon, J. X. 957
L'Heureux, J.-S. 509, 975
Li, J. 1117
Li, X.P. 1229
Liberati, A. 1529
Libric, L. 285
Lin, C.H. 893
Lin, C.P. 893
Lin, J. 1229, 1487

Liu, S.Y. 1229, 1487
Liyanapathirana, D.S. 273
Lo, S.R. 1423
Long, M. 831, 911, 917, 1193
Look, B. 181, 333, 899, 1099
López-Ausín, V. 323, 929, 1015
Lukiantchuki, J.A. 339, 401, 683
Lunne, T. 245, 389, 437
Lysdahl, A.O.K. 923

Ma, H. 497
Macari, R. 905
Maghous, S. 419
Mahler, A. 597
Mahmutovic, D. 779
Maia, P.C.A. 1029
Mantaras, F. 503
Marcellini, R. 1529
Marchetti, D. 825, 1051, 1417
Marchi, M. 615
Marks, D. 1099
Marques, E.A.G. 199, 809, 1105
Marques, M.E.S. 401
Martelli, L. 615
Martinez, A. 431
Martins, F. 1077
Mayne, P.W. 19, 461, 785, 1065
McCallum, A.B. 957
McGrath, T. 911
McKenna, G.T.C. 291
Mehdizadeh, A. 1353
Menq, F.M. 627
Mengé, P. 1235
Messaoud, F. 767
Minette, E. 809
Mirjafari, S.Y. 609
Młynarek, Z. 437, 1241
Monaco, P. 259, 395, 615, 1051, 1381
Monforte, L. 125
Monnet, J. 779
Montafia, A. 917
Moon, S.W. 1247
Moon, V. 1327
Mori, K. 99
Mörz, T. 383, 389
Moug, D.M. 81
Munter, S.K. 81

Narsilio, G.A. 1517, 1523
Nascimento, P.N.C. 1029
Nasrollahi, N. 677
Nejaim, P.F. 1009
Nery, G.G. 905
Newgard, J.T. 449
Nicotera, E. 1529
Nik, M.G. 1123
Nimbalkar, S. 1411
Nordal, S. 509, 1193, 1501
Novichkov, G.A. 1187
Nuñez, R.R. 345

O'Connor, P. 911
O'Loughlin, C.D. 583
O'Sullivan, C. 125
Odebrecht, E. 503
Ogunro, V.O. 941
Oh, E. 1087
Oh, M. 1513
Oliveira, J.R.M.S. 401
Orangi, A. 1517, 1523
Ørbech, T. 923
Orense, R.P. 609
Ortiz-Palacio, S. 323, 929, 1015
Osman, M.A. 1179
Ossig, B. 383
Ouyang, Z. 785

Page, P. 1327
Pagliaroli, A. 1051
Pando, M.A. 941
Paniagua, P. 509
Panzeri, R. 669
Parashar, S. 1057
Parida, S.S. 1459
Park, J. 135
Park, Y. 941
Parsons, M. 1033
Pascoe, D.M. 855
Pasqualini, B. 1529
Passeri, F. 425
Paul, D.K. 689
Pawar, N. 621
Peaker, S.M. 755
Pedersen, J.B. 923
Peiffer, H. 803, 1359
Peixoto, A.S.P. 345, 905
Penna, A.S.D. 1315
Penna, F.D. 547
Pereira, A.C. 407
Perez, F.C. 1291
Perlo, S. 843
Peuchen, J. 251, 351
Pfaffhuber, A.A. 917, 923
Phule, R.R. 621
Pineda, J.A. 191, 455, 883, 1021
Pinkert, S. 357
Piovan, T.T.C. 345
Plunket, T. 991
Porres-Benito, J.A. 323, 929, 1015
Povoa, L.M.M. 1029
Powell, J.J.M. 1253
Prakoso, W.A. 1259
Premstaller, M. 1365
Price, A.B. 81
Puppala, A.J. 1229, 1487
Purwodihardjo, A. 1033

Qin, H.Y. 1265

Rahardjo, P.P. 363
Rahiman, T. 1033
Rahman, M.M. 491, 1161
Rajkai, K. 479
Ramos, C. 217
Ramsey, N. 571
Randolph, M.F. 57, 1193
Read, K.J. 873
Reid, D. 369, 521
Reiffsteck, P. 443, 791
Reis, J.H.C. 683
Remund, T.K. 639
Rengifo, K. 729
Rice, R. 1057
Roberts, J.N. 627
Roberts-Kelly, S.L. 291
Robertson, P.K. 515, 711
Rocchi, I. 473
Rocha, B.P. 1129
Rodrigues, C. 633, 1077, 1137
Rodrigues, R.A. 1129
Rodriguez, T.G. 1071
Rollins, K.M. 639, 645
Rüegg, C. 991
Russell, A.R. 521

Saegusa, H. 553
Sakai, K. 99
Samang, L. 1349
Samani, E.G. 1123
Samim, A.S. 1143
Sandven, R. 917
Sandyutama, Y. 1349
Santamarina, J.C. 135
Sastre, C. 1465
Saswati, G. 413
Sauvin, G. 831, 923
Sawada, S. 651
Sawangsuriya, A. 717
Schmertmann, J.H. 797
Schnaid, F. 239, 419, 503
Schneider, J.A. 449

Schneider, S. 899
Schofield, N.B. 1039
Scott, B.T. 735
Sedran, G. 1417
Seitz, K.-F. 1271
Selänpää, J. 297
Sett, K. 1459
Shafiq, M.A. 819
Shah, M.V. 1369, 1535
Shahien, M.M. 663
Shahin, M.A. 1331
Shahnoory, A.M. 723, 1173
Shahrabi, M.M. 657, 879
Shammat, H. 1179
Shen, H. 803
Shi, W. 1149
Silva, T.Q. 809
Silvestri, V. 375
Simeoni, L. 615, 1381
Singla, P. 1459
Singui, V.S. 1029
Sirisak, S. 717
Sivakugan, N. 987
Skinner, W. 1507
Sloan, S.W. 1021, 1437
Smaga, A. 1481
Smebye, H.C. 923
Sosna, K. 1375
Stark, N. 69
Stefaniak, K. 1481
Stokoe, K.H. 627
Storteboom, O. 297
Stringer, M.E. 577
Styler, M.A. 1471
Su, J. 431
Suemasa, N. 609
Sugiyama, M. 535, 723, 1143, 1173
Suheriyatna, B. 1349
Sun, C.G. 935
Suto, K. 155
Suwal, L. 883, 1021
Syamsuddin, E. 735
Sylvain, M.B. 941

Tabib, C. 375
Tacita, J.-L. 843
Takechi, K. 861
Talbot, M. 645
Tallett-Williams, S. 849
Tanaka, M. 553
Teixeira, M.G. 401
Teoh, A. 1217
Terwindt, J. 351
Terzaghi, S. 1149
Thakur, V. 529
Thompson, T. 1045
Thorp, A. 303
Todd, J.K. 1117
Tomita, R. 553
Tonni, L. 473, 615
Totani, F. 1051, 1381
Totani, G. 1051, 1381
Trafford, A. 911
Tsai, C-C. 1443
Tschuchnigg, F. 315
Tuck, M. 1083
Tucker, N. 1117

Ünver, A.M. 1387
Ünver, İ.S. 1387

Vaillant, J.-M. 443
van Ballegooy, S. 627
Van den Broeck, M. 1235
Van Impe, P.O. 1235
Van Impe, W.F. 1235
Vasconcellos, C.A.B. 401
Verbeek, G. 1431
Viana da Fonseca, A. 217, 633
Vinck, K. 1235
Vöge, M. 923
von Ketelhodt, J.K. 947

Waarum, I.-K. 923
Wachiraporn, S. 717
Wang, Y. 627
Wang, Y.H. 1541
Ward, D. 911, 1253
Watanabe, K. 861
Watson, M. 873
Weemees, I. 1471
Whelan, M.J. 941
Wierzbicki, J. 173, 437, 1241, 1481
Wilke, D.N. 867
Williams, D.J. 1275
Williams, S. 887
Wilson, L.J. 455
Winter, R. 1327
Wirawan, A. 363
Withers, N.M. 1517, 1523
Wold, M. 1167
Wołyński, W. 1241, 1481
Woollard, M. 297
Wu, Y.X. 1541

Xu, T. 431

Yasrobi, S. 743
Yasuda, T. 1093
Yi, F. 1281
Yi, F.P. 1281
Yoon, H-K. 1287
Youd, T.L. 645

Záruba, J. 1375
Zhang, X. 1541
Zhou, M. 497
Zografou, D. 583
Zou, H.F. 1487

VOLUME 1

This volume comprises nine special/keynote lectures by world renowned experts in the field of in-situ site characterisation in addition to session reports and regular papers presented at the **Fifth International Conference on Geotechnical and Geophysical Site Characterisation** (ISC'5).

Topics covered in this volume include:

- Developments in technology and standards
- Penetration testing
- Interpretation of in-situ testing
- Laboratory testing and sampling
- Liquefaction assessment
- Pavements and fills
- Pressuremeter and dilatometer

Geotechnical and Geophysical Site Characterisation 5 is particularly aimed at academics and professionals interested in in-situ site characterisation. The conference was organised under the auspices of the Australian Geomechanics Society and the International Society for Soil Mechanics and Geotechnical Engineering (ISSMGE) Technical Committee TC102 (Ground Property Characterization from In-Situ Tests). ISC'5 is the latest in a series which began in Atlanta in 1985 (ISC'1), and was followed by conferences in Porto (ISC'2, 2004), Taipei (ISC'3, 2008) and Porto de Galinhas, Brazil (ISC'4, 2012).

AUSTRALIAN GEOMECHANICS SOCIETY
PO Box 955, St Ives, NSW 2075, Australia
www.australiangeomechanics.org

ISBN 978-0-9946261-1-0

GEOTECHNICAL AND GEOPHYSICAL SITE CHARACTERISATION 5

ISC'5

Lehane
Acosta-Martínez
Kelly
Editors

VOLUME 1